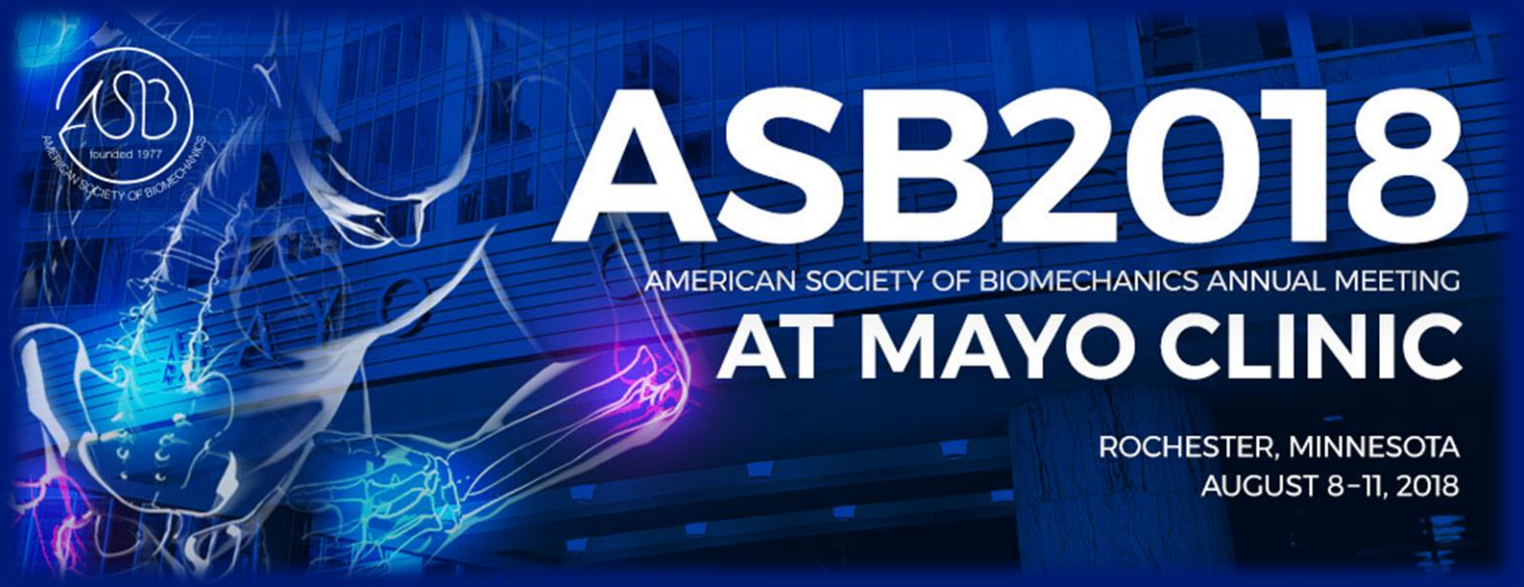
founded 1977
AMERICAN SOCIETY OF BIOMECHANICS
ASB2018
AMERICAN SOCIETY OF BIOMECHANICS ANNUAL MEETING
AT MAYO CLINIC
ROCHESTER, MINNESOTA
AUGUST 8-11, 2018

ABSTRACTS

ASB 2018

LEG STIFFNESS, JOINT STIFFNESS, AND RUNNING INJURY RATE: A PROSPECTIVE COHORT STUDY

John J. Davis IV, Jacob E. Vollmar, Ashley B. Nguyen, Emily G. Wagoner, Allison H. Gruber

Indiana University Bloomington, Bloomington IN, USA
email: jjd1@iu.edu website: https://iubiomechanicslab.weebly.com/

INTRODUCTION

Running is modeled as a spring-mass system, which gives rise to the concept of leg stiffness (i.e. "quasi-stiffness). Modulating leg and joint stiffness allows a runner to adapt to different surfaces, speeds, and cadences. Individuals self-select a wide range of stiffnesses for a given speed—two to four-fold differences in stiffness are not unusual (even when mass-normalized). Given the fundamental role of stiffness in gait, stiffness may be related to injury susceptibility among runners. Previous work has hypothesized that an "optimal" window of stiffness exists, and runners outside of this window may be predisposed to injury [1]. The purpose of this study was to examine the influence of leg and joint stiffness on running injury development. It was hypothesized that runners in the middle tertile of leg and knee joint stiffness would have the lowest incidence of injuries per 100 hours of running.

METHODS

Fifty-seven recreational runners free from injury in the previous three months volunteered for a cohort study with a maximum follow-up of 52 weeks. Upon enrollment, subjects completed a 3D kinematic and kinetic evaluation that involved five running trials at 4.0 m/s ± 5% on an 18 m runway. Motion data (Qualisys, Gothenburg, Sweden) and force data (AMTI, Watertown, MA) were captured at 240 Hz and 1200 Hz, respectively. Motion capture and force data were lowpass filtered in Visual 3D (C-motion, Germantown, MD) at 12 Hz and 50 Hz, respectively.

Subjects continued their typical training while filling out weekly surveys detailing their training habits and any injuries that occurred. Injuries were defined as "any physical pain located at the lower limbs or lower back region, sustained during or as a result of running practice and impeding planned running activity for at least one day" [2].

If cumulative survey compliance over the subject's follow-up period dropped below 75%, subsequent surveys were ignored and not included in the analysis. Subjects were excluded if they failed to report weekly training volume, completed zero surveys, dropped out prior to gait analysis, or had a pre-existing injury. Forty-one subjects remained after exclusion (16 males, 24 females, 31.7 ±9.9 yrs, 1.73 ± 0.09 m, 67.6 ± 10.8 kg).

Leg stiffness was calculated as the change in leg length from initial contact to the instant of maximum ground reaction force divided by peak vertical ground reaction force [3]. Knee stiffness was calculated as the slope of the least-squares linear regression line for the angle-moment plot from foot-ground contact to the time that peak joint flexion occurred [4]. Participants were stratified into tertiles according to leg stiffness and knee stiffness, both normalized and not normalized to body mass. Injury rate was calculated as injuries per 100 hours of running. Differences in injury rates were assessed using a Pearson χ^2 test ($\alpha = 0.05$). Rate ratios were used to determine the effect size of low and high leg stiffness on injury rates using the middle tertile as the reference group. Survey and gait data were processed using MATLAB (Mathworks, Natick, MA). Statistical analysis was conducted using R 3.4.3 (R Foundation, Vienna, Austria).

RESULTS AND DISCUSSION

Twenty-seven runners reported injury during the follow-up period (mean 14.5 weeks, range 1 - 52). The overall incidence rate of injuries was 2.22 per 100 hours of running (95% CI: 1.46 - 3.23) with a median survival time of 24.62 hours of running as derived from the Kaplan-Meier estimator.

The χ^2 test revealed no statistically significant difference in injury rates among the three leg stiffness tertiles and the three knee stiffness tertiles, regardless of whether stiffness was normalized to body mass (leg stiffness p = 0.15, normalized leg stiffness p = 0.16, knee stiffness p = 0.43, normalized knee stiffness p = 0.39).

Compared to the middle tertile, low and high leg stiffness were associated with an injury rate ratio (RR) of 2.50 (CI 0.94 - 7.40) and 2.18 (CI 0.80 - 6.53), respectively. Knee stiffness followed a similar trend (low RR 1.79, CI 0.70 - 4.50; high RR 1.22, CI 0.46 - 3.13). That is, the high and low leg stiffness tertiles had over twice as many injuries than the middle tertile per 100 running hours. Similarly, the low knee stiffness tertile experienced ~1.8 times more injuries than the middle tertile per 100 running hours. These trends provide merit to the hypothesis. However, after normalization to body mass, this trend did not hold for leg stiffness (low RR 0.49, CI 0.19 - 1.20; high RR 0.49, CI 0.18 - 1.24) or knee stiffness (low RR 1.39, CI 0.55 - 3.50; high RR 0.73, CI 0.27 - 1.87). These shifts can be seen graphically in **Figure 1**. In the case of both knee and leg stiffness, evidence supporting an increased rate of injury among the high and low stiffness groups diminished after normalizing stiffness to body mass.

Normalization was performed to avoid confounding by body mass [5]. However, mass-normalized stiffness may simply be a proxy measure for stride frequency, given the relationship between body mass, stiffness, and ground contact time implied by the mass-spring model. Future research should investigate whether the apparent decrease in injury risk at moderate stiffness levels is an artifact of body mass.

CONCLUSIONS

We are currently planning follow-up cohorts to evaluate the association between stiffness and injury with higher statistical power. This study did not find evidence supporting a relationship between leg stiffness and the rate of running-related overuse injury, regardless of whether leg stiffness was normalized to body mass. However, the higher rate ratios in the lowest and highest tertiles of leg and knee stiffness suggest more research is warranted into the relationship between stiffness and the development of running injuries.

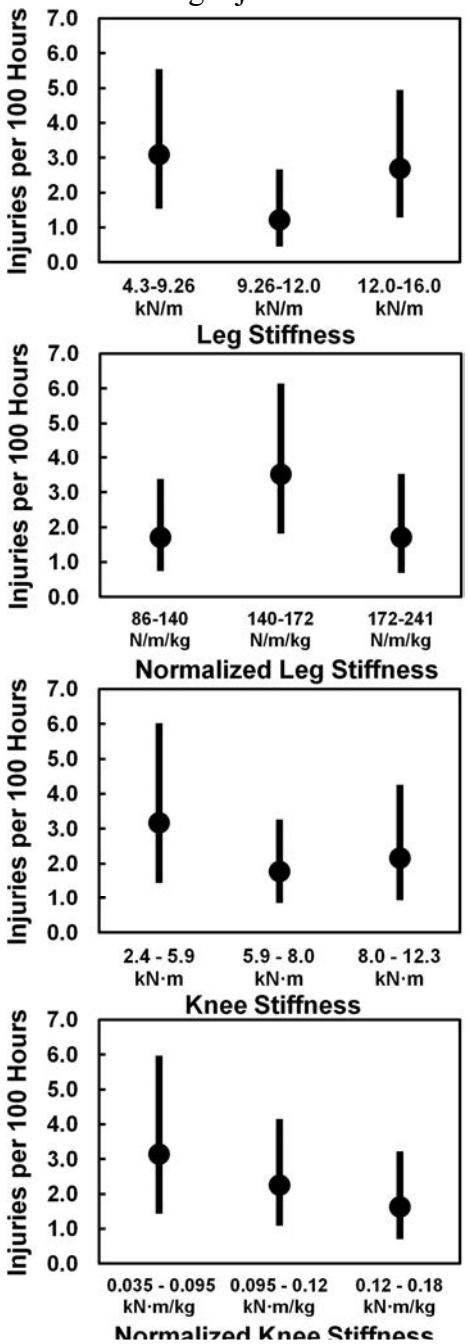

Figure 1. Injury rates and confidence intervals for the lowest, middle, and highest tertiles of stiffness variables.

REFERENCES

1. Butler et al., *Clin Biomech,* 2003;18(**6**):511-17.
2. Malisoux et al., *J Sci Med Sport,* 2015;18(**5**):523-28.
3. McMahon & Cheng, *J Biomech,* 1990;23:65-78.
4. Farley et al., *J Appl Physiol*, 1998; 85(3):1044-55.
5. Carruthers & Farley. *Proceedings of NACOB '98,* Waterloo, Canada, 1998.

THE INFLUENCE OF BODY MASS INDEX AND SEX ON FRONTAL AND SAGITTAL PLANE JOINT MOMENTS DURING WALKING.

[1] Steven A. Garcia, [2] Michael N. Vakula, [1] Skylar C. Holmes, [1] Brett K. Post, [1] Derek N. Pamukoff
[1] California State University, Fullerton, Fullerton, CA, USA, [2] Utah State University, Logan, UT, USA
Email: stegarcia@fullerton.edu

INTRODUCTION

Knee osteoarthritis (KOA) is one of the most common joint diseases in the US, and is characterized by a progressive degeneration of the articular cartilage [1]. While the direct cause of KOA progression is unclear, obesity and female sex are significant risk factors for KOA development [2, 3]. Higher body mass index (BMI) and body fat mass are associated with abnormal cartilage composition and higher compressive forces at the knee joint [1, 4, 5]. Additionally, sex specific anthropometrics, may contribute to altered gait mechanics and knee joint loading in females. Furthermore, alterations in gait mechanics are implicated in KOA incidence and progression [1]. Specifically, individuals with KOA exhibit larger peak external knee adduction moments (KAM) and smaller external knee flexion moments (KFM), which contribute to disease progression [5, 6]. As such, abnormal sagittal and frontal knee joint loading in conjunction with obesity and female sex may predispose individuals to early onset of KOA. However, few data are available on the interaction of sex and obesity in the younger population despite their independent contributions to KOA risk. Therefore, the purpose of this study was to examine the influence of sex and BMI on knee joint sagittal and frontal plane gait mechanics. Dependent variables included knee flexion moment (KFM) and the first knee adduction moment peak (KAM1).

METHODS

Table 1. Subject Demographics (mean ± SD)

Group	Normal	Obese
Age (years)	22 ± 2.89	22.25 ± 3.7
Height (cm)	168 ± 9.42	168 ± 9.78
Mass (kg)	61.48 ± 8.96	92.53 ± 15
BMI (kg/m^2)	21.48 ± 1.74	32.46 ± 3.67
% Female	56	55
Body Fat (%)	20.09±6.99	37.98±7.29

Gait biomechanics were assessed in 42 obese (BMI≥30.0) and 39 normal weight (BMI 18.0-25.0) participants that were cohort matched on age and sex. Marker position and force plate data were sampled using a 9-camera motion capture system (Qualysis, Göteborg, Sweden) and 2 force plates (AMTI, Germantown MD). Participants completed 5 over-ground walking trials in laboratory standard neutral cushion footwear (Nike Pegasus, Beaverton, OR) at a self-selected speed. Speed was maintained within ±5% and monitored using infrared timing gates (Tractronix, Belton, MO) placed 2m apart surrounding the force plates.

Marker position and force plate data were exported to Visual 3D, and low pass filtered using a 4th order zero-phase lag Butterworth at 6Hz and 50Hz, respectively. Stance phase was identified as the time-point between when the vertical GRF exceeded 20N and fell below 20N. A custom LabVIEW (National Instruments, Austin, TX) program was used to extract the peak external KFM during the first 50% of stance phase, and the first peak KAM. Joint moments were normalized to a product of bodyweight (N) and height (m) for analysis.

A 2 (BMI: normal, obese) by 2 (Sex: male, female) analysis of co-variance (α=0.05) was used to examine dependent variables (KFM, KAM,). Preliminary analyses indicated that self-selected gait speed was slower in the obese compared to normal weight group, and therefore, was used as a co-variate.

RESULTS AND DISCUSSION

The BMI by sex interaction was not significant for KAM1 ($F_{1,76}$=.146, p= .703) or KFM (df=1, F=.329, p=.073). A main effect was observed for sex in KAM1 (F=3.879, p=.05) and KFM (F=8.776, p=.004). After co-varying for gait speed, females exhibited larger KAM1 (.025 %BW•HT (95%CI: .022, .028) vs. .021 %BW•HT, (95%CI: .017, .024)

and lower KFM (0.052 %BW•HT, (95%CI: .047, .057) vs. .063 %BW•HT, (95%CI: .058, .069) compared to males.

There was no effect of BMI on KFM or KAM1 after co-varying for gait speed. This is contrary to previous findings in which obese individuals exhibited reduced peak knee extensor torque and larger KAM compared to normal weight participants at self-selected speed [4, 7]. Additionally, the discrepancy in findings may be explained by the difference in samples. Our obese sample is younger and with no previous clinical diagnosis of KOA. However, our results agree with a previous study in which no differences were found between younger obese individuals and normal controls [8].

Additionally, there was a significant main effect of sex on KFM and KAM1. Female sex is a significant risk factor for KOA incidence and aberrant biomechanics may be a key contributor. Females exhibited larger peak KAM1 compared to males, which contributes to preferential loading across the medial knee compartment. Previous studies have attributed lesser KAM in females to a more valgus knee alignment [9]. Additionally, greater KAM is attributed to greater varus alignment. However, we did not control or measure knee joint alignment, which may explain the discrepancies in our findings. Furthermore, females exhibited lower external KFM compared to males, which may indicate a quadriceps avoidance gait strategy [10] that is common among individuals with KOA. A quadriceps avoidance gait strategy may be explained by decreased quadriceps strength and muscle activity [10], which leads to decreased knee joint loading in the sagittal plane. A moderate amount of mechanical loading applied to the articular cartilage is necessary to maintain joint health, particularly in a normal joint environment absent of injury. [1]. Conversely, overloading or under-loading the cartilage may lead to degeneration of cartilage and development of OA [1]. As such, females may be at higher risk of OA due to lower sagittal and higher frontal plane knee joint loading regardless of the presence of obesity [3].

CONCLUSIONS

We observed no interaction between sex and BMI on KFM or KAM1. Furthermore, no differences were found in KFM or KAM1 between obese and normal weight participants. However regardless of BMI, females exhibited aberrant gait mechanics that are indicative of OA progression. Future studies should investigate the relationship between altered gait in females and knee cartilage morphology

REFERENCES

1. Griffin, T.M. and F. Guilak, *Exerc Sport Sci Rev*, 2005. **33**(4): p. 195-200.
2. Toivanen, A.T., et al., *Rheumatology (Oxford)*, 2010. **49**(2): p. 308-14.
3. Silverwood, V., et al., *Osteoarthritis and Cartilage*, 2015. **23**(4): p. 507-515.
4. Brisson, N.M., et al., *J Orthop Res*, 2017. **35**(11): p. 2476-2483.
5. Harding, G.T., et al., *Clin Biomech (Bristol, Avon)*, 2016. **31**: p. 79-86.
6. Astephen, J.L. and K.J. Deluzio, *Clinical Biomechanics*, 2005. **20**(2): p. 209-217.
7. DeVita, P. and T. Hortobagyi,. *J Biomech*, 2003. **36**(9): p. 1355-62.
8. Pamukoff, D.N., M.D. Lewek, and J.T. Blackburn, *Clin Biomech (Bristol,Avon)*, 2016. **33**: p. 61-65.
9. Wise, B.L., et al., *Arthritis Care Res (Hoboken)*, 2012. **64**(6): p. 847-52.
10. Berchuck, M., et al., *Journal of Bone and Joint Surgery-American Volume*, 1990. **72a**(6): p. 871-877.

ACKNOWLEDGEMENTS

This study was supported by the California State University Fullerton Intramural Research Grant Program.

SEX DIFFERENCES IN RUNNING, CUTTING AND DROP-LANDING BIOMECHANICS POST-ACL RECONSTRUCTION

[1] JJ Hannigan, [1] Brian Newcomb, [1] Justin Ter Har, and [1] Christine Pollard

[1] Oregon State University – Cascades, OR, USA
email: jj.hannigan@osucascades.edu, web: https://osucascades.edu/force-lab

INTRODUCTION

The anterior cruciate ligament (ACL) is the most commonly injured knee ligament, with approximately 250,000 anterior cruciate ligament ruptures occurring each year. Approximately two-thirds of ACL injuries occur without direct contact to the leg during either a cutting or drop-landing task [1]. Several biomechanical factors have been identified that may predispose an athlete to tearing their ACL, particularly greater hip adduction and knee valgus during either cutting or drop-landing compared to uninjured participants [1].

Patients hoping to return to their sport or activity typically choose to undergo surgical reconstruction of the ACL (ACLR) using a patellar, hamstring, or cadaver graft to replace the torn ligament. Approximately 80,000 to 100,000 patients undergo an ACL repair each year, which generally involves a 9-12 month rehabilitation process before being cleared for full activity [2]. However, recent evidence suggests that even after full rehabilitation, ACLR patients still display the biomechanical patterns during these tasks that would place them at risk of re-injury, which may explain why re-injury rates are as high as 50% after surgery [2].

Males and females display markedly different running, cutting, and jumping biomechanics compared to healthy [3-4]. It is currently unclear whether there are sex differences in these biomechanics upon return-to-sport following ACLR. Any sex differences in biomechanics in ACLR patients could mean that sex is an important factor to consider during ACLR rehabilitation. Thus, the primary purpose of this study was to compare running, cutting, and jumping biomechanics between males and females following ACLR.

METHODS

Nine females (age = 29.5 ± 7.5 yrs) and eight males (age = 30.4 ± 4.8 yrs) who had previously torn their ACL, underwent reconstructive surgery, and returned to sport have participated in this study. All subjects signed an informed consent form approved by IRB at Oregon State University prior to participating. Twenty-one reflective markers and six marker clusters were placed on subjects who performed 3 tasks in the lab: 1) overground running, 2) cutting at a 45° angle on their reconstructed limb, and 3) drop landing from an elevated platform. Five successful trials for each task were collected at 250 Hz with an 8-camera 3-D motion capture system (Vicon Motion Systems, Oxford UK). Two embedded force plates collected ground reaction forces and were used to determine heel strike and toe-off (AMTI, Watertown MA).

Joint kinematics were calculated using Visual3D software (C-Motion, Germantown MD). Variables of interest included peak angles for hip flexion, hip adduction, hip internal rotation, knee flexion, knee valgus, and ankle eversion for each task. Differences between sexes were calculated using independent sample *t*-tests with the alpha-level set to 0.5.

RESULTS AND DISCUSSION

During running, females displayed greater peak hip adduction (females: 14.6 ± 4.1°; males: 8.8 ± 4.9°, p = .024) and a trend towards greater peak knee valgus (females: 5.4 ± 4.3°; males: 1.9 ± 3.8°, p = .094)

During cutting, females displayed greater peak hip adduction (females: 2.1 ± 7.3°; males: -4.4 ± 4.1°, p = .043) and peak knee valgus (females: 9.8 ± 4.5°; males: 5.1 ± 3.0°, p = .025).

No differences were seen for other variables during running or cutting or for any variables during drop-landing.

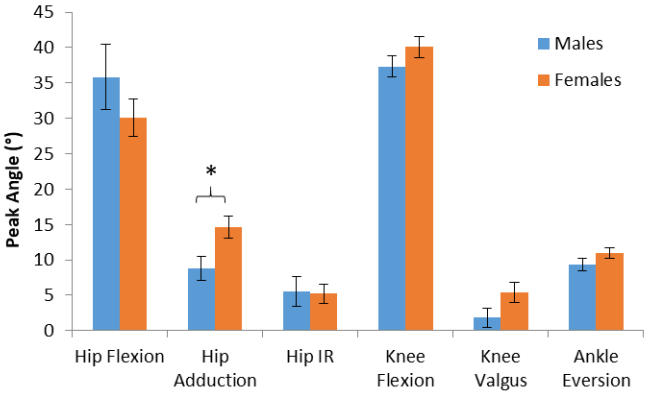

Figure 1: ACLR females displayed significantly greater peak hip adduction compared to ACLR males during running.

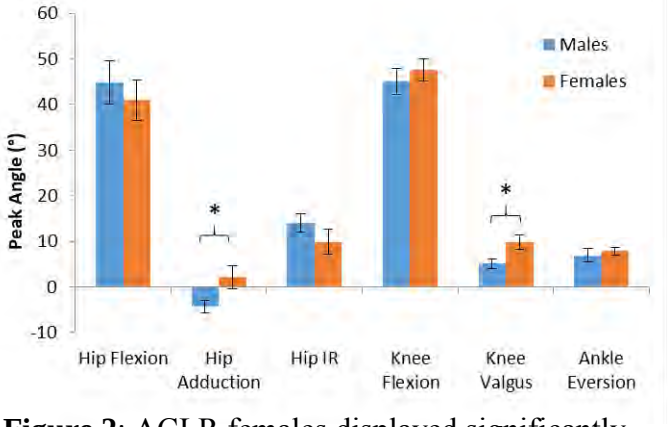

Figure 2: ACLR females displayed significantly greater peak hip adduction and peak knee valgus compared to ACLR males during cutting.

Greater peak hip adduction and peak knee valgus during cutting in females is concerning, as these are known risk factors for ACL tears [1]. The fact that females still display these poor frontal plane hip and knee mechanics after rehabilitation illustrates that females particularly may be at increased risk for re-injuring their ACL after return to sport. Based on these findings, current rehabilitation protocols may be insufficient, particularly for females.

Elevated peak hip adduction during running is a risk factor for developing patellofemoral pain [5], which appears to be a precursor to developing patellofemoral osteoarthritis later in life [3]. This finding may help explain why chronic anterior knee pain and the eventual development of knee osteoarthritis is particularly common among female ACLR patients [2].

CONCLUSIONS

Females displayed running and cutting mechanics that place them at an increased risk for an ACL re-injury and anterior knee pain.. Current ACL rehabilitation programs may not be sufficient in correcting poor biomechanics that likely contributed to the initial ACL injury, particularly in females.

REFERENCES

1. Goerger et al. *Br J Sports Med.* 49(3): 2015.
2. Shelbourne et al. *Am J Sports Med*. 37(2): 2009.
3. Ferber et al. *Clin Biomech*. 18(4): 2003.
4. Pollard et al. *Clin J Sport Med*. 17(1): 2007.
5. Noehren B, et al. *Clin Biomech*. 27(4): 2012.

ACKNOWLEDGEMENTS

The authors would like to acknowledge OSU-Cascades undergraduate students Jacqueline Diulio, Matthew Holmes, and David Schumacher for their assistance during data collection and processing.

SEX DIFFERENCES IN MOTOR UNIT BEHAVIOUR DURING FORCE DEVELOPMENT

[1] J. Greig Inglis, Justin Parro and David A. Gabriel

[1] Brock University, St. Catharines, ON, Canada
email: ginglis@brocku.ca

INTRODUCTION

Inglis et al. [1] previously reported that differences between males and females in the peak rate of force development (RFD) could be accounted for by using maximal strength as a covariate. However, there were significant differences in the rate of muscle activation and electromechanical delay, suggesting underlying differences in motor unit (MU) activity patterns. Therefore, the purpose of the current research was to quantify MU activity patterns during the force development phase of submaximal and maximal effort contractions, to identify potential sex-related differences in MU behavior associated with the peak RFD.

METHODS

Forty-eight (Females=24; Males=24) college-aged individuals free from any orthopedic abnormalities and neurological disorders were seated in a testing chair with their hip and knee fixed at 90^{o} and the ankle fixed at 20^{o} plantarflexion. A foot plate and padded bar across the distal metatarsal was used to perform isometric dorsiflexion. Force was recorded from a load cell (JR3 Inc., Woodland, CA) beneath the distal metatarsals. An oscilloscope (Tetronix, TDS 460A, Beaverton, OR) was used to provide real-time feedback about the quality of the EMG signal from the needle electrode. A second oscilloscope (Hitachi, VC-6525, Woodbury, NY) provided real-time force feedback with ± 2.5% error bars around the desired force. Surface EMG (sEMG) was recorded from the tibialis anterior (TA) electrically identified motor point with monopolar Ag/AgCl electrodes (Grass F-E9, Astro-Med Inc., West Warwick, RI). An intramuscular quadrifilar needle electrode (Viasys Healthcare UK; Surrey, England) was inserted 2 cm distal to the surface electrode. Myoelectric activity was amplified (Grass P511; Astro-Med Inc., West Warwick, RI) and band-pass filtered (sEMG: 3 & 1000 Hz; intramuscular EMG (iEMG): 1 & 10 kHz). Force and EMG were sampled at 25.6 kHz and stored for offline analysis (DASYLab; DASYTEC National Instruments, Amherst, NH, USA).

Anthropometric measurements and force target practice occurred on day 1. Day 2 all participants completed 3 isometric dorsiflexion contractions at 20, 40, 60, 80 and 100% of a maximal voluntary contraction (MVC). The submaximal contractions were arranged for both males and females in a balanced design with 100% MVC contractions taking place both pre and post submaximal trials. Each contraction was eight seconds in duration with three minutes rest in-between. Surface and intramuscular EMG signals were reduced in Matlab (The Mathworks Inc.; Natick, MA, USA). Measures were calculated during force development. Motor unit action potentials were identified using EMGlab (www.emglab.net) (Figure 1.).

RESULTS AND DISCUSSION

Sex differences in the peak RFD were observed from 20 to 100% MVC. On average males were 197.22 ± 118.11 N/sec greater than females (Δ=33.6% difference, $P<0.01$). There was a significant sex by force level interaction term ($p<0.01$). The incidence of doublet discharges during the RFD was 44.54% greater in females, during submaximal contractions ($P<0.01$). At maximum, males had a 9.42% greater incidence of doublets ($P<0.01$). Interestingly, there were no sex differences in time to peak RFD ($P>0.05$). However, there was an increase in the time to peak RFD as the percent of MVC increased (11.66 ms, Δ=89.1%, $p<0.01$). Likewise, there was a progressive increase in doublets for both groups from 20 to 100 percent MVC (Δ=20.2%, $P<0.01$).

Manal and colleagues [2] showed that the pennation angle-muscle length relationship is different between males and females. We believe that the specific ankle joint angle used for testing in this study produced a less optimal pennation angle for females compared to males.

Therefore, sex differences in motor unit behavior during the RFD may be a result of a sex-related compensation mechanism to overcome a sub-optimal muscle length and pennation angle during submaximal levels of force production in females. Placing the ankle joint at an optimal angle to create the appropriate muscle length and pennation angle to maximize motor unit activation efficiency could assist in the development of specific training modalities for both athletic and older populations.

REFERENCES

1. Inglis et al. *Eur J Appl Physiol*. 117: s00421-016-3495-7, 2017.
2. Manal et al. *J Appl Biomech*. 22: jab.22.4.255, 2006.

ACKNOWLEDGEMENTS

This work was funded by the Natural Sciences and Engineering Council of Canada.

Figure 1: Representation of decomposed intramuscular EMG data from a 100% of MVC trial. The top red trace is the surface interference pattern. Bottom 3 red traces are the intramuscular interference pattern recorded from each channel. The Black line represents the force trace. Vertical blue lines represent each identified discharge from each motor unit. The motor unit action potential shapes are of five motor units with the lowest coefficient of variation throughout the trial. The greyed portion is the shimmer of each discharge of the motor unit throughout the entire trial. The darkened black line is the average of all of the discharges of the motor unit.

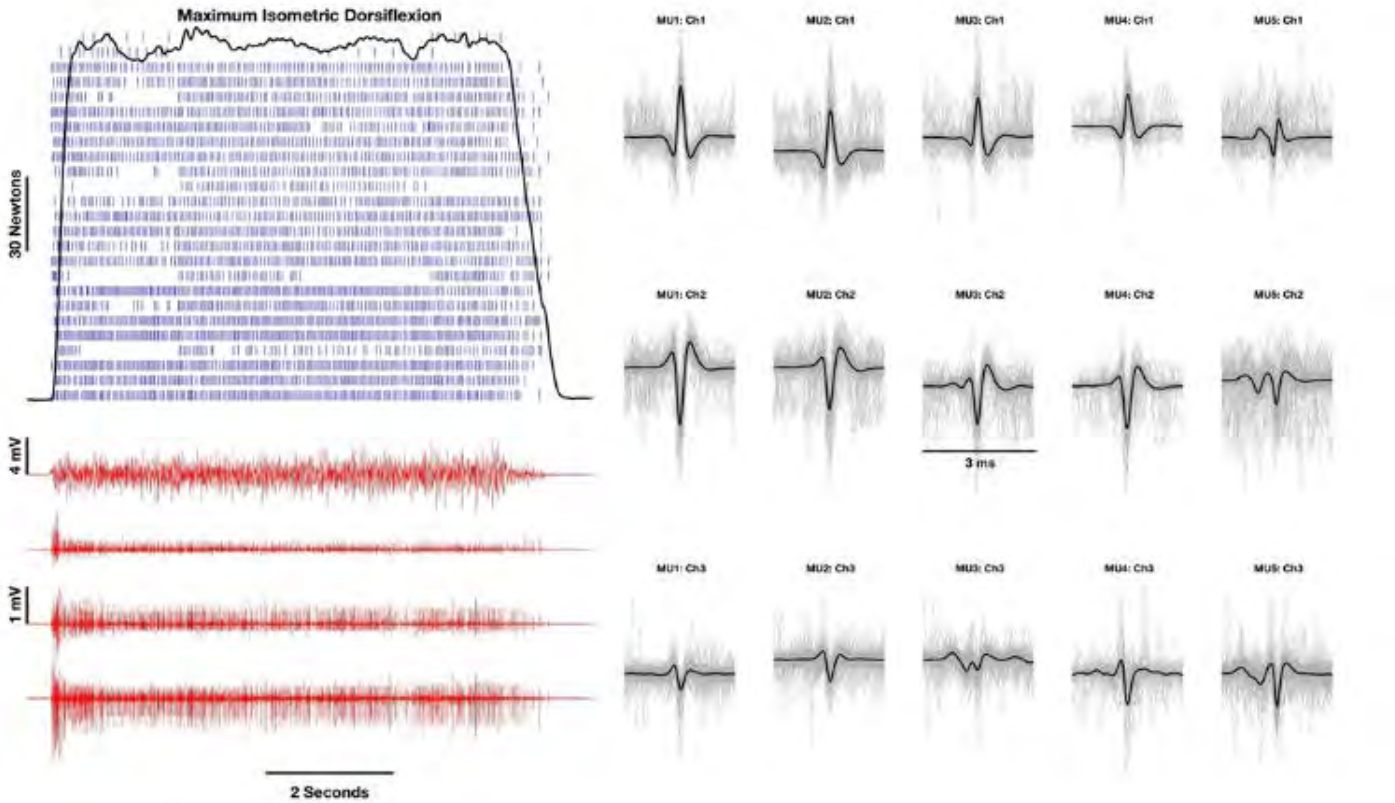

Sex and mechanism of injury (MOI) influence knee mechanics after anterior cruciate ligament reconstruction (ACLR)

Naoaki Ito, Jacob J. Capin, Ashutosh Khandha, Kurt Manal, Thomas S. Buchanan, Lynn Snyder-Mackler

University of Delaware, Newark, DE, USA
email: nito@udel.edu, web: http://sites.udel.edu/pt/

INTRODUCTION

Anterior cruciate ligament (ACL) injuries and ACLR are linked to altered knee gait mechanics and asymmetry in athletes [1]. Gait asymmetries, such as medial compartment tibiofemoral underloading, are associated with early joint degeneration and radiographic OA five years after ACLR [2,3,4].

Sex influences ACL injury risk and it can also influence outcomes. Women are more susceptible to ACL injuries than men [5]. Women are especially at risk for non-contact ACL injury, as around 70% of all ACL injuries in women are non-contact, compared to 52% in men [5]. The relationship between sex, mechanism of injury (MOI), and gait mechanics in athletes after ACLR has not been examined. The purpose of this study was to quantify gait mechanics after ACLR in male and female athletes who sustained contact versus non-contact ACL injury.

METHODS

This is a secondary analysis of prospectively collected data from an ongoing clinical trial. Testing was conducted 5.9 ± 1.9 months after ACLR. We included 28 contact (18 male [M]/10 female [F]) and 39 non-contact (19 M/20 F) participants between ages 13-54 who were recruited from the University of Delaware Physical Therapy clinic and the community. All participants sustained a primary ACL injury, were involved in level 1 or 2 sports (sports involving jumping, cutting, or pivoting) [6] ≥50 hours/year at the time of injury, planned on returning to activity at their pre-injury level and had ≥80% quadriceps strength index and effusion of trace or less [7]. Participants were excluded if they had an osteochondral defect >1cm^2 or a history of a previous ipsilateral/contralateral limb injury, combined grade III ligament injury or previous lower extremity surgery. MOI was self-reported by the participants.

We used an 8 camera motion capture system (Vicon, Oxford, UK; 120Hz) to track 39 retroreflective markers during overground walking at self-selected gait speeds maintained throughout testing. Ground reaction forces were collected at 1080Hz using a force plate (Bertec Corporation, Columbus, OH). Kinetic and kinematic variables were calculated using Visual 3D (C-Motion, Germantown, MD). Variables of interest included: peak knee flexion angle (pKFA), peak knee flexion moment (pKFM), and peak knee adduction moment (pKAM).

Surface electromyography (EMG) (MA-300 EMG System, Motion Lab systems, Baton Rouge, LA) data were collected bilaterally on 7 lower extremity muscles (rectus femoris, vastus medialis, vastus lateralis, medial and lateral hamstrings, medial and lateral gastrocnemius) at 1080Hz. The data were high-pass filtered using a 2nd order butterworth filter at 30Hz, rectified, and low-pass filtered at 6Hz to create a linear envelope, then normalized to maximum voluntary isometric contractions collected prior to gait.

The EMG data were then used to derive knee flexor (FlexpKFM) and extensor muscle force (ExtpKFM) at pKFM. Peak medial compartment contact force (pMCCF) and total contact forces (pTCF) were calculated using a validated musculoskeletal model [8]. Three trials per limb per participant were selected by minimizing the root mean square error and maximizing the R^2 value between the curves of the inverse dynamics knee flexion moment and the forward dynamics knee flexion moment, derived through simulated annealing to optimize muscle parameters. pMCCF was calculated using the Winby frontal plane moment algorithm that balances external pKAM with internal knee moments [9].

pMCCF and pTCF were then normalized to each participants' body weight [8].

Statistics were run using SPSS Version 24.0 (IBM Corp, Armonk, NY). We used a 2×2×2 (sex by MOI by limb) ANOVA (α=0.05) to analyze pKFA, pKFM, pKAM, FlexpKFM, ExtpKFM, pMCCF and pTCF. Demographic characteristics were evaluated using Pearson Chi-squared and Univariate ANOVA.

RESULTS AND DISCUSSION

Height, weight, and BMI were higher in male participants. Patellar tendon grafts (1contact:7non-contact) tended to be used more frequently in the non-contact group for men compared to hamstring grafts (11contact:7non-contact) or allografts (6contact:5non-contact). Other variables showed no significant difference among sex or MOI.

A 3-way interaction effect was observed among limb, sex, and MOI for pMCCF (Figure 1; p=0.001). In men, athletes who sustained non-contact injuries underloaded their involved knee approximately 6 months after ACLR, whereas female athletes who sustained non-contact injuries tended to overload their involved knee. In contrast, female athletes who sustained contact injuries underloaded their involved knee. No interlimb difference was observed in the male contact group. Previous studies have found links between knee underloading and early OA development [3,4]; our findings suggest sex and MOI may influence medial tibiofemoral joint loading, a risk factor for early OA development after ACLR, although long-term follow-up is needed.

Additionally, main effects of limb were observed in pKFA (p=0.000), pKFM (p=0.000), pTCF (p=0.027), and ExtpKFM (p=0.000), where all values were lower in the involved versus uninvolved limb. No other significant main or interaction effects were observed.

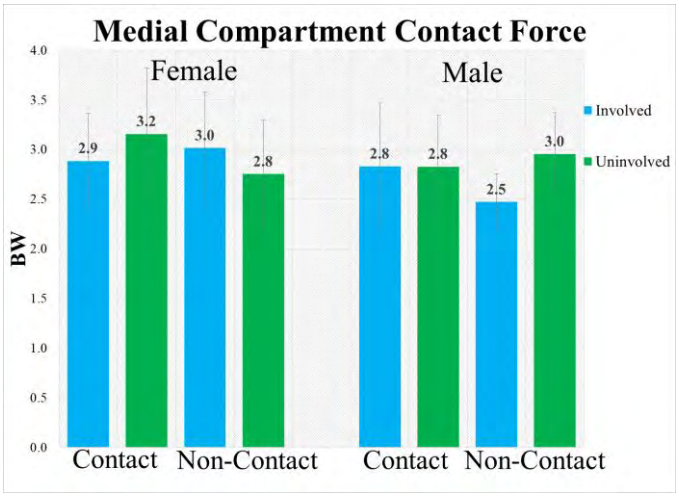

Figure 1: pMCCF grouped by limb, sex, and MOI.

CONCLUSIONS

The combination of sex and MOI may influence gait mechanics after ACLR. There is limited evidence on the effect of MOI on outcomes after ACLR, such as gait mechanics or early onset knee OA. It may be important to further investigate the influence of MOI on gait in athletes after ACLR, as targeted rehabilitation interventions may need to differ based on sex and MOI. Ultimately, these findings may lead to future studies emphasizing rehabilitation protocols aimed towards specific sex and MOI groups.

REFERENCES

1. Kaur et al., JSM, 2016
2. Wellsandt et al., AJSM, 2016
3. Pietrosimone et al., JOR, 2017
4. Saxby et al., OARSI, 2016
5. Kobayashi et al., JSSM, 2010
6. White et al., BMC, 2013
7. Sturgill et al., JOSPT, 2009
8. Manal and Buchanan, JOBE, 2013
9. Winby et al., JOB, 2009

ACKNOWLEDGEMENTS

Funding was provided by the National Institutes of Health: R01-AR048212, R37-HD037985, R01-HD087459, P30-GM103333, U54-GM104941, and T32-HD00749. This work was supported in part by a Promotion of Doctoral Studies (PODS) – Level I Scholarship from the Foundation for Physical Therapy (JJC) and a University of Delaware Doctoral Fellowship Award (JJC).

SEX DIFFERENCE IN HUMAN ANKLE STIFFNESS

[1] Jessica Trevino, [1] Thurmon E. Lockhart, [2] Timothy E. Hewett, and [3] Hyunglae Lee

[1] School of Biological and Health Systems Engineering, Arizona State University, Tempe, AZ, USA
[2] Department of Orthopedic Surgery, Mayo Clinic, Rochester, MN, USA
[3] School for Engineering of Matter, Transport, and Energy, Arizona State University, Tempe, AZ, USA

email: hyunglae.lee@asu.edu, web: http://faculty.engineering.asu.edu/hlee

INTRODUCTION

Ankle stiffness has been known as one of the most important components contributing to the maintenance of lower body stability during postural balance and locomotion. It has been repeatedly shown that women have lower stability and increased risk of injury when compared to men participating in similar sports activities, yet sex difference in neuromuscular control of the ankle, including the modulation of ankle stiffness, and its contribution to lower body stability remains unknown [1].

As a first step to fill this knowledge gap, we investigated sex difference in ankle stiffness in a multi-dimensional space spanning the sagittal and frontal plane and over a range of muscle activation levels. Based on previous findings on higher incidence of musculoskeletal injury at the ankle joint in females as well as higher anatomical risk factors (higher joint laxity, lower Young's modulus, and greater range of motion) in females, we hypothesized that ankle stiffness in females is significantly lower than males in both the sagittal and frontal planes and across all muscle activation levels.

METHODS

To identify sex difference in human ankle stiffness, this study quantified multi-dimensional ankle stiffness in 20 young men and 20 young women (age: 20−32 with the mean age of 23) with no reported history of neuromuscular or biomechanical disorders. Subjects gave written informed consent prior to participation.

A wearable ankle robot (Anklebot, Bionik Laboratories, Canada) capable of actuating 2 degree-of-freedom (DOF) of the ankle, was used to reliably quantify ankle stiffness in a 2-dimensional space spanning the sagittal plane and the frontal plane. Ankle stiffness was quantified at 3 different muscle activation levels: relaxed (0%), 10%, and 20% of maximum voluntary co-contraction (MVC) of ankle muscles. To this end, electromyographic (EMG) signals of tibialis anterior (TA) and soleus (SOL) were measured using differential surface electrodes (Trigno, Delsys, MA). Amplitudes of EMG signals were estimated and normalized with respect to MVC measurements.

During experiments, subjects sat in a chair with their ankle held by the ankle robot in a neutral position, defined as zero dorsiflexion-plantarflexion (DP) and inversion-eversion (IE) angles from the horizontal plane. A visual feedback was used to inform the subjects of real-time muscle activation of TA and a target activation level in %MVC. To control the constant level of co-contraction, subjects were instructed to simultaneously maintain the target activation level of TA and the neutral ankle position. A total of 3 repeated trials were performed for each muscle activation level. The order of target muscle activation was randomized. In each trial, mild random torque perturbations were applied to the ankle for 20 seconds, and the corresponding ankle angles in 2 DOFs (DP and IE) were recorded at 1 kHz. A minimum rest period of 3 minutes was provided between trials. All experimental protocols were approved by the Arizona State University Institutional Review Board.

Multi-dimensional ankle stiffness was quantified by applying the multi-input multi-output stochastic system identification method to the measured torques and angles at the ankle [2]. Ankle stiffness in the sagittal plane (DP stiffness) and ankle stiffness in the frontal plane (IE stiffness) were quantified. In addition, a spatial structure of ankle

stiffness was investigated by quantifying three parameters defining the stiffness ellipse of the ankle: area, aspect ratio, and orientation.

Sex difference in ankle stiffness was evaluated by running a mixed ANOVA where muscle activation level is a within-subjects factor and sex is a between-subjects factor. Separate analyses were completed for DP stiffness, IE stiffness, ellipse area, ellipse aspect ratio, and ellipse orientation. Following the mixed ANOVA, unpaired, independent, two-tailed t-tests were performed to identify sex difference at each muscle activation level. All tests were made at a significance level of $p<0.05$.

RESULTS AND DISCUSSION

First, significant sex difference in ankle stiffness was observed (Fig. 1). In all muscle activation levels, DP stiffness and IE stiffness were significantly lower in females than males. In detail, for DP stiffness, $p=0.001$, $p=0.001$, and $p=0.004$ for 0, 10, 20 %MVC, respectively. For IE stiffness, $p=0.001$, $p=0.003$, and $p=0.008$ for 0, 10, 20 %MVC, respectively. Furthermore, the sex difference of ankle stiffness increased with the increase of ankle muscle co-contraction.

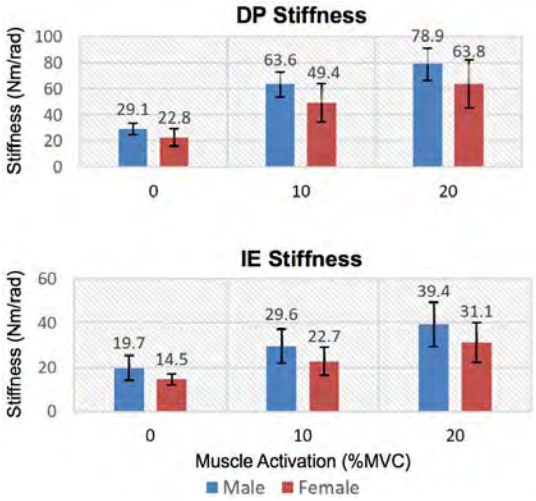

Figure 1. Group results of DP stiffness and IE stiffness. Error bars denote mean±1 standard deviation.

Next, while a significant sex difference was identified for the area of stiffness ellipse, no statistical sex difference was observed in the aspect ratio or orientation (Fig. 2). In detail, for the area, $p=0.000$, $p=0.003$, $p=0.008$ for 0, 10, 20 %MVC, respectively.

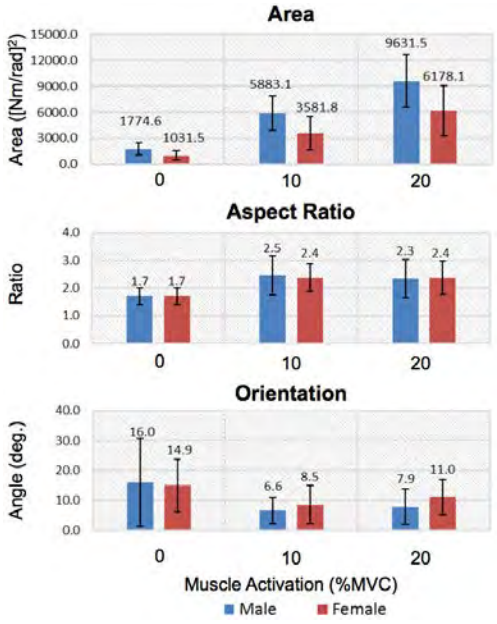

Figure 2. Group results of area, aspect ratio, and orientation of stiffness ellipse in a 2-dimensional space.

For the aspect ratio and angle, no significant main effect was found for the between-subjects factor: $p=0.91$ and $p=0.50$ for the aspect ratio and angle, respectively.

CONCLUSIONS

Clear sex difference in the magnitude of multi-dimensional ankle stiffness was observed, evidenced by significantly higher DP stiffness, IE stiffness, and the area of stiffness ellipse in males than females. These results are relevant to previous studies demonstrating that women have higher joint laxity, larger range of motion, and lower Young's modulus values. Contrary to the magnitude of ankle stiffness, no significant sex difference was observed for other structural information on the shape of stiffness ellipse, specifically aspect ratio and orientation. The sex difference in this study would shed lights on our understanding of sex difference in risk of ankle injury and contribute to the implementation of sex-specific exercise training programs to prevent ankle injuries.

REFERENCES

1. Almeida et al. *Medicine and Science in Sports and Exercise,* 31(12)**,** 1807-1812
2. Lee et al. *IEEE Trans. Neural Systems and Rehabilitation Engineering,* 22 (6)**,** 1104-1114, 2014

CHARACTERIZING MULTISCALE *IN VIVO* MUSCLE ARCHITECTURE CHANGES FOLLOWING STROKE

[1, 4, 5] Amy Adkins, [1,3] Lindsay Garmirian, [1,3]Christa Nelson, [1,3]Julius Dewald, and [1, 2, 3, 4, 5] Wendy Murray

Departments of [1] BME, [2] PM&R, and [3] PTHMS, Northwestern University, Chicago, IL, USA
[4] Shirley Ryan AbilityLab (formerly the Rehabilitation Institute of Chicago), Chicago, IL, USA
[5] Edward Hines, Jr. VA Hospital, Hines, IL, USA
email: adkins@u.northwestern.edu

INTRODUCTION

Seven million Americans have survived a stroke. Unfortunately, at six months post-stroke, 75% of these individuals report that their motor impairment significantly impedes their ability to perform activities of daily life. Muscle architecture is indicative of a muscle's force-generating capacity. Understanding changes in the overall capability for force generation in individual muscles following stroke may aid in the development of more effective, targeted rehabilitation protocols.

Comprehensive *in vivo* muscle architecture studies involving impaired populations do not exist. Despite many exciting and important advances in recent years, there is currently no *in vivo* muscle imaging study that measures all of the critical architectural parameters for any upper limb muscle, in any population. Here we combined multiple novel imaging techniques to directly measure each parameter needed to calculate optimal fascicle length and physiological cross sectional area in the biceps brachii, a parallel-fibered muscle. We compare inter-limb differences in a single subject with hemiparetic stroke to a nonimpaired, age-matched control subject.

METHODS

Sarcomere length (l^S), fascicle length (l^F), and muscle volume (V) of the biceps brachii were measured *in vivo* (Fig. 1) in both arms of two subjects under passive conditions; one subject with chronic hemiparetic stroke (male, 59 yrs old, Fugl-Meyer = 24, 8 yrs post-stroke) and one control subject with no history of musculoskeletal disease or injuries of the upper limb (male, 61 yrs old). Both subjects provided informed consent; Northwestern University's Institutional Review Board approved this study's procedures.

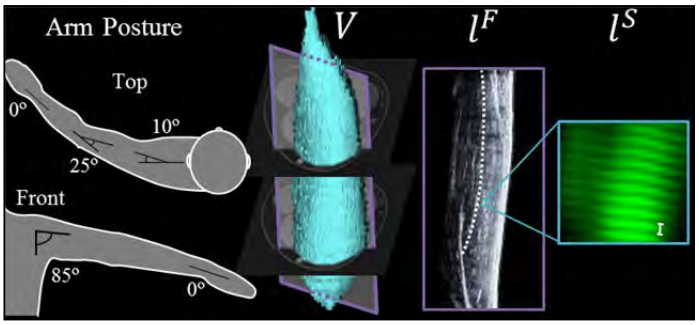

Figure 1: Multiscale muscle imaging.

To image sarcomeres *in vivo*, a microendoscopic needle was inserted into the long head of the biceps brachii with its optical lenses aligned parallel to the fascicle direction. A microscope (Zebrascope, Zebra Medical Technologies, Palo Alto, CA) which uses second-harmonic generation to capture the intrinsic striation pattern of sarcomeres was attached to the needle for imaging. Mean sarcomere length per image was calculated offline with an average of 15 images per arm [1]. In a separate session, extended field-of-view ultrasound (EFOV-US) images of the long head of the biceps were obtained [2]; 3 images were obtained per arm, 4 fascicles were measured per image. In both studies, subjects were seated, secured to a chair, with their arms supported in a controlled posture (Fig. 1). Surface EMG was obtained simultaneously; data collected while the biceps was active was excluded.

In a third imaging study, the Dixon method, a fat suppression MRI sequence, was used to acquire MR images of the biceps brachii (3D GRE, TR = 7ms, TE of 2.39ms and 4.7ms, flip angle = 12°, matrix size = 256x216, slice thickness = 3mm) [3]. Manual segmentation of the combined long and short heads of the biceps brachii was performed using Analyze 12.0 (AnalyzeDirect, Overland Park, KS). Volume of muscle contractile material was calculated as the volume of intramuscular fat subtracted from the total biceps volume, as described previously [3].

Optimal fascicle length (l_o^M) and (PCSA) were calculated for both arms of both subjects using the following equations:

$$l_o^M = l^F * \frac{2.7\mu m}{l^S} \qquad PCSA = \frac{V}{l_o^M}$$

where 2.7μm is optimal sarcomere length.

RESULTS AND DISCUSSION

Inter-limb differences in the volume of the biceps brachii and the average fascicle length of the long head were markedly more pronounced in the subject with chronic stroke (Table 1). For the nonimpaired subject, absolute differences between limbs were <5% for all parameters (Fig. 2). Biceps sarcomere lengths in the paretic limb of the stroke subject were ~6% longer than those in the nonparetic limb. Inter-limb differences in fascicle length and sarcomere length resulted in an optimal fascicle length that was 22.6% shorter in the paretic limb of the stroke subject (Fig. 2). A concomitant 23.1% decrease in muscle volume resulted in remarkably comparable muscle PCSAs across limbs, the only architectural parameter that was not more different between limbs in the subject with hemiparetic stroke than the corresponding measure in the control subject.

Our data for individual parameters are similar to previously reported values from studies that focused on measuring only a subset of muscle architectural parameters. For example, our measurement precision and mean sarcomere length are consistent with previously reported values for the biceps [1]. In addition, l_o^M values for both of the healthy individual's arms and the non-paretic arm of the stroke individual are within the range of values reported in cadaveric studies (e.g., [4]).

The inter-limb differences observed in this individual with stroke are greater than established accuracy and precision measures for each of the imaging modalities we implemented. EFOV-US applied to fascicle length measurement in the upper limb has been shown to result in absolute error <5% [5]. Measurement error of microendoscopic measures are reported to be about 1% of mean sarcomere length [6]. MRI volume measures have been shown to be accurate to within 4% [7].

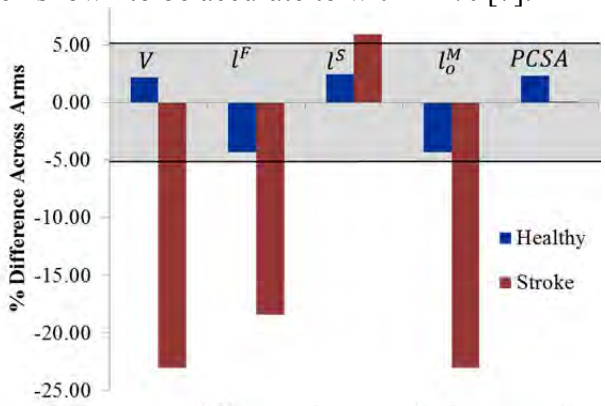

Figure 2: Percent difference between limbs, normalized to nonparetic (or dominant) arm. Negative indicates the value from the paretic (or non-dominant) arm is smaller.

CONCLUSIONS

This study demonstrates the feasibility of collecting comprehensive, *in vivo* muscle architecture data sets in individuals with severe motor impairments. Strikingly, our initial data suggests that in this subject with chronic hemiparetic stroke, the excursion capacity of the paretic long head of the biceps brachii is substantially decreased while the force generating capacity is similar to that of his non-paretic limb.

REFERENCES

1. Sanchez et al. *Neuron.* 88: 2015.
2. Nelson et al. *J Biomech.* 49(9): 2016.
3. Garmirian et al. *Proceedings of ASB '17*, Boulder, CO, USA, 2017.
4. Murray et al. *J Biomech.* 33: 2000.
5. Adkins et al. *J Biomech.* 63: 2017.
6. Chen et al. *J Biomech.* 49: 2016.
7. Tingart et al. *Clin Ortho Relat Res.* 415: 2003.

ACKNOWLEDGEMENTS

This work is supported by the National Science Foundation Graduate Research Fellowship Program under Grant No. DGE-1324585, as well as NIH R01D084009. Any opinions, findings, and conclusions or recommendations expressed in this material are those of the authors and do not necessarily reflect the views of the National Science Foundation or NIH.

Table 1: *In vivo* muscle architecture measures.

Subject	Humerus length (cm)		Volume (cm^3)		Fascicle Length (cm) (±SD)		Sarcomere Length (μm) (±SD)		Optimal Fascicle Length (cm)		PCSA (cm^2)	
	L	R	L	R	L	R	L	R	L	R	L	R
Healthy	38.4	38.1	241.5	246.8	13.9(0.6)	14.5(0.6)	3.10(0.09)	3.03(0.11)	12.1	12.7	19.9	19.5
Stroke	31.2	31.2	166.5	128.1	14.2(0.6)	11.6(0.4)	3.08(0.07)	3.26(0.13)	12.4	9.6	13.4	13.4

MOTOR MODULE GENERALIZATION ACROSS WALKING AND BALANCE IS ASSOCIATED WITH BETTER WALKING PERFORMANCE POST-STROKE

[1] Jessica L. Allen, [2] Trisha M. Kesar, [2,3] Lena H. Ting

[1] West Virginia University, Morgantown, WV, USA
[2] Emory University, Atlanta, GA, USA
[3] Georgia Institute of Technology, Atlanta, GA, USA
email: jessica.allen@mail.wvu.edu, web: http://www.neuromoblab.com

INTRODUCTION

Motor module (a.k.a muscle synergy) analysis related to mobility performance in clinical populations commonly focuses on walking behaviors. Although recruiting a larger number of modules has been associated with faster walking speeds post-stroke [1], differences in speed remain in individuals who recruit an identical number of modules. Maintaining balance is critical for mobility tasks such as walking, yet little is known about motor modules recruited for balance and how they compare to those recruited for walking. We recently demonstrated that recruiting common motor modules across walking and balance (i.e., motor module generalization) may be related to motor performance. For example, improved motor performance due to long-term training in healthy young adults is accompanied by increases in motor module generalization [2]. Similarly, gains in motor performance after rehabilitation in individuals with Parkinson's disease are accompanied by gains in motor module generalization [3]. Thus, our overall hypothesis is that motor module generalization across walking and balance is a neuromuscular strategy for producing well-coordinated walking. We posit that motor module recruitment for walking and balance are differently affected after stroke, and thus predict that 1) fewer common modules are recruited across behaviors post-stroke, which is 2) associated with reduced motor performance.

METHODS

Nine individuals post-stroke (3 male, 57.2±12.7 years, 6 right hemiparesis, 46.3±23.1 months post-stroke, Fugl-Meyer lower extremity score 23.7±3.7) and eight sex-, and age-similar neurotypical controls (3 male, 62.0±6.6 years) participated in the current study. Electromyography (EMG) was recorded from each subject while they (1) walked over-ground at self-selected speed for ~25ft, and (2) responded to ramp-and-hold translations of a support surface during standing that translated in 12 equally-spaced directions in the horizontal plane. For walking, at least 10 gait cycles were collected to ensure adequate capture of step-to-step variability. For balance, three trials in each direction were collected in random order, all subjects were exposed to the same level of perturbation, and subjects were instructed to maintain balance without stepping.

Motor modules were found using nonnegative matrix factorization [2] using EMG recorded from 12 muscles spanning the hip, knee, and ankle of each leg. For reactive balance, EMG data were analyzed during four different time bins: one before the perturbation and three during the automatic postural response. For walking, EMG data were analyzed as a function of time. To capture trial-by-trial / step-by-step variability, trials for each condition were concatenated together end to end. A total of four EMG data matrices were created for each subject [2 legs x 2 conditions]. Assembled EMG data matrices were normalized to the maximum activation observed during walking at self-selected speed.

The number of motor modules independently extracted in each leg (control, nonparetic, paretic) were compared using separate Kruskall-Wallis tests for walking and reactive balance (α =0.05). The number of motor modules recruited during each condition was chosen such that lower bound of the 95% confidence interval of variability accounted for was greater than 90% [2].

Motor module generalization was defined as the percentage of common motor modules across walking and reactive balance [3] and was compared across legs using a one-way ANOVA. The number

of common motor modules was identified using Pearson's correlations. A pair of motor modules were considered "common" if $r \geq 0.708$, which corresponds to the critical value of r^2 for 12 muscles at $p = 0.01$. The number of common motor modules was expressed as a percentage of total motor module number to account for the fact that each subject recruited a different number of modules (Fig. 1A).

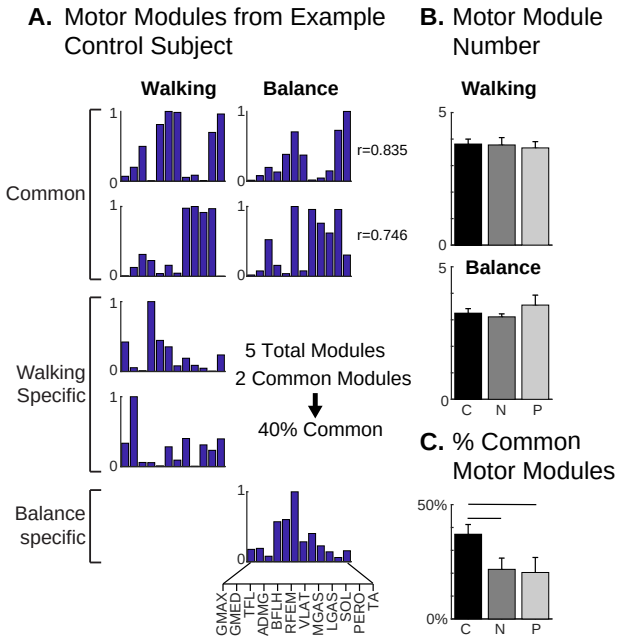

Figure 1: A) Motor modules from a representative subject illustrating motor modules recruited across walking and reactive balance. B) Motor module number was similar across control and stroke subjects. C) The percentage of common motor modules across walking and balance was reduced post-stroke in both the paretic and nonparetic legs. (legend: C = control legs, N = nonparetic legs, P = paretic legs)

RESULTS AND DISCUSSION

We found no difference in motor module number (Fig. 1B) recruited between control, non-paretic, or paretic legs for either walking ($p=0.801$) or reactive balance ($p=0.486$). The median number of motor modules recruited for walking was 4 [range 2- 5] in control legs, 4 [3-5] in nonparetic legs, and 4 [3-5] for paretic legs. The median number recruited for reactive balance was 3 [2-4] in control legs, 3 [3-4] in nonparetic legs, and 4 [2-5] in paretic legs.

Consistent with our prediction, motor module generalization was reduced post-stroke. The percentage of common modules across walking and reactive balance was 37.0±17.0% in control legs, 21.7±14.8% in nonparetic legs, and 20.3±1.7% in paretic legs (Fig. 1C). There was a trend for reduced generalization in both paretic ($p=0.066$) and nonparetic legs ($p=0.098$) compared to controls, but no difference between legs post-stroke ($p=0.984$).

In addition, higher levels of generalization post-stroke were associated with faster walking speeds. The percentage of common motor modules recruited in stroke subjects was positively correlated with walking speed ($r=0.45$). The most commonly recruited module across behaviors was composed of the ankle plantarflexors (e.g. Fig 1A, 2nd row). This module was recruited in both conditions in 13/16 control legs, 8/9 nonparetic legs, but only 4/9 paretic legs. Regression analysis identified presence of this common plantarflexor module in the paretic leg as a significant predictor of walking speed ($p=0.028$), pointing to this module as a potentially critical pattern of muscle coordination.

CONCLUSIONS

Here we show that motor module generalization (e.g. recruiting common motor modules) across walking and balance is related to motor performance post-stroke. Taken together with our prior results in young adults [2] and individuals with Parkinson's disease [3], this provides further evidence that motor module generalization is a neuromuscular strategy for producing well-coordinated walking. Therefore, examining how muscles are coordinated across walking and balance behaviors may have important implications for rehabilitation aimed at improving motor control in those with reduced mobility.

REFERENCES

1. Clark et al. *J Neurophys*. 103(2):844-57. 2010
2. Sawers et al., *J Neurophys*. 114(6):3359-73. 2015
3. Allen et al., *J Neurophys*. 118(1):363-73. 2017.

ACKNOWLEDGEMENTS

This work was supported by NIH grants R01-HD46922, F32-NS087775, and K01-HD079584.

MERGED PLANTARFLEXOR MODULE PREDICTS POOR WALKING PERFORMANCE IN POST-STROKE HEMIPARETIC SUBJECTS

Lydia G. Brough [1], Steven A. Kautz [2, 3], Mark G. Bowden [2, 3], Chris M. Gregory [2, 3] and Richard R. Neptune [1]

[1] Department of Mechanical Engineering, The University of Texas at Austin, Austin, TX, USA
[2] Ralph H Johnson VA Medical Center, Charleston, SC, USA
[3] Department of Health Sciences & Research and Division of Physical Therapy, Medical University of South Carolina, Charleston, SC, USA
email: lydia.brough@utexas.edu, web: http://www.me.utexas.edu/~neptune

INTRODUCTION

Stroke is the leading cause of long-term disability in the United States with approximately 795,000 people experiencing a stroke each year [1]. The ankle plantarflexors (PFs) are often impaired post-stroke [e.g., 2], which can have significant consequences as the PFs are critical to walking performance by being primary contributors to body support, forward propulsion and leg swing initiation [3].

Prior studies have shown that well-coordinated walking in healthy subjects can be produced by five co-activation modules: 1) hip and knee extensors in early stance, 2) PFs in late stance, 3) tibialis anterior and rectus femoris in swing, 4) hamstrings in late swing and early stance, and 5) hip flexors in pre- and early swing [4, 5]. Research has found that in post-stroke hemiparetic walking, modules in the paretic leg can merge or become co-activated, which prevents the independent activation of specific muscles and causes suboptimal execution of biomechanical functions [5].

Considering the critical biomechanical roles the PFs have in unimpaired walking, we hypothesized that a merged PF module would result in 1) increased paretic leg braking and nonparetic leg propulsion, 2) reduced paretic leg body support, and 3) increased stance and stepping asymmetry.

METHODS

Kinematic, kinetic and electromyography (EMG) data were collected from 45 hemiparetic post-stroke individuals (16 left hemiparesis, 18 female; age: 56 ± 13 years) and 16 healthy controls (8 female, age 53 ± 7 years) during 30 second treadmill walking trials at a self-selected speed.

EMG data were processed and analyzed using nonnegative matrix factorization (NNMF) as in [5]. NNMF determined the minimum number of muscle modules required to account for >90% of the EMG variability. Subjects were classified as having an independent PF module if NNMF produced a module composition with a Pearson's correlation coefficient of 0.8 or greater compared to weighted muscle contributions in the average healthy control PF module. If that criterion was not met, the subject was classified as having a merged PF module with other muscle groups.

Body support, braking and propulsion were calculated from the time integral of the vertical and anterior/posterior GRF and normalized by body weight. Braking and propulsion were also normalized by walking speed. For these quantities, paretic leg ratios were defined as the paretic value divided by the sum of the paretic and nonparetic values, with 0.5 being perfectly symmetric. Stance symmetry was defined as the percentage of total stance on the paretic and nonparetic legs.

Independent samples t-tests were used to test for significant differences between each group with Bonferroni-Holm corrections for multiple comparisons (uncorrected $p<0.05$).

RESULTS AND DISCUSSION

Twenty-nine of the hemiparetic subjects had a merged PF module and sixteen hemiparetic subjects had an independent PF module. The merged group's self-selected walking speeds were significantly

slower than the independent and control groups' ($p < 0.001$), while the difference between the independent and control group was not significant (Table 1).

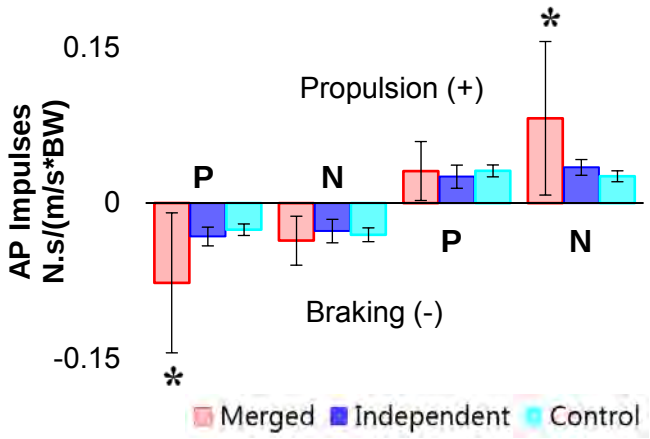

Figure 1: Paretic (P) and nonparetic (N) braking and propulsion for each group. (* denotes a significant difference between both other groups).

We hypothesized that the merged group would have increased paretic leg braking due to premature PF co-activation with the knee extensor and/or hamstring modules in early stance [e.g., 3]. As expected, merged paretic braking was higher than the independent ($p=0.002$) and control ($p<0.001$) groups. To maintain a constant walking speed (i.e., produce net zero anterior/posterior impulse), the merged group also produced higher nonparetic propulsion than the independent ($p=0.002$) and control ($p<0.001$) groups (Fig. 1).

The reduced paretic body support ratio in the merged group is consistent with a shorter stance time of the paretic leg compared to the nonparetic leg ($p<0.001$, Table 1). The merged group also had greater step length asymmetry than the independent ($p=0.002$) and control groups ($p<0.001$) (Table 1).

Paretic braking and propulsion ratios were the only significant differences between the independent and control groups ($p<0.001$). Notably, the independent group often performed more closely to the control group than to those in the merged group (Fig. 1, Table 1). Future work will use synergy-based control in musculoskeletal simulations to better understand the role of merged PF modules on walking performance measures.

CONCLUSIONS

These results indicate that gaining independent function of the plantarflexors is a crucial component of stroke rehabilitation in terms of walking speed and symmetry. Prior research has shown that stroke patients can gain additional modules [6]. Thus, patients who receive targeted rehabilitation of the PFs may be able to gain an independent PF module and improve walking performance.

REFERENCES

1. Benjamin EJ et al. *Circulation 135*, 146-603, 2017.
2. Higginson JS et al. *J Biomech 39*, 1769-77, 2006.
3. Neptune RR et al. *J Biomech 34*, 1387-98, 2001
4. Neptune RR et al. *J Biomech* 42, 1282-87, 2009.
5. Clark DJ et al. *J Neurophys 103*, 844-57, 2010.
6. Routson RL et al. *Gait Posture* 38, 511-17, 2013.

ACKNOWLEDGEMENTS

This work was supported in part by NIH P20HD109040, VA RR& D 1I01RX001935 and the Rehabilitation Research & Development service of the VA.

Table 1: Each group's walking performance assessments. ('*' denotes a significant difference between both other groups. '‡' denotes a significant difference between the paretic and nonparetic legs).

		Paretic Ratio (%)				Stance % of Gait	
Group	**Speed (m/s)**	**Braking**	**Propulsion**	**Body Support**	**Step Length**	**Paretic**	**Nonparetic**
Merged	0.27±0.12*	63±18	33±23	43±4*	58±8*	70±3‡	78±3‡
Independent	0.64±0.12	58±9	39±10	48±2	52±3	67±2	70±2
Control	0.75±0.22	46±6*	55±5*	50±0	50±1	67±2	67±2

POST-STROKE STIFF KNEE GAIT IS LINKED TO MIS-TIMED BRAKING FORCES

[1,2] Jesse C. Dean, [1,2] Mark G. Bowden, and [1,2] Steven A. Kautz

[1] Ralph H. Johnson VAMC, Charleston, SC, USA
[2] Medical University of South Carolina, Charleston, SC, USA
email: deaje@musc.edu

INTRODUCTION

Forward propulsion, a primary mechanical sub-task of human walking, is often altered following a stroke. The magnitude of post-stroke propulsive deficits has commonly been quantified using *propulsive impulse*, calculated by integrating the anterior component of the ground reaction force (GRF) during late stance [1]. In comparison to controls walking at matched speeds, stroke survivors typically walk with reduced propulsive impulses from the paretic leg, but near-normal impulses from the non-paretic leg [2-3].

In addition to post-stroke changes in propulsion magnitude, propulsion timing also appears to shift. Most notably, anteriorly directed GRFs tend to begin later in the stance phase for the paretic leg, and earlier for the non-paretic leg [1-2].

Beyond the primary effects of propulsion on anterior progression, an altered propulsive pattern could also affect motion of the swing leg. Deficits in paretic propulsion have been suggested to contribute to reduced knee flexion during the swing phase [4], often termed "stiff-knee gait". In turn, this may require greater circumduction to safely clear the ground. While not as commonly investigated, changes in the timing of propulsion could also influence swing phase mechanics [5].

This study investigated whether post-stroke changes in paretic propulsion magnitude or timing influence paretic swing phase kinematics. We hypothesized that reduced propulsion magnitude and delayed propulsion timing would predict reduced swing phase knee flexion and increased circumduction.

METHODS

The present study involved 29 chronic stroke survivors (11 F / 18 M; age = 59±12 yrs). Inclusion criteria were: hemiparesis secondary to a unilateral stroke > 6 months prior; daily home walking; self-selected treadmill walking speed of ≥0.3 m/s. Exclusion criteria were: orthopedic or neurologic conditions beyond stroke that would be expected to influence gait; impairments contraindicative to walking. All participants provided informed consent using a form approved by the University Institutional Review Board.

Participants performed 30-second walking trials on an instrumented treadmill at their self-selected and fastest-comfortable speeds. For each stride, we calculated several metrics based on anteroposterior GRF (see Fig. 1). We calculated paretic propulsive impulse as the area under the positive portion of the GRF-time trajectory, surrounding the point of maximum anterior GRF. We calculated paretic late braking impulse as the area under the negative portions of this trajectory that followed the propulsive impulse, an unusual pattern observed in a subset of participants. We identified the paretic propulsion onset time, quantified relative to contralateral initial contact. In addition, we identified

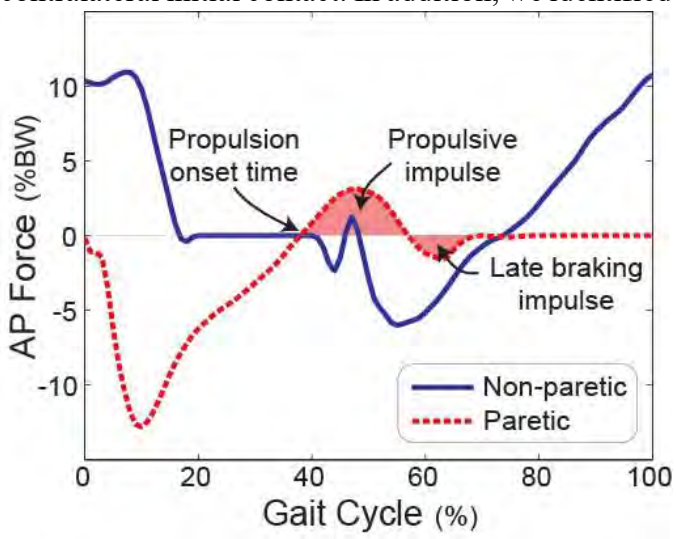

Figure 1: Metrics quantifying paretic propulsion, illustrated for a single participant. Forces are plotted for one stride, defined by paretic leg initial contact.

the peak paretic knee flexion angle from marker kinematic data, and quantified paretic circumduction as the maximum lateral displacement of the paretic heel relative to its location at the start of swing.

We used multiple regressions to determine whether paretic knee flexion and circumduction were predicted by various aspects of the paretic leg propulsive pattern. Specifically, independent variables in these regressions were: walking speed; propulsive impulse magnitude; late braking impulse magnitude; and propulsion onset time. We quantified the overall prediction ability of this combination of variables using R^2 magnitude, and the unique predictive contribution of each individual variable using partial η^2 value (a measure of effect size).

RESULTS AND DISCUSSION

Across participants, paretic knee flexion was predicted by a combination of walking speed and late braking forces (Table 1). Specifically, greater knee flexion was observed with faster walking speeds (η_p^2 = 0.11) and smaller late braking impulses (η_p^2 = 0.39). Neither propulsive impulse nor propulsion onset time made a significant unique contribution to the intersubject variance in knee flexion.

Paretic swing leg circumduction was similarly predicted by the preceding gait characteristics, although to a lesser extent than knee flexion (Table 1). Greater paretic circumduction was observed with larger late braking impulses (η_p^2 = 0.13). Neither gait speed nor the propulsion metrics made a significant unique contribution to variance in circumduction.

The single best predictor of both paretic knee flexion and paretic circumduction was the magnitude of the late braking impulse, contradicting our hypothesis. While the magnitude of propulsive forces has been extensively investigated in the chronic post-stroke population [1-3], little attention has been paid to the unusual braking forces observed here. Such forces may be linked to increased leg flexor activity in late stance [6], a potential outcome of disrupted post-stroke coordination.

The present results suggest that posteriorly directed GRFs just before the paretic foot leaves the ground may be particularly detrimental to achieving typical swing phase kinematics. Speculatively, this may be due to an inability to rapidly unload the paretic leg, causing this foot to "drag". Future research will more directly investigate whether interventions focused on reducing these late braking forces have beneficial effects on swing phase kinematics.

CONCLUSIONS

Many individuals who have experienced a stroke exhibit both propulsive deficits and altered swing phase kinematics. The present study revealed a link between unusual braking forces late in the paretic stance phase, and atypical paretic swing phase motion. The results suggest the importance of eliminating these late posterior forces in order to restore a typical gait pattern.

REFERENCES

1. Bowden et al. *Stroke.* **37**:872-876, 2006.
2. Combs et al. *Clin Biomech.* **27**, 887-892, 2012.
3. Raja et al. *Clin Biomech.* **27**, 1023-1030, 2012.
4. Campanini et al. *Gait Posture.* **38**, 165-169, 2013.
5. Malcolm et al. *J NeuroEng Rehab.* **12**, 21, 2015.
6. Turns et al. *Arch Phys Med Rehab*. **88**, 1127-1135.

Table 1: Regression results predicting swing phase gait behavior. Each row presents the results of a multiple regression predicting the indicated metric. For each predictor, the regression coefficient is presented, followed by the [95% confidence interval]. Significant ($p<0.05$) contributing factors are indicated with asterisks.

	Walking speed (m/s)	**Propulsive impulse (Ns/BW)**	**Late braking impulse (Ns/BW)**	**Propulsion onset time (%GC)**	**Constant term**	**Total model fit**
Swing phase knee flexion (degrees)	*20 * [4 36]*	3.1 [-4.1 10.2]	*-36 * [-48 -23]*	-0.06 [-0.58 0.46]	39 [29 49]	R^2=0.60 ($p<0.0001$)
Swing leg circumduction (mm)	-15 [-39 9]	-8.2 [-19.1 2.6]	*27 * [8 45]*	-0.14 [-0.93 0.65]	37 [22 52]	R^2=0.37 ($p<0.0001$)

Methodology to Estimate Voluntary Activation of the Paretic Elbow and Wrist Muscles in Chronic Hemiparetic Stroke Using Twitch Interpolation

[1]Lindsay R. P. Garmirian, [1]Ana Maria Acosta and [1]Julius P. A. Dewald

[1]Northwestern University, Chicago, IL, USA
Email: Lindsay.Garmirian@u.northwestern.edu

INTRODUCTION

Approximately 50-70% of stroke survivors experience long-term upper-extremity functional impairments[1]. Paresis, a decrease in the voluntary activation of muscles, causes weakness, and makes it difficult for stroke survivors to complete activities of daily living (ADLs). The amount of paresis that occurs at specific joints in the upper extremity has not been quantified. This paper will describe the methodology and preliminary results for using twitch interpolation to quantify the ability to fully activate the elbow and wrist flexors and extensors in the paretic upper limb post chronic hemiparetic stroke.

METHODS

The ability to fully activate elbow and wrist flexors and extensors volitionally was assessed in the paretic and non-paretic limbs of two individuals with chronic hemiparetic stroke. The individuals were 56 and 62 years old, 4 and 29 years post-stroke and scored a 24/66 and 16/66 on the upper-extremity portion of the Fugl-Meyer, respectively.

Participants were seated in a Biodex chair (Biodex, Shirley, NY) and the tested arm was rigidly attached to an isometric setup to measure elbow and wrist joint torques. A 6 degree-of-freedom load cell (JR3, Woodland, CA) was used to measure elbow flexion and elbow extension torque while a single axis torque sensor (Futek, Irvine, CA) mounted at the wrist was used to measure wrist torque. The subject was positioned with 15° shoulder flexion, 20° shoulder abduction, 90° elbow flexion and in neutral with respect to pronation/supination and wrist and finger posture.

A standard twitch interpolation protocol[2] was used with the following specifications and modifications to optimize measurement of the paretic upper extremity. A monopolar stimulation setup with a motor point pen (Compex, Guildford, UK) and a reference electrode (anode) was used to find the location for each muscle where the lowest amplitude of stimulation triggered the largest visible muscle contraction. Two self-adhesive electrodes (Dura-Stick, Hanover, Germany) were placed on each muscle group, one over the muscle specific motor point (cathode) and the other distal to the motor point (anode).

For each of the four muscle groups, participants were asked to generate at least six voluntary maximum contractions (MVC), with additional MVC trials collected if needed, to ensure that the six greatest torque values were within 10% of each other and that the last trial was not the greatest value.

The electrical stimulus consisted of a single monophasic pulse with duration of 100μs to maximize motor recruitment while minimizing activation of pain (Aδ and C) fibers. The maximal stimulation amplitude was set at the 1mA increment where the measured joint torque plateaued or began to decrease. This is in contrast with standard twitch interpolation protocols in the lower limb that employ 110% of the maximal stimulation amplitude. Due to the reduced muscle and limb size in the arm and forearm, using those supramaximal amplitudes will result in current spread to antagonist muscles decreasing the net joint torque production. Participants were asked to relax followed by a maximum voluntary contraction held for 4 seconds. A stimulus of maximal amplitude was applied after 250 ms of sustained contraction level within 10% of the target effort. A second stimulus was applied after the first stimulus, with the limb at rest (see Figure 1). This was repeated for 6 trials. Between trials, participants were asked to activate the antagonist muscle group, to eliminate residual torque from the previous trial. This is an important consideration since individuals post stroke often

have hypertonicity and difficulty relaxing the flexor muscles, thus the use of reciprocal inhibition is needed to minimize any potential residual torques from the previous trial.

Elbow joint torque was calculated offline from the measured forces and moments at the forearm through a Jacobian-based transformation. The wrist torque was obtained directly from the torque sensor based on its calibration equation determined previously.

For each of the four muscle groups, voluntary activation was estimated for each trial using the following formula (1):

Voluntary Activation = $(1-\tau_A/\tau_R)*100\%$ (1)

Where τ_A, the twitch torque, represents the torque produced by electrical stimulation during MVC and τ_R, the resting twitch torque, represents the torque produced by electrical stimulation with the limb at rest (Figure 1).

RESULTS AND DISCUSSION

Fig. 1 shows example data from an elbow flexion twitch interpolation trial for the paretic limb of one of the subjects. Electrical stimulation, shown in grey, has been superimposed on the elbow extension torque data, shown in black. The percent activation calculated for this trial was 48%.

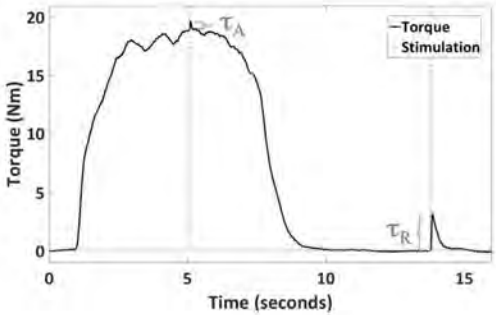

Figure 1. Example data from an elbow flexion twitch interpolation trial for the paretic limb.

Voluntary activation of the non-paretic limb in both participants was similar across muscle groups, ranging from 90.5% for the wrist extensors up to 96% for the elbow flexors (Fig. 2). Preliminary results show decreased ability to fully activate muscle groups in the paretic, compared to the non-paretic upper limb (Fig. 2). For the paretic limb, voluntary activation of the wrist muscles appears to be less than the elbow muscles, however, conclusions must be made cautiously due to small sample size (Fig. 2).

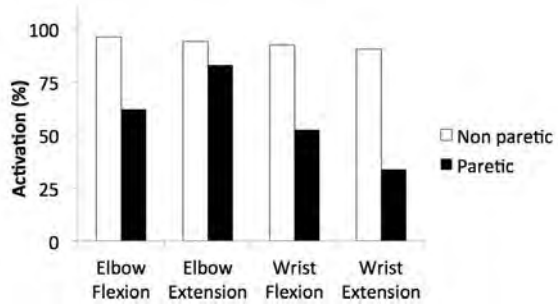

Figure 2. Voluntary activation of the paretic and non-paretic limb for elbow and wrist flexors and extensors (mean for two subjects).

CONCLUSIONS

This study shows that it is feasible to quantify voluntary activation of the elbow and wrist flexors and extensors in individuals with chronic hemiparetic stroke and describes methods to do so. The use of the twitch interpolation method to quantify deficits in voluntary activation in the paretic upper extremity of stroke subjects will help us determine differences between proximal and distal muscles and between flexors and extensors. It will also allow us to explore whether these activation impairments parallel losses in rate coding also observed in this cohort[3] and may impact development and assessment of rehabilitation approaches that seek to overcome upper extremity paresis in hemiparetic stroke.

REFERENCES

1. Faria-Fortini I, et al. Upper extremity function in stroke subjects: relationships between the international classification of functioning, disability, and health domains. *J Hand Ther*. 2011;24(3)..
2. Klein CS, et al. Voluntary activation failure contributes more to plantar flexor weakness than antagonist coactivation and muscle atrophy in chronic stroke survivors. *Journal of Applied Physiology*. 2010;109(5).
3. McPherson LM, et al. Properties of the motor unit action potential shape in proximal and distal muscles of the upper limb in healthy and post-stroke individuals. *Conf Proc IEEE Eng Med Biol Soc*. 2016; 335-339.

THE EFFECTS OF FALL-RECOVERY TRAINING ON SINGLE- AND MULTIPLE-STEPPING THRESHOLDS IN INDIVIDUALS WITH CHRONIC STROKE

[1] Jamie Pigman, [1] Darcy S. Reisman, [1] Ryan T. Pohlig, and [1] Jeremy R. Crenshaw

[1] University of Delaware, Newark, DE, USA
email: crenshaw@udel.edu

INTRODUCTION

Individuals with chronic stroke have a fall risk that is twice that of age- and sex-matched controls [1]. A third of falls in this population are from a trip or a slip [2]. An impaired ability to recover from anterior and posterior falls [3] likely contributes to this high risk of trip- and slip-related falls. We previously demonstrated that fall recovery is modifiable in this population through task-specific training [4,5]. Within-training modifications included improvements in step and trunk kinematics, the proportion of successful recoveries, and the highest disturbance magnitude from which a successful recovery was achieved. It is not clear, however, how this within-training adaptation transfers to other evaluations of balance and mobility.

The Berg Balance Scale (BBS) [6] and the Functional Gait Assessment (FGA) [7] are both established clinical measures of balance and mobility that are sensitive to stroke impairment. These measures, however, do not specifically evaluate the response to an external postural disturbance. Single-stepping (SST) and multiple-stepping (MST) thresholds, defined as the anterior and posterior disturbance magnitudes that consistently elicit one or more steps, are a reliable and objective measure of fall-recovery ability [8]. These assessments differ from fall-recovery training in the size of the disturbances and by including instructions that constrain the number of steps.

The purpose of this study was to determine if, within a single group of individuals receiving fall-recovery training, measures of balance and mobility improve after training. We hypothesized that performance on all assessments would improve. However, we expected that compensatory stepping thresholds, an assessment specifically evaluating fall-recovery ability, would demonstrate the largest training effects. In order to understand the biomechanical mechanisms that underlie observed changes in stepping thresholds, we evaluated the minimum margin of stability (MoS) [9] of feet-in-place responses and the step kinematics [10,11] of single-stepping responses.

METHODS

We recruited six participants with chronic stroke (mean (SD) age: 60 (7) years, BMI: 29.5 (4.6) kg/m^2, Fugl-Meyer LE 23 (9)) for this IRB-approved study. First, balance and mobility were evaluated using the BBS and FGA. Then, fall-recovery ability was measured with anteroposterior SST and MST tests using a computer-controlled treadmill (ActiveStep®, Simbex, Lebanon, NH). Participants were instructed to "try not to step" or "try to recover in a single step". Within each test progression, the disturbance magnitude was increased by 0.5 m/s^2 until four consecutive failures were observed, indicating the anterior or posterior threshold. During the SST and MST tests, failure was defined as taking one step or taking more than one step, respectively. Failure was also considered if more than 20% of body weight was supported by an instrumented harness system (Dillon, Fairmont, MN) [12]. Using a simple inverted pendulum model of standing, thresholds were expressed as the destabilizing moment caused by the treadmill acceleration [8].

Participants then underwent six fall-recovery training sessions consisting of simulated trips and slips. Within each session, four progressively challenging, 10-minute series of disturbances were delivered for anterior and posterior falls. The disturbance magnitude was incremented depending on recovery success. After training, participants repeated all assessments on a separate visit.

Whole-body motion during stepping threshold tests was recorded using motion capture technology (Qualisys., Sweden; 120 Hz). In order to compare response kinematics before and after training, we

selected successful responses at the highest common disturbance magnitude across evaluations. For the feet-in-place response of the SST, we determined the minimum MoS in the anteroposterior direction. For the stepping response of the MST, we evaluated the anteroposterior and lateral distances between the stepping foot and whole body CoM at foot strike. All measures before and after training were compared using repeated measures t-tests and effect sizes (Cohen's *d* for repeated measures).

RESULTS AND DISCUSSION

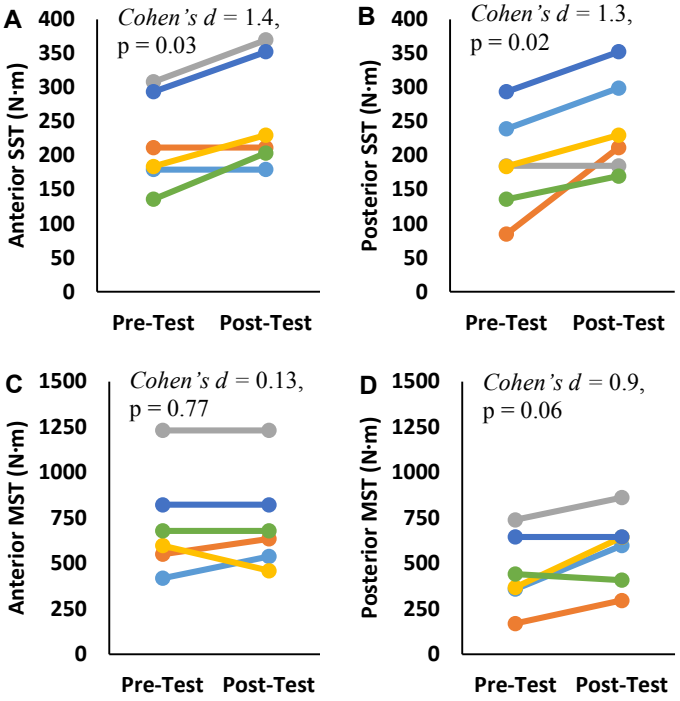

Figure 1: Stepping thresholds from pre- and post-training evaluations. With training, SST improved in anterior (**A**) and posterior (**B**) directions. The MST did not improve in the anterior direction (**C**), but there were effects of training in the posterior direction (**D**).

With training, both SST measures, as well as posterior MST measures, improved (Figure 1). Training was accompanied by moderate effects in the BBS (mean (SD) pre-test = 50/56 (6); change = +2 (3); d = 0.5, p = 0.3) and the FGA (pre-test = 18/30 (7); change = +2 (4); d = 0.6, p = 0.2).

We anticipated that, with training, participants would increase resistance to the destabilizing effects of the perturbation. In other words, we expected the minimum MoS to become *less negative*. However, when comparing the feet-in-place response at the same anterior disturbance magnitude, participants recovered from *more dynamic instability* after training (pre-test = -3.7 (4.4) cm; change = -1.6 (1.2) cm; d = 1.6, p = 0.3). This result suggests that, with training, participants altered their ability or willingness to recover from dynamic instability. There was no effect on the minimum MoS in the posterior direction (pre-test = 0.6 (1) cm; change = +0.3, d = 0.43, p = 0.36).

For the posterior stepping response of the MST assessment, medium effects of training were observed on foot placement. Steps became longer (pre-test = 15.8 (8.6) cm; change = +3.3 (8) cm) and narrower (pre-test = 7.6 (4.2) cm; change = -2.9 (7) cm; d = 0.41-0.43, p = 0.34-0.36). Although such moderate benefits in foot placement may have benefitted posterior thresholds, it could also be that participants learned to prevent second steps that weren't necessary for stability maintenance (i.e. steps due to low efficacy or fear).

CONCLUSIONS

Training had beneficial transfer to some, but not all stepping threshold measures. Kinematic analyses suggest that participants altered their ability or willingness to recover from dynamic instability. In response to a posterior slip-like disturbance, there was a trend of improved initial step placement.

To a lesser extent, training improved scores on the clinical measures of balance and mobility. This smaller effect may be due to limited transfer between a fall-recovery task and self-initiated balance and mobility.

REFERENCES

1. Jorgensen L, et al. *Stroke* **33,** 542-7, 2002.
2. Schmid A, et al. *J Rehabil Res Dev* **50,** 1277-86, 2013.
3. de Kam D, et al. *Neurorehabil. Neural Repair* **31,** 708-16, 2017.
4. Pigman J, et al. *Proceedings of ASB'16,* Raleigh, NC, USA, 2016,
5. Pigman J, et al. *Proceedings of ASB'17,* Boulder, CO, USA, 2017.
6. Berg T, et al. *Arch. Phys. Med. Rehabil.* **73,** 2-5, 2009.
7. Wrisley DR, et al. *Phys. Ther.* **84,** 906-18, 2004.
8. Crenshaw J, et al. *Gait Posture* **39,** 810-15, 2014.
9. Hof AL. *J Biomech* **38**, 1-8, 2005.
10. Troy KL, et al. *Gait Posture* **28,** 461-65, 2008.
11. Crenshaw J, et al. *J Biomech* **45,** 129-33, 2012.
12. Cyr MA-A, et al. *J Biomech* **42,** 1566-9, 2009.

ACKNOWLEDGEMENTS

This project was supported by the University of Delaware Research Foundation, the ASB Junior Faculty Research Award, and a grant from the National Institute of General Medical Sciences (2P20 GM103446) from the National Institutes of Health.

RESTORING PROPULSIVE FORCES IN ELDERLY GAIT DOES NOT IMPAIR DYNAMIC STABILITY

Michael G. Browne and Jason R. Franz

University of North Carolina at Chapel Hill and North Carolina State University, Chapel Hill, NC, USA
email: mgbrowne@email.unc.edu, web: http://abl.bme.unc.edu

INTRODUCTION

Older adults are at an exceptionally high risk of falls, and most of these falls occur during locomotor activities such as walking. Older adults may thus opt to walk slower to improve their resilience to unexpected balance challenges and mitigate their risk of falls. However, prior to eliciting slower preferred speeds, advanced age is accompanied by a precipitous reduction in propulsive forces (F_P) exerted during the push-off phase of walking [1]. Winter et al. (1990) originally proposed that many of the hallmark biomechanical features of elderly gait, including reductions in F_P generation during push-off, reflect the adoption of a safer, more stable pattern of movement [2]. Contrary to that perspective, we recently found that a diminished push-off during walking severely compromises dynamic stability, at least in young adults [3]. Indeed, our findings alluded to unfavorable consequences of reduced F_P generation on dynamic stability that could themselves precipitate slower speeds.

Together, these results suggest that mitigating age-related reductions in F_P may increase dynamic stability during walking toward values seen in young adults. Indeed, although interventions often aim to restore push-off intensity (e.g., F_P) in older adults, it remains unclear how these changes would affect dynamic stability – a major gap in our understanding with important translational implications. Do older adults decrease propulsive force generation to attenuate their risk of falls or can we enhance push-off intensity without unfavorable effects on dynamic stability? In this exploratory study, we investigated the extent to which older adults prioritize dynamic stability in selecting their preferred push-off intensity (i.e. F_P generation). We hypothesized that increasing F_P generation in older adults would improve dynamic stability while decreasing F_P generation would worsen dynamic stability.

METHODS

16 older adult subjects (5 males/11 females, mean ± SD, age: 75.3 ± 3.6 years) participated this study. We first calculated subjects' preferred walking speed (PWS: 1.23 ± 0.19 m/s) using a photo cell timing system and a 10 m walkway (Bower Timing Systems, Draper, UT, USA). We then implemented a visual biofeedback paradigm based on real-time force measurements from a dual-belt force measuring treadmill (Bertec, Corp., Columbus, OH) (Fig. 1A). Specifically, for trials involving biofeedback, a custom Matlab (Mathworks, Natick, MA) script continuously computed the average bilateral peak F_P during push-off from each set of four consecutive steps and projected a visual representation of those values as dots in real-time to a screen positioned in front of the treadmill (Fig. 1A).

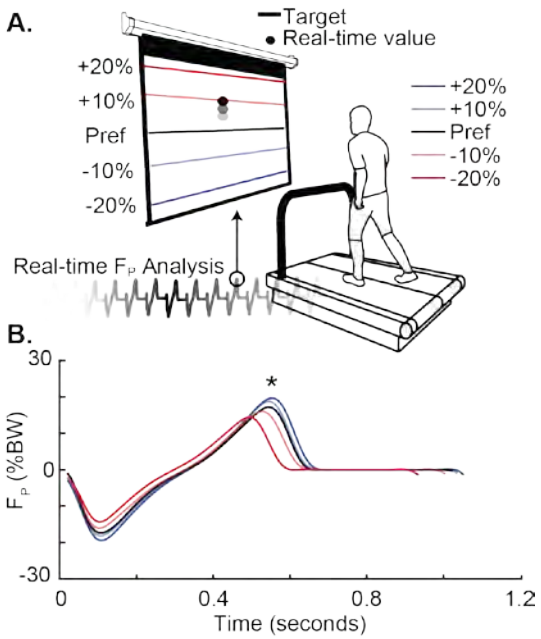

Figure 1: A.) Experimental design using real-time peak propulsive force measurements projected in front of participants with targets representing ±10 and 20% different from preferred. **B.)** Group average anterior-posterior ground reaction force by condition across time. Asterisks (*) denote a significant main effect of F_P biofeedback ($p<0.05$).

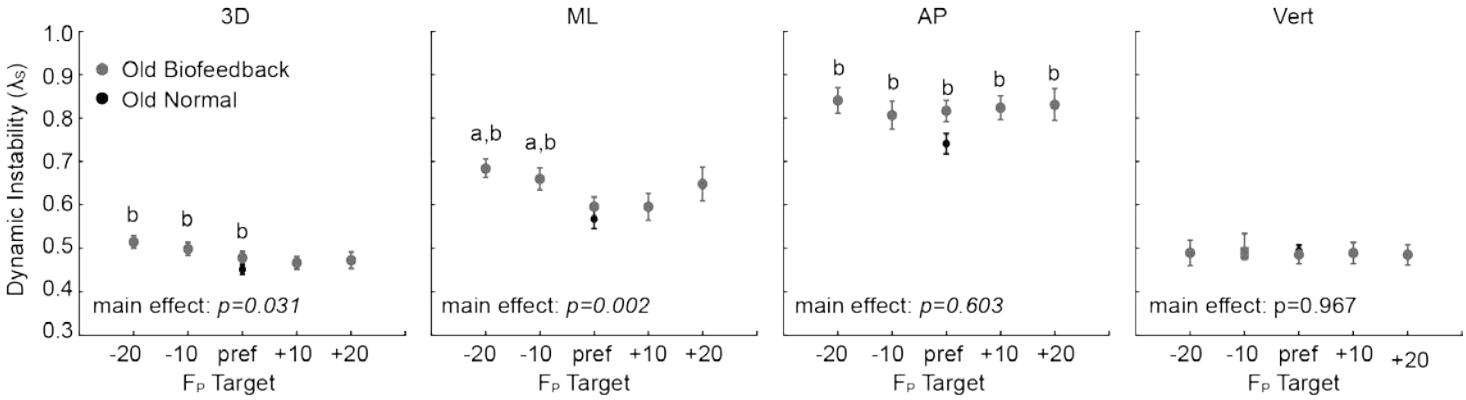

Figure 2: Group mean ± SE short-term maximum divergence exponents (λ_S) defined using three-dimensional (3D), mediolateral (ML), anterior-posterior (AP) and vertical (Vert) C7 velocities. 'a' and 'b' indicate significant ($p<0.05$) pairwise difference of biofeedback trial from preferred F_P biofeedback and normal walking, respectively.

Subjects walked at their PWS while matching their instantaneous F_P to target values representing ±10 and ±20% of preferred F_P (Fig. 1B). Using motion capture data, we constructed a state vector from the time series of C7 velocity in the anterior-posterior (AP), mediolateral (ML), and vertical directions to calculate short-term maximum divergence (i.e., Lyapunov, λ_s) exponents. Finally, we analyzed the variability of C7 kinematics given its complement to dynamic stability within the context of balance control (Data not shown).

RESULTS AND DISCUSSION

Older adults walked with a 10% F_P deficit compared to previously reported values in young adults walking at similar speeds ($p<0.05$) [4]. Older adults successfully modulated their F_P to target values, reaching +14% and -14% when targeting +20% and -20% different from preferred F_P. Older adults walked with progressively longer, wider steps across the range of presented F_P targets (i.e., from -20% to +20% F_P). Biofeedback alone (i.e. biofeedback of preferred F_P) increased AP dynamic instability, and thereby, 3D instability (Fig. 2). This effect of biofeedback on divergence in the AP direction is perhaps unsurprising considering that participants have to continually modulate F_P along the AP axis. Targeting decreases in F_P of as little as 10% worsened (i.e., increased) ML dynamic instability compared to preferred F_P biofeedback and normal walking. We posit that this is clinically meaningful; previous work suggests that older adults may be more prone to impairments in ML dynamic stability [5] and reducing F_P may further exacerbate those consequences. Compared to walking with smaller than preferred F_P, dynamic instability was much less susceptible to walking with larger than preferred F_P. Interestingly, increasing F_P generation in older adults, and thereby restoring push-off intensity to values seen in young adults, had no significant effect on dynamic stability. While we must reject our hypothesis that increasing F_P generation in older adults would improve their dynamic stability, the absence of a negative impact when restoring older adults F_P generation remains an exciting finding.

CONCLUSIONS

Our findings suggest that restoring propulsive force generation in older adults does not negatively impact their dynamic stability. These potentially favorable results may be combined with our previous work to paint an interesting story associated with restoring push-off intensity in old age. Increasing push-off intensity in old age appears to elicit beneficial changes in joint-level biomechanics without compensatory tradeoffs in whole-body measures of balance control (i.e. dynamic stability). As such, our study builds confidence toward continued efforts to restore push-off intensity during walking in old age.

REFERENCES

1. Franz JR, Kram R. *J Biomech* **46**, 535-40, 2013.
2. Winter D, et. Al. *Phys Ther.* **70(6)**, 340-7, 1990.
3. Browne M & Franz J. *RSOS*. 4(11): e171673, 2017.
4. Browne M & Franz *J Biomech* **55**, 48-55, 2017.
5. Cofré E, et. Al. *Gait & Posture* **42**, 79-84, 2015.

Young adults are surprisingly bad at walking: Sex differences in the circumstances associated with falls

[1]HyeYoung Cho, [2]Michel J. H. Heijnen, [3]Bruce A. Craig, [1]Shirley Rietdyk

[1]Health and Kinesiology, Purdue University, West Lafayette, IN, USA
[2] Health and Applied Human Sciences, University of North Carolina Wilmington, Wilmington, NC, USA
[3]Statistics, Purdue University, West Lafayette, IN, USA
email: cho273@purdue.edu

INTRODUCTION

Falls are not a trivial problem for young adults [1-3], and fall-related fractures have increased in young adults [3]. However, there are only a few studies of falls in young adults, and most of this information is from medical reports. For example, a higher proportion of fall injuries occur on stairs for young females as compared to males [2], and fall-related fractures in young females (aged 16-19 years) increased 59% from 2000 to 2010 [3]. However, it is still unclear whether young adult females are injured more because they fall more, or if they are more likely to sustain injuries from falls.

The purpose of this abstract is to determine if the frequency and circumstances of falls in young adults are associated with sex.

METHODS

Undergraduate students (N=230, 19.8 ±0.9 years, 74 males) participated in either the fall semester (106 students, 33 males) or the spring semester (124 students, 41 males).

Two surveys were distributed via email:

1. Initial survey (distributed once): Included participant demographics, number of falls in the past year, number of medications, and physical activity level with Leisure-Time Exercise Questionnaire (LTEQ) [4].
2. Daily survey (distributed daily for 16 weeks): Participants were asked if they had slipped, tripped or fallen in the past 24 hours. When participants reported a fall, follow-up questions regarding the circumstances and injuries were asked. If a participant had more than one fall a day, they were asked to report the most serious fall.

A generalized linear mixed model was used (GLIMMIX in SAS 9.3, Cary, NC, USA) to quantify differences between males and females. The odds of falls associated with fall frequency, primary cause, activity, injury, and medications were compared for men versus women. Significance level was set at $p = 0.05$. Insufficient observations were available to compare types of injuries and activity at time of injury, so these comparisons are described without statistics.

RESULTS AND DISCUSSION

1. Response Rate: The average response rate was 91%. The response rate demonstrated a linear decrease of 0.7% per week ($p<0.001$). Ten participants (4%) were excluded from the results because the response rate was less than 35%. The response rate ranged from 46-100% for the analyzed participants.

2. Fall frequency: A total of 260 falls were reported, circumstances were provided for 193 falls, so the following analysis focuses on those reports. One hundred ninety three falls were reported by one hundred six fallers (36 males). 52% of males and 46% of females fell at least once, and are henceforth termed fallers. 28% of males (n=19) and 23% of females (n=34) fell more than once, and are henceforth termed frequent fallers. (Fig. 1). There was not a significant difference in the frequency of falls between males and females (odds ratio (OR) 1.04; confidence interval (CI) 0.70-1.53; p=0.86; Fig. 1). The high fall frequency supports the observation that falls are not a minor issue, even for 20 year-old adults [1-3].

3. Causes of falls: The three main causes of falls for males were slip (40%), trip (32%), and hit/bump

(13%). Similarly, the three main causes of falls for female were slip (33%), trip (32%), and hit/bump (9%). No differences were observed between sexes on the causes of falls. The main causes of falls, slips and trips, are similar to observations for community dwelling older adults [5], highlighting the prevalence of these perturbations across all age groups.

4. Activity at time of fall: The three main activities for males were sports (58%), walking (35%), and transfer (3%). The three main activities for females were walking (48%), sports (40%), and transfer (5%). Males were more likely to fall during sports activities than females (OR 2.29; CI 1.04-5.02; p=0.04); no other differences were observed. For sports activities, it is expected that people will fall due to exposure to environmental and task-related hazards. However, a substantial number of falls occurred during walking, and walking was the main activity for females, which highlights the inherent instability of bipedal locomotion [1].

5. Physical activity (LTEQ score): No differences in physical activity level were observed between male and female fallers (p=0.68).

6. Injuries from falls: Injuries were reported as follows: males, 17% of falls (n=6); females, 37% (n=26). The number of injuries were not significantly different (p=0.12). The types of injury in males were 2 contusions (25% of injuries), 4 abrasions (50%), 2 sprain/strain (25%), and all of the injuries were due to sports-related falls. Females reported 14 contusions (45%), 10 abrasions (32%), 4 sprain/strain (13%), two concussions (6%), and one fracture (3%). The fall-related injuries were due to sports (n=15), walking (n=10), and transfer (n=1).

The number of injuries were not different between males and females, but all injuries sustained by males were sports-related, while 38% of injuries sustained by females were walking-related. Further, the most serious injuries, concussions and fractures, were only observed in females.

7. Prescribed medications: Female fallers took more medications than male fallers (p<0.001). Since this finding was unexpected, we also compared number of medications as a function of sex in the non-faller group; the number of prescribed medications was not significantly different across sex in the non-faller group (p=0.12). While it is well known that prescribed medications increase fall risk in older adults [6], this is the first observation of fall-risk related to medications in young female adults.

This study is limited by the relatively small and homogeneous subject sample.

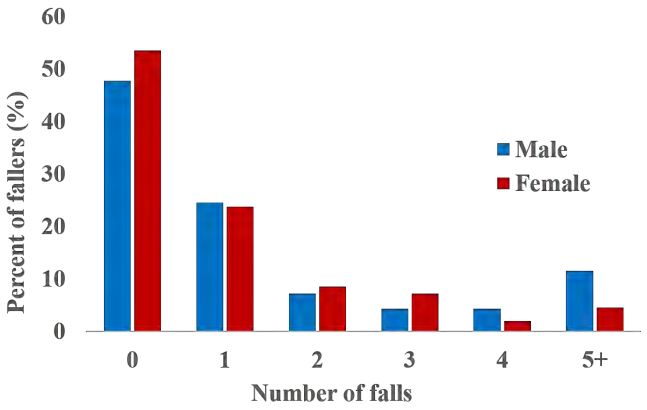

Figure 1: Percentage of participants described as a function of the number of falls; ten subjects with a response rate less than 35% were excluded.

CONCLUSIONS

The high fall rate and number of frequent fallers in 16 weeks reinforces the finding that falls are not a trivial problem for young adults [1-3]. Frequency of falls and fall-related injuries were not different for young adult males and females. While males sustained no injuries during walking, females did, and the types of injuries were more serious in females. Therefore, at 20 years of age, we provide preliminary support that females fall at the same rate as males, but they appear more likely to sustain injuries during less challenging activities and also appear to suffer more serious injuries.

REFERENCES

1. Heijnen & Rietdyk. *Hum Mov Sci,* 46, 86-95, 2016.
2. Timsina et al. *Plos One,* 12(5), p.e0176561, 2017.
3. Court-Brown et al. *Injury*, 48, 819–824, 2017.
4. Godin & Shephard. *Can J Appl Sport Sci*, 10(3), 141-146, 1985.
5. Berg et al. *Age and Aging*, 26, 261-268, 1997.
6. Yip & Cumming. *Med J Aust*, 160(1), 14-18, 1994.

DOES FOOT POSITION AFFECT MUSCLE FUNCTION DURING GAIT IN CEREBRAL PALSY?

[1] Amy K. Hegarty, [2] Max J. Kurz, and [1] Anne K. Silverman

[1]Department of Mechanical Engineering, Colorado School of Mines, Golden, CO, USA
[2]Physical Therapy Dept., Munroe-Meyer Institute, University of Nebraska Medical Center, Omaha, NE, USA
email: ahegarty@mymail.mines.edu, web: fbl.mines.edu

INTRODUCTION

Altered gait patterns in children with cerebral palsy (CP) are often characterized in the sagittal plane; however, altered transverse plane kinematics are also common. For example, previous work found 61% of children with CP walk with internal foot progression angles (FPAs) and another 21% of children with external FPAs [1]. The source of altered FPAs is often a combination of excessive femoral anteversion, tibial torsion, and dynamic hip rotation, among others. Surgical interventions and physical therapy can be prescribed to address differences in FPAs; however, the effect of FPA on muscle function during gait is unclear. Only 25% of FPA variance can be attributed to femoral anteversion and tibial torsion [2], therefore a clear understanding of these musculoskeletal deficits on muscle function can augment current treatment planning decisions.

Previous work found excessive tibial torsion reduces the capacity for muscles to accelerate the knee and hip joints by 10% [3]. However, the effects of internally and externally rotated FPAs on muscle function remains unclear.

Therefore, the purpose of this study was to characterize the effect of both internally and externally rotated FPA gait strategies for children with CP on the capacity of muscles to accelerate the body center of mass (COM).

METHODS

Three dimensional gait analysis was completed for 18 children with spastic CP (Gross Motor Function Classification System: level II, age: 12.5 ± 2.9 yrs., height: 1.52 ± 0.15 m, weight: 45.5 ± 14.9 kg). Lower body kinematics (120 Hz) and ground reaction forces (1200 Hz) were collected for each child walking overground at their self-selected walking speed, and low-pass filtered with a cutoff frequency of 6 Hz. Joint kinematics were calculated using a least-squares optimization algorithm in Visual3D (C-Motion, Inc., Germantown, MD).

A generic musculoskeletal model with 14 segments, 23 degrees of freedom, and 92 Hill-type musculo-tendon actuators was scaled to match each child's body size and mass (simtk.org). Contributions from lower-limb muscles to whole body COM acceleration were analyzed using an induced acceleration analysis with a rolling without slipping kinematic constraint for foot-ground contact.

Three walking trials for each participant were normalized to the gait cycle, and the root-mean-square (RMS) values of the muscle's capacity to accelerate the body center of mass were calculated over the stance phase of gait. Each participant's FPA was identified as the average value during stance, and used to characterize the limb as *internally rotated* (FPA < 0° external rotation), *externally rotated* (FPA > 17° external rotation), or *standard* (FPA 0 - 17° external rotation). A linear mixed effect model was used to predict the effect of foot position on muscle function for several lower limb muscles for each acceleration direction with two fixed effects (Foot Position x Muscle). Statistically significant effects were assessed using an ANOVA F-test, and pairwise comparisons with Tukey multiple comparison adjustments were completed when significant main effects or interactions were indicated.

RESULTS AND DISCUSSION

Significant main and interaction effects in each anatomical direction ($F>3.05$, $p<0.044$ for all tests) indicate FPA affects the capacity of muscles to produce COM acceleration. Posthoc pairwise comparisons were completed for each muscle group and each acceleration direction.

We found significantly greater forward COM acceleration capacity from individuals walking with internal FPA compared to external FPA for the hamstrings (HAM, p=0.012), and between internal, standard, and external FPAs for the vasti (VAS, p<0.001, p=0.007, p=0.016, Fig. 1A).

We found significantly greater vertical COM acceleration capacity from individuals walking with internal FPA compared to external FPA for the gastrocnemius (GAS, p=0.001), soleus (SOL, p=0.006), and VAS (p=0.069), and from individuals walking with standard FPA compared to external FPA for the GAS (p=0.031, Fig. 1B).

We also found significantly greater medial/lateral COM acceleration capacity from individuals walking with internal FPA compared to external FPA for the gluteus maximus (GMAX, p=0.044), and SOL (p=0.021), and between internal and standard FPA, and internal and external FPA for the gluteus medius (GMED, p<0.001, p<0.001, Fig. 1C).

Our data suggest that increasingly externally rotated gait patterns result in reduced muscle capacity to accelerate the COM, similar to previous work that examined tibial torsion [3]. The capacity of muscles to produce COM accelerations provides insight into whole body metrics such as walking speed and balance. Muscle induced accelerations are influenced both by muscle mechanics such as muscle length and moment arm, and by the skeletal posture dictating the distribution of intersegmental forces throughout the lower-limbs. We suspect the observed trend seen within our results is primarily caused by altered posture for those walking with internally rotated FPA. Kinematic differences are seen in hip abduction and frontal plane pelvis rotation during stance. We speculate that an internally rotated foot position provides a mechanism for sagittal plane joints to accelerate the hip into abduction and to increase acceleration of frontal plane pelvis rotation.

CONCLUSIONS

Foot progression angle is likely an important factor to consider when treating gait deficits for children with CP because it affects the capacity of muscles to accelerate the body during gait. This highlights the substantial effect that transverse plane kinematics can have on sagittal plane mechanics (e.g., forward and vertical acceleration of the body COM), which are likely critical for improving clinical outcomes such as walking speed. Future work will investigate whether internally rotated gait patterns may be used as a compensation for low force producing muscles.

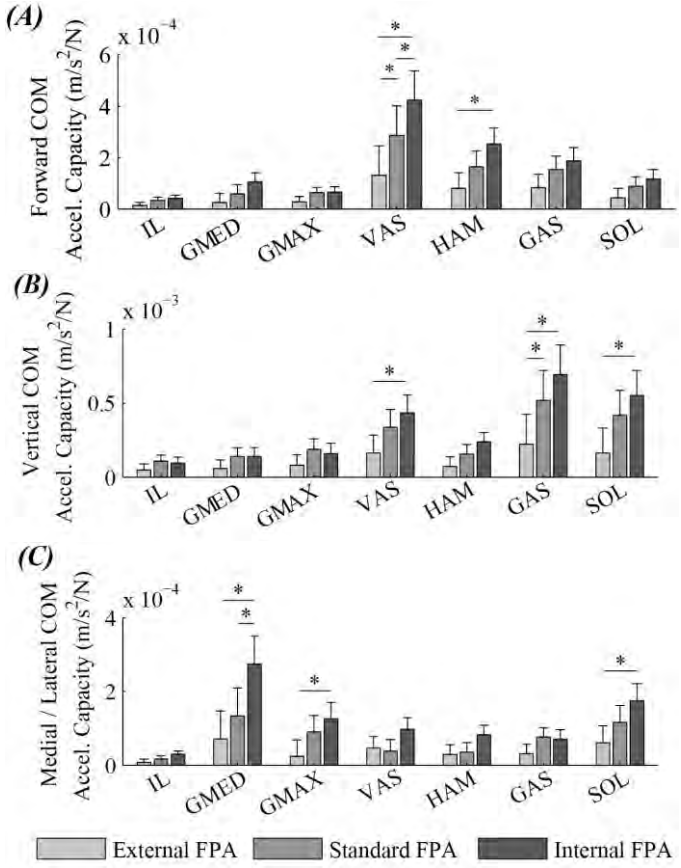

Figure 1: Capacity of major lower limb muscles to accelerate the body center of mass (COM), reported as RMS over the stance phase of gait (p<0.05*).

REFERENCES

1. Simon A. et. al. *J Pediatr Orthop* **35**, 576-82. 2015
2. Lee K. et. al. *J Neuroeng Rehabil*. **15**, 10-56. 2013
3. Hicks J. et. al. *Gait Posture*.**26**, 546-52. 2007.

ACKNOWLEDGEMENTS

This work was partially supported by the NSF GRFP (DGE-1057607).

ISOLATING EFFECTS OF TOE AND FOOT LENGTH ON BIPEDAL WALKING

Eric C. Honert, Gerasimos Bastas and Karl E. Zelik

Vanderbilt University, Nashville, TN, USA
email: eric.c.honert@vanderbilt.edu, web: http://my.vanderbilt.edu/batlab/

INTRODUCTION

The purpose of this ongoing study is to quantify the effects of toe length and foot length on walking biomechanics. Computational simulations [1, 2] and experimental motion analysis studies [1] have shown how varying the length of a rigid foot can affect gait mechanics. However, less is known about the effects of varying sub-segments of the foot; for example, varying the distance from the heel to the toe joint (hereafter referred to as *sole length*), or varying the distance from the toe joint to the distal end of the toes (hereafter referred to as *toe length*). We seek to address this knowledge gap using a custom-designed, adjustable prosthesis to systematically and independently vary toe and sole lengths. We expect the results to provide insight into how biological foot proportions (sole vs. toe length) affect walking, which in turn will inform the design of prosthetic and robotic feet.

METHODS

We designed and fabricated a pair of adjustable ankle-toe prostheses (Fig. 1A) to systematically quantify the effects of toe and sole length on bipedal walking biomechanics. Three healthy, able-bodied subjects (2 males, 1 female, 23±4 yrs, 79±10 kg, 1.8±0.5 m) have thus far consented and participated in this two-session gait analysis study. Subjects wore the adjustable ankle-toe prostheses bilaterally below simulator boots (which immobilize the biological ankles). The first session (~1 hour) served to acclimate individuals to walking on the ankle-toe prostheses with seven different conditions that would subsequently be evaluated in the experimental data collection.

Subjects returned within one week of the training session to participate in an experimental data collection. Subjects walked at 1.0 m/s on a split-belt, instrumented treadmill while we recorded ground reaction forces (GRFs) and lower-limb kinematics. Each subject walked with 25 different toe length and sole length combinations. We tested five toe lengths from 50 to 90 mm in 10 mm increments and five sole lengths from 170 mm to 230 mm in 15 mm increments. The overall lengths of the feet (ranging from 220 mm to 320 mm) are typical for persons ranging from 1.6 to 1.9 m tall. The ankle stiffness and toe joint stiffness were held constant. GRFs were used to compute center-of-mass (COM) power through the individual limbs method [3]. COM Collision and Push-off work were computed as key outcome metrics, based on prior literature (e.g., [4]).

RESULTS AND DISCUSSION

Increasing sole length from 170 mm to 230 mm (with a fixed toe length of 70 mm, Fig. 1B, left) resulted in an increase of 29% (4 J) in COM Push-off work and decrease of 23% (2 J) in COM Collision work magnitude. These trends were fairly consistent across all three subjects (Fig. 1B), and also for different fixed toe lengths (not shown here).

Unlike increasing the sole length, increasing the toe length did not initially reveal clear trends in COM Push-off or Collision work (Fig. 1B, right). At a sole length of 200 mm (Fig. 1B), the maximum COM Push-off work was attained at the 80 mm toe length (17 J). However, there was little difference (~1 J) in COM Push-off work between this toe length and all other toe lengths. Similarly, toe length appeared to have only a small influence (~2 J) on COM Collision work. Thus far, trends have been fairly consistent across all subjects and across different nominal sole lengths.

We plan to extend this toe and sole length study to 10 subjects and examine lower limb kinematics and kinetics. We will perform ANCOVA statistical analyses to examine trends in outcome metrics with

increasing toe and sole length. We expect the results of this study, in conjunction with a prior study we performed on toe joint stiffness and toe shape (manuscript in review), to inform our scientific understanding of biological feet and applications such as foot prostheses and walking robots.

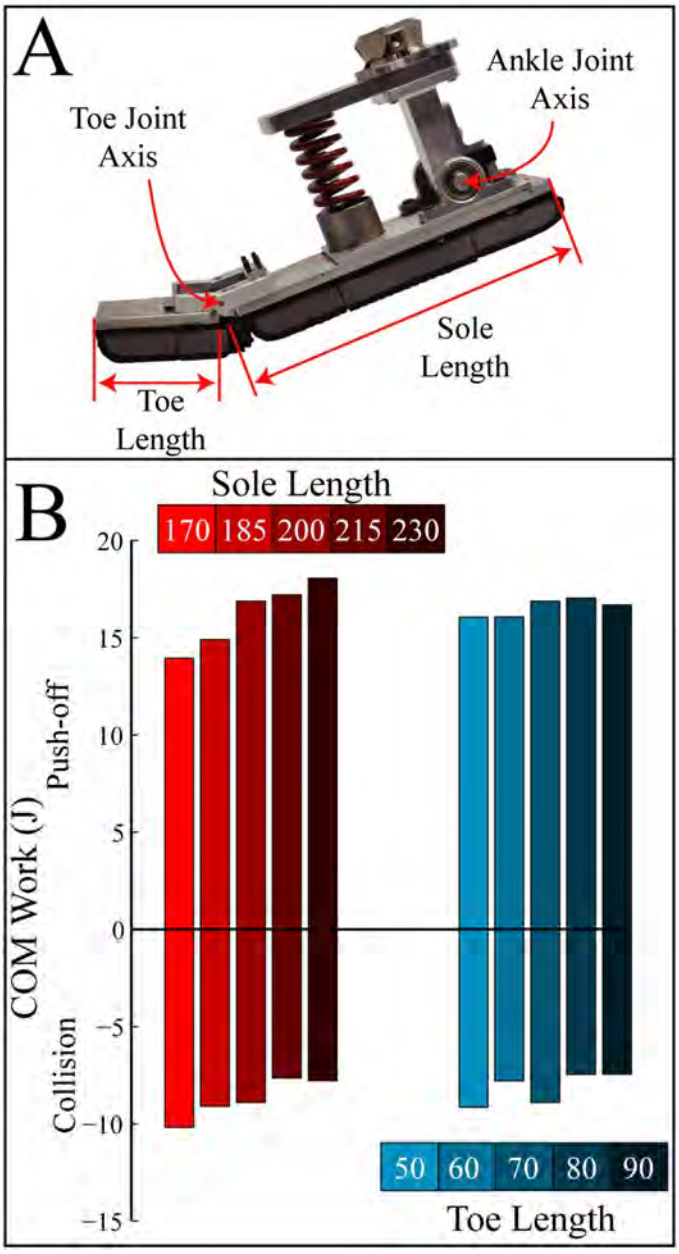

Figure 1: A) Adjustable ankle-toe prosthesis. B) Average COM Collision and Push-off work. Left: Vary sole length with a fixed toe length of 70 mm. Right: Varying toe length, with a fixed sole length of 200 mm. Dimensions are in mm, and work in Joules. Subjects walked at 1.0 m/s. Preliminary data (N=3), thus statistical analyses not yet performed.

CONCLUSIONS

This study is the first to systematically vary toe and sole lengths, and to isolate their effects on gait biomechanics. Thus far, sole length appears to have a greater effect than toe length on key metrics such as COM Push-off and Collision work. More comprehensive kinematic and kinetic analysis on a larger sample size is forthcoming.

REFERENCES

1. Adamczyk and Kuo. *J EXP BIOL*, **216**: 2722-2731, 2013.
2. Zelk, et al. *IEEE T NEUR SYS REH*, **19**: 411-419, 2011.
3. Donelan, et al. *J BIOMECH*, **35**: 117-124, 2002.
4. Caputo and Collins. *SCI REP*, **4**: 2045-2322, 2014.

ACKNOWLEDGEMENTS

This research was supported by NSF (1605200) and NIH (K12HD073945).

CORRELATION BETWEEN GAIT ASYMMETRY AND MOTOR VARIABILITY

[1] Cherice Hughes-Oliver, [2] Divya Srinivasan, [3] Matthew McCullough, [1,4]Robin Queen

[1] Department of Biomedical Engineering and Mechanics, Kevin Granata Biomechanics Lab, Virginia Tech, Blacksburg, VA, USA
[2] Department of Industrial Systems Engineering, Virginia Tech, Blacksburg, VA, USA
[3] Department of Chemical, Biological, and Bioengineering, North Carolina A&T, Greensboro, NC, USA
[4]Department of Orthopaedic Surgery, Virginia Tech Carilion School of Medicine, Roanoke, VA
email: cnh4ph@vt.edu, web: www.BEAM.vt.edu/granatalab

INTRODUCTION

Gait asymmetry and motor variability have both been associated with pathologic gait changes and increased injury risk [1, 2]. While both gait variability and asymmetry have been evaluated concerning injury risk and pathology, the direct relationship between motor variability and gait asymmetry has not yet been studied. Understanding this relationship may enable a deeper understanding of their respective roles with respect to injury and pathology during gait.

This study examined the correlation between gait asymmetry and motor variability in a healthy control population. We hypothesized that gait asymmetry and motor variability would be positively correlated in treadmill walking.

METHODS

Fifty-one recreationally active adults ages 18 to 35 were recruited (Table 1). Exclusion criteria included history of major lower extremity surgery, currently seeking medical treatment for any musculoskeletal disease/injury, and any lower extremity injury in the past 3 months that limited physical activity for more than 1 day.

Table 1: Participant demographics. Mean (SD).

	Age	Height (m)	Weight (kg)
Men (n = 23)	24.17 (4.84)	1.80 (0.07)	78.81 (14.76)
Women (n = 24)	24.54 (2.50)	1.70 (0.05)	66.90 (9.44)
p-value	0.620	<0.001	<0.001

An 8-camera Miqus MI system (Qualisys, Gothenburg, Switzerland) and a fore-aft split belt instrumented treadmill (AMTI, Watertown, Massachusetts) were used to collect motion capture (120Hz) and loading (1440Hz) data, respectively. Participants wore form fitting shorts, a shirt, and Nike Zoom neutral cushioning athletic running shoes. Reflective markers were placed bilaterally on lower extremity bony landmarks. Participants completed a five minute walking trial at 1.5m/s on the instrumented treadmill. All spatial and temporal time-series data was calculated using Visual 3D software (C-Motion, Bethesda, Maryland).

Step length, single support time (% stride), and swing time (% stride) asymmetry was quantified using a limb symmetry index (Equation 1) [3]. Stride-to-stride standard deviation was calculated for step length, stride length, step width, stride time, support time (% stride), and swing time (% stride). Standard deviation was used to quantify variability on the dominant (D) and non-dominant (ND) limbs.

$$\text{LSI} = \frac{|X_D - X_{ND}|}{0.5*(X_D + X_{ND})} * 100\% \qquad (1)$$

Pearson correlation coefficients between each pair of asymmetry and variability metrics were calculated in JMP Pro 13 (Table 2). An alpha level of 0.05 indicated significance and coefficients of below 0.34, 0.37-0.67, 0.67-0.9, and above 0.9 were considered poor, moderate, high, and very high respectively.

RESULTS AND DISCUSSION

Gait asymmetry and motor variability were significantly correlated. Increases in swing and single support time asymmetries were positively correlated with temporal variability. Increases in step length asymmetry were negatively correlated with variability of step length and step width. Spatial and temporal asymmetry were only significantly related to spatial and temporal variability, respectively.

Correlations between temporal measures were stronger than those between spatial measures.

Motor variability has been described as both noise in the motor control system and as serving to increase adaptability [4]. Similarly, gait asymmetry can be both functional and pathologic (**); the context of this observation is crucial. In active young adults, gait asymmetry may allow each limb to be utilized uniquely for propulsion and balance [5]. Results suggest this asymmetry would be correlated with increased temporal and decreased spatial variability. These potential changes in motor variability may also be functional and indicative of increased system adaptability. In a pathologic older adult population, gait asymmetry and related alterations to motor variability are less likely functional and more likely pathologic or reflective of some increased risk. In older adults with lower extremity pathology, higher variability may indicate decreased motor control and compromised balance that may increase fall risk [1].

The main limitation of this study was that only temporal and spatial correlations between gait asymmetry and motor variability were investigated. Spatial and temporal parameters are more commonly studied in variability literature than are kinetic and other kinematic measures, which drove this focus. However, the scope could be expanded to include kinetic and other kinematic measures in future studies. This study also only included healthy young adults. Since variability is so heavily studied in older adults and pathologic patients, this limited population decreases broad applicability back to the populations of interest. A similar study in older adults and individuals with injuries and/or pathology would widen the represented population.

CONCLUSIONS

The relationship between gait asymmetry and motor variability provides additional information to better understand the role of motor variability in gait. This relationship is another tool to differentiate between functional and pathologic asymmetry and variability. Gait retraining based on this relationship may be useful to decrease fall risk in older adults. Gait asymmetry and motor variability should not be thought of independently and should be investigated in tandem when possible.

REFERENCES

1. Hausdorff, J.M., et al. Arch Phys Med Rehabil. **82**(8). 2001.
2. Queen, R.M., et al. Clin Biomech. **29**(4). 2014.
3. Herzog, W., et al. Med Sci Sports Exerc. **21**(1). 1989.
4. Newell, K.M. and A.B. Slifkin. Motor behavior and human skill: A multidisciplinary perspective. 1998.
5. Sadeghi, H., et al. Hum Mov Sci. **16**(2). 1997

Table 4: Correlation Coefficient and p-values for each set of asymmetry and variability measures. Dominant limb (D) and Non-dominant limb (ND) are reported for visual comparison. R: very high (green), high (yellow), moderate (orange), poor (red). P-values: <0.05 (green), ≥0.05 (red).

Measures of Interest	Step Length LSI		Swing Time LSI		Single Support Time LSI	
	R	p-value	R	p-value	R	p-value
Step Length - D	-0.588	<0.001	0.162	0.262	0.044	0.761
Step Length – ND	-0.566	<0.001	0.237	0.097	0.107	0.460
Stride Length – D	0.186	0.195	-0.023	0.876	0.241	0.093
Stride Length – ND	0.198	0.168	-0.065	0.652	0.217	0.130
Stride Time – D	-0.237	0.098	0.824	<0.001	0.115	0.425
Stride Time – ND	-0.234	0.101	0.825	<0.001	0.116	0.421
Support Time - D	-0.226	0.115	0.933	<0.001	0.295	0.038
Support Time - ND	-0.248	0.082	0.931	<0.001	0.291	0.040
Swing Time – D	-0.165	0.252	0.844	<0.001	0.138	0.338
Swing Time – ND	-0.189	0.188	0.901	<0.001	0.173	0.230
Step Width	-0.387	0.006	0.275	0.053	0.185	0.199

CHANGES IN FORCE-DEFORMATION PATTERNS OF THE FOOT WITH WALKING SPEED

[1]Thomas Hulcher and [1,2] Elisa Arch

[1] Biomechanics and Movement Science Interdisciplinary Program, [2] Department of Kinesiology and Applied Physiology
University of Delaware, Newark, DE, USA
Email: thulcher@udel.edu

INTRODUCTION

Walking is one of the most important motor abilities a person can possess, allowing for transportation, exercise, socialization and participation in society. Loss of walking ability leads to physical inactivity which has been shown to increase mortality [1]. Depending on the injury or disability, an orthotic device may be prescribed to help an individual regain walking ability. Orthoses are common, with almost 2.5 million orthotic and prosthetic devices approved by Medicare in 2015 [2].

Ankle-foot orthoses are the most commonly prescribed category of orthotic devices [3]. Many foot and ankle-foot orthoses use a solid, rigid footplate which inhibits the natural deformation of the foot. In particular, during the latter part of the stance phase, the forefoot naturally deforms under force. Interestingly, this forefoot deformation absorbs power [4]. Use of a rigid footplate with a toe rocker has been shown to minimize the overall power loss of the ankle-foot complex [5], demonstrating the energetics of the ankle-foot system can be manipulated through control of the foot's deformation. Harnessing this knowledge, we theorize it may ultimately be possible to augment the power profile of the ankle-foot system, particularly for patients with impairments, through a deformable footplate that harnesses the natural loading and unloading pattern of the foot. In order to design such a footplate, the force-deformation patterns of the natural foot need to be characterized, especially in the latter part of stance during which the forefoot (toes) dorsiflex. We hypothesized that, in typical gait, as walking speed increases, the vertical ground reaction force and amount of forefoot foot deformation will both increase. Furthermore, we hypothesized that these increases will be similar in value, leading to a constant forefoot stiffness (ratio of force to displacement/deformation) across walking speeds.

METHODS

Motion capture data from nine healthy subjects walking barefoot, overground at four scaled speeds (0.4, 0.6, 0.8, 1.0 statures/second) were analyzed. These data were captured using a six camera optical motion analysis system (Motion Analysis Corporation, Santa Rosa, CA) and four force plates (AMTI, Watertown, MA, USA). A six-degree-of-freedom marker set was used to track lower extremity segments. Outcome measures were calculated for each subject at each speed for trials that had at least one foot completely in contact with a force plate. Each of these measures were then averaged across trials within each walking speed, for each subject. Primary outcome measures were the change in (1) vertical ground reaction force (GRF) and (2) the vertical center of pressure (COP), referenced to the foot coordinate system, over the period of interest (approximately the phase of toe dorsiflexion in late stance). To indicate the start and end of this period of interest, the time at which the vertical COP had an inflection point during the latter half of stance and the maximum COP value, respectively were used. The change in vertical GRF and vertical COP (forefoot deformation) were calculated as the measure's value at the second time point minus the value at the first time point. Finally, these measurements were used to determine forefoot stiffness according to the function $k = F/\delta$ where k is the stiffness value (N·foot-length/kg), F is the force (N/kg) and δ is the forefoot deformation (1/foot-length).

RESULTS AND DISCUSSION

On average, the forefoot deformation and vertical GRF increased at a seemingly steady rate as speed increased (Table 1.) Average forefoot stiffness increased from 0.4 to 0.8 stat/s. There was a slight decrease in stiffness from 0.8 to 1.0 stat/s (Table 1.)

These data supported our hypotheses across all speeds for the deformation and vertical GRF. Contrary to our hypothesis, the stiffness increased but then decreased as speed changed.

0.8 stat/s is generally considered to be a comfortable walking speed for healthy individuals. Trends in these data were consistent from slow to comfortable walking speeds but seem to change at a faster than comfortable speed (1.0 stat/s). This observation may indicate that the mechanics of the ankle/foot complex is altered at faster-than-comfortable speeds, perhaps as a preparatory transition from walking to running.

CONCLUSIONS

The goal of this study was to characterize how the foot, specifically the forefoot, naturally deformed at various walking speeds in order to take the first steps toward developing an orthotic footplate that mimics that deformation. The results showed that the deformation, GRF, and stiffness changed as walking speed changed although they do not all increase with increased walking speed. This work is the first step towards ultimately aiming to harness energetics of the ankle-foot system to improve gait function and mobility of patients with ankle-foot impairments.

REFERENCES

[1] A. H. Mokdad, *JAMA*, 2005.
[2] Department of Health & Human Services, "2016 CMS Statistics," 2016.
[3] S. Whiteside, *Certif. Orthotics, Prosthetics Pedorth.*, 2007.
[4] K. Z. Takahashi, *J. Biomech.*, 2012.
[5] E. S. Arch, *J. Appl. Biomech.*, 2016.

Table 1: Foot deformation, vertical GRF, and forefoot stiffness during approximate ~ period of toe dorsiflexion in stance for nine subjects and average at 0.4, 0.6, 0.8 and 1.0 stat/s

	Deformation (1/foot-length)				Vertical GRF (N/kg)				Forefoot Stiffness (N·ft-length/kg)			
	0.4 stat/s	0.6 stat/s	0.8 stat/s	1.0 stat/s	0.4 stat/s	0.6 stat/s	0.8 stat/s	1.0 stat/s	0.4 stat/s	0.6 stat/s	0.8 stat/s	1.0 stat/s
Sub 1	0.286	0.320	0.375	0.410	0.781	1.059	1.152	1.123	2.558	3.414	3.150	2.758
Sub 2	0.310	0.359	0.329	0.326	0.806	1.033	1.116	1.072	2.453	2.902	3.502	3.788
Sub 3	0.327	0.364	0.376	0.408	0.872	0.978	1.200	1.331	2.442	2.579	3.441	3.282
Sub 4	0.215	0.269	0.293	0.366	0.682	0.997	1.050	1.097	3.524	4.632	3.789	3.038
Sub 5	0.257	0.285	0.365	0.418	0.824	0.896	1.069	1.211	2.873	3.125	2.945	2.942
Sub 6	0.330	0.372	0.320	0.359	0.974	1.076	1.088	1.180	2.997	2.957	3.439	3.321
Sub 7	0.321	0.366	0.387	0.429	0.890	1.026	1.136	1.197	2.771	2.819	3.006	2.799
Sub 8	0.352	0.485	0.444	0.434	0.898	1.094	1.199	1.197	2.581	2.343	2.716	2.767
Sub 9	0.302	0.352	0.366	0.409	0.903	1.038	1.144	1.140	3.030	3.040	3.129	2.817
Avg	**0.300**	**0.352**	**0.362**	**0.395**	**0.843**	**1.022**	**1.128**	**1.172**	**2.803**	**3.090**	**3.235**	**3.057**

A NEW KINEMATIC-BASED GAIT EVENT DETECTION ALGORITHM DURING TREADMILL LOCOMOTION

[1]Alexander M. Morgan, [1]Stephen Cobb, [1]Emily Gerstle, [2]Bryan Heiderscheit, [2]Mikel Stiffler-Joachim, and [1]Kristian M. O'Connor

[1]University of Wisconsin-Milwaukee, Milwaukee, WI, USA
[2]University of Wisconsin-Madison, Madison, WI, USA
email: morgan28@uwm.edu

INTRODUCTION

Detection of gait events is typically reliant upon kinetic data from force plates. However, in the absence of force plate data as is typical for treadmill-based gait, algorithms using kinematic data are necessary to estimate these gait events. Numerous treadmill coordinate-based algorithms for detecting initial contact and toe off during the stance phase of the gait cycle have been developed and assessed for accuracy and reliability [1,2,3]. These algorithms have primarily examined the positions of heel and toe reflective markers, often in relation to a pelvis marker. However, not all motion capture methods utilize these markers. As such, it would be beneficial to be able to identify gait events using a single landmark.

Tracking the anterior-posterior position of the ankle joint center does not require placing markers on specific foot locations, and it is a point that all kinematic methods generally have access to. Such a method could be beneficial across different walking and running speeds if appropriate temporal offsets can be determined with adequate precision. Methods using foot-based markers have been reported for walking [4] and running [5], but no study has established using a single landmark across walking and running speeds. Therefore, the purpose of this study was to examine the validity of a new gait event detection method using the anterior-posterior position of the ankle joint center.

METHODS

Eighty subjects (43 male and 37 female) participated in this study (average: 40.9 years, 1.7 m, 70.5 kg). Written informed consent was obtained from all subjects prior to participation in accordance with the Institutional Review Board of the University of Wisconsin-Milwaukee. Three-dimensional kinematic data were collected using an MPT Series-2.0 motion capture system (Metria Innovation, Inc., Milwaukee, WI) at 180 Hz. Kinetic data were collected using Bertec instrumented force treadmill (Columbus, OH) at 1800 Hz.

Tracking targets were placed on the pelvis and bilaterally on the posterior aspect of the thigh, shank, and heel. Relevant anatomical landmarks, including bilateral ASIS, PSIS, greater trochanters, lateral and medial epicondyles and malleoli, and the head of the first and fifth metatarsals, were identified. The ankle joint center was identified as the midpoint of the malleoli.

Fifteen-second trials for six different gait speeds were collected. Subjects walked on the instrumented treadmill at 2 and 3 mph, and ran at 5, 6, 7, and 8 mph. The anterior-posterior position of the ankle joint center relative to the pelvis was used in the algorithm for detecting gait events. The most anterior and posterior relative positions of the right and left ankle joint center were determined for each step. The instants of initial contact and toe off were determined from the force data using a 20-N threshold. The temporal difference between the most anterior ankle position and initial contact, and the difference between the most posterior ankle position and toe off were determined. Positive reported offsets indicated that the actual gait event occurred later than the kinematic event.

Statistical analyses were performed using SPSS (v19.0 SPSS Inc., Chicago, IL). Within-subject differences in gait event offsets across the six different speeds were assessed using a one-way

repeated measures ANOVA ($p<0.05$). Within subject differences in gait event times between walking and running were assessed using a paired-samples t-test ($p<0.05$).

RESULTS AND DISCUSSION

For both walking and running, initial contact occurred on average between five and six frames after the most anterior ankle position, with a significant difference of a half frame between walking and running (Table 1).

The instant of toe off occurred nine frames after the most posterior ankle position for walking and 14 frames before this event for running (Table 1). For walking, the ankle joint begins to move forward as the ankle plantarflexes before toe off, while for running the leg continues to move backwards after toe off. Within each mode of gait, there were significant differences in gait event detection across speeds for both walking and running (Table 2). However, many of the speed related differences were relatively small.

The between-subjects standard deviations of the offset for walking are less than two frames for initial contact and slightly more than two frames for toe off, which is similar to previous reports [1]. These values for running are about two frames for initial contact and between two and four frames for toe off. These standard deviations are between two to eight times less than previously shown in other studies [1,2,6].

CONCLUSIONS

This study presents a kinematic algorithm using the ankle joint center to detect gait events across gait speed and type. Applying the offsets listed in Table 1 to the times of most anterior and posterior positions of the ankle joint provided an accurate representation of initial contact and toe off. In addition, the present algorithm appears to perform better than other, similar kinematic algorithms with regards to between subjects variation for running [1,2,6]. Furthermore, our findings concur with previous work suggesting that gait type does impact event offsets [5]. These results support the use of this algorithm for walking and running gait studies.

REFERENCES

1. De Witt J. *J Biomech* **43**(15), 3067-3069, 2010.
2. Smith L, et al. *Gait Posture* **41**(1), 39-43, 2015.
3. Zeni J, et al. *Gait Posture* **27**(4), 710-714, 2008.
4. Kiss R. *Med Eng Phys* **32**(6), 662-667, 2010.
5. Alvim F, et al. *J Appl Biomech* **31**(5), 383-388, 2015.
6. Sinclair J, et al. *Int J Sci Eng* **5**(3), 188-192, 2011.

Table 1: Average frame offsets between kinematic- and kinetic-based gait events for walking and running. Data presented as mean (SD). * indicates a significant difference between gait speed ($p<0.05$).

	Initial Contact	Toe Off
Walk	5.9 (1.2)*	9.4 (1.9)*
Run	5.4 (1.8)	-13.9 (3.0)

Table 2: Average frame offsets across gait speeds for walking and running. Data presented as Mean (SD). Letters indicate significant differences from the following: [a] 3 mph, [b] 6 mph, [c] 7 mph, and [d] 8 mph.

Walking		
Speed (mph)	Initial Contact	Toe Off
2	6.8 (1.7)[a]	10.2 (2.2)[a]
3	5.0 (1.1)	8.6 (2.3)
Running		
	Initial Contact	Toe Off
5	5.3 (2.3)[d]	-12.5 (4.2)[b,c,d]
6	5.2 (1.8)[c,d]	-14.1 (3.2)[c]
7	5.6 (2.3)	-14.7 (3.2)
8	5.8 (1.7)	-14.2 (2.6)

THE EFFECTS OF SUBTALAR AXIS ORIENTATION ON KINEMATICS AND KINETICS DURING DYNAMIC MOTION

[1] Julia M. Noginova, [1] Hunter J. Bennett, [2] Michael A. Samaan, and [1] Stacie I. Ringleb

[1] Old Dominion University, Norfolk, VA
[2] University of California-San Francisco, San Francisco, CA
email: Sringleb@odu.edu

INTRODUCTION

The ankle and subtalar joint (STJ) provide primary dorsiflexion/plantarflexion and inversion/eversion during gait, respectively. Frequently, the subtalar joint is overlooked in biomechanical models. These two joints are often grouped together as one ankle-subtalar-joint complex or the models focus on the ankle, keeping the subtalar joint locked. Further, when the STJ is included in the model, like in the commonly used OpenSim model, Gait2392 [1], the subtalar joint is treated as a one degree-of-freedom joint with the axes orientation angles set at the low range as reported by Inman [2]. According to Inman [2], the subtalar joint lies on an oblique axis with inclination and deviation angles that range from 68.5-20.5° and 4-47°, respectively. In the Gait2392 model, the orientation of the subtalar joint axis is set at 37.2° from the horizontal plane and 8.7° from the midline of the foot. While these lie within the range, these values are lower than the average inclination and deviation angles of 42° and 23° as reported by Inman [2].

The purpose of this study was to determine how varying the subtalar joint axes orientation to reflect Inman's average axes affect kinematics and kinetics of the ankle and subtalar joint during dynamic motion in OpenSim.

METHODS

Three-dimensional marker position and ground reaction force (GRF) data of three dynamic tasks: walking, running, and a one-leg jump, were obtained for five subjects (3 male, 2 female, mean age 23.4 ±3.43, average BMI 26.49 ± 3.48) as part of an IRB approved study after informed consent was obtained. The data were imported into OpenSim (SimTK, Stanford, CA, v3.3) and used to scale the default Gait2392 model for each subject. Marker data were filtered at 6 Hz for walking, running, and jumping prior to dynamics comparisons.

To determine the impact of Inman's axis on STJ dynamics, inverse kinematics and dynamics were computed using OpenSim in two STJ conditions: 1) the standard scaled model and 2) a scaled model with the subtalar joint orientation matching Inman's average inclination and deviation angles. A custom Matlab (The Mathworks, Natick, MA, R2014a) program was used to normalize stance phase of the right leg for all five subjects during walking and running. The one-leg jump task was separated into three parts and normalized for stance, in air, and land phases. A two-tailed paired t-test was used to compare max, min, and range values for kinematics and kinetics of the original Gait2392 subtalar joint axis orientation and Inman's mean axis. Significance was set at $p<0.05$ for all analyses.

RESULTS AND DISCUSSION

The mean ankle and subtalar joint kinematics patterns for both Inman and default Gait2392 subtalar joint models were similar to in vivo bone pin studies for walking [3]. Modifying the subtalar joint orientation from Gait2392 to match Inman's mean inclination and deviation angles resulted in a statistically significant change in the range of ankle angle values ($p=.049$) seen in the kinematics during walking (Gait2392: 28.95° ± 4.41°; Mean Inman: 29.42° ± 4.54°). No other changes in kinematics were seen in other joints or motions.

Varying the orientation of the subtalar joint axes caused a significant increase in peak subtalar joint moments in all three dynamic motions (Table 1): walking (peak 1: $p=.001$, peak 2: $p<.001$), running ($p=.005$), and one-leg jump (peak 1: $p=.009$, peak 2:

p<.001). Looking at the three motions (Figure 1), we can see that Inman's mean subtalar joint axes produce higher average subtalar joint moments throughout each motion. The more dynamic the task, with jumping being the most extreme, we see a larger difference in subtalar joint moment between the two models.

Changing the subtalar joint orientation also resulted in large changes of the subtalar joint moment patterns during walking. The average Inman's mean axes produces two large peaks during the stance cycle, one at 30% stance and the second around 80% of the gait cycle. The axis used by Gait2392 produced a much smaller second peak, seen later at around 90% of the stance (Figure 1a).

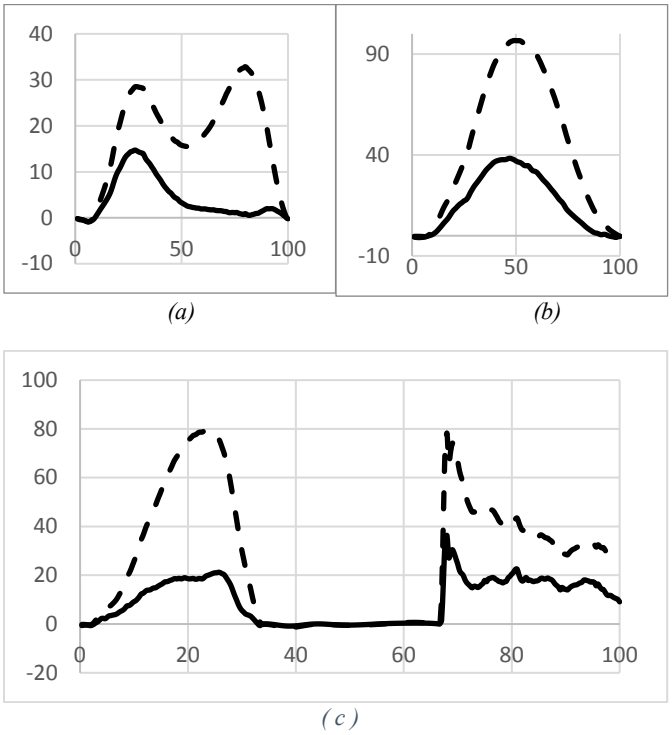

Figure 1: Average subtalar joint moment (Nm) comparing Gait2392 (solid) vs Inman (dotted) subtalar joint orientation during (a) walking (b) running (c) and one-leg jumping tasks.

Comparing the results from all five subjects, the subtalar joint moments during walking show subject-to-subject variability, which is consistent with prior studies [4]. The model with Inman's mean axes has a double-peak curve for all 5 subjects while the model with Gait2392 subtalar joint angles shows a slight double-peak for only 2/5 subjects. This is similar to the literature that showed a double-peak for only 1/3 subjects [4]. A limitation of this study is that due to lack of studies and the variability in subject specific differences, we are not able to verify which model is correct.

Another limitation of this study is that the knee, ankle, and subtalar joint are all modeled as one DOF joints. This restricts the observation to only one plane of motion. In order to see how the changes to the subtalar joint axes affects all planes of motion, the model should include 3DOF in the knee and ankle.

Since the net joint moments affects muscle force calculations, future studies should evaluate how changes to the subtalar joint inclination and deviation angles affect muscle activation and muscle force during dynamic tasks. In this study, walking, running, and a one-leg jump were investigated, but future work should also investigate more complex dynamic tasks like cutting maneuvers, which elicit more motion at the subtalar joint.

CONCLUSIONS

Changing the subtalar joint axes to match Inman's mean inclination and deviation angles produces different subtalar joint moments in various dynamic tasks. Future works should determine how these changes in subtalar joint moments affects muscle forces as well as the kinematics and kinetics at the hip and knee seen in dynamic motions, such as cutting.

REFERENCES

[1] Delp, et al. IEEE Trans Biomed Eng 37,757-767,1990.
[2] Inman, The Joints of the Ankle.Williams & Wilkins, 1976.
[3] Arndt, A., et al. Foot Ankle Int 25,357-364, 2004
[4] Scott, et al. J. Biomech, 24, 743-752,1991.

Table 1. Average STJ peak moments (Nm) during dynamic tasks

	Gait 2392	Mean Inman	p-value
Walk 1	14.7 ± 11.5	14.8 ± 28.1	0.001
Walk 2	11.9 ± 8.6	25.± 32.9	0.0007
Run	38.3 ± 40.6	96.7 ± 46.1	0.005
Jump 1	21.2 ± 69.4	79.7 ± 72.7	0.009
Jump 2	36.3 ± 38.7	78.2 ± 56.2	0.0008

DOES LOCAL DYNAMIC STABILITY DURING UNPERTURBED WALKING PREDICT THE RESPONSE TO BALANCE PERTURBATIONS?

Mu Qiao, Kinh N. Truong, and Jason R. Franz

University of North Carolina and North Carolina State University, Chapel Hill, NC, USA
email: jrfranz@email.unc.edu, web: http://abl.bme.unc.edu

INTRODUCTION

Older adults are at high risk of falls, and most falls occur during locomotor activities such as walking. Reduced local dynamic stability in old age is often interpreted to suggest a lessened capacity to respond to more significant balance challenges encountered during walking and future falls risk [1]. However, it remains unclear whether local dynamic stability during normal, unperturbed walking predicts the response to larger external balance disturbances. Indeed, local dynamic stability quantifies resilience to small, naturally occurring kinematic deviations arising normally during walking, and may not reflect resilience to larger external perturbations that could elicit a fall [1]. Predicting one's resilience to external balance challenges using measurements acquired during normal, unperturbed walking may be clinically desirable, enabling the targeted prescription of preventive care. We hypothesized that larger values of local dynamic instability during unperturbed walking would positively correlate with larger changes due to optical flow perturbations – a hypothesis that we tested in subjects coalescing to provide a spectrum of walking balance integrity: young adults, older non-fallers, and older fallers.

METHODS

We recruited 11 young (5M/6F), 11 older adult non-fallers (5M/6F), and 11 older adults with at least one fall in the last year (4M/7F) to walk on an instrumented dual-belt treadmill (Bertec, Corp.). Young adults walked at 1.25 $m \cdot s^{-1}$ while both older fallers (1.03±0.22 $m \cdot s^{-1}$) and non-fallers (1.19±0.20 $m \cdot s^{-1}$) walked at their preferred overground speed. While walking, subjects watched a speed-matched, virtual hallway rear-projected onto an immersive semi-circular curved screen surrounding the treadmill (Fig. 1A) both with and without continuous oscillations of optical flow designed to elicit the visual perception of lateral instability [2]. In randomized order, subjects walked for 2 min normally and with optical flow perturbations at amplitudes of 20, 35, and 50 cm. A 14-camera motion capture system (Motion Analysis Corp., 100Hz) recorded the 3D trajectories of heel markers and the C7 vertebrae (filtered with a low-pass cutoff of 8 Hz). We quantified local dynamic stability by estimating maximum exponential rates of divergence (*i.e.*, λ, bits·stride^{-1}) from 3D C7 marker velocity time series (Eqn. 1). We constructed a state space, $\boldsymbol{S}(t)$, as:

$$\boldsymbol{q}(t) = (\dot{x}, \dot{y}, \dot{z}) \quad (1)$$

$$\boldsymbol{S}(t) = [\boldsymbol{q}(t), \boldsymbol{q}(t + 1 \cdot \tau), \cdots, \boldsymbol{q}(t + (d_E - 1)\tau)] \quad (2)$$

where, $\dot{x}, \dot{y},$ and $\dot{z}$ are the C7 velocity components in the anterior-poster, medio-lateral, and vertical directions, respectively. By convention [1,2], we computed the maximum rates of divergence of initially neighboring trajectories from $\mathbf{S}(t)$ using an embedding dimension (d_E) of 4 and a time delay (τ) equal to one quarter of subjects' average stride time. We time normalized the divergence curves to account for differences in stride period and calculated short-term (i.e., λ_S, 0 to 1 stride) and long-term (i.e., λ_L, 4 to 10 stride) divergence exponents for each condition, where larger positive values indicate larger local dynamic instability. A mixed 2-way factorial ANOVA first tested for main effects of group and condition on λ_S and λ_L using α=0.05. Linear regressions then estimated the relation

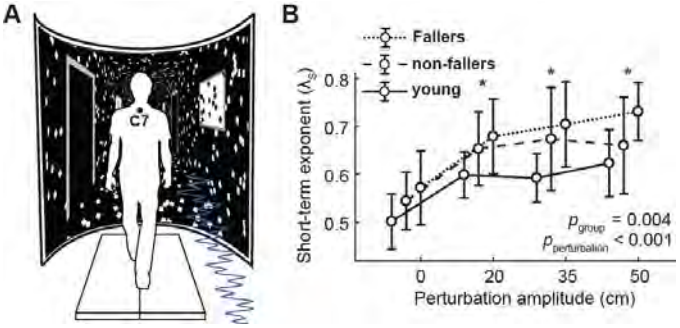

Figure 1: (A) Virtual environment. (B) The effects of group (*e.g.,* young adults, non-fallers, and fallers) and perturbation amplitude on short-term local divergence exponents (λ_S).

between local dynamic stability during unperturbed walking ($\lambda_{unperturbed}$) and the average change thereof in response to perturbations (i.e., $\bar{\lambda}_{perturbed}$-$\lambda_{unperturbed}$).

RESULTS AND DISCUSSION

Aging and falls history effects on dynamic instability

We observed a significant effect of group on short-term (λ_S, p=0.004, Fig. 1B) but not long-term local dynamic instability - an effect governed by instability due to age, independent of falls history. However, neither age nor falls history significantly affected dynamic instability during unperturbed walking. Compared to unperturbed walking, optical flow perturbations significantly increased short-term (λ_S, p<0.0001, Fig. 1B) local dynamic instability – which affected all subject groups (young: p<0.001, non-fallers: p=0.009, fallers: p<0.001, Fig. 1B).

Perturbations revealed between-group differences in local dynamic instability that were not apparent during unperturbed walking. Age alone did not increase local dynamic instability during walking for any optical flow perturbation amplitudes. In contrast, fallers exhibited larger local dynamic instability than young adults for all three perturbation amplitudes (fallers *vs*. young: p<0.009, Fig. 1B). We observed no difference in local dynamic instability between fallers and non-fallers for the two smallest amplitude perturbations (p≥0.445, Fig. 1B). However, although not statistically significant, fallers tended to have larger local dynamic instability than non-fallers at the largest amplitude (50cm: p=0.059, Fig. 1B).

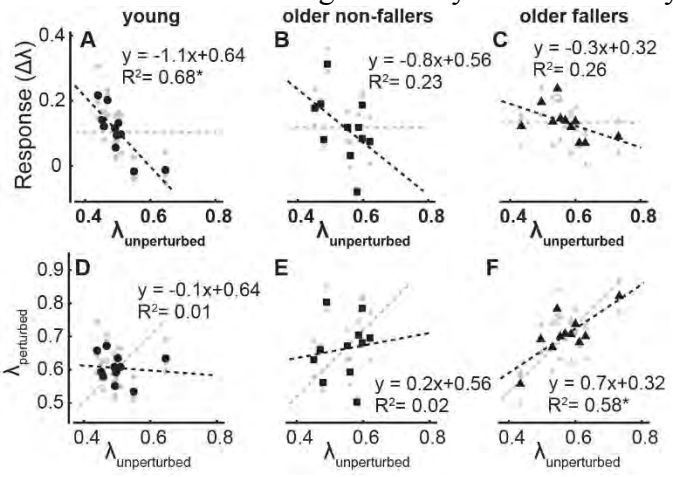

Figure 2. Top row; correlations between λ_S during unperturbed walking ($\lambda_{unperturbed}$) and the average change thereof in response to perturbations ($\Delta\lambda$=$\lambda_{perturbed}$-$\lambda_{unperturbed}$) for (A) young adults, (B) older non-fallers, and (C) older fallers. Bottom row; correlations between $\lambda_{unperturbed}$ and the average in response to optical flow perturbations ($\lambda_{perturbed}$) for (D) young adults, (E) older non-fallers, (F) and older fallers. The black dashed line is the best linear fit; the solid gray line has a slope of zero (top row) or one (bottom row) indicating, in both, a response to perturbations that is independent of subjects' baseline stability.

Predicting the response to balance perturbations

The relation between λ_S during unperturbed walking and changes due to optical flow perturbations differed across individual groups (Fig. 2). Young adults had the only significant. and by far the strongest and steepest, negative correlation between local instability during unperturbed walking and response to perturbations (R^2=0.68, Fig. 2A). Compared to young adults, this relation was similarly steep but much less well correlated in older non-fallers (R^2=0.23, Fig. 2B). Finally, older fallers exhibited by far the most shallow regression between λ_S during unperturbed walking and changes thereof due to optical flow perturbations (R^2=0.26, Fig. 2C). Indeed, the relation between λ_S during perturbed and unperturbed walking reached significance and approximated the line of unit only for older fallers, indicating a uniform response that emerged only in older adults with a history of falls (Fig. 2F).

CONCLUSIONS

Although modest, our data first suggest that older adults with a history of at least one fall have a more pervasive susceptibility to optical flow perturbations than older non-fallers during walking. Second, in surprising contrast to our hypothesis, a significant negative correlation indicated that young adults with higher local dynamic instability during unperturbed walking exhibited *smaller* responses to optical flow perturbations. One interpretation is that young adults may self-regulate their response to balance perturbations based on a self-perception of risk guided by their baseline level of dynamic instability. In contrast, particularly among older fallers, the response to optical flow perturbations appeared completely independent of their baseline level of dynamic instability. We conclude that understanding the response to balance perturbations, especially among older fallers, may require measuring that response directly rather than relying on measures collected during normal, unperturbed walking

ACKNOWLEDGEMENTS

Supported by a grant from NIH (R56AG054797)

REFERENCES

[1] Kang and Dingwell, J Biomech 14; 2008.

[2] Franz et al., Hum Mov Sci 40; 2015.

PREDICTING MEASURES OF PHYSICAL PERFORMANCE FROM GAIT MECHANICS IN PATIENTS WITH ANKLE OSTEOARTHRITIS

[1,2] Robin Queen, [1]Kristen Renner, [1]Shyam Ranganathan and [1]Divya Srinivasan

[1] Virginia Tech, Blacksburg, VA, USA
[2] Department of Orthopaedic Surgery, Virginia Tech Carilion School of Medicine, Roanoke, VA, USA
email: rmqueen@vt.edu, web: https://www.beam.vt.edu/granatalab/

INTRODUCTION

Measures of physical performance are often used in orthopaedic patient populations and older adults to understand function and determine changes over time [1, 2]. Two measures of physical performance which are often used in the clinical and older adult settings are the timed up and go (TUG) and the sit to stand (STS) tests. These two measures have been used extensively to monitor both functional decline in adults as well recovery following surgical interventions. Gait mechanics have also been used to assess post-operative recovery and functional status in these same populations. Although measures of physical performance and gait mechanics are both important for understanding functional changes, the association between these two paradigms has not been assessed on orthopaedic patients.

In order to examine the association between gait mechanics and physical performance, this study examined an end-stage ankle osteoarthritis (A-OA) cohort. A-OA has been associated with limitations in gait mechanics and physical performance [3]. Therefore, the purpose of this study was to determine whether, and which, gait mechanics measures during self-selected speed level walking can predict physical performance on the TUG and STS tests in an A-OA cohort.

METHODS

A prospective cohort study was completed during which 112 end-stage A-OA patients (**Table 1**). A-OA Patients were included in this study if they had unilateral disease and were able to walk without the use of an assistive device. All patients provided informed written consent prior to participation in this study.

Each patient completed a standard gait assessment with a modified Helen-Hayes marker set using an 8 camera motion analysis system (120Hz) (Motion Analysis Corporation, Santa Rosa, CA) and 4 embedded force plates (1200Hz) (AMTI, Watertown, MA) [3]. Seven barefoot walking trials were collected at a self-selected walking speed. Visual 3D (C-Motion, Bethesda, MD) was used to calculate joint kinematics and kinetics. In addition to the gait assessment, each participant completed a 5 time STS test and a TUG [3].

STS and TUG scores were sorted, and patients in the bottom 25% and the top 25% were identified independently and their data were used for further analysis (**Table 1**). A total of 200 variables characterizing gait including averages, peaks, and stride-to-stride variability (SD) on the affected side, and asymmetry (ASYM) using the formula from Herzog et al [5], were computed:

1. Spatiotemporal characteristics (28 variables - means and variability);
2. Joint Kinetics (60 variables quantifying peak flexion (FLEX)/extension (EXT) as well as abduction (ABD)/ adduction (ADD) of hip, knee, and ankle moments and powers, SD of moment and power trajectories, and ASYM in peak FLEX/EXT and ABD/ADD moments and powers)
3. Stance phase joint kinematics (56 variables characterizing FLEX/EXT and ABD/ADD peaks, range of motion (ROM), SD of joint trajectories and ROM, ASYM across limbs in FLEX/EXT and ABD/ADD peaks and ROM, mean coordination and SD of hip-knee and knee-ankle joint couples quantified through vector coding in sagittal and frontal planes);
4. Swing phase joint angle kinematics (same 56 variables as stance phase)

Four different regression models were used to predict performance on the TUG from gait characteristics from each of the above categories. Due to the large number of potential predictor variables, regularized regression is required to avoid overfitting. Least Absolute Shrinkage and Selection Operator (LASSO) was used to fit logistic regression models

to the data. Five-fold cross-validation was used to ensure low out-of-sample prediction error. Since the high number of variables may result in instability of the results, an additional variable selection step was used by iterating the LASSO algorithm multiple times and selecting only those variables that were selected in more than 95% of the model iterations. The same approach was implemented to predict STS performance using the same four gait variable categories. All statistical analysis was completed using R (R Foundation for Statistical Computing, Vienna, Austria).

RESULTS AND DISCUSSION

The full Ankle-OA cohort of 112 participants was divided into the top and bottom 25% on the STS and the TUG test independently (**Table 1**).

Performance on both the TUG and STS tests could be predicted with 0% mis-classification error, meaning that a logistic regression LASSO model could correctly classify all 55 subjects into the lower or upper quartile. TUG was predicted best using the joint kinetics variables: 7 of the 60 variables input into the model achieved 100% classification accuracy (**Table 2**). Models using stance and swing kinematics performed poorly (i.e. less than 50% classification accuracy), and the best model using gait spatiotemporal characteristics achieved only 65% accuracy.

STS performance was predicted best by swing phase kinematics: 14 of the 56 variables input into the model achieved 100% classification accuracy (**Table 2**). STS was predicted poorly by the stance phase kinematics and gait spatiotemporal models (less than 50% accuracy) but 88% accuracy using 11 variables was achieved through the joint kinetics model.

These results indicate that variability in measures of physical performance were high in A-OA patients. The best 25% of these A-OA patients were able to achieve similar physical performance outcomes to age matched healthy control for both the TUG 5.6 ± 1.0s and the STS 9.9 ± 1.4s tests.

Table 2: LASSO model selected variables for 100% accuracy in physical performance prediction

TUG	Joint Kinetics	Sagittal Knee Extension Moment Sagittal Knee Flexion Moment Frontal Hip ADD Moment Frontal Hip ADD Power Sagittal Hip Moment SD Sagittal Ankle Power SD Sagittal Hip Power Asymmetry
STS	Swing phase kinematics model	Sagittal Knee Extension Sagittal Knee Flexion Sagittal Ankle ROM Sagittal Hip-Knee coordination Frontal Knee SD Frontal Hip SD Frontal Ankle SD Sagittal Knee SD Sagittal Ankle ROM SD Sagittal Knee-Ankle Coordination SD Sagittal Ankle dorsiflexion Asymmetry Sagittal Knee Extension Asymmetry Sagittal Hip Flexion Asymmetry Sagittal Hip ROM Asymmetry

CONCLUSIONS

While the STS and TUG are clinically accessible and reliable methods for physical performance testing, they do not provide mechanistic insights on the source of a patient's deficits. Our work demonstrates that STS and TUG are able to be predicted by different sets of biomechanical variables, which might serve as good targets for therapeutic intervention.

REFERENCES

1. Bade, et al. JOSPT 40(9): 559-567, 2010.
2. Christiansen and Stevens-Lapsley. Arch Phys Med Rehabil. 91: 1524-1528, 2010.
3. McConnell and Queen. *Foot Ankle Int*. 38(2): 115-123, 2017
4. Queen et al. *Foot Ankle Int*. 33(7): 535-542, 2012.
5. Herzog et al. MSSE. 21(1): 110-114, 1989.

Table 1: Patient Demographics

	Total Cohort	TUG Top 25%	TUG Bottom 25%	STS Top 25%	STS Bottom 25%
Age	62.67 (9.62)	59.81 (11.35)	64.00 (9.70)	60.79 (1.67)	61.61 (8.65)
BMI	28.98 (5.48)	28.65 (5.65)	28.55 (4.65)	28.17 (5.81)	29.47 (4.51)
Gender	F: 69, M: 43	F:14, M:13	F:17, M:10	F:20, M: 8	F:14, M:14
STS Time	16.85 (6.05)	13.60 (4.30)	22.54 (7.02)	10.71 (1.28)	25.26 (4.79)
TUG Time	9.36 (3.44)	6.27 (0.65)	13.88 (3.83)	7.62 (1.60)	11.48 (3.81)

DISCREPANCY IN MODULAR CONTROL DERIVED FROM EXPERIMENTAL AND SIMULATED ACTIVATION PATTERNS

[1,3]Sarah A. Roelker, [2,3]Elena J. Caruthers, [3]Laura C. Schmitt, [3]Ajit M.W. Chaudhari, [3]Robert A. Siston

[1]The University of Texas at Austin, Austin, TX, USA; [2]Otterbein University, Westerville, OH, USA;
[3]The Ohio State University, Columbus, OH, USA
email: schloemer.sarah@utexas.edu

INTRODUCTION

Motor control of gait is thought to be governed by a reduced set of principal activation patterns (modules) [1]. Musculoskeletal modeling and simulation techniques are commonly used to characterize the underlying muscle activation patterns that control gait. Modular control of gait has been identified from electromyography (EMG) in young and older adults [1,2] and a combination of EMG and simulation-derived activation patterns in older adults [2,3]; yet, it remains unknown if activations derived from simulation alone would reduce to the same set of modules as those derived from EMG. Therefore, this study explored the modular control estimated from experimental and simulated muscle activation patterns in young and older adult gait.

METHODS

Ten young (23.9±2.8 years) and ten older (63.1±2.6 years) adults provided IRB-approved written informed consent prior to walking at a self-selected speed while 3D kinematic and kinetic data were collected. Surface EMG was collected from rectus femoris, vastus lateralis, vastus medialis, biceps femoris, medial hamstrings, lateral gastrocnemius, medial gastrocnemius, and soleus on the dominant leg. The EMG was demeaned, passed through a sixth order Butterworth bandpass filter (10-300 Hz), rectified, and then passed through a sixth order Butterworth low-pass filter (6 Hz).

Simulations of one gait cycle were generated for each subject in OpenSim 3.1 [4]. A generic model with 23 degrees-of-freedom and 92 musculotendon actuators [4] was scaled using a least squares approach to minimize the distance between the experimental and corresponding virtual model markers [5]. A least squares approach was used to determine the model's generalized coordinates that reproduced the experimental gait marker data [5]. A residual reduction algorithm slightly adjusted model mass properties and joint kinematics to achieve more dynamically consistent kinematics and kinetics [5]. Static optimization resolved the joint torques into individual muscle forces using an objective function that minimized the sum of the squared muscle activations [6]. The agreement between the normalized EMG and static optimization's simulated (SIM) activation patterns was quantified using RMS error. Each muscle's EMG was normalized by scaling the EMG pattern by the ratio of the muscle's peak SIM activation to the peak EMG activation in the trial [7,8]. A 40ms delay was applied to the EMG to account for electromechanical delay [9].

For each subject, separate non-negative matrix factorizations (NMF) [10] extracted modules from the original activation patterns (EMG_o; SIM_o). The number of modules required to produce adequately reconstructed activation patterns (EMG_r; SIM_r) was determined by the variability accounted for (VAF) by the modules. The VAF is calculated as, for example, $VAF=1-((SIM_o-SIM_r)^2/SIM_o^2)$. The NMF began by extracting one module. If VAF was greater than 0.9 for each muscle, additional modules were not needed to represent the data. Otherwise, the number of modules extracted by NMF was increased by one until VAF of all muscles was greater than 0.9 or until VAF was greater than 0.8 and adding another module did not increase the VAF of the muscle with the lowest VAF by more than 5% [11]. Each subject's principal patterns were normalized to the peak value. Muscle weights were normalized to the maximum weight of the muscle across all modules. Principal patterns and muscle weights were averaged within each age group for each activation source.

RESULTS AND DISCUSSION

All RMS errors between SIM_o and EMG_o were less than 0.31, with soleus having the largest errors in both age groups (Figure 1).

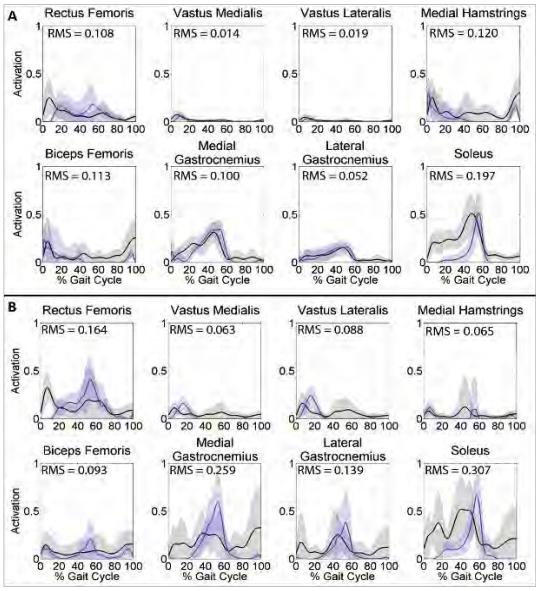

Figure 1: Average EMG_o (grey) and SIM_o (blue) activation patterns in A) young and B) older adults. Shaded areas represent ± one standard deviation.

The number of modules required to reconstruct the original activation patterns was greater with SIM_o (young: 6.8±1.2; older: 5.2±1.0) than EMG_o (young: 3.6±0.7; older: 3.6±0.8). Five young adults' SIM_o could not be reduced to a modular organization (8 modules required to represent the activation of 8 muscles). Therefore, young SIM modules could not be defined and compared to their EMG modules.

The principal patterns of older adult SIM Modules 1, 2, and 4 were qualitatively similar to their EMG modules (Figure 2A); however, no SIM module was similar to EMG Module 3. The muscles primarily associated with each module differed between SIM and EMG (Figure 2B). In contrast to EMG modules, hamstring activity governed SIM Module 1, vasti activity governed SIM Module 4, and separate modules were required to capture plantarflexor activity (gastrocnemius in SIM Module 2; soleus in SIM Module 3). The additional SIM module (5) was required to capture SIM rectus femoris activity.

CONCLUSIONS

Modules extracted from SIM_o differed from those extracted from EMG_o and previously derived modules [1–3], suggesting muscle activations estimated by static optimization, without any activation constraints [12], are not ideal for deriving the modular control of gait. The static optimization objective function was chosen because it is associated with minimizing energy expenditure [13]. However, the discrepancies between the EMG and SIM modules in both young and older adults suggests an optimization function that prioritizes minimizing energy expenditure may not fully capture the neuromuscular control of gait and an alternative objective function may be needed to estimate muscle function. Future work should determine if modules identified from muscle activations estimated by an alternate optimization method or objective function are more consistent with EMG modules.

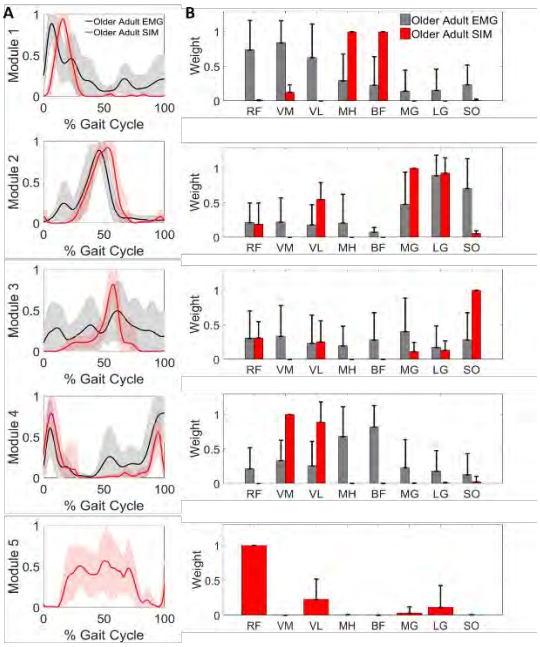

Figure 2: Older adult modules derived from EMG and SIM. A) Average principal patterns (solid line). Shaded area represents ± one standard deviation B) Average muscle weights. Error bar represents one standard deviation. Muscle abbreviations: rectus femoris (RF), vastus medialis (VM), vastus lateralis (VL), medial hamstrings (MH), biceps femoris (BF), medial gastrocnemius (MG), lateral gastrocnemius (LG), and soleus (SO).

REFERENCES

1. Ivanenko et al. *J Physiol* **556,** 267-82, 2004.
2. Neptune et al. *J Biomech* **42,** 1282-87, 2009.
3. Allen & Neptune. *J Biomech* **45,** 215763, 2012.
4. Delp et al. *IEEE Trans Biomed Eng* **37,** 757-67, 1990.
5. Delp et al. *IEEE Trans Biomed Eng* **54,** 1940-50, 2007.
6. Crowninshield & Brand. *J Biomech* **14**, 793-801, 1981.
7. van der Krogt et al. *Gait Posture* **36,** 113-9, 2012.
8. Thompson et al. *J Biomech* **46,** 2165-72, 2013.
9. Arnold et al. *J Exp Biol* **216,** 2150-60, 2013.
10. Lee & Seung. *Nature* **401,** 788-91, 1999.
11. Clark,et al. *J Neurophysiol* **103,** 844-57, 2010.
12. Steele et al. *J Neurophysiol* **113**, 2102-13, 2015.
13. Anderson & Pandy. *J Biomech* **34,** 153-61, 2001.

ACKNOWLEDGEMENTS

We thank Drs. Jackie Lewis and Greg Freisinger for their help with data collection. This research was supported by National Science Foundation Graduate Research Fellowship Program Grants DGE-1343012 (SAR) and DGE-0822215 (EJC).

AUDITORY AND VISUAL EXTERNAL CUES HAVE DIFFERENT EFFECTS ON SPATIAL BUT SIMILAR EFFECTS ON TEMPORAL GAIT VARIABILITY

[1] Joao R. Vaz, [1] Troy Rand, [1] Jessica Fujan-Hansen, [1] Mukul Mukherjee and [1,2] Nicholas Stergiou
[1]Department of Biomechanics, University of Nebraska at Omaha, Omaha, NE USA
[2]College of Public Health, University of Nebraska Medical Center, Omaha, NE USA
email: jvaz@unomaha.edu web: https://www.unomaha.edu/college-of-education/cobre/

INTRODUCTION

Sensorimotor synchronization deals with the coordination of a movement with an external rhythm. Specifically, external auditory or visual cues have been implemented in several populations: Stroke[1], Parkinson's Disease[2] and Aging[3]. Typically, the patient is instructed to synchronize their steps to an invariant stimulus that lack any temporal variability in their presentation. However, there is recent evidence indicating that such stimulus may not be optimal, as it does not incorporate the natural variability that is observed in the stride-to-stride fluctuations of the gait patterns of healthy adults[3]. Gait variability, the natural stride-to-stride fluctuations that are present in walking, is essential for adaptation and safe interaction with the ever-changing environment. Therefore, it has been recommended[3,4] to be incorporated in external cueing interventions. The selection of the type of cueing is also an important issue. In this study, we hypothesized that this selection should be based on our goal. We believe that if one would intend to alter stride length variability, spatial cueing should be provided (visual stimulus). Conversely, to manipulate stride time variability, temporal cueing (auditory stimulus) should be used. Therefore, we aimed to investigate the differences between a visual and an auditory stimulus on stride time and length variability. We also aimed to investigate the effect of incorporating the natural stride-to-stride fluctuations in the temporal structure of the stimulus used. We implemented a variable (pink-noise; a spectra/distribution that characterizes healthy natural gait[3]), a random (white-noise), an invariant, and a non-stimulus condition.

METHODS

Twenty subjects volunteered to participate in this study. The subjects were randomly assigned to an Auditory (AUD) or a Visual (VIS) group. Both groups started with a preferred walking speed familiarization trial. This was followed by four 10-min trials on an instrumented treadmill starting with a no external stimulus trial. From this trial, the preferred cadence was determined and embedded in the stimulus to be provided for the three stimulus conditions. The order of the three stimulus conditions was randomized: invariant (INV), variable (VAR) and random (RND). The VAR was generated using an approximation of a -10dB/decade filter with a weighted sum of first order filters; RND was generated using a normal distribution of random numbers. The subject's preferred cadence and standard deviation was incorporated in the stimulus. The INV stimulus was generated using each subjects' mean self-paced cadence and a standard deviation of zero. The auditory stimulus was provided through speakers as a single beat per step, and the visual stimulus was provided through the screen's projection of horizontal bars (GRAIL, Motek). For the latter, each subject's virtual footsteps were visible during the task on the screen. A high speed 8-camera Vicon system was used for spatiotemporal data calculations. Reflexive markers were placed on the heel, lateral malleolus and 2nd metatarsal. Means and SDs of stride time (ISIs) and stride length (ILIs) intervals were determined. The $\propto$-scaling of stride time ($\propto$-ISIs) and length ($\propto$-ILIs) time series was also calculated through Detrended Fluctuation Analysis (DFA)[5]. DFA estimates the autocorrelation behavior of the time series. An $\propto$ less than 0.5 indicates anti-persistence and greater than 0.5 indicates statistical persistence. To determine differences between groups and stimulus conditions a two-way ANOVA (group x conditions) was used. *Post hoc* analyses with Tukey's tests were used to highlight specific differences between conditions.

RESULTS AND DISCUSSION

A stimulus main effect was found for both ISIs (p<0.001) and ILIs (p<0.001). Further analysis revealed that the stimulus effect was present only for

the AUD group where INV was significantly lower compared to all the other conditions (p<0.05) (Table 1). A stimulus x group interaction was found for ∝-ILIs (p<0.001) but not for ∝-ISIs (p=0.887). A main effect was observed for stimulus both in ∝-ISIs and ∝-ILIs (p<0.01). Pairwise comparisons shown a significantly greater ∝-ISIs in non-stimulus compared to INV (p<0.001) and RND (p=0.010). Likewise, VAR showed greater ∝-ISIs compared to INV (p<0.001) and RND (p<0.001). For ∝-ILIs, significant differences were observed between non-stimulus compared to INV (p<0.001); and VAR compared to INV (p<0.001) and RND (p<0.001). A main effect of group was observed for ∝-ILIs (p=0.03). Further analysis revealed that the differences between groups were observed in INV (p<0.001) and RND (p<0.001) conditions, where ∝-ILIs was significantly smaller for VIS (Fig.1 and 2).

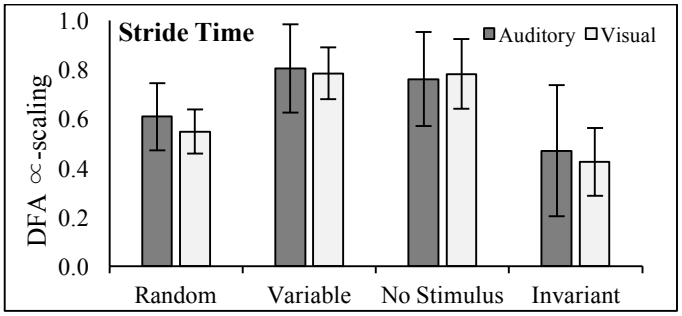

Figure 1. DFA ∝-scaling exponent of stride time (*ISIs*) for the all stimuli conditions for both auditory and visual groups.

The present study results showed that regardless of the type of stimulus provided (AUD or VIS), the variability of stride time and length was altered in a similar fashion. The structure of the RND and INV stimuli decreased the fractal scaling while VAR stimulus showed values similar to what was observed in the non-stimulus condition. A similar effect was previously observed with invariant cueing with both AUD and VIS cues [6]. We also found that the effect of the type of the stimulus on stride length variability was more evident when a VIS stimulus was provided, which partly corroborates our hypothesis that a VIS stimulus would affect the stride length more compared to an AUD stimulus. However, no differences between groups were observed in stride time variability. This finding can be partly explained by possibly the treadmill adding a temporal cueing effect. Therefore, the VIS group received both temporal and spatial cueing. Additionally, we also found that linear measures of ISIs and ILIs were altered in AUD group, particularly for INV condition.

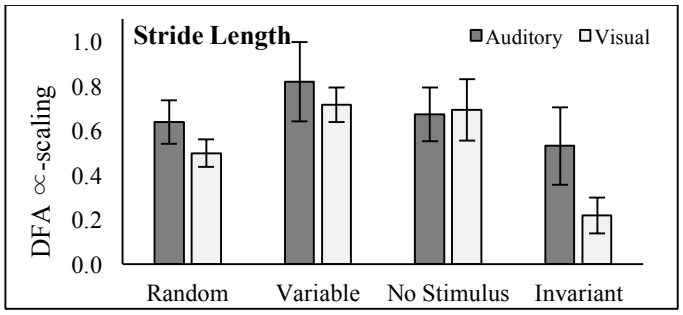

Figure 2. DFA ∝-scaling exponent of stride length (*ILIs*) for the all stimuli conditions for both auditory and visual groups.

CONCLUSIONS

This study shows that regardless of the stimulus (auditory or visual), the fractal scaling of stride time and length was decreased in the presence of a random or invariant stimulus, as compared to no stimulus. Interestingly, the modality of these stimuli affect the statistical persistence of spatial but not temporal gait variability. Conversely, the use of variable stimulus did not alter the variability of these spatiotemporal gait parameters. This further suggests that gait rehabilitation programs should incorporate this type of stimulus to achieve healthy values of gait variability.

REFERENCES

1. Hollands et al. *PLoS ONE. 10(10), 2015*
2. Baker et al. *Parkinsonism Relat Disord.* 14(4), 2008.
3. Kaipust et al. *Ann Biomed Eng. 41(8). 2013.*
4. Hove et al. *PLoS ONE*. 7(3), 2012.
5. Peng et al. *Chaos*. 5(1), 1995
6. Terrier. *Ann Biomed Eng*. 44(9), 2016

ACKNOWLEDGEMENTS

NASA EPSCOR, NIH-P20GM109090 and NIH R15HD08682.

Table 1: Stride time and stride length (mean ± SD) for auditory and visual groups in all stimulus conditions.

	Random		Variable		Non Stimulus		Invariant	
	Auditory	*Visual*	*Auditory*	*Visual*	*Auditory*	*Visual*	*Auditory*	*Visual*
Stride Time (s)	1.17 ± 0.05	1.22 ± 0.07	1.18 ± 0.06	1.22 ± 0.07	1.18 ± 0.06	1.22 ± 0.06	1.06 ± 0.08	1.22 ± 0.07
Stride Length (m)	1.14 ± 0.12	1.10 ± 0.03	1.14 ± 0.13	1.10 ± 0.04	1.14 ± 0.11	1.09 ± 0.05	1.04 ± 0.15	1.10 ± 0.03

REGULAR RUNNING IN MIDLIFE MAY BE PROTECTIVE OF PLANTARFLEXOR FUNCTION AFTER A PROLONGED WALK

[1] Erica M. Casto [2]Jocelyn F. Hafer and [1,3] Katherine A. Boyer

[1] University of Massachusetts Amherst, Amherst, MA
[2] University of Michigan, Ann Arbor, MI
[3] University of Massachusetts Medical School. Worcester, MA, USA
email: ecasto@kin.umass.edu, web: http://people.umass.edu/mobl/

INTRODUCTION

Aging is associated with declines in mobility and alterations in gait [1,2]. Muscle function and control may be a contributing factor to these mobility changes as midlife adults are shown to have altered muscle activation and co-activation patterns compared to young adults [2,3]. Greater muscle activation and co-activation may increase the economic cost of walking for midlife adults [2] and may also increase contact forces within the joint [4] increasing the risks for fatigue related falls and musculoskeletal injury.

There remains a need for a better understanding of factors influencing muscle activation with aging to develop targeted interventions for mobility. There is evidence to suggest that highly active midlife adults may be protected against both increases in cost of walking [5] and slowing gait speeds [6], as well as against knee extensor muscle fatigue from extended bouts of walking [7]. These findings may be explained by a mitigating effect of physical activity on altered muscle activation, but this has not been examined. Comparing midlife adults' muscle activation across physical activity level and in response to a bout of exercise may yield insight into how highly active midlife adults maintain the gait speed, cost of walking, and possibly gait mechanics of young adults.

Therefore, the aim of this study was to quantify the differences in muscle activity at the beginning and end of a prolonged treadmill walk in healthy young (Y), highly active midlife (RUN), and sedentary midlife (SED) females. It is hypothesized that sedentary midlife females will have longest duration of activation and greatest peak activation of the knee extensor and plantarflexors, and these differences will be larger following the prolonged walk.

METHODS

Twenty-eight female participants: 10Y (Age: 27.0 ± 3.5yrs; BMI: 23.19 ± 2.1kg/m^2; Speed: 1.41 ± 0.15m/s); 10 RUN who ran ≥15mi/wk (Age: 60.5 ± 3.9yrs; BMI: 21.2 ± 2.2kg/m^2; Speed:1.43 ± 0.12m/s;); and 8 SED exercising ≤ 2 times/wk (Age: 61.8 ± 1.4yrs; BMI: 23.9 ± 1.7kg/m^2; Speed: 1.34 ±0.10m/s); participated in this study. All participants completed an IRB approved informed consent prior to completing any study procedures.

Participants completed a 30 minute treadmill walk (30MTW) with intermittent "challenge" periods to simulate a bout of daily activity [8]. Electromyography (EMG) was collected during the 2nd and 30th minute of. Electrodes (Trigno, Delsys, Inc., Natick MA) were placed over 8 lower extremity muscles: vastus lateralis (VL), vastus medialis (VM), rectus femoris (RF), biceps femoris (BF), semitendinosus (ST), lateral gastrocnemius (LG), medial gastrocnemius (MG), and Tibialis Anterior (TA). EMG were bandpass filtered at 20-500Hz, full-wave rectified and then lowpass filtered at 20Hz to produce a linear envelope. Linear envelopes for each muscle were expressed as a percentage of the average stance phase signal for 10 consecutive strides from the 2nd minute of the 30MTW.

Peak, and duration of activation were calculated for each muscle from minutes 2 and 30 of the 30MTW. EMG time on/off for each muscle was determined by using a threshold set at 2 standard deviations from baseline. Duration was then calculated as the total time above this threshold throughout stance. A 2x3 (time*group) repeated measures ANOVA was used for each muscle to compare EMG peak, time of peak, and duration of activation between the three groups at the beginning and end of the 30MTW.

RESULTS AND DISCUSSION

Duration of activation in the knee extensors and flexors were not significantly different between groups across time. Peak activation of VM (Table 1) decreased significantly in SED ($p=0.041$) during early stance and in RUN during midstance ($p=0.033$). No differences were found between SED and RUN in VM peak activation throughout stance indicating that these changes are likely due to age rather than activity level.

Peak activation of the MG during late stance and LG in early stance decreased across time in all groups, with no difference between groups. In both early and midstance a group by time interaction was found for the MG ($p=0.034$ and $p=0.029$ respectively). Post-hoc testing showed no difference in peak activation of the MG between groups at the beginning of the walk, however, at the end, RUN had an increased peak activation while SED and Y decreased or had no significant change in the peak activation. These results suggest that regular running in midlife may protect women against the commonly observed distal to proximal shift in joint power during walking, thereby potentially limiting both slowing gait speed and increasing cost of walking.

The difference in response to the 30MTW for Y and SED as compared to RUN may be related to the onset of muscle fatigue at the end of the 30MTW. In a prior analysis of these participant groups we found both the Y and SED groups experienced knee extensor fatigue (defined as a decline in power) following the walk, while RUN did not [7] suggesting regular running in midlife adults may mitigate muscle fatigue in response to the 30MTW. While changes in plantarflexor power were not quantified in this prior study, a similar decrease in MG activation has been reported in a study [9] examining the gait and muscle activity of young adults following a unilateral plantarflexor fatigue protocol.

CONCLUSIONS

Peak activation in VM decreased throughout the walk in both early and midstance in midlife women regardless of activity level when compared to young women suggesting that this is an effect of aging rather than disuse. Peak activation of MG and LG show differences throughout stance for RUN when compared to both young and sedentary midlife women. This suggests that regular running in midlife may be protective against changes in plantarflexor function following a prolonged moderate intensity walk and should be explored more in future studies.

REFERENCES

1. Boyer, et al., *Exp. Gerontol* (95) 63-70. 2017.
2. DeVita & Hortobagyi, *J. Appl Physiol* 1804-11, 2000.
3. Hortobagyi et al., *Gait & Posture*, (29) 558-64, 2009.
4. DeMers, et al., *J Orthop Res* 32:769-76, 2014.
5. Ortega, et al., *PLOS ONE,* 9(11):e113471, 2014
6. Boyer et al., *Gait & Posture.*(36) 149-53, 2012.
7. Hafer, Kent, Boyer. *J Ortho Res,* Submitted.
8. Foulis., et al., *PLOS ONE,* 12(9):e0183483, 2017.
9. Hunt & Hatfield, *J Electromyogr Kinesiol,* (35)24-29, 2017.

ACKNOWLEDGEMENTS

The work was funded in part by Graduate student research grants to J. Hafer provided by ASB, ACSM, and University of Massachusetts Amherst Graduate School.

Table 1: Mean change in peak activation from beginning to end of walk in Y, RUN, and SED expressed as % of mean activation during stance at baseline, $\alpha=0.05$. *significant over time, ^Significant difference between groups over time.

	VM early	MG early	LG early	VM mid	MG mid	MG late	LG late
Y	-2.28 (1.5)	-0.91 (1.1)*^	-0.75 (0.6)*	0.76 (0.6)	-0.28 (0.2)	-0.29 (0.24)*	-0.71 (0.74)*
RUN	-2.54 (2.5)	0.98 (1.5)	0.41 (0.3)^	-1.2 (2.4)*	0.61 (0.6)^	-0.60 (0.61)^	-0.67 (0.9)^
SED	-2.63 (1.4)*	-0.66 (0.5)^	-0.36 (0.4)	-1.3 (1.2)	-0.40 (0.7)	-0.41 (0.7)	-1.05 (0.9)*^
p-value	p=0.013	p=0.028^	p=0.051	p=0.03	p=0.029	p=0.032	p=0.002

LOWER LIMB JOINT ANGLE VARIANCE AS A FUNCTION OF OBSTACLE HEIGHT DURING OBSTACLE CROSSING

[1]Chuyi Cui, [2]Brittney Muir, [1]Jeffrey Haddad, [3]Richard van Emmerik, [1]Shirley Rietdyk, [1]Satyajit Ambike
[1]Department of Health and Kinesiology, Purdue University, IN, USA
[2]Department of Occupational Therapy, The Sage Colleges, Troy, NY, USA
[3]Department of Kinesiology, University of Massachusetts, Amherst, MA, USA
email: cui111@purdue.edu, web: https://www.purdue.edu/hhs/hk/Biomechanics-MotorBehavior/

INTRODUCTION

Tripping is a main contributor to falls and fall related injuries. To ensure crossing an obstacle without tripping, one has to elevate the foot higher than the upper edge of the object. Typically, the trail foot (the foot that crosses second) contacts visible stationary obstacles more frequently than the lead foot (the foot that crosses first) [1].

The variability of foot clearance has been commonly used to quantify the risk of tripping during obstacle crossing [2]. During swing phase, lower limb segments from stance foot to swing toe form an open kinematic chain with multiple joint angles that influence the configuration of the swing foot. Foot variability clearly arises from the variability in joint angles. Although mean foot clearance and joint angles during obstacle crossing have been studied extensively, it is essential to study joint angle variances to understand toe height variability.

The purpose of this study is to (a) quantify the lead and trail toe height variability when crossing obstacles of different heights, and (b) investigate the source of the toe height variability by examining the lower limb joint angle variance.

METHODS

Ten young adults (age: 23.8±3.4 years, 3 females) walked along a 15 m walkway and stepped over an obstacle. Four obstacle heights were examined: unobstructed (no obstacle), 3, 10, and 26 cm. 10 trials of each condition were performed in block randomized order. Kinematic data were collected using the Qualysis Track Manager at 100 Hz.

Measures were calculated at the frame where tripping was most likely to occur: when the lead toe and the trail toe were above the obstacle, and at minimum toe clearance for unobstructed trials for both limbs.

We computed the across-trial standard deviation of the toe height (henceforth toe variability), the variances of lower-limb joint angles (sagittal hip, knee, and ankle of stance and swing limb), and the total joint angle variance as the sum of all six joint angle variances (henceforth total joint variance). Two-way mixed model ANOVA was conducted with *obstacle height* (unobstructed, 3, 10, 26 cm) and *limb* (lead, trail) as fixed factors. Tukey post hoc pairwise comparisons were conducted.

RESULTS AND DISCUSSION

Six of the 10 subjects contacted the obstacle one time (contact rate 2%; all with the 26 cm; five with the trail toe). Since contacting the obstacle modified gait in subsequent trials [3], data from the 26 cm condition was excluded from statistical analyses.

There was a significant interaction (*obstacle height by limb)* observed for toe variability ($F_{2,57}$=3.27; p=0.04; Fig. 1). Post hoc comparisons revealed that toe variability was not different for the lead and trail limbs for unobstructed and the 3 cm obstacle trials, but it was 72% higher for the trail limb for the 10 cm obstacle. Toe variability was 273% higher for 3 cm obstacle versus unobstructed ($p<0.01$). It was 80% higher for the 10 cm obstacle than the 3 cm obstacle, but only for the trail limb ($p<0.01$).

A significant interaction *(obstacle height by limb*) was observed for total joint variance ($F_{2,57}$=4.82; p=0.01; Fig. 2). Post hoc comparisons revealed that total joint variance with the trail crossing was 98% higher than the value of lead crossing for the 10 cm obstacle ($p<0.01$), whereas no difference for lead and trail crossing was observed for the unobstructed and 3 cm obstacle conditions. Total joint variance for trail

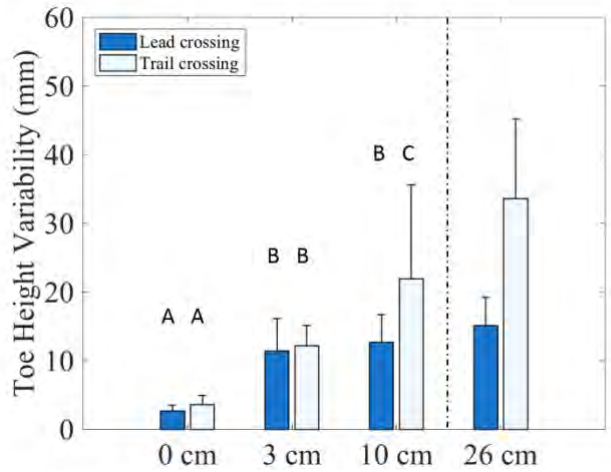

Figure 1: Effect of obstacle condition and limb for toe variability. 26 cm shown but not included in statistical analysis due to obstacle contacts. Letters A, B, C distinguish significantly different conditions.

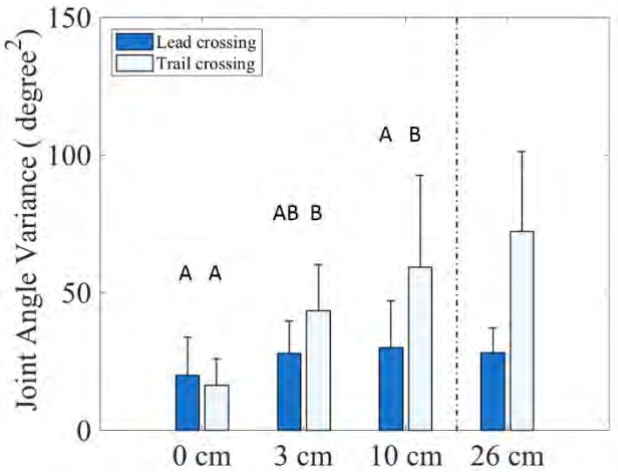

Figure 2: Effect of obstacle condition and limb for total joint angle variance.

crossing increased 164% for the 3 cm obstacle ($p<0.01$) and 259% for the 10 cm obstacle ($p<0.001$) compared with unobstructed walking; no significant obstacle effect was observed for lead crossing.

Overall, similar patterns were observed in toe variability and total joint variance (Fig. 1,2) as a function of obstacle height and limb: higher toe variability generally corresponded to higher total joint variance, consistent with the idea that total joint variance prescribes toe variability. There is an important exception – while toe variability and joint variance for the trail limb increased as a function of obstacle height, only toe variability increased for the lead limb. Future research should determine if the joint angles covary in a task-specific manner to control the variability in the toe height.

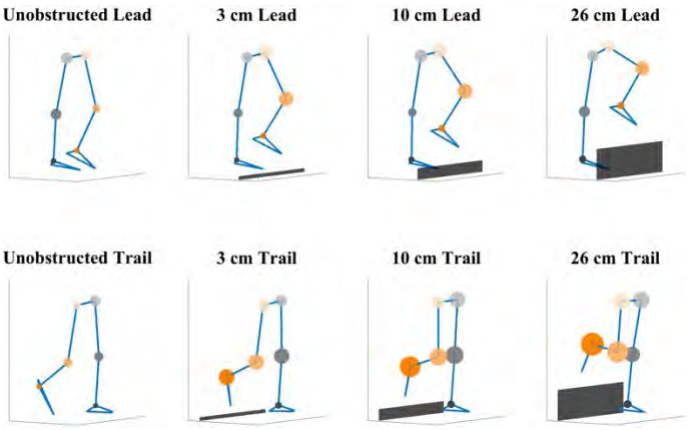

Figure 3: Individual joint angle variance marked on illustrative lower limb stick figures as circles. The area of circle reflects the amount of variance. Black rectangles are the obstacles.

We examined variances in each joint angle to locate the source of the toe variability. Qualitatively, variances in joint angles tended to be larger (quantified as larger circles on each joint, Fig. 3) during the trail crossing than lead crossing, and this pattern became more apparent for larger obstacles. The contribution from the stance limb joint angles to the toe variability is substantial. Although most research on obstacle crossing focus on the swing limb, stance limb behavior cannot be ignored.

CONCLUSIONS

Larger toe variability and total joint variance for the trail limb, especially for taller obstacles, is consistent with observations of greater failures with the trail foot [1]. Furthermore, the joint angle variances are distributed over the joints of both the swing and stance limb, indicating that the contribution of the stance limb to obstacle contacts must be considered. This suggests existence of compensatory covariance in the lower limb joint angles to control toe height. Further investigation into coordination between the individual joints of both limbs is necessary.

REFERENCES

1. Heijnen et al., Exp Brain Res, 2014
2. Mills et al. Gait Posture, 2008
3. Heijnen et al., Exp Brain Res, 2012

ESTIMATING GAIT EVENTS AND LOCOMOTION STATE WITH A BETA-PROCESS AUTO REGRESSIVE HIDDEN MARKOV MODEL

[1,2] Seth R. Donahue, [1,2] Li Jin, [1,2]Michael E. Hahn

[1] Bowerman Sports Science Clinic, [2] Neuromechanics laboratory, University of Oregon, Eugene, OR, USA
email: sethd@uoregon.edu, web: https://bssc.uoregon.edu/

INTRODUCTION

Identification of gait phase is important for many applications including control of active lower limb prostheses. One challenge for adaptive prostheses is accurate prediction of initial contact, toe off with minimal sensors and low sampling frequency. Previous work has used acceleration-based thresholds to identify initial contact and toe off [1]. These algorithms lack adaptability to different locomotion states and speeds. The beta-process auto-regressive hidden Markov model (BP-AR-HMM) has been shown to accurately identify different human movement patterns from motion capture data at low sampling frequency (10 Hz) [2]. Unlike other classification algorithms the BP-AR-HMM provides a statistical model for classification. The purpose of this exploratory data analysis is to determine the feasibility of the BP-AR-HMM to identify and estimate gait events and locomotion states from a single simulated accelerometer sampling at low frequency during two different gait transitions.

METHODS

Ten able-bodied subjects participated in the study (51 ± 6.0 years, 173 ± 11.4 cm, 70 ± 15.0 kg) (5 male, 5 female). Ground reaction force (GRF) and marker trajectory data were collected at 1200 Hz and 120 Hz, respectively. Subjects were asked to perform two different transitions: walk to run (WRT) and run to walk (RWT) transition on a force-instrumented treadmill (Bertec, Inc., Columbus, OH). The WRT protocol began with walking at 1.8 m s^{-1} for 30 seconds, then the treadmill was constantly accelerated at 0.1 m s^{-2} to 2.4 m s^{-1}. Subjects were asked to transition to running gait whenever they felt ready during the acceleration stage. After transitioning to a running gait, they ran at 2.4 m s^{-1} for another 30 seconds. The RWT protocol was the inverse of the RWT, starting at 2.4 m s^{-1} for 30 seconds, then the treadmill was constantly decelerated at -0.1 m s^{-2} to 1.8 m s^{-1}.

The GRF data were filtered with a low pass fourth order Butterworth filter (50 Hz cut off frequency). Ground contact state was determined when the vertical GRF values were above a threshold of 50 N. Motion trajectory data from a single marker on the dorsum of the left foot were extracted from a larger data set [3]. Three-dimensional (3D) acceleration values were calculated by taking the second derivative of the raw marker position data. The GRF and acceleration data were then down-sampled to 20 Hz. The algorithm was tested on a set of 17 trials. One trial was removed from the data set because the GRF data were incomplete for the present analysis

The BP-AR-HMM is composed of three major parts (2). The beta process determines the number of states available for each time series, based upon a Bernoulli probabilistic model. Vector autoregression implies acceleration throughout the gait cycle at any given time is a function of the previous acceleration values and random variation. The use of auto-regression also allows for features to be shared across different time series via the beta process. The hidden Markov model assumes a set of distributions and transitions between them follow a Markov process. The assumption of the Markov process is the probability of state change from i to j has a set probability π_{ij}, which does not depend on prior state. The algorithm also contains a parameter to limit state transitions at each time step. This parameter helps to ensure the estimated states are biomechanically relevant. The BP-AR-HMM algorithm used a data driven model to estimate and share states across each time-series.

The temporal differences between the change in the estimated state and the measured initial contact (IC) and toe off (TO) of the left foot were calculated. Duration of a state was calculated from the first

instance of desired state to the first instance of a different state. The duration of the state indicating stance phase was calculated to estimate whether the current gait was walking or running. With an effective sampling frequency of 20 Hz, the difference between two time steps corresponds to 50 msec. All analyses were performed post hoc.

RESULTS AND DISCUSSION

Example accelerations, foot contacts and estimated states are shown for a RWT and WRT condition in Figure 1. At Point 1 is the estimated event where swing phase terminates, and stance phase begins. State A occurs every gait cycle and is used as an estimator of stance phase. Transition out of State A is the time point used to determine the time until TO. Point 2 is indicative of the estimated termination of stance phase. State B occurs every gait cycle, indicating swing phase. The first point after State B is used to determine the time until IC.

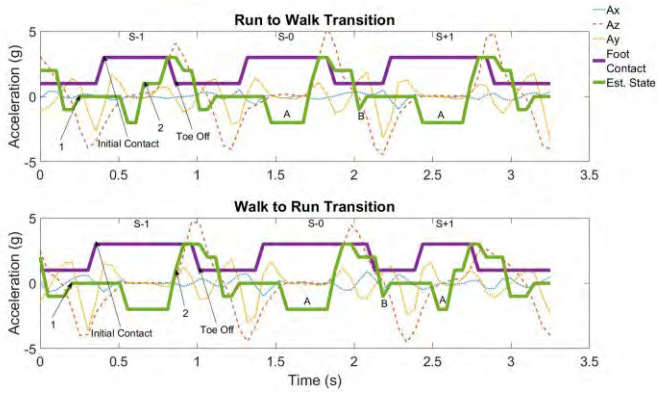

Figure 1: Accelerations, foot contacts and estimated states for RWT (top panel) and WRT (bottom panel) are shown for a single exemplar subject.

Figure 2 shows the natural transition points between walking and running locomotion states. Transition steps were verified by ground reaction force waveforms. The shaded area indicates foot ground contacts classified as running. The contacts in the unshaded area are classified as walking contacts.

Initial analysis indicates initial contact and toe off can be estimated for both the WRT and RWT from a single source of acceleration on the dorsum of the foot sampled at 20 Hz. Previous work has estimated that approximately 40 ms are required to adjust the prosthesis state [1]. The duration of state A, representing foot contact provides a basis to estimate the locomotion state of the subject as seen in Figure 2.

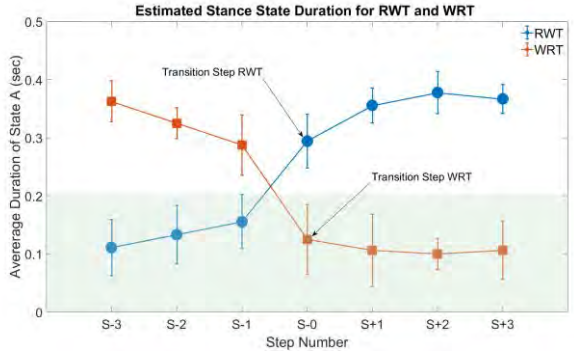

Figure 2: Average contact duration for WRT and RWT conditions. S-1 is the last step before the transition and S-0 is the actual transition step.

Table 1: Average time (sec) of estimated state change prior to actual gait event; mean (SD). The average duration of the states that approximate mid stance and mid swing are also shown; mean (SD).

	Initial Contact	Toe off	State A Duration	State B Duration
Walk	0.156 (0.037)	0.147 (0.068)	0.359 (0.048)	0.102 (0.036)
Run	0.180 (0.031)	0.126 (0.028)	0.103 (0.055)	0.081 (0.031)

CONCLUSIONS

The BP-AR-HMM provides a suitable basis for estimating initial contact, toe off, and locomotion state. Future directions of this work will include comparison of these results to over-ground transitions with self-selected accelerations, and a larger range of speeds. The final application of this work will be for use in a microcontroller of a lower limb prosthesis.

REFERENCES

1. Joshi et al., *IEEE J. Biomed. Health Inform.* 20(1): 2168-2194, 2014.
2. Fox, *Ann. Appl. Stat.* 8(3):1281-1313, 2014.
3. Jin, *PhD Dissertation*. U. Oregon, 2018.

ACKNOWLEDGEMENTS

We wish to thank Michael Hughes for his advice on use of the BP-AR-HM

A Novel Approach for Evaluating Compensatory Gait Strategies Using Mechanical Energetics

Anahid Ebrahimi, Jill S. Higginson, and Steven J. Stanhope

University of Delaware, Newark, DE, USA
E-mail: anahide@udel.edu

INTRODUCTION

Mechanical work is done about joints of the lower limb to move the body, subsequently changing the body's energy state. In gait, the limbs do mechanical work to rotate the center of mass (COM) upwards then downwards in a semicircular arc, theoretically following pendular mechanics [1]. Consequently, this leads to changes in gravitational potential energy and kinetic energy of the body.

With a joint impairment, mechanical work is redistributed among the limb yielding a compensatory gait strategy [2]. This is especially true for individuals with ankle impairment due to the key role of the ankle musculature in gait [3]. However, characterizing a compensatory strategy as "good" is complicated by the operational definition of the term.

Assessing if a strategy's energetics (work and energy) differ from the theorized pendular mechanics of gait in single support phase can help us to understand how and why certain gait strategies are used when there is an impairment. To explore compensatory gait strategies, we compared the mechanical energetics of healthy individuals walking with an artificially impaired ankle joint unilaterally and bilaterally to their typical gait (in shoes).

METHODS

Motion and force data were collected on 17 healthy subjects (8M/9F, 1.7 ± 0.2 m, 75.7 ± 15.1 kg) walking at 0.8 statures/s (1.4 ± 0.1 m/s) with shoes only, and with a custom ankle-foot orthotic on one limb (RiAFO) and on both limbs (BiAFO) which partially restricted ankle motion in dorsiflexion and plantar flexion. The summed net work and rate of change in energy for all segments of the body were integrated over two halves of single support: "single support rise" from left toe off to right midstance, and "single support fall" from right midstance to left heel strike. Average net work and change in gravitational potential energy, translational kinetic energy, and rotational kinetic energy of the whole body (W_{wb}, ΔGPE_{wb}, ΔTKE_{wb}, and ΔRKE_{wb}) are presented in bar charts with standard deviation bars.

Considering that the magnitude of energetics metrics would differ across conditions, relative metrics were calculated. Work or energy forms were calculated as a percentage of the largest energetics metric (see Fig. 1 for example). Statistical differences between conditions were assessed using one-way repeated measures ANOVA with Bonferroni corrections ($p < 0.05$). A † and ‡ denote a significant difference between Shoes and RiAFO conditions, respectively ($p < 0.05$).

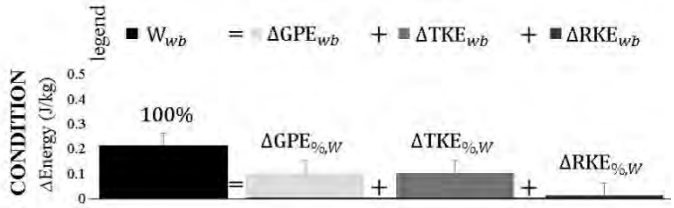

Fig 1. Example bar chart of energetics data. Note percentage values above bars are relative to the largest energetics metric (in this case W_{wb}).

RESULTS AND DISCUSSION

Subjects walked at the same scaled speed and did not significantly change their step lengths ($p = 0.065$) across conditions. The AFO successfully reduced the ankle work by an average 37-40% in the AFO conditions compared to shod walking.

In single support rise, ΔGPE_{wb} was the largest energy form. Individuals walking in the BiAFO condition had a significantly larger $W_{\%,\Delta GPE}$ (86%) compared to the Shoes condition (75%). In a conserved inverted pendulum, the $\Delta TKE_{\%,\Delta GPE}$ would be 100% such that translational kinetic energy and potential energy were equal in magnitude and opposite in sign. However, Fig. 2 shows 25% of the negative ΔTKE_{wb} was transferred to positive ΔGPE_{wb} to raise the COM in the Shoes condition, but only 14% transferred in the BiAFO condition.

Therefore, the BiAFO condition used less pendular mechanics (as evidenced by a smaller $\Delta TKE_{\%,\Delta GPE}$) to raise the COM compared to the Shoes condition.

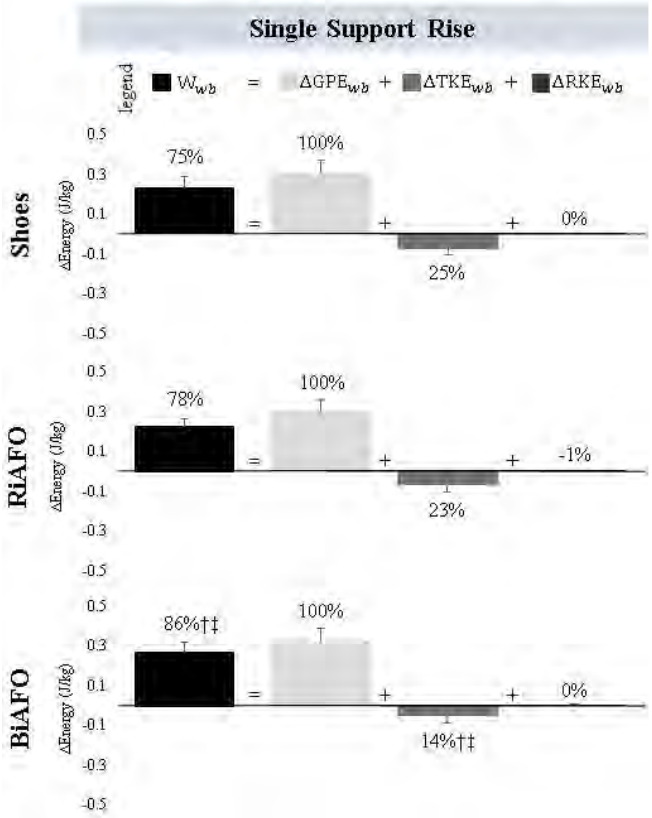

Fig 2. During single support rise, percentages are relative to ΔGPE_{wb}. The BiAFO condition results in significantly less $\Delta TKE_{\%,\Delta GPE}$ compared to Shoes.

In single support fall, W_{wb} was the largest metric. Individuals walking in the RiAFO condition had a significantly smaller $\Delta GPE_{\%,W}$ (-83%) compared to the Shoes condition (-87%). Interestingly, there is no evidence of pendular mechanics during this interval since ΔTKE_{wb} is not net positive. Thus, Fig. 3 shows that nearly all of the net work went into the form of negative ΔGPE_{wb} in all three conditions. While the body is doing a majority of net negative work to control the "fall" of the COM in all three conditions, the RiAFO condition led to altered energetic patterns (as evidenced by a smaller $\Delta GPE_{\%,W}$) to lower the COM compared to the Shoes condition. These results may support the necessity for lower limb prosthetic device design to provide control during this interval to reduce the risk of falls in individuals with amputations.

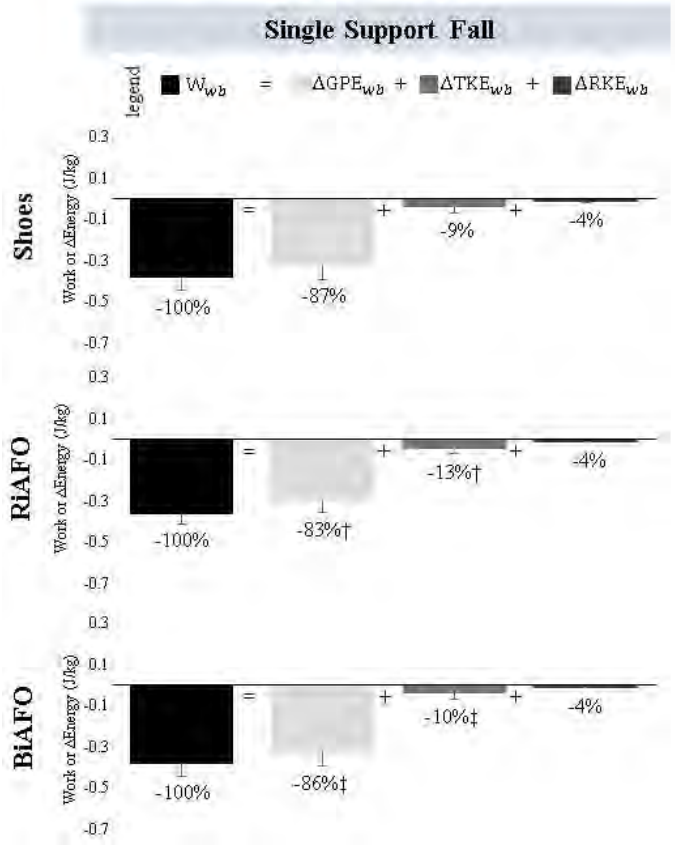

Fig 3. During single support fall, percentages are relative to W_{wb}. The RiAFO condition results in significantly less $\Delta GPE_{\%,W}$ compared to Shoes.

CONCLUSIONS

Individuals compensated with ankle impairment by walking with a similar stride length, yet evaluating the energetics revealed walking with an impairment required more work (as in the BiAFO condition in single support rise) and resulted in altered energy forms (as in the RiAFO condition in single support fall) compared to without impairment. Also, this analysis demonstrated that the limbs do not act like a conserved inverted pendulum, but rather do work to assist the rise and control the fall of the COM.

REFERENCES

1. Kuo, A. *Hu Mov Sci,* **26**(4): 617-656, 2007.
2. Ebrahimi et al. *Gait Pos,* **56**(April): 49-53, 2017.
3. Neptune et al. *J Biomech,* **34**(11): 1387-98, 2001.

ACKNOWLEDGEMENTS

This material was supported by the NSF GRFP (Grant #1247394) and the UD Helwig Fellowship. Data collection assisted by Teresa Ferrara, Michael Christensen, Independence Prosthetics & Orthotics.

INCONSISTENCIES IN STAIRCASE DIMENSIONS IMPACT UPON STAIR CLIMBING SAFETY

[1] Natasha Francksen, [1] Thijs Ackermans, [1, 2] Denis Holzer, [1] Constantinos Maganaris, [1] Mark Hollands, [3] Mike Roys, and [1] Thomas O'Brien

[1] Research to Improve Stair Climbing Safety (RISCS), Research Institute for Sport and Exercise Sciences, Liverpool John Moores University, Liverpool, UK
[2] Department of Biomechanics in Sports, Faculty of Sport and Health Sciences, Technische Universität München, Munich, Germany
[3] Rise and Going Consultancy, Watford, UK
Email: N.C.Francksen@2016.ljmu.ac.uk,

INTRODUCTION

Staircases are frequently associated with falls, over a million people were treated after falling on stairs in American emergency departments annually [1]. Injuries for the older individuals are more severe and require more hospitalisation [1]. In the UK, approximately ten fatalities per week are result from stair falls [2]. Treatment is costly for health care providers such as the National Health Service (NHS).

Inconsistent staircase dimensions are very common and are frequently associated with serious falls [3, 4]. Inconsistencies in rise result in an increased risk of tripping during stair ascent, where individuals are more likely to catch their toe. During stair descent variations in going (horizontal distance between the step edge and the next step) result in errors in stepping-length or over-stepping, which increases the potential for a slip to occur [4]. It is likely that inconsistencies in going also influence safety during ascent, and inconsistencies in rise also affect safety in descent. However, little is known about these and how they could affect fall risk [4].

The aim of this study, therefore is to investigate the influence of a small 1 cm change in going during ascent and 1 cm change in rise during descent on stepping parameters and risk factors for younger and older adults negotiating stairs. The local university's and NHS Ethics Committee approved this study (IRAS project ID: 216671).

METHODS

Twenty-six younger adults (YA; 24.4±3.4 yrs, 1.74±0.08 m, 71.4±11.0 kg, including of British, European and Asian origin, 15 male, 11 female) and thirty-three older adults (OA; 70.7±4.2 yrs, 1.68±0.08 m, 67.9±14.1 kg, of White British origin, 10 male, 23 female) negotiated a custom-built staircase set to three different dimensions: CONSISTENT, inconsistent GOING and inconsistent RISE. 1) The CONSISTENT staircase had uniform dimensions, where all steps had a 20 cm riser height and a 25 cm going length. 2) For the inconsistent GOING condition, Step3 was moved 1 cm inward, lengthening Step2 and shortening Step3 (Figure 1A). 3) For the inconsistent RISE condition, Step3 was raised 1 cm decreasing the riser height of Step4 and increasing the riser height of Step3 (Figure 1B). Participants were asked to leave the room and were not aware how the staircase had changed. GOING and RISE conditions were randomised.

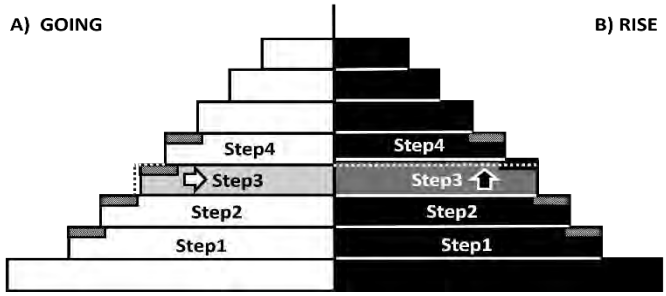

Figure 1: A) Ascent: GOING, Step3 moved 1 cm inward compared to CONSISTENT condition (dotted grey step edge. B) Descent: RISE, Step3 raised 1 cm compared to CONSISTENT condition (dotted white line).

Full-body 3D kinematics and kinetics were recorded (26 camera system: Vicon & 4 force plates: Kistler). Five CONSISTENT trials were averaged and only the first GOING trial during ascent and RISE trial during descent were used for analysis. Only leading limb foot clearances (Foot Clearance) and percentage of foot contact length (Foot Contact) were compared by mixed-methods ANOVAs. Alpha level, $P<0.05$.

RESULTS

There were no significant differences in Foot Clearances between the CONSISTENT and either RISE or GOING trials.

During stair ascent, there was a significant interaction effect between age group and stair configuration on Foot Contact on Step2 ($p = 0.004$), Step3 ($p = 0.013$) and Step4 ($p = 0.010$). YA increased their percentage of foot contact on Step2 in GOING whereas OA did not make this adjustment (Figure 2A). The OA however had a slight decreased Foot Contact on Step3 and the YA a slight increased Foot Contact (Figure 2B). Both groups had increased Foot Contact on Step4, YA more so than the OA (Figure 2C).

During stair descent, there were main effects of staircase configuration on Foot Contact (no age*step interactions). Main effects were recorded between CONSISTENT and inconsistent RISE conditions where both groups had less Foot Contact on Step3 and increased Foot Contact on Step2 ($p = 0.005$ & $p < 0.001$, respectively) (Figure 2D-E).

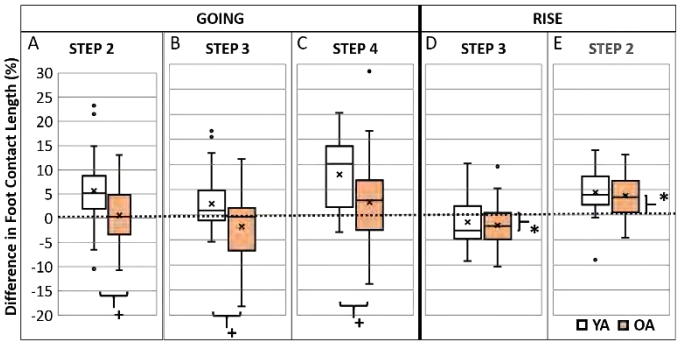

Figure 2: Difference in Foot Contact Length (%) during ascent GOING (A-C) and descent RISE (D-E) compared to CONSISTENT condition for YA (white box) and OA (shaded orange box). Dotted line = 0 % change, X = mean, middle line = median, * = condition effect; $p < 0.05$, $^{+}$ = age by condition effect; $p < 0.05$.

DISCUSSION

In stair ascent YA appear to make use of the longer going of Step2 by placing more of their foot on to the step, which carries forwards to a Foot Contact similar to CONSISTENT on Step3 (shorter going). However, OA did not make adjustments to increase Foot Contact on the longer Step2, nor appear to change their stepping pattern over the inconsistent step. Thus, they had a reduced Foot Contact and have an increased risk of slipping off the shorter Step3. On Step4 both groups had a positive increase in Foot Contact, potentially reducing their risk of slipping, but this could be too late. The interaction effect may be caused by the previously more forward position for the YA compared to the older adults. At this stage, the mechanism behind the YA adjustment on Step2 is unknown.

During stair descent, there were no apparent differences prior to the inconsistent step. Both groups had a reduced Foot Contact on the inconsistent Step3; creating a larger over-step. This in itself is associated with a higher fall risk [4]. Older individuals with larger variability in their stepping behaviour could be at greater risk from a fall.

Analysis of visual behaviour, full body kinetics and kinematics of both groups will help determine the mechanisms behind the changes to Foot Contact and the extent that a person's safety is compromised. The initial results presented could influence staircase regulations on tolerances, it could also justify the need to remodel existing staircases or develop visual cues that make inconsistencies more identifiable.

CONCLUSIONS

Inconsistencies in rise dimensions could increase the risk of over-stepping and slipping off the inconsistent step in descent, in a similar way to over-stepping onto a step with a shorter going dimension. In ascent, the OA did not adjust their stepping pattern to the inconsistent staircase which could increase the risk of slipping off the shorter step. This could be particularly dangerous for older adults' safety.

REFERENCES

1. Blazewick et al. *Am. J. Emerg. Med* (In Press): doi 10.1016/j.ajem.2017.09.034, 2017.
2. SHP online. Stair safety fact sheet, 2016
3. Nicol et al. Briefing paper: The cost of poor housing to the NHS. BRE, 2015
4. Roys. *Refurbishing stairs in dwellings to reduce…injuries*. BRE electronic publications, 2013.

A FULL-STATE CONTROLLER FOR THE SIMPLE INVERTED PENDULUM BIPED DERIVED FROM HUMAN PERTURBATION EXPERIMENTS

Varun Joshi and Manoj Srinivasan
The Ohio State University, Columbus, OH, USA
email: joshi.142@osu.edu

INTRODUCTION

Humans walk stably by using neural feedback control and perhaps some feedforward control. Characterizing the feedback controller might inform our understanding of falls and movement disorders, and inform the design of prosthesis and exoskeleton controllers. Here, we seek to characterize how humans balance themselves when subject to perturbations. We describe how human-subject response to Anterior-Posterior (AP) and Medio-lateral (ML) pulls applied at the hip [1] may be used to derive a full-state controller for a simple model of bipedal walking. We evaluate the feedback controller's perturbation rejection ability by determining the basin of attraction for this controller (set of perturbations that do not result in a fall). We also analyze the robustness of the feedback controller to noise in the control gains and biped body parameters.

METHODS

Subjects walked on a treadmill at constant speed for 10 bouts of 4 mins each. During each walking bout, the subjects were perturbed randomly, either in the AP direction (9 subjects, only backward pulls) or in the ML direction (7 subjects, randomly selected leftward or rightward pulls).

We collected kinematic data from 13 markers placed on the subject - 5 around the hip, 4 on each foot using 8 motion capture cameras (Vicon T20, 100 Hz). Subjects were manually pulled by the experimenters via cables tied at the hip. Forces from these cables were recorded using a load cell in series with them (Phidgets S-type 100Kg, 1000 Hz). A loose harness connected to the ceiling was provided for safety. Subjects wore blinders to block peripheral vision and headphones to muffle noise so that visual and audio cues could not be used to anticipate the onset of a perturbation. 20% of all perturbations were randomly assigned to be "fake" perturbations where the experimenter went through the action of pulling on the cable but the perturbing force was very small. These fake perturbations were used to prevent proprioceptive cues from being used to detect oncoming perturbations.

To determine the controller, we first calculate a linear equation that relates mid-stance state deviations of the human to the subsequent foot-placement deviation as outlined by Wang and Srinivasan [2]. Next we determine the Poincare map that relates mid-stance states for the human from one-step to the next:

$$\Delta\begin{bmatrix} X_{\text{torso}}(n+1) \\ \dot{X}_{\text{torso}}(n+1) \\ \dot{Y}_{\text{torso}}\ (n+1) \end{bmatrix} = J_1.\Delta\begin{bmatrix} X_{\text{torso}}(n) \\ \dot{X}_{\text{torso}}(n) \\ \dot{Y}_{\text{torso}}(n) \end{bmatrix}$$

For the simple inverted pendulum model shown in Fig. 1, we can write an equation relating the n+1th mid-stance states for the biped as a function of the mid-stance states during the nth step and the control actions during the nth step:

$$\Delta\begin{bmatrix} X_{\text{torso}}(n+1) \\ \dot{X}_{\text{torso}}(n+1) \\ \dot{Y}_{\text{torso}}\ (n+1) \end{bmatrix} = J_2.\Delta\begin{bmatrix} X_{\text{torso}}(n) \\ \dot{X}_{\text{torso}}(n) \\ \dot{Y}_{\text{torso}}(n) \end{bmatrix} + J_3.\Delta\begin{bmatrix} x_{\text{foot}}(\text{n}) \\ y_{\text{foot}}(\text{n}) \\ I_{\text{pushoff}}(\text{n}) \end{bmatrix}$$

If we select a biped controller of the form:

$$\Delta\begin{bmatrix} x_{\text{foot}}(\text{n}) \\ y_{\text{foot}}(\text{n}) \\ I_{\text{pushoff}}(\text{n}) \end{bmatrix} = J_4.\Delta\begin{bmatrix} X_{\text{torso}}(n) \\ \dot{X}_{\text{torso}}(n) \\ \dot{Y}_{\text{torso}}(n) \end{bmatrix}$$

Combining these equations, we get the following equation:

$$\Delta\begin{bmatrix} X_{\text{torso}}(n+1) \\ \dot{X}_{\text{torso}}(n+1) \\ \dot{Y}_{\text{torso}}\ (n+1) \end{bmatrix} = (J_2 + J_3.J_4).\Delta\begin{bmatrix} X_{\text{torso}}(n) \\ \dot{X}_{\text{torso}}(n) \\ \dot{Y}_{\text{torso}}(n) \end{bmatrix}$$

We solve for the value of J_4 that minimizes

$$J_1 - J_2 - J_3J_4$$

Since we already know the foot-placement gains from human data, the minimization only solves for the 3 impulse gains within J_4.

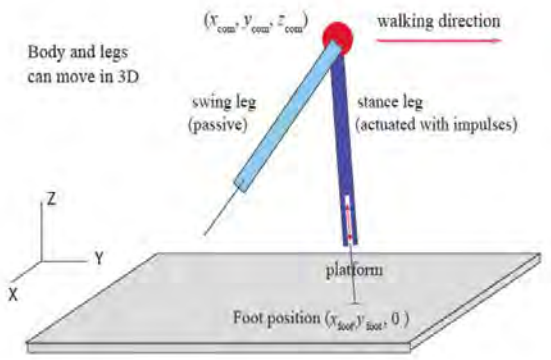

Figure 1: The inverted pendulum biped model

Once the gains are calculated, we simulated the biped for 20 steps with varying initial perturbations to determine the basin of attraction. Similarly, we simulated the biped with fixed initial perturbation and varying parameter noise to determine the parameter sensitivity of this controller.

RESULTS AND DISCUSSION

The feedback controller gains were determined to be as follows in non-dimensional terms:

$$J_4 = \begin{bmatrix} 1.85 & 1.99 & 0.22 \\ -0.49 & -1.65 & 0.85 \\ -0.18 & -0.69 & -0.52 \end{bmatrix}$$

This controller was found to be robust to changes in the gains and parameters, at least 10% in each non-zero parameter value, generally much more. The basin of attraction of the controller, seen in figure 2, was found to be 30-40 times larger than the standard deviation of mid-stance kinematic variability in normal walking. Such basins of attraction predictions can be tested in further large-perturbation experiments.

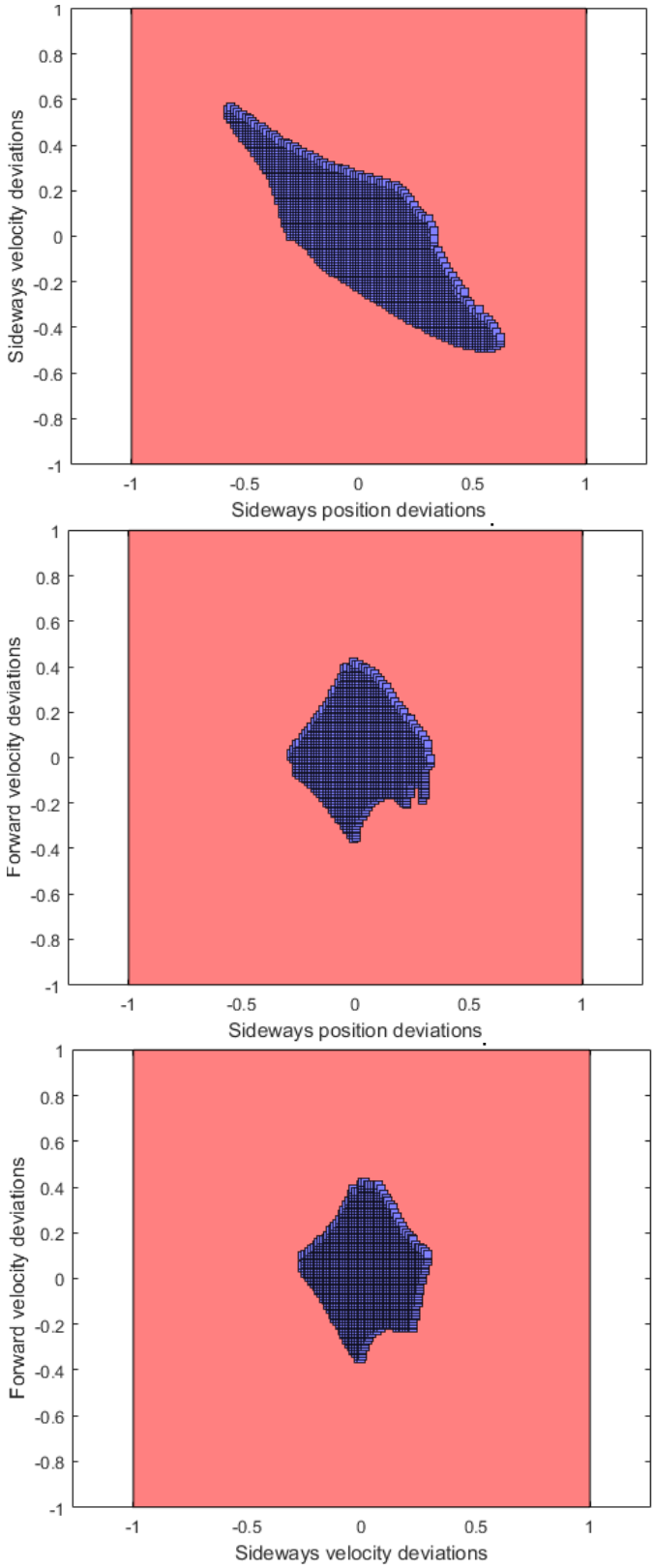

Figure 2: Basin of attraction for the simple inverted pendulum walker with a controller derived from human perturbation experiments. The dark patch represents the set of perturbations that do not result in a fall. All quantities non-dimensionalized.

REFERENCES

1. Vlutters, M., Van Asseldonk, E.H. and Van der Kooij, H., *J. Exp. Biol., 219(10), 1514-23, 2016.*
2. Wang, Y. and Srinivasan, M., *Biol. Lett.*, 10 20140405, 2014.

ACKNOWLEDGEMENTS

This work was supported by National Science Foundation grants number 1538342 and 1254842.

EFFECTS OF A NEW ADAPTIVE ANKLE PROSTHESIS ON LEVEL AND SLOPED WALKING

Erik P. Lamers, Maura E. Eveld and Karl E. Zelik

Vanderbilt University, Nashville, TN, USA
email: erik.p.lamers@vanderbilt.edu

INTRODUCTION

Sloped terrains can be challenging for individuals with lower limb amputation to navigate, in part because conventional prosthetic feet are aligned at a fixed angle and lack biological ankle joint articulation. The lack of ankle articulation may cause prosthesis users to adopt compensatory strategies on slopes [1]. To address this issue, various prosthetic feet have been developed to adapt their ankle angle based on the slope, partially restoring ankle articulation. There is evidence that this ankle articulation may help normalize certain gait biomechanics during level [2] and incline walking [3]. However, objective performance data on adaptive ankle prostheses is still limited, and the extent to which these devices benefit users on slopes requires additional investigation.

In this study we investigated a new microprocessor-controlled prosthetic ankle (MPA, Ossur premarket device), which uses a low-power motor to adapt its ankle angle to sloped terrain and to dorsiflex the ankle during swing to enhance toe clearance. We quantified the biomechanical effects of the MPA on unilateral transtibial prosthesis users during level and sloped walking, compared to the MPA with the ankle locked at the neutral position, and also compared to each user's prescribed prosthesis. The first comparison served as a controlled scientific study to isolate effects due specifically to ankle angle adaptation (since all other aspects of the MPA were unaltered). The latter comparison provided a more clinically-relevant assessment of the MPA against prostheses that users wear each day.

METHODS

Eight individuals with unilateral transtibial amputation participated in this study of level, incline and decline walking. These individuals (7 male, 1 female, height 1.78 ± 0.1 m, weight 92 ± 15 kg, age 45 ± 14 years) were all K3-K4 level ambulators, at least 6 months post amputation surgery. Six healthy controls (4 female, 2 male, height 1.78 ± 0.1 m, weight 69 ± 10.6 kg, age 21 ± 1.8 years) also performed identical walking conditions, to assist with results interpretation. All participants provided informed consent, according to Vanderbilt Institutional Review Board procedures.

Prosthesis users were fitted with the MPA by a certified prosthetist, and then users were educated on the functions of the device. After the fitting, prosthesis users wore the MPA for 2-3 weeks of at-home acclimation before returning for formal gait analysis testing.

Prosthesis users (and healthy controls) performed level (0°) and sloped (±7.5° incline/decline) walking on a treadmill at a fixed speed (either 0.8 or 0.9 m/s). Prosthesis users walked on: (i) the MPA, (ii) the MPA with the ankle locked at the neutral position (hereafter referred to as the MPA-locked condition), and (iii) their prescribed prosthesis (primarily higher profile energy storage and return prostheses). Ground reaction force data were collected under each foot at 1000 Hz using a split-belt force-instrumented treadmill (Bertec), and lower-body kinematics were recorded at 200 Hz via a synchronized motion capture system (Vicon). Joint level kinematics and kinetics, as well as center-of-mass power, were calculated using common gait analysis methods. Prosthesis power was estimated using a previously published method that computes power due to all structures distal to the prosthetic socket [4]. Statistical significance was evaluated via repeated measures ANOVA, α=0.05.

RESULTS AND DISCUSSION

This study resulted in a comprehensive biomechanical characterization of lower-limb kinematics and kinetics, and center-of-mass power. Various changes were only observed in prosthetic-side biomechanical outcomes. However, in many cases, these changes were observed within a subset of users. Changes in sound limb kinematics and kinetics across the prosthesis conditions were generally small in magnitude, and inconsistent across participants. For brevity, the focus of this abstract is limited to (i) reporting key trends that were observed to be consistent among multiple, or a majority of participants, and (ii) reporting on a subset of outcome metrics of interest based on previously published prosthetics studies. Additional/extended results and discussion will be presented at the conference itself.

MPA vs. MPA-locked Results

The MPA adapted its ankle angle by the programmed amount on slopes (6.0 ± 1.5° dorsiflexion for 7.5° incline, 2 ± 0.4° plantarflexion for 7.5° decline) and provided more toe clearance (minimum height of toe above ground between 75% and 85% of gait cycle) than the MPA-locked condition during level (1.39 ± 0.44 cm, $p<0.001$), incline (1.99 ± 0.40 cm, $p<0.001$) and decline walking (0.81 ± 0.46 cm, $p=0.005$).

MPA vs. Prescribed Results

The MPA provided more toe-clearance than prescribed prostheses during level (1.46 ± 0.7 cm, $p<0.001$), incline (1.84 ± 1.0 cm, $p=0.001$) and decline walking (1.17 ± 1.06cm, $p=0.012$. During incline walking, four users switched from a toe-landing gait pattern on their prescribed prosthesis to a heel-to-toe gait pattern on the MPA, which was more consistent with the gait pattern of the controls. The MPA stored and returned less elastic energy for 6 of 8 subjects during level walking, and for 5 of 8 subjects during both incline and decline walking.

Discussion

The MPA may provide benefits by reducing trip risk due to increased toe-clearance. This was anecdotally supported by one user who reported less "toe-catching" during the at-home acclimation period with the MPA compared to his prescribed prosthesis. For half the prosthesis users, the MPA also appeared to promote a more typical heel-to-toe gait pattern for incline walking (i.e., more similar in appearance to the controls); however, a trade-off was that elastic energy return was generally reduced relative to prescribed prostheses. One limitation of this study was that K2 users (limited community ambulators) were not tested, a group for whom large elastic energy storage/return may be less important, and for whom ankle articulation has been shown to benefit walking performance [2].

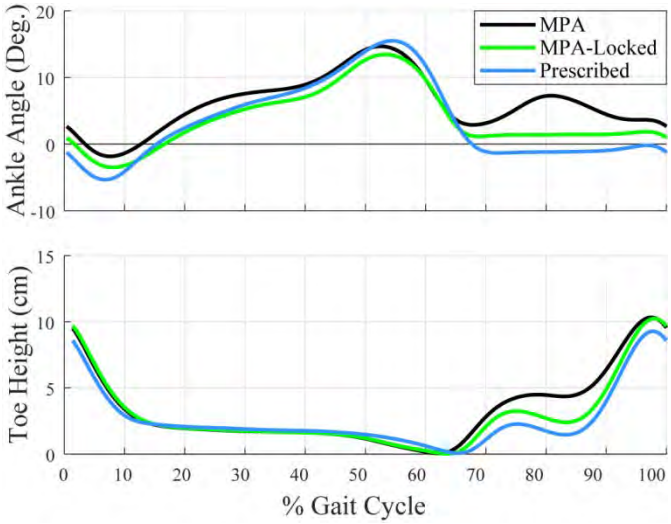

Figure 1: The MPA dorsiflexes the ankle during swing (~80% gait cycle) (top) to provide increased toe clearance (bottom), which may reduce trip risk. Representative subject depicted.

REFERENCES

1. Vrieling, A. H. et al. (2008). *Gait & Posture*.
2. Barnett et al. (2018). *J Prosthetics & Orthotics.*
3. Fradet, L. et al. (2010). *Gait & Posture.*
4. Takahashi, K. Z., et al. (2012). *J Biomechanics.*

ACKNOWLEDGEMENTS

Research was funded in part by Ossur. They had no role in analysis or interpretation of presented data.

RELIABILITY AND FEASIBILITY OF AN INERTIAL MEASUREMENT UNIT BASED DUAL-TASK GAIT BALANCE ASSESSMENT

[1]Will Pitt and [1]Li-Shan Chou

[1]Department of Human Physiology, University of Oregon, Eugene, OR, USA
email: chou@uoregon.edu, web: http://choulab.uoregon.edu

INTRODUCTION

Concussion in athletics, workplace, and everyday activities continue to occur at high rates leading to impaired dynamic balance control persisting up to two months post-injury [1]. Prolonged gait imbalance is currently detected using costly and time consuming camera-based whole body motion analysis under a dual-task paradigm (walking while performing a concurrent cognitive test). However, advances in commercially available wearable inertial measurement unit (IMU) technology offers an opportunity to perform objective post-concussion gait stability analysis in the clinical setting.

At present a clinically feasible dual-task gait balance assessment utilizing sensitive whole body center of mass (COM) biomechanical markers is not available. The development of such a clinical assessment requires design of a testing protocol, determination of its consistency in non-laboratory settings and across time, and establishment of inter-rater reliability and clinical feasibility.

This study has two main purposes: first, to examine the internal consistency and interrater reliability of an IMU-based dual-task gait balance control assessment. Second, to establish the clinical feasibility of the instrument in a Division I collegiate sports programs.

METHODS

This two part study consisted of 1) assessment of internal consistency and interrater reliability, and 2) assessment of clinical feasibility with a Division I female soccer team. Instrumentation consisted of an APDM OPAL IMU system (sensor placed over the L5 vertebrae as a COM proxy [2]) for kinematic data collection, Bluetooth headset/microphone for assessment instruction and cognitive test application, and Superlab 5 software for protocol automation. All hardware and software were controlled with a single MacBook Air laptop. In part one of the study subjects performed four walking trials in each of three conditions: walking only, walking while performing an auditory Stroop test, and walking while spelling a five letter word backwards or subtracting from a given number by 6s or 7s. Individuals walked at a self-selected pace over an eight meter level path, performed a 180° turn around a cone, and returned to the start. The conditions were repeated in two environments (laboratory and hallway representing a typical medical clinic), by two different raters, and on two separate days (separated by 7-10 days). The order of environment, rater, and walking condition was randomized for each testing session.

IMU data was sampled at 128Hz and filtered with a 2nd order, low-pass, Butterworth filter, with a 12Hz cutoff. The gait cycles beginning with the 5th heel strike during the walk out and the returning walk were analyzed. Peak linear accelerations along the vertical axis (10-30%, 30-50%, and 50-60% gait cycle) and medial-lateral axis (30-50%, 50-60%, and 60-75% gait cycle) were identified (Fig. 1).

The second part of the study consisted of a shortened clinical protocol implemented with the University Women's Soccer team. The protocol consisted of three walking trials in each of the three testing conditions with the conditions presented in a random order. Testing was performed in the University athletic medicine facility by a team athletic trainer. Total assessment time per athlete was collected to assess clinical feasibility. Additionally, the 10 linear acceleration metrics were collected and compared to our healthy, non-athlete female subjects from part one of the study.

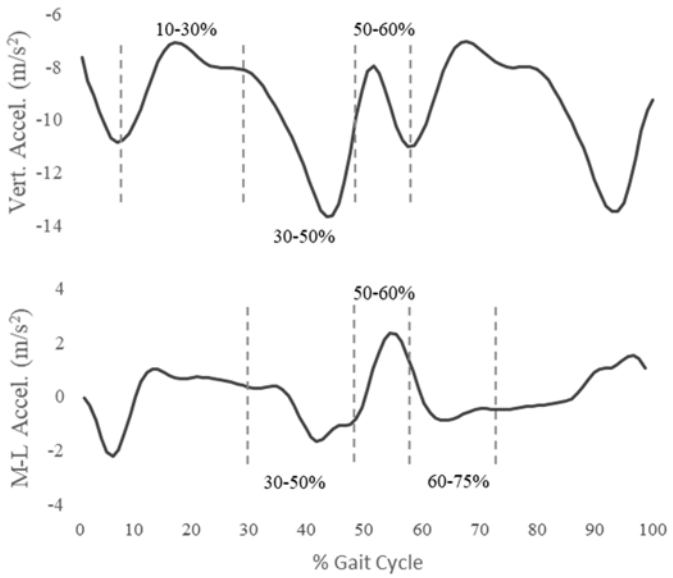

Figure 1: Representative plot of the A-P and M-L linear accelerations and 6 peak accelerations

An eight item Cronbach's α was used to establish the consistency of the measurement tool across time, environments, and raters. An Intraclass Correlation Coefficient and 95% CI was used to establish interrater reliability. Paired t-tests were performed for each outcome measure between female athletes and non-athlete controls. Statistical analyses were performed with SPSS version 24 (SPSS Inc., Chicago, IL).

RESULTS AND DISCUSSION

Twenty healthy subjects (10F) completed part one of the study (Age 22.2±2.8yrs, Wt. 71.0±12.0kg, Ht. 175.8±8.1cm). Internal consistency for the six outcome measures was excellent as established by Cronbach's α values between .904 and .980. Interrater reliability was also very good with ICC values ranging from .868 to .941 (Table 1).

Fourteen uninjured female athletes participated in part two of the study (Age 19.3±1.3yrs, Wt. 64.6±4.0kg, Ht. 168.4±7.1cm). Total assessment time including sensor placement and verbal instructions was 8:30 minutes ±35 seconds, demonstrating its clinical feasibility. Female athletes were compared to 10 non-athlete females from part one (Age 21.4±3.5, Wt. 62.5±7.6kg, Ht. 169.0±4.8cm). The magnitude of all M-L peak accelerations in all three walking conditions was

Table 1: Cronbach's α and ICC values for the 6 COM kinematic outcome measures

	Cronbach's Alpha			ICC	
Metric	Walk	Stroop	Q&A	r	95% CI
Vert. Accel 10-30%	.976	.942	.976	.920	.918±.022
Vert. Accel 30-50%	.951	.955	.980	.868	.865±.033
Vert. Accel 50-60%	.911	.914	.933	.876	.872±.034
M-L Accel 20-40%	.931	.963	.969	.931	.928±.020
M-L Accel 40-50%	.933	.904	.925	.902	.898±.027
M-L Accel 50-70%	.976	.969	.970	.941	.939±.016

greater than non-athlete females, however, only M-L Accel 20-40% and M-L Accel 50-70% reached a significant level (Table 2). This demonstrates the ability of the instrument to detect subtle differences in dynamic balance control.

Table 2: M-L peak accelerations (m/s^2) presented in mean±SD for non-athlete females and female soccer players. An * indicates $p < .05$

Metric	Group	Walking	Stroop
M-L Accel 20-40%	Non-Athlete	-2.24±0.52	-2.07±0.42
	Soccer	-2.91±1.14	-2.77±1.10 *
M-L Accel 40-50%	Non-Athlete	2.79±1.08	2.75±1.22
	Soccer	3.47±1.39	3.36±1.45
M-L Accel 50-70%	Non-Athlete	-1.39±0.70	-1.45±0.47
	Soccer	-2.07±1.01	-2.24±1.04 *

CONCLUSION

The high Cronbach's α and ICC values indicate our testing apparatus and protocol have excellent consistency and interrater reliability in a non-laboratory environment, across time, and with different evaluators. Furthermore, the instrument is both clinically feasible and sensitive to subtle differences in dynamic balance control. The results provide the necessary foundation for the development and implementation of a low-cost, accurate and sensitive, post-concussion gait stability assessment that is reliable in the clinical setting by minimally trained evaluators.

REFERENCES

1. Howell DR, et al. *Arch Phys Med Rehabil*., **94**(8), 513-1520, 2013
2. Howell DR, et al. *JOB*., **48**(23), 3364-8, 2015

Exploring Movement Variability and EEG Correlates During Motor Learning with a Smartpen: A Novel Method

[1,2] Jo Shattuck, [2] Matthew R. Johnson and [1]Jack W. Ransone

[1] University of Nebraska, Nebraska Athletic Performance Laboratory, Lincoln, USA
[2] University of Nebraska, Department of Psychology, Lincoln, NE, USA
email: joshattuck@huskers.unl.edu

INTRODUCTION

The optimal degree of movement variability during practice in the role of motor learning and ultimate performance outcome has been vigorously debated since Bernstein's degrees of freedom theory [1]. However, measuring movement variability with motion capture systems can be cumbersome, cost prohibitive and not suitable for smaller movements. Digital graphical tablets and touchscreens present one solution to capture smaller movements, but may not offer the flexibility of study design and the naturalistic feel of traditional pen and paper. Our solution was the use of an Echo Smartpen, which digitally stores every stroke of the pen on specialized LiveScribe paper, and image processing code with Matlab to record and analyze the movement variability over a timed drawing task with multiple training sessions spread over four days. Continual EEG data collection during the task was recorded with an EPOC 14 portable Bluetooth headset. The currently known neural substrates of motor learning have yet to offer a clear model of neural changes that occur over various brain regions through the learning stages. We intend to use the data collected via this novel method with non-linear analysis to pursue neural markers of performance outcomes and movement variability. This abstract describes the procedures, analysis and initial performance results in the timed drawing task.

METHODS

Nine females and eleven males from 19 to 30 years (M=21.35±3.65), completed 14 sets of a timed trail-making task. This timed drawing task required connecting 25 numbered circles on a page in a specific sequence. A 3-ring binder and timer button (Fig. 1) sat on the desk. The timer button and binder were attached; the left and right pages were equidistant to the timer button even if the subject repositioned the binder on the desk. Subjects were instructed to draw lines with the Echo Smartpen to connect the circles in sequence "as fast as possible without making mistakes." Fig. 2 shows Part A of the Trail Making Task in the Halstead Ralston Battery. (Part A was repeated 140 times over 4 days) Subjects pressed the timer button at the beginning and end of each page (trial), yielding a measure of speed; variability in movement was measured with custom Matlab code.

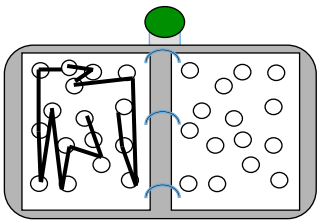

Figure 1: Binder and Timer Button

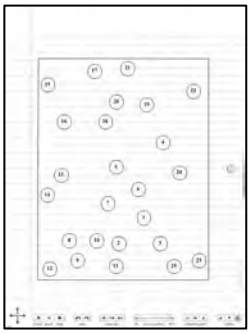

Figure 2: Trail Making Task

Each set containing ten pages (trials) was exported as a portable document format file (pdf), converted to black and white, inverted to show pen strokes as white, background as black, then overlaid into a single image. Fig. 3 shows the overlaid trials of Set 1 and Set 14.

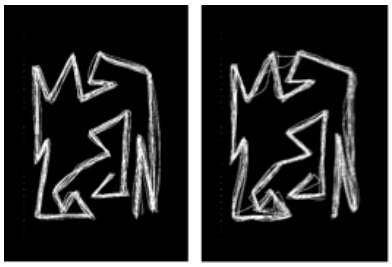

Set 1 Set 14

Figure 3: Overlaid Sets

Our variability code compared the distance of each white pixel to every other pixel to capture a quantitative measure of variability or Efficiency of movement. Figure 4 shows a low variability circle (top right inset), and a high-variability (bottom left

inset) for two 50 x 50 pixel areas (gray box) surrounding the numbered circles (dashed lines).

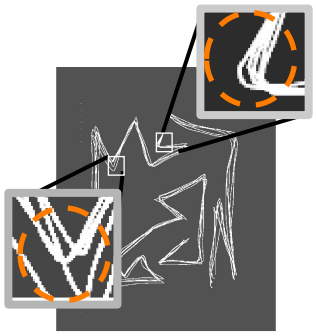

Figure 4: Examples of Different Levels of Variability

Each circle's coordinates surrounding the 23 circles (first and last were omitted) had been pre-determined from the original trail-making task. Variability was calculated on each circle in each set, from an image of the 10 overlaid trials in the set. Each subject completed 14 sets: four sets per day in Visits 1, 2, and 3, which all occurred on consecutive days, plus two sets in the Retention Visit, which occurred four days after Visit 3.

RESULTS AND DISCUSSION

Trial time retention (from set 1 to set 14) in the motor sequence improved 45%, in 4 days over 14 sets (M = 44.59±9.20). Variability improved 1.8% (M = 1.76±3.84). T-tests on the raw *variability scores* showed the mean difference in variability was significant (M=0.3212), p = 0.039). Recall variability (between set 12 to set 14, during which there was a four day delay) was not significantly different, suggesting the -1.06% efficiency gains were maintained and did not worsen over the delay, (M=-1.84, SD=4.74.)

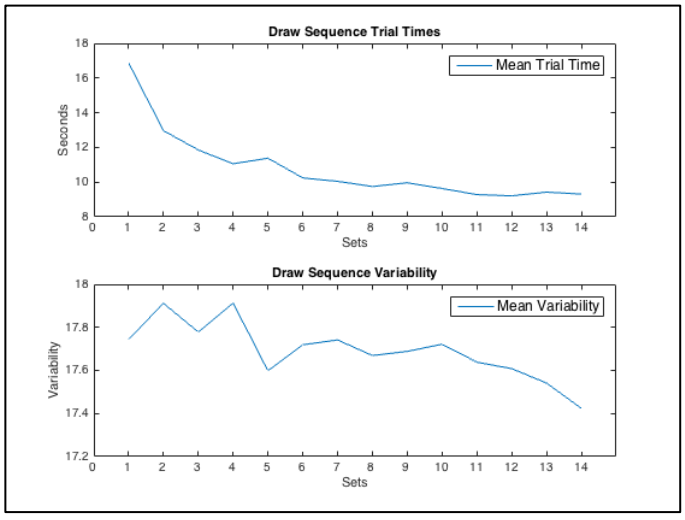

Figure 5: Trial Times (top) and Variability (bottom) per Set, n=20

Trial times decreased according to the law of practice, and the maximum speed/efficiency tradeoff occurred within the first 5 sets, the early (fast) stages of learning. The greatest change in trial times occurred in 1, after which trial times began to plateau; however, variability continued to decrease, (i.e. Efficiency improved, see Fig.5)

This method combined kinematics, a grapho-motor task and pen stroke capture, to produce a novel motor learning task and analysis method. While unable to capture force or pressure information as traditional digitizing tablets can, this method was a suitable alternative for studying 2 dimensional motor learning. The method was designed for a larger project for which the primary goal is to find neural correlations for different performance features of motor learning. Further analysis on continually recorded EEG data throughout the sessions was required to determine if neural activity shifts with movement variability and trial times. We intend to use a repeated measures non-linear multilevel model to examine between-set variability over the learning stages.

CONCLUSIONS

Stergiou and Decker stress the importance of studying variability to understand human movement: "Far from being a source of error, evidence supports the necessity of an optimal state of variability for health and functional movement" [2]. We explored the role of variability and its relationship with neural activity with this novel method in an attempt to improve movement pedagogy. Improved teaching techniques can benefit motor learning fields such as physical therapy, vocational training, and recreational and elite sport coaching.

REFERENCES

1. Bernstein NA (1967) *The co-ordination and regulation of movements.* Oxford, New York, Pergamon Press
2. Stergiou N, Decker LM (2011) Human movement variability, nonlinear dynamics, and pathology: is there a connection? *Hum Mov Sci* **30**:869–88.

GAIT VARIABILITY TO PREDICT MOTOR LEARNING OF A NOVEL MOTOR TASK

[1] Sophia Ulman, [2] Robin M. Queen, and [1] Divya Srinivasan

[1] Industrial and Systems Engineering, Virginia Tech, Blacksburg, VA, USA
[2] Kevin P. Granata Biomechanics Lab, Biomedical Engineering and Mechanics, Blacksburg, VA, USA
email: smu4@vt.edu

INTRODUCTION

Motor variability (MV) is a fundamental feature of movement that refers to the variation observed in the spatiotemporal dispersion of joint movements, inter-joint coordination patterns, and muscle activities, when an individual completes the same task numerous times. While variability is natural and inherent in any human movement, it was traditionally assumed to be undesirable, as it was thought to contribute to less accurate performance. However, basic motor control research has progressed in recent years, and now suggests that movement variability has important functional implications for the preservation of motor performance, both with respect to short-term adaptations of movement strategies and longer-term motor learning. Existing evidence of motor variability being predictive of motor learning has been reported during simple reaching tasks [1]. Whether this concept is generalizable to other kinds of movements such as gait is currently unknown.

The goal of this study was to assess whether motor variability in normal gait at a self-selected speed (baseline condition) was associated with motor learning in a young healthy population performing a novel motor task. The novel motor task involved clearing an obstacle course within a designated time while performing a dual task. We hypothesized that inter-individual differences in motor learning ability in the novel task would be explained by differences in baseline gait variability. As a secondary objective, we also aimed to determine which variability measures (stride characteristics. lower limb joint kinematics and inter-joint coordination as quantified by vector coding) were most discriminative of inter-individual differences in learning ability in our cohort of young healthy adults.

METHODS

Thirty-two participants (16 F, 16 M), aged 21.28 (SD 1.76) years, with no known history of musculoskeletal disorders or injuries were recruited. Each participant was asked to walk barefoot continuously at a comfortable, self-selected pace for six minutes in order to reliably capture baseline motor variability [2]. Gait kinematics were collected using a 10-camera motion capture system (Qualysis INC, Gothenburg, Sweden), and passive reflective markers placed at select anatomical landmarks on the pelvis and lower limbs. After baseline over-ground walking, each participant was asked to walk through an obstacle course barefoot while holding a bowl of colored water. In order to complete the course successfully, they needed to finish the course within a specified time constraint while not spilling the bowl of water. The course consisted of directional cones, an agility ladder, a low balance beam, and stepping stools to step over. “Performance” in the novel task was quantified by the number of trials taken by each participant to achieve success, i.e. obstacle course completion within the pre-set time.

Marker data were exported into Visual 3D (C-motion Inc., USA) for data processing. Spatiotemporal stride characteristics and hip, knee, and ankle joint angles in the sagittal and frontal planes, during the stance and swing phases of gait, were extracted for further analysis. Standard deviation of each joint angle trajectory was calculated as the root mean square of standard deviation obtained at each normalized time point across all trials, during the stance and swing phases (~35-40 strides). Inter-joint coordination was quantified through vector coding [3]: hip-knee and knee-ankle couples in the sagittal and frontal planes during stance and swing were computed, and the stride-to-stride SD of joint coupling angles were used to quantify coordination variability. Two stepwise linear regression models were estimated to assess the association between performance (response variable) and the following predictor variables:

1. Stride characteristics (mean and stride-to-stride SD);
2. Joint trajectory variability of hip, knee and ankle joints, and stride-to-stride SD of hip-knee and knee-ankle joint couples in the frontal and sagittal planes during stance and swing phases.

JMP (SAS Inst. Inc., USA) was used for all statistical analyses, and a type I error rate of 5% was considered to be acceptable for statistical significance in tests of each variable in the regression models.

RESULTS AND DISCUSSION

On average, the participants took 10.97 (range 2-21) trials to learn to clear the obstacle course. A model using only stride characteristics of baseline gait (top panel in table 1) to predict performance was not statistically significant. However, when joint kinematic variability measures were used as predictor variables (bottom panel of table 1), 95.6% of the variance in performance could be explained by the model. Thus, our results support the functional significance of joint kinematic variability in over-ground walking even for a homogenous group of young and healthy adults: inter-individual differences in the rate of learning a novel motor task was predicted by differences in kinematic variability between individuals. Specifically, individuals with the fastest learning rate exhibited increased variability in knee frontal and ankle sagittal joint angle trajectories during the stance phase, and increased knee-ankle coordination variability during the swing phase. Our results are also novel from the perspective of showing that swing phase joint kinematic variability is also meaningful to study in gait, as hip and knee joint variabilities as well as inter-joint coordination variabilities are predictive of performance.

CONCLUSIONS

Although the functional significance of motor variability has been demonstrated in various clinical populations and among older adults, ours is one of the first studies showing strong association between gait variability and short-term motor learning in a cohort of young and healthy individuals.

REFERENCES

1. Wu et al. *Nature neuro.* **17**, 312, 2014.
2. Konig et al. *Gait & Posture.* **39**, 615-617, 2014.
3. Heiderscheit et al. *J. Appl. Biomech.* **18**, 2002.

ACKNOWLEDGEMENTS

We would like to acknowledge the contributions of Melanie Kangelaris and Willow Ruud for their assistance with data collection and processing.

Table 1: Association between variability measures and performance.

	Input Variables to models		Model prediction
Spatiotemporal gait characteristics model	Speed Swing time: mean and SD Stance time: mean and SD Step time: mean and SD Cycle Time: mean and SD	Step length: mean and SD Stride length: mean and SD Stride width: mean and SD	Model not significant
Joint kinematics variability model	Sagittal Hip Angle SD stance Frontal Hip Angle SD stance Sagittal Knee Angle SD stance **Frontal Knee Angle SD stance * (r = - 0.18)** **Sagittal Ankle Angle SD stance * (r = - 0.35)** Frontal Ankle Angle SD stance Sagittal Hip-Knee SD stance Frontal Hip-Knee SD stance Sagittal Knee-Ankle SD stance **Frontal Knee-Ankle SD stance * (r = 0.03)**	Sagittal Hip Angle SD swing **Frontal Hip Angle SD swing * (r = 0.28)** **Sagittal Knee Angle SD swing* (r = 0.22)** Frontal Knee Angle SD swing Sagittal Ankle Angle SD swing Frontal Ankle Angle SD swing **Sagittal Hip-Knee SD swing* (r = 0.02)** **Frontal Hip-Knee SD swing * (r = 0.1)** **Sagittal Knee-Ankle SD swing * (r = - 0.1)** **Frontal Knee-Ankle SD swing * (r = - 0.1)**	Model R^2 = 95.6%, $p < 0.001$

REAL-TIME MUSIC-BASED BIOFEEDBACK TO REDUCE IMPACT LOADING DURING OVER-GROUND RUNNING

[1] Pieter Van den Berghe, [2] Valerio Lorenzoni, [1] Joeri Gerlo, [1] Bastiaan Breine, [1] Rud Derie, [2] Joren Six, [2] Marc Leman, [1] Dirk De Clercq

[1] Department of Movement and Sports Sciences, Ghent University, Belgium
[2] IPEM, Department of Arts, Music and Theatre Sciences, Ghent University, Belgium

email: pieter.vandenberghe@ugent.be, web: www.ugent.be/ge/bsw/en/research/biomechanics

INTRODUCTION

Running retraining through biofeedback on a measure of impact loading combined with simple instruction can decrease running related injuries [1]. Running retraining through real-time biofeedback on a direct measure of impact loading has been exclusively executed on treadmill [1,2]. For example, Peak Tibial Acceleration (PTA) was reduced by provision of simple auditory biofeedback within a single, treadmill-based retraining session [2]. Ecological validity could be improved by conducting retraining programs in an over-ground environment outside the laboratory and with a motivational bio-feedback approach.

In this 'proof of concept' study, retraining by means of real-time auditory biofeedback happened over-ground on an indoor running track in runners with elevated PTA. Impact loading was expected to be reduced within a single session.

METHODS

After screening 80 uninjured runners on PTA, 5 (3♂-2♀) high impact runners (height: 1.74 ± 0.02 m; weight: 71 ± 7 kg; age: 38 ± 11 years; weekly running volume: 25 ± 10 km; mean ± SD) were recruited in this ongoing study. These recreational, habitual rearfoot runners ran at least 15 km/week in non-minimalist footwear, were injury-free in the last 6 months and had no experience with gait retraining. They were instrumented with a wearable accelerometry system able to continuously detect PTA in real-time. Tibial skin was bilaterally pre-stretched before low-weight accelerometers (LSI 331, Sparkfun; 1000 Hz) were attached over the distal, anteromedial aspect of both tibia [3]. At an indoor track-and-field site (Flanders Sports Arena, 289 m/lap), participants were instructed to run at 3.2 ± 0.3 m/s. A warm-up of 4.5 min without bio-feedback was given while the average axial PTA was automatically determined for the leg bearing the highest tibial shocks. Lap times were used to give feedback on running speed. Real-time, music-based biofeedback was then provided for 20 min. in total (2*10 min. with ~ 5 min. intermittent rest). Music of a preferred genre was continuously synchronized to the runner's step frequency and was non-linearly distorted by superposition of pink noise according to the magnitude of elevated PTA [4]. To lower impact loading, runners were instructed to run with maximum music clarity and were not given any instructions on possible gait modifications. To account for any within-subject change in PTA during running, all PTAs were exported for further analysis using a custom MATLAB program. Wilcoxon signed-rank tests compared the mean running speed and mean PTA level between the no biofeedback and biofeedback (last 10 min. phase) conditions. The data were determined to be significant if $p < 0.05$. Mean ± SD are reported.

RESULTS AND DISCUSSION

Running speeds during the no biofeedback and biofeedback conditions were respectively 3.2 ± 0.1 and 3.1 ± 0.1 m/s ($p = 0.416$, $z = -0.813$), and thus speed had no confounding effect on PTA. Supporting our hypothesis, one retraining session with real-time biofeedback was enough to temporary decrease PTA in an over-ground setting (Table 1). The PTAs experienced by a representative runner during the over-ground running session are shown in figure 1. All subjects could decrease impact loading while listening to real-time biofeedback, and this without

any instruction on gait modification but simply by means of impact sonification. The reduction of -2.7 g or -26 % in PTA was more than the achieved reduction in other single retraining sessions by auditory biofeedback on treadmill [2, 5].

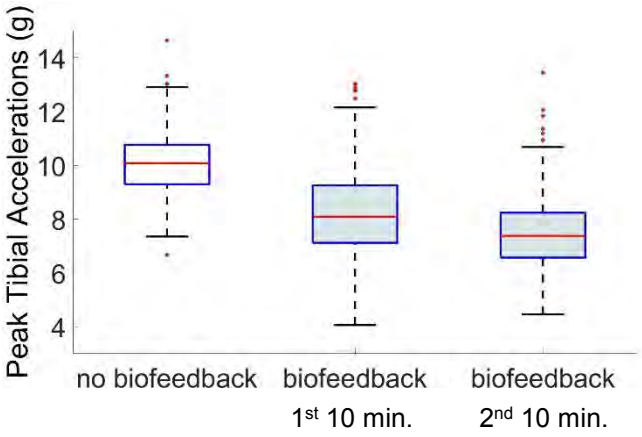

Figure 1: A Box-and-Whisker plot showing the distribution of peak tibial accelerations experienced by a representative participant.

The achieved reduction is arguably due to the more motivating form of the provided augmented feedback [6], consisting of music continuously synchronized to the runner's step frequency instead of simple beeps, and the cohort exhibiting high impacts along the lower leg's axial axis at baseline. Although other studies [2,5] demonstrated the effectiveness of auditory biofeedback by generating simple beeps for impact loading reduction on treadmill, this study is the first to show reduction in axial PTA in runners at-risk for the development of tibial stress injuries by applying more advanced and motivating real-time audio biofeedback and this in a non-lab environment. Besides the PTA acting along the axial axis, the impact shock severity along the other axes may also have altered and should be investigated in future and ongoing studies.

The feasibility of providing auditory information about clinically relevant biomechanical data per wearable biofeedback system eliminates the need of retraining exclusively in laboratory or clinic settings. This allows people to engage in gait retraining by means of impact sonification in their regular running environment (e.g. track-and-field, trail running) and is expected to increase the effectivity of and the adherence to a running retraining program.

CONCLUSIONS

High impact runners were able to temporarily decrease their PTAs during over-ground running by actively listening to and acting on music-based biofeedback without any instructions on gait modifications. Running retraining aiming at impact loading reduction by provision of augmented feedback on a direct measure of impact loading is possible in an ecologically valid environment.

REFERENCES

1. Chan et al. *Am J Sports Med*. 5, 36354651773627, 2017.
2. Wood and Kipp. *J Biom*. 47, 1739–41, 2014.
3. Van den Berghe et al. *Proceedings of WCB'18,* Dublin, Ireland, 2018.
4. Lorenzoni et al. *Proceedings of MOCO'18,* Genoa, Italy, 2018.
5. Morgan and Kipp. *Proceedings of ASB'15,* Columbus, OH, USA, 2015.
6. Maes et al. *Front. Neurosci*. 10, 548, 2016.

ACKNOWLEDGEMENTS

This ongoing investigation is funded by the Research Foundation – Flanders (FWO.3F0.2015.0048.01). We like to thank Gent Topsporthal Vlaanderen for the possibility of conducting a lab-in-the-field test.

Table 1: Comparison of peak tibial acceleration (g) between the no biofeedback and the biofeedback (2nd 10 min.) conditions. Mean number of steps analyzed per subject: 383, no biofeedback; 872, biofeedback.

	No biofeedback	**Biofeedback**
Mean	10.4	7.7
Std. Deviation	1.5	0.8
Minimum	8.8	6.5
Maximum	12.6	8.5
p-value	0.043	
z-value	-2.023	

LOAD EFFECTS ON PERFORMANCE FOR EXAMPLE OBSTACLES IN AN OUTDOOR COURSE

[1] Rachel Vitali, [1]Stephen Cain, [1]Michael Potter, [1]Lauro Ojeda, [1]Steven Davidson, [2]Alyssa Mendoza, [2]Leia Stirling, [1]Noel Perkins

[1] University of Michigan, Ann Arbor, MI, USA
[2] Massachusetts Institute of Technology, Cambridge, MA, USA
email: vitalir@umich.edu

INTRODUCTION

Modern warfare requires warfighters to carry increasingly heavy loads that include, for example, body armor, gear, electronics, food, and water. To optimize the magnitude and configuration of the load, the Marine Corps Load Effects Assessment Program (MC-LEAP) was developed to assess variations in soldier performance due to clothing and individual equipment (CIE) [1]. The program consists of an obstacle course representative of tasks warfighters encounter in combat. Historically, performance in the MC-LEAP (and variations of it) is quantified solely by the time required to complete each obstacle as often measured via timing gates. Although the time to complete an obstacle is one measure of performance, completion time alone does not reveal the technique(s) used or underlying biomechanics contributing to performance. As an alternative to video motion capture, recent studies employed inertial measurement units (IMUs) to measure underlying biomechanics that define performance for obstacles in the MC-LEAP [2-8]. The goal of this follow-up study is to understand how the IMU-derived performance metrics change when subjects carry different loads.

METHODS

A set of 22 subjects (7 females, 15 males) were recruited to complete a 10 obstacle abbreviated version of the LEAP-A a total of four times with a weight vest with 0% (2 repetitions), 15% (1 repetition), and 30% (1 repetition) of their body weight. All subjects wore an array of 13 IMUs (Opal, APDM, Portland OR) attached to the head, upper arms, forearms, sternum, sacrum, thighs, shanks, and feet. In addition, the subjects carried a mock plastic rifle (3.4 kg) with another attached IMU. The University of Michigan IRB approved the study and all subjects gave informed consent. The IMU data (accelerometer and angular rate) for each of the 14 IMUs was parsed into segments for each obstacle with custom activity identification code. The data for each obstacle was further analyzed with custom algorithms identifying key biomechanical measures of performance with examples detailed in [2-8].

Performance metric changes for a subset of obstacles is reported as a function of load. Thus, a repeated-measures analysis of variance (ANOVA) was conducted. Several subjects' data were eliminated because the subject did not complete all four testing sessions, data for one or more sensors was lost due to technical difficulties, or data was not properly parsed (i.e. falsely identified as another obstacle or failed to find anything). For the present analysis, the total number of subjects for the wall, window, and high crawl were 15, 13, and 14, respectively.

For each obstacle-specific performance metric, the normality assumption for the residuals is confirmed with Shapiro-Wilk normality tests, skewness and kurtosis calculations, and Q-Q plots. After conducting the repeated-measures ANOVA, a Mauchly's test for sphericity was conducted. Depending on the severity of the violation of this assumption, the ANOVA F-statistic was evaluated with adjusted degrees of freedom using a Greenhouse-Geisser correction. Then, Tukey post hoc analyses were conducted for performance metrics with significant results. All statistical tests are evaluated with a significance level of $\alpha = 0.05$.

Results are presented from the chosen subset of obstacles: 1) wall, 2) window, and 3) high crawl. The wall obstacle requires subjects to lift themselves up and over a 4ft tall wall. The window obstacle similarly requires subjects to lift themselves through a 3ft x 3ft opening 4ft off the ground. The high crawl requires subjects to crawl 30ft on elbows and knees while keeping their bodies as low as possible. The

ANOVA results include the F-statistic (and degrees of freedom), p-value, and effect size (η^2). For η^2, an effect size that is small is 0.01, medium is 0.06, and large is 0.14 [9]. The Tukey post hoc test results include the p-value and effect size (Cohen's **d**) for each pairwise comparison. Cohen's **d** indicates both the magnitude and direction of the comparison. (A negative **d** value indicates that the first group's average is less than that of the second group.) For Cohen's **d**, an effect size that is small is 0.2, medium is 0.5, and large is 0.8 [9].

RESULTS AND DISCUSSION

Performance on each obstacle is described by several performance metrics and a subset of three important metrics/obstacle are reported in Table 1 (all of which have normally distributed residuals). The ANOVA results show that load has a significant and large effect on the performance metrics in this subset of obstacles, whereas the post hoc results show these effects vary across metrics. As expected, the effect sizes for the 0%-30% comparison are larger in magnitude than either of the other two comparisons. However, there does not appear to be a common trend between the other two comparisons. For example, adding 15%BW from 0%BW has a larger effect on the wall's *Average take-off power* than adding 30%BW from 15%BW whereas adding 15%BW from 0%BW has a smaller effect on the wall's *Take-Off Speed* than adding 30%BW from 15%BW. These results imply potential metric-specific non-linear effects of adding weight. These differences could be the result of altering the underlying technique selected for the obstacle.

CONCLUSIONS

Load has large, significant effects on several performance metrics in this obstacle subset. The post hoc analyses indicate the increased load degrades performance, but in directions and magnitudes that vary across metrics and load conditions. These results suggest the IMU-derived metrics can be used to discriminate performance and technique in an outdoor setting that could potentially be extended to applications beyond warfighter performance.

REFERENCES

1. Smith and Kelley. *Statement before the Tactical Air and Land Forces Subcommittee,* 2013
2. Cain et al. *Gait & Posture*. 2016, 43, 65-69
3. McGinnis et al. *Jour. of Sports Eng*. 2016, 19(1), 21-34
4. Davidson et al. *Applied Ergonomics*. 2016, 26, 27-33
5. McGinnis et al. *Bio. Sig. Process.&Cont*. 2016, 32, 150-156
6. Tammana et al. *Applied Ergonomics*. 2018, 70, 68-76.
7. Zaferiou et al. *PLOS ONE*. 2017, 12(11)
8. Ojeda et al. *Sensors*. 2017, 17(11), 2647
9. Cohen J. 1988, Hillsdale, NJ:Erlbaum

ACKNOWLEDGEMENTS

This material is based upon work supported by the US Army Contracting Command-APG, Natick Contracting Division, Natick, MA, under contract W911QY-15-C-0053.

Table 1: Statistical results for the wall, window, and high crawl obstacles from the course. The effect sizes (η^2, **d**) are shaded according to how large the effect is [9]. Green indicates a large effect, yellow indicates a medium effect, and red indicates a small effect (as defined in the Methods section). *Significant at $\alpha = 0.05$.

	ANOVA			Tukey Post Hoc					
	F-Statistic	p-value	η^2	0%-15%		0%-30%		15%-30%	
				p-value	d	p-value	d	p-value	d
Wall									
Take-off Speed	F(2,28)=17.1	<0.001*	0.55	0.16	0.37	<0.001*	0.87	<0.001*	0.56
Average Take-off Power	F(2,28)=4.95	0.01*	0.26	0.48	0.67	0.05*	0.96	0.09	0.58
Take-off Work	F(2,28)=4.15	0.03*	0.23	0.19	0.58	0.05*	0.95	0.41	0.41
Window									
Approach Speed	F(2,24)=3.95	0.03*	0.25	0.31	0.32	0.02*	0.57	0.46	0.33
Take-off Speed	F(2,24)=3.91	0.03*	0.25	0.50	0.25	<0.01*	0.55	0.38	0.32
Window Time	F(1.01,11.1)=5.57	0.04*	0.34	0.10	-0.77	0.08	-0.88	0.07	-0.35
High Crawl									
Stride Time	F(2,26)=18.1	<0.001*	0.58	<0.01*	-0.68	<0.01*	-0.98	0.03*	-0.39
Opposite Side Coordination	F(2,26)=9.44	<0.001*	0.42	0.27	0.28	<0.01*	0.81	0.04*	0.49
Same Side Coordination	F(2,26)=4.25	0.03*	0.25	0.31	-0.32	0.07	-0.67	0.23	-0.33

CHANGES IN DYNAMIC MOTOR CONTROL FOLLOWING NEUROREHABILITATION FOR TRAUMATIC BRAIN INJURY: TREADMILL VS OVERGROUND WALKING

[1] Samuel A Acuña, [1] Mitchell E Tyler, [1] Yuri P Danilov, and [1] Darryl G Thelen

[1] The University of Wisconsin–Madison, Madison, WI, USA
email: saacuna@wisc.edu, web: http://uwnmbl.engr.wisc.edu

INTRODUCTION

Chronic gait deficits are often present in persons who have sustained a mild to moderate traumatic brain injury (TBI)—they tend to walk more slowly, take shorter steps and exhibit greater mediolateral sway [1]. Non-invasive neuromodulation of the cranial nerve has shown promise to enhance balance and gait in chronic TBI when coupled with rehabilitation exercises [2]. It is theorized this neuromodulation enhances neuroplasticity during rehabilitation, and thus improves the brain's ability to functionally compensate for damaged neural tissues [2]. However, it is unknown if the improvements in balance and gait arise from fundamental changes to the underlying motor control as a result of the neuromodulation.

One way to examine the underlying motor control during walking is with muscle synergy analysis. This has emerged as a quantitative tool to characterize the complexity of neuromuscular control patterns in neurologically impaired populations. The analysis typically involves the use of matrix factorization algorithms to identify low-dimensional patterns, or synergies, that can describe the variability inherent in an individual's measured muscle activations. A synergy then represents a group of muscles that are generally co-activated, which may represent simplified control. Hence, the variance in muscle activity accounted for by a given number of synergies can provide a measure of the complexity of control used by an individual. Prior synergy analysis studies have identified diminished complexity in the gait EMG patterns of stroke [3] and cerebral palsy [4] patients. Our previous work suggests that complexity is reduced for TBI subjects as well [5].

The objective of this study was to investigate if non-invasive cranial nerve neuromodulation during rehabilitation for a prior TBI can induce fundamental changes to the neuromuscular control of walking. We hypothesized that fundamental changes would manifest across a variety of walking tasks, such as walking overground and walking on a treadmill.

METHODS

Twenty healthy adults (25±3 years, 10 female) and forty-four ambulatory adults with a balance disorder due to a non-penetrative TBI participated in the study (53±9 years, 28 female). Each TBI participant was at least one year post-injury, had previously completed a focused physical rehabilitation program for their TBI, and were no longer seeing improvements from their gait rehabilitation. All TBI subjects had a dynamic posturography score at least 8 points below normal (Sensory Organization Test, NeuroCom®). The TBI subjects participated in 14-week neurorehabilitation program to train gait and balance. A portable electrotactile device stimulated cranial nerves V and VII throughout training via an electrode array placed on the human tongue, delivering three 0.4-60μs wide electric pulses at 5 ms intervals every 20 ms [2]. The rehabilitation program involved exercises 3x per day for two weeks in the clinic and then continued the exercises for 12 more weeks at home with the device.

Lower extremity electromyographic (EMG) signals were collected bilaterally from six muscles (tibialis anterior, medial gastrocnemius, soleus, vastus lateralis, rectus femoris, semitendinosus) during treadmill and overground walking (60 seconds). EMG was collected before rehabilitation (week 0), after the in-clinic training (week 2), after at-home training (week 14), and after a washout period without stimulation or exercises (week 26). Each chronic TBI subject walked at his/her pre-rehabilitation preferred speed (1.0±0.2 m/s). The

protocol was repeated on the healthy young adults walking at a speed of 1 m/s. EMG signals were rectified and then low-pass filtered at 10 Hz. Ensemble EMG patterns were created by averaging signals over all gait cycles and normalizing the data to each muscle's root-mean-squared EMG. Non-negative matrix factorization was used to derive the synergies. The walking dynamic motor control index (Walk-DMC) was then used to measure the complexity of neuromuscular control during gait [4]. A two-way repeated measures ANOVA tested for the effects of time (weeks 0, 2, 14, 26) and walking activity (treadmill, overground) on Walk-DMC score. For normative comparisons, exploratory Mann-Whitney tests compared Walk-DMC in TBI to the healthy adults.

RESULTS AND DISCUSSION

There was no significant effect of time (p = 0.581) or walking type (p = 0.307) on the Walk-DMC score of the TBI subjects (Fig. 1) During overground walking, the TBI subjects had a significantly lower Walk-DMC score than the healthy adults at every time point (p's < 0.01). However, the Walk-DMC score for TBI subjects on the treadmill was only significantly lower than the healthy adults before training (p = 0.018).

Changes in Walk-DMC for the TBI subjects were not consistent between treadmill and overground walking, suggesting that changes in neuromuscular complexity were different between the two walking tasks. This might suggest that the two walking tasks were sufficiently different and thus did not induce similar muscle activation patterns. Indeed, treadmill and overground walking may require different control strategies in this population [6]. However, as both walking activities have a lot of similarity, we may interpret our findings to suggest that the neurorehabilitation program did not create a fundamental change in the underlying control of walking. Rather, the improvements likely arose from proper training and increased familiarization of the treadmill walking task. Regardless, it is encouraging that neuromuscular complexity during treadmill walking improved to levels similar to the healthy adults after the in-clinic training, and then was maintained through the 12-week washout period. This suggests that the neurorehabilitation program may provide some level of meaningful change in walking control in a population of subjects who were no longer seeing improvements in gait and balance through traditional rehabilitation. Future research will examine individual subjects across time, as many TBI subjects started with healthy levels of neuromuscular complexity.

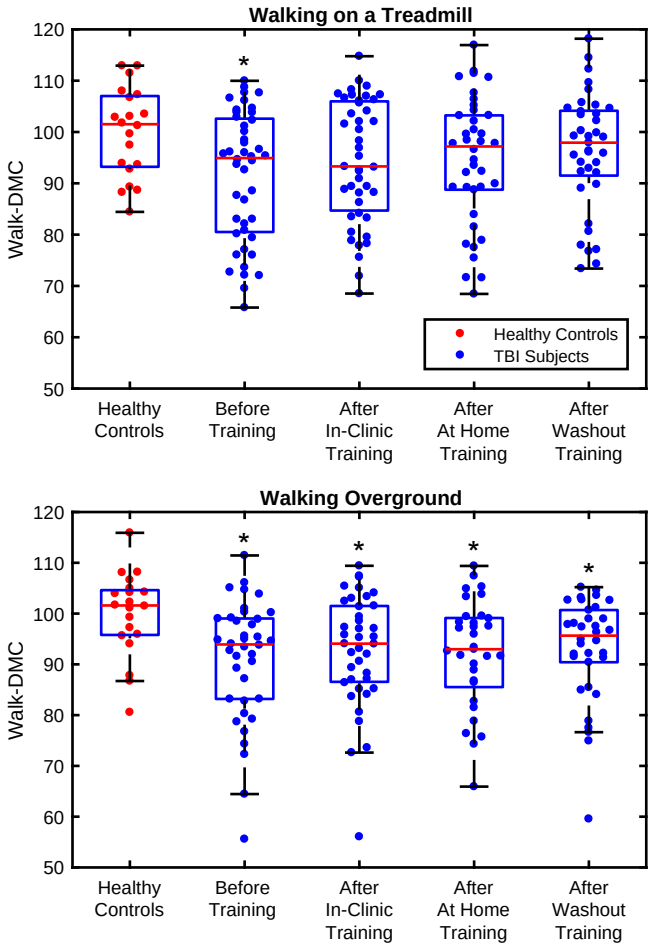

Figure 1: Walk-DMC scores for TBI and healthy controls. Asterisks indicate time points when the TBI subjects had a significantly lower Walk-DMC score than the controls.

REFERENCES

1. Vasudevan. *Neuro Phys Therapy.* 38(3), 2014.
2. Danilov. *Brain Neurotrauma*, CRC Press, 2015.
3. Clark et al. *Neurophysiology*. 103(2), 2015.
4. Steele et al. *Developmental Medicine & Child Neurology.* 57(12), 2015.
5. Acuña et al. ASB conference, Boulder, CO, 2017.
6. Brown et al. *Head Trauma Rehab.* 20(5), 2005.

ON-SITE REACTIVE BALANCE TRAINING AMONG RESIDENTS OF RETIREMENT COMMUNITIES

[1] Jessica Aviles, [1] Leigh Allin, [2] Neil Alexander, [1] Jennifer Van Mullekom, [1] Maury A. Nussbaum, [1] Michael L. Madigan

[1] Virginia Tech, Blacksburg, VA, USA
[2] University of Michigan, Ann Arbor, MI, USA
email: javiles@vt.edu

INTRODUCTION

Falls are a leading cause of injuries and injury-related deaths among older adults in the United States [1]. Up to half of all falls among older adults occur due to tripping [2-4]. Since the onset of tripping events may not be completely avoidable, enhancing the reactive balance response after tripping may be an effective approach for reducing falls among older adults. Reactive balance training (RBT) is a form of task-specific, perturbation-based balance training that has the potential to improve reactive balance performance. RBT involves repeatedly exposing individuals to trip-like perturbations in a safe, controlled manner to facilitate improvements in reactive balance performance.

The goal of this study was to evaluate the efficacy of RBT as an on-site balance training intervention for improving reactive balance among residents of retirement communities. This was done in comparison with Tai Chi, an active control demonstrated to reduce fall risk.

METHODS

Thirty-five older adults (age 70-92, 24 females) participated in the study. Subjects were initially required to pass a medical screening that included a history, physical, and bone mineral density assessment at the lumbar spine and proximal femur. Subjects were randomized to either RBT or Tai Chi. RBT was performed on a treadmill that was modified to elicit trip-like perturbations. Subjects stood quietly on the treadmill with a foam block placed in front of their feet. Perturbations were generated by accelerating the treadmill belt to a preselected walking speed over ~40 msec. This abrupt acceleration induced a forward fall similar to a trip while walking, and subjects subsequently attempted to take steps to recover balance (Fig. 1). RBT involved 30-minute sessions performed three times a week for four weeks. Each session consisted of 18-40 trials on the treadmill, with direction and speed pseudo-randomized and individualized based upon subject ability and improvement (with speeds between 0.5-2.4 mph). Tai Chi consisted of slow, controlled movements that focused on balance and like RBT, was performed three times a week for four weeks.

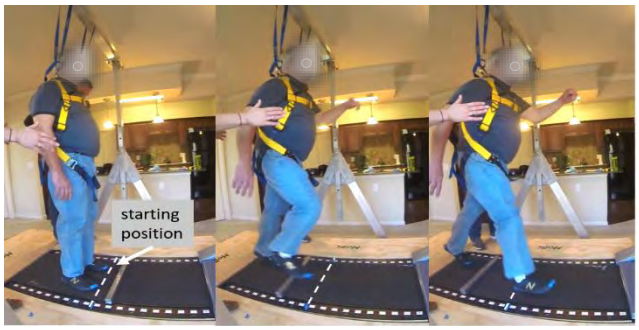

Figure 1. RBT subjects stood still on the treadmill (left) until the motorized treadmill suddenly accelerated, inducing a forward fall (middle). Subjects were asked to step over the block and establish a stable gait (right).

Outcome measures included metrics of reactive balance performance, along with standard clinical tests of balance and mobility. Outcome measures were assessed before (B) intervention, and one week (1W), one month (1M), three months (3M), and six month (6M) after intervention. Reactive balance performance was determined by accelerating the modified treadmill belt backward (to induce a forward fall) to 0.8, 1.6, and 2.4 mph. Outcomes measures were based on characteristics of the initial reactive step (measured from video recording) and sagittal plane trunk angle (measured using an inertial measurement unit). These measures included anterior/posterior length of the first reactive balance

step (step length), time from treadmill onset to lift-off of first recovery step (liftoff time), time from onset to touchdown of first reactive balance step (touchdown time), maximum sagittal plane trunk angle, and a reactive balance rating. Clinical tests included the time-up-and-go test (TUG), unipedal stance time, maximum step length, Berg Balance Scale, Performance-Oriented Mobility Assessment (POMA), and Activities-specific Balance Confidence Scale (ABC). Post-intervention differences between groups were investigated using a mixed model that accounted for fixed and random effects and within subject correlation. A $p \leq 0.05$ indicated significance.

RESULTS and DISCUSSION

RBT subjects performed better than Tai Chi subjects in a subset of reactive balance measures. Maximum trunk angle was 13.5 degrees smaller among RBT subjects one week after intervention ($p < 0.001$; Fig. 2). The reactive balance rating was 24% higher ($p = 0.016$; indicating better performance) at one week, 31% higher ($p = 0.023$) at one month, and 28% higher ($p = 0.029$) at six months after the intervention among RBT subjects compared to Tai Chi subjects. There were minimal differences in clinical tests between groups after intervention, though the POMA score was 5% higher (indicating better performance) among Tai Chi subjects one week after the intervention ($p = 0.040$).

CONCLUSIONS

Improvements in maximum trunk angle and reactive balance rating provide evidence for the ability of on-site RBT to improve reactive balance after trip-like perturbations. These results also support the use of the specificity of training principle among older adults for fall prevention.

REFERENCES

1. Centers for Disease Control and Prevention, *WISQARS*, National Center for Injury Prevention and Control [online], 2010.
2. Luukinen H, et al. *Osteoporos Int* **11**, 631-634, 2000.
3. Blake AJ, et al. *Age Ageing* **17**, 365-372, 1988.
4. Berg WP, et al. *Age Ageing* **26**, 261-268, 1997.
5. Owings TM, et al. *Clin Biomech* **16**, 813-819, 2001.

ACKNOWLEDGEMENTS

This research was supported by the National Science Foundation (HRD-1502335) and the NIH/NIA (R21 AG0457).

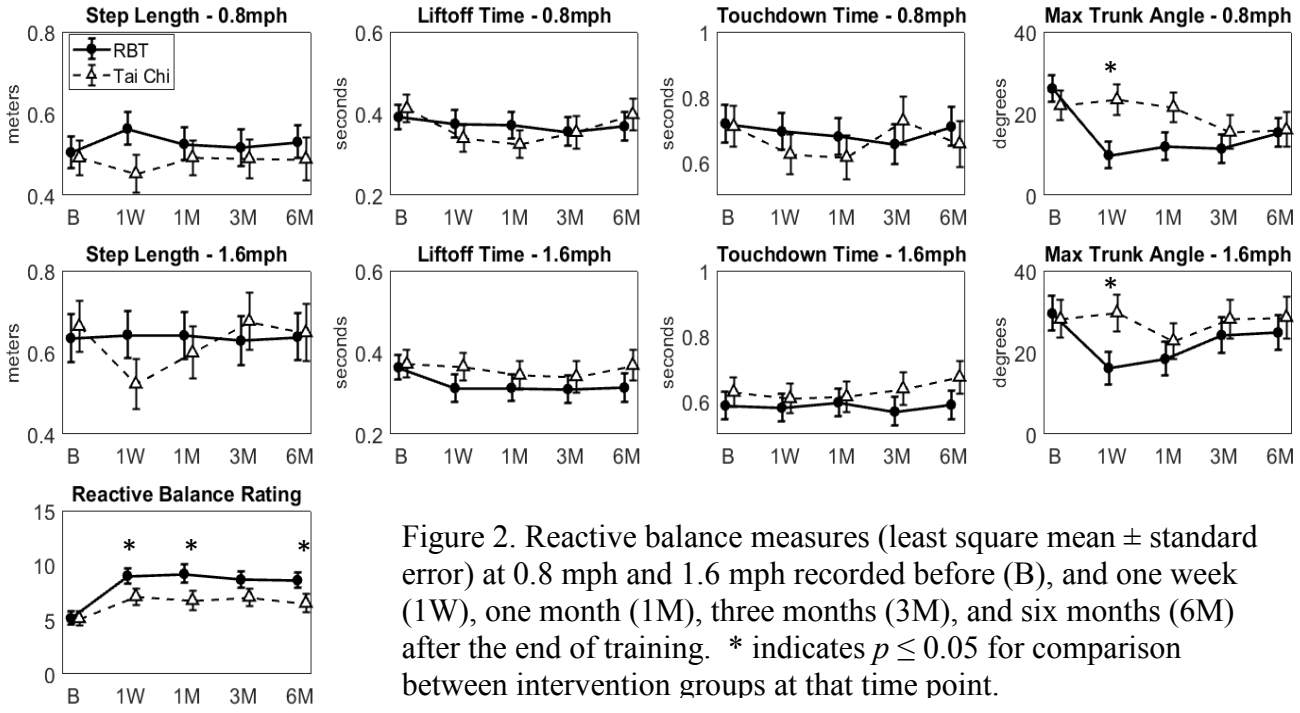

Figure 2. Reactive balance measures (least square mean ± standard error) at 0.8 mph and 1.6 mph recorded before (B), and one week (1W), one month (1M), three months (3M), and six months (6M) after the end of training. * indicates $p \leq 0.05$ for comparison between intervention groups at that time point.

PATIENTS WITH MEDIAL KNEE OA VARY IN THE KINETIC RESPONSE TO PLANTAR PRESSURE-BASED FEEDBACK

[1] Jade He, [1] Christopher Ferrigno, [1] Najia Shakoor, [1] Markus A. Wimmer
[1] Rush University Medical Center, Chicago, IL, USA
Email: Markus_A_Wimmer@rush.edu

INTRODUCTION

The knee adduction moment is a surrogate of medial compartment load during gait and is a regular target of conservative therapy for medial knee osteoarthritis (OA). In this study, we explore a gait retraining strategy that utilizes auditory cues based on real-time plantar pressure to inform individuals to medialize their center-of-pressure. After development and successful implementation of a gait retraining protocol on healthy subjects [1], we started a 6-week longitudinal clinical trial (NCT02955225) with patients with OA. This abstract reports on the initial gait retraining and investigates the immediate response of subjects to auditory cues.

The main purpose was to examine if patients were able to lower their knee adduction moment using pressure-based feedback. While 100% healthy subjects in a previous study responded favorably to pressure-based feedback [1], we anticipate that patients with OA will have more varied response with the training, prompting a secondary purpose to investigate gait variables that may differentiate responders from non-responders.

METHODS

Fifteen subjects with Kellgren-Lawrence (KL) grade 2 & 3) were recruited. The pressure-based auditory feedback system comprises a standardized, flexible shoe, a wireless, pressure-detecting shoe insole (Moticon GmbH, Munich, Germany), and a portable device for processing real-time plantar pressure and generating auditory cues (**Fig 1**). On the day of the visit, prior to the marker-based walks, subjects were fitted with the shoe and insole. Baseline plantar pressure was obtained from a 20-m walk at a self-selected, comfortable speed. A percentage (75-95% depending of actual performance of subjects) of the mean maximum of five steps of two lateral sensors were used as training thresholds. The sensors correspond to the time occurrence of the first and second peak of knee adduction moment.

Before gait retraining using pressure-based feedback, a motion capture (Baseline) acquired gait variables of subjects (**Fig 2**). After subjects were given an introduction on the pressure-based feedback system, they practiced walking while responding to the auditory cues under the supervision of a physical therapist. Once subjects were able to medialize center-of-pressure without triggering auditory cues from at least one of the two sensors for a few consecutive steps, they underwent another motion capture (Feedback).

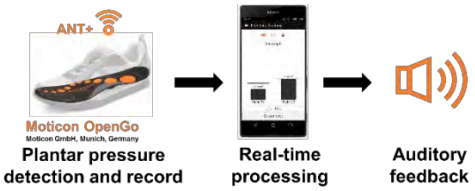

Figure 1: The pressure-based system was comprised of a flexible shoe, a wireless, pressure-detecting shoe insole, and a portable device.

Motion capture was performed using a ground embedded force plate (Bertec, Columbus, OH) to measure ground reaction forces and 12 optoeletric cameras (Qualysis, Gothenburg, Sweden) to capture lower extremities kinematics. A modified Helen Hayes marker-set was used. Raw kinetics and kinematics were processed in Visual 3D (C-Motion, Inc., Germantown, MD).

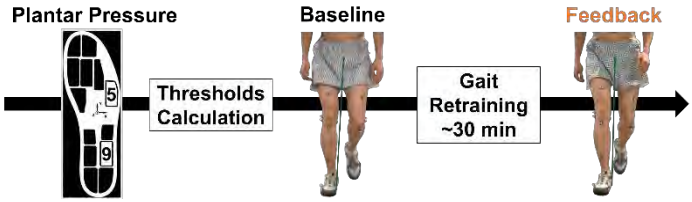

Figure 2: The gait retraining using pressure-based feedback happened between two marker-based walks, which captured gait variables before (Baseline) and after (Feedback) training.

Statistical analyses were performed using IBM SPSS Statistics 22 (SPSS Inc., Chicago, IL). Statistical significance was set to $\alpha = 0.05$. Binomial tests were used to evaluate if subjects were able to reduce the knee adduction moment. Paired t-tests were used to evaluate the training effects of pressure-based

feedback and independent sample t-tests were used to evaluate differences between subgroups. Linear regression was used to gauge a relationship between variables.

RESULTS

Characteristics of subjects recruited were 62 ± 11 yr, 85.4 ± 17.8 kg, 1.67 ± 0.09 m, and knee OA of 7 subjects was classified KL-2 and 8 subjects KL-3.

Ten subjects were able to reduce the overall and first peak of knee adduction moment, which was significant (p = 0.008 & 0.002, respectively). These ten subjects reduced the overall peak by 11.8% (0.31 %BW*Ht, p = 0.001) and the first peak by 12.7% (0.33 %BW*Ht, p < 0.001).

The responders to pressure-based feedback were separated from the non-responders based on whether or they were able to reduce the knee adduction moment (**Fig 3**). Between the subgroups, spatiotemporal variables were investigated since speed and its contributors stride length and cadence were shown to influence the knee adduction moment [2].

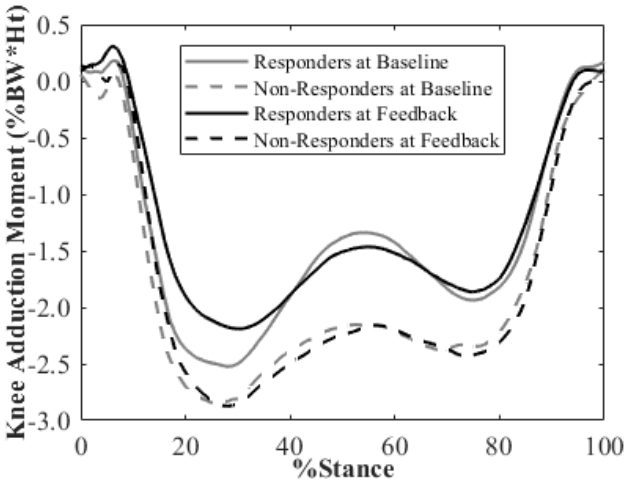

Figure 3: The average knee adduction moment at Baseline and Feedback across those who succeeded (responders) and failed (non-responders) to reduce knee adduction moment using pressure-based feedback.

At Baseline, responders showed longer stride length than non-responders (1.31 m > 1.13 m; t(13) = -2.13, p = 0.053). At Feedback, responders reduced stride length by 3.2% (0.41 m, p =0.001) (**Fig 4**) and increased cadence by 5.6% (3.13 step/min, p = 0.014). Reduced speed (8.9%, 0.11 m/s, p = 0.003) was also found in responders; however, there was no relationship between the reduction in speed and the reduction in knee adduction moment (r = 0.263, p = 0.464). In contrast, non-responders increased stride length by 9.7% (0.10 m, p = 0.336) without a significant change in cadence or speed at Feedback.

DISCUSSION

Two thirds of the OA subjects were able to follow auditory cues and lower their knee adduction moment within the 30-40 min training. According to Bernoulli statistics, it is unlikely that this happened by chance. A recent study revealed that stride length and cadence can have an impact on knee joint moments [2]. Starting with longer stride length, the responders might have more room of improvement, but by adjusting stride length a majority of the subjects with knee OA redistributed knee loads using pressure-based feedback.

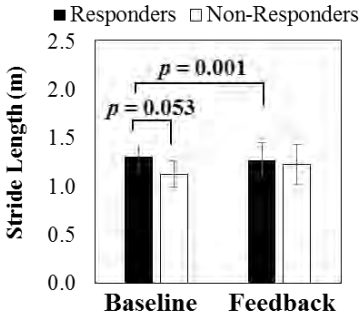

Figure 4: The responders who reduced knee adduction moment significantly reduced stride length after gait retraining using pressure-based feedback.

CONCLUSIONS

Pressure-based feedback was effective for a majority of subjects with medial knee OA to redistribute knee loads in the beginning of the clinical trial. How these subjects responded to pressure-based feedback to reduce knee adduction moment awaits more analyses. Difference in stride length at baseline and change in stride length and cadence that reflect a potential change in speed-regulating strategy post-training should deserve more attention when evaluating knee moments.

REFERENCES 1. Ferrigno et al. *J Biomech Eng.* 2016 Feb; **138**(2). 2. Ardestani et al. *Gait Posture*. 2016 May; **46**: 118-25.

ACKNOWLEDGEMENTS
Funding from the Arthritis Foundation is appreciated.

CERVICAL SPINE BIPLANAR FLUOROSCOPY: AUTOMATED SHAPE-MATCHING ALGORITHM VALIDATION

[1] Craig C Kage, [2] Mohsen Akbari-Shandiz, [1] Mary H Foltz, [1] Rebekah L Lawrence, [1] Taycia Brandon, [1] Eric Twohey, and [1] Arin M Ellingson

[1]University of Minnesota, Minneapolis, MN, USA
[2] Mayo Clinic, Rochester, MN, USA
email: ellin224@umn.edu, http://z.umn.edu/MRBL

INTRODUCTION

Current clinical assessment and diagnostic imaging techniques are unable to capture dynamic, three-dimensional (3D) motion of the spine at the segmental level. Understanding motion at the segmental level may help to better inform diagnosis, prognosis, and treatment for those with various musculoskeletal conditions. Biplane fluoroscopic imaging is a non-invasive and valid technique for quantifying 3D, dynamic bone motion at a segmental level in the spine [1,2]. Despite this technology being validated in other laboratory environments, it is important to validate each individual system's accuracy due to the complexity and customization of this developing technology. Moreover, because of the nature of radiographic imaging, the potential risk of radiation exposure must be balanced appropriately with the accuracy of the system, making the need for verification of each system's accuracy even more essential. Additionally, processing biplane fluoroscopic images into meaningful osteokinematic output (shape-matching) is manual and exceedingly labor-intensive with individual labs developing proprietary code to automate the process [1-3].

The purpose of this study was to validate our lab's biplane fluoroscopic system against the gold standard of radiostereometric analysis (RSA) for cervical spine kinematics using a custom, automated algorithm for shape-matching a cadaveric specimen.

METHODS

Data Collection

A fresh-frozen cadaveric specimen (male, 55 years of age), fully intact from the pelvis superiorly, was obtained for collection. Four tantalum beads were implanted into each of the anterior vertebral bodies of the cervical spine (C4-C6). Computed tomography (CT) images were obtained (Siemens Somaton Sensation 64; Germany; 120 kVp; voxel size: 0.23×0.23×0.60mm) from which bead centroids were identified and 3D bone models were reconstructed at each level (Mimics; Materialise, MI, USA). Anatomic-coordinates were labeled in Mimics: anterior, superior vertebral body and left and right lateral, superior vertebral notches (Figure 1). Bead traces were masked in the bone volumes to avoid shape-matching bias (ImageJ, NIH, MD, USA).

The specimen was thawed and dynamic fluoroscopic imaging was collected with our custom biplane system (Imaging Systems and Services Inc., OH, USA) using a long-handled apparatus to passively simulate neck motion from extension to flexion and from right to left lateral bending. The biplane system utilizes two 16″ image intensifiers (Thales 9447 QX; North American Imaging, OH, USA) and two high-speed cameras (Xcitex ProCapture, MA, USA). Figure 1 illustrates the system configuration with a 55-degree interbeam angle with one system parallel to the horizontal (flexion: lateral; bending: oblique) and the other oriented eight degrees above the horizontal inferior to superior (flexion and bending: oblique). Source-to-Image Distance (SID) was 152cm and the technique for acquisition was 70-74kV, 250-320mA, 3.5ms, 60Hz with a radiographic, wedge filter used for all trials (Ferlic Filter Co. LLC., MN, USA).

Data Analysis

Fluoroscopic images were undistorted, calibrated and dynamic bead positions were tracked for all visible frames using RSA (XMALab, Brown University, RI, USA). Prior to analysis all data were filtered with a low-pass, 4th order Butterworth Filter with a 3 Hz cutoff frequency [2]. To facilitate the automated shape-matching process, the position of

each vertebra (C4-C6) was manually set for the initial frame. All subsequent frames were tracked using an automated shape-matching algorithm, which incorporates a standard ray casting approach to generate digitally reconstructed radiographs (DRRs) and a 2D-3D image registration algorithm (Nelder-Mead Simplex optimization) which maximizes a correlation similarity measure to shape-match the DRR's onto the biplane radiographic projections (MATLAB, R2016B, The MathWorks, Inc., MA, USA). Three trials of flexion (565 total frames) and three trials of lateral bending (520 total frames) were analyzed. Output of the automated shape-matching algorithm was compared directly to RSA for rotations and translations at C4-C6 and for intersegmental kinematics (C4/C5, C5/C6). Bias, precision, and root mean square error (RMSE) were calculated at each level, averaged across all levels for that trial, then averaged across all three trials for each motion.

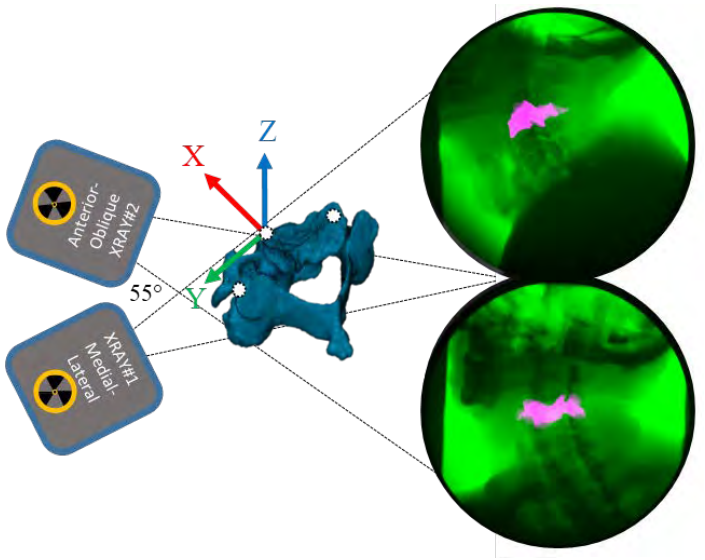

Figure 1: Biplane fluoroscopic set-up for flexion motion with reconstructed C4 CT bone model inset with local coordinate system and anatomic landmarks (white).

RESULTS AND DISCUSSION

Results of bias, precision, and RMSE calculations are displayed in Table 1. Briefly, average segmental RMSE for all levels (C4, C5, C6) of flexion trials was 0.78° rotation and 0.30 mm translation and average intersegmental RMSE (C4/C5, C5/C6) was 1.13° rotation and 0.33 mm translation. Average RMSE for all levels (C4, C5, C6) of lateral bending trials was 0.61° rotation and 0.21 mm translation and average intersegmental RMSE (C4/C5, C5/C6) was 0.85° rotation and 0.31mm translation. Rotations about the Y-axis (flexion/extension) demonstrated the greatest amount of error for both motions. Total RMSE was found to be below 1.70° degrees (rotation) and 0.50 mm (translation). Bias and precision values were similar to previously published works [1-3].

CONCLUSIONS

The results of this study demonstrate the appropriate accuracy of our biplane system, fluoroscopic technique, and the utility of an automated shape-matching algorithm for cervical motion analysis.

REFERENCES

1. McDonald CP, et al. *Spine J* **10**, 497-504, 2010.
2. Anderst WJ, et al. *Spine* **36**(6), E393-400, 2011.
3. Li G, et al. *J Biomech* **41**(7), 1616-1622, 2008.

ACKNOWLEDGEMENTS

This project was supported by NIH/NICHD K12HD073945, F31H087069, and Minnesota Partnership for Biotechnology and Medical Genomics (MNP IF #14.02).

Table 1: Summary of mean bias, mean precision, and mean RMSE for segmental and intersegmental kinematics across all trials and levels. Lateral Bending (LB), Flexion/Extension (FE), Axial Rotation (AR), Anterior-Posterior (AP), Medial-Lateral (ML), Superior-Inferior (SI).

	Flexion						**Lateral Bending**					
	Segmental Accuracy			Intersegmental Accuracy			Segmental Accuracy			Intersegmental Accuracy		
Rotation (degrees)	**LB (X)**	**FE (Y)**	**AR (Z)**	**LB (X)**	**FE (Y)**	**AR (Z)**	**LB (X)**	**FE (Y)**	**AR (Z)**	**LB (X)**	**FE (Y)**	**AR (Z)**
Bias	0.48	0.35	-0.49	-0.24	0.53	-0.34	0.29	-0.21	-0.15	-0.10	0.64	-0.12
Precision	0.34	0.53	0.35	0.38	0.76	0.48	0.23	0.57	0.23	0.34	0.83	0.31
RMSE	0.60	0.99	0.76	0.46	1.69	1.23	0.45	1.07	0.31	0.74	1.41	0.41
Translation (mm)	**AP (X)**	**ML (Y)**	**SI (Z)**	**AP (X)**	**ML (Y)**	**SI (Z)**	**AP (X)**	**ML (Y)**	**SI (Z)**	**AP (X)**	**ML (Y)**	**SI (Z)**
Bias	-0.46	0.11	-0.18	0.16	-0.24	-0.15	-0.07	-0.25	-0.04	0.26	-0.11	0.08
Precision	0.06	0.07	0.10	0.18	0.15	0.14	0.07	0.08	0.16	0.24	0.15	0.25
RMSE	0.46	0.22	0.21	0.40	0.28	0.30	0.17	0.27	0.20	0.45	0.20	0.29

THE EFFECT OF SCAPULOTHORACIC UPWARD ROTATION ON SUBACROMIAL PROXIMITIES

[1] Rebekah L. Lawrence and [1] Paula M. Ludewig
[1] Department of Rehabilitation Medicine, University of Minnesota, Minneapolis, MN, USA
email: lawre354@umn.edu

INTRODUCTION

Rotator cuff pathology is a prevalent finding on magnetic resonance (MR) images in individuals with shoulder pain. Subacromial rotator cuff compression has long been thought to be a primary mechanism of rotator cuff injury. Clinical theory suggests decreased scapulothoracic upward rotation (ST UR) increases risk for subacromial rotator cuff compression as it positions the acromion downward and presumably in closer proximity to the rotator cuff tendons. However, this clinical theory has not been fully tested *in vivo*. Therefore, the purpose of this study was to determine the impact of decreased ST UR on subacromial proximities.

METHODS

Sixty subjects were recruited to participate in this study. Of these, 30 had current shoulder symptoms consistent with a clinical diagnosis of "impingement syndrome" (32.4 ± 8.8 years, 46.7% male, 40% tested on dominant side) and 30 had no prior history of shoulder pain (32.7 ± 8.3 years, 46.7% male, 40% tested on dominant side).

Subjects underwent kinematic motion analysis using single plane fluoroscopy synced to a five-camera motion capture system. The camera system was used to track thorax motion, while the fluoroscopy was used to track humeral and scapular motion. Data was collected while subjects performed arm raising in the scapular plane. MR scans were also acquired, which was used to create 3D anatomical models of the humerus and scapula. Scapulothoracic and glenohumeral kinematics were tracked via manual 2D/3D image registration in JointTrack software. Kinematics were described using published recommendations [1, 2]. Subjects were ranked based on their magnitude of ST UR at 30° humerothoracic elevation, which corresponds to the range of closest subacromial proximities [3]. The 20 participants with the highest ST UR were classified as having "high" ST UR, while the 20 participants with the lowest ST UR were classified as having "low" ST UR. Classification in this manner allowed for the effect of ST UR on subacromial proximities to be tested directly. Demographic data for these subjects are provided in Table 1.

Table 1: Demographic Data for High and Low ST UR Groups (mean ± SD, or %)

	High (n=20)	**Low (n=20)**	**p-value**
Age (years)	30.7 ± 5.2	34.1 ± 10.1	0.20
Gender (% male)	25%	65%	0.01
Group (% asymptomatic)	45%	40%	0.75
Rotator cuff tendon thickness (mm)	5.5 ± 1.2	5.7 ± 0.9	0.59

The thickness of the rotator cuff tendon was measured at the articular margin on each subject's MR scan on the slice corresponding to the anterior/posterior midpoint of the tendon insertion. A plane was fit between the coracoid and acromion representing the coracoacromial ligament according to published anatomical descriptions [4].

Each subject's arm raising task was re-created by animating their humeral and scapular models using their glenohumeral kinematics. Subacromial proximities were quantified at 10° intervals of humerothoracic elevation by calculating the minimum distance between each pairwise set of vertices on the coracoacromial arch (i.e. acromion and the plane representing the coracoacromial ligament) and along the articular margin (**Fig. 1**). The minimum distance measures were constrained to the articular margin coinciding to where the rotator cuff thickness was obtained because the thickness cannot be assumed constant across the surface of the insertion site. All minimum distances were normalized to the subject's rotator cuff thickness value, which facilitated interpretation. For each

subject, the humerothoracic elevation position at which the normalized minimum distance was smallest was defined as the position of absolute minimum distance. Contact between the rotator cuff and coracoacromial arch was defined as a normalized minimum distance of <120%. This threshold accounts for approximately 1 mm of error in quantifying the minimum distance due to errors during 2D/3D image registration.

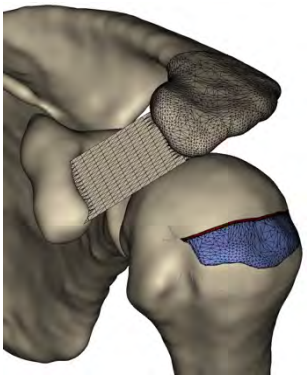

Figure 1: Definition of: 1) rotator cuff insertion (blue surface); 2) Articular surface region of interest (maroon line); and 3) coracoacromial ligament.

Data normality was tested prior to statistical analysis. The normalized minimum distance was skewed and subsequently log transformed for statistical analysis. The effect of ST UR on subacromial proximities was assessed using a two-factor mixed-model ANOVA with Toeplitz covariance structure. The model included a between-subject factor of group (low, high) and a within-subject factor of angle (arm at side, 30°, 60°, 90°). Follow-ups were calculated using Tukey adjustments. The position of absolute minimum distance was compared between groups using a two-sample independent t-test. The frequency of contact between the tendon was tested between groups using Chi-square analysis.

RESULTS AND DISCUSSION

Consistent with group assignment, the subjects in the low ST UR group had on average 11.9° less UR at 30° humerothoracic elevation than the subjects in the high ST UR group. In both groups, the normalized minimum distance was generally smallest below 90° humerothoracic elevation. There was a significant group-by-angle interaction, suggesting the difference between ST UR groups was dependent on the angle of humerothoracic elevation (p=0.047) (**Fig. 2**). However, group follow-ups were not significant at any angle of humerothoracic elevation. Although not statistically significant, the normalized minimum distance for the subjects in the low ST UR group was 15.2% lower than those in the high UR group at the minimum position, and 20% higher at the 90° humerothoracic elevation. The rotator cuff was closest to the coracoacromial arch an average of 8° lower in the range of motion in subjects in the low ST UR group. In total, only 38% of subjects had at least one humerothoracic position where the normalized minimum distance was <120% suggesting contact occurred.

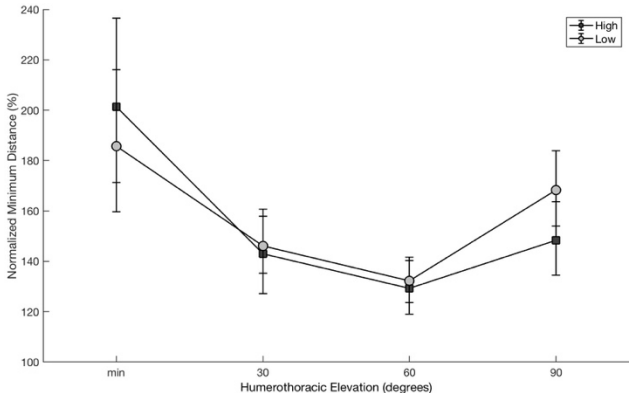

Figure 2: The normalized minimum distance for the high and low ST UR groups across angles of humerothoracic elevation.

CONCLUSIONS

Decreased ST UR shifts the range of risk for subacromial rotator cuff compression to lower angles. However, the clinical meaningfulness of the small magnitude of change in normalized minimum distance is unclear. Subacromial rotator cuff compression occurs in less than 40% of individuals during unweighted, non-fatigued arm raising, suggesting it may not be a predominant mechanism for rotator cuff injury.

REFERENCES

1. Ludewig et al. *Clin Biomech* 25:415-21, 2010.
2. Wu et al. *J Biomech* 38:981-92, 2005.
3. Lawrence et al. *J Orthop Res*. 37:2329-37, 2017.
4. Edelson et al. *Arthroscopy*. 11:715-9, 1995.

ACKNOWLEDGEMENTS

This study was funded by the NIH (F31HD087069) and the Foundation for Physical Therapy.

Changes in Hip Mechanics During Gait Modification to Reduce Knee Adduction Moment

[1]Bryndan Lindsey, [1]Oladipo Eddo, [1]Shane Caswell, [1]Matt Prebble, [1]Nelson Cortes

[1]George Mason University, Manassas, VA
email: ncortes@gmu.edu, web: https://smartlab.gmu.edu/

INTRODUCTION

First peak internal knee abduction moment (PKabdM) has been associated with knee osteoarthritis (OA) progression [1]. Gait modification strategies using real-time biofeedback (RTB) including lateral trunk lean (TL), medial knee thrust (MKT), and decreased foot progression angle (FPA) have reduced PKabdM in both healthy and OA populations [2]. Despite the success of these interventions in reducing PKabdM, the potential biomechanical effects on the kinetic chain remain poorly understood [3]. There is evidence suggesting that PKabdM partially depends on the magnitude of hip abduction moment [4, 5]. Greater internal hip abduction moment has been shown to be protective of medial knee OA development, reducing the odds of OA progression 50% for every additional unit of hip abduction moment [6]. Previous authors have suggested that increased hip abductor strength can be beneficial in controlling knee joint loads which is supported by reduction of knee OA symptoms after a hip strengthening intervention [7]. However, limited evidence suggests that common strategies to reduce PKabdM can reduce hip abduction moment [8]. Therefore, the purpose of this study was to investigate biomechanical changes at the hip during three previously studied gait modifications designed to reduce PKabdM.

METHODS

Twenty healthy individuals volunteered for this study (28.4 ± 3.8 years, 1.73 ± 0.1 m, 75.3 ± 12.5 kg). Mean and standard deviation (SD) for trunk angle, knee angle, and foot angle during stance was calculated from ten baseline trials using eight high-speed motion analysis cameras and four floor embedded force plates. Gait trials were conducted on a 6m long walkway with the last 2.4 meters containing the force plates. Trials were only valid with two full foot contacts of the experimental limb on the force plates and gait speed within ±5% of baseline speed. Five trials were completed for each gait strategy using RTB so that joint angles fell within a range of 3-5 SD greater than (FPA and TL) or less than (MKT) baseline. Visual 3D was used to project RTB on a 4.8m by 3.3m projection wall facing the walkway as a line graph displaying real-time joint angle during stance. Participants were instructed to modify their gait so that the line fell within a highlighted bandwidth representing the target ranges. Visual 3D was used to calculate joint angles (°) and internal moments (Nm/kgm) measured at PKabdM. Although, external joint moments are most commonly reported in knee OA literature, internal moments are equal but opposite. Repeated measures ANOVA was used to assess differences in hip moments and angles between conditions. Pairwise comparisons were conducted to compare changes between baseline walking and modification strategies ($p<0.05$).

RESULTS AND DISCUSSION

On average PKabdM was reduced in all strategies from baseline, however, significance was only reached for FPA ($p<0.05$) and MKT gait ($p<0.01$; Table 1). Compared to baseline, participants significantly reduced frontal plane hip angle during TL gait ($p<0.01$) and sagittal plane hip angle across all strategies ($p<0.01$; Table 1). Hip abduction moment was significantly decreased during TL and MKT gait compared to baseline ($p<0.01$) while hip extension moment was unchanged (Table 1). During TL gait participants walked with a more abducted and flexed hip and demonstrated decreased hip abduction moment at PKabdM (Figure 1).

Previous studies have shown that hip abduction moments are greater in patients with less severe medial compartment knee OA [4, 5, 6].

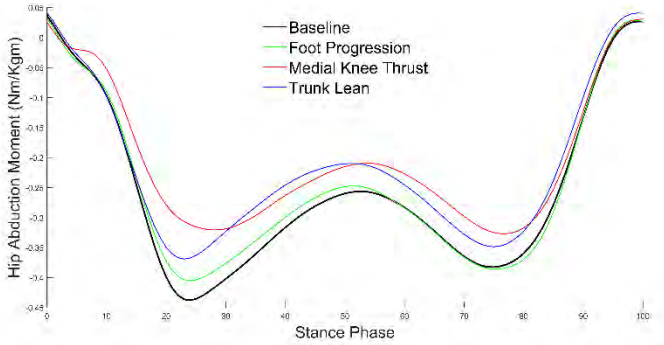

Figure 1: Mean hip abduction moment (Nm/kgm) across the stance phase.

A common gait strategy adopted by knee OA patients includes shifting the center of mass (COM) towards the involved limb while moving the trunk laterally [4]. This compensatory mechanism is similar to the TL strategy used in this study and has shown success in reducing medial knee joint load by shifting the GRF vector laterally, decreasing the magnitude of the moment arm [4].

Patients with more severe OA, however, may lack the hip abductor strength to maintain this altered trunk position during stance causing excessive pelvic drop in the contralateral leg. This shifts the COM away from the stance leg, increasing the PKabdM and subsequent medial compartment joint load [4, 6]. Even in patients with the prerequisite hip strength, this strategy may not be beneficial in the long-term as it decreases demand on the hip, weakening the musculature. This reduces the ability of the muscles to regulate medial/lateral knee load distribution, decreasing frontal plane stability [6]. Similar to TL gait, MKT gait resulted in participants walking with a more flexed hip and reduced hip abduction moment at PKabdM (Figure 1). The mechanism between the two strategies was similar; increased hip and knee abduction angle with reduced peak hip abduction moment potentially due to the shift of the COM closer to the joint centers.

CONCLUSIONS

Gait modifications designed to reduce PKabdM significantly changes hip mechanics in healthy individuals. TL and MKT strategies resulted in reduced hip abduction moment at PKabdM which may be detrimental to patients with more advanced knee OA. Therefore, future studies investigating gait modifications designed to slow the progression of OA should consider the effects on hip as well as knee mechanics.

REFERENCES

1. Miyazaki et al. *Annals of the Rheumatic Disease.* 2002;**61(**7):617-622.
2. Eddo et al. *International Journal of Kinesiology and Sports Science.* 2017;**5**(3):35-55.
3. Simic et al. *Arthritis Care & Research.* 2011;**63**(3):405-426.
4. Mündermann et al. *Arthritis & Rheumatology.* 2005;**52**(9):2835-2844.
5. Astephen et al. *Journal of Orthopaedic Research.* 2008;**26**(3):332-341.
6. Chang et al. *Arthritis & Rheumatology.* 2005;**52**(11):3515-3519.
7. Bennell et al. *Osteoarthritis and Cartilage.* 2010;**18**(5):621-628
8. Mündermann et al. *Journal of Biomechanics.* 2008;**41**(1):

Table 1: Descriptive statistics of (mean ± standard deviation) frontal and sagittal plane hip angles and moments across strategies. Significant difference from baseline is indicated by asterisk ($p<0.05$)

	Gait Strategy			
	Baseline	**FPA**	**MKT**	**TL**
PKabdM	-0.26 ± 0.05	-0.23* ± 0.06	-0.14* ± 0.10	-0.24 ± 0.10
Hip adduction angle	3.11 ± 2.90	2.71 ± 2.59	1.78 ± 4.09	0.56* ± 3.13
Hip flexion angle	13.14 ± 4.81	15.36* ± 4.69	20.27* ± 8.02	15.77* ± 6.44
Hip abduction moment	-0.41 ± 0.08	-0.38 ± 0.10	-0.29* ± 0.14	-0.34* ± 0.11
Hip Extension moment	-0.15 ± 0.11	-0.16 ± 0.12	-0.16 ± 0.14	-0.18 ± 0.15

COMPARISON OF JOINT KINETICS USING COMMON MODELS FOR BASEBALL PITCHING

Michael P. McNally, James A. Oñate, Ajit M.W. Chaudhari

The Ohio State University, Columbus, OH, USA
email: Michael.mcnally@osumc.edu

INTRODUCTION

Biomechanical analyses are more frequently being utilized to aid in achieving improved baseball pitching performance while minimizing joint loads on the body. Increased potential for injury at the shoulder and elbow have been associated with certain kinetic risk factors, which are calculated using standard inverse dynamics from a known force applied by the ball [1]. However, because of the complexity in measuring the pitching motion, different underlying modeling approaches have been used with varying constraints. In particular, three common models have been used in research, and are suggested for use in clinical throwing analysis, which include a 6 degree of freedom model (6DOF), an optimized model using inverse kinematics (IK), and a model that does not allow intersegmental translations (ASMI) [2]. Understanding the differences between these models is critical for understanding the biomechanics of the pitching motion, and how to interpret data relative to normative data expressed in the literature.

The purpose of this study was to determine the relationships between joint kinetic parameters as estimated by three different biomechanical models for baseball pitching, both in the absolute estimates as well as in the relative predictions of which individuals have elevated loading. We hypothesize that differences will exist in absolute joint kinetics between models, but that kinetic parameters will be correlated between models.

METHODS

15 right-handed male baseball pitchers from high school (n = 8), collegiate (n = 4), and professional (n = 3) baseball, who all learned to play in the United States, were analyzed for this study as part of an overarching study (age = 19.2±4.9 years, height = 1.85±0.06 m, mass = 83.5±12.1 kg, hand velocity = 23.6±1.38 m/s). After performing a self-selected warm-up, pitchers were recorded using an optical motion capture system (Vicon Inc., Oxford, UK) capturing at 300 Hz while throwing five fastballs from an instrumented pitcher's mound [3] at "game like effort" towards a target placed approximately 13m away. The first three pitches which contained complete marker data for the upper extremity were analyzed for each pitcher.

All analyses were performed using Visual3D software (C-Motion Inc., Germantown, MD, USA). Marker trajectories were filtered using a low-pass Butterworth filter with a cutoff frequency of 13.4 Hz [2]. Shoulder and elbow kinematics and kinetics were calculated in the global reference frame, and reported using 3 different methods. The first method utilized a 6 degree of freedom model, defined using recommendations of upper extremity kinematics described by the International Society of Biomechanics [4], and tracked each segment allowing full translation and rotation in all planes for each segment (6DOF model) [5]. The second method defined the upper extremity and the resulting kinematics and kinetics using the same ISB model, but utilized a global optimization technique to eliminate any translation at the wrist and elbow joint, varus/valgus motion at the elbow, and rotation at the wrist (IK model) [6]. The third method defines the distal end of the proximal segment and the proximal end of the distal segment to be coincident at the shoulder, elbow and wrist, thereby eliminating translations. It constrains the shoulder reference frame using the cross product of the long axis of the arm and vertical axis of the trunk to define the anterior axis, and the elbow reference frame using the cross product of the long axis of the forearm and long axis of the upper arm to define the anterior axis (ASMI model) [2]. As one of the critical instants, maximum shoulder external rotation (MER) was calculated as the point

when the shoulder is maximally externally rotated relative to the trunk.

Four kinetic variables were calculated using each method based on evidence suggesting a relationship to shoulder or elbow injury risk. Specific variables included peak elbow varus torque and elbow varus torque at MER, internal rotation torque at MER, and peak shoulder distraction force. A one-way ANOVA was used to detect a main effect of model for each kinetic variable, with Tukey's post hoc analysis to determine individual differences for any main effects. All variables were confirmed to be normally distributed, so Pearson correlation coefficients were calculated to determine the relationship in kinetic calculations between models. Significance for all statistical tests was set *a priori* at $p < 0.05$.

RESULTS AND DISCUSSION

Descriptive statistics and a summary of ANOVA's are listed in Table 1. Main effects of model were identified for all kinetic variables ($p < 0.001$). Peak elbow varus torque was significantly greater for IK and ASMI models compared to 6DOF ($p < 0.001$). Elbow varus torque at MER was different between all methods, with ASMI model estimating greater torque at MER than 6 DOF, which is greater than IK ($p < 0.001$). Shoulder internal rotation torque at MER was greater for IK and ASMI compared to 6DOF, and peak shoulder distraction force is greater for 6DOF and IK compared to ASMI ($p < 0.001$).

Elbow varus torque showed moderately strong correlations between methods (R = 0.696-0.777). Elbow torque at MER was moderately correlated between 6DOF and IK (R=0.541) and between 6DOF and ASMI (R=0.631), with no association between IK and ASMI models (R=0.078). Shoulder internal rotation torque at MER was weakly correlated (R=0.283-0.514), while peak shoulder distraction force showed only a strong correlation between 6DOF and IK, with no association between 6DOF and ASMI (R=0.137) and IK and ASMI (R=0.140).

While this research cannot differentiate which model is most accurate, it does suggest that results may not be generalizable between models, often making conclusions from research dependent on the model used. These differences are likely a result of both differing constraints and definitions of anatomical reference frames, as well as any resulting differences in the timing of MER using each method. When evaluating research or conducting performance evaluations on pitching, clinicians need to match the model they use to the available literature and normative values, otherwise inaccurate conclusions may be reached. Further study may help to better assess the validity and reliability of each model as it pertains to the pitching motion, identifying pitchers at risk, and in assessing interventions to improve performance while minimizing risk.

REFERENCES

1. Feltner ME, et al. *Int J Sport Biomech* **5**, 403-19, 1989.
2. Fleisig GS, et al. *J Appl Biomech* **12**, 207-24, 1996.
3. McNally, MP et al. *J Strength Cond Res* **29**, 2708-15, 2015.
4. Wu, G, et al. *J Biomech* **38**, 981-92, 2005.
5. Grood ES, et al. *J Biomech Eng* **105**, 136-44, 1983.
6. Lu TW, et al. *J Biomech* **32**, 129-34, 1999.

Table 1: Descriptive statistics and results of one-way analysis of variance between models.

Model	6DOF	IK	ASMI	ANOVA
Peak Elbow Varus Torque (Nm)	62.46 ± 19.39	86.00 ± 37.54	90.32 ± 21.33	6DOF < IK, ASMI
Elbow Varus Torque at MER (Nm)	41.81 ± 18.03	14.60 ± 19.97	77.13 ± 19.36	IK < 6DOF < ASMI
Shoulder internal rotation torque at MER (Nm)	20.29 ± 21.49	76.32 ± 55.44	75.90 ± 18.81	6 DOF < IK, ASMI
Peak shoulder distraction force (N)	857.44 ± 287.71	858.00 ± 243.25	124.98 ± 103.43	ASMI < 6DOF, IK

L5/S1 Joint Load Estimation during Lifting Using a Deep Learning Based Method

[1] Rahil Mehrizi, [1] Xi Peng, [2] Xu Xu, [3] Shaoting Zhang, [1] Dimitri Metaxas, and [1] Kang Li
[1] Rutgers University, Piscataway, NJ, USA
[2] North Carolina State University, Raleigh, NC, USA
[3] University of North Carolina at Charlotte, Charlotte, NC
email: rahil.mehrizi@rutgers.edu

INTRODUCTION

Occupational injuries are commonly observed among the workers involved in material handling tasks such as lifting. An important criterion to identify the non-ergonomic lifting task is the net force and moment values at L5/S1 joint. These values are mainly calculated in a laboratory environment, which utilizes marker-based motion capture systems and force plates. However, this method is usually a time-consuming process and needs expensive equipment. In this study, we propose and validate a novel marker-less method for L5/S1 joint load estimation, which address aforementioned limitations. The proposed method uses computer vision approaches, in particular Deep Neural Network (DNN), to estimate the 3D body pose from multi-view images and calculate the joint loads by an inverse dynamic algorithm. The results of our proposed method are compared with results obtained from a marker-based system as a reference and it is shown that the proposed method achieves promising results.

METHODS

Participants and Procedure. A group of 12 healthy males (age 47.50±11.30 years; height 1.74±0.07 m; weight 84.50±12.70 kg) participated in the experiment. Each participant performed various lifting trials in a laboratory while being filmed by two camcorders (positioned at 90 degree and 135 degree views) and a synchronized motion tracking system to measure the body movement. They lifted a plastic crate weighing 10 kg and placed it on a shelf without moving their feet. Each subject performed three vertical lifting heights (floor to knuckle, knuckle to shoulder, and floor to shoulder) combined with three end-of-lift angles (0, 30 and 60 degree). Lifting trials of subjects 1 to 10 were used as training dataset and subjects 11 and 12 were used for testing.

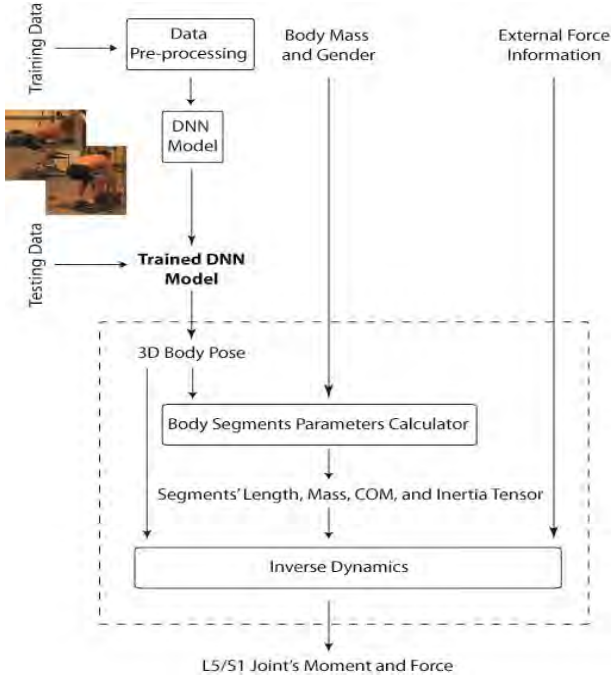

Figure 1: Workflow of the proposed DNN based method.

Methods. In this work, we aim to predict the 3D L5/S1 joint kinetic from a multi-view RGB image. As shown in figure 1, in the offline phase, the training dataset images are preprocessed and used to train a DNN model. In the online phase, given a new multi-view image (testing dataset), the trained DNN estimates its corresponding 3D body pose. The network architecture of the DNN model comprises of encoder and decoder. The encoder processes the input image with convolution and pooling layers to generate low resolution feature maps and the decoder processes low resolution feature maps with up-sampling and convolution layers to construct 2D joints coordination maps. The constructed 2D joints maps for each view are concatenated together and are processed more by another encoder. The neural network is ended with a fully connected output layer, which output the 3D coordination of each joint.

Next, the estimated 3D body pose along with the subject's anthropometric information are utilized to calculate body segments parameters including segments length, mass, position of the center of mass (COM), and inertia tensor based on the suggested values by [1].

Finally, L5/S1 joint kinetic is determined by a top-down inverse dynamic algorithm according to the estimated 3D body pose, body segments parameters and external force information. We applied a global equation of motion to estimate the net L5/S1 joint kinetic, as described by [2].

RESULTS AND DISCUSSION

L5/S1 Joint Moment. Results show a good agreement between the estimated L5/S1 joint moments in each of the three planes and the references (fig. 2). The grand mean (±SD) of the moment absolute errors across all the subjects and trials was 9.06 (±7.60) Nm. The R coefficient for all the lifting trials were high (above 0.94) and RMSE were small (mostly below 20 Nm).

Furthermore, Absolute peak values extracted from the moment time series of the proposed method were compared to the corresponding values of the reference across the whole lifting trials. In line with the small RMSE (6.14 Nm) and high R coefficient value (0.96), t-test showed no significant differences between the reference and the proposed method.

L5/S1 Joint Force. For all of the lifting trials, the correspondence between 3D L5/S1 joint force obtained from the reference and estimated from the proposed method was good with R values mostly above 0.90 and RMS mostly below 10 N (fig. 2). The grand mean (±SD) of the force absolute errors across all the subjects and trials was 4.85 (±4.85) N.

Absolute peak values extracted from force time series of the proposed method were also compared to the corresponding values of the reference across the whole lifting trials. In line with a small RMSE value (4.45 N) and high R coefficient value (0.99), t-test showed no significant differences between the reference and the proposed method.

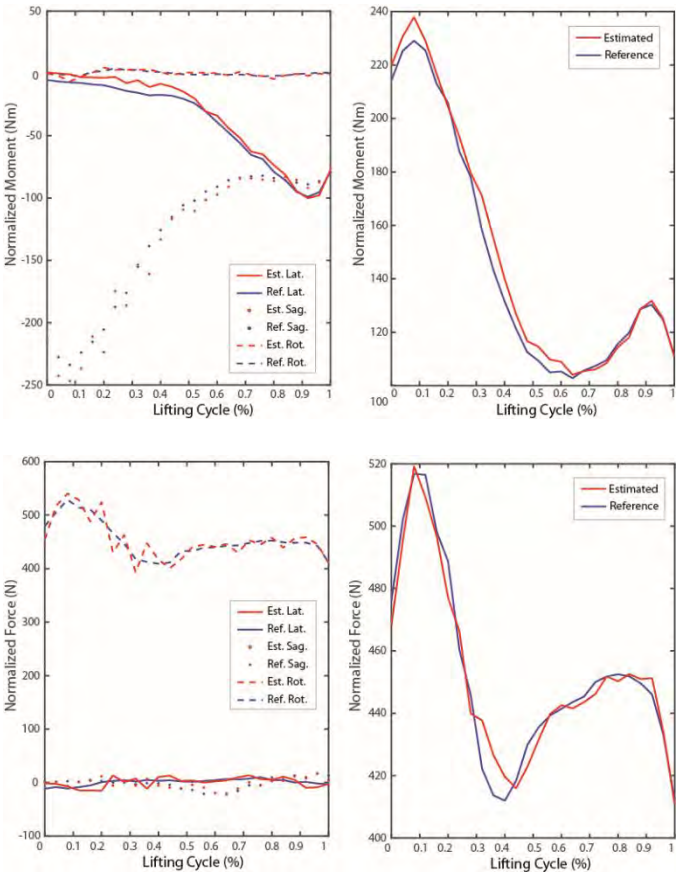

Figure 2: Estimated versus reference L5/S1 joint moment (top row) and L5/S1 joint force (bottom row) for floor-to-knuckle-height and 60 degree end-of-lift angle lifting trial. The total moment/force is the vector summation of the L5/S1 moments/forces at each three planes (right).

CONCLUSIONS

This study demonstrates the applicability of deep learning techniques in the context of biomechanical analysis and can provide a reliable tool for detecting the risk of lower back injuries during occupational lifting.

REFERENCES

1. P. De Leva, *Adjustments to Zatsiorsky-Seluyanov's segment inertia parameters*, Journal of biomechanics (**29**), 1996.
2. A. L. Hof, *An explicit expression for the moment in multibody systems*, Journal of biomechanics (**25**), 1992.

GAIT ASYMMETRIES 6 MONTHS POST-ACLR ASSOCIATE WITH INTER-LIMB T1ρ RATIOS 12 MONTHS POST ACLR

[1]Steven J. Pfeiffer, [1]Jeffrey Spang, [1]Daniel Nissman, [1,2]David Lalush, [1]Kyle Wallace, [3]Matthew S. Harkey, [1]Laura Stanley, [4]Randy Schmitz, [1]Troy Blackburn, [1]Brian Pietrosimone

[1] University of North Carolina at Chapel Hill, Chapel Hill, NC, USA, [2] North Carolina State University, Raleigh, NC, USA, [3]Tufts Medical Center, Boston, MA, USA, [4]University of North Carolina at Greensboro, NC, USA. email: stevenpf@email.unc.edu

INTRODUCTION

Individuals who sustain an anterior cruciate ligament injury and reconstruction (ACLR) are at heightened risk for posttraumatic knee osteoarthritis (PTOA).[1] The progression to PTOA following ACLR is theorized to result from an interaction between aberrant joint biomechanics during walking and deleterious biological changes to the knee cartilage.[2] Alterations in proteoglycan density within the cartilage matrix are hypothesized to be one of the initial cartilage changes that may be related to PTOA development.[3] T1ρ magnetic resonance imaging (MRI) relaxation times are sensitive to proteoglycan density changes and are elevated, indicating worse proteoglycan density, as early as one year post-ACLR.[4] The purpose of this study was to determine the associations between limb symmetry indices (LSI) for gait biomechanics measured six months post-ACLR and femoral T1ρ relaxation times twelve months post-ACLR. We hypothesized individuals with lesser loading of the ACLR limb six months following ACLR would demonstrate greater T1ρ MRI relaxation times on the ACLR limb twelve months following surgery.

METHODS

Twenty-four individuals (50% female, 21.92 ± 3.61 years old, 178.13 ± 11.30 cm, 75.35 ± 12.60 kg) with a unilateral bone-patellar-bone autograft ACLR participated in this study. Walking biomechanics [peak vertical ground reaction force (vGRF), vGRF loading rate (vGRF-LR), and peak internal knee extension moment (KEM)] were extracted from the first 50% of stance phase in both limbs during five trials of walking at self-selected speed six months following ACLR. LSI were used to normalize the biomechanical outcomes of the ACLR limb to the uninjured limb (ACLR Limb / Uninjured limb). Peak vGRF (BW) and vGRF-LR (BW/s) were normalized to body weight. vGRF-LR was calculated as the peak of the first derivative of the force-time curve. KEM was calculated using an inverse dynamics approach and was normalized to the product of body weight and height (BW*m). KEM was expressed as an internal moment and a negative value.

A 3-Tesla scanner was used to acquire images following 30 minutes of unloading the knee joint. T1ρ relaxation times were calculated (Figure 1) for the medial and lateral femoral condyles (MFC & LFC) using a five-image sequence created with a MatLab program with the following equation: $S(TSL) = S0 \exp(-TSL/T1\rho)$ where TSL is the duration of the spin-lock time, S0 is signal intensity when TSL equals zero, S corresponds to signal intensity, and T1ρ is the T1 relaxation time in the rotating frame. Prior to segmentation, affine and non-rigid deformable registration techniques were utilized to align the ACLR limb to the uninjured limb. The weight bearing portions of the cartilage of the MFC and LFC was manually segmented into posterior, central, and anterior regions of interest (ROI) based on the location of the meniscus in the sagittal plane.[5] Inter-limb T1ρ relaxation time ratios (T1ρ ILR = ACLR limb T1ρ / uninjured limb T1ρ) were calculated for each ROI.

Figure 1: Representative map of T1ρ relaxation times of an ACLR (L) and contralateral (R) knee.

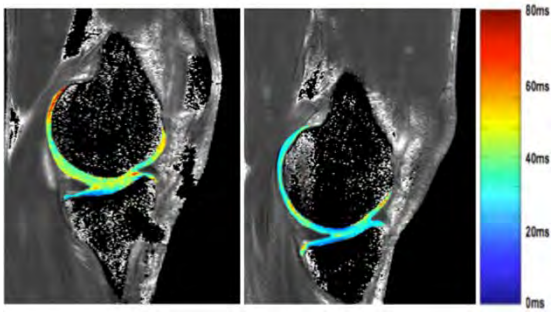

Separate, stepwise linear regressions were used to determine the unique associations between knee biomechanical outcomes and ILR for each ROI (ΔR^2, β, $P \leq 0.05$). Self-selected gait speed and the presence of a meniscal injury may influence T1ρ MRI relaxation times following ACLR. Therefore, these variables were entered into the regression model first followed by the biomechanical variable of interest. The presence of a medial or lateral meniscal injury was entered when specifically evaluating ILR of cartilage in either the medial or lateral compartment, respectively.

RESULTS

Lesser peak vGRF LSI six months following ACLR significantly associated with greater Posterior-LFC T1ρ ILR (ΔR^2=0.20, β=-0.48, P=0.04) twelve months following ACLR. Similarly, lesser peak vGRF-LR LSI six months following ACLR significantly associated with greater Posterior-MFC T1ρ ILR (ΔR^2=0.19, β=-0.45, P=0.05) twelve months following ACLR. Additionally, lesser peak KEM LSI six months following ACLR significantly associated with greater Central-MFC T1ρ ILR (ΔR^2=0.19, β=0.46, P=0.04) twelve months following ACLR.

DISCUSSION

Consistent with our hypothesis, individuals with lesser peak vGRF LSI, vGRF-LR LSI, and peak internal KEM LSI during walking six months following ACLR, demonstrated greater T1ρ ILR in the medial and lateral femoral condyles. These findings suggest that lesser mechanical loading of the ACLR limb compared to the uninjured limb early (i.e. 6 months) following ACLR may be related to deleterious changes in proteoglycan density of the ACLR limb compared to the uninjured limb at a later time point following ACLR (i.e. 12 months).

Both excessive and insufficient mechanical loading of the knee can lead to breakdown of tibiofemoral cartilage within the joint. Recent evidence[6,7] has demonstrated that excessive mechanical loading during walking early following ACLR associates with increased T1ρ relaxation times at early and later time points following ACLR. The findings of the current study are contrary to these studies but are consistent with previous findings demonstrating that lesser mechanical loading during walking following ACLR associates with changes in cartilage metabolism,[8] structure,[9] and future PTOA development.[10] Future work is needed to further understand the association between joint loading and deleterious changes to joint tissue metabolism following knee joint injury in order to develop interventions to optimally load the joint for the purpose of improving long-term joint health.

CONCLUSIONS

The findings of the current study illustrate that mechanical loading, specifically lesser loading, between limbs during walking early following ACLR may be related to deleterious changes of the cartilage matrix at later time points following ACLR, which may be related to the development of future PTOA. These findings illustrate the need for establishing optimal mechanical loading patterns during walking early in the rehabilitation process.

REFERENCES

1. Luc B, et al. *Journal of Athletic Training*. 2014;49(6):806-819.
2. Andriacchi TP, et al. *Annals of Biomedical Engineering*. 2015;43(2):376-387.
3. Regatte RR, et. al. *Academic Radiology*. 2002;9(12):1388-1394.
4. Regatte RR, et al. *Journal of Magnetic Resonance Imaging*. 2006;23(4):547-553.
5. Pfeiffer S, et al. *Arthritis Care and Research (Hoboken)*. 2017.
6. Kumar D, et al. *American Journal of Sports Medicine*. 2018;46(2):378-387.
7. Teng HL, et al. *American Journal of Sports Medicine*. 2017: 45(14): 3262–3271.
8. Pietrosimone B, et al. *Journal of Orthopedic Research*. 2017. 35(10): 2288–2297
9. Saxby DJ, et al. *Orthopedic Journal of Sports Medicine*. 2017;5(8).
10. Wellsandt E, et al. American Journal of Sports Medicine. 2016;44(1):143-151.

RUNNING-SPECIFIC PROSTHETIC MODEL AFFECTS TOP SPRINTING SPEED IN ATHLETES WITH UNILATERAL TRANSTIBIAL AMPUTATIONS

[1] Emily K. Southern, [2] Owen N. Beck, [3] Paolo Taboga, & [1,4] Alena M. Grabowski
[1] University of Colorado Boulder, CO, USA
[2] Georgia Institute of Technology, Atlanta, GA, USA
[3] Sacramento State University, Sacramento, CA, USA
[4] VA Eastern Colorado Healthcare System, Denver, CO, USA
email: emily.southern@colorado.edu

INTRODUCTION

Running-specific prostheses (RSPs), which are made of carbon fiber and passive-elastic, enable athletes with transtibial amputations (TTAs) to compete in running events. The stiffness and height of RSPs can be adjusted and likely affects users' performance. Additionally, RSP models are either C-shaped or J-shaped. C-shaped RSPs are attached beneath the socket and typically used for distance running, while J-shaped RSPs are attached posterior to the socket and more commonly recommended for sprinting. Despite the different attachments, both types of RSPs act in-series to the residual limb.

Faster sprinting speeds are achieved by applying greater average vertical ground reaction forces (vGRFs) to the ground during briefer contact times (t_c) for non-amputees [1]. However, athletes with unilateral TTAs who use an RSP have lower peak and stance average vGRFs for their affected leg (AL) than their unaffected leg (UL) [2], resulting in asymmetric forces between legs. Further, the use of a taller RSP results in more asymmetric peak vGRFs, which suggests that taller RSPs could prohibit faster sprinting speeds [3]. The purpose of our study was to quantify how RSP model, stiffness, and height affect top sprinting speed, stance average vGRF, and t_c in athletes with a unilateral TTA. We hypothesized that RSP model, stiffness, and height would affect top sprinting speed. We also hypothesized that stance average vGRF and t_c would be greater and shorter, respectively, and more symmetric using the optimal RSP configuration.

METHODS

Ten athletes with a unilateral TTA (7 M, 3 F; mean ± s.d. age: 28 ± 5 yr, mass: 76.0 ± 12.4 kg, height: 1.77 ± 0.12 m) gave written informed consent according to the COMIRB and USAMRMC Human Research Protection Office prior to participation. Each subject performed sets of running trials consisting of at least 10 strides per trial at a given speed on a 3D force measuring treadmill (Treadmetrix, Park City, UT). Each set of trials began at 3 m/s, rest was provided between trials, and each successive trial incremented treadmill speed by 1 m/s until the athlete approached top speed, when smaller speed increments were used. For each set of trials, subjects used 15 different combinations of RSP model, stiffness, and height. Models included the Freedom Innovations Catapult FX6 (FDM), Ottobock 1E90 Sprinter (OBK), and Össur Cheetah Xtend (OSR). FDM is C-shaped, while OBK and OSR are J-shaped. Stiffness conditions were the manufacturer recommended category (based on body mass) and ±1 stiffness categories. Height conditions were prosthetist-recommended and ±2 cm. For each model, height was only adjusted for the stiffness category that enabled the fastest speed.

We measured GRFs at 1000 Hz and filtered them using a 4th order low-pass Butterworth filter (30 Hz). We used these filtered data and a 30 N threshold to calculate stance average vGRF ($vGRF_{StA}$) and t_c for each step. For these variables (var), we calculated the average (AVG) of both legs (AL and UL) and the absolute value of the symmetry index (SI) between legs (Eq. 1):

$$SI = \left|\frac{var_{AL}-var_{UL}}{0.5(var_{AL}+var_{UL})}\right| * 100 \qquad Eq.\ 1$$

We used a linear mixed model to analyze the influence of RSP model, stiffness, and height on top sprinting speed. We used additional linear mixed models to analyze the influence of significant RSP configuration variables (model, stiffness, and/or height) on AVG and SI for the $vGRF_{StA}$ and t_c. We used a significance level of $p<0.05$.

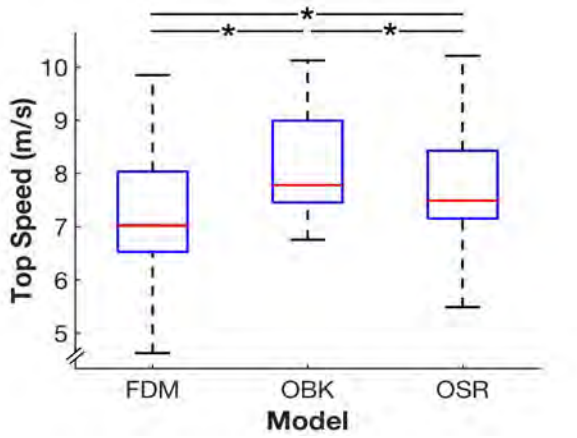

Figure 1: Mean ± s.d. top sprinting speed for each RSP model at all stiffness and height configurations. * indicates a significant difference between models.

RESULTS AND DISCUSSION

Compared to FDM, OBK and OSR resulted in 0.82 m/s ($p<0.0001$) and 0.37 m/s ($p<0.0005$) faster top sprinting speeds, respectively (Fig. 1). Additionally, OBK resulted in 0.46 m/s ($p<0.0005$) faster top sprinting speeds than OSR. Neither stiffness nor height influenced top sprinting speed ($p=0.72$ and $p=0.11$, respectively). There were no significant interactions among model, stiffness, and height for top sprinting speed.

RSP model had a significant effect on AVG and SI $vGRF_{StA}$ (Table 1). When controlling for speed, OBK resulted in 0.040*Body Weight (BW) greater $vGRF_{StA}$ than FDM ($p<0.01$). OSR resulted in 0.040*BW and 0.080*BW greater $vGRF_{StA}$ than OBK and FDM (both $p<0.005$). Additionally, OBK and OSR resulted in 5.1% and 6.7% lower SIs (more symmetric), respectively, for $vGRF_{StA}$ compared to FDM (both $p<0.001$). RSP model also had a significant effect on AVG and SI t_c (Table 1). When controlling for speed, OSR resulted in 0.003 s shorter t_c than both FDM ($p<0.005$) and OBK ($p<0.05$). In addition, OBK resulted in 2.5% and 3.5% higher SI (more asymmetric) for t_c than FDM and OBK, respectively (both $p<0.005$).

CONCLUSIONS

The data partially support our hypothesis that RSP model, stiffness, and height affect top sprinting speed. RSP model, but not stiffness or height, affects top sprinting speed in athletes with unilateral TTAs. Specifically, use of OBK resulted in the fastest top sprinting speed and use of FDM resulted in the slowest top sprinting speed.

We reject our hypothesis that stance average $vGRF_{StA}$ and t_c would be greater and shorter, respectively, using the optimal configuration. OSR resulted in the highest AVG $vGRF_{StA}$ and shortest AVG t_c, but did not elicit the fastest top sprinting speed. We partially reject our hypothesis that $vGRF_{StA}$ and t_c would be more symmetric using the optimal configuration. $vGRF_{StA}$ was more symmetric for OBK and OSR compared to FDM, and also elicited faster top sprinting speeds than FDM, suggesting that $vGRF_{StA}$ is important for top speed. In contrast, t_c was more asymmetric with OBK compared to FDM and OSR. Since OBK elicited the fastest top sprinting speed, this suggests that t_c symmetry may not influence top speed.

The underlying mechanisms for how J-shaped RSP models enable faster top sprinting speeds than a C-shaped RSP model could be due to relatively greater mechanical energy return, wider blades that enable greater stability, or a different alignment with respect to the residual limb [3,4]. Future studies are planned to assess the influence of prosthetic model on joint mechanics during top speed sprinting.

Table 1: Mean ± s.d. top sprinting speed, AVG and SI $vGRF_{StA}$, and AVG and SI t_c for each model.

		FDM	OBK	OSR
Top sprinting speed (m/s)		7.92 ± 1.53	8.78 ± 1.39	8.24 ± 1.42
$vGRF_{StA}$	AVG (BW)	1.88 ± 0.21	1.94 ± 0.19	1.96 ± 0.19
	SI (%)	15.18 ± 9.53	9.34 ± 7.39	8.44 ± 6.31
t_c	AVG (s)	0.13 ± 0.02	0.12 ± 0.02	0.12 ± 0.02
	SI (%)	5.87 ± 4.67	8.67 ± 4.76	5.15 ± 3.71

REFERENCES

1. Weyand et al. *J Appl Physiol* **89**, 1991-1999, 2000.
2. McGowan et al. *J R Soc Interface* **9**, 1975-1982, 2012.
3. Beck ON, et al. *J Appl Physiol* **123**, 38-48, 2017.
4. Beck ON, et al. *J R Soc Interface* **14**, 20170230, 2017.

LONGITUDINAL CHANGES IN CARTILAGE COMPOSITION ARE ASSOCIATED WITH ABNORMAL *IN VIVO* KNEE MECHANICS FOLLOWING ACL RECONSTRUCTION

[1]Michael F. Vignos, [1,2]Jarred Kaiser, [1]Richard Kijowski, [1]Geoffrey S. Baer, [1]Darryl G. Thelen
[1]University of Wisconsin-Madison, Madison, WI, USA; [2]Boston University, Boston, MA, USA
email: mvignos@wisc.edu, web: http://uwnmbl.engr.wisc.edu/

INTRODUCTION

Residual abnormalities in knee mechanics following ACL reconstruction (ACLR) may contribute to the high incidence of post-traumatic osteoarthritis (PTOA) in this patient population [1]. This theory is supported by *in vivo* studies that report abnormal kinematics in ACLR knees, which would lead to altered cartilage contact patterns [2]. Further, *ex vivo* cartilage testing and animal studies have shown that altered cartilage loading is related to the initiation and progression of PTOA [3]. However, prior studies have been unable to establish a direct link between altered knee mechanics and cartilage degeneration in ACLR knees. Thus, the objectives were (1) to determine bilateral differences in knee mechanics in ACLR patients using dynamic MR imaging, and (2) to investigate a link between altered cartilage contact patterns and signs of cartilage degeneration detected via quantitative MR imaging.

METHODS

We tested six subjects that underwent a primary, unilateral ACLR following completion of post-surgery rehabilitation (time point 1, TP1) (2F, 25.7±8.1 yrs, 14.9±4.2 months post-surgery, 3PT grafts) and at approximately one year after completion of rehabilitation (TP2, 29.7±5.2 months post-surgery). At both time points, bilateral static images were collected and manually segmented to obtain bone and cartilage geometries for the ACLR and contralateral knees. Quantitative MR imaging was then performed on the ACLR knees using an mcDESPOT multi-component T2 mapping sequence to obtain maps of the fraction of water bound to proteoglycan (FBW), with lower FBW representing loss of proteoglycan content in cartilage [4].

Post-rehabilitation (TP1), subjects lay supine in the MR scanner with their lower leg secured to an inertial loading device. They performed cyclic knee flexion-extension at 0.5 Hz, with the device inducing quadriceps loading similar to the weight-acceptance phase of gait. Dynamic 3D MR images were continuously acquired and reconstructed into 60 frames over the motion cycle [5]. Tibiofemoral kinematics and cartilage contact were computed by registering the bone and cartilage geometries to the dynamic images at each frame and measuring cartilage overlap. Contact maps were generated by computing the maximum contact depth across the tibial cartilage during knee extension. The tibial cartilage was divided into regions of interest (ROI). Contact and FBW maps were averaged within ROIs.

A two-factor repeated measures ANOVA (α=0.05) tested for differences in kinematics between ACLR and contralateral knees and across flexion angles (every 2.5°). Separate two-factor repeated measures ANOVAs (α=0.05) tested for differences in contact and changes in FBW. For significant interaction effects (α=0.05), post-hoc Bonferroni comparisons tested for differences across flexion angles (adjusted α=0.004) or ROIs (adjusted α=0.0013). Side-to-side differences (ACLR minus contralateral) in cartilage contact depth and changes in FBW (TP2 minus TP1) were computed across all ROIs for each subject. Geospatial analysis (bivariate local indicator of spatial association, BiLISA) was used to test for correlations between asymmetric cartilage contact and changes in FBW within each ROI (α=0.05) [6].

RESULTS AND DISCUSSION

ACLR knees exhibited abnormal tibiofemoral kinematics relative to contralateral knees (Fig. 1). Specifically, ACLR knees exhibited greater anterior tibial translation, medial tibial translation, and external tibial rotation during extension. We also observed abnormal cartilage contact in ACLR knees with greater contact depth than contralateral knees on both tibial plateaus (Fig. 2A). The greatest contact differences occurred on the posterior aspect of the medial plateau and along the medial tibial spine. We also found longitudinal changes in cartilage

composition in ACLR knees, with a reduced FBW in both plateaus between time points 1 and 2 (medial: TP1 = 22±8.8%, TP2 = 21±11%; lateral: TP1 = 22±8.1%, TP2 = 19±12%) (Fig 2B). The greatest reductions in FBW occurred in the posterior weight-bearing region of the medial plateau and the posterior-medial cartilage on the lateral plateau.

Bilateral differences in cartilage contact were linked to longitudinal reductions in FBW within ACLR knees (Fig. 3). In particular, there were weight bearing regions on both the medial and lateral tibial plateau where significant decreases in FBW were linked to greater contact (i.e. a high-low correlation).

Previous studies found that ACLR knees are externally rotated and medially translated, relative to healthy knees, during functional motion [2]. While we found similar kinematic asymmetries, ACLR knees also exhibited greater anterior tibial translation during knee extension. This may be due, in part, to the open-chain task causing internal kinematics to be more sensitive to changes in the ACL [7].

Many studies have been designed on the premise that a shift in cartilage loading initiates PTOA in ACLR knees [1]. We confirmed this theory by determining that increases in contact were correlated to signs of cartilage degeneration. Additionally, we found reduced contact was linked to degeneration along the lateral tibial spine. While this suggests that unloading of cartilage may also be problematic, it is important

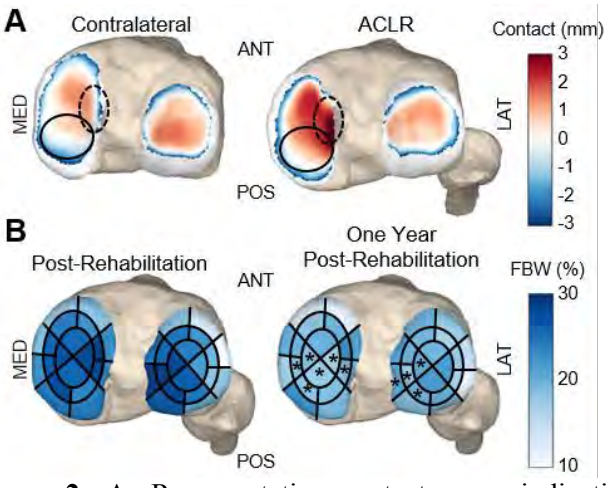

Figure 2: A. Representative contact maps indicating regions with greatest contact differences between ACLR and contralateral knees (ellipses). **B.** Average FBW (%) across all subjects for each ROI at both time points. * = significantly reduced FBW at one year post-rehab.

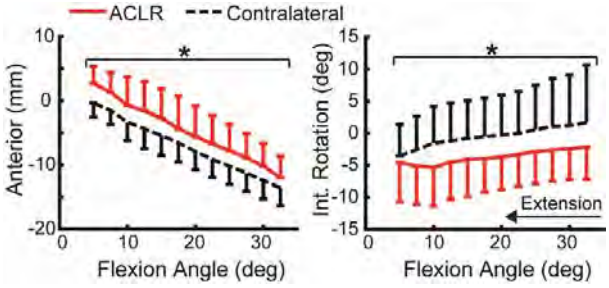

Figure 1: Anterior translation (mean ± SD) and internal rotation of the tibia relative to the femur during knee extension. * = a significant difference between ACLR and contralateral knees across all flexion angles.

to note that additional factors, such as subchondral bone bruising and joint inflammation, may also contribute to PTOA after ACL injury. Further work is needed to assess the sensitivity of the rate of cartilage degeneration to altered knee mechanics to determine the accuracy needed during ACLR.

CONCLUSIONS

This study provides striking evidence of early cartilage degeneration characterized by reductions in FBW one year after completing post-ACLR rehabilitation. Further, we provide evidence of an association between abnormal *in vivo* cartilage loading and cartilage degeneration. Taken together, these results provide evidence that failure to restore normal knee mechanics following ACLR contributes to cartilage degeneration within the knee.

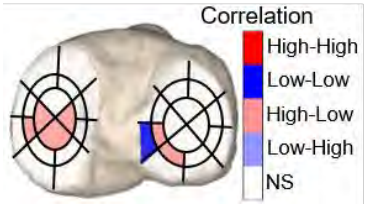

Figure 3: BiLISA summary map showing the correlation between cartilage contact and longitudinal changes in FBW for ROIs with reduced FBW (* in Fig. 2B). Colored ROIs indicate those with a significant correlation.

REFERENCES

1. Chaudhari AMW, et al. *MSSE.* 40, 2008.
2. Hofbauer M, et al. *Am J Sports Med.* 42, 2014.
3. Griffin TM, et al. *Exerc Sport Sci Rev.* 33, 2005.
4. Liu F, et al. *J Magn Reson.* 39, 2014.
5. Kaiser J, et al. *Magn Reson Med.* 69, 2013.
6. Anselin L, et al. *Geogr Anal.* 38, 2006.
7. Yack HJ, et al. *Am J Sports Med.* 21, 1993.

ACKNOWLEDGEMENTS

NSF GRFP (MFV): DGE-1747503, NIH EB015410, NIAMS R01 AR068373

ESTIMATES OF ACHILLES TENDON MOMENT ARM WITH AXIS OF ROTATION DETERMINED FROM ANKLE MOTION VERSUS ANATOMICAL LANDMARKS

[1]Francesca E. Wade, [2]Gregory S. Lewis, and [1]Stephen J. Piazza
[1]The Pennsylvania State University, University Park, PA
[2] Penn State College of Medicine & Milton S. Hershey Medical Center, Hershey, PA
email: piazza@psu.edu web: www.biomechanics.psu.edu

INTRODUCTION

Functional capacity of the ankle joint is influenced by the plantarflexion moment arm of the Achilles tendon (ATma). Experimentally, ATma may be found as the shortest distance from the ankle center of rotation (CoR) to the Achilles tendon line of action on planar magnetic resonance (MR) images [1], or ATma may be determined in three dimensions from MR imaging using ankle axes from instantaneous helical axis decomposition and a tendon path [2].

While MR imaging allows tracking of the bones and tendons, cost and accessibility are barriers to using an MR-based approach. An alternative method for finding ATma locates the Achilles tendon using an ultrasound probe fitted with motion capture markers [3,4]. Previous uses of this approach have typically assumed that the CoR lies at the midpoint between markers placed on the malleoli. This assumption, however, may not accurately represent ankle joint rotation [5].

The purpose of this work is to investigate how three different methods for locating the ankle center (or axis) of rotation influence estimates of 3D ATma during loaded and unloaded movements. We located the center (or axis) of rotation using the malleoli markers and finite helical axis decomposition of ankle motion. In each case the Achilles tendon was imaged with ultrasound. We hypothesized that ATma estimated from ankle motions would differ from those estimated from the malleoli landmarks, and would be more consistent with those previously measured using MR imaging.

METHODS

Fifteen participants (7M, 8F; 26 ± 2 y; 1.7 ± 0.07 m; 71 ± 12 kg) performed sets of three weight-bearing toe-raises in time to a 0.5 Hz metronome. This motion was repeated unloaded at the same frequency. Approval for all procedures was given by the Institutional Review Board of The Pennsylvania State University.

A linear 60 mm ultrasound probe (HL9.0/60.128Z-2; Telemed) imaged the Achilles tendon at the level of the malleoli. Four retroreflective markers were rigidly attached to the probe, with additional markers placed on the femoral epicondyles and the malleoli. Clusters of four markers were attached to the dorsum of the foot and the anterior shank. Ultrasound images were sampled at approximately 60 Hz, while marker motions were captured simultaneously using seven Eagle cameras (Motion Analysis Corp.) at 100 Hz.

Marker data were passed through a 4th order Butterworth low-pass filter with a cut-off frequency of 10 Hz. Image processing routines in MATLAB (Mathworks Inc.) were used to identify the midline of the Achilles tendon. ATma was calculated as the effective distance between this 3D line of action and either 1) a transmalleolar axis (TA), 2) the transmalleolar midpoint (TM), or 3) a 'functional' axis determined by finite helical decomposition of foot motion with respect to the shank (FA).

Moment arms were quantified over the range from 10° dorsiflexion to 20° plantarflexion (in 5° increments) by interpolating a second-order polynomial fit to ATma versus plantarflexion angle data. Ankle joint angles were computed using Cardan angle decomposition and a modified ISB joint coordinate system [6]. A three-way repeated measures ANOVA, followed by Bonferroni-corrected post-hoc comparisons as indicated by ANOVA results, was run to examine the effect of loading condition, ankle joint angle, and rotational axis/center on ATma.

RESULTS AND DISCUSSION

ATma calculated using FA were significantly larger than values calculated using TA or TM across all joint angles considered (all $p < 0.001$). TM values were slightly larger than TA values ($p = 0.008$). Values of ATma obtained with FA were commensurate with those reported in the literature from 2D and 3D MR data [1,2,7], and our TA and TM values were similar to those found by authors using a similar methods [3,4].

We found that ATma computed using FA increased with plantarflexion angle ($p < 0.001$), with an average increase of 7.5 mm over the range of ankle angles tested. No clear angle-dependent relationship was observed for TA or TM (Fig. 1). ATma has been found to increase with plantarflexion in 2D MR studies [1,7] but in 3D MR studies there is an increase from dorsiflexion to neutral followed by a plateau with increasing plantarflexion [2,7]. In studies employing TM, ATma has been found to increase with plantarflexion [3] and to remain constant with joint rotation [4].

Using FA, ATma were approximately 10% larger for loaded movements ($p < 0.001$) but did not differ with loading for TA and TM. Increases in moment arm with loading have been noted previously in MR studies [1,7].

The location of the FA qualitatively agrees with ankle axis of rotation described in previous studies of bone kinematics [5]. This agreement, along with the similarities between our ATma findings with published results from MR studies, suggest that FA may be a better choice when estimating ATma because FA provides a closer approximation of ankle axis of rotation than TA or TM. It must be noted, however, that our FA was a single axis fixed in the foot coordinate system (a choice we made for the sake of simplicity), and it is known that rotational axis of the ankle joint moves throughout a range of motion [5]. Future work will include use of an instantaneous helical axis to compute ATma with an axis of rotation that moves with respect to the local segment coordinate systems throughout the motion.

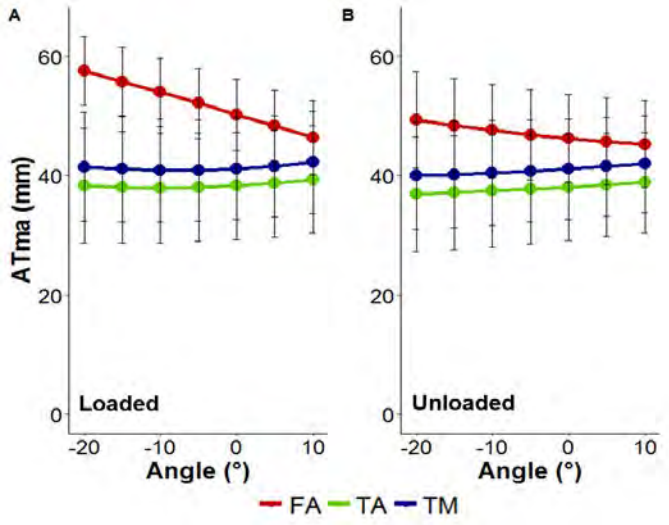

Figure 1: Achilles tendon moment arm, calculated using 'FA' in red, 'TA' in green, and 'TM' in blue, over plantarflexion (-) and dorsiflexion (+) in (A) the loaded condition, and (B) the unloaded condition.

CONCLUSIONS

The plantarflexion moment arm of the Achilles tendon approximated using a functional axis derived from the relative motions of the ankle and foot produces loading- and angle-dependent patterns similar to those with previously reported in MR studies. The results of this study suggest that location of the axis of rotation from measured motion may provide advantages over landmark-based methods when estimating ATma.

REFERENCES

1. Maganaris et al. *Journal of Physiology*. **510**(3): 977-985, 1998.
2. Sheehan. *Journal of Biomechanics*. **45**(2): 225-230, 2012.
3. Manal et al. *Physiological Reports*. **1**(6): e00139, 2013.
4. Rasske et al. *Computer methods in Biomechanics and Biomedical Engineering*. **20**(2): 201-205, 2017.
5. Lundberg. *Acta Orthopaedica Scandinavica*. **60**(233):1-24, 1989.
6. Wu et al. *Journal of Biomechanics*. **35**(5):453-548, 2002.
7. Hashizume et al., 2012. *Journal of Biomechanics*. **45**(2): 409-413, 2012.

FINGER MUSCLES INJECTED WITH BOTULINUM TOXIN DEMONSTRATE INCREASED PASSIVE STIFFNESS AND DECREASED PASSIVE RANGE OF JOINT MOTION IN INDIVIDUALS WITH CHRONIC HEMIPARETIC STROKE

[1,2,4]Benjamin I Binder-Markey, [1,2,3]Julius PA Dewald, and [1,2,3,4,5]Wendy M Murray

Departments of [1]Biomedical Engineering, [2]Physical Therapy and Human Movement Sciences, [3]Physical Medicine and Rehabilitation, Northwestern University, Chicago, IL, USA
[4]Shirley Ryan AbilityLab (Formerly RIC), Chicago, IL, USA
[5]Edward Hines, Jr. VA Hospital, Hines, IL, USA
Email: bbindermar@sralab.org, Website: https://www.sralab.org/research/labs/arms-lab

INTRODUCTION

In individuals with chronic hemiparetic stroke, botulinum toxin (BTX) is often used to reduce muscle hypertonicity and spasticity with the goal of improving passive range of motion (ROM), pain, and hygiene in the paretic limb [1, 2]. However, recent evidence suggests that BTX may increase the collagen content within rodent muscles [3, 4]. This could have devastating lasting effects on the passive mechanical properties of the muscle limiting the therapeutic effects of BTX.

Because of these findings in animal studies, we investigated the effects of BTX on the passive properties of the human extrinsic finger muscles following stroke. The extrinsic finger muscles were chosen because they are located in the flexor compartment of the forearm, a frequent target for BTX injection. In addition, we implemented an experimental design that exploits the multi-joint length-dependence of the extrinsic finger muscles across both wrist and finger posture to separate the torque they generate about the metacarpophalangeal (MCP) joints from those produced by other soft tissue structures at the MCP joint [5].

METHODS

The total passive flexion/extension torque generated about the four MCP joints, $T_t(\theta, \omega)$, was quantified in both hands of 16 subjects with chronic hemiparetic stroke and severe hand impairments. Seven subjects had previously received BTX injections in the flexor compartment of the forearm (Table 1).

$T_t(\theta, \omega)$ was quantified as a function of both MCP (θ) and wrist (ω) position using a custom built device [6]. Experimental conditions encouraged a sleep or near sleep state to mitigate hyperactivity of the paretic muscles; EMG monitoring ensured the absence of muscle activity. Data were collected in static 15° increments, spanning the range of motion of the MCP joints; measurements were repeated in 9 different wrist postures, with wrist posture randomized in 15° increments between 60° flexion to 60° extension. The passive ROM of the MCP joints within the torque-measurement device was determined by either the limits of the device or the subject's tolerance; the most extended and flexed postures of the MCP joints were recorded in each wrist posture. PIP & DIP joints were splinted to prevent movement.

For each subject, an exponential analytical model was fit to all of the torque data collected [5]:

$$T_t(\theta, \omega) = T_{sj}(\theta) + T_e(\theta, \omega)$$

The model is comprised of two components. The first component, $T_{sj}(\theta)$, assumes that the torques contributed by the single-joint structures (e.g., intrinsic muscles, skin, ligaments, joint capsules, etc.) vary as a function of MCP joint posture, θ, only. The second component, $T_e(\theta, \omega)$, assumes that torques that vary as a function of both MCP joint posture, θ, and wrist posture, ω, are produced by the extrinsic finger muscles. Data were analyzed using a linear-mixed model analysis.

Table 1: Subject demographics

	N	Age yrs (SD)	Time since Stroke yrs (SD)	CMHS (SD)	Mod. Ashworth (SD)	Time Since BTX yrs (SD)
BTX	7	56.7 (8.3)	10.7 (5.3)	2.8 (0.4)	2.7 (0.5)	4.5 (2.8)
No-BTX	9	60.3 (10.4)	17.1 (7.9)	2.4 (0.7)	2.2 (0.9)	NA

RESULTS AND DISCUSSION

We observed significant inter-limb differences ($p < 0.001$) in both $T_t(\theta, \omega)$ and $T_e(\theta, \omega)$ for both the BTX and the no-BTX groups. The largest differences between paretic and non-paretic limbs were observed in the BTX group when the wrist was extended (Fig. 1A). For the no-BTX group, the MCP passive torques were comparable across limbs in the same extended wrist posture (Fig. 1B).

When the wrist was flexed the differences in $T_e(\theta, \omega)$ between limbs were an order of magnitude smaller (Fig. 1C). In the no-BTX group, smaller inter-limb differences in $T_e(\theta, \omega)$ were observed across all postures (Fig. 1 B&D). No significant differences in $T_{sj}(\theta)$ were observed in either the BTX ($p=0.111$) or no-BTX ($p=0.131$) group in this study.

Large torque increase between limbs were only observed within the BTX group when the wrist was extended and the extrinsic finger flexor muscles were at their longest lengths (Fig 1A). These increases decreased as the wrist was flexed and the flexors shortened (Fig 1C). The increases were only observed in muscles that received the BTX injections and were not observed in muscles that did not receive BTX injections (Fig. 1B,C,&D).

The increased passive MCP flexion torque observed in the BTX group corresponded with a decreased ability to passively extend the MCP joint ($p<0.001$). This was especially evident when the wrist was extended, with an inter-limb decrease in passive extension of 68° for the paretic limb in the BTX group. This decrease in extension ROM was not present in individuals who did not receive BTX ($p=0.360$).

CONCLUSIONS

Paretic muscles located in the anatomical compartment where BTX injections were given demonstrated increased passive MCP flexion torques in joint postures associated with long muscle lengths. These effects were absent in individuals with comparably impaired hands who had never received BTX. These data, together with animal studies revealing increased muscle collagen following BTX injections, suggest that BTX may have long-term consequences opposing the desired treatment effect of increasing ROM.

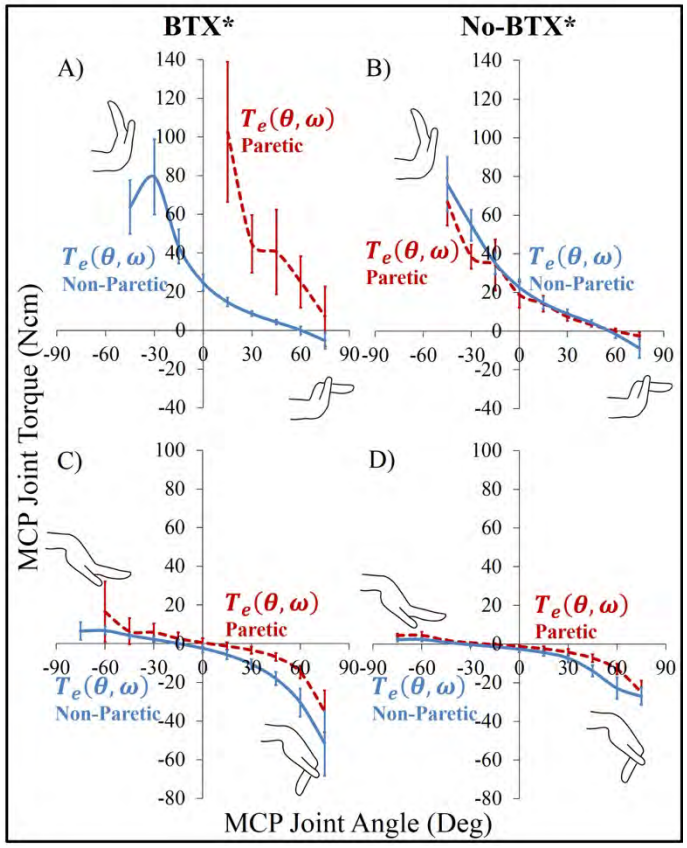

Figure 1: T_e vs MCP (θ) for the paretic (red dashed line) and non-paretic (blue solid) limb, with the wrist fully extended (A & B) and flexed (C & D). BTX (A & C) and No-BTX B groups with standard error bars. (+ flexion/- extension) (* $p<0.001$)

REFERENCES

1. Ozcakir, S. and K. Sivrioglu, Clin Med Res, 2007. **5**(2): p. 132-8.
2. Kaku, M. and D.M. Simpson, Drug Des Devel Ther, 2016. **10**: p. 1085-99.
3. Minamoto, V.B., et al., Muscle Nerve, 2015. 52(4): p. 649-57.
4. Ward, S.R., et al., Muscle Nerve, 2017.
5. Knutson, J.S., et al., J Biomech, 2000. 33(12): p. 1675-81.
6. Stienen, A., et al. *2011 IEEE International Conference on Rehabilitation Robotics*. 2011. Zurich , Switzerland.

ACKNOWLEDGEMENTS

This work was supported by a Promotion of Doctoral Studies (PODS) – Level II Scholarship from the Foundation for Physical Therapy, American Heart Association Pre-Doctoral Fellowship: 16PRE30970010, & NIH 1R01HD0840

OLDER ADULTS REVERSE THEIR DISTAL-TO-PROXIMAL REDISTRIBUTION USING BIOFEEDBACK

Michael G. Browne, Sarah N. Fickey, and Jason R. Franz

University of North Carolina at Chapel Hill and North Carolina State University, Raleigh, NC, USA
email: mgbrowne@email.unc.edu, web: http://abl.bme.unc.edu

INTRODUCTION

Compared to young adults, older adults walk slower and with a characteristic decrease in push-off intensity. This decreased push-off intensity stems from large reductions in mechanical power generated by the plantarflexor muscles (i.e. ankle power, P_A) and propulsive ground reaction forces generated during push-off (F_P) [1]. Seemingly in response to this decreased push-off intensity, older adults also rely more on positive mechanical power generated by the hip musculature. This phenomenon, known as the distal-to-proximal redistribution [2], may also contribute to increased metabolic energy costs during walking in older adults [3]. Conventional resistance training for improved mobility in older adults successfully improves maximal muscle strength and fast walking speed (FWS) but has minimal functional impact on habitual walking performance (i.e. preferred walking speed; PWS) or gait biomechanics (e.g., mechanical power generation).

Rehabilitative approaches that go beyond resistance training alone are needed, toward more direct means to elicit favorable biomechanical adaptations during habitual speed walking. As an important first step, we previously attempted to enhance push-off intensity in older adults using biofeedback to increase propulsive forces. While effective - older adults increased F_P with potentially favorable reductions in hip flexor power generation [4] – we were surprised to observe no concomitant increase in P_A. However, older adults can increase P_A in order to walk faster or uphill, revealing a translationally important gap in our understanding. Motivated by these findings, we tested here the primarily hypothesis that real-time ankle power biofeedback during walking can directly increase P_A in older adults. We also hypothesized that doing so would: (*i*) alleviate mechanical power demands at the hip and (*ii*) increase preferred but not fast walking speed.

METHODS

10 healthy older adults (mean±SD; age: 74.8±5.4 years, 3 males/7 females) participated in this study. We first assessed subjects' PWS (1.28±0.20 m/s) and FWS (1.79±0.20 m/s) using an instrumented walkway. Subjects then walked normally for 1-min on a dual-belt instrumented treadmill at their PWS. A custom Matlab script running a surrogate inverse dynamic model of the lower legs and feet estimated bilateral step-by-step P_A. Subjects walked again for 1-min each while watching a screen with visual biofeedback of their instantaneous P_A and targeting increases of +10% and +20% of normal (Fig. 1A). For all trials, a motion capture system recorded the

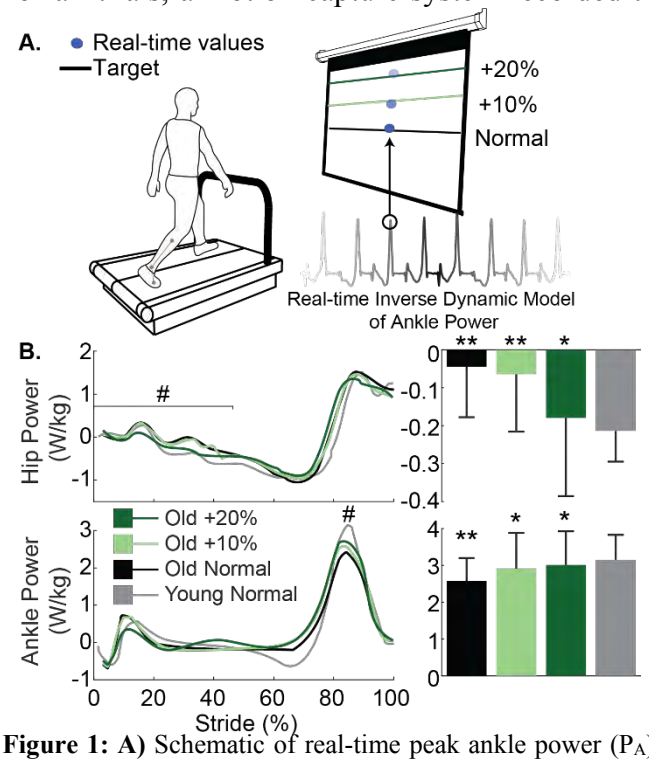

Figure 1: A) Schematic of real-time peak ankle power (P_A) biofeedback. **B)** Group-mean hip and ankle power plotted against an averaged gait cycle. Pound signs (#) denote a significant main effect of P_A biofeedback ($p<0.05$). Each graph is accompanied by bar graphs indicating group mean (±SD) peaks. Asterisks (*) and double asterisks (**) denote a significant pairwise difference from old and young adults walking normally, respectively.

trajectories of markers placed on subjects' pelvis and lower extremities for estimating joint kinetics. Data reported represents the 20 consecutive strides for which participants were most successful matching prescribed targets. Finally, we again assessed subjects' PWS and FWS to investigate recall. We additionally include normal walking data from 9 healthy young adults (age: 25.1±5.6 years, 4 males/5 females, PWS: 1.30±0.12 m/s) to serve as a reference for comparison.

RESULTS AND DISCUSSION

Our older adults walked with 21% lower P_A and 79% greater hip power during early to mid-stance compared to their younger counterparts ($p<0.034$). Older adults increased P_A by 13% and 17% when targeting increases of 10% and 20%, respectively (main effect, $p=0.006$), thereby attenuating their P_A deficit compared to young adults (Fig. 1B). Conceptually, older adults could increase P_A through changes in net moment or angular velocity at the ankle. Our older adult subjects increased P_A through modest (+3%) but significant changes to peak ankle moment ($p=0.008$) and nonsignificant changes to angular velocity (+7%, $p=0.157$) (Fig. 2). We also observed larger net ankle moments developed during early to midstance, which may have indirectly contributed to larger than preferred P_A through greater elastic energy storage and return. Greater P_A was also accompanied by up to a 300% reduction in the demand for positive hip power generation during early to mid-stance ($p=0.015$). P_A biofeedback also increased positive ankle joint work ($p=0.001$), total positive leg joint work ($p=0.002$), and F_P ($p<0.001$) (Fig. 2). This latter finding reveals an interesting disconnect in our understanding of push-off in walking: older adults increase F_P without related improvements in P_A [4], but increase P_A with related improvements in F_P. Finally, subjects walked overground with 11% faster PWS ($p=0.010$) but no change in FWS when recalling P_A biofeedback.

CONCLUSIONS

Our results reveal that older adults are capable of increasing P_A through the use of targeted ankle power biofeedback – effects that are accompanied by potentially favorable shifts in hip power generation during early to mid-stance. Moreover, the associated

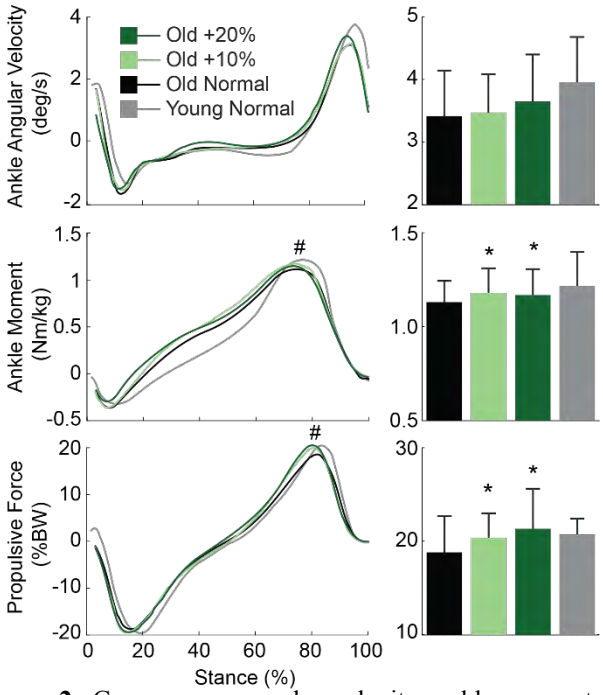

Figure 2: Group mean angular velocity, ankle moment, and propulsive force (F_P) against an average gait cycle. Asterisks (*) denote a significant main effect of biofeedback ($p<0.05$). Each graph is accompanied by bar graphs indicating group mean (±SD) peaks. Asterisks (*) denote a significant pairwise difference from old adults walking normally.

increase in PWS suggests a functional benefit to increased ankle power output during habitual speed walking. Further work will investigate whether ankle angular velocity alone may be sufficient feedback to modulate P_A, an approach more immediately translatable to novel rehabilitation approaches via wearable sensor technologies. Ultimately, targeted biofeedback may complement resistance training to reverse age-associated mobility decline.

REFERENCES

1. Franz, JR. *Exercise and sport science reviews,* 44(4):129-35, 2016.
2. DeVita, P & Hortobagyi, T. *J Appl Physiol*, 88(5):1804-11, 2000.
3. Ortega, JD & Farley, CT. *J Appl Physiol*. 102(6):2266-73, 2007.
4. Browne, MG & Franz, JR. *Plos One*. In Review, 2018.

ACKNOWLEDGEMENTS

This work was supported by grants from NIH (R01AG051748) and the UNC University Research Council.

TRICEPS SURAE MUSCLE-SUBTENDON INTERACTION DIFFERS BETWEEN YOUNG AND OLDER ADULTS

William H. Clark and Jason R. Franz

University of North Carolina and North Carolina State University, Chapel Hill, NC, USA
email: jrfranz@email.unc.edu, web: http://abl.bme.unc.edu

INTRODUCTION

Mechanical power generated via triceps surae muscle-tendon interaction during walking is largely responsible for the total power needed for forward propulsion and swing initiation [1]. This interaction is made complex by the biological architecture of the Achilles tendon (AT), which consists of distinct bundles of tendon fascicles, known as "subtendons", arising from the gastrocnemius (GAS) and soleus (SOL) muscles [2]. Comparative data and our own *in vivo* evidence alludes to a reduced capacity for sliding between adjacent subtendons compromising the AT in old age. This is functionally important, as subtendon sliding could facilitate independent actuation between individual triceps surae muscles, perhaps augmenting contributions to trunk support and forward propulsion. Indeed, our lab recently found that an age-associated reduction in the capacity for sliding between GAS and SOL subtendons correlated with smaller peak ankle moments and positive work performed during push-off, alluding to unfavorable functional consequences [3]. However, it remains unclear whether age-associated changes at the subtendon level unfavorably affect triceps surae muscle contractile dynamics. Recently, we introduced a novel dual-probe ultrasound imaging approach to reveal that length change differences between the GAS and SOL of young adults during force generation positively correlated with non-uniform tissue displacement patterns in the AT.

Therefore, the purpose of this study was to investigate aging effects on triceps surae muscle-subtendon interaction dynamics using dual-probe ultrasound imaging during a series of ramped isometric contractions. We hypothesized that, compared to young adults, older adults will have (*i*) more uniform Achilles subtendon tissue displacements that (*ii*) are accompanied by more uniform GAS and SOL muscle length change dynamics.

METHODS

We report data for 9 younger adults (age: 25.1 ± 5.6 years, weight: 69.8 ± 6.9 kg, height: 1.7 ± 0.1 m, 4 females) and, thus far, 6 older adults (age: 74.3 ± 3.4 years, weight: 67.2 ± 9.0 kg, height: 1.7 ± 0.1 m, 4 females). Subjects completed 3 ramped isometric voluntary contractions at each of 5 different ankle angles (spanning 30° plantarflexion to 10° dorsiflexion) using a Biodex (Biodex System 4 Pro), with the knee flexed to replicate that near the push-off phase of walking (~20º). We synchronized two linear array ultrasound transducers to simultaneously record GAS and SOL fascicle kinematics with tissue displacements in their associated tendinous structures (Fig. 1). A 60 mm Telemed Echo Blaster 128 transducer (LV7.5/60/128Z-2) placed over the medial gastrocnemius and soleus of subjects' right leg recorded cine B-mode images at 61 frames/s. Simultaneously, a 38-mm transducer (L14-5W/38, Ultrasonix Corporation, Richmond, BC) operating at 70 frames/s recorded ultrasound radiofrequency (RF) data from a longitudinal cross-section of the right free AT, distal to the SOL muscle-tendon junction and secured via a custom orthotic. Subjects' right foot was barefoot throughout the experiment to facilitate proper placement of the AT transducer.

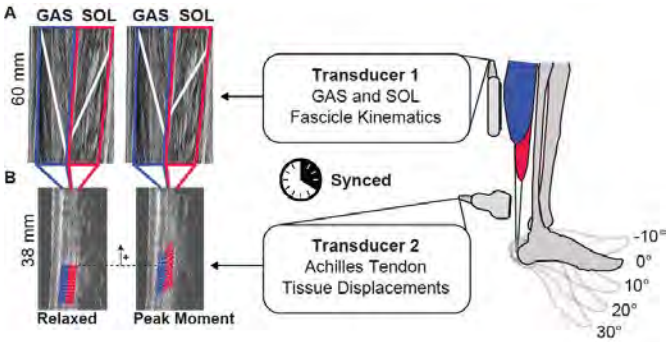

Figure 1. Simultaneous ultrasound imaging of the gastrocnemius (GAS), soleus (SOL), and Achilles free tendon. (A) Fascicle lengths and pennation angles derived from cine B-mode images. (B) Custom speckle-tracking of localized Achilles tendon tissue displacements.

Finally, motion capture tracked right ankle and knee joint kinematics and the positions and orientations of both probes.

Available MATLAB routines based on an affine extension to an optic flow algorithm quantified time series of GAS and SOL fascicle lengths and pennation angles (UltraTrack, [4]), which we combined to compute longitudinal muscle lengths. A custom 2D speckle-tracking algorithm estimated localized displacements of AT tendon tissue, which we averaged in two equally sized tendon depths - superficial and deep - corresponding to tendon tissue thought to arise from GAS and SOL, respectively [5]. A repeated measures ANOVA tested for, in part, significant main effects of and interactions between age and ankle angle on GAS-SOL differences in muscle shortening and tendon tissue displacement at peak ankle moment using an alpha level of 0.05.

RESULTS AND DISCUSSION

For young and older adults, peak isometric plantarflexor moment decreased progressively from dorsiflexion to plantarflexion across the angles tested (p<0.01). On average, older adults generated a 21% smaller peak isometric plantarflexor moment than young adults (p=0.014). Compared to young adults, average peak muscle shortening was 21% greater for SOL and 81% greater for GAS, while average peak tendon displacement was 18% greater for SOL and 50% greater for GAS in older adults (Fig. 2) – findings fully consistent with functional consequences of increased compliance in older tendon. In addition, consistent with our translational premise, GAS versus SOL differences in muscle contractile behavior and those in subtendon tissue displacements were significant in young but not in older adults. Indeed, as hypothesized, differences between peak GAS subtendon and peak SOL subtendon displacement averaged 44% smaller in older versus young adults (e.g., 77% at 0º, p<0.05). Also as hypothesized, differences between peak SOL and peak GAS muscle shortening averaged 58% smaller in older versus young adults (e.g., 65% at 0º, p<0.05) (Fig. 2).

CONCLUSIONS

We reveal that more uniform AT tissue displacements in older versus young adults extend to anatomically consistent and potentially unfavorable changes in muscle contractile behavior – evidenced by smaller differences between GAS and SOL peak shortening during isometric force generation. These findings provide an important biomechanical basis for previously reported correlations between more uniform AT subtendon behavior and reduced ankle moment generation during waking in older adults.

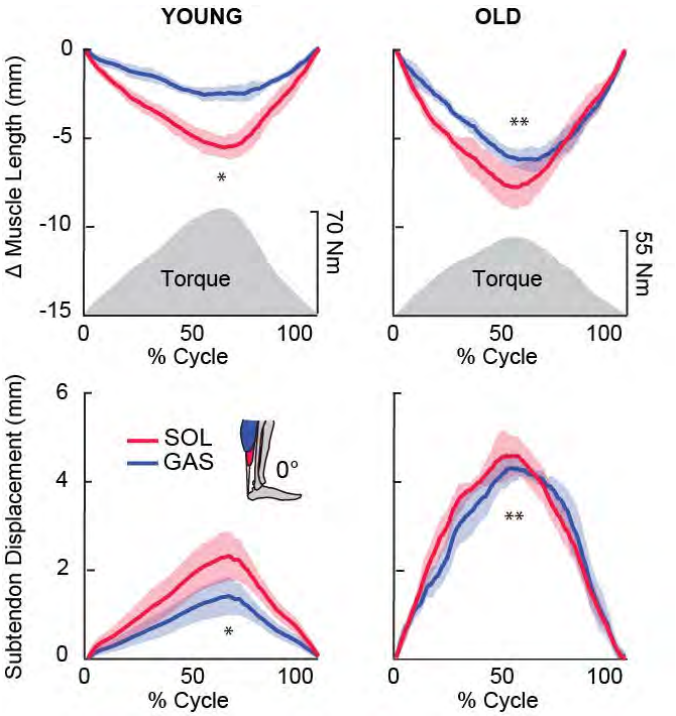

Figure 2. Group mean muscle shortening (above) and subtendon displacements (below; proximal positive). Gray shaded regions show the group mean net torque profile during a loading-unloading cycle. Single asterisks (*) indicate significant difference between peak GAS and peak SOL, Double asterisks (**) indicate significant difference between young and old. p<0.05 significant.

REFERENCES

[1] Zelik, K.E., et al. *J Theor Biol*, 2014.75-85.
[2] Szaro, P., et al. *Ann Anat*, 2009. (**6**):586-93.
[3] Franz, J.R., et al. *J Appl Physiol* (1985), 2015. (3):242-9.
[4] Farris, D.J., et al. *Comput Methods Programs Biomed*, 2016.111-8.
[5] Franz, J.R., et al. *Gait Posture*, 2015. (**1**):192-7.

ACKNOWLEDGEMENTS

We thank Ashish Khanchandani, Hannah Mckenney, and Michael Browne for their assistance with data collection. This study was supported by a grant from NIH (R01AG051748).

DOES FATIGUE AFFECT WRIST KINEMATICS DURING A REPETITIVE PICK-AND-PLACE TASK?

[1] Sarah P. DeDecker, [2] Bryan Piper, [1] Michele L. Oliver, and [1] Karen D. Gordon

[1] School of Engineering, University of Guelph, ON, Canada
[2] University of Toronto, ON, Canada
email: sdedecke@uoguelph.ca

INTRODUCTION

Carpal Tunnel Syndrome (CTS) is a common hand and wrist neuropathy. Increased risk for developing CTS is associated with extreme wrist posture during repetitive tasks, which is associated with some workplace occupations [1]. Ergonomic assessment is used to assess frequent flexion and extension motions of the wrist during repetitive tasks through various scoring methods. However, there is a lack of data regarding wrist kinematic alterations that may or may not occur as a worker becomes fatigued. If detectable differences in wrist kinematics with fatigue were present, this could provide an avenue for biofeedback mechanisms to inform preventative measures in the workplace.

The first objective of this study was to evaluate wrist posture during a repetitive pick-and-place task (e.g. task performed by a grocery cashier). The second objective was to quantify the effect of fatigue on wrist posture. It was hypothesized that wrist kinematics would be altered after fatigue.

METHODS

Ten healthy right-hand dominant subjects (four males and six females, age 21.1 ± 2.81 years) participated in this University of Guelph REB approved study. Seven retroreflective markers were mounted on the subject's right forearm and hand based on a previous model [2]. The markers were placed on the lateral epicondyle of the elbow, the medial epicondyle of the elbow, the ulnar styloid process, the radial styloid process, the capitate bone, the second metacarpal-phalangeal joint, and the third metacarpal-phalangeal joint. An eight camera VICON Bonita Motion Capture System (Vicon Motion System Ltd, Oxford, UK) was used to predict flexion-extension and radial-ulnar deviation angles of the wrist at a sampling frequency of 100 Hz. The subjects were instructed to perform a pick-and-place task. While seated, subjects used their right hand to move five objects (cans) from one end of a waist height table to the other and back (10 total cycles), while turning the cans over approximately 180 degrees each time. The cans weighed less than two kilograms and could be moved in any order selected by the subject. A fatiguing protocol described in [3] was followed to ensure subjects were fatigued prior to performing the pick-and-place task for a second time. Grip force data was collected using a hand dynamometer (Vernier, OR, USA) until grip force dropped to 70% or less of the subject's maximum grip force, as described in [3].

The range of motion (ROM) and mean angle were determined over the middle 5 pick-and-place cycles for both wrist flexion-extension (FE) and radial-ulnar deviation (RUD) angles. FE ROM, FE mean and RUD ROM were transformed using a Johnson transformation to meet data normality requirements prior to statistical analysis. RUD mean data was not transformed as it was normally distributed. A general linear model ANOVA ($p<0.05$) was performed on FE ROM, FE mean, RUD ROM, and RUD mean with factors of subject, sex, cycle, and fatigue included in the analysis. All statistical analyses were performed using Minitab 17 software (Minitab Inc., Chicago, Illinois, USA).

RESULTS AND DISCUSSION

FE and RUD ROM and mean angle for females and males pre- and post-fatigue are shown (Fig. 1 and Fig. 2).

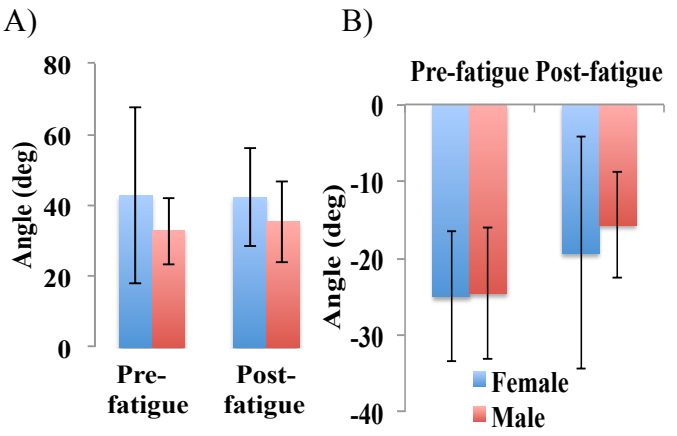

Figure 1: A) Mean ± SD flexion-extension ROM angle pre- and post-fatigue (left) and B) mean ± SD flexion-extension mean angle pre- and post-fatigue (right) for females and males (positive angles represent extension)

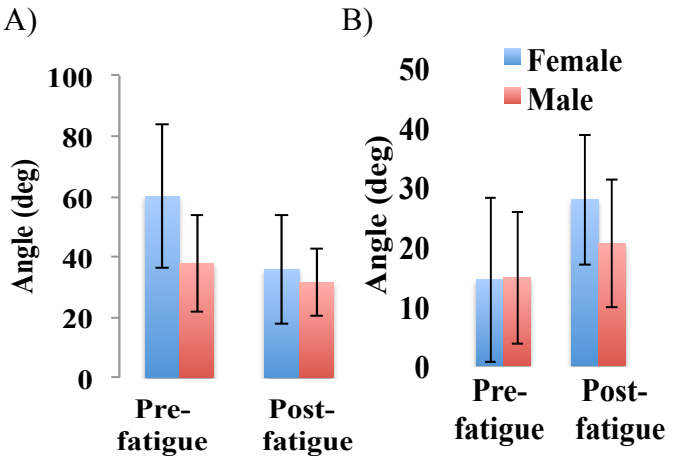

Figure 2: A) Mean ± SD radial-ulnar deviation ROM angle pre- and post-fatigue (left) and B) mean ± SD radial-ulnar deviation mean angle pre- and post-fatigue (right) for females and males (positive angles represent ulnar deviation)

There was a significant difference in pre- and post-fatigue for FE mean ($p=0.046$) and RUD ROM ($p=0.029$). The mean FE angle decreased indicating an increase in flexion angle post-fatigue. The RUD ROM increased significantly post-fatigue in both females and males. There was a significant difference in RUD ROM ($p=0.034$) between sexes. Females had a significantly larger RUD ROM compared to males.

CONCLUSIONS

Wrist posture changes significantly after fatigue during an everyday task for both wrist flexion-extension and radial-ulnar deviation. The changes detected post-fatigue were in the range of 5-10 degrees different for the mean angle measurement and 5-20 degrees for the ROM measurement. This information has potential applications in an ergonomic setting. To determine if wrist kinematic changes due to fatigue occur in the workplace, ongoing work in our laboratory is developing a wearable unobtrusive wrist device that could detect kinematic alterations without the need for motion capture or inertial measurement units. Ultimately, information determined from the current study coupled with an instrumented wrist device could help ergonomists and others improve hand-arm workplace risk evaluation by removing the ambiguity associated with common ergonomic risk assessment tools.

An interesting outcome of this study was that females had a larger RUD ROM than males. This result should be taken with caution due to the low number of subjects and subsequent low power to detect differences due to sex. However, tracking sex differences in biomechanical variables such as kinematics is a variable that has not previously been explored with respect to understanding the etiology of carpal tunnel syndrome. Though preliminary, results from the current work suggest that further work is needed.

REFERENCES

1. Fung et al. *Hand Surg.* **12**, 2007.
2. Murgia et al. *Clin. Biomech.* **19**, 2004.
3. Emge et al. *Neurosci. Lett.* **550**, 2013.

PATHOLOGICAL KNEE JOINT CONDITION IN CHILDREN WITH CEREBRAL PALSY IS ASSOCIATED WITH THE ACTIVE STATE MUSCULAR MECHANICS RATHER THAN PASSIVE

[1] Cemre Su Kaya, [2] Fuat Bilgili, [2,3] N. Ekin Akalan, [2] Yener Temelli, [1,4] Filiz Ates * and [1] Can A. Yucesoy

[1] Institute of Biomedical Engineering, Boğaziçi University, Istanbul, Turkey
[2] Istanbul School of Medicine, Department of Orthopaedics and Traumatology, Istanbul University, Turkey
[3] Department of Physiotherapy and Rehabilitation, Istanbul Kültür University, Turkey
[4] Mayo Clinic, Rochester, MN, USA, * presenting author
email: su.kaya@boun.edu.tr, ates.filiz@gmail.com; web: https://bme.boun.edu.tr/biomechanics-laboratory

INTRODUCTION

In individuals with cerebral palsy (CP), the knee joint is kept typically in a flexed position. Although the mechanism of the related pathological resistance against knee extension is unknown, this is ascribed to passive and active properties of spastic muscles. Yet, spastic muscle's passive forces at various joint angles have not been assessed. Hence, its contribution to the pathological condition cannot be judged objectively. Besides, intraoperative tests in which active state forces of spastic muscles were measured directly at the tendon indicate that spastic knee flexors produce only low forces in flexed knee positions [e.g., 1]. However, if co-activated with an antagonist, spastic Gracilis (GRA) muscle's overall mechanical characteristics change, with the peak force shifting to flexed knee positions hence resulting in a narrowed operational joint range of force exertion [2]. This was ascribed to epimuscular myofascial force transmission (EMFT) [e.g., 3] between activated muscles, which can be relevant for the unknown mechanism of the pathology. Additionally, as, unlike gait analyses, direct spastic muscle force measurements are very rare, the present literature remains insufficient to show the relationship between muscle's mechanical characteristics and the patient's gait.

The aim was to fill these gaps by combining intraoperative experiments with gait analyses and to test the following hypotheses: (i) spastic GRA shows high amplitudes of passive forces even in the flexed knee positions, (ii) active forces of spastic GRA are high, particularly within the gait relevant knee angle range, and (iii) this becomes more pronounced due to EMFT.

METHODS

Seven children with CP (mean age (SD)=9.1 (2.9) years; GMFCS scores level II) participated.

Pre-surgery gait analyses were performed using a motion analysis system (ELITE 2002, BTS Bioengineering, Milan, Italy) with six infrared cameras and two force plates (Kistler Instumente AG, Winterthur, Switzerland). Hip and knee joint angles and moments in the sagittal plane were used to relate the global gait metrics to intraoperative spastic muscle level mechanics.

Intraoperatively 10 limbs were tested. Isometric GRA forces (F_{GRA}) were measured per knee angle (KA) in four conditions: (I) passive state, after spastic GRA was stimulated (II) alone, (III) simultaneously with its synergists semitendinosus and biceps femoris, and (IV) also with its antagonist rectus femoris. Hip angle (HA) was set to 45° and 20°, and KA was changed from 120° to full extension (0°).

Two-way ANOVA (factors: KA and condition) and paired-t or Wilcoxon signed-rank test were used to test the effects of studied conditions on overall mechanical characteristics and Range-F_{GRA} (KA range between 120° and peak force exertion) ($P<0.05$).

RESULTS AND DISCUSSION

Passive and active state forces are shown in (Fig. 1).

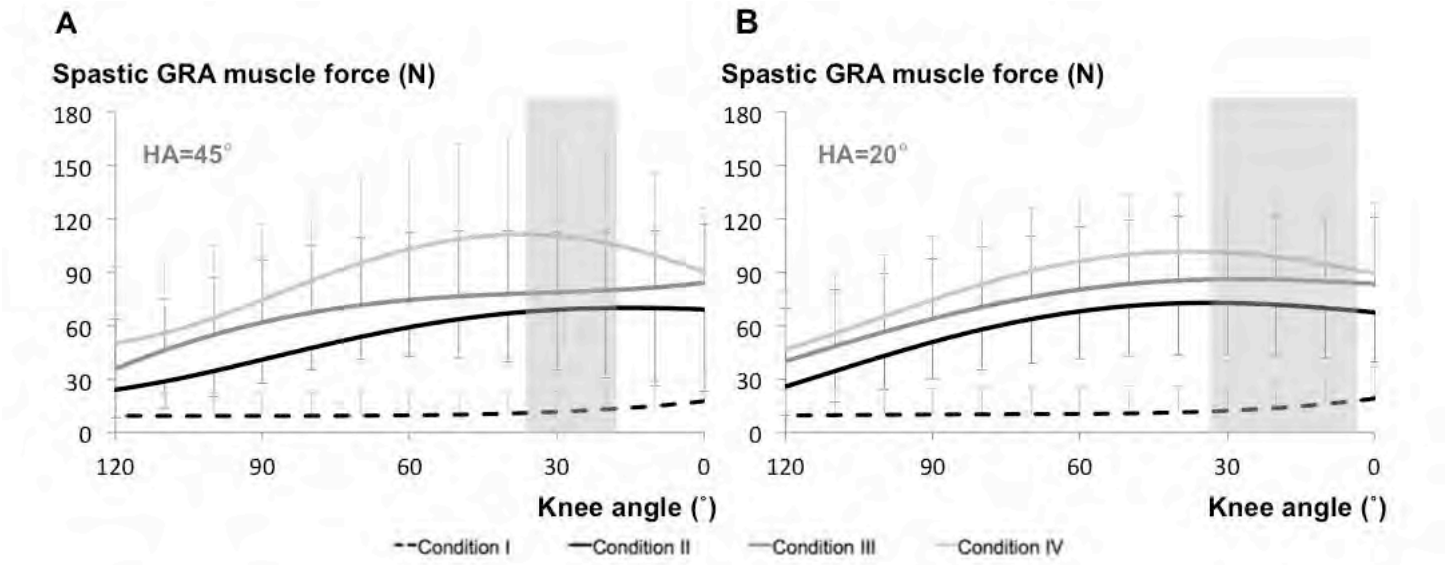

Figure 1: The mean of GRA forces of intraoperatively tested limbs per KA across the conditions tested at HA=45° and HA=20°. The gray shaded areas show the gait relevant KA-positions.

Passive force is low in flexed positions and increases towards knee extension. However, its peak value is only a small fraction of the peak total force (26%) measured in the active state.

ANOVA showed significant main effects of both factors on F_{GRA}, but no significant interaction. Compared to condition II, co-activation of other muscles caused F_{GRA} to increase substantially (on average, for HA=45° and 20°, by 32.8% and 71.9%, and 24.5% and 45.1% in conditions III and IV, respectively). Considering the muscle's overall mechanical characteristics in conditions III and IV, EMFT did cause major increases in spastic GRA forces. However, compared to condition II, no significant change in Range-F_{GRA} was shown in any co-activation condition.

Gait analyses indicated that intraoperative data for KA=36°-18° and KA=33°-3° (for HA=45° and 20°, respectively) are particularly relevant, where F_{GRA} in active state approximates its peak value. The elevated forces shown in conditions III and IV for gait relevant KA-ranges characterize an elevated contribution of the muscle to knee flexor moment during the patients' gait. Hence, the findings reflect an increasing effect on spastic muscle's mechanics of different components of EMFT. Since daily activities involve simultaneous activation of several muscles, such EMFT effects potentially have important implications for the poorly understood pathological joint condition in CP and its treatment.

CONCLUSIONS

The first hypothesis is rejected, while the second and the third are confirmed. Spastic muscle's passive forces measured directly for the first time in patients with CP do not show high amplitudes even in extended knee positions. In contrast, in the active state, the muscle's forces within the gait relevant KA-range are high. This gets much more pronounced due to EMFT. Therefore, the pathological knee joint condition can be ascribed to the active, rather than the passive state mechanics of spastic muscles effects of which, do elevate due to intermuscular mechanical interactions.

REFERENCES

1. Ates et al., *Clin Biomech*. **28**:48-54, 2013.
2. Ates et al., *Clin Biomech*. **29**:943-949, 2014.
3. Yucesoy, *Exerc Sport Sci Rev*. **38**:128-134, 2010.

ACKNOWLEDGEMENTS

TÜBİTAK Grant 113S293 to Can A. Yucesoy.

HOW DOES ACHILLES TENDON TWISTING INFLUENCE STRAIN AND ENERGY STORAGE?

[1] Katherine R. Knaus and [1] Silvia S. Blemker

[1] University of Virginia, Charlottesville, VA, USA
email: ker4e@virginia.edu, web: http:// bme.virginia.edu/muscle/

INTRODUCTION

The Achilles tendon (AT) transmits force from the triceps surae muscles during walking and other motion. It comprises three subtendons that originate from each muscle, twist around each other, then insert into the calcaneus. A recent investigation in 53 human cadavers sought to characterize the architecture of these subtendons and their variation between subjects [1]. The authors characterized the variation in torsion of the subtendons within the free AT, dividing subjects among three groups with Type 1 as the least twisted, Type 2 as moderately twisted, and Type 3 as extremely twisted. They also measured the torsion of the fibers within individual subtendons, which varied between the soleus (SOL) and the medial (MG) and lateral (LG) heads of the gastrocnemius, and tended to be greater than the twist of the subtendons about each other.

Sliding between subtendons is thought to explain non-uniform deformations of the Achilles observed with ultrasound during walking [2]. Measured differential displacements provide exciting insight into complex loading patterns by the triceps surae. However, conclusions about muscle-tendon behavior drawn from this imaging technique are dependent on several assumptions. Tissue displacements are tracked in a small 2D sagittal plane region of interest in the free AT, and while individual subtendons are not visually discernable, deep tissue is associated with the SOL and superficial tissue with the MG. Subjects exhibit varied amounts of AT torsion, though it is unknown if subtendons visible in the superficial and deep portions of the sagittal plane vary with twist type. In addition, tendon elongation is assumed to be longitudinal and estimated from in-plane displacements; however, this may misinterpret *in vivo* tendon strains due to out-of-plane stretch.

Ultrasound imaging combined with traditional force and motion capture can be used to quantify *in vivo* tendon dynamics, with displacement measurements of the free AT providing a more direct approach for approximating energy stored during walking [3]. These estimates are subject to assumptions about the force in the different subtendons as well as their strain, which may be altered by varied torsion.

The goal of this work is to understand how lengths of subtendon fibers with varied twist compare to free AT lengths. Using finite element models (FEM), we aim to decouple the influence of twisting architecture from other complexities of AT and triceps surae dynamics to assess how this anatomical feature and its variance may influence *in vivo* estimates of tendon stretch and energy storage.

METHODS

Three generic AT FEMs, representing the region of tendon from the calcaneus' superior border to SOL musculo-tendinous junction, were constructed with elliptical cross sections using average lengths and widths [1]. Models were divided into were divided into three parts to represent the subtendon architecture of each twist type. In order to focus on the effect of varied twist, the three models were identical in volume and subtendon proportions with amount of twist as the only distinguishing feature.

Tendon was modeled as transversely isotropic material with fiber direction vectors defined using Laplacian flow simulations [4]. Flow guides were used to match subtendon fiber torsion angles to twist types [1]. Flow results were used to determine subtendon fiber lengths.

Simulations of simplified walking conditions were defined to match deep and superficial measurements by prescribing either displacements [2] or forces [3] as boundary conditions to the proximal end. This end was constrained to only move proximal-distally. Frictionless contact was assigned to allow sliding between subtendons.

Subtendon along fiber strains were compared to longitudinal elongations estimated from proximal end displacements and the starting free tendon length. Subtendon strain energies were compared to stored energy estimated from integrals of force at the proximal end and length changes determined from displacements.

RESULTS AND DISCUSSION

Fiber lengths of all subtendons in each type were longer than the length of the AT. Fibers in the Type 1 model were the shortest while fibers in the Type 3 model were the longest. Fibers in the GM subtendon were shortest and the SOL subtendon were longest.

Along fiber strains were lower than estimated elongation in all subtendons, with Type 1 being the most similar (0.5% error) and Type 3 being the least (10% error) [Fig 1]. Subtendon strain energies were lower than estimated stored energy in the LG and MG and higher in the SOL, with Type 1 being the most similar in total energy stored (5% error) and Type 3 being the least (15% error) [Fig 1].

Larger amounts of twist lead to overestimation of tendon strain and energy storage. Twisting of subtendons created longer fiber lengths for the same give AT length and therefore more out-of-plane alignment. Interestingly, greater twist also contributed to having a greater portion of the LG subtendon in the deep distal region of the sagittal mid-plane [Fig 1], which is typically assumed to be occupied by SOL subtendon. Variations in twist architecture could contribute to higher rates of injury due to greater strains resulting from similar loading patterns.

CONCLUSIONS

While errors are not large enough to discount estimates of tendon dynamics made from sagittal plane ultrasound images, it does illuminate the necessity for considering architectural variation. This work demonstrates the utility of using 3D models to determine possible errors associated with 2D measurements. Models also provide the means to better calculate quantities that cannot be measured readily *in vivo*, like tendon strain energy, from those that can be measured, such as tendon length changes.

REFERENCES

1. Pekala et al. *Scand J Med Sports,* 27:1705-15,2017.
2. Zelik and Franz. *Plos One*. 12(7): e0179976, 2017.
3. Franz et al. *Gait & Posture,* 41:192-197, 2015.
4. Handsfield et al. Biomch Model Mechanobio 2017.

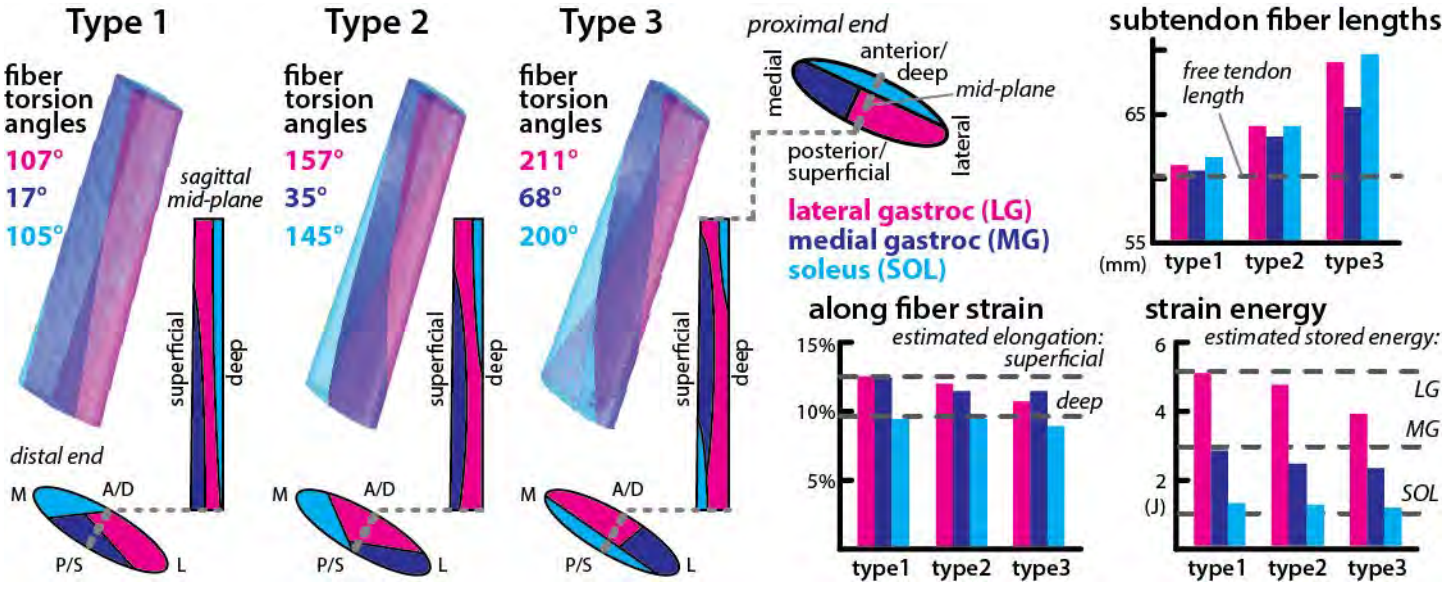

Figure 1: FEM of each type with increasing subtendon twist. The proximal end cross section was the same for all models and subtendon boundaries were lofted to varying distal end cross sections. Fiber directions were guided to match given torsion angles and subtendon fiber lengths were compared to free tendon length. Along fiber strains and strain energy were compared to elongation and energy estimated from displacements and forces.

POST-OPERATIVE FUNCTION AND MUSCLE MODULES DURING GAIT AT 6 AND 24 MONTHS FOLLOWING TOTAL KNEE ARTHROPLASTY

[1]Rebekah R. Koehn, [1,2]Sarah A. Roelker, [1]Elizabeth M. Leszcz, [1]Rachel K. Baker, [1,3]Elena J. Caruthers, [1,4]Jacqueline M. Lewis, [1,5]Gregory M. Freisinger, [1]Laura C. Schmitt, [1]Ajit M.W. Chaudhari, [1]Robert A. Siston

[1]The Ohio State University, Columbus, OH, USA; [2]The University of Texas at Austin, Austin, TX, USA; [3]Otterbein University, Westerville, OH, USA; [4]ARCCA, Inc. Penns Park, PA, USA; [5]United States Military Academy, West Point, NY, USA

email: koehn.19@osu.edu; web: https://nmbl.engineering.osu.edu/

INTRODUCTION

The theory of muscle modules (or synergies) suggests that groups of muscles are activated synergistically via a common neural command [1]. While this idea has provided insight into the control of simple tasks like locomotion [2], the clinical relevance of this theory has only recently begun to be explored. For example, patients with higher function at one year following a cruciate-retaining (CR) total knee arthroplasty (TKA) displayed a higher number of muscle modules (n=4-5) compared to patients with lower function (n=2-3) [3]. This relationship between number of modules and function suggests that if muscle modules are able to change over time, it may be possible to develop module-focused clinical programs to improve patient function.

The aim of this study was to determine muscle modules in patients with TKA during gait at 6 & 24 months post-operatively and to compare these modules to patient function. We hypothesized that (i) participants with a higher number of modules would demonstrate higher function and (ii) changes in patient function would be accompanied by changes in the number and characteristics of muscle modules.

METHODS

Fifteen participants (M/F 5/10; 60.3±6.8 y; 97.9 ±23.3 kg; 1.7±0.1 m) provided written informed consent prior to undergoing posterior-stabilizing TKA (Zimmer NexGen LPS Flex Knee) and were tested at 6 & 24 months post-operatively. Each participant performed 5 over-ground walking trials at self-selected speed. We collected passive motion capture data [4] at 150 Hz (10 Vicon MX-F40 cameras; Oxford, UK) and ground reaction force data at 1500 Hz (6 Bertec 4060-10 plates; Columbus, OH). We collected surface electromyography (EMG) data from the rectus femoris (RF), vastus medialis and lateralis (VM, VL), semitendinosis (ST), biceps femoris (BF), medial and lateral gastrocnemii (MG, LG), and soleus (SO) on the TKA-involved limb at 1500 Hz (Noraxon Telemyo DTS System; Scottsdale, AZ). To create linear envelopes for the EMG data , we used a 10-300 Hz 6th order bandpass Butterworth filter, rectified the data, smoothed the signals with a 6 Hz 6th order low-pass Butterworth filter, and normalized the signals to the maximum activations within each respective gait cycle.

For each trial, we used non-negative matrix factorization (NMF) to define muscle modules from the original EMG activations. Each module consisted of a principal activation pattern and weighting factors for the muscles within the module [5]. The product of the principal patterns and weights reconstructed individual muscle activation patterns. In order to ensure these reconstructions represented the original EMG, we calculated the variability accounted for (VAF) by the reconstructed signals and iteratively increased the number of modules from 1 to 8 in separate NMF calculations until the following criteria were satisfied: VAF > 0.9 for all muscles or VAF > 0.8 for all muscles and the addition of another module did not raise the minimum VAF by more than 5% [6].

To compare principal patterns and muscle weights between subjects and time points, we also performed NMF calculations the number of modules equal to the average for all gait trials. The principal pattern of each module was normalized to its peak and the weighting factors were normalized to the maximum within the module. We averaged the principal

patterns and weighting factors over the 5 walking trials to create ensemble averages for each participant at both 6 & 24 months. We used Wilcoxon signed-rank tests to compare muscle weights between 6 & 24 months in each of the modules and Spearman Rho tests to examine correlation in muscle weights in these modules (α=0.05).

We recorded the distance walked by each participant during a six-minute test (6MW) [7] and classified each participant as high- and low- functioning using a regression from Enright et al. that accounts for height, weight, and age [8]. We used paired t-tests to identify differences in 6MW performance at 6 & 24 months (α=0.05).

RESULTS AND DISCUSSION

The number of modules was consistent across time points and functional groups. At 6 months, 4 participants were high-functioning and had 2.5±0.4 modules (n=2, 2 modules; n=2, 3 modules), while 11 were low-functioning and had 2.7±0.6 modules (n=4, 2 modules; n=6, 3 modules; n=1, 4 modules). At 24 months, 6 participants were high-functioning and had 2.9±0.4 modules (n=2, 2 modules; n=4, 3 modules), while 9 participants were low-functioning and had 3.0±0.3 modules (n=2, 2 modules; n=8, 3 modules; n=1, 4 modules). We rounded the average number of modules in each group to 3.

Despite there being no significant change in 6MW tests between 6 & 24 months (p=0.902, 476.4±76.5m vs. 477.9±98.6 m), there were some differences in the modules of individual patients. There was a slight increase in the number of modules for 5 participants and a decrease for 2 participants. After performing the NMF calculations for each gait trial with the number of modules fixed at the average (n=3), each participant demonstrated modules at both 6 & 24 months in which the quadriceps (Q), hamstrings (H), and plantarflexors (PF) were primarily expressed (Fig. 1). However, the weights were related between 6 & 24 months for only 5 module-muscle pairs: the VM (ρ=0.779; p=0.001), BF (ρ=0.581; p=0.023), and LG (ρ=0.561; p=0.030) in the Q module and the VM (ρ=0.521; p=0.046) and LG (ρ=0.732; p=0.002) in the H module. Initial analysis indicated phase shifts in the three principal patterns between 6 & 24 months in individual participants. Such changes in timing and muscle weights contrast Shuman et al. who found greater consistency across modules between days in younger populations with and without cerebral palsy [9].

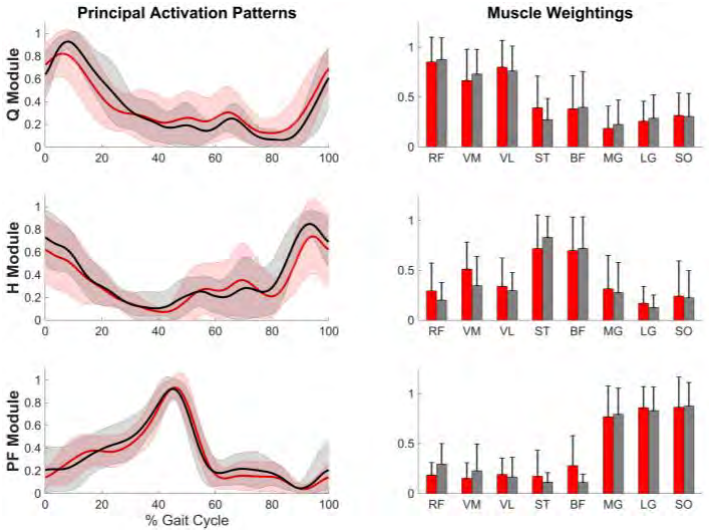

Figure 1. Average 6 month (red) & 24 month (gray) post-TKA principal patterns and muscle weights ± 1 standard deviation.

CONCLUSIONS

Our results did not indicate a relationship between function and either the number or characteristics of muscles modules. As part of a larger study, we have observed greater improvements in function between the pre- and post- TKA conditions. Additional investigation will examine the relationship between modular control and function pre-operatively as well as changes in modular control before and after TKA.

ACKNOWLEDGEMENTS

This project was supported by Grant Number R01 AR056700 from the National Institute of Arthritis and Musculoskeletal and Skin Diseases and an Ohio State University fellowship (RRK).

REFERENCES

1. Lee. *J Motor Behavior*. **16**(2): 135-70, 1984.
2. Ivanenko et al. *J Physiol*. **556**(1): 267-82, 2004.
3. Ardestani et al. *J Electromyogr Kines*. **37**: 90-100, 2017.
4. Andriacchi et al. *J Biomech Eng*. **120**:743-9, 1998.
5. Lee & Seung. *Nature*. **401**: 788-91, 1999.
6. Clark et al. *J Neurophysiol*. **103**(2): 844-57, 2010.
7. "ATS Statement." *Am J Respir Crit Care Med*. **166**(1): 111-7.
8. Enright et al. *Am J Respir Crit Care Med*. **158**:1384-7,1998.
9. Shuman et al. *Gait & Posture*. **45**: 127-32, 2016.

POST-STROKE WALKING MECHANICS USING A SPEED-ADAPTIVE MYOELECTRIC EXOSKELETON CONTROLLER

[1] Emily M. McCain, [1]Tracy N. Giest, [1]Katherine R. Saul, [2]Taylor J.M. Dick and [3]Gregory S. Sawicki

[1] North Carolina State University, Raleigh, NC, USA
[2] University of Queensland, St Lucia, QLD, Australia
[3] Georgia Institute of Technology, Atlanta, Georgia, USA
email: emmccain@ncsu.edu

INTRODUCTION

Reduced ankle function in post-stroke individuals limits the propulsive 'push-off' power of the paretic limb, resulting in asymmetric gait, reduced walking speed and higher metabolic cost [1]. Powered exoskeletons (exos) offer a promising opportunity to restore mechanical deficits by applying torque at the paretic ankle during the propulsive phase of gait. Previously, a proportional myoelectric ankle exo was shown to increase the paretic plantarflexion moment for stroke survivors walking at 75% of their comfortable overground speed [2]. Despite these improvements, the exos did not reduce the metabolic cost of walking. Researchers suggested exo performance could be limited because the walking speed was restricted to a pace at which exo assistance was not needed. In order to assess the impact of exo assistance on walking speed in stroke populations, we developed a novel, speed-adaptive exo controller [3]. This research extends previous work by: (i) exploring the efficacy of a myoelectric exo controller that automatically modulates the magnitude of propulsive assistance with changes in walking speed for post-stroke populations and (ii) assessing the ability of the controller to improve net average mechanical power output at the paretic ankle, knee and hip joints.

METHODS

We implemented a speed-adaptive controller designed to mitigate specific limitations of prior myoelectric controllers by including two independent adaptive gains: (1) a gain to map user's soleus muscle activity to peak exo torque (Koller) and (2) a gain to map peak exo torque capacity to walking speed (Giest) [3,4]. The speed-dependent gain ensures the exo outputs ~25% of the maximum normal biological ankle plantarflexion moment at the instantaneous treadmill velocity. The desired exo torque profile was applied by a benchtop motor (Baldor Electric Co) to the carbon-fiber ankle exo through a Bowden-cable transmission system.

Experimental data were collected from six stroke survivors (3 male, 3 female) walking on an instrumented split belt treadmill with and without an exo on their paretic limb. Subjects started by walking at 60% of their preferred speed (n00). At each consecutive minute, the treadmill speed was increased by 0.1 m/s (n01, n02, etc) until the subject's heart rate reached 60% of their heart rate reserve. Kinematic and kinetic data were processed in Visual3D (CMotion, USA) and MATLAB (Mathworks, USA) to determine joint angles and angular velocities. Inverse dynamics was used to calculate joint moments and powers at the ankle, knee, and hip. Average joint powers were calculated at the ankle, knee and hip for five strides [5]. Indirect calorimetry was used to determine metabolic cost during walking (OxyCon Mobile, Carefusion, USA). Statistical significance of peak average ankle power, and net average ankle, knee and hip powers were determined using paired t-tests (α=0.05).

RESULTS AND DISCUSSION

The speed-adaptive controller successfully amplified exo assistance as walking speed was increased, verifying efficacy of the speed-adaptive gain (Figure 1c). Subject averages for maximum paretic ankle power were significantly higher for the exo compared to the no exo condition at all speeds (Figure 1a and 1b) (paired t-test; p=0.04). Since subjects walked until reaching a specific heartrate, statistical power was reduced at high speeds for which the sample size was small (n<4 for n05-n07).

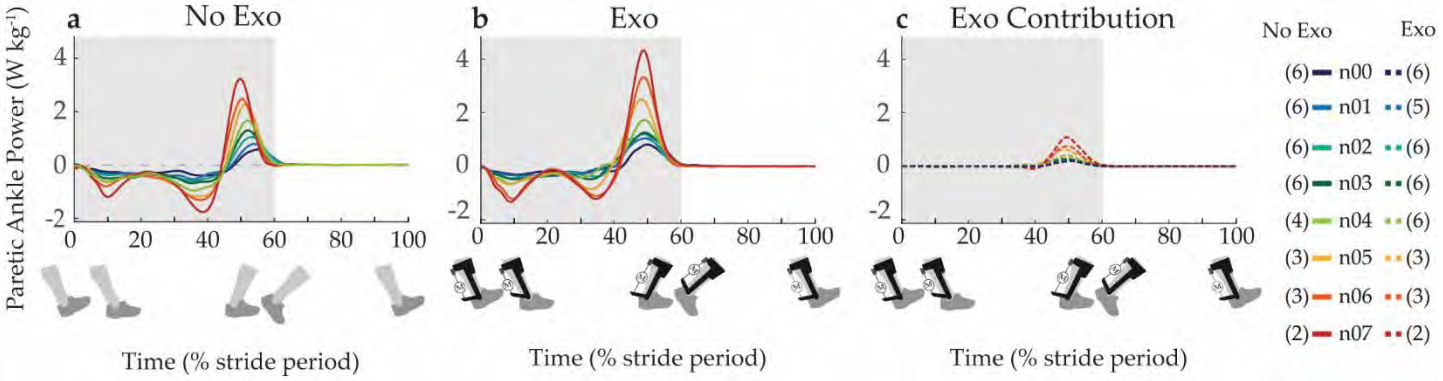

Figure 1.a Paretic ankle power in the no exo condition and **1.b** the exo condition with the **1.c** exo contribution isolated. The number of subjects is indicated in parenthesis. The shaded area represents the stance phase of gait.

Net average paretic ankle power was increased for all speeds while wearing the exo, demonstrating improved delivery of net energy at the ankle (paired t-tests; $p<0.05$ for n00-n04) (Figure 2).

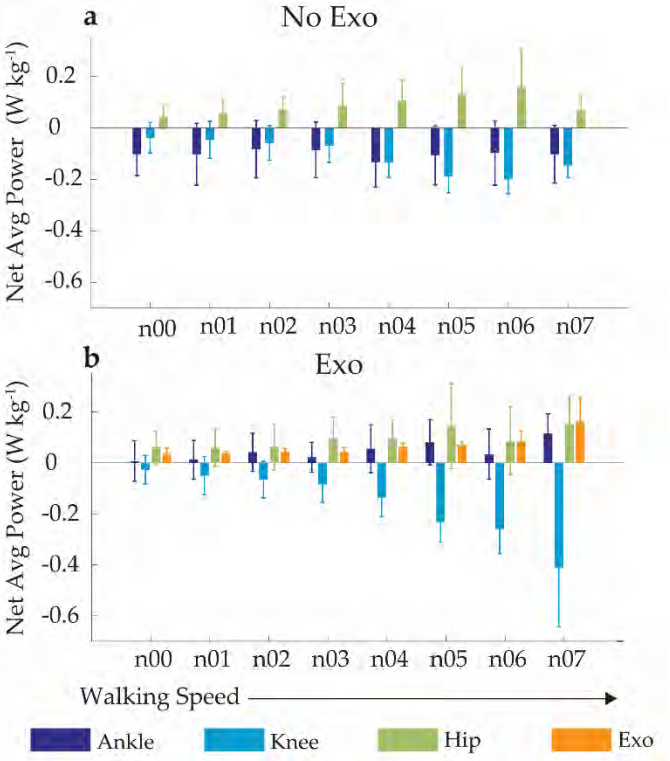

Figure 2.a Net average power averaged across subjects for the no exo and **2.b** exo conditions.

Despite these increases in net average ankle power, only two of the subjects experienced a decrease in metabolic cost while wearing the exo compared to the no exo condition, and no statistically significant change was found. One possible explanation is that assistance applied at the ankle may be absorbed by more proximal joints. This explanation is supported by the decrease in net average power seen at the knee in the exo compared to no exo condition (paired t-tests; $p<0.05$ for n00 and n02) (Figure 2).

CONCLUSIONS

Our speed-adaptive controller successfully increased exo assistance with changes in walking speed for post-stroke individuals. The exo assistance resulted in higher net average power at the paretic ankle. Though we found no significant change in metabolic cost, our exo controller demonstrates the potential of assistive devices to restore paretic limb propulsive power. Future work will examine the interaction between exo assistance, walking speed, distance travelled and gait symmetry between paretic and non-paretic limbs.

REFERENCES

1. Peterson, CL et al. *J Biomech*. 2010; 43:2348–55.
2. Takahashi, KZ et al. *J NeuroEng Rehab*.2015;12:23
3. Giest, TG et al. *ASB Abstract*, 2016.
4. Koller, JR et al. *J NeuroEng Rehab* 2015; 12:97.
5. Farris, DG et al. *J NeuroEng Rehab* 2015; 12:24.

ACKNOWLEDGEMENTS

We would like to acknowledge Dr. RW Nuckols for his assistance developing and implementing the controller. Funded by the National Institutes of Health, National Institute for Child Health and Human Development. NIH grant R21 HD072588-01A1 to GSS.

EVALUATING THE POSTURAL ERGONOMICS OF OPHTHALMOLOGISTS USING KINEMATIC MOTION ANALYSIS AND ELECTROMYOGRAPHY

[1] Safeer F. Siddicky, [2] Scott E. Olitsky and [1] Gregory W. King

[1] University of Missouri-Kansas City, Kansas City, MO, USA
[2] Children's Mercy Kansas City, Kansas City, MO, USA
Email: safeer.siddicky@umkc.edu

INTRODUCTION

Ophthalmologists often maintain static postures of the neck, shoulder, elbow and wrist during their routine clinical examinations, which may lead to work-related musculoskeletal diseases (MSDs) [1] and a decreased capacity for healthcare delivery. Ophthalmologists' posture, ergonomics and occupational discomfort are currently evaluated qualitatively using survey methods, such as the Visual Analog Scale (VAS) pain level reporting [2] or quantitatively using electromyography [3].

A combination of marker-based motion capture and electromyography may provide an objective, quantitative methodology to examine posture and suggest postural adjustments that will reduce the risk of developing MSDs. This study used motion analysis and electromyography to evaluate ophthalmologists' posture during routine exams and with alterations to exam setup.

METHODS

Ten pediatric ophthalmologists (5 male, 5 female, aged 40 ± 9.52 years old) performed retinoscopy, refraction and simulated retina exams using a slit lamp biomicroscope and a 90D lens on a child CPR manikin. Postural kinematics was tracked using 14 Optitrack Flex 13 cameras, with participants donning a conventional 27-marker upper body marker set [4]. Neck and shoulder muscle activity was recorded using Delsys Trigno surface electromyography electrodes placed bilaterally on the upper trapezius and anterior deltoid muscles.

Retinoscopy and refraction examinations were performed as is, and under a postural alteration which involved reclining the manikin to simulate patient viewing a raised eyechart. Non-neutral neck flexion (percentage of procedure time that neck flexion was outside 3 S.D. of upright neck posture) was compared among the postural alterations.

Slit lamp examinations were performed under 3 conditions: no postural adjustments, postural adjustment by altering slit lamp platform height and patient position, and postural adjustment with an elbow rest under arm holding the 90D lens. Sagittal plane neck flexion angle, upper trapezius muscle activation area and the percentage of procedure time that the anterior deltoid was active were compared among these 3 conditions for all ophthalmologists.

Neck flexion angles were calculated using the head and shoulder marker data and a Cardan rotation sequence. EMG data was rationalized using baseline data taken from upright static sitting. Muscle activation area was calculated as the area under the rectified EMG profiles. Paired t-tests were used for all comparisons (presented as mean ± 1 SEM).

RESULTS AND DISCUSSION

For the retinoscopy and refraction examinations, percentage of procedural time with non-neutral neck flexion decreased after reclining the manikin for loose lens retinoscopy (81.39 ± 2.57% vs. 69.45 ± 3.91%, $p = 0.038$*), lens bar retinoscopy (81.29 ± 1.83% vs. 70.62 ± 5.29%, $p = 0.095$), loose prism refraction (66.54 ± 3.80% vs. 64.47 ± 3.93%, $p = 0.741$) and prism bar refraction (74.57 ± 1.38% vs. 60.94 ± 7.54%, $p = 0.203$). These results are displayed in Fig. 1.

For the slit lamp examination, sagittal plane neck flexion angle range of motion decreased significantly after postural adjustment (41.4±3.3° vs. 36.4±2.8°, $p = 0.023$*) and elbow rest placement (41.4±3.3° vs. 35.8±2.8°, $p = 0.025$*). Upper Trapezius muscle

activity (procedural activation area) decreased after postural adjustment (106.1±52.9mV vs. 88.3±46.0mV, p = 0.137) and elbow rest placement (106.1±52.9mV vs. 87.6±45.0mV, p =0.186). Percentage of procedural time that the anterior deltoid was active decreased slightly after postural adjustment (38.8±3.7% vs. 37.43±4.3%, p = 0.756) and decreased significantly after elbow rest placement (38.8±3.7% vs. 31.37±3.9%, p = 0.037). These results are displayed in Fig. 2.

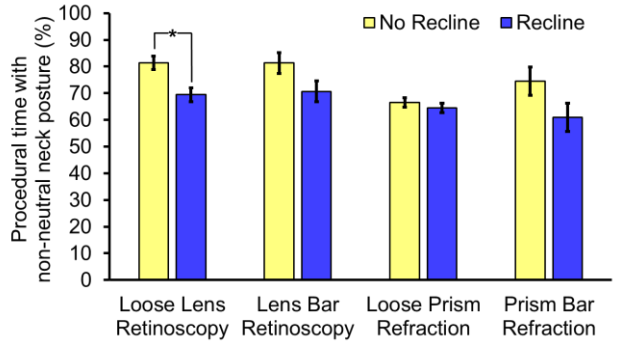

Figure 1: Percentage of procedural time with non-neutral neck flexion (no patient recline vs. recline).

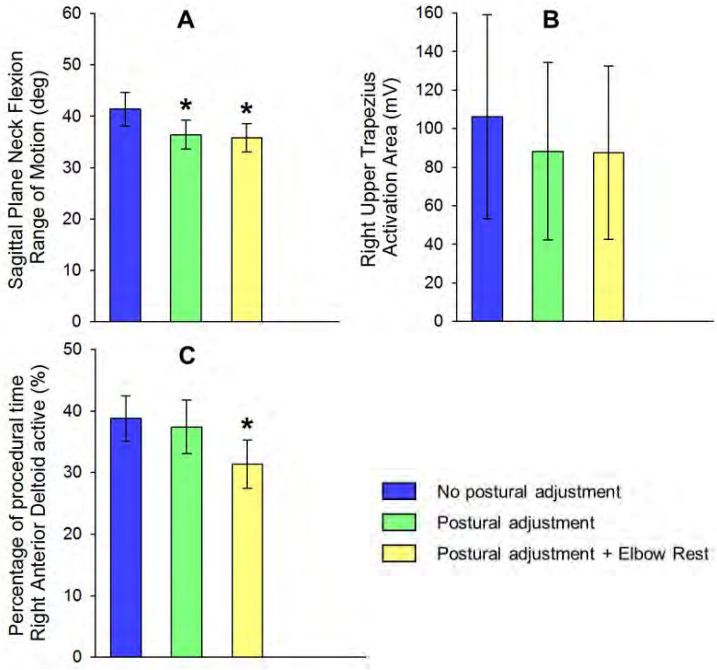

Figure 2: Sagittal plane neck flexion range of motion **(A)**, Activation area of the Right Upper Trapezius **(B)**, Percentage of procedural time that the Right Anterior Deltoid was active **(C)**.

The observed reduction in the percentage of procedural time with non-neutral neck flexion in the retinoscopy and refraction exams and the observed reduction in neck flexion and upper trapezius activity after postural adjustments in the slit lamp examination may indicate lower exposure to sustained non-neutral neck postures that can cause MSDs. The decrease in anterior deltoid activation after installing an elbow rest in the slit lamp examination may also indicate a practice that could lead to reduced stress related to prolonged, unsupported arm raise.

CONCLUSIONS

Easily implemented postural adjustments may decrease the possibility of occupational MSDs by reducing time spent by ophthalmologists in un-ergonomic postures. Preliminary analyses from this and future studies may help establish a quantitative standard for ergonomic postures in ophthalmic practice, lead to a wide scale re-design of ophthalmic equipment, and facilitate the development of postural ergonomics-focused training curriculums for current and future ophthalmologists.

This study only focuses on pediatric ophthalmologists, wherein a generalization of the procedural postural characteristics observed may not necessarily be accurate when applied to all practicing ophthalmologists. Future studies will include a wider subset of ophthalmologists as participants, leading to a more generalizable study and a larger sample size.

REFERENCES

1. NIOSH, NIOSH Publication 97-141, 2, 1997.
2. Kitzmann et. al., J Ophthalmol, 119(2): 213–20, 2012.
3. Fethke et.al., Int J Ind Ergon, 49: 53-59, 2015.
4. Leardini et. al. Clin. Biomech. 26, 562-71, 2011.

ACKNOWLEDGEMENTS

The authors would like to thank Children's Mercy Kansas City for the use of their pediatric ophthalmology clinic for testing, and the UMKC Center for Health Insights for the use of their Optitrack Flex 13 motion capture system.

IN VIVO RELATIONSHIP BETWEEN JOINT STIFFNESS, JOINT-BASED ESTIMATES OF MUSCLE STIFFNESS, AND SHEAR WAVE VELOCITY

[1] Andrew D. Vigotsky, [2] Elliott J. Rouse, and [1] Sabrina S.M. Lee

[1] Northwestern University, Evanston, IL, USA
[2] University of Michigan, Ann Arbor, MI, USA
email: vigotsky@u.northwestern.edu

INTRODUCTION

The underlying properties governing human joint mechanics, such as stiffness, are constantly regulated for effective, safe, and efficient interactions with the external environment. Joint stiffness (k_{joint}) is, in part, determined by the properties of the muscles surrounding the joint. The muscle-joint relationship can be thought of hierarchically, since there exists a lower level, muscle, and a higher level, joint. In light of this hierarchy, investigators often assess joint properties to make inferences about muscle-level changes. However, such approaches lack the specificity needed to understand the role of individual muscles.

Shear wave ultrasound elastography—which measures the velocity at which shear waves travel through tissue—has been increasingly used to assess the mechanical properties of muscle [2]. However, how shear wave velocity (SWV), measured at the muscle level, relates to k_{joint} and muscle stiffness *in vivo* remains poorly understood [2, 3]. Therefore, the purpose of this work was to quantify the relationships between 1) SWV of individual primary plantar flexors and ankle k_{joint}, and 2) SWV and joint-based estimates of muscle stiffness (k_{muscle}) in two muscles, medial gastrocnemius (MG) and soleus (SOL).

METHODS

Ten healthy, young adults (6 females, 4 males; age = 26 ± 4 years; body mass = 69 ± 16 kg; height = 171 ± 10 cm) participated in this study, which was approved by the Northwestern University Institutional Review Board. Ankle k_{joint}, SWV_{MG}, and SWV_{SOL} were measured in two positions (knee flexed, 90°; knee extended, 0°) and at three activation levels (0%, 20%, and 40% of maximum voluntary contraction, MVC) on two separate days. The ankle was positioned at 90° for all trials. The two knee positions permitted independent investigation of the MG, a bi-articular muscle, and the SOL, a uni-articular muscle.

Joint stiffness was measured using a custom dynamometer, by recording joint moment responses to 1° perturbations, collected over 27, 10-second trials for each activation. System identification analyses were used to isolate stiffness contributions to the ankle joint's resistance to rotation [4]. This approach differs from calculating the slope of the moment-angle curve, such that the measures are not strictly a function of the net moment demands of the task and are robust to inertial and damping components [1, 5]. Shear wave velocity was measured from the MG and SOL over six isometric trials for each condition (Aixplorer SuperSonic Imagine, Aix en Provence, France).

A biomechanical model was used to estimate k_{muscle} (Fig. 1). The ankle joint was modeled as a pin joint with two springs (k_{muscle} and k_{tendon}) acting in series about its center of rotation. Literature values for moment arm were used [6, 7], and k_{tendon} was measured experimentally by tracking the MG muscle-tendon junction with B-mode ultrasound during ramp (0–60%MVC), isometric contractions.

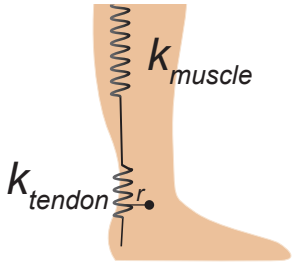

Figure 1: Biomechanical model to estimate muscle stiffness.

To understand the relationships between 1) SWV and k_{joint}, and 2) SWV and k_{muscle}, hierarchical linear statistical models were used. Trials were nested within participants, such that all relationships were within-subject.

RESULTS AND DISCUSSION

A strong, linear relationship was found between SWV_{MG}, SWV_{SOL}, and k_{joint} (R^2 = 0.96; RMSE = 14.6 N·m/rad) (Fig. 2A). SWV_{SOL} (when controlling for SWV_{MG}) had a greater slope in its relationship with k_{joint} than SWV_{MG} (when controlling for SWV_{SOL}). For example, if SWV_{SOL} and SWV_{MG} are 9 and 3 m/s, then $k_{joint} \approx 211$ N·m/rad. However, the inverse produces $k_{joint} \approx 113$ N·m/rad. Low collinearity between SWVs ($r = -0.331$) suggests that SOL and MG were independent regressors.

Shear wave velocity in both SOL and MG increased with ankle joint moment (Fig. 2B and C, R^2 = 0.88, R^2 = 0.95, respectively). The difference in slopes between flexion and extension in SWV_{MG} but not SWV_{SOL} reflect the biarticular nature of MG; SWV_{MG} increases more when it is in a kinematic position that facilitates greater force generation.

The strong relationship observed between SWV and k_{joint} is noteworthy and clinically relevant. Weak relationships between SWV and k_{joint} have been observed when assessed passively, between subjects, and using the moment-angle relationship to estimate k_{joint} [2]. However, our data suggest that *changes* in SWV are reflected on the joint level when assessed using more sophisticated measures of k_{joint} and taking into account inter-individual differences. Thus, researchers and clinicians may be able to use SWV as a guidepost for understanding joint stiffness changes with muscle-level specificity.

Surprisingly, no relationship was observed between SWV and estimates of k_{muscle} (R^2 = 0.10; RMSE = 10537.9 N/mm). Model outputs were highly sensitive to moment arm and k_{tendon} parameters. Moreover, the k_{tendon} estimates measured experimentally were likely low, as just the MG subtendon was assessed; low k_{tendon} inflates k_{muscle}. This is evidenced by non-monotonic within-subject k_{muscle} estimates over increasing activations. Future investigations may wish to model each triceps surae muscle-subtendon unit, while considering the specific properties of each, as has been done in the upper extremity [8].

CONCLUSIONS

Our results indicate that changes in muscle SWV are indicative of changes in k_{joint} in healthy, young adults, and suggest that SW ultrasound elastography may be useful for assessing the etiology of changes in k_{joint} by providing muscle-level specificity.

REFERENCES

1. Kearney, et al., *Crit. Rev. Biomed. Eng.* **18**(**1**), 55-87, 1990.
2. Jakubowski, et al., *Clin. Biomech.* **49** 48-55, 2017.
3. Eby, et al., *J. Biomech.* **46**(**14**), 2381-7, 2013.
4. Ludvig, et al., *IEEE Trans. Biomed. Eng.* **59**(**12**), 3541-9, 2012.
5. Rouse, et al., *IEEE Trans. Biomed. Eng.* **60**(**2**), 562-8, 2013.
6. Arnold, et al., *Ann. Biomed. Eng.* **38**(**2**), 269-79, 2010.
7. Hashizume, et al., *J. Biomech.* **47**(**12**), 3226-31, 2014.
8. Hu, et al., *J. Neurophysiol.* **105**(**4**), 1633-41, 2011.

ACKNOWLEDGEMENTS

This study was funded by the ASB Graduate Student Grant-In-Aid. The authors would like to thank Dr. Daniel Ludvig for his technical assistance.

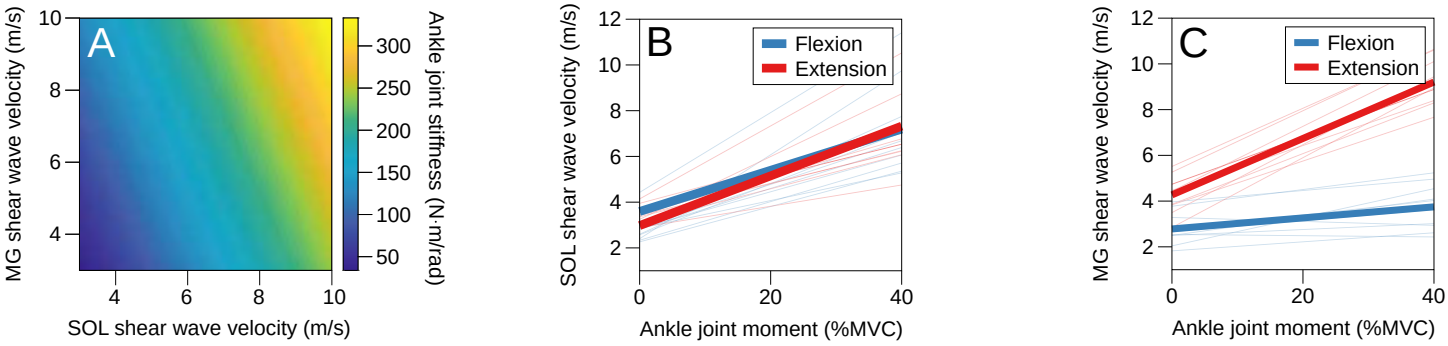

Figure 2: Relationships between shear wave velocity and joint-level measures. (A) Joint stiffness (color), soleus (SOL) shear wave velocity, and medial gastrocnemius (MG) shear wave velocity. Relative net joint moment and (B) SOL shear wave velocity and (C) MG shear wave velocity with the knee flexed (blue) and extended (red).

EFFECT OF LOCAL MUSCLE FATIGUE ON LOW-FREQUENCY COMMON INPUT TO BILATERAL AND UNILATERAL PLANTAR FLEXORS DURING QUIET STANDING

Tatsunori Watanabe[1,2] and Kotaro Saito[1]

[1]Department of Physical Therapy, Nagoya University Graduate School of Medicine, Nagoya-shi, Aichi JAPAN
[2]Japan Society for the Promotion of Science, Chiyoda-ku, Tokyo JAPAN
email: watanabe.tatsunori@h.mbox.nagoya-u.ac.jp

INTRODUCTION

Muscle fatigue is commonly defined as a reduction in the maximal force capacity of muscles, and can impair postural balance [1,2], possibly leading to injuries in not only sports but also leisure settings.

Control of posture is a complicated mechanism requiring efficient and effective muscular activation using the visual, somatosensory, and vestibular information. As the center of body's mass locates in front of the ankle joint during quiet standing, plantar flexor muscles play a primary role in maintaining balance, and many previous studies have assessed how these muscles are organized using time and frequency analyses. Mochizuki and colleagues, for example, have revealed that common input to motor units within soleus (SL) muscle as well as common input to motor units of bilateral SL muscles are stronger during standing than voluntary contraction [3]. Furthermore, recent studies have found electromyography (EMG)-EMG coherence, that quantifies common input to muscles, between bilateral homologous plantar flexor muscles and unilateral plantar flexor muscles in delta band (0-5 Hz) [4,5]. The origin of the comodulation has been suggested to be the subcortical systems [3].

Given a finding that muscle fatigue can influence the firing rate of motor units [6], this study examined whether localized muscle fatigue would affect the comodulation of bilateral and unilateral plantar flexor muscles during quiet standing, using the coherence analysis. It was hypothesized that muscle fatigue would decrease the delta-band coherences between bilateral homologous plantar flexor muscles and within unilateral plantar flexor muscles.

METHODS

Eleven healthy young male adults (mean age ± SD = 22.2 ± 0.8) participated in this study. They were asked to quietly stand on a force plate (Tec Gihan, Kyoto, Japan) with their bare feet parallel to each other for 40 seconds. The task was performed before and after fatigue protocol. The fatigue was induced by asking the subjects to raise their heels with knees extended until exhaustion.

The center of pressure (COP) was recorded from the force plate. EMG signals from bilateral medial gastrocnemius (MG) and SL muscles were also recorded using Trigno system (Delsys, MA, USA).

A customized Matlab script (Mathworks, MA, USA) was used to analyze the recorded data. We calculated SD and mean speed of COP displacement. Also, coherences between bilateral homologous plantar flexor muscles (MG-MG and SL-SL pairs) and within the unilateral muscles (MG-SL pair) for the right leg were estimated using the following equation:

$$|C_{xy}(f)|^2 = \frac{|P_{xy}(f)|^2}{P_{xx}(f) \cdot P_{yy}(f)},$$

where $P_{xx}(f)$ and $P_{yy}(f)$ are the auto-spectra of the signals x and y, and $P_{xy}(f)$ is the cross-spectra at the frequency f. They were calculated with a discrete Fourier transform of non-overlapping segments of 1024 data points. The coherence function is a number ranging from zero to one: zero indicates that two signals are completely independent, and one indicates that two signals are identical. For each analysis, 95% confidence limit was applied to identify the significant coherence.

Statistical analysis was performed with R. We compared the SD and mean speed of COP displacement between pre- and post-fatigue using a

paired t-test. In addition, we averaged z-transformed coherence over frequency ranges of 0-5 Hz (delta band). We compared the effect of fatigue on the bilateral coherence between the muscle pairs (MG-MG and SL-SL) using a two-way repeated measure analysis of variance (ANOVA). The effect of fatigue on the unilateral coherence (MG-SL) was assessed using a paired t-test. The significant level was 0.05.

RESULTS AND DISCUSSION

Results of COP parameters are presented in Figure 1. There was no significant difference in the SD of COP displacement between pre- and post-fatigue. The mean speed was greater in post- than pre-fatigue ($p = 0.0016$).

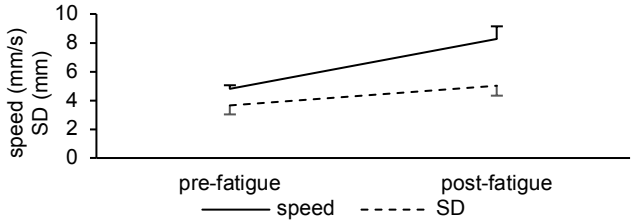

Figure 1: Effects of fatigue on COP parameters.

Pooled coherence spectra (95% confidence limit = 0.0047) and results of the z-transformed coherence are shown in Figure 2. A two-way repeated measure ANOVA on the delta-band coherence revealed a main effect of fatigue ($F_{1,10} = 11.0$, $p = 0.0078$) and interaction between fatigue and muscle pair ($F_{1,10} = 6.2$, $p = 0.032$). Post-hoc analysis showed that the delta-band coherence for the MG-MG pair was smaller in post- than pre-fatigue ($p = 0.0041$). There was no significant difference in the delta-band coherence for the SL-SL pair. Also, a paired t-test revealed that the delta-band coherence for the MG-SL pair was significantly smaller in post- than pre-fatigue ($p = 0.044$).

Consistent with a previous study [2], the speed of COP displacement was increased by the local muscle fatigue. The results regarding the coherence partly supported our hypothesis. The insignificant effect of muscle fatigue on the delta-band coherence for the SL-SL pair may be attributed to the fatigue protocol having the subjects raise their heels with knees extended. The gastrocnemius muscles might have been mainly fatigued by the protocol. The significant decrease in the delta-band coherence for the MG-MG and MG-SL pairs could be ascribed to an increase in the variability of motor unit firing rate [6]. This could have caused the comodulation less likely. Alternatively, it is also possible that a shift from ankle to hip postural control strategy has occurred after the muscle fatigue [8]. The ankle muscles could have been utilized less after the fatigue protocol.

A.

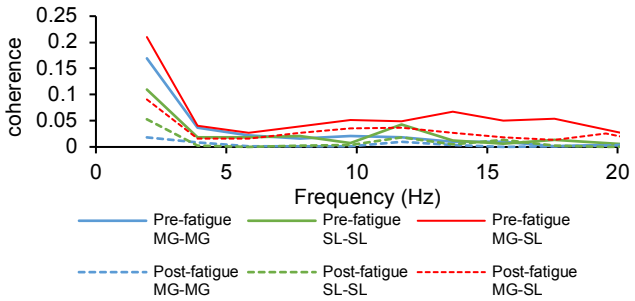

B.

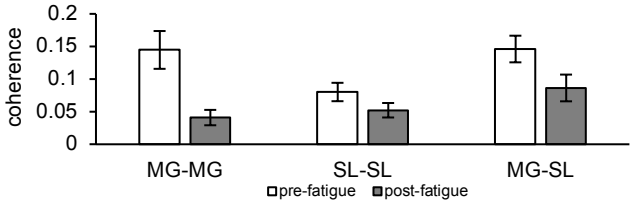

Figure 2: Pooled coherence spectrum (A) and effect of fatigue on coherence (B).

CONCLUSIONS

The local fatigue of plantar flexor muscles could decrease the low-frequency common input to these muscles. The current findings may provide guidance for developing interventions that mitigate fatigue-related problems, potentially in clinical populations.

REFERENCES

1. Nardone A, et al. *Arch Phys Med Rehab* **79**, 920-924, 1998.
2. Bisson EJ, et al. *Gait Posture* **32**, 482-286, 2010.
3. Mochizuki G, et al. *J Neurophysiol* **97**, 3917-3925, 2007.
4. Boonstra TW, et al. *J Neurophysiol* **100**, 2158-2164, 2008.
5. Obata H, et al. *Exp Bra Res* **232**, 1-11, 2014.
6. Taylor JL, et al. *Med Sci Sports Exerc* **48**, 2294-2306, 2016.
7. Grosse P, et al. *Clin Neurophysiol* **113**, 1523-1531, 2002.
8. Davidson BS, et al. *Gait Posture* **29**, 552-557, 2009.

COMPUTATIONAL MODEL OF MUSCLE INJURY VALIDATED WITH IN SITU EXPERIMENTS

[1] Amanda M. Westman, [1] Sarah Dyer, [1] J. David Remer, [1] Xiao Hu, [1] George J. Christ, [1] Silvia S. Blemker

[1] University of Virginia, Charlottesville, VA, USA
email: am5wk@virginia.edu

INTRODUCTION

Volumetric muscle loss (VML) injuries occur where there is a permanent loss of muscle function, and treatment of these injuries is challenging because the type of injuries and wound locations varies widely [1]. Regenerative medicine is a promising method for the treatment of VML injuries; however, within the literature, there is variability in the *in vivo* models used to study these injuries and the methods used to assess functional repair [2,3]. *In silico* analysis is a tool that can capture the variability of VML injuries' sizes and locations as well as simulate different experimental conditions.

In this study, we aimed to couple a finite element (FE) model with *in vivo* muscle functional analysis. The latissimus dorsi (LD) of rodents is a large flat muscle on the back that allows for a range of VML injury sizes and locations to be tested. Additionally, its complex muscle architecture of parallel and pennate fibers makes it complicated to understand the relationship between injury magnitude, location, and functional loss. Functional assessment of the LD can be tested using an *in situ* setup, which maintains the physiological conditions of the LD and captures the force of both parallel and pennate fibers. We developed a finite element model of the rat latissimus dorsi (LD) and used it as a predictive tool to focus our *in vivo* study and understand the complex biomechanics of force loss resulting from different injuries.

METHODS

The three-dimensional FE model of an intact rat LD was created based on measurements from dissected LDs of rats and was simplified to have a shape of one rectangle plus one fan [4]. The LD was modeled as a transversely isotropic, hyperelastic and quasi-incompressible material [5], and it was assigned fiber direction from the origin along the spine to the insertion at the humerus using computational fluid dynamics [6]. Boundary conditions were assigned to replicate *in situ* experimental testing conditions, and maximum muscle activation was set for all simulations. The native LD model was calibrated to fit native experimental data using a sensitivity analysis of the peak isometric stress parameter (Fig. 1C). Then an injury 11x15 mm was created at various locations within the muscle model and isometric contractions were simulated (Fig. 1A).

Experimentally, two injuries (11x15 mm) were created – the original injury and high injury – and then immediately tested using the *in situ* setup [3]. In this method, the LD muscle was minimally dissected and maintained in its native environment with blood supply and nerve innervation. A nerve cuff was placed around the motor nerve and the muscle's distal tendon was attached to the lever arm of a force transducer. The nerve was then stimulated and the peak isometric forces were measured at a range of stimulation frequencies.

RESULTS AND DISCUSSION

The isometric simulations of five different injuries demonstrated that the location of an injury has a dramatic impact on the LD's total force of contraction (Fig. 1B). The 36% reduction in force of the original injury compared to native LD was validated experimentally, as seen in Fig. 1C. An injury near the top of the muscle, labeled high injury, generated the largest decrease from native at 50% (Fig. 1B). The *in situ* testing of the high injury confirmed the model's force prediction (Fig. 1C). Using the FE model as a predictive tool, we were able to determine the preferred injury location to maximize the decrease between native and injured force production. For the development of novel therapies, an increased difference would help to

increase the margin of difference between treatments and better aid development.

The FE model can also be used to better understand the biomechanics of force production and the difference between the original and high injuries. A breakdown of the force production from each component of the LD showed that the original injury fan generated 3.204 N compared to only 2.269 N from the high injury fan portion. The increased number of intact fibers present in the original injury likely contributed to the increased force production of the original injury location. Analysis of along-fiber stretch shows that the high injury LD generated a larger along-fiber stretch within the region of intact fibers of the fan compared to the original injury. This indicates that the fibers of the high injury LD operate on the descending limb of the force-length curve and are unable to generate maximum force.

CONCLUSIONS

Using a computational and experimentally coupled framework, we were able to determine the best injury location to see the largest difference between native and injured rat LD muscles by creating, validating, and testing a model with three different data sets. This work demonstrates that combining these tools allows more focused and efficient *in vivo* studies to be designed which saves valuable time, money, and resources and has the potential to accelerate the development of regenerative therapies.

REFERENCES

[1] Corona et al. *JRRD*. 52(7): 2015.
[2] Baker et al. *Tissue Eng Part A*. 23(11-12): 2017.
[3] Chen and Walters. *J Plast Reconstr Aesthetic Surg*. 66(12): 2013.
[4] Hu et al. *Proc Am Soc Biomech*, 2016.
[5] Blemker et al. *J Biomech*. 38(4): 2005.
[6] Inouye et al. *Proc Am Soc Biomech*, 2015.

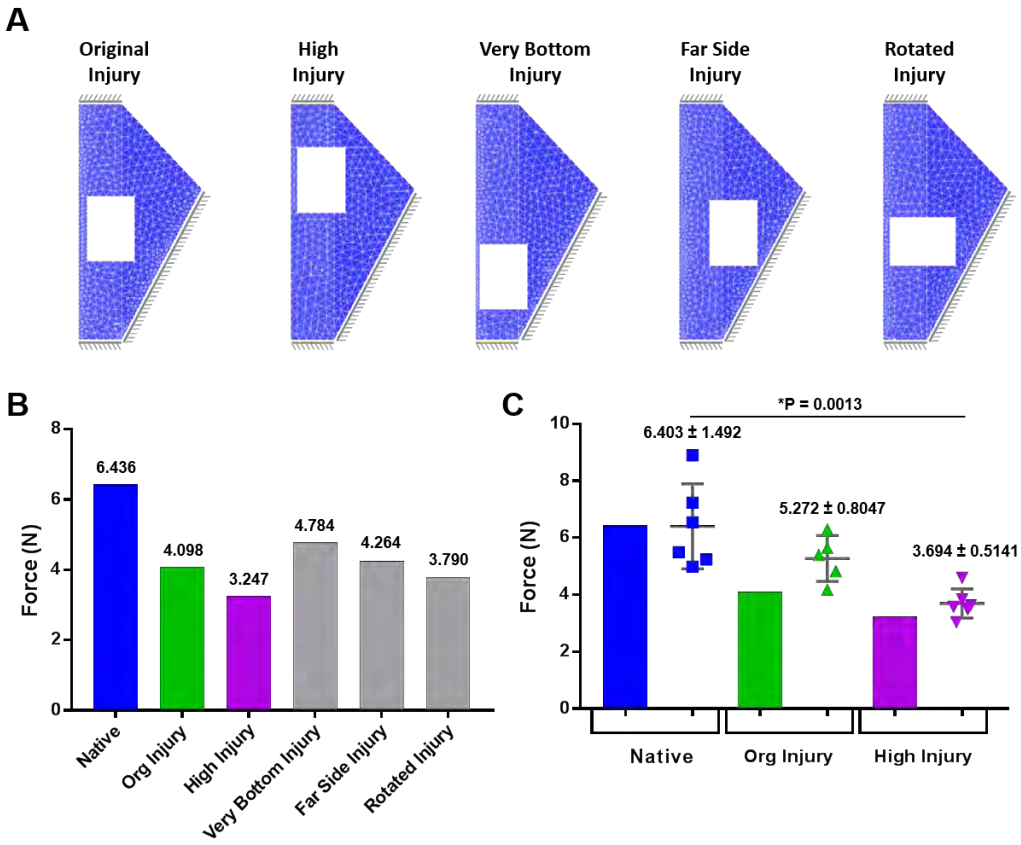

Figure 1: Five different injuries (11x15 mm) were created in the rat LD at varying locations within the muscle (A). Model simulations of the injuries showed that injury location has a dramatic effect on force production (B). Experimental *in situ* testing results of the original and high injury, shown as scatter plots, validate the model force predictions, shown as bars (C).

HIP EXTENSOR FATIGUE ALTERS HIP AND KNEE COUPLING DURING STEP DOWNS: A RANDOMIZED CONTROLLED TRIAL

Nicholas J. Beise, Michelle L. Fischer, Taylor L. Stecklein and John H. Hollman

Mayo Clinic College of Medicine and Science, Rochester, MN, USA
email: hollman.john@mayo.edu

INTRODUCTION

Impaired hip muscle function may contribute to movement coordination deficits (e.g., altered hip adduction or knee valgus) that increase lower extremity injury risks. In previous work [1] we reported hip extensor fatigue as a model of hip extensor impairment has little to no effect on hip and knee kinematics, as measured with linear measurement tools (mean and SDs of joint angles). Nonlinear measures of coupled hip and knee joint kinematics, however, may provide different insights into the effect of impaired hip muscle function on coupled lower extremity movement patterns.

We examined whether coupled dynamics of sagittal plane hip and frontal plane knee motion are altered during single-limb step-downs following a protocol that fatigues the hip extensors.

METHODS

30 healthy adults participated (10 men, 20 women, age = 23.5 ± 1.5 years, BMI = 24.3 ± 3.1 kg/m^2) in this randomized controlled trial. Each participant performed 20 repeated single-limb step-downs from a 19-cm step before and after completing either a Biering-Sorensen fatigue protocol or a sham fatigue protocol (push-ups to exhaustion).

Hip and knee kinematics during the step-down tests were acquired at 100 Hz with a Vicon MX motion analysis system and five MX20+ cameras. We used Vicon's Plug-in-Gait marker system to model lower extremity segments and Nexus software to quantify pelvis and lower extremity kinematics. Marker trajectories were filtered with a Woltring quintic spline filter (20-mm mean square error).

We analyzed peak sagittal and frontal plane hip and knee angles (i.e., hip and knee flexion, hip adduction, knee valgus or varus) across 20 repetitions of the step-down tests, including means and SDs.

To examine hip and knee coupling dynamics, we created cross recurrence plots and used cross recurrence quantification analyses (cRQA) as described by Webber & Zbilut [2]. Briefly, cRQA examines structural characteristics of two time series embedded in a reconstructed phase space containing sufficient dimensions to define the state of the system. According to Takens [3], that phase space may be reconstructed with time delayed copies of the series. We used a time delay of 60 samples based on average mutual information functions, 3 embedding dimensions based on global false nearest neighbors analyses, and set the radius at 20% of a SD to yield recurrence rates between 1% and 5%.

The following measures were quantified:

- Determinism (DET): proportion of recurrent points that fall on diagonal lines of 2 or more points; represents the predictability of coupling between two signals.
- Maximum line (L_{MAX}): length of the longest diagonal line of recurrent points; an indication of attractor strength between signals.
- Divergence (DIV): inverse of L_{MAX}, also related to the maximum positive Lyapunov exponent, estimates rates at which coupled trajectories in the phase space diverge; an indication of chaos in coupled signals.
- Mean line (L_{MEAN}): average length of diagonal recurrence lines; estimates average period during which signals are coupled.
- Shannon entropy (ENT): probability the length of diagonal recurrence lines will be repeated in the recurrence plot; estimates variety of patterns in which two signals are coupled.

Pre-to-post fatigue change scores in the linear hip and knee angle measures (means & SDs) and in the nonlinear coupled sagittal plane hip and frontal plane knee coordination measures were analyzed inferentially with independent t-tests ($\alpha = .05$).

RESULTS AND DISCUSSION

Overall, participants performed the step-downs with 52.9 ± 10.1° of hip flexion, 18.3 ± 5.9° of hip adduction, 72.2 ± 7.2° of knee flexion and 5.2 ± 13.0° of knee valgus. Neither the magnitude nor variability in sagittal and frontal plane hip and knee kinematics changed following the fatiguing protocol ($p > .05$). Based on cRQAs (Table 1), however, the determinism and entropy in coupled sagittal plane hip and frontal plane knee angle displacement patterns decreased in the control group and increased in the fatigue group ($p = .043$ and .044, respectively). Fig. 1 illustrates representative pre- and post-fatigue data.

Changes emanating from the coupled hip and knee angle trajectories can be interpreted. Namely, participants performed the step-down tests with altered coordination patterns in the fatigued state. Control participants performed the task with less irregularity, implying a learning effect in which they became more efficient at completing the task. Fatigued participants, in contrast, performed the step-downs with longer periods in which hip flexion and knee valgus were coupled (increased DET) and concomitantly performed the task with greater irregularity in the variety of patterns in which hip flexion and knee valgus were coupled (increased ENT). In the fatigued stated, overall hip flexion and knee valgus coupling was increased but that coupling occurred in a more irregular manner.

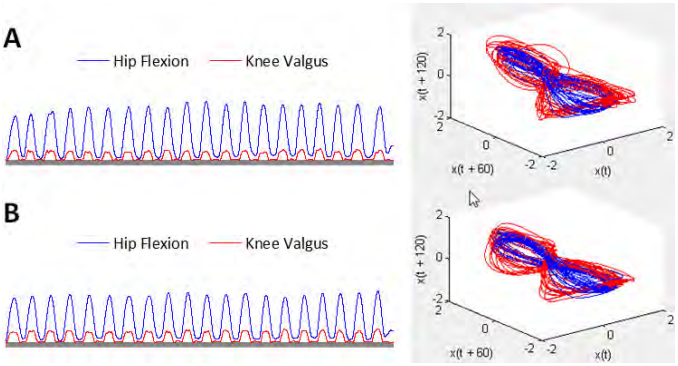

Figure 1: Time series of sagittal plane hip and frontal plane knee angles in (A) pre- and (B) post-fatigue conditions, with reconstructed phase spaces.

CONCLUSIONS

Fatiguing the hip extensors as a model of impaired hip muscle function altered coupled hip and knee motion patterns, suggesting that inter-joint coordination was impaired. This may have implications for pathomechanics that elevate lower extremity injury risks when hip extensor function is impaired. Furthermore, dynamical measures of inter-joint coordination may be more sensitive to examining consequences of changes in hip extensor function than are traditional linear measurements of lower extremity kinematics.

REFERENCES

1. Hollman et al. *Clinical Biomechanics*. 27(9): 903-909, 2012.
2. Webber & Zbilut. *Journal of Applied Physiology*. 76(2): 965-973, 1994.
3. Takens. In: Rand & Youngs (Eds.) *Dynamical Systems and Turbulence, Lecture Notes in Mathematics*, Springer-Verlag (898), 1981.

Table 1: Pre- and post-fatigue values of coupled sagittal plane hip and frontal plane knee dynamics.

Parameter	Pre-fatigue	Post-fatigue	Post – pre change	t	p
Determinism (%)					
Control group	99.83 ± .18	99.59 ± .49	-0.24 ± .38	2.131	.043
Fatigue group	99.56 ± .40	99.63 ± .43	+0.07 ± .36		
Entropy (bits/bin)					
Control group	4.86 ± .87	4.49 ± .90	-0.37 ± .54	2.113	.044
Fatigue group	4.27 ± .99	4.45 ± .99	+0.18 ± .82		

Learning Locomotor Stability in Novel Environments

[1,2] Mary A. Bucklin, [2] Mengnan/Mary Wu, [2] Geoffrey Brown, [2,3] Keith E. Gordon

[1] Northwestern University Department of Biomedical Engineering
[2] Northwestern University Department of Physical Therapy and Human Movement Sciences
[3]Edward Hines Jr. VA Hospital
Email: marybucklin2016@u.northwestern.edu

INTRODUCTION

Control of lateral stability is essential to prevent loss of balance and consequential falls during locomotion. This control is complex, demanding not only appropriate limb trajectories for foot placement, but also maintenance of a constantly shifting body center of mass (COM) [1]. Currently, our understanding of how and what the nervous system controls to create lateral stability during walking is poor.

Experiments utilizing robotic force fields to probe the sensorimotor system have been instrumental to our understanding of how the nervous system controls stable reaching movements [2]. When preforming a repetitive reaching task in a novel and consistent environment, people select motor control strategies that predict the effects of the force field. When the force field is unexpectedly removed, people exhibit movement errors, known as after-effects, which provide strong evidence that they have formed a predictive model of their environment.

While there is evidence that people form predictive models to control limb trajectories during walking, the same has not been shown for COM trajectories. Considering that previous research suggests that people plan walking paths in terms of COM trajectory it is likely that the nervous system also utilizes control strategies that predict COM dynamics [3]. Therefore, the purpose of this study was to investigate how people control COM trajectory while walking in a novel environment.

Specifically, we challenged stability by applying a laterally directed force field to participants' COM during a goal-directed walking task. We hypothesized that when lateral stability is altered by a novel but consistent force field, healthy young adults would form a predictive model of the environment that will be used to control lateral COM dynamics during walking.

METHODS

13 healthy young adult subjects (6 male, 7 female, 22.8 ± 2.1 years and 65.9 ± 8.5 kg, mean ± SD) participated in the study. Northwestern University's Institutional Review Board approved the protocol.

Participants preformed repetitions of a discrete walking task, moving from a static standing position to a 0.3 x 0.3 m target located 1.5 leg lengths in front of the start position. A cable robot was used to apply a novel external force field to the participant's COM. The applied forces were proportional in magnitude to forward walking velocity and directed laterally towards the participant's right side. Participants always began the task by stepping with their right foot first. A motion capture system recorded 3D coordinates of markers on the pelvis. This data was used to estimate COM dynamics.

Participants performed 110 total trials of the discrete walking task; 20 **Baseline** trials (no applied forces), 70 **Adaptation** (in the force field), and 20 **Washout** trials (no applied forces).

We quantified signed area deviation of the COM trajectory relative to a straight forward path originating from the lateral COM position at first toe-off (Fig. 1). Signed Deviation reflects directional biases in COM trajectory by taking the difference between areas on either side of the straight path.

We evaluated changes in COM trajectory by comparing COM Signed Deviation across the last

three trials of Baseline, the first three (early adaptation) and last three (late adaptation) trials of Adaptation, and the first three trials of Washout using a one-way repeated measures ANOVA with a Bonferroni correction.

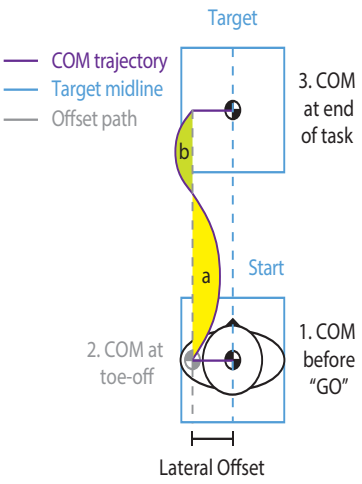

Figure 1: Lateral COM Offset calculated as the shift in COM position between the trial start and first toe-off. Signed Deviation is the net deviation of the COM from a straight path aligned with the Lateral COM Offset (the difference between areas "a" and "b").

RESULTS AND DISCUSSION

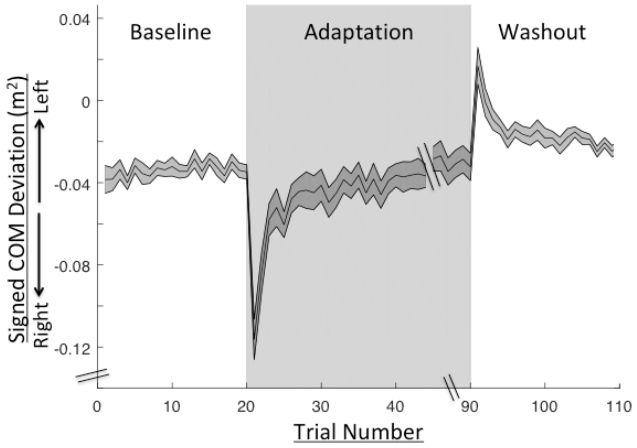

Figure 2: COM Signed Deviation and lateral offset. Mean and SEM calculated across all participants. During Early Adaptation COM Signed Deviation increased in the same direction as the force field. By Late Adaption, Signed Deviation was not different than Baseline. During Washout Signed Deviation increased in the opposite direction of the force field.

Our results revealed a significant difference in Signed Deviation across conditions (ANOVA; $p< 0.001$) (Fig. 2). Post hoc testing found that Signed Deviation was significantly different between Baseline and Early Adaptation ($p<0.001$), but not between Baseline and Late Adaptation ($p>0.99$). In addition we found that Signed Deviation was significantly different and in opposite directions between Early Adaptation and Washout ($p<0.001$). Overall, Early Adaptation movement in the perpendicular force field directed toward the participant's right side resulted in lateral deviations to the right. By Late Adaptation, participants had adjusted their control strategy such that lateral COM deviations were no longer different than Baseline. When the force field was unexpectedly removed during Washout, participants displayed large lateral COM deviations to their left, and after-effects that suggest that individuals were using predictive control strategies to offset the effects of the force field.

CONCLUSIONS

In support of our hypothesis we found that healthy young adults formed a predictive model of a novel-walking environment and used the model to adapt and control their COM trajectory during discrete goal-directed walking tasks. This finding suggests that people plan and control COM locomotor trajectories. Using force fields to probe sensory motor control of walking trajectories will be valuable for evaluating gait stability and identifying the underlying control objectives used to maintain COM stability.

REFERENCES

1. Patla, et al (1999). *Exp Brain Res*. (129)
2. Shadmehr, Mussa Ivaldi (1994) *J.Neurosci* (14)
3. Daley (2006). *Proc. Natl. Acad. Sci.* (103)

ACKNOWLEDGMENTS

Research supported by NIH (T32EB009406).

We would like to thank Mark Cummings and Jason Kwon for their help with data processing.

CONTACT STRESS OVER-EXPOSURE CORRELATES WITH OA DEVELOPMENT IN ACETABULAR FRACTURES

Kevin N. Dibbern, Tai C. Holland, Holly D. Thomas-Aitken, Tyler CarlLee, Michael C. Willey,
Jessica E. Goetz, J. Lawrence Marsh, Donald D. Anderson
University of Iowa, Iowa City, IA
email: kevin-dibbern@uiowa.edu

INTRODUCTION

Posttraumatic osteoarthritis (PTOA) is a common debilitating sequela of intra-articular fracture (IAF) [1]. Surgical reduction of IAFs aims to restore congruity of the disrupted joint surface to decrease articular contact stress and mitigate PTOA risk [2]. Elevated contact stress in mal-reduced IAFs of the ankle reliably predicts PTOA risk [3]. The effect of acetabular fracture on chronic hip contact stress and PTOA risk, however, is less well established. With up to a quarter of acetabular IAFs leading to PTOA, an investigation into the pathomechanical development of this condition is warranted.

Computational modeling of articular contact derived from CT images has been well validated for contact stress assessment. Discrete element analysis (DEA) is a specific modeling technique well suited for determining relationships between contact stress exposures and clinical outcomes, such as PTOA, in larger patient populations [6]. Mapping of the cumulative contact stress over-exposure on the articular surface across a complete gait cycle provides a means to identify those joints most prone to eventual development of PTOA.

METHODS

Eleven patients with operatively managed acetabular fractures were enrolled in this IRB-approved study. Patients were selected for having post-operative CT imaging and minimum two-year radiographic follow-up available. Femoral and pelvic anatomy for each patient was segmented from post-operative CT scans to produce DEA models using the validated method of Townsend et. al., 2018. The models were then aligned to the coordinate system defined by Bergmann et al. The walking gait data obtained in that study of instrumented total hips was discretized into 13 evenly spaced time increments. Patient specific forces were applied to each model based on body mass at the time of injury. DEA was used to compute deleterious contact stress exposure above a damage threshold ($P_d \geq 5$ MPa – defined as over-exposure) at each step in the gait cycle. For each patient, only the deleterious contact stress over-exposure was considered in our evaluation. These deleterious contact stresses were then computed at each of the 13 steps of the gait cycle and multiplied by the time spent in each of the steps to obtain a stress-time over-exposure metric. Summed over the gait cycle, the cumulative contact stress over-exposure experienced by the articular surface was compared to KL grades at 2 years post-operatively.

RESULTS AND DISCUSSION

Maximum values of contact stress over-exposure per gait cycle ranged from 0.23 - 2.91 MPa*s in the 11 acetabular cases analyzed in this study (Fig. 1). By design, KL grades were evenly distributed with 2 cases per grade except for grade 1 with 3 cases. Maximum per gait cycle contact stress over-exposure stress had a moderate positive correlation with KL grade ($R^2 = 0.426$). Qualitative assessment of the DEA derived post-operative models of this subset (cases 07, 08, and 10) reveals acetabular fractures with readily apparent joint incongruities flanked by areas of high contact stress over-exposure (Fig. 2). Cases with minimal or no radiographic evidence of osteoarthritis tended to exhibit better articular surface congruity. This corresponded with lower maximum contact stress over-exposure.

To our knowledge, this is the first study investigating the relationship between cumulative contact stress over-exposure and PTOA in acetabular fractures. The maximum per-gait cycle contact stress over-exposure cycle exhibited a

threshold above which all acetabular fractures progressed to PTOA.

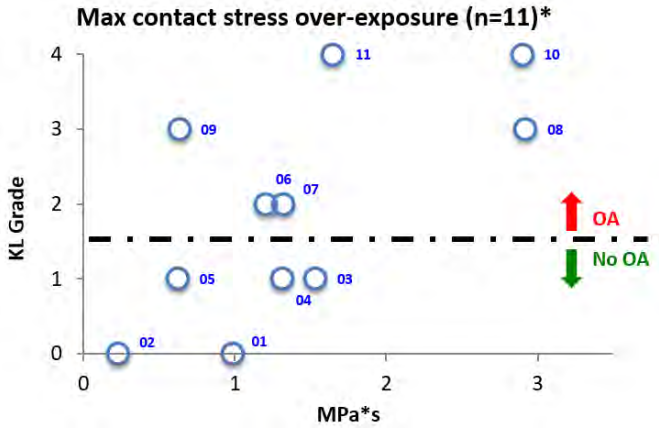

Figure 1: Maximum per gait cycle contact stress over-exposure.

CONCLUSION

The rate of PTOA development after surgical reduction and repair of acetabular fractures has remained stagnant over the years. Major efforts have focused on improving surgical technique to prevent PTOA, despite limited success and poor understanding of the pathogenesis of PTOA. Investigating how disruptions of articular surfaces can cause PTOA will likely provide insight on how to properly reconstruct them. The methods developed in this work allow precise and objective determination of the quality of acetabular fracture reduction. DEA techniques can quantify the mechanical impact of imperfect reduction via calculation of contact stress elevations throughout articular surfaces.

SIGNIFICANCE

The application of these techniques to acetabular fractures highlights the clinical value of this methodology in the hip joint. By identifying hips likely to degenerate due to a high level of residual incongruity, DEA-contact stress analysis may provide early prediction of joint failure and subsequent consideration of conversion to total hip arthroplasty.

REFERENCES

1. Anderson DD, et al. *Iowa Orthop J.* **31**, 1-20, 2011.
2. Buckwalter JA and Brown TD. *Clin Orthop Relat Res*. **423**, 7–16, 2004.
3. Anderson DD, et al. *J Orthop. Res.* **29**, 33-39, 2011.
4. Hadley NA, et al. *J Orthop. Res.* **8**, 504-513, 1990.
5. Townsend KC. *J Biomech*. **67**, 9-17, 2018.
6. Kern AM and Anderson DD. *J Biomech*. **48**, 3427-3432, 2015.

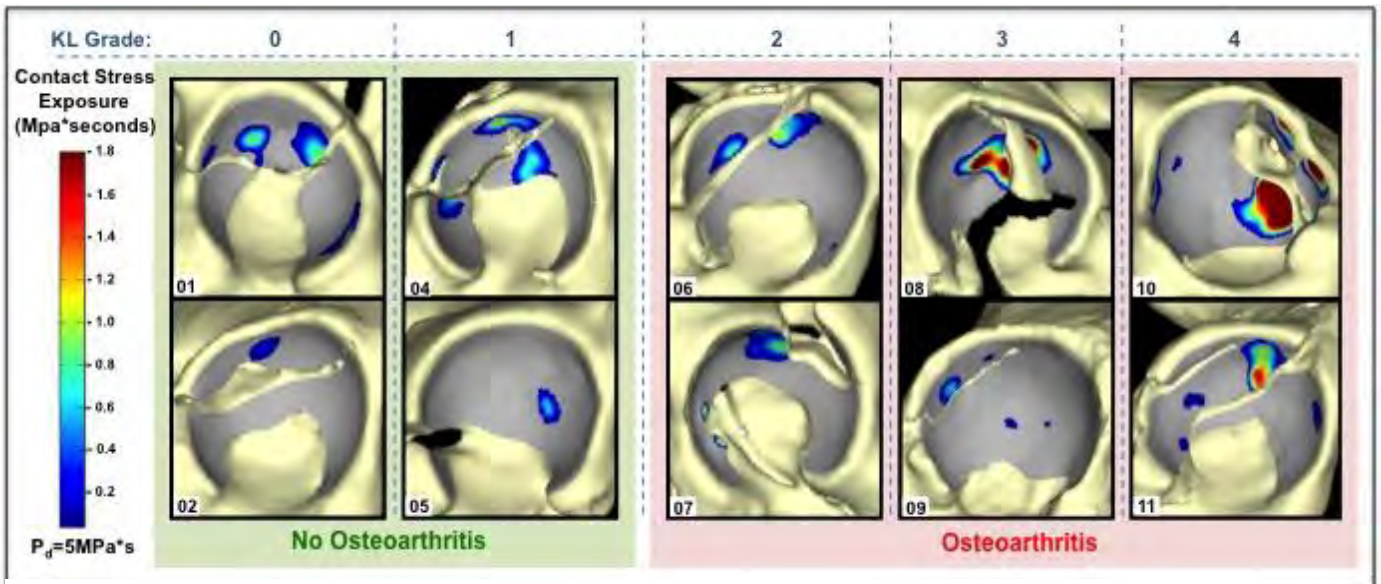

Figure 2: The distribution and magnitude of deleterious exposure (>5MPa*s) in acetabular fractures. Patient cases arranged by increasing KL grade and grouped by radiographic outcome.

KNEE ADDUCTION MOMENT IS GREATER WITH TIME SINCE INJURY IN INDIVIDUALS WITH LOWER LIMB LOSS

[1,2] Rebecca L. Krupenevich, [1] Ross H. Miller, [2] Lien T. Senchak, [2-4] Brad D. Hendershot, [2-4] Alison L. Pruziner

[1] University of Maryland, College Park, MD, USA
[2] Walter Reed National Military Medical Center, Bethesda, MD, USA
[3] DoD-VA Extremity Trauma and Amputation Center of Excellence, USA
[4] Uniformed Services University of the Health Sciences, Bethesda, MD, USA
email: rlkrup@umd.edu

INTRODUCTION

Individuals with unilateral lower limb loss often develop osteoarthritis (OA) in the knee of their contralateral limb [1]. OA is a leading cause of knee pain and disability, and is characterized by the progressive loss of articular cartilage, resulting in joint space narrowing. The high prevalence of OA in the limb loss population is posited to be due to large or abnormal loads on the contralateral limb during activities of daily living [1]. Specifically, features of the knee adduction moment (KAM) such as its peak, loading rate, and impulse during walking have been associated with narrow joint space [2] and cartilage volume loss [3].

In individuals with limb loss, we might therefore expect abnormal KAM profiles. For example, individuals living with limb loss for many years (14±10 yrs) demonstrate greater loading on the intact vs. prosthetic limb [4]. However, individuals with more recent limb loss (2±1 yrs) do not display unusually high KAM magnitudes [5], suggesting that individuals with limb loss may not alter their gait mechanics until there is a reason to do so (e.g., loss of fitness, pain from cartilage loss), which may occur years after sustaining the injury and after the joint has already begun to structurally deteriorate. These statements are largely speculative, but speculation serves to emphasize that fact that it is currently unknown how time since injury relates to joint space and knee mechanics during gait. This gap in knowledge is important because OA is not reversible, so we need to better understand how modifiable factors like joint mechanics affect joint health, prior to the initiation of OA.

Therefore, the purpose of this exploratory data analysis was to examine the cross-sectional relationships between time since injury vs. KAM peak, loading rate, impulse, and medial joint space in individuals with lower limb loss.

METHODS

Eleven individuals with unilateral lower limb loss (three transfemoral, eight transtibial; mean±SD age: 36±7 yrs, stature: 1.82±0.05 m, body mass: 100.9 ±14.1 kg, and time since injury: 10±2 yrs, range = 7-13 yrs) participated after providing written informed consent to study procedures approved by the local IRB. Participants walked at self-selected speed (1.34±0.15 m/s) along a 15-m walkway with biomechanical data captured using an 18-camera system and six force platforms embedded within the walkway. KAM was calculated using Visual3D software and scaled by bodyweight and height.

Outcome variables were KAM peak, impulse, and loading rate, the time since injury resulting in amputation, and joint space of the medial knee.

Figure 1: Example of radiographic assessment of joint space at the medial border of the knee (white arrows).

KAM impulse was calculated as the area under the moment-time curve. KAM loading rate was calculated as the slope during 20-80% of time from minimum KAM to first KAM peak.

Weight-bearing radiographs of the intact knee were obtained and evaluated by a trained musculoskeletal radiologist. Medial joint space was measured at the most medial border of the tibiofemoral joint (Fig. 1).

Pearson correlation coefficients (r) were used to examine relationships between time since injury vs. KAM peak, impulse, and loading rate, and medial joint space ($p < 0.05$). 95% confidence intervals on r (CI) were calculated via Fisher transformation. Due to the exploratory nature of these tests, reported p-values were not adjusted for multiple comparisons.

RESULTS AND DISCUSSION

Time since injury positively correlated with KAM peak ($r = 0.64$, $p = 0.03$, CI = [0.07, 0.90]; Fig. 2a) and impulse ($r = 0.62$, $p = 0.04$, CI = [0.03, 0.90], Fig. 2b). There was no correlation between time since injury and KAM loading rate ($r = 0.60$, $p = 0.05$, CI = [0.00, 0.90]; Fig. 2c) or time since injury and medial joint space ($r = 0.53$, $p = 0.09$, CI = [-0.10, 0.90]; Fig. 2d).

The significant correlations between peak KAM and KAM impulse with time since injury suggest that these individuals exhibit greater knee joint loading over time. Further, the insignificant correlation between time since injury and joint space suggests that changes in gait mechanics may precede cartilage degeneration and the resulting loss of joint space. Ongoing longitudinal data collection will further consider temporal relationships between knee joint loading, joint space narrowing, and the initiation/progression of OA.

CONCLUSIONS

The present study is the first to relate features of the KAM, joint space, and time since injury in the limb loss population. These exploratory results suggest a positive relationship between medial knee joint loading (as measured by KAM peak and impulse) and time since injury, but do not support an association between joint space narrowing and time since injury in this population. In other words, individuals with greater time since injury exhibit greater knee joint loading, which may place them at increased risk for future development of knee OA.

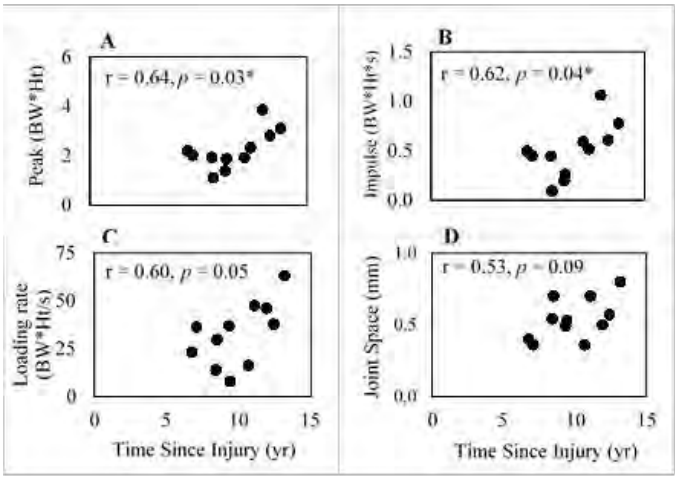

Figure 2: Correlations between time since injury and (A) KAM peak, (B) impulse, (C) loading rate, and (D) medial joint space. *p<0.05

REFERENCES

1. Morgenroth DC et al. *PM&R* **4**, S20-S27, 2012.
2. Sharma, L et al. *Arthritis Rheumatol* **7**, 1233-1240, 1998.
3. Bennell KL. *Ann Rheum Dis* **70**, 1770-1774, 2011.
4. Royer TD & Wasilewski CA. *Gait Posture* **23**, 303-306, 2005.
5. Esposito, E & Wilken, J. *Clin Biomech* **29** 1186-1192, 2014.

ACKNOWLEDGEMENTS

This work was funded by the CRSR at USU, award HU0001-15-2-0003, and supported by DoD-VA EACE. The views expressed in this abstract are those of the authors and do not reflect the official policy of the Departments of the Army/Navy/Air Force, Department of Defense, or U.S. Government.

BREAST CANCER TREATMENT TYPE AND POST-TREATMENT DURATION INFLUENCE PECTORALIS MAJOR RECRUITMENT

Tea Lulic, Bhillie D. Luciani, Rebecca L. Brookham and Clark R. Dickerson
Department of Kinesiology, University of Waterloo, Waterloo, ON, Canada
email: tlulic@uwaterloo.ca

INTRODUCTION

Pectoralis major is necessary for many daily tasks. It consists of two insertions: clavicular and sternal region, which contribute to shoulder adduction, flexion and humeral internal rotation. In women, this muscle is located beneath overlying breast and subcutaneous tissue and thus, it is commonly damaged iatrogenically during breast cancer treatment [BCT; 1-3]. BCT such as radiation therapy and mastectomy directly affect the pectoralis major [1], while the effects of chemotherapy affect the entire body and may cause indirect, widespread damage to the muscle. Subsequently, this damage contributes to upper limb disability in ~72% of breast cancer survivors [BCS; 4].

Most prior work quantified pectoralis major activity across patient groups and did not investigate the effect of treatment type and time post treatment on pectoralis major recruitment. This information is invaluable as the effects of treatment may differ between groups and mandate specific rehabilitative strategies. Additionally, the time post treatment may affect clavicular and sternal region engagement.

The purpose of this preliminary study was to investigate the effects of treatment type and time post treatment on pectoralis major activity in BCS during maximal voluntary contractions (MVC).

METHODS

50 female breast cancer survivors (59.4 ± 9.7 years) previously diagnosed with stage I, II or III unilateral breast cancer participated in this study. Participants completed treatment including surgery, radiation and/or chemotherapy at least 3 months prior to participation. 47 participants were right-hand dominant and 27 had cancer on the left breast. The average time since diagnosis was 74.9 ± 59.6 months.

Surface electromyography (sEMG) was collected from the clavicular and the superior part of the sternal region of the pectoralis major muscle bilaterally using disposable Ag/AgCl surface electrodes. EMG was collected at 3000 Hz using a Noraxon Telemyo 4200 T G2 telemetered system (Noraxon 2 USA Inc., Arizona, USA), with a band pass filter from 10-1500 Hz, input impedance > 100 MΩ, common mode rejection ratio > 100 dB and a base gain of 500.

Two sets of researcher-resisted maximal voluntary exertions (MVIC) were performed bilaterally against a dynamometer (ergoFET300TM, Utah, USA) using published techniques [5]. The duration of MVICs was 3 s with at least 2 minutes of rest between trials.

sEMG signals were high pass filtered at 30 Hz. A 200 ms RMS was calculated for both limbs and maximal values were extracted for clavicular and sternal regions. The data were then consolidated by quantifying the ratio of affected to unaffected limb peak sEMG for each region. Activations over 100% were defined as hyperactivated, while activations less than 100% were considered reduced. Participants were divided based on treatment type: a) radiation therapy only (9 BCS); b) mastectomy + chemotherapy (7 BCS); c) radiation + chemotherapy (12 BCS); and d) radiation, mastectomy and chemotherapy (13 BCS). Nine BCS received other treatment combinations and were excluded. Time post treatment was self-reported.

Spearman correlations were run for both, clavicular and sternal regions of the pectoralis major, to determine if a relationship existed between duration following treatment and muscle activation. Significance was set to $p = 0.05$.

RESULTS

A significant negative relationship existed in the radiation only group between the time post treatment

and sternal region muscle activation (r = -0.653, p = 0.05; *d* = -2.13). The sternal region of pectoralis major was overactivated in the first ~2 years following treatment, but this was reduced with increased duration following treatment (Fig. 1). This relationship did not exist for the clavicular region (r = - 0.084, p = 0.831). No relationship between time following treatment and regional muscle activity existed in the other treatment types (p > 0.05).

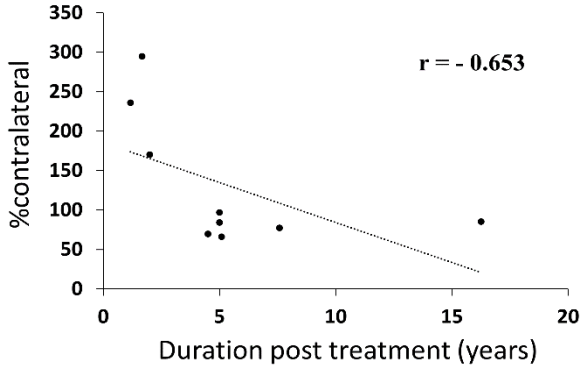

Figure 1: Significant moderate relationship between duration following radiation therapy and pectoralis major sternal activity ratio of affected: unaffected limb.

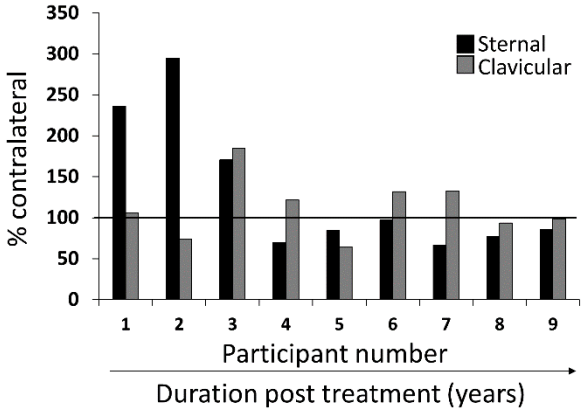

Figure 2: Representation of sternal and clavicular region activity in breast cancer survivors who received radiation therapy only.

Closer examination of the individual data showed that while the sternal region is hyperactive, the activity of the clavicular region is normal. However, when the sternal activity is reduced, the clavicular region became more active (Fig. 2).

DISCUSSION

A relationship existed between altered pectoralis major activity and duration post treatment only for the radiation therapy group. The hyperactivation of this region in the early stages following treatment may indicate fatigue sensitivity or inflamed and damaged tissue. With increased years following radiation therapy, the activity of the affected sternal region reduced relative to the unaffected side, supporting previous literature [2-3; 6]. The effects of radiation therapy on muscle and nerve tissue can continue up to 10 years following treatment [7-8]. Further, muscular scar tissue and fibrotic vasculature may result in decreased underlying muscular activity.

Additionally, preliminary findings suggest that the clavicular region may become hyperactive in some BCS in the later stages following treatment. This may partly be due to the reduction in the activity of the sternal region. However, the exact mechanism is ambiguous.

CONCLUSIONS

Treatment type and duration post treatment are factors that should be considered when investigating pectoralis major activity in BCS who underwent radiation therapy as a form of treatment. Specifically, rehabilitation in the earlier stages post BCT should focus on reducing activity of the sternal region of the pectoralis major, while later stages should focus on increasing activity of the sternal region while reducing activity of the clavicular region.

REFERENCES

1. Lipps et al. *Radiotherapy & Oncology. 122: 431-436, 2017.*
2. Shamley et al. *Breast Cancer Res. Treat.: 106, 19-27, 2007.*
3. Shamley et al. *Acta Oncol. (Madr.*), 51, 1045-1053, 2012.
4. Kwan et al. *J Clin Oncol., 20, 4242, 2002.*
5. Cram & Kasman. Aspen Publishers, 1998.
6. Brookham et al. *Clin Biomech, 52, 2018.*
7. Gillette et al. *Radiation Oncology Biol. Phys.* 31(5), 1995.
8. Schmitz et al. *American College of Sports Medicine*, 42(7), 2010.

GLENOHUMERAL JOINT STABILITY DURING DYNAMIC PUSHING AND PULLING

Daniel C. McFarland, Emily M. McCain, Michael N. Poppo, and Katherine R. Saul

North Carolina State University, Raleigh, NC, USA
email: dcmcfarl@ncsu.edu

INTRODUCTION

The glenohumeral joint is the most mobile joint in the human body and depends on active contributions of muscles to stabilize the resultant joint reaction force (JRF) within the glenoid fossa [1]. JRFs composed of large ratios of transverse to compressive forces destabilize the joint and pose a greater risk for shoulder dislocations. Prior dislocations can damage the fibrous structures surrounding the glenoid fossa [1] and reduce the stability index during hand-positioning tasks [2]. Therefore, to prevent degenerative wear to the joint, workspace design should consider glenohumeral instability to avoid motions that naturally place the shoulder at higher risk for instability. Pushing is a common industrial task that has been shown to have increased transverse to compressive forces [2,3]. Knowledge of whether these risks are spatial dependent with task target could be used to design safer workspaces. Our goal was to evaluate how task direction and task target during dynamic push-pull tasks influence joint reaction loads.

METHODS

Prior experimental data of 18 subjects (9M/9F) performing a series of push and pull tasks were used to inform computed muscle control (CMC) [4] simulations in OpenSim [5] to determine resultant JRFs at the glenohumeral joint. CMC tracked experimental kinematics of subjects pushing and pulling submaximal loads to 4 horizontal targets (0^o, 45^o, 90^o, and 135^o) at a sagittal angle of 90^o and 3 sagittal targets (20^o, 90^o, and 170^o) at the 90^o horizontal target for a total of 6 independent task targets (Figure 1). Individualized musculoskeletal models were developed for each subject by scaling a previously developed and validated upper extremity musculoskeletal model [6] to individual joint strength and anthropometry.

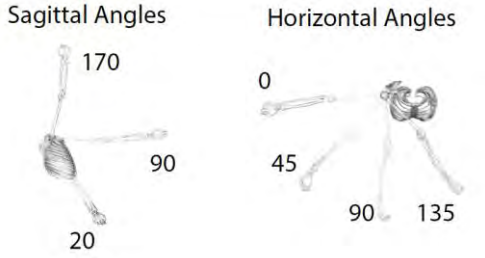

Figure 1: Task target location

Experimental electromyogram (EMG) recordings of surface muscles was used to inform on/off timing of the respective muscles, and thereby improve calculated activations for deep muscles. Furthermore, a penalty term was added to the static optimization stage of the CMC algorithm to constrain the resultant JRF to remain close to experimental limits of glenohumeral stability to prevent theoretical subluxation [7,8]. Differences in stability index, the ratio of transverse to compressive joint reaction forces at the glenohumeral joint, were analyzed across task direction and task target using a two-way ANOVA ($\alpha = 0.05$). If an interaction was present, simple main effects test was performed at each factor level.

RESULTS AND DISCUSSION

An interaction between task target and task direction was present ($p=0.0037$). Pulling stability index was more spatially dependent than pushing (Figures 2 and 3). However, pushing was significantly less stable than pulling for all task targets ($p<0.001$) except for the sagittal target of 20^o ($p=0.1113$) (Figure 3).

Pushing was found to result in less stable joint reaction forces, which agrees with previous studies [2,3]. However, the results suggest that there are limited stability benefits to optimizing push task location. Greater stability benefits would be seen by converting push task to pull tasks where possible

since pulling, except from the low target, was inherently more stable than pushing. Workspaces involving pulling tasks, however, could benefit from optimizing task location, mainly by avoiding placing pull tasks at low targets. Placing pulling tasks at more centrally located targets along the horizontal plane improves task stability.

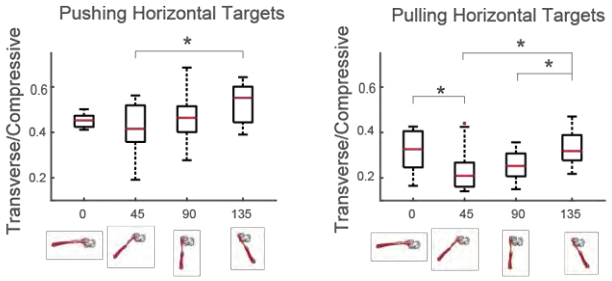

Figure 2: Stability index (transverse/compressive JRF components) across horizontal targets

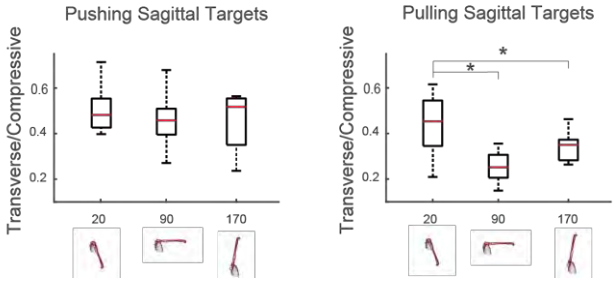

Figure 3: Stability index (transverse/compressive JRF components) across sagittal targets

Inherent task stability may influence muscle demand at the glenohumeral joint. Task targets identified as less stable in this study (i.e 20° for pulling and 135° for pushing) were reported to be significantly more demanding than other task targets [9]. Stabilization of the glenohumeral joint depends on active contributions of muscles, and this increase in demand may, in part, be due to an increased need to control the direction of the resultant joint reaction force.

One limitation of this research is that the kinematics of the handle in the experiment were not recorded. The direction of the applied loads was approximated from initial and final position of the hand's center of mass. Furthermore, strength data was only collected for shoulder abduction and elbow flexion, so strength scaling was limited to these measurements.

CONCLUSIONS

The primary findings have possible implications for arm function throughout the workspace:

1. Pushing places the glenohumeral joint at increased risk for instability; however, the stability index for pushing is similar across targets. Therefore, larger stability benefits may be seen from converting tasks like lever operation from push tasks to pull tasks rather than optimizing task layout.
2. Inherent glenohumeral stability may contribute to increased task demand. Additional work is needed to fully understand to what degree these features are linked.

REFERENCES

1. Lippitt and Matsen. *Clin Orthop Relat Res*, **291,** 20-28,1993.
2. Marchi et al. *Med Biol Eng Comput,* **52(3)**, 251-6, 2014.
3. Nimbarte et al. *Appl Ergon,* **44(5)**, 841-9, 2013.
4. Thelen et al. *J Biomech,* **36(3)**, 321-8, 2003.
5. Delp et al. *IEEE Trans Biomed Eng,* **54**, 1940-1950, 2007.
6. Saul et al. *Comput Methos Biomech Biomed Engin* **18(3)**, 1445-58, 2015.
7. Dickerson et al. *Comput Methos Biomech Biomed Engin* **10(6)**, 389-400, 2007.
8. Halder et al. *J Bone Joint Surg* **83(7),** 1062-1069, 2001.
9. McFarland et al. *Proceedings of ASB'17,* Boulder, CO, USA, 2017.

ACKNOWLEDGEMENTS

We would like to acknowledge CFD Research Corporation for funding and Alexander Brynildsen and Lauren Levine for their assistance in post-processing kinematic data.

WHAT ARE THE EFFECTS OF MUSCLE WEAKNESS ON THE SIT TO STAND TRANSFER?

[1,2] Elena J. Caruthers, [1, 3]Grant Schneider, [1]Laura Schmitt, [1]Ajit M.W. Chaudhari, and [1]Robert A. Siston

[1] The Ohio State University, Columbus, OH USA [2] Otterbein University, Westerville, OH USA
[3] Northwestern University, Evanston, IL USA
email: caruthers1@otterbein.edu

INTRODUCTION

Muscle strength declines in the elderly [1] and those with pathologies such as knee osteoarthritis [2], which leads to difficulty in performing daily tasks like rising from a chair [3]. The degree of weakness that can be tolerated, globally or in individual muscles, before the ability to rise from a chair is compromised is unknown. Previous work investigated this question for gait using dynamic simulations [4], but similar work has yet to be done for the sit to stand (STS) transfer. Such information could allow for better targeted rehabilitation for populations with muscle weakness. The purpose of this study was to investigate the effects of global and individual muscle weakness during the STS transfer and how other muscles compensate for the weakness.

METHODS

As part of a previous study by Caruthers et al. [5], six healthy individuals (4 males and 2 females, age: 23.0 ± 3.0 years) participated after providing IRB-approved informed consent. Each participant rose from a 55.2 cm high, hard-backed, armless chair three times with their arms crossed over their chest and each foot on a different force plate (Bertec, Inc); the chair did not contact the force plates. Motion data were collected at 150 Hz using an 8-camera Vicon MX-F40 system and the Modified Point Cluster Technique [6] while ground reaction forces were obtained from the force plates at 600 Hz. Bilateral surface EMG data were collected on the gluteus maximus, gluteus medius, rectus femoris, vastus lateralis, biceps femoris, tibialis anterior medial, gastrocnemius, and soleus at 1500 Hz using a 16-channel device (Noraxon Telemyo DTS).

Those data were previously used to create dynamic simulations that tracked one STS transfer per participant with the Full Body Model 2016 in OpenSim 3.1 [5, 7]. Muscle forces and activations were estimated by using static optimization (SO), which uses the cost function of minimizing the sum of muscle activations squared [7].

In this study, we began with full-strength simulations and weakened muscles by changing their peak isometric force for two cases. First, all lower extremity muscles were globally weakened by increments of 5% up to 70%. Second, the following individual or groups of muscles were weakened: gluteus maximus (GMAX), gluteus medius (GMED), iliopsoas (ILPS), hamstrings (HAM), rectus femoris (RF), vasti (VAS), quadriceps (QUAD, incl. RF and VAS), tibialis anterior (TA), gastrocnemius (GAS), soleus (SOL), and plantar flexors (PF, incl. GAS and SOL), in 5% increments up to 100% weakness, indicating the absence of a muscle. Using SO, we re-estimated muscle forces as the adjusted model tracked the original kinematics and kinetics, resulting in 932 simulations total.

A simulation was considered to have tracked the original STS transfer if: a) the simulation did not fail and b) the reserve actuators on any joint were less than 5% of peak joint moments [4]. For the simulations that met these criteria, changes in muscle forces and activations from the full-strength simulations were examined in the weakened muscle(s) and the remaining muscles in the dominant leg, which was the leg that had the largest peak vertical ground reaction force during the task. The overall demand placed on all muscles due to the respective muscle weakness was calculated across both legs by the muscle cost metric over time [4]:

$$\text{Muscle Cost} = \sum \text{Muscle Activation}^2$$

In this abstract, we only report global weakness and weakening of the QUAD, GMAX, and PF since Caruthers et al. demonstrated that they produce the largest forces and are main contributors to accelerating the COM up and out of the chair [5].

RESULTS AND DISCUSSION

The amount of global weakness that could be tolerated varied between participants. While three participants could not tolerate more than 35% weakness, the range of tolerable global weakness across all six participants was 20-65%. In all cases, the STS transfer was impaired due to insufficient torque at the knee. For the one participant who failed at 65% global weakness, muscle cost increased by 55% to 617% (relative to 0% weakness) as global weakness increased from 20 to 65%.

For individual weakness, muscle forces changed to maintain the same task kinematics and kinetics. For QUAD weakness, GMAX, biceps femoris long head (BFlh), and GAS reduced in force to oppose the weak QUAD less; the ILPS compensated for a weak RF (Figure 1). For 60% GMAX weakness, the BFlh and GMED forces increased by 183 ± 127% and 49 ± 23% to compensate for a weak GMAX; the RF and VAS forces changed by -5 ± 26% and 24 ± 13% to compensate for the change in BFlh and GMED forces. For 60% PF weakness, the TA decreased in force by 17 ± 23% to oppose the weak PF less.

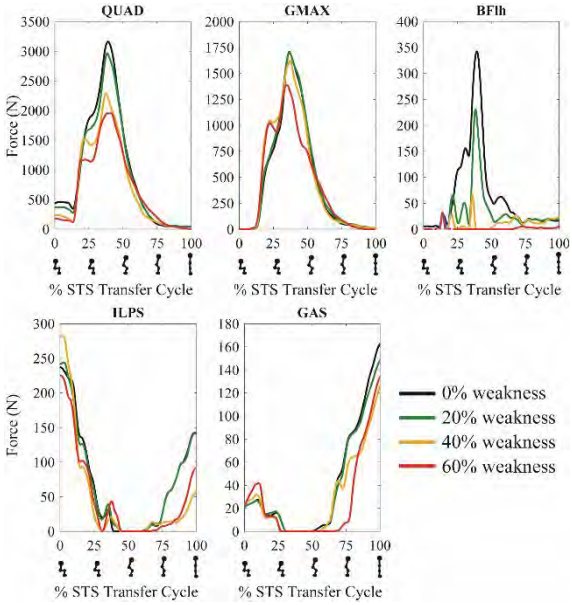

Figure 1. Example of the Effects of 0 – 60% QUAD Weakness on Muscle Forces in the Dominant Leg. Values were averaged across the dominant leg of the participants whose simulations passed the failure criteria for that weakness level.

The compensations that occurred with QUAD, GMAX, and PF weakness led to higher muscle cost, with the QUAD's increase in muscle cost being the highest (Table 1). Simulations with GMAX and PF weakness did not fail or failed later (60-80%) than those with QUAD weakness (20-60%).

Our findings contrast a study that examined how muscle weakness affects gait [4]. While 20-65% of global weakness could be tolerated during the STS transfer, 40-60% could be tolerated during gait [4]. In contrast to the STS transfer, gait was sensitive to PF weakness, but not to GMAX or QUAD weakness [4], which was reflected in muscle cost since the PF's change in muscle cost was the highest. These differences between studies are likely due to larger hip and knee torques but smaller ankle torques during the STS transfer in comparison to gait [9], demonstrating that task kinematics influence how a weakened muscle can contribute to the motion. In addition, more demand is placed on the weakened muscles to maintain the same kinematics and kinetics, which may lead to fatigue and make the task more challenging.

CONCLUSIONS

To our knowledge, this is the first study to examine the effects of muscle weakness on the STS transfer. Our results suggest this task may be most sensitive to weakness of muscles that span the knee, specifically the QUAD muscles, since they are the only muscles that can provide the necessary knee extension to rise from a chair [8]. While strengthening the knee extensors has been suggested to only add to their excess strength capacity during gait [4], such training appears to be essential to maintain a normal chair rise motion. The effects of muscle weakness on other tasks should be explored to inform rehabilitation programs for various populations.

REFERENCES

1. Skelton et al. *Age Ageing* **23**(5), 371-7, 1994.
2. Hurley and Newham.*Br J Rheum* **32**(2), 127-131, 1993.
3. Degens and Korhonen.*Maturitas* **73**(3), 197-201, 2012.
4. van der Krogt et al. *Gait Posture* **36** (1), 113-9, 2012.
5. Caruthers et al. *J Appl Biomech* **32**(5), 487-503, 2016.
6. Jamison et al. *J Biomech* **46**(13), 1881-1885, 2013.
7. Delp et al. *IEEE Trans Biomed Eng* **54**(11), 1940-1950, 2007.
8. Schultz et al. *J Biomech* **25**(12), 1383-1391, 1992.
9. Rodosky et al. *J Orthop Res* **7**(2), 266-271, 1989.

Table 1: Average Total Muscle Cost Increase for 60% Individual Muscle Weakness

	QUAD	GMAX	PF
Muscle Cost (Δ[a], %)	147.73 ± 94.56	51.99 ± 12.77	10.46 ± 14.85

[a] change relative to 0% weakness simulations and averaged across participants ± standard deviation

LATERAL STEPPING CONTROL IN OLDER ADULTS DURING MEDIOLATERAL PERTURBATIONS

[1,2] Meghan E. Kazanski, [2] Joseph P. Cusumano, and [1,2] Jonathan B. Dingwell

[1] University of Texas at Austin, Austin, TX, USA [2] Pennsylvania State University, University Park, PA, USA
email: mek79@psu.edu web: http://biomechanics.psu.edu/

INTRODUCTION

Falls among the elderly (aged ≥ 65) occur frequently, often resulting in injury and increased morbidity and mortality [1]. Most falls occur while walking, and sideways falls are especially hazardous [1-2]. Increased fall risk may be caused by greater gait variability, associated with walking situations that involve uneven terrain or perturbations [3]. Walking surface and visual field perturbations increase gait variability of young, healthy adults, particularly in the mediolateral (ML) direction [3-4]. It is not known how these ML perturbations affect gait parameters of older adults, who may be more susceptible to falls as the result of increased gait variability. Here, we examined the effects of ML visual and surface perturbations on the variability and step-to-step regulation of lateral stepping in healthy young and older adults.

METHODS

Thirteen healthy Young adults (5M/8F; aged 18-29) and thirteen healthy Older adults (6M/7F; aged 61-69) walked in a virtual-reality environment, on a treadmill at 90% of their preferred overground walking speed. Participants completed 3-min walking trials under 3 conditions: (i) Walking with no perturbations (NOP), or walking with continuous, pseudo-random oscillations of either the (ii) treadmill platform (PLA) or (iii) visual field (VIS), all in the ML direction (as in [3]). Participants were instructed to try to walk normally throughout all trials.

Kinematic data of participant and treadmill motion were recorded (Vicon) to compute ML stepping parameters (Fig. 1). Time series of left and right foot placements (z_L and z_R) were used to calculate means and standard deviations of absolute lateral position (z_B) and step width (w). We used Detrended Fluctuation Analysis (DFA) to compute scaling exponents (α) for each time series, $\alpha(z_B)$ and $\alpha(w)$, which quantified the amount of statistical persistence/ anti-persistence in each stepping parameter. Less statistical persistence is implied by α close to 0.5, and indicates stronger correction of deviations in the given stepping parameter from step-to-step [5].

Figure 1: Time series lateral stepping parameters:

- $\{z_L, z_R\} \equiv$ Left & Right lateral foot placements
- $z_B = (z_L + z_R)/2 \equiv$ Absolute lateral position of the body
- $w = z_R - z_L \equiv$ Step width
- $\Delta z_B = z_{Bn} + z_{Bn-1} \equiv$ Change in lateral position of the body (a.k.a., "heading").

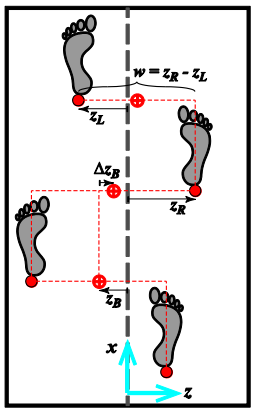

RESULTS

There were no significant differences in mean lateral position (z_B) between Young and Older adults, nor between conditions. Mean step widths (w) were not significantly different between Young and Older participants (p = 0.492; not shown), consistent with [6].

Participants exhibited significantly greater w variability during VIS and PLA perturbations than NOP ($p<0.001$; Fig. 2), also as expected [5]. Older adults tended to have slightly more variable step widths than Young adults, but not significantly (p = 0.089; Fig. 2). Participants exhibited significantly greater variability in z_B during both VIS and PLA perturbations compared to NOP ($p < 0.001$; Fig 2), but Young and Older adults were not significantly different (p = 0.192; Fig. 2).

All participants exhibited significantly decreased DFA α exponents during both VIS and PLA perturbations compared to NOP, for both step width (w; p

< 0.001) and lateral position (z_B; p < 0.001; Fig. 3). There were no differences between Young and Older adults for statistical persistence of either w (p = 0.526) or z_B (p = 0.573; Fig. 3).

DISCUSSION AND CONCLUSION

It was expected that mean step widths would be greater for perturbation conditions VIS and PLA, as increasing step width helps maintain lateral stability [3-4]. This is particularly relevant for fall prone populations [1-2]. Participants also demonstrated increased variability in w and z_B, confirming that young and older adults are far more variable in the lateral direction when subjected to perturbations [3].

DFA exponents $\alpha(z_B)$ were closer to 0.5 for PLA and VIS conditions than for NOP, suggesting that during these trials, participants more strongly corrected step-to-step lateral position-specific deviations with the subsequent stride. Thus, participants exhibited tighter step-to-step control [5] over their lateral position when perturbed (Fig. 3). These indications of greater lateral stepping variability and reduced statistical persistence are consistent with our predictions. It is noteworthy that, for all conditions, the $\alpha(w)$ were close to 0.5 than the $\alpha(z_B)$, demonstrating that participants exhibited stronger control of w than z_B. This suggests that participants prioritized maintaining step width for lateral stability [3-4]. Perturbations of the walking surface and visual field did increase Young and Older participant lateral gait variability, closely related to lateral balance control and sideways falling [2-4]. Further, perturbations encouraged a tighter stepping control strategy [5] for correcting w and z_B (Fig. 3).

The lack of significant group effects for variability (Fig. 2) may appear surprising, but was consistent with prior results from similarly *healthy* Older adults [7]. Likewise, the DFA results (Fig. 3) indicate that healthy older adults adopt similar strategies to regulate lateral stepping movements as young adults, despite slightly increased gait variability, consistent with what we found for sagittal plane stride-to-stride stepping control [8].

ACKNOWLEDGEMENTS

NIH / NIA Grant #: R01-AG049735

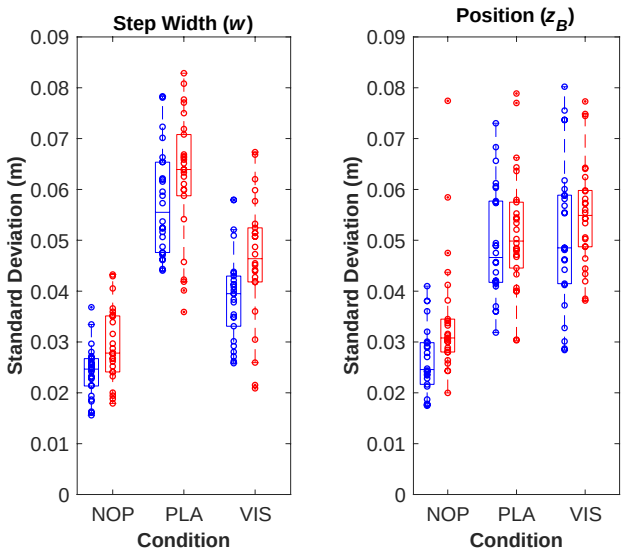

Figure 2: SD as a measure of Young (blue) and Older adult (red) stepping variability for w and z_B. Variability was greater for VIS and PLA compared to NOP.

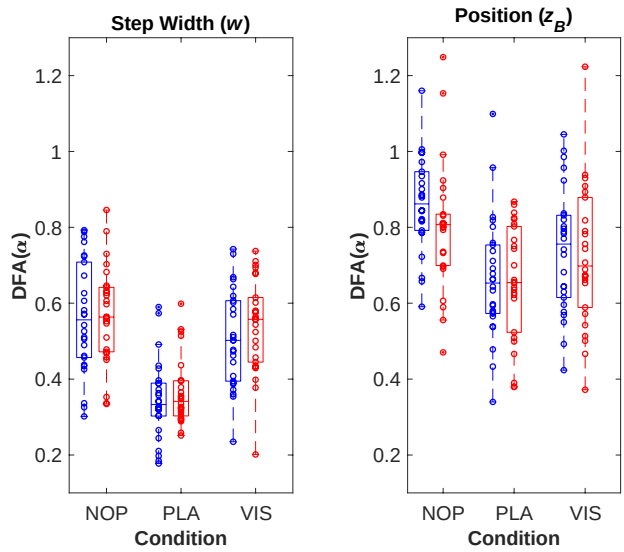

Figure 3: Statistical persistence of Young (blue) and Older adult (red) w and z_B. Group and condition DFA exponent values were closer to 0.5 for w, suggesting tighter regulation of this parameter for lateral stability.

REFERENCES

1. Robinovich SN, et al. *The Lancet* **381**, 47-54, 2013.
2. Mayhew PM, et al. *The Lancet* **366**, 129-35, 2005.
3. McAndrew PM, et al. *J Biomech* **43**, 1470-75, 2010.
4. Kuo AD. *Int. J Robotics Res* **18**, 917-30, 1999.
5. Dingwell JB, et al. *PLoS Comput. Biol.* **6**(7), 2010.
6. Kang KG et al. *J Biomech* **41**, 2899-2905, 2008.
7. Kang KG et al. *Gait Posture* **27**, 572-77, 2008.
8. Salinas MM et al. *Gait Posture* **55**, 131-37, 2017.

EFFECTS OF WEARING AN UPPER LIMB PROSTHESIS ON STANDING BALANCE

[1,2] Matthew J Major, [1] Tara Shirvaikar, [2] Rebecca Stine, and [1,2] Steven A Gard

[1] Northwestern University, Chicago, IL, USA
[2] Jesse Brown VA Medical Center, Chicago, IL, USA
email: matthew-major@northwestern.edu, web: http://www.nupoc.northwestern.edu/

INTRODUCTION

Whole-body composition influences the motor behavior required for controlling posture, with the arms playing a key role in standing balance [1, 2]. Consequently, this relationship has important implications for individuals who have lost all or part of an arm. Previous research has suggested that use of an upper limb prosthesis (ULP) can increase the likelihood of falling by six times [3], and that low levels of prosthetic embodiment can cause a postural disturbance to those with upper limb loss (ULL) [1]. A better understanding of the effects of wearing an ULP on balance may inform intervention strategies to enhance postural control. The purpose of this study was to evaluate the acute effects of wearing an UL prosthesis on standing balance, particularly the impact of matching the mass of the prosthetic limb to the sound limb. We hypothesized that this matching would improve bilateral weight symmetry, but have a negative effect on balance. We also expected persons with ULL who fell in the past 12 months to display worse standing balance than non-fallers based on similar observations in elderly persons [4].

METHODS

Eleven individuals with unilateral ULL (8 transradial level, 3 transhumeral level; 50±18 yrs; 175.1±7.4 cm; 79.6±22.6 kg) stood quietly and faced straight ahead for 30 seconds with each foot on a single force plate (AMTI, Watertown, MA) while instantaneous ground reaction forces and center-of-pressure (COP) were recorded. Three trials were collected under three conditions: 1) not wearing a prosthesis; 2) wearing their customary prosthesis; and 3) wearing a mock prosthesis which matched the mass and inertia of the sound limb (Fig 1). Subjects were classified in the 'Faller' group if they reported at least one fall in the 12 months prior to data collection, otherwise they were classified as 'Non-fallers'.

Data for the last 20 seconds of the trials were averaged for each condition and limb side (prosthetic, sound). A mixed three-way ANCOVA (side*condition*group, covariate: body mass index, stance width) was performed on anterior-posterior (AP) COP range, medial-lateral (ML) COP range, and COP sway area. Sway area was estimated using the Khachiyan Ellipsoid Algorithm with a tolerance of 0.001 cm. A mixed two-way ANCOVA (condition*group, covariate: body mass index, stance width) was performed on a Symmetry Index (= (sound side load - prosthetic side load) / (0.5*(sound side load + prosthetic side load))*100) to assess weight distribution symmetry for each condition. A Bonferroni adjustment was used for all multiple comparison post-hoc analyses. Natural log transformations were performed on AP COP range and sway area due to violations of normality as determined by the Shapiro-Wilk test. The critical α for all analyses was set at 0.05.

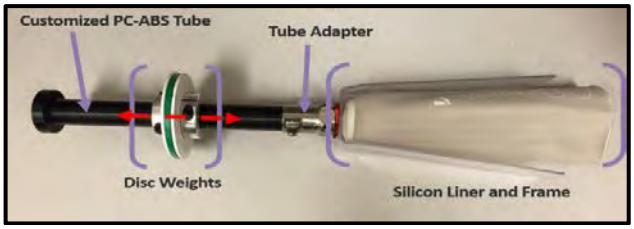

Figure 1: Image of the mock prosthesis allowing for addition and translation of distal mass.

RESULTS AND DISCUSSION

The main effect of prosthesis condition was significant for all COP parameters ($p \leq 0.028$), but post-hoc analyses were not significant ($p \geq 0.506$). COP range was greatest in the AP direction for the customary prosthesis condition, while COP range was greatest in the ML direction for the mock prosthesis condition (Fig 2). The sway area was generally larger for the mock and customary prosthesis conditions compared to not wearing a

prosthesis. Four subjects did not own a prosthesis and so the customary prosthesis was the mock prosthesis without added weight. The main effect of side was not significant for any parameter ($p \geq 0.315$). The main effect of prosthesis condition on weight symmetry was significant ($p=0.008$), with the mock prosthesis creating greater symmetry but a slight bias on the prosthetic limb side (Fig 3). The interaction effect of condition*group on symmetry was also significant ($p=0.042$) with differences between condition greater for the Faller group. There was no significant difference for any parameter between Fallers and Non-fallers ($p \geq 0.070$). Notably, 46% of subjects reported falling within the past year, which exactly matches the prevalence in a larger observation study on persons with ULL [3].

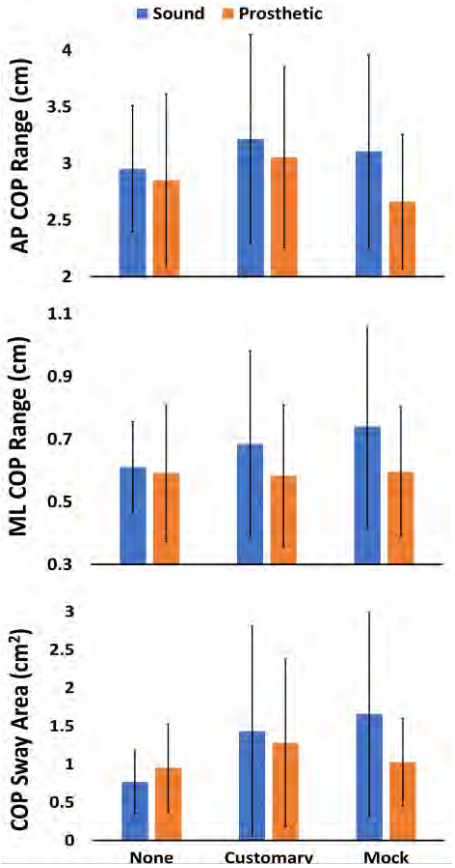

Figure 2: Average AP COP range (top), ML COP range (middle), and COP sway area (bottom) separated by side and condition. Error bars=95% CI.

The results support our hypotheses. Wearing an ULP with mass matched to the sound limb created more symmetric weight distribution, but wearing a prosthesis generally increased COP excursion. Increases in COP excursion represents greater sway of the whole-body center-of-mass and additional demands for postural control [5]. Accordingly, greater COP excursion has shown to be related to greater balance impairment in the elderly [4]. However, there was no significant difference in COP parameters between Fallers and Non-fallers. Given these inconsistent findings, further research is needed to define the relationship between COP excursion and fall risk in persons with ULL. Subjects in this study may have perceived wearing the ULP as a postural disturbance [1], which may help explain the observed acute increase in COP excursion.

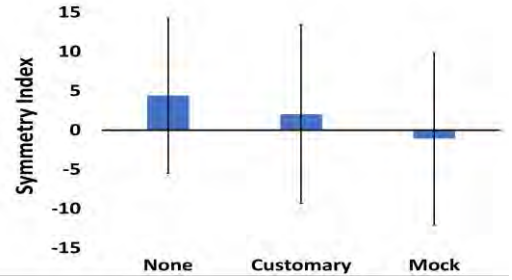

Figure 3: Average Symmetry Index separated by condition. Error bars=95% CI. 0=perfect symmetry, >0=sound side bias, <0=prosthetic side bias.

CONCLUSIONS

Wearing an ULP with mass matched to the sound limb may improve bilateral weight symmetry in persons with unilateral ULL, but acute periods of ULP wear may encourage need for greater postural control. The results do not suggest that an ULP should not be used given the functional benefits of these devices for reaching and grasping activities.

REFERENCES

1. Imaizumi S, et al. *Conscious Cogn* **45**, 75-88, 2016.
2. Shafeie M. *IEEE EMBS*, San Diego, CA, 2012.
3. Major MJ. *Proceedings of 16th ISPO World Congress 2017,* Cape Town, South Africa, 2017.
4. Pizzigalli L, et al. *J Bodyw Mov* **20**, 409-17, 2016.
5. Winter D. *Gait Posture* **3**, 193-214, 1995.

ACKNOWLEDGEMENTS

We thank John Brinkmann for helping design the mock prosthesis and Suzanne McConn for assistance with data collection. Work was supported by the U.S. Dept. of VA (#1I21RX001388 and 1IK2RX001322).

TIME-VARYING NATURE OF POSTURAL CONTROL DURING EYES CLOSED QUIET STANCE

[1] Scott M. Monfort, [2] Lise C. Worthen-Chaudhari, [3] Kimberly E. Bigelow, and [2]Ajit M.W. Chaudhari

[1] Montana State University, Bozeman, MT, USA
[2] The Ohio State University, Columbus, OH, USA
[3] University of Dayton, Dayton, OH, USA
email: scott.monfort@montana.edu website: http://www.montana.edu/biomechanics/

INTRODUCTION

Quiet stance with eyes closed (QEC) is an easy-to-implement and informative test condition for various neuromuscular impairments. Several descriptive balance measures (e.g., medial-lateral root-mean-squared excursion – RMS_ml) have been linked to fall risk, supporting their clinical relevance [1]. These descriptive center of pressure (CoP) measures typically analyze time-series data from entire trials; however, reports of CoP signal nonstationarity and acquisition time-dependency raise questions about what aspects of postural control are being analyzed (e.g., transient vs. quasi-steady-state vs. fatigue) [2]. Recommendations for longer acquisition durations are largely based on improving CoP measure reliability [3], without regard for potentially valuable transient characteristics. Identifying an initial transient response to the loss of visual information may be insightful for test design and interpretation of these clinically-relevant balance parameters. It may also provide new postural control outcomes to complement existing methods.

The purpose of this study was to investigate the dependence of clinically-relevant postural control parameters on acquisition time during QEC.

METHODS

Forty-five individuals participated in this study after providing IRB-approved informed consent. Data were collected at the 2017 American Society of Biomechanics Annual Meeting in Boulder, CO. Participants were generally healthy, without known neurological impairment, prior joint replacement, or lower extremity injury within the preceding 3 months (f/m=16/29; 29.3±7.8yr; 77.3±16.1kg; 1.76±0.10m).

Three 60-second QEC trials were collected. Participants stood as still as possible with the medial borders of their feet separated by 5 cm, looking forward with their arms at their sides. Participants counted down aloud '3-2-1-GO', where they closed their eyes as they said 'GO', which also marked the start of each 60 second trial. CoP data were recorded at 1000 Hz using a balance plate (Bertec Corp.), and low-pass 4th-order Butterworth filtered at 20 Hz.

Descriptive CoP parameters of RMS_ml, medial-lateral mean velocity (MVEL_ml), and 95% confidence ellipse area (EA) were calculated for 5-second epochs (n=12), with filtered CoP data demeaned separately for each epoch. Increases in these balance measures indicate worse balance.

Linear mixed models were used to identify the effects of epoch and trial number on these balance parameters (MINITAB). Participant was considered as a random effect, with epoch, trial number, and epoch*trial number as fixed effects. Natural logarithms were taken of balance parameters to satisfy normality and equal variance assumptions. Tukey post-hoc comparisons were made with a family error rate of α=0.05.

RESULTS AND DISCUSSION

The effect of epoch was significant for all balance measures (Table 1). The initial transient period following eyes closure was associated with worse balance for all three balance measures (Figure 1). The first 5 to 10 seconds (depending on the balance parameter) were significantly different from the remainder of the trial ($p<0.05$). The balance measures appeared to reach quasi-steady-state after 15 to 35 seconds, marked by epochs that were statistically similar to the final epoch (all pairwise comparisons, $p>0.05$).

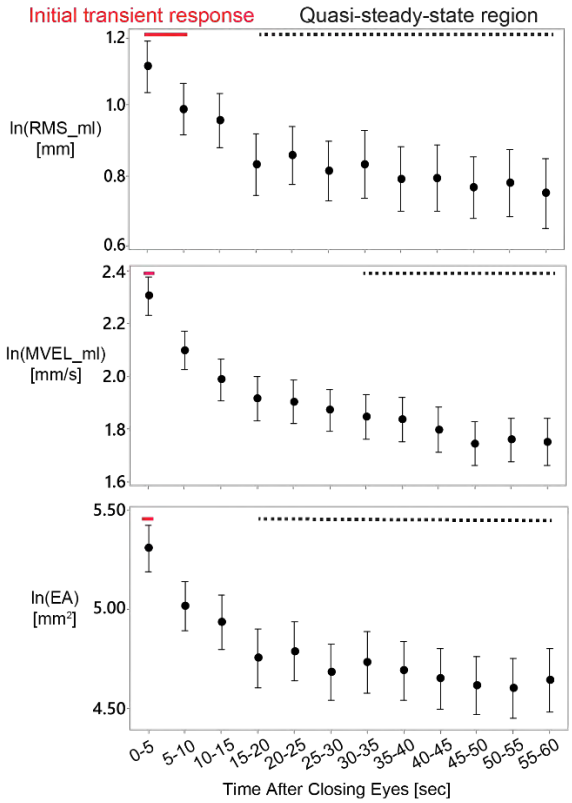

Figure 1. Time-varying behavior after closing eyes during quiet stance. **Solid red line** and the **dotted black line** correspond to epochs statistically similar to the first 5 seconds or last 5 seconds of the trial, respectively. Values correspond to mean ± SD.

Additionally, trial number had a significant effect on all measures, with worse balance observed during the first trial compared to the third (Table 1). An epoch*trial interaction was also observed for MVEL_ml. The greatest discrepancies between trials were during the transition from the transient to quasi-steady-state regions (Figure 2), with no differences detected between trials within the first or last epochs.

Table 1. P-values for model fixed effects.

	RMS_ml	MVEL_ml	EA
Epoch	**0.03**	**<0.001**	**0.02**
Trial	**<0.001**	**<0.001**	**<0.001**
Epoch*Trial	0.71	**0.03**	0.63

These findings demonstrate the transient effects that are prevalent in commonly used descriptive CoP measures during QEC. Increasing acquisition time may improve the reliability of these measures by increasing the relative weight of the reproducible quasi-steady-state response, but consequently removes the initial transient response. Notably, while the transition between the first epoch and quasi-steady-state was somewhat variable, all balance parameters gave repeatable estimates for the initial epoch.

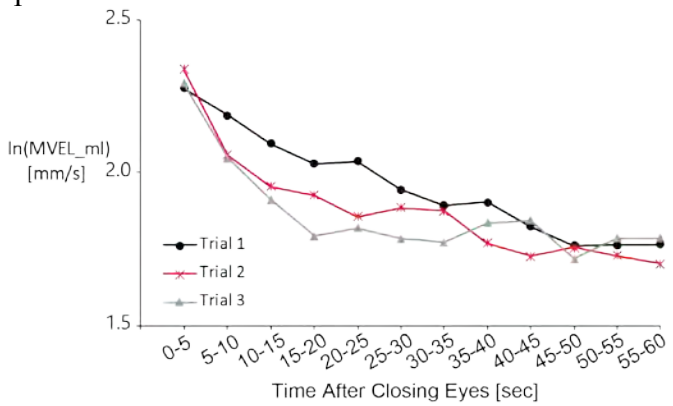

Figure 2. Effect of trial number on time-varying behavior of MVEL_ml. Mean values are presented.

The results of this study indicate that care should be taken when comparing descriptive CoP measures obtained using varying acquisition times, as the relative contribution of transient versus quasi-steady-state may influence estimates. Our ongoing work is investigating whether isolating aspects of the transient response (e.g., estimate for epoch 1, rate of decay to steady-state) provides valuable information.

CONCLUSIONS

Commonly used descriptive CoP measures demonstrate a repeatable transient period of relatively worse balance following closing one's eyes. Acknowledging this behavior may aid researchers in making decisions on acquisition time. Further work is needed to understand the potential value in isolating characteristics of the transient response when assessing postural control.

REFERENCES

1. Maki et al. *J Gerontology*. 49(2): M72-M84, 1994.
2. van der Kooij et al. *Gait & Posture*. 34: 19-24, 2011.
3. Carpenter et al. *Gait & Posture*. 13: 35-40, 2001.

ACKNOWLEDGEMENTS

We would like to thank the American Society of Biomechanics, ASB 2017 attendees who participated, and OSU and UD volunteers for their support of this ASB Quick Study.

ENVIRONMENT-DEPENDENT MODULATION OF HUMAN ANKLE STIFFNESS DURING UPRIGHT POSTURAL BALANCE

[1] Varun Nalam, [1] Tanner Bitz, and [1] Hyunglae Lee

[1] School for Engineering of Matter, Transport, and Energy, Arizona State University, Tempe, AZ, USA
email: hyunglae.lee@asu.edu, web: http://faculty.engineering.asu.edu/hlee

INTRODUCTION

Robotic lower limb exoskeletons have gained prominence in many fields including industrial, military, and clinical applications, for performance enhancement, assistance, and rehabilitation. For such devices, proper control of the robotic ankle joint in accordance with human ankle behavior is essential to achieve seamless and stable interaction of the human-robot system. Thus, it is imperative to understand how human ankle mechanics are controlled during interaction with the physical world, which is the main goal of this study.

Two main objectives of this study are: 1) to investigate how ankle stiffness, an integral component of ankle mechanics, is modulated when humans maintain upright posture against a wide range of physical environments, from compliant to rigid environments, and 2) to identify underlying mechanisms or contributing factors of environment-dependent modulation of ankle stiffness. Ankle stiffness was quantified in 2 degree-of-freedom (DOF) of the ankle, specifically, in dorsiflexion and plantarflexion (DP) in the sagittal plane and in inversion and eversion (IE) in the frontal plane.

METHODS

Five healthy male individuals (age: 18−28, height: 170−191 cm, and weight: 56−85 kg) with no reported history of neurological or biomechanical disorders were recruited for this study. This study was approved by the Institutional Review Board of Arizona State University and all experiments were performed after informed consent of the subjects.

In this study, a novel multi-axis robotic platform was used, which is capable of simulating a wide range of mechanical environments as well as providing precise perturbations to the ankle in 2 DOFs [1]. Surface electromyographic (EMG) signals of tibialis anterior (TA), soleus (SOL), peroneus longus (PL), and medial gastrocnemius (GAS), were also measured to estimate activation of major, superficial ankle muscles.

Each subject participated in two sets of experiments. First, subjects interacted with environments having different levels of compliance in order to investigate the environment-dependent modulation of human ankle stiffness. Next, subjects maintained upright posture in a rigid environment with different levels of muscle co-contraction in order to analyze the underlying mechanisms of stiffness modulation.

In the first experiment (compliant trials), subjects were instructed to stand upright in the simulated compliant environments and maintain the platform in a horizontal position. Three levels of compliant environments were simulated in each DOF of the ankle: 50, 150, 450 Nm/rad in DP and 16.7, 50, 150 Nm/rad in IE. These ranges were approximately from one third to three times the ankle stiffness in that particular DOF. When a compliant environment was simulated in one DOF, a rigid environment was implemented in the other DOF.

In the second experiment (rigid trials), in order to control the level of muscle co-contraction during standing, subjects were instructed to simultaneously maintain the target activation level of TA and the neutral position of the center-of-pressure (CoP) measured during quiet standing. Target muscle activation levels for TA were selected as 0, 10, and 20% of its maximum voluntary contraction (MVC).

For the quantification of ankle stiffness, brief ramp-and-hold perturbations (amplitude: 3°, speed: 40°/s) were applied to the ankle. Perturbations were applied in dorsiflexion, inversion, and eversion in a random order. Ten repeated trials were completed for each of 9 experimental conditions: 3 compliance levels x 3 perturbation directions for the first experiment, and 3 muscle co-contraction levels x 3 perturbation directions for the second experiment.

Ankle stiffness was quantified by fitting a linear 2nd order model, consisting of ankle stiffness, ankle damping, and foot inertia, to the measured ankle kinematics and torques.

RESULTS AND DISCUSSION

In the first experiment, ankle stiffness in DP (DP stiffness) was modulated in an environment-dependent manner. It linearly increased (from 56.4 to 90.1 Nm/rad) with increasing compliance of mechanical environment (Fig. 1A), which was highly correlated with notable increase in TA muscle activation (Fig. 2A). On the other hand, ankle stiffness in IE (IE stiffness) was not significantly influenced by the compliance of mechanical environment (Fig. 1B and 1C), consistent with no significant changes in activation of major, superficial ankle muscles (Fig. 2B).

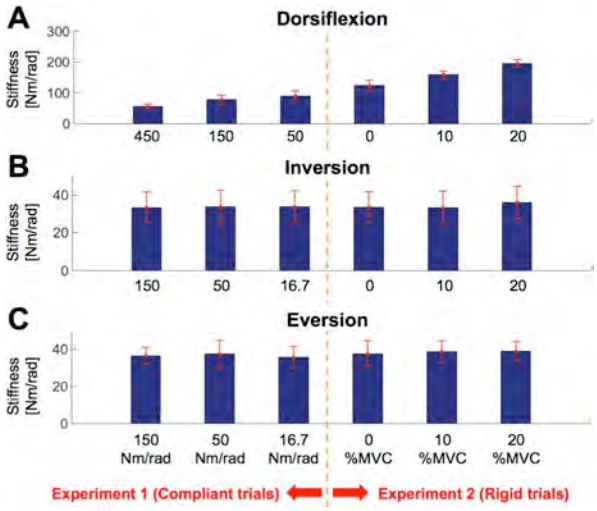

Figure 1 Ankle stiffness in compliant and rigid trials. **A**: dorsiflexion, **B**: inversion, **C**: eversion.

In the second experiment, co-contraction of ankle muscles effectively increased DP stiffness (Fig. 1A). It linearly increased (from 123.4 to 195.8 Nm/rad) with increasing muscle co-contraction. In contrast, IE stiffness was relatively invariant in all muscle co-contraction levels (Fig. 1B and 1C).

Notably, DP stiffness values in all compliant trials were lower than those in the rigid trials. Even the stiffness in the most compliant trial was lower than in the rigid trial during quiet standing (Fig. 1A), while overall activation of ankle muscles was significantly higher in the compliant trial than the rigid trial (Fig. 2A vs. 2C). This suggests that there exists additional factor involved in the modulation

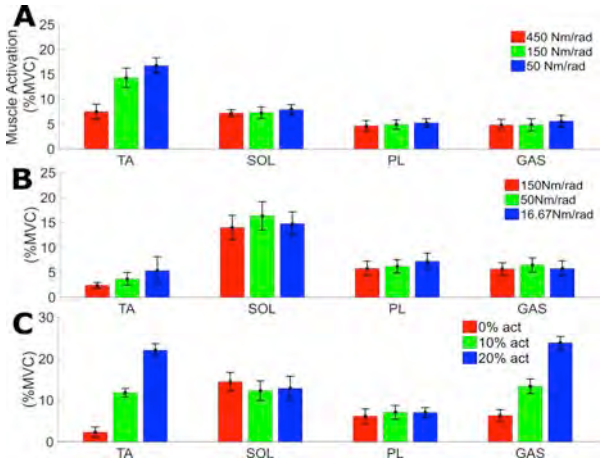

Figure 2 Muscle activation prior to the perturbation during (**A**) compliant DP trials, (**B**) compliant IE trials, and (**C**) rigid trials.

of DP stiffness apart from muscle activation of major, superficial ankle muscles.

Analysis of CoP demonstrated that there exists a positive correlation between DP stiffness and the location of CoP from the DP ankle axis. The CoP was about 53-56 mm in front of the DP axis in the rigid trials, while the CoP was close to the ankle axis (<1.5 mm) in the compliant trials.

Contrary to DP stiffness, IE stiffness values in all compliant trials were comparable to those in the rigid trials. Analysis of CoP in IE further supports the dependency of ankle stiffness on CoP. The location of CoP from the IE ankle axis was close to the ankle axis (<0.5 mm) in both rigid and compliant trials.

CONCLUSIONS

This study demonstrated that DP stiffness is modulated in an environment-dependent manner, while IE stiffness is not, at least in the given experimental conditions. Importantly, activation of superficial ankle muscles cannot fully account for the modulation of ankle stiffness, but it is necessary to incorporate CoP information to explain the modulation of ankle stiffness during upright postural balance. Knowledge gained in this study would aid in the development of a robust model-based controller for the robotic ankle joint.

REFERENCES

1. Nalam and Lee. *Proceedings of IEEE ICRA 2017,* Singapore, 511-516, 2017.

A PILOT STUDY OF ARGENTINE TANGO TO IMPROVE POSTURAL CONTROL AMONG CANCER SURVIVORS

[1] Lise Worthen-Chaudhari, [2]Marie Lamantia, [3]Scott M Monfort, [1]Ajit MW Chaudhari, [1]Maryam B Lustberg

[1] The Ohio State University, Columbus OH
[2] Ohio University Heritage College of Osteopathic Medicine, Dublin, OH
[3] Montana State University, Bozeman, MT
email: lise.worthen-chaudhari@osumc.edu, web: http://embeddedarts.tumblr.com/

INTRODUCTION

The most commonly reported serious adverse effect of cancer treatment, called chemotherapy-induced peripheral neuropathy (CIPN), impairs postural control [1] to the point that balance and walking become dysfunctional [2], risk of falling increases [3], and dose intensity of life saving chemotherapy is decreased which negatively impacts survival. CIPN has been reported to affect more than half of individuals who receive a neurotoxic chemotherapy agent and to persist chronically [4].

While balance training represents the best known medicine for neurotoxicity recovery [5], and has been proven feasible for cancer survivors to perform even during treatment [6], adherence and motivation to activity-based medicine represent challenges to participation [6]. Social, creative engagement in balance training has been proposed as an avenue to improve patient participation [7] but has received little study in cancer survivorship. Community-based social dance classes in Argentine Tango (ATango) – adapted for persons with movement disorders – were found previously to improve balance in populations with neurological disorders such as Parkinson Disease [8]. The purpose of this pilot study was to establish feasibility of ATango practice among cancer survivors and to characterize the effect of 5 weeks of practice on biomechanical measures of postural control among cancer survivors with demonstrated balance deficits. As an exploratory aim, we evaluated whether enrolling with a guest (e.g., friend, date, spouse) affected attendance.

METHODS

Participants: Twenty-two cancer survivors enrolled after providing IRB-approved informed consent (age 60.8 (9.2) years; 2 male). Nine enrolled with a partner (e.g., life partner or friend; 2 male). Six demonstrated impaired postural control at baseline (2 male); five completed chemotherapy treatment at least 3 months prior to baseline data collection and were included in this study (age 66.4 (11.7) years; 1 male).

Intervention: Partnered ATango, adapted for individuals with movement disorders [8]

Primary outcome: Postural sway amplitude (Root-Mean-Square amplitude of medial-lateral excursion during quiet standing with eyes closed; RMS_ml) was measured using a portable force platform (1000Hz, Bertec Corp) and custom software written in LabVIEW. Participants were assessed at baseline and at 5 weeks using the protocol reported by Monfort et al. This measure has shown sensitivity to identify changes in balance control associated with cancer treatment [1] and has been found to identify future fallers among elderly with and without neurologic impairment (71% overall accuracy; 81% sensitivity; 58% specificity) [9].

Postural control deficit categorization criteria: Participants were included in postural control change analysis if baseline RMSml was greater than the previously reported mean value for age matched healthy individuals at 75% CI (> 4.54mm) [10].

Secondary outcomes: Participant satisfaction per session; attendance; movement-to-music dose per class.

Statistical analysis: Student's t-test (2 tail, pairwise comparison) was used to evaluate the primary outcome measure (pre vs. post RMSml). Additionally, we report the count of participants for whom individual change exceeded typical within subject variability for the dynamic measure [10]. The MannWhitney U non-parametric statistical test was applied to evaluate the effect of enrolling with a partner on attendance. Descriptive statistics were calculated for secondary outcomes

RESULTS AND DISCUSSION

Participants with postural control deficits (n=5) showed improvement after 5 weeks of ATango practice (mean (SD) pre 7.9 (1.8) mm and post 4.4 (0.6) mm; p = 0.010). Individually, each of the 5 participants improved beyond what could be expected due to healthy, age-matched within-subject variability (Fig1A).

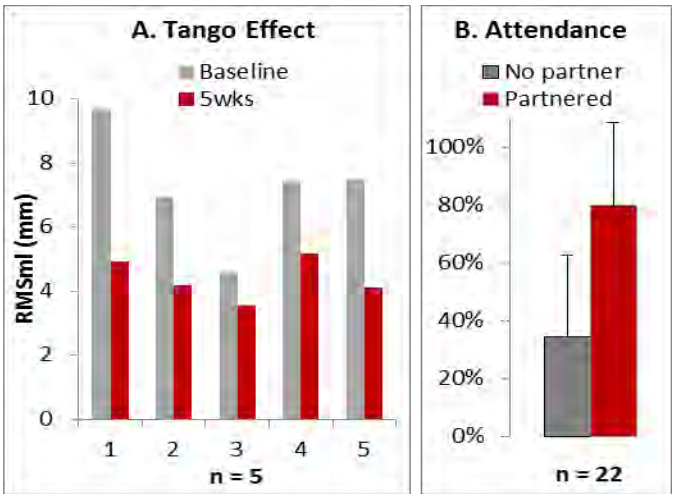

Figure 1: (A) Effect of Argentine Tango practice on postural control (RMSml) for 5 individuals who demonstrated postural control deficits at baseline and (B) effect of enrolling with a partner on attendance.

Those who enrolled with a partner (n=9) attended more classes (p=0.011; *U*-value = 20) with a mean rate of 80 (28) % attendance compared to 35 (28) % attendance for those who did not enroll with a partner (Fig 1B).

Satisfaction with the intervention was high (average = 1.2 +/- 0.5). A majority of participants attended at least half of classes offered (55%). Movement-to-music dose was calculated to be 32.9 (3.9) minutes per one hour class.

CONCLUSIONS

These data provide initial support for the idea that postural control function is recoverable among cancer survivors. In addition, the practice of Argentine Tango may be a candidate intervention for this population and attending with a life partner or friend may be a way to improve participation in the activity-based practice.

REFERENCES

1. Monfort et al. **164**(1): *G&P*. 2016.
2. Gewandter et al. **21**(7): *Support Care Canc* 2013.
3. Huang et al. **8**(4): *J Geriatr Oncol* 2017.
4. Stubblefield et al. **7**: *J Natl Comp Canc Net* 2009.
5. Streckmann et al. **25**(2): *Ann Onc* 2014.
6. Knols et a;. **23**(16) *J Clin Onc*, 2005.
7. Worthen-Chaudhari **33**(3): *NeuroRehab* 2013.
8. Hackney et al. **24**(4): *Neuroreh Neur Repair* 2010.
9. Maki et al. **49**(2): *J Geron Med Sci* 1994.
10. Worthen-Chaudhari et al.: *Proc ASB* 2017.

ACKNOWLEDGEMENTS

Thank you to The James Care for Life cancer survivorship program as well as to volunteers who supported this research: Courtney Bland, Shelia N. Zeng, Maureen Kleinhenz, Kelsey Kempner.

GUIDED PRE-CLASS ASSIGNMENTS ENHANCE STUDENT LEARNING AND INTEREST IN UNDERGRADUATE BIOMECHANICS

Hilary Becker and James Becker

Montana State University, Bozeman, MT, USA
email: james.becker4@montana.edu, web: http://montana.edu/biomechanics

INTRODUCTION

Several studies on biomechanics instruction have highlighted the benefits of using active learning strategies such as Just-in-Time Teaching [1], problem or challenge based learning [2], or inquiry based learning [3]. These approaches share the common theme of in-class lecture time being spent engaging students in the learning process rather than passively receiving content from the instructor, and result in improved student performance and learning over the course of the semester. However, to date, studies on the benefits of active learning have mainly focused on what happens during the actual in-class lecture time. In comparison, relatively little attention has been given to best methods for preparing students for in-class activities prior to class. Ensuring students have appropriate content knowledge prior to participating in active learning classes might further enhance the benefits of this approach to biomechanics education.

The purpose of this study was to compare student learning, interest in biomechanics, and perceptions of course difficulty when using two types of pre-class assignments: a traditional approach where assignments consisted of chapter readings and problem sets, and an approach which provided guided content based questions interspersed with applications and problems. We hypothesized the guided pre-class assignments would result in higher student learning over the semester and increased interest in biomechanics.

METHODS

This study was conducted during two successive semesters in an undergraduate biomechanics course. The course is a required component of the Exercise Science curriculum and is typically taken in either the junior or senior years. The course uses a problem based learning approach where the emphasis during in-class lecture time is working in groups to solve problems related to the days' topic.

The first semester used traditional (TRAD) weekly assignments consisting of reading assigned chapters in the textbook and problem sets featuring one or two problems integrating material from the readings and lecture content. Students were instructed to complete required readings before class. During the second semester the weekly readings were replaced with daily guided pre-class assignments (GUIDED). Rather than assign specific chapters from the textbook, these assignments outlined the required content and concepts and allowed students to obtain the information from any source they saw fit, provided they included appropriate citations. Each topic area was loosely grouped into a "chapter" with different sections of the chapter being due each day. The same problem sets used in the first semester were included as the last section of each "chapter".

The Biomechanics Concept Inventory, version 3 (BCI3) [4], was administered during the first and last weeks of both semesters. Student learning during the semester was evaluated by calculating the gain in BCI3 scores from beginning to end of semester, normalized by the maximum possible change [4]. A survey was administered at the end of each semester which, using 5 point Likert scales, asked students to rank their interest in biomechanics at the beginning and end of the semester, the perceived difficulty of the course compared to their expectations prior to the semester, and the extent to which they felt homework assignments contributed to their learning. Paired *t*-tests were used to evaluate differences between TRAD and GUIDED groups in BCI3 scores pre and post class and gain in BCI3 scores. Mann Whitney U tests were used to to compare differences in Likert scale survey

responses. An alpha of $p < .05$ was used for all statistical comparisons.

RESULTS AND DISCUSSION

Thirty eight and forty seven students completed pre and post semester BCI3 assessments and post-semester surveys in the TRAD and GUIDED semesters, respectively. Pre-semester BCI3 scores were not different between groups ($p = .138$). However, post-semester BCI3 scores were higher in the GUIDED group ($p = .005$). Gain in BCI3 scores was also higher in the GUIDED group ($p = .006$).

Table 1. Mean values for pre-semester, post-semester, and gain in BCI3 scores. * indicates significantly different at $p < .05$ level.

	TRAD	GUIDED
Pre BCI3 scores	12.5 (± 2.2)	13.2 (± 2.3)
Post BCI3 scores	14.3 (± 2.9)	15.6 (± 2.2)*
Gain in BCI3	0.22 (± 0.2)	0.35 (± 0.2)*

There were no differences between TRAD and GUIDED groups in student interest in biomechanics at the beginning of the semester ($p = .032$). However, at the end of the semester students in the GUIDED group indicated higher interest in biomechanics ($p < .001$). Students in the GUIDED group also indicated the course was easier than they expected ($p < .001$) and that pre-class assignments contributed more to their learning over the semester ($p = .004$).

There are several possible explanations for these finding. First, the guided pre-class assignments allowed students to organize information in a manner which best suited their individual learning style. There is evidence to suggest that learning improves when instruction is matched with students preferred learning styles [5]. Thus, the guided pre-class learning assignments may have allowed students to utilize their preferred learning style to a greater extent. This could also explain why students indicated the course was easier than expected and the assignments contributed more to their learning than textbook readings and problem sets. A second explanation is the guided pre-class assignments required students to engage with the content rather than passively read a textbook chapter. Numerous studies have shown this type of active engagement improves reading comprehension in college students [6]. Thus, the improved learning with guided pre-class assignments could have resulted from better comprehension and retention of any material students read. Finally, it has been shown that prior domain knowledge plays a role in student learning [5]. Compared to weekly textbook readings, the daily nature of the guided pre-class assignments may have resulted in greater domain knowledge on a day to day basis prior to class, thus resulting in deeper learning of material during in-class time.

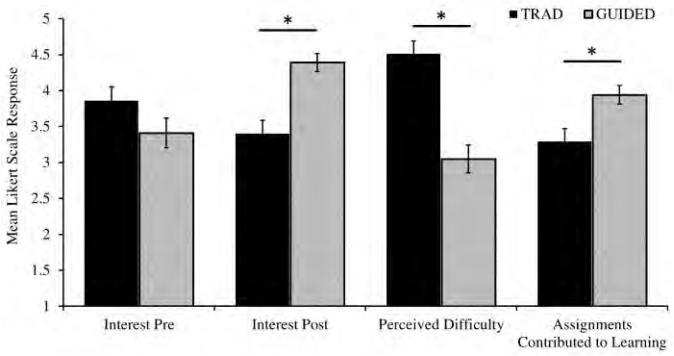

Figure 1. Mean Likert scale results for student interest pre-semester, post-semester, perceived course difficulty, and whether assignments contributed to their learning. Values of 1 indicate little interest, less difficult than expected and little contribution to learning. Values of 5 indicate highly interested, more difficult than expected, and substantially contributed to learning, respectively. * indicates significantly different at the $p < .05$ level.

CONCLUSIONS

Compared to weekly textbook reading and problem sets, daily guided pre-class assignments improve student learning in a problem based undergraduate biomechanics. Such assignments also make the course seem easier to students and increase students' overall interest in biomechanics.

REFERENCES

1. Riskowski, J. *Sports Biomech.* **14,** 168-179, 2015.
2. Roselli, R. et al. *J Engineering Education.* **95**, 311-324, 2006.
3. Duncan, M. *Practice Evidence Scholarship Teaching and Learning Higher Ed.* **3**,43-58, 2008.
4. Kundson, D. *Percept Motor Skills.* **103**, 81-82, 2006.
5. Hsieh, C., et al. *Sports Biomech*. **11,** 108-119, 2012.
6. Simon, A., et al. *Reading Improvement*. **47**, 30-43, 2010.

HANDS ON ACTIVITIES CAN IMPROVE LEARNING IN A LECTURE-ONLY QUALITATIVE BIOMECHANICS (FUNCTIONAL ANATOMY) COURSE

Robert D. Catena and Kira J. Carbonneau

Washington State University, Pullman, WA, USA
email: robert.catena@wsu.edu, web: https://labs.wsu.edu/biomechanics/

INTRODUCTION

A qualitative biomechanics (functional anatomy) course is a common course in a Kinesiology curriculum. While only a slight majority of biomechanics courses provide laboratory experiences [1], most instructors believe that laboratory experiences enhance learning outcomes in biomechanics. Even if there were significant evidence to suggest the inclusion of labs in qualitative biomechanics, most courses that don't incorporate a laboratory experience cannot because of administrative constraints (e.g. instructor cost and time) [1].

At the location of this research study, a single graduate teaching assistant will cost the department approximately $15,000 per year, on top of health benefits and tuition waivers provided by the university. Given class sizes, this university would need to offer a minimum of nine lab sections in a year to accommodate all students. That would require 2.25 graduate teaching assistants, putting the lab instructional cost at $33,750 per year.

Many programs may wish to include a hands on laboratory experience, but cannot do so in a cost-effective manner, supported by empirical evidence of the benefits. There is a critical need to determine (1) if hands on experiences do enhance student education in a qualitative biomechanics course and (2) an alternative method for providing hands on experiences applicable to qualitative biomechanics without the use of graduate teaching assistants or expensive equipment?

METHODS

Two hundred and fifty-four students were enrolled in a qualitative biomechanics course over five semesters taught by the same instructor (abstract author). The course has 45 contact hours. The sequential order of topics spread roughly evenly across the semester were: 1. Kinematics, 2. Kinetics, 3. Tissue mechanics, 4. Hand and wrist, 5. Elbow, 6. Glenohumeral, 7. Scapulothoracic, 8. Neck, 9. Thorax, 10. Pelvis, 11. Hip, 12. Knee, 13. Ankle and foot.

The sample of students were separated into two groups. Both groups were comprised of similar proportions of Athletic Training and Sport Science majors. One hundred and fifty-nine students made up the control group. The control group of students received content only through lecture, discussion and video examples. Ninety-five students made up the experimental group. The experimental group was taught by the same methods. However, three additional hands-on experiences were also included. Number 1 below was provided in conjunction with lecture. Numbers 2 and 3 replaced some (not all) video examples during the study semester:

1. Skeletal models corresponding to the joint lecture topic were provided to groups of students during lecture so that they could interact with the surrounding bones of a joint as it was taught. This was an unrestricted hands-on experience.
2. Two-channel electromyography (EMG) units (Backyard Brains) were provided to groups of students so that they could simultaneously measure muscle activity of two muscles during lower-extremity lectures. There were clear instructional procedure and outcome with this hands-on experience.
3. An isokinetic dynamometer (Isokinetic International) activity was used during one lower-extremity EMG activity to demonstrate how muscle activities correspond to joint torque production. There were clear instructional procedure and outcome with this hands-on experience.

The two groups were compared via correct answers from 22 multiple choice and short answer exam questions spread across three semester tests and subjective course evaluation questions completed after all but one test. Analyses were conducted through Chi-square tests with significance level for main effects was set to a p-value of 0.05. Post-hoc analyses were conducted though pairwise comparisons of adjusted residual z-scores with *Bonferroni* corrections.

Exam question results based on upper extremity lectures and lower extremity lectures were compared in the experimental group to determine if guided hands-on lab type experience provide any better education than unguided skeletal model use.

RESULTS AND DISCUSSION

Instructors at this university do not have access to student grade point averages to indicate if the two groups are dissimilar in overall abilities. However, there was no difference in grade point averages between the two groups as they were first certified into our program. There was one indication from student evaluations of potential differences between the makeups of the two groups. The experimental group gave significantly higher rating to the question of if they took responsibility for their learning in the course ($p=0.025$).

The results of the other course evaluation questions indicate that the two groups were not different in what they thought of the quality of the course, how much they learned, the difficulty of the course, or the variety of examples used in teaching. However, the experimental group reported the teacher's effectiveness ($p=0.021$), the encouragement for classroom participation ($p=0.027$), and the effectiveness of activities to encourage learning ($p=0.004$) as significantly higher compared to the control group.

On 22 exam questions, the experimental group did not perform significantly poorer than the control group on any test question. The experimental group performed better than the control group on 8 of the 22 questions, but 7 of the 13 questions specific to the lower extremity. However, when specifically comparing results of lower extremity test questions (EMG and dynamometry were used with skeletal models) and upper body questions (only skeletal model use) there was not a significant difference in test performance ($p=0.117$).

CONCLUSIONS

The findings from this study support the use of hands on activities embedded within a qualitative biomechanics lecture to improve education for kinesiology students and student evaluation of the course. There were some indications that guided hands on activities provide a better learning experience than unguided activities, but students at least have no change, and probably will have some benefit from unguided activities as well. The hands-on activities used in this study were easy to implement in the time allotted through lecture alone, with the exception of the dynamometry activity, which required us to split the classes up during one week.

The interaction of the physical activities and cognition is a theory rooted in cognitive science known as embodied cognition [2]. Having representations that accurately mimic the real thing in shape, and potentially also in force feedback, can significantly enhance learning in sciences foundational to biomechanics.

This study does not make any comparison in educational benefits to the official inclusion of a lab into a course. However, the one-time costs and yearly supply costs associated with the hands-on activities used in this study are significantly less than typical lab supply and instructor costs.

REFERENCES

1. Garceau et al. *Sports Biomechanics,* 2012.
2. Wilson. *Psychonomic Bulletin & Rev.* 2002.

ACKNOWLEDGEMENTS

This research was supported by a Berry Family Fellowship.

LESSONS FROM THE PAST: LEARNING ANATOMY IN THE ITALIAN RENAISSANCE

M. Melissa Gross

University of Michigan, Ann Arbor, MI, USA
email: mgross@umich.edu

BACKGROUND

Musculoskeletal modeling is an important aspect of contemporary biomechanics, and students need to know muscle attachments and functions to support their work with biomechanical models. Today, students learn musculoskeletal anatomy using print images, interactive digital media, plastic models, and plastinated cadaver materials. Undergraduate students rarely have the opportunity to dissect human cadavers, however, and the time spent in the cadaver laboratory is diminishing even in medical school [1]. As technology continues to advance, it is likely that future students will study musculoskeletal anatomy using 3D digital visualizations.

As the study of musculoskeletal anatomy in the 21st century promises to become even more virtual, pedagogical questions about the relationship between technology and anatomical visualization are inevitable. For example, should educators continue to structure anatomy learning experiences in the same way, in the absence of physical bodies? Are critical aspects of anatomical learning lost if students engage with digital materials exclusively? Scholars are tackling these pedagogical questions, especially with regard to anatomical education in professional schools [2]. These questions are also relevant for biomechanics faculty who want to help students visualize 3D muscle-tendon paths, length changes, moment arms and to understand muscle functions.

Scholars in the 21st century are not the first to grapple with the relationship between emerging technologies and anatomical visualization, and its impact on anatomical education [3]. During the Renaissance in Europe, new print technologies enabled reproduction of both anatomical texts and images on a broader scale, affecting where and how anatomical information was available. The public dissections hosted by prominent universities served both medical students eager to learn anatomy and anatomy professors interested in furthering their academic careers. University administrators invested in the construction of innovative buildings (i.e., anatomy theatres) to attract patrons and funding for their schools [4]. Later, wax anatomical models were introduced, valued for the realism and integrity of the anatomical representations.

Anatomical expertise did not reside solely in the academy, however, as artists played important roles in the advancement of anatomical sciences either through their own artistic work or as collaborators in the technical innovations of the time. Leonardo da Vinci used dissection to discover how the body functioned, and the artistic renderings of anatomy in his notebooks were representations of his thoughts and discoveries. Artists collaborated with anatomical scholars to create illustrations for the new, printed books; among the most well-known are the depictions of anatomy in Vesalius' *On the Fabric of the Human Body* published in 1543. The artists creating the anatomical wax models used for medical education innovated new techniques to form and color the wax, with each model based on dissections of many cadavers.

As the landscape of higher education today is shifting to emphasize hands-on and inquiry-based courses that leverage technological innovations, there may be lessons to be learned from considering how anatomy was studied and visualized in the distant past. Can students get insights into their own approach to learning anatomy by considering the Renaissance context for anatomical studies? With 21st century digital technologies for representing the human body and for teaching and learning anatomy, can students better understand how visualization technologies relate to learning by considering previous times of technological disruptions to established ways of knowing and learning? Exploring these questions may help to improve contemporary approaches to teaching and learning musculoskeletal anatomy.

GLOBAL STUDIES PROGRAM

To provide students with the opportunity to explore these issues while deepening their knowledge of musculoskeletal anatomy, a global studies program "Art and Anatomy in the Italian Renaissance" was created with stops in Rome, Florence, Bologna, Padua and Venice, offered in May 2018 through the School of Kinesiology at the University of Michigan. The goal of the program was to enable students to explore the intersection of art, anatomy and anatomical education during the expansion of humanistic thinking in the Renaissance, and to gain a new appreciation of the roles of art, technology and science in visualizing knowledge, then and now.

The program was designed to provide students with opportunities to: (1) expand their understanding of the cultural context for scientific discoveries while learning about the development of musculoskeletal anatomy knowledge by Renaissance artists and scientists, and (2) deepen their knowledge of surface anatomy by analyzing artworks and skeletal remains in museums, churches and public art. Because the course takes place in a global context, students could also develop important skills of autonomy and self-directed learning, improve their collaboration skills in team-based program activities, and engage with diverse others among program participants and in a global environment while immersing themselves in a non-English speaking culture by traveling in Italy.

Instruction will take place in both face-to-face (on site and in class sessions), and online (brief lectures and assignments) settings. Pre-departure academics included a session on Renaissance anatomy books by a curator from the U-M Special Collections Library, and an introduction to field notes session. In Italy, on site instruction will take place in art museums, anatomy theaters, anatomical wax museums, churches, catacombs, libraries, cultural sites and public places with art. Students participating in the program had basic anatomical knowledge since the prerequisite was a sophomore-level musculoskeletal anatomy course. Because surface anatomy is an important clinical skill [5], students will be encouraged to practice by applying their anatomical knowledge to the drawings, paintings, sculpture and wax models that they will encounter in Italy. To support students' understanding of Renaissance art, a History of Art scholar served as the course co-instructor.

Assignments include field notes, in which students collect, document and make visual records of their observations of musculoskeletal anatomy throughout the program. Students will also be asked to write short reflection papers about their observations and experiences, complete pre-work before visiting sites and give brief presentations to the group. Inspired by Leonardo's notebooks, the final project will be a compilation of their field notes, with embedded written reflections on the intersection of art and anatomy. Student perceptions of their learning will also be gathered using survey questions.

LEARNING ASSESSMENT

Student learning will be assessed on the assignments (IRB Exempt status). Qualitative analysis of their field notes, site-specific assignments and reflection papers will be used to assess the impact of the experience on their understanding of cultural contexts for visualizing musculoskeletal anatomy, especially with regard to technologies used for learning and demonstrating anatomy. It is expected that the students' knowledge of musculoskeletal anatomy will be reinforced by critical examination of artworks for anatomical correctness, as demonstrated in their field notes documents. It is also expected that students will be able to describe how anatomy was learned in the Renaissance, the relationship between anatomy and art in the Renaissance, and how the impact of technology on anatomical education in the Renaissance may relate to learning anatomy today.

REFERENCES

1. McLachlan and Patten. *Med Ed.* 40: 243, 2006.
2. Sugand et al. *Anat Sci Educ*. 3: 83, 2010.
3. Moxham and Plaisant. *Eur J Anat*. 18: 219, 2014.
4. Ferrari. *Past & Present* 117:50, 1987.
5. Standring S. *Clin Anat.* 25: 813, 2012.

INTRODUCING ENGINEERING AND BIOMECHANICS TO PREK-6 STUDENTS THROUGH A SERVICE LEARNING PARTNERSHIP

Stacie I Ringleb, Jennifer Kidd, Rachel Jones, Pilar Pazos
Old Dominion University, Norfolk, VA, USA
Email: sringleb@odu.edu

INTRODUCTION

Engineering education faces many persistent challenges including recruiting and retaining students, teaching engineering students to work successfully in groups, and communicating both within and outside their discipline.

Education majors are facing new challenges relevant to the field of engineering given the recent incorporation of engineering practices and core ideas into the Next Generation Science Standards (NGSS) at the elementary school level. Elementary preservice teachers can flourish if they are exposed to and learn content that is directly relevant to the science and engineering standards that they must teach in their own future classrooms [1].

The purpose of the described project was to tackle these challenges by grouping first year engineering students with pre-service teachers to develop and deliver engineering lessons to preK-6 students in Norfolk, VA. In this abstract, the experiences of three groups of students who developed and delivered lessons on prosthetics to 4-6th graders are described.

METHODS

First year mechanical engineering students were partnered with third year education students as part of existing courses within their disciplines. Small groups of 4-6 students developed prosthetic lessons which were taught to fourth graders (Fall 2016), fifth graders (Spring 2017) and sixth graders (Fall 2017). Google Sites were used to build a collaborative platform for each group that included templates and protocols designed to scaffold the lesson development process and facilitate collaboration and information sharing. The lessons were developed using the 5 E's principles (Engage, Explore, Explain, Extend, and Evaluate). After the lesson plan was drafted, students rehearsed their lessons in front of another group and a faculty member or graduate student. Lessons were finalized after students received feedback on their drafts and met with one of the course instructors. After the lesson was delivered, each student wrote a detailed reflection on the experience. The reflections were qualitatively analyzed to explore perceived benefits and challenges. In particular we wanted to determine what the college students learned from their experience and to ascertain the education students' comfort level teaching engineering.

RESULTS AND DISCUSSION

Three groups, including a total of eight engineering (6 male, 2 female) and nine education students (4 male, 5 female) developed lessons about prosthetics. Each team took a different approach. One team 3D printed prosthetic hands (Fig. 1) from plans obtained from the internet [2], while the other two groups designed their prosthetic hands with used materials such as clay, straws, and string (Fig. 2).

Six engineering and eight education students submitted post-project reflections. When asked what they learned from the experience, most (4/6) engineering students stated that they didn't learn anything about engineering. Few engineering (1/6) and most education (7/8) students discussed the experience of working with a group. Some comments about group work

were positive, for example, how working in groups was beneficial to increased idea generation. However, there were also some drawbacks discussed such as scheduling difficulties and lack of accountability.

Fig 1. Students building prosthetic hands

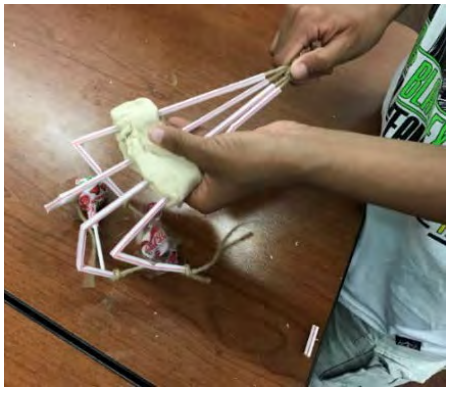

Fig 2. Prosthetic hand made with clay.

Most of the engineering students (4/6) explicitly stated that they had positive reactions to working with the students. One student wrote: "The most valuable part of this lesson was seeing how interested the kids were and how excited they were to try and come up with a solution."

Half of the education students explicitly stated that they have a new understanding and appreciation for engineering. Two students noted the creativity required to be an engineer. One student stated, "I was under the impression that engineers just built bridges and buildings, I was not aware that they also worked in medicine and computers." When asked how comfortable they would feel teaching an engineering lesson in the future, all the respondents said they would be willing to do so, but all but one said they would want support in order to do so.

Several things were learned from examining these groups. First, the engineering students perceived that they did not learn new content in engineering. We believe that is because they were not explicitly taught about the engineering design process and how their lesson development was an example of an iterative design experience. Future classes will receive this instruction, so they can draw a connection between this project and engineering. Secondly, education students were able to gain comfort with engineering from just one collaborative lesson with engineers. Partnerships such as the one described here could increase teachers' confidence with engineering, thereby increasing elementary students' exposure to (and interest in) engineering. Finally, cross disciplinary partnerships have the potential to cultivate communication and collaboration skills and increase understanding of engineering, but group work must be carefully scaffolded and supported. Even with such supports in place, many of these students reported challenges.

REFERENCES

[1] Steinberg et al. J College Science Teaching, 44(6): 51-57, 2015
[2] https://www.thingiverse.com/thing:1717809

ACKNOWLEDGEMENTS

This research was partially funded by an Improving Disciplinary Writing Action Project and a Service Learning Grant at ODU.

REQUIRED MUSCLE ACTIVATION DEPENDENCE ON MOMENT ARM AND MAXIMUM SHORTENING VELOCITY: A COMPUTER SIMULATION STUDY

Lauren J. Hickox and Stephen J. Piazza

The Pennsylvania State University, University Park, PA, USA
email: piazza@psu.edu, web: http://www.biomechanics.psu.edu/

INTRODUCTION

The leg muscle fascicles of sprinters have been shown to be longer than those of distance runners and sprinters have a higher percentage of fast-twitch muscle fibers [1,2]. Both of these properties would tend to reduce the attenuation of muscle force generation during muscle shortening that occurs due to the force-velocity property. In addition, previous studies have found that sprinters have smaller plantarflexor moment arms than non-sprinters, similarly reducing force-velocity effects by decreasing muscle shortening velocity for a given joint rotational velocity and thus increasing force generation [3,4].

Understanding muscle's capacity to produce movement requires knowledge of how limb and joint structure (e.g., muscle moment arm) interacts with muscle architecture and force-generating properties. The purpose of this study was to use computer simulation of a simple submaximal concentric plantarflexion task to determine how demand on the muscle (i.e., muscle activation) is affected by plantarflexor moment arm and composition. We hypothesized (1) that reducing muscle moment arm would reduce demand on the muscle (but only to a point) and (2) that increasing the maximum shortening velocity v_{max} in the force-velocity relation would also reduce the muscle demand.

METHODS

A simple 1-DOF planar musculoskeletal model was developed in Simscape Multibody (Mathworks, Inc., Natick, MA, USA) and used to simulate a submaximal plantarflexion task against an inertial load. The model consisted of two segments, a shank and a foot (properties based on [5]), and two Hill-type muscle-tendon actuators representing lumped plantarflexors (PF) and dorsiflexors (DF) (Fig. 1). The distal end of the foot segment was attached to a 50 kg mass by a revolute and the mass was allowed to slide along an incline. The task was to push the mass a distance of 10 cm along the incline in a fixed amount of time (0.5 s), with zero initial velocity and no constraint on terminal velocity.

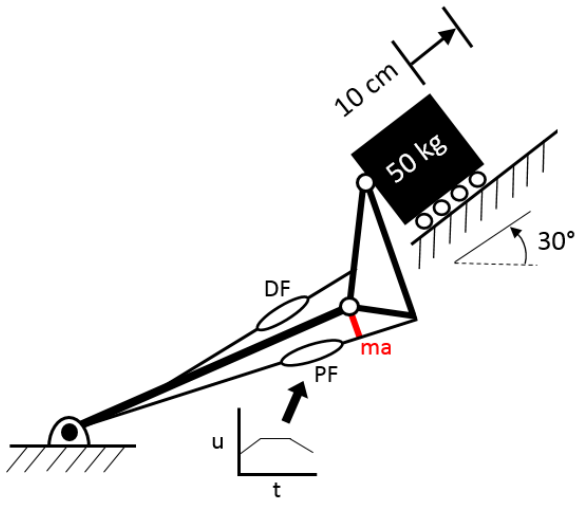

Figure 1: Schematic illustration of the model and the plantarflexion task. Plantarflexor moment arm (ma) was varied along with plantarflexor v_{max}.

Parameter optimization was used to find control strategies that minimized the area under the squared activation curves for both the PF and DF muscles. The fmincon() routine in MATLAB (Mathworks, Inc., Natick, MA, USA) was used to find excitations (11 evenly spaced nodes for each muscle actuator) that minimized activation.

Optimizations were repeated with the length of the plantarflexor moment arm varied from its default value by approximately -8, -4, 0, +4, and +8 mm by altering the length of the heel in the model. Sets of optimizations with these moment arm variations were run for different values of v_{max}, which was used as a surrogate for muscle composition. Increasing v_{max} was intended to represent muscles with a higher

proportion of fast-twitch muscle fibers. When v_{max} was changed (by -20%, -10%, 0, +10%, and +20%) the entire force-velocity curve was scaled in the velocity direction.

RESULTS AND DISCUSSION

Moment arms smaller and larger than the default value caused an increase in the PF activation required to complete the task (Fig. 2a). Minimum activation was achieved with a PF moment arm that was 3-4 mm smaller than the default. When maximum shortening velocities were varied, similar U-shaped patterns were seen over the range of moment arms simulated (Fig. 2b). The dependence of activation on moment arm was found to vary with v_{max}, however: Faster muscles with higher v_{max} produce a less pronounced minimum with lower activations required for the smallest and largest moment arms.

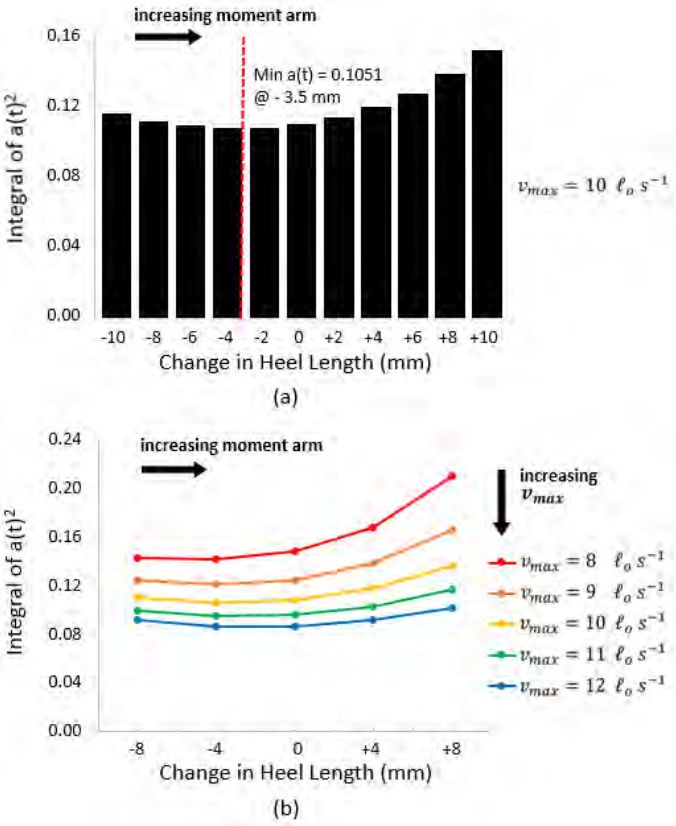

Figure 2: Integrated plantarflexor activation for varying moment arms (heel lengths) and maximum shortening velocity.

The interaction between these two musculoskeletal characteristics may affect the capacity for performing activities requiring rapid plantarflexion under load, such as sprinting. Consider two runners, one born with a high percentage of fast-twitch (faster maximum shortening velocity) fibers and one born with a lower percentage. The relative flatness of the high-v_{max} curves in Figure 2b, suggest that the runner with more fast-twitch fibers would be less affected by variation in PF moment arm. The runner with fewer fast-twitch fibers might still be an effective sprinter, but only with the right PF moment arm. With longer moment arms, this latter runner must activate the plantarflexors with twice the intensity as the first runner, and sprinting performance may thus be substantially limited.

This simulation study demonstrated an interaction between two PF muscle characteristics, moment arm and maximum shortening velocity in terms of their effect on required activation during a submaximal plantarflexion task. The results suggested that runners with a higher percentage of fast-twitch fibers may have greater potential as elite sprinters, regardless of the length of their PF moment arms. Muscle composition was also found to have a larger effect on required activation for runners with larger moment arms. The primary limitation of this study is that it involved only simulations and not experiments. Also, mathematical muscle models such as that used in this study fail to represent several important aspects of muscle-tendon behavior. Future work will focus on determining whether the same dependence on muscle moment arm and muscle composition exist in human subjects.

REFERENCES

1. Abe T, et al. *Med Sci Sports Exerc* **32**, 1125-1129, 2000.
2. Costill DL, et al. *J Appl Physiol* **40**, 149-154, 1976.
3. Baxter JR, et al. *Proc Biol Sci* **279**, 2018-2024, 2012.
4. Lee SSM and Piazza SJ. *J Exp Biol* **212**, 3700-3707, 2009.
5. Arnold EM, et al. *Ann Biomed Eng* **38**, 269-279 2010.

ACHILLES TENDON STRUCTURE DOES NOT CHANGE IN TRAINED DISTANCE RUNNERS

[1] Todd J. Hullfish, [1] Kenton L Hagan, [2] Ellen Casey, [1] Josh R. Baxter
[1] University of Pennsylvania, Philadelphia PA, USA
[2] Hospital for Special Surgery, New York, NY, USA
email: josh.baxter@uphs.upenn.edu, web: https://www.med.upenn.edu/motionlab/

INTRODUCTION

Achilles tendinopathy is a painful degeneration of the tendon that is ten-times more common in running athletes compared to age-matched peers [1]. Tendon loads in excess of twelve body weights are cyclically applied during running, which may be the driving factor in tendinopathy development in these athletes. However, the progression of asymptomatic and symptomatic tendinopathies is not well understood. Structural changes associated with symptomatic tendinopathy such as decreased collagen alignment – or 'organization' – and increased tendon thickness have both been reported in athletic populations. Previous work by our group has demonstrated that competitive collegiate distance runners have thicker and less organized tendons than their recreationally active peers (**Fig. 1**) even in the absence of signs or symptoms of tendinopathy [2]. However, it is unclear how tendon structure in highly-trained runners changes in response to prolonged bouts of training.

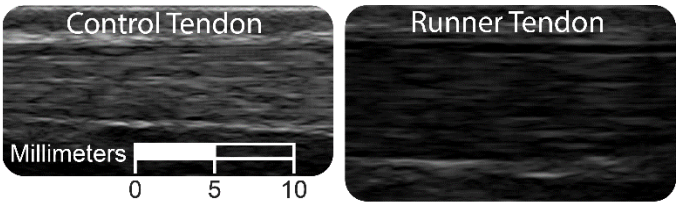

Figure 1. Competitive distance runners have thicker Achilles tendons that are darker in appearance when imaged using ultrasonography and are less organized [2].

Therefore, the aim of this study was to prospectively quantify Achilles tendon structure in competitive distance runners at the beginning and completion of a cross country season. We hypothesized that, in the absence of injury, there would be no significant changes in tendon thickness, organization, or echogenicity for a runner with a habituated tendon.

METHODS

Nineteen collegiate cross country runners (9 females; Age: 19 ± 1.5 years; Height: 172 ± 7 cm; Weight: 60.4 ± 8 kg) provided written consent in this IRB approved study. All participants had no signs or symptoms of Achilles tendinopathy before or after participation. Data were acquired one week prior to and one week following the competitive Division I NCAA Cross Country season. A self-reported assessment of tendon health and a quantitative ultrasound assessment was performed at each study visit. Subjects were asked to fill out a clinical outcome questionnaire (VISA-A [3]) to determine their level of health and function. The structure of the tendon was determined by measuring the level of organization present in its collagen fascicles through ultrasonography.

Longitudinal B-mode ultrasound images of the of the mid-substance of the right Achilles tendon were acquired while subjects lay prone on a treatment table with ankles placed in the resting position off the end of the table. Images were acquired using an 18 MHz transducer (L18-10L30H-4, SmartUs, TELEMED) with a scanning width of 3 cm (scan parameters: Dynamic Range: 72dB; frequency: 18 MHz; gain: 47 dB). Collagen organization was quantified in the ultrasound images using custom-written software [4]. This image processing algorithm is a computational analog to crossed polarizer imaging, which assesses collagen fascicle alignment and quantifies tendon 'organization' as the circular standard deviation (CSD) of these collagen structures and has been shown to be reliable in Achilles tendon [5]. These images were also used to quantify the longitudinal thickness and mean echogenicity of the tendon.

Tendon organization, thickness, and echogenicity as well as VISA-A scores were compared between the two study visits using two-way paired t-tests. This

study was powered ($\beta > 0.8$) to detect ultrasound differences of 15%. Additionally, effect sizes were determined for any differences found to be statistically significant ($P < 0.05$). Effect sizes were reported using Cohen's *d*, calculated as the mean difference divided by the pooled standard deviation.

RESULTS AND DISCUSSION

Achilles tendon symptoms did not develop in any of the runners, which were confirmed by no change in VISA-A scores between the pre- and post-season sessions ($P > 0.1$, **Table 1**). Similarly, tendon organization and echogenicity did not change over the course of the competitive season between the two sessions ($P > 0.05$, **Table 1**). Tendon thickness increased by 7% ($P < 0.001$, **Table 1**) but the effect size of this change was small ($d = 0.36$).

We confirmed our hypothesis that competitive distance runners have Achilles tendon structure that appears to be habituated to prolonged cyclic loading. These findings agree with previous work that showed collegiate distance runners do not undergo Achilles tendon hypertrophy throughout a competitive season [6]. This habituated tendon may be a protective adaptation, allowing trained runners to cyclically load their tendons without injury. Mechanically, the thicker-habituated tendon may undergo strain similar to what is observed in naïve tendon at lower levels of stress. This would result in similar maximal ankle torque generation potential while decreasing the impact of the rapid loading experienced during distance running.

The processes by which tendon remodels from a naïve to a habituated – and from a healthy to a pathologic state – are still not well understood. Exercise has been shown to increase levels of collagen synthesis in humans but the effects of this increase has not been directly linked to tendon remodeling. Additionally, different types of running demands appear to have different effects on tendon remodeling. Sprinters, for example, have stiffer Achilles tendons than distance runners and non-runners, though these findings have not been linked to tendon structure. As a result, there is a need to link the structural differences of habituated tendon with function to better understand the remodeling process and to elucidate the mechanisms that drive pathology.

CONCLUSION

Once habituated to the prolonged cyclic loading of distance running, cross-country athletes do not experience structural changes to the tendon in response to further training. The process by which a tendon becomes habituated remains unclear. Understanding the relationship between tendon structure and function is crucial to anticipating and preventing the development of pathology.

REFERENCES

1. Longo et al. *American Journal of Sports Medicine.* 37(7):1400–1405, 2009
2. Hullfish et al. *Proceedings of ORS '18*, New Orleans, LA, USA, 2018
3. Robinson et al. *British Journal of Sports Medicine*, 35(5):335–41, 2001
4. Riggin et al. *Journal of Biomechanical Engineering*, 136(2):021029, 2014
5. Hullfish and Baxter, *Epub ahead of print*
6. Sponbeck et al. *International Journal of Exercise Science*, 10(8):1226–1234, 2017

ACKNOWLEDGEMENTS

We would like to thank Annelise Slater and Neza Stefanic for assistance in data collection and Jamel Jones for subject recruitment.

Table 1. Subject reported tendon status and Ultrasound evaluation of tendon structure

	Pre-Season	Post-Season	% Change	*P*-value
VISA-A (0-100)	93 ± 8.1	94 ± 6.9	1.1	0.71
Organization (CSD)	9.4 ± 0.7	9.2 ± 0.4	2.5	0.21
Avg. Echogenicity (%)	14 ± 3.5	15 ± 5.8	4.5	0.56
Thickness (mm)	0.54 ± 0.1	0.56 ± 0.1	7.1	< 0.001

PREDICTION OF SOLEUS MUSCLE FASCICLE BEHAVIOR DURING WALKING USING A MULTISCALE COUPLED OPENSIM AND FEBIO MODEL

Brian K. Jones[1], Emily Y. Miller, Shayn Peirce-Cottler, and Silvia S. Blemker

Dept. of Biomedical Engineering , University of Virginia, Charlottesville, VA, USA
[1]email: bkj3f@virginia.edu

INTRODUCTION

One of the fundamental problems of musculoskeletal biomechanics is the accurate prediction of *in vivo* muscle behavior during whole-body dynamic motion. Recent advances in dynamic ultrasound imaging have allowed *in vivo* measurements of muscle fascicle length changes during movement. These data demonstrate the complex interplay between muscle fiber mechanics and in-series elasticity resulting from tendon and aponeurosis behaviors. Computational models provide a powerful paradigm for understanding muscle and tendon, however current approaches often utilize simple representations of muscle-tendon units that limit their predictive utility. The goals of this study were to: (i) develop a multiscale model of the soleus muscle by coupling the FEBio finite element and OpenSim biomechanical modeling softwares, and (ii) compare predictions from the model with ultrasound measurements [6] and lumped-parameter model predictions [1].

METHODS

OpenSim software (*opensim.stanford.edu*) was used to analyze a previously published [1] dynamic simulation of human walking motion. This model utilizes motion capture and force plate data to predict joint motions and the activations of 76 skeletal muscles in the torso and lower extremity. Results from the right leg of this model were utilized for the present study and included soleus activations, spatial locations of soleus origin and insertion, and kinematics of the pelvis, femur, tibia, talus, and calcaneus bones.

3D geometries of the right-side lower-extremity bones were taken from the OpenSim dataset and imported into the FEBio pre-processor PreView (*www.febio.org*). Each bone's global spatial location was then calculated from the *location_in_parent* field and generalized joint coordinates in the OpenSim model definition file. Predicted orientations and locations of the bones during the gait cycle were then obtained using the OpenSim *Analyze* tool, and a custom Matlab algorithm was written to convert Euler angles to rotation matrices and Euler vectors. This data was then formatted into rigid body translations and rotations for the FEBio model definition file.

Solidworks CAD software was used to create a simplified, unipennate soleus muscle with anterior and posterior aponeuroses based on origin, insertion, and pennation angle from the OpenSim model definition file. Additional soleus architecture and geometry data was taken from previously published literature [2].

Trelis software (*www.csimsoft.com*) was used to mesh the soleus CAD geometry using 8-node hex elements, and the mesh was then combined with the imported bone geometry in PreView. Bones were modeled as rigid bodies, the soleus muscle tissue was modeled as an nonlinear transversely isotropic mixture of muscle [3] and a Mooney-Rivlin material, and tendons were modeled as an elastic mixture of an exponential power law fiber and a Mooney-Rivlin material.

Muscle fiber directions were calculated using our previously published computational fluid mechanics approach [4]. Briefly, the soleus mesh domain was modeled as a Newtonian fluid using the FEBio fluid solver [5]. Aponeurosis attachment faces were given dilatation (pressure) boundary conditions to create a constant laminar fluid flow with Reynolds Number $<< 1$. Remaining exterior boundaries of the mesh domain were treated as slip surfaces (zero viscous traction and zero normal fluid velocity). Select interior mesh faces were also given slip conditions to serve as guides to fine tune the fluid velocity.

Fluid velocity vectors from this CFD analysis were used as muscle material fiber directions in the solid FEA model. In post-processing, a custom Matlab algorithm was used to calculate streamlines using the deformation gradient tensor **F** and this fiber direction vector field. These streamline lengths were reported as muscle fascicle lengths in the results below.

RESULTS AND DISCUSSION

The finite element model, shown in Fig. 1, was comprised of 5871 elements and required 4 minutes of solution time. Average fascicle stretch at a lateral, mid-sagittal, and medial location were calculated for a representative transverse mid-belly section of the soleus (Fig. 2). These calculations were compared with predictions of soleus fiber length changes from the lumped parameter prediction from John et al [1] and ultrasound measurements of soleus fascicle stretch during treadmill walking [6]. While the range of stretch magnitudes for all three datasets were similar, the OpenSim model over-predicts fascicle stretch during the stance phase. In contrast, the FEBio simulation follows the ultrasound measurements more closely, in particular during mid-late stance.

These results demonstrate the potential for finite-element models to predict *in vivo* muscle tissue behavior during whole-body motion. This approach has a wide variety of applications, including understanding how age- and disease-related changes in tendon and aponeurosis properties may influence plantar-flexor function and overall mobility.

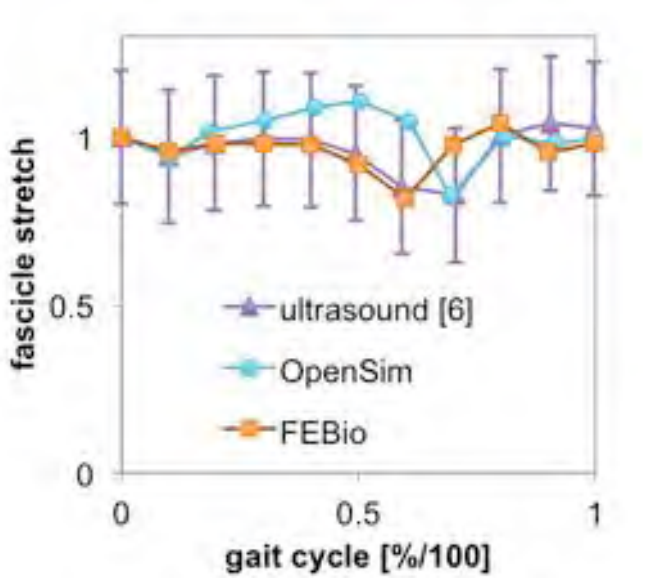

Figure 2: Comparison of fascicle stretch ultrasound data with the present study (FEBio) and the *gait2392* OpenSim model upon which the present model bone kinematics were based.

REFERENCES

1. John CT, et al. *J Biomech*. (**45**) 2012.
2. Agur AM, et al. *Clin Anat* (**16**) 2003.
3. Blemker SS, et al. *J Biomech.* (**38**) 2005.
4. Inouye J, et al. *Proc Conf Summer Comp Sim*, 2015
5. Ateshian GA, et al. *J Biomech Eng*. (**140**) 2018
6. Panizzolo FA, et al. *Gait Posture* (**38**) 2013

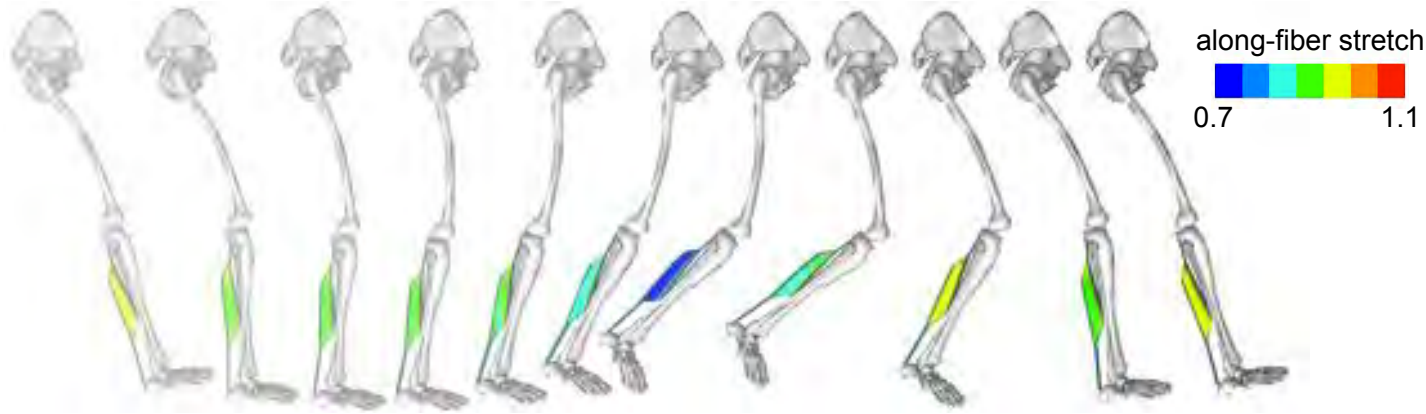

Figure 1: Full model throughout gait cycle. Soleus mesh is colored with element-wise along-fiber stretch.

NON-INVASIVE *IN VIVO* ACHILLES TENDON STRESS MEASUREMENT: POSTURE AND RATE DEPENDENCE

[1] Emily M. Keuler, [1] Jack A. Martin, [1] Joshua D. Roth, [1] Sarah C. Denning, [1] Darryl G. Thelen

[1] University of Wisconsin- Madison, Madison, WI, USA
email: emkeuler@wisc.edu, web: http://uwnmbl.engr.wisc.edu

INTRODUCTION

We are working on the development of a non-invasive shear wave sensor that could be used to track tendon loads during dynamic movement. The sensor is based on modeling and *ex vivo* studies that show shear wave propagation speed is directly dependent on axial tendon stress [1]. An *in vivo* version of the sensor uses skin-mounted miniature accelerometers and a tapping device to monitor wave speeds in superficial tendons. Initial collections have found a strong relationship between net joint moments and wave speed during walking [1]. However, to be suitable for use as a load sensor during movement, the relationship between wave speed and stress must be stable across different postures and load conditions. Hence, the purpose was to assess the relationship between Achilles tendon wave speed and loading metrics during voluntary ankle plantarflexion tasks performed at different limb postures and contraction rates.

METHODS

Twelve healthy subjects (6F, age: 23.6±2.8 years, height: 1.8±0.1 m, mass: 72.5±11.9 kg) were tested. Each subject's dominant foot was secured to the foot plate on an isokinetic dynamometer (Biodex System 4 Pro; Fig. 1). Subjects performed cyclic isometric exertions (0.5 Hz) up to maximum effort at eight postures: knee flexion of 20° and 90° and ankle angles of 10° dorsiflexion and 0°, 10°, and 20° plantarflexion. At the 20° knee and 0° ankle angle, exertions were performed at 3 cyclic contraction rates of 0.25, 0.50 and 1.00 Hz. Passive trials were also performed at each knee angle with the dynamometer rotating the ankle through a range of motion. Passive trial data was used to estimate the torque due to the weight of the foot and foot plate. Ankle plantarflexion torque was defined as the measured torque minus the torque due to gravity.

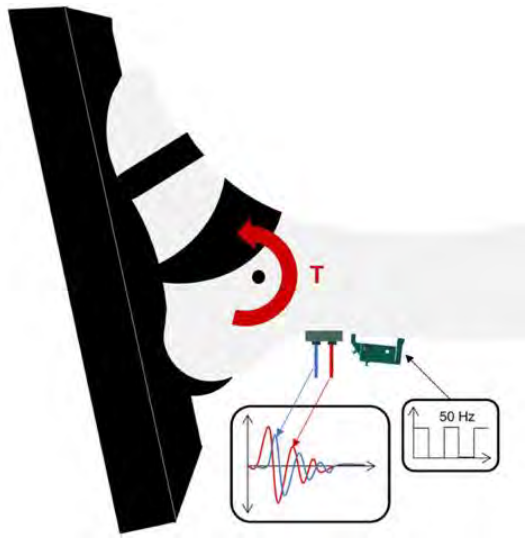

Figure 1: Subjects performed isometric exertions while a tapper induced shear waves that were observable on near (red) and far (blue) accelerometers.

MRI images of the calf and ankle were used to assess the tendon cross-sectional area, **A**. Coupled ultrasound and motion analysis was performed on these subjects to characterize the tendon moment arm, **r**, about the ankle as a function of ankle angle [2]. Tendon stress was then estimated from the ankle torque as $\sigma = \frac{T}{rA}$, which assumes the net torque arises entirely from tension in the Achilles.

Achilles tendon wave speed was measured using a custom shear wave tensiometer, consisting of a piezoelectric-actuated (20μm displacement, Thorlabs PK4JQP1) tapping device and two miniature accelerometers (Piezotronics 352C23) embedded in a platinum silicone mold (Smooth-On – Mold Star® 15 SLOW). The mold maintained constant 10 mm spacing between accelerometers. The tensiometer was strapped over the Achilles tendon, approximately 3.5 cm superior to the calcaneus. The tapper was driven with a 50Hz square

wave. Accelerometer, ankle angle, and torque data were collected at 50 kHz. For each tap, shear wave speed was calculated by finding the time delay that maximized the normalized cross-correlation between the two accelerometer signals [1].

The coefficient of determination (r^2) was used to assess the linear relationship between ankle torque and wave speed squared and was compared for all 12 subjects. Linear regressions of stress and wave speed squared were performed for each posture and contraction rate on the three subjects for which we had complete tendon image and moment arm measurements.

RESULTS AND DISCUSSION

Achilles tendon squared wave speed and ankle torque were highly correlated (r^2=0.95±0.06) at each of the 8 limb postures and 3 rates (Table 1). Correlation was weakest in the most plantarflexed posture where torque capacity is diminished.

Table 1: Coefficient of determination (r^2) mean (±1 s.d.) for posture specific linear regression correlation values over 12 subjects.

	Knee Flexion Angle	
Ankle Angle	**20°**	**90°**
10° DF	0.93 ± 0.08	0.95 ± 0.04
0°	0.96 ± 0.05	0.96 ± 0.03
10° PF	0.95 ± 0.04	0.95 ± 0.04
20° PF	0.91 ± 0.11	0.89 ± 0.11

Theoretical models suggest that wave speed squared should be proportional to tendon stress, as was seen in the three subjects for which this analysis was complete. Further, the slopes of the linear fits of stress to wave speed squared were relatively consistent across subjects, ankle angles, and speeds at the more extended knee posture (Fig 2). However, there tended to be a slight decrease in the computed slope when the ankle was dorsiflexed in the flexed-knee posture (Fig 2).

This observation could, in part, arise from non-uniform tendon stress due to a shortened gastrocnemius muscle. Further study is ongoing to assess if the slope of the stress-wave speed squared relationship remains consistent across additional subjects, or alternatively need to be calibrated by isometric trials of the type described in this study.

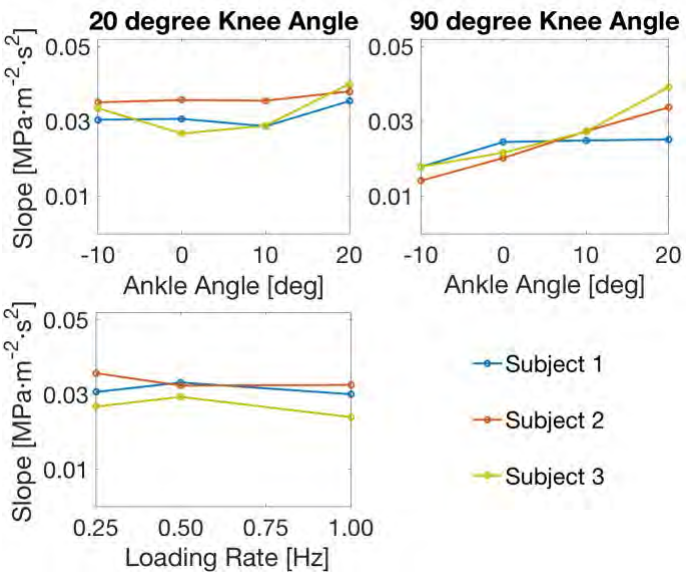

Figure 2: Linear fit slopes from squared wave speed-stress linear regression for three subjects over 8 postures and 3 cyclic contraction rates.

CONCLUSIONS

We observed strong relationships between ankle torque and squared wave speed over a broad range of limb postures and loading rates, supporting the use of shear wave tensiometry to assess internal tissue loading during dynamic movement. We previously showed that tensiometers of the type used in this study can monitor tendon wave speeds during dynamic activities such as running and walking [1]. Hence, shear wave tensiometry represents an exciting new tool that may be applicable for obtaining functional tissue load information that is relevant for a wide variety of orthopedic and rehabilitative applications.

REFERENCES

1. Martin, J.A., et al. *Nature Commun.* Accepted.
2. Manal, K., et al. *Appl Biomech*. 2010.

ACKNOWLEDGEMENTS

NIH AG051748, HD092697.

New insights into the mechanical behavior of the healthy, human Achilles tendon revealed by novel digital image correlation

[1]Nicholas Quirk, [1]Christopher Nagelli, [2]Alexander Hooke, [1]Consuelo Lopez De Padilla, [3]Timothy Hewett, [1]Christopher Evans, [2]Lawrence Berglund, and[1]Sebastian A. Müller

[1]Rehabilitation Medicine Research Center, [2] Materials and Structural Testing Resource Core, & [3] Orthopedic Biomechanics Laboratories and Sports Medicine Research Center, Mayo Clinic, Rochester, MN
email: nagelli.christopher@mayo.edu

INTRODUCTION

The Achilles tendon is the largest and strongest tendon in the human body, as it is loaded with more than 250%-390% body weight during functional tasks.[1, 2] Aberrant loading is thought to weaken the structure and make it vulnerable to injury. The majority of Achilles tendon ruptures occur as non-contact episodes and the primary location of tendon failure is 2-6 cm proximal to its insertion at the calcaneus.[3] Multiple risk factors are associated with an increased risk of injury, including overuse, age, sex, weight, and biomechanical abnormalities. Previous studies have investigated the mechanical properties of the Achilles tendons by stretching them to failure. However, most of these studies were conducted on tendons harvested from older individuals and used techniques that were not able to assess accurately the strain response under loading. This creates a significant gap in our understanding of the mechanical behavior of healthy tendons.

Digital image correlation (DIC) systems are an emerging state-of-the-art technology used to measure three-dimensional deformation and strains in real time with high precision. In combination with mechanical testing, DIC may provide invaluable insight into the properties of the tissue. Therefore, the purpose of this investigation is to utilize this novel methodology to study the mechanical behavior of healthy, human Achilles tendons.

METHODS

Eleven (n=11) Achilles tendons that included the calcaneus and a third of the gastrocnemius and soleus muscles were harvested from young, human cadavers with no prior history of lower extremity surgery (**Table 1**). The calcaneus was then wrapped in wire and secured in a metal fixture using bone cement such that the enthesis was free. The tendon's posterior surface was then coated with a black and white speckling pattern for the DIC system (GOM, Trillion Quality Systems, King Prussia, PA) to record, calculate, and analyze the strain and deformation response. The samples were then mounted to a servo-hydraulic testing machine (model 312, MTS, Minneapolis, MN) using a custom fixture with the calcaneus at a 30^o angle to simulate the anatomic position of a plantigrade foot in a neutral position. The other end of each sample, which included a third of the proximal muscles, was cryoclamped. Force and displacement data were collected at 128 Hz and the tendons underwent 10 cycles of pre-load to 2% strain. The tendons were loaded until failure at 5 mm/sec. After mechanical failure, standard histological analysis was performed on tissue adjacent to the rupture site to check for pre-existing histopathology. We analyzed the failure method, failure load, stiffness, and overall and regional peak strain.

Table 1: Subject demographics

Subjects (M/F)	Age (yrs±SD)	Weight (kg±SD)	Heigh (m±SD)
11(6/5)	42.1±9.8	83.3±22.3	1.78±0.1

RESULTS

Histological analysis of the tendon tissue showed healthy tissue with no pathohistological changes. There were five mid-substance tears, five calcaneus fractures, and one muscle tear during mechanical testing. The one muscle tear was excluded because it was an artifact of cryoclamping. T-tests were performed to determine differences between failure types (α=0.05). The failure load was significantly greater (p=0.02) in the group that sustained a mid-substance tear than the group that sustained a calcaneus fracture during tensile loading.

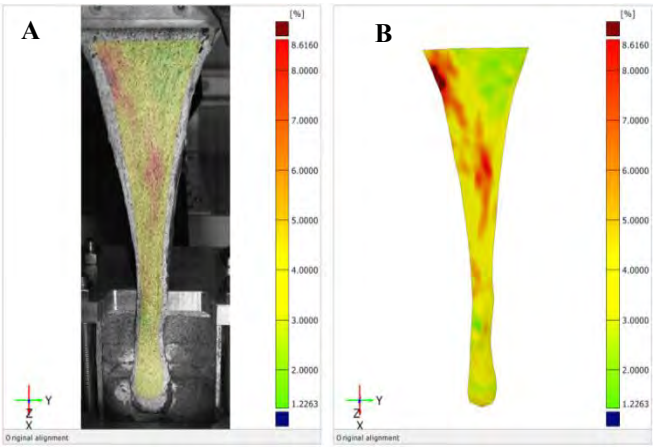

Figure 1: Experimental set-up (A) and percent strain distribution during testing (B).

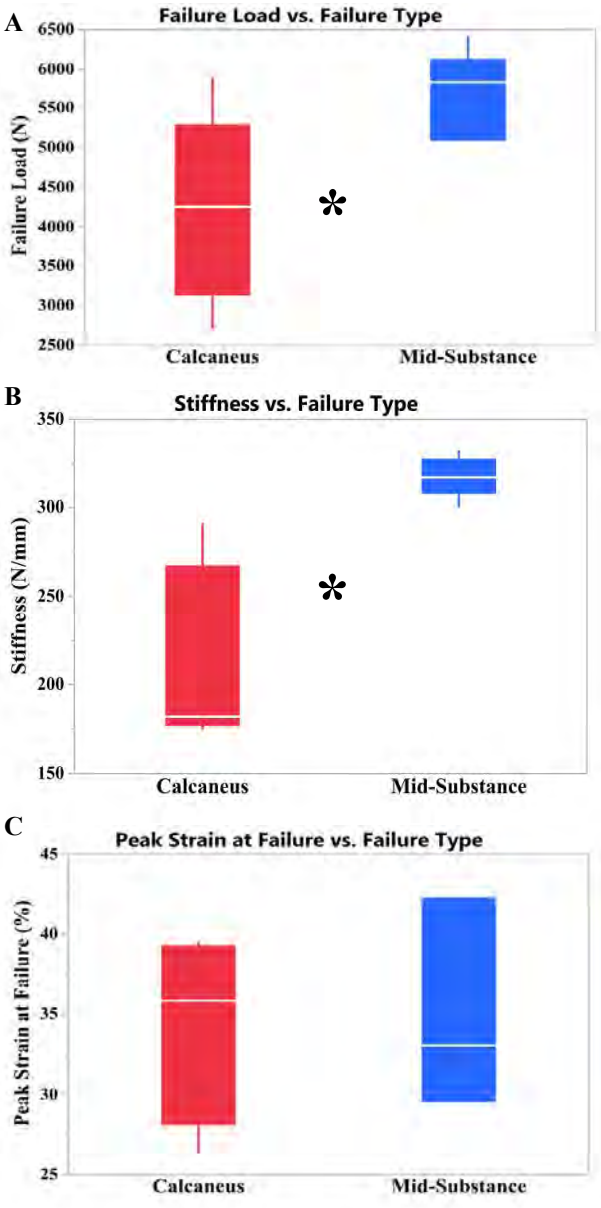

Figure 2: Differences between failure types in Failure Load (A), Stiffness (B), and Peak Strain at Failure (C). *Marks significant differences.

In addition, the mid-substance group was significantly (p=0.004) stiffer than the group which underwent a calcaneus fracture. There were no significant differences in peak strain (p=0.43) between the failure types. Since most Achilles tendons fail at the mid-substance, the tendons were divided into different regions to investigate local strains: distal (insertion to 2 cm proximal), mid-substance (2-4 cm from insertion), and (>4 cm from insertion). There were no significant differences between failure types across the same strain regions. However, within the calcaneus fracture group there were significant difference between the distal region and the mid-substance (p=0.03) and proximal (p=0.04). Also, within the mid-substance group, there was a significant difference between the distal region and the proximal region (p=0.03) (Table 2).

Table 2: Percent strain of the defined regions. Different symbols indicate significance across fracture types.

Failure Type	Distal (% strain)	Mid-Substance (% strain)	Proximal (% strain)
Calcaneus Fracture	17.6±10.0*	30.5±8.6^	34.4±7.4^
Mid-Substance	23.9±9.3*	30.1±8.8	33.7±6.0^

CONCLUSION

This is the first study to use a novel DIC system to measure entire surface deformation of the Achilles tendons. Mid-substance tears occurred at loads approaching 6,000N, which agrees with earlier data of Wren et al.[4] reporting a value of 5,000N. However, overall peak percent strain of nearly 35% observed in our study eclipses the previously reported peak strain values of 8.8% - 14.5%.[4] The results also demonstrate that the strain is not uniformly distributed. Because the tendons used in the present study were obtained from relatively young individuals and the tendons showed no degenerative changes by histology, the results of this study indicate that, healthy tendons are capable to be stretched to failure, despite requiring extremely high forces (700% body weight). This understanding may provide further insight into the load bearing of healthy, human Achilles tendons.

REFERENCES

[1] Perry, J. CORR, 1983
[2] Griddings VL. Med Sci Sport Med, 1999
[3] Saltzman CL. J Am Acad Ortho Surg, 1998.
[4] Wren et al., Clin Biomech, 2001

A model for internal elastic energy storage and recovery in deforming muscles

[1] Thomas J. Roberts, Carolyn Eng[1], R.L. Marsh[1], and E. Azizi[2]

[1] Brown University, Providence, RI, USA
[2] University of California, Irvine, CA, USA
email: thomas_roberts@brown.edu,

INTRODUCTION

Elastic structures within muscles have the potential to store and recover energy during movement. Intramuscular elasticity is typically represented in Hill-type models as parallel to the contractile element. This arrangement has two important implications. First, it dictates that energy can only be stored in the parallel elastic element when the contractile element is lengthened. Second, it suggests that elastic elements within muscles will be loaded only at long muscle lengths, where passive force is developed. These features of a Hill-type model conception of muscle elasticity have generally led to the conclusion that elastic energy storage and recovery within muscles is limited during normal movement.

Hill-type models typically do not account for muscle architecture. Most limb muscle are pennate, meaning that the fiber operates at an angle to the line of force generation of the whole muscle. As a result a portion of the force generated by the contractile element is oriented orthogonal to the line of action of the muscle (Fig. 1). This force tends to compress the muscle, and must be opposed by forces resisting compression within the muscle. Here we model this resistance as a spring element, and test the idea that compression and recoil of a transverse muscle spring could lead to elastic energy storage and recovery in the "parallel" elastic component of muscle, even when the muscle is not lengthening and not operating at long lengths.

METHODS

The model is constructed as a single muscle fiber operating at an angle (the pennation angle) to the line of action of the muscle (Fig. 1). A spring oriented orthogonal to the muscle line of action acts to balance the component of force tending to compress the muscle. The force and excursions of the model depend on the interaction between fiber force, fiber geometry, and transverse spring forces. Initial values of 30 degrees for theta and 30mm for L_f were used for all simulations.

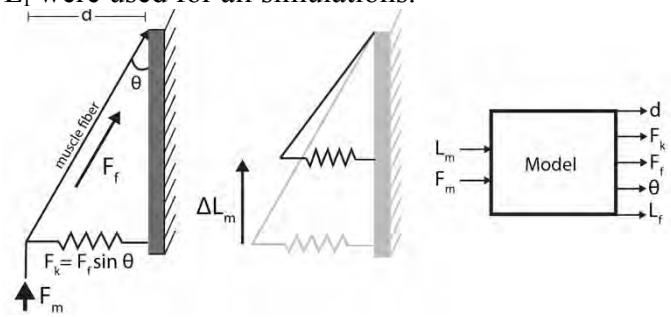

Figure 1. Modeled muscle at two time points, at rest (left) and contracted (middle). The muscle fiber operates at an angle (θ) to the muscle line of action (vertical). A spring generates a force, F_k, acting to resist compression (i.e., reducing of the pennation angle, θ). Simulations operate with an initial fiber length and pennation angle, and take inputs of muscle force and muscle length as a function of time. Outputs include muscle thickness (d), spring force (F_k), muscle fiber force (F_f), pennation angle (θ), and muscle fiber length (L_f).

RESULTS

We first tested whether the simple model could reproduce a phenomenon that has been observed in a number of unipennate muscles: variable gearing. The architectural gear ratio (AGR) of a muscle is defined as the ratio of muscle shortening velocity to fiber shortening velocity, and it has been observed to vary, with low force contractions operating with a high AGR and high force contractions operating with a low AGR. To test whether the model could produce variable gearing, we simulated contraction at a range of muscle forces but the same length trajectory. We optimized the spring stiffness for the high force condition, and then used the same spring constant for all simulations. Results from these simulations are shown in Fig. 2, along with previously measured values for AGR in isolated turkey gastrocnemius [1]. The model reproduced variable gearing (Fig. 2). This observation supports our hypothesis that intramuscular elastic elements

resist muscle compression and result in variable gearing.

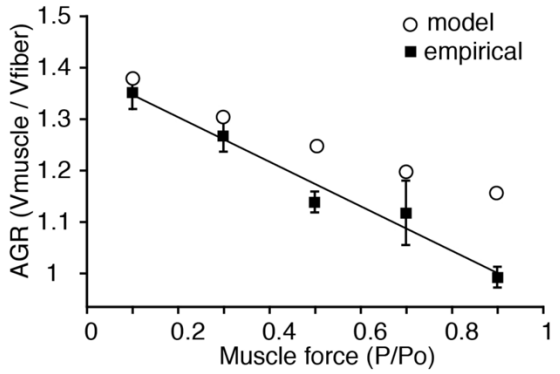

Figure 2. Results from modeled muscle (open circles) and empirical results from published data (closed circles, [1]) show similar patterns of variable gearing with force. Gear ratio was measured as the ratio of muscle velocity to fiber velocity during the constant force period of contraction.

Does the model have implications for elastic energy storage and recovery during ordinary movement? We aimed to test the idea that the springs that resist muscle compression might usefully store and recover energy cyclically by running the simulation with conditions meant to mimic those seen in some muscles during running. We drove the model with a half-sine pattern of muscle force and a half-sine stretch-shorten pattern of muscle length, with the goal of producing stretch-shorten cycles while muscle fibers were near-isometric. Figure 3 shows an example modeled contraction. In this example, nearly all of the excursion of the muscle-tendon unit is provided by fiber rotation (change in pennation angle), while fiber length remains nearly constant. Stretch-shorten cycles in muscles with near-isometric fibers have been observed in a number of systems [2, 3]. Calculated power shows that the majority of the power is associated with the transverse spring, which stores and recovers energy cyclically as the muscle compresses and then recoils.

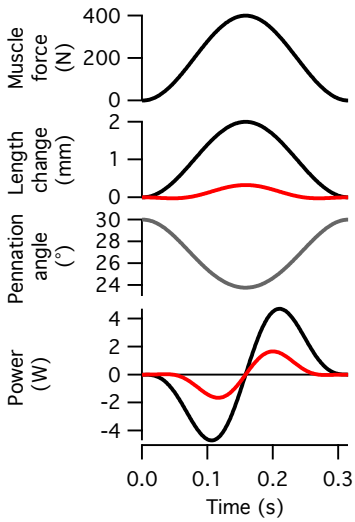

Figure 3. Simulated contractile mechanics for a stretch-shorten cycle. The model allows for significant length change in the whole muscle (black) with minimal length change in the muscle fiber (red). Changes in the pennation angle allow for cyclic energy storage and recover that does not require fiber length changes.

DISCUSSION

Results from a modeled muscle with a pennation angle and transverse spring demonstrate how this arrangement can produce variable muscle gearing. It also shows how a transverse spring can power cyclic stretch-shorten cycles in muscles. Like Hill-type models, our model is a simplified abstraction that does not include the morphological and mechanical reality of the complex, three-dimensional muscle deformations that we propose are associated with the loading of intramuscular elastic elements. It does demonstrate that a very simple modification to typical muscle models – orienting an elastic element orthogonal to the muscle line of action – can allow for the effective use of intramuscular elasticity. The modeled muscle allows for intramuscular energy storage at any muscle length and does not require muscle lengthening. We predict that further empirical measurements of three-dimensional muscle deformations will support the idea that intramuscular springs contribute significantly to muscle performance.

REFERENCES

1. Azizi, E. *et al.*. (2008). *Proc Natl Acad Sci U S A* **105**, 1745-50.
2. Fukunaga *et al.*. (2001). *Proc R Soc Lond B Biol Sci* **268**, 229-33.
3. Roberts, T. J., et al., (1997). *Science* **275**, 1113-5.

ACKNOWLEDGEMENTS

Support from NIH grant AR055295 is gratefully acknowledged.

COMPARISON OF 3DOF AND 6DOF WORK AND POWER FOR STANDING LONG JUMP

Blake M. Ashby and Gordon J. Alderink

Grand Valley State University, Grand Rapids, MI, USA
email: ashbybl@gvsu.edu, web: http:// www.gvsu.edu/biomechanicslab/

INTRODUCTION

Work and power measures at the whole body and joint level have commonly been used to study performance of human movements. The standing long jump is a common movement present in numerous sporting events. This movement has been thought to be primarily a 2D, sagittal-plane movement, but recent work has shown that 3D analysis allows for more complete accounting of work and power [1]. Accurate calculation of work and power is important for understanding and describing the fundamental mechanisms of human movement. Six degree-of-freedom (6DOF) joint power/work has been shown to more completely quantify the work and power in movements such as walking [2]. The purpose of the present study was to compare the total body and joint-level work and power in the standing long jump using three degree-of-freedom (3DOF) and 6DOF analyses.

METHODS

Seven healthy, adult, male volunteers (mean ± standard deviation: mass = 78.2 ± 5.5 kg; height = 1.796 ± 0.049 m; age = 24.7 ± 2.5 years) performed six standing long jumps for maximum distance. The 3D positions of 63 passive reflector markers were recorded (120 Hz) throughout the jumping movements using a 16-camera Vicon motion capture system (Vicon Motion Systems Ltd., Los Angeles, CA). Two in-ground AMTI force platforms (Advanced Mechanical Technology Inc., Watertown, MA) recorded (1200 Hz) the 3D ground reaction forces, free moments, and center of pressure locations for each foot during the propulsive phase of the jumps.

The body was modeled using a 12-segment, 11-joint model modified from previous work [1]. Inverse kinematics and dynamics analyses were performed using MATLAB R2017a (MathWorks, Natick, MA) to calculate segment angular velocities and accelerations and joint moments. The over-determinacy of the system of equations resulting from the use of force plate data was resolved by performing "bottom up" calculations for the ankle, knee, hip, and lower back moments and "top down" calculations for elbow and shoulder moments [3].

Traditional 3DOF powers were calculated for each joint according to:

$$P_{3DOF} = \vec{M}_p \cdot \vec{\omega}_p + \vec{M}_d \cdot \vec{\omega}_d \qquad (1)$$

where $\vec{M}_p$ and $\vec{M}_d$ represent the joint moments acting on the proximal and distal segments, respectively, and $\vec{\omega}_p$ and $\vec{\omega}_d$ represent the proximal and distal segment angular velocities. 6DOF powers [2, 4] were calculated for each joint by including terms which allow for relative translation between the segments at the joint with:

$$P_{6DOF} = P_{3DOF} + \vec{F}_d \cdot (\vec{v}_d - \vec{v}_p) \qquad (2)$$

where $\vec{F}_d$ represents the joint intersegmental force calculated from inverse dynamics acting on the distal segment and $\vec{v}_d$ and $\vec{v}_p$ represent the joint center velocities calculated from the distal and proximal segments, respectively.

Work was calculated for each joint by integrating the joint power over the 1.2 seconds prior to takeoff using both 3DOF and 6DOF methods. Total body work was estimated as the sum of the work performed at each of the 11 joints.

Left and right side values were combined for all joints except for the lower back. Two-way, repeated measures, ANOVA models developed with SAS 9.4 (SAS Institute Inc., Cary, NC) were used to compare the power and work values calculated using 3DOF and 6DOF methods. Results are presented as least square means ± 95% confidence intervals. Statistical significance was indicated for $p < 0.05$.

RESULTS AND DISCUSSION

Although the total body work calculated with the 3DOF method (515.3 ± 20.8 J) was not significantly different ($p = 0.3645$) than with the 6DOF method (517.2 ± 20.4 J), there were significant differences in the work done at the joints (Table 1). The lack of significant difference in total body work was due to 35.6 ± 5.4 J more ($p < 0.0001$) work at lower body joints (ankles, knees, hips, and lower back) while 33.7 ± 6.4 J less ($p < 0.0001$) work was calculated at upper body joints (shoulders and elbows) when using 6DOF methods. Looking at the joint powers during takeoff (Figure 1), the differences between 3DOF and 6DOF methods were relatively modest at the ankles, knees, and hips, but were much more apparent at the lower back, shoulders, and elbows.

It has been shown that errors in joint center estimation propagate into the joint power calculations using traditional 3DOF methods, but do not propagate when using 6DOF methods [4]. The large differences demonstrated in the results at the lower back, hip, and shoulder are perhaps reflective of the inherent challenges of properly locating these joint centers using motion capture technology and in modeling the lower back with a single joint.

The large work and power differences for the upper extremity joints might be further explained by the larger joint velocities in the arms just before takeoff. The joint center velocities calculated from the distal and proximal segments and used in Eq. (2) depend heavily on the segment angular velocities, which are considerably larger for the forearm and upper arm segments than for other segments. The results of this study highlight the value of using 6DOF methods for explosive movements such as jumping that involve significant upper body motion.

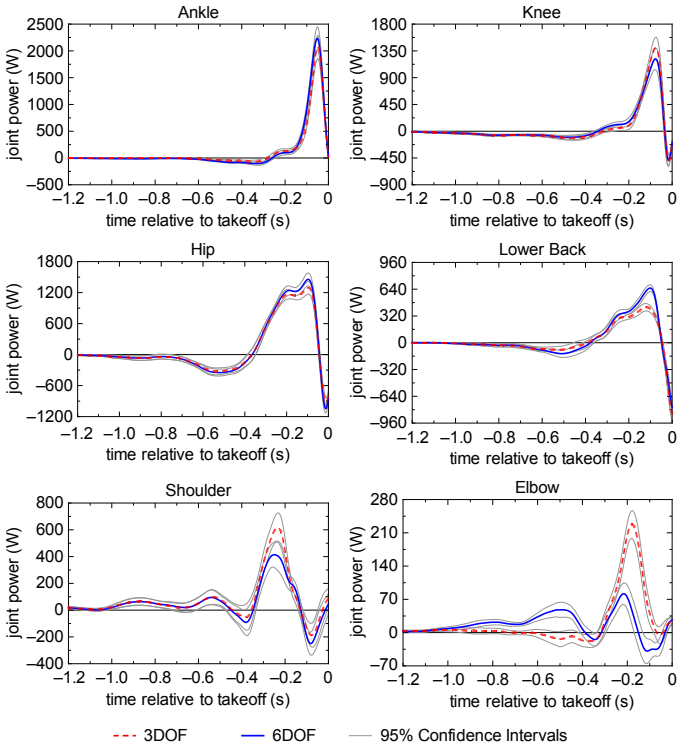

Figure 1: Joint power calculated using 3DOF and 6DOF methods.

REFERENCES

1. Hickox, et al. *J Biomech* **49**, 1085-1093, 2016.
2. Zelik, et al. *J Exp Biol* **218**, 876-886, 2015.
3. Ashby, et al. *39th Annual Meeting of ASB,* Columbus, OH, USA, 2015.
4. Buczek, et al. *J Biomech* **27**, 1447-1457, 1994.

ACKNOWLEDGEMENTS

Special thanks are given to Laura Sowatsky for her help with data collection for this study and to the Statistical Consulting Center at GVSU for their help with the statistical analyses.

Table 1: Joint work values calculated using 3DOF and 6DOF methods

	3DOF	6DOF	Difference	*p*-value
ankles	144.9 ± 8.7 J	148.2 ± 10.1 J	3.3 ± 1.9 J	0.0014
knees	69.0 ± 16.3 J	72.0 ± 17.4 J	3.0 ± 3.0 J	0.0517
hips	147.8 ± 9.2 J	158.2 ± 10.8 J	10.3 ± 3.3 J	<0.0001
lower back	35.7 ± 9.7 J	54.7 ± 7.2 J	19.0 ± 4.3 J	<0.0001
shoulders	91.4 ± 5.5 J	63.1 ± 5.1 J	-28.2 ± 5.3 J	<0.0001
elbows	26.4 ± 2.9 J	20.9 ± 3.5 J	-5.5 ± 2.9 J	0.0004

COUNTERMOVEMENT JUMP HEIGHT AND FORCE – TIME VARIABLES IN HIGH SCHOOL BASKETBALL PLAYERS

Rena Hale, Takashi Nagai, Nathan D. Schilaty, Nathaniel A. Bates, April L. McPherson, Alessandro Navacchia, and Timothy E. Hewett

Mayo Clinic Biomechanics Laboratories & Sports Medicine Center, Rochester & Minneapolis, MN, email: Hale.Rena@Mayo.edu

INTRODUCTION

Due to the increasing affordability and ease of use, force platforms are becoming one of the most commonly used biomechanical testing devices in clinical practice [1]. The countermovement jump (CMJ) is a common portion of athletic testing. It is quick to perform, non-fatiguing, and can inform the clinician of the athlete's neuromuscular control for strength and power training [2]. Plyometric intensity can be determined by calculation of rate of force development during the eccentric and concentric phases of a CMJ from force platform measurements [3]. However, the shape of the force-time curve is dependent upon expertise [2, 3, 4]. For clinical application and interpretation of force plate data, normative values of the CMJ are needed. Thus, the purpose of the study was to calculate Propulsion rate of force development (PRO-RFD), landing rate of force development (RFD), and jump height during a CMJ in high school basketball players. The hypothesis tested was that male athletes would jump higher than female athletes and as athlete's age, PRO-RFD and RFD would be greater in males than females.

METHODS

172 high school basketball athletes (males n=64, females n=108) 14 to 18 years old were recruited (Table 1). This study was approved by the Mayo Clinic IRB. Informed consents were obtained from each player and his/her parent if under 18 years old. Athletes were instructed to place hands on hips, stand feet shoulder width apart with each foot on the center of a force plate, (Bertec, Columbus, OH), and perform a max jump. Force plate data from three CMJs were collected.

Vertical ground reaction force (vGRF) was used to calculate jump height, PRO-RFD, and RFD for the right and left legs. PRO-RFD was calculated as the slope of the propulsion phase (eccentric loading) of the force-time curve. Propulsion phase began when vGRF exceeded body weight and ended when force was zero [3,4]. RFD was calculated as peak vGRF divided by the time from initial contact to peak vGRF during landing phase [4, 5]. Data was averaged by subject, sex, and age.

Table 1: High School Basketball Anthropometrics

	Height (m)		Weight (N)	
Age	Males	Females	Males	Females
14	1.73 (0.06)	1.68 (0.10)	681.13 (89.10)	618.73 (144.61)
15	1.78 (0.07)	1.70 (0.08)	652.84 (120.93)	651.33 (143.49)
16	1.83 (0.10)	1.68 (0.04)	722.20 (103.21)	661.92 (82.44)
17	1.84 (0.08)	1.74 (0.08)	772.36 (121.21)	675.36 (157.74)
18	1.84 (0.03)	1.71 (0.10)	792.04 (80.49)	654.96 (77.53)

Statistical analyses between sexes were performed with JMP 13 (SAS Institute Inc., Cary, NC) with matched pairs and one-way ANOVA with an alpha level < 0.05. A Tukey post hoc analysis was conducted to detect differences among age groups.

RESULTS AND DISCUSSION

Results showed significant differences ($P<0.05$) between male and female jump heights (Table 2), PRO-RFD (Table 3), and RFD (Table 4). Jump height was lower in females than males in all age groups (0.27m ± 0.02 vs. 0.37m ± 0.04). Within males, jump height significantly increased between 14 and 18-year-olds ($P<0.05$). No significant differences in jump height were determined within females. However, a deconditioning trend was seen in 18-year-old females. Results were consistent with previous studies, which report that male athletes jump 26.4% higher than female counterparts [6].

Overall average male PRO-RFD (2200 N/s ± 830) was higher than mean female PRO-RFD (1556 N/s ± 426). PRO-RFD in 16-year-old males was significantly higher than that of females. Significant difference was not found between sexes at any other age or within ages of each sex. PRO-RFD in elite basketball players has been reported as 3,370 N/s, which was 35% greater than the high school male and 66% higher than high school female basketball players analyzed in this study [6].

Table 2: Jump Height

Age	Male (m) mean (SD)	Female (m) mean (SD)	P- value
14	0.33 (0.10)	0.27 (0.08)	0.1401
15	0.39 (0.15)	0.28 (0.09)	0.0032
16	0.37 (0.07)	0.27 (0.06)	0.0002
17	0.35 (0.05)	0.29 (0.07)	0.008
18	0.44 (0.07)	0.24 (0.04)	0.0001

Table 3: Propulsion Rate of Force Development

Age	Male (N/s) mean (SD)	Female (N/s) mean (SD)	P- value
14	2426 (3076)	1625 (983)	0.2544
15	2176 (1879)	1734 (1539)	0.383
16	2098 (1076)	1324 (459)	0.0177
17	1971 (1034)	1580 (705)	0.1926
18	2329 (1612)	1518 (605)	0.1836

Table 4: Rate of Force Development Absorption

Age	Male (N/s) mean (SD)	Female (N/s) mean (SD)	P- value
14	42869 (19366)	26986 (12761)	0.0113
15	46157 (27785)	20769 (6984)	0.0001
16	38737 (13995)	18293 (5629)	0.0001
17	45134 (18460)	24111 (10804)	0.0002
18	45044 (13106)	19371 (5909)	0.0001

Differences in RFD between males and females were significant at all ages ($P<0.05$). Average male RFD was larger than in females (43,588 N/s ± 5,838 vs. 21,906 N/s ± 3,189). RFD was significantly different between males age 14 to 15, 14 to 16, and 14 to 18. No significant differences were found between ages in females. Interestingly, males experienced deconditioning at 16 years old, whereas females experienced deconditioning at 16 and 18 years old.

RFD is typically calculated for the first and second landings of a drop vertical jump (DVJ). Previously reported first and second landing RFD totals are 50,080 and 48,084 [4]. As expected, DVJ RFD values are higher than CMJs, since the DVJ landing is from 31 cm off the ground.

CONCLUSIONS

The purpose of this study was to calculate jump height, propulsion of force development (PRO-RFD), and landing rate of force development (RFD) of a CMJ in high school basketball players. Results demonstrate significantly higher jump height and RFD in males when compared to females. Results can be used to determine appropriate CMJ variables for other high school athlete populations. Coaches should be aware of potential deconditioning of male athletes at 16 years old and female athletes at 16 and 18 years old. Future work should look at the correlation of force-time variables to jump height.

REFERENCES

1. Peterson et al. *Sports Biomech,* 16.2, 2017.
2. Cormie *J Strength Cond Res,* 23.1, 2009.
3. Jensen, R. L., & Ebben, W. P *J Strength Cond Res,* 21.3, 2007
4. McMahon et al. *Strength Cond J*, 2017.
5. Bates, et al. *Clin Biomech,* 28.7, 2013
6. Laffaye et al. *J Strength Cond Res,* 28.4, 2014.

ACKNOWLEDGEMENTS

Funding from the NBA & GE Healthcare Orthopedics and Sports Medicine Collaboration, and NIH grant funding R01AR056259 & R01AR055563 and T32AR056950.

Sport-Specific Wearable: A Jump Monitor for Figure Skating

[1] Sarah T. Ridge, [1]Riley E. Reynolds, [1]Chris Adair, [2]Peter Zapalo, and [1]Dustin A. Bruening

[1] Brigham Young University, Provo, UT, USA
[2] United States Figure Skating, Colorado Springs, CO
email: sarah_ridge@byu.edu

INTRODUCTION

The sport of figure skating has become more technically demanding since the 1990s. While competitive skaters have increased their off-ice strengthening and training in this time, the number and difficulty of on-ice jumps performed has increased also. While the number of jumps skaters perform daily has never been formally quantified, it has been suggested that skaters perform at least 50, perhaps up to 100 jumps per training day [1].

Forces during performance of skating jumps have been estimated to be greater than 5 times the skater's body weight [1]. The magnitude of force, high loading rates, and frequent repetitions is likely a contributing factor to the injury rate of competitive skaters. As with many athletes, the trade-off between injury prevention and performance enhancement is difficult for skaters. Numerous jump repetitions are required in order to learn and improve technique. However, increasing the number of repetitions of jumps may increase the risk of injury to the skater. Increasing monitoring of the number of jumps performed by skaters may help decrease risk of injury, similar to the institution of pitch counts in youth baseball. In addition, wearable technology could help skaters and coaches monitor fatigue or performance degradation by measuring jump height and/or rotation speed.

Accelerometers are commonly used to monitor physical activity. While they are useful for counting steps during walking and running, figure skating involves a variety of movements that generate similar acceleration profiles, resulting in a number of false positives during jump identification. Figure skating movements are complex and occur in multiple planes, involve changes of direction, and are often performed at high speeds.

Therefore, the purpose of this study was to determine the feasibility of using an inertial measurement unit (IMU) to count the number of jumps performed by figure skaters and estimate flight time of those jumps.

METHODS

Seven healthy competitive figure skaters participated in this study (ages 12-27, 6 female, 1 male). All skaters (and parents, when necessary) signed assent/consent forms approved by the local Institutional Review Board.

Each skater wore an IMU affixed to the lower back while they performed a variety of isolated jumps and a complete competition routine, consisting of jumps, spins, and footwork. The isolated jumps were used to define the jump detecting algorithm, which was then tested on the competition routines. Data from all jumps and routines were recorded by the IMU (128 Hz). A high speed video camera (240 Hz) was used to identify take-off and landing for flight time calculations from isolated jumps.

MATLAB software was used to process and analyze the IMU data. All accelerometer signals were first low pass filtered (6th order Butterworth with 10Hz cutoff) prior to analysis. MATLAB's findpeaks() function was then used to identify jumps and implement jump height algorithms. Jump height was measured from the high speed video using Dartfish and from the IMU data using 4 algorithms - gravitational threshold (GT), peak to peak scaling (PPS), valley to valley scaling (VVS), and vertical/horizontal acceleration intersection (VHI).

RESULTS AND DISCUSSION

The isolated jumps were used to create a jump identification algorithm based on vertical acceleration data and gyroscope data. Using the video as reference, data were analyzed to specify

three factors that could be used in the algorithm to automatically identify jumps in future applications. The three factors were: 1) a jump had to have two acceleration peaks above 25 m/s^2, 2) the two peaks had to be separated by 0.3 – 0.85 s, and 3) a rotation above 688 deg/s had to occur between the two acceleration peaks (Figure 1).

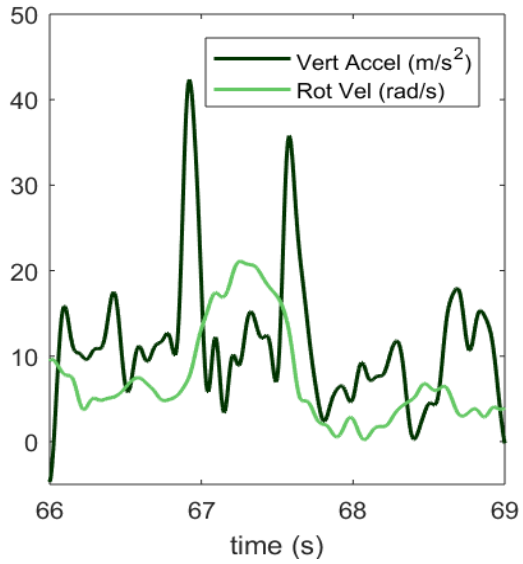

Figure 1. A 3 second section of IMU data from a competition routine. The large vertical acceleration peaks surrounding the rotational velocity peak indicate the jump (double flip).

These specifications were applied to the IMU data from the competition routines. The number of jumps identified by each step of the algorithm is shown in Figure 2. Forty-one total jumps with > 1 rotation in the air were performed during the competition routines. The algorithm performed very well; it identified a total of 40 jumps, missing only 2 jumps that were performed and including 1 ≤ 1 rotation jump.

Flight time and calculated jump height results can be seen in Table 1.

Method	Flight time (s)	Jump Height (cm)
Video	0.44 ± .060	24.4 ± 6.5
GT - error	0.098 ± 0.154	7.81 ± 10.8
PPS - error	0.031 ± 0.025	3.33 ± 2.75
VHI - error	0.165 ± 0.053	4.87 ± 3.87
VVS - error	0.047 ± 0.046	7.81 ± 10.83

Table 1. Algorithm errors for isolated jumps – absolute differences between each method and the gold standard video (mean ± standard deviation).

Further analysis with a greater variety of skaters should be done to determine if there are subject-specific characteristics that could help customize the algorithm to optimize accuracy of jump height calculations. However, it should be noted that, as a tool to monitor fatigue, skaters and coaches are likely more interested in decrease in jump height throughout a training day or session than precision of measurement relative to a gold standard.

CONCLUSIONS

A sport specific wearable to monitor the number and height of figure skating jumps performed during practice sessions is feasible. Future research will focus on finding a consumer-affordable IMU device and developing a user-friendly interface for skaters and coaches.

REFERENCES

1. Bruening & Richards. *J Biomech.* 22(4), 285-95, 2006

ACKNOWLEDGEMENTS

Partial funding for this project was provided by United States Figure Skating.

Figure 2: Flow chart showing the effect of each step of the jump identification algorithm on the competition routines.

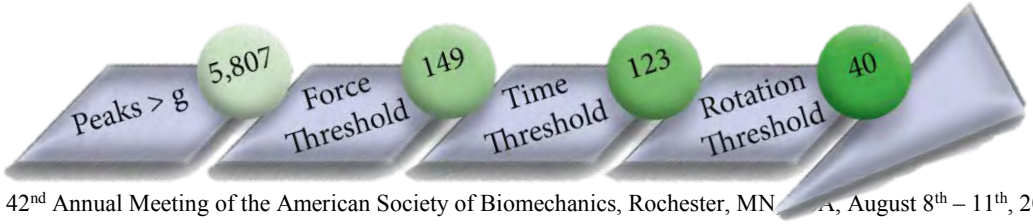

Impaired Jumping Performance Arising from Sedentary Growth is Recovered through Exercise in Adulthood

Matthew Q. Salzano[1], Suzanne M. Cox[2], Stephen J. Piazza[2], and Jonas Rubenson[1,2]

[1]Integrative and Biomedical Physiology, The Pennsylvania State University, University Park, PA, USA
[2] Kinesiology, The Pennsylvania State University, University Park, PA, USA
email: salzano@psu.edu, web: http://locomotionlab.net/

INTRODUCTION

Physical inactivity is known to contribute to a broad array of health problems throughout the lifespan, but biomechanical factors that limit physical activity are poorly understood. The musculoskeletal system is known to adapt to its activity-dependent loading, and is especially plastic during growth [1]. Studies of animal models have revealed differences in bone shape and joint structure between groups with different levels of physical activity during growth [2]. We have recently demonstrated using an avian, bipedal animal model that optimal fascicle lengths in hip and ankle muscles decrease substantially during growth (by ~15%) in sedentary compared to running-trained animals [3]. The shorter muscle lengths in the sedentary group may limit force generating capacity during dynamic movements due to force-length-velocity constraints [5]. Furthermore, preliminary data on ankle moment arms between these groups support the hypothesis that torque- and power-generating capacity will be compromised [5].

These morphological alterations over the growth span may reduce locomotor performance and increase effort when inactive animals with suboptimal musculoskeletal structure attempt to achieve a locomotor goal. The purpose of this study was to determine (1) the effects of growth-period inactivity upon locomotor performance immediately post-growth and (2) the extent to which these adaptations to inactivity can be reversed after a period of increased activity in adulthood.

This goal was addressed using an experimental design in which guinea fowl were grouped into 1) a control exercise group (EXE) where normal activity, including opportunities for running and jumping, was provided over the growth span and adulthood, 2) a disuse group (DIS) that was subject to limited movement and muscle disuse (using botulinum toxin) during growth and subsequently provided the same access to activity as the EXE group during adulthood.

METHODS

One-day old guinea fowl (*Numida meleagris*) were obtained from a regional breeder (Guineafarm, OH). At 4 weeks of age, guinea fowl were divided into EXE (n = 16) and DIS (n = 16) groups. EXE birds were housed in a large, circular pen that allowed ample room for locomotion and objects for jumping/perching. The DIS group were reared in small, square pens with low ceilings to restrict movement and jumping. Furthermore, the DIS groups was subjected to focal muscle disuse via injection of botulinum toxin-A (BTX-A) into the lateral (LG) and medial gastrocnemius (MG). This protocol created an enhanced disuse signal that was reversible.

Each animal received an initial BTX-A injection (4 units (LD50)/kg) at 7-8 weeks of age under general anesthesia (1.5% isoflurane). The animals received an additional injection every five weeks for a total of 4 injections over 20 weeks, by which time the animals had reached skeletal maturity. The EXE groups received sham injections of saline.

At 27-28 weeks of age (~6 months), a maximal jumping task was used to assess power capacity. Birds were placed on dual-force plates (AMTI 6x6; 20 lb. capacity each) that were surrounded by a vertical box (Fig 1). Birds were given 5 minutes to jump at least 3 times voluntarily or with encouragement. This was repeated across two days. Forces were recorded at 100 Hz and filtered using a

low-pass Butterworth filter with a cutoff frequency of 50 Hz. Peak vertical forces from the top three jumps were averaged and normalized to body weight (BW).

Following the 6 month testing, half of the animals from each group were sacrificed (pentobarbital >1.6 mg/kg) for morphological analyses (to be performed in a companion study). The remaining animals from the DIS group were housed in the same condition as those of the EXE group throughout adulthood. Adult animals were retested at 15 months of age.

Student t-tests were performed to assess group differences at an alpha level $p < 0.05$.

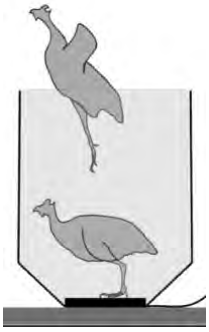

Figure 1. Schematic illustration of jumping task.

RESULTS AND DISCUSSION

The average maximum weight-normalized vertical force at the 6-month post-growth time point was ~6 N/BW in the DIS group vs. ~8 N/BW in the EXE group ($p < 0.05$). Upon retesting at the 15 month time point both the DIS and EXE groups average maximum weight-normalized vertical force was ~7 N/BW. The jumping force data are summarized in Fig. 2.

Not surprisingly, the jumping performance of DIS animals was markedly poorer than EXE birds after a growth period marked by both general and localized muscle disuse. Nevertheless, the magnitude of peak vertical force in the DIS group was remarkably high, reaching nearly 6x body weight. This value is comparable to the peak forces reported previously from cage-reared guinea fowl [6]. This suggests that localized muscle paralysis during growth is compensated for, possibly either through growing new muscle, or by increased growth and use of use of synergists. It also suggests that the difference in force observed between groups at 6 months is due primarily to the availability of exercise as opposed to a BTX-A effect.

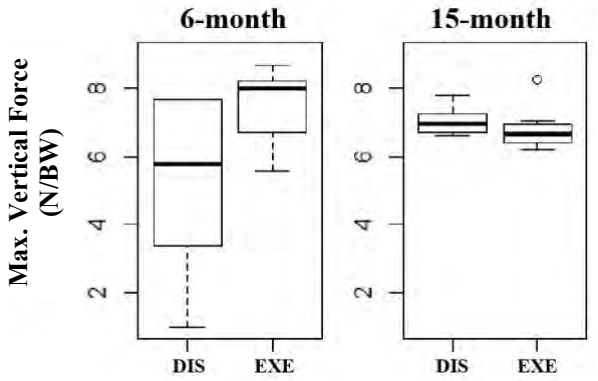

Figure 2. Box-and-whisker plots of max normalized vertical force at 6- (left) and 15-months (right).

To our knowledge, this is the first study to systematically assess whether movement impairment due to disuse during growth can be reversed. Our results suggest that maximal locomotor performance (jumping) can indeed be recovered after even severe locomotor and muscle disuse during growth. This finding has encouraging implications for exercise interventions for restoring function. How these findings correlate with morphological adaptations is currently being explored. The logical subsequent steps are to establish the exercise dose necessary to restore normal function and its timeframe, and if these findings relate generally across modes of movement and species.

REFERENCES

[1] Pearson OM & Lieberman DE. *Am J Phys Anthropol* **39**, 63-99, 2004.

[2] Green DJ, et al. *J Exp Zool* **318**, 621-638, 2012.

[3] Salzano MQ, et al. *40th Annual Meeting of ASB*, Raleigh, NC, USA, 2016.

[4] Lee SS & Piazza SJ. *J Exp Biol* **212(22)**, 3700-3707, 2009.

[5] Salzano MQ, et al. *41st Annual Meeting of ASB*, Boulder, CO, USA, 2017.

[6] Henry HT, et al. *J Exp Biol* **208(17)**, 3293-3302, 2005.

EFFECTS OF ERRONOUS MOVEMENT PREDISPOSITION ON JUMP LANDING

Mitchell L. Stephenson and Jason C. Gillette

Iowa State University, Ames, IA, USA
email: mistephe@iastate.edu, web: kin.hs.iastate.edu

INTRODUCTION

Non-contact anterior cruciate ligament (ACL) injury research is commonly implemented with protocols that include a reactive component. This is included to better reflect sports experience, whereas an athlete alters their movement direction in response to an opponent. Experimentally, this is often simulated with a discrete visual (often LED) stimulus indicating the movement direction moments before the participant lands from a jump or plants their foot before a cut [1-2].

Limited past research has relied on video of an opposing athlete as alternative visual stimuli [1]. Deceptive movements of the recorded athlete may predispose participants to assuming an erroneous movement direction. This study seeks to determine whether an erroneous predisposition may alter jump landing in a way that may increase ACL injury risk when the participant corrects to the proper movement direction. To limit other confounding variables that may be associated with video stimuli, this research implements predisposition using discrete LED directional stimuli.

METHODS

Ten physically-active, right-foot dominant, uninjured females that commonly participate in soccer, basketball, volleyball, tennis, or hockey (20.8±1.5 years; 1.63±0.09 m tall; 61.9±6.7 kg) have volunteered for this ongoing study. Participants provided informed consent, executed a warm-up protocol, and performed practice trials.

Participants jumped forward 50% of their height from a 30cm tall block, landed bilaterally on two force platforms (2000 Hz, AMTI, Watertown, MA), and then quickly and fluidly jumped to the left or right 60° from anterior for maximum speed and distance [2]. The jump direction was indicated by one of two LEDs (left or right) mounted in front of the participant. These indicators were illuminated in one of five conditions: The anticipated (AN) condition illuminated the LED before the trial began. The reactive conditions illuminated the LED either immediately after they jumped from the 30cm block (RE1) or the instant they landed on the force platforms (RE2). The predisposition conditions illuminated the incorrect LED before the trial began, and then switched to the correct LED at takeoff from the 30cm block (PRE1) or at landing (PRE2). Anticipated and predisposition trials were indistinguishable at the beginning of the trial.

Participants performed at least three successful trials in each direction in each condition. They performed more AN conditions than PRE, such that assuming the initially-indicated direction was correct would result in fewer repeated trials. Participants were informed of this before the data collection started.

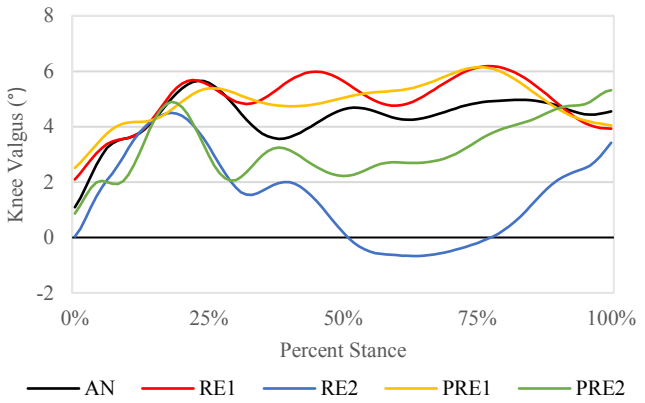

Figure 1: Ensemble mean knee valgus angle across percentage stance time for each condition while jumping left.

The jump direction and condition were computer-randomized to implement a double-blind design. Kinematics of 19 retroreflective markers placed on the right lower extremity, pelvis, and torso were recorded via 8 infrared cameras through Vicon Nexus 1.8.2 (200 Hz, Vicon Corp, Oxford, UK).

Peak knee valgus and flexion angles as well as the peak unilateral vertical ground reaction forces (VGRF) were extracted during the first 100ms of contact with the force platforms [3]. A repeated-measures ANOVA was performed to compare the effect of the condition on kinematics and landing VGRF for each jump direction.

RESULTS AND DISCUSSION

Significant main effects ($p < 0.01$) were identified in both movement directions for peak knee flexion angles and VGRF, but not peak knee valgus angles. Pairwise comparison results maintaining a false discovery rate of 0.05 are presented in Table 1.

Dependent variables were characteristically unique depending on jumping direction [2]. Left jumps demonstrated increased peak VGRF and decreased peak knee flexion angles in both the RE1 and PRE1 conditions compared to the AN, RE2, and PRE2 conditions. This may be interpreted as a stiffer, and possibly more dangerous [4], landing in the RE1 and PRE1 conditions.

Jumps to the right resulted in increased peak knee flexion angles in the RE1 and PRE1 conditions compared to the other conditions. Furthermore, the RE2 and PRE2 conditions demonstrated decreased peak flexion angles compared to the other conditions. Peak vertical ground reaction forces were highest in the RE2 and PRE2 conditions, and the PRE1 condition resulted in a smaller peak ground reaction force than the AN condition. The combination of increased VGRF and decreased knee flexion in the RE2 and PRE2 conditions again indicates a stiffer landing which may increase injury risk [4].

The RE1 condition did not significantly differ from PRE1, and RE2 did not differ from PRE2 in either jump direction for any reported variable. It appears that the effects of predisposition did not alter landing from the reactive conditions in the first 100ms of landing. However, Figure 1 does demonstrate frontal plane kinematic differences later in the landing phase. Qualitatively, researchers and participants noted increased difficulty in executing proper directional changes in the incorrectly predisposed conditions. Thankfully, these effects do not appear to affect the reported variables within the landing times expected to be consequential for ACL injury [3]. Participants reported after data collection that they did assume the initially-indicated direction was correct; we expect that it is unlikely that participants chose to ignore the stimuli until landing.

In conclusion, predisposing participants to an erroneous movement direction did not alter results within the first 100ms of landing, and therefore likely did not change ACL injury risk. It is possible that, in situations where erroneous predisposition is possible (such as deceptive opponents in sport), participants do not alter their pre-landing strategies in ways that may contribute to this lower extremity injury.

REFERENCES

1. Lee, MJC, et al. *Med Sci Sports Exerc*, **45**, 1740-1748, 2013
2. Stephenson, ML, et al. *Sports Biomech,* **17**, 67-82, 2018
3. Koga, H, et al. *Am J Sports Med*, **38**, 2218-2225, 2010
4. Leppanen, M, et al. *Am J Sports Med*, **45**, 386-393, 2017

Table 1: Peak knee angles and bodyweight-normalized vertical ground reaction force (VGRF) (Mean ± SD) for each condition and jump direction during the first 100ms of foot contact with the ground between jumps.

		AN	RE1	RE2	PRE1	PRE2
Jump Left	Flexion (°)	64.0 ± 6.7 ^{A}	61.5 ± 7.6 ^{B}	66.9 ± 8.9 ^{A}	60.5 ± 6.9 ^{B}	68.8 ± 8.9 ^{A}
	Valgus (°)	7.5 ± 5.0	8.0 ± 4.3	6.5 ± 5.5	7.9 ± 4.6	6.7 ± 4.5
	VGRF (BW %)	2.79 ± 0.48 ^{B}	3.14 ± 0.34 ^{A}	2.69 ± 0.49 ^{B}	3.15 ± 0.37 ^{A}	2.73 ± 0.47 ^{B}
Jump Right	Flexion (°)	70.4 ± 8.4 ^{B}	72.4 ± 8.2 ^{A}	67.6 ± 7.5 ^{C}	73.7 ± 7.8 ^{A}	67.5 ± 9.0 ^{C}
	Valgus (°)	7.1 ± 4.9	5.6 ± 5.9	5.7 ± 5.5	5.7 ± 4.9	6.7 ± 5.0
	VGRF (BW %)	2.21 ± 0.49 ^{B}	1.84 ± 0.57 ^{BC}	2.61 ± 0.47 ^{A}	1.67 ± 0.56 ^{C}	2.59 ± 0.37 ^{A}

Conditions grouped as A>B>C at a false discovery rate significant difference of 0.05

JOINT CONTRIBUTIONS TO TOTAL LOWER EXTREMITY POWER DURING A SINGLE-LEG HOP LANDING TASK AFTER ANTERIOR CRUCIATE LIGAMENT RECONSTRUCTION

[1]Rachel L. Tatarski, [1]Albert Chen, [2]Timothy E. Hewett, and [1,3]Stephanie Di Stasi
[1]Sports Medicine Research Institute, The Ohio State University Wexner Medical Center, Columbus, OH, USA
[2]Orthopedic Biomechanics Laboratories and Sports Medicine Center, Mayo Clinic, Rochester, MN, USA
[3]Division of Physical Therapy, The Ohio State University, Columbus, OH, USA
email: rachel.tatarski@osumc.edu

INTRODUCTION

The single-leg hop for distance (SLH) is often used to determine return-to-sport (RTS) readiness for patients recovering from anterior cruciate ligament reconstruction (ACLR) surgery. A limb-to-limb comparison of the hop distance with ≤5% asymmetry is considered clinically normal.[1] While hop distance symmetry is a valuable indicator of dynamic knee dysfunction, it does not capture abnormal mechanics that may confer injury risk. Sagittal plane knee extensor asymmetry during landing is a known predictor of second ACL injury even after ACLR.[2]

A deeper analysis into the force attenuation strategies during SLH landing after ACLR and patient-reported function may provide insight into compensations that are not necessarily apparent with hop symmetry. Thus, the purpose of this study was to compare the sagittal plane power absorption strategies between limbs during the landing phase of a SLH in individuals who have undergone ACLR and assess the relationships between joint contributions and patient-reported function. The hypotheses tested were 1) that the involved limb would demonstrate lower knee and higher hip power absorption during the SLH when compared to the uninvolved limb and 2) that knee contribution would be correlated with patient-reported function.

METHODS

Twenty individuals who had undergone ACLR gave written consent to participate in this study, which was approved by the university's IRB (Table 1). Participants had either completed physical therapy or were in the latest phases and were required to have full, pain-free knee range of motion, ≤1+ knee effusion on the effusion stroke test, and <30% hamstrings and quadriceps isokinetic strength deficits in order to perform the SLH. The symptoms, pain, and sports subscales of the Knee injury and Osteoarthritis Outcomes Score were used to assess patient-reported function (Table 1).[3]

Table 1: Participant demographics.

n	20 (9 males, 11 females)
Age (yrs)	20.6 ± 6.4
Height (cm)	172.3 ± 8.97
Mass (kg)	78.0 ± 16.8
Time since surgery (mon)	8.1 ± 3.6
KOOS – Sports	90.69 ± 11.13
KOOS – Pain	96.11 ± 4.97
KOOS – Symptoms	89.11 ± 7.81

Participants were fitted with 55 retro-reflective markers that were used to track body segments and define joint centers. Kinematics were captured at 240Hz with a 12-camera motion capture system (Motion Analysis Corp., CA) and ground reaction forces were captured at 1200Hz with an embedded force plate (Bertec, OH). Participants were instructed to begin the hop balanced on one foot, to hop as far forward as possible, and to land on the force plate with the same foot while maintaining balance. Hop distance was estimated during practice trials to ensure that the participant would land on the force plate.

The landing phase was defined as the first 0.5 seconds after initial contact (vertical ground reaction force >20N). Hop distance was calculated from the heel marker on the hopping foot. Limb symmetry index (LSI) was calculated as the percent of the involved limb to the uninvolved limb. Marker trajectory and force data were smoothed with a 6Hz and 50Hz low pass filter, respectively. Kinematic and kinetic data were imported into Visual 3D (v6 Pro., C-Motion Inc., MD) in which hip, knee, and ankle joint powers were calculated through inverse dynamics. The means of two successful trials on each limb were analyzed. Total limb negative power (TLP) was calculated as the sum of the hip, knee, and ankle negative joint powers. Hip, knee, and ankle

contributions at the time of the TLP peak were calculated as a percent of the TLP. Kinetic variables were normalized to body-weight*height.

The variables of interest were: hip, knee, and ankle joint contributions to TLP, peak TLP, and KOOS subscales. Paired t-tests were used to compare these variables on the involved and uninvolved limbs. Spearman's rho correlations were used to assess the relationship between KOOS subscales and knee contribution to the TLP. The alpha level was set to 0.05, *a priori*. Statistical analyses were carried out with Minitab (v17, PA).

RESULTS AND DISCUSSION

Participants hopped farther on the uninvolved limb (141.6 ± 23.2 cm) than the involved limb (149.3 ± 27.1 cm; p=0.02); however, the LSI was 95.0 ± 9.9%, which is considered within a normal range. Peak TLP was significantly greater on the uninvolved limb (p=0.001, Table 2). There were no significant differences between limbs for hip (p=0.334) or ankle (p=0.874) peak negative power; however, the peak power absorbed by the involved knee was significantly lower than the uninvolved knee (p=0.004; Table 2).

Table 2: Means and standard deviations for hip, knee, and ankle peak negative powers and the hip, knee, and ankle joint contributions to total lower extremity peak negative power for the involved and uninvolved limbs.

	Involved	Uninvolved
Hip Power	-5.87 ± 2.90	-6.39 ± 2.83
Knee Power	-7.39 ± 2.04*	-9.66 ± 0.87
Ankle Power	-2.22 ± 1.19	-2.16 ± 1.77
Peak Total Limb Power	-9.97 ± 2.85*	-12.33 ± 4.33

** denotes a significant difference, p < 0.05. Power is reported in W/kg*cm.*

Hip (p=0.089) and ankle (p=0.075) contributions to peak TLP absorption were not different between limbs (Figure 1). The knee contribution to TLP on the uninvolved side was significantly greater than on the involved side (p=0.028, Figure 1). In addition, the KOOS-Symptoms subscale was significantly related to the knee contribution to TLP (r=0.462, p=0.040), while the sports and pain subscales were not.

The data support the hypothesis that there would be a redistribution of power absorption away from the involved knee after ACLR.

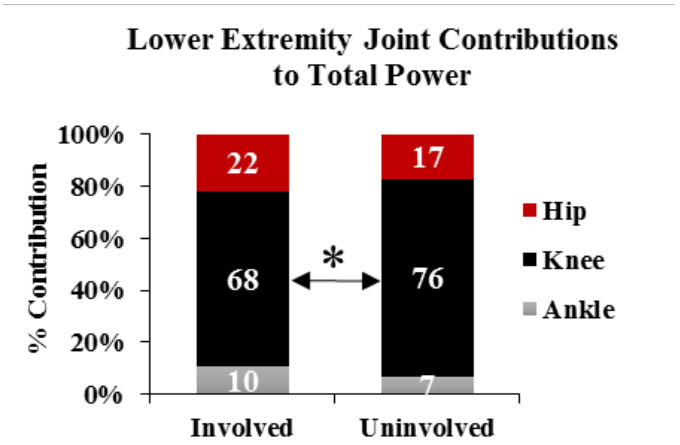

Figure 1: Hip, knee, and ankle contributions to total lower extremity negative power. Individual joint contributions were taken from the same frame as the peak for total joint power. (* indicates a significant difference between limbs, p < 0.05).

The reduction in knee contribution and peak power absorption on the involved knee indicates an "unloading" strategy and confirms power redistribution away from the involved knee.[4] Moreover, these data suggest a relationship between this redistribution landing strategy and function (symptoms).

Importantly, all participants had passed the clinical criteria to hop and LSI was well within normal limits, yet a different power absorption strategy on the involved limb remained, and was positively correlated with knee symptoms. Patient-reported function can be easily assessed by clinicians and should be considered when making RTS decisions.

CONCLUSIONS

Overall, the involved knee contributed significantly less to total limb power absorption which was significantly correlated to the KOOS-symptoms subscale score, despite clinically normal limb symmetry values in hop distance after ACLR.

REFERENCES

1. Paterno M V., et al. *Sport Heal A Multidiscip Approach*. 2017;ePub:1-6.
2. Paterno M V., et al. *Am J Sports Med*. 2010;38(10):1968-1978.
3. Roos EM, et al. *J Orthop Sport Phys Ther*. 1998;28(2):88-96.
4. Orishimo KF, et al. *Knee Surgery, Sport Traumatol Arthrosc*. 2010;18(11):1587-1593.

ACKNOWLEDGEMENTS

The authors acknowledge funding support from the Sports Physical Therapy Section of the American Physical Therapy Association.

STRIDE-TO-STRIDE FLUCTUATIONS OF CHILDREN'S GAIT FROM 2-10 YEARS OF AGE.

[1] Bryon C. Applequist and [2] Anastasia Kyvelidou

[1] The University of Scranton, Scranton, PA USA
[2] Creighton University, Omaha, NE, USA
email: bryon.applequist@scranton.edu

INTRODUCTION

Linear methods of variability are concerned with the magnitude of variability and often consider deviations from a central mean as error. Utilization of nonlinear tools to examine variability allows for the exploration and measurement of the patterns of variability displayed by the system or the structure of the variability. This explores the deterministic properties of gait, or how previous iterations within the gait cycle influence subsequent and future iterations. (1) Nonlinear analysis of gait variability of the joint angle time series has not been investigated in developing children. Differences in the structure of variability of the joint angle time series of children at different points in development should be able to be identified using nonlinear tools of analysis. Not only will this shed light on the potential control mechanisms being used and the refinement of gait throughout development but will give a launching point for comparison of the natural trajectory of gait development to be used to help understand various types of pathological gait in children.

The purpose of this study was to assess the development of kinematic gait variability in children from ages 2-10 years old using nonlinear methods of analysis. We hypothesized that with age and walking experience, children will have increased stride-to-stride fluctuations in their gait.

METHODS

Our study involved 28 boys and girls split into four separate age groups. The age groups consisted of 2-3-year-old (n = 7), 4-5-year-old (n = 7), 6-7-year-old (n = 7), and 8-10-year-old (n = 7) (Table 3.1). Prior to participation in the study, parental informed consent and child assent was obtained as approved by the University's Institutional Review Board. Children were excluded from the study if they had any neurological disorders or musculoskeletal injuries that may affect gait.

Subjects were provided with a standard laboratory shoe (Nike Free 5.0). Retro-reflective markers were then placed on the subject at specific anatomical locations of the foot, shank, thigh and pelvis. Lower extremity marker locations were acquired for one three-minute walking trial at 100Hz using an 8-camera motion capture system. The walking trial consisted of at least 3-minutes of walking at self-selected comfortable walking speed while wearing the lab provided footwear. Data was left unfiltered to not affect or influence potential biological signals within the data. It has been shown that filtering the data can lead to altered nonlinear results.(2)

Joint angle time series in the sagittal plane of the ankle, knee and hip joints were computed using Visual 3D software (C-Motion Inc., Germantown, MD). Data processing and analysis were conducted using custom Matlab scripts (The Mathworks Inc, Natick, MA). Stride-to-stride fluctuations during the walking trials were evaluated using the largest Lyapunov Exponent (LyE). A one-way ANOVA with four factors (4 age groups) was performed to determine statistical significance for the dependent variable for the Ankle, Knee, and Hip joint angle time series respectively. The dependent variable included The Largest Lyapunov Exponent. When significant effects were determined, post-hoc comparisons were performed using the Tukey method.

RESULTS AND DISCUSSION

There were significant effects of age group for LyE of the ankle, knee, and hip joint time series $p < .05$. (Fig. 1) Post hoc comparison results for each joint among the age groups can be found in Table 1.
Nonlinear analysis of the joint angle time series

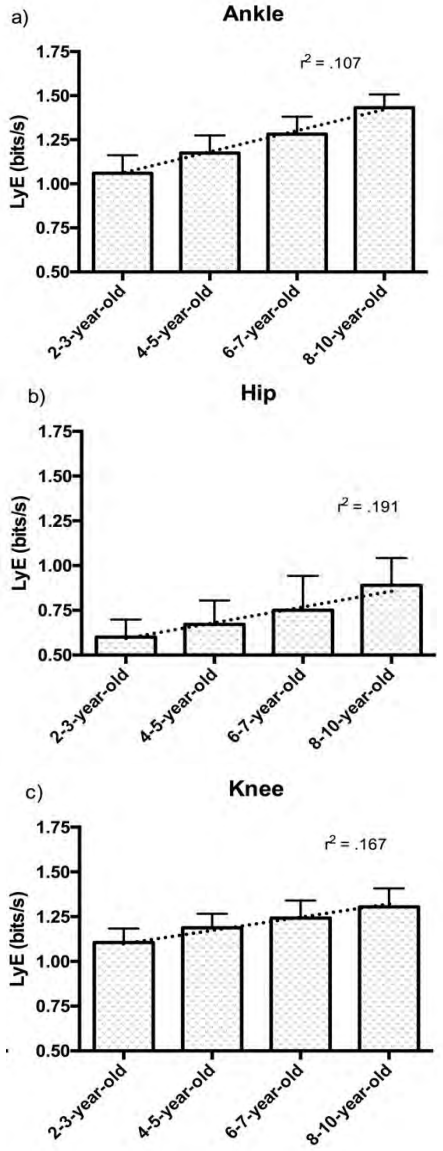

Figure 1: Bar charts showing the mean and standard deviation for Largest Lyapunov Exponent of the Ankle, Hip, and Knee joint time series. Data are reported for age group.

showed that the structure of gait variability in children is age dependent. There was an age effect on the LyE of the joint angle time series at the ankle, hip, and knee. All three joints showed an increase with age from youngest to oldest for the LyE. As children get older and gain more experience walking, their neuromuscular system and overall motor control are also maturing. The combination of maturation of the systems and gained experience leads to an overall better organization of movements. The increase in divergent patterns makes for a more robust movement system that is capable of dealing with small perturbations with little flaw. When we get older and become more experienced walkers, we can navigate our environment with ease. Small increases in rise or bumps in a path that could elicit falls in the youngest of walkers, are hardly noticed to the more adept, experienced walker.

CONCLUSIONS

Our results indicate that the nonlinear variability of children's gait increases as children age. The combination of a decrease in linear variability, or a refining and improved stability of gait, as well as an increase in nonlinear variability, or an increase in the complexity and quality of movement patterns, suggest an overall maturation of the neuromuscular system. Our results show that there is a refining of gait with age and motor maturation that is accompanied by an increase in complexity that speaks to the overall multifaceted organization of systems that is the maturation of gait.

REFERENCES

1. Stergiou et al. *JNPT*. 2006;30(3):120-9.
2. Rapp et al. *Physical review E*. 1993;47(4):2289.

ACKNOWLEDGEMENTS

Footwear provided by the Under Armour Innovation Research Footwear Fellowship (BA)

Table 1: Mean and Standard Deviation for the Largest Lyapunov Exponent for each of the age groups are reported. Significant differences ($p < .05$) between groups are denoted by the following symbols: * (2-3 and 4-5), ^ (2-3 and 6-7), ‡ (2-3 and 8-10), ŧ (4-5 and 6-7), § (4-5 and 8-10).

	Largest Lyapunov Exponent				
	2-3 (N=7)	4-5 (N=7)	6-7 (N=7)	8-10 (N=7)	Sig.
Ankle	1.06±0.10	1.17±0.10	1.28±0.10	1.43±0.08	^‡§ ç
Knee	0.60±010	0.67±0.13	0.75±0.19	0.89±0.15	‡§
Hip	1.11±0.08	1.19±0.08	1.24±0.10	1.30±0.10	^‡

ANKLE JOINT STIFFNESS OF CHILDREN WITH CEREBRAL PALSY AFTER SELECTIVE DORSAL RHIZOTOMY

[1] Filiz Ates, [2,3,4] Joline E. Brandenburg, [1]Kenton R. Kaufman

[1] Motion Analysis Lab. Department of Orthopedic Surgery, Mayo Clinic, Rochester, MN, USA
[2]Department of Physical Medicine and Rehabilitation, Mayo Clinic, Rochester, MN, USA
[3]Department of Pediatrics and Adolescent Medicine, Mayo Clinic, Rochester, MN, USA
[4]Department of Neurology, Mayo Clinic, Rochester, MN, USA
E-mail: ates.filiz@mayo.edu

INTRODUCTION

Selective dorsal rhizotomy (SDR) is a neurosurgical technique performed to reduce muscle spasticity and improve motor functions in children with cerebral palsy (CP) [1]. Combined with physiotherapy, SDR reduces pain, improves joint range of motion (ROM), and enhances gait performance. Even though improvement in patient mobility has been reported after SDR to last for many years, SDR has not prevented contracture formation [2]. To understand what is contributing to muscle contracture formation, it is necessary to assess the effects of SDR on ankle joint stiffness. We hypothesized that SDR (i) increases passive ankle ROM and (ii) decreases ankle joint quasi-stiffness.

METHODS

The Institutional Review Board of Mayo Clinic approved the study. 10 patients with CP (median age 6 years 2 months at the time of surgery) who had previously undergone SDR were included. Patients were studied 3 months (range 1 - 8 months) before (Pre-SDR) and 1 year 1 month (range 10 - 17 months) after (Post-SDR) surgery. The Gross Motor Functional Classification System (GMFCS) was used to classify the mobility of the patients. Ankle passive range of motion (ROM) was recorded with the knee angle at 0º (knee extension) and 90º (knee flexion).

3D gait analysis (Raptor-12HS, Motion Analysis Corp, Santa Rosa, CA), force plates (Model 9281B, Kistler Instrument Corp, Amherst, NY; Model BP400600, Advanced Mechanical Technology, Inc., Watertown, MA) and surface EMG (MA300, Motion Lab Sys, Inc., Baton Rouge, LA) were synchronized. The peak plantar flexion (PF) and peak dorsiflexion (DF) angles during walking were calculated for each participant. The phasic gastrocnemius activity was scored as follows: 0 = Phasic; 1 = Increased Phasic Activity; 2 = Continuous Low Level Activity; 3 = Continuous with Phasic Pattern; 4 = Continuous High Level Activity. Ankle joint quasi-stiffness [3] was calculated as the slope of the ankle moment vs ankle angle for the time interval from max DF to max PF during the gait cycle. Generalized estimating equations were used to evaluate changes in the ankle passive and dynamic characteristics pre- and post-SDR. Differences were considered significant if $p<0.05$.

RESULTS AND DISCUSSION

Pre-SDR GMFCS levels ranged from I to III. GMFCS levels of half of the children improved post-SDR.

Ankle joint passive ROM increased when measured with the knee flexed (Pre- and post-SDR median = 10º and 15º, interquartile range: 10º and 10º, respectively) ($p < 0.0001$) and knee extended ($p < 0.0001$) (Pre- and post-SDR median = 0º and 10º, interquartile range: 13.75º and 12.5º, respectively). This confirmed our first hypothesis.

After SDR, max PF during walking decreased ($p < 0.0001$) (Pre- and post-SDR median = -29.54º and -13.10º, interquartile range: 26.89º and 7.90º, respectively) and max DF increased ($p < 0.0001$) (Pre- and post-SDR median = 7.15º and 11.93º, interquartile range: 17.04º and 11.95º, respectively). This shift in ankle kinematics during walking indicates a reduction in equinus gait after SDR. Phasic gastrocnemius activity improved substantially post-SDR ($p < 0.0001$).

Ankle joint quasi-stiffness decreased ($p = 0.0017$) after SDR (Fig1A) (Pre- and post-SDR median = 0.056 Nm/kg/º and 0.051 Nm/kg/º, and interquartile

range: 0.031 Nm/kg/º and 0.019 Nm/kg/º, respectively). This confirmed our second hypothesis. Moreover, even though the total time of the gait cycle (Pre- and post-SDR median = 0.868 s and 0.935 s, and interquartile range: 1.308 s and 0.284 s, respectively) did not change (p = 0.99), the time interval from max DF to max PF (Pre- and post-SDR median = 0.125 s and 0.156 s, and interquartile range: 0.153 s and 0.253 s, respectively) increased significantly (p = 0.0068) after SDR (Fig 1B).

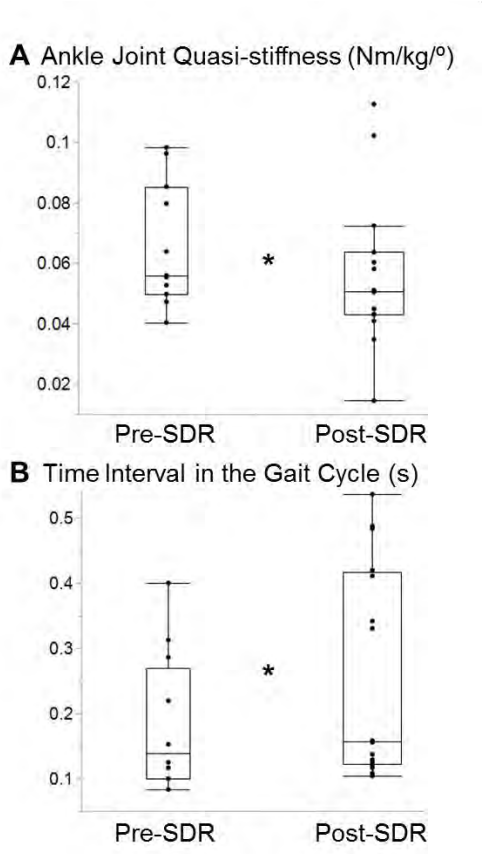

Figure 1: Box-and-whisker plot of **(A)** the ankle joint quasi-stiffness and **(B)** the time interval from max DF to max PF for Pre- and Post-SDR.
* indicates significant differences.

Decreased joint ROM and increased joint stiffness that characterize spastic CP are associated with changes in the material properties of contractile and non-contractile structures. Spastic contractions that cause muscle shortening are typically accepted as the main cause of muscle contracture formation. It has been reported that the active neural contribution of the plantar flexor muscles is a major source of higher ankle joint stiffness in CP [4]. In line with these works, our study demonstrates that SDR diminishes the neural source of spasticity and improves ankle joint quasi-stiffness. Therefore, the main reason of long term post-SDR contracture formation [2] is probably not be the active component. Previously, the increased passive tension that is unrelated to the stretch reflex was demonstrated for the spastic vastus lateralis [5]. Moreover, the extracellular matrix of biopsied hamstring muscles of children with spastic CP has been shown to be stiffer than age-matched controls [6]. Together with these previous data, our findings suggest that further research to understand muscle contractures should focus on mechanical alterations of non-contractile structures.

CONCLUSIONS

The present study shows that ankle joint characteristics during passive and dynamic conditions improve after SDR. Significant changes in ankle joint quasi-stiffness and in the time interval from max DF to max PF indicate better motor control together with other outcomes which reveal progress in dynamic joint parameters. Further research on muscle contracture following SDR is suggested to focus on mechanical alterations of intramuscular non-contractile structures as well as non-muscular tissues.

REFERENCES

1. Steinbok et al. *Dev Med Child Neurol* 1997; 39:178-84.
2. Tedroff K, et al. *Dev Med Child Neurol* 2015; 57: 484-90.
3. Davis RB and DeLuca PA. *Gait Posture* 1996; 4:224-31.
4. Sheean G, and McGuire JR. *PM&R*. 2009; 1:827-33.
5. Olsson MC, *J Physiol*. 2006; 577:339-52.
6. Smith LR, et al. *J Physiol.* 2011; 589:2625-39.

ACKNOWLEDGEMENTS

Scientific and Technical Research Council of Turkey (TUBITAK) 2219 International Post-doctoral Research Fellowship Programme grant to Filiz Ates.

WALKING BALANCE ON A TREADMILL CHANGES DURING PREGNANCY

[1] Robert D. Catena, [1] Daniel Flores, [1] Christopher P. Connolly, and [2] Nigel Campbell

[1] Washington State University, Pullman, WA, USA
[2] Moscow/Pullman OBGYN, Pullman, WA, USA
email: robert.catena@wsu.edu, web: https://labs.wsu.edu/biomechanics/

INTRODUCTION

An estimated 17%-39% of women fall during pregnancy, making falls a leading cause of accident-related injury during pregnancy [1]. There has been extensive research into standing balance changes during pregnancy. However, static balance measures may be inadequate for predicting dynamic balance change in a pregnant population [2]. In order to properly measure dynamic balance changes while walking, body center of mass (bCOM) location must be obtained.

We previously compared methods for determining the torso COM (tCOM) change and mass distribution changes throughout the body during pregnancy [3]. In this current study, we (1) tracked walking balance changes during pregnancy and (2) determined if the method for calculating bCOM significantly influences the balance measures.

METHODS

Fifteen pregnant women, ages 22 to 36 years at the start of testing, were tested in 4-week intervals from approximately 12 weeks gestation until delivery. Thirty-two anthropometric measurements were conducted for identifying volumes of 13 body segments. Fifty-four reflective markers were then attached for motion analysis.

Participants first performed a ten second standing static trial on a force plate. Participants then walked on a treadmill at a comfortable self-selected walking pace for a duration of sixty seconds. The final task required participants to lay supine on a backboard spanning two force plates for a duration of ten seconds.

A 10-camera motion capture system (Motion Analysis Corp.), recorded marker data at 100Hz. All motion capture data were filtered with a 6Hz low-pass Butterworth filter.

With assumed densities, 13 body segment masses and 12 COMs were identified [4]. We then compared the tCOM (13^{th} segment in our model) change through gestation using three methods: (A) through use of static force plate poses, (B) from Pavol anthropometry measurements [4], and (C) and combination using anterior and lateral locations from (A) and long axis location from (B). Whole-body center of mass (bCOM) was then calculated as the weighted sum of all segment COMs.

Strides were separated at right heel strike and balance measures averaged across strides. Control of balance was identified as the motion of the bCOM in three dimensions, and the bCOM angular motion relative to the ankle joint center. To measure the mechanical potential for fall, the minimum distances of the bCOM to the base of support edges were measured. Time of pregnancy (categorized by 4-week intervals) and model type (A. Force plate, B. Pavol, and C. Combined) were used as repeated-measure independent variables, and balance measures were used as depended variables in a generalized linear mixed model.

RESULTS AND DISCUSSION

We found that some balance control strategies started changing at the beginning of our study, indicating that they may have even started during the 1st trimester, prior to the start of our testing. Pregnant women started reducing their anterior-posterior motion (reduced AP angle changes) immediately during testing, corresponding with immediate and gradual reductions in preferred walking speed. This indicates previously noted changes in spatiotemporal gait measures between the second and third trimesters of pregnancy may

start even sooner, as a gradual reduction throughout gestation.

We found that step width starts to increase in the middle of the 2nd trimester (Table 1A). Correspondingly, the minimum distance between the center of gravity (COG) and lateral boarders of the stance foot start to increase (Table 1D). This change indicates a positive effect on balance, as it indicates that the bCOM is less likely to fall outside of the lateral edges of the base of support, reducing the need for corrective actions like body lean or crossover steps to avoid a lateral fall.

Going into the second trimester, pregnant participants had increased mediolateral bCOM angular motion (Table 1B) and liner motion (Table 1C). ML bCOM motion continued to increase through the third trimester even though step width decreased. Considering that we employed a treadmill for continuous gait, treadmill walking doesn't necessitate a decrease in step width of the average individual, but for pregnant women with increased abdominal volume, decreased step width may be employed on a treadmill to reduce the potential for waddling gait outside of the confined lateral boundary of a treadmill. Future studies should examine potential differences in treadmill vs. over-ground walking in a pregnant population. Accompanying this ML bCOM motion increase, the distance between COG and lateral base of support edge decreased. This combination of findings support a mechanism for waddling gait in the third trimester, and indicate balance control deficits from the beginning of the 3rd trimester on.

Unique to walking on a treadmill vs over-ground walking, there should be no AP excursion of the bCOM. We asked our participants to stay in the middle of the treadmill so that they would not risk falling of the back of the treadmill, but also not get to close to the front instrument panel and have markers blocked from camera view. AP excursion increased from the mid-2nd trimester on; another indication of decreased ability to control the bCOM motion as a result of pregnancy.

Our findings suggest that both sagittal plane measures and coronal plane measures related to bCOM position in the base of support can be effected by the method used to determine the torso center of mass location during pregnancy. The force plate method for determining torso COM results in the bCOM more anterior and centered laterally during walking.

CONCLUSIONS

Our results indicate significant changes in the control of balance during pregnancy. The likelihood of a fall in the lateral direction also increases. It is therefore important for women to be cautious when performing activities of daily living during pregnancy. The results of this study also indicate that some measures of balance are sensitive to the method used to identify torso COM. The results of this study will inform clinicians and patients about the temporal changes associated with pregnancy that increase the risk of falling and injury.

REFERENCES

1. Dunning, K. et al. *Maternal and Child Health*. **14**(5), 2010.
2. McCrory, J. et al. *J Biomechanics*. **43**(12), 2010.
3. Catena, R. et al. *J Biomechanics*. In press.
4. Pavol, M. et al. *J Biomechanics*. **35**(5), 2002.

ACKNOWLEDGEMENTS

This research was supported by a Washington State University New Faculty Seed Grant and a College of Education Faculty Funding Award.

Table 1: bCOM measures over time, but averaged across models. All significantly change over time ($p<0.001$).

Gestation week	12-16	16-20	20-24	24-28	28-32	32-36	36-40
A. Step width (cm)	11.4	11.3	11.4	11.7	12.3	12.1	11.9
B. ML ROM (deg)	10.4	10.4	11.0	11.3	11.4	11.8	11.8
C. ML ROM (cm)	3.9	3.8	3.8	4.0	4.0	4.3	4.4
D. COG - lateral (cm)	9.8	9.7	9.9	10.1	10.3	10.0	9.9

SIMCP: A SIMULATION PLATFORM TO PREDICT GAIT PERFORMANCE FOLLOWING ORTHOPEDIC INTERVENTIONS IN CHILDREN WITH CEREBRAL PALSY

[1]Friedl De Groote,[1]Lorenzo Pitto, [1]Hans Kainz, [1]Antoine Falisse, [1]Mariska Wesseling, [1]Sam Van Rossom, [1,2]Kaat Desloovere and [1]Ilse Jonkers

[1]KU Leuven, Leuven, Belgium
[2]University Hospital Leuven, Pellenberg, Belgium
E-mail: ilse.jonkers@kuleuven.be

INTRODUCTION

Three-dimensional gait analysis is typically used in the clinical decision-making process in children with cerebral palsy (CP). However, decision-making is complicated by the fact that the pathologic gait pattern results from the complex interaction between changes in musculoskeletal geometry, muscle weakness and impaired motor control. Since musculoskeletal modeling in combination with simulations of motion has the potential to non-invasively predict the effect of an intervention on gait performance, it might be a useful tool to establish a more data-informed decision on treatment selection compared to experimental gait analysis alone.

First, we present a simulation platform that will enable clinicians to compare the effect of different treatment modalities on gait performance in order to identify the treatment that has the highest potential to result in a closer-to-normal gait pattern, using a musculoskeletal model containing personalized musculoskeletal geometry and control, as well as pre-operative gait analysis data. Second, we present a case study in which the simulation platform was used to investigate if pre-intervention motion capture data in combination with a musculoskeletal model containing personalized musculoskeletal geometry and control could be used to predict post-operative gait performance in a child with CP.

METHODS

The simulation framework uses individualized musculoskeletal models as well as the joint kinematics from a typically developing (TD) child to calculate the ability of the patient to perform a typical gait pattern. We quantify the ability of the patient by the capability gap, which is the difference between the joint moments the model representing the CP child can produce, and the joint moments required for a TD gait pattern [1]. Bony geometries and muscle paths are personalized based on magnetic resonance imaging (MRI) [2]. The patient-specific lack of selective motor control is modeled based on muscle synergies computed from EMG measured during the pre-operative gait analysis. [3]. We assume that the intervention does not affect the number of synergies and the relative weighting of different muscles within a synergy. We developed a GUI to create the post-operative model by modifying the musculoskeletal geometry of the pre-operative model to mimic the effect of dedicated surgical interventions (e.g. extension osteotomy).

The pre- and post-operative model are subsequently used to compute the capability gap. To this aim, a synergy-constrained static optimization procedure is performed based on the patient's model while imposing joint kinematics and kinetics from a TD child. The reserve actuators indicate the gap between the required joint torques and the joint torque the muscles can produce, and therefore represent the capability gap according to our definition. The capability gap is therefore a measure of the inability of the patient to perform a typical gait pattern. By comparing the capability gap pre- and post-treatment, as well as between different treatment options, the effect of the surgery on the patient's capability to perform a normal gait pattern can be assessed.

This workflow was applied for a 10-year old female child with mild spastic triplegic CP (GMFCS II). The patient underwent a single-event multilevel surgery including bilateral psoas lengthening, rectus femoris transfer, tibia derotation, femur derotation and extension, and patella distalisation. Clinical pre-operative assessment of the patient showed a triple flexion gait pattern with increased femoral

anteversion and increased muscle tone in the bilateral hip flexors, hip adductors, rectus femoris, hamstrings, soleus and gastrocnemius.

During the pre- and post-surgery gait analysis (12 months post-surgery), marker trajectories, EMG (8muscles/leg) and ground reaction forces were measured. Pre- and post-surgery musculoskeletal models were created as described above, and were used to evaluate the patient's pre- and post-surgery capability gap, the latter with and without the corrective effect of the rectus femoris transfer.

The predicted capability gap was validated against the post-surgery gait analysis data. To this aim, we compared the pre- and post- surgery model-based capability gap (root mean square value) to the root mean square difference (RMSD) between measured TD kinetics, and the patient's pre- and post-surgery kinetics.

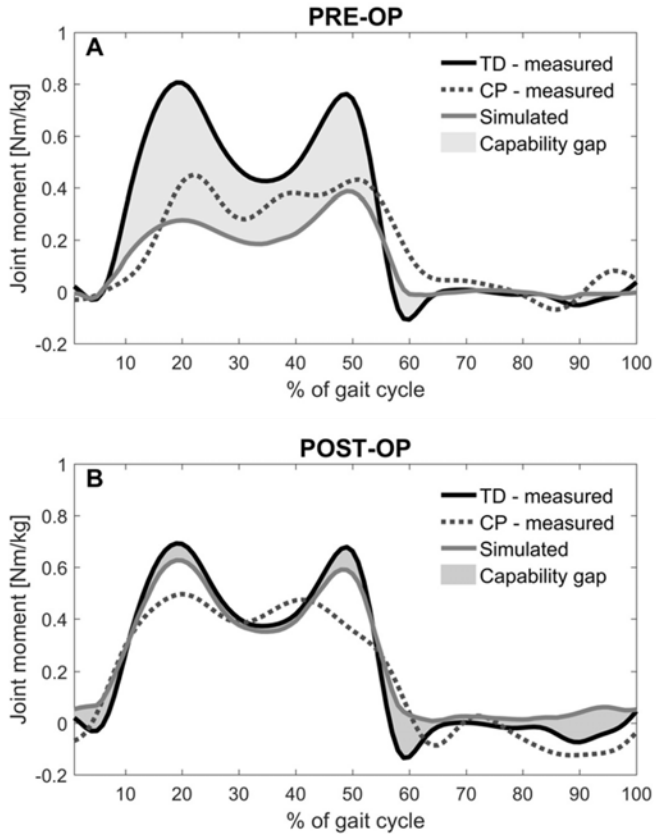

Figure 1. Experimental and model-based hip adduction joint moments and the capability gap pre- (A) and post-surgery (B).

RESULTS AND DISCUSSION

Post-operative joint kinetics during gait were more similar to TD gait kinetics than pre-operative gait kinetics. The post-surgery RMSD between patient and TD kinetics were smaller for six out of eight analyzed joints (average over all joints 0.28±0.18 Nm/kg and 0.17±0.10 Nm/kg for pre- and post-surgery, respectively). The pre- and post-surgery joint kinetics for the left hip adduction are shown in fig 1.

Our model-based simulations predicted a reduction of the root mean square capability gap post-surgery, indicating that the ability of the patient to produce normal gait kinetics increased. The RMS of the post-surgery capability gap was smaller for seven out of eight analyzed joints (average over all joints 0.14±0.06 Nm/kg and 0.10±0.03 Nm/kg for pre- and post-surgery, respectively), with the rectus femoris transfer further reducing the capability gap for hip and knee in the sagittal plane. The pre- and post-surgery capability gap for left hip adduction is shown in fig 1.

CONCLUSIONS

Our simulations predicted that the ability of the patient to produce healthy gait kinetics improved. This prediction is in accordance with the measured kinetics that was closer-to-normal after the intervention. At this stage, the simulation platform computes the theoretical capability and does not account for compensation strategies the patient adopts to overcome this capability gap. This might explain the difference between the capability gap and the RMSD between TD and CP kinetics. We are in the process of validating our framework by performing additional case studies. In addition, we will further improve model personalization by including changes in muscle-tendon properties and spasticity, and we are developing predictive simulations of movement kinematics. This first case study demonstrates the potential of our simulation platform to predict the effect of a surgical intervention on gait performance.

REFERENCES

1. Afschrift et al. *Biomed eng online,* **13**, 2014.
2. Bosmans et al. *J. Orthop Res*, **32(11)**, 2014.
3. Meyer et al. *Front Bioeng Biotechnol*, **4**, 20

ASYMMETRICAL STANCE DURING CHILD CARRYING: IMPLICATIONS FOR BACK PAIN

[1]Kathryn L. Havens, [2]Alexandra Kahney, [2,3*]Erin M. Mannen
[1] Division of Biokinesiology and Physical Therapy, University of Southern California, Los Angeles, CA;
[2]University of Denver, Denver, CO; [3]University of Arkansas for Medical Sciences, Little Rock, AR
*Corresponding Author: emannen@uams.edu

INTRODUCTION

Low back pain (LBP) affects nearly 80% of Americans at some point in their lifetime [1]. During periods of prolonged standing, individuals with LBP exhibit differences in their posture. Specifically, individuals with LBP spend more time in symmetrical stance, rather than shifting their body weight to one leg or another [2]. These body weight shifts may be altered by load carrying. While research has explored the effects of military backpack load carrying on back pain, little is known about the effects of carrying a baby.

During infancy and early toddlerhood, babies must be carried by a care giver. Babies are often held and carried in arms, but babywearing, the practice of carrying an infant or young child on the caregiver's body in a carrier, is becoming more common as parents reap the benefits of close-proximity to their children while remaining "hands-free." While babywearing has been shown to have numerous emotional, physical, and physiological benefits for babies [3], little work has been done to analyze the impact of child-carrying methods on the biomechanics of a woman's body.

The purpose of this study is to 1) characterize asymmetrical stance during prolonged standing and 2) compare the effects of infant carrying on these mechanics.

METHODS

Ten female subjects (age: 27.4 ± 4.1 years; BMI: 21.5 ± 2.5 kg/m^2) with no ongoing musculoskeletal problems and no previous babywearing experience were enrolled in the IRB-approved study. Men, pregnant women, or those with a pregnancy within the past nine months were excluded. Participants underwent testing in the Human Dynamics Lab at the University of Denver.

Each subject completed fifteen-minute quiet standing tasks with each foot placed on a separate force plate (Bertec Corporation, Columbus, OH) for three conditions: **unloaded**, holding a 9-month old infant sized mannequin (Dietz, Freiburg, Germany) **in-arms**, and wearing a 9-month old infant sized mannequin in a self-fit baby carrier (**in-carrier**; Ergobaby, Inc., Los Angeles, CA) (Figure 1). Subjects were instructed to quietly stand for the fifteen-minute trials while keeping each foot on its respective force plate. Subjects rested between fatigue trials, and conditions were performed in a random order.

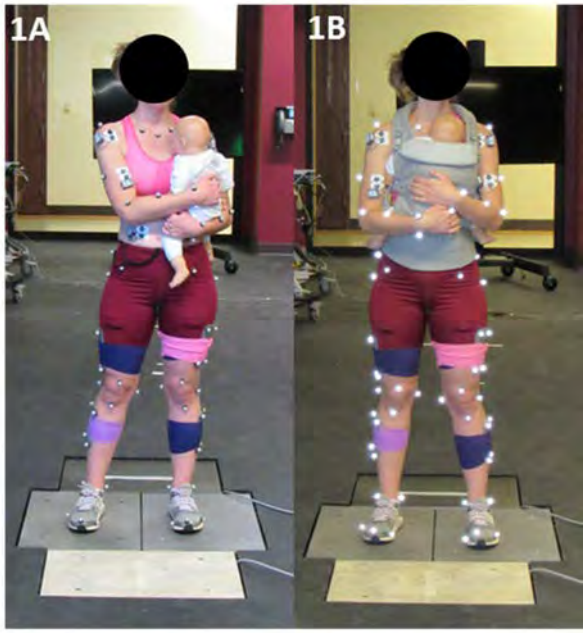

Figure 1: In-arms condition (1A) and in-carrier condition (1B).

Participants completed 100mm visual analog scales (VAS) to rank their pain and discomfort before and after the trials. Subjects were characterized as pain developers (PDs) if their VAS score increased by at least 10mm, and non-PDs if they had a <10mm increase during the unloaded condition.

Three-dimensional kinematics were collected using a 10-camera motion capture system (Vicon Motion Systems, Ltd., Oxford, UK), 250 Hz. Hip, trunk, and pelvis frontal plane angles were calculated (Visual3D, C-Motion, Inc., Rockville, MD, USA). Periods of asymmetrical stance were defined as time when at least 65% of the body weight was supported on one leg for at least one second, as determined by force plate recordings. Custom code (MathWorks, Natick, MA) was written to identify these periods and associated mechanics.

To characterize asymmetrical stance, descriptive statistics were used to demonstrate time in asymmetrical stance and number of body weight shifts. Peak hip, trunk and pelvis frontal plane angles were determined during periods of asymmetrical stance. These were compared to average angles during symmetrical stance using paired t-tests. To compare the effects of infant carrying, non-parametric Friedman tests were used to compare time in asymmetrical stance and number of body weight shifts, and kinematics during asymmetrical stance were compared using repeated measures ANOVA. Significance was set at $\alpha \leq 0.05$.

RESULTS AND DISCUSSION

Individuals spent about half of their time in asymmetrical stance. Wide variability between subjects in the total number of shifts and total time shifted was found. Hip angle, trunk lean and pelvic drop were all different between periods of asymmetrical stance compared to symmetrical stance. When subjects shift their weight onto one leg, they exhibited ipsilateral hip adduction, and contralateral trunk side-bending and pelvic drop ($p \leq 0.001$).

Significant differences between loading conditions were found for number of body weight shifts ($X2(2) = 7.467$, $p=0.024$) and total time in asymmetrical stance ($X2(2) = 10.903$, $p=0.004$) (Figure 2). When compared to the unloaded conditions, individuals spent more time in asymmetrical stance ($p=0.012$) during the in arms condition. Trends towards greater number of weight shifts were found in arms ($p=0.035$), and in carrier ($p=0.027$) compared to unloaded.

While individuals exhibited differences in kinematics during periods of weight shifting, no differences in hip, trunk or pelvis mechanics were found between loading conditions ($p>0.05$).

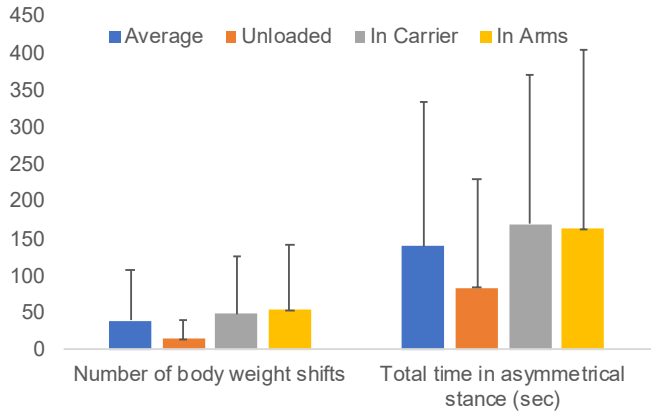

Figure 2: Weight shift characteristics

A preliminary analysis on 3/10 subjects who were characterized as PDs suggests that they significantly decreased both the number and time spent weight shifted. Additionally, the effect of the baby carrying method may be different for PDs v. non-PDs. This interesting finding warrants additional analysis.

CONCLUSIONS

Individuals shift their weight during prolonged standing and exhibit changes in their hip, trunk and pelvis posture. While holding a baby in arms and in carrier affects the shift time and duration, individuals use the same biomechanics under these varied loading conditions. However, individuals who develop pain during prolonged standing may benefit differently from carrying an infant in a carrier compared to those who do not develop pain.

REFERENCES

1. Walker BF, et al. *J Manip Physiol Ther*, **27**(4), 238-244, 2004
2. Gallagher KM, et al. *Gait Posture.* **32**, 490-495, 2011.
3. Anisfeld E, et al. *Child Dev* **61**, 1617-1627, 1990.

ACKNOWLEDGMENTS

This project was funded by Ergobaby, Inc.

LOWER EXTREMITY MUSCLE ACTIVITY OF HEALTHY INFANTS: IMPLICATIONS FOR HIP DYSPLASIA PATIENTS

[1*]Erin M. Mannen, [1]Akshay Krishnan, and [1]Brant C. Sachleben

[1]The University of Arkansas for Medical Sciences, Little Rock, AR, USA
*emannen@uams.edu

INTRODUCTION

Developmental dysplasia of the hip (DDH) refers to a group of disorders that can range from slight instability (Grades 1-3) to a severe dislocation (Grade 4) of the hip from the socket.[1] This condition occurs in 5.5 out of 1000 full-term babies within the first two days of life, and 10% of those patients continue to exhibit problems after 2 weeks of age.[2] In patients where DDH does not resolve on its own, infants are typically prescribed an orthopaedic brace or cast to aid in reducing the hip. In infants with DDH grades 1-3, the Pavlik Harness is the gold-standard of care and reduces hips with a 92% success rate.[3] Computational models have shown the positive impact of active adductor muscles on reducing DDH grades 1-3 when hips are placed in the optimal 90 degree flexion and 80 degree abduction position within the Pavlik Harness.[4]

Despite the success of the Pavlik Harness and the Rhino Cruiser, a similar orthopaedic brace, such restrictive devices are often uncomfortable for infants and problematic for parents to comply with as they require 24 hour/day usage for weeks to months. Babywearing, the act of carrying an infant in a device worn on a caregiver's body, often places infant hips in a flexed and abducted position (known as M positioning) that may be similar to the position provided by the orthopaedic devices. Furthermore, there is recent evidence showing that appropriate babywearing may prevent DDH.[5] However, no studies have evaluated the biomechanics of infant hips within these various devices.

The purpose of this study was to measure the lower-extremity muscle activity and hip positions of infants in common DDH devices compared to an inward-facing soft-structured baby carrier.

METHODS

Eight healthy full-term infants with no orthopaedic or neurological problems (5.0±1.5 months, 5 male) were enrolled in the IRB-approved study. Surface EMG (Delsys, Natick MA, USA) recorded muscle activity (1000 Hz) of bilateral gluteus medius, biceps femoris, quadriceps, and adductor muscle groups. Marker-based motion capture (Vicon, Oxford, UK) was used to track the lower extremity motion of the infants during four 30-second conditions: in a Pavlik harness, in a Rhino cruiser, held in an inward-facing soft-structured baby carrier (Boba, Inc., Boulder, CO, USA), and in a standard car seat. EMG data was rectified, filtered, and normalized to the Pavlik Harness condition via custom code (Matlab, Mathworks, Natick, MA, USA), and mean EMG signal and percent time that muscles were active at two standard deviations above the mean were calculated. Hip position data has not yet been analyzed, but hip flexion and hip abduction angles will be calculated for each condition. Paired t-tests were used to compare conditions to the Pavlik Harness condition ($p<0.05$).

RESULTS AND DISCUSSION

Lower limb muscle activity was *not* found to be significantly different in the Rhino cruiser or baby carrier (Boba) conditions when compared to the Pavlik harness, both in average signal (Figure 1) and in percent time above two standard deviations (Figure 2). Conversely, the car seat position resulted in approximately half of the mean muscle activity and five times less active time compared to the Pavlik harness condition.

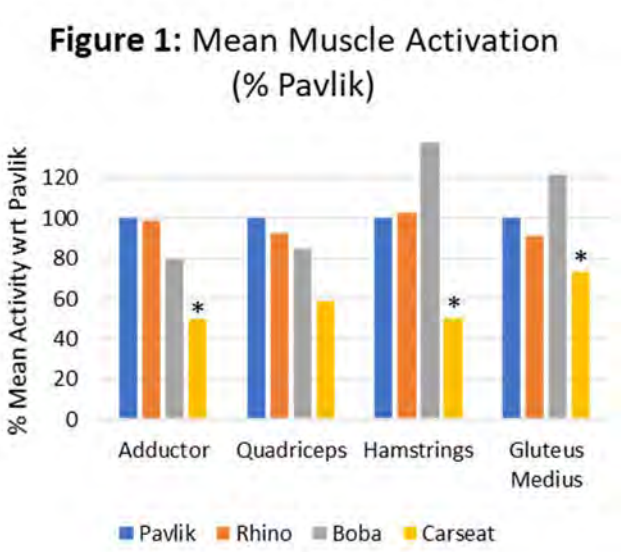

Figure 1: Mean muscle activity per condition as a percentage of mean muscle activity during the Pavlik harness condition. *p<0.05 v. Pavlik harness condition.

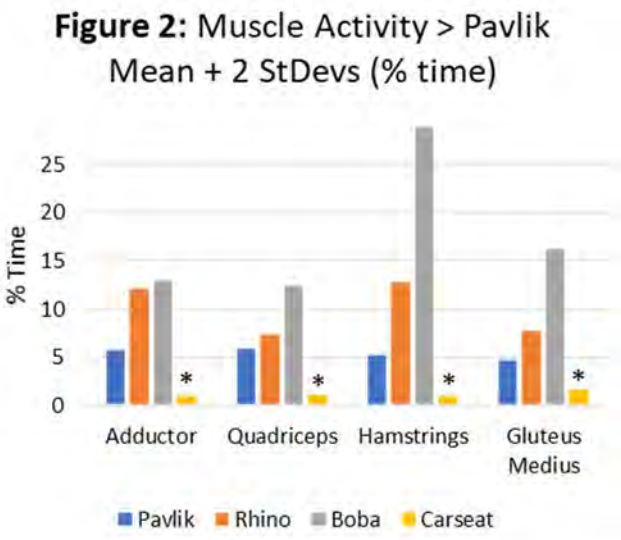

Figure 2: Percent time muscles were active above the mean + two standard deviations of the Pavlik harness condition. *p<0.05 v. Pavlik harness condition.

In agreement with previous computational models, the Pavlik harness and Rhino cruiser devices currently used to treat DDH in infants resulted in the highest levels of mean adductor muscle activity, supporting the use of the devices for reducing infant hips. The soft-structured infant baby carrier resulted in similar lower-extremity muscle activity for the infants in this healthy cohort, possibly indicating safe use in DDH populations. Conversely, the infants were significantly less active in the car seat, which may indicate that passive container-type of infant devices do not promote active lower-extremity muscles in healthy infants. However, hip positioning data for all conditions will be critical in assessing the appropriateness of use in healthy and DDH populations.

Limitations of the study include a small sample size, sometimes non-compliant subjects, and a data collection length of only 30 seconds per condition. Future work will include collection and analysis of 12 more subjects for both EMG and hip position during the various conditions. As parents continue to use infant devices, more research should be done on the musculoskeletal and biomechanical impact of infant positioning for both DDH and healthy infants.

CONCLUSIONS

Lower extremity muscle activity of healthy infants in a soft-structured baby carrier with M positioning of the hips was similar to the muscle activity of infants in orthopaedic devices used to treat patients with Developmental Dysplasia of the Hip. Furthermore, the car seat and other similar container-type of infant devices may not promote lower-extremity muscle activity.

REFERENCES

1. Marquez-Florez K, et al., *J Biomech Eng*, **138**:74501, 2016.
2. Alsaleem M, et al., *Clin Pediatr,* **54**:921-8, 2015.
3. Huayamave V, et al., *J Biomech*, **48:**2026-33, 2015.
4. Ardila O, et al., *J Biomech*, **46:**1501-7, 2013.
5. Graham S, et al., *J Pediatr Orthop*, **35:**57-61, 2015.

ACKNOWLEDGEMENTS

This research was funded by the International Hip Dysplasia Institute and Boba, Inc.

RELATIONSHIP OF SEGMENTAL ENERGY FLOW AND ELBOW VALGUS LOAD DURING BASEBALL PITCHING

[1] Arnel Aguinaldo and [2] Rafael Escamilla

[1] Point Loma Nazarene University, San Diego, CA, USA
[2] California State University, Sacramento, CA, USA
email: aaguinal@pointloma.edu

INTRODUCTION

Elbow valgus load is considered to be a significant predictor of baseball pitching-related elbow injuries. Consequently, the relationship between multi-segment mechanics and elbow valgus load during baseball pitching has been well examined using statistical methods [1], forward dynamics [2], and most recently, induced acceleration analysis [3]. However, the mechanisms by which the flow of mechanical energy across moving body segments influence elbow valgus load during pitching remain unclear. Therefore, the purpose of this study was to examine the relationship of intersegmental power with elbow valgus load during pitching in adult baseball players. It was hypothesized that elbow valgus load would be most affected by segmental powers supplied by trunk and shoulder torques.

METHODS

A sample of 20 male baseball pitchers (age = 21.9 ± 3.7 years; height = 1.88 ± 0.06 m, mass = 89.5 ± 9.0 kg) were recruited from the professional (n=13) and collegiate (n=7) ranks and participated in this study after providing written informed consents approved by the university's Institutional Review Board. A set of 38 reflective markers (1.4 cm DIA) were placed on the skin overlying specific anatomical landmarks according to a 16-segment rigid-body model described by Aguinaldo and Chambers [1]. Each participant threw 15 fastballs off a bullpen mound while the global locations of the markers were captured with an outdoor 3D motion analysis system (Motion Analysis Corp., Santa Rosa, CA) at a sampling rate of 300 Hz. The joint kinematics and kinetics of each participant's throwing motion were estimated based on the rigid model defined by the marker locations and inertial properties for healthy adult males [1]. The mechanical power of the trunk, upper arm, and forearm segments were calculated as the time rate-of-change in kinetic energy delivered into or out of each segment by muscular and non-muscular components during pitching [3,4]. Each segmental power at any instant in time (i) was presumed to be equivalent to the sum of the powers (P_t) due to joint forces (F_j) and torques (T_j):

$$P_t(i) = \sum_{j=1}^{N} [T_j(i)\omega_j(i) + F_j(i)v_j(i)]$$

where N is the number of joints adjacent to a segment, ω_j is joint angular velocity about the segment's longitudinal axis (y) for the trunk and shoulder and medio-lateral axis for the elbow (x), and v_j is the linear velocity of the segment. Peak magnitudes of individual segment powers were extracted and entered into a stepwise regression analysis to determine the best linear model that predicts maximum elbow valgus (MEV) torque at a significance level of 0.05. As an index of pitching performance, ball speed was also evaluated to determine its relationship with each segmental power using linear regression.

RESULTS AND DISCUSSION

The mean ball speed and MEV torque were 36.9 ± 3.3 m/s (82.7 ± 7.5 mph) and 76.7 ± 27.6 Nm (Figure 1), respectively. The peak rotational powers of the trunk (3249 ± 1057 W), upper arm (-1407 ± 707 W), and forearm (-1740 ± 651 W) occurred sequentially prior to maximum external rotation (MER) of the throwing shoulder during baseball pitching (Figure 1). The timing and pattern in segmental power generation and absorption indicated that energy flows from the trunk to the arm segments. Moreover, the segmental power delivered by shoulder external rotation torque in the

arm cocking phase accounted for 54% of the variance in MEV torque ($r = .734$, $p < .001$) while ball speed was significantly related to the segmental power of the trunk ($r = .868$, $p < .001$).

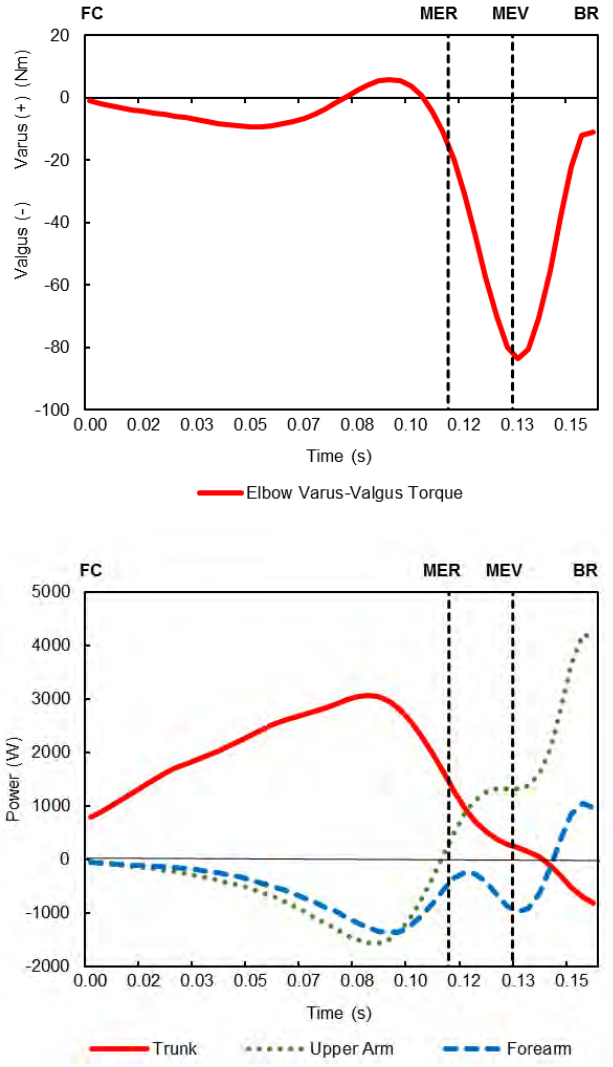

Figure 1: *Top:* Elbow varus (+) / valgus (-) torque during a baseball pitch; *Bottom:* Power histories of the trunk, upper arm, and forearm segments during a baseball pitch (FC = front-foot contact, MER = maximum external rotation, MEV = maximum elbow valgus torque, BR = ball release).

These findings suggest that the segmental energy flow that is associated with the lowest elbow valgus torques and the highest ball speeds represents the most efficient throwing mechanics. Subsequently, the loss of energy transferred from the trunk to the distal arm segments as a result of improper sequential body motion could lead to pitchers attempting to maintain optimal ball velocity by producing more internal torque at the throwing arm to compensate for this energy dissipation and thereby increasing their risk of a pitching-related injury at the elbow [1,3].

CONCLUSIONS

This segmental power analysis reinforces evidence previously presented by statistical methods [1] and induced acceleration analysis [3] that the rotational torque at the shoulder has the greatest effect on the development of elbow valgus load. The current findings support the notion that the transfer of segmental energy during baseball pitching generally follows a proximal-to-distal flow with power generated at the trunk by net muscular torques and absorbed at the upper arm and forearm. However, as this segmental power analysis is limited by the assumption that joint torques are produced by single-joint muscles [4], future research is needed to further decompose the energy transfer mechanisms by which moments from multi-joint muscles as well as from non-muscular components such as centrifugal, Coriolis, and velocity-induced forces influence valgus loading [2,3].

REFERENCES

1. Aguinaldo, A.L., et al., (2009). *American Journal of Sports Medicine*, **37**(10), 2043.
2. Buffi, J., et al., (2015). *Annals of Biomedical Engineering*, **43**(2), 404.
3. Naito, K., et al., (2017). *Proceedings of the Institution of Mechanical Engineers, Part P: Journal of Sports Engineering and Technology*, 175433711774523.
4. Gordon, D., et al., (1980). *Journal of Biomechanics*, **13**(10), 845.

ACKNOWLEDGEMENTS

The authors would like to thank graduate students, Sydney Dreaves, Caitlin Mazurek, Eric Burger, and Adam Bunn, for their assistance in data collection and processing.

KINEMATIC TIMING DIFFERENCES IN THE BASEBALL SWING IN VARIOUS TRAINING DRILLS

Christopher J. Curran, Nathaniel S. Harris, Caroline E. Yeomans, P. Rose Brock, Ryan P. Silberg, Patrick M. Rider, Nick P. Murray, Zachary J. Domire

East Carolina University, Greenville, NC, USA
email: curranch15@students.ecu.edu

INTRODUCTION

Baseball batting is one of the most difficult skills to develop in any sport and batters spend numerous hours refining the mechanics of their swing through repetition. These practice sessions are often performed alone or individually with a teammate or coach, and seldom involve hitting against a real pitcher. Perhaps the two most common training methodologies for the baseball swing are hitting a stationary ball placed on a tee and hitting a ball tossed from the side of home plate into the strike zone for a batter to hit forward, a drill commonly referred to as "soft toss". Other batting drill variations such as pop-up tees, various pitching machines, hitting balls of varying sizes and weights, and using bats of different barrel-widths and weights are frequently being introduced.

The kinetics and kinematics of the swing have been studied throughout the last 20 years, however most commonly only while batters hit a stationary ball on a tee [1, 2]. Welch et al. describe the separation of the biomechanics of the baseball swing into three phases: the lifting of the stride foot, the landing of the stride foot, and ball contact. While there have been several studies examining biomechanical parameters of swings at varying levels of competency [2] and others examining the effect of weighted bats [3], few studies have examined the effect of other batting drills on the kinetics and kinematics of the swing. **The purpose of this study was to evaluate kinematic and kinetic differences in the baseball swing between three common practice hitting drills.**

METHODS

Kinematic and kinetic data was collected for six male baseball batters (19.67 ± 1.37 years) in the Biomechanics Laboratory at East Carolina University. All participants had a history of playing competitive baseball at/after the age of 16. After providing informed consent, 58 reflective markers were applied to the participant. Glasses with six markers to track the position of the head were fitted to each participant, reflective markers were placed on the knob, midpoint, and end of the bat, and the ball was covered with reflective tape.

Participants were given time to warm-up prior to performing 5 practice hits and 10 collected hits in each of three commonly used practice batting drills: 1) a ball placed on a tee, raised to the height of the participant's mid-thigh, 2) soft-toss, and 3) a ball launched from a pop-up tee (Pop Toss Batting Tees) placed 0.85 m in front of home plate. Any trials in which participants swung and missed were discarded.

For each swing, the motion of the ball and reflective markers were measured by a ten-camera passive-marker motion capture system (360 Hz, Qualysis AB). Kinetic data was collected using two force platforms (1440 Hz, AMTI). Kinematic and GRF data were filtered using second-order low pass Butterworth digital filters with cut-off frequencies of 6 and 45 Hz, respectively, using Visual 3D software (C-Motion Inc.).

For each participant, the mean value for each biomechanical outcome variable was computed. Differences between mean values for each of the three batting conditions were analyzed using a paired t-test with a significance level of $p < 0.05$.

RESULTS AND DISCUSSION

Selected outcome variables are included in Table 1. The kinematics and timing of the swing appeared to

remain similar between batters hitting in the tee and soft-toss conditions, however batters demonstrated significant changes in the timing of their stride prior to swinging. Batters initiated their swing by lifting their stride foot closer to the time of ball contact in the pop-up tee condition compared to both the tee and soft-toss conditions ($p < 0.039$, $p < 0.036$). This change in stride initiation time led to a significantly shorter total stride time in pop-up tee compared to the tee and soft-toss conditions as well ($p < 0.024$, $p < 0.002$). Hitters also showed an altered timing of the sequence of the kinetic chain, reaching peak pelvic rotational velocity earlier compared to ball contact time in the pop-up tee condition compared to the soft-toss condition ($p < 0.011$).

The changes in stride timing were accompanied by a trend towards altered stride length and peak vertical ground reaction force produced by their rear leg during the stride. Batters demonstrated the longest stride length in the soft-toss condition compared to the tee and pop-up tee conditions and trended towards lower peak vertical ground reaction force in the pop-up tee condition compared to both the tee and soft-toss conditions.

CONCLUSIONS

Significant changes in the timing of baseball swing kinematics were seen in a pop-up tee hitting condition compared to a tee and soft-toss condition. The later initiation of the swing and shorter stride time may have led to a trend towards lower production of peak ground reaction force in the rear foot prior to ball contact.

It is unknown if the changes in swing mechanics seen while using the pop-up tee are either beneficial or detrimental as a training tool for baseball batters. While it may appear that hitting from a pop-up tee may have reduced hitting performance indicated by reduced peak vGRF, using a pop-up tee may in fact be more similar to facing a real pitcher, in which the batter's reaction time and the direction of travel of the ball are closest to that in the pop-up tee condition compared to hitting off of a tee or during soft-toss. Continued research is needed to evaluate the similarity of these three common baseball batting drills to in-game pitching.

REFERENCES

1. Dowling and Fleisig. *Sports Biomechanics*, 15(3): 255-269, 2011.
2. Welch et al. *Journal of Orthopaedic & Sports Physical Therapy*. 22(5): 193-201, 1995.
3. DeRenne et al. *Journal of Strength and Conditioning Research.* 9(4): 247-250, 1995

ACKNOWLEDGEMENTS

The authors thank Gustavo Sandri-Heidner and Ashley Moulder for assistance with data reduction.

Table 1: Selected kinematic variables of the baseball swing (mean ± SD).
* $p < 0.05$ – Tee compared to Pop-Up Tee
† $p < 0.05$ – Soft-toss compared to Pop-Up Tee

	Tee	Soft-Toss	Pop-up Tee
Foot Off, relative to Contact (s)*†	0.600 ± 0.10	0.576 ± 0.06	0.510 ± 0.06
Peak Pelvis Rotational Velocity, relative to Contact (s)†	0.066 ± 0.02	0.077 ± 0.02	0.082 ±0.02
Peak Back Foot vGRF (N)	798.902 ± 138.29	779.70 ± 161.47	746.545 ± 151.623
Stride Length (m)	0.135 ± 0.07	0.168 ± 0.066	0.137 ± 0.090
Stride Time (s)*†	0.330 ± 0.11	0.297 ± 0.098	0.218 ± 0.11

CHANGES IN YOUTH BASEBALL PITCHING BIOMECHANICS: A 7-YEAR LONGITUDINAL STUDY

[1] Alek Z. Diffendaffer, [1] Glenn S. Fleisig, [1] Brett Ivey, [1] Kyle T. Aune, [1] Tony Laughlin, [1] Dave Fortenbaugh, [1]Becky Bolt, [1] Wendy Lucas, [1] Kevin D. Moore and [1] Jeffrey R. Dugas

[1] American Sports Medicine Institute, Birmingham, AL, USA
email: alekd@asmi.org, web: asmi.org

INTRODUCTION

How does a youth athlete develop into a skilled adult athlete? This is a relevant question for a wide range of athletic activities, including baseball pitching. Previous research has quantified throwing mechanics for a sample of boys and girls, age 3 to 15 years, and showed component development levels, such as older children stepping forward with the contralateral leg and older children allowing the throwing arm to externally rotate at the side of the body instead of pushing the ball in front of the chest [1,2]. Additionally, there have been cross-sectional studies that have compared pitching biomechanics among various levels of competition [3,4]. Although these studies identified biomechanical differences among age groups, they did not show how or when specific changes occur within an individual. The ability to identify when these changes occur would allow athletes and coaches to use age-appropriate coaching techniques.

Thus, the purpose of this study was to examine biomechanical changes in baseball players during the first years of their pitching career. It was hypothesized that significant within-participant changes would be observed in pitching kinematics and kinetics as the pitchers grew older. Specifically, it was expected that joint forces, joint torques, and angular velocities would increase with age, while kinematics would change to be more similar to values of elite adult pitchers.

METHODS

Fifty-one youth baseball pitchers were recruited from the Birmingham community in early 2009 and 2010. Each pitcher came to the American Sports Medicine Institute (ASMI) biomechanics laboratory for initial testing during their first spring as a baseball pitcher. The pitcher was outfitted with 23 retro-reflective markers and was then instructed to warm-up. After conclusion of the warm-up, data for ten full-effort fastballs were collected. Each pitch was thrown from a pitching mound towards home plate located the league-appropriate distance away (typically 14.02 meters), while ball velocity was measured by a radar gun (Stalker Radar, USA). For all trials, three-dimensional motion data were tracked with a 12-camera automated motion analysis system sampling at 240 Hz (Raptor System, Motion Analysis Corp., USA).

Participants (and parents) were contacted each subsequent spring to return for biomechanical testing, and continued to be invited annually unless they were no longer pitching in organized baseball. After each biomechanical visit, no feedback was provided to the pitcher, his parents, or his coach about his pitching mechanics, per the study protocol.

Twenty kinematic and kinetic variables were calculated for each pitch as previously described [5]. Within-participant changes for each kinematic and kinetic parameter were tested with a mixed linear model with random effects. Least squares means for sequential ages were compared by use of Tukey's honestly significant difference test ($\alpha = 0.05$).

RESULTS AND DISCUSSION

Of the 51 pitchers enrolled, 35 participants were biomechanically tested a minimum of three years and were included in the analysis. For the 35 pitchers included into the analysis, 27 participants were 9 years old and 8 were 10 years old at the time of the initial testing. Due to the limited number of participants still pitching at the age of 16 years, the study was terminated at 15 years of age.

A significant increase in ball velocity was found each year when comparing to the previous. Significant kinematic differences with age were found for two of five velocity parameters as well as most (10/15) of the position parameters. Some of these are shown graphically in Figure 1. Several positional changes at the point of foot contact were noted with age, including stride length, lead foot position, and trunk separation. As a pitcher aged, they displayed less shoulder external rotation at foot contact but increased maximum shoulder external rotation during arm cocking.

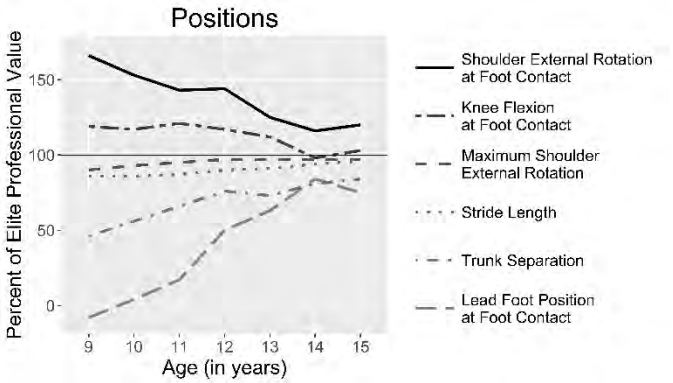

Figure 1: Some position parameters that had significant changes with age, with magnitudes expressed as percentage of mean value for elite professional pitchers.

All kinetic parameters increased significantly with age (Fig 2). Near the instant of maximum shoulder external rotation, shoulder internal rotation torque and elbow varus torque peaked to decelerate the arm cocking and initiate the arm's forward motion. Maximum shoulder horizontal adduction torque occurred as the arm cocked back and the upper trunk rotated to face the target. Near the instant of ball release, elbow flexion torque peaked to decelerate elbow extension. Maximum shoulder proximal force also occurred near this time to resist shoulder distraction.

As hypothesized, pitching kinematics and kinetics changed significantly during the first few years of pitching. The significant increases with age in all kinetic parameters were not surprising and were consistent with previous cross-sectional studies. Of particular note was the significant increase in normalized elbow varus torque from 13 to 14 years of age, and from 14 to 15 years, as varus torque is associated with tension (and tears) in the ulnar collateral ligament (UCL) which could explain the high rates of UCL injuries reported in baseball pitchers 15 years and older.

Figure 2: Significant kinetic changes with age, with magnitudes expressed as percentage of mean value for elite professional pitchers previously tested.

The most significant increases in kinematics occurred up until 12 or 13 years of age. The biggest changes appeared to be from 9 to 11 years of age for maximum shoulder external rotation, 10 to 11 years for trunk forward tilt, and 11 to 12 years for lead foot position and shoulder abduction.

CONCLUSIONS

Kinematic changes occur during the first few years of a youth pitcher's experience, particularly from ages 9 to 13 years. Forces and torques applied about the throwing shoulder and elbow increase with age, even when adjusted for height and weight, especially after 13 years of age which are likely attributed to strength changes after puberty. Improvements in kinematics and kinetics towards the magnitudes of professional pitchers were associated with increased ball velocity. Thus, prepubescent pitchers may work with their coaches to improve their motions, flexibility and arm paths. Once proper mechanics are developed, older adolescent pitchers can focus more on improving strength and power.

REFERENCES

1. Stodden et al. *Res Q Exerc Sport.* **77(4)**, 417-427, 2006.
2. Stodden et al. *Res Q Exerc Sport.* **77(4)**, 428-436, 2006.
3. Fleisig et al. *J Biomech.* **32(12)**, 1371-1375, 1999.
4. Fleisig et al. *Sport Biomech.* **15(2)**, 128-138, 2016.
5. Fleisig et al. *J of App Biomech.* **(12)**, 207-224, 1996.

PLANARITY OF THE SWING IN NCAA DIVISION I SOFTBALL PLAYERS

[1] Travis Ficklin, [2] Robin Lund, [1]Sutherland Wyatt, [1]Connor Meyerhoeffer

[1] Dixie State University, Saint George, UT, USA
[2] University of Northern Iowa, Cedar Falls, IA, USA
email: travis.ficklin@dixie.edu

INTRODUCTION

Swing plane is often discussed by baseball and softball practitioners, particularly as it relates to optimizing the chance of success when taking pitch path into account [1]. To hit the ball, the path of the incoming pitch must intersect, even if briefly, with the plane of the swing. Much discussion is further had about just how much the pitch path is contained in the bat plane, and the ensuing disputes likely stem to some measure from misunderstandings about the geometry of the swing plane.

Previous work has described the planarity of the field hockey hit [2], and the planarity of the golf swing [3], but a similar description is still lacking for baseball and softball swings. Because of the importance of first being able to describe swing planarity before understanding its importance or relevance, the purpose of this study was to develop a method of describing the planarity of swings made by NCAA Division-I softball players.

METHODS

Home run swings (n=27) made by NCAA Division-I players in games were captured by two video cameras recording at 100 Hz. Landmark data for the body, the tip and knob of the bat, and the ball were manually digitized in each camera view. A 3D calibration object and the Direct Linear Transformation method were used to reconstruct landmark locations in three dimensions, with a global frame of reference in which Y was the direction from home plate toward the pitcher, Z was vertically upward, and X was the cross product of the Y and Z directions. The location data were analyzed from the onset of the swing until contact was made. Onset was defined as the frame in which the bat tip began its final arc toward contact.

The locations of the bat tip during the swing (onset to contact) were resampled in equidistant sections of arc length toward contact, and then fitted with a plane using a least-squares fit in three dimensions. The plane was defined by its normal, expressed as a unit vector perpendicular to the plane.

The perpendicular distance from the plane to the bat tip in each frame was calculated (d_{PLANE}). This was done by projecting the location of the bat tip onto the normal of the plane. Because the normal was calculated using the least-squares fit, a projection onto this normal of zero was deemed to be exactly in the plane. The time-series data representing this projection were then normalized with respect to $d_{PLANE,}$ of the bat tip for the frame at impact. Mean d_{PLANE} and its standard deviations for the bat tip in and out of plane for each swing were calculated for each trial. Additionally, the normal direction defining the plane was compared to the direction of a vector defining the trunk to determine its alignment with the batter's body (θ_{TILT}) at contact.

RESULTS AND DISCUSSION

The descriptive statistics for the planarity of each swing can be found in Table 1. The visual representation of d_{PLANE} for the swings is depicted in Figure 1.

It is evident visually, that the bat tip proceeds from being above the average tilted swing plane to being in it when the values are normalized to distance from the plane at contact. The pattern seems to be bi-phasic. At about 50% of the swing duration, the bat tip becomes more in-the-plane every frame until contact.

The swing itself seems to be very planar. The average d_{PLANE} for the swings was 0.0038 +/- 0.0009 m as swings progressed, and the standard deviations in this value per swing were 0.0021 +/- 0.0005 m. The plane was tilted from the trunk of the batter with a

θ_{TILT} at contact of 28.4 +/- 13.9 degrees from the direction of the normal defining the plane.

The tight-fitting planarity of the swing may be best explained by the definition of swing onset in this study. Because the swing only contained the time during which the bat tip was in its final arc toward contact, it is reasonable that the plane was so well-defined and that the bat tip was so close to the plane during the swing. Defining swing time in other ways may change this result. More, because this sample included only successful swings, it cannot reveal whether there is more variability to d_{PLANE} in unsuccessful ones, and therefore whether such variability is problematic.

The tilt of the swing plane, θ_{TILT}, away from the trunk axis may be interesting to practitioners as they describe swing plane in terms of the body reference frame. However, other body references were not considered in this study, such as arm axes, leg axes, or other body references that practitioners may use as teaching cues. The current sample, however, demonstrates that the swing plane is not strictly formed about the trunk as contact is approached.

CONCLUSIONS

A method to describe the plane if the softball swing has been presented. The results of this study suggest that the plane of the softball swing is increasingly tightly followed as the bat follows its path to contact. This study only utilized the bat tip to define the plane, and it remains unknown if other definitions of the plane would yield similar results. Future studies should include a more heterogeneous sample of swings. Also, this method needs to be employed with baseball swings before it is known whether planarity is similar for them. Lastly, these variables must be investigated for predictive power in swing success, as well as explored for body movements that produce them.

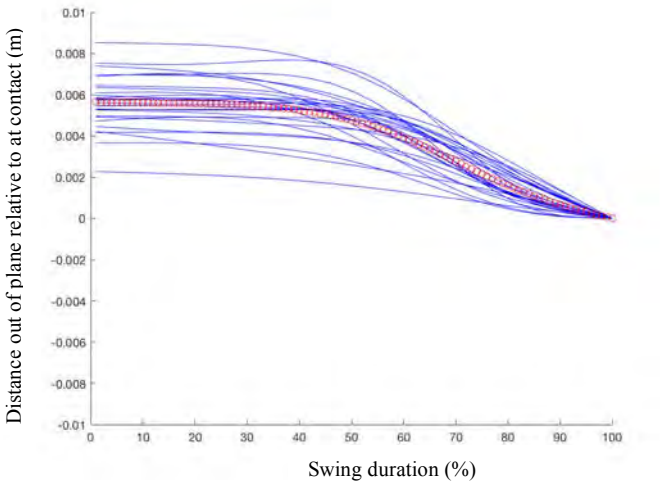

Figure 1. Time-series d_{PLANE} data normalized to swing time (100%) and compared to the value at contact. The swing proceeds from the bat tip being slightly out of plane early on to on-plane as contact is approached. The red circles represent average values for all swings during the swing duration.

REFERENCES

1. Williams, T, *The Science of Hitting*, Touchstone, 2013.
2. Willmott, AP & Dapena, J. *J Sports Sci* **30(4),** 369-77, 2012.
3. Kwon, YH, et al. *Sports Biomech* **11,** 127-48, 2012.

Table 1: Descriptive statistics for distance in and out of the plane (d_{PLANE}), variability in this measure during swings (SD d_{PLANE}), and tilt of swing plane with respect to the trunk (θ_{TILT}).

	MEAN		SD
d_{PLANE} (m)	0.0038	±	0.0009
SD d_{PLANE} (m)	0.0021	±	0.0005
θ_{TILT} (deg)	28.4	±	13.9

QUANTIFICATION OF SOFTBALL SWING PATTERNS AND RELATIONSHIPS TO SWING KINEMATICS FOR NCAA DIVIDION I SOFTBALL HITTERS

[1] Robin Lund, [2] Travis Ficklin, [2]Christina Kaady, [2]Connor Meyerhoeffer, [2]Miriam Lewis, [2]Susan Webb, [2]Tyson Banner

[1] University of Northern Iowa, Cedar Falls, IA, USA
[2] Dixie State University, Saint George, UT, USA
email: robin.lund@uni.edu

INTRODUCTION

It has been attempted to categorize baseball and softball swings based on generic movements such as a "push" pattern [1]. Players who adopt the push pattern use their arms to move the bat forward as the trunk is rotating during the swing.

This swing pattern is not considered to be an elite pattern for several reasons. First, the path of the barrel is downward as it moves towards the pitch and does not match the path of the pitch. In order to match the pitch path, the barrel should be moving slightly upward [2]. Second, because the barrel does not enter the path of the pitch until later in the swing, contact must be made further forward which means the hitter has less decision time to visually evaluate the quality of the pitch. Finally, this pattern will result in less acceleration of the bat during the initial moments of the swing [1].

Currently, there is no systematic way to quantify whether a swing exhibits the push pattern. The purpose of this study was to develop a method of quantifying "push" and to investigate the relationship of time spent in the push pattern during the swing to swing kinematics in Division-I softball players.

METHODS

In-game home run swings (n=27) were analyzed in 3D using the Direct Linear Transformation method. Video data were manually digitized from two cameras recoding at 100 Hz. Landmark location data for the body, the tip and knob of the bat, and the ball were reconstructed in three dimensions, with a global frame of reference in which Y was the direction from home plate toward the pitcher, and Z was vertically upward. The X direction was the cross product of the Y and Z directions. The location data were reconstructed from 0.25 s before contact until contact was made.

Several kinematic variables for this period were calculated: v_{BAT}, t_{SWING}, a_{BAT}, a_1 and a_2, where v_{BAT} was the speed of the bat tip at impact, t_{SWING} was the time from swing onset to contact (onset was determined as the initial start of the bat tip on its final arc toward contact), a_{BAT} was the average bat acceleration obtained by dividing v_{BAT} by t_{SWING}, and a_1 and a_2 were similarly calculated accelerations for the first and second halves of t_{SWING}, respectively.

Then, "push" (P) was quantified. First, for each frame, a vector from the rear shoulder to the front shoulder was formulated. Then, the location of the mid-grip by the hands on the bat was projected onto this vector. P was then expressed as a proportion of the distance of this projection from rear to front shoulder. A push value P of 0.00 would mean the hands were directly in front of the rear shoulder as the trunk rotated during swing. Positive values represent the hands moving forward with respect to the shoulder vector as the trunk rotated. All P values were then expressed with respect to the initial value for the onset of the swing. Last, t_P was then calculated as the percentage of t_{SWING} during which P was positive (i.e., pushing was occurring).

Pearson product-moment correlations were then calculated between t_P and the swing kinematic variables (v_{BAT}, t_{SWING}, a_{BAT}, a_1, and a_2). The level of significance was set at $p < 0.05$ for all inferential tests.

RESULTS AND DISCUSSION

Visual representation of P for all swings can be found in Figure 1. The correlation matrix can be found in Table 1.

A similar pattern was observed when P was plotted against time for all swings (Figure 1). The hands had a tendency to move back and then forward from the

initial position as contact was approached. Some of the swings featured hands that tended to stay behind the rear shoulder as the torso rotated during the swing whereas others moved forward sooner and spent more time in front of the rear shoulder which indicated the push pattern.

Significant positive relationships were observed between t_P and several of the swing kinematic variables. These relationships indicate that swings with more t_P tended to have greater v_{BAT} and a_{BAT}. This was unexpected because the push pattern is considered to a negative characteristic associated with the swing. It is possible that the homogeneity of a data set made up from only homeruns could explain this result. Each swing could be considered high quality based on the outcome and so adding swings with less favorable outcomes may change the nature of these relationships. A second reason to explain these unexpected results could be related to the nature of the bats used in softball compared to baseball. The moment of inertia is located much closer to the knob in a softball bat and they are significantly lighter than baseball bats making them easier to accelerate [3].

The significant relationship between t_P and a_2 (and the lack of a relationship between t_P and a_1) supports the theory that the push pattern swing makes it more difficult to accelerate the bat during the beginning of the swing.

CONCLUSIONS

A novel method of quantifying the extent to which a swing displays the push pattern was presented. Unexpectedly, as swings displayed more of this characteristic, certain beneficial swing kinematics increased. Future research should evaluate the effects of the push pattern in the sport of baseball. Additionally, a more heterogeneous sample of softball swings should be studied.

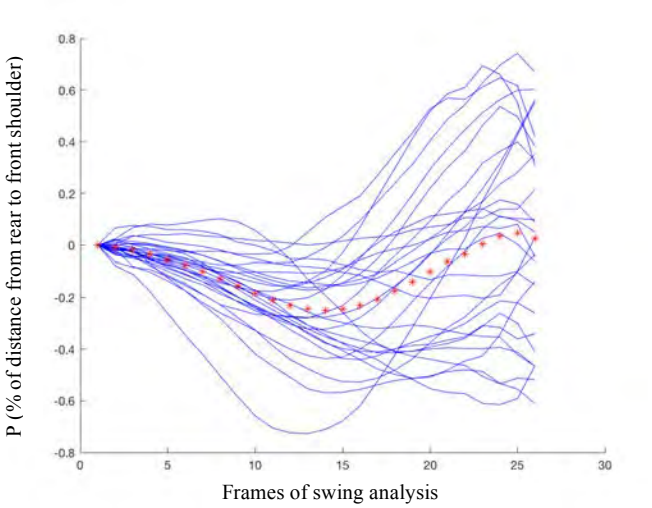

Figure 1. Push (P) as a percentage of the distance from rear to front shoulder. Blue lines represent individual swings, and red asterisks represent the average for all trials during the last 0.25 s (25 frames) of all swings.

REFERENCES

1. Tewksbary, R, *Elite Swing Mechanics* – Available from: http://tewkshitting.com
2. Williams, T, *The Science of Hitting*, Touchstone, 2013.
3. Russell, D, *Swing Weights of Baseball and Softball Bats* – Available from: www.acs.psu.edu/drussell/bats/Papers/TPT-October2010.pdf

Table 1. Correlation matrix.

	t_P (s)	v_{BAT} (m/s)	t_{SWING} (s)	a_{TOTAL} (m/s^2)	a_1 (m/s^2)	a_2 (m/s^2)
t_P (s)	1	0.422*	0.296	0.414*	0.057	0.382*
v_{BAT} (m/s)		1	0.094	0.286	-0.089	0.595**
t_{SWING} (s)			1	-0.843***	-0.397*	-0.168
a_{TOTAL} (m/s^2)				1	0.278	0.429*
a_1 (m/s^2)					1	0.497*
a_2 (m/s^2)						1

*p<0.05, **p<0.01, ***p<0.001

DXA-DRIVEN INVERSE DYNAMICS OF PITCHING ARM KINETICS IN YOUTH BASEBALL PLAYERS

Jay A. Sterner, Sofia R. Sanchez Porush, Scott K. Reaves, Scott J. Hazelwood, and Stephen M. Klisch

California Polytechnic State University: San Luis Obispo, CA, USA
email: sklisch@calpoly.edu

INTRODUCTION

Baseball pitching arm injuries in young athletes have steadily increased in recent years [1]. Ulnar collateral ligament (UCL) reconstructive (Tommy John) surgery rates in 15-19 year olds increased 9% per year from 2007 to 2011 [2]. Motion analysis studies of youth pitchers are aimed at developing a better understanding of, and identifying preventative strategies for, pitching-related injuries [3]. However, previous studies assumed body segment masses scaled from total body weight for the inertial properties in the equations of rigid body dynamics. Since the arm segments reach high accelerations during pitching, we hypothesized that DXA (dual energy X-ray absorptiometry)-driven inverse dynamics (ID) will predict different pitching arm kinetics than standard ID with scaled masses. The aims were to: 1) conduct DXA scans and motion analysis experiments of youth baseball pitchers and 2) compare elbow and shoulder kinetics calculated using scaled and subject-specific DXA masses for the pitching arms.

METHODS

All protocols were approved by Cal Poly's Human Subjects Committee. DXA scans and motion analysis studies were conducted with youth baseball pitchers (n=13) (aged 10.9 ± 0.4 years, height 148.0 ± 7.5 cm, weight 40.8 ± 8.6 kg). DXA scans were conducted using a Lunar iDXA scanner (GE Healthcare, WI, USA). The pitching experiment (Fig. 1) used a 9-camera motion analysis system with Cortex and PitchTrak software (Motion Analysis Corp., CA, USA). Following a 10-minute warming up exercise protocol, 48 markers were placed on anatomical landmarks based on the PitchTrak marker set. The pitcher then threw 10 pitches that were recorded in Cortex. The upper arm, forearm, and hand mass ratios used in PitchTrak were altered to: 1) standard scaled values [4] and 2) subject-specific values calculated from DXA total body and body segment masses.

Fig. 1: Youth pitcher with retroreflective markers.

PitchTrak analyses were used to obtain maximum values for shoulder compressive force (SCF), shoulder internal rotation torque (SIRT), elbow compressive force (ECF), and elbow varus torque (EVT). Scaled ID and DXA-driven ID predictions of each kinetic value were compared using paired t-tests ($p<0.05$). Also, percent differences between kinetic values were calculated in a subject-specific manner to report a range of "errors" when using standard scaled masses.

RESULTS AND DISCUSSION

Table 1: Mass ratio (%) of pitching arm segments used in PitchTrak (mean ± 1 S.D.)

	Scaled	**DXA**
Hand with ball	0.98± 0.08	1.03±0.11
Forearm	1.62± 0.00	1.50±0.10
Upper Arm	2.71± 0.00	3.33±0.30

The scaled and subject-specific DXA mass ratios were different for the hand with ball ($p<0.05$), forearm ($p<0.001$), and upper arm ($p<0.00001$) (Table 1).

The predictions of pitching arm kinetics using scaled and DXA masses were different for SCF ($p<0.05$), but not for SIRT ($p=0.097$), ECF ($p=0.37$), or EVT ($p=0.31$) (Fig. 1). The percent difference between calculated kinetics using scaled and DXA masses, in a subject-specific manner, ranged from -1.6 to 28.0% for SCF, -4 to 30% for SIRT, -6 to 30% for ECF, and -35 to 40% for EVT, with positive percentages indicating a larger value for DXA masses.

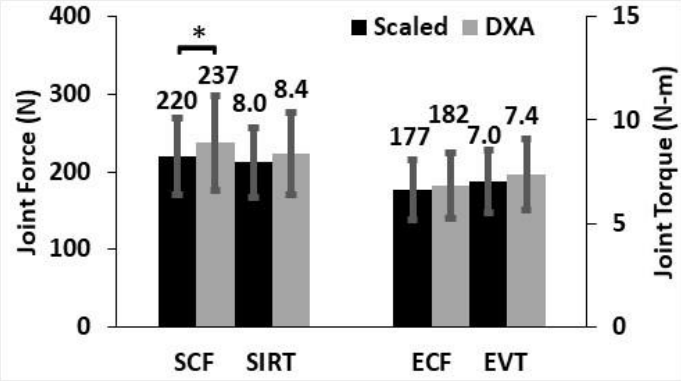

Fig. 1: Maximum compressive forces and torques for shoulder (left) and elbow (right) with scaled and DXA pitching arm segment masses. Means ± 1 S.D. shown. * = significant difference ($p\leq0.05$).

Interestingly, using the subject-specific DXA masses had a greater effect on calculated shoulder kinetics than calculated elbow kinetics. In contrast to elbow kinetic values, shoulder kinetic values depend additionally on upper arm mass, and upper arm masses exhibited the largest difference between scaled and DXA values. Although significant differences were only found for 1 of the 4 kinetic values, subject-specific differences were occasionally very high; thus, DXA driven ID is more desirable when the aim is to obtain accurate kinetic values for a single subject as opposed to a group of subjects. For example, our results suggest that ID analyses with scaled masses could be underestimating SIRT and EVT by 30 to 40% for youth baseball pitchers. One limitation of the study was that the size of the lab only allowed the pitchers to throw 30 feet instead of the entire regulation distance.

CONCLUSIONS

The major findings of this study were that 1) scaled and DXA-driven ID predictions of SCF values were significantly different for youth baseball pitchers and 2) subject specific errors in pitching arm kinetic values were as high as 40%.

These findings suggest future studies aimed at quantifying the effects of subject specific masses on adult pitchers. Adult pitchers have both larger masses and arm accelerations than youth pitchers, so differences between standard and DXA-driven ID may be even greater than those reported here. Thus, future studies should continue to quantify the effects of subject specific masses on adult pitching arm kinetics.

Although not described above, EMG muscle activation data was collected and will be used in ongoing studies to obtain muscle forces, joint contact forces, and loads carried by soft tissues, including those that are frequently injured (e.g. the elbow UCL).

REFERENCES

1. Fleisig et al. *Sports Health,* 4(5), 2012.
2. Erickson et al. *The American Journal of Sports Medicine,* 43(7), 2015.
3. Darke et al., *Orthopaedic Journal of Sports Medicine,* in press, 2018.
4. DeLeva. *Journal of Biomechanics*, 29(9), 1996.
5. Fleisig et al. *Journal of Biomechanics*, 32(12), 1999.

ACKNOWLEDGEMENTS

Supported by the W.M. Keck Foundation and the Donald E. Bentley Center.

MASS ADDED TO A RUNNING-SPECIFIC LEG PROSTHESIS INCREASES METABOLIC POWER DURING RUNNING

[1] Ryan S. Alcantara, [2] Owen N. Beck, [1,3] Alena M. Grabowski

[1] Department of Integrative Physiology, University of Colorado Boulder, Boulder, CO, USA
[2] Department of Mechanical Engineering, Georgia Institue of Technology, Atlanta, GA, USA
[3] Department of Veterans Affairs, Eastern Colorado Healthcare System, Denver, CO, USA
email: *ryan.alcantara@colorado.edu*

INTRODUCTION

Individuals with a unilateral transtibial amputation (TTA) are able to run with the use of a running-specific prosthesis (RSP). An RSP is comprised of carbon fiber, lacks an anatomical 'ankle' joint, and is lighter than a biological foot and partial shank. RSPs are attached in series to the residual limb of the affected leg (AL). During running, metabolic power increases by approximately 1% for every 100g added bilaterally to the feet of individuals without an amputation (P_{NA}) [1], but it is unknown how mass added to an RSP influences metabolic power or vertical ground reaction (vGRF) force symmetry between the AL and unaffected leg (UL) in individuals with TTAs.

The purpose of this study was to investigate the metabolic and biomechanical effects of mass added unilaterally to an RSP and bilaterally to the legs of individuals with a TTA during running. We hypothesized that when mass is added to the RSP or bilaterally to the legs, metabolic power will increase proportionally during running. We also hypothesized that peak and stance average vGRF would be more symmetric between legs when mass is added to the RSP compared with no added mass.

METHODS

We measured the metabolic rates and ground reaction forces (1000 Hz) of three subjects (1F) with a unilateral TTA (mean ± SD: 36.7 ± 3.8 years, 64.1 ± 4.5 kg, 1.72 ± 0.05 m). Subjects used their own RSP, reported no musculoskeletal injuries within the past 6 months, and had at least 1 year of experience using an RSP. This study was approved by the University of Colorado Boulder IRB and all subjects provided informed consent prior to participation.

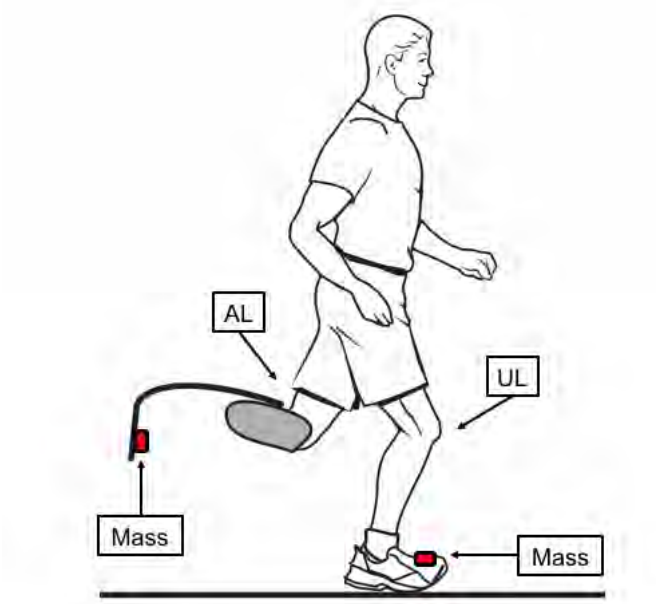

Figure 1: Added mass locations on subject's affected leg (AL) and unaffected leg (UL).

Subjects ran on a force-measuring treadmill (Treadmetrix, Park City, UT) at 2.5 m/s with randomized conditions of 0g, 100g, and 300g added unilaterally to their RSP or bilaterally to the legs. Each trial was 5 minutes long with 5 minutes rest between trials. We adhered mass 10 cm from the distal end of the RSP on the dorsal surface for the AL and 10 cm from the distal end of the foot on the laces of the shoe for the UL (Fig. 1). We measured rates of oxygen consumption and carbon dioxide production via indirect calorimetry (ParvoMedics TrueOne 2400, Sandy, UT), calculated average metabolic power from the final 2 minutes of each trial using a standard equation (Brockway, 1987), and normalized gross metabolic power to body mass including the RSP.

We used the symmetry index (SI) to determine peak and stance average vGRF symmetry between the AL

and UL [2,3]. Perfect symmetry between legs equals 0%.

$$SI = \left| \frac{(UL - AL)}{0.5(UL + AL)} \right| * 100$$

We constructed linear mixed effects models (α = 0.05) to determine the effect of added mass on metabolic power during running, peak vGRF SI, and stance average vGRF SI.

RESULTS AND DISCUSSION

For every 100 g of mass added to the RSP, gross metabolic power increased by 0.27 W/kg (p = 0.0040). For every 100g of mass added bilaterally to the legs (200g total), gross metabolic power increased by 0.32 W/kg (p=0.0047).

Adding mass to the legs had no effect on stance average vGRF SI (p = 0.2660) or peak vGRF SI (p = 0.0970). Additionally, there was no effect of whether the mass was added unilaterally to the RSP or to both legs on stance average or peak vGRF SI (p = 0.7001, p = 0.4969).

The data support our first hypothesis (Fig. 2). For every 100g of mass added to the RSP, metabolic power increased by 2.2% during running. We found that for every 100g of mass added bilaterally to the legs of people with a TTA, metabolic power increased by 2.6% during running. Previous studies have shown that adding 100g to both shoes of P_{NA} increases gross metabolic power by approximately 1% during running at 3.35 m/s [1] and our results suggest that mass added to both legs of individuals with unilateral TTAs has a 2.6 times greater effect than adding mass to both shoes of P_{NA} during running at 2.5 m/s.

Our data do not support our second hypothesis. Added mass to the RSP did not change peak vGRF SI or stance average vGRF SI. Future research is planned to increase the subject sample size.

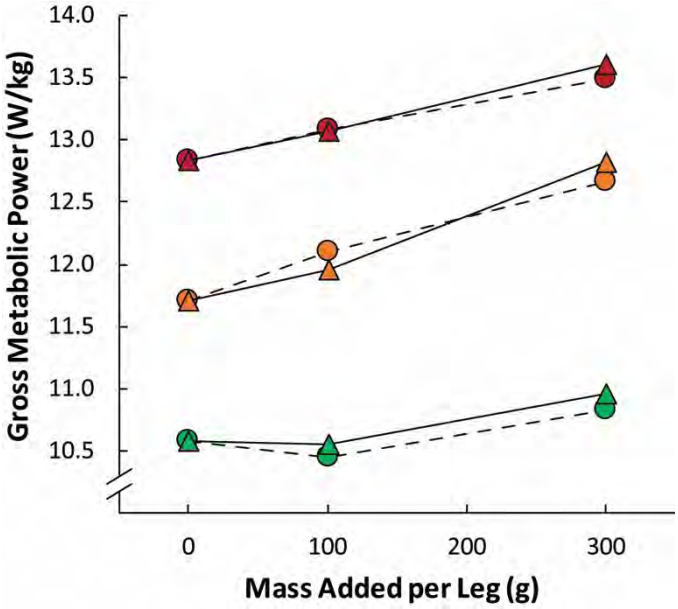

Figure 2: Subject-specific gross metabolic power of running with mass added unilaterally (*circles and dashed lines*) and bilaterally (*triangles and solid lines*).

CONCLUSIONS

Generally, decreasing the metabolic cost of distance running improves performance [4]. Our findings suggest adding mass to the legs of individuals with TTAs increases metabolic power during running. Thus, individuals with TTAs should not add mass to their RSP in an effort to improve distance running performance.

REFERENCES

1. Franz et al. *Med Sci Sports Exerc.* **44**(8), 2012.
2. Herzog et al. *Med Sci Sports Exerc.* **21**(1), 1989.
3. Beck et al. *J Appl Physiol.* **123**(1), 2017.
4. Hoogkamer et al. *Med Sci Sports Exerc.* 48(11), 2016.

INCREASING PUSH-OFF ENERGY FROM A PROSTHETIC FOOT MAY NOT REDUCE ENERGY LOSSES IN THE CONTALATERAL LEG DURING GAIT

Audra Davidson, Eston Walden, and Young-Hui Chang

Georgia Institute of Technology, Atlanta, GA, USA
email: yh.chang@ap.gatech.edu

INTRODUCTION

Patients with unilateral lower extremity limb loss are roughly 17 times more likely to develop knee osteoarthritis in their sound limb [1]. This elevated risk of knee osteoarthritis development is often tied to the increased loading of the sound limb that occurs in patients with unilateral limb loss [2]. Increased sound limb loading is strongly linked to the loss of plantarflexor musculature and subsequent reduction in push-off power in the affected limb [2, 3]. Dynamic walking principles predict that decreased power produced by the trailing (affected) limb during push-off should increase negative work done on the leading (sound) limb during heel strike, potentially resulting in overloading of the sound limb [3].

Powered ankle prostheses attempt to solve this problem by increasing the magnitude of a prosthetic ankle's push-off power, as increasing push-off is suggested to reduce sound limb loading [1, 3]. Thus far, these devices have been unsuccessful in restoring loading symmetry [4]. We reasoned that adjusting the timing of prosthesis power delivery could also modulate mechanical work done by the affected (trailing) limb. Notably, this could potentially reduce negative work done on the sound (leading) limb without increasing prosthesis power demands [5].

Our goal was to characterize the effects of adjusting the timing settings of a commercially available powered prosthesis to investigate its influence on ankle power delivery and, ultimately, on the negative work experienced by the leading (sound) limb in patients with unilateral limb loss during treadmill walking. We hypothesized that: 1) push-off power would increase as timing of power delivery occurs earlier in the gait cycle; and, 2) negative work of the intact leading limb would vary inversely with propulsive work performed by the amputated trailing limb.

METHODS

Five males with unilateral traumatic transtibial amputation (mean age 41±17.0yrs, mass 79.0±8.0kg, height 1.84±0.08m) gave informed consent prior to participating in this IRB-approved study.

Subjects were fitted with an emPOWER robotic ankle prosthesis (Ottobock, Bedford, MA) by a certified clinician. After a warm up, each subject walked on a treadmill at 1.1 m/s for 3 minutes for each of 7 randomized trials for a given timing condition (baseline, 3 late and 3 early). We used default tuning parameters suggested by the vendor as the baseline setting. Timing of ankle power delivery was adjusted using a wireless control interface (Ottobock, Bedford, MA). Kinetics data were obtained via force plates (AMTI, Watertown, MA) instrumented into a custom, dual-belt treadmill [5]. We collected lower body kinematics using an 8-camera motion capture system (Vicon, Centennial, CO; Visual 3D, C-Motion, Germantown, MD).

Prosthesis push-off timing was defined as the percent of the gait cycle when peak power was reached. Lower limb power output was calculated via Unified Deformable (UD) model analysis [7]. Energy delivered by the prosthesis during push-off was calculated by integrating the last positive region of the ankle power curve. Sound limb collisional work was calculated by integrating the first negative region of the COM work rate curve [8]. Pearson's correlations were used to determine the relationship between prosthesis timing and power with sound limb collisional work.

RESULTS AND DISCUSSION

No relationship was found between the device's timing settings and the measured timing of peak power delivery from the device ($R=-0.08$, $p=0.66$). The timing settings were significantly correlated

with prosthesis push-off work, however, with earlier timing conditions producing more power (R=-0.73, $p<0.001$). Neither timing condition nor calculated push-off timing were correlated with negative work on the lead leg ($p\geq0.197$). This suggests that altering the timing of power delivery via standard device tuning methods does not significantly alter push-off timing of the emPOWER prosthesis, but does influence positive prosthesis work produced by the device.

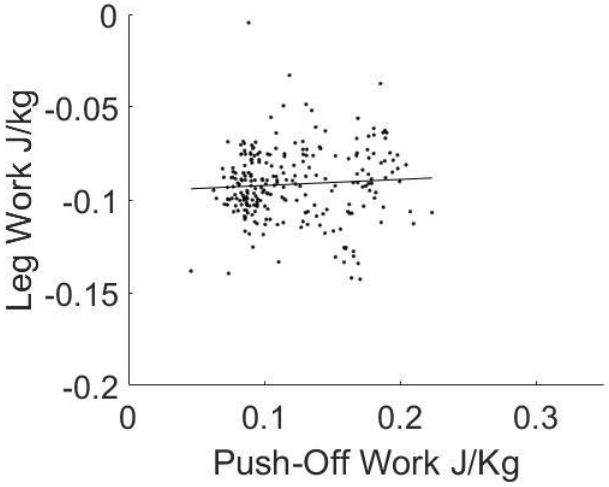

Figure 1: Relationship between prosthesis push-off work (J/Kg) and sound limb collisional work (J/Kg) across five male patients with unilateral limb loss.

Increasing push-off work to approximate or exceed physiological levels did not reduce loading on the sound limb. We saw no overall correlation between push-off work and sound limb collisional work across subjects (Fig. 1, R=0.29, p=0.31). These findings are consistent with previous studies, demonstrating that increasing ankle prosthesis power levels do not reduce sound limb collisional work or restore loading symmetry [4, 9].

This suggests that the positive work provided by the prosthesis was dissipated before reaching the COM, as positive prosthesis work was not correlated with sound limb collisional work. This could be due to power damping caused by the limb/socket interface, or altered joint control strategies when using a powered prosthesis. Only a short accommodation time with the device was provided to subjects for this study. Longer training times may help to promote full utilization of the delivered mechanical power. Each subject responded differently to increases in power, suggesting that personalized tuning and training may also be necessary.

CONCLUSIONS

The amount of push-off power rather than timing of power delivery is altered with standard suggested tuning methods of the emPower powered ankle prosthesis. Increasing the prosthesis push-off power does not immediately reduce sound limb collisional work. Due to possible damping and altered control strategies, a longer tuning and adaptation period with more extensive, personalized training may be required to alter sound limb collisional work.

REFERENCES

1. Struyf et al. *Arch Phys Med Rehabil.* 90, 2009.
2. Morgenroth et al. *Gait Post.* 34(4), 2011.
3. Adamczyk & Kuo. *IEEE Trans Neural Syst Rehabil Eng.* 23(5), 2015.
4. Esposito et al. *Clin Biomech*. 29, 2014.
5. Malcolm et al. *J Neuroeng Rehabil.* 12(21), 2015.
6. Kram et al., *J Applied Physiology* 85(2), 1998
7. Takahashi et al. *J Biomech.* 45, 2012.
8. Donelan et al. *Proc R Soc Lond.* 268, 2001.
9. Quesada et al. *J Biomech.* 49, 2016.

ACKNOWLEDGEMENTS

This work was funded by NIH HD075493 and supported indirectly by Ottobock GmbH via provision of time and use of the emPOWER foot ankle system. We thank Lee Childers for his clinical and scientific contributions to this work.

ABILITY TO PREDICT PERTURBATION TIMING DOES NOT IMPACT CENTER-OF-MASS DISPLACEMENT IN BELOW-KNEE PROSTHESIS USERS AND CONTROLS

[1,2] Matthew J Major, [1] Chelsi K Serba, and [1,3] Keith E Gordon

[1] Northwestern University, Chicago, IL, USA
[2] Jesse Brown VA Medical Center, Chicago, IL, USA
[3] Edward Hines Jr. VA Hospital, Chicago, IL, USA
email: matthew-major@northwestern.edu, web: http://www.nupoc.northwestern.edu/

INTRODUCTION

Over half of community living persons with lower-limb loss fall every year [1]. However, the factors that underlie this high fall prevalence have not been sufficiently explored. Our previous research suggests that *a priori* information of a lateral perturbation during walking influences the proactive mechanisms employed by below-knee prosthesis users (BKPUs) to resist this disturbance [2]. Specifically, providing information on the timing of a perturbation known to be directed towards the impaired limb encourages an increase in the margin-of-stability (MoS) on the impaired side just prior to the perturbation instance. The consequences of this control strategy on response dynamics have not yet been explored. The purpose of this study was to follow up our previous analysis to assess the effects of *a priori* information (direction, timing) of a lateral perturbation on response dynamics of BKPUs. We hypothesized that aligned with this BKPU proactive strategy when perturbation direction and timing were known, there would be a decrease in displacement of the body center-of-mass (BCoM) compared to when timing is unknown due to efforts to resist disturbance. We also hypothesize that due to a loss of an active ankle joint and critical forms of proprioception [3, 4], BKPUs' BCoM excursion would be greater on the impaired side with no difference in non-impaired controls.

METHODS

Six BKPUs (48±8yrs, 70±11kg, 1.7±0.1m) using their customary prostheses and 13 non-impaired controls (29±11yrs, 65±10kg, 1.7±0.1m) participated in the study. Subjects received lateral perturbations during a series of treadmill walking trials. *A priori* knowledge of the perturbation direction was provided, but timing was either not provided or provided through both visual and audio cues [2]. For this analysis, we examined four conditions of iterations of perturbation direction (impaired/non-dominant, sound/dominant) and timing (unknown, known). Subjects walked at their self-selected speed for all trials while perturbations of 12% bodyweight over 400 ms were generated by motorized cables attached to a waist harness [2]. Positions of markers on the pelvis were recorded at 100 Hz (Qualisys, Göteborg, Sweden), and used to define the BCoM position. BCoM displacement was estimated by subtracting the BCoM position at the start of the perturbation from the position at the end of the exposure, and averaged across trials for each condition. A mixed three-way ANOVA (α=0.05) tested the main and interaction effects of perturbation direction, perturbation timing, and group.

RESULTS AND DISCUSSION

A plot of representative BCoM trajectories with respect to time for the conditions of unknown time and when perturbations were directed towards either limb are displayed in Figure 1.

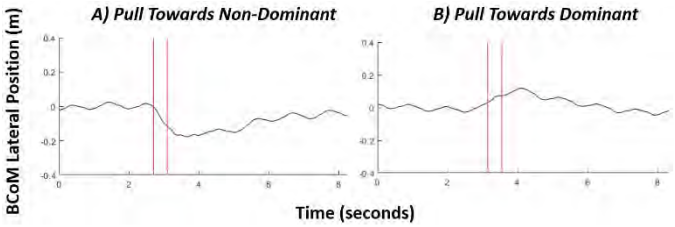

Figure 1: BCoM trajectories for one subject pulled towards the A) non-dominant and B) dominant limb. Vertical red lines=start and stop of perturbation. Positive to negative values indicate right direction.

The main effect of direction was significant (p=0.023), with BCoM displacement greater when perturbed toward the impaired/non-dominant limb

than the sound/dominant limb (Fig 2). No other main or interaction effects were significant ($p \geq 0.194$).

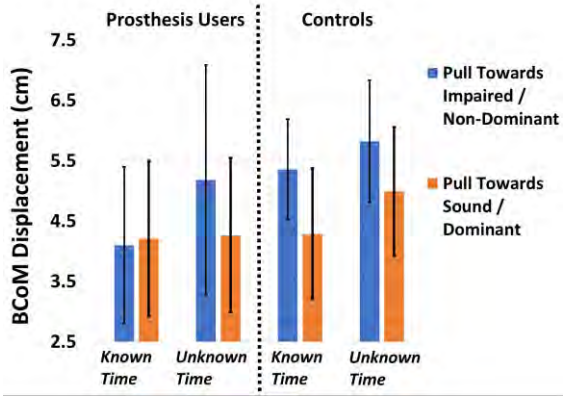

Figure 2: Average BCoM displacement separated by timing, direction, and group. Error bars=95% CI.

The results suggest that across both groups a larger lateral displacement of the BCoM is experienced when a perturbation is directed towards the control non-dominant limb and the BKPU impaired limb. The expectation that this increased BCoM displacement would be observed only in BKPUs was not supported as no interaction or group effects were significant. Additionally, both groups appear to experience similar displacements in BCoM during the perturbation exposure.

This finding may suggest that despite the unique unilateral lower limb impairment experienced by BKPUs, both BKPUs and non-impaired controls experience a bias in reactive control that favors the sound/dominant limb. However, given this impairment in BKPUs, the observed increase in MoS on the impaired limb side when timing of an expected perturbation is known [2] is reasonable to accommodate for this increase in BCoM displacement. Our previous results suggest that preceding MoS is not increased when timing is unknown to avoid prolonged exposure to elevated stability costs [2], although this strategy would likely benefit overall locomotor stability.

The results of this study suggest that across subjects BCoM displacement is not significantly affected by *a priori* knowledge of perturbation timing. Specifically, although this knowledge encourages an increase in MoS on the BKPU impaired limb side prior to the perturbation [2], there is no reduction in BCoM displacement. This finding did not support our hypothesis, as it was expected that BKPUs would employ a control strategy to minimize BCoM excursion and further enhance the distance between the base-of-support and extrapolated center-of-mass. Consequently, it may be that both controls and BKPUs do not employ control strategies that specifically minimize BCoM displacement following a lateral perturbation of this magnitude. Given our previous results [2], while BKPUs may partially rely on proactive strategies to enhance locomotor stability, non-impaired controls likely depend on reactive strategies. Subsequent analyses will focus on *a priori* knowledge effects on lateral BCoM velocity which may serve as an alternative means to maximize locomotor stability [2]. Additionally, the global maximum of BCoM displacement and time to reverse BCoM trajectory after perturbation will also be analyzed.

CONCLUSIONS

Non-impaired controls and unilateral BKPUs experience similar BCoM displacement when subjected to a lateral perturbation of 12% bodyweight. These displacements are not affected by *a priori* knowledge of timing, but both groups experience greater displacement with perturbations directed toward the impaired/non-dominant limb.

REFERENCES

1. Miller WC, et al. *Arch Phys Med Rehabil* **82**, 1031-1037, 2001.
2. Major MJ, et al. *Sci Rep* **8**, 1863, 2018.
3. Nadollek HS, et al. *Physiother Res Int* **7**, 203-214, 2002.
4. Vrieling AH, et al. *Gait Posture* **28**, 222-228, 2008.

ACKNOWLEDGEMENTS

We thank Geoffrey Brown, Sean Dwijendra, and Franklyn Ndubuisi-Obi for assistance with data collection and processing. Work was supported by the National Institutes of Health (#UL1TR001422) and the U.S. Department of Veterans Affairs (#1 IK2 RX001322-01A1, and #1 IK2 RX000717-01).

Comparison of Modular and Rigid Socket Systems for Lower Limb Amputees: A Preliminary Study

[1] Corey Pew, [2]Shane R. Wurdeman and [1]Richard R. Neptune

[1] Department of Mechanical Engineering, University of Texas, Austin, TX
[2] Department of Clinical & Scientific Affairs, Hanger Clinic, Austin, TX
email: Corey.Pew@utexas.edu, web: www.me.utexas.edu/~neptune/

INTRODUCTION

Lower limb amputees often express dissatisfaction with the fit of their prosthesis [1]. Prosthesis fit has been identified as a vital characteristic when evaluating a patient's prosthesis and often determines whether an individual will use their prosthesis effectively [2]. The fit of the socket system can also significantly affect amputee mobility, comfort, activity level, residual limb skin health, vocational success and safety [1–4].

The prosthetic socket plays a critical role in coupling the prosthesis to the residual limb. The current standard-of-care consists of a static exoskeleton socket secured to the residual limb through an elastomeric liner in combination with a mechanical locking pin or an element of negative pressure [5]. The residual limb, however, is dynamically changing shape and volume throughout the course of the day [6]. The impedance mismatch between the static, rigid socket and the dynamic, soft residual limb leads to the socket fit varying from ideal to poor throughout the day. The result of a poorly fitting socket is pain and discomfort that can limit the amputee's comfort and mobility.

Modular socket systems have recently become available that attempt to improve the coupling of the prosthesis to the user by providing components that can be manually adjusted. This allows the user to fine-tune the fit between the socket and limb as conditions vary throughout the day and over longer periods. This preliminary investigation sought to determine if one such modular system, the Hanger ComfortFlex Adapt system (Hanger Inc., Austin, TX), could provide improvements to user comfort, satisfaction, quality of life and mobility as compared to the standard-of-care (**Figure 1**).

Figure 1: Comparison of socket systems. A: Standard-of-care rigid exoskeleton socket, B: Hanger ComfortFlex Adapt modular socket.

METHODS

Utilizing a preliminary review of records provided by Hanger Clinic, we investigated differences between an adjustable, modular socket design (ComfortFlex Adapt) and the rigid, static sockets in above-knee prosthesis users using: 1) the Socket Comfort Score (SCS), 2) the Prosthesis Evaluation Questionnaire Well-Being subsection (PEQ-WB) modified to use a 10-point ordinal scale, and 3) the Prosthetic Limb Users Survey of Mobility (PLUS-M). This preliminary data utilized only the Well-Being subsection of the complete PEQ. The PEQ-WB consists of a satisfaction with amputation (PEQ-Sat) and a quality of life (PEQ-QoL) question. We were able to obtain data for 8 individuals with the modular socket (age: 46.1 ± 13.9 yrs., height: 176.9 ± 8.0 cm, mass: 85.5 ± 17.8 kg), which we then compared with 11 individuals using a conventional rigid socket (age: 49.3 ± 11.4 yrs., height: 172.7 ± 9.0 cm, mass: 87.7 ± 24.5 kg). Individuals with the rigid

socket were extracted from a large clinical outcomes database using an algorithm based on similar age, height, and mass. Groups were compared using independent t-tests to calculate associated p-values.

RESULTS AND DISCUSSION

When comparing results between the two socket types from the five scales, individuals with the modular socket reported increased socket comfort (SCS) (p=0.005), satisfaction (PEQ-Sat) (p=0.182), quality of life (PEQ-QoL) (p=0.141), overall well-being (PEQ-WB) (p=0.152), and mobility (p=0.003) (**Figure 2**).

These preliminary results highlight the potential differences that can exist between an adjustable, modular socket and a rigid, static socket design. While these initial results indicate that a modular socket has the potential to improve outcomes of comfort and mobility for lower limb amputees, more subjects are needed to increase our statistical power and determine if these outcomes can be generalized to the lower limb amputee population.

CONCLUSIONS

Modular socket systems may provide improvements to amputee comfort and mobility as compared to the standard-of-care rigid sockets. A future, in-depth study with a larger patient group is being designed to determine how modular sockets might benefit lower limb amputees. A study of socket systems could then be used to help guide clinical practice to determine when and how modular socket systems should be used with the lower limb amputee population.

REFERENCES

1. Dillingham, *Am. J. Med. Rehab.*, **80**(8), 2001.
2. Legro, *J. Rehab. Res. Dev.*,**36(**3), 1999.
3. Levy, *Pros. Orth. Int.*, **4**(1), 1980.
4. Millstein, *Pros. Orth. Int.*, **9**(2), 1985.
5. Safari, *J. Rehab. Res. Dev.*, **52(**5), 2015.
6. Sanders, *J. Rehab. Res. Dev.*, **49**(10), 2012.

ACKNOWLEDGEMENTS

The authors would like to thank the prosthetists for providing the clinical data for this preliminary analysis.

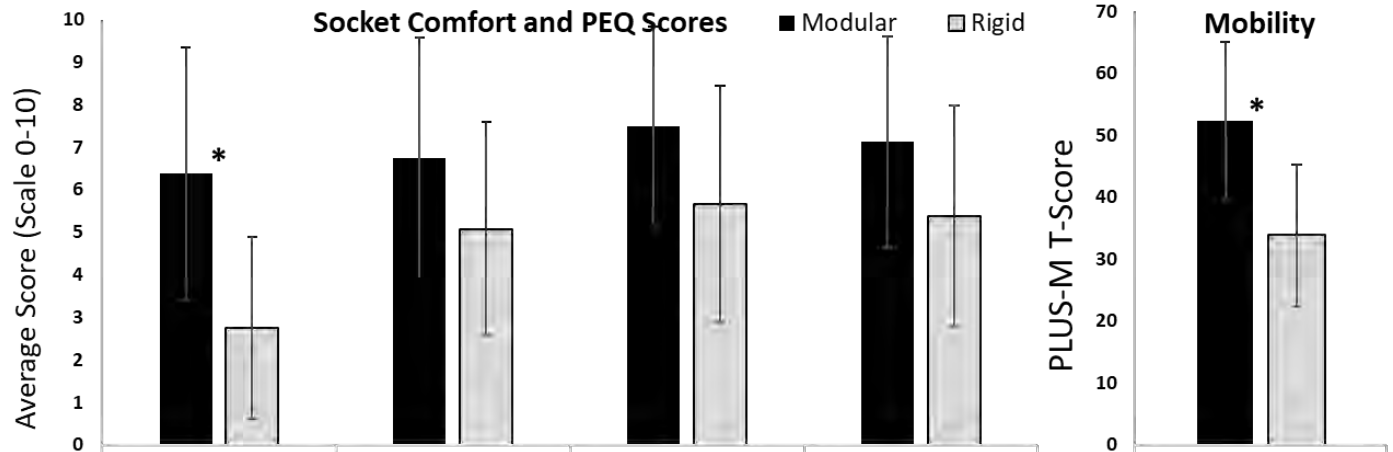

	Socket Comfort Score	PEQ-Sat	PEQ-QoL	PEQ-Well Being		PLUS-M
Modular	6.38±2.97	6.75±2.33	7.50±2.33	7.13±2.49	Modular	52.4±12.8
Rigid	2.75±2.14	5.08±2.50	5.67±2.77	5.38±2.60	Rigid	33.9±11.5

Figure 2: Average scores (± Standard Deviation) for the modular and rigid socket users from the Socket Comfort Score, PEQ-Satisfaction (Sat), PEQ-Qol (Quality of Life), PEQ-Well Being and PLUS-M. *Significant difference ($p<0.05$) between socket types for the available data.

COORDINATION OF FRONTAL-PLANE BALANCE DURING RAMP WALKING IN RESPONSE TO PROSTHETIC ANKLE POWER

[1,2]Nathaniel T. Pickle, [3,4]Jason M. Wilken, [3]Jennifer M.A. Whitehead, [2]Anne K. Silverman and [1,5]Nicholas P. Fey

[1] Depts. of Bioengineering and Mechanical Engineering, University of Texas at Dallas, Richardson, TX, USA
[2]Dept. of Mechanical Engineering, Colorado School of Mines, Golden, CO, USA
[3] Center for the Intrepid, Brooke Army Medical Center, JBSA Ft. Sam Houston, TX, USA
[4] Extremity Trauma and Amputation Center of Excellence, JBSA Ft. Sam Houston, TX, USA
[5]Dept. of Physical Medicine & Rehabilitation, UT Southwestern Medical Center, Dallas, TX, USA
email: nathaniel.pickle@utdallas.edu, web: www.sahmlab.org

INTRODUCTION

Mechanically-active ankle-foot prostheses for individuals with transtibial amputation (TTA) can produce mechanical power commensurate with the biological ankle during the push-off phase of gait [1]. Mechanical ankle power production can reduce metabolic energy expenditure [2,3] and increase prosthetic ankle range of motion compared to passive prostheses [1]. However, not all studies demonstrate a reduction in metabolic cost [4] and the range of whole-body angular momentum (*H*) can remain elevated compared to non-amputees [5].

These inconsistent findings may be due to active prostheses providing increased push-off power during terminal stance, but functioning similarly to passive prostheses during early stance [1]. Thus, the effects of an active prosthesis on whole-body coordination of balance may not be adequately captured by analyses such as range of *H*. A method for testing for statistically significant changes throughout the gait cycle, such as Statistical Parametric Mapping (SPM), is needed [6]. We used SPM to analyze segment contributions to frontal-plane *H* during uphill and downhill walking with passive and active prostheses.

METHODS

We evaluated data from 10 individuals with TTA (1F/9M, mean±SD: 30±5 years, 1.83±0.10 m, 96±7 kg) and 10 non-amputees (2F/8M, 24±5 years, 1.80±0.09 m, 91±10 kg). All individuals with TTA were Medicare Functional Classification Level K4. Trials were performed with the participants' clinically-prescribed passive prosthesis and the BiOM H2 Power Ankle (BiOM, Inc.). Participants acclimated to the BiOM over 43.4±18.1 days. Participants walked on a 16-foot ramp at slopes of 0°, ±5°, and ±10° at a fixed speed. Whole-body kinematics were tracked using 57 reflective markers (120 Hz, Motion Analysis Corp). Thirteen-segment full body models were created for each person using Visual3D (C-Motion, Inc.), with segment masses computed as a percentage of total body mass. The passive prosthesis shank mass was reduced by 30% and moved 30% more proximally. The BiOM was modeled with the same inertial properties as a biological shank and foot. We computed segment contributions to *H* as

$$\vec{H}_i = (\vec{r}_i - \vec{r}_{body}) \times m_i(\vec{v}_i - \vec{v}_{body}) + I_i\vec{\omega}_i$$

where $\vec{r}_i$, $\vec{v}_i$ and $\vec{\omega}_i$ are the position, velocity, and angular velocity of the i^{th} segment, $\vec{r}_{body}$ and $\vec{v}_{body}$ are the position and velocity of the whole-body COM, and m_i and I_i are the mass and inertia matrix of the i^{th} segment. H_i was normalized by body height, mass, and average horizontal walking velocity and expressed as a percentage of left or prosthetic limb gait cycle (gc).

Contributions of each arm, leg and the trunk to *H* were compared using spm1d [6] in MATLAB (The Mathworks, Inc.). A generalized linear model was created with ramp angle and group (non-amputee, passive, active) as fixed effects, and a random intercept for each subject. Using the SPM equivalent of ANOVA, we tested for significant fixed effects at each time step (α=0.05). Post hoc pairwise comparisons (α=0.0005 after Bonferroni correction) were performed during intervals in which significant main or interaction effects were found.

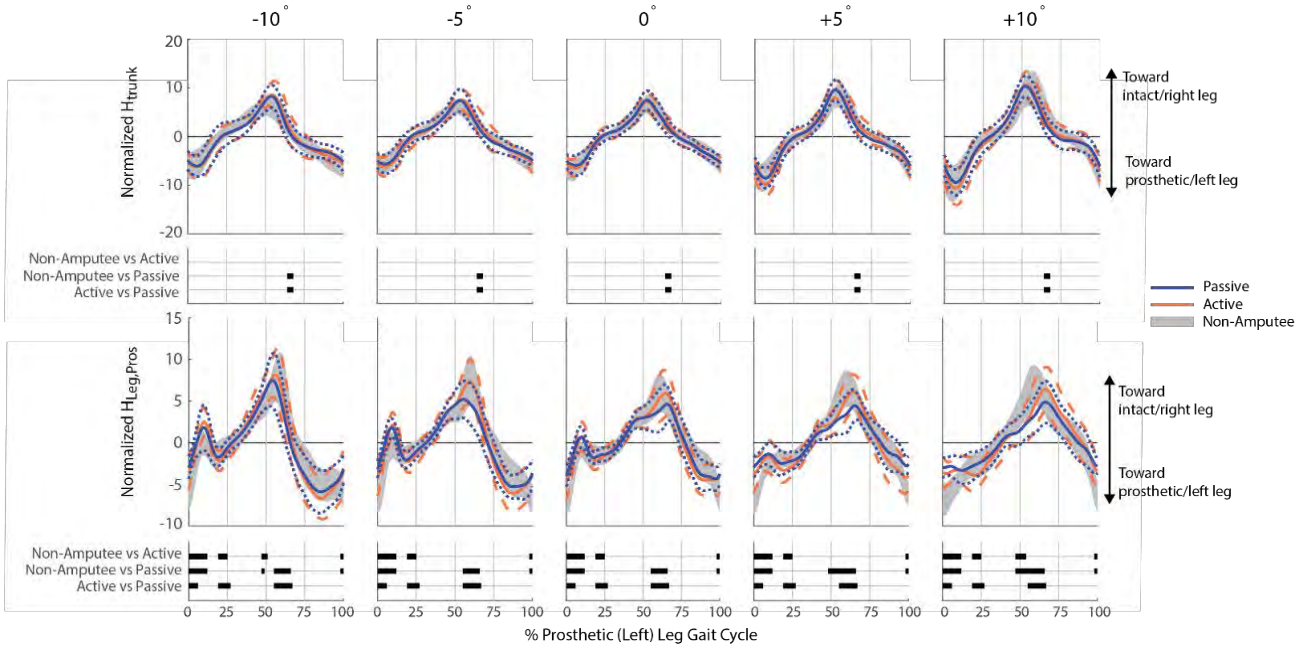

Figure 1: Mean (solid lines) ±1SD (dashed lines) normalized H_{trunk} and $H_{Leg,Pros}$. Mean±1SD non-amputee values are in shaded gray. Bars below each figure indicate significant differences between groups.

RESULTS AND DISCUSSION

There were significant differences in H_{trunk} just after toe-off (63-68% gc) on all slopes for the passive prosthesis compared to the other conditions, but not between the active prosthesis and non-amputees (Fig. 1). H_{trunk} was more positive when using the active compared to passive prosthesis, indicating greater angular momentum toward the intact leg at prosthetic leg toe-off (~63-68% gc). Similar differences were observed in $H_{leg,pros}$ at slopes of 0° and ±5° (Fig. 1), suggesting that ankle joint power contributes additional frontal-plane H_{trunk} and $H_{leg,pros}$ toward the intact leg.

Furthermore, the lack of differences between the active prosthesis and non-amputees suggests that the active prosthesis improves coordination of dynamic balance at toe-off. This finding is consistent with other studies demonstrating increased ankle push-off power [1,7] and trailing leg mechanical work [2,3] when using active compared to passive prosthetic ankles. Our findings also support simulations showing that the ankle plantarflexors contribute to frontal-plane H toward the contralateral leg in late stance [8]. We expand on these simulation results by identifying that ankle power generation primarily affects the ipsilateral leg and trunk, and has little effect on the intact leg.

Our analysis also indicated that both active and passive prostheses contributed a significantly lower magnitude of $H_{leg,pros}$ compared to non-amputees in early stance. This result is likely because active prostheses effectively function like passive prostheses during this portion of the gait cycle.

In conclusion, while the power produced by active prosthetic ankles during late stance appears to restore normative balance regulation at toe-off, the benefits of these devices are likely limited by user adaptation and/or device functionality during early stance.

REFERENCES

1. C.A. Rábago *et al.*, *PLoS One*, 2016, **11**, 1.
2. H.M. Herr and A.M. Grabowski, *Proc. Biol. Sci.*, 2012, **279**, 457.
3. E.R. Esposito *et al.*, *Prosthet. Orthot. Int.*, 2015.
4. R.E. Quesada *et al.*, *J. Biomech.*, 2016, **49**, 3452.
5. N.T. Pickle *et al.*, *J. Biomech.*, 2016, **49**, 3397.
6. T.C. Pataky *et al.*, *J. Biomech.*, 2013, **46**, 2394.
7. A.E. Ferris *et al.*, *Arch. Phys. Med. Rehabil.*, 2012, **93**, 1911.
8. R.R. Neptune and C.P. McGowan, *J. Biomech.*, 2016, **49**, 2975.

MEDIAL-LATERAL GAIT STABILITY IN PEOPLE WITH TRANSTIBIAL AMPUTATION ACROSS WALKING SPEEDS

Ryan D. Wedge, Andrew K. LaPrè, Frank C. Sup, and Brian R. Umberger
University of Massachusetts, Amherst, MA, USA
email: umberger@kin.umass.edu, web: www.umass.edu/locomotion, www.ecs.umass.edu/mie/mrrl

INTRODUCTION

People with lower limb amputation have a greater incidence of falling compared with people without amputation [1]. They are unable to produce as much force on the prosthetic side to recover from perturbations [2] and may adapt different strategies compared with the intact side to decrease the risk of falling. People with lower limb amputation demonstrate inter-limb asymmetries, such as a shorter step length on the intact side compared with the prosthetic side, which may be a functional adaptation to increase stability. Understanding the adaptations people with amputation make will enhance rehabilitation and prosthesis interventions and ultimately help decrease the risk of falling.

Gait stability in people with a unilateral transtibial amputation has been shown to vary between limbs. When using a global (i.e., center of mass) measure, such as margin of stability (MoS), there is greater stability on the intact side in the backwards (BW) direction [3,4] and greater stability on the prosthetic side in the medial-lateral (ML) direction [3]. The same trend for BW MoS remains across a range of speeds [4] but it is unknown how ML MoS varies beyond preferred speed.

When determining MoS, how the base of support (BOS) is defined can alter the magnitude of the MoS. The BOS was originally defined based on the center of pressure (COP) [5], though more recently investigators have used ankle markers to define the BOS [3]. Alternatively, the limits of the BOS could be defined using markers on the foot rather than on the ankle but the effects on ML MoS are unknown.

Gait stability across speeds is of interest because of the multiple speeds people use when walking, and may help quantify the capacity to avoid a fall at different speeds. How the base of support is defined when using markers is also important because it could the affect the magnitude of MoS and the conclusions of the study. The purpose of this study was to evaluate ML MoS across walking speeds using three different methods for defining BOS.

METHODS

Data were collected for seven subjects (2 females; mass: 74.3 ± 15.0 kg; height: 1.78 ± 0.09 m) with a unilateral transtibial amputation. All subjects were rated at a K3 or K4 level and used a standard pylon and a split toe flex-foot.

Minimum ML MoS during stance phase was calculated based on the extrapolated position of the center of mass (CoM) relative to the lateral margin of the base of support, which was defined three different ways based on markers on the lateral ankle (LANK), the lateral heel (LHL), and the fifth metatarsal (FMET). Kinematic data were captured using a high-speed motion capture system as subjects walked overground at three speeds: preferred (1.27 ± 0.04 m s^{-1}) and ±20% preferred (1.05 ± 0.04 m s^{-1} and 1.55 ± 0.07 m s^{-1}). CoM ML position was estimated from markers on the right and left anterior and posterior superior iliac spines, and then numerically differentiated to determine CoM velocity (vCOM).

Minimum ML MoS was determined during stance phase for both limbs (prosthetic and intact) for three trials at each of the three speeds. Dependent variables were tested for differences using 2 (limb) x 3 (speed) MANOVAs followed by post-hoc tests using the false discovery rate procedure with significance set at $\alpha = 0.05$.

RESULTS AND DISCUSSION

The magnitude of the minimum ML MoS was greater for the prosthetic side compared with the intact side across speeds for all three BOS definitions (Figure 1), with a significant main effect of limb. There were no significant speed effects or interactions. There were significant pairwise

differences between limbs at preferred (p=0.033) and fast (p=0.002) speeds for the FMET BOS definition, and all pairwise differences between limbs across speeds and BOS definitions had large effect sizes, except for LANK at the slow speed, which had a medium effect size (Figure 1).

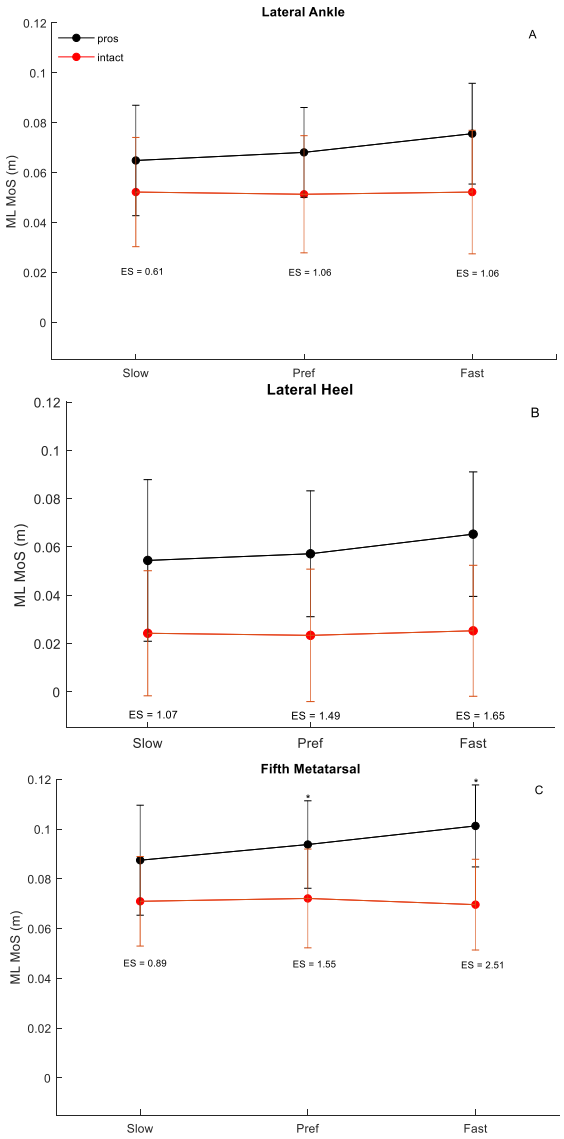

Figure 1: Minimum ML MoS during stance calculated using the LANK (A), the LHL (B), and the FMET (C) as the BOS for both limbs across speeds. The * symbol denotes a significant difference between limbs and ES = effect size.

The greater ML MoS on the prosthetic side compared with the intact side is consistent with previous findings [3] at the preferred speed, and was found to remain consistent across speeds (Figure 1). The lack of speed dependence for ML MoS differed from our previous finding that BW MoS at heel strike significantly increases with speed [4]. The greater ML MoS during stance on the prosthetic side may be a strategy to provide a greater margin of safety when the body is supported on the prosthetic limb, which is not able to produce as much force compared with the intact side [2].

The different methods for defining BOS using markers on the ankle and foot lead to similar general conclusions about the ML MoS across speeds. The main effects of limb and generally large effects sizes were consistent across methods. The BOS based on the FMET marker may have the advantage of greater sensitivity as it also identified statistically significant pairwise differences. Future work is needed to determine how the results obtained with different markers compare with the COP when defining the lateral BOS.

CONCLUSIONS

People with unilateral transtibial amputation demonstrate different stability patterns between limbs and in different directions. Rather than the increase in BW MoS previously observed with speed, ML MoS was maintained across speeds and was greater for the prosthetic limb. Taken together, these results may represent adaptations people with lower limb amputation make in response to a greater risk of falling in the mediolateral direction when the body is supported on the prosthetic limb, regardless of walking speed.

REFERENCES

1. Miller WC, et al. *Arch Phys Med Rehabil* **82**, 1031-1037, 2001.
2. Bolger D, et al. *Clin Biomech (Bristol, Avon)* **29**, 1039-1047, 2014.
3. Hak L, et al. *Arch Phys Med Rehabil* **94**, 2186-2193, 2013.
4. Wedge RD, et al. *Amer Soc Biomech*, Boulder, CO, 2017.
5. Hof AL, et al. *J Biomech* **38**, 1-8, 2005.

ACKNOWLEDGMENTS

Supported by grants from the National Science Foundation (IIS-1526986) and the National Center for Simulation in Rehabilitation Research.

POSTURAL INFLUENCES ON REGIONAL SUPRASPINATUS AND INFRASPINATUS ACTIVATION IN ISOMETRIC ARM ELEVATION EFFORTS

[1] Talia Alenabi [1] Rachel Whittaker, [2]Soo Kim, [1] Clark R. Dickerson

[1] Department of Kinesiology, University of Waterloo, Canada
[2] School of Rehabilitation, University of Saskatchewan, Canada
Email: cdickers@uwaterloo.ca

INTRODUCTION

Rotator cuff muscles stabilize the glenohumeral joint against humeral head translations and the suprapinatus (SUP) and infraspinatus (INF) can particularly contribute during arm elevation. Several EMG studies have quantified the activation of SUP and INF during different exercises and postures. In clinical settings, elevation posture is usually defined by thoraco-humeral elevation angle and elevation plane (sagittal, coronal, scapular). The activation patterns of SUP and INF in different elevation postures have scarcely been compared and very few studies considered the effect of elevation planes [1]and elevation angles[2] on muscle activation.

In addition, most EMG studies considered SUP and INF as a single muscle unit while anatomical studies suggested that there are two neuro-anatomically distinct regions within SUP (anterior, posterior) and three regions within INF (superior, middle, inferior) muscles. Only Kim et al. [3] reported the activation of both anterior and posterior SUP during some exercises and no EMG study evaluated the activation of the three regions of INF.

The aim of this study was to quantify the activation of different SUP and INF regions during resisted isometric arm elevations in different arm postures in order to explore the effect of elevation angle and elevation plane on muscle activation pattern.

METHODS

31 right-handed healthy individuals including 16 females (21.8 ± 1.6 years) and 15 males (23.2 ± 3.4years) participated in this study. EMG signals from anterior and posterior SUP were detected using indwelling electrodes as described by Soo Kim et al. [3]. Intramuscular electrodes were also placed into the superior, middle and inferior regions of infraspinatus muscles through a protocol validated in the local university. The data were collected using a Noraxon system with 3000Hz sampling rate.

The participants performed 18 isometric exertions against a robotic device that provided stationary resistance after completing 11 MVC exertions. The test postures included abduction, scaption and flexion at 30°, 90° and 150°of arm elevation in two load conditions: Maximal Voluntary Force (MVF) and 50% MVF. The force was exerted against a tri-axial force transducer, and sampled at 1500Hz before conversion to a digital signal using a Labview program. The participants could observe their %MVF on screen. Each trial lasted 6 sec and repeated once with 1-2 min rest between trials.

The raw EMG data were bandpass filtered, full wave rectified and linear enveloped using a low pass filter (fc = 2Hz). For each muscle, the maximum value across all MVC and MVF trials was extracted to represent the maximum voluntary excitation (MVE). All EMG data were presented as %MVE. The mean activation values were assessed using two-way repeated measure ANOVAs, with two independent variables: plane and angle of elevation, and their interaction effect.

RESULTS AND DISCUSSION

Supraspinatus (Figure 1): Changes in arm posture did not influence activation of the posterior region. This may indicate that the posterior region has mostly a stabilizing role. However, the effects of plane and angle were statistically significant for anterior SUP. At 50%MVF load condition, the activation of anterior SUP was in average 40.7%MVE and 38.9%MVE in scaption and abduction respectively, which were significantly higher than flexion (35.4%MVE). While applying

maximal force, the activation of anterior SUP was significantly lower in 30° of flexion (40.2%MVE) than abduction (53.2%MVE) and scaption (48.6%MVE). This indicates that anterior SUP contributes more prominently in lower regions of arm abduction.

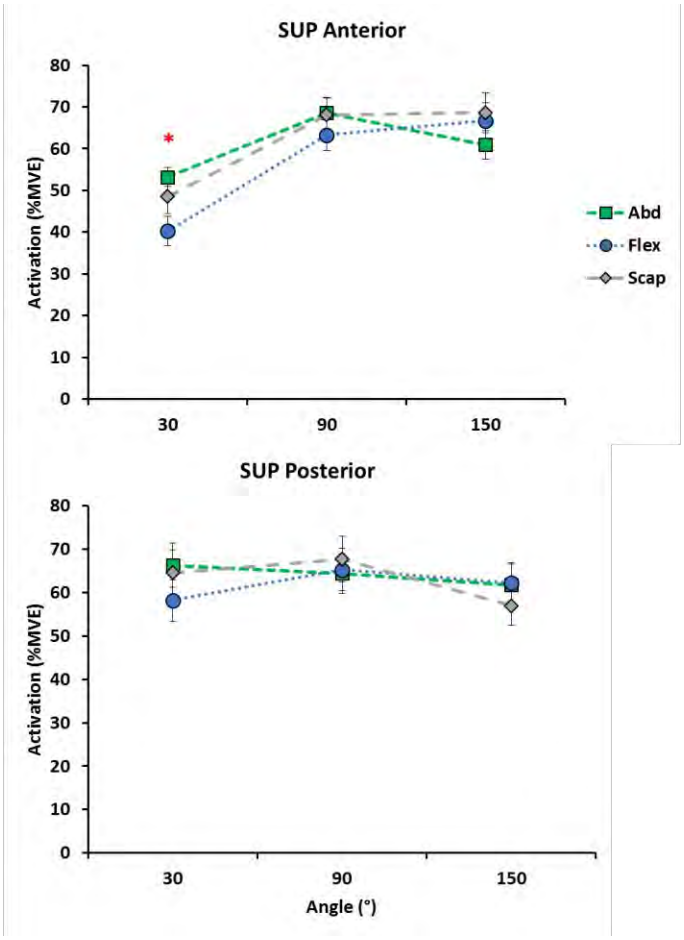

Figure 1: Activation of anterior and posterior regions of supraspinatus in different postures (maximal force), * = significant interaction ($p<0.05$)

Infraspinatus: The activation of superior INF was not affected by arm posture at low elevation angles (30°). However, in 90° of elevation, this region was more active during flexion. Likewise, the activation of middle INF was higher in flexion, irrespective to the elevation angles (Figure 2). This indicates that the superior and middle regions of INF are more involved in arm flexion. Irrespective to the plane of elevation, the inferior infraspinatus had higher activation in 90° (62%MVE) and 150° (58.6%MVE) of elevation than 30° (47.9%MVE) by applying maximal force.

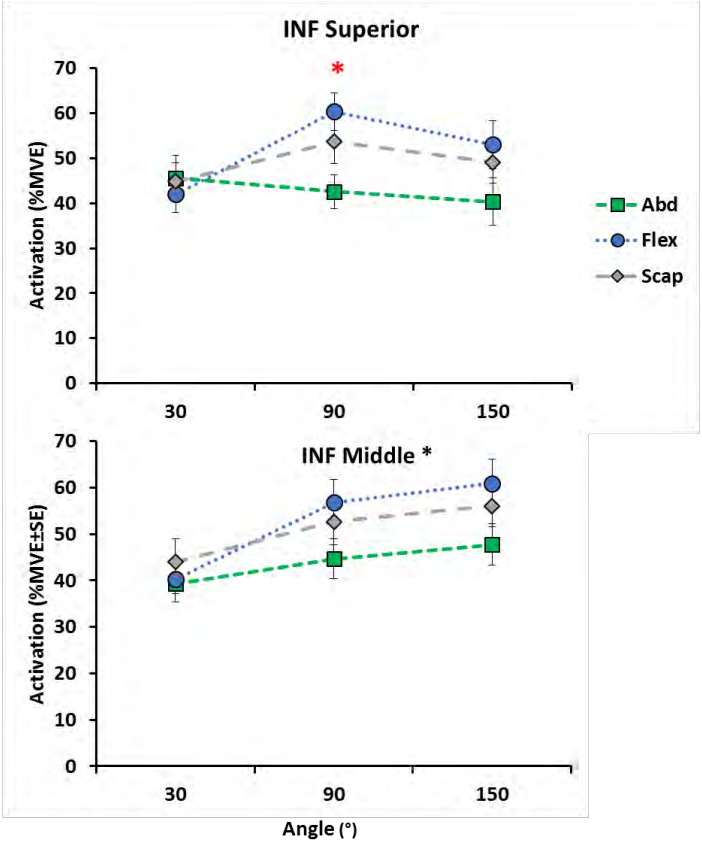

Figure 2: Activation of two infraspinatus regions in different postures (maximal force). *= significant interaction, *=Significant main effect ($p <0.05$)

CONCLUSIONS

Apart from posterior SUP, the contribution of the other regions of SUP and INF to arm elevation are influenced by plane and angle of elevation. The results of this study can help to identify the postures in which different regions of SUP and INF experience higher demand or exertion, and transfers directly to the development and modification of assessment and rehabilitation paradigms.

REFERENCES

1. Reed D et al. *J Man Ther* 21, 63-68, (2016)
2. Alpert SW et al. *Journal of Shoulder and Elbow Surgery* **9**, 47-58, (2000)
3. Kim SY et al. *International Biomechanics* **4**, 60-67 (2017)

SHOULDER KINEMATICS AND SUPRASPINATUS PROXIMITY DURING LEVEL AND SIMULATED RAMP PROPULSION

Beth A. Cloud, Stefan Madansingh, Emma Fortune, Melissa M. Morrow, and Kristin D. Zhao

Mayo Clinic, Rochester, MN, USA
email: cloud.beth@mayo.edu

INTRODUCTION

Individuals with spinal cord injury (SCI) report shoulder pain at rates up to 70% [1]. Imaging studies demonstrate that individuals with SCI have evidence of overuse shoulder pathology as early as 3.5 years after SCI [2]. Among the pathologies observed are rotator cuff tendinopathies and tears.

Certain scapular and humeral motions are suggested to be associated with subacromial impingement (SAI). In SAI rotator cuff tendons are impinged be between the humerus and scapula which can lead to tendon damage. Both level and ramp propulsion are characterized by scapular and humeral motions that have been associated with SAI [3].

The purpose of this study was to determine if shoulder kinematics and proximity of the supraspinatus insertion relative to scapular landmarks differ between level and simulated ramp propulsion.

METHODS

Individuals with SCI who use a manual wheelchair (MWC) as their primary mode of mobility were recruited to participate in this IRB approved study. Participants propelled on a custom set of rollers in two conditions (1) level and (2) simulated ramp (ramp). The ramp condition was simulated by raising support under the casters to create a 1:12 inclination (standard per the Americans with Disabilities Act (ADA) guidelines).

Unilateral shoulder kinematics were measured at 120 Hz with an electromagnetic system (Liberty, Polhemus). Thorax, scapula, and humerus local coordinate systems were defined using International Society of Biomechanics (ISB) standard landmarks [4]. Kinematics were quantified for the scapulathoracic (ST) joint, glenohumeral (GH) joint, and thorax relative to global (THOR). ST kinematics were quantified with the ISB standard rotation sequence (YX'Z"). GH kinematics were quantified with an alternative sequence (XZ'Y", [5]). THOR kinematics were quantified with a ZX'Y" sequence. Kinematic values were determined at 0, 25, 50, 75, and 100% of push and recovery propulsion phases.

Supraspinatus proximity relative to the coracoacromial (CA) arch (comprised of acromion, CA ligament, and coracoid) was determined by animating CT bone-models with GH kinematic data. The supraspinatus insertion site and inferior CA arch were defined as surface meshes. The minimum distance between the two surface meshes (supraspinatus proximity) was calculated by custom Matlab (Mathworks Ltd) code. The percentage of impingement time (%Supra) was quantified as the percentage of each phase that the supraspinatus insertion was within 5mm of the CA arch (Figure 1). Cadaver studies indicate the supraspinatus is about 5mm thick [6], therefore a space smaller than 5mm would suggest tendon impingement.

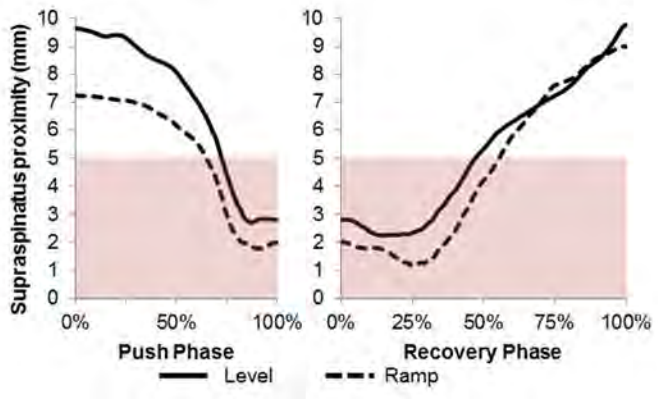

Figure 1: Supraspinatus time series for a sample participant. Push phase was ~40% of the total cycle. Pink shaded area denotes proximity <5mm

Five cycles from level and ramp propulsion were used for analysis. Analyses were performed within

each phase (push and recovery). %Supra was compared between the level and ramp conditions with a Wilcoxon signed-rank test. A series of linear mixed models for repeated measures were used to compare all GH and ST kinematics as well as THOR flexion between conditions and events.

RESULTS AND DISCUSSION

Ten individuals participated (age: 37±13yr, 9 male, SCI range: C5-T6, time since SCI: 10±11yr).

%Supra was significantly higher ($p<0.05$) in the ramp condition during recovery but not push (median difference (IQR): 9.1% (-0.7, 29.8); 5.5% (-5.3, 15.4), respectively; Figure 2). There was a main effect of event for all kinematics evaluated (as expected due to nature of the task). There was a main effect of condition in all 3 GH rotations, ST internal/external rotation, ST upward/downward rotation, and THOR flexion/extension in both push and recovery phases ($p<0.05$, Table 1). Condition-event interactions were seen in GH internal/external rotation in both phases and GH abduction during recovery ($p<0.05$).

Participants tended to be relatively more abducted, horizontally adducted, and externally rotated at the GH joint in the ramp condition. The difference in GH internal/external rotation was more pronounced at the end of push and beginning of recovery and in GH abduction at the beginning of recovery. Participants tended to be relatively more internally and upwardly rotated at the ST joint and use more thorax flexion during ramp propulsion.

CONCLUSIONS

GH, ST, and THOR kinematics differ by propulsion condition. The differences in each GH rotation are each small in magnitude but together have an effect on the impingement of the supraspinatus during propulsion, as evidenced by the %Supra changes.

The differences seen at the ST joint and thorax are likely repositioning the GH joint relative to the push rim and necessitating a change in GH kinematics. Work is ongoing to determine if the differences seen in the propulsion conditions can be leveraged to change an individual's percentage of time in impingement within a particular condition (i.e., training to propel with less ST internal rotation).

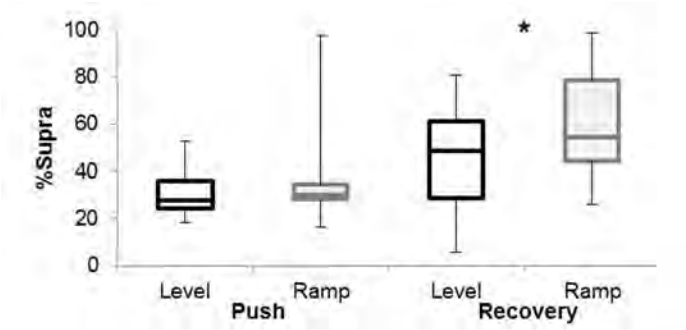

Figure 2: %Supra by condition and phase. Box plots show median, IQR, and min to max (error bars).

Table 1: Mean differences (95% CI) in kinematics between conditions (ramp–level; *, $p<0.05$)

	Push	Recovery
GH Abduction(-) [X]	-0.8* (-1.6, -0.1)	-1.5* (2.3, -0.6)
GH Horizontal Abd(-), Add(+) [Z']	2.6* (1.8, 3.4)	3.1* (2.2, 4.0)
GH External(-), Internal(+) Rotation [Y"]	-2.6* (-3.4, -1.9)	-3.9* (-4.7, -3.0)
ST Internal Rotation (-) [Y]	7.0* (5.8, 8.3)	6.8* (5.5, 8.0)
ST Up(-), Down(+) Rotation [X']	3.0* (2.2, 3.8)	3.2* (2.4, 4.0)
ST Anterior(-), Posterior(+) Tilt [Z"]	-0.5 (-1.0, 0.1)	-0.2 (-0.7, 0.3)
THOR Flex(-), Extension(+) [Z]	-6.0* (-6.8, -5.1)	-5.3* (-6.1, -4.4)

REFERENCES

1. Dyson-Hudson & Kirshblum. *J Spinal Cord Med.* 27(1), 2004.
2. Morrow et al. *BioMed Res Int*. 2014.
3. Morrow et al. *Clin Biomech*. 26(4), 2011
4. Wu et al. *J Biomech*. 38(5), 2005.
5. Phadke et al. *J Biomech*. 44(4), 2011.
6. Matsuhashi et al. *Clin Anat*. 27(5), 2014.

ACKNOWLEDGEMENTS

Funding provided by: Mayo Clinic Rehabilitation Medical Research Center, on behalf of the Craig H. Neilsen Fund for Spinal Cord Injury Care and Research Honoring Robert D. Brown Jr., M.D.
CT bone models collected under: NIH K01 HD042491 (P. Ludewig, University of Minnesota).

ANTERIOR AND POSTERIOR SUPRASPINATUS ACTIVATION AFFECTED BY PLANE OF ELEVATION AND PHASE OF MOTION USING INDWELLING ELECTROMYOGRAPHY

Alan C. Cudlip and Clark R. Dickerson

University of Waterloo, Waterloo, ON, CANADA

INTRODUCTION

The rotator cuff includes four muscles, and the supraspinatus is the most common site for injury initiation within this muscle group. The supraspinatus has a complex morphology, consisting of anterior and posterior regions, attaching to different sections of the supraspinatus tendon [1]. Recent research has determined that these two regions have divergent distributions of fiber types, and these regions may have different mechanical functions that are influenced by arm posture [2, 3].

Differences in activation patterns between the two regions of supraspinatus are minimally described. Previous research investigated both regions in static arm postures with a single hand load [3]. Accurate representation of differences in regional activations can elucidate recruitment strategies with increased resolution. This study quantified activation patterns of the anterior and posterior regions of the supraspinatus through different humeral ranges of motion and manual force intensities.

METHODS

15 participants [26 ± 3.7 years; 1.71 ± 0.05m height; 78.2 ± 13.1 kg body weight] completed 42 arm elevation tasks with 2 factors: plane of elevation (0/15/30/40/60/75/90°) and 3 intensities (unloaded/ 20%/40% of maximal elevation strength), each completed twice using a fixed cadence (Figure 1). Each trial consisted of one arm elevation and lowering, with 2 seconds to complete each phase of movement. Indwelling electromyography was recorded from anterior and posterior supraspinatus regions and a surface electrode over supraspinatus at 3000Hz (Noraxon Telemyo 2400 T G2), linear enveloped and normalized to muscle-specific maximal outputs. Motion capture was collected for the torso and right upper extremity using an 8 camera VICON MX20 system (VICON, Oxford, UK) at 50Hz. Kinematic analysis consisted of data filtering, marker reconstruction and local joint coordinate system reconstruction and shoulder angles were determined using ISB standards [4]. Activation levels at elevation angles were extracted in 5° increments from 5-135° for both ascending and descending motions. Multiple 2 way repeated measures ANOVAs using 4 factors (muscle region, plane of elevation, elevation angle, intensity) with each 2-way interaction examined activity changes.

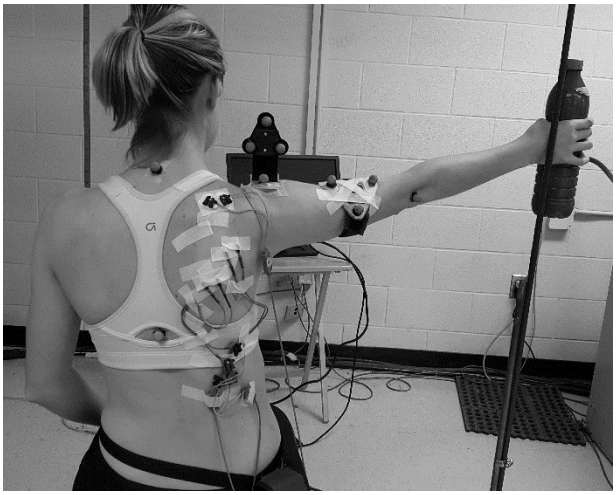

Figure 1. Arm elevation was completed at 3 hand force intensities in 7 planes of elevation.

RESULTS AND DISCUSSION

Elevation angle*Muscle region interactions were present for all EMG signals ($p<0.01$, Figure 2). All peak activations occurred during the ascending phase of motion, while posterior supraspinatus had a more consistent level of activation throughout arm elevation and depression, with standard deviations in activation that were ~50% smaller than the anterior region between 30-135° of elevation. Previous research has indicated similar persistent activation of posterior supraspinatus throughout the range of motion [3], though activation differences between these regions were smaller than previously reported.

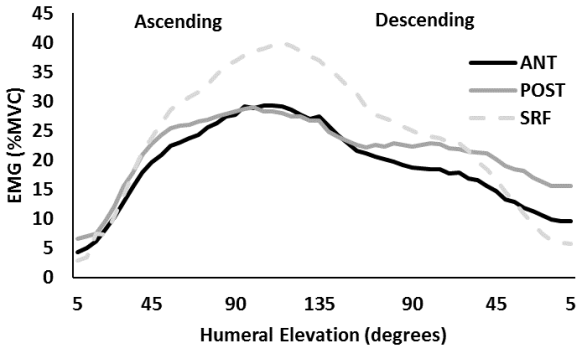

Figure 2. Elevation Angle*Muscle region effected existed ($p<0.01$), with higher elevation angles typically increasing activation.

An interaction between elevation angle and plane of elevation was present, with peak activation occurring between 90-115° in each plane, and increasing activation occurring in more sagittal planes of elevation ($p<0.01$, Figure 3). Differences between planes of elevation at the same angle ranged from 2.9 %MVC at 5° elevation to 14.3 %MVC at 55° elevation. Comparing the sagittal plane to more coronal planes of elevation consistently decreased activation at the same elevation angle, with some exceptions. The supraspinatus likely has a greater mechanical advantage in the coronal plane due to changes in 3D glenohumeral joint configurations and increasing moment arms in these postures [5].

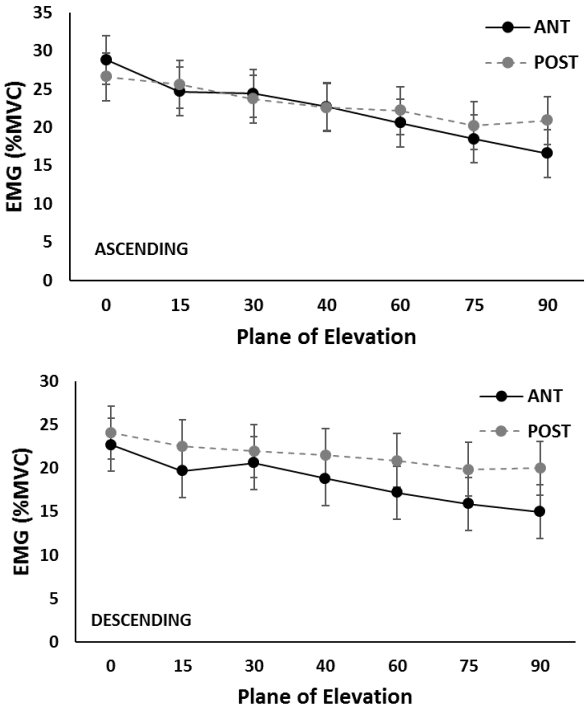

Figure 3. Plane of elevation*Muscle interactions lowered activation in more sagittal planes, and relative activations between anterior and posterior supraspinatus altered within movement phases.

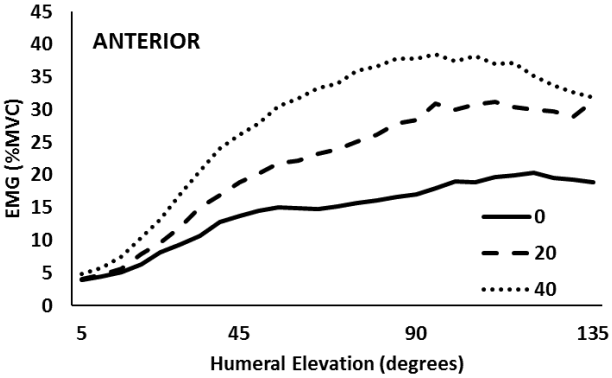

Figure 4. Angle*Load interactions ($p<0.01$) indicated greater muscle activation with increasing abduction angle and load (0/20%/40%).

Load and elevation angle interactions indicated higher elevation angles and loads increased activity by >40 %MVC ($p<0.01$, Figure 4). Muscle region and plane of elevation interactions increased activity in the anterior region in sagittal movements ($p<0.01$).

CONCLUSIONS

This research provides novel anatomical insights into supraspinatus activation across an extended shoulder range of motion. The findings from this study indicate that the supraspinatus has a complex activation pattern, and is heavily modulated by arm posture and phase of motion. Future research examining *in vivo* or *in vitro* responses of supraspinatus will need to examine the entire shoulder range of motion, as specific muscular responses are strongly influenced by posture and type of motion.

REFERENCES

1. Roh et al. *The Journal of Shoulder and Elbow Surgery,* 6(5):429-439. 2000.
2. Gates et al. *Journal of Orthopaedic Research,* 28(1):12-17. 2010.
3. Kim et al. *International Biomechanics,* 4(2):60-67. 2017.
4. Wu et al. *Journal of Biomechanics,* 38(5):981-992. 2005.
5. Kuechle et al. *Journal of Shoulder and Elbow Surgery*, 6(5):429-439. 1997.

CUMULATIVE SHOULDER IMPINGEMENT DURING FREE-LIVING MANUAL WHEELCHAIR PROPULSION

Emma Fortune, Beth Cloud, Stefan Madansingh, Meegan Van Straaten, Dennis Murphree, Kristin Zhao, Melissa Morrow

Mayo Clinic, Rochester, MN, USA
email: Fortune.Emma@mayo.edu

INTRODUCTION

The shoulder is the most common musculoskeletal pain site for manual wheelchair (MWC) users [1]. Shoulder pain can limit function and quality of life, and is often caused by rotator cuff tears and tendinopathies resulting from impingement of the supraspinatus tendon within the subacromial space [2]. Overuse is thought to be a major causal factor [3]. However, little is known regarding cumulative impingement exposure.

Wearable sensors have been used to identify WC propulsion [4]. A method using upper arm IMUs to objectively quantify MWC users' daily propulsion activity combined with estimations of shoulder impingement exposure could further the understanding of the link between MWC propulsion and shoulder impingement. This study presents data demonstrating the use of lab-based tendon impingement estimations with field-based propulsion detection to estimate cumulative supraspinatus impingement in MWC users.

METHODS

For this IRB-approved study, four MWC users with spinal cord injuries (SCIs) (29±6 yrs, injury levels T4-T6, 1 F) performed multiple MWC-related activity trials including propulsion on a ramp on rollers for 15 cycles and on level rollers for two minutes. Tri-axial acceleration data were collected from upper arm Opal IMUs (APDM Inc, USA; 128 Hz) while video data (60 Hz) and humeral and scapular kinematics (using electromagnetic sensors (Liberty, Polhemus; 120 Hz)) were collected.

Activity and peak detection algorithms were applied to the acceleration data [5] in MATLAB (Mathworks, USA). Activity cycles were identified as the acceleration data between consecutive peaks. A neural network model, with inputs of activity cycle acceleration features, was developed and validated from lab data (by video comparison) to identify propulsion activity. The supraspinatus proximity to the acromion (SPA) was calculated by determining the minimum distances between the supraspinatus tendon insertion site and the underside of the acromion using a generic reconstructed bone surface model (Fig 1). Each task's supraspinatus impingement % time was determined (Fig 2) by quantifying the % of time when the SPA was less than 5 mm [6].

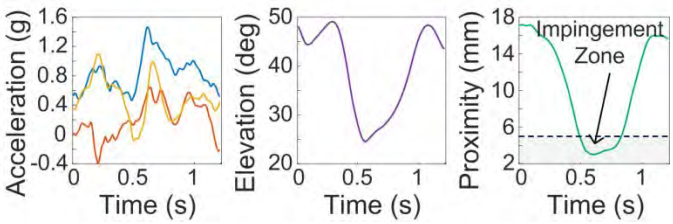

Figure 1: Right arm tri-axial acceleration, humerothoracic elevation and supraspinatus proximity to the acromion (SPA) for one propulsion cycle from a sample lab trial from subject 2.

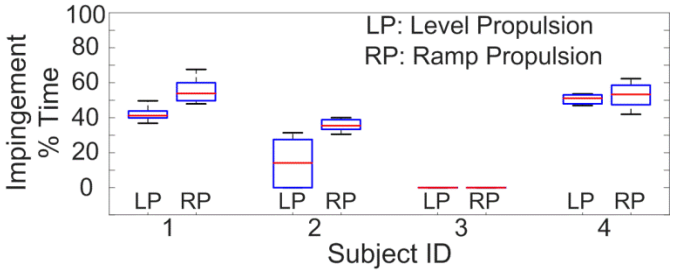

Figure 2: Supraspinatus impingement % time calculated for lab-based propulsion. Boxplots represent % time ranges across each subject's trials.

Subjects wore the IMUs for 1 to 3 days in their natural environment and propulsion time was estimated (Fig 3). Each subject's supraspinatus impingement % time during propulsion was estimated by multiplying their field-based propulsion time by their lab-based propulsion impingement % time. As the IMU algorithm cannot

yet separate level from ramp propulsion, cumulative impingement % times were calculated assuming (1) all level propulsion and (2) all ramp propulsion.

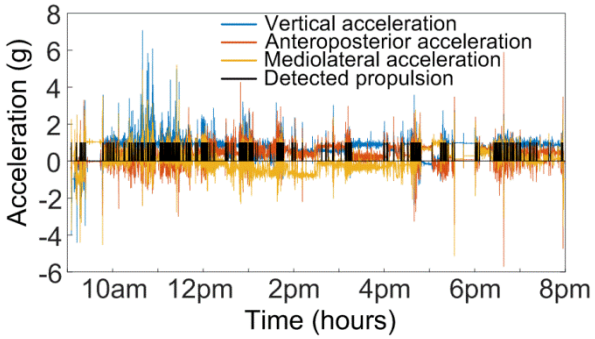

Figure 3: Right arm acceleration during a sample day for subject 2 with detected propulsion periods.

RESULTS AND DISCUSSION

The lab-derived elevation angles and associated SPA values were similar to previous reports [7]. Subjects' estimated daily propulsion time (39-88 mins), propulsion cycles (1956-4282) and associated supraspinatus impingement time (0-48 mins) are presented in Table 1. Previous WC studies have reported less than one hour of average daily wheeling time [8], which is similar to our observations. To place the impingement % time in context, in a rat shoulder overuse model, supraspinatus tendon pathology was observed in rats after 4 weeks of performing 1 hour of overuse activity for 5 days/week resulting in 7500 strides/day [9]. Based on our preliminary data, after ~60 days, MWC users would reach an equivalent number of propulsion cycles and impingement % time as in the rat study. These preliminary results highlight the potential of significant cumulative damage over multiple months of MWC use.

CONCLUSIONS

These preliminary results illustrate the potential of this method to estimate shoulder injury risk time in the field. Further, these results suggest that there is significant cumulative time spent in supraspinatus impingement from propulsion alone, and the inclusion of additional activities involving elevation and loading will further compound impingement time.

REFERENCES

1. Cooper R et al. *Team Rehab Rep,* **9**, 35-8, 1998.
2. Ludewig P et al. *Man Ther*, **16**, 33-39, 2011.
3. Soslowsky L et al. *Ann Biomed Eng*, **30**, 1057-63, 2002.
4. Nooijen C et al. *J NeuroEng Rehab*, **12**, 11, 2015.
5. Fortune E et al. *Physiol Meas*, **36**, 2519, 2016.
6. Collinger J et al. *Acad Radiol*, **16**, 1424-32, 2009.
7. Dal Maso F et al. *Manual Therapy*, **25**, 94-9, 2016
8. Sonenblum S et al. *Med Eng Phys*, **89**, 486-491, 2012.
9. Soslowsky L et al. *J Shoulder Elbow Surg*, **9**, 79-84, 2000.

ACKNOWLEDGEMENTS

Funding is provided by the Mayo Clinic Rehabilitation Medical Research Center, on behalf of the Craig H. Neilsen Fund for Spinal Cord Injury Care and Research Honoring Robert D. Brown Jr., M.D. and the NIH (R01 HD84423). CT bone models collected under: NIH K01 HD042491 (P. Ludewig, University of Minnesota).

Table 1: Number of days of field data collected, self-reported shoulder pain, tendinopathy, and mean (SD) daily propulsion cycle number, time spent in propulsion and in the risk zone (<5mm) for supraspinatus impingement % time during propulsion in cases where all propulsion occurs on level ground or all on a ramp of 5˚ incline.

Subject	Days	Shoulder Pain (past week)	Supraspinatus Tendinopathy	Number of Propulsion Cycles	Propulsion Time (mins)	Supraspinatus Impingement Time (mins)	
						Level	Ramp
1	1	No	No	4282	87.68	36.83	48.22
2	2	Yes	No	1956 (159)	32.75 (4.05)	4.58 (0.57)	11.46 (1.42)
3	3	Yes	No	2689 (1045)	47.64 (19.32)	0.00 (0.00)	0.00 (0.00)
4	2	Yes	Moderate	2349 (1486)	39.27 (22.23)	20.03 (11.34)	20.81 (11.78)

UPPER LIMB JOINT CONTROL DURING ACTIVITIES OF DAILY LIVING

[1] Meghan E. Vidt, [2] Dirk Marshall, [2] Dattaraj Sansgiri, [2] Joshua Sarbolandi, [2] Natalia V. Dounskaia

[1] Pennsylvania State University, University Park, PA, USA
[2] Arizona State University, Phoenix, AZ, USA
email: mzv130@psu.edu, web: https://sites.psu.edu/mvidt

INTRODUCTION

Upper limb function is critical for performing activities of daily living (ADL) and maintaining independence [1]. Natural, three-dimensional (3D) upper limb movement requires coordination of multiple degrees of freedom (DOF). Unconstrained movement enables DOF redundancy, allowing tasks to be completed by adoption of several different postures [2]. Understanding the ways in which healthy adults control upper limb DOF during performance of ADLs will enable future exploration of the mechanisms underlying movement control deficits in other groups, like older adults or those with a musculoskeletal injury. The goal of this study is to identify normative upper limb control strategies used by healthy adults during ADL performance.

METHODS

Fourteen ostensibly healthy, right hand dominant young adults (7M/7F, mean age 21.7±2.2yrs) were studied. Participants performed 7 ADL tasks selected to represent a variety of daily tasks and arm postures within the upper limb workspace. Tasks included: forward reach with an empty soda can, upward reach with an empty soda can to a shelf at two heights (shoulder height, eye level), empty cup to mouth, hair comb, turning a book page, pledge (right hand to left side of chest), and tooth brushing. Three trials of each task were performed and averaged. Movement of 12 passive reflective markers placed on anatomical locations on the upper limb and torso were tracked at 200Hz with 8 Kestrel motion capture cameras (Motion Analysis Corp., Santa Rosa, CA). Data was post-processed and filtered using a 6Hz low-pass 2nd order Butterworth filter using Cortex (Motion Analysis Corp., Santa Rosa, CA) software. A custom Matlab (The MathWorks, Natick, MA) program was used to calculate the kinematics and kinetics for 7 DOF (shoulder flexion/extension, abduction/adduction, internal/external rotation, elbow flexion/extension, forearm pronation/supination, wrist flexion/extension, radial/ulnar deviation) using previously reported methods [3]. Kinetics at the shoulder, elbow, and wrist were decomposed into contributions from muscle torque (MT), interaction torque (IT), gravitational torque (GT), and net torque (NT) bounded by Eq. 1.

$$NT = MT + GT + IT \quad (1)$$

The role of active control and passive factors (gravity, inter-segmental dynamics) was explored at each joint by computing the contribution of MT to NT. A two-dimensional (2D) representation of each joint's 3D torque was calculated by computing the scalar projection of MT, IT, and GT vectors upon the NT vector [2]. It was hypothesized that a leading pattern [4] would be observed across ADLs, whereby the shoulder rotates actively while the elbow rotates passively, or the elbow rotates actively while the shoulder rotates passively.

RESULTS AND DISCUSSION

Assessment of torque contributions to NT demonstrated distinct phases of shoulder and elbow control (Fig.1). Each phase is demarcated by the transition of either shoulder or elbow MT projection on NT from positive contribution (positive value) or zero contribution (negative value signifying that MT opposes NT). For example, with the hair comb task, MT contributes to NT both at the shoulder and elbow in phase 1 (cf. orange line, Fig.1A,B). During phase 2, the shoulder leads the movement actively while the elbow moves passively with MT opposing elbow movement. Both joints move passively in phase 3 (MT projection on NT is negative at both joints), and the elbow is rotated actively while the shoulder is rotated passively in phase 4.

This analysis identified three patterns of shoulder

and elbow coordination that were present in all tasks, except tooth brushing, despite the variety of movements and postures tested, supporting our hypothesis. These patterns included: 1) active shoulder rotation, passive elbow rotation; 2) passive shoulder rotation, active elbow rotation; and 3) passive shoulder rotation, passive elbow rotation. In addition, some tasks included a phase of active rotation of both the shoulder and elbow at the beginning (e.g. Fig. 1) or end of the movement, or both. These phases served to overcome gravity at the beginning of the movement or compensate for gravity at the end of the movement when the limb had to be stopped. Assessments at the wrist suggest that MT mainly compensates for passive torque to adjust wrist motion according to task requirements.

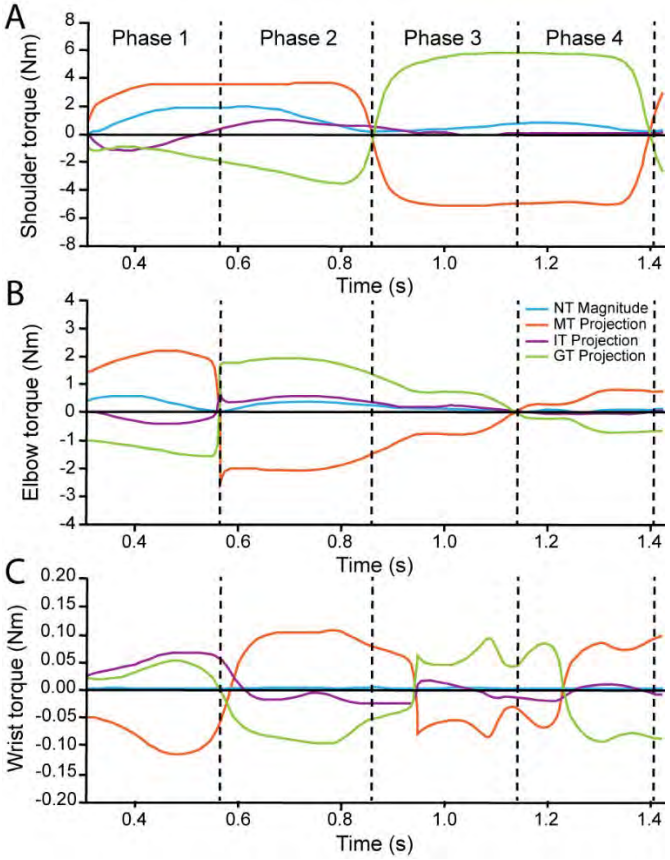

Figure 1: Torque projections at shoulder (A), elbow (B), and wrist (C) joints for hair comb task. MT (orange), IT (purple), and GT (green) vectors have been projected onto the NT vector; NT magnitude is shown in blue.

Identification of 3 shoulder-elbow control patterns, whereby at least one joint rotated passively, represent joint control primitives that direct performance of upper limb movements that are habitual. A lower prevalence of these joint control primitives was observed in ADL tasks that were less habitual, like tooth brushing; during tooth brushing, participants were asked to brush in a medial-lateral direction, which may conflict with typical tooth brushing movements used by the participant. The presence of identified control primitives suggests that the central nervous system prioritizes minimization of neural effort for joint coordination in order to reserve neural resources for other, higher-level cognitive tasks [4].

CONCLUSIONS

This study expands assessment of control mechanisms of upper limb tasks to include ADLs in 3D. Previous research of planar, line drawing tasks has identified that one joint typically leads the movement, while remaining upper limb joints follow largely passively [4]. Results have identified that despite the diversity of joint postures required across ADL tasks, 3 joint control primitives emerged for performance of unconstrained 3D tasks, supporting the leading joint theory previously proposed for planar tasks [2]. These findings suggest that healthy young adults adopt more simplified movement control strategies that rotate a single joint actively, which initiates movement at the trailing joints through mechanical coupling with IT and GT contributions. This suggests that the central nervous system prioritizes resources to other cognitive tasks during the performance of well-learned tasks, like ADLs. Ongoing work seeks to examine how identified joint control strategies change in the context of aging or musculoskeletal injury.

REFERENCES

1. Covinsky, K et al. *J Am Geriatr Soc*. **51**(4): 451, 2003.
2. Dounskaia and Wang. *J Neurophysiol*. **112**(5): 1040, 2014.
3. Hirashima, M et al. *J Biomech* **40**(4): 871, 2007.
4. Dounskaia and Shimansky. *Exp Brain Res*. **234**(6): 1335, 2016.

ACKNOWLEDGEMENTS

Support for this study was provided by an ASU-Mayo Clinic Seed Grant (Dounskaia, Vidt) and start-up funds (Vidt) from Arizona State University.

MAXIMAL VOLUNTARY ISOMETRIC CONTRACTION PRESCRIPTION FOR SUPRASPINATUS AND INFRASPINATUS REGIONS

[1] Rachel Whittaker, [1] Talia Alenabi, [2]Soo Kim, [1] Clark R. Dickerson

[1] Department of Kinesiology, University of Waterloo, Canada
[2] School of Rehabilitation, University of Saskatchewan, Canada
Email: cdickers@uwaterloo.ca

INTRODUCTION

Conventional electromyography (EMG) evaluation of supraspinatus and infraspinatus often relies on a single paired intramuscular electrode in each muscle, which assumes a singular mechanical function. However, studies have defined two architecturally distinct regions in the supraspinatus (anterior and posterior) [1] and three regions in the infraspinatus (superior, middle, and inferior) [2]; each region is also innervated by a distinct nerve branch of the suprascapular nerve [3]. EMG analysis of these muscle regions is emerging; however, a set of test exertions that generates maximal activations in all muscular regions is undefined. The purpose of this study was to quantify the activation of two anatomically distinct regions within the supraspinatus (anterior, posterior) and infraspinatus (superior and middle) during different MVIC exertions and identify optimal combinations of tests for normalizing these EMG data.

METHODS

31 right-handed healthy individuals (15 M, 16 F, age=22.5±2.5 y) participated. Information from the four regions of the infraspinatus and supraspinatus were obtained by fine wire electrodes. Participants performed 15 MVIC tests in a randomly assigned order against manual resistance. The MVIC tests selected were those recommended for normalizing shoulder EMG, or slight variations of these postures [5,6]. Each MVIC test was performed once for 5 seconds (s) and 2 minutes of rest separated tests to minimize muscle fatigue. Raw EMG signals were collected at 3000Hz.

The raw EMG data were digitally bandpass filtered using a 2nd order Butterworth filter (10-1000Hz). Then, all signals were full wave rectified and linear enveloped using a low pass filter (fc = 2Hz). The peak activation of each muscle during each MVIC trial was normalized to the maximum value across all MVIC trials (%MVIC). For each muscle, the MVICs for which activation of >90%MVIC occurred were identified. An optimal set of MVIC combinations, defined as those which elicited >90% MVIC activation in the muscles of interest in >90% of the population, were defined. These sets were identified for regions of the infraspinatus and supraspinatus muscles as well as both combined.

RESULTS AND DISCUSSION

Rotator cuff muscle activation exhibited large variability across MVICs and no single test achieved maximal activation of both regions of either the supraspinatus or infraspinatus. The highest, and lowest mean activations obtained during the MVICs ranged from 70-79% MVIC and 42-47% MVIC respectively (Figure 1). A total of 5-8 MVICs were needed to obtain >90% activation in 90% of the participant population for individual muscular regions. The criterion can be met for all 4 regions studied using a set of 10 MVICs (Table 1).

The results coincide with previous studies, indicating that a combination of MVICs are required to normalize EMG data from either a single muscle or a group of shoulder muscles across a population [4,5]. Although these studies investigated 1-3 rotator cuff muscles, none evaluated the regional activation. The current results both reiterate the importance of selecting MVICs based on the muscle(s) of interest and show that consideration of the specific muscular regions of interest is required.

High mean activity observed in both regions of the infraspinatus and supraspinatus muscles is consistent with the stabilizing role of the rotator cuff muscles

(Figure 1). In contrast to prime movers, the rotator cuff muscles are active across the large range of motion at the shoulder. The data from this study add to this construct, demonstrating that although anatomically distinct from one another, the regions of the supraspinatus and infraspinatus muscles likely share a stabilizing role at the GH joint as high levels of activation were observed across several MVICs performed in various postures.

The most important contribution is establishment of a basis for continued EMG research of the distinct regions of these muscles by outlining reliable MVIC test combinations to normalize intramuscular EMG data. Identifying the codependence or independence of muscular activation and control requires deliberate comparison of EMG from the various regions. This will help to precisely identify the overall and regional functions and contributions of these complex muscles, including providing clarification regarding proposed rotator cuff pathology pathways.

CONCLUSIONS

Robust normalization of EMG data for individual regions of the supraspinatus and infraspinatus muscles requires 5-8 MVIC exertions to generate >90% activation across 90% of the test population. Proposed combinations can reduce inter-participant variability in generating maximal activation for the several muscle partitions. To generate optimal MVIC data across all regions, a combination of 10 MVICs is required.

REFERENCES

1. Kim et al. *Clinical Anatomy*, 20, 648-55, 2007
2. Fabrizio and Clemente, *J. Bodywork Movement Therapies* 18, 228-32, 2014
3. Hermenegildo et al. *FASEB J.* 27, 745-9, 2013
4. Dal Maso et al. *APMR* 97, 1542-51, 2016
5. Schwartz et al. *J Electromyo Kines* 37, 1-8, 2017

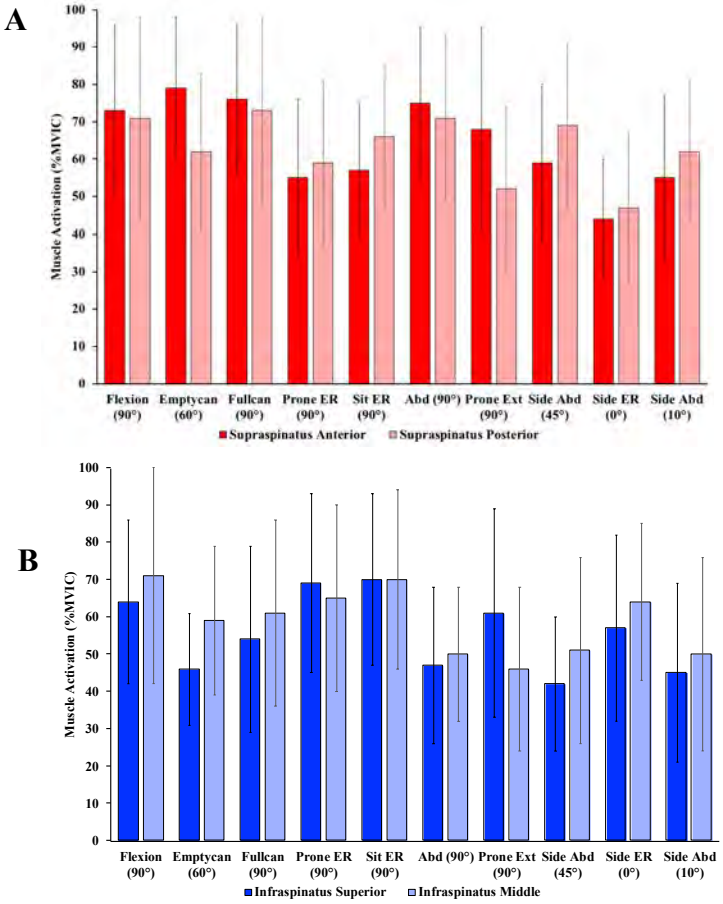

Figure 1: Mean activation (± standard deviation) of the supraspinatus (A) and infraspinatus (B) regions during MVIC exertions.

Table 1: Optimal MVICs which elicited >90% activation in >90% of the sample population for the supraspinatus anterior (SA), supraspinatus posterior (SP), infraspinatus superior (IS), and infraspinatus middle (IM). Acronyms: emptycan (EC), fullcan (FC), abduction (abd), external rotation (ER), extension (ext), flexion (flex).

	Flex (90°)	Prone Ext (90°)	EC (90°)	FC (90°)	Prone ER (90°)	Abd (90°)	Sit ER (0°)	EC (60°)	Side Abd (45°)	Side ER (0°)	Sit ER (110°)	Sit ER (90°)	Sit ER (45°)	# of MVICs
SA	×	×		×		×		×						5
IM	×		×	×	×		×						×	6
IS	×	×	×		×		×			×		×		7
SP	×	×	×	×	×	×			×		×			8
All	×	×		×	×	×	×	×	×	×		×		10

SENSITIVITY OF HIP LOADING TO PERIACETABULAR OSTEOTOMY REORIENTATION

[1]Brecca M. M. Gaffney and [1]Michael D. Harris
[1]Program in Physical Therapy, Washington University School of Medicine, St. Louis, MO, USA
email: brecca.gaffney@wustl.edu

INTRODUCTION

Developmental dysplasia of the hip (DDH) is characterized by abnormal acetabular and femoral geometries, which provide insufficient coverage and stabilization of the hip joint [1]. As a result, the mechanical loading and stress on the articular cartilage within the hip is altered, which can damage the cartilage and labrum [2]. Due to the altered hip loading mechanics, DDH is a major etiological factor of hip osteoarthritis (OA) development, which increases the risk of OA by 4.3 fold [3].

Periacetabular osteotomy (PAO) is the most common surgical treatment in the U.S. for DDH, and involves reorienting the acetabulum to provide more complete coverage of the femoral head [4]. Although PAO effectively improves short-term pain and function [4], long-term reports indicate that 71% of PAO hips progress to advanced hip OA or arthroplasty [5]. One potential explanation for the long-term inefficacy of PAO is the limited understanding of the effect of PAO on joint mechanics. Specifically, the influence of the individual degrees of freedom of PAO reorientation on hip mechanics remains unknown. Probabilistic analyses provide the most comprehensive approach for assessing the effect of input variability on biomechanical calculations [6]. Accordingly, the objective of this investigation was to determine the sensitivity of hip joint mechanics to PAO reorientation within a probabilistic framework.

METHODS

One female patient with diagnosed DDH scheduled for PAO (age: 32 years; BMI: 22.3 kg/m^2; lateral center edge angle (LCEA): -4.1°; acetabular inclination: 33.6°) participated by walking on an instrumented treadmill at a self-selected speed (1.42 m/s) while whole-body kinematics and ground reaction forces were recorded (100 Hz and 2000 Hz sampling frequencies, respectively). A subject-specific musculoskeletal model was created by scaling a model scaled to body segment dimensions and mass that included female pelvis geometry [7] and detailed hip and knee musculature [7, 8] The model was modified to include four degrees of freedom at the hip socket to simulate PAO reorientation (Fig. 1). A residual reduction algorithm was performed to improve dynamic consistency between measured external forces and the forces produced by the model by making minor perturbations to the torso center of mass and model kinematics.

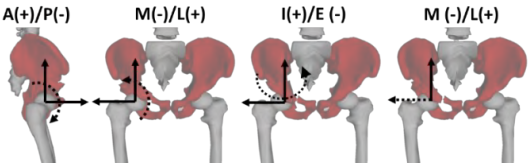

Figure 1. PAO was simulated within the musculoskeletal model by adding four degrees of freedom to the acetabulum: anteroposterior (AP) rotation, mediolateral (ML) rotation, internal/external (IE) rotation, and ML translation. Dashed line indicates positive direction for each DOF.

The sensitivity of hip joint reaction force (JRF) to PAO reorientation was assessed using a Monte Carlo (MC) simulation with 2,000 iterations. Within each MC iteration, each degree of freedom was randomly perturbed relative to the hip joint center within bounds specified within the model: AP rotation [-30° to 30°]; ML rotation [-20° to 30°]; IE rotation [-20° to 30°]; ML translation [-3 mm to 3 mm]. Hip mechanics (muscle forces and joint reaction forces) were determined within each MC iteration using static optimization and joint reaction analysis. The range of hip mechanics were estimated using 0.5 and 99.5% confidence bounds (99% probability the value lies between the bounds). The timing of peak hip resultant JRF during early stance (JRF1: ~14% gait cycle) and late stance (JRF2: ~47% gait cycle) were determined. Sensitivity factors between peak hip mechanics in each direction at JRF1 and JRF2 and each degree of freedom of PAO reorientation were calculated using correlation factors.

RESULTS AND DISCUSSION

Confidence Bounds: Acetabular orientation had a larger influence on hip JRF in the superoinferior (SI)

and AP directions than the ML direction during both the stance (0-61% gait cycle) and swing period (62-100% gait cycle), as indicated by the differences in bound sizes (Fig. 2). As an example, the maximum bound size of the SI hip JRF was 506.4 N (79.1% BW) and the maximum bound size of ML hip JRF was 216.5 N (33.8% BW).

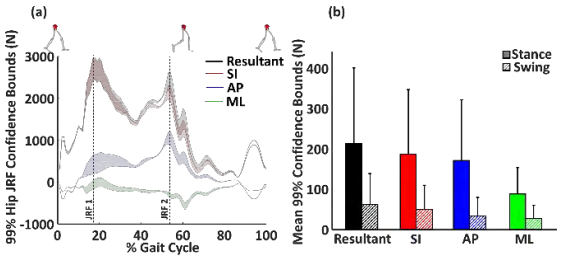

Figure 2. (a) Ensemble average and (b) mean ± 1SD of 99% hip JRF confidence bounds.

Sensitivity Factors: During early stance (JRF1), hip JRF was moderately ($0.5 \leq r \leq 0.75$) sensitive to socket ML and IE rotation (Fig. 3). Specifically, these results indicate that as the lateral rotation of the socket is increased, the magnitude of the resultant hip JRF during early stance is decreased ($r = -0.64$). This finding is of particular interest given DDH is most commonly diagnosed using the lateral coverage of the femoral head (LCEA), making this degree of correction one of the most common in PAO. During late stance (JRF2), the hip JRF was strongly ($r \geq 0.75$) sensitive to AP socket rotation (Fig. 3). Specifically, in late stance when the hip is in extension, the hip joint reaction force in the anterior direction is increased as the orientation of the socket becomes more anteriorly rotated. As the anterior rotation of the socket is increased, the length and moment arm of the rectus femoris is decreased, thus reducing the active force generating capabilities of this muscle, which is associated with an increase in anterior joint reaction force [9]. As a result, the optimization criterion increased recruitment in hip surrounding hip flexors (psoas and iliacus) in order to restore muscle balance within the hip joint. Conversely, because degenerative changes are often observed in the anterosuperior acetabulum prior to surgery, patients with DDH adopt pain avoidance movement compensations to shift joint loading away from this region. The increase in JRF following anterior socket reorientation may indicate that the hip joint is more suitable to support loading patterns more consistent with healthy normal patterns (i.e. normal hip extension).

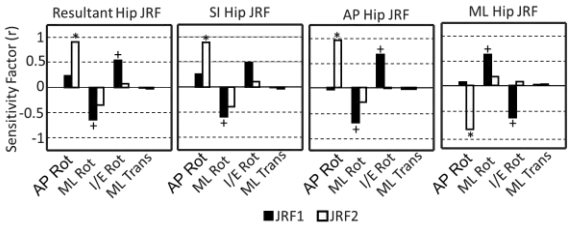

Figure 3. Sensitivity factors correlated between peak hip JRF (JRF1 and JRF2) and acetabular orientation. * Indicates strong correlation ($r \geq 0.75$) and + indicates moderate correlation ($0.5 \leq r \leq 0.75$). Sensitivity factors were calculated with a level of significance of $p \leq 0.05$ and considered statistically significant of the 95% confidence interval did not cross zero.

CONCLUSIONS

A musculoskeletal modeling analysis of the impact of simulated PAO on hip joint reaction force identified the AP alignment of the socket to have the greatest impact on the magnitude and direction of hip JRFs throughout the entire stance period. Furthermore, lateralization of the socket orientation was associated with a decrease in hip JRF. Socket position has a direct effect on muscle moment arms and lines of action because it alters their position relative to the hip joint center. Understanding the sensitivity of the hip joint reaction force to specific alignment can be used to help facilitate optimal alignment of the acetabulum to reduce or shift the hip JRF in patients with DDH. Future work will implement input distributions based on the degree of PAO orientation, and their associated change on hip joint center location, taken from post-operative radiographs.

REFERENCES

1. Cooperman, *Clin Orthop Relat Res.* 175, 1983.
2. Clohisy, *Clin Orthop Relat Res.* 467(1), 2009.
3. Reijman, *Arthritis Rheum*. 52(3), 2005.
4. Clohisy, *J Bone Joint Surg*. 87(2), 2005.
5. Lerch, *Clin Orthop Relat Res.* 475(4), 2017.
6. Laz, *Proc Inst Mech Eng*, 224(8), 2010.
7. Shelburne, *Trans Annu Meet Orthop Res Soc*, 0149, 2010.
8. Ackerman, *Proc IEEE,* 86(3), 1998.
9. Navacchia, *J Orth Res*, 34(9), 2016.
10. Valente, *J Biomech,* 46(13), 2013.

ACKNOWLEDGEMENTS

This project was supported by the National Institutes of Health (Grant No. T32 HD007434 and P30AR057235).

ASSOCIATION OF WALKING SPEED WITH GAIT MECHANICS FOLLOWING TOTAL ANKLE ARTHROPLASTY

[1,2] Robin Queen, [1]Kristen Renner, [1]Jiafeng Zhu, and [1]Laura Sands

[1] Virginia Tech, Blacksburg, VA, USA
[2] Department of Orthopaedic Surgery, Virginia Tech Carilion School of Medicine, Roanoke, VA, USA
email: rmqueen@vt.edu, web: https://www.beam.vt.edu/granatalab/

INTRODUCTION

Walking speed has been determined to be an excellent predictor of physical performance and function in older adults [1]. Walking speed in healthy control subjects has been strongly correlated with most kinematic and kinetic variables including range of motion (ROM), joint angles, ground reaction forces and joint moments [2]. In older adults, certain walking speed cut-offs have been determined in order to be able to determine patient safety with various ambulatory tasks. In order to be able to be considered a safe community ambulator, patients need to achieve a walking speed of 0.8 m/s [3], while those who are able to walk at 0.9 m/s or greater are able to safely complete housework independently [4]. Finally, patients who are able to walk at 1.1m/s are able to successfully and safely carry groceries and complete light yard work [5], while being able to walk at 1.3m/s or faster is an indication of patients being able to cross the street safely [3].

Total ankle arthroplasty (TAA) is a surgical option for the treatment of end-stage ankle osteoarthritis (A-OA). A-OA has been associated with limitations in gait mechanics and walking speed and previous work has indicated that following TAA walking mechanics and walking speed are not returned to the level of age matched controls [6]. Therefore, the purpose of this study was to determine whether TAA patients are able to achieve walking speed benchmarks by one year post-TAA as well as determining what biomechanical measures are correlated with walking speed and finally determining gait mechanics cut-offs that predict the ability for TAA patients to achieve a 0.9m/s walking speed post-TAA.

METHODS

A prospective, pretest/posttest mixed model cohort study was completed during which 197 patients were assessed prior to surgery as well as 1 year following surgery (**Table 1**). Patients were included in this study if they had unilateral A-OA, were able to walk without the use of an assistive device. All patients provided informed written consent prior to participation in this study.

Table 1: Patient Demographics

	Male (n=90, 45.7%)	Female (n=107.54.3%)
Age at Surgery	63.13 ± 8.85	61.73 ± 9.94
Height (m)	1.78 ± 0.7	1.64 ± 0.6
Weight Pre (kg)	90.94 ± 14.96	81.03 ± 18.93
Weight 1yr (kg)	90.78 ± 15.37	81.07 ± 18.67
Surgical Side	R: 40, 44.4% L: 50, 55.6%	R: 58, 54.2% L: 49, 45.8%

Each patient then completed a standard gait assessment with a modified Helen-Hayes marker set using an 8 camera motion analysis system (120Hz) (Motion Analysis Corporation, Santa Rosa, CA) and 4 embedded force plates (1200Hz) (AMTI, Watertown, MA) [6]. Seven barefoot walking trials were collected at a self-selected walking speed with a focus on the surgical limb. Visual 3D (C-Motion, Bethesda, MD) was used to calculate joint kinematics and kinetics. Matlab (Mathworks, Natick, MA) was then used to identify variables of interest including: ankle ROM (A-ROM), peak plantar flexion (PF) moment (Nm/kg), peak plantarflexion (PPF) angle, peak PF power (W/kg), peak weight acceptance (WA-vGRF) and peak propulsive vertical ground reaction forces (P-vGRF).

Correlations between the biomechanical variables of interest and walking speed at 1 year post-TAA was completed using the statistical package R ($p<0.05$ considered significant). Finally, ROC curves were generated to determine the biomechanical outcomes 1 year post-TAA that predict the ability to achieve a 0.9m/s walking speed. Variables with an area under the curve (AUC) >0.8 are considered to have good to excellent prognostic value for the outcome, in this cases a walking speed of 0.9 m/s.

RESULTS AND DISCUSSION

Of the 197 patients, 91.8% achieved a walking speed of at least 0.8 m/s, 85.3% were able to walk at 0.9m/s or greater, 65.0% walked at 1.1 m/s or greater, while only 24.4% achieved a walking speed of 1.3 m/s. Many of the biomechanical variables were correlated 1 year following TAA, however, most of these variables were weakly correlated with the exception of the peak PF moment and the propulsive vGRF. Following TAA, A-ROM was correlated with PPF, and peak PF power, while peak PF moment was correlated with peak PF power, WA-vGRF and P-vGRF. Finally, peak PF power was correlated with WA-vGRF and propulsive vGRF, while, the WA-vGRF and the P-vGRF were also weakly correlated. All variables of interest, except for A-ROM, were weakly correlated with walking speed at 1 year post-TAA (**Table 2)**.

ROC curves were generated for each biomechanical variable to determine cutoff values that needed to be achieved in order to achieve a post-TAA walking speed of 0.9 m/s (**Figure 1)**. The area under the curve (AUC) was used to determine excellent, good, fair and poor ability to predict who could achieve a walking speed of 0.9m/s. The peak PF moment and WA-vGRF demonstrate good AUC results, while the P-vGRF and peak PF power have fair results (**Table 2)**.

The results of this study indicate that following TAA, less than 32% of patients are able to achieve a walking speed of 1.27±0.2 m/s during over ground ambulation, the average walking speed for age matched healthy older adults [7].

In addition, the associations between walking speed and gait mechanics that have been typical in healthy controls do not appear to apply when examining TAA patients, therefore, we cannot assume that changes in specific mechanics will drive changes in walking speed as we are looking to develop post-TAA interventions. For example, A-ROM has been associated with walking speed in healthy control subjects [2], while there is no correlation between these two measures in TAA patients. These patients use varying compensatory patterns to control pain and deal with limited joint motion. This variability could account for some of the challenges in finding measures with good sensitivity and specificity to predict post-TAA walking speed. Therefore, additional measures such as symmetry and proximal joint mechanics should be investigated.

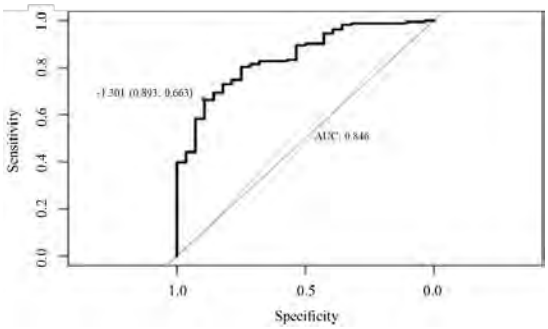

Figure 1: Sample ROC curve results for peak PF moment with a good AUC.

CONCLUSIONS

Associations between walking speed and gait mechanics are affected by pathology and therefore when developing intervention strategies in these populations we cannot assume that changing specific mechanics will change walking speed based on the associations that are present in healthy control subjects.

REFERENCES

1. Middleton et al. *J Aging Phys Act.* 23(2):314-322, 2015.
2. Cech, D. Functional Movement Development across the Life Span. 3rd Edition: 288-308, 2012.
3. Perry et al. *Stroke*. 26(6): 982-989, 1995.
4. Ainsworth et al. *Med Sci Sports Exerc.* 43(8):1575-1581, 2011.
5. Studenski. *J Nutr Health Aging*. 13(10):878-880, 2009.
6. Queen et al. *Foot Ankle Int*. 33(7): 535-542, 2012.
7. Watt et al. *Clin Biomech*. 25: 444-449, 2010.

Variable	Mean (SD)	Correlation		ROC Analysis			
		R	p-value	Cutoff Value	AUC	Specificity	Sensitivity
Range of Motion (deg)	13.77 (4.13)	0.08	0.28	14.16	0.66	0.82	0.53
Peak PF Angle (deg)	-5.97 (4.31)	-0.16	0.03	-3.83	0.63	0.54	0.74
Peak PF Moment, Nm/kg*	-1.34 (0.27)	-0.48	<0.001	-1.30	0.85	0.89	0.66
Peak PF Power, W/kg+	-0.58 (0.28)	-0.24	<0.001	-0.43	0.72	0.68	0.71
WA vGRF, BW*	1.05 (0.09)	0.58	<0.001	1.03	0.81	0.96	0.61
Propulsive vGRF, BW+	1.03 (0.08)	0.31	<0.001	1.02	0.73	0.93	0.55

Table 2: Correlation of 1yr post-op variables of interest to walking speed 1yr post-TAA and ROC analysis walking speed of 0.9m/s 1yr post-TAA (*good AUC, + fair AUC)

HOW DOES INTERNAL-EXTERNAL ROTATION OF THE FEMORAL COMPONENT IN TKA CHANGE PATELLOFEMORAL BIOMECHANICS DURING STAIR ASCENT?

[1] Joshua D. Roth, [1] Colin R. Smith, and [1] Darryl G. Thelen
[1] University of Wisconsin-Madison, Madison, WI, USA
email: jdroth2@wisc.edu web: http://uwnmbl.engr.wisc.edu/

INTRODUCTION

Up to 25% of patients are not satisfied after mechanically aligned (MA) total knee arthroplasty (TKA). One of the common sources of dissatisfaction is post-operative pain[1]. For example, the incidence of anterior knee pain is approximately 8%[2]. While anterior knee pain is a multifactorial problem, internal-external (I-E) rotation of the femoral component is an important intraoperative factor due to its effect on the trochlear groove location and resulting patellofemoral mechanics. Anterior knee pain may arise when an abnormally placed groove alters patellofemoral (PF) motion, giving rise to elevated ligament tension (e.g. the medial, mPFL, and lateral, lPFL, patellofemoral ligaments, also known as medial and lateral retinaculum) and/or elevated PF contact forces.

Accordingly, the objective was to determine how sensitive the tension in the mPFL and lPFL and PF contact forces are to I-E malrotation of the femoral component during stair ascent, which is an activity that often exacerbates anterior knee pain.

METHODS

TKA was virtually performed on a validated, multibody model of the knee[3]. This model included 6 degree-of-freedom tibiofemoral and patellofemoral joints, elastic foundation contact, and bundles of nonlinear spring elements to represent the ligaments. Components were aligned to restore the native joint lines (i.e., kinematically aligned) in the reference rotation because it most closely restored the native anatomy. To account for different alignment targets and possible surgical errors, the I-E malrotation of the femoral component was randomly varied from the reference alignment, which was parallel to the posterior femoral joint line, based on a uniform distribution between ±16°[4] (Figure 1). To account for variability in the soft tissue properties between patients, the stiffness and resting length of the soft tissue restraints of the knee were also randomly varied[5] (Figure 1). This knee model was incorporated into a lower extremity musculoskeletal model with 35 muscles spanning the hip, knee and ankle[6].

Using a high throughput computing grid, a total of 1000 probabilistic simulations of stair ascent were performed with variable I-E malrotation of the femoral component and variable soft tissue

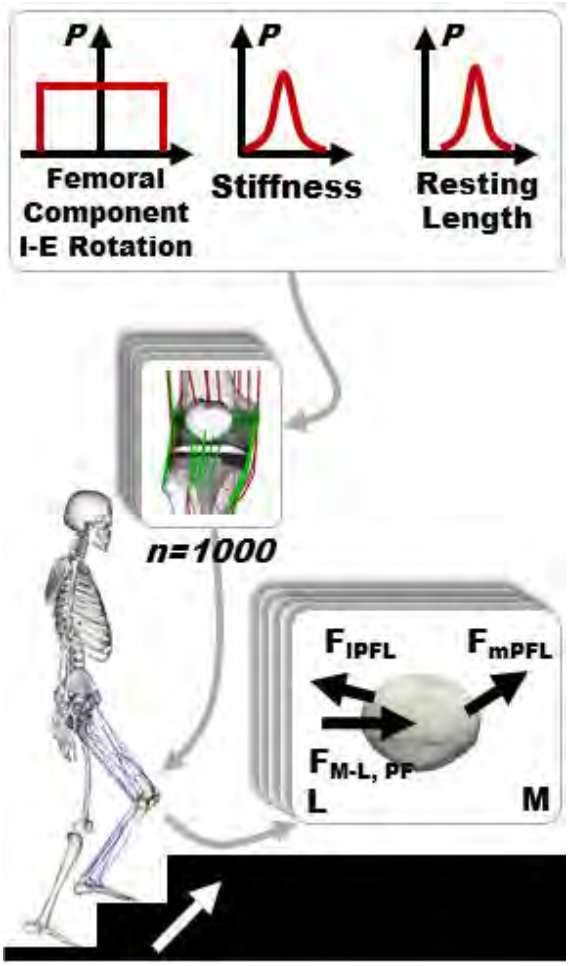

Figure 1. Schematic provides overview about how internal-external (I-E) malrotation of the femoral component along with ligament properties were varied to study the effect of I-E malrotation of the femoral component on patellofemoral biomechanics.

properties. The Concurrent Optimization of Muscle Activations and Kinematics (COMAK) simulation routine was used to calculate the muscle forces and internal knee mechanics needed to generate measured whole body dynamics and ground reactions at each frame of /motion[5].

At peak patellar contact during stance (25% stance, knee flexion = 45°), linear regression was used to assess the sensitivity of (1) the tension in the mPFL and lPFL and (2) the medial-lateral (M-L) component of the patellar contact force to I-E malrotation of the femoral component. Because the mPFL and lPFL became slack over some range of the I-E malrotations of the femoral component, the regressions were performed over the range where the structure was engaged.

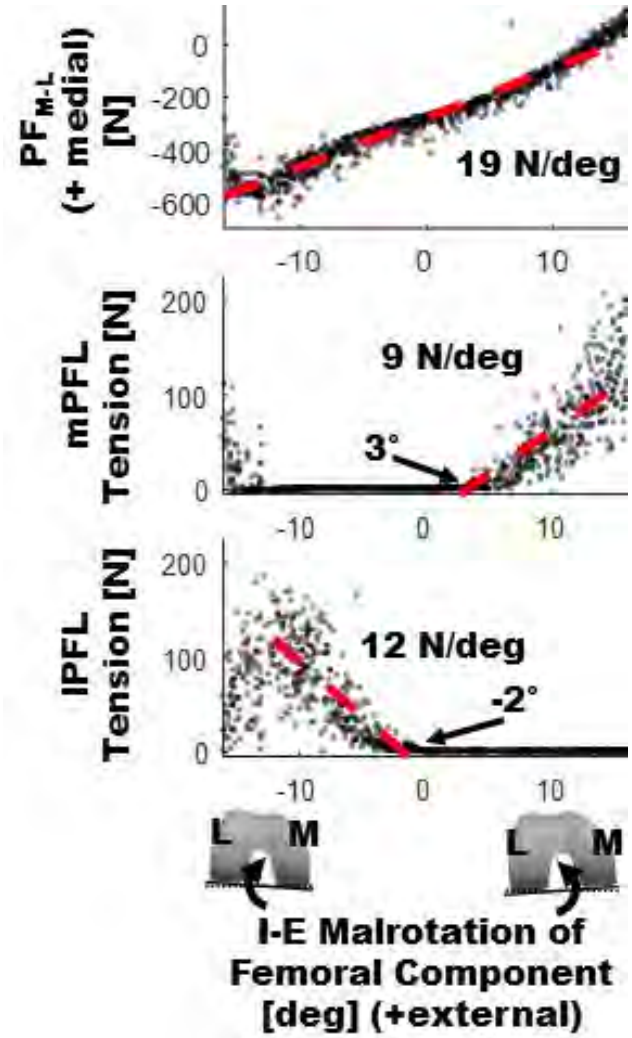

Figure 2. Scatter plots show the sensitivities of the M-L component of the PF contact force (PF_{M-L}), mPFL tension, and lPFL tension to the FC I-E malrotation.

RESULTS AND DISCUSSION

Tension in the mPFL and lPFL and the M-L component of the PF contact force were all highly sensitive to I-E malrotation of the femoral component. External malrotation decreased the M-L component of the PF contact force (19 N/deg, r^2 = 0.8), but engaged the mPFL starting at 3° of external malrotation (9 N/deg, r^2 = 0.7). Internal malrotation both increased the M-L component of the PF contact force and engaged the lPFL starting at 2° of internal malrotation (12 N/deg, r^2 = 0.7). Beyond 12° of internal malrotation, lateral subluxation of the patella began to occur, which is reflected by a drop in the lPFL tension and an increase in mPFL tension.

A major strength of the proposed computational approach is the ability to determine a tolerance for I-E rotation of the FC that results in tolerable tissue loads. These findings indicate that I-E rotations closer to the native posterior femoral joint line might reduce the risk of elevated tensions in the mPFL and lPFL and elevated PF contact forces. Our future work will incorporate variables such as femoral component design, patellar component thickness, and q-angle into our analyses.

CONCLUSIONS

We found high sensitivities of PF biomechanical metrics to I-E malrotations of the femoral component, which is important given that the rotational variability we considered reflects the ranges observed surgically. Moving forward, our probabilistic framework holds promise to determine causal links between I-E rotation of the femoral component and post-operative anterior knee pain to complement clinical observational studies.

REFERENCES

1. Nashi, Knee Surg Sports Traumatol Arthrosc, 2015. **2.** Petersen, Int Orthop, 2014. **3**. Lenhart, Ann Biomed Eng, 2015. **4.** Siston, J Bone Joint Surg Am, 2005. **5.** Smith, J Biomech Eng, 2016. **6.** Arnold, Ann Biomed Eng, 2010.

ACKNOWLEDGEMENTS

THINK Surgical Inc., NIH (5 T32 AG 213-26)

BIOMECHANICAL EVALUATION OF MINIMALLY INVASIVE STABILIZATIONS OF PELVIS WITH ACETABULAR LESION

[1] Sean M Tutton, [1]David M King, [1]William B Lea, [1]John C Neilson,
[1]D Ian English, [2]Sebastian Schafer, [2]Randolph M Setser, [1,3]Mei Wang
[1] Medical College of Wisconsin, [3]Marquette University, Milwaukee, WI, USA
[2] Siemens Healthineers, Hoffman Estates, IL, USA
email: meiwang@mcw.edu

INTRODUCTION

Osteolytic metastatic lesions frequently occur around the acetabulum in cancer patients and can cause structural weakening of the pelvis, leading to pathologic fractures. Acetabular reconstruction through minimally invasive percutaneous techniques has demonstrated clinically efficacy, allowing most patients to achieve full weight-bearing status [1, 2]. Biomechanically, little is known of the effectiveness of these procedures in restoring stability and strength to the pelvic segment during load-bearing activities. The purpose of this study was to evaluate the biomechanical behaviors of three distinct methods of percutaneous acetabular stabilization in the setting of lytic metastatic disease.

METHODS

A customized composite hemipelvis model based on an actual patient's CT-scans was created for this study (Pacific Research Laboratories, Vashon, WA). The model contained a 13 ml defect in the medial and superior acetabulum partially involving the medial and superior acetabular walls consistent with a Harrington type III [3]. Ten identical models were assigned to four study groups: 1) cementoplasty (n=2), 2) percutaneous screws fixation (n=2), 3) cement-augmented percutaneous screws fixation (n=2), and 4) untreated control (n=4). With the aid of a soft tissue torso surrogate, models were stabilized using minimally invasive, fluoroscopically guided percutaneous techniques [1]. For group 1, a cement cannula was advanced into the lesion from a posterior superior iliac spine (PSIS) access site. For group 2, an 8.0x155 mm cannulated, partially threaded ischial screw (Stryker, Asnis III) was placed from an ischial access superiorly through the posterior column and a second 8.0x150 mm posterior-anterior (PA) screw was placed from a PSIS access anteriorly, through the lesion, to the anterior inferior iliac spine (AIIS), bridging the anterior and posterior columns. For group 3, identical screws were placed, with cement injected into the lesion through the PA screw prior to advancing it into the AIIS (Fig.1).

Figure 1: CT-images showing screws trajectories.

Compressive load-to-failure tests were conducted on a servo hydraulic loading frame (MTS Landmark 370, MTS Systems, Eden Prairies, MN). Dental cement was used to pot the iliac wing in a configuration that mimics single-leg support of the mid-stance phase of a gait with 15-degree flexion and 10-degree adduction of the hip. Lateral shift of 5cm was added to the loading point to simulate the lateral displacement of the pelvis as the center of gravity moves closers to the stance leg. A fourth-generation composite femur (proximal half) with good fit to the acetabular socket of the hemipelvis was used to deliver the load to the acetabulum (Fig.2).

Load-to-failure tests were carried out in a series of displacement-controlled ramp loading and unloading runs with incremental displacement, until a failure was observed. Based on pilot tests, displacement steps of 3mm, 7mm, and if needed 10mm were selected. The loading rate was kept at a quasi-static rate of 0.1mm/sec. The axial force and displacement data were measured using MTS built-in loadcell and LVDT sensor and recorded at 100Hz. Yield force, maximum axial deformation, and fixation stiffness

were obtained from the load-displacement plot. Linear regression analysis and Dunnett's test were used to assess the effects of stabilization procedure in comparison to the non-treated controls ($p<0.05$).

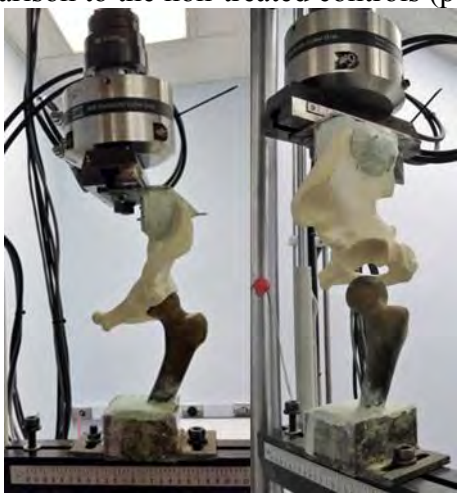

Figure 2: Testing setup.

RESULTS

The ultimate strength of cementoplasty group was the highest, at 4022±1032N, and was 46% higher than the non-treated control ($p=0.048$). Augmented screws fixation was a close second, at 3778±125N, and 37% higher than the control ($p=0.10$). Screws only group was at the same level as the control. Similar pattern was observed with yield strength (Fig.3). All three treatments improved axial stiffness of the hemipelvis, with the highest stiffness from augmented screws fixation, at 1061±123N/mm and was 45% stiffer than the control ($p=0.055$). The improvement in stiffness over the non-treated control was 24% in cementoplasty and 15% in screws fixation ($p>0.10$).

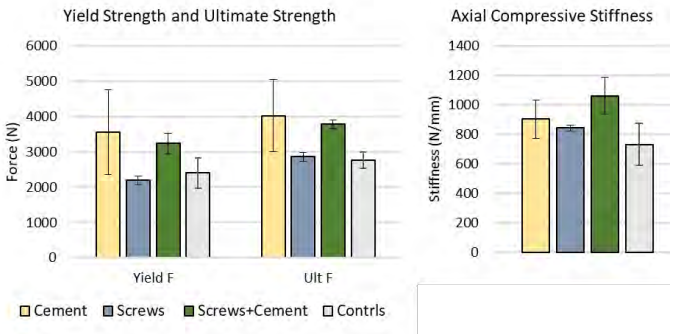

Figure 3: The mean (sd) strengths and stiffness of the three treatment groups and non-treated control.

When visually examining post-test acetabular fracture patterns, it was noted that fractures were initiated at the acetabular dome near the site of lesion and propagated anteriorly to split the acetabular rim. A slight difference was that multiple crack lines formed near the lesion in the non-treated controls, causing partial collapse through the lesion. While in the treated groups, especially ones with cementing, a single crack line ran through center of the dome. However, protrusion of the femoral head was not observed in any of the specimens.

DISCUSSION

Augmented screws fixation demonstrated the highest stability under single-leg weight bearing condition and the least deformation at failure point compared to the other fixation methods. Both cementoplasty and augmented screw fixation were able to restore the axial strength of the hemipelvis to withstand forces up to 5-times of average bodyweight. Screw fixation without cement augmentation showed improvement in stability but not in strength. Findings from the study suggest that percutaneous cement injection improves weight bearing strength by effectively filling the bone defect to prevent collapse of the acetabular wall, while greater segmental stabilization of the pelvis is achieved with screw fixation of the anterior and posterior columns of the acetabulum.

This study was the first to use a customized composite model for biomechanical comparison of percutaneous pelvic stabilization techniques for lytic acetabular metastases. While the loading scenario was simple and quasistatic and sample sizes are limited, consistency in mechanical behaviors was demonstrated, suggesting a reasonable model to evaluate more complex stabilization techniques.

REFERENCES

1. Hartung et al. *J Vasc Interv Rad* 27:682-8, 2016.
2. Cazzato et al. *Cardiovasc Intervent Radiol* 39: 1455-63, 2016
3. Harrington et al. *J Bone Joint Surg [Am]* 63-A:653-64, 1981.

ACKNOWLEDGEMENTS

This study was supported by a research grant from Siemens Healthineers. The concepts and information presented in this paper are based on research and commercial availability cannot be guaranteed.

IS KNEE BIOMECHANICS DIFFERENT DURING UPHILL WALKING OF DIFFERENT SLOPES BETWEEN OLDER ADULTS WITH AND WITHOUT TOTAL KNEE REPLACEMENT?

[1]Chen Wen, [2]Harolds E. Cates, [1]Songning Zhang
[1]Biomechanics/Sport Medicine Lab, The University of Tennessee, Knoxville, TN, USA
[2]Tennessee Orthopedic Clinics, Knoxville, TN, USA

INTRODUCTION

Uphill walking is an inevitable part of daily living and causes higher knee joint loading compared to level walking [1]. Previous gait analyses during uphill walking have only focused on young healthy populations [2,3]. Currently, no studies have explored knee kinematics and kinetics for uphill walking in total knee replacement (TKR) patients. Furthermore, uphill walking has been integrated into rehabilitation protocols after TKR surgery [4]; therefore, a comprehensive biomechanical analysis of its benefit for this population is warranted. The purpose of this study was to compare knee biomechanics of the replaced limb to the non-replaced limb of TKR patients and healthy controls during walking on level ground and inclined surfaces of 5°, 10° and 15°. The information from such a study may help physical therapists creating appropriate rehabilitation protocols and optimizing total knee prosthesis designs.

METHODS

Twenty-five TKR patients were recruited from a local orthopedic clinic (68.8 ± 4.9 years, 1.70 ± 0.11m, 83.2 ±15.6 kg, 22.1 ± 11.72 months since surgery). The inclusion criteria for TKR patients were having a unilateral total knee replacement (conducted by a single surgeon) between 6 months and 60 months and between the ages of 50 and 75 years. Potential participants were excluded if they had any additional lower extremity joint replacements, any additional diagnosed osteoarthritis (OA) of the hip or ankle, severe OA at the contralateral knee of TKR, BMI greater than 38, or neurological diseases. Ten older adults between the ages of 50 and 75 years without any lower extremity pathology participated in the study as healthy controls (69.1 ± 4.5 years, 1.74 ± 0.12 m, 75.0 ± 23 kg).

Three dimensional (3D) kinematic data were collected using a 12-camera motion capture system (240 Hz, Vicon). A customized instrumented ramp system consists of a walkway that is 1 m wide and 3 m long and with two separate walking surfaces/structures bolted on to two force platforms (1200 Hz, AMTI). The inclined angle of ramp surfaces can be adjusted to 5°, 10° and 15°. Gait speeds were monitored by two sets of photocells and two electronic timers (Lafayette Instrument Inc.), placed 3 meters apart for level walking, and 1.5 meters apart at shoulder height for ramp walking. Visual 3D (C-Motion) was used to compute 3D kinematics and kinetics. Kinematic and GRF data were smoothed at a cutoff frequency of 8 Hz using a fourth-order zero-lag Butterworth low-pass filter. All joint moments were computed as internal moments.

A 2 x 2 x 4 (limb: replaced, non-replaced limb x group: TKR and healthy controls x incline slope: 0°, 5°, 10° and 15°) mixed model ANOVA was used to examine the interactions and main effects of selected dependent variables ($p<0.05$, SPSS 24.0). When the ANOVA showed a significant three-way interaction, two-way ANOVAs were followed. When two-way ANOVAs showed significant interaction or main effect, post-hoc comparisons with Bonferroni adjustments were used to detect differences between limbs and slopes.

RESULTS AND DISCUSSION

There were no differences of age, height, and mass between TKR and healthy groups. TKR patients had greater BMI than healthy controls ($p=0.014$). Participants walked significantly faster on level ground than on 5°, 10° and 15° ramp, respectively ($p<0.002$). No differences of speed in all slope conditions were found between TKR and healthy groups.

A significant limb×slope×group interaction was detected in knee extension range of motion (ROM) ($p=0.01$, Table 1). In follow-ups, a significant limb×slope interaction was found for TKR patients

(p=0.015) and a significant slope×group interaction for replaced limb (p=0.019). Post hoc comparisons showed that non-replaced knees had greater extension ROM than replaced knees in 10° uphill walking (p=0.049). Knee extension ROM increased significantly as the incline angle increased in both TKR replaced and non-replaced limbs and both limbs of healthy controls (p<0.002 for all comparisons). Both TKR replaced and non-replaced limbs had smaller knee extension ROM than their respective matched limbs of healthy controls in all uphill conditions (p<0.016).

Significant limb×slope interaction (p=0.006), group (p=0.019) and limb (0.008) main effects were found for peak knee extension moment (KEM, Table 1). In replaced limbs, the peak KEM was greater in 15° compared to level and 5° uphill walking (p<0.012) and was greater in 10° compared to 5° uphill walking (p=0.002). In TKR non-replaced limbs, the moment was greater in 15° uphill compared to level walking, 5°, and 10° uphill walking respectively (p<0.009 for all comparisons). The moment was also greater in 10° compared to level and 5° uphill walking, respectively (p<0.001 for all comparisons). It was also smaller in replaced limbs compared to non-replaced limbs in 10° (p=0.002) and 15° (p<0.001) uphill walking. TKR patients had lower peak KEM than healthy controls (p<0.021). A significant slope main effect was observed for peak loading-response knee abduction moment (KAbM, p=0.009, Table 1). The peak loading-response KAbM was greater in level walking compared to 10° (p=0.013) and 15° (p=0.003) uphill walking.

The results from this study demonstrated that TKR patient had lower knee extension ROM and peak KEM than healthy controls during uphill walking. In addition, knee extension ROM increased significantly as the incline angle increased. The peak KEM was greater in uphill walking compared level uphill walking. The peak loading-response KAbM was greater in level walking compared to uphill walking. Uphill walking may have the potential to become a safe rehabilitation exercise for unilateral TKR patients. But it should be avoided walking on a 10° or steeper slope in rehabilitation exercises.

REFERENCES

1. Alexander N, Schwameder H. (2016). *Gait Posture*, **45**:137-42.
2. Lay AN, Hass CJ, Gregor RJ. (2006). *J Biomech*., 39(9):1621-8.
3. McIntosh AS., et al. (2006). *J Biomech*., 39(13):2491-502.
4. Meier W, et al. (2008). *J Orthop Sports Phys Ther*. 38(5):246-56.

Table 1. Selected knee kinematics (°) and moments (Nm/kg) during uphill walking (mean ± stdv).

Variable	Group	Limb	0°	5°	10°	15°
Knee extension ROM $^{\wedge YZ}$	TKR	Replaced	-	4.4±6.6$^{\& bc}$	17.3±7.8$^{\& c}$	29.8±6.8$^{\&}$
		Non-replaced	-	3.9±6.1$^{\& bc}$	19.8±8.0$^{\&\$ c}$	31.5±7.6$^{\&}$
	Healthy	Limb one	-	10.9±6.8	28.4±5.4	40.1±7.5
		Limb two	-	11.3±6.0	26.5±6.7	39.4±6.9
Peak KEM $^{Z\,*@\#}$	TKR$^{\&}$	Replaced	0.33±0.21^{c}	0.30±0.22^{bc}	0.39±0.27	0.45±0.28
		Non-Replaced	0.35±0.24^{bc}	0.32±0.28^{bc}	0.52±0.32$^{c\$}$	0.61±0.33$^{\$}$
	Healthy	Limb one	0.49±0.29	0.52±0.31	0.67±0.39	0.73±0.43
		Limb two	0.57±0.26	0.58±0.30	0.72±0.30	0.84±0.34
Peak loading-response KAbM $^{*\,\beta\,\gamma}$	TKR	Replaced	-0.36±0.12	0.34±0.10	-0.32±0.10	-0.31±0.11
		Non-Replaced	-0.43±0.15	-0.38±0.18	-0.37±0.18	-0.36±0.18
	Healthy	Limb one	-0.43±0.14	-0.42±0.11	-0.39±0.13	-0.37±0.14
		Limb two	-0.43±0.15	-0.38±0.15	-0.38±0.18	-0.36±0.17

$^{\wedge}$: significant limb x slope x group interaction; ^{Y}: significant slope x group interaction; ^{Z}: significant limb x slope interaction; *: Significant slope main effect; $^{@}$: Significant group main effect; #: Significant limb main effect; ^{b}: significantly different from 10°, ^{c}: significantly different from 15°; $^{\$}$: significantly different from replaced limb; $^{\&}$: significantly different from healthy controls; $^{\beta}$: significantly different between 0° and 10°; $^{\gamma}$: significantly different between 0° and 15°; -: no comparable values

A CROSS RECURRENCE QUANTIFICATION ANALYSIS OF HIP MUSCLE EMG COUPLING DURING STEP-DOWNS

John H. Hollman, Nicholas J. Beise, Michelle L. Fischer and Taylor L. Stecklein

Mayo Clinic College of Medicine and Science, Rochester, MN, USA
email: hollman.john@mayo.edu

INTRODUCTION

Neuromuscular control, operationally defined as the non-consciously regulated recruitment of muscles in preparatory anticipation of or reactionary response to joint movements or loading conditions for the purpose of maintaining functional joint stability [1], may be assessed in part with electromyography (EMG). Impaired neuromuscular control of hip muscles may contribute to movement coordination deficits of the lower extremity.

We reported previously that gluteus maximus (GMax) recruitment and hip extensor strength modulate transverse plane hip and frontal plane knee kinematics during a jump-landing task [2]. Similar EMG findings are corroborated by others [3]. We propose that examining coupled GMax and gluteus medius (GMed) recruitment may provide a greater understanding of the extent to which hip neuromuscular control influences lower extremity kinematics than merely examining muscle strength or EMG recruitment magnitudes.

We examined coupled GMax/GMed recruitment using cross recurrence quantification analyses and their contribution to variability in frontal plane hip kinematics during single-limb step-downs.

METHODS

30 healthy adults (20 women and 10 men, mean age 23.5 ± 1.5 years, mean BMI 24.3 ± 3.1 kg/m^2) participated. Isometric hip extensor strength was measured with a handheld dynamometer. Hip and knee kinematics during 20 step-downs from a 19-cm step were acquired at 100 Hz with a Vicon MX system. We used the Plug-in-Gait marker system to model lower extremity segments and Nexus software to quantify pelvis and lower extremity kinematics. Marker trajectories were filtered with a Woltring quintic spline filter (20-mm mean square error). GMax and GMed EMG signals were captured at 1000 Hz with bipolar surface electrodes and a Bagnoli-16 amplifier. Signals were band-pass filtered between 20 and 450 Hz with a fourth-order Butterworth filter and processed through a root-mean-square (RMS) algorithm with 100 msec time constants and sliding windows with 90% overlap.

To examine GMax/GMed recruitment coupling, we used cross recurrence quantification analyses (cRQA) described by Webber & Zbilut [4]. Briefly, cRQA examines characteristics of two time series embedded in a reconstructed phase space containing sufficient dimensions to define the system's state. According to Takens [5], that phase space may be reconstructed with time delayed copies of the series. We used a time delay of 60 samples based on average mutual information functions, 3 embedding dimensions based on global false nearest neighbors analyses, and a radius at 20% of a SD.

We examined the following measures:

- Determinism (DET): proportion of recurrent points that fall on diagonal lines of 2 or more points in a cross recurrence plot; represents the predictability of coupling between two signals.
- Divergence (DIV): estimates rates at which coupled trajectories in the phase space diverge; an indication of chaos in coupled signals.
- Shannon entropy (ENT): probability the length of diagonal recurrence lines will be repeated in the cross recurrence plot; estimates variety of patterns in which two signals are coupled.

Multiple regression ($\alpha = .05$) and partial correlation coefficients were used to examine relationships between variability in frontal plane hip data (SD of peak hip adduction angles) and (1) isometric hip extension strength, (2) mean GMax and GMed recruitment, normalized to maximal voluntary

isometric contraction (% MVICs) and (3) DET, DIV and ENT in coupled GMax/GMed recruitment patterns.

RESULTS AND DISCUSSION

Participants performed the task with 52.9 ± 10.1° of hip flexion, 18.3 ± 5.9° hip adduction, 72.2 ± 7.2° knee flexion and 5.2 ± 13.0° knee valgus. Mean GMax and GMed recruitment was 15.4 ± 9.9 and 18.1 ± 11.6% MVIC, respectively. The coupled GMax/GMed recruitment patterns were 74.4 ± 9.9% deterministic with a divergence exponent of .05 ± .03 and a Shannon entropy of 2.11 ± .51 bits/bin (see Fig. 1 for representative example).

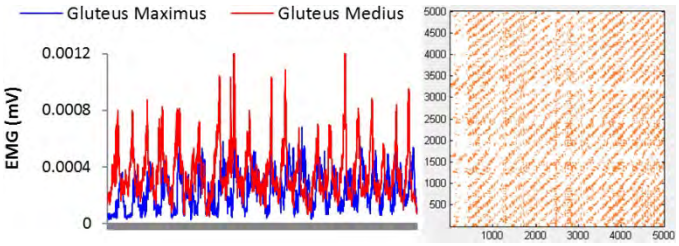

Figure 1: GMax and GMed EMG signals, with cross recurrence plot.

The multiple regression model accounted for 39.4% of the variance in peak hip adduction SDs during the step-downs (cumulative R^2 = .394, p = .044). Per Fig. 2, variance in hip adduction correlated with ENT (r = .554, p = .011) and DET in coupled GMax/GMed recruitment (r = -.487, p = .029). Variance in adduction SDs was not significantly correlated with hip extensor strength, mean GMax recruitment or mean GMed recruitment (partial r = .148, .351 & .019; p = .534, .130 & .937, respectively).

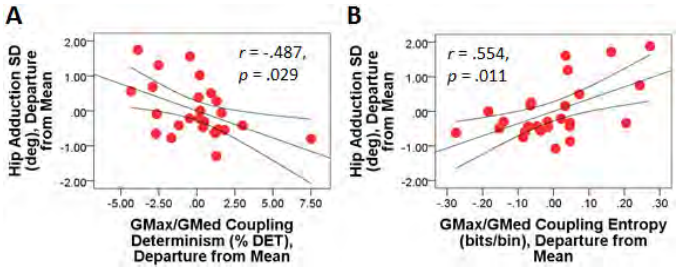

Figure 2: Partial correlation between hip adduction variability and GMax/GMed coupling determinism (A) and entropy (B).

Hip extensor strength, GMax recruitment and GMed recruitment suppressed the zero-order correlations between variability in peak hip adduction angles and entropy and determinism in the coupled GMax and GMed recruitment patterns. When strength and recruitment magnitudes were controlled, however, those relationships increased. Participants with greater variability in peak hip adduction performed the step-downs with greater entropy and lesser determinism in coupled GMax/GMed recruitment. Lesser predictability (decreased DET) and greater irregularity in the variety of patterns in which GMax and GMed recruitment patterns are coupled (greater ENT) may give rise to greater variation in frontal plane hip motions and may have implications for neuromuscular control mechanisms that contribute to movement coordination deficits.

CONCLUSIONS

Variability in peak hip adduction during single-limb step-downs correlated more strongly with determinism and entropy in coupled GMax and GMed recruitment patterns than with participants' hip extensor strength or their magnitudes of muscle recruitment. Examining coupled GMax and GMed recruitment patterns through cross recurrence quantification may provide a greater understanding of the extent to which neuromuscular control of hip muscles modulates lower extremity kinematics than merely examining muscle strength or EMG recruitment magnitudes.

REFERENCES

1. Riemann & Lephart. *Journal of Athletic Training*. 37(1): 71-79, 2002.
2. Hollman et al. *Journal of Sport Rehabilitation*. 22: 184-190, 2013.
3. Zazulak et al. *Journal of Orthopaedic and Sports Physical Therapy*. 35(5): 292-299, 2005.
4. Webber & Zbilut. *Journal of Applied Physiology*. 76(2): 965-973, 1994.
5. Takens. In: Rand & Youngs (Eds.) *Dynamical Systems and Turbulence, Lecture Notes in Mathematics*, Springer-Verlag (898), 1981.

CARTILAGE CONTACT IN OBESITY INDIVIDUALS WITH AND WITHOUT KNEE PAIN

[1,2,3] Jing-Sheng Li, [4] Tsung-Yuan Tsai, [2] Guoan Li, [3] David T. Felson, [1,3] Cara L. Lewis

[1]College of Health and Rehabilitation Sciences: Sargent College, Boston University, Boston, MA
[2]Orthopaedic Biomechanics Laboratory, Newton-Wellesley Hospital and Harvard Medical School, Boston, MA
[3] Clinical Epidemiology Research and Training Unit, Boston University School of Medicine, Boston, MA
[4] School of Biomedical Engineering, Shanghai Jiao Tong University, Shanghai, China
email: jsli1@bu.edu

INTRODUCTION

Obesity is a well-documented risk factor for knee osteoarthritis (OA) [1]. Among obese individuals, knee pain is prevalent. How the knee pain, in addition to existing obesity, contributes to the cartilage contact characteristics, such as cartilage contact deformation and cartilage contact area of the knee will provide insight into the pathomechanics of knee OA and may help us determine potential modifiable factors targeting the obese individuals with or without knee pain. In this study, we aimed to investigate the articular cartilage contact deformation in obese individuals with and without knee pain.

METHODS

Eighteen obese individuals knee pain on most days (15 females, 3 males; age: 42.4±9.4yrs; body mass index (BMI): 39.5±2.5 kg/m^2; pain level (0-100): 63.8±17.4) and seven obese individuals without knee pain (6 females, 1 male; age: 40.1±9.8yrs; BMI 37.1±2.1 kg/m^2) were recruited for this study. This study protocol was approved by the Institutional Review Board at Boston University. Each subject provided written informed consent.

One knee from each subject was selected for MR scan using a 3-Tesla machine (Philips, Achieva, Eindhoven, The Netherlands). The imaging protocol was a Proton Density-Weighted (PDW), Spectral Attenuated Inversion Recovery (SPAIR) sequence with a slice thickness of 1mm and image resolution of 512x512. For an individual with knee pain, the knee with more pain was scanned; for an individual without knee pain, the knee was chosen randomly. The MR images were reviewed and manually segmented to construct the 3-dimensional (3D) subject-specific bone and cartilage surface models for each subject.

Each subjects walked on a treadmill at 1.5 mph (0.67 m/s), and the MR-scanned knee was imaged by a dual fluoroscopic imaging system (Philips, BV Pulsera, Eindhoven, The Netherlands) at 30 Hz with 8ms pulse width. The knee position was processed through a 2-Dimensional to 3D registration procedure. The femoral and tibial cartilage models were mapped to the corresponding bone models at each knee position for cartilage contact analysis. The cartilage contact was represented by the overlapped surfaces of the tibial and femoral cartilage models. In this fashion, we were able to calculate cartilage contact deformation, cartilage contact area (mm^2), and thickness at the contact location [2]. Cartilage deformation was calculated by the amount of penetration of the cartilage surface models divided by the thickness of cartilage models at the same location (mm/mm) [2]. Cartilage thickness (mm) was calculated in the regions of contact.

Independent t tests were used to test the difference in the contact deformation, contact area, and cartilage thickness at contact locations between the obese groups with and without knee pain using MATLAB 2014b (MathWorks, Natick, MA). The analyses for medial and lateral compartments were performed separately. All tests were considered statistically significant when the p-value was less than 0.05.

RESULTS AND DISCUSSION

The cartilage deformation in both medial and lateral compartments was about 0.3 mm/mm (~30%) during the stance phase of the gait cycle. There was no significant difference between obese individuals

with and obese individuals without knee pain **(Fig 1A, 1B).**

In the cartilage thickness analysis, there was no significant difference between the two groups, suggesting that during the stance phase of the gait cycle the loading was consistently transmitting through the regions with similar thickness on both tibial and femoral cartilage **(Fig 1C-1F)**.

In terms of contact area, the two groups with obesity had similar contact area in both medial and lateral compartment at heel strike **(Fig 1G, 1H)**. Thereafter, the obese group without knee pain showed a tendency to increase the contact area and maintain the increase until the end of the stance phase when compared with the obese group with knee pain. This suggests that obese individuals without knee pain may distribute the joint load better than those with knee pain.

CONCLUSIONS

Obese individuals with knee pain had less cartilage contact area during the stance phase of the gait cycle than obese individuals without knee pain, but were not different in terms of the cartilage contact deformation or the thickness at contact location. These contact characteristics explain partly why some obese individuals experience knee pain while others do not..

REFERENCES

1. Felson DT. *Arthritis Rheum* **41**:1343-1355, 1998.
2. Van de Velde SK. *J Bone Joint Surg Am.* **91**:167-75. 2009.

ACKNOWLEDGEMENTS

This work has been supported by the National Institutes of Health under award numbers P60 AR47785 and K23 AR063235.

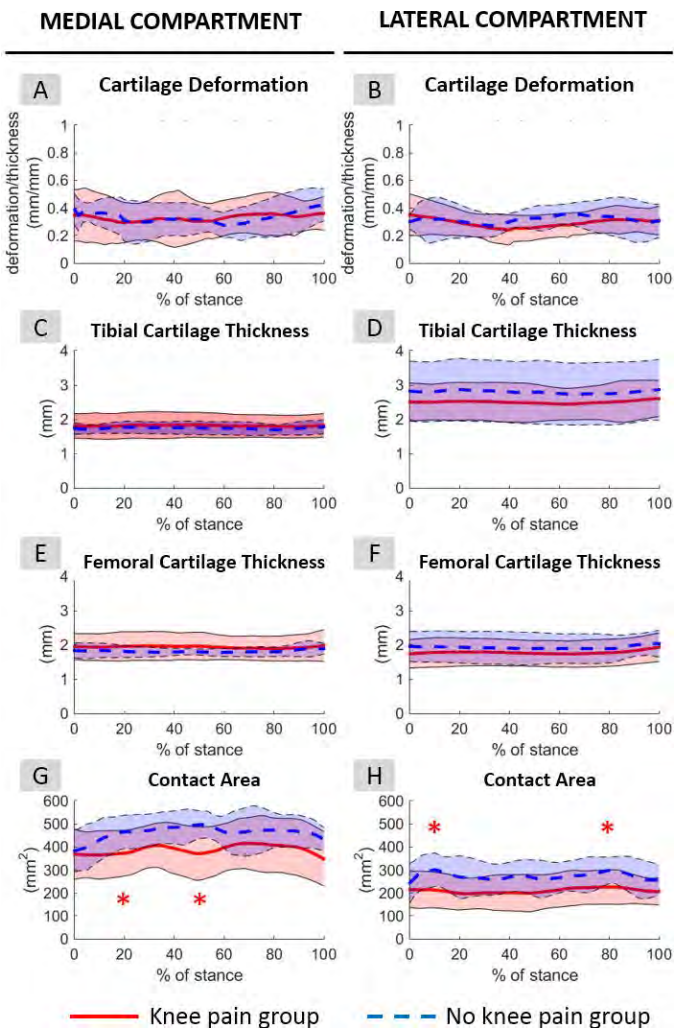

Fig 1. Cartilage contact characteristics during the stance phase of the gait cycle. Cartilage contact deformation in the medial compartment (A) and lateral compartment (B). Tibial and femoral cartilage thickness at contact location (C-F). Cartilage contact area in the medial compartment (G) and lateral compartment (H).

EVALUATION OF AN ACTIVE UNLOADER BRACE FOR MEDIAL KNEE OSTEOARTHRITIS

[1,2] Dylan Reinsdorf, [1,2]Anthony Anderson, [2] Chris Richburg, and [1,2] Patrick M. Aubin
[1]Department of Mechanical Engineering, University of Washington, Seattle, WA, USA
[2] VA Puget Sound RR&D Center for Limb Loss and MoBility (CLiMB), Seattle, WA, USA
email: dreinsdo@uw.edu, web: http://faculty.washington.edu/paubin/wordpress/

INTRODUCTION

Knee Osteoarthritis (KOA) is a painful and debilitating disease associated with mechanical loading in the medial compartment of the knee joint [1]. Unloader braces, a prevalent conservative treatment option for KOA, apply a brace abduction moment (BAM) to reduce the knee adduction moment (KAM) which is associated with medial compartment knee loading. While benefits of knee braces have been demonstrated in multiple studies, their efficacy is potentially limited by tolerable BAM magnitude, and/or brace discomfort leading to poor patient compliance [2]. Considering that the BAM is intended to reduce knee load during a small portion of the total time a brace is worn (stance phase), and that larger BAMs cause user discomfort leading to poor compliance, modulating the BAM so that it is present only during stance may improve comfort and compliance. With the advent of wearable lower limb exoskeletons, and robotic orthoses, it follows that an active robotic unloader brace may better control the KAM and improve patient comfort and brace use. The purpose of this study was to design and develop an offboard controlled robotic unloader knee brace and to measure the range of BAMs it can produce during steady state walking. Development of such a brace will provide a tool for exploring the effects of active knee joint unloading on KOA to inform the investigation of novel treatment methods.

METHODS

Active Brace System Design

The system is conceptualized as a three-point bending brace actuated via an offboard actuation system through a Bowden cable. An unloading mechanism was designed and fit to a modified off-the-shelf (OTS) brace (Fig. 1). The offboard actuation system, comprised of a motor, controller, gearing stage, and chassis, was designed to meet the performance criteria required for modulating knee brace load through a range of 0 to 10 Nm during the gait cycle (GC). The brace was instrumented with a load cell located at the brace condyle pad to directly measure the force transmitted through the brace to the user and to calculate the BAM.

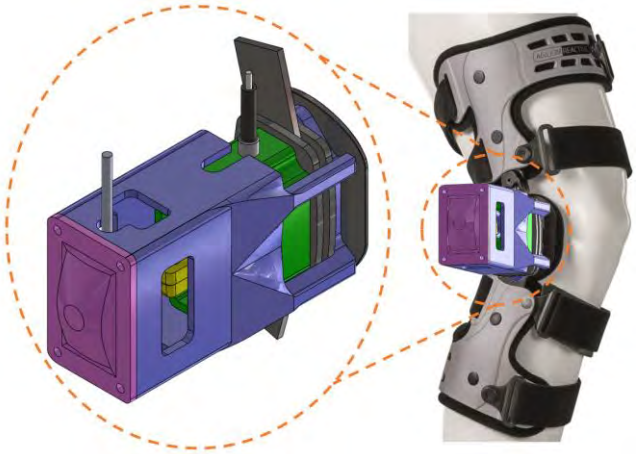

Figure 1: Mechanical design of active knee brace. The knee condyle pad is driven medially to produce a frontal plane KAM that is measured with a load cell in series with the condyle pad.

Human Subject Testing

One male subject diagnosed with medial knee osteoarthritis was recruited for this IRB approved study at the VA Puget Sound Health Care System. Following informed consent, the subject was fitted with the active brace and underwent walking trials. While wearing the active brace, the subject walked at self-selected speed on a split-belt instrumented treadmill under four active BAM conditions: (1) minimum, (2) low, (3) medium, and (4) high. For the fifth (5) condition, the active brace was decoupled from the offboard system and set to operate like a commercially available OTS brace. A constant electrical current command (manual input of Fig. 2) was sent to the motor during walking trials in conditions (1-4). For the minimum condition, the input was tuned to the lowest current level that yielded a non-zero load at the brace. Low, medium, and high levels were scaled from the minimum level, and selected to encompass the abduction moment range of commercially available passive braces.

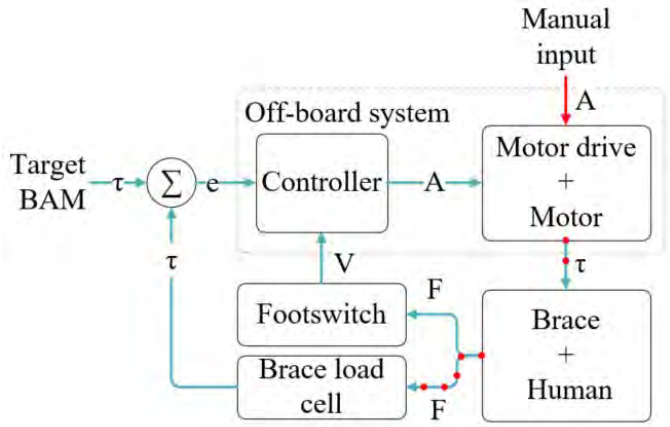

Figure 2: Open-loop and closed-loop brace control schemes, where V=volts, e=error, A=amps, τ=torque, F = force. The open-loop scheme (red, red/blue lines) was used in this experiment.

Condition (5), the passive mode, is representative of the current standard in bracing, where the unloading mechanism was fixed, and the brace tuned to a static position using the native OTS functionality of the brace. The brace force was adjusted to approximate the magnitude of the medium active condition (condition 3). Ground reaction force and brace load cell data were collected at 1200 Hz and filtered using a 4th-order low-pass Butterworth filter with 60 and 40 Hz cutoff frequencies, respectively. BAM was calculated from load cell measurements and brace geometry with the following equation:

$$BAM = F_m(L_{ls} - \frac{L_{ls}^2}{L_b})$$

where F_m is the force measured at the load cell, L_b the brace length, and L_{ls} the length from the lower strap to the condyle pad.

RESULTS AND DISCUSSION

Minimum, low, medium high, and passive conditions resulted in mean ± 1 standard deviation BAMs of 0.004±0.001, 0.028±0.002, 0.048±0.005, 0.073±0.006, and 0.047±0.002 Nm/kg, where means are calculated for first to second peak GRF, 20-50% of GC (Fig. 3). The minimum condition exhibited desirable mechanical transparency, maintaining a near zero BAM. The results indicate that a range of current inputs yielded a proportional range of BAM output. Although current input commands were constant within conditions, the BAM magnitude notably fluctuated over the GC. Bowden cable friction, frontal plane knee kinematics, and muscle contraction (soft tissue compliance under the straps) are likely factors that contributed to the shape of the BAM across the GC. A closed loop control scheme (Fig. 2) will subsequently be implemented for real-time intra step BAM control.

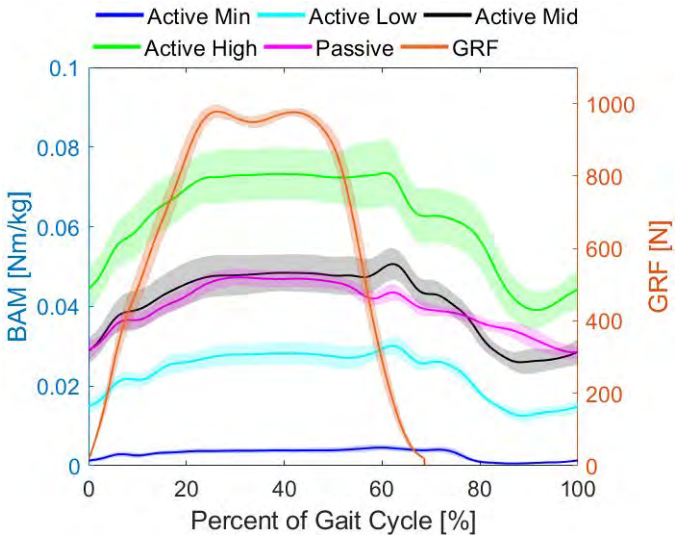

Figure 3: Average ± one standard deviation BAM and vertical GRF for the five study conditions.

In previous studies, mean BAMs of 0.065 Nm/kg for first peak GRF, 0.064 Nm/kg for second peak GRF [3], and 0.04 Nm/kg for first to second peak GRF [4] have been reported for OTS braces. The active brace system therefore achieved BAM magnitudes comparable to commercially available braces.

CONCLUSIONS

The realized active brace varied BAM on a KOA subject proportional to a range of inputs transmitted by an offboard actuation system. The system therefore exhibited desirable performance for a closed-loop active brace capable of exploring the effects of BAM modulation for KOA.

REFERENCES

1. A. Schmitz and B. Noehren, *Knee*, vol. 21, no. 6, pp. 1077–1083, 2014.2.
2. E. Squyer, et al., *Clin. Orthop. Relat. Res.*, vol. 471, no. 6, 2013.
3. C.H. Fantini Pagani, et al., *Arch. Phys. Med. Rehabil.*, vol. 91, no. 12, pp. 1936–1941, 2010.
4. T Schmalz, et al., *Rehabil. Res. Dev.*, vol. 47, no. 5, p. 419, 2010

EFFECTS OF DYSPLASTIC PELVIS MORPHOLOGY ON HIP MUSCLE LINES OF ACTION, MOMENT ARM LENGTHS, AND CONTRIBUTIONS TO JOINT REACTION FORCES

Ke Song, Brecca M. M. Gaffney, Cecilia Pascual-Garrido, and Michael D. Harris

Washington University School of Medicine, St. Louis, MO, USA
Email: harrismi@wustl.edu

INTRODUCTION

Developmental dysplasia of the hip (DDH) is characterized by abnormal pelvic morphology, including a shallow acetabulum, insufficient femoral coverage, and lateralized hip joint center (HJC) [1]. Such deformities result in altered hip intra-articular loading, which leads to damage in the labrum and articular cartilage, and increases the risk of early development of hip osteoarthritis [1].

In addition to bony deformity, hip joint loading is also affected by the force and torque generation of muscles spanning the hip. Specifically, joint reaction forces (JRF) are dependent upon muscle lines of action (LoA) and the corresponding moment arm lengths (MAL) [2]. However, the effects of abnormal pelvis morphology on these parameters in patients with DDH remains unknown. Because muscle paths and forces are difficult to measure *in vivo*, musculoskeletal models can be used to analyze their biomechanical roles in hips with deformity. Our objective was to quantify the effects of dysplastic pelvis morphology on hip muscle LoAs, MALs, and force contributions to JRFs during gait. We hypothesized that compared to healthy hip, a dysplastic hip with more lateral HJCs would have smaller abductor MALs, more medially-directed LoAs, higher medial muscle forces and hip JRFs.

METHODS

First, a musculoskeletal model was created with pelvis morphology of a representative healthy young adult. Specifically, 3D pelvis geometry, HJC locations and hip muscle paths were derived from CT images of a healthy subject [3], who had no previous lower extremity pathology or injury, and had pelvis radiographic measures in normal ranges (**Table 1; Fig. 1A**). An established OpenSim model with 23 degrees of freedom (DoF) and 96 muscle-tendon units (simtk.org/projects/hip_muscles) was modified by incorporating the subject-specific pelvis geometry, HJCs and muscle paths. Kinematic and force data from barefoot gait for this healthy subject were used to calculate muscle forces and JRFs during a gait cycle via inverse kinematics, residual reduction analysis and static optimization, as documented [3].

Table 1: Demographics & hip geometric characteristics.

	Age /Sex	BMI	LCEA	AI	ACEA	HJC (cm)		
						AP	SI	ML
Healthy	28/M	24.3	31.7°	4.8°	32.5°	-6.1	-6.8	8.8
DDH	23/M	26.2	-2.7°	35.9°	-2.5°	-6.1	-7.2	9.7

LCEA = lateral center-edge angle; AI = acetabular inclination; ACEA = anterior center-edge angle. HJC are from pelvis origin to right hip (affected side of DDH; matched side of healthy).

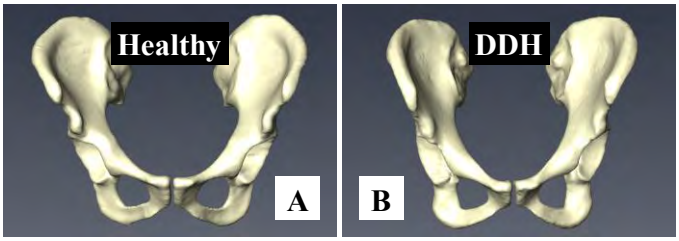

Figure 1: Pelvis geometry of (**A**) a representative healthy young adult and (**B**) a patient with DDH, characterized by a shallow, upwardly sloped acetabulum (high AI) and poor antero-lateral femoral coverage (low LCEA and ACEA).

Next, a representative DDH model was created using 3D geometry from a patient with DDH [3] (**Table 1; Fig. 1B**). Pelvis geometry and HJC locations of the healthy subject were substituted for the DDH pelvis; muscle paths, optical fiber lengths, and tendon slack lengths were then updated accordingly. To directly assess the effects of DDH pelvis morphology on LoA, MAL, muscle force and JRF, model inertial properties were maintained from the healthy model, and analyses were re-run with experimental kinematic and force data from the healthy subject.

Effective muscle LoAs were computed with wrapped paths taken into account [4]. LoA was expressed as a unit vector in antero-posterior (AP), supero-inferior (SI), medio-lateral (ML) components of the pelvis frame, which represented a muscle's potential to

contribute force in these directions (directional contribution) [2]. Muscle forces were then resolved by each LoA component. Lastly, muscle MALs in each hip DoF were computed using a generalized force method [5]. MALs, directional contributions, and estimated forces of iliopsoas, rectus femoris, tensor fascie latae, and gluteal muscles were compared between healthy and DDH models.

RESULTS

Results from the 3 muscle-tendon units that contributed more than 10% of hip JRF peak (Jp) are reported: anterior fibers of gluteus medius (GMedAnt), rectus femoris (RF), and iliacus (IL).

Hip muscle MALs in DDH differed from healthy mainly in hip flexion and adduction (**Fig. 2**). Flexion MAL of RF and abduction MAL of GMedAnt both decreased. Additionally, both RF and IL switched from abduction to adduction roles during stance.

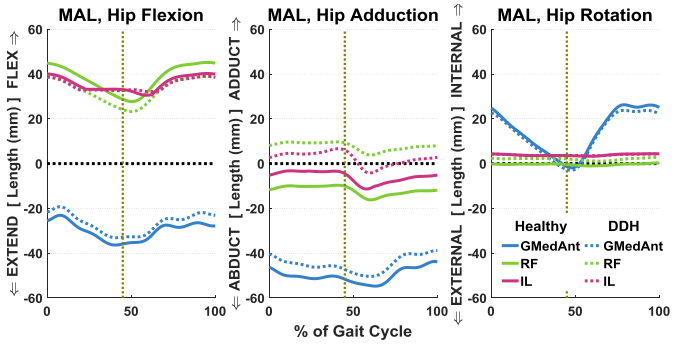

Figure 2: MALs for hip flexion, adduction, and rotation. Vertical band = time of Jp (JRF peak).

Muscle directional contributions in DDH differed from healthy primarily for IL and GMedAnt, with little changes for RF (**Fig. 3**). Most notably, both GMedAnt (0.05 to 0.20 at Jp) & IL (0.03 to 0.09 at Jp) became more medially directed.

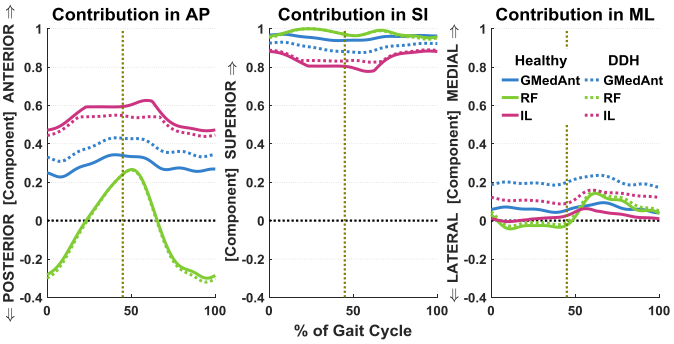

Figure 3: Hip muscle force directional contributions. Vertical band = time of Jp (JRF peak).

All muscle force components in DDH increased (**Fig. 4**). In particular, medial IL and GMedAnt forces raised by 308% and 535% respectively at time of Jp. Correspondingly, hip JRF and its components also increased (by 43% in resultant, 183% medially at Jp).

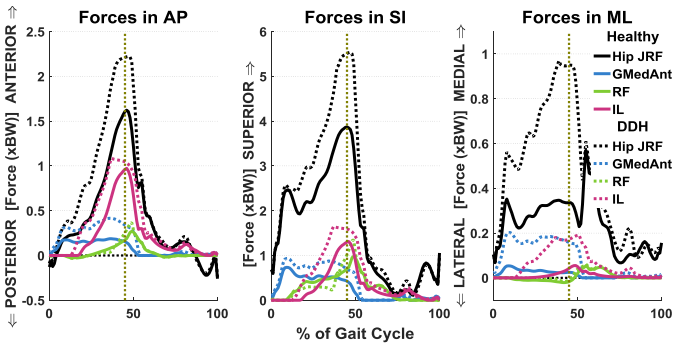

Figure 4: Hip muscle forces and JRFs. Vertical band = time of Jp (JRF peak). Note different vertical scales.

DISCUSSION AND CONCLUSIONS

DDH pelvis morphology had considerable effects on muscle LoAs, MALs, and force contributions to JRFs during gait. Reduced flexion MALs demanded higher force from hip flexors (e.g. by 45% at Jp for RF), which also switched to adduction MALs in the frontal plane due to a lateralized HJC. Consequently, the flexors could tend to abnormally adduct the hip during stance, while the abducting MAL of GMedAnt decreased simultaneously. Both required the hip-stabilizing abductor force to be also higher. As a result, increased forces from both hip flexors and abductors raised hip JRFs in multiple directions. Additionally, lateralized HJC caused muscles with shorter LoAs (e.g. GMedAnt and IL) to direct and contribute force more medially. This could further increase ML hip muscle forces and JRF, which supports our hypothesis and a recent DDH study [3]. To conclude, dysplastic pelvis morphology altered hip muscles' directional force contributions and ability to generate torques, which corresponded to higher hip JRFs on the acetabulum. Despite limited by 1-on-1 comparison, these representative findings provide insights to pathomechanics of DDH and may inform interventions aimed at establishing a normal hip biomechanical environment.

REFERENCES

1. Wyles et al. *CORR.* **475**(2): 336-50, 2017.
2. Yanagawa et al. *J Biomech Eng.* **130**(2): 021024, 2008.
3. Harris et al. *J Biomech.* **54**: 80-7, 2017.
4. van Arkel et al. *J Orthop Res.* **31**(8): 1172-9, 2013.
5. Sherman et al. *Proc ASME DETC.* Portland, OR, 2013.

IMPACT OF EXERCISE-INDUCED PAIN ON TIBIOFEMORAL CONTACT FORCES IN KNEE OA

[1] Ethan Steiner and [1, 2] Katherine A Boyer

[1] University of Massachusetts Amherst, Amherst, MA, USA
[2] University of Massachusetts Medical School. Worcester, MA, USA
Email: esteiner@umass.edu

INTRODUCTION

Knee osteoarthritis (OA) is a chronic degenerative condition marked by pain and stiffness that can fluctuate widely over time, often as a result of weight bearing activity [1]. Pain fluctuations brought on by weight bearing activity have been associated with inferior physical performance and increased risk of falling [2]. As this exercise-induced pain represents a significant component of the overall pain experienced by individuals with OA, there is a need to understand the associated biomechanical response to determine the potential consequences on physical function and knee joint health.

One of the challenges of quantifying the relationship between gait mechanics and pain in OA is that gait mechanics may be a stimulus for pain and/or change as a result of the motor system's response to pain. Prior work has found an association between the knee adduction moment and overall symptom severity [3], suggesting greater joint loading results in more severe symptoms. However, it's also possible that greater structural changes from tissue degeneration in those with more severe disease leads to greater loading. Therefore, to probe the relationship between pain and gait mechanics in knee OA, the aim of this study was to examine the effects of pain induced by multiple bouts of treadmill walking on the joint moments and forces in patients with symptomatic knee OA.

METHODS

Six adults with mild-to-moderate physician diagnosed symptomatic knee OA were included in this analysis. Inclusion criteria were ages 50-75 years, BMI < 35 kg/m^2, good general health, ability to walk unaided, and have no history of cardiovascular or neurological disorders. Participants completed an IRB approved informed consent document prior to starting the study.

Treadmill protocol: Participants completed two separate 20 minute treadmill walks at: 1) preferred walking speed; and 2) faster than preferred speed. In between, participants rested for 40 minutes. The protocol was designed to simulate walking that occurs during daily living with a rest time to minimize fatigue. Perceived knee pain was evaluated on an 11 point numerical pain rating scale at the start and end of the treadmill protocol with a change in pain level ≥ 1 considered to be clinically significant.

Data Collection: Overground walking mechanics were quantified before and after the treadmill protocol. Participants completed 3 overground walking trials over a 25m walkway at a preferred pace, while kinematic and kinetic data was collected. Electromyography (EMG) was collected during the treadmill protocol for the rectus femoris, vastus lateralis, vastus medialis, biceps femoris, and semitendinosus.

Data Processing: A custom MATLAB program was used to calculate external knee joint moments via inverse dynamics for each trial. OpenSim was then used to estimate tibiofemoral force [5]. A musculoskeletal model consisting of 23 degrees of freedom and 92 muscles [6] was scaled to a static trial for each participant. The three walking trials before and after the treadmill protocol were processed using inverse kinematics. Next, a residual reduction algorithm was performed to ensure dynamic consistency between model kinematics and ground reaction forces. Static optimization was then performed for each trial to estimate muscle forces. Following static optimization, OpenSim's JointReaction analysis tool was used to estimate tibiofemoral compressive forces. Experimental EMG was compared visually to estimated muscle activation produced by OpenSim to improve confidence in the simulation results. Paired t-test were used to assess the changes in peak knee joint moments and forces pre and post exercise ($p \leq 0.05$).

RESULTS AND DISCUSSION

All participants experienced clinically significant increases in knee pain (2.33 ±0.33). There were significant increases in the peak external knee flexion moment ($p = 0.025$) but no differences in 1st or 2nd peak knee adduction moments following the treadmill protocol (Figure 1). The external knee flexion moment has been considered as a surrogate measure for the total joint forces [7], thus suggesting an increase in the joint forces in early stance. However, analysis of the musculoskeletal modelling results indicated that there was no significant change in the 1st peak tibiofemoral joint force but there was significant increase in the 2nd peak force ($p = 0.016$) following the treadmill protocol (Figure 2).

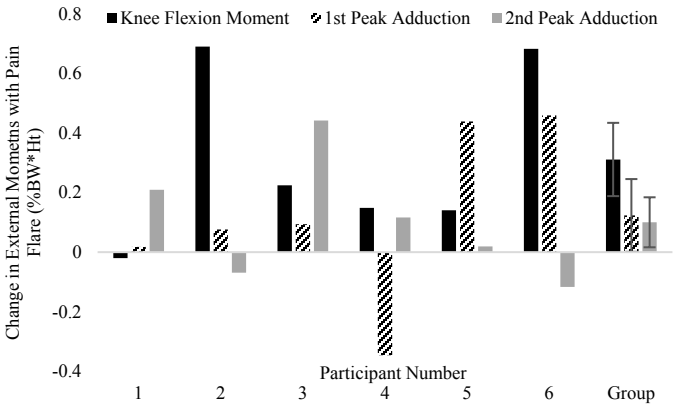

Figure 1: Change in external knee joint moments in response to the treadmill protocol for each participant as well as mean and SE for the group.

Both the lack of a consistent compensatory gait adaption to offload the knee joint in early stance and the increase in joint forces in late stance, with the increase in pain response, are surprising. Experimental knee pain studies have consistently shown a reduction in both knee flexion and adduction moments with the onset of pain [8]. There is also evidence to suggest more severe OA patients develop a compensatory gait strategy to offload the 2nd peak knee contact force, compared to less severe patients, as a way to lessen knee force duration at high loading [4]. The unexpected response in the participants may suggest an inability to successfully adapt to increases in pain following serial bouts of activity due to factors such as reduced proprioception, movement control or as a result of muscle fatigue. Numerous prospective studies have supported a causal relationship between knee joint kinetics and the rate of structural progression, suggesting there may be an increased risk for disease progression following serial bouts of moderate activity.

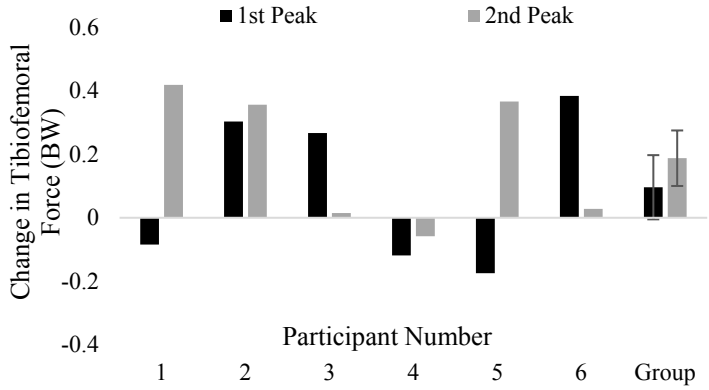

Figure 2: Changes in the 1st and 2nd peak tibiofemoral contact force following the treadmill protocol for each participant as well as mean and SE for the group.

CONCLUSIONS

The increases in knee flexion moment and tibiofemoral forces following the treadmill walks suggest that most participants did not develop a compensatory strategy to offload knee forces in response to the exacerbation of pain. Understanding the factors contributing to the lack of biomechanical pain response may provide insight for new rehabilitation targets.

ACKNOWLEDGMENTS

The study was funded by a University of Massachusetts Faculty Research Grant.

REFERENCES

1. Hutchings et al. *J. Rhe*um. **34**, 2291-2300, 2007.
2. Cruz-Almeida et al. *Exp. Gero.* **98**, 186-191, 2017.
3. Bennell et al. *Ann Rheum Dis.* ***70***, 1770-1774, 2011
4. Richards et al. *J of Biomech.* **43**, 2595-2600, 2010
5. Delp et al. *IEEE TBME.* ***54***, 1940-1950, 2007.
6. Saxby et al. 2016. *Gait & Posture*. **49**, 8-85
7. Walter et al. *J. of Ortho Res*. **10**, 1348-54, 2010
8. Henriksen et al. *Arth Care & Res.* **62**, 501-09, 2010

MUSCLE ACTIVITY DURING SIDELYING HIP ABDUCTION: A BIOMECHANICAL ANALYSIS

Sherry Yan, Anne Khuu, and Cara L. Lewis

Boston University, Boston, MA, USA
email: lewisc@bu.edu, web: http://sites.bu.edu/movement/

INTRODUCTION

Weakness of the hip abductor muscles is thought to contribute to lower extremity musculoskeletal problems, including patellofemoral pain and non-arthritic hip pain. In particular, weakness of the posterior portion of the gluteus medius (GlutMed), which has an extension and an external rotation moment arm, and dominance of the tensor fasciae latae (TFL), which has a flexion and internal rotation moment arm, have been implicated for the faulty movement pattern of hip adduction and internal rotation during weight-bearing. Therefore, it is common to prescribe sidelying hip abduction with the hip in external rotation to strengthen the GlutMed to address this fault. However, based on a few electromyography studies [1-3], it seems that external rotation promotes TFL activation while internal rotation promotes GlutMed activation. One potential explanation for this counter-intuitive finding is that the hip external rotation results in a hip flexion muscle moment during this exercise while the hip internal rotation results in a hip extension moment.

Thus, the purpose of this study was to evaluate the hip moments and muscle activity during sidelying hip abduction with three different hip rotation positions: internal, neutral, and external.

METHODS

Ten healthy adults (5 males, 5 females, 20.4±0.7yrs, 1.7±0.1m, 64.6±8.0kg) provided written informed consent and participated in the study.

A surface electromyography (EMG) system (Delsys Inc.) was used to obtain muscle activity. Electrodes were placed over the muscle bellies of the gluteus maximus (GlutMax), posterior portion of the GlutMed, middle portion of the GlutMed, and TFL on the participant's dominant side. Maximum voluntary isometric contractions (MVICs) were measured using standardized manual muscle testing techniques [4].

Kinematic data of the pelvis and lower limb were collected using a 10-camera motion capture system (VICON®). Markers were place bilaterally on the participant's pelvis, and unilaterally on the participant's dominant lower limb [5]. Participants were in sidelying on a treatment table, and instructed to raise their leg up to a bar positioned at approximately 30° of hip abduction. Participants completed five trials of sidelying hip abduction under three hip rotation conditions: internal, neutral, and external. For each condition, participants were instructed in the desired hip rotation and given verbal cues to maintain that position throughout the movement. Participants were also instructed to maintain the same position of the pelvis for each condition and given verbal feedback if the pelvis position was visibly different.

EMG and kinematic and kinetic data were analyzed using Visual3D. Raw EMG signals were band-pass filtered between 10 Hz and 390 Hz using a 4^{th} order Butterworth filter with zero phase lag. Filtered EMG signals were processed using root-mean squared (RMS) smoothing with a moving window of 100 msec. Average RMS activation was normalized using MVICs and extracted for two phases of movement: ascent (start of movement to peak hip abduction) and descent (peak hip abduction to end of movement). Participant-based mean activation, hip angles, pelvic segment angles, and hip moments of the five trials for each condition were exported for further analysis.

Repeated measures ANOVA was used to compare the mean muscle activation, kinematics, and kinetics within subjects for the three hip rotation positions. When the ANOVA was significant, additional pairwise comparisons were performed.

RESULTS AND DISCUSSION

Muscle activation, hip and pelvis kinematics, and hip kinetics (Table 1) were affected by the hip rotation position during sidelying hip abduction.

Muscle Activation: Individuals had different mean gluteal muscle activity for the three positions. For the GlutMax, the activity during ascent and descent in the external rotation condition was greater than activity in either the neutral ($P \leq .02$) or the internal rotation condition ($P \leq .03$). For the posterior GlutMed, activity during ascent and descent in the neutral condition was less than in the external rotation ($P \leq .03$) or internal rotation condition ($P \leq .02$). For the middle GlutMed, during the ascent phase, activity was greater in the internal rotation condition than in either the external rotation ($P = .03$) or the neutral condition ($P < .001$). During the descent phase, the middle GlutMed activity during the internal rotation condition was higher than the neutral condition ($P = .01$). There were no differences in TFL activity during the ascent or descent phases ($P \geq .65$) among the three conditions.

Kinematics: The mean hip rotation angle was different among the three conditions (Table 1, $P < .001$). As expected, the hip was in the most external rotation during the external rotation condition and the least in the internal rotation condition. The peak hip abduction angle was slightly different among the three conditions ($P = .01$). The mean hip flexion angle was not different among the conditions ($P = .11$). The mean pelvic position in the transverse plane (forward / backward rotation) was different among the three positions ($P < .001$). The pelvis in the internal rotation condition was in more forward rotation (toward prone) than in the neutral or external rotation conditions.

Kinetics: The mean hip moment in the sagittal plane was different among the conditions ($P < .001$). In the internal rotation condition, there was a hip flexion muscle moment, while the moment was in the direction of extension for both the neutral and external rotation conditions. The mean hip abduction and rotation moments were not different among the conditions ($P \geq .27$).

CONCLUSIONS

These preliminary findings suggest that hip rotation position during the sidelying hip abduction exercise affects the hip moment in the sagittal plane and may help explain previously reported differences in muscle activity. The position of the pelvis in the transverse plane likely contributes to the differences in hip moments. Based on these findings, it may be appropriate to perform sidelying hip abduction with the hip in neutral rotation and the pelvis rotated forward when the goal of the exercise is to elicit GlutMed activity in a more functional position.

REFERENCES

1. Lee et al. *J Sport Rehab.* 22, 301-307, 2013.
2. Lee et al. *J Electromyogr Kinesiol*. 24, 318-324, 2014.
3. McBeth et al. *J Athl Train.* 47, 15-23, 2012.
4. Hislop and Montgomery. *Daniels and Worthingham's Muscle Testing,* Elsevier, 2007.
5. Lewis et al. *PLoS One*. 10, e0126258, 2015.

ACKNOWLEDGEMENTS

This work was supported by the NIAMS of the NIH under Award Numbers R21 AR061690 and K23 AR063235, and Boston University's Undergraduate Research Opportunities Program.

Table 1: Hip and pelvis kinematics and hip kinetics during sidelying hip abduction (mean (SD)).

	Hip Angle (°)			Pelvic Angle (°)	Hip Moment (Nm)		
Hip rotation position	External rotation*	Abduction*	Flexion	Transverse plane†	Flexion†	Abduction	External rotation
Internal	-1.6 (10.1)	20.9 (4.9)	18.9 (11.0)	3.0 (4.9)	-2.5 (3.3)	32.0 (6.8)	10.3 (5.3)
Neutral	8.0 (10.9)	23.2 (3.7)	20.7 (11.2)	-2.5 (4.5)	1.1 (3.0)	31.8 (6.9)	10.6 (5.2)
External	22.1 (9.5)	25.1 (3.8)	19.8 (11.1)	-3.2 (4.6)	1.7 (2.8)	32.1 (6.7)	9.8 (5.0)

*All conditions were significantly different ($P < .05$); † Internal rotation condition was significantly different from the neutral and external rotation conditions ($P \leq .01$).

MUSCULOSKELETAL MODEL-BASED CONTROL PERFORMANCE IS CONSISTENT ACROSS STATIC UPPER LIMB POSTURES

[1,2,3] Dustin L. Crouch, [2,3] Lizhi Pan, [3] William Filer, [2] Jonathan W. Stallings, and [2,3] He (Helen) Huang

[1] University of Tennessee, Knoxville, TN, USA
[2] North Carolina State University, Raleigh, NC, USA
[2] University of North Carolina at Chapel Hill, Chapel Hill, NC, USA
email: dustin.crouch@utk.edu

INTRODUCTION

Electromyograms (EMG) are commonly used to estimate movement intent for control of human-machine interfaces (HMIs), such as prosthetic limbs. Emergent algorithms that aim to restore more life-like control can estimate simultaneous and independent movements across multiple joints [e.g. 1]. These algorithms typically require that each EMG is associated with only one primary biomechanical function (e.g. wrist extension). Recording such EMG is challenging in some HMI applications. For instance, EMG is susceptible to crosstalk when muscles are close to one another and overlapping (as in the proximal forearm of people with transradial amputation) and when it is recorded using surface electrodes (currently the only clinically-approved method for recording EMG for prosthesis control) [2]. Limb posture changes may also shift the location of surface electrodes relative to the underlying muscles and reduce the functional specificity of EMG [3]. We previously developed an EMG-driven, musculoskeletal model-based control algorithm that estimates simultaneous wrist and hand movements [4]. Using our algorithm, we conducted two studies to preliminarily evaluate the consistency of subjects' performance of a real-time control task across different limb postures and the extent to which performance could be improved with EMG processing and recording methods expected to provide more function-specific EMG.

METHODS

Musculoskeletal Model-Based Controller. Our 2-degree-of-freedom (wrist and metacarpophalangeal (MCP) flexion/extension) model with four virtual muscles [4] was implemented for real-time EMG-driven control in MATLAB, as previously described [5]. Briefly, EMG were recorded from four forearm muscles that primarily contribute to wrist and/or MCP movement. EMG data were smoothed and normalized by EMG collected during maximum voluntary contractions (EMG-MVC) to estimate muscle activation state (0 = inactive, 1 = maximally active). Activations were applied to the virtual muscles during a forward dynamics simulation to estimate joint kinematics for real-time control of a 2-segment planar virtual hand on a video monitor.

Real-Time Virtual Control Task. In each trial, subjects attempted to move the virtual hand to each of four different target hand postures (Fig.1A) in a randomized order. For each target, subjects were first required to move both joints of the virtual hand to within 8° of a resting (relaxed) posture for 0.25 consecutive seconds, then to within 5° of the target posture for 0.5 consecutive seconds. We computed three task performance measures: task duration (**TD**), normalized path length (**NPL**, path length divided by minimum path length, in joint angle space), and number of overshoots (**NO**, overshoot= virtual hand moved in then out of target range).

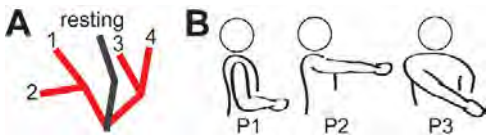

Figure 1: (A) Hand posture targets. (B) Static upper limb postures in which virtual task was performed.

Study 1: EMG processing (normalization) method: Seven able-bodied subjects (6 male, ages 21-32 years) gave their informed consent to participate. In each of 4 blocks of trials (12 trials per block), 4 trials were performed in each of 3 static upper limb postures in a randomized order: neutral arm with elbow at 90° flexion (P1), forward reach (P2), and contralateral reach (P3) (Fig.1B). Subjects assumed a neutral (F1) and pronated (F2) forearm posture in blocks 1/3 and 2/4, respectively. EMG were recorded using surface electrodes (sEMG). In blocks 1/2, EMG were normalized by EMG-MVC recorded in P1F1 (p1MVC); in blocks 3/4, EMG

were normalized by EMG-MVC recorded in the tested posture (psMVC). We performed a 3-way ANOVA to determine the effect of factors "upper limb posture", "forearm posture", and "EMG normalization method" on task performance.

Study 2: EMG recording method: Four able-bodied subjects from Study 1 (3 male, ages 21-25 years) and one transradial amputee (female, age 23) gave their informed consent to participate. In two sessions, EMG were recorded using either sEMG or fine-wire intramuscular electrodes (iEMG). iEMG were placed with ultrasound guidance in approximately the same muscles from which sEMG were recorded. For each electrode type, subjects performed 4 virtual task trials in each of 2 forearm postures (F1 and F2) in a randomized order. The amputee, unable to pronate the residual forearm, only performed trials in F1. We compared task performance between sEMG and iEMG trials using a Generalized Linear Mixed Model.

RESULTS AND DISCUSSION

Study 1. TD (p=.005) and NPL (p=0.019) were statistically significantly worse (i.e. higher) in F2 than in F1; all other differences were not statistically significant (p>0.05). Notably, normalizing by psMVC, which was expected to improve the accuracy of computed muscle activation states, did not significantly improve task performance compared to trials in which EMG was only normalized by p1MVC (Fig.2). Analysis of EMG (not shown) indicated that subjects adapted their contraction effort to overcome differences in EMG magnitude across postures.

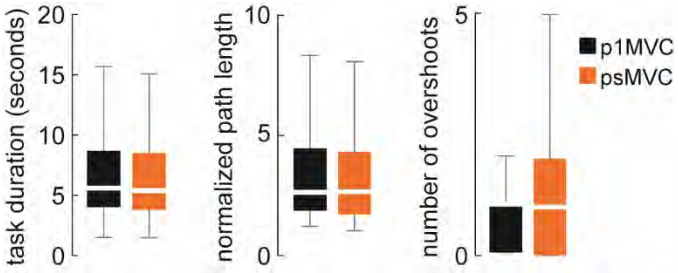

Figure 2: Box plot comparison of task performance measures between the two EMG-normalization conditions for able-bodied subjects (Study 1).

Study 2. There was a trend of more consistent, but not better, values of NPL with iEMG than sEMG (Fig.3). However, there was no statistically significant effect of electrode type or forearm posture (p>0.05). Qualitatively, for the subject with transradial amputation, all three task performance measures were worse with iEMG than sEMG.

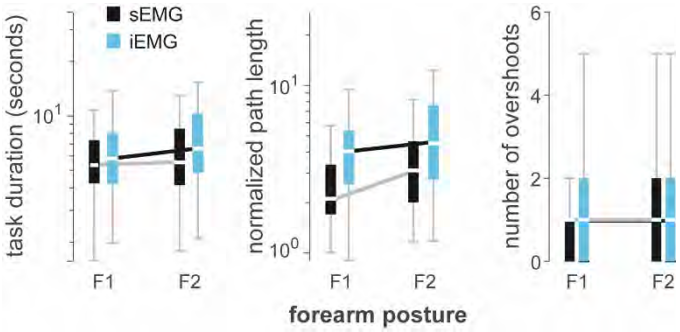

Figure 3: Box plot comparison of task performance measures between electrode type and between forearm postures for able-bodied subjects (Study 2).

CONCLUSIONS

Our results suggest that sEMG and normalizing EMG to MVC from only one posture may be sufficient for providing reliable control of 2 degrees of freedom. This was surprising since both normalizing EMG by psMVC and iEMG recording were expected to provide better function-specific EMG and, thus, enable better real-time control performance. Some limitations of our study were the small sample size (only 1 amputee) and that testing conditions differed from those of real-world tasks (no physical prosthesis/socket, virtual tasks performed in static postures). Some subjects also verbally reported that iEMG felt unusual and/or uncomfortable, which may have confounded the effect of iEMG signal quality on task performance. Our results motivate future work to further evaluate our algorithm's potential to enable more natural control of prosthetic hands and other EMG-driven HMIs.

REFERENCES

1. Smith et al. *IEEE Trans BME*, 63(4),2016.
2. Mogk & Kier. *J Electromyog Kinesio*, 13(1),2003.
3. Fougner et al. *IEEE TNSRE*, 19(6),2011.
4. Crouch & Huang. *J Biomech*, 49(16),2016.
5. Crouch & Huang. *J Neural Eng*, 14,2017.

ACKNOWLEDGEMENTS

DARPA (N66001-16-2-4052), NSF (1527202, 1637892), DHHS/NIDILRR (90IF0064), DOD (W81XWH-15-C-0125, W81XWH-15-1-0407).

Mapping Together Thumb Kinetic and Kinematic Function

Joshua P. Drost, Tamara Reid Bush
Michigan State University, East Lansing, MI, USA
email: drostjos@msu.edu, reidtama@msu.edu

INTRODUCTION

Hands are used for daily interactions with multiple devices ranging from keyboards to food. When hand function is reduced, it is critical that we understand how much function was lost and where it was lost to insure the best possible treatment. Currently, loss in hand function is determined using subjective methods such as surveys, pain scales and radiological exams; *objective* methods to quantify changes in hand function are critically needed [1, 2]. A hand model that includes complete *force and motion* abilities of an individual will allow comparisons of the changes in hand function and improved rehabilitation and treatment strategies.

Previously, the authors modeled changes in the motion abilities of the hand [3]. This model included the full range of motions of the fingers. However, the movement of the thumb and the forces it can generate have not yet been studied and mapped together. The thumb is critical for understanding the hand.

Thus, the goal of this work was to develop a protocol to measure the kinematic and kinetic abilities of the thumb and map them together.

METHODS

Seven participants (three female and four male, average age 22.6 years, SD 2.1 years) without any reported injury or arthritis were included in this study. Movement was measured using a seven-camera motion capture system and force was measured using a six-axis load cell with a custom interface device.

Full range of motion of the thumb was determined using three motions. 1) Full extension of the thumb to full flexion of the metacarpalphalange (MCP) and interphalangeal (IP) joint (Figure 1a). 2) Radial abduction of the carpometacarpal (CMC) joint and opposition to pinky MCP joint (Figure 1b). 3) Radial adduction of the carpometacarpal (CMC) joint and opposition to pinky MCP joint.

Maximum forces were measured in two directions in each of eight positions (Figure 1c-1d). The positions were based on varying rotation of the palm and abduction of the thumb. The palm was tested at four angles relative to the ground: 0°, 30°, 60° and 90°. At each rotation, the thumb was tested in two positions: full adduction (touching the palm) and maximal

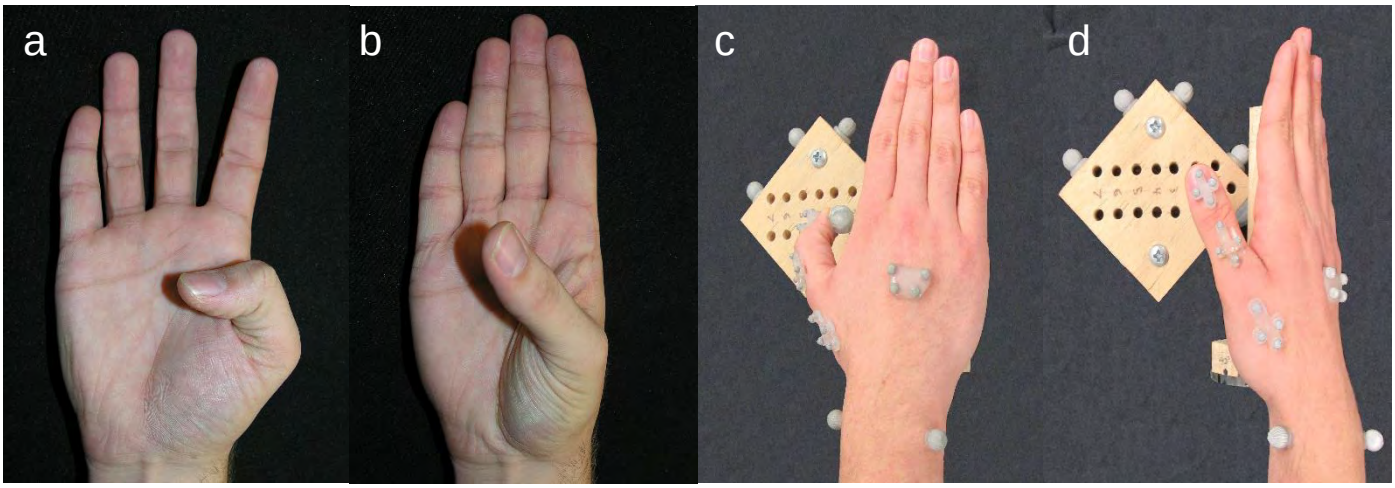

Figure 1: Testing procedure. Range of motion was measured through a) full flexion of the MCP and IP joints of the thumb and b) full ranges of opposition. Force capabilities were measured at multiple positions and directions; shown are palm at c) 0° (horizontal) and force directed medially d) and palm at 60° with respect to horizontal with force directed towards ground.

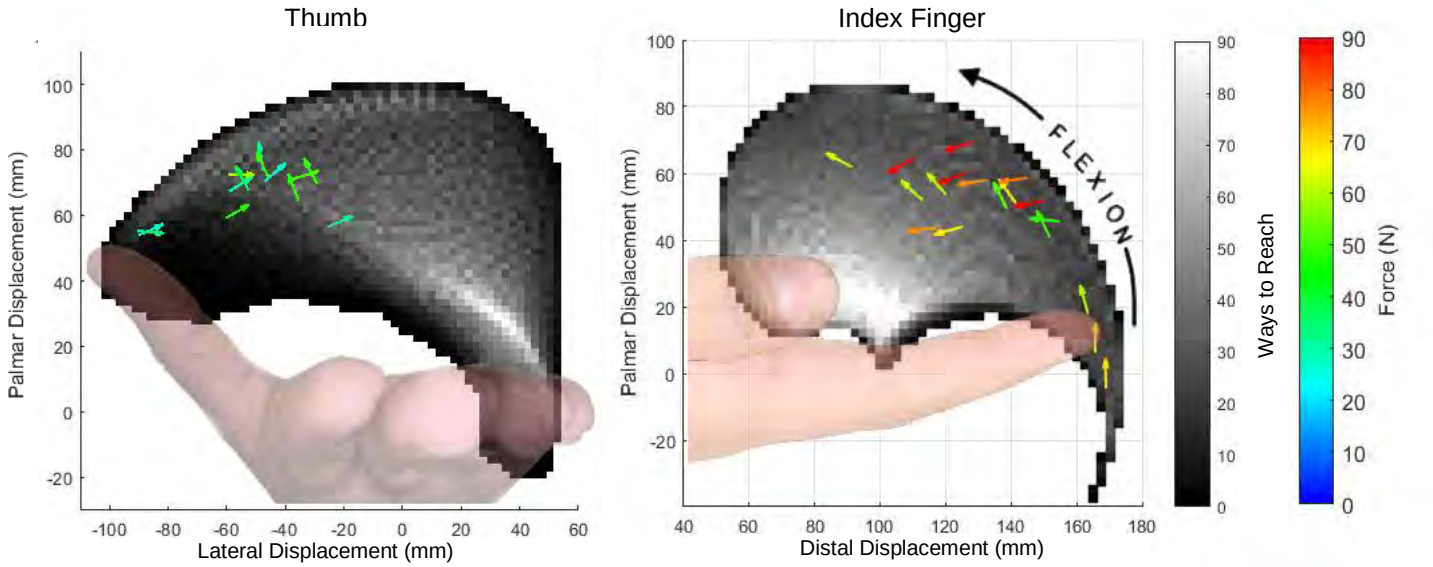

Figure 2: Finger function maps for the thumb and index finger. Greyscale background describes number of ways to reach each point. Colored arrows describe the force actions measured. The transparent hands show the orientation of the hand.

abduction of the thumb. At each position the participant was asked to apply maximal force towards the ground and then towards the hand.

After collection, the data were analyzed in three steps: determining the range of motion, the force data, and mapping the forces to the range of motion. The kinematic abilities of the thumb were determined by finding the full range of motion of each joint: the IP and MCP joints were treated as hinge joints and permitted to move in flexion/extension; the CMC was treated as a saddle joint and was measured using radial abduction (thumbs up motion) and palmar abduction (gripping motion). The thumb posture during each possible angle combination was identified and the full range of motion computed. Force data were analyzed in terms of the 1) fingertip posture (x, y, z coordinate) 2) the direction of the force applied, and 3) force magnitude. The force data were mapped to the range of motion by determining the rotation matrix between the coordinate systems of the load cell and motion capture system and computationally aligning both the motion and force data to the same coordinate system, relative to the CMC joint of the thumb.

RESULTS AND DISCUSSION

Figure 2 displays the motion and force abilities of the thumb and index finger. Due to the 3D nature of the thumb movement and to the complexities of presenting the data in 3D, the thumb motion and forces have been projected onto a 2D plane for visualization. The range of motion is described by the grayscale background, with the scale representing number of joint angle combinations that can be used to reach each point on the grid. The forces are represented as colored arrows, with the color indicating force magnitudes. As can been seen in Figure 2, the current methodology is able to measure forces over half the range of motion. Future work will include an additional protocol to measure the forces during full opposition to the fifth MCP joint.

There is a need for an objective method for diagnosing loss of hand function. This work provides a significant step in moving towards a full model of hand function by addressing the complicated movement pattern of the thumb. Future work will combine the thumb and fingers to understand interactions and investigate how function of the thumb changes due to hand osteoarthritis.

ACKNOWLEDGEMENTS

The authors would like to thank the Pearl J. Aldrich Endowment for funding this project.

REFERENCES

[1] Chung K C., et al The Journal of Hand Surgery, 575-587. 1998.

[2] Katz S, et al. Journal of the American Medical Association, 914-919. 1963.

[3] Leitkam S, Bush TR. ASME Journal of Biomechanical Engineering. 2015.

TASK CHARACTERISTICS AFFECT MOTOR ADAPTATION TO MUSCLE ASSISTANCE

[1] Hien Nguyen, [1,2] Billy C. Vemillion, and [1,2,3] Sang Wook Lee

[1] Catholic University of America, Washington, DC, USA
[2] MedStar National Rehabilitation Hospital, Washington, DC, USA
[3] National Institute on Neurological Disorder and Stroke, Bethesda, MD, USA
email: leesw@cua.edu (or leeb@cua.edu)

INTRODUCTION

Stroke affects about 600,000 people annually in the United States [1], resulting in significant functional impairment of those affected. While both upper and lower extremity functions are compromised, the recovery of upper extremity appears to be more limited [2]. Restoration of the hand function should be prioritized due to its functional importance, and its recovery is well correlated to the overall recovery of the overall upper extremity function. Typically repetitive movements of the hand (in a functional context) are prescribed for patients, instead of strength training, since resisted activities may increase flexor spasticity, interfering with a proper coordination of the hand muscles. Recent studies, however, suggest that resisted strength training may be beneficial for improving function post-stroke.

While the effectiveness of strength training has been demonstrated mostly in gait training, its benefit in upper-extremity (hand) function remains unclear [4]. Most manual tasks require complex spatiotemporal coordination of many muscles, thus focusing on proper muscle coordination during movements could be more beneficial. However, as extensor weakness is commonly observed post-stroke, strength training (of weakened finger extensor) could be helpful. As these two trainings typically involve different task types (static force exertion vs. movement) and muscle contraction types (isometric vs. concentric), different patterns of motor adaptation to assistance (provided during task) may also emerge.

In this study, therefore, we aim to examine the effects of task characteristics (force production vs. multi-joint movement) on the motor adaptation to assistance in healthy subjects. Here, we focused on the between-task difference in the muscle activation patterns and their adaptation to assistance.

METHODS

Twenty-four healthy subjects (age: 21 – 43 yrs) participated in the experiments, in which two different types of assisted finger extension task were performed (Exp 1. vs. Exp. 2).

Exp. 1: Twelve subjects (5 males) performed static finger extension tasks by producing a submaximal dorsal fingertip force against a load cell. Subjects wore an exotendon device, a modified version of a biomimetic device (BiomHED) [3] (Fig. 1). An exotendon that mimics the anatomy of the extensor digitorum communis (EDC) tendon were actuated by an electric motor (A-max 16, Maxon AG, Switzerland) to provide targeted assistance to the EDC muscle. Subjects first produced the dorsally-directed fingertip force (40% of their maximal voluntary force) with no assistance (10 trials), then with the targeted EDC assistance provided by BiomHED (10 trials).

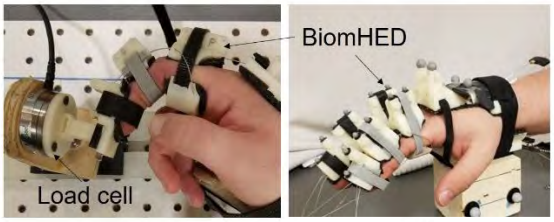

Figure 1. Experimental setup: (a) movement

Exp. 2: Another group of twelve subjects (8 males) performed 'timed' finger extension movements, which consisted of a preparation (2-sec), opening movement (3-sec), and sustaining of the open hand position (3-sec). A custom graphical user interface (LabView, National Instruments, Austin, TX) provided visual cues regarding the timing of different phases in the form of sliding bar with marks. Similar to Exp. 1, the task was performed without assistance (10 trials) first, then with assistance (10 trials).

Recording: Three pairs of disposable, self-adhesive silver/silver chloride surface electrodes (Noraxon, Scottsdale, AZ, USA) were used for surface EMG recordings from an intrinsic hand muscle (first dorsal interosseous; FDI), and two extrinsic muscles (EDC and flexor digitorum superficialis; FDS). EMG signals were inspected while subjects performed several finger/wrist motions related to the target muscles, and the location was adjusted if crosstalk was detected. The EMG signals were sampled at 1000 Hz and band-pass filtered (5Hz - 400Hz).

RESULTS AND DISCUSSION

Two distinct types of muscle coordination pattern were found to be employed for the two tasks. The activation level of the extrinsic extensor muscle (EDC) was not significantly different, while the activation level of the extrinsic flexor (FDS) and intrinsic (FDI) muscles were significantly smaller during movement (Task 2) than static task (Task 1) ($p < 0.04$ for FDS and FDI; see Fig. 2a). The observed between-task difference in the two muscles is likely due to their different primary roles during finger tasks (FDI: directional control of fingertip force; FDS: stability of multi-link system; [4]).

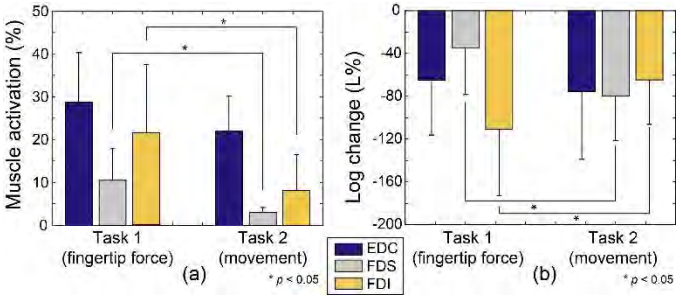

Figure 2. Between-task difference in (a) muscle activation level; (b) relative change in activation level

More importantly, the effects of targeted assistance of the extrinsic extensor muscle (EDC) were different between the two types of tasks (Fig. 2b). Under the targeted EDC assistance, the degree of reduction in the EDC activation were similar between the two tasks. However, the degree of FDS reduction was greater during movement ($p = 0.02$), while a significantly greater decrease in the FDI activation was observed during isometric task ($p = 0.05$; Fig. 2b).

The between-task difference in the motor adaptation to assistance was signified in the coordination of the muscle pairs (i.e., cocontraction ratios), as they showed contrasting patterns: under assistance, the CCR values of EDC-FDS and FDI-FDS pairs decreased during force production, but increased during movements. Contrastingly, EDC-FDI CCR increased during isometric task, but decreased during movement. The FDI-FDS CCR showed the largest between-task difference ($p < 0.001$). Overall, a greater degree of change was observed in Task 1.

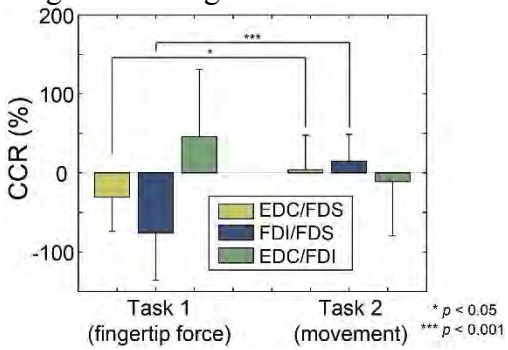

Figure 3. Between-task difference in cocontraction ratio

The results of this study suggest that the type of task should be carefully determined based on specific impairment characteristics of individuals and corresponding training goal (e.g., strengthening extrinsic extensor muscles vs. intrinsic muscles). While the targeted muscle assistance did not cause any substantial change in the muscle coordination (Fig. 2b) during movements, the assistance decoupled (and reduced) the activation of the intrinsic muscle during isometric force production, thus more suitable for those with extensor weakness. Assisted movement training may be desirable for those with severe intrinsic impairment, as the task does not require its activation much. We will test the same experimental protocol with stroke patients to examine whether they exhibit similar between-task difference in their motor adaptation patterns.

REFERENCES

1. Mozaffarian et al. *Circulation* 133: e38-360, 2016.
2. Nakayama et al. *Arch Phys Med Rehabil* 75: 394-98, 1994.
3. Lee et al. *IEEE Trans Neural Syst Rehabil Eng* 26:619-28, 2018.

ACKNOWLEDGEMENTS

This work was supported by NSF (CBET-1452763)

DECOMPOSED ELECTROMYOGRAPHY PREDICTS CLINICAL ASSESSMENT OF FINGER EXTENSOR WEAKNESS

[1]Nathan D. Schilaty, [2]Filippo Savoldi, [2]Zahra Nasr, [2]Adriana M. Delgado,
[1]Lawrence J. Berglund, and [2]Brian G. Weinshenker

[1]Mayo Clinic Biomechanics Laboratories & Sports Medicine Center, Rochester & Minneapolis, MN, USA
[2]Mayo Clinic Department of Neurology, Rochester, MN, USA
Email: schilaty.nathan@mayo.edu

INTRODUCTION

In 1987, O'Neill et al. reported a patient with multiple sclerosis (MS) who experienced rapid reversible deterioration in gait and increase in degree of pyramidal weakness of the lower limbs with neck flexion; this phenomenon was so prominent that affected patients had to hyperextend their necks in order to walk. [1] This manifestation was named McArdle's sign (McS) after M.J. McArdle who recognized this sign. [1] This sign has since been largely overlooked and the mechanism of is poorly understood. McS may have potential diagnostic value, especially in challenging cases of myelopathy, and possibly even therapeutic implications as an indicator of mechanically-induced conduction block, and thereby a reflection of the presence of spinal cord demyelination.

The aim of this study was to quantify neuromotor activation via decomposed electromyography (dEMG) of patients chosen because they had detectable finger extension weakness, a sensitive and easily testable muscle group; patients enrolled were classified by diagnosis: MS, other myelopathies and peripheral neuropathies. Additionally, 17 healthy controls were tested. We hypothesized that neuromotor activation as measured by dEMG would predict clinically diagnosed weakness.

METHODS

Informed consent was obtained from all study participants (n=48; 21M:27F, age 49.0±13.1). McS is detectable in muscle groups sensitive to upper motor neuron lesions. We specifically evaluated finger extensor strength (extensor digitorum) since it is both a sensitive and convenient indicator of McS. Clinical McS was rated by a clinician with head in extension and flexion positions. McS is graded 0-3 (0=Not detectable; 1=Barely detectable; 2=Moderate; 3=Prominent). A dEMG electrode (Delsys; Natick, MA) placed on the belly of the extensor digitorum measured surface EMG as each patient extended their four fingers isometrically. A 40 second rest interval was utilized in between individual contractions to allow for proper recovery of muscle force. Three 'baseline trials' with the neck in neutral position were obtained to determine subject maximal voluntary isometric contraction (MVIC). Afterward, three successive trials (with rest periods) were then performed in each neck position (head/neck in randomized order of flexion, neutral, or extension position) at 25% MVIC. Neck position was recorded by two gyroscopic sensors affixed to a headband (**Fig. 1**). EMG data was post-processed with Delsys dEMG Analysis software.

Figure 1. McArdle Biomechanical Test Setup. Subject's arm is secured in the device. Torque cell (blue arrow) measures torque as subject pushes on padded black bar. Two gyroscopes in headband measure neck flexion/extension (yellow arrow).

ANOVA and receiver operator curves (ROC) were performed in JMP 13 (SAS Institute Inc., Cary, NC). dEMG variables included in the model were: number of firings, recruitment, derecruitment, and average firing rate. A p-value <0.05 was considered statistically significant.

RESULTS AND DISCUSSION

Characteristic findings of dEMG were a decrease in function for Grade 1 McS, a recovery for Grade 2, and then a further loss of function for Grade 3 (**Fig. 2A**). Consequently, the ROC of dEMG as a predictor for McS demonstrates 'good' diagnostic accuracy for McS Grade 3, 'fail' for Grade 2, 'fair' for Grade 1, and 'poor' for Grade 0 (χ^2=1028.53; p<0.0001; **Fig. 2B**). For Grade 3, dEMG was 0.81 sensitive and 0.82 specific (χ^2=609.75; p<0.0001) for clinical McS.

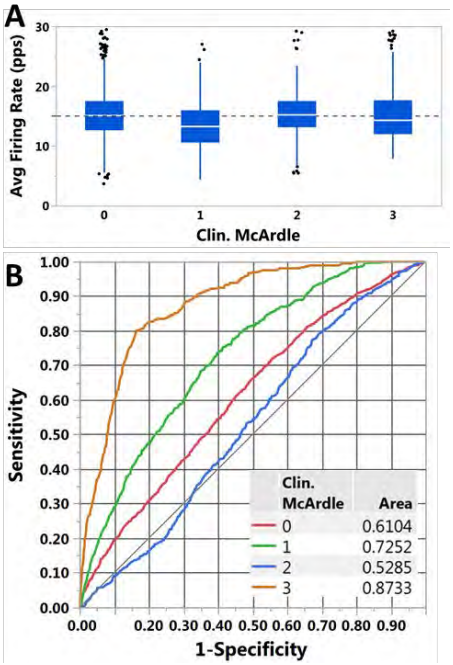

Figure 2. dEMG characteristics of clinical McS and ROC curve of dEMG as a predictor of clinical McS. Respective area under the curve (AUC) is provided for each McS grade.

Specifically evaluating the differences of neck position, there was excellent diagnostic effects of dEMG in neutral position for McS Grade 3 (χ^2=426.87; p<0.0001). With neck flexion, there was improved clinical diagnostic accuracy (χ^2=523.27; p<0.0001; **Fig. 3**); 'excellent' for McS Grade 3, 'poor' for Grade 2, 'fair' for Grade 1, and 'poor' for Grade 0. Neck extension was the least diagnostic of the three neck positions (χ^2=296.67; p<0.0001).

When divided by neck position and sex, females demonstrated improved diagnostic prediction of clinical McS than males for Grade 3. However, these criteria reverse for Grade 1 and 2. With all neck positions, females demonstrated 'excellent' diagnostic accuracy for McS Grade 3 (**Table 1**).

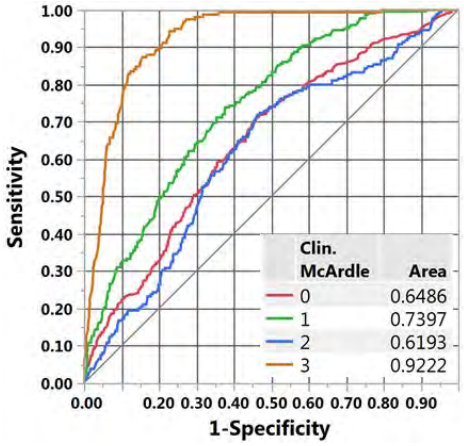

Figure 3. ROC curve of dEMG with subjects in neck flexion as a predictor of clinical McS. Respective area under the curve (AUC) is provided for each McS grade.

CONCLUSIONS

This data demonstrates that neuromotor activation as measured by dEMG is both sensitive and specific to clinically observed muscle 'weakness,' especially with neck flexion as observed with McS. This is an important objective measure that coincides with subjective clinical interpretation and could prove useful for confirming or predicting diagnosis of MS. Future work should determine specificity and sensitivity of dEMG to MS vs other peripheral neuropathies or myelopathies.

REFERENCES

1. O'Neill et al. *J Neurol. Neurosurg. Psychiatry*. 50:1691-1693.

ACKNOWLEDGEMENTS

Funding include NIH K12HD065987 and L30AR070273 and Mayo Clinic Kelly Orthopedic Fellowship.

Table 1: AUCs for each neck position by sex compared to Grade 0 McArdle Sign. 'Excellent' prediction is in **bold.**

	Neutral			Flexion			Extension		
McArdle Grade	**1**	**2**	**3**	**1**	**2**	**3**	**1**	**2**	**3**
Males	0.83	0.80	0.84	0.71	0.74	**0.90**	0.66	0.76	0.76
Females	0.71	0.74	**1.00**	0.73	0.59	**0.97**	0.76	0.63	**0.92**

ROLE OF COGNITIVE AGENCY IN REACH-TO-GRASP MOVEMENT PERFORMANCE

[1,2]Aniket Shah, [1,2]Sean Sanford, [1,3]YongQi Chen, and [1,2]Raviraj Nataraj (PI)

[1] Movement Control Rehabilitation (MOCORE) Laboratory, [2]Department of Biomedical Engineering, [3]Department of Electrical and Computer Engineering, Stevens Institute of Technology, Hoboken, NJ, USA
email: ashah97@stevens.edu, web: http://www.mocorelab.com

INTRODUCTION

Neuromuscular disorders such as stroke and spinal cord injuries can lead to severe movement disability and compromise the ability to perform activities of daily living. Physical rehabilitation involving repetitive movement task execution is a primary method to re-train and recover neuromuscular functionality. Virtual reality (VR) environments have been previously utilized to facilitate greater cognitive engagement with unique, colorful displays and task gamification [1]. In this study, we investigate employing a VR environment to systematically vary operation of a visualized virtual hand prosthesis [2] to alter sense of agency. Cognitive agency is the perception that one is the true author of one's actions [3]. We hypothesize that with greater agency, individuals will improve functional movement performance. In turn, such findings may provide a foundation to design VR-based paradigms that identify agency and correlate it to operational conditions which accelerate rehabilitation.

In this study, we investigate the potential role of agency in reach to precision pinch grasp. Precision pinch involves dexterous manipulation of small objects and greater cognitive attention. In VR, the virtual hand prosthesis moves with that of a subject's real hand. But visualized operation of the virtual hand is systematically modified to potentially alter sense of agency. Operational parameters include speed, addition of random noise, and a condition for automated task completion once initiated. These parameters are chosen to consider common operational issues for assistive devices often tuned by a clinical-level engineer.

METHODS

A. Subjects

Ten volunteers (8 male, 2 female, 21 ± 3 years in age) have participated according to protocols approved by the local Institutional Review Board. Subjects were screened to be able-bodied, right-hand dominant, and to have no previous injury or surgery to the upper extremities, no cited neuromuscular disease, and correctable-to-normal vision.

B. Motion capture system

Hand movements were tracked using retro-reflective motion capture of marker clusters placed on the index finger, thumb, and wrist using nine infrared cameras (*Prime17, OptiTrack, Natural Point, Inc.,* Corvallis, OR). Motion capture data were sampled at 120Hz with *Motive* (*Natural Point, Inc*.) and then streamed over a broadcast ethernet network to a remote computer running *MATLAB 2017a* (*Mathworks, Inc.*, Natick, MA).

C. Virtual reality environment

The physics engine displaying the hand prosthesis was *MuJoCo* (*Multi-joint dynamics with Contact, Roboti LLC*, Redmond, WA). Using *MATLAB*-compatible API code, streaming motion data were used to drive motions of the virtual hand in real-time.

D. Protocol

Each subject participated in a single, two-hour experiment session. After donning marker clusters on the motion hand, each subject would wear a VR headset (*BestFace 3D VR, Nibiru OS, Japan*) to visualize the *MuJoCo* display. A single trial involved moving the motion hand from a calibrated starting position, while observing the virtual hand move towards a target sphere (**Figure 1**). Each subject was asked to take the most efficient (shortest path-length) trajectory. To complete the 'action' for the trial, the target had to be contacted by the virtual hand thumb and index finger to undergo a color change (green to black). The subject was made aware of a sound (short beep) as a sensory 'consequence' of the 'action' at a variable time-interval (0 to 1 sec) following contact. To indicate intentional binding between action and consequence as a measure of agency [3], the subject

would estimate the time-interval. It was inferred that with greater agency one would perceive a compressed (shorter) time-interval [4].

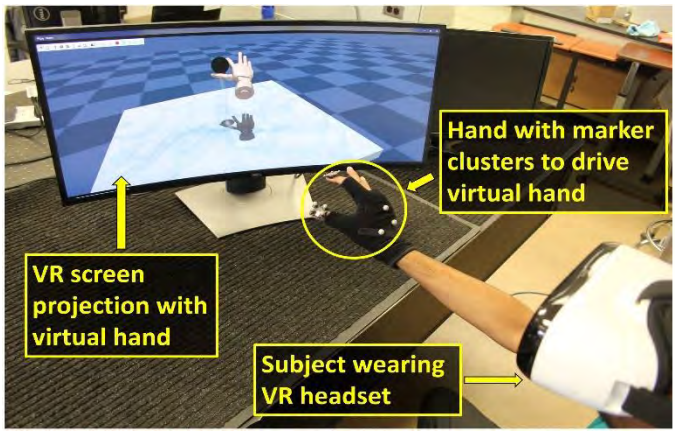

Figure 1: Subject reaching and pinching through to ensure virtual hand contacts sphere target.

Twenty trials were done for each of six virtual hand operation conditions. The conditions were: (1) 'normal' (control) - VR hand motion matched that of subject's real hand, (2) 'slow' - VR hand moved 50% slower than real hand, (3) 'fast' - VR hand moved 50% faster than real hand, (4) 'noisy' - VR hand had added random noise, up to 10% the expected total path-length, (5) 'auto' - VR hand was gradually under greater preset control in approaching the target instead of subject control, (6) '1-phase grasp' - no reaching (transport phase) as hand initially placed near target prior to contact.

RESULTS AND DISCUSSION

All conditions showed significant changes in agency relative to 'normal', except 'noisy' (**Table 1**). 'One-phase' had the greatest increase in agency, strongly implicating the role of transport in attenuating agency for grasp contact. 'Slow' and 'auto' had the greatest decreases in agency, suggesting a sense of control loss when operation lags or is automated. Desirable performance was taken as lower variability in path length. Performance was significantly lower for 'fast' and 'auto' but higher for 'slow'. Performance and agency appear correlated with automation, but not by variations in speed. Moderate visual noise appears tolerable in having had no apparent effect on performance or agency. This study serves as an able-body concept protocol whereby visualized motions are altered and mis-matched against intact proprioception and no haptic feedback.

The next phase of this research will build upon the principles identified in this study that relate agency, performance, and operation condition. We expect this versatile platform can be used to develop "customized" control systems for hand grasp assistive devices or rehabilitation paradigms for specific pathology groups. We seek to optimize controller operation not only for better performance but to leverage agency for accelerating functional gains. Applications of this platform may include the development of better hand neuroprostheses [5] following spinal cord injury, sensorimotor prostheses following upper-limb amputation [6], and exoskeleton-assisted stroke rehabilitation [7].

REFERENCES

1. Rose et al. *CyberPsych&Beh*, 8(3): 241-262, 2005.
2. Fifer et al. *IEEE Trans Neur Syst Rehab Eng*, 22(3): 695-705, 2013.
3. Moore et al. *Cons&Cogn*,18(4): 1056–1064, 2009.
4. Caspar et al. *Plos One*, 11(10): e0163892, 2016.
5. Peckham et al. *Arch Phys Med*, 82(10): 1380-1388, 2001.
6. Kuiken et al. *Lancet*, 369(9559): 3-9, 2007.
7. Schabowsky et al. *J NeuroEng Rehab*, 7: 36, 2010

ACKNOWLEDGEMENTS

We would like to thank the Schaefer School of Engineering and Science at the Stevens Institute of Technology for providing faculty start-up support.

Table 1: Performance (path length variability) and agency (estimation time offset) per operation condition

* $p < 0.05$	REACH-TO-GRASP RESULTS RELATIVE TO NORMAL					
	Normal	**Slow**	**Fast**	**Noisy**	**Auto**	**1-phase**
PERFORMANCE	3.6 cm (0%)	+31%*	-98%*	+7%	-89%*	N/A
AGENCY	73 msec (0%)	-89%*	+16%*	-3%	-47%*	+83%*

INCREASE IN MEDIAN NERVE LONGITUDINAL MOBILITY BY TRANSVERSE WRIST COMPRESSION IN PATIENTS WITH CARPAL TUNNEL SYNDROME

[1]Yifei Yao, [1]Emily Grandy, [2]Peter J. Evans, [2]William H. Seitz, Jr., [1,2,3]Zong-Ming Li
Hand Research Laboratory, Departments of [1]Biomedical Engineering, [2]Orthopaedic Surgery, and [3]Physical Medicine and Rehabilitation, Cleveland Clinic, Cleveland, OH, USA
email: liz4@ccf.org web: http://handlab.org/

INTRODUCTION

The carpal tunnel in the wrist is formed by the dorsal interconnected carpal bones and the volar transverse carpal ligament. Median nerve, one of the tunnel contents, is vulnerable to entrapment in the space-limited tunnel leading to compression neuropathy called carpal tunnel syndrome (CTS). It has been shown that patients with CTS have restricted median nerve excursion in the transverse direction at the distal [1] and proximal [2] level of the carpal tunnel, and in the longitudinal direction [3,4]. Nerve gliding exercises were developed for the purpose of increasing the mobility of the median nerve as treatment for CTS [5]. Recent studies support that the carpal tunnel space can be augmented by narrowing the carpal arch width [6-9]. Furthermore, it has been shown that applying radioulnar wrist compression (RWC) decreases median nerve flattening in patients with CTS [9]. The augmented carpal tunnel space might induce less flattening of median nerve thus leading to increase in median nerve mobility. However, the implications of RWC on median nerve mobility in CTS patients have not been examined. Therefore, the purpose of this study was to investigate the effects of RWC on the median nerve longitudinal mobility in the carpal tunnel in patients with CTS. It was hypothesized that the longitudinal median nerve mobility would be enhanced in CTS patients under RWC.

METHODS

Eleven (n=11) patients diagnosed with CTS (51.5±16.3 years; 7 female, 4 male; 8 right hands, 3 left hands) participated in this study. The subjects were recruited based on a history of paresthesia, pain, aching, tingling, dull, weakness, clumsiness and/or numbness in the median-innervated hand territory for at least three months, at least one positive physical examination of Tinel's sign, Phalen's test or carpal compression test, and a mean CTS Severity Score greater than 1.5 [10]. All subjects provided written informed consent for the study approved by the Institutional Review Board. Each patient lay supine on a testing bed with the arm abducted and hand supinated, while the wrist fit in a custom-made RWC system. The thumb was fixed in 45° extension and the proximal/distal interphalangeal joints of the four fingers were fixed in anatomical neutral position (Figure 1), but the metacarpophalangeal joints are free to move.

Figure 1. Experimental setup of in vivo ultrasound imaging

The RWC system applied transverse compressive forces of 0, 10 and 20 N across the distal carpal tunnel level for 3 minutes and then high-frequency (17 MHz) dynamic ultrasound images with 0.062 mm resolution captured the longitudinal median nerve within the carpal tunnel during finger flexion/extension. Each force condition was repeated three times in a randomized order. A 3-minute rest was provided between consecutive trials. Angular finger motion at the metacarpophalangeal joints were recorded by an electrogoniometer which was synchronized to ultrasound image capture. Cyclic finger flexion/extension was conducted between neutral (0°) and 90° flexion at a pace of 0.3 Hz. Longitudinal median nerve displacement was analyzed by a custom LabVIEW program using speckle cross-correlation algorithm [11]. The program defined regions of interest (ROIs) (6.2×1.8 mm) at a 0.62 mm increment along the midline of the median nerve ranging from proximal to distal boundaries of the tunnel. Each ROI frame by frame

corresponding to individual finger flexion angles. Median nerve displacement in the carpal tunnel was calculated as the mean value of individual displacements of all ROIs. Least-squares linear regression was performed for median nerve displacement as a function of finger flexion angle. The slope of the linear equation was used to quantify the mobility of the nerve. One-way Friedman repeated measures ANOVAs were performed to examine the effect of force magnitude (0, 10, and 20N) on the median nerve mobility. Post-hoc Tukey's tests were used for pairwise comparisons and p-value less than 0.05 was considered statistically significant.

RESULTS

R-square values of the linear regression on the median nerve displacements in the carpal tunnel as a function of finger flexion from all subjects were 0.9 ± 0.01. Median nerve mobility was significantly affected by the RWC levels ($p<0.05$, Figure 2). Pairwise comparisons showed that the median nerve mobility under 10N RWC (0.0053 ± 0.0022 mm/degree) was significantly greater than the no compression condition (0N) (0.0034 ± 0.0015 mm/degree, $p<0.05$). However, the median nerve mobility did not differ between 0N and 20N conditions ($p=0.23$) nor between 10N and 20N conditions ($p=0.47$).

DISCUSSION

This study revealed that compression applied to the wrist in the radioulnar direction could enhance the median nerve longitudinal mobility in CTS patients. Previous studies have demonstrated that CAW can be narrowed with increasing carpal arch area [6, 7], and that this narrowing can be achieved in vivo [8, 9]. The increase in median nerve mobility of CTS patients from wrist compression in the current study might due to the increase of carpal arch area and decompression of median nerve. Surprisingly, 20N wrist compression didn't increase the median nerve mobility as 10N wrist compression did. The increase of transverse wrist compression did not necessarily increase the median nerve longitudinal mobility. The excessive compression could increase more carpal tunnel area but might hinder the median nerve mobility. Median nerve mobility might be dependant on multiple surrounding biomechanical factors. Moderate wrist compression may provide relief of nerve compression in patients and restore the median nerve mobility with CTS. One limitation of this study was that tracking of the median nerve might be inaccurate due to the same tracked nerve region moving out of the image plane. Experimental and image processing methods can be improved to accurately track nerve motion with dynamic imaging in 3D.

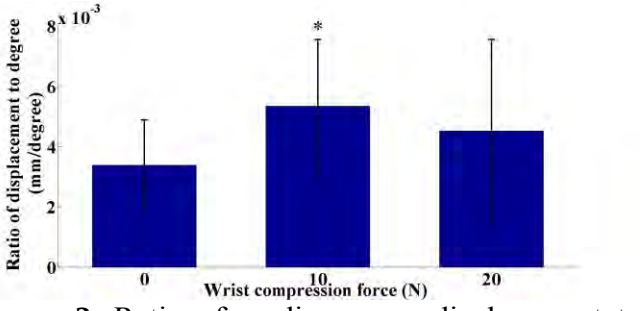

Figure 2. Ratio of median nerve displacement to the finger flexion degree (median nerve mobility) under the force magnitudes of 0, 10, and 20N. (* $P<0.05$).

ACKNOWLEDGEMENT

NIH/NIAMS R01AR068278

REFERENCES

[1]. Nakamichi and Tachibana. J Hand Surg [Br] 20.4 (1995): 460-464. [2]. Kuo et al. PLoS one 11.1 (2016): e0147051. [3]. Hough et al. Arch Phys Med Rehabil 88.5 (2007): 569-576. [4]. Filius et al. J Orthop Res 33.4 (2015): 483-487. [5]. Akalin et al. Am J Phys Med Rehabil. 2002; 81(2):108-113. [6]. Li et al. J Biomech Eng (2009) 131(8):p. 081011. [7]. Li et al. Clin Biomech (2013) 28(4): p.402-7. [8]. Marquardt et al. Clin Biomech (2015) 30(3), pp.248-253. [9]. Marquardt et al. J Orthop Res (2016) 34(7), pp.1234-1240. [10]. Levine et al. J Bone Joint Surg Am. (1993) 75 (11):1585-92. [11]. Dilley et al. Ultrasound Med Biol, 27 (2001): 1211–1218.

A Texture-Based Supervised Learning Framework For Morphology Of Plantar Soft Tissue

[1,2] Lynda Brady, [2]Christina Stender, [3]Yak-Nam Wang, [2]Matthew Kindig, [1,2,4]William Ledoux

Departments of [1]Mechanical Engineering and [4]Orthopaedics & Sports Medicine, and
[3]Applied Physics Laboratory, University of Washington, Seattle, WA, USA
[2] Center for Limb Loss and MoBility, VA Puget Sound, Seattle, WA, USA
email: lybrady@uw.edu

INTRODUCTION

The structure of biological tissue has been shown to affect its function. In the case of plantar soft tissue, the unique structure of the fat chambers is hypothesized to play a vital role in force dissipation and energy absorption during walking. [1,2] Prior work used dissection and histological methods to define the structure of typical healthy plantar soft tissue. [1,2] However, there are inherent limitations to histological morphological analysis.

Typically, manual morphological analysis is time-intensive, prohibiting comprehensive analysis of a large-scale study. Recent advances in computer vision have enabled rapid automated tissue identification. Using texture-based tissue classification methods could be an efficient and accurate way to obtain comprehensive morphological information in large-scale structure-function investigations.

METHODS

Kather's open-source texture-based multiclass classification framework originally developed for preliminary histopathological prostate cancer diagnosis [3] was expanded to include 14 texture-based feature detectors, 5 feature set reduction strategies, and 9 classification algorithms (Table 1).

Plantar soft tissue specimens were obtained from nine fresh cadaveric feet (age range: 61-79 years) and prepared for histological analysis using standard methods for modified Hart's stain for elastin. Large, whole-slide images of resolution 2.43 um/px were obtained using a Nikon Eclipse i80. 3500 smaller single-tissue training images were extracted from a subset of images obtained. The training images were comprised of five unequal groups of single tissue classes (adipose n=885, dermis n=540, epidermis n=361, muscle n=464, sepate n=522) and background (n=727) for six total classes. Feature detection algorithms were applied to these training images to reduce each image into vectors of textural information. These vectors stored the unique textural features of each tissue for identification and of the six tissue and background classes in the whole-slide images.

Following feature identification, feature set reduction strategies were employed to reduce the number of features applied to the classification to only those features most relevant to each texture; this decreases the likelihood of overfitting the classification model. Reduced feature sets were used to train classifiers, and the trained classifiers were then tested on the training data using 10-fold cross validation. Classifier accuracy was assessed using the multiclass Matthews Correlation Coefficient (MCC) to account for both false positive and false negative error across all six classes. After training, the best classifiers were identified using the multiclass MCC score. These classifiers were applied tile-wise to the whole-slide images in order to segment the whole-slide images into tissue sections. Segmented images were compared to ground-truth whole-slide images which were manually segmented by a trained histologist.

RESULTS AND DISCUSSION

The three best MCC scores achieved for classification of the training images were obtained using sequential backward selection-reduced RGB color space histogram features with radial basis SVM (MCC=0.96), f-IOCLBP all features with linear SVM (MCC=0.958), and stepwise multilinear regression-reduced f-IOCLBP features and radial basis SVM (MCC=0.957) (see Table 1 for

abbreviations). These accuracy measures are expected to be larger than those of a new data set given the reuse of training and testing data. In the more difficult task of whole-slide image segmentation, preliminary results indicate that the f-IOCLBP algorithm with all 342 features and linear SVM classification yielded the highest accuracy of 80.21% (Figure 1). This segmentation accuracy may be improved by changing the size of tiles used in tile-wise comparison, combining feature sets, or further feature reduction to alleviate overfitting errors.

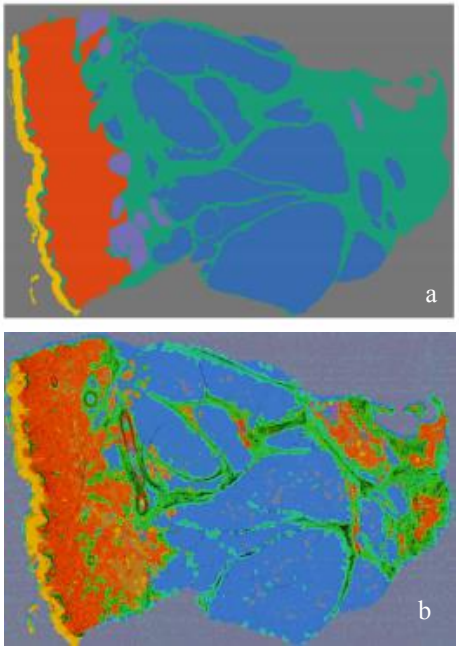

Figure 1: a. Manually-segmented ground-truth b. Classification segmentation of the same whole-slide image with all 342 f-IOCLBP features and linear SVM classification.

CONCLUSIONS

Many machine learning methods developed for cancer histopathology are applicable to issues in biomechanics. Rapid quantification of tissue morphology can enable large-scale study of structure-function relationships when coupled with classic *in vitro* mechanical testing. Additionally, the comprehensive study of entire histomorphological specimens without sacrificing information through statistical sampling could provide insight into the bias introduced using sampling methods or regional microscopic morphological variation within tissues. This texture-based classifier is a promising first step toward rapid morphological analysis. Optimized tile size, more tissue classes, and better feature reduction strategies should be investigated to improve the segmentation accuracy of this framework.

REFERENCES

1. Bleschmidt, E. *Foot Ankle.* (1982) **2**(5): 260-83.
2. Buschmann, W.R., et al. *Foot Ankle Int*. (1995) **16**(5):254-8.
3. Kather, J.N., et al. *Scientific Reports*. (2016) **6**.27988

ACKNOWLEDGEMENTS

Thank you to Alyssa Ricketts for help with image acquisition and Kara Lee for slide preparation.

Table 1: Feature detection methods with number of features generated per tissue, feature set reduction strategies, and classification algorithms.

Feature detection *(num. features)*	**Feature Set Reduction**	**Classification**
Histogram lower-order *(5)*	Correlation	1st-nearest neighbor
Histogram higher-order *(10)*	ReliefF	Linear support vector machine (SVM)
Fourier-reduced local binary pattern *(38)*	Stepwise multilinear regression	Radial basis support vector machine (SVM)
Gray-level co-occurrence matrix (GLCM) *(10)*	Sequential forward selection	RUSBoost
Gabor filter *(9)*	Sequential backward selection	ADABoost
Perceptual *(5)*		Bag
Undirected graphical mode (UGM) *(5)*		Subspace
Color space lower-order histograms *(75, 15 each for native and transformed color spaces: RGB, LaB, YIQ, YCbCr, HSV)*		Naïve-Bayes
Fourier-reduced improved opponent color local binary pattern (f-IOCLBP) *(342)*		Optimized nearest-neighbor

FORCE, DISPLACEMENT, AND WORK PROFILES OF STRUCTURES DISTAL TO THE SHANK

[1] Erica A. Hedrick, [2] Steven J. Stanhope, [1]Kota Z. Takahashi
[1] Department of Biomechanics, University of Nebraska at Omaha, Omaha, NE USA
[2] Department of Kinesiology & Applied Physiology, University of Delaware, Newark, DE USA
email: ehedrick@unomaha.edu, web: https://www.unomaha.edu/college-of-education/cobre/

INTRODUCTION

An objective understanding of human foot and ankle function can drive innovations and development of 'bio-inspired' wearable devices, such as prostheses, and exoskeletons. Specifically, knowledge regarding how mechanical force and work are produced within the biological foot-ankle structures can help determine what type of materials (e.g., elastic or viscous) or components (e.g., battery-powered actuators) are required to engineer biomimetic devices. A recent study of human walking found that the biological foot-ankle structures (when accounting for contributions from all anatomical subsections) produce near equal magnitudes of negative and positive work [1]. In other words, the biological foot-ankle structures are mechanically similar to an elastic unpowered device that can store and return energy. This knowledge may facilitate the optimization of unpowered devices that are inexpensive, yet highly functional.

For future designing or customization of wearable foot-ankle devices, a generalized technique to synthesize mechanics of structures distal to the shank is warranted, such as quantifying the total force, displacement, and work. For example, displacement of the center-of-pressure relative to the shank during stance in normal walking has been used to quantify the 'net deformation' of the foot-ankle system [2]. Such information has yielded novel approaches for prescribing prosthetic foot-ankle components that attempts to preserve a natural 'roll-over shape' [2]. Yet, to prescribe elastic devices that can store and return mechanical energy, a comprehensive knowledge regarding the force, displacement, and work of the biological foot-ankle system is needed.

The purpose of this study was two folds. First, we aimed to quantify the total force, displacement, power, and work of all structures distal to the shank in normal walking. Second, we tested the hypothesis that subject's body height and mass are strong predictors for the individual variability of force, displacement and work. This knowledge would facilitate creation of a simple data-driven model that could predict idealized force, displacement and work profiles (distal to the shank) that may be used to customize unpowered wearable foot-ankle devices, such as prostheses and exoskeletons.

METHODS

Eleven healthy subjects (6 females, 5 males, ages 24.2 ± 2.9 yrs, height 1.72 ± 0.08m, and body mass 75.3 ± 21.8 kg) participated in a fully-instrumented gait analysis. Prior to data collection, subjects were instrumented with a 6 degrees-of-freedom marker-set [3] to estimate the motions of the lower extremity during walking. The subjects walked barefoot at four walking velocities: 0.4, 0.6, 0.8 and 1.0 statures/s. The data from one walking velocity (0.8 statures/s) was included in this abstract. Data was processed and analyzed using Visual3D software (C-Motion Inc., Germantown, MD). A second-order dual-pass low-pass Butterworth filter (6Hz for kinematic data and 25Hz for kinetic data) was applied to the raw data.

To quantify force and displacement relative to the shank during stance, we transformed the ground reaction force and center-of-pressure (COP) data from the laboratory coordinate system to the shank's coordinate system (SCS), respectively [2]. To quantify mechanical power due to all structures distal to the shank, we used a unified deformable segment analysis [4]. To quantify mechanical work, we integrated power over time.

Multiple regression analyses were performed to determine if body height and weight were related to measures of force, displacement and work. Specifically, we analyzed the peak force in the anterior-posterior (A-P) and superior-inferior (S-I) axes of the SCS, as well as the total displacement along the A-P and S-I axes. We also examined the positive and negative mechanical work.

RESULTS AND DISCUSSION

During the first ~75% of stance, the structures distal to the shank (i.e., foot-ankle) produced negative power, whereas during the last ~25% of stance, the structures produced positive power (Figure 1a). These structures produced slightly greater magnitude of negative work (-16.18 ± 8.05 J) than positive (13.14 ± 4.57 J), resulting in slight net negative work (-3.05 ± 5.63 J) (Figure 1b). Body height and body mass accounted for 66.1% of the variance in positive work ($p=0.013$) and 85.5% of the variance in negative work ($p<0.001$). Body mass significantly predicted positive work ($\beta=.789$, $p=0.014$) and negative work ($\beta=-.877$, $p=0.001$). However, body height was not significantly correlated to either.

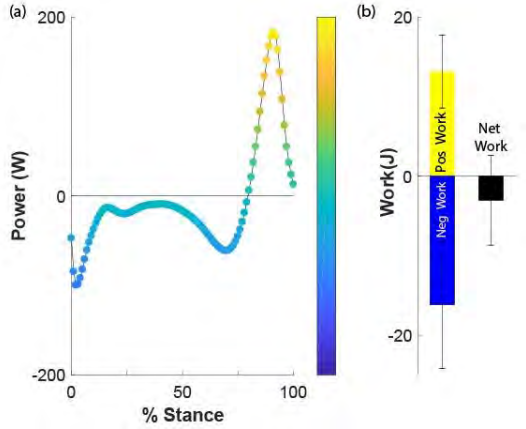

Figure 1. Average mechanical power (a) and work (b) distal to the shank during stance phase (N=11). The colors correspond to the intensity of the power. The magnitude of negative work (blue) is slightly greater than positive work (yellow), resulting in slight net negative work (black).

The COP in the SCS primarily displaced in the anterior direction during stance (Figure 2). The COP displaced in the superior direction in the presence of a superior-directed force through most of stance, which is analogous to a spring being compressed longitudinally (i.e., foot-ankle structures performing negative work) (Figure 2). During terminal stance, the COP displaced in the inferior direction in the presence of a superior-directed force, which is analogous to a spring recoiling after being compressed (i.e., foot-ankle structures performing positive work). Body height and body mass did not significantly account for the variance in displacement along the A-P and S-I axes. Body height and body mass explained 67.9% of the variance in the peak force along the A-P axis ($p=0.011$) and 99% of the variance in the peak force in the S-I axis ($p<0.001$). Body mass significantly predicted peak force in the A-P axis ($\beta=-.584$, $p=0.046$) and peak force in the S-I axis ($\beta=.986$, $p<0.001$), however body height was not significant.

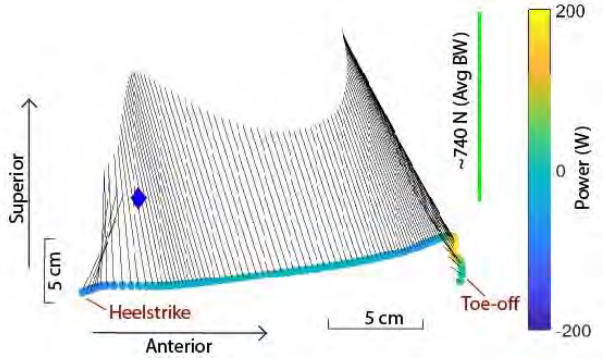

Figure 2: Displacement, force and power distal to the shank during stance phase. The colored circles indicate displacement of the COP in the shank coordinate system (SCS), and the colors of the circles represent power intensity at each point in stance. Black lines represent the ground reaction force in the SCS, in which the length of the vector denotes the magnitude of the force. Blue diamond represents the location of the ankle joint center in the SCS.

CONCLUSIONS

The force, displacement, and work characteristics of distal-to-shank structures in normal walking are largely predicted by body mass. These findings can inform the design and customization of unpowered foot-ankle devices (prostheses, exoskeletons) that can emulate biological functions during walking.

REFERENCES

1. Takahashi, K. Z.et al. *Sci Rep* **7**, 15404, 2017.
2. Hansen, A. H.et al. *Clin.Biomech.* **19**, 407-414, 2004.
3. Holden, J. P., & Stanhope, S. J. *Gait Posture* **7**, 1-6, 1998.
4. Takahashi, K. Z.et al. *J.Biomech.* **45**, 2662-2667, 2012.

ACKNOWLEDGEMENTS

This work was supported by the Center for Research in Human Movement Variability of University of Nebraska at Omaha, NIH (P20GM109090).

ANKLE KINEMATICS VARY WITH THE NUMBER OF SEGMENTS IN MULTI-SEGMENT FOOT MODELS

[1]Hoon Kim, [1]Marwan Aljohani, [1]William I. Wolf, and [1]Kristof Kipp

[1] Marquette University, WI, USA
email: hoon.kim@marquette.edu

INTRODUCTION

The biomechanical analysis of human movements depends on the use of appropriate musculoskeletal models. One important issue with respect to modeling the foot-ankle complex concerns the number of segments within the musculoskeletal model. For example, multi-segment foot models (MFM) produce results that are more realistic foot-ankle movements than single-segment foot models [1]. While MFM appears to be more appropriate, the number of foot segments and the definitions of segments differ greatly between models. The purpose of this study was to compare ankle joint kinematics derived from MFM with different number of segments (2-segment MFM (2MFM) vs. 5-segment MFM (5MFM)).

METHODS

Four male collegiate track and field athletes (22±0 years old, 1.85±0.05m, 79.8±5.0kg) participated in this study. All athletes signed an informed consent form, which was approved by the University's Institutional Review Board.

Fifty-one reflective markers (with at least 3 markers per segment) were attached to bony landmarks of all participants. The three-dimensional positions of the markers were recorded with a motion capture system (Vicon 612, Vicon, Los Angeles, CA, USA) at 100 Hz. Ground reaction forces were recorded from two force plates (OR6-6, AMTI, Watertown, MA, USA) at 1000 Hz. Kinematic data were filtered with a 4th order low-pass Butterworth filter at a cutoff frequency of 12 Hz.

Athletes performed vertical hopping tasks at three different frequencies (2.0 Hz, 2.2 Hz, and 2.4 Hz). After being familiarized with the tasks, subjects hopped at each frequency for approximately 10 seconds. The ground reaction force data were used to detect the stance phase during the hopping tasks. Five hops from each hopping tasks were selected for analysis.

Two MFMs (2MFM and 5MFM) were scaled to each athlete [1]. The 5MFM consists of five segments in the foot (talus, calcaneus, midfoot, forefoot, and toes). For the 2MFM, the articulations between calcaneus, midfoot, forefoot, and toes were locked such that only the talus and foot segments remained. Three-dimensional ankle joint kinematics were calculated using inverse kinematics (IK) procedures in OpenSim [2].

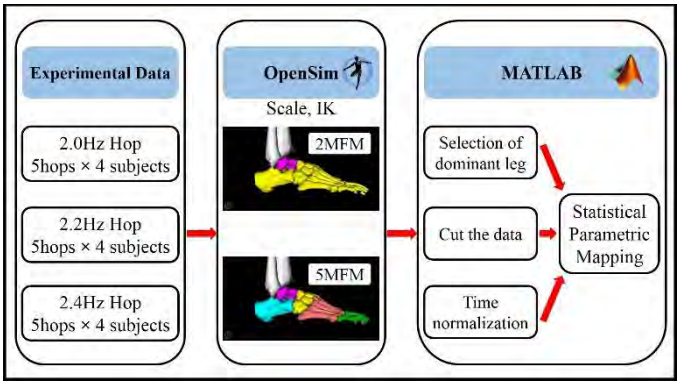

Figure 1: Workflow chart

Stance-phase ankle joint kinematics of the 2MFM and 5MFM in the frontal and sagittal plane were time-normalized and compared with Statistical Parametric Mapping (SPM) [3].

RESULTS AND DISCUSSION

The SPM analysis indicated significant effects between the 2MFM and 5MFM ankle kinematics in the sagittal and frontal plane for all hopping frequencies. Given that the effects were similar for all three hopping frequencies, only data from the 2.0 Hz will be discussed.

In the sagittal plane, the SPM analysis indicated significant differences in kinematics across almost the entire stance phase; identically smooth random time-series data would produce a cluster of this

breadth with a probability of $p = 0.001$ (Figure 2). In the frontal plane, the SPM analysis indicated significant differences in kinematics at the beginning and end of the stance phase; identically smooth random time-series data would produce clusters of this breadth with a probability between $p = 0.046$ and $p = 0.025$, respectively (Figure 2).

Model-based differences in dorsi-/plantar flexion at the talocrural joint occurred across most of ground contact, whereas differences in inversion/eversion at the subtalar joint occurred during the early phase and end phase of ground contact. However, the kinematic patterns at the talocrural joint are similar to each other. In contrast, the motions at the subtalar joint differed such that with the 2MFM there was more inversion during early and end phase and less inversion during the middle phase of hopping. Difference in frontal plane kinematics may have important clinical implications because excessive subtalar joint motion is purported risk factor for lateral ankle sprains.

Modeling the ankle-foot complex with an appropriate number of segments therefore seems to be important issue when researchers investigate kinematic characteristics associated with injury prevention and rehabilitation.

REFERENCES

1. Malaquias, T. M, et al. (2017). *Comput Methods Biomech Biomed Eng*, *20*(2), 153-159.
2. Delp, S. L, et al. (2007). *IEEE T Bio-Med Eng*, *54*(11), 1940-1950.
3. Pataky, T. C. (2010). *J Biomech*, *43*(10), 1976-1982.

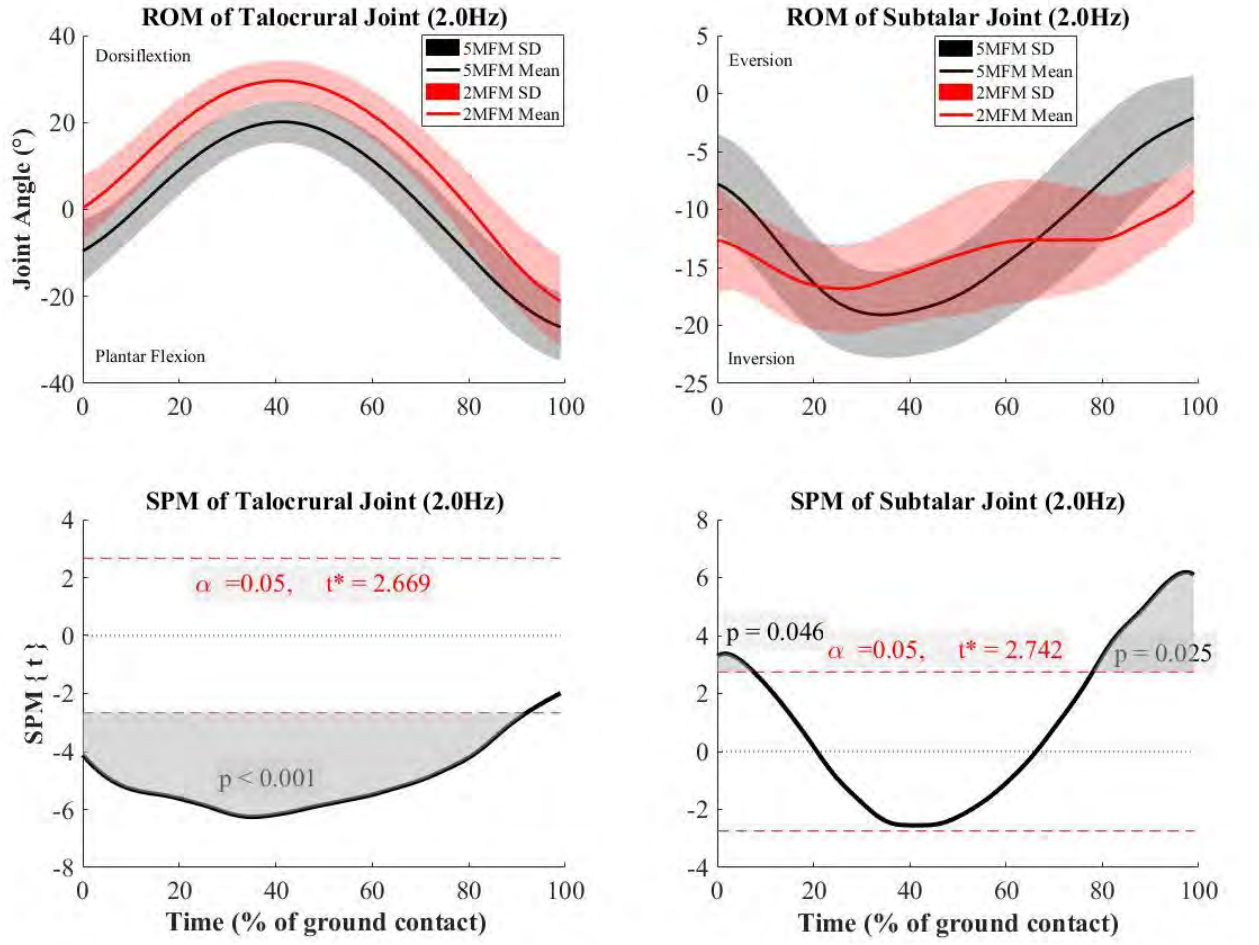

Figure 2: Mean ± SD (top row) and SPM analysis results (bottom row) of ankle kinematics in sagittal plane (first column) and frontal plane (second row) for the 2MFM and 5MFM.

SUBTALAR KINEMATICS AFTER TIBIOTALAR ARTHRODESIS

[1]Amy L. Lenz, [1] Koren E. Roach, [2]Jennifer A. Nichols,
[1]Alexej Barg, [1]Charles L. Saltzman, [1]K. Bo Foreman, [1] Andrew E. Anderson

[1] University of Utah, Salt Lake City, UT, USA
[2] University of Florida, Gainesville, FL, USA
email: amy.lenz@utah.edu
web: http://medicine.utah.edu/orthopaedics/research/labs/harold-dunn/dunn-research-groups/anderson-lab/

INTRODUCTION

Each year there are 100,000 new cases of tibiotalar osteoarthritis (OA) in the United States [1]. Tibiotalar OA is characterized by pain, difficulty walking, and a poor quality of life [1, 2]. Surgery, including tibiotalar arthrodesis and total ankle replacement, is the only reliable treatment option for end-stage tibiotalar OA [3]. Tibiotalar arthrodesis, which involves fusing the tibia and talus, is most commonly performed. This procedure alleviates pain, but nearly 50% of patients are unable to return to their desired activities due to complete restriction of the tibiotalar joint [4]. Eliminating tibiotalar motion may also contribute to secondary OA at the adjacent joints in the hindfoot, especially the subtalar joint [5]. Measurements of subtalar kinematics after tibiotalar arthrodesis would improve our understanding of the biomechanical effects of this surgery, and could identify the pathogenesis of OA at this joint.

The objective of this study was to quantify in-vivo, dynamic subtalar motion using dual-fluoroscopy (DF), which is a radiostereometric technique that accurately measures in-vivo bone motion without the use of markers adhered to the skin. We hypothesized that the subtalar joint of the arthrodesis limb would demonstrate increased motion relative to that of the contralateral, asymptomatic, non-surgical ankle.

METHODS

In this IRB-approved (University of Utah #65620) preliminary study, four asymptomatic patients who previously underwent unilateral tibiotalar arthrodesis were studied (2 men, 2 women; 53.8 ± 9.5 yrs; BMI 26.9 ± 3.2 kg/m^2, 2 right, 2 left). The mean time from surgery to testing was 4.0 ± 2.1 years. Plain film radiographs were collected prospectively to screen participants for subtalar deformities or degeneration on the arthrodesis limb and for OA and/or deformities on their contralateral limb. No subjects were excluded based on these criteria.

A validated high-speed DF system was used to measure subtalar kinematics [6]. All participants completed one trial of overground barefoot walking at a self-selected speed. A computed tomography (CT) scan of each patient was acquired (SOMATOM Definition AS; Siemens Medical Solutions) from mid-tibia through metatarsals at a 0.6 mm slice thickness. For each patient, the fused tibia/talus and calcaneus were segmented on the surgical side and the tibia, talus, and calcaneus were segmented on the contralateral side (Amira 6.0; Visage Imaging). Markerless tracking [7] was used to quantify in-vivo motion of the subtalar joint on the surgical and contralateral side. Subtalar joint angles were calculated using landmark based coordinate system definitions [8] and the Grood and Suntay method [9].

Given the small sample, the mean 95% confidence intervals (CIs) of the joint angles were plotted to visualize group profiles. Separate paired t-tests assessed subtalar joint angle differences between the arthrodesis and contralateral limbs. Comparisons were made between total ranges of motion (ROM) during stance and for the joint angle magnitude and direction at three separate time points (i.e., loading response, mid-stance, terminal stance) corresponding to 15%, 50%, and 85% of normalized stance.

RESULTS AND DISCUSSION

Arthrodesis and contralateral subtalar joint angles did not consistently differ when visualizing their 95% CI joint angle profiles during the entire stance phase (Figure 1). However, over the entire activity, the arthrodesis subtalar joint 5.5º (4.3º, 6.8º) exhibited significantly less inversion/eversion ROM ($p = 0.01$) than the contralateral limb 7.8º (6.7º, 8.8º) with a trend towards inversion. When analyzed at the discrete time points, significant differences were found in one instance. Specifically, during the

loading response, the arthrodesis subtalar plantarflexion angles were significantly greater than those of the contralateral limb (p=0.03). Clinically, the increased plantarflexion occurring at loading response indicates hypermobility. The hypermobility may be compensating for the fixed tibiotalar joint, which no longer allows for this typical motion as the limb transitions to weight-bearing.

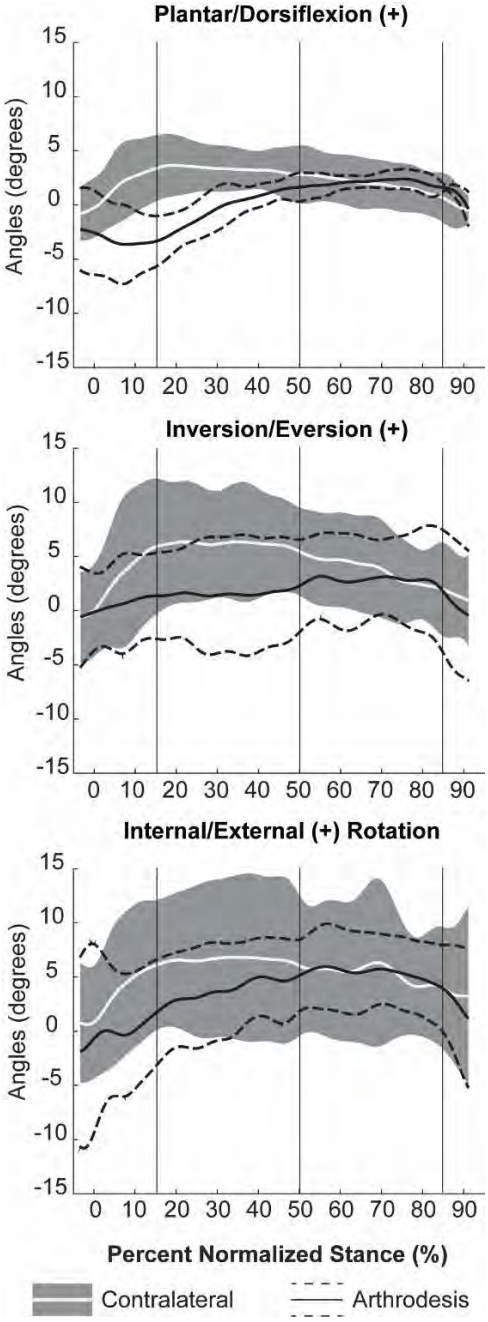

Figure 1: Mean (± 95% CI) subtalar joint angles for the surgically-altered limb (black) compared to the non-surgical contralateral limb (gray). Data are plotted per normalized percent stance. Vertical lines correspond to discrete time points that were analyzed.

Considering the small sample size, a post-hoc power analysis was conducted. For comparisons of Inv/Ev ROM and loading response plantarflexion, calculated power was 86% for Inv/Ev and 99.9% for loading response results. However, we recognize that our population size is a statistical limitation and are currently analyzing 6 additional asymptomatic tibiotalar arthrodesis subjects.

CONCLUSIONS

To our knowledge, this is the first study to investigate subtalar kinematics following arthrodesis using DF. We found altered subtalar joint angles in the arthrodesis limb, providing evidence that compensatory motion may induce OA in joints adjacent to the fusion site. Although only a preliminary study, our results are encouraging and warrant further investigation using a larger sample size. In the future, we intend to study patients undergoing arthrodesis pre- and post-surgical intervention to understand to what extent compensatory movements exist pre-operatively during the onset of OA. Clinically, patients may already demonstrate stiffness of their subtalar joint secondary to post-traumatic injuries which would not be addressed by fusing the tibiotalar joint. Ultimately, these data may provide the information necessary to develop novel treatment strategies aimed at alleviating pain and improving function.

REFERENCES

1. Brown et al. *J Orthop Trauma.* 20(10): 739-744, 2006.
2. Lawrence et al. *Arthritis Rheum.* 58(1): 26-35, 2008.
3. Ahmad et al. *Foot Ankle Clin.* 13(3): 381-400, 2008.
4. Ajis et al. *Foot Ankle Int.* 34(5): 657-665, 2013.
5. Easley et al. *J Bone Joint Surg Am.* 90(6): 1212-1223, 2008.
6. Wang et al. *Gait Posture.* 41(4): 888-893, 2015.
7. Bey et al. *J Orthop Surg.* 3(38): 1-8, 2008.
8. Roach et al. *J Biomech Eng.* 138(9): 1-9, 2016.
9. Grood and Suntay *J Biomech Eng.* 105:136-144, 1983.

ACKNOWLEDGEMENTS

Funding from the Orthopaedic Research Society and Orthopaedic Research Education Foundation (ORS/OREF Postdoctoral Fellowship), the National Institutes of Health (NIH R21 AR069773), and the L.S. Peery Discovery Program in Musculoskeletal Restoration is gratefully acknowledged.

INFLUENCE OF LIFETIME RUNNING EXPOSURES ON ANKLE KINETICS AND PLANTARFLEXOR MORPHOLOGY

[1]Ramzi M. Majaj, [1]Douglas W. Powell, [1]Max R. Paquette

[1] The University of Memphis, Memphis, TN, USA
email: rmmajaj@memphis.edu, website: http://www.memphis.edu/shs/research/mal.php

INTRODUCTION

Aging is associated with reductions in walking (1) and running (2) speeds. Older runners run with reduced preferred (2) and maximal (3) running speed accompanied by a reduction in step length (2,3) which may be the result of lower magnitudes propulsive forces and ankle kinetics observed with aging (2). Running experience (4), volume and intensity (5) may contribute to the preservation of ankle kinetics as runners age. Further, running training also appears to influence morphological properties of plantarflexors with age (6). However, the influence of lifetime running exposure on ankle kinetics during running and, morphological properties of plantarflexors is not well understood.

Considering the importance of training stimuli on endurance performance and muscle function in older adults, the purpose of this study was to examine the influence of lifetime running exposure on ankle kinetics during running, and medial gastrocnemius (MG) morphological properties in older runners. We hypothesized that older runners with higher lifetime running exposure would run with larger peak ankle moment and positive power compared to runners with low lifetime running exposure. We also expected that runners with high lifetime running exposure would have larger pennation angle, shorter fascicle length, and greater fascicle stiffness of the MG compared to runners with lower lifetime running exposure.

METHODS

Runners over 50 years of age with different lifetime running exposure participated in the study. Participants were grouped in low (LRE; 8834±3823 miles; n=12; 59±8 yrs) or high (HRE; 45984±14967 miles; n=9; 62±7 yrs) lifetime running exposure (Table 1). Lifetime training exposure was defined as the product of number of lifetime running years, average weekly lifetime running mileage, and average number of weeks running per year. During a single testing session, participants performed five successful over-ground running trials at 2.7m/s (±5%) while kinematic (240Hz Qualisys, Sweden) and ground reaction force (GRF) (1200Hz, AMTI, USA) data were collected simultaneously using Qualisys, Track Manager software. Using kinematic and GRF data, net joint moments were calculated using Newtonian inverse dynamics (Visual3D, C-Motion), and joint powers were calculated as the dot product of joint moment and angular velocity. The average peak joint moments and positive powers of the five trials was used in statistical analyses.

Following the running trials, right MG morphological characteristics were assessed using a linear array ultrasound transducer (L12-4MHz Philips, Lumify; USA), positioned along the longitudinal axis of MG at ~50% of muscle length, and secured using a custom-designed plastic mold. Ultrasound images where taken in both rested and dynamic conditions. During these measurements, participants were secured to a custom-built table with a strain gauge (Model MLP-1k, Transducer Techniques, Temecula, CA) in line with a chain and a custom foot pedal used to target plantarflexor tensile forces. Participants were in a prone position with the ankle joint angle at 90 degrees. The plantarflexor tensile forces corresponded to 25%, 50%, 75%, and 100% of previously reported forces of plantarflexors during running (7). MG imaging and analysis were conducted by the same sonographer using free online software (ImageJ, NIH). Pennation angle (θ) was measured as the angle of insertion of muscle fascicle into the deep aponeurosis. Fascicle length (FL) was then computed for rested and dynamic images using a previously reported equation (8). Stiffness was computed as the slope of tensile forces applied on strain gauge, and changes in FL between rested and dynamic

conditions (ΔL). Independent sample t-tests ($p \leq 0.05$) (SPSS 24.0, IBM) and Cohen's *d* effect sizes were used to compare all dependent variables.

RESULTS AND DISCUSSION

Our results reveal no differences in step length, ankle plantarflexors and knee extensor torques and positive powers, and hip flexion torque between older runners of different lifetime running exposure ($p>0.05$) (Table 2). Runners with HRE ran with greater concentric hip power compared to runners with LRE ($p=0.020$; $d=1.16$). These results are consistent with previous literature showing that individuals with higher overall capacity produce more hip power during walking (9). These results demonstrate that although middle-aged runners run with similar positive joint powers as young runners when weekly mileage is similar between groups (5), more lifetime running exposure does not appear to improve ankle joint kinetics within an older runner population.

Table 2: Peak lower limb joint torques and positive powers (mean±SD).

	LRE	HRE
Propulsive Force (BW)	0.21±0.03	0.21±0.04
Ankle Torque ($Nm \cdot kg^{-1}$)	-2.2±0.2	-2.3±0.4
Ankle Power ($Nm \cdot kg^{-1}$)	6.8±0.8	7.2±2.0
Knee Torque ($Nm \cdot kg^{-1}$)	1.98±0.35	1.91±0.50
Knee Power ($W \cdot kg^{-1}$)	3.03±0.84	3.11±0.98
Hip Torque ($Nm \cdot kg^{-1}$)	0.67±0.11	0.70±0.18
Hip Power ($W \cdot kg^{-1}$) *	2.19±1.31	3.14±1.0

Notes: *: $p<0.05$ with moderate Cohen's *d* effect size.

MG imaging revealed that pennation angles under rested and all dynamic tensile forces were smaller for the HRE group compared to runners with LRE ($p<0.05$; $d=0.96$-1.04), with no differences in MG stiffness ($p>0.05$; $d=0.01$) (Table 3). Runners tend to have larger MG pennation under resting conditions compared to non-active individuals (4) but contradicting literature reports no differences in MG pennation angle between older adults with different training exposures (10). Conflicting evidence may be the result of the cross-sectional nature of these studies and it is evidence that longitudinal studies are still needed to understand the influence of lifetime training exposures on morphological properties of muscles.

Table 3: Fascial length (FL) change between rested and dynamic conditions, tensile forces (TF), and stiffness for MG (mean±SD).

	LRE	HRE
25% ΔL (mm)	7.18±2.85	5.24±2.38
50% ΔL (mm)	9.42±3.10	8.92±3.38
75% ΔL (mm)	11.31±3.28	10.60±2.76
100% ΔL (mm)	13.86±4.70	11.46±3.00
TF 25% (N)	148.2±21.8	137.1±19.3
TF 50% (N)	264.0±44.0	234.4±38.4
TF 75% (N)	378.9±67.6	332.5±50.1
TF 100% (N)	495.6±89.7	434.1±66.9
Stiffness ($N \cdot mm^{-1}$)	39.5±18.8	39.8±22.7

CONCLUSIONS

Lifetime running exposure in older runners does not appear to influence ankle and knee kinetics but runners with HRE appear to run with greater hip concentric power compared to those with LRE. In addition, lifetime running exposure does not appear to influence mechanical properties of MG despite differences in pennation angles. However, this study was cross-sectional and longitudinal cohorts are necessary to truly understand how lifetime running exposure may influence joint kinetics during gait, and muscle morphology in older runners. Finally, we are currently studying the influence of lifetime running exposure on gait biomechanics and plantarflexor morphology in older adults to better understand the impact of running on walking function with aging.

REFERENCES

1. Bohannon et al, *Age Aging* 26: 15-19, 1997.
2. Devita et al, *MSSE*. 48(1): 2016.
3. Korhonen et al, *MSSE*. 41(4): 844-856, 2009.
4. Karamanidis et al, *Gait Posture.* 25(4): 590-6, 2007.
5. Paquette et al, *MSSE*. 50(3): 510-515, 2018.
6. Karamanidis et al, *J Exp Bio.* 208: 3907-23, 2005.
7. Besier et al, *JOB*. 42: 898-905, 2009.
8. Kubo et al, *Int J Sp Med*. 24(2): 125-130, 2003.
9. Kuhman et al, *JOB*. 69: 90-95, 2018.
10. Stenroth et al, *J App Phys*. 120: 63-69, 2016.

ROBOTIC APPROACH TO CHARACTERIZE ALTERED ANKLE MECHANICS AFFECTED BY STROKE AND MULTIPLE SCLEROSIS

[1] Varun Nalam, [2,3] Megan C. Eikenberry, [2] Carolyn L. Kinney, [4] Dean Wingerchuk, and [1] Hyunglae Lee

[1] School for Engineering of Matter, Transport, and Energy, Arizona State University, Tempe, AZ, USA
[2] Department of Physical Medicine and Rehabilitation, Mayo Clinic, Phoenix, AZ, USA
[3] Department of Physical Therapy, Midwestern University, Glendale, AZ, USA
[4] Department of Neurology, Mayo Clinic, Scottsdale, AZ, USA

email: hyunglae.lee@asu.edu, web: http://faculty.engineering.asu.edu/hlee

INTRODUCTION

Neurological disorders, such as stroke and multiple sclerosis (MS), are one of the leading causes of adult disability around the world. These disorders often impact lower limb function such as postural balance and locomotion. While mounting evidence suggests that the human ankle joint plays one of the most important roles in lower limb function at the interface between the neuromuscular system and the physical world [1], little is known about how neurological disorders alter ankle mechanics and how this alteration impacts the overall quality of patients' lower limb function. This is mainly due to the lack of appropriate characterization technology. In this study, we proposed a robotic approach to characterize ankle mechanics during upright standing, ran a pilot study with stroke and MS subjects, and evaluated its reliability.

METHODS

Two chronic stroke survivors (age: 54-60, weight: 60-65 kg) and two relapsing and remitting MS patients (age: 49-50, weight: 63-81 kg) participated in this pilot study. All subjects were affected on their right leg. In addition, three healthy subjects (age: 23-31, weight: 56-71 kg) were recruited to serve as a reference. This study was approved by the Institutional Review Board of Arizona State University and all experiments were performed after informed consent of the subjects.

We utilized a novel multi-axis robotic platform to quantify stiffness and damping components of the ankle mechanics during upright standing in 2 degree-of-freedom (DOF) of the ankle, specifically, dorsiflexion-plantarflexion (DP) and inversion-eversion (IE) [2] (Fig. 1).

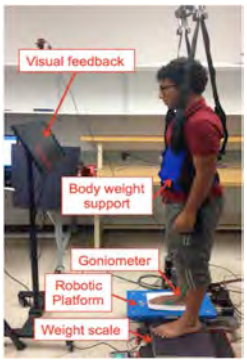

Figure 1 The experimental setup.

Each subject was instructed to stand upright with the right foot (affected side) on the robotic platform and the left foot on the weight scale, which was used to ensure equal weight distribution between legs. A dual-axis goniometer was attached to the subject's ankle to measure ankle angles in 2 DOFs. To encourage the subject to maintain the same upright posture, visual feedback was used, which displayed real-time center-of-pressure location in 2 DOFs as well as weight distribution between legs.

Once the subject maintained upright posture, ramp perturbations (amplitude: 3°, speed: 40°/s) were applied to the ankle in one of the 4 directions in random order: dorsiflexion, plantarflexion, inversion, and eversion. Ten repeated trials were completed for each perturbation direction.

Ankle stiffness and damping parameters in each DOF were quantified by fitting a 2nd order model (consisting of ankle stiffness, ankle damping, and foot inertia) to the measured kinematics and torques at the ankle. Reliability of quantification was evaluated by calculating the percentage variance accounted for (%VAF) between the measured ankle torques and estimated ankle torques from the best-fit 2nd order model.

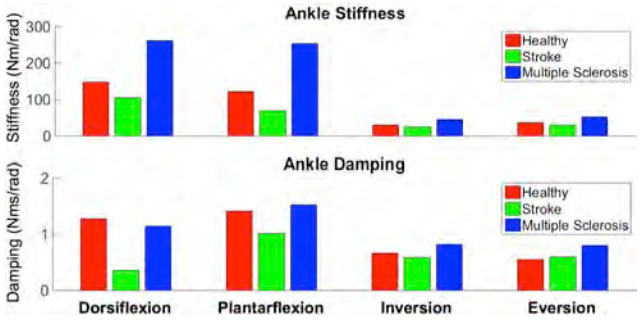

Figure 2: Comparison of ankle stiffness (A) and damping (B) of healthy, Stroke and MS subjects.

RESULTS AND DISCUSSION

In all stroke and MS subjects, the reliability for the characterization of ankle mechanics, i.e., %VAF, was higher than 98% in both DOF of the ankle and in any perturbation directions. This high reliability with a 2nd order model demonstrated that even altered ankle mechanics in stroke and MS patients could be accurately quantified by ankle stiffness and ankle damping parameters as in healthy subjects.

Ankle stiffness and damping in DP (DP stiffness and damping) of both stroke subjects were lower than those of healthy subjects (Fig. 2). In particular, DP stiffness of the first stroke subject was 2~3 times lower than the healthy human stiffness (Table I). Lower DP stiffness and damping could explain the prevalence of drop foot in stroke survivors.

Ankle stiffness in IE (IE stiffness) of both stroke subjects was lower than that of healthy subjects. However, the difference in IE stiffness between groups (stroke vs. healthy) was much smaller than DP stiffness. Ankle damping in IE (IE damping) was comparable to that of healthy subjects (Table I).

Contrary to the results in stroke subjects, DP stiffness of both MS subjects was higher than that of healthy subjects. In average, DP stiffness of MS subjects was about 2 times higher than the healthy human stiffness. This result may be due to higher spasticity and/or altered passive muscle properties in MS patients. DP damping of MS subjects was comparable to that of healthy subjects (Table I).

Both MS subjects exhibited higher IE stiffness and damping than those of healthy subjects. However, the difference in IE stiffness between groups was much smaller than DP stiffness (Table I).

CONCULSIONS

This study demonstrated that the proposed robotic approach based on a multi-axis robotic platform could be reliably used for the quantification of altered ankle mechanics in 2 DOFs in stroke and MS patients, evidenced by the high reliability measure in all experimental conditions.

This study also confirmed that altered ankle mechanics during upright standing are highly dependent on the type of neurological disorder. In addition, according to the results of this pilot study, both stroke and MS have higher impact on the alteration of ankle mechanics along DP in the sagittal plane than IE in the frontal plane.

Findings in this study support the need for individual characterization of altered ankle mechanics in order to deliver optimal patient-specific rehabilitation services. For example, the MS subjects in this study would need stretching exercises to increase joint flexibility, while the stroke subjects would need strengthening exercises to reduce weakness at the ankle joint.

REFERENCES

1. Winter. *Gait and Posture,* 3(4), 193-214, 1995
2. Nalam and Lee. *Proceedings of IEEE ICRA 2017*, Singapore, 511-516, 2017.

Table 1: Comparison of ankle stiffness and damping between healthy, stroke, and MS subjects.

Subject	Dorsiflexion		Plantarflexion		Inversion		Eversion	
	Stiffness Nm/rad	Damping Nms/rad	Stiffness Nm/rad	Damping Nms/rad	Stiffness Nm/rad	Damping Nms/rad	Stiffness Nm/rad	Damping Nms/rad
Healthy	147.99	1.27	121.53	1.41	29.23	0.66	37.20	0.54
Stroke 1	77.44	0.31	45.56	1.07	24.22	0.65	27.96	0.64
Stroke 2	132.45	0.41	91.95	0.95	25.12	0.51	31.38	0.55
MS 1	325.13	1.51	294.96	1.65	55.57	0.97	65.23	0.93
MS 2	198.22	0.77	211.54	1.39	35.65	0.67	40.23	0.68

REM sleep without atonia affects steady-state gait in early Parkinson's disease

Sommer Amundsen Huffmaster[1], Matthew Petrucci[1], Maria Linn[1], Michael Howell[1], Paul Tuite[1], Colum MacKinnon[1]

[1]Department of Neurology, University of Minnesota, MN, USA 55455
email: cmackinn@umn.edu, web: http://www.neurology.umn.edu/mackinnon_lab.html

INTRODUCTION

Advancing Parkinson's disease (PD) is associated with the emergence of postural instability and gait disturbances. These symptoms tend to occur earlier and be more severe in people that have PD and rapid eye movement (REM) sleep behavior disorder (RBD) [1]. RBD is a parasomnia characterized by dream enactment and elevated muscle activity during REM sleep (termed REM sleep without atonia, RSWA). People with RBD have a high probability of developing Parkinson's disease (PD) or a related neurodegenerative disorder [2,3], suggesting a link between the loss of REM sleep atonia and the neural system that controls gait and posture.

People with RBD and no diagnosis of neurodegenerative disease (e.g., PD) show abnormalities during steady-state gait. However, the variables affected were confined to those in the temporal domain including decreased velocity, cadence, and increased variability in double support and swing time [4]. For this reason, we tested the hypothesis that people with early PD who express RSWA would show significant changes in temporal measures of steady-state gait compared to those with PD without RSWA and matched controls.

METHODS

Thirty-three individuals with PD were tested (22 with RSWA+, age 65.1 ± 6.6, 11 females; 13 without RSWA-, age 62.5 ± 7.8, 7 females) along with 18 matched control subjects (age 60.8 ± 7.4, 12 females). Categorization of having abnormal levels of RSWA was based on the results of an overnight sleep test and assessment of REM sleep EMG activity from the polysomnographic recordings. PD subject's gait was tested after overnight withdrawal from Parkinson's disease medications. Steady-state gait was tested using a GaitRite walkway (CIR Systems, Inc, Franklin, NJ). Subjects were instructed to walk continuously at their comfortable walking pace around an oval course that included the GaiteRite walkway. A minimum of 35 full steps on the walkway were collected in each subject to ensure reliability [5]. Standard spatial and temporal gait characteristics were computed. Right and left leg variables were reassigned as being either more- (MA) or less-affected (LA) by Parkinson's disease (determined by summing their laterality scores from the Unified Parkinson's Disease Rating Scale). General linear model univariate ANOVAs were used to test for differences between groups (threshold for significance at $p < 0.05$).

RESULTS AND DISCUSSION

Significant main effects were observed for many of the temporal features of steady-state gait (Table 1). For follow-up comparisons of the PD-RSWA+ group to controls, gait speed ($p = 0.017$), and normalized speed (leg length/s; $p = 0.024$) were significantly slower while double-support time (MA: $p = 0.044$, LA: $p = 0.031$) and percent of gait cycle spent in double-support (MA: $p = 0.040$, LA: $p = 0.024$) were significantly longer. Similar effects were observed in lateralized variables. Percentage of the gait cycle spent in stance ($p = 0.004$) and swing ($p = 0.004$) with the LA leg were increased, and decreased, respectively, and the percentage of the cycle in single support of the MA leg was increased ($p = 0.004$) in the PD-RSWA+ group compared to controls. MA stride ($p = 0.038$) time variability was also significantly larger in the PD-RWSA+ group than controls. It is noteworthy that few differences in the temporal characteristics of gait were observed between the control and the PD-RSWA- groups, with the exception of LA stance time variability ($p = 0.003$). The only variables that showed significant differences between PD groups were LA stance ($p = 0.035$) and MA stride time variability ($p = 0.038$). Interestingly, PD-RSWA- had less variability compared to controls and PD-RSWA+. There were

no significant main effects of group across any of the spatial parameters of gait ($p > 0.05$).

CONCLUSIONS

Many of the timing variables associated with steady-state over-ground gait were different in the PD-RSWA+ group relative to matched controls subjects. In contrast, spatial variables were not significantly different across groups. Few differences were seen between those with PD-RSWA- and control subjects.

Our findings are consistent with the report that people with RBD, but no diagnosis of PD (although potentially in a prodromal stage of neurodegenerative disease), show significant changes in many temporal, but not spatial, gait variables [4]. This suggests that early pathophysiological changes in the brainstem circuitry controlling the regulation of muscle tone during REM sleep is associated with alterations in the timing of the locomotor cycle. Thus, simple temporal measures of gait may provide a biomarker of early or prodromal neurodegenerative process leading to postural instability and gait dysfunction. Individuals with these changes should be targeted for early exercise interventions to prevent or slow the evolution of gait impairment and perhaps slow disease progression.

REFERENCES

1. Postuma RB et al., *Neurology*. 66:845-851, 2006.
2. Schenck CH et al., *Sleep Med.* 14(8):744-8, 2013.
3. Boeve BF et al., *Brain*. 130:2770-2788, 2007.
4. McDade EM et al., *Movement Disorders.* 28(13):1847-53, 2013.
5. Galna et al., *Gait and Posture*. 375:580-5, 2013.

ACKNOWLEDGEMENTS

We acknowledge Josh DeKam for research coordination and Katia Rosenflantz for her assistance with data analysis. This study was funded by: Grant R01 - NS088679 from NINDS of the NIH. Additional support from: MnDRIVE, Udall Center of Excellence P50 NS09857, and UL1TR000114 from NCATS of the (NIH).

Table 1: Selected variables that exhibited significant main effects ($p < 0.05$) between groups.

	Controls (Mean ± SD)	PD-RSWA- (Mean ± SD)	PD-RSWA+ (Mean ± SD)	Main effects: F (*p*)	Post-hoc comparisons
Speed (cm/s)	133 ± 14	133 ± 13	120 ± 16	5.4 (*0.008*)	PD-RSWA+ < Controls
Normalized speed (leg length/s)	1.53 ± 0.18	1.47 ± 0.17	1.36 ± 0.20	4.1 (*0.023*)	PD-RSWA+ < Controls
Double support time (s)	MA: 0.29 ± 0.04 LA: 0.29 ± 0.04	MA: 0.30 ± 0.4 LA: 0.30 ± 0.4	MA: 0.33 ± 0.4 LA: 0.33 ± 0.4	MA: 3.6 (*0.035*) LA: 4.0 (*0.024*)	PD-RSWA+ > Controls
Double support %Cycle	MA: 27.1 ± 2.2 LA: 27.0 ± 2.4	MA: 28.2 ± 2.9 LA: 28.2 ± 2.9	MA: 29.3 ± 3.0 LA: 29.5 ± 3.0	MA: 3.3 (0.045) LA: 3.9 (*0.028*)	PD-RSWA+ > Controls
Single support %Cycle (MA)	36.4 ± 1.2	35.5 ± 1.5	34.9 ± 1.5	5.7 (*0.006*)	PD-RSWA+ < Controls
Stance %cycle (LA)	63.6 ± 1.2	64.4 ± 1.5	65.1 ± 1.5	5.7 (*0.006*)	PD-RSWA+ > Controls
Swing %cycle (LA)	36.4 ± 1.3	35.6 ± 1.5	34.9 ± 1.5	5.8 (*0.005*)	PD-RSWA+ < Controls
Stance time variability (std dev) (s) (LA)	0.022 ± 0.006	0.014 ± 0.006	0.020 ± 0.007	6.5 (*0.003*)	PD-RSWA- < Controls & PD-RSWA+
Stride time variability (std dev) (s) (MA)	0.21 ± 0.008	0.019 ± 0.006	0.28 ± 0.117	3.9 (*0.027*)	PD-RSWA+ > PD-RSWA-

ELECTROMYOGRAPHIC ASSESSMENT OF THE SHOULDER MUSCULATURE DURING PASSIVE REHABILITATION EXERCISES

[1] Janelle A Cross, [1] Mason Mocarski, [1] Nicholas Ketchum, [2] Eileen Craighead, [2] Matt Krimmer, [1] Carole Vetter

[1] Medical College of Wisconsin, Milwaukee, WI, USA
[2] Froedtert and the Medical College of Wisconsin Sports Medicine Center, Milwaukee, WI, USA
Email: jacross@mcw.edu

INTRODUCTION

Rotator cuff repair (RCR) surgery has a high rate of failure, with 25-94% re-tearing reported [1,2]. Failure is thought to be due to excessive strain on the surgical repair construct before proper healing has occurred, possibly through over activation of the rotator cuff muscles [3]. Persistent postoperative stiffness has been shown as a complication of RCR, with rates ranging up to or greater than 10% [4]. It is critical to engage the shoulder in passive range of motion exercises to avoid adhesions in the immobilized joint, while care is taken not to activate the muscles of the shoulder to avoid re-tearing of the surgical construct. The purpose of this study was to assess the activation of the shoulder muscles during passive exercises used in physical therapy immediately following RCR surgery using fine wire and surface electromyography (EMG).

METHODS

Approval was obtained from the Medical College of Wisconsin Institutional Review Board prior to beginning the study, and all subjects signed informed consent. 14 subjects, 8 females (24.9 ± 4.5 years) and 6 males (27.8 ± 3.1 years) were included in the study. Subjects were screened to determine eligibility. Exclusion criteria included: any history of shoulder injury, surgery, instability or pain, knowledge of rehabilitation exercises, as well as over the age of 50. The dominant hand shoulder was used for all subjects. All electrodes were applied by a board certified Physical Medicine and Rehabilitation physician. Four fine wire (fwEMG) electrodes were inserted into the supraspinatus (SUPR), infraspinatus (INFR), teres minor (TEMI) and subscapularis (SUBS) muscles, along with six surface (sEMG) electrodes placed on the biceps (BICE), posterior deltoid (PODE), lateral deltoid (LADE), anterior deltoid (ANDE), upper trapezius (UPTR) and the middle trapezius (MITR) following methods previously described [5,6].

EMG data were collected at 2000 Hz using a Delsys Trigno Wireless EMG system (Natick, MA) running EMGWorks 4.3.1 software. After EMG placement, maximum voluntary isometric contractions (MVIC) were recorded for each muscle. Using a Biodex System 3 to position the arm in the correct position, the subject was instructed to perform three maximal isometric contractions of each muscle for three second intervals, with ten seconds of rest between contractions. The peak amplitude during the three trials was defined as 100%.

Subjects were instructed by a licensed physical therapist in the proper technique of the following tasks: 1. Seated external rotation with a cane; 2. Standing towel slide into flexion; 3. Codman's pendulums; 4. Swiss ball rolls into flexion; 5. Seated towel slides into flexion; 6. Standing forward bows into flexion; 7. Seated pulleys into flexion; 8. Seated pulleys into scaption; 9. Seated pulleys into abduction; 10. Continuous Passive Motion (CPM) machine level 1 (30 to 50° abduction (ABD), 0 to 10° external rotation (ER)); 11. CPM level 2 (30 to 95° ABD, 0 to 25° ER); 12. CPM level 3 (30 to 140° ABD, 0 to 40° ER); 13. Donning a brace; 14. Doffing a brace; 15. Donning a brace with assistance; 16. Doffing a brace with assistance. Subjects practiced each task to the satisfaction of the therapist, and then EMG activity was recorded for all muscles during 3 repetitions of each task. The mean EMG activity values were calculated for each muscle for the entire duration of each task. All EMG data, including MVIC trials, were processed using a root-mean-square algorithm with a 0.625 second moving window. Muscle activation was normalized as %MVIC for each muscle for all tasks.

Two-sided Wilcoxon signed rank tests were applied using SAS version 9.4 (Cary, NC) and R 3.4 (www.r-project.org) statistical software to compare the %MVIC with 15%, which is considered a safe level of effort [5]. Exercises were classified into clinical groups by their statistical significance and the magnitude of their medians (Table 1).

Table 1: Safety score p-values

1	**Definitely Safe**: p-value < 0.001, median < 5%
2	**Safe**: p-value < 0.01, median < 10%
3	**Potentially Safe**: p-value < 0.05, median < 15%
4	**Borderline LOW**: p-value > 0.05, median < 10%
5	**Borderline**: p-value > 0.05, median between 10-20%
6	**Borderline HIGH**: p-value > 0.05, median > 20%
7	**Potentially Dangerous**: p-value <0.05, median> 15%
8	**Dangerous**: p-value < 0.01, median > 20%

RESULTS AND DISCUSSION

One hundred and sixty study outcomes were analyzed and categorized into a safety score (Table 2). The safety score aimed to attribute a level of risk associated with the corresponding exercise in terms of the level of muscle activation as measured by EMG. The average safety score for the fwEMG and sEMG were calculated, along with the overall score for each exercise. Three tasks (standing towel slides into flexion, standing forward bows into flexion, and donning a brace with assistance) showed a mean %MVIC greater than 15% and reached the peak safety score in the subscapularis muscle. No other muscles were over the 15% cutoff level for any task. Tasks such as exercises going into flexion (Ex 2, 4, 6), pulleys (Ex 7, 8, 9), and donning a brace (Ex13) show greater EMG activity, while the CPM machine at levels 1 and 2 (Ex 10, 11) showed the lowest EMG activity for the rotator cuff muscles. The main limitation of the current study was using subjects devoid of shoulder pathology. The activity of the shoulder muscles in healthy subjects may not be representative of the activity of individuals with a repaired rotator cuff muscle.

Overall, the goal of this study was to determine shoulder muscle activation during routinely prescribed rehabilitation tasks, to better inform clinicians on prescribing early post-operatively exercises. The bulk of the tasks demonstrated activation levels below the 15% cutoff. Though the supraspinatus, infraspinatus, and teres minor EMG activity was generally low, higher activity was observed in the subscapularis. Therefore, caution should be used when administering exercises to individuals with tears involving the subscapularis.

REFERENCES

1. Galatz L et al. *J Bone Joint Surg* 2004;**86**:219-24.
2. Thomazeau H et al. *Clin Orthop* 1997;344.
3. Koo SS, Burkhart SS. *Clin Sports Med* 2010;**29**:203-11.
4. Brislin KJ et al. *Arthroscopy: J Arthroscopic Related Surg* 2007;**23**:124-8.
5. Long JL et al. *J Orthop Sports Phys Ther* 2010;**40**:230-7.
6. Gurney AB et al. *J Orthop Sports Phys Ther* 2016;**46**:375-83.

Table 2: Safety Score of each muscle and exercise

	Ex1	Ex2	Ex3	Ex4	Ex5	Ex6	Ex7	Ex8	Ex9	Ex10	Ex11	Ex12	Ex13	Ex14	Ex15	Ex16
INFR	2	2	2	3	3	4	4	4	3	1	1	3	3	2	3	2
SUBS	6	8	6	7	7	8	7	7	7	6	6	7	7	7	8	7
SUPR	1	3	3	4	2	3	2	2	3	1	1	2	3	2	2	2
TEMI	3	4	3	4	4	3	3	4	4	3	3	3	4	4	3	3
fwEMG	**3.0**	**4.3**	**3.5**	**4.5**	**4.0**	**4.5**	**4.0**	**4.3**	**4.3**	**2.8**	**2.8**	**3.8**	**4.3**	**3.8**	**4.0**	**3.5**
ANDE	1	6	1	2	3	3	5	5	5	1	2	5	2	2	2	2
BICE	3	3	2	2	2	2	3	3	3	2	2	2	2	3	3	3
LADE	1	3	1	1	2	2	2	2	5	1	2	2	1	2	2	2
MITR	5	5	5	5	5	5	5	5	5	4	5	5	4	4	4	4
PODE	2	2	1	1	3	3	1	1	2	1	1	2	2	2	2	2
UPTR	1	2	1	3	2	3	3	3	3	1	2	2	2	2	2	2
sEMG	**2.2**	**3.5**	**1.8**	**2.3**	**2.8**	**3.0**	**3.2**	**3.2**	**3.8**	**1.7**	**2.3**	**3.0**	**2.2**	**2.5**	**2.5**	**2.5**
Overall	**2.5**	**3.8**	**2.5**	**3.2**	**3.3**	**3.6**	**3.5**	**3.6**	**4.0**	**2.1**	**2.5**	**3.3**	**3.0**	**3.0**	**3.1**	**2.9**

WALKING BIOMECHANICS IN INDIVIDUALS WITH KNEE OSTEOARTHRITIS AFTER QUADRICEPS STRENGTHING

[1]Hope C. Davis, [2]Brittney A. Luc-Harkey, [1]J. Troy Blackburn, [1]Brian Pietrosimone

[1]University of North Carolina at Chapel Hill, Chapel Hill, NC, USA
[2]Brigham and Women's Hospital, Boston, MA, USA
davishc@live.unc.edu

INTRODUCTION

Altered knee sagittal plane kinetics during walking are associated with worse pain outcomes in individuals with knee osteoarthritis (KOA) [1]. It is hypothesized that knee sagittal plane kinetics are influenced, in part, by quadriceps weakness [2]. Therefore, it is plausible that improving quadriceps strength may alter gait biomechanics. The primary purpose was to determine the association between baseline quadriceps strength and walking gait biomechanics linked to KOA onset and progression. The secondary purpose was to determine if individuals who increased quadriceps strength following 4-weeks of physical therapy (responders) demonstrated changes in gait biomechanics compared to individuals who did not increase quadriceps strength (non-responders).

METHODS

Physical Therapy for Knee Osteoarthritis
53 individuals with radiographic and symptomatic KOA (Kellgren-Lawrence grade 2-4, 47% female, 62.3±7.1 years, BMI = 28.5±3.9 kg/m^2) were enrolled in 10 sessions of supervised, progressive lower extremity strengthening directed by a licensed physical therapist over a 28-day period.

Quadriceps Strength
Maximum isometric quadriceps strength was measured on the involved limb (with bilateral KOA, the involved limb was defined as the more symptomatic limb) using a dynamometer at baseline and following the 4-week physical therapy protocol. 3-5 maximal strength practice trials were conducted to determine a target torque threshold. Then 2 maximal effort trials were conducted where participants were instructed to straighten their knee as fast as possible to reach or surpass the target torque threshold. Quadriceps strength was defined as peak torque and normalized to body mass (Nm/kg). The minimal detectable change (MDC) of quadriceps strength was calculated using the standard error of measurement and intraclass correlation coefficient from the baseline quadriceps strength measurements [3]. Individuals who increased quadriceps strength by ≥0.31 Nm/kg were classified as strength responders; those who did not increase by this amount were classified as non-responders for the secondary analysis.

Walking Gait Biomechanics
Participants were outfitted with retroreflective markers and walked at a self-selected comfortable speed down a 6m walkway that contained 2 staggered, embedded Bertec force plates and a 10-camera three-dimensional motion capture system (Vicon Nexus). 5 trials were collected where the participant walked at a pace within 5% of the average speed determined during previous practice trials. Vertical ground reaction force (vGRF), knee flexion angle, and internal knee extension moment were time-normalized to percent of stance phase (heel-strike to toe-off) using linear interpolation techniques. Moments were normalized to the product of body weight (BW) and height (m), and vGRF was normalized to BW. Peak vGRF, knee flexion displacement, peak knee flexion angle, and peak internal knee extension moment (a larger negative value = greater moment) were identified during the first 50% of the stance phase. Ensemble average waveforms were created by averaging the waveforms of each trial for each participant.

Statistical Analysis
For the primary aim, linear regression analyses were conducted to determine associations between baseline quadriceps strength and biomechanical variables after accounting for walking speed as a

covariate (ΔR^2). For the secondary aim, one-way ANCOVAs were conducted (percent change in walking speed from baseline to 4-weeks as the covariate) to determine differences between each biomechanical variable following 4-weeks of physical therapy between strength responders and non-responders. Next, ensemble average waveforms with 95% confidence intervals (CI) were plotted throughout the stance phase for responders and non-responders, and time points where 95% CI did not overlap were considered statistically different.

RESULTS

There were no differences in demographics between responders (n=21) and non-responders (n=32). Greater peak vGRF (R = 0.37 ΔR^2 = 0.08, p=0.02), peak knee flexion angle (R = 0.24, ΔR^2 = 0.12, p=0.01), and peak internal knee extension moment (R = 0.12, ΔR^2 = 0.08, p=0.04) all significantly associated with greater quadriceps strength after accounting for walking speed at baseline while knee flexion displacement (R = 0.11, ΔR^2 = 0.06, p=0.07) did not. Between strength responders and non-responders, there were no significant differences in the percent change of any biomechanical variable from baseline to 4-weeks (p-values ranged from 0.31 to 0.52). Visual examination of ensemble average waveforms with 95% confidence intervals between responders and non-responders showed no significant differences in any portion of the stance phase for any biomechanical variable (Figure 1).

DISCUSSION

Greater quadriceps strength associated with greater biomechanical variables at baseline; yet there were no differences in walking gait biomechanics between responders and non-responders to the strength intervention at either time point. Quadriceps strengthening may not be a mechanism directly responsible for an acute change in walking gait biomechanics in individuals with KOA. Future studies should consider directly targeting gait biomechanics with specific interventions to optimize gait in individuals with KOA, as quadriceps strengthening alone may not sufficiently influence adaptations in gait biomechanics.

REFERENCES

1. O'Connell et al. *Clin Biomech*. 31:40-6. 2016.
2. Murray et al. *Clin Biomech*. 30(10):1140-5. 2015.
3. Harkey et al. *Gait Posture*. 59:128-33, 2018.

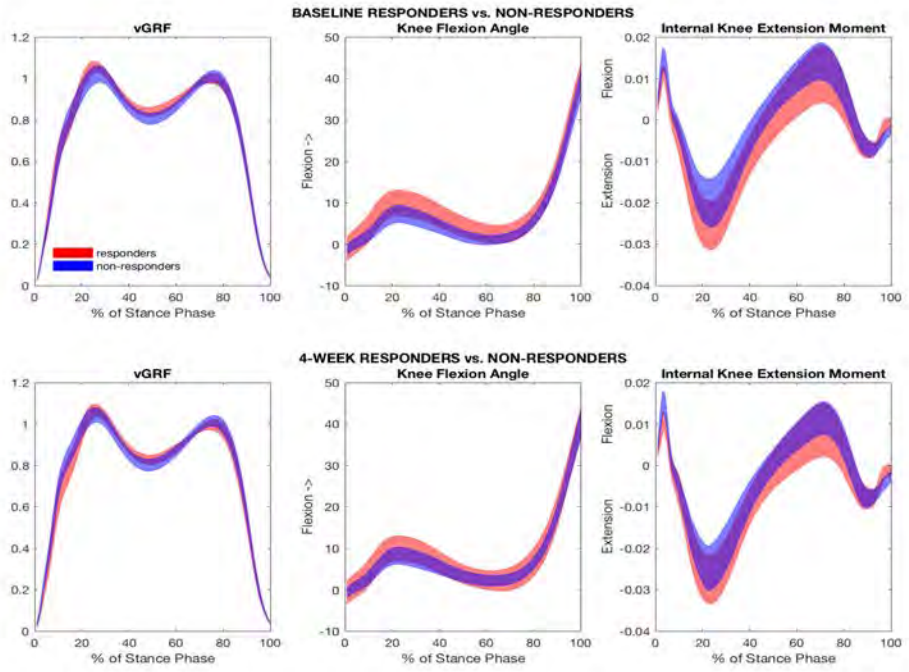

Figure 1. Ensemble average waveforms of vGRF, knee flexion angle and internal knee extension moment in individuals with KOA at baseline and 4-weeks following physical therapy.

DEVELOPMENT OF AN INTERVENTION-FOCUSED METRIC OF GAIT BALANCE

[1,2] Jesse C. Dean

[1] Ralph H. Johnson VAMC, Charleston, SC, USA
[2] Medical University of South Carolina, Charleston, SC, USA
email: deaje@musc.edu

INTRODUCTION

Many clinical populations, including chronic stroke survivors, exhibit deficits in gait balance. Such deficits can limit gait function due to an increased fall-risk and an increased fear of falling. The high prevalence of this problem has motivated the development of numerous metrics to quantify gait balance [1-2].

Several of these metrics have shown promise for identifying individuals with an increased fall-risk or fear of falling. However, few metrics provide clear justification for a specific intervention, and thus are of limited usefulness to clinicians. In contrast, an ideal gait balance metric would be one in which the identified deficit suggests the appropriate treatment.

For example, a metric quantifying muscle weakness could clearly be used to justify a strengthening intervention. A metric quantifying maximal aerobic capacity could be used to justify a cardiovascular-focused intervention. Conversely, a potential link between fall-risk and increased step width [1] would be unlikely to justify training a narrow step gait.

We propose that a metric quantifying the relationship between pelvis motion and foot placement [3] has the potential to serve as a gait balance metric with a direct link to treatment. Supporting this proposal, healthy controls actively adjust step width based on mediolateral pelvis motion. A failure to do so has been linked to post-stroke balance deficits [4].

The purpose of this study was to determine whether our metric of post-stroke gait balance is both valid and adaptable in response to targeted treatment. First, we validated this metric against measures of direct clinical interest. Second, we determined whether this metric can be experimentally manipulated. A promising balance metric would pass both tests.

METHODS

The gait metric of interest quantifies the mechanics-dependent step-by-step adjustments in step width [3]. Briefly, in healthy controls, the mediolateral pelvis displacement relative to the stance foot at the start of a step predicts step width (Fig. 1). We quantify the strength of this relationship by calculating the partial correlation between these two measures (ρ_{disp}), accounting for mediolateral pelvis velocity. The face validity of this metric is supported by the long accepted link between step width modulation and mediolateral gait stability [5].

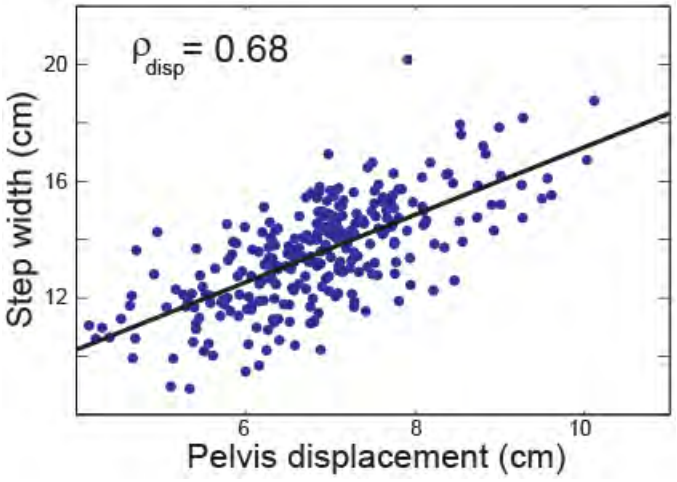

Figure 1. Relationship between pelvis displacement and step width. Each dot represents a single step.

The first component of this study involved 46 chronic stroke survivors (20 F / 26 M; 58 ± 14 yrs) able to independently walk at ≥0.2m/s. Participants provided informed consent using an IRB-approved form. We quantified ρ_{disp} using marker data collected from 3-minutes of treadmill walking at self-selected speed. We measured Functional Gait Assessment score (FGA; a common clinical test of gait balance) and self-selected overground walking speed (a common measure of general gait function). Finally, we recorded whether participants had fallen in the prior year, or had a self-reported fear of falling.

To test the criterion validity of our metric, we correlated ρ_{disp} with FGA score and overground speed. We also used receiver operator characteristic analysis to determine whether ρ_{disp} predicts individuals with a history or fear of falling.

The second component involved a subset of previous participants (n=18; 14 F / 4 M; 67 ± 10 yrs). Participants first walked normally on a treadmill at self-selected speed for 3-minutes. They then walked for 6-minutes while interfaced with a novel force-field, detailed previously [6]. The force-field applied mediolateral forces to the legs to influence step width on a step-by-step basis [7]. For the first 5-minutes, the force-field either *Assisted* balance (n=9) or *Perturbed* balance (n=9) by pushing step width either toward or away from mechanically-appropriate locations, respectively. For the final minute of walking, the force-field simply got out of the way.

We quantified the change in ρ_{disp} relative to baseline during *Assisted* and *Perturbed* modes (direct effects), as well as in the final minute of walking (after effects). We used paired t-tests to determine whether any of these changes reached significance ($p<0.05$).

RESULTS AND DISCUSSION

ρ_{disp} was positively correlated with both FGA score ($r=0.54$) and overground speed ($r=0.55$). ρ_{disp} was also related to an individual's likelihood of having a history or fear of falling, quantified with an area under the curve (AUC) value of 0.72. Following a suggested rule of thumb [8], all of these relationships would be classified as having a large effect size. Interestingly, the AUC value derived from ρ_{disp} exceeded the matching calculated values from FGA score (0.55) or overground speed (0.58). Our metric thus appears to be at least as valuable as common clinical measures for predicting negative consequences of poor gait balance in this population.

Participants appeared to increase ρ_{disp} while step width was *Assisted* by the force-field (Fig. 2), but this change did not reach the level of significance ($p=0.09$). When the assistance ceased, participants simply returned to their baseline ρ_{disp} level. In contrast, ρ_{disp} was significantly ($p<0.001$) reduced when step width was *Perturbed* (Fig. 2), followed by a significant ($p=0.04$) increase in ρ_{disp} for the next minute of walking. These results demonstrate that our metric of gait balance can be experimentally manipulated using methods focused on the step-by-step adjustment of step width.

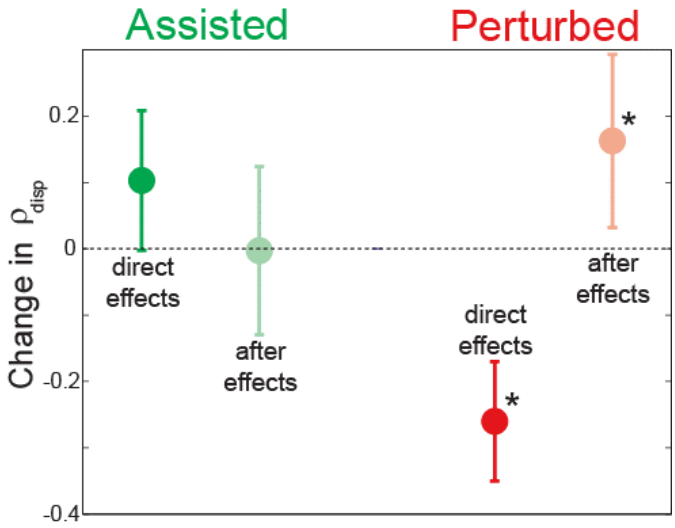

Figure 2. Direct effects and after-effects of walking with the force-field in *Assisted* and *Perturbed* modes.

CONCLUSIONS

Our proposed metric of gait balance (ρ_{disp}) focuses on one specific aspect of a stable walking pattern – the ability to appropriately adjust step width based on the mechanical state of the body. Despite this narrow focus, our results demonstrate that ρ_{disp} meets our dual goals of: 1) validity in comparison to measures of clinical interest; and 2) the potential to be experimentally manipulated. This combination of results has motivated an ongoing intervention (NCT02964039) to test whether repeated exposure to our force-field can improve post-stroke gait balance.

REFERENCES

1. Maki. *J Am Geriatr Soc*. **45**, 313-320, 1997.
2. Bruijn et al. *J Roy Soc Inter*. **10**, 20120999, 2013.
3. Stimpson et al. *J Biomech*. **68**, 78-83, 2018.
4. Dean et al. *J Rehab Res Dev*. **52**, 577-590, 2015.
5. MacKinnon et al. *J Biomech*. **26**, 633-644, 1993.
6. Nyberg et al. *IEEE TNSRE*. **25**, 1481-1488, 2017.
7. Bowman et al. *Proceedings of ASB'17*, Boulder, CO, USA, 2017.
8. Rice et al. *Law Hum Behav*. **29**, 615-620, 2005.

INTERNAL REPRESENTATION OF EXTERNAL PATIENT DYNAMICS DURING LOCOMOTOR REHABILITATION

[1] Sarah E. Goodman and [1,2,3] Christopher J. Hasson

[1] Departments of Bioengineering, [2] Physical Therapy, Movement and Rehabilitation Sciences, and [3] Biology
Neuromotor Systems Laboratory; Northeastern University, Boston MA [email: c.hasson@northeastern.edu]

INTRODUCTION

Locomotor impairments significantly reduce the quality of life and are typically addressed with locomotor rehabilitation. A key aspect of this therapy is that it involves simultaneous co-adaptation and learning: therapists must learn a patient's unique locomotor dynamics to apply forces effectively and elicit desired changes; patients must adapt to therapist force inputs to modify locomotor patterns in the way prescribed by the therapist. The current lack of understanding about this dynamic interaction may to some extent explain why a high percentage of patients retain locomotor impairments after rehabilitation [1].

In this work, we focus on the problem least explored: how do therapists learn patient locomotor dynamics? This is unknown in part due to the challenge of conducting controlled locomotor rehabilitation studies, as it can be difficult to quantify therapist adaptation if the patient is adapting in parallel.

Prior research using reaching tasks has shown that when faced with novel dynamics, e.g., artificial force fields, humans develop internal models of the field dynamics [e.g., ref. 2]. Here, we extrapolate this idea to investigate whether therapists develop internal models of *locomotor dynamics*, which constitutes a more dynamically complex model compared to standard velocity-dependent force fields.

In this work, we present a new paradigm that uses an interactive locomotor simulator to circumvent co-adaptation confounds and investigate how humans learn to modify a patient's locomotor dynamics. In this approach, subjects use a manipulandum (GeoMagic Touch; 3D Systems) to interact with a locomoting virtual patient (VP), which is given an instantaneous stroke. The stroke is rendered as an end-point impedance [3] that pulls the subject's hand into a typical stroke locomotor pattern, as would happen if subjects were holding onto the ankles of real stroke survivors. In this scenario, subjects must learn how to apply the correct forces to the VP's leg to restore healthy locomotor kinematics. Internal model formation is probed using a classic force-field approach with a locomotor twist: pathological locomotor dynamics are used as the force-field. The hypothesis is that humans adapt to novel external locomotor dynamics by developing internal models of the dynamics.

METHODS

The VP was modeled as a planar linked two-segment system representing the thigh and shank (foot omitted). Rigid body impedance contributions, i.e., gravity, Coriolis, and inertial forces, were based on manipulandum deviations from a reference locomotor pattern derived from pre-existing post-stroke locomotor kinematics [4] scaled down by 96.5%. Neuromuscular impedance contributions were represented by variable-stiffness rotational spring-dampers at the knee and hip joints, which modeled the spring-like behavior of muscle and geometric effects. The treadmill ground reaction forces were modeled using spring-dampers.

Healthy subjects practiced training the VP using the manipulandum under four conditions:

C1: Moving the VP's ankle to follow a healthy locomotor trajectory (80 steps).

C2: Adapting to a sudden stroke induced in the VP by applying forces to restore a healthy VP locomotor pattern (80 steps x 5 blocks).

C3: Adapting to the sudden elimination of the VP's stroke (40 steps).

C4: Adapting to a change in the VP's shank mass (40 steps).

In all conditions, the VP continuously walked in place as if on a treadmill. Intentionally, in the stroke condition (C2) the VP always tried to assume the same impaired locomotor pattern, i.e., it did not adapt. To probe internal model formation in C1 and C2 force channels [5] were applied during 8 randomly-selected 8 steps (out of 80). For these, the

stroke dynamics (if present) were turned off for one step and stiff springs applied orthogonal forces to keep the VP in a channel that followed the healthy kinematic trajectory. C3 probed after-effects by suddenly removing the VP's stroke (40 steps), and C4 tested generalization by changing a model parameter; shank mass increased by 50% (40 steps).

RESULTS AND DISCUSSION

Preliminary results are described here. When the VP was given a stroke the manipulandum generated forces that pulled the subject's hand (and VP's leg) towards the nominal stroke locomotor trajectory (Fig. 1; magenta line). With practice, subjects adapted by applying forces to counter this impedance (Fig. 1; red vectors), making the VP's leg follow the healthy trajectory (Fig 1; green line).

To probe adaptation, random force channels were imposed during the stroke practice condition (C2). During these trials, subjects exerted forces against the channel throughout almost the entire locomotor cycle, from mid-stance to heel-strike (Fig. 1; middle row; blue vectors). The presence of these forces reflect, in part, a subject's forward motor plan – at least during the first part of swing before significant feedback-driven modifications were possible.

A caveat in this force-channel interpretation is that a portion of the forces exerted during the force channels were due to subjects' inability to make the VP perfectly follow the healthy locomotor trajectory *without* the stroke dynamics imposed, especially during the rapid leg-swing. Therefore, the forces subjects exerted against the force channel during the healthy condition (C1) were subtracted from the stroke force-channel responses (C2; Fig. 1; middle row), which gives a clearer picture of a subject's adaptation to the *stroke* locomotor dynamics alone (Fig. 1; bottom row).

A significant aftereffect was observed after the stroke dynamics were switched off (C3), i.e., subjects made kinematic errors in the opposite direction. Subjects also showed generalization, as the kinematic errors with the parameter switch were smaller than during initial adaptation.

CONCLUSIONS

Together, the distinct patterns of forces that subjects exerted during the force channel trials, the presence of after-effects, and the generalization of performance lend support to the hypothesis that humans develop internal models of external patient locomotor dynamics. If these results hold for additional subjects, it will provide a theoretical foundation for future studies to explore ways of enhancing therapist effectiveness, such as speeding up and improving the accuracy of therapist internal models, and improving robotic gait rehabilitation control algorithms.

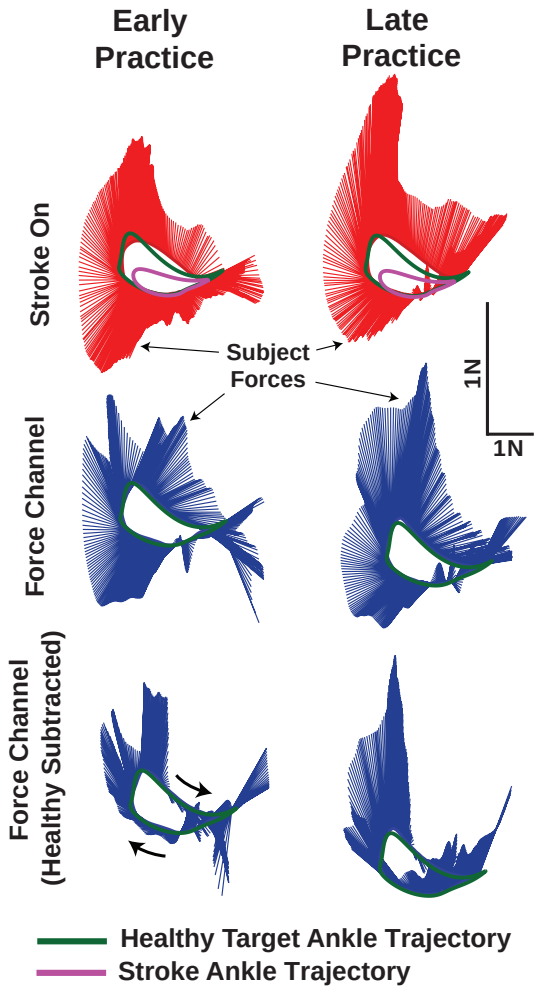

Figure 1. Exemplar kinematics and kinetics (applied forces) of subject adaptation to imposition of a stroke in the locomotor dynamics of a virtual patient. Adaptation to the stroke dynamics is shown in red, force-channel responses are shown in blue (see text for more details). Note scale is stretched vertically.

REFERENCES

1. Schaechter, *Progress in Neurobiology*, 2004. **73**(1): 61-72.
2. Shadmehr and Mussa-Ivaldi, *Journal of Neuroscience*, 1994. **14**(5): 3208-3224.
3. Tee, et al., *Biological Cybernetics*, 2004. **90**(5): 368-375.
4. Olney and Richards, *Gait & Posture*, 1996. **4**(2): 136-148.
5. Scheidt, et al., *Journal of Neurophysiology*, 2000, **84**(2), 853-862.

RELATIONSHIP BETWEEN NUMBER OF PHYSICAL THERAPY VISITS AND GAIT-RELATED OUTCOMES IN PATIENTS WITH BELOW-KNEE AMPUTATION

[1]Julianne Stewart, [1,2]Michael Marks, [1]Trevor Kingsbury, [1]Marilynn Wyatt

[1]Naval Medical Center San Diego, San Diego, CA, USA
[2]Improvement Path Systems, San Diego, CA, USA
E-mail: julianne.m.stewart.ctr@mail.mil

INTRODUCTION

The military healthcare system uses a well-structured, interdisciplinary approach to caring for service men and women who undergo amputation [1]. Patients who receive care at Naval Medical Center San Diego (NMCSD) have access to physical therapy (PT) five days per week once in the post-acute rehabilitation phase but use this resource to varying extents. Access to PT is far greater in the military healthcare setting than in the civilian healthcare system in the US, regardless of patient engagement with this resource [2].

As a part of the continuum of care for patients with amputation, instrumented gait analysis is available to help inform clinical decision-making and practice in physical therapy and prosthetic care. Patients have the option to undergo regular gait analysis throughout their rehabilitation at NMCSD beginning with a baseline (BL) gait study when deemed safe by a treating physical therapist to ambulate using a prosthesis without an assistive device. Each patient's BL gait study is then used to gauge the impact of further interventions and the patient's recovery during rehabilitation.

It is hypothesized that increased post-acute PT attendance in a group of patients with transtibial amputation, in the time frame between amputation and a gait study approximately six months (6mo) following the BL study, will lead to larger improvements in gait-related outcomes. Specifically, it is hypothesized that there will be a positive correlation between number of PT visits and percentage change in gait velocity, unaffected leg step length (SL), and affected leg stance time (StT). Additionally, it is hypothesized that there will be a negative correlation between number of PT visits and percentage change in affected leg SL, unaffected leg StT, and peak lateral trunk lean.

METHODS

A retrospective analysis of the NMCSD Gait Lab patient registry (IRB protocol #NMCSD.2014.0026) was performed and patients were selected for inclusion if they had a unilateral transtibial amputation between April 2012 and July 2017 and underwent both a BL and 6mo gait study in the NMCSD Gait Laboratory. Eight male patients were identified that fit these inclusion criteria. The patient group was aged 28.9±6.3 years. The number of post-acute physical therapy visits each patient attended was collected using the same patient registry.

During each gait study, retroreflective markers were applied to each patient's full body. Half of the included patients were markered using a modified Helen Hayes configuration throughout the duration of their care while the remaining patients were markered using a Six Degrees of Freedom (6DoF) configuration due to a change in lab procedures.

Three dimensional gait analysis was performed with a system of 12 Eagle motion capture cameras (Motion Analysis Corp., Santa Rosa, CA) and four force plates embedded into the laboratory floor (AMTI, Watertown, MA, USA). Data were collected using Cortex (Motion Analysis Corp., Santa Rosa, CA) and processed with Visual 3D (C-Motion Inc., Germantown, MD, USA) after a 4th order Butterworth filter was applied with a cutoff frequency of 6 Hz and 50 Hz for kinematic and kinetic data respectively.

Statistical analysis was performed using Excel (Microsoft, Redmond, WA, USA) and a Pearson's product-moment coefficient was calculated to

examine for correlation between number of physical therapy visits and each gait-related variable. Regression was performed for each variable.

RESULTS AND DISCUSSION

The only variable that was found to have a negative correlation with number of PT visits was affected leg step length (R = -0.83, R^2=0.68, p=0.01, Figure 1). Contrary to the authors' hypothesis, no variables were found to have a significant positive correlation with number of PT visits. However, several variables showed a trend toward correlation with number of PT visits. See Table 1 for details.

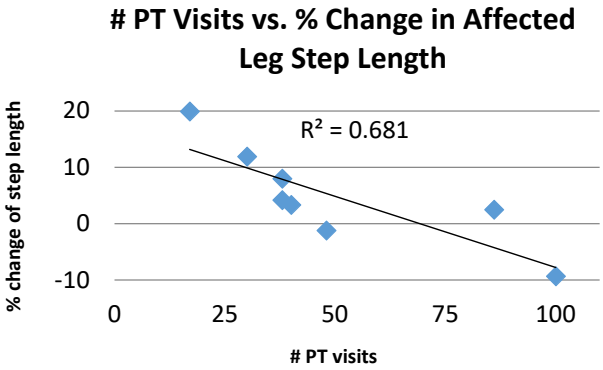

Figure 1: Scatterplot with number of PT visits on the horizontal axis and percentage change in affected leg step length from BL study to 6mo study on the vertical axis (trendline and R^2 value displayed).

The desired direction of change for affected leg step length can be patient-specific. A decrease may be the desired outcome for amputees who demonstrate large asymmetries in step length between affected and unaffected legs. However, affected and unaffected step length may both increase with increases in gait velocity, as demonstrated by the majority of positive changes in Figure 1.

Several caveats should be discussed when interpreting these results. The small sample size available for this analysis limits the ability to draw strong conclusions regarding the correlation between amount of physical therapy and gait-related outcomes. It should also be noted that many of these patients exhibited gait parameters within or very near the normal range for able-bodied individuals at the time of their BL studies and had engaged in 16.9±9.0 PT visits since final closure of amputation which might contribute to their excellent gait quality. Finally, two patients engaged in twice the amount of physical therapy visits of many of the other patients in this sample which may represent either difficult courses of care or very high levels of motivation. These two potential explanations would likely impact gait quality in very different ways and may skew the findings.

CONCLUSIONS

Understanding the relationship between amount of physical therapy after amputation and rehabilitation outcomes is crucial in order to optimize the function of patients and to ensure efficient use of resources. In addition to the finding of a negative correlation between number of PT visits and affected step length, trends between PT visits and multiple other variables should encourage further study of this relationship.

REFERENCES

1. Fitzpatrick and Pasquina. *Military Medicine.* 175(7):13-17, 2010.
2. Castillo et al. *Arch Phys Med Rehabil*. 86:1722-8, 2005.

ACKNOWLEDGEMENTS

The authors thank Katherine Sharp, Tatiana Djafar, Jenny Anne Maun, Kimberly Rowe, and John David Collins for assistance with data collection.

DISCLOSURE STATEMENT

The views expressed herein are those of the author(s) and do not necessarily reflect the official policy or position of the Department of the Navy, Department of Defense, or the U.S. Government.

Table 1: Correlation between number of PT visits and percentage change of each variable. Shading represents a significant correlation.

Variable	Velocity	Affected SL	Unaffected SL	Affected StT	Unaffected StT	Lateral Trunk Lean
Pearson's R	-0.53	-0.83	-0.58	0.50	0.51	-0.26
p-value	0.17	0.01	0.13	0.20	0.20	0.53

TRUNK MUSCLE FORCES AND SPINAL LOADS WHILE WALKING IN PERSONS WITH LOWER LIMB AMPUTATION BOTH WITH AND WITHOUT CHRONIC LOW BACK PAIN

[1]Julian C. Acasio, [1]Courtney M. Butowicz, [1-3]Christopher L. Dearth,
[4]Iman Shojaei, [4]Babak Bazrgari, and [1-3]Brad D. Hendershot
[1] Walter Reed National Military Medical Center, Bethesda, MD, USA
[2] DoD-VA Extremity Trauma and Amputation Center of Excellence, USA
[3] Uniformed Services University of the Health Sciences, Bethesda, MD, USA
[4] University of Kentucky, Lexington, KY, USA
Email: julian.c.acasio.ctr@mail.mil

INTRODUCTION

Low back pain (LBP) is a common musculoskeletal impairment among persons with lower limb amputation (LLA), capable of substantially reducing longer-term quality of life [1]. During activities of daily living, such as walking, altered trunk-pelvic motion with (vs. without) LLA impose greater mechanical loads on spinal tissues, and thus have been suggested as a risk factor for the development of LBP [2]. Moreover, in the presence of LBP, further alterations in trunk-pelvic motion have been identified [3-5], yet the effects of these altered motions with LBP on spinal loads remain unclear. The purpose of this study was to evaluate the influences of LBP on trunk-pelvic motion and spinal loads among persons with LLA. We hypothesized that there are differences in trunk-pelvic motions that are associated with larger spinal loads between persons with LLA with and without LBP, supporting a pathway wherein repeated exposure to abnormal spine mechanics can adversely affect spine health.

METHODS

Eighteen persons with LLA – 8 with LBP ("LLA-P") and 10 without LBP ("LLA-NP") – and 10 uninjured controls ("CTR"; without LBP) participated (Table 1). The LLA-P group reported chronic LBP (n=7; every day or nearly every day in the most recent 6 months, n=1; at least half of days in the most recent 6 months) [6]. Mean (standard deviation) pain in the past seven days = 3.8 (1.3). Participants walked overground across a 15m walkway at 1.3 m/s, with speed enforced by auditory feedback. An 18-camera motion capture system (Qualisys, Göteborg, Sweden) tracked (120Hz) trunk and pelvis kinematics via 10 reflective markers. Marker trajectories were low-pass filtered (Butterworth, 6Hz).

Table 1. Mean (SD) participant demographics.

	LLA-P	LLA-NP	CTR
Age (yr)	35.1 (8.7)	36.4 (6.8)	29.7 (8.9)
Stature (cm)	177.5 (8.0)	179.3 (5.9)	176.0 (6.3)
Mass (kg)	86.8 (11.5)	91.6 (14.6)	73.2 (13.4)
Time (yr)	5.2 (2.6)	10.5 (3.1)	N/A

Tri-planar (global) trunk and pelvis angles, and pelvis center of mass position were calculated in Visual3D (C-motion, Germantown, MD, USA), time-normalized to stride, and subsequently input to a non-linear finite element model of the spine [8]. A heuristic optimization procedure, controlled via MATLAB (Mathworks, Natick, MA, USA), estimated trunk muscle forces and spinal loads by minimizing the sum of squared muscle stress (i.e., the cost function) across 56 muscles. Individual muscle forces were summed across local (i.e., connecting individual lumbar vertebrae to the pelvis) and global muscles (i.e., connecting the thorax/rib cage to the pelvis). Spinal loads were compiled from the intervertebral level at which maximum spinal loads occurred (i.e., L5/S1). Peak spinal loads and muscle forces were determined and normalized to body mass. Trunk ranges of motion (ROM) were also determined. Separate one-way repeated-measure ANOVAs assessed the effect of group (LLA-P, LLA-NP, CTR) on all outcomes (P<0.05). Bonferroni-corrected t-tests (P<0.0167) assessed pairwise differences when main effects were observed.

RESULTS AND DISCUSSION

Main effects were observed in frontal (P=0.003) and transverse (P<0.001) plane trunk ROM (Table

1). In the frontal plane, trunk ROM were larger in LLA-P (P=0.001) and LLA-NP (P=0.011) vs. CTR. In the transverse plane, trunk ROM were larger in LLA-P versus both LLA-NP (P=0.015) and CTR (P<0.001), but were similar between LLA-NP versus CTR (P=0.022). No main effects were observed in peak spinal loads (P>0.078) or global muscle forces (P=0.076; Table 1). However, peak local muscle forces differed between groups (P=0.017); local muscle forces were larger in CTR vs. both LLA-P (P=0.012) and LLA-NP (P=0.016).

Despite larger trunk ROM in both the frontal and transverse planes, a lack of differences in spinal loads among LLA-P and LLA-NP vs. CTR are contrary to both our hypotheses (LLA-P ≠ LLA-NP) and prior work [LLA-NP > CTR; 8]. Nevertheless, larger transverse motions with vs. without LBP are consistent with prior work in persons with (transfemoral) LLA [4]. Interestingly, all persons in the LLA-P group had transtibial LLA while those in the LLA-NP group comprised a combination of both transtibial (n=7) and transfemoral (n=3) LLA. In the absence of LBP, alterations in the characteristics of trunk-pelvic motion are typically larger in persons with transfemoral vs. transtibial LLA [2]. It is therefore possible that presence of chronic LBP has concurrently increased trunk-pelvic motions in a group that is otherwise more similar to uninjured CTR. Also, while we identified group differences in local muscle forces, further consideration may be warranted for the model/optimization assumptions regarding muscle recruitment strategies with vs. without LBP [9]. Of note, despite categorization of chronic LBP, participants in the LLA-P group at the time of testing reported mean (standard deviation) numerical pain scores of 2.2 (1.3).

In summary, although prior work has identified larger spinal loads in persons with vs. without LLA, the current results do not necessarily support the notion that larger spinal loads during walking influence the persistence of LBP. It is however possible that individuals in the LLA-P group experienced larger spinal loads at some point prior to developing LBP and, thus, future work is needed to longitudinally characterize the temporal relationships in these outcomes with time since LLA to better elucidate the causal relationships.

REFERENCES

1. Devan, et al. *Phys Med Rehab* **9**; 949-59, 2017.
2. Hendershot and Wolf, *Clin Biomech*, **29**; 235-42, 2014
3. Devan, et al. *J Prosthet Orthot* **29**; 121-2, 2017.
4. Morgenroth, et al. *AJPMR* **89**; 635-43, 2010.
5. Fatone, et al. *AJPMR* **95**; 438-447, 2016.
6. Deyo, et al., *The J Pain* **15**; 569-585, 2014.
7. Bazrgari, et al. *Eur Spine J* **16**; 687-99, 2007.
8. Shojaei, et al. *Clin Biomech* **32**; 157-63, 2016.
9. Van Dieen, et al. *Spine* **28**; 834-41, 2003.

ACKNOWLEDGEMENTS

This work was funded in part by award W81XWH-14-02-0144. The views expressed are those of the authors and do not reflect the official policy of the Department of Army/Navy/Air Force, Department of Defense, or U.S. Government.

Table 1: Mean (SD) peak anteroposterior (AP) and mediolateral (ML) shear forces, compression forces, and global and local muscle forces, and tri-planar trunk ranges of motion (ROM) for LLA-P, LLA-NP, and CTR. * indicate statistically different than CTR , # indicate statistically different from LLA-NP.

	Spinal Loads (N/kg)			Muscle Forces (N/kg)		Trunk ROM (°)		
	AP Shear	ML Shear	Compression	Global	Local	Sagittal	Frontal	Transverse
LLA-P	5.4 (1.6)	8.7 (2.1)	22.3 (3.5)	11.1 (2.0)	8.6 (0.9)*	2.9 (1.1)	7.4 (1.5)*	9.5 (1.9)*#
LLA-NP	5.3 (3.4)	10.4 (5.8)	23.1 (3.6)	10.9 (2.6)	8.8 (1.0)*	2.8 (0.8)	6.3 (3.0)*	7.2 (2.3)
CTR	4.4 (0.8)	6.3 (2.3)	22.5 (2.8)	13.5 (3.1)	10.6 (2.3)	2.2 (0.7)	3.6 (1.6)	5.2 (1.2)

	Spinal Loads (N/kg)			Muscle Forces (N/kg)		Trunk ROM (°)		
	AP Shear	ML Shear	Compression	Global	Local	Sagittal	Frontal	Transverse
LLA-P	5.4 (1.6)	8.7 (2.1)	22.3 (3.5)	11.1 (2.0)	8.6 (0.9)*	2.9 (1.1)	7.4 (1.5)*	9.5 (1.9)*#
LLA-NP	5.3 (3.4)	10.4 (5.8)	23.1 (3.6)	10.9 (2.6)	8.8 (1.0)*	2.8 (0.8)	6.3 (3.0)*	7.2 (2.3)
CTR	4.4 (0.8)	6.3 (2.3)	22.5 (2.8)	13.5 (3.1)	10.6 (2.3)	2.2 (0.7)	3.6 (1.6)	5.2 (1.2)

EMG ANALYSIS OF AN UPPER BODY EXOSKELETON DURING AUTOMOTIVE ASSEMBLY

Jason C. Gillette and Mitchell L. Stephenson

Iowa State University, Ames, IA, USA
email: gillette@iastate.edu

INTRODUCTION

Shoulder injuries in the workplace result in the longest recovery time of any body part: 23 median days missed [1]. Common causes of shoulder pain include bursitis, tendinitis, impingement, instability, and arthritis [2]. Repetitive overhead postures are widely thought to increase the risk of shoulder injury. Threshold limit values (TLV) for upper limb fatigue have been developed that relate maximum voluntary contraction (MVC) to duty cycle [3]. Using this equation, a 39.5% MVC should not be exceeded with a 10% duty cycle, and a 16.5% MVC should not be exceeded with a 50% duty cycle.

When worksite modifications are impractical or impossible, robotic or passive assistive devices may be utilized in an attempt to prevent shoulder injuries. The Levitate Airframe is a passive exoskeleton designed to support arm weight during overhead shoulder postures. Previous testing with workers at John Deere indicated promising reductions of deltoid muscle activity when using this exoskeleton [4]. The purpose of this study was to assess this exoskeleton during overhead automotive assembly at Toyota Canada. Our hypothesis was that deltoid muscle activity would be reduced with the exoskeleton.

METHODS

Eleven experienced male workers (age 35±7 yr) volunteered for this study. Data were collected for ten overhead automotive assembly tasks. One participant performed three job tasks, five participants performed two job tasks, and five participants performed one job task. Eight job tasks were performed by two participants, and two job tasks were performed by one participant (18 comparisons). Approximately 12 minutes of data were collected per job task, with nine job tasks having ten repetitions (automotives completed), and one job task having three repetitions (multiple stations). Data for each job task were collected with and without use of the exoskeleton.

IRB-approved informed consent was obtained from all participants. Data were collected using a Delsys Trigno wireless electromyography (EMG) system at a sampling frequency of 1926 Hz using Delsys EMGworks software. EMG sensors were placed on eight muscles: right and left anterior deltoid, biceps brachii, superior trapezius, and lumbar erector spinae. Maximum voluntary isometric contractions (MVIC) were performed in the following postures: shoulder abduction empty can, seated elbow flexion, and prone spinal extension. EMG data were analyzed using custom written code in Matlab.

EMG signals were inspected to remove any non-physiological artifacts. The EMG data were bandpass filtered with a 4^{th}-order zero-lag Butterworth filter from 20-450 Hz and then rectified. Next, the EMG data were low-pass filtered at 10 Hz to create a linear envelope. A moving window was used to determine the maximum one second of sustained EMG amplitudes for the MVICs. The job task EMG amplitudes were divided into consecutive one second intervals. The highest 10% and 50% of EMG amplitudes were determined as a measure of 10% and 50% duty cycles.

Maximum 10% and 50% EMG amplitudes were normalized by the maximum one second MVICs (%MVIC). EMG amplitudes presented here are for the dominant arm anterior deltoid, biceps brachii, and trapezius muscles. The right and left side erector spinae muscle results were averaged. Paired t-tests were used to compare EMG amplitudes between conditions (with and without the exoskeleton) in all job tasks, with significance indicated at $p < 0.03$ (adjusted for 18 comparisons with 11 participants). Maximum 50% deltoid amplitudes are presented for individual job tasks (Figure 1) to explore if some tasks benefited differently from exoskeleton usage.

RESULTS AND DISCUSSION

Maximum 10% EMG amplitudes were significantly reduced for the deltoid (p=0.02), biceps brachii (p=0.01), and erector spinae (p=0.01) when wearing the exoskeleton (Table 1). There was not a significant change in trapezius EMG amplitudes (p=0.35). The deltoid demonstrated the greatest magnitude of EMG amplitude change: a 6.5% MVIC reduction with the exoskeleton. Deltoid EMG standard deviations exceeded the 39.5% TLV without the exoskeleton but fell below this level with the exoskeleton. Trapezius EMG standard deviations exceeded the 39.5% TLV both without and with the exoskeleton.

Maximum 50% EMG amplitudes were significantly reduced for the deltoid (p<0.01), biceps brachii (p<0.01), and erector spinae (p=0.03) when wearing the exoskeleton (Table 1). There was not a significant change in trapezius EMG amplitudes (p=0.61). The deltoid showed the greatest magnitude of EMG amplitude change: a 4.4% MVIC reduction with the exoskeleton. Deltoid EMG average exceeded the 16.5% TLV without the exoskeleton, but the average and standard deviation fell below this level with the exoskeleton. Trapezius EMG averages exceeded the 16.5% TLV both without and with the exoskeleton.

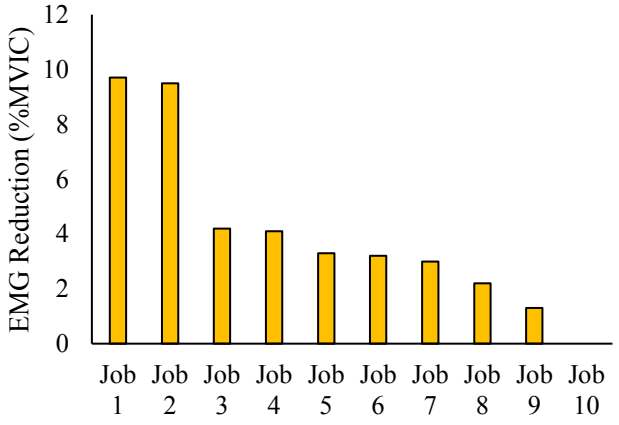

Figure 1: Reduction in maximum 50% EMG amplitudes for the deltoid as a function of job task.

Our hypothesis was supported by the significant reduction in deltoid EMG amplitudes when wearing the exoskeleton. Thus, the exoskeleton appeared to support the primary deltoid functions of shoulder flexion and abduction. Reductions in biceps brachii EMG may be due to exoskeleton stabilization of the shoulder to indirectly support elbow flexion. The unexpected reductions in erector spinae EMG may be explained by the exoskeleton reducing anterior lean and promoting a more upright posture. Effects on the trapezius were mixed, with possible benefits of shoulder abduction support mixed with possible shoulder strap restriction of scapular elevation.

We suggest assessing specific job tasks to determine potential benefits of assistive devices. The Levitate Airframe is most likely to benefit repetitive overhead movements that challenge the deltoid. When considering the different job tasks, there were tasks where the exoskeleton was more beneficial than others (Figure 1). We suggest that it is important to consider EMG amplitudes and standard deviations relative to TLVs as an indicator of fatigue and injury risk. In addition, analyzing maximum 10% and 50% EMG amplitudes may be useful for assessing risks associated with low vs. high repetition tasks.

REFERENCES

1. BLS. *Nonfatal occupational injuries and illnesses requiring days away from work*. 2016.
2. AAOS. *OrthoInfo*. 2010.
3. ACGIH. *Threshold Limit Values (TLVs)*. 2016.
4. Gillette and Stephenson. *ASB Proceedings*. Boulder, CO, USA, 2017.

ACKNOWLEDGEMENTS

The authors would like to acknowledge Terry Butler (Lean Steps Consulting), Seth Burt (Toyota), Alex Mason (Toyota), and Joseph Zawaideh (Levitate) for their assistance in coordinating this study.

Table 1: Maximum 10% and 50% EMG amplitudes with and without the exoskeleton

	Maximum 10% EMG Amplitude				Maximum 50% EMG Amplitude			
(%MVIC)	**Deltoid**	**Biceps**	**Trap**	**Spinae**	**Deltoid**	**Biceps**	**Trap**	**Spinae**
Without	31.8±8.2	14.9±4.2	28.0±12.9	26.0±9.5	16.6±6.9	8.3±2.6	17.8±9.3	16.8±6.3
Exoskeleton	25.4±6.4*	13.5±3.9*	30.8±13.9	21.9±6.6*	12.2±3.3*	7.3±2.5*	18.7±9.0	14.5±4.4*

*indicates significantly reduced EMG amplitude when wearing the exoskeleton ($p < 0.03$)

SKILL TRAINING VERSUS STRENGTH AND FLEXIBILITY EXERCISE IN PEOPLE WITH CHRONIC LOW BACK PAIN: EFFECTS ON KINEMATICS

[1] Quenten L. Hooker, [1] Kristen Roles, [1] Linda R. Van Dillen

[1] Washington University School of Medicine, St. Louis, MO, USA
Email : quenten.hooker@wustl.edu, vandillenl@wustl.edu

INTRODUCTION

An estimated 60-80% of all adults have experienced low back pain (LBP), and up to 75% of people with LBP fail to recover fully within one year [1, 2]. As LBP persists, people often have limitations in physical function [1]. Therefore, for many people LBP is a long-term function limiting condition.

The Kinesiopathologic Model (KPM) provides a theoretical framework for understanding the development or persistent course of LBP [3]. Specifically, the KPM suggests LBP may be a result of the repeated use of direction-specific movement patterns in the lumbar spine with functional activity performance [3]. For example, it has been documented that people with chronic LBP show repeated use of a movement pattern of early lumbar excursion during performance of functional activities [3,4]. The goal of treatment, therefore, would be to change the direction-specific movement pattern and introduce variability of movement across functional activities, in order to transfer tissue demands away from a sensitized and painful lumbar region.

Exercise is one of the primary non-surgical approaches for treating chronic LBP [5]. However, there is a lack of support for the benefits of one type of exercise over another [5]. Individualized movement training (i.e. skill training), utilizes patient specific instruction during functional activity performance to aid in the acquisition of new motor skills. Given skill training is individualized, it is likely that skill training is more effective at changing direction-specific movement patterns compared to general exercise (i.e. strength and flexibility).

The purpose of this study was to investigate the effects of skill training on early sagittal plane hip and lumbar spine excursion during a functional activity test of picking up an object (PUO). It was hypothesized that skill training would elicit *1)* greater changes in early hip and lumbar spine excursion and *2)* greater variability in hip and lumbar spine movement after treatment compared to strength and flexibility exercise.

METHODS

154 people (60 male, 94 female, 42.7 ± 11.7 years, 1.7 ± 0.1 meters, 73.8 ± 13.3 kg, 32.7 ± 9.8 mODI) with chronic non-specific LBP were included in a single-blind, prospective, randomized, controlled clinical trial. After completion of pre-treatment movement testing, participants were randomized to 1 of 2 treatment conditions: skill training or strength and flexibility exercise. Both conditions received 6, 1-hour treatment sessions (once/week for 6 weeks). Participants in the skill training condition received individualized training to modify pain-provoking, stereotypic patterns of movement used during functional activities. Participants in the strength and flexibility condition were prescribed general progressive, resistive trunk exercise (e.g. trunk curl ups) and trunk and limb flexibility exercise (e.g. hamstring stretching).

At baseline and immediately after the treatment phase, participants completed a functional activity test of picking up an object (PUO). 3-dimensional marker co-ordinate data were collected using 8 cameras (Vicon Motion Systems, LTD, Denver, CO) at 120 Hz. Joint kinematics for the hip and lumbar spine were calculated in Visual 3D (C-Motion Inc., Germantown, MD). Biomechanical variables of interest included early (1st half of the decent for a PUO task) sagittal plane hip and lumbar spine excursion.

Independent samples t-tests were used to determine if there were differences in hip or lumbar spine excursion between conditions at pre and post-

treatment data collection. Dependent samples t-tests were used to determine if there were changes in hip or lumbar spine excursion from pre to post-treatment for both conditions. Pearson product-moment correlations were used to examine the relationship of A) early lumbar excursion for pre and post-treatment and B) early hip excursion for pre and post-treatment for each treatment condition.

RESULTS AND DISCUSSION

Mean Values. Similar amounts of early hip and lumbar excursion were observed between treatment conditions at baseline (Table 1). The skill training condition had a significant increase (13.3%) in early hip excursion after treatment. No significant differences were found in early hip excursion for the strength and flexibility condition. No significant differences were found in early lumbar excursion from pre to post-treatment for either condition. Thus, the skill training condition increased early phase hip excursion to a greater extent than the strength and flexibility condition during a functional activity test of PUO (Table 1).

Table 1: Mean ± SD for early lumbar and hip excursion during a pick up an object task.

	ST	SF
Early Lumbar Excursion		
Pre-treatment	11.6 ± 3.7	11.9 ± 4.4
Post-treatment	11.7 ± 5.1	11.8 ± 4.3
Early Hip Excursion		
Pre treatment	$ 18.0 ± 7.3	17.1 ± 7.3
Post-treatment	*$ 20.4 ± 7.7	*17.1 ± 6.2

*Significantly different between treatments($p<0.05$)
$ Significantly different pre to post treatment ($p<0.05$)

Correlations. Pre-treatment early lumbar excursion explained 51% of the variance in post-treatment early lumbar excursion for the strength and flexibility condition, compared to 15% variance explained in the skill training condition (Figure 1A). A similar pattern of findings was observed for early hip excursion for each of the two treatment conditions (Figure 1B). These data suggest the strength and flexibility treatment has a more systematic effect on hip and lumbar spine movement from pre to post treatment. Alternatively, less variance explained in post-treatment movement in the skill training condition suggests this treatment induces a more variable hip and lumbar spine movement strategy. It is likely that the discrepancies in variability for post-treatment early hip and lumbar excursion are due to a more individualized treatment prescribed in the skill training condition.

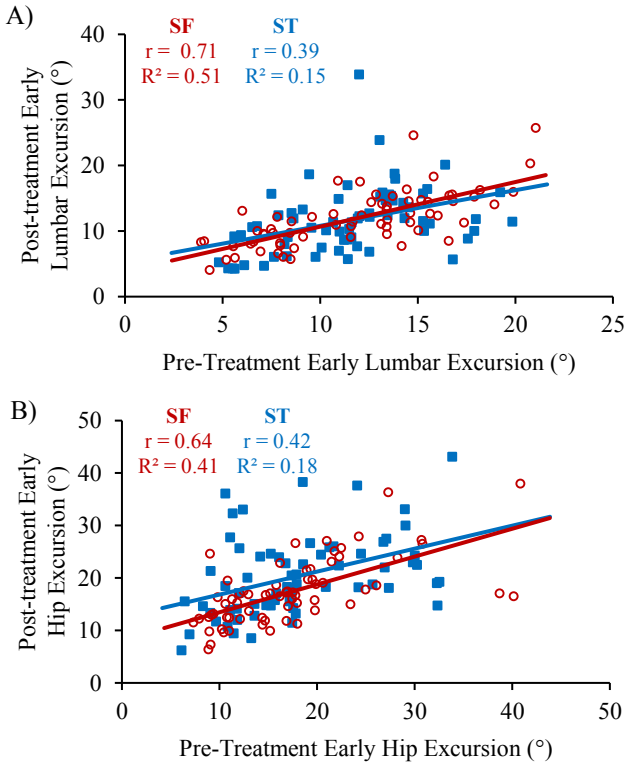

Figure 1: Relationship between A) pre vs. post-treatment early lumbar excursion and B) pre vs. post-treatment early hip excursion for skill training (ST) and strength and flexibility (SF) conditions

CONCLUSION

The skill training condition significantly increased early hip excursion and introduced greater early hip and lumbar spine movement variability after treatment in people with chronic LBP. Therefore, if the goal of treatment for people with chronic LBP is to modify direction-specific movement patterns and introduce greater variability of movement, our data suggest the skill training condition is superior to the strength and flexibility condition.

REFERENCES

1) Frymoyer JW, et al. *N Engl J Med* **318**, 291-300, 1988.
2) Croft PR, et al. *Br Med J.* **316**, 1356-9, 1998.
3) Sahrmann SA, Diag. Treat. Mov. Imp. Synd. 2002.
4) Marich AV, *Clin. Biom* **44**, 45-51, 2017.
5) Van Tulder M, et al. *Spine* **25**, 2784-96, 2000.
6) Tsao H, et al. *J Electro. Kines.* **18**, 559-69, 2008.

EFFECTS OF LOWER BACK AND HIP MORPHOLOGY ON WALKING KINEMATICS

[1]Russell T. Johnson, [2]Matthew C. O'Neill and [1]Brian R. Umberger

[1]University of Massachusetts Amherst, Amherst, MA, USA
[2]Midwestern University, Glendale, AZ, USA
email: umberger@kin.umass.edu, web: https://www.umass.edu/locomotion/index.html

INTRODUCTION

Bipedal walking is a fundamental aspect of human evolution. Humans are the only mammals that walk with an upright posture and extended limbs during stance. Chimpanzees, our closest living relatives, walk bipedally with flexed, abducted hind limbs, and a forward-leaning trunk [1]. Crouched walking should have a greater metabolic cost than upright walking, so why do chimpanzees walk on substantially flexed hind limbs?

Two main hypotheses have been proposed. First, chimpanzees lack a lumbar lordosis, so they are unable align the trunk over the pelvis when bipedal. Since their trunk is projected forward, chimpanzees may use a crouched posture to position their feet underneath their center of mass [2]. Second, due to their pelvis morphology (i.e., ischial length and orientation), chimpanzee hamstrings hip extension moment arm is near zero when the hip approaches full extension, which may preclude extended limb walking [3]. Experimental data alone are inadequate to isolate and test these hypotheses. However, musculoskeletal modeling and simulation techniques allow for the systematic manipulation of specific variables while others are held constant. Therefore, to test these hypotheses, we sought to determine if forward projection of the trunk and limitations on hip extension in a human musculoskeletal model would lead to crouched walking, similar to bipedal chimpanzees.

METHODS

A two-dimensional, 11 degree-of-freedom, 42 muscle human musculoskeletal model [4] was used within the OpenSim software package. Optimal control simulations of walking (1.3 m/s) were generated under ten different conditions using a direct collocation approach [5]. In the first set of five simulations, the model was modified such that the trunk was flexed 0, 15, 30, 45, or 60 degrees. This gradual progression of trunk flexion angles projected the trunk center of mass in front of the pelvis. In the second set of five simulations, the same five modified models were used to generate walking while constraining the hip to not pass 0 degrees of hip extension (i.e., no hyperextension). This constraint was a surrogate for the reduced hip extension moment capacity in chimpanzees. The optimization objective function was to minimize the sum of cubed muscle activations.

RESULTS AND DISCUSSION

In the first set of simulations, even substantial trunk flexion did not result in a chimpanzee-like crouched-limb gait (Table 1). At greater lumbar flexion angles, the model tilted the pelvis progressively posteriorly, resulting in less hip flexion, not more. For these conditions, the model did maintain a more flexed knee during stance, but the ankle was more plantar flexed (i.e., toe-walking), not more dorsiflexed. By tilting the pelvis posteriorly, the model was able to orient the trunk nearly perpendicular to the ground, positioning the whole-body center of mass over the base of support without flexing the hips. Thus, the minimum-activation solution for the first set of simulations did not involve walking with a crouched posture like a chimpanzee.

In the second set of simulations, restricting the hip to prevent hyperextension, combined with trunk flexion, resulted in the model walking with a slightly more chimpanzee-like crouched-limb gait, although differences still existed (Figure 1; Table 1). At greater lumbar flexion angles, the model still compensated with a more posteriorly tilted pelvis and a slightly more extended hip during stance, though to a lesser extent than in the first set of simulations. The adaptation most consistent with a crouched-limb gait was a progressively more flexed knee during stance at greater lumbar flexion angles, though by amounts considerably less than observed in chimpanzees [1]. There were small and inconstant effects at the ankle with increased lumbar flexion. Thus, while there were some elements of a crouched gait when trunk flexion and restricted hip extension were combined in the second set of simulations, it did not approximate walking like a chimpanzee.

The present results suggest that having a forward projected trunk does not necessarily lead to a chimpanzee-like couched-limb gait, even if restrictions are placed on hip extension. The gait patterns observed in chimpanzees are likely due as much to their specific pelvis and hind limb morphology as to the orientation of their trunk.

CONCLUSIONS

These results suggest that chimpanzee-like sagittal plane kinematics most likely arise from the interaction of multiple musculoskeletal traits. This may include pelvis and hind limb traits not studied herein. Future 3-D simulations of human and chimpanzee models will permit more direct testing of the effect of isolated musculoskeletal traits on bipedal walking kinematics.

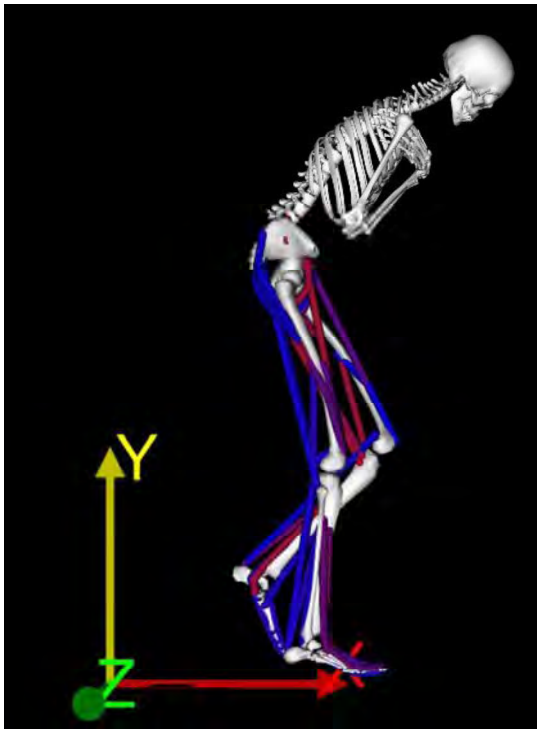

Figure 1: Midstance posture with lumbar flexion set at 60° and the hip restricted so as not to hyperextend.

REFERENCES

1. O'Neill MC, et al., *J. Hum. Evol.* **86,** 32-42, 2015.
2. Lovejoy CO & McCollum MA, *Philos Trans R Soc Lond B Biol Sci.* **365,** 3289-3299, 2010.
3. Fleagle JG & Anapol FC, *J. Hum. Evol*. **22,** 285-305, 1992.
4. Porsa S, et al., *Ann Biomed Eng.* **44,** 2542-57, 2015.
5. Lee LF & Umberger BR, *PeerJ.* **4,** e1638, 2016.

ACKNOWLEDGEMENTS

Support: UMass Amherst Robinson Fellowship, NSF-BCS 0935327 and 0935321.

Table 1: Average pelvis and lower limb joint angles during stance for each of the ten conditions. Positive values indicate posterior pelvis tilt, hip flexion, knee extension, and ankle dorsiflexion.

	Lumbar Flexion					**Lumbar Flexion and Hip Extension Restriction**				
	Lumbar 0°	Lumbar 15°	Lumbar 30°	Lumbar 45°	Lumbar 60°	Lumbar 0°	Lumbar 15°	Lumbar 30°	Lumbar 45°	Lumbar 60°
Pelvis	-11.6°	-5.0°	5.4°	14.8°	24.3°	-12.1°	-8.6°	0.5°	4.9°	6.8°
Hip	15.7°	5.6°	-4.2°	-13.8°	-23.7°	16.7°	11.3°	6.7°	4.5°	4.2°
Knee	-8.6°	-14.5°	-16.6°	-16.6°	-17.1°	-8.3°	-17.1°	-18.4°	-21.8°	-25.7°
Ankle	0.9°	-8.4°	-8.3°	-8.2°	-7.2°	0.5°	-3.8°	0.7°	-0.5°	-3.9°

DIRECT COMPARISON OF KINETICS AND LUMBAR FLEXION IN BARBELL BACK SQUATS AND DEADLIFTS

Joel L. Lanovaz, Corey P. Edington, Bart E. Arnold, Jonathan P. Farthing and Scotty J. Butcher

University of Saskatchewan, Saskatoon, SK, Canada
email: joel.lanovaz@usask.ca

INTRODUCTION

The barbell back squat and traditional deadlifts are common resistance training exercises utilized primarily by athletes to elicit muscular adaptations in strength, power and hypertrophy. Recently, these exercises are gaining popularity in rehabilitation settings and are being applied towards goals such as restoring motor function and increasing bone mineral density [1,2]. Understanding the kinematic and kinetic demands placed upon the lower limb and lumbar spine during these exercises can help ensure they are prescribed in such a way that produces the desired training outcomes without jeopardizing the safety of the lifter with excessive joint loading, especially in the lumbar spine.

With the exception of a few studies examining muscle activation [3], most of the research to date characterizing the biomechanics of heavy weight lifting have treated barbell back squats and deadlifts independently. While some general assertions can be made between studies, differences in participants and protocols can make direct comparisons challenging. To our knowledge, only one study has examined the kinematics of these two lift types in the same study population [4] and none have looked at kinetics. The goal of this study was to compare the lower limb and lumbar joint torques and lumbar kinematics between the conventional deadlift and the back squat.

METHODS

Seventeen healthy adults participated in this study (12 males; age: 27±5 years; height: 176±5 cm; mass: 97.7±19.3 kg). Participants were competitive powerlifters (n=9), weightlifters (n=7) and CrossFit athletes (n=1). All participants had competed in their respective sports within the past year (overall lifting experience: 5.7±3.5 years).

Prior to testing, each participant performed a warm-up of light aerobic exercise, dynamic stretching, and progressive squats and deadlifts up to 65% of their self-reported one repetition maximum (1RM). Each participant then performed three sets of single self-paced repetitions of the squat and deadlift at 85% of their self-reported 1RM for each type of lift. The order of lift type was alternated between participants. The techniques for each lift were standardized based on published protocols [5,6]. The deadlift was based on the conventional Olympic weightlifting technique with the initial bar position above the first metatarsal phalangeal joint and directly beneath the shoulders. The squat was a conventional "high bar" back squat (bar near the C6 vertebra) with depth controlled so that the hip crease was just below the top of the patella.

Kinematic data were collected for all trials using a 3D motion capture system (VICON, Centennial, CO, fs=100Hz) with 44 reflective markers. Ground reaction force (GRF) data were collected simultaneously using platforms located under each foot (AMTI OR7-6, Watertown, MA, fs=2000Hz). The 3D kinematics of the bar, lower limbs and pelvis were calculated using custom routines in Matlab (R2006b, Mathworks, Natick, MA). Lumbar spine curvature and the L5-S1 joint position were estimated using a custom planar kinematic model implemented in Matlab based on published geometry estimates for the lumbar vertebral bodies and spinous processes [7] and relative vertebral kinematics [8]. The model was scaled for each participant and positioning for each frame of data was driven by the matching the location of kinematic markers placed over the spinous processes of L1, L3 and L5 via an optimization approach. Using the GRF and kinematic data, quasi-static inverse dynamics were used to calculate joint torques for the ankles, knees, hips and L5-S1 joint. Joint torques were normalized to total load (body weight + lift load) x height and

flexion axis peak values extracted. Paired t-tests were used to compare between lift types with significance set at α=0.05 and effect sizes (d) reported.

RESULTS AND DISCUSSION

Almost all participants (15/17) had a higher self-reported deadlift 1RM compared to their squat. As a result, the deadlift (DL) load was significantly higher than the squat (SQ) load (DL: 1.56±0.31 x body weight, SQ: 1.33±0.27, $p<0.001$, d=0.8). Despite this, the squat produced a significantly higher peak normalized vertical GRF compared to the deadlift (DL: 1.10±0.03 x total load, SQ: 1.29±0.08, $p<0.001$, d=3.1) due to the upwards acceleration required to slow down and change direction at the bottom of the squat movement.

The peak knee extensor torque was significantly higher in the squat compared to the deadlift ($p<0.001$, d=4.5); however no differences were seen in peak ankle plantar-flexor, hip extensor or lumbar extensor torques between the lifts (Figure 1).

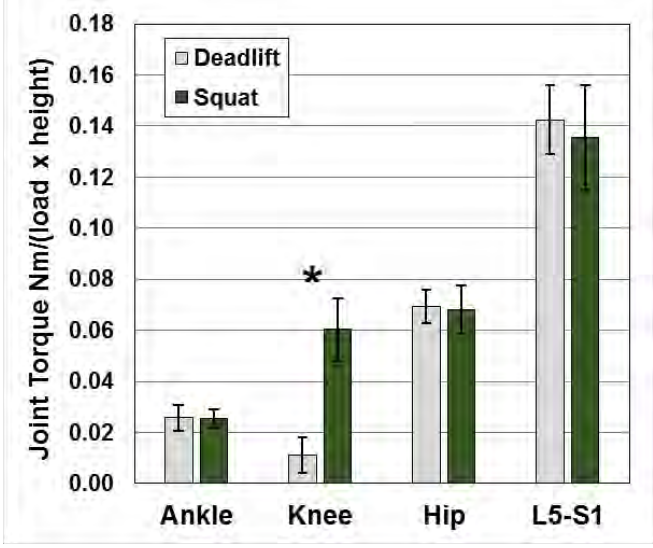

Figure 1: Mean peak joint torques (SD). Ankle, knee and hip torques are averages across legs. *significant difference between lift types

These data suggest that, for a given load, the back squat places much higher demands on the knee extensor mechanisms compared to the deadlift. This matches with what is generally believed in the training community and likely arises from the significantly increased forward lean of the tibia in the squat (unreported data).

Despite the differences in GRF and kinematics [4] between the deadlift and squat, the peak hip and lumbar torques in this study were similar. This may indicate an equivocal level of low back loading between the lift types but likely arising from different patterns of trunk muscle activation [3].

The spine model estimated significantly more lumbar flexion during the deadlift at the time of peak lumbar torque, however the effect size was relatively small (DL: 14.6±17.1°, SQ: 7.8±19.9°, p=0.001, d=0.3). Different lumbar angles could possibly affect the lines of action of the lumbar extensor muscles and result in different shear and compression loads at the L5-S1 joint even with similar joint torques.

Importantly, both the squat and deadlift have a number of technique variations that include different grips, foot positions, starting postures and movement ranges. This study focused on the more common techniques, but variations could have an impact on the lift kinetics.

CONCLUSIONS

This is the first study to directly compare lower limb and lumbar joint torques in the barbell back squat and deadlifts in the same population. Accounting for load, the main difference between the lifts is an increase in knee extensor torque in the squat. This should be kept in mind when prescribing these exercises.

REFERENCES

1. Watson et al. *Osteoporosis Int.*, 26:2889-2894, 2015.
2. Ebben et al. *Int J Sports Med*, 30:1-8, 2009.
3. Hamlyn et al. *J Strength Cond Res*, 21:1108-1112, 2007
4. Hales et al. *J Strength Cond Res*, 23:2574-2580, 2009
5. Wrettenberg et al. *Med Sci Sport Exer*, 28:218-224, 1996.
6. Hancock et al. *Int J Exerc Sci* , 5:183-195, 2012.
7. Panjabi et al. *Spine*, 17:299-306, 1992.
8. Christophy et al. *Biomech Model Mechanobiol*, 11:19-34, 2011.

Evaluating the Severity of Adult Spinal Deformity using Timed-Up and Go

[1,2] Victoria A. Smith, [1,2] Christopher W. Frames, [1] Jakub Godzik, MD, [1]Jay D. Turner, MD and [2] Thurmon Lockhart, PhD

[1] Barrow Neurological Institute, St. Joseph's Hospital and Medical Center, Phoenix, AZ, USA
[2] School of Biological and Health Systems Engineering, Arizona State University, Tempe, AZ, USA
email: vasmith5@asu.edu

INTRODUCTION

Adult spinal deformity (ASD) is a group of spinal pathologies that has a wide range abnormal radiographical patterns and is estimated to occur in up to 60% of the aging population [1]. Managing this patient population hinges on the balance of the amount of pain and disability each patient endures while correctional spinal surgery requires precision radiography [2,3].

Outcomes of these surgeries are assessed on post-operative questionnaires. The use of functional and quantitative measures can be used to accurately evaluate post-operative improvement in daily living activities instead of relying on subjective scales and perceived improvement from the patient. A simple battery of functional tests, e.g. walking, standing balance, and basic functions, such as rising from a chair, would provide more information about how the patient is functioning.

For example, the Timed-Up and GO (TUG) test is a simple and widely used clinical balance tool for assessing functional mobility [4,5]. In this test, the subject starts in a seated position and when told to "Go", they stand up, walk three meters, turn around, walk back to the chair, and sit back down. The TUG test can be subjective if only a visual assessment is performed, however, instrumented TUG testing can provide a wealth of quantitative data utilizing a single inertial measurement unit. The duration each subtask task and how well each task is performed can be evaluated.

We postulate that functional and quantitative measures can be used to better understand the effects of ASD on daily living activities before and after surgery. In this pilot study we ask eight ASD patients that are candidates for corrective spinal surgery to perform a TUG test.

METHODS

Eight patients with adult spinal deformity (ASD) were prospectively enrolled. Mean age was 65±4.2 years and 75% (6/8) of subjects are female. Subject must be diagnosed with ASD. Inclusion criteria for ASD using radiographic measurements: coronal cobb $\geq$ 20°, pelvic tilt $\geq$ 25°, Pelvic incidence-lumbar lordosis (PI-LL) mismatch >10°, and thoracic kyphosis $\geq$ 60°. Exclusion criteria: inability to stand, other confounding neurological conditions. In this study we asked subjects to perform a 3-meter TUG test while wearing four APDM sensors (APDM Portland, OR) using Mobility Lab. These sensor have a tri-axial accelerometer and tri-axial gyroscope. One sensor was place at the trunk, lumbar, and ankles of each foot.

The trunk acceleration data was denoised and filtered using a bandpass filter with cutoff frequencies between 2 Hz and 8 Hz. The time duration, range, root mean square (RMS) and jerk was calculated for the sit-to-stand and final stand-to-sit motions, respectively [6].

Standard radiographic measures, including lumbar lordosis (LL), pelvic incidence (PI), pelvic tilt, sagittal vertical axis, global coronal alignment, T1 and pelvic angle (TPA), and PI/LL mismatch were calculated for each patient using their preoperative x-rays. Correlation analyses between TUG parameters and radiographic measurements were performed using spearman's correlation. JMP Pro 13 was used for all analyses.

RESULTS AND DISCUSSION

We found several significant correlations between TUG parameters and radiographic measurements. Sit-to-stand and stand-to-sit duration increased as the pelvic tilt increased. As pelvic tilt increases, knee flexion increases resulting in retroversion of the pelvis as a compensatory mechanism to maintain the body's center of mass over its base of support. The Stand-to-sit duration also increased with the TPA. This angle is based on retroversion of the pelvis and the anteversion of the trunk; the larger the angle, the greater the deformity of the spine. The total duration of the TUG test increased as pelvic tilt and TPA increased. This is expected because pelvic tilt increases the duration of both sit-to-stand and stand-to-sit.

The Sit-to-Stand RMS in the anteroposterior direction increases as TPA, global coronal balance, sagittal vertical axis, and PI/LL mismatch increases. The RMS is a measure of variability, when RMS is low the movement is deemed to be smooth and more natural, while a greater RMS value evinces large amplitudes. In this case, the aforesaid radiographic measures increase as the spinal deformity worsens. Therefore, as the spinal deformity becomes more severe, the smoothness of the transition from sitting to standing becomes worse and requires greater effort.

Lastly, we found that the sit-to-stand jerk increased as the global coronal alignment decreased. In this instance, jerk can be used to evaluate efficiency of a motion. When jerk is high, the motion is easier and performed with less effort. Global coronal alignment is a measurement of decompensation of the spine. A higher absolute value of global coronal alignment is a sign of imbalance and scoliosis in the coronal plane. Therefore as the coronal scoliosis worsens the efficiency of standing from a seated position decreases.

CONCLUSIONS

We conclude that there is immense value in utilizing functional tests with inertial measurement unit data for increased understanding of how spinal deformities impact daily living activities and for evaluating post-operative improvements.

REFERENCES

1. Schwab FJ, Lafage V, Farcy JP, et al. *Spine.* 2008; 33:2243-7.
2. Bess S, Boachie-Adjei O, Burton D, et al. *Spine* 2009;34:2186-90.
3. Glassman SD, Bridwell K, Dimar JR, et al. *Spine* 2005; 30:1082-5.
4. Mancini M, Horak FB. *Eur J Phys Rehabil Med*. 2010;46(2):239-248.
5. Noohu MM, Dey AB, Hussain ME. *J Clin Gerontol Geriatr.* 2014;5(2):31-35.
6. Weiss A, Herman T, Plotnik M, et al. *Med Eng Phys.* 2010;32(10):119-25.

Table 1. Radiographic correlations with calculated TUG parameters

Variable	By Variable	Correlation	p-value
Sit-to-Stand Duration (s)	Pelvic Tilt	0.79	0.020
Stand-to-Sit Duration (s)	T1-Pelvic Angle	0.71	0.047
Stand-to-Sit Duration (s)	Pelvic Tilt	0.78	0.023
TUG Duration (s)	Pelvic Tilt	0.75	0.033
TUG Duration (s)	T1-Pelvic Angle	0.77	0.027
Sit-to-Stand RMS	T1-Pelvic Angle	0.71	0.047
Sit-to-Stand RMS	Global coronal alignment	0.96	0.0002
Sit-to-Stand RMS	Sagittal Vertical Axis	0.71	0.047
Sit-to-Stand RMS	PI/LL mismatch	0.74	0.037
Sit-to-Stand Jerk (g/s)	Global coronal alignment	-0.78	0.023

PI/LL mismatch – Pelvic Incidence/Lumbar Lordosis mismatch

IN SITU CALIBRATION OF THE TENDON SHEAR WAVE SPEED-STRESS RELATIONSHIP

[1] Jack A. Martin, [2] Christina J. Stender, [2] William R. Ledoux and [1] Darryl G. Thelen

[1] University of Wisconsin-Madison, Madison, WI, USA
[2] RR&D Center for Limb Loss and MoBility, VA Puget Sound Health Care System, Seattle, WA, USA
email: jamartin8@wisc.edu, web: http://uwnmbl.engr.wisc.edu/

INTRODUCTION

We recently developed a non-invasive technique for measuring *in vivo* tendon stress which could be useful in a variety of biomechanics applications [1]. This technique is based on a simple tensioned beam model for tendon, which predicts that shear wave speed is directly dependent on axial stress. We have previously shown that our model is valid for *ex vivo* tendons loaded in a mechanical testing machine, and have demonstrated the potential to track *in vivo* tendon wave speeds during dynamic activities, e.g., the Achilles tendon during walking. However, the precise relationship between stress and wave speed is dependent on the effective density of the tendon, which is influenced by surrounding tissues. It is unclear whether effective density can be calculated for different tendons using analytical methods. Accordingly, our objective was to calibrate the *in situ* Achilles and tibialis anterior (TA) tendon wave speed-stress relationships by applying dynamic loads representative of gait while concurrently measuring wave propagation speed.

METHODS

We simulated gait [2] on a fresh-frozen cadaveric lower limb specimen. A 6-DOF robot moved a force plate relative to the plantar surface of the foot to mimic relative tibia-to-ground motion and ground reaction forces observed during normal gait. Tendon forces were concurrently modulated to track dynamic force profiles that arise in gait. Gait simulations were performed at one sixth physiologic speed and at 50% body weight.

We synchronously measured tendon wave speeds using a novel surface-mounted sensor [1] comprised of: 1) a piezoelectric-actuated (Thorlabs PK4JQP1) tapping device that induces shear waves, and 2) a pair of miniature single-axis accelerometers (Piezotronics 352C23) aligned in series along the tendon (10 mm spacing). After each tap (50 taps/s), the induced wave sequentially passes the two accelerometers. Wave speed was calculated from a time delay determined by cross-correlation of the two acceleration signals. Tendon wave speed and applied force data were collected during three simulated stance phases both before and after removing the skin overlying the tendon. The skin-on and skin-off conditions were tested to examine the effects of superficial tissue on the effective density of the tendon.

Measured tendon stresses were obtained by normalizing applied force by the tendon cross-sectional areas obtained from a CT scan. Predicted stresses were calculated from wave speed based on the theorized wave speed-stress relationship [1]:

$$c^2 = \frac{k'\mu + \sigma}{\rho_{eff}} \qquad (1)$$

where c is shear wave speed, σ is axial stress, ρ_{eff} is effective density, μ is shear modulus, and k' (= 0.9) is a shear correction factor which accounts for the shape of the cross-section. It is unknown how shear modulus changes with axial load in tendon, so a constant value was chosen based on values obtained for ligament at a moderate shear strain (μ = 500 kPa) [3]. The effective density, ρ_{eff}, is theorized to account for an increased effective mass of the tendon caused by entrained motion of the surrounding tissue [1]. However, in this case, we first used the tendon density (ρ_t = 1060 kg/m^3) to demonstrate the resulting error in predicted stress. Subsequently, we determined effective densities that optimized agreement between predicted and measured stress in each of the tendons. Optimization was performed using data from periods of the gait cycle where stress exceeded 1 MPa, which is the loading regime at which axial

stress is believed to be a major determinant of shear wave speed. We assessed the fits between predicted and measured stresses using the coefficient of determination (r^2) and root mean squared error (RMSE).

RESULTS AND DISCUSSION

Predicted and measured stresses were highly correlated for both tendons and conditions (Table 1). Stresses were substantially under-predicted when using the tendon density, ρ_t, in Eqn. 1 (Fig. 1). The error between predicted and measured stress was low for all conditions when using the optimized effective density, ρ_{eff}, to calculate predicted stress (Table 1). The density that minimized error between predicted and measured stress ranged from 2060 to 3720 kg/m^3 (Table 1). The highest effective density was estimated for the TA tendon in the skin-on condition, which could reflect additional effective mass that arises when the subcutaneous tissue and overlying skin tether the motion of the tendon. The skin-off condition resulted in similar effective densities for both the TA and Achilles tendons.

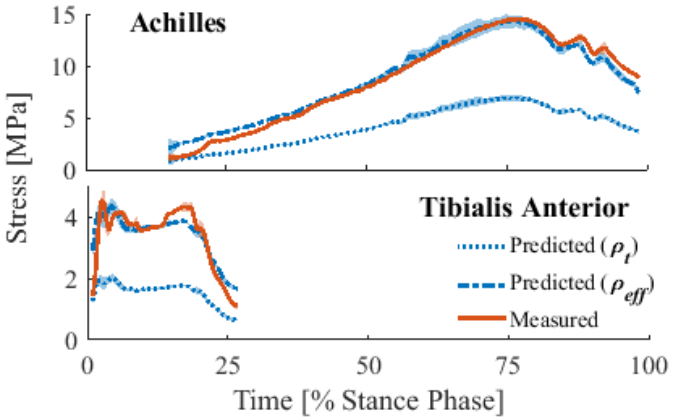

Figure 1: Predicted (using tendon density, ρ_t, and optimized effective density, ρ_{eff}) and measured stress across three trials for the skin-off conditions.

The excellent correlation between predicted and measured stress confirms that this technique can be useful for examining relative tendon loading under different conditions, even without consideration of uncertain parameters. However, absolute tendon stress estimates do require an estimate of effective density. These preliminary data suggest that effective density may be tendon dependent, and may be more affected by superficial tissue in the tibialis anterior tendon than in the Achilles.

Ongoing work is addressing the possibility of tendon specificity in calibration relationships. Ideally, calibration would not be necessary for *in vivo* applications since stress cannot be directly measured for such purposes. Future work will employ finite element modeling and *in situ* experimentation to investigate whether tendon and superficial tissue geometry modulate effective density in a predictable manner.

CONCLUSIONS

This work has demonstrated the potential for precisely estimating tendon stresses via non-invasive measurement of wave propagation speed. The availability of these data could lead to significant advances in a variety of applications in biomechanics, such as, guiding rehabilitative interventions by providing biofeedback on tissue loading, planning orthopedic procedures where tissue stresses are of high importance, and potentially examining the effects of tissue stresses on growth and remodeling.

REFERENCES

1. Martin et al. *Nat Commun*. Accepted.
2. Aubin et al. *IEEE Trans Robot* **28**(1):246-255,2012.
3. Weiss et al. *J Biomech*. **35**(7): 943-950, 2002.

ACKNOWLEDGEMENTS

NSF GRFP (DGE-1747503), NIH (HD092697).

Table 1: Coefficient of determination (r^2), empirical effective density (ρ_{eff}) and root mean squared error (RMSE) for wave speed-stress regressions on the Achilles and tibialis anterior (TA) tendons for each condition.

	Achilles, Skin-On	**Achilles, Skin-Off**	**TA, Skin-On**	**TA, Skin-Off**
r^2	0.96	0.97	0.85	0.82
ρ_{eff} [kg/m^3]	2110	2130	3720	2060
RMSE [MPa]	0.89	0.71	0.44	0.46

IDENTIFYING BIOMECHANICAL WRIST IMPAIRMENTS WITH MACHINE LEARNING: A FEASIBILITY STUDY

[1] Jennifer A. Nichols, [2] K. Supreet Alguri, and [1] Joel B. Harley

[1] University of Florida, Gainesville, FL, USA; [2] University of Utah, Salt Lake City, UT, USA
email: jnichols@bme.ufl.edu, web: http://www.bme.ufl.edu/labs/nichols/

INTRODUCTION

Traditional biomechanical methods often rely on the researcher to identify the key biomechanical features to analyze. For example, joint loading is frequently examined when studying osteoarthritis. Although analyzing a small number of pre-selected variables is sufficient for many biomechanics applications, it can be insufficient when studying complex, multi-joint systems, such as the wrist and hand. In these systems, the critical variables to analyze cannot always be readily identified.

Machine learning offers an alternative approach for analyzing large, multi-dimensional datasets without relying upon *a priori* assumptions regarding which variables are most important [1]. In biomechanics, machine learning has been applied in many different applications, such as analyzing gait [2], identify wrist ligament tears [3], and modeling EMG [4]. However, to our knowledge, machine learning has not yet been used to elucidate the complexity of the wrist/hand.

In this study, we examine how machine learning can guide analysis of the wrist and hand. We specifically evaluate whether three common machine learning algorithms can identify (i) wrist impairments and (ii) the features distinguishing those impairments. The wrist impairments studied represent two surgeries for wrist osteoarthritis (Fig. 1A). These surgeries are interesting, as their clinical outcomes are nearly identical [5]. Thus, identifying which surgery was performed given only biomechanical data is difficult.

METHODS

To evaluate whether machine learning can be used to identify wrist impairments, a biomechanical dataset was generated to simulate experimental motion capture data from nonimpaired, SE4CF, and PRC wrists. These simulations used published models and methods [6] to quantify dynamic changes in thumb-tip endpoint forces and posture during lateral pinch (Fig 1B). The 165 simulations represent unique combinations of lateral pinch force, model size, and wrist condition (Fig 2). Importantly, each simulation was dynamic, thereby providing time-varying data. Data-defined features were then used to train and test the machine learning algorithms (Fig. 2).

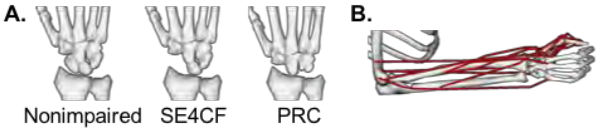

Fig. 1: We simulated (A) two surgeries for wrist osteoarthritis [scaphoid-excision four-corner fusion (SE4CF) and proximal row carpectomy (PRC)] performing (B) a lateral pinch task.

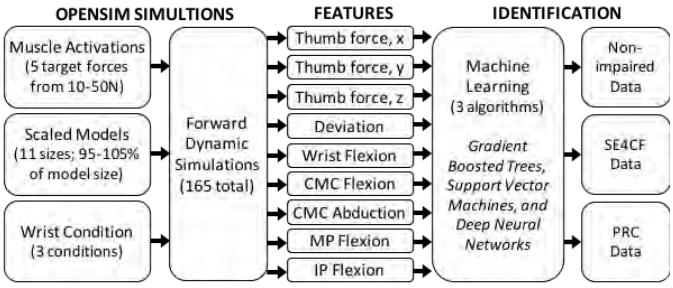

Fig. 2: Summary of machine learning approach.

Three common machine learning algorithms were evaluated for identifying data from nonimpaired, SE4CF, or PRC wrists. Multiple algorithms were examined, as differences in accuracy can inform future work. The algorithms are gradient boosted trees (GBT), support vector machines (SVM), and deep neural networks (DNN). Briefly, GBT uses layers of simple decision trees to model the relationship between features and categories [7]. Here, we employed 500 simple trees with a learning rate of 0.05 and a constraint that each node of each tree has at least 100 samples. SVM classifies data by identifying points (i.e., support vector) that optimally separates data from different categories and follows a known separation model, or kernel [8]. Here, we extend SVM for multi-category classification [8]. We use a Gaussian kernel with optimized scaling parameters. DNN use multiple layers to model and learn complex, non-linear relationships [9]. Here, our

DNN consists of an input layer, two hidden layers, and an output layer. The input layer is composed of input nodes corresponding to the number of features and is connected to a hidden layer with 16 tanh activated nodes. This hidden layer is then connected to a second hidden layer with 8 tanh activation nodes followed by an output layer with 3 output nodes, representing the three categories.

To evaluate each algorithm, we used a 20-fold cross-validation procedure [10], meaning each algorithm was trained with 80% of the data and tested with the remaining 20%. This procedure was repeated 20 times for each algorithm. The algorithm's accuracy is represented by the mean accuracy of all 20 tests. We performed this cross-validation procedure using all 9 features, the 2 most influential features, and the most influential feature. A feature's influence was determined as part of the GBT algorithm [7].

RESULTS AND DISCUSSION

The biomechanical dataset represents a wide range of dynamic behaviors. Importantly, the generated thumb-tip forces and joint angles overlap between the three wrist conditions (data not shown). Hence, distinguishing each condition from the simulated experimental data is a challenging problem. Optimal binary accuracies support this conclusion (Fig. 3). An optimal binary accuracy is the maximum accuracy for a single feature to categorize a single category versus all other categories. Some features classify one category well (accuracy > 0.95), but no feature accurately classifies all three categories.

The GBT algorithm indicates that radial-ulnar deviation followed by CMC ab/adduction are the most influential features for categorizing the three wrist conditions. This is an intriguing result, as the lead author's prior work [6] suggests that radial-ulnar deviation and wrist flexion-extension are the most important features differentiating these surgeries. CMC ab/adduction's substantial influence likely reflects its importance for producing well-directed thumb-tip endpoint forces. Examining different tasks that require varying wrist postures could lead to more insights regarding the role of wrist flexion/extension.

Regardless of whether one feature (deviation), two features (deviation and CMC abduction), or all nine features were used, the three machine learning algorithms performed well (Fig. 4). DNN achieved the highest accuracies, which is expected since DNN can learn the most complex relationships. As the number of features increased, the mean accuracy increased toward 100%. Although, this is not true for all test data, as evidenced by an outlier in SVM. The high accuracy results indicate that the presented algorithms can identify substantial musculoskeletal changes, such as those imposed by surgery. These results also suggest that these algorithms may be able to address more complex biomechanics problems.

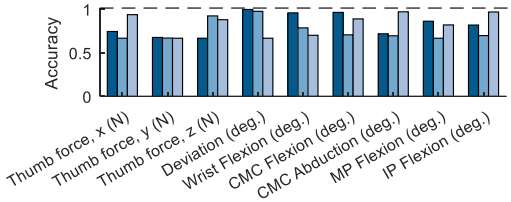

Figure 3: Optimal binary classification accuracies for each category and feature. The bars in each group (from dark to light) represents the accuracy of categorizing the nonimpaired, SE4CF, and PRC conditions versus all other conditions.

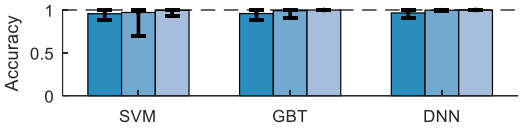

Figure 4: Mean accuracy (from left to right) using one, two, or nine features. Bars represent minimum and maximum accuracy.

CONCLUSIONS

This study demonstrates that it is feasible to use any of the three presented machine learning algorithms to identify simulated wrist impairments. Thus, this work lays the foundation for future analyses of the wrist and hand using machine learning. In the future, we plan to extend these algorithms to examine other biomechanical features, namely muscle parameters. This will inform our understanding of the relative importance of individual muscles for production of lateral pinch force. We also plan to evaluate how using experimental (instead of simulated) data influences the accuracy of each algorithm.

REFERENCES

1. Feber et al. *J Biomech*. 49(16): 2016
2. Phinyomark et al. *J Biomech.* 48(14): 2015.
3. Werner et al. *J Orthop Res*. 27(3): 2009.
4. Wang & Buchanan *IEEE Neur Syst Rehab Eng* 10: 2002.
5. Mulford et al. *J Hand Surg. Eur.* 34(2): 2009.
6. Nichols et al. *J Biomech* 58: 2017.
7. Z. Xu et al., Proc. of ACM SIGKDD, 2014.
8. Hsu et al., *IEEE Trans. Neural Netw.* 13(2): 2002.
9. LeCun et al., *Nature.* 521(7553): 2015.
10. Efron et al., *Am. Stat*. 37(1): 1983.

PREDICTION OF ACL STRAIN UNDER NON CONTACT SPORT-LOADING CONDITIONS: A DYNAMIC FINITE ELEMENT ANALYSIS

[1] Deniz U. Erbulut [1] Sara Sadaqi [1] Rodney Summer [2]Nathaniel A. Bates, [2]Nathan D. Schilaty, [2]Alessandro Navacchia [1] Vijay K. Goel [2]Timothy E. Hewett

[1]Engineering Center for Orthopaedic Research Excellence (E-CORE), Departments of Bioengineering and Orthopaedics, University of Toledo, Toledo, OH,

[2]Mayo Clinic Biomechanics and Sports Medicine Research Center, Mayo Clinic, Rochester & Min., MN

Deniz.erbulut@utoleod.edu

INTRODUCTION

Previously, our novel single validated -finite element (FE) model of the knee joint was used to investigate non-contact landing scenarios to understand the propagation of anterior cruciate ligament (ACL) injury [1]. In this study, the revised FE models, created using MR images of male and female subjects, were used to simulate more relevant scenarios for non-contact ACL injury. These FE models were validated against an *in vitro* study, undertaken by our group [2], designed based on *in vivo* driven biomechanical loading parameters. Validated FE models were then used to further investigate loading cases seen in the non-contact injury environment and sex related anatomical variations.

METHODS

MR images from four, healthy, 2 males and 2 females subjects were converted to 3D models of the bone and soft tissue across the knee joint using Mimics (Materialise, Leuven, Belgium). Meshes of C3D4 elements were constructed in Hypermesh (Altair, MI, USA) before final assembly in Abaqus/Explicit 6.14-5 (Simulia, RI, USA). Cruciate and collateral ligaments were modeled as Holzapfel-Gasser-Ogden hyperelastic materials with a Prony series defined viscoelasticity. The remaining joint capsule was modeled with uniaxial connector elements. Bone and cartilage were simulated as linear elastic materials, and menisci as transversely isotropic material.

FE models were subjected to different loadings using the explicit dynamic analysis. The joint was preconditioned (25° flexion with 441N quadriceps and 441N hamstrings loads) before the application of quasi-static loadings, Table 1. These loads were followed by an impact step that mimicked bipedal landing (half body- weight) from a height of 30cm. ACL strain was calculated post impact and compared with the experimental data.

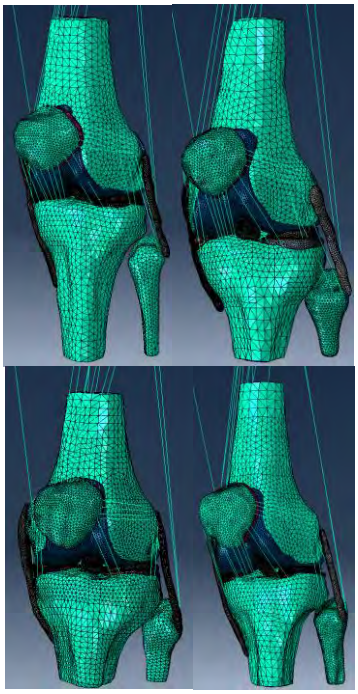

Figure 1: females (top) and males (bottom) FE models

RESULTS AND DISCUSSION

Table 2 shows the percent **c**hange in ligament strain at 100 ms post impact and wrt baseline (after 25° flexion). Cadaveric data are the mean percent change ACL strains for external sub failure loadings, knee abduction moment (KAM), anterior shear force (ASF), internal tibial rotation moment (ITR). Predictions were in good agreement with *in-vitro* data (close to and within 1.5SD) FE simulation predicted that ITR contribution to ACL strain was greater than ASF. ACL strain was up to 20% higher in case3 compared to case5, where KAM was held constant. Although, the loading magnitudes are not the same for comparisons of ITR and ASF, varying load magnitudes were matched to the corresponding

in vivo kinetics reported for the same percentile of the population.

ACL injury incidence was approximately six fold higher in female than male participating in jumping and cutting sports [3], However, relatively lesser ACL strain was predicted for female models compared to male models under the same loading cases. There are mainly two reasons for these findings. Our previous study [4] concluded that female athletes display greater valgus motion than males among basketball players during landing, which likely results in higher rates of knee injury in females. Similarly, our current FE model predicted higher abduction in female compared to male (Table 3). One can expect higher ACL strain in female models. However, as seen in Table 3, axial tibial translation was higher, meaning the joint is more compressed in female models, which would result in higher contact pressure on tibial cartilage. Therefore, ACL strain was much less in females compared to male models. In addition, the limited number of female and male models at present may contribute to this discrepancy as well.

CONCLUSIONS

FE models help understand how strain develops in the ACL due to multi-planar loading and moments seen in non-contact sport activities. Our validated models can predict engineering failure parameters for real case scenarios, which is not practical with *in vitro* and *in vivo studies*. Future studies will include more subject specific male and female models in combination with more loading protocols to conduct in-depth injury mechanism studies. The models will allow us to assess clinically relevant ACL injuries patterns using failure loading scenarios.

REFERENCES

1. Kiapour et al, J BiomechEng, 136(1), 2014
2. Hewett T.E. et al. *Clinical Biomech*. 44:36-4, 2017.
3. Malone, T.R. et al. *J. Southern Orthop. Assoc*. 2:36–39, 1993.
4. Hewett T.E. et al. *Med Sci Sports Exerc*. 35(10):1745-50. 2003

ACKNOWLEDGEMENTS

Supported in part by NIH (R01 AR056259-06-TEH) and by an allocation from the Ohio Supercomputer Center.

Table 1: Quasi-static loading protocols

	Knee abduction moment (KAM)(Nm)	Anterior tibial shear force (ASF)(N)	Internal tibial rotation moment (ITR)(Nm)
Case 1	57.34	80.35	9.73
Case 2	57.34	80.35	18.62
Case 3	57.34	80.35	53.71
Case 4	57.34	196.13	9.73
Case 5	57.34	196.13	18.62

Table 2: Percent change in ligament strain with respect to baseline (after 25^0 flexion) 100ms post impact

	Case1	Case2	Case3	Case4	Case5
Male FE model 1	1.32	1.65	2.00	0.55	1.62
Male FE model 2	-0.28	0.07	0.18	-0.24	0.14
Female FE model 1	0.27	0.09	0.25	0.31	0.20
Female FE model 2	-0.92	-1.01	-1.2	-0.93	-1.02
in vitro (mean(1SD))	3.64(3.10)	6.15(7.88)	3.93(3.02)	3.16(2.92)	3.69(3.00)

Table 3: Typical maximum kinematic values post impact for male and female models under loading Case 5.

	Knee abduction (deg)	Internal tibial rotation (deg)	Anterior tibial translation (mm)	Axial tibial translation (mm)
Male FE model 1	-1.78	3.30	0.12	1.14
Female FE model 1	3.14	4.92	3.03	2.42

EFFECTS OF KNEE KINEMATICS ON ACL STRAIN DURING SIMULATED LANDING

Rena Hale, Nathan D. Schilaty, Nathaniel A. Bates, Christopher V. Nagelli, Aaron J. Krych, and Timothy E. Hewett

Mayo Clinic Biomechanics Laboratories & Sports Medicine Center, Rochester & Minneapolis, MN, USA
email: Hale.Rena@Mayo.edu

INTRODUCTION

Approximately 75% of anterior cruciate ligament (ACL) ruptures occur in non-contact scenarios [1]. This injury is often the result of a high impulse force within the first 50 ms of initial ground contact during a rapid deceleration or change in direction landing [2]. Subsequently, it is important to understand the underlying mechanisms of ACL injury, specifically the knee kinematics that correlate to ACL strain. Previous studies have looked at how *in vivo* knee kinematics correlate to increase risk of ACL injury [3]. However, the exact change in knee kinematics due to high impulse forces have not been correlated to ACL strain. The purpose of this study was to determine how knee kinematics affect ACL strain when high external knee abduction moment (KAM) is applied. The hypothesis tested was that in high KAM impacts, greater change in knee abduction angle and internal rotation would increase relative ACL strain. Improved knowledge of knee kinematics will enhance ACL injury prevention and rehabilitation.

METHODS

A previously developed mechanical impact simulator was utilized to simulate landing from a drop vertical jump (DVJ) in the lower extremity of 35 specimen's age 24 to 52 [2]. Specimens showed no evidence of significant trauma or extended chemotherapy. Specimens were prepared according to published specifications [2] and were equipped with 3D triad markers mounted on the tibia and femur (Northern Digital, Ontario, Canada), and a differential variable reluctance transducer (LORD, Willison, VT) implanted on the ACL.

To replicate a DVJ landing, varied magnitudes of KAM, anterior tibial shear (ATS), and internal tibial rotation (ITR) were applied to the limb in a randomized order, while the foot was impacted with a vertical impulse force from a height of 31 cm. The varied magnitudes of externally applied KAM, ATS, and ITR resulted in 46 trial types and were derived from *in vivo* kinetics that were calculated from 67 athletes who performed DVJs during 3D motion analysis. In all trials quadriceps and hamstrings were co-contracted with a 1:1 ratio.

Triad marker data was used to build a skeletal model in Visual 3D (Germantown, MD). Data was filtered with a 4th order Butterworth 12 Hz low-pass filter. Knee angles and translations were calculated with respect to the femur. ACL strain was calibrated from the individual specimen's maximum and neutral points. Knee kinematics and relative ACL strain were normalized to the pre-loaded position, calculated as right limbs, and specimens were averaged across trial conditions.

Statistical analyses were performed with JMP 13 (SAS Institute Inc., Cary, NC) with matched pairs and one-way ANOVA with an alpha level < 0.05. The analysis determined the significance between change in ACL strain and knee kinematics at 33ms, 66ms, and 100ms after impact in each trial condition.

RESULTS AND DISCUSSION

When a KAM of 57.3 Nm was applied to the specimens, correlations between ACL strain and knee kinematics were statistically significant ($P<0.05$) at 33 ms (Table 1) and 66 ms (Table 2) after impact. At 33 ms after impact, change in knee abduction angle (3.58°± 0.67) and internal rotation (3.95° ± 0.27) correlated to change of relative ACL strain (3.79% ± 1.23%). At 66 ms after impact, knee abduction (1.66° ± 0.29) and internal rotation (3.90° ± 0.81) correlated to change in ACL strain (5.99% ± 1.3).

Previous *in vivo* studies correlated knee abduction angles greater than 5° at initial contact or 50 ms after impact to a higher risk of ACL injury [1, 3]. The current results demonstrated that knees with 3° or higher abduction and/or internal rotation had increased ACL strain at 33 ms. However, at 66 ms after impact, knee abduction decreased while internal rotation remained constant which yielded continual high ACL strain.

Change in anterior tibial translation (ATT) did not correlate to change in ACL strain at 33 ms after impact. However, in two testing conditions at 66 ms, ATT (0.03mm ± 5.09 and 0.73mm ± 4.24) correlated to ACL strain (5.99% ± 1.3).

CONCLUSIONS

Results from this study indicate during landing, ACL strain is correlated to knee abduction and internal rotation angles after impact, but not ATT. Future work should focus on the prediction of ACL strain from knee kinematics.

REFERENCES

1. Schilaty ND, et al. *Orthop J Sports Med*, **5**(8):1-8, 2017.
2. Bates, NA., et al. *Clinical Biomechanics* **44**:36-44, 2017.
3. Hewett TE, et al. *Am J Sports Med* **33**:492-501, 2005.

ACKNOWLEDGEMENTS

NIH funding include: R01AR049735, R01AR055563, R01AR056259, T32AR056950, K12HD065987, and L30AR070273.

Table 1: *in vitro* ACL strain and knee angles at 33ms after impact.

KAM (Nm)	ATS (N)	ITR (Nm)	ACL Mean (Std)	Extension/ Flexion Mean (SD)	Adduction/Abduction Mean (SD)	Internal/External Mean (SD)
57.3	64	9.7	2.77 (2.38)	-0.33 (2.43)	-3.90 (5.62) *	3.54 (3.52) *
57.3	64	18	2.30 (2.65)	-0.69 (1.98)	-2.54 (3.50)	3.21 (3.09) *
57.3	64	53.7	5.72 (9.31)	-0.25 (2.28)	-2.63 (3.44) *	3.82 (3.22)
57.3	80	9.7	2.90 (3.18)	-0.46 (2.20)	-2.94 (4.17)	3.24 (3.33)
57.3	80	18	4.04 (4.26)	-0.47 (1.98)	-3.24 (3.03) *	4.24 (3.24) *
57.3	80	53.7	3.69 (3.69)	-2.11 (8.09)	-3.72 (4.06) *	4.09 (2.75) *
57.3	196	9.7	2.71 (3.19)	-0.77 (1.90)	-4.39 (3.09) *	4.04 (2.69) *
57.3	196	18	3.47 (4.08)	-2.51 (8.96)	-3.52 (3.98)	4.62 (5.76)

* indicates significant difference (P<0.05)

Table 2: *in vitro* ACL strain and knee angles at 66ms after impact.

KAM (Nm)	ATS (N)	ITR (Nm)	ACL Mean (Std)	Extension/ Flexion Mean (SD)	Adduction/Abduction Mean (SD)	Internal/External Mean (SD)
57.3	64	9.7	5.05 (5.27)	5.05 (5.27)	-1.46 (2.40) *	-4.05 (5.76)
57.3	64	18	3.84 (4.55)	3.84 (4.55)	-1.62 (1.85)	-2.69 (3.59)
57.3	64	53.7	8.17 (9.97)	8.17 (9.97)	-1.34 (2.26)	-2.80 (3.88) *
57.3	80	9.7	4.36 (4.07)	4.36 (4.07)	-1.58 (2.01)	-3.33 (4.26)
57.3	80	18	6.92 (7.50)	6.92 (7.50)	-1.87 (2.65) *	-3.79 (3.57) *
57.3	80	53.7	4.95 (4.28)	4.95 (4.28)	-1.07 (1.81)	-4.54 (3.31) *
57.3	196	9.7	3.66 (3.51)	3.66 (3.51)	-1.51 (1.81)	-4.49 (3.17) *
57.3	196	18	4.51 (3.97)	4.51 (3.97)	-1.45 (2.08)	-3.07 (4.26)

* indicates significant difference (P<0.05)

KNEE JOINT AND QUADRICEPS DYSFUNCTION IN INDIVIDUALS WITH ANTERIOR KNEE PAIN, ACL RECONSTRUCTION, AND MENISCUS SURGERY

[1] Sungwan Kim, Daeho Kim, Yuyeon Roh, Minwook Kim, and Jihong Park

[1] Kyung Hee University, Yongin, Korea
email: jihong.park@khu.ac.kr

INTRODUCTION

Arthrogenous muscle inhibition (AMI) is common in patients with anterior knee pain (AKP) [1], anterior cruciate ligament reconstruction (ACLR) [2], and meniscus surgery [3]. Although AMI associated with knee injuries is evident, the relative magnitude of functional deficiency related to each individual knee pathology is unclear. A cross-sectional comparison using knee joint position sense (JPS), quadriceps maximal voluntary isometric contraction (MVIC), central activation ratio (CAR), and rate of torque development (RTD) in these populations would be beneficial. If a relative degree of AMI is observed, it would suggest a need for a particular intervention regarding each specific knee joint pathology.

Therefore, the purpose of this study was to examine knee joint (JPS at 15° and 75°) and quadriceps (MVIC, CAR, and RTD) function among knee joint pathologies, compared to healthy matched controls. Due to the presence of pain, we hypothesised that individuals with AKP would present higher deficits in knee joint and quadriceps function than individuals with other knee joint pathologies.

METHODS

Forty-four individuals with knee joint pathologies and 24 healthy matched controls participated in this study. Subjects with AKP were included if they felt pain during at least one of the following: 1) prolonged sitting, 2) step up and down, 3) patella compression, or 4) quadriceps voluntary isometric contraction. Subjects with AKP were excluded with history of lower extremity surgery within their lifetime. Subjects with ACLR and meniscus surgery were only included if there was no presence of current pain, isolated surgery and without other concomitant injuries and surgeries. Subjects with neurological disorder, cardiovascular disease, diabetes mellitus, or current pregnancy were excluded.

After a 10-min warm up on a stationary bike, subjects were performed three times each measurement in order (JPS at 15° and 75°, MVIC, CAR, and RTD).

Knee JPS was calculated by the absolute error of angle (°). Quadriceps MVIC was normalised to body mass (Nm/kg). The CAR was calculated by MVIC torque / superimposed burst torque (ratio). The RTD was calculated as voluntary torque of the torque-time curve, and the peak torque value was identified and normalised to body mass (Nm/s/kg).

Depending on normal distribution, we performed a parametric (mixed model analysis of variance and Tukey test) or a non-parametric test (Kruskal-Wallis and Duncan test) on each dependent measurement ($p<0.05$).

RESULTS AND DISCUSSION

The subject demographics are shown in Table 1. Age, height, mass, and body mass index were not statistically different ($p>0.16$). All pathology conditions had lower scores on the lower extremity functional scale ($\chi^2=43.02$, $p<0.0001$) than the healthy matched controls, but no relative differences were observed among them.

We did not observe differences on JPS 15° ($\chi^2=2.57$, $p=0.46$). However, AKP patients showed higher absolute errors on JPS 75° compared to other conditions ($\chi^2=8.71$, $p=0.03$, ES=1.00; Figure 1-A). The mechanisms behind this is unclear, but in speculation this is due to presence of current pain [4]. Although statistical differences were not observed, patients with ACLR (ES=0.74) and meniscus surgery (ES=0.55) showed joint function deficiency on JPS 75°.

Table 1. Subject demographics (mean ± 95%CIs).

	AKP (n=16)	ACLR (n=14)	Meniscus surgery (n=14)	Healthy controls (n=24)
Sex	14M, 2F	12M, 2F	12M, 2F	22M, 2F
Age	21.8 (1.3)	23.4 (1.4)	23.0 (1.2)	23.0 (1.0)
Height	174.4 (3.9)	175.9 (4.1)	175.2 (2.7)	175.7 (2.9)
Mass	74.3 (6.5)	75.0 (5.0)	75.8 (3.9)	74.8 (3.1)
BMI	24.3 (1.4)	24.2 (1.0)	24.6 (1.0)	24.4 (0.9)
MAI	33.6 (13.0)	32.2 (11.5)	50.1 (18.0)	N/A
MAS	N/A	31.6 (11.4)	45.4 (17.6)	N/A
LEFS	59.1 (5.5)	66.8 (5.7)	66.1 (5.1)	79.0 (1.0)

BMI: body mass index; LEFS: lower extremity functional scale; MAI: months after injury; MAS: months after surgery

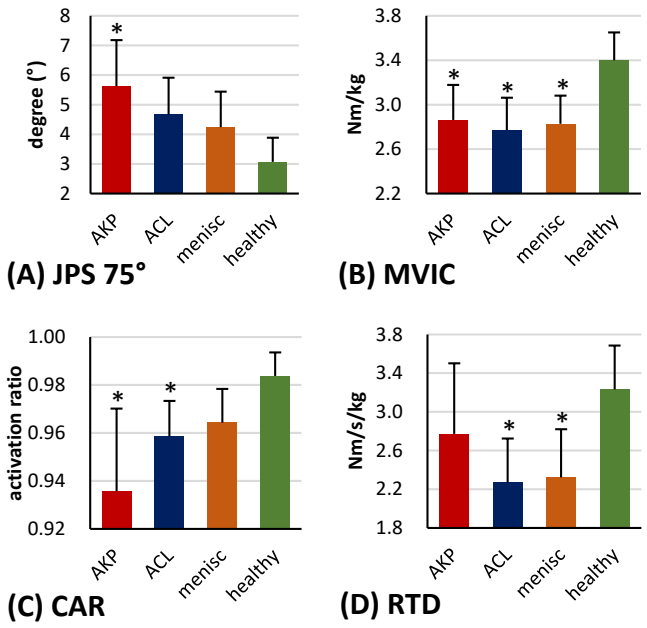

Figure 1: Changes in JPS at 75° (A), MVIC (B), CAR (C), and RTD (D). Error bars represent 95% CIs. * Indicate statistical differences from the healthy matched controls (p<0.05).

All conditions with knee pathologies showed quadriceps weakness ($F_{3,64}$=5.02, p=0.003; Figure 1-B), which is consistent with many previous observations. A relative magnitude of strength deficiency among knee pathologies were not observed.

Lower quadriceps CAR values (χ^2=13.94, p=0.003; Figure 1-C) were observed in patients with AKP (p=0.005, ES=0.99) and ACLR (p=0.02, ES=1.01) compared to the healthy matched controls. A longer time from injury (over four years) in patients with meniscus surgery may explain why this condition in our study did not show quadriceps activation deficiency.

Patients with ACLR (p=0.02, ES=0.92) and meniscus surgery (p=0.03, ES=0.85) showed lower values in quadriceps RTD than those in healthy matched controls (χ^2=11.28, p=0.01; Figure 1-D). Since RTD is related to force raise in a certain period of time, this may suggest that a surgical procedure, not presence of pain, can be a factor to reduce power output. More research is needed in this area.

CONCLUSIONS

Our data support previous evidence of AMI in knee joint pathologies. Restoration of joint function along with pain control in patients with AKP and power generating capacity in patients with ACLR and meniscus surgery should be addressed in rehabilitation process.

REFERENCES

1. Park et al. *J Sport Rehabil*. **21**(2): 119-126, 2012.
2. Pamukoff et al. *J Athl Train*. **52**(5): 422-428, 2017.
3. Ganderup et al. *Knee Surg Sports Traumatol Arthrosc*. **25**(2): 347-354, 2017.
4. Schaible et al. *Pain*. **55**(1): 5-54, 1993.

ACKNOWLEDGEMENTS

This work was supported by the Ministry of Education of the Republic of Korea and the National Research Foundation of Korea (NRF-2017S1A5A8022854).

INCREASED ANTERIOR TIBIAL ACCELERATION MEASURED DURING ACL INJURY TRIAL

Alessandro Navacchia, Nathan D. Schilaty, Nathaniel A. Bates, Christopher V. Nagelli, Aaron J. Krych, Timothy E. Hewett

Mayo Clinic Biomechanics Laboratories & Sports Medicine Center, Rochester & Minneapolis, MN
Email: navacchia.alessandro@mayo.edu

INTRODUCTION

Anterior cruciate ligament (ACL) injuries, particularly among young athletes, represent a substantial burden for the healthcare system and it can have devastating effects on quality of life, both in the short- and long-term [1]. These injuries occur during highly dynamic motor activities, such as landing from a jump and cutting [2]. The impact forces occurring during these activities produce high accelerations at the knee, which likely contribute to injury risk. Accelerometers have been previously used to measure impact accelerations and shock absorption during landing activities *in vivo* [3], but these measures during ACL injury have not been reported. Previous studies have developed impact test devices that simulate *in vitro* landing from a jump and are able to generate ACL rupture in the specimens with applied anterior tibial shear forces (ATS), knee abduction moments (KAM) and internal tibial rotation moments (ITR) associated with injury risk [4]. The goal of this study was to compare tibial and femoral accelerations and their rate of change (jerk) between tests that did and did not rupture the ACL. Our hypothesis was that higher anterior tibial accelerations would be observed during injury trials.

METHODS

Six fresh-frozen cadaveric lower limbs (44 ± 7 years; 81 ± 22 kg) were tested in a custom-designed impact simulator described in Bates et al. [4] to simulate landing from a 31-cm-high jump. Pneumatic actuators were used to apply *in vivo* kinetics at the knee collected from a cohort of 67 athletes divided into minimal (1st percentile), low (33rd percentile), middle (67th percentile), and high (100th percentile) risk categories. The specimens were subjected to a randomized series of sub-failure impacts of the aforementioned external tibial loading profiles. Two ±16g accelerometers (SPPDG, Mayo Clinic, Rochester, USA) [5] were fixed to the femur and tibia of every specimen to measure accelerations that occurred during the simulated impacts. The devices had an embedded 50 Hz upper 3 dB frequency limit. Tibial and femoral acceleration data were synchronized and transformed to a common coordinate system oriented as the tibia coordinate system. Jerk was quantified as the first derivative of acceleration in the three spatial directions. Positive (e.g. anterior) and negative (e.g. posterior) peaks, and ranges (difference between positive and negative peaks) were calculated for tibial and femoral acceleration and jerk at each impact. Ratios between femoral and tibial peaks and ranges were calculated (tibial / femoral) to quantify inter-segment relations. These results were compared between injurious impacts and impacts that did not result in an ACL tear (indicated as 'intact'). Since not every trial was common to all specimens due to load randomization and because certain specimens injured earlier than others, only the impacts with loads common to all specimens were used for the comparison to the injurious trial. The comparison was performed with one-way ANOVA and a Bonferroni correction was used to account for multiple comparisons.

RESULTS AND DISCUSSION

The ACL was completely disrupted in all specimens. Two specimens presented femoral avulsion. Seven load combinations common to all six specimens were identified and used for the comparison to the injurious trial. Tibial and femoral accelerations at impact presented a number of positive and negative spikes (Fig. 1). The number of spikes was generally larger in tibial accelerations when compared to femoral acceleration, indicating that the knee joint contributed to shock absorption.

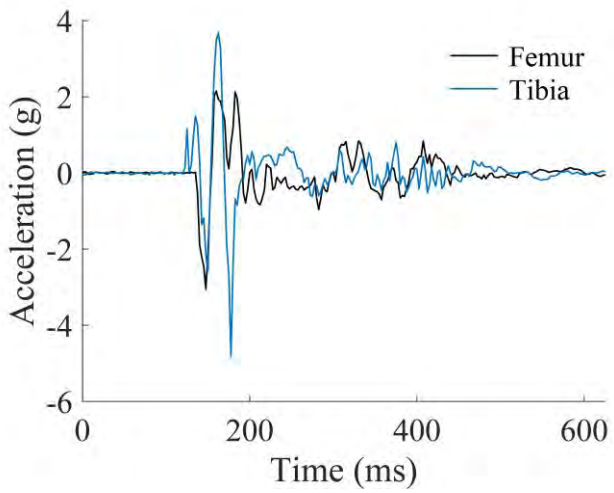

Figure 1: Example of femoral and tibial acceleration spikes during a simulated impact.

The comparison between anterior acceleration peak ratio (anterior tibial peak / anterior femoral peak) was the only one that resulted in a significant difference after the Bonferroni correction ($p < 0.004$, Fig. 2). Higher ratios during the ACL tear indicated that the anterior acceleration peak of the tibia was larger relative to the anterior peak of the femur during the injury. Ratios measured for 'intact' trials (black markers in Fig. 2b) ranged approximately between 1 and 2, whereas ratios during ACL tear presented a bimodal trend. Specifically, ratios were significantly larger at injury for four specimens, and similar to other impacts for the remaining two specimens. Larger anterior accelerations at the tibia and lower anterior accelerations at the femur (producing larger peak ratios) were expected during the injury, since the disruption of the ACL removes most of anterior restraint, and consequently deceleration, on the tibia.

CONCLUSIONS

The present study represents, to the authors' knowledge, the first attempt to measure acceleration and jerk on the femur and tibia during *in vitro* simulated landing and compare ACL-injurious impacts to intact 'impacts'. Additional specimens and work are required to establish whether the larger acceleration observed at the tibia was the cause or effect of ACL rupture.

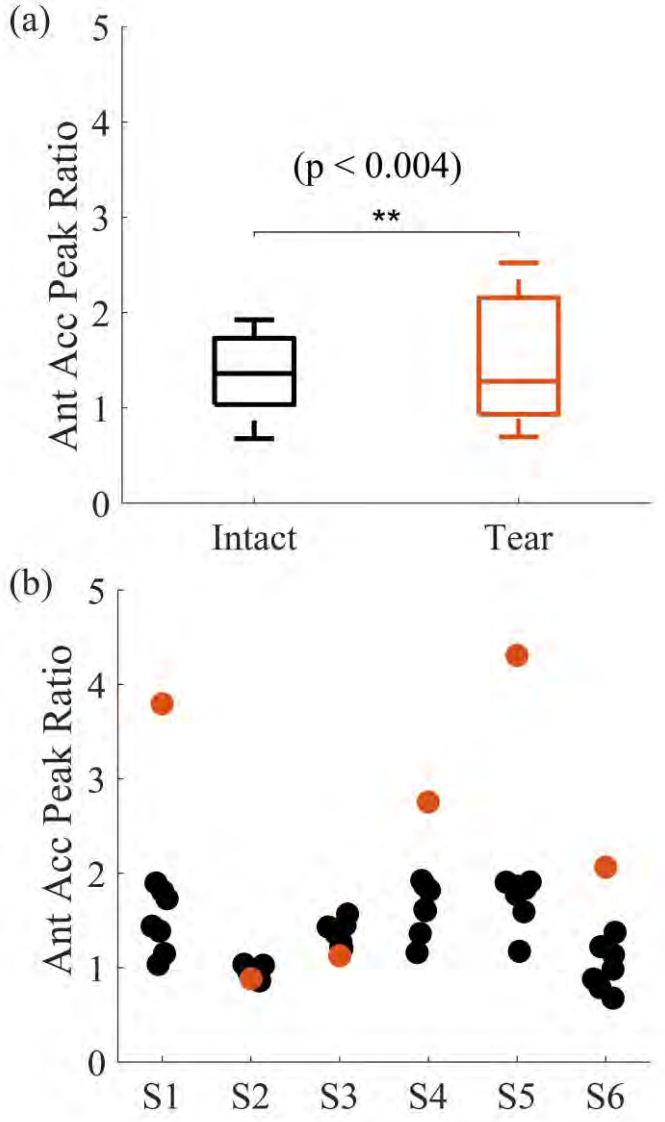

Figure 1: (a) Statistically significant difference between anterior acceleration peak ratios (tibia / femur) at injury ("tear") and "intact" trials. (b) Ratios for each specimen (S1 through S6): "intact" trials (black) vs. "tear" trials (red).

REFERENCES

1. Agel et al. *Am J Sports Med*, 33(4), 2005.
2. Boden et al. *Orthopedics*, 23(6), 2000.
3. Coventry et al. *Clin Biomech*, 21(10), 2006.
4. Bates et al. *Clin Biomech*, 44, 2017.
5. Gilbert et al. *Am J Biomed Eng*, 5(2), 2015.

ACKNOWLEDGEMENTS

NIH grant funding R01AR056259, R01AR055563, K12HD065987, T32AR056950, and L30AR070273.

MECHANICAL PROPERTIES OF PEDIATRIC ACLS AND TENDONS USED FOR RECONSTRUCTION

[1]Elaine C. Schmidt, [2]Theodore J. Ganley, [3]Kevin G. Shea, [1]Michael W. Hast

[1] Biedermann Lab for Orthopaedic Research, University of Pennsylvania; Philadelphia, PA
[2] Children's Hospital of Philadelphia; Philadelphia, PA
[3] St. Luke's Orthopaedics; Boise ID
email: hast@pennmedicine.upenn.edu, web: https://www.med.upenn.edu/biedermann/

INTRODUCTION

Cadaveric experiments have sought to characterize the mechanical properties of adult knee tendons and ligaments for many years [1]; however, relatively little is known about the pediatric population due to the rarity of these specimens. Extrapolating data back to pre-pubescent ages is inadequate, and the clinical need for this data has grown along with the recent increase in diagnosed anterior cruciate ligament (ACL) tears in skeletally immature patients [2]. Ideally, surrogate grafts should closely parallel the native pediatric ACL in both its biologic properties and mechanical durability. Thorough characterization of the ACL and potential autograft options will help to improve surgical outcomes in pediatric patients, which is particularly important, as injury frequency continues to accelerate.

The purpose of this study was to characterize the mechanical properties of ACLs and the most common tendons used for reconstruction in the pediatric knee. These properties were compared with existing information for the adult population.

METHODS

Five fresh-frozen knee specimens from separate donors were used in this study (3M, 2F, average age 9.2 years). ACLs, patellar ligaments, quadriceps tendons, and semitendinosus tendons were fine dissected free from the knee and subsequently cut into dog-bone shapes at the mid substance (ACL, patellar ligament) or distal third (quadriceps and semitendinosus tendon) with a custom-built jig (**Fig. 1A**). Initial cross-sectional areas of the prepared specimens were measured with a non-contact laser-based measurement system (**Fig. 1B**). Specimen ends were placed in custom aluminum clamps and attached to a 4500N load cell on a universal testing frame (ElectroForce 3550, TA Instruments, Eden Prairie, MN) to perform uniaxial tensile testing (**Fig. 1C**). Specimens were subjected to a standard preload, cyclic preconditioning, and stress-relaxation protocol before a ramp to failure at a constant quasistatic strain rate of 0.03%/s. Force displacement and stress-strain curves were fit using a bilinear constitutive model and least squares method to approximate the ultimate strain, ultimate stress, stiffness, toe modulus, transition point, Young's modulus, stiffness, and strain energy density.

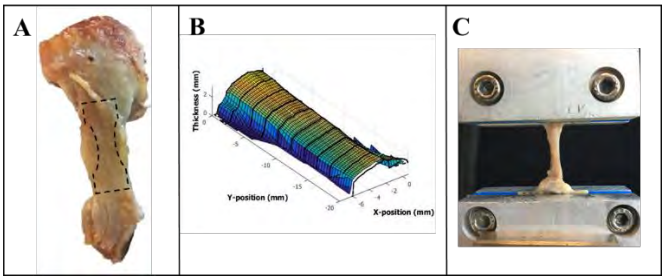

Fig. 1: A diagram summarizing A) the trimming of samples into dogbone shapes, B) laser measurement of cross-sectional area, and C) mechanical testing in a universal test frame.

RESULTS AND DISCUSSION

The patellar ligament exhibited mechanical properties that were most similar to that of the ACL, particularly for ultimate stress, ultimate strain, Young's modulus, and strain energy density (**Table 1**). The semitendinosus tendon provided the highest ultimate stress, but also had the lowest ultimate strain, while the quadriceps tendons provided the highest ultimate strain (**Fig. 2**).

The methods and results from different studies on the mechanical properties of adult knee tendons and ligaments vary markedly, which makes comparisons difficult. It is not surprising that the pediatric specimens have considerably weaker mechanical properties. In adults, hamstrings tendons have

previously been shown to exhibit significantly higher elastic modulus (1036±312 MPa) and ultimate stress values (120.1±30.0 MPa) than other graft candidates, including the patellar ligament (417±107 MPa, 76.2±25.1 MPa) [3]. This is in agreement with our data for a pediatric population, which showed that the semitendinosus tendons are stronger and less compliant than the quadriceps or patellar tendons.

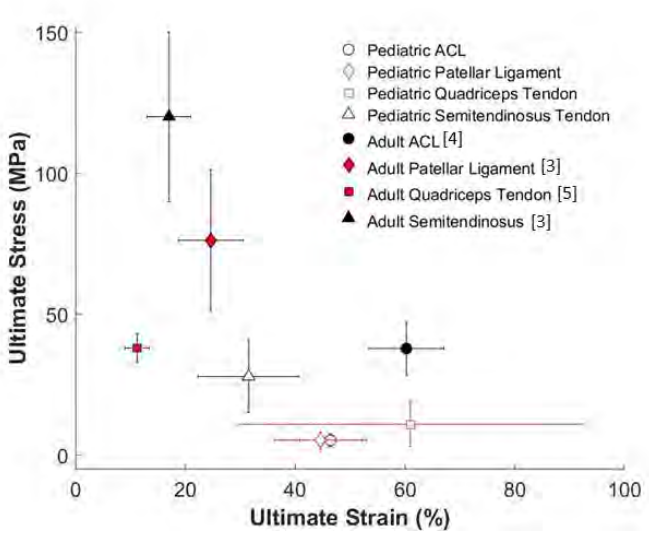

Fig. 2: Comparisons of ultimate stresses and ultimate strains for pediatric and adult specimens.

CONCLUSIONS

This suite of data can be used to inform the design and selection of grafts for reconstruction and also to develop constitutive computational models that can be applied to clinically relevant loading conditions that are difficult to test with bench-top experiments.

Based on the similarities of their material properties, the patellar ligament may be the better graft candidate for pediatric ACL reconstruction. However, it is important to take into consideration many factors can contribute to the strength and durability of an ACLR graft in vivo, including the extent of post-operative ligamentization and the femoral/tibial fixation method used [3]. Therefore, it may be more appropriate to utilize a hamstrings tendon graft, which is significantly stronger than the patellar ligament and could resist the loads that would otherwise lead to re-rupture.

REFERENCES

1. Kennedy et al. *JBJS* 58(3):350-355, 1976.
2. Gottschalk et al. *Sports Med Arthrosc Rev.*19(1):2-6, 2011.
3. Smeets et al. *Knee* 24(5):957-964, 2017
4. Noyes et al. *JBJS* 58(8): 1074-1082, 1976.
5. Staubli et al. *Am J Sports Med* 27(1):27-34, 1999.

ACKNOWLEDGEMENTS

This study was supported by the Penn Center for Musculoskeletal Disorders Histology Core (NIH P30-AR06919) and by the Electron Microscopy Resource Laboratory of the University of Pennsylvania.

Table 1: Summary of mechanical properties for ACLs and patellar ligaments

ACL

Specimen	Age	Ultimate Strain (%)	Ultimate Stress (MPa)	Toe Modulus (MPa)	Linear Modulus (MPa)	Transition Stress (MPa)	Transition Strain (%)	Stiffness (N/mm)	Strain Energy Density (MPa)
1	9	46.40	5.99	14.27	20.28	1.23	14.24	37.84	1.40
2	9	51.20	2.58	3.91	7.99	0.47	21.35	46.40	0.49
3	10	38.40	4.60	15.11	23.53	0.77	20.22	16.29	0.52
4	11	49.70	7.79	21.09	45.48	0.94	30.39	61.38	0.96
Mean	**9.75**	**46.43**	**5.24**	**13.59**	**24.32**	**0.85**	**21.55**	**40.48**	**0.84**
SD	**0.96**	**5.71**	**2.20**	**7.14**	**15.62**	**0.32**	**6.67**	**18.83**	**0.43**

Patellar Ligament

Specimen	Age	Ultimate Strain (%)	Ultimate Stress (MPa)	Toe Modulus (MPa)	Linear Modulus (MPa)	Transition Stress (MPa)	Transition Strain (%)	Stiffness (N/mm)	Strain Energy Density (MPa)
1	7	50.20	2.79	13.06	24.90	0.44	12.74	20.63	0.79
2	9	44.60	4.34	18.47	33.29	0.57	8.20	16.91	1.10
3	9	41.90	2.58	15.35	19.41	0.22	25.54	13.75	0.25
4	10	54.00	9.95	13.24	22.34	0.43	6.88	22.16	2.57
5	11	32.20	6.51	27.23	35.04	0.66	6.06	27.79	1.14
Mean	**9.20**	**44.58**	**5.23**	**17.47**	**27.00**	**0.46**	**11.89**	**20.25**	**1.17**
SD	**1.48**	**8.38**	**3.07**	**5.88**	**6.86**	**0.17**	**8.06**	**5.34**	**0.86**

ACL Loading During Unilateral Landing is Correlated to Dorsiflexion Range of Motion

[1]Joshua T. Weinhandl, [1]Shelby A. Peel & [2]Matthew C. Hoch
[1] University of Tennessee, Knoxville, TN, USA
[2] University of Kentucky, Lexington, KY, USA
email: jweinhan@utk.edu

INTRODUCTION

Anterior cruciate ligament (ACL) injury is one of the most frequent and debilitating lower extremity injuries experienced by physically active individuals. Approximately 250,000 ACL injuries occur annually in the United States alone with 50% occurring in athletes who are 15-25 years old [1]. Furthermore, female athletes have demonstrated a 4- to 6-fold increased risk of ACL injury compared to their male counterparts playing at similar levels in the same sports [2].

The ACL injury enigma is likely multifactorial and a variety of risk factors that may predispose an athlete to injury have been identified, which can be divided into two categories. Risk factors associated with anatomical (e.g., Q-angle, ligamentous laxity, ACL size and strength, boney geometry) and hormonal characteristics are considered to be non-modifiable. On the other hand, risk factors that can be manipulated through training are considered modifiable risk factors [1]. These include neuromuscular factors (e.g. relative muscle strength and recruitment, relative joint stiffness and stability, muscle fatigue, and flexibility) as well as biomechanical factors in all three planes of motion, which have been theorized as potential mechanisms related to ACL injuries [1].

Combining clinical and laboratory techniques may provide the best approach for advancement in the field. One such modifiable clinical measure is dorsiflexion range of motion (DROM). DROM is essential for completing several functional tasks, and decrements in DROM have been linked to an increased risk of several lower extremity injuries and conditions [3-5]. Recently, reduced DROM has been theorized to contribute to modified lower extremity movement patterns that could encourage ACL injuries [6-7]. These systematic reviews indicate that restricted DROM may increase an individual's risk of knee injury due to its association with frontal and sagittal plane knee movement. Therefore, restricted ankle mobility may create a defective base of support for knee stability at the knee during dynamic activity. By establishing a relationship between ankle function and knee biomechanics, we hope to identify a modifiable contributing factor to assist in ACL injury prevention.

METHODS

Nine recreationally active women (22.9±3.1 yr, 63.2±6.6 kg, 1.67±0.07 m) volunteered to participate in this study. Prior to data collection, participants were informed of study procedures and provided written informed consent in accordance with institutional guidelines. Participants first performed a modified knee-to-wall lunge test [8] to assess maximal weight-bearing DROM. Participants then performed unilateral landings from a box set equal to their maximum vertical jump height on to their dominant legs. Dominant leg was defined as the preferred kicking leg. Marker coordinate data (200 Hz, Vicon) and ground reaction force data (2000 Hz, Bertec) were collected synchronously for all trials.

OpenSim (v3.3 http://simtk.org) was used to simulate all landing trials [9]. An 8 segment, 23 degrees-of-freedom (*dof*) musculoskeletal model, with 92 Hill-type muscle actuators (modified from Gait2392), was scaled to match each participant's anthropometry based on experimentally measured anatomical landmarks. The knees were modified to be 3-*dof* joints (i.e., flexion-extension, adduction-abduction, internal-external rotation). Knee adduction-abduction and internal-external rotation *dof* were modeled as universal joints, with the same center of rotation as the flexion-extension *dof*, which was modeled as a planar joint. This allowed the tibia to translate relative to the femur as a function of knee flexion angle. Static optimization was used to calculate the muscle forces required to reproduce the

joint moments of each trial. The optimization minimized the sum of muscle activations to distribute muscle forces. Simulated knee joint reaction forces and moments, along with hamstrings, quadriceps and gastrocnemius muscle force estimates were input into a three-dimensional knee model to estimate ACL loading [10].

Pearson correlations (r) along with the coefficient of determination (r^2) were performed to examine the relationship between the DROM, and ACL loading.

RESULTS AND DISCUSSION

Participants exhibited an average DROM of 12.9±3.7 cm, which is consistent with previous reports of weight-bearing DROM in individuals with no history of lower extremity injury [8]. Participants also experienced a peak ACL loading of 0.57±0.16 BW at 44±6 ms after initial contact. Peak ACL loading was primarily due to loading in the sagittal plane (79%), followed by frontal plane (16%) and transverse plane (5%) contributions.

There was a strong, negative correlation between weight-bearing DROM and total ACL loading ($r = -0.81$, $r^2 = 0.66$), as well as sagittal plane ACL loading ($r = -0.91$, $r^2 = 0.82$). Moderate correlations were observed between DROM and time to peak ACL loading ($r = 0.48$, $r^2 = 0.23$), as well as between DROM and transverse plane ACL loading ($r = 0.59$, $r^2 = 0.35$). Finally, a weak correlation was observed between DROM and frontal plane ACL loading ($r = -0.27$, $r^2 = 0.07$).

CONCLUSIONS

The results of this study suggest that individuals with reduced DROM experience increased peak ACL loading during unilateral landings, primarily due to increases in sagittal plane loading. Although, DROM has been associated with frontal plane knee motion, it was not correlated with frontal plane ACL loading. This may be due to the sagittal plane nature of the experimental task. Future work should investigate the relationship between weight-bearing DROM and ACL loading during tasks such as sidestep cutting which produce greater frontal and transverse plane ACL loading. Additionally, future work is necessary to determine if modifications in weight-bearing DROM yield significant reductions in ACL loading during athletic tasks. Such information may lay the groundwork for novel ACL injury prevention strategies to be applied to athletes and physically active individuals

Table 1. Mean (SD) of weight-bearing dorsiflexion range of motion (DROM) and peak ACL loading (pACL) variables. Correlation coefficients between DROM and pACL variables are also presented.

	Mean (SD)	r
DROM (cm)	12.9 (3.7)	
pACL time (ms)	44 (6)	0.48
pACL (BW)	0.57 (0.16)	-0.81
pACL sagittal (BW)	0.45 (0.14)	-0.91
pACL frontal (BW)	0.09 (0.07)	-0.27
pACL transverse (BW)	0.03 (0.02)	0.59

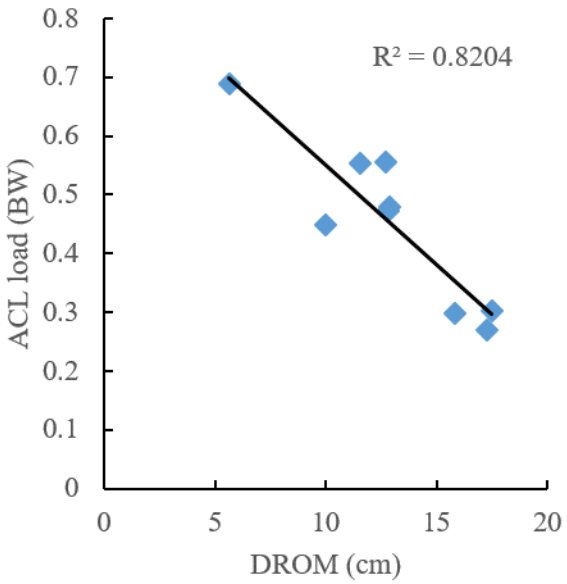

Figure 1. Relationship between weight-bearing DROM and sagittal plane ACL loading during unilateral drop landing.

REFERENCES

1. Hewett TE, et al., *AJSM*. **34**:299-311, 2006.
2. Agel J, et al., *CJSM*. **26**:518-23, 2016.
3. Malliaras P, et al., *JSMS*. **9**:304-9, 2006.
4. Riddle DL, et al., *JBJS*. **85-A**:872-7, 2003.
5. Whitting JW, et al., *MSSE*. **43**:706-13, 2011.
6. Lima YL, et al., *PTS*. **29**:61-9, 2018.
7. Mason-Mackay AR, et al., *JSMS*. **20**:451-8, 2017.
8. Hoch MC, et al., *JSMS*. **15**:574-9, 2012.
9. Delp SL, et al., *IEEE TBE*. **54**:1940-50, 2007.
10. Weinhandl JT, et al., *Clin Biomech*. **28**:655-63, 2013.

STATISTICAL SHAPE MODELING TO ESTIMATE COORDINATE SYSTEMS FOR PARTIAL CAPITATE MODELS

[1] Mohsen Akbari-Shandiz, [2] Ryan E. Breighner and, [1] David R. Holmes III, and [1] Kristin D. Zhao

[1] Mayo Clinic, Rochester, MN, USA, [2] Hospital for Special Surgery, NY, USA
email: shandiz.mohsen@mayo.edu

INTRODUCTION

High spatial and temporal resolution 4D (3D + time) CT technique (4DCT) has been used for accurate quantification of key metrics during wrist motion in patients with ligament injury [1]. However, due to limited FOV, the entirety of a wrist cannot always be imaged. The limited longitudinal coverage under the 4DCT technique (38.4mm), results in partial views of the capitate when imaging wrist motions (Fig1a). Principal axes, derived from surface models, have been used to define carpal coordinate systems [2]; however, principal axes determined from a partial capitate (resulting from limited longitudinal coverage) would result in a disparate coordinate system and thus inaccurate reporting and comparison of kinematic findings. To overcome this limitation, a conventional static CT of the whole wrist (Fig.1b) can be obtained to acquire the entire capitate and 3D-3D registration can be performed between the static and 4DCT to reconstruct dynamic capitate motion. However, this static CT alone contributes nearly one-third of the total radiation exposure in a 4DCT kinematic wrist analysis.

As an alternative, this study proposes the use of statistical shape modeling (SSM) as a means to estimate the full capitate surface model. We assess the viability of this technique using partial capitate geometry from simulated 4DCT flexion/extension scans.

METHODS

Statistical shape models of the capitate were built from a set of 25 wrist CT datasets (11 male and 14 female; Voxel sizes = 0.234 × 0.234 × 0.4 mm^3; resampled to isotropic), from which the capitate was semi-automatically segmented using AnalyzePro software (Mayo Clinic, Biomedical Imaging Resource, Rochester, MN).

The coordinate system of the capitate model was determined using the technique proposed by [2]. In this technique, the origin of the coordinate system is defined at the centroid of surface mesh vertices. Coordinate axes were defined by calculating the principal axes of the capitate model automatically, without manual intervention [2] (Fig. 1d).

To build the SSM, corresponding vertices across the training shapes were determined using the 'shape context' algorithm [3]. The SSM was computed as the mean shape plus a set of eigenvectors obtained by applying Principal Component Analysis (PCA) to the model vectors: $\mathbf{x} \approx \bar{\mathbf{x}} + \boldsymbol{\phi}\,\mathbf{b}$, where x is the shape model, $\bar{x}$ is the mean shape, ϕ is the matrix of modes of variation (eigenvectors of the covariance matrix), and b is the shape parameter vector. By varying b_i (elements of b), new instances of the shape were generated and by applying limits of $\pm 3\sqrt{\lambda_i}$ to the b_i (where λ_i is corresponding eigenvalues) it was ensured that the shape changes in a plausible manner.

For a given bone model, shape parameter vector (b) as well as 6 DOF rigid registration parameters were computed by optimizing an objective function measuring how well the estimated shape fit to the ground truth shape from CT scans. Optimization minimized the sum of surface-to-surface distance between the estimated shape and the ground truth shape, measured using the k-nearest neighbors algorithm. The optimization routine was a nonlinear multivariable function with linear equality constraints for the shape parameters (Matlab, R2016a). To validate the model, we used the first 10 (of 21) modes of variation which covered 90% of the total variation in capitate geometry. Therefore, in each registration we simultaneously optimized 10 shape and 6 rigid transformation parameters (3 translations and 3 rotations).

The performance of our statistical shape modeling was evaluated using two metrics:

1) Surface-to-surface distances: Mean absolute error (MAE) and standard deviation (SD) of the distances between the closest surface points of the

estimated SSM and the ground truth were used to measure the capability of the SSM to capture morphologic variation within the patient population. Distances were computed using CloudCompare (v2.6.3, http://www.cloudcompare.org/).

2) Error of coordinate system computation based on principal axes: Since the main objective of the SSM in this study was to estimate an accurate capitate coordinate system from a partial capitate model, the accuracy of the SSM reconstruction was also evaluated by computing the MAE and SD of translational and rotational errors in the estimation of coordinate systems, from SSM, compared to the the ground truth capitate model.

Experiment 1. To measure the capability of the SSM to capture capitate morphology within the patient population, we used a leave-one-out cross registration with the CT data. In each step, we left out one patient for testing, created the SSM from the remaining 24 patients, and registered the created SSM to the left-out CT. This process was repeated for all 25 datasets.

Experiment 2. To assess the ability of our SSMs to estimate full capitate models from partial geometry, partial capitates at the extrema of wrist flexion-extension in 4DCT scanning were simulated and used for the SSM registration. Three artificial cuts were performed at wrist flexion, extension and neutral position using axial planar cuts consistent with the longitudinal coverage in 4DCT (Fig.1c).

For this experiment, we studied 10 of the capitate models using leave-one-out technique. The SSMs were applied to the three cut capitate models to estimate the full capitate models (Fig.1e).

Table 1: Accuracy of SSM in estimating the capitate surface model and its coordinate system

Accuracy (MAE±SD)		Surface distance error (mm)	Coordinate system error	
			translation (mm)	rotation (deg)
SSM from full bone		0.05±0.3	0.2±0.1	2.9±2.1
SSM from flex. cut		0.2±0.5	0.3±0.2	3.9±2.9
SSM from neut. cut		0.1±0.4	0.2±0.1	2.3±1.6
SSM from ext. cut		0.2±0.4	0.3±0.2	2.6±1.8
Partial capitate	flexion cut		1.8±0.3	24.5±8.4
	neutral cut		0.9±0.2	4.6±3.0
	extension cut		1.7±0.2	17.5±9.2

RESULTS AND DISCUSSION

Our SSM models were able to provide sub-millimeter accuracy in terms of *surface-to-surface distance error* (MAE). For capitate coordinate system evaluation, the average translational errors were less than 0.3 mm and average rotational errors were less than 3.9° for the estimated SSM, compared to the 1.8 mm and 24.5° for the partial capitate models (Table 1).

CONCLUSIONS

Experimental results demonstrate that our SSM is accurate and robust to reconstruct capitate models for accurate coordinate system estimation from partial capitate models. Our results show that performance of SSM reconstructed capitates from registration to the neutral-cut, in sagittal view, was descriptively superior to flexion-cut and extension-cut. Ongoing research is aimed at developing SSM of the radius for estimating the full radius surface model from partial 4DCT scans, which is a crucial step for defining the wrist joint coordinate system. Replacing the static CT with SSM may potentially reduce the overall radiation dose of dynamic wrist imaging and may enable trials incorporating more or longer dynamic 4DCT trials.

REFERENCES

1. Zhao et al, J. Biomech. Eng. 137(7), 2015.
2. James et al, J. Biomech. 40(1), 2007.
3. Belongie et al, IEEE Trans. Pattern, 24(4), 2002.

ACKNOWLEDGEMENTS

R01AR071338; R21AR057902

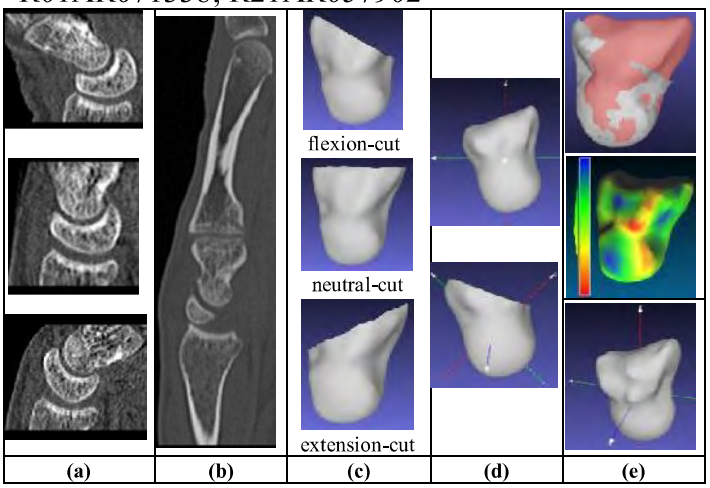

Figure 1: a) Static CT; b) flexion/extension 4DCT; c) simulated partial views of capitate; d) capitate coordinate system; and e) SSM estimation.

TIBIA CROSS-SECTIONAL ROUNDNESS IS RELATED TO AMBULATION, BUT NOT AGE, IN CHILDREN WITH MYELOMENINGOCELE

[1]Kyle P. Chadwick, [1]Nicole M. Mueske, [3]Rachel E. Horenstein, [3]Sandra J. Shefelbine, [1,2]Tishya A. L. Wren

[1]Children's Hospital Los Angeles, Los Angeles, CA
[2]University of Southern California, Los Angeles, CA
[3]Northeastern University, Boston, MA

INTRODUCTION

Skeletal loading through daily movement is important for normal development of bones. This loading is affected by the neurological and muscle deficits that result from myelomeningocele (MM). While children with MM have been shown to have atypical gait, decreased bone accrual, and increased fracture risk, it is still unclear what morphological bone differences exist and to what extent they relate to age and ambulation level. The objective of this study was to understand how tibia cross-sectional shape changes with age and how it differs in children with MM due to atypical and/or reduced ambulation.

METHODS

This study analyzed tibia computed tomography images from 77 children with MM and 169 typically developing (TD) children between the ages of 6 and 16yrs. Right tibias were segmented and isolated in OsiriX software [1]. The slices were aligned, thresholded, and analyzed in BoneJ [2]. To quantify bone cross-sectional "roundness", shape ratio (SR), defined as the ratio of minimum to maximum area moment of inertia (I_{min}/I_{max}), was calculated on cross-sectional slices along the length of the tibia. An SR value of 1 indicates a circular shape, and the degree of circularity decreases as SR changes from 1 towards 0. The SR values for all tibias were filtered and linearly interpolated to 200 slices to account for tibia length differences. The proximal and distal 20% were removed from all SR data to exclude the epiphyses. All analyses were performed on this diaphysis region, and are presented as 100% diaphysis length.

Ambulatory groups were defined based on Functional Mobility Scale (FMS) scores [3]; "non-ambulatory" was defined as crawling or using a wheelchair (score of 1) at all distances, "ambulatory with assistive devices" was defined as walking with a walker or crutches for one or more distances (2 or higher) without qualifying for "ambulatory independent", and "ambulatory independent" was defined as walking independently (5 or 6) for home and school distances. Differences in SR along the length of the tibias were examined across age groups (6-9, 10-13, 14-16 years) and ambulation level (all ages) using statistical parametric mapping (SPM), a methodology for making statistical inferences on spatially or temporally related datasets [4]. One-way SPM ANOVA was used to compare the three age groups and the four ambulatory groups; two-tailed SPM t-tests were used in comparisons of two groups (MM vs. TD and paired post-hoc comparisons). The significance level was set at $p<0.05$. For the post-hoc tests, Bonferroni adjustment was applied to adjust for multiple comparisons.

RESULTS

In TD children, tibia cross-sections became less round with age, particularly in the proximal 80% of the diaphysis (Fig 1a). However, tibia cross-sections of children with MM did not change shape with age (Fig 1b) and were rounder than those of TD children, particularly in the older age groups. Less ambulatory children with MM also had rounder tibia cross-sections (Fig 2). Even children with MM who walked independently had rounder tibia cross-sections than typically developing children.

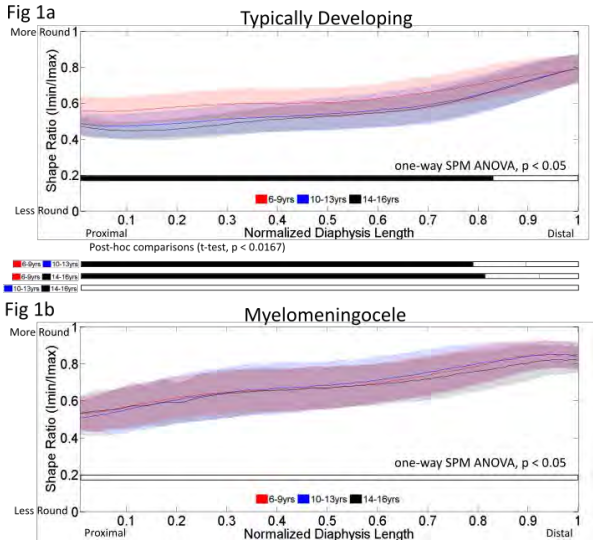

Figure 1: Comparison of shape ratio among age groups (all ambulatory levels)

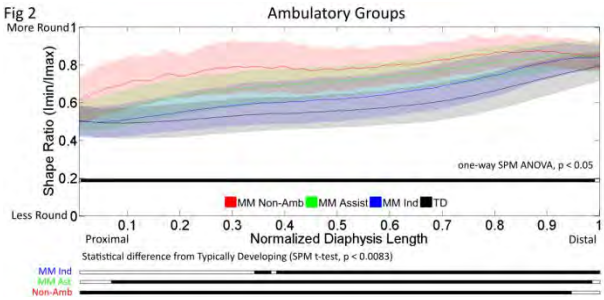

Figure 2: Comparison of shape ratio among ambulatory groups (all ages)

DISCUSSION

Loading associated with ambulation is needed to stimulate typical remodeling in tibia morphology. Children with MM have limited ambulation and atypical loading leading to the maintenance of rounder tibias compared to typically developing children. Bone cross-sectional shape greatly affects its bending strength. While circular cross-sections resist bending equally in all directions, more typical triangular or oval cross-sectional shapes can provide greater bending strength along common loading directions. This study emphasizes bone morphology's relationship with age throughout adolescence and the lasting impact of reduced and altered ambulation.

REFERENCES

1. Rosset A, Spadola L, Ratib O (2004) *Journal of digital imaging*, 17(3), 205-216.
2. Doube M, Kłosowski MM, Arganda-Carreras I, Cordelières FP, Dougherty RP, Jackson JS, Schmid B, Hutchinson JR, Shefelbine SJ (2010) *Bone*, 47(6), 1076-1079.
3. Graham HK, Harvey A, Rodda J, Nattrass GR, Pirpiris M (2004) *Journal of Pediatric Orthopaedics*, *24*(5), 514-520.
4. Pataky TC (2010) *Journal of biomechanics*, 43(10), 1976-1982.

ACKNOWLEDGEMENTS

Funding provided by NIH-NICHD Grant # 5R01HD059826

We would like to thank Djani Robertson for his help with data processing.

EFFECT OF BRACHIAL PLEXUS BIRTH INJURY LOCATION ON ALTERED GLENOHUMERAL MICROSTRUCTURE

[1,2] Emily B. Fawcett, [1]Nikhil N. Dixit, [1,2]Carolyn M. McCormick, [1,2]Ted A. Bateman, [1]Katherine R. Saul, and [1,2]Jacqueline H. Cole

[1] North Carolina State University, Raleigh, NC, USA
[2] University of North Carolina, Chapel Hill, NC, USA
email: ebfawcet@ncsu.edu, web1: http://www4.ncsu.edu/~ksaul/, web2: http://oml.web.unc.edu/

INTRODUCTION

Brachial plexus birth injury (BPBI) is the most common nerve injury in children, causing muscle paralysis and ultimately leading to joint deformities and lifelong impairment of arm function in up to 30% of these children [1]. The injury is known to cause both muscle weakness and gross morphologic changes in the glenohumeral joint [2]. However, little is known about the underlying microstructure of both bone and muscle and how that correlates to the gross morphologic changes, including how it differs due to injury location along the nerve. Postural deformity is more severe with injuries occurring distal to the dorsal root ganglion (postganglionic) rather than proximal (preganglionic) [3]. This study uses unique rodent models of both injuries to improve understanding of factors contributing to glenohumeral joint deformities with BPBI.

The purpose of the study is to examine microstructural abnormalities in the bones surrounding the glenohumeral joint following BPBI and the impact of nerve injury location on the severity of these changes. Findings will help elucidate the differential progression of preganglionic and postganglionic injuries, a key first step to develop more effective treatments for children with BPBI.

METHODS

All animal work was performed under an approved IACUC protocol. Male and female Sprague-Dawley rat pups were separated into three groups. The postganglionic neurectomy group (n=8) underwent C5 and C6 nerve root excision distal to the dorsal root ganglion [4]. The preganglionic neurectomy group (n=14) underwent C5 and C6 nerve root excision proximal to the dorsal root ganglion [5]. The sham control group (n=8) underwent sham surgery without nerve injury. Interventions were performed at postnatal day 3-5 on one side (affected) with the contralateral (unaffected) side serving as an additional control. At 8 weeks after surgery rats were sacrificed, and bones (humerus, scapula)were harvested from both affected and unaffected sides.

Bone microstructure was assessed in the distal scapula and proximal humerus using micro-computed tomography (micro-CT) (μCT 80, SCANCO Medical). Scans were reconstructed using a 10-μm isotropic voxel size, reoriented along anatomical planes, and calibrated for bone mineral density. Several volumes of interest (Fig. 1) were evaluated for standard trabecular bone metrics, including bone volume fraction (BV/TV), trabecular number (Tb.N), thickness (Tb.Th), and separation (Tb.Sp), and connectivity density (Conn.D). Analyses are ongoing, and a subset of data is presented here. Group comparisons were made on affected/ unaffected ratios using one-way ANOVA with Tukey's posthoc tests (α=0.05). The relationship between microstructural changes and

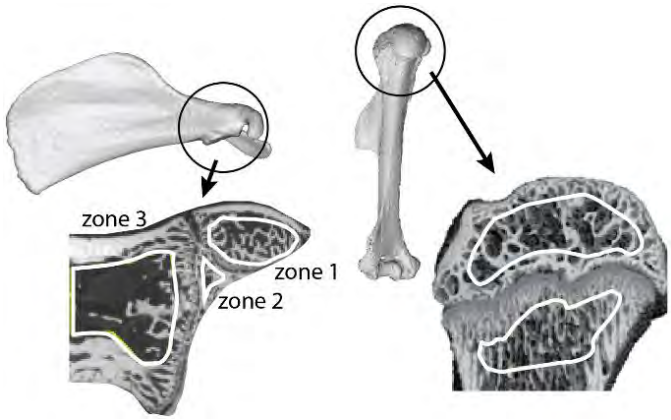

Figure 1: Micro-CT volumes of interest for the scapula (left) and humerus (right).

previously measured macrostructural changes in these animals will be examined with multivariate linear regressions (SAS).

RESULTS AND DISCUSSION

Trabecular bone microstructure in the scapular zone 3 region was significantly deteriorated in rats with postganglionic neurectomy compared with sham (Fig. 2). Bone volume fraction in the affected limb (relative to unaffected) was reduced more for the postganglionic neurectomy group than sham (-20.5%, p=0.0014). The same was true for trabecular number (-20.1%, p<0.0001) and connectivity density (-18.2%, p=0.0061). Relative trabecular separation was increased for postganglionic compared to sham (+34.8%, p<0.0001). The preganglionic group (n=2 preliminary data) also showed deficits in trabecular microstructure similar those observed in the postganglionic group.

We previously found, in these same groups of rats, macrostructural differences between the post- and preganglionic groups [6]. In particular, the glenoid inclination angle was significantly reduced in the postganglionic but not in the preganglionic group. These disparate effects with injury location for macrostructural (different pre- vs. postganglionic) and microstructural (similar pre- vs. postganglionic) properties suggests different drivers for these changes in the scapula following BPBI that warrants further study.

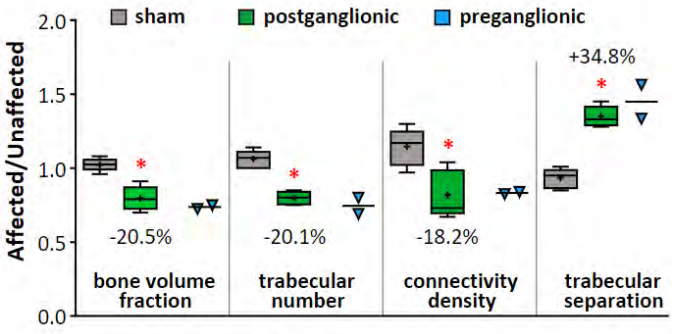

Figure 2: Compared to sham, postganglionic injury was associated with degenerated trabecular bone in scapula zone 3. Preganglionic rats (n=2) had similar changes compared to the sham group.
*p<0.05. + mean value.

CONCLUSIONS

Our work shows substantial losses in scapular trabecular bone within 8 weeks of neonatal post-ganglionic injury, and a trend for losses in preganglionic injury, relative to sham. Specifically, the trabeculae were fewer, less connected, and more sparsely arranged following neurectomy. Most notably, this study will provide new information on how bone microstructural changes correlate with the development of glenohumeral deformities following BPBI, and how injury location may modulate these relationships.

These results are limited by a small sample size for the preganglionic injury, but data analysis is ongoing. The current work also focuses only on changes in bone tissue; as part of a larger study we are also looking at parallel changes in muscle microstructure (morphology and fibrosis), as well as underlying cellular crosstalk between muscle and bone, to elucidate mechanisms contributing to the tissue- and joint-level changes observed post-injury. This knowledge will help guide future work in evidence-based treatment planning to improve the current wait-and-see approach used in clinical practice [7].

REFERENCES

1. Pondaag W (2004) *Dev Med Child Neurol* 46:138.
2. Crouch DL (2015) *J Bone Joint Surg Am* 97:1264.
3. Al-Qattan MM (2003) *Ann Plast Surg* 51:257.
4. Li Z (2010) *J Bone Joint Surg Am* 92:2583.
5. Nikolaou S (2015) *J Hand Surg* 40:2007.
6. Dixit NN (2018) *Orthop Res Soc Annual Meeting*
7. Hale HB (2010) *J Hand Su*rg 35:322.

ACKNOWLEDGMENTS

This study was funded by NIH R21HD088893. We thank Eric Livingston for micro-CT scanning.

CHARACTERIZATION OF GLENOID BASEPLATE FIXATION IN THE PRESENCE OF OSTEOPENIC BONE

Michael W. Hast, Matthew Chin, Anthony Cresap, Elaine Schmidt, and Andrew F. Kuntz

University of Pennsylvania, Philadelphia, PA, USA
email: hast@pennmedicine.upenn.edu, web: https://www.med.upenn.edu/biedermann/

INTRODUCTION

Reverse total shoulder arthroplasty (rTSA) has become a widely accepted solution for patients with various shoulder pathologies. Despite its popularity, complications are prevalent in the elderly population due to a limited amount of bone stock that may also be of poor quality (1). While research in baseplate stability is abundant, the vast majority of existing studies have utilized synthetic bones to model implant stability (e.g. 1-3). This approach effectively reduces variability within datasets, but it has also limited our understanding of baseplate fixation in osteopenic or osteoporotic bone.

This study introduces a novel cadaveric testing method that simulates physiologically relevant loads that may be responsible for baseplate loosening. The goal of the study was to utilize this new model to investigate how the central screw changes micromotion, subfailures, and catastrophic failure at the baseplate-bone interface. We hypothesized that the use of a central screw would improve bone-implant fixation when compared to specimens that omit it.

METHODS

Eight matched pairs of cadaveric scapulae with DEXA-confirmed osteopenia were implanted with rTSA baseplates and glenospheres (Titan, Integra LifeSciences, Plainsboro, NJ) and randomly divided into groups that used a central screw (CS+) and did not use a central screw (CS-).

The custom testing apparatus was designed to improve upon on the existing ASTM standard that imparts a compressive force of 750 N and alternating shear loads of 750 N (4) (**Fig. 1A**). The new test still uses bi-axial loading but simulates an arm loaded at 30° abduction (**Fig. 1B**), rather than 90° of abduction with high shear loads.

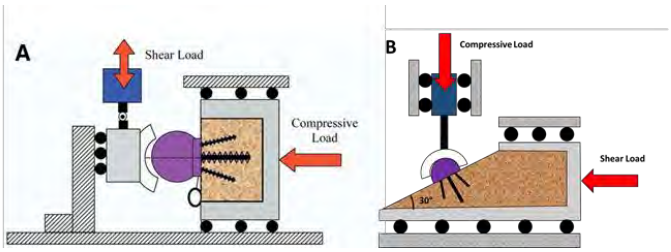

Figure 1: Diagrams of the ASTM standard (A), which does not apply physiologically relevant loads, and the current method (B), which simulates an activity similar to ambulating with a walker.

Each specimen was fatigue tested in the jig shown in **Fig. 2**. The glenoid and humeral stem were aligned to 30° abduction with a rotating vice (blue). 3-D marker clusters (inset) were fixed to the scapula and glenosphere to measure relative motions between the bone and implant. A vertical actuator applied monotonically increasing cyclic loads along the axis of the humerus (orange). The first cycle had a maximum load of 150 N, and 0.2 N of maximum load was added to each subsequent cycle. To simulate the compressive forces of muscles squeezing the joint, a pneumatic piston (pink) applied a constant 100 N load horizontally on the fixture, which was allowed to move freely on a linear bearing (brown). All tests were performed in a temperature-controlled circulating water bath and cyclically loaded until failure.

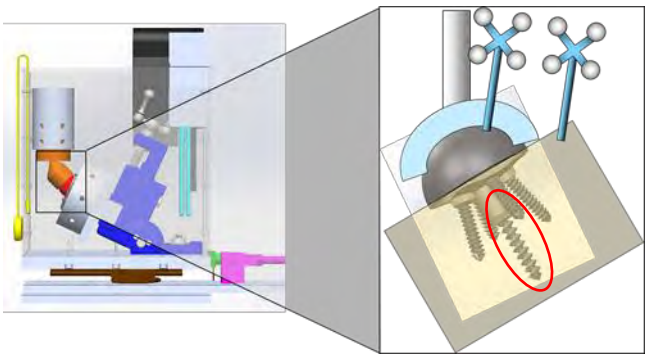

Figure 2: CAD representation of the test device with the central screw circled in red.

Deformation, load, relative 3-D displacement, and survived cycles were measured. Post-hoc analyses of sub-failure were defined as permanent creep between the bone-baseplate interface exceeding 1 mm. This was measured with actuator displacement and again with 3-D motion tracking. Groups were compared with 1-tailed paired student t-tests.

RESULTS AND DISCUSSION

Use of the central screw improved fatigue life before catastrophic failure, as the average maximum number of cycles survived for CS+ and CS- groups were 7281.88±2517.32 and 5911.63±2686.38 cycles, respectively (p=0.026) (**Fig. 3A**). There were no significant differences found between groups for subfailure when measured directly with actuator displacement (**Fig. 3B**) or with 3-D motion tracking (**Fig. 3C**). An analysis of cycle numbers survived as a function of DEXA T-score indicated no strong correlation, with R-squared values of 0.19 and 0.12 for the CS+ and CS- groups, respectively.

This study introduces a novel testing paradigm that successfully characterized the role of the central screw in baseplate fixation. Contrary to our hypothesis, the use of the screw did not improve the implant's resistance to 1 mm of creep. Interestingly, the use of a central screw improved the fatigue life of the implant before catastrophic failure.

There are several distinct differences between this experiment and previous experiments. The choice of 1mm of permanent deformation to determine subfailure is larger than previous reports of micromotion (on the scale of 0.15 mm) (1-3). Baseplate loosening in the clinic is typically determined with radiographic analyses and we believe that 1mm is the low threshold of implant motion that can be assessed with these techniques. Previous studies have used linear variable differential transformers (LVDTs), which provide high resolution measurements of micromotion. The use of cadaveric specimens, rather than bone blocks, precluded our ability to place LVDTs. We feel that 3-D motion capture with 0.2mm resolution was adequate to measure 1mm motions.

Optimizing baseplate fixation in poor quality bone is an important clinical issue that requires further

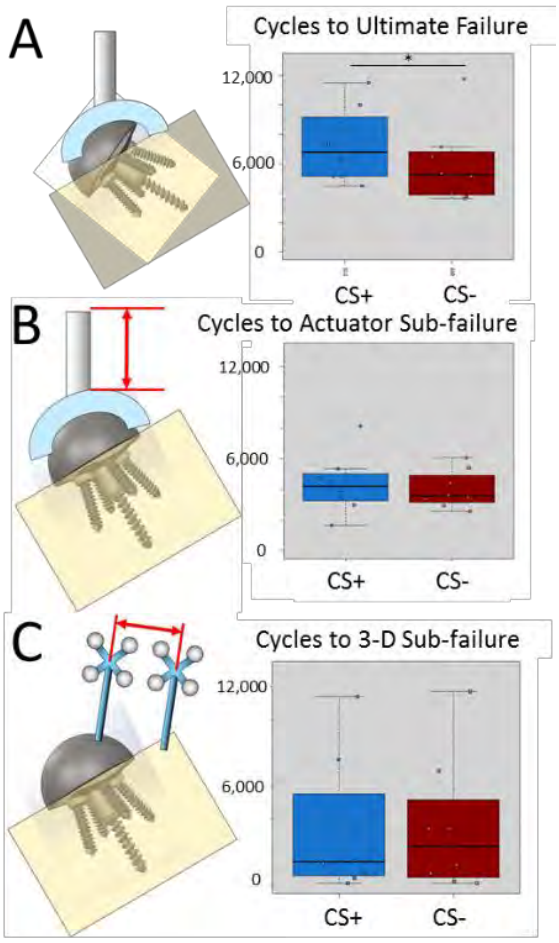

Figure 3: CAD images and boxplots of A) cycles to ultimate failure, B) cycles to actuator measured subfailure, and C) cycles to 3-D motion measured subfailure.

research. Our study suggests that central screw use is preferred, but omission of the central screw may be a reasonable tactic, especially if bone stock is sparse and the joint is only going to be exposed to small external forces.

REFERENCES

1. Codsi and Iannotti. *JSES.* 17(3):479-86, 2008.
2. Martin et al. *JSES.* 26(10):1748-1755, 2017.
3. Harman et al. *JSES* 14(1 Suppl S):162S-167S, 2005.
4. ASTM F2028-14 Standard Test Methods for Dynamic Evaluation of Glenoid Loosening or Disassociation. ASTM Int. 2014;

ACKNOWLEDGMENTS

This study was funded by Integra LifeSciences.

BEYOND GROUND REACTION FORCES: TOWARDS WEARABLE TECH TO MONITOR BONE LOADING & PREVENT INJURY

Emily S Matijevich, Lauren M Branscombe, Leon Scott and Karl E Zelik

Vanderbilt University, Nashville, TN, USA
email: emily.matijevich@vanderbilt.edu

INTRODUCTION

Bone stress injuries (BSI) can result from repeated submaximal bone loading that causes an accumulation of microdamage. There is a high prevalence of BSI, particularly tibia stress fractures, in military trainees, recreational runners, and certain industrial workers. BSI can result in pain, missed work, reduced physical activity, decreased productivity and substantial healthcare costs.

We predict that BSI could be prevented if one could monitor bone loading in daily life, identify potentially injurious loading conditions, and then intervene before an excessive accumulation of bone microdamage. However, monitoring bone loading is challenging, particularly if the goal is to do so in daily life outside of a motion analysis lab. An ideal solution would be a wearable, non-invasive device that serves as an injury prevention tool for military trainees, runners and industrial workers.

Various researchers have attempted to understand BSI by measuring ground reaction forces (GRFs), with the hope that GRF peaks or loading rates might reflect bone loading. GRFs are appealing because, in contrast to bone loading, they can be measured directly and non-invasively; however, it can be shown analytically (via Newton-Euler laws of motion) that bone forces are a function of more than just GRFs. Typically, the vast majority of bone loading is due to muscle contractions. GRF magnitude is generally only a small fraction of the total bone loading. For instance, during running peak GRFs are typically 2-3 times body weight (BW), whereas peak tibia bone forces are typically 8-12 times BW, as evidenced by gait analysis [1], cadaver [2] and modeling studies. Moreover, peak bone loading occurs in midstance, while GRF impact peaks occur near initial foot contact.

Nevertheless, it is plausible that for a certain subset of tasks (e.g., running over a limited range of speeds) that GRF might positively correlate with bone loading, and thus still be a useful indicator of increases/decreases in bone loading. Given the ability to measure GRFs directly with wearable sensors, this possibility is worth exploring before investigating more complex multi-sensor solutions.

The purpose of this study was to determine if increases in GRF peaks or loading rate were correlated with increases in peak tibia bone loading during running. We focused on running and tibia bone loading, because of the high prevalence of tibia stress fractures in runners. We hypothesized that increases in common GRF metrics (impact and active peaks, impact loading rate) would not be strongly correlated with increases in peak tibia loading as runners varied speed, step frequency and terrain slope (i.e., $r<0.8$). The absence of strong correlation would suggest the need to fuse data from additional/alternative sensors, moving beyond GRF measures, to non-invasively monitor bone loading.

METHODS

Three healthy subjects (2 M, 1 F, height 1.8 ± 0.1 m, weight 66.8 ± 7.0 kg, age 24.6 ± 1.5 years) have participated in this ongoing study. Subjects performed various running trials on a treadmill: (i) 20 total trials at 4 different speeds, ranging from 2.0-3.0 m/s, using self-selected step frequency at each speed, and 5 different slopes ranging from –6 to +6 degrees, (ii) 7 trials at 2.6 m/s but varying step frequency from -15% to +15% of their self-selected step frequency (enforced via metronome). Parameter ranges were selected to reflect variability that a recreational runner might encounter.

Data collection & processing: Unilateral lower-limb kinematics (100 Hz) and GRFs (1000 Hz) were collected. Subjects provided informed consent prior to participation. For each trial, data were collected for 20 seconds, individual steps were

parsed out, and outcome metrics were computed on a step-by-step basis and then averaged.

Tibia bone loading: An established inverse dynamics analysis was used to estimate the total tibia compression force (F_{total}, Fig. 1a), due to internal (muscle) and external (GRF) sources [1]. The external contribution (F_{ext}) was calculated as the measured GRF projected onto the long axis of the tibia. The internal force contribution (F_{int}) was calculated as the estimated ankle moment divided by the Achilles tendon moment arm (5 cm, assumed constant). Peak tibia force ($F_{total,max}$) was calculated as the maximum of F_{total} across stance. Forces were normalized by subject BW.

GRF: Three common GRF metrics were calculated: F_{active} (vertical GRF active peak), F_{impact} (vertical GRF impact peak) and VALR (vertical GRF average loading rate, Fig. 1b). For each subject, individual GRF metrics were linearly correlated to peak tibia force. The Pearson correlation coefficient (r) was computed for all trials, and also for each parameter sweep, then averaged across subjects.

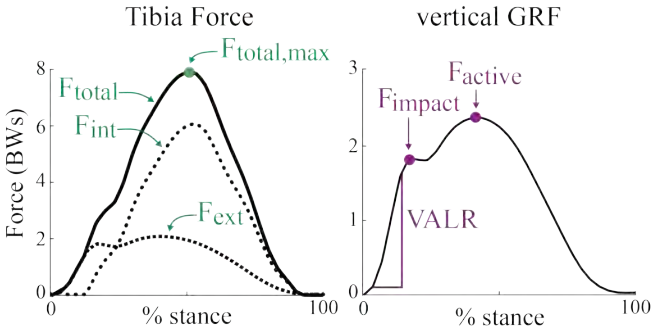

Figure 1. Running 2.8 m/s. (a) Total tibia load summation. (b) Vertical GRF metrics. Force in BWs

RESULTS AND DISCUSSION

All trials: GRF metrics were moderately or weakly correlated to F_{total} (Fig. 2). However, only the GRF active peak was positively correlated (F_{active}: r = 0.64 ± 0.26). Surprisingly, tibia bone force actually decreased with increases in GRF impact peak and loading rate (F_{impact}: r = -0.50 ± 0.29; VALR: r = -0.53 ± 0.28; Fig. 2). These preliminary results support our hypothesis. Increases in GRF metrics do not necessarily reflect increases in bone loading, signifying that GRFs alone may be of limited value in monitoring tibia loading or BSI risk. These findings complement prior evidence that higher impacts may not play a key role in the development of stress fractures [3].

Speed sweep: GRF metrics were strongly correlated to F_{total} (F_{active}: r = 0.86 ± 0.11; F_{impact}: r = 0.86 ± 0.10; VALR: r = 0.94 ± 0.10) with increasing speed on level ground. However, F_{total} was also strongly correlated to speed itself (r = 0.91 ± 0.10), which is generally easier to measure with wearable sensors.

Slopes sweep: F_{active} had a range of correlations with F_{total} (min r = -0.24; max r = 0.99), while F_{impact} and VALR were negatively correlated to F_{total} (F_{impact}: r = -0.75 ± 0.22; VALR: r = -0.78 ± 0.18). F_{active} had a range of correlations with slope itself (min r = -0.47; max r = 0.95). Even with this small sample size, large variability in correlation values indicates GRF may not adequately capture subject-specific running strategies or estimate bone loading trends.

CONCLUSIONS

Preliminary results suggest that trends in GRFs may be insufficient to track tibia bone loading. The most striking observation was that tibia loading tended to decrease with increasing GRF impact peaks and loading rates; though correlations were relatively weak. Additional or alternative measures may be needed to track tibia bone loading, with the long-term goal of predicting and preventing BSI risks.

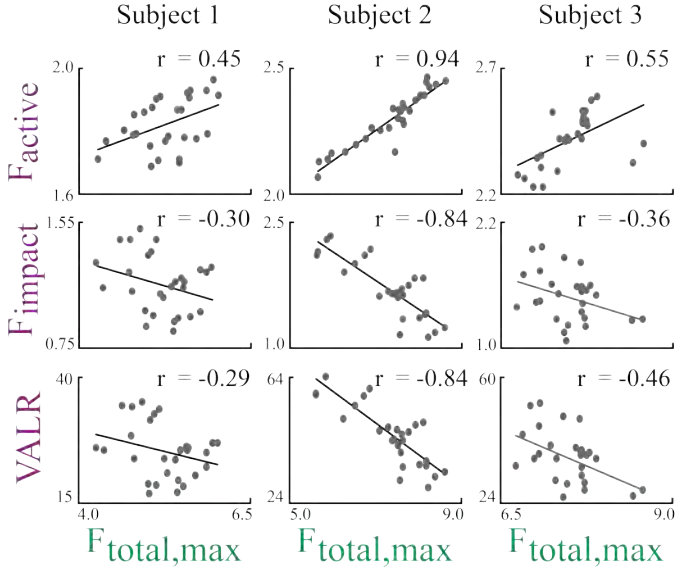

Figure 2. Each data point represents the average of one trial. Force in BWs. VALR in BWs/s.

REFERENCES

1. Scott and Winter. *Med. Sci. Sports Exerc*. 1990.
2. Sharkey and Hamel. *Clin Biomech.* 1998.
3. Loundagin et al. *J Biomech Eng.* 2018.

STATISTICAL SHAPE MODELING APPROACH TO PREDICT MISSING SCAPULAR BONE: APPLICATIONS IN PRE-SURGERY PLANNING AND MODELING

[1, 2]Asma Salhi, [1, 2]Valerie Burdin, [1,3]Sylvain Brochard, [4]Ashish Gupta, and [1,3]Bhushan Borotikar

[1] Laboratory for the Processing of Medical Information (LaTIM), INSERM, U1101, Brest, France
[2] Department of ITI, IMT Atlantique, Brest, France
[3]CHRU de Brest, Hospital Morvan, Brest, France
[4]Department of Orthopaedic Surgery, Greenslopes Hospital, Brisbane, Australia

email: bhushan.borotikar@gmail.com

INTRODUCTION

Shoulder joint disorders (arthritis or cuff tear arthropathies) lead to damaged bones, restricted function, and chronic pain. Shoulder joint replacement is regarded as a safe and effective procedure to relieve pain and help resume daily activities. Pre-planning software tools are prevalent in shoulder arthroplasties and play a vital role in successful surgical outcomes. However, any pre-surgery planning tool needs to create a 3D scapular shape from patient's complete shoulder images, which may not be available all the time.

The purpose of this study was to create and evaluate a statistical shape modeling (SSM) based pipeline that can accurately predict the missing part of the scapula bone due to incomplete image acquisitions.

METHODS

A: Scapula SSM building

An imaging database of dry bone samples and cadaveric scans (n = 81) was used for this study. CT scan images were acquired, manually segmented (Amira, FEI, Hillsboro, V5.4), and surface mesh models of each sample were created. Ten samples from this database were categorically selected for evaluation purpose and remaining samples were checked by the expert for anatomical normality and then used to build the SSM of scapula. The SSM pipeline can be summarized in three main stages: rigid alignment, non-rigid alignment to establish point-to-point correspondence, and principal component analysis. In this study, we used the Iterative Median Closest Point – Gaussian Mixture Model (IMCP-GMM) pipeline [1] to create the scapular SSM.

B: Virtual scapular defect creation

Two imaging defects were virtually created on ten external scapulae using 3D visualization software (Amira, FEI, Hillsboro, V5.4). These scapulae were selected to represent at least one type of anatomical classification of the scapular bone. For this purpose, shape of glenoid was classified as type 0, I, II, and III based on morphology of glenoid notch. Acromion was classified as type I, II and III based on flat, curved, and hooked morphology. Two samples each were selected to represent higher and lower critical shoulder angle (CSA) and glenoid ante- and retro-version. The virtual defects were represented in 1) Group 1: missing inferior part of the scapula (inferior scapular fossae), and 2) Group 2: missing superior part of the scapula (a part of the acromion and coracoid process).

C: Missing part prediction algorithm

The principal modes of variations that represented 95% of the population variability were retained and used in the missing part prediction algorithm. This algorithm was performed in three steps:

Step 1: Matching the centroids of the mean shape of the SSM (MS) and the target shape (TS).

Step 2: Rigid alignment: Depending on the group on which we are going to perform the fitting, a set of 5 or 10 landmarks were selected on both the MS and TS. Fifteen iterations of rigid Iterative Closest Point (ICP) algorithm were performed with a Procrustes analysis that applied the best rigid transform on the MS after each iteration.

Step 3: Model fitting: This non-rigid deformation algorithm aimed at finding the closest instance of the SSM to TS using following steps -

a) Find the identifiers (IDs) of the SSM: for each point in the TS, a closest point in the MS was found and corresponding IDs were recorded.

b) Create a posterior model (PM): The landmarks used for the rigid alignment in step 2 were used to create the PM [2] ,assuming a standard error for the landmark placement of 0.5mm. The landmark position of all the instances sampled from this posterior SSM were within the error parameter attributed to these landmarks.
c) Perform non-rigid ICP: 20 iterations of non-rigid ICP were executed. In each iteration, the algorithm suggested a candidate correspondence between the points of the PM associated to IDs, then a Gaussian process regression was performed based on the observed candidates and predicted shape was built.

D: Evaluation

Quality of the SSM was checked for its generality, specificity and compactness criteria. Each predicted shape was compared with the original shape using anatomical measures (glenoid inclination, glenoid version, glenoid center, and CSA), distance measures (mean, Hausdorff, RMS), and similarity measure (Dice coefficient).

RESULTS AND DISCUSSION

After checking for anatomical normality, five scapular shapes were discarded and SSM was built using n=66 scapulae. This number exceeds the required subjects to capture sufficiently the bone shape variation in the healthy population [3]. Generality of the SSM was found excellent for both the distance matrices (Hausdorff and RMS), whereas specificity and compactness criteria were well within the satisfactory levels.
Fifteen modes represented 95% variability in the SSM and were retained and used in the missing part prediction algorithm. Evaluation of predicted shapes revealed moderate to excellent outcomes (Table 1). All mean RMS metrics were predicted with high accuracy and predicted shape revealed excellent similarity index with the original shapes (Figure 1, Table 1). Results of the anatomical measures were encouraging and better than a recently published study [4] which predicted scapular glenoid shape.

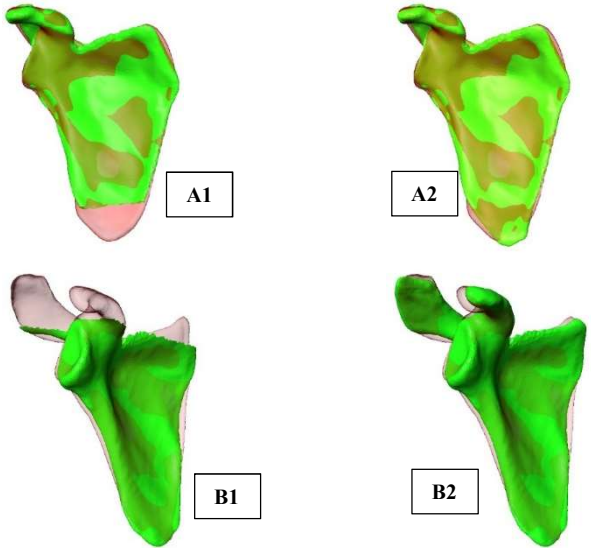

Figure 1: Sample data for missing part fitting. Green and translucent red scapulae indicate original and predicted shape respectively. A1 and B1 show imaging defects in inferior and superior parts whereas A2 and B2 show comparison with original.

CONCLUSIONS

Accurate scapular shape prediction is possible and can have strong applications in surgery planning and modeling.

REFERENCES

[1] T. Mutsvangwa et. al., *IEEE Trans. Biomed. Eng*., 2015.
[2] M. Lüthi et. al., *DAGM'11 Proc. 33rd Int. Conf. Pattern Recognition*, Berlin, 2011.
[3] G. Chintalapani et. al., *Med Image Comput Comput Assist Interv,* 2007
[4] K. Plessers et. al., *J Shoulder Elbow Surg*, 2017

Table 1: Evaluation of missing part prediction using anatomical, distance, and similarity measures. Values reported indicate mean deviations for ten external shapes from their original shapes.

	Anatomical Measures				**Distance Measures**			**Similarity Measures**
	Glenoid Inclination (°)	Glenoid Version (°)	Glenoid Center (mm)	CSA (°)	Mean(mm)	Hausdorff (mm)	RMS	Dice coefficient
Group 1	2.08	1.77	1.38	2.54	0.99	5.91	1.36	0.80
Group 2	1.47	1.70	2.02	2.73	0.84	5.40	1.17	0.82

DOES FOOT STRIKE PATTERN CHANGE DURING A MAXIMAL 800-METER RUN?

[1]Kathryn A. Farina, [1]Mark H. Langley, [1]Marco Meucci, [1]Alan R. Needle, [1] Natalie R. Kile, [1]Herman van Werkhoven
[1]Department of Health and Exercise Science, Appalachian State University, Boone, NC, USA
Email: farinak@appstate.edu

INTRODUCTION

Several studies have considered biomechanical differences between rearfoot (RF) and forefoot (FF) strike pattern during running. These differences include foot position, muscle activation, ground contact times, and ground reaction forces [1, 2, 3, 4]. It has also been suggested that the FF strike pattern is utilized more by faster runners and for faster running [5]. During a marathon, it has been shown that foot strike pattern (FSP) changes during the course of a race, with more runners initially running with a FF strike pattern, and then changing to a RF strike pattern [1].

During faster, shorter distances, such as an 800 m middle distance, it is unclear whether runners are able to maintain a certain FSP. Given the high intensity of the race, it is likely that onset of muscle fatigue would make it difficult for runners to maintain a given FSP throughout the race. The purpose of this study was to evaluate changes in FSP throughout a maximal 800 m run. We hypothesized that runners would not be able to maintain their initial FSP throughout the 800 m, and in general would move from a more FF strike pattern to a more RF strike pattern during the later stages of the run.

METHODS

21 healthy, trained subjects (14 female, 7 male; age: 24.29 ± 4.54 yrs) were recruited from the surrounding area running clubs, university, and collegiate track and field teams. The study was approved by the Appalachian State University Institutional Review Board. Subjects reported to the outdoor track where they completed an informed consent, health history, and training information form. Upon completion of a warm up, three sensors were placed on the subject's lower extremity. These sensors are equipped with a three 3-dimensional accelerometer, and 3-dimensional gyroscope, as well as unit capable of measuring electrical activity (BiostampRC, mc10, Lexington, MA, USA). One sensor was placed on the dorsal side of the right foot to measure accelerometer and gyroscope data. Although not reported here, additional sensors were placed on the lateral gastrocnemius and tibialis anterior to measure muscle electrical activity. A stopwatch was used to gather 100 m interval times over the course of the 800 m run.

To evaluate FSP, resultant acceleration peaks from the sensor attached to the foot were used to determine time of foot strike, similar to [6]. To quantify changes in FSP, FSP was evaluated on a continuum, instead of as a binary classifier (FF or RF). Two measures were calculated:

- Foot strike initial angular velocity **(ω_{FS})** – Sagittal plane gyroscope angular velocity over the first 30 ms after foot strike was averaged to get an indication of the direction of angular rotation directly after foot contact, with a more positive ω_{FS} indicating more RF strike pattern.
- Change in foot angle **($\Delta\theta$)** – Sagittal plane gyroscope data was integrated to get a change in foot strike angle. The difference in angle at foot strike and angle when the foot was deemed to be stationary on the ground (lowest mean resultant acceleration over a 50 ms interval after foot strike) was used to calculate a change in foot angle, with more positive $\Delta\theta$ indicating more RF strike pattern:

$$\Delta\theta = \theta_{STATIONARY} - \theta_{FOOTSTRIKE}$$

ω_{FS} and $\Delta\theta$ values for each foot strike was averaged across each 100 m interval ($\omega_{FS\text{-}ave}$ and $\Delta\theta_{ave}$). Only run was considered here (1st: 100m-200m, 2nd: 300m-400m, 3rd: 500m-600m, 4th: 700m-800m). One-way repeated measure analyses of variance (ANOVA) were used to (1) analyze time across each

100-meter straight interval and (2) investigate the factor of distance on i) $\omega_{FS\text{-}ave}$ and ii) $\Delta\theta_{ave}$ over each 100 m straight interval of the 800-meter run.

RESULTS and DISCUSSION

The 1st straight was run significantly faster than the other straights ($F[3, 60]=15.982$, $p<0.001$) (Fig. 1). The FSP indicator $\omega_{FS\text{-}ave}$ did not show significant differences between the 4 intervals ($F[3, 51]= 2.099$, $p=0.112$) (Fig. 2). Similarly, the FSP indicator $\Delta\theta_{ave}$ showed no significant differences between the different intervals ($F[3, 51]= 0.604$, $p=0.615$) (Fig. 3). It did appear that runners started with a more RF strike pattern (values less negative): 1st $\Delta\theta_{ave}$ = -2.04°; which them became more FF: 2nd $\Delta\theta_{ave}$ = -2.65°; 3rd $\Delta\theta_{ave}$ = -2.59° (Figure 3), however these differences were not significant.

Contrary to our hypothesis, runners did not move from a more FF strike pattern to a more RF strike pattern during the straight sections of the 800 m run. The runners in our study maintained a similar FSP throughout the run. The measure associated with initial angular velocity (ω_{FS}), as well as change in foot angle ($\Delta\theta$) both indicate that runners maintain a similar FSP. Further work is currently underway to determine to what extent muscle fatigue occur during the 800 m run. Understanding the potential mechanism whereby substantial muscle fatigue, which most like occur during an 800 m race, does not lead to changes in FSP, is of interest.

CONCLUSIONS

During a maximal 800 m, runners are able to maintain a relatively constant foot strike pattern throughout the duration of the run.

REFERENCES

1. Hasegawa et al. *J Strength Cond Res*, *21*(3), 888–893, 2007.
2. Ahn, et al. *J Sport Health Sci*, *3*(2), 102–112, 2014.
3. Cavanagh & Lafortune. *J Biomech*, *13*(5), 397–406, 1980.
4. Landreneau et al. *Int J Sports Phys Ther*, *9*(7), 888, 2014.
5. Novacheck. *Gait Posture*, *7*(1), 77–95, 1998.
6. Shiang et al. *J Sens,* 1–6, 2016.

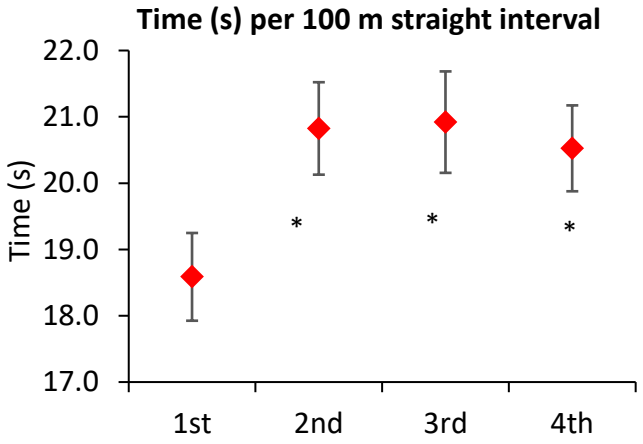

Figure 1: 100 m interval times over the 4 straights of the 800 m run. *: Sign. different from 1st interval.

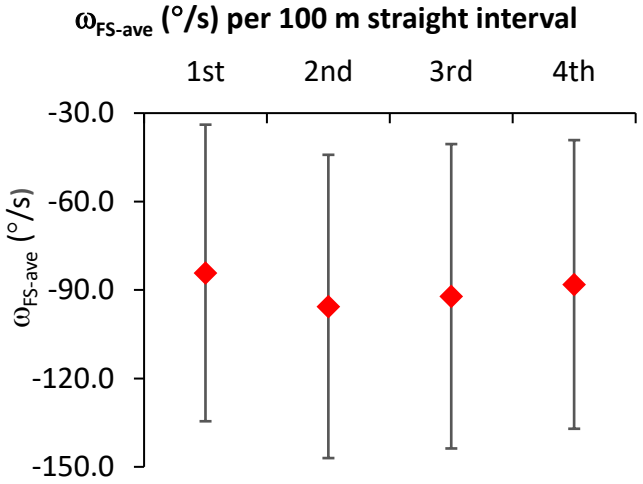

Figure 2: $\omega_{FS\text{-}ave}$ (°/s) over the 4 straights of the 800 m run. No significant differences were found.

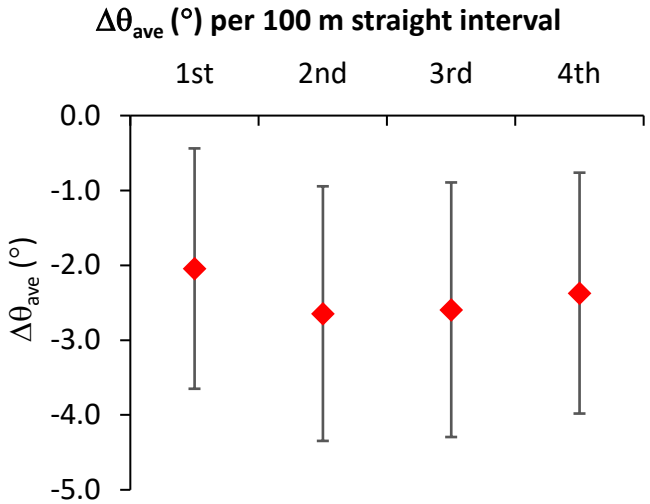

Figure 3: $\Delta\theta_{ave}$ (°) over the 4 straights of the 800 m run. No significant differences were found.

DIFFERENCES IN RUNNING BIOMECHANICS BETWEEN A MAXIMAL, MINIMAL, AND TRADITIONAL RUNNING SHOE

[1] JJ Hannigan, [1] Jacqueline Diulio, [1] Justin Ter Har, and [1] Christine Pollard

[1] Oregon State University – Cascades, OR, USA
email: jj.hannigan@osucascades.edu, web: https://osucascades.edu/force-lab

INTRODUCTION

Running shoes have traditionally been designed with the goal of cushioning the foot and protecting against injuries. However, despite significant advances in running shoe technology over the past 50 years, overall injury rates in runners have not significantly changed [1]. Within the past 10 years, two new types of shoes have gained popularity in the running community for their espoused benefits in injury-protection: a) minimal shoes, such as Vibram Five Fingers, and b) maximal shoes, such as the Hoka One One's.

Minimal shoes have been researched extensively over the past 10 years. In many runners, switching to a minimal shoe causes runners to switch from a rearfoot strike to a forefoot strike [2]. While wearing minimal shoes generally appears to decrease joint stress at the knee, minimal shoes have been shown to greatly increase joint stress and force at the ankle and calf muscles, respectively [2]. Consequently, injury rates for Achilles tendinopathy and calf strains are greater when consistently training in a minimal running shoe.

Maximal shoes, however, have received very little research since their inception less than 10 years ago. The Hoka One One company claims that maximal running shoes will decrease loading rates and impact forces, however, a recent study found the exact opposite trend [3]. No single study to date has looked at ground reaction forces and ankle kinematics in a minimal, traditional, and maximal running shoe. Also, no study has compared the effect of maximal and minimal shoes on both forefoot and rearfoot strikers. Thus, the purpose of this study was to investigate the effect of both a minimal and maximal shoe on vertical ground reaction forces (loading rate, impact peak, overall peak) and ankle kinematics (eversion and dorsiflexion) during running. It was hypothesized that rearfoot runners would display greater loading rates and impact peaks in the maximal shoe compared to the traditional and minimal shoe.

METHODS

Nineteen healthy females (age = 27.6 ± 5.2 yrs) and eight healthy males (age = 28.6 ± 5.8 yrs) participated in this study. All subjects signed an informed consent form approved by IRB at Oregon State University prior to participating. Twenty-one reflective markers and six marker clusters were placed on subjects who ran overground in the lab wearing three different types of custom-designed New Balance running shoes (Boston, MA): a) traditionally cushioned shoes, b) minimal shoes, and c) maximal shoes (Figure 1). Five successful running trials for each shoe were collected at 250 Hz with an 8-camera 3-D motion capture system (Vicon Motion Systems, Oxford UK). Two embedded force plates collected ground reaction forces and were used to determine heel strike and toe-off (AMTI, Watertown MA).

Figure 1: From left to right: minimal, traditional, and maximal cushioned New Balance shoes.

Ground reaction forces and ankle kinematics were calculated using Visual3D software (C-Motion, Germantown MD). Variables of interest included the impact peak, overall peak, and loading rate of the vertical ground reaction force (vGRF), as well as ankle eversion and dorsiflexion kinematics (angle at initial contact, peak angle, angle at toe-off, joint excursion). Because not all runners were rearfoot strikers (6 non-RF), data were analyzed using 2-way mixed effects ANOVA with shoe type as the within-subject effect and foot strike pattern (rearfoot or non-rearfoot) as the between-subjects effect. The alpha-level was set to 0.5 with appropriate Bonferroni corrections.

RESULTS AND DISCUSSION

No runners switched foot strike patterns between shoe conditions. The impact peak of the vGRF was higher in maximal shoes compared to traditional shoes (traditional: 2.3 ± 0.07 BWs; maximal: 2.4 ± 0.07 BWs, p = .039). There were no differences between shoes for any other ground reaction force parameter.

There was a significant shoe x foot strike interaction for peak eversion, with rearfoot strike runners displaying more peak eversion wearing maximal and minimal shoes compared to traditional (traditional: -10.6 ± 0.8°; maximal: -12.1 ± 0.8°; minimal: -12.6 ± 0.91°, p = .017).

There was a significant effect of shoe on the eversion angle at toe-off, with the maximal shoe displaying significantly less eversion at toe-off than the other two shoes (traditional: 1.8 ± 1.0°; maximal: 0.2 ± 1.0°; minimal: 2.9 ± 1.1°, p = .045).

There was a significant effect of shoe on peak ankle dorsiflexion, with greater dorsiflexion occurring in the minimal shoe compared to the maximal shoe (traditional: 21.4 ± 0.8°; maximal: 20.2 ± 0.7°; minimal: 21.8 ± 0.8°, p = .032). There was also a significant effect of shoe on dorsiflexion excursion, with the minimal shoe displaying significantly greater excursion than the traditional and maximal shoes (traditional: 17.9 ± 0.8°; maximal: 17.2 ± 0.8°; minimal: 21.0 ± 1.7°, p = .05).

The findings for the vGRF partially supported our hypothesis. While we did see a higher impact peak in maximal shoes compared to traditional shoes, we did not see a higher loading rate. Pollard et al. (2018) found that running in maximal shoes increased both the impact peak and loading rate compared to a traditional shoe [3]. This previous study only included rearfoot runners, and had runners wear Hoka shoes, which have markedly different midsole and heel construction than the shoes used in this study (Figure 2). Still, a greater impact peak during running may place runners at a greater risk of injury.

Figure 2: Difference in midsole and heel construction between the New Balance and Hoka One One maximal shoes.

Less eversion at toe-off may also be detrimental to injury risk. Becker et al. found that having less eversion at heel-off was a hallmark biomechanical pattern of runners suffering from Achilles tendinopathy and medial tibial stress syndrome [4].

CONCLUSIONS

Running in a maximal shoe may not be injury-protective. On average, running in the New Balance maximal shoe increased the impact peak and resulted in less eversion at toe-off, which may increase overall injury risk.

REFERENCES

1. Taunton et al. *Br J Sports Med.* 36 (2): 2002.
2. Sinclair. *Clin Biomech*. 29(4): 2014.
3. Pollard et al. *OJSM*: 2018 (in press).
4. Becker, et al. *AJSM*. 45(11): 2017.

RUNNING BIOMECHANICS IN 4% MORE ECONOMICAL MARATHON SHOES

Wouter Hoogkamer, Shalaya Kipp and Rodger Kram

University of Colorado, Boulder, CO, USA
email: wouter.hoogkamer@colorado.edu, web: https://tinyurl.com/wouter-colorado

INTRODUCTION

Previously, we showed that a new prototype shoe reduced the metabolic cost of running for all 18 participants, by an average of 4%, as compared to two well-established racing shoes [1]. Based on these findings, the now commercially available shoe has been named "Nike Vaporfly 4%". While running in the prototype shoes, the subjects generally ran with slightly greater peak vertical ground reaction forces, slower step frequencies, and longer contact times than in the control shoes, however these differences were small (~1% or less) and do not explain all the metabolic savings [1].

Here, we compared joint kinematics and mechanics between the Nike prototype shoes (NP) with those of baseline marathon racing shoes: the Nike Zoom Streak 6 (NS) and the shoes used to run the official marathon world record, the Adidas Adizero Adios BOOST 2 (AB) – the same models used as baselines in our metabolic study.

We hypothesized that the more compliant midsole of the NP shoes would allow the runners to run with less knee flexion and smaller peak knee moments [2]. Furthermore, we hypothesized that the carbon fiber plate in the NP shoes would reduce dorsiflexion and negative work in the metatarsal-phalangeal joint [3].

METHODS

To date, 6 male (aged 24.6±3.8 years, mass 64.9±4.8 kg) high-caliber runners ($\dot{V}O_2$max: 72.9±2.8 mL O_2/kg/min) who wear men's shoe size US10 completed the testing protocol. They gave written informed consent that followed the guidelines of the University of Colorado Boulder Institutional Review Board.

The runners wore three pairs of shoes (NP, NS and AB) in a randomized order. Shoe properties have been described in detail previously [1]. In short, the NP midsole comprises highly compliant and resilient ZoomX foam made with PEBA (polyether block amide), combined with a stiff embedded carbon-fiber plate. The NS midsole comprises lightweight EVA (ethylene-vinyl acetate) foam and a rearfoot Zoom air bag. The AB midsole comprises resilient BOOST foam made with TPU (thermoplastic polyurethane). All shoes were equilibrated to 250g/shoe (the mass of the AB shoe, size 10).

We placed 44 reflective markers on the subjects' legs using a modified Helen Hayes marker set. Markers were placed bilaterally on the hip, knee, ankle and metatarsal-phalangeal (MTP) joint centers and clusters were placed on each segment. Subjects performed 5-minute running trials at 16 km/hr in each shoe condition on a motorized, force-measuring treadmill (Treadmetrix, Park City, UT, USA). In between trials, subjects took a 5-minute break, while they changed shoes.

We collected ground reaction force (GRF) data at 1000 Hz and kinematics data at 200Hz during the last 30 seconds of each biomechanics measurement trial (Vicon 512 System, Oxford, UK) and analyzed 10 strides (20 steps). We used a Butterworth low-pass filter (14 Hz) to process both GRF and target-marker data. For the hip, knee, ankle and MTP joints, we calculated sagittal joint angles, angular velocities, moments, powers and work during the stance phase, using Visual 3D and MATLAB software (C-Motion Inc., Germantown, MD, USA; MathWorks Inc, Natick, MA, USA).

RESULTS AND DISCUSSION

Generally, joint angles, angular velocities, moments and powers were similar between shoes (Fig. 1). Specifically, opposite to our hypothesis, peak knee flexion and moments were similar between shoes ($p=0.80$ and $p=0.65$, respectively).

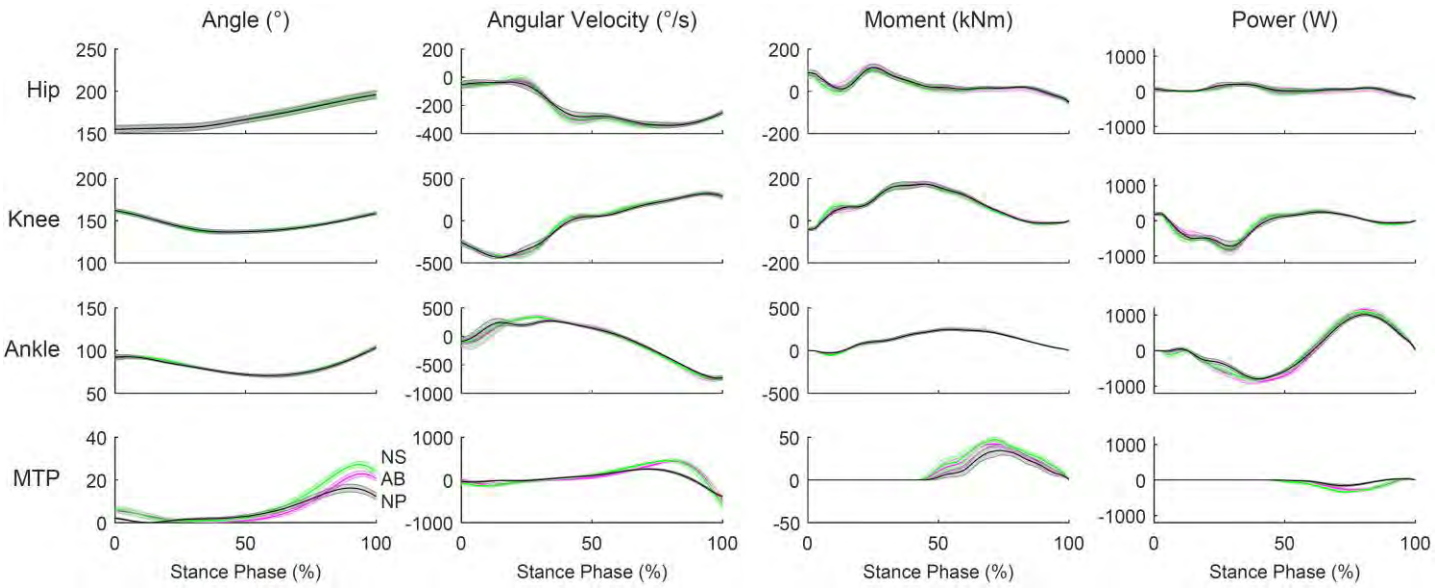

Figure 1: Joint kinematics and mechanics for running in the NP (black), NS (green) and AB (purple) shoes.

However, peak MTP dorsiflexion was significantly smaller in the NP shoes ($p<0.001$). Peak ankle and MTP moments were numerically lower in the NP shoes, but not statistically significant ($p=0.07$ and $p=0.15$, respectively). Furthermore, negative work at the ankle and MTP joints was significantly lower in the NP shoes (Table 1, both $p<0.001$).

CONCLUSIONS

Joint kinematics and mechanics were slightly different for running in the highly compliant and resilient prototype shoes as compared to running in the two other established marathon shoes. Differences were most prominent around the ankle and MTP joint, but knee mechanics were similar, suggesting that the earlier observed metabolic savings of 4% are not related to differences in knee mechanics.

REFERENCES

1. Hoogkamer et al. *Sports Med*, Epub ahead of print, 2017
2. Kerdok et al. *J Appl Physiol*. 92: 468-76, 2002
3. Willwacher et al. *J Appl Biomech*. 29: 583-92, 2013

ACKNOWLEDGEMENTS

We thank Jesse H. Frank and Claire Denny for help with data collection, Owen N. Beck and Stephen Allen for help with data analysis, and Geng Luo and Emily M. Farina for fruitful discussions.

Table 1: Running mechanics and joint work for running in the NP, NS and AB shoes. * indicates significantly different from NP, † indicates significantly different from NS

	NP	NS	AB	p-value
Step Frequency (steps/s)	2.92 ± 0.11	2.96 ± 0.10*	2.95 ± 0.10	**0.032**
Contact Time (ms)	193 ± 5	191 ± 5	191 ± 6	0.315
Peak Vertical Force (BW)	3.03 ± 0.15	2.98 ± 0.13	2.98 ± 0.15	0.092
Negative Hip Work (J/step)	5.27 ± 5.40	7.20 ± 8.29	8.85 ± 8.97	0.087
Positive Hip Work (J/step)	15.54 ± 10.71	13.20 ± 10.02	15.16 ± 11.46	0.305
Negative Knee Work (J/step)	33.36 ± 8.67	35.66 ± 9.07	33.30 ± 7.58	0.562
Positive Knee Work (J/step)	14.24 ± 4.58	15.52 ± 4.58	15.72 ± 5.68	0.129
Negative Ankle Work (J/step)	43.08 ± 3.47	47.86 ± 3.83*	52.94 ± 3.28*†	**<0.001**
Positive Ankle Work (J/step)	49.26 ± 5.55	55.34 ± 8.08	55.15 ± 4.16	0.087
Negative MTP Work (J/step)	5.89 ± 3.02	16.35 ± 2.96*	12.97 ± 3.77*	**<0.001**
Positive MTP Work (J/step)	0.57 ± 0.62	0.63 ± 0.82	0.24 ± 0.26	0.468

ACCUMULATED RUNNING LOADS ARE SIMILAR ACROSS TRAINING PROGRAMS

Jessica G. Hunter, Gina L. Garcia, Jae Kun Shim, and Ross H. Miller

University of Maryland, College Park, MD, USA
email: jghunter@umd.edu, web: http://sph.umd.edu/neuromechanics

INTRODUCTION

The forces due to vertical and torsional loading of the tibia during running are associated with injuries in general, and tibial stress fracture specifically [1, 2]. Runners with history of tibial stress fracture show higher per-step vertical average loading rate and absolute free moment than previously uninjured runners [1, 2]. However, per-step magnitudes of vertical loads increase as running speed increases in healthy runners [3], and interval training has been shown to have a protective effect on injury development [5]. Higher per-step loads associated with faster running may be beneficial when combined with slower speeds elsewhere in training.

Recent studies have investigated the accumulation of loads over a specific distance, rather than per-step comparisons. Per-step knee loads increased but cumulative loads were similar between walking and running [4]. At faster speeds, longer step lengths mean fewer steps are required to travel a distance, and may not necessarily lead to increases in accumulated load. The question of how speed distribution within a training program affects cumulative load (and ostensibly injury risk) is important because speed distribution is an easily modifiable factor of training.

Therefore, the purpose of this study was to compare the accumulated vertical average loading rate (accumulated LR), accumulated peak absolute tibial free moment (accumulated FM), and accumulated peak compressive tibial load (accumulated TL) between two distributions of speeds: i) all mileage at normal speed (N) and ii) a combination of slow and fast speeds with the same average speed as normal (ASN). We hypothesized that all accumulated loads would be greater for ASN than N program due to a larger proportion of fast running.

METHODS

Approval was obtained from the local Institutional Review Board. We recruited 56 healthy, recreational runners (age: 25±8 yrs, mass: 67.2± 13.0 kg, height: 1.70±0.12 m). Subjects wore 33 reflective markers on the pelvis and lower limb. They ran around a 50-m indoor track for three laps each at three speeds: self-selected slow, normal, and fast paces. Kinematic data were captured using a 13-camera motion capture system sampling at 200 Hz. Ten embedded force plates recorded ground reaction forces (GRF) at 1000 Hz.

For each self-selected speed, velocity (VEL), step length (SL), steps per kilometer (SPK), loading rate (LR), peak absolute free moment (FM), and peak tibial compressive load (TL) was calculated. Steps per kilometer were calculated by dividing 1000m by step length in meters. Loading rate was calculated as the slope of the vertical GRF between 20-80% of the time period from initial contact to impact peak and scaled by body weight [5]. Free moment was calculated according to Milner et al. [5]. TL was calculated by: i) estimating the Achilles tendon (AT) moment arm length [6], ii) dividing the resultant ankle moment during stance by the moment arm estimate to get AT force, iii) summing AT force with proximal foot forces, iv) identifying the peak value. Because subjects' speeds were self-selected, within-subjects repeated measures ANOVA was performed to compare the VEL, SL, SPK, LR, TL, and FM. For variables with significant main effects, post-hoc analysis using Tukey's contrasts were calculated with a Bonferroni adjustment for multiple comparisons.

Per-kilometer accumulated load was calculated for N by multiplying the normal speed SPK by the per step load for LR, TL, and FM. ASN was calculated by determining the fractions of slow and fast speeds required to average normal speed and multiplying

these fractions by the respective SPK. These slow and fast SPK were combined and multiplied by the per-step LR, TL, and FM. A paired-samples Wilcoxon test was performed to compare accumulated LR, accumulated FM, and accumulated TL between N and ASN speed distributions. Effect sizes for significant differences were calculated as Cohen's *d.* Significance between speed distributions was determined at $p < 0.05$.

RESULTS AND DISCUSSION

There was a main effect of speed for VEL, SL, LR, FM, and SPK (all $p < 0.001$). Post-hoc analysis showed that each variable increased with speed ($p < 0.01$) except FM, which was similar between *slow-normal.* Self-selected speed outcomes are shown in Table 1. The hypothesis that accumulated loads would be greater in the ASN than AN program was not supported. The comparisons of accumulated LR, accumulated TL, and accumulated FM showed no differences between the speed distributions (Fig. 1).

The proportions of slow and fast speed required to average the normal speed condition were nearly equal, at 51% and 49%, respectively (Fig. 1). The per-step FM was similar between slow and normal, therefore we expected the proportion of fast speed in the ASP distribution to lead to even greater accumulated FM in particular. However, the large contribution of fast running was insufficient to lead to increased accumulation of loads for any variable.

CONCLUSIONS

These results suggests runners can include substantial fractions of fast speeds in their training without accumulating significantly greater loads (Fig. 1). Nonetheless, too much "intensity", typically defined as too much fast running, is commonly suspected to cause injuries. Further research is therefore needed to determine the association between accumulated loads and injury development.

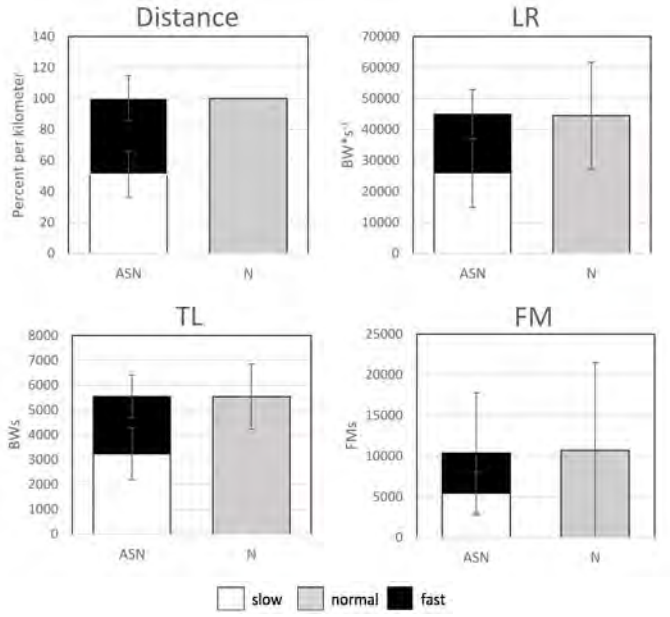

Figure 1. Per-km comparisons of distance proportions, and accumulated variables (LR, TL, and FM) for two speed distributions.

REFERENCES

1. Milner, CE, et al. *Med Sci Sports Exerc* **38**, 323–328, 2006.
2. Milner, CE, et al. *J. Biomech.* **39**, 2819–2825, 2006.
3. Hamill, J, et al. *Mov. Sci.* **2**, 47–56 (1983)
4. Miller, RH, et al. *Med Sci Sports Exerc* **46**, 572–579, 2014.
5. Hespanhol Junior, LC, et al. *J Physiother* **59**, 263–269, 2013.
6. Giddings, VL, et al. *Med Sci Sports Exerc* **32,** 627-634, 200

Table 1: Mean±SD of kinematics and kinetics at self-selected speeds.

Speed	VEL (m/s)	SL (m)	LR (BW/s)	TL (BWs)	FM	SPK
Slow	2.73±0.35*	1.01 ±03*	42.6±10.1*	6.43±1.31*	9.97±6.95	1002±119*
Normal	3.27±0.42*	1.19±0.16*	49.7±12.2*	6.47±1.34*	10.03±5.16	856±108*
Fast	4.09±0.55	1.40±0.18	64.3±17.6	6.53±1.32	17.83±22.97*	728±94

*Significantly different from all other speeds, all $p < 0.01$

INITIAL CONTACT AND TOE OFF EVENT IDENTIFICATION FOR TREADMILL RUNNING AT DIFFERENT SPEEDS

[1] Deborah L. King, [2] Maura McCartney, and [1] Eoghan Trihy

[1] Ithaca College, Ithaca, NY, USA
[2] University of Rochester, Rochester, NY, USA
email: dking@ithaca.edu

INTRODUCTION

Stride rate and foot strike pattern are common parameters examined as a profile of a runner's biomechanics. Accurately measuring stride rate and foot strike position requires precise determination of initial contact (IC) and toe-off (TO). Preferably, these variables are determined from a force plate / instrumented treadmill. However, studies performed in the field or on a standard treadmill rely on identification of IC and TO from kinematic data.

Kinematic based algorithms for determining IC and TO are available, but are often specific to a runner's foot strike pattern [1,3,4,5] or a limited range of speeds [2,3,4,5]. Developing a reliable method of identifying initial contact and toe-off for all foot strike patterns and over a large range of speeds is beneficial for running gait analysis based on kinematic data. Thus, the purpose of this study was to determine the validity of previously published kinematic based IC and TO algorithms across foot strike patterns and a range running speeds for treadmill running.

METHODS

As part of another study, 10 healthy active participants, five males and five females between the ages of 20 and 55 (age 29 ± 11 y; 170 ± 6.74 cm; 69.8 ± 9.24 kg), gave their written informed consent to participate and completed 6 treadmill running trials (20-60s depending on speed) at 6 speeds: 2.24, 2.69, 3.14, 3.5, 4.03, and 4.48 ms^{-1}.

Reflective markers were placed on the lower extremities and pelvis using the Plug-In-Gait marker set (Vicon, Centennial CO, USA). Participants wore their own running shoes and completed a three-minute warm up of light jogging. Data were collected for the last 20 s of each trial using a Vicon Nexus 2.5 (Vicon, Centennial, CO, USA) motion capture system (200Hz). Two force plates (AMTI, Watertown, MA, USA) sampling at 1000Hz were placed under the front of the treadmill for identification of IC and TO. Data were analyzed in Visual 3D (C-motion, Baltimore, MD, USA).

Two algorithms for finding IC, Alvim [1] and Milner [4], and one algorithm for finding toe off, Fellin [2], were chosen for analysis. IC and TO time from the three algorithms (IC_{Alvim}, IC_{Milner}, TO_{Fellin}) were compared to IC and TO times as determined from the forces from the force plates (IC_{FP} and TO_{FP}). Foot strike pattern, RFS versus nRFS, was determined from foot angle at initial contact.

Two-way repeated measures analyses of variance (ANOVA) were used to compare algorithm and force plate IC and TO identification times (JASP V0.8.1.2). Alpha = 0.05. Algorithm accuracy by foot strike pattern was examined using root mean square errors (RMSe).

RESULTS AND DISCUSSION

Seven RFS and three nRFS runners were identified totaling 3218 foot contacts (2468 RFS and 750 nRFS). IC_{Alvim} was identified 0.089 ±0.061 s before IC_{FP} ($p<0.011$). There was not a significant speed effect ($p=0.867$). IC_{Milner} was not significantly different from IC_{FP} ($p=0.155$) and was identified 0.010±0.040 s before IC_{FP}. $TO_{Fellin.}$ was not significantly different from TO_{FP} ($p=0.555$) and there was no significant speed effect on TO_{Fellin} accuracy ($p=0.610$).

IC_{Alvim} RMSe tended to be smaller for RFS runners (0.075±0.0.36 s) as compared to nRFS runners (0.086 ± 0.063 s); this difference was greater at faster

running speeds (Figure 1a). IC_{Milner} RMSe was similar for both RFS (0.015±0.008 s) and nRFS (0.015±0.008 s) decreasing in a linear pattern with running speed (Figure 1b). RMSe between TO_{Fellin} and TO_{FP} ranged from 0.012 to 0.014 s (Figure 1c).

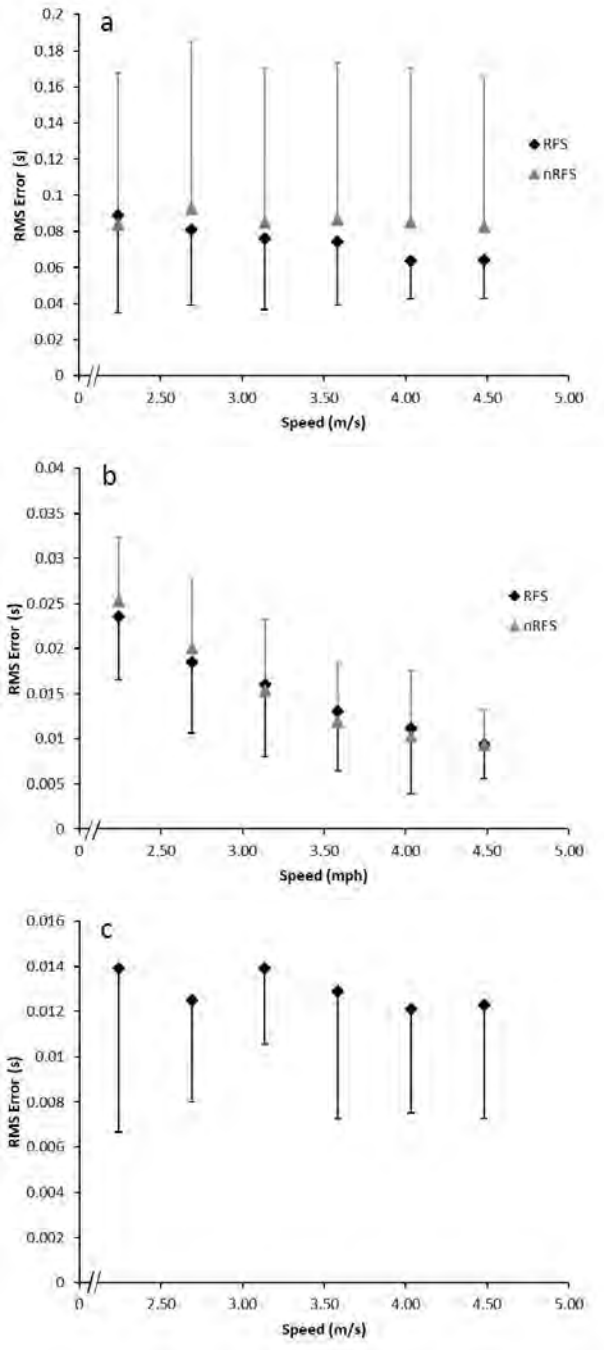

Figure 1: (1a) RMSe for IC_{Alvim} for RFS and nRFS, (1b) RMSe for IC_{Milner} for RFS and nRFS, (1c) RMSe for TO_{Fellin}. Values are means ±SD.

A linear regression analysis of 1598 randomly selected ICs provided a speed correction to IC_{Milner} of -0.0064 × speed + 0.0348 with $R^2 = 0.976$. This equation applied to the remaining 1598 ICs identified 98% of ICs within 20 ms, 4 frames at 200 fps, of IC_{FP} and 68% of IC within 10ms, 2 frames at 200 fps, of IC_{FP}.

IC_{Milner} outperformed IC_{Alvim} regardless of running speed and worked equally well for RFS and nRFS. IC_{Milner} accuracy depended on running speed. Based on the regression equation developed in the current study, the slowest speed of 2.24 ms^{-1} needed to be adjusted by 20 ms. At the fastest speed of 4.47 ms^{-1}, IC_{Milner} needed to be adjusted by 6 ms. IC_{Milner} was developed with RFS and nRFS over-ground running at 3.7 ms^{-1} [4]. The RMSe of 13 ms at 3.58 ms^{-1} in the current study agrees with the three frame (15 ms) offset reported for the similar 3.7 ms^{-1} over-ground running speed [4]. Of importance, at least for treadmill running, is that the offset observed with IC_{Milner} linearly decreased with speed. However, the linearity of the algorithm's accuracy at slower or faster running speeds than those tested in the current study should not be assumed.

CONCLUSIONS

The IC_{Milner} algorithm adjusted with the speed based linear regression equation and TO_{Fellin} are recommended for RFS and nRFS treadmill running between 2.2 and 4.5 m/s when IC and TO must be determined from kinematic data. The range of speeds used in this study, while broad, does not cover running speeds often performed by top competitive runners. Future research should validate the algorithm at faster speeds and for both treadmill and over-ground running.

REFERENCES

1. Alvim et al. *Journal of Applied Biomechanics*, **31**(5), 383–388, 2015.
2. Fellin et al. *Science and Medicine in Sport*, **13**(6), 646–650, 2010.
3. Leitch et al. *Gait and Posture*, **33**(1), 130–132, 2011.
4. Milner & Paquette. *Journal of Biomechanics*, **48**(12), 3502–3505, 2015.
5. Osis et al. *Journal of Biomechanics*, **47**(11), 2786–2789, 2014.

WHAT DETERMINES THE METABOLIC COST OF HUMAN RUNNING ACROSS A WIDE RANGE OF VELOCITIES?

Shalaya Kipp[1], Alena M. Grabowski[1,2] and Rodger Kram[1]

[1]University of Colorado, Boulder, CO, USA
[2] Colorado Healthcare System, Department of Veterans Affairs, Denver, CO
email: shalaya.kipp@colorado.edu

INTRODUCTION

The cost of generating force hypothesis [1] proposes that the metabolic rate during running is determined by the rate of muscle force development ($1/t_c$, t_c = contact time) (Eq. 1). Roberts et al. [2] assumed that the recruited muscle volume remains constant and reported that the rate of force development alone explains ~70% of the increase in metabolic rate for human runners across a moderate velocity range (2-4 m s^{-1}).

$$\frac{\dot{E}_{met}}{W_b} = c \cdot \frac{1}{t_c} \qquad \text{(Eq. 1)}$$

The Effective Mechanical Advantage (EMA) is the ratio of the muscle moment arm (r) to the ground reaction force moment arm (R); EMA= r/R [3]. EMA determines the muscle force (F_m) required and thus the amount of active muscle volume (V_m) recruited for running.

We hypothesized that: 1. over a wider range of velocities, the EMA of the lower leg would overall decrease at faster velocities, necessitating a greater volume of active muscle recruitment and 2. $1/t_c$ and V_m together would better explain the metabolic cost of running (Eq. 2).

$$\frac{\dot{E}_{met}}{W_b} = k \cdot \frac{1}{t_c} \cdot V_m \qquad \text{(Eq.2)}$$

METHODS

10 high-caliber male runners (VO_2max = 72.7 ± 3.9 mlO_2/kg/min) participated over two visits. During the first visit subjects ran at 8, 10, 12, 14, 16, 18 km hr^{-1} in a randomized order, each for 5 min. We measured O_2 uptake and CO_2 production to determine metabolic rate for each velocity [4]. We determined blood lactate concentration following the 14, 16 and 18 km hr^{-1} trials to assure a primary reliance on the oxidative metabolism. During a second visit, subjects ran at the same 6 velocities, in the same randomized order as visit 1, for 2-min. We measured ground reaction (1000Hz) forces and joint kinematics (200Hz). Then, we calculated net internal joint moments (M_{joint}) and muscle force (F_m) using published [3] moment arm (r) data.

$$F_m = M_{joint} / r$$

We calculated V_m at each joint using published [3] fascicle length (L) data and assuming muscles exert an isometric force/unit of cross sectional area (σ=20N/cm^2) [5].

$$V_m = L \cdot F_m/\sigma$$

RESULTS AND DISCUSSION

From 8 to 18 km hr^{-1}, metabolic rate increased 132% from 9.01 to 20.92 W kg^{-1} (Fig 1).

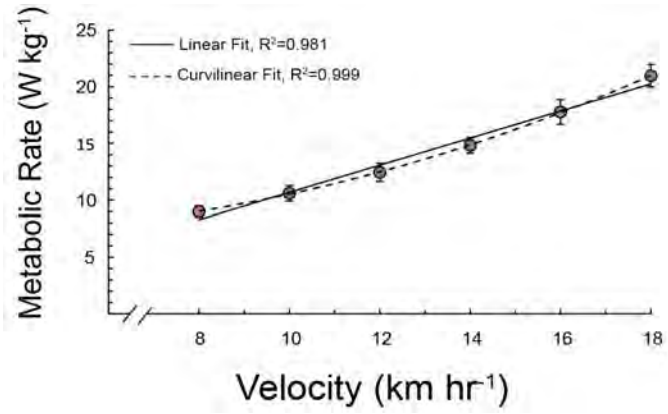

Figure 1: Metabolic rate vs. velocity. Error bars indicate ±1 SD.

Contact time (t_c) decreased from 0.280 sec to 0.190 sec, and thus the rate of force development ($1/t_c$) increased by 48%.

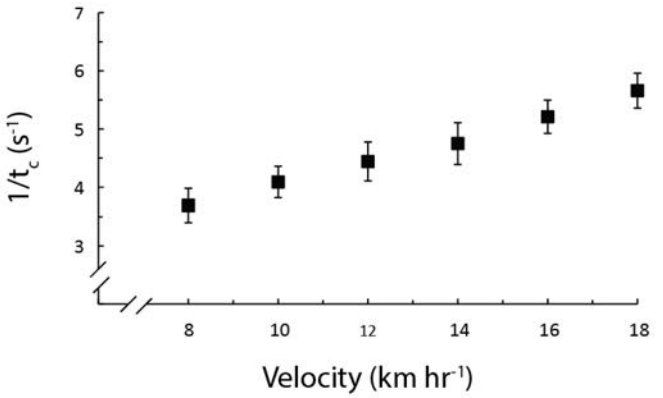

Figure 2: The rate of force production ($1/t_c$) vs. velocity. Error bars indicate ±1 SD.

Ankle EMA decreased by 19.7±11%, knee EMA increased by 11.1±26.9% and hip EMA decreased by 60.8±11.8%. Thus, active muscle volume increased by 65.5±28.7% at the ankle, 19.0 ± 14.3% at the knee and 102.3 ± 23.3% at the hip (Fig. 2). Overall, across the velocity range, total active muscle volume per leg increased 54.1% from 1663±152 cm^3 to 2550±169 cm^3. 86% of the increase in metabolic rate could be accounted for by the rate of force production ($1/t_c$) alone. 98% of the increase in metabolic rate could be accounted for by using both $1/t_c$ and V_m (Fig 3.).

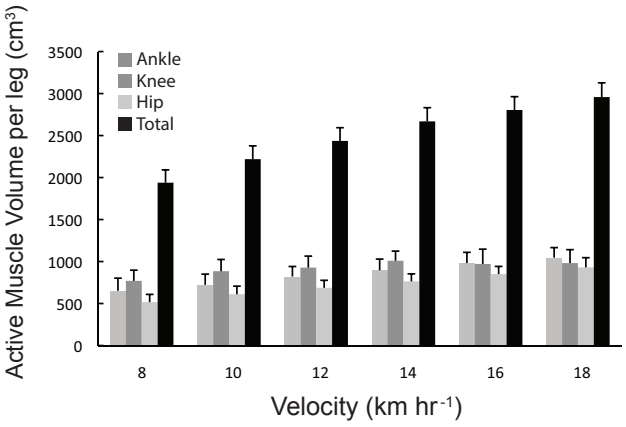

Figure 3: Mean estimated active muscle volume per leg across velocity for ankle, knee, and hip extensor muscles. Error bars indicate ±1 SD.

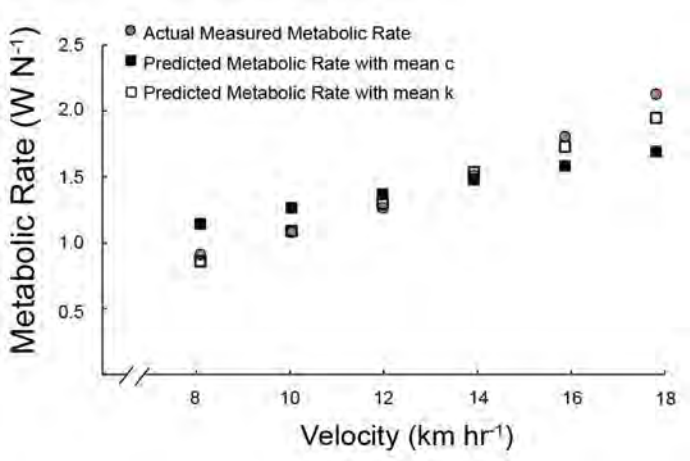

Figure 4: Measured metabolic rate (solid circles), predicted metabolic rate using mean c (closed squares), and predicted metabolic rate using mean k (open squares) vs. velocity in km hr^{-1}.

These results link the biomechanics and metabolic costs of running and may give greater insight into individual differences in metabolic rate.

CONCLUSIONS

We accept both of our hypotheses. Over the wider range of velocities tested, EMA of the lower limb joints overall decreased contributing to the increased volume of activated muscle. The rate of force production ($1/t_c$) and active leg muscle volume (V_m) together almost completely account for the increased metabolic requirements of human running across the entire aerobic velocity range.

REFERENCES

1. Kram, R., and Taylor, C.R. 1990 *Nature*. 346, 265-267.
2. Roberts, T. J., et al. 1998 *J Exp Biol*. 201, 2745-2751.
3. Biewener, A. A., et al. 2004 *J Appl Physiol*. 97, 2266-2274.
4. Brockway, J. M. 1987 *Hum Nutr Clin Nutr*. 41, 463-471.
5. Perry, A. K., et al. 1988 *J Exp Biol.* 137, 207-219.

SEX IMPACTS LEG STIFFNESS WHEN INCREASING STRIDE LENGTH TO RUN WITH BODY BORNE LOAD

[1] Nicholas J. Lobb, [1]AuraLea C. Fain, [1]Kayla D. Seymore, and [1]Tyler N. Brown
[1] Boise State University, Boise, ID, USA
email: nicklobb@u.boisestate.edu

INTRODUCTION

During military training, personnel are often required to run at a fixed cadence with heavy body borne loads. These loads routinely weigh between 20 kg and 40 kg, and alter lower limb biomechanics leading to increased risk of musculoskeletal injury (MSI) [1]. When running with load, personnel increase leg stiffness to attenuate larger GRFs and prevent collapse of the lower limb. Increased stiffness may elevate risk of MSI by transmitting GRFs to the lower limb's soft-tissues [2]. When running without load, individuals purportedly decrease leg stiffness by increasing lower limb flexion as stride lengthens [3]. Military personnel, however, may not possess the lower limb strength to similarly decrease leg stiffness as they lengthen their stride to run at a fixed cadence with heavy body borne loads. Female military personnel, who are purportedly weaker than males [4], may be especially at risk for injury as they may not possess the strength to safely attenuate large GRFs. The purpose of this study was to quantify leg stiffness for male and female participants as they lengthened their stride to run with body borne load.

METHODS

Seventeen male and ten female participants (21.2 ± 2.3 yrs, 1.7 ± 0.1 m, 75.5 ± 11.3 kg) had 3D lower limb biomechanics quantified while running with four load conditions: 20 kg, 25 kg, 30 kg, and 35 kg. For each load, participants wore a helmet, weighted vest, and carried a mock weapon. The vest weight was systematically adjusted to apply the load necessary for each condition. For the run task, participants were required to run at 4 m/s ± 5% using one of three stride lengths: preferred stride length (PSL), 15% shorter than PSL (SSL), and 15% longer than PSL (LSL). Participants performed five successful trials at each stride length. A successful trial required participants run with the correct stride length and speed, and only contact the force platform with their dominant leg.

During each running trial, lower limb biomechanics were quantified from the 3D trajectories of 34 reflective markers. A kinematic model with seven segments (bilateral foot, shank, and thigh and pelvis) and 24 DoF was created from a static trial. Synchronous GRF data and marker trajectories were low pass filtered with a fourth-order Butterworth filter (12 Hz). Then, filtered marker trajectories were processed using Visual 3D (C-Motion, Rockville, MD) to solve joint rotations at each instant.

Leg stiffness was calculated as the GRF vector directed from the center of pressure through the hip joint center (F_e) divided by the maximum change in leg length (L_e). Leg length was calculated as the linear distance between the center of pressure and the hip joint center.

$$\text{Leg Stiffness: } K_l = \frac{F_e}{\max(\Delta L_e)}$$

For analysis, peak of stance (PS, 0%-100%) leg stiffness, vertical GRF (vGRF), change in leg length, and hip, knee, and ankle flexion angles were quantified. Each variable was submitted to a RM ANOVA to test the main effect and interaction between load (*20 kg, 25 kg, 30 kg, 35 kg*), stride length (*SSL, PSL, LSL*), and sex (*Male, Female*). Significant interactions were submitted to a simple effects analysis, and a Bonferroni correction was used for multiple comparisons. Alpha was $p < 0.05$.

RESULTS AND DISCUSSION

Body borne load increased leg stiffness (P=0.006) and risk of MSI during running. Specifically, leg stiffness increased 12% with the 35 kg load compared to the 20 kg load (P=0.002). Participants may have increased leg stiffness to prevent collapse of the limb and help attenuate the larger peak vGRFs

evident with the addition of load (Fig. 1, $P<0.001$). These large vGRFs may increase strain on both the passive and active soft-tissue structures of the lower limb, increasing risk for MSI.

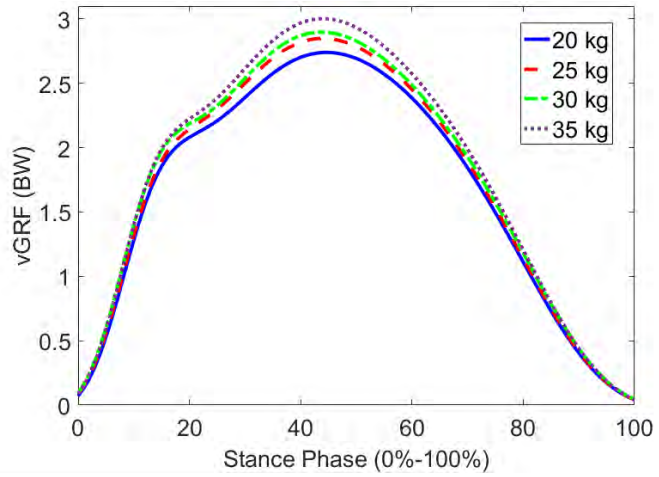

Figure 1: Depicts vGRF during stance for each load configuration (20 kg, 25 kg, 30 kg, 35 kg).

Risk of MSI may further increase when running with longer strides. Participants increased peak vGRF with LSL compared to PSL ($P<0.001$) and SSL ($P<0.001$). But, males may possess the ability to attenuate these larger vGRFs and decrease leg stiffness with longer strides (Fig. 2). Specifically, males decreased leg stiffness when using LSL compared to PSL ($P<0.001$) and SSL ($P<0.001$), and PSL compared to SSL ($P=0.026$). Whereas, females exhibited no significant difference in leg stiffness between strides ($P>0.05$). The discrepancy in leg stiffness may be attributed to a sex dimorphism in lower limb biomechanics as stride lengthens. Although, females adopted greater PS hip and knee flexion compared to males with SSL ($P=0.013$; $P=0.001$), only male participants significantly increased PS hip and knee flexion as stride length increased from SSL to PSL ($P=0.008$; $P=0.001$) and from PSL to LSL ($P=0.041$; $P<0.001$). Males may possess lower limb strength that affords them the ability attenuate the larger vGRF evident with longer strides by using greater lower limb flexion and reduced leg stiffness. Females, who are reportedly weaker [4], may not possess the strength to allow for greater lower limb flexion and, subsequently a reduction in leg stiffness when running with longer strides. Further, a significant stride by load interaction was evident for PS knee flexion angle ($P=0.028$). Participants increased PS knee flexion with LSL compared to PSL when carrying 20 kg ($P=0.001$), 25 kg ($P<0.001$), and 30 kg ($P=0.004$), but not 35 kg ($P=0.760$). The current participants may not have the lower limb strength to increase lower limb flexion, and attenuate the larger vGRF evident with longer strides, when running with heavy body borne loads.

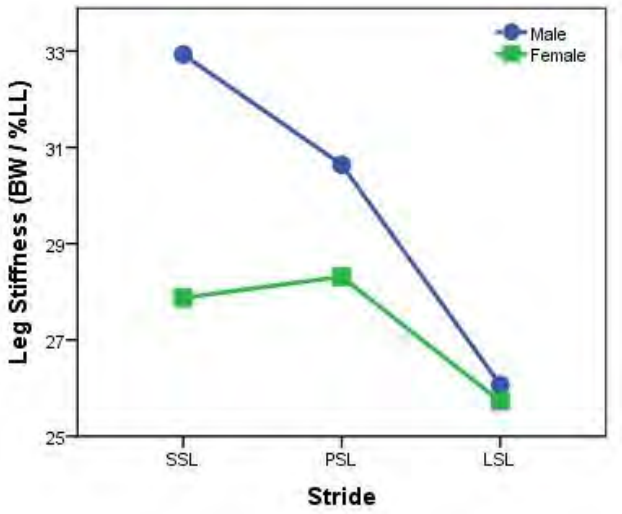

Figure 2: The leg stiffness exhibited by male and female participants running with SSL, PSL and LSL.

CONCLUSIONS

Body borne load increased leg stiffness and potential risk of MSI during running. This increased stiffness may help attenuate the greater peak vGRFs and prevent collapse of the lower limb when running with heavy body borne loads. Only male participants, however, demonstrated the ability to reduce leg stiffness and potentially risk of MSI by increasing hip and knee flexion when running with longer strides. Further study is warranted to determine if lower limb strength, rather than sex, determines the ability to adjust leg stiffness and lower limb biomechanics when altering stride length to run with heavy body borne load.

REFERENCES

1. Patton JF, et al. *Eur J Appl Physiol*, **63**:89-93, 1991.
2. Silder A, et al. *J Biomech*, **48**:1003-1008, 2015.
3. Farley CT, et al. *Clin. Biomech*, **26**: 23-28, 1998.
4. Miller A, et al. *Eur J Appl Physiol*, **66**: 254-262, 1993

Minimum Number of Strides to determine Stable Symmetry during Running

Shane P. Murphy, Zach B. Barrons, and Jeremy D. Smith

University of Northern Colorado, Greeley, CO, USA
email: shane.murphy@unco.edu, twitter: @UNCBiomechanics

INTRODUCTION

Gait symmetry is often used to characterize the quality of gait in both healthy and clinical populations [1]. In running, generally a mean of two to ten strides has been used to characterize symmetry [2,3]. Consecutive strides are often considered in these analyses, but in others, particularly overground studies, the strides are not consecutive.

Due to differences in study methodologies and the inherent variability of gait, it is not understood how the number of strides influence the outcomes of a given study. Further, it is not fully understood if a stable mean is only found in consecutive strides, or if subsets of strides will result in different mean symmetries.

The purpose of this study was to determine how many strides should be used to quantify the mean symmetry of a lower extremity variable during running. An additional purpose of this study was to determine if the order of strides analyzed would alter findings.

METHODS

Ten participants free of lower extremity injury for six months and no history of surgery (F = 6, 1.73 ± 0.12 m, 66.0 ± 12.0 kg, 25 ± 3 years, 326 ± 178 min/week of activity) completed two sessions of running at 2.5 $m \cdot s^{-1}$. Each session consisted of running for nine minutes (3 minutes of acclimation and 6 minutes of collection), in which 60 seconds of data were collected at the three and five minute marks. The last 75 strides of each 60 second trial were analyzed. Motion (100 Hz) and ground reaction force (2000 Hz) data were captured using a ten camera system (VICON, Englewood, CO) and an instrumented treadmill (AMTI, Watertown, MA), respectively.

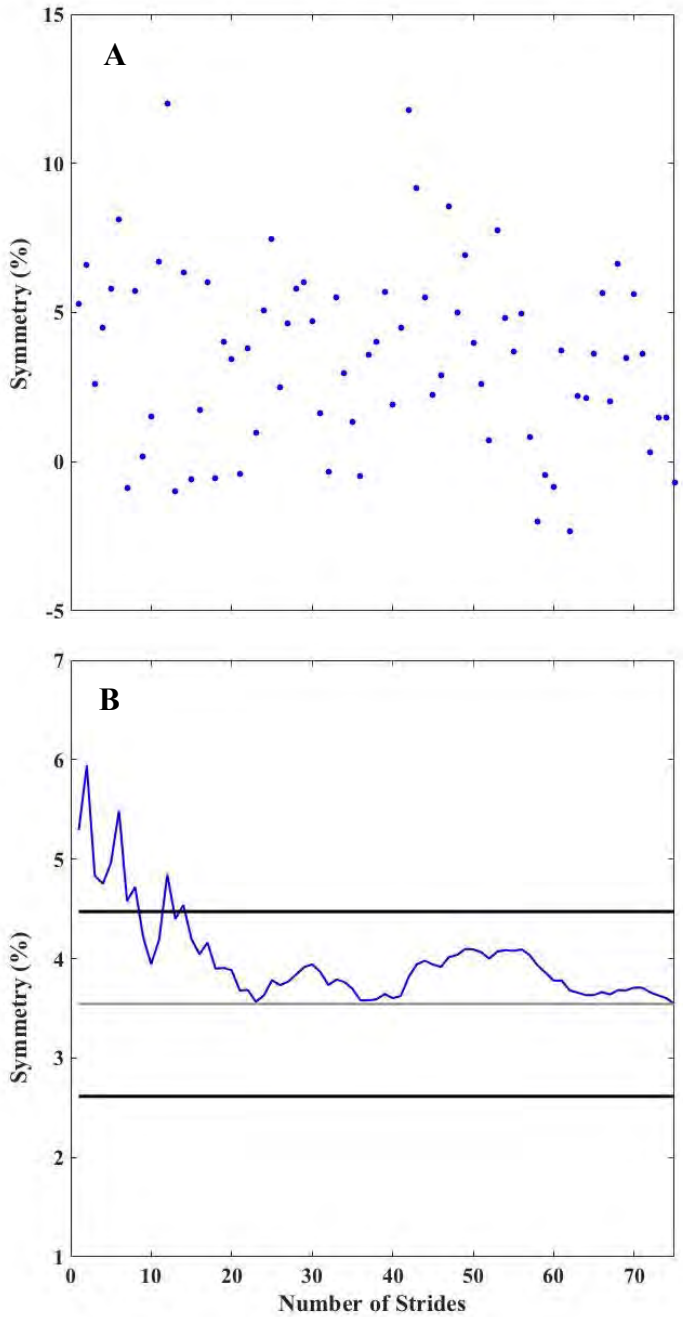

Figure 1: Symmetry of hip angular position at initial foot contact. **A)** Symmetry index for each stride and **B)** Mean symmetry indices with an increasing number of strides used in the mean (blue line). The mean of all stride symmetries (gray line) with a window of ±2SD (black lines) was used as a window to determine how many strides were needed to create a stable mean.

Data were filtered with a lowpass 4th order, zero lag, Butterworth filter at 10 Hz for ground reaction force data and 6 Hz for motion data. Spatiotemporal, joint kinematic and joint kinetic variables were determined in Visual 3D (C-Motion, Germantown, MD).

Symmetry for each measure was determined as the difference between each leg's values, and then divided by the average value of both legs (Fig. 1a) [4]. Mean symmetry for each running trial was determined by computing an average with an increasing number of strides until all strides from that trial were included. To determine the stable point for a variable's mean, the value had to fall within 2 standard deviations of the overall mean (Fig. 1b) [5].

Trials were removed prior to analysis if extreme values of symmetry were calculated. Fifteen stride symmetries were selected randomly to compare the first, middle, and last fifteen stride symmetries of each trial. Multiple repeated measure analyses of variance were used to determine if differences between random, first, middle, last, and all stride symmetries were statistically significant (SPSS 24, IBM, Armonk, NY), with each trial treated as individual subjects. An alpha of 0.05 was used to determine significance.

RESULTS AND DISCUSSION

A stable mean for all variables was achieved with an average of 16.4 ± 6.3 strides. This average includes variables, such as ankle angle at initial contact and minimum knee angle, which had a large variance in calculated symmetry values. This large variance was due to magnitudes of the variables being close to zero prior to determining symmetry. For variables near zero, on average 27.5 ± 5.3 trials were required to reach a stable mean. Without these highly variant variables, a stable mean was met in 14.1 ± 3.2 strides. Therefore, 15 strides were used to determine if order of strides analyzed would alter findings. No differences were found between all bins of strides, for all variables ($p < 0.05$; Table 1 presents the spatiotemporal outcomes).

In previous literature, 200 strides of continuous walking were required to describe variability in kinematics [5]. It is possible that the current findings do not fully capture the variability of symmetry between limbs during running, but instead provides a reference to how many strides are necessary to describe differences between means.

Future research should examine if the number of strides necessary for a stable mean changes between different symmetry calculations, and if the number of strides necessary for a stable mean changes with a smaller window about the mean.

CONCLUSIONS

Fifteen strides of running data, regardless of order, is sufficient to produce a stable mean symmetry index for lower extremity variables. Data collection procedures looking at limb symmetry should allow for at least 15 strides, regardless of overground or treadmill running. Caution should be used with variables with averages near zero, even when analyzed with upwards of 30 strides.

REFERENCES

1. Sadeghi et al., *Gait and Posture*, 2000.
2. Sanderson & Martin, *Gait and Posture*, 1997.
3. Bredeweg et al., *Gait and Posture*, 2013.
4. Herzog et al., *Med Sci Sports Exerc*, 1989.
5. Owings & Grabiner, *J Biomech*, 2003.

Table 1: Mean symmetry for common spatiotemporal measures in bins of 15 strides of data, except for the last column, which averaged all strides. Negative values represent a greater value on the left limb.

	First 15 Strides	Middle 15 Strides	Last 15 Strides	Random 15 Strides	All 75 strides
Step Length (%)	0.51 ± 1.80	0.48 ± 1.71	0.58 ± 1.95	0.62 ± 1.80	0.62 ± 1.65
Step Frequency	-0.10 ± 1.42	-0.10 ± 1.72	-0.21 ± 1.92	-0.40 ± 1.60	-0.28 ±1.45
Stance Time	-0.47 ± 2.21	-0.53 ± 2.35	-0.38 ± 2.49	-0.43 ± 2.31	-0.58 ± 2.25
Step Time	0.10 ± 1.42	0.10 ± 1.72	0.21 ± 1.92	0.33 ± 1.67	0.28 ± 1.45
Flight Time	0.35 ± 1.45	0.34 ± 1.56	0.30 ± 1.63	0.25 ± 1.60	0.38 ± 1.51

AN EXPLORATION OF MUSCLE ACTIVITY IN YOUNG AND OLDER RUNNERS AND THE RELATIONSHIPS WITH RUNNING ECONOMY

[1] Barbara J. Schornstein, [2] Kevin D. Dames, and [1] Gary D. Heise

[1] University of Northern Colorado, CO, USA
[2] SUNY Cortland, NY, USA
email: Barbara.schornstein@gmail.com

INTRODUCTION

While there have been studies comparing homogenous groups of runners and the relationship between their running economy (RE) and the duration of muscular activity of lower extremity muscles, there is an unclear relationship between the two [1,2,3]. Studies have shown both positive [3] and negative [1,2] relationships between RE and the duration of muscular activity. In these studies, the participants have been of a younger age group (mean ages of 22-34 years). The purpose of this exploration was to compare two age groups of runners and the relationship between their RE and the duration of muscular activity in the lower extremity biarticular muscles.

METHODS

This study was approved by the Institutional Review Board. Participants (9 young (22±2 years, range 18-24 years): 7 women, 2 men; 13 older (37±8 years, range 27-50 years): 4 women, 9 men) ran for 5 minutes at three speeds (3.3, 3.5, 3.7 $m \cdot s^{-1}$) on an instrumented force-measuring treadmill while motion (Vicon, 100 Hz), forces (AMTI, 2000 Hz), electromyographic (EMG, DELSYS, 2000 Hz), and metabolic (Parvo Medics) data were collected. EMG data were collected from rectus femoris (RF), biceps femoris (BF), and lateral gastrocnemius (LG) from the right leg only.

Motion and force data were imported into Visual 3D (C-Motion) to determine stance phase for five consecutive foot strikes. These data were then imported into MATLAB (MathWorks) for determining the percentage of stance that muscles were active. The EMG data were analyzed after full-wave rectification and a low pass filter (f_c=15 Hz), using manual determination of on- and off-set [1].

For each speed, the durations of activity in both the individual muscles and pairs of muscles were correlated with each participant's RE using Spearman's Rank correlations. Spearman's Rank correlations were used since the group membership was not equal and historic studies also used this measure [1,2,3].

RESULTS AND DISCUSSION

Age was different between the groups; however, height, mass, maximal oxygen consumption, heart rate at maximal oxygen consumption, and RE at the three speeds were not different between the age groups. One difference between the age groups was demonstrated in respiratory exchange ratio during the maximal oxygen test ($p \leq .05$; young:1.02 ± .04, old: 1.06 ± .04).

Younger runners appear to have shorter durations of muscular activity and coactivity than the older runners (Table 1). Younger runners also demonstrated more significant relationships between RE and RF, LG, and the corresponding RFLG. Older runners only showed relationships between RE and muscular activity/coactivity at 3.5 $m \cdot s^{-1}$ in RF, BF, RFBF and BFLG.

The significant relationships for the younger runners were all negative correlations, while the older runners' significant relationships were all positive. Eighteen relationships were studied in each group of runners. When considering all relationships, even the non-significant ones, the young runners had 16 negative relationships, leaving 2 positive; while older runners showed 3 negative relationships, leaving 15 positive.

The contrasting direction of relationships between the age groups is significant; as young runners have more activity in their muscles, there is an association with decreased metabolic cost. Older runners, however, have more muscle activity associated with increased metabolic cost. This may have an interaction with elastic energy use. In future studies with a larger and more distinctive age group difference, it is possible to see more of a disparity between the relationships of muscular activity and RE. In addition, the number of women and men runners in each age grouping was not equal as the younger group had more women and the older group had more men.

CONCLUSIONS

This is an exploration, as the groups were not balanced in number, nor in the gender split; however, there needs to be further studies in this area as there appear to be meaningful differences between younger and older runners. These differences in younger and older runners, that young runners show negative relationship between RE and muscular activity while older runners show positive relationships, may have implications on how physiology and neuromuscular adaptations to physical training occurs as a runner ages.

REFERENCES

1. Heise, Morgan, Hough, & Craib. *Int J Sports Med,* **17(2)**:128-133, 1996.
2. Heise, Morgan, & Binks. *Int J Sports Med*, **29(8)**: 688-691, 2008.
3. Moore, Jones, & Dixon. *J Sci Med Sport,* **17(6)**:671-676, 2014.

Table 1: Muscular activity and coactivity duration as a percent of stance phase during all three speeds in Young and Older participants, correlation with running economy (RE), and *p*-values for all subjects.

		Young		Older	
Speed	Muscles	Duration (SD)	ρ (*p*-value)	Duration (SD)	ρ (*p*-value)
3.3	RF	68.0 (10.2)	**-.66 (.05)**	74.0 (7.0)	.24 (.44)
	BF	63.2 (14.8)	.08 (.83)	76.6 (11.5)	.38 (.20)
	LG	83.7 (11.5)	-.41 (.27)	88.8 (6.9)	-.38 (.20)
	RFLG	65.6 (12.8)	**-.78 (.01)**	71.2 (6.7)	.18 (.57)
	RFBF	54.5 (14.8)	-.04 (.92)	65.0 (8.8)	.20 (.51)
	BFLG	59.4 (15.4)	-.06 (.88)	72.4 (10.3)	.13 (.67)
3.5	RF	69.3 (9.7)	***-.65 (.06)***	72.5 (6.8)	**.55 (.05)**
	BF	78.4 (6.4)	.02 (.97)	73.8 (14.1)	***.48 (.10)***
	LG	86.4 (12.4)	**-.70 (.04)**	90.8 (7.9)	-.19 (.53)
	RFLG	68.5 (9.5)	**-.78 (.01)**	70.1 (5.9)	.32 (.29)
	RFBF	63.8 (10.3)	-.45 (.22)	63.4 (8.5)	**.65 (.02)**
	BFLG	74.4 (8.4)	-.40 (.29)	72.5 (9.4)	***.54 (.06)***
3.7	RF	69.4 (11.3)	**-.68 (.04)**	74.0 (9.7)	.47 (.11)
	BF	76.2 (11.9)	-.18 (.64)	79.7 (8.0)	.23 (.46)
	LG	86.4 (13.5)	**-.82 (.01)**	89.9 (6.7)	-.15 (.62)
	RFLG	69.1 (11.1)	**-.68 (.04)**	72.1 (7.9)	.44 (.13)
	RFBF	62.3 (9.9)	-.23 (.55)	67.3 (7.1)	.46 (.12)
	BFLG	72.7 (11.8)	-.23 (.55)	77.2 (7.4)	.10 (.75)

Note: Speed = $m \cdot s^{-1}$; RF = rectus femoris, BF = biceps femoris, LG = lateral gastrocnemius; Duration = % on time during stance; **Bold** = significant $p \leq .05$, ***Bold Italic*** = significant $p \leq .1$

HIP WORK DURING RUNNING USING DAILY-USE AND RUNNING-SPECIFIC PROSTHESES

[1] Lauren A. Sepp, [2] Brian S. Baum, [2] Erika Nelson-Wong, and [1] Anne K. Silverman

[1] Department of Mechanical Engineering, Colorado School of Mines, Golden, CO, USA
[2] School of Physical Therapy, Regis University, Denver, CO, USA
email: lsepp@mines.edu, web: fbl.mines.edu

INTRODUCTION

Running has many health benefits, but can be difficult for people with a unilateral transtibial amputation (TTA). Running-specific prostheses (RSPs) can be cost-prohibitive, and thus people with TTA often run with their daily-use prosthesis (DU). However, biomechanical differences between using RSPs and DUs are unclear.

During walking, people with TTA compensate for the functional loss of the ankle plantarflexors with greater amputated and intact leg hip work compared to people without TTA [1]. In addition, people with TTA have a greater peak hip moment in the intact leg compared to the amputated leg during running [2]. However, differences in hip biomechanics have not been compared when using different types of prostheses during running. Similar to prior results during walking, we hypothesized that people with TTA would have greater positive hip work as compared to people without TTA at all speeds and regardless of leg. As RSPs are specifically designed for running, we expected that use of an RSP would reduce asymmetric biomechanics. Thus, we also hypothesized that positive hip work would be greater for TTA using DUs compared to RSPs at all speeds and regardless of leg. Finally, also similar to prior results during walking, we hypothesized that amputated side hip work would be greater than intact side hip work in people with TTA at all speeds, regardless of prosthesis type used.

METHODS

Sixteen participants (nine with TTA: (5F/4M), 32 years old (yrs) ± 8.8yrs, 69.0kg ± 10.9kg, 1.75m ± 0.073m, seven without TTA: (4F/3M), 28yrs ± 6.3yrs, 69.0kg ± 4.57kg, 1.70m ± 0.071m) ran at five speeds (2.5, 3.0, 3.5, 4.0, 5.0 m/s) on a force-sensing treadmill (2000 Hz, Bertec Corporation, USA). People with TTA performed trials twice, once with their prescribed RSP and once with their prescribed DU. Kinematics were collected using a whole-body marker set (100 Hz, Northern Digital Inc., Canada). Kinematics and ground reaction forces were filtered using a fourth-order Butterworth filter, with cutoff frequencies of 10 Hz and 15 Hz, respectively. An inverse dynamics analysis was performed to compute net hip joint power. Hip joint work was computed as the integral of sagittal hip joint power over the running gait cycle and normalized by body mass.

Hip work differences were assessed using three, three-factor ANOVAs with main effects of running speed, prosthesis type (DU vs. control, RSP vs. control, or DU vs. RSP), and leg (amputated/left vs. intact/right). The speed and leg main effects were all within-subjects comparisons. The prosthesis type main effect was a within-subjects comparison for RSP vs. DU, and a between-subjects comparison when comparing control participants (people without TTA) to people with TTA using either type of prosthesis. Tukey's correction factor for multiple comparisons was used for post-hoc pairwise comparisons when significant main or interaction effects were found (α=0.05).

RESULTS AND DISCUSSION

Our first hypothesis was partially supported. Positive hip work was greater for people with TTA using DUs compared to people without TTA, regardless of leg at 3.0 m/s, 3.5 m/s, and 4.0 m/s ($p \leq 0.040$) and increased with speed for people with and without an amputation ($p<0.01$). There were no differences between people with TTA using RSPs and people without TTA.

There was a significant group effect ($p<0.01$) for people with TTA wearing DUs as compared to RSPs.

People with TTA using DUs had greater positive hip work compared to using RSPs at every running speed ($p \leq 0.025$), consistent with our hypothesis.

Positive hip work was greater in the intact leg compared to the amputated leg for people wearing RSPs at 3.5 m/s, 4.0 m/s, and 5.0 m/s ($p \leq 0.024$), contrary to our hypothesis. People with TTA wearing DUs did not have any differences in positive hip work between amputated and intact legs, contrary to our hypothesis.

Over the running gait cycle, positive work results from the hip extension moment in early to mid-stance and a flexion moment in early to mid-swing. In addition, an extensor moment in late swing as the hip is extending in preparation for heel strike creates another period of positive work. The differences in hip work were driven by hip extension power in early stance and hip flexion power in late stance and swing.

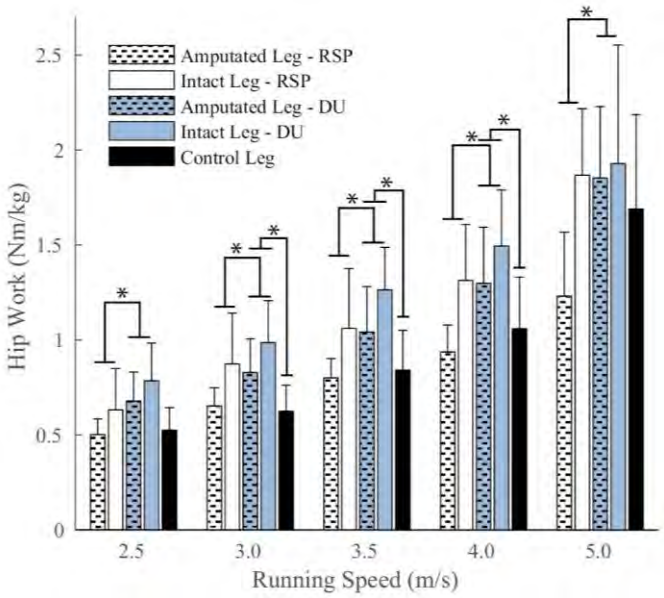

Figure 1. Positive hip work over the gait cycle for people without TTA (control) and for people with TTA using running-specific prostheses (RSPs) and daily-use (DU) prostheses (significance '*').

Energy storage and return (ESAR) prostheses provide more energy return during late stance compared to non-ESAR feet [3-5]. The RSPs and DUs included in this study were all ESAR designs, although RSPs do not have a heel and can also return more energy during late stance as compared to DUs [3-5]. Greater energy storage and return from RSPs may reduce the overall required hip extensor work on the amputated leg compared to DUs. Hip extensor work in early stance has been associated with a lack of positive ankle work in late stance during walking [1], which may also be reflective of running with an amputation. In addition, the hip moment in the intact leg has been shown to be greater than the amputated leg in people with TTA using RSPs [2]. Thus, greater energy return from the RSP may reduce the demand from the hip extensors in early stance.

The hip flexors are important for generating energy to the leg for swing initiation during walking [6], and this demand likely increases with running as speed increases. The RSPs in our study were generally lighter than the DUs, and thus could reduce the demand from the hip flexors for leg swing initiation.

CONCLUSIONS

Using RSPs reduces overall positive hip work during running compared to using DUs. Increased energy return from RSPs compared to DUs may reduce the demand at the hip during running. Differences in biomechanics of running between people with and without amputation, and between RSPs and DUs, should be further investigated to understand how individual muscles work with different device designs to achieve running mechanics.

REFERENCES

1. Silverman, A.K., et al., *J Biomech,* **28**, 602-609, 2008.
2. Hobara, H., et al., *J Biomech,* **46**, 2483-2489, 2013.
3. Nolan, L., *Foot and Ankle Surgery,* **14**, 125-129, 2009.
4. Czerniecki, J.M., et al., *J Biomech*, **24**, 63-75,1991.
5. Buckley, J.G., *Clinical Biomech.,* **15**, 352-358, 2000.
6. Neptune, R.R., et al., *J Biomech*, **34**, 1387-1398, 2001.

ACKNOWLEDGEMENTS

DoD Award #W81XWH-15-1-0518.

SENSORY FEEDBACK CONTROLS GROUND CONTACT VARIABILITY IN RUNNING

[1] Melissa Thompson, [1] Kyle Curtin, [1] Amanda Owens, [1] Lucas Rowton and [2,3] Kristine Hoffman

[1] Fort Lewis College, Durango, CO, USA
[2] Denver Health Medical Center, Denver, CO, USA
[3] University of Colorado School of Medicine, Denver, CO, USA
email: mathompson@fortlewis.edu

INTRODUCTION

Several lines of evidence indicate that sensory feedback plays a role in various mechanical aspects of running. In particular, the plantar surface of the foot provides essential afferent information regarding the nature of the foot's contact with the ground during running. It is thought that peripheral sensory feedback plays a key role in adjusting step-to-step limb trajectories in order to maintain balance during locomotion, and is essential for adjusting ground contact to avoid uncomfortable stimuli [1]. However, the integration of plantar afferent information and the mechanical control of running is a complex process, and many aspects remain to be elucidated.

A primary area that has seen little attention in the literature is the relationship between sensory feedback and gait variability. Normal variability in the foot's contact with the ground may be indicative of the successful integration of plantar sensory feedback and neuro-mechanical control of the running gait. Alternatively, absence or disorders of this sensory-motor integration may lead to reduced variability in the foot-ground contact during running and subsequently result in localized tissue loading that may potentially lead to injury. For example, it has been suggested that individuals with peripheral sensory deficits (such as diabetic peripheral neuropathy) have a less variable gait than those with intact sensory feedback, and this reduced variability may lead to abnormal tissue loading and subsequent ulceration [2]. Further, it has been hypothesized that shoes limit sensory feedback [3], and therefore individuals may run with a less variable gait when running shod as compared to running barefoot.

The aim of our research was to eliminate plantar sensory feedback by anesthetizing the feet in order to further understand the role of plantar sensory feedback in controlling the variability of foot-ground contact during running. We hypothesized that with the loss of sensory feedback from the plantar surface of the foot, individuals would run with less variable ground contact when both barefoot and shod.

METHODS

12 healthy active subjects (5 female, 7 male); mass: 62.6±12.2 kg; age: 28±7.3 years, participated in this study. Subjects completed 4 trials that consisted of 3 minutes of treadmill running in each of two sensory conditions: normal (NORM) and anesthetized (ANEST). For each sensory condition the participant's gait was analyzed while running both barefoot (BF) and shod (SHOD). For the ANEST conditions bilateral tibial nerve blocks were performed, which consisted of injecting 3 mL of 2% lidocaine surrounding the posterior tibial nerve according to the procedure of Fiolkowski et al. [4].

Following the anesthetic procedure, sensation was evaluated by standard clinical sensory testing techniques, including the Semmes–Weinstein monofilament and vibratory sensation tests. According to the Semmes–Weinstein monofilament test, anesthesia was confirmed when the subject did not have sensation when a 10 g monofilament was pressed on the foot sole with enough pressure to buckle. The vibratory sensation test was used to evaluate deep sensation of the plantar foot (sensory receptors located deep in the dermal layer and subcutaneous tissue, and/or free nerve endings located in joints and the calcaneal fat pad) and anesthesia was confirmed when the subject could not sense a vibrating 128 Hz tuning fork placed against the plantar surface.

For the treadmill running trials velocity was set at the subject's preferred running speed (mean velocity 2.41 $\pm$ 0.41 m/s), which was determined in the NORM SHOD condition and maintained for all other trials. Data was recorded for the 2nd minute of each 3 minute treadmill running trial. Variability in ground contact was evaluated as the standard deviation of stride time and stance time for all strides completed during the 1 minute of data collection. Stance and stride times were measured via footswitches sampling at 1,000 Hz that were located on the plantar surface of each subject's right foot.

Repeated measures ANOVA tests were performed to compare the differences in the standard deviation of stride and stance times among the four conditions. Statistical significance was defined as $p<0.05$.

RESULTS AND DISCUSSION

The tibial nerve block procedure eliminated superficial and deep sensory feedback in all subjects as evidenced by the lack of sensation when evaluated with the Semmes-Weinstein monofilament and vibratory sensation tests.

In support of our hypothesis, in both the BF_ANEST and SHOD_ANEST conditions participants exhibited significantly decreased variability in stride and stance time, as compared to the intact sensory conditions (SHOD_NORM *vs.* SHOD_ANEST, $p=0.04$; BF_NORM *vs.* BF_ANEST, $p=0.03$) (Fig. 1). Despite the hypothesis that shoes inhibit sensory feedback, there was no statistically significant difference in the standard deviation of stride or stance time between the BF and SHOD running conditions ($p>0.05$, Table 1). It is possible that shoes may reduce or alter sensory feedback when running, but the remaining sensory feedback is adequate for maintaining stride and stance time variability.

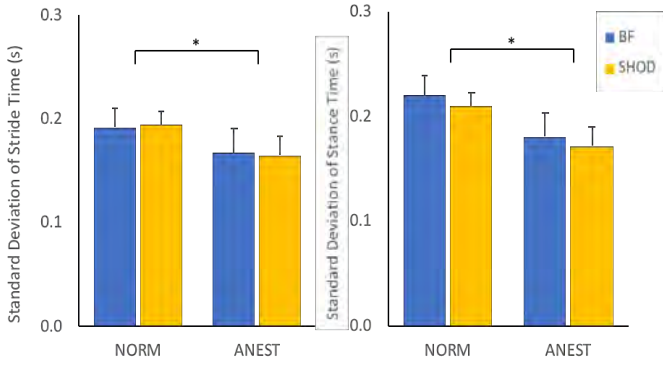

Figure 1: Standard deviation of stride time and stance time for both BF and SHOD running in the NORM and ANEST conditions. *Significant difference between NORM and ANEST condition, for a given shoe condition (BF or SHOD) $p<0.05$.

CONCLUSIONS

The results of the present study indicate that plantar sensory feedback plays an important role in controlling the variability of ground contact in running. With intact sensory feedback the timing of ground contact and the stance duration was more variable, indicating that plantar sensory feedback is integrated into the neuro-mechanical control of the running gait. The finding that there was no difference in stride or stance time between BF and SHOD running, indicates that shoes do not limit sensory feedback to the extent that gait variability is affected.

REFERENCES

1. Dingwell et al. *Gait Posture*. 10(1): 21-29, 1999.
2. Wu et al. *Vasc Health Risk Manag*. 3(1):65-76, 2007.
3. Robbins et al. *J Test Eval*. 16(4): 412-416, 1988.
4. Fiolkowski et al. *Clin Biomech*. 20: 952-958, 2005.

Table 1: Stride-to-stride variability as measured by the standard deviation (SD) of stride and stance time, in the four shoe (BF and SHOD) / sensory (NORM and ANEST) conditions. Data are reported as mean (SD). *Significant difference between the NORM and ANEST condition, for a given shoe condition (BF or SHOD) $p<0.05$.

	BF_NORM	BF_ANEST	SHOD_NORM	SHOD_ANEST
SD of stride time (s)	0.192 (0.013)	0.167 (0.018)*	0.194 (0.019)	0.165 (0.023)*
SD of stance time (s)	0.210 (0.019)	0.172 (0.009)*	0.220 (0.016)	0.181 (0.010)*

THE INFLUENCE OF PROLONGED RUNNING AND FOOTWEAR ON LOWER EXTREMITY BIOMECHANICS

[1]Gillian Weir, [1]Carl Jewell, [1]Hannah Wyatt, [2]Matthieu B. Trudeau, [2]Eric Rohr, [3]Gert-Peter Brüggeman and [1]Joseph Hamill

[1]Biomechanics Laboratory, University of Massachusetts, Amherst
[2]Brooks Running Inc., Seattle
[3] Institute of Biomechanics and Orthopedics, German Sports University, Cologne
email: gweir@umass.edu

INTRODUCTION

A number of studies have investigated the influence of maximal isolated muscle fatigue [1] and cardiovascular fatigue [2] on lower extremity biomechanics during running. However, the majority of runners do not run to exhaustion regularly. As such, researchers and footwear companies are interested in the biomechanical changes over the course of a typical prolonged run. Studies have shown that runners choose their habitual motion path (i.e. preferred joint kinematics) during running to either minimize energy cost and/or reduce stress on the tissues [3]. However, it is uncertain whether the same optimization strategies exist over the entire course of a run. Additionally, stability shoes with medial posting have been shown to reduce rear-foot eversion angle [4]. However, it is unknown as to whether this is beneficial to reducing injury risk and whether this can be maintained throughout a run.

The purpose of this study was to investigate the influence of a 42-minute prolonged treadmill run on lower extremity biomechanics during which footwear were changed from a neutral to a stability shoe at the midpoint of the run. It was hypothesized that: 1) lower extremity biomechanics would differ between sessions in the second half of the run (*intervention* run) where runners wore either neutral or stability running shoes and 2) lower extremity biomechanics would change over the course of the prolonged treadmill run.

METHODS

Fourteen male (age 24.1 ± 4.4 years, height 1.8 ± 0.1 m, mass 71.2 ± 8.3 kg) habitual rear-foot recreational runners participated in two 42-minute prolonged treadmill running sessions at their preferred speed (3.3±0.4 m/s) one week apart.
During the first 21 minutes (*baseline* run) of both sessions, participants ran in a neutral shoe. Following this, they changed into either another neutral shoe of the exact same construction but in a different colour (Session A) or a stability shoe of the same construction with an added medial post (Session B) and ran for another 21 minutes (*intervention* run). Three-dimensional kinematic data were recorded with an 8-camera motion capture system (Qualysis, Inc., Gothenburg, Sweden) sampling at 200Hz synchronously with ground reaction forces from the instrumented treadmill at 2000Hz (Treadmetrix, Park City, UT). Data were collected for 30 seconds at minutes 1, 21, 24 and 44. Ratings of perceived exertion (RPE) and percentage of maximum heart rate (%HR_{max}) were collected at the same time intervals. Two-way repeated measures ANOVAs (time/shoe) were implemented using statistical parametric mapping to compare joint angle and moment waveforms over stance [5].

RESULTS AND DISCUSSION

This study investigated lower extremity biomechanics during prolonged running in neutral and stability shoes. Exertion increased over the course of baseline and intervention runs where both HR_{max} (Min_1: 74±6%, Min_{21}: 85±6%, Min_{24}: 75±5%, Min_{44}: 84±4%) and RPE (Min_1: 10±2, Min_{21}: 12±2, Min_{24}: 10±0, Min_{44}: 12±2) increased (P<0.001) with no differences observed between sessions.

Influence of footwear. As a group, no differences in lower extremity biomechanics were observed during the *intervention* run for the neutral and stability shoes. However, runners do not all respond to

footwear conditions similarly [3]. Individual and subgroup analyses from these data have revealed some runners did have a beneficial effect of stability shoes (lower deviation from habitual motion path), while others did not.

Influence of time. To support our second hypothesis, there were differences in biomechanics at the hip, knee and ankle over the course of the prolonged run (Figure 1). Hip extension angle increased just prior to toe off during the baseline (95-100%, P=0.049) and intervention (94-100%, P=0.041) runs. Hip internal rotation angle increased during the baseline run (18-40%, P=0.019 and 46-55%, P=0.042) and intervention run (21-31%, P=0.041 and 50-66%, P=0.028). Knee flexion angle increased during the baseline and intervention runs for 26-32% (P=0.047) and 62-82% (P=0.021) of stance respectively. Knee abduction angle and internal rotation angles increased during the baseline run for 20-62% (P=0.001) and 22-66% (P=0.002) of stance respectively. Dorsiflexion angle decreased during the baseline and intervention runs for 0-14% (P=0.025) and 0-13% (P=0.027) of stance. Foot eversion angle increased during the baseline run for 16-69% of stance (P<0.001). The kinematic changes observed at the knee and foot are in agreement with the literature and are a likely mechanism to reduce effective mass of the leg [2]. However for every 5º increase in knee flexion at mid-stance, there is an approximate 25% increase in oxygen cost [6]. Knee abduction moment decreased during the baseline run for 25-42% of stance (P=0.001). Ankle plantarflexion moment increased during the baseline and intervention runs for 12-23% (P=0.009) and 45-58% (P=0.009) of stance respectively. While reducing effective mass may be a strategy to minimize stress applied to the tissues (i.e. peak knee moments did not increase) over the course of a prolonged run, this may come at a cost of running economy and may also be the product of changes in muscle coordination.

CONCLUSIONS

Runners deviate from their habitual motion path over the course of a prolonged run. Particularly, increased knee flexion and rear-foot eversion observed during mid-stance may exhibit a strategy to reduce the effective mass and minimize joint loads applied to the foot and knee. Additionally, individuals respond to footwear differently. With respect to the changes observed in kinematics throughout a prolonged run, running shoe design should focus on: 1) materials to allow runners to maintain baseline kinematics (i.e. habitual motion) for longer; and/or 2) materials for greater energy return when kinematics are altered and the muscles may not be performing optimally.

REFERENCES

1. Christina et al. *Hum. Mov. Sci.* **20**, 257–276, 2001.
2. Derrick et al. *Med. Sci. Sports Exerc.* **34,** 998–1002, 2002.
3. Nigg et al. *Med. Sci. Sports Exerc*. **49,** 1641–1648, 2017.
4. Clarke et al. *Med. Sci. Sports Exerc*. **15**, 376–381, 1983.
5. Pataky et al. *J. Biomech.* **46**, 2394–2401, 2013.
6. Valiant et al. *Biomechanics of Distance Running: Human Kinetics.* 225-247, 1990.

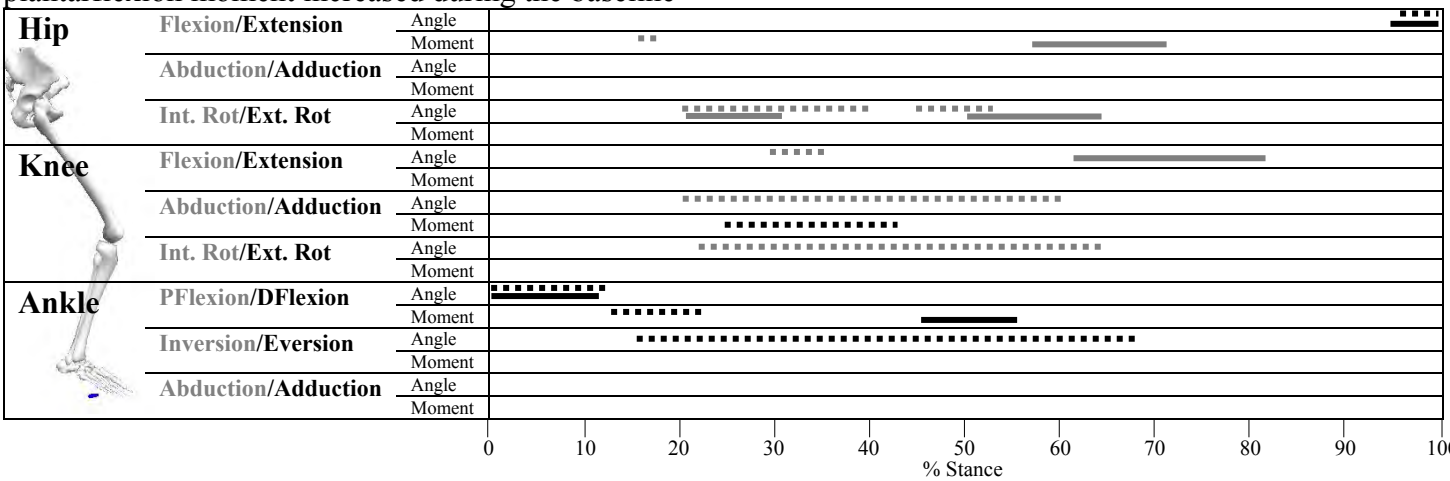

Figure 1. Significant differences in lower extremity biomechanics found over stance from SPM for the main effect of time (P < 0.05). Color (black/grey) is associated with direction. Dashed lines represent change from Min_1 to Min_{21} in the *baseline* run and solid lines represent change from Min_{24} to Min_{44} in the *intervention* run.

A SENSOR FUSION ALGORITHM FOR ESTIMATING CENTER OF MASS KINEMATICS IN HUMAN WALKING AFTER SPINAL CORD INJURY

[1] Musa L. Audu, [1] Naji Alibeji, [1] Brooke Odle and [1,2] Ronald J. Triolo
[1] Case Western Reserve University, Cleveland, OH, USA,
[2] Cleveland VA Medical Center, Cleveland, OH, USA
email: mxa93@case.edu

INTRODUCTION

Spinal cord injury (SCI) is a debilitating condition that results in loss of function due to paralysis of muscles of the body. Functional Neuromuscular Stimulation (FNS) is a technology that can be used to restore the activity of muscles paralyzed by SCI. This is achieved by applying low-level electric currents to the peripheral motor nerves to elicit contractions of the muscles and thus restore some or all of the lost functions. Restoring stable walking is an important desire expressed by individuals with SCI [1]. Reciprocal stepping motions are possible with either cyclic patterns of neural stimulation, or switch based triggering of pre-programmed stimulation for successive stance and swing phases [2]. The stability of these feed-forward walking systems needs to be significantly improved by developing and implementing feedback control systems to appropriately modulate stimulation for balance and propulsion. Such controllers depend on robust sensor signals that accurately reflect the state of the system.

Common walking stability measures include whole body kinematic/kinetic quantities such as center of mass position (CoMP) and acceleration (CoMA), center of pressure (CoP) and angular momentum. Inertial measurement units (IMUs) are ubiquitous in a wide variety of human motion and rehabilitation studies [3] and are a suitable choice to provide feedback information for stabilizing human walking with FNS because of their low cost and small size. Our laboratory is developing a completely implanted stimulation system, the Networked Neural Prosthesis System (NNPS) that contains IMUs embedded in its internal modules [4].

The main goal of this study was to design a sensor fusion algorithm based on the Kalman Filter (KF) for estimating the kinematics of whole body CoM using signals from IMUs mounted/implanted at strategic locations on the body.

METHODS

One subject with SCI (T4, AIS A) walked within the work volume of 16-camera Vicon motion capture system (Oxford Metrics, UK) with six Xsens (Xsens Technologies, BV, Enschede the Netherlands) wireless IMUs attached to the body at the chest (sternum), back, flanks, and posterior thighs. Retroreflective markers were affixed to the body in accordance with the Vicon Plug-in Gait marker set [5]. CoMP was computed analytically from the marker coordinates and segmental mass properties.

The underlying structure of the stochastic system defining the dynamics and measurement on which the KF is defined is given by equations (1) and (2):

$$x_k = Ax_{k-1} + Bu_k + w_{k-1} \quad (1)$$

$$z_k = Cx_k + v_k \quad (2)$$

Here, x is the state vector, z the measurement vector and A, B and C are the coefficient state transition matrices. w and v are independent white noise processes that are normally distributed as follows: $p(w) \sim N(0, Q)$ and $p(v) \sim N(0, R)$. Q is the state noise covariance and R the measurement noise covariance. Equation (1) specifies how the system state is propagated while equation (2) specifies the relationship between the state and the measurement. Details of the KF equations are available in most textbooks on systems theory and KF design [6].

It has been well documented that during normal walking, *changes* in all 3 components of whole body CoMP follow a sinusoidal profile [7] thereby making it possible to define each with an equation of form:

$$X(t) = F\sin(\omega t) \quad (3)$$

From this, V(t) and $\dot{V}(t)$ can be computed as:

$$V(t) = \omega F\cos(\omega t) \quad (4)$$

$$\dot{V}(t) = -\omega^2 F\sin(\omega t) = -\omega^2 X(t) \quad (5)$$

The discretized equations for displacement and velocity for each component of CoM are defined as:

$$X(t+\Delta t) = X(t) + \Delta t V(t) \quad (6)$$

$$V(t+\Delta t) = V(t) + \Delta t\dot{V}(t) \qquad (7)$$

Thus if we define the state vector as: $\vec{x}_k = [X_k \quad V_k]^T$ the unforced state equation (1) takes the form:

$$\underbrace{\begin{bmatrix} X_k \\ V_k \end{bmatrix}}_{x_k} = \underbrace{\begin{bmatrix} 1 & \Delta t \\ -\omega^2\Delta t & 1 \end{bmatrix}}_{A} \underbrace{\begin{bmatrix} X_{k-1} \\ V_{k-1} \end{bmatrix}}_{x_{k-1}} + \underbrace{\begin{bmatrix} w^X_{k-1} \\ w^V_{k-1} \end{bmatrix}}_{w_{k-1}} \qquad (8)$$

The measurement, z, which is hypothesized to be related to the *acceleration* measure from the sensors, can be written as:

$$Z(t) = G\dot{V}(t) = -\omega^2 GX(t) \qquad (9)$$

That is, the measurement equation (2) can be written as:

$$z_k = -\omega^2 G x_k + v_k = \underbrace{\begin{bmatrix} -\omega^2 G & 0 \end{bmatrix}}_{C} x_k + v_k \qquad (10)$$

Here v_k is the measurement noise and G an estimation gain. To improve estimation accuracy, 3 backpropagation artificial neural networks (ANNs) were designed to estimate CoMA from a pair of sensors each selected at random. The outputs of the ANNs were then fused using the time-invariant KF designed with matrices A and C and vectors w and v in equations (8) and (10) replicated for each of the 3 components.

RESULTS AND DISCUSSION

Figure 1 shows the results of the sensor fusion algorithm combining the outputs of the ANN and KF for each of the 3 components of CoMP. These results show the anterior posterior (AP) and the inferior-superior (IS) components with the trends/means removed from the plots to emphasize the changes that occur in these variables. From the results, the estimates from the KF matched the actual CoMP data with regression coefficients as high as 0.92 with the best fit obtained in the medial-lateral (ML) direction.

While good estimates are obtained with a sensor fusion algorithm that combines KF and ANNs, a preferred algorithm will be one that uses only a KF. This will minimize training effort for the ANNs. In addition, better estimates may be possible with a time varying KF rather than a time-invariant filter defined by equations (8) and (10). Time variance can be introduced by assuming that the frequency ω is a time-varying quantity to be estimated in an adaptive version of the KF. In addition, higher estimation accuracy may be possible by using a sum of sines for the CoMP defined by equation (3).

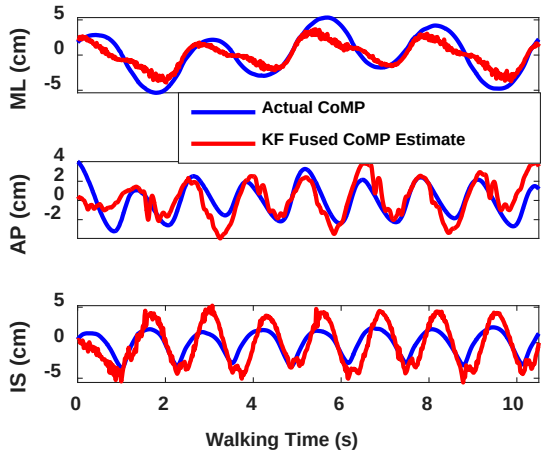

Figure 1: Changes in ML, AP* and IS* components of CoM Position as estimated by a Kalman Filter for SCI walking over 4 cycles of gait. Regression coefficients between the actual and estimated CoMP were 0.92, 0.68 and 0.78 respectively. *(*-detrended)*

CONCLUSIONS

With a simplified sensor fusion algorithm made up of a Kalman filter and backpropagation ANNs we have successfully extracted good estimates of whole body CoM position from multiple independent and anatomically distributed IMUs. The estimates will be invaluable in developing feedback control systems for stabilizing walking in individuals with SCI using FNS systems.

REFERENCES

1. Anderson K.D., *J.Neurotrauma*, 2004; 21 (10) :1371-1383.
2. Kobetic et al., *Human Walking*, Rose and Grimble, eds., 1994.
3. Patel et al. *J. of NeuroEngineering and Rehabilitation* 2012, 9:21.
4. Crish T, et al., US Patent No. 7,260,436, 2007.
5. Plug-In Gait Reference Guide, Vicon Motion Systems Limited, 2016-2017.
6. Brown et al., *Introduction to random signals and applied Kalman filtering.* J. Wiley and Sons., NY, 2012.
7. Lee et al, *Electronics Letters,* 43(20), 2007.

ACKNOWLEDGEMENTS

This work was supported by the following grant: NIH NS040547-03.

ACTIVITY RECOGNITION FOR A MILITARY-STYLE OBSTACLE COURSE USING BODY-WORN IMUS

[1]Stephen M. Cain, [1]Rachel V. Vitali, [1]Michael V. Potter, [1]Steven P. Davidson, [1]Lauro Ojeda, [2]Leia A. Stirling and [1]Noel C. Perkins

[1]University of Michigan, Ann Arbor, MI, USA
[2] Massachusetts Institute of Technology, Cambridge, MA, USA
email: smcain@umich.edu

INTRODUCTION

Warfighter performance is inherently challenging to quantify due to task complexity, technique variation, warfighter environment, and limited knowledge of measures that truly characterize task performance beyond simple success or failure. Obstacle courses are one approach to assess the effects of fatigue and/or load on warfighter performance [1-2], but typically measures of the total time to complete an obstacle course or time required to complete each obstacle are the only quantitative metrics obtained from such tests. To address this shortcoming, we have employed inertial measurement units (IMUs) to measure the underlying biomechanics that define performance for obstacles in the Marine Corps Load Effects Assessment Program (MC-LEAP) [3 – 5]. Because each obstacle requires different algorithms to calculate performance metrics from the IMU data, the IMU data must first be parsed according to obstacle before analysis. The goal of this study is to develop and test an algorithm that accurately and automatically identifies when a participant begins and finishes each obstacle in an obstacle course using only the data from body-worn IMUs.

METHODS

A total of 39 participants (16 females, age = 20.1 ± 2.0 years, mean ± standard deviation) were recruited to complete an abbreviated version of the MC-LEAP [2] consisting of 11 obstacles: functional calibration movements (needed for data analysis), sprint, vertical jumps, casualty drag, window, balance beam, wall, agility run, bounding rush, high crawl, and vertical transfer. All subjects wore an array of 13 IMUs (Opal, APDM, Portland OR) attached to the head, upper arms, forearms, torso, sacrum, thighs, shanks, and feet. Participants carried a mock plastic rifle (3.4 kg) with another attached IMU and an additional IMU was placed in the load used for the vertical transfer obstacle [5]. Data was manually marked by depressing a binary switch synchronized with the IMUs at the beginning and end of each obstacle, which provides the ground truth data for the automated algorithm developed herein. The University of Michigan IRB approved the study and all subjects gave informed consent.

Data from the participants were collected during two different phases of our research project, and therefore belongs to two different data sets: data set 1 (DS1) and data set 2 (DS2). DS1 contains data from 19 participants (9 females, age = 20.4 ± 1.8 years, weight = 68.1 ± 13.2 kg, height = 1.73 ± 0.11 m) who completed the MC-LEAP a single time without added load for a total of 19 trials. DS2 contains data from 20 participants (7 females, age = 19.9 ± 2.1 years, weight = 78.0 ± 15.5 kg, height = 1.78 ± 0.13 m) who completed the MC-LEAP four times with varying amounts of added load (2×0%, 1×15%, and 1×30% body weight) for a total of 80 trials. DS2 was used to develop and test the obstacle parsing algorithm and DS1 was used to further validate the obstacle parsing algorithm.

Our basic approach was to utilize the distinctive kinematic features of the obstacles that can be derived from the body-worn IMUs (Table 1) to parse the data. The approach was implemented using the following steps:

1. Define the obstacle course (included obstacles and order of obstacles).
2. Identify the functional calibration movements, bounding rush, high crawl, and vertical transfer by using obstacle specific kinematic features for both data segmentation and data classification.

3. Use the sum of the magnitudes of the acceleration from the feet, sacrum, and torso-mounted IMUs to define an activity measure to identify candidate data segments.
4. Identify sprint and agility run data segments using obstacle specific kinematic features (Table 1).
5. For remaining candidate data segments, calculate the kinematic features listed for casualty drag, wall, window, vertical jump, and balance beam (Table 1).
6. Using obstacle specific support vector machine models [6] trained using DS2 and using obstacle order, classify the remaining data segments as casualty drag, wall, window, vertical jump, balance beam, or none.

Table 1: Kinematic features used for classification.

Obstacle	Kinematic features
Functional calibration	Foot angular velocity when contralateral foot is still (unilateral pedaling motions)
	Torso angular velocity when feet are still (toe touches)
	Low angular velocity of all segments (quiet standing)
Sprint	Maximum sum of magnitude of acceleration from feet, sacrum, and torso
Agility run	Duration of data segment
Bounding rush	Estimated orientation of torso (five transitions from prone to upright)
High crawl	Estimated orientation of torso (prone)
	Upper arm acceleration impact peaks
Vertical transfer	Acceleration of the load-embedded IMU
Casualty drag	Distance between foot trajectory start and end point
	Area enclosed by foot trajectory
	Length of foot trajectory
	Width of foot trajectory
	Height of foot trajectory
Wall	Maximum vertical velocity of sacrum
	Minimum vertical velocity of sacrum
Window	Time difference between locations of maximum and minimum sacrum vertical velocity
Vertical jump	Slope of curve between maximum and minimum sacrum vertical velocity
Balance beam	Slope of velocity curve prior to minimum sacrum vertical velocity
	Estimated drop height of sacrum
	Minimum sacrum vertical velocity that occurs after maximum sacrum vertical velocity
	Number of times the sacrum heading angle passes through -45 degrees
	Maximum sum of magnitude of acceleration from feet, sacrum, and torso
	Duration of data segment

We tested our obstacle parsing algorithm on both DS1 and DS2. A successful obstacle identification was defined by an overlap in the start and end times identified by our activity recognition algorithm and the start and end times manually marked using the binary switch.

RESULTS AND DISCUSSION

DS1 contained 573 data segments and DS2 contained 2461 data segments for classification. Our algorithm was able to correctly identify obstacles with a high rate of success (Table 2), with error rates below 0.87% for both data sets. Some errors were caused by missing sensor data, incorrect protocol during completion of the course, and obstacle repeats.

Table 2: Obstacle parsing results for both data sets.

Obstacle	Data set 1 (DS1)		Data set 2 (DS2)	
	False positive	Missed	False positive	Missed
Calibration	0	0	0	1
Sprint	0	0	0	0
Agility run	1	1	1	1
Bounding rush	0	0	1	1
High crawl	0	0	0	2
Vertical transfer	1	0	0	1
Casualty drag	0	0	0	0
Wall	1	1	1	1
Window	0	0	0	0
Vertical jump	0	0	4	0
Balance beam	0	0	0	0
Error rate	5/573 = 0.0087		14/2461 = 0.0057	

Our obstacle parsing approach can accurately identify when a participant begins and finishes each of 11 obstacles in an obstacle course using solely data from body-worn IMUs. We implemented this algorithm as part of an automated measurement system for warfighter performance quantification. Future work will test our approach on new data sets and add additional error checking capabilities.

REFERENCES

1. Pandorf et al. *Can J Appl Physiol.* 28, 27-37, 2003.
2. Mitchell et al. NSRDEC, Natick, MA, 2015.
3. Cain et al. *Gait & Posture*. 43, 65-69, 2016.
4. Zaferiou et al. *PLoS ONE.* 12(11): e0188184, 2017.
5. Tammana et al. *Appl Ergon.* 70, 68-76, 2018.
6. Christianini and Shawe-Taylor. *An Introduction to Support Vector Machines and Other Kernel-Based Learning Methods*. Cambridge Univ. Press, 2000.

ACKNOWLEDGEMENTS

This material is based upon work supported by the US Army Contracting Command-APG, Natick Contracting Division, Natick, MA, under contract W911QY-15-C-0053.

WEARABLE TECHNOLOGY TO MONITOR HAND MOVEMENT DURING CONSTRAINT-INDUCED MOVEMENT THERAPY FOR CHILDREN WITH CEREBRAL PALSY

[1]Brianna M. Goodwin, [2]Emily Sabelhaus, [2]Kristie F. Bjornson, [2]Kelly Pham, [2]William Walker, and [1]Katherine M. Steele
[1] University of Washington, Seattle, WA, USA
[2] Seattle Children's Research Institute, Seattle, WA, USA
email: kmsteele@uw.edu, web: http://depts.washington.edu/uwsteele/

INTRODUCTION

Cerebral palsy (CP) is a non-progressive neurologic disorder of movement and posture that affects approximately 2 in every 1000 children in the United States [1]. Of these children, 40% have unilateral or hemiplegic CP, with abnormal tone, decreased strength, dystonia, and other muscle impairments impacting movement on one side of the body [2].

Constraint-Induced Movement Therapy (CIMT) is an evidence-based treatment for children with hemiplegic CP [3]. CIMT uses a constraint, typically a rigid cast, to restrict motion of the unimpaired hand, forcing the child to use their impaired hand during therapy and daily life. While CIMT has been shown to improve hand function, the protocols and results are often variable [4, 5]. CIMT is both time and resource intensive for the children, their families, and providers. Understanding the extent to which casting influences hand use both in therapy and in daily life, as well as the outcomes after therapy are critical to optimizing treatment protocols.

Wearable technology, including accelerometers, has been used to quantify hand movement and evaluate hand function for both children with CP and adult stroke survivors [6, 7]. The goal of this research was to use accelerometry metrics to quantify hand use in clinical and home environments before, during, and after CIMT for children with CP and compare it to typically-developing (TD) peers.

We hypothesized that (1) paretic hand use would increase during CIMT, both at home and in the clinic, and (2) that increased paretic hand use during CIMT would be associated with enhanced bimanual use in daily life after CIMT.

METHODS

We recruited eight children with hemiplegic CP undergoing CIMT (age: 3yr 5m – 9yr 2m, 4 boys/4 girls) and five TD children (age: 2yr 8m – 9yr 10m, 1 boy/4 girls) from a pediatric tertiary care facility.

Per the institution's CIMT protocol, the non-paretic hand of each child in the CP cohort was placed in a cast for three weeks. Unilateral hand training of the paretic hand occurred in the clinic for 2 hours/day, 4 days/week. On Fridays, the cast was removed and the children received bimanual training for 2 hours before replacing the cast. The CP cohort wore ActiGraph GT9X Link (ActiGraph Corp., Pensacola, FL) tri-axial accelerometers on both wrists for 3 consecutive days during three time periods: 1-week before, during, and 6-8 weeks after CIMT. Functional tests (grip strength and Box & Blocks) and the Canadian Occupational Performance Measure (COPM) were completed before and after CIMT. The TD cohort did not receive therapy, but wore the Actigraph accelerometers on both wrists for three consecutive days at home, on three occurrences temporally aligned with the CP cohort time periods.

Accelerometry data were analyzed using the magnitude ratio (MR) and bilateral magnitude (BM) [6]. The MR is the natural log of the vector magnitude of the paretic limb divided by the non-paretic limb. Values outside of the range ±7 were set to ±7 to constrain the range of values, similar to prior research. The BM is the sum of the vector magnitude of the paretic and non-paretic hands. Density plots were created to compare MR and BM before, during, and after CIMT, with the centroid of these plots as the primary outcome metric (Fig.1.).

RESULTS AND DISCUSSION

The MR results in Table 1 suggest that although CIMT encouraged children with CP to use their paretic hand more compared to their non-paretic hand during therapy, they returned to baseline values 6-8 weeks post CIMT. Although the BM decreased for children during CIMT, the increase after CIMT demonstrated that children were using their hands together at the same magnitude as the TD cohort. This may be reflective of the non-paretic hand being casted and therefore not being able to move. Similarly after CIMT, the CP cohort scored higher on paretic hand functional measures: grip strength increased by 7.5±4.9 lbs. and the number of blocks transferred in 60 seconds increased by 3.5±6.6 blocks. Furthermore, COPM scores increased 5±2.8 points, indicating that children in the CP cohort felt more confident achieving specific self-identified goals.

The combination of the baseline MR levels with increased BM levels and functional scores suggest that although the CIMT cohort is not using their paretic hand as much as their non-paretic hand in daily life after CIMT, they are using both hands in combination more.

CONCLUSIONS

The increase in MR levels and functional measure scores suggests that children feel more confident using their paretic hand following CIMT. However, the subsequent return to pre-intervention BM values, as measured by accelerometry data, indicates that further interventions (*i.e.*, a larger dose of CIMT and/or weekly follow-up therapy sessions) and strategies may be needed to maintain increased daily paretic hand use after CIMT.

REFERENCES

1. Cans et al. (2008) J Pediatr Child Health
2. Holmeffur et al. (2009) Dev. Med. Child Neurol.
3. Novak et al. (2013) Dev. Med. Child Neurol
4. DeLuca et al. (2017) Pediatr Rehabil
5. Brauers et al. (2017) Pediatr Rehabil
6. Lang et al. (2017) JoVE
7. Gordon et al. (2007) Dev. Med. Child Neurol

ACKNOWLEDGEMENTS

We thank the Seattle Children's Hospital Academic Enrichment Fund, Seattle Children's Hospital Occupational Therapists, and CIMT team for their help integrating this research into clinical care.

Table 1: Comparison of Magnitude Ratio and Bilateral Magnitude for TD and CP participants

	Magnitude Ratio		Bilateral Magnitude	
	Mean ± Standard Deviation	**Range**	**Mean ± Standard Deviation**	**Range**
Typically Developing	-0.3 ± 0.2	-0.7 – 0.3	92.9 ± 22.3	43.2 – 119.6
CP – Before CIMT	-1.9 ± 0.4	-2.3 – -1.2	73.4 ± 21.4	45.4 –109.8
CP – During CIMT	1.9 ± 0.4	1.1 – 2.5	48.2 ± 15.6	23.5 – 70.9
CP – After CIMT	-2.0 ±0.3	-2.2 – -1.6	95.0 ± 28.3	74.6 – 127.3

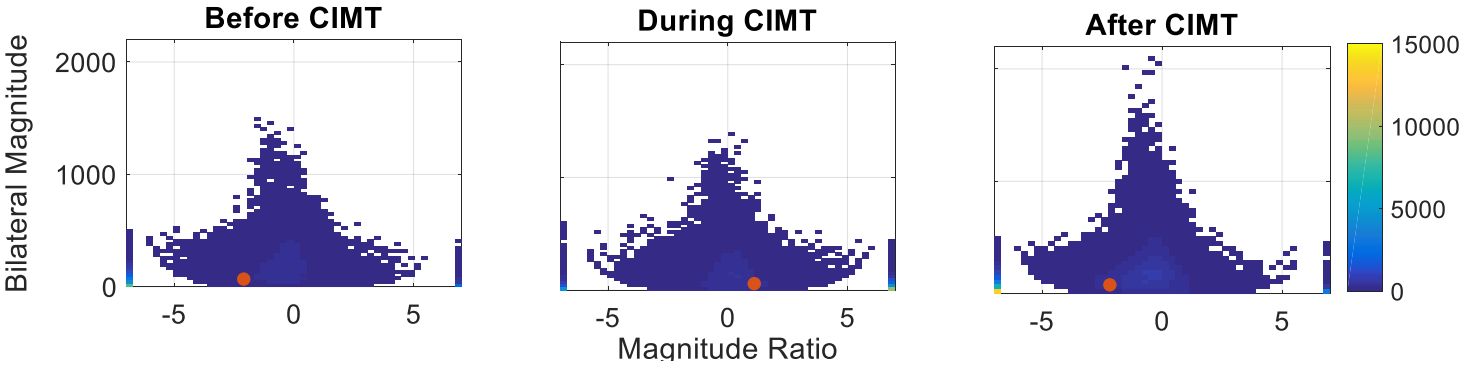

Figure 1: Density plots before, during, and after CIMT. The Magnitude Ratio compares how much the paretic hand is used compared to the non-paretic hand and Bilateral Magnitude compares the overall magnitude of both hands, with negative values indicating greater non-paretic hand use. The red dot is the shape's centroid.

PREDICTING VERTICAL GROUND REACTION FORCES WITH ACCELEROMETERS AND ARTIFICIAL NEURAL NETWORKS

Alec C. Miller, Marwan Aljohani, Hoon Kim, Kristof Kipp

Marquette University, Milwaukee, WI, USA
email: alec.miller@marquette.edu

INTRODUCTION

The repetitive nature of distance running often results in high incidence of overuse injury [7]. Variables related to the vertical ground reaction force (vGRF) are often used to assess risk of overuse injury, and are targeted during interventions [6]. However, measuring vGRF requires expensive, and often inaccessible, force platforms or instrumented treadmills.

Researchers have used a video-based kinematic data in combination with a two-mass model (i.e., lower leg and rest of the body) to predict vGRF during running [8]. Other researchers have used wearable technologies (i.e., accelerometers) to predict vGRF during locomotion [3,5]. However, most studies have only attempted to predict the peak vGRF during running from trunk and tibia accelerations.

Machine learning techniques, such as Artificial Neural Networks (ANN), have been used to predict entire vGRF time-series data during walking with great accuracy [1,2]. To date, no study has tried to predict vGRF time-series from accelerometer data during running. The combination of wearable technology and ANN may provide a low cost alternative to predict vGRF during running. The purpose of this study was to develop and train an ANN to predict the vGRF time-series from tibial and sacral accelerometry during running.

METHODS

The current study was approved by the Institutional Review Board at Marquette University. All subjects were informed of the study's purpose and signed an informed consent document before participation in the study.

Seven well-trained female distance runners (age: 21.4 ± 2.7 years; body-mass: 56.2 ± 6.7 kg; average weekly mileage: 37.9 ± 9.1 miles) participated in this study. Accelerometers were securely attached to the skin over the first sacral vertebrae and medial aspect of the distal tibia of the dominant leg.

Runners were then asked to run on a pressure treadmill at the speed where they spend most of their training time. After a six-minute warm-up, runners confirmed their pace as long-slow distance pace. vGRF and triaxial accelerations of the sacrum and distal tibia were recorded for 30 s at 100 Hz and 200 Hz, respectively. Collection of vGRF and accelerometer data was synched via an electrical pulse. All data were exported to Matlab for processing.

Cutoff frequencies for the vGRF and triaxial accelerations were determined with a residual analysis. Data were filtered with a dual-pass, fourth order low-pass Butterworth filter at cutoff frequencies of 14 Hz and 36 Hz, respectively.

Triaxial accelerations of the distal tiba were used to calculate the resultant tibial acceleration (RTA).

$$RTA = (X^2 + Y^2 + Z^2)^{0.5}$$

Heel strike and toe-off were defined by vGRF thresholds of 10 N. vGRF, RTA, and vertical sacral acceleration were time-normalized and averaged over the stance-phase of the first ten strides.

A nonlinear autoregressive ANN with external input was developed and trained for each subject. The ANN had one input layer, one hidden layer with 10 neurons, and one output layer. Average stance-phase RTA and vertical sacral acceleration were fed into the input layer, and used to predict the vGRF in the output layer (Figure 1). Performance of the ANN was

evaluated based on the root mean square error (RMSE) and Pearson correlation coefficient. In addition, the percent difference between actual and predicted peak vGRF were calculated to provide pragmatic interpretations of the ANN performance.

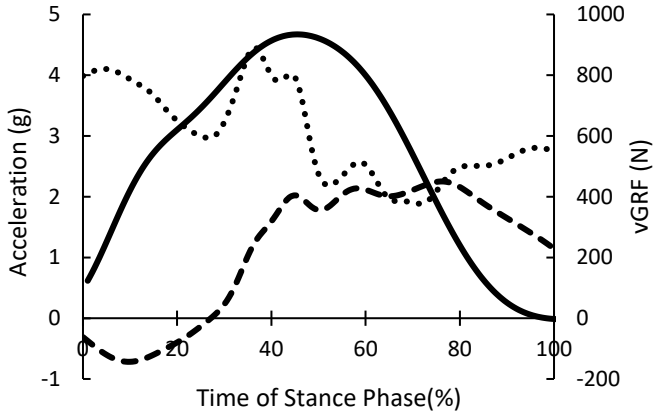

Figure 1: Vertical sacral acceleration (dashed line) and RTA (dotted line) were ANN inputs and used to estimate output vGRF (solid line).

RESULTS AND DISCUSSION

The RMSE for all ANN were very low (Mean ± SD: 0.71 ± 0.06 [N]). Linear regression analysis showed that the group average actual and predicted peak vGRF from all runners were highly correlated (r = 0.992; p = 0.0001; Figure 2). Furthermore, the percent difference between actual and predicted peak vGRF was 0.004%.

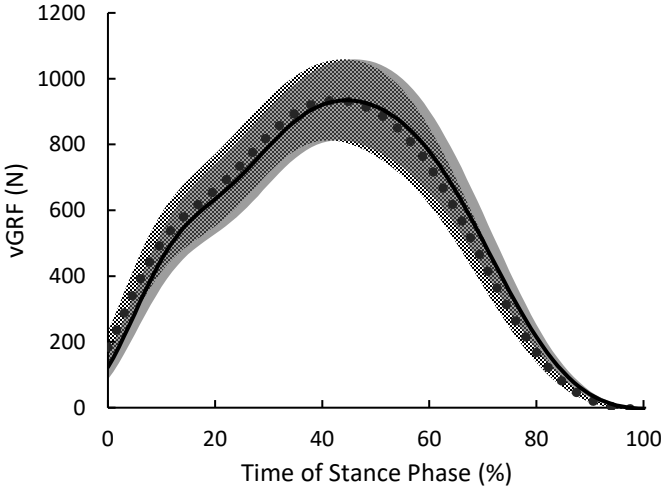

Figure 2: Ensemble average (Mean ± SD) of actual vGRF (solid line ± solid shade) and predicted vGRF (dotted line ± patterned shade).

The performance and prediction capacity of the ANN developed and trained in the current study is much better than previously reported for peak vGRF during running [4]. Niemelä et al. (2017) reported mean standard errors of 0.107 bodyweights in their ANN prediction of peak vGRF. The discrepancy in these results may stem from the difference in input parameters, as Niemelä and colleagues (2017) used primarily stride parameters (e.g., contact time, stride length) as ANN inputs, whereas the current study accelerometer data. Given the close relationship between tibial accelerations and GRF parameters during running [4], the use of accelerometers may present a better option to predict vGRF than stride parameters

The results of this study suggest that wearable technology (i.e., accelerometers) and machine learning techniques can be used to accurately predict vGRF during running. In combination, accelerometers and ANN may therefore provide a simple and cost effective alternative to force plates or an instrumented treadmill for researchers who strive to obtain vGRF data during running. One limitation of this study is that vGRF were collected while runners ran on a treadmill, which may not replicate over-ground running. Future studies should extend the current research into field-based testing.

REFERENCES

1. Begg RK. *J Med Eng Technol*, **30**, 315-322, 2006.
2. Eel Oh S, et al. *J Biomech*, **46**, 2372-2380, 2013.
3. Hennig EM, et al. J App Biomech, 9, 306-314, 1993.
4. Neugebauer JM, et al. *PLoS ONE*, **9**, e99023, 2014.
5. Niemelä M, et al. *Sports Eng*, **20**, 213-219, 2017.
6. Schubert AG, et al. *Sports Health*, **6**, 210-217, 2014.
7. van Gent RN, et al. *Br J Sports Med*, **41**, 469-480, 2007.
8. Weyand PG, et al. *J Exp Biol*, **220**, 247-258, 2017.

EFFECT OF FOOT-MOUNTED IMU DESIGN ON IMU-ESTIMATED RUNNING GAIT ACCURACY

Michael V. Potter, Lauro V. Ojeda, Noel C. Perkins, and Stephen M. Cain

University of Michigan, Ann Arbor, MI, USA
email: mvpotter@umich.edu

INTRODUCTION

Body-worn inertial measurement units (IMUs) are increasingly becoming a viable technology for measuring biomechanical parameters outside of traditional laboratory environments. While kinematic measurements obtained from IMUs can be subject to large integration drift errors, such errors can also be minimized through appropriate algorithms. One example is zero-velocity update (ZUPT) algorithms used to estimate full three-dimensional foot trajectories from foot-mounted IMUs [2]. These algorithms exploit the fact that in human walking, the foot reaches nearly zero velocity at some instance during each stance phase. Thus, drift in velocity estimates can be corrected on each stride. While these algorithms are validated for human walking, little validation exists for running speeds. One major barrier to obtaining accurate foot trajectory estimates from such algorithms is understanding the limitations of the inertial sensors that constitute the IMUs.

Bailey, et al. [1] investigated the effect of sampling frequency and accelerometer range on some stride parameter estimates for speeds up to 3.4 m/s, that is speeds much lower than those found in competitive distance running. Additionally, only two accelerometer ranges were considered. This work advances beyond that by simultaneously considering multiple ranges for both the accelerometers and the angular rate gyros and for speeds commensurate with walking through competitive running. In particular, we investigate how various accelerometer and gyroscope ranges typically found in commercial IMUs affect estimates of the total distance travelled at various speeds up to 6.5 m/s.

METHODS

Six subjects (3 male) were recruited for this University of Michigan IRB approved study. Each subject was equipped with one IMU (Opal, APDM, 128 Hz, ±200g, ±2000 deg/s) on each foot. Each subject was asked to complete ten 100-meter walks/runs. A straight 100-meter section of pavement was marked for this study. For each trial, subjects started with both toes on the starting line and were asked to finish with both toes on the finish line. Subjects completed each trial at self-selected paces, but were asked to complete the first trial at a slow walk and gradually increase their speed on each successive trial until completing their tenth trial at a maximal sprint.

For each trial, the subject's average speed was estimated using the time it took a subject to get from the start line to the finish line. Trajectory estimates for each foot were calculated from raw IMU data using a ZUPT foot trajectory algorithm similar to that described in [2]. For each foot, the total distance traveled was then estimated by summing the calculated stride lengths during that trial. The total distance travelled by the subject was then computed as the average of the total distance estimated from the left and right foot-mounted IMUs. The error in the average estimated distance was then reported as the percent deviation from the known 100-meter distance (negative error implying underestimated distance).

We hypothesize that the accelerometer range must be sufficiently large to resolve the major dynamical characteristics of the foot acceleration signal. To investigate this hypothesis, we consider the effects of systematically decreasing the accelerometer range on the aforementioned estimated total distance travelled. In particular, the raw accelerometer data was numerically saturated by setting all values outside a prescribed range to the limits of that range (e.g. to simulate a 6 g accelerometer, all readings above +6 g and below -6 g were set to +6 g and -6 g respectively). The resulting data (including saturated values) were used to estimate the total distance

travelled by the subject using the same method described above. This process was repeated by considering seven accelerometer ranges; namely, 100, 75, 50, 24, 16, 10, and 6 g. Similarly, we repeated the same study considering the effects of decreasing gyroscope range by considering five ranges; namely, 2000, 1500, 1000, 750, and 500 deg/s. The selected ranges in both accelerometers and gyroscopes are typical of commercially available MEMS sensors.

RESULTS AND DISCUSSION

The results for modifying accelerometer range are presented in Fig. 1. Note that even at moderate running speeds, the estimated distance travelled degrades greatly with insufficient accelerometer range. Additionally, for a given accelerometer range, degradation in estimated distance is approximately linear with speed. Best fit lines to the data confirm that errors increases with speed and with smaller acceleration range. For example, the slope of the linear fit for a 100 g accelerometer yields an error rate of -0.4 %/(m/s) while the slope (error rate) for 6 g accelerometer is -6.1 %/(m/s); that is, more than an order of magnitude increase in error rate.

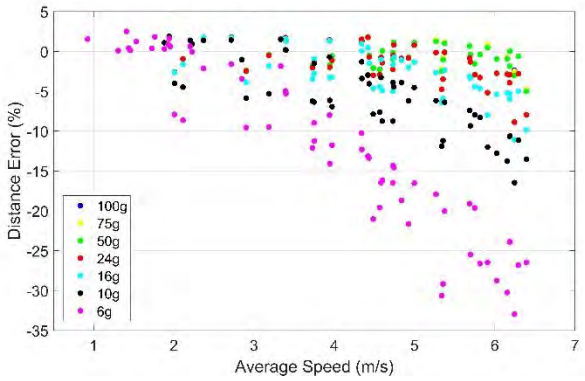

Figure 1: Distance error vs. speed for each accelerometer range investigated.

The results for modifying gyroscope range are presented in Fig. 2. Note again the significant errors in the estimated distance with decreasing gyroscope range and with increasing running speed. Linear fits yield slopes of -0.4 %/(m/s) for a 2000 deg/s gyroscope and -3.5 %/(m/s) for a 500 deg/s gyroscope.

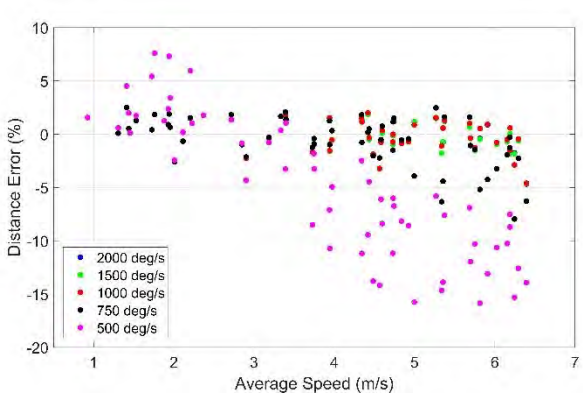

Figure 2: Distance error vs. speed for each gyroscope range investigated.

CONCLUSIONS

The accuracy of the total distance travelled derived from foot-mounted IMUs depend critically on the ranges of the constituent accelerometer and angular rate gyros. In general, accuracy degrades with increased running speed and decreased accelerometer and gyroscope ranges. For the speeds considered in this study (up to 6.5 m/s), the estimates converge for accelerometers having a range of 50 g or higher and a gyroscope having a range of 1000 deg/s or higher. Conversely, significant degradation in accuracy arises when these ranges are at or below 16 g and 750 deg/s respectively, especially at higher running speeds. Future work should investigate the effect of sensor design at even higher speeds such as those observed in elite sprinting. Additional work should also further investigate the cause of the slight degradation observed in estimates with increased speed despite accelerometer and gyroscope ranges that were large enough to prevent saturation.

REFERENCES

1. Baile, et al. *icSPORTS*, 2014.
2. Ojeda and Borenstein. *J. Navig.* **60**, 2007.

ACKNOWLEDGEMENTS

This material is based upon work supported by the US Army Contracting Command-APG, Natick Contracting Division, Natick, MA, under contract W911QY-15-C-0053.

FEASABILITY OF USING THE HTC VIVE SYSTEM TO COLLECT KINEMATIC DATA

[1]Kate A. Spitzley, [1]Kieley Trempy and [1]Andrew R. Karduna

[1]University of Oregon, Eugene, OR, USA
email: kspitzle@uoregon.edu

INTRODUCTION

Recent improvements in Virtual Reality (VR) technology have exciting implications for the research and rehabilitative sciences. Various modes of VR have been used successfully as intervention modalities in these settings with great success [1,2]. However, VR systems have not yet been used as a method of kinematic data collection. The use of these systems for both intervention and collection has the potential to greatly lower cost and increase portability of motion capture.

The HTC VIVE VR system currently costs $600, a fraction of the cost of research grade optical motion capture systems. Additionally, the entire setup consists of two small lighthouse boxes (about 9 cm x 9 cm x 6 cm), two lightweight handheld controllers and a fully immersive headset. While previous studies have looked at using the VIVE headset as a tracking method with little success, use of the handheld controllers has not yet been explored [3].

The aim of this study is to gather preliminary data to investigate the feasibility of using the VIVE VR handheld controllers to collect position and orientation data. To do so, we will compare the VIVE Virtual Reality sensors and Polhemus Liberty sensors to determine whether kinematic data can be accurately collected from this VR system. The Liberty system has been robustly validated for scientific data collection, we therefore feel comfortable using it as a gold standard for comparison.

METHODS

The VR system was setup as dictated by the VIVE owner's manual, with the lighthouses 6 m apart and connected by the sync cable. Lighthouses were mounted directly to the wall at a height of 2.1 m and angled downward at an angle of 30°, as recommended by the manufacturer. The VIVE headset was placed on a stable shelf within the calibrated space. The magnetic tracking system (Polhemus Liberty, Colchester, VT) transmitter was placed approximately 0.5 m from the sensor. All metal was cleared from the area to eliminate interference. Both systems sampled at a rate of 120Hz.

The VIVE controller and Liberty sensor were mounted to opposite ends of a rigid segment with a common central point of rotation. The rigid segment was mounted to a stable surface with a pegboard setup dictating five angular positions at approximately 0°, 20°, 50°, 70°, and 90°. The rigid segment was moved through fifty permutations of these angular targets. Data were collected from both sensors simultaneously using a customized Unity program.

In order to account for the difference in coordinate systems between the Liberty and VIVE systems, helical axis calculations were used to quantify the angular change in position. This calculation uses the α, β, and γ components of the signal to determine a rotation about a helical axis between trials. As long as the two sensors were rotated about the same axis, they should register the same rotation.

Angular measurement error between the two sensors was quantified as the absolute value of the difference in helical angles as measured by the Liberty sensor and the VIVE sensor in each trial. Additionally, an RMS calculation was used to quantify drift in the signal when the sensors were held in a stable position. Measures of angle and position were taken from ten different trials, two at each of the five angular targets.

RESULTS AND DISCUSSION

Helical angles calculated from Liberty sensor and the VIVE sensor data were similar over the fifty rotations tested (Figure 1).

The average helical angle measurement error between the two sensors was 0.2°± 0.1° and the largest error was 0.5°. Errors were then broken down by degree of angular movement (Figure 2). The highest average errors were seen at 90° of rotation and the lowest at 0° of rotation.

Average RMS over the ten trials did show some differences between sensors (Table 1). The VIVE demonstrated consistently higher measures of drift than the Liberty. However, both systems exhibited translational drift in the sub-millimeter range and rotational drift in the sub-degree range.

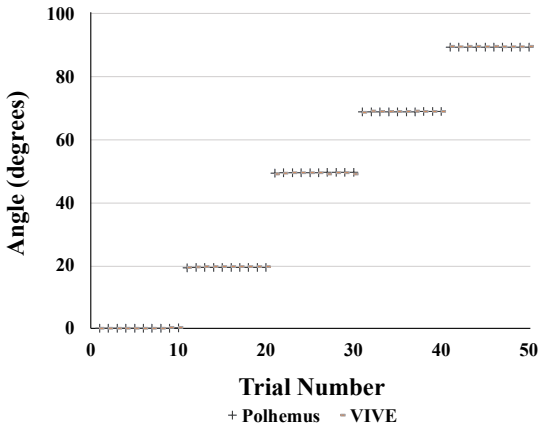

Figure 1: Helical angle of the Liberty and VIVE sensors throughout a series of rotations to angular targets of 0°, 20°, 50°, 70°, and 90°.

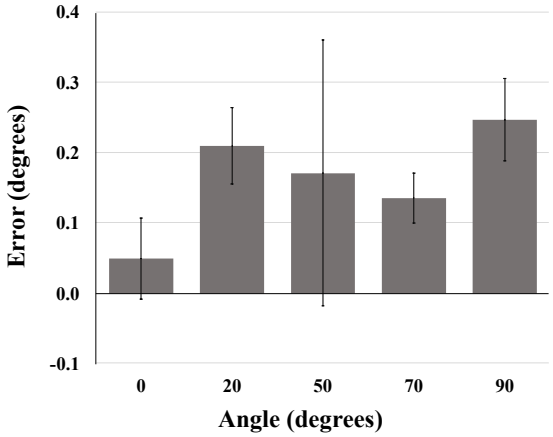

Figure 2: Difference in helical angle measurement between Liberty and VIVE sensors throughout a series of rotations to angular targets of 0°, 20°, 50°, 70°, and 90° (mean +/- sd).

CONCLUSIONS

While previous studies have used the VIVE headset as a tracking mechanism with little success, the handheld controllers are yet to be validated as a viable mode of data collection. Although the data presented here are preliminary in nature, they show promise for future measures of accuracy. It is our hope that with further validation, these controllers will be usable for kinematic data collection.

REFERENCES

1. Rose, T., Nam, C., Chen, K. *Applied Ergonomics,* **69**, 153-161, 2018
2. Rodrigues Severiano, M., et al., *Arq Neuropsiquiatr,* **76**, 78-84, 2018
3. Niehorster, D., Li, L., Lappe, M., *i-Perception,* **8**, 1-23, 2018

Table 1: Average RMS drift of the x, y, z, α, β, and γ signals of the Liberty and VIVE systems across a sample of 10 trials at five angles.

	Average RMS (mm)			Average RMS (degrees)		
	x	**y**	**z**	**α**	**β**	**γ**
Polhemus Liberty	0.02 ± 0.02	0.03 ± 0.02	0.02 ± 0.01	0.0 ± 0.0	0.0 ± 0.0	0.0 ± 0.0
HTC VIVE	0.61 ± 0.18	0.42 ± 0.12	0.60 ± 0.27	0.02 ± 0.02	0.01 ± 0.01	0.01 ± 0.0

PATTERNS OF ERECTOR SPINAE ACTIVATION AND TRUNK-PELVIS KINEMATICS IN PERSONS WITH LOWER LIMB AMPUTATION: INFLUENCES OF LOW BACK PAIN

[1]Julian C. Acasio, [1]Courtney M. Butowicz, and [1-3]Brad D. Hendershot
[1] Walter Reed National Military Medical Center, Bethesda, MD, USA
[2] DoD-VA Extremity Trauma and Amputation Center of Excellence, USA
[3] Uniformed Services University of the Health Sciences, Bethesda, MD, USA
Email: julian.c.acasio.ctr@mail.mil

INTRODUCTION

A higher prevalence of low back pain (LBP) is reported in persons with lower limb amputation (LLA) vs. uninjured individuals; moreover, persons with LLA often report that LBP negatively impacts quality of life [1]. In uninjured persons, movement impairments at the trunk and pelvis during gait, as well as altered trunk muscle activities, have been associated with increased risk for LBP [2]. However, there has yet to be a comprehensive study which examines both trunk kinematic and electromyographic (EMG) data while walking in persons with LLA, and more specifically, compares the influences of spine health (i.e., presence/severity of LBP). Therefore, the purpose of this study is to examine the relationship between patterns of trunk/pelvis kinematics and trunk muscle activations while walking, specifically comparing individuals with LLA with and without LBP.

METHODS

Seventeen persons with traumatic unilateral LLA – 9 with LBP (BP; 8 transtibial (TT), 1 transfemoral (TF), mean±standard deviation age (yrs): 34.7±7.8, stature (cm): 176.8±7.8, mass (kg): 85.4±11.6, and time since injury (yrs): 5.1±2.5) and 8 without LBP (NP; 5 TT, 3 TF, age: 36.8±7.6, stature: 179.9±5.4, mass: 91.8±15.8, and time since injury: 10.0±3.2) – and 6 uninjured controls (CTR, age: 28.2±9.0, stature: 174.5±4.5, and mass: 68.9±7.8) participated in this study. LBP was characterized via the NIH recommended minimal dataset [3]. Individuals walked across a 15m overground walkway at 1.3 m/s, with speed enforced by auditory feedback. An 18-camera motion capture system (Qualisys, Göteborg, Sweden) tracked (120Hz) trunk and pelvis kinematics via 10 reflective markers. Kinematic data were low-pass filtered (Butterworth, 6 Hz). Tri-planar trunk and pelvis angles and angular velocities were calculated in Visual3D (C-motion, Germantown, MD). Global trunk and pelvic ranges of motion (ROM) were determined and trunk-pelvic continuous relative phases (CRP) were calculated in MATLAB (Mathworks, Natick, MA). EMG data were collected (1200 Hz, Motion Lab Systems, Baton Rouge, LA) bilaterally at two levels of the erector spinae (T9 (TES) and L2 (LES)), high-pass filtered (Butterworth, 20 Hz), and full-wave rectified. A 50ms RMS smoothing window was then applied. EMG data were normalized to the signal mean and down-sampled to match kinematic capture rate. EMG data were processed bilaterally for individuals with LLA (i.e., on both the intact and affected side) and for the right side of CTR as no differences were observed between left and right sides. Both kinematic and EMG data were time-normalized to stride. Cross-correlations related EMG and trunk and pelvic rotation time series during both intact and affected strides. Separate one-way repeated measures ANOVAs assessed the effect of group (CTR, BP, NP) on ROM, mean CRP, and magnitudes of cross-correlation coefficients (R), with significance concluded at $P<0.05$. Bonferroni-corrected t-tests assessed pairwise differences ($P<0.0167$).

RESULTS and DISCUSSION

Larger frontal plane trunk ROM were observed in both BP and NP vs. CTR ($P<0.008$). Transverse plane trunk ROM were larger in BP than CTR ($P<0.001$) and tended to be larger than NP ($P=0.032$). A main effect was observed in frontal plane mean CRP, with NP exhibiting smaller (i.e., more in-phase) CRP than CTR ($P=0.013$). Main effects were observed in the R-values of both intact and affected side LES and sagittal trunk angles (Figure 1). Affected-side LES activations more strongly correlated with sagittal trunk angles in BP

and NP vs. CTR (P<0.003). Intact-side LES more strongly correlated with sagittal trunk angles in NP vs. CTR (P=0.005), and with transverse trunk angles in NP vs. BP (P=0.010). R-values of affected -side LES and sagittal pelvis angles were greater in NP vs. CTR (P=0.011) and tended to be larger in BP vs. CTR (P=0.023). R-values of trunk and pelvis angles and TES did not differ between groups.

The observed changes in frontal plane CRP are consistent with prior work and posited to be a trunk stiffening strategy to prevent injury and/or mitigate pain [4]. Though sagittal plane kinematics were similar between groups, R-values of LES activation patterns and sagittal plane trunk and pelvis angles were larger in both BP and NP vs. CTR. This suggests persons with LLA utilize LES to control sagittal plane trunk and pelvis motion during walking. Such an active control strategy may be especially important in the BP group as they tended to walk with more anterior trunk lean than CTR (P=0.023); this anterior shift in center of mass has been associated with an increased risk of falls [5]. While increased LES contributions may compensate for decreases in passive stability, the increased demand on the muscles may contribute to LBP development. NP may minimize this risk by using LES bilaterally to regulate sagittal trunk motions, and distributing the associated demand across both sides. BP, meanwhile, seems to rely more heavily on affected-side LES, which may increase the risk of injury on that side. In the transverse plane, smaller trunk ROM and stronger correlations between intact LES and trunk angles were observed in NP vs. BP. This suggests NP individuals are better able to control transverse plane trunk rotations, likely using LES to limit axial rotations. As increases in trunk and pelvic rotations are associated with increased spinal loads [6], the observed reductions in transverse plane trunk ROM may help mitigate the risk of LBP in the NP group. Thus, interventions training low-back musculature and enhancing trunk postural control strategies in persons with LLA are likely warranted.

REFERENCES

1. Ehde, et al. *APMR*, **86**, 731-34, 2001.
2. Lamoth, et al. *Gait Posture*, **23**, 230-39, 2006.
3. Deyo, et al. *J Pain*, **15**, 569-85, 2014.
4. Esposito, et al. *Gait Posture*, **40**, 640-46, 2014.
5. Pavol, et al. *J Gerontology*, **56A**, M428-37, 2001
6. Hendershot, et al. *J Biomech*, In Press, 2017.

ACKNOWLEDGEMENTS

Supported by award: W81XWH-14-02-0144. The views expressed herein are those of the authors and do not reflect the official policy of the Department of Army/Navy/Air Force, Department of Defense, or U.S. Government.

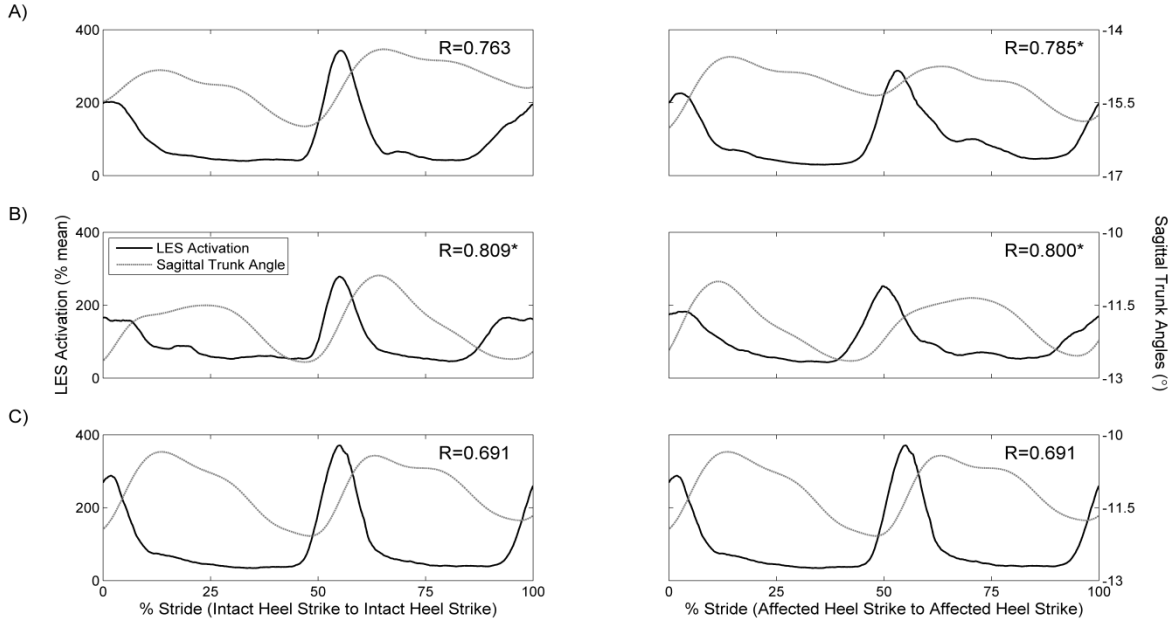

Figure 1: LES activation patterns (black), sagittal trunk angles (gray) and corresponding cross-correlation coefficients (R) for LBP (A), NP (B), and CTR (C) on the intact (left) and affected (right) sides. Asterisks (*) indicate statistically different from CTR.

Gait Restoration After a Spinal Cord Injury: A Simulation and Experimental Study of the Double Support Phase

[1]Naji A. Alibeji, [1]Brooke Odle, [1]Musa Audu, and [1,2]Ronald Triolo
[1]Case Western Reserve University, Cleveland, OH, USA
[2]Cleveland VA Medical Center, Cleveland, OH, USA
email: naa57@case.edu

INTRODUCTION

Paraplegia due to a spinal cord injury (SCI) results in an impairment of walking function and drastically lowers the quality of life of the affected persons. The use of Functional Neuromuscular Stimulation (FNS) to reanimate lower-limbs to restore walking function is highly desired by the affected population [1]. FNS is the application of an electric field across a nerve to produce a desired muscular contraction and is prescribed as an intervention to rehabilitate or restore gait function in individuals with mobility impairments. Currently, most research efforts focus on using FNS to restore swing phase [2], but little research has been undertaken on the double support phase (DSP) of gait.

During the DSP, when the body is supported by both legs in tandem stance configuration, the body weight load transfers from the trailing leg to the leading leg in anticipation of the subsequent swing phase in able bodied individuals. However, for subjects with SCI using FNS to restore gait, preprogrammed stimulation patterns only keep the subjects standing upright during DSP and does not actively help with weight shifting. This results in the subjects relying more heavily on their upper extremities (UE) to maintain balance and propel the body forward. Normalizing the DSP in FNS driven walking would stabilize transitions between the gait phases and help reduce the voluntary UE effort required, thus prolonging walking durations.

The main goal of this study was to explore the potential of improving the stability of the DSP of gait to reduce UE effort by modulating the stimulation to the available hip and back extensor muscles to actively shift the weight from the trailing leg to the forward leg.

METHODS

The load transfer during DSP in able-bodied subjects was analyzed by asking a male subject to stand in a tandem stance, feet shoulder width apart and one foot in front of the other. He was then asked to shift his weight forward from trailing to leading leg. Using smart insole sensors (iEE, Luxembourg), which measure contact forces at eight points of the foot (as shown in **Figure 1**), the ground reaction forces (GRFs) and center of pressure (CoP) of each foot were captured. The CoP is an epiphenomenon that occurs as a result of the position and movement of the center of mass (CoM) over the base of support and is often used as an indicator for balance.

To explore the potential of recreating the shift in DSP in individuals with SCI, extensive simulations were carried out with an anatomically realistic 3D musculoskeletal model of human standing developed in OpenSim [3]. The model is characterized by 35 degrees of freedom in the lower extremities, torso, and arms and 68 muscle actuators. Passive muscle dynamics were included to account for the hyper flexion and hyper extension restraints. Eight Hunt Crossley contact spheres where included at each foot (same location as the insole sensors) to model ground interaction and provide the GRFs and CoP measurements. Model simulations along with dynamic optimizations were performed to solve for a stimulation paradigm that achieves anterior-posterior (AP) shift of the CoM during tandem stance. To find a stimulation paradigm that is translatable to an FNS system, only 12 muscles that are readily accessible to stimulation, the hip/knee extensor/flexor muscles and the erector spinae bilaterally, were included in the simulations.

The optimization objective cost was to minimize the whole body CoM position error between the actual CoM and the desired shifted CoM to achieve that AP shift by modulating the stimulation inputs to the model.

The stimulation profiles obtained from optimizations were tested on a subject with a C5

tetraplegia (AIS C) and the recipient of a 16-channel implanted FNS system for standing. While standing in a tandem stance the stimulation was modulated in a feed forward manner to coincide with the activation profiles computed through optimizations, which specified increasing activation of the hip extensors. The GRFs and CoP were monitored using the smart insole sensors.

RESULTS AND DISCUSSION

The body weight normalized GRFs and CoP trace from the simulation and human subject experiments are displayed in **Figure 1**. The plots in the Figure show the progression of the CoP and GRF of each foot as the subjects shifted their weight forward. From the able-bodied data, a clear transition of the GRF between the trailing foot and the leading foot can be seen, i.e. the force decreases in the trailing foot (left) and increases in the leading foot (right). This weight transition trend was replicated in the simulation results and in the preliminary testing in the subject with an SCI and implanted FNS system.

As for the CoP profiles, in the able bodied subject (solid blue line) there is a lateral-medial shift of the CoP in the trailing leg and an posterior-anterior shift of the CoP in the leading leg. However, this is not the case for the simulation result (dotted cyan line) and experiments with the SCI subject (dashed red line). For these cases the AP shift of the CoP occurred in the trailing leg and the CoP in the leading leg remained near the heel of the foot. The differences in the CoP traces between the SCI and able bodied subject can be attributed to the limitations of the current system, i.e., the lack of activity of the ankle/foot (i.e., plantarflexor) muscles and limited control of how the foot interacts with the ground.

The preliminary data also demonstrate the feasibility of using the smart insole sensors to provide CoP measurements as feedback for closed-loop control to help maintain balance in real-time.

CONCLUSIONS

Through the appropriate modulation of the stimulation we have successfully produced a more dynamic DSP in subjects using an implanted FNS system. The inclusion of such stimulation paradigms, along with appropriate activation of the ankle/foot muscles, may improve the DSP in a walking neuroprosthesis and should greatly improve the gait stability of individuals with SCI walking with FNS. In addition, the potential extension of these results could lead to the development of a closed-loop control system to further stabilize walking in this population.

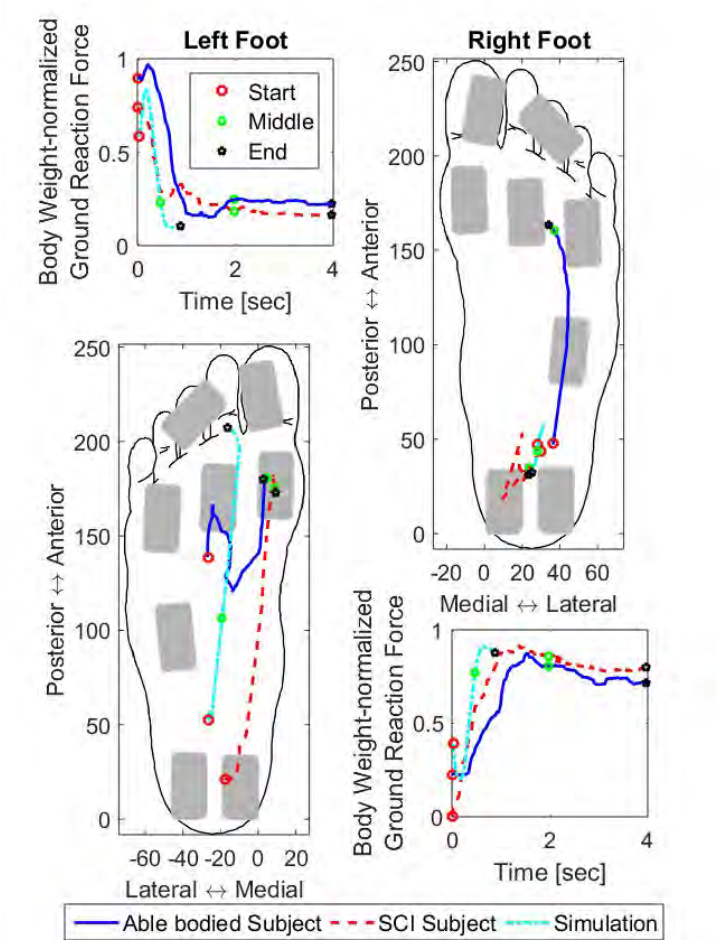

Figure 1: Experimental and simulated body weight normalized GRFs and CoP of each foot in tandem stance pose. The sensing locations of the smart insole sensors are indicated by rectangular grey regions.

REFERENCES

1. Yarkony et al, *Arch Phys Med Rehabil*, 73(1): 78-86, 1992.
2. Popovic et al., *IEEE Transactions on Rehab Eng,* 7(1):,69-79, 1999.
3. Delp et al., *IEEE Trans Biomed Eng*, 54(11): 1940-1950, 2007

A REACTIVE BALANCE RATING METHOD TO ASSESS PERFORMANCE AFTER TREADMILL-INDUCED TRIP-LIKE PERTURBATIONS

[1] Leigh J. Allin, [1] Jessica Aviles, [2] Maury A. Nussbaum, [3] Neil B. Alexander, and [2] Michael L. Madigan

[1] Department of Biomedical Engineering and Mechanics, Virginia Tech, Blacksburg, VA, USA
[2] Grado Department of Industrial and Systems Engineering, Virginia Tech, Blacksburg, VA, USA
[3] Division of Geriatric and Palliative Medicine, Department of Internal Medicine, University of Michigan and Ann Arbor Veterans Affairs Health Care System Geriatric Research Education and Clinical Center, Ann Arbor, MI, USA
email: lallin@vt.edu, web: ise.vt.edu/madigan

INTRODUCTION

Task-specific, perturbation-based balance training has emerged as a method to address the problem of falls among older adults, and it has been shown to improve reactive balance following large postural perturbations [1]. Several studies have implemented this type of training using treadmills to elicit trip-like perturbations [2,3]. In these studies, common outcome measures to assess reactive balance include trunk and stepping kinematics measured using a motion capture system [2,3]. A more "low-tech" method to assess reactive balance, that does not require a motion capture system, may help facilitate this training approach outside of the research setting.

The goal of this study was to develop and validate a low-tech reactive balance rating (RBR) method in the context of trip-like treadmill perturbations. RBR was validated as a surrogate measure of reactive balance by evaluating the strength of association of RBR with kinematic measures that discriminate between falls and successful balance recoveries, and as an indicator of fall risk by evaluating the strength of association with clinical tests that predict fall risk.

METHODS

Thirty-five independent-living residents of senior congregate housing facilities completed the study (24 women, mean age = 82 years). This study was approved by the university Institutional Review Board, and written consent was obtained from all subjects prior to participation.

Trip-like perturbations were induced using a treadmill (Freemotion 800, Freemotion Fitness, Logan, UT). The treadmill was modified to elicit a sudden (~40ms) change in treadmill belt speed (from stationary to an operator-selected walking speed) to induce a forward loss of balance (Figure 1). The RBR protocol involved six posterior treadmill perturbations, including two at each of three speeds (0.36, 0.72, and 1.07 m/s). At the start of each perturbation, subjects stood on the stationary treadmill belt. A rectangular foam block (4×4 cm cross section) was positioned 3-7 cm in front of the toes to elicit a step over an obstacle. Subjects were instructed to, upon treadmill movement, take steps to clear the obstacle to prevent a fall into a safety harness and establish a consistent gait. Subjects were also instructed to take their first step over the block with a particular foot. The safety harness, supported by an overhead gantry, was used to prevent knee or hand contact with the treadmill in the event of an unsuccessful attempt to recover balance.

Figure 1. Example of a treadmill perturbation

Each perturbation was rated using video recordings (recorded at 100 Hz), based upon the quality of the stepping response and the amount of harness or spotter support. For each perturbation, the overall reactive response was rated on a three-point scale (0, 1, or 2; Table 1). These ratings were then summed across the six perturbations to arrive at the RBR, which ranges from zero (worst) to 12.

Table 1: Reactive balance rating rubric

0	substantial harness and/or spotter support **OR** no attempt to step is made **OR** block remains in front of toe after first attempt to step
1	all other cases
2	minimal harness and spotter support **AND** correct foot clears block during first attempt to step (without shuffling) **AND** second step clears block

Four measures of reactive balance kinematics were determined for each perturbation using video recordings (100 Hz) and an inertial measurement unit (APDM, Inc., Portland, OR) worn inferior to the suprasternal notch. These measures included the time from treadmill movement to liftoff of the recovery step (step LO time), time from the onset of treadmill movement to touchdown of initial step over the block (step TD time), length of initial step over the block (step length), and maximum sagittal plane trunk angle from vertical.

Six clinical tests of balance and mobility that predict fall risk were also obtained, including: timed-up-and-go test (TUG), unipedal stance time (UST), maximum step length (MSL), Berg Balance Scale (Berg), Performance-Oriented Mobility Assessment (POMA), and Activities-specific Balance Confidence Scale (ABC).

The strength of association between RBR, reactive balance kinematics, and clinical tests were determined using Spearman rank correlation coefficients. These coefficients were compared using the method described by [4].

RESULTS AND DISCUSSION

RBR had a median of 4 (range 0-11). RBR was significantly associated ($p < .05$) with reactive balance kinematics (Spearman's rho correlations 0.19-0.55), suggesting RBR to be a valid surrogate measure of reactive balance kinematics. RBR had a stronger association with clinical tests than reactive balance kinematics had with these same tests (Table 2), and RBR was 42-60% lower for subjects predicted to be at a high risk of falling, suggesting RBR to be a promising indicator of fall risk.

In conclusion, a reactive balance rating method was developed that associates with important reactive balance kinematics after tripping, and with clinical tests that are predictive of fall risk. RBR has the added benefit over kinematic measures in that it requires minimal research equipment (only a video camera), minimal training, and encompasses multiple aspects of reactive balance after tripping. Therefore, RBR may provide a low-tech, valid measure to assess reactive balance kinematics and indicate fall risk after trip-like postural perturbations.

REFERENCES

1. Mansfield et al. *Phys Ther*. 95: 700-709, 2015.
2. Owings et al. *Clin Biomech*. 16: 813-819, 2001.
3. Grabiner et al. *Med Sci Sports Exerc*. 44:2410-2414, 2012.
4. Myers and Sirois *Wiley StatsRef: Statistics Reference Online*: John Wiley & Sons, Inc; 2006

Table 2: Spearman rank correlation coefficients between RBR, kinematic measures and clinical measures

		TUG (s)	UST (s)	MSL (in)	Berg	POMA	ABC (%)
RBR		-.45	.51	.47	.44	.44	.43
Step length	0.36 m/s	-.12*	.06**	.18*	.08*	-.08*	.21
	0.72 m/s	-.01**	.28	.07**	.06**	.12*	.24
Step LO time	0.36 m/s	-.34	.15**	.09**	.19	.28	.12*
	0.72 m/s	-.32	.42	.14*	.32	.47	.29
Step TD time	0.36 m/s	-.35	.17*	.25	.18	.21	.24
	0.72 m/s	-.48	.34	.36	.37	.46	.24
Max trunk angle	0.36 m/s	-.01**	.05**	-.07**	-.02**	.14*	.11*
	0.72 m/s	-.22	.23*	-.01**	.11*	.30	.16

* Correlation is smaller than RBR correlation with same clinical measure ($p < 0.1$)
** Correlation is smaller than RBR correlation with same clinical measure ($p < 0.05$)

POSTURAL STABILITY IN UNILATERAL TRANSTIBIAL AMPUTEES USING TWO SUSPENSION SYSTYEMS: SMARTPUCK™ VS LOCK AND PIN

Ashley N. Alunan, Vanessa A. Kellems, Gabby M. Rentuma, Jeremy D. Smith & Abbie E. Ferris
School of Sport and Exercise Science, University of Northern Colorado, Greeley, CO
alun3924@bears.unco.edu; www.unco.edu/biomechanics

INTRODUCTION

Individuals with transtibial amputation (TTA) are at an increased risk of falling in comparison with non-amputees due to increased center of pressure (COP) displacements and velocities during quiet standing [1-3]. Quiet standing is often assessed to understand postural stability deficits associated with fall risk in this population [4].

One factor that may contribute to stability is choice of socket suspension system used to attach the residual limb to the prosthetic [5]. Most commonly, lock and pin (PIN) and elevated vacuum systems are prescribed. Research has examined differences in functional outcomes between vacuum and PIN suspension systems and found an improvement in balance, gait, and transfers with vacuum systems [5]. However, differences in postural stability have not been thoroughly examined. Improvements in functional measures may be due to the interaction between the socket and residual limb and an improved fit of the residual limb in the socket.

Furthermore, current vacuum systems tend to experience small leaks which can lead to limb volume fluctuations and ultimately poor socket fit. The SmartPuck™ (PUCK) is a newly developed elevated vacuum suspension system. The PUCK is unlike traditional vacuum systems in that it is housed within the socket and vacuum levels are controlled with a smart phone. Housing the PUCK internally to the socket helps to address the flaw in current vacuums: loss of pressure. The purpose of the present study was to compare postural control of individuals with unilateral TTA using PUCK and PIN socket suspension systems.

We established the null hypothesis there would be no differences in COP displacements, velocities, or frequencies between PUCK and PIN under multiple surface and vision conditions. We hypothesized that stability would decrease as surfaces changed from rigid to compliant and visual input was removed.

METHODS

Four individuals with TTA (71.34 ± 41.52 kg, 1.39 ± 0.08 m; 49.2 ± 27.79 years, K3 - K4) have participated in this study thus far. Inclusion criteria included: amputation resulting from trauma (and otherwise healthy), currently wearing a PIN or PUCK suspension system, at least 6 months of experience in their current prosthesis, healthy residual limb, no neurological cardiac, vascular problems that could limit their function, and able to walk continuously for 10 minutes without assistance.

Two visits occurred in a random order with participants wearing 1) PUCK and 2) PIN. Before each visit participants had at least one week accommodation time for each suspension system.

Participants stood shod with a self-selected stance, with each foot positioned on a separate force plate (AMTI, Watertown, MA). Foot location was measured to ensure similar placement between trials/visits. For each trial, COP and vertical ground reaction forces (GRF, 1000 Hz) were collected. Participants maintained a quiet standing position for 30s for four separate conditions: 1) rigid surface eyes open (RSEO), 2) rigid surface eyes closed (RSEC), 3) compliant surface eyes open (CSEO), 4) compliant surface eyes closed (CSEC). The compliant surface consisted of a viscoelastic mat placed on each force plate. The middle 20s of each trial were analyzed. Dependent variables were calculated according to methods described by Prieto et al. [4]. Vertical GRF was expressed as a percentage of body weight (% BWT) supported by each limb. Due to the small sample size and preliminary nature of the data, statistical analyses were not performed.

RESULTS AND DISCUSSION

Asymmetries in loading of each limb existed between systems and conditions. The intact limb was loaded ~5% more during the rigid surface conditions with both systems. However, the amputated limb was loaded more than the intact limb for the compliant surface conditions. While, asymmetries (~5% BWT) persisted in the PIN across conditions, the PUCK became more symmetrical and only a ~2% BWT difference was seen during the CSEO and CSEC conditions. Proprioception from the feet contributes to maintaining postural control during quiet standing [6]. Amputees experience some loss of proprioceptive feedback due to the absence of one foot. Therefore, the intact foot might assume more responsibility in maintaining balance as seen in the RSEO condition. Interestingly, the amputated limb, in both systems (especially the PUCK), loaded a greater %BW than the intact limb during CSEC which may facilitate proprioceptive feedback in this population.

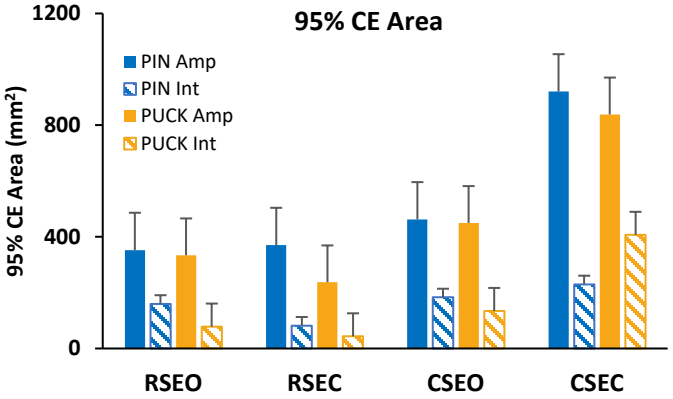

Figure 1. Mean (sd) 95% CE Area for each condition.

In general, the amputated limb had larger 95% confidence ellipse (95% CE) areas than the intact limb regardless of suspension system or condition. It is not unexpected to see increased 95% CE areas in the amputated limb as proprioception has been altered [6]. However, the PUCK amputated limb showed smaller 95% CE areas during the RSEO and CSEC conditions compared to the PIN (Figure 1). Smaller 95% CE areas in PUCK, may suggest improved COP control in the conditions with removed vision, and a lower fall risk [3].

Anteroposterior (AP) velocities increased across eye and surface conditions regardless of suspension type; the amputated limb AP velocities were generally 2-3 times larger than the intact limb. The PUCK showed smaller inter-limb asymmetries and smaller intact mediolateral (ML) COP velocities than the PIN across all conditions except for the RSEO condition (Figure 2). Reduced ML velocities observed in PUCK intact limbs compared to PIN, may also translate to a lower fall risk [3].

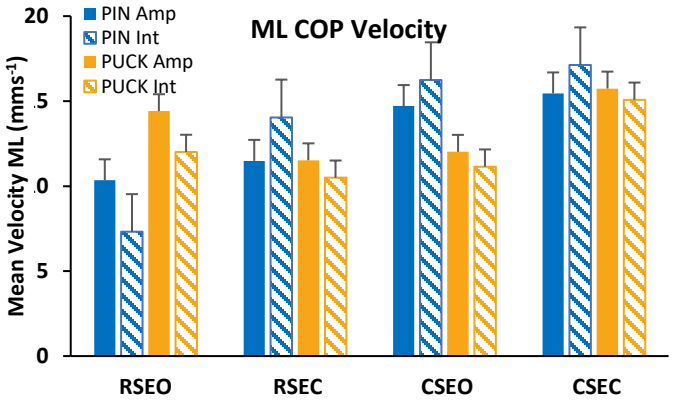

Figure 2. Mean (sd) COP ML velocities for each condition.

CONCLUSION

Our hypotheses were partially supported. Our data did show an increase in 95% CE and velocities as surfaces changed from rigid to compliant and from eyes open to eyes closed. However, a few trends were seen which may suggest differences exist between the PUCK and PIN systems. The decreases in 95% CE and ML velocity may suggest the PUCK improved postural control compared to the PIN systems as surfaces changed from rigid to compliant and from eyes open to eyes closed. The improvement in these measures may be linked to a better fit between the residual limb and the socket. Patients commonly report that the PUCK "feels like a part of me." This sensation may enhance proprioceptive feedback resulting in improvements in postural control. As more participants are added to the current dataset, these trends may become more clear.

REFERENCES

1. Buckley, J.G., *et al.* AM J Phys Med Rehabil, 2002. **81**(1): p. 13-20
2. Hlavackova, P., *et al.* PLOS ONE, 2011. **6**(5): p. e19661
3. Bigelow K.E., & Berme, N., J Gerontolog, 2011. **66**(2): p. 228-33
4. Prieto, T.E., *et al.* IEEE Trans Biomed Eng, 1996. **43**(9): p. 956-66
5. Samitier, C.B., *et al.* Pros Orth Int, 2016. **40**(1): p. 83-88
6. Magnusson, M., *et al.* Acta Otolaryngol, 1990(3-4): p. 182-8

Effects of Sound on Static Postural Stability

[1]Chad Anderson, [1]James Aubrey, [1]Alyssa Haley, [1]Thuy-Vi Le and [1]Rahul Soangra

[1] Department of Physical Therapy, Crean College of Health and Behavioral Sciences, Chapman University, Orange, CA, USA
email: soangra@chapman.edu, web: https://www.chapman.edu/our-faculty/rahul-soangra

INTRODUCTION

According to the C.D.C., 800,000 patients a year are hospitalized because of fall injuries. Falls are a significant health concern in the US, and can be life-threatening for the most fall-prone population groups.Human beings use several body systems to maintain balance. These include our vision, somatosensory, vestibular, and musculoskeletal systems.

In addition to the sensory input and efferent cues mentioned above, there is also some data indicating that we also utilize our hearing system to maintain our equilibrium or balance in a static state. Kanegaonkar et al. (2017) found that a decrease in auditory input in subjects led to greater postural sway as measured with a Nintendo Wii with a balance board. Rumalla et al. (2015) found that people wearing hearing aids scored significantly higher in both the Romberg on foam test and the tandem stance test than those unaided by hearing aids. In addition to the absence or presence of sound impacting our balance, there has also been some research showing that sound input can have a positive impact on our ability to maintain balance. Ross et al. (2016) found that white noise reduced the radius of the sway patterns of both younger participants and participants over the age of 65. Ross, et al. (2015) also found that the introduction of white noise reduced the sway pattern radius in participants in both vision and non-vision conditions.

There is some paucity in research regarding the effects of white noise and pink noise on postural stability. This study explores the effect of white and pink noise with and without vision. We hypothesize that white noise and pink noise may not affect sway radius, circular area of sway, and ellipse area of sway. The independent variables for this study were: i) ambient noise, ii) no noise, iii) white noise, iv) pink noise, with and without vision.

METHODS

Four healthy subjects, two male and two female, who were recruited from Chapman University. All participants were healthy with no orthopedic, neurological, or balance issues. Also, participants reported no problems with hearing. The protocol for this study was approved by Chapman University Institutional Review Board (IRB#1718H020). All participants provided written informed consent prior to the experiment.

Table 1: Anthropometrics

	Mean	***Standard Deviation***
Age (years)	27.5	+/- 7.77
Height (in.)	66.75	+/- 4.03
Weight (lb.)	158.75	+/- 34.73

Participants were instructed to stand on a force plate in a comfortable position with their hands down to their sides and looking forward. They were instructed to focus on a spot 2 meters infront and fix their gaze on that during trials. The conditions included a combination of either Eyes Open (EO) or Eyes Closed (EC) for vision and either Ambient Noise (AN), No Noise (NN), White Noise (WN), or Pink Noise (PN). Three trials were conducted for each condition. The trials were one minute in duration with 3 minutes in between trials to rest. Each participant completed all twenty-four trials consecutively. The order of the trials and participants were randomized. This eliminated learning effect to some degree and also eliminated the anticipatory ability to prepare for any particular forthcoming trial conditions. The participants used headphones, Sony Model MDR-7506, for the WN, PN and the NN condition. The sound levels were set to 65dB. A 40cm by 60cm Bertec force plate (BP4060, Bertec, Columbus, OH 43229 USA) was used with Motion Analysis Cortex software to

measure center of pressure (COP) displacement over 60 seconds of participants.

RESULTS AND DISCUSSION

Some of the measured COP variables include: range, mean radius, circular area, ellipse area, and mean power frequency. The Romberg ratio (EC/EO) was computed.

We found 18% higher COP sway ranges with pink noise as shown in figure 1a but 13% lower COP way ranges with white noise when compared to ambient noise. We also found that exposure to pink noise increased sway area by 28% while the elliptical sway area decreased by 23% when exposed to white noise from that of ambient noise. We also found that no noise condition increased postural sway area by 19% (Figure 1b).

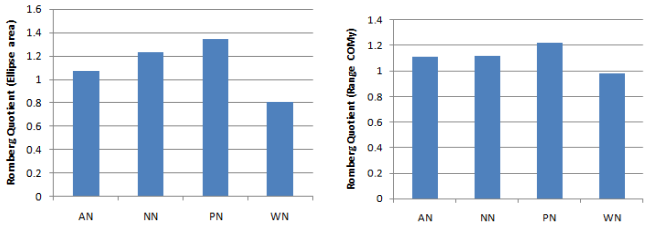

Figure 1: Romberg Quotient

Figure 2: Experiment picture of postural sway

We found improved postural stability for white noise and ambient noise conditions while no noise and pink noise conditions were found unstable.

We found that the trends of Romberg ratios for the white noise condition similar to ambient noise condition. These results corroborate previous study conducted by Bateni, et al. (2013), which found no statistical difference in subjects' COP maintenance between white noise and environmental noise conditions. We also found that the pink noise exposure deteriorated postural stability among the participants. We found that exposure to auditory white noise had improved postural sway variability similar to ambient noise in the subjects and may be useful in therapeutic and rehabilitative settings. These results are consistent with previous studies that assessed the effects of white noise on balance and found a reduced sway variability in the presence and absence of visual information (Ross et al., 2015). Similarly, Lockhart et al. (2011) researched the effects of varying frequencies of sounds on postural swaying during static standing and found that the frequency of sound was directly correlated with swaying in the anterior-posterior direction. Additionally, we also found that the no noise condition induced instability, thus eliminating any environmental noise decreases the amount of information the body is receiving about where it is in space and thus makes it more difficult to maintain balance. Contrary to this, the pink noise consistently showed increased in postural sway or instability. This is an interesting result to note because it is worth investigating whether environments with pink noise are associated with greater losses of balance. For populations that are at an increased fall risk, this is a possibly dangerous environmental factor. A study conducted by Dozza, et al. (2007) found that auditory biofeedback improved postural sway significantly in individuals with bilateral vestibular interruptions when the environment presented with minimal amounts of somatosensory and visual information. Thus, elderly individuals who have reduced visual and vestibular capabilities could be more at-risk of a fall if they are exposed to pink noise at a level or intensity that blocks out some of the natural yet subtle auditory biofeedback that one experiences with ambient noise.

CONCLUSIONS

This is the first study investigating the relationship between pink noise and its effect on postural stability both with eyes open and eyes closed. While previous studies have looked at white noise and no-noise relationship (Ross et al. 2015; Ross et al. 2016), this specific study provided new information on the effects of types of sound on postural stability. Although the sample size is small, it was shown that pink noise was often as dangerous as no noise and deteriorated postural control, especially with eyes closed.

REFERENCES

1. Azevedo R, Teixeira N, Abade E, Carvalho A. *Work* May 2016;54(1):87-91.Bach et al. *Plos One*. 10(3): e0118797, 2015.

PRELIMINARY INVESTIGATION ON THE EFFECTS OF XBOX 360 KINECT TRAINING ON GAIT AND LIKELIHOOD OF INITIATING A LOSS OF BALANCE

[1] Sara L. Arena, [2] Kevin R. Ford, and [2] Jeffrey B. Taylor

[1] Virginia Polytechnic Institute and State University, Blacksburg, VA, USA
[2] High Point University, High Point, NC, USA
email: sarena@vt.edu

INTRODUCTION

Falls are a major source of injury among adults over the age of 65. Over 57% of falls in older adults are due to slips and trips, which may be due, in part, to an increased likelihood of initiating a loss of balance [1]. Commercially available video gaming systems, such as the Nintendo Wii and Xbox 360 Kinect, have potential as a fall prevention intervention among older adults. Previously, older adults who participated in a training program playing Xbox 360 Kinect games were shown to improve functional balance scores [2] as well as modulate declines in HG strength and improve TUG scores [3] compared to controls. It is possible that these improvements in balance and physical function may also translate to changes in gait and decrease the likelihood of initiating a loss of balance. Therefore, the purpose of this study was to examine the effect of a 6-week Xbox Kinect training program on gait, slip propensity, and trip propensity in older adults.

METHODS

Twelve subjects (78.6 ± 4.7 years; 5 males and 7 females) participated in this study and were randomly assigned to a control group (79.7 ± 5.3 years; 3 males and 3 females) or a treatment group (77.2 ± 4.6 years; 2 males and 4 females).

All participants reported to the laboratory twice for measurement of gait and physical function (baseline and post intervention). Results on physical function have been reported previously [3]. Participants completed three gait trials down a walkway at a self-selected speed. The position of select anatomical landmarks were sampled at 200 Hz using a 14-camera motion capture system (Motion Analysis Corporation, Santa Rosa, CA, USA). Ground reaction forces (GRF) were sampled at 1200 Hz using in-line force platforms (AMTI, Watertown, MA, USA).

The required coefficient of friction (RCOF), the ratio of resultant shear to vertical GRF generated during gait, was used to quantify slip propensity. A higher RCOF value implies a greater shear force is needed to keep the foot from slipping [4]. Minimum toe clearance (MTC), the lowest vertical position of the foot during the swing phase of gait, was used to quantify trip propensity. A smaller toe clearance value implies an increased risk of tripping [5].

The treatment group participated in a 6-week Xbox 360 Kinect training program in which each participant completed 3 training sessions per week, each session lasting 30 minutes. Participants played 6 different games from Kinect Adventures!, with game order randomized for each training session. In brevity, the games challenged participants to squat, move around the room, and reach with arms and legs to control their avatar for the various game objectives.

Dependent variables included gait speed, step length (normalized to body height), cadence, RCOF, and minimum tow clearance (normalized to foot length). Independent t-tests were performed on pre-intervention data to ensure groups (control, treatment) had similar gait characteristics and propensities prior to implementation of the intervention. Differences between pre and post intervention were then calculated for each dependent variable. Independent t-tests were used to examine the influence of group (control, treatment) on change in all dependent variables. Statistical analyses were performed using JMP Pro 13 (SAS Institute, Inc., Cary, NC) with a significance level of $p \leq 0.05$.

RESULTS AND DISCUSSION

No significant differences were found between the control and treatment group prior to the implementation of the intervention ($p > 0.28$).

Minimum toe clearance was found to decrease in the treatment group (6.66 ± 4.47 %FL) while minimally changing in the control group (0.02 ± 2.83 %FL) (p=0.01; Figure 1). Treatment and control groups had similar changes in gait speed, step length, step width, cadence, and RCOF (p>0.31).

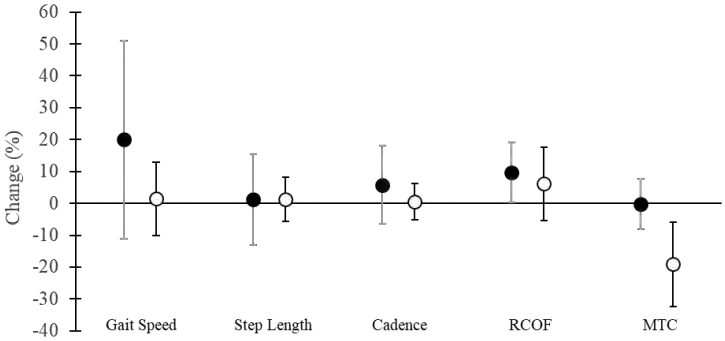

Figure 1: Change in dependent variables for control (black) and treatment (white) participants as a percentage of pre-intervention measurement.

Previous work has demonstrated a change in clinical measure of balance and physical function in older adults with the implementation of an Xbox 360 Kinect training program [2, 3]. Our results suggest that despite improvements in these clinical measures, training on the Xbox 360 Kinect for 6 weeks may not translate to activities of daily living, such as gait, and may not positively influence risk factors for falling. In contrast, Lee and Shin [6] found gait speed and cadence to increase with longer training sessions (50 minutes) and program (10-weeks) in older adults with diabetes mellitus. It is possible that a longer training program with longer sessions could result in changes in mobility and likelihood of initiating a fall, but it is not clear if the results of Lee and Shin [6] are applicable to otherwise healthy older adults.

Interestingly, MTC was found to decrease with Xbox 360 Kinect training, indicating a greater risk of initiating a trip. This may be due to an unintended training effect. The selected games require sudden, and quick movements, and repeated exposure to these games may have lead participants to adopt smaller amplitude motion in order to achieve the goal in the desired time. Additionally, we have previously found higher Xbox 360 Kinect game scores were associated with a higher RCOF, indicating a greater risk of initiating a slip [7]. In contrast, in the current study, RCOF did not change significantly with training on these games despite an increase in game scores (data not shown), and indicates that the training does not influence the likelihood of initiating a slip.

Several limitations warrant discussion. First, all participants were highly functioning older adults and it is possible that our participants exhibited a ceiling effect. Second, 6-weeks may not have been a long enough program to generate changes in gait or likelihood of initiating a fall. Third, the small sample size limits the statistical power of our results.

CONCLUSIONS

A 6-week training program utilizing the Xbox 360 Kinect resulted in an increased likelihood of initiating a trip and no significant changes in gait speed, step length, cadence, or likelihood of initiating a slip. Our results imply benefits previously demonstrated by an Xbox 360 Kinect training program may not translate to changes in mobility or frequency of initiation of a loss of balance. Future research should explore if a longer program and session time may achieve desired changes in a healthy older adult population and if higher risk populations may incur a more positive effect of such training programs.

REFERENCES

1. Schiller et al. *CDC and Prevention, National Center for Health Statistics*, 2007.
2. Bieryla K, et al. *Aging Clin Exp Res*, 28(3), 2016.
3. Hutcheson J, et al. *40th Annual Meeting of ASB*, Raleigh, NC, USA, 2016.
4. Buczek FL, et al. *International Symposium on Slip Resistance* - the Interaction of Man, Footwear, and Walking Surfaces 353-358, 1995.
5. Rietdyk S, et al. *Clin Biomech*, **20**, 2005.
6. Lee & Shin. *Diabetes Technol Ther,* 15(6), 2015.
7. Gould LM, et al. *40th Annual Meeting of ASB*, Raleigh, NC, USA, 2016.

ACKNOWLEDGEMENTS

The authors would like to acknowledge Lacey Gould, Melissa Savas, Jordan Hutcheson, and Alyssa Walker for their contributions in data collection and processing.

POSTURAL STABILITY, VERTICAL STIFFNESS, AND LOWER-EXTREMITY JOINT MOTION DURING MULTI-DIRECTION SINGLE-LEGGED JUMP-LANDINGS

Colin W. Bond [1], Alexander J. Hron [1,2], Benjamin C. Noonan [1]

[1] *Sanford Health, Fargo, ND, USA*
[2] *University of North Dakota, Grand Forks, ND, USA*
email: colin.bond@sanfordhealth.org

INTRODUCTION

Diminished time to stabilization (TTS) may be a risk factor for ACL injury [1]. While TTS does not directly evaluate the biomechanical mechanisms associated with ACL injury, the kinetic profile displayed during a jump-landing task serves as a surrogate measure of the capacity of the lower-extremity neuromuscular system to achieve stability during a shift from a dynamic movement to a stationary position over the base of support. High vertical stiffness (K_{vert}) during a jump-landing may indicate poor attenuation of ground reaction forces through controlled sagittal plane knee flexion, which may challenge the lower-extremity's passive stability and increase the risk for ACL injury [2]. The purpose of this study was to compare TTS, K_{vert}, and knee joint motion during a backward, forward, medial, and lateral single-legged jump-landing. It was hypothesized that TTS and K_{vert} would be greatest during the backward jump-landing.

METHODS

Seventeen male and female recreational athletes (22.2 ± 3.0 yr, 1.75 ± 0.08 m, 73.4 ± 12 kg) participated in this study. A randomized, repeated measure design was used so that three trials of a backward, forward, medial, and lateral single-legged jump-landing were completed barefoot on the non-dominant leg.

Landings were performed on an in-ground force plate and three-dimensional motion capture was used to quantify lower-extremity kinematics. For the forward direction, participants took two steps, hopped on the test leg over a 15-cm hurdle placed equidistant to their leg length from the center of the force plate, and landed on the same leg on the force plate. For the other directions, the hurdle was placed directly next to the force plate, and the participants hopped over the hurdle on the test leg and landed on the same leg on the force plate. Participants were instructed to keep their hands on their hips, stabilize as quickly as possible, and remain motionless for the remainder of the 10 s sampling period.

Initial contact and peak vertical ground reaction force (vGRF) were identified to determine sagittal plane knee angles during weight acceptance. TTS was quantified as the time it took for the vGRF to stabilize within 5% of the subject's body mass for 1 s after landing. K_{vert} was calculated as the relative peak vGRF divided by the change in the participant's center of mass vertical position during the weight acceptance period. Separate one-way repeated measures ANOVA were used to examine the effect of jump-landing direction on TTS, K_{vert}, and knee angles. Tukey corrected pairwise comparisons were used where appropriate to identify the source of the effect. P was initially set to < 0.05.

RESULTS AND DISCUSSION

There was a significant effect of jump-landing direction on TTS ($F = 3.45$, $P = 0.03$)(Fig. 1). Participants took longer to stabilize during the medial jump-landing direction than during the forward direction ($P < 0.01$). A significant effect for jump-landing direction on K_{vert} was also identified ($F = 55.0$, $P < 0.01$)(Fig. 2). Participants landed with greater stiffness during the forward jump-landing than during the other three directions ($P < 0.01$). Finally, a significant effect of jump-landing direction on knee angle excursion during weight acceptance was identified ($F = 45.8$, $P < 0.01$)(Fig. 3). Participants had less weight acceptance knee flexion excursion during the backward jump-landing than during the forward ($P < 0.01$), lateral ($P < 0.01$), and medial ($P < 0.01$) directions.

Participants had greater weight acceptance knee flexion excursion during the forward jump-landing direction than during the lateral ($P < 0.01$) and medial ($P < 0.01$) directions.

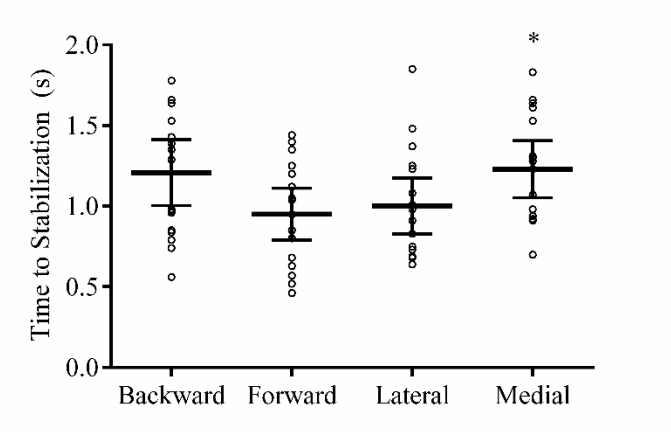

Figure 1. Time to stabilization for the backward, forward, medial, and lateral single-legged jump-landing directions. Thick lines: means; whiskers: 95% confidence interval; circles: participants. * significantly different from forward direction.

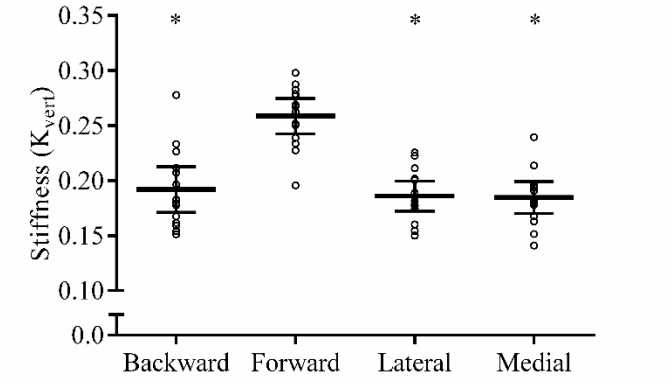

Figure 2. Vertical stiffness for the backward, forward, medial, and lateral single-legged jump-landing directions. Thick lines: means; whiskers: 95% confidence interval; circles: participants. * significantly different from forward direction.

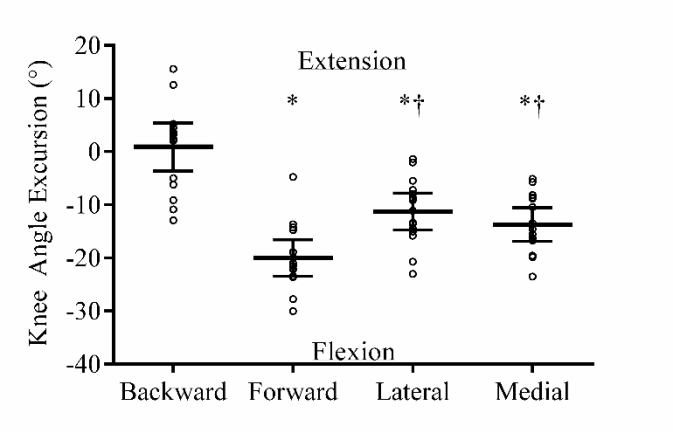

Figure 3. Change in sagittal plane knee angle between initial contact and peak vertical ground reaction force. Positive values indicate movement towards extension, negative values indicate movement towards flexion. Thick lines: means; whiskers: 95% confidence interval; circles: participants. * significantly different from backward direction. † significantly different from forward direction.

Different jump directions appear to challenge different aspects of landing biomechanics. Although TTS seems to be the best during the forward jump-landing, participants tended to land with greater stiffness than in the other directions. This is possibly due to greater horizontal velocity of the center of mass at take-off. Despite demonstrating comparable stiffness to the lateral and medial directions, participants' weight acceptance knee flexion excursion was close to 0° during the backward jump-landing. This may be due to the unique proprioceptive demands of a backward jump-landing.

Jumps should be performed from multiple directions in order to fully elucidate potentially injurious landing biomechanics. This is because one injury mechanism may be displayed for a given direction while others are not.

REFERENCES

1. DuPrey et al. *The American journal of sports medicine*, **44(6)**, 2016.
2. Butler, Crowell, & Davis. *Clinical biomechanics*, **18(6)**, 2003.

PERTURBATION-EVOKED LATERAL STEPS IN OLDER ADULTS: WHY TAKE TWO STEPS WHEN ONE WILL DO?

[1] James R. Borrelli, [1] Robert A. Creath, [1] Douglas Pizac, [1] HaoYuan Hsiao, [1] Ozell Sanders, [1] Mario Inacio, [1] Douglas N. Savin, [1] Mark W. Rogers

[1] University of Maryland School of Medicine, MD, USA
email: jborrelli@som.umaryland.edu, web: http://asb2018.asbweb.org/

INTRODUCTION

Many older adults at risk for falls have difficulties stepping sideways as a protective response to a lateral loss of balance. Younger adults tend to use a single lateral step while older adults are more prone to taking multiple steps [1]. Multistep strategies are associated with an increased risk of inter-limb collisions, more complex step trajectories [2], and an increased risk of falls [3]. The first step of a multistep strategy has been suggested to be preparation for executing a subsequent lateral step with the ipsilateral leg, relative to the fall direction [4]. Although the first step of a multistep strategy has been proposed to be less stable [4,5], it may be easier to execute due to passive unloading that facilitates more rapid swing-foot lift off [4]. The characteristics of the second step in a multistep step strategy are largely unknown.

The primary purpose of this study was to characterize: 1) the spatio-temporal step parameters; and 2) the stability of single and multi-step strategies of older adults to unpredictable lateral waist-pull perturbations. We hypothesize that the first step of a multistep strategy is less stable than a single lateral sidestep. Furthermore, we hypothesize that the first step of a multistep strategy is preparation for a subsequent lateral step. Therefore, we expect lateral steps to have similar spatio-temporal and stability characteristics whether they are the first or second step.

METHODS

This study focused on strategies that consisted of a medially directed sidestep (MSS) followed by a lateral sidestep (LSS2) or a single lateral sidestep (LSS1, 19 and 14 of 51 trials respectively). The stepping strategies were evoked from seventeen community dwelling older adults (11 females and 6 males; 72.7±5.7 years old; 165±2 cm; 72±3 kg) out of a group of 21 subjects that received 36 randomly applied, motor-driven lateral waist-pull (described previously [6]) perturbations at six displacements (5, 8.6, 12.1, 15.7, 19.3, 22.8 cm), velocities (9, 18, 27, 36, 45, 54 cm/s), and accelerations (180, 360, 540, 720, 900, 900 cm/s^2). Trials with a leftward pull at the perturbation level at which the mean protective stepping response became a multistep reaction were considered for analysis.

Three-dimensional motion-capture (Vicon) was used to collect kinematic data (sampling rate = 120 Hz, low-pass filtered at 6 Hz using a dual-pass fourth-order digital filter). Forty-four retro-reflective markers were used to calculate whole-body center of mass (COM) position [7]. Step initiation was defined as the time that the lateral ankle marker's vertical velocity exceeded 0.07 m/s [8] and was verified visually. Step termination was defined as the 2nd zero crossing of the lateral ankle vertical velocity.

Stability was quantified using the margin of stability (MOS) defined by Hof [9],

$$MOS = BOS - \left(x + \dot{x}/\sqrt{g/L}\right),$$

where BOS is the base of support, g is gravitational acceleration, L is the average body COM height prior to perturbation, and x and $\dot{x}$ are the COM displacement and velocity. Positive MOS values indicate a stable state while negative values imply instability. The MOS and COM velocity were calculated at step initiation, during swing (maximum COM velocity and minimum MOS), and at step termination. The lateral limit of the BOS was the most lateral marker of the toe, lateral malleolus, or 5th metatarsophalangeal joint depending on the orientation of the foot.

A one-way repeated measures analysis of variance was used to test the effect of step type (LSS1, MSS, and LSS2) on the dependent variables (pull magnitude, step initiation, swing time, step length, COM displacement, COM velocity, and MOS). Data were rank transformed to avoid violating the underlying assumptions of the ANOVA. The method of Benjamini and Hochberg [10] was used to control for multiplicity of testing.

RESULTS AND DISCUSSION

Step initiation, step length, COM displacement, COM velocity during swing, and MOS were significantly affected by step type (Table 1). Step length was shorter, COM displacement and COM velocity during swing were smaller, and the MOS was larger at step initiation and during swing for MSS compared to LSS1. The MOS at step termination was smaller for MSS compared to LSS1. Step initiation occurred later, COM displacement and COM velocity during swing, and MOS at step initiation were smaller for LSS2 compared to LSS1. The MOS for LSS1 was smaller than LSS2 during swing.

The results do not entirely support our hypothesis. A MSS is less stable than a LSS1 only at step termination. Even though all three step types do not reach the limit of stability (the point at which a step must be taken) at step termination, a LSS2 was required to regain balance following a MSS. The MOS at step termination is comparable between a LSS1 and a LSS2, which is likely an important factor in avoiding additional compensatory steps. This result is consistent with previous studies of lateral balance that reported stepping may occur before the limit of stability is reached (e.g. [11]).

While a MSS may be taken in preparation for a LSS2, a MSS also appears to modify the subsequent LSS2 (delayed step initiation, shorter COM displacement, slower COM velocity during swing, and improved MOS during step initiation and swing) compared to a LSS1. Taking a MSS then a LSS2 extends the time it takes to recover balance and achieve a MOS sufficient to terminate compensatory stepping, introducing the risk of inter-limb collisions, more complex step trajectories [2], and increased incidence of falls [3] compared to LSS1.

REFERENCES

[1] Mille, et al. *Clin Biomech*, 20(6), 2005
[2] Maki, et al. *J Gerontol:* Med Sci, 55(5), 2000
[3] Johnson-Hilliard, et al. *Arch Phys Med Rehabil*, 89(9), 2008
[4] Maki et al. *J Biomech.* 29(3), 1996
[5] Patton, et al. *Conf Proc IEE Eng Med Biol Soc*, 2006
[6] Pidcoe and Rogers. *J Biomech*, 31(4), 1998
[7] Eames, et al. *Human Mvmnt Sci*, 18(5), 1999
[8] Hurt, et al. *Exp Brain Res*, 214(4), 2011
[9] Hof, et al. *J Biomech*, 38(1), 2005
[10] Benjamini and Hochberg. *J R Stat Soc Ser B*, 57(1), 1995
[11] Pai, et al. *J Biomech*, 31(12), 1998

ACKNOWLEDGEMENTS

NIH/NIA R01AG033607, the University of Maryland Claude D Pepper-OAIC NIH/NIA P30AG028747, the UMANRRT Program (NIDRR 90AR50280, NIDILRR 90AR5004 formerly H133P100014). The assistance of the Baltimore VA Medical Center, Geriatric Research, Education and Clinical Center is gratefully acknowledged.

Table 1: Mean (standard error of the mean) of the outcome measures. Significant Tukey-Kramer post-hoc differences (α=0.05) are denoted with † (LSS1 and MSS) and ‡ (LSS1 and LSS2). Note: step termination often occurred briefly after step initiation of the second step (LSS2).

		LSS1	MSS (followed by LSS)	LSS2 (after MSS)	*p*-value
	Pull Magnitude	4.79 (0.26)	4.21 (0.22)	4.21 (0.22)	0.39
	Step Initiation (ms)	399 (31)‡	399 (26)	625 (42)‡	**0.0007**
	Swing Time (ms)	423 (16)	376 (18)	430 (18)	0.13
	Step Length (%height)	21.9 (1.9)†	6.1 (0.9)†	19.3 (1.4)	**<0.0001**
	COM Displacement (%height)	14.5 (1.1)†,‡	6.2 (0.6)†	10.2 (0.9)‡	**0.0002**
Step Initiation	COM velocity (%height/s)	13.1 (1.8)	8.1 (1.2)	12.9 (1.5)	0.19
Swing	COM velocity (%height/s)	41.6 (3.4)†,‡	24.2 (1.6)†	30.5 (2.0)‡	**0.013**
Step Termination	COM velocity (%height/s)	25.5 (3.3)	23.6 (2.0)	20.4 (1.7)	0.54
Step Initiation	MOS (cm)	8.7 (1.6)†,‡	12.1 (1.0)†	6.3 (1.0)‡	**0.0221**
Swing	MOS (cm)	-57.0 (2.5)†,‡	1.3 (1.1)†	-45.3 (1.8)‡	**<0.0001**
Step Termination	MOS (cm)	17.8 (1.5)†	6.6 (0.8)†	18.5 (1.2)	**<0.0001**

INVESTIGATION OF EXPOSURE TIME ON DYNAMIC STABILITY MEASURES DURING COMMON ASSESSMENT TASKS

K. Otto Buchholz, Sara Nash, Arastoo JahanAfrooz, Gary D. Heise and Jeremy D. Smith

University of Northern Colorado, Greeley, CO, USA

INTRODUCTION

Dynamic stability is the postural control system's "ability to maintain balance while transitioning from a dynamic to a static state" [1]. Commonly used in clinical and research settings, dynamic stability assessment tasks include the forward hop (FWH), drop landing (DPL), and lateral hop (LAH). Differences between testing protocols, particularly the amount of exposure individuals have to the task prior to data collection, may influence the measures used to quantify stability in many of these tasks. In many instances, the amount of exposure to the task provided prior to the data collection is not reported. For example, in a forward hop landing task the same research group in one article [1] described that participants were given as many practice trials as they needed without providing the number of trials, but in a subsequent article [2] reported that participants completing the same task on average used ~5 practice trials. In the latter paper [2], the dynamic stability indices were slightly lower than the first for the same task [1].

Other measures of hopping performance have been shown to improve with further exposure to the task, such as total hop distance [3, 4]. In addition, rarely is landing velocity (LV) reported in dynamic stability studies. The combination of exposure time and landing velocity at impact may provide insights into differences in stability measures across studies. Thus, the purpose of this study was to determine whether measures of dynamic stability, such as Time to Stabilization (TTS) and the Dynamic Postural Stability Index (DPSI), are influenced by the amount of exposure to the task and landing velocity at impact.

METHODS

Seventeen healthy participants (10 males: 24 ± 3 years, 174 ± 9 cm, 80.1 ± 15.4 kg; and 7 females: 23 ± 2 years, 167 ± 8 cm, 65.2 ± 5.2 kg) from the general population who were not currently participating in any formal stability training were recruited for this study. All subjects were injury-free for six months prior to the study.

Each participant performed 30 barefoot repetitions of one hop task (DPL, FWH, LAH) per day, with a different task each day. At least 24 hours were required between collection sessions to allow for recovery. No practice trials were allowed prior to collection. The foot the participant would use to kick a ball determined leg dominance. Each repetition required jumping from both feet and landing on their dominant leg to balance for 20 seconds. The participant repeated the trial if balance was lost. The DPL was performed from a 30 cm box placed at the edge of the force plate. Participants stepped off of the box and landed to stabilize. For FWH and LAH tasks, subjects started at a line 70 cm from the center of the force plate, clearing a 15 cm hurdle. For FWH, their toes were at the line and the lateral edge of their dominant foot for the LAH. Each task was performed in 3 sets of 10 repetitions with five-minutes of seated rest after each set.

The DPSI (based on 3 s) [1] and TTS (vertical force) [5] trial means were analyzed for trend as 30 individual trials using a second order polynomial, as well as being grouped into bins (3 or 5 means per bin) and tested with a repeated measures ANOVA ($\alpha < 0.05$). Individual scores were also assessed with ICC. LV was analyzed as a correlation with each measure.

RESULTS AND DISCUSSION

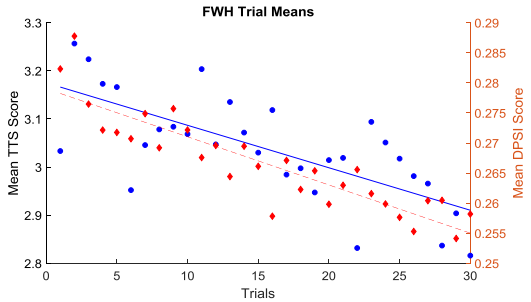

Figure 1: TTS and DPSI trial means of all participants

Individual trials were examined for trend (Fig. 1). The derivative of the second order polynomial fit to the DPSI trial means indicated the minimum of the curve occurred at trial 20 (DPL), 35 (FWH) and 23 (LAH). This indicates that the overall trend was decreasing up until that point, with FWH not reaching a minimum within the protocol.

Means were then grouped into bins (Fig. 2), which did not show a significant decrease in score (RM-ANOVA) between bins, except within DPSI scores for FWH (Table 1).

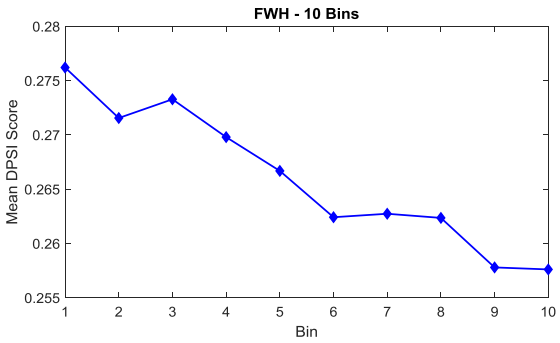

Figure 2: DPSI mean score grouped by 3 means per bin

Model Significance	DPL	FWH	LAH
6 Bins	0.100	0.025*	0.287
10 Bins	0.156	0.043*	0.128

Table 1: Model significance (p-value) in two different analysis methods by task using DPSI

Using individual participant scores per trial, overall ICCs were calculated to assess reliability of the scores over each protocol. The ICC dot plot for FWH DPSI is shown in Figure 3.

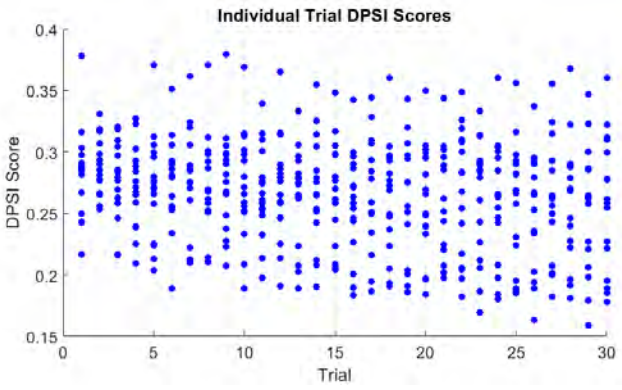

Figure 3: ICC (0.197) dot plot of FWH DPSI calculation

ICC values indicated very low reliability for both TTS (0.015 - 0.191) and DPSI (0.048 - 0.197) over the course of the 30-trial protocol for all conditions. Thus, these low ICCs indicate that data from trial to trial were not repeatable. Previous researchers [2–4] have also suggested continued score improvement with more trials, with Bolgla et al. [3] indicating that after three practice trials (FWH) subjects still consistently improved over the five test trials. They suggested that optimal performance may require more than eight trials. Our results were consistent with this trend, but more importantly indicated that this improvement continued over the course of 30 trials.

Correlations between DPSI, TTS and landing velocity are shown in Table 2.

Correlations	DPSI Vs. TTS	DPSI Vs. LV	TTS vs. LV
DPL	0.656	0.759	0.612
FWH	0.553	0.768	0.576
LAH	0.207	0.467	0.210

Table 2: Correlations (Pearson's r) between scores and each score with landing velocity

Landing velocity showed moderate to strong correlations with the TTS and DPSI scores. This indicates that an increased landing velocity was related to worse stability (higher DPSI and TTS). When testing stability indices of dynamic tasks, landing velocity should either be controlled for or accounted for during the analysis phase.

CONCLUSIONS

These results indicate that exposure time to the task influences DPSI and TTS. If using these measures, every participant should have the same amount of practice and test trials to ensure equal task familiarity between participants. In addition, landing velocity influenced these stability measures and should be controlled for when using these measures to assess stability. One other interpretation of these outcomes might be that DPSI and TTS are not quality measures of stability given the lack of repeatability from trial to trial.

REFERENCES

[1] Wikstrom et al., *J. Athl. Train.*, **40**, 2005.
[2] Wikstrom et al., *J. Sci. Med. Sport*, **11**, 2008.
[3] Bolgla and Keskula, *J. Orthop. Sports Phys. Ther.*, **26**, 1997.
[4] Booher et al., *J. Sport Rehabil.*, **2**, 1993.
[5] Ross and Guskiewicz, *Athl. Ther. Today*, **8**, 2003.
[6] Ross et al., *J. Strength Cond. Res.*, **16**, 2002.

INFLUENCES OF LOW BACK PAIN ON THE ENERGY CONTRIBUTIONS OF THE HIP AND SPINE DURING GAIT AMONG PERSONS WITH LOWER LIMB LOSS

[1] Courtney M. Butowicz, [1,2] Rebecca L. Krupenevich, [1] Julian C. Acasio, and [1,3,4] Brad D. Hendershot
[1] Walter Reed National Military Medical Center, Bethesda, MD, USA
[2] University of Maryland, College Park, MD, USA
[3] DoD-VA Extremity Trauma and Amputation Center of Excellence, USA
[4] Uniformed Services University of the Health Sciences, Bethesda, MD, USA
Email: courtney.m.butowicz.ctr@mail.mil

INTRODUCTION

Persons with vs. without unilateral lower limb loss (LL) walk with altered trunk-pelvic mechanics that, with repeated exposure, presumably represent a mechanistic pathway for low back pain (LBP) [1,2]. Specifically, persons with LL walk with increased lateral trunk motion over the stance limb, posited as an adaptive strategy to compensate for absent or weak musculature in the lower extremity. Moreover, hip ab/adduction moments may compensate for increased lateral trunk motion over the stance limb, suggesting an altered motor pattern that redistributes energy/power during gait [3]. Among uninjured individuals, impaired hip abductor strength is associated with LBP, suggesting impaired load/energy transfer between the lower extremity and lumbar spine. While persons with vs. without LL demonstrate increased positive phases of joint powers at L5/S1 in the frontal plane, the contributions of the unaffected hip powers to lumbar spine mechanics are unknown. Further, to date, no study has compared frontal plane low back and hip movement strategies among persons with limb loss and varying degrees of disability associated with LBP. Thus, the objective of the current study was to determine the contributions of hip and low back joint powers (L5/S1) to LBP-related disability among persons with limb loss, hypothesizing that persons with greater LBP disability will demonstrate larger power generation through the unaffected hip and low back.

METHODS

Nineteen persons with traumatic unilateral lower LL (n = 7 transfemoral, n = 12 transtibial; mean ± standard deviation age: 31.9 ± 12.5 yrs, stature: 1.8 ± 0.1 m, body mass: 89.1 ± 13.7 kg, and time since injury: 8.6 ± 7.0 yrs) participated in this cross-sectional study after providing written informed consent to study procedures approved by the local IRB. Acute LBP was characterized using a Visual Analog Scale. The presence of chronic LBP was determined via self-report using the Oswestry Disability Index (ODI; "I have 'chronic pain' or pain that has bothered me for 3 months or more"), and was further quantified using ODI percent disability. Participants walked at 1.3 m/s (±10%) along a 15m walkway with full-body biomechanical data captured using an 18-camera system (Qualisys, Göteborg, Sweden) and six force platforms (AMTI, Watertown, MA) embedded within the walkway. Marker positions and ground reaction forces (GRF) were smoothed using a fourth-order dual-pass Butterworth filter with cutoff frequencies of 6 Hz and 45 Hz, respectively. L5/S1 and hip joint powers were calculated as the product of joint moment and angular velocity using 6DOF inverse dynamics in Visual3D (C-motion, Germantown, MD) and normalized to body mass. Positive/negative work at the L5/S1 and hip joints, calculated as the total areas under the joint power curves, respectively indicate mechanical energy generation/absorption.

Multiple regression was used to determine the influences of frontal plane L5/S1 and hip joint powers on ODI percent disability among persons with LL. Independent t-tests were used to determine differences in work between persons with and without chronic LBP at L5/S1 and hip joints throughout the gait cycle ($P < 0.05$).

RESULTS AND DISCUSSION

After controlling for time since amputation and stride width, the total positive and negative powers for both L5/S1 and hip joints significantly predicted

LBP-related disability ($F_{(6,18)}$ = 5.11, P = 0.008), with all but positive hip power significantly contributing to the prediction. Total positive and negative work through the unaffected hip and low back explain 58% of the variance in the model. While there were no significant (P > 0.11) differences in the total work at L5/S1 or hip joints between persons with LL whom identified themselves as having chronic LBP (acute pain = 1.4 ± 1.7, ODI percent disability = 26.5 ± 24.7) and those who did not (acute pain = 0.1 ± 0.3, ODI percent disability = 11.3 ± 12.4), there were distinct differences in joint power waveform characteristics throughout the gait cycle. At L5/S1, persons with LL and chronic LBP demonstrate greater energy absorption during loading response, whereas those without LBP demonstrate greater energy absorption just prior to toe-off (Figure 1). Persons with LL and chronic LBP walk with greater trunk motion during early stance yet demonstrate larger energy absorption at the hip. Although not reported here, this is likely the result of greater hip joint angular velocity, counteracting larger trunk lateral flexion and contralateral pelvic drop during early stance, as a means to maintain mediolateral balance. Such a hip dominant strategy could also have implications for the increased joint loading and prevalence of hip osteoarthritis among persons with LL [5]. The two distinct negative power phases at L5/S1 among persons with LL without chronic LBP are similar to previous reports [4]; in contrast, persons with LL and chronic LBP demonstrate a smaller L5/S1 negative peak power at toe-off that is coupled with a larger positive peak power at the hip. The larger power generation at the hip suggests an active hip strategy to control the mediolateral movement of the center of mass as it moves from peak lateral flexion over the stance limb towards the subsequent heel-strike of the affected limb. Thus, persons with limb loss and LBP may adopt a compensatory strategy to avoid pain and/or to account for impaired neuromuscular control of the trunk. Future research should focus on developing interventions geared towards improving neuromuscular control strategies of the trunk-pelvic-hip complex, thereby reducing possible mechanisms of LBP-related disability.

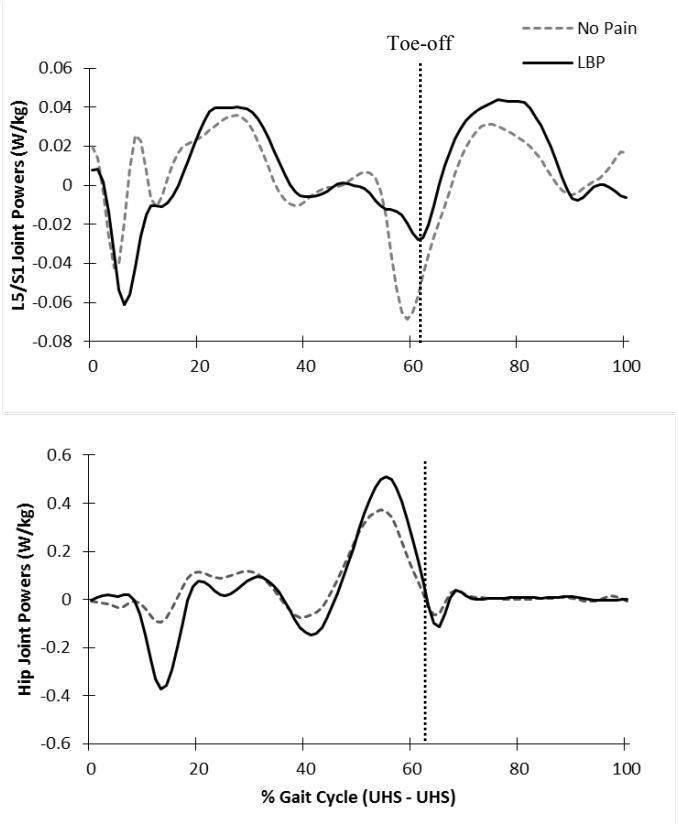

Figure 1: L5/S1 (top) and unaffected hip joint (bottom) powers during the gait cycle (unaffected heel strike (UHS) to unaffected heel strike (UHS)) among persons with limb loss with vs. without self-identified chronic LBP.

REFERENCES

1. Hendershot, et al *Clin Biomech* **29:** 235-242, 2014.
2. Hendershot, et al. *J Biomech* in press: 2018.
3. Rueda, et al. *Gait & Posture* **37:** 436-439, 2013.
4. Hendershot, et al. *APMR* **96:** 154-157, 2015.
5. Hurwitz, et al. *J Biomech* **31**: 919-925, 1998.

ACKNOWLEDGEMENTS

Supported by Award: W81XWH-14-2-0144. The views expressed herein are those of the authors and do not necessarily reflect the official policy or position of the Departments of the Army or Defense, nor the United States Government.

UNWINDING THE CONTROL OF WALKING TURNS

[1] Carolin Curtze

[1] Oregon Health and Science University, Portland, OR, USA
email: curtze@ohsu.edu

INTRODUCTION

The concept of the extrapolated center of mass (XcoM) suggests a simple rule for stable walking: at initial contact the foot is placed at a certain distance behind and lateral to the XcoM, thereby redirecting the movement of the XcoM into a sinusoidal trajectory [1]. In a simulation of walking turns, Hof [1] showed that turns can be achieved by rotating these forward and lateral offsets over a certain angle.

The goal of this study is to experimentally test the proposition that turning is controlled by changes in the mediolateral foot placement relative to the XcoM. It was hypothesized that an increase in lateral foot placement leads to a change in walking direction during the subsequent step.

METHODS

Three healthy participants (2 male / 1 female, age 66-76 years, height 1.62-1.77 meter, and weight 63-78 kg) were recruited for this study.

Participants performed preplanned turns to the left and right, at different turn angles (45, 90, 135, and 180 degrees) while walking at normal and fast speeds. Floor markings similar to a clock face consisting of a turning point in the center and turn angle marks in the periphery were used to indicate turn angle. The experimental protocol was approved by the local Medical Ethics Committee. All participants gave their informed consent.

Full-body kinematics were acquired using 12 infrared motion capture cameras (Report-H (8) and Osprey (4), Motion Analysis Inc.) sampling at a frequency of 120 Hz. A total of 30 reflective makers were attached bilaterally to the following bony landmarks: head (front, back, and lateral), thorax and arms (acromion, sternum, offset, lateral epicondyle of humerus, and distal radius), pelvis (sacrum, anterior superior iliac spine (ASIS)), legs (thigh, lateral epicondyle of the femur, shank, lateral and medial malleolus), and feet (1st and 5th metatarsal head, and posterior calcaneus). All data were low-pass filtered at 6Hz using a fourth-order Butterworth filter.

The position of the XcoM [1] was defined based on the inverted pendulum model:

$$\mathrm{XcoM} = \mathrm{CoM} + v_{\mathrm{CoM}} / \omega_0$$

in which CoM denotes the positon of the center of mass, and v_{CoM} the velocity of the CoM. The eigenfrequency of a pendulum is denoted as

$$\omega_0 = \sqrt{g/l},$$

where l is the effective pendulum length defined as mean CoM height.

During straight walking the mediolateral direction can be defined as perpendicular to the overall walking direction. During turning, the coordinate frame changes with the arc of the walking path. This constant change in reference frame is accounted for by transforming position data from a global (Figure 1) to a local/pelvis based coordinate system. Subsequently, the offset between the center of mass of the foot and XcoM in mediolateral (b_{ml}) and anteroposterior (b_{ap}) direction was determined.

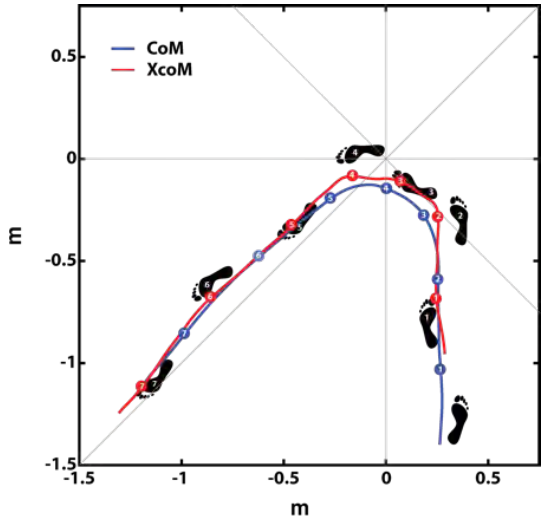

Figure 1: Planar view of the stepping pattern with CoM and XcoM trajectory for a 135-degree turn.

To determine the relationship between mediolateral foot placement on the change in walking direction, linear regression models were fit for the outside and inside limb for each of the participants.

RESULTS AND DISCUSSION

Figure 2 describes the phase dependent offset between the center of mass of the left and right foot and the XcoM throughout the gait cycles. To execute the 135-degree turn to the left, both feet are placed with an offset lateral to the right of the XcoM.

At initial contact, participants placed their outside limb more lateral to the XcoM, than the inside limb (β_0, Table 1; Figure 3). By linear regression it was found the for larger changes in walking direction participants place their outside and inside limb further lateral to the XcoM (β_1, Table 1). Participant #3, however, maintained a large margin of stability (β_0, Table 1) for the inside limb with only a marginal effect of turn angle (β_1, Table 1), suggesting a more conservative, mediolaterally stable turning strategy.

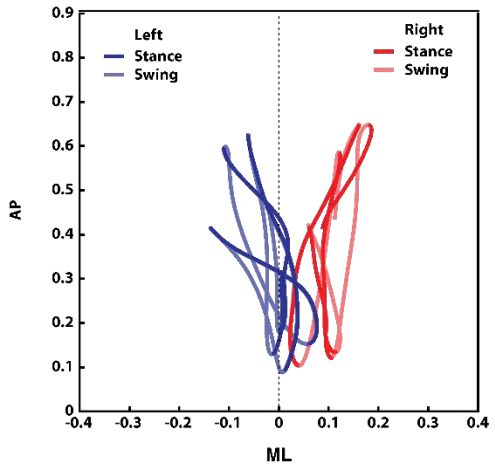

Figure 2: Phase-plot of b_{ml} and b_{ap} for a 135-degree turn to the left (Figure 1).

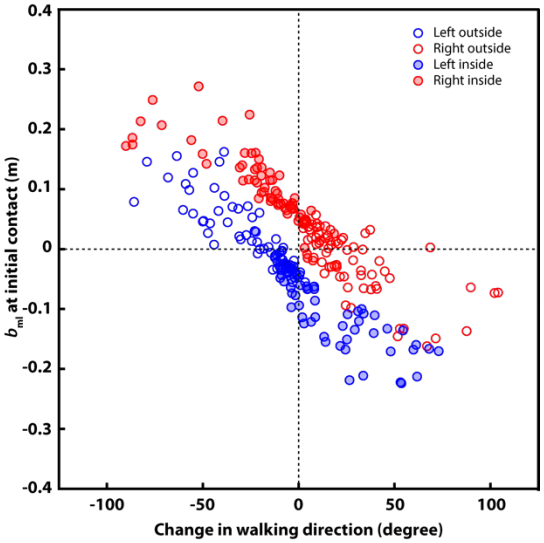

Figure 3: Mediolateral offset (b_{ml}) at initial contact against the change in walking direction during the subsequent step. Limbs are categorized as either outside or inside, based on the overall direction of a turn. Experimental data of participant #1.

CONCLUSIONS

Walking in turns requires a tradeoff between mediolateral stability and ability to change walking direction.

REFERENCES

1. Hof. Hum Mov Sci. 27(1):112-25. 2008.

ACKNOWLEDGEMENTS

This study was supported by the Medical Research Foundation of Oregon.

Table 1: Linear regression models of b_{ml} at initial contact and change in walking direction.

Participant	Outside limb		Inside limb	
	Slope (β_1)	Intercept (β_0)	Slope (β_1)	Intercept (β_0)
#1	-0.0021	0.0621	-0.0019	-0.0305
#2	-0.0008	0.0634	-0.0017	-0.0285
#3	-0.0011	0.0634	-0.0004	-0.0511

REACTION TIME OF YOUNG ADULT AND MIDDLE-AGED MEN AND WOMEN DURING A FORWARD FALL

Margo Donlin, Kurt DeGoede, Ph.D., Dan Panchik, Ph.D.

Elizabethtown College, Elizabethtown, PA 17022
Email: donlinm@etown.edu, degoedek@etown.edu, panchikd@etown.edu

INTRODUCTION

Middle-aged (MA) women fracture their wrists more than twice as frequently as MA men, partly due to falling more frequently [1, 5]. A potential reason for this disparity is that MA women may have slower reaction times than MA men, leading to increased falls and an increased risk for wrist fractures. However, few studies have used MA subjects, resulting in a gap in scientific knowledge. The purpose of this study was to test for differences in reaction time (RT) to initiate a recovery step during a forward fall (trip).

METHODS

The tether-release method, which has been shown to be a consistent fall simulator, was used to initiate a forward fall in young adult (YA, 18-30 years old) and MA (40-59 years old) men and women [2, 4]. PASCO Force Plates and a load cell collected data at 2 kHz, and a MotionNode accelerometer collected data at 100 Hz during the fall trials. Subjects were suspended at a 15±2° forward lean and were released at a random time within 30 seconds of the beginning of data collection.

Reaction times in milliseconds (ms) were calculated by the difference between the release time and the initiation of a recovery step. Release time was determined to be when the load cell registered less than 50% of the voltage that the subject initially generated. Step time was determined to be when the force plate under the subject's dominant foot registered less than 40% of the force on that plate at the time of release. Each subject performed one practice trial, two undistracted trials, and two distracted trials. Subjects were given a maze with a washer on it and told to maneuver the washer along a printed path while leaning for the distracted trials. The reaction times were averaged into one undistracted reaction time and one distracted reaction time.

RESULTS AND DISCUSSION

Average undistracted and distracted reaction times are shown in Figure 1. Two-tailed t-tests showed that there was no difference between the reaction times of YA and MA females in distracted or undistracted scenarios (p=0.355, p=0.153). Average undistracted and distracted reaction times for males and females are shown in Figure 2. There was no difference between reaction times of MA males and MA females in undistracted or distracted scenarios (p=0.221, p= 0.288).

Paired t-tests showed that there was no difference between undistracted and distracted reaction times in YA subjects (p=0.189), MA subjects (p=0.067), or overall (p=0.750). However, MA subjects tended to have slightly faster distracted reaction times than undistracted reaction times.

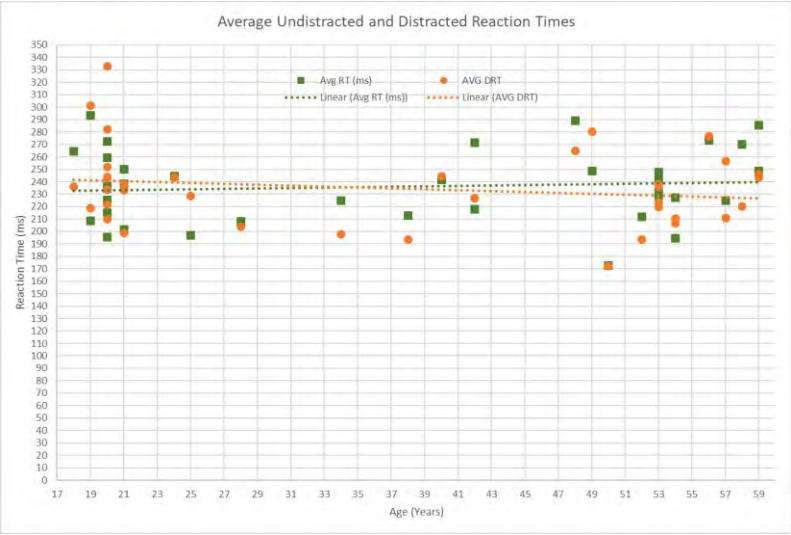

Figure 1: Graph showing age of subject plotted against their average undistracted and distracted reaction times. YA reaction times were not faster than MA reaction times in undistracted or distracted conditions (p=0.656, p=0.165).

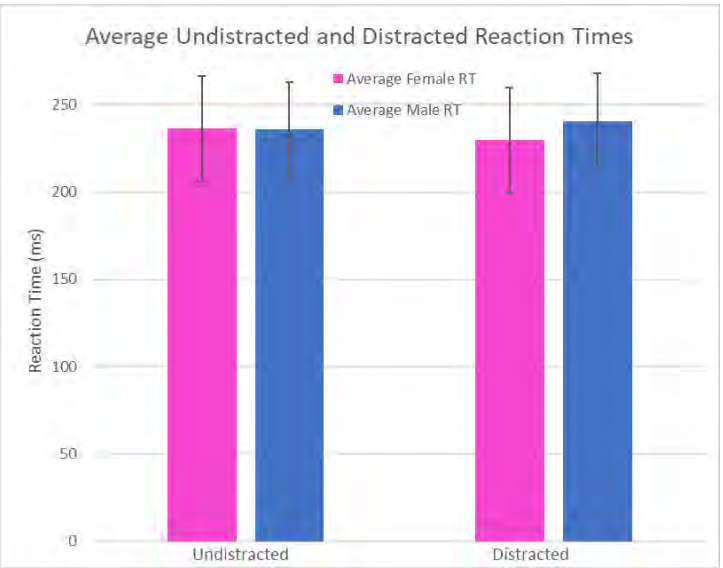

Figure 2: Graph showing male and female average distracted and undistracted reaction times and standard deviation. Male and female undistracted and distracted reaction times did not differ.

Although more MA women fall than MA men (5), reaction time is not why MA women fall more frequently. However, it is still unknown why MA women experience this phenomenon that puts them at greater risk for wrist fractures. Although osteoporosis would be a logical assumption for why MA women fracture their wrists more frequently than MA men, osteoporosis was found to be infrequent in women under 65 years old; therefore, osteoporosis cannot be the main reason that MA women experience more wrist fractures than MA men [3].

Since undistracted and distracted reaction times did not differ across all subjects, the distraction clearly did not affect the vestibular system, which is responsible for maintaining balance and spatial positioning. Although the mind and body were distracted by the maze task, the vestibular system was still able to respond to the impending fall in the same amount of time, indicating that a someone who trips while walking in a distracted state should have the same potential to recover from that trip as if they were not distracted.

The variability of the data was very large, and it is difficult to determine if that variation was due to natural differences in reaction time or due to age differences or the maze distraction. The average difference in a subject's undistracted reaction times was 3.816 ms, and the average difference between distracted trials was 2.355 ms. The average difference between the average undistracted and distracted times was 1.362 ms, indicating that the subjects responded to the simulated trip very consistently. The distraction caused no more variation in the trials than a subject's natural variation between trials.

Furthermore, the consistent angle of lean may have affected the reaction times, specifically for the YA subjects. Pierre's study used increasing lean angles to determine the maximum recoverable lean angle and showed that MA subjects could recover from a less severe lean than YA subjects (4). Using the same lean angle for all subjects may have resulted in differing levels of urgency for the different age groups. A more threatening lean for the MA age group may have resulted in faster MA reaction times compared to YA reaction times. In order to rectify this, an additional study could be performed using a lean angle based off the subject's age.

CONCLUSIONS

The primary conclusion from this study was that for mild trips with mild distractions, there is no noticeable age or distraction effect on reaction time. However, more serious trips or more involved distractions may show an effect on reaction time.

REFERENCES

1. Graven, A.R. (2013, April 16). Women at higher risk of wrist fractures. Retrieved on June 1, 2016 from http://sciencenordic.com/women-higher-risk-wrist-fractures
2. Hsiao-Wecksler, E.T. (2008, April). Biomechanical and age-related differences in balance recovery using the tether-release method. *Journal of Electromyography and Kinesiology, 18*(2). 179-187.
3. Lashin, H. & Davie, M.W.J. (2008, March). DXA scanning in women over 50 years with distal forearm fracture shows osteoporosis is infrequent until age 65 years. *International Journal of Clinical Practice, 62*(3). 388-393.
4. Pierre, M. (2016, January). Effect of age on the forward perturbation threshold line for lean releases, lean releases with surface translations and surface translations in younger, middle-aged and older adults. Unpublished master's thesis, Sherbrooke University, Quebec.
5. Talbot, L.A., Musiol, R.J., Witham, E.K., & Metter, E.J. (2005). Falls is young, middle-aged, and older community dwelling adults: perceived cause, environmental factors, and injury. *BMC Public Health, 5*(86).

THE EFFECT OF SPINAL DECOMPRESSION SURGERY ON THE GAIT EFFICIENCY AND BALANCE OF CERVICAL MYELOPATHY PATIENTS THROUGH SIX-MONTH FOLLOW-UP

Emily Dooley, Jason Horowitz, Hamid Hassanzadeh M.D., and Shawn Russell Ph.D.
University of Virginia, Charlottesville, VA, USA
email: sdr2n@virginia.edu

INTRODUCTION

Cervical myelopathy is a condition caused by compression of the spinal cord in the neck that results in difficulty walking and sensory loss at the extremities.[1] This difficulty walking is characterized by a shuffling gait pattern and a wider base of support during the stance phase. These characterizations stem from postural and dynamic instability, which can result from reduced sensation and motor control in the legs. To prevent further disability and spinal cord deterioration surgical decompression of the spinal cord can be performed.[2] Multiple studies have been conducted characterizing this difficulty walking and noting gait improvements following decompressive surgery.[2,3] However, in this population, gait and energy expenditure during normal walking is not well defined and could influence future therapy and rehabilitation.

Specifically, for this study we hypothesize that cervical decompression and stabilization:

(1) results in improved gait parameters during the first six months of follow-up with associated improvement in energy expenditure;
(2) results in improved postural stability

The overall aim of this study is to fully characterize stability, gait, and energy expenditure during the first six months following decompressive surgery and stabilization in patients with Nurick grade 2 or 3 cervical spondylotic myelopathy, as defined by walking difficulty that does not require assistance.

METHODS

Experimental data was collected for 12 subjects: 6 controls (4 female and 2 male, 57 ± 7.4 y.o.) and 6 subjects with cervical myelopathy (4 female and 2 male, 58 ± 13.4 y.o.). The myelopathy group was tested at -1, 3, and 6 months after surgery. Subjects were instructed to complete two tasks:

(1) stand as still as possible for 30-seconds
(2) walk at a self-selected comfortable speed

Walking trials were completed on a 15m walkway. A minimum of five standing sway trials and six walking trials were used for analysis. Subjects were recorded using Vicon Nexus and five Bertec force plates. Kinematic and kinetic data were exported for Matlab analysis.

To characterize gait we looked at the spatio-temporal parameters of walking speed, percent of gait cycle in double support, and stride length. Gait efficiency was determined by measuring the total mechanical work during walking. Balance was assessed with two methods: path length normalized by time, and area of 95% confidence ellipses of that path. Path length refers to the path of the center of pressure of the subject's stance on a single force plate as the person attempts to stand as still as possible for 30-seconds.

RESULTS AND DISCUSSION

The myelopathy group tended to have slower walking speeds than the control population. After surgery this group tended to increase their walking speed and develop more efficient gait. Differences

Table 1. Summary of results on cohorts thus far. Significant differences are denoted with *.

	Path Length (mm/s)		**Ellipse Area (mm^2)**		**Walking Speed (m/s)**		**Double Support (% gait cycle)**		**Stride Length (m/LL)**		**Total Body Work (J/kg*m)**	
	Mean	*St. Dev.*	*Mean*	*St. Dev.*	*Mean*	*St. Dev.*	*Mean*	*St. Dev.*	*Mean*	*St. Dev.*	*Mean*	*St. Dev.*
Control	11.0 *	1.79	253	143.8	1.08	0.04	16	1	1.27	0.03	3.19	0.10
Baseline	17.7 *	2.88	740	320.0	0.96	0.07	18	1	1.23	0.03	3.21	0.12
Three Month	13.5	1.74	471	137.9	0.94	0.04	19	2	1.20	0.04	3.08	0.12
Six Month	14.1	1.39	381	97.9	0.98	0.04	20	4	1.24	0.08	2.79	0.12

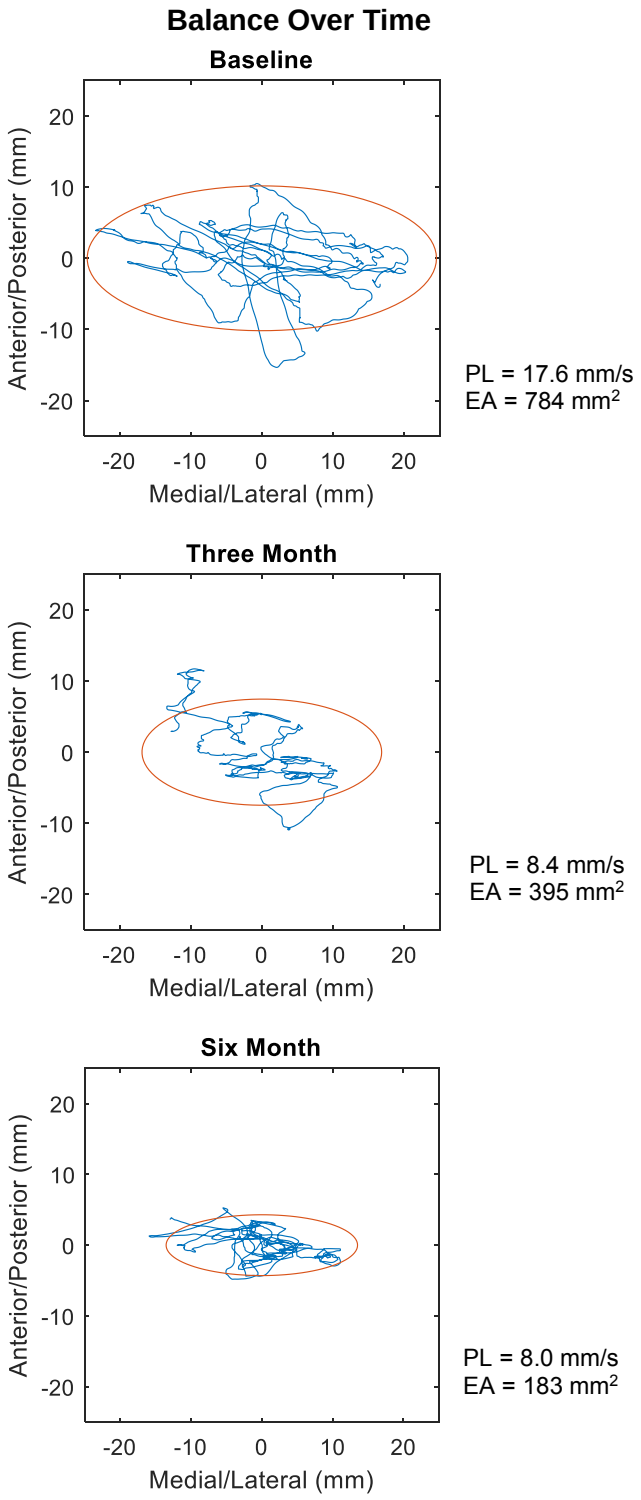

Figure 1. Best balance plot for one myelopathy subject at baseline, three month, and six month visits. Best meaning shortest path and smallest ellipse. The blue line is the path of the center of pressure over the duration of the trial. Total length per time is PL. The red oval is 95% confidence ellipse for the given path. The analyzed ellipse area (EA) is the area inside of the red oval.

seen in the time spent in double support and stride length were at the resolution of collection. With only six subjects in each group this study has not yet achieved full power. We anticipate these trends to become significant when the study is fully powered with 26 subjects in each group.

Despite the study not being fully power, significant differences in balance were found (*Figure 1*). The path length of the center of mass is significantly longer in the baseline population than the control group ($p < 0.05$). When looking at the area of the 95% confidence ellipse of that path differences are approaching significance between the control and both the baseline and the three-month post-surgery groups, as well as between the three-month post-surgery and the six-month post-surgery groups ($p = 0.07$).

CONCLUSIONS

The above results suggest that spinal decompression surgery improves the patient's stability and gait efficiency. This result was anticipated as difficulty with walking and balance are characteristic markers of cervical myelopathy.[4] Increased differences between the controls and the earlier time points of the myelopathy patients shows that the patients are approaching the control measures for balance and gait efficiency by six-months post-surgery.

REFERENCES

1. Ono et al. *Spine*. 1977, 2: 109-25.
2. Fehlings et al. *J. Bone and Joint Surgery*. 2013, 95:1651-8.
3. Singh et al. *Spine*. 2009, 34:1296-300.
4. Kuhtz-Buschbeck et al. *Gait & Posture*. 1999, 9:184-9.

ACKNOWLEDGEMENTS

The authors would like to thank Clayton Tondreau, Rachel Newman, and the rest of the UVA Motion Analysis and Motor Performance Lab for their continued assistance with data processing.

Age-related kinetic imbalances during gait

Eranda Ekanayake, William Estep, Osama Ramadan and Jerome Hausselle

BAMM Lab, Mechanical & Aerospace Engineering, Oklahoma State University, Stillwater, OK, USA
email: jerome.hausselle@okstate.edu, web: https://bammlab.okstate.edu/

INTRODUCTION

Muscle co-contractions in the lower limbs correlate with high joint contact forces, which in turn increases the risk of osteoarthritis (OA) onset [1]. Since half of Americans older than 65 suffer from this disease [2], there is no denying that age plays a significant role. Thus, assessing age-related effects on biomechanical parameters leading to increased joint contact forces is critical to prevent OA progression.

Although many studies have focused on analyzing single gait cycles, only a few have studied the fluctuations of variables related to imbalance over hundreds of cycles. Our aim was to quantify age-related variations in muscle co-contractions and mediolateral peak vertical ground reaction forces.

METHODS

The 18-25 control group consisted of eight younger subjects (age: 22 ± 1 years old), whereas the 50-60 study group consisted of eight older subjects (age: 57 ± 3 years old). The protocol was approved by the Institutional Review Board and each participant signed an informed consent form. Subjects walked barefoot at a self-selected speed on an instrumented treadmill (Noraxon, Scottsdale, AZ, USA) for 10 minutes. Vertical ground reaction forces (vGRF) were recorded at 100 Hz, as well as EMG signals of eight muscles of the right leg: rectus femoris (RF), vastus lateralis (VL), vastus medialis (VM), biceps femoris (BF), semitendinosus (ST), tibialis anterior (TA), lateral (LG) and medial (MG) gastrocnemius.

The vGRF signals were filtered using a 4th-order lowpass Butterworth filter (cutoff frequency: 20 Hz) [3]. To study side-to-side imbalances, we computed a GRF index using the peak vGRF during heel strike for two consecutive steps:

$$GRF\ index = 100 * \frac{|Right\_GRF - Left\_GRF|}{Right\_GRF}$$

EMG data was filtered using a 4th order Butterworth filter at 40-400 Hz, rectified, RMS-smoothed (50 ms window) [4,5], and normalized using the maximum value over the 10-minute trial. Co-contractions were computed during the stance phase for the thigh muscles (RF+VM+VL vs. BF+ST) and leg muscles (TA vs. LG+MG) by using the areas under the EMG envelopes for agonist and antagonist muscles (*Area* 1 and *Area* 2) and the common area [6].

$$Co\text{-}contraction = 100 * \frac{2*common\ area}{Area\ 1+Area\ 2}$$

We used Matlab to test for differences in the GRF index between genders and in the GRF and co-contraction indices between age groups. The Jarque-Bera test was used to test for normality. Normal data was analyzed using F-test to determine variance relationship of samples and independent 2-sample t-test to compare means. Non-normal data was analyzed using Mann-Whitney U test. *p*-values were set at 0.05.

RESULTS

The average number of gait cycles was 543 ± 25 for the 18-25 group, and 458 ± 127 for the 50-60 group. There was no significant differences in the GRF indices between sides for any of the subjects and between genders. We thus combined left and right data for each subject and sorted solely by age.

The mean GRF index was higher for older subjects (Fig. 1), but the difference was not significant ($p = 0.86$). The interesting finding is the larger range of values found for older subjects (4.4%) than for younger subjects (2.3%). This finding highlights that aging may hinder force modulation during the heel strike phase, due to impaired joint proprioception or potential emerging pain [7]. This kinetic imbalance may result in the consistent overloading of a particular side, thus increasing joint contact forces and the risk of potential OA onset.

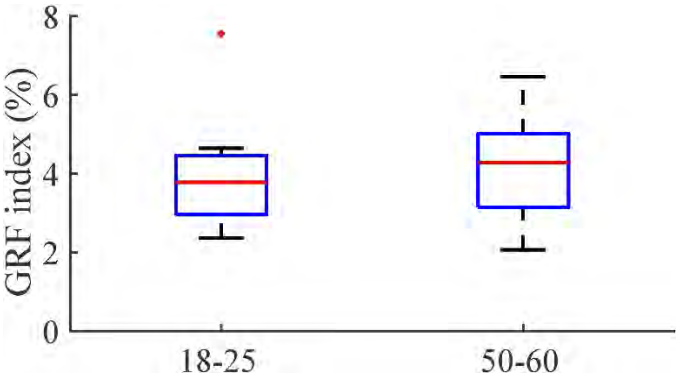

Figure 1. GRF Indices for each age group. Red lines represent median values, top and bottom of boxes represent 25th and 75th percentiles, respectively. Whiskers represent maximum and minimum values and cross displays outliers (1.5*Interquartile range [IQR], away from box limits).

The co-contraction index for thigh muscles was not significantly different between age groups ($p = 0.22$). However, it was significantly higher for older subjects in the leg muscles ($p < 0.01$) (Fig. 2). Since older subjects exhibit less plantarflexion muscle force [8], eccentric co-contraction of the TA may be a strategy to increase the propulsive force necessary to progress forward. Though not significant, the higher co-contraction index found for the thigh muscles of older subjects is a cause for higher-than-normal joint contact forces

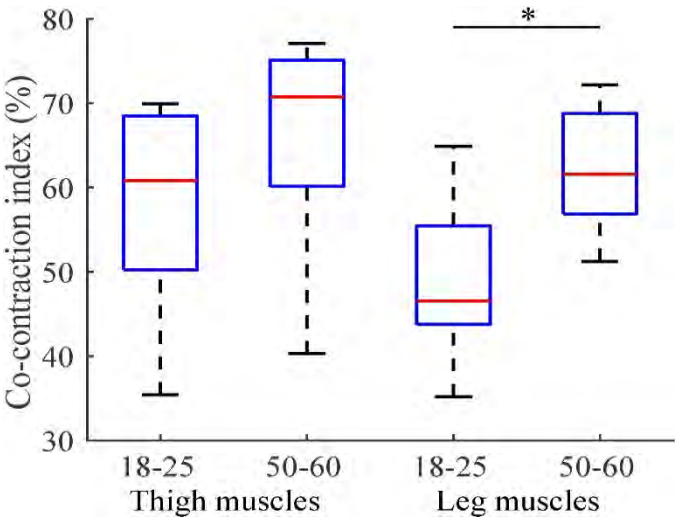

Figure 2. Co-contraction indices for each muscle and age groups. Symbols are similar to figure 1. The asterisk represents a significant difference ($p < 0.05$).

Even if not individually significant, combining higher side-to-side peak vGRF and muscle co-contractions should lead to higher-than-normal joint contact forces for older subjects. We are currently developing musculoskeletal models to estimate joint contact forces and confirm that these kinetic imbalances lead to increased forces and thus potential long-term cartilage damage.

One limitation of this study is the low number of subjects. Future work will target a larger population. Based on the data already collected, we will also select a gait speed suitable for all subjects to eliminate any potential speed-related effects.

CONCLUSIONS

Though not statistically significant, older subjects exhibited larger kinetic imbalances than younger subjects, even while walking at a self-selected speed. If confirmed by testing a larger population, our results indicate that older subjects may be at higher risk of overloading one side of their body, thus leading to increased joint contact forces and potential OA onset.

This study is the first critical step towards the development of efficient screening protocols to detect older adults at risk of developing OA in one or more of their lower limb joints.

REFERENCES

1. Tsai et al. *Journal of Orthopaedic Research*. 30(12): 2007-2014, 2012.
2. Barbour et al. *MMWR Morbidity and Mortalility Weekly Report*. 66: 246-253, 2017.
3. Kiss, R.M. *Medical Engineering & Physics*. 32(6): 662-667, 2010.
4. Shiavi et al. *Journal of Rehabilitation Research*. 24(2): 13-23, 1987.
5. Burden et al. *Journal of Electromyography and Kinesiology*. 13(6): 519-532, 2003.
6. Lo et al. *Gait and Posture*, 53: 110-114, 2017.
7. Knoop et al. *Osteoarthritis and Cartilage*. 19(4): 381-388, 2011.
8. Anderson and Madigan. *Journal of Biomechanics*. 47(5): 1104-1109, 2014.

POSTURAL CONTROL MEASURES BETWEEN INDIVIDUALS WHO FALL AND RECOVER AFTER AN UNEXPECTED SLIP

[1]John Garner, [2]Paul Donahue, [2]Caleb Williams, [2]Christopher Hill, [2]Lauren Luginsland,

[2]Dwight Waddell, [3]Harish Chander & [2]Sam Wilson.

[1]Troy University, Troy, AL, USA
[2]University of Mississippi, University, MS, USA
[3]Mississippi State University, Mississippi State, MS, USA
Email: jcgarner@troy.edu web: https://trojan.troy.edu/healthandhumanservices/khp/

INTRODUCTION

Disruptions to balance are alarmingly regular occurrences on a daily basis. Whether it is being bumped walking down a busy street, traversing an icy sidewalk, tripping over an unexpected obstacle, or encountering a slippery contaminant, there are countless situations that can result in a loss of balance, and a subsequent fall. Thus, it is no surprise that falls account for large rates of injury in multiple populations. The process of an unexpected slip is divided into four distinct phases (environment, initiation, detection, and recovery) [1]. Researchers have commonly classified slips in a severity range based on the magnitude of this heel slip distance, as well as the velocity of the heel slip [2-4]. Though, more recent work has attempted to quantify the slip response as a fall or recovery through the use of a force criterion in the fall arrest harness system [5]. Previous research using equilibrium scores during sensory organization tests have suggested that individuals with decreased EQ scores slipped longer when exposed to unexpected slips [1]. The purpose of this study was to examine postural control parameters between those classified as a fall, or recover during an unexpected slip.

METHODS AND PROCEDURES

This study was conducted in a case-controlled design, with 40 healthy adults (20 male, 20 female; age: 21.96 ± 3.178; height: 171.37cm ± 13.79; weight: 75.69kg ± 16.51), who had no history of musculoskeletal, orthopedic, neurological, or vestibular abnormalities. Standing postural control measures were recorded using the six conditions of the Neurocom® sensory organization test (SOT) [eyes open (EO), eyes closed (EC), eyes open with sway referenced vision (EOSRV), eyes open with sway referenced support, (EOSRP), eyes closed with sway referenced support (ECSRP), and eyes open with sway referenced vision and support (EOSRVP). The variables were the sway velocity components in the medial-lateral (M/L) and anterior-posterior (A/P) directions, and root mean square (RMS) of CoP displacement in the anterior-posterior (A/P) and medial-lateral (M/L) directions. An 8 camera Vicon Nexus (Oxford, UK) 3D motion capture system was used to collect and analyze kinematic gait data. A lower body plug-in gait model from the Helen–Hayes marker system was used for the participant configuration and the kinematic data was sampled at 100 Hz and collected using the Vicon Nexus software. A back-pack type fall arrest system with a movable trolley was used to prevent any undesired falls. Glycerol mixed with water in the ratio of 75% glycerol and 25% water was used as the slippery agent [3]. During the slip trials, glycerol was applied and evenly distributed on a force plate for contact of the leading left leg. Participants were strapped to a harness and performed multiple gait trials until normal self-selected pace walking with appropriate foot positioning onto the force plate was achieved. Participants turned away and listened to music on noise cancellation head phones for about 1 minute between each of these normal gait trials. One trial was then chosen to be the unexpected slip (US) and the contaminant was applied. Each slip trial was classified based on a force criterion using a digital crane scale inline with the overhead harness system. The slip was classified as a fall if the peak body weight measured by the scale exceeded 30% of body weight during the slip, and confirmed with visual inspection. After classification, sway

parameters were analyzed for each SOT condition, using independent samples t-tests between falls and recovers.

RESULTS AND DISSCUSSION

For the postural control measures, we have evidence of significant differences in the EO condition for ML velocity ($t(38) = -2.200$, $p = 0.034$), and AP velocity ($t(38) = -2.246$, $p = 0.031$). For ML velocity, fallers presented with increased sway velocity compared to those who recovered during the slip (mean sway velocity of 0.879 ± 0.11 vs. 0.791 ± 0.13). Similarly, for AP velocity, increased sway velocity was found in fallers, compared to those who recovered from the slip (mean sway velocity of 1.16 ± 0.24 vs 1.00 ± 0.20). No other statistically significant findings were observed for the sway parameters. Previous research using equilibrium scores during sensory organization tests have suggested that individuals with decreased equilibrium scores slipped longer when exposed to unexpected slips [1]. Other previous findings have suggested that adults with one or more sensory impairments have increased odds of having dysfunctional balance [6] Our findings using postural sway measures, and classified slip outcomes corroborate those findings. Suggesting that individuals who were unable to recover after a slip, have increased sway velocity, suggesting worse balance performance compared to those who were able to recover.

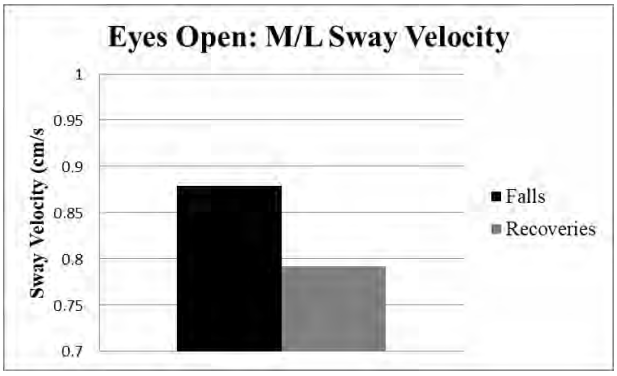

Figure 1: Medial/Lateral Sway Velocity in the EO condition between those who fell, and those who recovered.

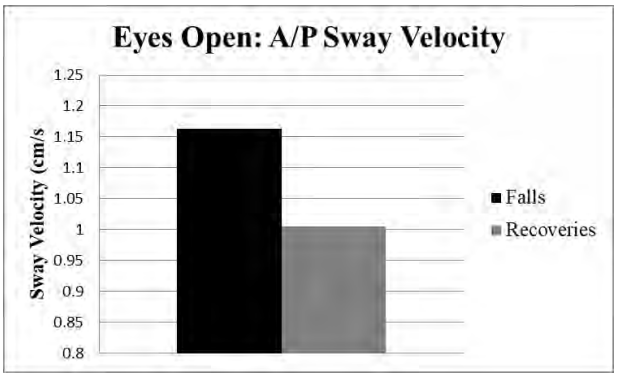

Figure 2: Anterior/Posterior Sway Velocity in the EO condition between those who fell, and those who recovered.

CONCLUSION

Our findings suggest that possible decrements in standing balance, as measured through postural sway parameters could be indicative of an individuals inability to recover following an unexpected slip. This could be due to an impairment in slip detection, leading to an increased propensity of a subsequent fall.

REFERENCES

1. Lockhart, T.E., J.L. Smith, and J.C. Woldstad, *Effects of aging on the biomechanics of slips and falls.* Human factors, 2005. **47**(4): p. 708-729.
2. Chander, H., J.C. Garner, and C. Wade, *Heel contact dynamics in alternative footwear during slip events.* International Journal of Industrial Ergonomics, 2015. **48**: p. 158-166.
3. Redfern, M.S., et al., *Biomechanics of slips.* Ergonomics, 2001. **44**(13): p. 1138-1166.
4. Cham, R. and M.S. Redfern, *Lower extremity corrective reactions to slip events.* Journal of biomechanics, 2001. **34**(11): p. 1439-1445.
5. Sawers, A., et al., *Neuromuscular responses differ between slip-induced falls and recoveries in older adults.* Journal of neurophysiology, 2017. **117**(2): p. 509-522.
6. Wilson, S.J., J.C. Garner, and P.D. Loprinzi, *The influence of multiple sensory impairments on functional balance and difficulty with falls among US adults.* Preventive medicine, 2016. **87**: p. 41-46.

THE IMPACT OF OBESITY ON GAIT STABILITY IN OLDER ADULTS

[1] Michael Gonzalez, [2] Noah J. Rosenblatt and [1] Deanna H. Gates

[1] University of Michigan, Ann Arbor, MI, USA
[2] Rosalind Franklin University of Medicine and Science, North Chicago, IL, USA
email: gatesdr@umich.edu, web: http://rehab-biomech-lab.kines.umich.edu/ /

INTRODUCTION

Falls are common in adults over the age of 65, and can result in injury or even death. Older adults who are also obese are at a higher risk of falling and have a greater risk of disability after a fall [1]. However, the mechanisms to explain falls by obese older adults are unclear. There is a growing body of evidence that obesity interferes with postural stability [e.g. 2]. However, the relationship between postural stability and falls is also not necessarily clear. In addition, the majority of falls by community dwelling adults occur during gait and not from standing postures [3].

Obese gait can be characterized by reduced walking speed, a longer stance phase duration and a greater period of double support compared with normal-weight individuals [4]. These characteristics are generally thought to be compensatory strategies to increase stability when dynamic balance has been compromised. However, these are not direct measures of stability – i.e. the ability of the system to respond to small perturbations – and these metrics have had limited ability to predict falls. Measures of local dynamic stability based on trunk motion, which directly quantify the stability of the system, have been able to identify older adults with and without high fall risk [5] as well as older adults with and without a fear of falling (FOF), which is a risk factor for falls [6].

The purpose of this study is to determine the impact of obesity on gait stability in older adults. Secondarily, we determined whether walking stability was related to history of falls in older adults.

METHODS

A total of 12 obese older adults (73 ± 5 yrs, BMI: 34.8 ± 4.2) and 12 age and gender matched healthy weight controls (74 ± 7 yrs, BMI: 23.7 ± 0.9) participated in this IRB approved study. As part of a larger study, participants walked on a treadmill at self-selected walking speed. Up to 10 minutes of walking was recorded in 30 second trials, 6 trials of which were used for analysis. We tracked the position of a marker placed on the C7 vertebra at 100 Hz throughout all walking trials using motion capture (Vicon, Oxford Metrics, Oxford, UK). In addition, participants completed several test of functional mobility including the 10 meter walk test (at maximum speed) and the timed-up-and go (TUG). They also completed the Survey of Activities and Fear of Falling (SAFE) which asks if they regularly perform a series of activities of daily living; if so it asks for their level of FOF while completing the activity (0-4 point scale); if not it asks whether or not the activity is avoided due to FOF. Participants also completed the SF-12 to quantify mental and physical health [7].

Local dynamic stability was quantified using short-term local divergence exponents (λ_s*) which indicate the rate of divergence of neighboring trajectories. Positive exponents indicate local instability, with larger exponents indicating greater instability [8]. State spaces were constructed from five time delayed copies of the C7 marker velocity for each direction of motion. We then calculated λ_s* for each state space using previously published methods [8]. The average λ_s* across 6 trials of 20 strides (120 total strides) was calculated for each individual in each plane of motion [9].

We used a two-factor ANOVA to test for differences in λ_s* between weight groups (obese, healthy-weight) and fall history (yes/no). Walking speed is known to influence local stability, and as such we first compared the self-selected speeds between the groups. The obese participants tended to walk slower (0.78 ±0.23 m/s) than the healthy weight controls (0.94 ±0.24 m/s). Therefore, walking speed was

included as a covariate in the ANOVA. This covariate was significant in the M-L direction, only. All other measures were compared using single-factor ANOVAs to test for differences between healthy-weight and obese older adults. All statistical analyses were performed in SPSS v 24 (IBM, Armonk, NY) with an $\alpha = 0.05$.

RESULTS AND DISCUSSION

Obese and control participants had a similar incidence of falls in the prior year (5/12 per group). They also had similar fear of falling ($p = 0.228$). The obese participants generally performed worse on functional tests. They had a significantly longer TUG time ($p = 0.002$), and trends toward slower 10-m walk ($p = 0.087$, figure eight walk ($p = 0.071$), and four-square step ($p = 0.119$) times. Obese participants were not able to stand on one leg for as long as healthy weight controls ($p = 0.001$).

Obese participants were less stable in the medial-lateral (M-L) direction ($p = 0.002$) compared to healthy-weight controls. However, there were no significant differences in stability between groups in the anterior-posterior (A-P: $p = 0.888$) or vertical (VT: $p = 0.632$) directions (Fig. 1). There were no significant effects of fall history or significant fall history x weight group interactions for any comparison.

CONCLUSIONS

Older adults who are obese have decreased medial-lateral stability compared to their healthy weight counterparts. They also have decreased functional performance measures, but not a greater fear of falling. Future work will include a larger sample size and incidence of falls after assessment. This data is essential to determine the factors related to fall risk in this population

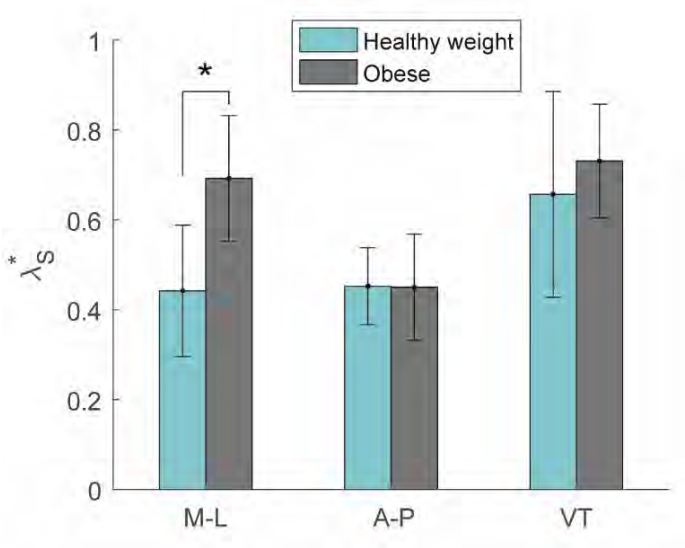

Figure 1: Average λ_s* for Obese (black) and Healthy-Weight (cyan) subjects in the medial-lateral (M-L), anterior-posterior (A-P), and vertical (VT) directions.

ACKNOWLEDGEMENTS

Research reported in this abstract was supported by the National Institute of Arthritis and Musculoskeletal and Skin Diseases award number 1R03AR066326-01A1

REFERENCES

1. Himes, CL and Reynolds, SL. *J Am Geriatrics Soc,* 60, 124-129, 2012.
2. Teasdale, N. et al. *Int J Obesity* (31): 153–160, 2007.
3. Berg, W. P. et al. *Age ageing*, 26(4): 261-268, 1997.
4. DeVita, P. *J Biomech* **(36)**: 1355–1362, 2003.
5. Lockhart, T. *Ergon,*51(12):1860-1872, 2008.
6. Toebes, M. J. *Gait posture*, *41*(1), 76-80, 2015.
7. Lachman, M. E. et al. *J Gerontol* (53):43-50, 1998.
8. Dingwell, J. & Marin, L., *J Biomech* 39 (3): 442-452, 2006.
9. van Shooten, K et al. *Gait Posture* (39): 695-699, 2004.

LOCOMOTOR STABILITY EFFORT CHANGES MANEUVER EXECUTION IN INCOMPLETE SPINAL CORD INJURY

[1,2] Keith E. Gordon, [1] Mengnan/Mary Wu, [1] Geoffrey Brown, [1,3] Jane Woodward, [4] Tara Cornwell, [4] Wendy Boehm
[1] Northwestern University, Physical Therapy and Human Movement Sciences, Chicago, IL, USA
[2] Edward Hines Jr. Veterans Administration Hospital, Hines, IL, USA
[3] Shirley Ryan Ability Lab, Chicago, IL, USA
[4] Northwestern University, Department of Biomedical Engineering, Chicago, IL, USA
email: keith-gordon@northwestern.edu

INTRODUCTION

The recovery of locomotor *stability* – the ability to maintain a desired walking trajectory amid perturbations – and *maneuverability* – the ability to change walking trajectory – are major gait rehabilitation challenges for ambulatory individuals with incomplete spinal cord injury (iSCI). Although essential for community ambulation, it is difficult for people with impaired sensory motor function to effectively control both. Instead, they may select conflicting locomotor control strategies that are either stable or maneuverable. For example, increasing lateral margins of stability (MOS) increases resistance to lateral perturbations and also increases resistance to volitional efforts to move laterally [1]. We sought to quantify the interaction between stability effort and maneuver performance in an iSCI population. We hypothesized that following walking practice in a force field that increased effort required to maintain straight walking, individuals would adopt gait patterns that are more resistive to lateral maneuvers, and, conversely, following practice in a force field that decreased stabilization effort, individuals would adopt less resistive gait patterns during maneuvers.

METHODS

12 ambulatory individuals with iSCI (age: 54.9 ± 8.2, 10 males, 2 females) provided informed written consent and participated in the study. We quantified lateral maneuvers during treadmill walking immediately following three straight-ahead walking conditions during which a cable robot [2] applied external force fields to the center of mass (COM) to modify the effort required to control lateral motion (Figure 1). The conditions were:

Null: No external forces.

Damping: Force field proportional in magnitude and opposite in direction to lateral COM velocity. This field made it easier to control mediolateral COM position.

Amplification: Force field proportional in magnitude and in the same direction as lateral COM velocity. This field made it more difficult to control mediolateral COM position.

During all walking, real-time mediolateral COM position was projected along the length of the treadmill surface (Figure 1). To ensure that participants were trying to control lateral COM motion during straight walking in each force field condition, they were tasked with maintaining their COM projection within a dynamic target lane. The width of the lane updated every 10 seconds based on performance (narrowing if the participant was successful or widening if they were not) to maximally challenge the participant's ability to control lateral COM motion. After 2 minutes of straight walking, the force-field shut off and the center of the target lane immediately jumped to the left side of the treadmill. Participants were instructed to maneuver to the new target lane as quickly as possible. This was followed by three more lateral maneuvers with the target lane moving to either the left or right (target centers located 0.45m apart) one second after each maneuver was completed.

We quantified minimum step width and minimum lateral margin of stability [3] during the first maneuver on the side ipsilateral to the direction of the maneuver. One-way repeated measures ANOVAs tested for differences in gait measures. When significant differences were found Bonferroni-corrected pairwise comparisons were made between conditions.

Figure 1: Experimental Setup. During straight walking a cable robot applied lateral forces to a pelvic harness. During all walking mediolateral COM position was projected on the treadmill surface. Participants were instructed to maintain their COM within a dynamic target lane.

RESULTS AND DISCUSSION

We found significant differences between conditions for minimum left step width (repeated measures ANOVA; $p < 0.0005$), and minimum left lateral margin of stability (repeated measures ANOVA; $p = 0.001$) during the first maneuver performed to the left immediately after straight walking (Figure 2). Post hoc tests revealed that compared to maneuvers performed immediately after the Null condition, both step width ($p = 0.006$) and lateral margin of stability ($p < 0.031$) were significantly larger during maneuvers after straight walking in the Amplification field. Conversely, when compared again to maneuvers performed immediately after the Null condition, both left step width and left lateral margin of stability tended to decrease after straight walking in the Damping field. This change was only significant for minimum left step width ($p = 0.015$).

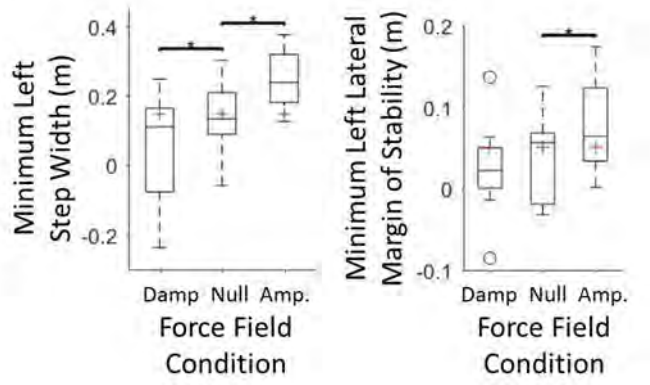

Figure 2: Minimum left step width and minimum left lateral margin of stability during maneuvers performed to the left immediately after two minutes of straight walking in three different force fields: Damping, Null, and Amplification.

These results support our hypotheses. When the effort required to maintain lateral COM stability during straight walking was altered in a force field, we observed changes in how individuals with iSCI executed lateral maneuvers after the field was removed. Following straight walking in the Amplification field, individuals demonstrated increased step width and lateral margin of stability during maneuvers compared to the Null condition. These changes likely increased lateral stability – resistance to perturbations – but also resisted the participants' own volitional efforts to change direction [1]. Conversely, after walking in the Damping field that reduced the effort required to stabilize lateral COM motion during straight walking, individuals decreased step width and lateral margin of stability during lateral maneuvers. These changes should decrease resistance to both lateral perturbations and volitional changes in direction.

CONCLUSIONS

Our results suggest that the control strategies used by individuals with incomplete spinal cord injury to create stability have consequences for maneuvering. During community ambulation there are instances when it is necessary to be both stable and maneuverable. Developing interventions that improve the ability to either rapidly switch between control strategies or to learn alternative strategies that facilitate simultaneous control of both stability and maneuverability [4] would expand the variety and complexity of environments in which individuals with iSCI can safely and effectively walk.

REFERENCES

1. Acasio, J., et al. Gait Posture, 2016. 52.
2. Brown, G., et al. Conf Proc IEEE Eng Med Biol Soc. 2017.
3. Hof, A.L., et al. J Biomech, 2005. 38(1).
4. Wu, et al. Plos One, 2015. 10(7).

ACKNOWLEDGEMENTS

Supported by Merit Review Award #I01RX001979 from the United States Department of Veterans Affairs Rehabilitation Research and Development Service, and the Northwestern University Undergraduate Research Assistant Program.

THE RELATIONSHIP BETWEEN STAR EXCURSION BALANCE TEST JOINT ANGLES LIMB ASYMMETRY AND NORMALIZED REACH DISTANCE IN 12 WEEKS POST HIP ARTHROSCOPY PATIENTS

Rena Hale, Allison Mumbleau, Aaron J. Krych, and Timothy E. Hewett

Mayo Clinic Biomechanics Laboratories & Sports Medicine Center, Rochester & Minneapolis, MN, USA
email: Hale.Rena@Mayo.edu

INTRODUCTION

Due to the recent advancements in clinical examination skills and diagnostic imaging, the number of hip arthroscopies (HA) performed in the United States increased nearly 6-fold from 2004 to 2009 [1]. HA can include but are not limited to labral debridement and repair, femoroacetabular impingement correction, chondroplasty, osteoplasty, microfracture, synovectomy, repair of the ligamentum teres, and treatment for capsular hyperlaxity [2]. Previous studies have shown promising functional outcome improvements in short and mid-term patient follow ups after HA [3]. Despite this progress, recommendations for postoperative rehabilitation are minimal [3, 4].

Multiple metrics are available to assess patient performance after HA. The modified Star Excursion Balance Test (SEBT) is a reliable and low cost functional test commonly performed to assess lower extremity dynamic stability and neuromuscular control. The SEBT measures performance via limb symmetry of reach distance. Despite the clinical utility of the SEBT, performance standards to determine patient readiness to advance with rehabilitation activities for patients post HA have not been defined. The purpose of this study was to correlate sagittal plane trunk, hip, knee kinematics and reach distances of the surgical and nonsurgical limb during a modified SEBT with 12 week postoperative HA patients. The first hypothesis tested was that sagittal plane trunk, hip, and knee flexion would be decreased on the surgical limb when compared to nonsurgical limb. The second hypothesis tested was that reach distance asymmetries would correlate to sagittal plane kinematic asymmetries.

METHODS

Nine patients 12 weeks post HA (15-50 years old) were recruited for participation in this study. Average participant height and weight were 155.3cm ± 33.4 and 67.5kg ± 11.4. Patients with bilateral HA were excluded. Prior to participation, informed consents were obtained. The study was reviewed and approved by the Mayo Clinic Institutional Review Board.

3D motion analysis (Motion Analysis Corp, Santa Rosa, CA) was collected on patients while the SEBT was performed. Patients wore compression shorts and spandex tops. Twenty-nine reflective markers were placed on anatomical landmarks following the Helen Hayes marker set. For the SEBT, participants were instructed to balance on one leg while using their free leg to reach as far as possible with the reach indicator. Three reaches on the injured then uninjured limb were performed in the anterior, posterolateral, and posteromedial direction relative to the stance leg.

A musculoskeletal model (Visual3D, Germantown, MD) was developed to calculate trunk, hip, and knee angles. Kinematics at maximum reach were reported. Limb asymmetry (surgical/nonsurgical) was calculated for joint kinematics and reach distance. Paired t-tests were used to determine significance of reach distance between reach directions. Linear regressions were used to examine the correlation of sagittal plane kinematics with limb asymmetries in reach distances for each test direction. Significance was set at $p < 0.05$.

RESULTS AND DISCUSSION

Mean reach distances for the surgical limb were significantly shorter in the anterior reach than the

posterolateral or posteromedial directions (P<0.05; Figure 1) when compared to nonsurgical limb.

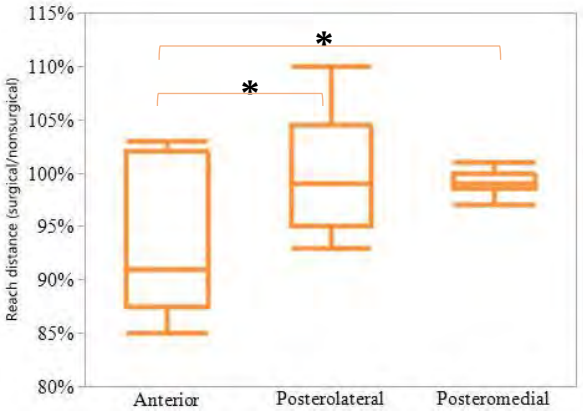

Figure 1 Average and standard deviation reach distance limb asymmetries. Asterisk denotes significant correlation between reach directions (P<0.05).

Hip (R_2 0.49) and knee flexion (R_2 0.47) of the surgical limb when compared to the nonsurgical limb were significantly less in the anterior reach direction of the SEBT (P<0.05; Figure 2). Joint kinematics in neither the posterolateral (R_2 0.36) nor the posteromedial (R_2 0.12) directions correlated to reach distance limb asymmetries.

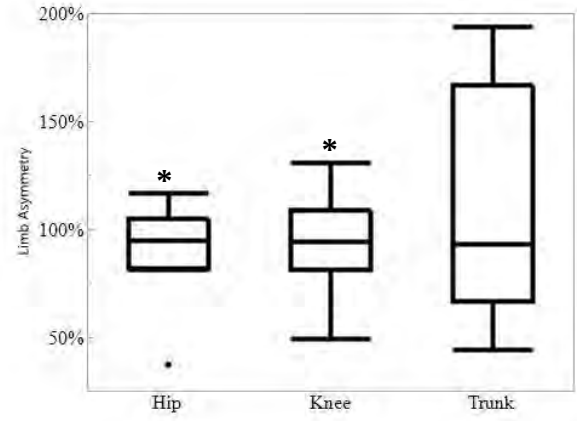

Figure 2 Average and standard deviation anterior reach limb kinematics represented as limb asymmetries. Asterisk denotes significant correlation with reach distance (P<0.05).

Clinically, a reach asymmetry with magnitude < 90% as compared to the uninvolved limb has been associated with increased lower extremity injury risk. Interestingly, most (7 of 9) of the current patients had limb symmetry reach distances ≥ 90% the uninvolved limb, which would qualify them as low injury risk. However, kinematic limb asymmetry analysis of individual patients showed that over half were below 90% asymmetry threshold in hip flexion in all three reach directions.

These results agree with previous literature that correlates hip and knee flexion with reach distance [6]. Movement patterns with limited sagittal plane flexion are undesirable, as decreased sagittal plane excursion during jump landing is associated with increased ground reaction forces and increased injury risk [7].

CONCLUSIONS

Though decreased reach distance in the anterior direction correlated to decreased hip and knee flexion angles, kinematics in the posteromedial and posterolateral directions did not correlate to reach distance in the surgical limb. Results from this study indicate that reach distance asymmetries alone may not describe the underlying movement mechanics of the patient specifically in the posterior reach directions. Future studies should compare absolute reach distances and joint kinematics between HA patients and a healthy cohort, as well as measure HA patient's limb asymmetries at six and twelve month follow-ups.

REFERENCES

1. Montgomery, et al. *Arthroscopy,* 29.4B, 2013.
2. Cheatham, et al. *J Sport Rehabil,* 24.4, 2015.
3. Khan, et al. *Arthroscop,* 32.1, 2016
4. Grzybowski, et al. *Frontiers in surgery* 2, 2015.
5. Plisky, et al. *NAJSPT,* 4.2, 2009
6. Robinson & Gribble *Arch Phys Med Rehabil.,* 89, 2008.
7. Devita & Skelly. *Med Sci Sports Exerc* 24.1, 1992.

ACKNOWLEDGEMENTS

Mayo Clinic Clinical Outcomes Research Coordinator (CORC) Program, T32AR0569

REPEATED MOTOR CONTROL TESTING DECREASES CO-CONTRACTION INDEX IN HEALTHY YOUNG ADULTS

[1]Christopher M. Hill, [1]Sam Wilson, [1]J. Grant Mouser, [1]Paul Donahue, [1]Caleb Williams, [1]Lauren Luginsland, & [2]Harish Chander

[1]University of Mississippi, University, MS, USA
[2]Mississippi State University, Mississippi State, MS, USA
Email: cmhill1@go.olemiss.edu web: hesrm.olemiss.edu

INTRODUCTION

Automatic postural responses are the first line of defense against environmental disturbances to postural equilibrium. Rapid adaptation of the neuromuscular system's reactive and anticipatory mechanisms to novel perturbations decreases the possibility of fall and musculoskeletal injury [1]. In order to react to balance perturbations, co-contraction of agonist antagonist pairs of the lower extremity muscles increases to create stability around a joint, by generating stiffness in the agonist and antagonistic muscles [2]. The postural control system modifies neuromuscular responses and habituates with repeated exposure to surface perturbations. Previous literature has demonstrated a decrease in muscular co-contraction index with repeated exposure to balance perturbations suggesting the adoption of a feedforward control after initial exposure [3, 4]. A commonly used device to elicit balance perturbations in research and clinical settings is the Neurocom® EquiTest®'s Motor Control Test (MCT). Novel laboratory equipment has been used in previous studies to disturb postural equilibrium, yet no study has evaluated the effect of repeated MCTs on automatic postural responses. Thus the purpose of this study was to determine whether exposure to repeated MCTs elicit changes to neuromuscular responses in the lower extremities of healthy young adults.

METHODS AND PROCEDURES

The study was conducted in a repeated measures design with twenty healthy adults (10 male, 10 female age: 25 ± 4.73 years; height: 183.8 ± 8.5 cm; mass: 85.2 ± 15.6 kg) with no history of musculoskeletal, orthopedic, neurological, and vestibular abnormalities. Data collection procedures included an initial familiarization that consisted of a single, full MCT. Following familiarization, participants performed five fully randomized MCTs over six testing sessions, in which they were not given knowledge of the direction or magnitude of the perturbations. The first five sessions occurred on consecutive days, with the sixth occurring two days after the fifth. Muscle activity was collected on medial gastrocnemius (Plantar Flexor-PF), tibialis anterior (Dorsi Flexor-DF), vastus medialis (Q) and semitendinosus (H) using the Noraxon TelemyoTM T2400 G2 wireless EMG system (Scottsdale, Arizona) with a sampling frequency of 1500 Hz. Response times were assessed using Motor Control Test (MCT) (backwards small [BWS], medium [BWM] and large [BWL], and forward small [FWS], medium [FWM], and large [FWL]). Co-contraction between of muscle pairs were calculated using the Co-Contraction Index (CCI) with mean muscle activity agonist-antagonist pairs of Q & H and DF & PF using the following equation [6]:

$$(EMG_{Least} + EMG_{Most}) x EMG_{Least} / EMG_{Most}$$

The first trial of a perturbation on each testing day was analyzed using a 1 (Participant) x 6 (Day) repeated measures ANOVA at an alpha level of 0.05 using SPSS25.

RESULTS AND DISSCUSSION

Significant main effect was found for Q-H CCI Day-Trial 1 BWM [F (1.949, 14) =4.037, p= 0.027, η^2 =0.175] and Day-Trial 1 FWM (1.949, 14) =4.037, p= 0.027, η^2 =0.175]. Day-Trial 1 BWM Q-H CCI Day 1 was significantly higher than Day 3 (p=0.017), Day 4 (p=0.024), Day 5 (p=0.024), and Day 6 (p=0.023) but not Day 2 (p=0.160). Day-Trial 1 FWM Q-H CCI Day 1 was significantly her than Day 2 (p=0.160), Day 4 (p=0.014), Day 5 (p=0.017), and

Day 6 (p=0.012), but not Day 3 (p=0.063). Day 3 was significantly higher than 4 (p=0.034), Day 5 (p=0.01), and Day 6 (p=0.01), but not Day 2 (p=0.113).

Significant main effect was found for PF-DF CCI in Day-Trial 1 BWS [F (3.290, 14) =3.204, p= 0.025, η^2 =0.144], Day-Trial 1 FWL [F (3.342, 14) =3.679, p= 0.014, η^2 =0.185], and Day-Trial 1 FWM [F (2.056, 14) =6.535, p= 0.003, η^2 =0.256]. Day-Trial 1 BWS PF-DF CCI Day 1 was significantly higher than Day 6 (p=0.019). Day-Trial 1 FWL PF-DF CCI Day 1 was significantly higher than Day 2 (p=0.011), Day 3 (p=0.003), Day 4 (p=0.015), Day 5 (p=0.005), and Day 6 (p=0.008). Day-Trial 1 FWM revealed Day 1 was significantly higher than, Day 3 (p>0.001), Day 4 (p>0.001), Day 5 (p>0.001), and Day 6 (p>0.001) but not Day 2 (p=0.257).

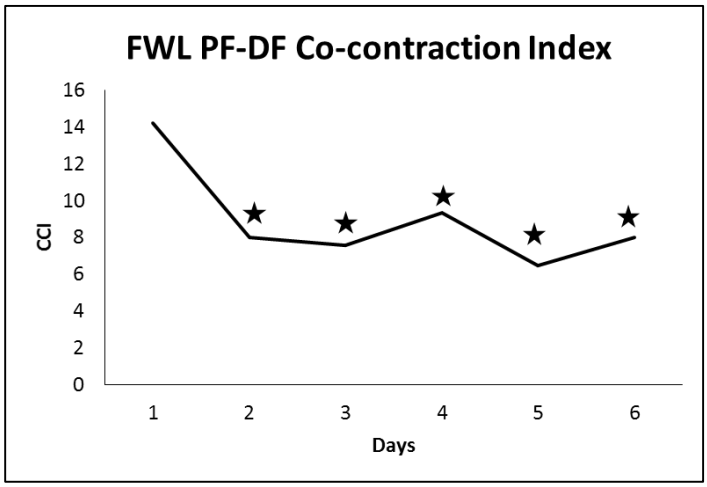

Figure 1: Muscle co-contraction index for backward medial gastrocnemius (PF) and tibialis anterior (DF). ★ denotes significant differences from Day 1.

Initial exposure to the postural perturbations of the MCT increased co-contraction indices across both sets of agonist and antagonist muscle pairs. However a decrease was noted after the third testing session and was maintained after a two day retention period. Previous literature has described similar findings as "The First Trial Effect" in which postural responses shift from feedback control to feedforward [5]. Exposure to the novel perturbations of MCT activates the lower extremity musculature via a proprioceptive feedback loop. After the initial encounter with a particular type of perturbation, the need to utilize feedback from the lower extremity is diminished, thus resulting in a decrease co-contraction between the agonist and antagonist pairs. The Q-H muscle pair decreased in their co-contraction when repeatedly exposed MCT. Paradigms utilizing repeated postural perturbations have demonstrated a decrease in the activation of proximal musculature [1, 6]. The hip and knee fixed support strategy requires the activation of proximal lower extremity muscles to maintain balance. However, after repeated exposure and upright stance is maintained successfully, the postural control system shifts to the more efficient ankle fixed support strategy to decrease muscle exertion.

After two days of non-exposure to the MCT balance perturbations, a similar CCI to that found during the repeated exposure was maintained. Previous findings have noted that participants with prior experience with a postural disruptions, decrease CCI when exposed to the perturbation again suggesting a change in pre-perturbation anticipatory control [1, 3]. Prior experience with the MCT perturbations allowed the central nervous system to implement a more efficient anticipatory control strategies to counteract the upcoming perturbations.

CONCLUSION

Reactive postural response are needed to maintain balance and must rapidly adapated to meet enviormental demands. Perturbing balance with MCT elicits lasting changes to reactive balance responses via feedforward control and alterations to anticpatory mechanisms via prior experinance. Such changes create more efficent postural control strategies that decrease muscle exertion of the lower exterimity.

REFERENCES

1. Welch, T. & Ting., *PloS One,* ***9****(5),* 2014
2. Winter, D. A., Patla, A. E., Prince, F., Ishac, M., & Gielo-Perczak, K. *J of Neurophy*, ***80*****,** 1211-122, 1998.
3. Schinkel-Ivy, A. & Duncan, C. A. *J of Electomy Kin,* ***39****, 42-48,* 2018.
4. Fryler, K. et al. *PloS One,* ***11*** *(12), 2016.*
5. Pai, Y.C. & Bhatt, T.S., *Phys Ther,* ***87****, 1478-1491,* 2007.
6. Horak, F. B., & Nashner, L. M. *J of Neurophy* ***55,*** *1369-1381,* 1989.

Texting while walking influences Step Width

[1] Tyler Hofstee, [1]Don Hoang, [1]Cory Barella, [1]Justin DeGuia and [1]Rahul Soangra*
[1] Department of Physical Therapy, Crean College of Health and Behavioral Sciences, Chapman University, Orange, CA, USA
email: soangra@chapman.edu, web: https://www.chapman.edu/our-faculty/rahul-soangra

INTRODUCTION

Dual tasking has become a necessity in today's fast-paced society. Nowadays it seems as though it's more preferable to perform multiple tasks with a limited focus of attention rather than perform each task individually and give each task your full focus and attention. Walking and texting is something which we commonly see or perform in our daily lives. The ownership of a mobile smartphone has increased significantly over the course of the last few years along with the individual use of emailing, social media scrolling, internet browsing, and above all texting. Specifically, texting while walking can have a profound impact on an individual's gait and fall risk. The dual task of texting and walking carries with it the risk of normal gait deviation which can lead to variances in gait pattern, destabilization, tripping, colliding and can result in an injury to the person texting or an innocent bystander. License and Smith's studied the effect that texting had on gait characteristics while negotiating common pedestrian obstacles such as curbs and steps *(License et al. 2015).* Agostini et. al. studied gait modifications due to texting on a smartphone while walking, with an emphasis on distal motor control *(Agostini et al. 2015).* This study looks into effects of dual-tasking on fall risk. We hypothesize that walking while texting with a cell phone will increase stride width and reaction time, and decrease stride length and stride interval in comparison to normal gait tendencies. The inclusion of the Stroop test will rule out that the significant differences in gait are due to the cognitive tasks of texting, rather than the motor tasks of flexion of the head, elbows and fingers.

METHODS

Four healthy adult males aged 22-34 from Chapman University Department of Physical Therapy were recruited. The protocol for this study was approved by Chapman University Institutional Review Board (IRB#1718H020). All participants provided written informed consent prior to the experiment. The participants were devoid of any other neurological or musculoskeletal conditions and had previous experience using their cellular device.

Participants were assessed in the Gait Real-time Analysis Interactive Lab (GRAIL) and were instructed to wear comfortable, tight-fitting clothing for walking without any reflective material. Twenty-five reflective markers were placed on several bony landmarks of these participants.

The preferred pace of the participant was found and recorded for each participant, and held constant for each of their trails. Participants were instructed when to start and stop walking and data was collected for three minutes using the VICON motion capture and D-Flow programs in the GRAIL lab for assessing stride length, stride width, stride interval, and reaction time after perturbation. The participants used www.typingtest.com using the parameters: 3 minutes, English, and "Zebra - Africa's striped horse" script and "Rules of Baseball" script. The typing test assess the typing speed in words per minute, the amount of errors made, and the adjusted typing speed.

Figure 1: Participant walking on Split belt treadmill with a virtual reality environment

RESULTS AND DISCUSSION

We found that Step width of participants increased significantly while performing dual-task (texting with walking) (p=0.018). Average step width for subjects was 0.195m with no texting, 0.2003m with texting. Average Step length was 0.67 meters when no texting and reduced to 0.66 meters in dual task condition. We also found that during dual tasking the participants decreased their gait speed.

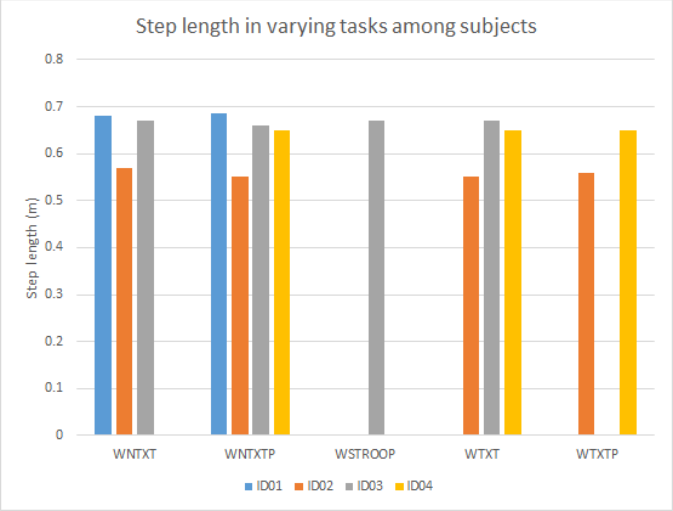

Figure 2: Measurement of average step length (in meters) per gait cycle among participants in WNTXT, WNTXTP, WSTROOP, WTXT, WTXTP.

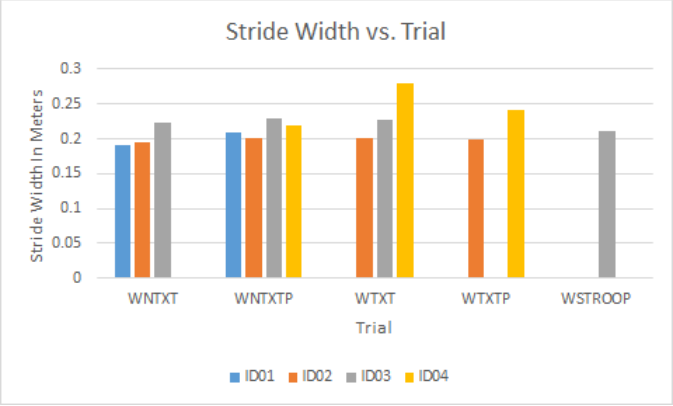

Figure 3: Measurement of average stride width (in meters) per gait cycle among participants in WNTXT, WNTXTP, WSTROOP, WTXT, WTXTP

CONCLUSIONS

This study examined the effects of dual tasking more specifically, texting on a phone on gait. We hypothesized that texting while walking will increase the step width in comparison to normal gait tendencies. *Licence et al.* and *Plummer et al.* found that a decrease in gait velocity during dual tasking (*Licence et al., 2015)*. We also found decrease in gait speed during dual tasking.

In *Texting and Walking:* We found that when the participants were walking and texting they had an increased step width. This is similar to the findings in Schabrun et al. This increase in stride width was due to the human body's natural response to being off balance while in the single-limb support phase of gait; the body will compensate by increasing the base of support to prevent the person from falling over. With a decrease in spatial awareness due to increased prioritization in texting (brain executive function), it seems that the body tries to protect itself from any harm of not being aware of the surrounding, and in this case, it does that by increasing stride width (*Jongil et al., 2015)*.

REFERENCES

1. Agostini, V., Lo Fermo, F., Massazza, G., Knaflitz, M. (2015) *Does texting while walking really affect gait in young adults.* Journal of NeuroEngineering and Rehabilitation. 2015. 12(1). Bach et al. *Plos One*. 10(3): e0118797, 2015.
2. Frankel, V. H., Nordin M., Basic Biomechanics of the Musculoskeletal System 4th Ed. Philadelphia, Lippincott Williams & Wilkins 2012
3. Jongil L., Avelino A., Leo S., Richard, E.A., Van, E. Dual task interference while walking: the effects of texting on situational awareness and gait stability, In Gait & Posture Volume 42, Issue 4, 2015 pp. 466-471
4. Lamberg, E. M., Muratori, L. M. *Cell phones change the way we walk, In Gait & Posture*, Volume 35, Issue 4, 2012, Pages 688-690
5. Licence, S., Smith, R., McGuigan, M., Earnest, C.P. *Gait pattern alterations during walking, texting and walking and texting during cognitively Distractive tasks while negotiating common pedestrian obstacles,* PLoS One (2015)
6. Lin, M B. Huang, Y P. *The impact of walking while using a smartphone on pedestrians awareness of roadside events,* Accid Anal Prev. 2017
7. Neumann, D. A. *Kinesiology of the Musculoskeletal system: Foundations for Rehabilitation 2nd Ed.* St. Louis, Mosby Inc. 2010

Smartphone Technology Can Measure Postural Stability and Distinguish Fall Risk in Older Adults

[1]Katherine L. Hsieh, [1]Kathleen L. Roach, [2]Douglas A. Wajda, and [1]Jacob J. Sosnoff

[1]University of Illinois at Urbana Champaign, Urbana, IL, USA
[2]Cleveland State University, Cleveland, OH, USA
Email: klhsieh3@illinois.edu

INTRODUCTION

Falls are the leading cause of injury related death in older adults [1]. One in three older adults 65 years or older fall once per year [1]. Given the frequency and severity of falls, research in the past decade has focused on identifying factors that predict and prevent falls. Impaired postural stability is a consistent predictor of falls in older adults but is rarely assessed in clinical settings [2]. Clinical tests are subjective and lack sensitively, while objective measures require expensive equipment (i.e. force plates, motion capture cameras) and lack of expertise.

Mobile technology such as smartphones are emerging as a tool to measure postural stability. Because smartphones are commercially available and owned by a large proportion of the population across all age groups, they may serve as a solution to measure postural stability in clinical or home settings [3]. The purpose of this study was to determine if a smartphone can measure static postural stability and distinguish between fall risk in older adults compared to a force plate. We hypothesized that smartphone measures would be comparable to force plate measures during progressive, static balance conditions, and that smartphone measures would be able to distinguish between older adults with low and high risk of falling.

METHODS

Thirty healthy, older adults (age=67.17 ± 6.00) underwent static balance tests while standing on a force plate (Bertec Inc, Columbus, OH) and holding a Samsung Galaxy S6 (Samsung, Seoul, South Korea smartphone) with their dominate hand medially against the chest and along the sternum. Seven static balance tests were conducted in the following order: 1) eyes open, 2) eyes open with concurrent cognitive challenge (dual task), 3) eyes closed, 4) eyes closed with dual task, 5) semi tandem stance, 6) tandem stance, and 7) single leg stance. Two trials of each static balance task were performed. During the dual-task, participants simultaneously subtracted by seven from a random number between 100 and 200.

Center of pressure (COP) data from the force plate was extracted, and various parameters including velocity in the anterioposterior (AP) and mediolateral (ML) directions and 95% confidence ellipse were calculated. Acceleration from the smartphone was extracted and peak acceleration and root mean square (RMS) in ML, AP and vertical directions were calculated. To maximize reliability data was averaged across two trials for each condition. Spearman rank-order correlations were conducted between the force plate and smartphone measures, and receiver operating curves (ROC) and the area under the curves (AUC) were constructed to distinguish between low and high fall risk. Per guidelines, a physiological profile assessment score, a test that measures fall risk, of above one was considered high risk and below one was considered low risk [4].

RESULTS AND DISCUSSION

Peak acceleration ML ranged from 0.403-0.841 m/s^2, peak acceleration vertical ranged from 10.051-10.403 m/s^2, and peak acceleration AP ranged from

1.754-1.998 m/s^2. RMS ML ranged from 0.072-0.120 m/s^2, RMS vertical was 9.81 m/s^2, and RMS AP ranged from 0.181 m/s^2 to 0.242 m/s^2. COP velocity AP ranged from 9.628 mm/s to 27.050 mm/s and COP velocity ML ranged from 3.817 mm/s to 27.612 mm/s. COP 95% confidence ellipse ranged from 172.440 mm to 1135.500 mm. These values are similar to previously reported values of older adults.

Spearman's correlations found moderate correlations between COP measures from the force plate and acceleration measures from the smartphone. There were significant correlations between COP velocity from the force plate and RMS from the smartphone during eyes open dual task, eyes close dual task, semi-tandem, tandem, and single leg stance (ρ=0.423-0.812; p<0.01-0.05). Correlations were greater with more challenging balance conditions.

Table 1 indicates the AUC from constructed ROCs. For brevity, the first five conditions are included. The AUC for COP velocity in the AP direction ranged from 0.61-0.82 and in the ML direction ranged from 0.70-0.75. The AUC for RMS AP ranged from 0.58-0.77, RMS ML ranged from 0.47-0.72, and RMS vertical direction ranged from 0.60-0.82.

CONCLUSIONS

Our results support our hypothesis that acceleration from a smartphone is a valid measure of postural sway in older adults. In addition, RMS AP from a smartphone was capable of distinguishing between older adults at a low and high risk of falling.

This study provides evidence that smartphones are a valid way to measure postural stability and assess fall risk in older adults. Because smartphones are portable, cost-effective, and commercially available, there is potential for smartphones to be used in clinical or home settings to help provide objective, balance assessments for older adults. Future work should measure postural stability with a smartphone in a non-laboratory setting and determine the usability of smartphone technology to measure fall risk in older adults.

REFERENCES

1. Centers for Disease Control and Prevention. Ten Leading causes of Death (Charts). 2014 [02/01/2016]
2. Ambrose AF, Paul G, Hausdorff JM. Risk factors for falls among older adults: a review of the literature. *Maturitas.* 2013;75(1):51-61.
3. Anderson MO, Perrin AN. Technology use among seniors. Washington, DC: Pew Research Center for Internet & Technology. 2017 May 17.
4. Lord SR, Menz HB, Tiedemann A. A Physiological Profile Approach to Falls Risk Assessment and Prevention. *Physical therapy.* 2003;83(3):237-2.

Table 1. Area under the curve (AUC) of receiver operating curves for center of pressure (COP) measures from the force plate and root mean square (RMS) measures from the smartphone. *Indicates $p \leq 0.05$

Condition	COP Velocity AP		COP Velocity ML		RMS AP		RMS Vertical		RMS ML	
	AUC	*p*-value	AUC	*p* -value	AUC	*p* -value	AUC	*p* -value	AUC	*p* -value
Eyes Open	0.66	0.21	0.72	0.07	0.76	0.03*	0.63	0.28	0.47	0.79
Eyes Open Dual Task	0.82	0.08	0.71	0.09	0.72	0.07	0.75	0.04*	0.63	0.30
Eyes Closed	0.62	0.34	0.70	0.12	0.84	<0.01*	0.69	0.13	0.71	0.07
Eyes Closed Dual Task	0.71	0.09	0.75	0.05*	0.60	0.39	0.58	0.50	0.52	0.82
Semi Tandem	0.71	0.39	0.71	0.12	0.82	<0.01*	0.77	0.02*	0.72	0.07

THE EFFECT OF SURGICAL ALIGNMENT ON STANDING BALANCE IN ADULT DEFORMITY PATIENTS – INVARIANT DENSITY APPROACH

[1] Pilwon Hur, PhD, [1] Yi-Tsen Pan, [3] Isador H. Lieberman, MD MBA FRCSC, [2] Theodore Belanger, MD, and [4] Ram Haddas, PhD

[1]Texas A&M University, College Station, TX, USA
[2]Texas Back Institute, Rockwall, TX, USA
[3]Texas Back Institute, Plano, TX, USA
[4]Texas Back Institute Research Foundation, Plano, TX, USA
email: {pilwonhur,yitsenpan}@tamu.edu, rhaddas@texasback.com

INTRODUCTION

Adult degenerative scoliosis (ADS) patients comprise a variety of conditions that affect the normal spinopelvic alignment in the coronal and or sagittal planes. In spinal deformity patients a variety of postural changes in the spine, pelvis and lower extremities are observed in their effort to compensate for the anterior shift in the gravity line. Spinal alignment surgery was found to improve balance and overall function. Balance is defined as the ability of the human body to maintain its center of mass within the base of support with minimal postural sway. Sway can be measured as the center of pressure (COP) movement when a person is standing in a static position.

Objective of this study is to investigate the effect of surgical alignment on postural sway in ADS patients both before and 3-months-after-surgery.

METHODS

Clinical gait analysis was performed on eighteen ADS patients. Each patient performed a series of functional balance tests one week prior (Pre) and 3 months post-surgery (Post) one week prior and 3 months post-surgery. The functional balance test was similar to a Romberg's test in which the patients were asked to stand quietly with each foot on a force platform (i.e., total two force platforms) in a self-selected posture with eyes open for a full minute. Force platform data were used to compute COP measures in both anterior-posterior (AP) and medial-lateral (ML) directions. Two postural sway assessment techniques were used for analysis: 1. traditional summary COP descriptive measures [1]; and 2. invariant density analysis [2] which describes the dynamic COP distribution over time.

Traditional COP measures, *Range* and *Mean Velocity* of COP were also examined to provide statistical description. The stochastic structure of postural sway was analyzed using a reduced-order finite Markov-chain model [2]. The location of the COP can be categorized as different states emanating from the centroid. It has been shown that the distribution of COP over the state space converges to a unique steady state distribution π, known as invariant density [2]. Therefore, by understanding the invariant density, we can observe the long-term postural sway behavior. Five parameters were used to characterize the invariant density to better understand the system dynamics. This technique is called Invariant Density Analysis (IDA) [2]. In this study, we examined five IDA parameters: *Ppeak*, *MeanDist*, *D95*, *EV2*, and *Entropy*. *Ppeak* is the largest probability of π. *MeanDist* is the average location of the COP. *D95* is the largest state at which there is a 95% probability of containing the COP. *EV2* is the 2nd largest eigenvalue of the transition matrix and describes the convergence rate of the system to the invariant density. *Entropy* is the measure of randomness.

In addition to the existing IDA parameters, we introduced one more new metric that provides insight into the control mechanisms of the postural control system. As suggested in [3], the eigenvector corresponding to the second largest eigenvalue is of our interests. Hur [3] noted that investigation of the second eigenvector has the potential to provide a complete understanding of the embedded dynamics

in the reduced order model. Recently, [48] reported that the state space could be subdivided into two subsets depending on the sign of the corresponding second eigenvector (i.e., positive vs. negative). Each subset shows different dynamic behavior. Using this idea, we will investigate the zero crossing point of the second eigenvector, *ZeroCross*, to measure how much the central nervous system (CNS) is actively involved in the control of the standing balance. We report only the results in the AP direction, which showed statistical significance. A paired *t*-test was performed. Level of significance was set to p=0.05 (SPSS, v21, Chicago, IL).

RESULTS AND DISCUSSION

Surgical alignment revealed a significant decrease in the *ZeroCross* from the IDA. The *ZeroCross* in AP were Pre: 10.43±5.82 vs. Post:8.49 ± 3.78mm (*p*-value: 0.05) (Table 1, Fig. 1). The other variables did not detect the significant differences (Table 1).

CONCLUSIONS

The smaller *ZeroCross* from IDA post-surgery indicates that the surgical intervention and re-alignment allows the human postural control system to provide more active and robust balance. In other words, the CNS became more actively involved in the control of standing balance and thus the patients regain more efficient standing balance after the surgical re-alignment. The only significant change in *ZeroCross* and the insignificances from all the other measures suggest that 3 months after surgery may not be a sufficient time for ADS patients to fully recover. A long term follow-up is required. Objective motor performance measures such as *ZeroCross* from IDA will improve the evaluation and understanding of the biomechanical effects of spinal disorders on locomotion.

REFERENCES

1. Prieto et al., *IEEE Trans. Biomed. Eng.*, **43(9), pp956–966, 1996.**
2. Hur et al., *IEEE Trans Biomed Eng*, **59 pp1094–1100, 2012.**
3. Hur, *Ph.D. dissertation, University of Illinois at Urbana-Champaign*, **2010**

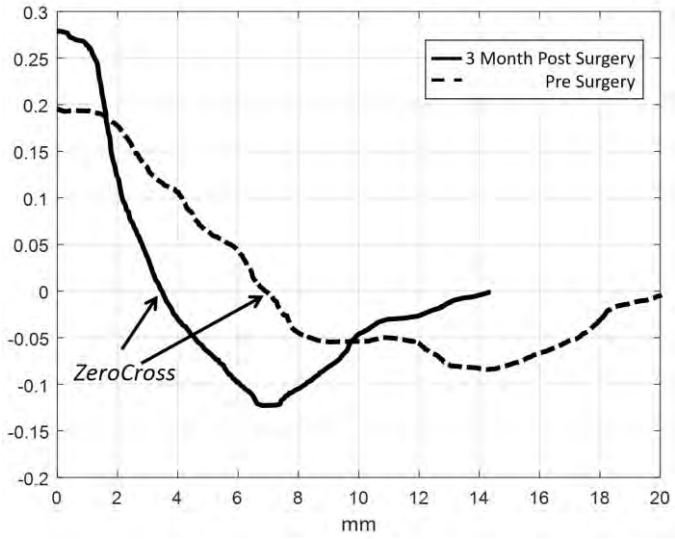

Fig. 1: A representative plot of the second eigenvector of the transition matrix for both pre-surgery (dashed) and 3 month post surgery (solid). The *ZeroCross* point happens earlier when subjects received surgery (3 Month Post).

Table 1: Required number of walking synergies pre- and post-surgery, and *t*-test results (Mean ± SD).

	Pre-surgery	Post-Surgery	*p*-value
Range	42.51 ± 18.89	39.45 ± 15.06	0.25
Mean Velocity	9.97 ± 4.02	9.62 ± 4.28	0.56
Ppeak	0.038 ± 0.038	0.040 ± 0.026	0.82
MeanDist	6.70 ± 3.41	5.93 ± 2.60	0.29
D95	16.69 ± 8.60	14.80 ± 6.34	0.29
EV2	0.985 ± 0.025	0.986 ± 0.021	0.71
Entropy	5.92 ± 0.84	5.71 ± 0.83	0.24
ZeroCross	10.43 ± 5.82	8.49 ± 3.78	**0.05**

MOVING BEYOND TRIPS AND SLIPS WITH PROXIMAL DETERMINANTS OF FALLS IN OLDER ADULTS: THE MOBILIZE BOSTON STUDY

Hyun Gu Kang*, Jonathan Hsu, Jasper Angeles

California State University San Marcos, San Marcos, CA, USA

email: hkang@csusm.edu, web: http://faculty.csusm.edu/hkang

INTRODUCTION

Although falls are common in older adults, the immediate circumstances surrounding a fall, particularly its biomechanics, are not well known [1]. The biomechanics of some types of falls, such as trips and slips, are well characterized, but it is clear if some types of falls are also common or need to be characterized better.

Distal risk factors for falls as such as age, gender, fall history, medical history, disability, gait speed, gait variability, etc. are often collected in large epidemiological studies of falls. Unfortunately, almost always all falls are studied as a single outcome, even though the biomechanics of each fall is unique. This is because it has been difficult to determine biomechanics of falls *in situ*, because the immediate circumstances of a fall are often difficult to measure in real life. Understanding the wide range of biomechanical and environmental factors that influence the immediate circumstances of a fall would allow for better preventative strategies.

Therefore, our goal was to determine (1) the immediate circumstances surrounding the falls, the *proximal* determinants of falls from an interview narrative, (2) our reliability in determining these determinant, and (3) their relationship with traditional *distal* risk factors, in order to better understand the specific biomechanics related to each fall.

METHODS

We used a structured interview data of self-reported falls from the MOBILIZE BOSTON STUDY database. The MOBILIZE Boston Study (MBS), which stands for "Maintenance of Balance, Independent Living, Intellect, and Zest in the Elderly of Boston" is a prospective study examining risk factors for falls, including pain, cerebral hypoperfusion, and foot disorders in the older population [2]. The study includes a representative population sample of 765 elderly volunteers age 70 or above from the Boston area. They were 77.9±5.3 years old, with height of 1.63±0.10 m and weight of 74.1±19.7 kg. 64% were female. The dataset is available to the public.

Standing postural data was collected on a Kistler force place. Participants stood 30 seconds at a time, eyes open. Postural sway and stiffness (Ke) were calculated per Winter's method [3].

Falls data was collected through monthly mail-in fall calendars, where the participant marked the days when a fall occurred. Once the calendars were received, the participant completed a structured interview over the phone. The circumstances, injuries, and the type of fall was recorded from the interview. Over the study period, a total of 1425 verified falls and narratives were identified.

Proximal determinants of falls were determined through (1) reading and sorting of fall narratives into categories by the investigators, (2) refining the categories, definitions, and the classification algorithm then iterating the process, (3) training two naïve readers to categorize the narratives, and (4) comparing the reliability of the algorithm. Each fall was allowed to enter multiple categories.

The incidence rates of these proximal determinants were compared to distal risk demographic, medical, functional, and biomechanical factors, such as age, gender, cognitive function, disability, gait speed, and postural sway, stiffness and damping. Negative

binomial regression was used, using R software 3.4.1.

RESULTS

Trips and slips: Of the 1425 verified falls, 581 (41%) were self-reported trips, 315 (22%) slips, and 529 (37%) neither. 49% of trips occurred outdoors and 51% indoors. 70% of slips occurred outdoors, and 30% indoors. 39% of other falls occurred outdoors and 60% indoors. Lower postural stiffness (p=.05) and damping (p=.004) predicted trips. Lower damping (p=.05) predicted slips. Increased sway predicted other falls. (p<.004).

Proximal determinants: 14 proximal determinants and frequencies were identified (Table 1). 74.67% of falls had only one proximal determinant. The classification algorithm produced 89% agreement between the raters.

Table 1: Proximal Determinants

Proximal determinant of fall	**Count / %**	**Associated with**
Obstacles	378/ 21%	
Texture change	272/ 15%	
Platform Height	358/ 20%	AP Ke
Perturbation	22/ 1%	AP sway
Impaired Vision	30/ 2%	
Sit-to-stand	87/ 5%	AP sway, ML sway
Push-pull	21/ 1%	
Carrying Object	42/ 2%	
Bending over / Reaching overhead	43 /2%	ML Ke
Dual-task	170 /10%	
Absentmindedness	90 /5%	
Speed (too slow or fast)	78 /4%	
Rotation	43 /2%	
Internal (felt dizzy, etc.)	140 / 8%	AP Ke, AP sway, ML sway

Distal Factors:
Falls due to internal issues were negatively associated with AP Ke (p = .003) and positively with AP and ML sway (p = .003, .001). Platform height changes were negatively associated with AP Ke (p = .03). Perturbations were positively associated with AP sway (p = .03). Sit-to-stand was positively associated with AP sway (p = .01). Sit-to-stand was positively associated with ML sway (p = .003). Bending-over-reaching-overhead was positively associated with ML stiffness (p = .01).

As shown previously, postural sway was positively associated with fall rates, and postural stiffness was negatively associated with fall rates.

DISCUSSION

Our goal was to determine the proximal determinants of falls. A greater variety of proximal determinants were identified given that 37% of falls were neither slip or trip. The most common proximal determinants were obstacles (21%), platform height change (20%), texture change (15%), and dual tasking (10%). Postural stiffness appears to be protective of platform height changes and internal issues, suggesting that these situations particularly require the ability to stabilize the body. However, postural sway is predictive of falls due to perturbations, internal issues, and sit-to-stand, which require better COM control. Further work is needed to understand specific physiologic and biomechanical reasons for these associations.

Although the proximal determinants were derived from verbal rather than video or inertial sensors, the falls data were collected from a representative community-dwelling population and therefore the results have strong external validity. Our work suggests that the biomechanics and neurophysiology of falls due to platform heights and dual tasking need further study, beyond obstacles/trips, and texture changes/slips.

REFERENCES

1. Crenshaw J. et al *ASB 2015.*
2. Leveille SG et al. *BMC Geriatr* 8:16, 2008.
3. Kang HG et al. J Neurophysiol 104(6) 2010.

ACKNOWLEDGEMENTS

NIAP01AG004390, Marg Bryant for help with the dataset

Ethnic differences in lower extremity static and dynamic postural measures as a potential risk factor for Anterior Cruciate Ligament (ACL) Injury

Chang-Young Kim [1,2], Sae-Yong Lee [1,2]

Integrated Sports Science Research Laboratory (ISSRL) [1]
Yonsei Institute of Sports Science & Exercise Medicine (YISSEM)[2]
E-mail: cykim1204@gmail.com

INTRODUCTION

More than 70% of Anterior Cruciate Ligament (ACL) injury is related to sports with incidence of 1 per 3000 for the general population and injury rate for female is as much as eight times the higher as male in the United States[4]. However, Korean National Health Insurance Service (KNHIS) data analysis reported that, male have higher knee injury rate as compared to female in South Korea[3]. The risk factor of anterior cruciate ligament (ACL) injuries is generally associated with quick deceleration, hyperextension or rotation, muscle fatigue, and gender differences. It is well known that female has different kinematics and kinetics during landing and cutting, as compared to male in the United States[1,2]. However, there is a lack of study regarding ethnic differences in static and dynamic LEAs. Therefore, the purpose of this study is to determine whether ethnic differences exist in lower extremity static and dynamic postural measures between Caucasian female and Asian female.

METHODS

A total of 30 subjects were voluntarily participated. 15 Caucasian female (age: 21.3 ±1.58 yrs; weight: 63.9±7.42 kg; height: 169.6±4.60 cm) and 15 Asian female (age: 20.4±1.20 yrs; weight: 57.8±3.86 kg; height: 164.0±2.72 cm). Without any past history of lower extremity surgery. The definition caucasian includes persons of Scottish, New Zealander, Greek, English, Canadian, Welsh, Irish, and-in the United State[5]. This research choose the subject who parents were born in above countries.

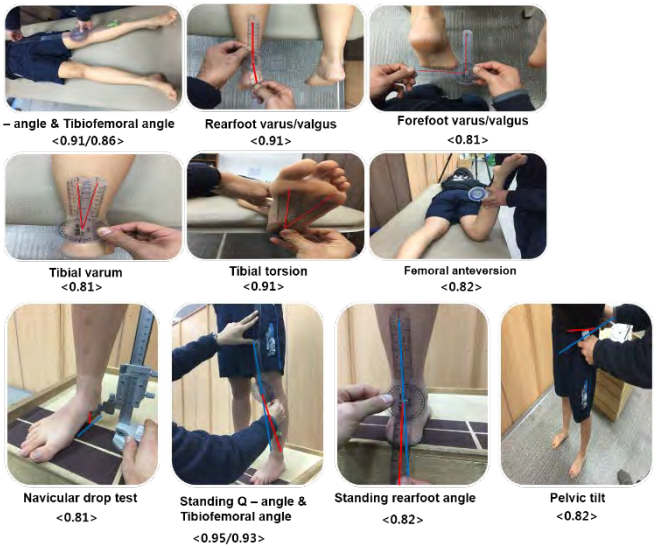

Figure 1. Static alignment measures. <ICC Level>

All subjects performed drop jump and static alignment measure. Drop jump was performed a 30cm-box, which was set at the half of their height distance away from the force plate. A single investigator measured the static alignment variables with lying and standing from all subjects.

Three-dimensional knee joint kinematics were extracted from 2 different type of motion analysis system (Vicon Inc, Oxford, UK; BTS Bioengineering, Milano, Italy).

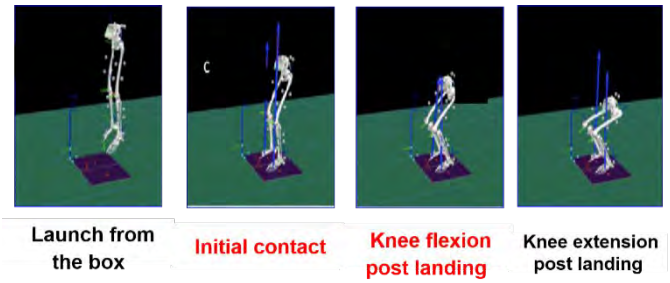

Figure 2. 3D motion capture during drop jump from a 30cm box.

All joint kinematics were analyzed at one discrete point which was 30° knee flexion during Drop jump from a 30cm-box. Independent sample t-test was performed to analyze mean differences between ethnicity.

RESULTS

<Static>

There were significant differences between Caucasian and Asian female at static lower extremity alignment measure. Asian female had significantly greater Q-angle (t= -3.782, p=0.00), Anteversion angle (t=.263, p=0.00), Rear, Fore foot angle (t= 2.020, p=0.00) compared to Caucasian female. Caucasian female had significantly greater TF-angle (t= 3.435, p=0.00), Tibial-varus angle (t=2.351, p=0.00), Tibial torsion angle (t= 2.645, p=0.00) compared to Asian female.

Variable	Caucasian		Asian		Effct size (η^2)
	Female (n = 43)		Female (n = 43)		Ethnic effect
	M	SD	M	SD	
Q-angle	15.3	2.79	19.01	4.40	1.01 (0.23~1.79)
TF angle	19.66	3.44	12.92	1.95	-2.41 (-3.01~-1.82)
Anteversion	7.15	2.36	10.19	6.52	0.62 (-0.42~1.66)
Rear-foot	1.14	4.08	5.98	4.26	1.16 (0.28~2.04)
Fore-foot	15.23	4.55	18.16	6.41	0.53 (-0.65~1.71)
Tibial-varus	5.27	1.6	3.51	1.97	0.98 (-1.36~ 0.61)
Tibial-torsion	19.66	4.58	16.58	6.44	-0.55 (-1.73~0.63)
Q-angle(WB)	7.05	2.68	10.58	3.6	1.11 (0.44~1.78)

Table 1. The variables from static alignment of Caucasian female and Asian female (p<.05).

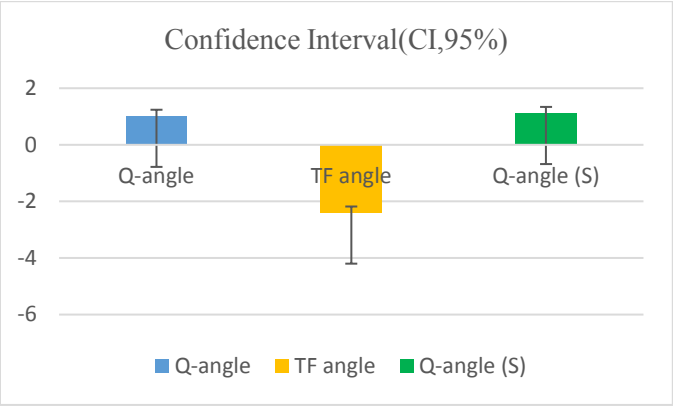

Table 2. The confidence interval from static alignment of Caucasian female and Asian female (p<.05).

<Dynamic>

There were statistically significant differences between Caucasian and Asian female at max angle during initial contact to 30° knee flexion. Caucasian female had significantly greater knee valgus angle (t= -3.293, p=0.03, Caucasian: -3.15°±6.12°; Asian: 3.19°±3.94°) and knee internal rotation (t= 2.143, p=0.41, Caucasian: 12.58°±9.54°; Asian: 5.05°±9.35°) compared to Asian female in drop jump from a 30cm-box.

Variable	Caucasian		Asian		Effct size (η^2)
	Female (n = 15)		Female (n = 15)		Ethnic effect
	M	SD	M	SD	
Hip Flexion	44.7	8.12	39.8	5.00	0.73 (-0.01~1.47)
Hip Adduction	-5.60	4.48	-5.88	4.36	0.06 (-0.65~0.78)
Hip Internal rotation	-9.22	9.31	-2.26	10.28	-0.71 (-1.45~0.03)
Knee Flexion*	31.2	3.15	29.0	2.48	0.78 (0.03~1.52)
Knee Valgus*	-3.15	6.12	3.19	3.94	-1.23 (-2.01~-0.45)
Knee Internal rotation*	12.6	9.54	5.05	9.35	0.8 (0.06~1.54)
Ankle Dorsi Flexion	-5.99	8.60	-6.12	8.69	0.02 (-0.7~0.73)
Ankle Eversion	1.31	2.25	.92	2.29	0.17 (-0.55~0.89)
Ankle Internal rotation	-4.08	8.11	-6.17	10.9	0.22 (-0.5~0.94)

Table 3. The variables from drop jump of Caucasian female and Asian female at max angle during initial contact to toe off (p<.05).

CONCLUSION

Our results showing that significantly differences between Caucasian female and Asian female in static and dynamic alignment. Greater knee valgus and internal rotation in a Caucasian female may support the difference of ACL injury rates between Caucasian female and Asian female. The difference of dynamic angle between Caucasian and Asian may one of the key factor for ACL injury rate. Possibly reducing knee valgus and internal rotation may drop the injury rate of female to similar with a male as found in South Korea. Further study is necessary to investigate the relation between static and dynamic angles in different ethnic and whether static LEAs contribute to dynamic LEAs or not in dynamic movements during numerous sports event.

REFERENCES

1. Arendt E, Dick R. Knee injury patterns among men and women in collegiate basketball and soccer NCAA data and review of literature. The American journal of sports medicine. 1995;23(6):694-701.
2. Messina DF, Farney WC, DeLee JC. The Incidence of Injury in Texas High School Basketball A Prospective Study Among Male and Female Athletes. The American journal of sports medicine. 1999;27(3):294-299.
3. KOSIS (Korean Statistical Information Service) http://kosis.kr/statisticsList/statisticsList_01List.jsp?vwcd=MT_ZTITLE&parmTabId=M_01_01#SubCont
4. Gwinn DE, Wilckens JH, McDevitt ER, et al: The relative incidence of anterior cruciate ligament injury in men and women at the United States Naval Academy. Am J Sports Med. 2000;28: 98–102.
5. Bhopal R, Donaldson L. White, European, Western, Caucasian, or :What? Inappropriate Labeling in Research on Race, Ethnicity, and Health. Am J Public Health. 1998; 88(9): 1303–1307.

BALANCING HUMAN DRIVER POSTURE IN VEHICLE UNDER LATERAL MOTION

[1, 2] Hideyuki Kimpara, [1] Kenechukwu C. Mbanisi, [1] Jie Fu, [1] Zhi Li, [1] Karen L. Troy, and [1] Michael A. Gennert

[1] Worcester Polytechnic Institute, Worcester, MA, USA
[2] Toyota Research Institute N.A. (TRI-NA), Ann Arbor, MI, USA
email: hkimpara@wpi.edu, web: https://www.wpi.edu/academics/departments/robotics-engineering

INTRODUCTION

More human-like driver models could realize improved driving in various driving environments and could be useful for advanced safety design of human-operated vehicles as well as autonomous vehicles [1]. We attempted to implement a robotics-based control algorithm on the OpenSim [2] human model with a driver-vehicle feedback system [1, 3] to simulate human-like posture control in a moving vehicle as Figure 1.

Although Proportional, Integral and Differential (PID) control is widely accepted for many purposes, PID allows feedback control only for a single-input-single-output (SISO) system, e.g. independent joint control. Some studies have applied PID control for occupant balancing problem, however, simulated postures could not fully predict the postural response of braking drivers due to limitation of SISO [3]. On the other hand, motion control algorithms for a human driver may require multiple inputs, such as positions and contact forces, and produce multiple outputs, one for each actuated degree of freedom. In addition, since human body is modeled as a coupled multi-body system, a single link of a human body may receive forces and torques from adjacent or connected other links. As a result, the control system for a human driver requires a multiple-input-multiple-output (MIMO) feedback system. Therefore, this study employed the inverse dynamics control algorithm to enable MIMO feedback system.

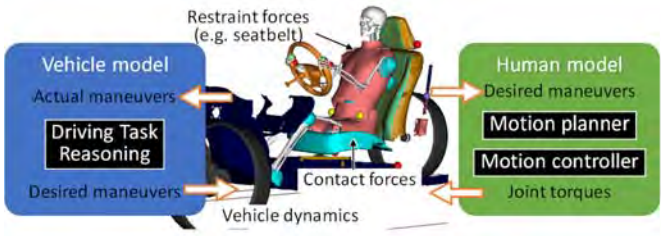

Figure 1: Driver-vehicle feedback system with OpenSim model.

This paper presents balancing driver's posture with consideration for dynamics.

METHODS

The OpenSim driver-vehicle model has more than 90 bodies and around 200 state variables. Human driver model consists of head/neck [5], lumbar/torso [6], upper extremity [7], and lower extremity [8] models. Muscle elements were replaced with ideal torque actuators at the joints for the simplicity. Anthropometry of the model is assumed as height of 1.8 m and weight of 77.4 kg. The OpenSim vehicle model represents 2012 Toyota Camry. Model geometry and inertial properties were obtained from a finite element (FE) model of Toyota Camry [9]. This model includes major components of vehicular exterior and interior such as driver seat, pedals, and steering wheel. Joint center, mass center, inertial properties for all components were estimated from properties of FE models. Elastic foundation definition of OpenSim is used in modeling the contacts of lower extremities against brake/gas pedals, floor of vehicles as well as upper bodies against steering wheel and interior components. In particular, the contact geometry of foot is obtained from shoes model of Hybrid III 50th percentile male dummy [10], and contact forces are validated against sole impact test data [11].

The inverse dynamics control is valid in a system with known mass, Coriolis, and gravity [12] as following equation:

$$M(q)\ddot{q} + C(q,\dot{q}) + N(q) = \tau \qquad (1)$$

where q is the state variables in joint space, $M(q)$ is mass matrix, $C(q,\dot{q})$ is velocity vector which is the product of Coriolis matrix and velocity of state variables, $N(q)$ is gravity vector, and τ is the joint torques. We utilized SimBody API [13] to extract dynamics parameters from OpenSim model during runtime. For the dynamic system as in equation (1),

the inverse dynamics control in joint space will compute the joint torque τ via the coefficients K_P and K_D and designed control law as following:

$$\tau = M(q)a_q + C(q,\dot{q}) + N(q) \quad (2)$$

$$a_q = -K_P(q - q^d) - K_D(\dot{q} - \dot{q}^d) \quad (3)$$

where a_q is a new transformed input term, q^d is desired joint state variables. In case of balancing control, initial joint angles set q^d with $\dot{q}^d = 0$. Because we desire the error to converge to zero, this control law will make the system asymptotically stable when K_D is positive.

The base body of vehicle model was enforced to move as desired acceleration pulses. The 2 DOF acceleration data in lateral translational motion and yaw rotation were obtained from a linear driver – vehicle model [3] to express vehicle dynamics of slalom driving. Custom joint between seat cushion and pelvis performs as free joint, however, pelvic motions are constrained by contacts with friction and non-linear point-to-point forces which represent seatbelt tensions. The inverse dynamics control in balancing upper body was operated with 50 Hz of feedback frequency. The utilized gains for K_P and K_D were 200 and 20 respectively.

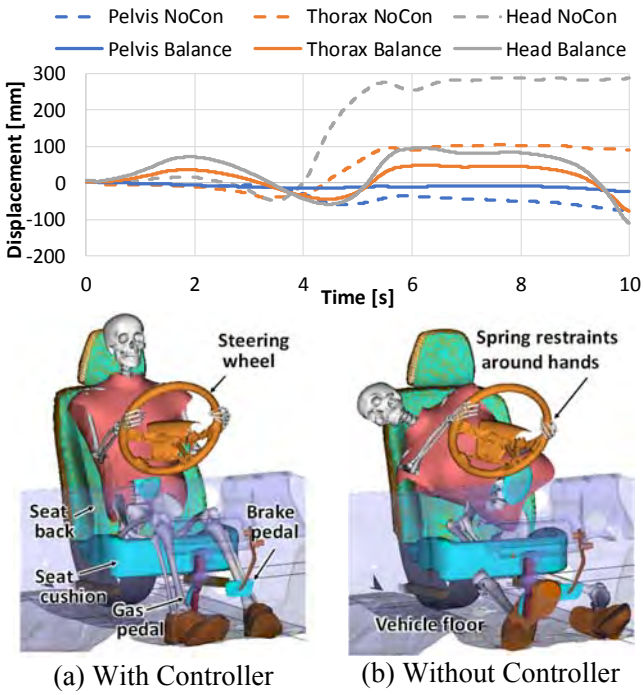

(a) With Controller (b) Without Controller

Figure 2: Comparison of relative displacements on head, thorax, and pelvis against vehicle frame during slalom lateral vehicle motions (upper), and driver model kinematics at 5 [s] (lower).

RESULTS AND DISCUSSION

Figure 2 shows body kinematics of human driver model in vehicular lateral motions. Human driver model with no controller fold up the upper body during vehicular lateral motions because of no active joint torques. On the other hand, the controller maintained the human body in human-like upright posture. The balancing controller reduced the maximum displacements.

Although lateral motions of vehicle would create non-linear body kinematics of human driver, the balancing controller based on inverse dynamics control with gravity compensation succeeded in maintaining upper body balance during lateral vehicular motion. The results of balancing control indicate that extracted parameters using SimBody API from the model were appropriate for requirements of the inverse dynamics control. Previous studies published occupant response data using real human volunteer subjects in moving cars. Further simulation with similar simulation setup as previous study would be necessary for validation of system and assumed parameters.

REFERENCES

1. Mbanisi et al. *IROS 2017 Workshop*, 2017.
2. Delp et al. *IEEE Tran. Biomed. Eng.*, **54**(11), 2007.
3. Saigo S. *Ph.D. dissertation, Tokyo University of Agriculture and Technology*, 2014.
4. Östh et al. *Gait & Posture*, **40**, pp.664-669, 2014.
5. Vasavada et al. *Spine*, **23**(4):412-422, 1998.
6. Christophy et al. *Biomechanics and Modeling in Mechanobiology*, **11**:19-34, 2011.
7. Saul et al. *Computer Methods in Biomechanics and Biomedical Engineering*. **18**:1445-58, 2015.
8. SimTk. https://simtk-confluence.stanford.edu/display/OpenSim/Gait+2392+and+2354+Models.
9. Reichert et al. *SAE 2016–01–1534*, 2016.
10. LSTC. http://www.lstc.com/download.
11. Manning et al. *ESV Conf.*, pp.1960-98, 1998.
12. Spong et al. *Robot modeling and control (Vol. 3)*. New York: Wiley, 2006.
13. Sherman et al. *Procedia Iutam*, *2*, 2011.

JOINT ANGLE COORDINATION STRATEGIES DURING ROTATIONS IN DANCE

Melanie B. Lott

Denison University, Granville, OH, USA
email: lottm@denison.edu

INTRODUCTION

The motion of any rigid body is fully characterized by the sum of two independent components: translational motion of the center of mass (CM) and rotational motion of the body around the CM. Previous work on step and spin turns has shown that these movements require larger ranges of motion outside of the sagittal plane and different muscular demands than straight-line gait [1]. Given the prevalence of rotational maneuvers in everyday life, more studies on whole-body rotations and balance maintenance in particular are needed.

A pirouette is a whole-body rotation in which rotational momentum is generated from a double stance, then some number of revolutions are completed about a vertical axis on a single support. It has been shown that dancers are likely to make adjustments for balance maintenance during pirouettes [2]; however, the nature of these adjustments has yet to be measured.

The goal of this study was to perform principal components analysis (PCA) on joint angle data of dancers performing pirouettes to determine whether joint angle coordination strategies were utilized. Previously, PCA has found relative contributions of body segments' motion to postural control in quiet standing [3]. It is hypothesized that dancers utilize coordination strategies in pirouettes, but the particular joints and directions involved in these strategies may vary between individuals.

METHODS

Six injury free, advanced female dancers (20.2 ± 5.5 years) participated after giving informed consent (parental consent). Dancers performed triple-turn pirouettes until 4-5 clean trials were obtained, i.e. the dancer landed after three complete revolutions (1080°). Position data of 70 reflective markers attached to dancers were recorded with a 6-camera system (100 Hz; Oqus 5+, Qualisys). Marker data were low-pass Butterworth filtered (6 Hz) and used to define and track body segments.

Lower extremity joint angles (ankle, knee, hip) and pelvis-trunk angle were determined from LCS orientations of adjoining segments. The Cardan sequence of rotations was performed in Visual3D (C-Motion) to compute flexion/extension (X), abduction/adduction (Y), and internal/external rotation (Z). To isolate the turning phase, joint angle data were time-normalized, beginning at 360° and ending at 900° (1.5 revolutions).

PCA was performed on the joint angle time series data for each dancer (4 or 5 trials x 21 joint angles) using R Studio. Eigenvalues of the covariance matrix, mean centered and normalized to unit trace, were computed and provided the proportion of variance in the data explained by each PC (Table 1). Coefficients of the corresponding eigenvectors were determined and indicate the contributions of each joint angle to the PC (Fig. 2).

RESULTS AND DISCUSSION

Evolution of the data along PC1 and PC2 show two distinct patterns (Fig. 1). One PC had a clear upward trend ("PC_{Drift}") and the other PC exhibited oscillatory behavior ("$PC_{Oscillate}$"). The period of oscillation of $PC_{Oscillate}$ was calculated from the time between the global minimum and peak maximum (average = 66 ± 5%). In time normalized units, the period of oscillation of the pirouette is 66.7% (1/1.5 rev^{-1}). The movement characteristic of $PC_{Oscillate}$ (average eigenvalue = 0.2514) is joint angle oscillations near the characteristic frequency of the pirouette. A Fourier analysis is necessary to further determine the frequency spectrum. The joint angles contributing most greatly to $PC_{Oscillate}$ vary by dancer (Fig. 2).

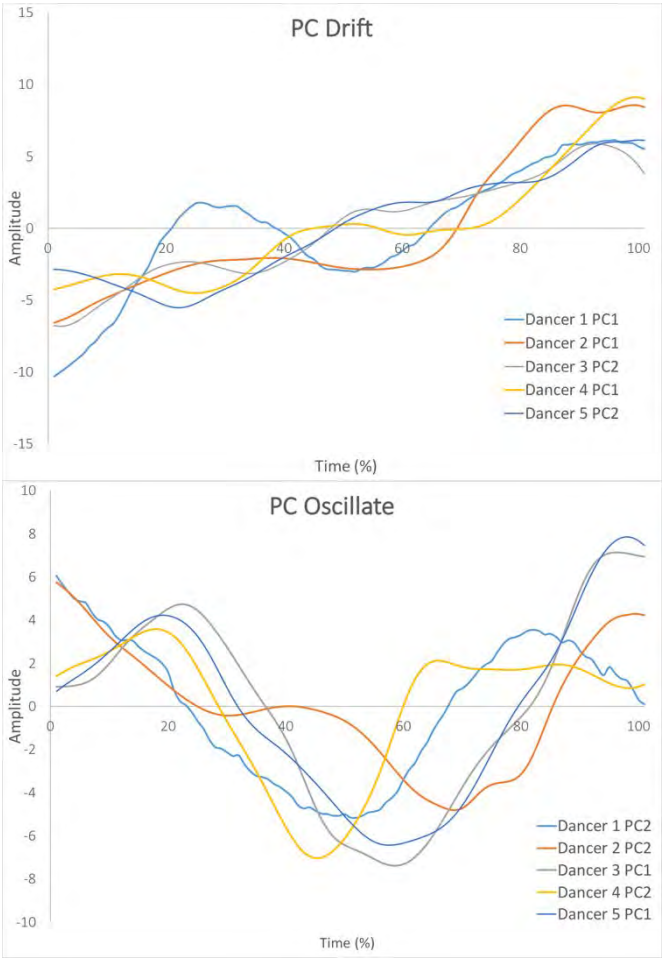

Figure 1: Evolution of the data along the first two PCs (i.e., "eigenmodes). Note that PC2 (PC1) for Dancers 3 and 5 is included in PC_{Drift} ($PC_{Oscillate}$).

Fewer joint angles typically contributed meaningfully to PC_{Drift} than $PC_{Oscillate}$. For example, AnkleX, KneeZ, and Pelvis-TrunkZ had the most significant contributions to PC_{Drift} for Dancer 5. This dancer employed a strategy to descend from "demi-pointe" (ankle plantarflexion) in coordination with pelvis-trunk external rotation. She also experienced knee external rotation during this maneuver. The movements characterized by PC_{Drift} often captured early landing mechanics.

Further research on joint coordination strategies, and in particular which strategies are correlated with CM motion, could provide dancers with methods for enhancing pirouette performance and could potentially lead to understanding of balance maintenance strategies during whole body rotations more generally.

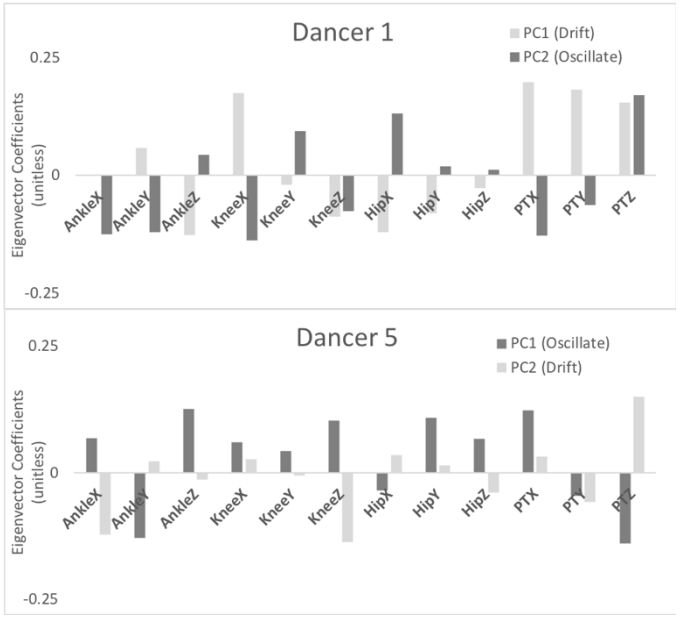

Figure 2: Coefficients of the eigenvectors of PC1 and PC2 for Dancer 1 and Dancer 5.

REFERENCES

1. Taylor MJD, et al. *Percept Mot Skills*. **102**, 576-588, 2006.
2. Lott MB & Laws KL. *J Dance Med Sci*. **16**, 167-174, 2012.
3. Pinter IJ, et al. *J Neurophysiol.* **100**, 3197–3208, 2008.

ACKNOWLEDGEMENTS

The author thanks Arleen Sugano, Annie Oyler, Gemma Aldana, and Gan Xu.

Table 1: Eigenvalues, or proportion of variance explained by each PC.

	PC1	PC2	PC3	PC4	PC5	Cumulative
Dancer 1	0.3859	0.2249	0.1612	0.0750	0.0470	**0.8940**
Dancer 2	0.4839	0.1750	0.1203	0.0873	0.0713	**0.9378**
Dancer 3	0.3411	0.2185	0.1367	0.0914	0.0880	**0.8757**
Dancer 4	0.3106	0.2094	0.1561	0.0874	0.0714	**0.8349**
Dancer 5	0.3064	0.2280	0.1667	0.0898	0.0607	**0.8516**

A POWERED 3D COMPASS WALKER: ENERGETICS AND STABILITY OF PERIOD-1 GAITS

Soumyabrata Maiti, Jonathan B. Dingwell, and Joseph P. Cusumano

The Pennsylvania State University, University Park, PA, USA
Email: sxm710@psu.edu

INTRODUCTION

Simple anthropomorphic models play an important role in research on human locomotion, particularly for studies concerned with energy consumption and stability. Kuo's analysis of a 3D passive dynamic walker [1] showed that lateral stability may present an inherently greater challenge to the nervous system than sagittal plane stability, a prediction supported by experiments with humans [2]. In other studies, an open-loop stable, impulse-driven planar walker was used to examine the relationship between preferred speed and step length [3], and to compare the energetics of toe-off impulses to hip actuation [4]. To date, however, a powered version of the 3D "compass" walker has not been studied. We here present such a model, find its period-1 gaits, and examine their basic dynamic and energetic properties.

METHODS

Following [1], governing equations in the angles q_1, q_2, and q_3 (see Fig. 1) are derived using angular momentum balance about the ground contact point, O, the joint between the foot and stance leg, A, and the hip of the swing leg, B.

Conservation of angular momentum across the heel strike can be written in matrix form as

$$[H]^{+}\begin{bmatrix}\dot{q}_1^{+}\\ \dot{q}_2^{+}\\ \dot{q}_3^{+}\end{bmatrix} = \begin{bmatrix}h_{\mathrm{O}}^{-}\\ h_{\mathrm{A}}^{-}\\ h_{\mathrm{B}}^{-}\end{bmatrix} + \begin{bmatrix}M_{\mathrm{O}}\\ M_{\mathrm{A}}\\ 0\end{bmatrix} \qquad (1)$$

where: $-/+$ superscripts denote before/after impact; $h_{\mathrm{O}}, h_{\mathrm{A}}, h_{\mathrm{B}}$ are angular momentum components about O, A and B in the n_3, f_1 and i_3 directions, respectively (Fig. 1); $\dot{q}_i$ $(i = 1, 2, 3)$ are angular velocities; and $[H]^{+}$ is a state-dependent matrix. Impulsive moments M_{O} and M_{A} in the sagittal and frontal planes, respectively, arise from the toe-off impulse P (Fig. 1). During application of P we assume an impulsive moment acting at the ankle to counteract M_{A}.

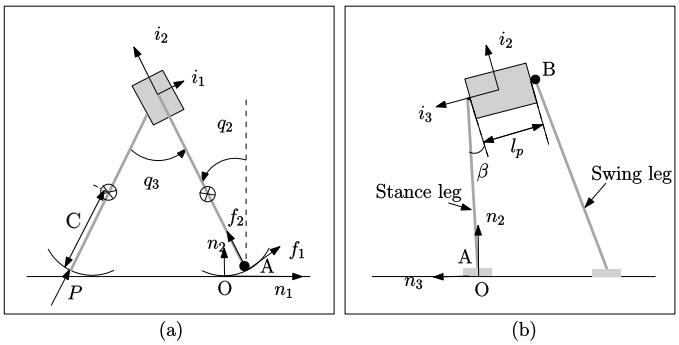

Figure 1: Powered 3D walker at heel strike/toe off: point O is the ground contact, B the hip joint, and A the stance foot "ankle" (see Eq. 1). Center of mass of each leg is a distance C from each foot. Just before toe-off, impulse P is applied along swing leg.

Simulations of the governing equations were carried out using `ODE15s` in Matlab to find the time evolution of the system during the single support (i.e., swing) phase, that is, between visits to the Poincaré section determined by heel strike [1]. A shooting method and arc-length continuation were used to study the system's behavior as a function of P.

RESULTS AND DISCUSSION

Period-1 gaits (i.e., fixed points of the impact Poincaré map) of the powered walker are shown in Fig. 2. The stability properties at each point on the curve were also determined via eigenanalysis, as required for controller design. All solutions shown were found to be open-loop unstable, with each possessing an unstable roll mode; some have additional unstable modes that stabilizing control must account for. Also shown are bifurcation points corresponding to saddle node (I,III, V), period doubling (II, IV, VII), and secondary Hopf (VI) bifurcations. At these points, the number of unstable directions that need to be controlled changes.

As in [1], splay angle control is used to stabilize the roll direction of the long period gait, however, for gaits possessing a sagittal plane instability we implemented

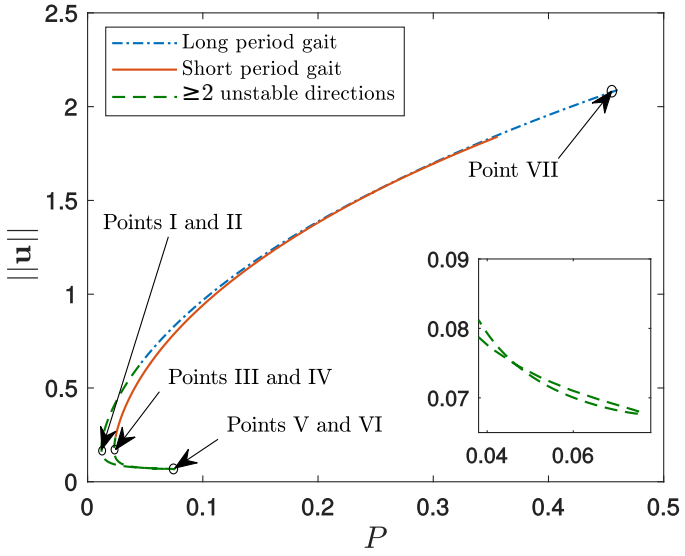

Figure 2: Magnitude $\|\mathbf{u}\|$ of period-1 fixed points vs. toe-off impulse P. Without feedback control, all solutions have at least one unstable mode. Bifurcation points I–VII are also shown (see text).

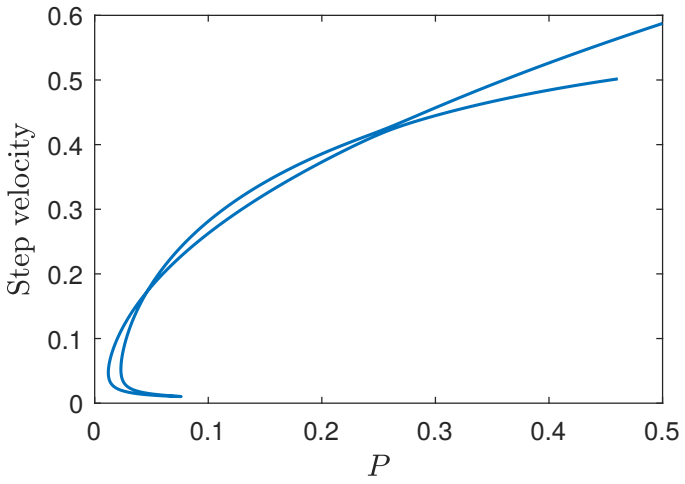

Figure 3: Step velocity (step length/step time) vs. P for system, corresponding to the steady state solutions displayed in Fig. 2.

an additional toe-off impulse controller. Figure 3 shows the step velocity (step length divided by step time) along the curve of Fig. 2.

Figure 4 shows the work done by the toe-off impulse P for the period-1 gaits of Figs. 2, normalized by the maximimum leg swing kinetic energy. For a given toe-off impulse, we find the short period gait (Fig. 2) is more efficient than the long period gait, dissipating less energy during heel strike. The relative power requirement is lowest for the portion of the solution

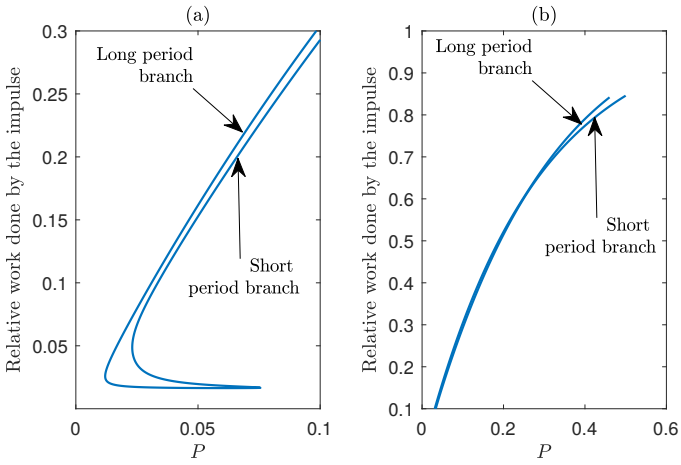

Figure 4: Work per step done by P, relative to the maximum kinetic energy during swing phase along solutions of Fig. 2.

curve connecting long and short period gaits, at the expense, however, of a low step velocity (see Fig. 3).

CONCLUSIONS

We presented a variant of the 3D compass walker powered by toe-off impulses, and found its period-1 gaits as a function of impulse strength. Stability analyses showed that all of these gaits are open-loop unstable, and also identified seven bifurcation points where the number of unstable directions change. Thus, we find that some period-1 gaits (those with a higher number of unstable directions) are relatively more difficult to stabilize than others. We also computed the energy cost for the period-1 gaits: for a given value of toe-off impulse, we found that the short period gait is energetically more efficient.

ACKNOWLEDGMENTS

NIH/NIA Grant #R01AG049735.

REFERENCES

1. A. D. Kuo. *Int J Robot Res*, 18(9):917–930, 1999.
2. P. M. McAndrew et al. *J Biomech*, 44(4): 644–649, 2011.
3. A. D. Kuo. *J Biomech Eng*, 123(3):264–269, 2001.
4. A. D. Kuo. *J Biomech Eng*, 124(1):113–120, 2002.

EQUILIBRIUM DURING SINGLE-LEG STANDING WITH HEEL RAISED UP IN INDIVIDUALS WITH ANKLE INSTBILITY

Morikawa M, Urabe Y, Takeuchi T, Hashimoto R, Maeda N

Hiroshima University, Hiroshima, Japan
email: m-masanori@hiroshima-u.ac.jp, web: https://yurabelab.wixsite.com/sportsrehabilitation

INTRODUCTION

Lateral ankle sprain is the most common injury in sports. Since the frequency of recurrent is also high, athletes suffer from chronic symptoms such as swelling, pain and ankle instability. Wikstrom *et al.* reported individuals with ankle instability had exhibited less postural stability during single-leg and found that less single-leg standing ability developed ankle injury risk [1]. Therefore, the evaluation of single-leg standing plays an important role for clinicians.

Although ankle sprain tends to occur with plantar flexed, there is no consideration about ankle joint during single leg standing. Therefore, it is possibility that evaluation of single-leg standing with heel raised up is more useful. The purpose of this study was to clarify whether COP variables can discriminate individuals with ankle instability during single-leg standing with heel raised up.

METHODS

A total of 9 men participated in this study and undertook Cumberland Ankle Instability Tool to divide into 2 groups of individuals with and without ankle instability (CAI and Control) [2]. The cut-off score were more than 25 points. The demographic characteristics was showed as follow; [CAI group - 5 men, age 24.3 ± 1.0 years old (mean ± SD); height 1.76 ± 0.05 m; body weight 74.3 ± 9.72 kg, Control – 4 men, age 25.0 ± 1.0 years old (mean ± SD); height 1.71 ± 0.02 m; body weight 60.8 ± 1.95 kg]. Study procedures were carried out in accordance with the Declaration of Helsinki.

All subjects conducted single-leg standing with heel raised up on a force platform (T.K.K.5810; Takei Scientific Instruments Co., Ltd., Japan) during 5 seconds. Subjects wore T-shirts, spats, no sox and no shoes. The authors instructed each subject to flex the knee at 30 degrees and raise up your heel as high as possible within not losing upright posture. The knee flexion angle of contralateral side set at 90 degrees. Both of hands placed on the hip. Finally, subjects were called to look forward and to maintain posture as stably as possible.

A total of 5 successful trials were recorded, and COP data was collected in 100 Hz. Then, total length (TL) [mm], speed [mm/s], root-mean-square (RMS) amplitude [mm] and RMS speed [mm/s] in anterior-posterior (A-P) and medial-lateral (M-L) directions were calculated respectively.

The unpaired t-test was used for testing the difference between CAI and control. The statistical analysis was performed in SPSS for Windows, version 20.0 (IBM Japan Co., Tokyo, Japan). The significance level was set at 5%.

RESULTS AND DISCUSSION

The total length and RMS amplitude in M-L direction statistically increased in CAI compared to control (Fig.1,2). On the other hand, the other variables showed no significant (Table.1). Results suggested total length, RMS amplitude and RMS speed in M-L allowed to discriminate CAI by single-leg standing with heel raised.

The reason why total lengths and RMS amplitude increased may be related to characteristics of ankle joint. While dorsiflexion position in talocrural joint stabilizes ankle joint, plantarflexion makes talocrural joint lose joint stability [3].

The increased total length after instructing to maintain posture as stably as possible indicated less postural stability [4]. Also, increased RMS amplitude shows to fail maintain COP in same position [4].

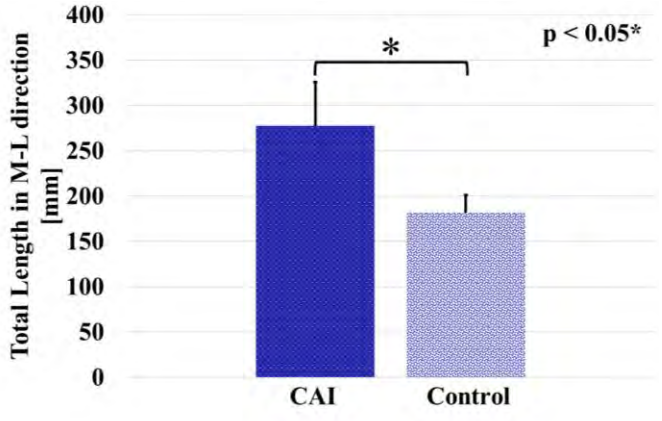

Figure1: Total length in M-L direction during single-leg standing with heel raised up [mm]. M-L, medial-lateral.

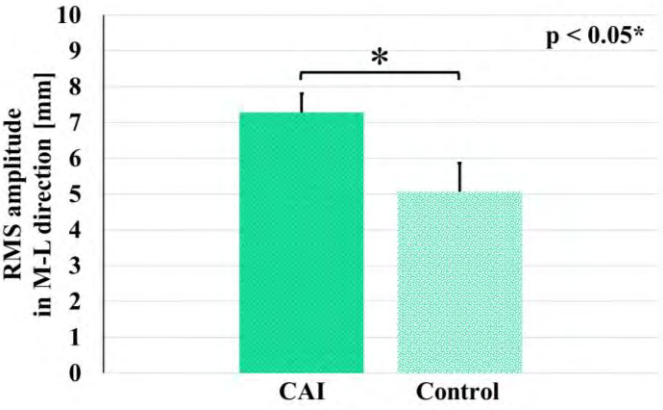

Figure2: RMS amplitude in M-L direction during single-leg standing with heel raised up [mm]. RMS, root-mean-square; M-L, medial-lateral

It is worth mentioning about significant changes of total length and RMS amplitude in only M-L direction. Yota *et al.* found that there was no significant response in total length and RMS amplitude in M-L direction between sprain and control group during single-leg standing without heel raised up. Therefore, single-leg standing with heel raised up may allow to distinguish between CAI and heathy individuals.

CONCLUSIONS

- This study investigated whether single-leg standing with heel raised up can discriminated the individual of chronic ankle instability or healthy.
- Single-leg standing with heel raised up can distinguish individuals of chronic ankle instability by total length and RMS amplitude in M-L direction, in different to previous study.
- Single-leg standing with heel raised up may be effective to evaluate postural stability for chronic ankle instability.

REFERENCES

1. Wikstrom E. scand j med sci sports. 34(3), 2000.
2. Kunugi S. Disabil Rehabil. 39(1), 2017
3. Abe Y. J Phys Ther sci. 26(3), 2014
4. Stormont D. Am J Sports Med. 13(5), 1985

Table1: Values for RMS amplitude according to knee orthoses with and without strap

Variable [mm]	Group		p-value
	CAI (n=5)	Control (n=4)	
Total Length, A-P	209.1 ± 32.0	164.3 ± 12.8	0.053
Total Length, M-L	277.8 ± 48.1	164.3 ± 12.8	p < 0.05*
Speed, A-P	27.5 ± 2.0	26.3 ± 1.3	0.365
Speed, M-L	27.0 ± 3.2	24.7 ± 1.3	0.279
RMS amplitude, A-P	6.2 ± 1.4	6.3 ± 1.5	0.869
RMS amplitude, M-L	7.3 ± 0.5	5.1 ± 0.8	p < 0.05*
RMS speed, A-P	22.9 ± 1.9	21.2 ± 1.1	0.201
RMS speed, M-L	21.8 ± 2.3	20.2 ± 0.8	0.294

A-P, Anterior-Posterior; M-L, Medial-Lateral; RMS, root-mean-square;
*Indicate a significant difference between CAI and control (p < 0.05)

THE EFFECT OF MENTAL FATIGUE ON POSTURAL STABILITY

Amanda Morris and Anita D. Christie

University of Oregon, Eugene, OR, USA
email: amorris8@uoregon.edu

INTRODUCTION

Fatigue is a multidimensional concept that has both physical and psychological components. While neuromuscular fatigue is a transient reduction in the ability of the muscle to produce force or power in response to contractile activity [1], mental fatigue is a psychophysiological state that occurs after or during prolonged periods of cognitive activity [2]. As mental fatigue can negatively affect the ability to simultaneously allocate attention and respond to unexpected stimuli [3], it may impact motor functions such as balance control. This could be especially important in older individuals, as their attentional resources and cognitive processing abilities are more limited than younger adults. However, the effect of mental fatigue on postural stability has not been studied. The purpose of this study was to examine the effect of a mentally fatiguing, sustained attention task on postural stability in young and older women.

METHODS

Thirty-two women (16 young 22.4 ± 3.72 years, 16 older 72.6 ± 6.50 years) participated in this study. Testing was divided into two sessions involving postural perturbations; one mental fatigue session (sustained attentional task) and one control session (scenery video without sound). The order of the protocols across the two visits was randomized across participants.

Perturbations. Hydraulically activated, dual force plates that translated forward and backward were used for postural perturbations. Platform translations were 15 cm at a velocity of 30 cm/s. Trials were randomized and, to account for any learning effect, 20 perturbations (5 forward, 15 backward) were provided in random order at baseline. During both the mental fatigue and control sessions, 5 perturbations (1 forward, 4 backward) occurred at the beginning (1 minute) and end (18 minutes) of the session for a total of 10 perturbations (2 forward, 8 backward) over the 20–minute session. Only backwards perturbation trials were analyzed, forward perturbations were used to avoid an anticipation effect. Force data was sampled at 1kHz then low pass filtered at 10 Hz. Total displacement of center of pressure (COP) and COP velocity in the anterior-posterior direction were used to assess postural stability in response to backward perturbations . . All data were analyzed with custom-written programs using MATLAB software (MathWorks Inc., Natick, MA, USA).

Mental Fatigue Task. During the mental fatigue session, participants were asked to perform the psychomotor vigilance task (PVT; Biotechnology HPC Software Applications Institute) for twenty minutes, which was run using MATLAB. The PVT is based on simple reaction time (RT) to stimuli that are presented at random intervals. Slower reaction times during this task are associated with subjective measures of physical fatigue and decline in energy. Increases in reaction time throughout the protocol indicated the presence of mental fatigue.

Statistical Analyses
Repeated-measures ANOVAs were used to examine the impact of each protocol on each variable. If significance was found, the Bonferroni procedure was used for post-hoc testing. Linear regression was used to determine if there was a significant relationship between percent change in PVT reaction time and percent changes in COP displacement and COP velocity.

RESULTS AND DISCUSSION

Reaction Time. Older women had significantly slower reaction times (325.17 ± 30.90 ms) than young (287.95 ± 29.53 ms) at baseline (p=0.002) (Figure 1). Reaction time significantly increased

over the 20-minute period only for the young women (p=0.001; 287.95 ± 29.5 vs. 320.3 ± 35.05 ms), indicating the presence of mental fatigue (Figure 1).

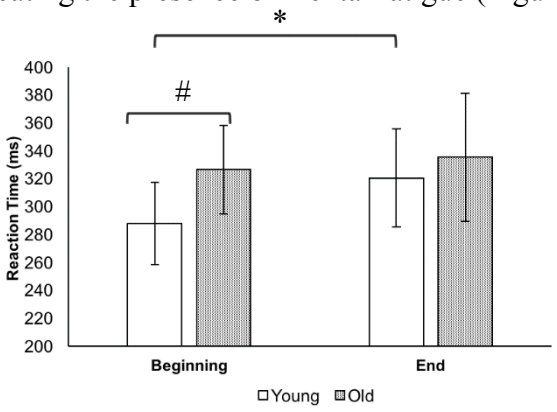

Figure 1. Reaction time from first 5 minutes (Beginning) and last 5 minutes (End) of the PVT. *p=0.001, #p=0.002.

Postural Stability. Older women had significantly larger anterior-posterior COP displacement (p=0.001; 6.89 ± 0.96 cm vs. 5.74 ± 0.96 cm) and significantly faster COP velocity (p=0.04; 41.14 ± 12.29 cm/s vs. 31.51 ± 12.30 cm/s) than young women. Young women had significantly faster COP velocity during the mental fatigue condition (p=0.009; 36.27 ± 16.74 cm/s vs. 26.75 ± 10.68 cm/s) than the control condition

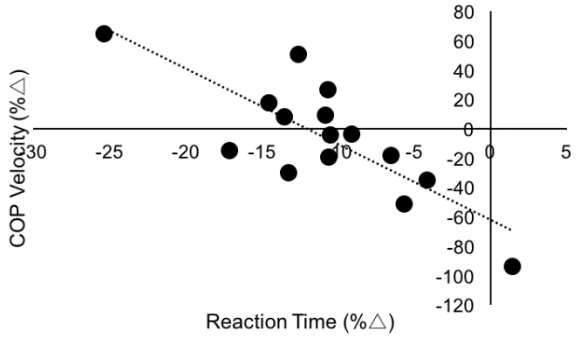

Figure 2. The relationship between percent change in RT and percent change in COP velocity in young women.

Relationship Between Reaction Time and Stability. There was no significant relationship between percent change in reaction time during the PVT and percent change in COP displacement in either the young or older women. Percent change in reaction time during the PVT significantly predicted percent change in COP velocity (r=-0.80, p=0.001) in young women only (Figure 2). The magnitude of this effect was large, explaining 64% of the variance in percent change in COP velocity (p=0.001) in young women only (Figure 2).

CONCLUSIONS

Older women had slower reaction time, larger COP displacement, and faster COP velocity than young women, suggesting that the neuromuscular system in older women may be less efficient in braking the forward movement of the body in response to backward perturbations. Only the young women experienced significant increases in RT and COP velocity during the mental fatigue condition. This could be because the older women were already near their threshold for efficiently allocating attentional resources in response to postural threats and adding a mentally fatiguing, sustained attention task resulted in constraint of the postural response for both safety and to manage the additional attentional demand. This resulted in older women having similar COP displacement and velocity in both conditions. Younger women, however, were still trying to effectively allocate attentional resources to both tasks and maintain RT performance. As young women became mentally fatigued, more attentional resources were redirected to maintaining RT and efficiency of the neuromuscular system's response to postural threats was reduced resulting in increased COP velocity to maintain COP displacements like those seen in the control condition.

While older women did not seem to experience any decrements in performance with mental fatigue, this research can be used to develop intervention strategies to improve attentional efficiency. Cognitive and postural tasks can be practiced simultaneously in to simulate the effect of mental fatigue and improve the ability to efficiently allocate attentional resources and improve the neuromuscular system response to postural perturbation.

REFERENCES

1. Gandevia, SC. *Physiological Reviews* **81**(4),1725-89, 2001.
2. Boksem & Tops. *Brain Res Rev.* **59**(1), 125-139, 2008.
3. Rankin, JK, et al. *Journals Gerontol Ser.*, **55**(3), 112-119, 2000.

CHANGES IN PROSTHETIC ALIGNMENT AFFECT GROUND REACTION FORCE SYMMETRY AND PAIN DURING SIT-TO-STAND

[1] Luis A. Nolasco, [2] Anne K. Silverman, and [1] Deanna H. Gates

[1] School of Kinesiology, University of Michigan, Ann Arbor, MI, USA
[2] Department of Mechanical Engineering, Colorado School of Mines, Golden, CO, USA
email: lnolasco@umich.edu, web: rehab-biomech-lab.kines.umich.edu

INTRODUCTION

People with a transtibial amputation (TTA) can navigate their environments successfully with use of a prosthetic device. The success of the prosthesis is dependent on numerous factors, one of which is the alignment of the prosthetic socket and pylon. Prosthetists alter the alignment of a prosthesis such that the patient has a normal (symmetric) gait pattern, assessed through observation and patient feedback. Misaligned prostheses can cause pressure changes in the socket, increased intact limb loading when standing, and increased asymmetry during walking [1-3]. In particular, anterior and posterior misalignment can increase pressures on the end of the residual limb, which can lead to tissue damage and/or pain [1]. TTA are also at greater risk for secondary conditions such as osteoarthritis [4] and low back pain [5], and this risk may be further elevated by use of a misaligned prosthesis. During sit-to-stand (STS) motions, people with TTA have asymmetric ground reaction forces [6] and greater lateral trunk lean [7] relative to non-amputees, which could be related to a higher risk for low back pain [5]. The purpose of this study was to determine how altering sagittal plane prosthetic alignment affects pain in the residual limb and low back as well as ground reaction force (GRF) symmetry during STS in people with TTA.

METHODS

A prosthetist adjusted the prosthesis of five participants with a unilateral transtibial amputation (1F/4M, 44.8±16.8 yrs, 1.77±0.10 m, 88.7±15.4 kg) by translating the prosthetic foot by 10 mm in the anterior and posterior directions, relative to the prescribed alignment. After each of the three alignment conditions, participants rated pain in their residual limb and back on a Visual Analog Scale (VAS) and performed five self-paced STS trials from a backless chair. Each trial began with hips, knees, and ankles at 90° of flexion and feet hip-width apart. The participants' arms were folded across their chest during the movement. Feet were placed on separate force plates (AMTI) recording at 1200 Hz.

Ground reaction forces (GRFs) were low-pass filtered using a 4th-order Butterworth filter with a cutoff frequency of 10 Hz. We then computed a Symmetry Index (SI) of the peak GRF between the prosthetic and intact limbs for each direction using:

$$SI\ (\%) = \frac{(GRF_{Intact} - GRF_{Prosthetic})}{(GRF_{Intact} + GRF_{Prosthetic})} * 100\%$$

where GRF values were taken at the time of peak vertical GRF within the STS lift phase (0-50%).

We used a single-factor, repeated-measures ANOVA to test for differences in GRF symmetry and pain scores between alignment conditions. Effect sizes were then computed using Cohen's d.

RESULTS AND DISCUSSION

There was no significant main effect for alignment for back ($p = 0.23$) or residual limb pain ($p = 0.18$; Fig. 1). However, there were medium and large effects for pain in the residual limb which increased from prescribed for the anterior ($d = -1.03$) and posterior ($d = -0.59$) alignments. For back pain, there was a trend for decreased pain in the anterior condition compared to prescribed ($d = 0.46$) while it tended to increase in posterior condition compared to prescribed ($d = 0.29$). All participants who scored above the 'No Pain' category had decreased back

pain in either alignment that was not their prescribed alignment. Unlike back pain, the change from the prescribed alignment in residual limb pain was different for every participant (Fig. 1).

The difference in GRF symmetry in the anterior-posterior (A/P) direction across conditions was significant ($F = 5.96$; 2; $p = 0.026$; Fig. 2). The posterior alignment had more symmetric A/P GRFs compared to the prescribed alignment ($d = -0.81$). Differences in GRF symmetry across conditions for the vertical and M/L directions were not significant. However, anterior and posterior alignments had decreased M/L and Vertical GRFs during STS, for both limbs, compared to the prescribed alignment.

These results suggest that using a different alignment than prescribed may reduce the load placed on the intact limb during STS, which may have implications for joint disorders and pain associated with increased intact limb loading [e.g., 4]. While these outcomes may point to more reliance on the prosthetic limb during STS, it is unclear whether TTA can benefit from different alignments as all parameters do not respond to alignment changes in the same way. More work is needed to verify these effects.

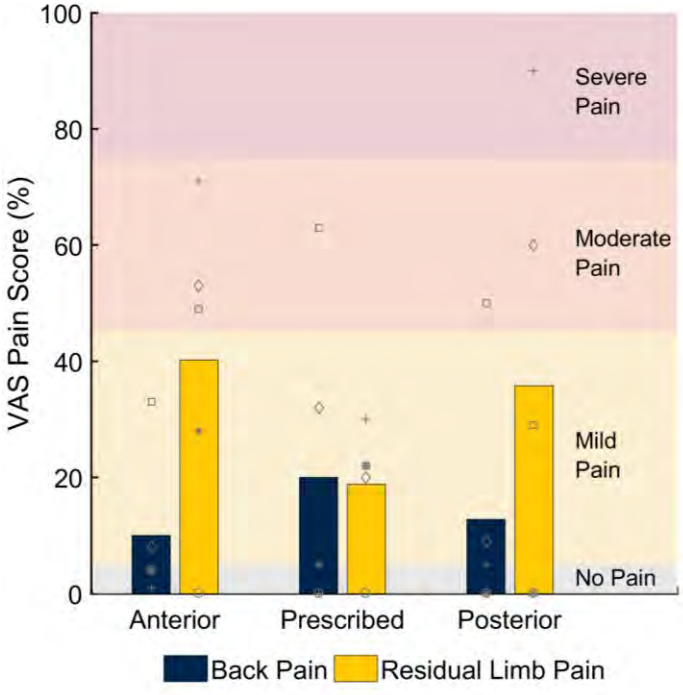

Figure 1: Average VAS scores for back pain and residual limb pain for different alignments (bars). Different gray symbols represent the pain scores for individual participants.

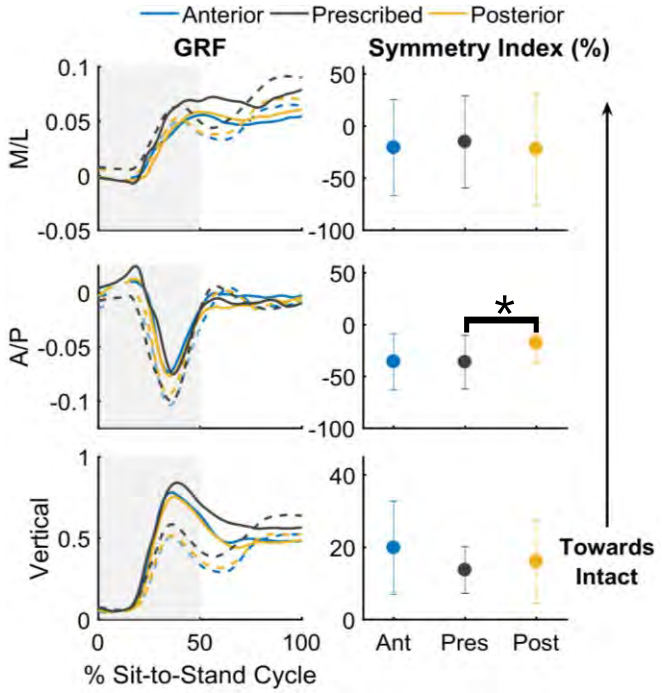

Figure 2: Left: 3D ground reaction forces (GRF) across the sit-to-stand (STS) cycle for all alignment conditions (Anterior (Ant), Prescribed (Pres), Posterior (Post)). Dashed lines represent the prosthetic limb; solid lines represent the intact limb. Right: Average Symmetry Index of peak GRF during the lift off phase (0-50%). Asterisk (*) denotes significance with $\alpha = 0.05$.

CONCLUSIONS

While there was large variation in VAS pain scores and GRF symmetry, decreases in overall GRF and peak GRF asymmetry suggest that STS may require a different alignment from prescribed. Additionally, while changes in back pain across conditions were consistent for all participants, the large variation in residual limb pain suggests that patient feedback alone should not be used in the prosthetic prescription process. Future work will investigate medial/lateral alignment conditions during STS and the effects of alignment on other common tasks.

REFERENCES

1. Seelen, HA., et al. *Clin Rehab,* **17**, 787-796, 2003.
2. Isakov, E., et al. *Clin Biomech,* **9**, 258-262, 1994.
3. Fridman, A., et al. *Prost Orthot,* **27**, 17-22, 2003.
4. Struyf, MD. *Arc Phy Med*, **90**, 440-446, 2009
5. Kulkarni, J. *Clin Rehab*, **19**, 81-86, 2005.
6. Agrawal, V., et al. *Ergonomics,***54**, 656-664, 2011.
7. Actis, JA., et al. *J Biomech,* **85,** 1-9, 2018.

PROTOCOL FOR REALISTIC VIRTUAL REALITY ENVIRONMENT THAT PERTURBS BALANCE

Caitlin O'Connell, Gustavo Sandri Heidner, J.C. Mizelle, Nicholas Murray, Patrick Rider, Zachary Domire

East Carolina University, Greenville, NC, USA
email: oconnellca17@ecu.edu

INTRODUCTION

Virtual reality (VR) can be utilized to challenge balance control by manipulating the visual environment. Studies have demonstrated balance perturbations using VR including increased postural sway [1], alterations in center of pressure (COP) displacement [2] and increased COP approximate entropy [3]. Previous research examining the impact of VR on balance have implemented entirely digital scenes, however a more realistic environment, such as a reproduction of an individual's environment may produce greater perturbations to balance. The objective of this study was to establish parameters, specifically amplitude and frequency, of a sinusoidal movement of a realistic VR environment to induce altered balance, as defined by increased sway displacement, velocity and approximate entropy.

METHODS

Twelve young adults (aged 22.1 ± 2.3 years, 2 male) were recruited. Individuals with conditions affecting balance were ineligible. Participants donned a VR headset (Oculus VR, USA) in which a 360° picture of the lab was projected (Figure 1). During data collection, participants were asked to stand still and look at the "X" on the wall in front of them. Prior to introducing balance challenges, a baseline trial was collected while participants wore the VR headset. Balance was challenged by an anterior-posterior sinusoidal movement of the lab within the VR headset. Four different amplitudes of the sinusoidal movement were tested: 1 cm, 5 cm, 10 cm and 20 cm, with each amplitude being presented at two frequencies were tested: 0.5 Hz and 0.25 Hz. The presentation order of sinusoidal amplitude was randomized to account for adaptation effects; and participants were presented first with a movement at 0.5 Hz and then 0.25 Hz within each amplitude. Center of pressure (COP) data was collected for 30s at 1000Hz.

Figure 1: Projection of laboratory environment as seen in VR headset.

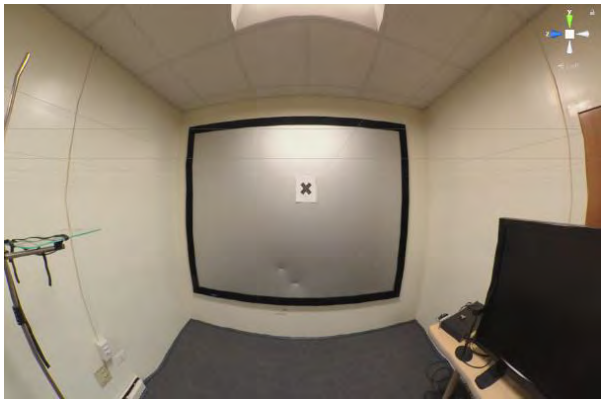

COP data was low-pass filtered with a cutoff frequency of 5 Hz. Balance performance was assessed using anterior-posterior COP displacement (root mean square), mean velocity and approximate entropy (length = 2, tolerance window = 0.2 x standard deviation of time series). Paired t-tests (α = 0.05) were performed to determine whether the mean COP displacement, mean velocity and approximate entropies during each sinusoidal movement was greater than during baseline (no movement).

RESULTS AND DISCUSSION

COP mean velocity was significantly greater than baseline when the sinusoidal movement of the VR scene had a frequency of 0.5 Hz and amplitudes of 10 cm (p=0.04) and 20 cm (p=0.007). There were no significant differences when the sinusoidal movement had a frequency of 0.25 Hz or smaller amplitudes (Figure 2).

Sinusoidal movement at 0.5 Hz and 20 cm amplitude was the only condition in which COP approximate

entropy was greater than baseline (p=0.01). Smaller amplitudes and 0.25 Hz frequency did not alter COP approximate entropy compared to baseline standing (Figure 3).

There were no differences in COP displacement between baseline and sinusoidal movement conditions for any of the tested amplitudes or frequencies.

Figure 2: COP mean velocity during varying amplitudes and frequencies of sinusoidal movement of VR environment. Conditions in which the mean velocity was significantly greater than baseline (0 cm, 0 Hz) are denoted (*).

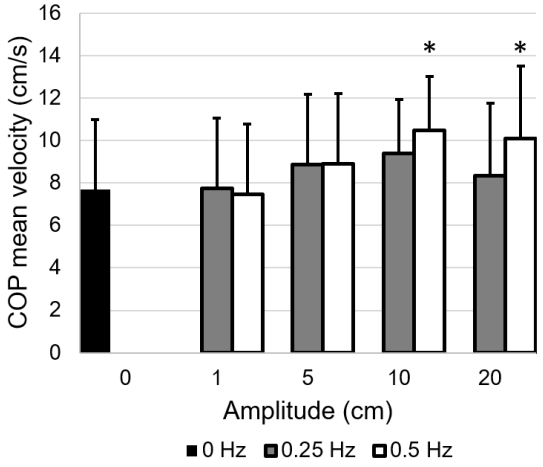

Figure 3: COP approximate entropy during varying amplitudes and frequencies of sinusoidal movement of VR environment. Conditions in which the approximate entropy was significantly greater than baseline (0 cm, 0 Hz) are denoted (*).

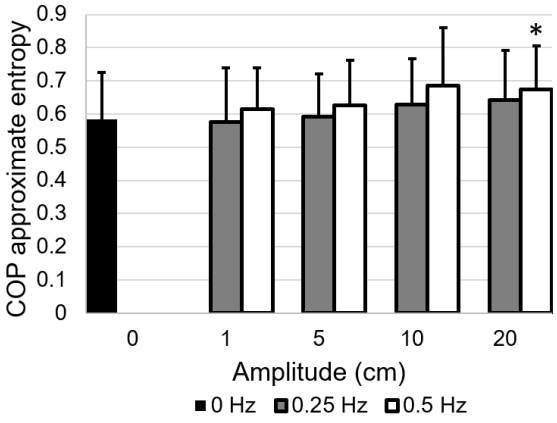

The results suggest that sinusoidal movement of a realistic VR environment produces altered balance compared to baseline standing, but only under specific movement parameters. Specifically, mean velocity and approximate entropy increase under large amplitudes and a frequency of 0.5 Hz. It is likely that the postural control system filters out sinusoidal movement at smaller amplitudes and frequencies so that balance is not altered. Thus, there seems to be a threshold of amplitude (>10cm) and frequency (0.5 Hz) of movement that will induce balance deficits. Interestingly, sway displacement was not impacted by movement of the VR environment. This suggests that the postural control system is able to maintain balance, but must make more adjustments to remain stable, as demonstrated by increased sway velocity and approximate entropy.

One limitation to this study is that a wide range of amplitudes and frequencies were not tested. Future studies should include larger amplitudes (>20 cm) and frequencies (>0.5) to determine if balance deficits increase with amplitude and frequency or if there is a threshold where the postural control system stops responding to the sinusoidal movement. Additionally, future analyses should account for presentation order of amplitude conditions to explore whether there is an adaptation effect when participants are repeatedly exposed to the sinusoidal stimulus.

CONCLUSIONS

This study established parameters of a realistic moving VR environment that perturbs balance. Future directions for this study include comparing response to the moving environment between healthy adults and individuals with impaired balance, such as individuals with concussion.

REFERENCES

1. Horlings et al. *Neuroscience Letters*, 2009.
2. Chiarovano et al. *Front Neurol*, 2015.
3. Luo, et al. *Front Neurol*, 2018.

ACKNOWLEDGEMENTS

Funding provided by the Office of Naval Research (N00014-17-1-272).

DIRECTION AND MODALITY SENSITIVITY OF WALKING BALANCE TO VISUAL PERTURBATIONS

Shawn M. O'Connor, Paula S. Baluyut, Danae C. Narvaza, Jose M. Sanchez, Arianne J. Soriano

San Diego State University, San Diego, CA, USA
email: soconnor@sdsu.edu

INTRODUCTION

Three-dimensional biomechanical walking models suggest that the walking task is passively stable in the sagittal plane direction but unstable in the frontal plane direction [1], indicating that visual information pertaining to frontal plane movement may be more useful for actively controlling balance than information about sagittal plane movement. Previous studies have demonstrated this result for linear visual perturbations; subjects effectively ignore anterioposterior (AP) visual balance perturbations but significantly modify step width in response to mediolateral (ML) perturbations [2].

Since walking is a pendular motion, we hypothesized that pendulum-like visual perturbations (Roll, Pitch) would have greater impact on active balance control compared to linear perturbations, and therefore be more likely to induce step length balance corrections.

It is also unclear how step width adjustments are controlled by the neuromuscular system. Modification of swing leg motion may be an efficient strategy for such control. We hypothesized that variations in hip adduction-abduction would be a significant mechanism for step width adjustment.

To test these hypotheses, we used a virtual reality environment to induce visual perturbations and measured foot placement and muscle activity variability during walking.

METHODS

Nine healthy subjects (aged 22 ± 1.7 yrs., mean ± s.d.) received visual information through a head-mounted display while walking on a large (5x7 ft) instrumented treadmill at a comfortable speed. The display consisted of a virtual dark hallway tiled with randomly placed white rectangles [3] synchronized with the walking speed.

Subjects were exposed to sinusoidal visual perturbations that were categorized as frontal or sagittal plane, linear or pendular modality, and at four amplitudes (Fig. 1). The effect of the perturbations was assessed by measuring variability in foot placement (step length and step width) and variability in root-mean-squared muscle activity (RMS-EMG) recorded from at least 300 steps. Surface EMG was recorded from hip muscles (Adductor Longus, Gracilis, Gluteus Medius) potentially responsible for step width adjustment.

To measure the foot placement sensitivity to the visual perturbations, we calculated the slopes of the step placement variability vs perturbation amplitude trends. Muscle activity sensitivity was calculated as the slope of the RMS-EMG variability vs perturbation amplitude trends.

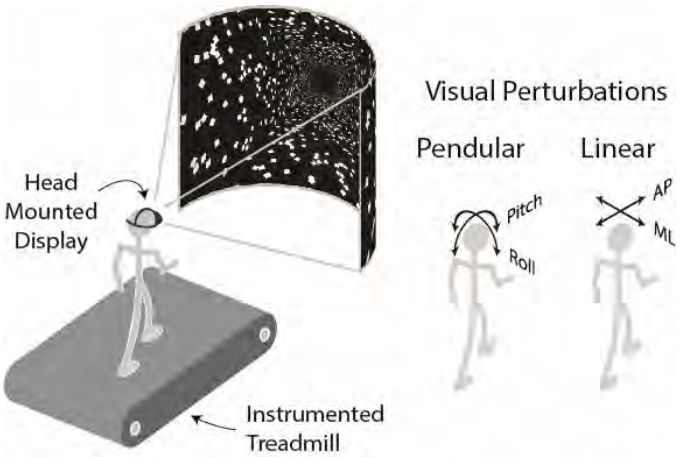

Figure 1: Depiction of experimental setup with instrumented treadmill and head mounted display. Subjects were visually perturbed in either the frontal or sagittal plane and with linear or pendular modality, producing four unique perturbations (Roll, Pitch, Mediolateral (ML), and Anteroposterior (AP).

RESULTS AND DISCUSSION

Results from a two-way ANOCOVA test revealed a significant main effect of perturbation plane on step placement sensitivity (Fig. 2,3). Subjects were 9.3 times more sensitive to frontal than sagittal plane perturbations (P<1.0e-10). This result indicates that greater emphasis is generally placed on side-to-side visual information than front-to-back for controlling walking balance, regardless of the modality of perturbation.

The ANOCOVA also revealed no significant main effect (P=0.54) of perturbation modality (linear vs. pendular), suggesting both perturbation modalities equivalently induced active balance corrections (Fig. 2,3).

Results from a one-way ANCOVA test revealed a significant main effect of Roll perturbation amplitude on RMS-EMG variability (P=7.0e-6). The ANCOVA also revealed no significant main effect (P=0.30) of hip muscle type (Adductor Longus, Gracilis, Gluteus Medius), suggesting that variations in both adductor and abductor activations contribute to active step width adjustment.

CONCLUSIONS

The demonstrated visual sensitivity may be generally explained by needs for maintaining balance during walking, which requires active step width adjustments. These adjustments are controlled by the neuromuscular system through equivalent variations in both hip adduction and abduction muscle activity. The neuromuscular system also appears to rely on sagittal passive balance provided by the limb biomechanics to a significant degree. These findings establish normative balance control behavior and may lead to improvements in clinical assessments for detecting balance impairment.

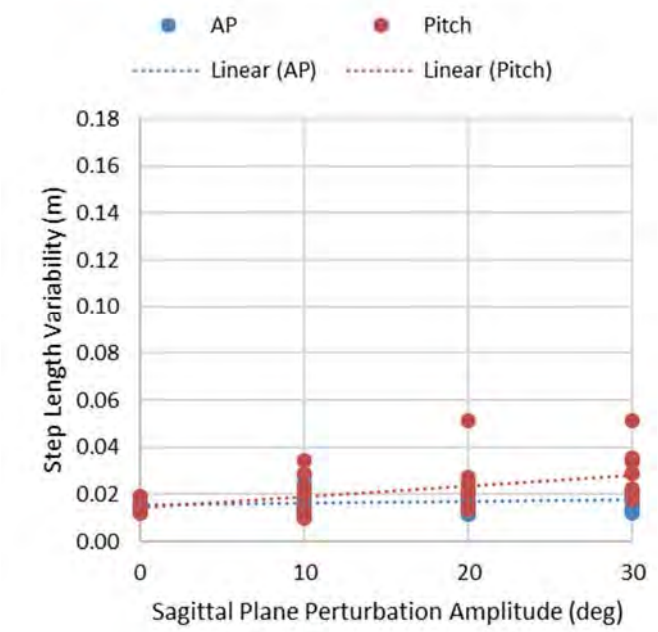

Figure 2: Comparison of sagittal plane visual perturbations (AP, Pitch) with increasing amplitude on step length variability.

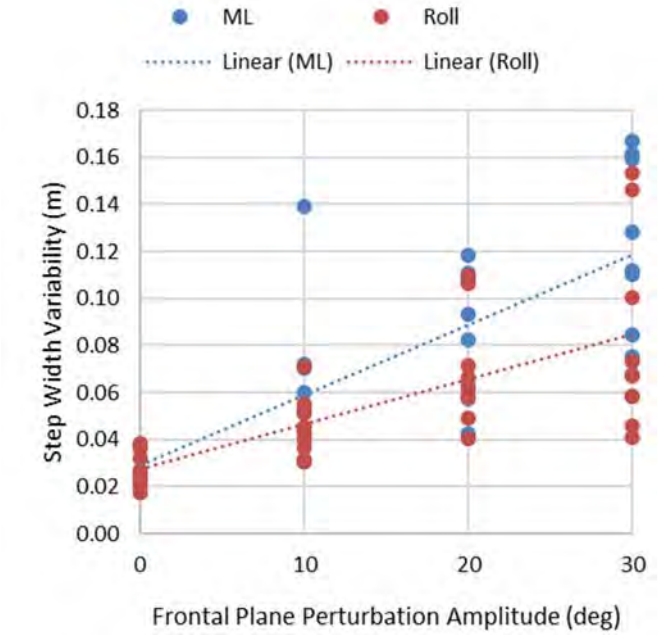

Figure 3: Comparison of frontal plane visual perturbations (ML, Roll) with increasing amplitude on step width variability.

REFERENCES

1. Kuo, AD. *Int. J Robotics Research*, 18, 1999.
2. O'Connor, SM., Kuo, AD. *J of Neurophysiology*, 102(3), 2009.
3. Warren, WH., et al. (1996). *J Exp. Psych.*, 22, 1996.

DECREASED DIVERGENCE OF THE TRUNK MOVEMENT TRAJECTORIES DURING TREADMILL WALKING IS NOT RELATED TO TRUNK FLEXION OF YOUNG SUBJECTS FOLLOWING TREADMILL-DELIVERED DISTURBANCES MIMICING A TRIP

Simisola O. Oludare[1], Nicholas Stergiou[2], Mark D. Grabiner[1]
1. University of Illinois at Chicago, Chicago, Illinois, USA
2. University of Nebraska at Omaha, Omaha, Nebraska, USA
email: soluda2@uic.edu

INTRODUCTION

Trips are a major cause of falls by older adults during walking [1]. Trunk kinematics at recovery step completion following a laboratory-induced trip and following a treadmill-delivered disturbance that mimics a trip discriminates those who fall from those who do not fall following the disturbances [2]. Given their ability to discriminate falls from recoveries in this manner and the demonstrable responsiveness to specific, targeted training, trunk kinematics following a trip appear to qualify as a biomarker for trip-related falls.

Measures of divergence of the trunk movement trajectories during walking have been suggested as estimators of all-cause fall risk of older adults [3,4,5]. These measures, have been associated with retrospectively determined all-cause falls by older adults [6,7] and prospectively determined time to first all-cause fall by older adults [8].

In this study we determined if the movement trajectory of the trunk, measured as the largest Lyapunov exponent (LyE) during unperturbed treadmill walking, could estimate trunk kinematics following increasingly challenging treadmill-delivered disturbances that mimic a trip which discriminate between fallers and non-fallers [2]. LyE reflects the continuous response of a system to disturbances. We expected the largest LyE exponent in the sagittal plane during unperturbed treadmill walking to be positively and significantly correlated to trunk flexion following increasingly challenging treadmill-delivered disturbances that mimic a trip.

METHODS

Following informed consent, eight healthy young adults (6 females, 23.1±2.5 years old, 165.4±10.7 cm, and 60.9±14.1 kg) walked on a microprocessor controlled treadmill for 10 minutes at 2.5 mph before being subjected to eight randomized disturbances from a static upright posture. The disturbance magnitudes reflected treadmill belt motion, under constant acceleration of 14 ms^{-2} to peak velocities of 0.84 m/s, 1.12 m/s, 1.4 m/s, 1.68 m/s, 1.96 m/s, 2.24 m/s, 2.52 m/s and 2.8 m/s.

An eight camera motion capture system operating at 120 Hz tracked the motions of reflective markers placed beneath the left scapula, over the shoe at the heel and 2nd metatarsal phalangeal joints (MTPJ), the acromion processes, the anterior superior iliac spines and on the sacrum at S2.

The time series of the sagittal plane movement trajectory of the trunk, represented by the scapula marker, was used to calculate the largest LyE via the Wolf et al's algorithm and the methods of time delay to reconstruct the state space. Briefly, the state space was constructed by determining the appropriate time delay and embedding dimension via the average mutual information method and the far nearest neighbors methods, respectively [9,10]. Following the state space reconstruction, Wolf et al's algorithm was implemented to compute the divergence of the sagittal plane trajectories in state space. The maximum divergence was determined to be the largest LyE [10] based on 150 consecutive steps.

The recovery response to each perturbation was characterized as the trunk angle at the instant of recovery step completion. Recovery step completion was determined from the markers on the shoe. The trunk angle was calculated using the segment defined from the midpoint of the line between the markers placed over the acromion processes and the midpoint of the line between the

markers placed over the anterior superior iliac spines. For each subject, the computed trunk angles were fit using a second-order polynomial (MATLAB, R2012a) after which each trunk angle at a given disturbance was represented as the point estimate using the subject-specific regression. Correlations and regression analysis (SPSS, V24) were used to describe the relationships between the largest LyE and disturbance-specific point estimates of the trunk angle at recovery step completion

RESULTS AND DISCUSSION

The linearly increasing peak disturbance velocities, intended to increase the difficulty of the recovery, resulted in a quadratic increase (R^2= 0.77, p<0.001) of the trunk angle at recovery step completion (Figure 1).

For the eight participants, the largest LyE of the scapula marker during unperturbed treadmill walking was 0.90±0.57 (range: 0.22-1.86).

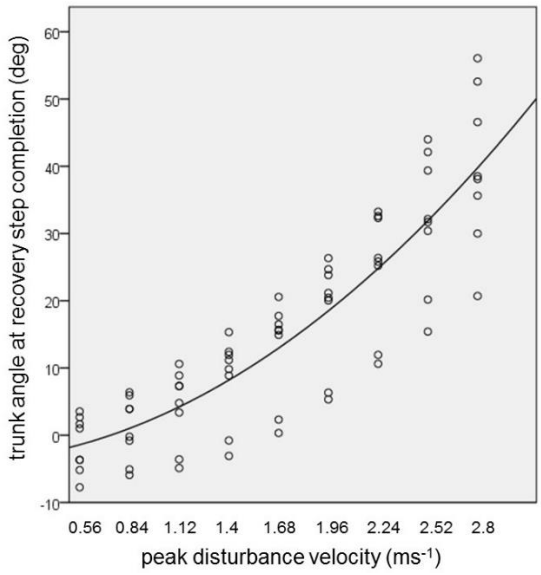

Figure 1: Trunk flexion angle at the instant of recovery step completion following a treadmill-delivered disturbances that mimicked a trip. The disturbance magnitude was manipulated using by increasing the peak velocity of treadmill belt motion. Individual subject data (open circles) and the line of best fit are shown.

Contrary to our expectations, the largest sagittal plane LyE of the scapular marker during unperturbed treadmill walking was not significantly correlated to trunk flexion following the increasingly challenging treadmill-delivered disturbances. The correlations, the values of which ranged from 0.19 to 0.36 (all p>0.38), accounted for a maximum of 13 percent of the shared variance.

The result merits consideration in the context of its representing only a small sample of healthy young subjects who participated in a novel protocol. In light of these limitations, it seems premature to conclude that divergence of sagittal plane trunk movement trajectories during unperturbed treadmill walking is, or is not, a risk factor for trip-related falls by older adults.

CONCLUSIONS

The growth of the population of older adults ensures that the magnitude of the multifaceted problem of falls by older adults will grow proportionately. In our view, replication of the experiment with young subjects and repeating the experiment using older adults merit consideration.

REFERENCES

1. Luukinen H et al. *Osteoporosis Int* 11, 631-634, 2001.
2. Grabiner MD et al. *Exerc Sport Sci Rev* 42, 161-168, 2014
3. Roos PE and Dingwell JB. *Hum Mov Sci* 32, 984-996, 2013
4. Bruijin SM et al. *J R Soc Interface* 10, doi:20120999, 2013
5. Stergiou N and Decker LM. *Hum Mov Sci* 30, 869-888, 2011
6. Lockhart TE and Liu J. *Ergonomics.* 51, 1860 – 1872, 2008
7. Granata KP and Lockhart TE: *J Electromyogr Kinesiol*, 18:172-178, 2008.
8. Van Schooten et al. PLOS One, DOI:10.1371/journal.pone.0158623, 2016
9. Kurz MJ et al. *Nonlinear Dynamics Psychol Life Sci*. 14, 151 – 164, 2010
10. Kennel MB et al. Phys Rev A 45, 3403-3411, 1992

TEST-RETEST RELIABILITY OF THE SENSORY ORGANIZATION TEST AND CENTRAL SENSORIMOTOR INTEGRATION (CSMI) TEST

[1,2] Lucy Parrington, [1,2] Peter C. Fino, [1,2] Robert J. Peterka, [1,2] Nicholas Kreter, and [1,2] Laurie A. King

[1] Oregon Health & Science University, Portland, OR, USA
[2] Veterans Affairs Portland Health Care System (VAPORHCS), Portland, OR, USA
email: parringt@ohsu.edu

INTRODUCTION

The collection and integration of information from the vestibular, visual and somatosensory systems are an integral aspect of balance control. Balance dysfunction can arise from damage to sensory systems (e.g. somatosensory decline following lower limb injury) or from central integration issues (e.g. neuromotor impairment following mild traumatic brain injury). Tests such as the Sensory Organization Test (SOT), and the Central Sensorimotor Integration (CSMI) Test [1] have been developed to try to identify contributions to balance dysfunction in patients. Both of these tests collect anterior-posterior sway data under different sensory conditions (e.g. moving surface, moving visual surround, eyes open or closed). One of the key differences between the two tests, is that the surface or visual surround movement during the SOT is dependent upon an individual's sway, and thus the amplitude of surface or visual surround movement is not fixed, while movement of the surface and visual surround in the CSMI is determined by continuous pseudorandom stimuli at fixed peak-to-peak amplitudes of 2° and 4°.

Although the SOT has been recognized as a reliable tool for the assessment of sensory contribution to balance in a number of populations [2,3], one of the recognized limitations is the effect of learning with repeated exposures [4]. Comparatively, there is limited information about the test-retest reliability of the CSMI test, and whether or not the CSMI test is subject to learning effects. In this abstract we present preliminary data on the test-retest reliability of the SOT and CSMI test measures focusing on four comparable conditions across the two tests: 1) surface movement with eyes closed, 2) surface movement with eyes open, 3) visual surround movement, and 4) both surface and visual surround movement. We hypothesize that a) both the SOT and the CSMI will have good to excellent reliability, and b) that the participants will improve on the SOT, but will not improve on the CSMI – suggesting learning effects occur in the SOT but not CSMI test.

METHODS

Participants were 14 healthy volunteers (26.3 ± 2.8 years) recruited from Oregon Health & Science University (OHSU). Exclusion criteria included any history of injury, surgery or medical condition that would impair cognition or motor ability. All participants gave written informed consent, and procedures were approved by the OHSU Institutional Review Board. Participants completed two testing sessions, conducted six-weeks apart –a timeline chosen to reflect a reasonable test-retest interval in a balance intervention program. Participants completed the SOT and the CSMI test in a custom modified SMART Balance Master (Neurocom International Inc.), adapted to collect CSMI test data (Figure 1). For the SOT, participants completed the standard SOT clinical protocol of three 20-s trials per six conditions. For the CSMI test, participants completed randomly ordered trials at amplitudes of 2° and 4°, making eight total trials. Outcome measures were the Equilibrium Score (E, SOT) and the Sensory Weight presented as sensory weight*100 (W, CSMI) per condition.

Figure 1: Custom modified SMART Balance Master

Test-retest reliability was assessed using Intraclass Correlation Coefficients (ICCs) using a 2-way mixed effects model ($ICC_{3,1}$) with absolute agreement. 95% confidence intervals were calculated, and interpretations (<.5=poor; .5-.75=moderate; .75-.9=good; >.9=excellent) were based off Koo & Li [5]. Paired t-tests were also assessed to evaluate any mean differences between testing sessions.

RESULTS AND DISCUSSION

Except for the 2° visual condition, the ICC values for the CSMI were on average higher than the SOT (Table 1). SOT equilibrium score significantly improved in the visual movement condition (mean±SD, E_1=92±3, E_2=94±2, p=.041), and the surface plus visual movement condition, (E_1=64±18, E_2=74±15), p=.001), but no significant changes to performance in the surface movement with eyes open condition (E_1=86±5, E_2=88±6, p=.050) or surface movement with eyes closed condition (E_1=66±14, E_2=72±12, p=.168).

Table 1: ICC values, 95% confidence intervals and interpretation of ICC for each condition tested.

			95% CI		
		$ICC_{3,1}$	Lower	Upper	Interpretation
SOT	S, EC	0.475	-0.46	0.83	Poor
	S, EO	0.733	0.20	0.91	Moderate
	V	0.451	-0.36	0.81	Poor
	S + V	0.867	0.10	0.97	Good
CSMI	S, EC 2°	0.854	0.55	0.95	Good
	S, EC 4°	0.655	0.03	0.89	Moderate
	S, EO 2°	0.557	-0.46	0.86	Moderate
	S, EO 4°	0.878	0.61	0.96	Good
	V 2°	0.392	-0.69	0.80	Poor
	V 4°	0.705	-0.05	0.91	Moderate
	S + V 2°	0.849	0.52	0.95	Good
	S + V 4°	0.882	0.61	0.96	Good

*S = surface movement; V = visual movement; EC = eyes closed; EO = eyes open

The only significant change in performance for the CSMI test was in the 4° visual movement condition, W_1=5±3, W_2=3±1, p=.004. No significant changes in performance occurred in any other condition (2° surface movement, eyes closed condition, W_1=49±8, W_2=50±7, p=.448; 4° surface movement, eyes closed condition, W_1=39±10, W_2=35±4, p=.063; 2° surface movement, eyes open condition, W_1=72±4, W_2=72±5, p=.697; 4° surface movement, eyes open condition, W_1=19±4, W_2=19±3, p=.864; 2° visual movement condition, W_1=10±5, W_2=8±2, p=.178; 2° surface and visual movement condition, W_1=53±7, W_2=54±6, p=.814; 4° surface and visual movement condition, W_1=44±9, W_2=41±7, p=.063).

Our results suggest better test-retest reliability of the CSMI than the SOT for the surface movement with eyes closed condition, while being comparable for surface movement with eyes open, and surface plus visual surround movement. Test-retest reliability was low for the SOT visual condition and the low amplitude CSMI visual movement condition. Repeat test performance improved in the SOT visual movement and surface plus visual movement conditions, while for the CSMI a decrease in the sensory weight occurred in the visual movement condition. Overall reliability of the SOT and CSMI were somewhat lower than expected. This may be an outcome of the repeat trial occurring six weeks following the initial testing block. The general improvement in SOT performance is consistent with a learning effect.

CONCLUSIONS

Test-retest reliability ranged from poor to good for both the SOT and CSMI test, with the CSMI test performing slightly better overall. The observed test-retest changes in performance in healthy young adults provide a benchmark for judging whether rehabilitation interventions are effective in improving balance function in patients.

REFERENCES

1. Peterka. *Journal of Neurophysiology*. 88(3), 2002
2. Murray et al. *J Athl Train.* 49(4), 2014
3. Ford-Smith et al. *Arch Phys Med Rehabil.* 76(1), 1995
4. Wrisley et al. *Arch Phys Med Rehabil.* 88(8), 2007
5. Koo and Li. *J Chiropr Med.* 15(2), 2016

ACKNOWLEDGEMENTS

Funding was provided by the US Department of Defense (W81XWH-15-1-0620). Thank you to Ms. Alexa Beeson for her assistance with data collection.

EFFECT OF SPEED CONTROL ON GLOBAL STABILITY OF A POWERED COMPASS WALKER

Navendu S. Patil, Jonathan B. Dingwell, and Joseph P. Cusumano

The Pennsylvania State University, University Park, PA, USA
Email: nsp129@psu.edu

INTRODUCTION

Identifying the risk of falling is intimately related to characterizing the dynamic stability [1] of neuromuscular control of human walking. However, *global* stability is hard to measure in practice, and data-driven measures of local stability alone may not predict the risk of falling. Conversely, the dynamical systems analysis of simple mechanical models of human walking, which has the issue of stability at its core, can provide crucial insights into the global stability of locomotion in response to external disturbances. We here use a compass walker capable of walking on a level ground using toe-off impulse actuation [2] to study the global stability of its periodic gait. A recent experimental study of humans walking on a treadmill [3] showed that humans primarily regulate their stepping variability by controlling speed rather than by maintaining some constant absolute position on the treadmill. However, the implications of such regulation on global stability have not been examined. For the powered compass walker, we show that a nonlinear state-feedback speed regulator that optimally adjusts the toe-off impulse at each step dramatically enlarges the basin of attraction (BoA) of its periodic gait, i.e., the set of initial "postures" (i.e., states) yielding transient gaits that asymptotically approach a stable periodic motion. Our results thus suggest a functional connection between motor regulation and global stability, and further reinforce the potential importance of speed control as a strategy to regulate intrinsic physiological motor fluctuations in human walking.

METHODS

The step-to-step dynamics is described using the stance leg angle, θ^+, and its time derivative, $\dot{\theta}^+$. The dynamics itself has two phases: In the first, the stance leg swings from a previous heel strike (Fig. 1a), past the vertical, to just before the next heel strike (Fig. 1b) without any energetic cost while the swing leg rotates

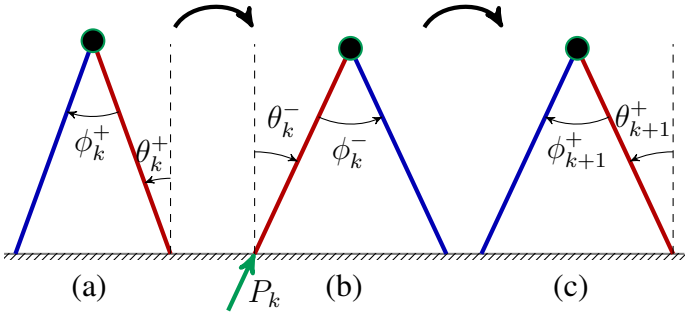

Figure 1: Three snapshots of powered compass walker [2]: (a) just after k^{th}, (b) at $(k+1)^{\text{st}}$, and (c) just after $(k+1)^{\text{st}}$ heel strike. The walker has massless stance (*red*) and swing (*blue*) legs, and a mass at (*black dot*) the hip. At heel strike, $\phi = 2\theta$. The walker's state just after heel strike is $(\theta^+, \dot{\theta}^+)$. The toe-off impulse, P, applied just before the heel strike, allows controlled walking steps on an even ground.

freely, about the hip, past the stance leg. In the second, the toe-off impulse P, applied to the stance foot, compensates for the impending energy loss during the impact of the swing leg with the ground. Finally, the stance and swing legs are switched to prepare for the next walking step (Fig. 1c).

First, we estimated the BoA of the stable fixed point, $(\theta^*, \dot{\theta}^*) \approx (0.30518, -0.31744)$ for a fixed $P^* = 0.1$, by simulating trajectories on a $16501\times$ 1000 grid of initial states in the region where the walker takes at least one step. This region is bounded by two curves, Ω_{low} and Ω_{high} (Fig. 2, top), which we found numerically using a continuation procedure. We restricted our attention to $\theta^+ \in [0.23, 0.56]$. For a given θ^+, $\Omega_{\text{low}}(\theta^+)$ gives the minimum speed for the stance leg to swing past vertical, while $\Omega_{\text{high}}(\theta^+)$ is the maximum speed for a step without falling forward. We simulated trajectories for a maximum of 100 steps and classified a given initial state to lie in the BoA if the distance of states along its trajectory approached the fixed point monotonically for its last 10 steps.

We then imposed our optimal nonlinear speed-

controller that actively sets the toe-off impulse P_k to P_k^{opt} (Eq. 1 below) so as to make the walking speed at the next step, v_{k+1}, as close to the desired speed, $v^* \approx 0.15633$ (of the stable periodic gait), as possible:

$$P_k^{\text{opt}} := \underset{P_k}{\text{argmin}} \left[v_{k+1}(P_k) - v^*\right]^2, \qquad (1)$$

$$v_k := L_k/T_k, \qquad (2)$$

where the step length $L_k := \sin(\theta_k^+) - \sin(\theta_k^-)$, and T_k is the step period. The function $v_{k+1}(P_k)$ is not known explicitly and requires numerical integration of equations of motion and event detection. Thus, the optimization in Eq. (1), if carried out at every walking step, significantly slows down trajectory computation. We addressed this issue by calculating P_k^{opt} offline for several thousand θ_k^-'s in parallel, using MATLAB's `fminbnd` function, and then interpolated the required result as needed during simulations. Furthermore, we simulated the trajectories to a maximum of 50 steps.

RESULTS AND DISCUSSION

The BoA (Fig. 2) of the stable periodic gait of the powered walker with *no active control* is quite thin and has a complicated geometric structure in the state space, with possible "holes" and multiple, disconnected boundaries. Our nonlinear speed-regulator, which pushes the states in each step as close as possible to the *constant-speed GEM* [3] (i.e., the goal-equivalent manifold passing through the operating point on which $v = v^*$), not only regulates the speed of the aforementioned open-loop walker, but also enlarges the BoA 10-fold. Also, the BoA is geometrically much simpler: in the region of the computation it possesses only two disconnected basin boundaries and no holes.

CONCLUSIONS

We have shown that a speed regulator dramatically improves the global stability of the compass walker's periodic gait, as quantified by the area of the set of initial states that can be stabilized (that is, by the size of its BoA). Our results further support [3] the importance of speed-control as a strategy to regulate intrinsic physiological motor fluctuations, and may suggest the future design of assistive devices that would not only regulate walking speed but also reduce fall risk.

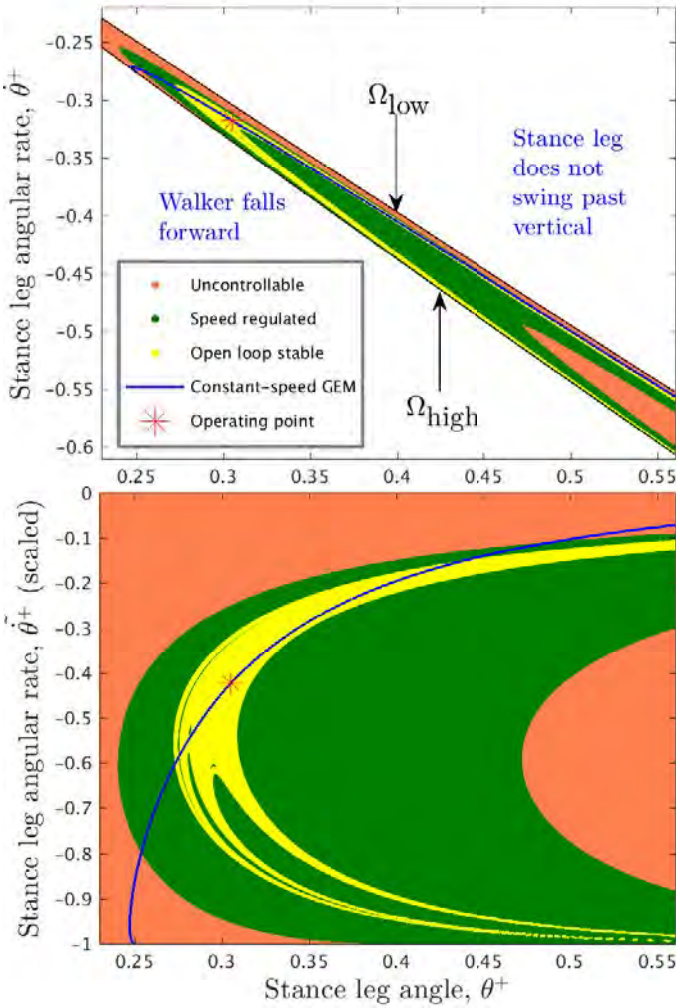

Figure 2: Effect of speed regulation on the basin of attraction (BoA): (*top*) original state space $(\theta^+, \dot{\theta}^+)$; (*bottom*) zoomed-in view using scaled angular velocity $\tilde{\dot{\theta}}^+ := [\dot{\theta}^+ - \Omega_{\text{low}}(\theta^+)]/[\Omega_{\text{low}}(\theta^+) - \Omega_{\text{high}}(\theta^+)]$. Uncontrolled walker has a stable periodic gait at the *operating point* with BoA (yellow) marked *open loop stable*. In contrast, *speed regulated* BoA (green) is ten times bigger than the open-loop BoA, and has a more regular boundary.

ACKNOWLEDGMENTS

NIH/NIA Grant #R01AG049735.

REFERENCES

1. J. B. Dingwell and J. P. Cusumano. *Chaos*, 10(4): 848–863, 2000.
2. Kuo AD. *ASME. J Biomech Eng.*, 124(1):113–120, 2001.
3. J. B. Dingwell and J. P. Cusumano. *PLOS ONE*, 10(4): e0124879, 2015.

EFFECTS OF WEIGHTED BELT ON LIMIT OF STABILITY DURING STANDING

[1] Jimmy Phan, [1] Kaylen Wakumoto, [1] Jeffrey Chen, [2] Woochol Joseph Choi

[1] Department of Physical Therapy, Chapman University, Irvine, CA, USA
[2] Injury Prevention and Biomechanics Laboratory, Department of Physical Therapy, Yonsei University, Wonju, South Korea
email: wcjchoi@yonsei.ac.kr

INTRODUCTION

Hip fractures in older adults are a big health problem, and more than 90% of hip fractures are due to a fall [1]. While efforts have been made to address this issue, it is still an ongoing problem due to fast growing aging population. As individuals age, they develop an increased risk of falling due to natural changes in the body, activity level, and other characteristics. A simple but effective balance training method that might slow down the progress of age-related changes, or improve one's balance, especially for frail population, should help to reduce incidence of falls and associated injuries in older adults.

A recent study theorized that for every 1% rise in height of COM, there is a 37% increase in the risk of falls [2]. Furthermore, a study has shown that subjects who wore an 8lb cervical halo performed more poorly in sling-legged stance and functional reach tests than a control group who did not wear a halo, suggesting that the halo raised the COM and decreased performance on balance tests [3]. These studies provide an idea that individual's balance may be improved more effectively if trained with the lowered COM.

We conducted balance tests with young adults while lowering the COM with a weighted belt, which could be a useful training tool to improve one's balance.

METHODS

Twenty healthy individuals (mean age 26 (SD = 2.43)) participated in the Limit of Stability (LOS) test. After calculating each participant's center of mass with a reaction board, a weighted belt was fastened ten centimeters below the COM. The SMART Blance Master (Natus, San Carlos, CA, USA) was utilized to quantify changes in each participant's LOS under five weighted belt conditions: 0%, 2%, 4%, 6%, and 8% of the participant's body weight. The order of presentation of weight condition was randomized. In each trial, subjects were asked to move toward each of the four targets (Figure 1).

LOS outcome measures included reaction time, movement velocity, endpoint excursion, maximum excursion, and directional control in 4 cardinal directions (mediolateral and anteroposterior).

A two-factor ANOVA was used to test whether these outcome variables associated with the weighted belt and moving direction.

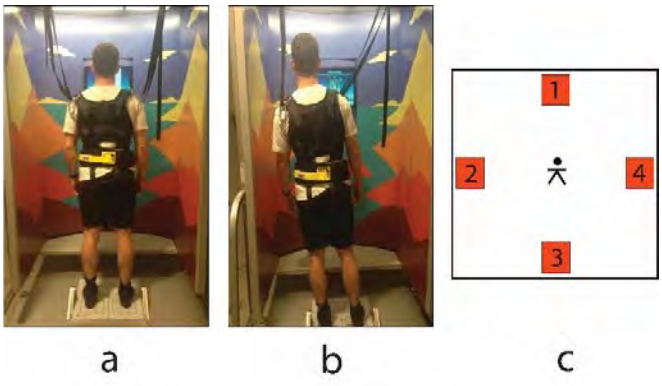

Figure 1: A participant standing with harness (a), moving toward a target on his left (b), and display of targets that participant can monitor during trials.

RESULTS AND DISCUSSION

Surprisingly, none of our outcome variables associated with weighted belt ($p > 0.075$), but all of them associated with moving direction ($p < 0.01$) (Table 1, Figure 2). On average, movement velocity of the COM (degrees per second) and maximum

excursion (maximum displacement as a percentage of maximum LOS distance) were 31% and 18% greater, respectively, in mediolateral than anteroposterior direction (5.4 versus 4.1 °/s; 97.5 versus 82.6 %). There were no interactions between the weighted belt and moving direction ($p > 0.31$).

Biomechanically, postural stability requires that the vertical line passing through the COM locates within the base of support formed by the feet. In theory, postural stability is improved when the height of the COM is decreased. This is, in part, due to a. that a greater angle (perturbation) is required to cause instability and b. a smaller recovery torque is needed to recover balance if the height of the COM is decreased. However, our data from healthy young adults suggest that there is no effect on balance of decreased height of the COM caused by increasing weight of the belt at 10 cm below the COM.

A goal of this study was to examine how balance performance is affected by the lowered COM, and discuss potential benefits of weighted belt as a training strategy to improve balance for individuals at high risk of a fall. Balance is largely affected by neuromuscular responses (i.e., reaction time, muscle strength), which likely decline with age. Therefore, future studies are warranted to confirm our results with older adults.

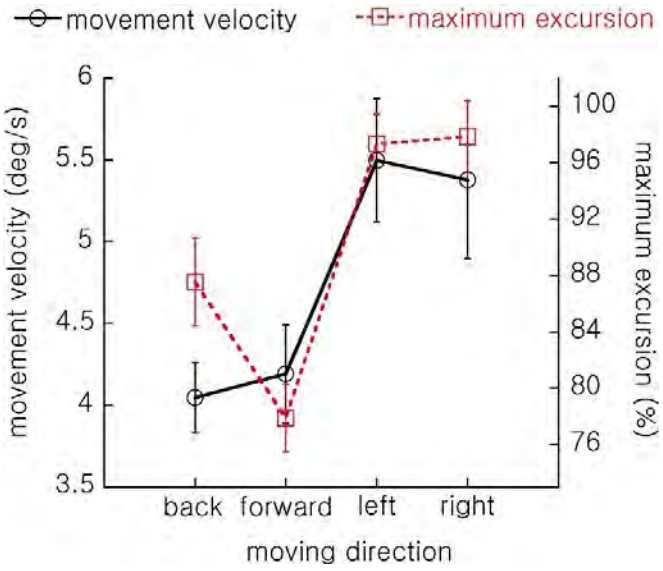

Figure 2: Effect of moving direction on Limit of Stability (movement velocity and maximum excursion).

REFERENCES

1. Grisso et al., J Am Geriatr Soc. **38**:1326-1331. 1990.
2. Almeida et al., Gait and Posture. **34**:208-12. 2011.
3. Richardson et al., Arch Phys Med Rehabil. **81**:255-257. 2000.

Table 1: Average values of outcome variables (with SE shown in parentheses).

belt weight (% of body weight)	0%	2%	4%	6%	8%
reaction time (sec)	0.76 (0.04)	0.77 (0.03)	0.76 (0.04)	0.82 (0.05)	0.84 (0.05)
movement velocity (deg/s)	4.66 (0.32)	4.82 (0.34)	4.85 (0.33)	4.73 (0.35)	4.84 (0.35)
endpoint excursion (%)	81.6 (1.9)	84.0 (1.5)	83.3 (1.7)	81.6 (1.8)	81.5 (2.1)
maximum excursion (%)	89.8 (1.9)	90.9 (1.9)	91.0 (1.6)	89.9 (2.0)	89.2 (2.1)
directional control (%)	88.0 (0.9)	88.1 (0.7)	86.9 (0.9)	88.4 (0.5)	88.5 (0.6)

CENTER OF PRESSURE RESPONSE TO VISUAL PERTURBATIONS IN VIRTUAL REALITY

David Phillips, PhD and Markus Santosa, PhD

Montclair State University, NJ, USA
email: phillipsdav@montclair.edu, web: https://www.montclair.edu/cehs/academics/departments/espe/

INTRODUCTION

The loss of postural control can lead to falls and injury. In older adults the treatment of these injuries incurs direct medical expenses exceeding $31 billion annually. The average hospital bill is estimated at $30,000 [1]. Other than the financial cost, falls are the leading cause of fatal injuries and often lead to loss of independence or a reduced quality of life.

Maintaining balance requires sensory input from the visual, proprioceptive, and vestibular systems. Deficiencies or perturbations in any of these systems may reduce an individual's ability to anticipate or respond to environmental conditions. Inducing perturbations in each system comes with unique challenges. The vestibular system can be stimulated with electrodes behind the ear and ankle proprioception can manipulated through different types of muscle contractions to induce temporary muscle damage or fatigue. Creating visual distortions requires that the entire field of view be manipulated. This can potentially be accomplished by using glasses or by building complex and immersive environments. Glasses are restricted to manipulating incoming visual information and constructing environments requires both space and expense.

Virtual reality (VR) is becoming a popular method to conduct balance training and rehabilitation. Virtual environments do not require physical constructs and the equipment is highly portable. However, VR has not been used to induced visual perturbations to study balance and balance recovery. In previous studies where the physical walls of a room were displaced either anteriorly or posteriorly, subjects leaned in the direction of the displacement [2, 3]. The purpose of this study was to investigate the effects of visual motion (direction and velocity) of corridor walls in VR on the center of pressure. We hypothesized that center of pressure (COP) displacement will be greater after the visual perturbation and that the initial response of the COP will be to move in the direction of the visual displacement.

METHODS

Six subjects (4 males and 2 females) volunteered for the pilot study. Subjects stood barefoot on a Bertec force plate (Bertec Corporation, Columbus, OH) sampling at 1000Hz with custom LabVIEW software (LabVIEW v2017, Austin, Tx) and downsampled to 200Hz. The subjects wore an Oculus Rift VR headset (Oculus VR). The VR environment consisted of a corridor with a width of 16m and a height of 12m (Fig 1) and was developed with Unity3D software (Unity Technologies v2017.2, San Francisco, CA). Subjects stood barefoot with both feet on the force plate facing the computer monitor in the lab and a closed wall of the corridor in VR.

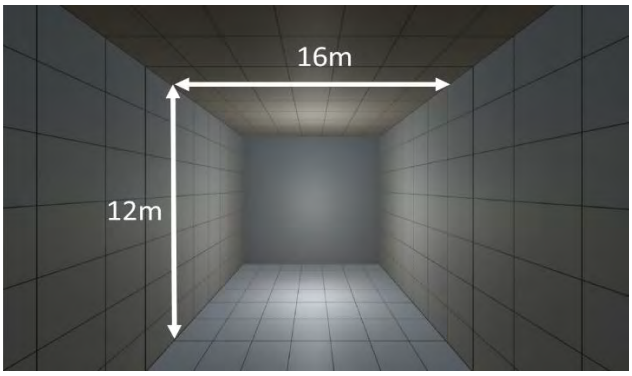

Figure 1: Corridor simulated in VR

The subjects were not aware of when a perturbation would occur. The experimenter initiated a perturbation by pushing a key. Ten seconds of data were collected before the perturbation and 10s after. When the key was pressed the room would displace 3m either anteriorly or posteriorly, at 1m/s, 3m/s, or 5m/s. Three trials were collected for each velocity in the anterior and posterior directions for a total of 18 trials. The 'time zero' (T_0 = 0s, moment the key is pressed) was used to align all trials.

Center of pressure (COP) in the anterior-posterior direction was calculated from ground reaction forces and moments using previous literature [4]. Peak-to-peak displacement was calculated 3s before and after T_0. The peak directional displacement was determined by subtracting the mean COP -3s before T_0 from the peak displacement within +3s of T_0. This indicates both the magnitude of displacement from starting position and the direction of the displacement. This magnitude must be greater than 3SD of the COP position -3s before T_0 to be considered a response (Fig 2).

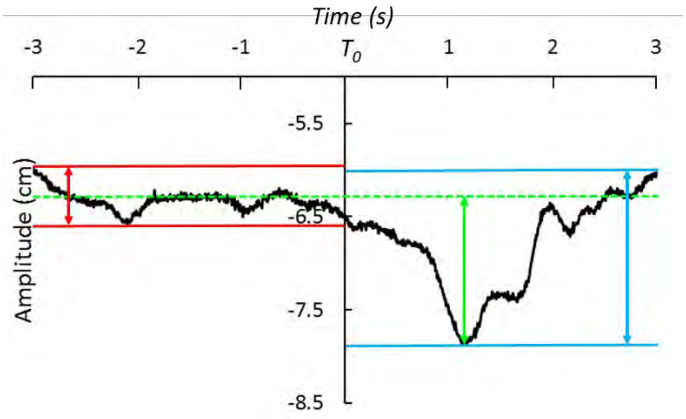

Figure 2: Visual depiction of data analysis of COP in the anterior-posterior direction. Green dashed line is COP mean position prior to perturbation, vertical green line indicates peak COP displacement from mean, blue and red horizontal bars indicate peak-to-peak displacement before and after perturbation.

RESULTS AND DISCUSSION

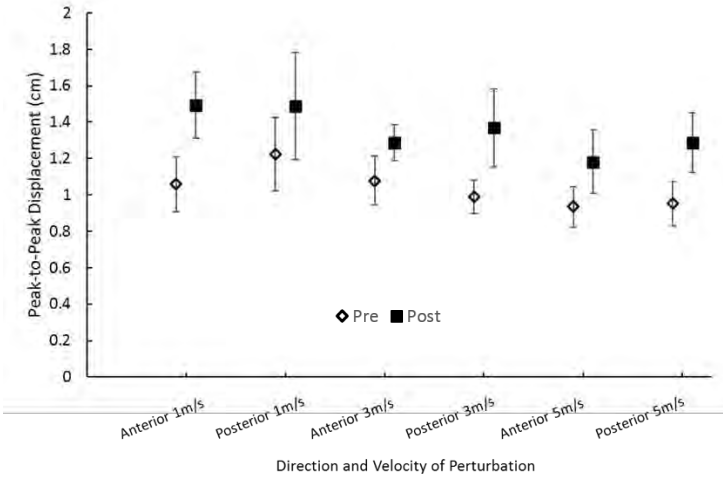

Figure 3: Peak-to-peak COP displacement before and after visual perturbations**.**

In all conditions, the peak-to-peak displacement of the COP after the visual perturbation was greater than the displacement before the perturbation ($p < 0.05$) (Fig 3). Greater displacement is indicative of reduced postural control. Subjects therefore had more difficulty maintaining their balance after the visual perturbation. The magnitude of the peak-to-peak displacement also increased with velocity ($p < 0.05$). The velocity of movement in the visual field likely plays a role in how much postural stability is perturbed.

However, we classified a discrete response to the perturbation as when COP displacement was more than 3 standard deviations from the mean COP position before the perturbation. Only 59% of the trials met this criterion. This may indicate that the visual perturbation was sufficient to require corrective action but it was not sufficient to consistently introduce a response beyond what is normally required to maintain balance. It may be necessary to make the task more challenging in this population by balancing on one foot. Because there were so many trials that did not meet this criterion, we also did not evaluate if subjects' initial COP response was to move in the direction of the perturbation. However, creating visual perturbations in VR may be a useful method to study the role of vision in conditions leading up to falls.

CONCLUSIONS

Creating a visual perturbation in VR increases postural instability but not enough to induce a potential loss of balance in healthy subjects standing on both feet.

REFERENCES

1. Burns, Stevens & Lee. *J Safety Res.* 58, 2016
2. Lee & Aronson. *Percept Psychophy*. **15**(3), 1974
3. Lee & Lishman. *Agressologie*. **18**, 1975
4. Winter. *Biomechanics of Motor Control and Human Movement,* Wiley & Sons, 1996.

LONGITUDNAL ASSOCIATION OF STANDING BALANCE AND NEURODEGENERATIVE BIOMARKERS IN A CONCUSSED ATHLETE: A CASE STUDY

Moira K. Pryhoda, Julie Campbell, Aurelie Ledreux, Kim Gorgens, Lotta Granholm-Bentley, and Bradley S. Davidson

University of Denver, Denver, CO, USA
Email: moira.pryhoda@du.edu

INTRODUCTION

A concussion, or mild traumatic brain injury (mTBI), is a complex sports injury that can possibly lead to long-term disability including chronic traumatic encephalopathy (CTE) and Alzheimer's disease (AD) [1]. Elevated blood biomarker concentrations such as total Tau (t-Tau) are commonly associated with neurodegeneration, and also serve as a strong indicator of secondary injury mechanisms in mTBI [1]. Loss of balance function is a well-known factor in post-concussion syndrome (PCS) that arises from a disruption in sensorimotor integration and may also remain long after the acute phase of recovery is complete [2]. However, it is unclear whether any measures associated with PCS can be used as indicators of concussion severity or long-term consequences including neurodegeneration.

The objective of this case study was to examine whether longitudinal associations exist between various measures of balance and Tau pathology following an acute mTBI through 6 months after injury. These data provide an initial indication of which balance measures are candidates for inclusion in more comprehensive, sensitive, and relevant clinical protocols for mTBI management and could be predictors of long-term neurodegenerative conditions such as CTE or AD.

METHODS

A 20-year-old female student athlete at the University of Denver (DU) with no previous history of concussion was hit on the temporal right side of the head with a volleyball on 11/3/16. She visited the training room that day with a headache. Clinical balance (BESS) and cognitive tests (Immediate Post-Concussion and Cognitive Test; ImPACT) were unimpaired. She returned to the training room on 11/4/16 with elevated symptoms and reported trouble falling asleep the previous night. She was removed from all activity and placed on DU's concussion protocol. She was given full clearance for return to play (RTP) on 11/9/16.

The athlete participated in instrumented standing balance testing (Balance Error Scoring System; BESS) and blood sampling prior to the concussion event (baseline), acutely (within 3 days of concussion), 1 week, 1 month, and 6 months post-concussion (PC). BESS clinical score errors (number of balance errors from 0-10, where 0 is no balance errors and 10 is the greatest number of errors) were recorded simultaneously with force platform data for single, double, and tandem stance on firm and foam surfaces. Center of pressure (COP) total, mediolateral (ML), and anterior-posterior (AP) average velocity, as well as 95% elliptical sway area were calculated for each task. The blood sample was analyzed for t-Tau concentration in plasma, a blood biomarker associated with neurodegeneration. Each biomechanical balance measure and t-Tau across the five data collection time points were plotting on the same axis for visual assessment of simultaneous changes in balance dysfunction and brain neurobiological dysfunction.

RESULTS AND DISCUSSION

t-Tau concentration, a marker of brain health, increased acutely post-concussion (PC) followed by a decrease 1 week PC. t-Tau increased again by 1 month PC and remained elevated as long as 6 months PC. BESS single leg errors, a commonly performed balance test following mTBI was associated with t-Tau concentration for 1 week PC (Fig. 1A). While t-Tau concentration remained elevated up to 6 months PC, BESS clinical score decreased after 1 week PC, which is reflected in prior BESS literature [3].

Among the force platform-based variables, the longitudinal trends of single leg COP total (Fig. 1D) and AP (Fig. 1E) average velocities were the most similar to t-Tau concentration through 6 months PC, indicating possible long-term utility. Double leg stance COP total average velocity, a common biomechanical measure of standing balance, did not follow the longitudinal trend acutely PC (Fig. 1B). However, the long-term trend between 1 week and 6 months PC was associated with t-Tau. If these outcomes hold in larger populations, these may be possible for use long-term associations with brain health after mTBI.

Single leg COP ML average velocity was associated with t-Tau concentration up to 1 week PC (Fig. 1C). 95% elliptical sway area was not associated with t-Tau during any task.

CONCLUSIONS

Total COP velocity during single leg stance provided the best association with t-Tau concentration and has potential to be a sensitive measure that is translational to the clinic and concussion management programs. This case study highlights early data from a large prospective investigation (n=262), which includes additional of clinical domains such as symptoms and neurocognitive function. We will continue to investigate these trends presented here along with additional analyses on functional balance measures during specific movement tasks, which are potentially more applicable as an indicator of readiness for RTP.

REFERENCES

1. Moszczynski et. al. *Neurology*. 90(5):1-8, 2018.
2. Harmon et. al. *British Journal of Sports Medicine*. 47:15-26, 2012.
3. Murray et. al., *Brain* Injury. 26(4):1-8, 2014.

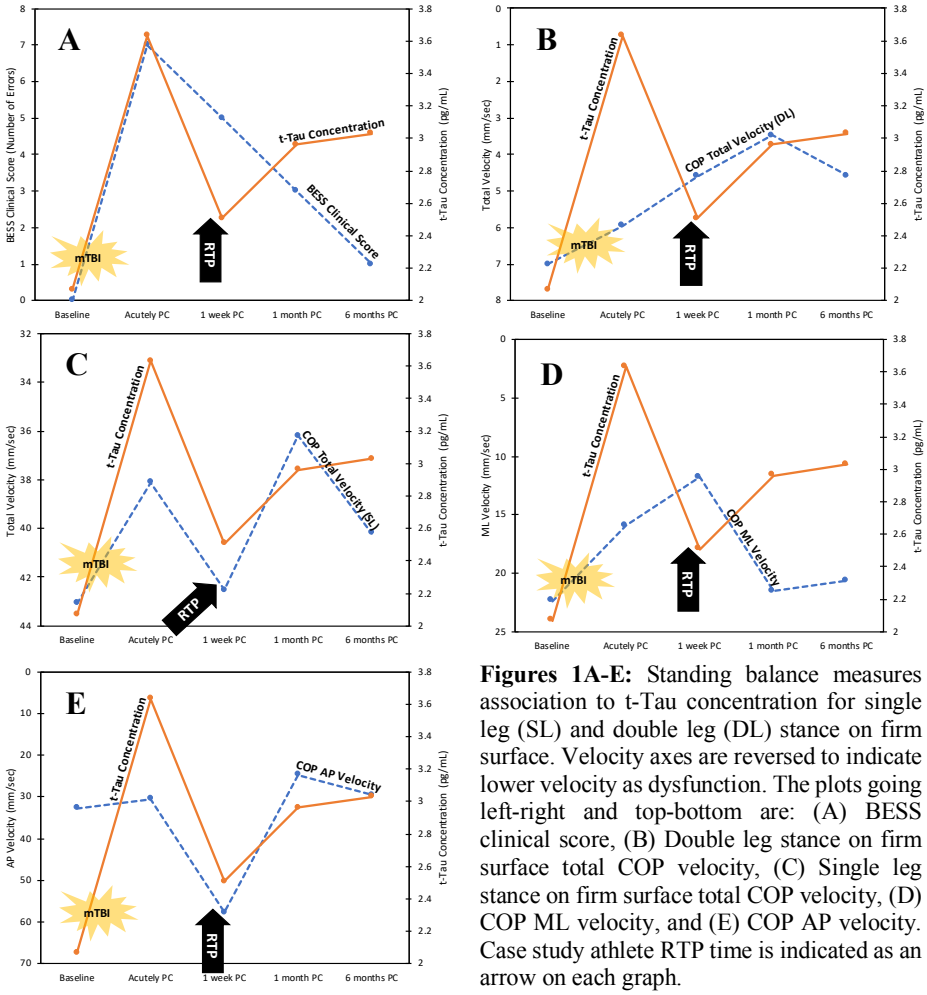

Figures 1A-E: Standing balance measures association to t-Tau concentration for single leg (SL) and double leg (DL) stance on firm surface. Velocity axes are reversed to indicate lower velocity as dysfunction. The plots going left-right and top-bottom are: (A) BESS clinical score, (B) Double leg stance on firm surface total COP velocity, (C) Single leg stance on firm surface total COP velocity, (D) COP ML velocity, and (E) COP AP velocity. Case study athlete RTP time is indicated as an arrow on each graph.

VISUOMOTOR ERROR AUGMENTATION AFFECTS MEDIOLATERAL HEAD AND TRUNK STABILIZATION DURING WALKING

Mu Qiao, Jackson T. Richards, and Jason R. Franz

University of North Carolina and North Carolina State University, Chapel Hill, NC, USA
Email: jrfranz@email.unc.edu, web: http://abl.bme.unc.edu

INTRODUCTION

Humans regulate lateral balance in walking through coordinated adjustments between the continuous control of posture (*i.e.*, head and trunk stabilization) and the discrete (step-to-step) control of foot placement (*i.e.*, step width). These corrective adjustments strongly depend on the integration of reliable sensory feedback. Accordingly, walking balance is acutely susceptible to optical flow perturbations designed to elicit the visual perception of lateral imbalance. Specifically, in response to those perturbations, we recently discovered that head and trunk kinematics during walking instinctively synchronize (*i.e.*, entrain) to a broad range of driving frequencies of perceived mediolateral (ML) motion [1]. In that study, we speculated that this entrainment acted to minimize errors between the visual perception of motion and the actual motion of the head and trunk, thereby unifying visual with vestibular and somatosensory feedback. However, we lacked direct evidence that minimizing these 'visual prediction errors' was a control goal for head and trunk stabilization during human walking.

Therefore, we investigated the role of visual prediction errors in governing the control of mediolateral head and trunk position during human walking as a means to explain the acute postural response to optical flow perturbations. Specifically, we used a visuomotor error augmentation paradigm in which optical flow was synchronized to instantaneous head and trunk kinematics recorded via motion capture. We hypothesized that minimization of visual prediction errors, achievable during the task by reducing lateral head and trunk movement, is an important and instinctive feature governing walking balance control. The alternative hypothesis would be that visual feedback overrides other sensory modalities and is itself an independent control parameter in regulating head and trunk position. We also tested the hypotheses that the response to error-augmented optical flow would: (*i*) scale (*i.e.*, increase) with larger feedback gains and (*ii*) exhibit tuning via time-dependent adaptation following prolonged exposure.

METHODS

Twelve subjects participated (8M/4F, age: 24.1±4.7 yrs, body mass: 73.3±13.0 kg; height: 176±9 cm, mean±S.D.). All subjects walked at their preferred walking speed (1.36±0.14 $m \cdot s^{-1}$) on an instrumented split-belt treadmill (Bertec Corp., Columbus, OH) while watching a speed-matched, virtual hallway rear-projected onto a semi-circular screen surrounding the treadmill (1.45 m radius × 2.54 m height, Fig. 1). A 3D motion capture system (Motion Analysis Corp., 100 Hz) recorded the trajectories of markers placed on subjects' pelvis, legs, and 7th cervical (C7) vertebra. In real-time, a Simulink® controller prescribed the mediolateral (ML) position of the virtual hallway for all trials based on the instantaneous ML position of subjects' C7 marker, which we selected as the highest point on the trunk that is not affected by head orientation. In some trials, we introduced errors between the visual perception of self-motion (via optical flow) and actual ML motion of head and trunk using a position gain, *G* (Fig. 1). Across different conditions, *G* took

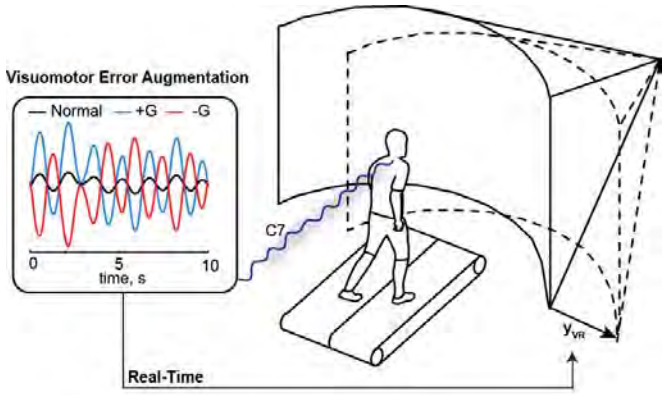

Figure 1. Subjects walked in a virtual environment with visuomotor error augmentation based on instantaneous measurements of their mediolateral (ML) C7 position.

4 values (±2.5 and ±5.0), the largest of which determined in pilot testing to ensure that the virtual hallway remained on the projection screen. Positive/negative values indicate the ML motion of the virtual hallway was in the same/opposite direction of the measured ML C7 motion. Subjects first walked for 1 min with the normal oncoming optical flow (G=0, baseline). Subjects then walked for 10 min with the error-augmented optical flow with one of the four gains. Each of these trials ended with 1 min of walking with the normal oncoming optical flow (G=0, post). Dependent variables included the step-to-step range of ML trunk motion (intra-step measure), and the root mean square (RMS) of ML trunk position (inter-step measure).

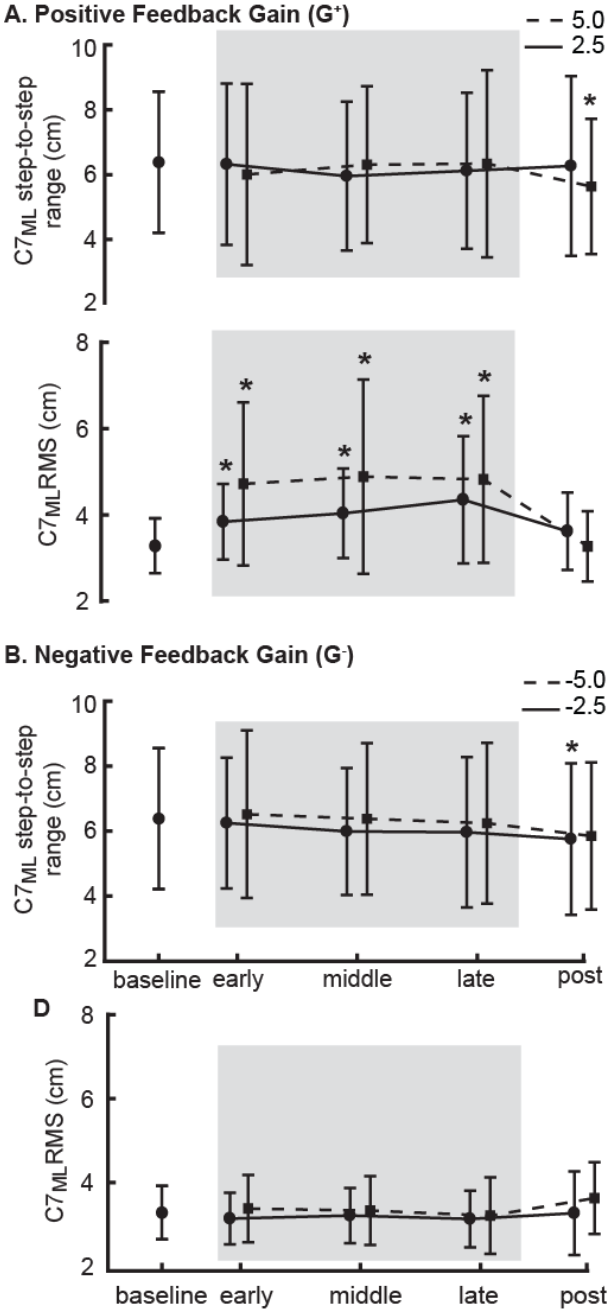

Figure 2. Intra- and inter-step mediolateral trunk motion from all steps across the protocol. Asterisks (*) indicate different from baseline (p<0.05).

RESULTS AND DISCUSSION

In contrast to our hypothesis, neither intra- nor inter-step measures of ML trunk motion amplitude decreased in the presence of error-augmented optical flow (Fig. 2). Rather, larger positive visual prediction errors increased the RMS of ML trunk position – an effect that scaled in proportion to feedback gain amplitude (early vs. baseline, p<0.05, Fig. 2A). These early responses to error-augmented optical flow persisted with prolonged exposure; we found no significant effects of time (i.e., early, middle, late) on step-to-step ML trunk range of motion (G^+: p=0.856, G^-: p=0.124) nor the RMS of ML trunk motion (G^+: p=0.204, G^-: p=0.552) (Fig. 2). Following 'release' of error-augmented optical flow, the RMS of ML trunk position returned to baseline values within one minute. However, despite no apparent effects of time during exposure, the step-to-step trunk range of motion decreased significantly following exposure compared to baseline walking (-12% for G=+5.0, p=0.002, Fig. 2A; -10% for G=-2.5, p=0.002, Fig. 2B). Those after-effects were also accompanied by longer and wider steps, but only following walking with positive feedback gains.

CONCLUSIONS

Subjects did not instinctively minimize errors between the visual perception of movement and actual movement of the head and trunk. Our results are instead more consistent with our alternative hypothesis – that visual feedback can override other sensory modalities and independently compel adjustments in head and trunk position. Our results also allude to a recalibration of head and trunk stabilization toward more tightly regulated postural control following exposure to error-augmented optical flow. Although this study focused on young adults, lasting reductions in ML postural sway evident in our data may have important implications for enhancing the integrity of walking balance control through training, for example in older adults.

ACKNOWLEDGEMENTS

Funded by a grant from NIH (R56AG054797).

REFERENCES

[1] Franz et al., IEEE TNSRE 2017: 25(8).

EFFECTIVENESS OF SIT TO STAND WORKSTATIONS: A SYSTEMATIC REVIEW

Ahmed Radwan[1], PT, DPT, Ph.D., **Savannah Bernardin[1]** PT, DPT, **Nicholas Ball[1]** PT, DPT, **Julia Primps[1]** PT, DPT, **Spencer Simmons[1]** PT, DPT

1: Physical Therapy Program, Utica College, New York, USA.

1600 burrstone road, Utica, NY, 13502

Email: aradwan@utica.edu

INTRODUCTION

On average, employees spend more than half of the workday in the seated position. Even more, computers are becoming increasingly mainstream in the work place causing workers to spend as much as 10-11 hours sitting throughout the day (Graves, Murphy, Shepherd, Cabot, & Hopkins, 2015). This sedentary behavior has been linked to office workers acquiring negative health conditions including, obesity, insulin resistance, cardiovascular disease, depression and chronic back and neck pain. [1]

In combining the current knowledge on sustained sitting and standing, it is suggested that office workers receive bouts of both sitting and standing time during working hours. A solution to facilitate movement and contest the associated effects of sitting among the office worker population is a sit to stand work station.

The sit to stand workstation can provide office workers with a versatile desk that can adjust the computer screen and keyboard independently of one another in order to fit each individual's ergonomic needs. These stations promote comfort, good health and maintain productivity by giving workers the option to alternate between sitting and standing positions.

Current evidence surrounding sit to stand workstations, is limited. At this point research has not identified significant differences in productivity when using a sit to stand workstation versus the traditional desk environment [2]

The aim of this systematic review was to determine the benefits of sit to stand workstations, both physically and psychologically, on seated workers. This review provides useful knowledge to healthcare professionals regarding ergonomics, health and wellness of employees.

METHODS

Evidence surrounding sit to stand workstations and their ability to reduce physical discomfort and improve cognitive ability was searched over multiple databases. The included databases were CINAHL, PubMed, ScienceDirect, and Google Scholar. Keywords including sit to stand workstation, ergonomics, posture, discomfort, and occupation were divided among two search groups.

Four independent reviewers, broken into two groups, used a combination of search terms in screening the databases. The term sit to stand was used in conjunction with either ergonomics and/or posture, or discomfort and/or occupation. Search limits were peer reviewed, randomized controlled trials published in the English language or translation readily available, articles published within the last 5 years, participants' age range of 18-65 years old, and articles had to focus on the effects of sit to stand workstations on improving workers' physical/psychological well-being.

Articles were excluded if they did not meet the aforementioned criteria. Initial database search led to a peak number of 275 articles. Titles and abstracts of the search results were screened by two independent raters and in case of discrepancy in their inclusion findings, a third rater interfered or raters' consensus was utilized. Titles and abstracts were screened down to 15 articles. Full version of the searched articles were acquired and those without a

full version were excluded. Upon further review, articles that did not meet the criteria based on the study design were excluded. A total of 5 articles met the inclusion criteria.
Two independent reviewers appraised the articles using both the PEDro scale and the risk of bias. Differences in scores led to a third reviewer appraising the article and collaboration to determine an appropriate score.

RESULTS AND DISCUSSION

After critiquing the five RCT's notable trends were identified, including participant demographics, methodological quality of articles, musculoskeletal discomfort, cognitive ability, and productivity.
The mean participant ages for the five articles were 38.4, 38.8, 39.0, 43.2, 46.2, 47.8, and 48.2 with one group having an outlier mean of 22.7. The PEDro scale was used to appraise the strength and quality of the included RCT's. The PEDro scores given to the five articles included within this systematic review were all rated between 5/10 and 7/10. This trend occurred due to a lack of subject blinding, assessor blinding, therapist blinding and the inability to conceal group allocation
The Cochrane Collaboration's Tool for assessing risk of bias (ROB) was used in conjunction with the PEDro to further evaluate the level of bias for each study. The articles were categorized as either unclear or high risk of bias
Measurements of pain and discomfort were discussed within three of the included articles. The most significant areas of reduced pain or discomfort were musculoskeletal which included the low back, shoulders and neck. Cognition was only assessed in one of the included studies, which concluded that the use of sit to stand workstations does not cause a deficit in cognitive ability. Finally, implementation of sit to stand workstations improved or caused no change in work productivity in two of the studies included in this systematic review

CONCLUSIONS

The sit to stand work environment has the ability to decrease musculoskeletal discomfort without compromising productivity and cognitive ability, in the adult office worker population. This systematic review establishes a need for more high quality randomized controlled trials that pay careful attention to methodological quality and risk of bias within the study design.
Employers are encouraged to consider sit to stand workstations because of its affordability and potential benefits to employees.

REFERENCES

1.Thorp, A. A., Kingwell, B. A., Owen, N., & Dunstan, D. W. (2014). Breaking up workplace sitting time with intermittent standing bouts improves fatigue and musculoskeletal discomfort in overweight/obese office workers. *Occupational & Environmental Medicine*, *71*(11), 765-771 7p. doi:10.1136/oemed-2014-102348
2.Hall, J., Mansfield, L., Kay, T., & McConnell, A. K. (2015). The effect of a sit-stand workstation intervention on daily sitting, standing and physical activity: protocol for a 12-month workplace randomized control trial. *BMC Public Health*, *15*, 152.

ACKNOWLEDGEMENTS

Acknowledgments are optional.

DYNAMICS OF POSTURAL CONTROL IN ELITE SPORT RIFLE SHOOTERS

[1,2] Peter C. Raffalt, [2] Ida Fillingsnes Marker, [3] Andreas Top Adler and [2] Tine Alkjaer

[1]Julius Wolff Institute for Biomechanics and Musculoskeletal Regeneration, Charité – Universitätsmedizin Berlin, Berlin, Germany
[2]Department of Biomedical Sciences, University of Copenhagen, Copenhagen, Denmark
[3]Team Denmark, House of Sport, Brondby, Denmark
email: peter-christian.raffalt@charite.de

INTRODUCTION

During uni- and bilateral upright stance the center of pressure (CoP) trajectory reflects the postural control executed to maintain balance. In two recent studies, Ko and colleagues [1,2] observed that skilled sport pistol shooters had lower variability and complexity in their center of pressure movements compared to novices during a shooting-like bilateral stance task. This indicates that extensive practice of stable upright stance reduces the complexity of postural control. However, it is unknown if this alteration in postural control is specific to the nature of the trained task (bilateral standing) or it can be incorporated to other balance task (unilateral). The purpose of the present study was to investigate if the dynamics of postural control during bilateral and unilateral stance differed between elite sport rifle shooters who are exposed to extensive postural control training and healthy non-athletes. We hypothesized that the dynamics of postural control during both bilateral and unilateral stance in elite sport rifle shooters would be characterized by higher predictability, lower rate of trajectory divergence, lower dimensionality, longer time dependency, and lower variability compared to non-athletes.

METHODS

Thirteen skilled sport rifle athletes (mean±SD age: 20.2±4.0 yrs, body mass: 71.0±14.0 kg and body height: 1.74±0.11 m) and eleven non-sport shooters (mean±SD age: 28.1±4.9 yrs, body mass: 71.1±10.5 kg and body height: 175.2±9.0 m) performed 90s of 1) barefooted shoulder wide bilateral stance and 2) unilateral (on each feet) stance on a force plate (AMTI OR6-7) with hands kept akimbo. Anterior-posterior (AP) and mediolateral (ML) CoP trajectories were extracted, filtred using a Daubechies wavelet and down sampled to 100Hz. To assess the dynamics of the postural control, four different nonlinear methods were applied to the CoP trajectories: sample entropy to quantify regularity (input parameters: m=2, r=0.2), the largest Lyapunov exponent (LyE) to quantify rate of trajectory divergence (using Wolf's algorithm and delayed embedding method to reconstruct state space), the correlation dimension (CoD) to quantify dimensionality, and entropic half-life (Ent) to quantify the level of time dependency [3]. Additionally, body sway variability was quantified by the elliptical area of the standard deviation of the CoP trajectories in both directions (elliptical area = pi x SD_{AP} x SD_{ML}). To investigate the effect of group and task on the dependent variables, a two way mixed-design ANOVA was applied. In case of an overall effect of group or task or the interaction, a Holm-Sidak post hoc test was applied. Level of significance was set at 5%.

RESULTS AND DISCUSSION

There was a significant effect of group on SaEn AP ($p<0.001$), SaEn ML ($p<0.001$), LyE ML ($p<0.001$), CoD AP ($p<0.001$), CoD ML ($p<0.001$) and Ent ML ($p=0.005$). While the sport rifle shooters had significantly lower SaEn, LyE and CoD, they had significantly higher Ent compared to the non-athletes (figure 1 and 2). There was a significant effect of task for all extracted variables except CoD ML. In general, the SaEn, LyE and CoD of the CoM were significantly different during bilateral stance compared to unilateral stance. In contrast, the Ent was significantly higher during bilateral stance. There was a significant group-task interaction for SaEn AP ($p<0.001$), SaEn ML ($p=0.003$), LyE ML ($p<0.001$) and Ent ML ($p<0,026$). The post hoc tests revealed that significant group differences were only present during unilateral stance (figure 1 and 2). There was a significant effect of group

($p<0.001$), task ($p<0.001$), and group-task interaction ($p=0.001$) on the body sway variability. The post-hoc test revealed that the sport rifle shooters had lower variability during the unilateral stance tasks (table 1).

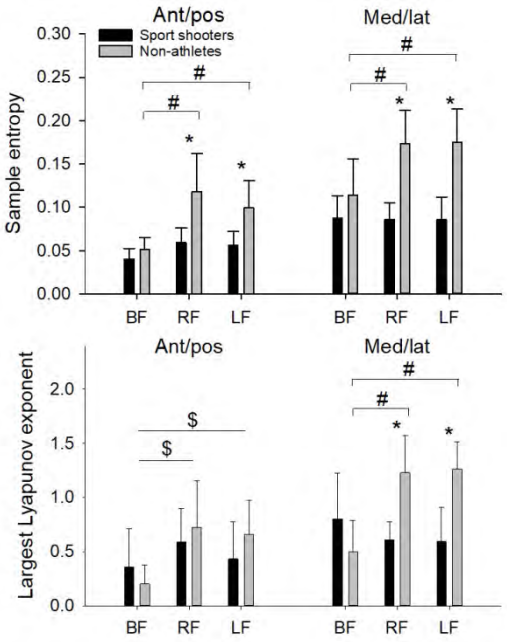

Figure 1: SaEn (top) and LyE (bottom) in anterior/posterior and mediolateral direction for bilateral stance (BS), unilateral (right foot: RF, left foot: LF), *) indicates significant group difference, $ indicates overall significant task difference and # indicates significant task difference within a group.

The raised hypothesis could partly be confirmed as we observed higher predictability, lower rate of divergence, lower dimensionality, longer time dependency, and lower variability in the sport rifle shooters compared to the non-athletes during unilateral stance but not during bilateral stance. Thus, the present study supports previous observations by Ko and colleagues [1,2] suggesting that the postural control in highly skilled sport rifle shooters were characterized by less complexity. Additionally, we observed that the group differences in variability and dynamics only were present during unilateral stance tasks.

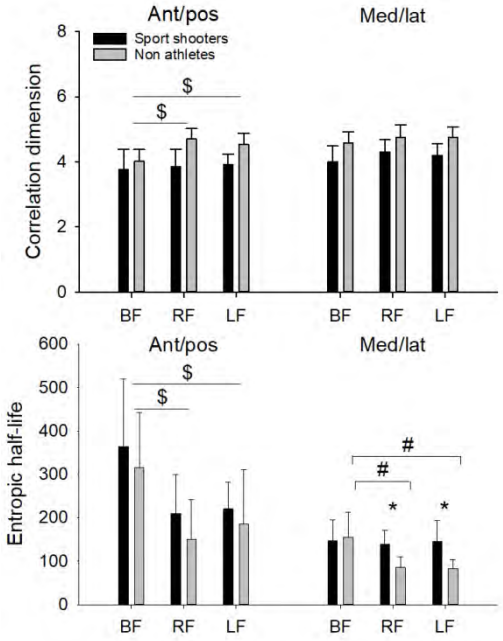

Figure 2: CoD (top) and Ent (bottom) in anterior/posterior and mediolateral direction for bilateral stance (BS), unilateral (right foot: RF, left foot: LF), *) indicates significant group difference, $ indicates overall significant task difference and # indicates significant task difference within a group.

CONCLUSIONS

The present study suggests that extensive training background in maintaining upright quite standing may be associated with altered postural control during unilateral standing task. Thus, sport rifle shooters solved the challenging nature of the unilateral task by use of a less complexed movement pattern compared to the non-athletes.

REFERENCES

1. Ko et al. *Hum Mov Sci*. 55: 255-263, 2017.
2. Ko et a. *J Sports Sci.* 36(7): 809-816, 2018.
3. Federolf, P. *Exp Brain Res.* 233(12): 3507-15, 2015.

ACKNOWLEDGEMENTS

The authors thank The Danish Sport Shooting Association for helping with subject recruitment.

Table 1: Body sway variability during the three balance task. * indicates significant group differences.

	Elliptical area of center of mass trajectory		
	Bilateral stance	Unilateral stance – right foot	Unilateral stance – left foot
Sport pistol shooters (mm^2)	12.2 ± 5.1	119.0 ± 74.6*	103.7 ± 45.2*
Non-athletes (mm^2)	18.1 ± 9.1	193.8 ± 62.3	210 ± 53.0

DYNAMICS OF POSTURAL CONTROL IN INDIVIDUALS WITH LATERAL ANKLE SPRAIN

Peter C. Raffalt, Marios Chrysanthou, Georg N Duda and Alison N Agres

Julius Wolff Institute for Biomechanics and Musculoskeletal Regeneration, Charité – Universitätsmedizin Berlin, Berlin, Germany
email: peter-christian.raffalt@charite.de

INTRODUCTION

The center of pressure (CoP) trajectory reflects the neuromuscular processes executed to maintain postural control. Thus, the dynamics of the CoP trajectory has been related to the development of balance in infants and the superior postural control in elite sport pistol shooters [1,2]. It has previously been suggested that individuals with ankle instability rely more on visual input to maintain postural control during unilateral stance compared to healthy individuals [3]. The present study tested this notion by assessing the dynamics of CoP trajectory in individuals with previous lateral ankle sprain (LAS) and ankle instability, as well as healthy controls during unilateral stance with and without visual input. We hypothesized that the CoP dynamics of individuals with LAS during unilateral stance with no visual feedback would be characterized by lower regularity, higher dimensionality and shorter time dependency compared to healthy controls. In contrast, the characteristics of the CoP dynamics during unilateral stance with visual input were expected not to differ between groups.

METHODS

Sixteen individuals with previous LAS (males/females: 9/7, mean±SD age: 30.9±4.7 yrs, body mass: 73.4±11.9 kg and body height: 176.4±9.5 m) and nine healthy controls (CON) (males/females: 7/2, mean±SD age: 29.3±4.5 yrs, body mass: 72.5±11.3 kg and body height: 178.6±11.5 m) performed 30 seconds of shod unilateral stance (on the affected leg for the LAS individuals and preferred leg for the healthy controls) with 1) eyes open (EO) and 2) eyes closed (EC). Anterior-posterior (AP) and mediolateral (ML) CoP trajectories were extracted from the middle 20 seconds of each trial, filtered using a Daubechies wavelet and down sampled to 100Hz. To assess the dynamics of the postural control, three different nonlinear methods were applied to the CoP trajectories: sample entropy to quantify regularity (input parameters: m=2, r=0.2), the correlation dimension (CoD) to quantify dimensionality (delayed embedding method to reconstruct state space), and entropic half-life (Ent) to quantify the level of time dependency (input parameters: m=2, r=0.2) [4]. To investigate the effect of task (EO vs EC), group (LAS vs CON), and the task-group interaction on the dependent variables, a two way mixed-design ANOVA was applied. In case of an overall effect, a Holm-Sidak post hoc test was applied. Level of significance was set at 5%.

RESULTS AND DISCUSSION

There was a significant effect of task ($p=0.003$) and group ($p=0.028$) on SaEn in the AP direction and a significant interaction ($p=0.019$) on the SaEn in the ML direction. The post hoc test revealed that CON had a significant lower regularity (higher SaEn) compared to LAS for the eyes open task ($p=0.013$, Figure 1). There was a significant effect of task ($p=0.001$) on CoD in the ML direction, indicating that the CoP trajectory during EC had lower dimensionality compared to during EO (Figure 1). There was a significant effect of task ($p=0.001$) on Ent in the AP direction, indicating that the CoP trajectory during EC had shorter time dependency compared to during EO. There was a significant interaction ($p=0.028$) on the Ent in the ML direction. The post hoc test revealed that CON had significantly shorter time dependency ($p=0.024$) during EO compared to LAS.

We could not confirm our hypothesis as we did not observe concomitant group differences in the CoP dynamics during EC and no group differences during EO. Thus, we could not support the previously suggested notion that individuals with ankle instability rely more on visual input during unilateral stance. In contrast, the significantly lower regularity and shorter time dependency in the AP

direction and lower dimensionality in the ML direction during EC compared to EO across groups indicate that the lack of visual information affects the postural control of both groups.

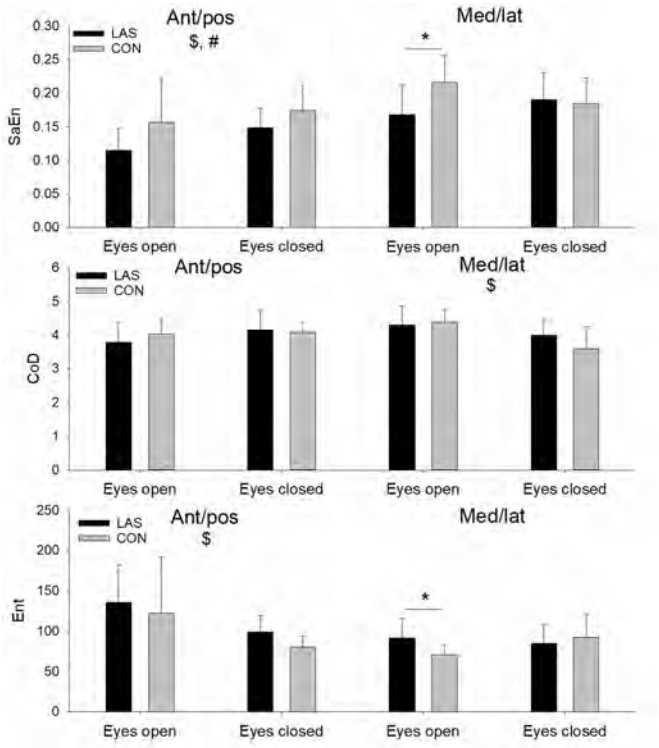

Figure 1: SaEn (top), CoD (middle), and Ent (bottom) in anterior/posterior and mediolateral direction for unilateral stance with eyes open and eyes closed for the CAI and CON group. $) indicates a significant effect of task, #) indicates a significant effect of group, and *) indicates a significant interaction effect and a significant group difference within a task.

The significant effect of visual information for Ent in the AP direction but not in the ML direction suggests that visual feedback plays a more pronounced role for AP postural control.

The higher regularity in the AP direction for the individuals with LAS and in the ML direction during EO, suggest that fewer functional degrees of freedom are available to establish a stable movement pattern [5]. This could be due to impaired motor control in muscles surrounding the ankle joint and increased passive joint laxity, which result in reduced adaptability during unilateral stance.

CONCLUSIONS

The present study did not support the notion that individuals with LAS rely more on visual input during unilateral stance compared to healthy controls. However, higher regularity in the CoP trajectory was observed suggesting that the motor control system of LAS individuals rely on fewer functional degrees of freedom to maintain postural control.

REFERENCES

1. Harbourne and Stergiou *Dev Psychobiol.* 42: 368-377.
2. Ko et at. *J Sports Sci.* 36(7): 809-816, 2018.
3. Song et al. *Med Sci Sports Exerc*. 48: 2046-2056, 2016.
4. Federolf, P. *Exp Brain Res.* 233(12): 3507-3515, 2015.
5. Newell, KM. *Erlbaum.* 63-84, 1998.

ACKNOWLEDGEMENTS

The authors acknowledge Lena Castel-Wohnlich for assisting with data collection.
This work was funded by the German Federal Ministry of Education and Research (BMBF 13GW0104B).

RELIABILITY OF SENSITIVE PARAMETER ESTIMATES IN HEAD POSITION TRACKING

[1] Ahmed Ramadan, [1] Jacek Cholewicki, [1] John M. Popovich, Jr., [1,2] N. Peter Reeves, [1] Clark J. Radcliffe, and [3] Jongeun Choi

[1] Michigan State University, East Lansing, MI, USA
[2] Sumaq Life LLC, East Lansing, MI, USA
[3] Yonsei University, Seoul, Republic of Korea
email: ramadana@msu.edu, web: http://orthopedicresearch.msu.edu

INTRODUCTION

Parametric modeling of human movement provides an insight into the relative contribution of neuromuscular control pathways. Researchers have developed complex dynamical models that describe human movement; therefore, these models usually have many parameters to be estimated. Although different system identification techniques were used to estimate these parameters, the reliability of these estimates received little attention.

Reliable parameter estimates are essential for these models to be useful in clinical and biomechanical applications. With the limited data, usually consisting of gross measurements such as kinematics, estimating many parameters leads to relatively less precise, hence less reliable, estimates. A sensitive parameter selection method [1] reduces parameter variability by selecting only sensitive parameters to be estimated while fixing the remaining parameters to preliminary values. Therefore, we hypothesized this method can provide reliable estimates of the selected sensitive parameters.

METHODS

Ten healthy subjects (Table 1) were recruited for this study. They did not have any history of neck pain lasting more than three days or any neurological motor control impairment. The Michigan State University's IRB approved the test protocol. The subjects signed an informed consent before participating.

The subjects performed a head position tracking task in the horizontal plane (Figure 1) on two visits separated by one day. The subject wore a helmet with

Table 1: Subjects' demographic characteristics.

	Females	**Males**
N	7	3
Height (m)	1.66±0.11	1.78±0.07
Weight (kg)	55.3±11.8	87.7±17.7
Age (years)	22.3±1.2	34.0±11.8

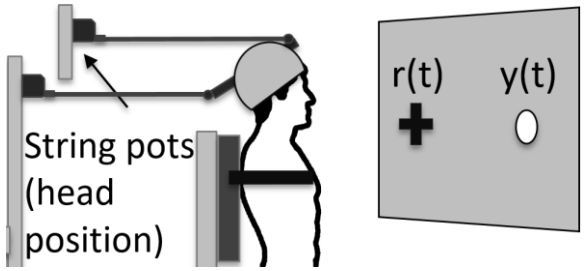

Figure 1: Head position tracking task.

strings attached to two potentiometers (Celesco SP2-50, Chatsworth, CA) to measure the head rotation. Two markers were displayed on a monitor (Samsung SyncMaster SA650; height 27 cm, width 47.5 cm) located 1 m away from the subject: the reference r(t) and the head position y(t) markers. The reference signal consisted of pseudo-random sequence with random step durations (0.3-0.9 s) and amplitudes such that the maximum amplitude was ±4° from the neutral head position. Each subject performed two 15-second practice trials then three 30-second full trials. Data were collected using a data acquisition system (cDAQ-9172, National Instruments, Austin, TX) and sampled at 60 samples per second.

The parametric model describing this task (Figure 2) was augmented from published models of neuromuscular pathways (visual, vestibular, proprioceptive, and intrinsic) [2, 3]. The model parameters were divided into candidate parameters for estimation $\Theta = \{K_{\text{vis}}, K_{\text{vcr}}, K_{\text{ccr}}, \tau, \tau_{1\text{A}}, \tau_{\text{CNS1}}, \tau_{\text{c}}, \tau_{\text{CNS2}}, \tau_{\text{MS1}}, \tau_{\text{MS2}}, B,\ K\}$ and fixed parameters $\Theta_{\text{fixed}} = \{J, T_c\}$. Using the Fisher Information Matrix

(FIM) method for sensitive parameter selection [1], we selected the parameters that have less variability across subjects and visits. Sensitive parameters were estimated using nonlinear least squares while fixing the insensitive parameters to preliminary estimated values. Goodness of fit was measured by Variance Accounted For (VAF).

Between-visit reliability of the selected sensitive parameters was assessed using Intraclass Correlation Coefficients ICC(A, k). The ICCs were classified as poor (<0.40), fair (0.40-0.59), good (0.60-0.74), or excellent (0.75-1.00).

RESULTS AND DISCUSSION

The selected sensitive parameters were $\{K_{\text{vis}}, \tau, \tau_{1A}, \tau_c\}$ that represent visual and vestibular pathways only. Selecting the visual pathway validates the published simplified models that used visual feedback without vestibular and proprioceptive feedbacks (e.g., [3]). Estimates of the sensitive parameters yielded good fit (VAF>78%) (Table 2). By comparison to the case of estimating all 12 parameters (Θ) (VAF>80%), goodness of fit was not sacrificed by estimating only the 4 sensitive parameters.

The ICCs of the sensitive parameter estimates varied between fair and excellent (Table 2). In case of estimating all 12 parameters (Θ), the ICCs of some parameters were negative (e.g., ICC(τ_c)=-0.50). Therefore, estimating many parameters may lead to unreliable parametric models. The FIM method of selecting sensitive model parameters yields more reliable parameters besides providing less parameter variability.

Table 2: Selected sensitive parameters.

	Visit 1	Visit 2	ICC
$K_{\text{vis}}\left[\frac{Nm}{rad}\right]$	388±107	362±74	0.70
$\tau[s]$	0.213±0.027	0.206±0.029	0.81
$\tau_{1A}[s]$	0.077±0.061	0.055±0.038	0.61
$\tau_c[s]$	1.93±1.01	2.17±1.12	0.48
VAF (%)	78.42±7.93	80.33±6.94	-

CONCLUSIONS

The FIM method of selecting sensitive parameters can improve reliability of parametric models, making the parametric models useful for clinical and biomechanical applications.

REFERENCES

1. A. Ramadan et al. *Journal of Biomechanical Engineering*, 2018.
2. G. Peng et al. *Biological Cybernetics*. **75**:309-319, 1996.
3. K. Chen et al., *Journal of Vestibular Research*. **12**(1):25-33, 2002.

ACKNOWLEDGEMENTS

This work has been supported in part by grant number U19AT006057 from the National Center for Complementary and Integrative Health (NCCIH) at the National Institutes of Health. Its contents are solely the responsibility of the authors and do not necessarily represent the official views of NCCIH.

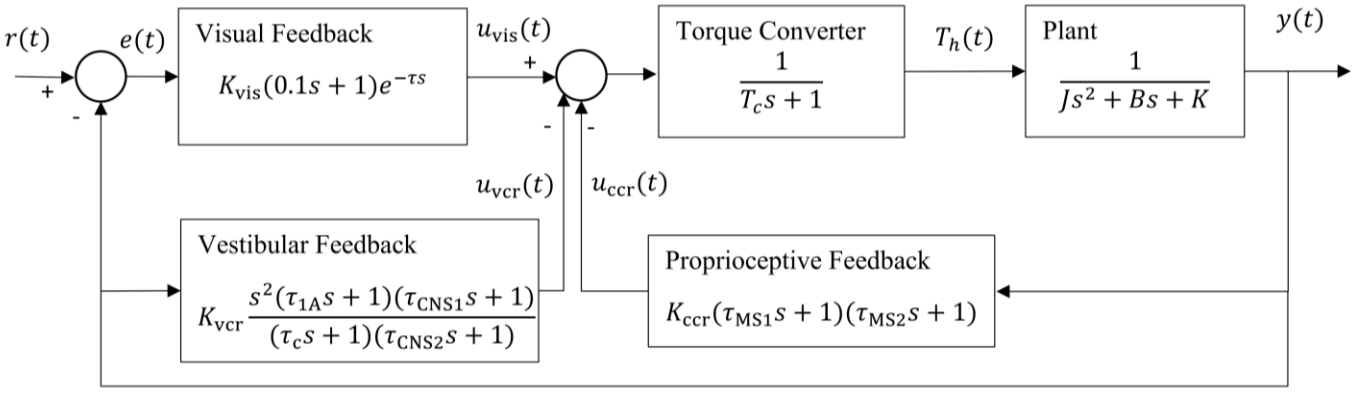

Figure 2: The parametric model of head position tracking in the horizontal plane.

MEDICINE BALL THROW TO EVALUATE POSTURAL STABILITY IN PERSONS WITH AMPUTATION

Kimberly Rowe, Julianne Stewart, Katherine Sharp, Jenny Anne Maun, and Marilynn Wyatt
Naval Medical Center San Diego, San Diego, CA USA
email: kimberly.l.rowe.ctr@mail.mil

INTRODUCTION

Rehabilitation of service members with lower limb amputation is of utmost importance. The military medical system has worked to impart interdisciplinary rehabilitation methods in order to bring this population to its highest possible level of function [1]. One of the most significant deficits this population struggles with is postural instability [2]. This is important because postural instability poses an increased risk of falling [3]. Many patients have goals to participate in high level activities, and one of the ways to evaluate dynamic postural control during such activities is to monitor the center of pressure total excursion (CoP TE), CoP velocity, and trunk excursion [4]. A chest pass medicine ball throw is one such movement which mimics activities of everyday life, as it requires dynamic postural stability and demands use of both hands.

This study cohort consisted of five subjects, each with a different level of amputation: unilateral transtibial (TTA), bilateral TTA, unilateral transfemoral (TFA), TTA and TFA, and bilateral TFA. CoP TE, CoP velocity, and trunk excursion were identified between limbs within subjects during a chest-pass medicine ball throw. In this study, we considered small CoP and trunk excursion measurements indicators of good postural stability. Therefore, we predict that postural instability increases with the number affected joints.

METHODS

Medicine ball throws were collected using a portable 12 Raptor-E camera setup (Motion Analysis Corp., Santa Rosa, CA, USA), and four portable force plates (Kistler Instrument Corp., Amherst, NY, USA). Target and analog data were processed using Visual 3D (C-Motion Inc., Germantown, MD, USA), and a 4th order, low-pass Butterworth filter with a cutoff frequency of 8 Hz and 50 Hz for kinematic and kinetic data respectively was used. Five retired U.S. Marine Corps service members (age 28.53 ± 1.17 yrs; height 1.76 ± 0.057 m; weight 81.65 ± 16.17 kg) were markered using a full-body, 6 degrees of freedom marker set, with additional markers placed on the 9.07 kg medicine ball for tracking. All participants provided written informed consent prior to the study (CIP #NMCSD-2014.0026).

All subjects were instructed to stand with each foot on two adjacent force plates, bring the ball to their chest, and throw it as far as they could in front of them. The movement was divided into two phases in post-processing: windup and forward throw. A WINDUP event was placed when the ball is closest to the trunk segment in the sagittal plane, and RELEASE was identified at the point of ball release by a custom Visual 3D script.

RESULTS AND DISCUSSION

CoP TE and velocity were calculated between WINDUP and RELEASE (Table 1). These two events marking the beginning and end of the medicine ball throw (Fig. 1).

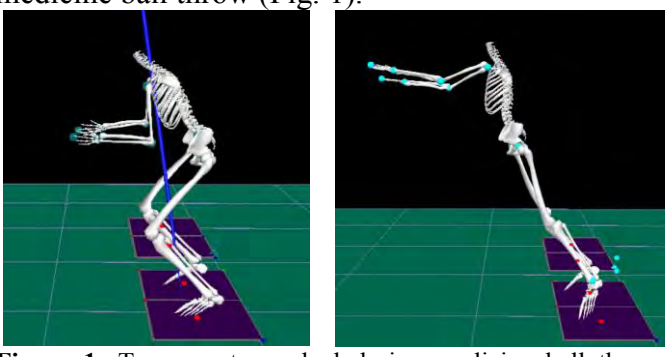

Figure 1: Two events marked during medicine ball throw: WINDUP (left) and RELEASE (right).

Left and right foot CoP trajectories from WINDUP to RELEASE are depicted on respective halves of the graph (Fig. 2), and are represented numerically in Table 1. The time between WINDUP and RELEASE was 0.51 ± 0.04 s, establishing that the CoP

trajectories presented take place over similar amounts of time.

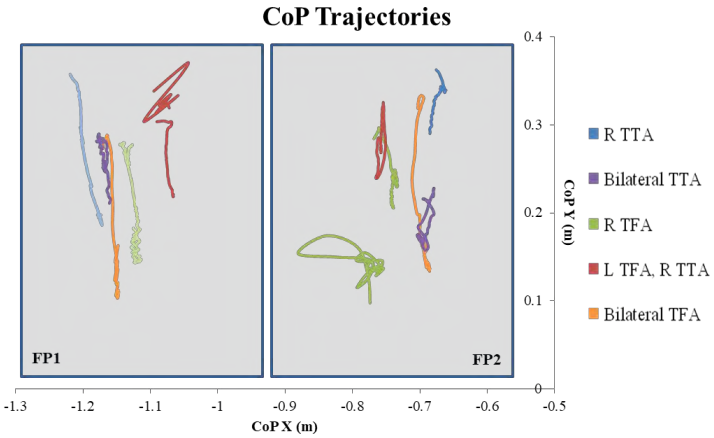

Figure 2: CoP TE for each subject. Data for affected limb(s) are more brightly colored than unaffected limb for comparison purposes. Non-continuous trajectories show a loss of contact between the foot and force plate.

The data follow a trend that CoP TE and velocity increase with the number of major joints amputated and/or number of limbs affected. The Right TTA subject's data does not follow the trend; CoP TE and velocity for the unaffected side was much larger than the affected side. This is likely because this subject spent the entire movement in an athletic position on the toe of his prosthetic foot, and was able to rock back and forth on his intact foot, as confirmed by reference video. It is notable that the two subjects with bilateral, symmetrical amputation (TTA; TFA) exhibit CoP TE and velocity values very close to symmetrical.

In general, subjects with unilateral or asymmetrical amputation demonstrate smaller CoP TE and velocity on their (less involved) intact limb, suggesting greater stability on that side. Gaps in CoP trajectories (Fig. 2) indicate a loss of contact between the foot and the force plate, which may be noteworthy in evaluating stability as well, as losses of contact are present only on affected limbs. Data also show a positive trend of trunk excursion with level of amputation (Table 1). To note: The subject with bilateral TTA has an upper limb injury that requires increased trunk motion for windup and ball release.

CONCLUSIONS

As the population of service members with amputation progresses through rehabilitation, performance of high-level tasks with safety and stability is an important step toward achieving high functional goals. The CoP and trunk excursion trends shown in this subset of subjects support our hypothesis, indicating that use of these measures to evaluate dynamic postural stability during activity is valid. This study and future related work is beneficial because there is limited research regarding postural stability and its role in functional movements for amputee populations. Future work should evaluate larger numbers of subjects, and consider similar variables for other functional movements.

REFERENCES

1. Cecere et al. *Mil Med*, **181**, 11-12, 2016.
2. Buckley et al. *Am J Phys Med Rehab*, **81**, 13-20, 2002.
3. Miller et al. *Arch Phys Med Rehab*, **82**, 1031-1037, 2001.
4. Palmieri et al. *J Sport Rehabil*, **11,** 51-66, 2002.

ACKNOWLEDGEMENTS

The authors would like to thank John-David Collins, Tatiana Djafar, and Trevor Kingsbury for their technical, intellectual, and emotional support! Thanks to Bobbi Bricks for her help and direction in this study. This work was supported in part with resources provided by the Extremity Trauma & Amputation Center of Excellence.

DISCLOSURE STATEMENT: The views expressed herein are those of the authors and do not necessarily reflect the official policy or position of the Department of the Navy, Department of Defense, or the U.S. Government.

Table 1: Light cell shading indicates affected limb in subject with unilateral or asymmetrical amputation, while darker shading indicates symmetrical bilateral amputation.

Amputation Level	CoP TE (m)			CoP Velocity (m/s)		Trunk Excursion (deg)
	Left	Right	% Difference	Left	Right	
R TTA	0.212	0.067	103.90	0.372	0.117	7.01
R TFA	0.359	0.912	87.02	0.749	1.900	11.28
L TFA; R TTA	0.523	0.209	85.79	1.112	0.445	18.44
Bilateral TTA	0.263	0.243	7.91	0.530	0.492	36.52
Bilateral TFA	0.341	0.320	6.35	0.643	0.604	23.59

RAMBLING-TREMBLING DECOMPOSITION IS NOT SENSITIVE TO INTENTIONAL POOR BALANCE

Gustavo Sandri Heidner, Caitlin O'Connell, J.C. Mizelle, Patrick Rider, Zachary Domire, Nicholas Murray

East Carolina University, Greenville, NC, USA
email: sandriheidnerg17@students.ecu.edu

INTRODUCTION

An important step in balance testing of concussed patients is the determination of sincerity of effort. Performing poorly intentionally on a balance baseline test, also known as 'sandbagging,' is a practice that can potentially alter the results and compromise the sensitivity to detect the presence of concussion [1]. Rambling-trembling (RT) decomposition of the center of pressure (COP) is a methodology based on the migration of the COP reference point (rambling) and its deviation away from that point (trembling) [2]. Previous research has suggested that rambling (RM) is representative of supraspinal components, more pronounced during voluntary control of balance [3]. Therefore, we have hypothesized that the RM component would be more pronounced in the signal when a participant was sandbagging. The objective of this study was to investigate if RM was a sensitive measurement of balance-test sandbagging in quiet standing by analysis of COP anterior-posterior displacement, and RMS error deviation from the trajectory (RMSe) by implementing RT decomposition.

METHODS

Eleven ($N = 11$) young adults (aged 23.3 ± 4.4 years, 5 males) participated in the study. Individuals with conditions affecting balance were ineligible. Participants performed a balance test that consisted of two vision conditions: eyes open (EO) and eyes closed (EC); and two types of balance conditions: (1) participants were instructed to stand on the force platform naturally (baseline), and (2) to sandbag the test without being detected by the naked eye (poor balance). Sway was assessed by COP displacement in the anterior-posterior direction (COP_{a-p}) and COP spline by the RT method. Rambling was determined as the cubic spline of the zero-time lag points where anterior-posterior force equals zero (Figure 1a,b). The correlation coefficient (r) and the RMSe between the COP_{a-p} trajectory and the RM were used for comparison between conditions.

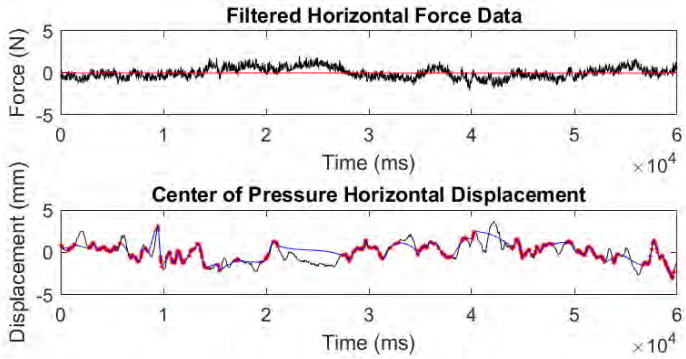

Figure 1a: Example of the RT decomposition analysis of one trial of good balance, with eyes closed. Spline connecting dots represents the rambling component, plotted over the COP_{a-p} displacement.

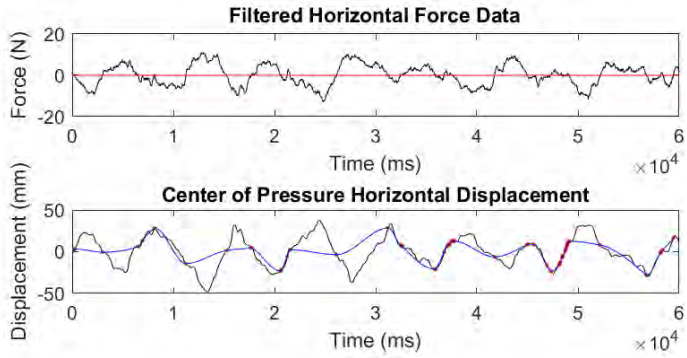

Figure 1b: Example of the RT decomposition analysis of one trial of poor balance, with eyes closed. Spline connecting dots represents the rambling component, plotted over the COP_{a-p} displacement.

COP trajectory data was collected for 60-sec. at 1000 Hz and low-pass filtered with the cut-off frequency of 20 Hz. Two 2-by-2 Factorial ANOVAs were conducted to compare the main effects of type of balance and vision conditions, and the interaction

effect between type of balance and vision conditions on the RT correlation coefficient and on RMSe between COP_{a-p} trajectory and RM spline, respectively. Level of significance was set *a priori* at $\alpha = .05$.

RESULTS AND DISCUSSION

There were no significant main effects of vision condition ($p = .094$) and balance type ($p = .309$) or the interaction between balance type and vision ($p = .701$) on the correlation coefficient (Figure 2).

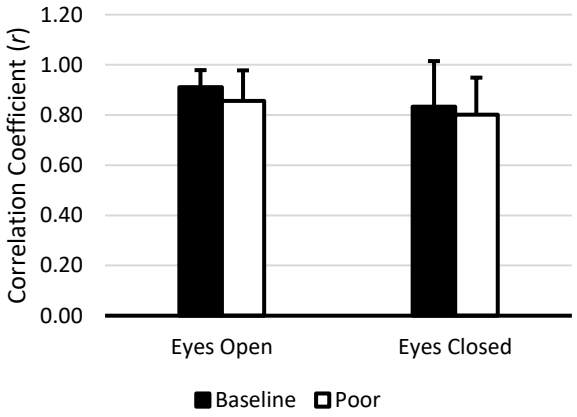

Figure 2: COP mean correlation coefficient during baseline and poor balance, with eyes open and eyes closed.

A significant main effect of vision condition on RMSe was found, $F(1, 10) = 11.61$, $p = .007$, $\eta p^2 = .537$, more specifically, the RMSe of the COP_{a-p} trajectory and the RM spline was lower with eyes open (Figure 3). The main effect of balance type ($p = .280$) and the interaction between balance type and vision condition on the RMSe ($p = .587$) were not significant.

These results suggest removal of visual feedback of balance, i.e. closing your eyes, produce COP_{a-p} alterations that can be detected by RT decomposition analysis if we focus on the RMS error between the COP trajectory and rambling spline, i.e. anterior-posterior COP oscillations induced by superior spinal processes. The correlation coefficients were surprisingly high across all conditions, suggesting that those are not interesting markers for the specific purpose of detecting balance-test sandbagging using RT decomposition.

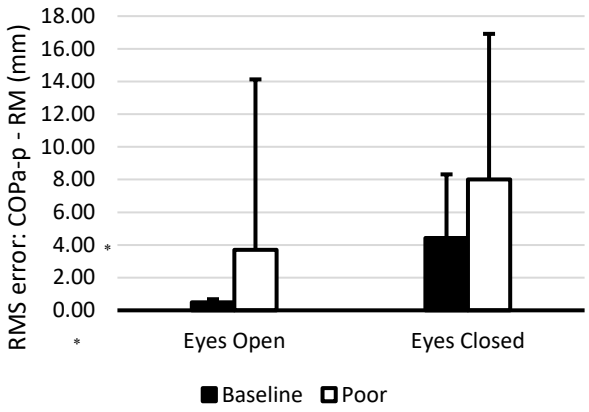

Figure 3: COP_{a-p} mean RMSe during baseline and poor balance, with eyes open and eyes closed. The * denotes greater than Eyes Open.

One limitation to this study is the small sample size in face of the large *SD*s in RMSe. Future studies should target larger sample size to address the large *SD*s, and consider investigating the sensitivity of other balance measures, for instance approximate entropy.

CONCLUSIONS

The correlation coefficient (rambling) and RMSe between the anterior-posterior COP trajectory and rambling spline (trembling) are not good measurements to detect sandbagging of balance tests. Future endeavors should focus on different measures.

REFERENCES

1. Erdal, K. *Arch Clin Neurophsychol*, 27(5), 2012.
2. Zatsiorsky, V.M. and Duarte, M. *Motor Control*, 4(2), 2000.
3. Shin, S. et al. *Motor Control*, 15, 2011.

ACKNOWLEDGEMENTS

Funding provided by the Office of Naval Research (N00014-17-1-272).

A SIMPLE CONTROLLER FOR RUNNING DERIVED FROM STEP-TO-STEP VARIABILITY

[1] Nidhi Seethapathi and [1] Manoj Srinivasan

[1] The Ohio State University, Columbus, OH, USA
email: seethapathi.1@osu.edu, web: www.movement.osu.edu

INTRODUCTION

Constant-speed human running is not exactly periodic. For instance, the body states of the person at mid-flight fluctuate about a mean value. Despite these noise-like deviations, people are able to run without falling down. Here, we examine how these natural fluctuations are controlled using ground reaction forces. As in [1,2], we use step-to-step variability to infer such control. In contrast to [2], which attempted to explain running stability with variants of a spring-mass model, we focus on ground reaction force modulations. We show how classic spring-mass based models of running are incomplete. Our work has implications to mathematical measures of running stability and controllers for running prostheses, exoskeletons and robots.

METHODS

Subjects (N = 8, 5 male, 3 female) ran on a treadmill at 2.5. 2.7 and 2.9 m/s while motion of the hip, motion of the foot and ground reaction forces were collected for a few minutes. Using linear least squares methods similar to those used in [1], we derive a linear model by mining the variability in the data. Using this linear model, we study whether the deviations in control variables like leg force, foot placement, stance duration and leg length during stance are explained by the deviations in the body states at mid-flight. The inputs to the controller and coordinate notation are shown in Figure 1. We implement this derived controller on a simple point mass telescoping leg model by finding the model gains that best match the step-to-step map in the data. We apply these gains to the simple model during stance to control for any perturbations added during flight. We perturb the sideways velocity, fore-aft velocity and vertical position of the model at flight apex, one or two at a time. We obtain the basin of attraction for the model by using a 200 x 200 grid of perturbations and letting the model simulate for 20 steps at each grid point. A fall is defined as when the model's center-of-mass goes below the ground.

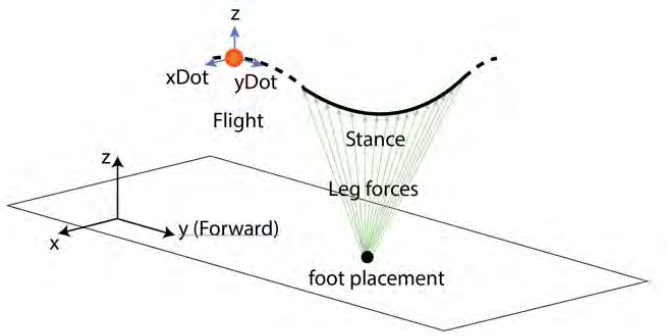

Figure 1. A linear map from flight states to stance controls is inferred.

RESULTS AND DISCUSSION

Experiment Results: The linear model obtained from experimental data found that a sideways velocity perturbation at flight apex is, on average, completely corrected by the sideways impulse during the next step (R^2=0.55). Around 80% of fore-aft velocity deviation at flight apex is corrected by the fore-aft impulse during the next step (R^2=0.35). Impulses can be modulated by modulating leg forces and stance duration. However, we find that stance duration does not play a role in correcting velocity deviations. Stance duration decreases in response to an upward vertical perturbation and increases in response to a downward vertical perturbation at flight apex. The phase-dependent ground reaction force modulation gains are shown in Figure 2. We find that, in response to fore-aft velocity deviations, the negative part of the GRF is modulated more than the positive part. People place their foot in the direction of the velocity perturbation. This foot placement control is more exaggerated in the sideways than in the fore-aft direction. Finally, we find that the landing leg length is changed proportionally in response to a vertical perturbation at flight apex. All gains were independent of running

speed and maintaining horizontal planar position was not found to be a priority for the controller inferred. All experimentally obtained gains are statistically significant with $p<10^{-4}$.

Model Results: The simple point mass telescoping leg model was first simulated with experimentally obtained control gains and some perturbations were applied. These gains were then adjusted to make sure that the step-to-step map for the model matched that from experiment. The adjusted model gains were found to be similar to experimental gains and are shown in Figure 2 below.

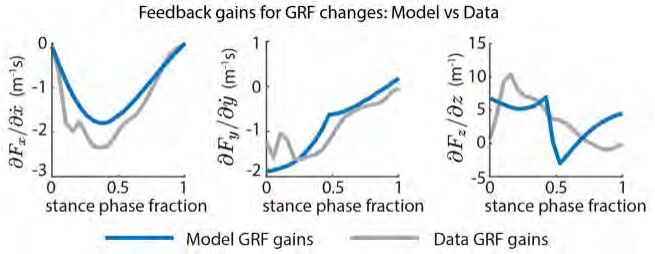

Figure 2: Experimental and model gains for GRF control. The model gains are similar to experimentally-obtained gains.

With the control present, the model has an asymptotically stable running motion. It recovers from fore-aft and sideways velocity perturbations and from vertical position perturbations, as shown in Figure 4. Although not explicit in the model's controller, it discovers a steeper leg angle in response to an upward perturbation. The model's basin of attraction (Figure 3) shows that it recovers from perturbations almost four times larger than the experimental variability size. We find that the basin of attraction is wider for fore-aft than for sideways perturbations. We also find that the model is more robust to upward than to downward perturbations.

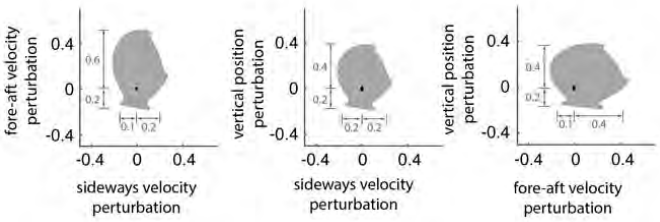

Figure 3: Basin of attractions for the simple model.

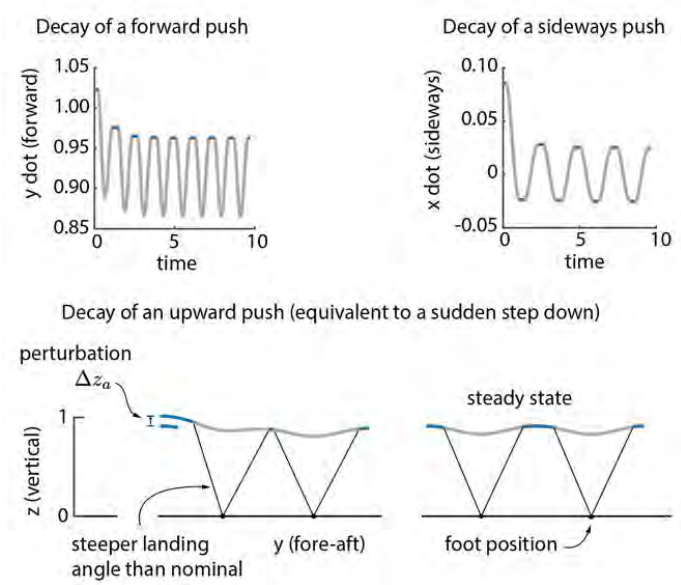

Figure 4: The model is stable to perturbations in fore-aft and sideways velocities and vertical position.

CONCLUSIONS

The control strategies found here are obtained from actual human running data and provide an empirical basis for the running controllers currently in use. The foot placement control found here appears to be qualitative similar to that used by people when walking as found in [1]. Our simple model discovers a steeper leg angle in response to an upward perturbation and this has previously been reported in papers with step-up and step-down perturbations for running birds and humans. An energy-conservative spring cannot explain the control gains observed here. Thus, we find that spring-mass assumptions for running control are insufficient to explain human running stability for even small steady-state perturbations such as those in our experiments. Since our controller is primarily derived from human running data, it can be used to make exoskeletons and prosthetic legs respond to the users in a more natural and seamless manner.

REFERENCES

1. Wang and Srinivasan. *Biology Letters,* 10.9 20140405, 2014.
2. Maus et al. *J. Roy. Soc. Interface*. 12.103 20140899, 2015.

EFFECT OF PROPHYLACTIC ANKLE BRACING ON DYNAMIC BALANCE

Mitchell L. Stephenson and Jason C. Gillette

Iowa State University, Ames, IA, USA
email: mistephe@iastate.edu, web: kin.hs.iastate.edu

INTRODUCTION

Due to the prevalence of ankle injuries in sport and exercise, many athletes choose to wear prophylactic ankle braces in an attempt to prevent injury. Previous research attempted to identify whether lace-up or hinged ankle braces affected dynamic balance in the Star Excursion Balance Test (SEBT) but did not identify any performance changes from the control condition [1].

More recently a new type of ankle brace has become popular: This hybridized design combines rigid sub-structures stabilized against the ankle with compressive strapping. As many manufacturers tout this new semi-rigid design as a technological advancement, the current study was implemented in order to determine if these new braces affect dynamic balance.

METHODS

Twenty physically-active, uninjured recreational athletes (9 females and 11 males; 21.1±1.9 years; 1.67±0.04 m tall; 76.1±14.0 kg) provided informed consent, performed a warm-up, and completed the following as part of a larger study. Four braces were tested: A lace-up and hinged ankle brace were tested to compare to previous research, and two new semi-rigid designs from different manufacturers.

Participants performed a modified SEBT [2] in unbraced and four braced conditions in a counterbalanced order. All participants stood on their right (braced) leg and attempted to reach their left toe as far along guiding vectors as possible. These guiding vectors were marked with tape on the ground, and were oriented anteriorly, posteriolateral to the stance leg at 45°, and posteriomedially at 45° (Figure 1).

Participants performed seven successful repetitions in each direction: six served as practice and the seventh was recorded [3]. An attempt was successful if the participant kept their arms folded across their chest, performed the movement with a smooth continuous motion, did not transfer weight to the reach leg, and kept the stance foot firmly and flatly planted on the ground.

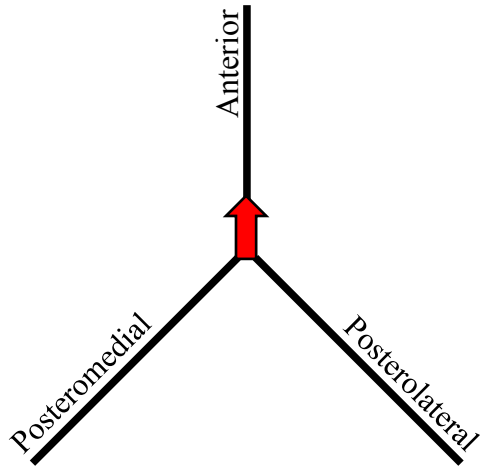

Figure 1: Modified SEBT protocol. Participants stood with their right foot on the red arrow. With their left foot, they attempted to reach their toe as far along the anterior, posterolateral, and posteromedial axes.

Kinematics of retroreflective markers placed on both feet were recorded via 8 Vicon cameras at 160Hz through Vicon Nexus 1.8.2 (Vicon Corp, Oxford, UK). Peak displacement of the left (reach limb) toe marker from the right (stance limb) toe marker (in anterior reaches) or heel marker (in posterior reaches) along the aforementioned axes was calculated and normalized to leg length. A repeated-measures analysis of variance was performed to compare the effect of the braces on the reach distances. An alpha value of 0.05 was utilized to evaluate statistical significance.

RESULTS AND DISCUSSION

No significant main effects were identified for any reach direction ($p > 0.60$). As seen in Table 1 below, participants attained further reach distances in both the posterolateral and posteromedial directions than the anterior direction, but reach distances were similar for all braces and the unbraced condition within each direction.

The lack of significant differences between the braces is similar to previous research [1]. The lace-up and the hinged braces were selected to match the designs in that investigation; as such, a lack of differences was not surprising. But the semi-rigid design is a more recent development in the prophylactic bracing market. Given multiple manufacturers' claims that these braces are more effective than previous models, we expected they may affect dynamic balance. Results indicate this was not the case.

Participants did qualitatively differentiate the perceived effect of certain braces on their performance, indicating in post-performance surveys that the semi-rigid braces were more restrictive than the lace-up brace. Some participants described this restrictiveness as beneficial, providing stability and support which may have facilitated their performance in the modified SEBT. But other participants believed the opposite, suspecting that the restriction may have hindered their range of motion. *Post hoc* exploratory analyses did not identify differing effects on dynamic balance based on these survey results, however.

It is possible that participants' performance was not altered due to the investigation's participant delimitations: Participants were required to be healthy and fit, which may mitigate the effect of a brace. It may be beneficial to investigate these possible effects on athletes with chronic ankle instability. Modern brace designs may affect the dynamic balance of this population, in contrast to the previously-tested lace-up designs [4].

CONCLUSIONS

It appears that prophylactic ankle bracing, independent of the brace's design, may not significantly affect dynamic balance in recreationally-athletic, uninjured populations. Given that athletes have an adequate level of dynamic balance, braces are therefore not likely to hinder balance and increase injury risk. In contrast, individuals within this population that would benefit from enhanced balance should not attempt to rely on ankles braces to augment such performance.

REFERENCES

1. Hardy, L, et al. *J Athl Train*, **46**, 347-351, 2008
2. Hertel, J, et al. *J Orthop Sport Phys Ther*, **36**, 131-137, 2006
3. Hertel, J, et al. *J Sport Rehabil*, **9**, 104-116, 2006
4. Gribble, P, et al. *Phys Ther Sport*, **11**, 3-7, 2010

ACKNOWLEDGEMENTS

The authors would like to thank United Sports Brands for providing the braces for testing.

Table 1: Modified SEBT reach distances (mean ± standard deviation) while wearing ankle braces, normalized to reach leg length

	No brace	Lace-up	Hinged	Semirigid I	Semirigid II
Anterior (%)	0.44 ± 0.07	0.47 ± 0.20	0.43 ± 0.08	0.43 ± 0.06	0.43 ± 0.09
Posterolateral (%)	1.08 ± 0.24	1.13 ± 0.11	1.03 ± 0.25	1.11 ± 0.09	1.11 ± 0.10
Posteromedial (%)	1.21 ± 0.09	1.20 ± 0.10	1.14 ± 0.25	1.21 ± 0.08	1.19 ± 0.11

No significant differences detected ($p > 0.60$)

ASSESSMENT OF POSTURAL CONTROL IN MULTIPLE SCLEROSIS: IDENTIFICATION OF CORE OUTCOME VARIABLES

[1]Ruopeng Sun, [2]Salma Musaad, and [1]Jacob J. Sosnoff

[1]University of Illinois at Urbana-Champaign, Department of Kinesiology and Community Health, IL, USA
[2]University of Illinois at Urbana-Champaign, Interdisciplinary Health Sciences Institute at Illinois, IL, USA
email: rusun@illinois.edu

INTRODUCTION

Balance impairment in individuals with multiple sclerosis (MS) is very common and associated with increased risk of falling. Although posturography is the gold standard of balance assessment, the vast number of metrics it yields presents a daunting challenge for clinicians and researchers to properly interpret data and provide actionable insights. Numerous postural sway metrics (i.e. sway path, sway area, sway amplitude, frequency domain measures, and sway entropy, etc.) have been shown to be sensitive to balance impairment in individuals with MS [1]. Yet there is limited data to inform guidelines on the most appropriate postural sway metrics for impairment tracking and fall risk evaluation. This investigation assessed the accuracy and feature importance of various postural sway metrics to differentiate MS individuals as a function of physiological fall risk.

METHODS

This secondary data analysis included 153 participants (50 controls and 103 individuals with MS). Participants were further classified into four subgroups based on individual's physiological fall risk - Physiological Profile Assessment (PPA): controls (n=50, 64.9 ± 4.9 years old, PPA < 1); low-risk MS (n=34, 54.0 ± 13.1 years old, PPA < 1, EDSS: 4.3 ± 1.5); moderate-risk MS (n=27, 58.3 ± 8.3 years old, 1 ≤ PPA < 2, EDSS: 5.3 ± 1.5); high-risk MS (n=42, 56.8 ± 9.7 years old, PPA ≥ 2, EDSS: 6.0 ± 0.9). Participants also completed balance confidence questionnaires (Activities-specific Balance Confidence Scale - ABC, Falls Efficacy Scale – International - FES)

All participants were instructed to stand upright for 30 s on a force platform (Bertec Corp, Columbus, OH) with their feet shoulder width apart, and eyes open, fixating at a target at 2 m away. Forceplate data were sampled at 1000 Hz and low-pass filtered (4th order Butterworth) at 10 Hz. The mediolateral and anteroposterior components of center of pressure (COP) were calculated using standard equations. Twenty common sway metrics (i.e. sway path length, 95% confidence sway ellipse area, mean sway velocity, sway range, root mean squared sway amplitude, sway frequency, sway entropy, etc.) were derived following standard procedure[2,3]. These sway metrics were subsequently used to train a set of random forest (RF) classification algorithms (70-30 training/test split, holdout validation) to predict individuals' fall risk grouping (low, moderate, high). The feature importance from the RF algorithms was used to select the strongest sway metric for fall risk prediction. All COP analysis were performed with MATLAB R2015b (The Mathworks, Inc., Natick, MA, USA), and statistical analyses were performed with Python Scikit-learn [4].

RESULTS AND DISCUSSION

Overall, as shown in Table 1, using sway metrics, the RF classification accuracy was high for discriminating controls from MS individuals (>90%) and discriminating low-risk MS individuals from high-risk individuals (78.9%). Whereas the classification accuracy for discriminating moderate-risk MS individuals from low/high-risk MS individuals were low (≤ 60 %).

Table 1: Classification accuracy based-on sway metrics

Classification Accuracy %	low-risk MS	moderate-risk MS	high-risk MS
controls	90.4	90.0	91.3
low-risk MS		60.0	78.9
moderate-risk MS			52.9

Sway sample entropy, a sway regularity metric, was identified as the strongest feature for classification of low-risk MS individuals from healthy controls. Whereas for all other comparisons, the mediolateral sway range was identified as the strongest predictor for fall risk groupings.

Additionally, when adding the balance confidence scale into the model, the RF algorithm improved its classification accuracy for discriminating controls from MS individuals (≥95%), while decreased its classification accuracy for MS individuals grouping (Table.2).

Table 2: Classification accuracy based-on sway metrics and balance confidence scale

Classification Accuracy %	low-risk MS	moderate-risk MS	high-risk MS
controls	95.2	95.0	95.7
low-risk MS		60.0	73.7
moderate-risk MS			47.1

CONCLUSIONS

Overall, the findings indicate that sample entropy is a sensitive sway metric for differentiating healthy controls and MS individuals without elevated fall risk, whereas mediolateral sway range can be used as a hallmark for increased fall risk in moderate to high-risk MS individuals. Self-reported balance confidence can improve the fall risk classification accuracy between healthy controls and MS individuals, but does not add value toward fall risk classification among MS individuals. These findings may set the foundation for the development of guidelines for accurate assessment of balance impairment in individuals with MS.

REFERENCES

1. Cameron MH & Lord S. *Curr Neurol Nerurosci Rep,* 10 (5), 2010
2. Prieto TE, et al. *IEEE Trans Biomed Eng*, 43 (9), 1996
3. Yentes JM, et al. *Ann Biomech Eng,* 41(2), 2013
4. Pedregosa F, et al. *JMLR* 12, pp2825-2830, 2011

ACKNOWLEDGEMENTS

The studies in this analysis were in part funded by the National Multiple Sclerosis Society, Consortium of MS Centers.

Reliability of A Novel, Clinically-Oriented Approach to Quantify Ankle Proprioception

[1]Rachel H. Teater, [2]Scott M. Monfort, [3]Kim E. Bigelow, [1,4]Ajit M.W. Chaudhari

[1]The Ohio State University, Columbus, OH, USA; [2]Montana State University, Bozeman, MT, USA;
[3]University of Dayton, Dayton, OH, USA; [4]Perfect Practice, Inc.
email: rachelteater21@gmail.com, web: http://u.osu.edu/osusportsbiomechanics

INTRODUCTION

Proprioception is an essential component of balance and postural control, as it provides information relating to the sense of movement (kinesthesia), the position of joints (joint position sense), velocity of muscular contraction, and the force associated with muscular contractions. Proprioception is at risk of deterioration with factors such as aging, peripheral neuropathy, osteoarthritis, and ligament injury [1]. Being able to measure proprioception in the clinic is important as rehabilitation in patients with decreased proprioception may mitigate declines in their functional stability [2].

Proprioception is often evaluated using a Biodex isokinetic dynamometer or custom-built devices. These methods have cost, space, ease-of-use, and portability barriers that impede the ability of clinicians to measure proprioception in populations that are at risk of having deficits. Because of these challenges, mobile device applications have increasingly been investigated as an alternative method of measuring human movement and proprioception. CoreX Therapy (Perfect Practice, Inc.) is an iOS app that has previously demonstrated utility for quantifying core stability through the measurement of pelvic tilt [3]. Recent research has investigated using this application as a clinically-relevant tool for measuring ankle joint position sense (JPS), a component of proprioception [4], but the reliability of this novel tool has not been established.

The purpose of this study was to establish the reliability of the CoreX Therapy app as a tool for assessing ankle proprioception in the clinic. Number of trials and post-processing considerations were examined to determine the most reliable protocol for clinical implementation.

METHODS

Forty-five healthy participants (16 females, 29.3 ± 7.8 yrs, 1.76 ± 0.10 m, 76.0 ± 15.7 kg) were recruited at the 2017 Annual Meeting of the American Society of Biomechanics at the University of Colorado Boulder in August 2017. Data were collected by a number of undergraduate, graduate, and faculty researchers, to demonstrate the approach's ease of use.

Figure 1: Ankle joint position sense assessment using CoreX Therapy iPod application.

Each participant's ankle JPS was evaluated using the CoreX Therapy application. Participants' more unstable ankle (self-reported) was tested. If neither ankle was reported to be unstable, the ankle of the dominant leg was tested. An iPod was strapped to participants foot, as they lay supine on a table (Figure 1). Each participant performed ten trials of active ankle repositioning. For each trial, the participant started with their sole perpendicular to the ground then actively plantarflexed their foot until they reached the target angle of 15 degrees and were instructed to stop by the researcher. The participant held this position for 5 seconds to learn the angle. The participant then repeated the movement and indicated when they thought they had reached the target angle once again. The researcher recorded the

error from target angle of the participant's ankle for each trial.

Intraclass correlation coefficients (ICCs) were used to assess the trial-to-trial reliability of participants' absolute error in active joint reposition sense. To determine how the reliability changed with the available number of trials, an iterative analysis was performed. ICCs were calculated considering the first five through all ten trials. The reliability of each number of trials was assessed with and without the most and least accurate trials included.

RESULTS AND DISCUSSION

The ICCs for five through ten trials are shown below in Figure 2. The reliability of using the CoreX Therapy app as a measure of ankle active JPS generally increased with increasing number of trials included. The reliability was always greater with the most and least accurate trial excluded. When analyzing only the first five and six trials and not excluding the most and least accurate trials, the test had poor reliability (ICC(1, k) < 0.50). All other scenarios resulted in moderate reliability. The most reliable measure of JPS was achieved by collecting ten trials then excluding the most and least accurate trial with an ICC(1, k) of 0.741.

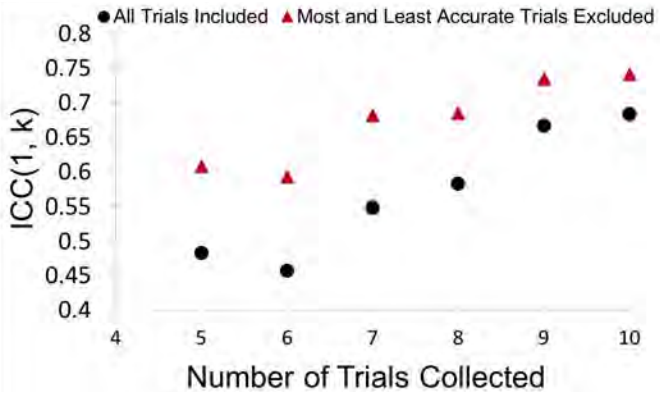

Figure 2: ICCs for the absolute error of five through ten trials of active ankle reposition tests.

This tool reduces the barriers to widespread clinical assessment of proprioception as it is low-cost and easy to operate. Materials necessary only include an iPod and a way of securing the iPod to the patient's foot, such as a Velcro strap. Widespread clinical assessment of proprioception can lead to increased implementation of rehabilitative interventions for patients who have impaired proprioception. Additionally, this tool provides improved ability for researchers to directly test relationships between ankle proprioception and other variables of interest rather than inferring proprioception from indirect measures such as nerve conduction velocity or self-reports.

CONCLUSIONS

The CoreX Therapy app is a moderately reliable tool that can be used to evaluate ankle JPS and proprioception by both clinicians and researchers. The low cost, high portability, and simplicity of this method allows proprioception assessment to be easily implemented in clinical settings. For best reliability, ten trials of active joint position sense should be collected and the most and least accurate trial should be excluded before determining the average absolute error.

REFERENCES

1. Deshpande N, et al. *Arch Phys Med Rehabil* **84**, 883-889, 2003.
2. Lee AJY et al. *Clinical Biomech* **23**, 1065-1072, 2008.
3. Chaudhari AM, et al. *J Strength Cond Res* **25**, 2127 - 2132, 2011.
4. Monfort SM, et al. *Proceedings of 2017 ASB* **41**, 2017.

ACKNOWLEDGEMENTS

The authors gratefully acknowledge the support of the Organizing Committee of the 2017 American Society of Biomechanics Annual Meeting and the Ohio State University College of Engineering Undergraduate Research Grant. Due to author AMWC's relationship with Perfect Practice, Inc., he was not involved in recruiting or consenting participants, or in performing the data collection or analysis.

DYNAMIC STABILITY DURING WALKING IN CHILDREN WITH AND WITHOUT CEREBRAL PALSY: A PILOT STUDY

[1] James B. Tracy, [1] Drew A. Petersen, [1] Jamie Pigman, [2] Benjamin C. Conner, [3] Christopher M. Modlesky, [1,4] Freeman Miller, [1] Curtis L. Johnson, [1] Jeremy R. Crenshaw

[1] University of Delaware, Newark, DE, USA, [2] University of Arizona, Tucson, AZ, USA, [3] University of Georgia, Athens, GA, USA, [4] Nemours/A.I. DuPont Hospital for Children, Wilmington, DE, USA
email: crenshaw@udel.edu, web: http://sites.udel.edu/kaap/crenshaw-lab/

INTRODUCTION

Cerebral palsy (CP) is associated with a high risk and rate of falling, 55% of which occur during walking [1]. Gait abnormalities associated with CP include a "stiff" knee during swing, knee hyperextension (i.e. recurvatum) or excessive flexion (i.e. crouch) in stance, limited dorsiflexion (i.e. equinus), leg crossing in swing (i.e. scissoring), intoeing, internal hip rotation, and excessive hip adduction [2]. These abnormalities likely alter the trajectory of the whole-body center of mass (COM) during gait and foot placement in a way that increases the risk of falling forward or to the side.

Previous analyses of gait stability in children with CP demonstrate that it is dependent on speed and direction. By evaluating step placement relative to a "foot placement estimator", one study suggested that those with CP are *more unstable* anteriorly, especially at fast speeds and when stepping with the more affected limb [3]. By evaluating the inclination angle between the COM and center of pressure, another study suggested that children with CP are *more stable* anteriorly, likely achieved through slower speeds as a protective means against falling [4]. Both studies, however, noted lateral instability in children with CP compared to typically developing (TD) counterparts [3, 4]. These results align with other studies that determined that children with CP have larger mediolateral COM excursions and velocities relative to the center of pressure [5, 6].

The "margin of stability" (MOS) represents the distance between the edge of the base of support and the vertical projection of the extrapolated center of mass (xCOM), which is determined by the position and velocity of the whole-body COM [7]. The MOS has distinct advantages in that it is a dynamic measure (i.e. it accounts for velocity), and it can be evaluated at distinct time points in the gait cycle. In addition, the magnitude of the MOS is proportional to the impulse needed to change stability states, so it has explicit biomechanical meaning [7].

The purpose of this study was to compare the anterior and lateral MOS of children with and without CP. We hypothesized that (1) children with CP would be less stable than TD children, (2) group differences would be greater when bearing weight with the non-dominant limb, and (3) group differences would be greater at fast speeds than at preferred speeds.

METHODS

A group of 5 children with CP (3 boys and 2 girls, mean = 8.4 (standard deviation = 2.2) years old, 4 GMFCS level I, 1 GMFCS level II) were age-matched with 5 TD children (3 boys and 2 girls, 8.4 (2.2) years old).

Using motion capture technology (Qualisys, Göteborg, Sweden, 120 Hz) and a full-body marker set, the overground gait of all participants were recorded at preferred and fast speeds.

The MOS [7] was calculated as follows:

- The anterior MOS was evaluated immediately before foot strike as the anterior distance between the trailing stance toe and the xCOM. This measure represents the maximum anterior instability that the child allowed.
- The anterior MOS at mid-swing was evaluated as the anterior distance between the stance toe and the xCOM. This measure represents the state of stability when a trip is likely to occur.
- The minimum lateral MOS was evaluated as the minimum lateral distance between the stance toe and the xCOM during stance. This measure is proportional to the minimum impulse needed to induce frontal plane instability.

The average of each measure over two complete gait cycles was calculated for each participant. Mixed factorial ANOVA's were used to evaluate the effects and interactions of GROUP (CP or TD), LIMB (dominant or non-dominant, as per reported kicking preference), and SPEED (preferred or fast) (SPSS, IBM Corp, New York, USA). Given the small sample size, results were interpreted using effect sizes (large: $f = 0.40$, medium: $f = 0.25$, small: $f = 0.10$).

RESULTS AND DISCUSSION

Gait Speed

A large effect of commanded SPEED ($f = 3.39$, $p < 0.001$) indicated that participants walked faster when instructed to do so (Table 1). Small main effects and interaction containing GROUP ($f < 0.07$, $p > 0.86$) suggested that children with CP did not walk slower than TD children.

Anterior Margin of Stability before Foot-Strike

There were medium-to-large effects of LIMB ($f = 0.35$, $p = 0.357$) and SPEED ($f = 3.44$, $p < 0.001$) on anterior stability, such that faster speeds were more unstable and participants allowed themselves to be more unstable when pushing off of their dominant limb (Table 1). All other main effects and interactions were weak ($f < 0.23$, $p > 0.53$).

Anterior Margin of Stability at Mid-Swing

There was a medium effect of SPEED x LIMB x GROUP ($f = 0.33$, $p = 0.381$). In post-hoc comparisons, only small between-group differences were observed (Cohen's $d < 0.24$, $p > 0.72$).

Minimum Lateral Margin of Stability

There was a large SPEED x LIMB x GROUP effect ($f = 0.41$, $p = 0.285$). At fast speeds, as well as when bearing weight on the non-dominant limb at preferred speeds, children with CP were more stable than TD children (Cohen's $d = 0.78 – 2.00$, $p = 0.015 – 0.17$, Table 1).

CONCLUSIONS

This high-functioning group of children with CP exhibited a more conservative lateral stability strategy, especially on the non-dominant limb and at fast speeds. Despite a worse response to anterior perturbations (*in review)*, no group differences in anterior stability during walking were observed. This discrepancy could increase the risk of falling should an anterior perturbation, such as a trip, occur during walking.

REFERENCES

1. Morgan et al. *Rehab Research Practice*. 196395, 2015.
2. Wren et al. *J Pediatr Orthop*. **25**:79–83, 2005.
3. Bruijn et al. *Res Dev Disabil.* **34**:1689-1699, 2013.
4. Chang et al. *Biomed Eng Appl Basis Commun* **23**:509-517, 2011.
5. Hsue et al. *Gait Posture*. **29**:465-470, 2009.
6. Hsue et al. *Gait Posture*. **29**:471-476, 2009.
7. Hof et al. *J Biomech*. **38**:1-8, 2005.

ACKNOWLEDGEMENTS

This work was supported by the Delaware INBRE program with a grant from the NIGMS (P20-GM103446) and the State of Delaware, and by 1R01HD090226.

Table 1: Mean (SD) for each measure of the margin of stability (MOS), displayed by speed, limb, and group.

MOS (cm)	Preferred Speed: 1.23 (0.17) m/s				Fast Speed: 2.01 (0.20) m/s			
	Dominant Limb		Non-Dominant Limb		Dominant Limb		Non-Dominant Limb	
	CP	TD	CP	TD	CP	TD	CP	TD
Anterior MOS before foot strike	-48.4 (10.5)	-45.8 (11.4)	-47.3 (11.1)	-46.1 (11.7)	-78.0 (11.6)	-76.5 (12.2)	-76.5 (11.2)	-75.7 (14.3)
Anterior MOS at mid-swing	-25.0 (7.4)	-23.3 (7.0)	-25.4 (7.3)	-23.7 (7.1)	-48.5 (7.7)	-48.1 (8.5)	-49.2 (7.5)	-47.0 (11.4)
Lateral minimum MOS	2.0 (1.0)	2.0 (0.5)	2.8 (1.0)*	1.1 (0.9)	2.1 (0.8)*	1.0 (1.4)	4.3 (1.3)*	0.8 (2.2)

*Large between-group differences (Cohen's d =0.78—2.00).

Posture assessment of a chiropractor performing side posture adjustments: a pilot study using an inertial measurement unit system

[1] Michael Weiner, [1] Brent Russell, [1] Linda Mullin, [1] Ronald Hosek and [1] Edward Owens

[1] Life University, Marietta, GA, USA
email: brent.russell@life.edu

INTRODUCTION

Chiropractic is the third-largest health care profession in the United States. As of 2012, based on data from the National Health Interview Survey, approximately 8.4% of U.S. adults (19.1 million) had seen a chiropractor within the past 12 months, and 24% (54.6 million) during their lifetime. [1]

While the therapeutic method most commonly associated with chiropractic is spinal manipulation, also known as manual "adjustment", there has here has been limited investigation into the mechanical characteristics of how chiropractors perform adjustments. More knowledge of how chiropractors *do* perform manual adjustments could contribute to a more ambitious effort of determining how they *should* perform them. Most chiropractic care involves performance of "high-velocity, low-amplitude" thrusts (HVLA), which is considered to be physically demanding. Improper technique is thought to contribute to injury in chiropractic practitioners; documented common complaints include pain in the low back, neck, shoulders, hands, and wrists. [2,3] Furthermore, the educational process is largely dependent on instructors' subjective assessments of students' performance; objective measurement methods and educational standards is an emerging area of investigation.

One of the more commonly-known chiropractic methods is the side-posture adjustment (SPA). The aim of the present study, using a single chiropractor (Doctor of Chiropractic, or DC), was to develop a protocol to track postural angles and angular velocities during the performance of SPAs.

METHODS

All procedures were approved by our institution's IRB. An email was sent to students in the DC program who had recently completed a 3rd-level technique class, had an established clinical file, and were known to have no contraindications to receiving HVLA chiropractic care. Potential participants were included if an SPA of the lumbar spine was deemed appropriate the day of data collection; they were to be excluded if HVLA was deemed inappropriate for any reason, or if their health & examination records were not available. The first 10 students who responded were examined and included in the study.

One chiropractor, with 23 years of practice and teaching experience, was outfitted with MyoMotion inertial measurement unit (IMU) sensors (Noraxon, Scottsdale Arizona, USA), on the back of her head, overlying the C7 and T12 vertebra and upper sacrum, on the lateral aspects of both upper arms, and on the distal thighs. System calibration was done before each adjustment, using the manufacturer's proprietary system, with the doctor standing still in an upright neutral posture for approximately 30 seconds. She then performed a Gonstead-style lumbar SPA on each patient.

The first author examined motion recordings to identify the moment of maximum execution of each adjustment thrust. Data were exported to an algorithm developed in Excel by the fourth and fifth authors and analyzed for a period from one-half second before to one-half second after the thrust. We have thus far limited our analyses to spinal motions, specifically maximum values of angular measurements and rates of change for flexion-extension, lateral bending, and rotation of the cervical, thoracic, and lumbar regions.

RESULTS AND DISCUSSION

Data collection was successful for all trials, though the SPA was repeated on one trial in which the chiropractor felt that her first attempt was not optimally executed.

Relative to neutral calibration, the DC's spinal regions were flexed during the entirety of set-up and thrust. The cervical region also remained in right lateral bending and rotation; the lumbar spine was mostly in slight left rotation. Otherwise, the patterns of thoracic lateral bending and rotation and lumbar lateral bending were small in magnitude and clustered around the calibrated zero position.

The general patterns of all motions were consistent, trial-to-trial, though peak angles varied in their magnitudes and in when they occurred relative to the thrusts. Figure 1 presents cervical flexion-extension as an example of one regional motion pattern.

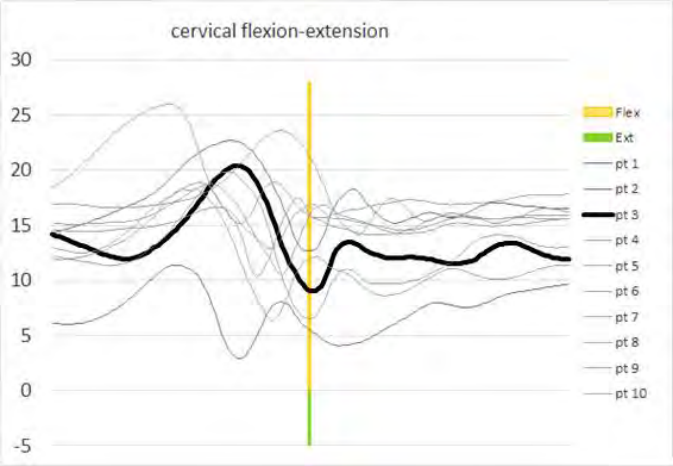

Figure 1: Cervical flexion-extension motion patterns around time of peak thrusts in side-posture adjustments (SPAs). The bold line highlights one pattern felt to be typical; those for other patients are sequentially similar, though they differ in magnitudes, and in timing of peak motions relative to the moment of peak thrust (vertical line).

Around the times of peak thrust, angular velocities during acceleration for the cervical, thoracic, and lumbar regions were, on average, 111.8, 73.5, and 38.7 degrees per second (deg/s), respectively; one period of cervical flexion reached 137.3 deg/s. Angular velocities in the frontal plane for the cervical, thoracic, and lumbar regions were, on average, 83.5, 66.5, and 48.6 deg/s, respectively; one period of thoracic lateral bending reached 140.3 deg/s. Angular velocities during transverse plane rotation for the cervical, thoracic, and lumbar regions were, on average, 124.7, 61.7, and 32.1 deg/s, respectively; the fastest was during one period of cervical rotation, at 205.8 deg/s.

The motion capture system and our data analysis method both worked well. Our patient recruitment was successful, but this was a small study and may not work for an expanded version. The patients were relatively young and healthy, and the findings could be different for older patients and those with pain, stiffness, or degeneration. The study also involved only one chiropractor, who may or may not be typical.

CONCLUSIONS

The methods appear to be feasible for identifying similarities and differences in motion patterns. Future studies will include additional chiropractors and should draw patients from other populations. These efforts may contribute to chiropractic student education and the understanding of occupational injuries of chiropractors.

REFERENCES

1. Adams J, et al. Spine. 2017;42(23):1810-6.
2. Holm SM, et al. J Manipulative Physiol Ther. 2006; 29(7): 518-23.
3. Ndetan HT, et al. J Manipulative Physiol Ther. 2009;32(2):140-8.

Table 1: Mean maximum values of angular motions for 10 patient-participants. The top row indicates either movement toward flexion (flex-ext columns) or toward the left (lateral bending or transverse plane rotation). The bottom row indicates either movement toward extension or toward the right. Relative to neutral calibration, positive numbers indicate flexion, right lateral bending or right transverse rotation.

C flex-ext	C lat bend	C trans rot.	T flex-ext	T lat bend	T trans rot.	L flex-ext	L lat bend	L trans rot.
19.7°	2.2°	6.0°	19.8°	-3.6°	-0.7°	34.0°	-2.2°	-12.8°
10.0°	7.0°	16.9°	11.9°	1.3°	3.9°	29.6°	0.6°	-8.5°

LEAD LEG RECOVERY RESPONSES BETWEEN INDIVIDUALS WHO FALL AND RECOVER AFTER AN UNEXPECTED SLIP

[1]Sam Wilson, [1]Paul Donahue, [1]Caleb Williams, [1]Christopher Hill, [1]Lauren Luginsland,

[1]Dwight Waddell, [2]Harish Chander, & [3]John Garner.

[1]University of Mississippi, University, MS, USA
[2]Mississippi State University, Mississippi State, MS, USA
[3]Troy University, Troy, AL, USA
Email: sjwilso2@go.olemiss.edu web: hesrm.olemiss.edu

INTRODUCTION

Falls are a major health and economic burden in the United States. Peoples over the age of 65 contribute to over 80% of all fall related deaths in the United States [1], and within this older population, fall-related injuries account for approximately $19 billion in annual medical costs [2]. Falls are also a major hazard in occupational settings, and represent another robustly studied area of fall research. Occupational injuries related to slips, trips, and falls resulted in a direct cost of over $16 billion in the United States. The process of an unexpected slip is divided into four distinct phases (environment, initiation, detection, and recovery) [3]. Researchers have commonly classified slips in a severity range based on the magnitude of this heel slip distance, as well as the velocity of the heel slip [4-6]. Though, more recent work has attempted to quantify the slip response as a fall or recovery through the use of a force criterion in the fall arrest harness system [7]. The kinetic analysis during slip events has generally focused its attention on the GRFs and the corrective joint moments during the slip response [4-6, 8-10]. These responses have been reported to be scaled to the severity of the slip, but have yet to be analyzed between groups of fallers and non-fallers. Thus the purpose of this study was to examine lead leg slip recovery parameters between those classified as a fall, or recover during an unexpected slip.

METHODS AND PROCEDURES

This study was conducted in a case-controlled design, with 32 healthy adults (16 male, 16 female; age: 21.66 ± 3.156; height: 170.24cm ± 13.86; weight: 74.62kg ± 16.60), who had no history of musculoskeletal, orthopedic, neurological, or vestibular abnormalities. An 8 camera Vicon Nexus (Oxford, UK) 3D motion capture system was used to collect and analyze kinematic and kinetic gait data. A lower body plug-in gait model from the Helen–Hayes marker system was used for the participant configuration and the kinematic data was sampled at 100 Hz and collected using the Vicon Nexus software. Variables of interest are mean sagittal moments about the ankle, knee, and hip, during stance phase (ANKm, KNEm, HIPm). Peak moments (ANK_PFp/DFp, KNE_Ep/Fp, HIP_Ep/Fp), and time to peak moments (ANK_PFttp/DFttp, KNE_Ettp/Fttp, HIP_Ettp/Fttp). A back-pack type fall arrest system with a movable trolley was used to prevent any undesired falls. Glycerol mixed with water in the ratio of 75% glycerol and 25% water was used as the slippery agent [3]. During the slip trials, glycerol was applied and evenly distributed on a force plate for contact of the leading left leg. Participants were strapped to a harness and performed multiple gait trials until normal self-selected pace walking with appropriate foot positioning onto the force plate was achieved. Participants turned away and listened to music on noise cancellation head phones for about 1 minute between each of these normal gait trials. One trial was then chosen to be the unexpected slip (US) and the contaminant was applied. Each slip trial was classified based on a force criterion using a digital crane scale inline with the overhead harness system. The slip was classified as a fall if the peak body weight measured by the scale exceeded 30% of body weight during the slip, and confirmed with visual inspection. After classification, recovery kinetics were analyzed, using independent samples t-tests between falls and recovers.

RESULTS AND DISSCUSSION

For the slip recovery measures, we have evidence of significant differences for the average ankle moment ($t(30) = 2.878$, $p = 0.007$), peak knee extension moment ($t(30) = -2.125$, $p = 0.042$), and knee extension time to peak moment ($t(30) = 2.051$, $p = 0.049$). Our results suggest a decreased average ankle moment over stance phase, likely due to the fall eliminating the progression into toe-off and the propulsion phase of gait. Our data also suggest an increased knee extension peak for fallers, but a decreased knee extension time to peak. Previous research has shown that after a slip has been initiated, a series of corrective responses attempt to rescue the fall and maintain locomotion. The primary response identified during a slip is an increased flexion knee moment, and extension moment about the hip [6]. This is followed by a secondary response consisting of a knee extension moment and hip flexion moment. These portions on average, represented approximately 190ms to 350ms after heel contact. Our findings also observed a peak knee flexion moment at approximately 200ms (201.8 in recoveries vs 198.7 in falls), however our data further suggest that a greater, premature knee extension peak similar to the previously observed secondary response may contribute to a fall as opposed to a recovery.

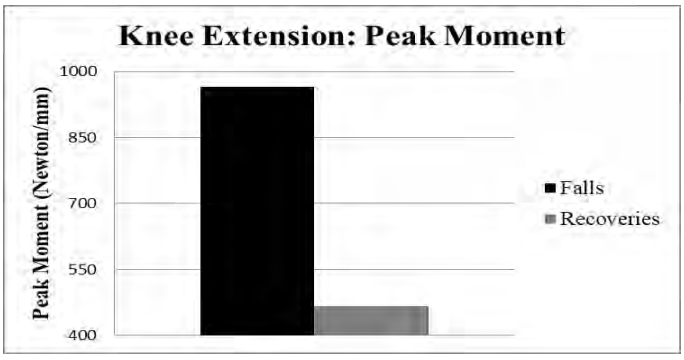

Figure 1: Peak knee extension moments between those who fell, and those who recovered.

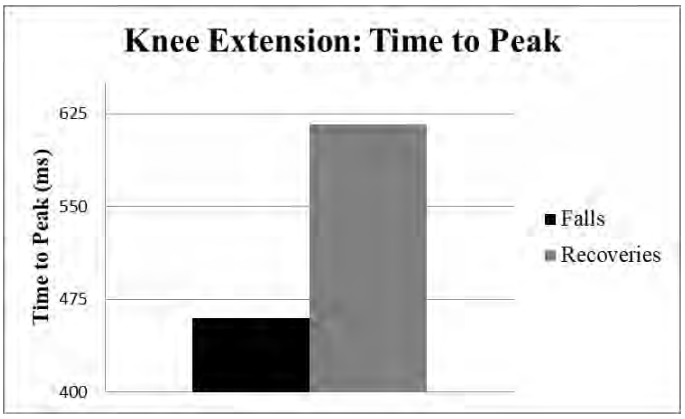

Figure 2: Time to peak knee extension moments between those who fell, and those who recovered.

CONCLUSION

The findings of this study suggest that differences in knee extension during the secondary response of slip recovery may contribute to the likelihood of a slip induced fall. These temporal differences could be due to co-contraction responses at the knee during slip responses, or different muscle synergy underpinnings within the slip recovery response.

REFERENCES

1. Control, C.f.D. and Prevention, *National center for injury prevention and control. Web-based injury statistics query and reporting system (WISQARS); 2010.* Accessed January, 2014.
2. Merrill, Z., A.J. Chambers, and R. Cham, *Arm reactions in response to an unexpected slip—impact of aging.* Journal of Biomechanics, 2017.
3. Lockhart, T.E., J.L. Smith, and J.C. Woldstad, *Effects of aging on the biomechanics of slips and falls.* Human factors, 2005. **47**(4): p. 708-729.
4. Chander, H., J.C. Garner, and C. Wade, *Heel contact dynamics in alternative footwear during slip events.* International Journal of Industrial Ergonomics, 2015. **48**: p. 158-166.
5. Redfern, M.S., et al., *Biomechanics of slips.* Ergonomics, 2001. **44**(13): p. 1138-1166.
6. Cham, R. and M.S. Redfern, *Lower extremity corrective reactions to slip events.* Journal of biomechanics, 2001. **34**(11): p. 1439-1445.
7. Sawers, A., et al., *Neuromuscular responses differ between slip-induced falls and recoveries in older adults.* Journal of neurophysiology, 2017. **117**(2): p. 509-522.
8. Cham, R. and M.S. Redfern, *Heel contact dynamics during slip events on level and inclined surfaces.* Safety Science, 2002. **40**(7): p. 559-576.
9. Chander, H., J.C. Garner, and C. Wade, *Ground Reaction Forces in Alternative Footwear during Slip Events.* International Journal of Kinesiology & Sports Science, 2015. **3**(2): p. 1.
10. Chander, H., J.C. Garner, and C. Wade, *Slip outcomes in firefighters: A comparison of rubber and leather boots.* Occupational Ergonomics, 2016. **13**(2): p. 67-77.

RELATIONSHIP BETWEEN MUSCLE ACTIVATION AND POSTURAL STABILITY IN PERSONS WITH MULTIPLE SCLEROSIS

[1] Silvia Zanini, [1]Derek Tolbert, and [1] Bradley J Bowser

[1] South Dakota State University, Brookings, SD, USA
email: silvia.zanini@sdstate.edu, web: http://www.sdstate.edu/health-and-nutritional-sciences

INTRODUCTION

Multiple sclerosis (MS) is a chronic neurological disease that affects millions of people worldwide and may significantly affect activities of daily living [1,2]. Peersons with MS (PwMS) often exhibit poor postural control [3], likely contributing to the high rate of falls in this population. For example, 56% of PwMS in one study fell at least once in a three-month period [4].

Surface electromyography (EMG) records the summed electrical activity of the individual motor unit action potentials. These data give insight into the magnitude of muscle activation as well as the temporal characteristics of the muscular activation. Postural stability can be assessed by tracking the center of pressure (COP) on a force plate. By combining EMG and COP data, we can determine which muscles are most active during quiet standing and how muscle activation differs between PwMS who exhibit varying degrees of postural stability.

Thus, the aim of this study was to determine the relationship between muscle activation and postural stability in MS patients. We hypothesized that there will be positive correlations between postural sway and muscular activity in the lower extremities.

METHODS

Thirteen patients with a physician's diagnosis of MS and an expanded disability status score (EDSS) ≤ 6.5 participated in the study (age 5.7±9.4, mass 78.1±20.6, height 1.68±0.1, EDSS score 3.65±2.1). Participants who experienced an MS flare-up or had a change in medication during the 3 months prior to enrollment were excluded from the study.

Following a light warm up (3-minutes of walking), participants performed 5 trials of a sit-to-stand-to-sit movement. With arms folded across the chest, participants stood up from a chair at a self-selected speed, stood quietly for 10 seconds, then sat back down. A 90-120 second rest period was given between trials. Muscle activation and postural stability were assessed during the middle 5 seconds of the quiet standing phase.

After prepping the skin, surface EMG electrodes were placed bi-laterally on the following muscles: vastus medialis, vastus lateralis, tibialis anterior, medial and lateral gastrocnemius, and medial soleus. EMG data was captured at 2000Hz. A 2nd-order recursive high-pass filter (20Hz) followed by a 2nd-oder recursive low-pass filter (500Hz) was applied to the EMG data to remove any DC bias. The EMG signals were then filtered using a moving-root mean square (RMS) filter with a 101ms window. The mean and max RMS values from the 5s window were then calculated from the filtered EMG signals. Both meanRMS and maxRMS values were scaled to the maxRMS of the entire sit-to-stand-to-sit movement.

Ground reaction forces were collected at 1000 Hz. Participants stood with their feet on separate adjacent force platforms (figure 1). After filtering the force data (50Hz 4th-order recursive low-pass), Net COP data was calculated from both force plates using the methods described by Chung et al. [5]. Finally,

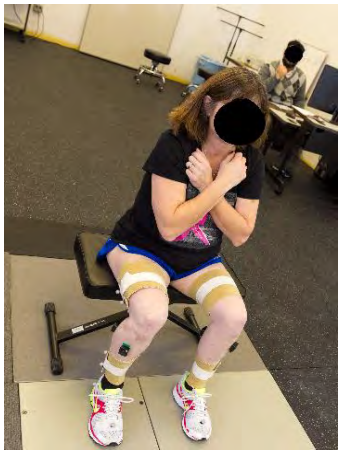

Figure 1: Participant starting position.

absolute path length and peak sway velocity were calculated in the anterior- posterior and medial-lateral directions. All variables of interest were averaged across the 5 movement trials.

Pearson correlation coefficients were calculated to determine the relationships between postural sway variables and the mean and maxRMS of each muscle.

RESULTS AND DISCUSSION

Results from the correlation analysis are shown in Table 1. Several significant correlations were found between the postural variables and the muscle activation.

Table 1: Correlation table between postural stability and muscle activation

		AbsLength AP	AbsLength ML	AP Velocity Max	ML Velocity Max
sVL	Mean	0.14	0.10	0.16	0.21
	Max	0.21	0.15	0.22	0.26
wVL	Mean	-0.09	-0.17	-0.04	-0.19
	Max	-0.08	-0.20	-0.01	-0.20
sVM	Mean	0.41	0.31	0.46	0.39
	Max	0.49	0.39	**0.55***	0.49
wVM	Mean	**0.58***	**0.62***	**0.61***	**0.63***
	Max	**0.61***	**0.65***	**0.63***	**0.66***
sTA	Mean	0.54	0.47	**0.58***	0.54
	Max	0.51	0.44	0.55	0.50
wTA	Mean	0.34	0.16	0.34	0.11
	Max	**0.59***	0.43	**0.56***	0.45
sLatG	Mean	0.50	0.48	0.49	0.41
	Max	**0.73****	**0.74****	**0.73****	**0.73****
wLatG	Mean	-0.04	-0.03	0.02	-0.05
	Max	**0.69****	**0.69****	**0.71****	**0.65***
sMedG	Mean	0.27	0.41	0.24	0.40
	Max	0.44	**0.60***	0.40	**0.58***
wMedG	Mean	0.30	0.36	0.29	0.40
	Max	**0.57***	**0.63***	0.51	**0.67***
sMedS	Mean	0.08	0.22	0.00	0.12
	Max	0.38	0.47	0.31	0.39
wMedS	Mean	-0.19	-0.14	-0.12	-0.12
	Max	0.34	0.35	0.40	0.38

*p <0.05; **p<0.01; s: stronger limb; w: weaker limb; VL: vastus lateralis; VM:vastus medialis; TA: tibialis anterior; Lat G:lateral gastrocnemius; MedG: medial gastrocnemius; MedS: medial soleus.

As hypothesized, several significant positive correlations between muscle activation and measures of postural stability were identified. Both the mean and maxRMS of the vastus medialis of the weaker limb displayed significant correlations with each of the stability measures. In addition, the maxRMS of both the strong and weak gastrocnemius (both medial and lateral head) were found to be significantly related to several of the postural stability variables. These findings are consistent with other studies where the muscle activity of the vastus medialis of the weaker limb was reported to be greater ie. patients with Osteoarthritis [6] or Stroke [7]. This confirms our results, and shows that the VM in the affected leg is highly involved in stability. Similar to patients who have experienced a stroke, persons with MS displayed increased sway [7]. One may speculate that the greater maxRMS suggests that participants compensate for muscle weakness by increasing muscle activity of the muscles that will help maintain control of their body. Because it is energetically costly, this mechanism may lead to fatigue, a common symptom of MS.

CONCLUSIONS

Several significant correlations were found between the postural sway variables and muscle activation. Out of those, the vastus medialis of the weaker limb and the gastrocnemius of both limbs appears to demonstrate the strongest correlations to postural stability. Because of the small sample size, more research is needed to confirm and these findings.

REFERENCES

1.Trapp et al. *Annu Rev Neurosci*. **31**, 247-69, 2008.
2.Frohman et al, *N Engl J Med*. **354**, 942-55, 2006.
3.Grassi et al. *Journal of Neuro Eng Rehabil* **14**, 2007.
4.Nilsagård et al. *Multiple Sclerosis Journal* **21**, 92–100, 2015.
5.Chung et al. *Med Sci Sports Exerc.* **40,** 1717-24, 2008.
6.Lyytinen et al. *J Electromyogr Kinesiol.***20**, 1066-74, 2010.
7.Wen et al. *Top Stroke Rehabil*. **21**, 163-72, 2014.

DEVELOPMENT OF A MUSCULOSKELETAL FINITE ELEMENT ANALYSIS METHOD FOR DYNAMIC BONE STRESS ANALYSIS OF PROXIMAL FEMUR

[1] Kazuhiko Adachi, [1]Nungna Wi and [2]Mitsuaki Noda

[1] Department of Mechanical Engineering, Chubu University, Kasugai, Aichi, Japan
[2]Orthopedics, Nishi Hospital, Kobe, Hyogo, Japan
email: kazuhiko@isc.chubu.ac.jp

INTRODUCTION

Proximal femur fractures due to osteoporosis are one of the serious health issues in aging societies. The fractures happen as a result of an accidental fall that would not usually cause the fracture for younger people. In stable fractures, osteosynthesis with pin / screw / plate type fixations, such as Hansson pin (Stryker) and Dual SC Screw (KiSCO), is widely used for femoral neck fracture treatment in Japan. Unfortunately, some complications such as secondary fractures may occur during postoperative rehabilitation period. In order to reveal the potential cause of the postoperative fracture from the viewpoint of the biomechanics, authors had already performed the dynamic stress analysis of the treated proximal femur based on finite element (FE) analysis. The final goal of our study is to establish the reliable postoperative bone fracture risk assessment method in response to the daily activity including mainly walking. The aim of this study is to propose a novel musculoskeletal finite element (MS-FE) analysis method for proximal femur biomechanics.

METHODS

This study was approved by the Ethical Review Board of the Konan Hospital. Patient was provided with a written informed consent. A new patient-specific 3D left hip joint FE model was constructed from the CT images of an elderly female volunteer. The model consists of the pelvis, proximal femur, cartilage, and Dual SC Screw (DSCS). The fracture surface was modeled an inclined surface with an angle 50 degrees as Pauwels type II classification [1]. The model was meshed into 4-noded tetrahedral elements and then assembled as multi bodies shown in Fig.1. The mechanical properties, Young's modulus and Poisson's ratio, were shown in Table 1 which obtained from the literature [2]. The mass densities both cortical and cancellous bone were calculated from their Young's modulus by using the expression shown in the literature [3]. All materials were assumed to be homogeneous, isotropic, and linear elastic feature. Each muscle was modeled in a straight line element. The dynamic muscle loading, joint reaction force and boundary conditions were applied to the model for simulating a gait motion.

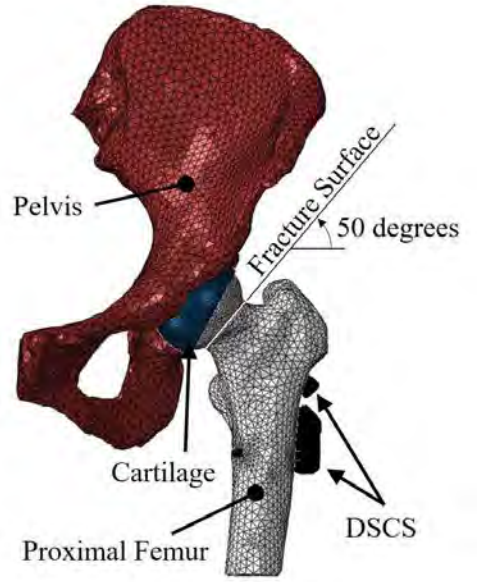

Figure 1: Three dimensional left hip joint FE model; DSCS treated model.

Table 1: Material properties.

	Young's modulus MPa	**Poisson's ratio**	**Mass density** kg/m^3
Cortical bone	13,300	0.3	1,141
Cancellous bone			
Head	440	0.3	138.8
Neck	320	0.3	120.1
Distal	150	0.3	85.1
Pelvis	13,300	0.3	1,141
Cartilage	10	0.4	100
Implant	110,000	0.3	4,620

Direction and magnitude of the loads varies in response to the gait motion. The time dependent loading forces; hip contact, gluteus medius, gluteus maximus, tensor fasciae latae and adductor, acting around the hip joint was obtained by inverse dynamic analysis of a human gait using in-house lower-limb musculoskeletal (MS) model. These loading and boundary conditions for simulating the gait motion are the major technical advantages of the proposed MS-FE analysis comparing with the conventional static FE analysis. Time varying stress distribution during the gait was evaluated by using dynamic explicit method via ABAQUS.

RESULTS AND DISCUSSION

Obtained stress distributions shown in Fig.2. The figure successfully demonstrated the detailed time varying cortical bone stress distribution and the excessive local stress concentration. The stress distribution fields indicate significant increase of the stresses around the proximal lateral insertion holes for DSCS treatment model comparing with the intact model. Maximum stress values are good agreement with previous static FE analysis [4]. It is indicated that the proposed method is feasible to support the better pre- and postoperative clinical decisions, which is the main contribution of this study.

CONCLUSIONS

In this study, we proposed a novel MS-FE analysis method for proximal femur biomechanics. The dynamic loading and boundary conditions for simulating the gait motion are the major technical advantages of the proposed method. The simulation results successfully demonstrated the detailed time dependent stress distribution and excessive local stress concentration that is the potential cause of sub-trochanteric fractures during postoperative rehabilitation period. It is proved that the proposed method is effective to assess the postoperative fracture risk of the osteosynthesis with implants.

REFERENCES

1. Pauwels. *Z Orthop Ihre Grenzgeb: Der Schenkelhalsbruch ein mechanisches Problem*, **63**: 1935.
2. Simpson et al. *Proceedings of the Institution of Mechanical Engineers, Part H: Journal of Engineering in Medicine*, **222**(3): 2008.
3. Keyak et al. *Journal of Biomechanics*, **31**: 1998.
4. Noda et al. *Archives of Trauma Research*, **4**(3): e23167, DOI:10.5812/atr.23167, 2015.

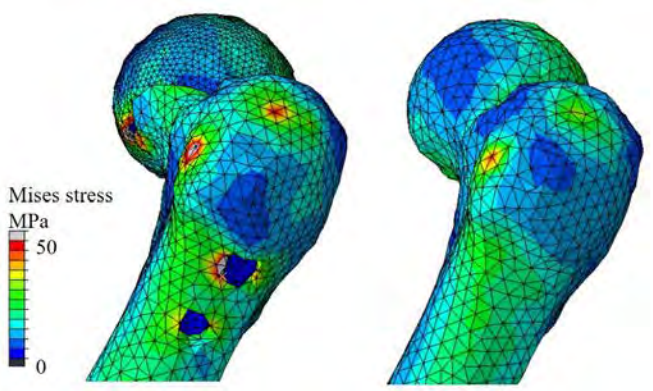

(a) 41.6 %Gait

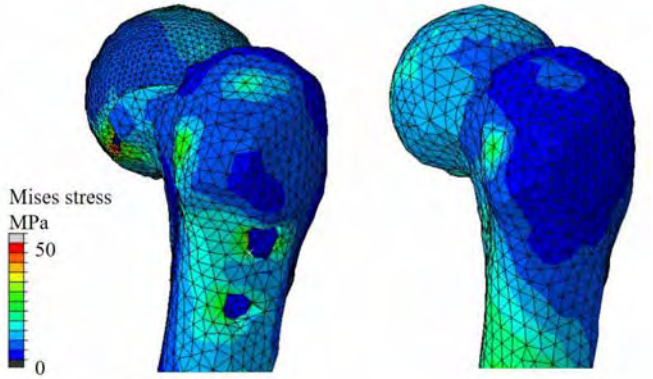

(b) 62.9 %Gait

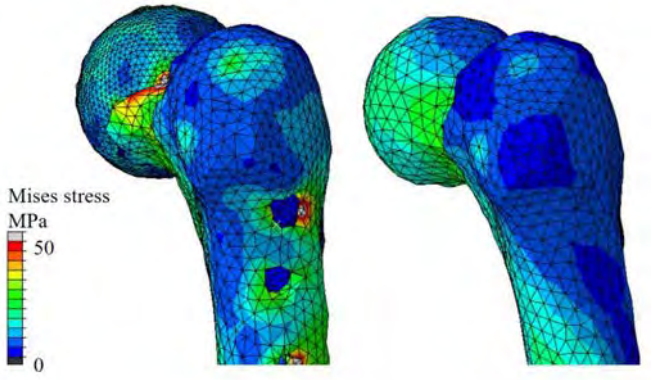

(c) 84.7 %Gait

Figure 2: Lateral view of color-coded von Mises stress fields on the cortical surface of proximal femur at (a) maximum flexion, (b) flexion 0 degree and (c) maximum extension; DSCS treated (left) and intact (right) models.

DEVELOPMENT OF A STRUCTURAL STOCHASTIC FINITE ELEMENT MODEL OF CANCELLOUS BONE

Saif Alrafeek[1,4] , James R. Jastifer[2,3] and Peter A. Gustafson[1,2]

[1] College of Engineering and Applied Sciences, Western Michigan University, Kalamazoo, MI, USA
[2] Homer Striker M.D. School of Medicine, Western Michigan University, Kalamazoo, MI, USA
[3]Borgess Hospital, MI, USA
[4]Al Khwarizmi College of Engineering, University of Baghdad, Baghdad, Iraq
email: saifghazyfais.alrafeek@wmich.edu, web: http://wmich.edu

INTRODUCTION

Bone can be described as a multi-level composite arranged in a hierarchical form. At the macrostructure scale, bone is grouped into two types: cortical bone (also known as compact bone or dense bone) and trabecular bone (known as cancellous bone or spongy bone) [1]. Generally, cortical bone surrounds trabecular bone. While cortical bone has a porosity of five to fifteen percent, trabecular bone has a porosity that varies from forty to more than ninety percent [1]. Because cortical bone has low porosity, continuum based finite element methods have been used for most FE modelling. Similarly, homogenized continuum methods have been used for trabecular bone. Recent FE approaches have meshed the trabecular architecture (i.e., non-homogenized) using continuum elements, however, these meshes are difficult to produce, may require detail CT or MRI imaging, and are costly to solve. The proposed paper studies a representation of the trabecular micro-architecture using beam elements. The proposed approach may permit lower meshing and computational cost while capturing the behavior sought with detailed trabecular models. Further, the proposed approach readily admits stochastic analysis incorporating both porosity level and other inputs and model outputs.

METHODS

Trabecular bone consists of a three-dimensional network structure mainly composed of rod-shaped and plate-shaped fundamental units named "trabeculae." In this work, the trabeculae were modelled as beam elements.

The method assumed randomly oriented beams over a cubic trabecular bone specimen with 4 mm sides. The beams were created algorithmically so that beam properties could be applied stochastically, Fig. (1).

The algorithm is general to apply a stochastic approach to all beam properties. However, in this article, stochastic properties included length and orientation while the cross section was assumed to be a square shape with a side length ranges between (0.07 – 0.25) mm. For both methods, the beam element type was a 2–node linear beam element (B31). Abaqus (V. 6.16, Simulia Ltd) was used as an FE solver.

Boundary conditions were consistently applied on the "cube surfapce" nodes of the beam structure to attain successful axial and shear loadings on the specimen. For axial loading, these constraints were placed on two parallel faces of the specimen. All degrees of freedom were fixed for nodes of one face and a small displacement was perpendicularly imposed on the nodes of the opposite face. For shear loading, the constraints were placed on four orthogonal faces of the specimen in opposing pairs. All degrees of freedom were fixed for nodes of the lower left edge of the specimen. A small displacement was imposed on the nodes of each face and parallel to the face; such that pure shear is consistently applied to the specimen. Apparent stress was calculated by dividing the applied force by the apparent area of the relevant face. Apparent strain was obtained by calculating the ratio of resulting displacement of the moving nodes to the original side length of the specimen (i.e., change in length over length) figure (1). Apparent moduli were computed from apparent stress and apparent strain. Apparent densities were calculated by obtaining the ratio of the beams' mass to the volume of the unit cube.

The Individual FE model created in this study exhibited the apparent mechanical properties listed in Table (1). The model demonstrated effective moduli and apparent density within published ranges of trabecular bone [1, 2]. Anisotropic material moduli were extracted and the three normal-normal stress-strain relationships are presented here.

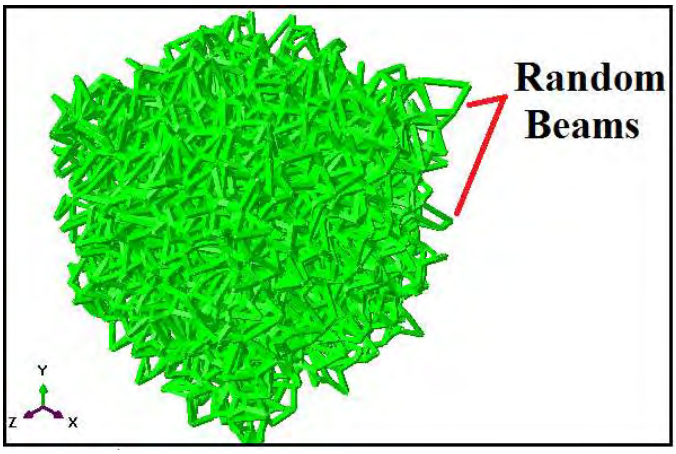

Figure 1: Trabecular bone (representative model).

RESULTS AND DISCUSSION

The Individual FE models created in this study exhibited the mechanical properties listed in Table (1). Each model demonstrated effective moduli within published ranges of trabecular bone [1]. The similarity on average of the three elastic constants suggests a lack of bias in the random algorithm, though bias could be intentionally introduced. The difference among the elastic constants within a single model exhibits anisotropy consistent with the localized trabecular architecture. The apparent densities of the current models were also within the published ranges [1, 2]. In the models, apparent density strongly correlates with the elastic moduli as would be expected in cancellous bone. Cancellous bone preferred directionality can be introduced into the stochastic model by controlling the parameters such that they are not fully random. Rather, they should follow some stochastic process with a distribution of properties that result the preferred anisotropy on average. For example, the beam elements can have a distribution of orientations centered on a preferred orientation. The apparent densities of the FE models are dependent on the number of beams and on their cross sections which were dissimilar between the models. Future models will emphasize cross sections and lengths that are consistent with the nominal (and stochastic) geometry of physical trabecular architecture.

Table 1: Young moduli, Apparent density, Beam section area and Anisotropy ratio.

	Random FE Model Mean (SD)	**Bartel, D.L. [1]**
Exx (MPa)	256.7343 (±57.6553)	237
Eyy (MPa)	258.1053 (±59.9611)	309
Ezz (MPa)	257.4531 (±61.6275)	823
App. Den. (g/cm3)	0.8782 (±0.1295)	0.09 ~ 1
Ab (mm2)	0.1665 x 0.1665 (±0.06 x 0.06)	-
Anisotropy Ratio	1.2075 (±0.2067)	-

CONCLUSIONS

The stochastically driven beam element approach may prove useful for efficiently modeling trabecular bone, structural open cell foams, grid stiffened core composites, and other structures. The need for efficiencies in meshing and computation are particularly relevant for current areas of interest to the composites and medical communities including the modeling of mechanical fasteners and bonding, damage evolution, and the modeling of aging. The proposed paper may provide a detailed description of the methodology in future research.

REFERENCES

[1] Bartel, D.L. *Orthopedic Biomechanics*, Pearson Education, Inc., New Jersey, USA, 2006.
[2] C.J. Hernandez. *Handbook of Biomaterial Properties*, Springer Science, New York, USA, 2016.

A COMPREHENSIVE TESTING SUITE FOR MECHANICAL CHARACTERIZATION OF ARTICULAR CARTILAGE WITH DOCUMENTED REPEATABILITY

Snehal K. Chokhandre and Ahmet Erdemir

Dept. of Biomedical Eng., Lerner Research Institute, Cleveland Clinic, Cleveland, OH 44195, USA
email: chokhas@ccf.org, web: https://simtk.org/projects/openknee

INTRODUCTION

Reliable mechanical characterization of cartilage is essential for finite element (FE) analysis that can provide a predictive platform to improve treatments options and to identify prevention strategies targeting cartilage pathologies. The literature on cartilage material characterization is vast and diverse with large variations in documented mechanical response of the tissue. There is also a lack of specimen-specific cartilage characterization to determine the extent and need for specimen-specific information [1]. An important limitation of the testing results is associated with the reproducibility and fidelity of the experimental procedures that are often not very well documented or addressed. The repeatability of the experimental procedures and subsequently the usefulness of obtained material properties are paramount for dependable analysis.

The goals of this study were to develop a testing suite for extensive characterization of articular cartilage from a human knee specimen and to provide cartilage mechanical response with quantified repeatability. This comprehensive testing suite and accompanying data sets encompass various testing types conducted on samples from multiple locations of cartilage within the knee.

METHODS

Specimen and samples: Cartilage samples were obtained from a cadaver left knee of a 25 years old female Caucasian donor with a body mass index of 22.8. One compression sample (5 mm diameter, full cartilage thickness) and one tensile sample (5 mm length by 1 mm width, close to superficial region) were taken from the load bearing regions of patella, patellar groove, medial and lateral femoral condyle, and medial and lateral tibial plateau (a total of 12 samples).

Mechanical testing: The six compression samples were tested under unconfined (UC) and confined conditions (CC). Each test was repeated three times. Including the repeatability tests for six tensile (T) samples, a total of 54 tests were conducted. All tests were performed at room temperature and the samples were immersed in phosphate buffered saline (PBS) during the entire test. Sample thicknesses were measured using an optical thickness measurement system designed in house.

Testing protocol included: (i) A 10 g initial load applied to either establish contact (compression) or to find reference length (tensile), (ii) ramp load-unload to 15% strain at 20%/s strain rate, (iii) 1000 preconditioning cycles between 10-15% strain at 2 Hz, (iv) ramp load-unload to 15% strain at 20%/s strain rate followed by a full unload, (v) 10 g force applied to establish contact or find reference length. (vi) stress-relaxation test at 5-10-15% target strains at 20%/s strain rate with a 30 minutes wait after each step.

For convenience, the displacement at 10 g force was used as reference. Nonetheless, a 300 micron offset was adapted before the preconditioning and stress relaxation stages of testing to capture the full range of loading and deformation included the unloaded state.

Analysis: For the 18 repeatability sets (6 confined compression, 6 unconfined compression, and 6 tension), average instantaneous (AIM) and equilibrium moduli (AEM) were calculated by the mean of the full range moduli at the three strain levels. Coefficient of variation (COV) was calculated for each of these sets to assess variability within the set.

RESULTS AND DISCUSSION

For all the unconfined compression test sets the COV was < 10% except for the lateral femur (COV, AIM: 31.37%; COV, AEM: 23.41%). For the tension test sets the COV was < 6% for all sets. For the confined compression test sets the COV ranged from 1.5% - 31.46% with most sets with COV < 15%. The larger discrepancies in repeatability of confined compression tests may be due to the challenges associated with misalignment of sample in the confined compression test chamber or its position relative to the moving indentor head. Non-uniformities of the dissected samples may have also resulted in non-uniform deformation of the sample during confined compression. The equilibrium moduli values for compression tests (0.205 - 0.63 MPa) were within the range reported in literature [2, 3] indicating these results are within the envelope of previously reported values.

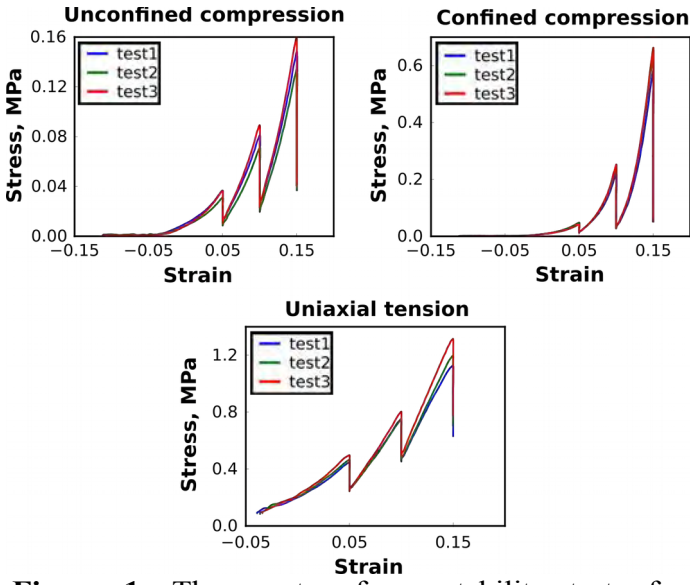

Figure 1: Three sets of repeatability tests for samples taken from the patella cartilage.

The results of these repeatability tests were encouraging (Fig. 1). As per our knowledge this is the first study to document experimental repeatability for cartilage mechanical characterization in a comprehensive manner, including multiple test types. The inter-sample variability (e.g., 4.85 – 26.18 MPa AEM for tensile tests) supports that there exists a large range of location dependent properties for cartilage within the specimen [4]. This is significant when location dependent intervention is required. A further in-depth analysis of this data set will be conducted to capture overall experimental repeatability to understand its relevance to compare regions and different knees. Availability of this extent of specimen-specific material information, may allow a better understanding of its need.

The primary motivation behind this study was to obtain repeatable and reliable cartilage material properties to support specimen-specific finite element model development of the knee. This is a part of the Open Knee(s) project (https://simtk.org/projects/openknee). However, the utility of this testing suite, including the accompanying data and the repeatability assessment may have a significant impact on dependable cartilage characterization methods. This study will be extended to other tissues of the knee and to additional knee specimens. Our approach and documentation will likely be helpful in developing testing standards for soft tissue characterization.

REFERENCES

1. Chokhandre et. al. *Plos one.* 10(**9**):e0138226, 2015.
2. Jurvelin et. al. *Proc. Inst. Mech. Eng. [H]* **217,** 215–219, 2003.
3. Treppo et. al. *J. Orthop. Res. Off. Publ. Orthop. Res. Soc.* **18,** 739–748, 2000.
4. Denewith et. al. *J. Orthop. Res. Off. Publ. Orthop. Res. Soc.* **31**, 370–375, 2013.

ACKNOWLEDGEMENTS

This study was funded by NIGMS, NIH (R01GM104139, PI: Erdemir).

Temporal response of muscle-bone deformities at the shoulder following brachial plexus birth injury

[1] Nikhil Dixit, [1,2] Jacqueline H. Cole, and [1]Katherine Saul

[1] North Carolina State University, NC, USA
[2] University of North Carolina-Chapel Hill, NC, USA
email: ndixit2@ncsu.edu

INTRODUCTION

Brachial plexus birth injury (BPBI) is a traumatic perinatal neuromuscular injury causing muscle paralysis, shoulder contracture, and deformed growth of the scapula and humerus [1-3]. The resulting lifelong impairment greatly limits critical activities of daily living, such as eating and bathing. Almost nothing is known about the timing and mechanisms of changes in underlying bone and muscle structure following nerve injury occurring at birth to provide a foundation for clinical decision-making. As a result, there is currently no consensus on optimal timing or approach for therapy after injury [4], leading to inconsistent clinical outcomes. When the brachial plexus is injured in children outside of the neonatal period, there is limited contracture compared to BPBI, providing a unique opportunity to explore why the same injury in a similar period of rapid musculoskeletal growth avoids marked deformity.

Understanding the timing and mechanism of deformity initiation is essential for developing treatments that prevent bone and postural deformities from developing, rather than correcting deformity after formation. The objective of this work is to identify whether deformity is initiated first in muscle or bone by examining gross bone and muscle structure and contracture, and to explore how tissue response to injury depends on timing of injury.

METHODS

The study protocol was approved by the NC State IACUC. We used an existing rat model of BPBI developed in our group [5]. Because contracture and bone deformity are known to depend clinically on whether the nerve injury is proximal or distal to the dorsal root ganglion [6], we explored these effects in models of both injuries. Nerve injuries were created under isoflurane anesthesia using standard aseptic technique [7]. For preganglionic neurectomy, the C5 and C6 nerve roots were excised proximal to the dorsal root ganglion, partially preserving afferent innervation and muscle spindle function [8], which produces nerve damage without marked postural shoulder contracture. For postganglionic neurectomy, the C5 and C6 nerve roots were excised distal to the dorsal root ganglion, resulting in nerve damage and associated increases in shoulder contracture.

The progression of shoulder deformity after neonatal injury was examined by intervention at postnatal day 4 (P4), and progression was examined using 3 timepoints (2, 4, and 5 weeks post injury). The effect of injury timing (neonatal vs. postnatal) was examined by using a 4-week postnatal injury age (P4wks). Rats were provided water and rat chow *ad libitum* and sacrificed at the respective timepoints via CO_2 asphyxiation. To assess changes in muscle and bone structure and deformity, we measured passive external rotation range of motion (ROM) to analyze shoulder contracture ($n_{preganglionic} = 16$, $n_{postganglionic} = 22$) [5], glenoid inclination angle using micro-computed tomography, and optimal muscle fiber length of biceps long head (BICLong) using a laser diffraction technique (P4 postganglionic: $n_{2wks} = 1$, $n_{4wks} = 4$ for glenoid inclination angle and 1 for BICLong fiber length, $n_{5wks} = 1$; P4 preganglionic: $n_{4wks} = 1$; P4wks: $n_{postganglionic} = 1$; $n_{preganglionic} = 1$) [7]. Due to challenges in the preganglionic procedure, we looked only at the 4-week post-injury timepoint. Measures in the affected limb were compared relative to those in the contralateral unaffected limb.

RESULTS AND DISCUSSION

Our analyses of muscle and bone structure in rats following P4 pre- and postganglionic neurectomy support early changes to muscle and bone when

nerve injury is inflicted in the neonatal period (Figure 1, P4). Range of motion at 4 weeks post-neurectomy indicated more contracture in the postganglionic group compared to preganglionic group, consistent with previous studies [6]. Glenoid inclination measured at 2, 4, and 5 weeks tended to be more declined in the affected shoulder, with deformity values increasing with time for the postganglionic group. Biceps long head in the affected limb tended to be shorter than the contralateral limb at the same timepoints for postganglionic injury.

In contrast, analyses of bone and muscle following postganglionic neurectomy at P4wks showed that limited deformity to bone and muscle was observed when neurectomy occurred postnatally. Minimal changes to glenoid inclination and muscle length were observed at 2 and 4 weeks post-neurectomy (Figure 1, P4wks). Our results in rats are consistent with another study of the elbow following postganglionic injury in mice [9]. In that study, elbow contracture following postganglionic neurectomy at P4wks (n=17) was nearly absent, with no contractures more than 10°, and significantly lower ($p<0.001$) than in mice with neonatal postganglionic injury (n=42) [9], with elbow contractures up to 40°.

CONCLUSIONS

Our preliminary work shows gross alterations in both muscle and bone by 4 weeks after neonatal injury in rats (~1 year in infants [7]), suggesting early tissue changes at odds with the wait-and-see approach in clinical practice [5]. The observed bone and muscle deformities due to a neonatal injury become more severe over time. However, severe deformities do not occur when the injury occurs postnatally. This study provides new information about the effect of time progression and timing of BPBI.

The current work is limited by a small sample size and limited time points for preganglionic injury; data collection is ongoing. Further, the current work identifies structural changes alone; ongoing work examines the underlying changes in metabolism, microstructure, and mechanics to explicate the observed macrostructural changes.

REFERENCES

1. Hogendoorn (2010) *J Bone Joint Surg Am* 92:935.
2. Pearl (1998) *J Bone Joint Surg Am* 80:659.
3. Poyhia 2005) Pediatr Radiol 35:402.
4. Belzberg (2004) *J Neurosurg* 101:365.
5. Li (2008) *J Hand Surg* 33(3):308-12.
6. Al-Qattan (2003) *Ann Plast Surg* 51:257.
7. Crouch (2015) *J Bone Joint Surg Am* 97:1264.
8. Nikolaou (2015) *J Hand Surg* 40:2007.
9. Weekley (2012) *J Orthop Res* 30:1335.

ACKNOWLEDGMENTS

The study was funded by NIH R21HD088893. Contributions were made by Eric Warren in muscle sarcomere length measurements and Dr. Ted Bateman and Eric Livingston in micro-CT scans.

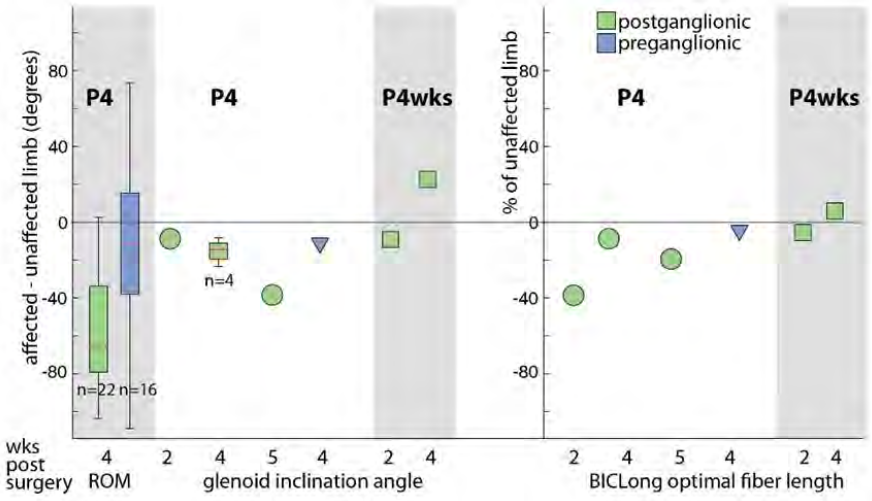

Figure 1: ROM, glenoid inclination angle, and biceps long head optimal fiber length for P4 and P4wks neurectomy at multiple timepoints. n=1 per timepoint unless noted.

A Comparison of the Mechanical Properties of Trabecular Bone Between Micro-Finite Element and Meshless Models

[1,3] Kenneth K.C. Ip, [1,3,4] Nikolas K. Knowles, and [2,3,4] Louis M. Ferreira

[1]Graduate Program in Biomedical Engineering, The University of Western Ontario, London, ON, CAN
[2]Department of Mechanical and Materials Engineering, The University of Western Ontario, London, ON, CAN
[3]Roth|McFarlane Hand and Upper Limb Centre, St. Josephs Health Care, London, ON, CAN
[4]Collaborative Training Program in MSK Health Research, and Bone and Joint Institute, The University of Western Ontario, London, ON, CAN
email: kip32@uwo.ca

INTRODUCTION

Accurate modeling of trabecular architecture in computational simulations is essential when evaluating joint replacement components and pathologic bone disease. Although significant advancements have been made in micro finite element (FE) modeling of trabecular bone, models are generally limited to small cores, due to the computational expense of these high-resolution models. As such, FE modeling whole bones that maintain trabecular architecture are seldom utilized and are limited to models that oversimplify the boundary conditions [1].

The reduction in computational resources provided by meshless methods has the potential to overcome these shortcomings. This allows for whole bone modeling while maintaining trabecular architecture and complex boundary conditions. In order to evaluate if meshless methods are comparable to micro-FE models that have been extensively validated, comparative analysis is necessary.

The objectives of this study were to: i) compare the apparent modulus of trabecular bone using μFE and meshless models, ii) evaluate if models derived from different μ-CT spatial resolutions affect model apparent modulus, and iii) compare FE element type to meshless models.

METHODS

Two separate micro-CT scans (Nikon XT H 225 ST, Nikon Metrology, NV, 95 kVp, 64 μA, 3141 projections, 1000 ms exposure) at 32 μm and 64 μm spatial resolutions were acquired for 14 cadaveric scapulae (7 male; 7 female; mean age 67 ± 8 years). The raw DICOM images were filtered to remove high frequency noise (Gaussian filter: $\sigma = 1.25$, support = 2). Virtual bone cores were extracted from the glenoid vault, medial to the subchondral bone, maintaining the recommended 2:1 aspect ratio [2]. Custom code was used to generate finite element models (FEMs) with 8-node hexahedral elements (HEX8) at both 32 μm and 64 μm. Stereolithography (STL) models were created to maintain the bone volume fraction (BV/TV) of each HEX8 model (BV/TV=0.24±0.10). These STLs were used to generate 10-node tetrahedral (TET10) FEMs and are the direct input to the meshless software (Simsolid, Simsolid Corporation). A homogeneous tissue modulus of 20 GPa was applied to all models. All FEMs and meshless models were constrained with identical boundary conditions and compressed to 0.5% apparent strain. The apparent modulus of each model was calculated and compared.

RESULTS AND DISCUSSION

The "gold standard" apparent modulus in this study is provided by the HEX8 32 μm FEMs. Across the volume fraction range of cores tested, the meshless models generated from 64 μm scans most accurately matched the E_{app} of the HEX8 32 μm FEMs (Table 1). The TET10 32 μm FEMs and Meshless 32 μm were generated from the same STLs, but interestingly the Meshless 64 μm models were a closer match over the volume fraction range of cores tested (Table 1).

The Meshless 32 μm models tended to over-estimate E_{app}, while the Meshless 64 μm models under

estimated E_{app} (Figure 1). This was most pronounced at the extreme bone volume fractions (0.40 < BV/TV < 0.20). There was no significant difference (p=0.633; Kruskal-Wallis One-Way ANOVA, Sigmaplot 11.0, Systat Software Inc., San Jose, CA, USA) between the apparent modulus of any of the models tested (Figure 1): however, due to the large variability in apparent modulus due to large variations in BV/TV, significant differences may have occurred with a larger sample size, or cores that had less variation in BV/TV.

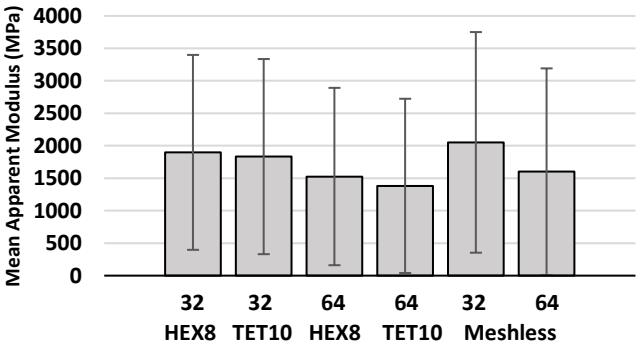

Figure 1: Mean apparent modulus for 14 trabecular cores with different modeling parameters. HEX8 refers to 8-node hexahedral µFEMs, TET10 to 10-node tetrahedral µFEMs, Meshless to meshless models, and 32 and 64 to models derived from 32 µm or 64 µm spatial resolution µ-CT scans. There was no significant difference between model types (p=0.633)

Inherently, at lower resolution (64 µm) and lower BV/TV (< 0.20), STL generation loses trabecular connectivity [3]. This has a marked effect on E_{app}. It is therefore recommended that for lower BV/TV bone, higher resolution scans be acquired to provide optimal trabecular architecture during model generation. This is necessary in both µFEMs and meshless models, but is perhaps less necessary in meshless models, as was shown by the ability of the lower resolution (64 µm) meshless model to closely match the E_{app} of the HEX8 32 µm "gold standard" µFEMs.

Future comparisons of whole bone meshless models to empirical bone testing has the potential to validate meshless methods for use in accurately replicating the non-linear and complex boundary conditions native to *in-vivo* and *in-vitro* joints, as well as joint replacement component loading.

CONCLUSIONS

This study compared to apparent modulus of trabecular cores among hexahedral and tetrahedral finite element, and meshless models. The results suggest that meshless methods can accurately model the mechanical properties of trabecular bone. This is important because meshless methods significantly reduce computational resources, allowing for whole bone models to be generated with trabecular architecture. This allows for complex boundary conditions to be implemented and non-linear models to be evaluated. This has the potential to significantly improve understanding of joint replacement components and pathologic bone disease.

REFERENCES

1. Chevalier et al. J Biomech; 49:1724-1733. 2016
2. Helgason et al. J Biomech; 23:135-146. 2008
3. Bevill and Keaveny. Bone; 44:579-584. 2009

Table 1: Linear regression results for apparent modulus and volume fraction for FEM and Meshless models.

$E_{app} = m\frac{BV}{TV} + b$	r^2	m	b	SE	SE/mean
HEX 8 – 32 µm	0.88	13685	-1433	383	20.2%
TET10 – 32 µm	0.89	13830	-1430	360	19.6%
HEX8 – 64 µm	0.89	12373	-1488	338	22.1%
TET10 – 64 µm	0.88	11701	-1228	310	22.4%
Meshless – 32 µm	0.91	15752	-1678	375	18.3%
Meshless – 64 µm	0.89	13739	-1398	336	21.0%

ESTABLISHING A RELATIONSHIP BETWEEN BONE MINERAL DENSITY AND DAILY DYNAMIC SKELETAL LOADING IN POST-MENOPAUSAL WOMEN

[1] Stefan Madansingh, [2] Dennis Murphree, [3] Kenton Kaufman, and [2] Emma Fortune

[1]Assistive and Restorative Technology Laboratory, Mayo Clinic, Rochester MN
[2] Robert D. and Patricia E. Kern Center for the Science of Health Care Delivery, Mayo Clinic, Rochester, MN
[3]Motion Analysis Laboratory, Department of Orthopedic Surgery, Mayo Clinic, Rochester, MN
Email: Fortune.Emma@mayo.edu

INTRODUCTION

Osteopenia (low bone mass) and the disease of osteoporosis are of concern for a significant population in the U.S. including 50% of adults >50 years of age and 30% of postmenopausal women [1]. Hip fractures, which increase exponentially with age and occur disproportionally in women [2], account for the majority of the disability and financial burden associated with osteoporosis [3], and often lead to premature death.

Estimates of bone mineral density (BMD) are an important factor in the identification of fracture risk, however provide no insight into identifying modifiable causal factors. To date, physical activity with low and high impact forces continues to be the primary behavioral modifier for the prevention of osteoporotic fractures [4]. Unfortunately, a well-defined relationship between physical activity and hip BMD has not been determined. We hypothesize that cumulative estimates of dynamic skeletal loading in the free-living environment could provide a biomarker for tracking and prescribing physical activity changes in high risk patients.

METHODS

Sixty nine post-menopausal women (age: 61.3±7.4 years, BMI: 25.9±4.3 kg/m^2) were included in this study. Exclusion criteria included: current use of prescribed medication which could result in BMD changes, assistive device use while walking, any amputations or orthotics use, a history of hip surgery or hip or knee joint replacement on the non-dominant side. The study protocol was approved by the Mayo Clinic IRB and written informed consent was obtained prior to subject participation.

Under laboratory conditions, participants performed a minimum of 5 bare-foot walking trials at each of three self-selected walking speeds categories (slow, normal and fast) to simultaneously collect bilateral ankle acceleration (ActiGraph GT3X+, ActiGraph LLC, USA; 100 Hz) and ground reaction forces (GRFs) using five floor-embedded force plates (3 AMTI, USA and 2 Kistler Instruments, Switzerland; 600 Hz). Linear regression and cross-validation techniques yielded a model to predict bodyweight normalized vertical GRFs (1) with low average mean absolute error (6.8±5.5%) and low root-mean-square error (0.087±0.006) suggesting strong predictive qualities [5].

$$\mathrm{GRFbw} = 0.1118(Az) + 0.7865 \qquad (1).$$

where Az is the peak vertical component of ankle acceleration identified during foot-strike on the laboratory force plates.

All participants received DXA scans (Lunar iDEXA, GE Medical Systems, USA) to measure total hip BMD on the non-dominant side and wore the Actigraph activity monitors on both ankles for 7 days in their free-living environments. Steps taken in the free-living environment were detected from ankle acceleration data using our previously developed and validated step detection algorithm [5] in MATLAB 2016b (Mathworks, USA). Peak vertical GRF, in units of body weight (GRFbw), was calculated for each step using equation (1). A bone density index (BDI), an index of cumulative loading, for each day was determined as the cumulative sum of the peak vertical GRF estimated for each detected step [7]:

$$\mathrm{BDI} = [\textstyle\sum_{i=1}^{n}(\beta.GRF_i)^m]^{1/2m} \qquad (2)$$

where β is the ratio of the individual subject's

bodyweight (BW) to the cohort's mean BW and n is the daily step count. The exponent m weights the relative importance of force magnitude and loading cycles and was set to a value of 6 [6]. Mean BDI ($\overline{BDI}$) was calculated across the 7 days of activity monitoring for each participant.

Mean BDI, age, BMI and mean step count were entered into stepwise multiple regression to identify the significant predictors of BMD and estimate the strength of the relationship among these variables.

RESULTS AND DISCUSSION

All participants successfully completed 7 days of activity monitoring resulting in the capture of over 7 million steps, producing a population representative range of peak accelerations from detected steps (Fig.1).

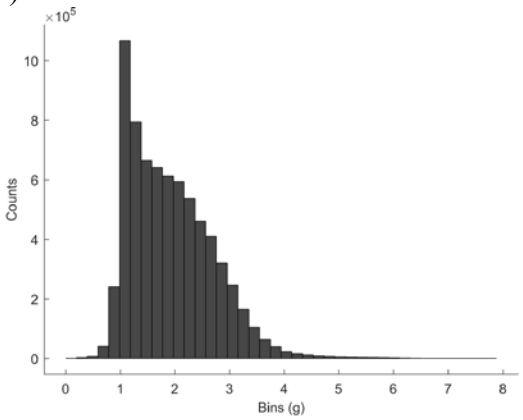

Figure 1: Histogram of peak acceleration (g) values identified at each detected step throughout 7 days of activity monitoring.

The mean±SD daily step count across participants estimated was 14485 (4334), which is in line with ActiGraph algorithms producing mean estimates of 10565±4313 and 15792±5284 using default and "Low Frequency Extension" settings, respectively.

Of the four factors entered, stepwise linear regression revealed $\overline{BDI}$ and age to be significant predictors of BMD ($F_{2,66}$=12.60, $p < 0.001$) (Fig. 2).

$$\text{BMD} = 0.312(\overline{BDI}) - 0.005(age) + 0.533 \quad (3)$$

With a standardized beta of 0.392 ($p < 0.05$) mean BDI was the strongest predictor of BMD, accounting for 19.5% of the variance in BMD. Age accounted for an additional 8.2% of the variance in BMD, with a beta of -0.29 ($p < 0.05$). Overall, the multiple regression model explains 27.6% of the variance in BMD (R = 0.526), suggesting a stronger relationship than previous studies using simple linear regression (R = 0.437) [7,9].

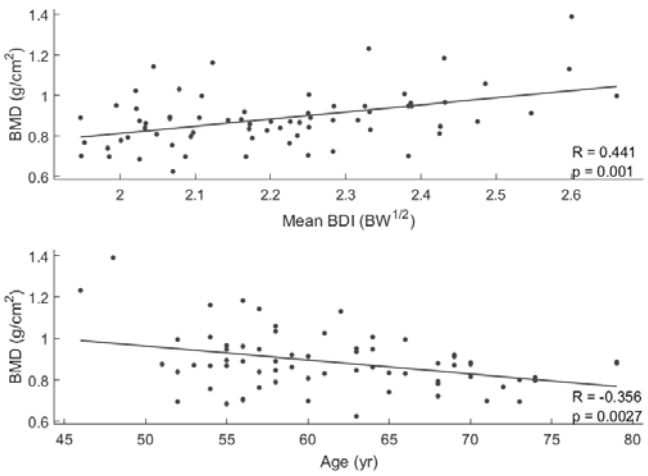

Figure 2: Partial regression plots highlighting the significant linear relationships among mean bone density index (BDI) and age with bone mineral density (BMD) in the free-living environment.

CONCLUSIONS

These results provide evidence to support the use of cumulative dynamic loading estimates captured through daily PA observation as a biomarker of total hip BMD. Future PA interventions can leverage this relationship to improve outcomes in postmenopausal women at high risk of hip fracture.

REFERENCES

1.Lim L et al. *Am J Prev Med,* **36**, 366-75, 2009
2.Khosla S. *New Eng J Med*, **356**, 2293-300, 2007
3.Johnell O. *Am J Med,* **103**, S20-S26, 1997
4.Bassey E. *Age Ageing*, **30**, 29-31, 2001
5.Lowndes B et al. *Proc.ASB'17*, Boulder,CO, 2017
6.Fortune E et al. *Physiol Meas*, **36**, 2519, 2016
7.Boyer K et al. *Osteoporos Int*, **22**, 2981-8, 2011
8.Fortune E et al. *JAppl Biomech*, **30**, 668-74, 2014
9.Bowley S, Whalen R, *Ortho Res Soc*, 0063, 2001

ACKNOWLEDGMENTS

Funding is provided by NIH R21 AR066643. Stacy Loushin assisted with recruitment and data collection. This project is supported by CTSA UL1 TR002377 from the National Center for Advancing Translational Sciences.

ESTIMATION OF MECHANICAL LOAD *in-vivo* BASED ON THE TRABECULAR BONE IN THE VERTEBARAL BODY

[1] Teppei Mano and [2] Masafumi Machida, [1] Yoshimori Kiriyama

[1] Kogakuin University, Tokyo, Japan
[2] Yokohama Brain and Spine Center, Kanagawa, Japan

email: kiriyama@cc.kogakuin.ac.jp

INTRODUCTION

The bone remodeling mechanism requires an adequate mechanical load surrounding the bone. The loading condition *in-vivo* could be different individually, therefore the individual structure of the trabecular bone could be affected by the load *in-vivo*. Especially, the trabecular bone in the vertebral body shows the optimized configuration against the magnitude and direction of the mechanical loads *in-vivo* [1]. This means that it could be possible to estimate the loading condition by evaluation of the configuration on the trabecular bone. In this study, we've developed an estimation method of the loading condition *in-vivo*. We evaluated the bone configuration based on the analysis of stress distribution by using the finite element model of the trabecular bone constructed from MDCT.

METHODS

We estimated the mechanical load *in-vivo* from the trabecular bone as the following two procedure: (1) Modeling process to extract the trabecular bone from MDCT and calculate the value of the yield stress as shown in Fig. 1, (2) Estimation process to decide the three dimensional load applied to the trabecular bone (Fig. 2).

The IRB of the institute approved all methodological procedures and the subject gave an informed written consent prior to participation.

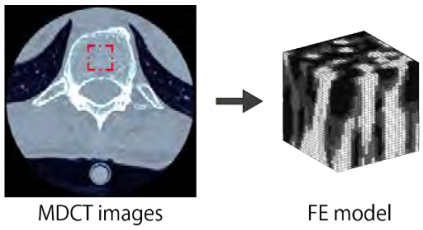

Figure 1: Extraction procedure of analysis region

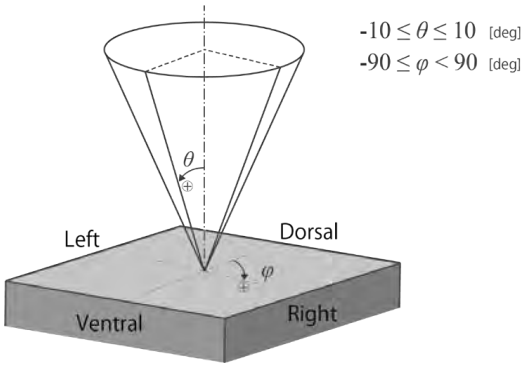

Figure 2: *in-vivo* load direction of the estimation procedure

(1) Modeling process: we extracted the trabecular bone in the vertebral body from MDCT, and constructed the finite element model. Subject was a 75-year-old female, who was diagnosed osteoporosis. We took the MDCT images of the L1 vertebra. We used a phantom in the measurement to compensate CT value and convert it to bone mineral density (BMD). And then, the BMD values were converted to Young's modulus based on the literature by Kayak et al. [2] as the following equation,

$$E = \begin{cases} 0.001 & (\rho = 0.0) \\ 33900\rho^2 & (0.0 < \rho \le 0.27) \\ 5307\rho + 469 & (0.27 < \rho < 0.6) \\ 10200\rho^{2.01} & (0.6 \le \rho) \end{cases} \quad (1)$$

where E is Young's modulus [MPa], ρ is BMD [g/cm^3].

This conversion from BMD to Young's modulus was applied to a rectangular region (10.14 × 10.14 × 10.20 [mm^3]) in the center of the vertebral body.

(2) Estimation process of the loads; Because the trabecular bone should not be destroyed in daily life, we assumed that the maximum limitation of the bone was the yield stress σ_y of the cancellous bone. By using the BMD ρ, we calculated the magnitude of the load *in-vivo*. The yield stress σ_y was calculated based on the following equation by Keyak [2].

$$\sigma_y = \begin{cases} 137\rho^{1.88} & (\rho < 0.317) \\ 114\rho^{1.72} & (0.317 \leq \rho) \end{cases} \quad (2)$$

Simultaneously, we assumed that the cancellous bone in the vertebral body was remodeled to withstand loading condition *in-vivo* and the configuration was optimized to reduce the stress against a specific loading direction. Hence, we applied a load of 300 N to the fem model of the trabecular bone. In finite element analysis, the load was applied to the top surface on the bone model (Fig. 1). In this study, the surface was modeled as a rigid plane, and the load was assumed as a plane load. The various loading direction were evaluated as shown in Fig. 2. The direction of the load was decided by two parameters of θ and φ. Here θ is inclined against the vertical downward direction, and φ is the axial rotated angle around the model as Fig. 2.

RESULTS AND DISCUSSION

Previous to the *in-vivo* load estimation, we evaluated the estimation process. We calculated the direction when we applied loads to the uniform inclined beam of 0, 5, 10 [deg.]. As the results, the process has an error of ±1 [deg.] in both the inclination and rotation angles.

We obtained the median value of the yield stress in each element of 2.96 [MPa]. These value is regarded as the mechanical load per unit area applied to the cancellous bone in the vertebral body.

Figure 3 shows the typical stress distribution when adequate (a) or inadequate directions of the loads(b) were applied to the trabecular model. Even when the same magnitudes of the loads were applied to the model, different direction of the loads showed the different patterns of stress distribution and adequate direction of the load should be able to reduce the averaged von Mises stress over the model.

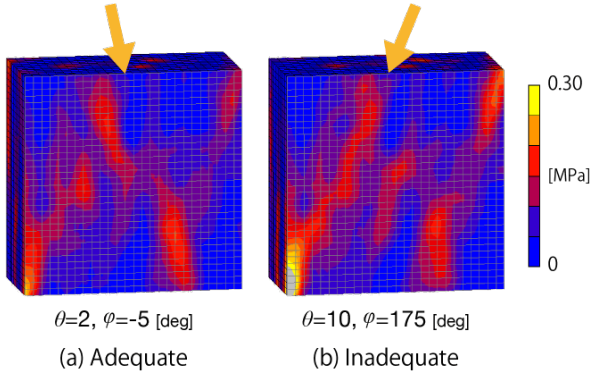

Figure 3: Typical stress distribution

From our estimation, we obtained the load direction of θ =2, ϕ =-5 [deg.]. This direction is slightly inclined from vertical direction, i.e. the posterior to the anterior.

Since the healthy L1 vertebra is usually extended, the loading direction should be inclined from ventral to dorsal relatively. However, our estimation was opposite to it. Considering our estimation method with an error of 1 [deg.] about the direction, the subject could show kyphotic posture as a patient of spine osteoporosis, and the result of the direction could be acceptable enough.

Our limitation was that we didn't investigate the subject or X-ray images. Also, we just estimated the loading condition applied to the cancellous bone. However, our method has a possibility to expect an individual loading condition, and it could be useful to estimate the bone remodeling *in-vivo*.

CONCLUSIONS

In this study, we showed the estimation method of mechanical load *in-vivo* consisted of (1) modeling process to extract the trabecular bone, (2) estimation process to decide the load applied to the trabecular bone. This method could estimate individual loading condition *in-vivo*.

REFERENCES

1. Wolff *Springer*, 1986.
2. Keyak et al. *J Biomech* 31(2), 1998.

EFFECTS OF EXERCISE AND POSTURE ON SUBCHONDRAL BONE THICKNESS

[1,2]Munsur Rahman, [1]Anna Alvarez, [1,3]John D. Polk, [2]Mariana E. Kersh

[1]Department of Anthropology, [2]Department of Mechanical Science and Engineering, [3]Department of Biomedical and Translational Sciences
University of Illinois at Urbana-Champaign, Urbana, IL, USA
email: mkersh@illinois.edu, web: http://uitbl.mechse.illinois.edu/

INTRODUCTION

Subchondral bone is the thin layer of cortical bone found at the ends of long bones and underlies articular surface that provides an interface transmitting loads between the articular cartilage and trabecular bone. Changes in subchondral properties enable identification of differences in joint loading conditions in comparative biology, and in biomedical studies of the etiology of joint diseases such as osteoarthritis (OA). Previous studies have examined the subchondral bone apparent density and used it to infer differences in joint load orientation and magnitude in humans [1,2] and primates [3]. However, considerable uncertainty remains to determine how and where the osteological changes occurs due to habitual loading; and the choice of analytical methods also greatly influence the results.

The primary goal of this study is to test whether subchondral thickness responds to experimentally induced differences in knee postures, and exercise.

METHODS

We included 15 juvenile sheep ($\bar{x} = 60\ d$) divided into three group: (i) incline treadmill exercise (15% grade; n=3), (ii) flat treadmill exercise (0% grade; n=3), and (iii) control (n=3). Sheep were housed at the University of Illinois Sheep and Beef Cattle facility. All the procedures were approved by the UIUC IACUC. Sheep from groups (i) and (ii) were first trained to walk on a motorized treadmill (Star Trac 4000HR, Star Trac, Irvine, CA) at moderate walking speeds and were exercised twice daily at 1.12m/s for 20 min/bout for 60 days. The duration of exercise has been shown a significant osteogenic response in sheep and other mammals [3, 4]. The control sheep were not exercised. All sheep were housed in a large indoor pen and were able to move freely. Access to food and water was not limited.

Three-dimensional (3D) limb kinematic data were measured with a 6-camera Qualisys (qualisys.com) motion capture system at 160Hz. Kinematic data were collected for group (i) and (ii) only, since control group was not trained to walk on treadmill. Reflective markers were placed on standard hindlimb landmarks (Fig. 1). Joint angles were measured at mid-stance (the hoof is beneath the hip) when peak loads are experienced. All subjects were euthanized humanely, limbs were dissected, muscles and ligaments were removed, and their limb bones segments were frozen.

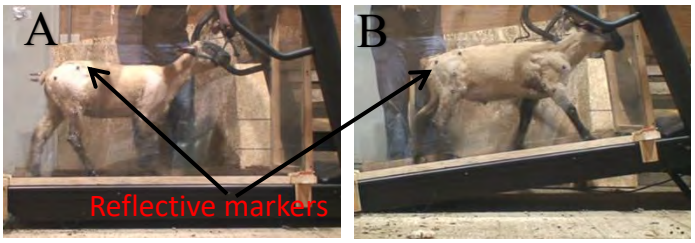

Figure 1. Sheep walking on treadmill: (a) Flat, and (b) Incline (10° grade)

Subchondral bone thickness measurement was evaluated on the medial femoral condyle (MFC). Femora were microCT scanned at 50µm voxel size using a Siemens Inveon microCT scanner (siemens.com/inveon). Noise was removed using MATLAB (MathWorks Natick, MA, USA), and 3D representations created using AMIRA (v 6.4, Thermo Fisher Scientific, MA, USA). Each specimen was resliced through the long axis of the MFC to obtain images along the axis of the joint. Thickness data were obtained using the BoneJ plugin from imageJ. The thickness values were then extracted by fitting a contour line to the joint

surface. The coordinate values were plotted in 3D surface plot in MATLAB by putting the thickness as a color matrix. Differences between groups were assessed using nonparametric Mann-Whitney U tests. All statistics were calculated in Minitab (v.16, Minitab, Inc. PA, USA), with a type one error rate of α=0.05.

RESULTS

Exercised sheep experienced around 3600 more loading cycles per day than did non-exercised sheep. On the incline walking, sheep used significantly more flexed knees (n=10; $p < 0.0001$) postures at mid-stance than on flat treadmills (Fig. 2). The difference of mean knee joint angle was 8° between these two groups. A similar pattern of difference is observed when comparing the position of subchondral bone thickness between the groups of sheep. The position of the maximum subchondral thickness moved more posteriorly for the Inclined group compared to Flat group (Fig. 3). The mean angular positions difference between the Flat and Inclined groups was 10° (n=3, p=0.08). The difference is close to our kinematically measure angular difference. The angular difference between Flat and Control, and Inclined and Control groups was 5° (n=3, p=0.38) and -4° (n=3, p=0.66) respectively. Average of peak subchondral thickness were 1.77 mm, 1.58mm, and 1.38mm, respectively, for flat, inclined, and control group.

DISCUSSION

The main goal of this study was to test whether the patterns of subchondral bone thickness could be used to infer differences in joint posture. Overall, there is good correspondence between thickness-based measurement and kinematic results, suggesting that the selected characteristics can be used to infer differences in joint posture. As expected, we observed higher subchondral thickness in exercised group compared to control group. However, more subjects experiment is required to make statistically strong conclusion on maximum thickness.

This study has direct application to questions of behavioral inference in anthropology, paleontology, and for clinical debates concerning the bony changes that precede osteoarthritis. For example, the relationship between the spatial patterns of subchondral bone thickness and kinematic measurement should permit the reconstruction of habitual posture used by extinct hominins and other primates, particularly for those in museum collections.

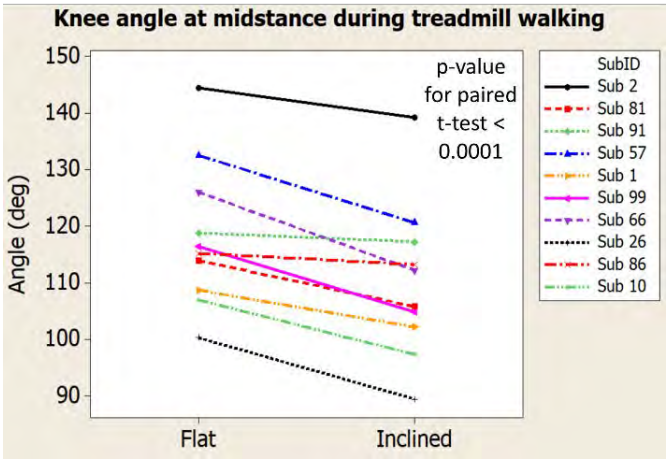

Figure 2. Pairwise comparison of midstance knee joint angle for individual subject during Flat and Incline treadmill walking

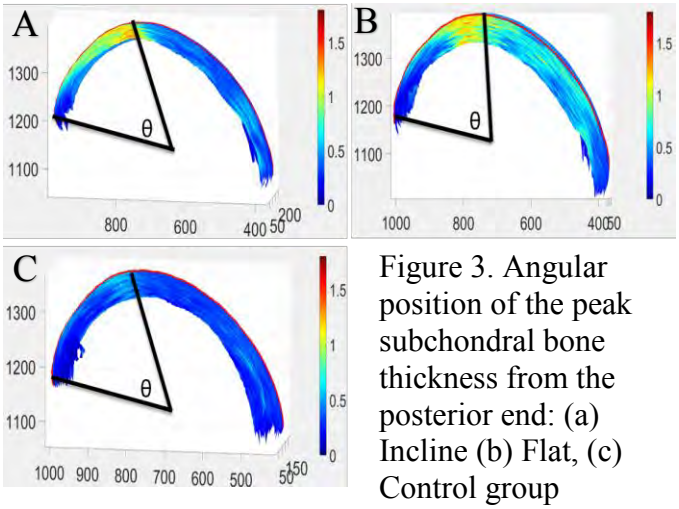

Figure 3. Angular position of the peak subchondral bone thickness from the posterior end: (a) Incline (b) Flat, (c) Control group

REFERENCES

1. Schulz, et al. Clinical Orthopaedics and Related Research 423:259-263, 2004.
2. Schulz, et al. Journal of Shoulder and Elbow Surgery 11:174-181, 2002.
3. Polk, et al. Anat Rec 291:293–302, 2008.
4. Robling, et al. J Bone Miner Res 17:1545–1554, 2002.

EFFECT OF TUMOR SIZE AND LOCATION WITHIN VERTEBRAL BODY ON FRACTURE RISK

[1]Asghar Rezaei, [2]Hugo Giambini, [1,2]Lichun Lu.

[1] Department of Physiology and Biomedical Engineering, Mayo Clinic, Rochester, MN, USA
[2]Department of Orthopedic Surgery, Mayo Clinic, Rochester, MN, USA
Email: lu.lichun@mayo.edu

INTRODUCTION

In 2017, new cancer cases were estimated to be 1,688,780 in the United States [1]. Spinal metastases are expected to occur in up to one-third of all cancer patients [2]. A metastatic disease reduces the structural integrity of the spine leading to vertebral fracture which can lead to pain and neurologic manifestations that significantly affects the quality of life. Unfortunately, there is no objective method to assess fracture risk in patient with metastatic disease in the spine. To target this problem, we have developed a non-invasive and quantitative technique that integrates quantitative computed tomography (QCT) imaging and finite element analysis (FEA). This method (QCT/FEA) estimates vertebral fracture loads in vertebral bodies with metastatic lesions, and has the ability to evaluate vertebral fracture properties based on various tumor characteristics (shape, size, and location). While tumor size has been considered as the most important risk factor for vertebral pathologic fractures, the effect of tumor location within vertebral bodies has not been previously addressed appropriately. A main goal of this pilot study was to assess the effect of lesion size and location within vertebral bodies on vertebral fracture strength using QCT/FEA.

METHODS

Three cadaveric spines were obtained and the L3 vertebral bodies were dissected. The L3 vertebrae were intact and did not present any lesions. The specimens were potted in PMMA and CT scan imaging was then performed. Specimens were mechanically tested in compression to fracture to measure the fracture properties. The QCT/FEA process is shown in **Fig. 1**; first, QCT images (**Fig. 1A**) are segmented to obtain a 3D model (**Fig. 1B**); then, the volume of the vertebra is meshed using voxel elements (**Fig. 1C**), and material properties, Young's modulus, are assigned to each element based on the specific grey values of the CT image determined by the Hounsfield units (HU) (**Fig. 1D**). Boundary conditions mimicking the experimental process, as well as a failure criterion, are then applied to the models (**Fig. 1E**), with a final analysis of predicted fracture properties outcomes (**Fig. 1F**).

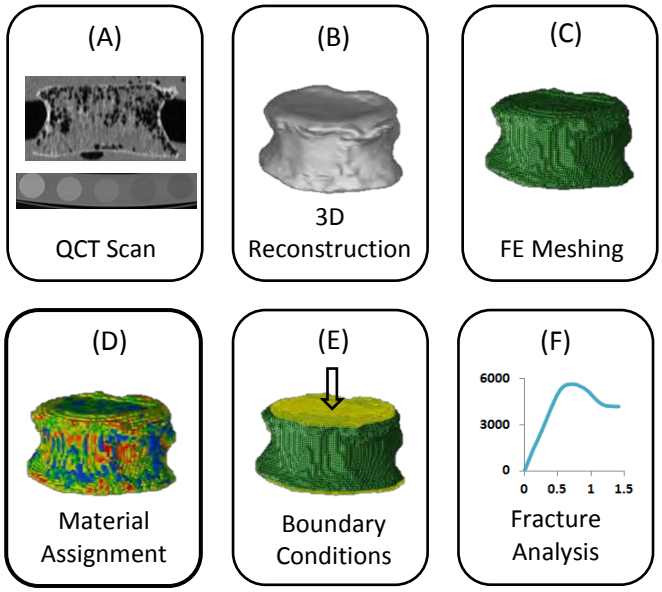

Figure 1. Overview of QCT/FEA process

For each intact vertebral body, thirteen QCT/FEA model scenarios were created; **1)** intact (with no virtual lesion), **2)** virtual spherical osteolytic lesion at the center, **3)** in the anterior, and **4)** at the pedicle of the vertebral body. The lesion sizes consisted of 1.5, 5, 12, and 24 % of the total vertebral volume **Figure 2** shows a QCT/FEA model of a vertebral body with a spherical lesion at the center. PMMA was also modeled and included in the simulations to mimic the experimental testing setup. Colors represent varying material properties.

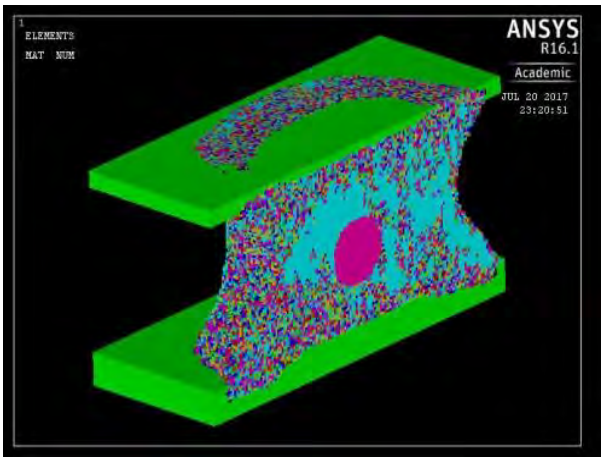

Figure 2. QCT/FEA model of a vertebral body with a simulated lytic lesion at the center.

RESULTS AND DISCUSSION

Experimentally measured vertebral fracture forces showed close agreement with their respective QCT/FEA-estimated outcomes) **Fig. 3A** (R^2=0.94)).

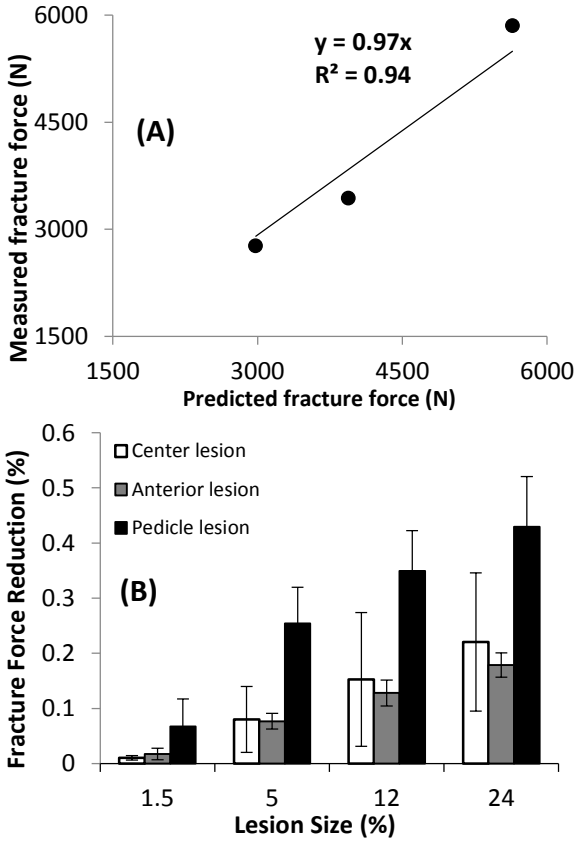

Figure 3. (A) Experimentally measured fracture force vs QCT/FEA predicted fracture force in intact specimens; (B) fracture force reduction with lesion size at three different locations.

QCT/FEA results showed that the effect of a lesion size of about 5% of the total vertebral volume, in the pedicle region, reduced the fracture load by more than 20%. This reduction was considerably lower when the lesion was located at either the center or anterior side of the vertebral body (**Fig. 3B**). Although with increasing lesion size the fracture load decreased dramatically, a lesion at the pedicle showed the largest decrease in the load bearing capacity of the vertebrae, up-to 50% when the lesion size was 24% of the total volume.

CONCLUSIONS

Osteolytic lesion size has been considered as one of the most significant risk factors leading to vertebral fracture [3]. Tumor location is also an important risk factor. When considering tumor location, a vertebra is divided in three locations; 1) the body, irrespective of the location of a lesion within the body; 2) the pedicles and 3) the posterior elements [3]. Interestingly, the location of the lesions within the vertebral body has not been highlighted sufficiently in previous studies. The results of the current study suggest that the destruction of bony tissue in the pedicle of a vertebral body by a lytic lesion can have significant negative effects in the load bearing capacity of the vertebrae when compared to a lesion size with same volume either at the anterior or at the center of the vertebral body. Our results highlight the importance of location inside vertebral bodies as a risk factor for vertebral fracture.

REFERENCES

[1] R.L. Siegel, K.D. Miller, A. Jemal, Cancer Statistics, 2017, A cancer journal for clinicians 67 (2017) 7-30.

[2] D.A. Wong, V.L. Fornasier, I. MacNab, Spinal metastases: the obvious, the occult, and the impostors, Spine 15(1) (1990) 1-4.

[3] H. Taneichi, K. Kaneda, N. Takeda, K. Abumi, S. Satoh, Risk factors and probability of vertebral body collapse in metastases of the thoracic and lumbar spine, Spine 22(3) (1997) 239-245.

ACKNOWLEDGEMENTS

This work was supported by a grant from the NIH (R01 AR56212) and an award from the National Institute of Biomedical Imaging and Bioengineering (F32 EB023723).

Strain rate dependent responses of the engineered and native cartilage

Alireza Seifzadeh[1]
[1]Biomedical Engineering, Islamic Azad University Khomeinishahr branch, Khomeinishahr, Isfahan Iran
Email: seifzadeh@iaukhsh.ac.ir

INTRODUCTION

To gain insights into the osteoarthritis initiation and progress, the study of changes in the material properties of tissue engineered cartilage and functional consequences after implantation that accounts for tissue associated non-linearities, as well as intrinsic viscous effects, fiber reorientation and dispersion at higher strains (~20%) is inevitable. It is, however, anticipated that knowledge of the stress-strain state of both cartilage collagen and in chondrocytes under repeated cartilage deformation will aid the understanding of how osteoarthritis begins and progresses. Prediction of changes in the material properties of soft hydrated tissue engineered, its behavior under loading, and associated consequences after implantation, is challenging. Therefore, using a model that accounts for tissue non-linearities at higher strains (~20%), is inevitable. In this work, Fibrillar stiffness and transient compressive stiffness of cartilage at various strain rates of both native and implanted ovine cartilage in biphasic construct in vitro and implanted into sheep for 3 and 9 months, were determined. Stiffening of both solid matrix and collagen fibers of cartilage in higher strains and strain rates were modeled.

METHODS

The indentation data for 10 native cartilage samples harvested from knee joints of 6-9 month old sheep as well as 10 engineered cartilage samples (at various times from implantation) on calcium polyphosphate (CPP) scaffolds were analyzed and compared to determine changes in material properties [1]. To determine material properties of both the native and engineered samples, the non-linear biphasic fiber-reinforced poro-hyper-visco-elastic (BFPHVE) model proposed by Seifzadeh et. al. [2], along with the coupled FE-optimization proposed by Seifzadeh et. al. [3] were performed using experimental indentation data for extracted cartilage samples at different growth stages (i.e., time periods after implantation) and different loadings. The transient and equilibrium stiffness, for both solid matrix and collagen fibers were determined for both native and engineered cartilage for strain rates ranging from zero to 20% s^{-1}.

RESULTS

Figure 1 shows the computed transient compressive stiffness in the radial direction for a 3 month native specimen (N-3) for different strain rates, and for two values of solid matrix shear modulus, 0.254 MPa to 0.370 MPa. Figure 1 shows that the stiffness increased more with an increase in solid matrix shear modulus values at the higher strain rates than the lower ones. As seen in the figure 2, the collagen fibers stiffen rapidly initially followed by a soft region at low and intermediate stretches. Only a small force is needed to achieve significant extension in the intermediate strains. Finally, there is a sharp increase in collagen fiber stiffness at higher stretches, the magnitude of which strongly depends on the value of the collagen stiffness κ_1.

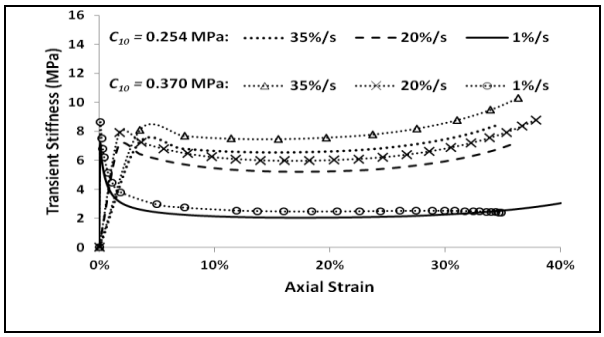

Figure 1: Transient compressive stiffness of cartilage

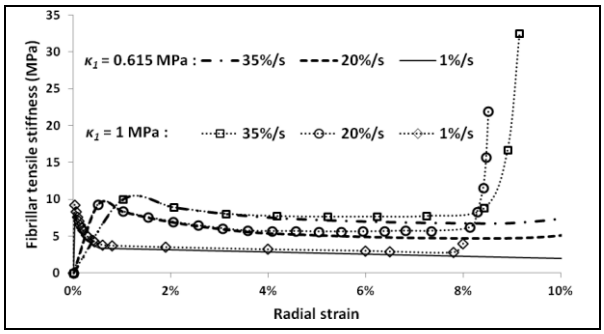

Figure 2: Fibrillar stiffness for a native sample

DISCUSSION / CONCLUSIONS

The strain rate dependent responses of the engineered and native cartilage in unconfined compression were investigated using a constitutive model that captures the response of cartilage over the whole experimental time and incorporates all included non-linearities. It was found that the non-linear BFPHVE is useful for modeling the transient and equilibrium responses of cartilage in tension and compression and dynamic tests to diagnose and evaluate cartilage quality. Osteoarthritis results in simultaneous changes in the solid matrix and collagen quality and interaction of these constituents impairs both the dynamic and static properties of cartilage. This study can be used to gain insights into the damage process in cartilage and determine load bearing.

REFERENCES

[1] Seifzadeh A. et al. (2012). *Journal Clinical Biomechanics,* Vol 27 (8); p. 852-859

[2] Seifzadeh A. et al. (2011). *ASME Journal of Biomechanical Engineering* Vol 133; (8pp)

[3] Seifzadeh A. et al. (2012). *Computer Methods and* Programs *in Biomedicine,* 102 (2); p. 315-326

FUNDING

"Not Funded"

EXPERIMENTAL MEASUREMENT OF THE CUTTING FORCES GENERATED DURING A ROBOT-DRIVEN GLENOID REAMING PROCEDURE

[1,2,3] Mayank Sharma [1,2,3] Louis M. Ferreira and [1] O. Remus Tutunea-Fatan

[1] Western University, London, ON, CANADA
[2] Roth|McFarlane Hand and Upper Limb Centre, London, ON, CANADA
[3] Lawson Health Research Institute, St. Joseph's Health Care Center, London, ON, CANADA
email: msharm@uwo.ca

INTRODUCTION

Total shoulder arthroplasty (TSA) aims to surgically restore the lost functionality of a degenerated shoulder joint. TSA involves implantation of a prosthesis on the glenoid bone for which the native bone must be resurfaced to ensure its optimal contact with the mating implant surface. Due to significant natural variability in the anatomy of the glenoid among patients, pre-operative planning, surgical technique, and skill play a significant role in a surgeon's ability to successfully place the glenoid implant in a suitable position [1].

To determine if the reaming process has been performed to an adequate depth, a virtual simulator with augmented-feedback was developed to mimic the TSA procedure for surgical training purposes. One of the core features of the intended simulator is to convey appropriate reaming force levels to the user to tune his/her surgical decisions based on the feedback. The generation of the appropriate reaming force levels is strongly dependent on the adequate calibration of the bone removal model, which in turn depends on experimental data collected with varying levels of bone densities.

METHODS

An electric surgical reamer (DePuy Synthes, West Chester, USA) was retrofitted to a light-weight robot (Kuka Robotics, Augsburg, Germany) (Fig. 1). The robot was programmed to apply preset levels of reaming thrust force (36 N) corresponding to an experienced surgeon's reaming practice. Five synthetic bone specimens (Sawbones, Vashon Island, USA) each of densities 0.16 g/cm^3, 0.24 g/cm^3 and 0.32 g/cm^3 - replicating different human cancellous bone - were reamed to a 5 mm depth.

Figure 1: Experimental setup of the KUKA robot retrofitted with a Synthes glenoid reamer and an optical tracker.

Labview (National Instruments, Austin, USA) was used in conjunction with a 6 degrees-of-freedom load cell to collect and filter the load data during reaming. An optical tracker (Northern Digital Inc, Waterloo, Canada) was used to evaluate the linear motion of the reamer relative to the specimen. Peak force, reaming speed, and force as a function of displacement (stiffness) were evaluated. One-way ANOVA followed by Tukey's post-hoc were performed to assess differences between various specimen density groups.

RESULTS AND DISCUSSION

An increase in the peak force was noted as the specimen density increased (Fig. 2). The 0.16 g/cm^3, 0.24 g/cm^3 and 0.32 g/cm^3 samples exhibited a mean peak force (MPF) of 16.45 ± 0.79 N, 26.15 ± 2.69 N, and 34.51 ± 1.23 N, respectively. Peak force increased significantly with material density ($p < 0.001$)

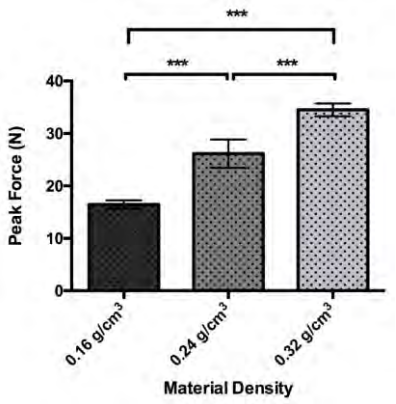

Figure 2: MPF recorded during reaming Sawbone specimens of various densities (*** $p < 0.001$).

For a given thrust force, reaming through a denser material should result in a slower reamer translation. In accordance, the average speed of the reamer through 5 mm specimen depth was recorded as 2.87 ± 0.30 mm/s, 1.95 ± 0.23 mm/s, and 1.29 ± 0.11 mm/s for the 0.16 g/cm^3, 0.24 g/cm^3 and 0.32 g/cm^3 specimens, respectively (Fig. 3). The decrease in reamer speed with increasing material density was significant ($p < 0.001$).

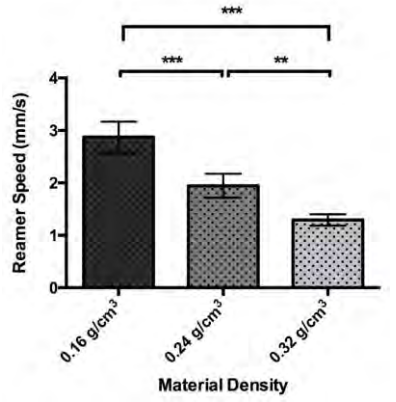

Figure 3: Average speed of the reamer while reaming Sawbone specimens of various densities (*** $p<0.001$, ** $p<0.01$).

Reaming force as a function of displacement was also evaluated (Fig. 4). This dependence could be related to the stiffness of the medium used in the simulator. For the five samples of each density tested, the average force-displacement rate was 3.72 ± 0.88 N/mm, 6.25 ± 0.73 N/mm, and 8.50 ± 0.41 N/mm for the 0.16 g/cm^3, 0.24 g/cm^3 and 0.32 g/cm^3 specimens, respectively. As expected, the perceived stiffness of the reamed material was directly proportional with its density ($p<0.001$). This implies that while advancing into the material, the reaming force will increase faster for denser specimens.

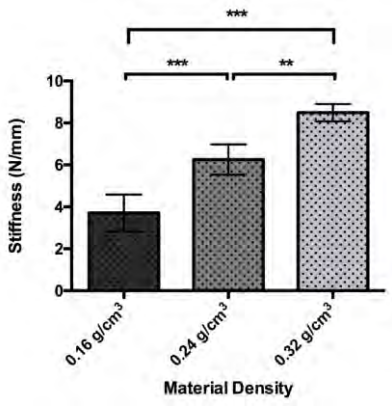

Figure 4: Average stiffness while reaming Sawbone specimens of various densities (*** $p<0.001$, ** $p<0.01$).

CONCLUSIONS

The results obtained suggest that greater reaming forces are required in cortical bone when compared to the cancellous bone (former has a higher density than the latter). Future tests will be conducted on human glenoid samples to verify this hypothesis.

ACKNOWLEDGEMENTS

The financial support provided in part by Natural Sciences and Engineering Research Council (NSERC) of Canada and Canadian Institutes of Health Research (CIHR) is gratefully acknowledged.

REFERENCES

1. Schrumpf et al. *The Glenoid in Total Shoulder Arthroplasty*, Current Reviews in Musculoskeletal Medicine 4(4): 191–199, 2011.

LOCAL THICKNESS OF THE HUMAN SKULL AFFECTS PATTERNS OF CRANIAL FRACTURE

[1,2] Paul Snyder, [2] Steven Rundell, [3] Todd Fenton, [1] Roger Haut, and [1] Feng Wei

[1] Orthopaedic Biomechanics Laboratories, Michigan State University, East Lansing, MI, USA
[2] Explico Engineering Company, Novi, MI, USA
[3] Department of Anthropology, Michigan State University, East Lansing, MI, USA
email: weifeng@msu.edu, web: http://www.obl.msu.edu/

INTRODUCTION

Differences in skull thickness of more than 300% have been documented in the adult human population [1]. While the effects of global skull thickness on cranial fracture tolerance have been investigated in the literature, computational models have yet to demonstrate the variability of cranial fracture patterns that are observed experimentally under the same mechanical inputs [2, 3]. Such variability may be explained in part, among several factors, by differences in the local thickness distribution of the skulls. It was hypothesized that variations in fracture patterns arising from the same mechanical input would present in areas of reduced skull thickness on a specimen-by-specimen basis.

METHODS

Blunt impacts were administered to the parietal bone of eighteen unembalmed, adult male human crania. Prior to impact, each specimen underwent a high-resolution computed tomography (CT) scan (GE 750HD; 120 kVp; 125 mAs; 0.625-mm slice thickness; 0.49-mm pixels; 512x512 matrix). Sample preparation involved removal of the scalp on the ipsilateral side of impact, with the exception of an island of scalp at the location of impact. Specimens were secured between the third and sixth cervical vertebrae to a horizontal mounting plate (located on the x-y plane) that allowed translation in the x- and y-directions as well as rotation about the z-axis during impact. A positioning collar with breakaway tethers was affixed around the neck to suspend the head in an upright posture.

A custom-built pneumatic striker applied fracture-initiating impacts to the temporoparietal region. Three different aluminum impactor geometries were tested: a flat 1-inch diameter implement ("hammer" n = 7), a flat 3-inch diameter implement ("brick" n = 5), and a cylindrical curved 2.5-inch diameter implement ("bat" n = 6). Mass of the impact trolley ranged from 6.048 to 9.593 kg, and impact velocities ranged from 4.968 to 6.280 m/s. Slightly increased velocities were used to ensure fracture initiation in the "brick" and "bat" impacts. Forensic anthropologists hand-diagrammed the resulting fracture patterns post-impact.

Three-dimensional models of each skull were generated from the CT data using thresholding and segmentation operations in Mimics (Materialise NV; Leuven, Belgium). Wrapping operations were performed to eliminate cavities in the diploë layer, allowing a consistent thickness measurement between the cortical layers. Heat map thickness analyses were then scaled and overlaid onto the corresponding fracture diagrams to evaluate the effects of local skull thickness distribution on fracture pattern presentation arising from three different impacting implements.

RESULTS AND DISCUSSION

Local thickness maps from specimens showing typical fracture patterns of each implement were closely overlaid with their corresponding fracture diagrams (Fig. 1). "Hammer" specimens tended to exhibit a focal fracture pattern consistent with the implement's 1-inch diameter at the point of impact. Typically, secondary fracturing propagated anteriorly into the areas of reduced thickness. The thickest "hammer" specimen (17-3757) did not experience focal fracture at the point of impact but fractured remotely in an area of reduced thickness near the external auditory meatus. One of the thinnest "hammer" specimens (17-2071) experienced a diffuse pattern of fracture in the temporoparietal region of reduced thickness. No

"hammer" specimens fractured superiorly towards areas of increased thickness.

"Brick" specimens tended to exhibit diffuse fracture patterns in the temporoparietal region. The outline of the diffuse area of fracture tracked along transition regions of reduced thickness to regions of increased thickness. One specimen (17-2035) experienced linear type fractures near the point of impact anteriorly towards regions of reduced thickness in the sphenoid. The thickest specimen (16-3817) fractured remotely in the sphenoid region in an area of reduced thickness.

"Bat" specimens tended to exhibit the widest variety and span of diffuse and linear fractures. "Bat" impacts were the only to travel anteriorly into the frontal bone (16-3803, 17-2067, 17-2081), as well as the only to experience significant superior propagation towards the sagittal suture (17-2118). While "bat" specimens 16-3803 and 17-2081 experienced more focal fracture near the point of impact with anterior linear fracture propagation, specimens 17-2067, 17-3758, and 17-2118 experienced more diffuse fracture in the area of impact, and 17-4813 experienced more remote linear fracture. In general, "bat" fracture occurred in relative regions of reduced thickness.

CONCLUSIONS

Fractures tend to occur in, and propagate through, regions of reduced thickness. While "hammer" impacts are likely to exhibit focal fracture near the point of impact, "brick" and "bat" impacts are likely to exhibit more diffuse fracture patterns that track along locally thin areas of the skull.

In general, the results of the current study have confirmed the hypothesis. Intrinsic skull properties, specifically thickness distribution, play an important role in the patterns of cranial fracture. These findings are important when determining the cause of a skull fracture in a forensic setting.

ACKNOWLEDGEMENTS

NIJ 2015-DN-BX-K013, Explico Engineering Company, and Mr. Clifford Beckett.

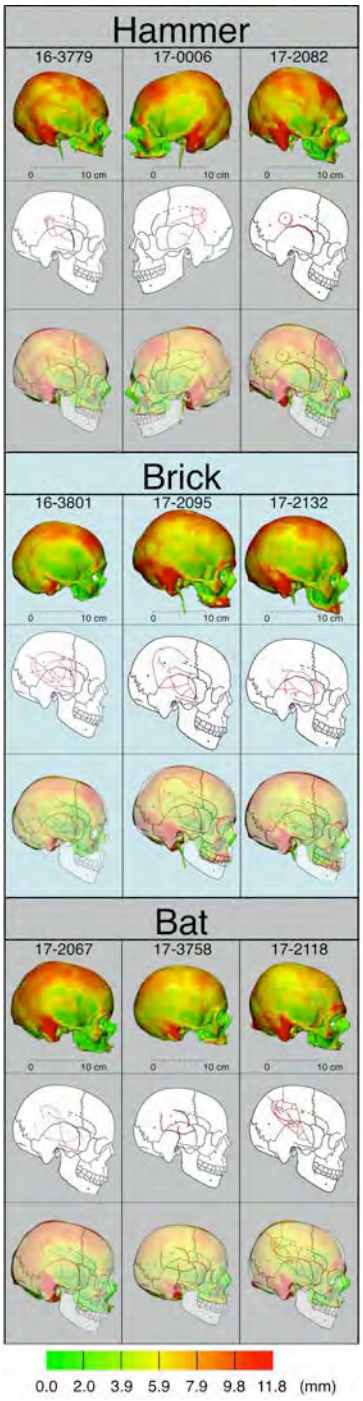

Figure 1: Representative sample of thickness distribution maps compared to typical fracture pattern diagrams of each implement.

REFERENCES

1. Got, C., et al. *SAE Technical Paper*, No. 831619, 1983.
2. Ruan and Prasad. *Stapp Car Crash J*, 45.11 p395-414, 2001.
3. Yoganandan, et al. *Clinical Biomechanics*, 19.3 p225-239, 2004.

Relating Gait and Bone Growth in Rat Tibia

[1] Hyunggwi Song and [1,2] Mariana E. Kersh

[1] Department of Mechanical Science and Engineering, [2] Beckman Institute for Advanced Science and Technology
University of Illinois at Urbana-Champaign, Urbana, IL, USA
email: hsong41@illinois.edu

INTRODUCTION

Material and mechanical properties of bone are optimized via modeling during growth – when mass and size increase significantly – in order to sustain the loading cycles from everyday movement [1, 2]. However, the mechanisms of this optimization are not clear. Using rats as a model system for bone development, the aim of this study was to understand how rodent bone morphology, apparent density, and bone volume fraction respond to the everyday movements during growth, and if they are related to changes in joint kinematics and gait dynamics.

METHODS

Data was collected from 5 healthy female Sprague-Dawley rats beginning at the age of 7 weeks. All protocols were approved by the IACUC at UIUC. Computed tomography data and gait biomechanics data was collected at seven time points: weekly from age 8 weeks to 12 weeks, 14 weeks, and 20 weeks.

The hindlimbs were scanned using in vivo microCT with a resolution of 35.8 μm. The right hindlimb was segmented semi-automatically using Amira 5.6. The apparent density along the length of the bone was calculated by Hounsfield unit to apparent density conversion using hydroxyapatite phantoms placed within the scan field of view [3]. The length of the bone and transverse cross-sectional area were calculated using custom Matlab code.

Next, rat gait analysis was performed. A custom walkway was developed with an in-ground force plate to record ground reaction forces (GRF). Each rat was trained to walk on the walkway before collecting the data. Kinematics of the hindlimb during walking were measured using two high-speed cameras (Fig 1). Key anatomical landmarks were marked with a non-toxic permanent marker. Each rat was placed upon the walkway and marker positions and the GRF were collected at 240 Hz frequency when the right foot hit the force plate correctly. The knee marker position was estimated in 3D by measuring the length of the femur and the tibia to minimize skin movement error [4].

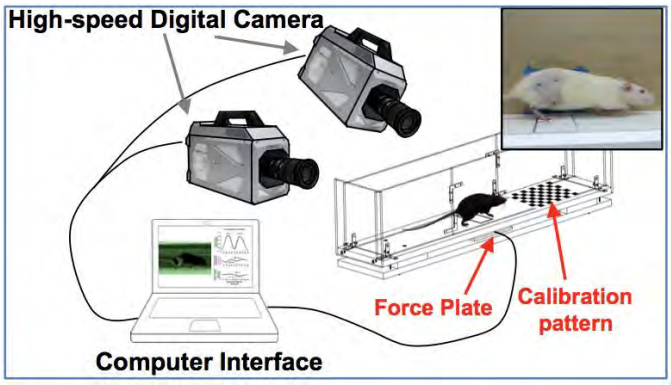

Figure 1: Schematic of rat walkway platform for gait data.

RESULTS AND DISCUSSION

Ground reaction forces and hip, knee, and ankle joint angles were obtained at each time point along one gait cycle. Peak GRF and joint angles at the time of the peak GRF were averaged at each time point (Fig. 2). Mean peak GRF increased during growth, but the rate of increase decreased over time. At 11 weeks, the GRF increased and remained relatively constant until it increased again at 20 weeks ($p<0.05$). The joint angles decreased at ten weeks after which they again remained constant beyond ten weeks of age (Fig. 2).

As expected, tibia bone length followed a power law increase with age and converged by the end of the experiment (93% of skeletal maturity). The proximal portion had a larger cross-sectional area, but smaller

apparent density compared to the middle and distal regions of the bone over time (Fig. 3).

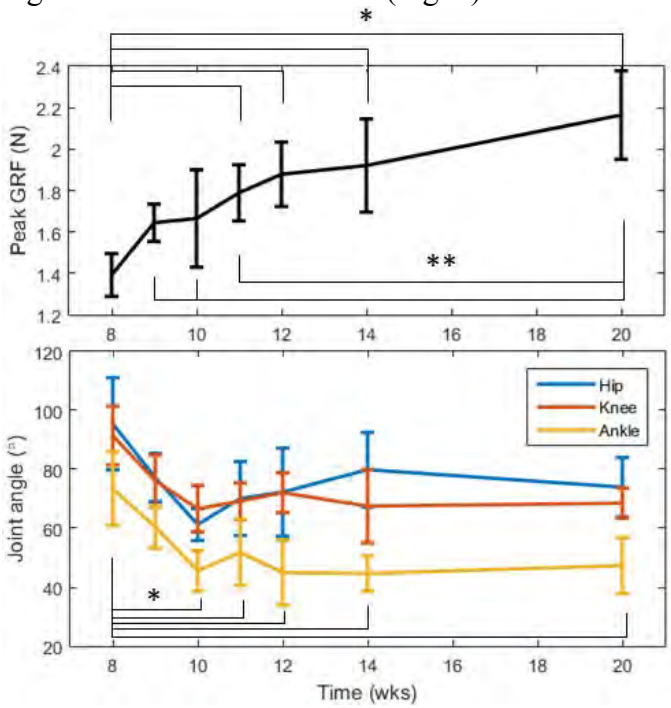

Figure 2: Mean peak ground reaction forces and standard deviations, and Hip, knee, and ankle joint angle trajectories when peak GRF at each age.

Proximal CSA kept increasing, whereas distal and middle CSA did not change over time. However, density in all three regions increased and then converged at the end of experiment similar to the trend observed in bone volume fraction.

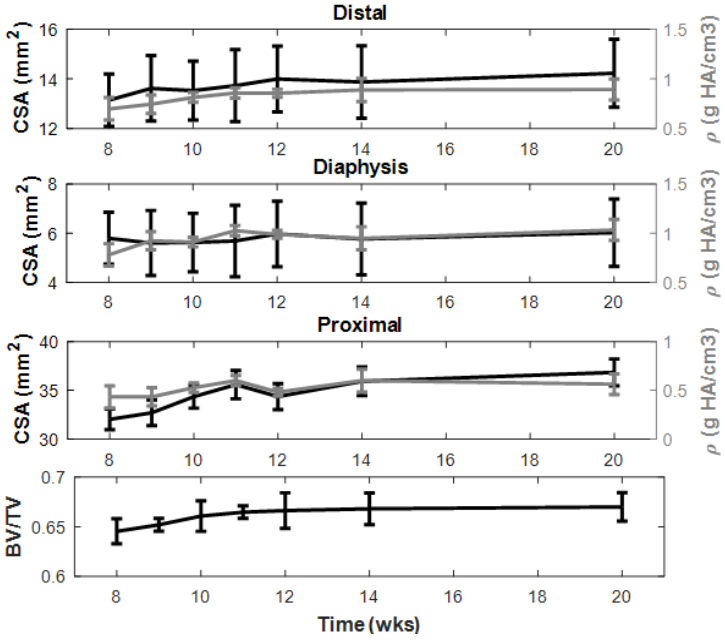

Figure 3: Cross-sectional area and apparent density of distal, middle, and proximal ends, and bone volume fraction at each age.

The peak ground reaction forces correlated with respect to body mass over time when rats walked naturally during growth. To generate the ground reaction forces, each joint angle decreased until week 10 and then converged. This trend was also observed from the proximal CSA, the apparent density of whole regions of the bone, and the bone volume fraction, but one week shifted. The shift may represent the time bone needs to undergo bone modeling in response to the change in motion.

The proximal end had a larger CSA and lower apparent density because it has more trabecular bone. Unchanged CSA and increased density at the distal and middle ends imply that the distal and middle regions of the bone are getting denser and stronger than other regions during growth. Generally, the ankle joint has higher moments and force during walking and this loading condition may initiate the need to increase the strength of the distal tibia.

At the age of 20 weeks, rodents are almost mature in terms of CSA, apparent density, and bone volume fraction that are about to converge, even though ground reaction forces keep increasing over time.

CONCLUSIONS

This study shows how bone properties change during the growth period and that those properties are related to gait strategy. The specific role of muscle forces during growth remains to be understood, and is the subject of future work.

REFERENCES

1. Warden, Stuart J., et al. *Proceedings of the National Academy of Sciences*, *111*(14), 2014.
2. Turner, C. H., and Robling, A. G. *Journal of bone and mineral metabolism*, *23*(1), 2005.
3. Cory, E., et al. *Journal of biomechanics*, *43*(5), 2010.
4. Bauman, J. M., & Chang, Y. H. *Journal of neuroscience methods*, 186(1), 2010.

TENDON ALLOGRAFT PROCESSING AND RECONSTITUTION INCREASES FLEXURAL STIFFNESS

[1] Andrew Thoreson, [2] Chun Bi and [1] Chunfeng Zhao

[1] Mayo Clinic, Rochester, MN, USA
[2] Shanghai Jiao Tong University, Shanghai, China
email: zhao.chunfeng@mayo.edu

INTRODUCTION

Tendon grafts play a critical role in functional recovery of Zone II tendon repairs and have been sourced from both intrasynovial and extrasynovial sites. Intrasynovial tendon (e.g. flexor digitorum profundus (FDP) tendon) is a preferred source because of its smooth surface, low friction; however, its supply is limited. Extrasynovial tendon is readily available and is often sourced as an allograft for tendon repair. Clinical outcomes of graft repair will be partly dependent on mechanical properties of the processed graft.

Differences in mechanical properties between intrasynovial and extrasynovial tendon have been previously documented [1, 2]. However, mechanical characterization of tendon allograft has largely been limited to compressive, tensile and frictional properties. While these properties are relevant to the functional performance of tendon, its flexural stiffness will also affect performance, a parameter which has been largely neglected in prior studies. The tendon's ability to bend will impact the gliding resistance as the tendon traverses through the pulley of a flexing digit. Each mechanical property could be completely independent of the others, requiring a more robust characterization to appreciate in vivo performance of the graft.

The objective of this study was to first develop an approach to quantify the flexural modulus of tendon, then determine how this property differs between extrasynovial and intrasynovial tendon, between regions within intrasynovial tendon, and between the freshly harvested and rehydrated lyophilized conditions. We hypothesized that extrasynovial and intrasynovial tendon have different flexural moduli and lyophilization would increase flexural moduli of both fibrocartilaginous and non-fibrocartilaginous regions.

METHODS

A custom-fabricated apparatus was designed based on the 3-point bend test methods traditionally used for evaluating flexural properties of materials [3]. The device consisted of a recessed well that retained a room temperature saline bath, two vertical 3.2-mm-diameter pins that served as simple supports for the tendon and a mechanical actuator instrumented with a load cell and linear potentiometer that extended into the saline bath with another vertical 3.2-mm pin to load the tendon (Fig 1). The tendon was flexed in the horizontal plane to negate the effects of gravity. The span between pins was set to 12.5 mm.

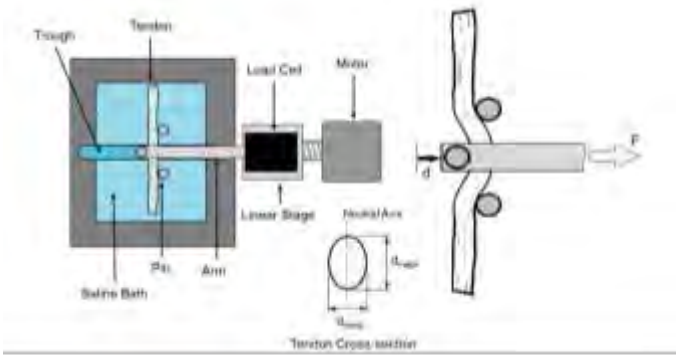

Figure 1: Schematic of custom apparatus to test tendon flexural modulus in a saline bath.

Twenty hind paws were harvested from 10 adult mongrel dogs which were sacrificed for other Institutional Animal Care and Use Committee approved studies. Second digit flexor digitorum profundus (FDP) intrasynovial tendons and peroneus longus (PL) extrasynovial tendons were harvested. Intrasynovial and extrasynovial tendons were each randomly divided into two groups of ten

tendons each, one to be tested as harvested and the other to be processed as allografts.

Allografts were processed starting with 5 cycles of liquid nitrogen immersion and thawing in 37°C saline (0.9%), lyophilization for 12 hours (Benchtop Manifold Freeze Dryer, Millrock Technology, Kingston, NY). and rehydration in saline solution (0.9%) at 4°C for twenty-four hours. The middle 20 mm was cut from each PL tendon or tendon allograft and 40-mm FDP tendon/allograft samples were cut that included fibrocartilaginous (fc) and non-fibrocartilaginous (nfc) regions. The major and minor diameters of each tendon cross-section were measured with a digital caliper.

Tendons were placed on the device and at a constant rate of 0.05 mm/s for 2 mm for two cycles. Data from the 2nd cycle was used for property calculations as the first cycle was applied to stabilize the tendon. Flexural modulus (E) was calculated using classic mechanical equations for beam deflection (Eq 1), assuming tendon cross-section was elliptical, where F is the force loading the tendon, L is the span, d is the tendon deflection, and a and b are the major and minor tendon diameters, respectively.

$$E = \frac{FL^3}{12ab^3\pi d} \qquad \text{(Eq 1)}$$

Student's t-tests were performed to compare the flexural modulus between groups. A p value of 0.05 or less was considered statistically significant.

RESULTS AND DISCUSSION

Lyophilization and rehydration significantly increased flexural modulus of PL tendon and FDP tendon in both the fibrocartilage and non-fibrocartilage regions ($P<0.001$ for all). Flexural modulus was significantly different between fibrocartilaginous and non-fibrocartilaginous regions in fresh tendon, and this difference remained significant after lyophilization ($P < 0.001$ for both comparisons) (Fig. 2).

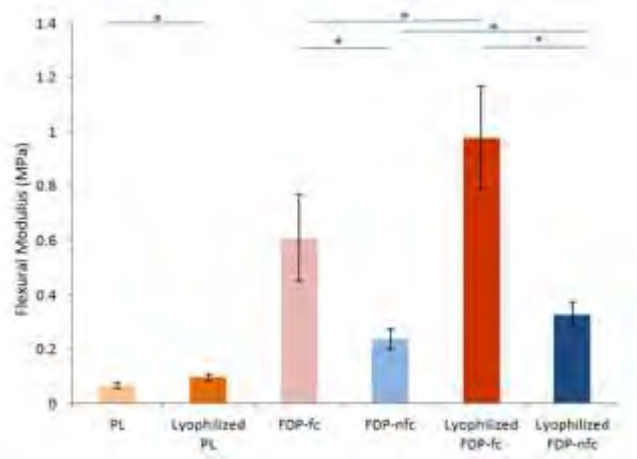

Figure 2: Mean flexural modulus of different tendon types and preparation. Bars connect groups that are significantly different.

Gliding resistance and longitudinal stiffness represent only two relevant properties of tendon. This new characterization shows yet another manner in which graft processing technique can alter mechanical properties of the tendon and potentially affect clinical outcomes.

CONCLUSIONS

Lyophilization and reconstitution of tendon allografts can alter flexural properties compared to the native state. This may increase tendon gliding and wear on the tendon surface. Methods to reconstitute allografts without increasing stiffness should be investigated further.

REFERENCES

1. Uchiyama S et al. *J Bone Joint Surg Am:* 79, 1997.
2. Zhao C et al. *J Orthop Res*. 20: 2002.
3. Thubikar, M et al. *J Biomech,* 15: 1982.

ACKNOWLEDGEMENTS

This study was supported by a grant from the National Institutes of Health/National Institute of Arthritis and Musculoskeletal and Skin Diseases (AR057745).

DEVELOPMENT OF PELVIS MODEL FOR BIOMECHANICAL EVALUATION OF MINIMALLY INVASIVE ACETABULAR RECONSTRUCTION

[1] Sean M Tutton, [1]David M King, [1]D Ian English, [1]William B Lea,
[1]John C Neilson, [2]Randolph M Setser, [2]Sebastian Schafer, [1,3]Mei Wang

[1] Medical College of Wisconsin, [3]Marquette University, Milwaukee, WI, USA
[2] Siemens Healthineers, Hoffman Estates, IL, USA
email: meiwang@mcw.edu

INTRODUCTION

Bone is the third most common site for cancer metastases behind the lung and liver, while pelvis is the second most common site of bone metastasis (second to the spine). Goals of the reconstruction are to achieve full weight-bearing post-op and to provide durable construct to last expected lifetime of patient. Harrington established guidelines for treatment of type III and IV lesions [1]. Image-guided minimally invasive percutaneous acetabular stabilization using augmented screws combined with thermal ablation is newer treatment approach that avoids the morbidity of open surgical reconstruction and allows patients undergo earlier chemotherapy and radiation [2]. However, there is a lack of suitable model for biomechanical evaluations of these minimally invasive fixation procedures. The standard 4th-generation composite hemipelvis model was almost twice as stiff as that of the cadaver specimens.

The purpose of this study was to develop a composite model of hemipelvis with metastatic acetabular lesions that mimic the biomechanical properties of human cadaver, and a surrogate soft tissue torso to perform percutaneous augmented screw fixation. Composite model contained a defect in the acetabulum partially involving the medial and superior acetabular walls consistent with a Harrington type III.

METHODS

The CT images of a patient with Harrington III bone defect in the medial and superior acetabulum were selected. Based on these images, prototypes of composite hemipelvis were developed for this study in collaboration with Pacific Research Laboratories (Vashon, WA). In addition, a surrogate soft tissue torso with skin from waist to upper thigh was custom-made (Fig.1). The torso surrogate was used to house the sawbone hemi-pelvis and to be strapped onto the patient table of an angiography system for the percutaneous stabilization procedures. The torso was designed for repeated utilization, with a Velcro opening on the side for the insertion and removal of composite hemipelvis.

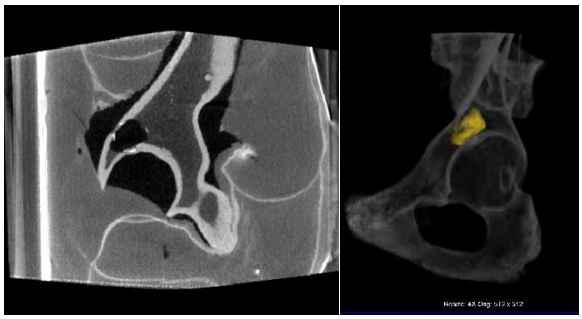

Figure 1: Fluro-image of hemipelvis model inside foam torso (left) and CT-scan of the model (right).

To characterize the biomechanical behaviors of the prototypes, compressive force up to 1200N and then load to failure tests were conducted with the hemi-pelvis being in a configuration that mimic single-leg mid stance phase of a gait. Servo hydraulic loading frame (MTS Landmark 370, Eden Prairie, MN) was used to apply axial load through a 4th-generation composite femur (proximal half) at a rate of 0.1mm/s for both tests. The hip was positioned with 15-degree flexion and 10-degree adduction [3]. Lateral shift of 5cm from the sagittal midline was also added to the loading point when mounting the pelvis to the actuator. This was to simulate lateral displacement of the pelvis as the center of gravity moves closer to the stance leg. Two marker triads from a motion tracking system (Optotrak Certus, NDI, Waterloo, Canada) were each placed on the pubic tubercle and anterior margin of the iliac crest to track movement of the hemipelvis and deformation in response to loading. Marker triads data and axial force and displacement

data from MTS built-in sensors were synchronized and collected at 100Hz.

From the non-destructive test, compressive stiffness was obtained from the linear portion of the load-displacement plot, while maximum deformation under 1200N was identified from the motion tracking data. Mechanical yield strength, ultimate strength, and stiffness were obtained from the load-to-failure test. After finalizing the model, four samples of the selected hemipelvis prototype were fabricated for mechanical evaluation. Mechanical variables of these samples were compared to the previously published data from cadaver testing where was available [4].

Figure 2: Configuration for axial compression test.

RESULTS

After two rounds of modification (tuning elastic module of the cortical shell and altering cortical thickness) and testing, the finalized model was a composite model consisted of cortical shell made of 20pcf rigid foam with thickness varying between 1-2 mm, and cancellous core made of 8pcf rigid foam. The volume of superior lateral acetabular wall defect was 13ml (Fig.1).

Results of axial compression tests showed that the mean stiffness of the hemipelvis was 730±141N/mm, 12% lower than the 832±62N/mm obtained from cadaver hemipelvis from healthy elderly donors [4]. The mean yield strength and ultimate strength was 2400±432N and 2758±230N respectively. The mean corresponding yield and ultimate deformations were 4.3±1.2mm and 6.2±0.9mm respectively. At 1200N compression, the deformation across the acetabular area was relatively small, with the mean rotational deformations ranged from 0.12 to 0.17 degree around the three axes, and the mean axial deformation of 0.59mm.

DISCUSSION

A composite model of hemipelvis with simulated metastatic acetabular lesion was developed based on previously treated patient scans. Biomechanical testing of the model in a single-leg loading configuration showed that its stiffness, at 730N/mm, was more comparable to the cadaver specimens (at 832N/mm) than the standard 4th-generation composite model (at 1448±54N/mm). The 12% reduction over the intact cadaver specimens in stiffness also supports its suitability as an acetabular lesion model. There is no previous data on compressive strength on cadaver pelvis except under high-speed impact loading, but the yield and ultimate strengths of the current model, at 3-4 times of bodyweight, represents good estimations for patients in this population.

CONCLUSIONS

The composite sawbone Harrington III hemipelvis developed in this study provides a reasonable model to be used for comparative studies of minimally invasive technique of percutaneous acetabuloplasty and screw fixations for metastatic lesions of the acetabular area.

REFERENCES

1. Harrington et al. *JBJS* 63-A:653-64, 1981
2. Hartung et al. *J Vasc Interv Rad* 27:682-8, 2016.
3. DiMattia et al. *J Sport Rehabil* 14:108-23, 2005.
4. Giradi et al. *J Biomech* 49:537-42, 2016.

ACKNOWLEDGMENTS

This study was supported by a research grant from Siemens Healthineers. The concepts and information presented in this paper are based on research and commercial availability cannot be guaranteed.

EFFECT OF SURFACES WITH DIFFERENT STIFFNESS ON BODY KINEMATICS WHILE ROLLING

[1] Rahul Agrawal [2] Mahdi Hassan and [1] Nils Hakansson

[1] Wichita State University, KS, USA

[2]University of Nebraska at Omaha, Omaha, NE, USA

email: nils.hakansson@wichita.edu, web: http://www.wichita.edu/thisis/home/?u=bme

INTRODUCTION

Rolling is an activity that most people perform repeatedly on a daily basis without knowing. This complicated movement requires the coordinated motion of body segments, i.e., trunk and upper and lower extremities [1]. Rolling and repositioning in bed serves to improve comfort, circulation, sleep quality, and prevent pressure sores. People who cannot roll or have difficulty rolling may receive training from a physical therapist based on a standard or norm. To date, no standard or norm exists. Previous research on autonomous rolling kinematics has been limited to rolling on an exercise mat [1-2] or firm surface [3]. Thus, rolling on surfaces with different stiffness could provide further insight into understanding the biomechanics of rolling and offer new training options. The goal of this research is to determine the body kinematics when rolling from the supine position to the side-lying position on three surfaces with different stiffness (i.e., a stiff surface, exercise mat, and a mattress) under two rolling conditions to mimic independent rolling and assisted rolling by a caregiver: (1) arms free to move naturally and (2) arms crossed over the chest (constrained arms), respectively. The objective of this study was to determine the effect of rolling surface stiffness and arm conditions on the body kinematics as defined by the body segment (shoulder vs. pelvis) that initiates and concludes the roll.

METHODS

Data were collected from 18 participants (12 males and 6 females; mean weight 76.3 ± 13.9 kg; mean height 173.6 ± 7.6 cm; mean age 24.6 ± 3.4 yrs.) who were not limited in their ability to roll after receiving informed consent as defined by the WSU Institutional Review Board. Participants were instructed to roll to their right from the supine to a side-lying position on three different surfaces (stiff floor, 2-inch exercise mat, 8-inch memory foam mattress) using two types of rolling conditions: arms free to move naturally and arms crossed over the chest, to mimic autonomous and caregiver assisted rolling respectively. Five trials were collected for each type of rolling for a total of 30 trials per participant.

The data collection order was randomized by surface and by arm condition within each surface. Shoulder and pelvis kinematics were recorded at 50 Hz using an eleven-camera, high-resolution motion analysis system (Motion Analysis Corp., Santa Rosa, CA) and reflective spherical markers positioned on the left and right acromia and anterior superior iliac spine (ASIS). Shoulder and pelvis angles were calculated from the inverse tangent of the horizontal and vertical components of the vector formed from the right to left shoulder (AB) and the right to left ASIS (CD) markers, respectively (Figure 1). Initiation and cessation of the rolling motion was based on the shoulder and pelvis angular velocities [3].

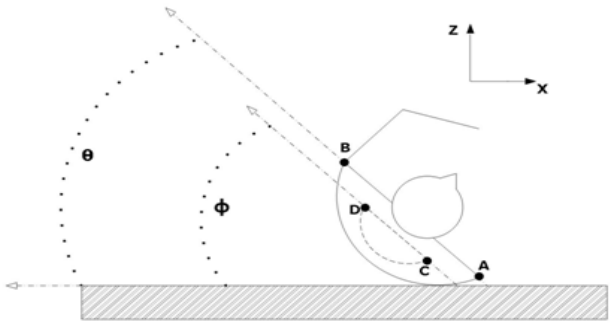

Figure 1: Shoulder (θ) and pelvis (ϕ) angles.

The dependent variables studied are listed in Table 1. Friedman's nonparametric tests for repeated measures were used to test for differences in the initiating and ending segment for each surface and rolling condition. Two-way repeated-measures ANOVA (α=0.05) tests were performed to examine the effect of rolling surface stiffness and arm

condition had on shoulder and pelvis kinematics during the rolling motion. When significant main effects were identified, *post hoc* pairwise t-tests with Bonferroni correction (p = 0.05/n where n is 5) were performed.

RESULTS AND DISCUSSION

No significant difference was observed for the segment (shoulder or pelvis) that initiated or concluded the roll, the timing of the peak angular velocity of the shoulders, the peak angular velocity of shoulders, or the duration of the roll. There was a significant interaction between conditions and surfaces for both the timing of the peak angular velocity of the pelvis (p=0.034) and the magnitude of the peak angular velocity of the pelvis (p=0.006). The rolling condition had a significant ($p<0.001$) effect on the pelvis peak angular velocity. Across all rolling combinations, the shoulder initiated 61.3% and ended 50.5% and the pelvis initiated 37.8 % and ended 45.1 % of the rolls.

An important finding of this study was neither the constraint imposed on the arms nor the rolling surface stiffness affected the majority of dependent variables that were examined. This information could be useful to a therapist teaching a patient to roll. The consistency of the initiating and concluding segments across conditions and surfaces supports the motor control theory that a movement is planned prior to initiation [4]. The mean peak angular velocity for the arms-uncrossed condition appears to be higher, yet there was not a significant difference in the duration of the roll, indicating that the average angular velocity was similar for all rolling conditions. This characteristic is consistent with previous research that upper extremity and torso rotation is smooth and steady [2-5]. The decrease in peak pelvis angular velocity when rolling on a compliant surface with arms crossed suggests that subjects generated less peak kinetic energy with the pelvis segment. The increase in peak angular velocities of shoulder with arm uncrossed condition could be associated with an increase in momentum generated by arms to assist in rolling on compliant surface.

CONCLUSIONS

The application of motion constraints that do not alter segment coordination patterns could facilitate future biomechanical analyses of human rolling. To this end, we found that constraining the arms surface stiffness did not affect most rolling kinematic measures. This result provides confidence that future research work on rolling, for example the creation of a musculoskeletal simulation of rolling, can be performed with constrained arms and on varying surface stiffness's without altering the basic rolling movement.

REFERENCES

1. Richter RR, et al. *Phys. Ther* 69:63-71, 1989.
2. Sekiya N, et al. *J. of Jpn. Phys. Ther. Assoc* 7, 1-6, 2004.
3. Vu, LQ, et al. *39th ASB Conf., Columbus, OH*, 2015.
4. Rosenbaum, DA, *J. of Experimental Psychology.* 109(4): 444-474, 1980.
5. Davies, PM, Springer Science & Business Media, 2008.

Table 1: Descriptive Statistics of kinematic (dependent) variables. (p-value indicates interaction)

Dependent Variables	Arm Crossed						Arm Uncrossed						p- value
	Hard Surfaces		Exc. Mat		Mattress		Hard Surfaces		Exc. Mat		Mattress		
	Average	S.D.	Average	S.D.	Average	S.D.	Average	S.D.	Average	S.D.	Average	S.D.	
Initiating Segment	1.4	0.5	1.4	0.5	1.4	0.5	1.5	0.5	1.4	0.5	1.3	0.5	0.308
Ending Segment	1.5	0.6	1.4	0.6	1.5	0.6	1.6	0.6	1.6	0.6	1.6	0.5	0.331
Time of peak pelvis angular velocity (% roll)	51.3	10.6	50.1	11.0	50.4	11.3	48.5	9.5	51.2	10.9	52.7	10.9	**0.034**
Time of shoulder peak angular velocity (% roll)	43.0	8.9	41.3	9.6	41.9	9.0	42.6	9.1	42.1	7.9	44.2	8.5	0.092
Peak pelvis angular velocity (deg/s)	88.5	15.9	88.2	15.6	85.8	15.6	89.5	16.5	93.8	17.5	93.5	20.8	**0.006**
Peak shoulder angular velocity (deg/s)	98.3	22.0	99.6	21.0	103.1	22.2	106.3	21.6	110.1	21.6	112.3	23.1	0.532
Duration of roll	3.1	0.7	3.1	0.8	3.1	0.7	3.2	0.7	3.2	0.6	3.1	0.6	0.102

DIFFERENCES IN MECHANICAL ENERGY OF HUMAN ROLLING ON DIFFERENT SURFACES

[1] Rahul Agrawal, [2] Mahdi Hassan and [1] Nils A. Hakansson

[1,3]Wichita State University, Wichita, KS, USA
[2]University of Nebraska at Omaha, Omaha, NE, USA
email: nils.hakansson@wichita.edu, web: http://www.wichita.edu/thisis/home/?u=bme

INTRODUCTION

Rolling is a milestone in human development. Rolling serves to improve comfort and prevent ischemic-associated injuries to the tissues (i.e., pressure sores), facilitate a healthy quality of sleep, and reduce the potential for long-term health complications. Previous research provides some knowledge on how people roll on a firm surface [1-3]. A goal of our research is to determine fundamental characteristics of rolling and evaluate whether environmental factors (e.g., rolling surface) or movement constraints (e.g., crossing the arms over the chest as employed in an assisted roll) changes the rolling motion. This information would be useful to a therapist working to evaluate or train a patient's rolling. The objective of the study was to determine mechanical energy requirements of the body when rolling from the supine position to the side-lying position on surfaces with three different stiffness: a) firm surface, b) exercise mat, and c) mattress under two rolling conditions: (1) constrained arms (arms crossed over the chest) and (2) arms uncrossed (arms free to move naturally).

METHODS

Written informed consent, as defined by the Wichita State University Institutional Review Board, was obtained from 18 healthy participants (12 males and 6 females; mean weight 76.3 ± 13.9 kg; mean height 173.6 ± 7.6 cm; mean age 24.6 ± 3.4 yrs) prior to their participation in the study. Subjects were instructed to cross their arms over their chest, to prevent the effects of varying arm motions from influencing the results [4].

The data collection order was randomized by surface order and by arm condition within surface. Whole body kinematics were recorded at 50 Hz using an eleven-camera, high-resolution motion analysis system (Motion Analysis Corp., Santa Rosa, CA). The eleven cameras recorded the three-dimensional positions of reflective spherical markers positioned on the body. Twenty-two retro-reflective markers were placed on bony landmarks to define different body segments.

Participants were instructed to lay supine and roll to their right to a right side-lying position in a controlled and comfortable manner under two different conditions: (1) arms crossed, and (2) arms uncrossed, as shown in (Figure 1). Subjects were asked to roll under these two conditions five times on three different surfaces (stiff floor, exercise mat, and memory foam mattress).

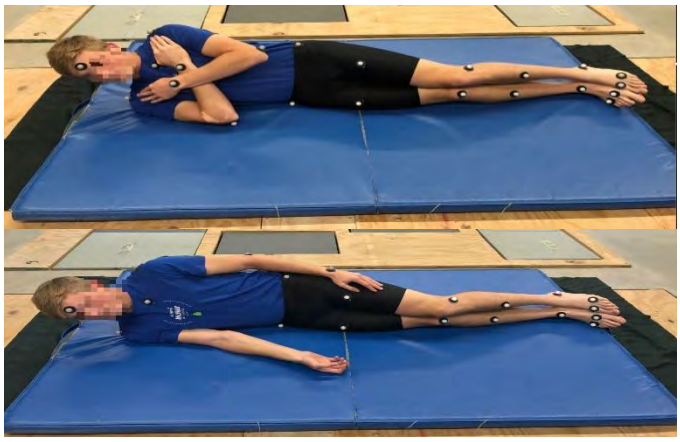

Figure 1: Rolling with arms crossed (upper figure) and arms uncrossed (lower figure).

The marker position x, y, z data were imported into a musculoskeletal simulation software (OpenSim version 3.3) [5] to calculate the body kinematics, including linear (v) and angular (ω) velocities and individual body segment center of mass positions. The total mechanical energy is the sum of potential energy (Ep) and kinetic energy (Ek), which were calculated as:

$$Ep = mgh$$

$$Ek = \frac{1}{2}mv^2 + \frac{1}{2}I\omega^2$$

where m is the mass of the body segment, g is the gravitational acceleration, h is the height of the segment COM in the lab reference frame, *v* is the velocity of the segment COM, I is the mass moment of inertia of the segments, and ω is the angular velocity of the segment. Total energy (Etot) was calculated by summing all positive increments in Ep and Ek [6].

RESULTS AND DISCUSSION

The mean total mechanical energy (E_{tot}) measures across all subjects for arms-crossed rolling on three different surfaces including hard surface, exercise mat, and mattress were 78.4 ± 21.6J, 77.1 ± 20.7J, and 77.7 ± 22.2J, respectively. Similarly, for the arms-uncrossed condition on three different surfaces including hard surface, exercise mat, and mattress, E_{tot} measures were 91.3 ± 23.8J, 88.8 ± 24.0J, and 87.9 ± 26.3J, respectively (Figure 2). There was a significant difference observed for main effects of rolling conditions (p<0.01) for total mechanical energy. No statistically significant difference was observed between the rolling conditions and the surfaces (p=0.403) or in the main effects of the surfaces (p=0.053) for total mechanical energy. For the mean total mechanical energy, potential energy comprised about 90% and kinetic energy comprises 10%, which is consistent for all surfaces and rolling conditions.

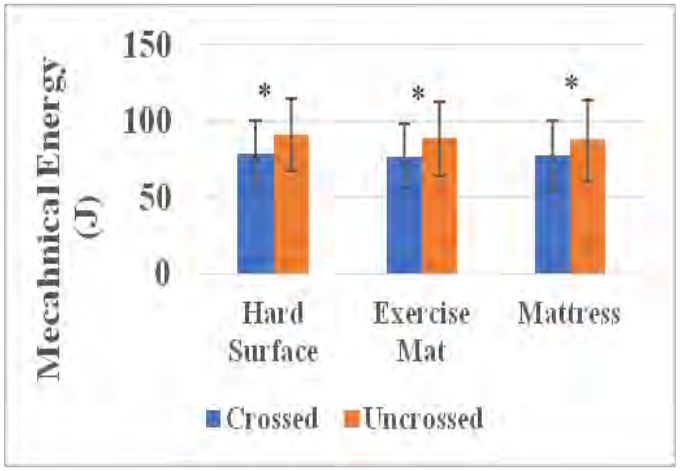

Figure 2: Mean body total mechanical energy across condition and surfaces. Asterisks indicate significant differences between rolling conditions.

Potential energy comprised the majority of energy generated to roll for surfaces and conditions tested [7]. This energy represented the energy required to raise the body center of mass. Kinetic energy is comprised of two components: translational energy and rotational energy. Across all trials, the mean translational kinetic energy was 99% and rotational kinetic energy was 1%, which was consistent for the two rolling conditions and three different surfaces. Constraining the arms over the chest reduces the energy demands to roll from the supine to side-lying position. This finding is very important from the perspective of healthcare workers who reposition individuals with immobility in bed. Since crossing the arms of the patient may reduce the energy required by healthcare providers to roll a patient, which in turn may reduce their risk of low back injury.

CONCLUSIONS

This study provided insight about the mechanical energy requirements of the body when rolling on different surfaces with arms crossed and arms-uncrossed conditions. The arm segments were the major contributor to the difference observed in the mechanical energy. This information will further help to simplify the musculoskeletal models and simulations in order to understand energy absorbed by the compliant surface during rolling. Rolling on the compliant surface is more difficult as some amount energy is being absorbed by the surface, leading to more requirement of energy as input to roll.

REFERENCES

1. Hassan M, et al. *BMES Conf Proc*, 2015.
2. Hassan M, et al. *ASB Conf Proc,* 2016.
3. Agrawal R,et al.*ASB Conf Proc,* 2016.
4. Richter RR, et al. *Phys. Ther* 69:63-71, 1989.
5. Delp SL, et al. *IEEE Trans Biomed Eng,* 54:1940-1950, 2007
6. Cavagna GA et al. J Physio 262, 639-657, 1976.
7. Hassan M, et al. *ASB Conf Proc,* 2015

ACKNOWLEDGEMENT

This study was supported by Regional Institute of Aging.

Development of a Pelvic Model for Study of Surgical Errors in the Midurethral Sling Procedure

[1] Md A. Arif, [2]Fizza Mahmud, [1] Gregory W. King, [2] Gary Sutkin, [1] Antonis P. Stylianou

[1] Department of Civil & Mechanical Engineering, University of Missouri – Kansas City, MO, USA
[2] Department of Obstetrics & Gynecology, University of Missouri – Kansas City, MO, USA
Email: maa5g8@mail.umkc.edu, web: http://s.web.umkc.edu/stylianoua/

INTRODUCTION

Surgical procedures always involve an element of risk and even a minor error can lead to serious complications. Recent data suggests that over 200 million surgeries are performed annually worldwide and about 3 to 22% of these surgeries involve some sort of complications. Surgical errors can be caused by both technical errors and cognitive errors which may happen to even an experienced surgeon. However, resident surgeons are more prone to surgical errors as they start their surgical career with less experience and skills [1]. In order to reduce errors and accelerate the learning experience of surgeons, we propose a method that can identify, model and prevent surgical errors by using biomechanical motion analysis and a high-fidelity 3-D surgery simulator.

Our work targets a complex, common, and high-risk surgery for stress urinary incontinence called the midurethral sling (MUS) procedure. The procedure involves using a sharp steel trocar to place a mesh underneath the urethra to control its mobility. For this surgery, the surgeon has to guide the sharp steel trocar blindly past the bladder, bowel and some major blood vessels that require the surgeon to have distinct surgical skills (bimanual dexterity, ability to envision a blind 3-D space, strong knowledge on the complex anatomy of the periurethral and perivesical spaces etc.) [2].

Surgical errors occurring during trocar passage procedure could be described and therefore predicted and/or prevented by discrete changes in the kinematics of the surgeon's shoulder, arm, hand and the spatio-temporal characteristics of the trocar [3]. The main goal of this study is to create a high fidelity 3-D pelvic simulator to study the kinematics of on particular high-risk step of the MUS surgery.

METHODS

The first step in this work is to create a high fidelity 3-D model of the pelvic anatomy. The Virtual Pelvic Surgery model (VPS) was developed from segmentation of high resolution magnetic resonance images (MRI) of a 57-year-old female patient with stress urinary incontinence. Structures of pelvic anatomy including bone, muscle, blood vessels, bladder, uterus, urethra, vaginal wall, and skin were segmented from MRI using 3D Slicer (www.slicer.org). The 3-D geometries were post-processed using MeshLab (http://www.meshlab.net/) and Artec Studio (www.artec3d.com). Post-processing of 3-D geometries included reduction of artifacts and noise, and decimation to reduce the file sizes. Finally, all individual geometries were combined to form the complete 3-D virtual pelvis model.

The VPS was then used to construct a physical pelvic model. All the structures of the pelvic anatomy were 3-D printed using a Dimension bst1200es series 3D printer. Individual physical structures are assembled and encased to construct the complete 3-D physical pelvis model.

The next step will be to use biomechanical motion analysis (www.vicon.com) to measure surgeon shoulder, hand, and arm kinematics, as well as the kinematics of the surgical instrument during simulated trocar passages. The kinematics of the most common surgical errors (injury of the bladder, urethra, bowel, or external iliac vessels) will be analyzed using this procedure.

RESULTS AND DISCUSSION

High resolution T2 MR Image sequences were used to segment the bowel, urethra, vaginal wall, ureter,

levator muscle and rectus abdominus muscles. Muscles such as obturator, quad, vastus, adductor, tensor fasciae latae, sartorius, iliopsoas, rectus femoris, piriformis, pectineus, gracillis, semimembranus and semitendinosus were more clearly visible from out-phase MR image sequences. In-Phase MR image sequences were used to segment the skin (with fat layer), part of bowel and urethra. Major blood vessels (external iliac vein and artery, femoral vein and artery), fascia and bowel were segmented from the Water MR Image sequences. Femur, pelvic bone, bladder, rectum and uterus were segmented from all five sequences (T2, In-Phase, Out-Phase, Water and Fiesta) and merged to finalize these geometries.

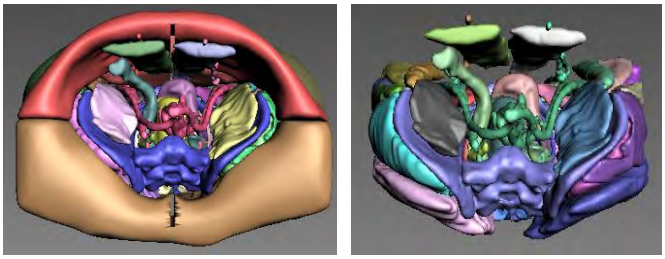

Figure 1: Pelvic Model (after post-processing)

High resolution Out-Phase MR image sequences have been used to extract the peritoneum membrane to provide us with a proper indicator of surgeon's performance. In ideal cases, it is expected that the surgeon will maintain minimum distance between the trocar and peritoneum membrane while performing this surgery.

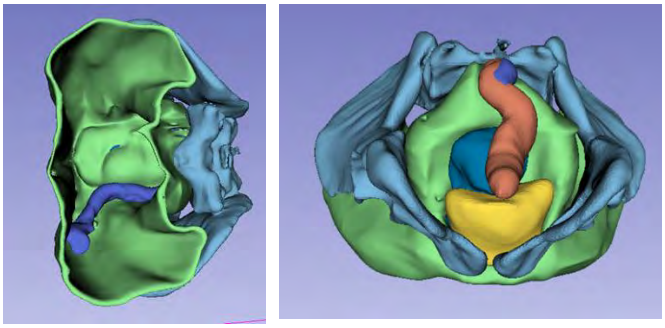

Figure 2: Pelvic Model with Peritoneum

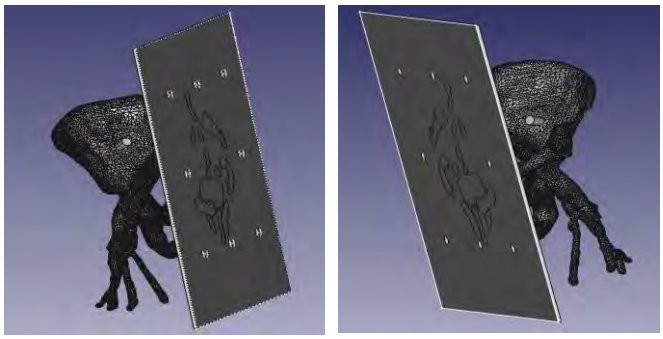

Figure 3: Virtual CAD model with mid-plates

During the procedure, the trocar will never cross through the mid-plane of the pelvic anatomy. This novel model includes two thin plates (3mm thickness) in the middle to attach the soft tissues and blood vessels from both sides, and two mid-pates have been mounted on each other using 8 small posts (3mm radius for each of them). After post-processing, small posts and pockets (5mm radius) have been created on individual geometries using FreeCAD (www.freecad.com) to attach them on the physical model based on correct anatomical orientation.

CONCLUSIONS

The aim of this research project is to create a realistic anatomical platform on which surgical trainees can practice their skills and get effective feedback on their overall surgical errors through kinematic analysis.

REFERENCES

1. WHO Guidelines for Safe Surgery 2009: Safe Surgery Safe Lives. 2009, World Health Organization: Geneva.
2. Ford et al., Mid-urethral sling for stress urinary incontinence. Cochrane Database, 2015
3. Siddicky, S., Use of Biomechanical Motion Analysis to Evaluate Endotracheal Intubation Skill, UMKC, 2015

ACKNOWLEDGEMENTS

University of Missouri Research Board (UMRB)

(IRB Protocol ID: 17-310; PI: Gary Sutkin, M.D.)

INFLUENCE OF INCREASED FORWARD TRUNK FLEXION DURING STAIR ASCENT ON THE AVERAGE RATE OF PATELLOFEMORAL JOINT STRESS DEVELOPMENT

[1]Lee T. Atkins, [1]Cevan Smithson, [1]Daniel Grimes, [1]Nancy Heuer

[1]Angelo State University, San Angelo, TX, USA
email: lee.atkins@angelo.edu

INTRODUCTION

Patellofemoral pain (PFP) is a common yet complex, multifactorial condition that affects women more frequently than men [1]. One theory assumes that increased patellofemoral joint (PFJ) stress is a contributing factor to PFP onset and exacerbation [2]. In particular, a recent study reported that the average rate of patellofemoral joint (PFJ) loading was significantly and positively associated with the rate of change in PFP ($r=0.42$, $p=0.02$) [3]. Thus, it has been recommended that clinicians utilize treatments that minimize the average rate of PFJ loading during provocative functional tasks for patients with PFP.

Stair ambulation has been identified as an activity that evokes symptoms for persons with PFP [4]. Furthermore, it has been reported that while running a 7° increase in forward trunk flexion was associated with a reduction in peak PFJ stress ($p<0.01$) [5]. Although feasible, it is not known if the same strategy (i.e. increased forward trunk flexion) causes a decrease in the average rate of PFJ stress development during stair ambulation. Therefore the purpose of this study was to test the hypothesis that increasing forward trunk flexion during stair ascent would cause a decrease in the average rate of PFJ stress development.

METHODS

Twenty female subjects (age: 23.4 ± 2.5 yr; height: 164.4 ± 7.9 cm; mass: 63.0 ± 12.2 kg) participated in this study. To be included subjects must have been free of lower limb and low back pain at the time of testing and must have reported no prior lower limb or low back surgery.

Each subject performed 5 trials of stair ascent (tread height: 12 cm, tread depth: 26.5 cm) using their self-selected (SS) and a forward flexed trunk posture (FLX) for a total of 10 trials. The velocity of each trial was controlled by having subjects step to the beat of a metronome (96 steps/min). Sagittal trunk and knee kinematics (200 Hz) and ground reaction force (2000 Hz) data were collected using an 8 camera Vicon motion capture system and Bertec forceplate (embedded in the first step of the staircase) respectively. Patellofemoral joint stress was estimated using a previously described PFJ model [5]. Subject-specific model inputs included sagittal knee angle and moment data obtained during the stance phase of each trial. Additional model inputs, not specific to subjects, were calculated using data from previous studies and included quadriceps lever arm length, quadriceps muscle force, PFJ contact area, and a constant that described the ratio of the quadriceps force to patellofemoral joint reaction force (PFJRF) as a function of knee flexion angle [6, 7, 8].

The primary dependent variable was the average rate of PFJ stress development. Secondary dependent variables included the average rate of change of the PFJRF, PFJ contact area, knee extensor moment, and knee flexion angle. All dependent variables were calculated during the time from initial contact to the point of peak PFJ stress. Paired t-tests were used to evaluate for differences in dependent variables between conditions.

RESULTS AND DISCUSSION

The average sagittal plane trunk angle was significantly greater during the FLX condition ($p<0.01$, 45.4 ± 22.4°) compared to the SS condition (14.6 ± 8.3°). Additionally a concomitant decrease in the average rate of PFJ stress development was observed during the FLX condition ($p<0.01$, 51.0 ± 16.3 MPa/sec) compared to the SS condition (33.2 ± 15.5 MPa/sec) (Figure 1).

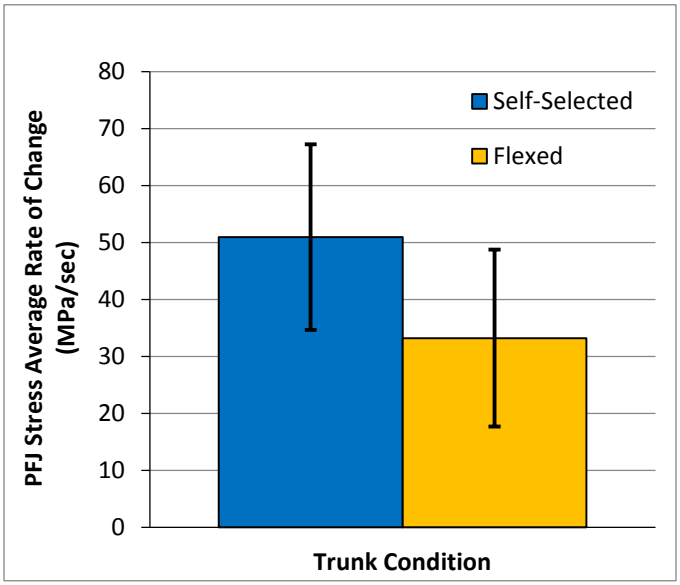

Figure 1. Average rate of change in patellofemoral (PFJ) stress during the self-selected and forward flexed trunk conditions. Error bars represent one standard deviation.

The observed decrease in average rate of PFJ stress development was the result of a significant decrease in the average rate of PFJRF development ($p<0.01$) from the FLX to the SS condition (Table 1) as the average rate of change in PFJ contact area was similar for both conditions ($p=0.48$) (Table 1). Furthermore, the observed decrease in average rate of PFJRF development was caused by a decrease in the average rate of change in knee extension moment ($p<0.01$) from the SS to FLX condition (Table 1). The knee flexion angle did not contribute to the change in PFJRF rate as the knee extended at a more rapid rate during the SS condition compared to the FLX condition ($p<0.01$) (Table 1).

CONCLUSIONS

Findings from this study indicate that increasing forward trunk flexion during stair ascent is effective for minimizing the average rate of PFJ stress development. Clinicians should consider teaching patients with PFP to utilize increased forward trunk flexion during stair ascent as this may be effective for minimizing symptom exacerbation. However, additional studies are needed to confirm these findings in PFP patients. Additionally, the effects of increasing forward trunk flexion on PFP should be examined as well.

REFERENCES

1. Boling et al. *Scand J Med Sci Sports*. 20: 725-30, 2009.
2. Heino-Brechter, Powers. *Med Sci Sports Exerc*. 34(10): 1582-93, 2002.
3. Atkins et al. *Clin Biomech*. 53: 31-6, 2018.
4. Schwane et al. *J Athl Train*. 49(3), 2014.
5. Teng and Powers. *J Orthop Sports Phys Ther*. 44(10): 785-92, 2014.
6. van Eijden et al. *Acta Anat*. 129: 310-14, 1987.
7. van Eijden et al. *J Biomechanics*. 19(3): 219-29, 1986.
8. Powers et al. *Clin Biomech*. 13: 616-24, 1998.

Table 1: Effect of trunk posture on secondary dependent variables of interest.

	Self-Selected	Forward Flexed	P-value
Patellofemoral Joint Reaction Force Average Rate of Change (N/kg/sec)	192.4 ± 56.8	122.0 ± 50.4*	<0.01
PFJ Contact Area Average Rate of Change (mm^2/sec)	-22.7 ± 20.7	-25.9 ± 16.2	0.48
Knee Extension Moment Average Rate of Change (Nm/kg/sec)	8.1 ± 2.2	5.4 ± 2.1*	<0.01
Knee Flexion Angle Average Rate of Change (deg/sec)	-60.2 ± 14.5	-31.1 ± 21.1*	<0.01

Values are mean ± SD. * indicates a significant difference from the self-selected condition ($\alpha = 0.05$).

TRUNK KINEMATICS DURING SIMULATED ROOF SHINGLE INSTALLATION

[1,2] Robert E. Carey, [1]Erik W. Sinsel, [1]John Z. Wu, [1]Christopher M. Warren, and [1]Scott P. Breloff

[1] Health Effects Laboratory Division, National Institute for Occupational Safety and Health, Morgantown, WV, USA
[2] Department of Mechanical Engineering and Materials Science, University of Pittsburgh, Pittsburgh, PA, USA
email: RCarey@cdc.gov, web: https://www.cdc.gov/niosh/

INTRODUCTION

There are more than 146,000 roofers in the United States of America, and that number is expected to increase to more than 162,000 by 2026 [1]. Roofers are required to bend and twist their bodies repetitively in a kneeling, crouching, stooping or crawling position for 75% of their work time, and when combined with excessive loading, these postures may contribute to the development of musculoskeletal disorders (MSDs) [2]. From 2013 to 2016, the occurrence of MSDs in the roofing industry has more than doubled from 340 to 850 reported cases per year [2], resulting in a median of 10 days away from work in 2016 [3].

The lower back is largely affected by MSDs in the roofing industry, evidenced by a greater back injury rate among roofers than the average construction sector [2]. Workers who experienced back pain in more physically demanding work settings and in awkward postures were 300% more likely to retire prematurely than those involved in less physically challenging work [4]. The goal of the current study is to investigate whether the roof pitch and task performed during simulated shingle installation significantly influences trunk joint angles.

METHODS

Eight male subjects (age: 27.6 ± 5.9 years, height: 181.0 ± 6.6 cm, weight: 89.5 ± 9.8 kg) participated in the National Institute for Occupational Safety and Health's (NIOSH) Institutional Review Board (IRB) approved study after providing informed consent.

Three dimensional kinematic data were collected using a 14-camera motion capture system (Vicon, Oxford, England), sampled at 100 Hz, using spherical skin-surface reflective markers placed on body segments using clusters, as well as bony anatomical landmarks. Subjects were asked to simulate roof shingle installation five times at three randomly ordered roof pitch angles (0°, 15°, and 30°) for a total of 15 trials. The subjects used their dominant hand during trials (all but one were right-handed), and the nail gun was not loaded or powered.

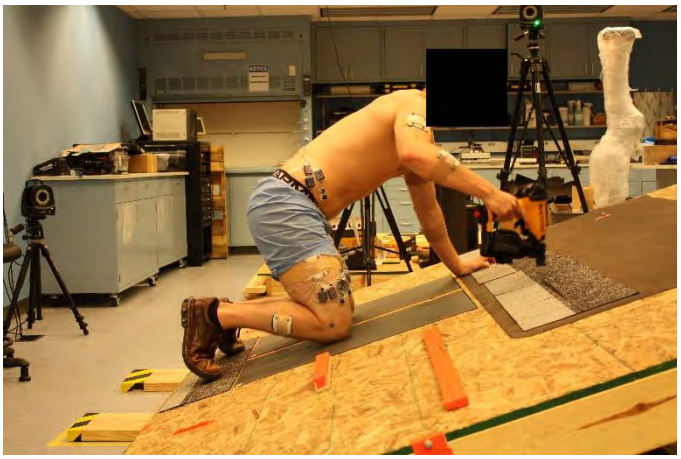

Figure 1: Subject using a nail gun to simulate affixing roof shingles at a 15° pitch.

Kinematic data were modeled to obtain six degree of freedom trunk joint angles (flexion/extension, left/right lateral bending, left/right axial rotation) using commercially available biomechanics analysis software (Visual 3D, C-Motion, Germantown, MD, USA). The simulated roof shingle installation was analyzed in four sequential phases: (1) beginning from an upright kneeling posture, picking up and placing the shingles, (2) picking up and positioning a nail gun, (3) using the nail gun to affix the shingles (Fig. 1), and (4) returning the nail gun to its original position, going back to an upright kneeling posture. For each trial, the maximum angle for each degree of freedom was found within each phase. Two-way repeated measures analysis of variance tests were performed to determine statistical significance ($p<0.05$) between different phases and

roof pitch angles, using the Greenhouse-Geisser correction when sphericity was violated.

RESULTS AND DISCUSSION

Statistical significance was found for the following main effects: (1) flexion pitch and phase ($p \leq 0.001$), (2) left lateral bending phase ($p \leq 0.001$), (3) right lateral bending pitch ($p=0.003$) and phase ($p \leq 0.001$), (4) left axial rotation phase ($p \leq 0.001$), and (5) right axial rotation phase ($p=0.011$). Significant differences were also seen in the interaction effect between pitch and phase for right lateral bending ($p \leq 0.001$), right axial rotation ($p=0.016$), and left axial rotation ($p \leq 0.001$). Pairwise comparisons between different pitch angles and phases for each kinematic variable produced significant results (Table 1 & 2). One interesting result is that as the pitch angle of the roof increased, the maximum flexion angle of the roofer's trunk decreased (0°: 81.1°±6.3°; 15°: 68.1°±4.7°; 30°: 61.1°±5.7°). Our results suggest that trunk posture is influenced by differences in roof pitch and shingle installation tasks.

CONCLUSIONS

Postural changes in the trunk induced by different roof pitch angles and roof shingle installation phases suggest the necessity of wearable interventions. Devices such as knee pads and knee savers may reduce joint angles in the trunk; however, there are no such devices currently designed exclusively for roofing work. Future studies will examine the effects of such devices.

REFERENCES

1. Bureau of Labor Statistics (BLS), *Employment Projections*, https://data.bls.gov/projections.
2. Center for Construction Research and Training (CPWR), *The Construction Chart Book: The U.S. Construction Industry and Its Workers*, Silver Spring, MD, USA, 2013.
3. Bureau of Labor Statistics (BLS), *Nonfatal cases involving days away from work: selected characteristics (2011 forward)*, https://www.bls.gov/data/#injuries.
4. Welch et al. *American Journal of Industrial Medicine*. 53(6): 552-560, 2010.

DISCLAIMER

The findings and conclusions in this report are those of the authors and do not necessarily represent the official position of the National Institute for Occupational Safety and Health, Centers for Disease Control and Prevention.

Table 1: Significant differences ($p \leq 0.05$) between maximum trunk joint angles for flexion (*), right lateral bending (‡), and right axial rotation (╫) at different roof pitch angles.

Pitch angle (°)	Pitch angle (°)	
	15	30
0	*,‡,╫	*
15		*,‡

Table 2: Significant differences ($p \leq 0.05$) between maximum trunk joint angles for flexion (*), left lateral bending (†), right lateral bending (‡), left axial rotation (╪), and right axial rotation (╫) at different roof shingle installation phases.

Phase	Phase		
	2	3	4
1	†,‡,╪	*,†,‡,╪,╫	*,†,╪,╫
2		*	†,‡
3			*,†,‡

RELATIONSHIP BETWEEN MEDIAL LONGITUDINAL ARCH ANGLE AND FIRST RAY MOTION DURING WALKING

Christopher Casillas, Linnea Zavala, and James Becker

Montana State University, Bozeman, MT
email: james.becker4@montana.edu; web: http://www.montana.edu/biomechanics

INTRODUCTION

Abnormal motion of the first ray has been associated with several foot disorders, including metatarsalgia, hallucis valgus, and hallucis rigidus [1]. In clinical settings, static measurements of first ray mobility are commonly used to assess risk for these disorders. However, static measurements of the first ray do not seem to fully represent the motion of the first ray during walking [2]. Thus, the use of both static and dynamic measurements of first ray motion are important to gain a further understanding of the relationship between foot disorders and first ray motion.

A "gold standard" method for assessing dynamic motion of the first ray requires the use of detailed foot models and three-dimensional motion capture, options which are not available in most clinical settings. However, in clinical settings it is feasible to use two-dimensional video analysis to quantify the medial longitudinal arch (MLA) angle. The MLA encompasses the structures composing the first ray and could potentially be a simplified method of assessing first ray motion. A relationship between MLA and first ray motion would provide clinicians a practical option for describing first ray motion.

Therefore, the aim of this study was to explore the relationship between first ray motion and MLA. We specifically examined the relationship between both static measures of MLA taken during quiet standing and dynamic measures of MLA during gait, and dynamic first ray motion. We hypothesized that a strong relationship exists between MLA angle and the mobility of the first ray.

METHODS

All participants provided IRB-approved informed consent. Participants consisted of 10 physically active individuals (sex: 5 M, 5 F; age: 21.8 ± 3.0 years; mass: 71.4 ± 9.9 kg; height: 1.74 ± 0.90 meters). All participants were free from any lower extremity injuries at the time of testing. A 12-camera motion capture system (Motion Analysis) was used to record foot kinematics 200 Hz. Participants completed a static trial of quiet standing with feet shoulder width apart followed by three walking trials for both left and right feet. The subjects were asked to walk at a self-selected walking speed. Stance phase was determined using an AMTI force plate sampling at 1200 Hz.

A multi-segment foot model was used to calculate sagittal plane movement of the first metatarsal relative to the midfoot [3]. MLA angle was determined by calculating angle between the medial heel, navicular, and first metatarsal head marker. For the quiet standing trial, mean MLA across the trial was calculated. For the walking trials range of motion (ROM), peak, and minimum angles for MLA during stance phase were calculated. First ray motion was quantified as ROM across the walking trials. The three trials from each foot were averaged with the average value being used for the regression analysis (n = 20 trials).

Linear regressions were used to analyze the relationship between first ray motion and peak, minimum, ROM, peak, and static MLA angles.

RESULTS AND DISCUSSION

Average first ray ROM across all subjects during the walking trials was 7.8 (± 2.5°). The results from the multiple regressions varied among the different measures of MLA. The first ray and MLA share components; therefore, it was hypothesized that the MLA angle would move in tandem with the first ray. However, there was no relationship between first ray ROM and MLA angle ROM ($R^2 = 0.05$, $p = 0.36$, Figure 1). There was a statistically significant but weak relationship between first ray ROM and

peak MLA angles ($R^2 = 0.21$, $p = 0.04$, Figure 1). A similar significant but weak relationship existed between first ray ROM and minimum MLA angle ($R^2 = 0.29$, $p = 0.01$, Figure 2). The static measurement of MLA angle unexpectedly had the strongest relationship with first ray ROM. ($R^2 = 0.41$, $p = 0.002$, Figure 2).

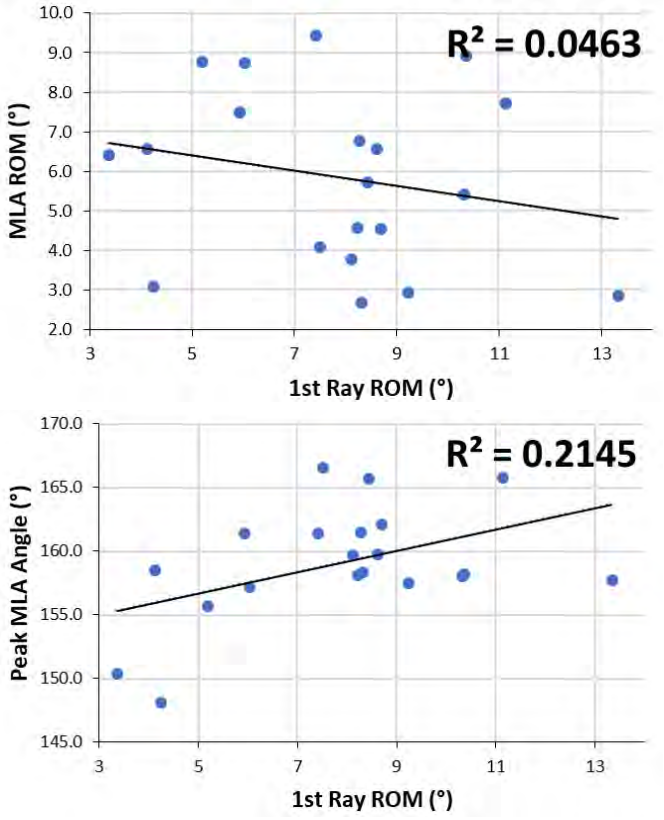

Figure 1. Relationship between first ray ROM and MLA ROM during stance phase (top) and peak MLA angle during stance phase (bottom).

The results were unexpected, as previous literature has shown that static first ray measures do not accurately reflect dynamic first ray motion [2]. As such, it was hypothesized that dynamic measurements of MLA angle would have a stronger relationship to the dynamic motion of the first ray. However, dynamic measures only had weak relation to first ray motion compared to the moderate relation between static MLA angle and first ray motion. This might indicate that during dynamic task MLA and first ray motion are quantifying different aspects of foot function. Further research is necessary to determine the relationship between MLA and the first ray using both static and dynamic measures.

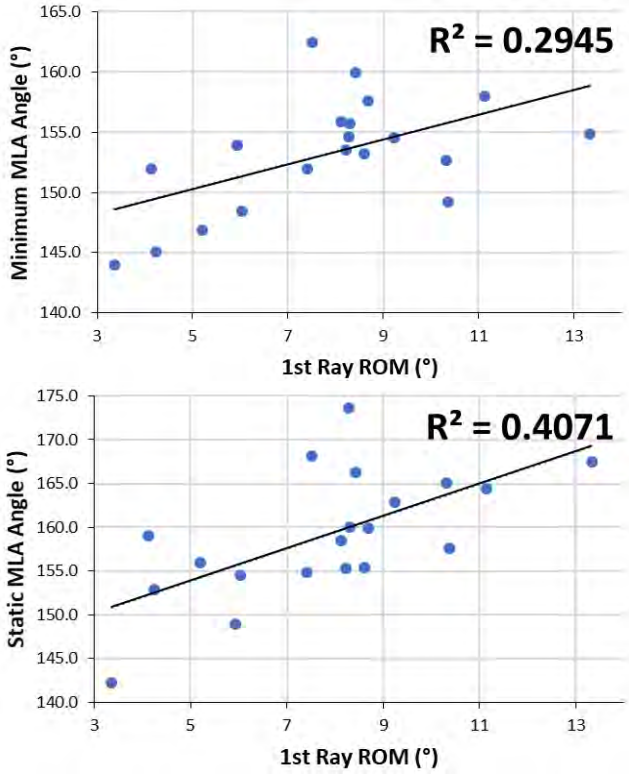

Figure 2. Relationship between first ray ROM and minimum MLA angle during stance phase (top) and static MLA during quiet standing (bottom).

In interpreting our results, it is important to note that our measurement of MLA angle was different from what is commonly used in clinical settings in two ways. First, three-dimensional motion capture was utilized instead of two-dimensional video, and secondly, the marker on the first metatarsal head was placed on the distal dorsal aspect of the metatarsal instead of the distal medial aspect. While previous studies have quantified MLA using similar marker placements [3], it is not clear whether marker placement influenced the relationships examined in the current study.

CONCLUSIONS

Static measures of MLA angle during quiet standing are able to predict movement of the first ray during gait better than dynamic measures of MLA. Static measures may be clinically useful for quantifying potential abnormalities in first ray motion

REFERENCES

1. Greisberg et al. Foot Ankle Int. **33**, 44-49, 2012.
2. Allen et al. Foot Ankle Int. **25**, 391-396, 2004.
3. Leardini et al. Gait Posture, **25**, 453-462, 2

MOVING OUT OF THE LABORATORY AND IN TO THE REAL WORLD: USING INERTIAL MEASUREMENT UNITS TO ASSESS LONG-TERM RECOVERY AFTER TOTAL KNEE ARTHROPLASTY

[1] Ryan M. Chapman, [2]Wayne E. Moschetti, and [1]Douglas W. Van Citters

[1] Dartmouth College, Thayer School of Engineering, Hanover, NH, USA
[2] Dartmouth Hitchcock Medical Center, Department of Orthopaedics, Lebanon, NH, USA
email: rmchapman.th@dartmouth.edu, web: http://engineering.dartmouth.edu/dbec/

INTRODUCTION

Maximum knee range of motion (ROM) is typically the metric cited when attempting to establish dysfunction prior to total knee arthroplasty (TKA) and recovery following TKA [1, 2]. However, this measure is traditionally captured at discrete time points (e.g. 1-week pre- or 6-weeks post-TKA) in ideal settings (e.g. clinic or laboratory) while performing idealized movements (e.g. passive ROM via goniometry). This idealized measurement technique may not accurately represent knee function during activities of daily living (ADL). Moreover, simply because an individual can achieve a large ROM, does not mean they will actively utilize that ROM during ADL. As such, a novel method for continuously monitoring long-term knee function was developed and validated using inertial measurement units (IMUs). Then, a prospective study was completed to evaluate long-term knee function before and after TKA and the results compared to a cohort of healthy individuals.

METHODS

Two distinct IMU sensors (Fig. 1) were affixed to the thigh (superior to lateral epicondyle) and shank (inferomedial to tibial tuberosity), respectively. Relative motion between the two IMUs was utilized to calculate knee flexion continuously.

This method was validated in a laboratory via comparison to optical motion capture (MOCAP) with two subjects during repeated walking trials on a treadmill at 1.5, 2.0, and 2.5 MPH.

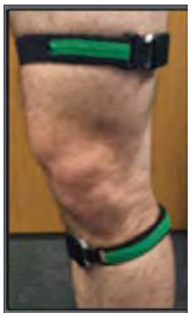

Fig 1. IMU placement for knee ROM

Following validation and IRB approval, 17 patients (10M, 65±6 years) undergoing TKA wore the sensors on the affected leg for 1-week pre-TKA, 6 weeks immediately post-TKA, and 1 week at 1 year post-TKA. Additionally, 10 control subjects (5M, 50±18 years) wore sensors on the dominant leg for 1 week. Subjects donned/doffed the IMUs upon waking/prior to sleeping each day for the duration of their required participation in the study. Daily average and maximum knee flexion were computed. Additionally, knee flexion during periods of gait was averaged across strides each day and normalized as a percentage of the gait cycle. IMU-based metrics were averaged weekly and weekly average metrics were averaged across subjects. Finally, patient reported outcome measures (PROMs) and clinical maximum ROM were captured from all subjects at all time points.

RESULTS AND DISCUSSION

Validation via comparison to optical MOCAP showed good agreement between MOCAP and IMU-based measures with average error of 1° for all both subjects at all walking speeds (Fig. 2).

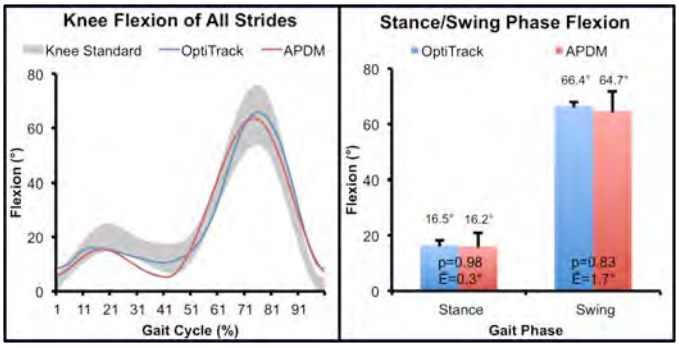

Fig 2. Validation of IMU-based ROM algorithm via comparison with optical MOCAP.

Subject demographics are contained in Table 1. Only one significant difference was noted between cohorts with respect to age ($p<0.05$). Average

flexion (Fig. 3) was increased during post-TKA weeks 2/3 and subsequently decreased thereafter. Maximum flexion (Fig. 4) was not significantly different between cohorts at any time point. When assessing flexion during stance phase (Fig. 5), patients were reduced below controls pre-TKA and during post-TKA weeks 1 and 2. However, from post-TKA week 3 onward controls and patients were indistinguishable with steady improvement for patients week after week. In contrast knee flexion during swing phase of gait (Fig. 6) was reduced for patients pre-TKA and during all six immediate post-TKA weeks. However, when analyzed at one-year post-TKA patients and controls were equal.

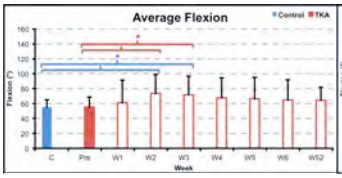

Fig 3. Average flexion

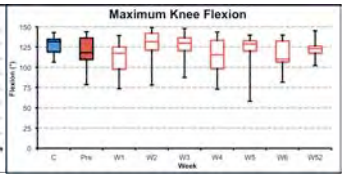

Fig 4. Maximum flexion

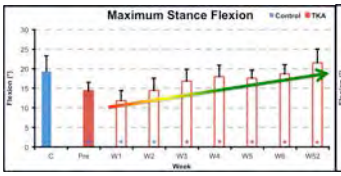

Fig 5. Maximum stance flexion

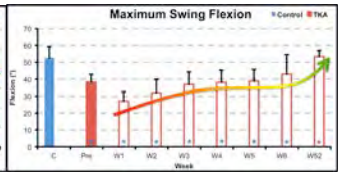

Fig 6. Maximum swing flexion

Despite many advances in orthopaedics (e.g. patient specific implants), pre- and post-operative monitoring has remained homogenous. As such, we developed and validated a novel IMU-based method for continuously (8-12 hours/day) monitoring long-duration (weeks at a time) knee ROM before and after TKA. The method was validated with average error of 1°.

In more detail, we found average flexion rose and subsequently fell and is likely not useful for assessing function following TKA. Our results with respect to maximum knee flexion are well aligned with previous work indicating pre-TKA maximum flexion is the greatest predictor of post-TKA maximum flexion. Specifically, we noted maximum flexion was not significantly different between cohorts at any time. As such, maximum knee flexion is likely not well suited for assessing knee function following TKA. Despite the limited utility of average and maximum flexion, we found significant improvements in stance and swing flexion following TKA. More specifically, given the relatively short time to recovery for stance flexion we believe this can be used to assess basic gait function. In addition, because swing flexion needed one year to fully recover we believe this metric can be used to quantify gait quality post-TKA.

CONCLUSIONS

Our method provides far more clarity on expected pre- and post-TKA knee biomechanics in real-world environments. More specifically, the method allows extension beyond well-controlled laboratory studies while maintaining the precision and accuracy afforded by those methods. Additionally, this study further elucidates what metrics are critical to monitor before and after TKA. Clinical ROM is often used as the metric to assess function, however our work highlights that knee flexion during both phases of gait are more sensitive for capturing knee function before and after surgical intervention.

REFERENCES

1. Ryu, J. et al. 1993, *Factors influencing the postoperative range of motion in total knee arthroplasty*, Bulletin Hospital for Joint Diseases, **53**(3), pp. 35-40.
2. Callaghan, J. J. et al., 2000, *Cemented rotating-platform total knee replacement: A nine to twelve-year follow-up study*, JBJS, **82**(5), pp. 705-711.

ACKNOWLEDGEMENTS

We are grateful for the efforts of Dan Ressler and Lisa Davis of the Clinical Research Unit.

Table 1: Subject demographics for both control and patient cohorts

	Subjects	Gender	Age	Footedness	Sensor Side	Days	Hours/Day
Controls	10	5M, 5F	50±19	0.7±0.5	8R, 2L	7±0	12.0±4.7
Patients Pre-	17	10M, 7F	65±6	0.7±0.5	9R, 8L	6±1	11.2±3.2
Patients Post-6W						36±4	11.0±0.8
Patients Post-1Y						6±1	12.8±3.4

ASSESSING RECOVERY IN TOTAL & REVERSE SHOULDER ARTHROPLASTY VIA INERTIAL MEASUREMENT UNITS: WHAT METRICS ARE IMPORTANT TO MEASURE?

[1] Ryan M. Chapman, [2]Michael T. Torchia, [2]John-Erik Bell, and [1]Douglas W. Van Citters

[1] Dartmouth College, Thayer School of Engineering, Hanover, NH, USA
[2] Dartmouth Hitchcock Medical Center, Department of Orthopaedics, Lebanon, NH, USA
email: rmchapman.th@dartmouth.edu, web: http://engineering.dartmouth.edu/dbec/

INTRODUCTION

Shoulder arthroplasty (SA) is the fastest growing arthroplasty procedure in the United States (US). However, because the total volume of SA procedures is significantly less than that of total knee (TKA) and hip arthroplasty (THA), little is known about the typical recovery process after surgical intervention. Generally, clinicians utilize maximum shoulder elevation to measure recovery. Unfortunately, this metric is typically captured at discrete time points (e.g. 1-week pre-SA, 6-weeks post-SA) in controlled settings (e.g. clinic) while performing prescribed movements (e.g. passive ROM via goniometry). These idealized measures may not represent 'real-world' shoulder function during activities of daily living (ADL). Moreover, an individual that can achieve a large shoulder range of motion (ROM) may not actively utilize the entirety of such ROM during ADLs. As such, a novel method for continuously monitoring long-term shoulder function was developed and validated using inertial measurement units (IMUs). A prospective study was then undertaken to evaluate long-term shoulder function before and after total shoulder arthroplasty (TSA), before and after reverse shoulder arthroplasty (RSA), and the results compared to a cohort of healthy individuals.

METHODS

Two IMU sensors were rigidly attached to the sternum (xyphoid process) and humerus (deltoid tuberosity), respectively. Relative motion between the two IMUs was used to continuously calculate shoulder elevation. This method was validated in a laboratory via comparison to optical motion capture (MOCAP) with two subjects during repeated upper extremity movements including forward flexion, abduction, external rotation at 0° abduction, and external rotation at 90° abduction.

Following validation and IRB approval, 10 patients (7M, 70±7 years) undergoing TSA and 10 patients undergoing RSA (1M, 82±5 years) wore the sensors on the affected arm for 1 week pre-SA, 6 weeks beginning at 3 months post-SA, and 1 week at 1 year post-SA (at time of submission, all RSA patients have not returned for one year follow up and are thus omitted from analyses). Additionally, 10 control subjects (4M, 69±20 years) wore sensors on the dominant arm for 1 week. Subjects donned & doffed the IMUs upon waking & prior to sleeping each day, respectively, for the duration of their required study participation. Average and maximum shoulder elevations were computed daily. Additionally, shoulder elevation was broken in to 5° angle bins and the percentage of each day spent in each angle bin (e.g. 0-5°, 5-10°, etc.) was computed. Each IMU-based metric was averaged weekly and weekly average metrics were averaged across subjects. Finally, patient reported outcome measures (PROMs) and clinical maximum ROM were captured from all subjects at all time points.

RESULTS AND DISCUSSION

Validation via comparison to optical MOCAP showed good agreement between MOCAP and IMU-based measures (R^2=0.98) with average error of 1.4° for all aforementioned movements (Fig. 1).

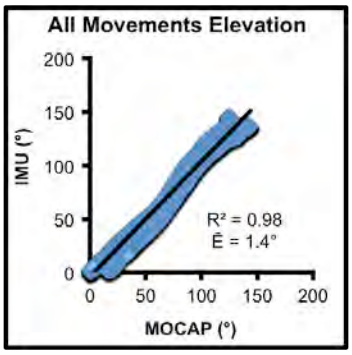

Fig 1. Validation of IMU-based ROM algorithm via comparison with optical MOCAP.

Average elevation (Fig 2) was equal between controls and TSA patients at all times. For the RSA cohort, average elevation was greater than controls at weeks 1 and 3 but was equal at all other times. Maximum elevation (Fig 3) was significantly reduced for TSA patients compared to control subjects during the preoperative week as well as week 1 but was equal thereafter. The RSA cohort showed reduced maximum elevation at all times.

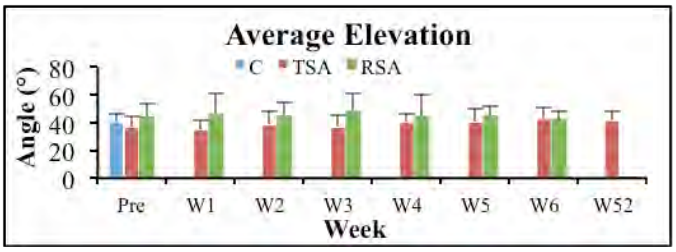

Fig 2. Average elevation

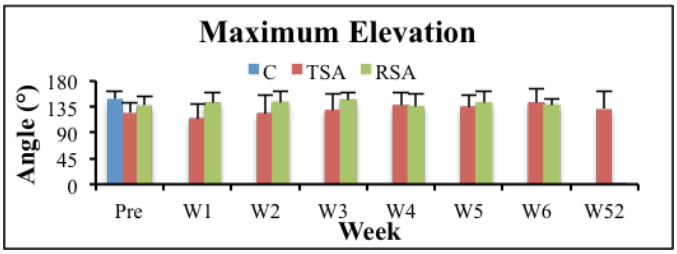

Fig 3. Maximum elevation

Binned elevation showed percentage of day spent below (Figure 4) and above 90° elevation (Figure 5) were similar between cohorts preoperatively. Following surgery, TSA patients showed a consistent decrease in the percentage of the day spent between 0-30° and a corresponding increase in the percentage of day spent between 90-180°. Interestingly, the RSA cohort showed decreasing percent of the day in 0-30° during post-RSA weeks 1-3 and corresponding increases in percent over 90° of elevation but that trend reversed in weeks 4-6.

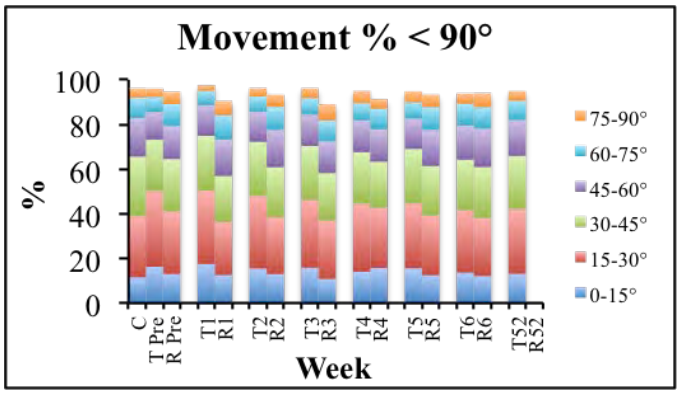

Figure 4. Movement percent < 90°

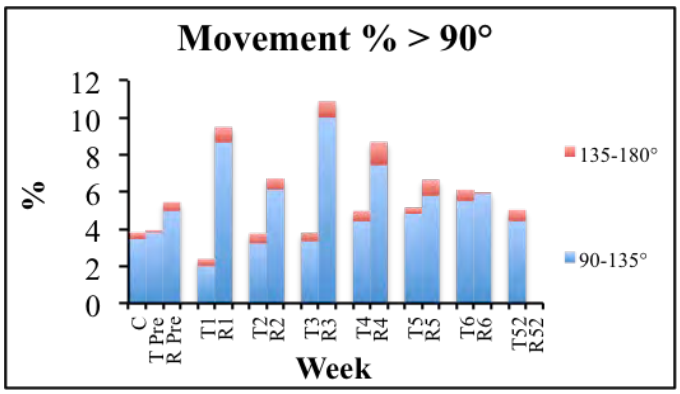

Figure 5. Movement percent > 90°

Although significant improvements have been made in orthopaedics, pre- and post-operative patient monitoring continues to lag. Accordingly, we developed a novel IMU-based method for capturing continuous (8-12 hours) long duration (weeks at a time) shoulder ROM before and after TSA and RSA, respectively. The method was validated with average error of 1.4°.

Through our prospective study, we found that patients undergoing TSA showed steady improvement with respect to movement percentage spent above 90°. In contrast, this study did not elucidate a suitable metric for assessing post-RSA function.

CONCLUSION

Our method provides more nuanced information on our expectations about shoulder function before and after shoulder arthroplasty. Our IMU-based method allows clinicians, patients, and scientists alike the opportunity to capture high-precision biomechanics information outside of the well-controlled laboratory and clinical environments.

ACKNOWLEDGEMENTS

We are grateful for the efforts of Lisa Davis and Dan Ressler of the Clinical Research Unit.

INDIVIDUALS WITH MULTIPLE SCLEROSIS EXHIBIT MORE REGULAR CENTER OF MASS ACCELERATIONS AFTER PHYSICAL THERAPY

[1, 2] Brenda L. Davies, [2]Min Liu, [2]Raschelle M. Hoffman, [2]Heidi Reelfs, [2]Kathleen G. Volkman, [2]Kathleen Healey, [2]Rana Zabad, and [2]Max J. Kurz

[1] Concordia University St Paul, St Paul, MN, USA
[2] University of Nebraska Medical Center
email: mkurz@unmc.edu

INTRODUCTION

Multiple sclerosis (MS) is a progressive, demyelinating disease that affects both the sensory and motor pathways, which disrupts an individual's balance and can also affect mobility [1]. There is a prevailing consensus that neurologic health is associated with a gait pattern that exhibits an optimal amount of variability and that alterations to this variability may serve as a biomarker for disease [2]. Recent investigations have displayed that individuals with MS often have uncharacteristic gait variability [3]. However, it is currently unknown if this uncharacteristic variability can be changed after undergoing a therapeutic exercise intervention and if this change is related to improved mobility.

Therefore, the purpose of this investigation was to explore the influence of a therapeutic exercise intervention upon the variability of the center of mass (COM) accelerations of individuals with MS during a walking task. Secondarily, we evaluated how changes in the spatiotemporal kinematics and walking endurance were related to the changes in COM variability after the intervention. We hypothesized that the COM variability would become more similar to that of a healthy population following the intervention and that these changes would be related to the improved spatiotemporal kinematics and walking endurance.

METHODS

Fifteen individuals (7 female; mean age: 54.8 ± 9) with relapsing-remitting or secondary progressive MS were enrolled in this study. Additionally, 15 healthy, age-matched adults (10 female; mean age: 53.5 ± 7 years) were enrolled and acted as a healthy control group for the gait variables. All experimental procedures were reviewed and approved by the UNMC Institutional Review Board. All subjects provided written informed consent before participating in the experimental procedures.

The subjects with MS completed the experimental procedures before and after the therapeutic intervention and the healthy control subjects completed all outcome measures once. All subjects completed a 6-minute walk test in a hallway ~40 m long. Accelerations of the COM were measured using a tri-axial accelerometer (Delsys Inc., Natick, MA) that was positioned over the L2 vertebra and attached to a neoprene belt. The subjects completed two self-paced walking trials where the spatiotemporal kinematics of gait were measured with a digital mat (GAITRite®, CIR Systems Inc., Sparta, NJ). The spatiotemporal kinematic variables of interest were velocity (m/s), step width (m), step length (m), and cadence (steps/minute).

The unfiltered resultant accelerometer signal was used to evaluate the changes in the gait variability. Standard deviation (SD) was used to quantify the amount of variability present in the acceleration signal. Sample entropy (SampEn) was also calculated to quantify the regularity of the time dependent changes in the resultant accelerometer time series [4]. More regular time dependent changes in the accelerometer time series will have a SampEn closer to zero, while completely irregular time dependent changes will have a SampEn that approaches infinity.

The total physical therapy intervention period was six weeks with the therapy being performed twice a day for five consecutive days each week. Each therapy session consisted of 15 minutes of strength and flexibility exercises, 15 minutes of postural balance exercises, and 15 minutes of treadmill walking.

RESULTS AND DISCUSSION

Thirteen subjects completed the entire six weeks of the therapeutic program. Before the therapeutic intervention, the accelerometer time series for the individuals with MS had a lower SD ($p=0.008$) and a higher SampEn ($p<0.001$) than the healthy control group. Hence, indicating that the individuals with MS had less overall variability and less regular time dependent changes in the accelerations than the healthy control group (Figure 1A & B). After the therapeutic program, there was an increase in SD ($p=0.008$) and decrease in SampEn ($p=0.01$) for the group with MS. These results implied that the amount of variability of the acceleration time series increased and the time dependent changes became more regular for the individuals with MS after the intervention. However, the individuals with MS still had a lower SD ($p=0.05$) and higher SampEn ($p=0.02$) post-intervention than the healthy control group.

After the therapeutic exercise program, there was an improvement in the distance walked during the 6-minute walk (Pre: 298.8 ± 23m; Post: 318.0 ± 24m; $p = 0.04$); however, the improvement did not match the healthy control subjects ($ps<0.001$). Additionally, after the intervention, the individuals with MS improved their walking velocity (Pre: 0.83 ± 0.06 m/s; Post: 0.90 ± 0.06 m/s; $p = 0.05$) and step lengths (Pre: 0.51 ± 0.02m; Post: 0.54 ± 0.02m; $p=0.03$). Even though velocity was still different between the groups post-intervention (Control: 1.17 ± 0.02 m/s; $p<0.001$), the step lengths of the subjects with MS normalized to those of the healthy individuals (Control: 0.58 ± 0.01 m; $p=0.11$).

There was a negative correlation between the percent change in SampEn and the percent change in the distance walking during the 6-minute walk test ($r=-0.64$; $p=0.02$). This indicates that the subjects who had a greater improvement in the distance walked after the therapeutic intervention also tended to exhibited a greater improvement in the regularity of the COM accelerations. There was a negative correlation between the percent change in SampEn and the percent change in the walking velocity ($r=-0.56$; $p=0.05$), indicating that subjects who exhibited greater improvements in walking speed after the therapeutic intervention also tended to have a greater improvement in the regularity of the COM accelerations.

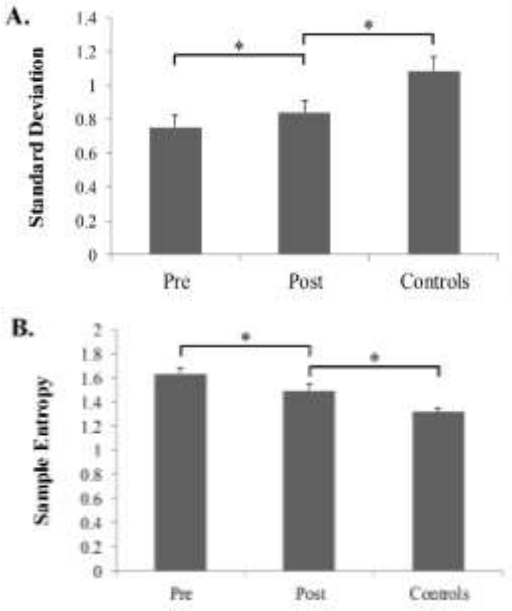

Figure 1: The SD **(A)** and SampEn **(B)** of the resultant accelerations during the 6-minute walk test before and after the therapeutic intervention and for the healthy control group.

CONCLUSIONS

Altogether, these outcomes indicate that after a six week high-frequency therapeutic exercise program, individuals with MS not only exhibited improved walking speeds, step lengths, and walking endurance but also displayed more normal amounts of COM variability and more regular COM accelerations during walking. These improvements in COM accelerations were related to the improvements in walking velocity and endurance. Altogether these results suggest that therapeutic exercise may improve the ability of individuals with MS to control their gait.

REFERENCES

1. Campbell et al. *Mult Scler Relat Disord.* 3(2): 227-36, 2014.
2. Stergiou & Decker. *Hum Mov Sci.* 30(5): 869-888, 2011.
3. Craig et al. *Clin Biomech*. 49: 16-21, 2017.
4. Richman & Moorman. *Am J Physiol Heart Circ Physiol.* 278(6): H2039-2049, 2000.

INERTIAL LOADING OF THE PEDIATRIC HEAD EXCEEDS NECK INJURY TOLERANCE PRIOR TO HEAD INJURY TOLERANCE

[1] Mark A. Davison, [2] Keith D. Button, [2] Brian T. Weaver, and [2]Steve A. Rundell

[1] Rush University Medical Center, Chicago, IL
[2] Explico Engineering Co. Novi, MI
email: kbutton@explico.com, web: www.explico.com

INTRODUCTION

Shaken Baby Syndrome (SBS) has been thought to occur as a result of inertial loading of the head resulting in retinal hemorrhaging, cerebral hemorrhaging, and encephalopathy with little or no sign of external trauma. Recent findings suggest that inertial loading alone is not sufficient to cause these symptoms and that cervical trauma will precede head injury [1,2].

The objective of the current study was to evaluate pediatric neck and head injury potential during purely inertial loading of the head. Both real-world and empirically derived data from automobile collisions provides valuable information related to pediatric injury patterns during pure inertial loading of the head, which is similar to violent shaking. Specifically, frontal collision events involving forward-facing children provide a biomechanical environment analogous to violent shaking. Thus, publicly available full-scale vehicle collision tests and laboratory sled test data from the National Highway Traffic Safety Administration (NHTSA) were analyzed.

The objective of the current study was to evaluate pediatric neck and head injury potential during purely inertial loading of the head. Given the anatomical and biomechanical properties of the pediatric cervical spine, we hypothesized that inertial loading of the pediatric head provides a greater risk of injury to the cervical spine when compared with closed-head injury.

METHODS

Each of the tests considered in the current study involved Hybrid III, 3-year-old anthropometric test devices (ATDs) seated in age-appropriate, forward-facing child restraint systems. The full-scale crash tests utilized in the current study were conducted in accordance with NHTSA's New Car Assessment Program (NCAP), an ongoing program that evaluates new automobiles for occupant safety. Specifically, the NCAP tests involve rigid frontal barrier impacts at barrier equivalent speeds of 35 mph. The laboratory sled testing utilized in the current study was conducted in accordance with FMVSS No. 213. Specifically, the tests consisted of 30 mph deceleration sled tests. 131 New Car Assessment Program (NCAP) test reports were reviewed in addition to 32 sled tests.

Head Injury Criterion 15 (HIC_{15}), and upper neck peak tension force measurements from the reviewed technical reports were documented for each of the ATDs (n=234). The collected values were then evaluated in the context of published and accepted Injury Assessment Reference Values (IARVs) for the Hybrid III, 3 year-old ATD. The IARVs for HIC_{15} and upper neck peak tension force were 570 and 1,430 N for the 3 year-old ATD. The percentage of data points that exceeded either IARV was calculated. Additionally, HIC_{15} was plotted against peak neck tension in order to investigate the presence of a correlation and to graphically depict each data point in relation to the IARVs.

RESULTS AND DISCUSSION

A total of 190 individual data points were obtained from 131 NCAP full-scale vehicle crash tests. The average HIC_{15} was 480.9 (SD = 164.9). The average upper neck peak tension force was 1933.1 N (SD = 275.3). Of these tests, 161 (96%) exceed the upper neck peak tension IARV and 37 (22%) surpassed the HIC_{15} IARV (Figure 1).

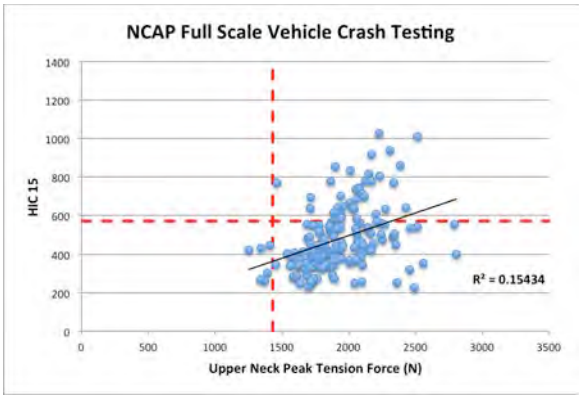

Figure 1: NCAP full-scale vehicle crash testing of the Hybrid III, 3 year-old ATD compared to head and neck IARVs.

A total of 38 separate occupant data points were obtained from 32 laboratory sled test runs. The average HIC_{15} was 306.9 (SD = 120.5). The average upper neck peak tension force was 1723.2 N (SD = 337.7). Of the 33 data points garnered from the laboratory sled testing reports, 27 (82%) exceeded the upper neck peak tension IARV while only 1 test (3%) surpassed the HIC_{15} IARV (Figure 2).

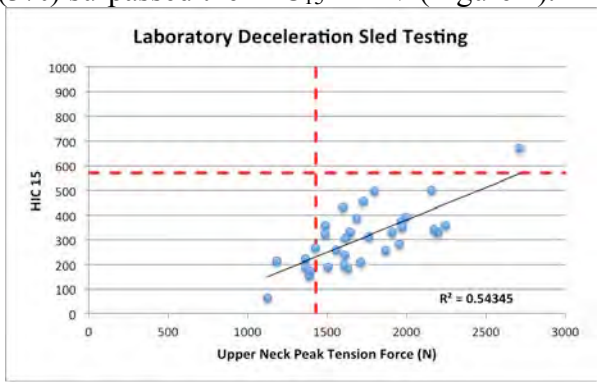

Figure 2: Laboratory deceleration sled testing of the Hybrid III, 3 year-old ATD compared to the head and neck IARVs.

The objective of this study was to investigate the injury potential associated with the pediatric neck and head during pure inertial loading. ATDs in the current study were subjected to injurious levels of neck tension, yet HIC_{15} values tended to remain below the IARV. These findings support the original hypothesis that inertial loading of the head provides a greater risk of injury to the cervical spine when compared with closed-head injury. At minimum, these data indicate a clear coupling of head and neck injury risk for the pediatric population in the absence of head impact.

In the current study, ATDs that underwent full-scale NCAP crash testing were subjected to mean peak head accelerations of 740 m/s^2 (SD = 213). Similarly, ATDs that were tested in laboratory sled tests measured average peak head accelerations of 602 m/s^2 (SD = 142.2). For comparison, previous studies involving young pediatric biofidelic surrogates have reported head accelerations associated with a shaking event to range between 90 m/s^2 and 272 m/s^2 [1,4]. Consequently, frontal collisions occurring at speeds in the range of 30 to 35 mph result in more severe inertial loading conditions to the head and neck than violent, maximum-effort shaking by an adult. Regardless of the magnitude of the inertial forces involved, the findings indicate that an infant's neck is the most vulnerable anatomical structure under these loading conditions. It is only after the ATDs surpassed injury tolerance thresholds for the cervical spine that they even began to measure injurious head accelerations.

CONCLUSIONS

The findings indicate that the pediatric neck is the most vulnerable structure under inertial loading conditions. It is only after the ATDs surpassed injury tolerance thresholds for the cervical spine that they experienced injurious head accelerations. These data support the hypothesis that inertial loading of the head provides a greater risk of injury to the cervical spine when compared with closed-head injury. The results indicate that the traditional triad of symptoms associated with infant shaking should be revised to include the presence of neck injury in cases of suspected shaking.

REFERENCES

1. Duhaime AC, et al. *J Neurosurg* 66(3):409-415, 1987.
2. Prange MT, et al. *J Neurosurg* 99(1):143-153, 2003.
3. Mertz, HJ. et al. *Stapp Car Crash* J, 47, pp. 155–188, 2003.
4. Jenny C et al. *Inj.* Biomech. Res., pp. 129–141, 2002.

RELATIONSHIP BETWEEN SIMPLE GAIT PARAMETERS AND PATIENT FUNCTION BEFORE AND AFTER TOTAL KNEE ARTHROPLASTY

[1]Brooke K. Delventhal, [1]Rachel K. Baker, [1,2]Elena J. Caruthers, [3]Jacqueline M. Lewis, [4]Gregory M. Freisinger, [1]Laura C. Schmitt, [1]Ajit M.W. Chaudhari, [1]Robert A. Siston

[1]The Ohio State University, Columbus, OH, USA; [2]Otterbein University, Westerville, OH, USA
[3]ARCCA, Inc. Penns Park, PA, USA; [4]United States Military Academy, West Point, NY, USA

Email: delventhal.6@osu.edu; web: https://nmbl.engineering.osu.edu/

INTRODUCTION

Human gait can change as a function of age and disease. The onset of knee osteoarthritis (OA) is associated with muscle weakness and knee instability, and results in a decreased knee range of motion compared to healthy controls [1]. Advanced cases of OA require a total knee arthroplasty (TKA) in attempt to relieve pain and improve function; however, suboptimal outcomes are very common. Patients often report knee instability and walking abnormalities, such as reduced range of motion in the knee joint and irregular muscle co-activation [2].

While previous studies have investigated a large number of gait variables (e.g., speed, joint kinematics, torques, etc.), insight into gait changes following surgery may be complex and challenged by the number of comparisons that are necessary to compare these gait changes between different populations. Conversely, Ivanenko et al. introduced the idea that human locomotion can be represented by a footpath trajectory, which they defined as the path that the foot travels over one gait cycle with respect to the hip forms an elongated ellipse [3]. Their investigation demonstrated that this footpath trajectory changes in different walking conditions, indicating different neuromuscular control strategies. Given recent work that has suggested the importance of neuromuscular control in patient function following TKA (e.g.[4]), parameters of this footpath could characterize patient function with fewer parameters than what is generated from a more traditional motion analysis.

The purposes of this study were to determine if there are differences in the footpath ellipse during gait before and after TKA and to determine if characteristics of the footpath ellipse were related to a patient's function.

METHODS

Twenty-two subjects (7 male, 15 female, age=60.6±6.8 years, height=1.66±0.86 m, mass=92.9±16.5 kg) provided IRB approved written informed consent to participate. Each completed the Knee Injury and Osteoarthritis Outcome Score (KOOS) [5], the 6 Minute Walk (6MW) Test [6], and motion analysis at three different time periods: pre-operatively, 6-months post-surgery, and 24-months post-surgery. Markers were applied to subjects following the modified point-cluster technique [7]. Motion capture data were collected at 150 Hz using 10 Vicon MX-F40 cameras (Vicon; Oxford, UK) and filtered using a fourth-order Butterworth filter at 6 Hz. Subjects completed multiple (at least 3) walking trials at self-selected speed.

Vicon software and custom MATLAB code were used to process gait trials. Footpath trajectory was calculated by extracting the locations of the marker on the 5th metatarsal with respect to the marker on the greater trochanter and plotting the horizontal location versus vertical location throughout the gait cycle. The resulting trajectory data were normalized according to subject height and evaluated according to length (maximum toe excursion), and angle (with respect to the horizontal). The area of the ellipse was calculated with numerical trapezoidal integration (Fig 1).

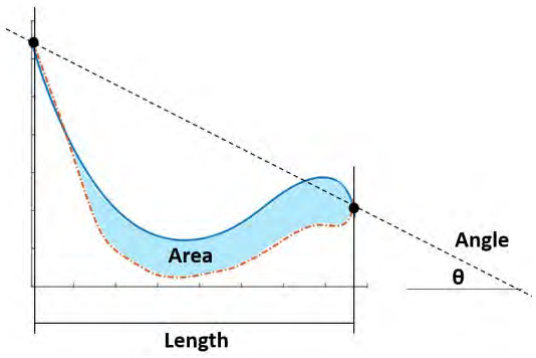

Figure 1: Representative footpath and characteristics

A repeated measures analysis variance was used to determine differences in these characteristics at the different time points, with post-hoc tests performed as appropriate. Spearman's rho was used to identify how the footpath characteristics were related to Activity of Daily Living (ADL) and Quality of Life (QOL) KOOS sub-scales. Pearson's correlations were used to relate footpath characteristics to the 6MW distances.

RESULTS AND DISCUSSION

The angle, length, and area of the footpath were different across the 3 time points ($p=0.03$, $p=0.007$, $p=0.002$, respectively). Despite non-significant post-hoc tests for all measures, average ellipse angles pre-operatively trended towards being larger (9.91±2.07°) than angles both at 6 months (7.99±1.15°) and 24 months (7.23±0.65°) after surgery. Additionally, average non-dimensional ellipse lengths at 6 months post-operatively trended towards being larger (0.42 ±0.11) than lengths before (0.36 ±0.16) and 24 months after surgery (0.41 ±0.11). Average non-dimensional ellipse areas at 6 months post-op also trended towards being larger (0.39 ±0.11) than before (0.33±0.17) and 24 months (0.38 ± 0.027) after surgery.

Changes in the 6MW test were associated with some characteristics of the footpath. 6MW distance was greater 6 months post-operatively (449.7±79.6m) than before surgery (400.4±87.7m, $p=0.001$). This distance at 24 months after surgery (467.0±75.1m) was not significantly different than at 6 months post-operation ($p=0.504$). Longer ellipse lengths and areas were significantly associated with a greater 6MW distance pre-operatively ($r=0.640$, $p=0.001$; $r=0.623$, $p=0.001$) and at 6 months after surgery ($r=0.537$, $p=0.008$; $r=0.494$, $p=0.016$). However, this relationship was not significant at 24 months post-operatively ($r=0.323$, $p=0.143$; $r=0.276$, $p=0.214$). Pre-operatively, longer ellipse length was related to a better KOOS ADL sub-scale score ($\rho=0.440$; $p=0.035$). There were no significant relationships to KOOS sub-scales in either category at 6-months and 24-months post-operatively.

CONCLUSIONS

This exploratory study suggests that the length and area of the path of the toe relative to the hip may be related to patient function before and 6 months after TKA. Future work should investigate this footpath trajectory in healthy older and younger adults and relate characteristics of the footpath to more traditional gait analysis variable to clarity its clinical utility.

REFERENCES

[1] Childs, J.D., et al., Clin Biomech, 19(1): p. 44-49, 2004

[2] Andersson, G B. J., et al. *Acta Orthopaedica Scandinavica* 52.5, 569-73, 1981.

[3] Ivanenko, Y.P., et al., Jl of Neurophysiology 87(6): p. 3070-3089, 2002.

[4] Ardestani MM, et al. *J Electromogr Kines* **37**, 90-100, 2017.

[5] Roos, E. M., et al. *Health and Quality of Life Outcomes* 1:64, 2003

[6] "ATS Statement." American Journal of Respiratory and Critical Care Medicine, 166(1), pp. 111–117, 2002

[7] Andriacchi TP, et al. J Biomech Eng 120:743-749, 1998.

AKNOWLEDGEMENTS

This project was supported by Grant Number R01 AR056700 from the National Institute of Arthritis and Musculoskeletal and Skin Diseases.

EFFECTS SEMITENDINOSUS TENDON STIFFNESS ON ISOKINETIC FORCE AND TORQUE: IMPLICATIONS FOR ACL REPAIR

Zachary J Domire, Clara Amat Fernandez, Anthony S Kulas

East Carolina University, Greenville, NC, USA
email: domirez@ecu.edu

INTRODUCTION

The Semitendinosus Tendon (ST) regenerates following harvest for an ACL reconstruction. While there is evidence that the tendon physically regenerates, little is known about the quality of this regeneration. Evidence from elastography studies conducted in our lab [1] has shown that tendon stiffness is highly reduced following ACL reconstruction. Having information about the quality of the regenerated tendon is crucial as the stiffness of a tendon can have a large effect on muscle force output under dynamic situations [2]. As the hamstrings are protective of the ACL, any reductions in muscle function from this change in stiffness would potentially increase the risk for re-injury. Furthermore, changes in knee joint loading could contribute to an increased risk for the development of osteoarthritis.

The purpose of this study was to investigate the functional consequences of the change in the ST stiffness due to harvest for ACL reconstruction using a computer simulation model of an isokinetic strength test.

METHODS

Isokinetic, concentric knee flexion was simulated at 60º/sec using a custom MATLAB program (MathWorks, Natick, MA). The simulation model included the semitendinosus as a separate muscle and the other hamstrings grouped into a single muscle with respective force-length and force-velocity properties. Maximum active state was assumed throughout the entire motion. The simulation used was similar to past simulations [3]. Model parameters for the simulation are presented in Table 1. These parameters seem reasonable based upon comparison with measurements from various cadaver studies [4].

Simulations were performed with the model representing the healthy state, with a 65% decrease in ST tendon stiffness. This value is consistent with experimental findings measured using ultrasound elastography [1].

Net hamstrings moment and isolated ST force were calculated to assess functional outcomes of tendon compliance.

Table 1: Model parameters

Model parameter	Semitendinosus	Other Hamstrings
Optimal Fiber Length (cm)	17.8	17.8
Spread of the force-length curve	0.56	0.56
Maximum isometric force (N)	1100	3900
Resting tendon length (cm)	26.3	26.3
Tendon stiffness (N/m)	73333	260000
Maximum shortening velocity (optimal fiber lengths per second)	5.2	5.2
Force-velocity curvature	2.439	2.439
Pennation Angle (°)	10	15

RESULTS AND DISCUSSION

The overall effect of ST tendon stiffness on knee flexor moment was relatively modest (Figure 1). The peak knee flexor moment decreased from 140.8 Nm to 139.3 Nm. There was also a shift in the joint angle where the peak occurred from 33.8° to 26.1°.

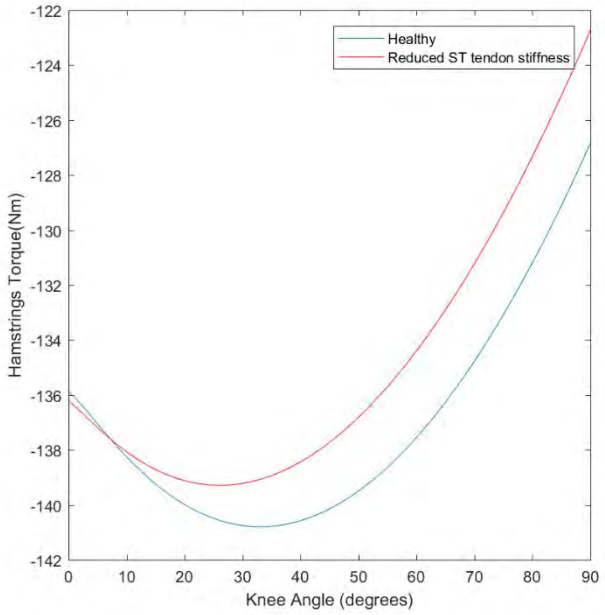

Figure 1: Net hamstrings isokinetic torque plotted vs. knee angle for healthy and reduced stiffness conditions.

The effect of reduced tendon stiffness was more apparent when looking at isolated ST muscle force (Figure 2). The reduction in peak ST force was only 12 N. However, the pattern of force production across the range of motion was highly altered. The angle of peak force shifted from 28.3° to 1.4°. Additionally, the force was significantly lower throughout most of the range of motion.

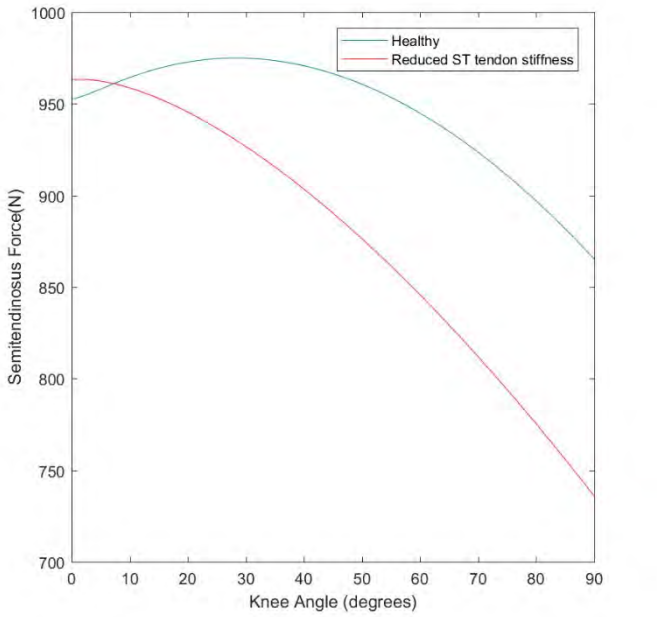

Figure 2: Net semitendinosus isokinetic force plotted vs. knee angle for healthy and reduced stiffness conditions.

CONCLUSIONS

While the change in total torque is relatively small. This would result in any deficits from reduced tendon stiffness being very difficult to measure with strength testing.

The pattern of ST force across the range of motion is highly altered. This is a result of the increased tendon stretch shifting the fiber force length relationship. While this change is likely to produce negligible effects on movement performance, the change in loading pattern could alter cartilage loading. Additional research is needed to examine the possible effects on the progression of osteoarthritis.

REFERENCES

1. Amat Fernandez et al. *SEACSM Annual Meeting*, Chattanooga, TN, USA, 2018.
2. Domire ZJ and Challis JH. *J Sp. Sci.* 25, 2007.
3. Domire et al. *Clin Biomech.***24**: 807-11. 2009.
4. Yamaguchi et al. in *Multiple Muscle Systems,* Springer-Verlag, 1990.

ANTICIPATORY NECK MUSCLE ACTIVITY IN AUTOMATIC AND MANUAL EMERGENCY BRAKING

[1] Ethan C. Douglas, [1]Valentina Graci, [1]Thomas Seacrist, [2]Jason Kerrigan, [3]Julie Mansfield, [3]John Bolte, [4]Rini Sherony, [4]Jason J. Hallman, and [1]Kristy B. Arbogast.

[1]Center for Injury Research and Prevention, Children's Hospital of Philadelphia, USA
[2]Center for Applied Biomechanics, University of Virginia, USA
[3]Injury Biomechanics Research Center, The Ohio State University, USA
[4]Collaborative Safety Research Center, Toyota Motor North America
email: douglase1@email.chop.edu

INTRODUCTION

Up to 80% of automobile crashes are preceded by pre-crash maneuvers such as emergency braking [1]. Braking may influence passenger kinematics and lead to less optimal positioning at the moment of impact. As the automotive field moves to more active safety technologies, the method by which braking is achieved is changing – from driver-applied manual braking to vehicle-triggered automatic braking. Previous research has investigated head and sternum kinematics and muscle activity during automated braking; however, only adult drivers were examined, and muscle activity prior to the maneuver was not reported [2]. Anticipatory cervical muscle activation has been found to alter the kinematic response of the head to impulsive loading [3], and it could decrease muscle strain and whiplash injury risk in simulated rear impacts [4]. Thus, it is important to understand how varied muscular activation strategies prior to and during braking maneuvers influence occupant kinematics. Therefore, we examined the effect of anticipatory neck muscle activity on head kinematics for pediatric and adult rear seat passengers in automatic emergency braking (AEB) and manual emergency braking (MEB) via closed-course testing.

METHODS

18 male participants age 10 – 33 (17.1 ±5.6) years old were restrained in a lap/shoulder belt in the rear right passenger seat of a modern 4-door sedan. The pre-crash maneuvers were performed at the Transportation Research Center Inc. (East Liberty, Ohio) by a professional driver. For MEB an average deceleration of ~1 g was achieved by the driver pressing the brake pedal with maximum effort while the vehicle was moving at 50 km/h with cruise control. The AEB was triggered by the vehicle radar detecting a 3D Soft Car (Dynamic Research, Inc.) while travelling at 50 km/h with cruise control, achieving an average deceleration of ~0.8g. Vehicle dynamics were collected with an Inertial and GPS Navigation system (Oxford RT 3003, 200Hz Oxford Technical Solutions Ltd.), kinematics were collected with an eight-camera 3D motion capture system (Optitrack 200Hz, NaturalPoint, Inc.), and muscle activity was collected with surface electromyography (EMG) sensors (2000 Hz Delsys, Inc.). Photo reflective markers were placed on the participant's head and sternum, while EMG sensors were placed bilaterally on the participant's sternocleidomastoid. Participants were instructed to initially sit relaxed with their hands on their lap as a starting position, and then to react naturally during the maneuver. Muscle activity was normalized to a 5 second static trial in which participants were instructed to sit in the vehicle with their initial position as described above. Pre-maneuver muscle activity and during-maneuver activity are defined for AEB in the below graph (Fig. 1). The EMG activity for the MEB maneuver was quantified in the same way.

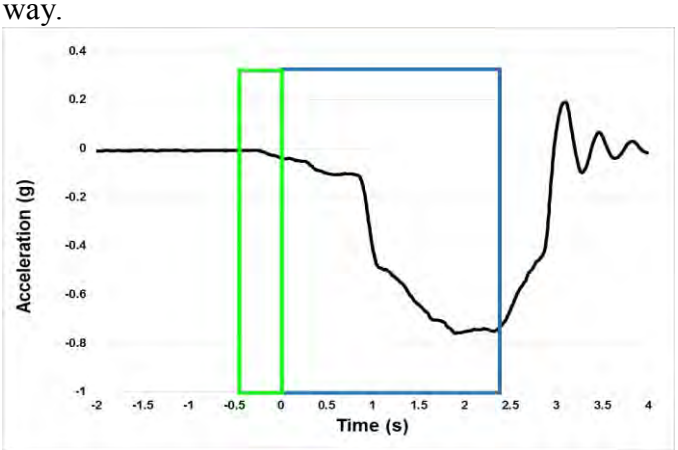

Figure 1: Graph of vehicle acceleration (g) over time for the AEB maneuver. Pre-maneuver EMG activity was collected for 0.5 seconds before the onset of the maneuver (green box), while during-maneuver EMG

activity was collected from onset of the maneuver until the end of steady-state braking (blue box).

A repeated measure 2-way ANOVA was performed to understand the differences in pre and during maneuver muscle activities between AEB and MEB. Tukey's post hoc test was performed to analyze significant main effects. Product-moment correlation tests were performed to understand the relationship between occupant age and muscle activity pre- and during-maneuvers, and, the relationship between head kinematics and pre-maneuver muscle activity in both AEB and MEB.

RESULTS AND DISCUSSION

Paired t-tests found no significant differences between right and left sternocleidomastoid, therefore the average of the two sides is presented. A significant main effect was found between pre-maneuver and during-maneuver muscle activity. In AEB, sternocleidomastoid muscle activity during the maneuver (1.97 ±1.78) was significantly greater than pre-maneuver muscle activity (p=0.048, 1.48 ± 1.07). In AEB, pre-maneuver sternocleidomastoid muscle activity had a moderate negative correlation with head excursion (r = -0.67, p=0.001, Fig. 2).

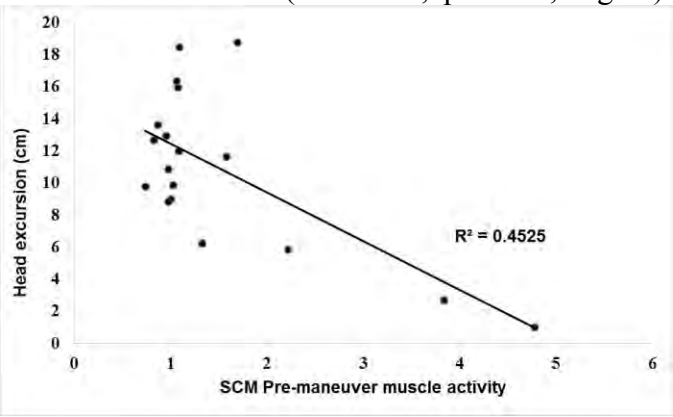

Figure 2: Scatterplot of head excursion (cm) versus sternocleidomastoid (SCM) pre-maneuver muscle activity during automatic emergency braking (AEB).

For MEB, during-maneuver sternocleidomastoid muscle activity (11.34 ±19.92) was significantly greater than pre-maneuver activity (p=0.022, 1.43 ±0.97), but there were no significant correlations between sternocleidomastoid muscle activity and head excursion. Age had no effect on muscle activity in both MEB (p=0.650) and AEB (p=0.440). Lastly, there were no significant differences between AEB and MEB in the pre-maneuver activity (p=0.719), while MEB during-maneuver activity was significantly greater than AEB during-maneuver activity (p=0.046)

During-maneuver muscle activity was greater than pre-maneuver activity for both MEB and AEB, indicating increased muscle activation to resist the forward acceleration. However, despite no significant differences in pre-maneuver muscle activity between AEB and MEB, greater anticipatory muscle activity in AEB was related to reduced head excursion, while no such relationship was found for MEB. Participants experienced a lower acceleration and a longer time to maximum acceleration during the AEB maneuver than the MEB maneuver, and thus their sternocleidomastoid muscles may have been better able to resist the forward motion of the head. Safety countermeasures such as auditory warning systems have been found to increase muscle activity before an impact and reduce important kinematic variables such as head excursion and head acceleration [4]. Given that pre-maneuver muscle activity correlated with reduced head excursion in AEB, these countermeasures could potentially be useful in optimizing occupant position during pre-crash maneuvers such as automatic emergency braking.

CONCLUSION

For AEB test conditions, pre-maneuver anticipatory muscle activation in the sternocleidomastoid muscles was associated with greater muscle activation during the maneuver and reduced head excursion. Similar observations were not seen in MEB test conditions. Active safety technology could alert participants to impending maneuvers, reducing the amount the occupant is out of position prior to an impact. Future work should investigate the effect of anticipatory muscle response on kinematics in a variety of pre-crash maneuvers, and examine other muscle groups that control occupant kinematics.

REFERENCES

1. Seacrist et al. (2017). *Traffic Injury Research Prevention*.
2. Osth et al. *Stapp Car Crash Journal*, ***57,*** 1-41.
3. Eckner et al. (2014). *American Journal of Sports Medicine*.
4. Mang et al. (2015). *The Spine Journal,* ***15***(1), 153-161

CAPSULOTOMY AND REPAIRS ON TORSIONAL STABILITY OF THE HIP

[1] Demetrio Douros, [1] Scott Smith, [1] Preston Easterday, [1] Melinda Choi,
[1,2] Linda McGrady, [3]Patrick M Birmingham, [1,2] Mei Wang

[1] Medical College of Wisconsin, [2] Marquette University, Milwaukee, WI, USA
[3]NorthShore Orthopaedics, Chicago, IL, USA
email: meiwang@mcw.edu

INTRODUCTION

Arthroscopic hip preservation is one of the fast-growing fields in orthopaedic surgery. One of its frequent applications is the treatment of symptomatic femoral acetabular impingement (FAI). To gain access to the joint to visualize the morphology and perform joint preserving procedures, a capsulotomy must be performed. Two of the most commonly used approaches are interportal capsulotomy and T-capsulotomy. Interportal capsulotomy allows good viewing of the central compartment, including the labrum, acetabular rim, and articular cartilage. T-capsulotomy, with additional incision perpendicular to the interportal capsulotomy, allows the viewing of the peripheral compartment such as the proximal femoral head-neck junction. The necessity of capsular repair after arthroscopic procedure has been debated. The decision to leave the capsulotomy open, or perform a complete or partial repair, is typically made depending on factors such as patient age, BMI, gender, and degree of chondral damage [1].

Quantitative studies into biomechanical effects of capsulotomy are limited. Wuers et al. compared the joint stability after 4-cm vs. 6-cm interportal capsulotomy and found increased motions with the larger sized procedure, but repair effectively restore the joint motion to the intact level [2]. The purpose of this study was to determine the biomechanical impacts of two common capsulotomy procedures on the stability of the hip joint during external rotation, and to evaluate the effects of partial and full capsular closures on the restoration of hip joint stability.

METHODS

Eight fresh-frozen cadaveric specimens of hemi-pelvis with proximal femur attached were procured from musculoskeletally normal donors (mean age 59.4 yrs). Mechanical tests were conducted on an axial-torsion servo hydraulic testing system (MTS Landmark 370, Eden Prairie, MN). The pelvis was secured at the iliac wings using bolts and dental cement and mounted onto the MTS base with ASIS and the pubic symphysis were aligned in the same frontal plane for an upright alignment. The end of the proximal femur was bolted to a pair of angle plates and mounted to the MTS actuator in neutral position. Torque in the external rotation direction was applied under load-control with maximum torque limited to 5Nm for the intact capsular condition and 3Nm for the operated conditions. Five cycles at a rate of 2deg/sec for loading and 5deg/sec for unloading were completed in each trial, with the last cycle used for data analysis and the first four cycles for pre-conditioning. Two marker triads from a motion analysis system (Optotrak Certus, NDI, Waterloo, Canada) were fixed on the proximal femur and the superior pubic ramus to track the relative hip joint motion while the torsional load was applied (Fig.1). Two additional markers were attached to the MTS actuator to synchronize data from the MTS and motion analysis systems. Data from both systems were sampled at the rate of 100Hz.

Each specimen was sequentially tested in five capsular conditions: 1) intact, 2) 4-cm interportal capsulotomy, 3) T-capsulotomy, 4) partial repair (3-stitch suture closure of T-branch), 5) full repair (additional 4-stitich suture closure of interportal cut). All repairs were made with FiberWire#2 sutures (Arthrex, Naples FL). For each specimen, data from four capsule-operated conditions were normalized with respect to their intact condition. Three outcome variables were compared: 1) range of motion (ROM) of the hip joint at 3Nm, 2) neutral zone motion (NZ), a metric for joint laxity determined by amount of motion prior to rapid stiffening point on the load-displacement plot, and 3) structural stiffness and

structural stiffness obtained from the linear region of the MTS load-displacement plot for each condition. Analysis of variance (ANOVA) was performed on the normalized data with post-hoc comparisons using Dunnett's method. All tests were completed using statistical software JMP (v.13, SAS Institute, Cary NC), with level of significance set at 0.05.

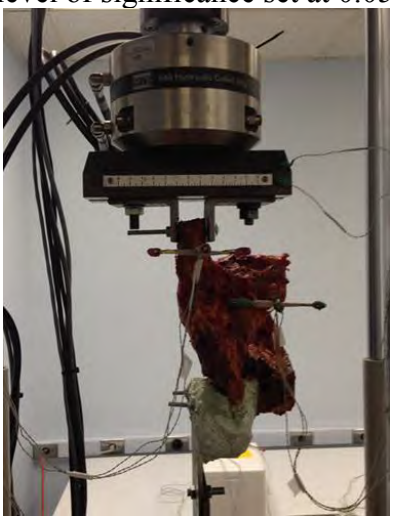

Figure 1: Experimental setup of a hemipelvis.

RESULTS

The mean ROM at 3Nm external rotation torque was 15.0±4.2 degrees for the intact capsular. The mean normalized increase over the intact was 134±20% and 149±25% for interportal and T-capsulotomy respectively, and 145±23% and 138±22% for partial and full repairs respectively (Fig.2). There were no statistically significant differences between any of the four operated groups, while mean ROMs of all four operated groups presented were significantly higher than the intact group ($p<0.006$).

The mean NZ result was 6.8±3.9 degrees for the intact group. The mean normalized NZ increase over the specimen's intact stage was 162±26% and 186±31% for interportal and T-capsulotomy respectively, and 179±30% and 151±32% for partial and full repairs respectively (Fig.3). Comparisons of the means found that the increases in the interportal capsulotomy stage and full repair stage did not reach the level of statistical significance ($p=0.18$ and $p=0.12$ respectively), while mean increases for T-capsulotomy and partial repair were ($p=0.02$) over the intact stage.

The mean stiffness obtained from the MTS load-displacement plot were similar among the five capsular conditions. The differences of the four operated stages were within 6% of the intact stage without reaching statistical significance.

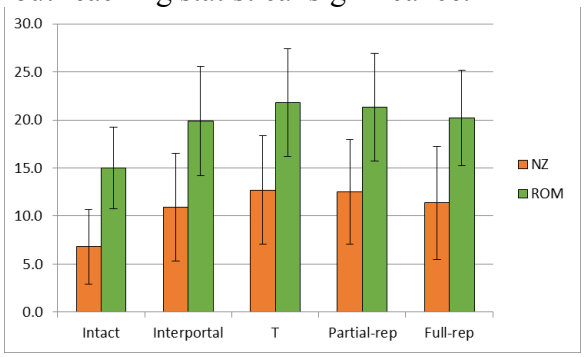

Figure 2: Mean (sd) NZ and ROM (unit:degree)

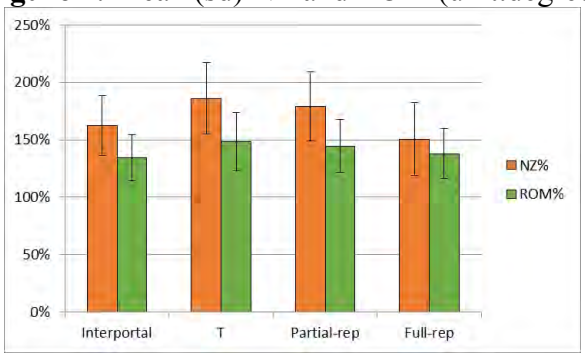

Figure 3: Mean (sd) normalized NZ and ROM

DISCUSSION

Results from this study show that capsulotomy affects joint laxity, as measured by NZ, the most, and only full repair of the capsule can restore it close to intact level. Once the hip as loaded beyond the laxity zone, the joint with all capsular altered conditions responded similarly to the intact joint under external rotation loading, as demonstrated by insignificant changes (<6%) in construct stiffness among all tested conditions.

Limitation of the study includes the sequential testing protocol designed to optimize the use of cadaver specimens. The true effect of the repair of interportal capsulotomy was hampered by the creation of T-capsulotomy.

REFERENCES

1. Domb et al. *Arthroscopy* 31:643-50, 2015.
2. Wuers et al. *Arthroscopy* 32:1571-80, 2016.

An Upper-Extremity Function Dual-task to Identify Cognitive Status of Older Adults

[1] Hossein Ehsani, [1] Jane Mohler, [2] Kathy O'Connor, [2] Edward Zamrini, [1] Genevieve Wahlert, [2] Sarah Fakhoury, [2]Daniel Gaytan-Jenkins and [1] Nima Toosizadeh
[1] Arizona Center on Aging, Biomedical Engineering, University of Arizona, Tucson, AZ, USA
[2] Banner Sun Health Research Institute, Sun City, AZ, USA
email: hehsani@email.arizona.edu

INTRODUCTION

The need to coordinate concurrent motor and cognitive tasks (e.g., "dual tasks") occurs constantly in our daily life. Dual tasks place demands on attentional resources, and reflect increasing cognitive challenge for older adults and those with cognitive impairment. Understandably, performing dual-task actions is accompanied with a decline in performance when compared to single task performance (e.g., dual task "cost"). As this decline becomes more evident with increasing age, and with cognitive decline, researchers have tried to find meaningful associations between the state of cognition in older adults and how it is reflected in their dual-task performance.

Our objective, in this study, was to develop a novel dual-task cognitive function test incorporating a validated upper-extremity function (UEF) motor test [1], which was simultaneously performed with counting backwards as a cognitive challenge. Unlike gait, UEF is an uncommon motor activity and during its performance possible skill learning may evolve. Further, counting backward was selected, since it involved working memory and its rhythmic structure would interfere with repetitive elbow flexion.

METHODS

Older adults (≥65 years of age) were recruited and stratified into three clinically confirmed groups: 1) cognitively healthy (CH), 2) mild amnestic cognitive impairment (MCI, presumed due to Alzheimer's disease), and 3) early dementia due to Alzheimer's disease (AD) according to National Institute of Aging – Alzheimer's Association (NIA-AA) criteria. According to our previously validated UEF method [1], wearable motion sensors (tri-axial gyroscope sensors, sample frequency = 100 Hz, BioSensics LLC, Cambridge, MA) were employed to measure forearm and upper-arm motion, and ultimately the relative elbow angular velocity. Participants completed four trials of dual-task UEF: NDT1: Normal-paced elbow flexion while counting backwards by one; NDT2: Normal-paced elbow flexion while counting backwards by three; FDT1: Fast-paced elbow flexion while counting backwards by one; and, FDT2: Fast-paced elbow flexion while counting backwards by three. Normal-paced and fast-paced trials were performed for 60s and 20s, respectively. In addition to the number of flexions, using the coefficient of variation, we computed the variability of the following UEF parameters for each trial: 1) speed (elbow angular velocity range that is the maximum minus minimum speed); 2) range of motion (elbow flexion range); 3) rise time (the required time to reach the maximum angular velocity), 4) semi-period (time distance between two consecutive maximum angular velocity).

Separate multivariable ANOVA models were used to assess differences in UEF parameters between the three groups. Age, body mass index (BMI), and gender were considered as covariates in these analyses. In case a significant difference was observed among the groups, we performed multiple comparisons correcting for family-wise error rates using Tukey's test.

Using the same procedure explained previously [2], within each dual-task condition a logistic regression model was developed to predict cognitive status via the selected demographic and UEF parameters. For all models, area under curve (AUC) was estimated using receiver operator characteristic (ROC) curves. All analyses were done using JMP (Version 11, SAS Institute Inc., Cary, NC, USA), and statistical significance was concluded when $p < 0.05$.

RESULTS AND DISCUSSION

A total of 30 participants were recruited, 10 in each group (CH: age=86.3±2.9, MCI: age=87.2±3.0, and AD: age=86.5±5.3; 40% male in each group).

Results from ANOVA models for UEF dual-tasks demonstrated that in all trials the number of flexion, semi-period and rise time variability were significantly different among the groups (Table 1). Also, range of motion (ROM) variability was significantly different between the groups within both normal-paced trials. Speed variability was non-significant among the groups in all trials except NDT1.

Multiple comparisons within NDT1 trial showed that all parameters could differentiate between CH and AD groups (Table 1). However, not all UEF parameters were different between MCI and AD or CH and MCI. Results suggest that rise time and semi-period variability differed more noticeably between MCI and AD groups. On the other hand, the number of flexions, especially within the FDT2 was the only parameter that was different between CH and MCI individuals.

Based on the ANOVA results and the procedure explained in [2], number of flexions, ROM, semi-period and rise time variability were chosen as the independent variables of the logistic models. Also, we incorporated sex, age, and BMI in these models. Using these models, MCI and AD group assignment was predicted. The receiver operating characteristic area under curve of these predictions were shown in Fig. 1.

While the performance of all logistic models are satisfactory, slight differences between the trials can be observed. Within fast-paced dual task trials, counting backwards by three led to a superior dual-task function compared to counting backwards by one. Also, all models showed better performance to identify AD compared to MCI group. As expected, similar trends were observed in the ANOVA results (Table 1).

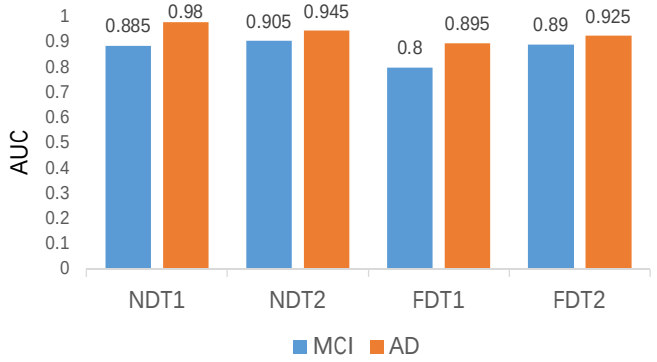

Figure 1: Area under curve (AUC) in predicting MCI and AD group assignment

CONCLUSIONS

Accurate, objective, and rapid cognition screening strategies are needed for use in research and clinical settings. Although several previous studies have reported associations between dual-task gait and cognitive assessment, we propose a new gait-free method that can be implemented more easily in clinical settings, especially for older adults with mobility problems. The reported method has high screening potential, and could be likewise employed to measure change over time. Our preliminary findings should be further explored in a larger clinical study.

REFERENCES

1. Toosizadeh et al, Front. Aging Neurosci., 8(167), 2016.
2. Toosizadeh et al, BMC Geriatrics, 17(1), 2017.

Table 1: ANOVA results between the cognition groups. In the pairwise columns only results with a significant difference are shown.

	NDT1		NDT2		FDT1		FDT2	
	All	Pairwise	All	Pairwise	All	Pairwise	All	Pairwise
Speed variability	0.0139*	0.0105[a]	0.0699	-	0.9874	-	0.2337	-
ROM variability	0.0258*	0.0321[a]	0.0136*	0.0152[a]	0.2691	-	0.0797	-
Rise time variability	0.0004*	0.0004[a] 0.0085[b]	0.0062*	0.007[a] 0.0325[b]	0.0186*	0.0144[b]	0.0065*	0.0058[a] 0.0475[b]
Semi-period variability	0.0002*	0.0003[a] 0.0024[b]	0.0473*	0.0473[a]	0.0175*	0.0155[b]	0.0074*	0.0054[a]
Number of flexions	0.0084*	0.0071[a]	0.0038*	0.0028[a]	0.0019*	0.0013[a]	0.0002*	0.0002[a] 0.0102[c]

* Significant difference; a: CH vs AD; b: MCI vs AD; c: CH vs MCI

MUSCLE AND JOINT CONTACT FORCES WHILE ROWING ON AN ADAPTED ERGOMETER

[1] Ying Fang and [1] Karen L. Troy

[1] Worcester Polytechnic Institute, Worcester, MA, USA
Email: yfang3@wpi.edu

INTRODUCTION

Individuals with spinal cord injury (SCI) experience rapid and profound bone loss in the legs, which is partly attributed to mechanical disuse [1]. Functional electrical stimulation (FES) on an adapted ergometer is used by SCI population to improve musculoskeletal health. During the activity, knee extensors and flexors are stimulated to help SCI rowers to accomplish a smooth rowing movement [2]. Muscle contraction and reaction force at the foot initiate joint loading, which potentially prevents bone loss. Adaptations made to the ergometer constrain rower's trunk movement and knee range of motion (ROM), which affect rowing biomechanics in a manner that hasn't been well established. Quantifying joint loading in FES rowing is a key step to making it more effective for the prevention of bone loss. As a first step, we developed a rowing musculoskeletal model based on able-bodied rowers, and calculated joint contact and muscle forces during able-bodied rowing on an adapted ergometer. We also examined factors that affect knee loading.

METHODS

10 male and 10 female able-bodied subjects with no rowing experience participated in this study (age: 26.5±3.8, height: 1.7±0.1 m, mass: 70.0±14.8 kg). They rowed on an adapted ergometer (Concept2, model D. Morrisville, VT) at 40 strokes per minute, with a knee ROM from 45° to 135°. Kinematics were collected using a motion capture system (100 Hz; Vicon Motion Analysis Inc., UK), and the force under the right foot was collected using a six-axis force sensor (1000 Hz; MC3A-1000lb, AMTI, Watertown, MA). Data were used as the basis for calculating muscle force versus time curves using OPENSIM (3.3, SimTK, Standford, CA).

To accomplish this, a generic lower body rowing model (**Figure 1**) was developed by constraining the subtalar joint and metatarsophalangeal joint, increasing the range of knee, hip, and ankle angles, and adjusting the path of the knee muscles in an existing model [3]. The generic model was then scaled by weight, and by the marker positions of each subject to generate subject-specific models (total error: 1.5±0.6%, RMS error: 2.9±0.9%). Marker trajectories were applied to the model to replicate the kinematics, and measured foot force was added to the right foot. We assumed that subjects generated symmetrical forces at their feet, therefore measured foot force was also applied to the left foot. The force beyond the hip joint (seat force, hand pulling force) was applied at the pelvis as a reaction force. We ran the residual reduction algorithm (RRA) considering pelvis force and foot force at both feet, to get updated kinematics and model. The maximum residual forces and moments were acceptable (Fx: -11.6±7.2 N, Fy: 8.2±12.3 N, Fz: 7.0±15.2 N, Mx, My, Mz: <1 Nm). Muscle forces were calculated by static optimization.

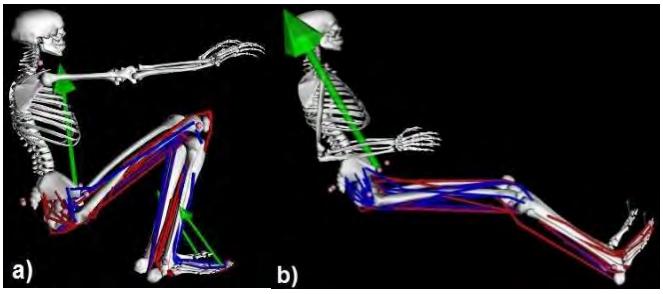

Figure 1: Musculoskeletal model of an able-bodied rower at the start (a) and end (b) of a rowing cycle. Green arrows indicate external forces applied at both feet and at the pelvis.

Summed forces were calculated for hip extensors and flexors, knee extensors and flexors, and ankle plantarflexors and dorsiflexors. Mean foot reaction force during the driving phase and resultant joint contact forces (JCF) were calculated. Peak forces were calculated on the mean of 4 rowing cycles for all variables. Joint contribution (%) was calculated by dividing the joint extensor muscle force by the total of hip, knee, and ankle extensor muscle forces.

We observed two patterns in the foot reaction force curves (**Figure 2**). Subjects were categorized based on the presence (pattern 1) or absence (pattern 2) of a second peak during the drive phase. All variables was compared between the two patterns using

independent t-tests. Correlation between knee JCF and other variables was tested for all subjects (IBM SPSS Statistics 22, Chicago, IL).

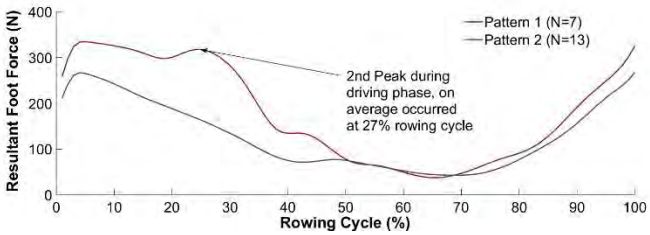

Figure 2: Average foot force curves showing two patterns. Both had a peak at the very beginning of the drive, but pattern 1 also showed a 2nd peak.

RESULTS AND DISCUSSION

Rowers with pattern 1 (N=7) generated significantly higher mean foot force during the driving phase than rowers with pattern 2 (N=13). Joint contact and muscle forces were significantly higher in rowers with pattern 1, except for knee muscle forces (**Table 1**). Knee JCF was positively correlated with mean foot force during driving phase, and was negatively correlated with ankle joint contribution (**Figure 3**).

Table 1: External foot force, joint contact force (JCF), summed muscle force, and joint contribution of subjects with two patterns (mean ± standard deviation). *p<0.05, and **p<0.01.

	Pattern 1	Pattern 2
Peak Foot Force (N/kg)	3.9±1.0	4.2±0.7
Mean Foot Force (N/kg)	3.3±0.4	2.6±0.4**
Hip JCF (N)	3755±1172	2392±876**
Knee JCF (N)	3429±706	1994±851**
Ankle JCF (N)	2408±255	1622±410**
Hip Extensor (N)	2839±868	1917±635*
Hip Flexor (N)	1784±583	973±431**
Knee Extensor (N)	2546±956	1741±861
Knee Flexor (N)	1883±694	1366±574
Ankle Plantarflexor (N)	1717±309	1433±353
Ankle Dorsiflexor (N)	1294±367	547±345**
Hip Contribution (%)	39.8±8.0	37.5±4.9
Knee Contribution (%)	35.4±9.5	33.6±5.8
Ankle Contribution (%)	24.8±5.6	28.8±2.9**

It's not surprising that both groups have similar knee muscle forces, since the knee is the main power generator during rowing. We found that the more one relies on the ankle joint, the lower the knee loading. And, people with pattern 2 had significantly higher ankle contribution, which led to lower knee and hip contributions. They also had lower ankle muscle force, indicating the higher ankle contribution may be the result of weaker or less active proximal joints. People who were able to engage relatively more proximal muscles generated higher mean force at the foot, and also had higher knee loading (**Figure 4**).

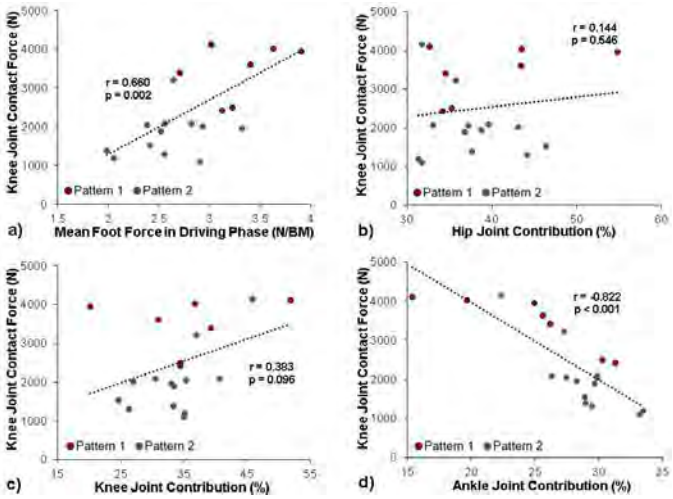

Figure 3: Correlation between knee contact force and mean foot force, and between knee contact force and joint contributions.

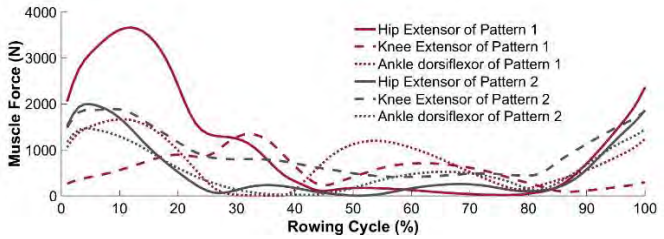

Figure 4: Joint extensor muscle force curves of two subjects with two pattern. Hip extensor muscle was much higher in rower with pattern 1 than pattern 2.

CONCLUSIONS

Knee contact force was affected by external foot reaction force and joint contribution. Relying more on hip and knee joints, and less on the ankles, may increase knee loading. For SCI rowers, stimulating hip extensors muscles during rowing may potentially benefit to bone health.

REFERENCES

1. Tan et al. *Int J Phys Med Rehabil*, 1, 2013. 2. Gibbons et al. *Spinal Cord.,* 52, 2014. 3. Lai et al. *Ann Biomed Eng.* 45(12), 2017.

ACKNOWLEDGEMENT

This study was supported by ASB grant-in-aid.

How Does Ergometer Setup and Rowing Speed Affect Biomechanics during Rowing on an Adapted Ergometer Designed for People with Spinal Cord Injury

[1] Ying Fang and [1] Karen L. Troy

[1] Worcester Polytechnic Institute, Worcester, MA, USA
Email: yfang3@wpi.edu

INTRODUCTION

Functional electrical stimulation assisted rowing (FES-rowing) is used in spinal cord injury (SCI) rehabilitation to improve musculoskeletal and cardiovascular health [1]. A primary goal is to mechanically load the bones in the legs as a means of preventing disuse osteoporosis. In FES-rowing, a normal rowing ergometer is adapted to ensure the safety of SCI users. Specifically, two stoppers are added on the seat rail to limit the seat movement, which prevents knee hyperextension; a seat backrest is added and the user wears a seatbelt with shoulder straps for stabilization; and a knee stabilizer is placed between the legs during rowing to prevent knees from separating apart (**Figure 1a**).

The amount of force that is delivered to bone is a major determinant of whether a given exercise is beneficial or harmful. Recent data show that SCI rowers generate only 20% of the foot force produced during able-bodied (AB) rowing [2,3]. The low loads (0.22–0.25 body weight (BW)) may be attributed to less muscle engagement by SCI users, and/or to the altered rowing mechanics, which can be affected by different setup on the adapted ergometer. If an optimized setup exists to passively maximize loading, SCI rowers could benefit from it. Therefore, our **purpose** was to investigate the effect of rowing speed, knee range of motion (ROM), and seat position on lower extremity loading when AB users row on an adapted ergometer.

METHODS

Ten male and ten female subjects with no rowing experience participated in this study (age: 26.5±3.8, height: 1.7±0.1 m, mass: 70.0±14.8 kg). Upon arrival to the lab, subjects practiced rowing on the adapted ergometer after receiving instructions on basic technique. A researcher set the stopper location based on subject's knee angle. The front stopper was adjusted such that the angle was 45°, 70°, or 95°; and the rear stopper was adjusted such that the angle was 115°, 135°, 140°, or 165°. In this way, knee ROM and seat position could be independently adjusted. Each subject rowed for 90 to 120 seconds at each of the 12 conditions, which included 3 speeds (25, 35, and 40 strokes per minute (SPM)), 3 knee ROM (70°, 90°, and 120°), and 3 seat positions (forward, middle, and rear) (Table 1). Data were collected for 30 s starting at 30 s into the bout of rowing.

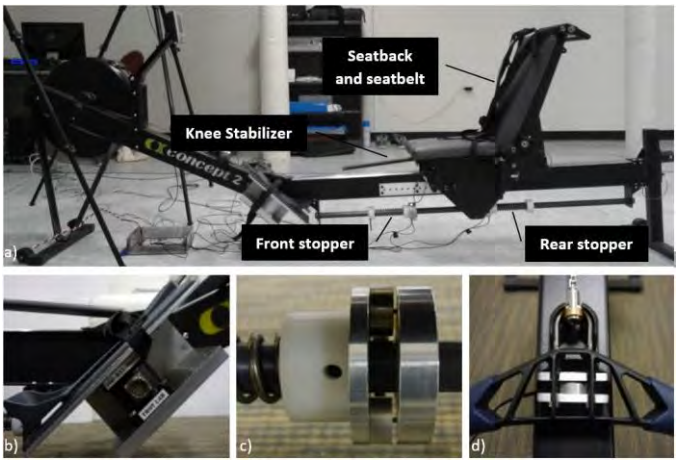

Figure 1: Instrumentation and experimental setup with a) adapted rowing ergometer, b) six-axis force sensor, c) two single load cells on the stopper, and d) one single load cell on the handle.

An adapted rowing ergometer (Concept2, model D. Morrisville, VT) was used for the rowing test (Figure 1a). A ten-camera motion capture system (100 Hz; Vicon Motion Analysis Inc., UK) was used to collect kinematics data. A six-axis force sensor (1000 Hz; MC3A-1000lb, AMTI, Watertown, MA) was mounted under the right foot stretcher of the ergometer (**Figure 1b**). Single-axis load cells (Phidgets Inc., Alberta, Canada) were mounted at the stoppers (**Figure 1c**) and the handle (**Figure 1d**) to measure the hand pulling force and the impact force between the seat and stoppers.

The raw kinematics and force data were filtered using a low-pass 4th order Butterworth filter with zero lag at a cutoff frequency of 1 Hz. Joint angles, moments, and forces were calculated based on ISB recommendations and a recursive Newton-Euler

approach [4,5]. Peak forces and moments were calculated by averaging the peaks of at least five rowing cycles, which began at the start of pulling. All analyses were done using customized code in Matlab (MathWorks, Natick, MA). Three repeated measures analyses of variance were used to examine the each of the three factors (speed, ROM, position). If a main effect was significant, post hoc analysis was performed using pairwise t-tests with Bonferroni adjustments. An alpha level of 0.05 was set as a priori (IBS SPSS Statistics 22, Chicago, IL).

RESULTS AND DISCUSSION

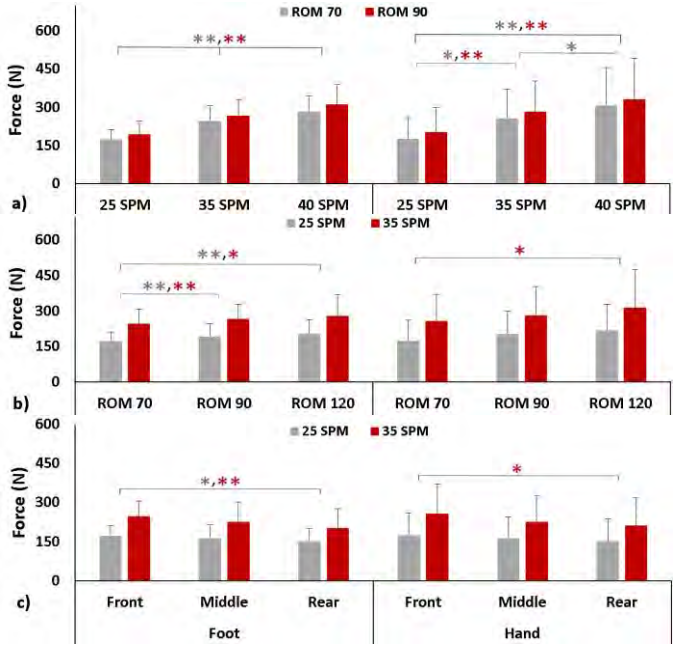

Figure 2: Resultant foot reaction forces and hand forces at different a) rowing speed, b) knee ROM, and 3) seat position. *p<0.05, and **p<0.01.

There was no sex effect in any variable. Peak foot reaction force reached 0.45 BW, and rowing setup could change loading by 0.23 BW. Rowing at higher speeds generated significantly larger foot force, hand force, and peak extension moments at the hip, knee, and ankle. Rowing with larger knee ROM led to significantly larger foot force, and peak extension moments at the knee and hip. Rowing with a forward seat position caused significantly larger foot force, and peak extension moment at ankle and knee (**Table 1**, **Figure 2**).

We observed two patterns in the foot force versus time curve among all subjects. One pattern showed continuously large force throughout the first 30% of the cycle (n=7), while another showed a peak at the beginning of the rowing cycle (n=13) (**Figure 3**). Further analyses indicated that the use of hip extensor muscles may contribute to lasting force generation at the foot (pattern 1).

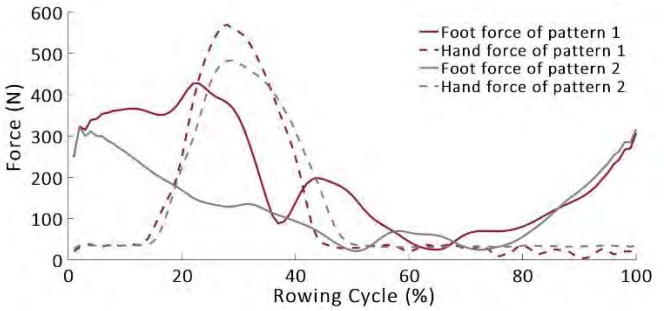

Figure 3: Resultant foot force and hand force curves of two subjects, who showed different patterns in the foot force curve.

CONCLUSIONS

Ergometer setup has a large effect on lower extremity loading. However, even with the optimal setting, foot force was 50% less than rowing on non-adapted ergometers [6]. The added seat back and seatbelt constrained trunk extension, which may be the factor that limits foot force production. This knowledge can be transferred to the SCI population to further improve the FES-rowing program.

REFERENCES

1. Gibbons et al. *Spinal Cord.,* 52, 2014. 2. Draghici et al. *J Biomech*. 53, 2017. 3. Halliday et al. *Arch Phys Med Rehabil*. 85(8), 2004. 4. Wu et al. *J Biomech*. 35(4), 2002. 5. Winter, D.A. 2009. 6. Cerne et al. *Measurement. 44,* 2011

ACKNOWLEDGEMENTS

This study received support from ASB grand-in-aid.

Table 1: The two conditions that generated the most and least force and moments (mean ± standard deviation). BM is short for body mass (kg), BW is short for body weight (N), and Ht is short for height (m).

Speed (SPM)	Knee ROM (°)	Seat Position	Foot Force (BW)	Hand Force (BW)	Hip Moment ($Nm \cdot BM^{-1} \cdot Ht^{-1}$)	Knee Moment ($Nm \cdot BM^{-1} \cdot Ht^{-1}$)	Ankle Moment ($Nm \cdot BM^{-1} \cdot Ht^{-1}$)
40	**90**	**Front**	0.45±0.08	0.49±0.19	0.42±0.11	0.42±0.18	0.29±0.06
25	**70**	**Rear**	0.22±0.07	0.23±0.13	0.17±0.10	0.08±0.07	0.11±0.05

THE EFFECT OF TRANSITIONING FROM A REARFOOT STRIKE TO A NON-REARFOOT STRIKE ON RUNNING IMPULSES PER STEP

Gregory Freisinger, Nathaniel Schlosser, Daniel Watson, Erin Miller, Donald Goss

United States Military Academy, West Point, NY, USA
Email: Gregory.freisinger@usma.edu; Web: http://www.usma.edu/cme/

INTRODUCTION

Over 19 million people consistently run as a form of exercise in the United States alone. Annually, approximately 50% of these runners will experience an injury detrimental to performance [1]. A recent approach to mitigating running injuries is modification of a runner's foot strike pattern (FSP).

Transitioning runners from a rearfoot strike (RFS) to a non-rearfoot strike (NRFS) pattern has been shown to influence several factors related to running injuries, to include a reduction in average vertical loading rate (AVLR) [2]. This idea is well established, but there are likely other factors influencing running related injuries, such as running cadence and different impulses during each stance phase.

The purpose of this study was to analyze the effect of a transitional NRFS running program on the magnitude of impulse per step. We hypothesized that impulse per step will decrease in the vertical, anterior, and posterior directions following the running program due to increased cadence. We hypothesized that medial and lateral impulses will remain unchanged after the treatment protocol.

METHODS

Twenty-seven runners recovering from lower extremity injuries at the United States Military Academy were recruited to participate in this study after providing IRB approved consent. All participants had previous running experience (14 males, 13 females; mean age: 25.3 ± 9.9 yrs; mean height: 172.1 ± 10.3 cm; mean weight 73.0 ± 12.0 kg).

Participants met each of the following six inclusion criteria: 1) previously a RFS runner; 2) recovering from a lower extremity injury; 3) able to walk pain free for 2 miles; 4) dorsiflexion range of motion of at least 80% symmetry; 5) capable of performing 20 unassisted single leg heel raises; 6) able to perform a single leg hop for distance with at least 80% symmetry. The participants were clinically diagnosed and recovering from lower extremity injuries including, but not limited to: patellofemoral pain syndrome, lower leg stress injury, lower leg fracture, plantar fasciitis, and anterior cruciate ligament reconstruction.

The running transition program began with a private 30 minute training session to initiate transition from a RFS to a NRFS running pattern. Training focused on soft landing off of the heel, a cadence of approximately 180 steps/minute, forward trunk lean, and strict adherence to a gradual walk to run progression. Participants met with their study assigned medical provider once a week post-training for the first 4 weeks, then again at weeks 6, 8, and 10 during which the training focuses were reinforced.

Initial and 10 week assessments were conducted before and after the 10-week training program. Assessments consisted of subjects running on an instrumented treadmill at a self-selected pace for five minutes. Speed was kept constant for both evaluations. Two-dimensional video was collected at 240 Hz [Casio, EX-ZR200; Tokyo, Japan] in the sagittal plane to confirm FSP. Ground reaction force data was collected via the instrumented treadmill [Bertec; Columbus, OH] at 1000 Hz, low-pass Butterworth filtered at 35 Hz, and normalized to bodyweight.

Impulse was then calculated in vertical, anterior, posterior, medial, and lateral directions based on ground reaction forces for five stance phases on each foot. The ensemble averages of left and right impulse values were calculated for use in further analysis. Cadence in steps per minute was also determined based on ground reaction force data.

Subjective measures of running ability were taken initially and at 10 weeks. Metrics used were the PSFS (Patient Specific Functional Scale) and SANE (Single Assessment Numeric Evaluation) which assess functional running ability and self-reported normalcy of the injured body part, respectively.

Paired t-tests with a significance level of alpha = 0.05 were used to identify differences between the initial and 10 week assessments for the impulse, cadence, PSFS, and SANE measures.

RESULTS AND DISCUSSION

All subjects successfully transitioned from a RFS to NRFS pattern based on high speed video data. Cadence increased from 168.7 ± 8.2 steps/min to 173.6 ± 7.5 steps/min following the treatment ($p<0.01$). PSFS and SANE scores also increased significantly after 10 weeks ($p<0.01$) (Table 1).

In accordance with our hypotheses, vertical impulse per step decreased by 2.1% following the protocol ($p<0.05$); while medial impulse failed to demonstrate a change after 10 weeks ($p=0.14$) (Table 1).

Anterior and posterior impulse per step both showed significant changes; however contrary to the hypothesis, they increased following the training protocol. Anterior impulse per step grew by 8.7% ($p<0.05$), while posterior impulse increased by 8.5% ($p<0.001$). Additionally, lateral impulse grew by 79.7% ($p<0.01$), which conflicts with the original hypothesis. These changes are displayed in Table 1 and Figure 1.

These results indicate that the transition from RFS to NRFS alter not only loading rate, as has been previously reported, but also impulse per step. The reduction in vertical impulse may be offset over a given distance due to the significant increase in cadence, while by the same logic the increase in anterior, posterior and lateral impulses may be magnified.

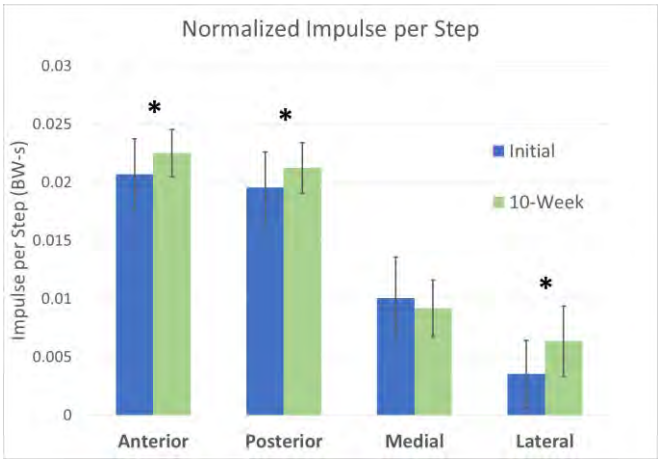

Figure 1. Changes normalized impulse per step after 10 week NRFS program. Asterisks indicate statistically significant changes ($p<0.05$).

CONCLUSIONS

The 10 week NRFS program increased the subjective functional running ability of participants, indicated by higher PSFS and SANE scores. Impulses in the medial direction were unaffected by this protocol. Vertical impulse per step decreased as hypothesized, while anterior, posterior, and lateral impulses all increased per step.

Further research is required to determine the specific characteristics of the ground reaction force leading to these changes in impulse. Long-term effects of altered impulses following transition to NRFS pattern and the effect on overall runner health are also unknown.

REFERENCES

1. Goss, et al. *J Ath Train* 50.6: 603-611, 2015.
2. Van Gent RN, et al., *Br J Sports Med* 41, 469-480, 2007.

Table 1. Normalized impulse per step (BW-s) and clinical scores before and after running foot strike transition program

	Vertical		Anterior		Posterior		Medial		Lateral		SANE		PSFS	
	Mean	StDev	Mean	StDev	Mean	StDev	Mean	StDev	Mean	StDev	Mean	StDev	Mean	StDev
Initial	0.3572	0.0180	0.0207	0.0030	0.0196	0.0030	0.0101	0.0035	0.0035	0.0029	79.4	18.2	7.5	2.8
10-Week	0.3498	0.0171	0.0225	0.0020	0.0212	0.0022	0.0092	0.0025	0.0063	0.0030	93.6	10.1	9.4	2.0
% Change	-2.1		8.7		8.5		-9.0		79.7		17.8		24.2	
p-value	**<0.05**		**<0.05**		**<0.001**		0.14		**<0.01**		**p<0.001**		**p<0.001**	

EFFECTS OF PROSTHETIC SOCKET SUSPENSION ON KNEE PROPRIOCEPTION AND DYNAMIC BALANCE IN TRANSTIBIAL AMPUTEES

Fan Gao
University of Kentucky, Lexington, KY, USA
Email: fan.gao@uky.edu

INTRODUCTION

Prosthetic socket suspension offers a critical means to intimately integrate the prosthetic device with the human body. Though several studies highlighted the benefits of using vacuum assisted socket system (VASS), the outcomes have been shown only marginal and/or amputee dependent. The limited scientific evidence fails to justify its clinical necessity. To further extend our knowledge base on the effectiveness of VASS, studies addressing aspects closely related to amputee's functional performance when using VASS are strongly needed. In this study, we systematically evaluated and compared three prosthetic socket suspensions: 1) locking-pin; 2) suction; 3) VASS. It was hypothesized that VASS will improve knee proprioception and dynamic balance when compared to other suspensions.

METHODS

Participants

Unilateral transtibial amputees, who have amputations due to either trauma or PVD for more than a year without neuromuscular disorders and can walk independently (K level ≥ 2, 15 male and 1 female; mean (std); age: 63.4 (7.9) yrs; body mass: 85.5 (22.4) kg; body height: 1.77 (0.10) m), participated in the study. With one-way expulsion valve and/or vacuum pump, we were able to obtain two other types of suspension (i.e. suction and VASS) for five participants who were originally using locking-pin suspension. Participants were placed in three groups according to the suspension types used: 1) locking pin (n = 10); 2) suction (n = 9); 3) VASS (n = 7).

Instrumentation

A custom electrical goniometer (Bourns AMS22U non-contacting analog rotary position sensor, linearity: 0.5%; supply voltage: 5VDC) was used to measure knee joint position. A custom LabVIEW GUI was used for data acquisition and signals were collected via an NI PCIe6363 data acquisition card at a rate of 100 Hz (National Instrument, Inc., Austin, TX, USA). A three-dimensional wireless IMU sensor (YEI Technology, 3-Space Sensor Wireless 2.4 GHz) was used to register the acceleration (at a range of ±2 g) of the center of mass of the body during treadmill walking. The signal was streamed to a desktop PC at a rate of 100 Hz. A NordicTrack™ treadmill was used for walking trial. For the five participants who originally used locking-pin suspension, a battery-powered air-pump (vacuum level up to 25 inHg) was used to convert the test suction socket to VASS.

Knee position sense

A custom electrical goniometer was used to measure knee joint position. Knee position sense was tested with and without weight bearing across joint positions ranging from 5 to 25 degrees with 5 degrees of increment. The matching errors were calculated using root mean squared error (RMSE) over a window size of 100 samples.

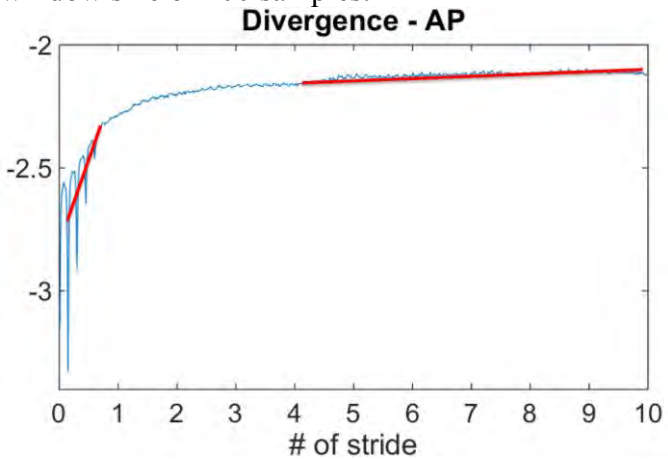

Figure 1: Sample divergence curve as a function of number of strides.

Dynamic balance

Participants walked on a treadmill at their self-selected speed with a tri-axial accelerometer attached

to the lower back for three 3-min walking sessions with break in between. Local dynamic stability (LDS) was estimated using Lyapunov exponents in mediolateral, anteroposterior and vertical directions. Data were processed in MATLAB (Mathworks, Inc. MA).

Statistics

One-way ANOVA with repeated measures was conducted with alpha level set at 0.05.

RESULTS AND DISCUSSION

Knee joint proprioception

The performance of knee joint proprioception was assessed using joint target position matching error. The matching errors of knee joint position are 2.02±0.57 deg, 2.20±0.60 deg and 2.02±0.68 deg (mean±SE) for locking-pin, suction and VASS respectively and there is no statistical difference between suspensions (P=0.97). The matching errors of knee joint position are 2.63±0.44 deg and 1.53±0.35 deg for non-weight-bearing and weight-bearing respectively (P=0.004). Target position shows significant effect and the matching errors are 1.50±0.32 deg, 2.78±0.46 deg, 2.50±0.37 deg, 1.74±0.33 deg and 1.87±0.66 deg for target positions of 5, 10, 15, 20 and 25 degrees respectively (P= 0.004). In addition, sound side shows slightly better performance than affected side (1.82±0.29 deg v.s. 2.35±0.52 deg) though the difference does not reach significant level.

Dynamic balance

No significant effect is revealed on long term LLE. The short term local dynamic stability in the anteroposterior direction are 0.38±.04, 0.52±0.04 and 0.44±0.04 (mean±SE) for locking-pin, suction and VASS respectively. The effect of suspension shows statistical significance (P=0.047) only in the AP direction and the AP short-term LLE of locking-pin is significantly less than that of suction (P=0.036).

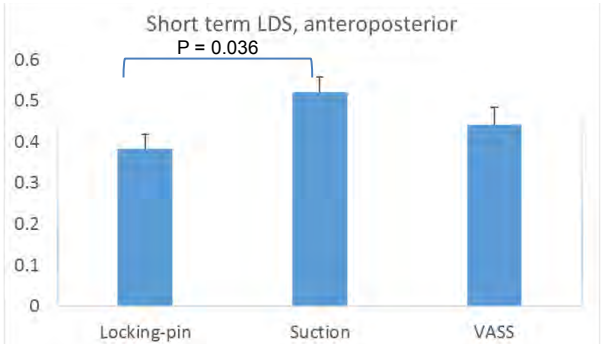

Figure 2: Short term LDS in anteroposterior direction.

The outcome of this study indicates that prosthetic socket suspension does not influence knee joint sense and locking-pin is superior to other means particularly suction in dynamic stability. The study is limited by a relatively small sample size and the fact that some of the participants have not used other suspensions (i.e suction or VASS) before. Further study with larger sample size and suction/VASS suspension of original users is needed.

CONCLUSIONS

Socket suspension does not appear to influence knee joint sense and locking-pin is superior to other means particularly suction in local dynamic stability. The benefits of using VASS are hence not supported by this study.

REFERENCES

1. Hilfiker R et al. BMC Res Notes; 6(1), 260, 2013
2. Clark FJ et al. J Neurophysiol; 42(3), 877-88, 1979
3. Board WJ et al. Prosthet Orthot Int;25(3), 202-9, 2001

ACKNOWLEDGEMENTS

This work was supported by AOPA Research Award administered by the Center for Orthotics and Prosthetics Learning and Outcomes/Evidence-based Practice.

DEVELOPMENT OF A CHARGED OPF HYDROGEL-SCAFFOLD SYSTEM FOR THE TREATMENT OF VERTEBRAL FAILURE IN METASTATIC SPINES

[1]Hugo Giambini, [2]Asghar Rezaei, [1]A. Lee Miller II, [1,2]Xifeng Liu, [1,2]Michael J. Yaszemski, [1,2]Lichun Lu.

[1] Department of Orthopedic Surgery, Mayo Clinic, Rochester, MN, USA.
[2] Department of Physiology and Biomedical Engineering, Mayo Clinic, Rochester, MN, USA
email: lu.lichun@mayo.edu

INTRODUCTION

Multiple pathologies affect vertebral bodies in the spine, including tumors and fractures, reducing spinal stability and increasing the risk for additional vertebral or nervous tissue injury [1]. There were about 1.6 million new cancer cases estimated in the U.S. in 2017 [2]. Up-to one third of all cancer cases will eventually develop secondary bone metastasis, usually to the spine. Vertebral body injury has historically been treated with corpectomy of the affected body and adjacent intervertebral discs. The defect can then be replaced with autografts, allografts, or a variety of fixed and expandable titanium or polymeric cages. However, these approaches have been either associated with complications such as pseudoarthrosis, graft collapse, kyphotic deformity, and graft extrusion; or require both an anterior and a posterior surgical exposure, or the modulus is much higher compared to natural bone, leading to injury of adjacent vertebral bodies. To overcome these shortcomings, we developed a novel biodegradable polymeric hydrogel scaffold to replace the missing vertebral body and intervertebral discs. These scaffolds could potentially enable a less invasive posterior-only surgical approach.

METHODS

Oligo poly(ethylene glycol) fumarate (OPF) was synthesized using fumaryl chloride and polyethylene glycol (PEG) with average molecular weight of 2,000 Da. Gel permeation chromatography (GPC) was then performed to evaluate its molecular weight. The synthesized OPF was used to fabricate scaffolds of 8mm in internal diameter. Briefly, a solution containing OPF, and Bis-acylphosphine oxide (BAPO, photoinitiator) were combined into a flask, vortexed, and placed into a mold in a UV oven. After 2h, the scaffolds were removed from the oven and placed in a laminar flow fume hood at room temperature overnight to fully dry. The effect of negative charge on swelling of the scaffolds was studied by physically infiltrating sodium methacrylate (SMA) into the network. The cross-linked OPF scaffolds were soaked for 8h in ddH_2O containing 0.5% SMA. The expansion rate was evaluated on the final scaffolds containing charge by immersing them in phosphate buffered saline (PBS) solution at 37 °C. Mass, length and diameter were measured at serial time points from 0-100 min. Compressive force-displacement curves for OPF cages before and after swelling were obtained and the stiffness was calculated from the linear portion of the curve.

RESULTS AND DISCUSSION

A sample image of the expanded and charged scaffold is shown in **Fig 1**. The expanded scaffolds were malleable while presenting consistent diameter along its length. Average cross-sectional area (CSA) of the dry and expanded scaffolds were 20.6 (2.4) and 107.1 (3.5) mm^2, respectively. There was a significant radial and longitudinal expansion over time of the scaffold when immersed in the PBS solution. Scaffolds showed a significant increase in their length, wall thickness, internal diameter (ID) , volume, and mass during the first 20 min. All measurements tended to plateua after the initial 20 minutes. **Fig. 2** shows the ratios (based on initial dimension) for the ID, length, and wall thickness. Average stiffness outcomes of the dry and expanded scaffold were 109 N/mm and 0.25 N/mm, respectively. It can be clearly observed that expansion of the hydrogel scaffold reduced the mechanical properties significantly. As a proof of

concept and to mimick the potential *in vivo* application where a vertebral body, containing a defect, and the adjacent intervertebral discs are removed, we conducted a simplified *in vitro* study. Briefly, a metal mold with two metal rods, mimicking vertebral bodies, was manufactured. A gap distance was set to create an artificial defect, mimicking vertebra and disc removal, and the mold was immersed in PBS. The dry OPF cages were then inserted into the defect and allowed to expand. Once expanded inside the defect and between the rods (mimicking adjacent vertebrae), polymethyl methacrylate (PMMA) was injected inside the lumen of the scaffold to allow for mechanical stability. The OPF scaffold, acting as a containment system, allowed for PMMA to cross-link inside the lumen without leaking and preventing potential damage to adjacent tissues (**Fig. 3**).

Figure 1: The expanded hydrogel scaffold is malleable and shows consistent longitudinal morphology.

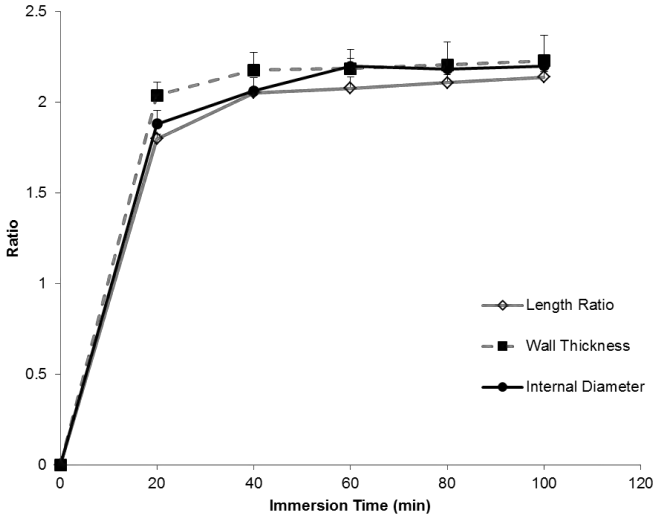

Figure 2: Length, wall thickness and internal diameter changes over time. All measurements tended to plateau after approximately 20 minutes of immersion, reaching a 2-fold change in values.

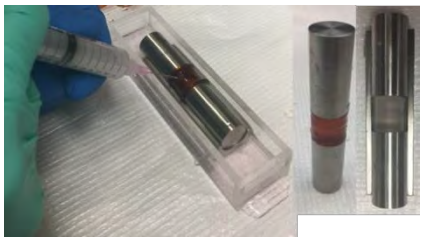

Figure 3: In-situ swelling and injection. A mold consisting of metal rods and a liquid container were used to mimic a lesion. Swelling of the OPF and injection of PMMA allowed for rigidity and stability of the construct.

CONCLUSIONS

The spine is a load-bearing structure and vertebral fragility and vertebral body collapse due to metastatic disease significantly decreases the patient's quality of life. Longtime survival in some cancer types, as well as the existing demographic shift toward an elderly population, places a significant importance in trying to develop new treatment strategies that can not only minimize the likelihood of vertebral failure and adjacent tissue injury, but also minimize surgical intervention and reduce the cost of treatment.

The developed OPF polymeric hydrogel scaffold plays a key role in this process. Its' cost is cheap, could potentially be delivered via a posterior-only surgical procedure, which is much less invasive compared to the combined anterior and posterior approaches, and, upon augmentation, would provide the necessary structural stability to the spine. Because vertebral geomery varies along the length of the spine, the scaffolds could potentially be developed in different sizes to accommodate these various morphological differences.

REFERENCES

[1] Acosta, F.L. et al. Neurosurg Spine 8, 341, 2008.

[2] R.L. Siegel, er al. Cancer Statistics, 2017, A cancer journal for clinicians 67 (2017) 7-30.

ACKNOWLEDGEMENTS

This work was supported by a grant from the NIH (RO1-AR56212) and an award from the National Institute of Biomedical Imaging and Bioengineering (F32 EB023723).

ESTABLISHING NORMS FOR WEIGHT-BEARING HIP ROTATION RANGE OF MOTION

Heather Gulgin, Lindsey Remski, Brittany Sugg, Josie Freybler, Alexis Van Dusen
Dalton Payton, Jake Sommers

Grand Valley State University, Allendale, MI, USA
email: gulginh@gvsu.edu

INTRODUCTION

Range of motion (ROM) is typically measured in a non-weight-bearing (NWB) status, however we participate in most activities of daily living (ADL's) and sport activities in a weight-bearing (WB) status. Thus, the primary purpose of this study was to establish normative values for WB hip rotation ROM. The secondary purpose was to compare WB hip rotation ROM values for younger (age 18-35 years) and older (age 36-55 years) adults.

METHODS

135 participants were separated into two different age categories: 18-35 (20.7 ± 3.3 yrs., 173.4 ± 9.7 cm, 74.3 ± 18.4 kg, 24.2 ± 3.9 BMI) and 36-55 (45.2 ± 6.0 yrs., 173.0 ± 9.7 cm, 76.8 ± 19.9 kg, 25.4 ±4.8 BMI) and had hip internal and external rotation measured on the Functional Footprint® device (Figure 1-2). Statistical analysis was completed using SPSS version 24 (IBM Corp, Raleigh, NC). The average of three trials for each measure were entered for data analysis. A One-way ANOVA tested for significant differences ($p < 0.05$) between the two groups for internal and external rotation. Additionally, to test for any side-to-side differences within each age category, separate paired t-tests were conducted for internal and external rotation.

RESULTS & DISCUSSION

Participant background information is reported in Table 1. Average internal and external WB ROM for right and left sides are reported by group in Table 2. There was no significant difference between hip internal or external rotation between the two groups. When examining side-to-side differences between right and left sides for internal rotation, there was no significant difference in younger group ($p = 0.089$), but there was a significant difference for the older group ($p = 0.006$). For external rotation, there was a significant side-to-side difference (Table 2) for both younger group ($p = 0.002$) and older group ($p = 0.003$). While statistically significant the differences were generally 2-4°, which would not be considered clinically significant (< 5 degrees). Most of the existing literature on hip rotation ROM has been measured actively or passively, but measured in a NWB condition. Sports occur with athletes in load-bearing or weight-bearing condition. Thus, it is important to determine normative values for WB ROM. One previous study [1] did examine hip rotation in a load-bearing condition, but it was not a full WB condition. For internal rotation, they found average values of 22.6 ± 2.7 and 21.1 ± 2.1 for right and left sides respectively and the current study found internal rotation values ranging from 19.8-21.2 (right) and 22.6-22.7 (left) depending on age category. For external rotation, Aefsky [1] found average values of 27.8 ± 2.1 and 25.8 ± 1.7 for right and left respectively and our current study found values ranging from 41.5 (right) and 37.2-38.7 (left). While the internal rotation values were similar between studies, it appears our values for external rotation were quite higher than Aefsky [1]. This could be due to the difference in position of pelvis being slightly tilted in frontal plane for Aefsky [1] measurements. In comparison to other literature on active, prone hip rotation ROM measures, our study found lower internal and external rotation than Simoneau [2], but we found similar values for internal rotation and slightly higher external rotation than Ellenbecker [3].

CONCLUSION

Normative values for healthy adults were established and may be used to compare to actual hip rotation range of motion used in various sports.

REFERENCES

1. Aefsky, B., Fleet, N., Myers, H., Butler, R.J. (2016). Reliability and validity of a novel approach to measure hip rotation. *Journal of Sport Rehabilitation*, 25:330-337.

2. Simoneau, G.G., Hoenig, K.J., Lepley, J.E., Papanek, P.E.(1998). Influence of hip position and gender on active hip internal and external rotation. *J Orthop Sport Phys*, 28:158-164.

3. Ellenbecker, T.S., Ellenbecker, G.A., Roetert, E.P., et al. (2007). Descriptive profile of hip rotation range of motion in elite tennis players and professional baseball pitchers. Am J Sport Med, 35:1371-1376.

Figure 1: WB Internal Rotation

Figure 2: WB External Rotation

Table 1: Participant Background (Percent)

Group (n = 135)	PA	Yoga	Rot Sport	Ethnicity	Leg Dom	Hand Dom
Percent	77.8	11.9	48.1	85.2 Cauc. 4.4 Latino 5.9 Afr-Am. 3.0 Asian 1.5 other	88.9 (R)	91.1 (R)

Table 2: WB Hip Rotation ROM

Group (n)	R Int Rot	L Int Rot	R Ext Rot	L Ext Rot
Ages 18-35 (91)	21.2 ± 10.1	22.6 ± 9.6	41.5 ± 9.9	38.7 ± 9.3*
Ages 36-55 (44)	19.8 ± 9.4	22.7 ± 10.6*	41.5 ± 9.9	37.2 ± 12.1*

*Significant difference ($p<0.05$) between right and left sides
+Significant difference between groups

HOW FEMORAL VERSION CHANGES JOINT LOADING IN PATIENTS WITH DEVELOPMENTAL DYSPLASIA OF THE HIP

Michael D. Harris, Ke Song, Brecca M.M. Gaffney

Washington University School of Medicine, St Louis, MO, USA
email: harrismi@wustl.edu

INTRODUCTION

Femoral version (FV) describes torsional changes in shape between the proximal and distal femur (**Fig 1**). FV deformities are found in several disorders (e.g. cerebral palsy, FAI) and may detrimentally affect hip joint mechanics [1]. FV is also an important surgical consideration in total hip arthroplasty and derotational osteotomies when correcting lower extremity alignment [2].

Development dysplasia of the hip (DDH) is a major etiologic factor in hip osteoarthritis, and is diagnosed primarily using measures of acetabular geometry [3]. However, there is growing interest in the role of femoral deformities in damage within DDH [4], but their mechanical influence in this population is unknown. Accordingly, the objective of this study was to compare how FV variation alters hip joint reaction forces (JRFs) and muscle forces during gait in patients with DDH.

METHODS

Joint angles and ground reaction forces during gait were used from nine previously reported patients with DDH (6F, 26.4±7.2 y/o, 22.7±3.1 BMI) [5]. A baseline model with 23 degrees of freedom and 96 musculotendon actuators was modified in OpenSim (v3.3) by adding subject-specific pelvis geometries, hip joint center locations, and pelvis muscle attachments using CT-based reconstructions as described previously [5,6].

To simulate variations in FV, the femurs of each patient were divided into proximal and distal sections 1 cm inferior to the lesser trochanter. Next, a rotation-only joint was created at the junction of the femur sections. The joint was rotated to create three models per patient: Neutral (15° anteversion [7], matching native OpenSim geometry), ANTE (35° anteversion), and RETRO (7° anteversion), based on FV reports from patients with DDH [4] and an internal DDH database (**Fig 1**). After

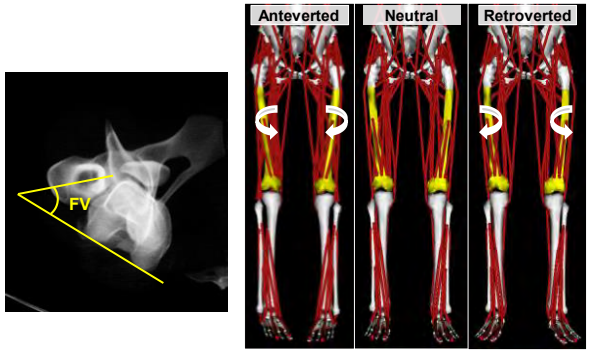

Figure 1: *Left* - FV is the angle between the femoral neck and posterior condyles. *Right* – FV variation was simulated by rotating the distal femur (yellow) relative to proximal femur.

rotation, the custom joint was locked and muscle forces during a full gait cycle were calculated using residual reduction analysis (maintaining original kinematics) and static optimization. JRFs were calculated for each subject's symptomatic hip and presented in a pelvic coordinate frame to reflect the direction and magnitude relevant to the acetabulum.

JRFs and forces for muscles spanning the hip were normalized to bodyweight (BW), peak resultant JRF times during early and late stance (JRF1, JRF2) were identified, and JRFs and muscle forces at those times were reported. Resultant JRF; anteroposterior (AP), superoinferior (SI) and mediolateral (ML) JRF components; and muscle forces in Neutral, ANTE, and RETRO were compared across models using repeated measures ANOVA with Bonferroni correction (initial α=0.05).

RESULTS AND DISCUSSION

Compared to Neutral, ANTE femurs resulted in significantly smaller ML JRFs at JRF1 (p=0.002), with smaller forces in the posterior gluteus medius (p=0.02), but larger forces in the long head of biceps-femoris (**Fig 2, Table 1**). At JRF2, ANTE caused larger AP JRFs (p=0.004) with larger forces in the anterior gluteus minimus and tensor fascia latae (TFL), but a smaller rectus femoris force.

RETRO femurs caused larger ML JRFs at JRF1 (p=0.01) and larger posterior gluteus medius forces compared to Neutral (**Fig 2, Table 1**). At JRF2, RETRO SI and resultant JRFs were smaller than Neutral (p=0.02, 0.01, respectively). Anterior gluteus medius, anterior gluteus minimus, and TFL forces were smaller at JRF2 in RETRO versus Neutral, but rectus femoris forces were larger.

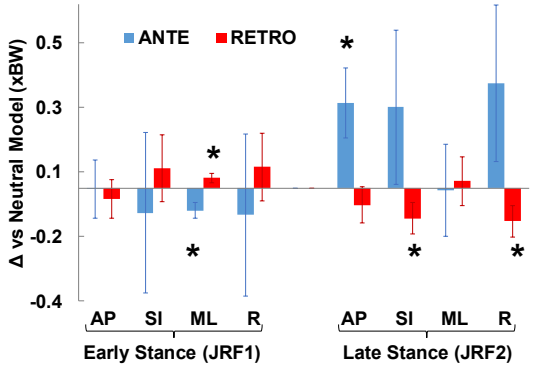

Figure 2: Mean and 95% CI JRF differences (Δ) of ANTE and RETRO models versus Neutral. * indicate p<0.05.

In addition to the statistically significant changes, resultant JRFs in late stance were 40% higher in ANTE models compared to Neutral (p=0.09). Anteversion is more common in DDH [4], and the increased anterior JRFs, and increased superior JRFs, in ANTE cases may contribute to patterns of damage on the superoanterior acetabulum where bony support is lacking and the labrum experiences greater than normal loading [6]. While the magnitude of changes caused by ANTE were much greater than RETRO, it is interesting that each caused an equal number of significant changes to JRFs and muscle forces given the relatively small FV change applied to the RETRO models. Thus, either type of deformity may have important mechanical ramifications on joint loading, with their impact being greatest in late stance.

ANTE increased the role of TFL on pelvis stabilization in late stance. Muscles in these models were not weakened, and the patients did not walk with grossly abnormal patterns. However, if TFL and other abductors were weak, (as found in some DDH patients), the increased demand from anteversion could reasonably lead to the Trendelburg gait and lateral pain some patients manifest. Changes in abductor demand were also evident in the anterior gluteus minimus, which had altered forces in ANTE and RETRO, despite not being directly affected by the FV rotation. Finally, the effect on rectus femoris was opposite TFL, with its activity diminished in ANTE and enlarged in RETRO. While rectus femoris makes a large contribution to hip flexion during transition from stance to swing, in cases of RETRO it may also assist with stabilization to compensate for the mechanically disadvantaged TFL during late stance.

CONCLUSIONS

This study represents the first reported combination of pelvic and femoral bony abnormalities (pelvic shape, lateralized hip joint center, and FV) for investigating musculoskeletal biomechanics in patients with DDH. ANTE and RETRO both caused significant changes to JRFs and muscle forces and may help explain patterns of intra-articular damage found in DDH. The femoral junction was chosen at a location commonly used for rotational correction surgery [8]. However, the location of FV deformities in DDH is not well known and is a topic of our ongoing work. Future work will investigate the effect of changes to proximal FV (i.e. head/neck or inter-trochanteric) and femur neck-shaft angles.

REFERENCES

1. Tonnis D. and Heinecke A. *JBJS*, **81**, 1998.
2. Myers et al. *Clin Biomech*, **53**, 2018.
3. Gala et al. *JBJS*, **98**, 2016.
4. Wells et al. *Clin Ortho Rel Res*, **475**, 2017.
5. Harris et al. *J Biomech*, **54**, 2017.
6. Henak et al. *Osteo Cart*, **22**, 2014.
7. Tayton E. *JBJS Br*, **89**, 2007.
8. Matsuda et al. *Arthrosc. Tech.* **3**, 2014.

ACKNOWLEDGEMENTS

NIH P30AR057235. NIH R01AR05344.

Table 1. Significantly different muscle forces (xBW) at JRF1 and JRF2 versus Neutral. Mean [95% CI]. Bold indicates p<0.05.

	Early Stance (JRF1)		Late Stance (JRF2)			
	GMED_post	Bi.FemLH	GMED_ant	GMIN_ant	TFL	Rec.Fem
ANTE	**0.16 [0.12,0.20]**	**0.05 [0.01,0.09]**	0.96 [0.82,1.1]	**0.25 [0.16,0.34]**	**0.34 [0.26,0.42]**	**0.77 [0.45,1.09]**
Neutral	0.18 [0.14,0.22]	0.03 [0.00,0.07]	0.80 [0.57,1.03]	0.17 [0.11,0.23]	0.26 [0.18,0.34]	1.12 [0.78,1.46]
RETRO	**0.19 [0.15,0.23]**	0.03 [0.00,0.06]	**0.70 [0.46,0.94]**	**0.14 [0.08,0.20]**	**0.23 [0.16,0.30]**	**1.28 [0.94,1.62]**

DETERMINING CERVICAL DISC INJURY POTENTIAL IN MOTOR VEHICLE COLLISIONS

Rami Hashish, Omid Komari, Manon Limousis-Gayda

National Biomechanics Institute, Los Angeles, CA, USA
email: rhashish@nationalbi.com, web: https://nationalbi.com/

INTRODUCTION

More than 6 million motor vehicle collisions (MVCs) occur annually in the United States, resulting in 3.9 million injures and $23 billion of medical expenses. The most common type of MVC is a rear-end, whilst 65 percent of all claimed injuries following low speed MVCs are to the cervical intervertebral discs. Despite such a high prevalence, the potential and mechanism for cervical intervertebral disc injuries in response to low-speed rear-end MVCs is frequently debated in medicolegal circumstances. Accordingly, biomechanics experts are commonly tasked to provide professional opinion with regards to whether an incident was sufficient in severity to cause the medically diagnosed injuries. In order to connect said injuries to the subject incident, experts should rely on valid and reliable methods and criterions. Thus, the purpose of this paper is to provide a qualitative analysis of the current biomechanical approach to evaluating the potential for cervical intervertebral disc injuries in low-speed rear-rend MVCs.

METHODS

Research papers examining rear-end MVCs between 1960 and 2018 were analyzed. For the purpose of this analysis, a low-speed MVC was operationally defined as when the bullet (i.e. impacting) vehicle was traveling between one and 25 mph at impact. Ultimately, 300 peer-reviewed manuscripts were appraised, 20 of which included a biomechanical analysis of injury. A qualitative analysis of these 20 papers was conducted to evaluate the current biomechanical approach for determining cervical intervertebral disc injury potential in low speed rear-end MVCs.

RESULTS AND DISCUSSION

The current biomechanical approach to determine injury potential in a low-speed rear-end MVC is as follows:[1]

1. Accident reconstruction experts determine the magnitude and direction of impact forces at the time of the accident. This step is commonly conducted using computational tools and software such as the EDSMAC4 or GATB models.

Table 1: Injury criteria methods and issues.

Injury criteria	Based on	Method	Issue(s)
Nij (Neck Protection Criterion)	Function of the dynamic loads at the occipital condyles.	Concept of linear combination of axial loads and bending moments initially developed on pigs for frontal crashes.	Relies on pig's skeletal structure for frontal impacts. Risk curves show injury risk greater than zero when Nij equals zero.
NIC (Neck Injury Criterion)	Relative acceleration and velocity of the occipital condyles v. 1st thoracic vertebra.	Assuming relationship between pressure changes inside spinal canal and injury based on animal tests.	The first 150 ms are the only reasonable values obtained during tests, only enabling evaluation of the retraction phase.

2. Biomechanics expert relate the findings as determined from the accident reconstruction to the forces experienced by the occupant(s).
3. Biomechanics experts compare the magnitude of forces experienced by the occupant(s) to research-established injury tolerances and / or criteria, such as Nij or NIC (Table 1).

There appears to be (at least) three issues / flaws to this approach.

Firstly, relating tolerance limits to human injury is not considered externally valid. Tolerance limits have largely been ascertained through an analysis of cadaveric responses and / or tests conducted in healthy youth subjects. Therefore, comparisons of these findings across populations of different ages, genders, sizes, BMIs, and/or pre-existing injuries / conditions (e.g. elderly or obese populations) can lead to an over (or under) estimation of injury tolerance.

Secondly, a simple comparison of force magnitude does not (fully) take into consideration the viscoelastic characteristics of human tissue / intervertebral discs. The crash pulse duration during rear-end impacts is approximately 80-120 milseconds.[2] The resulting occupant kinematic profile is characterized by approximately 350-500 milliseconds of total movement, with only a fraction of that movement being composed of the initial rearward thrust. Research papers examining tolerance limits for the cervical spine, however, have commonly applied loads to cadaveric interverbal discs for time durations ranging from 300 milliseconds to 1 second. Because intervertebral discs are viscoelastic – i.e. they demonstrate time dependent resistance to strain – the loading rate affects the potential for tearing and / or protrusion of the disc(s). Therefore, the tolerance to injury as determined from research may theoretically overestimate the threshold to injury during a rear-end impact.

Thirdly, injury criterions have commonly been developed using cadavers, dummies and / or animals such as piglets used as human surrogates.[3] The inherent issue with using human surrogates is their inability to mimic how humans respond to impact. Accordingly, such data may not accurately reflect intrinsic human responses (such as muscle tensing / contractions that may occur during anticipated MVCs).

CONCLUSION

There are a variety of parameters that affect injury potential, including, past medical history, weight, age, gender, and the magnitude, duration, location and direction of applied forces. However, the current biomechanical approach to determine injury potential in low-speed rear-end MVCs appears to be relegated to a comparison between the magnitude of experienced forces to injury tolerance metrics. This is despite such tolerance metrics may overestimate the force required to cause injury. It is thus encouraged that future biomechanical analyses consider other parameters – such as loading rate, passive / active muscle contraction, and pre-existing condition – when making conclusions regarding injury potential. Simulation technologies and computational models based on response data obtained from laboratory studies could also help improve the validity of the conclusions made by experts. Further research is also encouraged to determine new neck injury criteria and tolerance limits of cervical discs injuries that consider these parameters.

REFERENCES

1. Nahum and Gomez. *Injury Reconstruction: The Biomechanical Analysis of Accidental Injury*. SAE Technical Paper; 1994.
2. Linder et al. *Change of Velocity and Pulse Characteristics in Rear Impacts: Real World and Vehicle Tests Data*. Proc 18th Enhanced Safety of Vehicles Conference. 2003:1-9.
3. Svensson et al. *Pressure Effects in the Spinal Canal during Whiplash Extension Motion: A Possible Cause of Injury to the Cervical Spinal Ganglia.* Int IRCOBI Conf Biomech Impacts. 1993;(1986):189-200.

SINGLE LEG LAND PROVIDES UNIQUE INSIGHT INTO LANDING MECHANICS IN FEMALE ATHLETES POST-ACL/R

[1] Courtney C. Hatcher, [1] Fred Baldwin, [1] Christy Conroy, and [1, 2] Emily J. Fox

[1] Brooks Rehabilitation, Jacksonville, FL, USA
[2] Department of Physical Therapy, University of Florida, Gainesville, FL, USA
email: courtney.hatcher@brooksrehab.org

INTRODUCTION

Over 200,000 athletes sustain anterior cruciate ligament (ACL) injuries every year, half of which require surgery and/or rehabilitation. Athletes who have undergone ACL reconstruction (ACL/R) surgery are 15 times more likely to re-injure themselves within the first year of surgery and 5 times more likely to re-injure themselves within 24 months of surgery [1]. Previous research has highlighted the importance of limb symmetry during clinical testing for return to participation clearance in athletes post-ACL/R, but because re-injury rates remain high, biomechanical testing is now recommended as an additional method of detecting limb asymmetries [2].

Biomechanical tasks that include double-leg jump landings, such as the drop vertical jump, have been used most often in return to participation protocols [3]. The outcome measures from this task identify compensatory techniques that athletes often develop during the course of rehabilitation, offering valuable information about their landing strategies. However, these outcomes provide limited insight about individual limb capabilities. The single leg land is a task that is understudied but may be useful for identifying key information about individual limb characteristics that is not available through evaluation of the drop vertical jump. Outcome measures from the single leg land have previously been reported, but limited research has compared outcomes between the two tasks [4]. This comparison may be useful in understanding the effectiveness of the single leg land for identification of individual limb capabilities that are not detected using the drop vertical jump.

Therefore, the purpose of this case series is to compare outcome measures between the single leg land and drop vertical jump in athletes post-ACL/R. By evaluating the outcomes from these tasks, we may gain insight into the potential usefulness of the single leg land to identify information about individual limb capabilities in injured athletes.

METHODS

Return to participation testing in three collegiate female soccer players post-ACL/R (Age: 21 ± 1 year; Time post-surgery: 30 ± 7 weeks) was conducted using a combination of clinical and biomechanical testing. Clinical testing consisted of isometric strength, y-balance, and single leg hop testing. For biomechanical testing, individuals were assessed using three dimensional kinematics and kinetics. Individuals performed five repetitions of the single leg land where they stood on an 8" box in single limb support, dropped onto one foot, and held for approximately 2-3 seconds. Individuals also performed five repetitions of the drop vertical jump where they stood on a 12" box in double limb support, dropped onto both feet simultaneously, immediately performed a maximum vertical jump, and landed on both feet simultaneously again. Kinematic and kinetic data were then used to compare symmetry across subjects, and the symmetry index (SI) was defined:

$$SI = \frac{Uninvolved\ Limb - Involved\ Limb}{Uninvolved\ Limb} \times 100\%,$$

where an increase in SI represents greater asymmetry. Limb symmetry for peak vertical ground reaction force (vGRF), peak knee flexion angle, and peak internal knee extensor moment were compared across tasks as these outcomes have been identified as biomechanical risk factors for re-injury [2].

RESULTS AND DISCUSSION

As expected at an average of 30 weeks post-surgery, individuals passed all clinical tests (Table 1), demonstrating limb symmetry during this aspect of return to participation testing. However, limb asymmetries were evident in the outcomes from the biomechanical tasks (Fig. 1). For the single leg land, the average SI for individuals was increased for the peak knee flexion angle (11.3%) and peak knee extensor moment (23.2%). For the drop vertical jump, the average SI for individuals was increased for the peak vGRF (1st land: 21.9%, 2nd land: 26.0%) and peak knee extensor moment (1st land: 25.7%, 2nd land: 34.4%).

The outcomes from both biomechanical tasks revealed increased limb asymmetries for the peak knee extensor moment. However, the contributing factors to these asymmetries varied between tasks. During the drop vertical jump, while the peak knee flexion angles were nearly symmetrical, the peak vGRF values were asymmetrical during both landings, indicating that individuals shifted their weight to one side. Because ground reaction forces are used to calculate joint moments, it is likely that the increased joint moment asymmetries during the drop vertical jump were due to asymmetric weight distribution. Therefore, these drop vertical jump outcomes reflect how athletes functionally use their involved and uninvolved sides simultaneously. However, during the single leg land, individuals are required to land with all of their weight on a single limb, reflecting the capacity of the limb to absorb landing forces. The outcomes from this task resulted in symmetrical landing forces (peak vGRF SI: 7.45%) and asymmetrical peak knee flexion angles. This highlights a key difference in what the outcomes from these tasks can provide: the increased joint moment asymmetry during the single leg land could not be due to weight shifting to the opposite limb, but instead was likely due to a difference in landing strategies between limbs, suggesting different limb capabilities.

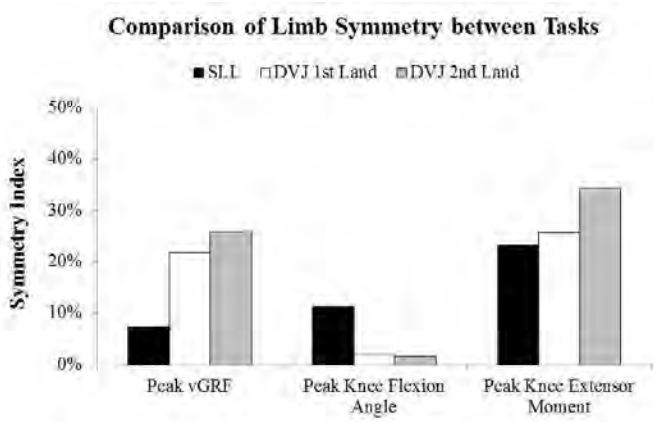

Figure 1: Average limb symmetry indices for athletes during the single leg land (SLL) and both landings of the drop vertical jump (DVJ).

To further understand the athletes' landing strategies, quadriceps strength symmetry was examined, as this has previously been reported as a predictor of knee flexion angle and extensor moment symmetry [5]. Interestingly, individuals demonstrated symmetric quadriceps strength but were asymmetric in peak knee flexion angle and extensor moment. This suggests that although muscle strength has been restored post-surgery, athletes may have neuromuscular deficits that are affecting individual limb capabilities [6].

In summary, the results from this case series highlight the usefulness of the single leg land for identification of individual limb capabilities in injured athletes. By understanding the value of this task, a more comprehensive return to participation protocol can be developed to help reduce the risk of re-injury in athletes post-ACL/R.

REFERENCES

1. Paterno MV. *J Athl Train* **50**, 2015.
2. Chmielewski TL. *JOSPT* **41**, 374-376, 2011.
3. Hewett TE, et al. *Am J Sports Med* **33**, 2005.
4. Taylor JB, et al. *Orthop J Sports Med* **4**, 2016.
5. Palmieri-Smith RM, et al. *Am J Sports Med* **43**, 1662-1669, 2015.
6. Hewett TE, et al. *Br J Sports Med* **39**, 347-350, 2005.

Table 1: Limb symmetry indices for athletes during return to participation clinical tests.

Return to Participation Clinical Tests	SI Pass Criteria	ACL 01	ACL 02	ACL 03
Quadriceps Isometric Strength	≤ 10%	6.44%	7.25%	3.26%
Hamstring Isometric Strength	≤ 10%	4.76%	7.79%	3.37%
Y-Balance Anterior Reach	< 4 cm	1.5 cm	2.0 cm	0.5 cm
Single Leg Hop for Distance	< 15%	6.78%	1.47%	0.00%

MECHANICAL CHARACTERIZATION AND BIOMECHANICAL COMPUTAIONAL MODELING OF SHORT BOWEL SYNDROME

[1] Hadi S. Hosseini, [1] Jordan S. Taylor, [1] AL. Thomas and [1] James C. Y. Dunn

[1] Department of Surgery, Stanford University, Palo Alto, CA, USA
email: hh2@stanford.edu

INTRODUCTION

Intestinal failure (IF) is a rare multifactorial clinical condition that results in patients' inability to sustain normal growth and nutritional and hydration status. Short bowel syndrome (SBS) is the most common cause of IF which is a devastating condition owing to loss of significant intestinal length thereby affecting the organ's ability to absorb nutrients. The incidence of SBS is approximately 25 per 100,000 live births per year in the US [1]. SBS is a congenital or acquired condition affecting the small intestine, hallmarked by loss of intestinal absorptive capacity with resultant malabsorption, dehydration, and malnutrition. This is due to the loss of absorptive surface area, as the human intestinal tract requires a massive surface area to effectively absorb nutrients to support a growing and living organism. Current treatment strategies for SBS involve parenteral nutrition and small bowel transplantation; various transit slowing and bowel lengthening procedures have been employed in highly selected subpopulations [2]. However, these therapies have shown limited success and are associated with high rates of sepsis, intestinal failure-associated liver disease, and mortality [2].

Intestinal lengthening by distraction enterogenesis from use of mechanical forces has been studied as a potential treatment for SBS. [3]. Our previous studies have shown successful lengthening of jejunum using self-expanding springs in rats and pigs for both metal and biodegradable springs [4,5]. However, mechanisms that generate lengthening remains poorly understood from a biomechanical perspective. Main aim of this study was to determine the mechanism behind intestine lengthening as well as optimizing spring implementation and characterization to have maximum intestine lengthening using both finite element modeling and experimental approach.

METHODS

Experimental method: female juvenile (age 4 to 6 weeks) Yucatan pigs (S&S Farms), weighing at least 5kg were used for all experiments. Animals were kept alive for 1-2 weeks on a normal solid food diet prior to sacrification. Immediately after euthanizing the animal, a laparotomy was performed to remove 10-20cm segment of small intestine. Specimen was rinsed with saline to remove intestinal content and the specimen was placed in phosphate buffered saline (PBS) on ice. Segments of freshly harvested porcine small intestine were stored in PBS prior to uniaxial tensile testing. Cylindrical intestinal tract was cut open, and longitudinal cuts were made to obtain the Elastic Modulus of the small intestine in the longitudinal direction. Tensile tests were performed using an Instron type 5565 (Fig. 1A), with a 1kN load cell to measure the Elastic Modulus. Specimens were clamped using special custom-made anti-slip grips to counteract any slipping (Fig. 1B). A pre-load of 2N is then applied at a displacement of 0 mm to eliminate slack within the sample.

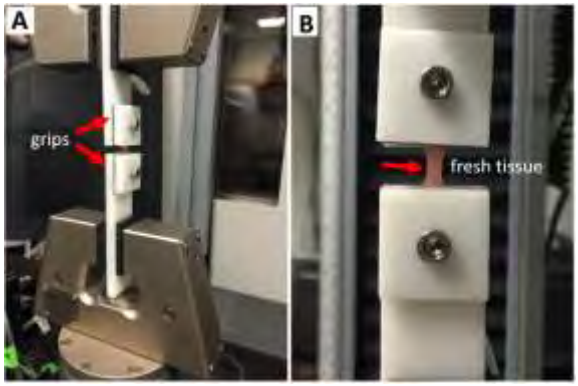

Figure 1: Tensile test performed using an Instron type 5565 with anti-slip grips.

Computational method: To study mechanics involved in the intestinal tract lengthening, finite

element analysis (FEA) was used. Three-dimensional models were created using ABAQUS (D. S. Simulia) where initial geometry was matched to geometry of real intestinal tracts which was a hollow cylinder and for nonlinear material behavior, new-hooking model was taken.

RESULTS AND DISCUSSION

For every specimen ($n = 12, length = 22.6 \pm 6\ mm, width = 7.2 \pm 0.7 mm$), tensile test with rate of 0.4 mm/min was performed and a force-displacement curve was obtained (Fig. 2A). From this, once a linear line was fit to the data, stress was calculated by dividing the force by the undeformed cross-sectional area (width × thickness) of the specimen and strain was calculated by dividing the displacement of the specimen by the initial length (ΔL/L). Finally, Young's modulus (E) was characterized by dividing the stress by strain, $E = 1.54 \pm 0.26$ (MPa) (Fig. 2B).

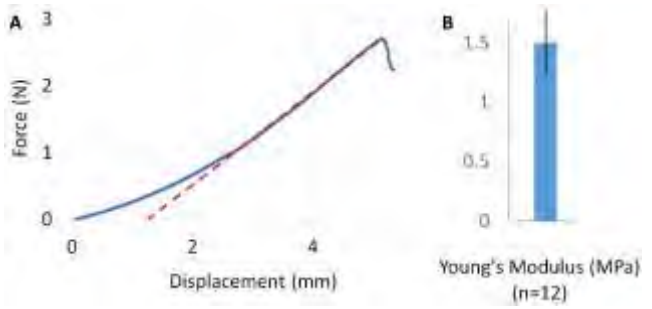

Figure 2: Mechanical testing of intestinal tissue: (A) Representative force-displacement plot, dashed-red line shows the linear fit. (B) Average Young's module of specimens, $E = 1.54 \pm 0.26$ (MPa).

As previously mentioned in introduction section, an effective way to apply mechanical force is use of self-expanding springs for successful lengthening of jejunum but with variable intestinal sizes, it is critical to determine safe, translatable spring characteristics in differently sized animal models before clinical use. To this goal, finite element modeling was used where models in different size in radius and thickness was made (Fig. 3A) and mechanical forces was applied at both ends of the cylindrical hollows with fixed boundary condition for midline. In different models (size was changed while other features of models kept unchanged), scaled forces based on the cross-sectional area predicted same lengthening ratio (Fig. 3B). Further investigation proved robustness of model in prediction for lengthening ratio when different range of material properties was chosen.

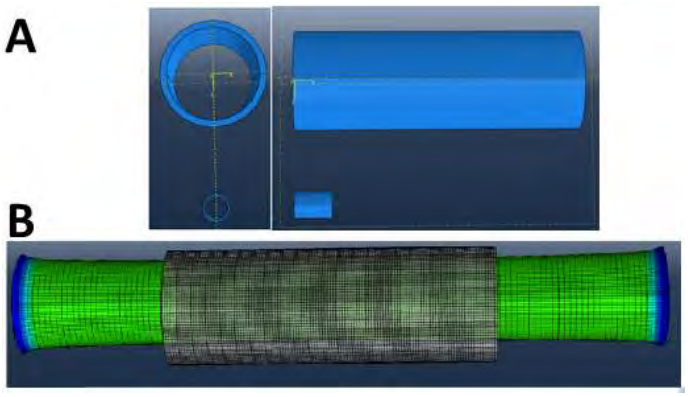

Figure 3: Computational model for intestinal lengthening due to applied mechanical force: model results confirm cross-sectional area as an appropriate parameter for force scaling for variable intestinal sizes.

CONCLUSIONS

Experimental results provided required material properties of intestinal tract while computational models suggests cross-sectional area as a proper parameter to rescale the required mechanical force in variable intestinal sizes. However future work will include additional complications (tissue growth and tissue lengthening due to growth in response to stress experienced by tissue) for the further investigations.

REFERENCES

1. Wales et al. *J Pediatr Surg* 39(690–5), 2004.
2. Thompson et al. *Surg Clin North Am*. 91(3):493-510, 2011.
3. Sullins et al. *J Pediatr Surg* 49(971–5), 2014.
4. Scott et al. *J Pediatr Surg* 50(954–7), 2015
5. Sullins et al. *J Pediatr Surg* 49(109–13), 2014.

AN INVESTIGATION OF BUCKLING COMPLICATIONS IN SPINAL ANESTHESIA ADMINISTRATION PROCEDURES

[1] Tessa C. Hulburt, [2]Jessica M. Booth, [2]Peter Pan, [1]Philip J. Brown

[1] Biomedical Engineering, Wake Forest Baptist Health
[2] Anesthesiology, Wake Forest Baptist Health
Email: thulburt@wakehealth.edu

INTRODUCTION

In an effort to reduce the most common complication of spinal anesthesia administration procedures, post-dural puncture headaches (PDPH), small diameter spinal anesthesia needles are used. Though effective in reducing PDPH prevalence, the use of small diameter needles has increased complications due to needle buckling [1]. While a mechanical evaluation of needle deviation during advancement as well as a clinical understanding of needle fracture have been documented, buckling behavior is not well understood [1,2]. Therefore, it is clinically relevant to quantify changes that occur from uninterrupted needle insertion, axial loading during barrier contact and buckling. Furthermore, due to the large variety of spinal needles used clinically, it is appropriate to compare performance of different needle types in their ability to resist buckling. The goal of this study was to quantify the buckling behavior of spinal anesthesia needles with respect to the relative contribution of needle brand, gauge (G), and tissue depth.

METHODS

A repeatable spinal anesthesia administration procedure and buckling complication was simulated using a novel test fixture (**Figure 1**). The needle shaft was clamped to advance it through a ballistics gelatin tissue surrogate to a barrier using a servohydraulic Landmark material testing machine [MTS, Eden Prairie, MN]. This setup simulated Euler buckling in an elastic medium with fixed-pinned boundary conditions to match needle advancement in a clinical setting. Needles were tested in 50mm and 70mm tissue depths to represent average and obese bodyweights, respectively [3]. Varying gauges of needles manufactured by four different companies were selected for testing (see **Figure 3**). Four phases of buckling were analyzed (**Figure 2**): uninterrupted needle insertion into the gelatin tissue surrogate, axial loading of the needle once the barrier was met, critical buckling point (X_2 in **Figure 2**) and the buckling region where buckling continues as the needle is further advanced into the tissue. An analysis of variance (α=0.05; β=0.8) was conducted to compare results.

Figure 1. Test fixture diagram. 1) Force applied by MTS. 2) Needle grip that simulates physician's grip. 3) Ballistics gelatin tissue surrogate. 4) Needle. 5) Barrier.

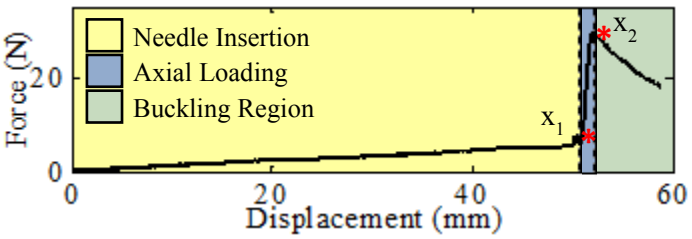

Figure 2. F-D plot of a buckling test defining four buckling phases

RESULTS AND DISCUSSION

F-D data showed consistent results within different needle testing groups, verifying reproducibility. Needle deformation occurred closer to the barrier, suggesting minimal lateral movement at the needle

hub. This is likely due to lateral support from the gelatin on the needle. Therefore, we propose that buckling is better detected from axial force or displacement.

Critical buckling loads (CBL) collected at different tissue depths did not vary significantly for most needle types. CBL is the force at the critical buckling point. It was observed that the force increased linearly as the needle was advanced (see **Figure 2**) due to friction created by the tissue surrogate on the needle. When performing this procedure, it is possible that increased resistance from barrier contact could feel like expected proportional resistance increase as the needle is further inserted into the tissue, especially for larger tissue depths. **Table 1** compares the force change when a barrier is met (ΔF) at the two tissue depths. Smaller ΔF were found for all same gauge needles at the larger tissue depth, supporting our theory that buckling is more challenging to detect at larger tissue depths due to the smaller ΔF, rather than from CBL alone.

Table 1. ΔF (N) = CBL – Force at x_1

	22G	27G
50mm	23.54 ± 0.63	7.700 ± 0.01
70mm	21.18 ± 0.65	5.737 ± 0.16

Analyses of axial loading and buckling regions found large stiffness and minimal energy values during axial loading and large energy values during continued buckling. These results indicate that buckling is better detected with axial force feedback, rather than displacement due to the needle's limited ability to displace axially. Due to the minimal energy that is able to be absorbed when loaded axially, needles are prone to buckling. Therefore, the needle will fail under much smaller loading than the material ultimate failure load. While the needle will buckle easily, far more energy is required to fracture the needle as indicated by the large buckling region energy results.

When analyzing different needle types, larger diameter needles produced overall larger CBL. Differences in CBL for different brand needles of a single gauge were far less than CBL differences between needle gauges (**Figure 3**). Statistically significant variations were found between CBL from all same-brand-different-gauge and different-brand 22G and 24G needles, but not for all different-brand 25G and 27G CBL comparisons. These data show that needle gauge effects buckling behavior significantly and that needle brand is less influential overall, particularly for smaller needles.

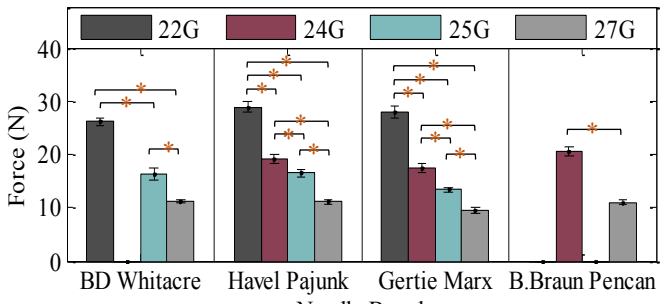

Figure 3. CBL Results Collected in 50mm Tissue. * = p<0.001. Each bar represents n=8-12 needles tested.

CONCLUSIONS

Our results indicate the use of axial force feedback as the primary metric to detect buckling. Barrier contact may be challenging to detect before buckling occurs, but the large stiffness increase that occurs during needle axial loading may be used to prevent permanent needle damage. To choose a needle best equipped to resist buckling complications, special consideration for needle gauge should be taken. Needle brand should also be considered, especially if a larger gauge needle is appropriate. We expect the results of this study and further analyses of spinal needle yield and failure point to help us achieve our long-term goal of improving spinal anesthesia procedure safety.

REFERENCES

[1] Martinello et al., *J Clin Anesth,* 2014, 26(4).
[2] Sitzman and Uncles, *Anesth Analg,* 1996, 82(2).
[3] Meikle, *Reg Anesth Pain Med,* 1983, 62(10).

SAMPLE SIZES OF STATISTICAL MODEL FOR THE ELDERLY

Eunjoo Hwang, Sven Holcombe, Susumu Ejima, Kristen Cunningham and Stewart Wang

University of Michigan Health System, Ann Arbor, MI, USA
email: ejhwang@umich.edu

INTRODUCTION

To prevent serious injury from repetitive low-intensity usage or sudden high-energy impact, various computational models have been developed and used to reveal the injury biomechanics. For injury biomechanics during high-energy impact such as motor vehicle crashes, whole-body-level human body models (HBMs) have been developed and examined under diverse impacting scenarios. As a result, a few commercialized subject-specific HBMs have been presented to represent midsize male, small female, and large male [1, 2].

Recently, HBMs for the elderly, which is a vulnerable and growing population, have been actively studied. With concerns about the representation of subject-specific HBMs and the efficiency of developing procedure, elderly HBMs are developed mainly by a mesh morphing process to fit statistically-determined geometries. However, sample sizes of statistical models for the entire age spectrum were ranged between less than 50 and 350 [3, 4]. These wide variances in sample sizes may have an effect on the statistically-determined geometry. There might be recommendable sample sizes that represent the elderly population properly. Thus, this study was to designed to address these issues by generating multiple thorax-skin statistical models from diverse sample sizes of subjects.

METHODS

Geometries of thorax skin were obtained from CT scans which were collected and processed by a high-throughput in-house program in the International Center for Automotive Medicine/ Morphomic Analysis Group. For the adult thorax skin model, CTs were collected only from subjects older than 18 years of age who had all images between highest thoracic vertebrae (T1) and lowest lumbar vertebrae (known as L5). For each CT, individual vertebral levels between T1 and L5 were divided into four levels, and the circumference of each level was demonstrated as 200 data points. Due to arm posture during CT imaging, gradually fewer data points were extracted from the levels above the T8 vertebrae.

For this study, massive asymmetric data points per subject were processed to be symmetric in sagittal plane and condensed into 1/20 ratio. Data points in left and right body sides were averaged in each vertical level. Among 66 vertical levels, data points in every other vertical level were used. In one vertical level, every tenth data point was used to represent the thorax skin.

The thorax skin statistical models were generated through principal component (PC) analysis and multivariate regression analysis. As predictors, age, body mass index (BMI), and height of the subject were used for separate models for male and female cases. Based on thorax skin data points matrix, the covariance and PC scores were calculated. In all statistical models, the numbers of PC scores cover more than 99% of the variance in each set of sample data. This study tested diverse sample sizes; 100, 200, 300, 500, 800, 1000, 1200, and 1500 subjects per sex. For each sample size, the mean age, BMI, and height for men fell at approximately age 45, BMI 28, height 178 cm, and for women, the mean age was 51, BMI 30, and height 163 cm.

To compare the statistically-determined geometry, individual statistical models predicted 27 different thorax skins. 3 values for age (20, 45, and 70 years), BMI (20, 30, and 40), and height (145, 160, and 175 cm for female; 160, 175, and 190 cm for male) were combined. On all vertebrae levels, the anterior-posterior and lateral-medial distances passing the center of the spinal canal (total 34 values) were obtained. The differences from reference in those 34 measurements were calculated and averaged among individual thorax skins. Reference measurements

were the predicted values by the statistical model using 1500 subjects. The ability to predict thorax skin by the statistical model based on 1500 subjects was previously tested by direct comparison to the 27 subject-specific thorax skins. The averaged differences in both male and female models were less than 1% (0.7 ± 0.2%) which was not strongly related to subjects' age, BMI, and height.

RESULTS AND DISCUSSION

The thorax skin to represent the mid-age, mid-BMI, and mid-height subject was not as varied as thorax skin representing subjects at both the lower and upper ends of age, BMI, and height, regardless of sex. The smallest difference in the midsize subject among 27 subjects was observed in all of statistical models in this study, even the model with only 100 sample sizes.

The mean and standard deviation of the difference in geometry were decreased with increasing sample sizes in both sexes. In the thorax skin of the subject representing both the lower and upper ends in age, BMI, or height, the benefit of using larger sample sizes for the statistical models was demonstrated. Averaged difference among three female thorax skins representing mid-age, mid-BMI, or mid-height was 5.49, 5.72, 4.25 in 100 sample sizes, and reduced to 0.34, 0.42, 0.29 in 1000 sample sizes. However, averaged difference among three female thorax skins for young, low BMI, or shorter height were 8.97, 9.48, 7.11 in 100 sample sizes reduced to 0.51, 0.65, 0.36 in 1000. The negative relationship between sample sizes and difference in geometry was also observed in the male statistical models.

With specific attention to the elderly, the isolated age factor on the negative relationship was presented in Figure 1. Figure 1 shows that the mean difference in thorax skin geometry was reduced by around 1% when the sample sizes reached 500 for the 45-year-old cases, and 1000 for the 20-year-old and 70-year-old cases. The variations in the difference for 70-year-olds were almost double the variations in the difference for 45-year-olds, especially in the statistical models taking smaller sample sizes than 800. Furthermore, the negative relationship stabilizes when the statistical model is based on more than 1000 sample sizes. Thus, the sample sizes of a robust statistical model for the elderly were recommended to be greater than 1000.

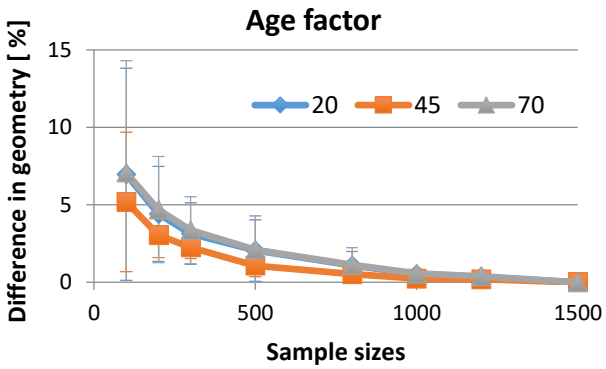

Figure 1: The mean and standard deviation of the difference in geometry as a function of sample sizes in each age group.

This study tested only for the thorax skin. The skin was defined by the soft tissues, so that more variation may be presented than in the geometry defined by the bone tissues. The current study sampled subjects across the adult age population (18 years and above). For the elderly HBMs, the sample could be selected from a more limited age group; smaller sample sizes then might capture the variations.

CONCLUSIONS

This study generated thorax skins by statistical models based on different numbers of subjects. The thorax skin representing a midsize subject experienced the minimum influence based on sample size among individual sets of 27 thorax skins. However, the difference in the statistically-determined thorax skin from the reference for subjects who are not mid value in age, BMI, or height significantly decreased with increasing sample size. Thus, this study suggests more than 1000 for each sex as the sample size for the robust statistical thorax skin model.

REFERENCES

1. Gayzik et al. *Ann Biomed Eng.* 39: 2568-83, 2011.
2. Iwamoto et al. *Proceedings of IRCOBI'02,* Munich, Germany, 2002.
3. Klein et al. *Ann Biomed Eng.* 43: 2503-14, 2015.
4. Weaver et al. *J Anat.* 225:246-61, 2014.

RADIOULNAR WRIST COMPRESSION FOR CARPAL TUNNEL SYNDROME TREATMENT: A PRELIMINARY CLINICAL STUDY

[1]Lenicia N. Jenkins, [1]Emily Grandy, [1]Carli Norman, [2]Peter J. Evans, [3]Juliet Hou, [2]William H. Seitz, Jr., [1,2,3]Zong-Ming Li

Hand Research Laboratory, Departments of [1]Biomedical Engineering, [2]Orthopaedic Surgery, [3]Physical Medicine and Rehabilitation, Cleveland Clinic, Cleveland, OH, USA

email: liz4@ccf.org web: http://handlab.org/

INTRODUCTION

Carpal Tunnel Syndrome (CTS) is the most common compressive neuropathy, causing pain, paresthesia, numbness, and tingling in median nerve innervated digits. Routine treatment for CTS involves surgically transecting the transverse carpal ligament, however this procedure is associated with several complications. Conservative treatment methods such as physical therapy, corticosteroid injection, and splinting are also commonly used as a first line of defense, but lack scientific and clinical efficacy. As an alternative, we have developed a method to enlarge the carpal arch using radioulnar wrist compression (RWC) as a means to decompress the median nerve [1, 2]. The purpose of this study was to evaluate the RWC treatment efficacy in relieving hand symptoms and improving hand function in CTS patients. It was hypothesized that daily RWC intervention would alleviate CTS symptoms and improve hand function.

METHODS

Nine patients (6 females, 3 males; 53.67 ± 16.46 years old) were recruited for this study. Individuals were eligible if they were over age 18, clinically diagnosed with CTS, experienced nocturnal pain, numbness or tingling, demonstrated one positive provocative maneuver (Tinel's sign, Phalen's test, or carpal compression test) and/or abnormal nerve conduction finding for the median nerve at wrist. Patients were excluded for any systemic disease (i.e. rheumatoid arthritis, diabetes, osteoarthritis), history of major injury to the wrist or hand, BMI over 30, or were currently pregnant.

The RWC was implemented by an intervention device (Fig. 1) consisting of a thermoformable Exos Wrist Brace with Boa (DJO, Vista, CA), inflatable bladder, and aneroid sphygmomanometer dial and bulb assembly. The brace was molded to stabilize the patient's wrist in an anatomically neutral position. The air bladder, measuring 50mm x 50mm when deflated, was attached with Velcro to the inside of the brace. The bladder was centered on the medial side of the wrist and at the level of hook of hamate to apply radial-ulnar wrist compression, achieving compression forces similar to that implemented in our previous experimental studies [1, 2].

Fig. 1: RWC bracing device worn on the hand (A) and inside view with inflated bladder (*) (B)

Patients performed three RWC bracing sessions daily. Each bracing session consisted of three 5-minute pressurized intervals, with a 1-minute rest between each application. To apply pressure, subjects were instructed to inflate the bladder and maintain the pressure at 140 mmHg. Patients participated over an 8 week period which was subdivided into three phases: pre-intervention (Week 0), intervention (Weeks 0-4), and follow-up (Week 8). Laboratory data collection was performed at weeks 0, 2, 4, and 8. Primary outcome measures used to evaluate intervention effectiveness included (a) Boston Carpal Tunnel Syndrome Questionnaire (BCTQ) [3] including Symptom Severity Score (SSS), Functional Severity Score

(FSS), and Overall Score (OS), and (b) pain, numbness, and tingling intensity using a 0-10 visual analog scale (VAS).

One-way repeated measures ANOVAs or the non-parametric equivalent were performed to determine differences in FSS, SSS, OS and individual VAS scores across intervention time points. Post-hoc Tukey's tests were used for all pairwise comparisons. A significance level of $\alpha = 0.05$ was used for statistical comparisons.

RESULTS

Outcome scores (mean ± SD) are summarized in Table 1. By the second week of intervention, patients' numbness and tingling had significantly decreased ($p<0.05$), as had SSS and OS ($p<0.05$), however pain and FSS had not improved significantly. At Week 4, patients' SSS and OS had decreased by 0.52 ($p<0.05$) and 0.40 ($p<0.01$), respectively, compared to pre-intervention, however FSS reduction (by 0.25) was not significant. Similarly, worst pain ($p<0.05$), numbness ($p<0.001$) and tingling ($p<0.05$) improved between baseline and Week 4. At Week-8 follow-up, SSS remained 0.39 lower compared to pre-intervention, as did FSS and OS (0.1 and 0.26 points lower, respectively), however these BCTQ score changes relative to the baseline were not statistically significant. Worst pain ($p<0.05$), numbness ($p<0.05$), and tingling ($p<0.01$) had all significantly decreased at Week-8 follow-up in comparison to pre-intervention.

Table 1: Clinical outcome scores (mean ± SD) at individual assessment time points

Outcome	Week 0	Week 2	Week 4	Week 8
BCTQ OS	2.50 ± 0.46	2.11 ± 0.50	2.10 ± 0.56	2.24 ± 0.95
BCTQ SSS	2.83 ± 0.45	2.29 ± 0.70	2.31 ± 0.62	2.44 ± 1.03
BCTQ FSS	2.06 ± 0.52	1.86 ± 0.46	1.81 ± 0.52	1.96 ± 0.88
Worst Pain	6.33 ± 3.84	4.44 ± 3.06	4.22 ± 3.27	3.89 ± 3.86
Worst Numbness	7.56 ± 2.19	4.89 ± 1.45	4.56 ± 2.07	3.78 ± 2.91
Worst Tingling	6.44 ± 3.17	4.00 ± 2.00	3.89 ± 2.62	3.33 ± 2.69

DISCUSSION & CONCLUSION

In this study, we utilized radioulnar wrist compression to alleviate symptoms and improve functional performance in patients suffering from CTS. After two and four weeks of 3x daily treatment consisting of 15 minutes of bracing, subjects noted marked symptom improvement. When compared to 8 hours of nightly splinting over a similar time period (1 month), our treatment, 45 min of daily wear, achieved comparable reductions in functional severity (compression -0.25 ± 0.52 vs splinting -0.21 ± 0.34) , and achieved even greater improvements in symptom severity (-0.52 ± 0.53 vs -0.38 ± 0.47) and overall scores (-0.40 ± 0.49 vs -0.29 ± 0.35) [4]. Compared to surgical intervention, in which a BCTQ raw score decrease of 0.47 is considered clinically significant [5], our non-surgical, biomechanical intervention demonstrated comparable overall score reductions between baseline and the end of intervention, indicative of active symptom relief and functional improvement. These results were further supported by patients' diminished worst pain, numbness and tingling after four weeks of intervention. Although BCTQ scores increased between Weeks 4 and 8, follow-up scores did not return to baseline measures, suggesting positive lasting effects of our treatment even after four weeks of no device use. In addition to our objective outcomes, we also received favorable written feedback from participating patients. Several months post follow-up, one patient contacted us to report her CTS symptoms remained 'greatly relieved'. Another subject appreciated that a non-surgical treatment for CTS was in development. One limitation of this study is the relatively short intervention phase and low daily dosage. A long-term intervention with a higher daily dosage may provide added benefits of radioulnar compression for CTS symptom relief. Based on these findings, we can conclude that radioulnar wrist compression may be an effective means to relieve symptoms associated with CTS.

ACKNOWLEDGEMENT

NIH/NIAMS R01AR068278

REFERENCES [1] Marquardt et al. Clin Biomech 2015, 30(3):248-53 [2] Marquardt et al. J Orthop Res 2016, 34(7):1234-40 [3] Levine et al J Bone Joint Surg Am 1993 75(11):1585-92 [4] So et al Int J Rheum Dis. 2018 Jan; 21(1):102-107 [5] Amirfeyz et al. Int Orthop 2009, 33(1):181-5

BIOMECHANICAL RESPONSE TO ACUTE PATELLOFEMORAL PAIN IN RUNNING

[1] Carl Jewell, [1]Joseph Hamill and [1] Katherine A. Boyer

[1] University of Massachusetts, Amherst, MA, USA
email: cjewell@kin.umass.edu, web: people.umass.edu/mobl, twitter: @carlmjewell

INTRODUCTION

Patellofemoral pain syndrome (PFPS) is the most common lower limb injury in runners, comprising 20 percent of all running injuries [1]. PFPS is marked by persistence and frequent reoccurrence [2]. Despite our current depth of knowledge of PFPS and its resulting impairments in muscle function and gait mechanics, PFPS treatment often remains ineffective. Altered gait and muscular function may contribute to PFPS but may also result from PFPS-related pain. Thus, there is a need to understand the relationship between pain and altered gait and muscular function with PFPS in order to improve treatment efficacy and patient outcomes. The aim of this study was to examine the impact of a 21-minute treadmill run on self-reported pain, frontal and sagittal plane knee mechanics, and muscle activation intensity in both healthy runners and runners with PFPS.

METHODS

Twenty-two active individuals (11 healthy, 11 PFPS) completed a 21-minute moderate, self-selected paced treadmill run. Rating of perceived exertion (RPE) on a modified Borg scale and knee pain on a Verbal Numeric Rating Scale were measured every two minutes of the run.

Kinematic data were collected unilaterally at 200 Hz. Ground reaction forces were measured using an instrumented treadmill at 1000 Hz. Electromyograms (EMG) were collected from six muscles (medial and lateral gastrocnemii, biceps femoris, lateral and medial vastii and gluteus medius) using a wireless Delsys Trigno system at 2000 Hz. Data for all measures were collected on the same computer for 30 seconds one minute into the run, and during the final 30 seconds.

Angle and moment data were filtered using an 8 Hz low pass, second-order Butterworth Filter. Joint moments presented are internally referenced to the proximal segment. EMG data were wavelet-transformed using 13 non-linearly spaced wavelets and the activation intensity was calculated as the sum of all wavelets for each muscle for each time sample. The net activation intensity (sum of activation intensity over time) was determined for three time windows: pre-contact (50 ms before foot strike), weight acceptance (first 50% of stance), and propulsion (final 50% of stance).

Two-way repeated measures ANOVAs were used to test for differences in the knee angles and moments and in the EMG intensity of each time window at the beginning of the run and in the change over time between PFPS and healthy controls. For kinematic and kinetic measures, testing was performed on waveforms using one-dimensional Statistical Parametric Mapping [3]. Across all outcomes, significance was defined as $p \leq 0.05$.

RESULTS AND DISCUSSION

An increase in pain was found for the PFPS group (2.2±1.8) but not the healthy group with the 21-minute run. Eight out of the 11 participants with PFPS had a clinically significant increase in pain (> 1 point). Each group had a mean change in RPE of 3.1. The healthy group ran at a faster speed (3.30 vs 2.97 $m \cdot s^{-1}$, $p = 0.04$) compared to the PFPS group.

Kinematics

A significant main effect for group was found in knee flexion angle between 34-64% of stance ($p = 0.006$). The PFPS group had a lessor knee flexion angle in this window compared to the healthy group. This may be due to an avoidance strategy to prevent further increases in pain as an increased knee flexion angle can lead to increased patellofemoral joint stress [4]. A significant main effect for run time was found in the knee adduction angle from 20-64% stance ($p =$

0.002). This indicates that over the course of the 21-minute run, knee adduction angles decreased in both groups. No group*time interactions were present in either plane.

Kinetics

For joint moments, there was a significant main effect for group in the sagittal plane between 0-5% stance ($p = 0.043$) and 20-44% stance ($p < 0.001$). This indicated a greater initial knee flexion moment at footstrike and a larger extension moment in midstance in the PFPS group relative to healthy controls. This result is in contrast to previous work investigating healthy individuals' response to experimental knee pain that found decreased knee extension moments with greater pain severity [5]. The PFPS group, despite an increase in pain, showed no adjustment in knee extension moment. It is possible that some form of long term adaptation to unsuccessful pain reduction blunted this response.

There was much greater variance for the PFPS group relative to healthy in the frontal plane moments, with a significant main effect for group in the final 10% of stance (p=0.034). This was marked by a small adduction moment in the healthy group and a small abduction moment in the PFPS group. This increased variance in this moment could be due to a lack of control in frontal plane loading due to PFPS. No group*time interactions were present in either plane.

Electromyography

There were no significant group differences found in EMG. There were also no significant differences found for time in the pre-contact window. During weight acceptance, there was a significant main effect for time (p=0.002) indicating a decrease in total gluteus medius activity between the beginning and end of the run. During propulsion, there was also a main effect for time (p=0.024), indicating a decrease in total biceps femoris activation between the beginning and end of the run. These results indicate that despite differences in kinematics and kinetics between healthy runners and those with PFPS, the muscles included in this investigation showed no difference in net activation intensity. It is possible that other metrics of EMG, such as timing or duration of activity, may uncover differences between groups related to a pain response.

CONCLUSIONS

Individuals with PFPS have different kinematic and kinetic patterns at the knee at baseline compared to healthy runners. Those with PFPS do not appear to adapt their mechanics in response to an acute change in pain, suggesting that the gait differences observed may arise in part from an adaptation to chronic pain or that the abnormal mechanics are what leads to the observed pain increase.

REFERENCES

1. Taunton et al. *British J Sport Med.* 36, 95-101. 2002.
2. Collins et al. *BMC muscular disorders.* 11:11. 2010.
3. T.C. Pataky et al. *J Biomech.* 46, 2394–2401. 2013.
4. Y-J Chen et al. *J Applied Biomech.* 30. 2014.
5. Henriksen et al. *Arth Care & Research.* 62, 501-509. 2010.

ACKNOWLEDGEMENTS

Research reported in this abstract was supported by a grant from the De Luca Foundation. The content is solely the responsibility of the authors and does not necessarily represent the official views of the De Luca Foundation.

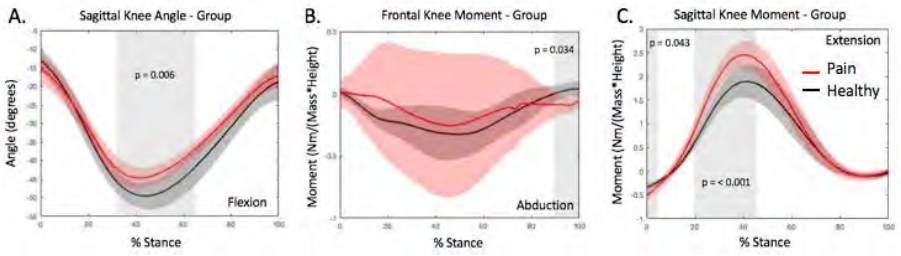

Figure 1. A-C show the mean waveforms (mean±SD) for the PFPS group (red) and the healthy group (black). The shaded vertical regions mark the significant differences between waveforms and their respective p-values.

GAIT PERFORMANCE IN BIPOLAR DISORDER: A 6-MONTH PILOT LONGITUDINAL STUDY

[1*] Gu Eon Kang, [2] Brian J. Mickey, [1] Melvin G. McInnis, [1] Barry S. Krembs and [1] M. Melissa Gross

[1] University of Michigan, Ann Arbor, MI, USA
[2] University of Utah, Salt Lake City, UT, USA
[*]email: guekang@umich.edu

INTRODUCTION

Bipolar disorder is a severe mood disorder that is characterized by periods of (hypo)mania and depression, with euthymia, a relatively normal mood state [1], for which objective biomarkers have not been developed yet. In the United States, lifetime prevalence of bipolar disorder is 4.4% among adults [2]. Diagnoses of bipolar disorder are based on evaluating clinical criteria such as abnormal motor behavior [1]. However, the evaluation of the behavioral symptoms depends on qualitative self-report only and lacks objective basis, resulting in subjective assessments with limited reliability.

Gait performance can be measured quantitatively and expresses emotional state [3]. In addition, gait performance can be easily tested in clinics, thus may have potential as objective clinical criteria; however, too little information about gait performance and bipolar disorder has been established until now. Therefore, the purpose of this study was to investigate gait variables in bipolar patients (BP) across mood states and healthy controls (HC) over the course of a 6-month period.

METHODS

BP and HC were recruited from the Heinz C. Prechter Longitudinal Study of Bipolar Disorder Cohort [4]. BP had no history of neurological or orthopedic conditions. HC had no history of psychiatric, neurological or orthopedic conditions. Participants completed baseline (31 BP; 14 HC) and 6-month follow-up sessions (24 BP; 13 HC). Manic and depressive symptoms were assessed using the 5-item Altman Self Rating Mania Scale (ASRM; total score of 20; on a score of 0-4 per item) [5] and the 9-item Patient Health Questionnaire (PHQ-9; total score of 27; on a score of 0-3 per item) [6]. Baseline mood symptoms for BP were categorized into hypomania (n=5; ASRM≥6; PHQ-9<6), euthymia (n=14; ASRM<6; PHQ-9<6) and depression (n=12; ASRM<6; PHQ-9≥6).

Participants performed gait trials on an 8-meter walkway five times at each of comfortable, slow and fast speeds. Preliminary analyses revealed gait performances were similar in slow or fast speeds in BP and HC [7], thus this study included only data from comfortable speed. Data from marker and ground reaction forces (GRFs) were collected at 120 and 1200 Hz, respectively, using a 16-camera motion capture system (Motion Analysis, Santa Rosa, CA) and two force plates (AMTI, Watertown, MA), and were low-pass filtered at 6 and 50 Hz, respectively. Visual3D (C-Motion, Germantown, MD) was used to compute gait speed during one gait cycle, and peak anterior-posterior and vertical GRFs in the first half of stance. Mean values for baseline anthropometric and gait data were compared among BP-hypomania, BP-euthymia, BP-depression and HC using one-way ANOVA with Tukey correction. Correlations between baseline mood scores and gait data were determined for BP using coefficient of determination (R^2). Changes in anthropometric and gait data between baseline and 6-month follow-up sessions were compared between BP and HC using independent t-test. Correlations between changes in mood scores and gait data between baseline and 6-month follow-up sessions were determined using coefficient of determination. A $p<0.05$ value was used to detect significant differences among means.

RESULTS AND DISCUSSION

Baseline results showed that age and body mass index were not significantly different among BP-hypomania (45.2±15.1 years; 26.5±5.5 kg/m^2), BP-euthymia (38.7±10.5 years; 26.5±4.1 kg/m^2), BP-depression (38.4±9.3 years; 27.0±6.9 kg/m^2) and HC (42.2±12.6 years; 25.6±5.1 kg/m^2) (all $p>0.05$).

Mean gait speed was greater for BP-hypomania (1.48±0.21 m/s) than for BP-euthymia (1.21±0.15 m/s), BP-depression (1.14±0.26 m/s) and HC (1.22±0.12 m/s) (all $p<0.05$). Mean values in peak anterior-posterior and vertical GRFs in the first half of stance (fraction of body weight) were greater for BP-hypomania (0.25±0.07 and 1.22±0.18, respectively) than for BP-euthymia (0.18±0.03 and 1.09±0.09, respectively), BP-depression (0.16±0.05 and 1.06±0.09, respectively) and HC (0.18±0.03 and 1.07±0.06, respectively) (all $p<0.05$). Within BP, gait speed and peak anterior-posterior and vertical GRFs were significantly correlated with manic scores (R^2=0.247, 0.347 and 0.333, respectively) (all $p<0.05$), but not with depressive scores (R^2=0.034, 0.069 and 0.037, respectively) (all $p>0.05$).

For both BP and HC, body mass index was not significantly different between baseline and 6-month follow-up sessions (all $p>0.05$). Changes in gait speed (m/s), and peak anterior-posterior and vertical GRFs were not significantly different between BP (-0.02±0.17, 0.00±0.04 and -0.01±0.12, respectively) and HC (-0.03±0.16, 0.01±0.03 and 0.03±0.09, respectively) (all $p>0.05$). Within BP, changes in peak vertical GRFs between baseline and 6-month follow-up sessions showed significant negative correlation with changes in depressive scores (R^2=0.180) ($p<0.05$) but not with changes in manic scores (R^2=0.047) ($p>0.05$). Changes in mood scores, and gait speed and peak anterior-posterior GRFs were not significantly correlated with manic (R^2=0.001 and 0.082, respectively) and depressive scores (R^2=0.098 and 0.018, respectively) (all $p>0.05$).

CONCLUSIONS

Results suggest that gait speed and peak GRFs may reflect mood symptoms in BP. Changes in GRFs were associated with changes in mood symptoms over the longitudinal course. Monitoring speed and GRF-related variables (i.e., foot contact pressure) in the community and clinic using wearable equipment could help detect and predict mood symptoms. In conclusion, gait variables may have potential as behavioral biomarkers for BP

REFERENCES

1. American Psychiatric Association, *DSM-V*, 2013.
2. Merikangas et al. *Arch Gen Psychiatr*. 64(5): 543-552.
3. Kang and Gross. *J Biomech*. 49, 4022-4027, 2016.
4. McInnis et al. *Int J Epidemiol*. 47(1): 28-28n, 2018.
5. Altman et al. *Biol Psychiatry*. 42(10): 948-955, 1997.
6. Kroenke et al. *J Gen Intern Med*. 16(9): 606-613, 2001
7. Kang et al. *Proceedings of ASB'17*, Boulder, CO, USA 2017.

ACKNOWLEDGEMENTS

The American Society of Biomechanics (GIA), Blue Cross Blue Shield of Michigan Foundation, and Rackham School at University of Michigan supported this study. The authors thank Dr. Deanna Gates for help with data collection.

Wearable Sensors for Assessment of Varus Thrust in Knee Osteoarthritis: A Proof of Concept

[1] Deepak Kumar, PT, PhD; [1]Victoria Brus; [1]Chun Jui Lin; [1]Julie Osipow, BA; [1]Alex Geronimo, MS; [2]Jim Richards, PhD

[1] Movement & Applied Imaging Lab, Boston University, Boston, MA, USA
[2] University of Central Lancashire, Preston, UK
email: kumard@bu.edu, web: https://sites.bu.edu/kumarlab/

INTRODUCTION

Knee osteoarthritis (OA) affects 12% of American adults over the age of 55 years, and is the leading cause of disability in the US. There is no available treatment to slow the progression of knee OA. Up to 50% of people with knee OA exhibit a varus (adduction) thrust during walking. Varus thrust is associated with knee pain and stiffness,[1] measures of knee loading including KAM,[2] and most importantly, a 4x greater risk of medial knee OA progression.[3] It may be possible to reduce the varus thrust by means of devices (braces), exercises (gait retraining, neuromuscular exercise), or surgery. However, previous research has been based on either visual determination of presence/absence of varus thrust, or quantification of angular knee kinematics in an expensive gait lab. An inexpensive technique to quantify the presence and magnitude of varus thrust is acutely needed for clinical research on interventions to reduce varus thrust.

The objective of this study was to evaluate the feasibility of using gyroscopes within wearable inertial sensors for assessment of the angular knee velocity in the frontal plane,[4] a known biomechanical marker of varus thrust, in people with medial knee OA.

METHODS

So far, data from 10 participants (Age = 65.8±7.1 years; BMI = 28.7±4 kg/m^2; 5 men, 5 women) are included in these analyses. The participants were recruited from the community using advertisements. The inclusion criteria were age between 45 and 80 years, BMI ≤ 35 kg/m^2, frequent knee pain, and radiographic medial knee OA. Exclusion criteria were use of walking aid, inflammatory arthritis, total knee replacement, neurological disorders, and other conditions that could affect gait. All participants underwent weight-bearing fixed flexion radiographs for Kellgren-Lawrence Grading (KLG) and joint space width measurements and long-limb radiographs for measurement of alignment. All participants also completed the Knee injury and Osteoarthritis Outcome Score (KOOS).

All participants completed 3D gait analyses while walking at their self-selected pace and their fastest pace. Kinematic data were collected with a 12 camera passive motion capture system @ 250 Hz and ground reaction forces were collected using floor-imbedded force platforms @ 2000 Hz. A cluster-based marker set was used and high-resolution 2D color video was also recorded during all trials. Marker and GRF data were processed to calculated knee joint angles, angular velocities, and moments. Additionally, inertial sensors (@ 148 Hz, upsampled to 2000 Hz) were placed on the shank and thigh clusters, and distal lateral tibia. The sensors included tri-axial accelerometer (± 16g), triaxial gyroscope (± 2000 deg/s) and triaxial magnetometer (± 1000 μT)(Delsys Inc, Natick, MA, USA). For these analyses, only the gyroscope signal was used. Peak knee angular adduction velocity was calculated from motion capture data, as well as, the three gyroscopes, during loading response phase (initial contact to peak knee flexion). Correlations were assessed between the gyroscope and motion capture data across all participants.

RESULTS AND DISCUSSION

There was 1 participant with KLG2, 6 with KLG3 and 3 with KLG4. Mean medial joint space width was 2.3±1.2 mm and mean alignment was

175.3±3.3° (<180° = varus). KOOS scores for the participants were as follows – Pain = 66.8±10.6, Symptoms = 57.8±9.4, Activities of Daily Living = 66.2±16.3, Sports/Recreation = 46±17.1, and Quality of Life = 41.9±11.8.

Correlations between knee angular velocity from motion capture and gyroscope data during the two tasks are shown in Table 1. Lateral tibia gyro accounted for 53% and 73% of the variability in knee angular velocity during the self-selected and fast pace conditions.

CONCLUSIONS

These preliminary findings suggest that a single inexpensive gyroscope sensor on the distal lateral shank may allow for assessment of varus thrust during walking in people with medial knee OA. This approach could allow for clinical identification of the presence and magnitude of varus thrust without reliance on 2D video or expensive gait labs. Hence, this technology could be used in future clinical trials to evaluate the efficacy of interventions to reduce varus thrust and slow the progression of knee OA.

REFERENCES

1. Fukutani N, Iijima H, Fukumoto T, et al. Association of Varus Thrust With Pain and Stiffness and Activities of Daily Living in Patients With Medial Knee Osteoarthritis. *Phys Ther.* 2016;96(2):167-175.
2. Kuroyanagi Y, Nagura T, Kiriyama Y, et al. A quantitative assessment of varus thrust in patients with medial knee osteoarthritis. *Knee.* 2012;19(2):130-134.
3. Chang A, Hayes K, Dunlop D, et al. Thrust during ambulation and the progression of knee osteoarthritis. *Arthritis Rheum.* 2004;50(12):3897-3903.
4. Chang AH, Chmiel JS, Moisio KC, et al. Varus thrust and knee frontal plane dynamic motion in persons with knee osteoarthritis. *Osteoarthritis Cartilage.* 2013;21(11):1668-1673.

Table 1: Correlations between knee angular velocity from motion capture and gyroscope data.

CORRELATIONS			Thigh Cluster Gyro	Shank Cluster Gyro	Lateral Tibia Gyro
Self-Selected	Knee Adduction Velocity	r	0.84	0.58	0.73
		P-value	0.005	0.076	0.039
Fast		r	0.62	0.68	0.85
		P-value	0.076	0.029	0.007

Relating functional task performance to rotator cuff pain in a breast cancer survivor population

[1] Angelica E. Lang, [2]Soo Y. Kim, [2]Stephan Milosavljevic and [3] Clark R. Dickerson

[1] Department of Health Sciences, University of Saskatchewan, Saskatoon, SK, Canada
[2] School of Rehabilitation Sciences, University of Saskatchewan, Saskatoon, SK, Canada
[3]Department of Kinesiology, University of Waterloo, Waterloo, ON, Canada

INTRODUCTION

Breast cancer survivors (BCS) may encounter upper limb morbidities post-surgery. Impairments such as reduced range of motion, reduced strength, pain, and lymphedema are commonly reported post-treatment [1]. BCS have a higher occurrence of other secondary morbidities, including rotator cuff disorders (RCD). It is currently unclear how these impairments affect arm kinematics, particularly during functional task performance, and how possible changes affect future injury risk or RCD development.

Limited documentation of BCS shoulder kinematics suggests conflicting results for scapular motion. In the first year after treatment, increased protraction and decreased anterior tilt have been reported, but there is no indication that these alterations remain longer term [2]. Past the first year of treatment, BCS with no indication of RCD may have higher scapular upward rotation than controls during arm elevation [3], but it is unknown if these alterations affect functional tasks performance.

The purpose of this investigation was to examine upper body kinematics during a waist to overhead lift for BCS and an age matched control group.

METHODS

Breast cancer survivors between the ages of 35 and 65, who had undergone mastectomy at least six months prior to participation, and were able to lift their arms above shoulder height were recruited from community advertisements. A control group of women in the same age range with no known upper limb impairments also participated.

Prior to task performance, all participants completed consent forms and the Quick Disability of Arm Shoulder and Hand (QuickDASH) questionnaire and were evaluated with three impingement tests (Neer, Hawkins-Kennedy, and empty can). A positive on any test warranted exclusion from the control group. For the waist to overhead lift, a shelves set at approximate waist and forehead heights. Participants lifted a weighted standard size milk crate (total load: 6.2 kg) between these two shelves 5 times in row. After a rest period, this was repeated twice. Motion of the torso and upper limbs was tracked with 10 VICON MX-T40 (Vicon Motion Systems, Oxford, UK) optoelectronic infrared cameras and reflective markers were placed on the skin near anatomical landmarks per ISB standards.

Torso, scapular, and thoracohumeral angles were calculated for all trials and split into cycles. A cycle was defined from the first upward movement of the hands to when the hands reached maximum height. Mean and maximum angles were calculated for each cycle and averaged within each participant. Torso and upper arm angles were compared between groups and to normative values from young, healthy adults performing the same lift [4]. Differences between the three groups were determined via one-way ANOVAs ($p<0.05$) and confirmed with Tukey HSD. For scapular angular kinematics, BCS were split into 2 groups based on pain in impingement tests and compared to age-matched controls with one-way ANOVAs ($p<0.05$).

RESULTS AND DISCUSSION

BCS reported significantly higher QuickDASH scores. Out of 16 BCS, 11 reported pain on at least one impingement test (Table 1).

Compared to younger controls, BCS presented with higher average torso flexion (-5.0 compared to 4.9, $p = .037$) and less peak arm abduction during the waist

to overhead lift (126.1 compared to 137.0, p = .027). Age-matched controls did not differ from either group. However, both BCS and age-matched controls had more horizontal flexion than the younger group (Figure 1).

While trends indicated BCS and age-matched controls differences, i.e. humeral abduction and axial rotation, none were significant. However, dividing BCS by impingement test status identified lower peak scapular upward rotation for BCS with pain than controls (-27.8 vs -35.8, p = .016) (Figure 2).

Kinematic alterations of BCS suggest impingement pathways. Increased torso flexion throughout the lift may reflect a kyphotic thorax commonly observed in BCS [5]. This torso position combined with decreased humeral abduction and scapular upward reduction may decrease available subacromial space, thereby raising rotator cuff tendon impingement risk [6]. Further, an average decrease of peak humeral external rotation of 7 degrees existed in BCS with impingement pain, which is also associated with RCD. The collective effects of BCS and RCD status indicate important pathological kinematics existed during functional task performance.

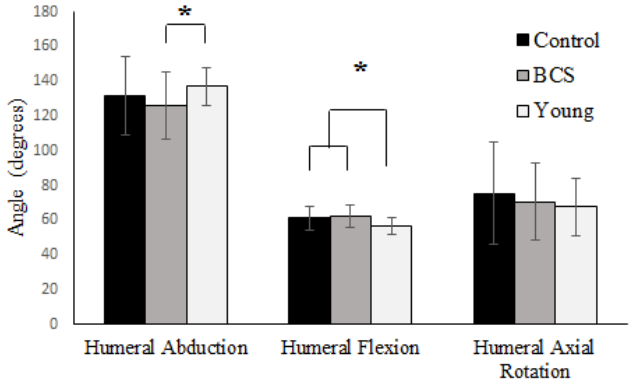

Figure 1: Peak humeral angles for BCS, age-matched controls, and young controls (+ve values for axial rotation represent external rotation).

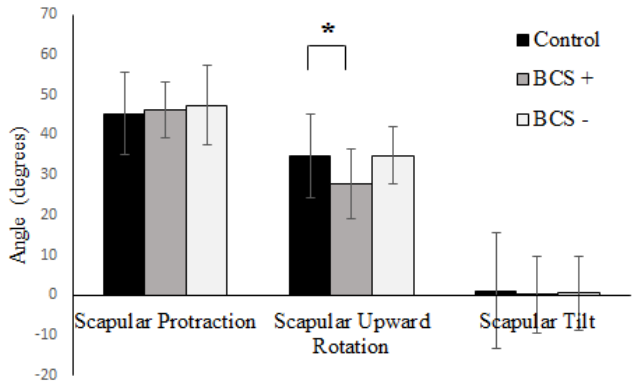

Figure 2: **Peak scapular angles with impingement test results (+ve vales represent protraction, upward rotation and anterior tilt, respectively). BCS + = 1+ positive impingement test; BCS – = 0 positive tests; Control = age-matched.**

CONCLUSIONS

Breast cancer survivors past the initial recovery stage demonstrated kinematic alterations in overhead lift performance. However, these alterations appear to be more strongly influenced by presence of RCD in BCS. It is not currently clear if these alterations are the cause or result of the pain.

REFERENCES

1. Hack et al. *J. Clin Oncol. 17*(1), 1999.
2. Borstad & Szucs. *Hum Move Sci. 31*(2), 2012.
3. Crosbie et al. *Phys Ther. 90*(5), 2010.
4. Lang & Dickerson, *Work, 58*(2), 2017.
5. Malicka et al. *Orto Taum Rehab, 12*(4), 2010.
6. Ludewig & Reynolds. *J Ortho Spor Phys Ther. 39*(2), 2009.

ACKNOWLEDGEMENTS

Natural Sciences and Engineering Research Council for funding the project and the U of S Ergonomics Lab for sharing their research lab.

Table 1: Demographic and clinical information for BCS, age-matched controls, and young controls.

	N	Age	Height	Weight	DASH	Clinical	Time since
BCS	16	55.0 (5.1)	1.60 (0.05)	71.9 (14.3)	15.3 (8.7)	11	66.6 (43.4)
Age-match control	22	52.7 (6.4)	1.63 (0.07)	69.0 (12.4)	5.3 (6.5)	0	n/a
Young control	15	22.9 (1.7)	1.63 (0.07)	62.9 (8.7)	4.1 (4.7)	0	n/a

DEVELOPMENT AND ASSESSMENT OF A LOW-COST CLINICAL GAIT ANALYSIS SYSTEM

[1,2] M. Emily Littrell, [1] Young-Hui Chang, and [1,3] Brian P. Selgrade

[1] Georgia Institute of Technology, Atlanta, GA, USA
[2] Hanger Clinic, Birmingham, AL, USA
[3] North Carolina State Univ/Univ of North Carolina, Chapel Hill, NC, USA

email: m.littrell3@gmail.com

INTRODUCTION

In the clinic, it can be useful to measure gait kinematics and kinetics to determine the outcome measures and effectiveness of treatment. Maintaining and operating a research-grade gait analysis system, however, can be time consuming and cost-prohibitive. A low-cost gait analysis system would allow higher reliability of quantitative assessment that could be more broadly utilized in clinical settings to promote evidenced based outcomes (Rathinam et al, 2012).

Our objective was to validate the performance of a portable gait analysis system that utilizes widely available, affordable technology. We hypothesized that a low-cost system could perform comparably to a popular laboratory grade gold standard system in terms of forces (within ±5% bodyweight) and kinematics (within ±3°).

METHODS

Five healthy, recreationally fit subjects (163.9±11.9 cm, 62.7±19.2 kg, 2 males) gave informed consent prior to participating in this Georgia Tech IRB approved protocol.

The low-cost gait analysis system consisted of four major parts. A Wii Balance Board (WBB, Nintendo, Kyoto) provided ground reaction force (GRF) data and was embedded within a custom wooden walkway (731.5 cm x78.7 cm). We obtained sagittal plane video data (60 Hz) using a portable camera (GearPro GDV285, New York). We performed kinematics analysis using an open source motion-tracking software (Kinovea.org). The total cost of this system was under $300.

The research grade system consisted of a force platform (AMTI, Watertown, MA) and a six-camera motion analysis system (Vicon, Oxford) sampled at 1080 Hz and 120 Hz, respectively. The WBB was mounted on top of the force platform within the walkway to allow simultaneous collection of all data for a given trial. Only vertical ground reaction forces were compared since the WBB only measures this one component of force.

We performed static calibration trials with known weights (25-126 lbs) and a rigid phantom with a known angle (90^{o}) to record and compare the two systems. We also collected data from both systems simultaneously as subjects walked on the walkway. We used high contrast 2D markers for the low-cost system and retroreflective spherical markers for the Vicon system. Ground reaction forces (GRF) and sagittal plane segment angles were collected and analyzed.

We used custom MATLAB software to analyze the GRF and segment angle data from the laboratory grade system. We used standard spreadsheet software (Microsoft Excel) to analyze the data from our low-cost system and compared the two systems with percent error and absolute error metrics using a paired t-test (alpha=0.05). Bland-Altman plots were used to visualize the means and differences between the two systems.

RESULTS AND DISCUSSION

In static validation trials, the WBB measured weights to be 2.0-3.7% heavier than the force plate. Human walking trials showed similar GRF trajectories across the two systems (Figure 1). Across subjects, the difference in vertical GRF at the first peak GRF was non-significant, with the average difference across trials being ≤3.04%BW.

Maximum GRF errors measured across the gait cycle for each subject were between 25-53%BW, which largely occurred at the end of stance phase.

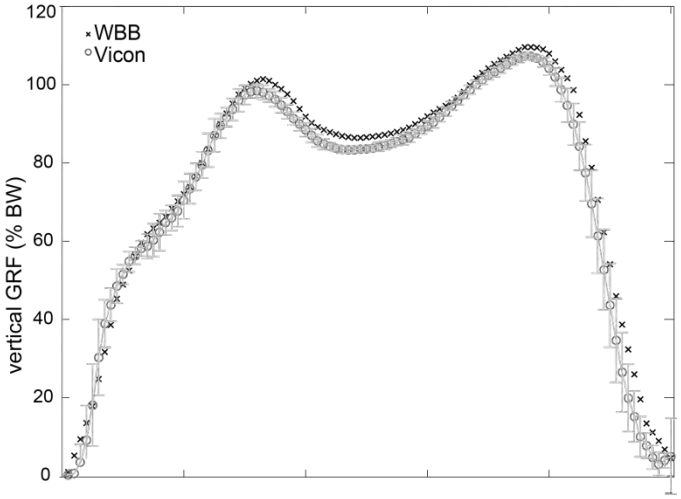

Figure 1: Vertical ground reaction forces from a representative trial measured with WBB (x's) and AMTI force plate (circles).

We accepted our hypothesis that the WBB could measure peak GRF during gait within 5% of a research-grade force plate. The greatest errors in GRF data occurred at times when force values changed rapidly but were consistent with previous studies [2]. The larger errors in GRF during highly dynamic periods of stance suggest an inconsistent sampling rate of the WBB as the cause rather than inaccurate force measurement.

Segment angles measured in Kinovea were similar to Vicon-measured angles for the shank, thigh, and, to a lesser extent, the foot (Figure 2). For the foot, the largest average difference between systems for any subject was 3.2° while the largest differences for the shank and thigh were 2.8° and 2.2°, respectively. The pelvis exhibited the largest errors, with maximum differences between 4.8° and 11.0°. The foot, thigh, and shank angles were more accurate than the pelvis angle for both individual subjects and the group average.

The hypothesis that the Kinovea/GearPro system could measure segment angles within 3° of the Vicon system was partially supported. The higher errors of the pelvis and foot segment angles were likely due to placement of the Vicon pelvic and toe markers relative to the low-cost markers. The high contrast markers taped to the skin for Kinovea (e.g. over the ASIS) were not as clearly visible in the sagittal plane view of the video camera.

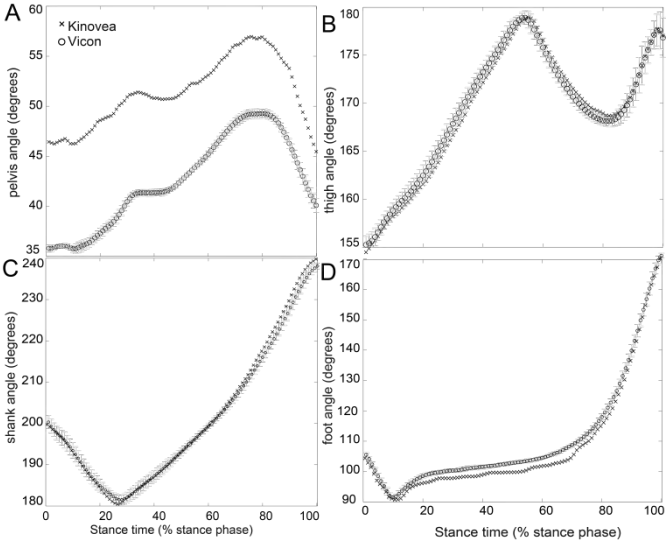

Figure 2: Sagittal plane segment angles for the pelvis (A), thigh (B), shank (C), and foot (D) from a representative walking trial measured by the low-cost system (x's) and by the Vicon system (circles).

CONCLUSIONS

The proposed system has the potential to provide a low-cost, quantitative gait analysis system to inexpensively measure gait kinetics and kinematics. The system was particularly accurate for key parameters such as peak force during gait and thigh and shank segment angles. It can be used to aid in determining effectiveness of various clinical approaches in prosthetics and orthotics without the need for a costly laboratory grade motion analysis system. This system could also provide an affordable solution for classrooms and outreach.

REFERENCES

1. Rathinam C, et al. *Gait & Post.* 2012; 40: 279-285.
2. Bartlett et al. *Gait & Post.* 2014; 39(1): 224-228

ACKNOWLEDGEMENTS

This research was supported by NICHD T32HD055180, NINDS R01NS069655, NSF BCS-0847325 and a Georgia Tech President's Undergraduate Research Award.

3D MODELS OF NECK STRENGTH IN 3 PLANES OF MOTION

[2]John M Looft, [3]Chris DeBlois, [1]Laura A. Frey Law

[1] University of Iowa, Iowa City, IA, USA
[2] University of Minnesota, Minneapolis MN, USA
[3]Johnson Health Tech, Madison, WI, USA.
email: laura-freylaw@uiowa.edu

INTRODUCTION

Musculoskeletal neck pain is a significant healthcare problem. One-year prevalence rates for neck pain are between 20-40% and nearly two-thirds of the general population will experience some form of neck pain in their lifetime [1]. Muscle strength and endurance are common targets for neck pain rehabilitation and deficits may be contributory risk factors for its development. Indeed, reduced cervical muscle endurance was a significant predictor of first-time onset of neck pain in a prospective study of office workers [2]. Additional loads, such as military helmet attachments (i.e. night vision goggles) create higher cervical muscle activity to accommodate the increased head mass and altered center of mass [3], thereby potentially elevating the risks of developing neck pain.

Unfortunately, it is unclear what level of neck strength is needed to reduce risk levels. Further to predict high-risk levels of neck torque during functional tasks, high quality normative neck strength data is required. However, relatively few studies of normative strength are available in the literature for the cervical spine compared to other joints, and none assessing 3 planes of motion, considering multiple isometric angles and isokinetic velocities. This information is important for predicting strength requirements for functional tasks, ergonomic applications, or helmet design.

Thus, the primary goals of this project were to 1) comprehensively assess cervical strength for each cardinal plane of cervical spine motion, considering multiple angles and velocities in healthy men and women and 2) develop normative mathematical models to represent cervical strength. Secondarily, we aimed to differentiate capital neck strength (i.e., head on neck caption) from full cervical neck strength in the sagittal plane (i.e., flexion and extension).

METHODS

56 participants (28M, 28F) completed 2 visits assessing peak neck strength. All subjects provided written informed consent, as approved by the Western Institutional Review Board. Isometric and isokinetic neck peak torque (Nm) was assessed using the Biodex System 3 Isokinetic Dynamometer (Biodex Medical Systems, Shirley, New York) in the sagittal (flexion/extension, FE), frontal (side-bending, SB), and transverse (rotation, RO) planes of motion. Custom attachments were built for each test, and secured to the head with Velcro straps. For the FE and SB testing, participants were seated and securely strapped into a chair to minimize unwanted movement. RO testing was performed supine on a plinth. For each plane, isometric strength was assessed prior to isokinetic strength (**Table 1**). During capital FE, only isokinetic strength was tested.

Table 1: *Neck strength protocol.*

	Angle (deg)	Velocity (deg/s)
Cervical FE	-25, -15, 0, 15, 30	30, 60, 90, 120
Capitol FE	-15, 0, 15	60, 75, 90, 120
Lateral SB	-25, -15, 0, 15, 25	30, 60, 90, 120
RO	-30, -15, 0, 15, 30	30, 60, 90, 120

Note: +/- angles represent flexion/extension for FE and left/right for SB and RO, respectively.

Mean peak torques for each angle and velocity combination (4 velocities, 3 to 5 angles), for each test plane were determined for men and women separately. These mean data were plotted as 3D strength surfaces, with peak torque as a function of joint angle and movement velocity. Mathematical models of the 3D strength surfaces were curve fit using logistic regression (TableCurve 3D, SYSTAT) [4].

RESULTS AND DISCUSSION

Normative neck strength models were fit for male and female cervical and capitol FE, SB, and RO. Only cervical flexion and extension are shown in **Figures 1 and 2** due to space constraints. Extension stre[illegible] me[illegible] vel[illegible]

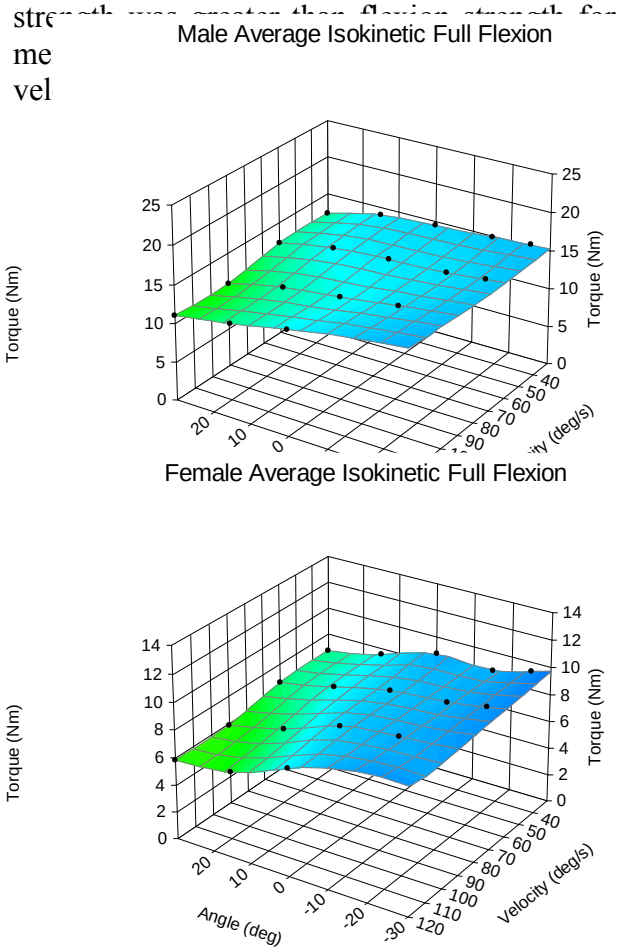

***Figure 1**: Examples of 3D strength surfaces, showing cervical flexion for men (top panel) and women (bottom panel).*

Logistic models provided reasonably good fits to the data (R^2 > 0.6 across models), but with less curvature than observed at other hinge joints [5]. This may be a result of a reduced range of motion available at the neck and consequently slower peak velocities. None-the-less, sex differences observed at other joints [5] were maintained at the neck.

A limitation of this study was the challenges associated with reducing trunk motion, particularly at end ranges of motion during isometric contractions. Due to the long moment arm from the neck to the base of the lumbar spine, even restricted trunk movements likely influenced measured cervical torques. As a result, we analyzed strength surfaces with and without these end range isometric da[illegible]n he[illegible]

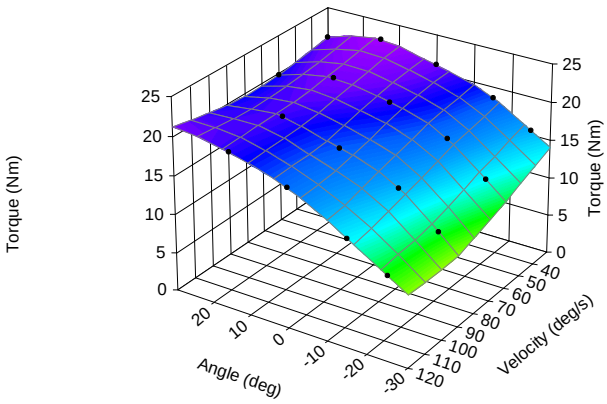

***Figure 2**: 3D strength surface for cervical extension for men only (women looked similar, but lower).*

CONCLUSIONS

Comprehensive normative neck strength has received limited attention in the literature despite the prevalence of neck pain. This may in part be due to the difficulty in which neck strength is assessed. However, these results are needed to parallel advances in biomechanical analyses of neck loads to better estimate relative task intensities and improve risk assessment for neck pain.

REFERENCES

1. Fejer R, Kyvik KO, Hartvigsen J, "The prevalence of neck pain in the world population: a systematic critical review of the literature." *Eur Spine J,* vol. 15, pg. 834–848, 2006
2. Shahidi B, Curran-Everett D, Maluf, K, "Psychosocial, Physical, and Neurophysiological Risk Factors for Chronic Neck Pain: A Prospective Inception Cohort Study" *Journal of Pain*, vol 16, pg 1288-1299, 2015
3. Thuresson M, Ang B, Linder J, "Mechanical load and EMG activity in the neck induced by different head-worn equipment and neck postures." *International Journal of Industrial Ergonomics*, vol 35, pg 13-18, 2005
4. Looft, JM. and Frey Law LA. "Modeling Three-Dimensional Human Strength Surfaces: Logistic vs. Polynomial Equations." *Int. J. of Human Factors Modelling and Simulation (IJHFMS)* vol 5, pg. 5-18, 2015
5. Frey-Law LA, Laake A, Avin, KG, Heitsman J, Marler T, Abdel-Malek K, "Knee and Elbow 3D Strength Surfaces: Peak Torque-Angle-Velocity Relationships." *Journal of Applied Biomechanics,* vol 28, pg 729-737, 2012

ACKNOWLEDGEMENTS

Funded in part by Viztek, through the Department of Defense Office of Naval Research (ONR) and a Heartland Fellowship (Graduate Student Funding)

CHARACTERIZATION OF DYNAMIC ANKLE STIFFNESS IN INDIVIDUALS WITH SPASTICITY

Stacy R. Loushin, Krista A. Coleman Wood, and Kenton R. Kaufman

Motion Analysis Laboratory, Department of Orthopedic Surgery, Mayo Clinic, Rochester, MN, USA
email: loushin.stacy@mayo.edu

INTRODUCTION

Dynamic joint stiffness is defined as the resistance that a joint offers during gait in response to an applied moment. Davis and DeLuca quantified ankle stiffness as the slope of the ankle joint moment-angle curve over the gait interval of the second rocker [1]. The second rocker interval is defined explicitly as the period of the gait cycle from the first relative maximum plantar flexion (PF) in early stance to maximum dorsiflexion (DF) in midstance [2] (A to B Figure 1).

However, shortening, stiffness, or spasticity of the gastrocnemius may interfere with this second rocker, resulting in absence of DF and a biphasic pattern of ankle moment (Figure 2) [3]. This disruption of the second rocker prevents the execution of the method proposed by Davis and DeLuca for individuals with pathological gait, specifically cerebral palsy (CP) with equinus or jump gait. The stiffness calculations also do not account for the initial peak PF moment in jump gait which is of greater magnitude than the second terminal stance peak. Therefore, current dynamic stiffness metrics need to be modified to allow for implementation in individuals with pathological gait.

The main goal of this study is to develop a new method of evaluating dynamic ankle stiffness in individuals with pathological gait who lack a second rocker interval.

METHODS

The Institutional Review Board approved this study consisting of 20 unimpaired ambulators, between the ages of 18 and 36, and 9 individuals with CP, between the ages of 5 and 8. Kinematic data from a 10 camera system (Motion Analysis Corp, Santa Rosa, CA; 120 Hz) and kinetic data from force plates (2 AMTI, Watertown, MA and 3 Kistler, Amherst, NY 600 Hz) embedded in the walkway were processed in Visual3D (C-Motion, Inc, Germantown, MD).

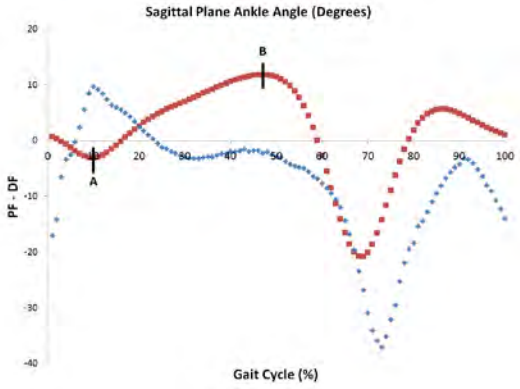

Figure 1: Sagittal plane kinematic ankle data for an unimpaired ambulator (red) with the second rocker interval from point A to B. This interval is absent for an individual with spastic diplegia (blue).

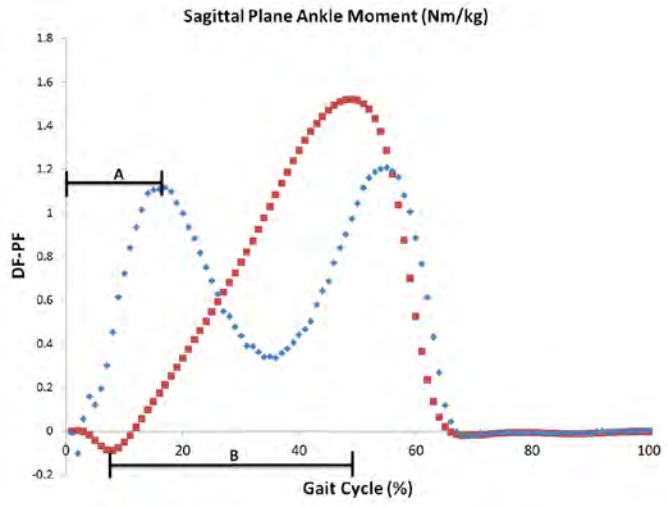

Figure 2: Sagittal plane kinetic ankle data for individuals with CP (blue) with a decreased time of initial peak, line A, of only 1-15% of the gait cycle. This is significantly reduced from the unimpaired ambulators (red) with a time to peak from ~3-48% of the gait cycle.

Dynamic ankle stiffness was evaluated using two methods. Kinematic data was utilized for the method described by Davis and DeLuca, taking the period of the first relative maximum PF in early stance to maximum DF in midstance. Kinetic data was utilized for a new method devised by the authors, taking the period of the first relative maximum DF moment to first relative maximum PF moment.

Stiffness was quantified over each period as the slope of a linear regression between the sagittal-plane ankle angle and moment. Method differences were explored using an equivalence test ($\alpha = .05$).

RESULTS AND DISCUSSION

The methods for calculating dynamic ankle stiffness were found to be equivalent in unimpaired individuals ($p = 0.000$). Although the new method utilizes kinetic data to determine the stiffness interval, maximum DF to maximum PF moment represents the second rocker in unimpaired individuals. In individuals with CP, the methods were not equivalent ($p = 0.958$) with the method described by Davis and DeLuca resulting in a decreased stiffness (0.047 (0.023) Nm/kg/°) compared to the method devised by the authors (0.066 (0.028) Nm/kg/°). Using kinetic data to determine the stiffness interval more accurately describes the physiological increased joint stiffness due to muscle spasticity in individuals with CP.

The mean time to initial PF moment peak for individuals with CP was found to be 0.177 (0.10) seconds. Due to the biphasic ankle moment pattern, the CP population has a time to peak corresponding to ~1-15% of the gait cycle as opposed to ~3-48% of the gait cycle in unimpaired ambulators (Figure 2).

The metric developed by the authors was successfully applied to all 9 individuals with CP and produces a stiffness value that more accurately describes the physiological increased joint stiffness present in CP, which is an improvement from the previously described method from Davis and DeLuca. This metric could prove critical to represent clinical improvement after treatments aimed to improve gait kinematics and kinetics and allow clinicians to evaluate their outcomes.

CONCLUSIONS

This study establishes a method for quantifying the dynamic joint stiffness in individuals with pathological gait lacking a second rocker interval. Future work in this area should investigate application of this method in other populations with pathological gait.

REFERENCES

1. Davis, R.B, DeLuca, P.A. *Gait & Posture*. 4(3), 224-231, 1996.
2. Perry, J. *Gait Analysis: Normal and Pathological Function,* Slack Incorporated, 1992.
3. Boyd, R.N. el al. *Developmental Medicine & Child Neurology*. 42, 32-41. 2000.

MUSCLE COMPARISONS AND RELIABILITY OF A NOVEL METHOD TO ASSESS RATE OF FORCE RELAXATION

[1]Ryan Mathern, [2]Mitchel Anhorn, and [2]Mehmet Uygur

[1] Cooper Medical School of Rowan University, Camden, NJ, USA
[2] Rowan University, Glassboro, NJ, USA
email: uygurm@rowan.edu, web: https://works.bepress.com/mehmet-uygur/

INTRODUCTION

The ability to generate quick sub-maximal muscle forces followed by quick relaxations is not only important in cyclical activities that require consecutive agonist and antagonist contractions (e.g. walking and sprinting), but also is crucial for postural control and fall prevention. Recently, rate of force development scaling factor (RFD-SF) has been introduced as a robust measure of neuromuscular quickness that reliably quantifies an individual's ability to scale her/his rate of force development across a range of sub-maximal force levels [1,2]. While rate of force development (RFD) has been studied extensively [3], the rate of force relaxation (RFR) following a muscle contraction has mainly been neglected. As a result, an individual's ability to quickly relax muscle forces after quick force productions has yet to be quantified. Our aims were to 1) develop a kinetic variable (rate of force relaxation scaling factor; RFR-SF) that can quantify an individuals ability to relax their muscle forces quickly and to compare it with the RFD-SFs obtained from the same muscle, 2) to test within and between session reliability of RFR-SF, and 3) to explore the correlations of RFR-SFs obtained among the tested muscle groups.

METHODS

Grip force muscles (GF), elbow (EE) and knee extensors (KE) of thirteen healthy individuals (6 females and 7 males, mean age 23.38±4.72 yrs, 74.66±16.20 kg, and 173.1±11.5 cm) were tested isometrically in two different testing sessions separated by 48 hours. In GF, participants grasped an instrumented handle by employing a precision grip where only the tips of the four fingers and thumb were in contact with the grasping surfaces [2]. In EE, the distal arm of standing participants was cuffed to a transducer while their elbow was at 90^0 of flexion. In KE, a distal lower leg of the seated subjects was coupled with a force transducer while their knee was at 70^0 of flexion (Fig 1a).

In each session and muscle group tested, subjects provided around 120 brief isometric force pulses that varied between 20-80% of their maximum capacities under the instruction to produce each pulse as quickly as possible followed by a quick relaxation (Fig. 1b). A feedback monitor displayed four horizontal lines representing 20, 40, 60, and 80 % of the MVC of the tested muscle groups. The areas between 20-40%, 40-60%, and 60-80% were referred to as small, medium, and large forces, respectively. Experimenters used these amplitudes as a verbal command to instruct the subjects to produce the desired force amplitude. A familiarization block was completed before each tested muscle group.

For every participant and tested muscle group, RFD-SF and RFR-SF were calculated from the kinetic analysis of the brief force pulses as the slope of the linear relationship between the peak values of the force produced and the corresponding peak RFD (RFD-SF) and peak RFR (RFR-SF), respectively. The R^2 obtained from the same relationships was also studied and valued as a measure of consistency of force control (Fig. 1c).

A two-way repeated measure ANOVA was used to test the differences across the tested muscle groups and scaling factors. The within and between session reliability of RFR-SF was assessed by using intraclass correlation ($ICC_{3,1}$). Pearson correlation coefficients were used to determine the relationships among the tested RFR-SFs from three different muscles.

RESULTS AND DISCUSSION

Results of a two-way repeated measures ANOVA (3 muscles and 2 scaling factors) indicated that RFR-SF was smaller than RFD-SF in all of the selected muscles ($p<0.001$). Regarding the muscle comparisons, RFR-SF was comparable between the tested muscles of upper extremity (i.e. GF and EE) and both were higher than the RFR-SF in KE ($p<0.05$). RFD-SF was similar between GF and KE and both were smaller than RFD-SF in EE ($p<0.001$) (Fig. 2).

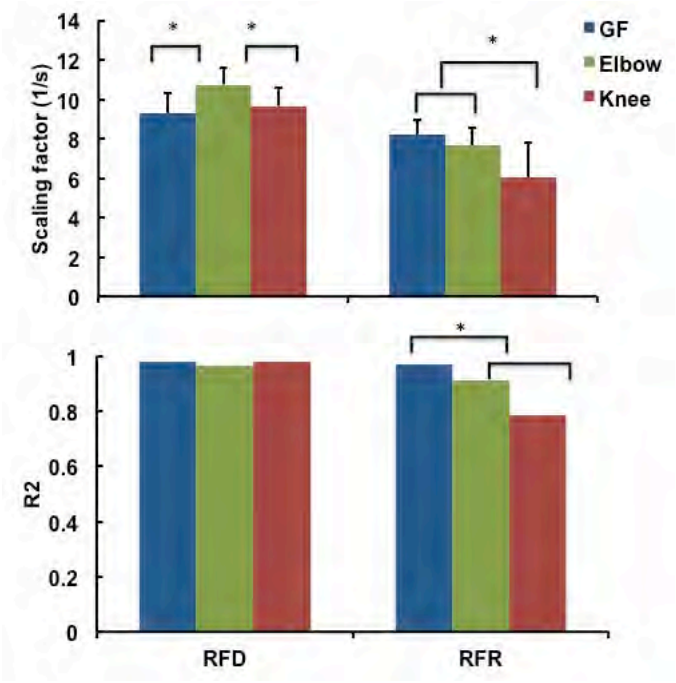

Figure 2: The regression parameters obtained from the peak Force-RFD (RFD-SF) and peak Force-RFR (RFR-SF)

The within and between session reliability of RFR-SF obtained from the studied muscle groups was found to be fair to high ($ICC_{(3,1)}$s of GF, EE, and KE were 0.67, 0.6, and 0.74, respectively). There were no significant correlations in RFR-SFs among the tested muscle groups (correlations were between 0.087 and 0.396).

CONCLUSIONS

The ability of relaxing a muscle force quickly could be quantified reliably through RFR-SF in brief submaximal force production tasks. The differences found between RFD-SF and RFR-SF across the tested muscles indicate that they assess different properties of the neuromuscular system and, therefore, future studies should include both of these variables. The lack of correlation among RFR-SFs across the tested muscle groups might indicate the need to test RFR-SF separately for each of the muscle group of interest. Future studies that aim to explore the functional relevance of RFR-SF across various healthy and neurological populations are needed.

REFERENCES

1. Bellumori M, et al. *Exp Br Res*. **212**, 359-369, 2011.
2. Haberland K and Uygur M. *Exp Br Res*, **235**, 321-329.
3. Maffuiuletti N, et al. *Eur J Appl Physiol*. **116**, 1091-1116

Figure 1: (a) The tested muscle groups; GF (circles represents digits), EE, and KE. (b) a sample of recorded brief force pulses performed to various submaximal levels and its RFD and RFR. (c) linear relationships between peak force and RFD (upper) and peak force and RFR (lower). Slopes represent RFD-SF and RFR-SFs.

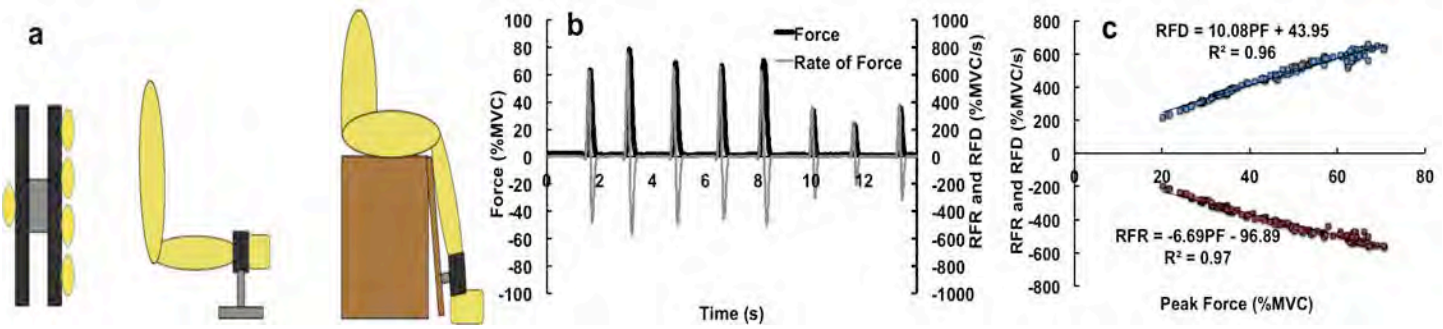

TRUNK COMPENSATORY STRATEGIES PERSIST TWELVE MONTHS FOLLOWING TOTAL KNEE ARTHROPLASTY

[1] Jodie A. McClelland [2] Joshua D. Winters [3]Julian A. Feller [1]Kate E. Webster

[1] La Trobe University, Melbourne, Australia
[2] University of Kentucky Sports Medicine Research Institute, Lexington, KY, USA
[3]OrthoSport Victoria, Epworth Richmond, Melbourne, Australia
email: j.mclelland@latrobe.edu.au

INTRODUCTION

Patients who undergo Total Knee Arthroplasty in the management of end-stage knee osteoarthritis report significant improvements in pain and quality of life following TKA. Most patients report an improvement in their capacity to complete daily functional activities within 6 months of surgery, but continue to experience difficulty in simple tasks such as rising from a chair [1,2]. More detailed motion analysis has revealed that patients following TKA adopt altered movement strategies to complete daily functional activities. For example, when rising to stand from a seated position, patients with TKA tend to shift their weight away from the operated limb and towards the non-operated limb [3]. Continued preferential loading of the non-operated knee is likely to contribute to the development of secondary pathology, including acceleration in the progression of osteoarthritis in lower limb joints of the contralateral limb. To date, post-operative rehabilitation does not successfully restore normal movement following TKA, therefore greater understanding of the specific movement strategies that are associated with this weightbearing asymmetry is warranted. It is likely that patients with TKA use movements of the trunk to alter loading in the lower limbs, however this has not yet been investigated in this population. Therefore, the aim of this study was to investigate the relationship between lower limb loading and trunk movements during a sit-to-stand task in patients with TKA.

METHODS

Forty consecutive patients of a single experienced knee surgeon were recruited 12 months following TKA. All patients underwent TKA in the management of a primary diagnosis of osteoarthritis, and all received a posterior stabilized knee implant with patellar resurfacing. Forty control participants who were matched to the age and sex of TKA patients were also recruited.

All participants had three dimensional kinematics and kinetics recorded during 6 repetitions of a sit-to-stand task. Trajectory data was collected using a 10 camera Vicon MX System (Vicon Motion Systems Pty Ltd) at a frequency of 100 Hz. Two embedded force platforms collected ground force at a frequency of 4000Hz. Participants were asked to sit on a stool of standard seat height (45cm) without a back or arm rests. The stool was positioned directly adjacent to two embedded force platforms so that participants placed one foot on each force platform. Participants were asked to rise from sitting to standing with arms folded, and pause before stepping forward off the platforms. A Woltering filter (MSE 20) was applied to trajectory data prior to calculation of kinematics based on Euler angles.

The maximum vertical component of the ground reaction force (GRF) and the maximum angle of the trunk in the coronal plane (trunk lean) were extracted from each repetition of the movement and combined to form an average that represented each participant. The GRF was compared between limbs using paired t-tests, and GRF and trunk lean were compared between groups using independent t-tests.

RESULTS AND DISCUSSION

The demographic information of participants is summarized in Table 1.

Table 1 Demographic information about participants

	TKA		Controls	
	Mean	*(SD)*	*Mean*	*(SD)*
Age *(years)*	69.1	(8.0)	69.6	(8.3)
Sex *(%Female)*	55%		55%	
BMI	31.6	(6.2)	28.0	(4.6)

Three participants with TKA were unable to complete the task without the assistance of armrests, and therefore their data was omitted from analysis.

The maximum vertical ground reaction force was reduced in the operated limb compared to the non-operated limb for all TKA participants ($p<0.001$, Figure 1). In 63% of TKA participants, the GRF on the operated limb was at least 10% less than the non-operated limb. This difference was not present in control participants ($p=0.51$).

86% of participants with TKA completed the sit-to-stand task with trunk lean in the coronal plane that was away from the operated limb. Figure 1 summarizes the direction of trunk lean for TKA participants who either (i) loaded the non-operated limb by more than 10% of the operated limb (63% of TKA participants), (ii) had similar loads (within 10%) in the operated and non-operated limbs (29% of TKA participants) and (iii) loaded the operated limb by more than 10% of the non-operated limb (8%).

Figure 1 Direction of trunk lean (blue or orange) indicates direction of trunk lean for TKA participants based on the limb loading preference.

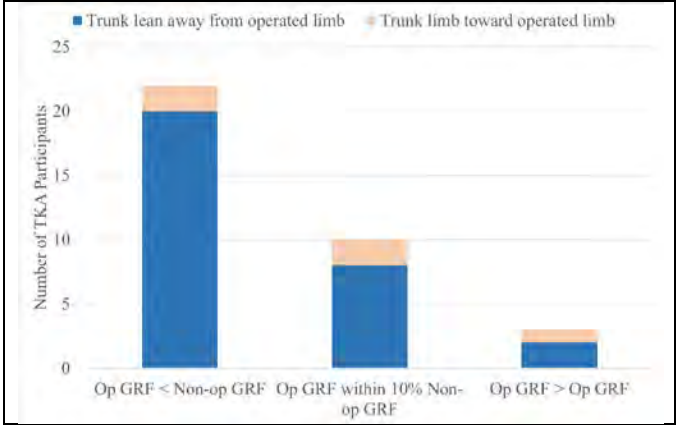

CONCLUSIONS

This was the first study to investigate and find an association between trunk movements and lower limb loading that persist at 12 months following surgery. These findings suggest that patients with TKA adopt abnormal trunk movements during a sit-to-stand task that also reduce loading on the operated limb and increase loading on the non-operated limb. This strategy was not seen in the majority of control participants, and could be a contributory factor in the rising incidence of a second TKA in the contralateral knee following a primary TKA.

This preferential loading strategy has been reported up to six months following TKA, but this is the first study to report similar strategies up to 12 months following surgery. The findings of this study suggest that rehabilitation that aims to restore more normal movement patterns should extend beyond the knee and, in particular, address control of the trunk during functional movements.

REFERENCES

1. Noble et al. *Clini Orthop Related Res,* 452:35-43, 2005.
2. Mizner et al. *J Arthroplasty,* 26(5):728-37, 2011.
3. Alnahdi et al. *Knee Surg Sports Traumatol Arthrosc.,* 24(8):2587-94, 2016.

RESULTANT LOWER LIMB ACCELERATION AND GROUND REACTION FORCES ARE CORRELATED IN THE TIME AND FREQUENCY DOMAINS

[1,2] Michael A. McGeehan, [1,2] Evan R. Day, [1,2] Michael E. Hahn

[1] Bowerman Sports Science Clinic, [2]Neuromechanics Lab, University of Oregon, Eugene, OR, USA
email: mmcgeeha@uoregon.edu web: http://bssc.uoregon.edu

INTRODUCTION

Biomechanical impact measures such as ground reaction forces (GRF) and resultant acceleration (RA) are common variables of interest in investigation of running-related injuries. Increased vertical GRF and RA have been identified as risk factors for running-related injuries [1,2]. Recent advancements in microelectromechanical systems (MEMS) have extended the ability to measure RA outside of the laboratory using wearable accelerometers and inertial measurement units (IMU). Compared to GRFs, which are typically measured within the confines of a laboratory, IMU-derived measures such as RA may be more desirable for quantifying impact loads during running, as IMUs are relatively low-cost, widely available, and can collect data in a multitude of environments**.** While RA offers considerable advantages compared to GRF for quantifying impact load during outdoor running, an evaluation of the time and frequency characteristics of the two measures is necessary if they are to be considered comparable. The objective of this study is to assess the agreement between resultant lower limb acceleration and ground reaction force in time and frequency domains during running.

METHODS

Seven trained male runners (21 ± 1 y, 176.4 ± 5.4 cm, 62.5 ± 3.5 kg) were analysed in this comparative investigation as part of a larger study. Three-axis lower limb accelerations were measured via two IMUs (Vicon, f_s: 500 Hz) placed bilaterally 2 cm proximal to the lateral malleolus. The long axis of each IMU was aligned with the long axis of the lower leg. Three-axis GRFs were measured using a force plate-instrumented treadmill (Bertec, f_s: 1000 Hz). Prior to running, subjects completed a vertical jump on the stationary treadmill to provide a time lock signal for the GRF and IMU signals. Subjects ran at 3.83 m/s (moderate velocity) and 5.36 m/s (fast velocity) for ~20 gait cycles at each pace.

Resultant GRF (RGRF) and RA of the lower leg were calculated [3]. The RGRF and RA signals were time-locked to the impact peak of the vertical jump. Both data records were then low-pass filtered using a 4th order zero-lag Butterworth filter (f_cGRF: 50 Hz, f_cRA: 30 Hz). Individual stance phases were defined using a threshold of 5% body mass. Each stance phase was interpolated to 150 data points using a cubic spline and concatenated into a single RGRF and a single RA data record containing 139 stance phases from all subjects. Relationships between RGRF and RA were characterized in frequency and time domains using magnitude-squared coherence and cross correlation functions, respectively.

Coherence data were derived from a power spectral density analysis with 1 Hz resolution and represents the linear relationship between two variables across a range of frequencies ($0 < r > 1$). The cross correlation function was used to quantify an associative pattern between the two variables in the time domain. Correlation coefficients ($-1 < r > 1$) were calculated at each time point of stance phase.

RESULTS AND DISCUSSION

Consistent with previous findings, power spectral density analysis showed the RGRF and RA signals to be composed primarily of frequencies below 15 and 25 Hz, respectively [4]. For the moderate velocity, RGRF and RA demonstrate weak, moderate, and strong correlations from 16-36 Hz, 8-15 Hz, and 1-7 Hz, respectively (Figure 1). For the fast velocity, weak, moderate, and strong correlations were exhibited from 4-5 Hz and 13-31 Hz, 3 Hz, and 1-2 Hz, respectively. These data indicate that RA may be comparable to RGRF across their relevant operational bandwidths when running at moderate

and fast velocities. Coherence values for the fast velocity exhibited no correlation from 5-12 Hz, before returning to a weak correlation above 13 Hz.

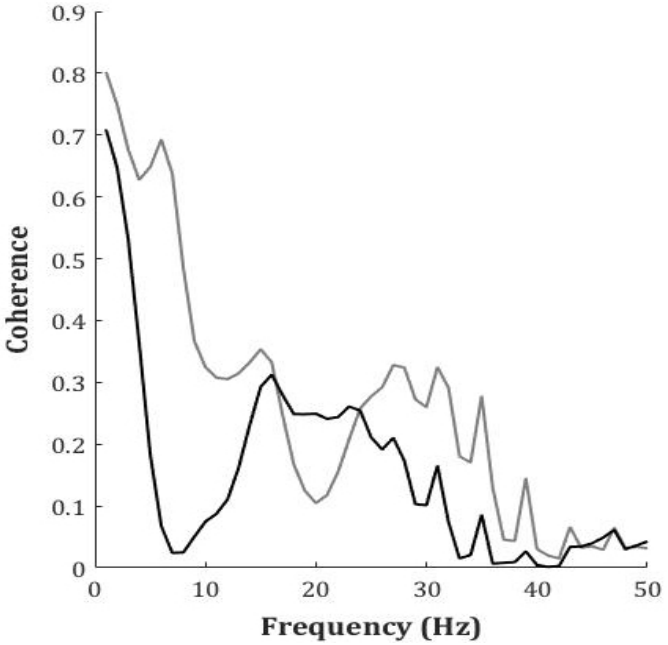

Figure 1: Coherence between RA and RGRF across a 50 Hz bandwidth during moderate (grey) and fast (black) running velocities.

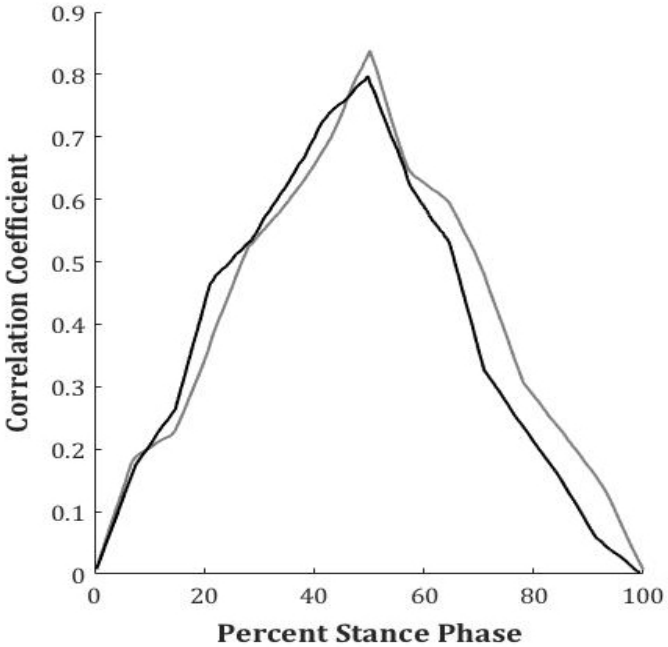

Figure 2: Correlation coefficients in the time domain for RA compared to RGRF during moderate (grey) and fast (black) running velocities.

In the time domain, RGRF and RA were correlated from 3-97% stance phase during the moderate and fast running conditions (Figure 2). For the moderate velocity RGRF-RA comparison, weak ($0.10 < r > 0.29$), moderate ($0.30 < r > 0.49$), and strong ($r > 0.50$) correlations were seen from 4-20% and 81-96%, 21-27% and 72-80%, and 28-71% stance phase, respectively. For the fast velocity (Figure 2), weak, moderate, and strong correlations were seen from 4-16% and 74-96%, 17-25% and 68-73%, and 26-67% stance phase, respectively. These data indicate that RA provides similar information compared to RGRF regarding biomechanical loading during the weight acceptance and propulsion portions of stance phase. However, RA and RGRF may not be comparable before full weight acceptance or near toe-off.

CONCLUSIONS

Preliminary results support the utility of RA for quantifying impact load during running. In the frequency domain, RA may be a comparable measure to RGRF at frequencies below 30 Hz. In the time domain, RA provides similar information compared to RGRF during the weight acceptance and propulsion portions of stance phase at moderate and fast running velocities. However, there is no association between the signals early and late in stance phase when RGRF is near zero, indicating that RA may not provide comparable loading information compared to RGRF when RGRF is minimal. Further investigation is necessary to determine if these patterns are consistent between treadmill and over-ground running, which would establish the value of RA as a proxy to RGRF outside of the laboratory.

REFERENCES

1. Brayne et al. *33rd Int Symp Biomech Sport*. 540-543, 2015.
2. Zifchock et al. *J Biomech*. 39(15): 2792-2797, 2006.
3. Sheerin et al. *Sport Biomech*. 3141:1-10, 2017.
4. Hennig and Lafortune, *Int J Sport Biomech*. 7:303-309, 1991.

ACKNOWLEDGEMENTS

This work was supported by a grant from the Pac12 Conference, as part of the IBIS collaboration group.

PASSIVE HAMSTRING MUSCLE STIFFNESS ASSESSED IN HIGH SCHOOL ATHLETES USING SHEAR WAVE ELASTOGRAPHY

[1]April L. McPherson, [1]Takashi Nagai, [1]Nathaniel A. Bates, [1]Nathan D. Schilaty, [1]Rena F. Hale, and [1]Timothy E. Hewett

[1]Mayo Clinic Biomechanics Laboratories & Sports Medicine Center, Rochester & Minneapolis, MN, USA
email: mcpherson.april@mayo.edu

INTRODUCTION

Shear wave elastography (SWE) is an emerging ultrasound imaging technology that quantifies tissue stiffness properties. Skeletal muscle tissue properties can be attributed to contributions from both passive and active stiffness. A previous study using SWE has identified differences in passive skeletal muscle stiffness due to age, activity level, and sex.[1] However, that study was performed on the biceps brachii in a sample of adults ranging from 21-94 years old and not specifically an athletic population. Therefore, the purpose of this study was to characterize lower extremity passive muscle stiffness in a young, athletic population differs between age and sex. It was hypothesized that males would exhibit greater stiffness than females and stiffness would increase with age.

METHODS

The study was approved by the Mayo Clinic IRB. Informed consents were obtained from each high school basketball player and his/her parent if under 18 years old. Hamstring flexibility was first assessed by a clinician using an active knee extension test and a digital inclinometer; ipsilateral hip and knee flexion both positioned at 90° were considered neutral.[2] 40%, 60%, and 80% of the maximum flexibility were calculated. The greater trochanter and femoral condyle were then marked and the midpoint was identified by the clinician for repeatable placement of the ultrasound transducer both within and between subjects. While lying supine, the clinician moved and held the athlete's leg at each position to assess biceps femoris muscle stiffness using SWE at each position (GE LOGIQ E9, 9L-D transducer, GE Healthcare, Wauwatosa, WI). Three SWE images were acquired while surface EMG provided real-time feedback to ensure measurement of passive muscle stiffness and no muscle activation. Muscle stiffness (kPa) was measured from the SWE color map using custom Matlab software (**Fig. 1**).

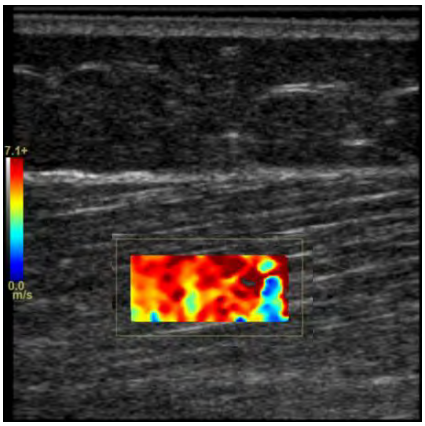

Figure 1: Representative example of shear elastic modulus color map used to calculate hamstring muscle stiffness

One-way ANOVA was used for between sex comparisons for each angle and within sex differences between age groups. A 2x5 ANOVA was used to investigate significant interactions between sex (female, male) and age groups (14, 15, 16, 17, 18) ($p < 0.05$) (JMP 13, SAS Institute Inc., Cary, North Carolina). Tukey *post-hoc* tests were used to assess sex differences between age groups.

RESULTS AND DISCUSSION

Male (n=59) and female (n=106) subjects were significantly different for height (180.0±8.1 cm vs. 170.1±8.3 cm) and weight (72.8±11.9 kg vs. 65.7±13.1 kg). Hamstring stiffness was significantly different between males and females for every angle on both the right and left sides ($p < 0.05$) (**Table 1**). As hypothesized, hamstring stiffness was greater in males compared to females for each angle comparison.

There was no significant interaction between sex and age for right or left side for any angle ($p > 0.05$). There were significant differences between sexes for individual age groups. When these occurred, males typically demonstrated higher stiffness values than females (**Table 2**). There were no significant within-sex differences between age groups. This was interesting and countered our anticipated hypothesis as there are significant maturational changes in the musculoskeletal system between 14 and 18 years of age in both males and females.[3,4,5] However, sex differences in pubertal timing and different developmental characteristics during pubertal stages may help explain the differences in muscle tissue stiffness between sex for the adolescent age groups.

CONCLUSIONS

This study represents passive hamstring muscle stiffness for a young, healthy athletic cohort. Future studies may investigate what factors contribute to the large variability observed in muscle stiffness in a healthy, similar aged population.

REFERENCES

1. Eby et al. *Clin Biomech*. 30(1):22-7, 2015.
2. Reurink et al. *Am J Sports Med*. 41(8):1757-61, 2013.
3. Malina, et al. *Growth, Maturation, and Physical Activity*, Human Kinetics, 2004.
4. Quatman et al. *J Sci Med Sport*. 11(3):257-63, 2008.
5. Hewett et al. *J Bone Joint Surg Am*. 86-A(8):1601-8.

ACKNOWLEDGEMENTS

Funding from the NBA & GE Healthcare Orthopedics and Sports Medicine Collaboration, and NIH grant funding R01AR056259 & R01AR055563.

Table 1: Hamstring stiffness (kPa) for each sex

	40%		60%		80%	
	Left	Right	Left	Right	Left	Right
Male	53.8 ± 33.6^{+}	51.4 ± 32.0^{+}	61.3 ± 42.0^{+}	61.8 ± 41.4^{+}	54.7 ± 38.1^{+}	52.5 ± 38.3^{+}
Female	43.9 ± 27.0*$^{+}$	36.6 ± 21.7*$^{+}$	40.6 ± 25.6^{+}	40.3 ± 28.2^{+}	32.1 ± 20.5^{+}	30.2 ± 20.2^{+}

*indicates significant difference within sex between right and left; +indicates significant difference between sex for same percentage

Table 2: Hamstring stiffness by sex and age (kPa)

	Age		Right			Left	
			Male	**Female**		**Male**	**Female**
40%	**14**		43.3 ± 9.0	32.1 ± 5.0		47.6 ± 10.2	36.1 ± 5.7
	15		63.5 ± 6.2	39.7 ± 4.4*		73.0 ± 7.2	49.5 ± 5.0
	16		35.8 ± 6.8	34.0 ± 6.6		43.8 ± 7.7	40.8 ± 7.5
	17		53.2 ± 7.4	36.7 ± 5.4		39.6 ± 8.3	44.3 ± 6.2
	18		61.2 ± 9.6	41.7 ± 8.1		61.0 ± 10.9	49.6 ± 9.1
60%	**14**		76.4 ± 11.8	35.9 ± 6.6*		48.0 ± 10.3	36.7 ± 5.7
	15		72.6 ± 8.1	42.1 ± 5.8*		70.5 ± 7.1	46.3 ± 5.1*
	16		46.1 ± 8.9	40.2 ± 8.6		47.0 ± 7.8	33.3 ± 7.5
	17		49.8 ± 9.7	42.3 ± 7.1		54.7 ± 8.4	40.7 ± 6.2
	18		71.8 ± 12.7	42.0 ± 10.6		69.3 ± 11.0	42.4 ± 9.2
80%	**14**		51.7 ± 10.0	30.2 ± 5.6		59.6 ± 9.6	28.5 ± 5.3*
	15		53.4 ± 6.9	31.3 ± 4.9*		57.7 ± 6.6	36.5 ± 4.7*
	16		44.3 ± 7.6	25.4 ± 7.3		39.5 ± 7.3	26.4 ± 7.0
	17		48.0 ± 8.2	28.2 ± 6.0		50.0 ± 7.9	32.1 ± 5.8
	18		63.4 ± 10.7	38.4 ± 9.0		68.2 ± 10.3	34.8 ± 8.6*

*indicates significant difference between sex for that age group

ORBITAL STABILITY DURING DUAL-TASK TREADMILL WALKING IN CANCER PATIENTS

[1] Scott M. Monfort, [2] Xueliang Pan, [3] Charles L. Loprinzi, [2] Maryam B. Lustberg, and [3] Ajit M.W. Chaudhari

[1] Montana State University, Bozeman, MT, USA; [2] The Ohio State University, Columbus, OH, USA;
[3] Mayo Clinic, Rochester, MN, USA
email: scott.monfort@montana.edu website: http://www.montana.edu/biomechanics/

INTRODUCTION

Improved diagnoses and treatments for cancer have contributed to increased survival rates [1]. These improvements have enabled greater focus to be placed on survivors' quality of life after cancer treatment. Notably, cancer survivors often report peripheral and central nervous system adverse effects from chemotherapy (e.g., chemotherapy-induced peripheral neuropathy (CIPN), executive dysfunction) that can negatively influence quality of life [2]. Cancer survivors are reported to be at an increased risk of falling [3] and demonstrate altered gait [4]; however, little is known about the potential contributing factors that may drive these impairments in this population. Additionally, to our knowledge, no prior studies have used nonlinear dynamical systems measures, such as Floquet multipliers, to characterize gait stability in this population.

The purpose of this pilot study was to explore the effects of central and peripheral nervous system impairments on orbital stability in cancer patients. We hypothesized that deficits in executive function and self-reported sensory symptoms of CIPN would be associated with decreased orbital stability.

METHODS

Twenty cancer patients participated in this study after providing IRB-approved informed consent. Participants enrolled into one of three groups: (1) no chemotherapy exposure (**CON;** 0f/6m; 59.3±9.6yr; 78.0±14.1kg; 1.62±0.05m), (2) recently completed taxane- or oxaliplatin-based chemotherapy, but asymptomatic for CIPN (**-CIPN;** 1f/7m; 55.9 ±9.0yr; 77.1±11.1kg; 1.68±0.04m), and (3) recently completed taxane- or oxaliplatin-based chemotherapy and symptomatic for CIPN (**+CIPN;** 2f/4m; 50.0±15.0yr; 91.6±21.6kg; 1.71±0.06m).

Participants walked on a split belt instrumented treadmill (Bertec Corp.). Bilateral lower extremity kinematics were recorded at 60 Hz (Metria Innovation, Inc.) and processed in Visual 3D (C-Motion). Marker data were 4th order Butterworth low-pass filtered at 10 Hz.

Treadmill walking consisted of an acclimation period and two 5-minute recorded trials. After identifying participants' self-selected speed, participants took a 2-minute break before the first of two 5-minute self-selected walking trials, one single-task (ST) and one dual-task (DT). Trial order was randomized between participants, and a 2-minute break was given between tasks. The DT condition consisted of a serial 7's subtraction from 1,000. Participants were instructed to do their best to maintain focus on the serial 7's task throughout the duration of the trial. Accuracy of the serial 7's task was not recorded, and one participant refused to count by 7's and instead counted down by 4's. The ST trial consisted of walking with minimized distractions as participants were instructed to maintain their gaze straight ahead.

A 12-dimensional state space consisting of time delayed copies (1/4 stride) of pelvis 3D linear accelerations and 3D angular velocities was used for analysis [5]. All trials were trimmed to 145 strides and normalized to 14,500 data points. Orbital stability was defined by calculating the maximum Floquet multiplier (maxFM) for each percent of the gait cycle (0-100%). The average of 101 maxFM (maxFM_all) and the maxFM for initial contact (maxFM_IC) were defined as the primary dependent variables to represent orbital stability. Higher maxFM indicates worse orbital stability.

A Groton Maze Learning Test was administered as part of a computerized test battery (Cogstate, Ltd.) to gain insight into gross executive function deficits.

The primary outcome of this test was the total errors in attempting to learn the same hidden pathway that connected two targets over five trials.

Kruskal-Wallis tests were used to identify where at least one between-group difference was likely ($p<0.05$). Nonparametric tests were deemed necessary because group data were often not normally distributed. Pairwise comparisons between groups were then made with Wilcoxon Rank Sum tests on gait parameters with significant differences indicated by the Kruskal-Wallis test (SAS).

Spearman's Rank Order correlations ($\alpha=0.05$) were also performed between executive function and the gait parameters for single-task, dual-task, and dual-task cost (percent change between single- and dual-tasks). We did not correct for multiple comparisons due to the exploratory nature of this study.

RESULTS AND DISCUSSION

Decreased orbital gait stability during dual-task walking was observed for the -CIPN group, with a similar trend for the +CIPN group (Table 1). Notably, two of the +CIPN participants (and no other participants) required a stop of their first attempt at the dual-task condition because they slowed their walking at the onset of the counting task to a point of nearing the rear of the treadmill. This behavior was not observed during their recorded second attempt, which may have artificially improved the +CIPN groups' orbital stability estimate from what was observed with the novel exposure to the counting task. However, the inability to appropriate devote cognitive resources in response to a distraction may in itself indicate a potential hazardous response.

Table 1. maxFM_IC values. Median (IQR)

	CON	-CIPN	+CIPN
Single Task	0.45 (0.06)	0.48 (0.06)	0.45 (0.22)
Dual Task	0.35 (0.04)	**0.56 (0.20)***	0.42 (0.05)†

$^{*}p<0.05$ compared to CON; $^{\dagger}p<0.1$ compared to CON

Additionally, for the +CIPN group, worse executive function was associated with improved orbital stability during single-task gait ($\rho = -0.94$, $p = 0.017$). Conversely, worse executive function was also associated with a more substantial dual task cost on orbital stability ($\rho = 0.94$, $p = 0.017$) (i.e., greater decreases in orbital stability during dual-task walking compared to single task). One interpretation of these relationships is that patients with self-reported sensory symptoms (i.e., +CIPN) tend to compensate for impaired sensory feedback with increased cognitive attention placed on gait control. Participants in this group who also had lower cognitive capacity were affected the most in distracting gait scenarios (e.g., dual-task walking).

CONCLUSIONS

The findings of this pilot study suggest that receiving neurotoxic chemotherapy can decrease orbital gait stability in cancer survivors. Impaired orbital stability was observed in the group that was asymptomatic for sensory CIPN symptoms, which suggests the importance for physical function interventions even in survivors who do not experience noticeable symptoms. Additionally, combined peripheral and central nervous system impairments appear to be particularly problematic for survivors during divided attention tasks. Further work is warranted to better understand these relationships and how they may be used to improve survivorship quality of life.

REFERENCES

1. Howlader et al., *SEER Cancer Statistics Review 1975-2014*, 2017.
2. Ferguson and Ahles, *Curr Neurol Neurosci Rep*, **3**(3): 215-222, 2003.
3. Spoelstra et al., *Oncol Nurs Forum*, **40**(2): E69-E78, 2013.
4. Monfort et al., *Breast Cancer Res Treat,* **164**(1): 69-77, 2017.
5. Bruijn et al., *Ann Biomed Eng*, **38**(8): 2588-2593, 2010.

ACKNOWLEDGEMENTS

We would like to thank our funding sources:

- NCI R03 CA182165-01
- NSF GRF DGE-13430

PASSIVE AND ACTIVE KNEE JOINT STIFFNESS DURING HIGH-VELOCITY THRESHOLD TO DETECT PASSIVE MOTION TEST IN ACL-RECONSTRUCTED SUBJECTS

Takashi Nagai, Nathaniel A. Bates, Timothy E. Hewett, and Nathan D. Schilaty

Mayo Clinic Biomechanics Laboratories & Sports Medicine Center, Rochester & Minneapolis, MN, USA
Email: nagai.takashi@mayo.edu

INTRODUCTION

Disruption of the ACL can result in mechanical instability as well as sensory deficits as it contains an extensive network of neural tissues and mechanoreceptors inside the ligament [1]. Those neural tissues may not be fully returned to the original level even years after ACL-reconstruction (ACLR) surgeries, compromising joint stability [2]. This is a concerning issue as a high percentage of athletes with ACLR suffer secondary ACL injuries to either reconstructed or contralateral limb [3].

Proprioceptive feedback influences the resting tension (muscle tone) and the threshold of alpha-motor-neuron activation, resulting in higher or lower passive or active joint stiffness [4]. Previous research has focused on various proprioception tests, rate of muscular force development tests, and stiffness to quantify the sensorimotor function in ACLR subjects (see a review article [5]); however, different procedures from various studies make it almost impossible to know one's sensorimotor function in ACLR subjects.

Recently, we developed a sensorimotor test to examine both proprioception with high-velocity threshold to detect passive motion (hvTTDPM) and reactive knee flexion (hamstrings) muscular strength [4]. The purpose of the current study was to examine the difference of sensorimotor characteristics between ACLR subjects and controls and between reconstructed limb and contralateral limb in the ACLR group. It was hypothesized that ACLR subjects and reconstructed limb would exhibit slower hvTTDPM and less joint stiffness when compared with controls and contralateral limb, respectively.

METHODS

Fifteen subjects with ACLR (9 males / 6 females, age: 20.1 ± 6.7 years, height: 173.8 ± 7.8 cm, weight: 76.2 ± 11.1 kg, days from ACLR to the current test: 281.5 ± 89.6 days) and 17 control subjects (7 males / 10 females, age: 22.1 ± 4.9 years, height: 175.3 ± 9.6 cm, weight: 69.7 ± 11.8 kg) participated in the study. Subjects with ACLR were cleared by their doctors at the time of testing. Prior to their participation, informed consents were obtained from each subject. The study was reviewed and approved by the Institutional Review Board.

Subjects were seated on a HumacNORM dynamometer (CSMi; Natick, MA) with the knee joint axis rotation aligned to the axis of rotation of the dynamometer. The leg of the subject was then comfortably strapped to the dynamometer arm. The leg was then extended and anatomic zero recorded in the machine. The dynamometer acceleration was set for 500°/s and torque limit set to 60 Nm. For safety reasons, both mechanical and hardware limits of rotation were set at 30 and 70 degrees. The subject's leg was then rested on the 30 degree stop and a blindfold was placed over the subject's eyes.

The subject was instructed to relax the leg completely. The subject was instructed to resist forward motion as quickly and forcefully as possible when they became aware of acceleration. Then, the dynamometer accelerated at random points in time. The subject had 3 trials of randomized time intervals to respond to the perturbation. Based on previous piloting data, it was determined that subjects failed to react about 20% of time; therefore, only successful trials were used for analyses.

Joint position and torque values were collected at 1000 Hz with customized LabVIEW (National

Instruments; Austin, TX) on a USB-1608G (Measurement Computing; Norton, MA). Data was post-processed in customized LabVIEW software to determine joint position and torque values at each of four time points: initiation, 100ms, hvTTDPM, and peak torque). Time point at hvTTDPM was defined as the point in which acceleration of the dynamometer began decreasing and when torque deflected greater than 10% over a 5ms interval. The passive and active stiffness was calculated by the changes in torque values over the changes in position values from initiation to 100ms and from hvTTDPM to peak torque, respectively (Figure 1).

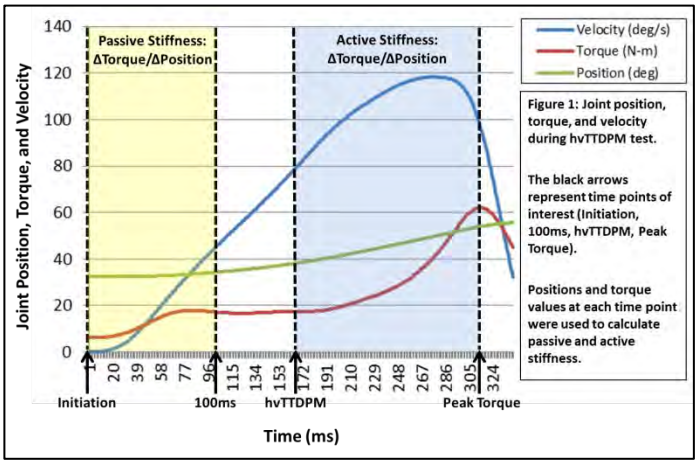

Descriptive statistics (means and standard deviations) were calculated on both reconstructed limb and contralateral legs in ACLR group while both right and left legs in control group were reported. For group differences, independent *t*-tests or nonparametric tests were used to compare between constructed limb of ACLR subjects and right limb in control subjects and between the contralateral limb in ACLR group and left limb in control group. Within-subjects analyses in ACLR subjects were conducted using a paired *t*-tests or nonparametric tests. Significance was set at $p<0.05$.

RESULTS AND DISCUSSION

Descriptive statistics are shown in Table 1 and 2. Contrary to the hypothesis, ACLR subjects had higher passive stiffness in the current study when compared to the control subjects (Passive Stiffness: Reconstructed Limb: 5.7 ± 1.0 Nm/°, Control Right Limb: 5.0 ± 1.4 Nm/°, $p = 0.030$). The rest of the variables in both passive and active stiffness were not significant ($p > 0.05$), rejecting hypotheses.

Table 1: Descriptive Statistics and Group Differences during Passive Stiffness

	ACLR	Control	*p*-value
Torque at Initiation Recon/R	3.6 ± 3.7 Nm	3.4 ± 2.8 Nm	0.835
Torque at Initiation Contra/L	3.9 ± 2.2 Nm	5.2 ± 4.7 Nm	0.720
Torque at 100ms Recon/R	14.9 ± 3.8 Nm	14.2 ± 2.8 Nm	0.575
Torque at 100ms Contra/L	15.4 ± 2.9 Nm	14.4 ± 4.5 Nm	0.480
Passive Stiffness Recon/R	5.7 ± 1.0 Nm/°	5.0 ± 1.4 Nm/°	0.030
Passive Stiffness Contra/L	5.7 ± 1.5 Nm/°	5.4 ± 1.6 Nm/°	0.249

Recon and Contra: Reconstructed and Contralateral limbs in ACLR subject.
R and L: Right and Left limbs in control subject.

For within-subject comparison (reconstructed limb vs. contralateral limb) in ACLR group, there were no significant differences ($p > 0.05$), rejecting the tested hypotheses. It is speculated that return-to-sport rehabilitation/training had positive influence on knee passive stiffness.

Table 2: Descriptive Statistics and Group Differences during Active Stiffness

	ACLR	Control	*p*-value
Time at hvTTDPM Recon/R	143.0 ± 17.1 ms	139.1 ± 20.0 ms	0.556
Time at hvTTDPM Contra/L	143.3 ± 18.3 ms	138.4 ± 25.6 ms	0.762
Torque at hvTTDPM Recon/R	15.8 ± 4.1 Nm	15.5 ± 2.7 Nm	0.844
Torque at hvTTDPM Contra/L	16.3 ± 2.9 Nm	16.2 ± 4.5 Nm	0.952
Time at Peak Torque Recon/R	312.6 ± 32.7 ms	330.4 ± 26.7 ms	0.100
Time at Peak Torque Contra/L	316.0 ± 31.8 ms	320.8 ± 42.0 ms	0.850
Peak Torque Recon/R	56.2 ± 15.4 Nm	61.4 ± 6.1 Nm	0.299
Peak Torque Contra/L	61.6 ± 1.9 Nm	62.4 ± 4.6 Nm	0.093
Active Stiffness Recon/R	2.4 ± 1.0 Nm/°	2.3 ± 0.6 Nm/°	0.781
Active Stiffness Contra/L	2.7 ± 0.7 Nm/°	2.9 ± 1.1 Nm/°	0.556

CONCLUSIONS

Additional subjects are needed to confirm the current findings. A few methodological limitations (potential ceiling effect and learning effect) should also be addressed in future studies.

REFERENCES

1. Hewett et al. *Clin Orthop*, 2002: 76-94
2. Young et al. *Orthop J Sports Med*, 2016.
3. Schilaty et al. *Am J Sports Med,* 2017: 1567-1573.
4. Nagai et al. *Sports Med,* 2018.
5. Nyland J et al. *Knee Surg Sports Traumatol Arthrosc,* 2017: 1461-1474.

ACKNOWLEDGEMENTS

Funding from the NIH R01AR056259, R01AR055563, L30AR070273, K12HD065987, and the Mayo Clinic Kelly Orthopedic Fellowship.

Prophylactic Ankle Bracing Alters Lower Extremity Kinematics during Landing

Alexis K. Nelson, Rachael A. Arnwine, Hannah Nelson, Jake A. Malero, Alex M. Carnall, Ramzi Majaj, Max R. Paquette, Douglas W. Powell

[1] University of Memphis, Memphis, TN, USA
email: knelson6@memphis.edu

INTRODUCTION

Lateral ankle sprain is the most common ankle ligament injury in sport and is typically caused by excessive inversion during ankle plantarflexion (1, 3). Ankle sprains can have long lasting effects with 79% of athletes experiencing a recurrence of ankle sprain and 59% of athletes exhibited functional disability and significant residual symptoms (2). Two common ways to mechanically stabilize the ankle joint are bracing and taping. One advantage of ankle bracing over taping includes constant mechanical stability with bracing without the loss of mechanical properties over the course of training or competition. Other advantages are that the brace is reusable and adjustable. Research has demonstrated the effects of ankle bracing on ankle joint motion and kinetics, but few studies have investigated secondary effects of bracing on more proximal joints. Limiting ankle range of motion during a dynamic loading task may have secondary effects in the sagittal and transverse planes as well as at the knee and the hip joints. The purpose of this exploratory project is to quantify changes in three-dimensional ankle, knee and hip joint angles in response to prophylactic ankle bracing.

METHODS

Eleven recreational athletes (6 M; 5 F) performed five step off landing trials from a height of 16" with their dominant limb in an ankle brace (ASO). Three-dimensional kinematics (240 Hz, Qualisys Inc., Sweden) and ground reaction forces (960 Hz, AMTI, MA, USA) were collected simultaneously. Visual 3D was used to calculate joint angles and custom software (MATLAB, MathWorks, MA, USA) was used to determine discrete variables. Data were analyzed during a 100 ms period following initial contact. Paired samples t-tests were used to compare outcome variables.

RESULTS AND DISCUSSION

Peak ankle dorsiflexion angles were smaller in the BRACED compared to UNBRACED limb while no differences were observed in peak eversion or adduction angles (Table 1). Peak knee abduction and internal rotation angles were greater in the BRACED compared to UNBRACED limb, however, no differences in peak knee flexion were observed. No differences in peak hip flexion, adduction or internal rotation angles were observed between the BRACED and UNBRACED limbs. For clinical relevance, the lack of differences in frontal plane ankle motion may mean that we are not limiting ankle range of motion and protecting the joint. Therefore, for future studies we should investigate the energy absorption values in multi-planar motion and kinetics at the ankle, knee and hip.

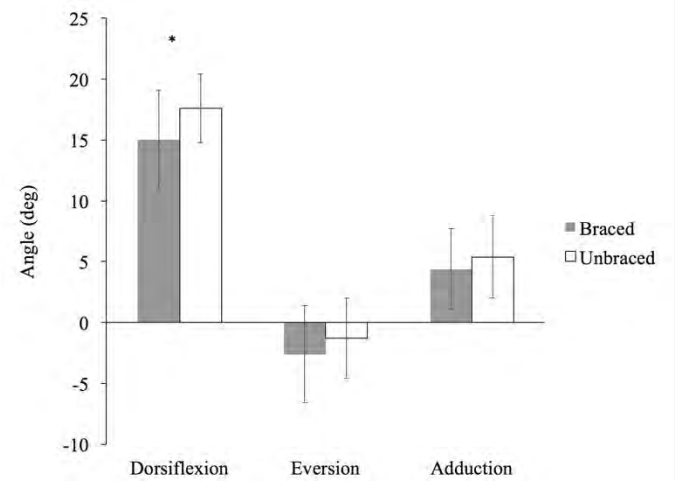

Figure 1: Ankle Results. * indicates a statistically significant p-value > 0.05.

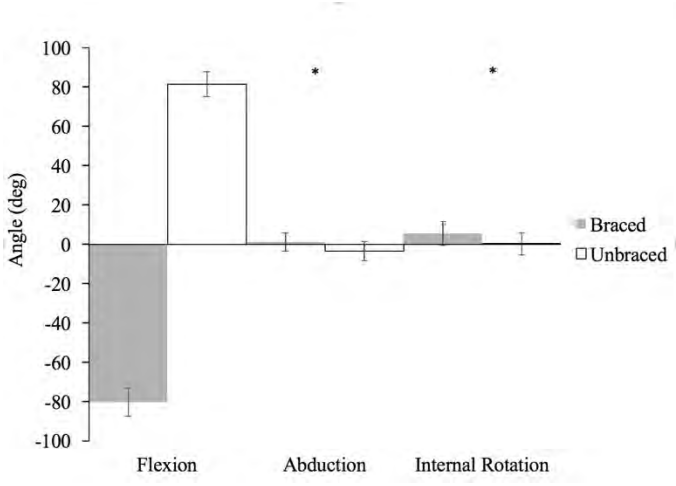

Figure 2: Knee Results. An * indicates a statistically significant p-value > 0.05.

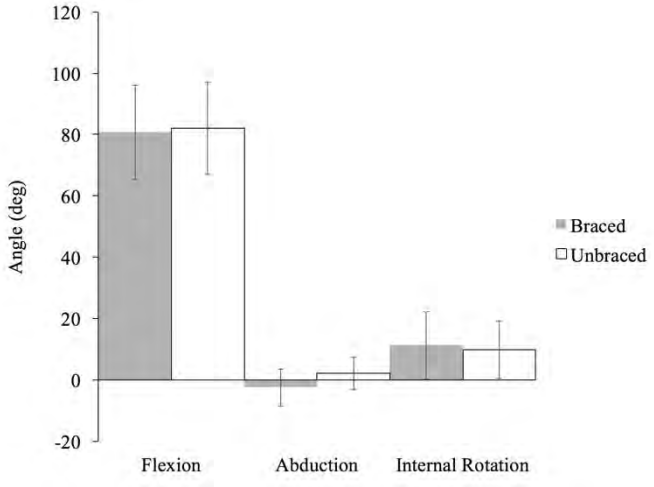

Figure 3: Hip Results. An * indicates a statistically significant p-value > 0.05.

CONCLUSIONS

Though ankle bracing is commonly used in sports medicine as a means to prevent and rehabilitate injury, these data demonstrate that mechanical load is shifted to other structures in other planes. Further research is required to determine that the prophylactic use of ankle bracing does not place other structures at an increased risk of injury.

REFERENCES

1. Yeung MG, Chan DK, So CH, Yuan WY. An epidemiological survey on ankle sprain. Br J Sports Med 1994; 28(2): 112-116.
2. De Clercq D.L. Ankle bracing in running: the effect of a Push type medium ankle brace upon movements of the foot and ankle during the stance phase. Int J Sports Med. 1997; 18 (3): 222-228.
3. Zhang, S. N., Bates, B. T., & Dufek, J. S. (2000). Contributions of lower extremity joints to energy dissipation during landings. Medicine and Science in Sports and Exercise, 32, 812–819.

Table 1: Joint Movements in the Braced and Unbraced conditions. A significant value is a p value > 0.05 indicated in bold lettering.

Joint	Movement	Braced	Unbraced	P	d
Ankle	DF	15.0 (4.1)	17.6 (2.8)	***0.022***	0.74
	Ev	-2.6 (4.0)	-1.3 (3.3)	0.149	0.35
	Add	4.4 (3.3)	5.4 (3.4)	0.208	0.32
Knee	Flex	80.3 (7.2)	81.4 (6.4)	0.293	0.14
	Abd	1.3 (4.6)	-3.3 (4.8)	***0.015***	0.99
	IR	5.7 (6.2)	0.1 (5.6)	***0.034***	0.95
Hip	Flex	80.7 (15.3)	82.0 (15.2)	0.266	0.09
	Add	-2.5 (6.1)	2.2 (5.2)	0.472	0.04
	IR	11.2 (11.0)	9.8 (9.3)	0.323	0.14

IN VITRO REDUCTION OF WRIST PRESSURE DURING ANTEBRACHIAL TISSUE MANIPULATION

[1]Carli Norman, [1]Rakshit Shah, [1]Hui Zhang, [4]Pauline Luong, [4]Jae Son, and [1,2,3]Zong-Ming Li
Hand Research Laboratory, Departments of [1]Biomedical Engineering, [2]Orthopaedic Surgery, and [3]Physical Medicine and Rehabilitation, Cleveland Clinic, Cleveland, OH, USA
[4]Pressure Profile Systems, Inc., Los Angeles, CA, USA
email: liz4@ccf.org web: http://handlab.org/

INTRODUCTION

Carpal tunnel syndrome (CTS) is associated with elevated carpal tunnel pressure which leads to compression of the median nerve. CTS is routinely treated by transecting the transverse carpal ligament which increases the cross-sectional area of the carpal tunnel [1] and decreases carpal tunnel pressure [2], thereby decompressing the nerve. Recently, an unobtrusive and non-invasive device was developed to non-surgically treat CTS by relieving pressure on the median nerve. This carpal tunnel manipulation device (CTMD) attaches to the volar aspect of the wrist and applies negative pressure by lifting the underlying tissue. In a pilot study, 4 weeks of daily CTMD use resulted in significant improvements in CTS symptom severity, with improvement seen as early as 2 weeks [3]. However, the effect that the device has on pressure within the wrist remains unknown. The purpose of this study was to investigate changes of pressure within the wrist in response to wrist manipulation applied by volarly lifting the tissues. It was hypothesized that pressure would decrease with the application of wrist tissue manipulation.

METHODS

Eight (n = 8) fresh frozen cadaveric hands (5 males, 3 females; 6 left, 2 right; age 52±12 years; BMI 23±3 kg/m^2) were used in this study. Tissue manipulation was implemented with a custom apparatus consisting of a robotic arm (Denso Robotics, VM-G) and a CTMD modified to fit the curvature of the wrist. The robotic arm interfaced with the device via a wire woven through slots in the CTMD and an eyelet on the robotic end-effector.

Pressures within the wrist were measured using a 12-element tactile pressure transducer (DigiTact Strip Sensor, Pressure Profile Systems, Inc., Los Angeles, CA). The DigiTact was inserted via an incision into the lumen of the carpal tunnel and under the median nerve. Along with the sensor, a PTA Balloon Dilation Catheter (AT-120184, Atlas, Tempe, AZ) was inserted for standardization of the baseline pressure beneath the CTMD. The wrist regions under investigation include the carpal tunnel (distal wrist), beneath the CTMD (proximal wrist), and the region between the two (middle wrist) (Fig. 1).

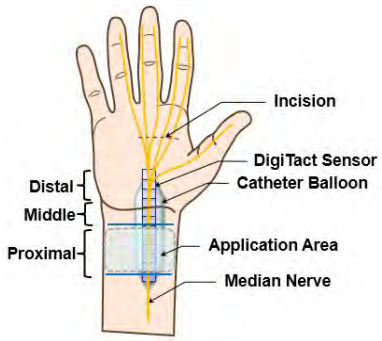

Fig. 1. Experimental setup for in vitro simulation and measurement of wrist pressure

Following insertion of the sensor, the specimen was positioned in a supinated, anatomically neutral position within a splint that was affixed to a wooden base using Velcro. The CTMD was attached to the wrist using double-sided adhesive located in the center of the concave side of the device. The CTMD was pressed down and adhered to the distal forearm with the distal edge of the CTMD located 1 cm proximal to the distal wrist crease. Once attached, the balloon within the specimen was inflated with water via a syringe until the elements under the CTMD reached an average of 100 mmHg, a pressure level commonly reached in CTS patients. The CTMD was lifted in 1 mm increments up to 6 mm and returned to its original position, pausing for 5 seconds at each lifting distance. Pressure was recorded simultaneously at 50 Hz. The lifting

procedure was repeated for 20 trials on each specimen.

A two-way repeated measures ANOVA was used to examine the dependence of pressure on lifting distance (0-6 mm) and wrist location. We also examined the effects of repetitive trials on pressure drop at 6 mm lifting distance by two-way repeated measures ANOVA (factors as Trial and Location). Post-hoc Tukey's tests were used for all pairwise comparisons. Statistical analysis was completed using SigmaStat 3.5 (Systat Software Inc., San Jose, CA, USA) with a significance level of $\alpha = 0.05$.

RESULTS

The application of tissue manipulation had a significant effect on pressure within the wrist ($p<0.001$). In general, as the magnitude of lifting distance increased, pressure decreased. Pairwise comparisons within the proximal wrist revealed significant differences between baseline pressure (0 mm) and pressures at 3-6 mm lifting distance; a maximum decrease of 25 mmHg was observed at the 6 mm when compared to baseline (Fig. 2). Pressure in the proximal wrist at the 6 mm lifting distance was also significantly different from that at 1 mm. For pressure within the middle wrist region, significant decreases up to 20 mm were observed at the 6 mm lifting distance when compared to 1 mm and baseline (Fig 2). Despite changes in other wrist segments, the distal wrist pressure was not significantly affected by the tissue manipulation, remaining relatively unchanged with increasing lifting distance (Fig. 2).

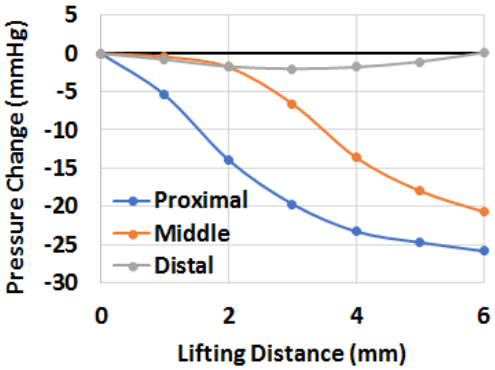

Fig. 2. Pressure change (average across specimens) within the proximal, middle, and distal wrist as a function of lifting distance

When further analysis was conducted on the pressure data at the 6 mm lifting distance for factors of trial and location, it was found that there was a significant location - trial interaction. Both the main effect of wrist location and trial were significant ($p < 0.001$). Although the distal wrist pressure was not significantly affected by lifting distance, pairwise comparisons of distal pressure at 6 mm lifting distance revealed that there were significant differences between distal wrist pressures at trials 6-20 when compared to the first trial (Trial 1 vs 8-20: $p < 0.001$, Trial 1 vs 6 & 7: $p < 0.05$)(Fig. 3).

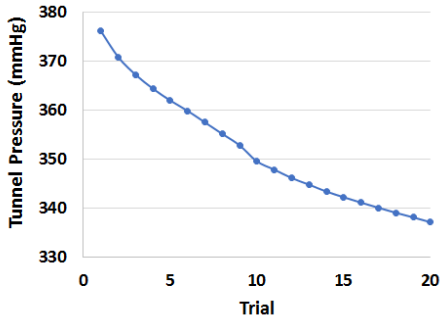

Fig 3. Pressure at the tunnel region (at 6mm lifting) over repeated trials

DISCUSSION

There is a well-established association between CTS and increased carpal tunnel pressure. In this study, we examined a non-surgical strategy to alleviate carpal tunnel pressure by lifting the tissues on the volar aspect of the wrist. Tissue manipulation significantly reduced pressure under the CTMD and just distal to the device with a small lifting distance of 3 mm. Although the carpal tunnel pressure was not significantly affected by lifting distance, the pressure significantly decreased after 6 trials suggesting that with repeated use, carpal tunnel pressure may be reduced.

REFERENCES

[1] Kato et al., J Hand Surg [Am], 1994. 19(3): p. 416-9. [2] Gelberman et al., J Bone Joint Surg Am, 1981. 63(3): p. 380-3. [3] Luong et al., Arthritis Rheumatol. 2017; 69 (suppl 10).

ACKNOWLEDGEMENTS

NIH/NIBIB1R44EB024713

DIFFERENCES IN RESULTANT JOINT FORCES AND MOMENTS AT L4/L5 BETWEEN PARTICIPANTS WITH AND WITHOUT BACK PAIN

Nunez, M.A., Hasan, M., Avalos, M., Hung, C., Kwon, Y.H

Texas Woman's University, Denton, Texas, USA

email: mnunez3@twu.edu webpage: https://twu.edu/kinesiology/graduate-programs/biomechanics/

INTRODUCTION

According the World Health Organization, a very large number of adults are affected by lower back pain and the etiology of these issues is limitless and range from chronic debilitating ailment to an acute annoyance and are difficult to assess (1). With many causes, the pain is a multifaceted condition which is influenced by varying factors such as socio-environmental, predispositions, and individual personalities (4). A communal problem in all pain studies is the variability of the level of self-reported pain; being it is a subjective measure described by the individual (2). One of the factors that contributes to the physiological process of disk degeneration are the forces deposited on the disks (5). More specific, the compressional forces are a contributing risk factor for injury at the joint between lumbar disk 4 and 5 (L4/L5) (6). When we stand moments and forces must be generated by the tissues around the intervertebral joint, these moments in turn are compensatory the moments created by the upper body segmental masses, gravitational, and inertial forces (3)

The aim of this study is to examine if there are differences in the forces and torques at the lumbar L4/L5 joint between participants with self-reported back pain versus non-pain in every day movements, such as standing from a seated position.

METHODS

Using a Vicon 10 camera motion capture system and 4 AMTI force plates, 41 participants (22 pain, 19 non-pain) were fitted with 56 reflective markers to record two trials of a sit to stand motion. The data was then analyzed with Kwon 3D XP to calculate kinetic and kinematic data. The McKinnon estimation method for the L4/L5 was used to assess the moments and forces about the joint. The participants (ages 18-27) were asked to stand from a seated position without any assistance.

KWON 3D XP v.5.0 software was used to calculate the resultant joint moment (RJM) in the sagittal plane (- flexion/ + extension) and the resultant joint force (RJF) along the longitudinal axis (+ compression/ - decompression). Mass normalization to both parameters was performed for the group analysis. The peak torque and force were assessed using SPSS v.22 (sig > .05) to compare the results of RJM and RJF between the two groups.

RESULTS AND DISCUSSION

The average of two trials per participant were analyzed and then the group averages were calculated. The RJM between the pain (-.2025 Nm/kg) and non-pain group (-.1657 Nm/kg) showed that participants with back pain statistically ($p=.004$) exhibit a greater moment when compared to the non-pain group; this can be interpreted as a greater *flexion* moment for the pain group (Fig 1). The resultant joint force also showed a significant ($p=.011$) difference between the pain (1.9325 N/kg) versus the non-pain group (1.8354 N/kg), which can be interpreted as a greater compression force at L4/L5 for the pain group (Fig 2).

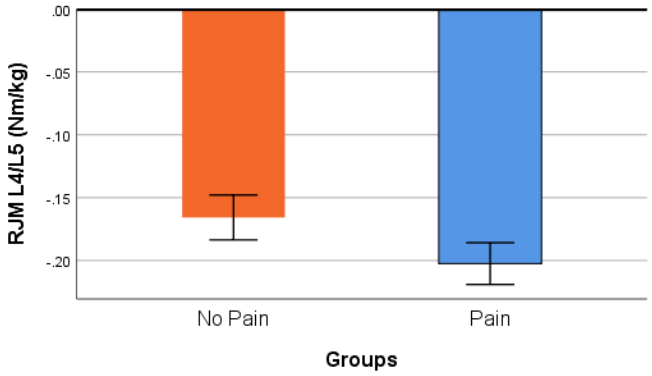

Figure 1: The comparison between groups for the RJM at L4/L5 (- flexion moment).

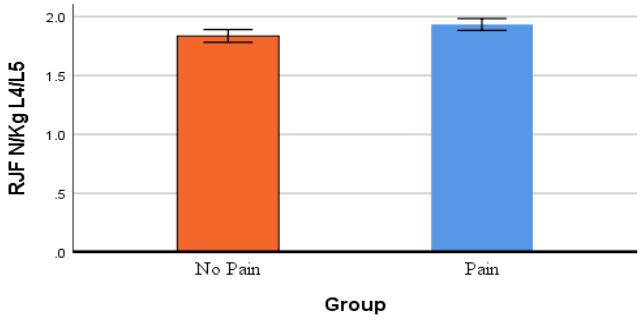

Figure 2: The comparison between groups for the RJF at L4/L5 (+ compression force).

What this means is that there exists a difference between the pain and non-pain group that must be further investigated. Limitations of this exploratory evaluation were that only female participants were assessed, therefore male evaluations must also be completed. Another limitation was that as stated previously, the biomechanical differences are only a part of the lumbar back pain contributing conglomerate. Further investigation with EMG analysis and mathematical modeling is needed to find out why there is a difference between the two groups in RJM and RJF.

CONCLUSIONS

With the results demonstrating that there are significant differences in the resultant joint moment and forces at the L4/L5 joint, further investigation into the causation of these differences should next be addressed. Since strengthening lumbar extensor muscles exclusively has shown a decrease in reported lower back pain patients (4), the next step is to investigate if such a program would even the resultant joint moment and forces at L4/L5 after treatment.

REFERENCES

1. Duthey. (2013) Low Back Pain. *Priority Medicines for Europe and the World Update Report, Back Ground Paper,* **(6)**24.
2. Coghill (2010) Individual differences in the subjective experience of pain: New insights into mechanisms and models. *Headache*, **50**(9).
3. Potvin et al. (1991) Trunk muscle and lumbar ligament contributions to dynamic lifts with varying degrees of trunk flexion. *Spine*, **16**(9).
4. Risch et al. (1993) Lumbar strengthening in chronic low back pain patients. Physiologic and psychological benefits. *Spine*, **18**.
5. Vieira et al. (2018). Influence of lifestyle characteristics and VDR polymorphisms as risk factors for intervertebral disc degeneration: A case-control study. *European Journal of Medical Research*, **23**(1).
6. Wettenschwiler et al. (2017). Loading of the lumbar spine during backpack carriage. *Computer Methods in Biomechanics and Biomedical Engineering*, **20**(5).

ACKNOWLEDGMENTS

Thank you to all the TWU Biomechanics team for all the help.

Comparison of Ground Reaction Forces and Knee Joint Moments between Parkinson's Disease and Healthy Older Adults using a Kinect-Driven Musculoskeletal Gait Analysis Model

[1] Jeonghoon Oh, [1] Moataz Eltoukhy, [2] Christopher Kuenze, [3] Michael S. Andersen, and [1] Joseph Signorile

[1] University of Miami, Coral Gables, FL, USA
[2] Michigan State University, East Lansing, MI, USA
[3] Aalborg University, Fibigerstraede, Denmark

email: jxo130@miami.edu

INTRODUCTION

The gait impairment is commonly observed in people with Parkinson's disease (PD). It is caused by the progressive loss of dopamine-producing cells of the central nervous system. Clinically, it is characterized by rigidity and freezing of the gait, which causes significant loss of independence and increased incidences of falls [1].

Despite the large increase in the number of PD patients in the US, clinicians are still using subjective measures to assess the level of the disease. But, these methods often produce inconsistent diagnoses. At the same time, gait analysis using a laboratory-based motion capture system provides a quantitative assessment of the rate of the disease progress. Yet, due to its high cost, technical difficulty, lack of portability, need for larger spaces, and the large requirements for setup time, it is very difficult to adopt this technology in clinical settings.

According to the literature, measurement of kinetics, such as the vertical ground reaction forces (vGRF) pattern during gait in PD patients is often used to monitor the stage of the disease. In addition, many researchers used GRF in order to develop ways to automatically classify gait patterns in PD patients. Other studies have also indicated that an abnormality in the pattern of the kinetics was more pronounced than in the kinematics in PD patients during gait.

Therefore, the purpose of this study was to compare the GRFs and knee joint flexion moments during gait between PD and healthy individuals using a full-body musculoskeletal model driven by the Microsoft Kinect v2.

METHODS

Nine elderly patients diagnosed with PD (71.0±5.6 yrs) and eleven healthy age-matched control participants (71.1±7.5 yrs) were recruited for this study. We recruited PD patients who were impaired with mild to moderate (H&Y stages I-III) and had a score of 24 or above on the Folstein Mini-Mental State Examination.

The Kinect v2 was located at 2.5 m from the subject, at a height of 0.75 m from the ground. This location was determined by formerly published research which involved measuring gait parameters using the Kinect sensor. The subjects performed three walking trials at their normal walking speeds without wearing any type of footwear. The Kinect's depth data was analyzed by subtracting the background depth information and tracking the subjects' movement using anthropometric models in order to extract 26 joint trajectories using a customized MATLAB code [2].

The musculoskeletal GaitFullBody model (AnyBody Technology, Aalborg, Denmark), generated the gait GRFs and knee joint flexion moment using a modified version of the method proposed by Fluit et al. and Skals et al. [2-3]. This is attained by 25 artificial muscle-like actuators which are connect to under each foot.

We used an unpaired Student *t*-test analysis to compare the mean kinetic data between PD patients and control healthy subjects. The ensemble curves and associated 90% confidence intervals (CI_{90}) of the vGRF were compared between both groups.

RESULTS AND DISCUSSION

Table 1 shows the kinetic data of the PD and control groups. A significantly lower vGRF ($P<.05$) and $_{AP}$GRF ($P<.05$) was found in both the braking and propulsion phases of the PD group. At the knee joint, however, the maximum flexion moment generation in the stance phase did not significantly differ from that of the controls.

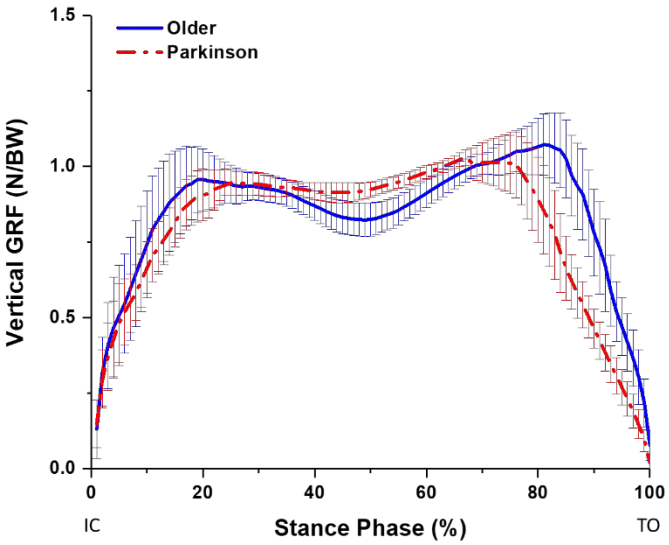

Figure 1: The ensemble curve of estimated vGRF from Kinect-driven musculoskeletal gait model for the Parkinson's group (red) and healthy control group (blue).

In the PD group, subjects appear to walk flat-footed, with minimal push-off with plantar flexion, so the two peaks of vGRF is lower than the control groups'. Also, the vGRF curve in the PD did not show the two distinct peaks and showed a more pronounced valley which then became more of a plateau. It indicates that the PD subjects utilized more load at the mid-foot when compared with the healthy subjects. The vGRF pattern of the PD group is similar to the findings reported by Nieuwboer et al [4]. Additionally, patients with PD showed less $_{AP}$GRF braking and propulsion impulse, due to their inability to generate sufficient braking impulse followed by a decline in the propulsion impulse, than those generated by the healthy control group.

This was the first study to compare the differences in the vGRF and knee joint moment between PD and healthy subjects using a Kinect-driven musculoskeletal modeling. The ability of the model to effectively estimate gait kinetics was apparent in its ability to effectively assess PD gait abnormalities characterized by a reduction in the vGRF second peak.

CONCLUSIONS

The findings of this study confirm that both vGRF and $_{AP}$GRF generated by the PD patients are significantly different than the healthy group. On the other hand, statistically no significant difference was found in the maximum knee flexion moment. In addition, the gait-related kinetic outcomes obtained using our Kinect-driven musculoskeletal model, proves that Kinect has the potential to be an effective, accurate gait analysis tool for the PD population.

REFERENCES

1. Halliday et al. *Gait & Posture.* 8(1):8-14, 1998.
2. Skals et al. *Multibody System Dynamics.* 41(4):297-316, 2017
3. Fluit et al. *Journal of Biomechanics*. 47(10):2321-2329, 2014
4. Nieuwboer et al. *Scandinavian journal of rehabilitation medicine*, 31(3):185, 1999

Table 1: Comparison between Parkinson's and older groups kinetics variables during the stance phase.

	Max vertical GRF (N/BW)		Max horizontal GRF (N/BW)		Max knee flexion moment (Nm/BW)
	Braking	**Propulsion**	**Braking**	**Propulsion**	
Parkinson's group	1.02±0.03	1.10±0.04	-0.13±0.03	0.16±0.04	0.75±0.15
Older group	1.09±0.11	1.18±0.12	-0.16±0.05	0.19±0.06	0.77±0.14
***P*-value**	.009*	.041*	.042*	.037*	.716

PHASE OFFSET ERROR ATTENUATION IN PATTERN BASED FEEDBACK FOR GAIT RETRAINING

[1,2] Nuno Oliveira, [1,2] Naphtaly Ehrenberg and [1,2] Peter Barrance

[1] Human Performance and Engineering Lab, Kessler Foundation, West Orange, NJ
[2] Research Department, Children's Specialized Hospital, Mountainside, NJ
email: noliveira@kesslerfoundation.edu

INTRODUCTION

Successful use of visual feedback based gait training for normalization of knee flexion patterns relies on the sensory integration of visual signals. Visual feedback that only focuses on individual gait cycle parameters does not target deviations in other parts of the cycle and may induce new deviations into the learned pattern. Alternatively, pattern based training with whole cycle feedback provides the user with quantitative information about the deviation from the target. However, this value might be affected by small phase offsets between the patterns that result from normal gait variability, and are not relevant for overall gait pattern retraining. Therefore, it is important for pattern based feedback relying on overall cycle error to develop measures that attenuate phase offset errors.

In a previous study [1], our research team investigated knee flexion modifications during pediatric gait using visual feedback. The visual feedback provided the users with information about the error between their real time knee flexion pattern and a target knee flexion pattern. This study reported that while participants were able to direct maximum knee flexion toward the target, overall cycle error was not reduced. This was in part due to timing offsets between the actual pattern and the target during swing. This phase error increased overall cycle error while the user was responding appropriately to the target knee flexion.

The purpose of this study was to investigate the potential of dynamic time warping (DTW) [2] to attenuate temporal offsets between measured knee flexion patterns and the target, and highlight the magnitude of spatial errors driving overall cycle error. DTW is a method used to measure the similarity between two temporal sequences by generating two warped signals maximally aligned in time.

METHODS

The current study reanalyzed data from a previous study that tested the effect of visual feedback on knee flexion patterns during gait [1]. Research procedures relative to the data analyzed in this study are summarized below.

Twelve typically developing children and adolescents (6M, 6F; 11.9±2.7 yrs old) participated in the study. All research procedures were approved by the Kessler Foundation Institutional Review Board. Knee flexion angle data were collected using Inertia Measurement Units (Xsens MTw, Enschede, The Netherlands). Three sensors were fixed to each participant's dominant lower limb (anterior thigh, posterior shank, and the posterior surface of the shoe). Data recorded by the sensors was processed and integrated into a display for real-time visual feedback using MATLAB (MathWorks Inc., Natick, MA). The swing phase of a normal averaged gait cycle was amplified and reduced by 20 and 40%, resulting in four different target gait cycles. Participants were asked to use the primary full cycle error display to score 'points', and were also provided two assistive cues on peak flexion, and timing error.

All analyzed cycles were normalized in time. The following measures were calculated (Fig. 1): mean absolute cycle error ('MACE') was calculated as the mean absolute difference between the measured cycle and the target cycle; peak error ('MAX') was calculated as the absolute error between the measured maximum angle and the target maximum angle; peak local minimum error ('MIN') was calculated as the absolute error between the

measured minimum angle and the target minimum angle; peak timing error ('MAXT') was calculated as the absolute error between the measured maximum angle time point (%) and the target maximum angle time point (%); swing curve length ('WIDTH') was calculated as the absolute error between the measured and target durations of swing, measured as the time point difference between the two minima before and after maximum knee flexion. Mean absolute cycle error of the dynamically time warped signals ('MACEdtw') was calculated a posteriori as the mean absolute difference between the dynamically time warped measured cycle and the dynamically time warped target cycle.

Multiple regression analysis was used to test if MAX, MAXT, MIN, and WIDTH significantly predicted participants' MACE and MACEdtw. A total of 6521 gait cycles were included in two linear regression models. One model tested the relationship between the predictors and the 'MACE' response. A second model tested the relationship between the same predictors and the 'MACEdtw' response. Standardized regression coefficients (β) were calculated by assigning all measures a variance of 1 (z-scores). This allowed for a quantitative comparisons between coefficients.

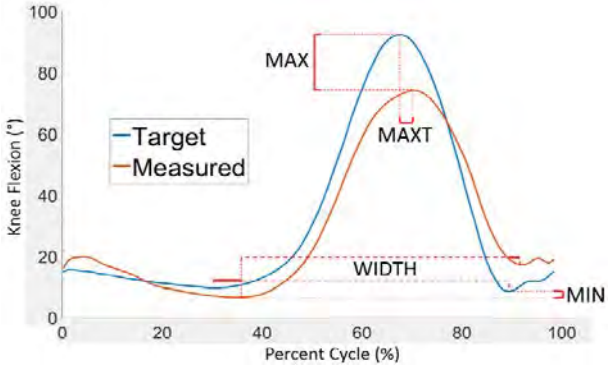

Figure 1: Example of a target pattern and a measured pattern with predictor error measures.

RESULTS AND DISCUSSION

The results of the regression indicated the four predictors explained 51% of variance in MACE (R^2 = 0.51, p<0.001), and 61% of the variance in MACEdtw (R^2 = 0.61, p<0.001). MAX (β = 0.40, p<0.001), MAXT (β =0.33, p<0.001), MIN (β = 0.41, p<0.001), and WIDTH (β = 0.02, p<0.001) significantly predicted MACE. When tested as predictors of MACEdtw, MAX (β = 0.51, p<0.001), MIN (β = 0.53, p<0.001) and WIDTH (β = 0.04, p<0.001) coefficients increased, while MAXT (β = 0.10, p<0.001) decreased (Fig.2). Small predictive values were observed for WIDTH in both MACE and MACEdtw models.

Compared with MACE, MACEdtw was more highly associated with pattern deviations in MAX and MIN error. This was associated with the reduced phase offset due to dynamic time warping of the signals. Therefore, pattern based biofeedback training that aims to normalize joint motions with large amplitude of movement and tolerated phase error could benefit from the use of dynamic time warping. This will provide the user with more functionally relevant measures of whole cycle error.

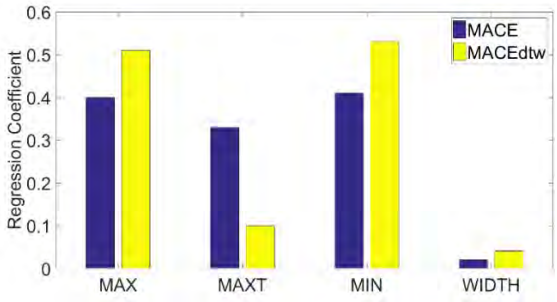

Figure 2: Regression standardized coefficients (β) for the predictors used in the MACE and MACEdtw regression models.

CONCLUSIONS

This study demonstrated the potential for DTW to attenuate phase offset errors in visual feedback based on knee flexion patterns during gait. This approach also increased the relative contribution of magnitude deviations for whole cycle error. This has been implemented in the feedback system previously reported [1], and is currently being tested.

REFERENCES

1. Oliveira et al. *Proceedings of ASB'17,* Boulder, CO, USA, 2017.
2. Sakoe, H., & Chiba, S. *IEEE transactions on acoustics, speech, and signal processing, 26*(1), 43-49, 1978.

ACKNOWLEDGEMENTS

Support for this study was provided by Children's Specialized Hospital (New Brunswick, NJ) and Kessler Foundation (West Orange, NJ).

POST-TRIAL FEEDBACK USING A PORTABLE CLINICAL SYSTEM MAY ALTER LANDING PERFORMANCE

[1] Jessica E. Onsager, [1] Jeremie J. Schiedermayer, [1,2] Becky L. Heinert, [1] Drew N. Rutherford, [1] Thomas W. Kernozek

[1] Department of Health Professions – Physical Therapy Program, University of Wisconsin-La Crosse, La Crosse, WI, USA
[2] Sports Medicine Department, Gundersen Health System, Winona, MN, USA
email: drutherford@uwlax.edu ; web: www.uwlax.edu/grad/physical-therapy/la-crosse-institute-for-movement-science-lims/

INTRODUCTION

Clinicians appear to desire easy to use, cost-effective, transportable, and flexible functional assessment systems that can be used in clinical settings that can provide either real-time feedback or rapid post-trial feedback [1]. This may reduce injury incidence and improve training within both prevention and rehabilitation based on motor learning principles. Our aim was to use a low-cost, portable clinical system to screen and train regional female athletes participating in jumping and landing related sports based on vertical ground reaction force (vGRF), loading symmetry, and qualitative video performance for reducing knee injury risk.

METHODS

Seventy-three adolescent females competing in high school and middle school sports programs (Age: 14.9 ± 1.8 years, Height: 166 ± 8 cm, Mass: 58.9 ± 10.6 kg, BMI: 21.3 ± 3.2 kg/m^2) participated. Each landed from a 50 cm height onto two force platforms using their own athletic footwear for a total of 30 trials. Kinetic data were obtained from custom, high-impact force platforms designed and purpose-built for these in situ data collections. Bilateral vGRF data were sampled at 2000 Hz. Frontal plane videos were recorded from a high-speed camera at 100 Hz (DFK 23UV024, The Imaging Source, LLC, Charlotte, NC, USA). Custom software (Innovative Sports Training, Inc., Chicago, IL, USA) displayed on a projection screen provided post-trial feedback of peak total vGRF in multiples of bodyweight (BW), symmetry of loading from the peak vGRF of each platform, and the frontal plane video (Fig. 1).

Participants performed a baseline block of 6 Pre-test trials blinded without feedback, followed by two Training blocks of 6 trials (Training1, Training2) each where participants received post-trial feedback and verbal instructions on how to use the feedback to improve their landing performance. Upon completion of a Training trial, researchers provided the augmented vGRF feedback and scanned through the video to demonstrate key frames at the moment of impact, greatest frontal plane knee angle, and greatest squat depth. Participants were instructed to decrease the peak total vGRF by "landing softly" and with a greater squat depth, landing symmetrically by "keeping a teeter-totter bar level" with equal weight on each leg, and avoiding a valgus knee angle by "controlling knee movement and keeping the knees over the toes". Following Training, a Post-test block of 6 trials was performed without feedback or instruction. Participants completed the session by performing 6 trials of a dual-task Transfer activity in which they were required to catch a ball in mid-air from a randomly chosen throw or fake throw.

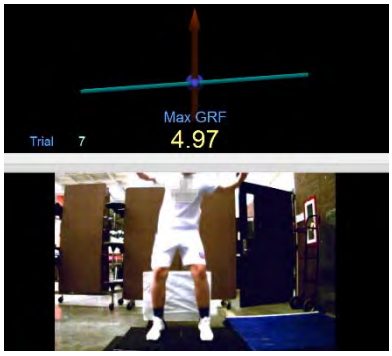

Figure 1: Post-trial feedback display for participant.

Means for peak total vGRF (BW) were calculated for the Pre-test, Training1, Training2, Post-test, and the Transfer dual-task trial blocks. A repeated measures

ANOVA (alpha set to 0.05) was performed on total peak vGRF to analyze differences between trial blocks, with Bonferroni correction on post-hoc comparisons. Effect sizes (Cohen's *d*) were calculated between comparisons. Statistical tests were completed using SPSS, version 25 (IBM Corporation, Armonk, NY, USA).

RESULTS AND DISCUSSION

Improvement from the Pre-test peak total vGRF (4.46 ± 1.04 BW) was demonstrated for the first Training block (-17.1%, 3.70 ± 0.71 BW, $p < 0.001$, $d = -0.87$). The second Training block continued to show improvement from Training1 (-6.25%, 3.47 ± 0.65 BW, $p < 0.001$, $d = -0.34$). Performance also did not change from Training2 to the Post-test ($p > 0.05$), demonstrating retention. The Transfer task demonstrated loss of improvement from the Post-test (3.43 ± 0.67 BW) (+19.2%, 4.09 ± 0.94 BW, $p < 0.001$, $d = +0.82$); however, this was still improved from the Pre-test (-8.38%, $p = 0.005$, $d = -0.38$), demonstrating positive transfer of learning in the dual-task scenario. Overall training retention improved from the baseline Pre-test to Post-test (-23.2%, $p < 0.001$, $d = -1.21$).

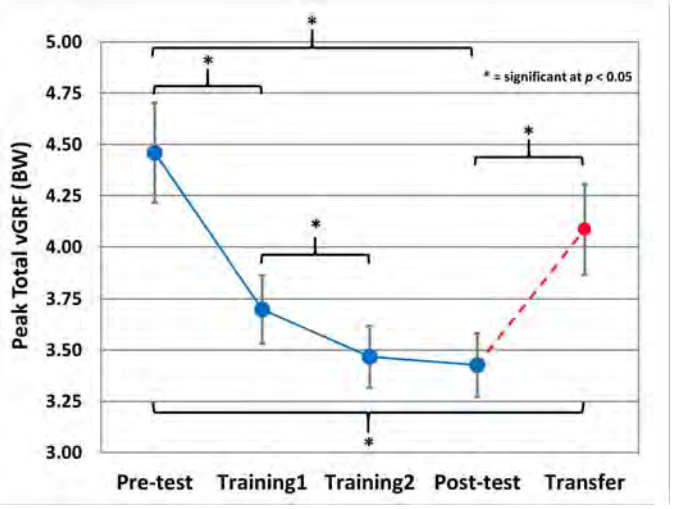

Figure 2: Peak total vGRF performance learning curve for the feedback training and transfer tasks.

Participants completed and retained all improvements in landing performance within a total of 12 trials (Fig. 2). Training effect size was similar, but greater, to prior work performed in a laboratory setting with college-aged females using the same peak total vGRF feedback variable (Cohen's $d = 0.8$) [2].

Motor learning principles related to the use of augmented feedback or knowledge of results appear to have a direct application to clinical practice [3]. Either intrinsic feedback presented on a visual display or final results can be presented from data obtained from force platforms and high-speed cameras. Such data produce implicit cues to the performer, promoting them to have an internal focus and facilitating more effective learning of a motor task [4]. Performance-based feedback has been shown to be effective in modifying neuromuscular risk factors in drop landings [5]. Many have used expensive and more elaborate laboratory-based methods to provide such feedback [6,7,8]. The high cost of such laboratory-based systems is prohibitive for in situ data collections.

CONCLUSIONS

Post-trial feedback using a low-cost, portable clinical system appears to alter landing performance. Further work appears warranted.

REFERENCES

1. Bonnechère, et al. *J Biomech*, 49(13), 2561-2565, 2016.
2. Rutherford, et al. *Proceedings of ASB'17,* Boulder, CO, USA, 2017.
3. Winstein. *Phys Ther*, 71(2), 140-149, 1991.
4. Wulf, et al. *J Motor Behav*, 34(2), 171-182, 2002.
5. Onate, et al. *Am J Sports Med*, 22(8), 831-842, 2005.
6. Herman, et al. *Am J Sports Med*, 37(7), 1301-1308, 2009.
7. Myer, et al. *Am J Sports Med*, 41(3), 669-677, 2013.
8. Olbrantz, et al. *J Appl Biomech*, 34(1), 82-87, 2018.

ACKNOWLEDGEMENTS

The authors wish to thank Gundersen Medical Foundation for funding and Brenda and Terry Bricco and Erik Kernozek for assistance with portable force platform development.

INTERNAL KNEE JOINT ABDUCTION MOMENTS OF ACL RECONSTRUCTION PATIENTS DURING GAIT AND CYCLING USING OPENSIM

[1]Megan V. Pottinger, [2]Otto J. Schueckler, [1]Scott J. Hazelwood, and [1]Stephen M. Klisch

[1] California Polytechnic State University, San Luis Obispo, CA, USA
[2] Central Coast Orthopedic Medical Group, San Luis Obispo, CA, USA
email: sklisch@calpoly.edu

INTRODUCTION

Studies have found that patients who have undergone anterior cruciate ligament reconstruction (ACLR) have high incidence of knee osteoarthritis (OA) [1,2]. Knee joint contact forces and moments from Inverse Dynamics (ID) may be used to estimate cartilage tissue loads. Previous studies have used the external knee adduction/internal knee abduction moment (KAM) to estimate medial contact forces and have linked large peak values to rate of OA progression [1,3]. No studies have analyzed KAM in cycling, a well-known rehabilitation exercise for ACLR patients due to reduced knee contact loads [4].

The long-term goal of this study is to assess rehabilitation exercises for ACLR patients that maintain knee joint loading at safe levels and, thus, minimize the risk of OA development. The hypothesis was that peak KAMs are significantly lower during cycling than gait for ACLR patients. The aims were to: (1) conduct motion analysis experiments and perform ID (OpenSim, Stanford, CA, USA) analyses for gait and cycling, and (2) compare peak contact KAMs between gait and cycling at moderate and high resistances.

METHODS

Equipment. Kinematic data were captured using a 12-camera motion analysis system with Cortex software (Motion Analysis Corp., CA, USA). Kinetic data were collected using 4 force plates (Accugait, AMTI, MA, USA) for gait experiments, and a stationary bike (Lifecycle GX, Life Fitness, IL, USA) retrofitted with custom pedals containing 6-axis load cells (AMTI, MA, USA).

Experimental Study. Protocols were approved by Cal Poly's Human Subject Committee. Six female subjects (aged 18-45, BMI=23.4±1.7) underwent ACL anatomic single bundle reconstruction with an autograft by a board certified orthopedic surgeon (OJS), and were tested 9-31 months post-op. Kinematic data were tracked using 32 retroreflective markers placed on anatomical positions following an enhanced Helen Hayes marker set. Subjects performed 3 gait trials at self-selected walking speeds, and 3 cycling trials at 70 RPM with moderate (10) and high (15) machine resistance levels. A static trial was captured for reference knee angles and to perform scaling in OpenSim.

Data Analysis. Kinematic and kinetic data were processed in Cortex and filtered (4^{th} order Butterworth, cutoff frequency 6 Hz). Data were outputted and formatted using Matlab (MathWorks, MA, USA). In OpenSim, a musculoskeletal model was scaled to each subject [5]. Marker kinematics were used in the Inverse Kinematics (IK) tool to obtain kinematic data. Kinematic and kinetic data were used in the Residual Reduction Algorithm (RRA) to correct segment masses and optimize kinematics. Static Optimization (SO) was run to output a force file, which is then used to run Joint Reaction (JR) analysis. JR produced joint contact forces and internal moments which were normalized by body mass and height and trimmed to one full gait cycle (0% = 1^{st} heel strike, 100% = 2^{nd} heel strike), and one full crank revolution (0 deg. = 1^{st} top dead center, 360 deg. = 2^{nd} top dead center).

Statistics. Two-way repeated measures ANOVA and post-hoc Tukey tests were used to compare ACLR and contralateral peak KAMs between gait and cycling at both resistances. Significance was defined by $p < 0.05$

RESULTS AND DISCUSSION

Results showed a significant difference of peak contact KAMs between gait and cycling at either resistance (Fig. 1). Similar peak KAMs were found between the contralateral and ACLR knees during gait and cycling at either resistance.

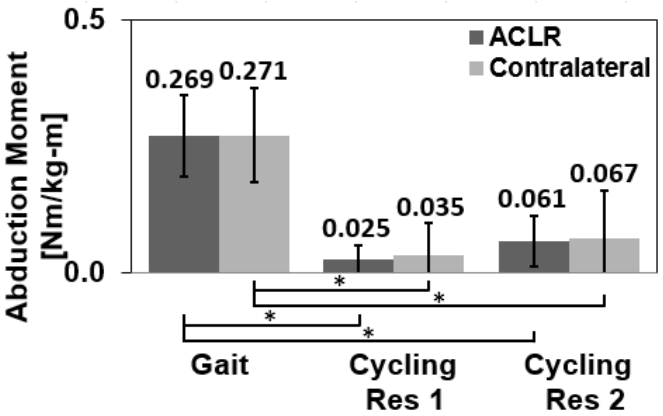

Figure 1: ACLR and contralateral peak contact knee abduction moments during gait, cycling resistance 1 (Res 1), and cycling resistance 2 (Res 2) (n=6). Mean ±1 S.D. shown. *=significant difference ($p<0.05$).

Studies have found OA to be most common in the medial compartment for ACLR patients [6]. This is likely due to altered biomechanics that increase loading on the medial compartment. KAM calculated in JR is an internal moment supported primarily by cartilage and ligaments and, thus, estimates medial to lateral cartilage loading. The reduced peak KAM found in cycling suggests reduced medial knee loading compared to gait, making cycling a preferred exercise for limiting OA development in ACLR patients.

CONCLUSIONS

Previous analyses found significantly lower tibiofemoral (TF) knee joint contact forces, as well as lack of posterior shear, in cycling compared to gait for ACLR patients [7]. Those findings provided evidence for cycling as a preferred exercise for ACLR patients due to the lack of strain on the ACL and minimized knee loading, which are beneficial for graft healing during rehabilitation.

Although no significant difference in peak contact KAMs were found between ACLR and contralateral knees, including additional subjects may lead to significant differences. Additionally, this study only included female subjects due to their higher incidence of ACL injuries [2]; thus, future studies should consider inclusion of male subjects.

The results from this and previous studies provide evidence of cycling being a preferred exercise for ACLR patients, because lower peak contact KAMs translate to lower medial cartilage loading which is preferable for those at risk for OA development. With no significant difference between ACLR and contralateral knees, these results suggest cycling is a preferred exercise for all populations at risk for OA development. Future analyses may include EMG-driven ID with muscle activation data to better estimate how muscle forces contribute to KAMs during various rehabilitation and fitness sustainment exercises.

REFERENCES

1. Butler RJ et al., *British Journal of Sports Medicine,* 43:366-370, 2009.
2. Lohmander LS et al., *Arthritis & Rheumatism,* 50:3145-3152, 2004.
3. Chang AH et al., *Osteoarthritis and Cartilage,* 23:1099-1106, 2015.
4. Neptune R et al., *Clinical Biomechanics,* 15:528–535, 2000.
5. Anderson F et al., *Journal of Biomechanical Engineering*, 123:381-390, 2001.
6. Barenius B et al*., The American Journal of Sports Medicine,* 42:1049-1057, 2014
7. Mavrommati K et al., *BMES Conference Transactions*, 2017.

ACKNOWLEDGEMENTS

Donald E. Bently Center, W.M. Keck Foundation, and the Defense Health Program through the DoD Broad Agency Announcement for Extramural Medical Research Program #W81XWH-BAA-14-1 under Award No. W81XWH-16-1-0051. Opinions, interpretations, conclusions, and recommendations are those of the authors.

SHEAR LAG IN A PARTIALLY FAILED IN FIBERWIRE SURGICAL SUTURE

Arz Y. Qwam Alden[1], Andrew G. Geeslin[2]; MD; Peter A. Gustafson, PhD [1,3]

[1]Western Michigan University, Department of Mechanical and Aerospace Engineering, Kalamazoo, MI, USA
[2]Borgess Orthopaedics, Kalamazoo, MI, USA
[3]Western Michigan University Homer Stryker M.D. School of Medicine, Kalamazoo MI, USA
email: arzyahyarzayy.qwamalden@wmich.edu, web: http://wmich.edu/

INTRODUCTION

The "shear-lag" phenomenon is frequently used to describe the interplay between axial and shear stress around fracture points or geometric discontinuities and provides ongoing load transfer after the initial compromise of a structure. Suture is a generic term for a class of thread-like materials used to bring severed body tissues together in aid of tissue healing. Suture fails for various reasons, e.g., mechanical trauma in use can result in a discontinuity in the suture material [1]. Several biomechanical studies have reported the importance of suture material on the strength of soft tissue repair [2]. However, it is difficult to fully describe the mechanics of the driving shear lag phenomenon using traditional tensile testing (neither in vivo nor ex vivo). Numerical simulation provides a useful tool to examine the governing mechanics of load transfer, but has not previously been applied to multifilament suture such as FiberWire surgical suture.

The study aims are: first, apply the finite element method to describe the shear lag phenomenon of suture failure by examining the distribution of normal and shear stresses along a partially failed FiberWire suture. Second, to describe the clinical implications of the shear-lag phenomenon.

METHODS

Braided non-absorbable suture materials No.2 FiberWire (Arthrex, Naples, FL) was tested to failure to obtain data for finite element model validation. Uniaxial tests were reported previously and were found to have a fail/reload/fail pattern where load was transferred between suture core and jacket via the shear lag mechanism [3].

Knowledge of the stress distribution at the failure site is essential for predicting the effects of the governing mechanics of load transfer. Therefore, Abaqus (Version 6-16) was used as the finite element solver in creating two models of the suture: (1) suture with an intact core and (2) suture with a broken core. The jacket and the core of the suture were created using reduced integration axisymmetric quadrilateral elements (CAX4R). The materials were assumed to be homogeneous and isotropic elastic. Displacement control was applied at 0.1 mm/sec on a reference point on one side of the suture model. All degrees of freedom were constrained on the opposing side.

RESULTS AND DISCUSSION

Mechanical properties and gross load to failure of the suture were determined experimentally and compared to published literature and were found to be consistent [3].

Cylindrical coordinates are used in reporting model results. The models show detailed stress and strain within the suture: the shear stress (in the core and the jacket) varies significantly over their cross-section and along the axis of the suture. The predicted stresses and strains occurred in locations that are qualitatively consistent with expectations based on shear lag theory. Fig. 1 provides an example of the results of the finite element models, a broken core.

Figs. 2 and 3 show the normal and shear stresses predicted by finite element models of the broken and intact core subjected to axial loading. At the broken core site, the models show that the core filament locally stops carrying the normal load and sheds it to the surrounding jacket via shear lag. Also, the load in the jacket surrounding the broken core builds via shear, and transfers that load across the broken site as normal stress. Subsequently, the load transfers back

to the core again via shear. Referring to Fig. 2, the normal stresses in the core approaches zero (limited by mesh convergence) at the fracture location. The stress distribution asymptotically approaches the intact suture stress distribution over a long distance. Normalizing axial position from the point of failure with respect to the total suture diameter (Z/D), the load transfer occurs over approximately Z/D = 35%. The jacket filaments carry the complete load despite complete failure of the core filament.

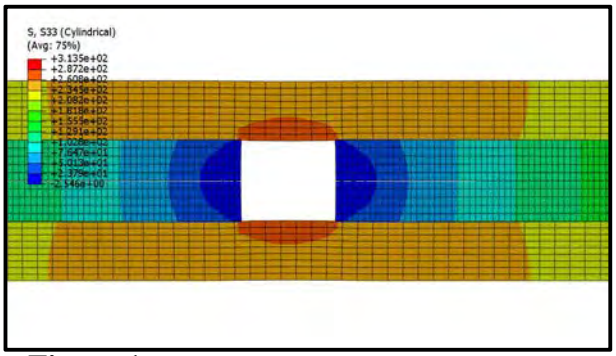

Figure 1: Normal stresses of the suture model, broken core

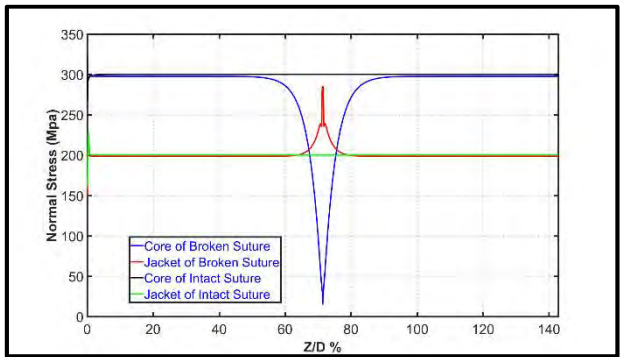

Figure 2: Normal stresses along the suture model

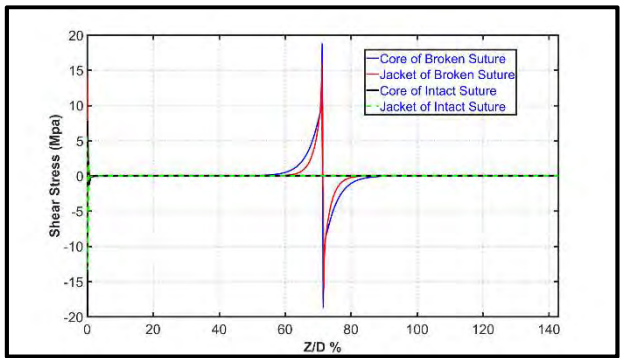

Figure 3: Shear stresses along the suture model

CONCLUSIONS

In this article, a finite element model to describe the shear lag phenomenon in surgical suture has been developed. It predicts the stress distribution and load transfer around the core fracture site. The finite element results are qualitatively consistent with existing shear lag theory and also with experimental results for the subject composite suture. Thus, the finite element model describes a biomechanical phenomenon by which failed suture can appear to be competent during a surgical procedure. Hence, a clinician should be aware of the possible failure mode and consider remedial actions when such failures are suspected.

ACKNOWLEDGEMENTS

This work was supported by The Higher Committee for Education Development in Iraq. Additional support was provided by: Western Michigan University College of Engineering and Applied Sciences and Homer Stryker M.D School of Medicine.

REFERENCES

[1] Surgical Knot Tying Manual, Third Edition.
[2] Rawson, S. D., et al., Biomech. Model. Mechanobiol., 14(1),123–33, 2015.
[3] Qwam Alden AY, et al., *ASME, Volume 3: Biomedical and Biotechnology Engineering*, 2017

EVIDENCE BEHIND ALTERNATIVE COMPUTER MOUSE DESIGNS: A SYSTEMATIC REVIEW OF CONTROLLED TRIALS

Ahmed Radwan[1], Tyler Kallasy[1], Abigail Monroe[1], Emily Chrisman[1], and Orrin Carpenter[1]

1: Physical Therapy Program, Utica College, New York, USA.

1600 burrstone road, Utica, NY, 13502

Email: aradwan@utica.edu

INTRODUCTION

Previous research has shown that the prolonged use of a standard computer mouse is associated with musculoskeletal symptoms. Many alternative designs may reduce this risk by optimizing posture, decreasing undesirable muscle activity and improving subjective response.

Purpose: To provide professionals with an in-depth analysis of the literature regarding the evidence behind computer mouse designs and their ability to reduce pain and discomfort in computer users

METHODS

Multiple data bases were searched by independent researchers to identify high quality controlled trials that evaluated the use of alternative and standard computer mouse designs. Databases searched were PubMed, Science direct, CINAHL, Google Scholar and specific ergonomics journals

The search was performed by four blinded researchers who were assigned specific search criteria by an independent, unbiased academic advisor. The text search terms were: computer mouse, pain, fatigue, discomfort, repetitive stress injuries (RSI). The criteria for inclusion in the review were as follows: Peer-reviewed, controlled-trial (CT) or randomized control-trial (RCT), English language (or translation), published within the last 10 years, and comparison of alternative and standard computer mouse designs with impact on pain/discomfort, biomechanics, productivity and psychological symptoms.

Each title and abstract was screened by two researchers. Disagreements regarding inclusion were rectified either by consensus or decision by an unbiased third party.

RESULTS AND DISCUSSION

Articles that met the inclusion criteria (18 total) were then evaluated for methodological quality using both the Cochrane Risk of Bias tool (ROB) and PEDro scale. Two reviewers independently assessed the quality of each study.

The ROB tool assesses 6 domains of bias including: selection, performance, detection, attrition, reporting and other with an assignment of high, low or unclear risk. All items of the ROB tool were scored yes, no or unclear (ie. insufficient information was available) and each item's scoring was compared between the two reviewers. According to current research, the ROB has been widely accepted and recommended for use in systematic reviews [1].

The PEDro uses 11 items to assess the external validity, internal validity and interpretability of studies in terms of allocation, randomization, key outcomes, blinding, intention to treat, and statistical comparisons. Using items 2-11, the sum of 'yes' responses creates a score of 0-10, with '0' representing the least amount of quality and '10' representing the most. This scale has been widely used among systematic reviews. Studies have shown that the PEDro has the ability to discriminate between higher- and lower-quality physical therapy research [2] [3].

In case of disagreement, consensus was reached during a meeting between the two

researchers. If disagreement persisted, a decision was made by an unbiased third party reviewer.

Evaluation of mouse efficiency included objective measures of muscle activities and range of motion and subjective measures of pain, discomfort, preference, and productivity. Alternative computer mouse designs such as biofeedback, roller-bar, slanted and vertical mice were effective in reducing muscle activity in comparison with the standard mouse. In terms of comfort and user preference, the standard mouse was still considered superior by most users.

CONCLUSIONS

Mild to moderate quality of evidence supported the use of alternative mouse designs to reduce neck/shoulder discomfort, promote a more neutral posture and decrease the amount of muscle activation within the neck and upper extremity. Ergonomic education will enhance the benefits of using alternative mouse designs.
Mouse selection should be an individualized process that is preceded by careful analysis of each individual's needs and occupational demands. Mild to moderate quality of evidence supported the use of alternative mouse designs to reduce physical and mental stress symptoms in most users especially if combine with appropriate ergonomic training

REFERENCES

1. Savovic, J., Weeks, L., Sterne, J., Turner, L., Altman, D., Moher, D., & Higgins, J. (2014). Evaluation of the Cochrane Collaborations tool for assessing the risk of bias in randomized trials: Focus groups, online survey, proposed recommendations and their implementation. Systematic Reviews, 3 (37). Doi: 10.1186/2046-4053-3-37Bach et al. *Plos One*. 10(3): e0118797, 2015.
2. Moher D, Liberati A, Tetzlaff J, Altman DG, The PRISMA Group (2009). Preferred Reporting Items for *S*ystematic Reviews and Meta-*A*nalyses: The PRISMA Statement. *PLoS Med* 6(7): e1000097. doi:10.1371/journal.pmed1000097.
3. Macedo LG, Elkins MR, Maher CG, Moseley AM, Herbert RD, & Sherrington C. (2010). There was evidence of convergent and construct validity of Physiotherapy Evidence Database quality scale for physiotherapy trials. *Journal Of Clinical Epidemiology, 63*(8),920-5.doi:10.1016/j.jclinepi.2009.10.005

ACKNOWLEDGEMENTS

Acknowledgments are optional.

PREDICTION OF FEMALE INJURY IN AUTOMOTIVE CRASH ENVIRONMENTS

[1] Carolyn W. Roberts, [1]Jason L. Forman, and [1]Jason R. Kerrigan

[1] Center for Applied Biomechanics, University of Virginia, Charlottesville, VA, USA

email: cwr2tn@virginia.edu, web: http://www.centerforappliedbiomechanics.org/

INTRODUCTION

The odds of a belt-restrained female occupant sustaining a serious to fatal injury are 47% higher than a belt-restrained male of the same age, height, and weight for a similar automotive crash [1]. While several studies have shown females have higher injury risk in the lower extremity, a recent study by Forman et al examined injury risk in different body regions, and demonstrated that total increased risk of female injury is primarily driven by an increased risk of injuries to the lower extremity [2, 3]. Development of injury prediction tools (crash test dummies and computation models) has historically focused on mid-sized males. Therefore, most of the available fundamental post-mortem human surrogate (PMHS) injury biomechanics data is male. As a result, efforts to predict injury risk for females have mostly relied on using dimensional analysis based scaling on data from male PMHS tests [4]. Despite the fact that scaling is the currently the primary methodology used to predict female injury, its accuracy has not been well validated with measured female data. The goal of this study to generate an injury dataset for female lower extremities that match previous male testing, and to use these matched datasets to perform an initial evaluation of the effectiveness of scaling in predicting female injury.

METHODS

Thirty-four small female PMHS (age= 64.5 ± 6.3 years, height= 159.4 ± 4 cm, weight= 48.3 ± 6.0 kg) lower extremities (matched pairs) were tested under three dynamic loading conditions: axial loading through the heel (n=14), and 2000 N axial preload (applied with a spring) in combination with inversion (n=10) or eversion loading (n=10). Half of the PMHS were tested with a shoe, the other half were barefoot. Only barefoot specimens were used in this scaling analysis. Joint ankle moments were calculated using data from: CT scans, implanted tibia and fibula load cells, footplate load cells, and tri-axis accelerometers and angular rate sensor arrays. Following testing, a combination of CT scans and dissections were performed to define injury location and type. Strain gages and acoustic sensors were affixed to the distal third of the tibia and fibula, and data from these sensors were used to determine time of injury. Axial load and inversion/eversion test configurations are depicted in Figure 1, below.

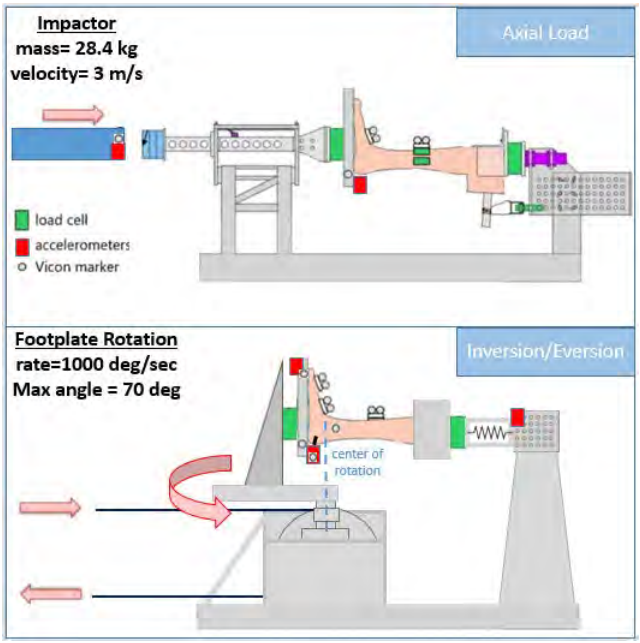

Figure 1: Axial loading through the heel test setup (top) and inversion/eversion test setup with 2000 N axial preload (bottom) are depicted above.

Axial force measured in the tibia for the axial loading tests, and the subtalar joint moment for the inversion and eversion tests were determined at the time of injury. The failure forces and moments determined for all subjects in this study, and any additional female tests in the literature with the same boundary conditions, were scaled to a 5th percentile female target anthropometry (mass: 49.12 kg, height: 149.86 cm) [5, 6]. This target anthropometry was selected

as because it is the most commonly used for female crash test dummies in vehicle crashworthiness evaluations. Scale factors were created from ratios of total mass and total standing height for each subject. This dimensional analysis scaling was also performed on data from matched male datasets [5, 6] also to predict the injury force and moment for the 5th percentile female anthropometry. The average scaled forces and moments at the time of injury and their standard deviations for both male and female datasets for axial loading, inversion, and eversion were calculated, and are reported in Table 1, below.

RESULTS AND DISCUSSION

Using scaled male data to predict the 5th percentile female response consistently overestimated the force and moment at failure (percent error between average response between 7.0% and 62.5%). For the examined test conditions, neither mass nor length based scaling of male data consistently produced a more accurate response; in fact, these two different scale factors resulted in different injury predictions when using male data (up to 22% difference). Conversely, scaled female data predicted similar average failure force and failure moment when comparing both length and mass based scaling factors (less than 9.6% difference between average failure force and moment). Scaling female data to a single anthropometry also resulted in decreased variance from the original measured female dataset, suggesting that the use of dimensional analysis based scaling is effective within same sex data for the examined test conditions.

CONCLUSIONS

This study has shown that scaling is ineffective in predicting female injury from male data for loading cases involving loading across the ankle joint. In order to better leverage the large volume of existing male data to predict female response, a deeper understanding of differences between the sexes (such as bony and cartilage geometry, material properties, and bone mineral density), and how these differences affect injury, is necessary to create a technique to predict female injury response from male data. As new prediction techniques are developed, the PMHS dataset described in this abstract provides necessary data to validate new methodologies and evaluate their accuracy to predict response across the sexes.

REFERENCES

1. Bose et al. *American Journal of Public Health,* **101 (12)**, 2011.
2. Ye et al. *Accident Analysis and Prevention*, **83**, 2015.
3. Forman et al. *Traffic Injury Prevention,* 2018.
4. Eppinger, Rolf. *International Conference on the Experimental Safety Vehicles*, 1976.
5. Funk et al. *Journal of Biomechanical Engineering*, **124.6**, 2002.
6. Funk et al. *Stapp Car Crash Journal*, **46**, 2002.

ACKNOWLEDGEMENTS

This work was supported by a grant from the National Highway Traffic Safety Administration (NHTSA), for which we thank them.

Table 1: Average tibia axial force or inversion/eversion moment at the subtalar joint and standard deviation at failure are reported for measured and scaled male (blue) and female (pink) PMHS data, (pink). All scaled data are scaled to 5th percentile female anthropometry values.

Dataset Info:	Axial Load Tests (N)	Inversion Tests (Nm)	Eversion Tests (Nm)
Female Dataset: measured	Fail Force = 3052.7 Standard Dev = 1356.6	Fail Moment = 58.3 Standard Dev = 25	Fail Moment = 46.8 Standard Dev = 18.7
Female Dataset: total mass scaling	Fail Force = 2886.9 Standard Dev=1007.0	Fail Moment = 45.3 Standard Dev=17.0	Fail Moment=40.1 Standard Dev=14.9
Female Dataset: standing height scaling	Fail Force = 2607.9 Standard Dev=1050.3	Fail Moment = 43.4 Standard Dev=17.2	Fail Moment=37.2 Standard Dev=14.3
Male Dataset: measured	Fail Force = 5873.3 Standard Dev = 296.5	Fail Moment = 81.3 Standard Dev = 25.2	Fail Moment = 194 Standard Dev = 44
Male Dataset: total mass scaling	Fail Force = 4690.3 Standard Dev=989.74	Fail Moment = 48.5 Standard Dev=21.4	Fail Moment = 56.23 Standard Dev=27.4
Male Dataset: standing height scaling	Fail Force = 3840.8 Standard Dev=641.0	Fail Moment = 49.5 Standard Dev=12.1	Fail Moment = 68.8 Standard Dev=46.0

WORK ENVELOPE IN NATIVE AND NON-NATIVE SIGNERS

[1,2] Gretchen Roman, [1] Daniel Peterson, and [3] Meghan E. Vidt

[1]Exercise Sciences and Health Promotion, Arizona State University, Phoenix, AZ, USA
[2]Physical Therapy, Midwestern University, Glendale, AZ, USA
[3]Biomedical Engineering, PM&R, Pennsylvania State University, University Park, PA, USA
email: garoman@asu.edu

INTRODUCTION

Previous literature [1,2] and anecdotal evidence supports a higher report of musculoskeletal (MSK) pain in non-native signers. However, the factors contributing to increased MSK pain in non-natives compared to natives have not been fully examined. Previous research has observed the work demands and style of interpreters [3] and identified work envelope as one of the 5 biomechanical considerations unique to sign language interpreters [4]. Work envelope is the area of optimal signing. A prior study revealed that interpreters with pain had more frequent lateral work envelope excursions per minute compared to interpreters without pain [3]. Despite recognition of the importance of work envelope on MSK injury risk, little work has quantified this metric for signers. The objective of this study was to quantify work envelope in natives and non-natives while signing, and compare outcomes with the Occupational Health and Safety for Sign Language Interpreters' recommended norms. We hypothesize the work envelope of natives will be within the recommended norm, while the work envelope of non-natives will be larger than the recommended norm; non-natives will also use a larger work envelope when compared to natives.

METHODS

Six participants (mean age 36.7±9.0yrs; mean height 1.72±0.06m; 2F/4M; 4 deaf/2 hearing; 1 left-/5 right-hand dominant) interpreted 3 trials of a 7min video source in sign language while standing. Participants were assigned to native and non-native groups based on whether they were born to hearing, non-signing parents (non-native), or deaf, signing parents (native). An 8 Kestrel camera motion capture system tracked the location of a surface marker on the dominant-side 2nd metacarpophalangeal (MCP) joint and Cortex software was used for post-processing (Motion Analysis, Santa Rosa, CA). A custom Matlab program (MathWorks, Natick, MA) was used to quantify the work envelope in three-dimensions (3D) by measuring linear motion (maximum – minimum marker location) along the x- (medial-lateral), y- (anterior-posterior), and z-axes (superior-inferior). Medial-lateral and superior-inferior measures were compared to norms of the Occupational Health and Safety for Sign Language Interpreters, which quantifies normal work envelope as a two-dimensional (2D) space, or a 25cm x 25cm area of hand movement in front of the body while signing in a seated position [4,5].

Group differences between natives and non-natives were evaluated using separate Mann Whitney U tests for work envelope along the x-, y-, and z-axes, 2D area (x-axis*z-axis), and 3D volume (x-axis*y-axis*z-axis). All analyses were performed using SPSS (v.24, IBM, Armonk, NY).

RESULTS AND DISCUSSION

No significant differences were observed between natives and non-natives for work envelope along the x-, y-, and z-axes (all $p=0.827$), 2D area ($p=0.827$), and 3D volume ($p=0.127$).

Mean measures for work envelope along x-, y-, and z-axes, 2D area, 3D volume, and %difference relative to the 25cm x 25cm norm were separately calculated (Table 1). Since overall excursion was greatest along the y-axis (non-natives=81.77cm, natives=83.43cm), a heightened concern now surrounds the potential impact of work envelope depth and breadth on MSK injury risk. Non-native signers had greater linear motion for work envelope along the x-axis (52.63cm), 2D area (1851.27cm^2), and 3D volume (152431.42cm^3), which was consistent with our hypothesis.

Qualitative assessment was performed by visualizing individual participants' usage of the 3D work

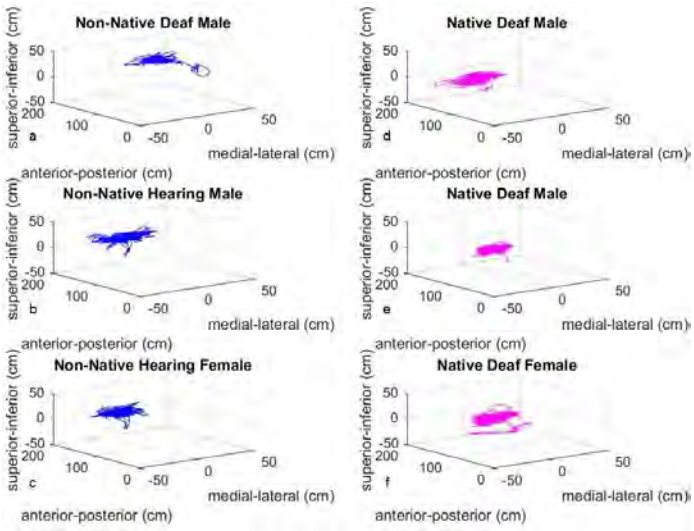

Figure 1: 3D plot of dominant-side 2nd MCP joint surface marker location for non-native (a-c) and native (d-f) participants.

envelope (Fig. 1). While native deaf male (Fig. 1e) was right-hand dominant, his motions were well-balanced along the x-axis. Versatility between dominant and non-dominant hands is a typical feature of a native signer [6]. Native deaf male (Fig. 1e) had the smallest work envelope (2D=1066.16cm^2, 3D=84923.59cm^3) and non-native hearing female (Fig. 1c) had the second smallest work envelope (2D=1238.34cm^2, 3D=97422.10cm^3). Native deaf female (Fig. 1f) had the greatest medial-lateral (60.87cm) and anterior-posterior (92.20cm) excursions with the largest 2D area (2283.01cm^2) and 3D volume (210491.49cm^3). Non-native deaf male (Fig 1a) was the only left-hand dominant signer. He had the greatest superior-inferior (40.32cm) excursion with the second largest 2D area (2246.08cm^2) and 3D (191078.53cm^3) volume. While mean height of non-natives (1.69m) was less than natives (1.75m), collectively, they used more superior regions of the work envelope (Fig. 2). A consistent pattern of work envelope size and dimension between natives and non-natives has yet to emerge, but ongoing analyses seek to explore the source of possible underpinning factors.

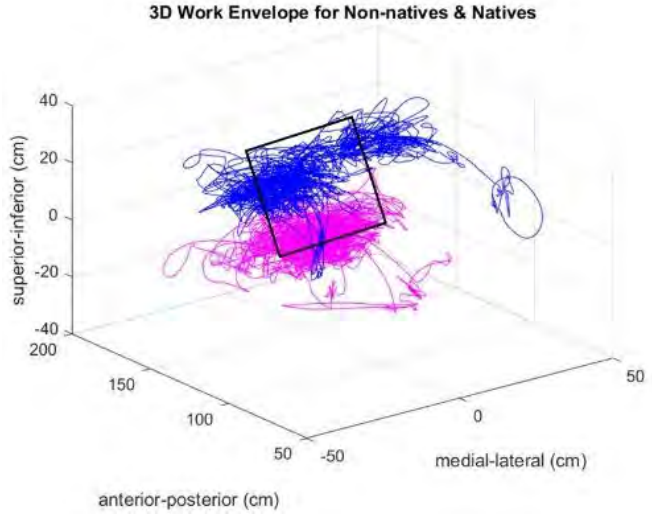

Figure 2: 3D plot of dominant-side 2nd MCP joint surface marker location for non-natives (blue) and natives (magenta) with 25cm x 25cm normal work envelope (black square).

CONCLUSIONS

No previous literature exists using motion capture to quantify the differences in 3D work envelope between natives and non-natives. The greater mean work envelope along the x-, z-axes and the greater mean 2D area compared to the norm suggests a change in work envelope when signing in a standing compared to a seated position. The area of optimal signing was based on work space specifications for seated work [7]. Results from this research will help to establish standing work envelope norms and inform how standing work envelope may relate to MSK injury risk in natives and non-native signers. Lack of significant findings between groups was likely due to the small sample size. Ongoing work will expand these results to include a larger sample of 25 participants, which will further inform the relationships between these variables.

REFERENCES

1) Podhorodecki, A.D. et al. *Arch Phys Med Rehab* 74(3): 261-2, 1993.
2) Roman, G. et al. E*rgonomics.* Manuscript in review, 2018.
3) Feuerstein, M. et al. *JOM.* 34(3):257-64, 1992.
4) Cumulative Trauma Disorder. Rochester, NY, USA:RIT, 2005.
5) Woodcock, K. et al. OHS for SLIs. Toronto, ON, Canada:RU, 2008.
6) Williamson, A. http://digitalcommons.wou.edu/theses/22, 2015.
7) Ayoub, M. *Hum Factors.* 15:265-68, 1973.

ACKNOWLEDGEMENTS

Funding for this project was provided by Arizona State University start-up funds (Vidt) and the Adopt-a-Doc Scholarship from the American Physical Therapy Association (Roman).

Table 1: Mean work envelope measures and % difference relative to the 25cm x 25cm norm for native and non-native groups.

	Envelope x-axis (cm)	Envelope y-axis (cm)	Envelope z-axis (cm)	2D area (cm^2)	3D volume (cm^3)
Non-native signers (n=3)	52.63, 111%	81.77	34.69, 39%	1851.27, 196%	152431.42
Native signers (n=3)	50.45, 102%	83.43	35.07, 40%	1801.88, 188%	152232.40

INTERVERTEBRAL DISC HERNIATION RISK DURING LOW-SPEED LATERAL COLLISIONS

[1] Stephanie Rossman, [1] David Sproule, [1] Keith Button, [1] Brian Weaver, [1] Steve Rundell

[1] Explico Engineering, Novi, MI, USA
email: srossman@explico.com, web: www.explico.com

INTRODUCTION

Intervertebral disc herniations account for a major portion of spine-related surgeries. Although temporal consistency between symptomology and a relatively minor automobile collision is a common factor for establishing causation, this may yield a false-negative diagnosis given the prevalence of disc herniations in the asymptomatic population [1]. Several biomechanical studies have previously documented the biomechanical environment associated with disc herniations [2,3]. These studies definitively demonstrate that axial compressive loading is essential in the causation of, or significant contribution to, a disc herniation. Therefore, the objective of the current study was to evaluate the potential for intervertebral disc herniation during lateral collisions by specifically evaluating spinal compression. We hypothesized that low-speed lateral collisions generate minimal spinal compression, and are therefore not associated with intervertebral disc herniations.

METHODS

Low-speed lateral sled tests have previously been performed for belted, far-side volunteers and anthropomorphic test devices [4]. Articulated Total Body (ATB) was utilized to simulate the published lateral sled tests. Two collision pulses matching the previous tests were applied in the simulations. The first collision pulse was characterized by a peak acceleration of 4 g and a velocity change (delta-V) of 6 kph, and the second collision pulse had a peak acceleration of 4 g and a delta-V of 10 kph. Both pulses were simulated in ATB for two male volunteers, one female volunteer, and a 50th percentile male Hybrid III dummy (Table 1).

Each of the volunteers and the ATD was represented by a series of ellipsoids linked together with joints scaled to each respective height and weight. The models were placed in a seat modeled using a series of contact planes, and were belted using a three-point harness belt. Lateral head displacement and cervical and lumbar loads were evaluated for each test condition.

RESULTS AND DISCUSSION

ATB generally predicted early-phase occupant kinematics for all occupants and restraint configurations. During late-phase of occupant motions (after 200 msec) ATB grossly over predicted the motion.

Results of the ATB simulations for volunteer 1 and volunteer 2 for each pulse are shown in Figure 1 and Figure 2. During the 6 kph and 10 kph pulses, peak cervical compression occurred during the early-phase motion and averaged 76 ± 27 N and 86 ± 30 N, respectively, for all volunteers. During the early-phase motion, compression in the lumbar spine was negligible. At the onset of the collision pulse, the peak lumbar compression for all volunteers was 285 ± 67 N and 283 ± 66 N, respectively, consistent with a neutral seated position.

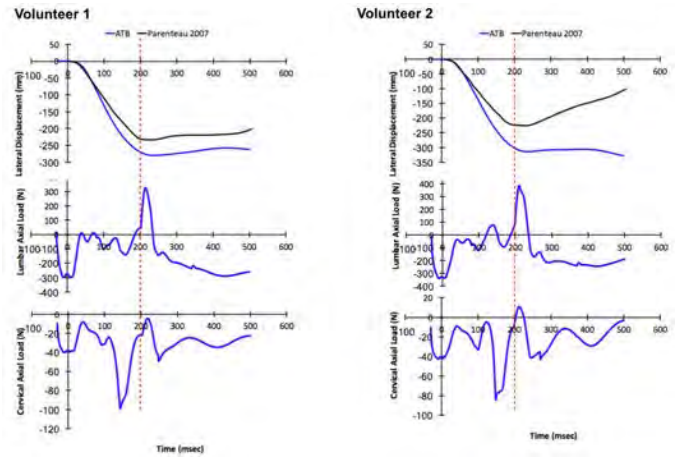

Figure 1: ATB results for volunteer 1 and 2 for pulse 1 (peak of 4g, delta-V of 6 kph) for lateral head displacement and cervical and lumbar axial loads.

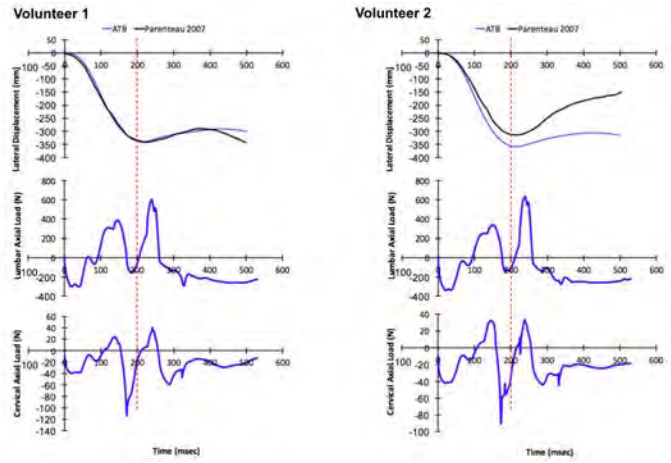

Figure 2: ATB results for volunteer 1 and 2 for pulse 2 (peak of 4g, delta-V of 10 kph) for lateral head displacement and cervical and lumbar axial loads.

The compression in the spine during the ATB simulation was consistent with results obtained from previously conducted lateral impacts with volunteers [5]. Results of the current study indicate that low-speed lateral collisions do not generate a biomechanical environment consistent with what has been shown to cause intervertebral disc herniations. Specifically, the compression experienced by the spine during these events was less than simple physical activity, such as sitting quickly in a chair, and significantly less than injury assessment reference values.

REFERENCES

[1] Matsumoto M, Fujimura Y, Suzuki N, Nishi Y, Nakamura M, Yabe Y, et al. *MRI of cervical intervertebral discs in asymptomatic subjects*. J Bone Joint Surg Br 1998;80:19–24. doi:10.1097/BRS.0b013e3181c17067.

[2] Adams MA, Hutton WC. *Gradual disc prolapse*. Spine (Phila Pa 1976) 1985;10:524–31.

[3] Adams MA, Hutton WC. *The mechanics of prolapsed intervertebral disc.* Int Orthop 1982;6:249–53.

[4] Parenteau C. *Far-side occupant kinematics in low speed lateral sled.* Traffic Inj Prev 2006;7:164–70. doi:10.1080/15389580500482005.

[5] Mkandawire C, Mazzucco D, Vijayakumar V, Scher I, Heller M, Morrison H. *Head Kinematics and Upper Neck Loading during Simulated Low-Speed Lateral Impact Collisions.* Int Fed Automot Eng Soc 2006;Paper # F2.

Table 1: All ellipsoid human models were scaled to the anthropometrics of the volunteers [4].

	Sex	Height (cm)	Weight (kg)	Age (years)
Volunteer 1	Male	175	72	32
Volunteer 2	Male	183	78	31
Volunteer 3	Female	158	48	25
HBM 50th-male	-	174	75.5	-

BIOMECHANICAL INDICATORS OF MOVEMENT DISORDERS IN PARKINSONS DISEASE

[1]Serge H. Roy, [1]Bhawna Shiwani, [1]Joshua C. Kline, [2]Marie Saint-Hilaire, [2]Cathi A. Thomas, Raveena H. Ravi[1] and Gianluca De Luca [1]Delsys, Inc and Altec, Inc, Natick, USA
[2]Department of Neurology, Boston University Medical School, Boston, USA
email: sroy@delsys.com, web: http://www.delsys.com/altec/

INTRODUCTION

Parkinson's disease (PD) is associated with a complex progression of involuntary movements that vary throughout the day in response to dopamine replacement medication and physical activity. The significant inter- and intra-patient variability of these motor fluctuations requires an autonomous monitoring capability with sufficient temporal resolution to guide therapeutic interventions for effective management. Unlike current rater-dependent assessments that use self-report motor diaries in the home in conjunction with standardized motor scales in the clinic, wearable sensor-based technologies offer numerous possibilities for objective, remote, and continuous monitoring of the health and quality of human movement. A key challenge in developing a sensor-based approach to autonomous detection of PD movement disorders is the ability to quantify and accurately track biomechanical indicators of movement disorders in the context of changing daily activities. In this work, we developed an autonomous activity-dependent system for detecting body bradykinesia, tremor, and dyskinesia in PD patients by monitoring sensor-based metrics that are capable of quantifying the symptomatic state of each movement disorder throughout unscripted activities of daily living.

METHODS

Patients (n=29, 17 male, 12 female, mean age 60.8 ±11) with mild to moderate Parkinson's disease (Hoehn and Yahr 1-3; mean duration = 6.5 years) presenting a range of PD motor symptoms that included body bradykinesia, tremor, and dyskinesia participated in experiments involving a 2-3 hour period of unscripted activities of daily living in a home-like setting. Trigno™ IM wireless sensors (Delsys, Inc. Natick, USA) were placed on the extensor digitorium longus (EDL) muscle of the forearm and on the tibialis anterior (TA) muscle of the leg to record inertial measurements (IMUs) and surface electromyographic (sEMG) data for quantifying changes in movement characteristics throughout the session. Video recordings of the experiments were annotated offline by movement disorder experts to provide a truth file of different activity states (i.e. sitting, standing, walking, etc) and movement disorder symptoms based on UPDRS [1] guidelines.

We designed algorithms to automatically detect different activity states and classify the manifestations of different movement disorders based on biomechanical indicators of impairments in human movement. The activity classifier consisted of a single-hidden layer feedforward neural network trained using feature vectors incorporating different activity subclasses under the presence and absence of each motor symptom of PD. For each activity state, separate multilayered feed-forward Dynamic Neural Networks (DNNs) were developed to track the presence and absence of PD movement disorders. Changes in severity for each disorder were informed by the temporal changes in biomechanical indicators of each motor symptom.

RESULTS AND DISCUSSION

An example of the outcomes achievable using this approach are summarized in Figure 1 for body bradykinesia, one of the three movement disorders monitored in this study. Our algorithms were able to automatically detect walking and non-walking activity states with an accuracy of 99.5% and track changes in the manifestations of bradykinesia specific to each activity with an average accuracy of 94.6% using a set of biomechanical metrics that directly captured UPDRS-based motor symptoms. The biomechanical indicators included reduced directional magnitude of arm and leg swing for walking activities and poverty (duration) of

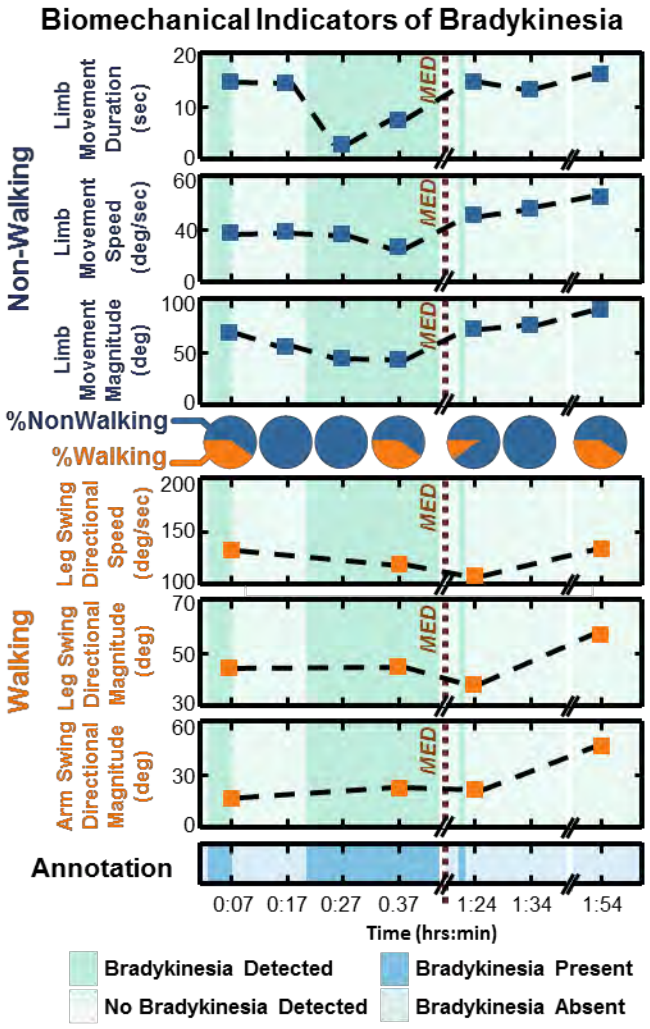

Figure 1: Results of autonomous body bradykinesia detection for one PD subjects taken before and after dopamine replacement medication ("MED").

movement as well as reduced speed and magnitude of limb movement for non-walking activities. When we tracked changes in the movement biomechanics during dopamine replacement treatment, we observed two major outcomes of our system:

1) the algorithms were able to track changes in the presence and absence of body bradykinesia (dark and light green areas, respectively) that are in agreement with presence and absence classifications from video annotations (dark and light blue areas, respectively) from movement disorder experts,

2) the biomechanical metrics we quantified were able to indicate the degree of improvement in PD motor symptoms after administration of the medication dose ("MED").

CONCLUSIONS

Our system provide an activity-dependent approach for detecting movement disorders in PD and monitoring their severity based on biomechanical indicators of motor impairments extracted from data recorded using a single sEMG/IMU hybrid sensor per symptomatic limb. When integrated with algorithms under development for detecting tremor and dyskinesia, the complete wearable system will provide continuous tracking of accurate and clinically relevant metrics of PD symptoms. This information is crucial for healthcare providers to better manage medication titration, adjust DBS settings, and establish efficacy for new interventions undergoing clinical trials.

REFERENCES

1. Goetz CG, *Mov Disord* **22(1)**:41–47, 2007.

ACKNOWLEDGEMENTS

Research reported in this abstract was supported in part by the De Luca Foundation and by a grant from the National Institute of Neurological Disorders and Stroke (NINDS) of the National Institutes of Health under award R44NS083098.

SPATIAL DIFFERENCES IN NERVE MECHANICAL PROPERTIES USING SHEAR WAVE ELASTOGRAPHY

Chelsea L. Rugel[1], Collin K. Franz[2], and Sabrina S.M. Lee[1]

[1]Northwestern University, Chicago, IL, USA
[2]Shirley Ryan Ability Lab, Chicago, IL, USA
Email: chelsearugel2022@u.northwestern.edu

INTRODUCTION

Peripheral neuropathy is a very common group of conditions that are characterized by damage to peripheral nerves. It affects approximately three million Americans annually [1]. However, despite its prevalence, it remains difficult to determine the extent of nerve damage, as well as monitor for the efficacy of treatments, due to the challenge of assessing nerve function *in vivo.*

Measurements of architecture (e.g. cross-sectional area (CSA)) and structure (e.g. connective tissue and axon number) are frequently studied and can correlate with *in vivo* measures of nerve function, but this is not always the case [2]. Additionally, measures of structure are invasive and typically require biopsies. Other aspects of nerves, such as mechanical properties, have been less frequently studied, and thus, their relationship to nerve function remains largely unknown. It is likely that mechanical properties, such as stiffness, could indicate salient changes in connective tissue or loss of axons and therefore, could be a correlative measure of nerve function.

Shear wave (SW) ultrasound elastography is a non-invasive *in vivo* technique that induces and measures SW velocity [3] from which tissue stiffness can be inferred. Our preliminary data from patients who received nerve reconstruction revealed that SW velocity was higher distal to the nerve injury site compared to the proximal site. This suggested that increased connective tissue or loss of axons in the distal nerve could be related to the increased stiffness. Although these preliminary data demonstrate the potential of relating mechanical properties and function, examination of mechanical properties, as measured using SW ultrasound elastography, of upper extremity nerves is needed. Previous studies of nerve SW velocity (median [4], tibial [5], sciatic [6]) only report measures at one location. As the long-term goal is to use mechanical properties as a clinical assessment, the first step was to identify spatial differences in the stiffness of three healthy nerves: median (MN), radial (RN), and ulnar (UN), by examining them at proximal and distal locations along the upper extremity. Nerve CSA and thickness were examined to assess the relationship between stiffness and architectural properties.

METHODS

Twelve subjects participated in this study (7 males and 5 females; mean ± std, age: 27.09 ± 4.46 yrs; mass: 68.25 ± 10.69 kg; height: 1.76 ± 0.07 m). Participants were in a supine position with their dominant arm relaxed. Arm positions for each nerve were based on standard clinical tests (MN: elbow at 180°, whole arm supinated; RN: elbow at 180°, whole arm pronated; UN: elbow at 90°, whole arm supinated). Wrist was at neutral flexion/extension for all positions.

Nerves were imaged (shear wave ultrasound: Aixplorer, SuperSonic Imagine, Aix en Provence, France; linear transducer array, 4–15 MHz, SuperLinear 15–4, Vermon, France) longitudinally at two locations: proximal (lower third of upper arm) and distal (middle third of forearm). A custom-written software (Matlab, Mathworks, Natick, USA), was used to process and analyze the SW velocity data. The mean SW velocity value was calculated from a manually cropped region of interest (ROI) containing only the area of the nerve. Thickness and CSA of the nerve were measured from B-mode ultrasound images.

Student's paired t-tests were conducted to compare the SW velocity, CSA, and thickness of each nerve

between proximal and distal locations. A two-way analysis of variance was used to compare the SW velocity of the three examined nerves. Regression analyses were conducted to evaluate correlations between nerve SW velocity, CSA, and thickness.

RESULTS AND DISCUSSION

Our main finding was that in each of the examined nerves, SW velocity was at least 20% greater at distal locations than proximal locations (all $p<0.05$; MN: 20.5%, RN: 27.5%, UN: 36.0%; Figs. 1 and 2). Additionally, SW velocity between the three nerves was significantly different ($p=0.003$). SW velocity of the distal MN was similar to those reported at the wrist in previous studies [4]. This has implications for interpreting measures made in patients with nerve reconstruction, as single location measurements could lead to inaccurate assessments.

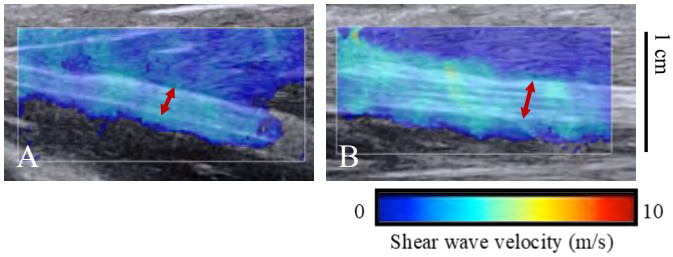

Figure 1: Shear wave ultrasound images of the radial nerve, longitudinally at proximal (A) and distal (B) locations. Red arrows indicate nerve.

We found no difference in nerve thickness between distal and proximal locations (Table 1), and CSA was only significantly different between distal and proximal locations for the MN (distal: 9.00±1.75mm^2, proximal: 7.21±1.81mm^2; $p=0.008$). There were also no significant correlations between nerve CSA or thickness and SW velocity (all $R^2<0.4$). These findings indicate that although SW velocity, and therefore stiffness, is greater in distal locations compared to proximal locations, this difference is not due to macroscopic nerve properties such as CSA. It is possible that this difference in stiffness is related to changes in more microscopic properties such as nerve structure (e.g. ratio of axon number to collagen density).

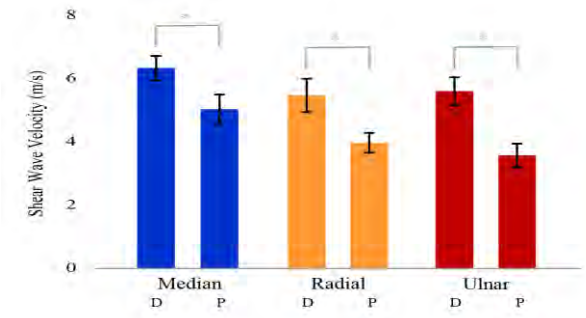

Figure 2: Shear wave velocity of nerves at distal (D) and proximal (P) locations.

CONCLUSIONS

These results demonstrate that nerves have spatial differences in mechanical properties, as measured with SW velocity. Specifically, these measures suggest greater stiffness distally along the upper extremity. These differences in SW velocity do not appear to be related to differences in nerve architectural properties such as CSA or thickness. Although this work demonstrates the feasibility of SW ultrasound to quantify mechanical properties of nerve, further investigation on why spatial differences occur is needed.

REFERENCES

1. Watson & Dyck. *Mayo Clin Proc,* 90(7): 940-951, 2015.
2. Logician et al. *Muscle Nerve,* 17(9): 1010-1020, 1994.
3. Bercoff et al. *IEEE Trans Ultrason Ferroelectr Freq Control,* 51(4), 396-409, 2004.
4. Kantarci et al. *Eur Radiol,* 24(2):434-440, 2014
5. Dikici et al. *Radiology,* 282(2): 494-501, 2017
6. Andrade et al. *J Biomech,* 49(3): 326-331, 2016

Table 1: Mean and standard deviation of cross-sectional area (CSA) and thickness of nerves.

	Median nerve	P value	Radial nerve	P value	Ulnar nerve	P value
Distal CSA (mm^2)	9.00±1.75	**0.008**	8.79±2.69	0.605	8.00±1.67	0.220
Proximal CSA (mm^2)	7.21±1.81		7.80±1.75		7.36±1.70	
Distal thickness (mm)	2.58±0.24	0.118	2.20±0.49	0.384	2.21±0.31	0.445
Proximal thickness (mm)	2.32±0.46		2.04±0.43		2.14±0.34	

THE EFFECT OF EXCISING A SUPRA-SCAPULAR SPINE LIPOMA ON SCAPULAR KINEMATICS

Peter J. Rundquist, Whitney Markson, Amanda Nosbush, Alexandra Zuleger, and Sanjay Sarkar

Concordia University, St. Paul, MN, USA
email: rundquist@csp.edu
web: http:// http://www.csp.edu/academic-programs/doctor-of-physical-therapy-program/

INTRODUCTION

Lipomas, encapsulated fat nodules consisting of mature adipose cells, are the most common type of benign connective tissue tumor. They occur in adults over 39 years old and increase in size over time. Locations include abdomen, arms, neck, and thighs. They are the most frequently observed shoulder tumors [1-3].

Lipomas are typically painless. However, they have been implicated in the etiology of periscapular muscle and nerve dysfunction [3-5].

The purpose of this case study was to determine the effect of a periscapular lipoma on scapulothoracic kinematics. Due to the location of the lipoma, an increase in scapular upward rotation was hypothesized.

METHODS

The participant was a 52 year old male with a 3 year history of progressive periscapular pain originating at the supero-medial aspect of the spine of the scapula which radiated proximally to the occiput, laterally along the spine of the scapula, and distally along the vertebral border of the scapula. The participant noted an increase in discomfort and perceived size of the mass over the 6 months prior to initial data collection. A general surgeon excised the 3 x 1.5 cm mass which was sent to pathology. The diagnosis of lipoma was confirmed.

The Concordia University, St. Paul IRB approved this case study.

The participant completed two sessions of data collection. The first session was completed 3 days prior to the surgical excision of the lipoma. The second session was completed 6 weeks afterward. This was to allow the participant to heal from the procedure.

Before each data collection session, the patient went through objective data collection including cervical range of motion, shoulder range of motion and manual muscle testing, and shoulder impingement tests. Prior to the excision, there was approximately a 25% limitation in cervical left side bending and some discomfort in cervical left rotation. All humerus to trunk ranges of motion were normal. Manual muscle testing was 5/5 throughout with the exception of external rotation which was 4/5 with pain. The impingement tests were negative. After the excision and healing time, the participant demonstrated full cervical and shoulder range of motion. Subject reported minimal pain with left cervical side bending. Shoulder MMT was 5/5 bilaterally. Both impingement tests were negative.

At both data collection sessions, scapulothoracic kinematics during flexion, scapular plane abduction, and abduction were collected using the Polhemus G4 3-D electromagnetic motion capture system (Colchester, VT). Three repetitions of each motion were collected during each session. Changes in ST upward rotation, internal rotation, and posterior tilting were calculated between 30 and 90 degrees of elevation in each plane.

RESULTS AND DISCUSSION

The participant demonstrated more ST UR, more ST IR, and less ST PT 6 weeks post-lipoma excision than he demonstrated 3 days prior to the excision.

Scapulothoracic upward rotation demonstrated the largest amount of increase between sessions. During abduction there was a 4.5 degree increase. During flexion, there was a 10 degree increase. During scapular plane abduction, there was a 9.5 degree increase. Table 1 outlines all of the data.

This case study revealed the effects a lipoma can have on scapulothoracic kinematics. The participant reported decreased symptoms during range of motion and strength screening post-surgery, and only reported experiencing tightness at the end range of left side bending of the cervical spine. Moreover, the patient demonstrated increased motion in scapulothoracic kinematics in flexion, scapular plane abduction, and abduction after surgical excision of the supra-scapular spine lipoma. These findings support the implications that a lipoma has a role in the etiology of periscapular muscle dysfunction.

CONCLUSIONS

Scapular upward during elevation in the coronal and scapular planes demonstrated the largest change between pre- and post-op scapulothoracic kinematics. These greater than 9 degree changes may lead to the shoulder dysfunctions associated with lipomas in the literature. Addressing the altered may alleviate the symptoms patients with periscapular lipomas present with.

REFERENCES

1. Sitartz et al. Lipomas – A health condition that cannot be ignored. *Family Medicine and Primary Care*. 18(4):473-476, 2016.
2. Beggs, I. *Musculoskeletal Ultrasound* (1st ed.). Wolters Kluwer/ Lippincott Williams & Wilkins Health, 2014.
3. Lenza et al. Subdeltoid lipoma causing shoulder impingement syndrome – a case report. *Einstein (Sao Paulo)*. 12(3):351-4, 2014.
4. Hazrati et al. Suprascapular nerve impingement secondary to a lipoma. *Clinical Orthopedics and Related Research*. 411:124-8, 2003.
5. Murray and Pelet. Subacromial impingement syndrome caused by a voluminous subdeltoid lipoma. *Case Reports in Orthopedics*. 2014(3), 2014.

Table 1: Scapulothoracic Range of Motion During Humerus to Trunk Elevation.

ST Motion	Abduction 30-90°			Flexion 30-90°			Scapular Plane 30-90°		
	Pre	Post	Change	Pre	Post	Change	Pre	Post	Change
Upward Rotation	19.6	24.1	4.5	15.8	25.8	10	18.2	27.7	9.5
Internal Rotation	-8	-5.3	2.7	7.9	9.1	1.2	0	.7	.7
Posterior Tilt	19.3	10.7	-8.5	12.5	4.2	-8.3	14.6	4.2	-10.3

DEVELOPMENT OF LOW COST 3D PRINTED ANATOMICAL MODELS FOR PRE-SURGICAL PLANNING

David Salazar[1], Drew Dudley[1], James Pierce[1], Keaton Young[1], Justin Cramer[2], Trevor Huff[3], Gabe Linke[4], Jorge Zuniga[1]
[1]Department of Biomechanics, University of Nebraska at Omaha, Omaha, NE USA
[2]Department of Radiology, University of Nebraska Medical Center, Omaha, NE USA
[3]Creighton University, Omaha, NE USA
[4]Children's Hospital, Omaha, NE USA
email: dsalazar@unomaha.edu

INTRODUCTION

Three-dimensional (3D) printing is a process of making a 3D solid object of virtually any shape from a digital model. 3D printing is achieved using an additive process, in which successive layers of material, such as plastic, are laid down in different arrangements. Previous investigations have demonstrated the feasibility and utility of 3D printing in a wide range of subspecialties of medicine, such as the development of low-cost 3D prostheses [1]. Modeling and printing techniques have also been used in the development of various anatomical structures such as organs and skeletal structures [2].

The goal of this research is to develop a methodology explaining how to create low-cost anatomical models for pre-surgical planning of highly complex surgeries. This low-cost production has a high potential impact in underserved medical populations, especially those with less access to resources and advanced technologies. Additionally, the anatomical models developed in the processes will be shown to licensed radiologists and surgeons to assess the potential benefit of using these tools to help improve surgical methods.

METHODS

In order to produce the models, a 3D representation of the structure must be created with a specified software, and then printed by a 3D printer. Unidentified computed tomography (CT) imaging data of an unidentified participant was converted to 3D printing specific stereolithography (STL) files using specified software. Then, the STL files were processed for a specific printer before being 3D printed (see Figure 1). To compare the different model possibilities, structures were prepared by 2 different types of software (industrial and open-source), and 3 different types of printers (high-end, intermediate level, and low-cost). Models were produced using each type of software and each type of printer, resulting in 6 total models of the same anatomical structure.

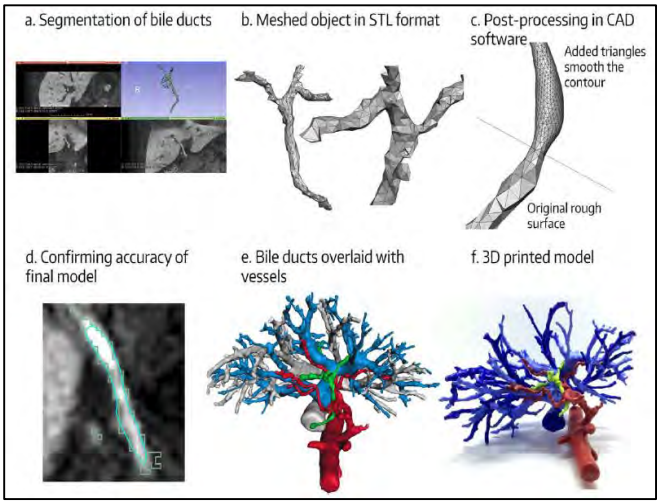

Figure 1: 3D printing workflow example. A) Segmentation process, B) STL file creation, C) Triangulation and smoothing techniques, D) visual inspection of the slicing process, E) virtual CAD model, and F) Final 3D printed model [2].

The proprietary software used to develop the model files was the Mimics program (Materialise Interactive Medical Image Control System; Materialise, Leuven, Belgium: $32,000 per year), and the open-source software used was the 3DSlicer program (Brigham and Women's Hospital, Boston, MA: free).

Various quality printers and materials ranging from high-end, intermediate level, and low-cost were used to produce the models for accurate comparison. The high-end professional 3D printer used was the

OBJET260 Connex3 (Stratasys, Inc. Eden Prairie, MN; cost $158,900.00). The intermediate level 3D printer used was the uPrint SE Plus (Stratasys, Inc. Eden Prairie, MN; cost $26,934). The low-cost 3D printer used was the Ultimaker 2 extended (Ultimaker B.V., Geldermalsen, The Netherlands; cost $ $2,999). In addition, different materials were used for the manufacturing process, such as resin base materials (high-end professional 3D printing material $530, per pack of 3.6 kg), Acrylonitrile Butadiene Styrene (ABS; intermediate level 3D printing material $50 per pack of 1 kg), and Polylactic acid (PLA; low-cost 3D printing material $20 per 1 pack of 1 kg).

Once all the 3D models were produced, they were presented to a licensed radiologist in a single-blind study for accuracy of representation of the region of interest, overall quality, and potential usefulness in the operating room.

RESULTS AND DISCUSSION

Using the various printer and software types, we were able to significantly reduce production cost of these unique structures. Our methodology of using low-cost printers in combination with open-source software rather than high-end printers and proprietary software resulted in a significant cost reduction from $30,000 to $1,000. The cost estimations are rough approximations of the software, equipment, and material costs for a single model.

In a blind preliminary analysis of the 3D printed models, a licensed radiologist was asked to review all of the models at once and rank which he felt to be a “better representation of the region of interest”. His observation found that the models printed by the free open-source 3DSlicer software were preferred to those prepared by the proprietary (Mimics) software.

One pitfall of the initial examination of the models was that all of the structures were presented at the same time. In future examinations, the anatomical models will be shown individually but in a randomized order, and then scored independently. This will help to prevent any bias based on seeing models side by side.

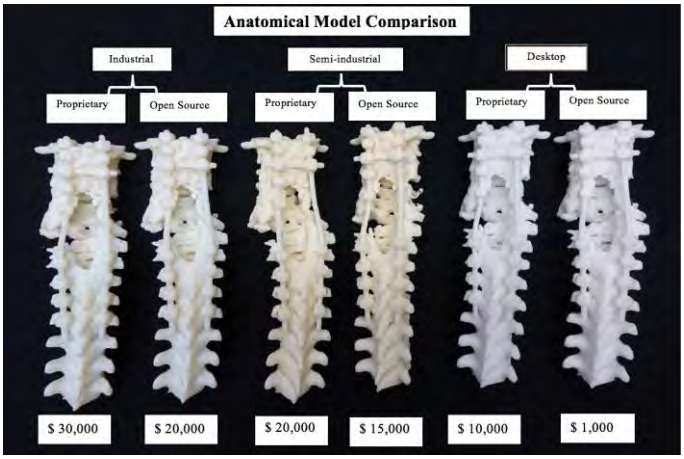

Figure *2*: Low-cost methodology for the development of anatomical models for pre-surgical planning. From left to right: Anatomical models of a section of the spine using proprietary versus open source software and industrial 3D printers, semi-industrial, and desktop (low-cost) 3D printers. Engineering time not included in pricing.

ANTICIPATED RESULTS

For future evaluations, a clinical team including radiologists and surgeons will validate, evaluate, and compare the anatomical models against original clinical imaging data. Models will be produced as similar to one another as possible to prevent software differentiations. Each anatomical model will be scored in terms of preference of use in the operating room, effect on surgery time, and a number of other different parameters based on previously developed surveys [3].

In the blind preliminary analysis, the licensed radiologist expressed that the open-source software produced a more accurate model, which could be a potential indicator that the low-cost development is not only useful for surgical planning, but also as good as or even superior to the proprietary software.

REFERENCES

1. Zuniga JM, Carson AM, Peck JM, Kalina T, Srivastava RM, Peck K. Prosthetics and Orthotics International. Apr 2016.
2. Ripley B, Levin D, Kelil T, et al. Journal of Magnetic Resonance Imaging: JMRI. Nov 2016
3. Bagaria V, Chaudhary K. Injury. Aug 2017

FINGER EXTENSOR MUSCLE STIFFNESS PREDICTS CLINICAL ASSESSMENT OF EXTENSOR WEAKNESS

[1]Nathan D. Schilaty, [2]Filippo Savoldi, [2]Zahra Nasr, [2]Adriana M. Delgado,
[1]Lawrence J. Berglund, and [2]Brian G. Weinshenker

[1]Mayo Clinic Biomechanics Laboratories & Sports Medicine Center, Rochester & Minneapolis, MN, USA
[2]Mayo Clinic Department of Neurology, Rochester, MN
Email: schilaty.nathan@mayo.edu

INTRODUCTION

In 1987, O'Neill et al. reported a patient with multiple sclerosis (MS) who experienced rapid reversible deterioration in gait and an increase in the degree of pyramidal weakness of the lower limbs with neck flexion; this phenomenon was so prominent that affected patients had to hyperextend their necks in order to walk. [1] This manifestation was named McArdle's sign (McS) after M.J. McArdle who recognized this sign. [1] This sign has since been largely overlooked. The mechanism of the sign is also poorly understood. McS may have potential diagnostic value, especially in challenging cases of myelopathy, and possibly even therapeutic implications as an indicator of mechanically-induced conduction block, and thereby a reflection of the presence of spinal cord demyelination.

The aim of this study was to evaluate the presence of McS clinically and to quantify McS with a device that precisely measured muscle stiffness in a cohort of patients chosen because they had detectable finger extension weakness, a sensitive and easily testable muscle group; patients enrolled were classified by diagnosis: MS, other myelopathies and peripheral neuropathies. Additionally, 19 healthy controls were tested. We hypothesized that muscle stiffness would accurately predict clinically diagnosed weakness.

METHODS

Informed consent was obtained from all study participants (n=74; 18M:56F). McS is detectable in muscle groups sensitive to upper motor neuron lesions. We specifically evaluated finger extensor strength (extensor digitorum) since it is both a sensitive and convenient indicator of McS. Clinical McS was rated by a clinician with head in extension and flexion positions. McS was graded 0-3 (0=Not detectable; 1=Barely detectable; 2=Moderate; 3=Prominent). A torque cell (TRT-25; Transducer Techniques, Temecula, CA) measured produced torque from the finger extensors as each patient extended their four fingers isoinertially (patient extended fingers against constant resistance generated by continuous downward movement of the bar by a technician – similar to a clinical manual muscle test). A 40 second rest interval was utilized to allow for proper recovery of muscle force. Three 'baseline trials' with the neck in neutral position were obtained to determine subject maximal voluntary isometric contraction. Five paired successive trials were then performed with neck in extension and flexion. Neck position was recorded by two gyroscopic sensors affixed to a headband (**Fig. 1**).

Figure 1. McArdle Biomechanical Test Setup. Subjects arm is secured in the device. Torque cell (blue arrow) measures torque as subject pushes on padded black bar. Two gyroscopes in headband measure neck flexion/extension (yellow arrow).

Statistical analysis was performed in JMP 13 (SAS Institute Inc., Cary, NC). ANOVA and receiver operator curve (ROC) were utilized to assess the diagnostic properties for muscle stiffness. A *p*-value <0.05 was considered statistically significant.

RESULTS AND DISCUSSION

Muscle stiffness compared to clinical McS grading scale demonstrated significance across groups ($F_{3,715}$=37.83, p<0.0001). Dunnett's post-hoc analysis demonstrated differences in Table 1.

Clinical McArdle Sign	Mean* (SD)	*p*-value
0	-1.64 (1.14)	1.0000
1	-2.16 (1.43)	**<0.0001**
2	-1.26 (0.97)	**0.0024**
3	-0.24 (0.16)	**<0.0001**

* Units of stiffness are Nm/deg.

The ROC of muscle stiffness as a predictor for McS demonstrates 'good' diagnostic accuracy for McS Grade 3 (χ^2=123.86; p<0.0001; **Fig. 2**). The ROC curve is 'poor' for Grade 1 and 'fail' for Grade 2 and Grade 0. For Grade 3, the stiffness measure was 94% sensitive and 75% specific (χ^2=97.03; p<0.0001).

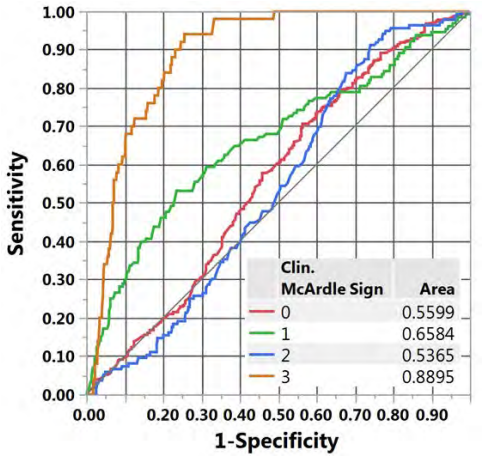

Figure 2. ROC curve of muscle stiffness as a predictor of clinical McArdle Sign. Respective area under the curve (AUC) is provided for each McS grade.

As neck flexion is where the characteristic weakness of McS becomes apparent, the analysis was divided by neck position (extension, flexion). With extension, the ROC of muscle stiffness as a predictor for McS demonstrates 'good' diagnostic accuracy for McS Grade 3 (χ^2=57.11; p<0.0001; **Fig. 3A**). The ROC curve is 'poor' for Grade 1 and 'fail' Grade 2 and Grade 0. With flexion, the ROC of muscle stiffness as a predictor for McS demonstrates 'excellent' diagnostic accuracy for McS grade 3 (χ^2=67.62; p<0.0001; **Fig. 3B**). The ROC curve is 'poor' for Grade 1 and 'fail' Grade 2 and Grade 0. For Grade 3, the stiffness measure was 100% sensitive and 82% specific (χ^2=62.15; p<0.0001).

CONCLUSIONS

This data demonstrates that muscle stiffness as measured by a torque cell is both sensitive and specific to clinically observed muscle 'weakness,' especially with neck flexion as observed with McS. The specificity and sensitivity directly coincides with the clinical grading scale. This is an important objective measure that coincides with subjective clinical interpretation.

REFERENCES

1. O'Neill et al. *J Neurol. Neurosurg. Psychiatry*. 50:1691-1693.

ACKNOWLEDGEMENTS

Funding include NIH K12HD065987 and L30AR070273 and Mayo Clinic Kelly Orthopedic Fellowship.

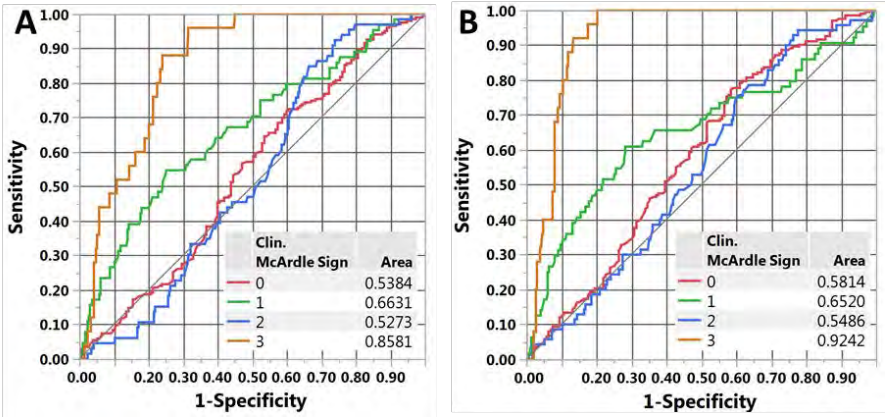

Figure 3. ROC curve of muscle stiffness as a predictor of clinical McArdle Sign with neck extension (A) and flexion (B). Respective area under the curve (AUC) is provided for each McS grade.

EFFECTS OF VISUAL FEEDBACK ON PATELLOFEMORAL JOINT REACTION FORCE DURING SQUATTING IN PEOPLE WITH PATELLOFEMORAL PAIN SYNDROME

[1] Michael Schiller, Amanda Smith, Thomas Kernozek, Drew Rutherford, Chris Durall

[1] University of Wisconsin-La Crosse, La Crosse, WI, USA
email: tkernozek@uwlax.edu

INTRODUCTION

Patellofemoral pain syndrome (PFPS) is common, occurring in 7.3% of those seeking medical care [1]. Patellofemoral joint loading is important in PFPS [2]. Visual feedback has previously been shown to alter mechanics in those with PFPS [3].

Our purpose was to determine if real-time visual feedback could reduce patellofemoral joint reaction force (PFJRF) while squatting in those with PFPS.

METHODS

Sixteen subjects with PFPS (average age = 20.9; 13 female, 3 male; average Tegner Scale = 6/10) were identified based on clinical evaluation by the same physical therapist. Kinetic and kinematic data were collected using two force platforms (1800 Hz) and a 15-camera motion analysis system (180 Hz) where 47 markers were being tracked and used in an 18 segment musculoskeletal model. Muscle forces were calculated with static optimization (HBM, Motekforce Link, Amsterdam, Netherlands) in real-time and then used in a custom patellofemoral joint model to determine PFJRF.

Each subject performed multiple squats during 3 conditions: pre-training, training, and post-training. During pre-training, 5 trials were performed to a squat depth to the onset of knee pain where an analog trigger was pressed to record this position. During training, each subject performed 10 squats to 80% of that depth. Participants were instructed to squat and hold using the feedback display to minimize their PFJRF (Fig. 1). When the participant felt they had maximally reduced their PFJRF, they pressed an analog trigger. The PFJRF value at the time the trigger was pressed was displayed during the next trial giving the participant an idea of their previous performance. During post-training, 5 squats were performed without feedback to a depth at which their knee pain was felt. Participants were instructed to use any strategy they discovered during training that allowed them to keep their PFJRF low.

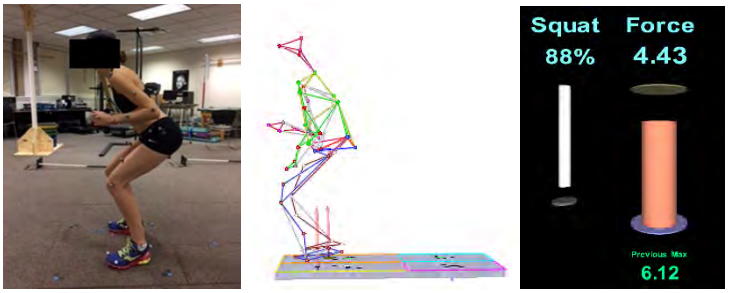

Figure 1: Example of PFJRF and squat depth feedback (right) provided to participant (left) while squatting. The middle image represents the musculoskeletal model created by HBM.

Dependent variables included quadriceps force, peak ankle dorsiflexion, knee flexion and hip flexion, peak moments at the ankle, knee and hip, and PFJRF. To examine differences between conditions a repeated measures multivariate analysis was performed (α=0.05) with follow-up tests on each dependent variable as warranted. SPSS (ver. 25, IBM, Armonk, NY, USA) was used for statistical calculations. Cohen's d was calculated to represent effect size.

RESULTS AND DISCUSSION

Multivariate analysis identified differences across conditions (Wilks' Lambda = 0.032, p=0.00). Follow-up univariate tests identified differences in pre-training and training conditions, as well as between pre-training and post-training conditions (Table 1).

Compared to the pre-training condition, quadriceps force decreased during training (mean difference = 1.2 BW, p=0.00) and in the post-training condition (mean difference = 0.5 BW, p=0.008). Compared to

the pre-training condition, the hip moment increased during training (mean difference = 0.02 Nm/kg BW, p=0.01) and in the post-training condition (mean difference = 0.01 Nm/kg BW, p=0.04). Compared to the pre-training, PFJRF decreased during training (mean difference = 1.2 BW, p=0.00) and post-training (mean difference = 0.6 BW, p=0.01) (Fig. 2).

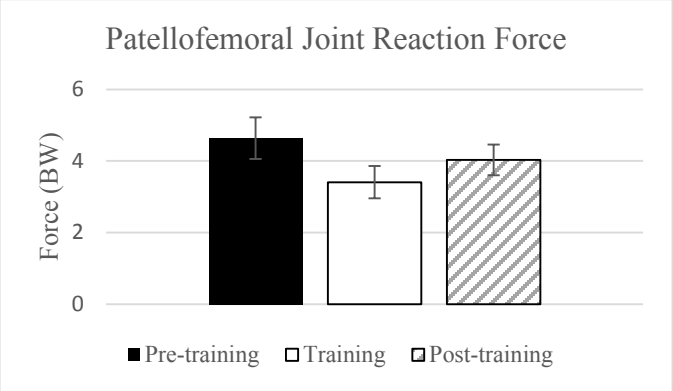

Figure 2: Peak PFJRF for each squat condition.

PFJRF may be a factor in the pain associated with PFPS [4]. Reducing PFJRF without excessive increases in knee flexion angle may decrease pain. The results of this study demonstrate that feedback can be used to reduce PFJRF in those with PFPS by altering squatting mechanics. Cueing to squat with an increased hip moment may be an effective way to decrease PFJRF.

REFERENCES

1. Glaviano et al. *Int J Sports Phys Ther,* **10**(3), 281-290, 2015.
2. Rothermich et al. *Clin Sports Med,* **24**, 313-327, 2015.
3. Willy et al. *Clin Biomech,* **27**(10), 1045-1051, 2015.
4. Vannatta et al. *Med Sci Sports Exerc,* **47**, 1001-1008, 2015.

ACKNOWLEDGEMENTS

This study was funded by a University of Wisconsin – La Crosse Research, Service and Education Leadership grant.

Table 1: Mean and Standard Deviation (in parentheses) peak variables during the three squat conditions with pairwise comparisons between pre-training and training, and pre-training and post-training. MD is mean difference and ES is effect size.

	Squat Conditions (Mean (SD))			Pre-training / Training			Pre-training / Post-training		
Variable	**Pre-training**	**Training**	**Post-training**	**MD**	**p-value**	**ES**	**MD**	**p-value**	**ES**
Quad Force (BW)	4.71 (1.09)	3.52 (0.89)	4.19 (0.99)	1.19	0.00	0.92	0.52	0.01	0.40
Dorsiflexion (deg.)	36.10 (7.68)	32.58 (7.81)	35.31 (8.15)	3.52	0.00	0.37	0.79	0.15	0.08
Knee Flexion (deg.)	104.49 (19.39)	85.57 (18.20)	100.43 (20.11)	18.92	0.00	0.79	4.06	0.10	0.17
Hip Flexion (deg.)	92.59 (16.61)	78.46 (16.54)	89.17 (14.11)	14.13	0.00	0.73	3.42	0.20	0.18
Ankle Moment (Nm/kg BW)	-0.001 (0.001)	0.002 (0.01)	0.0003 (0.01)	0.003	0.10	0.42	0.001	0.43	0.18
Knee Moment (Nm/kg BW)	-0.11 (0.02)	-0.10 (0.02)	-0.11 (0.02)	0.01	0.00	0.50	0.007	0.17	0.29
Hip Moment (Nm/kg BW)	-0.06 (0.04)	-0.04 (0.03)	-0.05 (0.03)	0.02	0.01	0.44	0.01	0.04	0.22
PFJRF (BW)	4.64 (1.16)	3.41 (0.90)	4.03 (0.86)	1.23	0.00	0.94	0.61	0.01	0.47

THE EFFECT OF DISTRACTION ON DERMAL PATCH RECONSTRUCTION OF THE HIP CAPSULE

Patrick J. Schimoler[1,2], Alexander Kharlamov[1], Stephen Jacobsen[1], Mark Carl Miller[1,2], John Christoforetti[1]
[1]Allegheny General Hospital, Pittsburgh, PA, [2]University of Pittsburgh, Pittsburgh, PA
email: mark.c.miller@ahn.org

INTRODUCTION

Hip arthroscopy may include capsulotomy or and capsulectomy, with uncertain consequences. Hip stability depends in part on the integrity of the hip capsule and reconstruction after arthroscopic damage may restore the native behavior. Dermal patches have shown success in shoulder repairs and the possibility that a similar repair could help in hip surgery forms the basis of the current study. This work seeks to test the use of a patch on the ability of the hip capsule to constrain distraction loads at different internal/external rotations. The null hypotheses were that

- the hip capsule in intact, capsulotomized, capsulectomized, and repaired conditions would not differ in the load created by 5 mm of distraction; and,
- 30 degrees of external and 20 degrees of internal rotation applied to the intact, capsulotomized, capsulectomized, and repaired hip capsule would have no effect on the load created by 5 mm of distraction.

METHODS

The capsule in five cadaveric hemi-pelvises was exposed and the pelvis and distal femur of each specimen were bound in custom fixturing with polyester resin filler (3M) and cancellous bone screws. The specimens with the fixtures were mounted into a biaxial load frame (Bionix 858, MTS) with the hip aligned at neutral flexion / extension and neutral abduction / adduction orienations.(Figure 1) Distractions of 5 mm along the femoral axis of each specimen were at neutral internal / external rotation, at 30° of external rotation and 20° of internal rotation. The distraction load during the each movement was monitored at 100 Hz. Each specimen was first tested with the capsule intact, followed by three more conditions. A 4 cm capsulotomy at the level of the labrum was performed, followed by removal of an equilateral triangular capsulectomy. Lastly, repair with a dermal patch (ArthroFLEX, Arthrex) was performed using two acetabular anchors and two distal sutures at the corners of a rectangular patch.

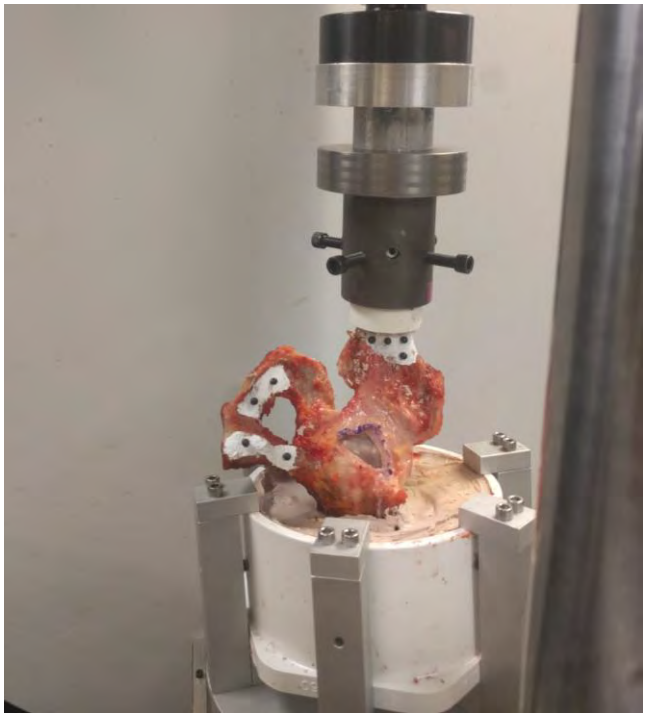

Figure 1: Specimen mounted for testing

Statistical analysis was conducted using a two-way repeated measures ANOVA with distraction load as the dependent variable and with hip internal / external rotation orientation angle and capsule condition as independent variables. If the ANOVA was found to be significant, Tukey's post-hoc test was applied to an independent variable.

RESULTS

The damage caused by capsulotomy and capsulotomy led to lower loads required to produce 5 mm of distraction. The repair with a dermal patch

increased the required load (Figure 2). The different conditions, however, produced no significant differences among the distraction loads ($p = 0.17$).

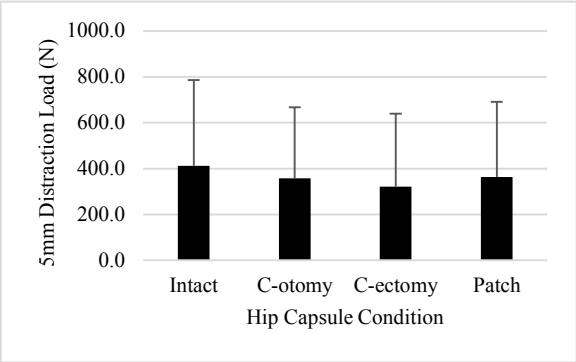

Figure 2: Distraction loads by condition

The different hip internal / external orientations led to significant differences due to 5 mm distraction (Figure 3, $p < 0.001$): all three conditions were different from each other with the load at 30° external rotation loading higher than that at 20° internal rotation loading which was higher than the load at the neutral orientation. No differences among the cases were found by post-hoc testing.

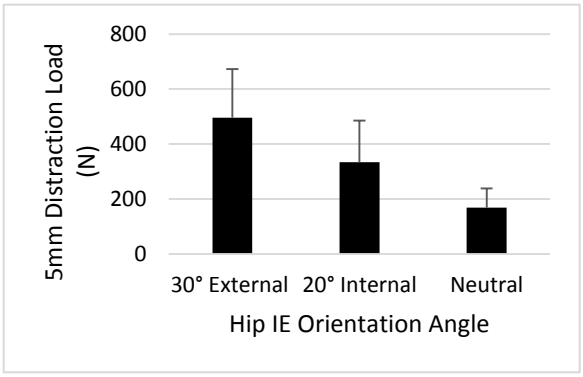

Figure 3: Distraction loads by I/E orientation

DISCUSSION

As indicated by the difference due to internal-external orientation, the capsule ligaments could tighten and stiffen the joint despite the damage. Although the capsular damage and the dermal patch repair did not have statistically significant effects, the resulting distraction loads ordered the cases with respect to the amount of damage. Namely, the load in the native case was greater than that in case of capsulotomy; the capsulotomy load was greater than that of the capsulectomy; and, the load after repair with a patch was greater than both the capsulotomy or capsulectomy loads.

Ito et al. [1] studied the contributions to hip stability of the capsule and zona orbicularis, finding a 5mm distraction load of approximately 300±150N in an intact hip in a neutral orientation. While smaller than the neutral load recorded here, Ito's value is well within one standard deviation of our values. Although Ito found significance between intact and vented conditions, they had two additional specimens.

Femoral rotation increased capsular stiffness and surgical condition did not affect these increases. Thus, the capsule could transmit load despite the damage and patients should therefore be able to perform normal daily activities that do not interfere with healing. The current research, however, did not study the integrity of the patch/capsule construct to quantify movements of the patch relative to the capsule caused hip movements: any movements of the patch relative to the capsule could impair healing.

The study does have limitations. Foremost, additional specimens could change the statistical outcome. Additionally, a reduction in the fixture compliance would ensure that inadvertent femoro-acetabular motion was more limited. Comparison of movements using tracked three-dimensional markers found no difference between cases and affirmed the 5 mm of distraction. Nonetheless, a stiffer fixture might reduce variability.

SIGNIFICANCE/CLINICAL RELEVANCE
Dermal patch reconstruction may increase stability in hip capsular repair.

ACKNOWLEDGEMENTS
Thanks to Anne Smolinski for assistance with experimentation and data processing and to Arthrex for the materials.

[1] H Ito, et al., JOR. 2009; 27(8): 989-995.

CHRONOLOGICAL COMPARISON OF WALKING GROUND REACTION FORCE IN INDIVIDUALS WITH ANTERIOR CRUCIATE LIGAMENT RECONSTRUCTION

[1]Matthew K. Seeley, [2]Christopher Johnston, [2]Steven J. Pfeiffer,
[2]Jeffrey T. Spang, [2]J. Troy Blackburn & [2]Brian G. Pietrosimone

[1] Brigham Young University, Provo, UT, USA
[2] University of North Carolina at Chapel Hill, Chapel Hill, NC, USA
email: matt_seeley@byu.edu

INTRODUCTION

Vertical ground reaction force (vGRF) is a fundamental measure of external load transmitted to lower extremity joints, including the knee. Walking vGRF is linked to multiple indicators of knee cartilage health, including knee tissue metabolism and cartilage composition, and patient reported function following anterior cruciate ligament reconstruction (ACLR) [1]. Approximately 40% of ACLR patients report clinically relevant knee symptoms years after ACLR [2], and these symptoms are associated with aberrant movement biomechanics [3], which may influence the long-term health of knee joint tissue. The association, however, between persistent clinically relevant knee symptoms and aberrant biomechanics, post-ACLR, is unclear. The purpose of this project was to compare walking vGRF transmitted to the involved leg of clinically symptomatic and asymptomatic ACLR patients, at three clinically relevant time periods: 6-11, 12-24, and > 24 months post-ACLR. We hypothesized that, relative to the asymptomatic patients, symptomatic patients would exhibit decreased walking vGRF at 6-11 months post-ACLR, but increased vGRF at 12-24 and > 24 months post-ACLR.

METHODS

vGRF were measured for 5 walking trials, for 128 post-ACLR patients (Table 1). All procedures were approved by the appropriate institutional review board before data collection. Patients were classified as clinically symptomatic or asymptomatic using the Knee Injury and Osteoarthritis Outcome Score, as previously defined [4]. Patient descriptors (Table 1) were compared, between groups, for each time, using *t* tests ($\alpha = 0.05$). Multiple 2 × 2 functional ANOVAs were used to evaluate effects of group (symptomatic and asymptomatic) and time post-ACLR (6-11 months, 12-24 months, and > 24 months) on walking vGRF. This functional statistical approach allowed for detection of statistical differences throughout stance, rather than only at certain discrete time points (e.g., peak vGRF). Estimates of pairwise comparison functions were plotted for the symptomatic and asymptomatic groups, for each of the three different time periods (Figures 1A-C), as well as 95% confidence intervals, to determine significant differences (Figures 1D-F); vGRF were considered to be statistically different when confidence intervals did not cross zero (Figures 1D-F).

Table 1: Descriptions of six different subgroups of ACLR patients included in this analysis.

	6-11 Months	
	Symptomatic	Asymptomatic
n (females)	28 (16)	24 (14)
Age (Years)	22 ± 3	22 ± 4
BMI (kg/m^2)	24.9 ± 4.0	25.0 ± 4.0
Gait Speed (m/s)	1.23 ± 0.15	1.25 ± 0.13
	12-24 Months	
	Symptomatic	Asymptomatic
n (females)	15 (11)	15 (10)
Age (Years)	20 ± 3	22 ± 4
BMI (kg/m^2)	23.4 ± 3.6	25.4 ± 4.2
Gait Speed (m/s)	1.22 ± 0.11	1.21 ± 0.14
	>24 Months	
	Symptomatic	Asymptomatic
n (females)	13 (13)	33 (22)
Age (Years)	19 ± 2	21 ± 2
BMI (kg/m^2)	24.2 ± 3.3	24.9 ± 4.5
Gait Speed (m/s)	1.31 ± 0.26	1.18 ± 0.19

RESULTS AND DISCUSSION

None of the patient descriptors reported in Table 1 differed between the symptomatic and asymptomatic patients, for any of the time periods. For the 6-11 months time period, walking vGRF were less for the

symptomatic group, during most of the first and final third of stance, but greater during most of the middle third of stance (Figures 1A and 1D). Between-group differences diminished for the 12-24 months time period, and only existed between 5 and 8%, and 92 and 95% of stance (Figures 1B and 1E). Between-group differences also existed for the > 24 months time period, when walking vGRF were greater for the symptomatic group during most of the first and final third of stance, but less during most of the middle third of stance (Figures 1C and 1F). Although not presented here, between-time comparisons, for each group, indicated that the variation in between-group differences, across the three observed time periods, was due more to between-time differences for the symptomatic groups, while asymptomatic vGRF was similar between indiviudals at different time points.

It is possible that vGRF differences observed during the first year post-ACLR are due to kinesiophobia or inability to bear weight on the ACLR limb, while the latter differences (> 24 months) might be more related to inadequate lower-extremity muscular capacity to control the limb during gait. We further speculate that presently observed vGRF differences may reflect differences in knee joint loading patterns that are detrimental to joint tissue health at the knee. Additionally, it should be emphasized that this analysis involved 128 different ACLR patients, each at various times post-ACLR; a longitudinal study of the same symptomatic and asymptomatic patients, and associated biomechanics, is warranted.

CONCLUSIONS

The present analyses indicate that symptomatic and asymptomatic ACLR patients utilize different loading patterns during walking, and that these differences vary depending upon time post-ACLR. Symptomatic ACLR patients appear to unload their affected leg, during the first year, post surgery; however, these abnormal loading patterns appear to reverse later in time, > 24 months post surgery.

REFERENCES

1. Pietrosimone et al. *J Orthop Res.* 35(10), 2288-2297, 2017.
2. Wasserstein et al. *Osteoarthritis Cartilage.* 23(10), 1674-1684, 2016.
3. Pietrosimone et al. *J Orthop Res.* In Press.
4. Englund et al. *Arthritis Rheum.* 48(8), 2178-2187, 2003.

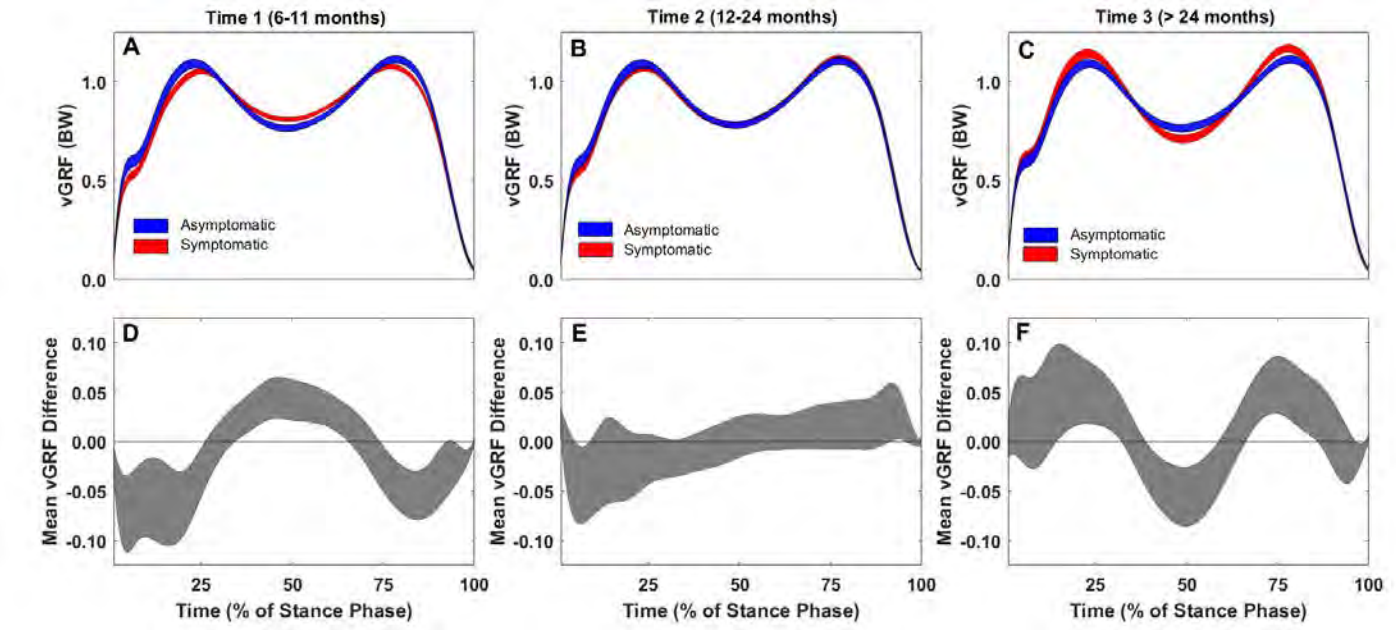

Figure 1: Mean walking vGRF for 128 different ACLR patients (A-C), at three different time periods, and the corresponding mean differences and estimated effect sizes (D-F). Relative to the asymptomatic patients, peak vGRF was usually less ($\alpha = 0.05$) for the symptomatic patients at 6-11 months, but greater at > 24 months (differences are indicated whenever the effect sizes did not overlap zero in D-F).

IN VITRO SIMULATION OF TORQUE-INDUCED ROTATOR CUFF TEARS

[1]John F. Shanley IV, [2]Rick Goding, and [1]Mariana E. Kersh

[1] University of Illinois at Urbana-Champaign, Urbana, IL, USA
[2]Joint Preservation Institute of Iowa, West Des Moines, IA, USA
email: mkersh@illinois.edu, web: http://uitbl.mechse.illinois.edu/

INTRODUCTION

Rotator cuff tears are the most common cause of shoulder pain, appearing in over 20% of the population and increase in prevalence with age [1,2,5]. High torque loading during sports has been associated with rotator cuff weakness and injury, and we hypothesize that a similar mechanism occurs in occupations using drills [9]. While many studies have examined the mechanical properties of the rotator cuff in vitro [3,4,11], there are no studies that simulate the injury mechanism. Therefore, we developed a test apparatus to simulate and evaluate the mechanics of the rotator cuff tendons during repeated exposure to adduction torques. Understanding the mechanism of injury during sudden torques may inform repair and rehabilitation techniques for rotator cuff tears.

METHODS

A custom apparatus for dynamic load measurements of supraspinatus, the primary muscle used in humeral abduction [6,7,8], during sudden adduction was developed (Fig 1). Four fresh frozen shoulder specimens (proximal humerus, scapula, and clavicle) were used (mean age = 55.3 ± 4 years). All soft tissue, except for supraspinatus, was removed. The coracoid process and acromion were removed to allow uninhibited access to the supraspinatus. The supraspinatus was severed along the scapular origin, leaving the distal insertion to the humeral head intact.

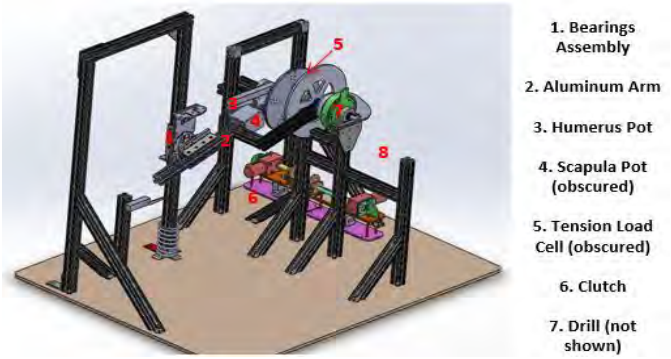

Figure 1: Custom apparatus used for testing, with key features described.

A drill (Makita 18-Volt LXT) was coupled to the humerus via a clutch (Ogura) and an aluminum arm system. A frame held the scapula at a fixed position. The humeral head was centered on the drill rotational axis and secured. The supraspinatus was clamped at the distal muscle-tendon junction and loaded to a desired pretension based on rigid body musculoskeletal calculations of supraspinatus force required to lift the arm [10] (Fig 2, Phase 1).

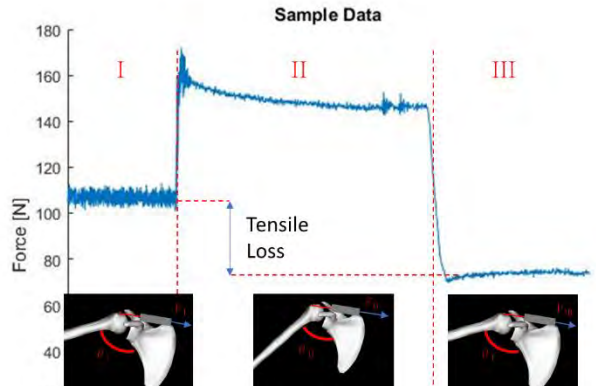

Figure 2: Stages of a test cycle--Specimen is held in tension (I), the clutch engages, the arm adducts and settles (II), and is manually returned to the initial position (III).

The drill was then activated to full speed, at which time the clutch engaged, resulting in sudden torque to the shoulder (30˚ of powered adduction measured using an accelerometer attached to the arm). A load cell was used to monitor the tension in supraspinatus during testing. Upon completion of the test, the specimen came to rest (Fig 2, Phase II) before being raised back up to its original position and (if necessary) re-tensioned to the target value (Fig 2, Phase III). This process was repeated 30 times at two-minute intervals for all specimens.

The peak load ratio (PLR = maximum load normalized to the initial load for each cycle) was calculated. Tendon damage was defined as a decrease in PLR over the course of the test. Tensile strength maintenance was quantified by comparing

the initial supraspinatus tensile force during phase I to the force when the specimen was returned to the initial position in phase III.

RESULTS & DISCUSSION

Over the 30˚ of travel after clutch engagement, specimens reached an average of 2.55 G's of peak acceleration. Over the course of testing, no specimen showed visible signs of tearing.

During the first few cycles, most specimens lost ~15%-35% of the tensile strength upon return to their initial positions but leveled out to minor tensile losses (~<5%) as testing progressed (Fig 3). There was a noticeable change in the amount of tension lost as testing progressed across all specimens.

The peak load ratio (PLR) showed varying degrees of decay across the specimens (Fig 4). The initial immediate increase in PLR suggests that as testing progressed the collagen fibers initially bearing the bulk of the load were tearing, and consequently different fibers began to bear load.

While all specimens showed a gradual decrease in force in the latter cycles, one specimen had a moderate increase in PLR but began with relatively low initial (first 5-8) PLR values. This may be due to the re-tensioning of the tendon.

All specimens were visually evaluated for tearing; however, the degree of micro-tearing and subject-specific geometry was not quantified and may explain the varying response initially to sudden adduction. A limitation of the study is the lack of a quantitative measures of the initial anatomical state of the supraspinatus tendon and low sample size.

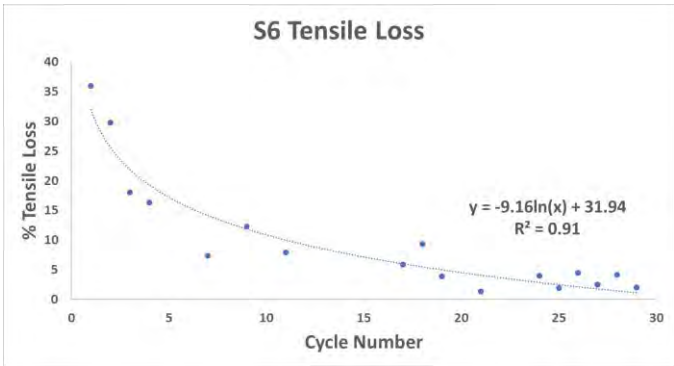

Figure 3: Decaying tensile losses for a specimen as cycles increase.

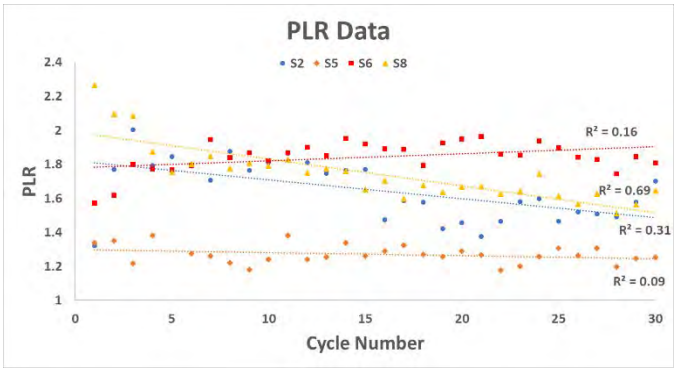

Figure 4: PLR data with linear fits shown; general trends show decreasing ability to bear load

CONCLUSIONS

We have demonstrated that there is a decay in the supraspinatus tendon's ability to support load during sudden adduction motions. Rotator cuff tears may be fatigue-driven where repeated trauma gradually weakens the tissue prior to failure rather than the result of a blunt immediate trauma. However, the immediate decrease in load capacity suggests that the damage associated with decreased tendon strength occurs relatively early in the fatigue cycle. Our data suggests that preventative methods to protect the shoulder from fatiguing via a brace or other ergonomic considerations should be employed to mitigate this risk factor. Further work is needed to determine how shoulder biomechanical function *in vivo* is affected by repeated exposure to torques and to relate tissue microstructure to macroscopic tendon properties.

REFERENCES

1. Minagawa H et al., J of Orthopaedics, 10 (2013): 8-12.
2. Tashjian R, Clin Sports Med, 31 (2012): 589-604.
3. Miller R et al., Orthopaedic Research Society, (2014).
4. Itoi E et al., J of Orth Research,13.4 (1995): 578-584.
5. Reilly P et al., Ann R Coll Engl, 88 (2016): 116-121.
6. McMahon P et al. J Shoulder and Elbow Surgery, 4.3 (1995) 199-208.
7. Wu W et al., J of Biomechanics, 49.15 (2016): 3626-3634.
8. Järvholm U et al., Clin Orth and Related Research, 245 (1989) 102-109.
9. Anton D. et al., Ergonomics, 5 (2001): 489-501.
10. Shanley J et al., Midwest ORS 2017 Abstracts.
11. Rahman H et al., J Biomech Eng, 139 (2017).

ACKNOWLEGMENTS

Special thanks to Tissue Biomechanics Lab member Hafizur Rahman for his assistance during testing.

DEVELOPMENT OF FORCE-SPACE NAVIGATION FOR SURGICAL ROBOTICS

[1,2,3] Corey D. Smith [2,3] George S. Athwal and [1,2,3] Louis M. Ferreira

[1] University of Western Ontario, London, ON, CANADA
[2] Roth|McFarlane Hand and Upper Limb Centre, London, ON, CANADA
[3] Lawson Health Research Institute, St. Joseph's Health Care, London, ON, CANADA
email: csmit424@uwo.ca

INTRODUCTION

Shoulder replacement is a common procedure that replaces bone in the shoulder joint with implants to help relieve chronic pain [1]. In this procedure, a surgeon removes bone in the shoulder socket, referred to as the glenoid. The surgeon uses a large reaming tool to remove the bone but the tool obscures their view and the shoulder blade moves within the body complicating the procedure. Poor reaming can lead to improper tilt and version of the implant and excessive bone loss causing implant loosening which will require revision surgery [2].

Surgical robots have been used to help improve implant accuracy but currently none exist for shoulder replacement. This work presents a new surgical robot system that utilizes reaction force feedback from flexible strips that tether the robot to the patient for navigation. This allows the robot to "feel" its way around.

METHODS

To validate the system, the surgical robot was tested against a fellowship-trained shoulder surgeon on shoulder analog models. Both the robot and the surgeon simulated glenoid preparation and implant placement procedures. Two different types of shoulder analogs were tested: one with standard anatomy and the other with asymmetric bone loss referred to as a Walch type B2.

Before the procedures, using 3D computer models from CT scans, the surgeon virtually placed appropriate implants on each shoulder model in the correct surgical location to create a pre-operative plan as a target for both surgical methods. The robot (Figure 1) and the surgeon were both tested on 6 standard and 6 B2 shoulders.

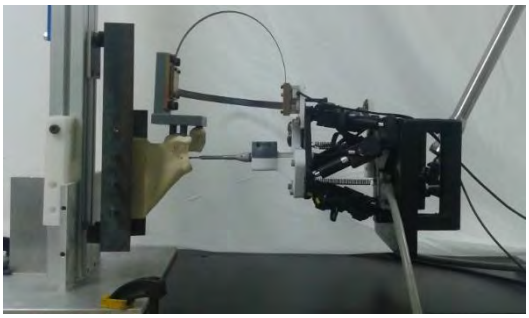

Figure 1: Surgical robot test set-up.

Following implant placement, shoulder analogs were CT scanned, and 3D computer models were created to quantify final implant placement compared to the pre-operatively planned targets, in terms of position and orientation. These results were analyzed using a one-way MANOVA with $p<0.05$.

RESULTS AND DISCUSSION

Comparing the tests, x, y and z directions were defined as superior-inferior, anterior-posterior and lateral-medial respectively. Based on these tests, the robot's net implant position error for the standard shoulder was 1.47 ± 0.48 mm compared to the surgeon's 1.61 ± 0.29 mm ($p=0.674$) seen in (Figure 2). The net implant orientation error for the robot in the standard shoulder tests was 2.57 ± 2.30° compared to the surgeon's 5.04 ± 1.92° ($p=0.063$).

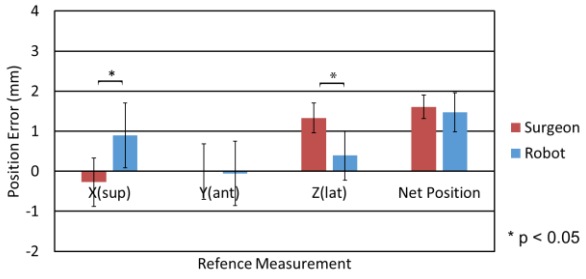

Figure 2: Standard scapula implant position error of robot vs. surgeon.

For Walch type B2 shoulders, the robot's net implant position error was 2.16 ± 0.36 mm compared to the surgeon's 3.01 ± 0.42 mm (p=0.002) seen in (Figure 3). The net implant orientation error for the robot in the B2 shoulder tests was 2.89 ± 0.88° compared to the surgeon's 4.54 ± 1.49° (p=0.121).

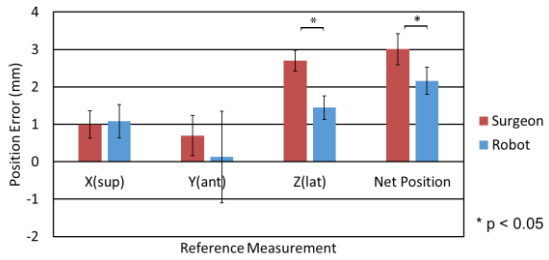

Figure 3: B2 scapula implant position error of robot vs. surgeon.

For the standard anatomy (Figure 4), and B2 anatomy (Figure 5) the robot was able to leave peripheral bone that the surgeon did not. This may add implant support that could prevent loosening but future work is still needed.

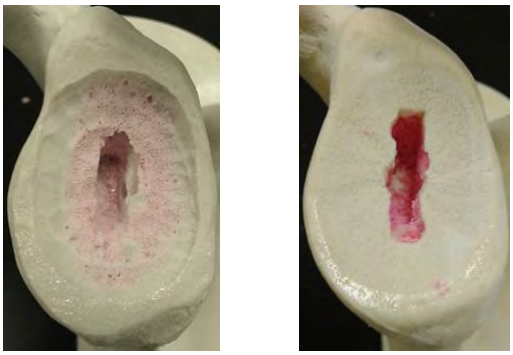

Figure 4: Standard shoulder analog robot cut (left) versus surgeon cut (right).

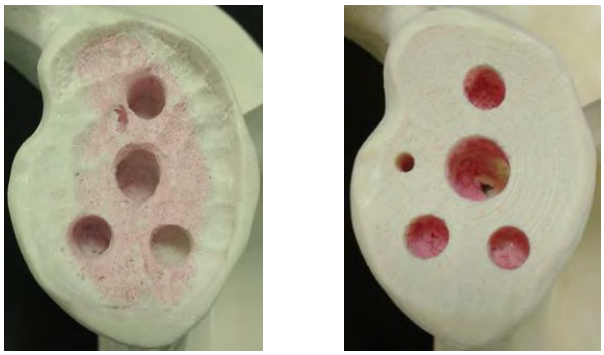

Figure 5: B2 shoulder analog robot cut (left) versus surgeon cut (right).

The robot could match or outperform the surgeon in most measurements. The robot maintained relatively high accuracy. As well, the robot only required the bone burring tool for either anatomy while the surgeon required a number of surgical tools. For more complex anatomy and implant designs, the surgeon needs more complex tools while the robot can use the same tool with a new programmed path.

CONCLUSIONS

Overall, the study showed that the reaction force navigation system could be effectively used for a surgical robot. This tracking system and robot are relatively inexpensive compared to current systems.

The robot proved to be versatile in adapting to different implant designs with only slight changes to the system. This removes the need for large number of tools and the sanitization that follows.

With the validation of the system on shoulder analogs, the next steps will be to test the robot on cadaveric shoulders. As well, the system does not need to be restricted to shoulder orthopaedics. Other surgical fields have been identified that this system may be tested on in the future including: elbow replacement, finger joint replacement, ear reconstruction and craniofacial reconstruction.

REFERENCES

1. E. M. Padegimas, *"Future patient demand for shoulder arthroplasty by younger patients: national projections.," Clin. Orthop. Relat. Res.*, vol. 473, no. 6, pp. 1860–1867, Jun. 2015.
2. A. Karelse et al, "*A glenoid reaming study: How accurate are current reaming techniques?,*" *J. Shoulder Elb. Surg.*, vol. 23, no. 8, pp. 1120–1127, 2014.

ACKNOWLEDGEMENTS

The authors would like to thank Wright Medical Group Inc., for allowing the use of their B2 shoulder analog molds and for providing the surgical tooling.

SIMULATION OF OCCUPANT KINEMATICS IN LOW-SPEED LATERAL COLLISIONS USING ARTICULATED TOTAL BODY

[1] David Sproule, [1] Stephanie Rossman, [1] Keith Button, [1] Brian Weaver, [1] Steve Rundell

[1] Explico Engineering, Novi, MI, USA
email: dsproule@explico.com, web: www. explico.com

INTRODUCTION

There is limited data available for occupant kinematics during low-speed, lateral collisions when compared to frontal and rear-end collisions. Simulation software can be a valuable tool in the prediction of occupant dynamics when properly verified and validated. The multibody, dynamic physics software Articulated Total Body (ATB) specifically simulates the human body's response to dynamic environments, but has not been previously evaluated for low-speed lateral collisions. The objective of the current study was to evaluate the ability of ATB to simulate occupant kinematics during low-speed lateral collisions utilizing previously conducted sled tests.

METHODS

Low-speed lateral sled tests have previously been performed for belted, far-side volunteers and anthropomorphic test devices [1]. Two collision pulses matching the previous tests were applied in the simulations. The first collision pulse was characterized by a peak acceleration of 4 g and a velocity change (delta-V) of 6 kph, and the second collision pulse had a peak acceleration of 4 g and a delta-V of 10 kph. Both pulses were simulated in ATB for two male volunteers, one female volunteer, and a 50th percentile male Hybrid III dummy (Table 1).

Each of the volunteers and the ATD were represented by a series of ellipsoids, scaled to their respective height and weight, linked together with joints. The models were placed in a seat modeled using a series of contact planes, and were belted using a three-point harness. Lateral head displacement was evaluated for each simulation and compared to the previously conducted low-speed lateral sled tests.

RESULTS AND DISCUSSION

The early-phase occupant kinematics during the low-speed lateral sled tests were accurately predicted by ATB (Figure 1).

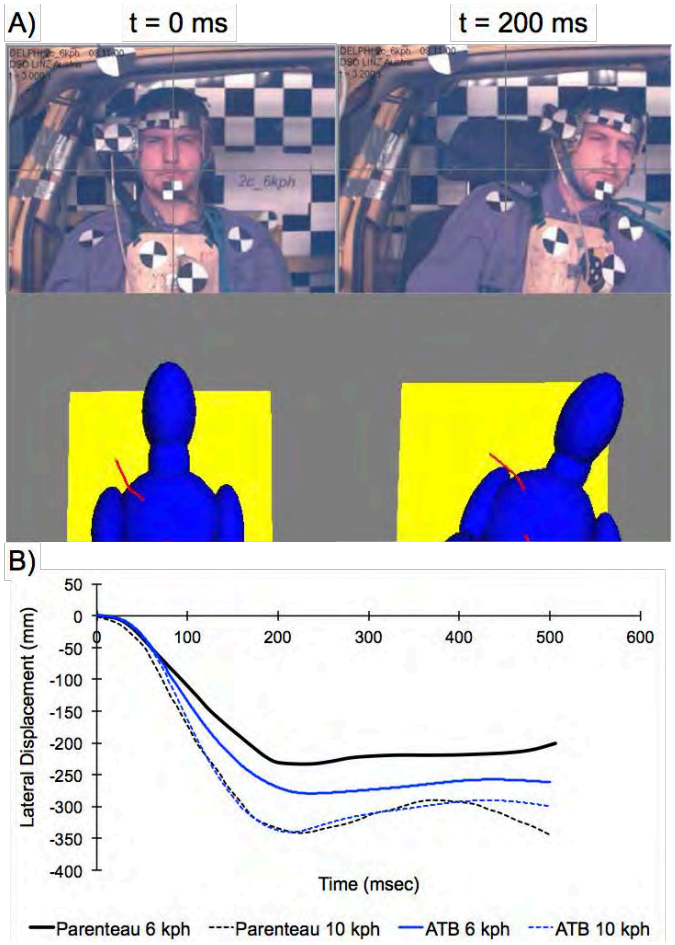

Figure 1: (A) Volunteer and simulation occupant motion during a 6 kph pulse (B) ATB simulation of lateral head displacement in comparison to sled test data for one subject with both a 6 kph and 10 kph pulse.

When compared to the sled tests, the 6 kph simulations produced an average error in peak lateral head displacement of 80 ± 56 mm, and the 10

kph simulations produced an average error in peak lateral head displacement of 56 ± 41 mm. Generally, the ATB simulations over-predicted the occupants' motion when compared with physical sled tests. Although ATB was generally over-predictive of peak displacements, these peak displacements occurred in late-phase motion.

ATB can effectively predict the initial occupant kinematics in low-speed lateral collisions, where peak occupant forces are likely to occur. However, ATB fails to accurately predict late-phase occupant motions, likely due to idealized compartment geometry and a lack of active muscle forces. Similarly, a lack of active muscle control has previously been found to influence the prediction of late-phase occupant kinematics in low-speed rear end impacts [2]. These data indicate that ATB provides a valuable tool when evaluating early phase occupant kinematics during low-speed lateral collisions for belted occupants.

REFERENCES

1. Parenteau, C., (2006). Traffic Inj. Prev., **7**(2), pp. 164–70.
2. Fisher, J., et al., (2013), *Summer Bioengineering Conference*, Vail, Colorado.

Table 1: All ellipsoid human models were scaled to the anthropometrics of the volunteers [1].

	Sex	**Height (cm)**	**Weight (kg)**	**Age (year)**
Volunteer 1	Male	175	72	32
Volunteer 2	Male	183	78	31
Volunteer 3	Female	158	48	25
HBM 50th-male	-	174	75.5	-

COMPARISON OF DYNAMIC JOINT KINEMATICS DURING SHOULDER ELEVATION IN HEALTHY CONTROLS AND INDIVIDUALS DIAGNOSED WITH MULTIDIRECTIONAL INSTABILITY

[1]Justin L Staker, [1]Rebekah L Lawrence, [1]Arin M Ellingson, [2]Scott N Haglund, [1]Jonathan P Braman, [1]Paula M Ludewig
[1]University of Minnesota, Minneapolis, MN, USA
[2]St. Catherine University, Minneapolis, MN, USA
email: stak@umn.edu

INTRODUCTION

Glenohumeral multidirectional instability (MDI) is thought to particularly affect competitive swimmers due to the repetitive strain the shoulder experiences during an overhead swim stroke. Excessive joint translations or joint instability and resulting strain to surrounding structures are thought to lead to injury. No studies have investigated if swimmers diagnosed with MDI demonstrate joint instability during an overhead reaching activity. Therefore, the purpose of this study was to determine if any differences in glenohumeral translations are present in swimmers with clinically diagnosed MDI compared to matched controls during scapular plane abduction.

METHODS

Twenty-three symptomatic, competitive swimmers were compared to 21 matched controls who were not swimmers. Swimmers with shoulder pain were included in the study if they were judged to possess increased glenohumeral joint laxity as determined by subjective scoring of 1.5 or greater on a composite laxity score from the sulcus and anterior/posterior drawer laxity tests. The composite laxity score was calculated as the average subjective grade from each of the three laxity tests [1]. Further, swimmers were required to have one additional finding indicating excessive joint laxity from either a positive apprehension test or a Beighton score of two or greater. Humerothoracic range elevation greater than 120 degrees was required for both groups. Matched controls participants were excluded if they had a composite laxity score of greater than 1.5 or any history or clinical signs of glenohumeral MDI.

Figure 1. C-arm orientation during scapular plane elevation. Start position (left), middle position (center), and end position (right)

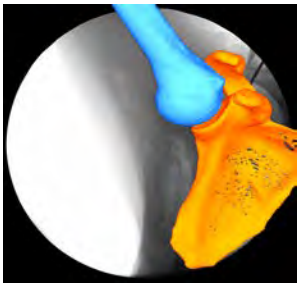

Figure 2. Example of 2D/3D shape matched scapula and humerus utilizing JointTrack software

Each subject had dynamic images recorded during scapular plane abduction using single-plane fluoroscopy (Figure 1). These images were manually shape matched by the primary investigator to 3D reconstructions of the scapula and humerus obtained from magnetic resonance images. Images were shape matched every 3% of motion, therefore each subject had 36 images to shape match from the rest position to the completion of humeral movement. Kinematic data derived from the shape matching process in JointTrack software underwent filtering with a fourth order, low pass Butterworth filter using a custom Matlab code.

Joint stability was described utilizing four dependent variables; helical axis parameters (total translation, displacement of the instantaneous center of rotation, variance in orientation of the helical axes), and joint contact path lengths. Three, two-way repeated measures ANOVAs were performed to analyze helical axis parameters. Contact path length comparisons between groups were performed with a two sample independent t-test.

RESULTS AND DISCUSSION

On average, swimmers reported onset of symptoms 149 ± 56 weeks prior to data collection. The average greatest pain in the past one month (out of 100) reported on the numeric pain rating scale was 51.5 ± 3.9. Consistent with inclusion criteria, swimmers (n=23) had significantly ($p<0.01$) higher composite laxity observational scores (mean 1.74 ± 0.3 SD, standard deviation) than controls (n=21, mean 0.98 ± 0.25 SD); and significantly higher Beighton's Index scores (3.48 ±1.7 SD) than controls (0.67 ± 0.91 SD, $p<0.01$). Additionally, swimmers had significantly ($p<0.05$) larger (105° ± 12° SD) passive external rotation range of motion compared to controls (98° +/- 10° SD).

There were no differences in measures of instability between groups during active, non-resisted scapular plane abduction. There was no effect of group for total translation ($p=0.29$, $F(1,42)=1.1$), displacement of the instant center of rotation translation ($p=0.32$, $F(1,42)=1.0$), variance in the helical axis translation ($p=0.16$, $F(1,42)=2.1$), or contact path length ($p=0.32$, $t(42)=1.0$).

All of the passive clinical findings, in addition to pain, identified in this study have been associated with MDI diagnostic criteria in previous work [2, 3]. However, there were no differences in any of the four measures of dynamic stability.

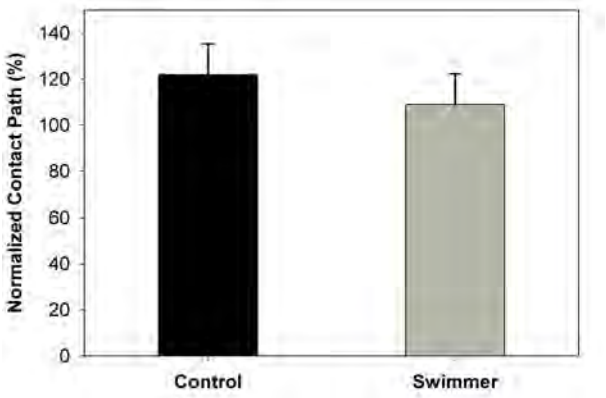

Figure 1. Contact path length of the centroid of minimum distances up to 150% of the absolute minimum distance. Contact path length is normalized to the sum of the height and width of the glenoid. $p=0.32$, $t(42)=1.0$

The lack of difference between swimmers and controls in this study is likely multifactorial. Shoulder elevation in the scapular plane without resistance may not have adequately challenged the swimmers' ability to stabilize the joint. If the impact of relative fatigue levels and external loads on swimmers during practice had been reproduced for this study, it is possible joint kinematics would have been affected and differences in glenohumeral stability may have become evident. An additional reason for the lack of significant differences between groups in joint stability may be that the inclusion criteria were not discrete enough to produce significantly distinct patterns of glenohumeral motion between controls and swimmers thought to have MDI in this study

CONCLUSIONS

No differences in joint stability were found between swimmers diagnosed with MDI and matched controls. To detect differences in glenohumeral stability between groups, tested movements may need to more closely simulate forces, positions and exposures thought to be associated with the diagnosis of multidirectional instability

REFERENCES

1. Staker, J.L., et al., *Three-dimensional kinematics of shoulder laxity examination and the relationship to clinical interpretation.* International Biomechanics, 2017. **4**(2): p. 77-85.
2. Longo, U.G., et al., *Multidirectional Instability of the Shoulder: A Systematic Review.* Arthroscopy : The Journal of Arthroscopic & Related Surgery, 2015. **31**(12): p. 2431-2443.
3. Ogston, J.B. and P.M. Ludewig, *Differences in 3-dimensional shoulder kinematics between persons with multidirectional instability and asymptomatic controls.* The American Journal of Sports Medicine, 2007. **35**(8): p. 1361-1370.

ACKNOWLEDGEMENTS

APTA Orthopaedic Section Grant: New Investigator Award (Staker)

OVERGROUND WALKING KNEE BIOMECHANICS OF DISSATISFIED TOTAL KNEE REPLACEMENT PATIENTS

[1] Kevin A. Valenzuela, [2] Lauren E. Schroeder, [3] Harold E. Cates, and [2] Songning Zhang

[1] California State Polytechnic University, Pomona, CA, USA
[2] University of Tennessee, Knoxville, TN, USA
[3] Tennessee Orthopaedic Clinics, Knoxville, TN, USA
email: kvalenzuela1@cpp.edu

INTRODUCTION

Patient dissatisfaction after total knee replacement (TKR) procedures is likely influenced by both subjective and objective aspects. Current literature on dissatisfied patients has focused primarily on survey and functional test data, indicating both increased pain [1] and reduced performance on clinical tests [2] for dissatisfied patients. . However, it is unknown how overground walking kinematics and kinetics are different between dissatisfied and satisfied TKR patients and how this relates to dissatisfaction. Therefore, the purpose of this study was to compare knee kinematics and kinetics of dissatisfied TKR patients to satisfied patients and healthy controls during level walking.

METHODS

Nine dissatisfied TKR patients (age: 68.0±4.2 years, height: 1.69±0.07 m, weight: 80.99±18.59 kg, months from surgery: 34.6±14.3 months), fifteen satisfied TKR patients (age: 66.6±6.3 years, height: 1.76±0.10 m, weight: 90.19±16.98 kg, months from surgery: 29.3±12.8 months), and fifteen healthy individuals (age: 60.7±9.2 years, height: 1.75±0.09 m, weight: 77.74±11.75 kg) were recruited from a local orthopaedic clinic (TKR patients) and the community (healthy individuals).

All subjects performed five successful walking trials at their preferred walking speed. A preferred speed range (mean speed ±5%) was established during practice trials. A numerical visual analogue scale was used to assess pain in both knees for all subjects at the end of the five trials. Standardized running shoes (Adidas Noveto) were worn by all subjects. A 12-camera motion capture system (240Hz, Vicon, UK) and two force platforms (1200Hz, AMTI, USA) were used to collect 3D kinematic and ground reaction force (GRF) data, respectively. Anatomical and tracking markers were placed bilaterally on the shoes, shanks, thighs, pelvis, and trunk for kinematic data collection.

Kinematic and GRF data were filtered at 8 Hz using a fourth-order zero-lag low-pass Butterworth filter for kinematic and internal joint moment calculations. Raw GRFs were filtered separately at a cut-off frequency of 50 Hz using the same filter for GRF variables. Visual3D (version 5.0, C-motion, Inc.) was used for 3D kinematic and kinetic data computations. Internal joint moments were reported in the proximal reference system and normalized to body mass (Nm/kg). GRF variables were normalized to body weight (BW). A 2 x 3 (limb x group) mixed model analysis of variance (ANOVA, $p<0.05$) was performed to detect differences between limbs and groups for all kinematic and kinetic variables (SAS, version 9.4).

RESULTS AND DISCUSSION

Significant interactions were present for 1st and 2nd peak VGRF, knee flexion ROM, and the loading-response knee abduction moment. The dissatisfied patients showed reduced 1st and 2nd peak VGRFs, knee flexion ROM, and knee loading-response abduction moments compared to healthy controls (Table 1). First and 2nd peak VGRFs and flexion ROM were reduced in replaced limbs of the dissatisfied patients compared to their non-replaced limbs. A return to VGRF symmetry between the two limbs has been previously shown to occur in TKR patients 12 months post-operatively [5], which is not evident here in dissatisfied patients who are closer to three years post-operative. Increased asymmetry in limb loading can further impact the non-diseased limb through increased compensation.

Reductions in loading-response extension moments were evident in the dissatisfied group compared to both the satisfied patients and the healthy group. This reduction has been suggested as being indicative of a quadriceps avoidance pattern with compensations being employed at other joints [5], thereby requiring targeted therapy to remedy. However, improvement in sagittal knee movement has been linked to a return to a bimodal knee extension moment pattern post-operatively, which is already evident in all but one of the patients. This suggests progress in the right direction for the dissatisfied patients and increasing the quadriceps strength may further contribute to the improvement.

The reduced knee function was further evident in the reduced knee flexion ROM (which could potentially require compensations in other areas). This is not in agreement with previous research that found similar levels of knee flexion during stance between TKR patients and healthy subjects [3, 5]. The reduced knee flexion ROM and extension moments are also likely related to the increased pain levels and reduced gait speed.

Dissatisfied patients presented both increased knee joint pain ($p<0.0001$) and reduced preferred gait speed ($p=0.0063$; 1.15±0.17 m/s compared to 1.32±0.11 m/s for satisfied patients and 1.33±0.13 m/s for healthy subjects). Gait speed for the dissatisfied patients is similar to pre-operative values previously reported for TKR patients [3]. This suggests reduced improvement in functional ability, which may in part be related to the increased pain levels experienced by the dissatisfied patients. While the pain may manifest at the surgery site (i.e. the knee) and subsequently contribute to dissatisfaction, additional factors have been shown to contribute to patient dissatisfaction, including the need for outside assistance, lack of social interaction, or presence of comorbidities, all of which have been shown to contribute to reduced satisfaction levels [4]. Additionally, the pain may have contributed to the observed reductions in kinematics and kinetics of replaced limbs in the dissatisfied group, even at 34 months after TKR procedure.

CONCLUSIONS

Asymmetrical loading appears evident given the differences in side loading in the dissatisfied patients. Correcting the loading imbalances, adding to the strength to improve walking speed, and managing the pain may help to alleviate dissatisfaction and improve walking ability.

REFERENCES

1. Beswick, et al. *BMJ Open.* 2(1): e000435, 2012.
2. Noble, et al. *Clin Orthop Relat Res*. 431: 2005.
3. Levinger, et al. *J Arthroplasty*. 28(6): 2013.
4. Anderson, et al. *J Arthroplasty*. 11(7): 1996.
5. Yoshida, et al. *Clin Biomech.* 23(3): 2008.

ACKNOWLEDGEMENTS

This study was partially funded by the Matching Dissertation Grant of the International Society of Biomechanics and the Department of Kinesiology at the University of Tennessee, Knoxville.

Table 1: Peak VGRF (BW), knee joint moments (Nm/kg), and knee angle and ROM (°): Mean ± SD.

	Dissatisfied Replaced	Dissatisfied Non-Replaced	Satisfied Replaced	Satisfied Non-Replaced	Healthy Dominant	Healthy Non-Dominant	Interaction p value
1st Peak VGRF#*	1.03±0.07^{AC}	1.08±0.07^{C}	1.08±0.06^{AC}	1.13±0.08	1.15±0.06	1.14±0.06	**0.0041**
2nd Peak VGRF#*	1.01±0.05^{ABC}	1.04±0.05	1.07±0.05	1.09±0.05	1.10±0.08	1.09±0.07	**0.0440**
LR Extension Moment*	0.42±0.18^{BC}	0.56±0.32^{BC}	0.55±0.20	0.70±0.24	0.74±0.22	0.74±0.22	0.1739
PO Extension Moment	0.16±0.08	0.20±0.10	0.26±0.09	0.26±0.08	0.20±0.11	0.21±0.11	0.0721
Flexion LR ROM#*	-11.1±6.4^{AC}	-15.4±3.3	-12.7±5.0^{AC}	-17.0±5.1	-18.1±4.1	-17.8±4.2	**0.0136**
Adduction LR ROM*	2.6±1.4	2.7±1.2	2.3±2.4^{C}	0.9±1.4^{C}	3.3±1.9	2.2±1.6	0.3317
LR Abduction Moment	-0.42±0.17^{C}	-0.50±0.08	-0.48±0.13	-0.48±0.14	-0.55±0.13	-0.42±0.13	**0.0248**
PO Abduction Moment	-0.29±0.15	-0.35±0.10	-0.33±0.09	-0.38±0.13	-0.33±0.10	-0.32±0.12	0.1982

#Limb main effect, *Group main effect
^{A} Significantly different from contralateral leg of same TKR group, ^{B} Significantly different from same leg of satisfied TKR group, ^{C} Significantly different from same leg of healthy group
LR=Loading Response, PO=Push Off

ESTIMATING WALKING SPEED USING A SINGLE CAMERA IN THE PLANE OF PROGRESSION

[1]Mathew Sunil Varre, [2]Jessica DeBerardinis, [1]Daniel E. Lidstone, [1]Ashley Trotter, [2]Mohamed B. Trabia, and [1]Janet S. Dufek
[1]Department of Kinesiology and Nutrition Sciences, [2]Department of Mechanical Engineering
University of Nevada, Las Vegas, Las Vegas, NV, USA
email: varre@unlv.nevada.edu

INTRODUCTION

Walking speed (WS) is a commonly used spatiotemporal measure to evaluate and identify differences between pathological and non-pathological gait [1]. Current measurement techniques include stopwatch and tape measure, instrumented walkway, automated timers, accelerometry and, two-dimensional (2-D) video techniques [1-3]. Previous 2-D videography studies placed cameras perpendicular to the sagittal plane to measure walking speed [3]. However, this approach cannot be used when experiments are conducted in long and narrow corridors or other constrained spaces. In this work, we present a video-based analysis technique to quantify walking velocity using a single camera placed along the line of progression of the participant, which can be used in limited spaces.

The purpose of our study was to introduce and demonstrate the utility of a novel and reliable approach to quantify walking speed using a single fixed camera, aligned along the plane of progression, as individuals walked away from the camera in a linear fashion. Single camera calibration was used to correct for lens distortion, minimize projection errors in a still image, and map pixels with real world measurements [4].

METHODS

A video camera (Nikon 1 J4; Lens: NIKKOR 10-30 mm; f/3.3 - 5.6; 60 Hz, Nikon, JP) was used in this research. The video camera was calibrated using 'Camera Calibrator' in the Computer Vision Toolbox application in MATLAB 2017b (MathWorks, USA) and a black and white checkerboard pattern (1.2 m x 0.9 m) consisting of 100 mm squares for given locations along the line of progression of walking. The camera was placed on a tripod at a distance of 1.5 m from the walkway and at height of 2 m tilted forward 60° to the line of

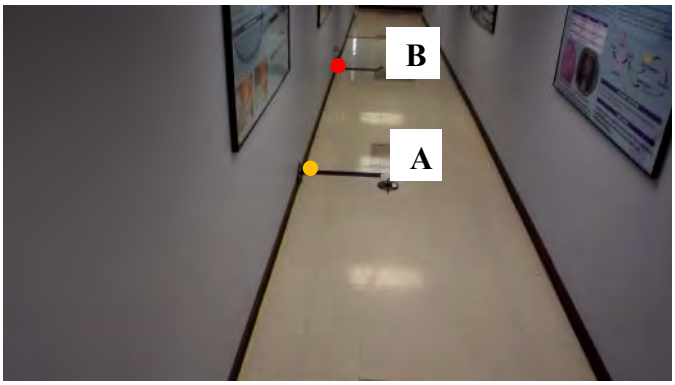

Figure 1: Experimental setup demonstrating the start and end point of the walkway. A: 3m tape location; B: 7m tape mark location.

of progression of walking (Fig 1). A calibration video was recorded using the camera with the checkerboard pattern orientated in different positions at 3m, 5m and 7m depth locations along a 10m illuminated walkway (Fig 1). Still images of the checkerboard in different positions were extracted from the video using the 'Video Viewer' tool in MATLAB. These images were used for calibrating the camera.

The camera calibration process yielded intrinsic and extrinsic parameters of the camera. The intrinsic parameters provided the focal length, principal point, radial and tangential distortions of the lens and, skew coefficient of the camera. The extrinsic parameters of the camera provided the translation and rotation vectors that were used to transform the pixels within a still image into global coordinates [4]. The origin of the global coordinate system was defined using a flat checkerboard pattern in the middle of the walkway. A re-projection error of <1 pixel was used as criteria for accurate calibration.

The extrinsic parameters provided the locations of the pattern with respect to the fixed camera.

High definition videos of fifty adults including 23 males and 27 females (59.5 ± 12.2 years; 1.7 ± 0.1 m; 96.5 ± 25.6 kg) were recorded during five consecutive walking trials at a self-selected pace for a distance of 10m along an illuminated walkway. Informed consent was obtained from the participants before the session (IRB#777036). A calibration video was recorded before every participant session.

Each participant's walking speed was analyzed for steps between locations A and B. These locations were used to reduce the effects of acceleration and deceleration phases of walking. Black contrasting tape was used to identify A and B.

Figure 2: Depiction of heel contact at first step (red circle) and last step (red dotted circle) during a walking trial considered for analysis. A: 3m tape mark location, B: 7m tape mark location.

Pixel coordinates of the walkway at 3m and 7m from the start point were obtained for each walking trial during individual participant sessions. For each walking trial, heel contact as the subject passed the 3m mark was considered as the first step and the pixel coordinates of the heel during this step were recorded (Fig 2). Similarly, heel contact of the step before the 7m tape marker was considered as last step and the pixel coordinates of the heel during this step was recorded. The difference between the video frame numbers of the first and last steps was used to calculate the time elapsed.

Using the camera parameters, the pixel coordinates of the first and last steps of each walking trial were transformed to global coordinates. The change in position of the heel from the first step to last step and the time elapsed were used to compute the walking velocity of the participant during the walking trial. A custom MATLAB code was written to detect the steps, perform the coordinate transformations, measure the distance between the two steps and, compute the velocities, based upon on the procedures described.

Statistical analysis was performed to obtain descriptive statistics using SPSS 24 (IBM, USA). Test-retest reliability of the measurement technique (N=49) was performed to measure the variations in the walking speeds of the participants among five walking trials using a two-way mixed model for absolute agreement.

RESULTS AND DISCUSSION

Participants walked with an average WS of 0.91 ± 0.19 m/s. The technique was found to have good test-retest reliability (across 5 walking trials) with an ICC of 0.93 (95% CI: 0.856-.963). This is comparable to WS measured using automatic timers and stop watches in 10m walk tests which showed excellent test-retest reliability (ICC: 0.96-0.98) [2].

CONCLUSIONS

2-D analysis of WS for individuals in a constrained setting while moving away from a fixed calibrated video camera placed in the plane of progression has been successfully demonstrated. The measurement technique described estimated the walking speed of participants with good reliability.

REFERENCES

1. Middeleton et al. *J Aging Phys.* **23**(2), 2015.
2. Peters et al. *J Geriatr Phys Ther*. **36**, 2013.
3. Nigg and Skleryk, *Clin Biomech*. **3**, 1988.
4. Zhang, Z. *IEEE Trans. Pattern Anal. Mach. Intell*. **22**(11), 1998.

ACKNOWLEDGEMENTS

The project described was supported by a grant from the National Institute of General Medical Sciences (GM 103440).

CHARACTERIZING UPPER EXTREMITY FUNCTION USING REAL WORLD EVIDENCE

Christina M. Webber, Alexander Y. Shin, Kenton R. Kaufman

Mayo Clinic, Rochester, MN, USA
email: kaufman.kenton@mayo.edu

INTRODUCTION

Recently, the U.S. Food and Drug Administration (FDA) has begun emphasizing the importance of real world data (RWD) and real world evidence (RWE). RWD comes from various sources, including electronic health records, billing data, and patient mobile devices used everyday life [1]. RWE is derived from RWD and applied to clinical practice.

While the information gained from traditional laboratory based studies is valuable, it is important to acknowledge its limited perspective. The use of RWD and RWE strengthens typical evidence generated by clinical trials required for medical device approval and development of clinical practice guides [1,2]. Activity monitoring using triaxial accelerometers provides the opportunity to collect RWD that assesses function in the free living environment [3]. Development of quantitative functional outcome measures from RWD is key to better understanding the effects of surgical intervention. This is particularly the case for upper extremity (UE) trauma, especially brachial plexus injuries (BPI). These injuries are devastating and often result in a complete loss of sensory and motor function in the affected UE [4]. Function is typically evaluated using a muscle grading system [5]. This approach focuses on muscle activation, range of motion, and strength, but does not necessarily prove functionality.

In an effort to move towards the use of RWD in clinical practice as a functional outcome measure, this study analyzed bilateral UE activity in patients who have undergone surgery to restore arm function after a BPI. It was hypothesized that subjects with BPI surgical reconstruction would exhibit more symmetrical UE activity compared to those individuals who had yet to receive surgical treatment for BPI.

METHODS

Twenty five subjects (Table 1) participated in this IRB approved study. Upon providing consent, subjects wore four +/-6g triaxial accelerometers (ActiGraph, Pensacola, FL) on bilateral forearms and upper arms for four days. Activity data was collected at 50 Hz.

Table 1: Subject demographics

	Sex (Male:Female)	Age (years±StDev)
Control	8:1	39±12
Pre-	7:3	34±12
Post-	6:0	39±14

Acceleration data were exported from the device using ActiLife software (ActiGraph, Pensacola, FL). Custom MATLAB code (MathWorks, Natick, MA) was used to filter the data and partition it into 60 second epochs. Methods presented by Hurd et al. [3] were used to calculate the asymmetry index between limbs (Equation 1). Group differences were explored using the Tukey-Kramer method. Statistical significance was set at $p \leq 0.05$.

Equation 1. Asymmetry index (A_x), where U is the activity of the uninvolved limb and I is the activity of the involved limb

$$\text{If } U \geq I, \text{ then } A_x = \frac{U}{I} - 1$$
$$\text{If } U < I, \text{ then } A_x = 1 - \frac{I}{U}$$

RESULTS AND DISCUSSION

An asymmetry index closer to 0 indicated more symmetrical UE use between sides, as evident in the control subjects (Table 2).

Table 2: Asymmetry index (standard deviation)

	Forearm	Upper Arm
Control	0.09(0.07)	0.07(0.05)
Pre-	2.03(0.63)	0.82(0.24)
Post-	0.16(0.65)	0.55(0.27)
Shoulder [3]	0.13(0.20)	0.17(0.17)

Both subject groups with BPI had asymmetry indices significantly different than controls (Figure 1). However, forearm asymmetry decreased in the post-surgery group as compared to the pre-surgery group.

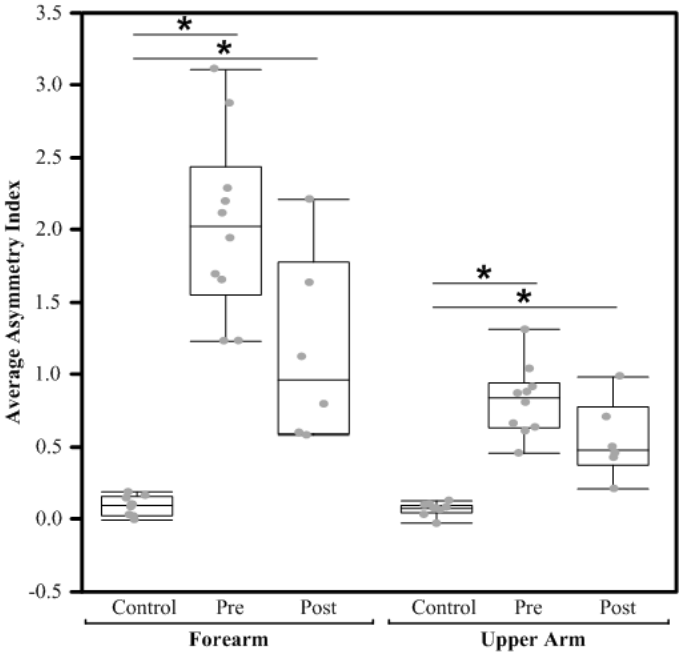

Figure 1. Asymmetry index plotted in quartiles, with individual subject values as grey dots. Statistically significant ($p \leq 0.05$) differences are indicated with a star (*).

Given that surgical reconstruction options first aim to restore elbow flexion, this observation provides real world evidence supporting anecdotal patient reports of increased usage of the affected forearm after surgery. Asymmetry index has been used previously to evaluate patients with shoulder pathology [3], making this a viable, objective functional outcome measure.

CONCLUSIONS

Analyzing the activity of the upper extremities following treatment of a BPI provides objective real world evidence of functional in daily life. Further studies comparing the activity before and after treatment can provide insight into the efficacy of the surgical treatment and aid in guiding clinical practice.

REFERENCES

1. U.S. FDA. Use of real-world evidence to support regulatory decision-making for medical devices. 2017.
2. Sherman RE, et al. *N Engl J Med* **375**(23): 2293-2297, 2016.
3. Hurd WJ, et al. *J Electromyogr Kinesiol* **23**: 924-929, 2013.
4. Barrie KA, et al. *Neurosurg Focus* **16**(5): Article 8, 2004.
5. Riddoch A, et al. War Memorandum No. 7. 1943.

ACKNOWLEDGEMENTS

Fellowship funding (Webber) was provided by NIH T32-AR056950 and Mayo Clinic Graduate School of Biomedical Sciences.

EFFECTS OF TRUNK MOVEMENT RETRAINING ON GAIT MECHANICS OF A PATIENT WITH TRANSTIBIAL AMPUTATION

[1,2] Adam J. Yoder, MS, [1,2] Brittney Mazzone, PT, DPT, [1,2] Shawn Farrokhi, PT, PhD

[1] Extremity Trauma & Amputation Center of Excellence, San Diego, CA
[2] Naval Medical Center San Diego
email: adam.j.yoder.civ@mail.mil, web: https://health.mil/EACE

INTRODUCTION

Patients with a lower limb amputation can present with multiple movement deviations, in some cases with suspected relations to reported musculoskeletal pain and decreased function. Methods to change aberrant movement patterns using sessions of biofeedback-based retraining have shown promise in able-bodied populations [1], yet implementations with limb amputation patients are relatively scarce. Obstacles with prosthetic device management, multiple limb amputations and pain involvement sites, or fear of movement, all may pose barriers to systematically learning and retaining a new movement strategy.

One means to address a portion of these challenges is to focus on faulty trunk movement. Abnormal trunk motion during walking has suspected associations with a number of secondary complications, such as back pain and susceptibility to falls [2,3]. Additionally, trunk kinematics are relatively simple to measure in real-time and explain to patients in terms of a feedback target. Although how well persons with lower limb amputation can modulate trunk motion and coordination without supplemental strengthening and prosthetic interventions is unclear [2,3]. The aim of this study is to report treatment effects for a patient with transtibial amputation who underwent movement retraining to reduce lateral trunk lean.

METHODS

The patient was a 29 year old male, active duty United States Marine Corp service member (Ht=175cm, Wt=69kg), referred to the Movement Retraining Clinic at the Naval Medical Center San Diego. Initial injury was due to high-energy blast trauma that resulted in right transtibial amputation and left knee patellar fracture (8 years prior), with later surgical revision of the residual, right fibular head (1.7 years prior). At referral, the patient's stated goals were to improve his walking and to address low back and right knee pain he felt were associated with his movement. A biomechanical walking evaluation was performed with the patient wearing his own passive prosthetic foot using a 14-camera passive-optical system (120Hz), a full body six-degree-of freedom marker set, and a force-instrumented treadmill (1200Hz). The treating physical therapist identified exaggerated lateral trunk range of motion (ROM) as a primary deviation, further exacerbated by a variable right toe-in \ toe-out strategy – used occasionally to alleviate right knee pain, per patient self-report.

The patient was prescribed eight training sessions (S1-S8) with an aim to limit peak-to-peak lateral trunk motion during walking. Frontal plane trunk angle relative to the lab was continuously displayed on a television screen relative to a 0.0 ± 3.0^{o} target range, with green coloration indicating adherence and red indicating limits exceeded (Visual3D). Similar to [1], total walk time was incrementally increased each session (S1=10min → S8=20min), while total time viewing feedback was faded over S5 to S8. Follow up evaluations were completed immediately after (POST) and one month after (FU) the final session. Changes in trunk kinematics were assessed using peak-to-peak ROM, and trunk-pelvis continuous relative phase (CRP) calculated per [4], using a 20 second recording (≈15 strides) taken after eight minutes of walking. Metrics were first calculated per prosthetic limb stance phase then compiled to session inter-cycle mean and standard deviation. Patient self-report outcomes were also taken at each evaluation, including the Visual Analog Pain Scale (VAS, 0-10cm) and Single Assessment Numeric Evaluation (SANE, 0-100%).

RESULTS AND DISCUSSION

The patient successfully completed all eight treatment sessions, with self-report measures notably improved at POST and FU. The SANE, which measures 0-100% ability to move the affected body regions increased from 50% PRE to 70% at POST, and was retained at 75% at FU (Table 1). Pain measured by VAS decreased by 2.4cm and 1.8cm at POST and FU, relative to PRE.

The primary retraining target of frontal plane trunk ROM decreased in inter-cycle mean from 7.3^o at PRE to 3.4^o at POST, with FU retention at 3.8^o (Table 1). Less side-to-side trunk motion may lessen net demand on trunk-pelvis musculature and lower limb joints for lateral stabilization and have positively influenced this patient's reported back/knee pain. However modifying habitual trunk motion could also influence trunk-pelvis segmental coordination – a measure prior shown sensitive to low back pain status in able-bodied persons [4]. PRE to POST, mean frontal CRP decreased from 143^o to 104^o with increased inter-cycle variability – changes that persisted through FU. For reference, a range of 120^o(±15^o) during walking has been reported for frontal CRP in able-bodied persons with no current or prior low back pain [4], and increasing CRP variability is generally associated with greater motor adaptability and flexibility to perturbations [3,4]. Clinically important CRP change magnitudes are challenging to ascertain, regardless the concurrent within-patient changes observed here in frontal peak-to-peak trunk ROM, trunk-pelvis CRP, and pain/function may suggest a relationship among these measures to explore further in this patient population.

Lateral trunk lean in the gait of patients with lower limb amputation is frequently discussed in relation to low back and hip strength/endurance deficits as possible, causative factors [2]. In this single case, a patient with transtibial amputation was able to immediately limit their lateral trunk motion when provided kinematic feedback, and to maintain those changes for up to 20 minutes of continuous walking without concomitant strengthening or manual physical therapy interventions. While every patient will have unique treatment needs, this demonstrates that these added interventions may not always be a requisite to resolve a trunk lean deviation.

CONCLUSIONS

This preliminary clinical case demonstrated that a session-based movement retraining program can be successfully applied to decrease lateral trunk motion of a patient with transtibial amputation during walking. Self-reported pain and physical function were also improved after treatment. Supplementary analyses suggested that frontal trunk-pelvis coordination was also influenced by the intervention. Future study should assess broader efficacy of the treatment methods across a larger sample of patients with lower limb amputation and trunk lean deviation.

REFERENCES

1. Crowell, et al. J Orth Sprt. 40(4) 206–213, 2010.
2. Devan et al. Medical. Hyp. 82(1) 77–85, 2014.
3. Russell Esposito et al. Gait P. 40(4) 640–6, 2014.
4. Seay, et al. Clin. Biomech. 26(6) 572–8, 2011.

Table 1: Trunk and pelvis kinematics before (PRE), after (POST), and at one month (FU) following treatment, after 8 minutes of 1.2m/s walking; 15 prosthetic stance phases were used to compute inter-cycle mean (standard deviation). For continuous relative phase (CRP), a 0^o magnitude represents in-phase trunk-pelvis coordination, and 180^o anti-phase. VAS=Visual Analog Scale, SANE=Single Assessment Numeric Scale.

			Trunk ROM (Deg.)			Trunk-Pelvis CRP (Deg.)		
	VAS Pain (0-10cm)	SANE (0-100%)	Frontal	Transverse	Sagittal	Frontal	Transverse	Sagittal
PRE	4.5	50	7.3(0.9)	12.8(2.4)	4.9(1.7)	143(18)	98(23)	98(34)
POST	2.1	70	3.4(1.3)	8.9(2.1)	4.4(0.9)	104(47)	113(31)	101(30)
FU	2.7	75	3.8(1.0)	9.9(1.1)	4.2(0.9)	116(31)	109(34)	103(37)

VALIDATION OF MICRO SPIKES FOR MOUNTING AN IMPLANT TO A TENDON

Won Suk You, Justin Casebier and Ravi Balasubramanian

Oregon State University, Corvallis, OR, USA
email: ravi.balasubramanian@oregonstate.edu, web: http://web.engr.oregonstate.edu/~balasubr/

INTRODUCTION

In previous work, we have shown that it is biomechanically beneficial to use implantable passive mechanisms to re-engineer the mechanics of force and movement transmission within the body [1]. Specifically, we have shown that a surgically constructed differential mechanism using biological tendons and a simple strut in the tendon-transfer surgery for high median ulnar palsy enables adaptive movement between fingers even when all four finger tendons are driven by one muscle. Overall, the new implant-based surgery provides increased finger flexion over the conventional surgery during physical-interaction tasks such as the grasping of objects.

The current embodiment of this implant requires the tendons to be sutured to the implant. It has been seen in an avian animal model that the suture creates too much trauma to the tendon, which then instigates a fibrotic healing response and long-term scarring [2]. This paper seeks to re-design the implant so that sutures are not necessary for long term adhesion. This paper presents preliminary designs of the implant, attachment method using micro spikes, and its durability via cycle testing.

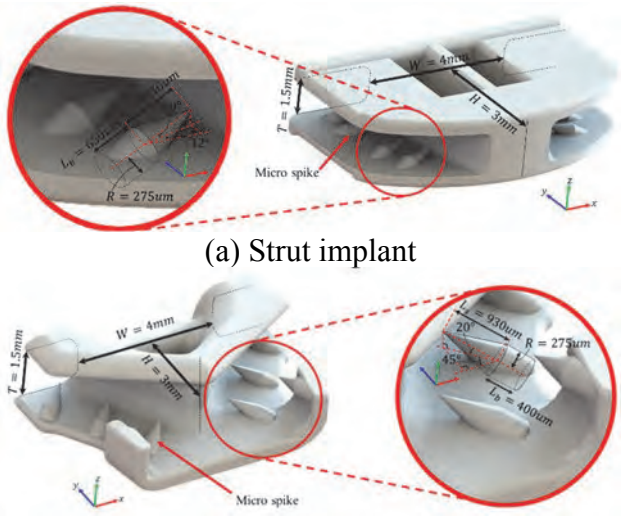

(a) Strut implant

(b) V-shape implant

Figure 1: New implant design use either (a) micro spikes, or (b) both micro spikes and structural locking method to secure the tendon to the implant.

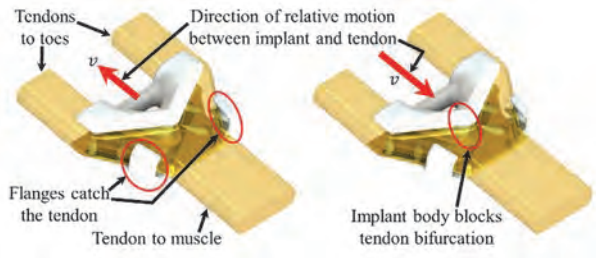

Figure 2: Depiction of structural locking mechanism of 'V-shape implant'.

METHODS

The key requirement of the new implant design is to secure the implant to the tendon using a method that will promote secure attachment while mitigating foreign body response. To achieve this, two implant designs were chosen (see Fig. 1). The first design uses multiple micro spikes and sits between the tendons (Fig. 1(a)). The second design also uses spikes and adds a structural locking method to the design (Fig. 2(b)). After a survey of prior work that designed spikes for attaching implants to tendons, we chose the following spike dimensions: 275um base radius (R), 930um spike length (L_s), and 20° inclination from x-y plane. The spikes are angled toward the center of the implant to secure the tendon to the implant.

The only difference between two designs is that the 'V-shape implant' use flanges to structurally prevent relative motion between the tendon and the implant as shown in Fig. 2. The implants were 3D-printed through 3D systems, Inc. (M2R-WT, Acrylate, Tensile strength 35-45MPa). Two samples of each implant were attached to the extensor digitorum longus in chicken cadavers approximately 8.5 mm distal of the natural bifurcation (one implant per leg)

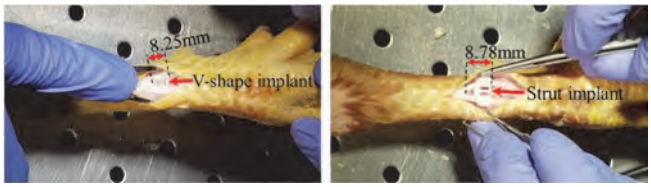

Figure 3: The implants in chicken cadaver legs.

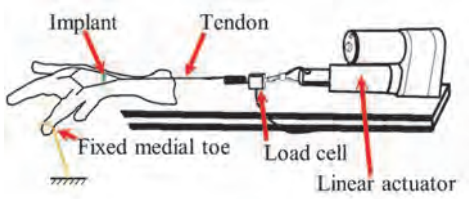

Figure 4: Experimental setup of the cycling test.

Table 1: Parameters of cycle test.

No.	Implant type	Cycle	Avg. pulling forces (N)	Std. of forces (N)
1	V-shape	2000	8.0153	1.5123
		2000	11.7622	3.0705
		1000	19.9331	0.8046
2	V-shape	2000	7.4169	0.8127
		2000	10.9744	0.6778
		1000	20.87	0.9035
3	Strut	2000	8.0228	0.7737
		2000	11.6285	3.5959
		1000	21.2655	3.5602
4	Strut	2000	7.3164	0.5169
		2000	12.1309	2.8325
		1000	20.5877	1.4079

(Fig. 3). Surgeries were performed by Dr. Jennifer J. Warnock, DVM (Oregon State University, College of Veterinary Medicine).

The implant's endurance in mechanically attaching to the tendon is validated by cycling the implanted legs as in Fig. 4. Each leg was cycled for a total of 5000 cycles (Table 1). The cycles were split up as follows: The first 2000 cycles were pulled with a force of 8N. This is the force required to fully extend a chicken foot under no load [3]. Next, the tendon is pulled with 11~12N for 2000 cycle to see how the implant and micro spikes endure a force higher than natural full extension. Finally, a 20N force is applied to the tendon for 1000 cycle to see whether it can withstand the extreme force. After conducting the cycle test, tendons and implants were dissected from the chicken legs and checked visually for any signs of wear or damage.

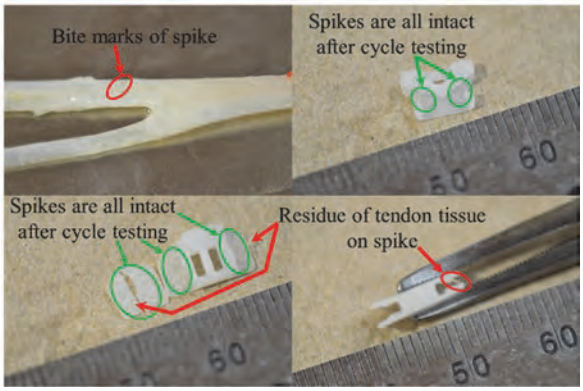

Figure 5: Tendon and implants after cycling test.

RESULTS AND DISCUSSION

Fig. 5 shows small marks on the tendon which signifies that the micro spikes engaged mechanically with the tendon. Tissue residuals were also found on the micro spikes. Although some spikes showed wear, all the spikes survived the 5000 cycles. Therefore, we conclude the micro spikes enable a secure mechanical attachment between biological tendon and implant. Future work includes validating the spike-based implants in vivo.

REFERENCES

1. Homayouni et al. *IEEE Transactions on Biomedical Engineering,* **62**(9), 2208-2214, 2015.
2. Le et al. *Proceedings of 44th VOS Conference*, Snowbird, Utah, 2017.
3. Gilbert et al. *Journal of biomedical materials research*. **19**(5), 601-605, 1985.

ACKNOWLEDGEMENT

This work was supported in part by the Office of the Assistant Secretary of Defense for Health Affairs, through the Joint Program Committee 8 (JPC8), Clinical and Rehabilitative Medicine Research Program (CRMRP), Neuromusculoskeletal Injuries Research Award (NIRA), Funding Opportunity Number: W81XWH-15-JPC-8/CRMRP-NMSIRA, under Award No. W81XWH-16-1-0794. Opinions, interpretations, conclusions and recommendations are those of the author and are not necessarily endorsed by the Department of Defense.

HOPPING PERFORMANCE IN INDIVIDUALS WITH ACHILLES TENDON RUPTURE: APPLYING A CONSTITUENT LOWER EXTREMITY WORK APPROACH

[1] Jennifer A. Zellers, [1]Anahid Ebrahimi and [1] Karin Grävare Silbernagel
[1] University of Delaware, Newark, DE, USA
email: jzellers@udel.edu

INTRODUCTION

Achilles tendon rupture results in permanent calf strength deficits along with altered jumping and running biomechanics observed at least 5-7 years following injury[1]. One of the challenges in this patient population is quantifying patient performance during common functional tests, such as the repetitive hopping task, in a way that is easily interpreted and captures compensatory strategies at the ankle and more proximal lower extremity joints.

Recently, the constituent lower extremity work (CLEW) approach[2] has been proposed as a clinically applicable way to quantify and display constituent-level contributions to absolute limb work during a cyclic movement task. This approach seems to hold the potential of describing performance on a hopping task in individuals with Achilles tendon rupture, however, it has only been used in healthy individuals and an individual with unilateral amputation during a walking task. Therefore, the purpose of this study was to apply the CLEW approach to individuals with Achilles tendon rupture to quantify hopping performance and identify constituent-level compensations in the context of impaired ankle function.

METHODS

This study describes two cases of individuals with unilateral Achilles tendon rupture with surgical repair. Morphological measures of the triceps surae musculotendinous unit included Achilles tendon length[3], soleus thickness[4], and gastrocnemius cross sectional area[5] were taken using B-mode ultrasound imaging. Participant self-reported symptoms and function was assessed using the Achilles tendon Total Rupture Score (ATRS)[6] with higher scores indicating better symptoms and function.

Kinematic and kinetic data were collected using an 8-camera motion capture set-up (Nexus, Vicon, UK) and force plate (Bertec Corporation, USA). After static calibration, participants were asked to perform a repetitive hopping task, similar to jumping rope on one foot. Twenty-five hops were performed, of which 10 hops from the middle of the trial were used for analysis. 6 degree-of-freedom powers were calculated at four constituents (distal foot, ankle, knee, hip) of the stance limb[2]. Positive and negative portions of each constituent power curve were integrated over three intervals to attain positive and negative work, respectively: landing (initial contact to peak knee flexion), takeoff (peak knee flexion to toe off), and air (toe off to initial contact). Absolute limb work was the sum of all positive and absolute negative constituent work over the three intervals. Relative constituent work was the positive or negative constituent work as a percentage of absolute limb work.

RESULTS AND DISCUSSION

Case information is described in Table 1. Findings from the CLEW analysis are displayed in Figure 1 and Table 2.

Table 1: Case study descriptions.

	Case 1	**Case 2**
Sex	Female	Male
Age (years)	46	28
Time from surgery (months)	26	13
Achilles tendon elongation (cm)	2.2	3.1
Muscle cross sectional area LSI (%)		
Lateral Gastrocnemius	90	110
Medial Gastrocnemius	117	68
Soleus muscle thickness LSI (%)	90	82
ATRS (out of 100)	91	96

In an individual with 2.2 cm of tendon elongation and recovered muscle cross-sectional area (case 1), we found nearly symmetrical absolute work and relative constituent work during hopping (Table 2). Conversely, an individual with more asymmetrical musculotendinous structure (case 2) performed less absolute limb work on his ruptured side. Also in case 2, we found the ankle did less relative positive work

during takeoff on the ruptured side compared to the intact side, with the knee appearing to increase in relative positive work as a compensation for ankle dysfunction. Although we do not present the data here, we found the non-standing limb in both cases to contribute relatively little to the hopping task, with contributions coming primarily from the hip.

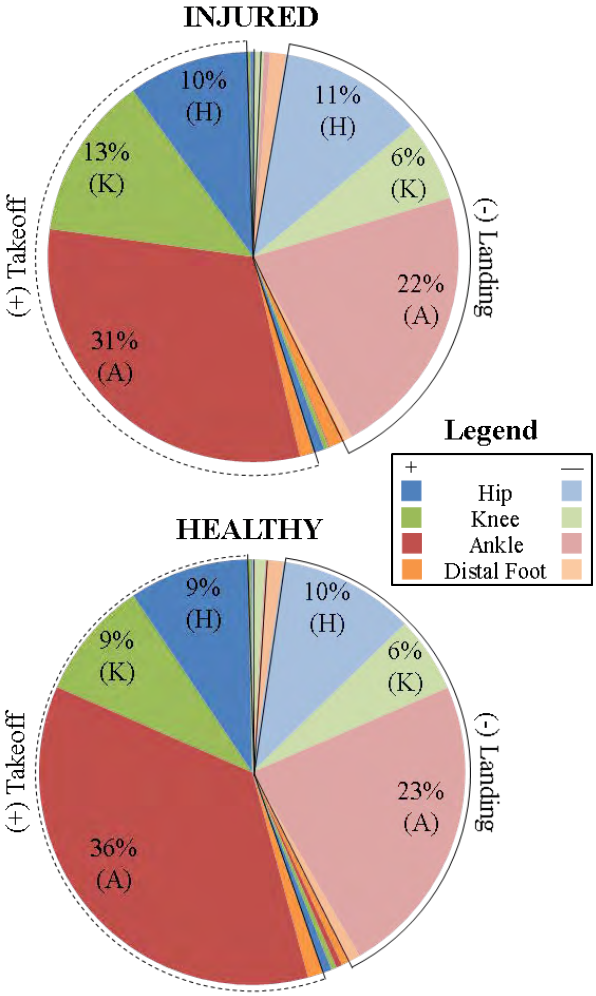

Figure 2. Relative work pie charts for case 2. Note size of pie chart is scaled by absolute limb work.

These findings are consistent with prior work that has described peak power generation during a hopping task to shift away from the ankle and toward the knee[1]. Greater asymmetries in ankle kinetics and kinematics have been previously associated with tendon elongation and calf strength deficits, respectively[7]. Using the CLEW approach, we saw relatively less ankle and more knee contribution to overall work in an individual with greater tendon elongation and smaller calf cross sectional area.

CONCLUSIONS

This study utilized a novel approach to quantifying and reporting biomechanical data to identify adaptations during a hopping task in individuals with unilateral Achilles tendon rupture with surgical repair. An individual with more structural asymmetries was found to have relatively lower ankle and greater knee work contributions to absolute limb work compared to an individual with less structural asymmetries.

Although only a descriptive case series, this study supports the application of the CLEW approach on injured populations and supports the use of the approach to cyclic tasks outside of walking.

REFERENCES

1. Willy et al. *Am J Sport Med.* 45(5):1124-33, 2017.
2. Ebrahimi et al. *Gait and Posture*. 56:49-53, 2017.
3. Silbernagel et al. *Muscles, Lig, Tendons J*. 6(1):104-10, 2016.
4. Dudley-Javoroski et al. *Ultrasound Med & Biol*. 36(10):1594-1607, 2010.
5. Park et al. *Yonsei Med J*. 55(4): 1115-22, 2014.
6. Nilsson-Helander et al. *Am J Sport Med*. 35(3):421-6, 2007.
7. Brorsson et al. *Am J Sport Med*. 45(13):3060-8, 2017.

ACKNOWLEDGEMENTS

Research reported in this publication was supported by the National Institutes of Health under Award numbers P30-GM103333 and R21AR067390, the NSF GRFP (Grant #1247394), the Foundation for Physical Therapy, and the University of Delaware Research Foundation.

Table 2: Absolute limb work and relative work in two individuals with Achilles tendon rupture.

			Takeoff			Landing		
		^{abs}Work	$^{+}RW_{hip}$	$^{+}RW_{knee}$	$^{+}RW_{ankle}$	$^{-}RW_{hip}$	$^{-}RW_{knee}$	$^{-}RW_{ankle}$
Case 1	Injured Hop	3.41 J/kg	4%	15%	33%	8%	9%	24%
	Healthy Hop	3.32 J/kg	7%	15%	29%	11%	8%	21%
Case 2	Injured Hop	2.61 J/kg	10%	13%	31%	11%	6%	22%
	Healthy Hop	3.38 J/kg	9%	9%	36%	10%	6%	23%

REGULAR RUNNING IN MIDLIFE MAY BE PROTECTIVE OF PLANTARFLEXOR FUNCTION AFTER A PROLONGED WALK

[1] Erica M. Casto [2]Jocelyn F. Hafer and [1,3] Katherine A. Boyer

[1] University of Massachusetts Amherst, Amherst, MA
[2] University of Michigan, Ann Arbor, MI
[3] University of Massachusetts Medical School. Worcester, MA, USA
email: ecasto@kin.umass.edu, web: http://people.umass.edu/mobl/

INTRODUCTION

Aging is associated with declines in mobility and alterations in gait [1,2]. Muscle function and control may be a contributing factor to these mobility changes as midlife adults are shown to have altered muscle activation and co-activation patterns compared to young adults [2,3]. Greater muscle activation and co-activation may increase the economic cost of walking for midlife adults [2] and may also increase contact forces within the joint [4] increasing the risks for fatigue related falls and musculoskeletal injury.

There remains a need for a better understanding of factors influencing muscle activation with aging to develop targeted interventions for mobility. There is evidence to suggest that highly active midlife adults may be protected against both increases in cost of walking [5] and slowing gait speeds [6], as well as against knee extensor muscle fatigue from extended bouts of walking [7]. These findings may be explained by a mitigating effect of physical activity on altered muscle activation, but this has not been examined. Comparing midlife adults' muscle activation across physical activity level and in response to a bout of exercise may yield insight into how highly active midlife adults maintain the gait speed, cost of walking, and possibly gait mechanics of young adults.

Therefore, the aim of this study was to quantify the differences in muscle activity at the beginning and end of a prolonged treadmill walk in healthy young (Y), highly active midlife (RUN), and sedentary midlife (SED) females. It is hypothesized that sedentary midlife females will have longest duration of activation and greatest peak activation of the knee extensor and plantarflexors, and these differences will be larger following the prolonged walk.

METHODS

Twenty-eight female participants: 10Y (Age: 27.0 ± 3.5yrs; BMI: 23.19 ± 2.1kg/m^2; Speed: 1.41 ± 0.15m/s); 10 RUN who ran ≥15mi/wk (Age: 60.5 ± 3.9yrs; BMI: 21.2 ± 2.2kg/m^2; Speed:1.43 ± 0.12m/s;); and 8 SED exercising ≤ 2 times/wk (Age: 61.8 ± 1.4yrs; BMI: 23.9 ± 1.7kg/m^2; Speed: 1.34 ±0.10m/s); participated in this study. All participants completed an IRB approved informed consent prior to completing any study procedures.

Participants completed a 30 minute treadmill walk (30MTW) with intermittent "challenge" periods to simulate a bout of daily activity [8]. Electromyography (EMG) was collected during the 2nd and 30th minute of. Electrodes (Trigno, Delsys, Inc., Natick MA) were placed over 8 lower extremity muscles: vastus lateralis (VL), vastus medialis (VM), rectus femoris (RF), biceps femoris (BF), semitendinosus (ST), lateral gastrocnemius (LG), medial gastrocnemius (MG), and Tibialis Anterior (TA). EMG were bandpass filtered at 20-500Hz, full-wave rectified and then lowpass filtered at 20Hz to produce a linear envelope. Linear envelopes for each muscle were expressed as a percentage of the average stance phase signal for 10 consecutive strides from the 2nd minute of the 30MTW.

Peak, and duration of activation were calculated for each muscle from minutes 2 and 30 of the 30MTW. EMG time on/off for each muscle was determined by using a threshold set at 2 standard deviations from baseline. Duration was then calculated as the total time above this threshold throughout stance. A 2x3 (time*group) repeated measures ANOVA was used for each muscle to compare EMG peak, time of peak, and duration of activation between the three groups at the beginning and end of the 30MTW.

RESULTS AND DISCUSSION

Duration of activation in the knee extensors and flexors were not significantly different between groups across time. Peak activation of VM (Table 1) decreased significantly in SED ($p=0.041$) during early stance and in RUN during midstance ($p=0.033$). No differences were found between SED and RUN in VM peak activation throughout stance indicating that these changes are likely due to age rather than activity level.

Peak activation of the MG during late stance and LG in early stance decreased across time in all groups, with no difference between groups. In both early and midstance a group by time interaction was found for the MG ($p=0.034$ and $p=0.029$ respectively). Post-hoc testing showed no difference in peak activation of the MG between groups at the beginning of the walk, however, at the end, RUN had an increased peak activation while SED and Y decreased or had no significant change in the peak activation. These results suggest that regular running in midlife may protect women against the commonly observed distal to proximal shift in joint power during walking, thereby potentially limiting both slowing gait speed and increasing cost of walking.

The difference in response to the 30MTW for Y and SED as compared to RUN may be related to the onset of muscle fatigue at the end of the 30MTW. In a prior analysis of these participant groups we found both the Y and SED groups experienced knee extensor fatigue (defined as a decline in power) following the walk, while RUN did not [7] suggesting regular running in midlife adults may mitigate muscle fatigue in response to the 30MTW. While changes in plantarflexor power were not quantified in this prior study, a similar decrease in MG activation has been reported in a study [9] examining the gait and muscle activity of young adults following a unilateral plantarflexor fatigue protocol.

CONCLUSIONS

Peak activation in VM decreased throughout the walk in both early and midstance in midlife women regardless of activity level when compared to young women suggesting that this is an effect of aging rather than disuse. Peak activation of MG and LG show differences throughout stance for RUN when compared to both young and sedentary midlife women. This suggests that regular running in midlife may be protective against changes in plantarflexor function following a prolonged moderate intensity walk and should be explored more in future studies.

REFERENCES

1. Boyer, et al., *Exp. Gerontol* (95) 63-70. 2017.
2. DeVita & Hortobagyi, *J. Appl Physiol* 1804-11, 2000.
3. Hortobagyi et al., *Gait & Posture*, (29) 558-64, 2009.
4. DeMers, et al., *J Orthop Res* 32:769-76, 2014.
5. Ortega, et al., *PLOS ONE,* 9(11):e113471, 2014
6. Boyer et al., *Gait & Posture.*(36) 149-53, 2012.
7. Hafer, Kent, Boyer. *J Ortho Res,* Submitted.
8. Foulis., et al., *PLOS ONE,* 12(9):e0183483, 2017.
9. Hunt & Hatfield, *J Electromyogr Kinesiol,* (35)24-29, 2017.

ACKNOWLEDGEMENTS

The work was funded in part by Graduate student research grants to J. Hafer provided by ASB, ACSM, and University of Massachusetts Amherst Graduate School.

Table 1: Mean change in peak activation from beginning to end of walk in Y, RUN, and SED expressed as % of mean activation during stance at baseline, $\alpha=0.05$. *significant over time, ^Significant difference between groups over time.

	VM early	MG early	LG early	VM mid	MG mid	MG late	LG late
Y	-2.28 (1.5)	-0.91 (1.1)*^	-0.75 (0.6)*	0.76 (0.6)	-0.28 (0.2)	-0.29 (0.24)*	-0.71 (0.74)*
RUN	-2.54 (2.5)	0.98 (1.5)	0.41 (0.3)^	-1.2 (2.4)*	0.61 (0.6)^	-0.60 (0.61)^	-0.67 (0.9)^
SED	-2.63 (1.4)*	-0.66 (0.5)^	-0.36 (0.4)	-1.3 (1.2)	-0.40 (0.7)	-0.41 (0.7)	-1.05 (0.9)*^
p-value	p=0.013	p=0.028^	p=0.051	p=0.03	p=0.029	p=0.032	p=0.002

LOWER LIMB JOINT ANGLE VARIANCE AS A FUNCTION OF OBSTACLE HEIGHT DURING OBSTACLE CROSSING

[1]Chuyi Cui, [2]Brittney Muir, [1]Jeffrey Haddad, [3]Richard van Emmerik, [1]Shirley Rietdyk, [1]Satyajit Ambike
[1]Department of Health and Kinesiology, Purdue University, IN, USA
[2]Department of Occupational Therapy, The Sage Colleges, Troy, NY, USA
[3]Department of Kinesiology, University of Massachusetts, Amherst, MA, USA
email: cui111@purdue.edu, web: https://www.purdue.edu/hhs/hk/Biomechanics-MotorBehavior/

INTRODUCTION

Tripping is a main contributor to falls and fall related injuries. To ensure crossing an obstacle without tripping, one has to elevate the foot higher than the upper edge of the object. Typically, the trail foot (the foot that crosses second) contacts visible stationary obstacles more frequently than the lead foot (the foot that crosses first) [1].

The variability of foot clearance has been commonly used to quantify the risk of tripping during obstacle crossing [2]. During swing phase, lower limb segments from stance foot to swing toe form an open kinematic chain with multiple joint angles that influence the configuration of the swing foot. Foot variability clearly arises from the variability in joint angles. Although mean foot clearance and joint angles during obstacle crossing have been studied extensively, it is essential to study joint angle variances to understand toe height variability.

The purpose of this study is to (a) quantify the lead and trail toe height variability when crossing obstacles of different heights, and (b) investigate the source of the toe height variability by examining the lower limb joint angle variance.

METHODS

Ten young adults (age: 23.8±3.4 years, 3 females) walked along a 15 m walkway and stepped over an obstacle. Four obstacle heights were examined: unobstructed (no obstacle), 3, 10, and 26 cm. 10 trials of each condition were performed in block randomized order. Kinematic data were collected using the Qualysis Track Manager at 100 Hz.

Measures were calculated at the frame where tripping was most likely to occur: when the lead toe and the trail toe were above the obstacle, and at minimum toe clearance for unobstructed trials for both limbs.

We computed the across-trial standard deviation of the toe height (henceforth toe variability), the variances of lower-limb joint angles (sagittal hip, knee, and ankle of stance and swing limb), and the total joint angle variance as the sum of all six joint angle variances (henceforth total joint variance). Two-way mixed model ANOVA was conducted with *obstacle height* (unobstructed, 3, 10, 26 cm) and *limb* (lead, trail) as fixed factors. Tukey post hoc pairwise comparisons were conducted.

RESULTS AND DISCUSSION

Six of the 10 subjects contacted the obstacle one time (contact rate 2%; all with the 26 cm; five with the trail toe). Since contacting the obstacle modified gait in subsequent trials [3], data from the 26 cm condition was excluded from statistical analyses.

There was a significant interaction (*obstacle height by limb)* observed for toe variability ($F_{2,57}$=3.27; p=0.04; Fig. 1). Post hoc comparisons revealed that toe variability was not different for the lead and trail limbs for unobstructed and the 3 cm obstacle trials, but it was 72% higher for the trail limb for the 10 cm obstacle. Toe variability was 273% higher for 3 cm obstacle versus unobstructed ($p<0.01$). It was 80% higher for the 10 cm obstacle than the 3 cm obstacle, but only for the trail limb ($p<0.01$).

A significant interaction *(obstacle height by limb*) was observed for total joint variance ($F_{2,57}$=4.82; p=0.01; Fig. 2). Post hoc comparisons revealed that total joint variance with the trail crossing was 98% higher than the value of lead crossing for the 10 cm obstacle ($p<0.01$), whereas no difference for lead and trail crossing was observed for the unobstructed and 3 cm obstacle conditions. Total joint variance for trail

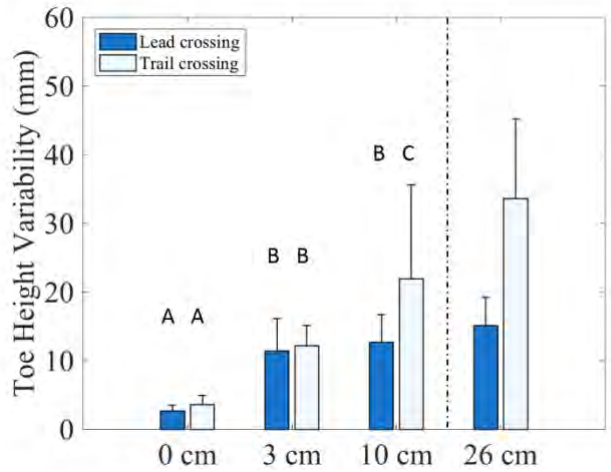

Figure 1: Effect of obstacle condition and limb for toe variability. 26 cm shown but not included in statistical analysis due to obstacle contacts. Letters A, B, C distinguish significantly different conditions.

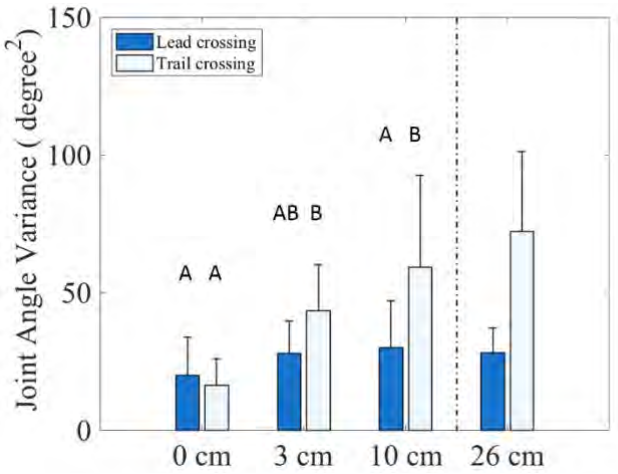

Figure 2: Effect of obstacle condition and limb for total joint angle variance.

crossing increased 164% for the 3 cm obstacle ($p<0.01$) and 259% for the 10 cm obstacle ($p<0.001$) compared with unobstructed walking; no significant obstacle effect was observed for lead crossing.

Overall, similar patterns were observed in toe variability and total joint variance (Fig. 1,2) as a function of obstacle height and limb: higher toe variability generally corresponded to higher total joint variance, consistent with the idea that total joint variance prescribes toe variability. There is an important exception – while toe variability and joint variance for the trail limb increased as a function of obstacle height, only toe variability increased for the lead limb. Future research should determine if the joint angles covary in a task-specific manner to control the variability in the toe height.

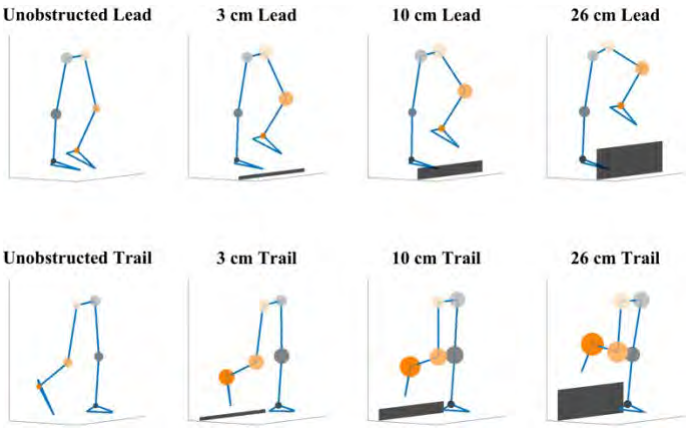

Figure 3: Individual joint angle variance marked on illustrative lower limb stick figures as circles. The area of circle reflects the amount of variance. Black rectangles are the obstacles.

We examined variances in each joint angle to locate the source of the toe variability. Qualitatively, variances in joint angles tended to be larger (quantified as larger circles on each joint, Fig. 3) during the trail crossing than lead crossing, and this pattern became more apparent for larger obstacles. The contribution from the stance limb joint angles to the toe variability is substantial. Although most research on obstacle crossing focus on the swing limb, stance limb behavior cannot be ignored.

CONCLUSIONS

Larger toe variability and total joint variance for the trail limb, especially for taller obstacles, is consistent with observations of greater failures with the trail foot [1]. Furthermore, the joint angle variances are distributed over the joints of both the swing and stance limb, indicating that the contribution of the stance limb to obstacle contacts must be considered. This suggests existence of compensatory covariance in the lower limb joint angles to control toe height. Further investigation into coordination between the individual joints of both limbs is necessary.

REFERENCES

1. Heijnen et al., Exp Brain Res, 2014
2. Mills et al. Gait Posture, 2008
3. Heijnen et al., Exp Brain Res, 2012

ESTIMATING GAIT EVENTS AND LOCOMOTION STATE WITH A BETA-PROCESS AUTO REGRESSIVE HIDDEN MARKOV MODEL

[1,2] Seth R. Donahue, [1,2] Li Jin, [1,2]Michael E. Hahn

[1] Bowerman Sports Science Clinic, [2] Neuromechanics laboratory, University of Oregon, Eugene, OR, USA
email: sethd@uoregon.edu, web: https://bssc.uoregon.edu/

INTRODUCTION

Identification of gait phase is important for many applications including control of active lower limb prostheses. One challenge for adaptive prostheses is accurate prediction of initial contact, toe off with minimal sensors and low sampling frequency. Previous work has used acceleration-based thresholds to identify initial contact and toe off [1]. These algorithms lack adaptability to different locomotion states and speeds. The beta-process auto-regressive hidden Markov model (BP-AR-HMM) has been shown to accurately identify different human movement patterns from motion capture data at low sampling frequency (10 Hz) [2]. Unlike other classification algorithms the BP-AR-HMM provides a statistical model for classification. The purpose of this exploratory data analysis is to determine the feasibility of the BP-AR-HMM to identify and estimate gait events and locomotion states from a single simulated accelerometer sampling at low frequency during two different gait transitions.

METHODS

Ten able-bodied subjects participated in the study (51 ± 6.0 years, 173 ± 11.4 cm, 70 ± 15.0 kg) (5 male, 5 female). Ground reaction force (GRF) and marker trajectory data were collected at 1200 Hz and 120 Hz, respectively. Subjects were asked to perform two different transitions: walk to run (WRT) and run to walk (RWT) transition on a force-instrumented treadmill (Bertec, Inc., Columbus, OH). The WRT protocol began with walking at 1.8 m s^{-1} for 30 seconds, then the treadmill was constantly accelerated at 0.1 m s^{-2} to 2.4 m s^{-1}. Subjects were asked to transition to running gait whenever they felt ready during the acceleration stage. After transitioning to a running gait, they ran at 2.4 m s^{-1} for another 30 seconds. The RWT protocol was the inverse of the RWT, starting at 2.4 m s^{-1} for 30 seconds, then the treadmill was constantly decelerated at -0.1 m s^{-2} to 1.8 m s^{-1}.

The GRF data were filtered with a low pass fourth order Butterworth filter (50 Hz cut off frequency). Ground contact state was determined when the vertical GRF values were above a threshold of 50 N. Motion trajectory data from a single marker on the dorsum of the left foot were extracted from a larger data set [3]. Three-dimensional (3D) acceleration values were calculated by taking the second derivative of the raw marker position data. The GRF and acceleration data were then down-sampled to 20 Hz. The algorithm was tested on a set of 17 trials. One trial was removed from the data set because the GRF data were incomplete for the present analysis

The BP-AR-HMM is composed of three major parts (2). The beta process determines the number of states available for each time series, based upon a Bernoulli probabilistic model. Vector autoregression implies acceleration throughout the gait cycle at any given time is a function of the previous acceleration values and random variation. The use of auto-regression also allows for features to be shared across different time series via the beta process. The hidden Markov model assumes a set of distributions and transitions between them follow a Markov process. The assumption of the Markov process is the probability of state change from i to j has a set probability π_{ij}, which does not depend on prior state. The algorithm also contains a parameter to limit state transitions at each time step. This parameter helps to ensure the estimated states are biomechanically relevant. The BP-AR-HMM algorithm used a data driven model to estimate and share states across each time-series.

The temporal differences between the change in the estimated state and the measured initial contact (IC) and toe off (TO) of the left foot were calculated. Duration of a state was calculated from the first

instance of desired state to the first instance of a different state. The duration of the state indicating stance phase was calculated to estimate whether the current gait was walking or running. With an effective sampling frequency of 20 Hz, the difference between two time steps corresponds to 50 msec. All analyses were performed post hoc.

RESULTS AND DISCUSSION

Example accelerations, foot contacts and estimated states are shown for a RWT and WRT condition in Figure 1. At Point 1 is the estimated event where swing phase terminates, and stance phase begins. State A occurs every gait cycle and is used as an estimator of stance phase. Transition out of State A is the time point used to determine the time until TO. Point 2 is indicative of the estimated termination of stance phase. State B occurs every gait cycle, indicating swing phase. The first point after State B is used to determine the time until IC.

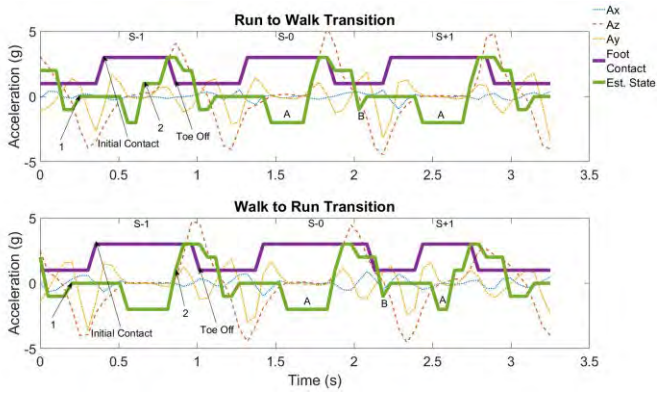

Figure 1: Accelerations, foot contacts and estimated states for RWT (top panel) and WRT (bottom panel) are shown for a single exemplar subject.

Figure 2 shows the natural transition points between walking and running locomotion states. Transition steps were verified by ground reaction force waveforms. The shaded area indicates foot ground contacts classified as running. The contacts in the unshaded area are classified as walking contacts.

Initial analysis indicates initial contact and toe off can be estimated for both the WRT and RWT from a single source of acceleration on the dorsum of the foot sampled at 20 Hz. Previous work has estimated that approximately 40 ms are required to adjust the prosthesis state [1]. The duration of state A, representing foot contact provides a basis to estimate the locomotion state of the subject as seen in Figure 2.

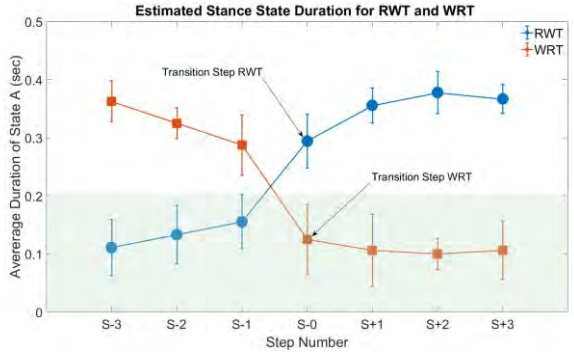

Figure 2: Average contact duration for WRT and RWT conditions. S-1 is the last step before the transition and S-0 is the actual transition step.

Table 1: Average time (sec) of estimated state change prior to actual gait event; mean (SD). The average duration of the states that approximate mid stance and mid swing are also shown; mean (SD).

	Initial Contact	Toe off	State A Duration	State B Duration
Walk	0.156 (0.037)	0.147 (0.068)	0.359 (0.048)	0.102 (0.036)
Run	0.180 (0.031)	0.126 (0.028)	0.103 (0.055)	0.081 (0.031)

CONCLUSIONS

The BP-AR-HMM provides a suitable basis for estimating initial contact, toe off, and locomotion state. Future directions of this work will include comparison of these results to over-ground transitions with self-selected accelerations, and a larger range of speeds. The final application of this work will be for use in a microcontroller of a lower limb prosthesis.

REFERENCES

1. Joshi et al., *IEEE J. Biomed. Health Inform.* 20(1): 2168-2194, 2014.
2. Fox, *Ann. Appl. Stat.* 8(3):1281-1313, 2014.
3. Jin, *PhD Dissertation*. U. Oregon, 2018.

ACKNOWLEDGEMENTS

We wish to thank Michael Hughes for his advice on use of the BP-AR-HM

A Novel Approach for Evaluating Compensatory Gait Strategies Using Mechanical Energetics

Anahid Ebrahimi, Jill S. Higginson, and Steven J. Stanhope

University of Delaware, Newark, DE, USA
E-mail: anahide@udel.edu

INTRODUCTION

Mechanical work is done about joints of the lower limb to move the body, subsequently changing the body's energy state. In gait, the limbs do mechanical work to rotate the center of mass (COM) upwards then downwards in a semicircular arc, theoretically following pendular mechanics [1]. Consequently, this leads to changes in gravitational potential energy and kinetic energy of the body.

With a joint impairment, mechanical work is redistributed among the limb yielding a compensatory gait strategy [2]. This is especially true for individuals with ankle impairment due to the key role of the ankle musculature in gait [3]. However, characterizing a compensatory strategy as "good" is complicated by the operational definition of the term.

Assessing if a strategy's energetics (work and energy) differ from the theorized pendular mechanics of gait in single support phase can help us to understand how and why certain gait strategies are used when there is an impairment. To explore compensatory gait strategies, we compared the mechanical energetics of healthy individuals walking with an artificially impaired ankle joint unilaterally and bilaterally to their typical gait (in shoes).

METHODS

Motion and force data were collected on 17 healthy subjects (8M/9F, 1.7 ± 0.2 m, 75.7 ± 15.1 kg) walking at 0.8 statures/s (1.4 ± 0.1 m/s) with shoes only, and with a custom ankle-foot orthotic on one limb (RiAFO) and on both limbs (BiAFO) which partially restricted ankle motion in dorsiflexion and plantar flexion. The summed net work and rate of change in energy for all segments of the body were integrated over two halves of single support: "single support rise" from left toe off to right midstance, and "single support fall" from right midstance to left heel strike. Average net work and change in gravitational potential energy, translational kinetic energy, and rotational kinetic energy of the whole body (W_{wb}, ΔGPE_{wb}, ΔTKE_{wb}, and ΔRKE_{wb}) are presented in bar charts with standard deviation bars.

Considering that the magnitude of energetics metrics would differ across conditions, relative metrics were calculated. Work or energy forms were calculated as a percentage of the largest energetics metric (see Fig. 1 for example). Statistical differences between conditions were assessed using one-way repeated measures ANOVA with Bonferroni corrections ($p < 0.05$). A † and ‡ denote a significant difference between Shoes and RiAFO conditions, respectively ($p < 0.05$).

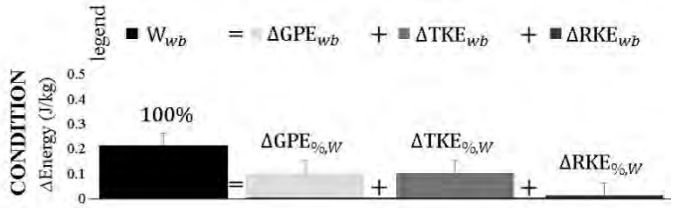

Fig 1. Example bar chart of energetics data. Note percentage values above bars are relative to the largest energetics metric (in this case W_{wb}).

RESULTS AND DISCUSSION

Subjects walked at the same scaled speed and did not significantly change their step lengths ($p = 0.065$) across conditions. The AFO successfully reduced the ankle work by an average 37-40% in the AFO conditions compared to shod walking.

In single support rise, ΔGPE_{wb} was the largest energy form. Individuals walking in the BiAFO condition had a significantly larger $W_{\%,\Delta GPE}$ (86%) compared to the Shoes condition (75%). In a conserved inverted pendulum, the $\Delta TKE_{\%,\Delta GPE}$ would be 100% such that translational kinetic energy and potential energy were equal in magnitude and opposite in sign. However, Fig. 2 shows 25% of the negative ΔTKE_{wb} was transferred to positive ΔGPE_{wb} to raise the COM in the Shoes condition, but only 14% transferred in the BiAFO condition.

Therefore, the BiAFO condition used less pendular mechanics (as evidenced by a smaller $\Delta TKE_{\%,\Delta GPE}$) to raise the COM compared to the Shoes condition.

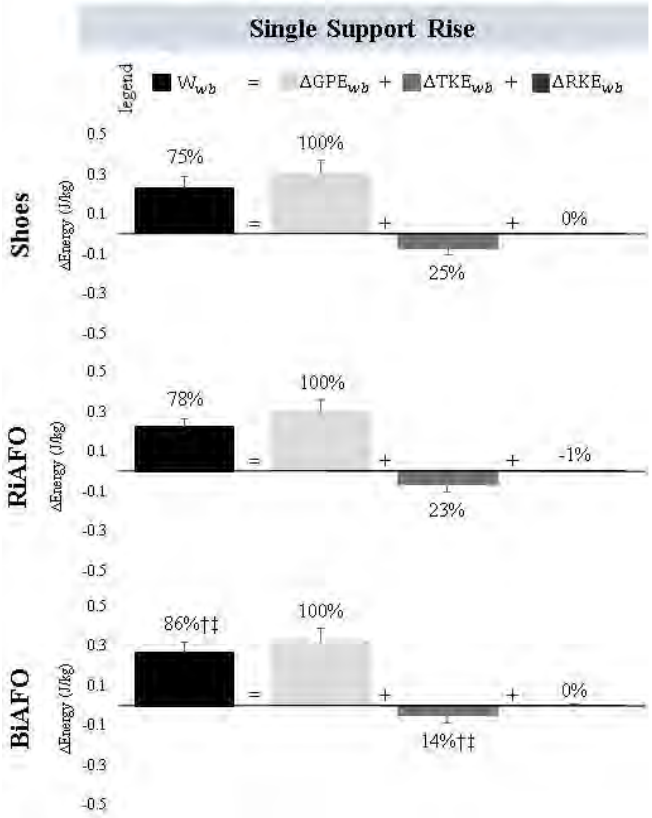

Fig 2. During single support rise, percentages are relative to ΔGPE_{wb}. The BiAFO condition results in significantly less $\Delta TKE_{\%,\Delta GPE}$ compared to Shoes.

In single support fall, W_{wb} was the largest metric. Individuals walking in the RiAFO condition had a significantly smaller $\Delta GPE_{\%,W}$ (-83%) compared to the Shoes condition (-87%). Interestingly, there is no evidence of pendular mechanics during this interval since ΔTKE_{wb} is not net positive. Thus, Fig. 3 shows that nearly all of the net work went into the form of negative ΔGPE_{wb} in all three conditions. While the body is doing a majority of net negative work to control the "fall" of the COM in all three conditions, the RiAFO condition led to altered energetic patterns (as evidenced by a smaller $\Delta GPE_{\%,W}$) to lower the COM compared to the Shoes condition. These results may support the necessity for lower limb prosthetic device design to provide control during this interval to reduce the risk of falls in individuals with amputations.

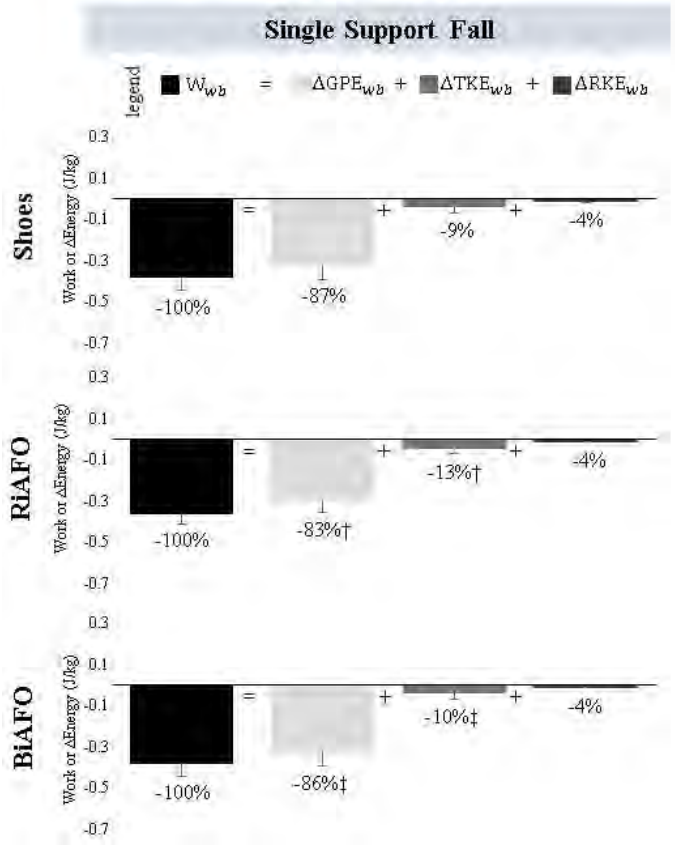

Fig 3. During single support fall, percentages are relative to W_{wb}. The RiAFO condition results in significantly less $\Delta GPE_{\%,W}$ compared to Shoes.

CONCLUSIONS

Individuals compensated with ankle impairment by walking with a similar stride length, yet evaluating the energetics revealed walking with an impairment required more work (as in the BiAFO condition in single support rise) and resulted in altered energy forms (as in the RiAFO condition in single support fall) compared to without impairment. Also, this analysis demonstrated that the limbs do not act like a conserved inverted pendulum, but rather do work to assist the rise and control the fall of the COM.

REFERENCES

1. Kuo, A. *Hu Mov Sci,* **26**(4): 617-656, 2007.
2. Ebrahimi et al. *Gait Pos,* **56**(April): 49-53, 2017.
3. Neptune et al. *J Biomech,* **34**(11): 1387-98, 2001.

ACKNOWLEDGEMENTS

This material was supported by the NSF GRFP (Grant #1247394) and the UD Helwig Fellowship. Data collection assisted by Teresa Ferrara, Michael Christensen, Independence Prosthetics & Orthotics.

INCONSISTENCIES IN STAIRCASE DIMENSIONS IMPACT UPON STAIR CLIMBING SAFETY

[1] Natasha Francksen, [1] Thijs Ackermans, [1, 2] Denis Holzer, [1] Constantinos Maganaris, [1] Mark Hollands, [3] Mike Roys, and [1] Thomas O'Brien

[1] Research to Improve Stair Climbing Safety (RISCS), Research Institute for Sport and Exercise Sciences, Liverpool John Moores University, Liverpool, UK
[2] Department of Biomechanics in Sports, Faculty of Sport and Health Sciences, Technische Universität München, Munich, Germany
[3] Rise and Going Consultancy, Watford, UK
Email: N.C.Francksen@2016.ljmu.ac.uk,

INTRODUCTION

Staircases are frequently associated with falls, over a million people were treated after falling on stairs in American emergency departments annually [1]. Injuries for the older individuals are more severe and require more hospitalisation [1]. In the UK, approximately ten fatalities per week are result from stair falls [2]. Treatment is costly for health care providers such as the National Health Service (NHS).

Inconsistent staircase dimensions are very common and are frequently associated with serious falls [3, 4]. Inconsistencies in rise result in an increased risk of tripping during stair ascent, where individuals are more likely to catch their toe. During stair descent variations in going (horizontal distance between the step edge and the next step) result in errors in stepping-length or over-stepping, which increases the potential for a slip to occur [4]. It is likely that inconsistencies in going also influence safety during ascent, and inconsistencies in rise also affect safety in descent. However, little is known about these and how they could affect fall risk [4].

The aim of this study, therefore is to investigate the influence of a small 1 cm change in going during ascent and 1 cm change in rise during descent on stepping parameters and risk factors for younger and older adults negotiating stairs. The local university's and NHS Ethics Committee approved this study (IRAS project ID: 216671).

METHODS

Twenty-six younger adults (YA; 24.4±3.4 yrs, 1.74±0.08 m, 71.4±11.0 kg, including of British, European and Asian origin, 15 male, 11 female) and thirty-three older adults (OA; 70.7±4.2 yrs, 1.68±0.08 m, 67.9±14.1 kg, of White British origin, 10 male, 23 female) negotiated a custom-built staircase set to three different dimensions: CONSISTENT, inconsistent GOING and inconsistent RISE. 1) The CONSISTENT staircase had uniform dimensions, where all steps had a 20 cm riser height and a 25 cm going length. 2) For the inconsistent GOING condition, Step3 was moved 1 cm inward, lengthening Step2 and shortening Step3 (Figure 1A). 3) For the inconsistent RISE condition, Step3 was raised 1 cm decreasing the riser height of Step4 and increasing the riser height of Step3 (Figure 1B). Participants were asked to leave the room and were not aware how the staircase had changed. GOING and RISE conditions were randomised.

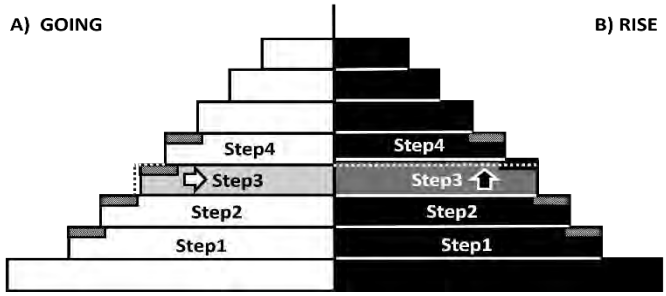

Figure 1: A) Ascent: GOING, Step3 moved 1 cm inward compared to CONSISTENT condition (dotted grey step edge. B) Descent: RISE, Step3 raised 1 cm compared to CONSISTENT condition (dotted white line).

Full-body 3D kinematics and kinetics were recorded (26 camera system: Vicon & 4 force plates: Kistler). Five CONSISTENT trials were averaged and only the first GOING trial during ascent and RISE trial during descent were used for analysis. Only leading limb foot clearances (Foot Clearance) and percentage of foot contact length (Foot Contact) were compared by mixed-methods ANOVAs. Alpha level, $P<0.05$.

RESULTS

There were no significant differences in Foot Clearances between the CONSISTENT and either RISE or GOING trials.

During stair ascent, there was a significant interaction effect between age group and stair configuration on Foot Contact on Step2 ($p = 0.004$), Step3 ($p = 0.013$) and Step4 ($p = 0.010$). YA increased their percentage of foot contact on Step2 in GOING whereas OA did not make this adjustment (Figure 2A). The OA however had a slight decreased Foot Contact on Step3 and the YA a slight increased Foot Contact (Figure 2B). Both groups had increased Foot Contact on Step4, YA more so than the OA (Figure 2C).

During stair descent, there were main effects of staircase configuration on Foot Contact (no age*step interactions). Main effects were recorded between CONSISTENT and inconsistent RISE conditions where both groups had less Foot Contact on Step3 and increased Foot Contact on Step2 ($p = 0.005$ & $p < 0.001$, respectively) (Figure 2D-E).

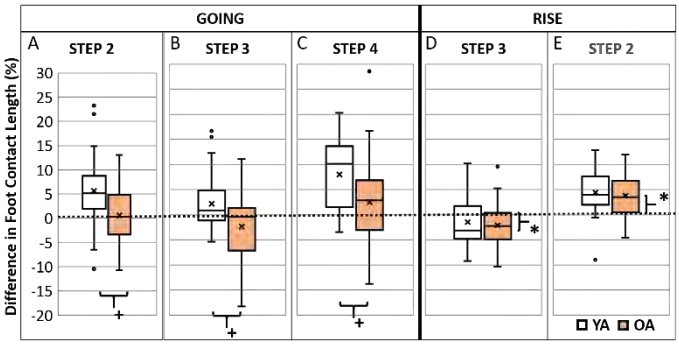

Figure 2: Difference in Foot Contact Length (%) during ascent GOING (A-C) and descent RISE (D-E) compared to CONSISTENT condition for YA (white box) and OA (shaded orange box). Dotted line = 0 % change, X = mean, middle line = median, * = condition effect; $p < 0.05$, $^{+}$ = age by condition effect; $p < 0.05$.

DISCUSSION

In stair ascent YA appear to make use of the longer going of Step2 by placing more of their foot on to the step, which carries forwards to a Foot Contact similar to CONSISTENT on Step3 (shorter going). However, OA did not make adjustments to increase Foot Contact on the longer Step2, nor appear to change their stepping pattern over the inconsistent step. Thus, they had a reduced Foot Contact and have an increased risk of slipping off the shorter Step3. On Step4 both groups had a positive increase in Foot Contact, potentially reducing their risk of slipping, but this could be too late. The interaction effect may be caused by the previously more forward position for the YA compared to the older adults. At this stage, the mechanism behind the YA adjustment on Step2 is unknown.

During stair descent, there were no apparent differences prior to the inconsistent step. Both groups had a reduced Foot Contact on the inconsistent Step3; creating a larger over-step. This in itself is associated with a higher fall risk [4]. Older individuals with larger variability in their stepping behaviour could be at greater risk from a fall.

Analysis of visual behaviour, full body kinetics and kinematics of both groups will help determine the mechanisms behind the changes to Foot Contact and the extent that a person's safety is compromised. The initial results presented could influence staircase regulations on tolerances, it could also justify the need to remodel existing staircases or develop visual cues that make inconsistencies more identifiable.

CONCLUSIONS

Inconsistencies in rise dimensions could increase the risk of over-stepping and slipping off the inconsistent step in descent, in a similar way to over-stepping onto a step with a shorter going dimension. In ascent, the OA did not adjust their stepping pattern to the inconsistent staircase which could increase the risk of slipping off the shorter step. This could be particularly dangerous for older adults' safety.

REFERENCES

1. Blazewick et al. *Am. J. Emerg. Med* (In Press): doi 10.1016/j.ajem.2017.09.034, 2017.
2. SHP online. Stair safety fact sheet, 2016
3. Nicol et al. Briefing paper: The cost of poor housing to the NHS. BRE, 2015
4. Roys. *Refurbishing stairs in dwellings to reduce…injuries*. BRE electronic publications, 2013.

A FULL-STATE CONTROLLER FOR THE SIMPLE INVERTED PENDULUM BIPED DERIVED FROM HUMAN PERTURBATION EXPERIMENTS

Varun Joshi and Manoj Srinivasan
The Ohio State University, Columbus, OH, USA
email: joshi.142@osu.edu

INTRODUCTION

Humans walk stably by using neural feedback control and perhaps some feedforward control. Characterizing the feedback controller might inform our understanding of falls and movement disorders, and inform the design of prosthesis and exoskeleton controllers. Here, we seek to characterize how humans balance themselves when subject to perturbations. We describe how human-subject response to Anterior-Posterior (AP) and Medio-lateral (ML) pulls applied at the hip [1] may be used to derive a full-state controller for a simple model of bipedal walking. We evaluate the feedback controller's perturbation rejection ability by determining the basin of attraction for this controller (set of perturbations that do not result in a fall). We also analyze the robustness of the feedback controller to noise in the control gains and biped body parameters.

METHODS

Subjects walked on a treadmill at constant speed for 10 bouts of 4 mins each. During each walking bout, the subjects were perturbed randomly, either in the AP direction (9 subjects, only backward pulls) or in the ML direction (7 subjects, randomly selected leftward or rightward pulls).

We collected kinematic data from 13 markers placed on the subject - 5 around the hip, 4 on each foot using 8 motion capture cameras (Vicon T20, 100 Hz). Subjects were manually pulled by the experimenters via cables tied at the hip. Forces from these cables were recorded using a load cell in series with them (Phidgets S-type 100Kg, 1000 Hz). A loose harness connected to the ceiling was provided for safety. Subjects wore blinders to block peripheral vision and headphones to muffle noise so that visual and audio cues could not be used to anticipate the onset of a perturbation. 20% of all perturbations were randomly assigned to be "fake" perturbations where the experimenter went through the action of pulling on the cable but the perturbing force was very small. These fake perturbations were used to prevent proprioceptive cues from being used to detect oncoming perturbations.

To determine the controller, we first calculate a linear equation that relates mid-stance state deviations of the human to the subsequent foot-placement deviation as outlined by Wang and Srinivasan [2]. Next we determine the Poincare map that relates mid-stance states for the human from one-step to the next:

$$\Delta\begin{bmatrix} X_{\text{torso}}(n+1) \\ \dot{X}_{\text{torso}}(n+1) \\ \dot{Y}_{\text{torso}}\ (n+1) \end{bmatrix} = J_1.\Delta\begin{bmatrix} X_{\text{torso}}(n) \\ \dot{X}_{\text{torso}}(n) \\ \dot{Y}_{\text{torso}}(n) \end{bmatrix}$$

For the simple inverted pendulum model shown in Fig. 1, we can write an equation relating the n+1th mid-stance states for the biped as a function of the mid-stance states during the nth step and the control actions during the nth step:

$$\Delta\begin{bmatrix} X_{\text{torso}}(n+1) \\ \dot{X}_{\text{torso}}(n+1) \\ \dot{Y}_{\text{torso}}\ (n+1) \end{bmatrix} = J_2.\Delta\begin{bmatrix} X_{\text{torso}}(n) \\ \dot{X}_{\text{torso}}(n) \\ \dot{Y}_{\text{torso}}(n) \end{bmatrix} + J_3.\Delta\begin{bmatrix} x_{\text{foot}}(\text{n}) \\ y_{\text{foot}}(\text{n}) \\ I_{\text{pushoff}}(\text{n}) \end{bmatrix}$$

If we select a biped controller of the form:

$$\Delta\begin{bmatrix} x_{\text{foot}}(\text{n}) \\ y_{\text{foot}}(\text{n}) \\ I_{\text{pushoff}}(\text{n}) \end{bmatrix} = J_4.\Delta\begin{bmatrix} X_{\text{torso}}(n) \\ \dot{X}_{\text{torso}}(n) \\ \dot{Y}_{\text{torso}}(n) \end{bmatrix}$$

Combining these equations, we get the following equation:

$$\Delta\begin{bmatrix} X_{\text{torso}}(n+1) \\ \dot{X}_{\text{torso}}(n+1) \\ \dot{Y}_{\text{torso}}\ (n+1) \end{bmatrix} = (J_2 + J_3.J_4).\Delta\begin{bmatrix} X_{\text{torso}}(n) \\ \dot{X}_{\text{torso}}(n) \\ \dot{Y}_{\text{torso}}(n) \end{bmatrix}$$

We solve for the value of J_4 that minimizes

$$J_1 - J_2 - J_3J_4$$

Since we already know the foot-placement gains from human data, the minimization only solves for the 3 impulse gains within J_4.

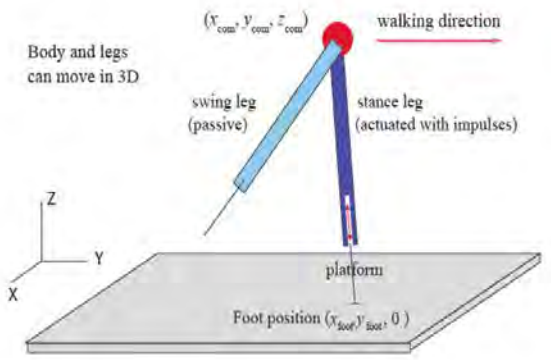

Figure 1: The inverted pendulum biped model

Once the gains are calculated, we simulated the biped for 20 steps with varying initial perturbations to determine the basin of attraction. Similarly, we simulated the biped with fixed initial perturbation and varying parameter noise to determine the parameter sensitivity of this controller.

RESULTS AND DISCUSSION

The feedback controller gains were determined to be as follows in non-dimensional terms:

$$J_4 = \begin{bmatrix} 1.85 & 1.99 & 0.22 \\ -0.49 & -1.65 & 0.85 \\ -0.18 & -0.69 & -0.52 \end{bmatrix}$$

This controller was found to be robust to changes in the gains and parameters, at least 10% in each non-zero parameter value, generally much more. The basin of attraction of the controller, seen in figure 2, was found to be 30-40 times larger than the standard deviation of mid-stance kinematic variability in normal walking. Such basins of attraction predictions can be tested in further large-perturbation experiments.

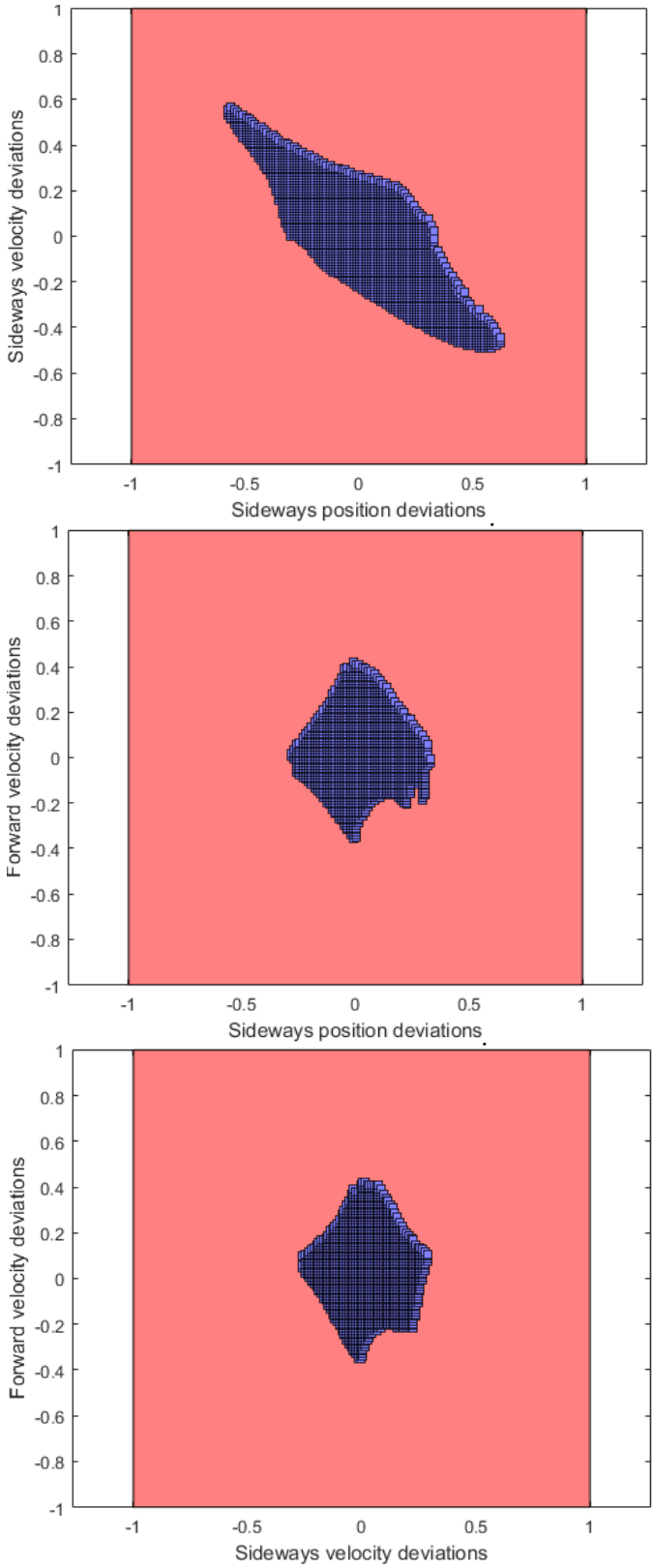

Figure 2: Basin of attraction for the simple inverted pendulum walker with a controller derived from human perturbation experiments. The dark patch represents the set of perturbations that do not result in a fall. All quantities non-dimensionalized.

REFERENCES

1. Vlutters, M., Van Asseldonk, E.H. and Van der Kooij, H., *J. Exp. Biol., 219(10), 1514-23, 2016.*
2. Wang, Y. and Srinivasan, M., *Biol. Lett.*, 10 20140405, 2014.

ACKNOWLEDGEMENTS

This work was supported by National Science Foundation grants number 1538342 and 1254842.

EFFECTS OF A NEW ADAPTIVE ANKLE PROSTHESIS ON LEVEL AND SLOPED WALKING

Erik P. Lamers, Maura E. Eveld and Karl E. Zelik

Vanderbilt University, Nashville, TN, USA
email: erik.p.lamers@vanderbilt.edu

INTRODUCTION

Sloped terrains can be challenging for individuals with lower limb amputation to navigate, in part because conventional prosthetic feet are aligned at a fixed angle and lack biological ankle joint articulation. The lack of ankle articulation may cause prosthesis users to adopt compensatory strategies on slopes [1]. To address this issue, various prosthetic feet have been developed to adapt their ankle angle based on the slope, partially restoring ankle articulation. There is evidence that this ankle articulation may help normalize certain gait biomechanics during level [2] and incline walking [3]. However, objective performance data on adaptive ankle prostheses is still limited, and the extent to which these devices benefit users on slopes requires additional investigation.

In this study we investigated a new microprocessor-controlled prosthetic ankle (MPA, Ossur premarket device), which uses a low-power motor to adapt its ankle angle to sloped terrain and to dorsiflex the ankle during swing to enhance toe clearance. We quantified the biomechanical effects of the MPA on unilateral transtibial prosthesis users during level and sloped walking, compared to the MPA with the ankle locked at the neutral position, and also compared to each user's prescribed prosthesis. The first comparison served as a controlled scientific study to isolate effects due specifically to ankle angle adaptation (since all other aspects of the MPA were unaltered). The latter comparison provided a more clinically-relevant assessment of the MPA against prostheses that users wear each day.

METHODS

Eight individuals with unilateral transtibial amputation participated in this study of level, incline and decline walking. These individuals (7 male, 1 female, height 1.78 ± 0.1 m, weight 92 ± 15 kg, age 45 ± 14 years) were all K3-K4 level ambulators, at least 6 months post amputation surgery. Six healthy controls (4 female, 2 male, height 1.78 ± 0.1 m, weight 69 ± 10.6 kg, age 21 ± 1.8 years) also performed identical walking conditions, to assist with results interpretation. All participants provided informed consent, according to Vanderbilt Institutional Review Board procedures.

Prosthesis users were fitted with the MPA by a certified prosthetist, and then users were educated on the functions of the device. After the fitting, prosthesis users wore the MPA for 2-3 weeks of at-home acclimation before returning for formal gait analysis testing.

Prosthesis users (and healthy controls) performed level (0°) and sloped (±7.5° incline/decline) walking on a treadmill at a fixed speed (either 0.8 or 0.9 m/s). Prosthesis users walked on: (i) the MPA, (ii) the MPA with the ankle locked at the neutral position (hereafter referred to as the MPA-locked condition), and (iii) their prescribed prosthesis (primarily higher profile energy storage and return prostheses). Ground reaction force data were collected under each foot at 1000 Hz using a split-belt force-instrumented treadmill (Bertec), and lower-body kinematics were recorded at 200 Hz via a synchronized motion capture system (Vicon). Joint level kinematics and kinetics, as well as center-of-mass power, were calculated using common gait analysis methods. Prosthesis power was estimated using a previously published method that computes power due to all structures distal to the prosthetic socket [4]. Statistical significance was evaluated via repeated measures ANOVA, α=0.05.

RESULTS AND DISCUSSION

This study resulted in a comprehensive biomechanical characterization of lower-limb kinematics and kinetics, and center-of-mass power. Various changes were only observed in prosthetic-side biomechanical outcomes. However, in many cases, these changes were observed within a subset of users. Changes in sound limb kinematics and kinetics across the prosthesis conditions were generally small in magnitude, and inconsistent across participants. For brevity, the focus of this abstract is limited to (i) reporting key trends that were observed to be consistent among multiple, or a majority of participants, and (ii) reporting on a subset of outcome metrics of interest based on previously published prosthetics studies. Additional/extended results and discussion will be presented at the conference itself.

MPA vs. MPA-locked Results

The MPA adapted its ankle angle by the programmed amount on slopes (6.0 ± 1.5° dorsiflexion for 7.5° incline, 2 ± 0.4° plantarflexion for 7.5° decline) and provided more toe clearance (minimum height of toe above ground between 75% and 85% of gait cycle) than the MPA-locked condition during level (1.39 ± 0.44 cm, $p<0.001$), incline (1.99 ± 0.40 cm, $p<0.001$) and decline walking (0.81 ± 0.46 cm, $p=0.005$).

MPA vs. Prescribed Results

The MPA provided more toe-clearance than prescribed prostheses during level (1.46 ± 0.7 cm, $p<0.001$), incline (1.84 ± 1.0 cm, $p=0.001$) and decline walking (1.17 ± 1.06cm, $p=0.012$. During incline walking, four users switched from a toe-landing gait pattern on their prescribed prosthesis to a heel-to-toe gait pattern on the MPA, which was more consistent with the gait pattern of the controls. The MPA stored and returned less elastic energy for 6 of 8 subjects during level walking, and for 5 of 8 subjects during both incline and decline walking.

Discussion

The MPA may provide benefits by reducing trip risk due to increased toe-clearance. This was anecdotally supported by one user who reported less "toe-catching" during the at-home acclimation period with the MPA compared to his prescribed prosthesis. For half the prosthesis users, the MPA also appeared to promote a more typical heel-to-toe gait pattern for incline walking (i.e., more similar in appearance to the controls); however, a trade-off was that elastic energy return was generally reduced relative to prescribed prostheses. One limitation of this study was that K2 users (limited community ambulators) were not tested, a group for whom large elastic energy storage/return may be less important, and for whom ankle articulation has been shown to benefit walking performance [2].

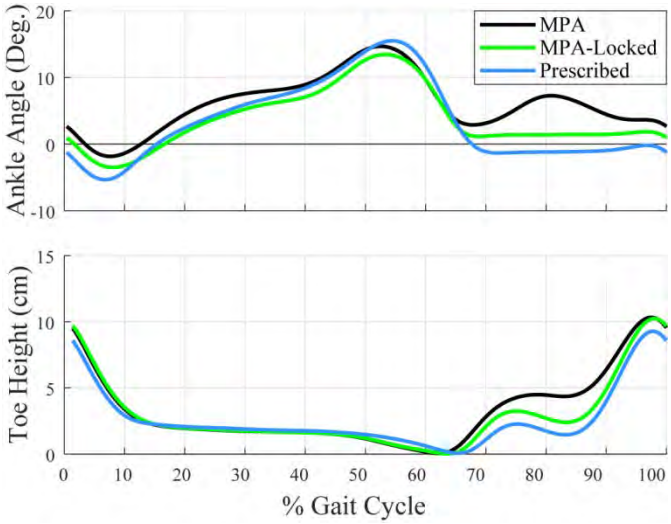

Figure 1: The MPA dorsiflexes the ankle during swing (~80% gait cycle) (top) to provide increased toe clearance (bottom), which may reduce trip risk. Representative subject depicted.

REFERENCES

1. Vrieling, A. H. et al. (2008). *Gait & Posture*.
2. Barnett et al. (2018). *J Prosthetics & Orthotics.*
3. Fradet, L. et al. (2010). *Gait & Posture.*
4. Takahashi, K. Z., et al. (2012). *J Biomechanics.*

ACKNOWLEDGEMENTS

Research was funded in part by Ossur. They had no role in analysis or interpretation of presented data.

RELIABILITY AND FEASIBILITY OF AN INERTIAL MEASUREMENT UNIT BASED DUAL-TASK GAIT BALANCE ASSESSMENT

[1]Will Pitt and [1]Li-Shan Chou

[1]Department of Human Physiology, University of Oregon, Eugene, OR, USA
email: chou@uoregon.edu, web: http://choulab.uoregon.edu

INTRODUCTION

Concussion in athletics, workplace, and everyday activities continue to occur at high rates leading to impaired dynamic balance control persisting up to two months post-injury [1]. Prolonged gait imbalance is currently detected using costly and time consuming camera-based whole body motion analysis under a dual-task paradigm (walking while performing a concurrent cognitive test). However, advances in commercially available wearable inertial measurement unit (IMU) technology offers an opportunity to perform objective post-concussion gait stability analysis in the clinical setting.

At present a clinically feasible dual-task gait balance assessment utilizing sensitive whole body center of mass (COM) biomechanical markers is not available. The development of such a clinical assessment requires design of a testing protocol, determination of its consistency in non-laboratory settings and across time, and establishment of inter-rater reliability and clinical feasibility.

This study has two main purposes: first, to examine the internal consistency and interrater reliability of an IMU-based dual-task gait balance control assessment. Second, to establish the clinical feasibility of the instrument in a Division I collegiate sports programs.

METHODS

This two part study consisted of 1) assessment of internal consistency and interrater reliability, and 2) assessment of clinical feasibility with a Division I female soccer team. Instrumentation consisted of an APDM OPAL IMU system (sensor placed over the L5 vertebrae as a COM proxy [2]) for kinematic data collection, Bluetooth headset/microphone for assessment instruction and cognitive test application, and Superlab 5 software for protocol automation. All hardware and software were controlled with a single MacBook Air laptop. In part one of the study subjects performed four walking trials in each of three conditions: walking only, walking while performing an auditory Stroop test, and walking while spelling a five letter word backwards or subtracting from a given number by 6s or 7s. Individuals walked at a self-selected pace over an eight meter level path, performed a 180° turn around a cone, and returned to the start. The conditions were repeated in two environments (laboratory and hallway representing a typical medical clinic), by two different raters, and on two separate days (separated by 7-10 days). The order of environment, rater, and walking condition was randomized for each testing session.

IMU data was sampled at 128Hz and filtered with a 2nd order, low-pass, Butterworth filter, with a 12Hz cutoff. The gait cycles beginning with the 5th heel strike during the walk out and the returning walk were analyzed. Peak linear accelerations along the vertical axis (10-30%, 30-50%, and 50-60% gait cycle) and medial-lateral axis (30-50%, 50-60%, and 60-75% gait cycle) were identified (Fig. 1).

The second part of the study consisted of a shortened clinical protocol implemented with the University Women's Soccer team. The protocol consisted of three walking trials in each of the three testing conditions with the conditions presented in a random order. Testing was performed in the University athletic medicine facility by a team athletic trainer. Total assessment time per athlete was collected to assess clinical feasibility. Additionally, the 10 linear acceleration metrics were collected and compared to our healthy, non-athlete female subjects from part one of the study.

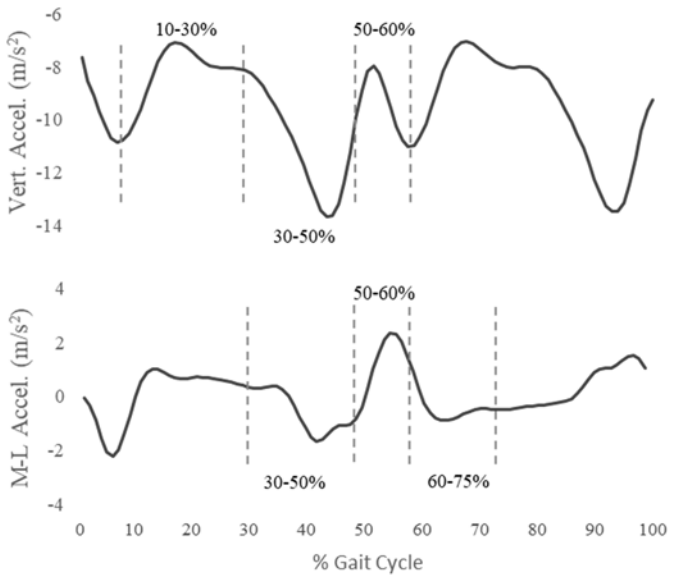

Figure 1: Representative plot of the A-P and M-L linear accelerations and 6 peak accelerations

An eight item Cronbach's α was used to establish the consistency of the measurement tool across time, environments, and raters. An Intraclass Correlation Coefficient and 95% CI was used to establish interrater reliability. Paired t-tests were performed for each outcome measure between female athletes and non-athlete controls. Statistical analyses were performed with SPSS version 24 (SPSS Inc., Chicago, IL).

RESULTS AND DISCUSSION

Twenty healthy subjects (10F) completed part one of the study (Age 22.2±2.8yrs, Wt. 71.0±12.0kg, Ht. 175.8±8.1cm). Internal consistency for the six outcome measures was excellent as established by Cronbach's α values between .904 and .980. Interrater reliability was also very good with ICC values ranging from .868 to .941 (Table 1).

Fourteen uninjured female athletes participated in part two of the study (Age 19.3±1.3yrs, Wt. 64.6±4.0kg, Ht. 168.4±7.1cm). Total assessment time including sensor placement and verbal instructions was 8:30 minutes ±35 seconds, demonstrating its clinical feasibility. Female athletes were compared to 10 non-athlete females from part one (Age 21.4±3.5, Wt. 62.5±7.6kg, Ht. 169.0±4.8cm). The magnitude of all M-L peak accelerations in all three walking conditions was

Table 1: Cronbach's α and ICC values for the 6 COM kinematic outcome measures

	Cronbach's Alpha			ICC	
Metric	Walk	Stroop	Q&A	r	95% CI
Vert. Accel 10-30%	.976	.942	.976	.920	.918±.022
Vert. Accel 30-50%	.951	.955	.980	.868	.865±.033
Vert. Accel 50-60%	.911	.914	.933	.876	.872±.034
M-L Accel 20-40%	.931	.963	.969	.931	.928±.020
M-L Accel 40-50%	.933	.904	.925	.902	.898±.027
M-L Accel 50-70%	.976	.969	.970	.941	.939±.016

greater than non-athlete females, however, only M-L Accel 20-40% and M-L Accel 50-70% reached a significant level (Table 2). This demonstrates the ability of the instrument to detect subtle differences in dynamic balance control.

Table 2: M-L peak accelerations (m/s^2) presented in mean±SD for non-athlete females and female soccer players. An * indicates $p < .05$

Metric	Group	Walking	Stroop
M-L Accel 20-40%	Non-Athlete	-2.24±0.52	-2.07±0.42
	Soccer	-2.91±1.14	-2.77±1.10 *
M-L Accel 40-50%	Non-Athlete	2.79±1.08	2.75±1.22
	Soccer	3.47±1.39	3.36±1.45
M-L Accel 50-70%	Non-Athlete	-1.39±0.70	-1.45±0.47
	Soccer	-2.07±1.01	-2.24±1.04 *

CONCLUSION

The high Cronbach's α and ICC values indicate our testing apparatus and protocol have excellent consistency and interrater reliability in a non-laboratory environment, across time, and with different evaluators. Furthermore, the instrument is both clinically feasible and sensitive to subtle differences in dynamic balance control. The results provide the necessary foundation for the development and implementation of a low-cost, accurate and sensitive, post-concussion gait stability assessment that is reliable in the clinical setting by minimally trained evaluators.

REFERENCES

1. Howell DR, et al. *Arch Phys Med Rehabil*., **94**(8), 513-1520, 2013
2. Howell DR, et al. *JOB*., **48**(23), 3364-8, 2015

Exploring Movement Variability and EEG Correlates During Motor Learning with a Smartpen: A Novel Method

[1,2] Jo Shattuck, [2] Matthew R. Johnson and [1]Jack W. Ransone

[1] University of Nebraska, Nebraska Athletic Performance Laboratory, Lincoln, USA
[2] University of Nebraska, Department of Psychology, Lincoln, NE, USA
email: joshattuck@huskers.unl.edu

INTRODUCTION

The optimal degree of movement variability during practice in the role of motor learning and ultimate performance outcome has been vigorously debated since Bernstein's degrees of freedom theory [1]. However, measuring movement variability with motion capture systems can be cumbersome, cost prohibitive and not suitable for smaller movements. Digital graphical tablets and touchscreens present one solution to capture smaller movements, but may not offer the flexibility of study design and the naturalistic feel of traditional pen and paper. Our solution was the use of an Echo Smartpen, which digitally stores every stroke of the pen on specialized LiveScribe paper, and image processing code with Matlab to record and analyze the movement variability over a timed drawing task with multiple training sessions spread over four days. Continual EEG data collection during the task was recorded with an EPOC 14 portable Bluetooth headset. The currently known neural substrates of motor learning have yet to offer a clear model of neural changes that occur over various brain regions through the learning stages. We intend to use the data collected via this novel method with non-linear analysis to pursue neural markers of performance outcomes and movement variability. This abstract describes the procedures, analysis and initial performance results in the timed drawing task.

METHODS

Nine females and eleven males from 19 to 30 years (M=21.35±3.65), completed 14 sets of a timed trail-making task. This timed drawing task required connecting 25 numbered circles on a page in a specific sequence. A 3-ring binder and timer button (Fig. 1) sat on the desk. The timer button and binder were attached; the left and right pages were equidistant to the timer button even if the subject repositioned the binder on the desk. Subjects were instructed to draw lines with the Echo Smartpen to connect the circles in sequence "as fast as possible without making mistakes." Fig. 2 shows Part A of the Trail Making Task in the Halstead Ralston Battery. (Part A was repeated 140 times over 4 days) Subjects pressed the timer button at the beginning and end of each page (trial), yielding a measure of speed; variability in movement was measured with custom Matlab code.

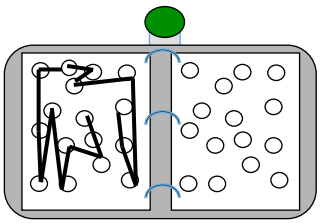

Figure 1: Binder and Timer Button

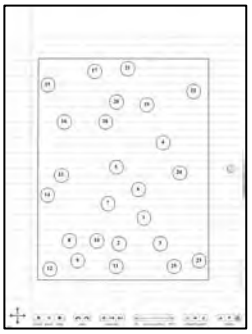

Figure 2: Trail Making Task

Each set containing ten pages (trials) was exported as a portable document format file (pdf), converted to black and white, inverted to show pen strokes as white, background as black, then overlaid into a single image. Fig. 3 shows the overlaid trials of Set 1 and Set 14.

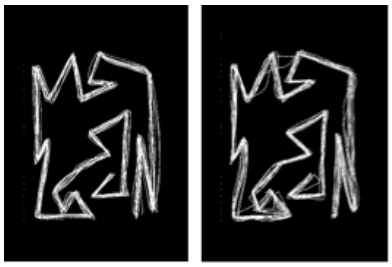

Set 1 Set 14

Figure 3: Overlaid Sets

Our variability code compared the distance of each white pixel to every other pixel to capture a quantitative measure of variability or Efficiency of movement. Figure 4 shows a low variability circle (top right inset), and a high-variability (bottom left

inset) for two 50 x 50 pixel areas (gray box) surrounding the numbered circles (dashed lines).

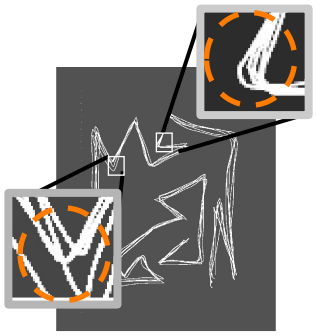

Figure 4: Examples of Different Levels of Variability

Each circle's coordinates surrounding the 23 circles (first and last were omitted) had been pre-determined from the original trail-making task. Variability was calculated on each circle in each set, from an image of the 10 overlaid trials in the set. Each subject completed 14 sets: four sets per day in Visits 1, 2, and 3, which all occurred on consecutive days, plus two sets in the Retention Visit, which occurred four days after Visit 3.

RESULTS AND DISCUSSION

Trial time retention (from set 1 to set 14) in the motor sequence improved 45%, in 4 days over 14 sets (M = 44.59±9.20). Variability improved 1.8% (M = 1.76±3.84). T-tests on the raw *variability scores* showed the mean difference in variability was significant (M=0.3212), p = 0.039). Recall variability (between set 12 to set 14, during which there was a four day delay) was not significantly different, suggesting the -1.06% efficiency gains were maintained and did not worsen over the delay, (M=-1.84, SD=4.74.)

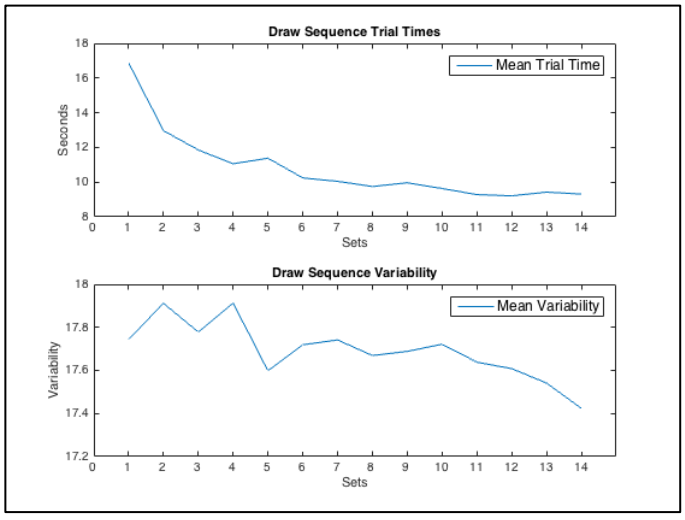

Figure 5: Trial Times (top) and Variability (bottom) per Set, n=20

Trial times decreased according to the law of practice, and the maximum speed/efficiency tradeoff occurred within the first 5 sets, the early (fast) stages of learning. The greatest change in trial times occurred in 1, after which trial times began to plateau; however, variability continued to decrease, (i.e. Efficiency improved, see Fig.5)

This method combined kinematics, a grapho-motor task and pen stroke capture, to produce a novel motor learning task and analysis method. While unable to capture force or pressure information as traditional digitizing tablets can, this method was a suitable alternative for studying 2 dimensional motor learning. The method was designed for a larger project for which the primary goal is to find neural correlations for different performance features of motor learning. Further analysis on continually recorded EEG data throughout the sessions was required to determine if neural activity shifts with movement variability and trial times. We intend to use a repeated measures non-linear multilevel model to examine between-set variability over the learning stages.

CONCLUSIONS

Stergiou and Decker stress the importance of studying variability to understand human movement: "Far from being a source of error, evidence supports the necessity of an optimal state of variability for health and functional movement" [2]. We explored the role of variability and its relationship with neural activity with this novel method in an attempt to improve movement pedagogy. Improved teaching techniques can benefit motor learning fields such as physical therapy, vocational training, and recreational and elite sport coaching.

REFERENCES

1. Bernstein NA (1967) *The co-ordination and regulation of movements.* Oxford, New York, Pergamon Press
2. Stergiou N, Decker LM (2011) Human movement variability, nonlinear dynamics, and pathology: is there a connection? *Hum Mov Sci* **30**:869–88.

GAIT VARIABILITY TO PREDICT MOTOR LEARNING OF A NOVEL MOTOR TASK

[1] Sophia Ulman, [2] Robin M. Queen, and [1] Divya Srinivasan

[1] Industrial and Systems Engineering, Virginia Tech, Blacksburg, VA, USA
[2] Kevin P. Granata Biomechanics Lab, Biomedical Engineering and Mechanics, Blacksburg, VA, USA
email: smu4@vt.edu

INTRODUCTION

Motor variability (MV) is a fundamental feature of movement that refers to the variation observed in the spatiotemporal dispersion of joint movements, inter-joint coordination patterns, and muscle activities, when an individual completes the same task numerous times. While variability is natural and inherent in any human movement, it was traditionally assumed to be undesirable, as it was thought to contribute to less accurate performance. However, basic motor control research has progressed in recent years, and now suggests that movement variability has important functional implications for the preservation of motor performance, both with respect to short-term adaptations of movement strategies and longer-term motor learning. Existing evidence of motor variability being predictive of motor learning has been reported during simple reaching tasks [1]. Whether this concept is generalizable to other kinds of movements such as gait is currently unknown.

The goal of this study was to assess whether motor variability in normal gait at a self-selected speed (baseline condition) was associated with motor learning in a young healthy population performing a novel motor task. The novel motor task involved clearing an obstacle course within a designated time while performing a dual task. We hypothesized that inter-individual differences in motor learning ability in the novel task would be explained by differences in baseline gait variability. As a secondary objective, we also aimed to determine which variability measures (stride characteristics. lower limb joint kinematics and inter-joint coordination as quantified by vector coding) were most discriminative of inter-individual differences in learning ability in our cohort of young healthy adults.

METHODS

Thirty-two participants (16 F, 16 M), aged 21.28 (SD 1.76) years, with no known history of musculoskeletal disorders or injuries were recruited. Each participant was asked to walk barefoot continuously at a comfortable, self-selected pace for six minutes in order to reliably capture baseline motor variability [2]. Gait kinematics were collected using a 10-camera motion capture system (Qualysis INC, Gothenburg, Sweden), and passive reflective markers placed at select anatomical landmarks on the pelvis and lower limbs. After baseline over-ground walking, each participant was asked to walk through an obstacle course barefoot while holding a bowl of colored water. In order to complete the course successfully, they needed to finish the course within a specified time constraint while not spilling the bowl of water. The course consisted of directional cones, an agility ladder, a low balance beam, and stepping stools to step over. “Performance” in the novel task was quantified by the number of trials taken by each participant to achieve success, i.e. obstacle course completion within the pre-set time.

Marker data were exported into Visual 3D (C-motion Inc., USA) for data processing. Spatiotemporal stride characteristics and hip, knee, and ankle joint angles in the sagittal and frontal planes, during the stance and swing phases of gait, were extracted for further analysis. Standard deviation of each joint angle trajectory was calculated as the root mean square of standard deviation obtained at each normalized time point across all trials, during the stance and swing phases (~35-40 strides). Inter-joint coordination was quantified through vector coding [3]: hip-knee and knee-ankle couples in the sagittal and frontal planes during stance and swing were computed, and the stride-to-stride SD of joint coupling angles were used to quantify coordination variability. Two stepwise linear regression models were estimated to assess the association between performance (response variable) and the following predictor variables:

1. Stride characteristics (mean and stride-to-stride SD);
2. Joint trajectory variability of hip, knee and ankle joints, and stride-to-stride SD of hip-knee and knee-ankle joint couples in the frontal and sagittal planes during stance and swing phases.

JMP (SAS Inst. Inc., USA) was used for all statistical analyses, and a type I error rate of 5% was considered to be acceptable for statistical significance in tests of each variable in the regression models.

RESULTS AND DISCUSSION

On average, the participants took 10.97 (range 2-21) trials to learn to clear the obstacle course. A model using only stride characteristics of baseline gait (top panel in table 1) to predict performance was not statistically significant. However, when joint kinematic variability measures were used as predictor variables (bottom panel of table 1), 95.6% of the variance in performance could be explained by the model. Thus, our results support the functional significance of joint kinematic variability in over-ground walking even for a homogenous group of young and healthy adults: inter-individual differences in the rate of learning a novel motor task was predicted by differences in kinematic variability between individuals. Specifically, individuals with the fastest learning rate exhibited increased variability in knee frontal and ankle sagittal joint angle trajectories during the stance phase, and increased knee-ankle coordination variability during the swing phase. Our results are also novel from the perspective of showing that swing phase joint kinematic variability is also meaningful to study in gait, as hip and knee joint variabilities as well as inter-joint coordination variabilities are predictive of performance.

CONCLUSIONS

Although the functional significance of motor variability has been demonstrated in various clinical populations and among older adults, ours is one of the first studies showing strong association between gait variability and short-term motor learning in a cohort of young and healthy individuals.

REFERENCES

1. Wu et al. *Nature neuro.* **17**, 312, 2014.
2. Konig et al. *Gait & Posture.* **39**, 615-617, 2014.
3. Heiderscheit et al. *J. Appl. Biomech.* **18**, 2002.

ACKNOWLEDGEMENTS

We would like to acknowledge the contributions of Melanie Kangelaris and Willow Ruud for their assistance with data collection and processing.

Table 1: Association between variability measures and performance.

	Input Variables to models		Model prediction
Spatiotemporal gait characteristics model	Speed Swing time: mean and SD Stance time: mean and SD Step time: mean and SD Cycle Time: mean and SD	Step length: mean and SD Stride length: mean and SD Stride width: mean and SD	Model not significant
Joint kinematics variability model	Sagittal Hip Angle SD stance Frontal Hip Angle SD stance Sagittal Knee Angle SD stance **Frontal Knee Angle SD stance * (r = - 0.18)** **Sagittal Ankle Angle SD stance * (r = - 0.35)** Frontal Ankle Angle SD stance Sagittal Hip-Knee SD stance Frontal Hip-Knee SD stance Sagittal Knee-Ankle SD stance **Frontal Knee-Ankle SD stance * (r = 0.03)**	Sagittal Hip Angle SD swing **Frontal Hip Angle SD swing * (r = 0.28)** **Sagittal Knee Angle SD swing* (r = 0.22)** Frontal Knee Angle SD swing Sagittal Ankle Angle SD swing Frontal Ankle Angle SD swing **Sagittal Hip-Knee SD swing* (r = 0.02)** **Frontal Hip-Knee SD swing * (r = 0.1)** **Sagittal Knee-Ankle SD swing * (r = - 0.1)** **Frontal Knee-Ankle SD swing * (r = - 0.1)**	Model R^2 = 95.6%, $p < 0.001$

REAL-TIME MUSIC-BASED BIOFEEDBACK TO REDUCE IMPACT LOADING DURING OVER-GROUND RUNNING

[1] Pieter Van den Berghe, [2] Valerio Lorenzoni, [1] Joeri Gerlo, [1] Bastiaan Breine, [1] Rud Derie, [2] Joren Six, [2] Marc Leman, [1] Dirk De Clercq

[1] Department of Movement and Sports Sciences, Ghent University, Belgium
[2] IPEM, Department of Arts, Music and Theatre Sciences, Ghent University, Belgium

email: pieter.vandenberghe@ugent.be, web: www.ugent.be/ge/bsw/en/research/biomechanics

INTRODUCTION

Running retraining through biofeedback on a measure of impact loading combined with simple instruction can decrease running related injuries [1]. Running retraining through real-time biofeedback on a direct measure of impact loading has been exclusively executed on treadmill [1,2]. For example, Peak Tibial Acceleration (PTA) was reduced by provision of simple auditory biofeedback within a single, treadmill-based retraining session [2]. Ecological validity could be improved by conducting retraining programs in an over-ground environment outside the laboratory and with a motivational bio-feedback approach.

In this 'proof of concept' study, retraining by means of real-time auditory biofeedback happened over-ground on an indoor running track in runners with elevated PTA. Impact loading was expected to be reduced within a single session.

METHODS

After screening 80 uninjured runners on PTA, 5 (3♂-2♀) high impact runners (height: 1.74 ± 0.02 m; weight: 71 ± 7 kg; age: 38 ± 11 years; weekly running volume: 25 ± 10 km; mean ± SD) were recruited in this ongoing study. These recreational, habitual rearfoot runners ran at least 15 km/week in non-minimalist footwear, were injury-free in the last 6 months and had no experience with gait retraining. They were instrumented with a wearable accelerometry system able to continuously detect PTA in real-time. Tibial skin was bilaterally pre-stretched before low-weight accelerometers (LSI 331, Sparkfun; 1000 Hz) were attached over the distal, anteromedial aspect of both tibia [3]. At an indoor track-and-field site (Flanders Sports Arena, 289 m/lap), participants were instructed to run at 3.2 ± 0.3 m/s. A warm-up of 4.5 min without bio-feedback was given while the average axial PTA was automatically determined for the leg bearing the highest tibial shocks. Lap times were used to give feedback on running speed. Real-time, music-based biofeedback was then provided for 20 min. in total (2*10 min. with ~ 5 min. intermittent rest). Music of a preferred genre was continuously synchronized to the runner's step frequency and was non-linearly distorted by superposition of pink noise according to the magnitude of elevated PTA [4]. To lower impact loading, runners were instructed to run with maximum music clarity and were not given any instructions on possible gait modifications. To account for any within-subject change in PTA during running, all PTAs were exported for further analysis using a custom MATLAB program. Wilcoxon signed-rank tests compared the mean running speed and mean PTA level between the no biofeedback and biofeedback (last 10 min. phase) conditions. The data were determined to be significant if $p < 0.05$. Mean ± SD are reported.

RESULTS AND DISCUSSION

Running speeds during the no biofeedback and biofeedback conditions were respectively 3.2 ± 0.1 and 3.1 ± 0.1 m/s ($p = 0.416$, $z = -0.813$), and thus speed had no confounding effect on PTA. Supporting our hypothesis, one retraining session with real-time biofeedback was enough to temporary decrease PTA in an over-ground setting (Table 1). The PTAs experienced by a representative runner during the over-ground running session are shown in figure 1. All subjects could decrease impact loading while listening to real-time biofeedback, and this without

any instruction on gait modification but simply by means of impact sonification. The reduction of -2.7 g or -26 % in PTA was more than the achieved reduction in other single retraining sessions by auditory biofeedback on treadmill [2, 5].

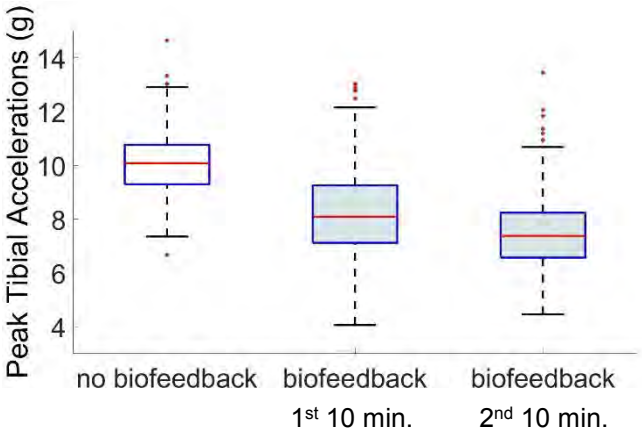

Figure 1: A Box-and-Whisker plot showing the distribution of peak tibial accelerations experienced by a representative participant.

The achieved reduction is arguably due to the more motivating form of the provided augmented feedback [6], consisting of music continuously synchronized to the runner's step frequency instead of simple beeps, and the cohort exhibiting high impacts along the lower leg's axial axis at baseline. Although other studies [2,5] demonstrated the effectiveness of auditory biofeedback by generating simple beeps for impact loading reduction on treadmill, this study is the first to show reduction in axial PTA in runners at-risk for the development of tibial stress injuries by applying more advanced and motivating real-time audio biofeedback and this in a non-lab environment. Besides the PTA acting along the axial axis, the impact shock severity along the other axes may also have altered and should be investigated in future and ongoing studies.

The feasibility of providing auditory information about clinically relevant biomechanical data per wearable biofeedback system eliminates the need of retraining exclusively in laboratory or clinic settings. This allows people to engage in gait retraining by means of impact sonification in their regular running environment (e.g. track-and-field, trail running) and is expected to increase the effectivity of and the adherence to a running retraining program.

CONCLUSIONS

High impact runners were able to temporarily decrease their PTAs during over-ground running by actively listening to and acting on music-based biofeedback without any instructions on gait modifications. Running retraining aiming at impact loading reduction by provision of augmented feedback on a direct measure of impact loading is possible in an ecologically valid environment.

REFERENCES

1. Chan et al. *Am J Sports Med*. 5, 36354651773627, 2017.
2. Wood and Kipp. *J Biom*. 47, 1739–41, 2014.
3. Van den Berghe et al. *Proceedings of WCB'18,* Dublin, Ireland, 2018.
4. Lorenzoni et al. *Proceedings of MOCO'18,* Genoa, Italy, 2018.
5. Morgan and Kipp. *Proceedings of ASB'15,* Columbus, OH, USA, 2015.
6. Maes et al. *Front. Neurosci*. 10, 548, 2016.

ACKNOWLEDGEMENTS

This ongoing investigation is funded by the Research Foundation – Flanders (FWO.3F0.2015.0048.01). We like to thank Gent Topsporthal Vlaanderen for the possibility of conducting a lab-in-the-field test.

Table 1: Comparison of peak tibial acceleration (g) between the no biofeedback and the biofeedback (2nd 10 min.) conditions. Mean number of steps analyzed per subject: 383, no biofeedback; 872, biofeedback.

	No biofeedback	**Biofeedback**
Mean	10.4	7.7
Std. Deviation	1.5	0.8
Minimum	8.8	6.5
Maximum	12.6	8.5
p-value	0.043	
z-value	-2.023	

LOAD EFFECTS ON PERFORMANCE FOR EXAMPLE OBSTACLES IN AN OUTDOOR COURSE

[1] Rachel Vitali, [1]Stephen Cain, [1]Michael Potter, [1]Lauro Ojeda, [1]Steven Davidson, [2]Alyssa Mendoza, [2]Leia Stirling, [1]Noel Perkins

[1] University of Michigan, Ann Arbor, MI, USA
[2] Massachusetts Institute of Technology, Cambridge, MA, USA
email: vitalir@umich.edu

INTRODUCTION

Modern warfare requires warfighters to carry increasingly heavy loads that include, for example, body armor, gear, electronics, food, and water. To optimize the magnitude and configuration of the load, the Marine Corps Load Effects Assessment Program (MC-LEAP) was developed to assess variations in soldier performance due to clothing and individual equipment (CIE) [1]. The program consists of an obstacle course representative of tasks warfighters encounter in combat. Historically, performance in the MC-LEAP (and variations of it) is quantified solely by the time required to complete each obstacle as often measured via timing gates. Although the time to complete an obstacle is one measure of performance, completion time alone does not reveal the technique(s) used or underlying biomechanics contributing to performance. As an alternative to video motion capture, recent studies employed inertial measurement units (IMUs) to measure underlying biomechanics that define performance for obstacles in the MC-LEAP [2-8]. The goal of this follow-up study is to understand how the IMU-derived performance metrics change when subjects carry different loads.

METHODS

A set of 22 subjects (7 females, 15 males) were recruited to complete a 10 obstacle abbreviated version of the LEAP-A a total of four times with a weight vest with 0% (2 repetitions), 15% (1 repetition), and 30% (1 repetition) of their body weight. All subjects wore an array of 13 IMUs (Opal, APDM, Portland OR) attached to the head, upper arms, forearms, sternum, sacrum, thighs, shanks, and feet. In addition, the subjects carried a mock plastic rifle (3.4 kg) with another attached IMU. The University of Michigan IRB approved the study and all subjects gave informed consent. The IMU data (accelerometer and angular rate) for each of the 14 IMUs was parsed into segments for each obstacle with custom activity identification code. The data for each obstacle was further analyzed with custom algorithms identifying key biomechanical measures of performance with examples detailed in [2-8].

Performance metric changes for a subset of obstacles is reported as a function of load. Thus, a repeated-measures analysis of variance (ANOVA) was conducted. Several subjects' data were eliminated because the subject did not complete all four testing sessions, data for one or more sensors was lost due to technical difficulties, or data was not properly parsed (i.e. falsely identified as another obstacle or failed to find anything). For the present analysis, the total number of subjects for the wall, window, and high crawl were 15, 13, and 14, respectively.

For each obstacle-specific performance metric, the normality assumption for the residuals is confirmed with Shapiro-Wilk normality tests, skewness and kurtosis calculations, and Q-Q plots. After conducting the repeated-measures ANOVA, a Mauchly's test for sphericity was conducted. Depending on the severity of the violation of this assumption, the ANOVA F-statistic was evaluated with adjusted degrees of freedom using a Greenhouse-Geisser correction. Then, Tukey post hoc analyses were conducted for performance metrics with significant results. All statistical tests are evaluated with a significance level of $\alpha = 0.05$.

Results are presented from the chosen subset of obstacles: 1) wall, 2) window, and 3) high crawl. The wall obstacle requires subjects to lift themselves up and over a 4ft tall wall. The window obstacle similarly requires subjects to lift themselves through a 3ft x 3ft opening 4ft off the ground. The high crawl requires subjects to crawl 30ft on elbows and knees while keeping their bodies as low as possible. The

ANOVA results include the F-statistic (and degrees of freedom), p-value, and effect size (η^2). For η^2, an effect size that is small is 0.01, medium is 0.06, and large is 0.14 [9]. The Tukey post hoc test results include the p-value and effect size (Cohen's **d**) for each pairwise comparison. Cohen's **d** indicates both the magnitude and direction of the comparison. (A negative **d** value indicates that the first group's average is less than that of the second group.) For Cohen's **d**, an effect size that is small is 0.2, medium is 0.5, and large is 0.8 [9].

RESULTS AND DISCUSSION

Performance on each obstacle is described by several performance metrics and a subset of three important metrics/obstacle are reported in Table 1 (all of which have normally distributed residuals). The ANOVA results show that load has a significant and large effect on the performance metrics in this subset of obstacles, whereas the post hoc results show these effects vary across metrics. As expected, the effect sizes for the 0%-30% comparison are larger in magnitude than either of the other two comparisons. However, there does not appear to be a common trend between the other two comparisons. For example, adding 15%BW from 0%BW has a larger effect on the wall's *Average take-off power* than adding 30%BW from 15%BW whereas adding 15%BW from 0%BW has a smaller effect on the wall's *Take-Off Speed* than adding 30%BW from 15%BW. These results imply potential metric-specific non-linear effects of adding weight. These differences could be the result of altering the underlying technique selected for the obstacle.

CONCLUSIONS

Load has large, significant effects on several performance metrics in this obstacle subset. The post hoc analyses indicate the increased load degrades performance, but in directions and magnitudes that vary across metrics and load conditions. These results suggest the IMU-derived metrics can be used to discriminate performance and technique in an outdoor setting that could potentially be extended to applications beyond warfighter performance.

REFERENCES

1. Smith and Kelley. *Statement before the Tactical Air and Land Forces Subcommittee,* 2013
2. Cain et al. *Gait & Posture*. 2016, 43, 65-69
3. McGinnis et al. *Jour. of Sports Eng*. 2016, 19(1), 21-34
4. Davidson et al. *Applied Ergonomics*. 2016, 26, 27-33
5. McGinnis et al. *Bio. Sig. Process.&Cont*. 2016, 32, 150-156
6. Tammana et al. *Applied Ergonomics*. 2018, 70, 68-76.
7. Zaferiou et al. *PLOS ONE*. 2017, 12(11)
8. Ojeda et al. *Sensors*. 2017, 17(11), 2647
9. Cohen J. 1988, Hillsdale, NJ:Erlbaum

ACKNOWLEDGEMENTS

This material is based upon work supported by the US Army Contracting Command-APG, Natick Contracting Division, Natick, MA, under contract W911QY-15-C-0053.

Table 1: Statistical results for the wall, window, and high crawl obstacles from the course. The effect sizes (η^2, **d**) are shaded according to how large the effect is [9]. Green indicates a large effect, yellow indicates a medium effect, and red indicates a small effect (as defined in the Methods section). *Significant at $\alpha = 0.05$.

	ANOVA			Tukey Post Hoc					
	F-Statistic	p-value	η^2	0%-15%		0%-30%		15%-30%	
				p-value	d	p-value	d	p-value	d
Wall									
Take-off Speed	F(2,28)=17.1	<0.001*	0.55	0.16	0.37	<0.001*	0.87	<0.001*	0.56
Average Take-off Power	F(2,28)=4.95	0.01*	0.26	0.48	0.67	0.05*	0.96	0.09	0.58
Take-off Work	F(2,28)=4.15	0.03*	0.23	0.19	0.58	0.05*	0.95	0.41	0.41
Window									
Approach Speed	F(2,24)=3.95	0.03*	0.25	0.31	0.32	0.02*	0.57	0.46	0.33
Take-off Speed	F(2,24)=3.91	0.03*	0.25	0.50	0.25	<0.01*	0.55	0.38	0.32
Window Time	F(1.01,11.1)=5.57	0.04*	0.34	0.10	-0.77	0.08	-0.88	0.07	-0.35
High Crawl									
Stride Time	F(2,26)=18.1	<0.001*	0.58	<0.01*	-0.68	<0.01*	-0.98	0.03*	-0.39
Opposite Side Coordination	F(2,26)=9.44	<0.001*	0.42	0.27	0.28	<0.01*	0.81	0.04*	0.49
Same Side Coordination	F(2,26)=4.25	0.03*	0.25	0.31	-0.32	0.07	-0.67	0.23	-0.33

CHANGES IN DYNAMIC MOTOR CONTROL FOLLOWING NEUROREHABILITATION FOR TRAUMATIC BRAIN INJURY: TREADMILL VS OVERGROUND WALKING

[1] Samuel A Acuña, [1] Mitchell E Tyler, [1] Yuri P Danilov, and [1] Darryl G Thelen

[1] The University of Wisconsin–Madison, Madison, WI, USA
email: saacuna@wisc.edu, web: http://uwnmbl.engr.wisc.edu

INTRODUCTION

Chronic gait deficits are often present in persons who have sustained a mild to moderate traumatic brain injury (TBI)—they tend to walk more slowly, take shorter steps and exhibit greater mediolateral sway [1]. Non-invasive neuromodulation of the cranial nerve has shown promise to enhance balance and gait in chronic TBI when coupled with rehabilitation exercises [2]. It is theorized this neuromodulation enhances neuroplasticity during rehabilitation, and thus improves the brain's ability to functionally compensate for damaged neural tissues [2]. However, it is unknown if the improvements in balance and gait arise from fundamental changes to the underlying motor control as a result of the neuromodulation.

One way to examine the underlying motor control during walking is with muscle synergy analysis. This has emerged as a quantitative tool to characterize the complexity of neuromuscular control patterns in neurologically impaired populations. The analysis typically involves the use of matrix factorization algorithms to identify low-dimensional patterns, or synergies, that can describe the variability inherent in an individual's measured muscle activations. A synergy then represents a group of muscles that are generally co-activated, which may represent simplified control. Hence, the variance in muscle activity accounted for by a given number of synergies can provide a measure of the complexity of control used by an individual. Prior synergy analysis studies have identified diminished complexity in the gait EMG patterns of stroke [3] and cerebral palsy [4] patients. Our previous work suggests that complexity is reduced for TBI subjects as well [5].

The objective of this study was to investigate if non-invasive cranial nerve neuromodulation during rehabilitation for a prior TBI can induce fundamental changes to the neuromuscular control of walking. We hypothesized that fundamental changes would manifest across a variety of walking tasks, such as walking overground and walking on a treadmill.

METHODS

Twenty healthy adults (25±3 years, 10 female) and forty-four ambulatory adults with a balance disorder due to a non-penetrative TBI participated in the study (53±9 years, 28 female). Each TBI participant was at least one year post-injury, had previously completed a focused physical rehabilitation program for their TBI, and were no longer seeing improvements from their gait rehabilitation. All TBI subjects had a dynamic posturography score at least 8 points below normal (Sensory Organization Test, NeuroCom®). The TBI subjects participated in 14-week neurorehabilitation program to train gait and balance. A portable electrotactile device stimulated cranial nerves V and VII throughout training via an electrode array placed on the human tongue, delivering three 0.4-60μs wide electric pulses at 5 ms intervals every 20 ms [2]. The rehabilitation program involved exercises 3x per day for two weeks in the clinic and then continued the exercises for 12 more weeks at home with the device.

Lower extremity electromyographic (EMG) signals were collected bilaterally from six muscles (tibialis anterior, medial gastrocnemius, soleus, vastus lateralis, rectus femoris, semitendinosus) during treadmill and overground walking (60 seconds). EMG was collected before rehabilitation (week 0), after the in-clinic training (week 2), after at-home training (week 14), and after a washout period without stimulation or exercises (week 26). Each chronic TBI subject walked at his/her pre-rehabilitation preferred speed (1.0±0.2 m/s). The

protocol was repeated on the healthy young adults walking at a speed of 1 m/s. EMG signals were rectified and then low-pass filtered at 10 Hz. Ensemble EMG patterns were created by averaging signals over all gait cycles and normalizing the data to each muscle's root-mean-squared EMG. Non-negative matrix factorization was used to derive the synergies. The walking dynamic motor control index (Walk-DMC) was then used to measure the complexity of neuromuscular control during gait [4]. A two-way repeated measures ANOVA tested for the effects of time (weeks 0, 2, 14, 26) and walking activity (treadmill, overground) on Walk-DMC score. For normative comparisons, exploratory Mann-Whitney tests compared Walk-DMC in TBI to the healthy adults.

RESULTS AND DISCUSSION

There was no significant effect of time (p = 0.581) or walking type (p = 0.307) on the Walk-DMC score of the TBI subjects (Fig. 1) During overground walking, the TBI subjects had a significantly lower Walk-DMC score than the healthy adults at every time point (p's < 0.01). However, the Walk-DMC score for TBI subjects on the treadmill was only significantly lower than the healthy adults before training (p = 0.018).

Changes in Walk-DMC for the TBI subjects were not consistent between treadmill and overground walking, suggesting that changes in neuromuscular complexity were different between the two walking tasks. This might suggest that the two walking tasks were sufficiently different and thus did not induce similar muscle activation patterns. Indeed, treadmill and overground walking may require different control strategies in this population [6]. However, as both walking activities have a lot of similarity, we may interpret our findings to suggest that the neurorehabilitation program did not create a fundamental change in the underlying control of walking. Rather, the improvements likely arose from proper training and increased familiarization of the treadmill walking task. Regardless, it is encouraging that neuromuscular complexity during treadmill walking improved to levels similar to the healthy adults after the in-clinic training, and then was maintained through the 12-week washout period. This suggests that the neurorehabilitation program may provide some level of meaningful change in walking control in a population of subjects who were no longer seeing improvements in gait and balance through traditional rehabilitation. Future research will examine individual subjects across time, as many TBI subjects started with healthy levels of neuromuscular complexity.

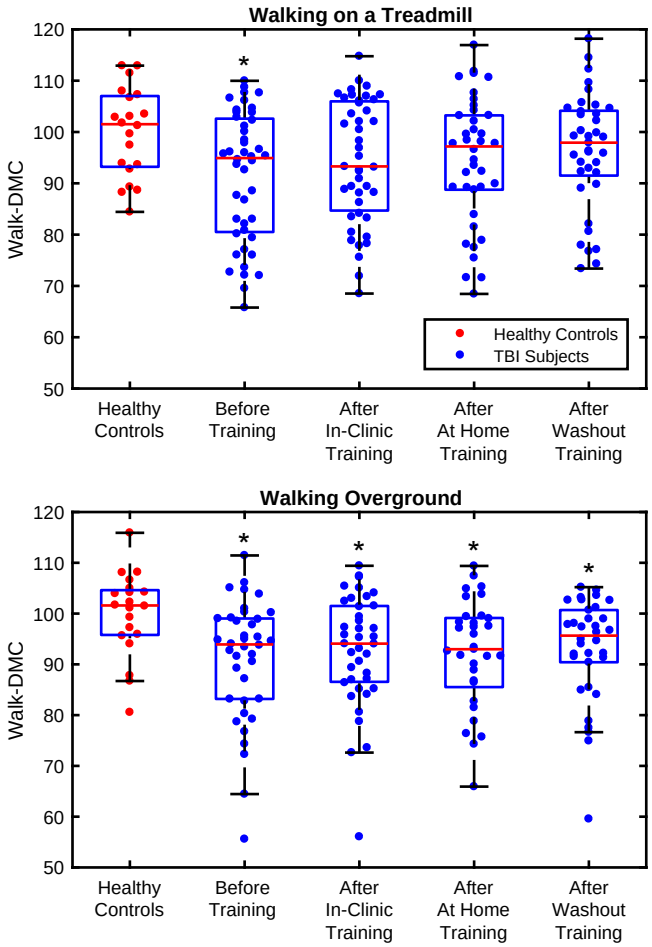

Figure 1: Walk-DMC scores for TBI and healthy controls. Asterisks indicate time points when the TBI subjects had a significantly lower Walk-DMC score than the controls.

REFERENCES

1. Vasudevan. *Neuro Phys Therapy.* 38(3), 2014.
2. Danilov. *Brain Neurotrauma*, CRC Press, 2015.
3. Clark et al. *Neurophysiology*. 103(2), 2015.
4. Steele et al. *Developmental Medicine & Child Neurology.* 57(12), 2015.
5. Acuña et al. ASB conference, Boulder, CO, 2017.
6. Brown et al. *Head Trauma Rehab.* 20(5), 2005.

ON-SITE REACTIVE BALANCE TRAINING AMONG RESIDENTS OF RETIREMENT COMMUNITIES

[1] Jessica Aviles, [1] Leigh Allin, [2] Neil Alexander, [1] Jennifer Van Mullekom, [1] Maury A. Nussbaum, [1] Michael L. Madigan

[1] Virginia Tech, Blacksburg, VA, USA
[2] University of Michigan, Ann Arbor, MI, USA
email: javiles@vt.edu

INTRODUCTION

Falls are a leading cause of injuries and injury-related deaths among older adults in the United States [1]. Up to half of all falls among older adults occur due to tripping [2-4]. Since the onset of tripping events may not be completely avoidable, enhancing the reactive balance response after tripping may be an effective approach for reducing falls among older adults. Reactive balance training (RBT) is a form of task-specific, perturbation-based balance training that has the potential to improve reactive balance performance. RBT involves repeatedly exposing individuals to trip-like perturbations in a safe, controlled manner to facilitate improvements in reactive balance performance.

The goal of this study was to evaluate the efficacy of RBT as an on-site balance training intervention for improving reactive balance among residents of retirement communities. This was done in comparison with Tai Chi, an active control demonstrated to reduce fall risk.

METHODS

Thirty-five older adults (age 70-92, 24 females) participated in the study. Subjects were initially required to pass a medical screening that included a history, physical, and bone mineral density assessment at the lumbar spine and proximal femur. Subjects were randomized to either RBT or Tai Chi. RBT was performed on a treadmill that was modified to elicit trip-like perturbations. Subjects stood quietly on the treadmill with a foam block placed in front of their feet. Perturbations were generated by accelerating the treadmill belt to a preselected walking speed over ~40 msec. This abrupt acceleration induced a forward fall similar to a trip while walking, and subjects subsequently attempted to take steps to recover balance (Fig. 1). RBT involved 30-minute sessions performed three times a week for four weeks. Each session consisted of 18-40 trials on the treadmill, with direction and speed pseudo-randomized and individualized based upon subject ability and improvement (with speeds between 0.5-2.4 mph). Tai Chi consisted of slow, controlled movements that focused on balance and like RBT, was performed three times a week for four weeks.

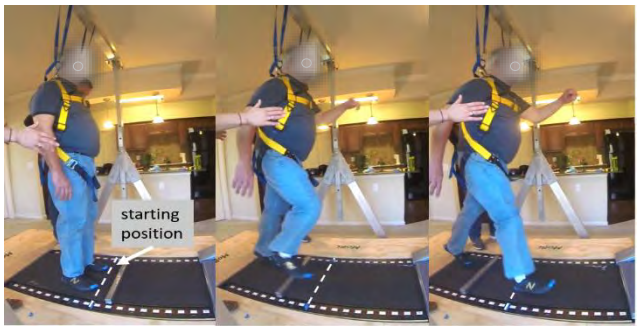

Figure 1. RBT subjects stood still on the treadmill (left) until the motorized treadmill suddenly accelerated, inducing a forward fall (middle). Subjects were asked to step over the block and establish a stable gait (right).

Outcome measures included metrics of reactive balance performance, along with standard clinical tests of balance and mobility. Outcome measures were assessed before (B) intervention, and one week (1W), one month (1M), three months (3M), and six month (6M) after intervention. Reactive balance performance was determined by accelerating the modified treadmill belt backward (to induce a forward fall) to 0.8, 1.6, and 2.4 mph. Outcomes measures were based on characteristics of the initial reactive step (measured from video recording) and sagittal plane trunk angle (measured using an inertial measurement unit). These measures included anterior/posterior length of the first reactive balance

step (step length), time from treadmill onset to lift-off of first recovery step (liftoff time), time from onset to touchdown of first reactive balance step (touchdown time), maximum sagittal plane trunk angle, and a reactive balance rating. Clinical tests included the time-up-and-go test (TUG), unipedal stance time, maximum step length, Berg Balance Scale, Performance-Oriented Mobility Assessment (POMA), and Activities-specific Balance Confidence Scale (ABC). Post-intervention differences between groups were investigated using a mixed model that accounted for fixed and random effects and within subject correlation. A $p \leq 0.05$ indicated significance.

RESULTS and DISCUSSION

RBT subjects performed better than Tai Chi subjects in a subset of reactive balance measures. Maximum trunk angle was 13.5 degrees smaller among RBT subjects one week after intervention ($p < 0.001$; Fig. 2). The reactive balance rating was 24% higher ($p = 0.016$; indicating better performance) at one week, 31% higher ($p = 0.023$) at one month, and 28% higher ($p = 0.029$) at six months after the intervention among RBT subjects compared to Tai Chi subjects. There were minimal differences in clinical tests between groups after intervention, though the POMA score was 5% higher (indicating better performance) among Tai Chi subjects one week after the intervention ($p = 0.040$).

CONCLUSIONS

Improvements in maximum trunk angle and reactive balance rating provide evidence for the ability of on-site RBT to improve reactive balance after trip-like perturbations. These results also support the use of the specificity of training principle among older adults for fall prevention.

REFERENCES

1. Centers for Disease Control and Prevention, *WISQARS*, National Center for Injury Prevention and Control [online], 2010.
2. Luukinen H, et al. *Osteoporos Int* **11**, 631-634, 2000.
3. Blake AJ, et al. *Age Ageing* **17**, 365-372, 1988.
4. Berg WP, et al. *Age Ageing* **26**, 261-268, 1997.
5. Owings TM, et al. *Clin Biomech* **16**, 813-819, 2001.

ACKNOWLEDGEMENTS

This research was supported by the National Science Foundation (HRD-1502335) and the NIH/NIA (R21 AG0457).

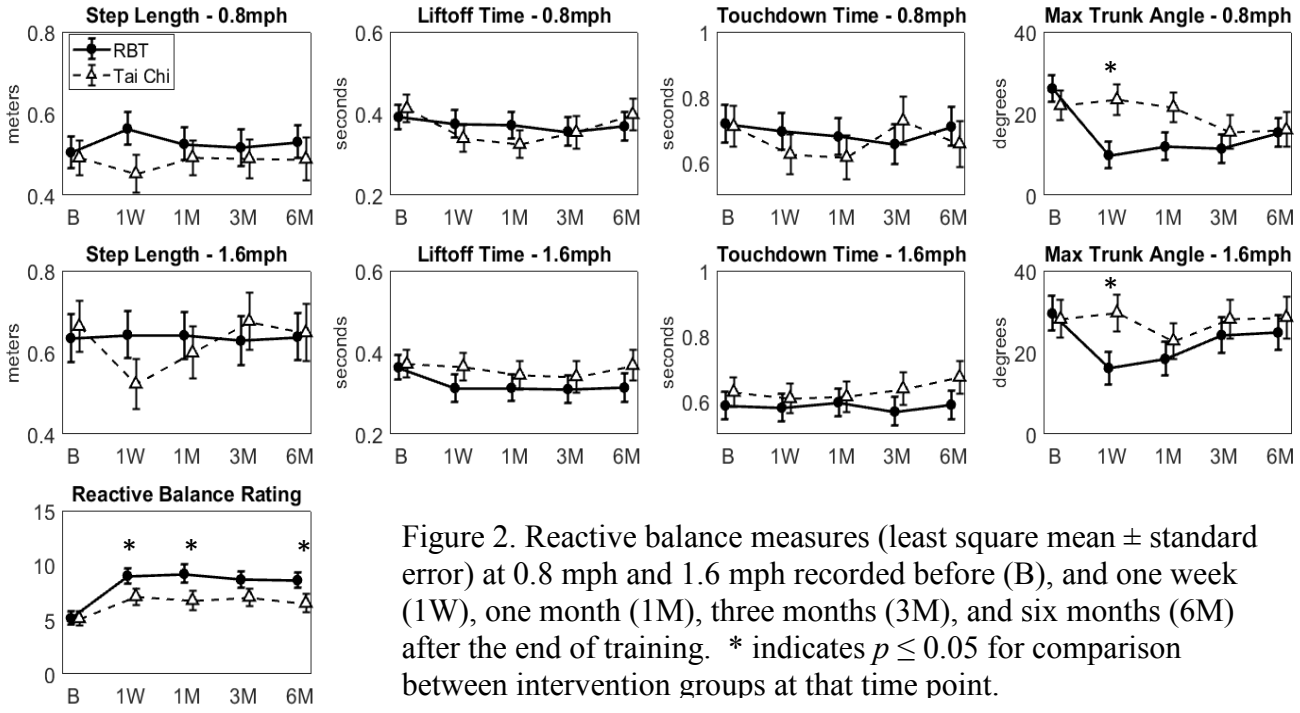

Figure 2. Reactive balance measures (least square mean ± standard error) at 0.8 mph and 1.6 mph recorded before (B), and one week (1W), one month (1M), three months (3M), and six months (6M) after the end of training. * indicates $p \leq 0.05$ for comparison between intervention groups at that time point.

PATIENTS WITH MEDIAL KNEE OA VARY IN THE KINETIC RESPONSE TO PLANTAR PRESSURE-BASED FEEDBACK

[1] Jade He, [1] Christopher Ferrigno, [1] Najia Shakoor, [1] Markus A. Wimmer
[1] Rush University Medical Center, Chicago, IL, USA
Email: Markus_A_Wimmer@rush.edu

INTRODUCTION

The knee adduction moment is a surrogate of medial compartment load during gait and is a regular target of conservative therapy for medial knee osteoarthritis (OA). In this study, we explore a gait retraining strategy that utilizes auditory cues based on real-time plantar pressure to inform individuals to medialize their center-of-pressure. After development and successful implementation of a gait retraining protocol on healthy subjects [1], we started a 6-week longitudinal clinical trial (NCT02955225) with patients with OA. This abstract reports on the initial gait retraining and investigates the immediate response of subjects to auditory cues.

The main purpose was to examine if patients were able to lower their knee adduction moment using pressure-based feedback. While 100% healthy subjects in a previous study responded favorably to pressure-based feedback [1], we anticipate that patients with OA will have more varied response with the training, prompting a secondary purpose to investigate gait variables that may differentiate responders from non-responders.

METHODS

Fifteen subjects with Kellgren-Lawrence (KL) grade 2 & 3) were recruited. The pressure-based auditory feedback system comprises a standardized, flexible shoe, a wireless, pressure-detecting shoe insole (Moticon GmbH, Munich, Germany), and a portable device for processing real-time plantar pressure and generating auditory cues (**Fig 1**). On the day of the visit, prior to the marker-based walks, subjects were fitted with the shoe and insole. Baseline plantar pressure was obtained from a 20-m walk at a self-selected, comfortable speed. A percentage (75-95% depending of actual performance of subjects) of the mean maximum of five steps of two lateral sensors were used as training thresholds. The sensors correspond to the time occurrence of the first and second peak of knee adduction moment.

Before gait retraining using pressure-based feedback, a motion capture (Baseline) acquired gait variables of subjects (**Fig 2**). After subjects were given an introduction on the pressure-based feedback system, they practiced walking while responding to the auditory cues under the supervision of a physical therapist. Once subjects were able to medialize center-of-pressure without triggering auditory cues from at least one of the two sensors for a few consecutive steps, they underwent another motion capture (Feedback).

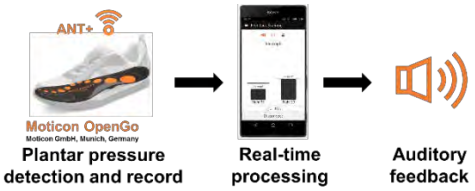

Figure 1: The pressure-based system was comprised of a flexible shoe, a wireless, pressure-detecting shoe insole, and a portable device.

Motion capture was performed using a ground embedded force plate (Bertec, Columbus, OH) to measure ground reaction forces and 12 optoeletric cameras (Qualysis, Gothenburg, Sweden) to capture lower extremities kinematics. A modified Helen Hayes marker-set was used. Raw kinetics and kinematics were processed in Visual 3D (C-Motion, Inc., Germantown, MD).

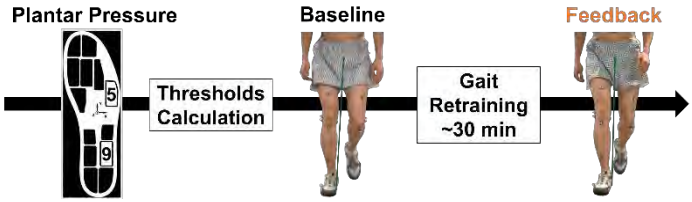

Figure 2: The gait retraining using pressure-based feedback happened between two marker-based walks, which captured gait variables before (Baseline) and after (Feedback) training.

Statistical analyses were performed using IBM SPSS Statistics 22 (SPSS Inc., Chicago, IL). Statistical significance was set to $\alpha = 0.05$. Binomial tests were used to evaluate if subjects were able to reduce the knee adduction moment. Paired t-tests were used to evaluate the training effects of pressure-based

feedback and independent sample t-tests were used to evaluate differences between subgroups. Linear regression was used to gauge a relationship between variables.

RESULTS

Characteristics of subjects recruited were 62 ± 11 yr, 85.4 ± 17.8 kg, 1.67 ± 0.09 m, and knee OA of 7 subjects was classified KL-2 and 8 subjects KL-3.

Ten subjects were able to reduce the overall and first peak of knee adduction moment, which was significant (p = 0.008 & 0.002, respectively). These ten subjects reduced the overall peak by 11.8% (0.31 %BW*Ht, p = 0.001) and the first peak by 12.7% (0.33 %BW*Ht, p < 0.001).

The responders to pressure-based feedback were separated from the non-responders based on whether or they were able to reduce the knee adduction moment (**Fig 3**). Between the subgroups, spatiotemporal variables were investigated since speed and its contributors stride length and cadence were shown to influence the knee adduction moment [2].

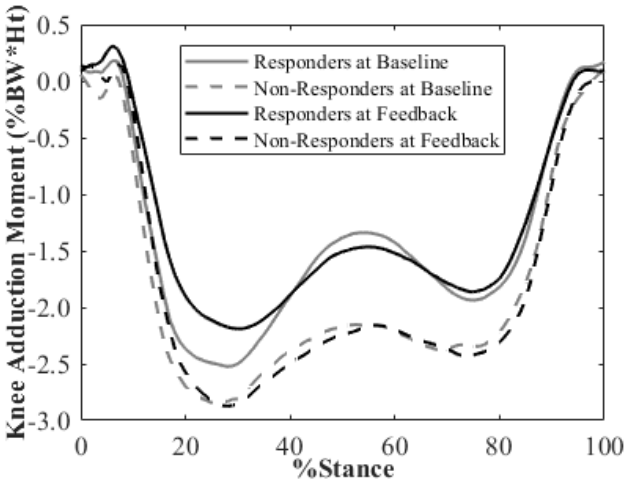

Figure 3: The average knee adduction moment at Baseline and Feedback across those who succeeded (responders) and failed (non-responders) to reduce knee adduction moment using pressure-based feedback.

At Baseline, responders showed longer stride length than non-responders (1.31 m > 1.13 m; t(13) = -2.13, p = 0.053). At Feedback, responders reduced stride length by 3.2% (0.41 m, p =0.001) (**Fig 4**) and increased cadence by 5.6% (3.13 step/min, p = 0.014). Reduced speed (8.9%, 0.11 m/s, p = 0.003) was also found in responders; however, there was no relationship between the reduction in speed and the reduction in knee adduction moment (r = 0.263, p = 0.464). In contrast, non-responders increased stride length by 9.7% (0.10 m, p = 0.336) without a significant change in cadence or speed at Feedback.

DISCUSSION

Two thirds of the OA subjects were able to follow auditory cues and lower their knee adduction moment within the 30-40 min training. According to Bernoulli statistics, it is unlikely that this happened by chance. A recent study revealed that stride length and cadence can have an impact on knee joint moments [2]. Starting with longer stride length, the responders might have more room of improvement, but by adjusting stride length a majority of the subjects with knee OA redistributed knee loads using pressure-based feedback.

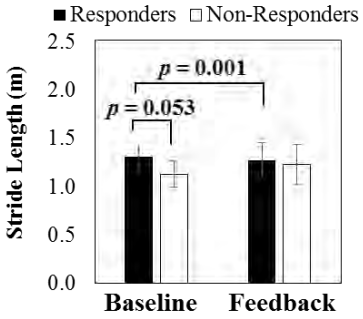

Figure 4: The responders who reduced knee adduction moment significantly reduced stride length after gait retraining using pressure-based feedback.

CONCLUSIONS

Pressure-based feedback was effective for a majority of subjects with medial knee OA to redistribute knee loads in the beginning of the clinical trial. How these subjects responded to pressure-based feedback to reduce knee adduction moment awaits more analyses. Difference in stride length at baseline and change in stride length and cadence that reflect a potential change in speed-regulating strategy post-training should deserve more attention when evaluating knee moments.

REFERENCES 1. Ferrigno et al. *J Biomech Eng.* 2016 Feb; **138**(2). 2. Ardestani et al. *Gait Posture*. 2016 May; **46**: 118-25.

ACKNOWLEDGEMENTS
Funding from the Arthritis Foundation is appreciated.

CERVICAL SPINE BIPLANAR FLUOROSCOPY: AUTOMATED SHAPE-MATCHING ALGORITHM VALIDATION

[1] Craig C Kage, [2] Mohsen Akbari-Shandiz, [1] Mary H Foltz, [1] Rebekah L Lawrence, [1] Taycia Brandon, [1] Eric Twohey, and [1] Arin M Ellingson

[1]University of Minnesota, Minneapolis, MN, USA
[2] Mayo Clinic, Rochester, MN, USA
email: ellin224@umn.edu, http://z.umn.edu/MRBL

INTRODUCTION

Current clinical assessment and diagnostic imaging techniques are unable to capture dynamic, three-dimensional (3D) motion of the spine at the segmental level. Understanding motion at the segmental level may help to better inform diagnosis, prognosis, and treatment for those with various musculoskeletal conditions. Biplane fluoroscopic imaging is a non-invasive and valid technique for quantifying 3D, dynamic bone motion at a segmental level in the spine [1,2]. Despite this technology being validated in other laboratory environments, it is important to validate each individual system's accuracy due to the complexity and customization of this developing technology. Moreover, because of the nature of radiographic imaging, the potential risk of radiation exposure must be balanced appropriately with the accuracy of the system, making the need for verification of each system's accuracy even more essential. Additionally, processing biplane fluoroscopic images into meaningful osteokinematic output (shape-matching) is manual and exceedingly labor-intensive with individual labs developing proprietary code to automate the process [1-3].

The purpose of this study was to validate our lab's biplane fluoroscopic system against the gold standard of radiostereometric analysis (RSA) for cervical spine kinematics using a custom, automated algorithm for shape-matching a cadaveric specimen.

METHODS

Data Collection

A fresh-frozen cadaveric specimen (male, 55 years of age), fully intact from the pelvis superiorly, was obtained for collection. Four tantalum beads were implanted into each of the anterior vertebral bodies of the cervical spine (C4-C6). Computed tomography (CT) images were obtained (Siemens Somaton Sensation 64; Germany; 120 kVp; voxel size: 0.23×0.23×0.60mm) from which bead centroids were identified and 3D bone models were reconstructed at each level (Mimics; Materialise, MI, USA). Anatomic-coordinates were labeled in Mimics: anterior, superior vertebral body and left and right lateral, superior vertebral notches (Figure 1). Bead traces were masked in the bone volumes to avoid shape-matching bias (ImageJ, NIH, MD, USA).

The specimen was thawed and dynamic fluoroscopic imaging was collected with our custom biplane system (Imaging Systems and Services Inc., OH, USA) using a long-handled apparatus to passively simulate neck motion from extension to flexion and from right to left lateral bending. The biplane system utilizes two 16″ image intensifiers (Thales 9447 QX; North American Imaging, OH, USA) and two high-speed cameras (Xcitex ProCapture, MA, USA). Figure 1 illustrates the system configuration with a 55-degree interbeam angle with one system parallel to the horizontal (flexion: lateral; bending: oblique) and the other oriented eight degrees above the horizontal inferior to superior (flexion and bending: oblique). Source-to-Image Distance (SID) was 152cm and the technique for acquisition was 70-74kV, 250-320mA, 3.5ms, 60Hz with a radiographic, wedge filter used for all trials (Ferlic Filter Co. LLC., MN, USA).

Data Analysis

Fluoroscopic images were undistorted, calibrated and dynamic bead positions were tracked for all visible frames using RSA (XMALab, Brown University, RI, USA). Prior to analysis all data were filtered with a low-pass, 4th order Butterworth Filter with a 3 Hz cutoff frequency [2]. To facilitate the automated shape-matching process, the position of

each vertebra (C4-C6) was manually set for the initial frame. All subsequent frames were tracked using an automated shape-matching algorithm, which incorporates a standard ray casting approach to generate digitally reconstructed radiographs (DRRs) and a 2D-3D image registration algorithm (Nelder-Mead Simplex optimization) which maximizes a correlation similarity measure to shape-match the DRR's onto the biplane radiographic projections (MATLAB, R2016B, The MathWorks, Inc., MA, USA). Three trials of flexion (565 total frames) and three trials of lateral bending (520 total frames) were analyzed. Output of the automated shape-matching algorithm was compared directly to RSA for rotations and translations at C4-C6 and for intersegmental kinematics (C4/C5, C5/C6). Bias, precision, and root mean square error (RMSE) were calculated at each level, averaged across all levels for that trial, then averaged across all three trials for each motion.

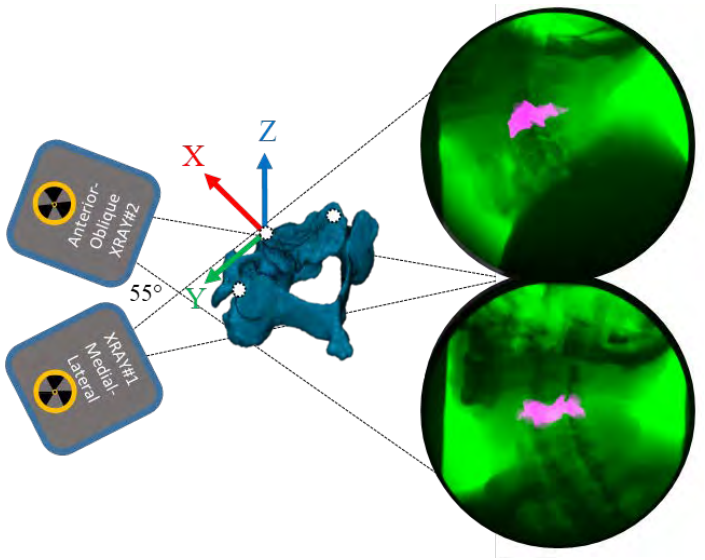

Figure 1: Biplane fluoroscopic set-up for flexion motion with reconstructed C4 CT bone model inset with local coordinate system and anatomic landmarks (white).

RESULTS AND DISCUSSION

Results of bias, precision, and RMSE calculations are displayed in Table 1. Briefly, average segmental RMSE for all levels (C4, C5, C6) of flexion trials was 0.78° rotation and 0.30 mm translation and average intersegmental RMSE (C4/C5, C5/C6) was 1.13° rotation and 0.33 mm translation. Average RMSE for all levels (C4, C5, C6) of lateral bending trials was 0.61° rotation and 0.21 mm translation and average intersegmental RMSE (C4/C5, C5/C6) was 0.85° rotation and 0.31mm translation. Rotations about the Y-axis (flexion/extension) demonstrated the greatest amount of error for both motions. Total RMSE was found to be below 1.70° degrees (rotation) and 0.50 mm (translation). Bias and precision values were similar to previously published works [1-3].

CONCLUSIONS

The results of this study demonstrate the appropriate accuracy of our biplane system, fluoroscopic technique, and the utility of an automated shape-matching algorithm for cervical motion analysis.

REFERENCES

1. McDonald CP, et al. *Spine J* **10**, 497-504, 2010.
2. Anderst WJ, et al. *Spine* **36**(6), E393-400, 2011.
3. Li G, et al. *J Biomech* **41**(7), 1616-1622, 2008.

ACKNOWLEDGEMENTS

This project was supported by NIH/NICHD K12HD073945, F31H087069, and Minnesota Partnership for Biotechnology and Medical Genomics (MNP IF #14.02).

Table 1: Summary of mean bias, mean precision, and mean RMSE for segmental and intersegmental kinematics across all trials and levels. Lateral Bending (LB), Flexion/Extension (FE), Axial Rotation (AR), Anterior-Posterior (AP), Medial-Lateral (ML), Superior-Inferior (SI).

	Flexion						**Lateral Bending**					
	Segmental Accuracy			Intersegmental Accuracy			Segmental Accuracy			Intersegmental Accuracy		
Rotation (degrees)	**LB (X)**	**FE (Y)**	**AR (Z)**	**LB (X)**	**FE (Y)**	**AR (Z)**	**LB (X)**	**FE (Y)**	**AR (Z)**	**LB (X)**	**FE (Y)**	**AR (Z)**
Bias	0.48	0.35	-0.49	-0.24	0.53	-0.34	0.29	-0.21	-0.15	-0.10	0.64	-0.12
Precision	0.34	0.53	0.35	0.38	0.76	0.48	0.23	0.57	0.23	0.34	0.83	0.31
RMSE	0.60	0.99	0.76	0.46	1.69	1.23	0.45	1.07	0.31	0.74	1.41	0.41
Translation (mm)	**AP (X)**	**ML (Y)**	**SI (Z)**	**AP (X)**	**ML (Y)**	**SI (Z)**	**AP (X)**	**ML (Y)**	**SI (Z)**	**AP (X)**	**ML (Y)**	**SI (Z)**
Bias	-0.46	0.11	-0.18	0.16	-0.24	-0.15	-0.07	-0.25	-0.04	0.26	-0.11	0.08
Precision	0.06	0.07	0.10	0.18	0.15	0.14	0.07	0.08	0.16	0.24	0.15	0.25
RMSE	0.46	0.22	0.21	0.40	0.28	0.30	0.17	0.27	0.20	0.45	0.20	0.29

THE EFFECT OF SCAPULOTHORACIC UPWARD ROTATION ON SUBACROMIAL PROXIMITIES

[1] Rebekah L. Lawrence and [1] Paula M. Ludewig
[1] Department of Rehabilitation Medicine, University of Minnesota, Minneapolis, MN, USA
email: lawre354@umn.edu

INTRODUCTION

Rotator cuff pathology is a prevalent finding on magnetic resonance (MR) images in individuals with shoulder pain. Subacromial rotator cuff compression has long been thought to be a primary mechanism of rotator cuff injury. Clinical theory suggests decreased scapulothoracic upward rotation (ST UR) increases risk for subacromial rotator cuff compression as it positions the acromion downward and presumably in closer proximity to the rotator cuff tendons. However, this clinical theory has not been fully tested *in vivo*. Therefore, the purpose of this study was to determine the impact of decreased ST UR on subacromial proximities.

METHODS

Sixty subjects were recruited to participate in this study. Of these, 30 had current shoulder symptoms consistent with a clinical diagnosis of "impingement syndrome" (32.4 ± 8.8 years, 46.7% male, 40% tested on dominant side) and 30 had no prior history of shoulder pain (32.7 ± 8.3 years, 46.7% male, 40% tested on dominant side).

Subjects underwent kinematic motion analysis using single plane fluoroscopy synced to a five-camera motion capture system. The camera system was used to track thorax motion, while the fluoroscopy was used to track humeral and scapular motion. Data was collected while subjects performed arm raising in the scapular plane. MR scans were also acquired, which was used to create 3D anatomical models of the humerus and scapula. Scapulothoracic and glenohumeral kinematics were tracked via manual 2D/3D image registration in JointTrack software. Kinematics were described using published recommendations [1, 2]. Subjects were ranked based on their magnitude of ST UR at 30° humerothoracic elevation, which corresponds to the range of closest subacromial proximities [3]. The 20 participants with the highest ST UR were classified as having "high" ST UR, while the 20 participants with the lowest ST UR were classified as having "low" ST UR. Classification in this manner allowed for the effect of ST UR on subacromial proximities to be tested directly. Demographic data for these subjects are provided in Table 1.

Table 1: Demographic Data for High and Low ST UR Groups (mean ± SD, or %)

	High (n=20)	**Low (n=20)**	**p-value**
Age (years)	30.7 ± 5.2	34.1 ± 10.1	0.20
Gender (% male)	25%	65%	0.01
Group (% asymptomatic)	45%	40%	0.75
Rotator cuff tendon thickness (mm)	5.5 ± 1.2	5.7 ± 0.9	0.59

The thickness of the rotator cuff tendon was measured at the articular margin on each subject's MR scan on the slice corresponding to the anterior/posterior midpoint of the tendon insertion. A plane was fit between the coracoid and acromion representing the coracoacromial ligament according to published anatomical descriptions [4].

Each subject's arm raising task was re-created by animating their humeral and scapular models using their glenohumeral kinematics. Subacromial proximities were quantified at 10° intervals of humerothoracic elevation by calculating the minimum distance between each pairwise set of vertices on the coracoacromial arch (i.e. acromion and the plane representing the coracoacromial ligament) and along the articular margin (**Fig. 1**). The minimum distance measures were constrained to the articular margin coinciding to where the rotator cuff thickness was obtained because the thickness cannot be assumed constant across the surface of the insertion site. All minimum distances were normalized to the subject's rotator cuff thickness value, which facilitated interpretation. For each

subject, the humerothoracic elevation position at which the normalized minimum distance was smallest was defined as the position of absolute minimum distance. Contact between the rotator cuff and coracoacromial arch was defined as a normalized minimum distance of <120%. This threshold accounts for approximately 1 mm of error in quantifying the minimum distance due to errors during 2D/3D image registration.

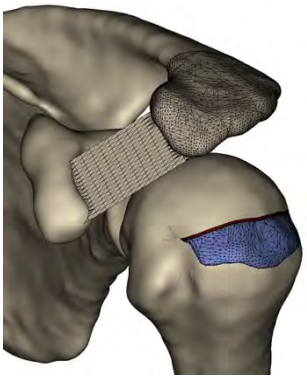

Figure 1: Definition of: 1) rotator cuff insertion (blue surface); 2) Articular surface region of interest (maroon line); and 3) coracoacromial ligament.

Data normality was tested prior to statistical analysis. The normalized minimum distance was skewed and subsequently log transformed for statistical analysis. The effect of ST UR on subacromial proximities was assessed using a two-factor mixed-model ANOVA with Toeplitz covariance structure. The model included a between-subject factor of group (low, high) and a within-subject factor of angle (arm at side, 30°, 60°, 90°). Follow-ups were calculated using Tukey adjustments. The position of absolute minimum distance was compared between groups using a two-sample independent t-test. The frequency of contact between the tendon was tested between groups using Chi-square analysis.

RESULTS AND DISCUSSION

Consistent with group assignment, the subjects in the low ST UR group had on average 11.9° less UR at 30° humerothoracic elevation than the subjects in the high ST UR group. In both groups, the normalized minimum distance was generally smallest below 90° humerothoracic elevation. There was a significant group-by-angle interaction, suggesting the difference between ST UR groups was dependent on the angle of humerothoracic elevation (p=0.047) (**Fig. 2**). However, group follow-ups were not significant at any angle of humerothoracic elevation. Although not statistically significant, the normalized minimum distance for the subjects in the low ST UR group was 15.2% lower than those in the high UR group at the minimum position, and 20% higher at the 90° humerothoracic elevation. The rotator cuff was closest to the coracoacromial arch an average of 8° lower in the range of motion in subjects in the low ST UR group. In total, only 38% of subjects had at least one humerothoracic position where the normalized minimum distance was <120% suggesting contact occurred.

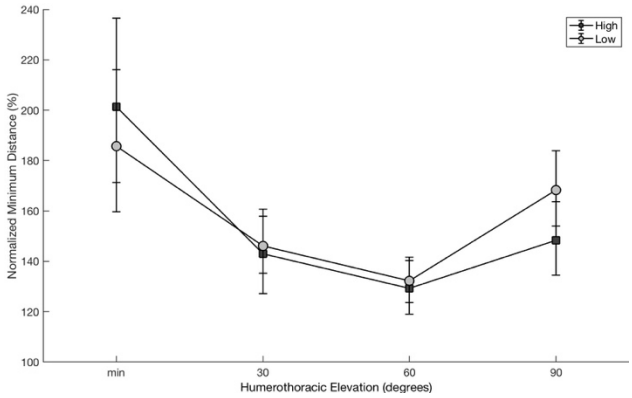

Figure 2: The normalized minimum distance for the high and low ST UR groups across angles of humerothoracic elevation.

CONCLUSIONS

Decreased ST UR shifts the range of risk for subacromial rotator cuff compression to lower angles. However, the clinical meaningfulness of the small magnitude of change in normalized minimum distance is unclear. Subacromial rotator cuff compression occurs in less than 40% of individuals during unweighted, non-fatigued arm raising, suggesting it may not be a predominant mechanism for rotator cuff injury.

REFERENCES

1. Ludewig et al. *Clin Biomech* 25:415-21, 2010.
2. Wu et al. *J Biomech* 38:981-92, 2005.
3. Lawrence et al. *J Orthop Res*. 37:2329-37, 2017.
4. Edelson et al. *Arthroscopy*. 11:715-9, 1995.

ACKNOWLEDGEMENTS

This study was funded by the NIH (F31HD087069) and the Foundation for Physical Therapy.

Changes in Hip Mechanics During Gait Modification to Reduce Knee Adduction Moment

[1]Bryndan Lindsey, [1]Oladipo Eddo, [1]Shane Caswell, [1]Matt Prebble, [1]Nelson Cortes

[1]George Mason University, Manassas, VA
email: ncortes@gmu.edu, web: https://smartlab.gmu.edu/

INTRODUCTION

First peak internal knee abduction moment (PKabdM) has been associated with knee osteoarthritis (OA) progression [1]. Gait modification strategies using real-time biofeedback (RTB) including lateral trunk lean (TL), medial knee thrust (MKT), and decreased foot progression angle (FPA) have reduced PKabdM in both healthy and OA populations [2]. Despite the success of these interventions in reducing PKabdM, the potential biomechanical effects on the kinetic chain remain poorly understood [3]. There is evidence suggesting that PKabdM partially depends on the magnitude of hip abduction moment [4, 5]. Greater internal hip abduction moment has been shown to be protective of medial knee OA development, reducing the odds of OA progression 50% for every additional unit of hip abduction moment [6]. Previous authors have suggested that increased hip abductor strength can be beneficial in controlling knee joint loads which is supported by reduction of knee OA symptoms after a hip strengthening intervention [7]. However, limited evidence suggests that common strategies to reduce PKabdM can reduce hip abduction moment [8]. Therefore, the purpose of this study was to investigate biomechanical changes at the hip during three previously studied gait modifications designed to reduce PKabdM.

METHODS

Twenty healthy individuals volunteered for this study (28.4 ± 3.8 years, 1.73 ± 0.1 m, 75.3 ± 12.5 kg). Mean and standard deviation (SD) for trunk angle, knee angle, and foot angle during stance was calculated from ten baseline trials using eight high-speed motion analysis cameras and four floor embedded force plates. Gait trials were conducted on a 6m long walkway with the last 2.4 meters containing the force plates. Trials were only valid with two full foot contacts of the experimental limb on the force plates and gait speed within ±5% of baseline speed. Five trials were completed for each gait strategy using RTB so that joint angles fell within a range of 3-5 SD greater than (FPA and TL) or less than (MKT) baseline. Visual 3D was used to project RTB on a 4.8m by 3.3m projection wall facing the walkway as a line graph displaying real-time joint angle during stance. Participants were instructed to modify their gait so that the line fell within a highlighted bandwidth representing the target ranges. Visual 3D was used to calculate joint angles (°) and internal moments (Nm/kgm) measured at PKabdM. Although, external joint moments are most commonly reported in knee OA literature, internal moments are equal but opposite. Repeated measures ANOVA was used to assess differences in hip moments and angles between conditions. Pairwise comparisons were conducted to compare changes between baseline walking and modification strategies ($p<0.05$).

RESULTS AND DISCUSSION

On average PKabdM was reduced in all strategies from baseline, however, significance was only reached for FPA ($p<0.05$) and MKT gait ($p<0.01$; Table 1). Compared to baseline, participants significantly reduced frontal plane hip angle during TL gait ($p<0.01$) and sagittal plane hip angle across all strategies ($p<0.01$; Table 1). Hip abduction moment was significantly decreased during TL and MKT gait compared to baseline ($p<0.01$) while hip extension moment was unchanged (Table 1). During TL gait participants walked with a more abducted and flexed hip and demonstrated decreased hip abduction moment at PKabdM (Figure 1).

Previous studies have shown that hip abduction moments are greater in patients with less severe medial compartment knee OA [4, 5, 6].

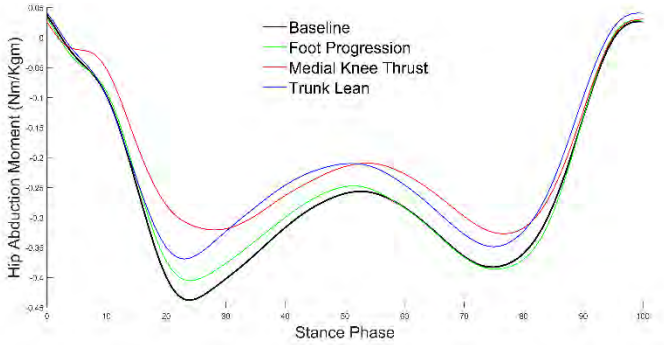

Figure 1: Mean hip abduction moment (Nm/kgm) across the stance phase.

A common gait strategy adopted by knee OA patients includes shifting the center of mass (COM) towards the involved limb while moving the trunk laterally [4]. This compensatory mechanism is similar to the TL strategy used in this study and has shown success in reducing medial knee joint load by shifting the GRF vector laterally, decreasing the magnitude of the moment arm [4].

Patients with more severe OA, however, may lack the hip abductor strength to maintain this altered trunk position during stance causing excessive pelvic drop in the contralateral leg. This shifts the COM away from the stance leg, increasing the PKabdM and subsequent medial compartment joint load [4, 6]. Even in patients with the prerequisite hip strength, this strategy may not be beneficial in the long-term as it decreases demand on the hip, weakening the musculature. This reduces the ability of the muscles to regulate medial/lateral knee load distribution, decreasing frontal plane stability [6]. Similar to TL gait, MKT gait resulted in participants walking with a more flexed hip and reduced hip abduction moment at PKabdM (Figure 1). The mechanism between the two strategies was similar; increased hip and knee abduction angle with reduced peak hip abduction moment potentially due to the shift of the COM closer to the joint centers.

CONCLUSIONS

Gait modifications designed to reduce PKabdM significantly changes hip mechanics in healthy individuals. TL and MKT strategies resulted in reduced hip abduction moment at PKabdM which may be detrimental to patients with more advanced knee OA. Therefore, future studies investigating gait modifications designed to slow the progression of OA should consider the effects on hip as well as knee mechanics.

REFERENCES

1. Miyazaki et al. *Annals of the Rheumatic Disease.* 2002;**61(**7):617-622.
2. Eddo et al. *International Journal of Kinesiology and Sports Science.* 2017;**5**(3):35-55.
3. Simic et al. *Arthritis Care & Research.* 2011;**63**(3):405-426.
4. Mündermann et al. *Arthritis & Rheumatology.* 2005;**52**(9):2835-2844.
5. Astephen et al. *Journal of Orthopaedic Research.* 2008;**26**(3):332-341.
6. Chang et al. *Arthritis & Rheumatology.* 2005;**52**(11):3515-3519.
7. Bennell et al. *Osteoarthritis and Cartilage.* 2010;**18**(5):621-628
8. Mündermann et al. *Journal of Biomechanics.* 2008;**41**(1):

Table 1: Descriptive statistics of (mean ± standard deviation) frontal and sagittal plane hip angles and moments across strategies. Significant difference from baseline is indicated by asterisk ($p<0.05$)

	Gait Strategy			
	Baseline	**FPA**	**MKT**	**TL**
PKabdM	-0.26 ± 0.05	-0.23* ± 0.06	-0.14* ± 0.10	-0.24 ± 0.10
Hip adduction angle	3.11 ± 2.90	2.71 ± 2.59	1.78 ± 4.09	0.56* ± 3.13
Hip flexion angle	13.14 ± 4.81	15.36* ± 4.69	20.27* ± 8.02	15.77* ± 6.44
Hip abduction moment	-0.41 ± 0.08	-0.38 ± 0.10	-0.29* ± 0.14	-0.34* ± 0.11
Hip Extension moment	-0.15 ± 0.11	-0.16 ± 0.12	-0.16 ± 0.14	-0.18 ± 0.15

COMPARISON OF JOINT KINETICS USING COMMON MODELS FOR BASEBALL PITCHING

Michael P. McNally, James A. Oñate, Ajit M.W. Chaudhari

The Ohio State University, Columbus, OH, USA
email: Michael.mcnally@osumc.edu

INTRODUCTION

Biomechanical analyses are more frequently being utilized to aid in achieving improved baseball pitching performance while minimizing joint loads on the body. Increased potential for injury at the shoulder and elbow have been associated with certain kinetic risk factors, which are calculated using standard inverse dynamics from a known force applied by the ball [1]. However, because of the complexity in measuring the pitching motion, different underlying modeling approaches have been used with varying constraints. In particular, three common models have been used in research, and are suggested for use in clinical throwing analysis, which include a 6 degree of freedom model (6DOF), an optimized model using inverse kinematics (IK), and a model that does not allow intersegmental translations (ASMI) [2]. Understanding the differences between these models is critical for understanding the biomechanics of the pitching motion, and how to interpret data relative to normative data expressed in the literature.

The purpose of this study was to determine the relationships between joint kinetic parameters as estimated by three different biomechanical models for baseball pitching, both in the absolute estimates as well as in the relative predictions of which individuals have elevated loading. We hypothesize that differences will exist in absolute joint kinetics between models, but that kinetic parameters will be correlated between models.

METHODS

15 right-handed male baseball pitchers from high school (n = 8), collegiate (n = 4), and professional (n = 3) baseball, who all learned to play in the United States, were analyzed for this study as part of an overarching study (age = 19.2±4.9 years, height = 1.85±0.06 m, mass = 83.5±12.1 kg, hand velocity = 23.6±1.38 m/s). After performing a self-selected warm-up, pitchers were recorded using an optical motion capture system (Vicon Inc., Oxford, UK) capturing at 300 Hz while throwing five fastballs from an instrumented pitcher's mound [3] at "game like effort" towards a target placed approximately 13m away. The first three pitches which contained complete marker data for the upper extremity were analyzed for each pitcher.

All analyses were performed using Visual3D software (C-Motion Inc., Germantown, MD, USA). Marker trajectories were filtered using a low-pass Butterworth filter with a cutoff frequency of 13.4 Hz [2]. Shoulder and elbow kinematics and kinetics were calculated in the global reference frame, and reported using 3 different methods. The first method utilized a 6 degree of freedom model, defined using recommendations of upper extremity kinematics described by the International Society of Biomechanics [4], and tracked each segment allowing full translation and rotation in all planes for each segment (6DOF model) [5]. The second method defined the upper extremity and the resulting kinematics and kinetics using the same ISB model, but utilized a global optimization technique to eliminate any translation at the wrist and elbow joint, varus/valgus motion at the elbow, and rotation at the wrist (IK model) [6]. The third method defines the distal end of the proximal segment and the proximal end of the distal segment to be coincident at the shoulder, elbow and wrist, thereby eliminating translations. It constrains the shoulder reference frame using the cross product of the long axis of the arm and vertical axis of the trunk to define the anterior axis, and the elbow reference frame using the cross product of the long axis of the forearm and long axis of the upper arm to define the anterior axis (ASMI model) [2]. As one of the critical instants, maximum shoulder external rotation (MER) was calculated as the point

when the shoulder is maximally externally rotated relative to the trunk.

Four kinetic variables were calculated using each method based on evidence suggesting a relationship to shoulder or elbow injury risk. Specific variables included peak elbow varus torque and elbow varus torque at MER, internal rotation torque at MER, and peak shoulder distraction force. A one-way ANOVA was used to detect a main effect of model for each kinetic variable, with Tukey's post hoc analysis to determine individual differences for any main effects. All variables were confirmed to be normally distributed, so Pearson correlation coefficients were calculated to determine the relationship in kinetic calculations between models. Significance for all statistical tests was set *a priori* at $p < 0.05$.

RESULTS AND DISCUSSION

Descriptive statistics and a summary of ANOVA's are listed in Table 1. Main effects of model were identified for all kinetic variables ($p < 0.001$). Peak elbow varus torque was significantly greater for IK and ASMI models compared to 6DOF ($p < 0.001$). Elbow varus torque at MER was different between all methods, with ASMI model estimating greater torque at MER than 6 DOF, which is greater than IK ($p < 0.001$). Shoulder internal rotation torque at MER was greater for IK and ASMI compared to 6DOF, and peak shoulder distraction force is greater for 6DOF and IK compared to ASMI ($p < 0.001$).

Elbow varus torque showed moderately strong correlations between methods (R = 0.696-0.777). Elbow torque at MER was moderately correlated between 6DOF and IK (R=0.541) and between 6DOF and ASMI (R=0.631), with no association between IK and ASMI models (R=0.078). Shoulder internal rotation torque at MER was weakly correlated (R=0.283-0.514), while peak shoulder distraction force showed only a strong correlation between 6DOF and IK, with no association between 6DOF and ASMI (R=0.137) and IK and ASMI (R=0.140).

While this research cannot differentiate which model is most accurate, it does suggest that results may not be generalizable between models, often making conclusions from research dependent on the model used. These differences are likely a result of both differing constraints and definitions of anatomical reference frames, as well as any resulting differences in the timing of MER using each method. When evaluating research or conducting performance evaluations on pitching, clinicians need to match the model they use to the available literature and normative values, otherwise inaccurate conclusions may be reached. Further study may help to better assess the validity and reliability of each model as it pertains to the pitching motion, identifying pitchers at risk, and in assessing interventions to improve performance while minimizing risk.

REFERENCES

1. Feltner ME, et al. *Int J Sport Biomech* **5**, 403-19, 1989.
2. Fleisig GS, et al. *J Appl Biomech* **12**, 207-24, 1996.
3. McNally, MP et al. *J Strength Cond Res* **29**, 2708-15, 2015.
4. Wu, G, et al. *J Biomech* **38**, 981-92, 2005.
5. Grood ES, et al. *J Biomech Eng* **105**, 136-44, 1983.
6. Lu TW, et al. *J Biomech* **32**, 129-34, 1999.

Table 1: Descriptive statistics and results of one-way analysis of variance between models.

Model	6DOF	IK	ASMI	ANOVA
Peak Elbow Varus Torque (Nm)	62.46 ± 19.39	86.00 ± 37.54	90.32 ± 21.33	6DOF < IK, ASMI
Elbow Varus Torque at MER (Nm)	41.81 ± 18.03	14.60 ± 19.97	77.13 ± 19.36	IK < 6DOF < ASMI
Shoulder internal rotation torque at MER (Nm)	20.29 ± 21.49	76.32 ± 55.44	75.90 ± 18.81	6 DOF < IK, ASMI
Peak shoulder distraction force (N)	857.44 ± 287.71	858.00 ± 243.25	124.98 ± 103.43	ASMI < 6DOF, IK

L5/S1 Joint Load Estimation during Lifting Using a Deep Learning Based Method

[1] Rahil Mehrizi, [1] Xi Peng, [2] Xu Xu, [3] Shaoting Zhang, [1] Dimitri Metaxas, and [1] Kang Li
[1] Rutgers University, Piscataway, NJ, USA
[2] North Carolina State University, Raleigh, NC, USA
[3] University of North Carolina at Charlotte, Charlotte, NC
email: rahil.mehrizi@rutgers.edu

INTRODUCTION

Occupational injuries are commonly observed among the workers involved in material handling tasks such as lifting. An important criterion to identify the non-ergonomic lifting task is the net force and moment values at L5/S1 joint. These values are mainly calculated in a laboratory environment, which utilizes marker-based motion capture systems and force plates. However, this method is usually a time-consuming process and needs expensive equipment. In this study, we propose and validate a novel marker-less method for L5/S1 joint load estimation, which address aforementioned limitations. The proposed method uses computer vision approaches, in particular Deep Neural Network (DNN), to estimate the 3D body pose from multi-view images and calculate the joint loads by an inverse dynamic algorithm. The results of our proposed method are compared with results obtained from a marker-based system as a reference and it is shown that the proposed method achieves promising results.

METHODS

Participants and Procedure. A group of 12 healthy males (age 47.50±11.30 years; height 1.74±0.07 m; weight 84.50±12.70 kg) participated in the experiment. Each participant performed various lifting trials in a laboratory while being filmed by two camcorders (positioned at 90 degree and 135 degree views) and a synchronized motion tracking system to measure the body movement. They lifted a plastic crate weighing 10 kg and placed it on a shelf without moving their feet. Each subject performed three vertical lifting heights (floor to knuckle, knuckle to shoulder, and floor to shoulder) combined with three end-of-lift angles (0, 30 and 60 degree). Lifting trials of subjects 1 to 10 were used as training dataset and subjects 11 and 12 were used for testing.

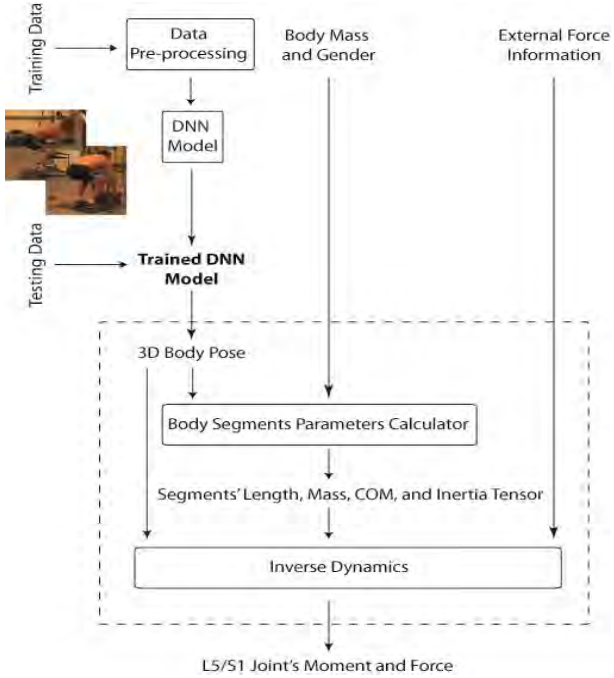

Figure 1: Workflow of the proposed DNN based method.

Methods. In this work, we aim to predict the 3D L5/S1 joint kinetic from a multi-view RGB image. As shown in figure 1, in the offline phase, the training dataset images are preprocessed and used to train a DNN model. In the online phase, given a new multi-view image (testing dataset), the trained DNN estimates its corresponding 3D body pose. The network architecture of the DNN model comprises of encoder and decoder. The encoder processes the input image with convolution and pooling layers to generate low resolution feature maps and the decoder processes low resolution feature maps with up-sampling and convolution layers to construct 2D joints coordination maps. The constructed 2D joints maps for each view are concatenated together and are processed more by another encoder. The neural network is ended with a fully connected output layer, which output the 3D coordination of each joint.

Next, the estimated 3D body pose along with the subject's anthropometric information are utilized to calculate body segments parameters including segments length, mass, position of the center of mass (COM), and inertia tensor based on the suggested values by [1].

Finally, L5/S1 joint kinetic is determined by a top-down inverse dynamic algorithm according to the estimated 3D body pose, body segments parameters and external force information. We applied a global equation of motion to estimate the net L5/S1 joint kinetic, as described by [2].

RESULTS AND DISCUSSION

L5/S1 Joint Moment. Results show a good agreement between the estimated L5/S1 joint moments in each of the three planes and the references (fig. 2). The grand mean (±SD) of the moment absolute errors across all the subjects and trials was 9.06 (±7.60) Nm. The R coefficient for all the lifting trials were high (above 0.94) and RMSE were small (mostly below 20 Nm).

Furthermore, Absolute peak values extracted from the moment time series of the proposed method were compared to the corresponding values of the reference across the whole lifting trials. In line with the small RMSE (6.14 Nm) and high R coefficient value (0.96), t-test showed no significant differences between the reference and the proposed method.

L5/S1 Joint Force. For all of the lifting trials, the correspondence between 3D L5/S1 joint force obtained from the reference and estimated from the proposed method was good with R values mostly above 0.90 and RMS mostly below 10 N (fig. 2). The grand mean (±SD) of the force absolute errors across all the subjects and trials was 4.85 (±4.85) N.

Absolute peak values extracted from force time series of the proposed method were also compared to the corresponding values of the reference across the whole lifting trials. In line with a small RMSE value (4.45 N) and high R coefficient value (0.99), t-test showed no significant differences between the reference and the proposed method.

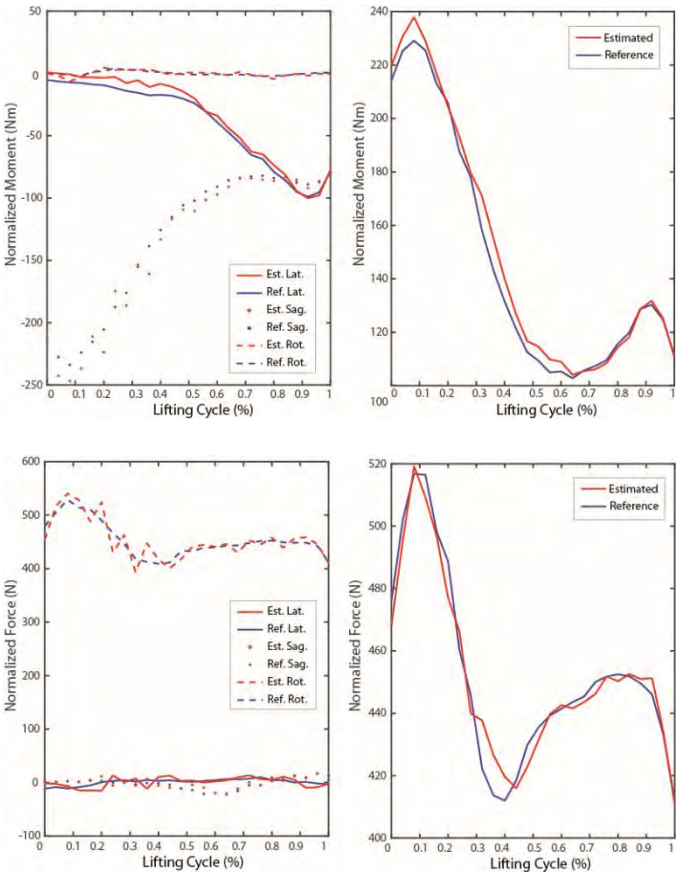

Figure 2: Estimated versus reference L5/S1 joint moment (top row) and L5/S1 joint force (bottom row) for floor-to-knuckle-height and 60 degree end-of-lift angle lifting trial. The total moment/force is the vector summation of the L5/S1 moments/forces at each three planes (right).

CONCLUSIONS

This study demonstrates the applicability of deep learning techniques in the context of biomechanical analysis and can provide a reliable tool for detecting the risk of lower back injuries during occupational lifting.

REFERENCES

1. P. De Leva, *Adjustments to Zatsiorsky-Seluyanov's segment inertia parameters*, Journal of biomechanics (**29**), 1996.
2. A. L. Hof, *An explicit expression for the moment in multibody systems*, Journal of biomechanics (**25**), 1992.

GAIT ASYMMETRIES 6 MONTHS POST-ACLR ASSOCIATE WITH INTER-LIMB T1ρ RATIOS 12 MONTHS POST ACLR

[1]Steven J. Pfeiffer, [1]Jeffrey Spang, [1]Daniel Nissman, [1,2]David Lalush, [1]Kyle Wallace, [3]Matthew S. Harkey, [1]Laura Stanley, [4]Randy Schmitz, [1]Troy Blackburn, [1]Brian Pietrosimone

[1] University of North Carolina at Chapel Hill, Chapel Hill, NC, USA, [2] North Carolina State University, Raleigh, NC, USA, [3]Tufts Medical Center, Boston, MA, USA, [4]University of North Carolina at Greensboro, NC, USA. email: stevenpf@email.unc.edu

INTRODUCTION

Individuals who sustain an anterior cruciate ligament injury and reconstruction (ACLR) are at heightened risk for posttraumatic knee osteoarthritis (PTOA).[1] The progression to PTOA following ACLR is theorized to result from an interaction between aberrant joint biomechanics during walking and deleterious biological changes to the knee cartilage.[2] Alterations in proteoglycan density within the cartilage matrix are hypothesized to be one of the initial cartilage changes that may be related to PTOA development.[3] T1ρ magnetic resonance imaging (MRI) relaxation times are sensitive to proteoglycan density changes and are elevated, indicating worse proteoglycan density, as early as one year post-ACLR.[4] The purpose of this study was to determine the associations between limb symmetry indices (LSI) for gait biomechanics measured six months post-ACLR and femoral T1ρ relaxation times twelve months post-ACLR. We hypothesized individuals with lesser loading of the ACLR limb six months following ACLR would demonstrate greater T1ρ MRI relaxation times on the ACLR limb twelve months following surgery.

METHODS

Twenty-four individuals (50% female, 21.92 ± 3.61 years old, 178.13 ± 11.30 cm, 75.35 ± 12.60 kg) with a unilateral bone-patellar-bone autograft ACLR participated in this study. Walking biomechanics [peak vertical ground reaction force (vGRF), vGRF loading rate (vGRF-LR), and peak internal knee extension moment (KEM)] were extracted from the first 50% of stance phase in both limbs during five trials of walking at self-selected speed six months following ACLR. LSI were used to normalize the biomechanical outcomes of the ACLR limb to the uninjured limb (ACLR Limb / Uninjured limb). Peak vGRF (BW) and vGRF-LR (BW/s) were normalized to body weight. vGRF-LR was calculated as the peak of the first derivative of the force-time curve. KEM was calculated using an inverse dynamics approach and was normalized to the product of body weight and height (BW*m). KEM was expressed as an internal moment and a negative value.

A 3-Tesla scanner was used to acquire images following 30 minutes of unloading the knee joint. T1ρ relaxation times were calculated (Figure 1) for the medial and lateral femoral condyles (MFC & LFC) using a five-image sequence created with a MatLab program with the following equation: $S(TSL) = S0 \exp(-TSL/T1\rho)$ where TSL is the duration of the spin-lock time, S0 is signal intensity when TSL equals zero, S corresponds to signal intensity, and T1ρ is the T1 relaxation time in the rotating frame. Prior to segmentation, affine and non-rigid deformable registration techniques were utilized to align the ACLR limb to the uninjured limb. The weight bearing portions of the cartilage of the MFC and LFC was manually segmented into posterior, central, and anterior regions of interest (ROI) based on the location of the meniscus in the sagittal plane.[5] Inter-limb T1ρ relaxation time ratios (T1ρ ILR = ACLR limb T1ρ / uninjured limb T1ρ) were calculated for each ROI.

Figure 1: Representative map of T1ρ relaxation times of an ACLR (L) and contralateral (R) knee.

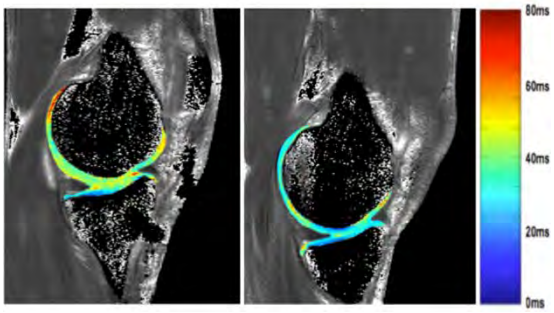

Separate, stepwise linear regressions were used to determine the unique associations between knee biomechanical outcomes and ILR for each ROI (ΔR^2, β, $P \leq 0.05$). Self-selected gait speed and the presence of a meniscal injury may influence T1ρ MRI relaxation times following ACLR. Therefore, these variables were entered into the regression model first followed by the biomechanical variable of interest. The presence of a medial or lateral meniscal injury was entered when specifically evaluating ILR of cartilage in either the medial or lateral compartment, respectively.

RESULTS

Lesser peak vGRF LSI six months following ACLR significantly associated with greater Posterior-LFC T1ρ ILR (ΔR^2=0.20, β=-0.48, P=0.04) twelve months following ACLR. Similarly, lesser peak vGRF-LR LSI six months following ACLR significantly associated with greater Posterior-MFC T1ρ ILR (ΔR^2=0.19, β=-0.45, P=0.05) twelve months following ACLR. Additionally, lesser peak KEM LSI six months following ACLR significantly associated with greater Central-MFC T1ρ ILR (ΔR^2=0.19, β=0.46, P=0.04) twelve months following ACLR.

DISCUSSION

Consistent with our hypothesis, individuals with lesser peak vGRF LSI, vGRF-LR LSI, and peak internal KEM LSI during walking six months following ACLR, demonstrated greater T1ρ ILR in the medial and lateral femoral condyles. These findings suggest that lesser mechanical loading of the ACLR limb compared to the uninjured limb early (i.e. 6 months) following ACLR may be related to deleterious changes in proteoglycan density of the ACLR limb compared to the uninjured limb at a later time point following ACLR (i.e. 12 months).

Both excessive and insufficient mechanical loading of the knee can lead to breakdown of tibiofemoral cartilage within the joint. Recent evidence[6,7] has demonstrated that excessive mechanical loading during walking early following ACLR associates with increased T1ρ relaxation times at early and later time points following ACLR. The findings of the current study are contrary to these studies but are consistent with previous findings demonstrating that lesser mechanical loading during walking following ACLR associates with changes in cartilage metabolism,[8] structure,[9] and future PTOA development.[10] Future work is needed to further understand the association between joint loading and deleterious changes to joint tissue metabolism following knee joint injury in order to develop interventions to optimally load the joint for the purpose of improving long-term joint health.

CONCLUSIONS

The findings of the current study illustrate that mechanical loading, specifically lesser loading, between limbs during walking early following ACLR may be related to deleterious changes of the cartilage matrix at later time points following ACLR, which may be related to the development of future PTOA. These findings illustrate the need for establishing optimal mechanical loading patterns during walking early in the rehabilitation process.

REFERENCES

1. Luc B, et al. *Journal of Athletic Training*. 2014;49(6):806-819.
2. Andriacchi TP, et al. *Annals of Biomedical Engineering*. 2015;43(2):376-387.
3. Regatte RR, et. al. *Academic Radiology*. 2002;9(12):1388-1394.
4. Regatte RR, et al. *Journal of Magnetic Resonance Imaging*. 2006;23(4):547-553.
5. Pfeiffer S, et al. *Arthritis Care and Research (Hoboken)*. 2017.
6. Kumar D, et al. *American Journal of Sports Medicine*. 2018;46(2):378-387.
7. Teng HL, et al. *American Journal of Sports Medicine*. 2017: 45(14): 3262–3271.
8. Pietrosimone B, et al. *Journal of Orthopedic Research*. 2017. 35(10): 2288–2297
9. Saxby DJ, et al. *Orthopedic Journal of Sports Medicine*. 2017;5(8).
10. Wellsandt E, et al. American Journal of Sports Medicine. 2016;44(1):143-151.

RUNNING-SPECIFIC PROSTHETIC MODEL AFFECTS TOP SPRINTING SPEED IN ATHLETES WITH UNILATERAL TRANSTIBIAL AMPUTATIONS

[1] Emily K. Southern, [2] Owen N. Beck, [3] Paolo Taboga, & [1,4] Alena M. Grabowski
[1] University of Colorado Boulder, CO, USA
[2] Georgia Institute of Technology, Atlanta, GA, USA
[3] Sacramento State University, Sacramento, CA, USA
[4] VA Eastern Colorado Healthcare System, Denver, CO, USA
email: emily.southern@colorado.edu

INTRODUCTION

Running-specific prostheses (RSPs), which are made of carbon fiber and passive-elastic, enable athletes with transtibial amputations (TTAs) to compete in running events. The stiffness and height of RSPs can be adjusted and likely affects users' performance. Additionally, RSP models are either C-shaped or J-shaped. C-shaped RSPs are attached beneath the socket and typically used for distance running, while J-shaped RSPs are attached posterior to the socket and more commonly recommended for sprinting. Despite the different attachments, both types of RSPs act in-series to the residual limb.

Faster sprinting speeds are achieved by applying greater average vertical ground reaction forces (vGRFs) to the ground during briefer contact times (t_c) for non-amputees [1]. However, athletes with unilateral TTAs who use an RSP have lower peak and stance average vGRFs for their affected leg (AL) than their unaffected leg (UL) [2], resulting in asymmetric forces between legs. Further, the use of a taller RSP results in more asymmetric peak vGRFs, which suggests that taller RSPs could prohibit faster sprinting speeds [3]. The purpose of our study was to quantify how RSP model, stiffness, and height affect top sprinting speed, stance average vGRF, and t_c in athletes with a unilateral TTA. We hypothesized that RSP model, stiffness, and height would affect top sprinting speed. We also hypothesized that stance average vGRF and t_c would be greater and shorter, respectively, and more symmetric using the optimal RSP configuration.

METHODS

Ten athletes with a unilateral TTA (7 M, 3 F; mean ± s.d. age: 28 ± 5 yr, mass: 76.0 ± 12.4 kg, height: 1.77 ± 0.12 m) gave written informed consent according to the COMIRB and USAMRMC Human Research Protection Office prior to participation. Each subject performed sets of running trials consisting of at least 10 strides per trial at a given speed on a 3D force measuring treadmill (Treadmetrix, Park City, UT). Each set of trials began at 3 m/s, rest was provided between trials, and each successive trial incremented treadmill speed by 1 m/s until the athlete approached top speed, when smaller speed increments were used. For each set of trials, subjects used 15 different combinations of RSP model, stiffness, and height. Models included the Freedom Innovations Catapult FX6 (FDM), Ottobock 1E90 Sprinter (OBK), and Össur Cheetah Xtend (OSR). FDM is C-shaped, while OBK and OSR are J-shaped. Stiffness conditions were the manufacturer recommended category (based on body mass) and ±1 stiffness categories. Height conditions were prosthetist-recommended and ±2 cm. For each model, height was only adjusted for the stiffness category that enabled the fastest speed.

We measured GRFs at 1000 Hz and filtered them using a 4th order low-pass Butterworth filter (30 Hz). We used these filtered data and a 30 N threshold to calculate stance average vGRF ($vGRF_{StA}$) and t_c for each step. For these variables (var), we calculated the average (AVG) of both legs (AL and UL) and the absolute value of the symmetry index (SI) between legs (Eq. 1):

$$SI = \left|\frac{var_{AL}-var_{UL}}{0.5(var_{AL}+var_{UL})}\right| * 100 \qquad Eq.\ 1$$

We used a linear mixed model to analyze the influence of RSP model, stiffness, and height on top sprinting speed. We used additional linear mixed models to analyze the influence of significant RSP configuration variables (model, stiffness, and/or height) on AVG and SI for the $vGRF_{StA}$ and t_c. We used a significance level of $p<0.05$.

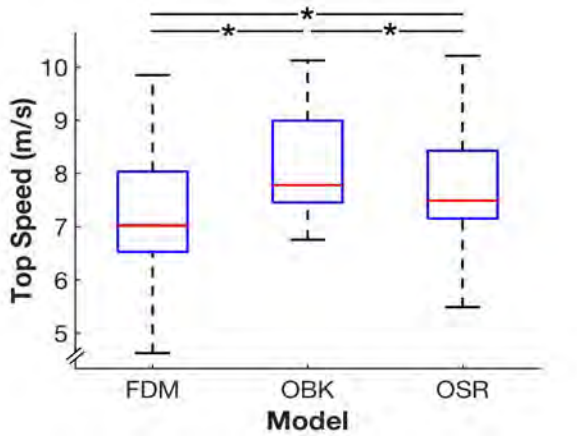

Figure 1: Mean ± s.d. top sprinting speed for each RSP model at all stiffness and height configurations. * indicates a significant difference between models.

RESULTS AND DISCUSSION

Compared to FDM, OBK and OSR resulted in 0.82 m/s ($p<0.0001$) and 0.37 m/s ($p<0.0005$) faster top sprinting speeds, respectively (Fig. 1). Additionally, OBK resulted in 0.46 m/s ($p<0.0005$) faster top sprinting speeds than OSR. Neither stiffness nor height influenced top sprinting speed ($p=0.72$ and $p=0.11$, respectively). There were no significant interactions among model, stiffness, and height for top sprinting speed.

RSP model had a significant effect on AVG and SI $vGRF_{StA}$ (Table 1). When controlling for speed, OBK resulted in 0.040*Body Weight (BW) greater $vGRF_{StA}$ than FDM ($p<0.01$). OSR resulted in 0.040*BW and 0.080*BW greater $vGRF_{StA}$ than OBK and FDM (both $p<0.005$). Additionally, OBK and OSR resulted in 5.1% and 6.7% lower SIs (more symmetric), respectively, for $vGRF_{StA}$ compared to FDM (both $p<0.001$). RSP model also had a significant effect on AVG and SI t_c (Table 1). When controlling for speed, OSR resulted in 0.003 s shorter t_c than both FDM ($p<0.005$) and OBK ($p<0.05$). In addition, OBK resulted in 2.5% and 3.5% higher SI (more asymmetric) for t_c than FDM and OBK, respectively (both $p<0.005$).

CONCLUSIONS

The data partially support our hypothesis that RSP model, stiffness, and height affect top sprinting speed. RSP model, but not stiffness or height, affects top sprinting speed in athletes with unilateral TTAs. Specifically, use of OBK resulted in the fastest top sprinting speed and use of FDM resulted in the slowest top sprinting speed.

We reject our hypothesis that stance average $vGRF_{StA}$ and t_c would be greater and shorter, respectively, using the optimal configuration. OSR resulted in the highest AVG $vGRF_{StA}$ and shortest AVG t_c, but did not elicit the fastest top sprinting speed. We partially reject our hypothesis that $vGRF_{StA}$ and t_c would be more symmetric using the optimal configuration. $vGRF_{StA}$ was more symmetric for OBK and OSR compared to FDM, and also elicited faster top sprinting speeds than FDM, suggesting that $vGRF_{StA}$ is important for top speed. In contrast, t_c was more asymmetric with OBK compared to FDM and OSR. Since OBK elicited the fastest top sprinting speed, this suggests that t_c symmetry may not influence top speed.

The underlying mechanisms for how J-shaped RSP models enable faster top sprinting speeds than a C-shaped RSP model could be due to relatively greater mechanical energy return, wider blades that enable greater stability, or a different alignment with respect to the residual limb [3,4]. Future studies are planned to assess the influence of prosthetic model on joint mechanics during top speed sprinting.

Table 1: Mean ± s.d. top sprinting speed, AVG and SI $vGRF_{StA}$, and AVG and SI t_c for each model.

		FDM	OBK	OSR
Top sprinting speed (m/s)		7.92 ± 1.53	8.78 ± 1.39	8.24 ± 1.42
$vGRF_{StA}$	AVG (BW)	1.88 ± 0.21	1.94 ± 0.19	1.96 ± 0.19
	SI (%)	15.18 ± 9.53	9.34 ± 7.39	8.44 ± 6.31
t_c	AVG (s)	0.13 ± 0.02	0.12 ± 0.02	0.12 ± 0.02
	SI (%)	5.87 ± 4.67	8.67 ± 4.76	5.15 ± 3.71

REFERENCES

1. Weyand et al. *J Appl Physiol* **89**, 1991-1999, 2000.
2. McGowan et al. *J R Soc Interface* **9**, 1975-1982, 2012.
3. Beck ON, et al. *J Appl Physiol* **123**, 38-48, 2017.
4. Beck ON, et al. *J R Soc Interface* **14**, 20170230, 2017.

LONGITUDINAL CHANGES IN CARTILAGE COMPOSITION ARE ASSOCIATED WITH ABNORMAL *IN VIVO* KNEE MECHANICS FOLLOWING ACL RECONSTRUCTION

[1]Michael F. Vignos, [1,2]Jarred Kaiser, [1]Richard Kijowski, [1]Geoffrey S. Baer, [1]Darryl G. Thelen
[1]University of Wisconsin-Madison, Madison, WI, USA; [2]Boston University, Boston, MA, USA
email: mvignos@wisc.edu, web: http://uwnmbl.engr.wisc.edu/

INTRODUCTION

Residual abnormalities in knee mechanics following ACL reconstruction (ACLR) may contribute to the high incidence of post-traumatic osteoarthritis (PTOA) in this patient population [1]. This theory is supported by *in vivo* studies that report abnormal kinematics in ACLR knees, which would lead to altered cartilage contact patterns [2]. Further, *ex vivo* cartilage testing and animal studies have shown that altered cartilage loading is related to the initiation and progression of PTOA [3]. However, prior studies have been unable to establish a direct link between altered knee mechanics and cartilage degeneration in ACLR knees. Thus, the objectives were (1) to determine bilateral differences in knee mechanics in ACLR patients using dynamic MR imaging, and (2) to investigate a link between altered cartilage contact patterns and signs of cartilage degeneration detected via quantitative MR imaging.

METHODS

We tested six subjects that underwent a primary, unilateral ACLR following completion of post-surgery rehabilitation (time point 1, TP1) (2F, 25.7±8.1 yrs, 14.9±4.2 months post-surgery, 3PT grafts) and at approximately one year after completion of rehabilitation (TP2, 29.7±5.2 months post-surgery). At both time points, bilateral static images were collected and manually segmented to obtain bone and cartilage geometries for the ACLR and contralateral knees. Quantitative MR imaging was then performed on the ACLR knees using an mcDESPOT multi-component T2 mapping sequence to obtain maps of the fraction of water bound to proteoglycan (FBW), with lower FBW representing loss of proteoglycan content in cartilage [4].

Post-rehabilitation (TP1), subjects lay supine in the MR scanner with their lower leg secured to an inertial loading device. They performed cyclic knee flexion-extension at 0.5 Hz, with the device inducing quadriceps loading similar to the weight-acceptance phase of gait. Dynamic 3D MR images were continuously acquired and reconstructed into 60 frames over the motion cycle [5]. Tibiofemoral kinematics and cartilage contact were computed by registering the bone and cartilage geometries to the dynamic images at each frame and measuring cartilage overlap. Contact maps were generated by computing the maximum contact depth across the tibial cartilage during knee extension. The tibial cartilage was divided into regions of interest (ROI). Contact and FBW maps were averaged within ROIs.

A two-factor repeated measures ANOVA (α=0.05) tested for differences in kinematics between ACLR and contralateral knees and across flexion angles (every 2.5°). Separate two-factor repeated measures ANOVAs (α=0.05) tested for differences in contact and changes in FBW. For significant interaction effects (α=0.05), post-hoc Bonferroni comparisons tested for differences across flexion angles (adjusted α=0.004) or ROIs (adjusted α=0.0013). Side-to-side differences (ACLR minus contralateral) in cartilage contact depth and changes in FBW (TP2 minus TP1) were computed across all ROIs for each subject. Geospatial analysis (bivariate local indicator of spatial association, BiLISA) was used to test for correlations between asymmetric cartilage contact and changes in FBW within each ROI (α=0.05) [6].

RESULTS AND DISCUSSION

ACLR knees exhibited abnormal tibiofemoral kinematics relative to contralateral knees (Fig. 1). Specifically, ACLR knees exhibited greater anterior tibial translation, medial tibial translation, and external tibial rotation during extension. We also observed abnormal cartilage contact in ACLR knees with greater contact depth than contralateral knees on both tibial plateaus (Fig. 2A). The greatest contact differences occurred on the posterior aspect of the medial plateau and along the medial tibial spine. We also found longitudinal changes in cartilage

composition in ACLR knees, with a reduced FBW in both plateaus between time points 1 and 2 (medial: TP1 = 22±8.8%, TP2 = 21±11%; lateral: TP1 = 22±8.1%, TP2 = 19±12%) (Fig 2B). The greatest reductions in FBW occurred in the posterior weight-bearing region of the medial plateau and the posterior-medial cartilage on the lateral plateau.

Bilateral differences in cartilage contact were linked to longitudinal reductions in FBW within ACLR knees (Fig. 3). In particular, there were weight bearing regions on both the medial and lateral tibial plateau where significant decreases in FBW were linked to greater contact (i.e. a high-low correlation).

Previous studies found that ACLR knees are externally rotated and medially translated, relative to healthy knees, during functional motion [2]. While we found similar kinematic asymmetries, ACLR knees also exhibited greater anterior tibial translation during knee extension. This may be due, in part, to the open-chain task causing internal kinematics to be more sensitive to changes in the ACL [7].

Many studies have been designed on the premise that a shift in cartilage loading initiates PTOA in ACLR knees [1]. We confirmed this theory by determining that increases in contact were correlated to signs of cartilage degeneration. Additionally, we found reduced contact was linked to degeneration along the lateral tibial spine. While this suggests that unloading of cartilage may also be problematic, it is important

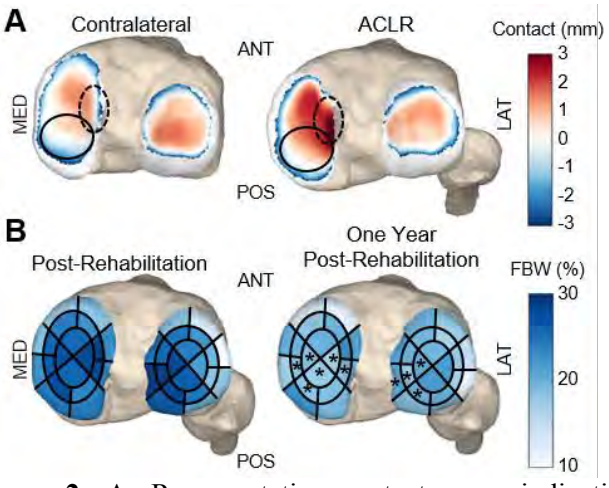

Figure 2: A. Representative contact maps indicating regions with greatest contact differences between ACLR and contralateral knees (ellipses). **B.** Average FBW (%) across all subjects for each ROI at both time points. * = significantly reduced FBW at one year post-rehab.

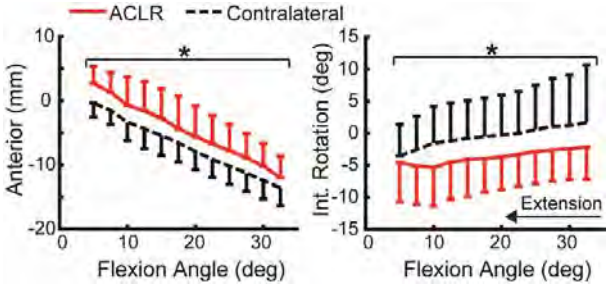

Figure 1: Anterior translation (mean ± SD) and internal rotation of the tibia relative to the femur during knee extension. * = a significant difference between ACLR and contralateral knees across all flexion angles.

to note that additional factors, such as subchondral bone bruising and joint inflammation, may also contribute to PTOA after ACL injury. Further work is needed to assess the sensitivity of the rate of cartilage degeneration to altered knee mechanics to determine the accuracy needed during ACLR.

CONCLUSIONS

This study provides striking evidence of early cartilage degeneration characterized by reductions in FBW one year after completing post-ACLR rehabilitation. Further, we provide evidence of an association between abnormal *in vivo* cartilage loading and cartilage degeneration. Taken together, these results provide evidence that failure to restore normal knee mechanics following ACLR contributes to cartilage degeneration within the knee.

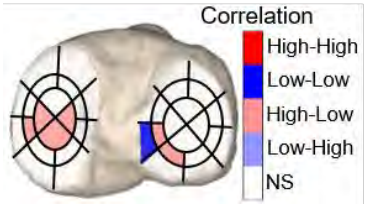

Figure 3: BiLISA summary map showing the correlation between cartilage contact and longitudinal changes in FBW for ROIs with reduced FBW (* in Fig. 2B). Colored ROIs indicate those with a significant correlation.

REFERENCES

1. Chaudhari AMW, et al. *MSSE.* 40, 2008.
2. Hofbauer M, et al. *Am J Sports Med.* 42, 2014.
3. Griffin TM, et al. *Exerc Sport Sci Rev.* 33, 2005.
4. Liu F, et al. *J Magn Reson.* 39, 2014.
5. Kaiser J, et al. *Magn Reson Med.* 69, 2013.
6. Anselin L, et al. *Geogr Anal.* 38, 2006.
7. Yack HJ, et al. *Am J Sports Med.* 21, 1993.

ACKNOWLEDGEMENTS

NSF GRFP (MFV): DGE-1747503, NIH EB015410, NIAMS R01 AR068373

ESTIMATES OF ACHILLES TENDON MOMENT ARM WITH AXIS OF ROTATION DETERMINED FROM ANKLE MOTION VERSUS ANATOMICAL LANDMARKS

[1]Francesca E. Wade, [2]Gregory S. Lewis, and [1]Stephen J. Piazza
[1]The Pennsylvania State University, University Park, PA
[2] Penn State College of Medicine & Milton S. Hershey Medical Center, Hershey, PA
email: piazza@psu.edu web: www.biomechanics.psu.edu

INTRODUCTION

Functional capacity of the ankle joint is influenced by the plantarflexion moment arm of the Achilles tendon (ATma). Experimentally, ATma may be found as the shortest distance from the ankle center of rotation (CoR) to the Achilles tendon line of action on planar magnetic resonance (MR) images [1], or ATma may be determined in three dimensions from MR imaging using ankle axes from instantaneous helical axis decomposition and a tendon path [2].

While MR imaging allows tracking of the bones and tendons, cost and accessibility are barriers to using an MR-based approach. An alternative method for finding ATma locates the Achilles tendon using an ultrasound probe fitted with motion capture markers [3,4]. Previous uses of this approach have typically assumed that the CoR lies at the midpoint between markers placed on the malleoli. This assumption, however, may not accurately represent ankle joint rotation [5].

The purpose of this work is to investigate how three different methods for locating the ankle center (or axis) of rotation influence estimates of 3D ATma during loaded and unloaded movements. We located the center (or axis) of rotation using the malleoli markers and finite helical axis decomposition of ankle motion. In each case the Achilles tendon was imaged with ultrasound. We hypothesized that ATma estimated from ankle motions would differ from those estimated from the malleoli landmarks, and would be more consistent with those previously measured using MR imaging.

METHODS

Fifteen participants (7M, 8F; 26 ± 2 y; 1.7 ± 0.07 m; 71 ± 12 kg) performed sets of three weight-bearing toe-raises in time to a 0.5 Hz metronome. This motion was repeated unloaded at the same frequency. Approval for all procedures was given by the Institutional Review Board of The Pennsylvania State University.

A linear 60 mm ultrasound probe (HL9.0/60.128Z-2; Telemed) imaged the Achilles tendon at the level of the malleoli. Four retroreflective markers were rigidly attached to the probe, with additional markers placed on the femoral epicondyles and the malleoli. Clusters of four markers were attached to the dorsum of the foot and the anterior shank. Ultrasound images were sampled at approximately 60 Hz, while marker motions were captured simultaneously using seven Eagle cameras (Motion Analysis Corp.) at 100 Hz.

Marker data were passed through a 4th order Butterworth low-pass filter with a cut-off frequency of 10 Hz. Image processing routines in MATLAB (Mathworks Inc.) were used to identify the midline of the Achilles tendon. ATma was calculated as the effective distance between this 3D line of action and either 1) a transmalleolar axis (TA), 2) the transmalleolar midpoint (TM), or 3) a 'functional' axis determined by finite helical decomposition of foot motion with respect to the shank (FA).

Moment arms were quantified over the range from 10° dorsiflexion to 20° plantarflexion (in 5° increments) by interpolating a second-order polynomial fit to ATma versus plantarflexion angle data. Ankle joint angles were computed using Cardan angle decomposition and a modified ISB joint coordinate system [6]. A three-way repeated measures ANOVA, followed by Bonferroni-corrected post-hoc comparisons as indicated by ANOVA results, was run to examine the effect of loading condition, ankle joint angle, and rotational axis/center on ATma.

RESULTS AND DISCUSSION

ATma calculated using FA were significantly larger than values calculated using TA or TM across all joint angles considered (all $p < 0.001$). TM values were slightly larger than TA values ($p = 0.008$). Values of ATma obtained with FA were commensurate with those reported in the literature from 2D and 3D MR data [1,2,7], and our TA and TM values were similar to those found by authors using a similar methods [3,4].

We found that ATma computed using FA increased with plantarflexion angle ($p < 0.001$), with an average increase of 7.5 mm over the range of ankle angles tested. No clear angle-dependent relationship was observed for TA or TM (Fig. 1). ATma has been found to increase with plantarflexion in 2D MR studies [1,7] but in 3D MR studies there is an increase from dorsiflexion to neutral followed by a plateau with increasing plantarflexion [2,7]. In studies employing TM, ATma has been found to increase with plantarflexion [3] and to remain constant with joint rotation [4].

Using FA, ATma were approximately 10% larger for loaded movements ($p < 0.001$) but did not differ with loading for TA and TM. Increases in moment arm with loading have been noted previously in MR studies [1,7].

The location of the FA qualitatively agrees with ankle axis of rotation described in previous studies of bone kinematics [5]. This agreement, along with the similarities between our ATma findings with published results from MR studies, suggest that FA may be a better choice when estimating ATma because FA provides a closer approximation of ankle axis of rotation than TA or TM. It must be noted, however, that our FA was a single axis fixed in the foot coordinate system (a choice we made for the sake of simplicity), and it is known that rotational axis of the ankle joint moves throughout a range of motion [5]. Future work will include use of an instantaneous helical axis to compute ATma with an axis of rotation that moves with respect to the local segment coordinate systems throughout the motion.

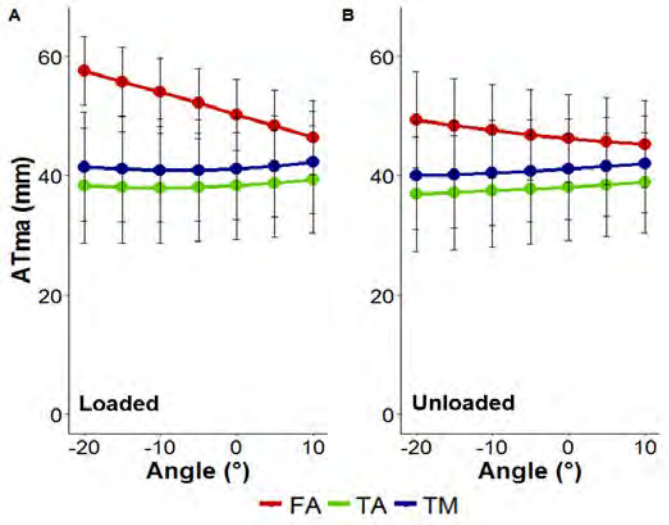

Figure 1: Achilles tendon moment arm, calculated using 'FA' in red, 'TA' in green, and 'TM' in blue, over plantarflexion (-) and dorsiflexion (+) in (A) the loaded condition, and (B) the unloaded condition.

CONCLUSIONS

The plantarflexion moment arm of the Achilles tendon approximated using a functional axis derived from the relative motions of the ankle and foot produces loading- and angle-dependent patterns similar to those with previously reported in MR studies. The results of this study suggest that location of the axis of rotation from measured motion may provide advantages over landmark-based methods when estimating ATma.

REFERENCES

1. Maganaris et al. *Journal of Physiology*. **510**(3): 977-985, 1998.
2. Sheehan. *Journal of Biomechanics*. **45**(2): 225-230, 2012.
3. Manal et al. *Physiological Reports*. **1**(6): e00139, 2013.
4. Rasske et al. *Computer methods in Biomechanics and Biomedical Engineering*. **20**(2): 201-205, 2017.
5. Lundberg. *Acta Orthopaedica Scandinavica*. **60**(233):1-24, 1989.
6. Wu et al. *Journal of Biomechanics*. **35**(5):453-548, 2002.
7. Hashizume et al., 2012. *Journal of Biomechanics*. **45**(2): 409-413, 2012.

FINGER MUSCLES INJECTED WITH BOTULINUM TOXIN DEMONSTRATE INCREASED PASSIVE STIFFNESS AND DECREASED PASSIVE RANGE OF JOINT MOTION IN INDIVIDUALS WITH CHRONIC HEMIPARETIC STROKE

[1,2,4]Benjamin I Binder-Markey, [1,2,3]Julius PA Dewald, and [1,2,3,4,5]Wendy M Murray

Departments of [1]Biomedical Engineering, [2]Physical Therapy and Human Movement Sciences, [3]Physical Medicine and Rehabilitation, Northwestern University, Chicago, IL, USA
[4]Shirley Ryan AbilityLab (Formerly RIC), Chicago, IL, USA
[5]Edward Hines, Jr. VA Hospital, Hines, IL, USA
Email: bbindermar@sralab.org, Website: https://www.sralab.org/research/labs/arms-lab

INTRODUCTION

In individuals with chronic hemiparetic stroke, botulinum toxin (BTX) is often used to reduce muscle hypertonicity and spasticity with the goal of improving passive range of motion (ROM), pain, and hygiene in the paretic limb [1, 2]. However, recent evidence suggests that BTX may increase the collagen content within rodent muscles [3, 4]. This could have devastating lasting effects on the passive mechanical properties of the muscle limiting the therapeutic effects of BTX.

Because of these findings in animal studies, we investigated the effects of BTX on the passive properties of the human extrinsic finger muscles following stroke. The extrinsic finger muscles were chosen because they are located in the flexor compartment of the forearm, a frequent target for BTX injection. In addition, we implemented an experimental design that exploits the multi-joint length-dependence of the extrinsic finger muscles across both wrist and finger posture to separate the torque they generate about the metacarpophalangeal (MCP) joints from those produced by other soft tissue structures at the MCP joint [5].

METHODS

The total passive flexion/extension torque generated about the four MCP joints, $T_t(\theta, \omega)$, was quantified in both hands of 16 subjects with chronic hemiparetic stroke and severe hand impairments. Seven subjects had previously received BTX injections in the flexor compartment of the forearm (Table 1).

$T_t(\theta, \omega)$ was quantified as a function of both MCP (θ) and wrist (ω) position using a custom built device [6]. Experimental conditions encouraged a sleep or near sleep state to mitigate hyperactivity of the paretic muscles; EMG monitoring ensured the absence of muscle activity. Data were collected in static 15° increments, spanning the range of motion of the MCP joints; measurements were repeated in 9 different wrist postures, with wrist posture randomized in 15° increments between 60° flexion to 60° extension. The passive ROM of the MCP joints within the torque-measurement device was determined by either the limits of the device or the subject's tolerance; the most extended and flexed postures of the MCP joints were recorded in each wrist posture. PIP & DIP joints were splinted to prevent movement.

For each subject, an exponential analytical model was fit to all of the torque data collected [5]:

$$T_t(\theta, \omega) = T_{sj}(\theta) + T_e(\theta, \omega)$$

The model is comprised of two components. The first component, $T_{sj}(\theta)$, assumes that the torques contributed by the single-joint structures (e.g., intrinsic muscles, skin, ligaments, joint capsules, etc.) vary as a function of MCP joint posture, θ, only. The second component, $T_e(\theta, \omega)$, assumes that torques that vary as a function of both MCP joint posture, θ, and wrist posture, ω, are produced by the extrinsic finger muscles. Data were analyzed using a linear-mixed model analysis.

Table 1: Subject demographics

	N	Age yrs (SD)	Time since Stroke yrs (SD)	CMHS (SD)	Mod. Ashworth (SD)	Time Since BTX yrs (SD)
BTX	7	56.7 (8.3)	10.7 (5.3)	2.8 (0.4)	2.7 (0.5)	4.5 (2.8)
No-BTX	9	60.3 (10.4)	17.1 (7.9)	2.4 (0.7)	2.2 (0.9)	NA

RESULTS AND DISCUSSION

We observed significant inter-limb differences ($p < 0.001$) in both $T_t(\theta, \omega)$ and $T_e(\theta, \omega)$ for both the BTX and the no-BTX groups. The largest differences between paretic and non-paretic limbs were observed in the BTX group when the wrist was extended (Fig. 1A). For the no-BTX group, the MCP passive torques were comparable across limbs in the same extended wrist posture (Fig. 1B).

When the wrist was flexed the differences in $T_e(\theta, \omega)$ between limbs were an order of magnitude smaller (Fig. 1C). In the no-BTX group, smaller inter-limb differences in $T_e(\theta, \omega)$ were observed across all postures (Fig. 1 B&D). No significant differences in $T_{sj}(\theta)$ were observed in either the BTX ($p=0.111$) or no-BTX ($p=0.131$) group in this study.

Large torque increase between limbs were only observed within the BTX group when the wrist was extended and the extrinsic finger flexor muscles were at their longest lengths (Fig 1A). These increases decreased as the wrist was flexed and the flexors shortened (Fig 1C). The increases were only observed in muscles that received the BTX injections and were not observed in muscles that did not receive BTX injections (Fig. 1B,C,&D).

The increased passive MCP flexion torque observed in the BTX group corresponded with a decreased ability to passively extend the MCP joint ($p<0.001$). This was especially evident when the wrist was extended, with an inter-limb decrease in passive extension of 68° for the paretic limb in the BTX group. This decrease in extension ROM was not present in individuals who did not receive BTX ($p=0.360$).

CONCLUSIONS

Paretic muscles located in the anatomical compartment where BTX injections were given demonstrated increased passive MCP flexion torques in joint postures associated with long muscle lengths. These effects were absent in individuals with comparably impaired hands who had never received BTX. These data, together with animal studies revealing increased muscle collagen following BTX injections, suggest that BTX may have long-term consequences opposing the desired treatment effect of increasing ROM.

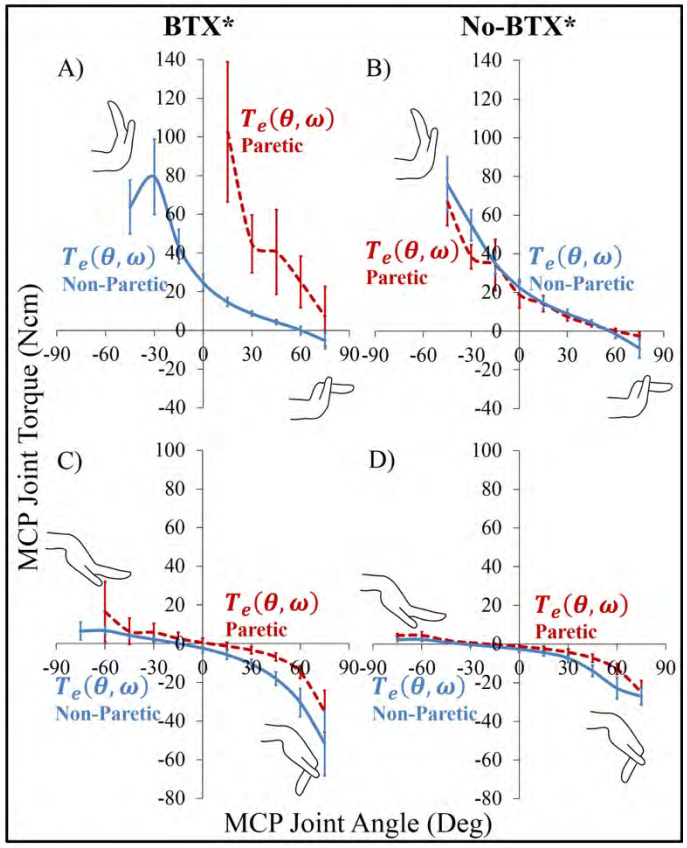

Figure 1: T_e vs MCP (θ) for the paretic (red dashed line) and non-paretic (blue solid) limb, with the wrist fully extended (A & B) and flexed (C & D). BTX (A & C) and No-BTX B groups with standard error bars. (+ flexion/- extension) (* $p<0.001$)

REFERENCES

1. Ozcakir, S. and K. Sivrioglu, Clin Med Res, 2007. **5**(2): p. 132-8.
2. Kaku, M. and D.M. Simpson, Drug Des Devel Ther, 2016. **10**: p. 1085-99.
3. Minamoto, V.B., et al., Muscle Nerve, 2015. 52(4): p. 649-57.
4. Ward, S.R., et al., Muscle Nerve, 2017.
5. Knutson, J.S., et al., J Biomech, 2000. 33(12): p. 1675-81.
6. Stienen, A., et al. *2011 IEEE International Conference on Rehabilitation Robotics*. 2011. Zurich , Switzerland.

ACKNOWLEDGEMENTS

This work was supported by a Promotion of Doctoral Studies (PODS) – Level II Scholarship from the Foundation for Physical Therapy, American Heart Association Pre-Doctoral Fellowship: 16PRE30970010, & NIH 1R01HD0840

OLDER ADULTS REVERSE THEIR DISTAL-TO-PROXIMAL REDISTRIBUTION USING BIOFEEDBACK

Michael G. Browne, Sarah N. Fickey, and Jason R. Franz

University of North Carolina at Chapel Hill and North Carolina State University, Raleigh, NC, USA
email: mgbrowne@email.unc.edu, web: http://abl.bme.unc.edu

INTRODUCTION

Compared to young adults, older adults walk slower and with a characteristic decrease in push-off intensity. This decreased push-off intensity stems from large reductions in mechanical power generated by the plantarflexor muscles (i.e. ankle power, P_A) and propulsive ground reaction forces generated during push-off (F_P) [1]. Seemingly in response to this decreased push-off intensity, older adults also rely more on positive mechanical power generated by the hip musculature. This phenomenon, known as the distal-to-proximal redistribution [2], may also contribute to increased metabolic energy costs during walking in older adults [3]. Conventional resistance training for improved mobility in older adults successfully improves maximal muscle strength and fast walking speed (FWS) but has minimal functional impact on habitual walking performance (i.e. preferred walking speed; PWS) or gait biomechanics (e.g., mechanical power generation).

Rehabilitative approaches that go beyond resistance training alone are needed, toward more direct means to elicit favorable biomechanical adaptations during habitual speed walking. As an important first step, we previously attempted to enhance push-off intensity in older adults using biofeedback to increase propulsive forces. While effective - older adults increased F_P with potentially favorable reductions in hip flexor power generation [4] – we were surprised to observe no concomitant increase in P_A. However, older adults can increase P_A in order to walk faster or uphill, revealing a translationally important gap in our understanding. Motivated by these findings, we tested here the primarily hypothesis that real-time ankle power biofeedback during walking can directly increase P_A in older adults. We also hypothesized that doing so would: (*i*) alleviate mechanical power demands at the hip and (*ii*) increase preferred but not fast walking speed.

METHODS

10 healthy older adults (mean±SD; age: 74.8±5.4 years, 3 males/7 females) participated in this study. We first assessed subjects' PWS (1.28±0.20 m/s) and FWS (1.79±0.20 m/s) using an instrumented walkway. Subjects then walked normally for 1-min on a dual-belt instrumented treadmill at their PWS. A custom Matlab script running a surrogate inverse dynamic model of the lower legs and feet estimated bilateral step-by-step P_A. Subjects walked again for 1-min each while watching a screen with visual biofeedback of their instantaneous P_A and targeting increases of +10% and +20% of normal (Fig. 1A). For all trials, a motion capture system recorded the

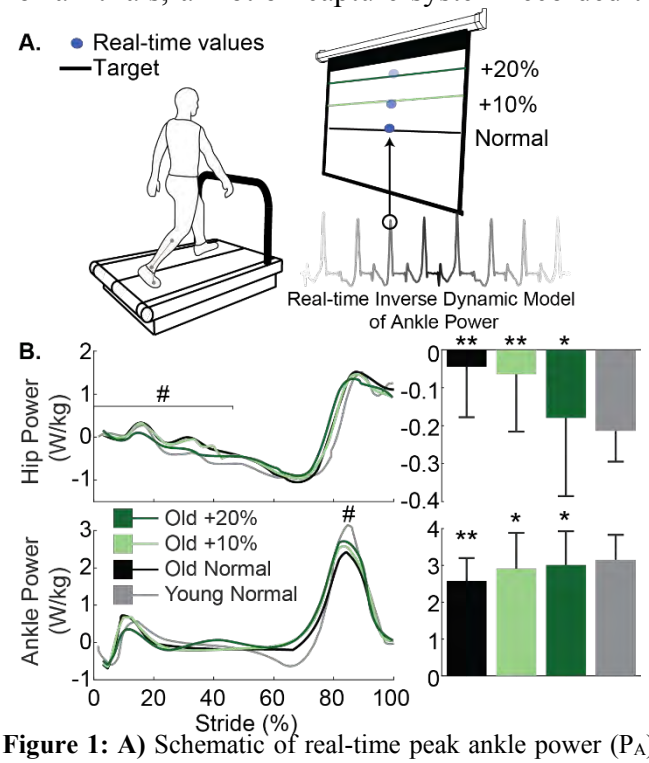

Figure 1: A) Schematic of real-time peak ankle power (P_A) biofeedback. **B)** Group-mean hip and ankle power plotted against an averaged gait cycle. Pound signs (#) denote a significant main effect of P_A biofeedback ($p<0.05$). Each graph is accompanied by bar graphs indicating group mean (±SD) peaks. Asterisks (*) and double asterisks (**) denote a significant pairwise difference from old and young adults walking normally, respectively.

trajectories of markers placed on subjects' pelvis and lower extremities for estimating joint kinetics. Data reported represents the 20 consecutive strides for which participants were most successful matching prescribed targets. Finally, we again assessed subjects' PWS and FWS to investigate recall. We additionally include normal walking data from 9 healthy young adults (age: 25.1±5.6 years, 4 males/5 females, PWS: 1.30±0.12 m/s) to serve as a reference for comparison.

RESULTS AND DISCUSSION

Our older adults walked with 21% lower P_A and 79% greater hip power during early to mid-stance compared to their younger counterparts ($p<0.034$). Older adults increased P_A by 13% and 17% when targeting increases of 10% and 20%, respectively (main effect, $p=0.006$), thereby attenuating their P_A deficit compared to young adults (Fig. 1B). Conceptually, older adults could increase P_A through changes in net moment or angular velocity at the ankle. Our older adult subjects increased P_A through modest (+3%) but significant changes to peak ankle moment ($p=0.008$) and nonsignificant changes to angular velocity (+7%, $p=0.157$) (Fig. 2). We also observed larger net ankle moments developed during early to midstance, which may have indirectly contributed to larger than preferred P_A through greater elastic energy storage and return. Greater P_A was also accompanied by up to a 300% reduction in the demand for positive hip power generation during early to mid-stance ($p=0.015$). P_A biofeedback also increased positive ankle joint work ($p=0.001$), total positive leg joint work ($p=0.002$), and F_P ($p<0.001$) (Fig. 2). This latter finding reveals an interesting disconnect in our understanding of push-off in walking: older adults increase F_P without related improvements in P_A [4], but increase P_A with related improvements in F_P. Finally, subjects walked overground with 11% faster PWS ($p=0.010$) but no change in FWS when recalling P_A biofeedback.

CONCLUSIONS

Our results reveal that older adults are capable of increasing P_A through the use of targeted ankle power biofeedback – effects that are accompanied by potentially favorable shifts in hip power generation during early to mid-stance. Moreover, the associated

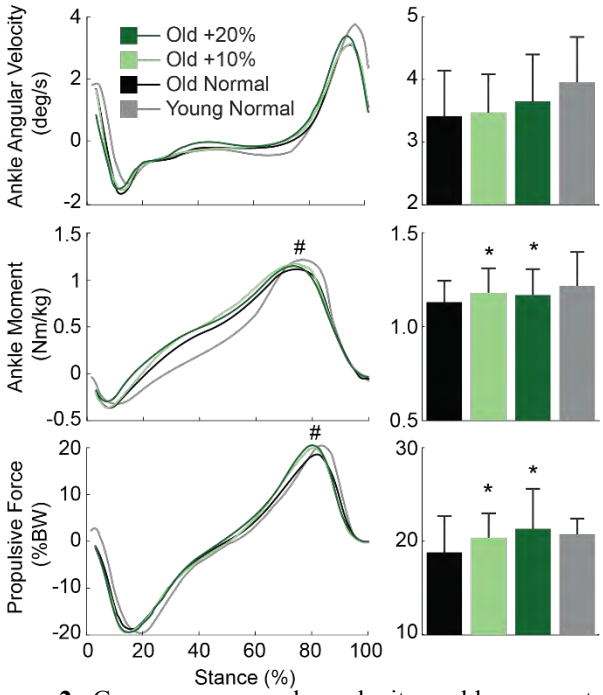

Figure 2: Group mean angular velocity, ankle moment, and propulsive force (F_P) against an average gait cycle. Asterisks (*) denote a significant main effect of biofeedback ($p<0.05$). Each graph is accompanied by bar graphs indicating group mean (±SD) peaks. Asterisks (*) denote a significant pairwise difference from old adults walking normally.

increase in PWS suggests a functional benefit to increased ankle power output during habitual speed walking. Further work will investigate whether ankle angular velocity alone may be sufficient feedback to modulate P_A, an approach more immediately translatable to novel rehabilitation approaches via wearable sensor technologies. Ultimately, targeted biofeedback may complement resistance training to reverse age-associated mobility decline.

REFERENCES

1. Franz, JR. *Exercise and sport science reviews,* 44(4):129-35, 2016.
2. DeVita, P & Hortobagyi, T. *J Appl Physiol*, 88(5):1804-11, 2000.
3. Ortega, JD & Farley, CT. *J Appl Physiol*. 102(6):2266-73, 2007.
4. Browne, MG & Franz, JR. *Plos One*. In Review, 2018.

ACKNOWLEDGEMENTS

This work was supported by grants from NIH (R01AG051748) and the UNC University Research Council.

TRICEPS SURAE MUSCLE-SUBTENDON INTERACTION DIFFERS BETWEEN YOUNG AND OLDER ADULTS

William H. Clark and Jason R. Franz

University of North Carolina and North Carolina State University, Chapel Hill, NC, USA
email: jrfranz@email.unc.edu, web: http://abl.bme.unc.edu

INTRODUCTION

Mechanical power generated via triceps surae muscle-tendon interaction during walking is largely responsible for the total power needed for forward propulsion and swing initiation [1]. This interaction is made complex by the biological architecture of the Achilles tendon (AT), which consists of distinct bundles of tendon fascicles, known as "subtendons", arising from the gastrocnemius (GAS) and soleus (SOL) muscles [2]. Comparative data and our own *in vivo* evidence alludes to a reduced capacity for sliding between adjacent subtendons compromising the AT in old age. This is functionally important, as subtendon sliding could facilitate independent actuation between individual triceps surae muscles, perhaps augmenting contributions to trunk support and forward propulsion. Indeed, our lab recently found that an age-associated reduction in the capacity for sliding between GAS and SOL subtendons correlated with smaller peak ankle moments and positive work performed during push-off, alluding to unfavorable functional consequences [3]. However, it remains unclear whether age-associated changes at the subtendon level unfavorably affect triceps surae muscle contractile dynamics. Recently, we introduced a novel dual-probe ultrasound imaging approach to reveal that length change differences between the GAS and SOL of young adults during force generation positively correlated with non-uniform tissue displacement patterns in the AT.

Therefore, the purpose of this study was to investigate aging effects on triceps surae muscle-subtendon interaction dynamics using dual-probe ultrasound imaging during a series of ramped isometric contractions. We hypothesized that, compared to young adults, older adults will have (*i*) more uniform Achilles subtendon tissue displacements that (*ii*) are accompanied by more uniform GAS and SOL muscle length change dynamics.

METHODS

We report data for 9 younger adults (age: 25.1 ± 5.6 years, weight: 69.8 ± 6.9 kg, height: 1.7 ± 0.1 m, 4 females) and, thus far, 6 older adults (age: 74.3 ± 3.4 years, weight: 67.2 ± 9.0 kg, height: 1.7 ± 0.1 m, 4 females). Subjects completed 3 ramped isometric voluntary contractions at each of 5 different ankle angles (spanning 30° plantarflexion to 10° dorsiflexion) using a Biodex (Biodex System 4 Pro), with the knee flexed to replicate that near the push-off phase of walking (~20º). We synchronized two linear array ultrasound transducers to simultaneously record GAS and SOL fascicle kinematics with tissue displacements in their associated tendinous structures (Fig. 1). A 60 mm Telemed Echo Blaster 128 transducer (LV7.5/60/128Z-2) placed over the medial gastrocnemius and soleus of subjects' right leg recorded cine B-mode images at 61 frames/s. Simultaneously, a 38-mm transducer (L14-5W/38, Ultrasonix Corporation, Richmond, BC) operating at 70 frames/s recorded ultrasound radiofrequency (RF) data from a longitudinal cross-section of the right free AT, distal to the SOL muscle-tendon junction and secured via a custom orthotic. Subjects' right foot was barefoot throughout the experiment to facilitate proper placement of the AT transducer.

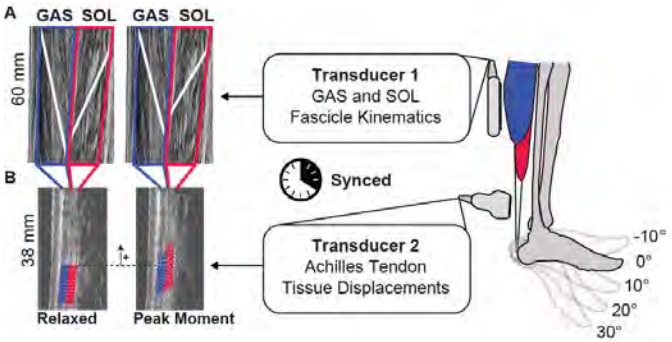

Figure 1. Simultaneous ultrasound imaging of the gastrocnemius (GAS), soleus (SOL), and Achilles free tendon. (A) Fascicle lengths and pennation angles derived from cine B-mode images. (B) Custom speckle-tracking of localized Achilles tendon tissue displacements.

Finally, motion capture tracked right ankle and knee joint kinematics and the positions and orientations of both probes.

Available MATLAB routines based on an affine extension to an optic flow algorithm quantified time series of GAS and SOL fascicle lengths and pennation angles (UltraTrack, [4]), which we combined to compute longitudinal muscle lengths. A custom 2D speckle-tracking algorithm estimated localized displacements of AT tendon tissue, which we averaged in two equally sized tendon depths - superficial and deep - corresponding to tendon tissue thought to arise from GAS and SOL, respectively [5]. A repeated measures ANOVA tested for, in part, significant main effects of and interactions between age and ankle angle on GAS-SOL differences in muscle shortening and tendon tissue displacement at peak ankle moment using an alpha level of 0.05.

RESULTS AND DISCUSSION

For young and older adults, peak isometric plantarflexor moment decreased progressively from dorsiflexion to plantarflexion across the angles tested (p<0.01). On average, older adults generated a 21% smaller peak isometric plantarflexor moment than young adults (p=0.014). Compared to young adults, average peak muscle shortening was 21% greater for SOL and 81% greater for GAS, while average peak tendon displacement was 18% greater for SOL and 50% greater for GAS in older adults (Fig. 2) – findings fully consistent with functional consequences of increased compliance in older tendon. In addition, consistent with our translational premise, GAS versus SOL differences in muscle contractile behavior and those in subtendon tissue displacements were significant in young but not in older adults. Indeed, as hypothesized, differences between peak GAS subtendon and peak SOL subtendon displacement averaged 44% smaller in older versus young adults (e.g., 77% at 0º, p<0.05). Also as hypothesized, differences between peak SOL and peak GAS muscle shortening averaged 58% smaller in older versus young adults (e.g., 65% at 0º, p<0.05) (Fig. 2).

CONCLUSIONS

We reveal that more uniform AT tissue displacements in older versus young adults extend to anatomically consistent and potentially unfavorable changes in muscle contractile behavior – evidenced by smaller differences between GAS and SOL peak shortening during isometric force generation. These findings provide an important biomechanical basis for previously reported correlations between more uniform AT subtendon behavior and reduced ankle moment generation during waking in older adults.

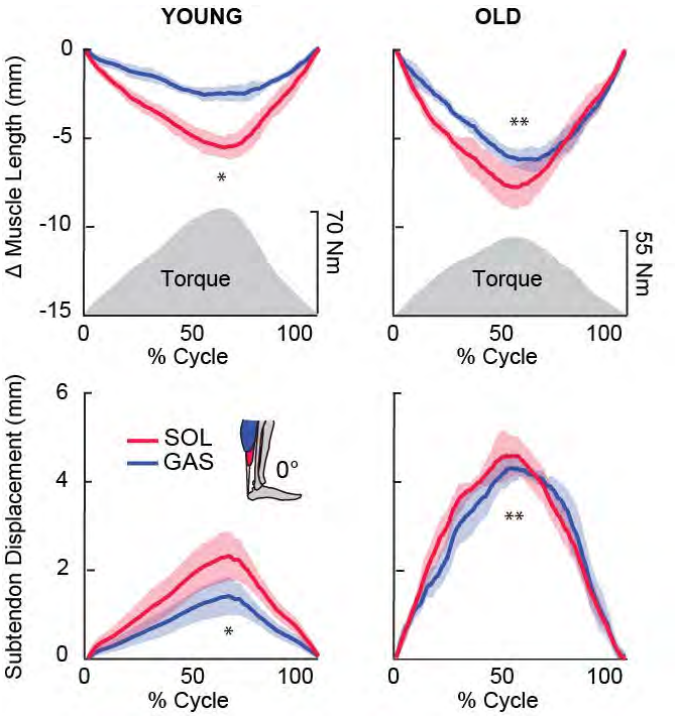

Figure 2. Group mean muscle shortening (above) and subtendon displacements (below; proximal positive). Gray shaded regions show the group mean net torque profile during a loading-unloading cycle. Single asterisks (*) indicate significant difference between peak GAS and peak SOL, Double asterisks (**) indicate significant difference between young and old. p<0.05 significant.

REFERENCES

[1] Zelik, K.E., et al. *J Theor Biol*, 2014.75-85.
[2] Szaro, P., et al. *Ann Anat*, 2009. (**6**):586-93.
[3] Franz, J.R., et al. *J Appl Physiol* (1985), 2015. (3):242-9.
[4] Farris, D.J., et al. *Comput Methods Programs Biomed*, 2016.111-8.
[5] Franz, J.R., et al. *Gait Posture*, 2015. (**1**):192-7.

ACKNOWLEDGEMENTS

We thank Ashish Khanchandani, Hannah Mckenney, and Michael Browne for their assistance with data collection. This study was supported by a grant from NIH (R01AG051748).

DOES FATIGUE AFFECT WRIST KINEMATICS DURING A REPETITIVE PICK-AND-PLACE TASK?

[1] Sarah P. DeDecker, [2] Bryan Piper, [1] Michele L. Oliver, and [1] Karen D. Gordon

[1] School of Engineering, University of Guelph, ON, Canada
[2] University of Toronto, ON, Canada
email: sdedecke@uoguelph.ca

INTRODUCTION

Carpal Tunnel Syndrome (CTS) is a common hand and wrist neuropathy. Increased risk for developing CTS is associated with extreme wrist posture during repetitive tasks, which is associated with some workplace occupations [1]. Ergonomic assessment is used to assess frequent flexion and extension motions of the wrist during repetitive tasks through various scoring methods. However, there is a lack of data regarding wrist kinematic alterations that may or may not occur as a worker becomes fatigued. If detectable differences in wrist kinematics with fatigue were present, this could provide an avenue for biofeedback mechanisms to inform preventative measures in the workplace.

The first objective of this study was to evaluate wrist posture during a repetitive pick-and-place task (e.g. task performed by a grocery cashier). The second objective was to quantify the effect of fatigue on wrist posture. It was hypothesized that wrist kinematics would be altered after fatigue.

METHODS

Ten healthy right-hand dominant subjects (four males and six females, age 21.1 ± 2.81 years) participated in this University of Guelph REB approved study. Seven retroreflective markers were mounted on the subject's right forearm and hand based on a previous model [2]. The markers were placed on the lateral epicondyle of the elbow, the medial epicondyle of the elbow, the ulnar styloid process, the radial styloid process, the capitate bone, the second metacarpal-phalangeal joint, and the third metacarpal-phalangeal joint. An eight camera VICON Bonita Motion Capture System (Vicon Motion System Ltd, Oxford, UK) was used to predict flexion-extension and radial-ulnar deviation angles of the wrist at a sampling frequency of 100 Hz. The subjects were instructed to perform a pick-and-place task. While seated, subjects used their right hand to move five objects (cans) from one end of a waist height table to the other and back (10 total cycles), while turning the cans over approximately 180 degrees each time. The cans weighed less than two kilograms and could be moved in any order selected by the subject. A fatiguing protocol described in [3] was followed to ensure subjects were fatigued prior to performing the pick-and-place task for a second time. Grip force data was collected using a hand dynamometer (Vernier, OR, USA) until grip force dropped to 70% or less of the subject's maximum grip force, as described in [3].

The range of motion (ROM) and mean angle were determined over the middle 5 pick-and-place cycles for both wrist flexion-extension (FE) and radial-ulnar deviation (RUD) angles. FE ROM, FE mean and RUD ROM were transformed using a Johnson transformation to meet data normality requirements prior to statistical analysis. RUD mean data was not transformed as it was normally distributed. A general linear model ANOVA ($p<0.05$) was performed on FE ROM, FE mean, RUD ROM, and RUD mean with factors of subject, sex, cycle, and fatigue included in the analysis. All statistical analyses were performed using Minitab 17 software (Minitab Inc., Chicago, Illinois, USA).

RESULTS AND DISCUSSION

FE and RUD ROM and mean angle for females and males pre- and post-fatigue are shown (Fig. 1 and Fig. 2).

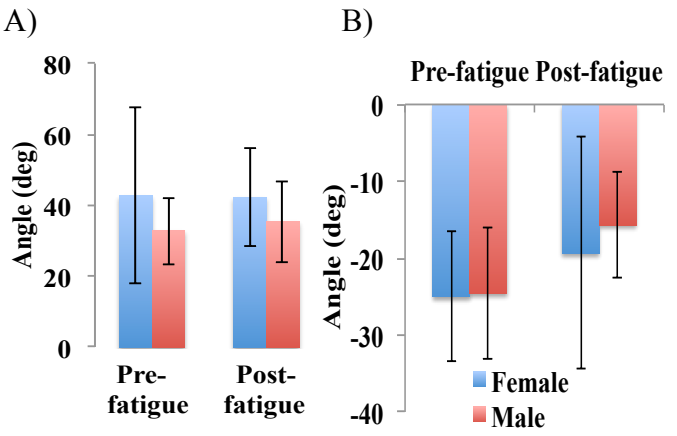

Figure 1: A) Mean ± SD flexion-extension ROM angle pre- and post-fatigue (left) and B) mean ± SD flexion-extension mean angle pre- and post-fatigue (right) for females and males (positive angles represent extension)

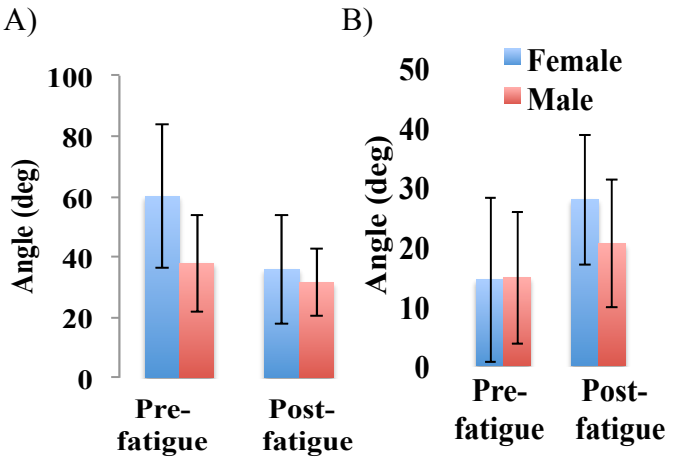

Figure 2: A) Mean ± SD radial-ulnar deviation ROM angle pre- and post-fatigue (left) and B) mean ± SD radial-ulnar deviation mean angle pre- and post-fatigue (right) for females and males (positive angles represent ulnar deviation)

There was a significant difference in pre- and post-fatigue for FE mean ($p=0.046$) and RUD ROM ($p=0.029$). The mean FE angle decreased indicating an increase in flexion angle post-fatigue. The RUD ROM increased significantly post-fatigue in both females and males. There was a significant difference in RUD ROM ($p=0.034$) between sexes. Females had a significantly larger RUD ROM compared to males.

CONCLUSIONS

Wrist posture changes significantly after fatigue during an everyday task for both wrist flexion-extension and radial-ulnar deviation. The changes detected post-fatigue were in the range of 5-10 degrees different for the mean angle measurement and 5-20 degrees for the ROM measurement. This information has potential applications in an ergonomic setting. To determine if wrist kinematic changes due to fatigue occur in the workplace, ongoing work in our laboratory is developing a wearable unobtrusive wrist device that could detect kinematic alterations without the need for motion capture or inertial measurement units. Ultimately, information determined from the current study coupled with an instrumented wrist device could help ergonomists and others improve hand-arm workplace risk evaluation by removing the ambiguity associated with common ergonomic risk assessment tools.

An interesting outcome of this study was that females had a larger RUD ROM than males. This result should be taken with caution due to the low number of subjects and subsequent low power to detect differences due to sex. However, tracking sex differences in biomechanical variables such as kinematics is a variable that has not previously been explored with respect to understanding the etiology of carpal tunnel syndrome. Though preliminary, results from the current work suggest that further work is needed.

REFERENCES

1. Fung et al. *Hand Surg.* **12**, 2007.
2. Murgia et al. *Clin. Biomech.* **19**, 2004.
3. Emge et al. *Neurosci. Lett.* **550**, 2013.

PATHOLOGICAL KNEE JOINT CONDITION IN CHILDREN WITH CEREBRAL PALSY IS ASSOCIATED WITH THE ACTIVE STATE MUSCULAR MECHANICS RATHER THAN PASSIVE

[1] Cemre Su Kaya, [2] Fuat Bilgili, [2,3] N. Ekin Akalan, [2] Yener Temelli, [1,4] Filiz Ates * and [1] Can A. Yucesoy

[1] Institute of Biomedical Engineering, Boğaziçi University, Istanbul, Turkey
[2] Istanbul School of Medicine, Department of Orthopaedics and Traumatology, Istanbul University, Turkey
[3] Department of Physiotherapy and Rehabilitation, Istanbul Kültür University, Turkey
[4] Mayo Clinic, Rochester, MN, USA, * presenting author
email: su.kaya@boun.edu.tr, ates.filiz@gmail.com; web: https://bme.boun.edu.tr/biomechanics-laboratory

INTRODUCTION

In individuals with cerebral palsy (CP), the knee joint is kept typically in a flexed position. Although the mechanism of the related pathological resistance against knee extension is unknown, this is ascribed to passive and active properties of spastic muscles. Yet, spastic muscle's passive forces at various joint angles have not been assessed. Hence, its contribution to the pathological condition cannot be judged objectively. Besides, intraoperative tests in which active state forces of spastic muscles were measured directly at the tendon indicate that spastic knee flexors produce only low forces in flexed knee positions [e.g., 1]. However, if co-activated with an antagonist, spastic Gracilis (GRA) muscle's overall mechanical characteristics change, with the peak force shifting to flexed knee positions hence resulting in a narrowed operational joint range of force exertion [2]. This was ascribed to epimuscular myofascial force transmission (EMFT) [e.g., 3] between activated muscles, which can be relevant for the unknown mechanism of the pathology. Additionally, as, unlike gait analyses, direct spastic muscle force measurements are very rare, the present literature remains insufficient to show the relationship between muscle's mechanical characteristics and the patient's gait.

The aim was to fill these gaps by combining intraoperative experiments with gait analyses and to test the following hypotheses: (i) spastic GRA shows high amplitudes of passive forces even in the flexed knee positions, (ii) active forces of spastic GRA are high, particularly within the gait relevant knee angle range, and (iii) this becomes more pronounced due to EMFT.

METHODS

Seven children with CP (mean age (SD)=9.1 (2.9) years; GMFCS scores level II) participated.

Pre-surgery gait analyses were performed using a motion analysis system (ELITE 2002, BTS Bioengineering, Milan, Italy) with six infrared cameras and two force plates (Kistler Instumente AG, Winterthur, Switzerland). Hip and knee joint angles and moments in the sagittal plane were used to relate the global gait metrics to intraoperative spastic muscle level mechanics.

Intraoperatively 10 limbs were tested. Isometric GRA forces (F_{GRA}) were measured per knee angle (KA) in four conditions: (I) passive state, after spastic GRA was stimulated (II) alone, (III) simultaneously with its synergists semitendinosus and biceps femoris, and (IV) also with its antagonist rectus femoris. Hip angle (HA) was set to 45° and 20°, and KA was changed from 120° to full extension (0°).

Two-way ANOVA (factors: KA and condition) and paired-t or Wilcoxon signed-rank test were used to test the effects of studied conditions on overall mechanical characteristics and Range-F_{GRA} (KA range between 120° and peak force exertion) ($P<0.05$).

RESULTS AND DISCUSSION

Passive and active state forces are shown in (Fig. 1).

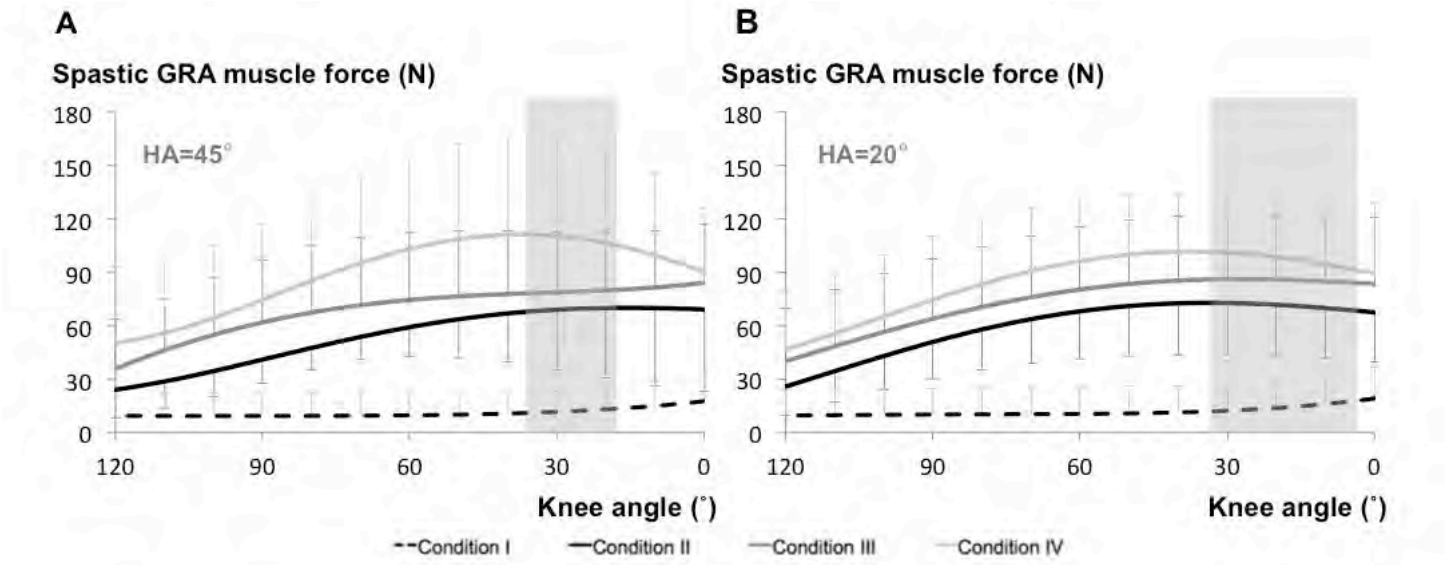

Figure 1: The mean of GRA forces of intraoperatively tested limbs per KA across the conditions tested at HA=45° and HA=20°. The gray shaded areas show the gait relevant KA-positions.

Passive force is low in flexed positions and increases towards knee extension. However, its peak value is only a small fraction of the peak total force (26%) measured in the active state.

ANOVA showed significant main effects of both factors on F_{GRA}, but no significant interaction. Compared to condition II, co-activation of other muscles caused F_{GRA} to increase substantially (on average, for HA=45° and 20°, by 32.8% and 71.9%, and 24.5% and 45.1% in conditions III and IV, respectively). Considering the muscle's overall mechanical characteristics in conditions III and IV, EMFT did cause major increases in spastic GRA forces. However, compared to condition II, no significant change in Range-F_{GRA} was shown in any co-activation condition.

Gait analyses indicated that intraoperative data for KA=36°-18° and KA=33°-3° (for HA=45° and 20°, respectively) are particularly relevant, where F_{GRA} in active state approximates its peak value. The elevated forces shown in conditions III and IV for gait relevant KA-ranges characterize an elevated contribution of the muscle to knee flexor moment during the patients' gait. Hence, the findings reflect an increasing effect on spastic muscle's mechanics of different components of EMFT. Since daily activities involve simultaneous activation of several muscles, such EMFT effects potentially have important implications for the poorly understood pathological joint condition in CP and its treatment.

CONCLUSIONS

The first hypothesis is rejected, while the second and the third are confirmed. Spastic muscle's passive forces measured directly for the first time in patients with CP do not show high amplitudes even in extended knee positions. In contrast, in the active state, the muscle's forces within the gait relevant KA-range are high. This gets much more pronounced due to EMFT. Therefore, the pathological knee joint condition can be ascribed to the active, rather than the passive state mechanics of spastic muscles effects of which, do elevate due to intermuscular mechanical interactions.

REFERENCES

1. Ates et al., *Clin Biomech*. **28**:48-54, 2013.
2. Ates et al., *Clin Biomech*. **29**:943-949, 2014.
3. Yucesoy, *Exerc Sport Sci Rev*. **38**:128-134, 2010.

ACKNOWLEDGEMENTS

TÜBİTAK Grant 113S293 to Can A. Yucesoy.

HOW DOES ACHILLES TENDON TWISTING INFLUENCE STRAIN AND ENERGY STORAGE?

[1] Katherine R. Knaus and [1] Silvia S. Blemker

[1] University of Virginia, Charlottesville, VA, USA
email: ker4e@virginia.edu, web: http:// bme.virginia.edu/muscle/

INTRODUCTION

The Achilles tendon (AT) transmits force from the triceps surae muscles during walking and other motion. It comprises three subtendons that originate from each muscle, twist around each other, then insert into the calcaneus. A recent investigation in 53 human cadavers sought to characterize the architecture of these subtendons and their variation between subjects [1]. The authors characterized the variation in torsion of the subtendons within the free AT, dividing subjects among three groups with Type 1 as the least twisted, Type 2 as moderately twisted, and Type 3 as extremely twisted. They also measured the torsion of the fibers within individual subtendons, which varied between the soleus (SOL) and the medial (MG) and lateral (LG) heads of the gastrocnemius, and tended to be greater than the twist of the subtendons about each other.

Sliding between subtendons is thought to explain non-uniform deformations of the Achilles observed with ultrasound during walking [2]. Measured differential displacements provide exciting insight into complex loading patterns by the triceps surae. However, conclusions about muscle-tendon behavior drawn from this imaging technique are dependent on several assumptions. Tissue displacements are tracked in a small 2D sagittal plane region of interest in the free AT, and while individual subtendons are not visually discernable, deep tissue is associated with the SOL and superficial tissue with the MG. Subjects exhibit varied amounts of AT torsion, though it is unknown if subtendons visible in the superficial and deep portions of the sagittal plane vary with twist type. In addition, tendon elongation is assumed to be longitudinal and estimated from in-plane displacements; however, this may misinterpret *in vivo* tendon strains due to out-of-plane stretch.

Ultrasound imaging combined with traditional force and motion capture can be used to quantify *in vivo* tendon dynamics, with displacement measurements of the free AT providing a more direct approach for approximating energy stored during walking [3]. These estimates are subject to assumptions about the force in the different subtendons as well as their strain, which may be altered by varied torsion.

The goal of this work is to understand how lengths of subtendon fibers with varied twist compare to free AT lengths. Using finite element models (FEM), we aim to decouple the influence of twisting architecture from other complexities of AT and triceps surae dynamics to assess how this anatomical feature and its variance may influence *in vivo* estimates of tendon stretch and energy storage.

METHODS

Three generic AT FEMs, representing the region of tendon from the calcaneus' superior border to SOL musculo-tendinous junction, were constructed with elliptical cross sections using average lengths and widths [1]. Models were divided into were divided into three parts to represent the subtendon architecture of each twist type. In order to focus on the effect of varied twist, the three models were identical in volume and subtendon proportions with amount of twist as the only distinguishing feature.

Tendon was modeled as transversely isotropic material with fiber direction vectors defined using Laplacian flow simulations [4]. Flow guides were used to match subtendon fiber torsion angles to twist types [1]. Flow results were used to determine subtendon fiber lengths.

Simulations of simplified walking conditions were defined to match deep and superficial measurements by prescribing either displacements [2] or forces [3] as boundary conditions to the proximal end. This end was constrained to only move proximal-distally. Frictionless contact was assigned to allow sliding between subtendons.

Subtendon along fiber strains were compared to longitudinal elongations estimated from proximal end displacements and the starting free tendon length. Subtendon strain energies were compared to stored energy estimated from integrals of force at the proximal end and length changes determined from displacements.

RESULTS AND DISCUSSION

Fiber lengths of all subtendons in each type were longer than the length of the AT. Fibers in the Type 1 model were the shortest while fibers in the Type 3 model were the longest. Fibers in the GM subtendon were shortest and the SOL subtendon were longest.

Along fiber strains were lower than estimated elongation in all subtendons, with Type 1 being the most similar (0.5% error) and Type 3 being the least (10% error) [Fig 1]. Subtendon strain energies were lower than estimated stored energy in the LG and MG and higher in the SOL, with Type 1 being the most similar in total energy stored (5% error) and Type 3 being the least (15% error) [Fig 1].

Larger amounts of twist lead to overestimation of tendon strain and energy storage. Twisting of subtendons created longer fiber lengths for the same give AT length and therefore more out-of-plane alignment. Interestingly, greater twist also contributed to having a greater portion of the LG subtendon in the deep distal region of the sagittal mid-plane [Fig 1], which is typically assumed to be occupied by SOL subtendon. Variations in twist architecture could contribute to higher rates of injury due to greater strains resulting from similar loading patterns.

CONCLUSIONS

While errors are not large enough to discount estimates of tendon dynamics made from sagittal plane ultrasound images, it does illuminate the necessity for considering architectural variation. This work demonstrates the utility of using 3D models to determine possible errors associated with 2D measurements. Models also provide the means to better calculate quantities that cannot be measured readily *in vivo*, like tendon strain energy, from those that can be measured, such as tendon length changes.

REFERENCES

1. Pekala et al. *Scand J Med Sports,* 27:1705-15,2017.
2. Zelik and Franz. *Plos One*. 12(7): e0179976, 2017.
3. Franz et al. *Gait & Posture,* 41:192-197, 2015.
4. Handsfield et al. Biomch Model Mechanobio 2017.

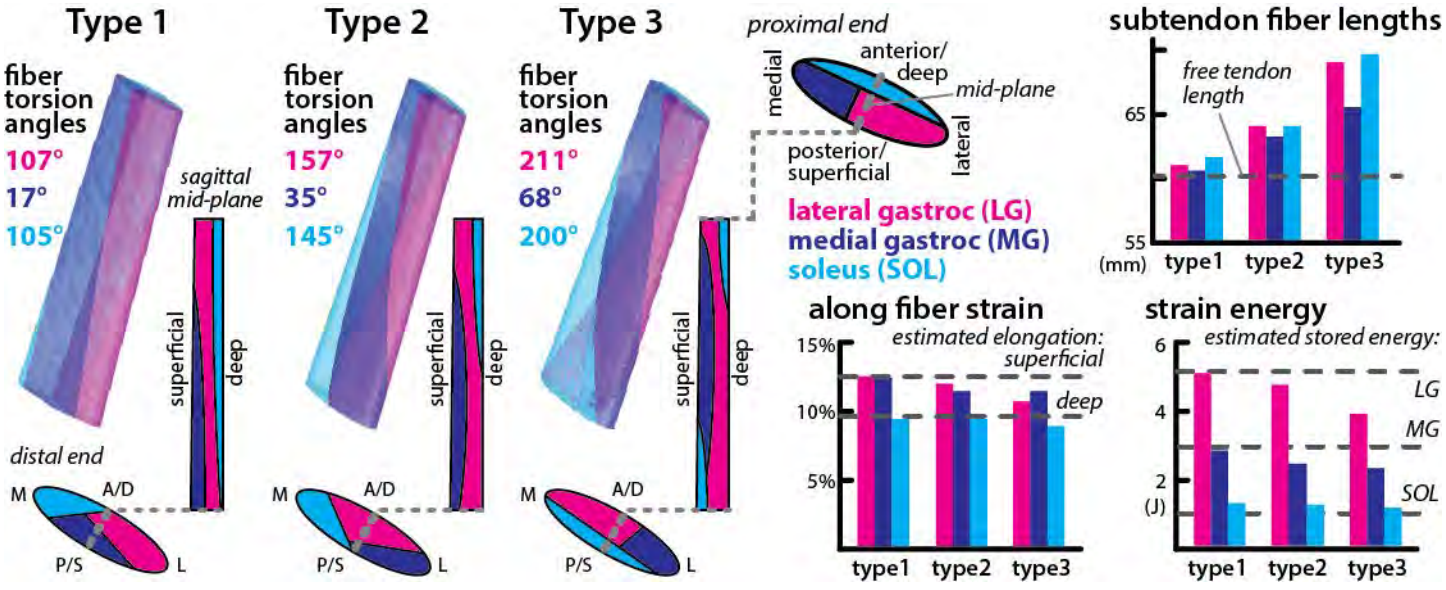

Figure 1: FEM of each type with increasing subtendon twist. The proximal end cross section was the same for all models and subtendon boundaries were lofted to varying distal end cross sections. Fiber directions were guided to match given torsion angles and subtendon fiber lengths were compared to free tendon length. Along fiber strains and strain energy were compared to elongation and energy estimated from displacements and forces.

POST-OPERATIVE FUNCTION AND MUSCLE MODULES DURING GAIT AT 6 AND 24 MONTHS FOLLOWING TOTAL KNEE ARTHROPLASTY

[1]Rebekah R. Koehn, [1,2]Sarah A. Roelker, [1]Elizabeth M. Leszcz, [1]Rachel K. Baker, [1,3]Elena J. Caruthers, [1,4]Jacqueline M. Lewis, [1,5]Gregory M. Freisinger, [1]Laura C. Schmitt, [1]Ajit M.W. Chaudhari, [1]Robert A. Siston

[1]The Ohio State University, Columbus, OH, USA; [2]The University of Texas at Austin, Austin, TX, USA; [3]Otterbein University, Westerville, OH, USA; [4]ARCCA, Inc. Penns Park, PA, USA; [5]United States Military Academy, West Point, NY, USA

email: koehn.19@osu.edu; web: https://nmbl.engineering.osu.edu/

INTRODUCTION

The theory of muscle modules (or synergies) suggests that groups of muscles are activated synergistically via a common neural command [1]. While this idea has provided insight into the control of simple tasks like locomotion [2], the clinical relevance of this theory has only recently begun to be explored. For example, patients with higher function at one year following a cruciate-retaining (CR) total knee arthroplasty (TKA) displayed a higher number of muscle modules (n=4-5) compared to patients with lower function (n=2-3) [3]. This relationship between number of modules and function suggests that if muscle modules are able to change over time, it may be possible to develop module-focused clinical programs to improve patient function.

The aim of this study was to determine muscle modules in patients with TKA during gait at 6 & 24 months post-operatively and to compare these modules to patient function. We hypothesized that (i) participants with a higher number of modules would demonstrate higher function and (ii) changes in patient function would be accompanied by changes in the number and characteristics of muscle modules.

METHODS

Fifteen participants (M/F 5/10; 60.3±6.8 y; 97.9 ±23.3 kg; 1.7±0.1 m) provided written informed consent prior to undergoing posterior-stabilizing TKA (Zimmer NexGen LPS Flex Knee) and were tested at 6 & 24 months post-operatively. Each participant performed 5 over-ground walking trials at self-selected speed. We collected passive motion capture data [4] at 150 Hz (10 Vicon MX-F40 cameras; Oxford, UK) and ground reaction force data at 1500 Hz (6 Bertec 4060-10 plates; Columbus, OH). We collected surface electromyography (EMG) data from the rectus femoris (RF), vastus medialis and lateralis (VM, VL), semitendinosis (ST), biceps femoris (BF), medial and lateral gastrocnemii (MG, LG), and soleus (SO) on the TKA-involved limb at 1500 Hz (Noraxon Telemyo DTS System; Scottsdale, AZ). To create linear envelopes for the EMG data , we used a 10-300 Hz 6th order bandpass Butterworth filter, rectified the data, smoothed the signals with a 6 Hz 6th order low-pass Butterworth filter, and normalized the signals to the maximum activations within each respective gait cycle.

For each trial, we used non-negative matrix factorization (NMF) to define muscle modules from the original EMG activations. Each module consisted of a principal activation pattern and weighting factors for the muscles within the module [5]. The product of the principal patterns and weights reconstructed individual muscle activation patterns. In order to ensure these reconstructions represented the original EMG, we calculated the variability accounted for (VAF) by the reconstructed signals and iteratively increased the number of modules from 1 to 8 in separate NMF calculations until the following criteria were satisfied: VAF > 0.9 for all muscles or VAF > 0.8 for all muscles and the addition of another module did not raise the minimum VAF by more than 5% [6].

To compare principal patterns and muscle weights between subjects and time points, we also performed NMF calculations the number of modules equal to the average for all gait trials. The principal pattern of each module was normalized to its peak and the weighting factors were normalized to the maximum within the module. We averaged the principal

patterns and weighting factors over the 5 walking trials to create ensemble averages for each participant at both 6 & 24 months. We used Wilcoxon signed-rank tests to compare muscle weights between 6 & 24 months in each of the modules and Spearman Rho tests to examine correlation in muscle weights in these modules (α=0.05).

We recorded the distance walked by each participant during a six-minute test (6MW) [7] and classified each participant as high- and low- functioning using a regression from Enright et al. that accounts for height, weight, and age [8]. We used paired t-tests to identify differences in 6MW performance at 6 & 24 months (α=0.05).

RESULTS AND DISCUSSION

The number of modules was consistent across time points and functional groups. At 6 months, 4 participants were high-functioning and had 2.5±0.4 modules (n=2, 2 modules; n=2, 3 modules), while 11 were low-functioning and had 2.7±0.6 modules (n=4, 2 modules; n=6, 3 modules; n=1, 4 modules). At 24 months, 6 participants were high-functioning and had 2.9±0.4 modules (n=2, 2 modules; n=4, 3 modules), while 9 participants were low-functioning and had 3.0±0.3 modules (n=2, 2 modules; n=8, 3 modules; n=1, 4 modules). We rounded the average number of modules in each group to 3.

Despite there being no significant change in 6MW tests between 6 & 24 months (p=0.902, 476.4±76.5m vs. 477.9±98.6 m), there were some differences in the modules of individual patients. There was a slight increase in the number of modules for 5 participants and a decrease for 2 participants. After performing the NMF calculations for each gait trial with the number of modules fixed at the average (n=3), each participant demonstrated modules at both 6 & 24 months in which the quadriceps (Q), hamstrings (H), and plantarflexors (PF) were primarily expressed (Fig. 1). However, the weights were related between 6 & 24 months for only 5 module-muscle pairs: the VM (ρ=0.779; p=0.001), BF (ρ=0.581; p=0.023), and LG (ρ=0.561; p=0.030) in the Q module and the VM (ρ=0.521; p=0.046) and LG (ρ=0.732; p=0.002) in the H module. Initial analysis indicated phase shifts in the three principal patterns between 6 & 24 months in individual participants. Such changes in timing and muscle weights contrast Shuman et al. who found greater consistency across modules between days in younger populations with and without cerebral palsy [9].

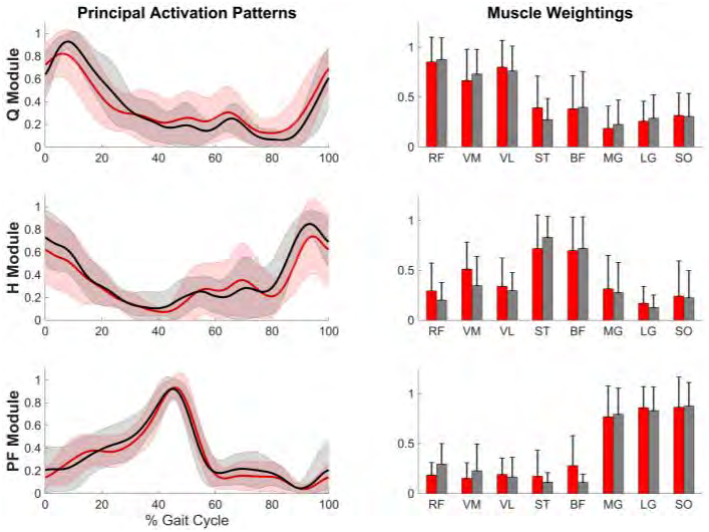

Figure 1. Average 6 month (red) & 24 month (gray) post-TKA principal patterns and muscle weights ± 1 standard deviation.

CONCLUSIONS

Our results did not indicate a relationship between function and either the number or characteristics of muscles modules. As part of a larger study, we have observed greater improvements in function between the pre- and post- TKA conditions. Additional investigation will examine the relationship between modular control and function pre-operatively as well as changes in modular control before and after TKA.

ACKNOWLEDGEMENTS

This project was supported by Grant Number R01 AR056700 from the National Institute of Arthritis and Musculoskeletal and Skin Diseases and an Ohio State University fellowship (RRK).

REFERENCES

1. Lee. *J Motor Behavior*. **16**(2): 135-70, 1984.
2. Ivanenko et al. *J Physiol*. **556**(1): 267-82, 2004.
3. Ardestani et al. *J Electromyogr Kines*. **37**: 90-100, 2017.
4. Andriacchi et al. *J Biomech Eng*. **120**:743-9, 1998.
5. Lee & Seung. *Nature*. **401**: 788-91, 1999.
6. Clark et al. *J Neurophysiol*. **103**(2): 844-57, 2010.
7. "ATS Statement." *Am J Respir Crit Care Med*. **166**(1): 111-7.
8. Enright et al. *Am J Respir Crit Care Med*. **158**:1384-7,1998.
9. Shuman et al. *Gait & Posture*. **45**: 127-32, 2016.

POST-STROKE WALKING MECHANICS USING A SPEED-ADAPTIVE MYOELECTRIC EXOSKELETON CONTROLLER

[1] Emily M. McCain, [1]Tracy N. Giest, [1]Katherine R. Saul, [2]Taylor J.M. Dick and [3]Gregory S. Sawicki

[1] North Carolina State University, Raleigh, NC, USA
[2] University of Queensland, St Lucia, QLD, Australia
[3] Georgia Institute of Technology, Atlanta, Georgia, USA
email: emmccain@ncsu.edu

INTRODUCTION

Reduced ankle function in post-stroke individuals limits the propulsive 'push-off' power of the paretic limb, resulting in asymmetric gait, reduced walking speed and higher metabolic cost [1]. Powered exoskeletons (exos) offer a promising opportunity to restore mechanical deficits by applying torque at the paretic ankle during the propulsive phase of gait. Previously, a proportional myoelectric ankle exo was shown to increase the paretic plantarflexion moment for stroke survivors walking at 75% of their comfortable overground speed [2]. Despite these improvements, the exos did not reduce the metabolic cost of walking. Researchers suggested exo performance could be limited because the walking speed was restricted to a pace at which exo assistance was not needed. In order to assess the impact of exo assistance on walking speed in stroke populations, we developed a novel, speed-adaptive exo controller [3]. This research extends previous work by: (i) exploring the efficacy of a myoelectric exo controller that automatically modulates the magnitude of propulsive assistance with changes in walking speed for post-stroke populations and (ii) assessing the ability of the controller to improve net average mechanical power output at the paretic ankle, knee and hip joints.

METHODS

We implemented a speed-adaptive controller designed to mitigate specific limitations of prior myoelectric controllers by including two independent adaptive gains: (1) a gain to map user's soleus muscle activity to peak exo torque (Koller) and (2) a gain to map peak exo torque capacity to walking speed (Giest) [3,4]. The speed-dependent gain ensures the exo outputs ~25% of the maximum normal biological ankle plantarflexion moment at the instantaneous treadmill velocity. The desired exo torque profile was applied by a benchtop motor (Baldor Electric Co) to the carbon-fiber ankle exo through a Bowden-cable transmission system.

Experimental data were collected from six stroke survivors (3 male, 3 female) walking on an instrumented split belt treadmill with and without an exo on their paretic limb. Subjects started by walking at 60% of their preferred speed (n00). At each consecutive minute, the treadmill speed was increased by 0.1 m/s (n01, n02, etc) until the subject's heart rate reached 60% of their heart rate reserve. Kinematic and kinetic data were processed in Visual3D (CMotion, USA) and MATLAB (Mathworks, USA) to determine joint angles and angular velocities. Inverse dynamics was used to calculate joint moments and powers at the ankle, knee, and hip. Average joint powers were calculated at the ankle, knee and hip for five strides [5]. Indirect calorimetry was used to determine metabolic cost during walking (OxyCon Mobile, Carefusion, USA). Statistical significance of peak average ankle power, and net average ankle, knee and hip powers were determined using paired t-tests (α=0.05).

RESULTS AND DISCUSSION

The speed-adaptive controller successfully amplified exo assistance as walking speed was increased, verifying efficacy of the speed-adaptive gain (Figure 1c). Subject averages for maximum paretic ankle power were significantly higher for the exo compared to the no exo condition at all speeds (Figure 1a and 1b) (paired t-test; p=0.04). Since subjects walked until reaching a specific heartrate, statistical power was reduced at high speeds for which the sample size was small (n<4 for n05-n07).

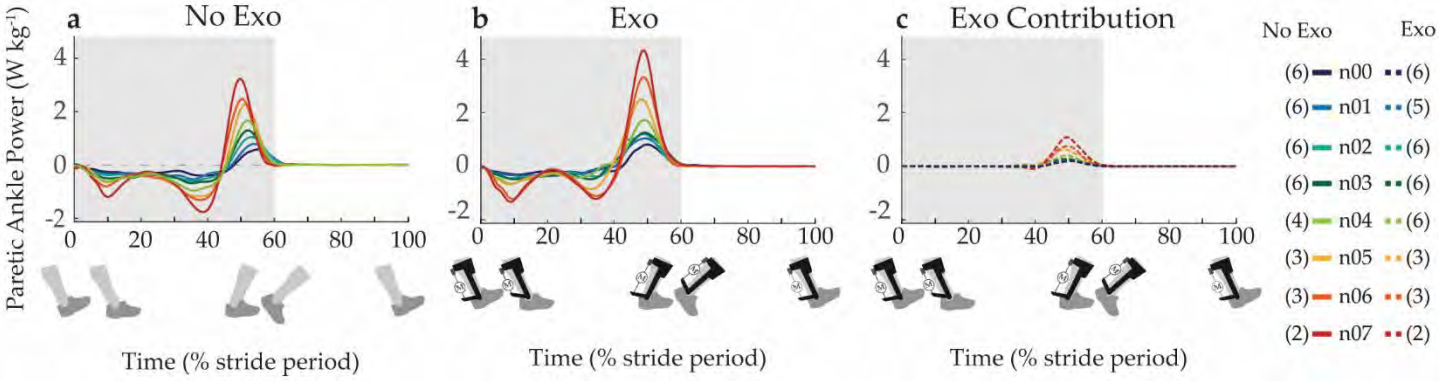

Figure 1.a Paretic ankle power in the no exo condition and **1.b** the exo condition with the **1.c** exo contribution isolated. The number of subjects is indicated in parenthesis. The shaded area represents the stance phase of gait.

Net average paretic ankle power was increased for all speeds while wearing the exo, demonstrating improved delivery of net energy at the ankle (paired t-tests; $p<0.05$ for n00-n04) (Figure 2).

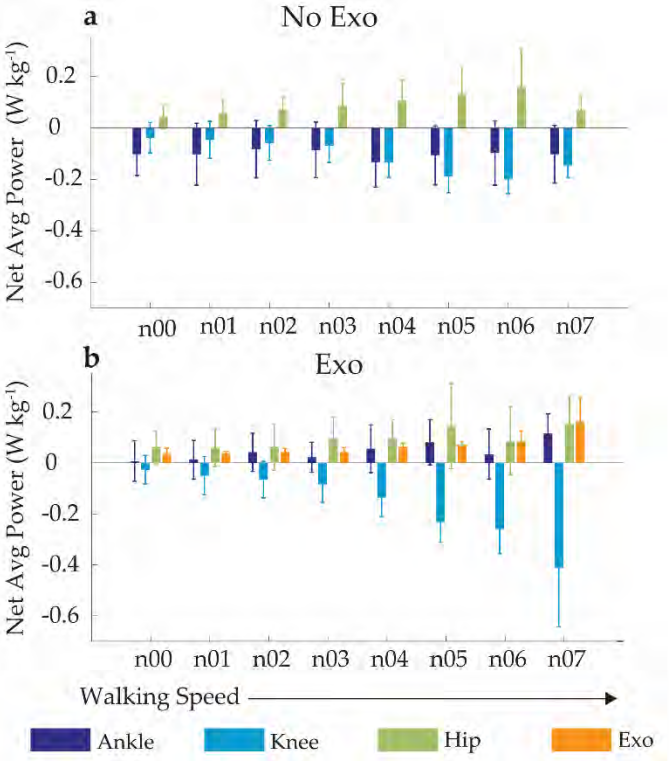

Figure 2.a Net average power averaged across subjects for the no exo and **2.b** exo conditions.

Despite these increases in net average ankle power, only two of the subjects experienced a decrease in metabolic cost while wearing the exo compared to the no exo condition, and no statistically significant change was found. One possible explanation is that assistance applied at the ankle may be absorbed by more proximal joints. This explanation is supported by the decrease in net average power seen at the knee in the exo compared to no exo condition (paired t-tests; $p<0.05$ for n00 and n02) (Figure 2).

CONCLUSIONS

Our speed-adaptive controller successfully increased exo assistance with changes in walking speed for post-stroke individuals. The exo assistance resulted in higher net average power at the paretic ankle. Though we found no significant change in metabolic cost, our exo controller demonstrates the potential of assistive devices to restore paretic limb propulsive power. Future work will examine the interaction between exo assistance, walking speed, distance travelled and gait symmetry between paretic and non-paretic limbs.

REFERENCES

1. Peterson, CL et al. *J Biomech*. 2010; 43:2348–55.
2. Takahashi, KZ et al. *J NeuroEng Rehab*.2015;12:23
3. Giest, TG et al. *ASB Abstract*, 2016.
4. Koller, JR et al. *J NeuroEng Rehab* 2015; 12:97.
5. Farris, DG et al. *J NeuroEng Rehab* 2015; 12:24.

ACKNOWLEDGEMENTS

We would like to acknowledge Dr. RW Nuckols for his assistance developing and implementing the controller. Funded by the National Institutes of Health, National Institute for Child Health and Human Development. NIH grant R21 HD072588-01A1 to GSS.

EVALUATING THE POSTURAL ERGONOMICS OF OPHTHALMOLOGISTS USING KINEMATIC MOTION ANALYSIS AND ELECTROMYOGRAPHY

[1] Safeer F. Siddicky, [2] Scott E. Olitsky and [1] Gregory W. King

[1] University of Missouri-Kansas City, Kansas City, MO, USA
[2] Children's Mercy Kansas City, Kansas City, MO, USA
Email: safeer.siddicky@umkc.edu

INTRODUCTION

Ophthalmologists often maintain static postures of the neck, shoulder, elbow and wrist during their routine clinical examinations, which may lead to work-related musculoskeletal diseases (MSDs) [1] and a decreased capacity for healthcare delivery. Ophthalmologists' posture, ergonomics and occupational discomfort are currently evaluated qualitatively using survey methods, such as the Visual Analog Scale (VAS) pain level reporting [2] or quantitatively using electromyography [3].

A combination of marker-based motion capture and electromyography may provide an objective, quantitative methodology to examine posture and suggest postural adjustments that will reduce the risk of developing MSDs. This study used motion analysis and electromyography to evaluate ophthalmologists' posture during routine exams and with alterations to exam setup.

METHODS

Ten pediatric ophthalmologists (5 male, 5 female, aged 40 ± 9.52 years old) performed retinoscopy, refraction and simulated retina exams using a slit lamp biomicroscope and a 90D lens on a child CPR manikin. Postural kinematics was tracked using 14 Optitrack Flex 13 cameras, with participants donning a conventional 27-marker upper body marker set [4]. Neck and shoulder muscle activity was recorded using Delsys Trigno surface electromyography electrodes placed bilaterally on the upper trapezius and anterior deltoid muscles.

Retinoscopy and refraction examinations were performed as is, and under a postural alteration which involved reclining the manikin to simulate patient viewing a raised eyechart. Non-neutral neck flexion (percentage of procedure time that neck flexion was outside 3 S.D. of upright neck posture) was compared among the postural alterations.

Slit lamp examinations were performed under 3 conditions: no postural adjustments, postural adjustment by altering slit lamp platform height and patient position, and postural adjustment with an elbow rest under arm holding the 90D lens. Sagittal plane neck flexion angle, upper trapezius muscle activation area and the percentage of procedure time that the anterior deltoid was active were compared among these 3 conditions for all ophthalmologists.

Neck flexion angles were calculated using the head and shoulder marker data and a Cardan rotation sequence. EMG data was rationalized using baseline data taken from upright static sitting. Muscle activation area was calculated as the area under the rectified EMG profiles. Paired t-tests were used for all comparisons (presented as mean ± 1 SEM).

RESULTS AND DISCUSSION

For the retinoscopy and refraction examinations, percentage of procedural time with non-neutral neck flexion decreased after reclining the manikin for loose lens retinoscopy (81.39 ± 2.57% vs. 69.45 ± 3.91%, $p = 0.038$*), lens bar retinoscopy (81.29 ± 1.83% vs. 70.62 ± 5.29%, $p = 0.095$), loose prism refraction (66.54 ± 3.80% vs. 64.47 ± 3.93%, $p = 0.741$) and prism bar refraction (74.57 ± 1.38% vs. 60.94 ± 7.54%, $p = 0.203$). These results are displayed in Fig. 1.

For the slit lamp examination, sagittal plane neck flexion angle range of motion decreased significantly after postural adjustment (41.4±3.3° vs. 36.4±2.8°, $p = 0.023$*) and elbow rest placement (41.4±3.3° vs. 35.8±2.8°, $p = 0.025$*). Upper Trapezius muscle

activity (procedural activation area) decreased after postural adjustment (106.1±52.9mV vs. 88.3±46.0mV, p = 0.137) and elbow rest placement (106.1±52.9mV vs. 87.6±45.0mV, p =0.186). Percentage of procedural time that the anterior deltoid was active decreased slightly after postural adjustment (38.8±3.7% vs. 37.43±4.3%, p = 0.756) and decreased significantly after elbow rest placement (38.8±3.7% vs. 31.37±3.9%, p = 0.037). These results are displayed in Fig. 2.

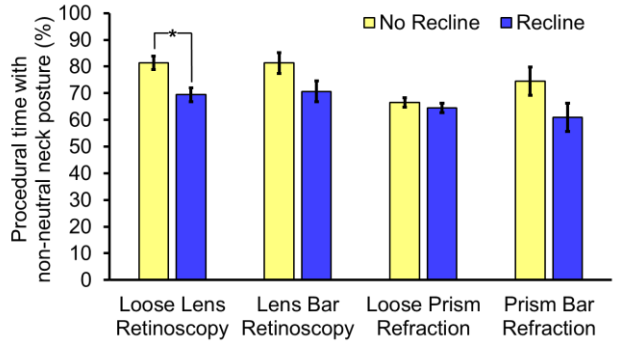

Figure 1: Percentage of procedural time with non-neutral neck flexion (no patient recline vs. recline).

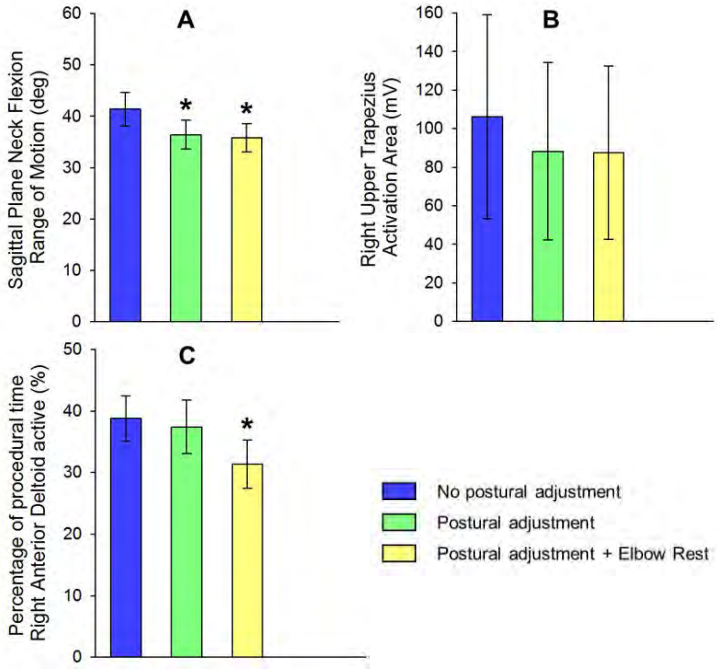

Figure 2: Sagittal plane neck flexion range of motion **(A)**, Activation area of the Right Upper Trapezius **(B)**, Percentage of procedural time that the Right Anterior Deltoid was active **(C)**.

The observed reduction in the percentage of procedural time with non-neutral neck flexion in the retinoscopy and refraction exams and the observed reduction in neck flexion and upper trapezius activity after postural adjustments in the slit lamp examination may indicate lower exposure to sustained non-neutral neck postures that can cause MSDs. The decrease in anterior deltoid activation after installing an elbow rest in the slit lamp examination may also indicate a practice that could lead to reduced stress related to prolonged, unsupported arm raise.

CONCLUSIONS

Easily implemented postural adjustments may decrease the possibility of occupational MSDs by reducing time spent by ophthalmologists in un-ergonomic postures. Preliminary analyses from this and future studies may help establish a quantitative standard for ergonomic postures in ophthalmic practice, lead to a wide scale re-design of ophthalmic equipment, and facilitate the development of postural ergonomics-focused training curriculums for current and future ophthalmologists.

This study only focuses on pediatric ophthalmologists, wherein a generalization of the procedural postural characteristics observed may not necessarily be accurate when applied to all practicing ophthalmologists. Future studies will include a wider subset of ophthalmologists as participants, leading to a more generalizable study and a larger sample size.

REFERENCES

1. NIOSH, NIOSH Publication 97-141, 2, 1997.
2. Kitzmann et. al., J Ophthalmol, 119(2): 213–20, 2012.
3. Fethke et.al., Int J Ind Ergon, 49: 53-59, 2015.
4. Leardini et. al. Clin. Biomech. 26, 562-71, 2011.

ACKNOWLEDGEMENTS

The authors would like to thank Children's Mercy Kansas City for the use of their pediatric ophthalmology clinic for testing, and the UMKC Center for Health Insights for the use of their Optitrack Flex 13 motion capture system.

IN VIVO RELATIONSHIP BETWEEN JOINT STIFFNESS, JOINT-BASED ESTIMATES OF MUSCLE STIFFNESS, AND SHEAR WAVE VELOCITY

[1] Andrew D. Vigotsky, [2] Elliott J. Rouse, and [1] Sabrina S.M. Lee

[1] Northwestern University, Evanston, IL, USA
[2] University of Michigan, Ann Arbor, MI, USA
email: vigotsky@u.northwestern.edu

INTRODUCTION

The underlying properties governing human joint mechanics, such as stiffness, are constantly regulated for effective, safe, and efficient interactions with the external environment. Joint stiffness (k_{joint}) is, in part, determined by the properties of the muscles surrounding the joint. The muscle-joint relationship can be thought of hierarchically, since there exists a lower level, muscle, and a higher level, joint. In light of this hierarchy, investigators often assess joint properties to make inferences about muscle-level changes. However, such approaches lack the specificity needed to understand the role of individual muscles.

Shear wave ultrasound elastography—which measures the velocity at which shear waves travel through tissue—has been increasingly used to assess the mechanical properties of muscle [2]. However, how shear wave velocity (SWV), measured at the muscle level, relates to k_{joint} and muscle stiffness *in vivo* remains poorly understood [2, 3]. Therefore, the purpose of this work was to quantify the relationships between 1) SWV of individual primary plantar flexors and ankle k_{joint}, and 2) SWV and joint-based estimates of muscle stiffness (k_{muscle}) in two muscles, medial gastrocnemius (MG) and soleus (SOL).

METHODS

Ten healthy, young adults (6 females, 4 males; age = 26 ± 4 years; body mass = 69 ± 16 kg; height = 171 ± 10 cm) participated in this study, which was approved by the Northwestern University Institutional Review Board. Ankle k_{joint}, SWV_{MG}, and SWV_{SOL} were measured in two positions (knee flexed, 90°; knee extended, 0°) and at three activation levels (0%, 20%, and 40% of maximum voluntary contraction, MVC) on two separate days. The ankle was positioned at 90° for all trials. The two knee positions permitted independent investigation of the MG, a bi-articular muscle, and the SOL, a uni-articular muscle.

Joint stiffness was measured using a custom dynamometer, by recording joint moment responses to 1° perturbations, collected over 27, 10-second trials for each activation. System identification analyses were used to isolate stiffness contributions to the ankle joint's resistance to rotation [4]. This approach differs from calculating the slope of the moment-angle curve, such that the measures are not strictly a function of the net moment demands of the task and are robust to inertial and damping components [1, 5]. Shear wave velocity was measured from the MG and SOL over six isometric trials for each condition (Aixplorer SuperSonic Imagine, Aix en Provence, France).

A biomechanical model was used to estimate k_{muscle} (Fig. 1). The ankle joint was modeled as a pin joint with two springs (k_{muscle} and k_{tendon}) acting in series about its center of rotation. Literature values for moment arm were used [6, 7], and k_{tendon} was measured experimentally by tracking the MG muscle-tendon junction with B-mode ultrasound during ramp (0–60%MVC), isometric contractions.

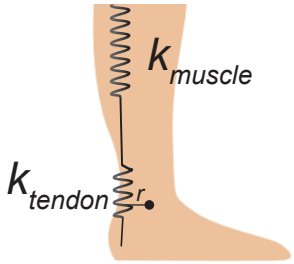

Figure 1: Biomechanical model to estimate muscle stiffness.

To understand the relationships between 1) SWV and k_{joint}, and 2) SWV and k_{muscle}, hierarchical linear statistical models were used. Trials were nested within participants, such that all relationships were within-subject.

RESULTS AND DISCUSSION

A strong, linear relationship was found between SWV_{MG}, SWV_{SOL}, and k_{joint} (R^2 = 0.96; RMSE = 14.6 N·m/rad) (Fig. 2A). SWV_{SOL} (when controlling for SWV_{MG}) had a greater slope in its relationship with k_{joint} than SWV_{MG} (when controlling for SWV_{SOL}). For example, if SWV_{SOL} and SWV_{MG} are 9 and 3 m/s, then $k_{joint} \approx 211$ N·m/rad. However, the inverse produces $k_{joint} \approx 113$ N·m/rad. Low collinearity between SWVs ($r = -0.331$) suggests that SOL and MG were independent regressors.

Shear wave velocity in both SOL and MG increased with ankle joint moment (Fig. 2B and C, R^2 = 0.88, R^2 = 0.95, respectively). The difference in slopes between flexion and extension in SWV_{MG} but not SWV_{SOL} reflect the biarticular nature of MG; SWV_{MG} increases more when it is in a kinematic position that facilitates greater force generation.

The strong relationship observed between SWV and k_{joint} is noteworthy and clinically relevant. Weak relationships between SWV and k_{joint} have been observed when assessed passively, between subjects, and using the moment-angle relationship to estimate k_{joint} [2]. However, our data suggest that *changes* in SWV are reflected on the joint level when assessed using more sophisticated measures of k_{joint} and taking into account inter-individual differences. Thus, researchers and clinicians may be able to use SWV as a guidepost for understanding joint stiffness changes with muscle-level specificity.

Surprisingly, no relationship was observed between SWV and estimates of k_{muscle} (R^2 = 0.10; RMSE = 10537.9 N/mm). Model outputs were highly sensitive to moment arm and k_{tendon} parameters. Moreover, the k_{tendon} estimates measured experimentally were likely low, as just the MG subtendon was assessed; low k_{tendon} inflates k_{muscle}. This is evidenced by non-monotonic within-subject k_{muscle} estimates over increasing activations. Future investigations may wish to model each triceps surae muscle-subtendon unit, while considering the specific properties of each, as has been done in the upper extremity [8].

CONCLUSIONS

Our results indicate that changes in muscle SWV are indicative of changes in k_{joint} in healthy, young adults, and suggest that SW ultrasound elastography may be useful for assessing the etiology of changes in k_{joint} by providing muscle-level specificity.

REFERENCES

1. Kearney, et al., *Crit. Rev. Biomed. Eng.* **18**(**1**), 55-87, 1990.
2. Jakubowski, et al., *Clin. Biomech.* **49** 48-55, 2017.
3. Eby, et al., *J. Biomech.* **46**(**14**), 2381-7, 2013.
4. Ludvig, et al., *IEEE Trans. Biomed. Eng.* **59**(**12**), 3541-9, 2012.
5. Rouse, et al., *IEEE Trans. Biomed. Eng.* **60**(**2**), 562-8, 2013.
6. Arnold, et al., *Ann. Biomed. Eng.* **38**(**2**), 269-79, 2010.
7. Hashizume, et al., *J. Biomech.* **47**(**12**), 3226-31, 2014.
8. Hu, et al., *J. Neurophysiol.* **105**(**4**), 1633-41, 2011.

ACKNOWLEDGEMENTS

This study was funded by the ASB Graduate Student Grant-In-Aid. The authors would like to thank Dr. Daniel Ludvig for his technical assistance.

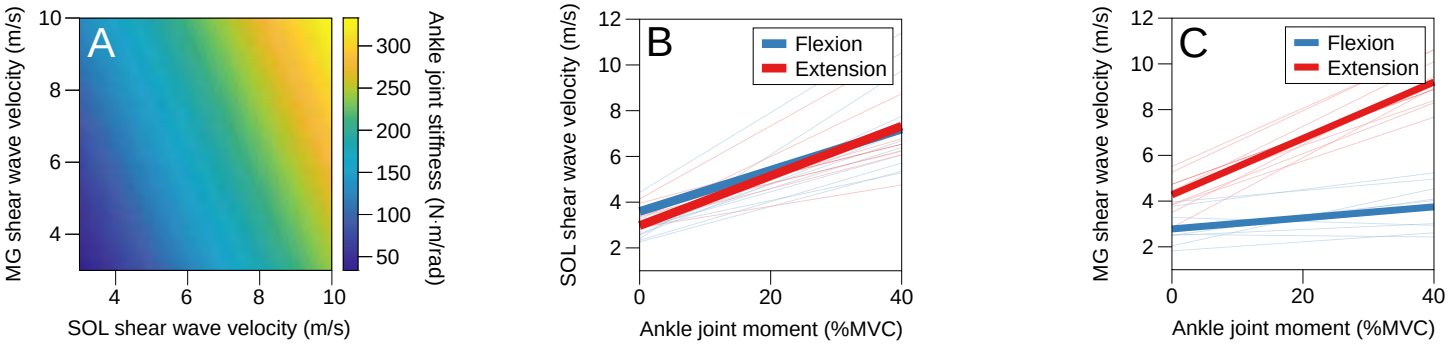

Figure 2: Relationships between shear wave velocity and joint-level measures. (A) Joint stiffness (color), soleus (SOL) shear wave velocity, and medial gastrocnemius (MG) shear wave velocity. Relative net joint moment and (B) SOL shear wave velocity and (C) MG shear wave velocity with the knee flexed (blue) and extended (red).

EFFECT OF LOCAL MUSCLE FATIGUE ON LOW-FREQUENCY COMMON INPUT TO BILATERAL AND UNILATERAL PLANTAR FLEXORS DURING QUIET STANDING

Tatsunori Watanabe[1,2] and Kotaro Saito[1]

[1]Department of Physical Therapy, Nagoya University Graduate School of Medicine, Nagoya-shi, Aichi JAPAN
[2]Japan Society for the Promotion of Science, Chiyoda-ku, Tokyo JAPAN
email: watanabe.tatsunori@h.mbox.nagoya-u.ac.jp

INTRODUCTION

Muscle fatigue is commonly defined as a reduction in the maximal force capacity of muscles, and can impair postural balance [1,2], possibly leading to injuries in not only sports but also leisure settings.

Control of posture is a complicated mechanism requiring efficient and effective muscular activation using the visual, somatosensory, and vestibular information. As the center of body's mass locates in front of the ankle joint during quiet standing, plantar flexor muscles play a primary role in maintaining balance, and many previous studies have assessed how these muscles are organized using time and frequency analyses. Mochizuki and colleagues, for example, have revealed that common input to motor units within soleus (SL) muscle as well as common input to motor units of bilateral SL muscles are stronger during standing than voluntary contraction [3]. Furthermore, recent studies have found electromyography (EMG)-EMG coherence, that quantifies common input to muscles, between bilateral homologous plantar flexor muscles and unilateral plantar flexor muscles in delta band (0-5 Hz) [4,5]. The origin of the comodulation has been suggested to be the subcortical systems [3].

Given a finding that muscle fatigue can influence the firing rate of motor units [6], this study examined whether localized muscle fatigue would affect the comodulation of bilateral and unilateral plantar flexor muscles during quiet standing, using the coherence analysis. It was hypothesized that muscle fatigue would decrease the delta-band coherences between bilateral homologous plantar flexor muscles and within unilateral plantar flexor muscles.

METHODS

Eleven healthy young male adults (mean age ± SD = 22.2 ± 0.8) participated in this study. They were asked to quietly stand on a force plate (Tec Gihan, Kyoto, Japan) with their bare feet parallel to each other for 40 seconds. The task was performed before and after fatigue protocol. The fatigue was induced by asking the subjects to raise their heels with knees extended until exhaustion.

The center of pressure (COP) was recorded from the force plate. EMG signals from bilateral medial gastrocnemius (MG) and SL muscles were also recorded using Trigno system (Delsys, MA, USA).

A customized Matlab script (Mathworks, MA, USA) was used to analyze the recorded data. We calculated SD and mean speed of COP displacement. Also, coherences between bilateral homologous plantar flexor muscles (MG-MG and SL-SL pairs) and within the unilateral muscles (MG-SL pair) for the right leg were estimated using the following equation:

$$|C_{xy}(f)|^2 = \frac{|P_{xy}(f)|^2}{P_{xx}(f) \cdot P_{yy}(f)},$$

where $P_{xx}(f)$ and $P_{yy}(f)$ are the auto-spectra of the signals x and y, and $P_{xy}(f)$ is the cross-spectra at the frequency f. They were calculated with a discrete Fourier transform of non-overlapping segments of 1024 data points. The coherence function is a number ranging from zero to one: zero indicates that two signals are completely independent, and one indicates that two signals are identical. For each analysis, 95% confidence limit was applied to identify the significant coherence.

Statistical analysis was performed with R. We compared the SD and mean speed of COP displacement between pre- and post-fatigue using a

paired t-test. In addition, we averaged z-transformed coherence over frequency ranges of 0-5 Hz (delta band). We compared the effect of fatigue on the bilateral coherence between the muscle pairs (MG-MG and SL-SL) using a two-way repeated measure analysis of variance (ANOVA). The effect of fatigue on the unilateral coherence (MG-SL) was assessed using a paired t-test. The significant level was 0.05.

RESULTS AND DISCUSSION

Results of COP parameters are presented in Figure 1. There was no significant difference in the SD of COP displacement between pre- and post-fatigue. The mean speed was greater in post- than pre-fatigue ($p = 0.0016$).

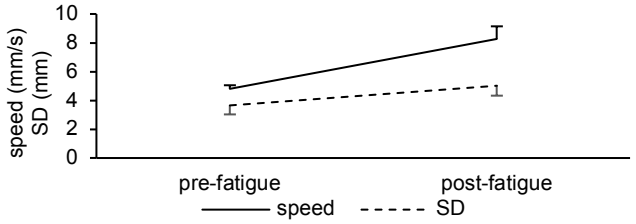

Figure 1: Effects of fatigue on COP parameters.

Pooled coherence spectra (95% confidence limit = 0.0047) and results of the z-transformed coherence are shown in Figure 2. A two-way repeated measure ANOVA on the delta-band coherence revealed a main effect of fatigue ($F_{1,10} = 11.0$, $p = 0.0078$) and interaction between fatigue and muscle pair ($F_{1,10} = 6.2$, $p = 0.032$). Post-hoc analysis showed that the delta-band coherence for the MG-MG pair was smaller in post- than pre-fatigue ($p = 0.0041$). There was no significant difference in the delta-band coherence for the SL-SL pair. Also, a paired t-test revealed that the delta-band coherence for the MG-SL pair was significantly smaller in post- than pre-fatigue ($p = 0.044$).

Consistent with a previous study [2], the speed of COP displacement was increased by the local muscle fatigue. The results regarding the coherence partly supported our hypothesis. The insignificant effect of muscle fatigue on the delta-band coherence for the SL-SL pair may be attributed to the fatigue protocol having the subjects raise their heels with knees extended. The gastrocnemius muscles might have been mainly fatigued by the protocol. The significant decrease in the delta-band coherence for the MG-MG and MG-SL pairs could be ascribed to an increase in the variability of motor unit firing rate [6]. This could have caused the comodulation less likely. Alternatively, it is also possible that a shift from ankle to hip postural control strategy has occurred after the muscle fatigue [8]. The ankle muscles could have been utilized less after the fatigue protocol.

A.

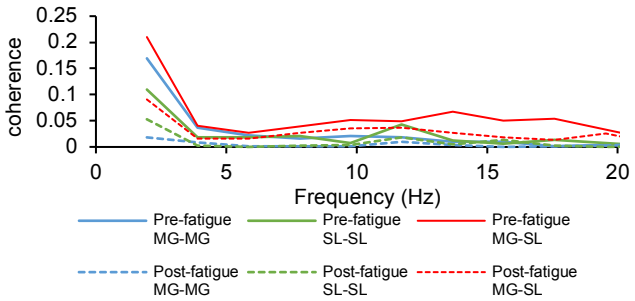

B.

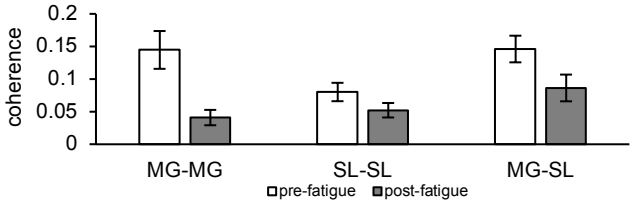

Figure 2: Pooled coherence spectrum (A) and effect of fatigue on coherence (B).

CONCLUSIONS

The local fatigue of plantar flexor muscles could decrease the low-frequency common input to these muscles. The current findings may provide guidance for developing interventions that mitigate fatigue-related problems, potentially in clinical populations.

REFERENCES

1. Nardone A, et al. *Arch Phys Med Rehab* **79**, 920-924, 1998.
2. Bisson EJ, et al. *Gait Posture* **32**, 482-286, 2010.
3. Mochizuki G, et al. *J Neurophysiol* **97**, 3917-3925, 2007.
4. Boonstra TW, et al. *J Neurophysiol* **100**, 2158-2164, 2008.
5. Obata H, et al. *Exp Bra Res* **232**, 1-11, 2014.
6. Taylor JL, et al. *Med Sci Sports Exerc* **48**, 2294-2306, 2016.
7. Grosse P, et al. *Clin Neurophysiol* **113**, 1523-1531, 2002.
8. Davidson BS, et al. *Gait Posture* **29**, 552-557, 2009.

COMPUTATIONAL MODEL OF MUSCLE INJURY VALIDATED WITH IN SITU EXPERIMENTS

[1] Amanda M. Westman, [1] Sarah Dyer, [1] J. David Remer, [1] Xiao Hu, [1] George J. Christ, [1] Silvia S. Blemker

[1] University of Virginia, Charlottesville, VA, USA
email: am5wk@virginia.edu

INTRODUCTION

Volumetric muscle loss (VML) injuries occur where there is a permanent loss of muscle function, and treatment of these injuries is challenging because the type of injuries and wound locations varies widely [1]. Regenerative medicine is a promising method for the treatment of VML injuries; however, within the literature, there is variability in the *in vivo* models used to study these injuries and the methods used to assess functional repair [2,3]. *In silico* analysis is a tool that can capture the variability of VML injuries' sizes and locations as well as simulate different experimental conditions.

In this study, we aimed to couple a finite element (FE) model with *in vivo* muscle functional analysis. The latissimus dorsi (LD) of rodents is a large flat muscle on the back that allows for a range of VML injury sizes and locations to be tested. Additionally, its complex muscle architecture of parallel and pennate fibers makes it complicated to understand the relationship between injury magnitude, location, and functional loss. Functional assessment of the LD can be tested using an *in situ* setup, which maintains the physiological conditions of the LD and captures the force of both parallel and pennate fibers. We developed a finite element model of the rat latissimus dorsi (LD) and used it as a predictive tool to focus our *in vivo* study and understand the complex biomechanics of force loss resulting from different injuries.

METHODS

The three-dimensional FE model of an intact rat LD was created based on measurements from dissected LDs of rats and was simplified to have a shape of one rectangle plus one fan [4]. The LD was modeled as a transversely isotropic, hyperelastic and quasi-incompressible material [5], and it was assigned fiber direction from the origin along the spine to the insertion at the humerus using computational fluid dynamics [6]. Boundary conditions were assigned to replicate *in situ* experimental testing conditions, and maximum muscle activation was set for all simulations. The native LD model was calibrated to fit native experimental data using a sensitivity analysis of the peak isometric stress parameter (Fig. 1C). Then an injury 11x15 mm was created at various locations within the muscle model and isometric contractions were simulated (Fig. 1A).

Experimentally, two injuries (11x15 mm) were created – the original injury and high injury – and then immediately tested using the *in situ* setup [3]. In this method, the LD muscle was minimally dissected and maintained in its native environment with blood supply and nerve innervation. A nerve cuff was placed around the motor nerve and the muscle's distal tendon was attached to the lever arm of a force transducer. The nerve was then stimulated and the peak isometric forces were measured at a range of stimulation frequencies.

RESULTS AND DISCUSSION

The isometric simulations of five different injuries demonstrated that the location of an injury has a dramatic impact on the LD's total force of contraction (Fig. 1B). The 36% reduction in force of the original injury compared to native LD was validated experimentally, as seen in Fig. 1C. An injury near the top of the muscle, labeled high injury, generated the largest decrease from native at 50% (Fig. 1B). The *in situ* testing of the high injury confirmed the model's force prediction (Fig. 1C). Using the FE model as a predictive tool, we were able to determine the preferred injury location to maximize the decrease between native and injured force production. For the development of novel therapies, an increased difference would help to

increase the margin of difference between treatments and better aid development.

The FE model can also be used to better understand the biomechanics of force production and the difference between the original and high injuries. A breakdown of the force production from each component of the LD showed that the original injury fan generated 3.204 N compared to only 2.269 N from the high injury fan portion. The increased number of intact fibers present in the original injury likely contributed to the increased force production of the original injury location. Analysis of along-fiber stretch shows that the high injury LD generated a larger along-fiber stretch within the region of intact fibers of the fan compared to the original injury. This indicates that the fibers of the high injury LD operate on the descending limb of the force-length curve and are unable to generate maximum force.

CONCLUSIONS

Using a computational and experimentally coupled framework, we were able to determine the best injury location to see the largest difference between native and injured rat LD muscles by creating, validating, and testing a model with three different data sets. This work demonstrates that combining these tools allows more focused and efficient *in vivo* studies to be designed which saves valuable time, money, and resources and has the potential to accelerate the development of regenerative therapies.

REFERENCES

[1] Corona et al. *JRRD*. 52(7): 2015.
[2] Baker et al. *Tissue Eng Part A*. 23(11-12): 2017.
[3] Chen and Walters. *J Plast Reconstr Aesthetic Surg*. 66(12): 2013.
[4] Hu et al. *Proc Am Soc Biomech*, 2016.
[5] Blemker et al. *J Biomech*. 38(4): 2005.
[6] Inouye et al. *Proc Am Soc Biomech*, 2015.

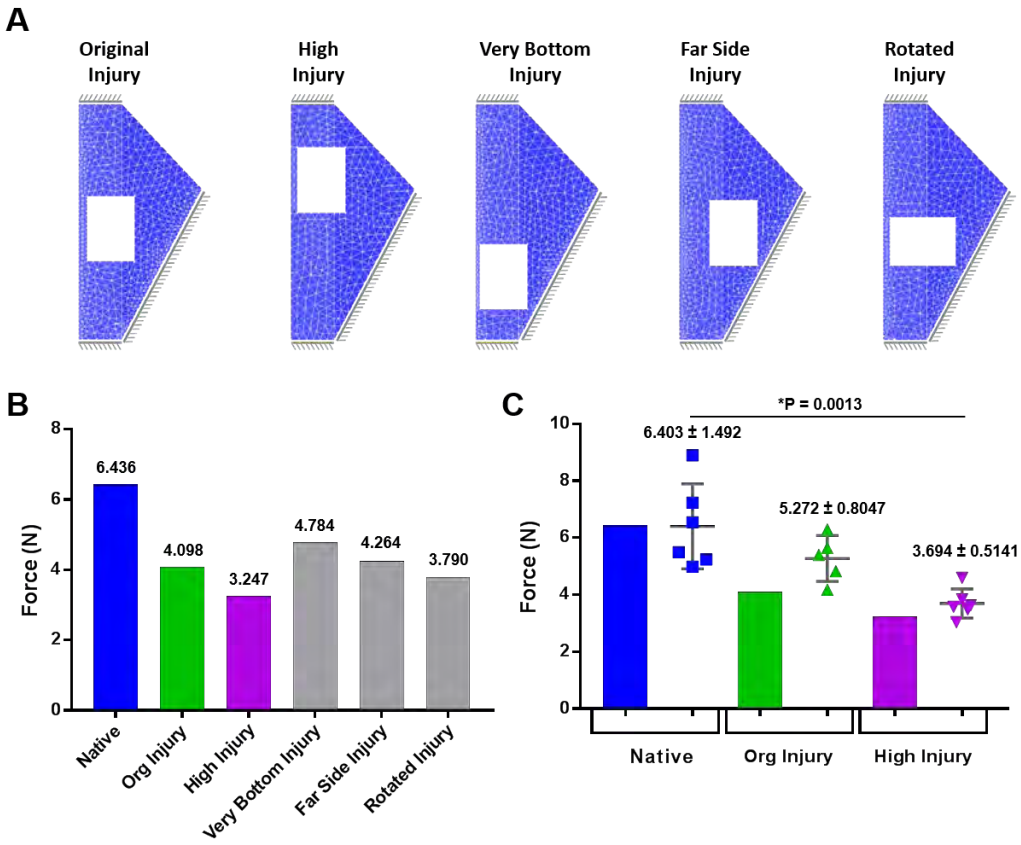

Figure 1: Five different injuries (11x15 mm) were created in the rat LD at varying locations within the muscle (A). Model simulations of the injuries showed that injury location has a dramatic effect on force production (B). Experimental *in situ* testing results of the original and high injury, shown as scatter plots, validate the model force predictions, shown as bars (C).

The Effect of Mid-flight Whole-Body and Trunk Rotation on Landing Mechanics

Meghan Critchley, Daniel Davis, Michaela Keener, Jacob Layer, and Boyi Dai

Division of Kinesiology and Health, University of Wyoming, Laramie, WY, USA
email: mcritch1@uwyo.edu, web: http://www.uwyo.edu/kandh/

INTRODUCTION

The anterior cruciate ligament (ACL) reconstruction surgery is one of the most commonly performed orthopedic surgeries in the United States [1]. ACL injuries are commonly observed when individuals perform jump-landing and cutting tasks. A combination of increased knee valgus and internal rotation moments may increase the risk of an ACL rupture [2].

Lateral trunk bending was associated with increased external knee valgus moment in a single-leg landing [3]. In an examination of vertical jumps with and without rotation, greater anterior-posterior and medial-lateral force couples were observed during the rotated condition and may have induced greater shear joint forces [4]. This force-coupling was enacted to reduce the angular momentum to zero at landing to prevent further rotation. However, this previous study was limited to a force analysis, and only whole body rotation was performed.

The purpose of the current study was to quantify the effect of whole body and trunk rotation on the biomechanics of jump-landings. It was hypothesized that landing with trunk rotation would result in knee kinematics and kinetics associated with increased ACL loading compared with landing without rotation or with whole body rotation.

METHODS

Twelve male and 8 female recreational athletes participated in this study (21.5 ± 2.68 years, 1.73 ± 0.10 m, and 73.0 ± 12.29 kg). Participants performed three jump-landing-jump trials in each of 5 conditions. For all conditions participants were asked to jump forward from the box, reach and hold the basketball as early as possible, land with the testing foot on the center of the force plate, and then perform a maximum vertical jump. In the Forward condition, no body or trunk rotation was performed (Figure 1).

In whole body conditions, participants rotated the whole body 90 degrees towards (WBI) or away (WBC) from the testing leg to land on the force plate (Figure 2). In trunk rotated conditions, participants rotated their trunk towards (TRI) or away (TRC) from the testing leg to land on the force plate (Figure 3). Participants' landing kinematics and vertical ground reaction force (VGRF) were captured using eight Vicon cameras and a Bertec force plate.

Participants' jump height, stance time, peak VGRF, knee flexion angle, knee valgus angle, and knee internal rotation angle during the first 100 ms of landing were extracted for analysis. Repeated-measure ANOVAs with the landing condition were performed for each dependent variable. A significant ANOVA test was followed by paired-wise comparisons. A type I error rate was established at 0.05 for statistical significance.

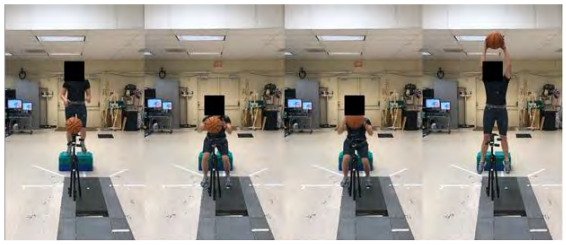

Figure 1: Forward condition

Figure 2: Whole body rotation

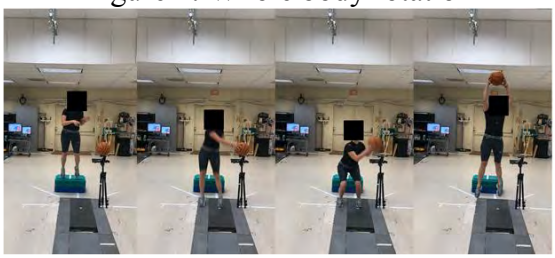

Figure 3: Trunk rotation

RESULTS AND DISCUSSION

ANOVAs showed significant condition effects for all the variables, excepted for jump height (Table 1). Paired-wise comparisons showed significant increases in initial trunk rotation and trunk rotation at 100 ms after landing in the TRC and TRI conditions. The TRI condition resulted in increased stance time, increased peak VGRF, decreased knee flexion angles, increased knee valgus and internal rotation angles during the first 100 ms of landing compared with most other conditions. Compared with the Forward condition, a significant decrease in knee valgus angle was demonstrated in the TRC condition. Increased Peak VGRF was also found in the WBC condition.

In the TRI condition, as the participant rotated the body towards the testing leg, a greater percent of body weight was shifted to the testing leg, resulting in increased impact GRF. In addition, because the trunk and lower extremity act as a closed kinetic chain during landing, increased trunk rotation caused the thigh rotating externally and resulted in increased knee internal rotation. The findings were consistent with previous studies, which have analyzed videos of ACL events and found that landing with the trunk rotated may increase the risk of an ACL rupture [5].

CONCLUSIONS

The TRI condition resulted in landing biomechanics associated with increased ACL loading and injury risk [6]. The results may help researchers to better understand trunk rotation in relation to ACL injury risk. Athletes should be coached to be more aware that trunk rotation during mid-flight may result in a more dangerous landing position. Training and intervention programs incorporating landing technique and core stability training may help athletes re-align their trunk before landing.

REFERENCES

1. Ferretti A, et al. *Knee Surgery, Sports Traumatology, Arthroscopy,* 19, 2011.
2. Shin CS, et al. *Medicine & Science in Sports & Exercise,* 43, 2011.
3. Kimura Y, et al. *British Journal of Sports Medicine,* 48, 2014.
4. Harry JR, et al. *Journal of Strength and Conditioning Research,* 31(7), 2017.
5. Stuelcken MC, et al. *Journal of Sports Sciences*, 2015.
6. Kim SY, et al. *The American Journal of Sports Medicine*, 43, 2015.

Table 1: Means ± Standard Deviations of Biomechanical and Performance Variables

	Forward	WBC	WBI	TRC	TRI
Jump height (m)	0.41 ± 0.12	0.39 ± 0.40	0.40 ± 0.10	0.39 ± 0.11	0.39 ± 0.11
Stance time (ms)	504 ± 72.8^{c}	475 ± 94.6^{d}	530 ± 77.8^{b}	566 ± 93.9^{a}	572 ± 109.7^{a}
Initial Trunk rotation (deg)	0.08 ± 3.9^{b}	-7.35 ± 4.1^{c}	-4.89 ± 3.8^{c}	28.81 ± 7.3^{a}	29.41 ± 7.6^{a}
Trunk rotation 100 ms (deg)	0.25 ± 3.61^{b}	-3.1 ± 3.85^{c}	-5.58 ± 3.79^{c}	28.87 ± 5.79^{a}	29.95 ± 5.94^{a}
Knee flexion 100 ms (deg)	78.61 ± 7.7^{a}	71.27 ± 7.6^{c}	75.78 ± 6.3^{b}	78.68 ± 7.9^{a}	75.92 ± 6.3^{b}
Knee Valgus (-) 100 ms (deg)	-5.54 ± 5.8^{b}	-5.75 ± 5.6^{b}	-4.88 ± 6.3^{b}	-2.86 ± 6.7^{c}	-8.54 ± 7.2^{a}
Knee internal Rotation (deg)	9.52 ± 6.07^{b}	9.62 ± 5.40^{b}	5.61 ± 5.89^{c}	8.73 ± 5.85^{b}	12.03 ± 6.40^{a}
Peak VGRF (Body Weight)	2.19 ± 0.58^{b}	2.59 ± 0.62^{a}	2.14 ± 0.46^{b}	2.05 ± 0.69^{b}	2.67 ± 0.63^{a}

Note*: a>b>c>d* at a significance level set at 0.05

MODULAR CONTROL OF THE TIMED-UP-AND-GO TEST IN STROKE SURVIVORS

Hannah D. McDonald, Jessica L. Allen

West Virginia University, Morgantown, WV, USA
e-mail: jessica.allen@mail.wvu.edu, web: http://neuromoblab.com

INTRODUCTION

Characterizing impairments in muscle coordination after stroke across various movement behaviors important for mobility may inform the prescription of rehabilitation to match individual-specific impairments and maximize mobility gains. Here, we use motor module (a.k.a. muscle synergy) analysis to examine muscle coordination during the Timed-Up-and-Go (TUG) test [1], a clinical test designed to assess a patient's mobility. We chose to analyze the TUG test because it includes several different movement behaviors important for mobility: standing up from a chair, walking 3 meters at either a self-selected or fast pace, turning around to walk back to the chair, and then sitting back down. We have recently shown that recruiting common motor modules across different behaviors is important for mobility performance [2]. We hypothesize that having a stroke impairs the ability to selectively recruit patterns of neuromuscular control appropriate for a given movement behavior, and thus predict that fewer common motor modules are recruited across the sub-behaviors of TUG in stroke survivors vs. otherwise healthy age-matched controls.

METHODS

Electromyographic (EMG) and kinematic data were collected from 7 healthy older adults (HOAs, 62.3±7.1 years old, 3 males) and 5 chronic stroke survivors (58.0±15.2 years old, 1 male, 47.8±22.3 months post-stroke, 3 left-side hemiparesis) during the TUG test. TUG timing was determined based on visual inspection of kinematic data. Each trial began with the first forward progression of the trunk in the sagittal plane and ended when the trunk reached a lower plateau in the vertical plane. The TUG trial was further divided into four sub-behaviors: (1) sit-to-stand, (2) walking [in which both walking phases were combined], (3) turning, and (4) stand-to-sit.

Motor modules were extracted independently for each subject and leg usig EMG collected from 12 muscles spanning the hip, knee, and ankle. Each subject completed at least two TUG trials (range: 2-4), and processed EMG from all trials were concatenated together to get a single matrix for each subject and leg. EMG from each muscle was then normalized to maximum observed across all trials. For each subject and leg, a total of five sets of motor modules were extracted using non-negative matrix factorization: the full TUG trial plus the four sub-behaviors. The primary criterion used to select number of modules, n, was that the 95% confidence interval (CI) of the overall variance accounted for (VAF) was > 90% [2]. The secondary criterion was VAF > 75% for each muscle. In cases where overall VAF CI was > 90%, but a muscle VAF was low, we selected the next highest number of modules if it increased the muscle's VAF by > 5% [3].

For each subject, a hierarchical cluster analysis was performed to determine (1) the percentage of common modules recruited during the TUG test and (2) the similarity in motor modules recruited between walking and each sub-behavior. The modules independently extracted for each sub-behavior were pooled together and the minimum number of clusters was selected such that each cluster contained at most one module from each sub-behavior. The percentage of common motor modules across all sub-behaviors was defined as 100 x [1- number of clusters / sum of module numbers across all sub-behaviors]. The cluster results were then used to determine the percentage of modules shared between walking and each sub-behavior, defined as 100 x [n_{common} / (n_{walk} + $n_{sub\text{-}behavior}$ − n_{common})].

RESULTS AND DISCUSSION

Despite taking a significantly longer time to complete the TUG test (17.0±3.47s vs. 8.03±0.95s,

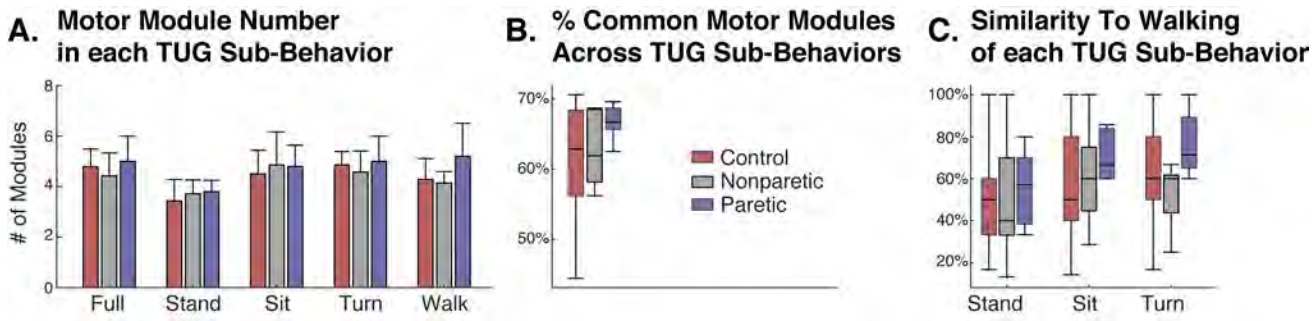

Figure 1: (A) The number of motor modules recruited during each sub-behavior of the TUG test, (B) the percentage of common motor modules across all sub-behaviors and (C) similarity between motor modules recruited in walking and the other sub-behaviors.

$p<0.001$), motor module number post-stroke was comparable to the number in HOAs (Fig. 1A). Across the full TUG test, HOAs recruited 4.79±0.70 modules, whereas stroke survivors recruited 4.60±0.89 in the nonparetic and 5.00±1.00 in the paretic leg. A similar number of motor modules were identified in each sub-behavior of TUG.

Similarly, the percentage of unique motor modules recruited during the TUG test post-stroke was comparable to the values observed in HOAs (62.1±7.53% for HOAs, 64.5±5.62% for nonparetic leg, and 66.8±2.68% for paretic leg, Fig. 1B). In HOAs the number of clusters was 6.50±1.65 out of a total number of 17.1±1.90 possible clusters. In the nonparetic leg, the number of clusters was 6.60±1.14 out of total number of 17.80±2.17 possible clusters. In the paretic leg, the number of clusters 6.20±0.84 out of a total number of 18.80±3.35 possible clusters. This is in contrast to our prediction and suggests that many of the motor modules are shared between the movement behaviors included in the TUG test even after a stroke. However, it is still possible that the recruited modules post-stroke are "inappropriate" for successful TUG performance. Further analysis of the actual motor module composition is needed.

Interestingly, the percentage of motor modules in each sub-behavior shared with those recruited for walking may indicate possible differences post-stroke (Fig. 1C). For turning, 63.5±26.7% of motor modules were shared with walking in HOAs versus 52.3±16.4% in the nonparetic and 76.8± 16.1% in the paretic leg. The percentages that sit-to-stand and stand-to-sit shared with walking were generally comparable across HOAs and stroke survivors. These results suggest a difference in turning strategy between the HOAs and stroke, which may explain why falls often occur during turning post-stroke [4].

CONCLUSIONS

Here we provide initial evidence that motor module numbers both within and across the movement behaviors of walking, stand-to-sit, turning, and sit-to-stand (as evaluated during the TUG test) are similar between HOAs and stroke survivors with hemiparesis. Our results also demonstrate a difference in turning strategy post-stroke, indicating that this may be a potential critical focus for rehabilitation efforts. Further analysis of module composition may provide more insight into the reasons for differences between HOA and stroke TUG test performance. Including additional factors such as leg dominance and turning direction may also help clarify some of the differences in performance observed between groups. A larger study is needed to confirm these initial results.

REFERENCES

1. Podsiallo and Richardson. *J Am Geriatr Soc,* 39:142-144, 1991.
2. Allen et al. *J Neurophys*. 118:363-73. 2017.
3. Clark et al. *J Neurophys*. 103:844-57. 2010
4. Hyndman et al. *Arch Phys Med Rehabil.* 83:165-170. 2005.

ACKNOWLEDGEMENTS

This work was supported by NIH grant F32-NS087775 and the WVU Research Corporation.

TIME-COURSE CHANGES OF TREADMILL RUNNING KINEMATICS IN DIFFERENT FOOTWEAR

[1]Jake A. Melaro, [2]Isabel S. Moore, [1]Megan R. Briley, [1]Quvilo V. Sherrod, [1]Max R. Paquette

[1] University of Memphis, Memphis, TN, USA
[2] Cardiff Metropolitan University, Cardiff, UK
email: mrpqette@memphis.edu, web: http://www.memphis.edu/shs/research/mal.php

INTRODUCTION

Using treadmills for running biomechanics research is useful when measuring several continuous gait cycles. When assessing the influence of novel footwear on running biomechanics during treadmill running, acute footwear familiarization periods between studies vary tremendously (e.g., not reported, 2min, 5min, 6min) [1-3]. Early work by Schieb [4] reported that step length (and cadence) and center of mass (COM) vertical oscillation changed between the first and eighth minute of a run but not between the eighth and fourteenth minute when trained runners with limited treadmill running experience ran at a set speed. However, stabilization of these variables may occur before the eighth minute of a treadmill. Assessing more time points during a run would provide valuable information regarding the stabilization of kinematics variables.

Since many biomechanical studies investigate footwear effects during running, assessing time to stability for running biomechanics variables is of importance. During overground running, approximately 7 trials over a 30m runway seem appropriate to ensure stable kinematic and kinetic variables in novel and familiar footwear types [7]. It would be worthwhile to understand differences in kinematic variable time to stability when novel footwear are used in during treadmill running. Therefore, the purpose of this study was to assess the time to stability of selected running kinematic variables during treadmill running in three types of footwear. We expected longer times to stability of kinematic variables in novel footwear compared to habitual neutral cushion footwear.

METHODS

Seven runners (three women; 25±6 yrs; 74.1±13.7 kg; 1.72±0.16 m; 23.6±12.2 miles·week^{-1}) attended three testing sessions separated by 24 to 48hrs. Each testing session was completed in one of three footwear conditions presented in a randomized order: 1) minimal (KSO, FiveFinger, Vibram), 2) neutral cushion (1080, New Balance), and 3) highly cushioned (Bondi 5, HOKA ONE ONE). During each testing session, reflective markers were placed on the pelvis and right lower limb. Anatomical marker position was marked with a black ink pen to ensure good placement reliability between testing sessions. A 9-camera 3D motion capture system (240Hz, Qualisys AB) was used to collect a static calibration trial, and ten seconds of kinematic data at the end of each minute throughout a 10-min treadmill run (Excite+ RUN 900, TechnoGym). Visual3D software (C-Motion) was used to compute the following kinematic dependent variables: cadence, pelvis COM vertical oscillation, and peak ankle dorsiflexion, peak ankle eversion and peak knee flexion.

The test-retest intra-class correlation coefficient (ICC, 3, k) was used to detect time to stability [5] for all kinematic variables. Time to stability for each variable was calculated for the population for each footwear condition using ICC for the first two 10s time points. Then, ICC was repeated by iteratively adding the averages from the subsequent time points. The time point needed to achieve an ICC greater than 0.90 was used to identify time to stability since this value represents a nearly perfect correlation [6].

RESULTS AND DISCUSSION

With the ICC method, time to stability for the selected kinematic variables ranged from 1 to 3min. Average ICC values ranged between 0.80 and 1.00. Vertical oscillation, peak dorsiflexion, peak eversion and peak knee flexion all showed nearly perfect correlation by minute two in all three footwear types (**Table 1**). Cadence showed nearly perfect correlation by minute two while wearing the highly

cushioned shoes while an ICC of > 0.90 was observed at minute three for the minimal and neutral cushion footwear (**Fig. 1**). Early work has reported that cadence and vertical oscillation are different between 1 and 8min of treadmill running [4]. This previous work did not collect data between 1 and 8min but our results indicate that stability in these kinematic variables may actually occur after only 1 to 3min. Using the sequential averaging method [8], ~7 to 7.5 trials of overground running over a 30m runway were reported to be necessary to achieve stability in selected kinematic and kinetic variables [7]. Assuming a step length of ~1m and ~30 steps per trial, a total of ~210 steps were required to reach stability. In the current study, with an average cadence of ~170 steps/min, runners took between 170 and 510 steps which is comparable to the total number of steps needed to reach stability during overground running in novel and familiar footwear types [7].

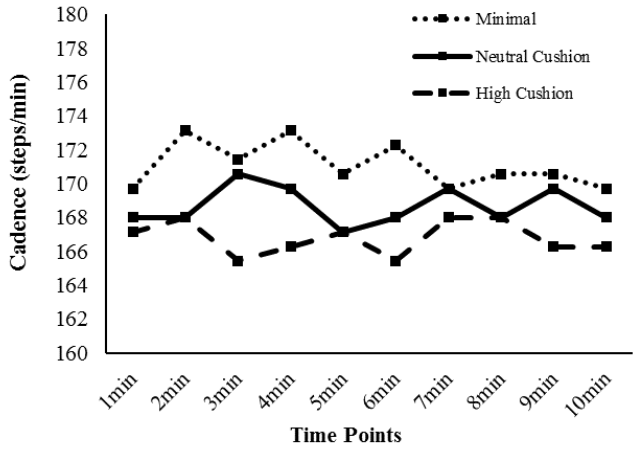

Figure 1: Average cadence during all ten 10s trials during the treadmill run in all footwear types.

Finally, most ICC values in the current study were similar to ICC values reported during overground running [9]. It is also important to note that other methods such as the sequential averaging method [8] have been used to identify time to stability in biomechanical variables during gait. We chose the ICC method since the sequential averaging method may be too conservative and the one-quarter standard deviation threshold from the mean is arbitrarily chosen.

CONCLUSIONS

Our findings suggest that, regardless of footwear type, 1 to 3min, or 170 to 510 steps, is sufficient for kinematic variables to stabilize during treadmill running studies. Next, we plan to assess if running experience influences time to stability for these running kinematic variables.

REFERENCES

1. Butler et al. *Gait Posture*, 26:219-225, 2007.
2. Fredericks et al. *J Sp Sci Med*, 14:276-283, 2015.
3. Divert et al. *Orth & Biomech*, 26:593-598, 2005.
4. Schieb. *Res Qu Ex Sp*, 57:1-7, 1986.
5. Portney & Watkins, *Foundations of clinical research: Applications to practice*, 2000.
6. Hopkins. New View of Statistics: http://www.sportsci.org/resource/stats/
7. Gittoes & Moore, *Proc of ISBS*, 2015.
8. Bates et al. *JOB*. 16(3):181-191, 1983.
9. Moore & Gittoes. *Proc of Footwear Biomech Symp*, 2015.

Table 1: ICC (95% CIs) value beyond 0.90 and time point of kinematic variable stabilization during the treadmill run and average time to stabilization per variable and per footwear type (mean±SD).

		Kinematic Variables					
Footwear		**Cadence**	**Oscillation**	**Ankle DF**	**Ankle EV**	**Knee FL**	**Time (min)**
Minimal	ICC	0.92 (0.72-0.99)	0.93 (0.65-0.99)	1.00 (0.97-1.00)	0.99 (0.97-1.00)	0.99 (0.95-1.00)	-
	Time Point (n^{th} min)	3	2	2	2	2	2.2±0.4
Neutral Cushion	ICC	0.92 (0.71-0.98)	0.98 (0.91-1.00)	1.00 (0.99-1.00)	0.99 (0.96-1.00)	1.00 (0.96-1.00)	-
	Time Point (n^{th} min)	3	2	2	2	2	2.2±0.4
High Cushion	ICC	0.98 (0.89-1.00)	0.99 (0.97-1.00)	0.97 (0.77-1.00)	1.00 (0.97-1.00)	0.99 (0.96-1.00)	-
	Time Point (n^{th} min)	2	2	2	2	2	2.0±0.0
	Time (min)	2.7±0.6	2.0±0.0	2.0±0.0	2.0±0.0	2.0±0.0	

Notes: Oscillation: pelvis COM vertical oscillation; Ankle DF: peak dorsiflexion; Ankle EV: peak eversion: Knee FL: peak knee flexion.

CHANGES IN STRUCTURE AND LOADING CONDITIONS OF THE EQUINE PROXIMAL PHALANX DURING GROWTH

Sara G. Moshage, Rebecca Vining, Annette M. McCoy, John Polk, and Mariana E. Kersh

University of Illinois at Urbana-Champaign, Urbana, IL, USA
email: moshage1@illinois.edu

INTRODUCTION

The metacarpophalangeal, or fetlock, joint experiences the highest joint forces in the distal forelimb [1], and is the site of most fatal musculoskeletal injuries in racing horses [2]. The proximal phalanx (P1) bone in the fetlock accounts for 23% of all distal forelimb fractures in racing Thoroughbreds [3], and up to 29% in Standardbred racehorses [4]. It is unknown how the distal forelimb is loaded during the two-year growth to racing age timeframe when loading may, or may not, predispose the P1 to fracture. This study aims to understand how equine P1 bone morphology and density changes during growth, and whether this is related to changes in gait.

METHODS

One uncastrated male Standardbred horse (DOB 03/26/17) free of disease and lameness was used as a subject for this study. All protocols were approved by the Institutional Animal Care and Use Committee at University of Illinois at Urbana-Champaign. The subject was put under anesthesia at four time points: ages 10, 18, 28, and 35 weeks. Body mass was measured at each time point. The distal left forelimb was imaged using computed tomography (CT) (LightSpeed-16, GE Medical Systems, 120kVp, 250 mA, 50 cm field of view, 512 x 512 matrix, and a 0.625 mm slice thickness). The proximal phalanx was segmented from the DICOM files using Amira 5.6 (Thermo Fisher Scientific). Hounsfield unit to density (ρ_{QCT}) conversions were calculated for each scan based on HA phantoms (Model 092, CIRS). Custom Matlab (R2016b, Mathworks) code was used to calculate whole bone cross-sectional area, cortical area, and densities at each slice within the P1 at each age.

Kinematic data of the left forelimb at several gaits were collected at age 12, 23, 29, and 36 weeks. Motion capture data was acquired with a six-camera system (Qualysis Oqus) while the subject walked, trotted, and cantered over an AMTI equine force plate. The kinematic data were post-processed in Qualysis Track Manager (Qualysis) to calculate joint angles and gait speed. Force data were analyzed using custom Matlab code.

RESULTS AND DISCUSSION

The P1 bone increased in length by 4.4% during the first 35 weeks of growth, but showed a larger (36%) increase in cross-sectional area in the diaphysis (Fig. 1, between 20% from the distal end and 35% from the proximal end).

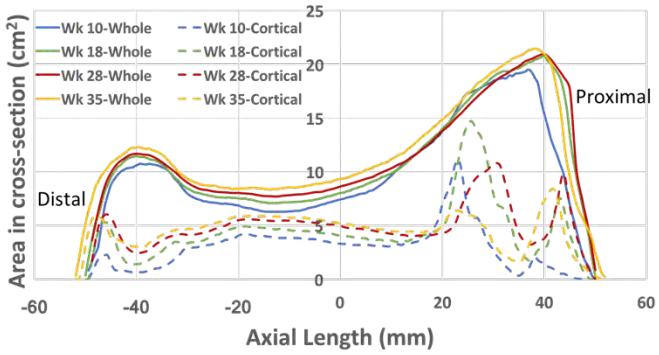

Figure 1. Area within cross sectional slices, with proximal end to the right. Age groups were aligned with 50% of total length plotted at 0 mm.

Cross-sectional cortical area increased by 50% in the diaphysis over the 35-week period. The fluctuation in cortical area at the proximal end is due to the proximal growth plate, which has mostly closed by 35 weeks of age.

Over the four CT time points, body mass was 163, 214, 268, and 319 kg. Cortical area at 20% from the distal end closely followed the isometric scaling expectation (slope =2/3) [5], with a log-log scaling exponent of 0.63 (Fig 2). This relationship suggests that the cortical bone is scaling appropriately with mass. However, total CSA exhibited significant

negative allometry (slope= 0.45), which may be affected by the size of the medullary cavity.

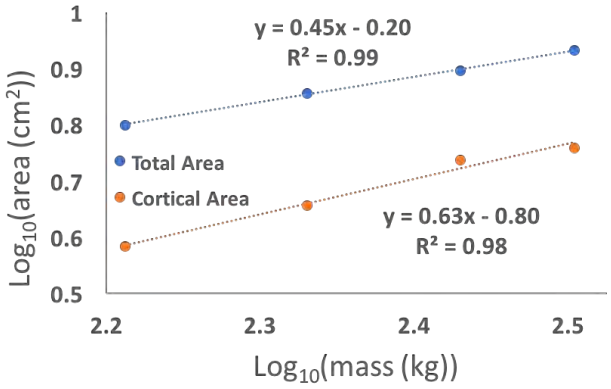

Figure 2. Log-log plot of cross-sectional area (total and cortical bone) with respect to mass. The slope of the linear fit represents the scaling exponent.

Although total CSA and cortical area increased with age and mass, particularly in the diaphysis, this trend did not hold for cortical density (Fig. 3).

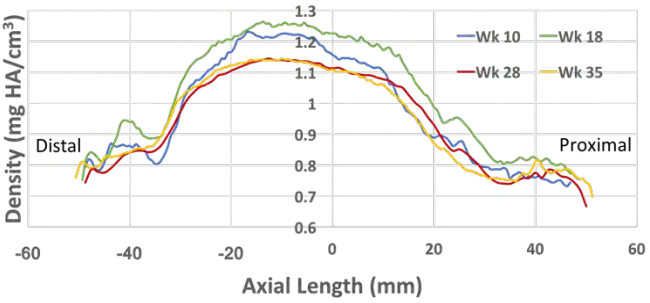

Figure 3. Average cortical density per cross-sectional slice. Same alignment as Fig. 1.

The highest cortical density throughout the entire length of the bone occurred at 18 weeks and was most evident in the diaphysis (-30 mm to 15 mm). Foals go through a playful, rambunctious phase, especially when they are housed with peers. Increased play and trotting would have resulted in increased moments on the bone, possibly leading to the peak in cortical density for the 18-week foal. Cortical density at 28 and 35 weeks was very similar, especially in the diaphysis, but lower than the density at 10 and 18 weeks. The difference in density may be tied to weaning, as the foal was weaned just prior to the 18-week scan.

Joint angles during walking were not significantly different during growth, while angles at the trot increased significantly until 29 weeks of age ($p<0.05$) (Fig. 4). Peak GRF increased significantly ($p<0.05$) with both speed and mass, resulting in higher bending moments on the P1 during trotting.

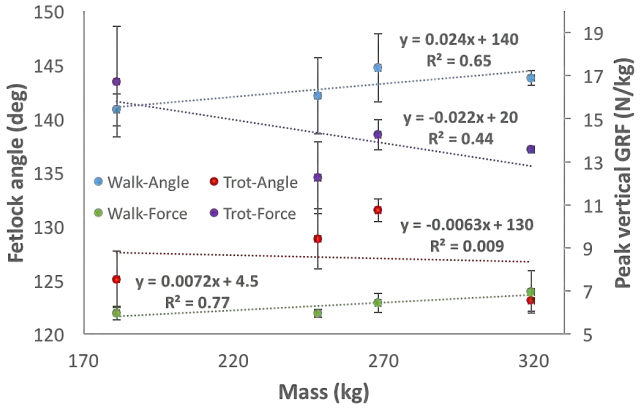

Figure 4. Fetlock angle and peak GRF at mid-stance. Standard deviation bars shown for angles.

CONCLUSION

Early exercise in foals is controversial. Rapid growth occurs from birth to 5 months, and to a lesser degree until 11 months [6]. During this time, structures resistant to repair later in life, such as articular cartilage and tendon, show a high capacity to regenerate [6]. These results indicate that there may be a window during the first year of growth where the musculoskeletal system may be primed for a later career. Based on the results of this study, the equine proximal phalanx may peak in cortical density by 18 weeks of age, indicating that an intervention strategy may need to be implemented around that time, in order to alter the growth trajectory of the bone for optimal strength. As a next step, regional differences in size and density (palmar, dorsal, medial, and lateral) will be analyzed.

REFERENCES

1. Harrison et al., (2010). *J. of Exp. Biol.,* **213** p3998
2. Parkin et al., (2004). *Vet. Record*, **154** p493
3. Verheyen et al., (2004). *Equine Vet. J.*, **36**(2) p167
4. Bertgulia et al., (2014). *BMC Vet. Res.*, **10**(11)
5. Biewener, A., (2005). *J. of Exp. Biol.*, **208** p1665
6. Barnveld et al., (1999). *Equine Vet. J. Suppl.,* **31** p112

REDUCING THE METABOLIC COST OF FAST WALKING THROUGH STIFF INSOLES

Samuel F. Ray and Kota Z. Takahashi
University of Nebraska Omaha, Omaha, NE, USA
Email: sfray@unomaha.edu, web: https://www.unomaha.edu/college-of-education/cobre/

INTRODUCTION

Metabolic cost of human locomotion is largely determined by the amount of force and work muscles generate [1,2], which are influenced by force-length and force-velocity relationships of muscle fibers [3]. During walking, the ankle plantarflexors operate near isometric contraction speeds, landing in favorable portions of the force-velocity region [4], thereby optimizing force production and helping to minimize metabolic cost. One factor that affects plantarflexor force-velocity operating region is the ankle-foot "gear ratio" [5], defined as the ratio between ground reaction force and Achilles tendon moment arms about the ankle. Modulating gear ratio changes the force-velocity characteristics of the plantarflexors throughout stance [5], helping to maintain a favorably low shortening velocity.

Adding stiffness to the foot (via shoes and insoles) has been previously explored as a method of altering ankle-foot gear ratio and augmenting plantarflexor muscle mechanics in walking [6]. In Takahashi et al."s study, added foot stiffness increased gear ratio, increased soleus muscular force output, and decreased fascicle shortening velocity. However, despite this „favorable" shift in the force-velocity region, walking with stiff feet led to an unchanged or increased metabolic cost at normal speeds [6]. We believe this is due to the added stiffness" *disadvantageous increase* in muscle force demand outweighing the *beneficial decrease* in fascicle velocity at normal walking speeds. In particular, increases in overall force output of plantarflexors lead towards higher metabolic cost; meanwhile, decreases in plantarflexor shortening velocity should have a metabolic benefit of greater force generation at similar activation levels. These competing effects may have no metabolic benefit in normal walking speed, however, added foot stiffness could have metabolic benefits in tasks where muscles may not operate economically, such as during fast walking.

At fast walking speeds, both musculoskeletal modeling simulations and *in vivo* imaging data of plantarflexor muscles reveal fast plantarflexor shortening velocities [7,8]. This places the muscles in unfavorable force-velocity relationships, reducing force output and requiring greater activation levels to maintain walking gait. Following Takahashi et al."s study [6], we propose that adding foot stiffness in fast walking could be a mechanism for the ankle plantarflexors to "shift gears", i.e., to improve force-velocity relationships toward those in normal speeds and ultimately reduce metabolic cost.

The purpose of our study is to determine if added foot stiffness can be used to reduce the metabolic cost of fast walking, and to determine the effects of shifting plantarflexor force-velocity operating range on the energetics of locomotion. We hypothesize that there will be a fast walking speed where overall metabolic cost will be lower with greater foot stiffness, due to an increased moment arm of the ground reaction force and a shift in plantarflexor force-velocity operating region.

METHODS

15 young adults aged 19 to 35 (n=12 males, 3 females, mean±SD mass 76.4±12.4 kg, height 176±7 cm) walked at a total of nine combinations of three walking speeds (1.25, 1.75, and 2.0 m/s) and three different foot stiffness conditions – shoes only (k=7.2±1.3 N/mm), shoes with 1.6mm carbon fiber insoles (32.4±8.7 N/mm), and shoes with 3.2mm insoles (85.2±25.9 N/mm). Subjects completed data collection across two visits in a randomized order. In one visit, subjects walked for 7 minutes at each of the three stiffness and speed conditions (9 total conditions), while breath-by-breath gas exchange measurements recorded metabolic cost (Parvo Medics, UT). For the other visit, subjects performed the nine walking conditions while three-dimensional limb kinematic data (VICON, Oxford, UK) and kinetic data through an instrumented treadmill (Bertec, Columbus, OH) were recorded.

Additionally, subjects wore electromyography sensors (Delsys, MA) recording muscle activity of the soleus, medial/lateral gastrocnemius, and tibialis anterior muscles of the left leg. Lastly, an ultrasound probe (Telemed, UK) placed on the right leg captured *in vivo* soleus muscle contractions over time. Two-way repeated measures ANOVA tests were used to determine significant main effects of added foot stiffness and walking speed on the outcome measures of peak ankle plantarflexion moment, ankle work, gear ratio, and metabolic cost.

RESULTS/DISCUSSION

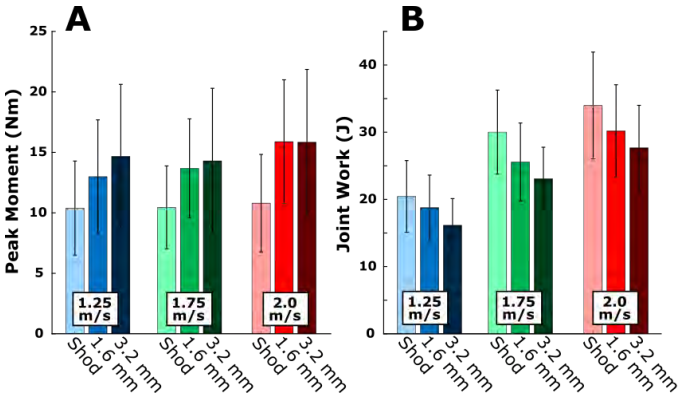

Figure 1: Peak ankle plantarflexion moment (A) and ankle positive work (B) over stride across speed/stiffness conditions (N=15).

We found a significant increase in ankle plantarflexion moment at faster walking speeds ($p=0.023$) and with added stiffness ($p<0.001$) (Fig. 1A). Ankle positive work increased at faster walk speeds ($p<0.001$), but decreased with added stiffness ($p<0.001$) (Fig. 1B). This simultaneous increase in ankle plantarflexion moment and decrease in ankle joint work (with added foot stiffness) likely supports the hypothesis that the force-velocity operating region of the plantarflexors has shifted to a slower shortening speed. We are currently processing the ultrasound imaging data of the soleus muscle to confirm this hypothesis. This is also corroborated by gear ratio increasing an average of 15.4% between shod and 3.2mm insole conditions ($p<0.001$).

We found a significant main effect of speed ($p<0.001$) but not stiffness ($p=0.068$) on metabolic cost (Fig. 2), and a significant stiffness*speed interaction ($p<0.001$). One-factor repeated measures ANOVAs performed at each speed revealed that stiffness had a significant effect at 1.25 ($p=0.005$) and 2.0 m/s ($p=0.027$) speeds, but not at 1.75 m/s ($p=0.173$). At 1.25 m/s, 3.2mm carbon fiber insoles increased metabolic cost by 9.6%, while at 2.0 m/s, the same insoles decreased cost by 7.1%.

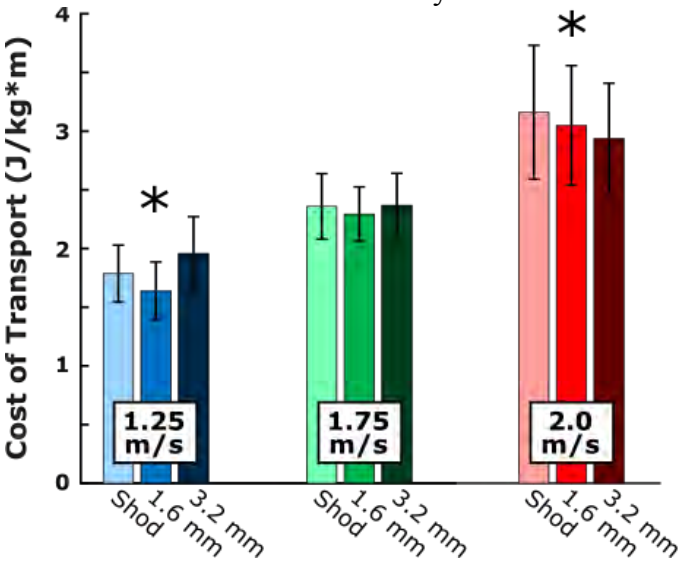

Figure 2: Metabolic cost of transport across speed/stiffness conditions (N=15) (* = denotes a significant effect of stiffness within a speed condition, $p<0.05$).

CONCLUSIONS

This study utilized a simple, passive device (i.e., insoles) that takes advantage of ankle-foot gearing effect to reduce the metabolic cost of fast walking by 7.1%, comparable to results garnered by passive ankle exoskeleton devices at normal speed [9].

REFERENCES

1. Farris DJ and Sawicki GS (2012a). *J. R. Soc. Interface* **9**, 110–118.
2. Kram R and Taylor CR (1990). *Nature* **346**, 265–267.
3. Hill AV (1953). *Proc. R. Soc. Lond. B Biol. Sci.* **902**, 104-195.
4. Ishikawa M et al. (2005). *J Appl Phys*, **99**(2), 603-608.
5. Carrier DR et al. (1994). *Science*. **265**. 651-653
6. Takahashi KZ et al. (2016). *Sci. Rep.* **6:29870**
7. Neptune RR and Sasaki K. (2005). *J. Exp. Biol*. **208**, 799–808.
8. Farris DJ and Sawicki GS (2012b) *Proc. Natl. Acad. Sci. U. S. A.* **109**, 977–982.
9. Collins SH et al. (2015). *Nature*. **522**(7555) 212-215

ACKNOWLEDGEMENTS

This work was supported by the Center for Research in Human Movement Variability of University of Nebraska at Omaha, NIH (P20GM109090).

Wearable Technology Measures Manual Tactile Forces during Activities of Daily Living

[1] Michael Riddle, [1]Kevin MacDermid-Watts, [1]Sara Holland [1]Emily Lalone, [1,2]Joy MacDermid and [1,2] Louis Ferreira

[1] Western University, London, ON, Canada
[2] Hand and Upper Limb Centre, St. Joseph's Hospital, London, ON, Canada
Email: mriddle@uwo.ca

INTRODUCTION

Hand Osteoarthritis (H-OA) affects approximately 10% of the population and results in pain and stiffness of the fingers [1, 2]. Clinicians often prescribe Joint Protection Programs (JPP), self-management strategies to manage hand pain and deformity during the performance of activities of daily living (ADL). Current JPP offer outdated recommendations and are not evidence based or definitively described in literature.

In order to develop and improved JPP, finger forces experienced during various ADL need to be established. However, current methods for determining the applied forces in the hand during activities of daily living rely on the use of grip dynamometers or force-measurement gloves. These tools however are limited in their ability to isolate individual finger forces and interfere with the sense of touch. Therefore, the objective of this study was to develop a portable measuring system that would be able to measure individual finger forces during activities of daily living and that would not occlude the volar dermis and interfere with physiological tactile sensation.

METHODS

Tactile finger force sensors were created to measure the applied load in the fingers during five activities of daily living involving the hand. Foil-type strain gauges (350 Ohm wired in a quarter-bridge circuit) were secured to an acrylic nail substrate and attached to the finger nails of the thumb, index, ring, and middle fingers and on the radial and ulnar side of the middle phalanges of the index and ring fingers (Fig. 1).

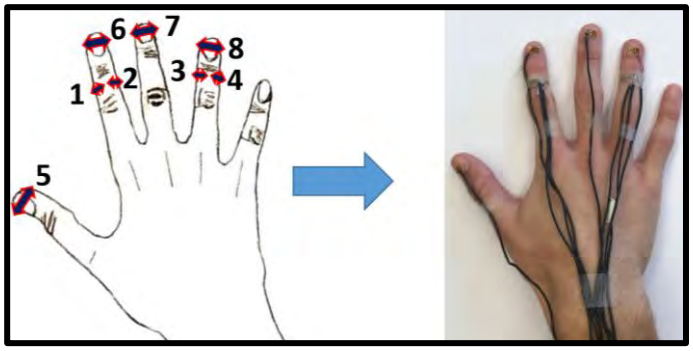

Figure 1: A total of eight sensors were placed on the dominant hand of each participant. The arrows in the sketch on the left indicate the measurement axis of the sensors, as they measure transverse bending strains on the nail and middle phalanges dorsal aspects.

Each strain gauge sensor was calibrated using a load cell to allow for the conversion of microstrain to forces (N). Eight healthy control participants (four female: 21-55 years old, four male: 22-52 years old) were recruited for testing. Tasks were chosen to include power and precision grip as well as point loading of individual fingers and included: zipper, snap button, pouring a kettle, opening a jar, and press button microwave.

RESULTS AND DISCUSSION

From the calibration technique used for each of the tactile sensors, a function was created to convert the microstrain data recorded for each activity to force data to allow for comparisons of applied forced during the activities performed (Fig. 2). The sensors were found to be sensitive enough to measure forces as small as 0.17 N and did not saturate during high force tasks (above 15N). For the precision grip tasks, the highest forces occurred in the thumb and index finger (42% of the overall measured force for the zipper and 31% in the snap button. Conversely, for the power grip tasks, the force was distributed

primarily to the fingertips/phalanges depending on the task. For the pouring task, 60% of the overall force was in the phalanges, and 62% was in the fingertips for the jar. This preliminary data demonstrates the tactile sensors ability to reliably distinguish which fingers/segments are used in various tasks.

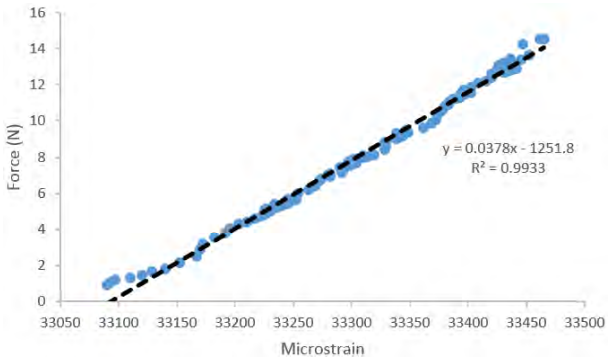

Figure 2. Each sensor was calibrated after being installed on the subject. Subjects were instructed to press each finger instrumented finger segment against a load cell with up to 15 N of force on their volar surface. Force output in Newtons from the load cell was synchronized with microstrain from the finger sensor to produce a calibration equation, which was used subsequently to convert the microstrain data from all trials into units of force. The fit for this sensor was linear with and R^2 value of 0.993.

The system used in this study provides a new type of low-cost wearable technology to monitor forces in the hands without interfering with the contact surface of the hand. They are able to measure applied forces throughout the full range of forces expected during normal activity and are able to provide information about finger recruitment and the use of different finger segments during activities. This will provide clinicians with quantifiable measurements of finger forces to provide objective treatment plans for patients with H-OA and other hand problems.

CONCLUSIONS

These sensors applied to the dorsal aspect of the fingers are capable of providing quantifiable measurements of finger contact forces during functional tasks without occluding the volar dermis and address a number of issues with current measurement devices. With continued work being performed to improve the calibration process, these sensors will find several applications in quantifying touch and dexterity.

Future work with these sensors will involve determining the effectiveness of JPP at reducing forces in the hands during the performance of a variety of ADL in individuals with osteoarthritis. This data will allow hand therapists to develop and updated, evidence-based JPP for patients with osteoarthritis.

REFERENCES

1. Haugen et al. *Annals of Rheumatic Diseases*. **70(9)**.
2. Chen et al. *Gait and Posture*. **32(4)**.

ACKNOWLEDGEMENTS

This research was funded by The Arthritis Society. This study was approved by the Health Science Research Ethics Board at Western University (protocol ID no. 108625).

Reliability of Radiographic Evidence of Glenohumeral Subluxation and the Relationship to Shoulder Joint Motion

[1] Matt Topley, [2] Stephanie Russo, [1]Elizabeth Rapp van Roden, [3]R. Tyler Richardson, [4]Ross Chafetz, [4]Scott Kozin, [4]Dan Zlotolow, [1]Jim Richards

[1] University of Delaware, Newark, DE, USA
[2] UPMC Hamot, Pittsburgh, PA, USA
[3] Pennsylvania State University Harrisburg, Middletown, PA, USA
[4]Shriners Hospital for Children Philadelphia, Philadelphia, PA, USA
email: topley@udel.edu

INTRODUCTION

Brachial plexus birth injuries (BPBI) cause long-term effects in approximately 1 of every 1000 live births[12]. Deficits include range of motion limitations and glenohumeral (GH) dysplasia, marked by deformity of the glenoid, deformity of the humeral head, and posterior subluxation of the humerus. Internal rotation contractures of the shoulder are common among children with BPBI and are associated with development of GH dysplasia[3–5].

Management goals for children with BPBI include preventing, halting, or reversing GH dysplasia. Surgical options include anterior GH joint releases and tendon transfers of latissimus dorsi and teres major or teres major alone. The amounts of correction and/or recurrence of GH dysplasia are thought to be variable. The prevailing theory is that a more congruent GH joint will result in better joint function than a less congruent GH joint, so the patients who present with less congruent joints post-surgery are expected to exhibit more severe limitations in joint function, especially the ability to abduct or elevate the humerus[4]. We hypothesized that patients with mild, moderate, and severe GH dysplasia would demonstrate differences in GH and humerothoracic (HT) elevation.

METHODS

Forty-nine children with BPBI (age 8.9 +/- 4.1 years, 22 male, 27 female) who previously had transfer of latissimus dorsi and teres major or teres major alone along with closed or surgical GH reduction were recruited for this study. A three-dimensional motion capture system was utilized to measure GH and HT joint angles in the 15 positions listed in Table 1. The GH and HT elevation displacements from the neutral position to each of the tested motions were calculated. An axillary radiograph of the shoulder was also obtained. Motion capture was completed within one year of radiographic evaluation.

To classify the severity of the GH dysplasia, two hand surgeons used a modified classification for GH dysplasia based on Waters et al. (1998). The scale was organized into three categories: mild, moderate, and severe (Figure 1). The mild category is represented by the A2 image of a concentric glenoid, the moderate category is represented by the A1 or B1 images of a flat glenoid and/or posterior subluxation, and the severe category was represented by the B2 or C images as a biconcave or pseudoglenoid fossa.

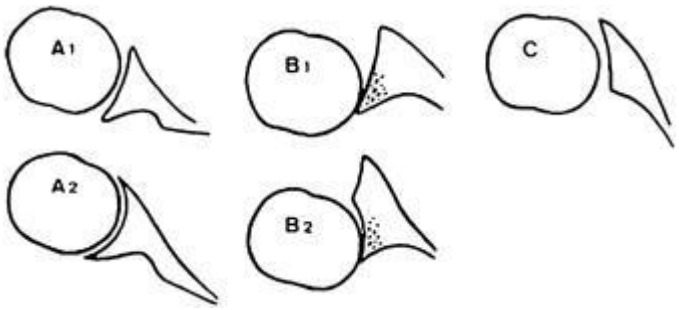

Figure 1: Modified Waters classification of glenohumeral dysplasia[6].

The surgeons independently reviewed the axillary shoulder x-rays and graded the severity of the GH deformity. Approximately two weeks later, the image order was randomized and images were independently reviewed a second time. The scores were then compared using polychoric correlation to determine inter and intra-rater reliability.

The GH and HT elevation displacements for each of the 15 positions yielded 28 variables. Therefore, a backward stepwise discriminate function analysis (DFA) was used to reduce the number of variables by determining a combination, if any, that could differentiate GH dysplasia group membership (mild, moderate, or severe).

RESULTS AND DISCUSSION

The inter- and intra-rater reliability showed strong correlations between the surgeons' first viewings and their second viewings. Surgeons 1 and 2 had intra-rater correlations of .869 and .986, respectively, and inter-rater correlations of 0.777 on the first reading, and 0.998 on the second reading. The inter/intra-rater correlations suggest that x-rays were consistently categorized by experienced hand surgeons into categories of dysplasia based on a modified Waters et al. (1998) classification. For this study, the second readings were used to categorize subjects into dysplasia groups.

The DFA produced two significant functions containing 17 variables. Sixty-eight percent of cases were correctly identified in a "leave one out" cross-validation analysis. Seventy-one percent of the mild cases, 71% of the moderate cases, and 62% of the severe cases were correctly identified.

Results of the DFA indicate that subjects exhibiting different levels of GH dysplasia can be differentiated by the ability to elevate their GH joint and humerus. Unexpectedly, when elevation displacements were averaged across all variables in the DFA, the mild group displayed the smallest average displacement at 33.7º, and the severe group displayed the greatest displacement at 42.9º. The moderate group showed 35.4º of displacement.

CONCLUSIONS

Radiographic assessment of GH joint dysplasia severity demonstrated high inter- and intra-rater reliability. Additionally, GH and HT elevation displacements from the positions tested in this study were found to be associated with and predictive of GH dysplasia severity. Surprisingly, there was an inverse relationship between GH dysplasia severity and GH and HT elevation displacements. Children with severe GH dysplasia demonstrated, on average, the largest GH and HT elevation displacements. Further investigations are needed to better define the relationship between GH joint preservation procedures and functional outcomes.

REFERENCES

1. Buterbaugh KL, Shah AS. *Curr Rev Musculoskelet Med*. 2016;9(**4**).
2. Hoeksma AF, Wolf H, Oei SL.*Clin Rehabil*. 2000;14(**5**)
3. Pearl ML, Edgerton BW. *J Bone Joint Surg Am*. 1998;80(**5**)
4. Kozin SH. *J Hand Surg Am*. 2011;36(**8**)
5. Kozin SH. *J Pediatr Orthop*. 2004;24(**2**)
6. Walch G, Badet R, Boulahia A, Khoury A. *J Arthroplasty*. 1999;14(**6**).

Table 1: Functional Positions used for Analysis

Pos	Description	Pos	Description	Pos	Description
1	Neutral position with arm by side	6	Full internal rotation at 90º abduction	11	Forward reach
2	Full abduction in coronal plane	7	Full external rotation at 90º abduction	12	Hand to nape of neck
3	Full external rotation at 0º abduction	8	Full humeral elevation	13	Full humeral extension
4	Full internal rotation at 0º abduction	9	Full humeral flexion	14	Abduction in the scapular plane at 45º
5	Hand to most superior point on spine	10	Hand to mouth	15	Full abduction in the scapular plane

THE ROLE OF CYCLE-TO-CYCLE VARIABILITY IN THE DEVELOPMENT OF SHOULDER PAIN IN MANUAL WHEELCHAIR USERS

[1] Shelby L. Walford, [2] Philip S. Requejo, [2] Sara J. Mulroy, and [1] Richard R. Neptune

[1] The University of Texas at Austin, Austin, TX, USA
[2] Rancho Los Amigos National Rehabilitation Center, Downey, CA, USA
email: shelbywalford@utexas.edu, web: http://www.me.utexas.edu/~neptune/

INTRODUCTION

There are currently 3.2 million manual wheelchair users in the United States [1,2]. Because of the consistently high muscle demand on the upper limbs during manual wheelchair propulsion, shoulder pain and injury are prevalent, which often leads to a decreased quality of life [3]. Studies have shown that wheelchair users with shoulder pain have lower cycle-to-cycle variability in peak total shoulder joint force [4], peak total handrim force and push time [5]. Although recent work has shown differences in intra-individual variability between groups of wheelchair users with and without shoulder pain [4,5], it is not yet known if variability is a predictor of shoulder pain development.

The purpose of this study was to determine whether cycle-to-cycle variability in manual wheelchair propulsion is a predictor of the development of shoulder pain. Specifically, we hypothesized that those with lower variability are likely to develop future shoulder pain.

METHODS

Experimental data from 102 subjects with paraplegia were analyzed (93 men; age: 36.2±9.6 yrs; time from injury: 9.5±6.5 yrs; height: 1.74±0.09 m; mass: 73.9±15.9 kg). All subjects were initially free of upper extremity pain and participated in three lab visits at 0, 18 and 36 months. During each visit, subjects self-reported shoulder pain, which placed them into either a "pain" or "no pain" group. Participants propelled their own wheelchair on a stationary ergometer for a 10-sec trial at their comfortable, self-selected speed. Kinematic data from the wheel, trunk and right upper extremity were recorded using a 4-scanner CODA motion analysis system at 100 Hz (Charnwood Dynamics Ltd.). Right-side handrim forces were collected using an instrumented handrim (SmartWheel; Three Rivers Holdings) at 200 Hz, which allowed identification of the propulsion cycle contact and recovery phases. A transition phase was identified as the last 10% of contact and first 10% of recovery. Joint kinetics were calculated using inverse dynamics in Visual 3D (C-Motion, Inc.) and normalized by bodyweight.

Spatiotemporal, joint kinematics and kinetics and handrim kinetic variables were exported and analyzed with custom Matlab code (Mathworks Inc.). Cycle-to-cycle variability was measured for each subject by calculating the absolute variability as standard deviation (SD) and relative variability as coefficient of variation (CV=SD/mean*100) of the shoulder joint ranges of motion, handrim forces, contact time, angle and percentage, net radial thickness (NRT) and total radial thickness (TRT) [6], peak and average moments about the shoulder joint, and positive and negative shoulder joint work. All joint kinetic parameters were analyzed over the full cycle as well as in the contact, transition and recovery phases.

To determine which parameters predict shoulder pain development, a forward stepwise binary logistic regression was conducted in SPSS Statistics (SPSS Inc.). The p-value for entry was 0.05 and the p-value for removal was 0.10.

RESULTS AND DISCUSSION

The variables in the final logistic regression model that significantly predicted shoulder pain development were plane of elevation ROM CV ($p=0.007$), average radial force CV ($p=0.005$), average fraction effective force (FEF) CV ($p=0.022$), positive shoulder joint work CV ($p=0.010$), and flexion/extension moment about the shoulder joint SD during the contact phase ($p=0.044$) (Table 1). The model was statistically significant ($p<0.001$), and explained 41.8% (Nagelkerke R^2) of the variance in the development of shoulder pain. Those who would

develop shoulder pain had more cycle-to-cycle variability in the plane of elevation ROM (CV) and positive shoulder joint work (CV) and less cycle-to-cycle variability in the minimum trunk angle (CV), average radial force (CV), average FEF (CV) and average flexion/extension moment about the shoulder joint during the contact phase (SD).

In support of our hypothesis, three of the five predictors of shoulder pain were higher in the no-pain group than the pain group. These variables are all kinetic measures, suggesting that applying force to the handrim in a more variable manner, which in turn should increase variability in the shoulder reaction moment, might help decrease the likelihood of developing shoulder pain.

Contrary to our hypothesis, the plane of elevation ROM CV and positive shoulder joint work CV were higher in individuals who developed shoulder pain. To our knowledge, variability of shoulder joint kinematics has not yet been assessed in manual wheelchair propulsion. One study analyzed the kinematic spatial variability of the wrist motion and found that intra-individual variability was higher in those who currently had shoulder pain [7]. This finding may be related to our kinematic measure of plane of elevation ROM CV being higher in individuals who will develop shoulder pain.

It is unclear why the variability in positive shoulder joint work is higher in individuals who develop shoulder pain. A potential limitation of this study was that we assessed variability during a short time period (10-sec trial). Future work should assess variability across a longer time period to see if the relationship between the short-term cycle-to-cycle variability and the development of shoulder pain still holds. Additionally, because of the small group mean differences, future work is needed to determine if differences in shoulder joint work variability are clinically meaningful.

CONCLUSIONS

These results suggest that relative variability (CV) of the plane of elevation ROM, average radial force, average FEF, positive shoulder joint work and absolute variability (SD) of the average flexion/extension moment during contact are important predictors of shoulder pain development. In general, these results suggest that using more variable force application might decrease the risk of developing shoulder pain. However, future work is needed to analyze variability over a longer time period to see if these same relationships hold.

REFERENCES

1. Brault, *Americans with disabilities: 2010,* Washington, D.C, 2012.
2. Kaye, et al. *Mobility Device Use in the United States Disability Statistics Report*. Washington, D.C, 2000.
3. Requejo, et al., *Top Spinal Cord Inj Rehabil* **13**, 86-119, 2008.
4. Moon, et al., *Clin Biomech* **28**, 967-972, 2013.
5. Rice, et al. *Arch of Phys Med and Rehabil* **95**, 699-704, 2014.
6. Slowik et al., *Clin Biomech* **30**, 927-932, 2015.
7. Jayaraman et al., *PLoS One* **9**, e89794, 2014.

ACKNOWLEDGEMENTS

This study was supported by NIH Grant R01 HD049774.

Table 1: Variables included in the final regression model. '*' indicates a significant correlation. Group averages are mean ± SD. Moment SD is normalized by bodyweight (e.g. N-mm/N).

	β Estimate	p-value	No Pain Group Average	Pain Group Average
Plane of Elevation ROM CV [%]*	0.257	0.007*	5.630 ± 2.918	6.756 ± 4.701
Minimum Trunk Angle CV [%]	0.073	0.050	-8.905 ± 20.549	5.829 ± 40.070
Average F_{rad} CV [%]*	0.138	0.005*	-16.831 ± 12.766	-11.274 ± 5.770
Average FEF CV [%]*	-0.030	0.022*	56.765 ± 41.109	48.411 ± 26.365
Positive Shoulder Joint Work CV [%]*	0.153	0.010*	12.006 ± 4.792	13.128 ± 6.234
Average Flexion/Extension Moment during Contact SD [mm]*	-1.309	0.044*	1.328 ± 0.560	1.223 ± 0.459
Intercept	0.878	0.407		

THE EFFECTS OF FOOTWEAR ON BARBELL BACK SQUAT MECHANICS IN EXPEREIENCED FEMALE SQUATTERS

Sara J. Walker, Vanessa Kellems, Ashley Alunan and Jeremy D. Smith

University of Northern Colorado, Greeley, CO, USA
email: sara.walker@unco.edu

INTRODUCTION

The barbell back squat is a key component in competitive powerlifting, athletic performance development, and rehabilitation. Manipulating footwear is one way to aid in performance and reduce injury risk during squatting [1,2]. The most common footwear conditions are traditional athletic shoes, barefoot, and weightlifting shoes. Weightlifting shoes are costly, which may discourage recreational lifters from using them. A simple heel lift may be an inexpensive alternative to weightlifting shoes if the heel lift results in similar lifting mechanics. Weightlifting shoes during squatting, reduce anterior trunk lean, maintain a more vertical shank position, increase knee flexion, decrease ankle dorsiflexion, and increase excitation of the quadriceps muscles [2]. Barefoot squatting results in significantly less squat depth, knee flexion, and rectus femoris activation, accompanied by a greater forward trunk lean [1]. The purpose of this study was to determine whether squat mechanics were similar between athletic shoes, barefoot, and a simulated heel-lift condition.

METHODS

Recreationally trained females (n =15, 24 ± 3 years, 1.67 ± 0.06 m, 65.77 ± 9.20 kg) with at least 5 years of squatting experience participated in the study. At visit 1 the participants completed a 1 repetition maximum test (1RM). During visit 2, a 20 kg barbell was loaded to 60% of the predetermined 1RM. Retroreflective markers were placed bilaterally on the participant using a full-body cluster marker set. Markers were also placed on each end of the barbell to track bar velocity. Participants completed five repetitions of the three conditions in a randomized order (barefoot = BF, shod = SH, and heel-lift = HL) with a constant base of support. The barefoot condition was done without socks. For the shod condition, participants were instructed to bring their own athletic shoes. The heel-lift condition was done with the participants placing their heels on a 2.8 cm heel-lift, while wearing their own althletic shoes to simulate the average height of a weightlifting shoe. Throughout data collection, velocity of movement was not controlled as this may have been a possible difference between shoe conditions. For each condition, force data were collected with the participants placing one foot on a seperate force plate embedded in the floor (2000 Hz, AMTI, Watertown, MA). Motion data were also collected using a 10-camera motion capture system (100 Hz, VICON, Englewood, CO)..

Using a recursive Butterworth digital filter, marker position coordinates (Fc = 6 Hz) and ground reaction forces (Fc = 10 Hz) were filtered in Visual 3D (C-Motion). The middle three squats of each condition were used for analysis. All lower extremity data analyses were performed on the right limb. For each dependent variable, a series of one factor (footwear with three levels: barefoot, heel-lift, or shod) ANOVAs with repeated measures were used to test for differences among footwear conditions (α = 0.05). Post-hoc analysis with a Bonferroni adjustment was used to determine where differences occurred when the ANOVA was significant.

RESULTS AND DISCUSSION

Bar velocity was not significantly different between conditions or between ascent and descent phases of the squat. Squatting with a HL resulted in reduced peak ankle dorsiflexion compared to SH and BF. BF squatting significantly decreased peak knee flexion in comparison to both the SH and HL conditions. There were no significant differences observed at the hip or trunk. The only significant finding in the joint angular velocity data occurred during squat ascent, where BF squatting resulted in a decreased ankle angular velocity compared to SH (Figure 1).

Squatting with a HL significantly decreased the peak ankle dorsiflexor moment compared to SH, but not compared to BF (Figure 1). The peak knee extensor moment increased significantly using the HL in comparison to both SH and BF (Figure 1). In addition, knee power generation with the HL was greater during ascent compared to BF. During squat descent, SH produced a significantly more negative joint work at the ankle than HL. Positive work at the knee was also greater in the HL during ascent compared to BF.

In comparing squat depth, our results were consistent with previous literature in that BF squatting resulted in decreased squat depth and knee flexion [1]. Since the knee extensors are a targeted muscle group in this lift, this would imply BF squatting decreases the effectiveness of the back squat as a training exercise for the quadriceps. In comparing our HL data to existing results from weightlifting shoes, both conditions resulted in increased max knee flexion and squat depth [2]. In addition, the HL in this study and previous literature utilizing weightlifting shoes both led to less ankle dorsiflexion [2]. The increased knee moment and increased positive knee work observed in the HL condition observed in the current study, suggests a greater involvement of the knee extensors when using a HL. This is consistent with previous weightlifting shoe research that observed an increase in knee extensor moment in weightlifting shoes compared to athletic shoes [2].

In conclusion, squatting with a heel-lift placed more emphasis on the knee extensors to produce power, while squatting barefoot relied less on the knee and more on the ankle. As the quadriceps are the primarily muscles being targeted in this lift and the magnitudes of the joint kinetics at the knee are within safe ranges, squatting with a heel-lift is more beneficial than squatting barefoot or shod. Finally, squatting using a low cost heel-lift produces many of the same positive outcomes on mechanics that are associated with expensive weightlifting shoes

REFERENCES

1. Sato et al. *Journal of Strength and Conditioning.* **26(1)**, 2012.
2. Legg et al. *Journal of Sports Science*. **35(5),** 2017.

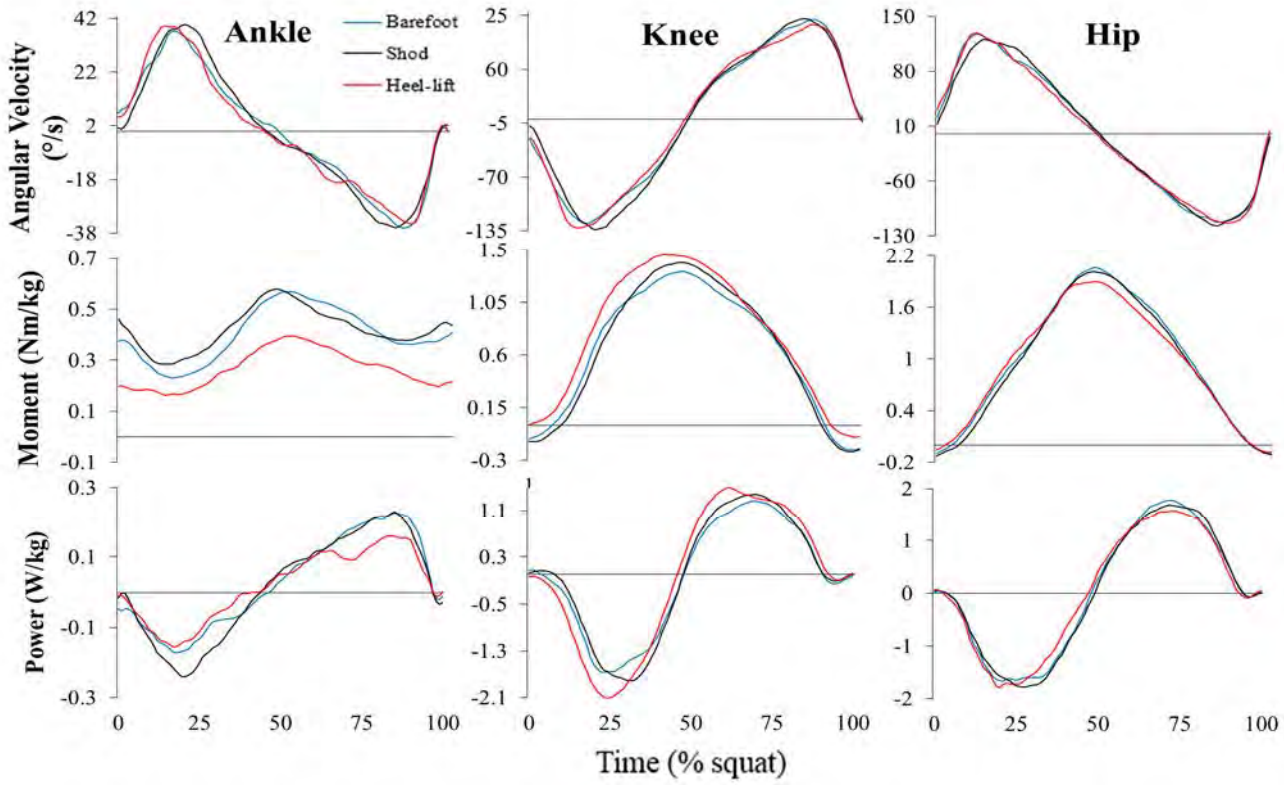

Figure 1: Graphs represents group averages across squats for angular velocity, joint moment, and joint power over percent squat cycle for the right leg.

UTILIZING INERTIAL SENSORS TO EVALUATE HUMAN WALKING DURING A LONG OUTDOOR FOOT MARCH

[1] Rachel Wathen, [2] Clifford Hancock, [1] Rachel Vitali, [1] Stephen Cain,
[1] Noel Perkins and [1] Lauro Ojeda

[1] University of Michigan, Ann Arbor, MI, USA
[2] U.S. Army Natick Soldier Research, Development and Engineering Center, Natick, MA, USA
email: rwathen@umich.edu

INTRODUCTION

Understanding human walking performance in naturalistic environments is challenging as it remains difficult to measure human gait outdoors and on unknown and variable terrain. Nevertheless, there is ample motivation for doing so and particularly to understand the performance of warfighters who walk and operate on rugged outdoor terrain [1]. Laboratory experiments may not produce realistic results for understanding outdoor walking performance as demonstrated in [2]. A promising approach for measuring outdoor gait and thus understanding outdoor walking performance rests on the use of using foot-mounted inertial measurement units (IMUs) to deduce gait parameters.

IMUs are portable, unobtrusive, and unconstrained (e.g. do not need external references) measurement devices that incorporate accelerometers and angular rate gyros (and sometimes can be augmented by magnetometers and GPS). While IMUs provide reasonably accurate measurements of angular velocity and linear acceleration, further estimates of velocity and position suffer from several error sources (e.g. bias instability, scale factor errors, g-sensitivity, and temperature sensitivity). However, when IMUs are mounted to the feet, errors in velocity (and thus position) can be minimized by exploiting the fact that the feet achieve zero velocity at specific times during the stance phase. Estimation methods that embed this kinematic constraint are often referred to as zero velocity update (ZUPT) methods [3].

In this study, we employ the ZUPT strategy in custom algorithms that accurately estimate foot trajectories and relevant gait parameters. Specifically, we estimate stride length and width [3] in the context of a long outdoor march. The objective of this study is to further explore if the estimated stride length and width may reveal indicators of fatigue during a long (3-mile) foot march. We hypothesize that there may be increases in the variability of stride length or width at the end of the march compared to the beginning which may be indicators of fatigue [4].

METHODS

This study uses data from 11 young male participants (all infantrymen, age 23 ± 3.4 years, weight 82.1 ± 12.1 kg, height 1.78 ± 0.06 m) in a study conducted by the Natick Soldier Research Development and Engineering Center (NSRDEC). All participants provided written consent prior to testing which was approved by the United States Army Research Institute of Environmental Medicine institutional review board in Natick, MA. IMU data loggers (Opals, APDM, Portland OR) were attached to the feet of each subject used for this study and a third one attached to the sternum. The subjects individually walked a 3-mile outdoor march in approximately one hour. March speed was monitored by GPS watches (Garmin, USA) and was maintained at 3 mph. Checkpoints with study staff located at every mile and signposts displayed elapsed time and distance at every quarter mile also helped ensure participants maintained pace. Estimated foot trajectories were derived from the IMU data using a previously validated algorithm [3]. The algorithm uses the gyroscope and accelerometer data to estimate IMU orientation, and then integrates the acceleration data to estimate foot velocity and position. Drift and other inertial sensor errors were reduced by applying the aforementioned ZUPT algorithm [3].

Using the computed foot trajectory and orientation estimates, the data is segmented into individual strides. A stride is defined as the foot motion that occurs between two footfalls of the same foot [5]. For each stride, we define a local frame with the forward direction determined by the best fit (least squares) line through three successive footfalls. Each foot trajectory is examined with respect to this local frame to study the variation of the stride length (forward distance) and width (lateral distance); see Fig 1. We pool left and right foot strides assuming left and right stride symmetry.

To eliminate the confounding influences of sloped and curved portions of the course, we examine 100 seconds of data only from straight and level portions at the start and end of the march. We then test for differences in the mean and standard deviations of the (normally-distributed) of the stride parameters from the start versus the end of the march using paired t-tests with significance defined by $\alpha = 0.05$.

RESULTS AND DISCUSSION

The mean and standard deviation of the stride length at the start of the march are not significantly different from those at the end ($t(20) = -0.009$, $p = 0.99$ and $t(20) = -0.259$, $p = 0.80$, respectively); these results are expected since the march was paced. The mean stride width showed no significant difference ($t(20) = 0.005$, $p = 0.99$), since the data being analyzed was taken from a straight path this is to be expected. However, the standard deviation of stride width is nearing significance ($t(20) = -1.905$, $p = 0.07$) which suggests that it may be indicative of fatigue. This is a preliminary finding however and further studies should seek to validate this finding through independent measures of fatigue (e.g. VO2 max) as well as the significance of variation in stride length or width during walking that is not paced. If the standard deviation of stride width is successfully validated as a fatigue indicator, this measure could act as an input into an overall soldier physical status. Alternatively, this measure, along with other performance indicators, could help the Army better assess the impact of newly developed individual equipment on the soldier.

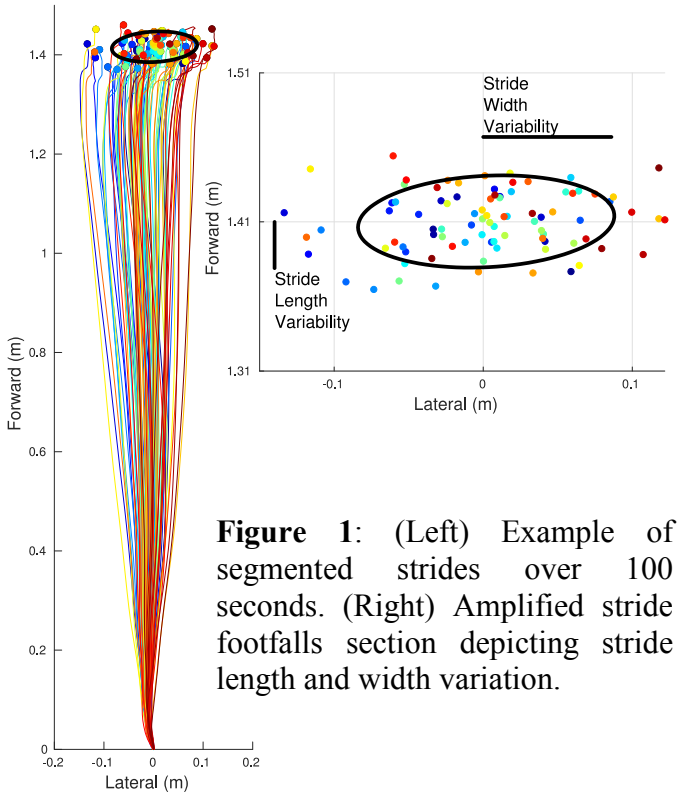

Figure 1: (Left) Example of segmented strides over 100 seconds. (Right) Amplified stride footfalls section depicting stride length and width variation.

REFERENCES

1. Hancock and Hasselquist, *ASB 2017*, Boulder, CO, USA, 2017.
2. Ojeda et al., *Med Eng Phys* 37(10): 929-936, 2015.
3. Ojeda and Borenstein, *J of Nav* 60(3): 391-407, 2007.
4. Qu and Yeo, J Biomechanics, 44(7): 1259-1263, 2011
5. Rebula, et al., *Gait Posture*, 38(4): 974-980, 2013.

ACKNOWLEDGEMENTS

This material is based upon work supported by the US Army Contracting Command-APG, Natick Contracting Division, Natick, MA, under contract W911QY-15-C-0053.

CENTER OF MASS MOTION DURING SIT-TO-STAND CHANGES THROUGH PREGNANCY

Sandra Alejandre-Rios and Robert D. Catena

Washington State University, Pullman, WA, USA
email: robert.catena@wsu.edu, web: http://labs.wsu.edu/biomechanics/

INTRODUCTION

Pregnant women experience physiological changes over the course of several months, which are thought to affect their standing balance and ability to perform daily activities [1]. Understanding balance related performance changes through pregnancy are crucial since falls are one of the main causes of injury during pregnancy [2]. Both joint kinematics and kinetics have been found to change during sit-to-stand (STS) motions. Trunk flexion becomes a more difficult task because abdominal volume increases, especially in the third trimester [3]. Consequently, pregnant women shift from greater hip flexion moments in the 1st trimester of pregnancy to greater knee flexion moments in the 3rd trimester [3]. However, these previous studies have eluded to the STS being a symmetric action through pregnancy without investigating movement outside of the sagittal plane.

We have previously developed a method to determine the person-specific COM during pregnancy [4]. In this current study, we examined how that center of mass (COM) motion changes in the STS over the course pregnancy. We were particularly interested in asymmetric lateral COM motions since these could indicate inefficient energy expenditure, the potential for loss of balance during STS, and a potential for increases in low-back injury.

METHODS

We have currently completed, and present here, the results of 5 women tested five times in 4-week intervals from 16 to 36 weeks gestation (1st: 16-20, 2nd: 20-24, 3rd: 24-28, 4th: 28-32, and 5th: 32-36).

Participants had body anthropometry measured to determine the individual masses of 13 body segments [5]. They then had 54 reflective markers placed on the body and performed a quite standing trial and a laying trial with markers tracked by a 10-camera motion capture system (MotionAnalysis Corp) to allow us to calculate COM locations of the 13 body segments [4]. In between standing and laying trials, they performed STS at a self-selected pace using a 45 cm height chair on a force plate. They repeated the movement for 60 seconds, pausing when they were both fully standing and quietly sitting for a second so that any rocking momentum was negated.

All markers were tracked at 100 Hz and filtered with a 6 Hz 4th order low-pass Butterworth filter. The body COM was calculated from the weighted-sum of the 13 body segments throughout the STS trial. The first seven STS cycles for each participant were split into 2 phases, before (STS1) and after (STS2) the moment of seat-off, as measured by the force plate under the seat. The average times to complete each phase were measured as dependent variables. The COM linear ranges of motion and peak velocities in three orthogonal directions were used as dependent variables. We also calculated the average coefficient of variation (COV) in lateral motion during each phase.

Four-week intervals of gestation were used as the independent variable. Dependent variable change over time was measured with a repeated-measures general linear model analysis, and follow-up pairwise comparisons with *Bonferonni* adjustments (alpha = 0.05).

RESULTS AND DISCUSSION

STS1

The amount of time to complete the STS1 significantly increased from the 1st to 3rd testings. The lateral COM range of motion (Table 1.) and peak velocity increased from the 1st to 4th testings. The upward peak velocity also increased during this time. In contrast, the anterior COM motion decreased from the 3rd testing to the 5th testing. In fact, all motions and velocities appear to decrease at the last testing.

STS2

Phase 2 of the STS also took significantly longer from 1st to 3rd testings, and increased again in the last test compared to previous testings. Lateral COM motion (range and COV) in STS2 displayed a similar pattern as STS1 (Table1): they increased to the 4th testing, and then decreased in the 5th testing. Vertical velocity in rising from the chair followed this same pattern over time.

There appear to be two unique phenomena occurring over time that result in the statistically significant changes described above. First, up to the beginning of the third trimester (4th testing), participants shifted from a symmetric forward motion to initiate standing to a lateral asymmetric rocking motion to initiate standing. This corresponded with significant volume increase in the torso. We believe that the change in strategy was adopted to provide sufficient momentum to push off the chair. Since the pregnant torso precludes enough trunk flexion to increase forward momentum, lateral rocking with limited trunk flexion creates enough forward momentum to rise from a chair later in pregnancy. Therefore, the adoption of a lateral COM rocking motion may be dependent on abdomen size, as not all women have similar abdominal change during pregnancy. This change in strategy can possibly increase the risk of balance changes and low back injury.

The second phenomena of reduced motion in the 5th testing corresponds with the time point of largest mass. We believe that at this time point, strength is particularly relied upon to complete the STS. Reduced motion in the 5th testing may be a result of insufficient strength to maintain normal STS motion. However, it is not clear why individuals would shift away from the rocking motion adopted in the 3rd and 4th testing to successfully complete the STS in the 5th testing. Lateral rocking seems like an appropriate alternative to generate assisting momentum even in the later stages of pregnancy. Perhaps lateral rocking became insufficient and a new method not analyzed here was adopted. This current analysis cannot discount a strategy shift that may include increased arm counter-reciprocal momentum to aid in propelling the body COM forward without relying merely on generating torso momentum. We also cannot discount a shift to generating upward momentum with hands pushing against the distal thighs. Our ongoing analyses will include a look at arm motions that correspond with our COM results.

CONCLUSIONS

Our results provide new perspectives on how pregnant women adapt to accomplish a common daily activity – the STS. The adaptation of lateral COM motions is beneficial in performance, but is not without potential consequence. Lateral COM motions can increase the possibility of a fall or the development of low back pain. Our findings clearly point out that the STS is increasingly asymmetric during pregnancy, and as such, future studies should consider the 3D nature during analyses.

REFERENCES

1. Takeda et al. *J. Phys. Ther. Sci.* 2012
2. Dunning et al. *Maternal Child Health J.*, 2010.
3. Lou et al. *Clinical Biomechanics*, 2001.
4. Catena et al. *J. Biomechanics,* in press.
5. Pavol et al. *J Biomechanics,* 2002.

ACKNOWLEDGEMENTS

The authors would like to acknowledge the help of Kathryn Lober, Hallie Music, Lexi Fredrickson, and Daniel Flores in data collection and processing.

Table 1: Average COM lateral range of motion (standard deviation) during each phase and each testing time.

	Testing time (weeks of gestation)					
Phase	**1st (16-20)**	**2nd (20-24)**	**3rd (24-28)**	**4th (28-32)**	**5th (32-36)**	**p-value**
STS1 (mm)	6.4 (3.6)	7.6 (4.2)	7.5 (3.9)	9.0 (4.6)	8.5 (3.9)	0.048
STS2 (mm)	11.8 (7.3)	9.9 (7.1)	10.0 (4.4)	12.1 (7.2)	8.4 (4.2)	0.025

The Effects of Hearing Loss on Gait Stability in Older Adults

[1]Tara Cornwell, [2,3]Jane Woodward, [1] Brennan Jackson, [2]Mengnan/Mary Wu, [3]Sumit Dhar, [3]Pamela Souza, [3]Jonathan Siegel, [2]Keith Gordon

[1] Northwestern University, Physical Therapy and Human Movement Sciences, Chicago, IL, USA
[2]Northwestern University, Physical Therapy and Human Movement Sciences, Chicago, IL, USA
[3] Northwestern University, Communication Sciences and Disorders, Chicago, IL, USA
[4]Shirley Ryan Ability Lab, Chicago, IL, USA
email: keith-gordon@northwestern.edu

INTRODUCTION

Cohort studies have identified a positive relationship between hearing loss and the probability of falling [1]. Even mild hearing loss (> 25 dB) is associated with a three-fold increase in fall rate [2]. Falls are the leading cause of fatal and non-fatal injuries in adults over the age of 65 [3], making it imperative to identify addressable fall risk factors. Currently, mechanisms linking hearing loss and falls are unclear. We examined the impact of auditory feedback on walking stability. **We hypothesized that self-generated sounds (e.g. footsteps) during walking enhance people's ability to locate their absolute and relative position in space**. These are critical factors for controlling walking stability. We also hypothesized that older adults who used gait-related auditory feedback to control stability would modify walking patterns in a manner consistent with a decreased ability to control their center of mass (COM) and limb trajectories when hearing is degraded. Specifically, when hearing ability is degraded we hypothesize that participants will increase lateral excursion of their COM, increase minimum lateral margins of stability, increase step width, and take shorter, faster steps.

METHODS

We observed walking in older adults without known hearing deficits during conditions that degraded hearing. We performed clinical tests to screen for visual and hearing acuity and assess walking balance using the Functional Gait Assessment (FGA).

We collected kinematic data from the pelvis and lower limbs to assess gait stability. Participants walked on an oversized treadmill at preferred speed for 3 minutes during three hearing conditions:

Normal – Unobstructed hearing
Ear Plugs – Environmental sounds attenuated using both foam earplugs and industrial hearing protection ear muffs
White Noise – White noise played at 75 dB through ear buds to mask ambient sounds

To evaluate whether the effects of hearing on gait stability would be more pronounced during walking conditions that challenge balance, each walking condition was performed twice: once with **Arms Free** and allowed to swing, and once with **Arms Crossed**. Removing arm swing has previously been shown to reduce lateral gait stability. Two-way repeated measures ANOVAs (hearing condition by arm swing) tested for differences in gait measures. Bonferroni-corrected pairwise comparisons were made between conditions when significant differences were found. Friedman's Two-Way tests were used when data were not normally distributed.

RESULTS AND DISCUSSION

Twenty healthy older adults (age: 76.9± 6.4 years, 7 males, 13 females) who do not use hearing aids and had not been diagnosed with hearing loss gave written informed consent and participated in the study.

We found no main effects of hearing condition on lateral COM excursion (ANOVA; $p = 0.558$), minimum lateral margin of stability (ANOVA; $p = 0.870$), or step width (Friedman's; $p = 0.453$). However, a main effect of arm swing was found for both lateral COM excursion (ANOVA; $p = 0.015$) and minimum lateral margin of stability (ANOVA; $p = 0.049$). Both lateral COM excursion and lateral margin of stability were greater during Arms Crossed vs. Arms Free (post-hoc; $p < 0.05$).

Step time was less (faster steps) in the Normal condition vs. the Ear Plug condition (ANOVA; $p = 0.032$, post hoc; $p = 0.025$). Step Length was shorter in the Normal condition vs. the Ear Plug condition (ANOVA; $p = 0.037$; post hoc $p = 0.045$) (Figure 1). Neither step time (ANOVA; $p = 0.243$) or step length (ANOVA; $p = 0.356$) showed a main effect of arm swing.

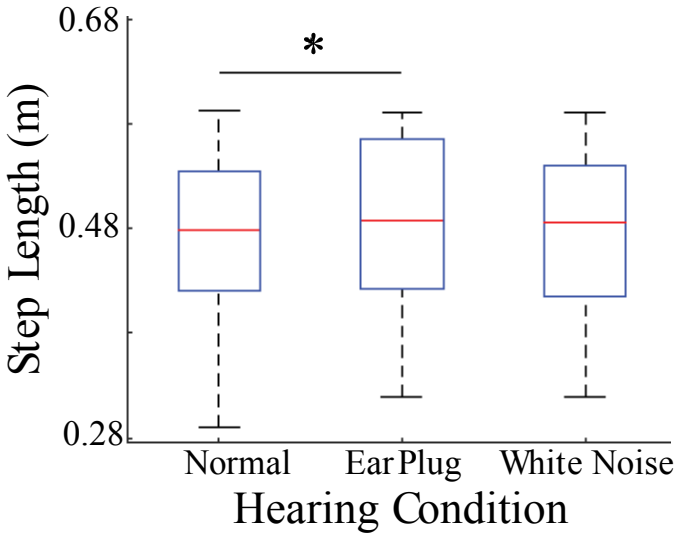

Figure 1: When participants wore ear plugs, step length was significantly longer than walking with normal unobstructed hearing.

Our findings did not support our hypothesis. Compared to normal walking, we found no differences in lateral COM excursion, lateral margin of stability, or step width when hearing was degraded using either ear plugs or white noise. The current findings suggest that continuous auditory feedback may have a limited role in controlling lateral gait stability for older adults who possess normal vision, vestibular function, and proprioception when walking in environments that present minimal challenges to balance.

Surprisingly, compared to normal walking, participants chose longer steps during the Ear Plug condition. Typically, in unstable walking environments people will adapt their gait patterns to create shorter, faster, and wider steps that increase mechanical stability. It is possible that the increase in step length during the Ear Plug condition may have been an intentional strategy to increase auditory feedback of gait-related events. The ear plugs and ear muffs may have created an occlusion effect resulting from relative movement of the mandible and skull that provided auditory feedback each time the foot contacted the ground. Increasing step length will result in greater vertical ground reaction forces at foot contact, which in turn should increase accelerations of the skull and potentially amplify the occlusion effect.

As a follow-up to this unexpected finding, we examined the relationship in individual changes in step length (between the Ear Plugs and Normal conditions) and FGA score. A Pearson's correlation found a moderate negative relationship that approached significance ($r = -0.44$; $p = 0.054$). **This relationship suggests that individuals with the poorest balance increased step length the most.** Although increasing step length may sacrifice mechanical stability, during the Ear Plug condition this adaptation may have been beneficial for providing additional feedback about when the foot contacted the ground.

CONCLUSIONS

These results suggest a limited role of auditory feedback for maintaining steady-state gait stability. However, our observation that step length increased during the Ear Plug condition and that this increase was greater for individuals with poorer balance may suggest that individuals actively seek out walking strategies that can enhance feedback about their relative position in the gait cycle and may even sacrifice some mechanical stability to do so.

REFERENCES

1. Viljanen, A., et al. Journals of Gerontology Series a-Biological Sciences and Medical Sciences. 64(2), 2009.
2. Lin, F.R. and L. Ferrucci. Archives of Internal Medicine. 172(4), 2012.
3. Houry, D., et al. American journal of lifestyle medicine. 10(1), 2016.

ACKNOWLEDGEMENTS

Supported by the Knowles Hearing Center and the Northwestern University Undergraduate Research Assistantship Program.

EFFECT OF NUMBER OF SEGMENTS IN A RUNNING-SPECIFIC PROSTHESIS MODEL ON HIP AND KNEE KINETICS

Abigail Eustace[1], Lauren A. Sepp[1], Brian S. Baum[2], Erika Nelson-Wong[2], and Anne K. Silverman[1]

[1]Department of Mechanical Engineering, Colorado School of Mines, Golden, CO, USA
[2]Department of Physical Therapy, Regis University, Denver, CO, USA
email: lsepp@mines.edu, web: http://fbl.mines.edu/

INTRODUCTION

Runners with a transtibial amputation often use running-specific prostheses (RSPs). RSPs are an energy storage and return (ESAR) prosthesis designed for running. The complex geometry and material properties of RSPs result in large device deformations during running. However, best modeling practices to characterize RSP deformation remain unclear. The number and location of kinematic markers are important decisions in developing an experimental protocol, as they will be used to define the number of rigid segments within an inverse dynamics model. The number of segments that define an RSP likely affects how device deformation is quantified and results of inverse dynamics calculations.

Previous studies have examined how RSP marker placement affects whole-body kinetics and recommend using more than one rigid segment to model RSPs as opposed to using simplified approaches [1]. The previous results suggest that the RSP should be modeled as a series of rigid bodies to represent the deflection of the device. Therefore, the purpose of this study was to investigate the effects of the number of segments used to represent an RSP on the joint moments and powers of the amputated leg during running.

METHODS

One participant with a unilateral transtibial amputation ran using her prescribed RSP (Össur Cheetah X-tend) at five speeds (2.5, 3.0, 3.5, 4.0, 5.0m/s) on a force-sensing treadmill (2000Hz, Bertec Corp., USA). Kinematics were collected using a whole-body marker set (100Hz, Northern Digital, Inc., Canada). The RSP keel was instrumented with six markers spanning from the most acute point of curvature of the RSP to the toe, in addition to fixed markers on the socket, and fixed markers to define the proximal end and width of the RSP (used to define the top section of the RSP, which is assumed to be rigid (Fig. 1)). Kinematics and ground reaction forces were low-pass filtered with a fourth-order Butterworth filter, with cutoff frequencies of 10Hz and 15Hz respectively.

Visual3D (C-Motion, Inc., USA) was used to develop four different RSP configurations increasing in complexity: 3, 4, 5, and 7-segment models (Fig. 1). Each model had the same proximal segment defined as the most proximal portion of the RSP connected to the amputated leg socket. From the proximal segment the remaining portion of the RSP was divided into 2, 3, 4, and 6 segments (Fig. 1). Mass of the RSP was measured at the time of the experiment. Inertial properties were estimated from a previous study [3].

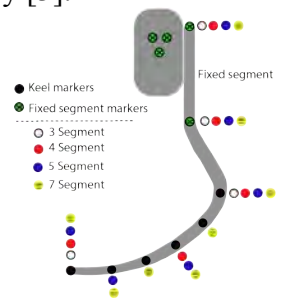

Figure 1. RSP with kinematic markers shown in addition to the points for each model configuration.

An inverse dynamics approach was used to determine joint moments and powers on the amputated leg. The amputated leg hip and knee moments and powers were compared at the slowest and fastest speeds (2.5m/s & 5.0m/s) across the different models. We calculated the root-mean-square (RMS) difference between RSP models in joint moment and power curves over the running gait cycle.

RESULTS AND DISCUSSION

RMS difference between the 5 and 7-segment models was the smallest for the hip and knee moments and powers (Table 1). As the number of segments in the RSP model increased, the difference in knee and hip moments decreased between model definitions. During swing phase, the 3 and 4-segment model definitions were similar in shape, and resulted in large flexion and extension moments calculated during swing. The greatest differences between models occurred during swing (~50-100% of the running gait cycle), but the curves also substantially differed in late stance phase (~30-40% of the running gait cycle) when the RSP returned energy that was stored in early stance.

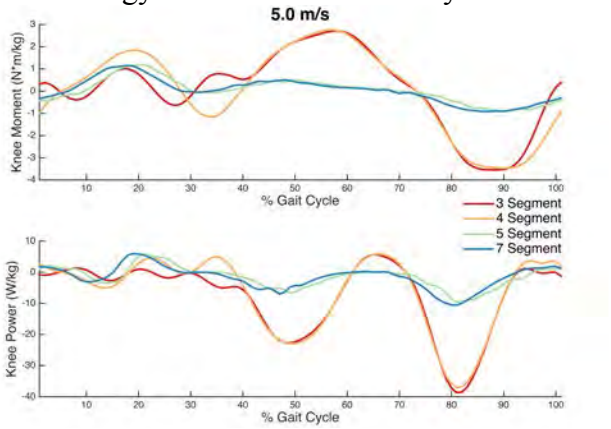

Figure 2. Amputated leg knee moment and power at 5.0 m/s for 3, 4, 5, and 7-segment models.

The greatest difference between models was between the 4- and 5-segment models for the knee moment and between the 4- and 7-segment models for the hip moment (Table 1). The greatest difference in joint power was between the 3- and 5-segment models for the knee and between the 4- and 7-segment models for the hip (Table 1). There were greater differences between models in net joint power, likely because of the large effects of different numbers of segments in characterizing angular velocity at "joints" throughout the RSP. Deformations in device structure are likely better characterized with a greater number of segments.

Our results suggest using more than five segments when modeling an RSP. As model complexity increased, additional joints were added distally (Fig. 1). More distal segments likely helps to better characterize the deformation of the RSP in addition to distributing the mass more realistically. Failure to characterize deformation at the toe section shifts the mass distribution more posterior, which may explain why knee moment and power are uncharacteristically large during swing phase. These results have implications for the number of markers that should be placed on the keel of an RSP to accurately capture the device deformation, and how many segments to use when modeling the device. Similar differences between models were seen at both 2.5m/s and 5.0m/s.

CONCLUSIONS

The number of segments representing RSPs in an inverse dynamics model affects net joint moments and powers at the knee and hip. We suggest that RSPs be modeled using five or more segments. Future work includes investigating additional participants and varied RSP designs. Furthermore, the addition of musculoskeletal models to investigate how the number of segments of a RSP model may influence muscle force estimation will provide further understanding of how model definition affects biomechanical results.

REFERENCES

1. Rigney, S., et al., *J Biom,* **49,** 3185-3193, 2016.
2. Fey, N.P., et al., *J Biom*, **46**, 637-644, 2013.
3. Baum, B.S., et al., *Arch Phys Med Rehab*, 2013.

Table 1: RMS differences in amputated leg knee and hip moment and powers at 5.0 m/s over the running gait cycle between RSP model definitions.

RMS Error	Models Compared (Number of Rigid Segments)					
	3 & 4	**3 & 5**	**3 & 7**	**4 & 5**	**4 & 7**	**5 & 7**
Knee Moment (Nm/kg)	0.75	1.43	1.40	1.47	1.46	0.18
Hip Moment (Nm/kg)	0.78	1.46	1.49	1.52	1.53	0.34
Knee Power (W/kg)	2.74	10.54	10.42	10.36	10.29	1.75
Hip Power (W/kg)	2.93	8.70	9.05	9.04	9.08	2.36

EFFECTS OF FIXED AND VARIABLE DAMPING ENVIRONMENTS ON ANKLE AGILITY AND STABILITY

[1] Harrison Hanzlick, [1] James Arnold, and [1] Hyunglae Lee
[1] School for Engineering of Matter, Transport, and Energy, Arizona State University, Tempe, AZ, USA

email: hyunglae.lee@asu.edu, web: http://faculty.engineering.asu.edu/hlee

INTRODUCTION

Increasingly, physically interactive robots are sought for use in conjunction with the human lower extremity. These lower extremity robots are already in use to augment strength and enhance precision in military and industry, and to assist and/or rehabilitate the lower extremity in clinics.

The human ankle is critical to everyday tasks as the primary joint responsible for transferring energy between the lower extremity and the physical world. For this reason, it is imperative to characterize how the human ankle behaves when coupled with a lower extremity robot. On the robotic side, proper control of damping properties is essential to maximize performance without compromising stability of the coupled human-robot system. This study explores 1) the trade-off between ankle agility and stability during interaction with fixed damping-defined environments, and 2) the potential benefits of interacting with variable damping-defined environments to improve the trade-off. Results of this study will be useful in the design and control of lower extremity robots, such as exoskeleton robots.

METHODS

This study consisted of two experiments approved by the Institutional Review Board of Arizona State University. Four young, healthy subjects (age: 19-28, weight: 53-82 kg) participated in the first experiment, and two young, healthy subjects (age: 21, weight: 53-82 kg) participated in the second experiment.

A wearable ankle robot (Anklebot, Bionik Laboratories, Canada) was used to simulate damping-defined mechanical environments. During experiments, subjects were seated and wore a knee brace, which supported the subject's leg and the robot. At the beginning of each experiment, the robot was calibrated to the neutral position of the ankle (the foot at 90° to the shank in sagittal plane and horizontal in frontal plane), and gravity compensation provided a constant torque to support the weight of the foot-ankle complex. This study focused on dorsiflexion-plantarflexion movement in the sagittal plane, and inversion-eversion movement was restricted. Subjects were provided real-time feedback on the current ankle position and target position via a graphical user interface (GUI).

In the first experiment, subjects were tasked with moving their ankle from the neutral position to a target indicated as efficiently as possible. This experiment simulated positive (+0.5 Nms/rad; dissipative) and negative (-1.0 Nms/rad; active) damping environments with 40 trials each. At the beginning of each trial, subjects maintained stability within ±0.5° of the neutral position for a randomized time interval between 3 and 5 sec. Once completed, the target was displayed 7° away from the neutral position and the subject moved to the target. Subject were required to maintain stability within ±0.5° of the target for a continuous 500ms window for the trial to conclude. Once the task was completed, subjects returned to the neutral position in preparation for the next trial. The direction of movement (dorsiflexion (DF) / plantarflexion (PF)) randomly alternated between trials.

The second experiment simulated positive (+1.0 Nms/rad), negative (-1.0 Nms/rad), and variable ([-1.0, +1.0] Nms/rad) damping environments with 40 trials each. Variable damping was calculated at 100 Hz using filtered velocity ($\dot{\theta}$) and acceleration ($\ddot{\theta}$) and simple intent recognition based on changes in kinetic energy scaled by the ankles inertia, $\dot{\theta}\ddot{\theta}$ [1]. Velocity was filtered using a 1st order Butterworth filter with a cutoff frequency of 5 Hz and acceleration was moving averaged over 50 ms.

$$b = \frac{-2}{1 + e^{-0.5 * \dot{\theta}\ddot{\theta}}} + 1.0$$

The target was 10° away from the neutral position, however the remainder of the experimental protocol was identical to the first experiment.

For both experiments, agility and stability were evaluated and compared. 'Maximum velocity' and 'maximum overshoot' were used as an analog for agility and stability, respectively. Maximum velocity was calculated based on maximum average velocity over a continuous 5 ms window, and maximum overshoot was computed by subtracting the subject's maximum angular displacement from the outermost bound of the target (10.5°).

RESULTS AND DISCUSSION

From the first experiment, we demonstrated that ankle agility was greater in the negative damping environment (active environment) and ankle stability was greater in the positive damping environment (dissipative environment) (Table 1).

Table 1: Relative agility and stability between dissipative and active environments.

	Max Velocity (deg/s)		Max Overshoot (deg)	
	Dissipative	**Active**	**Dissipative**	**Active**
DF	37.1 ± 9.4	57.5 ± 18.0	0.3 ± 0.3	1.0 ± 1.0
PF	42.3 ± 11.2	65.6 ± 20.0	0.4 ± 0.3	1.4 ± 1.4

These results were compelling and prompted the second experiment which included a variable damping environment in an attempt to achieve the agility benefits of negative damping and the stability benefits of positive damping.

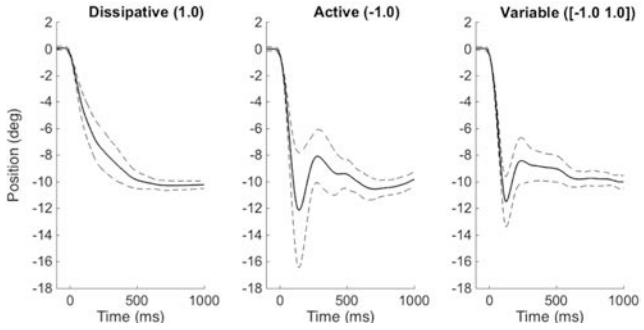

Figure 1: One representative subject's position responses for the plantarflexion trials. Solid lines represent the mean of all trials and dashed lines represent the mean ± 1 standard deviation (SD).

In the second experiment, subjects exhibited similar maximum velocity or agility in the variable damping environment as the negative damping (active) environment. While subjects still overshot the target in the variable damping environment, the overshoot was less severe and there was less variability in the position profile than in the negative damping environment (Fig.1).

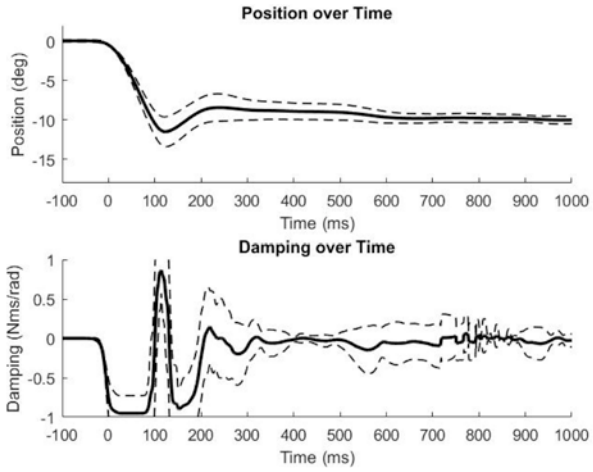

Figure 2: One representative subject's position responses along with associated damping responses in the variable damping environment. Solid traces represent the mean of all trials and dashed traces represent the mean ± 1 SD.

Both subjects could utilize the minimum and maximum bounds of the damping range (Fig. 2 bottom). This suggests that humans can get benefits of both assistance (negative damping) and stabilization (positive damping) from the selected variable damping environment in this task-specific scenario.

CONCLUSIONS

This study investigated the effects of fixed and variable damping-defined mechanical environments on ankle agility and stability. The experiment with fixed damping environments demonstrated that there exists trade-off between ankle agility and stability. Variable damping environments combined benefits of negative damping for agility and positive damping for stability, and our pilot study further confirmed that humans could get benefits of a wide range of damping-defined environments.

REFERENCES

1. Aguirre-Ollinger, et al. *Proceedings of the IEEE/RSJ International Conference on Intelligent Robots and Systems, San Diego, USA*. 2007.

CREATION OF SUBJECT-SPECIFIC SUBTALAR JOINT CONTACT MODELS FROM WEIGHT BEARING CT SCANS

[1] James Hiller, Kevin N. Dibbern, and Donald D. Anderson

[1] University of Iowa, Iowa City, IA, USA
email: kevin-dibbern@uiowa.edu

INTRODUCTION

Despite an abundance of research demonstrating the utility of understanding joint health through the mechanical marker of articular contact stress, there exists a paucity of research regarding the normal contact stress environment for the subtalar joint. When contact stress exceeds that of normal joints, the mechanical conditions can become unfavorable for chondrocytes, leading to a decline in cartilage health that predictably progresses to post-traumatic osteoarthritis (PTOA), a disabling condition.

Prior research in the subtalar joint has focused on direct physical measurement of contact stress in cadaveric tissues [1]. As the subtalar joint is narrow and tight when ligaments are healthy and intact, the insertion of stress detecting film or sensors can substantially alter the mechanical environment from that experienced in-vivo. Discrete element analysis (DEA) models present an alternative means to estimate subtalar contact stresses, as they have been demonstrated to provide accurate representations of the mechanical environment experienced by joints by modeling the articular cartilage as a bed of compressible springs arrayed over underlying assumed-rigid bone. The objective of this research was to create accurate subject-specific subtalar joint contact models from weight bearing CT scans to evaluate in-vivo contact stresses.

METHODS

Seven fresh frozen cadaveric ankle specimens were utilized in this IRB approved study. Each ankle was loaded along the long axis of the tibia with 100lbs and scanned in an upright standing position using a weight-bearing CT scanner (Figure 1). The talus and calcaneus bones were segmented from the CT scans to obtain their relative 3D positions in a loaded configuration. From these segmentations, average bone-to-bone distances were calculated for the middle and posterior facets of the subtalar joint.

Figure 1: pedCat weight bearing CT scanner used to obtain imaging used in this study

The cartilage thickness, which could not be directly measured in the CT scans, was extrapolated from bone-to-bone distance in the loaded configuration. This extrapolation was based on a loaded cartilage thickness model, which assumed that 50% of the bone-to-bone distance over the contacting area was the deformed cartilage thickness for each side. To generate an unloaded model of the articular surface, a 10% strain was taken as the static deformation of cartilage in the area where the bones were most closely apposed. This presumed deformation value was then added to the 50% bone-to-bone distance.

The DEA model of the subtalar joint contact used an elastic modulus for cartilage of 0.5MPa, while the Poisson's ratio was varied to determine the amount of compressibility that provided the most accurate result. The cartilage model was tested by moving the models of the foot out of contact and running DEA in load control. The model was allowed free movement in the vertical direction and free rotation in the frontal and axial planes.

Accuracy of the model was evaluated by mimicking the loading conditions of the scanned configuration and moving the models 4mm out of contact. An ideal model result would achieve 100lbs loading and settle into the scanned configuration. Therefore, a perfect result would have a 0mm deviation from its scanned position and achieve a loading of 100lbs upon convergence. From the results, the method for model creation was tested on an in-vivo case using the same protocol, except running to the half the patient's body weight.

RESULTS

All cartilage models generated converged at 100lbs with a Poisson's ratio between 0.488-0.496 (0.490±0.003). The final loading configuration for each model converged at 100lbs was within 0.1mm (0.094mm±0.027mm) of the scanned position. The test case obtained a loading equivalent to a body weight of 109.1kg for a 112.5kg subject (3.0% difference) and a final position of 0.076mm from the scanned configuration (Figure 2).

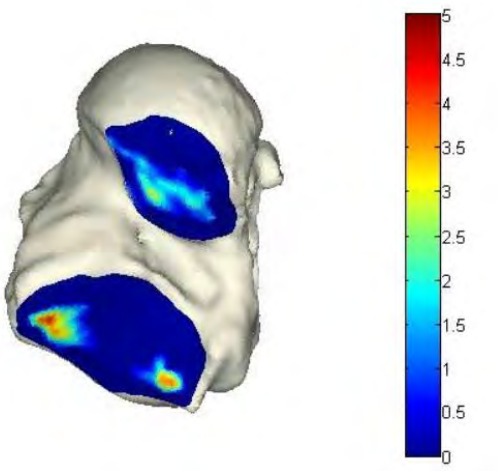

Figure 2. Inferior view of subtalar contact stresses (in MPa) in an in-vivo subject.

DISCUSSION

These results indicate that the methods are suitable for creating accurate DEA models of patient subtalar joint cartilage from weight bearing CT scans. The elastic modulus was selected to be 0.5MPa to correspond with statically loaded cartilage. The studied range of Poisson's ratio values corresponds well with previously published literature values. Future work will evaluate patient specific subtalar joint contact stress distributions from weight-bearing CT scans to determine average contact stresses seen in normal joints.

CONCLUSIONS

The findings of this study demonstrate that the subtalar joint model described can be used to evaluate joint loading and generate contact stress maps. The contact stress maps can be used to evaluate mechanical joint health by computing patient specific contact stress to determine if deleterious loading is occurring thereby providing prediction of symptomatic pathology.

REFERENCES

1. Wang, CL et al. *J Biomech.* 1995 Mar;28(3):269-79.
2. Wagner, UA et al. *J Ortho Research.* 1992 Jul; 10(4):535-543.

ACKNOWLEDGEMENTS

The authors would like to acknowledge the contributions of Jess Goetz and the University of Iowa Orthopedic Biomechanics Lab for supporting this research.

THE ACHILLES TENDON MOMENT ARM EXHIBITS INDEPENDENT AND COMBINATORY EFFECTS OF JOINT ROTATION AND MUSCLE LOADING

Ashish Khanchandani[1], Hannah McKenney[1], Brianna Arnold[2], William H. Clark[1], and Jason R. Franz[1]

[1]University of North Carolina and North Carolina State University, Chapel Hill, NC, USA
[2]Winston-Salem State University, Winston-Salem NC
email: jrfranz@email.unc.edu web: http://abl.bme.unc.edu

INTRODUCTION

The Achilles tendon moment arm (ATma), the distance from the tendon's line of action to the ankle joint center, is a critical component of the human musculoskeletal system, transforming triceps surae muscle forces into a moment about the ankle to power functional activities. In contrast to longstanding conventions, we recently discovered that the ATma exhibits highly dynamic variations during walking, which we interpreted to reflect combinatory effects of ankle joint rotation and increases due to triceps surae muscle loading [1] – the latter presumably governed by bulging during force generation. We posit that these variations are functionally meaningful; Lee and Piazza [2] reported that smaller AT moment arms estimated during isolated ankle rotation correlated with slower walking speeds in some older adults. As a biomechanical explanation, we more recently added that age-related reductions in peak ankle moment during push-off were correlated with smaller AT moment arms in older adults [3]. However, due to the complex neuromechanics of muscle-tendon and ankle joint function during walking, our mechanistic understanding of these ATma variations remains fundamentally incomplete.

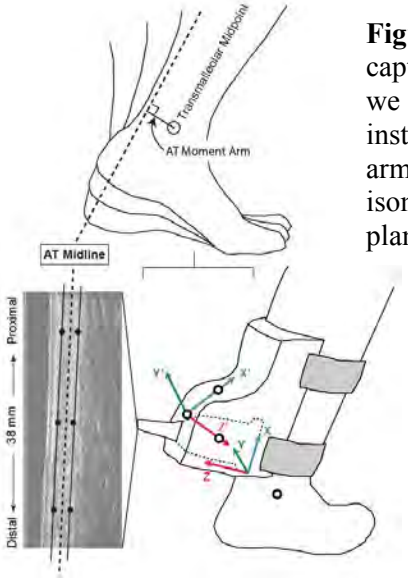

Figure 1. Using motion capture guided ultrasound, we estimated the instantaneous AT moment arm during isolated isometric and isotonic plantarflexor contractions.

Therefore, our purpose was to determine the kinematic (*i.e.,* ankle joint rotation) and kinetic (*i.e.,* triceps surae muscle loading) determinants of physiological variations in the Achilles Tendon (AT) moment arm during isolated plantarflexor contractions. We co-registered motion capture estimates of the transmalleolar midpoint with simultaneous cine ultrasound images of the instantaneous AT line of action. We tested the hypothesis that variations in the AT moment arm reflect independent and combinatory effects of ankle joint rotation and triceps surae muscle loading.

METHODS

11 young adults (age: 25.0 ± 5.4 years, 7F/4M) participated. Subjects were seated in a computer-controlled dynamometer (Biodex Medical Systems, Inc.) with their knee flexed to replicate that near the push-off phase of walking (i.e., ~20°). Subjects performed two series of isolated plantarflexor muscle contractions. In the first (effect of muscle loading while controlling for ankle angle), subjects performed three ramped isometric voluntary contractions at five ankle joint angles spanning 10º dorsiflexion to 30º plantarflexion, each separated by at least one minute and presented in random order. In the second (effect of ankle angle while controlling for muscle loading), subjects performed three isotonic concentric contractions over their range of motion at each of three ankle joint moments (i.e., 25%, 50%, and 75% of their peak 0° isometric ankle joint moment). During all trials, a custom orthotic positioned a 38 mm linear array transducer (L14-5W/38, Ultrasonix Corporation) over subjects' right Achilles free tendon, on average ~6 cm superior to the calcaneal insertion. We recorded ultrasound radiofrequency (RF) data from a longitudinal cross-

section of the AT. We manually tracked the AT midline from B-mode images created from the RF data using previously published procedures [2]. Finally, we calculated instantaneous variations in subjects' ATma as the perpendicular distance between the AT midline and the transmalleolar midpoint, estimated using marker data collected using eight cameras from a 14-camera motion capture system (Motion Analysis, Corp.).

RESULTS AND DISCUSSION

As hypothesized, and consistent with measurements made during walking, we found here that the Achilles tendon moment arm (ATma) exhibits independent and combinatory effects of ankle joint rotation and triceps surae muscle loading. In the absence of muscle loading during the isometric tasks, we found that the ATma became systematically smaller with increasing ankle plantarflexion ($p<0.001$, Fig. 2A). For example, at rest, the ATma was 7% smaller on average at 30° plantarflexion than at 10° dorsiflexion. In contrast, at maximum isometric activation, we found no significant effect of ankle joint angle on the ATma ($p=0.496$, Fig. 2B). We similarly found no significant main effect of ankle joint rotation across the range of motion tested during isotonic contractions performed at ≥25% maximum isometric torque ($p=0.218$, Fig. 2D). We interpret these findings to suggest that while ankle joint rotation systematically influences the ATma, a result fully consistent with prior reports, muscle loading substantially attenuates those effects. One possible explanation is that the effects of ankle joint rotation on the ATma, at least those with increasing plantarflexion, are governed primarily by tendon slack and tendon curvature – factors that are themselves both attenuated by triceps surae muscle loading. Indeed, we acknowledge that our range of dorsiflexion angles was limited.

Triceps surae muscle loading also independently increased the ATma. During ramped isometric contractions, the ATma increased by as much as 8% compared to resting values (Fig. 2C). However, this effect reached significance only for the two most plantarflexed ankle positions (i.e., 20° and 30°). We also found a significant main effect of muscle loading on the ATma during concentric isotonic contractions (Fig. 2D). Post-hoc comparisons revealed this was driven by modest but progressive increases in ATma from 25% maximum isometric torque to 50% ($p=0.032$) and again to 75% ($p=0.017$) – effects that held across the range of motion tested.

CONCLUSIONS

Our findings reveal that the Achilles tendon moment arm (ATma) exhibits complex independent and combinatory effects of ankle joint rotation and triceps surae muscle loading – results with clear implications for the study of elderly gait and the musculoskeletal modeling community. This outcome is also fully consistent with our earlier interpretations of the mechanisms governing physiological variations in the ATma observed during walking.

REFERENCES

1. Rasske et al., *CMBBE* **20(2)**: 201-5, 2017.
2. Lee and Piazza, *J Biomech* **45**, 1601-1606, 2012.
3. Rasske and Franz, *J Biomech* (in revision)

ACKNOWLEDGEMENTS

Funded by NIH (R01AG051748) and the National Center for Simulation in Rehabilitation Research.

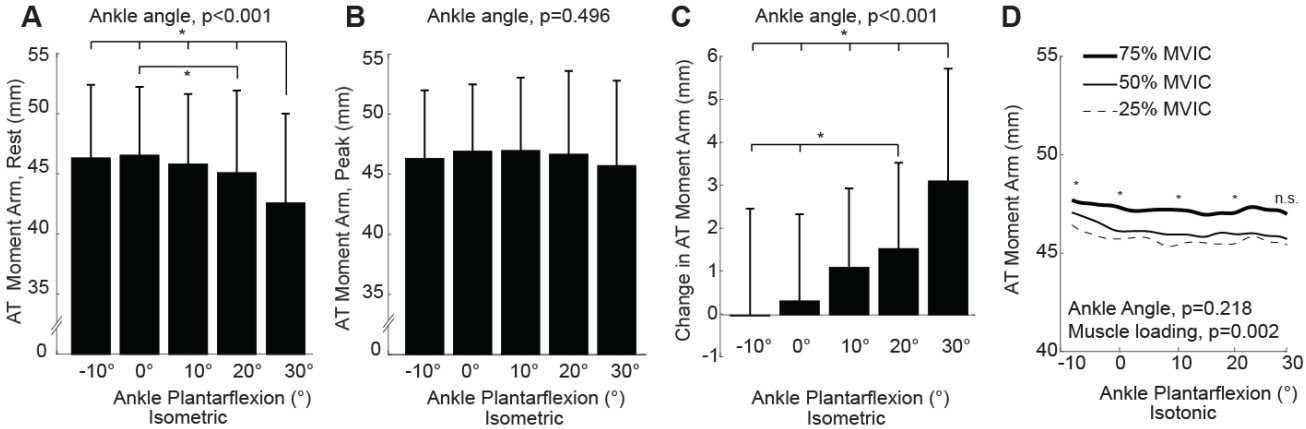

Figure 2. Group average (standard deviation) effects of ankle joint rotation and triceps surae muscle loading during maximum isometric (A-C) and concentric isotonic (D) contractions performed in isolation using a dynamometer.

Finite Element Analysis of the Rotator Cuff: A Systematic Review

[1] Drew H. Redepenning, [1]Paula Ludewig, [1] John M. Looft
Departments of Biomedical Engineering and Rehabilitation Medicine
[1] University of Minnesota, Minneapolis, MN, USA
email: jmlooft@umn.edu

INTRODUCTION

Finite element (FE) modeling has become an increasingly popular method for understanding biomechanical loading as well as impacts on novel orthopedic implant designs. FE is both low cost and easily adaptable to a wide range of applications for example: examination of rotator cuff tear propagation, kinematic loading, and impacts of glenoid implant designs [1]. Despite the recent advancements in FE modeling, validation and verification procedures have yet to develop into customary practice. Deficiencies in model development and reporting procedures limit model reliability and application to clinical practice. The aim of this project was to conduct a systematic review of rotator cuff FE models and assess model quality using a FE model grading procedure. The grading procedure includes specific aspects of model development including verification and validation methods.

METHODS

A comprehensive, electronic search strategy conducted between January 20th-March 3rd 2017 was used to elicit FE studies focused on the rotator cuff. The search protocol was implemented in Web of Science, PubMed, and Embase. No terms for health or health outcomes were included to ensure that all applications of FE modeling were identified. Bibliographies of primary studies and review articles meeting the inclusion criteria were searched manually to identify further eligible studies. Dissertations and any unpublished data were not included nor retrieved.

To be included in the review, finite element models needed to aim to model the rotator cuff including the tendons or muscular structure. This included: (1) models designed to improve diagnosis, investigation, monitoring and management of disease (2) models to assess geometrical differences between patients, (3) models for designing patient specific implants. Studies were excluded if analysis of the RC tendons were not included in the model.

Two independent review authors screened titles and abstracts of the resulting journal publications implementing the predefined inclusion/exclusion criterion. All studies meeting the inclusion/ exclusion criterion were subject to an additional full text review by each review author. The final decision for inclusion was determined from the consensus of the two review authors (Redepenning and Looft).

Following article retrieval, an in-depth FE model grading procedure presented by Erdemir et al. (2010), was performed on studies meeting the inclusion/ exclusion criterion. The grading procedure included 6 categories, each consisting of individual items: Model Identification (20 items), Model Structure (9 items), Simulation Structure (6 items), Verification (6 items), Validation (9 items), and Availability (5 items). Each item was weighted equally and was either marked as reported or not reported. Scores from groups were assessed both individually and collectively. Individual group scores were based on the percentage of items satisfied in the group. The collective score was calculated from the total percentage of items satisfied in each group with equal weight given to each group. The grading procedure was completed by two review authors independently. Disputes between scoring were resolved with the consultation of a third reviewer (Ludewig).

RESULTS AND DISCUSSION

A total of 22 articles were retrieved from the FE model literature search meeting the inclusion/ exclusion criterion (**Fig. 1**). 13 of the articles retrieved analyzed the supraspinatus as their primary region of interest. Remaining studies were focused on the complete structures of the rotator cuff or shoulder joint, which comprised 3 and 6 of the studies, respectively.

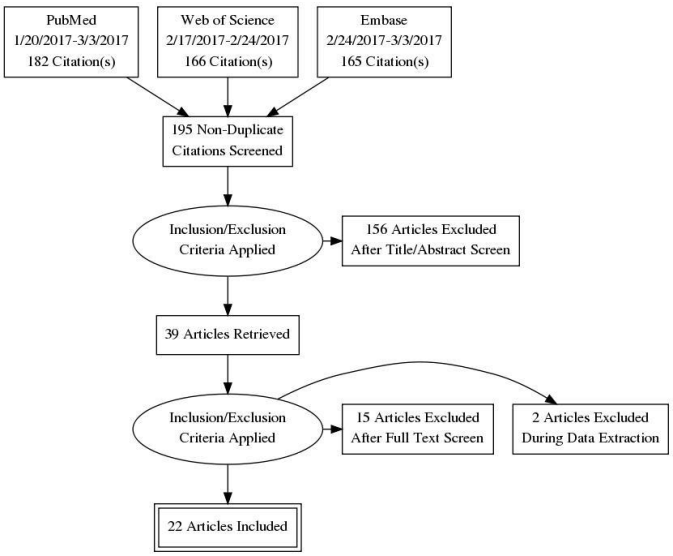

Figure 1: *Results of the literature search of the databases based on the inclusion search criterion.*

Grading results (**Fig. 2**) indicated a significant deficiency in validation and verification items in model and reporting procedures. Of the 22 articles, only 9 models satisfied over 50% of verification items and only 5 articles met over 50% of the required items for validation.

Mesh convergence, one of the more essential components for model optimization [3], was only reported in 7 of the articles under verification procedures. Furthermore, sensitivity to simulation settings was only reported in 3 articles. Absence of these and other verification items indicates either incomplete model development procedures or reporting procedures; suggesting the need for more in depth reporting requirements for FE modeling. Additionally, to allow for complete inclusion of verification items and additional items necessary for model reproducibility, separate reports for model development prior to experimental analysis should be encouraged.

Though many studies were deficient in specific verification items, validation items were more frequently exempt from model analysis and reporting practices with only 2 of the 22 studies satisfying the items: *"validation procedure"* and *"validated output"*. Additionally, sensitivity analyses of model parameters were only reported in 5 of the 22 studies.

CONCLUSIONS

Due to the inherent variability of human tissue, validation procedures are necessary to ensure model reliability. To the authors knowledge there exists no method to reliably determine a patient's specific tissue properties. Thus, models should be designed to simulate the variability in the population rather than aim to model a specific patient's values. Sensitivity analyses serve as a powerful tool to ensure the model's ability to simulate the subject variability [4]. Exclusion of sensitivity analysis and additional verification/validation practices compromises the quality of model outputs and indicates there is a need for better reporting procedure standards for FE modeling.

REFERENCES

[1] P. Favre, J. G. Snedeker, and C. Gerber, "Numerical modelling of the shoulder for clinical applications," *Philos. Trans. R. Soc. Lond. Math. Phys. Eng. Sci.*, vol. 367, no. 1895, pp. 2095–2118, May 2009.

[2] A. Erdemir, T. M. Guess, J. Halloran, S. C. Tadepalli, and T. M. Morrison, "Considerations for reporting finite element analysis studies in biomechanics," *J. Biomech.*, vol. 45, no. 4, pp. 625–633, Feb. 2012.

[3] H. B. Henninger, S. P. Reese, A. E. Anderson, and J. A. Weiss, "Validation of computational models in biomechanics," *Proc. Inst. Mech. Eng. [H]*, vol. 224, no. 7, pp. 801–812, 2010.

[4] J. E. Mottershead, M. Link, and M. I. Friswell, "The sensitivity method in finite element model updating: A tutorial," *Mech. Syst. Signal Process.*, vol. 25, no. 7, pp. 2275–2296, Oct. 2011.

ACKNOWLEDGEMENTS

Funded in part by NIH/NIAMS T32 AR050938 "Musculoskeletal Training Grant"

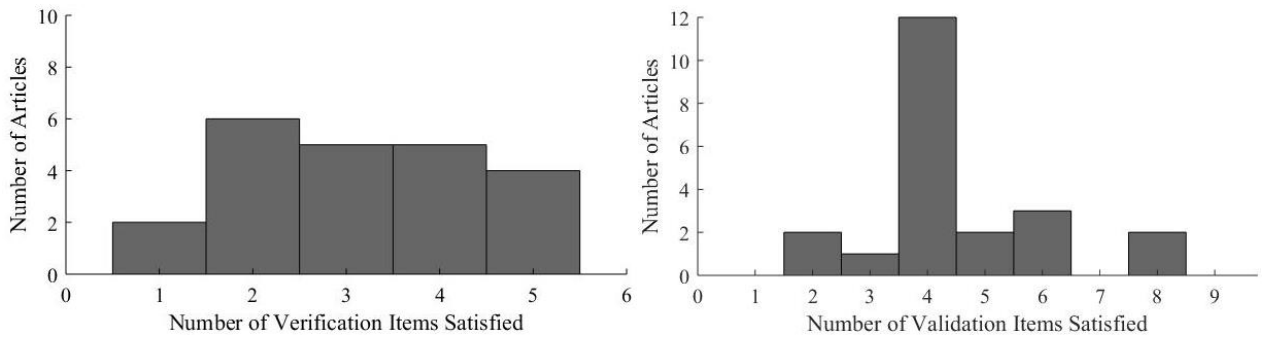

Figure 2: *Verification (Left) and Validation (Right) results from FEA grading procedure. No studies were found to have completely satisfied all 6 items for verification nor all 9 items for validation.*

Progressive Lateral Column Lengthening in a Cadaveric Flatfoot Model Increases Individual Bone Rotations in the Midfoot and Hindfoot

[1] Nicole Szabo, [2] John E. Femino, [1,2] Jessica E. Goetz

[1]Department of Biomedical Engineering, University of Iowa, Iowa City, IA, USA
[2]Department of Orthopedics & Rehabilitation, University of Iowa, Iowa City, IA, USA
email: nicole-szabo@uiowa.edu, web: https://uiowa.edu/uiobl/

INTRODUCTION

Flatfoot reconstruction often includes a surgical procedure called lateral column lengthening. This is an opening wedge osteotomy of the lateral calcaneus, which assists with the restoration of the arch as the soft tissues of the foot are tensioned during bony correction. This procedure corrects the overall alignment of the flat foot, however at the expense of the natural articulations of the joints in the mid- and hindfoot. The goal of this work was to use weightbearing CT scans of loaded cadaveric foot specimens to quantify individual bone rotations that occur during a lateral column lengthening to correct a flat foot. The secondary goal of this work was to determine if greater opening of the osteotomy resulted in greater rotations of individual bones or if there was a finite correction that could be achieved due to soft tissue tension.

METHODS

Eight cadaveric foot specimens were prepared for testing by implanting four 2-mm diameter metal beads in the talus, cuboid, and navicular, and eight beads (divided with 4 in the anterior region and four in the posterior region) in the calcaneus (Figure 1).

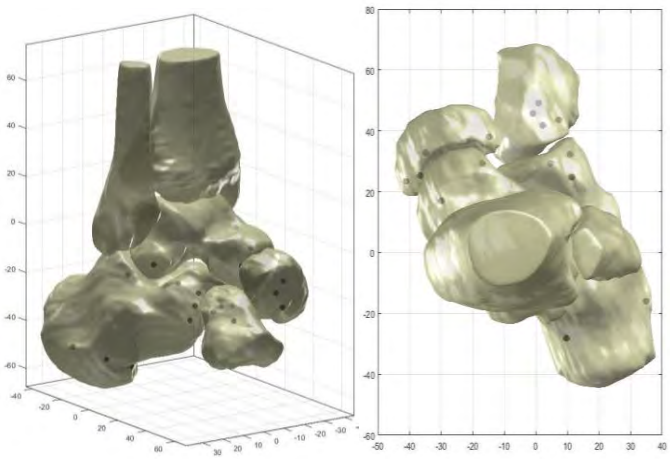

Figure 1: Oblique and superior-to-inferior view of bone surfaces illustrating bead placement in bones.

Specimens underwent serial weightbearing CT scans while loaded with 445 N (100 lbs.) (Figure 2). Specimens were scanned intact, after creation of a Type IIB flatfoot by cutting the spring, interosseous talo-calcaneal and cervical ligaments,[1] and after 6-mm, 8-mm, and 10-mm lateral column lengthening of the calcaneus.

Figure 2: Loaded cadaveric specimen in the weightbearing CT scanner

Metal beads and the distal tibia were segmented from CT scans using an automated segmentation program developed in Matlab. Any errors in automated segmentation from scatter due to the beads was manually corrected (www.itksnap.org) prior to segmentations being converted to Standard Triangle Language (.stl) files for analysis in Matlab. All ankle, mid- and hindfoot bone surfaces were similarly segmented from the intact CT scan, and all bone surfaces and bead clusters were transformed into a specimen-specific coordinate system established based on bony landmarks of the tibia and fibula.[2] The tibial surface from each of the

experimental CT scans was aligned to the tibial surface of the intact case using an iterative closest point algorithm. The rotations required to align the tibias were applied to the bead clusters from the experimental CT scans to align all data in a common coordinate system (Figure 3). Individual bone rotation from the different injury and repair scenarios were calculated by determining the rotation matrix needed to align bead sets between conditions to be compared, and then decomposing that rotation matrix into Euler angles.

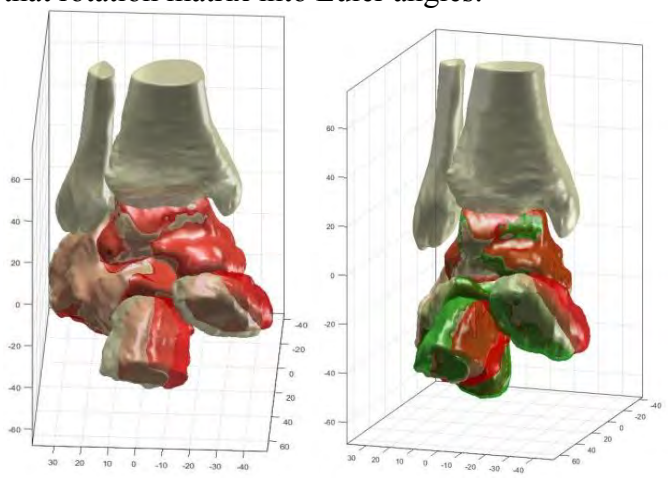

Figure 3: (Left) Rotation of bones from intact (tan) to flat (red). (Right) Rotation between intact bone (tan), flatfoot (red) and a 6-mm correction (green).

RESULTS AND DISCUSSION

Creation of the flatfoot condition caused the talus to dorsiflex and all other bones to plantar flex (Table 1). The talus rotated minimally in the coronal plane, and all other bones inverted with flatfoot creation. Flatfoot condition created adduction in all bones. After 6-mm, 8-mm and 10-mm lateral column lengthenings, the navicular, cuboid and anterior portion of the calcaneus had progressively less inversion and plantar flexion relative to the bone orientations in the flatfoot condition. Talar rotation in all three planes changed minimally with the different amounts of correction. The rotations of the other bones corrections reflect a general return back to the intact bony location (Table 2).

Table 1: Average (± standard deviations) bony rotation angles from intact to flatfoot conditions. Negative angles indicate inversion, adduction, and dorsiflexion.

Bone	Plantar/ Dorsiflexion	Inversion/ Eversion	Abduction/ Adduction
Talus	-2.8±1.4	0.1±0.7	-1.6±1.3
Navicular	1.6±0.6	-1.8±2.1	-2.1±8.9
Cuboid	0.8±0.5	-3.0±2.4	-5.5±2.6
Calcaneus	0.3±0.5	-1.6±1.5	-4.0±2.2

CONCLUSIONS

While overall flatfoot correction appears to plateau with increasing lateral column lengthening, larger and less reliable corrections of individual midfoot bone orientations occur with greater lateral column lengthening.

REFERENCES

1. Baxter JR, et al. *Foot Ankle Int*. 2015; **36**(6): 705-9.
2. Wu G, et al. *J Biomech*. 2002;35(4)543-548.

ACKNOWLEDGEMENTS

Thank you to Ross Schumer and Christopher Anthony for surgical assistance, and Andrew Kern, Elise Femino, and James Hiller for assistance performing image segmentations.

Table 2: Average (± SD) bone rotations relative to the intact case for 6, 8 and 10 mm corrections. Negative angles indicate inversion, adduction, and dorsiflexion, and smaller values are closer to the intact case.

	Abduction/Adduction			Plantar/ Dorsiflexion			Inversion/Eversion		
	6 mm	8 mm	10 mm	6 mm	8 mm	10 mm	6 mm	8 mm	10 mm
Talus	-1.9±1.8	-0.5±3.1	-0.3±5.0	-0.1±3.0	-0.6±4.7	0.3±3.2	-0.2±0.6	-0.5±0.9	-0.1±0.8
Navicular	0.8±5.1	-7.5±4.4	-0.2±4.2	0.3±1.4	0.2±1.9	0.7±2.4	2.7±1.6	-1.6±4.8	1.5±3.7
Cuboid	3.5±5.0	-5.7±8.5	3.5±2.9	-2.3±3.0	-0.03±6.2	-2.3±5.0	0.5±3.2	-0.1±5.1	-0.2±5.2
Anterior Calcaneus	1.6±4.2	-7.0±4.1	-1.0±9.4	0.7±1.6	-1.1±1.1	1.3±1.6	-2.4±1.2	3.3±1.4	-3.8±2.0
Posterior Calcaneus	-1.9±1.5	-0.5±0.6	0.8±3.7	1.7±2.1	-0.9±2.4	1.8±0.9	-0.7±0.9	-0.4±2.5	2.5±3.6

EVALUATION OF ANKLE PROPRIOCEPTION AND SELF-REPORTED ANKLE INSTABILITY USING A NOVEL, CLINICALLY-ORIENTED PROCEDURE

[1]Rachel H. Teater, [2]Scott M. Monfort, [1]Sarah E. Dowling, [3]Kim E. Bigelow, [1,4]Ajit M.W. Chaudhari

[1]The Ohio State University, Columbus, OH, USA; [2]Montana State University, Bozeman, MT, USA;
[3]University of Dayton, Dayton, OH, USA; [4]Perfect Practice, Inc.
email: rachelteater21@gmail.com, web: http://u.osu.edu/osusportsbiomechanics

INTRODUCTION

Lateral ankle strain is a common injury that has high rates of recurrence for reasons that are not well understood. Researchers have hypothesized that underlying functional ankle instability (FAI) predisposes individuals to re-injury after lateral ankle sprains and loss of proprioceptive input causes position-sense deficits leading to improper positioning of the foot just before foot contact [1].

Joint position sense (JPS) is a component of proprioception. JPS is often evaluated using a Biodex isokinetic dynamometer or custom-built devices. These methods have cost, space, ease-of-use, and portability barriers that impede the ability of clinicians to measure proprioception. Because of these challenges, recent research has investigated the use of a novel, clinically-oriented method to measure JPS [2].

Previous studies have investigated the connection between ankle joint position sense and ankle instability, but have reported varying results [1]. A targeted, quantifiable approach to establish the relationship between ankle proprioception and ankle instability is needed to provide further insight. Therefore, the goal of this research was to investigate the relationship between self-reported ankle instability and a quantitative measure of ankle proprioception using a novel, clinically-oriented proprioception test.

METHODS

Forty-five healthy participants (16 females, 29.3 ± 7.8 yrs, 1.76 ± 0.10 m, 76.0 ± 15.7 kg) were recruited at the 2017 Annual Meeting of the American Society of Biomechanics at the University of Colorado Boulder in August 2017.

Severity and history of ankle stability were assessed through a validated self-reported questionnaire, the Identification of Functional Ankle Instability (IdFAI). The IdFAI is a 10-item instrument that covers the severity and persistence of instability during various activities [3] and the instrument has shown superior ability to identify functional ankle instability in individuals compared to other existing questionnaires [4].

Each participant's active ankle JPS was evaluated using the iOS-based CoreX Therapy app (Perfect Practice, Inc.). Participants' more unstable ankle (self-reported from IdFAI) was tested. If neither ankle was reported to be unstable, the ankle of the dominant leg was tested. An iPod was strapped to the participant's foot as they lay supine on a table (Figure 1). Each participant performed ten trials of active ankle repositioning. For each trial, the participant started with their sole perpendicular to the ground then plantar flexed their foot until they reached the target angle of 15 degrees and were instructed to learn the position. The participant then repeated the movement and indicated when they thought they had reached the target angle once again. The researcher recorded the error from the target angle for each trial.

Participants were classified as having ankle instability if they scored eleven or greater on the IdFAI. This cutoff score has been established as a reliable threshold for identification of functional ankle instability [3]. The average absolute error in ankle repositioning with the most and least accurate trial excluded was used as the measure of ankle JPS. This method has been found to be moderately reliable with an ICC(1, k) = 0.741 [5].

An independent two-sided t-test (α=0.05) was used to test for a significant difference in active ankle position error between groups with and without ankle

instability. Additionally, the Pearson correlation between ankle position error and IdFAI was used to investigate a continuous relationship between ankle instability and JPS.

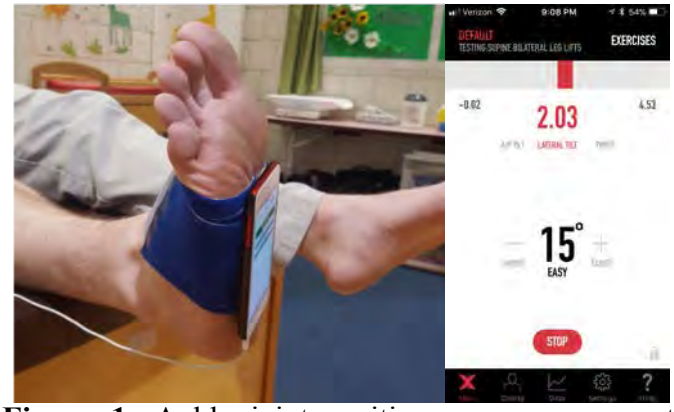

Figure 1: Ankle joint position sense assessment using CoreX Therapy iPod application.

RESULTS AND DISCUSSION

No significant difference (p=0.21) was observed in the average absolute ankle position error between participants with ankle instability (n=20; 2.54 ± 0.87°) and participants without ankle instability (n=25; 3.07 ± 1.63°). Additionally, the low Pearson correlation coefficient (r = -0.08) indicated no relationship between self-reported IdFAI score and ankle joint position error (Figure 2).

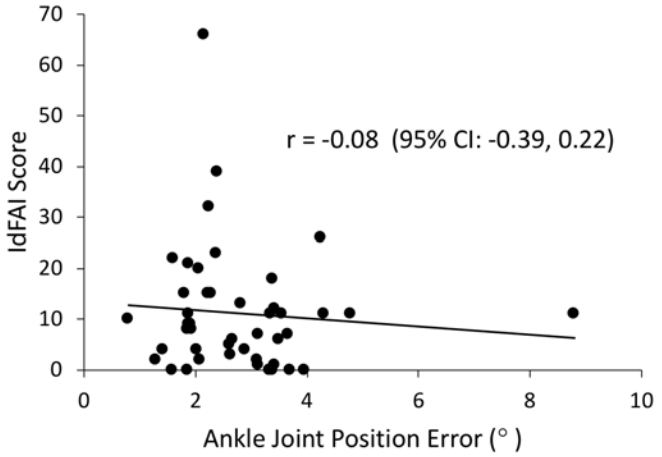

Figure 2: Pearson correlation results comparing ankle joint position error and ankle instability.

These results complement previous research investigating ankle instability and proprioception using various methods that also found no significant difference in active JPS between injured and uninjured ankles [1]. This is the first study investigating this relationship using a clinically-oriented test for proprioception and the IdFAI to characterize ankle instability.

CONCLUSIONS

Through the use of clinically-relevant tools for measuring both ankle joint position sense and functional ankle instability, this study demonstrated a lack of a relationship between ankle JPS and self-reported ankle instability. This result suggests indicates that functional ankle instability may be caused by factors other than proprioceptive deficits, such as strength deficits or impaired range of motion, and further research is necessary to investigate whether these or other factors are most important to address in individuals with ankle instability.

REFERENCES

1. Willems T et al, *J Athl Train* **37**, 487 – 493, 2002.
2. Monfort SM et al, *Proc. of 2017 ASB* **41**, 2017.
3. Simon J et al, *Foot Ankle Int* **33**, 755 – 763, 2012.
4. Simon J et al, *Phys Ther Sport* **15**, 97 -100, 2014.
5. Teater RH et al, *Proc. of 2018 ASB* (under review).

ACKNOWLEDGEMENTS

The authors gratefully acknowledge the support of the Organizing Committee of the 2017 American Society of Biomechanics Annual Meeting and the Ohio State University College of Engineering Undergraduate Research Grant. Due to author AMWC's relationship with Perfect Practice, Inc., he was not involved in recruiting or consenting participants, or in performing the data collection or analysis.

EFFECTS OF ANKLE BRACING ON KNEE AND HIP TORQUES DURING LANDING

Rachael A Arnwine, Alexis K Nelson, and Douglas W Powell

University of Memphis, Memphis, TN, USA
email: rarnwine@memphis.edu

INTRODUCTION

Ankle sprains can have long lasting effects; 79% of athletes experience a recurrence of ankle sprain and 59% of athletes exhibited functional disability and significant residual symptoms (2). A common form of ankle stabilization to prevent or treat ankle injuries is ankle bracing. Ankle Bracing results in altered loading patterns, which require neuromuscular compensation to complete the movement task. In the kinetic chain, the foot is the point of interaction with the ground, therefore forces are transmitted through the foot to the lower extremity. Though ankle bracing is known to protect the ankle against lateral sprains, little is known regarding the effects of ankle bracing on knee joint kinetics. It is assumed that if the ankle were to be altered by being braced, this would affect not only the ankle joint, but also the knee in hip joints. The purpose of this study was to determine the effects of ankle bracing on knee and hip joint moments during a landing task.

METHODS

Ten recreational athletes, aging 18-35, performed five step off landing trials from a height of 16" with their dominant ankle braced. Three-dimensional kinematics (240 Hz, Qualisys Inc., Sweden) and ground reaction forces (960 Hz, AMTI, MA, USA) were collected simultaneously. Visual 3D was used to calculate joint moments and custom software (MATLAB, MathWorks, MA, USA) was used to determine peak joint moments in the sagittal, frontal and transverse planes during the 100 ms period following initial contact. Paired samples t-tests were used to compare braced and unbraced limbs for each variable

RESULTS AND DISCUSSION

The braced limb had greater knee adduction moments compared to unbraced limb while no differences in peak knee extension or external rotation moments were observed. At the hip, the braced limb exhibited greater peak extension, abduction and external rotation moments. This suggests that prophylactic ankle bracing can increase knee and hip joint torques during jump landing.

This increase in overall load may yield potential injury risk for proximal joints.

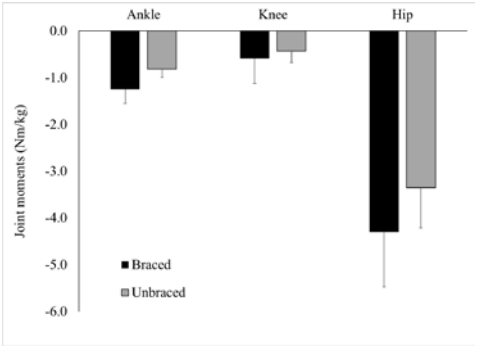

Figure 1: Sagittal plane moments.

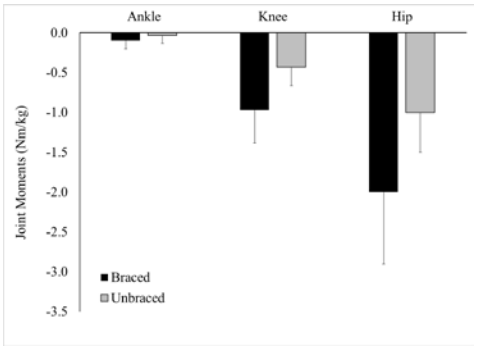

Figure 2: Frontal plane moments.

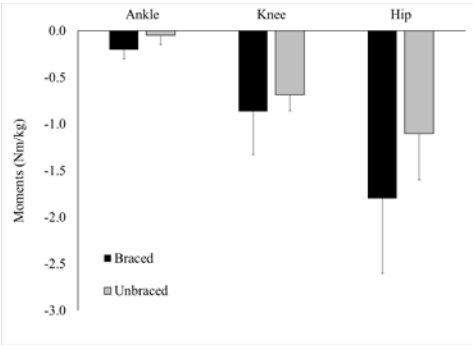

Figure 3: Transverse plane moments.

CONCLUSIONS

Ankle bracing increases multi-planar joint moments at the knee and hip, in addition to ankle, during a landing task. It is possible that prophylactic ankle bracing may place proximal structures at greater risk of injury.

REFERENCES

1. Yeung MG, Chan DK, So CH, Yuan WY. An epidemiological survey on ankle sprain. Br J Sports Med 1994; 28(2): 112-116.

2. De Clercq D.L. Ankle bracing in running: the effect of a Push type medium ankle brace upon movements of the foot and ankle during the stance phase. Int J Sports Med. 1997; 18 (3): 222-228.

3. Zhang, S. N., Bates, B. T., & Dufek, J. S. (2000). Contributions of lower extremity joints to energy dissipation during landings. Medicine and Science in Sports and Exercise, 32, 812–819

ACKNOWLEDGEMENTS

SPAHCC, Max R Paquette

Table 1: Peak ankle, knee and hip joint angles in the sagittal, frontal and transverse planes.

Joint	Movement	Braced	Unbraced	P	d
Knee	Ext	0.59 (0.54)	0.43 (0.25)	0.191	0.4
	Abd	0.97 (0.42)	0.43 (0.23)	***0.001***	1.6
	ER	0.87 (0.46)	0.69 (0.17)	0.109	0.5
Hip	Ext	4.3 (1.2)	3.3 (0.9)	***0.002***	0.9
	Abd	2.0 (0.9)	1.0 (0.5)	***0.001***	1.4
	ER	1.8 (0.8)	1.1 (0.5)	***0.010***	0.9

TIBIALIS ANTERIOR IN VIVO MUSCULAR ACTIVITY DECREASES WITH AGE

[1] Filiz Ates, [1]Krista Coleman-Wood, [2]William Litchy, [1]Kenton R. Kaufman

[1] Motion Analysis Lab. Department of Orthopedic Surgery, Mayo Clinic, Rochester, MN, USA
[2]Department of Neurology, Mayo Clinic, Rochester, MN, USA
E-mail: ates.filiz@mayo.edu

INTRODUCTION

Muscle weakness is a common result of many neuromuscular diseases as well as aging [1]. Detecting the course of change in strength is crucial, albeit challenging. In order to understand the relationship between neuromuscular structural changes and the observed functional loss, there is a need to quantify local mechanical properties of individual muscles. Intramuscular pressure is the fluid hydrostatic pressure generated within a muscle and directly reflects the mechanical forces produced by a muscle [2]. Previous *in situ* investigations qualitatively show a strong relationship between IMP and the active and passive muscle tension [3]. Recently, it was shown that IMP reflects *in vivo* voluntary activity of human muscles [4]. However, the relationship between the activity levels of muscles and IMP and how this changes with age has never been tested. The goal of this study was to test the following hypotheses on human tibialis anterior (TA) muscle *in vivo*: IMP (i) reflects the compound muscle action potential (CMAP) activity, (ii) follows the increase in muscle activity imposed by increasing rates of stimulation frequency, and (iii) is lower for older adults.

METHODS

The procedures were approved by the Mayo Clinic Institutional Review Board. Thirteen healthy young adults between the ages of 20-40 years old (7 females; mean (SD) age = 28.4 (4.9) with 25.5 (5.7) kg/m^2 body mass index) and seven healthy older adults between the ages of 60-80 years old (4 females; mean (SD) age = 68.8 (3.76) with 28.1 (4.1) kg/m^2 body mass index) were recruited. All participants provided written informed consent. Stimulation of the peroneal nerve provided the (i) CMAP and (ii) supramaximal stimuli at frequencies of 2 Hz, 5 Hz, 10 Hz, and 20 Hz. All stimulations were applied twice. Ankle torque and the TA IMP were measured simultaneously. All statistical tests were performed using JMP 10.0 software (SAS Institute, Inc., Cary, NC). Distribution normality was tested using the Shapiro-Wilk test and statistical tests were selected accordingly. A Kruskal-Wallis test was used to detect differences between the TA IMP of young and older adults during CMAP activity. The Spearman's rank correlation coefficient was calculated to analyze the relationship between the IMP and ankle torque. Two-way ANOVA (factors stimulation rates and age group) for repeated measures was used to detect differences between the IMP at different stimulation frequency rates for young and older adults. Statistical significance was set at P =0.05.

RESULTS AND DISCUSSION

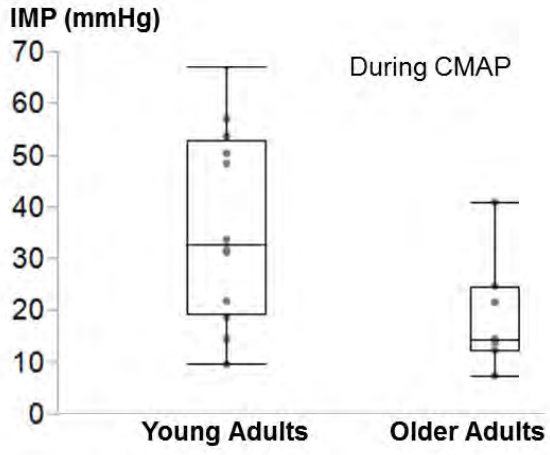

Figure 1: Box and whisker plot of the TA IMP of young and older adults during CMAP activity.

The TA IMP of young adults during CMAP activity (32.57 Nm (33.39 Nm)) was 47.2% higher than the TA IMP of older adults (14.36 Nm (12.38 Nm), P = 0.03) (Fig 1). Ankle torque during CMAP activity was not significantly different for young adults (median (interquartile range) = 6.14 Nm (2.25 Nm)) compared to older adults (6.01 Nm (2.21 Nm), P =

0.66). These indicate that (i) the IMP reflects local muscle activity that is not possible to be detected by ankle torque measurements and (ii) aging causes a decrease in IMP. These observations confirmed both our first and third hypotheses.

TA IMP and ankle torque was significantly correlated for both young ($\rho = 0.69$, $P < 0.0001$) and older adults ($\rho = 0.43$, $P = 0.02$). This also supports the first hypothesis.

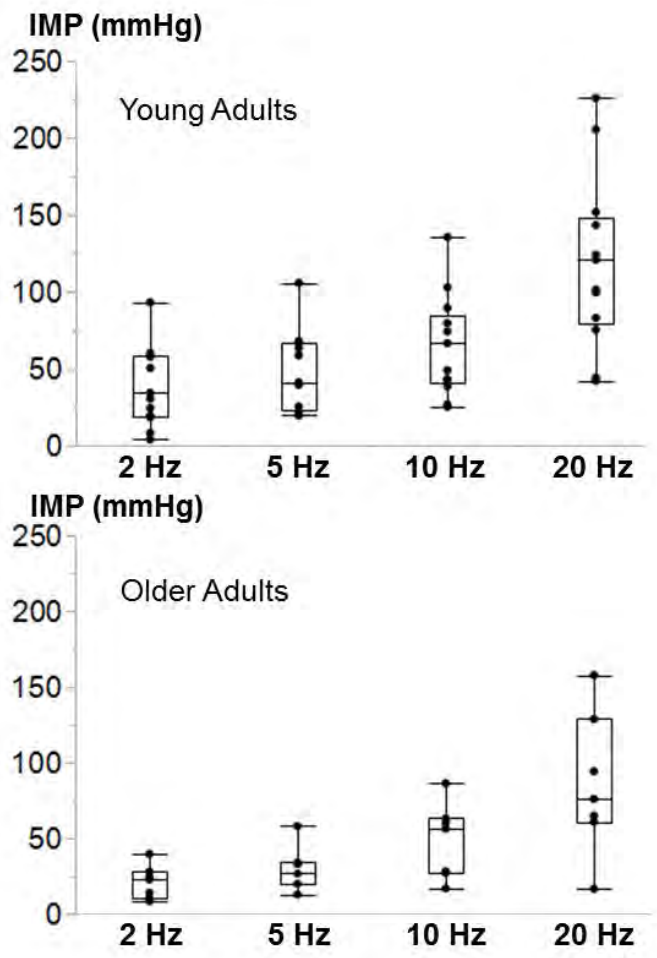

Figure 2: Box and whisker plot of the TA IMP of young (upper) and older adults (lower) at different stimulation frequency rates.

The main effect of stimulation rates ($P < 0.0001$) on ankle torque was significant. However, no significant effects of age group ($P = 0.20$) or interaction were found ($P = 0.34$). The main effects of both factors (age group ($P = 0.04$) and stimulation rates ($P < 0.0001$)) on TA IMP were significant. However, no significant interaction was found for IMP ($P = 0.74$) (Fig 2). The TA IMP of young adults was 33.20% higher than the TA IMP of older adults on average. Our second hypothesis was confirmed as well. This indicates that (i) IMP not only can detect the differences in local muscle response to various stimulation rates that are represented as ankle joint torque but also (ii) IMP detects the weakening effects of aging on muscle mechanics.

CONCLUSIONS

Our study shows that IMP increases with the increasing muscular activity imposed by nerve stimulation and reflects the mechanical response of muscle. Furthermore, the effects of aging on force production capacity of healthy human muscles *in vivo* are quantified using intramuscular pressure approach for the first time. Our findings suggest that IMP as a minimally-invasive approach can provide a new measure for muscle weakness. By providing accurate quantification of interstitial fluid pressure, IMP can be designed as a diagnostic tool to follow the weakening of muscles due to aging in order to treat sarcopenia as well as to detect the course of electromechanical pathophysiology of the skeletal muscle such as myopathies.

REFERENCES

1. Janssen I. et al., *J Am Geriatr Soc* 50: 889-896, 2002.
2. Baumann et al., *Clin Orthop Relat Res.* 145: 292-299, 1979.
3. Davis J. et al., *J Biomech* 36: 505-512, 2003.
4. Ates F. et al., Frontiers in Physiol 9:22, 2018.

ACKNOWLEDGEMENTS

National Institutes of Health under grant R01HD31476, and The Scientific and Technical Research Council of Turkey (TUBITAK) 2219 Programme.

LANDING BIOMECHANICS DIFFER BETWEEN PROFESSIONAL DANCERS AND NON-DANCERS: EXPERIMENTAL AND PRELIMINARY MODELING APPROACHES

[1,2]Ana M. Azevedo, [2]Qi Wei, [1]Raul Oliveira, [3]João R. Vaz, [2]Nelson Cortes

[1]Faculty of Human Kinetics, University of Lisbon, Portugal
[2]George Mason University, Manassas, VA, USA
[3]University of Nebraska at Omaha, NE, USA
email: ncortes@gmu.edu, web: http://smartlab.gmu.edu

INTRODUCTION

Jump-landing tasks place strenuous demands on the lower extremity. Professional dancers (PD) perform frequent multidirectional single-leg jump-landings. Biomechanical landing strategies are dependent on the movement direction. Previous research showed that jumps in the diagonal and lateral directions had decreased hip and knee flexion suggesting a higher injury risk than during a forward direction jump [1]. Conversely, an erect landing posture can employ an ankle plantarflexion strategy to attenuate the impact [2]. There is scarce evidence in applying musculoskeletal modeling in dance science, which could lead to comprehensive understanding of differential muscle contributions to landing between dancers and other populations. Therefore, the current study had two aims: 1. to investigate kinematic and kinetic differences between PD and non-dancers (ND) during multidirectional single-leg landings, and 2. to present preliminary data of musculoskeletal modeling.

METHODS

Biomechanical data of the dominant limb of 15 PD (27±7years, 1.69±0.1m, 57.8±9.3kg), and 15 ND (25±5 years, 1.69±0.1m, 66±10.2kg) were collected. The participants performed multidirectional single-leg jump-landings (diagonal, frontal, and lateral). A ten-camera motion capture system (200Hz, Opus, Qualisys AB, Gothenburg, Sweden), and a Bertec force plate (1000Hz, Bertec Corporation, Columbus, Ohio) were used to collect marker trajectories and ground reaction forces, respectively.

Visual 3D. Visual 3D (C-Motion, Inc., Rockville, USA) was used to create a kinematic model (pelvis, thigh, shank and foot) based on a static trial. Hip, knee, and ankle kinematics (sagittal and frontal plane joint angles, º) and kinetics (internal joint moments, Nm/Kgm; vertical ground reaction forces, BW), were calculated at initial contact (IC), peak knee flexion (PKF), and peak vertical ground reaction force. Landing phase was defined from IC to PKF. Repeated measures ANOVAs were conducted ($p<0.05$).

OpenSim. OpenSim (Simtk, Standford, CA, United States) was used for the preliminary musculoskeletal modeling. Two participants were randomly selected from our sample; one PD (22years, 1.60m, 46.3kg) and one ND (21years, 1.60m, 47.8kg). One trial of the lateral jump-landing was analyzed. Marker trajectories data were exported from Visual 3D to OpenSim. Gait2392 model was used in all simulations [3]. Each model was scaled to match participants' anthropometry. The inverse kinematic tool and static optimization were used to calculate sagittal joint angles (hip, knee and ankle) and gluteus maximus activation from the marker set data, respectively.

RESULTS AND DISCUSSION

An interaction effect between group and jumps, at IC, was statistically significant ($p<0.05$) for ankle, and hip angles in frontal and sagittal planes, respectively (Table 1). During the lateral jump, PD showed lower hip flexion than during their frontal jump and when compared to the three landing directions for ND. PD also exhibited lower hip flexion, during the diagonal jump, compared to the diagonal and frontal jumps of ND. PD had higher ankle eversion while performing the frontal jump when compared to ND completing the diagonal and lateral jumps. The preliminary assessment of our musculoskeletal modeling, demonstrated that the OpenSim results had similar outcomes as Visual 3D

(Figure 1). Further, it is visible that the non-dancer had increased estimated higher gluteus maximus activity during the early stance phase of the landing, whereas the professional dancer had increased muscle activity towards the end of the stance phase (Figure 2).

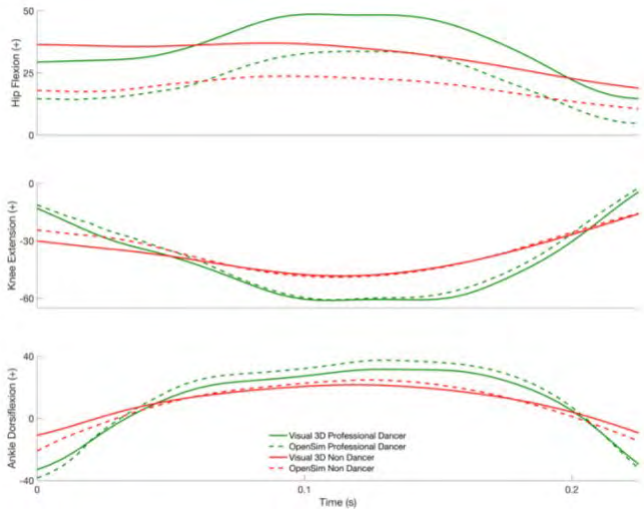

Figure 1: PD and ND hip, knee and ankle angles (º), during stance phase of the lateral jump-landing.

An overall decreased lower extremity flexion landing pattern is associated with an increase in sagittal and frontal plane loading at the knee. Moreover, the ability to maintain proper stability during landing depends on the hip abductors, external rotators, and extensors neuromuscular activity and strength. Thus, the PD' strategy, decreased hip flexion and increased ankle motion, can suggest the adoption of a distal stabilization strategy. While eversion can place greater stress on the medial border of the foot, the increased work of the evertors can act as stabilizers, protecting the ankle joint of excessive lateral motion (e.g., ankle sprains).

CONCLUSIONS

Differential proximal and distal stability landing strategies solicit distinct lower extremity neuromuscular muscle recruitment. The preliminary data of this study, presents an opportunity to continue integrating musculoskeletal modeling to estimate the relative muscular contributions in highly complex and skilled tasks in a unique population (i.e., professional dancers). Further investigation should explore proximal and distal muscular contribution during multidirectional jump-landing.

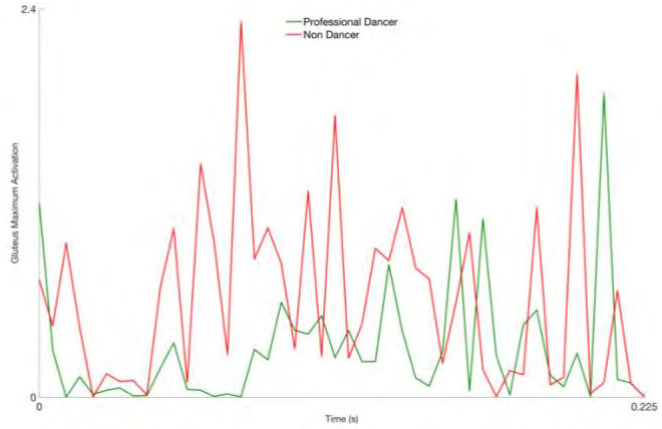

Figure 2: Preliminary analysis of Gluteus Maximus muscle activation in PD and ND participants during the stance phase.

REFERENCES

1. Sinsuri K. et al. Eur J Sport Sci, 2017. **17**(6): 699-709.
2. Decker MJ et al. Clin Biomec, 2003. **18**: 662-669.
3. Delp SL et al. IEEE Trans Biomed Eng, 2007. **11**: 1940-1950.

Table 1. Mean and standard deviation of the interaction effect between group and jumps, in degrees, at IC.

	Lateral Jump	Frontal Jump	Diagonal Jump	Total
Hip Flexion (+)				
Professional Dancers	25.7±4.3	35.1±5.7	31.9±5.7	30.9±5.2
Non-Dancers	35.6±7.4	40.9±4.7	39.5±6.2	38.7±6.1
Total	30.7±5.9	38.0±5.2	35.7±6.0	
Ankle Inversion (+)				
Professional Dancers	2.7±4.8	-2.3±4.4	0.4±4.3	0.3±4.5
Non-Dancers	4.8±4.7	2.1±3.8	3.6±5.2	3.5±4.6
Total	3.8±4.8	-0.1±4.1	2.0±4.8	

EXTERNAL LOAD CONTRIBUTIONS TO ACL STRAIN IN MULTIPLANAR LOADING DURING SIMULATED LANDINGS

Nathaniel A. Bates, Nathan D. Schilaty, Christopher V. Nagelli, Aaron J. Krych, and Timothy E. Hewett

Mayo Clinic Biomechanics Laboratories & Sports Medicine Center, Rochester & Minneapolis, MN, USA
email: bates.nathaniel@mayo.edu

INTRODUCTION

Anterior tibial shear (ATS), knee abduction moment (KAM), and internal tibial rotation (ITR) increase strain on the anterior cruciate ligament (ACL) in an intact knee [1]. However, debate continues over how these loads contribute to ligament mechanics leading up to and during an injury event. As over $2 billion is spent annually in ACL reconstruction and rehabilitation, understanding these underlying contributors is important such that investigators and clinicians can implement targeted injury prevention techniques with greater efficacy. Recently, the mechanical impact simulator was validated to replicate clinical presentation of ACL injuries in cadaveric specimens during simulated landing tasks [2]. The objective of this study was to quantify the influence of KAM, ATS, and ITR on ACL strain during simulated landings. The hypothesis tested was that combined loading would exhibit the greatest ACL strain during landing and that KAM would be the most significant individual contributor to this strain.

METHODS

45 cadaveric full lower extremities were tested in the mechanical impact simulator. Detailed description of the simulator protocol is available in the literature [3]. Briefly, the simulator delivered a series of gravity-driven impulse forces into a ground platform that was aligned with the tibia of lower-extremity cadaveric specimen flexed to 25º in order to mimic initial contact from a drop landing task. Pneumatic actuators simulated hamstrings and quadriceps muscle forces about the knee, then simultaneously applied KAM, ATS, and ITR loads to the knee joint. Each of these loads were applied in randomized increments relative to injury risk levels (baseline, low, medium, and high; Table 1) derived from *in vivo* biomechanical assessments of 67 healthy athletes who performed drop vertical jump tasks off a 31 cm box. A 6-DOF load cell aligned with the long axis of the femur reported loads at the knee and a DVRT strain gauge implanted on the anteromedial bundle of the ACL ligament measured strain. Specimens were included in this analysis only if they survived the entire randomized protocol of 46 impacts. 17 specimens were analyzed (age = 38.4±9.0 years; mass = 92.7±23.4 kg; height = 175.6±9.1 cm; 4F:13M). ANOVA was used to test for significance between increments of each individual loading factor ($\alpha<0.05$), and multivariate regression was used to examine the predictive relationship of each factor.

Figure 1: Heatmaps that demonstrate the influence of each external load (KAM [A], ATS [B], & ITR [C]) had on peak ACL strain throughout all 46 randomized simulations. The magnitude of each individual applied load increases from left to right, while the magnitude of the combined two loads increase from front to back. In all cases, the greatest ACL strain was experienced in peak combinatorial loading; however, KAM expressed the greatest individual effect as demonstrated by the left to right slope in that plot.

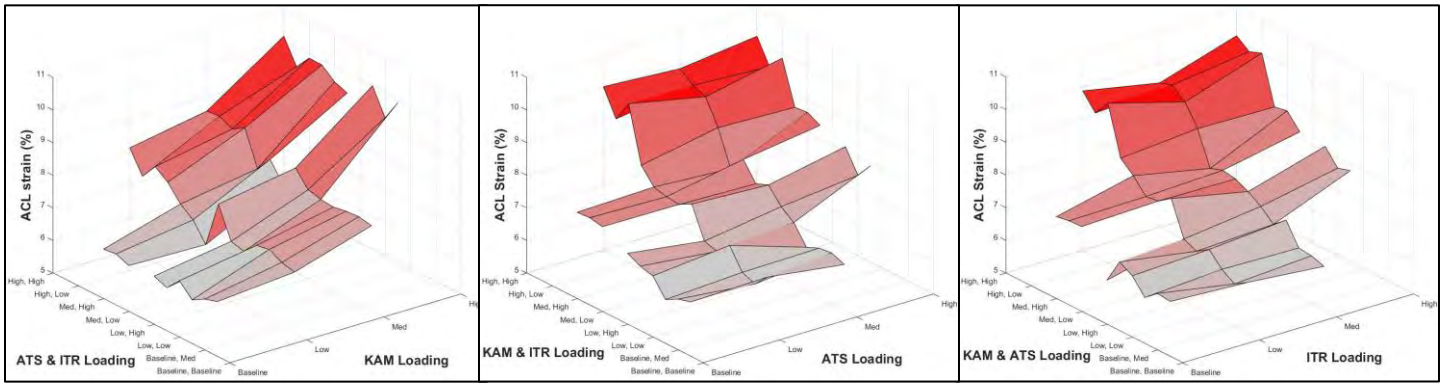

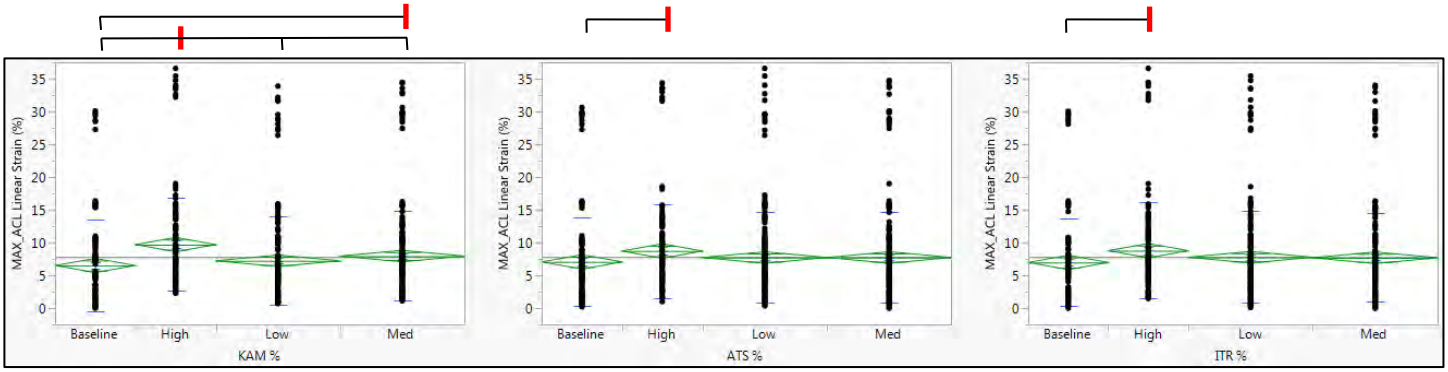

Figure 2: Peak ACL strain from every trial plotted against increments of KAM, ATS, and ITR. Significance between increments is indicated by bars above plots. Change in KAM increment effected the greatest change in ACL strain relative to baseline.

Table 1: KAM, ATS, and ITR load input magnitudes based on motion analysis from an *in vivo* population cohort

Risk Level	KAM (Nm)	ATS (N)	ITR (Nm)
Baseline	1.7	47	1.0
Low	13.5	64	9.7
Med	26.8	80	18.6
High	57.3	196	53.7

RESULTS AND DISCUSSION

Mean peak ACL strain was greater than baseline simulations (6.5±6.9%) during impacts with moderate (8.0±6.8%, P=0.04) and high KAM loads (9.7±7.1%, P<0.01; Figure 1 and 2). High KAM loads also exhibited greater peak strain than low (7.2±6.7%; P<0.01) or moderate KAM (P=0.01). ACL strain was greater during impacts performed at high ATS (8.7±7.2%) and ITR loads (8.8±7.3%) as compared to their baseline conditions (7.1±6.7%; P=0.04 & 7.0±6.7%; P=0.02, respectively). Multivariate regression using KAM, ATS, and ITR covariates significantly predicted ACL strain (P=0.02); however, KAM was the only significant individual covariate within that model (P<0.01, P=0.74, & P=0.57, respectively).

When external loads were applied in a high-low-low format, high ATS (3.9±3.5%) and high ITR (3.9±3.7%) effected less change in ACL strain from the baseline condition than did combined high loading from all three factors (6.6±3.2%; P≤0.03). No significant differences were observed between change in ACL strain from high KAM loading (5.7±3.6%) and high combined loading (P=0.47). These findings corroborate the influence of isolated tibial rotations applied to cadaveric specimens in robotically-controlled simulations of landing tasks [4].

Uni- and multi-planar loading in a previous drop-stand simulator demonstrated that combinatorial KAM, ATS, & ITR loading had a greater effect on ACL strain during landing than any component individually [5]. However, drop-stand loading was derived from a purely linear scale, not an *in vivo* cohort, which lead to far greater peak KAM and ATS loads than were applied in the present study. In the present study, after completion of the prescribed protocol, loads were linearly increased between trials until specimen failure was induced. Only three specimens reached the peak KAM load from the drop-stand prior to failure, which was insufficient for comparison between devices.

CONCLUSIONS

The hypothesis was supported. Combined loading increases ACL strain during simulated landings. During this loading, KAM was the most significant contributor to ACL strain. As such, preventive and rehabilitative measures to reduce ACL injury incidence should continue to focus on limiting frontal plane torques at the knee during landing.

REFERENCES

1. Bates NA, et al. *Clin Bio*, **30**(1), 2015.
2. Bates NA, et al. *Am J Sports Med*, Accepted: in-press.
3. Bates NA, et al. *Clin Bio,* **44**, 2017.
4. Bates NA, et al. *Clin Orthop Relat Res*, **475**(10), 2017.
5. Kiapour AM, et al. *Am J Sports Med*, **44**(8), 2016

ACKNOWLEDGMENTS

NIH grant funding R01AR056259, R01AR055563, K12HD065987, T32AR056950, and L30AR070273

INFLUENCE OF INJURY RISK PROFILES ON ACL STRAIN DURING SIMULATED LANDINGS

Nathaniel A. Bates, Nathan D. Schilaty, Christopher V. Nagelli, Aaron J. Krych, Timothy E. Hewett

Mayo Clinic Biomechanics Laboratories & Sports Medicine Center, Rochester & Minneapolis, MN, USA
email: batesna@gmail.com

INTRODUCTION

Varied levels of anterior cruciate ligament (ACL) injury risk have been established with *in vivo* cohorts largely based on peak knee abduction moment during landing [1]. Specifically, a threshold of >25.25 Nm of knee abduction moment (KAM) during a drop vertical jump (DVJ) landing is a predictor of high injury risk. In addition, anterior tibial shear (ATS) and internal tibial rotation (ITR) are known contributors to ACL strain [2]. Despite this, limited direct data in regards to how these relative levels of injury risk manifest in intra-articular biomechanics are available. Recently a mechanical impactor was developed to simulate DVJ landings and clinical presentations of ACL failure [3]. Therefore, the purpose of this investigation is to quantify how relative levels of injury risk simulated on cadaveric knees influence ACL strain during landing in the mechanical impact simulator. The hypothesis tested was that simulated landing profiles with >25.25 Nm of applied KAM would produce larger ACL strains than lower KAM profiles.

METHODS

45 cadaveric lower extremities were inverted and loaded into the mechanical impactor (Figure 1) to simulate the DVJ landings [4]. Briefly, an impulse force was delivered to each specimen's flat foot in direct alignment with the tibia by dropping a 75 lb weight sled from 31 cm to simulate landing from a DVJ. Immediately prior (~1 sec) to impulse delivery, pneumatic actuators delivered KAM, ATS, and ITR loads to the specimen through a custom designed fixture attached directly to the tibia. These loads were derived from an *in vivo* cohort of 67 healthy athletes who previously underwent full three dimensional motion analysis while they performed DVJ tasks. This *in vivo* cohort was stratified into injury risk levels (baseline, low, medium, and high risk) that corresponded to population percentage of loading (0^{th}, 33^{rd}, 67^{th}, 100^{th} percentile, respectively) as calculated by a Visual3D biomechanical model (Table 1). Loading conditions were applied in a randomized order across each of the three factors (KAM, ATS, ITR). For the present analysis, trials with consistent risk level across each of the three loading factors were used (i.e. low-low-low). As testing was concluded following failure in each specimen, only 20 specimens (age = 39.6±9.1 years;

Table 1: KAM, ATS, & ITR corresponding to load profiles.

Load Profile	KAM (Nm)	ATS (N)	ITR (Nm)
Baseline	1.7	47	1.0
Low-risk	13.5	64	9.7
Med-risk	26.8	80	18.6
High-risk	57.3	196	53.7

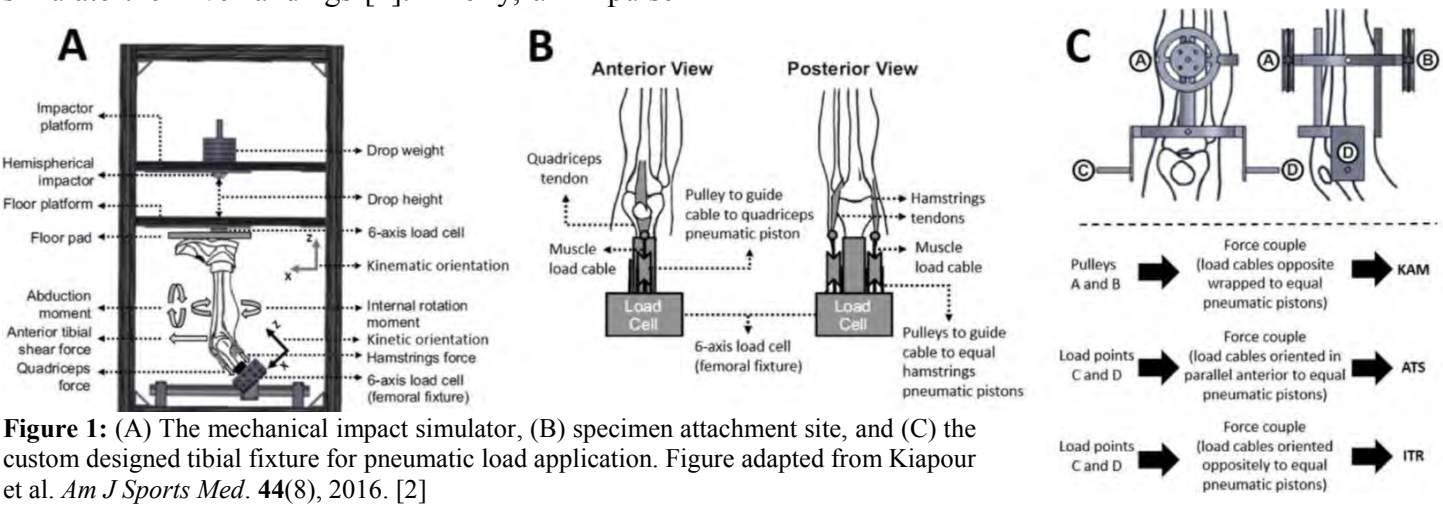

Figure 1: (A) The mechanical impact simulator, (B) specimen attachment site, and (C) the custom designed tibial fixture for pneumatic load application. Figure adapted from Kiapour et al. *Am J Sports Med*. **44**(8), 2016. [2]

Table 2: Mean ACL strain ± standard deviation (%) for each risk profile tested.

Completed Testing	Baseline	Low Risk	Med Risk	High Risk	Pre-Fail	Peak
Med Risk (N = 33)	8.4 ± 7.8¥ Æ	9.0 ± 7.5¥ Æ	9.5 ± 7.1¥ Æ	N/A	13.5 ± 8.0*#†	14.6 ± 8.5*#†
High Risk (N = 20)	6.2 ± 6.8¥ Æ£	6.6 ± 6.0¥ Æ£	7.5 ± 5.8¥ Æ	10.3 ± 6.6‡Δ	12.0 ± 7.0*#†	12.9 ± 6.9*#†

* = significantly different from No Risk; # = significantly different from Low Risk; † = significantly different from Med Risk; ¥ = significantly different from Pre-Fail; Æ = significantly different from Peak; ‡ = trend toward difference (α < 0.1) from No Risk; Δ = trend toward difference (α < 0.1) from Low Risk; £ = trend toward difference (α < 0.1) from High Risk

mass = 93.0±22.0 kg; height = 176.3±8.5 cm; 4F:16M) completed each the baseline, low, medium, and high-risk trials and, thus, were included for analysis. 35 specimens (age = 41.1±8.7 years; mass = 88.5±25.1 kg; height = 173.8±10.9 cm; 16F:19M) completed the baseline, low, and medium risk trials and were included in a subsequent analysis. ANOVA was used to assess ACL strain differences between individual trials for each group (significance = $\alpha<0.05$; trend = $\alpha<0.10$).

RESULTS AND DISCUSSION

Both the medium-risk and high-risk profiles simulated through the mechanical impact simulator exceeded the 25.25 Nm threshold of KAM. For the group that completed high-risk testing (N=20), the high-risk profile trended toward greater ACL strain than the baseline (P=0.05) or low-risk profiles (P=0.08; Table 2). Also, overall peak ACL strain and ACL strain in the trial immediately prior to specimen failure were both greater than the baseline (P<0.01), low (P<0.01), and medium-risk (P<0.03) profiles, but not the high-risk profile ($P\geq$0.21). For the group that completed medium-risk testing (N=35), there were no ACL strain differences between baseline, low, and medium-risk profiles ($P\geq$0.57). All risk profiles in this group exhibited lower ACL strain than the trial immediately prior to failure (P<0.03) as well as the overall peak ACL strain (P<0.01).

The hypothesis was partially supported in that the simulated high-risk profiles, which well exceeded the 25.25 KAM threshold, produced greater ligament strain and were closer to the peak strain before failure than the baseline or low-risk profiles. Conversely, the medium-risk profiles, which slightly exceeded the 25.25 KAM threshold, did not produce larger ACL strains than the baseline or low-risk profiles. However, these medium-risk profiles also did not exhibit lower strain than high-risk profiles.

Literature has documented that neuromuscular interventions effect the greatest biomechanical change on subjects with the highest relative injury risk [5]. The current data would support this notion in that the baseline, low, and medium-risk trials did not express significant changes in ACL strain from one another. The high-risk trials trended toward greater ACL strain, which may lead to greater effects of training interventions. Also, the trending differences of ACL strain likely would have been significant if not collected on DVRTs. The limitation of large between specimen variability in ligament strains collected from DVRTs has been discussed in the literature [6], and can consequently result in underestimated significance.

CONCLUSIONS

Athletes who present the highest levels of loading and relative potential injury risk are likely to place added strain on their ACL during controlled landing tasks. This added strain predisposes these individuals to ACL injury during athletic activity as their ACL is likely approaching near-failure strain during controlled tasks. Interventional training should be focused toward high-risk athletes to reduce the magnitude of strain their ACL experiences during athletic tasks.

REFERENCES

1. Bates NA et al. *J Knee Surg*. **29**(2), 2016.
2. Bates NA et al. *Clin Biomech*. **30**(1), 2015.
3. Bates NA et al. *Am J Sports Med*. Accepted: in-press.
4. Bates NA et al. *Clin Biomech*. **44**, 2017.
5. Hewett TE et al. *Am J Sports Med*. **45**(9), 2017.
6. Bates NA et al. *Clin Orthop Relat Res*. **475**(10), 2017.

ACKNOWLEDGEMENTS

NIH funding from R01AR055563, R01AR056259, K12HD065987, and L30AR070273

VIDEO ANALYSIS OF SECOND ACL INJURY EVENTS IN MALE PROFESSIONAL ATHLETES

[1]Nathaniel A. Bates, [1] Manuela Vargas, [1]Maria C. Mejia Jaramillo, [1]April L. McPherson, [1]Timothy E. Hewett

[1] Mayo Clinic Biomechanics Laboratories & Sports Medicine Center, Rochester & Minneapolis, MN, USA
email: batesna@gmail.com

INTRODUCTION

Annually, 250,000 anterior cruciate ligament (ACL) injures generate $2 billion in reconstructive and rehabilitative expenses. Significant effort has gone into the identification and quantification of the underlying mechanisms of primary ACL injury. Secondary ACL injury (sACL) is observed in approximately one-quarter to one-third of athletes who return to sport following ACL reconstruction [1], but little has been done to evaluate the mechanisms and playing circumstances surrounding these repeat injuries. The aim of the current study was to use publically available videos of sACL events to characterize the mechanics of non-contact sACL injuries including joint kinematics, playing situation and player attention at initial contact (IC), and immediately after. It was hypothesized that during sACL videos athletes would exhibit greater frontal plane hip and knee angles, but not greater hip and knee flexion, at 66 ms following IC than they would at IC.

METHODS

A total of 20 publically available videos of non-contact sACL injuries suffered by male professional and collegiate athletes across various sports that incorporate jumping and cutting maneuvers were identified for analysis. Videos were analyzed in both the frontal and sagittal planes dependent on the camera angles obtained for each athlete. Measurement tools within Kinovea v0.8.15 were used to estimate joint kinematics of an athlete's injured leg at IC, 33 ms after IC, and 66 ms after IC during the sACL event. As allowed by each video, measurements were taken of trunk flexion, trunk frontal plane sway, hip flexion and adduction, knee flexion and abduction, and ankle flexion. These measurements were standardized relative to bony anatomical landmarks on each subject's body. In addition to kinematic measurements, several categorical variables were independently assessed from each video by both raters. Playing situation was categorized as attacking, defending, or celebrating. Player action was categorized as single-leg landing, double-leg landing, cutting, or pivoting. Player attention was selected based on where the player's focus appeared to be immediately prior to injury and was categorized as on the ball, on the opponent, on the objective, or on landing.

RESULTS AND DISCUSSION

Ten videos were captured from American football, two from basketball, five from soccer, and one each from baseball and Australian rules football. Table 1 exhibits outcomes relative to playing situation, player action, and player attention. Average kinematic estimates for each joint at each time point across all videos are displayed in Table 2.

Table 1: Injury circumstances.

	N	%
Playing Situation		
Attacking	10	50
Defending	8	40
Celebrating	1	5
Indeterminate	1	5
Player Action		
Single leg landing	8	40
Double leg landing	0	0
Cutting/ Pivoting	12	60
Player Attention		
Ball	9	45
Opponent	7	35
Objective	3	15
Landing	1	5

No change was observed between IC and 33 ms for any variables of interest. The observed change in knee flexion at 66 ms from IC demonstrated the opposite of the hypothesis, with greater knee flexion observed at 66 ms. There was no significant change in frontal plane knee angle from IC to 66 ms.

Table 2: Joint kinematics during sACL injury event.

Joint	IC		33 ms		66 ms	
	Flexion	Frontal	Flexion	Frontal	Flexion	Frontal
Trunk	13 ± 30	11 ± 8	15 ± 31	12 ± 9	14 ± 30	15 ± 8
Hip	58 ± 29	33 ± 13	58 ± 31	30 ± 15	62 ± 32	20 ± 23
Knee	43 ± 19	5 ± 11	52 ± 22	8 ± 19	72 ± 25*	9 ± 19
Ankle	2 ± 17	---	-6 ± 23	---	-1 ± 26	---

Previous video analysis of primary ACL injury in males demonstrated no change in frontal plane knee angle during landing after initial contact, similar to the present study [2]. Variance in trends was observed in playing situation and player attention in the analysis of sACL injuries compared to primary injury video analysis [3]. In both studies, 25% of the videos analyzed player action involved a single-leg landing. However, primary injury video analysis reported that 33% of injuries occurred in double-leg landings, whereas 55% of cases involved a cutting movement during sACL injury analysis [3]. In both studies, a larger percentage of injuries occurred while the player was attacking compared to defending. In primary injury analysis, the player's attention was most commonly on the basket rim (38%), the opponent (28%), or the ball (23%) [3]. In sACL, the player's attention was most commonly on the ball (45%), followed by the opponent (35%). Rehabilitation and laboratory testing should incorporate these differences into simulations of playing situation and player attention in order to best prepare for return to sport after primary ACL injury.

In healthy drop vertical jumps, athletes demonstrate approximately 30° and 60° changes in hip and knee flexion on the first landing, then 20° and 50° on the second landing [4]. Elite healthy male athletes demonstrate an average flexion of 15.4° and 43.4° at the hip and knee [5]. During sACL events, mean flexion changes were 4° and 29° at the hip and knee. Compared to healthy landings, mean joint excursions for hip and knee flexion from IC to 66 ms during a sACL event were significantly lower. Video analysis of primary injury events also demonstrated greater change in frontal plane hip angle from IC to 66 ms (15°) compared to healthy landings (3°) [4]. Interestingly, changes in frontal plane knee angle were similar between both studies (6°), highlighting the importance of the difference in sagittal plane excursion during a landing that causes injury.

Video analysis has indicated that ACL rupture occurs within 50 ms of ground contact [13]. The results of the current investigation did not reveal statistically significant differences between IC and 33 ms; however, knee flexion angle was greater at 66 ms than at IC. In addition, frontal plane angles trended toward reduced hip adduction at 66 ms. This trend may indicate that the injury occurs between the 33 ms and 66 ms time points after IC; however, additional studies are necessary to determine the exact timing of an injury event.

CONCLUSIONS

Knee valgus collapse was identified in the majority of cases at the time of injury, with knee flexion angle increasing from IC to 66 ms. Athletes experiencing secondary ACL injury exhibited increasing knee and hip flexion after initial contact, which indicated that these ruptures were a product of combinatorial loading at the knee and not isolated frontal plane motion. No additional joint kinematic variables revealed a timing effect. Secondary ACL injuries occurred most frequently during landing and cutting movements. Injuries occurred in both attacking and defensive plays, and most commonly the player was determined to have an external focus, such as the ball or an opponent

REFERENCES

1. Wiggins et al. *Am J Sports Med*. **44**(7), 2016.
2. Hewett et al. *Br J Sports Med*. **43**(6), 2009.
3. Krosshaug et al. *Am J Sports Med*. **35**(3), 2007.
4. Bates et al. *Clin Bio*. **25**(2), 2013.
5. McPherson et al. *Phys Ther Sport*. **22**, 2016.

ACKNOWLEDGMENTS

NIH grant funding R01AR056259 & R01AR055563

KNEE LOADING CORRELATIONS WITH ACL GEOMETRIES DURING SIMULATED LANDINGS

Nathaniel A. Bates, Nathan D. Schilaty, Christopher V. Nagelli, Aaron J. Krych, Timothy E. Hewett

Mayo Clinic Biomechanics Laboratories & Sports Medicine Center, Rochester & Minneapolis, MN, USA
email: batesna@gmail.com

INTRODUCTION

The mechanical function of the anterior cruciate ligament (ACL) as a restraint to multiple degrees of freedom (DOF) in the knee is established [1,2]. However, these determinations were traditionally made under uni- and bi-directional loading, not during dynamic tasks and without consideration of ligament geometry. The objective of this investigation was to establish which geometric properties of the ACL correlated with peak loading at the knee during a simulated drop landing task. It was hypothesized that geometric parameters that increase ACL cross sectional area (CSA) would correlate with peak anterior, abduction, and flexion loads, but not with peak ACL strains.

METHODS

45 cadaveric lower extremity specimens were subjected to drop landing impulses in the mechanical impact simulator as described in the literature [3]. Briefly, a 34 kg weight sled delivered an impulse force to the foot of each specimen while pneumatic actuators applied loads about the knee joint that are associated with increased ACL strain (knee abduction moment (KAM), anterior tibial shear (ATS), internal tibial rotation (ITR)) [1,2]. The magnitudes of these loads were determined from *in vivo* motion analysis performed on 67 healthy athletes who performed drop vertical jump tasks and were stratified into the 0th, 33rd, 67th, and 100th percentile of that population cohort (Table 1). This stratification represented the anticipated distribution of injury risk (baseline, low-risk, medium-risk, high-risk) across the *in vivo* cohort [4]. The order in which stratification was applied was randomized for each load variable. A 6-axis load cell aligned with the femur collected knee joint loading, while implanted DVRT strain gauges recorded ACL strain. Prior to testing, an MRI was performed on the knee of each specimen and these DICOM images were used to calculate the width (transverse view, midsubstance), depth (sagittal view midsubstance), and length (sagittal view, midline) of the ACL. ACL CSA was then estimated as width*depth. Seven specimens were excluded for unsuitable tissue quality or complications from the experimental protocol, which left 38 specimens for analysis (19F:19M, age = 41.6±8.5 years; mass = 84.3±24.3 kg). Multivariate linear regression models were then used to correlate these four factors against peak knee joint loading in each DOF and peak ACL strain for each simulated condition. Significance was determined at $\alpha<0.05$.

Table 1: KAM, ATS, & ITR corresponding to load profiles.

Pop. Percentile	KAM (Nm)	ATS (N)	ITR (Nm)
0%	1.7	47	1.0
33%	13.5	64	9.7
67%	26.8	80	18.6
100%	57.3	196	53.7

RESULTS AND DISCUSSION

The geometric factors model was correlated with peak anterior force, compressive force, and flexion torque throughout testing ($P<0.05$; Table 2). ACL CSA was a significant factor for peak anterior force and peak flexion torque across all simulated conditions ($P<0.04$). ACL CSA also largely correlated with compressive/ distractive forces ($P<0.05$), and with KAM in select trials where the 100th percentile of KAM was applied ($P<0.03$). ACL width and depth individually mimicked the behavior of ACL CSA in that they correlated with anterior force, distraction force, and flexion torque at the knee ($P<0.05$). These similarities were unsurprising as width and depth are used to calculate ACL CSA. ACL length was significantly correlated with anterior knee force and knee flexion torque in simulations where applied KAM and ATS loading were under the 100th percentile ($P<0.05$). There were no significant correlations between any geometric factor and peak ACL strain ($P \geq 0.10$).

Table 2: R-squared values from the full linear model of geometric factors compared to knee loading in six DOFs for each simulation condition. Shaded cells indicate significant (P<0.05) correlation between ACL geometry and the indicated knee load variable.

ACL Geometry vs. Peak Anterior Force

ATS & ITR Applied \ KAM Applied	0%	33%	67%	100%
0%, 0%	0.47	0.59	0.56	NaN
0%, 33%	0.48	0.48	0.52	NaN
0%, 67%	0.50	0.51	0.48	NaN
33%, 0%	0.48	0.52	0.53	NaN
33%, 33%	0.48	0.53	0.45	0.65
33%, 67%	0.50	0.50	0.54	0.56
33%, 100%	NaN	0.65	0.45	0.56
67%, 0%	0.43	0.50	0.53	NaN
67%, 33%	0.54	0.46	0.59	0.46
67%, 67%	0.51	0.47	0.49	0.62
67%, 100%	NaN	0.61	0.61	0.68
100%, 33%	NaN	0.62	0.66	0.52
100%, 67%	NaN	0.64	0.64	0.65
100%, 100%	NaN	0.68	0.66	0.67

ACL Geometry vs. Peak Medial Force

ATS & ITR Applied \ KAM Applied	0%	33%	67%	100%
0%, 0%	0.90	0.93	0.98	NaN
0%, 33%	0.90	0.98	0.92	NaN
0%, 67%	0.85	0.95	0.95	NaN
33%, 0%	0.94	0.93	0.95	NaN
33%, 33%	0.94	0.96	0.99	0.50
33%, 67%	0.84	0.91	0.92	0.61
33%, 100%	NaN	0.51	0.94	0.19
67%, 0%	0.78	0.83	0.96	NaN
67%, 33%	0.67	0.99	0.98	0.50
67%, 67%	0.93	0.94	0.93	0.27
67%, 100%	NaN	0.90	0.92	0.33
100%, 33%	NaN	0.83	0.89	0.28
100%, 67%	NaN	0.69	0.88	0.18
100%, 100%	NaN	0.68	0.43	0.45

ACL Geometry vs. Peak Compression Force

ATS & ITR Applied \ KAM Applied	0%	33%	67%	100%
0%, 0%	0.36	0.40	0.37	NaN
0%, 33%	0.37	0.35	0.34	NaN
0%, 67%	0.36	0.36	0.32	NaN
33%, 0%	0.33	0.42	0.35	NaN
33%, 33%	0.34	0.35	0.33	0.69
33%, 67%	0.36	0.37	0.40	0.77
33%, 100%	NaN	0.42	0.46	0.75
67%, 0%	0.38	0.40	0.40	NaN
67%, 33%	0.39	0.36	0.39	0.65
67%, 67%	0.34	0.35	0.35	0.71
67%, 100%	NaN	0.32	0.45	0.67
100%, 33%	NaN	0.30	0.48	0.50
100%, 67%	NaN	0.42	0.44	0.76
100%, 100%	NaN	0.46	0.31	0.47

ACL Geometry vs. Peak Abduction Torque

ATS & ITR Applied \ KAM Applied	0%	33%	67%	100%
0%, 0%	0.11	0.18	0.20	NaN
0%, 33%	0.17	0.16	0.13	NaN
0%, 67%	0.11	0.13	0.13	NaN
33%, 0%	0.11	0.12	0.11	NaN
33%, 33%	0.16	0.20	0.12	0.38
33%, 67%	0.09	0.08	0.13	0.25
33%, 100%	NaN	0.09	0.14	0.36
67%, 0%	0.15	0.15	0.10	NaN
67%, 33%	0.12	0.11	0.30	0.25
67%, 67%	0.10	0.09	0.16	0.39
67%, 100%	NaN	0.22	0.17	0.53
100%, 33%	NaN	0.10	0.22	0.49
100%, 67%	NaN	0.09	0.32	0.39
100%, 100%	NaN	0.22	0.08	0.49

ACL Geometry vs. Peak Flexion Torque

ATS & ITR Applied \ KAM Applied	0%	33%	67%	100%
0%, 0%	0.49	0.55	0.55	NaN
0%, 33%	0.45	0.48	0.51	NaN
0%, 67%	0.50	0.51	0.48	NaN
33%, 0%	0.49	0.51	0.51	NaN
33%, 33%	0.49	0.53	0.43	0.61
33%, 67%	0.48	0.49	0.52	0.51
33%, 100%	NaN	0.52	0.45	0.50
67%, 0%	0.43	0.47	0.51	NaN
67%, 33%	0.50	0.49	0.56	0.47
67%, 67%	0.52	0.46	0.45	0.52
67%, 100%	NaN	0.57	0.51	0.55
100%, 33%	NaN	0.52	0.53	0.44
100%, 67%	NaN	0.52	0.51	0.55
100%, 100%	NaN	0.57	0.57	0.72

ACL Geometry vs. Peak Internal Torque

ATS & ITR Applied \ KAM Applied	0%	33%	67%	100%
0%, 0%	0.10	0.17	0.11	NaN
0%, 33%	0.11	0.10	0.09	NaN
0%, 67%	0.11	0.13	0.14	NaN
33%, 0%	0.07	0.13	0.17	NaN
33%, 33%	0.09	0.10	0.10	0.43
33%, 67%	0.11	0.10	0.09	0.44
33%, 100%	NaN	0.13	0.51	0.40
67%, 0%	0.09	0.11	0.10	NaN
67%, 33%	0.08	0.10	0.11	0.25
67%, 67%	0.11	0.10	0.08	0.41
67%, 100%	NaN	0.10	0.15	0.49
100%, 33%	NaN	0.09	0.27	0.32
100%, 67%	NaN	0.16	0.27	0.36
100%, 100%	NaN	0.19	0.10	0.31

The hypothesis was partially supported. As the ACL resists up to 85% of the anterior translation of the knee [1], it was expected that ligament geometry would significantly influence this DOF. Flexion is the primary DOF of knee function; therefore, larger ACL CSA was expected to better constrain the knee to the sagittal plane and increase the peak flexion moment during landing. The ACL resists KAM [3]; thus, a larger ACL CSA was expected to provide greater constraint to this DOF and limit the magnitude of frontal plane torque during landing. Such a relationship was not presently observed. As KAM plays an integral role in relative ACL injury risk [4], it would be interesting to examine whether there is variation in ACL CSA between ACL injured athletes and matched healthy controls. ACL length was not expected to exhibit significant correlation with knee loading as length does not influence ligament material properties. Correlation of anterior force and flexion torque with ACL length in lower load simulations likely was the product of longer ACLs achieving load bearing later in testing than shorter ACLs. In high load simulations, the ACL was immediately required to restrain the joint and correlations dissipated.

CONCLUSIONS

ACL geometry, primarily ACL CSA, influences anterior knee force and knee flexion torque during simulated landings; and, should have implications for injury risk and reconstruction graft selection.

REFERENCES

1. Nesbitt et al. *J Biomech*. **47**(9), 2014.
2. Bates et al. *Clin Biomech*. **30**(1), 2015.
3. Bates et al. *Clin Biomech*. **44**, 2017.
4. Bates et al. *J Knee Surg*. **29**(2), 2016.

ACKNOWLEDGEMENTS

NIH funding from R01AR055563, R01AR056259, K12HD065987, and L30AR070273

ADAPTATION OF LOWER LIMB JOINT WORK IN SINGLE LEG HOPPING AFTER UNILATERAL ANKLE FATIGUE

Elizabeth M. Bell, Edward Chu, Sara Honarvar, Kyung Koh, Ross H. Miller, and Jae Kun Shim

Neuromechanics Research Core, University of Maryland, College Park, MD, USA
email: lizbell@terpmail.umd.edu, web: http://www.sph.umd.edu/neuromechanics

INTRODUCTION

Performing voluntary movements is complex since the human motor system has more elements contributing to performance than what is necessary to "solve" a motor task (a problem referred to as motor abundancy [1]). Having many solutions to a motor problem may allow for flexibility in how the central nervous system (CNS) selects a motor task solution when dealing with perturbations. Fatigue, an internal perturbation, is an acute neuromuscular state and a term commonly used to describe the point where performance aspects, such as power production, are impaired [2]. Fatigue has neural (central) and muscular (peripheral) mechanistic causes. Neural fatigue is associated with the failure of the nervous system to excite the muscle maximally decreasing the ability of the nervous system to demand force [3]. Muscular fatigue is thought to be a result of metabolic inhibition and decreases the ability of muscles to produce force [3]. Both aspects of fatigue may reduce force production and change the strategy used by the CNS during movements which require high force production like single leg hopping. Distinguishing which aspects of neuromuscular fatigue may perturbate the CNS into selecting a different coordination strategy is difficult, as frequently neural and muscular causes are intertwined.

This study aimed to better understand the biomechanical response to neural and muscular fatigue by examining how joint work is coordinated during the motor task of repeated single leg hopping. Participants performed single leg hops bilaterally, before and after unilateral, exercised based fatigue of an ankle joint. This design allows for the effect of neuromuscular fatigue to be examined (exercised leg) as well as the effect of neural fatigue in the absence of muscular fatigue (non-exercised leg). With this experimental design, adaptations in joint work observed for the exercised leg but not for the non-exercised leg may be attributed to muscular fatigue. We hypothesized that, before exercise, both limbs would generate a similar distribution of joint work. After exercise, the work production strategy within the exercised limb would adapt to compensate for the reduced ability of the exercised ankle muscles to generate force, which would result in reduced ankle joint work. If the non-exercised limb also altered joint work production, then aspects of neural fatigue may also be influencing strategy used by the CNS.

METHODS

Fifteen healthy volunteers (7 male; 21.5 ± 2.7 years) participated after completing informed consent procedures approved by the local Institutional Review Board. Each participant hopped for 30 s on both legs before and after exercise procedures. During hopping participants matched their frequency to an audible metronome signal of 2 Hz. One (randomly selected) limb performed exercises to generate neuromuscular fatigue at the ankle. Exercise procedures consisted of 15 sets of 10 repetitions of single-leg calf raises, with 30 seconds of rest in between sets. Participants were instructed to perform each repetition with a smooth and controlled motion, and to hold the maximum plantarflexion at the top of the raise for 1 s. Calf raises were performed on an elevated surface to allow the exercised leg to perform full ankle range of motion dorsiflexion and plantarflexion, and the non-exercised leg to rest.

Four motion capture trials consisting of 60 hops each (13 cameras, Vicon, Oxford, UK) were collected for each participant. Kinematics (200Hz) were collected simultaneously with analog data (1000Hz; Kistler, Amherst, NY). Inverse dynamics procedures were performed with Visual3D software (C-Motion,

Germantown, MD). Vertical center of mass displacement was estimated by using the trajectory of the marker placed on the hopping limbs' anterior superior iliac spine. Ground contact times, hopping frequency and joint work values were calculated for each participant in a customized matlab script.

Paired t-tests were performed to test for within-limb differences in jump height, ground contact times and hopping frequency before and after exercise (α = 0.05). A two-way repeated measures ANOVA (α = 0.05) with Time (before and after exercise) and Leg (exercised and non-exercised) was conducted on net (Wnet), negative (Wneg), and positive (Wpos) joint work performed throughout a hopping cycle. Post hoc tests using the Bonferroni correction were used to determine simple main effect (within-limb and within-time point) differences in Wnet, Wneg, and Wpos.

RESULTS AND DISCUSSION

No statistically significant differences were found in within-limb hopping cycle frequency or ground contact time (all $p > 0.10$). However, mean jump height of the exercised limb significantly ($p < 0.01$) reduced (7.2 ± 2.6 cm to 5.9 ± 2.4 cm) after exercise.

At the ankle joint, significant interactions between Time and Leg were found in Wnet, Wneg and Wpos (all $p \leq 0.01$) with significant within-limb and within-time point differences exhibited after exercise (all $p \leq 0.01$). The exercised limb attempted to compensate for the significant reduction in ankle work by eliciting greater knee joint work. At the knee, significant interactions between Time and Leg were found in Wnet, Wneg and Wpos (all $p \leq 0.02$) and significant within-limb and within-time point differences were indicated after exercise (all $p \leq 0.01$; except for within-time Wneg p = 0.06). Analysis indicated no statistically significant interactions or main effect differences in hip joint work, within the non-exercised limb or between limbs at the pre-exercise time point.

CONCLUSIONS

Examining the coordination of joint work during the motor task of repeated single leg hopping before and after exercise established that neuromuscular fatigue significantly affects overall hopping behavior. Neuromuscular fatigue, significantly affected the work produced at the exercised ankle joint. However, the role of neural fatigue on its own did not significantly affect joint work strategy during hopping. These findings suggest that muscular fatigue is likely the major contributor to neuromuscular fatigue which affects overall hopping coordination, while neural fatigue may play a minimal role. Therefore, if fatigue is mostly due to muscular effects, then motor performance may be regained after muscle recovers from muscular fatigue.

REFERENCES

[1] Latash, M. Exp. Brain Res 217(1)1-5, 2012.
[2] Enoka RM J Physiol. 86(1):11-23, 2008.
[3] Taylor JL Clin Exp Pharml Physiol. 33(4):400-405, 2006.

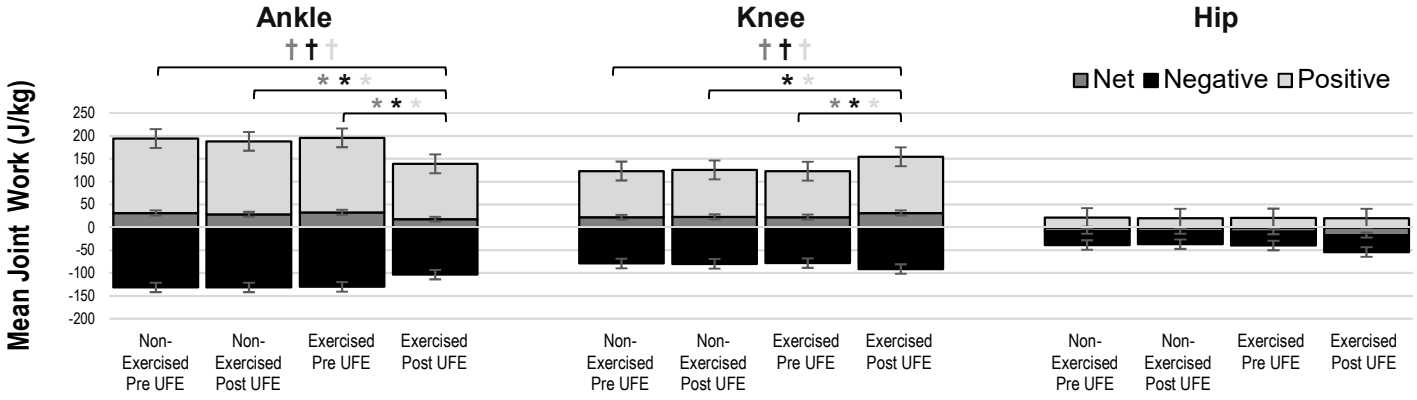

Figure 1: Mean (±SE) joint work for the ankle, knee, and hip before (Pre) and after (Post) unilateral fatiguing exercise (UFE) at the ankle joint. Crosses indicate a significant († $p < 0.05$) interaction within the joint and asterisks indicate a significant post hoc pairwise difference (* $p < 0.025$).

ZERO ECHO TIME (ZTE) IMAGING BONE and JOINTS

[1]Ryan Breighner, [1]Erin Argentieri, [1]Darryl Sneag, [1]Matthew F. Koff, and [1]Hollis G. Potter

[1] Radiology and Imaging, Hospital for Special Surgery, New York, NY, USA
email: breighnerr@hss.edu

INTRODUCTION

This paper presents findings of several studies employing the use of proton density-weighted zero echo time (ZTE) MRI of bone in the hip[1], shoulder[2], cervical spine[3], and ankle. ZTE is a radial MR acquisition that yields images at/near isotropic resolution, making them amenable to multiplanar reformats (MPR). Due to short tissue relaxation times and signal scarcity, routine MRI does not provide direct visualization of bone. However, ZTE affords the acquisition of the scarce signal present in bone and, with appropriate post-processing, provides positive, 'CT-like' contrast for bone. In particular, applications to hip dysplasia/FAI, shoulder stability and shoulder osteoarthritis, cervical neuroforaminal stenosis (NFS), and malleolar fractures of the ankle have been examined. Across these studies, ZTE MRI has been employed for bone imaging and provides an ionizing radiation-free means to image osseous tissues for clinical and research purposes. It is our contention that zero echo time MRI may mitigate the need for CT in some clinical cases.

In concert with clinical collaborators, we have conducted these studies to address scenarios in which MRI is clinically warranted for soft tissue assessment and concurrent CT is ordered to assess osseous pathology/injury. We have generally found 'good' to 'excellent' agreement in both subjective and quantitative measurements and grading obtained from CT and ZTE MRI, and, where applicable, we have similarly found comparable interrater agreement in ZTE grades and measurements to be comparable to interrater agreement in CT.

METHODS

As part of a larger IRB-approved study investigating improvements to musculoskeletal MRI, patient cohorts comprising of 24 hips, 34 cervical spines, 34 shoulders, and 14 ankles were recruited from institutional radiology schedules. Subjects were selected for the specific joint pathologies mentioned above and relevant concurrent imaging (CT or radiographs within a given time period of MRI, augmented with a ZTE pulse sequence).

General imaging parameters used were as follows: TR: 300ms, flip angle: 1°, receiver bandwidth: ±62.5 kHz, matrix size: 320, slice thickness: 1.2-1.5 mm, scan time: ~4-6 mins. MRI scanning was performed on clinical 3.0T or 1.5T scanners (Discovery MR750 or MR450W, GE Healthcare, Waukesha, WI). Standard patient positioning and commercial coils were utilized for all imaging (8-channel cardiac or 32-ch body coils for hip, 3-ch or 8-ch shoulder coils, 8-ch foot/ankle, and 32-ch head/neck/spine coil array).

Clinically relevant grading scales and measurements were established to assess the various pathologies. In particular, a 6-pt scale from 'none' to 'severe' was used to assess NFS. In the shoulder, osteoarthritis (OA), instability, injury, and available bone stock were assessed using Walch's classification for glenoid erosion, a subjective 4-pt scale for OA severity, as well as glenoid vault depth, Hill-Sachs and Bankart lesion sizes, and glenoid version angle. In the ankle, comparison to operative findings was utilized as a gold standard for diagnosis of malleolar fractures. Additionally, comparison of fracture length measurements was made in the subset of the ankle cohort (N = 3) for which concurrent CT was available. In the hip, an institutional standard battery of measurements was used for the assessment of FAI/dysplasia, consisting of center-edge-angles (CEA) in sagittal and coronal planes, axial acetabular version (AV) at 3 loci, femoral neck-shaft angle (FNS), Tönnis angle, and alpha and modified beta angles (assessing angles subtended by the femoral head-neck junction to the femoral neck axis and clearance between the head-neck junction and the acetabular rim, respectively).
Measurements and grading were performed by board-certified musculoskeletal radiologists in a blinded fashion. Binary grading task agreement (e.g.

ankle fracture presence/absence) was assessed using the Kappa statistic. Multilevel grading task agreement (Walch grade, NFS grade, subjective OA score, etc.), was assessed using Cohen's Kappa, and weighted Kappa, where appropriate. Intraclass correlation coefficients ($ICC_{2,1}$) were utilized to assess agreement among continuous measurements (linear and angular measurements such as shoulder lesion sizes and hip coverage angles).

RESULTS AND DISCUSSION

A summary of the agreement statistics utilized in the various studies is provided in table 1. Across all three types (multilevel, binary, and continuous grading/measurement), it has been shown that comparison to operative findings and CT image-based gold standards, ZTE MRI-based measurements and grading consistently agree.

Table 1. Summary of agreement statistics across ZTE MRI studies. Agreement ranges are listed when multiple measures of the same type were assessed. Measurement types are continuous measurement (CM), binary grading (BG), and multi-level grading (MLG). *agreement for was not significant for two measurements owing to lack of condition prevalence in the cohort (bankart lesion width and percent width loss).

Study *(Type)*	*agreement statistic* $icc_{2,1}$	κ	*agreement*
Hip (CM)	0.45-0.89	--	'moderate'-excellent'
Cervical Spine (MLG)	--	0.72-0.75	'substantial
Ankle (CM)	0.99	--	'excellent'
(BG)	--	0.84-1.00	'substantial' - 'excellent'
Shoulder (BG)	--	0.62-1.00	'substantial' - 'excellent'
(MLG)	--	0.63-1.00	'substantial' - 'excellent'
(CM)	0.79-0.98*	--	'substantial' - 'excellent'

In addition to the above summary, figures 1 shows comparable images generated in both CT and ZTE in the completion of the hip and shoulder studies discussed herein indicating the strong morphological agreement borne out in the above results. Figure 2 shows surface meshes derived from ZTE MRI using semi-automated segmentation approaches.

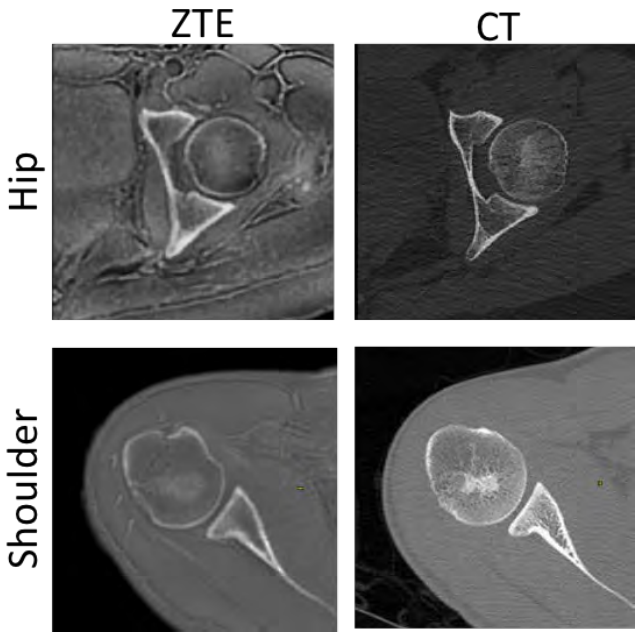

Figure 1. Axial ZTE and CT images acquired of the hip and shoulder. Note that slight postural variations between acquisitions account for the slight differences in humeral orientation.

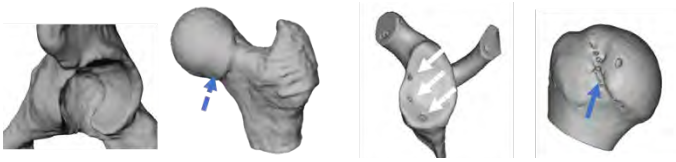

Figure 2. 3D surface meshes of hip and shoulder generated from ZTE MRI. From left to right, an acetabulum, proximal femur showing cam-type FAI lesion, en-face glenoid showing evidence of suture anchor tracks, and a humeral head revealing hill-sachs lesion.

CONCLUSIONS

Given the strong levels of agreement generally seen in the results presented, ZTE MRI exhibits some degree of diagnostic equivalence to CT for some grades and measures and may potentially be applied clinically or in research where CT-radiation dose is deemed too great a risk.

REFERENCES

1. Breighner et al. *Radiology,* 2018.
2. Argentieri et al. *Spine*, 2017.
3. Breighner et al. Paper #198 *ORS 2018, New Orleans, LA*.

SAGITTAL PLANE TRUNK AND LOWER EXTREMITY MOVEMENT DURING A SINGLE LEG DROP TASK AT 6 AND 12 MONTHS AFTER ANTERIOR CRUCIATE LIGAMENT RECONSTRUCTION

[1]Matthew S. Briggs, [1]Stephanie Di Stasi, [1]Joshua T. Hoffman, [1]Samuel C. Wordeman, [1]Laura C. Schmitt, [2]Mark V. Paterno, [3]Timothy E. Hewett

[1] The Ohio State University, Columbus, OH, USA
[2]Cincinnati Children's Hospital Medical Center, Cincinnati, OH, USA
[3]Mayo Clinic, Rochester, MN, USA
email: Matt.Briggs@osumc.edu

INTRODUCTION

Decreased trunk, hip, and knee flexion and increased ankle dorsiflexion during dynamics tasks have been associated with increased risk of anterior cruciate ligament (ACL) injury.[1-4] In addition, risk of second injury after ACL reconstruction (ACLR), to either the involved or uninvolved knee, is dramatically higher than risk of initial injury.[5,6] However, investigation of trunk, hip, knee, and ankle kinematics after ACLR during dynamic tasks is limited.

The objective of this study was to identify differences in sagittal plane trunk and lower extremity movement in patients during a single-leg landing task at 6 month and 12 months following ACLR and compare values to matched uninjured controls.

METHODS

Ten patients [7 males; 3 females] with landing data at 6 and 12 months following ACLR were included in this study and matched to 10 uninjured controls without ACL injury. The dominant limb of the control group was used for comparison during one testing session. Fifty-five retro-reflective markers were adhered to the skin at anatomical and tracking landmarks for testing sessions. Three-dimensional motion capture data was collected bilaterally for 3 successful single leg drop (SLD) landings off a 31cm tall box for all groups. During the SLD, participants balanced on one leg, dropped from the box and landed on the same limb. Marker trajectories were collected at 240Hz using a 12-camera motion capture system and filtered at 12Hz using a Butterworth low-pass filter. Sagittal plane peak angles for the trunk, hip, knee, and ankle were analyzed for the first 100 milliseconds after initial contact for each task. Discrete variables were taken from each subject's individual data and time series averages were calculated on a time-point by time-point basis. Statistical analyses included repeated analysis of variance and paired t-tests. Significance was set to $p<0.01$ after correction for multiple comparisons to evaluate simple effects.

RESULTS AND DISCUSSION

During the SLD, interactions of time and limb were present for peak hip flexion, peak knee flexion, and peak angle dorsiflexion angles. Overall, *post-hoc* testing demonstrated decreased hip and knee flexion and ankle dorsiflexion on the uninvolved limb at 12 months following ACLR compared to 6 months (Fig. 1). More specifically, at 12 vs. 6 months for the ACLR group there was decreased hip flexion on the uninvolved side [mean(SD), 27.28°(8.29), 38.17°(5.59); p=0.001)]; decreased knee flexion on the uninvolved side [45.77°(5.92), 49.84°(5.15); p=0.001)]; less ankle dorsiflexion on the uninvolved side [-13.07°(3.07),1.93°(8.55); p=0.001)], and less ankle dorsiflexion on the involved side [-13.45°(2.17), 1.01°(11.97); p=0.008)]. When comparing side to side differences there was less knee flexion on the involved side vs. the uninvolved side at 6 months for the ACLR group [43.67°(4.77), 49.84(5.15); p<0.001)]; less ankle dorsiflexion on the uninvolved side at 12 months compared to the involved side at 6 months for the ACLR group [13.07°(3.07), 1.01°(11.97); p=0.006)]; and less ankle dorsiflexion on the involved side at 12 months vs. the uninvolved side at 6 months for the ACLR

group [-13.44°(2.17), 1.92°(8.55); p=0.001)]. Finally, there was greater ankle dorsiflexion on the uninvolved side at 6 months vs. the control group [1.92°(8.55), -9.04°(4.05); p=0.009)]. There were no interactions or main effects for sagittal plane trunk excursion.

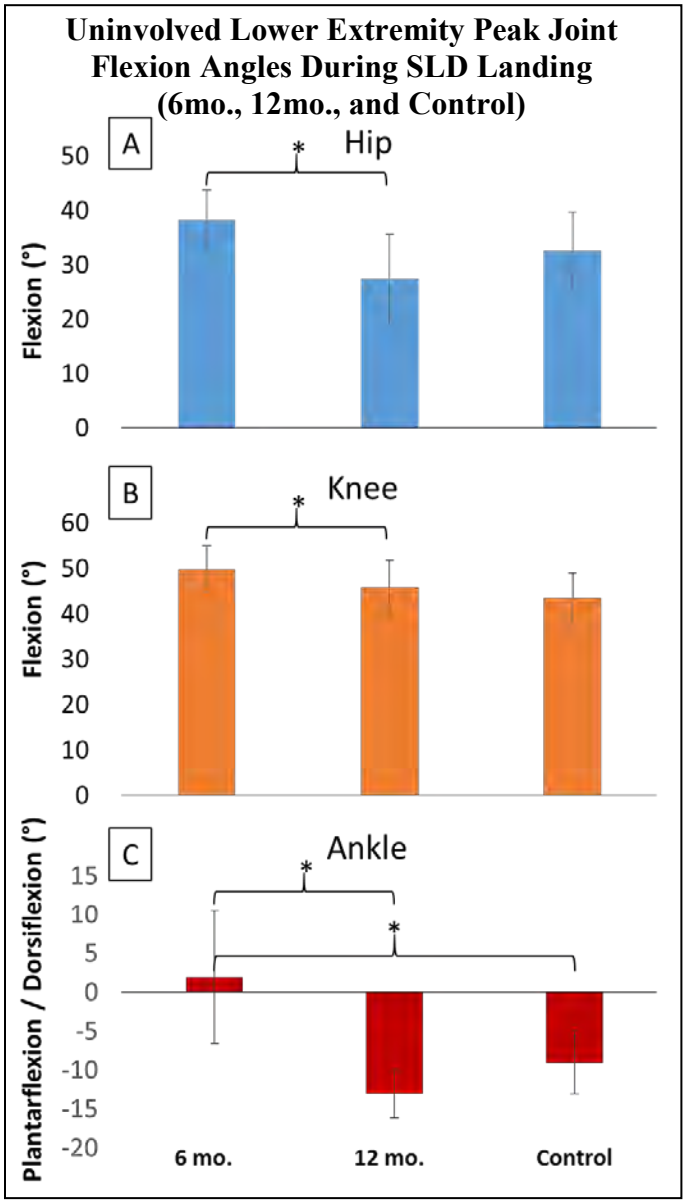

Figure 1: Mean sagittal plane peak angles for the uninvolved limb and control group during the first 100 milliseconds of landing for the A) Hip, B) Knee, and C) Ankle (dorsiflexion is positive and plantar flexion is negative). Single Leg Drop = SLD. *p<0.01. Error bars = standard deviation.

Increased hip and knee flexion during a drop jump has been shown to decrease anterior tibial shear forces thus reducing ACL stress.[7] Further, landing in more dorsiflexion has been associated with increased ground reaction forces, increased ACL peak forces, and ACL injury. [3,4,8,9] The results from the current data demonstrate overall decreased hip and knee joint flexion and less ankle dorsiflexion, in particular on the uninvolved limb, at 12 vs. 6 months following ACLR. The movement patterns at the hip and knee have potential to increased ACL stress based on previous evidence, whereas the decrease in dorsiflexion may serve to offset this stress.

Limitations of the current study include a small sample size and limited numbers of female patients, who have been shown to be at a higher risk of initial and second ACL injury.[5,6] Further evaluation of kinetics of the lower extremity will provide additional insight into joint loading patterns during the SLD. This information will provide valuable insights into sagittal plane trunk and lower extremity mechanics and potentially secondary ACL injury risk.

CONCLUSIONS

Overall, patients demonstrate decreased hip and knee flexion and ankle dorsiflexion on their uninvolved limb at 12 months following ACLR compared to 6 months. In general, decreased lower extremity joint flexion is viewed as a high risk movement pattern. Understanding these lower extremity movement patterns over time following ACLR may assist in designing interventions focused on minimizing the risk of second and contralateral ACL injury.

REFERENCES

1.Hewett TE, et al. *Br J Sports Med.***43** 2009.
2.Leppänen M, et al. *Orthopaedic journal of sports medicine.***5** 2017.
3.Koga H, et al. *Am J Sports Med.***46** 2017.
4.Boden BP, et al. *Am J Sports Med.***37** 2009.
5.Paterno MV, et al. *Clin J Sport Med.***22** 2012.
6.Paterno MV, et al. *Am J Sports Med.***42** 2014.
7.Tsai L-C, et al. *J Sports Sci.***35** 2017.
8.Heinrich D, et al. *Scand J Med Sci Sports.***24** 2014.
9.Fong C-M, et al. *Journal of athletic training.***46** 2011.

NUMBER OF SUCCESSIVE CRANK CYCLES NEEDED TO ACHIEVE STABLE PEDAL FORCES DATA

Harsh H. Buddhadev, Daniel L. Crisafulli, Jenny N. Duong, Jun G. San Juan, and David N. Suprak

Western Washington University, Bellingham, WA, USA
email: harsh.buddhadev@wwu.edu

INTRODUCTION

Cycling is frequently prescribed for rehabilitation of individuals with knee osteoarthritis (OA) because it is a low-weight bearing and non-impact form of physical activity. Few researchers have contrasted symmetry of pedaling power [1] and lower limb net joint moment variables [2] in individuals with knee OA and healthy controls over a range of submaximal power outputs and cadences.

Interestingly, the number of cycles of data analyzed in these studies varies drastically (ranging from 3 cycles [2] to 60 cycles [1]). This large range is understandable because no research has examined the number of successive crank cycles needed to achieve stable data for such analyses. Sequential average analysis is a common technique used to determine the trial size needed to obtain stable reaction force data for various activities such as running [3], walking [4], jumping [5], and landing [6].

The purpose of our study was to determine the number of successive crank cycles needed to achieve stable pedal force data in individuals with knee OA and healthy controls across submaximal power output and cadence conditions using the sequential average analysis method.

METHODS

Twelve individuals with knee OA (67.3 ± 7.6 years; 6 females and 6 males) and 12 age- and sex-matched healthy controls (66.1 ± 7.3 years) participated in the study. Each participant completed a single 1-hour testing session. Following a bicycle set-up procedure that standardized the cycling posture on a Velotron bicycle ergometer, participants completed a 5-minute warm-up ride at 50 W at self-selected cadence. They then completed 2 minutes of pedaling at 75W-60rpm, 75W- 90rpm, 100W-60 rpm, and 100W-90rpm. These conditions were interspersed by 3-5 minute rest intervals. Anterior-posterior (AP), medial-lateral (ML), and normal pedal reaction forces were sampled synchronously at 250 Hz using a strain gauge instrumented Sensix I-crankset force pedal system for 60 seconds. The pedal force data were low pass filtered at 4 Hz [1].

For the sequential analysis procedure, force data were analyzed from the more affected leg of the knee OA group and the dominant leg of the control group. Successive average pedal force values were computed by averaging each crank cycle's data with that of all previous crank cycles (i.e. moving average computation). Therefore, the successive average force value of 60th crank cycle will be equal to the average force value for the 60 cycles of data. Next, for each component of the force, mean and standard deviation (SD) values were calculated for 60 crank cycles of data. A stability criterion (mean ± 0.25 SD), identical to the one in previous studies [3-6], was applied to the successive average crank cycle data for each component of the force. Stability was determined as one crank cycle greater than the smallest crank cycle number for which all successive mean deviations were within ± 0.25 SD value for a given participant and component of force.

Two-way mixed model ANOVA with repeated measures on power output and cadence was used to examine the differences in the stable number of crank cycles needed for knee OA vs. the healthy control group. Significant differences were considered at $p < 0.05$. Small, medium, and large effect sizes correspond to partial eta squared (η_p^2) values of 0.01, 0.06, and 0.15, respectively [7].

RESULTS AND DISCUSSION

Across all the experimental conditions and different components of pedal forces, it is apparent that the

number of crank cycles needed to obtain stable data ranges from 25-33 crank cycles (figure 1).

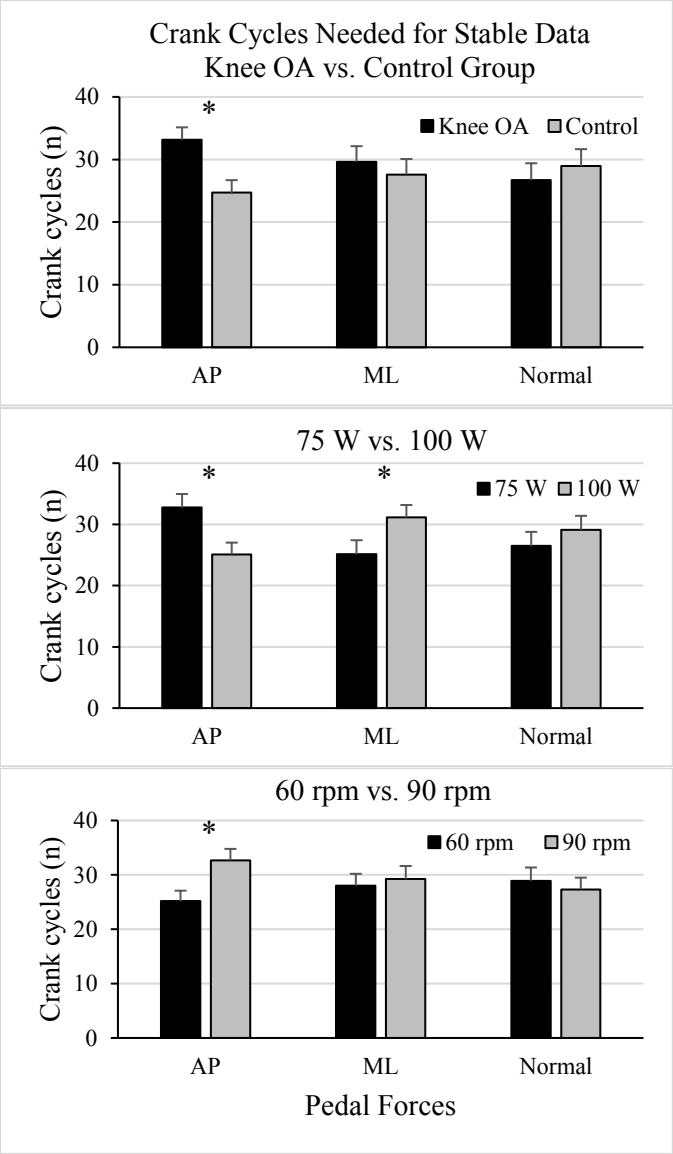

Figure 1. Number of crank cycles needed to achieve stable pedal force. Data presented as Mean ± standard error.

The AP component of pedal force was most affected by group differences and effects of power output and cadence. Conversely, the normal component of pedal force was not affected by any of these variables ($p > 0.05$). The knee OA group needed 8 additional crank cycles for stable data than the control group for the AP component of pedal force ($p = 0.007$; $\eta_p^2 = 0.291$). We speculate the higher interlimb asymmetry demonstrated by knee OA vs. the control group may be the underlying factor [1]. For the AP forces, fewer crank cycles (n = 8) were needed to obtain stable data when pedaling at lower cadence ($p = 0.020$; $\eta_p^2 = 0.291$) and higher power output ($p = 0.015$; $\eta_p^2 = 0.240$). Pedal force effectiveness is increased when cycling at lower cadence and higher power outputs [8]. We suspect pedal force effectiveness improvement under these conditions, could potentially explain why fewer crank cycles were needed to obtain stable AP pedal force data when pedaling at lower cadence and higher power output. Opposite to the results of AP forces, when pedaling at higher power output (100 W), 6 additional crank cycles were needed to achieve stable ML force data compared to lower power output (75 W; $p = 0.012$; $\eta_p^2 = 0.254$). The ML component of pedal force has a very small contribution towards pedal force effectiveness. We suspect this may be the reason for the results of ML forces not being aligned with those of AP forces for the effect of power output.

CONCLUSIONS

Data from successive 25-33 crank cycles would be needed to achieve stable three dimensional pedal force data during submaximal cycling. Individuals with knee OA would need greater number of crank cycles to attain stable data compared to healthy controls. Pedaling at lower compared to higher cadences, will require less crank cycles of data to achieve stable pedal force values. Finally, pedaling at higher power outputs will require fewer crank cycles to achieve stable pedal force data than pedaling at lower external power outputs.

REFERENCES

1. Buddhadev et al. *J Appl Biomech,* 2018 (in press).
2. Gardner et al. *Clin Biomech*, 30, 276-282, 2015.
3. Bates et al. *J Biomech*, 16(3), 181-191, 1983.
4. Hamill and McNiven. *Hum Mov Sci*, 9(2), 117-313, 1990.
5. Racic et al. *J Sports Sci Med,* 8, 39-647, 2009.
6. James et al. *J Sports Sci Med,* 6, 126-134, 2007.
7. Vincent, W. *Statistics in Kinesiology*. Human Kinetics, 1999
8. Bini et al. *J Sci Cycling*, 2(1), 11-24, 2013.

FRONTAL PLANE BIOMECHANICS DURING A SINGLE LEG HOP TASK ARE CORRELATED WITH QUALITY OF LIFE AND CONFIDENCE IN PATIENTS WITH ANTERIOR CRUCIATE LIGAMENT RECONSTRUCTION

[1]Albert J. Chen, [1]Rachel L. Tatarski, [2]Timothy E. Hewett, [1,3]Stephanie Di Stasi

[1]Jameson Crane Sports Medicine Research Institute, The Ohio State University, Columbus, OH, USA
[2] Orthopedic Biomechanics Laboratories and Sports Medicine Center, Mayo Clinic, Rochester, MN, USA
[3]Division of Physical Therapy, The Ohio State University, Columbus, OH, USA
Email: Albert.Chen@osumc.edu, web: https:// wexnermedical.osu.edu/sports-medicine/

INTRODUCTION

Anterior cruciate ligament (ACL) rupture is a devastating injury to the knee that affects 250,000 people in the US annually [1]. These injuries are frequently associated with long term sequelae, including increased risk of a second ACL tear, decreased activity levels due to fear of re-injury, and a dramatically increased risk of developing osteoarthritis (OA) [2, 3].

The Knee injury and Osteoarthritis Outcomes Score (KOOS) survey, in conjunction with radiographs, can be used to track symptomatic knee OA [4]. Patients after an ACL reconstruction tend to demonstrate altered biomechanics during gait, which has been shown to significantly correlate with KOOS outcomes [5]. It is unclear whether this relationship with KOOS outcomes exists with more dynamic tasks. The single leg hop landing (SHPLND) task is not only analogous to movements found in sports, but is regularly used by clinicians to determine return to sport readiness. The ACL Return to Sport after Injury (ACL-RSI) scale is used to determine the psychological impact of returning to sport after ACL reconstruction [6]. However, there has been little work done in analyzing how ACL-RSI scores might correlate with biomechanics during dynamic tasks.

Therefore, the purpose of this study was to determine if a correlation exists between frontal plane biomechanics during a SHPLND task and patient reported outcomes. We hypothesized that greater knee adduction moments and angles would correlate with worse KOOS and ACL-RSI scores.

METHODS

After obtaining approval from the Ohio State Institutional Review Board, 20 patients with an ACL reconstruction were recruited for this study (Table 1). To be included in this study, each patient must have demonstrated an isokinetic quadriceps strength deficit of less than 30%, pain free range of motion, and an effusion stroke test score of 1+ or less [7].

M:F	Age (yr)	Height (cm)	Mass (kg)	TSS (mo)
9:11	20.5 ± 6.4	172.3 ± 9.0	78.0 ± 16.8	8.1 ± 3.6

Table 1: Demographic data. TSS: Time since surgery.

Before the motion analysis portion of the data collection, each patient completed self-administered KOOS and ACL-RSI surveys. All 5 subscales (Symptoms, Pain, Activities of Daily Living (ADL), Sport, and Quality of Life (QOL)) were included for analysis. Each subscale was graded on a scale of 0-100, with 100 representing the optimal outcome.

Biomechanics were measured using a 12 camera 3-dimensional motion capture system (Motion Analysis, CA) with 4 embedded force plates (Bertec, OH). Each patient was fitted with 55 retro-reflective markers using a modified Helen-Hayes marker set. For the SHPLND task, each patient was instructed to jump as far forward as they could with one leg onto a specified force plate and maintain balance ("stick") after landing. Two successful trials were recorded on each limb and were exported for data analysis. Variables of interest included frontal plane knee angles and moments of the involved limb at peak vertical ground reaction force, and frontal plane knee moment impulse. Moments were normalized by bodyweight*height. Side-to-side differences between the uninvolved and involved limbs (defined

as uninvolved – involved) were also calculated for these variables. Moment impulse was calculated numerically using the MATLAB (Mathworks Inc., MA) *trapz* function from each patient's time-series curves. Due to the patient reported outcomes failing the normality assumption, Spearman's rank correlation coefficients were calculated for each biomechanical variable, each KOOS subscale, and the ACL-RSI (α = 0.05). Statistical analyses were performed in SPSS Statistics 25 (IBM, NY).

RESULTS AND DISCUSSION

There were significant correlations between frontal plane moment impulse and KOOS-QOL (R = 0.47, p = 0.04) and side-to-side difference in frontal plane angle and ACL-RSI (R = 0.49, p = 0.04). Correlations between all other biomechanical measures and patient reported outcomes were weak and not statistically significant (p > 0.05). These results indicate that patients who land in greater adduction on the involved limb relative to their uninvolved limb tend to score worse on ACL-RSI. Furthermore, greater knee adduction moment impulse on the involved limb correlated with better KOOS-QOL scores.

The KOOS-QOL subscale and ACL-RSI survey both focus on how confident the patient feels about their recovery and whether that inhibits them from participating in sport. The results of the present study could indicate a conscious effort by the patient to protect their knee via greater adduction during a relatively demanding task, an action which is emphasized throughout rehabilitation. Furthermore, emphasis on greater adduction during landing may, in fact, lead to OA development, in spite of the goal to decrease ACL injury risk. Future work should examine the relationship between KOOS-QOL and ACL-RSI and other dynamic tasks, such as the drop vertical jump.

A limitation of this study was the short follow-up time between surgery and biomechanical testing, which may have biased patient-reported outcomes to be better than what could be expected at longer follow-up.

CONCLUSIONS

Significant correlations were found between side-to-side differences in frontal plane knee angle and ACL-RSI, and frontal plane moment impulse and KOOS QOL.

REFERENCES

1. Griffin, LY et al. *AJSM*, **34(9)**, 1512–1532, 2006.
2. Lohmander, LS et al. *AJSM*, **35(10)**, 1756–1769, 2007.
3. Kvist, J et al. *KSSTA*, **13**, 393-397, 2005.
4. Lohmander, LS et al. *Arth. Rheum.,* **50(10)**, 3145-3152, 2004.
5. Erhart-Hledik, JC et al. *J. Orthop. Res.*, **35(3)**, 634–640, 2017.
6. Webster, KE et al. *Phys. Ther. Sport*, **9(1)**, 9-15, 2008.
7. Sturgill, LP et al. *J Ortho Sport PT*, **39(12)**, 845-849, 2009.

ACKNOWLEDGEMENTS

The authors would like to acknowledge the Sports Physical Therapy Section of the American Physical Therapy Association for their funding.

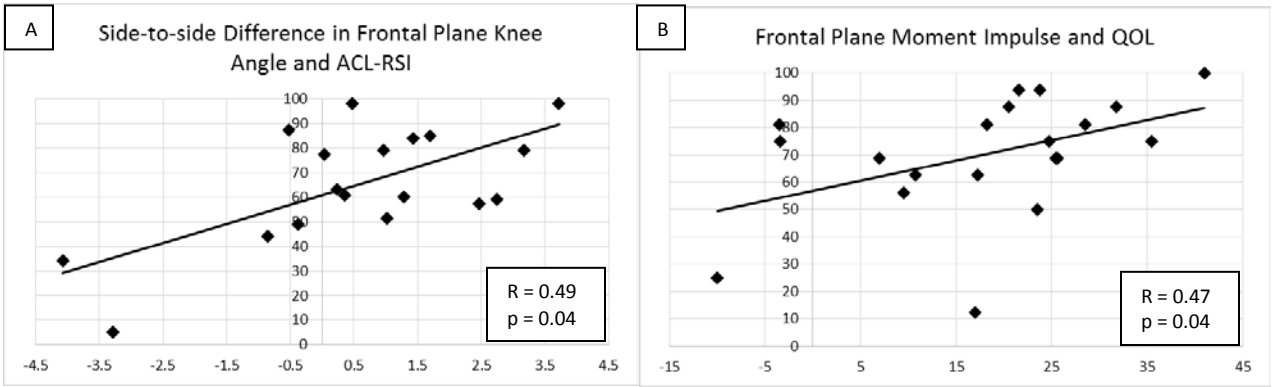

Figure 1: Correlations between (A) side-to-side difference in frontal plane knee angle during peak vertical ground reaction force and ACL-RSI; (B) frontal plane moment impulse on the involved limb during peak vertical ground reaction force and the KOOS QOL subscale. Both correlations were moderate and statistically significant ($p < 0.05$).

ACTIVATION-DEPENDENT CHANGES IN SOLEUS LENGTH-TENSION BEHAVIOR AUGMENT ANKLE JOINT QUASI-STIFFNESS

William H. Clark and Jason R. Franz

University of North Carolina and North Carolina State University, Chapel Hill, NC, USA
email: jrfranz@email.unc.edu, web: http://abl.bme.unc.edu

INTRODUCTION

The triceps surae (i.e., gastrocnemius and soleus) muscle-tendon units are functionally important in governing walking performance, acting to regulate mechanical behavior of the ankle joint through the interaction between active muscle and passive elastic structures [1]. Ankle joint quasi-stiffness, defined as the slope of the relation between ankle moment and ankle rotation, is a useful aggregate measure of this presumably complex mechanical behavior [2]. For example, quasi-passive lower limb prostheses with impedance control methods have garnered attention and their designs are benchmarked against the quasi-stiffness of the biological ankle joint [3]. In walking, ankle joint quasi-stiffness systematically changes with walking speed and positively correlates with positive work performed about the ankle during push-off [3]. Those findings reflect a fundamental assumption that the control of triceps surae muscle behavior can functionally augment ankle joint quasi-stiffness via changes in activation. However, while entirely intuitive, this assumption lacks direct empirical evidence that, in addition to its biological relevance, could be vital in designing appropriate control systems for powered prostheses [2].

The purpose of this study was to couple dynamic ultrasound imaging with electromyographic biofeedback to quantify activation-dependent modulation of soleus muscle length-tension behavior and its role in augmenting ankle joint quasi-stiffness. We first hypothesized that soleus muscle stiffness and ankle joint quasi-stiffness would increase with increasing muscle activation. We also tested the null hypothesis that activation-dependent changes in soleus muscle stiffness would be proportional to and correlate with those in ankle joint quasi-stiffness.

METHODS

We report data for 10 subjects (age: 24.5 ± 5.4 yrs, mass: 74.7 ± 12.7 kg, height: 1.8 ± 0.1 m, 4 females). Subjects first completed 3 isometric voluntary plantarflexor contractions (IVCs) at a neutral ankle (i.e., 0º) in a dynamometer (Biodex Medical Systems, Inc.), from which we extracted a reference maximum voluntary activation from a wireless electrode (Delsys, Inc.) placed over the soleus muscle. Subjects then completed 3 eccentric isokinetic plantarflexor contractions between 20º plantarflexion and 15º dorsiflexion at 30º/sec both passively and at each of 2 prescribed activation levels (25% and 75% reference maximum activation), all presented in fully randomized order. To match prescribed activations, subjects watched a screen on which we projected real-time visual electromyographic (EMG) biofeedback showing their instantaneous soleus activation (250 ms moving average) with target values based on the reference maximum activation determined earlier (Fig. 1). Subjects received at least one minute of rest between trials. A 60 mm Telemed Echo Blaster 128 transducer (LV7.5/60/128Z-2) placed over the mid-belly of subjects' right soleus recorded cine B-mode images of a longitudinal cross-section at 61 frames/s. Simultaneously, motion capture-guided ultrasound from a second transducer (L14-5W/38, Ultrasonix Corporation) placed over the Achilles free tendon estimated the moment arm of the line of action of

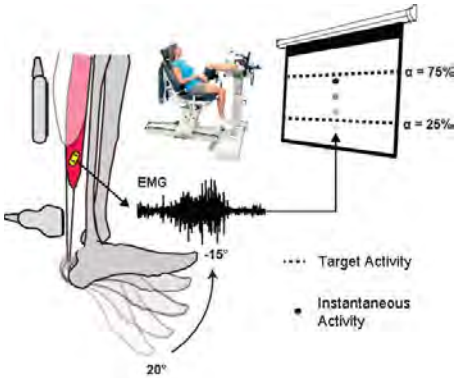

Figure 1. We used visual biofeedback to prescribed muscle activations (α) during eccentric isokinetic plantarflexor contractions while cine ultrasound imaging captured soleus muscle length changes.

soleus muscle force for each subject using previously published techniques [4]. Available MATLAB routines quantified time series of soleus fascicle length and pennation angle [5], which we combined to compute length change along the line of action of the soleus. To calculate "muscle stiffness", we resolved net triceps surae muscle force by dividing subjects' net ankle moment by their measured moment arm [4]. We then estimated soleus muscle force by scaling triceps surae force by the relative physiological cross-sectional area attributed to the soleus (i.e., 63%) [6]. For each subject, we defined: (*i*) muscle stiffness as the change in soleus muscle force divided by the change in muscle length, and (*ii*) ankle joint quasi-stiffness as the change in ankle moment divided by the change in ankle angle.

RESULTS AND DISCUSSION

In the absence of muscle activity, we found relatively negligible values of soleus muscle stiffness (k_M) and ankle joint quasi-stiffness (k_A) across the range of ankle rotation observed during walking. In contrast, k_M and k_A increased significantly with increased muscle activation ($p<0.05$). On average, k_M was 15 N/mm during passive rotation, 118 N/mm during the 25% IVC condition, and 204 N/mm during the 75% IVC condition (Fig. 2A). On average, k_A was 24 Nm/rad during passive rotation, 154 Nm/rad during the 25% IVC condition, and 213 Nm/rad during the 75% IVC condition (Fig. 2B). However, these activation-dependent changes were made complex by the interaction between active muscle and passive elastic structures. Conceptually, from 0% to 25% IVC, increased muscle activity should augment k_A directly by increasing k_M and indirectly by engaging series elastic tendon (i.e., $\Delta k_A > \Delta k_M$). Consistent with this premise, although highly correlated ($R^2=0.87$), we found that the sensitivity (i.e., slope) of k_A to altered activation averaged 25% greater than that of k_M from 0% to 25% IVC ($p=0.069$, Fig. 2C). Thereafter, the contribution of tendon stiffness to k_A is independent of activation; further increases in muscle activity should augment k_A only by increasing k_M. Indeed, compared to changes seen with 25% IVC, k_A was significantly less sensitive to further increasing activation to 75% IVC ($p=0.016$) – a change indistinguishable from that of k_M ($p=0.23$) (Fig. 2C). Surprisingly, k_M was also less sensitive to further increasing activation to 75% IVC ($p=0.025$).

CONCLUSIONS

We present *in vivo* evidence that ankle joint quasi-stiffness can be directly modulated via activation through changes in soleus muscle length-tension behavior. However, this modulation is more complex than previously appreciated – reflecting combinatory effects of active muscle and passive elastic tissues. Our findings have substantial implications for understanding human locomotor behavior and the design of impedance-based powered prostheses.

REFERENCES

[1] Zelik, K.E., et al. *J Theor Biol*, 2014.75-85.
[2] Rouse, E.J., et al. *IEEE Trans Biomed Eng*, 2013. 2:562-8.
[3] Shamaei, K., et al. *PLoS One*, 2013. (**3**):e59935.
[4] Rasske, K., et al. *Comput Methods Biomech Biomed Engin*, 2017. (2):201-205.
[5] Farris, D.J., et al. *Comput Methods Programs Biomed*, 2016.111-8.
[6] Morse, C.I., et al. *Acta Physiol Scand*, 2005. (**3**):291-8.

ACKNOWLEDGEMENTS

Supported by a grant from NIH (R01AG051748).

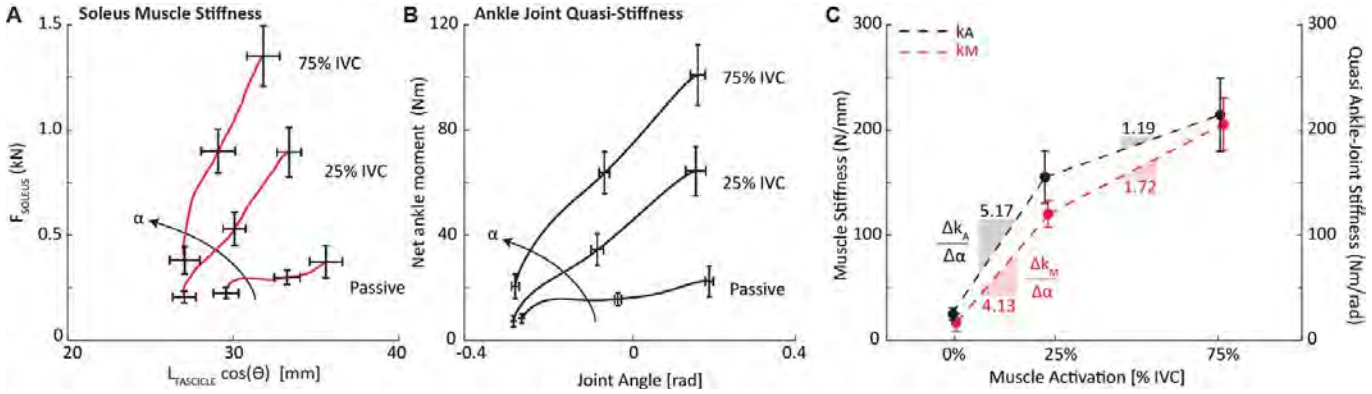

Figure 2. Activation-dependent changes in muscle (k_M) and quasi-ankle joint (k_A) stiffness. (A) Group mean change in soleus muscle force (F_{Soleus}) versus longitudinal soleus muscle length ($L_{fascicle}$ cos Θ) as a function of activation (Θ: pennation). (B) Group mean change in net ankle moment versus joint angle as a function of activation. (C) Activation-dependent k_M and k_A from 0% to 25% and 25% to 75% IVC. Bars represent ± standard error.

THE EFFECT OF HAMSTRING FOAM ROLLING ON KNEE AND HIP JOINT PROPRIOCEPTION

[1] Erin David, [1]Tal Amasay, [1]Kathryn Ludwig, and [1]Sue Shapiro

[1] Barry University, Miami Shores, FL, USA
email: tamasay@barry.edu

INTRODUCTION

Therapeutic interventions, such as massage [1, 2], have been shown to improve proprioception. Less is known about how other therapeutic interventions, such as foam rolling, affect proprioception. Only one study has examined the effect of foam rolling on proprioception. They found that foam rolling of the hamstring muscles once a day led to significant improvements in joint position sense of the hip one week after treatment [3]. The purpose of the current study is to determine the acute effect of two 1-minute bouts of hamstring foam rolling on proprioception at the knee and hip joints.

METHODS

Twenty-five healthy students (9 males, 16 females) served as subjects in this study (age 22.88 ± 2.24 yrs, height 169.38 ± 8.80 cm, weight 77.70 ± 20.63 kg). Subjects completed two tests on separate days, in a random order. Both sessions began with a 5-minute stationary bicycle warm-up.

For the joint position matching test (JPMT), subjects were verbally guided to a target lunge position in which the right knee and hip were flexed to a random angle 25˚-35˚ from the vertical plane. Once the target position was achieved, subjects held the position for six seconds while knee and hip joint positions were recorded with the motion capture system. Subjects then returned to the starting position for three seconds and were then asked to reproduce the target position without guidance and hold it for six seconds. This entire process was repeated two more times with 15 seconds of rest between trials. Subjects then completed the foam rolling intervention. This consisted of two 1-minute bouts along the right hamstring group, with 30 seconds between bouts. Subjects then completed a post-intervention JPMT at zero, 10, and 20 minutes.

In the force sense test (FST) session, subjects began with the same 5-minute warm-up. For the entire session, the isokinetic dynamometer was set to 30˚ of knee flexion and 55˚ of hip flexion. Prior to data collection, each subject's mean peak isometric torque was determined. Subjects applied maximal effort torque against the stationary dynamometer attachment in the direction of knee flexion for six seconds, followed by 30 seconds of rest. This procedure was repeated two more times, followed by a 5-minute break. The mean peak isometric torque for the three test trials was calculated, and 20% of this value served as the target torque for the FST [4].

Each FST consisted of three trials with visual feedback and three trials without visual feedback [4]. For visual feedback trials, subjects gradually applied torque on the dynamometer attachment in the direction of knee flexion until they reached their target torque, based on the torque graph on the computer screen. Once subjects reached their target torque, they maintained it for six seconds and then rested for six seconds. Two more trials with visual feedback were performed, followed by a one-minute rest period. Subjects then performed three more 6-second trials without visual feedback from the graph. For these trials, subjects would signal when they thought they had reached the target torque. At that point the six-second trial was recorded, followed by six seconds of rest between trials [4]. After all baseline trials had been completed, subjects carried out the same foam rolling intervention protocol as described previously. Subjects then repeated the FST at zero, 10, and 20 minutes post-intervention.

Angles and torques were calculated using the average value for the middle two seconds of each six second trial. For the JPMT, the mean absolute difference between each target angle and reproduced angle pair was determined for the hip and knee at all four testing times (absolute knee position matching error [AKPME] and absolute hip position matching

error [AHPME]). For the FST, the absolute difference between the average torque for the three visual feedback trials and all three trials without feedback was determined at all four testing times (absolute knee flexion torque [AKFT]). Three separate one-way repeated measures ANOVA tests were performed. When a significant main effect was found, a post hoc paired samples t-test was conducted. The alpha level was set at 0.05.

RESULTS AND DISCUSSION

There was a significant main effect for AKPME ($F(1.97, 47.36)$, $p = 0.004$) (Fig. 1). This illustrates the potential for foam rolling to improve proprioception for at least 20 minutes. It is unknown whether this improvement is enough to prevent an injury, but it may indicate that foam rolling could be an effective adjunct to proprioceptive exercises during rehabilitation.

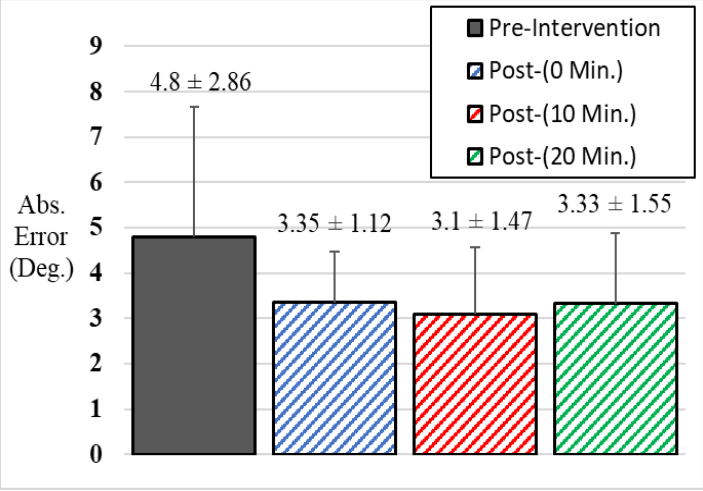

Figure 1: A striped pattern indicates significant difference from baseline ($p < 0.05$).

No significant main effects were found for AHPME ($F(2.42, 58.21)$, $p = 0.24$) or AKFT (Table 1). The lack of improvement in AHPME is in contrast with previous research, which found that post-intervention hip joint position sense improved significantly after one week of foam rolling [3]. The contrasting results are likely due to differences in methodology, especially the time frames of interest. Although AKPME improved, AKFT did not. Previous research found that force sense was not correlated with joint position sense, and suggested that the FST acts more on golgi tendon organs, while JPMT acts more on muscle spindles in the muscle belly [5]. Important to note is that although no improvements in AHPME or AKFT were found in the current study, there was also no significant deterioration of these variables.

CONCLUSIONS

It is not entirely clear whether foam rolling will consistently improve proprioception. The current study did find that foam rolling of the hamstrings can improve AKPME, and that it does not diminish proprioception. This makes probability of injury due to proprioceptive effects of foam rolling unlikely.

REFERENCES

1. Henriksen et al. *Advances in Physiotherapy*. **6**: 29-36, 2004.
2. Shin and Sung. *Journal of Strength and Conditioning Research*. **29(8)**: 2255-2260, 2015.
3. Cho and Kim. *The Journal of Physical Therapy Science*. ***28*(6)**: 1806-1808, 2016.
4. Torres et al. *Journal of Human Kinetics*. **34**: 33-39, 2012.
5. Li et al. *The Journal of Physical Therapy Science*. **28**: 478-482, 2016.

Table 1: Mean Absolute Hip Position and Knee Torque Matching Error over Time.

	Pre-Intervention	**Post-(0 min.)**	**Post-(10 min.)**	**Post-(20 min.)**
AHPME (± SD)	1.83 ± 0.98°	1.61 ± 0.81°	1.46 ± 0.67°	1.81 ± 0.71°
AKFT (± SD)	4.74 ± 3.10 N*m	3.71 ± 2.53 N*m	3.86 ± 2.81 N*m	3.69 ± 2.31 N*m

THE EFFECT OF MID-FLIGHT TRUNK FLEXION AND EXTENSION ON CENTER OF MASS REDISTRIBUTION AND LANDING MECHANICS

Daniel J. Davis, Taylour J. Hinshaw, and Boyi Dai

University of Wyoming, Laramie, WY, USA
email: bdai@uwyo.edu, web: http://www.uwyo.edu/kandh

INTRODUCTION

Anterior Cruciate Ligament (ACL) injuries are prevalent and can have devastating effects [1, 2]. While various landing conditions predispose an individual to these injuries, knee flexion angle and trunk motion appear to be significant risk factors [3, 4]. A stiff landing characterized by decreased knee and hip flexion and increased vertical ground reaction force (VGRF) is associated with increased ACL loading [5]. Mid-flight medial and lateral trunk bends influence landing mechanics [6], but the effect of trunk flexion and extension is unclear.

This study aimed to analyze the effect of mid-flight trunk flexion and extension on joint positions relative to whole-body center of mass (COM) and landing mechanics. Researchers hypothesized that mid-flight trunk extension would cause anterior motion of the hips and knees relative to the whole-body COM, resulting in a mechanically disadvantageous position for landing. Consequently, subjects would demonstrate a stiffer landing with decreased knee and hip flexion.

METHODS

Ten males and five female recreational athletes (age: 21.8 ± 1.6 years, height: 1.75 ± 0.11m; mass: 74.4 ± 28.7kg) participated. Forty-four reflective markers were attached to participants' body segments (Fig. 1). Kinetic and kinematic data were collected using eight Vicon cameras (160 Hz) and two Bertec force plates (1600 Hz).

After a static trial, participants completed three jump-landing trials in three randomly ordered conditions: reaching backward (Fig. 2), reaching up (Fig. 3), and reaching forward (Fig.4). Trials began with participant's feet on two separate force plates. The participants received instructions to jump vertically as high as possible for all conditions. Prior to jumping, participants were also instructed to reach as far backward, up, or forward as they felt comfortable after reaching their maximum jump height. A successful trial concluded when the participant landed with each foot on the force-plate on which it began.

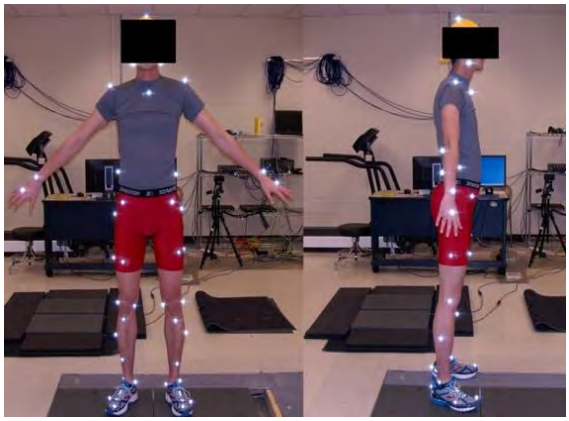

Figure 1. Marker set for data collection.

The positions of the hip, knee, and ankle joints relative to the whole-body COM at initial foot contact of landing were calculated and normalized to body height (Fig. 2, 3, 4). Positive positions represented joints anterior to whole-body COM. Hip, knee, and ankle flexion/extension angles were calculated at initial foot contact and 100 ms following initial contact of landing. Repeated-measure ANOVAs were performed for each dependent variable followed by pairwise comparisons. A type I error rate was established at 0.05 for statistical significance.

RESULTS AND DISCUSSION

ANOVAs (Table 1) showed significant differences among the three different conditions, except for VGRF. The reaching backward condition resulted in more anterior hip and knee positions from whole-body COM, smaller hip flexion angles at initial

contact, and smaller hip and knee flexion angles at 100 ms of landing compared to the other two conditions. The reaching forward condition demonstrated more posterior hip, knee, and ankle positions from whole-body COM and greater hip and knee flexion angles at initial contact and 100 ms of landing compared to the other two conditions.

Trunk flexion and extension resulted in altered joint positions related to whole-body COM and subsequent landing mechanics. In the reaching backward condition, the whole-body COM is placed posterior of the hip, resulting in an external hip extension moments. Consequently, an active internal hip flexion moment is needed to flex the hip and move the whole-body COM forward during early-landing. In addition, because of a posteriorly positioned whole-body COM, actively knee flexion may not be performed to avoid further moving the whole-body COM posteriorly to prevent falling. On the other hand, in the reaching forward condition, the whole-body COM is placed anterior of the hip, causing an external hip flexion moment to facilitate hip flexion. In the meantime, as the whole-body COM is moving forward due to hip flexion, an active knee flexion may be achieved during early-landing while postural stability is maintained.

CONCLUSIONS

COM redistribution elucidated by the reaching backward condition may predispose an individual to a stiffer landing posture that renders them at risk for ACL injury. The findings may provide information for understanding ACL injury mechanisms associated with trunk motion and developing effective landing strategies to decrease ACL injury risk after trunk perturbation.

REFERENCES

1. Kay et al. *Journal of Athletic Training,* 52(2), 2017.
2. Hootman et al. *Journal of Ath Train,* 42(2), 2007.
3. Stuelcken et al. *Journal of Sport Science,* 2015.
4. Walden et al. *British J of Sports Med,* 49(22), 2015.
5. Dai et al., *Am J of Sports Med,* 43(2) 2015.
5. Hinshaw et al. *Proceedings of ASB'17*, Boulder, CO, USA, 2017.

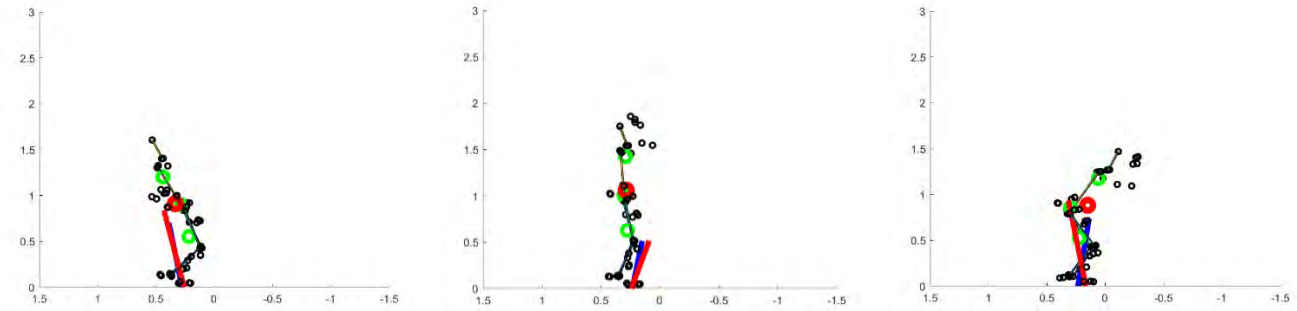

Figures 2, 3, and 4. Stick figures of participant with COM locations (red and green dots) and VGRF (red and blue lines) for reaching backward, up, and forward conditions respectively.

Table 1. Means ± Standard Deviations of Dependent Variables.

	VGRF (body weight)	Hip position at contact (body height %)	Knee position at contact (body height %))	Ankle position at contact (body height %))	Hip flexion at contact (degrees)	Knee flexion at contact (degrees)	Ankle plantar flexion at contact (degrees)	Hip flexion at 100 ms (degrees)	Knee flexion at 100 ms (degrees)	Ankle dorsiflexion at 100 ms (degree)
Backward	4.2±1.1	$3.0±1.6^{A}$	$4.6±1.7^{A}$	$-0.6±1.7^{A}$	$2.7±8^{C}$	$13.5±8.3^{B}$	$36.5±6^{B}$	$23.0±14^{C}$	$56.6±10^{C}$	$26.9±6.4^{A}$
Up	4.4±1.0	$-0.3±1.7^{B}$	$2.7±1.1^{B}$	$-1.3±1.2^{A}$	$12.8±7^{B}$	$13.5±8.9^{B}$	$37.2±10^{B}$	$37.0±12^{B}$	$60.6±11^{B}$	$25.7±4.8^{A}$
Forward	4.4±1.0	$-7.1±2.6^{C}$	$0.2±2.5^{C}$	$-2.5±1.8^{B}$	$34.8±13^{A}$	$21.7±9.5^{A}$	$40.3±9^{A}$	$60.6±17^{A}$	$66.5±12^{A}$	$20.5±6.4^{B}$

Note: A>B>C at a significance level of $p < 0.05$.

MEASUREMENT OF KNEE ANGLES AT LANDING AND PEAK GROUND REACTION FORCE USING WEARABLE SENSORS

Amanda Esquivel, Ruchika Tadakala and Jessica Buice
University of Michigan - Dearborn, Dearborn, MI, USA
email: aoe@umich.edu

INTRODUCTION

The incidence of anterior cruciate ligament (ACL) injury in female high school and collegiate athletes is 2-6 times higher than in male athletes when comparing athletes in the same sport, and the rate of ACL injury has also been reported to be increasing in recent years.[1] Many studies have demonstrated that there are sex differences in the kinematics and kinetics of the lower extremity during jump and squat tasks. In addition, laboratory research indicates that noncontact ACL injuries that occur in female athletes may be overuse injuries due to repeated strain on the ACL.[2]

Wearable sensors have been developed to monitor lower extremity motion using a variety of methods for several applications, including gait analysis and assistance with rehabilitation. The purpose of this study is to validate a wearable sensor that could monitor knee kinematics in the field and eventually identify knee motion that could place an individual at risk for ACL injury.

METHODS

Prior to commencement of the study, Institutional Review Board approval was obtained. Forty-eight spherical reflective markers were placed on the subject's body at key bony landmarks and five wearable sensors were placed on the lower body according to the sensor fusion algorithm generated by the opal APDM Inc. Data were collected using a 12-camera motion capture system (Prime 13 Optitrack, Corvallis, OR) and two 2000 lb force plates (FP4060-05-PT, Bertec, Columbus, OH). Joint angular position was calculated from the filtered 3D marker coordinate data.

Subjects were instructed to jump off of a 30 cm box onto force plates and then immediately perform a maximum vertical jump.

The time at initial landing and maximum ground reaction force was determined using the force plates and was also determined using the acceleration in the vertical direction of the wearable sensor located on the left lower leg. Knee angles were compared between the wearable sensors and motion capture system.

RESULTS AND DISCUSSION

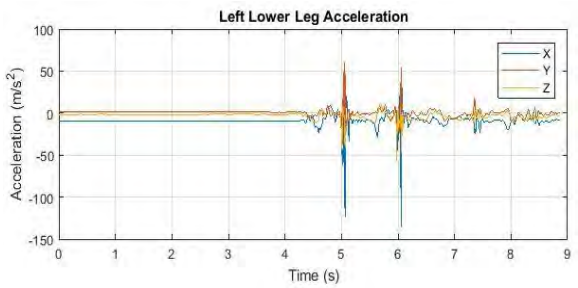

Figure 1. Leg Acceleration

The time at initial landing and maximum ground reaction force was determined using the acceleration data from wearable sensor located on the left lower leg. The figure above shows the output of the shank accelerometer for one subject. Two sharp spikes can be seen when the subject lands on the force plates and jumps off second time (Fig 1). The accelerometer data provided a distinct signal which can be used to identify and count the number of times the subject's foot lands from a jump task. The maximum ground reaction force occurred when acceleration was at maximum peak in the negative direction. (Fig 2)

Knee flexion was recorded at these time points and compared with values found from the motion capture system. (Tables 1 and 2) The average difference in measurement between the motion capture system and the wearable device was 5.22° at landing and 3.79° at peak GRF and the root mean square error was 7.3° and 6.9°, respectively.

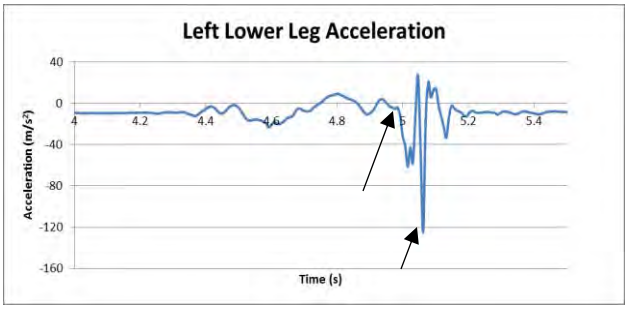

Figure 2. Leg acceleration at initial contact and peak vertical force

Angle measurements from the wearable sensors were somewhat different from those measured by the motion capture system. Knee angle estimation using IMUs faces notable challenges. Knee angles measurements are based on orientation estimates provided by the IMUs, which makes them sensitive to sensor-to-body calibration. To address this, a calibration routine to be carried out by subjects and eventually players in the field will need to be developed.

CONCLUSIONS

We have presented an analysis of the measurement of knee flexion angles at landing and peak ground reaction force using wearable sensors. Errors between the wearable devices and the motion capture system were identified. In addition, the use of these sensors may depend on various conditions if used in the field.

This study presents evidence of the validity of the IMU based measurement technique for measuring the knee angles at landing and peak ground reaction force. This device is easy to use, and provides required accelerometer, gyroscope and magnetometer data. In the future, we will continue to validate this device by comparing abduction/adduction and internal/external rotation angles and developing calibration procedures necessary for more accurate measurements.

REFERENCES

1. Gornitzky, A. L., A. Lott, J. L. Yellin, P. D. Fabricant, J. T. Lawrence and T. J. Ganley. Sport-specific yearly risk and incidence of anterior cruciate ligament tears in high school athletes: A systematic review and meta-analysis. Am J Sports Med 2015

2. Wojtys, E. M., M. L. Beaulieu and J. A. Ashton-Miller. New perspectives on acl injury: On the role of repetitive sub-maximal knee loading in causing acl fatigue failure. J Orthop Res 34: 2059-2068, 2016

Table 1: Comparison of Knee Flexion (+) and Extension (-) at Landing and Peak GRF for the Left Leg

Subject	Landing – Motion Capture	Landing – Wearable Sensor	Peak GRF – Motion Capture	Peak GRF – Wearable Sensor
1	**1.77°**	**-0.16°**	**31.94°**	**32.29°**
2	**25.75°**	**25.72°**	**47.27°**	**40.84°**
3	**16.85°**	**25.72°**	**46.59°**	**35.52°**
4	**24.89°**	**33.98°**	**49.72°**	**42.79°**
5	**14.54°**	**24.66°**	**38.74°**	**43.87°**

QUANTIFYING KNEE INJURY RISK DURING A WRESTLING TAKEDOWN

Zachary B. Fox[1] and Allison R. Altman-Singles[1,2]

[1] Kinesiology, Penn State Berks, Reading, PA, USA
[2] Mechanical Engineering, Penn State Berks, Reading, PA, USA
email: zzf5041@psu.edu

INTRODUCTION

The knee is the most commonly injured site in college wrestling and is the second most commonly injured site in high school wrestling (Kay et al., 2017; Yard et al., 2008). In total, knee injuries account for nearly 40% of all significant injuries in the sport of wrestling, and nearly 60% of knee injuries result in a sprain or tear of the anterior cruciate ligament (ACL), meniscus, medial collateral ligament (MCL), or lateral collateral ligament (LCL). (Estwanik et al., 1980; Wroble et al., 1986).

Due to the closed chain, flexed knee posture of the defensive wrestler while in the neutral position, the risk for knee injury is extremely high (Olsen et al., 2004). In the neutral position, if the attacking wrestler wants to perform a leg attack, there are two common approaches: head inside and head outside. Depending on the approach, force is applied at different places on the defensive wrestler's leg.

The purpose of this research was to quantify the knee mechanics during these two common wrestling takedowns. Motion analysis was used to compare knee adduction of the defensive wrestler from the initial takedown period. Knee adduction angle, knee adduction acceleration, knee linear acceleration and proximal tibia acceleration were compared between a head inside leg attack and a head outside leg attack during initial contact with the offensive wrestler.

METHODS

Eleven healthy male wrestlers between the ages of 18 and 35 with at least one year of wrestling experience were recruited for this experiment. To minimize injury risk and replicate a more realistic scenario, the participants recruited were in a 30-pound range of the offensive wrestler's weight (165-225 pounds). This experiment excluded athletes with significant musculoskeletal injury to the lower extremity and previous surgery to the lower extremity.

Fifty-three reflective markers were placed on the foot, shank, thigh and pelvic segments of both lower extremities. Marker placement was optimized to maximize cluster visibility during the head inside and head outside leg attacks. A standing calibration trial was performed using anatomical and tracking markers, then the anatomical markers were removed, leaving the tracking markers. An eight camera VICON Bonita Motion Analysis System (Vicon, Denver, CO) was used to capture marker trajectory data at 200 Hz.

The offensive wrestler performed 5-10 head inside and head outside practice shots on the participant in order to warm-up and re-acclimate the participant to the feeling of a leg attack. Once the participants were warmed-up, the participants were instructed to stand in a square wrestling stance. The offensive wrestler then proceeded to perform either head inside or head outside leg attacks on the participants until approximately 3-5 satisfactory trials of each shot type were collected.

Mean adduction, peak adduction and peak abduction values were extracted from the initial takedown period for knee adduction angle, knee adduction acceleration, knee linear acceleration and proximal tibia acceleration. These variables of interest calculated from the 3-5 trials for the head inside and head outside leg attacks were averaged and compared within subjects using a paired *t*-test. A *p*-value of 0.05 was considered a significant difference.

RESULTS AND DISCUSSION

Individual knee adduction angle differed substantially between subjects, which made it difficult to identify differences in knee kinematics

between the head inside and head outside leg attack. A representative knee adduction angle during a head inside (left leg) and head outside (right leg) leg attack is shown below (Figure 1).

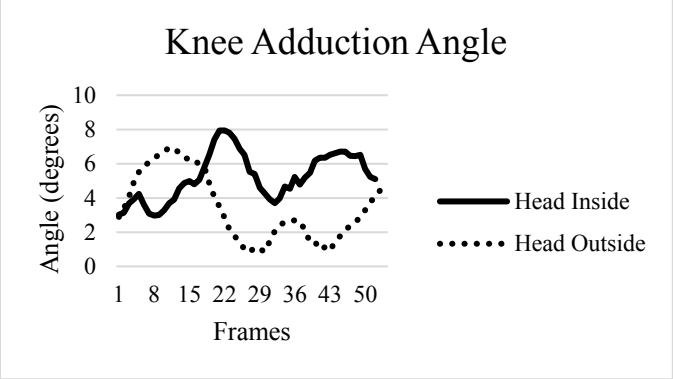

Figure 1. Representative Knee Adduction Angle

The head inside leg attack showed a 50% lower peak lateral knee linear acceleration (p=0.0023) and a 73% lower peak medial knee linear acceleration (p<0.001) than the head outside leg attack. No significant differences were found between the other variables of interest (Figure 2).

During the head inside leg attack, the defensive wrestler had a lower peak medial and peak lateral knee linear acceleration, suggesting there is an increased valgus force as well as an increased varus force at the knee during different times of a head outside leg attack. No difference was found in knee adduction angle and knee adduction acceleration between the head inside and head outside leg attack. The lack of significance of the knee adduction acceleration suggests no difference in net moment at the knee during a head inside and head outside leg attack.

Based on past cadaveric research looking at knee joint, ACL and MCL loads during athletic tasks, the ACL experienced significantly more loading than the MCL during drop vertical jump and sidestep cut maneuvers. During the drop vertical jump and sidestep cut maneuvers, the male knee peak adduction angle was roughly 2 to 9 degrees, respectively, corresponding to ACL strain of 6.1 to 7.0% (Bates et al., 2015). In this present study, the defensive wrestler had peak knee adduction angles during a head inside and head outside leg attack of 10.5 degrees and 12.7 degrees, respectively. This suggests that the ACL and MCL would experience more strain during the leg attacks than what the previous literature reported during the drop vertical jump and sidestep cut maneuvers. This likely explains the high incidence of knee injuries during the sport.

CONCLUSIONS

This study identified the initial takedown to be a high-risk period for the defensive wrestler regardless of the takedown type. By identifying this risk, better training programs and knee brace designs can be developed to minimize the incidence of knee injuries in wrestlers. This study also introduces a quantitative method for evaluating knee injury risk in wrestlers which is the first step in minimizing the high injury risk involved in the sport.

REFERENCES

[1] Bates NA, et al. *Am J Sports Med* **43**, 2259-2269, 2015.
[2] Estwanik JJ, et al. *Phys Sports Med* **8**, 111-121, 1980.
[3] Kay MC, et al. *J Athl Train* **52**, 117-128, 2017.
[4] Olsen O, et al. *Am J Sports Med* **32**, 1002-1012, 2004.
[5] Wroble RR, et al. *Am J Sports Med* **14**, 55-66, 1986.
[6] Yard EE, et al. *Am J Sports Med* **36**, 57-64, 2008

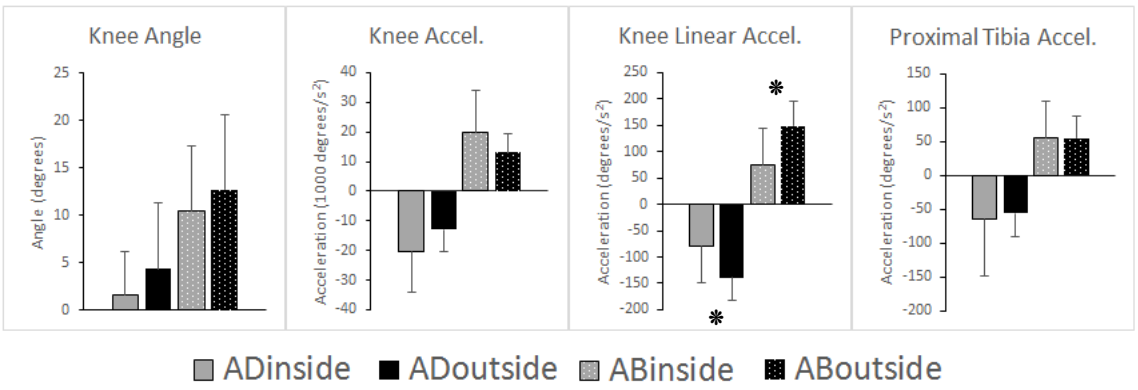

Figure 2. Variables of Interest for a Head Inside and Head Outside Leg attack (AD represents adduction, AB represents abduction, and * represents a significant difference of p<0.05)

SINGLE-JOINT STRENGTH CURVES FROM A MULTI-JOINT TASK

[1] John Fox, [2] Adam Jagodinsky, [3] Christopher Wilburn, [3] Lorraine Smallwood, and [3] Wendi Weimar

[1] Methodist University, Fayetteville, NC, USA
[2] Illinois State University, Normal, IL, USA
[3] Auburn University, Auburn, AL, USA
email: jfox@methodist.edu

INTRODUCTION

Activities of daily living involve the use of whole limbs. Utilizing the whole the limb to interact with an object or the environment entails coordinating multiple joints. Strength curves, which provide an estimate of capacity to execute a task, are typically expressed as single-joint strength curves or torque-angle curves [1, 2]. Although single-joint torque-angle curves provide insight into muscular mechanisms of joint torque [2], they may not provide precise estimates of multi-joint capacity. Research into multi-joint capacity measures force at the endpoint of the limb, and thereby, measures the result of a coordinated effort from multiple joints [3, 4]. However, these efforts have not evaluated the magnitude of endpoint force resulting from a particular joint within the multi-joint task. Therefore the purpose of this study was to construct strength curves for the whole limb, hip, knee, and ankle by evaluating the contribution of each to vertical endpoint force in a maximum effort isometric leg extension. It was hypothesized that the relationships would be linear.

METHODS

Sixteen female and 17 male participants (76.94±7.4kg; height, 1.73±0.07m; 19-35 years of age) volunteered for this study. Participants completed two protocols. First, participants performed the vertical jump protocol. In the vertical jump protocol participants performed 3 maximum height countermovement jumps. The trial in which the participant's center of mass achieved the greatest vertical height was kept for identifying postural configurations of interest for the maximum effort isometric leg extensions. Four postural configurations were obtained from each participant's vertical jump kinematics. The most flexed posture was defined by the position of maximum knee flexion in the vertical jump. The most extended posture was limited to a 160 degree knee angle, as this is the limiting knee angle measured by Hugh-Jones [3]. The other two postures were defined by equally spaced postures between the flexed and extended postures.

These postures were utilized in the multi-joint strength protocol, which involved 2 maximum effort isometric leg extensions at each of the 4 defined postures. Each participant stood over two AMTI OR6-1000 force platforms (Advanced Mechanical Technology, Inc., Watertown, MA) inside a squat rack. Safety bars were used as mechanical stops for an Olympic lifting bar. Retro-reflective markers were used for measuring kinematics with 10 Vicon T-series cameras (Vicon, Los Angeles, CA). Participants were instructed to push vertically with as much force as possible against the Olympic lifting bar at each postural configuration.

From kinematic and kinetic data joint angles and joint moments were computed in Visual 3d (C-motion, Bethesda, MD) and exported to Matlab (MathWorks, Inc., Natick, MA). The Jacobian matrix for each posture was computed and the contribution of each joint to vertical endpoint force was estimated using the following equation:

$$F = J^{-T}\tau$$

where F is the endpoint force, J is the Jacobian matrix, and τ is the vector of joint torques. The contributions of the whole limb, hip, knee, and ankle (WL, HF, KF, and AF, respectively) were normalized to the total force in each trial. The vertical force contributions from WL, HF, KF, and AF were checked for a linear relationship with leg extension. Leg extension was measured by the height

of the hip joint center from the floor, which was normalized to the height of the hip joint center in anatomical neutral. For each participant's data a line of best fit and R-squared value were computed using Microsoft® Excel®. This resulted in 33 R-squared values for WL, HF, KF, and AF. Distributions of R-squared values were evaluated for the most probable R-squared value.

RESULTS AND DISCUSSION

Median and ranges of R-squared values for the relative vertical force from the WL, HF, KF, and AF are reported in Table 1. Figure 1 shows cumulative mass functions of R-squared values. The median R-squared values were greatest for AF followed by HF, WL, and KF, respectively.

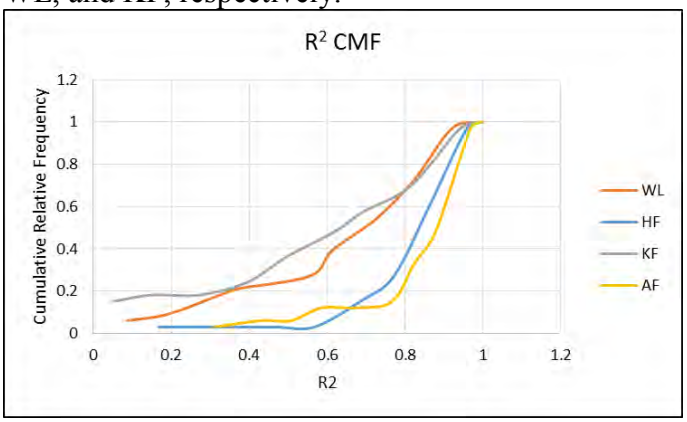

Figure 1. Cumulative mass functions (CMF) for WL, HF, KF, and AF. Note that HF and AF cross 0.5 at larger R-squared values.

Results indicate that a linear strength curve, in which normalized force is the dependent variable and normalized leg length is the independent variable, is more likely to occur for AF and HF compared to WL and KF. This study does not provide insight to a mechanism for the shape of a strength curve.
However, this study demonstrates that some individual joints (i.e. the hip and ankle) demonstrate a linear relationship between their contribution to endpoint force and limb extension. For example the contribution of the hip to vertical endpoint force decreased linearly as the limb was extended, conversely the contribution of the ankle increased linearly with limb extension. The knee contribution was less likely to demonstrate a linear relation with leg extension. This suggests that activities of daily living such as gait, which involves an extended posture, rely more heavily on the ankle to provide vertical ground reaction force compared to knee and hip. Such results corroborate Kepple and colleagues who stated that the ankle contributed the most to support during single limb support phase of gait [5]. However, these results must be interpreted with caution as not everyone demonstrated a strong linear relation between force and leg extension.

CONCLUSIONS

In this study normalized vertical endpoint force contribution from the whole limb, hip, knee, and ankle were examined in relation to normalized leg length. The most linear relationships were found for the hip and ankle. This data can be used to better understand the contribution of individual joints to activities of daily living involving the simultaneous use of multiple joints.

REFERENCES

1. Bober, T., et al. *Acta Bioengineering and Biomech,* **4**, 49-61, 2002.
2. Anderson, D., et al. *J Biomech,* **40**, 3105-3113, 2007.
3. Hugh-Jones, P. *J Physiol,* **105**, 358-386, 1947.
4. Hahn, D. *J Strength Cond Res,* **25**, 1622-1631, 2011.
5. Kepple, T., et al. *Gait Posture,* **6**, 1-8, 1997.

Table 1: Median, maximum, and minimum R-squared values for WL, HF, KF, and AF versus leg length.

	R-squared values			
	Whole Limb (WL)	**Hip Force (HF)**	**Knee Force (KF)**	**Ankle Force (AF)**
Median	0.754	0.884	0.672	0.934
Maximum	0.990	0.998	0.998	0.996
Minimum	0.500	0.167	0.003	0.310

COMPARING PATELLEFEMORAL JOINT STRESS OF VARIOUS MOVEMENTS

[1] Naghmeh Gheidi, Alexey A. Minaev, Sara M. Frank, Madeline Sandheinrich, Taviare L. Hawkins, Thomas W. Kernozek
[1] University of Wisconsin La Crosse, La Crosse, WI, USA
Email: ngheidi@uwlax.edu

INTRODUCTION

Patellofemoral pain syndrome (PFPS) is a major cause of anterior knee pain in young active people, accounting for 25% to 40% of all knee problems and 25% of knee problems in the general population [1]. Females have a higher incidence of PFPS in the general population, but when studying athletes, PFPS is more common in men [1].

Painful symptoms often occurs during movements such as running, squatting, lunging, and stair climbing hindering the ability to perform everyday tasks. Increases in patellofemoral joint stress (PFJS) often corresponds with an increases in PFPS [2]. There are many studies comparing PFJS in different exercises, but to the best of our knowledge, there is no published study comparing PFJS involved in high risk everyday movements. Our study aims to compare the peak PFJS, peak quadriceps force (QF), and Knee Range of Motion (KROM), between a walk, run, front lunge (FL), single leg stand (SLS), and single leg hop (Hop).

METHODS

16 males (Age: 22.00 ± 1.54 yrs.; Height: 178.40 ± 6.28 cm; Mass: 74.74 ± 9.93 kg) were selected as participants. All scored > 5 on the Tegner activity scale and had no previous knee pain associated with PFPS.

Subjects performed five repetitions for 5 movements including walk (at 1.4m/s±5%), run (at 3.5m/s±5%), front lunge (FL), single leg stand (SLS), and single leg hop over a 16 cm barrier (Hop) in a random order. Kinematic data were collected utilizing a 15-camera Motion Analysis (Motion Analysis Corp, Santa Rosa, CA) system (180Hz) and using 47 markers on anatomical landmarks. Bertec Force Platforms (Bertec Corp, Columbus, OH) (1800Hz) recorded the ground reaction forces.

Utilizing Human Body Model (HBM) (Motek Medical, Amsterdam, Netherlands), muscle forces were determined from a 44 degree of freedom musculoskeletal model with 16 segments via inverse dynamic based static optimization routine. Quadriceps force (QF) was calculated from the sum of the rectus femoris, vastus (medialis, lateralis, and intermedius) muscles forces from HBM. Patellofemoral joint reaction force (PFJRF) was the compressive component of the QF based on knee flexion angle and quadriceps muscle orientation [3]. The PFJS was then determined by dividing the PFJRF by patellofemoral joint contact area as a function of knee angle using data from Huberti and Hayes [4]. All data were clipped to the stance phase of each movement based on vertical ground reaction force > 10 N.

Using SPSS (Version 24, IBM, Armonk, NY, USA), a multivariate analysis of variance (MANOVA) with repeated measures (α=0.05) was used to examine differences in peak PFJS, peak QF and KROM between the 5 movements. Follow-up univariate tests were completed to detect differences between movements for each variable.

RESULTS AND DISCUSSION

The MANOVA revealed differences between the movements (Wilk's lambda<0.001, F=158.4, P-value<0.001). Univariate testing showed differences in PFJS, QF, and KROM. The mean and standard deviation, and pairwise comparisons between movements are shown in Table 1.

The pairwise comparisons indicated differences in peak PFJS, QF and KROM between almost all the movements, however, the peak PFJS magnitude was similar for the Run, FL, and Hop. Post-hoc comparison showed that PFJS could be placed into 3 groups (Figure 1A). SLS, had the lowest PFJS, QF, and KROM. These were around 10 times less than the highest magnitude grouping of movements. The stress was approximately the same during SLS (Figure 1B). Walk had the second lowest PFJS. Peak PFJS occurred during the first ~30% of the stance phase (Figure 1B). The final group contained Run,

FL, and Hop, with the most dynamic of the movements being the highest PFJS. The KROM was different between all three exercises despite having similar peak PFJS. Timing of peak PFJS was largely different, where the FL and Run had one peak occurring at ~50% of the activity whereas the Hop had two peaks in PFJS, one during landing and the other at takeoff (Figure 1A).

PFJS is due to compressive vector QF and the patellofemoral joint contact area both relative to knee angle. Relatively low impact activities, such as; SLS and Walk have low PFJS. These activities have low QF but varied KROM. There was a 3-fold increase in PFJS between Walk and SLS, indicating a corresponding increase in QF and KROM (Table 1). In walking, peak contact area is known to occur at ~20° knee flexion, around 60% gait cycle which supports our findings [5]. Peak PFJS has been shown to occur in FL when KROM is >75°, where the patellofemoral joint contact area begins to plateau and quadriceps activation is responsible for increased PFJS (6).

Table 1: Mean ± standard deviation (sd) of patellofemoral joint stress, quadriceps muscle force, and KROM for each movement and pairwise comparisons.

Movements	Peak PFJS (MPa)	Peak QF (BW)	KROM (°)
	Mean ± sd		
SLS	1.7±0.9	0.697 ± 0.395	1.64 ± 1.23
Walk	5.4±1.7	2.199 ± 0.706	25.75 ± 2.98
FL	19.8±2.2	7.783 ± 0.699	103.96 ± 7.43
Run	19.9±3.5	8.139 ± 1.422	35.88 ± 6.87
Hop	23.1±3	9.481 ± 1.286	44.92 ± 9.16
Exercises	Percentage changes (* Indicates p < 0.05)		
Run-Walk	*114.63	*114.92	*32.87
Run-FL	0.5	4.47	*97.37
Run-SLS	*168.52	*168.45	*182.52
Run-Hop	14.88	15.23	*22.38
Walk-FL	*114.29	*111.88	*120.59
Walk-SLS	*104.23	*103.73	*176.05
Walk-Hop	*124.21	*124.69	*54.25
FL-SLS	*168.37	*167.12	*193.79
FL-Hop	15.38	*19.67	*79.31
SLS-Hop	*172.58	*172.61	*185.91

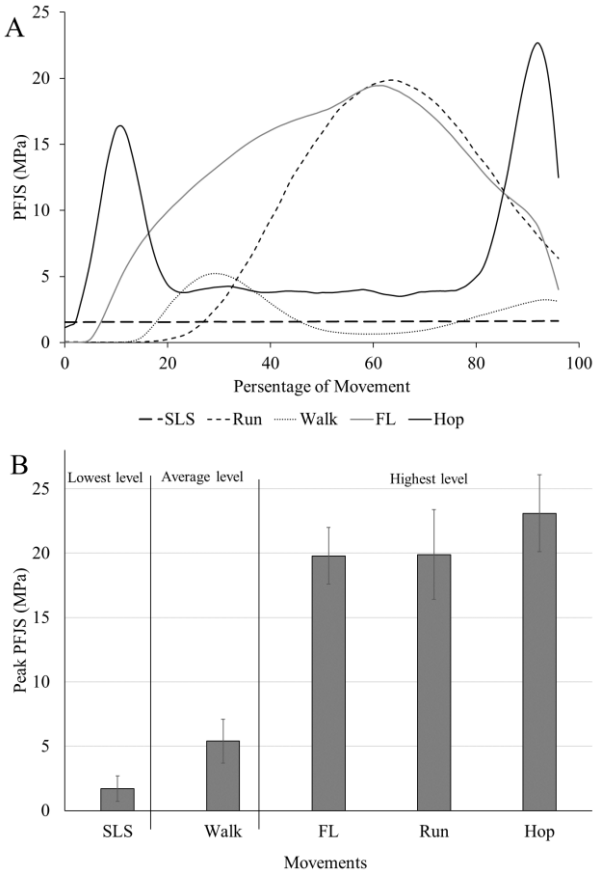

Figure 1: A) Ensemble average PFJS for each movement. B) Peak PFJS showing level of magnitude for the movements based on pairwise comparisons (3 main groups show the level of PFJS).

CONCLUSIONS

In general, PFJS increased with increased QF but KROM was also a factor. FL had a similar level of PFJS as a Run and Hop even though it could be viewed as a less dynamic and impact related movement.

REFERENCES

1. Clijsen R, et al. *Phys Ther*. **94**(12): 1697-1708, 2014.
2. Rodriguez-Merchan EC. *Arch Bone Jt Surg*. **2**(1): 4–6, 2014.
3. Vannatta CN & Kernozek TW. *Med Sci Sports Exerc*. **47**(5): 1001-1008, 2015.
4. Huberti HH & Hayes WC. *J Bone Joint Surg Am*, **66**(5): 715-724, 1984.
5. Powers CM, et al. *Am J Sports Med*. **32**(1): 224-31, 2004.
6. Escamilla RF, et al. *J Orthop Sports Phys Ther*. **38**(11): 681-690. 2008.

OPTIMIZING WHOLE BODY KINEMATICS TO REDUCE PEAK NON-SAGITTAL PLANE KNEE LOADS DURING SINGLE LEG JUMP LANDING TASK TO REDUCE RISK OF ACL INJURY

[1]Dhruv Gupta, [2]Jeffrey A. Reinbolt, [1]Jody L. Jensen and [3]Cyril J. Donnelly

[1] University of Texas at Austin, Austin, TX, USA
[2] University of Tennessee, Knoxville, TN, USA
[3] The University of Western Australia, Perth, Western Australia, Australia
email: dhruv.gupta@utexas.edu

INTRODUCTION

In the United States, every year over 200,000 anterior cruciate ligament (ACL) injuries occur [1, 2]. Approximately 60% of these are non-contact in nature, with >90% occurring during single-leg jump landing (SLJL) or sidestepping [3, 4]. Anterior tibial force in conjunction with non-sagittal plane (valgus, varus and internal rotation) knee moments has been shown to place the maximum strain on the ACL [5]. During landing and sidestepping the peak loads are typically observed during the weight acceptance or the impact phase of the movement [6].

Using the residual reduction algorithm (RRA) tool in OpenSim musculoskeletal modeling framework, optimized kinematics that reduce peak valgus knee moments can be solved for [7]. They used outer level optimization tool [8] which makes the simulations work with negligible residual forces not allowing the reduced knee loads to simply shift to the residual forces.

As acknowledged by Donnelly et al. (2012) [7], one of the primary limitations of their simulation work was the absence of a foot-contact model that would prevent inappropriate translations of the foot like breaking the plane of the floor. Use of zero-moment point (ZMP) computations [9] to give a dynamically consistent ground reaction force (GRF) for each simulation is a promising solution to this problem. A secondary limitation of this study [7] is that only peak valgus knee moment was reduced and not all the non-sagittal plane knee moments.

The purpose of this study is to a) integrate the ZMP computations [9] within outer level optimization tool [8] to produce simulations of SLJL task during weight acceptance phase, with dynamically consistent GRF using the RRA tool in OpenSim and b) using these simulations, find the optimal whole body kinematic pattern that reduces the non-sagittal plane knee moments to reduce ACL injury risk.

METHODS

Step 1: Producing simulations: Methods used by Donnelly et al (2012) [7] create joint torque driven simulations with negligible model residuals were integrated to ZMP computations [9]. This creates simulations with negligible residual forces and with dynamically consistent GRF (fig. 1). The cost function $J(x)$ of the outer level optimization tool was modified to not only reduce the errors in model kinematics, residuals and torque excitations, but also the foot translation errors, GRF errors and COP errors.

$$J(x) = \min_{x^R, x^T}[\sum_{i=1}^{n_q} w_{\ddot{q}_i}(\ddot{q}_i^{exp.} - \ddot{q}_i^{sim.})^2 + \sum_{j=1}^{6} w_R\left(\frac{R_j(x_j^R)}{R_j^{max}}\right)^2 + \sum_{k=1}^{n_T}\left(\frac{T_k(x_k^T)}{T_k^{max}}\right)^2 + \sum_{m=1}^{n_m} w_m(p_m^{exp.} - p_m^{sim.})^2 + \sum_{f=1}^{4} w_f(GRF_f^{exp.} - GRF_f^{ZMP})^2 + \sum_{c=1}^{2} w_c(COP_c^{exp.} - COP_c^{ZMP})^2]$$

Where, x^R and x^T are the excitation values for six residuals (R_j) and joint torques (T_k), $p_m$is the position of markers tracked on the foot and q_i are the model kinematics.

Step 2: Reducing non-sagittal knee moments: The maximum allowable joint torques of knee V/V and knee I/E rot were simultaneously reduced until the model crashes, but still producing reasonable simulations with consistent ground reaction forces. Our a priori definition of a reasonable simulation that it has negligible residuals, GRF errors < 10 N, GRF moment errors < 10 Nm and COP errors < 3 cm and foot translation errors < 3 cm compared to the simulations from the first step. This simulation gives

us the optimal kinematics that reduced peak non-sagittal plane knee moments for the SLJL task.

Figure 1: Reasonable simulation of SLJL task with dynamically consistent GRF.

We define non-sagittal plane knee moment as vector sum of knee V/V and I/E rot knee moments. Its peak value before and after step 2 was compared. Texas Advanced Computing Center at The University of Texas at Austin was used for all computations.

RESULTS AND DISCUSSION

Data analyzed was from male Australian-rules-football players. Five simulations with negligible residuals and consistent GRF for the SLJL task during the weight acceptance phase were produced. All simulations landed on right leg. The peak non-sagittal plane knee moment was reduced by an average of 30.18 ± 18.52 % (29.92 ± 15.16 Nm). Fig. 2 shows the changes in peak knee moments in all three axes individually and the non-sagittal plane knee moment. All simulations reduced the peak non-sagittal plane knee moment. The peak knee flexion/ extension moment remained approximately the same except for the first simulation, where the peak knee flexion moment increased. This however, does not increase risk of ACL injury as it is the non-sagittal plane knee moments that put heavy ACL strain [5].

For our SLJL simulations, the change in kinematics after the reduction of the non-sagittal plane knee moments were surprisingly small (a maximum of 1.46 degrees for left hip rotation in simulation 5). 11 out of the 22 significant kinematic differences observed were in sagittal plane, 3 in frontal plane and 8 in transverse plane. Sagittal plane displayed the most kinematic changes in previous side-stepping research as well [7]. Lack of big kinematic changes could be due to the additional tracking of the foot translation and the ZMP computations. This calls for a deeper study of load distribution with more data.

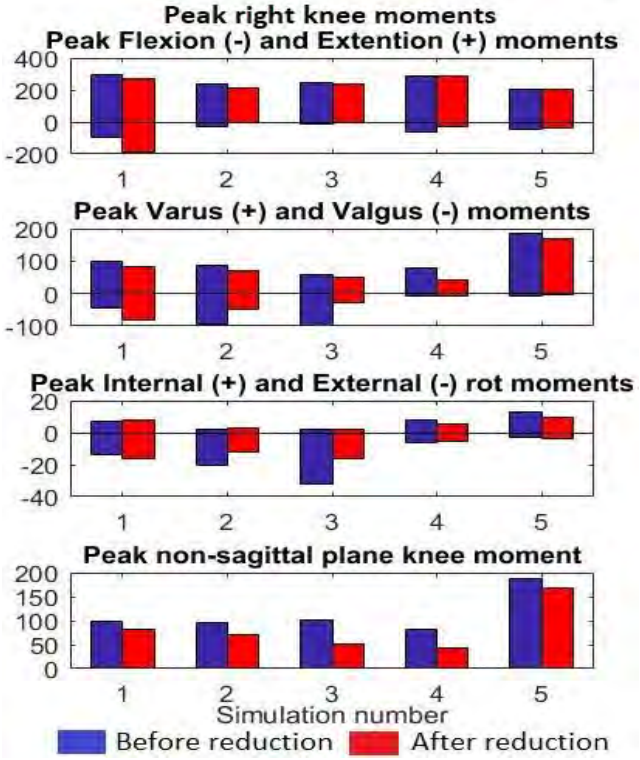

Figure 2: Peak right (landing) knee moments before and after optimizing whole body kinematics to reduce peak non-sagittal plane knee moments.

CONCLUSIONS

This is first time that simulations with negligible residuals and dynamically consistent GRFs have been produced. Optimizing whole body kinematics to reduce peak knee moments can help design training protocols [10] that can have huge implications in preventive medicine. Further research in load distribution in optimized simulations and muscle contributions is needed

REFERENCES

1. Arendt E and Dick R. *Am J Sports Med*,1995.
2. DeMorat G. et al. *Am J Sports Med*, 2004.
3. Ekegren CL, et al. *J Orthop Sports Phys Ther*, 2009.
4. Hewett TE, et al. *Am J Sports Med*, 1996.
5. Markolf KL, et al. *J Orthop Research*, 1995.
6. Cerulli G, et al. *Knee Surg, Sport Traumatology, Anthroscopy*, 2003.
7. Donnelly CJ et al. *J Biomechanics*, 2012.
8. Reinbolt JA, et al. *Simulation of human movement*, 2011.
9. Reinbolt JA and Donnelly CJ. *Int Society Biomech*, 2017.
10. Staynor JMD, et al., *Sports Biomechanics*, 2017.

SEGMENT COORDINATION VARIABILITY CHANGES DURING BACK SQUATS WITH BIOFEEDBACK

[1, 2] Kelci B. Hannan, [1]Jason Stone, [1]Daniel Arndts, [1]Anthony Anzalone, [1]Jonathan M. Oliver, [2]James Bothwell, [1]Adam C. King

[1] Texas Christian University, Fort Worth, TX, USA
[2]Ben Hogan Sports Medicine, Texas Health Resources, Fort Worth, TX, USA
email: k.besand@tcu.edu

INTRODUCTION

Fatigue is the decreased ability to produce force and plays an important role in all physical activity, dictating the duration and quality of movement. With the onset of fatigue often comes a breakdown of movement patterns in which the individual compensates with undesirable, and sometimes dangerous, movements. Biofeedback has the potential to encourage maintenance of safe, effective movement patterns. Previously, real-time feedback about peak velocity has been reported to improve performance of movement and sport-specific tasks [1]. Additionally, the provision of feedback encourages consistency in squat jump performance and increases in peak velocity [2, 3]. These qualities may also contribute to reduction of altered movement during fatiguing tasks.

In motor tasks, such as the back squat, the desired movement pattern is highly constrained to sagittal plane motion. Minimizing accessory movement in other planes may enhance performance by allowing the individual to focus force and energy production into the primary movement plane. Additionally, accessory movements in the frontal and transverse planes may increase injury risk. Reduction of movement in the frontal plane is also a common focus during rehabilitation. For example, anterior cruciate ligament reconstruction (ACLR) patients often use visual feedback to provide information about knee motion with the intent to decrease medial movement.

The primary purpose of the current investigation was to investigate changes in lower extremity coordination variability as a result of implementing biofeedback during back squats. A secondary purpose was to examine changes in lower extremity segment coordination as a function of fatigue and load. We hypothesized that an increase in load would alter accessory movement in the frontal plane due to a more rapid onset of fatigue compared to a lighter load. Additionally, we hypothesized that use of biofeedback would attenuate the altered movement pattern effects of fatigue. This is expected to manifest as a reduction in accessory movement in the frontal plane.

METHODS

Thirteen (n = 13) resistance-trained males (23.8 ± 4.9 years; 85.4 ± 17.3 kg; 14.4 ± 6.4% fat) were recruited to participate in this study. All participants underwent a familiarization session 48 hours prior to one-repetition maximum (1RM) testing. Seventy-two hours after 1RM testing, participants completed experimental testing under four conditions, ordered randomly, until voluntary fatigue. The conditions were 75% 1RM with and without biofeedback and 90% 1RM with and without biofeedback. Participants were instructed to move the load "as explosively as possible". Each experimental condition was separated by at least 72 hours. A linear position transducer attached to the right end of the barbell provided real-time feedback about peak bar velocity during each repetition of the biofeedback conditions.

Kinematic data were collected using a 10-camera Qualisys Motion Capture System (Qualisys AB, Göteborg, Sweden) and were filtered using a fourth-order Butterworth filter and 12 Hz cut-off frequency. Segment angles were calculated relative to the lab coordinate system and couplings were used to create relative motion (angle-angle) plots as a function of anatomical plane.

Data from three participants were excluded from analysis due to poor kinematic profiles. Modified vector coding [4] was used to bilaterally analyze frontal plane segment couplings: shank-foot, thigh-shank, and trunk-thigh. Circular statistics were used for the analysis of angular data comparing mean vector coding values for each independent variable (trial, biofeedback condition, and load) of squats ($p < 0.05$).

RESULTS AND DISCUSSION

The results of the HARRISON-KANJI test revealed significant differences in the right shank-foot ($p = 0.0449$), thigh-shank ($p = 0.0143$), and trunk-thigh ($p = 0.0001$) couplings and in the left trunk-thigh coupling ($p = 0.0006$) for biofeedback condition. Significant interactions between biofeedback condition and trial were observed in the left shank-thigh coupling ($p = 0.0018$) and left trunk-thigh coupling ($p = 0.0297$). Additionally, significant differences in load were observed for the right trunk-thigh coupling ($p = 0.0072$) and left shank-foot ($p = 0.0039$) and thigh-shank ($p < 0.0001$) couplings. No other significant differences were found.

The significant differences in load confirmed the fatiguing effects of back squatting at 90% 1RM versus 75% 1RM and the subsequent coordination changes. The change in coordination variability is likely related to the onset of fatigue, specifically for the right trunk-thigh, left shank-foot, and left thigh-shank couplings. A more detailed analysis is needed to identify the exact changes occurring among these segments, as well as those in which no significant difference between load conditions was observed. An investigation to identify the timepoint in the squat cycle at which differences in coordination variability occur would also be valuable in understanding the effects of fatigue on movement patterns. The interaction between use of feedback and load for left leg couplings suggests that implementation of biofeedback may attenuate movement pattern changes that commonly occur because of fatigue during heavy weight lifting.

Frontal plane movement is a primary focus during rehabilitation of knee injuries, as medial knee movement is a common mechanism of injury for serious injuries, such as ACL injury. Visual observation and feedback are typically used to make improvements in frontal plane motion, but this feedback is not readily available when the athlete returns to sport and is highly subjective. Implementing other forms of real-time feedback based on peak velocity or force production may lead to increasingly consistent movement patterns.

CONCLUSIONS

The results of feedback implementation suggest an effect of biofeedback on frontal plane segment coordination variability. These findings may suggest a potential value in implementing biofeedback during rehabilitation to alter movement patterns in the frontal plane, especially when combatting fatigue. This may be especially applicable following ACLR when reduction in frontal plane motion at the knee is desirable prior to return to sport. These results are preliminary and further investigation is needed to determine the full effect of biofeedback as a means of attenuating changes in coordination variability due to fatigue in a variety of sports-related and rehabilitation tasks.

REFERENCES

1. Randell et al. *Journal of Strength and Conditioning Research,* **25**(1), 87-93, 2011.
2. Randell et al. Effect of performance feedback during velocity based resistance training. *Journal of Strength and Conditioning Research*, 2010.
3. Randell et al. Reliability of velocity measures for jump squats under feedback and non-feedback conditions. *Sports Biomechanics,* 2009.
4. Sparrow et al. *Journal of Motor Behavior,* **19**, 115-129, 1987.

TESTING OF RUBBER BUMPERS FOR IMPROVEMENT OF THE SINGLE AXIS FOOT

[1,2]Emily Hein, [1]Eric Nickel, [1,2]Andrew Hansen, and [1]Sara Koehler-McNicholas

[1]Minneapolis VA Health Care System, Minneapolis, MN, USA
[2]University of Minnesota, Minneapolis, MN, USA
Email: Emily.Hein@va.gov

INTRODUCTION

Flexion and extension of a single-axis foot (SAF) is governed by the mechanical properties of rubber bumpers located in the front and rear of the prosthetic ankle joint. These bumpers determine the torque-angle relationship of the ankle joint and therefore, sub-optimal bumper selection can negatively impact gait biomechanics. Although the SAF has been in existence since 1861, there are still improvements to be made [1]. Many modern prosthetic feet attempt to mimic the roll-over shape demonstrated by the natural human ankle [2]. Some feet achieve this roll-over shape better than others. Hansen and Childress showed that the Otto Bock C-Walk more closely resembles the able-bodied ankle-foot roll-over shape than the Otto Bock Single-Axis foot [2]. The Otto Bock SAF is more rigid in the forefoot region than the C-Walk, and thus the center of pressure advances suddenly from the heel to the toe, rather than rolling gradually. According to a study by Raschke et al. [3], prosthesis users generally prefer mechanically compliant feet over stiff feet. By adjusting the rubber bumpers in the SAF, a more compliant foot could be created which would be cost-effective and low-maintenance, yet have a more natural feel than current SAF options. The long-term goal of this study is to construct a model that defines the force (F) on a bumper at a given Shore A durometer (D), resting height (l_o), and deflection (δ) to support the design of more biomimetic SAF prostheses.

$$F = f(D, l_o, \delta)$$

METHODS

Polyurethane rubber bumpers were linearly compressed on a dual column universal testing machine equipped with a 5 kN uniaxial load cell (Test Resources, Inc., Shakopee, MN). One-inch square rods with Shore durometers of 97A, 92A, 75A, 60A, and 40A were tested. Each rubber rod was cut into samples of five different heights: 20 mm, 30 mm, 40 mm, 50 mm, and 60 mm. Additional 40 mm samples were prepared for each durometer so that multiple trials of a single height could be performed, resulting in a total of 35 bumper samples.

After the samples had been prepared, each was loaded on the dual column universal testing machine and compressed at a constant rate of 254 mm/min to a force that is equal to or greater than the target force of 4250 N. Displacement and force data were collected from the testing.

RESULTS AND DISCUSSION

Understanding the relationship between force and displacement (Figure 1) is helpful in design applications of the SAF.

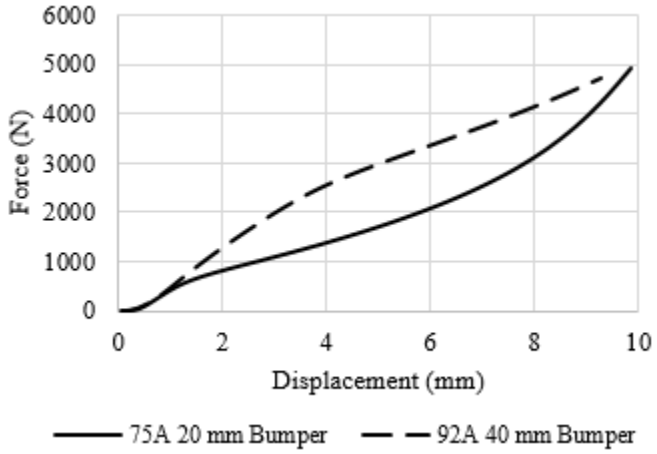

Figure 1: Example force-displacement curves for two bumper samples.

The displacements at a force of 4250 N were plotted for each durometer versus the initial bumper height (Figure 2).

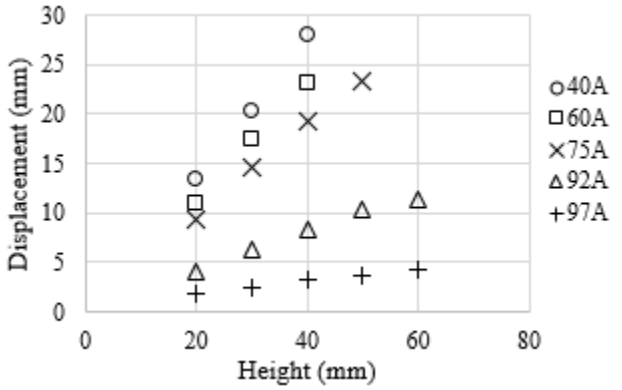

Figure 2: Displacement at which a force of 4250 N was reached. Samples that buckled were excluded from the graph (50 mm 40A and 60A, as well as 60 mm 40A, 60A, and 75A samples).

Samples that buckled were all taller than 40 mm. For this reason, bumpers that have a height ranging above 40 mm would not be recommended for implementation in the SAF.

The following example provides a design scenario in which the results of this study can be applied. Assuming that the moment arm of the dorsiflexion bumper from the ankle joint is 50 mm, the ankle torque and angle can be converted to force and displacement on the bumper. Winter [4] has shown that the peak torque during late stance of a natural human ankle is about 1.7 $N \cdot m \cdot kg^{-1}$ at normal self-selected walking speed, which is reached at an angle of approximately 10˚ of dorsiflexion. Given a user mass of 125 kg, the force applied to the bumper would approximate 4250 N. At 50 mm from the ankle, the 10˚ angle would correspond to a displacement of 8.8 mm. Based on this force-displacement requirement, Figure 2 can be used to select an appropriate bumper. In this case, the best choice of bumper is either the 20 mm tall bumper with a durometer of 75A, or the 40 mm tall 92A bumper (Figures 1 and 2).

All bumpers tested in this study had a uniform cross-sectional area of one square inch. It is important to note that changing the cross-sectional area will impact the force-displacement relationship. It is also important to note that no durometers in the range of 76-91A were tested. From the data collected, this appears to be a region of interest and further studies could expand into this range to find a durometer that better mimics the human ankle biomechanics. This model could also be validated in a future study by creating a SAF system and collecting the ankle kinematics/kinetics and preferences of prosthesis users while using different bumpers.

CONCLUSIONS

These data are currently being analyzed to achieve the project end goal: to create a model of the force-displacement relationship of the bumpers as a function of the initial height and Shore A durometer. This relationship could be used by designers to determine the durometer and initial height that would generate the most biomimetic ankle torque-angle relationship for their SAF designs. Improvements to the roll-over characteristics of SAF prostheses will support improved mobility and comfort for many prosthesis users.

REFERENCES

1. Goh et al. *Prosthet Orthot Int* **8**, 147-154, 1984.
2. Hansen and Childress. *J Prosthet Orthot* **21**(1): 48-54, 2009
3. Raschke et al. *J Biomech* **48**: 146-152, 2015.
4. Winter, D. *The Biomechanics and Motor Control of Human Gait: Normal, Elderly, and Pathological,* University of Waterloo (2), 1991.

ACKNOWLEDGMENTS

The authors would like to thank Steve Morin and Greg Voss for their assistance with preparing the compression plates for testing. This work was supported by Merit Review Award Number I01 RX002267 from the United States (U.S.) Department of Veterans Affairs Rehabilitation R&D (Rehab RD) Service. The views expressed are those of the authors and do not reflect the official policy of the Department of Veterans Affairs.

EFFECTS OF ANKLE TENDON VIBRATION ON POST-STROKE ANKLE PROPRIOCEPTION

[1] Amanda A. Herrmann and [2] Jesse C. Dean

[1] HealthPartners Neuroscience Center, St. Paul, MN, USA
[2] Medical University of South Carolina, Charleston, SC, USA
email: Amanda.A.Herrmann@HealthPartners.com

INTRODUCTION

Proprioception, or the sensory processes that contribute to the sense of movement and position, is often disrupted after a stroke [1]. Methods aimed at enhancing proprioception could thus be integrated with current rehabilitation methods to potentially improve functional outcomes after a stroke.

A possible method for enhancing proprioception involves stochastic resonance. Stochastic resonance is a phenomenon in which low-amplitude noise (e.g. through the application of low-amplitude vibration) increases the likelihood that weak signals will exceed the perceptual threshold, therefore enhancing signal detection [2].

Two recent studies [3-4] investigated stochastic resonance in healthy adults, quantifying ankle proprioceptive function using an isolated movement detection test. Both stochastic resonant tendon vibration [3] and electrical stimulation [4] improved the detection of ankle motion. However, it is unknown whether similar methods can enhance ankle proprioception in populations who are more likely to exhibit reduced mobility due to proprioceptive deficits. The primary goal of this study was to quantify the effect of stochastic resonant tendon vibration on the threshold to detect passive motion (an isolated joint proprioception test), in individuals with stroke and in healthy age-matched controls.

METHODS

Individuals with chronic stroke (n=12) and healthy controls (n=12) participated in this study. As a measure of baseline function, participants with stroke completed the motor and sensory components of the Fugl-Meyer Assessment for the Lower Extremity (FMA-LE). Participant characteristics are provided in Table 1, with no significant differences in demographic characteristics between groups.

Threshold to detect passive movement (TDPM) at the ankle joint (plantarflexion & dorsiflexion) was assessed for both ankles in random order, using a Biodex Multi-Joint System Pro dynamometer (Biodex Medical Systems, Shirley, NY USA). Participants were seated, wearing noise cancelling headphones and a sleep mask to eliminate other sensory cues. Participants were positioned with the knee as extended as possible, and the ankle at a consistent starting position of 10^{o} plantarflexion. The dynamometer passively moved the ankle joint at a constant velocity of 0.25°/s. Participants were instructed to press a hand-held push button as soon as they detected ankle movement and to verbally state the direction of the movement.

In some trials, vibration was delivered using C-2 tactors (Engineering Acoustics Inc., Winter Park, FL, USA), electromechanical devices designed to stimulate a sensory response through vibration. The tactors were securely strapped over the bilateral Achilles tendons for all trials.

The TDPM test was performed under four conditions: one with No Vibration, and three with Vibration of low amplitude. For each condition, TDPM was quantified three times each for plantarflexion and dorsiflexion motion, with trial order randomized.

We used a repeated measures three-way ANOVA with interactions to determine whether movement detection was influenced by vibration (Vibration vs. No Vibration), group (Control vs. Non-paretic vs. Paretic ankle), or ankle movement direction (Plantarflexion vs. Dorsiflexion). Post-hoc tests were performed as appropriate.

RESULTS AND DISCUSSION

No significant interactions were observed (p>0.32 for all comparisons), allowing us to simply present the statistical results as main effects.

Addressing our primary goal, vibration reduced (improved) the TDPM when compared to the no vibration condition (p=0.01; Fig. 1). This result is in agreement with the two previously mentioned studies, in which the application of low-amplitude tendon vibration [3] and electrical stimulation [4] improved ankle proprioception in healthy adults.

Group had a significant effect (p=0.02) on TDPM, with the paretic ankle exhibiting a significantly higher (worse) TDPM than controls. While this result was expected, the lack of an interaction between group and vibration condition indicates that stochastic resonance may be an equally valuable tool for improving proprioception in both groups.

Ankle movement direction also had a significant effect (p=0.002) on TDPM, with a higher TDPM in the dorsiflexion direction. While somewhat unexpected, this result may be partially due to our initial ankle position (10^o plantarflexion) making it easier to detect further plantarflexion motion.

To our knowledge, this is the first study to demonstrate the use of stochastic resonance to enhance lower extremity proprioception in a chronic stroke and healthy-aged matched adult population. Further research is warranted to determine the potential beneficial effects of ankle tendon vibration on post-stroke functional outcomes dependent on proprioception (e.g. postural control and gait).

Despite evidence for sensory deficits following a stroke, rehabilitation research and treatment is primarily focused on motor-based therapy, and sensory loss is often overlooked. The present study provides proof-of-concept for a potential intervention of stochastic resonant vibration applied to the Achilles tendon in individuals with stroke and in healthy older adults, which could be directly and easily transferred into a real-world environment.

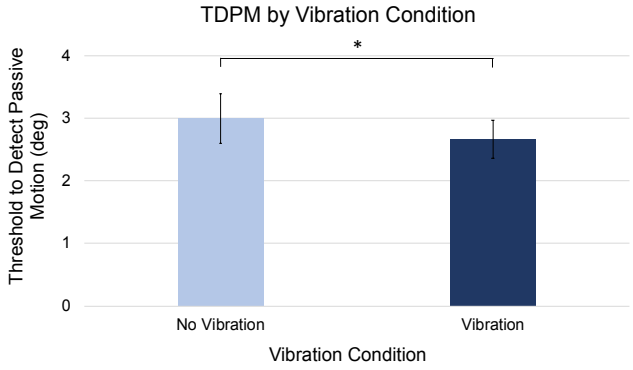

Figure 1: TDPM by Vibration Condition. The error bars represent 95% confidence interval.

REFERENCES

1. Connell et al. *Clinical Rehabilitation.* **22**(8), 2008.
2. Collins et al. *Nature.* **383**, 1996.
3. Ribot-Ciscar et al. *Experimental Brain Research.* **228**(4), 2013.
4. Toledo et al. *Neuroscience.* **358**, 2017.

Table 1: Participant Baseline Characteristics

	Stroke (n = 12)	**Control (n = 12)**	***p*-value**
Gender	7F, 5M	7F, 5M	N/A
Age (yrs)	54 ± 15	50 ± 14	0.08
Height (cm)	172 ± 13	169 ± 11	0.20
Mass (kg)	79 ± 11	79 ± 16	0.79
Time Since Stroke (mo)	64 ± 41	N/A	N/A
	Motor Function[a] / Sensory[b]		
FMA-LE	25 ± 4 / 11 ± 1	N/A	N/A

Notes: Data is presented as mean ± standard deviation; [a] Maximum Score: 34; [b] Maximum Score: 12

EVALUATION OF THREE DIMENSIONAL KNEE CRUCIATE & COLLATERAL LIGAMENT STRAIN WITH DIGITAL IMAGE CORRELATION

Alexander W. Hooke, Nathaniel A. Bates, Nathan D. Schilaty, Lawrence J. Berglund, Timothy E. Hewett
Mayo Clinic, Rochester, MN, USA
email: hooke.alaexander@mayo.edu

INTRODUCTION

Ultimate strain of knee ligaments has traditionally been limited to uniaxial failure tests that compare the overall change in length at the time of peak load to initial taught length [1]. Recently, ultimate strain has also been examined under more physiologic loading conditions through the simulation of landing tasks in cadaveric lower extremities [2]. Even these measurements are limited as they report strain relative to a singular point of strain gauge implantation. As ligaments are anisotropic [3], strain would best be assessed across the entire body of the structure. Recent video analysis technological advances have made such a surface assessment of strain possible in a controlled failure environment.

The aim of this investigation was to quantify strain across the surface of all four major knee ligaments during uniaxial failure tensioning. This study used a Digital Image Correlation system (DIC) (ARAMIS 4M, Trilion Quality Systems, Plymouth Meeting, PA) which records, calculates, and analyzes the strain and deformation response of a test specimen subjected to a load or force. This allowed the investigators to assess entire ligament surface strain through tensile failure testing to determine failure patterns and quantitative locations. The hypothesis tested was that strain would not be uniformly distributed across the surface of the ligamentous structures at the time of structural failure.

METHODS

Contralateral knees from a single male cadaveric specimen were used in this preliminary investigation [51 years, 81.6 kg, 170 cm]. All soft tissues surrounding the knee joint were removed except for the anterior/posterior cruciate and medial/lateral collateral ligaments which were left intact. The femur, tibia, and fibula were cut to separate the ligaments. Thus, each ligament plus its bony footprints at the origin and insertion were available to be tested independently. Each specimen was potted in a custom fixture such that the bony footprint was rigidly encased in bone cement leaving the ligament free.

A black and white speckling pattern was applied to each ligament surface using a combination of face and spray paint. The speckled sample was then mounted to a multi-axis servo-hydraulic test machine (MTS 312, MTS Systems Corporation, Eden Prairie, MN) such that the long axis of the ligament was parallel to the linear actuation axis of the machine and the surface of interest on each ligament was facing the DIC cameras. The following surfaces were captured: anterior surface of the ACL, medial surface of the MCL, lateral surface of the LCL, and posterior surface of the PCL.

Each of the four ligaments were tested individually using the following loading and data collection protocol. A 4 N preload was applied followed by a cyclical preconditioning of 10 cycles oscillating between 0% and 3% strain at 1 Hz. The ligaments were then linearly tensioned to failure at a strain rate of 20%/sec until failure. Load and displacement data were recorded by the MTS actuator at 64 Hz. The DIC system recorded the surface deformation at 64 Hz.

The load at failure and stiffness of the ligament was computed with the data in MATLAB. The surface strain maps of each ligament were analyzed with the ARAMIS software. The peak strain and its location on the surface of each ligament were extracted for the duration of east test.

RESULTS AND DISCUSSION

The 3D strain maps of the ligaments' surfaces indicate that the strain was not uniformly

distributed. Rather, the strain distribution varied across the surface with some areas strained approximately 20% more than others. This can be seen in the single-frame strain maps of each ligament presented in Figure 1. The failure load, stiffness, and peak surface strain at failure of each ligament is presented in Table 1.

Table 1: Results of load-to-failure testing on ACL, LCL, MCL, and PCL. Failure load, stiffness, and peak surface strain at failure are presented.

Ligament	Failure Load (N)	Stiffness (N/mm)	Peak Strain at Failure (%)
ACL	489.6	129.3	39.7
LCL	445.3	66.2	43.3
MCL	502.3	79.9	32.9
PCL	1153.9	199.0	46.1

All ligaments failed with a peak strain ranging from approximately 33-46%. The ACL and PCL were remarkably stiffer than the LCL and MCL. However, any conclusions drawn from this data set are limited due to its single-specimen nature. The development of a DIC system to capture accurate 3D strain maps of the knee ligaments will enhance understanding of the strain distribution during loading and failure.

CONCLUSIONS

Strain was not evenly distributed across the surface of each major knee ligament during uniaxial tensioning to failure. The peak reported surface strain for each ligament well exceeded the mean ultimate strain values reported in previous literature [1, 2].

REFERENCES

1. Woo, et al. *Am J Sports Med*. **19**(3), 1991
2. Bates, et al. *Am J Sports Med*. In-press, 2018
3. Kiapour, et al. *J Biomech Eng*. **136**(1), 2014

ACKNOWLEDGEMENTS

NIH grants R01AR055563, R01AR056259, K12HD065987, and L30AR070273 with support from the Materials and Structural Testing Research Core at Mayo Clinic.

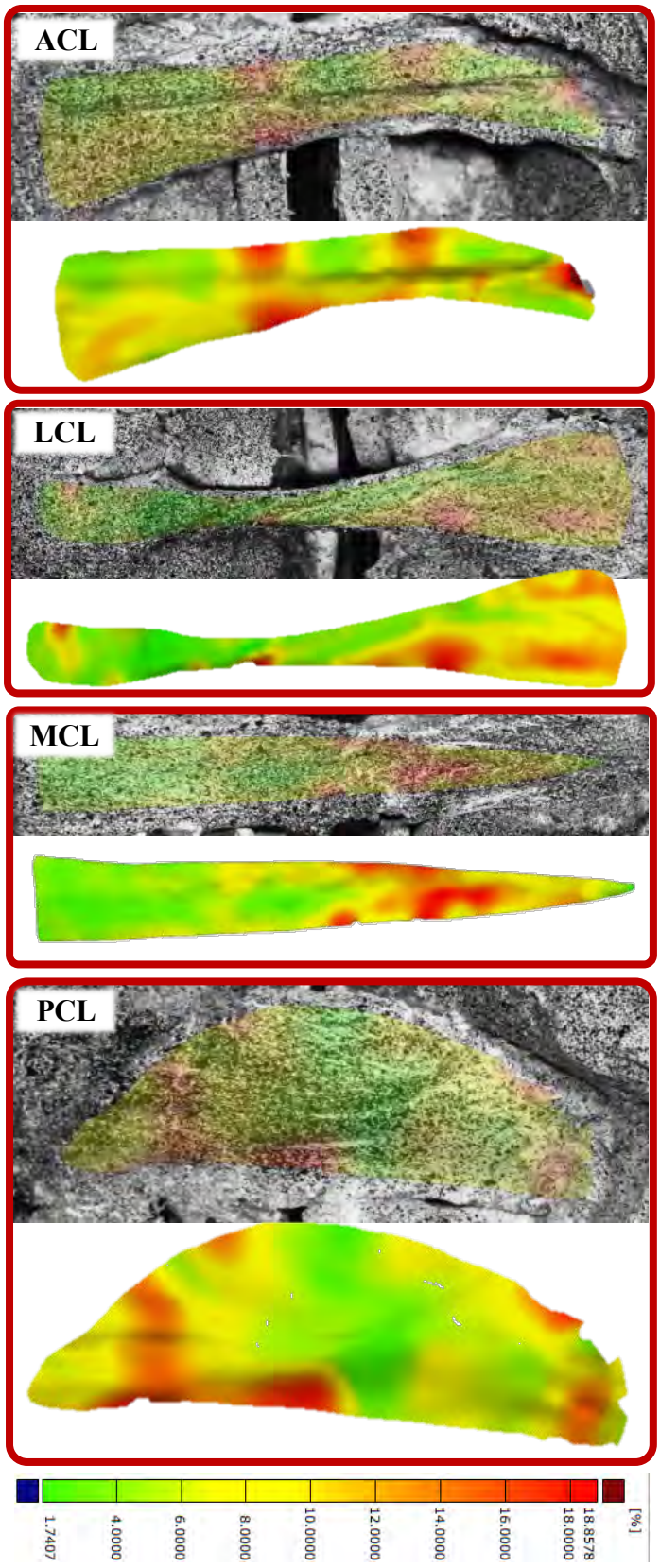

Figure 1: Strain maps of the ACL, LCL, MCL, and PCL during tension testing. Each image represents a single frame during pre-failure loading with the proximal side on the right and distal side on the left.

THE RELATIONSHIP BETWEEN GOLF STANCE AND THE LEAD LIMB PEAK KNEE ADDUCTION MOMENT

[1, 2] Quenten L. Hooker, [2] Robert Shapiro, [2] Terry Malone, [3] Michael B. Pohl

[1] Washington University, St. Louis, MO, USA
[2] The University of Kentucky, Lexington, KY, USA
[3] University of Puget Sound, Tacoma, WA, USA
Email : quenten.hooker@wustl.edu, mpohl@pugetsound.edu

INTRODUCTION

Golf is a popular sport that allows people to remain active during the later stages of life. Although it is widely considered to be a low impact activity, recent information suggests up to 72% of golfers have experienced an injury [1]. It has been speculated that the forces experienced at the knee during the golf swing are not large enough to cause acute injury [1, 2]. However, with repetitive use it is possible that forces and moments may be high enough to cause damage over time [2]. One load of particular interest is the external knee adduction moment, a measure that has been strongly associated with the progression of medial compartment knee osteoarthritis [3]. Moreover, given the external knee adduction moment has been reported to be 29% larger during the golf swing than gait, it seems pertinent to examine factors associated with this moment during the swing [4].

Deviations in stance have the potential to alter loading on the knee joint. For example, increasing foot angle (external rotation of the foot) or stance width has been shown to decrease the peak knee adduction moment during gait [3]. Similarly, Lynn et al. [4] found a reduction in the peak knee adduction moment during the golf swing when foot angle was increased from 0° to 30° in the setup. However, no prior study has examined the relationship between self-selected golf stance characteristics and the peak knee adduction moment during the golf swing.

Ground reaction forces (GRF) may also influence knee joint loading during the golf swing. Specifically, the vertical GRF has been reported to exceed two bodyweights during the golf swing [5]. However, the relationship between the peak vertical GRF and lead limb external knee adduction moment during the swing needs further investigation.

In summary, golf setup and GRF may be related to knee joint loading during the golf swing [4, 5]. Therefore, the purpose of the current study was to examine the association between the lead limb peak external knee adduction moment and self-selected foot angle, self-selected stance width, and peak lead limb vertical GRF. It was hypothesized that the peak external knee adduction moment would be negatively associated with foot angle and stance width, and positively associated with the peak vertical GRF.

METHODS

21 healthy participants (17 male, 4 females, age: 26.1 ± 7.0 years, handicap: 10.3 ± 6.8, height: 1.7 ± 0.1 meters, mass: 78.8 ± 13.3 kg) completed the study protocol. Retroreflective markers were placed on the spine and bilaterally on the pelvis and lower extremity. After a brief warm up period (5 min), participants were asked to hit three golf drives using their self-selected golf stance.

3D marker co-ordinate data were collected using ten high speed cameras (Motion Analysis Corp., Santa Rosa, CA) at 200 Hz. Ground reaction force data were collected using two Bertec Force Plates (Bertec Corp., Columbus, OH) at 1000 Hz. Self-selected foot angle was defined as the angular distance between the antero-posterior axis and longitudinal foot axis (i.e. toe and heel markers). Stance width was measured by the medio-lateral distance between the left and right heel markers. Joint dynamics were calculated in Visual 3D (C-Motion Inc., Germantown, MD).

Pearson product moment correlations were used to examine the relationship of the peak knee adduction

moment with self-selected foot angle, self-selected stance width, and peak lead limb vertical GRF. Correlations were considered significant at $p < 0.05$ and interpreted as either negligible ($0.0 \leq r < 0.2$), weak ($0.2 \leq r < 0.4$), moderate ($0.4 \leq r < 0.7$), strong ($0.7 \leq r \leq 0.9$), or very strong ($0.9 \leq r \leq 1.0$).

RESULTS and DISCUSSION

Participants had a mean self-selected foot angle of 10.2 ± 6.1° and stance width of 0.5 ± 0.1 meters. Mean peak lead limb vertical GRF and peak external knee adduction moment values were 2.2 ± 0.9 Nm/kg and 1.2 ± 0.6 Nm/kg respectively. The correlation results show that the peak knee adduction moment had a moderate positive relationship with the peak vertical GRF (Figure 1A), but negligible relationships with both self-selected foot angle (Figure 1B) and stance width (Figure 1C).

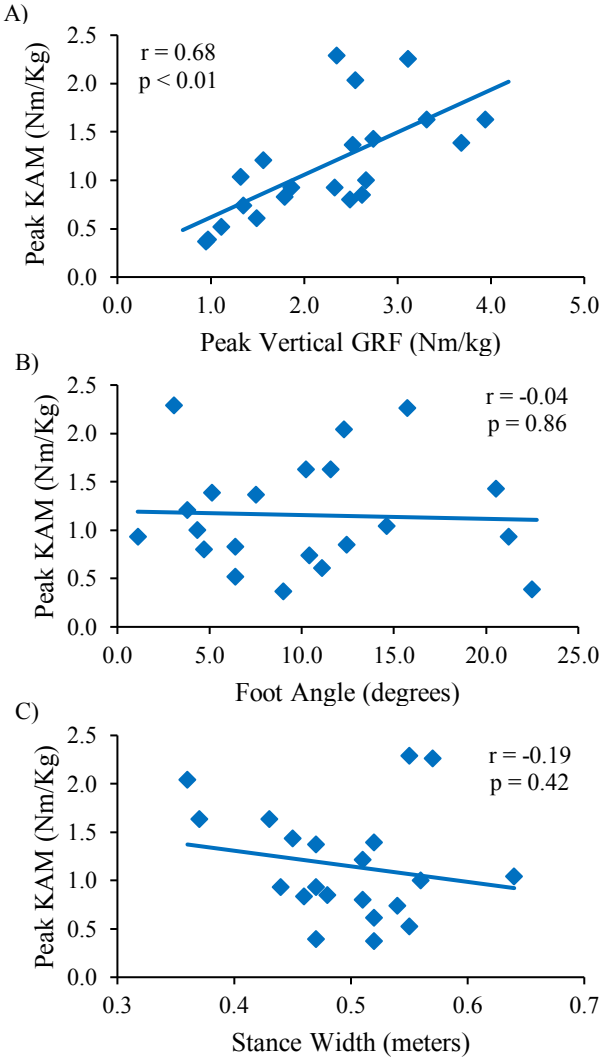

Figure 1: Relationship the peak external knee adduction moment (KAM) and A) peak vertical GRF (VGRF), B) foot angle, and C) stance width

Our results contradict the findings of previous research. Lynn et al. [4] reported significant reductions in the peak knee adduction moment when increasing foot angle from 0° to 30° in the setup, but we found negligible correlations between the peak external knee adduction moment and self-selected foot angle (Figure 1B). However, Lynn et al. [4] tested players during two fixed stance positions and did not assess knee moments during a self-selected golf stance. Our data indicates that a greater foot angle (more external rotation) is not associated with a reduced peak external knee adduction moment when players are allowed to adopt their self-selected stance.

To date, no prior study has investigated the relationship between the peak external knee adduction moment and self-selected foot angle and stance width during the golf swing. It has been proposed that an externally rotated foot position during the golf setup moves the GRF vector closer to the frontal plane axis of rotation and decreases the external adduction moment [4]. However, the external knee adduction moment could also be influenced by the magnitude of the GRF. Lynn et al. [4] did not report whether GRFs were altered during the stance modifications. Our data suggest that elevated GRFs may play a greater role in altering the external knee adduction moment than increases in foot angle or stance width.

CONCLUSIONS

Results show a positive moderate association between the lead limb peak external knee adduction moment and vertical GRF, whereas negligible correlations were observed for self-selected foot angle and stance width. Therefore, our data suggest GRFs during the golf swing contribute more to potentially harmful knee loads than stance variables.

REFERENCES

1) McHardy A, et al. *Sports Med* **36**, 171-87, 2006.
2) Baker M, et al. *Sports Med* **46,** 2621-39, 2017.
3) Favre et al. *J. Orth Res* **34**, 1547-56, 2016.
4) Lynn SK et al. *J. Sport Sci and Med* **9**, 275-81, 2010.
5) Hume et al. *J. Sports Med* **35**, 429-449.

Sex and Not Functional Ankle Instability Impact Peroneal Muscle Parameters

Wyatt D. Ihmels, Kayla D. Seymore, and Tyler N. Brown
Department of Kinesiology, Boise State University, Boise, ID USA
email: wyattihmels@u.boisestate.edu

INTRODUCTION

Ankle sprains are the most common recreational injury [1]. These sprains typically occur with inversion of the joint greater than 30°. Individuals who suffer an initial sprain may be predisposed to functional ankle instability (FAI), or recurrent injury from sensorimotor and mechanical deficits of the peroneal musculature [2]. During motions of the ankle, the peroneus longus prevents excessive inversion. Damage or injury to the peroneus longus may lead to changes in the muscle's function that can alter its effectiveness to prevent excessive inversion, as well as predispose the individual to repeated ankle sprains [3]. Recent advances in ultrasound technology have become a prominent way to measure specific muscle parameters *in vivo*, including physiological cross sectional area (PCSA) and muscle stiffness (MS). Yet, to our knowledge it is unknown if FAI participants exhibit differences in *in vivo* peroneal muscle parameters, or if these muscle parameters differ between sexes. This study sought to determine whether parameters of peroneal musculature differ between sexes or FAI participants, and whether these muscle parameters relate to ankle kinematics exhibited during a sudden inversion event.

METHODS

Eleven male and thirteen female recreationally active participants (ht: 1.72 ± 0.08 m, wt: 72.0 ± 11.4 kg, age: 20.9 ± 2.4 years) had muscle parameters and ankle kinematics quantified. Participants were also defined as FAI (n=9) or control (Con, n=15), based on their responses to the ankle instability instrument [5]. Each participant had MS and PCSA of the peroneus longus muscle measured using an ultrasound 9L4 transducer (Siemens Acuson S2000, Erlangen, Germany) while they stood with the dominant or effected ankle inverted to 30°. Measurements were taken at 50% length of the muscle. To quantify peroneal strength, participants completed three maximal isometric eversion contractions on an isokinetic dynamometer (System 2, Biodex Medical Systems, Inc., Shirley, NY). Peroneal eversion strength was the average maximum exhibited from each trial.

Each participant had ankle kinematics quantified during a sudden inversion event. For the inversion event, participants stood shoulder width apart on a wooden platform, which contained a trap door under each foot, that when dropped caused the ankle to invert to 30°. Participants performed five trials on each foot, however for purposes of this study only dominant or effected ankle kinematics were quantified. During each trial, subjects had the 3D trajectories of 32 anatomically placed lower-body reflective markers recorded by eight high-speed (240 fps) optical cameras (Vicon, Oxford, UK). Marker trajectories were low pass filtered using a fourth-order Butterworth filter (12 Hz) and then processed to solve ankle joint rotations at each instant using Visual 3D (C-Motion, Rockville, MD).

For analysis, MS and PCSA of the peroneus longus were quantified, peak ankle plantarflexion (PF) and inversion angle, and time to peak inversion were calculated during then sudden inversion event. Each muscle parameter was submitted to ANOVA to test main effect and interaction of group and sex. Each ankle kinematic variable was submitted to ANCOVA to test main effect and interaction of group and sex with muscle parameters considered as covariates. Alpha level was set to 0.05.

RESULTS AND DISCUSSION

Sex differences in muscle parameters were observed. Specifically, males exhibited grater maximum eversion strength ($p=0.044$) compared to females which may be attributed to the larger PCSA ($p<0.001$) of the peroneus longus musculature. But differences in MS were not observed between sexes ($p=0.138$). These differences in lower body

musculature are congruent with previous research showing equally trained women having smaller and weaker lower body muscles [4] The FAI group had greater, albeit non-significant, eversion strength (p=0.234), PCSA (p=0.421), and MS (p=0.124) compared to Con participants.

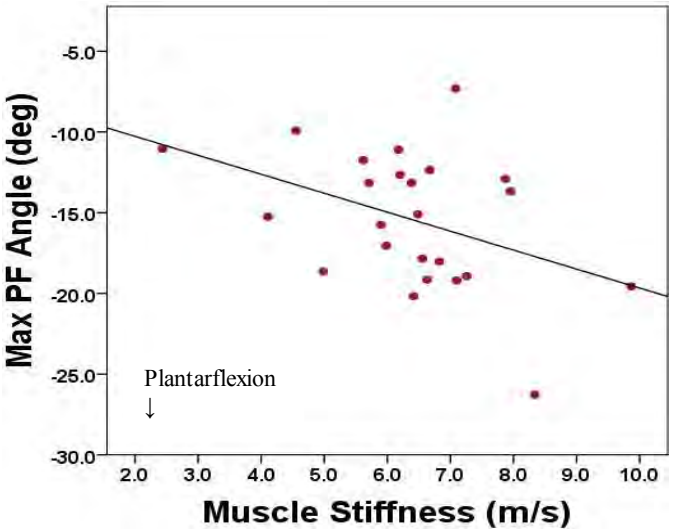

Figure 1: Depicts the relation between peak ankle inversion PF (deg) exhibited during the sudden inversion even and peroneal MS (m/s).

There was sex dimorphism in ankle kinematics observed during the sudden inversion event. During the sudden inversion event, females exhibited a significantly larger peak inversion angle (p=0.007), but no difference in in peak PF angle (p=0.504) or time to peak inversion (p=0.881) compared to males. Considering females have smaller and weaker peroneal musculature, future work is warranted to determine if these strength and size deficits limit their ability to prevent excessive inversion and increase their risk of ankle sprain.

Group difference in ankle kinematics were also observed during the sudden inversion event. In contradiction to previous research [2], the Con group exhibited greater peak ankle inversion (p=0.041) compared to FAI. However, no group differences were observed for peak PF angle (p=0.877) or time to peak inversion (p=0.179). Peroneal MS however, was a significant covariate of peak PF angle (Fig. 1; p=0.046) during the sudden inversion, with unit increase in stiffness predicting 1.4º increase in peak PF. Considering, the FAI participants exhibited a stronger, larger, and stiffer peroneal compared to Con group, future work is warranted to determine if initial or recurrent ankle injury, common to the FAI group, leads to changes in peroneal function that can alter ankle kinematics and increase risk of injury.

CONCLUSIONS

Males exhibited larger and stronger peroneal musculature compared to females. The weaker peroneal of females may limit their ability to prevent excessive ankle inversion and increase ankle sprain injury risk. The FAI group exhibited a significantly reduced peak ankle inversion during the sudden inversion event compared to Con. But, FAI participants also displayed a stronger, larger, and stiffer peroneal compared to Con. Peroneal stiffness however, exhibited a relation to peak PF during sudden inversion. Future work should look to determine how peroneal stiffness impacts ankle kinematics and relates to risk of ankle sprain.

REFERENCES

1. Garrick, JG. *AJSM,* **5**, 241-242. 1977
2. Delahunt, K., et al. *AJSM,* **21**, 168-174, 2006.
3. Butler RJ, et al. *Clin Biomechanics,* **6**, 511-517, 2003.
4. Bishop, P. *Ergonomics,* **30**, 685-687, 1987.
5. Docherty, C., et al. *J Athl Train*, **41**, 154-158, 2006

ACKNOWLEDGMENTS

We would like to thank Idaho Global Entrepreneurial Mission (IGEM) for providing funding for this work.

Table 1: Group means for muscle parameters.

	Male		Female	
	FAI	**Control**	**FAI**	**Control**
MS (m/s)	6.45 ± 0.21	5.67 ± 1.03	7.29 ± 1.13	6.49 ± 2.07
PCSA (cm^2)*	4.87 ± 0.99	4.38 ± 0.82	3.58 ± 0.35	3.54 ± 0.58
Eversion (N*m)*	16.47 ± 8.20	10.81 ± 6.46	8.43 ± 7.12	6.30 ± 5.31

*=Denotes significant effect of sex.
^=Denotes significant effect of group.

DOMINANT LIMB LOWER EXTREMITY WORK PREDICTS PERFORMANCE IN INDIVIDUALS WITH LOW BACK PAIN

[1] Alexa K Johnson, [1] Joshua D Winters, [1]Kathleen M Poploski, [1]Nicholas R Heebner, [1]Scott M Lephart, and [1]John P Abt

[1] The University of Kentucky, Lexington, KY, USA

email: johnson.alexa@uky.edu, web: https://www.uky.edu/chs/research/smri

INTRODUCTION

More than 80% of individuals will experience an episode of low back pain (LBP) at some time during their lives [1]. In active populations, up to 37% of athletes suffer from LBP [2] and military populations report 70% higher prevalence than the general population [3]. Those who experience LBP tend to adapt their movement patterns to avoid painful positions while still successfully completing a task. During running individuals with low back pain exhibit increased knee stiffness [4] and during walking, limb dominance has been reported to have an effect on lower extremity limb support in individuals with LBP [5]. Though, no information exists on how LBP affects more advanced functional performance such as hopping or jumping, in highly active populations. Dominant limb dependence may lead to asymmetrical movement patterns that may impede their overall performance during more complex tasks. Increased joint stiffness in individuals with LBP may also reduce the power generating capability at that specific joint, thereby reducing the amount of positive work they are able to produce during explosive movements.

The purpose of this project was to determine if there are differences in performance between those with low back pain and those without, and to determine if individuals with LBP demonstrated a greater dependence on the dominant limb than those without LBP during a stop jump task. We hypothesized that those with low back pain will have decreased jump height compared to controls and that lower extremity dominant limb work will be a better predictor of jump height in those with low back pain.

METHODS

Forty-three participants, 28 with a history of chronic low back pain (age 29.1±5.2yrs; height 1.78±0.06m; mass 85.4±9.0kg) and 15 healthy control participants (age 25.5±4.1yrs; height 1.81±0.05m; mass 84.9± 8.8kg), completed a double limb stop jump. Participants jumped forward onto two force platforms (Kistler Instrument Corp., Amherst, NY) from 40% of the subject's total body height. They were instructed to jump forward and then vertically as high as possible. Practice trials were given as needed and variables were averaged across three subsequent trials. Healthy control participants reported no history of back or lower extremity surgery, injuries, or back pain. The LBP group indicated they suffered from chronic LBP lasting at least six months and the first time in which they had to alter activity due to pain was an average 3.8 ± 3.3 years ago. All participants were currently highly physically active despite pain. Dominant limb was defined as the leg each subject would prefer to use to kick a ball.

Raw vertical ground reaction forces (VGRF) were sampled at 1200 Hz and filtered using a fourth order low pass Butterworth filter with a cutoff of 50Hz. An eight camera three-dimensional motion capture system (Vicon Motion Systems Ltd, Centennial, CO) was used to collect lower extremity reflective marker data. Reflective markers were placed on the participants using a plug-in gait model to collect bilateral sagittal plane kinematics and kinetics at the hip, knee, and ankle. Kinematic data were sampled at 200 Hz and marker trajectories were filtered using a low pass Butterworth filter with a cut-off at 6Hz. Visual 3D (C-Motion, Germantown, MD) was used to calculate dominant and non-dominant ankle, knee, and hip work. Individual joint work was calculated by taking the integral of joint power curves from the power generation phase of the jump. Total lower extremity work was calculated by summing ankle, knee, and hip work values.

Data were summarized using descriptive statistics including means and standard deviations. There was a significant difference in age between the LBP group and the control group (LBP: 29.2±5.2yrs; Control: 25.5±4.1yrs). Independent samples t-tests were used to examine differences in jump height

performance and joint work during the stop jump between the LBP and control group. Paired samples t-tests were used to determine within group differences between dominant and non-dominant ankle, knee, hip, and total lower extremity work. Multiple linear regression models were constructed using a backwards stepwise method to predict jump height, in each group, from dominant and non-dominant ankle, knee, and hip work. Additionally, because age is a known confounding variable in those with LBP, it was entered into each final model. A significance level of alpha = 0.05 was used. All data analyses were conducted using SPSS (SPSS 22 IBM Corp, Armonk, NY).

RESULTS AND DISCUSSION

There were no significant differences within groups, between dominant and non-dominant ankle, knee, hip, and total work. There were no differences between groups in ankle, knee, and hip work or jump height. There was a significant difference in total lower extremity work (Figure 1) in the dominant (LBP: 2.80 ± 0.35J Control: 3.14± 0.50J; p=0.014) and non-dominant (LBP: 2.78 ± 0.33J, Control: 3.06 ± 0.45J; p=0.049) limbs, between the LBP and control group. In the low back pain group, the final model included dominant limb ankle work, knee work, hip work, and age. This model predicted 61.4% (p=0.0001) of the variance in the data. In the control group, the final model included non-dominant limb ankle work, hip work, and age, this model predicted 41.2% (p=0.032) of the variance in the data.

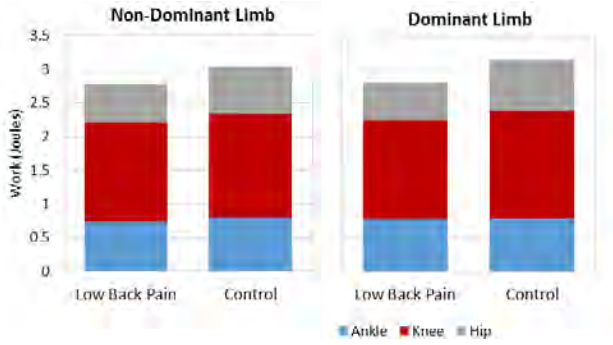

Figure 1: Bar graph representing individual joint work contributions in the low back pain and control group.

Our hypotheses were partially supported, in that there were no differences of jump height between groups, though the dominant limb was a strong predictor of jump height in the LBP group. Additionally, total lower extremity joint work was less in the LBP group compared to the control group, indicating that the LBP group may have small alterations at each joint, which collectively create a difference in lower extremity performance.

The different joint work variables that are present in the low back pain group model, compared to the control group model suggest that those with low back pain use a dominant limb dependence strategy to reach the same jump height as those without low back pain. The different lower extremity joint work strategies in individuals with low back pain may be from learned strategies and compensations due to pain that they have experienced for an extended amount of time [4]. This data indicates that limb dominance, may be driving lower extremity movement dysfunction in individuals with low back pain. Further, it has been indicated that those with LBP exhibit altered pelvis - trunk coordination during walking and running [6]. This intersegmental coordination may be present further down the kinetic chain, beyond the pelvis.

CONCLUSIONS

Those with LBP have decreased total lower extremity joint work compared to individuals without LBP. Although functional performance may not be altered between those with LBP and those without, differing strategies to functional performance may exist. Dominant limb dependent strategies may cause asymmetrical mechanics which, over time, may lead to an increased risk of secondary lower extremity injury.

REFERENCES

1. Rubin DI. *Neurol Clin*, **25,** 353-71, 2007.
2. Nadler SF et al. *Spine,* **23**, 828-33, 1998.
3. Clark L, Hu, Z. *MSMR*, **22**, 2015.
4. Hamill et al. *Res Sports Med,* **17**, 206-73, 2009.
5. Sung et al., *Hum Mov Sci,* **52,** 36-44, 2017.
6. Seay et al., *Clin Biomech,* **26,** 572-78, 2011.

ACKNOWLEDGMENTS

This research was supported by the Office of Naval Research N00014-1-15-0069. The content is solely the responsibility of the authors and does not necessarily represent the official views of the Office of Naval Research

LOWER LIMB BIOMECHANICS DURING SINGLE-LEG LANDINGS FOLLOWING ANTERIOR CRUCIATE LIGAMENT RECONSTRUCTION: A SYSTEMATIC REVIEW AND META-ANALYSIS

[1]Peta T. Johnston, [1]Jodie A. McClelland and [1]Kate E. Webster

[1]La Trobe University, Bundoora, VIC, AUS
email: 3579584@students.latrobe.edu.au

INTRODUCTION

Anterior cruciate ligament (ACL) rupture is a devastating knee injury with an annual incidence of 68.6 per 100,000 person-years [1]. Anterior cruciate ligament reconstruction (ACLR) surgery stabilizes the injured knee joint but may not restore knee biomechanics to a pre-injury level [2]. Exploring movement patterns during sports activities in athletes post ACLR surgery may identify modifiable biomechanical features. This is important as the risk of a second ACL injury is significantly higher in athletes who return to sport compared to the risk of a primary ACL injury [1,3].

The aim of this systematic review is to identify and evaluate differences in lower limb biomechanics, during high demand single-limb landings on the ACLR limb, when compared to the contralateral limb and healthy control participants.

METHODS

A systematic review of the literature was conducted using 6 electronic databases searched until April 2017 for published peer reviewed studies that compared lower limb biomechanics in the ACLR limb to either the contralateral limb or healthy control participants during single-limb landings.

Meta-analyses with standardized mean difference (SMD) were performed for peak angles and moments (hip and knee joints) in the sagittal plane during single-limb landing tasks comparing the ACLR limb to the contralateral limb and healthy control participants.

RESULTS AND DISCUSSION

35 studies met the inclusion criteria. Four different single-leg landing tasks were identified: forward hop (n= 24 studies), landing from a height (n= 9 studies), vertical hop (n= 4 studies), and diagonal leap (n= 1 study).

Peak knee flexion angle was reduced in the ACLR limb compared to the contralateral limb during a forward hop SMD= -0.39, 95% CI [-0.59, -0.18] and to a control group (SMD between -1.01 and -0.45) for all three single-leg landing tasks: forward hop, landing from a height, and diagonal leap (Figure 1). Stiffer single-leg landings potentially expose the knee joint to higher forces which may increase risk of injury [4].

Similarly, the peak knee internal extensor moment was reduced in the ACLR limb in comparison to the contralateral limb for all three landing tasks: forward hop, landing from a height, and vertical hop (SMD between -1.43 and -0.53); and in two out of three landing tasks when compared to a control group [SMD between -1.2 and -0.52; (Figure 2)]. Reduced knee moments may indicate ongoing knee muscle strength deficits after ACLR [5].

No significant differences in peak hip flexion angle or peak hip internal extensor moment were found in the ACLR limb compared to both the contralateral limb and a control group. However firm conclusions cannot be made due to the limited number of studies investigating hip biomechanics.

CONCLUSIONS

Participants performed single-limb landings on the ACLR limb with reductions in peak sagittal knee kinematics as well as peak joint moments compared to both the contralateral limb and a control group.

Findings may assist ongoing improvements in rehabilitation programs after ACLR surgery to focus on training landing techniques with greater amounts

of knee flexion to avoid stiff landings and help restore knee biomechanics.

REFERENCES

1. Sanders et al. *Am. J. Sports Med.* **44**, 2016.
2. Hewett et al. *Am. J. Sports Med.* **41**, 2013.
3. Paterno et al. *Clin J Sports Med.* **22**, 2012.
4. Meyer and Haut. *J Biomech.* **38**, 2005.
5. Schmitt et al. *Med. Sci. Sports Exerc.* **47**, 2015

ACKNOWLEDGEMENTS

This work was supported by an Australian Government Research Training Scholarship.

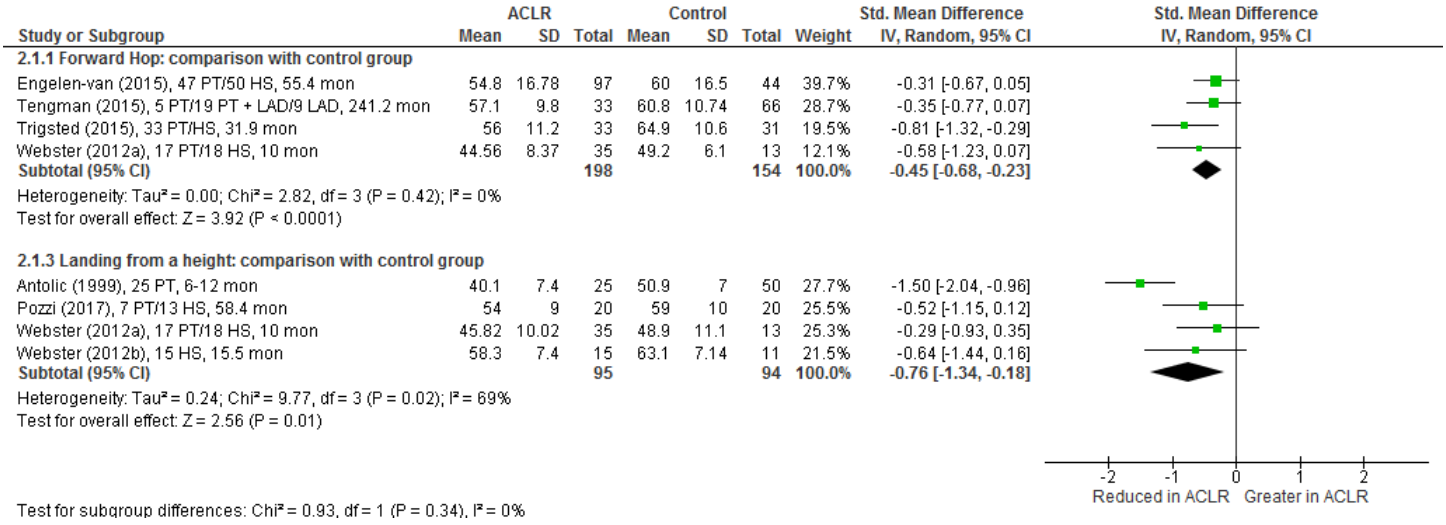

Figure 1. Effect sizes and 95% Confidence Intervals of ACLR limb to a control group for peak knee flexion angle. Abbreviations: PT, patellar tendon autograft; HS, hamstring tendon autograft; HS allograft, hamstring tendon allograft; mon, months post ACLR surgery; PT + LAD, patellar tendon autograft + ligament augmentation device; LAD, ligament augmentation device.

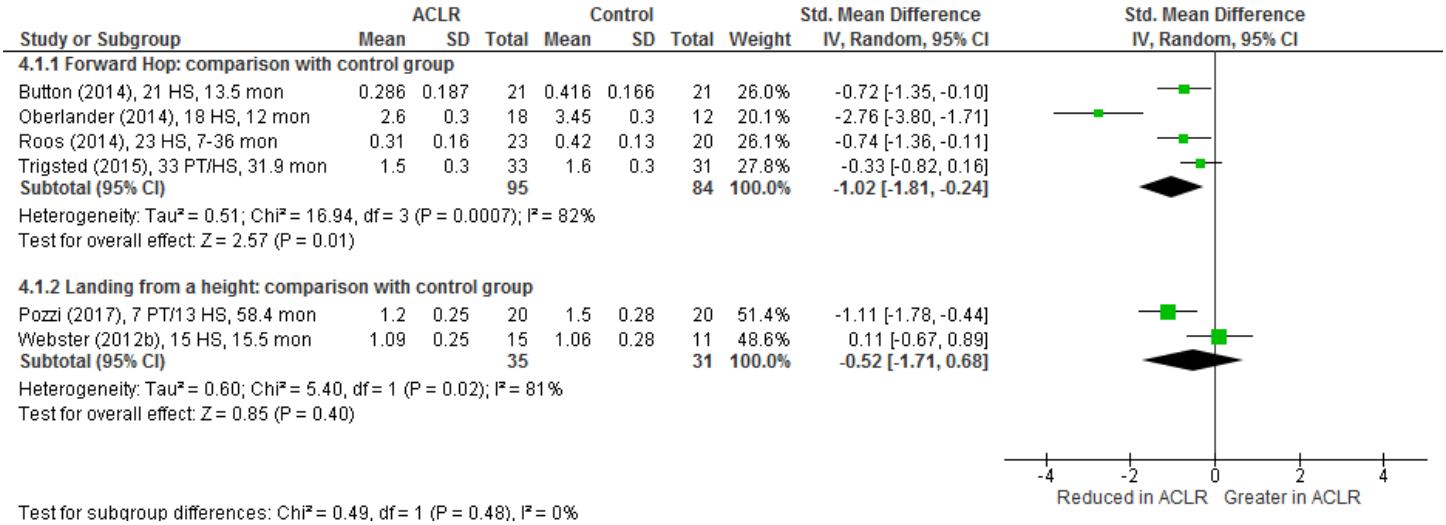

Figure 2. Effect sizes and 95% Confidence Intervals of ACLR limb to a control group for peak internal knee extensor moment. Abbreviations: PT, patellar tendon autograft; HS, hamstring tendon autograft; mon, months post ACLR surgery.

3D MOTION ANALYSIS OF SUCCESSFUL VERSUS FAILED SINGLE-LEG LANDINGS AFTER ACL RECONSTRUCTION

[1]Peta T. Johnston, [1]Jodie A. McClelland, [2]Julian A. Feller and [1]Kate E. Webster

[1]La Trobe University, Bundoora, VIC, AUS
[2] OrthoSport, Melbourne, VIC, AUS
email: 3579584@students.latrobe.edu.au

INTRODUCTION

Anterior cruciate ligament (ACL) rupture is a serious knee injury common in sports that involve sudden decelerations, such as, landing from a jump onto a single limb [1]. ACL injuries are more likely to occur during a poor or failed landing technique [2], however limited biomechanical data exists for failed landings. Greater understanding of failed landing biomechanics is especially important in athletes who return to sport after anterior cruciate ligament reconstruction (ACLR) surgery as the risk of a second ACL injury is significantly higher compared to the risk of a primary ACL injury [3].

The aim of this study was to compare differences in lower limb biomechanics between successful and failed single-leg landings in ACLR participants. Understanding failed landing biomechanics may help identify modifiable deficits that could be targeted with neuromuscular training, reducing the number of failed landings in ACLR participants, thereby reducing the potential for re-injury.

METHODS

22 male participants (17-40 years) who had undergone unilateral ACLR at a mean 10.1 (SD 2.0) months post-surgery were recruited. Three-dimensional motion analysis was used to collect data during single-limb landings onto both the ACLR limb and contralateral limb for each participant.

Joint angle and joint moment data were compared between ACLR limb successful and failed landing trials, and also between contralateral limb successful and failed landing trials using paired t-tests. A successful trial required participants to land and balance for 1 second. A failed trial was recorded when a loss of balance occurred causing the participant to move the landing foot and/or excessively swing the opposite limb.

RESULTS AND DISCUSSION

Most kinematic differences found between successful and failed single-leg landing trials in ACLR participants occurred at the pelvis and hip joints in the coronal plane (Table 1). A pattern for increased pelvic lateral tilt angle (contralateral hitch) at initial contact was shown in failed landing trials, however this was only statistically significant on the contralateral limb. An increased peak pelvic lateral tilt angle (contralateral hitch) during failed landing trials compared to successful landing trials was statistically significant for both ACLR and contralateral limbs. The peak hip abduction angle was also increased during failed landing trials compared to successful landing trials for both ACLR and contralateral limbs. Proximal joint positioning at initial contact appears to contribute to ACLR participants landing successfully.

There were no significant differences for hip and knee moments between successful and failed single-leg landing trials on either the ACLR limb or contralateral limb (Table 2).

CONCLUSIONS

Compared to successful landings, ACLR participants display significant kinematic differences, particularly in the coronal plane at the pelvis and hip joints during failed landings. Results suggest pelvis and hip joint positioning at the initial contact of landing onto a single-limb are important to complete a successful landing.

REFERENCES

1. Boden et al. *Orthopaedics,* **23***,* 2000.
2. Wikstrom et al. *Scand J Med Sci Sports,* **18**, 2008.
3. Wiggins et al. *Am J Sports Med,* **44**, 2016.

ACKNOWLEDGEMENTS

This work was supported by an Australian Government Research Training Scholarship.

Table 1. Coronal plane kinematics for successful and failed single-leg landings.

Dependent Variable	Limb	Angle at Initial Contact (degrees)			Peak Angle (degrees)		
		Failed Mean (SD)	Successful Mean (SD)	*P* value	Failed Mean (SD)	Successful Mean (SD)	*P* value
Pelvic Contralateral Drop	ACLR	-7.0 (3.8)	-6.8 (3.1)	0.657	*-9.2 (5.2)*	*-7.1 (3.0)*	*0.03*
	Contra	*-6.5 (2.6)*	*-5.5 (2.3)*	*0.003*	*-9.8 (4.4)*	*-6.1 (2.3)*	*<0.001*
Hip Adduction	ACLR	-7.8 (2.7)	-8.1 (3.5)	0.575	*-11.5 (5.2)*	*-8.9 (2.9)*	*0.006*
	Contra	*-8.0 (4.4)*	*-6.6 (4.8)*	*0.002*	*-12.8 (5.5)*	*-7.7 (4.0)*	*<0.001*
Knee Abduction	ACLR	3.0 (4.0)	2.9 (3.7)	0.619	8.2 (4.5)	7.7 (4.5)	0.224
	Contra	3.8 (3.3)	3.5 (3.6)	0.076	*9.4 (4.6)*	*8.0 (5.0)*	*0.002*

Pelvic contralateral drop, hip adduction, knee abduction are represented as positive values during initial contact and peak.
Abbreviations: ACLR, anterior cruciate ligament reconstruction; Contra, contralateral

Table 2. Peak external joint moments during successful and failed single-leg landings.

Dependent Variable	Limb	Moment (Nm/kg)		
		Failed Mean (SD)	Successful Mean (SD)	*P* value
Hip Flexion	ACLR	0.7 (0.5)	0.7 (0.5)	0.916
	Contra	0.5 (0.6)	0.5 (0.6)	0.794
Hip Adduction	ACLR	1.0 (0.3)	1.0 (0.3)	0.634
	Contra	1.0 (0.3)	1.1 (0.3)	0.230
Knee Flexion	ACLR	1.4 (0.4)	1.3 (0.3)	0.656
	Contra	1.6 (0.6)	1.6 (0.6)	0.941
Knee Adduction	ACLR	1.2 (0.4)	1.2 (0.3)	0.473
	Contra	1.5 (0.4)	1.5 (0.5)	0.632

Abbreviations: ACLR, anterior cruciate ligament reconstruction; Contra, contralateral

EFFECT OF ACL RECONSTRUCTION ON INTER-LIMB ASYMMETRIES AND LIMB DOMINANCE

[1] Rumit Singh Kakar, [1]Jamie Kronenberg, [1]Danielle Pasqualle, [2]Jenn McKeon, and [2]Patrick McKeon

[1]Department of Physical Therapy, Ithaca College, Ithaca, NY, USA
[2]Department of Exercise and Sports Sciences, Ithaca College, Ithaca, NY, USA
email: rkakar@ithaca.edu, web: https://www.ithaca.edu/hshp/clinics/movementlab/

INTRODUCTION

Over 33% of individuals with a history of anterior cruciate ligament (ACL) injury returning to cutting or pivot sports such as soccer suffer a reinjury.[1,2] Neuromuscular deficits presenting as kinematics and kinetic asymmetries can persist between the affected and unaffected limb following an ACL reconstruction (ACLR), long after they have been cleared to return to sports (RTS). In some cases, the deficits can last for as long as 2 years post reconstruction.[3] These asymmetries may predispose athletes to a recurrent ACL injury. Healthy, physically active individuals do not show limb asymmetries on.[4] Neuromuscular deficits during closed kinetic chain activities like jump landings that are apparent post ACLR can be identified with 3D motion analysis.[5] Although the 3D motion analysis is well established for its benefits, availability is limited and is not a common practice when making RTS decisions by clinicians. RTS tests have been in use but decisions for clearance by physician/ surgeons is based heavily on the functional outcomes/ performance on the tests rather than the neuromuscular control and mechanics of the movements. Functional testing results can provide information regarding landing mechanics but are not good predictors for probability of reinjury.[6] 2-dimensional (2D) motion analysis with the use of easily available video cameras and tablets (iPads®) is gaining popularity amongst clinicians. Studies have validated its use for sagittal and frontal plane kinematics analysis in healthy adults. There is extremely limited knowledge of use of 2D analysis for kinematic asymmetries post ACLR in athletes. If 2D analysis is proven sensitive to pick up inter-limb differences and help make decisions on existence or neuromuscular deficits, it would aid in screening patients for their readiness to RTS and in-turn possibly prevent secondary tears.

The purpose of this study is to examine inter-limb asymmetries during functional hop tests post ACLR using 2D motion analysis. It is hypothesized there will be greater inter-limb differences in individuals following ACLR that predispose them to an increased risk of re-injury compared to health controls.

METHODS

11 physically active ACLR participants (age: 21.1 ± 3.8yrs, height: 170.9 ± 5.2cm, weight: 70.9 ± 9.6kg) and 11 matched controls (age: 22.3 ± 1.9 yrs, height: 167.6 ± 5.8cm, weight: 70.9 ± 21.5kg) participated.

Series of hop tests in a randomized order were performed: functional hop tests- single leg hop, triple hop, crossover hop for distance, and 6-meter timed hop. Videos of hop tests were recorded using iPads and 2D kinematics for peak ranges of motion at hip, knee and ankle were analyzed using Kinovea® software. Reflective markers were placed on greater trochanter, midpoint of lateral joint line for knee, lateral malleolus, head of 5th metatarsals, and left and right anterior and posterior superior iliac spines. Markers were used to improve accuracy of 2D analysis and improve inter and intra rater reliabilities.

Limb symmetry indices (LSI = 100*(Affected/ Unaffected) for ACLR or 100*(Dominant/Non-Dominant) for controls) were calculated and group comparisons were made using univariate analysis of variance (ANOVA), ($p < 0.05$). An LSI < 85% or LSI > 115% is considered a clinically important difference.

RESULTS AND DISCUSSION

Group differences were found only in increased knee ROM for affected of ACLR vs dominant limb of control groups in triple hop (mean difference = 15.4º; $p = 0.009$) and ankle in cross-over hops (mean difference = 15.4º; $p = 0.009$).

Significant clinical asymmetries as per LSI were on the other hand observed for ankle in all 4 of the hop tests (27.1%- 62.1% average asymmetry) and for hip ROM during single leg hop (48.6%) and hip (26.1%)

and knee (22.2%) for 6-meter timed hop. (Table 1). No asymmetries were observed for healthy controls.

Neuromuscular deficits and altered mechanics were observed during landing on hop tests. These results support those available in the literature.[3-5] LSI results indicate that asymmetries between limbs exist based on limb dominance and neuromuscular control and these can in part but not completely be identified with 2D motion analysis. Healthy individuals use different neuromuscular strategies between limbs as well, but the extent of asymmetries is significantly greater post ACLR. These asymmetries when not focused on during post-surgical rehabilitation can be the major contributor to secondary tears. While minimal asymmetries were observed at the knee using 2D analysis, current literature provides plethora of evidence for their existence.[3,5] The fact that they were not evident in 2D could possibly stem from limitations in the sample sizes but also from the inherent limitations of the 2D motion analysis methodology in its sensitivity and specificity to capture such small but meaningful differences.

CONCLUSIONS

Neuromuscular deficits are present in the affected and unaffected limb post-ACLR that may lead to asymmetries and predispose either limb to injury. While not all but some of these can be observed with 2D analysis and clinicians should use this when 3D analysis is not accessible to make informed decisions for clearance to RTS along with functional performance of the battery of tests.

REFERENCES

1. Dekker, TJ. et al. *Surg Am* **99**, 897–904, 2017.
2. Wiggins, AJ et al. *Sports Med* **44**, 1861-76, 2016.
3. Ithurburn, MO et al, *Am J Sport Med* **45(11)**, 2604-13, 2017.
4. Lisee, C. *J Sport Rehabil* 1-26, 2018.
5. Hewett, TA. Et al. *Am J Sports Med* **45(9)**, 2142-2147, 2017.
6. Zwolski C, et al. *Am J Sport Med* **44(8),** 2030-2038, 2016

Table 1: Lower extremity kinematics and Limb Symmetry indices for the 4 functional hop tests. (*- statistical significance at $p < .05$, and ^ - clinically relevant significance)

		ACLR (°)		MC(°)		p value		Limb Symmetry Index (%)	
TASK	JOINT	Surgical	Non-Surgical	Dominant	Non-Dominant	ACL vs Dom	Uni vs NDom	ACL	MC
Triple Hop	Hip	50.3 ± 25.7	62.7 ± 17.7	68.0 ± 8.9	54.3 ± 11.5	0.313	0.513	101±25	103±6
	Knee	69.0 ± 6.1	69.4 ± 22.7	84.4 ± 1.4	88.0 ± 5.2	0.009*	0.233	98±21	104±32
	Ankle	11.7 ± 9.6	16.7 ± 13.8	9.2 ± 4.1	22.6 ± 9.3	0.7	0.549	162±23^	113±21
Cross-over Hop	Hip	57.2 ± 13.7	55.1 ± 17.0	66.9 ± 9.5	54.7 ± 14.6	0.347	0.977	104±11	100±7
	Knee	70.9 ± 6.4	67.5 ± 11.4	74.0 ± 17.6	83.9 ± 5.7	0.756	0.074	108±50	100±11
	Ankle	19.5 ± 9.8	19.1 ± 10.3	3.9 ± 2.1	23.6 ± 5.8	0.045*	0.525	123±78^	88±26
6m Timed hop	Hip	49.1 ± 20.9	33.2 ± 17.3	53.7 ± 17.0	41.9 ± 3.6	0.77	0.441	126±34^	100±10
	Knee	67.4 ± 7.0	74.9 ± 11.9	75.2 ± 10.2	82.7 ± 8.3	0.277	0.377	78±24^	104±10
	Ankle	13.2 ± 5.5	23.4 ± 2.5	17.3 ± 5.1	30.8 ± 10.4	0.355	0.216	73±61^	101±15
Single Leg hop	Hip	83.9 ± 30.4	51.5 ± 9.4	67.3 ± 3.5	72.3 ± 23.4	0.401	0.159	149±40^	100±10
	Knee	67.3 ± 15.7	64.8 ± 27.7	81.1 ± 9.7	94.7 ± 6.6	0.242	0.133	104±26	104±10
	Ankle	16.7 ± 13.2	22.7 ± 12.4	48.0 ± 3.2	52.0 ± 7.8	0.403	0.978	73±41^	101±15

VERBAL ENCOURAGEMENT DOES NOT PRODUCE ADDITIVE EFFECT ON QUADRICEPS FUNCTION AS LONG AS SUFFICIENT REST PEROID IS PROVIDED

Daeho Kim, Minwook Kim, Sungwan Kim, Yuyeon Roh, and Jihong Park

Kyung Hee University, Yongin, Korea
email: jihong.park@khu.ac.kr

INTRODUCTION

Verbal encouragement during strength training is commonly practiced to maintain maximal effort. Sudden loud sounds are strong sensory modification to stimulate central activation [1]. Although many studies reported its effectiveness, current supportive evidence [2, 3] is from the data collected on fatigued muscle. When performing a bout of exercise (e.g., sets of multiple repetitions), we normally take a sufficient rest between sets. If muscle fatigue from the first set of exercise is recovered prior to the second set, receiving verbal encouragement during the second set of exercise may results in an additional strength increase.

Hence, we manipulated verbal encouragement on a single bout of exercise with a rest interval between sets. The observation of quadriceps strength and activation changes would clarify if there is a summative effect when psychological recovery time (subjective feeling of readiness) is combined with verbal encouragement. We hypothesized that a rest interval is the main factor to maintain muscle function regardless of verbal encouragement.

METHODS

Thirty-one neurologically healthy adults (males=20, females=11) participated in this single blind randomised controlled trial. Independent variables were condition (non-verbal: n=15 & verbal encouragement: n=16) and time (base, and T1 to T5). Dependent variables were blood lactate (BLa) concentration and quadriceps isokinetic torque, strength (maximal voluntary isometric contraction: MVIC) and activation (central activation ratio).

After reading and signing on the informed consent from (approved by the intuitional review board), participants performed the baseline measurements (three trials in quadriceps strength and activation with a 1-min rest intervals). Quadriceps strength was normalised to body mass (Nm/kg); activation was calculated by voluntary strength torque divided by torque generated by burst superimposition. Prior to the first trial (base 1) and 5-min after the last trial (base 2), BLa was assessed.

A five-set of quadriceps endurance exercises (continuous isokinetic knee extensions at 60°/s) was performed on an isokinetic dynamometer. Each set of exercise was ended when three consecutive torque values were dropped less than 50% of the averaged MVIC recorded at baseline. Between each set, a 3-min rest interval was given.

At the beginning of the rest period, BLa was recorded to quantify level of physiological fatigue. Afterwards, quadriceps strength and activation were assessed twice in the same manner as baseline.

Several words (e.g. “kick, more, harder, good work”) in a same order were provided by the same tester to the condition with verbal encouragement. Visual feedback (looking a monitor for torque traces) was provided for both conditions.

To test condition effect over time, analysis of covariance (quadriceps strength and activation; baseline values as covariate), analysis of variance (BLa concentration, quadriceps isokinetic torque), and Tukey-Kramer tests were performed ($p<0.05$).

RESULTS AND DISCUSSION

BLa concentration measured at base 1 and 2 were not different ($p=0.16$), confirming that the quadriceps MVICs during the baseline measurements did not affect the first set of exercise. Compared to the baseline value, BLa was increased by 2.3 times ($p<0.0001$, ES=1.8) and 3.1 times

(p<0.0001, ES=1.8) after the first and second set of endurance exercise, respectively (Figure 1-A). There was no further change in BLa from T3 through T5 (p=0.14).

For the quadriceps endurance exercise, the largest difference in torques between two conditions was observed at T1 (ES=0.3; Figure 1-B). Torques at other time points were very similar, which simply indicates that receiving verbal encouragement did not produce an additive force. This also suggests that there may be no need for verbal encouragement as long as sufficient recovery time and visual feedback [4] are provided.

Quadriceps strength showed a 6.4% decrease at T2 (p=0.0002) and a 4.9% further decrease at T3 (p<0.0001). However, these changes are negligible (ES=0.2). Changes in quadriceps strength in both conditions were almost identical (Figure 1-C). This also supports the idea that recovery time after muscle fatigue is more important than additional sensory input during muscle contractions.

While quadriceps activation of 0.95 is considered as normal [5], both conditions in our study maintained normal activation throughout the exercise bout (Figure 1-D). Similar to other variables, quadriceps activation was maintained from T2 through T5.

We tried to select the duration of rest period between exercise sets that not only provides psychological recovery but it also does not exceed a typical rest interval in a bout of exercise. In our pilot study (n=4), we asked participants to report when they thought that they were ready for another set of exercise. The average time was 152-sec at T1 and 187-sec at T4. Based on these data, we chose 3-min as the rest interval.

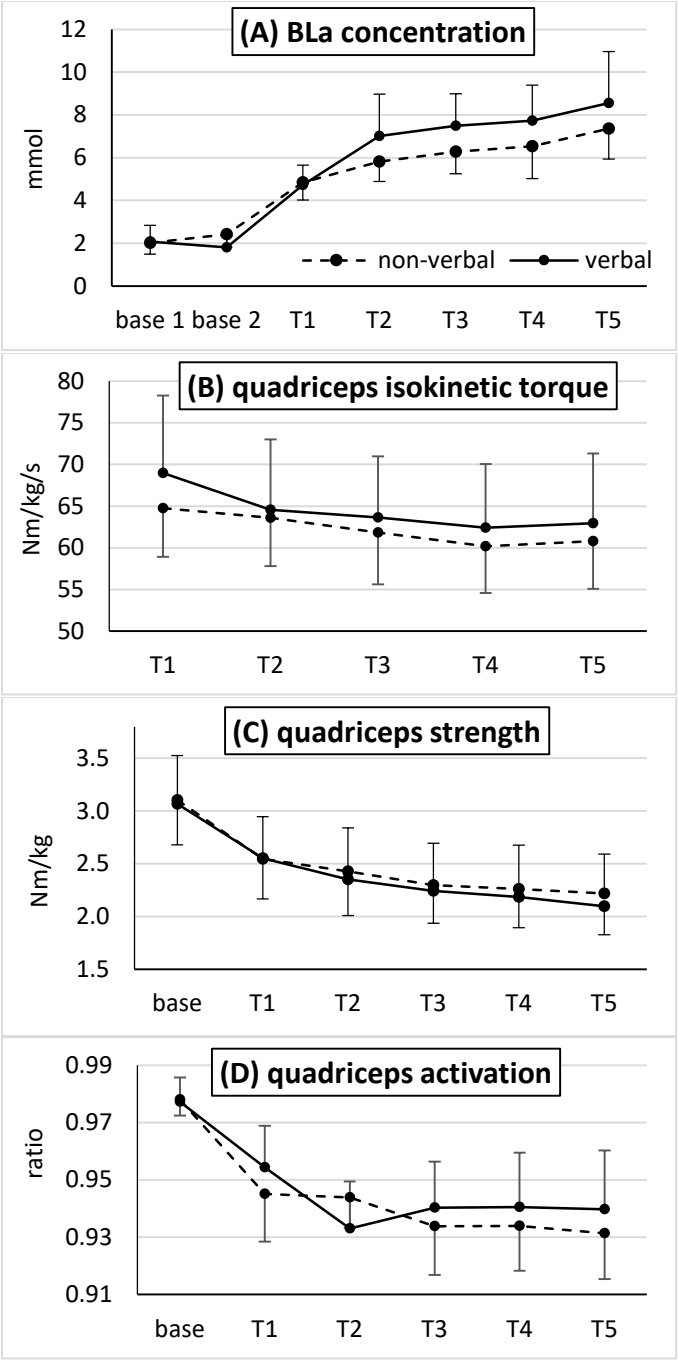

Figure 1: Mean of BLa concentration (A), quadriceps isokinetic torque (B), quadriceps strength (C), and quadriceps activation (D). Error bars represent 95% CIs.

ACKNOWLEDGEMENTS

This work was supported by the Ministry of Education of the Republic of Korea and the National Research Foundation of Korea (NRF-2017S1A5A802285.

REFERENCES

1. McNair et al. *Br J Sports Med,* **30**, 243-245, 1996.
2. Neto et al. *Acta Sci. Health Sci,* **37**, 25, 2015.
3. Bouillard et al. *J Neurophysiol,* **111**, 768-766.
4. Binboğa et al. *J sports sci,* **31**, 982-988, 2013.
5. Park and Hopkins. *J Electromyogr Kinesiol,* **21**, 136-140.

DEVELOPING THE SENSITIVITY OF A HUMAN ANKLE JOINT FINITE ELEMENT MODEL TO THE THICKNESS OF CARTILAGE

Jinhyuk Kim, Sebastian Y. Bawab, Stacie I. Ringleb
Old Dominion University, Norfolk, VA, USA
Email: sringleb@odu.edu

INTRODUCTION

Computational modeling of joints is used to investigate the effect of injuries, to plan surgeries, and to answer questions about joints that cannot be answered experimentally [1]. Ankle joint models are moving toward being patient specific, however, it is unclear which anatomy should be subject specific, and what anatomy can be generic, while still obtaining accurate results and minimizing computation time. Existing models tend to extrude the surface of the tibia and talus by a uniform amount to create cartilage [2] because it is hard to evaluate articular cartilage thickness using imaging techniques [3].

When modeling contact in finite element analysis (FEA), there are many considerations to make, including, but not limited to how contact is modeled (tied vs. sliding) and how many layers of elements are required to obtain accurate results. Sliding contact represents anatomical motion, however, modeling with sliding contact requires more restrictive boundary conditions, either through constraining the bones ore modeling ligaments with more than a single spring to get the model to converge. FEA theory suggests that more accurate results may be obtained with two or more layers of elements when modeling contact [4], which is a challenge when meshing a thin layer of ankle cartilage. The purpose of this study was to use sliding contact interface in a model of the ankle joint while evaluating: 1) the effect of cartilage thickness and 2) the effects of single layer and double layers of elements in the cartilage model.

METHODS

A quasi-static finite element model was developed using FEBio 2.4 (FEBio, Salt Lake City, UT) with the tibia, fibula, talus, and calcaneus previously segmented form CT images obtained from one cadaver. Cartilage from each bone was modeled by extruding the bone surfaces and rigidly fixing the cartilage to the bone. The cartilage was modeled as three different thickness within the ranges of measured ankle cartilage thickness [3] (i.e., 1mm, 1.3mm, or 1.6mm) with 4-node quadratic tetrahedral element (TET4) using LS-Prepost (Livermore, CA) and FEBio. The cartilage was assigned Neo-Hookean material properties (E = 12 MPa, ν = 0.42, and ρ = 1.93E-6 kg/mm^3) [2]. The bones modeled with quadrilateral shell element and bones were designated the homogeneous isotropic elastic materials (E=13GPa, ν=0.3, and ρ = 4.65E-6 kg/mm^3) [2]. The following ligaments were modeled as linear elastic springs with stiffness ranging from 20-80N/mm: anterior tibiotalar, posterior tibiotalar, anterior talofibular, posterior talofibular, tibiocalcaneal, calcaneofibular, anterior tibiofibular, and posterior tibiofibular. The ligaments were modeled as multiple parallel springs proportional to their cross sectional area (i.e., 1 spring = 0-25 mm^2, 2 springs 25-50 mm^2, 3 springs 50-65 mm^2, and 4 springs 65 – 80 mm^2) (Figure 1).

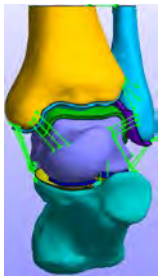

Figure 1: The 3D FE model investigated with parallel spring structures.

The top surface of tibia and fibula were fixed in X and Y, talus was fixed in X and Y, and calcaneus was fixed all translational directions. Contact was modeled between the tibia and talus, and fibula and talus, and talus and calcaneus using a sliding interface was. The tibia was loaded with a 600 N axial load. Peak pressure values between each model were compared at the anterior areas of pressure concentration on the surface of tibia base on the contact area.

RESULTS AND DISCUSSION

The peak pressures obtained from this model ranged from 2.90 MPa to 3.66 MPa depending on cartilages thickness. This is similar to pressures reported from ankle model, which ranged from 2.92 MPa to 3.69 MPa with 1.7 mm thick cartilage [2] or 3.95 MPa [5]. The contact area of peak pressure was ranged from 6.21mm^2 to 11.6mm^2. The models showed similar pressure patterns to the model by Rodrigues [5], however a model by Anderson et al. showed more pressure on the lateral side of the tibia [2]. There was a larger area of peak pressure with the thinner cartilage, and there was an increase in peak pressure with an increase in cartilage thickness. When two layers of elements was used to model contact, there was a difference between the peak pressure values ranging from 0.07 MPa to 0.48 MPa, when compared to the single layer of elements, and the peak pressure was lower than one layer only when the cartilages was 1.3 mm thickness and 1.6 mm thickness (Figure 2).

While this investigation shows that cartilage thickness and the layers of elements used does influence the values of contact pressure in a finite element model, it was not experimentally validated and all material properties were liner elastic. Future studies should investigate the effects of different cartilage thicknesses on the tibia vs. talus and the effects of cartilage non-uniformity [3]. Additionally, cartilage was modeled as a single phased material because it was a quasi-static model, however a biphasic model may be needed. Finally, the behavior of this model under different positions throughout the range of motion, as well as with additional loading, similar to what is experienced in daily life should be investigated. Therefore, further investigation of the uses of different cartilage thickness in this model must be conducted. This model was also limited because it was only axially loaded and should be tested with off axis loads, and all materials were modeled as linear elastic.

CONCLUSION

Cartilage thickness and the number of element layers influences peak pressure and the area of peak pressure in the ankle. However, it does not affect the overall pressure pattern in the ankle.

REFERENCES

1. Z. JIN, *Fundamentals of computational modelling of biomechanics in the musculoskeletal system*, Woodhead Pulishing Limited, p. 9, 2014.
2. Anderson D. D. at al., J. Biomech, **40**, 1662-1669, 2006.
3. S. A. Millington, Osteoarthritis Research Society International, 2007
4. H. Djabella, *Thin Solid Films*, **235**, 156-162, 1993
5. D. Rodrigues, "Biomechanics of the Total Ankle Arthroplasty: Stress Analysis and Bone Remodeling," p. 10.

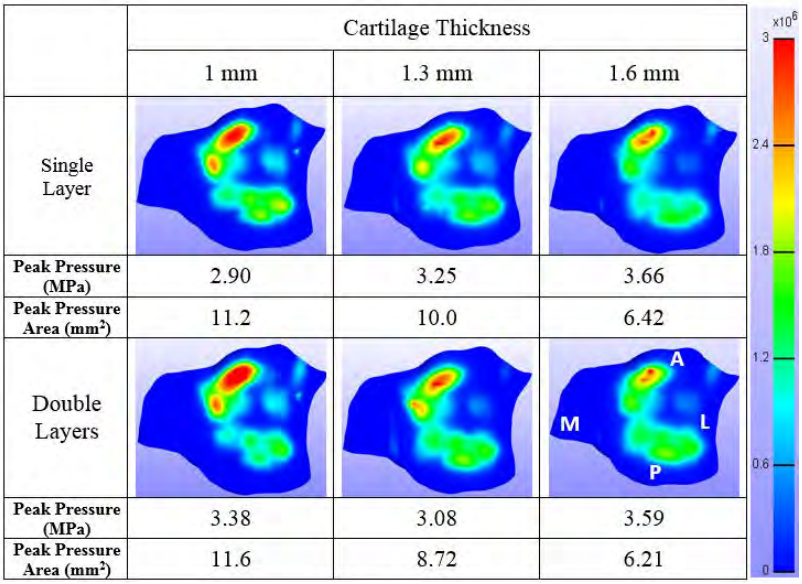

Figure 2: Inferior view of tibia, the 3D Fe results of pressure distribution are for three different thickness with single layer or double layers. Legend; A-Anterior; P-Posterior; L-Lateral; M-Medial

Biomechanical characteristics of subtalar joint axis of rotation individual with chronic ankle instability

[1] Byonghun Kim and [1] Saeyong Lee

[1] Yonsei Institute of Sports Science Exercise Medicine(YISSEM)
[1] Yonsei University, Seoul, Republic of South Korea
email: kimbyunghoon1986@gmail.com

INTRODUCTION

Ankle injuries are one of the most frequent and common injuries either in athletics or daily activities. This is due to a variety of risk factors that are generally divided into either functional or structural aspects with the former being much studied. To gain a broader perspective on the cause of the injuries for better treatment, this study saw a need to look at the less studied, the structural aspect. Specifically, a subtalar joint (STJ), one of the main ankle joints responsible for ankle injuries along with an ankle joint, has been the main focus of this study and its inclination has been investigated since its axis of rotation (AoR) helps determine and prevent the cause of injuries. Thus, in this study, we report a measurement tool we have developed to correctly measure the STJ AoR.

METHODS

In order to achieve the purpose of this study, the subjects were classified into two groups, i.e. CAI (N=19) and the control group (N=19).
The patient inclusion criteria for the CAI group was set if the subject satisfied any one condition of either FAAM 95% or lower than FAAM Sports 80%, who had an ankle sprain more than twice a year and showed the characteristics of repeated giving way behavior. (Custom made locator) For ease of measurement, a specially built STJ measurement device consisting of an anterior exit pointer, a posterior exit pointer and a basic bolt made from aluminum with a body manufactured from a light, firm acrylic material, was used. The foot size measurement was set up from 190mm to 330mm, taking into account gender as well as ethnic differences. Similarly, the device angular measurable range was designed up to ±60° to ease flexible measurement.

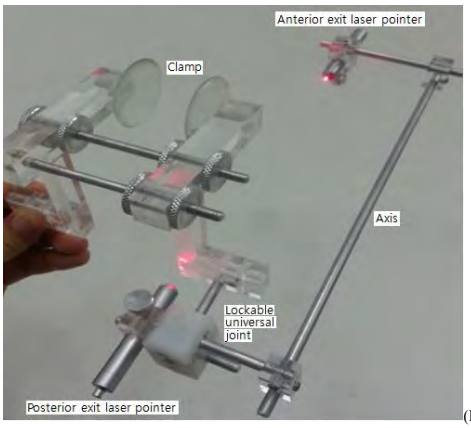

(Fig.1 Custom made locator)

(Measuring STJ AoR in sagittal plane with x-ray)
We used the x-ray in order to compare the validity test between the custom made locator and X-ray. In the present study, the STJ's AoR was measured by using the STJ locator. The angle was measured in the sagittal and transverse planes with the use of a digital inclinometer after positioning and securing the pointer to the anterior and posterior exits. An average was taken from 5 trials.

RESULTS

To investigate the reliability of the locator, static posture of STJ's sagittal and transverse planes was measured after at least 24 hrs. It was showed that higher correlation of ICC of sagittal plane .913 and transverse plane .748 was observed. The validity test yielded the result of Pearson's correlation with significantly higher correlation coefficient of .798 ($p<.01$). CAI group was observed with relatively higher inclination of STJ's sagittal and transverse planes when compared between the two groups.

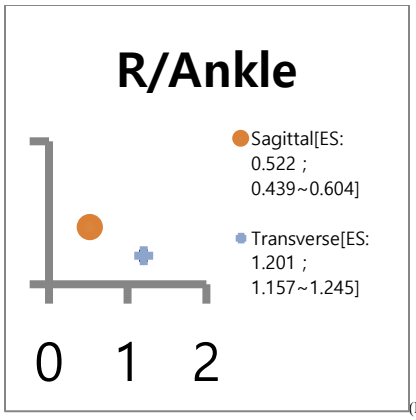

(Fig.2 Effect size between groups)

Fig.2 shows the effect size between groups from the Cohen's D analysis of lower limb alignment for each variables ($p<.05$).

DISCUSSION

The study aims to determine whether the custom-made STJ locator can be clinically used as well as aims to perform a comparative study on the inclination of STJ AoR between the CAI group and the control group. The results from the test of reliability showed consistency in the measurement of the two types of variables. Similarly, the results of the test of validity between the locator and x-ray showed a high correlation. The inclination of STJ AoR in both sagittal and transverse planes showed a larger angle in the CAI group in comparison to the control group. Even though most of the in-vivo related studies indicated a relatively low average inclination, the small sample size can be considered a limitation. A consistent average angle value was observed in three experiments conducted on the cadaver. So far, no clear connection has been observed regarding STJ's radiography. Hence, the aforementioned studies made use of generally known methods (McClay, and Bray 1996, 499-502). Through comparing the results of STJ AoR' sagittal plane inclination from this study, with respect to an actual in-vivo experiment, a relatively similar angle was indicated in one of the four (Angle.2) measuring methods. A larger inclination in the transverse plane signifies a medial deviation of AoR which can be considered as a condition for frequent ankle sprains. So far, studies related to the accurate measurement of STJ AoR's transverse plane have not been noticed. Kirby reported the reason for the occurrence of such a condition was due to the change in moment arm with respect to the STJ AoR's inclination (Spooner, S.K and K.A. Kirby 2006, 212-219). According to the results obtained from this study, it is more likely that the ankle structure of the majority of CAI subjects who participated in the study had a medial deviation of STJ AoR which increases the possibility of ankle sprain during the initial contact through an inversion moment i.e. Ground Reaction Force. Thus, it is considered that the inclination of STJ AoR and ankle sprain is closely associated. The inclination of STJ AoR in the sagittal plane was observed at a larger angle in the CAI group than in the control group. Also observed was a medial deviation of inclination in the transverse plane. Hence, the differences in results obtained can be defined as the differences in the biomechanical characteristics of STJ between the two groups.

CONCLUSION

According to the result of the present study, the effects of the differences in inclination of STJ AoR on ankle sprain can be observed. In addition, the study could play a role of an accurate parameter in determining the patient's condition with respect to different foot deformities i.e. flat foot, cavus foot. In conclusion, further studies need to be conducted not only on the inclination of STJ AoR but also on the specific characteristics of lower limb structure as well as on muscle movements.

REFERENCES

1. Spooner, S.K and K. A. Kirby. 2006. "The subtalar joint axis locator A preliminary report". Journal of American podiatric medical association, 96(3): 212-219.
2. McClay, I. and J. Bray. 1996. "The subtalar angle: a proposed measure of rearfoot structure". Foot & ankle international, 17(8): 499-502.

ACKNOWLEDGEMENTS

We Thank Dr. Na Young Moo at Sol hospital for his support for the experiments in this study.

THE EFFECTS OF MUSCULAR FATIGUE AND GENDER ON KNEE KINETICS AND KINEMATICS DURING THE FORWARD LUNGE

Ania Lipat, Amanda Stone, Hillary Holmes, Chris Hass, Ph.D.

University of Florida, Gainesville, FL, USA
email: ania.lipat@ufl.edu, web: http: web: http://hhp.ufl.edu

INTRODUCTION

The forward lunge is commonly used in knee rehabilitation to strengthen the quadriceps[1]. Due to its common use in knee rehab, the roles of the knee cruciate ligaments during the forward lunge have been widely investigated. Results from these investigations indicate the posterior cruciate ligament (PCL) stabilizes the knee during a forward lunge, whereas the anterior cruciate ligament (ACL) contributes very little[2].

These studies examined the role of cruciate ligaments based on performance during a single lunge. In reality, however, strength training and rehabilitation protocols involve many repetitions that can induce fatigue. Fatigue has been shown to alter knee mechanics by increasing knee laxity and decreasing joint stability under loading[3]. Moreover, fatigue promotes high ACL injury risk mechanics for activities such as stop-jump tasks by increasing knee abduction moment and proximal tibial anterior shear force[4]. Therefore, introducing fatigue may alter cruciate ligament loading patterns and increase risk for injury. Studies investigating the effect of fatigue on task performance have also noted gender differences in responses to fatigue. For instance, females have demonstrated greater knee adduction and abduction angles and moments in a fatigued drop-landing task in comparison to males, placing them at greater risk for ACL injury[5].

These studies demonstrate that both fatigue and gender can alter an individual's knee mechanics during lower extremity tasks, and increase risk for injury. The effects of fatigue and gender on knee mechanics during the forward lunge, however, remain unknown. Understanding these effects may identify potential knee injury risks associated with fatigue and gender for the forward lunge, and can help develop safer rehabilitation protocols for knee injury patients. Therefore, the purpose of this study is to investigate the effects of fatigue and gender on knee kinetics and kinematics during the forward lunge.

METHODS

Nineteen healthy, active, young adults (10 female, ages 18-22) participated in the study. Data were collected using a Vicon motion capture system (Vicon Motion Systems, Oxford, UK) and force plates (Bertec, Columbus, OH). Subjects first completed a warm up session consisting of 5 minutes of treadmill walking at 1 m/s and 10 practice lunges. Subjects were then asked to repeat a set of seven walking lunges across the lab and four stationary lunges on the force plates until fatigued. After each set, the participant scored their level of fatigue using a modified Borg RPE scale[6]. A fatigued state was identified as two consecutive sets that scored a 9 or a single set that scored a 10 (maximal).

Peak forward limb knee flexion, extension, adduction, abduction, internal rotation, and external rotation angles and internal moments for the stationary lunges were calculated. Average values were calculated for the baseline set and the last fatigued set for each individual. Main effects of gender and fatigue and their interaction were evaluated using a repeated measures ANOVA for each variable.

RESULTS AND DISCUSSION

No significant interactions between gender and fatigue were found. Significant main effects of fatigue and gender, however, were identified for several variables.

The fatigued set had a significantly greater peak knee flexor moment (baseline: 314.73 ± 90.97 Nmm/kg, fatigued: 421.38 ± 148.89 Nmm/kg, $p = 0.001$) and adductor moment (baseline: 92.37 ± 62.83, fatigued: 130.61 ± 75.23, $p = 0.037$), and a significantly lower knee extensor moment (baseline: 1153.93 ± 246.09 Nmm/kg, fatigued: 976.18 ± 256.13 Nmm/kg, $p < 0.001$) compared to baseline (Figure 2). The fatigued set also demonstrated significantly greater external rotation (baseline: 12.0 ± 7.20˚, fatigued: 14.4± 7.7˚, $p = 0.005$) than baseline.

When collapsing over sets, males exhibited greater knee flexion angles (males: 114.2 ± 3.2˚, females: 99.3 ± 3.1˚, $p = 0.004$) and adduction angles (males: 27.5 ± 2.8˚, females: 13.8 ± 2.7˚, $p = 0.003$) compared to females. Females also abducted their knees, whereas males did not (males: N/A, females: 2.59 ± 1.50˚, $p = 0.003$).

The decrease in knee extensor moment with fatigue may be due to quadriceps fatigue, given the important role the quadriceps play in the forward lunge. The increase in knee flexion moment may be clinically relevant, as knee flexion causes the tibia to translate posteriorly, which causes the PCL to become taught[7] An increase in knee flexion moment, therefore, could be increasing strain on the PCL. Actual PCL strain, however, should be measured to confirm this occurrence.

The increase in knee adduction moment with fatigue and the presence of knee abduction in females may also hold clinical value. High knee adduction moments and abduction angles during drop landing tasks have been shown to be predictive of ACL injury in female college athletes[8]. These increases, therefore, could be increasing an individual's risk for ACL injury, especially for females.

Figure 2: Average peak knee moments at baseline and fatigue. Knee flexor and abductor moments significantly increased with fatigue, while knee extensor moment significantly decreased.

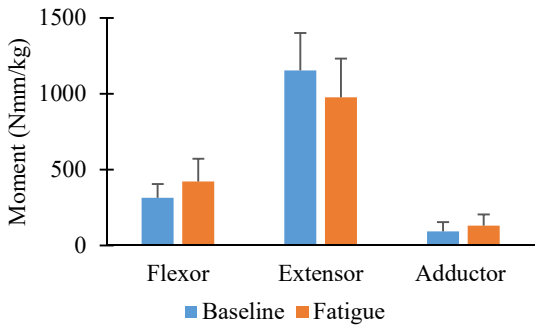

CONCLUSION

Performing the forward lunge to fatigue may put individuals in positions that increase strain on the PCL and increase risk for ACL injury. Therefore, clinicians should exercise caution when prescribing lunges in rehabilitation, especially for PCL or ACL injured patients.

REFERENCES

1. Begalle, RL et al. *J Ahtl Train* **47**, 2012
2. Alkjær, T et al. *J Anat* **221**, 590-7, 2012
3. Wojtys EM et al. *Am J Sports Med*, **24**, 1996
4. Chappell, JD et al. *Am J Sports Med*, **33**, 2005
5. McLean SG et al. *Med Sci Sports Excer* **39**, 2006.
6. Day ML et al. *J Strength Cond Res* **18**, 2004.
7. Li, G et al. *Am J Sports Med,* **32**, 2004
8. Hewett, TE. *Am J Sports Med* **33**, 2005

DECISION-MAKING INFLUENCES TIBIAL IMPACT ACCELERATIONS DURING LATERAL CUTTING

[1]Logan Lucas, [1]Benjamin England, [1]Travis Mason, [1]Christopher Lanning, [1]Taylor Miller, [2]Alexander Morgan, [1]Thomas Gus Almonroeder

[1]Trine University, Doctor of Physical Therapy Program, Fort Wayne, IN, USA
[2]University of Wisconsin – Milwaukee, Milwaukee, WI, USA
email: almonroedert@trine.edu

INTRODUCTION

Lower extremity musculoskeletal injuries are common in sports involving high-impact maneuvers such as landing and cutting (e.g. soccer, basketball). The high injury rate in athletes is not surprising considering the physical demands of sports. Even a routine maneuver such as a plant-and-cut can result in impact forces over three-times bodyweight. These impact forces generate a transient spike in acceleration that is transmitted throughout the musculoskeletal system from the foot to the head [1]. Although the lower extremity musculature can help to attenuate these impacts, passive tissues also play a prominent role (e.g. the meniscus, ligaments) [1, 2]. As a result, high impact accelerations may place excessive load on passive tissues, which could increase injury risk.

An additional challenging aspect of sports is that athletes are typically unable to pre-plan their movements, as they must maneuver in response to the actions of their opponents, teammates, etc. This requires athletes to perform the cognitive processing associated with decision-making (i.e. movement selection) under significant temporal constraints. Not allowing an athlete to pre-plan their movement appears to influence lower extremity joint kinematics and kinetics [3]. However, the influence on impact accelerations has not been explored.

The purpose of this study was to compare impact accelerations for pre-planned and un-planned lateral cutting. We hypothesized that impact accelerations would be higher and that there would be greater inter-trial variability for un-planned cutting. We also wanted to determine whether males and females respond in a similar manner when they are unable to pre-plan their movement.

METHODS

Thirty subjects (15 males, 15 females) between the ages of 18 to 35 years old took part in this study. Participants were active and had experience competing in sports that involve frequent landing and cutting. Individuals were excluded if they had a history of lower extremity surgery or a recent injury.

Following a warm-up, participants performed lateral cutting trials under pre-planned and un-planned conditions. For the pre-planned trials, participants would stride forward from a distance of 1.5 m, land with their non-dominant limb, and immediately cut laterally in the opposite direction. The initial cut (non-dominant limb) and subsequent landing (dominant limb) needed to occur within 40 cm x 50 cm areas outlined on the floor to ensure consistency among trials, conditions, and participants.

For the un-planned condition, participants were unaware of the maneuver to perform until after initiating a trial. For each trial they would stride forward and respond to the illumination of one of three stimuli presented on a screen. The stimulus illuminated approximately 250 ms before foot contact. The three stimuli corresponded with a lateral cut, single-leg landing, or vertical jump. When the stimulus corresponding with the lateral cut illuminated, the participants performed the same maneuver described for the pre-planned condition. If the stimulus corresponding with the single-leg landing illuminated they would land on their non-dominant limb and if the stimulus corresponding with the vertical jump illuminated they would land on both feet and jump vertically.

Subjects performed five lateral cut trials for both conditions (pre-planned, un-planned). The single-leg

landing and vertical jump trials were not analyzed, as these were included for the un-planned condition so participants could not pre-plan their movement. The order of the conditions was randomized.

Impact accelerations were recorded during the cutting trials using a tri-axial accelerometer that sampled at 500 Hz (range of ± 16 g) (Shimmer Sensing, Dublin, Ireland). The accelerometer was secured to the anterior-medial tibia of the participant's non-dominant limb (opposite of the leg used to kick a ball), 8 cm above the medial malleolus [4]. The vertical axis of the accelerometer was aligned with the longitudinal axis of the leg.

The vertical acceleration signal was filtered using a 4th order, zero lag, recursive, Butterworth filter with a cutoff frequency of 50 Hz. For each trial the peak vertical acceleration ('impact peak') was identified. In addition to the five-trial mean for these impact peaks, the coefficient of variation was calculated for each participant/condition as an indicator of the inter-trial variability ('impact variability').

For both dependent variables (impact peaks and impact variability), a mixed-model ANOVA with a between factor of sex (male, female) and a within factor of condition (pre-planned, un-planned) was performed using an alpha of .05.

RESULTS AND DISCUSSION

For the impact peaks, there was not a sex by condition interaction effect (p=.94); however there was a main effect of condition (p=.01). Impact peaks were 14.06% higher for the un-planned trials (9.25 ± 2.28 g vs. 8.11 ± 2.53 g) (Fig. 1).

For the impact variability, there was also not a sex by condition interaction effect (p=.56). There was a trend toward greater variability for the un-planned trials; however, this difference was not significant (p=.07) (Fig. 2).

The higher impact peaks for the un-planned cutting trials may indicate that the participant's ability to attenuate impact accelerations was compromised when they could not pre-plan their movement. These differences were independent of sex, as males and females responded in a similar manner as the cognitive demands progressed.

The un-planned condition was designed to simulate the dynamic nature of the sports environment, as participants were afforded limited time to re-direct their movement in response to the visual stimulus. Our findings appear to indicate that imposing temporal constraints on decision-making may place greater demands on the musculoskeletal system.

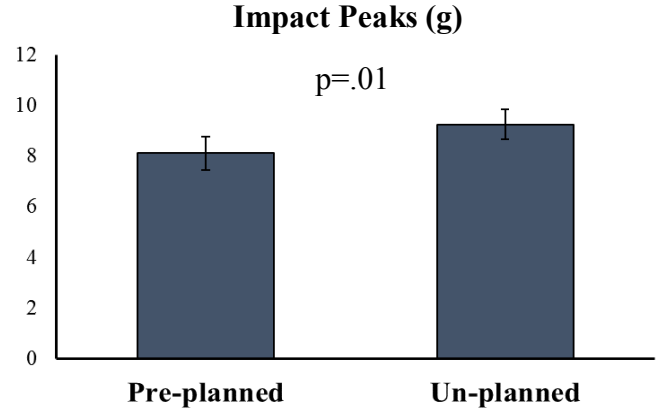

Figure 1: Impact peaks (g) for the pre-planned and un-planned lateral cutting trials. Error bars reflect the standard error.

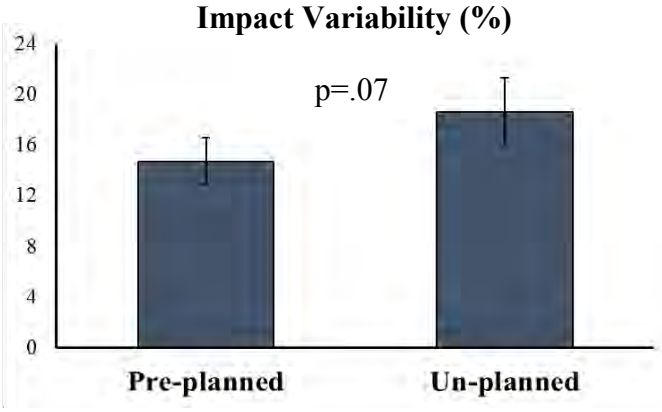

Figure 2: Impact variability (%) for the pre-planned and un-planned lateral cutting trials. Error bars reflect the standard error.

REFERENCES

1. Chu et al. *J Biomech*, **19(12)**, 1986.
2. Voloshin & Wosk. *J Biomech Eng,* **5(2)**, 1983.
3. Almonroeder et al. *Int J Sports Phys Ther,* **10(7)**, 2015.
4. Schutte et al. *Gait Posture*, **59,** 2018.

THE EFFECT OF JOINT HYPERMOBILITY ON HIP AND KNEE KINETICS AND STRENGTH IN ADOLESCENTS WITH JUVENILE FIBROMYALGIA

[1] Tiffany A. Marulli DPT, [1]Jennifer Perry MS, [1]Stephanie Di Stasi PhD, [2]Timothy E. Hewett PhD, [3]Gregory D. Myer PhD, and [3]Susmita Kashikar-Zuck PhD

[1] OSU Sports Medicine Research Institute, The Ohio State University, Columbus, OH, USA
[2]Mayo Orthopedic Biomechanics Laboratories and Sports Medicine Center, Mayo Clinic Rochester, MN, USA
[3]Cincinnati Children's Hospital Medical Center, Cincinnati, OH, USA
email: tiffany.marulli@osumc.edu

INTRODUCTION

Juvenile Fibromyalgia (JFM) is a complex non-articular rheumatic condition, characterized by diffuse musculoskeletal pain, tender points, fatigue, and significant impairments in physical and social function.[1] Altered biomechanics during functional tasks may propagate the cascade of pain exacerbation in JFM patients.[2] In addition, joint hypermobility (HM) is often evident among JFM patients,[3] and benign joint HM is associated with many similar symptoms reported in JFM including chronic pain, deficient physical performance, altered biomechanics and anxiety.[4,5] These symptomology similarities between HM and JFM might be indicative of common pathophysiological processes specific to these conditions;[3] however, the significance of joint HM in adolescents with JFM is unknown.

The purpose of this study was to evaluate the effects of joint HM on hip and knee strength and kinetics during a drop vertical jump (DVJ) in adolescents with JFM. The hypothesis tested was that hypermobile subjects would demonstrate muscle weakness and larger knee abduction, hip adduction and smaller hip flexion moments during the DVJ compared to non-hypermobile subjects.

METHODS

Twenty-five female subjects (15.48±1.46 years old) with JFM volunteered to participate in this study and provided written informed consent. A nine point Beighton-Horan Laxity Scale (BHLS) was performed on each subject to determine joint mobility status. Subjects were considered hypermobile if their BHLS score was greater ≥4 and non-hypermobile if their score was ≤3.

Isokinetic knee flexion and extension was assessed at 300°/second using the Biodex System II. Each subject performed 10 repetitions of maximal effort on each limb. Isokinetic hip abduction was assessed at 120°/second using the Biodex System III. Each subject performed 5 repetitions of maximal effort hip abduction on each limb.

Study participants were fitted with 47 retro-reflective markers. Maker data were collected at 240Hz by a ten camera motion-analysis system (Raptor-E; Motion Analysis Corp.). Each subject completed three DVJ trials from a 31 cm box. Unilateral ground reaction force data were collected for each limb, sampled at 1200 samples per second. Kinetic data reduction and analysis was performed using customized software (Visual3D v6, C-Motion Inc., Germantown, MD). Limb dominance of each subject was unknown so one limb was randomly selected for analysis for each subject. Data were normalized to height and mass for each subject.

Independent t-tests were performed to assess the effect of joint mobility on discrete measures of hip and knee strength and kinetics. Alpha was set to 0.05, *a priori*.

RESULTS AND DISCUSSION

There was a significant difference in peak knee abduction moment (**Figure 1**) ($p<0.05$) between hypermobile and non-hypermobile adolescents with JFM. No differences in sagittal plane knee moments were observed. There were no significant differences in peak frontal or sagittal hip moments between hypermobile and non-hypermobile subjects (**Figure 2**). In addition, there were no significant differences

in hip or knee strength between hypermobile and non-hypermobile subjects (**Table 1)**.

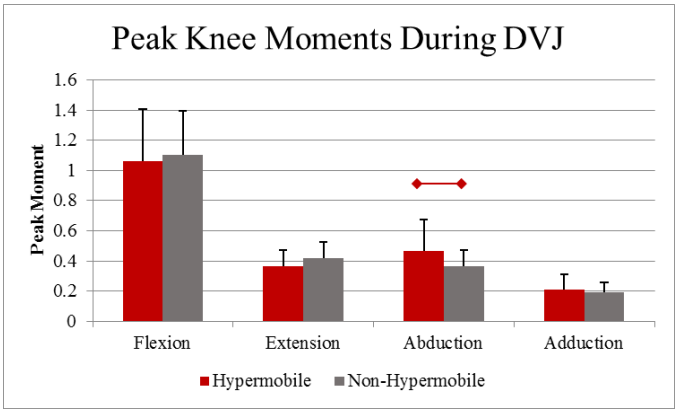

Figure 1: Peak knee moments during DVJ. Standard deviation denoted by error bars.

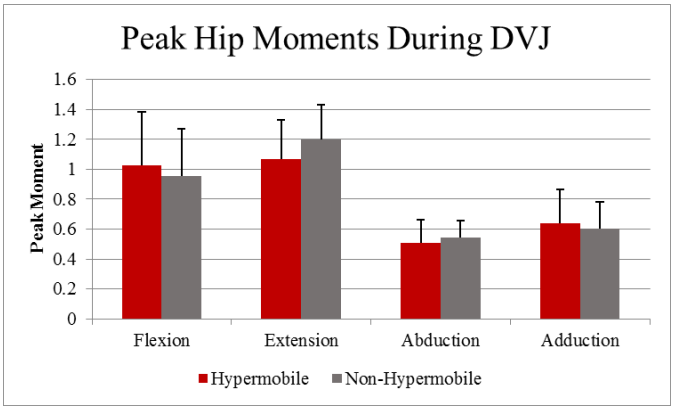

Figure 2: Peak hip moments during DVJ. Standard deviation denoted by error bars.

The purpose of this study was to determine the effect of joint HM on hip and knee strength and kinetics in adolescents with JFM. Hypermobile JFM subjects demonstrated greater knee abduction moments during the DVJ landing compared to non-hypermobile subjects. However, joint mobility did not affect hip moments, sagittal plane knee moments or lower extremity strength in this population. These results partially support the *a priori* hypothesis.

The results of this study indicate that joint hypermobility is associated with altered biomechanics during a functional task in adolescents with JFM. Hypermobile JFM subjects demonstrated significantly greater knee abduction moments during DVJ landing compared to non-hypermobile subjects despite no difference in hip or knee strength. This finding indicate that altered landing kinetics in HM JFM may be a result of deficient neuromuscular control and are less associated to absolute strength. Increased knee abduction has been previously shown to increase risk of lower extremity injury.[6] Although hypermobile subjects demonstrated greater knee abduction moments than non-hypermobile subjects it is still unclear if these biomechanical alterations contribute to pain, dysfunction and injury in this cohort. This study is limited by a small sample size and unknown limb dominance. Further research is needed with a larger sample size and to determine if biomechanical alterations are associated with pain and dysfunction in this cohort

CONCLUSIONS

Joint hypermobility is associated with larger knee abduction moment during DVJ landing. Further research is needed to determine if the observed biomechanical alterations contribute to pain and dysfunction in this cohort and if these biomechanical alterations are modifiable with neuromuscular training interventions.

REFERENCES

1. Zernikow et al. *Shermz,* 26(3), 318-330, 2012.
2. Sil et al. *Arthritis Care Res*, 67(1), 102-111, 2015
3. Gedalia et al. *Ann Rheum Dis*, 52(7), 494-496, 1993
4. Scheper et al. *BMC Musculoskeletal Disord,* 15(1), 243, 2014
5. Smith et al. *Rheumatol*, 53(1), 114-112, 2014
6. Paterno M, et al. *Am J Sports Med*, **38**(10), 1968-78, 2010.

ACKNOWLEDGEMENTS

The authors acknowledge funding support from the National Institutes of Health/National Institute of Arthritis and Musculoskeletal and Skin Diseases grant R21-AR-063412-01, Cincinnati Children's Hospital Medical Center and the OSU Sports Medicine Research Institute.

Table 1: Peak Hip and Knee Torque (Nm/kg)

	Knee Flexion	Knee Extension	Hip Abduction
Hypermobile	0.654 (.0123)	0.980 (0.119)	00670 (0.261)
Non-Hypermobile	0.633 (.0154)	1.014 (0.195)	0.715 (0.196)

POSTERIOR LATERAL TIBIAL CONTACT WITH LATERAL WEDGING IN MEDIAL OSTEOARTHRITIS

[1] Melvin Mejia, [2,3] Jeffrey L. Cole, [1,2] Peter Barrance

[1] Human Performance and Engineering, Kessler Foundation, West Orange, NJ, USA
[2] Rutgers, The State University of New Jersey, Newark, NJ, USA
[3] Kessler Institute for Rehabilitation, West Orange, NJ, USA
email: pbarrance@kesslerfoundation.org

INTRODUCTION

Knee osteoarthritis (OA) is a prevalent cause of disability that is associated with a high cost burden to the United States healthcare system [1]. Lateral insole wedging is a low cost conservative intervention for medial knee OA (MKOA) that has been associated with pain relief in some studies. However, recent reviews have not revealed a consensus on clinical effectiveness or evidence to support dosing decisions [2, 3]. Most biomechanical and clinical studies have investigated single levels of wedging, most often a 5° lateral wedge. The current report presents initial findings on the effects of three levels of lateral wedging on biomechanical parameters derived from MRI of the knee joint during active weight bearing. This is one component of a more comprehensive study that also explores lateral wedging using gait analysis methods [4].

METHODS

Initial results from three participants (n=3, male, 62.4±9.2 years) are reported. All research procedures were approved by the Institutional Review Board. Inclusion criteria included presentation of symptomatic, predominantly medial knee osteoarthritis as confirmed by examination and standing radiographs. Exclusions included: advanced knee OA, prior lower extremity joint replacement or osteotomy, and recent knee surgery, intra-articular injection, or wedged insole use. One knee was assigned for study based on clinical and radiological severity.

Testing was performed in standardized walking shoes (New Balance MW577). Four sets of custom insoles for each available adult shoe size were prepared by a professional pedorthist. The base insole was 5/16" thick neoprene (SpenCore®, Spenco Medical Corp., Waco, TX), with the neutral ('N') insole consisting only of this layer. Lateral wedging of 3°, 6°, and 9° was added using 1/8" and ¼" cork layers applied to the full width, tapering to zero thickness medially. Wedging was placed from the heel to the metatarsal head.

Scanning and data analysis methods as summarized below follow those reported previously [5]. MRI scanning was performed in a 0.6 T vertically open scanner (Upright MRI, Fonar, NY). Using high-definition reconstruction, sagittal view images through the knee joint were acquired with 0.483 mm pixel spacing, 1.0 mm slice spacing, 250 mm field of view, and a scan time of 1m35s. A custom fiber-optic sensor and feedback system were used to present the real time knee flexion angle, along with the 20° targeted angle to the participant. Testing order for footwear condition (N/3°/6°/9°) was randomized. Participants weight-shifted to allow insole exchange, and foot positioning was maintained by manual assistance to guide the shoe to an outline traced on the support surface.

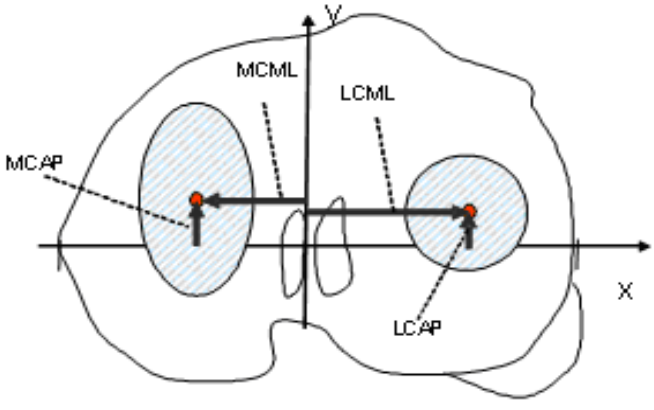

Figure 1: Coordinates of medial and lateral compartment contact centers.

Scan data were transferred to laboratory work stations and formatted for analysis. Femoral and tibial bone surfaces, along with medial and lateral compartment (MC and LC, respectively) cartilage surfaces were traced for each image using a digitizing tablet. Bone coordinate systems were placed on the 'N' condition scans, and surface matching was used to maintain consistent placement. Femoral and tibial cartilage points were projected relative to the tibial plateau coordinate system, and a cartilage contact proximity algorithm was used to measure medial/lateral (ML) and anterior/posterior (AP) centers of femoral contact relative to the tibial plateau (Fig. 1). Kinematic parameters of joint positioning were also calculated from the relative coordinate positions, as reported previously. Data for the index knee were analyzed, and descriptive statistics and relationships are reported for the initial study participants.

RESULTS AND DISCUSSION

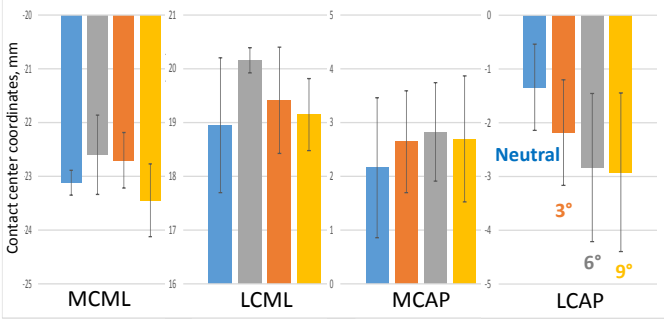

Figure 2: Contact center coordinates with the neutral insole and three lateral wedge conditions. Error bars represent SD.

Grouped results indicate a monotonically increasing trend of posterior translation of lateral compartment contact (LCAP, Fig. 2) with incremental wedging. With a single exception for a 6° to 9° increment, the monotonic increase was observed in individual data. MCAP changes were smaller and less consistent, and medial/lateral contact (MCML, LCML) changes were variable. Evidence of tibial external rotation with incremental lateral wedging was observed in data from two participants. Analysis of grouped data supported a correlative association of tibial external rotation with lateral compartment posterior contact translation (Fig. 3). This is consistent with the following link between parameters: external tibial rotation around a medial center of rotation is associated with anterior lateral tibial plateau

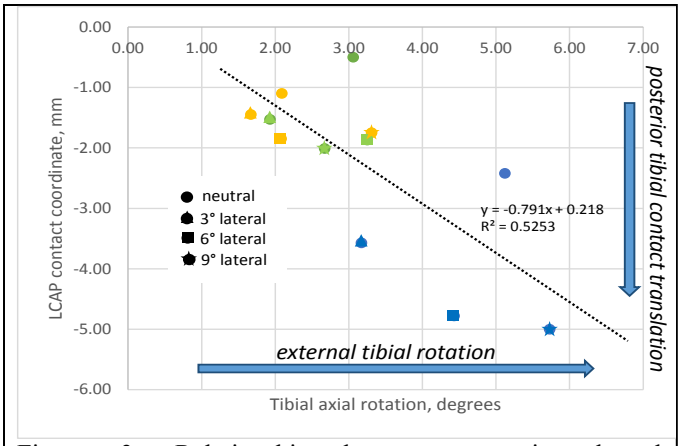

Figure 3: Relationship between posterior lateral compartment contact translation and external tibial rotation. Data from individual participants are grouped by colors.

movement and posterior migration of the tibial contact area. Data from two participants also exhibited a trend of anterior tibial translation with lateral wedging. Changes in frontal plane angulation were small with a maximum range of 0.74°. Data for two participants indicated an overall trend toward more varus angulation, contrasting with a first order effect of valgus angulation that might be expected with lateral wedging.

CONCLUSIONS

While mechanistic theories on lateral wedge effect in MKOA generally suggest alteration to the biomechanical environment of the medial compartment, these preliminary data did not support such changes. Ongoing work will explore the trend of lateral wedging on lateral compartment contact. It should be noted that past studies have associated lateral posterior contact with decreasing joint contact area, a potential risk factor for osteoarthritis.

REFERENCES

1. Wallace, I. et al. *Proc Natl Acad Sci* 114(35), 2017
2. Marks, R. et al. *Int J Clin Pract,* 58(1), 2004
3. Parkes, M et al. *JAMA,* 310(7), 2013
4. Mejia, M. et al., *Proceedings of American Society of Biomechanics, Boulder, CO,* 2017
5. Barrance, P. et al., *Clin Biomech*, 29(9), 2014

ACKNOWLEDGMENTS - This study was supported by NIDILRR grant 90IF0077 (formerly H133G140183). Additional funding was provided by Kessler Foundation.

Biomechanical Symmetry during Drop Jump and Single-Leg Hop Landing in Uninjured Adolescent Athletes

[1] Nicole Mueske, [1] Mia Katzel, [1] Kyle Chadwick, [1,2] Curtis VandenBerg, [3] J. Lee Pace, [1,2] Tracy Zaslow, [1] Bridget O'Callahan, [2] Haley Nakata, and [1,2] Tishya Wren

[1] Children's Hospital Los Angeles, CA, USA
[2] University of Southern California, Los Angeles, CA, USA
[3] Connecticut Children's Medical Center, Hartford, CT, USA
email: twren@chla.usc.edu

INTRODUCTION

Symmetry of quadriceps girth, strength and hop distance are often used as benchmarks for return to sport testing. The practice of using symmetry as a gold standard has been translated into biomechanical testing; however, whether normal kinematics and kinetics are symmetric is not well understood. The purpose of this study was to assess symmetry in uninjured adolescent athletes during double and single-leg landing tasks using a statistical method which considers the temporal characteristics of the data.

METHODS

36 uninjured athletes (ages 7-15 years, mean 12.4, SD 2.4; 47% female) completed vertical drop jump (DJ) and single-leg hop (SLH) for distance tasks; lower extremity kinematics and kinetics were collected through 3-D motion analysis using a 6 degree-of-freedom model; 2-3 trials per participant per side were included for analysis. Differences between dominant and non-dominant limbs from initial contact to peak knee flexion were examined using statistical parametric mapping (SPM), a methodology for making statistical inferences on spatially or temporally related datasets [4]. Two-tailed SPM t-tests were used to compare dominant and non-dominant limbs across the movement cycle.

RESULTS AND DISCUSSION

During both DJ (Figure 1) and SLH (Figure 2), the dominant limb tended to be more internally rotated at the hip throughout landing, but the asymmetry was significant only for short periods early in landing during the DJ ($p<0.05$) and at mid-landing in the SLH ($p=0.01$). Additionally, the dominant hip tended to have less abducted positioning throughout both tasks, but differed significantly only shortly after initial contact in the SLH landing ($p=0.04$). The dominant limb ankle was less inverted ($p<0.001$) with a lower external inversion moment ($p<0.001$) during early to mid-landing in the DJ, and less everted ($p=0.04$) with higher external inversion moment ($p\leq0.05$) early in SLH landing. The only asymmetry observed in the sagittal plane was slightly higher external ankle flexion moments ($p=0.05$) just after initial contact in the DJ. No asymmetries were detected in peak vertical ground reaction force or knee kinematics/kinetics for either task.

Uninjured adolescent athletes exhibited only slight asymmetries during double and single-leg landing, primarily at the hip and ankle in the frontal and transverse planes. The hip may perform larger adjustments to accommodate center of mass location, while the ankle fine-tunes the landing as the closest segment to the ground.

CONCLUSIONS

The SPM method allowed the significance of differences between dominant and non-dominant limbs to be evaluated at all time points throughout the landing movement. While only small regions of statistically significant asymmetry were identified, it is possible that greater asymmetries are present within individuals. In the grouped analysis, asymmetry towards the dominant side for one individual could offset asymmetry towards the non-dominant side of another individual. In future

analysis, we will examine the magnitude and significance of within-subject asymmetry.

REFERENCES

1. Rethlefsen et al. Dev Med Child Neurol 59:79-88, 2017.
2. Rethlefsen et al. J Pediatr Orthop 33:510-504, 2013.
3. Delp et al. IEEE Trans Biomed Eng 54:1940-1950, 2007.
4. Pataky, T. C. (2010). Generalized n-dimensional biomechanical field analysis using statistical parametric mapping. *Journal of biomechanics*, 43(10), 1976-1982.

ACKNOWLEDGEMENTS

We would like to thank our other Motion Lab sports team members – Bitte Healy and Henry Lopez.

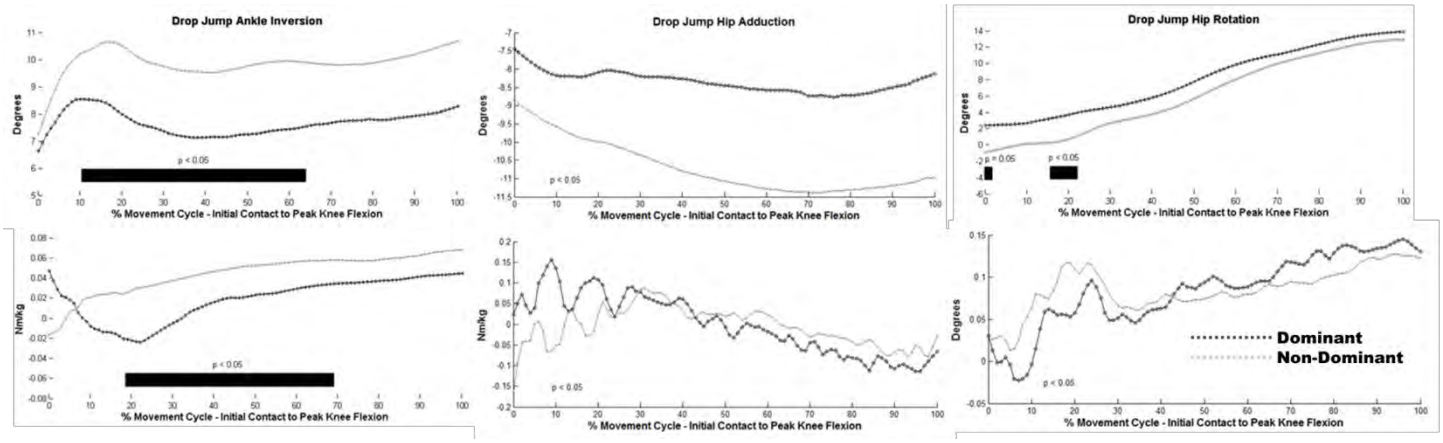

Figure 1: Select SPM results for drop jump; black bars indicate location of significant ($p \leq 0.05$) differences.

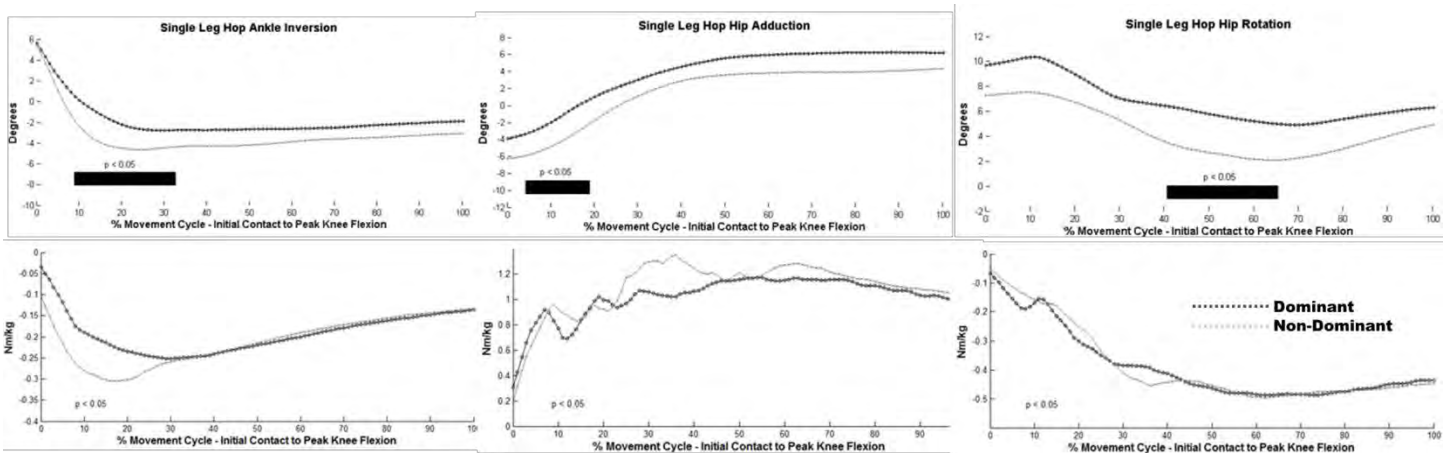

Figure 2: Select SPM results for single leg hop; black bars indicate location of significant ($p \leq 0.05$) differences.

SEX DIFFERENCES IN PASSIVE AND ACTIVE JOINT STIFFNESS DURING HIGH-VELOCITY THRESHOLD TO DETECT PASSIVE MOTION TEST

[1]Takashi Nagai, [1]Nathaniel A. Bates, [1]Timothy E. Hewett, [2] Hyunglae Lee, [3] Thurmon Lockhart, and [1]Nathan D. Schilaty

[1] Mayo Clinic Biomechanics Laboratories & Sports Medicine Center, Rochester & Minneapolis, MN, USA
[2] School for Engineering of Matter, Transport, and Energy, Arizona State University, Tempe, AZ, USA
[3] School of Biological and Health Systems Engineering, Arizona State University, Tempe, AZ, USA
Email: nagai.takashi@mayo.edu

INTRODUCTION

Anterior cruciate ligament (ACL) injuries are one of the most common orthopedic injuries in sports. It is also known that female athletes suffer ACL injuries at higher rates than their male counterparts in the same sports [1]. Modifiable neuromuscular risk factors such as muscular strength, flexibility, balance, landing biomechanics, and proprioception have been investigated in an attempt to screen at-risk athletes, to design preventive intervention program, and to monitor athletes' return-to-sport readiness [2]. In particular, proprioception is the primary regulator of both passive joint stiffness (by modulating the resting tone of muscles) and active joint stiffness (by informing the CNS) [3].

Threshold to detect passive motion (TTDPM) with a slow moving leg (usually less than 0.25°/s) is used for proprioception [4]. Reactive strength can be measured by the rate of torque development over position changes (active joint stiffness) using an isokinetic dynamometer. Recently, we developed a sensorimotor test to examine both proprioception with high-velocity TTDPM (hvTTDPM) and reactive knee flexion (hamstrings) muscular strength [3]. The purpose of the current study was to examine sex differences in this new test. It was hypothesized that females would exhibit slower hvTTDPM and less joint stiffness than males.

METHODS

Seven males (age: 19.7 ± 4.4 years, height: 184.7 ± 6.3 cm, weight: 80.5 ± 9.9 kg) and 10 females (age: 23.7 ± 4.8 years, height: 168.6 ± 4.5 cm, weight: 80.5 ± 9.9 kg) participated in the study. Prior to their participation, informed consents were obtained from each subject. The study was reviewed and approved by the Institutional Review Board.

Subjects were seated on a HumacNORM dynamometer (CSMi; Natick, MA) with the knee joint axis rotation aligned to the axis of rotation of the dynamometer. The leg of the subject was then comfortably strapped to the dynamometer arm. The leg was then extended and anatomic zero recorded in the machine. The dynamometer acceleration was set for 500°/s and torque limit set to 60 Nm. For safety reasons, both mechanical and hardware limits of rotation were set at 30 and 70 degrees. The subject's leg was then rested on the 30 degree stop and a blindfold was placed over the subject's eyes.

The subject was instructed to relax the leg completely. The subject was instructed to resist forward motion as quickly and forcefully as possible when they became aware of acceleration. Then, the dynamometer accelerated at random points in time. The subject had 3 trials of randomized time intervals to respond to the perturbation. Based on previous piloting data, it was determined that subjects failed to react about 20% of time; therefore, only successful trials were used for analyses.

Joint position and torque values were collected at 1000 Hz with customized LabVIEW (National Instruments; Austin, TX) on a USB-1608G (Measurement Computing; Norton, MA). Data was post-processed in customized LabVIEW software to determine joint position and torque values at each of four time points: initiation, 100ms, hvTTDPM, and peak torque). Time point at hvTTDPM was defined as the point in which acceleration of the dynamometer began decreasing and when torque

deflected greater than 10% over a 5ms interval. The passive and active stiffness was calculated by the changes in torque values over the changes in position values from initiation to 100ms and from hvTTDPM to peak torque, respectively (Figure 1).

Descriptive statistics (means and standard deviations) were calculated on both left and right

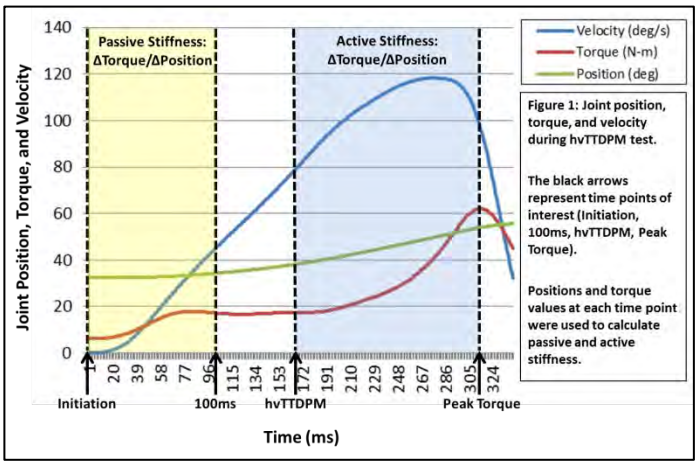

legs. For sex differences, independent *t*-tests or nonparametric tests were used to compare between males and females. Significance was set at $p < 0.05$.

RESULTS AND DISCUSSION

Descriptive statistics are shown in Tables 1 and 2. There were significant sex differences in torque at 100ms on both legs (Torque at 100ms Right: males: 15.9 ± 2.7 Nm, females: 13.1 ± 2.3 Nm, $p = 0.034$. Torque at 100ms Left: males: 17.1 ± 4.8 Nm, females: 12.5 ± 3.4 Nm, $p = 0.032$) and passive stiffness on right leg (males: 6.2 ± 1.2 Nm/deg, females: 4.1 ± 0.4 Nm/deg, $p = 0.003$). There were no sex differences in torque at initiation and all position at initiation and at 100ms ($p > 0.05$).

Table 1: Descriptive Statistics and Sex Differences during Passive Stiffness

	Males	Females	p-value
Torque at Initiation R	2.7 ± 2.7 Nm	4.0 ± 2.8 Nm	0.364
Torque at Initiation L	5.3 ± 4.8 Nm	5.2 ± 4.9 Nm	0.969
Torque at 100ms R	15.9 ± 2.7 Nm	13.1 ± 2.3 Nm	0.034
Torque at 100ms L	17.1 ± 4.8 Nm	12.5 ± 3.4 Nm	0.032
Passive Stiffness R	6.2 ± 1.2 Nm/deg	4.1 ± 0.4 Nm/deg	0.003
Passive Stiffness L	6.4 ± 1.9 Nm/deg	4.6 ± 0.7 Nm/deg	0.052

There were significant sex differences in torque at hvTTDPM in left leg (Torque at hvTTDPM Left: males: 18.8 ± 5.1 Nm, females: 14.3 ± 3.1 Nm, $p = 0.038$). The remaining variables during active stiffness were not statistically significant ($p > 0.05$).

Table 2: Descriptive Statistics and Sex Differences during Active Stiffness

	Males	Females	p-value
Time at hvTTDPM R	135.0 ± 27.0 ms	141.9 ± 14.2 ms	0.501
Time at hvTTDPM L	136.6 ± 10.7 ms	139.6 ± 32.9 ms	0.819
Torque at hvTTDPM R	17.0 ± 2.5 Nm	14.6 ± 2.4 Nm	0.065
Torque at hvTTDPM L	18.8 ± 5.1 Nm	14.3 ± 3.1 Nm	0.038
Time at Peak Tq R	329.0 ± 25.2 ms	331.4 ± 29.0 ms	0.858
Time at Peak Tq L	314.4 ± 43.1 ms	325.2 ± 42.9 ms	0.619
Peak Torque R	63.2 ± 5.6 Nm	60.1 ± 6.5 Nm	0.303
Peak Torque L	64.5 ± 3.2 Nm	61.0 ± 4.9 Nm	0.120
Active Stiffness R	2.4 ± 0.7 Nm/deg	2.2 ± 0.6 Nm/deg	0.583
Active Stiffnfess L	3.2 ± 1.3 Nm/deg	2.6 ± 1.0 Nm/deg	0.356

CONCLUSIONS

The current hvTTDPM findings revealed that females had less passive stiffness and less torque at 100ms and at hvTTDPM. This short-range passive stiffness may be considered as the first line of defense against joint perturbation [2]. The current test results may have suffered ceiling effects as males could have produced greater muscular torque than 60 Nm, which potentially may have resulted in higher active stiffness as represented in the previous study. The ability to detect joint movement as seen as the time at hvTTDPM was mostly similar between sexes. These preliminary results can shed light on the importance of early torque development. Future studies should examine the training effects on the passive and active stiffness and establish the association between stiffness and ACL injuries or return-to-sport readiness [5].

REFERENCES

1. Schilaty et al. *Am J Sports Med*, 2017: 1567-1573.
2. Hewett et al. *Am J Sports Med*, 2016: 3146-3151.
3. Nagai et al. *Sports Med,* 2018.
4. Nagai et al. *Knee Surg Sports Traumatol Arthrosc*, 2013: 2048-56.
5. Nagelli CV and Hewett TE, Sports Med, 2017: 221-232.

ACKNOWLEDGEMENTS

NIH grant funding R01AR056259, R01AR055563, K12HD065987, L30AR070273, and T32AR056950 and the Mayo Clinic Kelly Orthopedic Fellowship.

COMPARISON OF KNEE BIOCHEMICAL VARIABLES IN INVOLVED AND UNINVOLVED KNEES 6 MONTHS POST ANTERIOR CRUCIATE LIGAMENT RECONSTRUCTION (ACLR)

Kelsey Neal, Jack R. Williams, Ashutosh Khandha, Thomas S. Buchanan

University of Delaware, Newark, DE, USA
email: kaeneal@udel.edu

INTRODUCTION

Studies show that ~40% of individuals who undergo ACLR develop knee osteoarthritis (OA) within 8 years of surgery [1], with medial compartment OA being the most common occurrence [2]. About 100,000 ACLR surgeries occur in the United States annually, with a mean patient age in the mid to late 20s [3]. This results in a large population of individuals who develop knee OA at a young age. Quantitative magnetic resonance imaging (qMRI) can measure biochemical variables that can help identify OA onset earlier than X-rays. Chemical exchange saturation transfer (CEST) is a technique that can indirectly estimate glycosaminoglycan (GAG) content in knee cartilage. The loss of GAG in cartilage is an indicator of early onset OA [4]. Transverse relaxation (T2) time of cartilage, another biochemical variable measured using qMRI, has also been used to detect OA post ACLR. High T2 values indicate collagen matrix degradation. As the first step in a longitudinal study, we sought to investigate both GAG-CEST and T2 values at 6 months post-ACLR, in the medial compartment of the involved and uninvolved knees.

METHODS

16 subjects (8 women, mean age: 21 years) were studied at 6 months post unilateral ACLR. Each subject underwent supine bilateral knee MRI (3T, Siemens) using a segmented 3D radiofrequency spoiled sagittal gradient-echo GAG-CEST sequence (repetition time: TR = 452 ms, echo time: TE = 2.73 ms, voxel size 0.6 x 0.6 x 3.0 mm^3, acquisition time 9:51 minutes). All saturation parameters were specifically optimized to induce maximal GAG-CEST effects at 3T by simulation of Bloch equations [3]. GAG-CEST values were calculated by using the % magnetization transfer asymmetry ratio measurement [3] on a pixel-by-pixel basis. A sagittal T2 mapping sequence was also used (TR = 3090 ms, TE = 10, 20, 30, 40, 50, 60, 70 ms, slice thickness = 3 mm, acquisition time: 7:17 minutes). T2 values were also calculated on a pixel-by-pixel basis, by skipping the 1st echo to avoid stimulation artifacts. For both GAG-CEST and T2 measurements, three slices corresponding to the center of the medial compartment were analyzed. Each slice was segmented into six regions of interest (ROIs) (figures 1 and 2). These ROIs correspond to primary load-bearing regions during activities of daily living, such as gait.

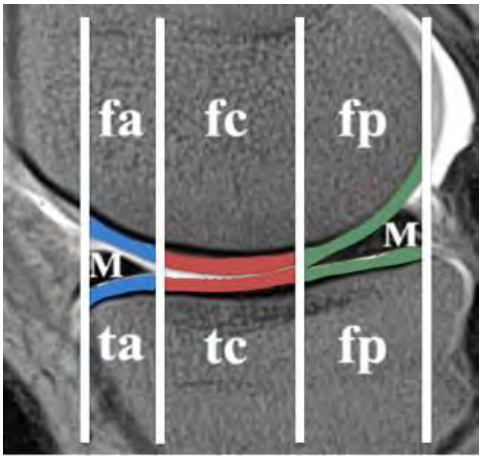

Figure 1: Regions of interest (ROIs) of the tibiofemoral joint, where f = femur, t = tibia, a = anterior, c = central, p = posterior, and M = medial meniscus. The solid lines represent meniscus boundaries.

The ROI included anterior, central, and posterior regions of both the femur and the tibia. The final value for each ROI was found by averaging across three slices. The mean values GAG-CEST and T2 values for each ROI were then compared for involved vs. uninvolved knee using students t-test.

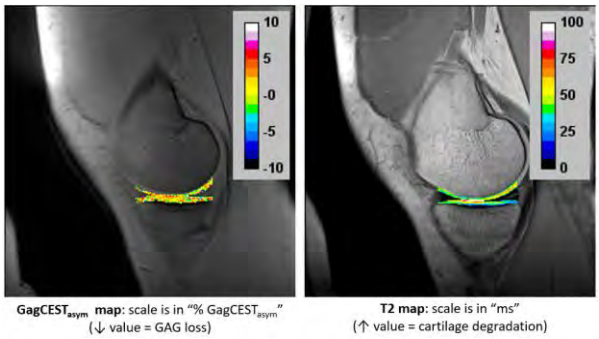

Figure 2: Sagittal GAG-CEST and T2 maps

RESULTS AND DISCUSSION

For GAG-CEST, four out of the six ROIs showed lower gag values in the involved (vs. uninvolved) knee, with the central tibial ROI having a statistically significant difference ($p = 0.029$, figure 3A). T2 values were higher in four out of the six ROIs, however, none of the differences were statistically significant (figure 3B).

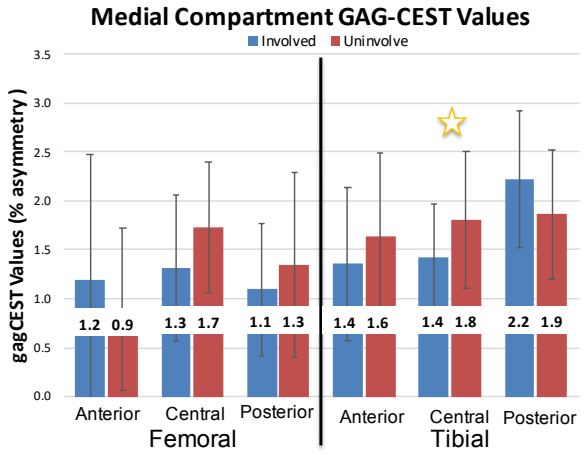

Figure 3A: Medial Compartment GAG-CEST

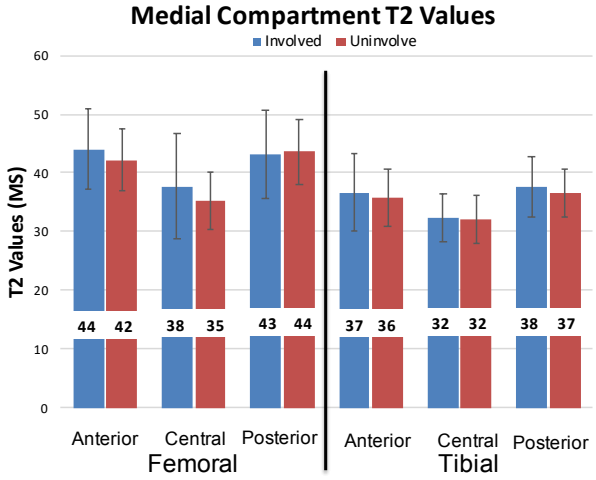

Figure 3B: Medial Compartment T2

Figure 3: Mean GAG-CEST values (Figure 3A) and mean T2 values (Figure 3B) showing one standard deviation for the six ROIs in the involved vs. uninvolved knees.

CONCLUSIONS

Quantitative MRI is a noninvasive technique that can help with the identification of early onset OA. In the early stages of OA, GAG loss typically occurs before collagen matrix degradation. Our results show statistically significant lower values for GAG-CEST in the medial compartment of the involved knee, 6 months after ACLR. These preliminary results warrant further investigation of these variables, with both a larger sample size and long-term follow-up. Evaluation of these biochemical variables in conjunction with biomechanical knee gait variables may help elucidate the relationship between OA-related changes in the knee joint cartilage and aberrant knee joint mechanics after ACLR [5]. Early identification of both biochemical and biomechanical aberrations may also be useful in the design of therapy aimed to delay OA progression post-ACLR.

REFERENCES

1. Li et al. *American Journal of Sports Medicine.* 39(12), 2011.
2. Barenius et al. *The journal of Sports Medicine.* 42(5), 2014.
3. Csintalan et al. *The Permanente Journal.* 12(3), 2008.
4. Rehnitz et al. *Osteoarthritis and Cartilage.* 22(10), 2014.
5. Wellsandt et al. *The American Journal of Sports Medicine.* 44(1), 2015.

ACKNOWLEDGEMENTS

NIH: R01-HD087459, P30-GM103333.

INERTIAL PARAMETER CHANGES OF THE SHANK AND THIGH DURING STAMPING

Matthew T.G. Pain[1], Dimitrios Voukelatos[1], Pui Wah Kong[2] and Laura-Anne M. Furlong[1]

[1]Loughborough University, United Kingdom
[2]National Institute of Education, Nanyang Technological University, Singapore
email: m.t.g.pain@lboro.ac.uk web: http://www.lboro.ac.uk/microsites/ssehs/biomechanics/

INTRODUCTION

During impacts the shape of a body segment can change due to a mechanical wave propagating through soft tissue. Changes in segment geometry are due to application of some force; assuming human limbs behave as rigid bodies ignores a real set of forces occurring within the human body. It has previously been reported that the inertial properties of the shank can change markedly solely due to active muscular contractions with moments of inertia increasing by 5% about the longitudinal axis and decreased by 8% about the two transverse axes [1]. High speed video evidence would indicate deformations are even larger during impacts, but no dynamic assessment of changes in body segment inertial parameters (BSIP) during impacts has been published. The aim of this study was to investigate changes in BSIP of the shank and thigh during a stamping task using high frequency 3D motion analysis.

METHODS

Following university ethical committee approval, seven healthy, recreationally active, males (age: 32 ± 7 years, height: 1.79 ± 0.07 m, mass: 80 ± 8 kg) provided written informed consent. They were instructed to stamp onto the center of a force plate sampling at 1500 Hz (Kistler 9281E, Kistler Group, Winterthur, Switzerland) from a starting posture which had hip flexion at approximately 135 degrees and their knee flexed until the foot was approximately 0.3 m off the ground. Marker positions were determined using a 16 camera high-speed motion analysis system (750 Hz, Vicon T20 and T20S, Oxford Metrics PLC., Oxford, UK). Standard rigid body motions of the lower limb were determined using inverse kinematics in Visual 3D (C–Motion Inc., Germantown, USA) from markers on the greater trochanter, anterior and posterior iliac spines, the medial and lateral femoral condyles and malleoli. The fixed segmental centers of mass, COM_{fixed}, of the shank and the thigh were then calculated from de Leva [2]. Soft tissue motion was tracked using arrays of markers. A 7×8 array covered the proximal 15-75% of the shank; a 7×9 array covered the proximal 25-85% of the thigh.

All processing was completed in Matlab (MathWorks, Natick, MA., USA). Data were low pass filtered at 100 Hz with a 4th order, zero lag Butterworth filter and then time histories of the changes in BSIP were calculated. Segment volumes within the marker arrays were calculated using a mesh of tetrahedra based on 3D Delaunay triangulation. The volume of each tetrahedron, V_i, was calculated using the Jacobian determinant of its vertex coordinate matrix, J, and used to find the mass assuming density of 1060 kg.m^{-3} (Figure 1).

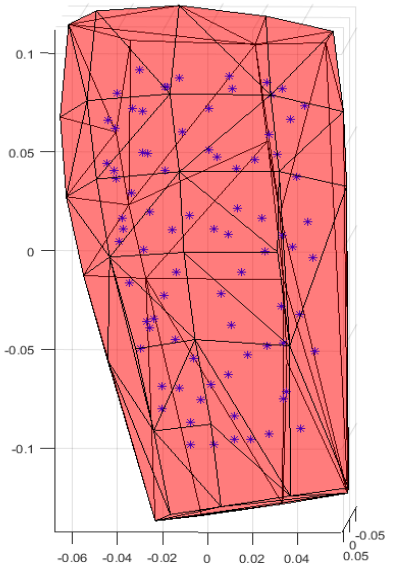

Figure 1. Delaunay triangulation tetrahedral representation of the shank: individual tetrahedron COM locations, blue stars. Axes in meters.

Subsequently the center of mass of the mesh, $COM_{mesh,}$ was established using the relationship:

$$COM_{mesh} = \frac{1}{M} \cdot \left(\sum_{i=1}^{N} m_i \cdot \boldsymbol{r}_i \right) \quad (1)$$

where $\boldsymbol{r}_i$ is the position vector of the i[th] tetrahedron's center of mass given by the mean of the four vertices. This allowed the calculation of the inertia tensor of the mesh, I^{mesh} with respect to COM_{mesh} using the method of Tonon [3]:

$$\boldsymbol{I}^{mesh} = \sum_{i=1}^{N} \boldsymbol{E}_i^Q = \begin{bmatrix} I_{xx}^{mesh} & I_{xy}^{mesh} & I_{xz}^{mesh} \\ I_{yx}^{mesh} & I_{yy}^{mesh} & I_{yz}^{mesh} \\ I_{zx}^{mesh} & I_{zy}^{mesh} & I_{zz}^{mesh} \end{bmatrix} \quad (2)$$

where N is the number of tetrahedra in the mesh, $\boldsymbol{E}_i^Q$ is the 3x3 inertia tensor of the i[th] tetrahedron of volume Vi and density μ. Specifically:

$$\boldsymbol{E}_i^{\boldsymbol{Q}} = \begin{bmatrix} a_i & -b_i' & -c_i' \\ -b_i' & b_i & -a_i' \\ -c_i' & -a_i' & c_i \end{bmatrix} \quad (3)$$

where moments and products of inertia are given from vertices locations:

$$a_i = \int_{V_i} \mu(y^2 + z^2) dV \,;\; b_i = \int_{V_i} \mu(x^2 + z^2) dV;\; c_i = \int_{V_i} \mu(x^2 + y^2) dV \quad (4)$$

$$a_i' = \int_{V_i} \mu yz dV; \qquad b_i' = \int_{V_i} \mu xz dV; \qquad c_i' = \int_{V_i} \mu xy dV \quad (5)$$

In order to quantify the effects of the soft tissue motion on the segmental inertia values, the mesh MoI values were expressed with respect to the segmental centers of mass, COM_{fixed}, for both the shank and thigh. Finally, the inertia tensor, $\boldsymbol{I}^{fixed}$, with respect to COM_{fixed}, was calculated using the parallel axis theorem equations

$$\boldsymbol{I}_{\boldsymbol{kl}}^{\boldsymbol{fixed}} = \boldsymbol{I}_{\boldsymbol{kl}}^{\boldsymbol{mesh}} + \boldsymbol{M}(|\boldsymbol{R}|^2 \cdot \boldsymbol{\delta_{kl}} - \boldsymbol{R_k} \cdot \boldsymbol{R_l}) \quad (6)$$

for *k, l* = x, y, z. $\boldsymbol{R}$ is the vector from COM_{mesh} to COM_{fixed} and I_{kl}^{fixed} is the general term for the elements of the 3×3 inertia tensor. Absolute and percentage variation during the impact were calculated for MoI values and the magnitude of $\boldsymbol{R}$.

RESULTS AND DISCUSSION

Group mean peak vertical impact force from the stamps was 2195 ± 1111 N, (2.8 bodyweights) comparable to running. The mass of the thigh and shank represented by the meshed volume in a static trial was 47% and 70% respectively. This is as expected from the length of the segment markered and the static mass distribution of the segments. This meant that the static mesh moment of inertias about the rigid COM were around 25% and 40%, thigh and shank, of the whole segment COM.

The mean group changes in BSIP were up to 1.3 cm for COM_{mesh} motion and between 7% and 16% for inertias (Table 1), with some peak individual values over 2 cm and over 25% respectively. The largest changes were seen with the highest impact forces, with one subject having a COM_{mesh} change of 1.8 cm for the shank with a peak force of 4500 N. Although an outlier in terms of values the ratio of COM change to peak force is the same as the mean values, indicating more forceful impacts result in greater changes. As the whole segment was not represented by the markers, extrapolating the changes in BSIP reported here to whole segment changes needs to be considered. For the thigh the area covered was representative in terms of tissue type and distribution of the whole segment and so these changes may be representative of the BSIP changes across the whole segment. For the shank this is more complex as although the remaining segment has less soft tissue the soft tissue segment includes the tibia which is rigid. These values are thus likely to more indicative of the upper bounds of the whole segment BSIP changes seen in this task.

This study has shown that meaningful changes in BSIP can be determined during even moderate impacts. Further examination of the affect these could have on the dynamics of the impact compared to rigid body calculations seems pertinent.

REFERENCES

1) Pain, MTG & Challis, JH. *Journal of Applied Biomechanics* 17 (4), 326-334, 2001.
2) deLeva, P. *J Biomech* 29 (9), 1223-1230, 1996.
3) Tonon, F. *Journal of Mathematics and Statistics* 1, 8-11, 2004.

Table 1. Changes in body segment inertial parameters of the soft tissue calculated from the mesh of markers.

	Thigh				Shank			
	Δ COM_{mesh} (cm)	**I_X (%)**	**I_Y %)**	**I_Z (%)**	**Δ COM_{mesh} (cm)**	**I_X (%)**	**I_Y (%)**	**I_Z (%)**
Stamp	1.3 ± 0.6	15.8 ± 5.6	15.7 ± 7.0	9.2 ± 4.7	0.8 ± 0.4	7.1 ± 2.7	8.9 ± 4.4	16.0 ± 5.5

THE INFLUENCE OF PATELLAR TILT ON PATELLAR TENDON STRESS: A SENSITIVITY ANALYSIS

Kyung-Mi Park[1], Tzu-Chieh Liao[2], Christopher M. Powers[1], and Joyce H. Keyak[3]

[1]University of Southern California, Los Angeles, CA, USA
[2]University of California, San Francisco, CA, USA
[3]University of California, Irvine, CA, USA
Email: powers@usc.edu, web: http://pt.usc.edu/labs/mbrl/

INTRODUCTION

Patellar tendinopathy is a common condition among jumping athletes. The prevalence rate of patellar tendinopathy has been reported to be as high as 45% and 30% among elite volleyball and basketball players, respectively [1].

Excessive patellar tendon loading has been considered to be the main causative factor for patellar tendinopathy [2-3]. It has been proposed that abnormal patellar position can contribute to increased patellar tendon loading. Specifically, lateral patellar tilt has been reported in persons with patellar tendinopathy suggesting that patellar mal-alignment may contribute to abnormal stresses in the patellar tendon [4]. Although altered patellar position in transverse plane may be a risk factor for patellar tendinopathy, a comprehensive analysis in the context of patellar tendon loading has not been performed.

The purpose of this study was to determine the influence of patellar tilt on peak maximum principal stress in the patellar tendon using three-dimensional (3D) subject-specific finite element (FE) modeling. We hypothesized that increased rotations of the patella in the transverse plane would result in increased peak maximum principal stress patellar tendon stress.

METHODS

A 3D FE model of the knee joint was developed from a healthy female participant (28 years of age). Subject-specific input parameters included 1) patellofemoral joint (PFJ) geometry, 2) weight bearing PFJ kinematics, and 3) quadriceps muscle forces (Fig. 1). Subject-specific PFJ geometry and morphology, weight-bearing PFJ alignment, and quadriceps muscle morphology were obtained from magnetic resonance (MR) imaging. Lower extremity kinematics, kinetics, and EMG were collected during a squatting task (45° of knee flexion). Quasi-static loading simulations were performed using a nonlinear FE solver in ABAQUS.

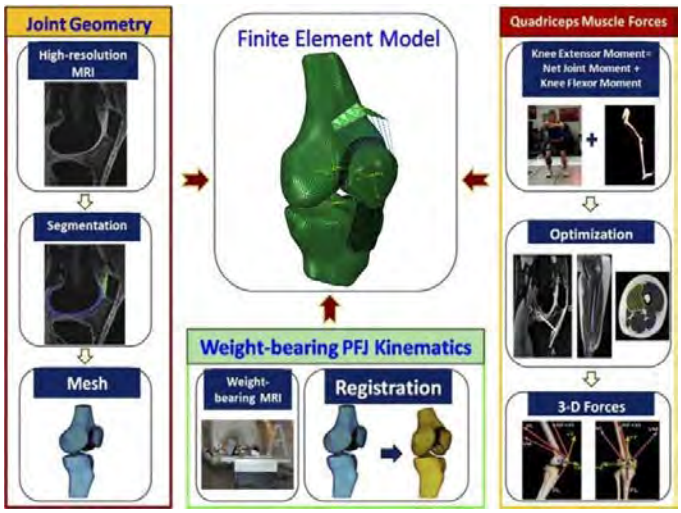

Figure 1: 3D subject-specific finite element model framework.

Detailed descriptions of subject-specific inputs for the FE model have been described in previous publications [5-6]. The patellar tendon was modeled as homogeneous elastic and transversely isotropic using tetrahedral continuum elements. Elastic constants for patellar tendon were determined based on the data obtained by Rawson et al. [7].

To examine the influence of patellar tilt on the patellar tendon stress, the patella was rotated about its axis (Fig. 2) in the transverse plane from the neutral weight-bearing position to 10° (2° increments). This was done for both the medial and lateral directions. (Fig. 3). A total of 10 different

models were created in addition to the neutral model.

Patellar tendon stress was quantified in terms of maximum principal stress. The peak maximum principal stress was at a node that exhibits the highest maximum principal stress.

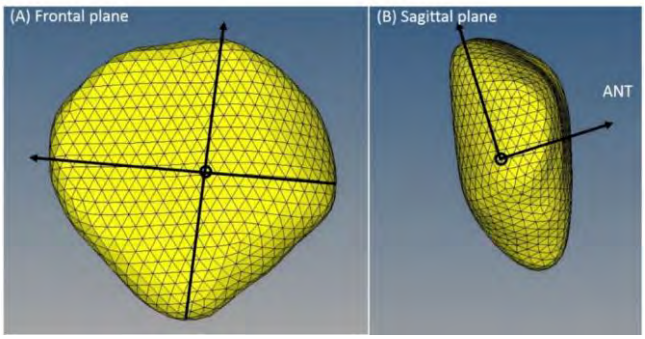

Figure 2: Local coordinate system of the patella. (A) Respective lines representing maximum patellar width and length on frontal plane. (B) Anteroposterior axis perpendicular to other 2 axes. ANT: anterior side.

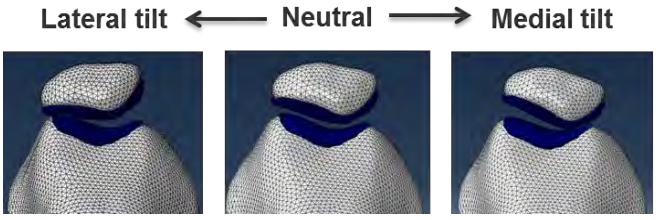

Figure 3: Finite element model simulation for patellar tilt in medial and lateral directions.

RESULTS AND DISCUSSION

Both medial and lateral patellar tilt resulted in a linear increase in peak maximum principal stress in the patellar tendon (2.9 and 3.3 MPa/°, respectively) when compared to the neutral position (Fig. 4). The finding of greater patellar tendon stress with increasing medial or lateral patellar tilt suggests that the orientation of the patella influences the mechanical behavior of the tendon.

CONCLUSIONS

Patellar tilt results in a linear increase in peak maximum principal stress in the patellar tendon stress. The findings of this study suggest that altered patellar tilt may be a risk factor for the development of patellar tendinopathy.

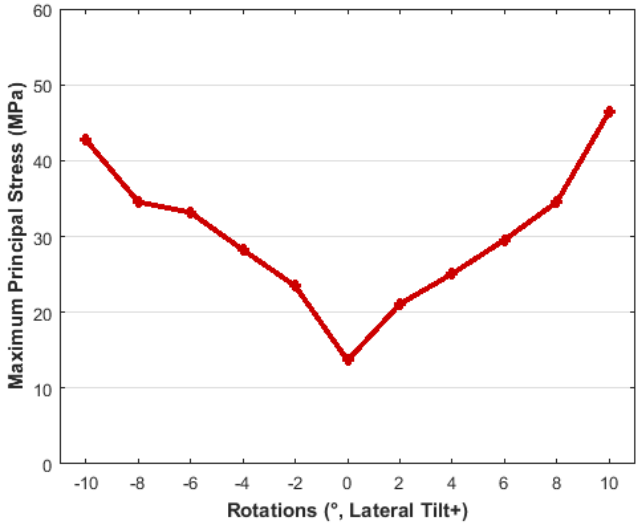

Figure 4: Peak maximum principal stress in patellar tendon resulting from medial and lateral tilt of patella.

REFERENCES

1. Lian OB, et al. *Am J Sports Med* ***33***, 561-567, 2005.
2. Edwards S, et al. *Med Sci Sports Exerc* ***42***, 2072-2080, 2010.
3. Janssen I, et al. *Med Sci Sports Exerc* ***45***, 927-934, 2013.
4. Allen MG, et al. *Skeletal Radiol* ***28***, 220-223, 1990.
5. Farrokhi S, et al. *Osteoarthritis Cartilage* ***19***, 287-294, 2011.
6. Liao TC, et al. *Med Sci Sports Exerc* ***47***, 1775-1780, 2015.
7. Rawson SD, et al. *Biomech Model Mechanobiol* ***14***, 123-133, 2015.

ACKNOWLEDGEMENTS

This study has been supported by the International Society of Biomechanics Matching Dissertation Grant, the American Society of Biomechanics Grant-in-Aid, and SC CTSI Voucher Program.

Effect of Foot Rotation on Knee Mechanics During an Anticipated Running and Cutting Task

[1] Shelby A. Peel, [1] Lauren E. Schroeder, [1] Joshua T. Weinhandl
[1] University of Tennessee, Knoxville, TN, USA
email: speel@vols.utk.edu

INTRODUCTION

Running and cutting is considered one of the "high-risk" sporting movements that can lead to ACL injury [1]. Cutting tasks have been shown to increase knee abduction angle as well has knee adduction moment [2,3]. This increase in knee abduction angle and adduction moment is commonly the result of a medial collapse of the knee, which is a strong characteristic of ACL injury movement patterns [4]. Because of this, much attention has been placed on kinematic and kinetic variables associated with cutting and how they relate to ACL injury risk. One such variable is foot progression angle (FPA).

Previous research has found landing with a "toe-in" position of 30˚ increases peak hip adduction, knee internal rotation angles and moments, as well as peak knee abduction angles, and decreases peak hip flexion angles [5]. However, to date, no study has observed how foot placement affected knee mechanics during a cutting task.

Therefore, the purpose of this study was to assess the effects of changing FPA on lower extremity mechanics during an anticipated run and cut task in healthy, recreationally active, males and females.

METHODS

Eight healthy, active participants (four females, four males) volunteered for the current study and provided written informed consent. Participants also completed the Lower Extremity Functional Scale to ensure they qualified to participate.

At the start of their testing session, participants were fitted with a standardized lab shoe (Nike Pegasus) and asked to complete a five-minute warm-up. After completing the warm-up, EMG sensors were placed on the quadriceps (vastus lateralis and vastus medials) and the hamstrings (biceps femoris and medial hamstrings). Three MVIC trials were collected for the quadriceps and the hamstrings. Anatomical markers and tracking marker clusters were then placed bilaterally on the participants, as well as the trunk and acromion processes. A three-second static calibration trial was collected, and data collection began.

Timing gates (Lafayette Instrument) were placed one-meter apart before and after the force plate. Participants were asked to complete an anticipated cutting movement, were the right foot was planted cleanly on the force plate, and the participants made a 45º cut to the left. While planting on the force plate, participants were asked to complete four FPA conditions: 0˚ neutral, 15˚ toe-in, 30˚ toe-in, and 15˚ toe-out. Cutting tasks were counterbalanced and five trials of each condition were collected. A customized MATLAB code (MathWorks) was used to provide real-time feedback of cutting FPA during the toe-in and toe-out conditions to eliminate a targeting effect.

A 12-camera motion capture system (200Hz, Vicon, Centennial, CO, USA) and a force platform (2000Hz, AMTI, Inc) were used to collect marker coordinate and GRF data, respectively. EMG data were collected using a wireless EMG system (Delsys Trigno). Visual3D biomechanical software (C-Motion) was used to process and analyze all kinematic and kinetic data, while EMG data were processed using a customized MATLAB code. Marker coordinate and GRF data were filtered using fourth-order Butterworth low-pass filters with cut-off frequency of 10Hz. 3D joint kinematics were calculated using a joint coordinate system approach. 3D internal joint moments were calculated using standard inverse dynamics techniques and expressed in the joint coordinate system. Joint moments were normalized to body mass.

A 2x4 (gender x task) repeated measures ANOVA was used to compare dependent kinematic and kinetic variables, as well as muscle activity co-contraction indices (v22.0, SPSS Inc). Significant

interactions and main effects were examined with *post hoc* pairwise comparisons with Bonferroni adjustments. Significance was set at $p < 0.05$.

RESULTS AND DISCUSSION

Initial contact knee abduction and knee internal rotation angle were found to be significant for task, but not gender ($p < 0.05$). Initial contact knee flexion angle, peak knee extension, knee adduction, and knee internal rotation moments, and pre and post initial contact quadriceps:hamstring activation ratios were not significant for any task or gender difference ($p > 0.05$).

Our results revealed that only initial contact knee abduction and internal rotation angles were significantly different between tasks. No gender effects were found in 3D knee kinematics, kinetics, or quadriceps:hamstring activation ratios. Initial contact knee abduction angle was greater at the TI30 condition compared to the TO15 condition. Surprisingly, participants displayed on average a knee adduction angle at TO15. Knee internal rotation angle was also found to be greater at the TI30 condition compared to the TO15 condition. These findings may suggest that a toe-in FPA of 30° could be more of a "high-risk" foot placement during a cutting task than a toe-out FPA.

3D knee joint kinetics showed no significance for gender or task. While knee abduction angle in combination with knee adduction moment is considered an ACL-injury risk mechanism, that was not shown in the current study. This could be due to the positioning of the ground reaction force vector in relation to the knee joint during the cutting task. However, further analysis is needed to investigate this phenomenon.

CONCLUSIONS

The results of this study reveal that an extreme toe-in position of 30° during a cutting task alters knee mechanics unfavorably for ACL injury risk. However, further analysis is needed to fully determine the effects of FPA on lower extremity mechanics during a cutting task. Such findings may provide insight regarding the relationship between foot positioning and ACL injury risk, which may help improve ACL injury prevention protocols for athletes who utilize a cutting task in their respective sport.

REFERENCES

1. Shimokochi Y et al. *J Athl Train.* **43**, 396-408, 2008.
2. Olsen et al. *Am J Sports Med.* **32**, 1002-1012, 2004.
3. Sigward et al. *Clin J Sport Med.* **25**, 529-534, 2015.
4. Kim et al. *Am J Sports Med.* **42**, 1985-1992, 2014.
5. Tran A et al. *J Exp Orthop.* **3**, 2016.

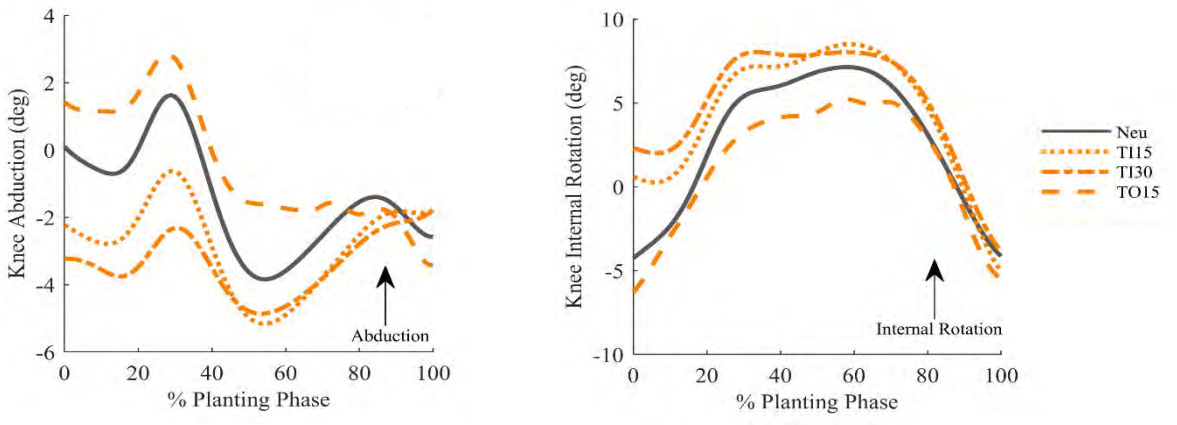

Figure 1. Mean ensemble curves for initial contact knee abduction and internal rotation angles during four cutting conditions: 1) neutral 0° FPA (Neu; grey solid line) 2) toe-in 15˚ FPA (TI15; orange dotted line), 3) toe-in 30˚ FPA (TI30; orange dot-dash line) 4) and toe-out 15˚ FPA (TO15; orange dash line).

REGULATION OF WHOLE BODY ANGULAR IMPULSE WHILE PERFORMING GOLF SWINGS WITH SHORT AND MID IRONS

[1] Travis Peterson and [2] Jill McNitt-Gray

[1] California Lutheran University, Thousand Oaks, CA, USA
[2] University of Southern California, Los Angeles, CA, USA
email: tjpeterson@callutheran.edu

INTRODUCTION

Successful performance of golf shots with different clubs allows players to either set up future shots or position the ball closest to the pin. Regulating distance is vital within the set of irons for optimal performance on the golf course. The set of irons provides a range of clubs that vary in length, loft, and lie characteristics. This allows players to produce golf shots of varying distances and trajectories where short irons (e.g. 9-iron) typically are designed to hit shorter distances than mid irons (e.g. 6-iron). Previous research has demonstrated that players will regulate their linear and angular impulse as golf shot distance is modulated [1,2]. Understanding how players regulate impulse between short and mid irons will provide insights into how players perform golf shots across the entire set of clubs.

Previous research has determined that reaction forces increase when increasing distance within (e.g. -10 yards versus normal with 6-iron) or between clubs (e.g. 6-iron versus driver) [1–4]. Multiple studies found vertical ground reaction forces to increase with shorter irons compared to the driver [4,5]. They also found horizontal reaction forces to increase when using the driver compared to irons, but there is a lack of consensus on whether there are differences in reaction forces between long, mid, and short irons [4,5]. The current landscape suggests there is a need to understand the regulation of reaction forces between clubs within the set of irons as players regulate angular impulse to successfully perform the golf swing.

This study aimed to determine how skilled golf players regulate angular impulse as they performed golf swings with a short iron (9-iron) and a mid iron (6-iron). We hypothesized that net angular impulse would increase with the 6-iron due to contributions from both the rear and target legs. We expected that these increases would be due to increases in RFh with minimal modification of the RFh-angle relative to the target line.

METHODS

Skilled players (n = 10, handicap < 5, 6 female, 4 male, 20 ± 1.24 years old) volunteered in accordance with the institutional review board. Each player performed four to six shots towards a target with a 9-iron (9I, TaylorMade-Adidas) and a 6-iron (6I). Shots were initiated with each foot fully supported by a force plate (Kistler, 1200 Hz). Magnitude and direction of the peak resultant horizontal reaction forces (RFh) at the artificial turf/plate interface and point of wrench application (PWA) were computed for each leg [6]. Reaction force magnitudes were expressed as a percentage of body weight (%BW). Moments about the vertical axis passing through the CM were calculated as the cross-product of the RFh and position vector from the CM to the PWA (moment arm) summed with the free moment for each leg [7]. Angular impulse (AI) normalized by body mass was calculated as the area under the moment curves for each leg during the period of net positive AI beginning near transition of backswing to downswing and ending near ball contact. Components of angular impulse (RFhs, RFh-angles, and moment arms) were represented as the mean value of the 10 samples measured before and after the maximum RFh. Between club differences across the group were determined using the Sign Test (α = 0.05).

RESULTS AND DISCUSSION

The net angular impulse was significantly greater across the group (Figure 1) when swinging with the 6-iron (0.285 N*m*s/kg) compared to 9-iron (0.275

N*m*s/kg, p = 0.002). The observed increase in net angular impulse between clubs did not occur with significant increases in angular impulse generation by a specific leg (target between club differences in AI (p = 0.088); rear leg (p = 0.088)). Although target leg angular impulse was not different between irons, target leg RFh (p = 0.002) and RFh-angle (p = 0.001) were significantly greater during swings with the 6-iron (27.64 %BW, 282°) compared to the 9-iron (25.78 %BW, 288°); whereas target leg perpendicular moment arm was comparable across club conditions. In contrast, rear leg RFh and RFh-angle were not significantly different between the irons, however, rear leg perpendicular moment arms were significantly greater during swings with the 6-iron (p = 0.013, 0.224 m) compared to the 9-iron (0.242 m). Stance width also increased by ~0.024m between clubs across the group (p = 0.001).

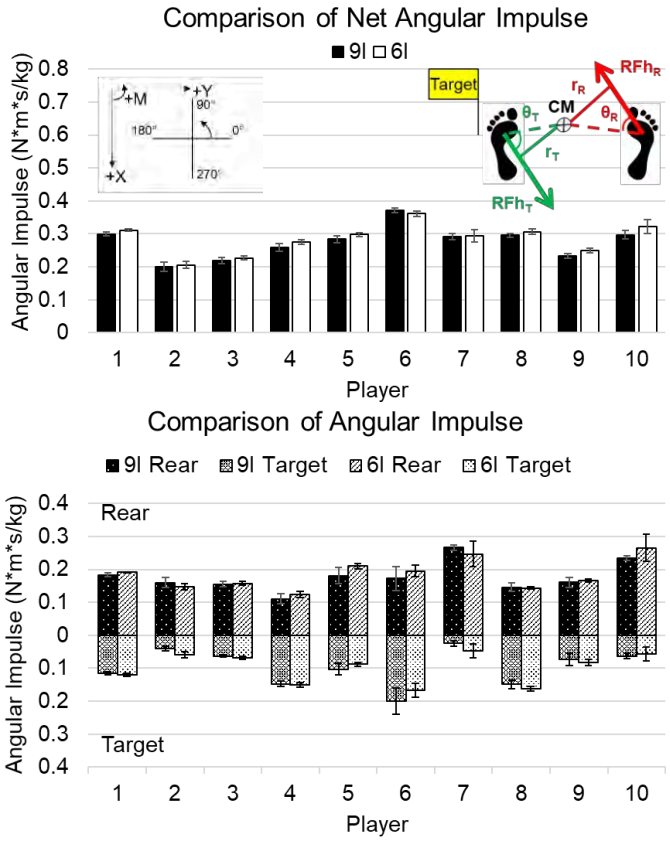

Figure 1: Mean angular impulse (AI, normalized by body mass) of each players' golf swings with the 9-iron (9I) and 6-iron (6I) during the interval of interest. Net AI was greater while swinging with a 6-iron (p = 0.002, above), however rear (p = 0.088) and target leg AI (p = 0.088, below) were not found significantly different. Error bars represent ±1 standard deviation. Positive AI values were plotted above and below zero for rear and target leg.

On average, players increased net angular impulse with the 6-iron compared to the 9-iron, but the differences were small and were not associated with consistent increases in target or rear leg angular impulse generation across players. The results indicate that achievement of between-club differences in net angular impulse generation involved player-specific modifications in rear and target leg angular impulse generation. The difference in net angular impulse magnitude between 9-irons and 6-irons were comparable to observed differences in net angular impulse generation when hitting normal and maximal shots within a driver, but substantially less than differences between the 6-iron and the driver (~0.046 N*m*s/kg) [2,8]. Across the group, players increased target leg RFh while maintaining rear leg RFh with the 6-iron as compared to the 9-iron as part of a net angular impulse regulation strategy. This finding is consistent with Hirano and colleagues who reported target leg RFh increases with a mid iron (6-iron) compared to a shorter iron (approach wedge), but rear leg RFh did not differ [4].

CONCLUSIONS

The results of this study indicate that highly skilled players performed golf shots with short and mid irons while generating comparable amounts of net angular impulse with different stance widths. Differences in angular impulse generation within leg and between clubs were found in target leg RFh magnitude and direction as well as rear leg moment arms. The net angular impulse generated using the short and mid irons was less than with a driver [2]. Knowledge of how players generate net angular impulse across a wide range clubs can assist with skill acquisition as well as performance on the course.

REFERENCES

1. McNitt Gray, JL, et al. *Sports Biomech* **12**(2), 121-31, 2013.
2. Peterson, TJ, et al. *J. App. Biomech* **32**(4), 342-49, 2016.
3. Barrentine, SW, et al. *WSCG Proceedings*, St. Andrews, Scotland, UK, 1994.
4. Hirano, T, et al. *ISBS Proceedings*, Cologne, Germany, 2017.
5. Worsfold, P, et al. *J. Sports Sci Med.* (6), 484-89, 2007.
6. Williams, K, et al. *Med. Sci. Sports Exer* **15**(3) 247-55, 1983.
7. Holden, JP, et al. *J. Biomech* **24**(10) 887-97, 1991.
8. Peterson, TJ, et al. *ASB Proceedings*, Raleigh, NC, USA, 2016.

BROAD JUMP PERFORMANCE AND BASKETBALL SHOE BENDING STIFFNESS

Bryan Picco, Nicholas S. Frank, Bryan P. Conrad

Nike Sport Research Laboratory, Beaverton, OR, USA
email: Bryan.Picco@nike.com

INTRODUCTION

Increasing basketball shoe bending stiffness has been proposed as a way to improve jump performance. Attempts to increase bending stiffness using carbon fiber plates inserted into midsole cushioning have resulted in mixed jump performance results. Stefanyshyn and Nigg [1] reported a 1.70 cm countermovement jump height increase when athletes jumped in stiff (bending stiffness = 0.25 Nm/º) compared to control shoes (0.04 Nm/º). Their explanation for this increased jump height was that a stiff plate reduces the energy lost at the metatarsophalangeal (MTP) joint during the jump's propulsive phase. Conversely, Worobets and Wannop [2] found no significant improvements in jump height with increased bending stiffness; however, their tested stiffness range was relatively small (0.22 Nm/º to 0.33 Nm/º).

More energy is typically lost at the MTP during standing maximum-effort horizontal jumps than during vertical jumps because of increased MTP extension [3]. For this reason, altering footwear bending stiffness may have a larger influence on broad jump (i.e. horizontal) performance compared to a vertical countermovement jump. Therefore, the purpose of this study was to determine if broad jump performance could be improved by increasing the bending stiffness of basketball footwear. It was hypothesized that an athlete-specific bending stiffness exists that improves broad jump distance.

METHODS

Nine male basketball players (self-reported shoe size 14, 30.7 ±5.1 yrs, 100.6 ± 15.1 kg, 1.92 ± 0.02m) performed 3 maximum effort broad jumps in 4 different shoe conditions. All conditions were assembled using identical uppers and foam midsoles. The distinguishing feature across the conditions was bending stiffness, manipulated using carbon fiber plate layers. A "Control" basketball shoe condition (12.8 Nm bending stiffness) was built without a carbon fiber plate. The other three conditions were classified as "Low" (20 Nm), "Medium" (24 Nm), and "High" 27.3 Nm) bending stiffness. Stiffness was measured using a three-point bending test.

For each jump, ground reaction forces and foot position were collected at 2000 Hz and 250 Hz respectively. Jump distance was calculated as the average location between left and right heel, from the start of the jump to the landing. Horizontal, vertical, and their resultant impulse was calculated from jump initiation, defined as the instant in time when less than 95% of body weight was crossed, to when both feet left the force plates.

Four one-way repeated measures ANOVAs were performed ($\alpha = 0.05$) to determine shoe bending stiffness effects on jump distance and horizontal, vertical, and resultant impulse. Additionally, control shoe outcome measures were compared to each athlete's best performing "stiff" condition using paired t-tests ($\alpha = 0.05$), defined as the shoe that enabled the furthest broad jump distance compared to the control.

RESULTS AND DISCUSSION

Eight out of nine athletes jumped farther in one of the carbon fiber conditions compared to the control shoe without a carbon plate, but none of these improvements, or any impulse outcome, were significantly different for any specific condition (Figures 1 and 2).

However, there seemed to be an optimal stiffness that was subject specific. Compared to the control shoe without a plate, athletes jumped significantly farther and generated significantly greater resultant and horizontal impulse while wearing their best stiff shoe (Table 1).

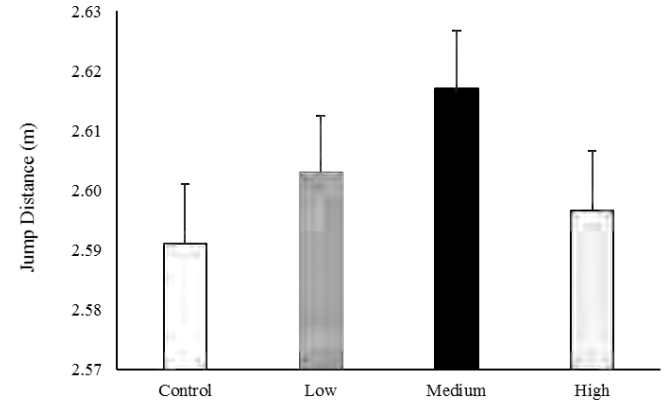

Figure 1: Broad jump performance across shoe conditions. Differences were not significant

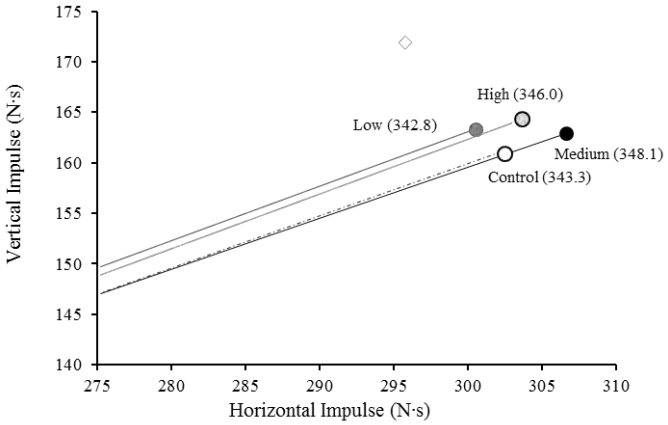

Figure 2: Resultant impulse generated across shoe conditions. Differences were not significant

Table 1: Jump performance and impulse comparisons between the control shoe and each athlete's best performing "stiff" shoe.

	Control	Optimal Plate	*p*
Jump Distance (m)	2.591 ± 0.254	2.641 ± 0.244	**0.012**
Resultant Impulse (N·s)	343.3 ± 34.8	348.0 ± 34.7	**0.045**
Horizontal Impulse (N·s)	302.5 ± 29.8	307.1 ± 29.6	0.078
Vertical impulse (N·s)	160.9 ± 26.2	162.5 ± 25.3	0.249

For the conditions with plates, three athletes jumped furthest wearing the low stiffness shoe, three jumped furthest wearing medium stiffness shoe, and three jumped furthest wearing the high stiffness shoe. This suggests that there may be an athlete-specific optimal bending stiffness that enables best broad jump performance. Similar findings of a subject-specific optimal stiffness has been found in gait and running [4,5]. Reasons for this specificity could include technique, ability to generate force, and athletes' muscle force-length/force-velocity relationships.

It was expected that bending stiffness effects on performance would be more prominent for horizontal jumping compared to vertical. The 5.0 cm performance improvement between the control shoe and the athletes' best stiff shoe supports this notion. Worobets and Wannop [2] suggest that previous studies that did not find bending stiffness-related jump performance gains did not vary stiffness enough. Additionally, the control shoe's stiffness impacts the likelihood of finding a difference. For example, Stefanyshyn and Nigg's [1] control shoe was very flexible (0.04 Nm/º) and Worobets and Wannop's [2] control was nearly as stiff as Stefanyshyn and Nigg's "stiff" shoe. The current study measured bending stiffness differently, but it is reasonable to hypothesize that a more flexible control shoe could have increased broad jump performance gains. Researchers instead chose to build a control shoe relevant for basketball. Collectively, these findings emphasize the importance of establishing relevant controls for testing and being diligent when reporting and measuring shoe bending stiffness to better inform future basketball footwear design.

CONCLUSIONS

Increasing shoe bending stiffness allowed eight of the nine tested athletes to broad jump farther than the control basketball shoe. However, the optimal bending stiffness was athlete-specific. The stiff plates allowed athletes to generate increased propulsive impulse compared to the control without sacrificing vertical impulse. These kinetic changes resulted in improved jump performance.

REFERENCES

1. Stefanyshyn and Nigg. *Med Sci Sports Excers,* 32.2, 471-476, 2000.
2. Worobets and Wannop. *Sports Biomech,* 14.3, 351-360, 2015
3. Stefanyshyn et al. *J Sports Sci,* 16, 177-186, 1998.
4. Willwacher et al. *J Appl Biomech,* 29, 583-592, 2013.
5. Stefanyshyn and Fusco. *Sports Biomech,* 3.1, 55-66, 2004.

INJURY PREVENTION BASED ON COMPUTER MODELING OF CLEAT TRACTION

[1]Justin L. Rittenhouse and [1,2]Peter A. Gustafson

[1] Western Michigan University, Mechanical and Aerospace Engineering, Kalamazoo, MI
[2] Western Michigan University Homer Stryker MD School of Medicine, Kalamazoo, MI
email: peter.gustafson@wmich.edu, web: https://wmich.edu

INTRODUCTION

Injuries related to foot traction are ubiquitous ranging from insufficient traction (slip and fall) to excessive traction (failure to release causing fracture or soft tissue damage). The existing literature on computational modeling of the footwear/ground interaction is limited and focused primarily on musculoskeletal dynamics simulation (i.e., the load transfer through the body) rather than on transfer into the body (through the ground/foot interface). Hence, there is opportunity to develop and/or enhance techniques for modeling footwear traction to reduce injury.

The most common NFL injury, excluding quarterbacks, is to the foot and ankle region accounting for 26% of all reported injuries [1]. Only 30% of injuries for non-quarterbacks happen above the waist [1]. Regardless of position, 53% of all injuries occur in the knee and low leg regions [1]. A significant but unknown number of these injuries are related to excessive traction. These injury trends show that understanding and accurately modeling turf is essential. The goal of this research is to determine whether the discrete element method can simulate the interaction between turf and studded footwear. The long-term goal is to optimize the interface between footwear and artificial turf to provide the safest possible environment for athletic participation while balancing demand for dynamic traction against the risk of injury. Related models could investigate footwear and granular materials, e.g. sand on a beach or climbing on gravelly hills.

METHODS

A bench level laboratory experiment used three football studs in a rigid bracket and used a rigid box to hold the artificial grass and infill. This set up can be seen in Figure 1. This set up was to provide validation data to a discrete element model of the same. The studded assembly was turned at 1 degree per second in artificial grass, rubber infill, and grass+infill artificial turf on a servo hydraulic load frame for 60 seconds. An increase of over 1200% in both max and average torque was found when comparing grass+infill to just infill. Results can be seen in Table 1 below. Torque and axial force were sampled at 100Hz.

Figure 1: Laboratory experiment set up.

These load frame results were used to calibrate a discrete element model. A trial and error approach was employed to calibrate the elastic modulus, Poisson's ratio, and density until it had a similar output to the hydraulic load frame. Subsequently, a series of simulations were run to determine the effects of stud geometry and pattern. The models applied 1 degree per second for 60 seconds or 2.58 meters per second for 0.4 seconds, as with published literature [2, 3]. Each model evaluated the torque/rotation load history and the

force/translation history in two directions. The three load scenarios were repeated on four common stud designs and three unique. Filtered torque, force, and kinetic energy were evaluated as indicators of stud grip.

RESULTS AND DISCUSSION

Round, square and hex shape studs were compared in just the rubber infill in the current study. In comparison to the round studs, max torque increased 17% while average torque increased 22% for the square. Changes in max and average torque for the hex studs were negligible. These results can be seen in Table 1 below.

The average torque of the discrete element model was within 2% of the bench experiment for the round cleat. Stud geometry appears to play a significant role in torque generation while interacting with turf. The forces/torques generated by the studs and footwear will transfer to the athlete, impacting performance and potential for injury. No ideal limit of load transfer has yet been established. Based on preliminary results, the discrete element method appears to provide a path for dynamic stud/turf interaction modeling.

REFERENCES

1. Andrews, W., Berkowitz, B. and Cuadra, A. *NFL injuries: Where does it hurt?,* The Washington Post, 2013
2. Da Corte, D. (2017). *Biomechanical analysis of the sidestep cutting maneuver in football players with OpenSim*.(2013/2014)
3. Kirk, R., Noble, I., Mitchell, T., Rolf, C., Haake, S. and Carré, M. *High-speed observations of football-boot-surface interactions of players in their natural environment,* Sports Engineering 10(3), 2007.

Table 1: Results of laboratory experiments versus DEM models.

Experiments	Laboratory Grass/Infill Round Studs	Laboratory Infill Round Studs	DEM Model: Infill Round Studs	DEM Model: Infill Square Studs	DEM Model: Infill Hex Studs
Average Torque [N-mm]	1061.5	81.3	82.4	100.7	82.1
Max Torque [N-mm]	1744.3	103.0	130.0	152.5	128.9

QUADRICEPS ACTIVATION AND STRENGTH CHANGES DURING REPETITIVE EXERCISE IN INDIVIDUALS WITH ANTERIOR KNEE PAIN

[1] Yuyeon Roh, Daeho Kim, Minwook Kim, Sungwan Kim, and Jihong Park

[1] Kyung Hee University, Yongin, Korea
email: jihong.park@khu.ac.kr

INTRODUCTION

Quadriceps weakness in patients with anterior knee pain (AKP) is common [1,2]. In terms of weakness, measurement of strength (e.g., maximal voluntary isometric contraction: MVIC) and activation (MVIC along with an exogenous electrical stimulation are broadly used. Although these measurements provide us sufficient evidence on quadriceps inhibition [2], the available data are still lacking of practicality. For example, we still do not know how these values would change during repetitive exercise (e.g. 5 sets of continuous muscle contractions).

Hence, we examined how quadriceps activation and strength changes during a bout of knee extension isokinetic exercise in patients with anterior knee pain. We then compared the results to comparing to matched healthy controls. We hypothesized that AKP patients would show further quadriceps dysfunction while controls would maintain as repetitive exercise goes.

METHODS

Twenty-two AKP patients (age: 22.4 ± 2.9 years; BMI: 22.0 ± 1.9 kg/m^2) and matched healthy controls (age: 22.9 ± 1.9 years; BMI: 21.6 ± 2.2 kg/m^2) participated in this study. Their mean time from pain onset was 38.6 months (range: 4-110 months). AKP was defined as checking "yes" to at least one of the following options: (i) pain during ascending or descending stairs, (ii) pain when sitting more than an hour, (iii) pain when giving force to the front thigh, or (iv) pain by pressing the patella while sitting with leg stretched.

After a 10-min warm-up on a stationary bike, the baseline values were assessed. Blood lactate level was recorded using lactate test strips. Maximal voluntary isometric contraction (MVIC) along with burst superimposition (with a 90-s resting interval) was performed on an isokinetic dynamometer.

The first set of isokinetic exercise (continuous knee extension at 60˚/s) was performed. Exercise was stopped when the three consecutive extension torques were below half of the MVIC value recorded at baseline. Immediate after the first set, blood lactate and quadriceps strength were recorded. The second through fifth set of measurements were performed in the same manner.

Quadriceps strength values were normalised by body weight (Nm/kg). Quadriceps activation was calculated by dividing the torque value of the MVIC by the torque produced by the burst superimposition. Isokinetic torques were normalised by body weight and time (Nm/kg/s).

To test condition effect over time, a mixed model ANCOVA (baseline values as covariates) and Tukey-Kramer post-hoc tests were performed for each dependent variables (SAS 9.4; $p<0.05$). Between-condition effect sizes (ES) were also calculated.

RESULTS AND DISCUSSION

Blood lactate levels for both conditions gradually improved over exercise sets (time main effect: $F_{4,156}=21.05$, $p<0.0001$; Figure 1-A). The healthy controls were slightly higher than AKP patients at every time point (ES ranged between 0.46 to 0.75). We believe that healthy controls produced higher isokinetic forces over time resulted in higher level in blood lactate [3].

At baseline, AKP patients produced less strength as compared to the healthy controls (ES: 0.71; Figure 1-B), which is consistent with previous observations [1,4]. Strength reduction rate over time for both

conditions were nearly identical (interaction: $F_{4,156}$=1.61, p=0.17), indicating that AKP patients have no further weakness in response to the exercise.

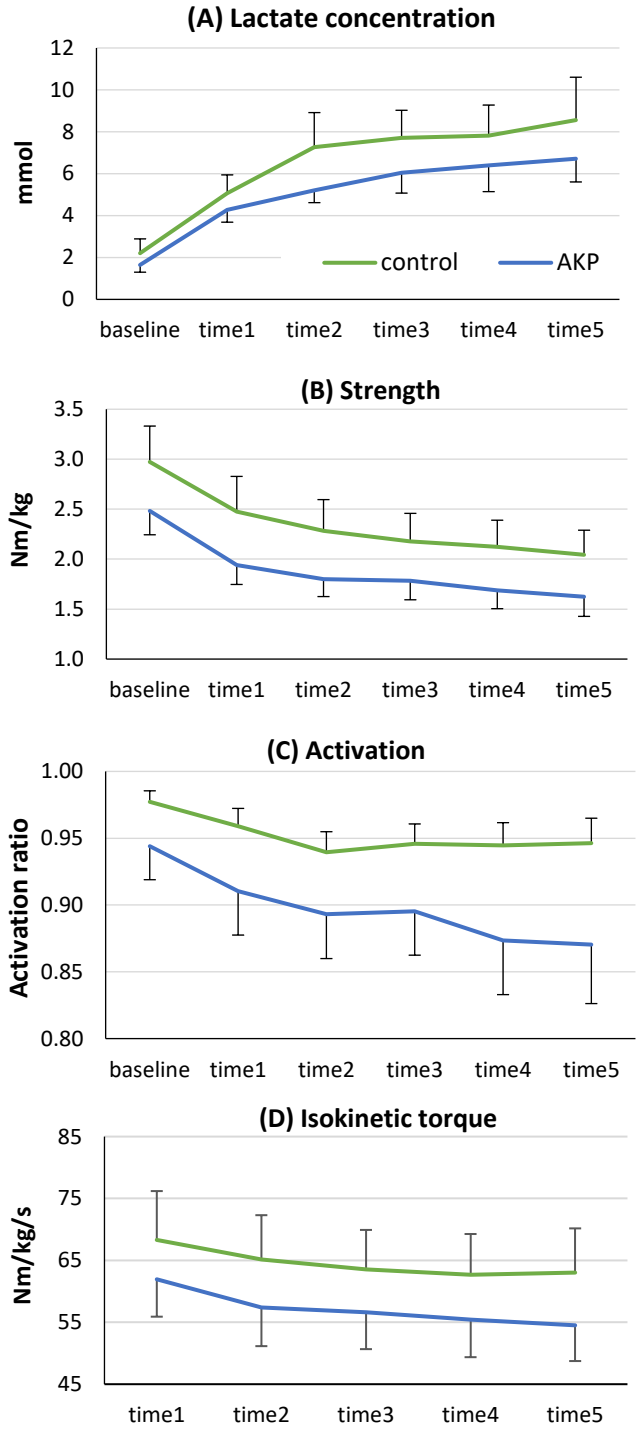

Figure 1: Changes in lactate concentration (A), strength (B), activation (C), and isokinetic torque (D). Error bars represent 95% CIs.

At baseline, the AKP patients had relatively less quadriceps activation (0.94) compared to the healthy control (0.98; ES: 0.75). Although 0.95 is considered normal, these results support previous reports [5]. While the control subjects maintained activation, the AKP patients showed further reduction throughout the exercise bout (Figure 1-C; ES at time 5: 0.95; interaction: $F_{4,156}$=2.01, p=0.10).

Isokinetic torques for both conditions were also parallel (interaction: $F_{4,156}$=0.34, p=0.85)—From baseline through time 5, the AKP patients had less endurance capacity (ES ranged between 0.40 to 0.57). There was no further reduction in patients with AKP.

For the healthy controls, strength and isokinetic torque values were dropped while activation was maintained. This could be interpreted as peripheral fatigue. For the AKP patients, all variables were decreased. Interestingly, the reduction rate of activation is not linearly related to quadriceps strength or endurance.

CONCLUSIONS

We observed trends that quadriceps strength and activation in patients with AKP were lower than the healthy matched controls. Muscular endurance in patients with AKP appears to be inhibited as compared with the healthy matched controls. Both AKP patients and healthy controls similarly responded to one bout of intentional exercise.

REFERENCES

1. Guney et al. *The Knee*. **23**, 610-615, 2016.
2. Park et al. *Clin J Sport Med*. **23**, 19-24, 2013.
3. Ishii et al. *J Phys Ther Sci*. ***25***, 1637-1642, 2013.
4. Callaghan et al. *Br J Sports Med*. **38**, 295-299, 2004.
5. Ingram et al. *Muscle & Nerve*. **53**, 280-286, 2016.

ACKNOWLEDGEMENTS

This work was supported by the Ministry of Education of the Republic of Korea and the National Research Foundation of Korea (NRF-2017S1A5A8022854

EFFECT OF MENISCECTOMIES ON ACL STRAIN: A DYNAMIC FINITE ELEMENT STUDY

[1]S Sadeqi, [1]RK Summers, [1]DU Erbulut, [2]TE Hewett, [1]VK Goel

[1] Engineering Center for Orthopaedic Research Excellence, Toledo, OH, USA
[2] Mayo Clinic Biomechanics Laboratory & Sports Medicine Center, Rochester, MN, USA
email: ssadeqi@rockets.utoledo.edu

INTRODUCTION

The Menisci play an important role in knee joint function, shock absorption, lubrication and load transition. Also, the anterior cruciate ligament (ACL) and menisci are significant in maintenance of knee stability[1, 2]. Meniscal injuries are often concomitant with ACL injuries, or activities that can lead to ACL injury. Knee meniscectomy is an old and yet common treatment for meniscal injuries.[3] Therefore, the purpose of this study was to simulate impact loading using dynamic finite element models of the knee joint with intact menisci, medial and lateral meniscectomy, and fully removed menisci to investigate the contribution of the menisci to ACL strains.

METHODS

Three finite element models of the human knee joint were reconstructed from MR images of two 23 year old healthy male subjects (models no.1&3) and one 23 year old healthy female subject (model no.2). Each model included all boney structures and soft tissues segmented in Mimics (Materialise, Leuven, Belgium), smoothed in Geomagic Studio (3D Systems, Rock Hill, South Carolina), and then meshed utilizing Hypermesh (Altair, MI, USA). The resulting C3D4 elements were then imported into Abaqus[4] 6.14-5 (SIMULIA, Providence, RI, USA) where cruciate and collateral ligaments were modeled as Holzapfel-Gasser-Ogden materials for the hyperelastic part and a time-based Prony series was used to model viscoelasticity. Bones and cartilages were modeled as Hookean materials. The menisci were modeled as transversely isotropic structures. Remaining capsules, muscles, tendons, and remaining ligaments were modeled as uniaxial, incompressible connector elements. Surface contacts were defined between all cartilage and meniscal surfaces. Simulations were done at 25° of knee flexion with muscle forces (441 N quadriceps and 441 N hamstrings). Multi-axial loads (Table 1), followed by an impact load of half-body weight, were applied to simulate bipedal landing from a jump from a height of 30 cm. To simulate the meniscectomy cases, the lateral meniscus, medial meniscus or both menisci were removed from the model (Figure 1).

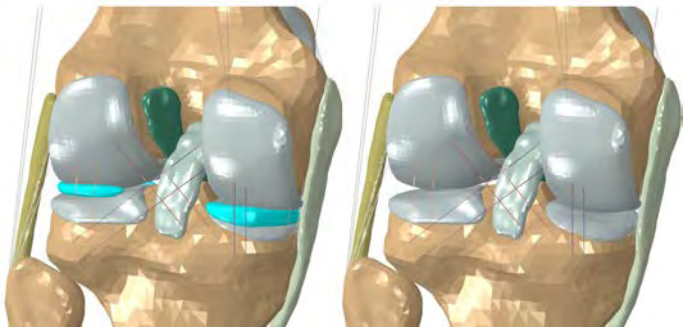

Figure 1: Finite element model of the knee. Left: including menisci (in blue), right: menisci removed.

Table 1. Simulated loads used to study impact of meniscectomies on ACL strains under dynamic loading conditions

Load Case No.	Knee Abduction Moment (Nm)	Anterior Shear Force (N)	Internal Tibial Rotation Moment (Nm)	Impact force (N)
1	26.76	80.35	18.62	0.5*BW
2	57.34	64.13	9.73	0.5*BW
3	13.54	196.13	9.73	0.5*BW

RESULTS AND DISCUSSION

ACL strain did not change significantly after removing the lateral meniscus, medial meniscus or both the menisci, showing only a small increase in 24 out of the 27 analyzed cases. Table 2 depicts the ratio of ACL strain after meniscectomy to the intact case for each model under the selected loading case.

Model no.3 showed a decrease in ACL strain after removing the lateral meniscus in all load cases, model 1 also showed a decrease in just one load case after removing the medial meniscus, while model 2 (female) showed increased strain for all cases.

Contact pressure increased up to 5% in cases without menisci, and this finding may also be indicative of more joint compression due to the removal of menisci from the joint space. Since ligaments do not take compression, a decrease, or no change, in the strain measured would be expected.

CONCLUSIONS

Although menisci are known contributors to knee stability, their presence does not appear to have significant influence on ACL strain. It is known that meniscectomy expedites knee degeneration. However, if it doesn't increase ACL strain, there are alternate scenarios on its ACL loading effects. The degeneration primary cause may be pressure and contact areas in this case. An alternative hypothesis is that the knee joint may be under-constrained and not experience sufficient contact throughout the range of motion. In our current models, kinematics (anterior tibial translation, knee valgus and internal tibial rotation) increased after removal of the menisci which should lead to increased strain; however, joint compression also increased, which increased the contact pressure on the cartilages and increased laxity in the ACL. This can lead to a decrease in the strain that develops throughout the ligament, even under higher loads known to lead to increased risk of non-contact ACL injury. Furthermore, this can help identify some of the pathomechanics that may lead to increased risk of post-traumatic osteoarthritis commonly seen in the ACL deficient population.

Future work will include utilization of three more models (two females, and one male) and a more robust set of loading conditions to further elucidate the impact of menisci on the ACL strains and joint contact pressures.

REFERENCES

1. Salata et al. Am J Sports Med. 38(9):1907-1916, 2010
2. Shelbourne et al. Am J Sports Med. 28(4):446-452, 2000
3. Englund et al, Rheumatology. 40(6):631-639, 2001
4. Ohio Supercomputer Center. 1987. Ohio Supercomputer Center. Columbus OH: Ohio Supercomputer Center. http://osc.edu/ark:/19495/f5s1ph73.

ACKNOWLEDGEMENTS

Study supported in part by NIH (R01 AR056259-06-TEH).

Table 2. Ratio of ACL strain after meniscectomy to the intact case. (WOLM: lateral meniscus removed. WOMM: medial meniscus removed. WOmenisci: both menisci removed. (m): male, (f): female)

	Model	WOLM	WOMM	WOmenisci
Load case 1	No.1 (m)	1.001	1.004	1.002
	No. 2 (f)	1.057	1.053	1.100
	No. 3 (m)	0.909	1.013	1.028
Load case 2	No.1 (m)	1.030	0.982	1.012
	No. 2 (f)	1.036	1.022	1.062
	No. 3 (m)	0.8	1.034	1.132
Load case 3	No.1 (m)	1.012	1.005	1.013
	No. 2 (f)	1.068	1.027	1.107
	No. 3 (m)	0.828	1.315	1.022

Initiation and Propagation of Microcracks in Collagen Networks of Cartilage

[1] Stephany Santos, [2] Nancy Emery, [2] Corey P. Neu, and [1] David M. Pierce

[1] University of Connecticut, CT, USA
[2] University of Colorado Boulder, CO, USA
email: dmpierce@engr.uconn.edu, web: http://im.engr.uconn.edu

INTRODUCTION

Articular cartilage is a heterogeneous tissue comprised of interstitial fluid, electrolytes, collagen fibers, proteoglycans, and chondrocytes. The tissue's impressive responses to mechanical loading depend on interactions among these constituents. The variation in orientation and distribution of the network of collagen fibers strongly contributes to the mechanical function of healthy cartilage. Near the articular surface, collagen fibers align parallel to the surface, with their local principal orientation characterized by the split-line direction (SLD).

In previous studies, we probed mechanical damage to the network of collagen by imaging the second harmonic generation (SHG) via confocal microscopy, and observed micron-scale cracks in the collagen network resulting from low-energy impacts [1, 2]. We defined microcracks as micron-scale cracks in the network of collagen with a width less than that of the lacunae (~30 μm). Using SHG, we also screened cartilage from total knee arthroplasties (TKAs) and found microcracks in human cartilage with very early-stage osteoarthritis.

In this study, we investigate the extent to which microcracks propagate during cyclic, mechanical loading which mimics walking. We initiated microcracks in the collagen network using single low-energy mechanical impacts, and tracked the propagation of microcracks after cyclic compression mimicking 12,000 steps. Using SHG microscopy we measured crack density after impact and after cyclic loading (relative to the pristine state), and quantified changes in crack morphology (length, width, and depth) and orientation.

METHODS

Sample Preparation. We extracted cylindrical cartilage-bone explants (3 mm Ø, full thickness) from load-bearing regions within the condyles of five skeletally mature bovine joints (18-30 months old) and marked the local SLD. We removed most of the subchondral bone while ensuring the bottom surface was visibly parallel to the articular surface, and measured the thickness of cartilage.

Mechanical Loading. We separated specimens from the lateral and medial femoral condyles, and assigned specimens to three different impact groups (no impact-*I0*, low impact-*IL*, high impact-*IH*), and to three different cyclic loading groups (no cyclic compression-*C0*, low cyclic compression-*CL*, high cyclic compression-*CH*). We tested all possible combinations per condyle. We performed impact tests using a custom drop-tower, with impact energy density as the independent variable. We selected *IL* = 1.5-2.5 mJ/mm^3 and *IH* = 2.6-4.0 mJ/mm^3 based on our previous results [2]. We performed unconfined cyclic compression tests using an LM1 Electroforce linear motor (Bose). We selected *CL*= 10% compression and *CH* = 15%. Cartilage deforms between 6% and 23% during walking [3, 4]; thus, we selected interval values of 10% and 15% of overall compressive thickness.

Imaging. We performed SHG imaging (Zeiss LSM 510, Nikon FN1) for three separate experimental phases (pristine-*P*, post-impact-*PI*, and post-cyclic compression-*PC*), cf. Fig. 1.

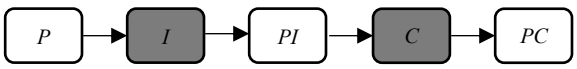

Figure 1: Experimental protocol with imaging (white boxes) and mechanical (gray boxes) experiments. *P*: Pristine, *I*: Impact, *PI*: Post-impact, *C*: Cyclic load, *PC*: Post-cyclic load.

We mounted specimens on a platen using cyanoacrylate adhesive and submerged the specimen in Phosphate Buffered Saline (PBS, pH~7.4) during imaging. We acquired tiled grids covering the full surface area for *P*, *PI*, and *PC*, and acquired axial *z*-stacks from the surface to 200 μm

deep with a 2.5 μm slice increment for *PI* and *PC*, only for central frames that were at least 1 mm from the specimen edge to avoid edge effects.

Data Processing. We measured the area density of cracks, as well as the crack lengths, widths, depths, and angles (relative to SLD) using Fiji image processing software, both *PI* and *PC*. In addition, from our mechanical tests we calculated the input impact energy density, the first P-K stress both *PI* and *PC*, and the specimen's compaction *PC*.

Statistical Analyses. We applied a mixed model ANOVA (SAS Institute, Inc.) with condyle, impact, and cyclic load as fixed main effects, and all possible interactions, with a significance level $p<0.05$. We also included phase (*P*, *PI*, or *PC*) as a fixed effect; phase × condyle, phase × impact, and phase × cyclic × load interactions; thickness as a covariate; and animal as a random effect.

RESULTS AND DISCUSSION

We completed a total of 48 impact tests and 72 cyclic tests using 76 samples from five skeletally mature bovine joints. We analyzed 76 area maps and 1368 image stacks totaling ~47,000 individual images. We show representative images in Fig. 2.

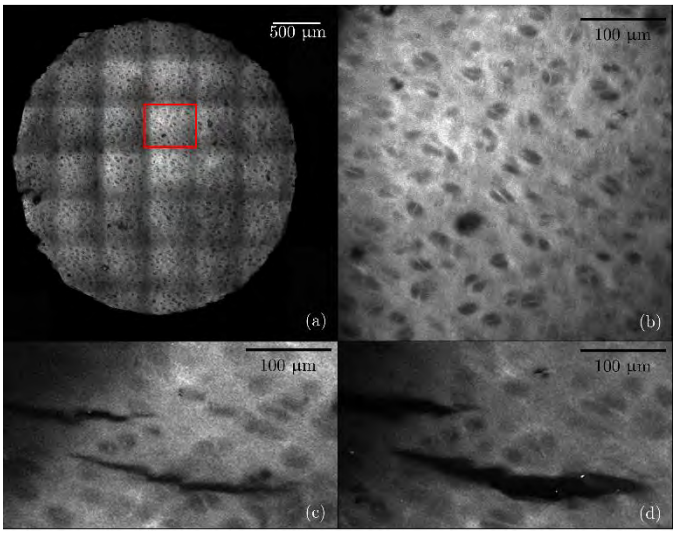

Figure 2: Representative initiation and propagation of microcracks in the collagen network of cartilage: (a) complete area map near the surface of a pristine specimen; (b) zoomed view of boxed red region showing no cracks prior to impact; (c) microcracks initiated after a single impact of 3.5 mJ/mm^3; and (d) the same microcracks propagate after 12,000 cycles of unconfined compression at 15% strain.

In both condyles we found significant differences in crack density for low vs. high cyclic compression after low, but not high, impact. Crack density was substantially greater for low impact followed by low vs. high cyclic loading ($p<0.003$). We found mean crack length was also greater under low vs. high cyclic loading ($p<0.05$), yet no difference in cracks formed under low vs. high single impacts ($p=0.14$).

Relative to impact only, impact plus cyclic loading resulted in a statistically significant increase in mean crack width ($p<0.05$) and no statistically significant differences in density ($p=0.47$), mean crack length ($p=0.76$), depth ($p=0.66$), or orientation ($p=0.90$). High impact resulted in larger mean crack depth at low vs. high cyclic loading $p<0.06$), and low impact resulted in larger mean crack depth at high vs. low cyclic loading ($p<0.005$). We also found mean crack angles formed via low impacts were ~40° from the SLD, while mean crack angles formed via high impacts were roughly perpendicular to the SLD.

Inter-condyle differences emerged in mean crack width, depth, and orientation. We found the largest mean crack width in the medial condyle after low impact and high cyclic loading vs. any other combination.

CONCLUSIONS

Microcracks propagate by increasing in width, as opposed to length or depth. Our results show key differences in the lateral and medial condyle, as well as significant differences in crack initiation and propagation behaviors under diverse loading conditions. Specifically, the effect of cyclic loading depends on prior impact loading.

REFERENCES

1. Kaplan+, *J Mech Behav Biomed Mat* **65**, 2017.
2. Kaleem+, *Osteoarthr Cartil* **25**(4), 2017.
3. Liu+, *J Biomech* **43**(4), 2010.
4. Harkey+, *Osteoarth Cartil* **25**(6), 2017.

ACKNOWLEDGEMENTS

NSF CAREER 1653358. Undergraduate students V. Blair, J. Clum-Russell, L. Contenta, J. Grosso, Z. Hall, H. Kackley, E. Miller, E. Loret de Mola, K. Morozov, B. Samolyk, P. Woods.

EFFECT OF FILTER CUTOFF ON IMPACT SIMULATOR DATA: ARTEFACT OR ARTEFICTION

Nathan D. Schilaty, Nathaniel A. Bates, Christopher V. Nagelli, Aaron J. Krych, and Timothy E. Hewett

Mayo Clinic Biomechanics Laboratories & Sports Medicine Center, Rochester & Minneapolis, MN, USA
Email: schilaty.nathan@mayo.edu

INTRODUCTION

Our mechanical impact simulator is unique in that it evaluates ligament strain and knee kinetics during multiplanar, dynamic simulations of ground contact when landing from a drop vertical jump (DVJ) as would occur *in vivo*. Invariably, these simulations are subject to high-frequency noise due to dynamic artefacts and vibrations that occur during foot-to-ground contact [1]. For this reason, the data are low-pass filtered to remove high-frequency noise prior to calculation of joint moments. In an environment of high impulse and rapid variation (such as with jump landing), data filtering is a balance between elimination of noise and truncation of the true signal for analysis.

The purpose of the current investigation was to determine the effects of different low cut-off frequencies (12 and 60 Hz) on knee kinetics and ligament strain of data reporting. We hypothesized that 60 Hz filtered data would be larger in magnitude, but correlate with 12 Hz filtered data. This information is important to understand the relevancy and validity of reported values from ground simulated impact simulators.

METHODS

A custom-designed cadaveric impactor was utilized to simulate athletic drop landings in 45 lower extremities specimens (22M:23F; ages 24-52). Exclusion criteria: 1) evidence of significant trauma/surgery to lower extremity and 2) evidence of chemotherapy ≥4 weeks as these would alter tissue biomechanics. Specimens were prepared according to previously outlined specifications [2].

In vivo kinetics/kinematics of 67 healthy athletic subjects were measured and categorized for application to cadaveric knees with three degrees of knee forces/moments [i.e. knee abduction moment (KAM), anterior tibial shear (ATS), and internal tibial rotation (ITR)]. Pneumatic cylinders applied designated knee forces/moments at the tibia, as determined from *in vivo* subjects (**Table 1**), and then a gravity-driven drop sled of 0.5 body weight (34 kg) was released from a height of 31 cm with quadriceps and hamstrings co-contracted at a 1:1 ratio. Knee flexion angle was set at 25°. Two DVRT strain gauges were implanted into the midsubstance of the medial collateral ligament (MCL) and anteromedial bundle of the anterior cruciate ligament (ACL), respectively, to measure ligament strains. Single- and 6-axis load cells measured ground reaction force and knee joint kinetics. Six specimens were excluded for unsuitable tissue quality or complications from the experimental protocol. 39 specimens remained for analysis (19M:20F). Specimen kinetic and ligament strain data was post-processed in a custom-built LabVIEW program to apply 60 or 12 Hz low-pass 4th order Butterworth filter to the data.

Table 1: KAM, ATS, and ITR load magnitudes based on *in vivo* population percentage.

Population Percentage	KAM (Nm)	ATS (N)	ITR (Nm)
0%	1.7	47	1.0
33%	13.5	64	9.7
67%	26.8	80	18.6
100%	57.3	196	53.7

Statistical analyses were performed with JMP 13 (SAS Institute Inc., Cary, NC) with utilization of matched pairs t-test and pairwise correlations.

RESULTS AND DISCUSSION

Baseline trials with no external knee loads applied exhibited significant differences in knee kinetics between 60 vs 12 Hz low-pass filters. Output values increased with 60 Hz data vs 12 Hz data (p<0.05, **Table 2**). However, even with significantly higher values for 60 Hz data, each of the kinetics also had a high degree of correlation

($p \leq 0.0004$) with the lowest correlation coefficient at 0.58 for Fy (lateral/medial translation; **Table 2**). As the baseline trial has no pre-defined directionality, it is likely that the limb could respond in multiple directions due to chance. However, the correlation of data remained valid.

For knee kinetics under the 'Pre-Failure' trial (referencing failure of the ACL), there was more variability along certain axes. Each of the kinetic variables were significantly higher with the 60 Hz data compared to the 12 Hz data. However, even with significantly larger magnitudes, each of the kinetics maintained a high degree of correlation ($p<0.0001$) with the lowest correlation coefficient at 0.79 for Fy (lateral/medial translation; **Table 3**).

Peak ACL strain during the 'Pre-Rupture' trial demonstrated a mean difference (60 Hz – 12 Hz) of 0.5% with 60 Hz significantly higher than 12 Hz ($p=0.035$). However, for peak ACL strain, the pairwise correlation coefficient of 60 Hz vs 12 Hz low-pass filter cutoff was 0.98 (0.96, 0.99) with $p<0.0001$. This correlation demonstrated that although the magnitude of the signal may vary with filter frequency, the data point relationships maintain a high degree of resemblance.

MCL maximum strain during the 'Pre-Rupture' trial demonstrated no mean difference of strain (0.0%; 60 Hz – 12 Hz; $p=0.105$). For MCL maximum strain, the pairwise correlation coefficient of 60 Hz vs 12 Hz low-pass filter cutoff is 0.99 (0.99, 1.00) with $p<0.0001$. This correlation demonstrated a near perfect data representation order for the data points of MCL data filtering.

CONCLUSIONS

These results demonstrate that there are significant differences between absolute data values after application of 60 and 12 Hz low-pass filter cutoff frequencies during impactor simulations across varied trial setups. Although values' magnitudes differed between these filter cutoffs, the data remained relative and highly correlated. Values reported at 60 or 12 Hz low-pass cut-off were both valid and reliable to one another.

REFERENCES

1. Roewer BD, et al. *Br J Sports Med*. 48(6):464-468, 2014.
2. Bates NA, et al. *Clin Bio*. 44:36-44, 2017.

ACKNOWLEDGEMENTS

NIH funding include: K12HD065987 and L30AR070273 to NDS, T32AR056950 to CVN, and R01AR055563 and R01AR056259 to TEH.

Table 2: Pairwise correlation values for kinetic variables comparing 60 to 12 Hz low-pass filter cutoff at baseline (no external loads). 95% confidence intervals are provided for the pairwise correlations in parentheses.

	Fx (ant./post.)	Fy (lat./med.)	Fz (dist./comp.)	Mx (int./ext.)	My (flex./ext.)	Mz (Abd./Add.)
Mean Diff.	400.0	194.3	88.9	76.6	71.2	151.6
***p*-value**	**<0.0001**	**<0.0001**	**<0.0001**	**<0.0001**	**<0.0001**	**<0.0001**
Pairwise Correlation	0.91 (0.83, 0.96)	0.58 (0.30, 0.77)	0.70 (0.47, 0.84)	0.91 (0.82, 0.95)	0.95 (0.90, 0.97)	0.64 (0.38, 0.81)
***p*-value**	**<0.0001**	**0.0004**	**<0.0001**	**<0.0001**	**<0.0001**	**<0.0001**

Table 3: Pairwise correlation values for kinetic variables comparing 60 to 12 Hz low-pass filter cutoff at 'Pre-Failure.' 95% confidence intervals are provided for the pairwise correlations in parentheses.

	Fx (ant./post.)	Fy (lat./med.)	Fz (dist./comp.)	Mx (int./ext.)	My (flex./ext.)	Mz (Abd./Add.)
Mean Diff.	339.4	140.8	60.2	58.8	50.6	116.3
***p*-value**	**<0.0001**	**<0.0001**	**<0.0001**	**<0.0001**	**<0.0001**	**<0.0001**
Pairwise Correlation	0.96 (0.92, 0.98)	0.79 (0.62, 0.88)	0.91 (0.84, 0.95)	0.88 (0.78, 0.94)	0.96 (0.93, 0.98)	0.86 (0.75, 0.93)
***p*-value**	**<0.0001**	**<0.0001**	**<0.0001**	**<0.0001**	**<0.0001**	**<0.0001**

MEDIAL COLLATERAL LIGAMENT STRAIN CHARACTERISTICS AT ANTERIOR CRUCIATE LIGAMENT FAILURE

Nathan D. Schilaty, Nathaniel A. Bates, Christopher V. Nagelli, Aaron J. Krych, and Timothy E. Hewett

Mayo Clinic Biomechanics Laboratories & Sports Medicine Center, Rochester & Minneapolis, MN, USA
Email: schilaty.nathan@mayo.edu

INTRODUCTION

Both the anterior cruciate ligament (ACL) and medial collateral ligament (MCL) bear loads along with musculature during athletic tasks of landing, cutting, pivoting, and twisting. The ACL is the primary restraint to anterior translation of the tibia with respect to the femur; the MCL is the main restraint of valgus movement (i.e. tibial abduction with respect to the femur) [1]. ACL injury is generally non-contact in nature, with estimates for the non-contact mechanism accounting for approximately 75% of all ACL injuries [2]. This injury mechanism indicates that ACL tears are likely influenced by deficits in neuromuscular control and risky movement strategies that include dynamic knee abduction (valgus), hip adduction, and internal rotation of the tibia and hip. Strong biomechanical and epidemiological evidence supports knee valgus as a primary mechanism of ACL injuries during landing tasks, yet controversy and debate continue as the MCL is the likely candidate for restraint of knee valgus (abduction). However, concomitant MCL injury occurs in a minority of ACL injuries (30-40%) [1].

Consequently, this study was designed to investigate the loading of the MCL that occurs with the presence of ACL failure during valgus collapse. The hypothesis tested was that cadaveric specimens would demonstrate a significant increase in MCL strain upon failure of the ACL at 25° knee flexion.

METHODS

A custom-designed mechanical impact simulator was utilized to simulate athletic drop landings in 45 cadaveric lower extremity specimens (22M:23F; ages 24-52). Exclusion criteria: 1) evidence of significant trauma/surgery to lower extremity and 2) evidence of chemotherapy ≥4 weeks as these both significantly alter tissue biomechanics. Specimens were prepared according to previously outlined specifications [3].

In vivo kinetics/kinematics of 67 healthy athletic subjects were measured to determine tertiles of injury risk (i.e. low, medium, and high) in three degrees of knee forces/moments [i.e. knee abduction moment (KAM), anterior tibial shear (ATS), and internal tibial rotation (ITR); each condition was designated as a percentage of loading KAM_ATS_ITR (e.g. 00_33_33)]. Pneumatic cylinders applied the designated knee forces/moments at the tibia determined from the *in vivo* subjects (**Table 1**) and then a gravity-driven drop sled of 0.5 body weight (34 kg) was released from a height of 31 cm with quadriceps and hamstrings co-contracted with a 1:1 ratio. Knee flexion angle was set at 25°. Two differential variable reluctance transducers (DVRTs) were implanted into the MCL midsubstance and anteromedial bundle of the ACL, respectively, to measure ligament strains during landing simulations with increasing magnitudes of knee abduction. Six specimens were excluded for unsuitable tissue quality or complications from the experimental protocol. 39 specimens remained for analysis (19M:20F). All concomitant MCL injuries were removed from the analysis to accurately depict intact MCL strain with ACL failure.

Table 1: KAM, ATS, and ITR load magnitudes based on *in vivo* population percentage.

Population Percentage	KAM (Nm)	ATS (N)	ITR (Nm)
0%	1.7	47	1.0
33%	13.5	64	9.7
67%	26.8	80	18.6
100%	57.3	196	53.7

Statistical analyses were performed with JMP 13 (SAS Institute Inc., Cary, NC) with utilization of

one-way ANOVA, matched pairs t-test, and Fisher's Exact Test.

RESULTS AND DISCUSSION

Specimen demographics were not significantly different between sexes for age, but there are significant differences in mass and height (**Table 2**). As ligament strain is a percentage calculated by displacement over initial length,

$$strain\ (\%) = \frac{displacement}{initial\ length} * 100$$

male vs female normalization was not possible.

Table 2: Summary Statistics by Sex.

	Males	Females	*p*-value
Age (yrs)	43.1 ± 7.7	40.0 ± 9.0	0.249
Mass (kg)	95.4 ± 19.3	76.5 ± 27.8	**0.019**
Height (cm)	181.7 ± 5.4	165.4 ± 7.5	**<0.001**

One-way ANOVA demonstrated significance of MCL strain in the 'ACL Failure' condition ($F_{4,119}$=3.812, p=0.006). Tukey *post-hoc* analysis demonstrated significance of MCL strain during the 'ACL Failure' condition vs 00_33_33 and 33_33_33 loading conditions (**Fig. 1**). During the control condition of no external loading (00_33_33), the mean MCL strain was 2.2 (1.1, 3.4). With the 33_33_33 condition, mean MCL strain was 2.5 (1.3, 3.7). With the 67_33_33 condition, mean MCL strain was 3.6 (2.0, 5.2). With the 100_33_33 condition, mean MCL strain was 4.3 (2.3, 6.3). In the 'ACL Failure' condition, mean MCL strain was 6.1 (3.7, 8.5).

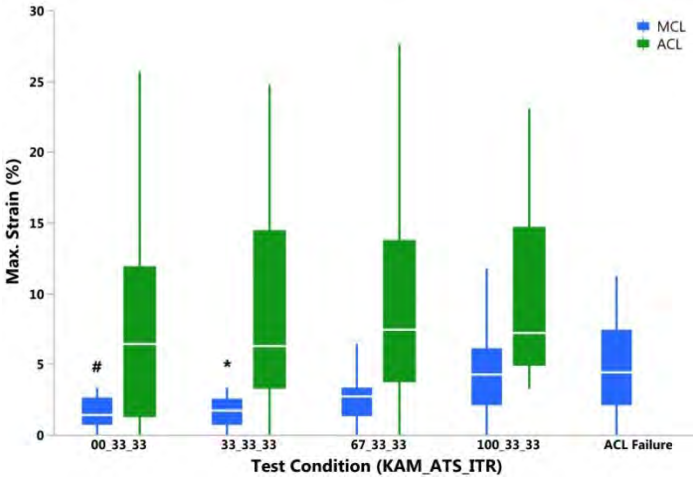

Figure 1. Maximum MCL and ACL Strain by Test Condition. Any concomitant MCL failures were removed for this analysis. (# denotes p=0.008 and * denotes p=0.014 compared to 'ACL Failure').

Matched pairs analysis compared ACL strain to MCL strain across all conditions by sex. Each condition yielded significantly higher values of ACL strain relative to MCL strain (p=0.001, p<0.001, p=0.001, and p=0.050 for 00_33_33, 33_33_33, 67_33_33, 100_33_33, respectively). In addition, females demonstrated higher strain differences between ACL and MCL (**Table 3**).

Table 3: Differences of strain (%; ACL-MCL) by sex and loading condition. Loading is designated as percentage KAM_ATS_ITR.

Loading Condition	Males	Females	*p*-value
00_33_33	3.4	8.1	**0.014**
33_33_33	3.9	8.7	**0.016**
67_33_33	4	7.6	**0.034**
100_33_33	4.1	9.8	0.351

CONCLUSIONS

The hypothesis tested was not supported as MCL strain post ACL failure did not significantly increase compared to the high load conditions. The ACL bears more strain than the MCL at increasing amounts of knee abduction at 25° knee flexion. Females showed significantly higher ACL strain than MCL strain compared to males at similar load conditions, though males have longer levers (height) and higher forces (mass) that should induce higher strain on viscoelastic structures. These sex differences of ACL vs MCL strain should be evaluated further with future research.

REFERENCES

1. Quatman CE, et al. *Am J Sports Med*. 42(1):177-186, 2014.
2. Schilaty ND, et al. *Orthop J Sports Med*. 5(8):1-8, 2017.
3. Bates NA, et al. *Clin Bio*. 44:36-44, 2017.

ACKNOWLEDGEMENTS

NIH funding include: K12HD065987 and L30AR070273 to NDS, T32AR056950 to CVN, and R01AR055563 and R01AR056259 to TEH.

ANKLE KINEMATICS AND KINETICS ARE ALTERED WHEN ROUNDING A RAISED BASE

Lauren E. Schroeder and Joshua T. Weinhandl

The University of Tennessee, Knoxville, TN, USA
email: Lschroe1@vols.utk.edu

INTRODUCTION

Fast-pitch softball has increased in popularity, with 19,628 NCAA Division I female athletes participating in the 2014-15 season [1]. However, increased participation results in increased chance of injuries. Contacting a raised, fixed base is one of the most common tasks in softball, occurring in almost every play of the game. Unfortunately, this movement is a main injury mechanism, resulting in approximately 9% of game day injuries. Additionally, almost 44% of the injuries that occur when contacting a raised, fixed base are lateral ankle sprains [2].

Approximately 85% of injuries at the ankle-foot complex are lateral ankle sprains, making the lateral ankle ligament complex the most frequently structure in the body [3]. Two primary mechanisms have been identified that increase the risk of lateral ankle sprains: excessive inversion and plantarflexion angles [3] and an external inversion moment that is greater than the internal eversion moment [4]. These risk factors are increased during a poorly executed cutting movement with an abnormal foot placement, such as stepping on someone's foot or possibly stepping on a raised, fixed base [3].

To date, no study has examined ankle kinematics and kinetics while contacting a raised, fixed base or how a fixed base may influence injury risk during game play. Therefore, the aim of this study was to determine the effect of rounding a raised, fixed base on ankle kinematics and kinetics in softball players.

METHODS

Eight recreationally active females with high school playing experience (age: 21.1±1.9yrs; height: 1.71±0.04m; mass: 66.68±12.97kg) and eight recreationally active females with college playing experience (age: 21.5±2.3; height: 1.71±0.03m; mass: 71.36±7.16kg) participated. Participants were required to have a minimum of two years high school softball experience to ensure they were familiar with the base running technique. Participants completed two base running conditions. In the first condition, a sidecut simulating rounding first base was performed with no base (NB) present on the force plate. For the second condition, the same route was performed with a base (WB) present on the force plate. Participants were required to stay within a range of 60°-90° from the original direction of motion. Entrance and exit speeds were monitored at 4.0 m/s ± 0.25 m/s and 3.75 m/s ± 0.25 m/s, respectively. During each trial, right leg 3-D kinematics and kinetics were collected using a 12-camera Vicon motion capture system (200 Hz), and ground reaction forces (GRF) were collected with an AMTI force plate (2000 Hz).

Right-leg raw 3D marker coordinate and raw GRF data were both low-pass filtered using a 4th order, Butterworth filter (20 Hz). 3D ankle angles were calculated using a joint coordinate system. Internally applied, 3D joint kinetics were calculated using a Newton-Euler approach, projected on to the joint coordinate system, and normalized to body mass. Dependent variables included initial contact (IC) dorsiflexion angle, peak dorsiflexion angle, IC inversion angle, peak inversion angle, peak plantarflexion moment, and peak eversion moment.

Separate 2 × 2 repeated measures ANOVAs (base × experience) were performed for each of the dependent variables. Experience was the between-subjects factor, and base condition was the within-subjects factor. The alpha level was set at $p \leq 0.05$.

RESULTS AND DISCUSSION

This study analyzed ankle kinematics and kinetics during two base running conditions. There were no experience main effects. Regarding kinematics, the WB condition increased IC dorsiflexion angle ($F_{1,14} = 8.552$, $p = 0.011$, Table 1), while also decreasing IC inversion angle ($F_{1,14} = 39.666$, $p < 0.001$, Table 1) and peak inversion angle ($F_{1,14} = 180.024$, $p <$

0.001, Table 1). For kinetics, the WB condition decreased peak plantarflexion moment ($F_{1,14}$ = 38.424, $p < 0.001$, Table 1) and eversion moment ($F_{1,14}$ = 109.617, $p < 0.001$, Table 1).

Overall, the base decreased frontal plane ankle biomechanics, a main risk factor in lateral ankle sprains [3]. The base placed the foot in a more dorsiflexed position at initial contact, as well as limiting the frontal plane range of motion the ankle could move through. The decrease in inversion range of motion subsequently reduced the internal eversion moment experienced at the ankle throughout the stance phase of the movement. These results suggest that contacting a raised, fixed base does not increase the risk of a lateral ankle sprain.

Because only trials with proper foot placement were accepted for analysis, the base may have created a banked surface, which resulted in the decreased frontal plane range of motion. Additionally, this banked surface potentially shifts the center of pressure laterally, thus reducing the external inversion moment experienced at the ankle [4]. Wannop et al. [4] found that a banking angle of 10° during a sidecut movement significantly reduced the amount of ankle inversion. It is suggested that the ankle and the shank are better aligned during touchdown, causing the force vector to be oriented in a more favorable way that decreases lateral ankle injury risk [4].

The current study found that a fixed base, with a controlled foot placement, reduced ankle inversion angle throughout the stance phase and peak ankle eversion moments, both of which have been identified as risk factors for lateral ankle sprains. Certain game-day factors, such as an abnormal foot placement on the base (i.e. misfooting), playing surface, and footwear type (i.e. rubber or metal cleats), may possibly explain the incidence rate of lateral ankle sprains that occur in softball while contacting a fixed base.

CONCLUSIONS

These findings suggest that contacting a raised, fixed base with a controlled foot placement decreases the risk of lateral ankle sprain injuries. Abnormal foot placement or shoe type may provide further insight as to why lateral ankle sprain injuries when contacting a raise, fixed base are so common during softball game-play.

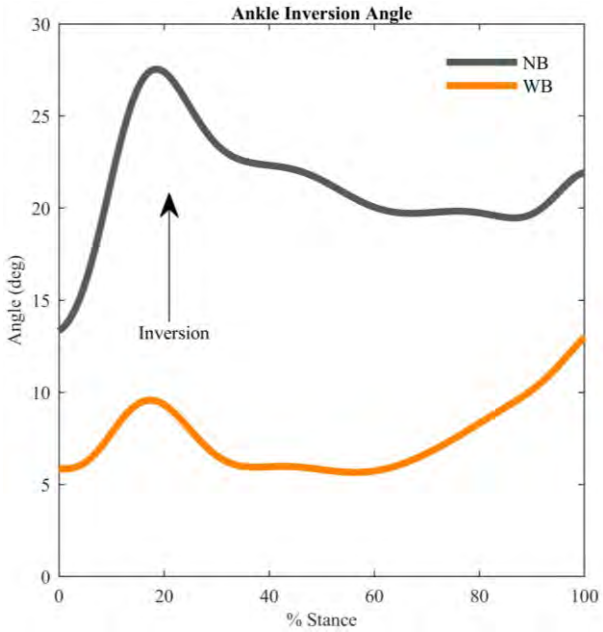

Figure 1: Ankle inversion angle of the NB and WB during 100% of the stance phase.

REFERENCES

1. *1981/82-2014/15 NCAA Sports Sponsorship and Participation Rates Report*. NCAA, 2015.
2. Marshall, S.W., et al. *J Athl Train* **42**:286-294. 2007.
3. Garrick, J.G. *Am J Sports Med* **5**:241-242. 1977.
4. Wannop, J.W., et al. *Hum Mov Sci* **33**:97-107. 2014.

Table 1. Mean ± SD ankle kinematic and kinetic variables of two base conditions and softball experience.

		No Base		Base		Int.	Base	Exp
		HS	College	HS	College	*p*	*p*	*p*
Ankle kinematics (°)	IC Dorsiflexion *	-3.8±11.8	-4.9±12.5	0.6±7.2	3.7±7.1	0.359	**0.011**	0.827
	IC Inversion *	12.1±7.6	14.6±7.1	6.0±4.2	5.7±3.5	0.252	**0.000**	0.701
	Peak Dorsiflexion	22.9±7.4	22.9±4.4	22.7±8.9	26.9±6.0	0.223	0.290	0.501
	Peak Inversion *	28.4±3.4	29.7±5.3	15.8±3.9	15.0±4.8	0.321	**0.000**	0.885
Ankle kinetics ($Nm \cdot kg^{-1}$)	Peak Eversion *	-0.47±0.17	-0.45±0.07	-0.25±0.15	-0.17±0.06	0.289	**0.000**	0.387
	Peak Plantarflexion *	-2.92±0.46	-2.97±0.33	-2.46±0.53	-2.59±0.30	0.555	**0.000**	0.667

* significant base effect ($p < 0.05$)

Material Properties of the Thigh: Body Position Matters

Justin Scott and Tamara Reid Bush
Michigan State University, East Lansing, MI, USA
email: scottju5@msu.edu, reidtama@egr.msu.edu

INTRODUCTION

When designing devices that interface with the human body, it is important to consider the loads that they exert on the body and the body's response. Since prolonged loading contributes to tissue breakdown, having accurate material property responses to compressive loads will lead to better interface designs for mobility devices, such as wheelchairs, where tissue breakdown is a significant issue [1].

Limited work has been conducted to determine the material properties of soft tissue in humans. Only a few studies have been able record *in vivo* force and deflections of soft tissue at the same time, however each study had significant limitations. For example, Affagard et. al were able to construct a force-deflection curve for a few individuals in one region of the body while the individuals were in the supine position [2]. While the supine position is an adequate analog for someone lying in bed, it does not reflect someone sitting in a chair. The goal of this study was to define material properties for multiple regions of soft tissue in multiple postures, so comparisons between postures and regions could be made.

METHODS

Eleven healthy, college-aged males (n=6) and females (n=5) consented to tissue deflection testing in three postures (IRB #15-889). A custom indenting tool was used to collect force and deflection data. The indenting surface was a 5 cm by 5 cm square attached to the top of a six axis load cell. And a linear potentiometer was attached to the load cell to measure deflection from a stationary reference. With the participant in one of the postures (i.e., seated, prone, crawling) we manually indented the soft tissue of the proximal thigh, using a constant loading rate, until a physiological resistance was felt, and the load was removed. This was repeated for the middle and distal thigh regions and for each posture. Force deflection curves resulted.

In the seated position, the participant sat on a chair with removable slats in order to give us access to the testing regions. In the crawling and prone position, the testing regions were not obstructed by any of the testing apparatus. All participants wore snug fitting, stretchy athletic pants; preliminary work was conducted to insure that the pants did not change the response in comparison to no clothing.

RESULTS AND DISCUSSION

Figure 1 a, b, and c presents the average force-deflection data curves for all participants. These data showed a consistent difference between the thigh tissue properties in the seated, crawling, and prone positions. The largest deflections were consistently seen in the crawling position for all three regions while the prone position had the least amount of deflection in the middle and distal thigh regions. The middle and distal thigh curves both indicated that the prone position had significantly stiffer (less deformation) thigh properties than the seated and crawling positions, producing less deflection given a comparable force.

Our work has shown that body posture plays a role in how thigh tissue responds under compressive loading. This suggests that posture should be taken into account when determining material properties of soft tissue. Further, when trying to design a device or develop a model of interface stresses for seated individuals, material properties derived from the seated position must be used..

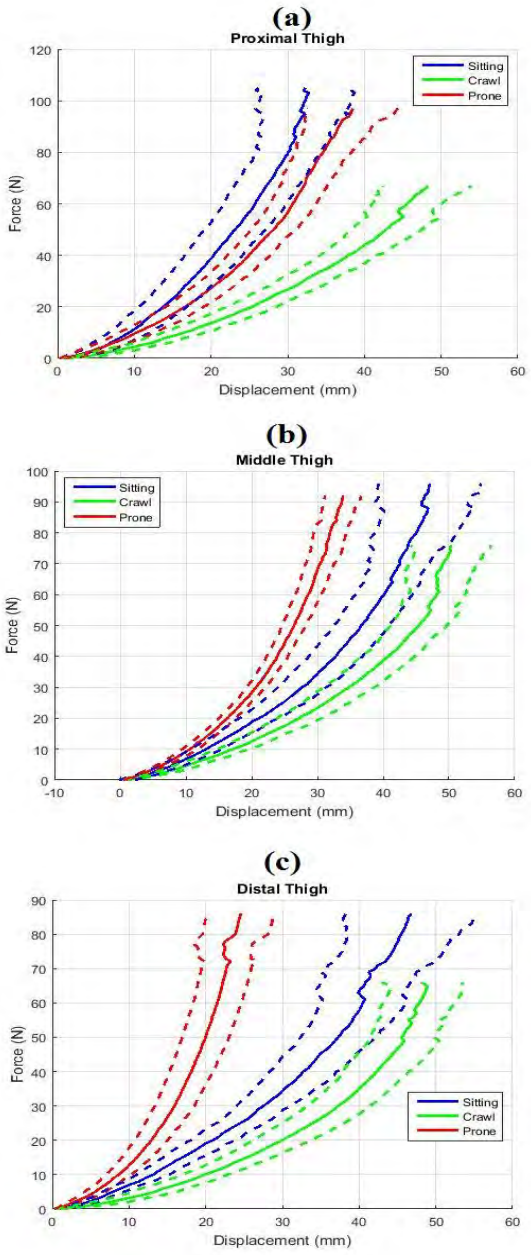

Figure 1. Force-Deflection Curves for the proximal thigh (a), middle thigh (b), and distal thigh (c) with 95% confidence intervals on the mean for a general population.

To that end, preliminary work has been conducted to fit these data to a non-linear elastic model using the Mooney-Rivlin strain energy function.

CONCLUSIONS

Today's mobility devices contribute to tissue breakdown, particularly in the buttocks and thigh regions of those who use them. Attempts to better design the surfaces with which the users interact are necessary; and for improved design, a knowledge of human body material properties is needed. In particular, understanding difference in the tissue properties based on the user's posture is imperative.

While all of our participants in this study were healthy, college-aged individuals, future work will include the measurement of tissue properties in individuals with disabilities, specifically those who use mobility devices in their everyday lives. Since the crawling position is a more accessible position and is used by physical therapists, this posture can be used to quantify the material properties. If consistent relations persist between the thigh tissue properties in the crawling position versus those in the seated position, then we can use the properties in the crawling position to estimate those while seated. This future work will allow us not only to improve mobility devices, but also understand if there are any differences in tissues between able bodied people and those with disabilities such as spinal cord injury.

REFERENCES

1. McKinley, WO et. al. *Archives of Physical Medicine and Rehabilitation* 80, 1999.
2. Affagard, J.-S. J. Biomechanical Engineering. 136, 2014.

ACKNOWLEDGEMENTS

This work is supported by NSF CBET, grant number 1603646.

RELIABILITY OF MOTOR VARIABILITY AMONG HEALTHY CONTROLS AND ATHLETES IN A SIDE-HOP TASK

[1] Sophia Ulman, [2] Charlotte Häger, and [1] Divya Srinivasan

[1] Department of Industrial and Systems Engineering, Virginia Tech, Blacksburg, VA, USA
[2] Department of Physiotherapy, Umeå University, Umeå, Sweden
email: smu4@vt.edu

INTRODUCTION

Motor variability (MV) is a fundamental feature of movement that refers to the variation observed when an individual completes the same task numerous times. While variability is natural in any human movement, there are still several unanswered questions about its actual functional significance, specifically in clinical, sports and training applications [1]. Although such questions on the functional significance of MV are being increasingly explored, the reliability of MV has been demonstrated only in a few simple tasks such as goal-directed movements and over ground walking [2, 3]. The reliability of MV in more challenging tasks such as the side-hop is currently unknown. Very few empirical studies, if any, have verified whether individuals within a homogeneous population with respect to gender, age, skill and health do, still, differ consistently in MV. Hence, the goal of this study was to determine the consistency of lower limb joint kinematic variability during side hops performed by a healthy control group and an age-matched athletic group.

METHODS

Thirteen healthy controls and twelve athletes (floor ball and soccer players) with no known history of musculoskeletal disorders or injuries were recruited. The testing session began with a 6-minute warm-up on a bicycle ergometer at moderate intensity. Then, the participant was asked to perform side hops on each leg. A side hop consisted of hopping on one foot laterally from a force plate, landing on a second force plate, and then hopping back to the starting medial force plate. If the participant put the opposite foot down or could not maintain balance for the entire jump, that hop was considered to be unsuccessful. Hops were performed until at least 5 successful hops were captured on each leg. Other hop and balances tests were conducted during the session, however, those were not considered for this study. Kinematics were collected using an 8-camera motion capture system (Qualysis INC, Gothenburg, Sweden), and passive reflective markers placed at select anatomical landmarks on the upper and lower limbs, pelvis, and head. Events used for analysis were determined using two force plates (Kistler, USA). These events identified two phases for investigation: (1) *Lateral take-off*, defined as beginning of data collection (when participant was asked to hop) to force signal registration < 20 N on the medial force plate, and (2) *Medial take-off*, defined as force signal registration > 20 N to < 20 N on the lateral force plate.

Marker data were exported into Visual 3D (C-motion Inc., USA) which was used for data processing. Hip, knee, and ankle joint angles in the sagittal and frontal planes were extracted for further analysis. Joint angle time series data were all time-normalized. Standard deviation of each joint angle trajectory was calculated as the root mean square of the standard deviation obtained at each normalized time point across all trials, during each phase. Additionally, inter-joint coordination was quantified through vector coding [4]: hip-knee and knee-ankle couples in the sagittal and frontal planes during each phase were computed, and the trial-to-trial SD of joint coupling angles were used to quantify coordination variability. A one-way random effects model with subjects as a random factor was resolved using ANOVA to partition the total variance in MV measures into between-subjects and between-days variance components. F tests were performed to determine whether the ratio of the between-subjects to within-subjects (i.e. between-days) variance component of each MV measure was significantly greater than 1. Alpha level was set at 0.05.

RESULTS AND DISCUSSION

Results (table 1) show that only specific joint trajectory and coordination variability measures are reliable, i.e. they show significant between-subjects differences within each group. In general, athletes seem to exhibit lower variability than controls in the sagittal plane and higher variability than controls in the frontal plane. Group differences in which variability measures are consistent suggest that athletes and controls seem to be utilizing different strategies for movement control in the take-off and landing phases.

CONCLUSIONS

Thus, documenting reliability of MV measures in specific tasks and populations seems to be a critical first step before designing or interpreting MV-related studies. Future research in clinical populations and sports applications must be cautious about comparing groups or studying the effects of specific interventions on MV, when using challenging tasks such as side-hops.

REFERENCES

1. Bartlett et al. *Sports Biomechanics.* 6, 2007.
2. Samani et al. *J Electromyogr Kinesiol.* 25, 2015.
3. Konig et al. *Gait & Posture.* 39, 615-617, 2014.
4. Heiderscheit et al. *J. Appl. Biomech.* 18, 2002.

ACKNOWLEDGEMENTS

We would like to acknowledge the contributions of Jonas Selling, Jonas Marklund, and Andrew Strong for their assistance with data collection and processing.

Table 1: Healthy control and Athlete groups (variables with significance shaded in gray)

Controls: Lateral Take-off	**Hip Sag SD**	**Knee Sag SD**	**Ankle Sag SD**	**Hip Front SD**	**Knee Front SD**	**Ankle Front SD**	**Hip-knee Sag SD**	**Knee-Ankle Sag SD**	**Hip-knee Front SD**	**Knee-Ankle Front SD**
Average SD across group (°)	**7.10**	**8.48**	**6.02**	3.42	2.44	3.82	**68.21**	**75.73**	81.26	93.90
Variance in SD across group (°)	**3.31**	**2.37**	**2.20**	0.89	0.58	0.77	**51.73**	**59.54**	46.14	33.12
Between subjects variance (°)	**1.60**	**1.30**	**1.67**	0.34	0.16	0.38	**28.48**	**41.29**	20.50	13.74
Within subjects variance (°)	**1.71**	**1.07**	**0.53**	0.55	0.42	0.39	**23.25**	**18.25**	25.64	19.38
ICC	**0.48**	**0.55**	**0.76**	0.38	0.28	0.50	**0.55**	**0.69**	0.44	0.41
Controls: Medial Take-off										
Average SD across group (°)	6.03	6.47	4.23	4.84	3.44	3.14	80.71	**80.09**	**85.68**	90.54
Variance in SD across group (°)	9.29	6.91	1.37	3.05	1.29	2.12	27.94	**62.93**	**31.10**	20.77
Between subjects variance (°)	0.80	0.44	0.00	0.38	0.10	0.70	11.47	**46.28**	**19.62**	7.16
Within subjects variance (°)	8.49	6.47	1.37	2.67	1.19	1.42	16.47	**16.65**	**11.84**	13.61
ICC	0.09	0.06	0.00	0.13	0.08	0.33	0.41	**0.74**	**0.62**	0.34
Athletes: Lateral Take-off										
Average SD across group (°)	5.56	7.38	4.08	2.75	**1.92**	2.98	67.55	75.74	81.04	92.61
Variance in SD across group (°)	1.72	2.50	1.16	0.73	**0.68**	1.31	110.87	107.33	51.29	55.51
Between subjects variance (°)	0.00	0.54	0.48	0.18	**0.56**	0.48	16.40	26.00	17.42	19.79
Within subjects variance (°)	1.72	1.96	0.68	0.55	**0.12**	0.83	94.47	81.33	33.87	35.72
ICC	0.00	0.22	0.41	0.25	**0.82**	0.37	0.15	0.24	0.34	0.36
Athletes: Medial Take-off										
Average SD across group (°)	3.82	4.10	3.30	**3.06**	**2.30**	**2.17**	80.23	**78.64**	86.08	89.55
Variance in SD across group (°)	1.18	1.12	0.61	**2.03**	**1.06**	**1.11**	6.65	**22.55**	28.29	21.21
Between subjects variance (°)	0.00	0.41	0.19	**1.57**	**0.76**	**0.83**	1.16	**19.72**	6.49	2.19
Within subjects variance (°)	1.18	0.71	0.42	**0.46**	**0.30**	**0.28**	5.49	**2.83**	21.80	19.02
ICC	0.00	0.37	0.31	**0.78**	**0.72**	**0.75**	0.17	**0.87**	0.23	0.10

INFLUENCE OF VIBRATION INTENSITY ON LOWER LIMB JOINT LOADING DURING STANDING

Margaret Underdahl & Feng Yang

Georgia State University, Atlanta, GA, USA
email: fyang@gsu.edu

INTRODUCTION

Controlled whole-body vibration (CWBV) training has been used as an alternative modality in rehabilitation sites, recreation centers, and clinical settings due to its inherent advantages, such as portability, safety, ease of operation, and low-cost [1, 2]. However, the current research of CWBV's effects has produced inconclusive results about the functional and neuromuscular improvements [3]. One of the possible contributors to such indecisive findings could be the inconsistent protocols used across studies. Various vibration protocols, leading to different vibration intensities, could account for the inconsistency of the current findings. Therefore, a systematic study is needed to examine how CWBV intensity affects the training outcomes.

During CWBV, joint loading could be used as an indicator of the stimulation level on the joints and their attached muscles. Thus, by examining how vibration intensity, determined by the combination of vibration frequency and amplitude, impacts the lower limb joint moments, additional insights could be gained into the efficacy of CWBV training. Whereas, no study has inspected this topic. It remains completely unknown how vibration intensity impacts joint loading. The primary purpose of this study was to quantify the effects of CWBV intensity in terms of vibration frequency and amplitude on the lower limb joint moments during stance among healthy young adults.

METHODS

Three healthy young adults (1 female and 2 male) participated in this study after providing written informed consent approved by the Institutional Review Board. The demographic information for these three participants were: age: 26.5 ± 2.53 years; body height: 1.74 ± 0.11 m; and body mass: 88.3 ± 5.9 kg.

In this study, all participants went through various vibration intensities that were dependent on the corresponding vibration frequency and amplitude. The frequency levels were 10, 20, and 30 Hz while the amplitudes were set at 1, 2, and 3 mm. Therefore, there were totally 9 experimental conditions (3 frequencies × 3 amplitudes) for each participant.

A side-alternating vibration platform (Galileo, German) was used in this study to generate the vibration. The platform oscillated around a horizontal sagittal axis, giving thrusts to the legs in an alternately upward and downward motion. During each condition, participants stood barefooted over clearly-marked positions on the platform. They were required to maintain stance on the platform with straight knees and the upright trunk. They were also instructed to try to distribute their body weight evenly over the forefoot and hindfoot bilaterally. Participants experienced two 20-sec trials for each experimental condition. The foot position was closely monitored to avoid any skidding of the feet from the desired positions.

The full-body kinematics were recorded from 26 reflective markers attached to the body using an 8-camera motion capture system (Vicon, UK) at 100 Hz. The bilateral vertical interaction force (GRF) and the center of pressure between the foot and the vibration platform were also recorded by a pair of insoles at 100 Hz, synchronized with the motion capture system. Marker paths and the GRF were low-pass filtered using fourth-order, zero-lag Butterworth filters. A customer-written Matlab program was developed to conduct the inverse dynamics for calculating joint moments based on the collected kinematic/kinetic and inertia parameters [4, 5]. The joint moments, normalized to the body mass, at the right ankle, knee, and hip joints were calculated

for the middle 10 seconds of each trial. Due to the symmetry between sides, we did not consider the joint moments on the left side. The peak value of each joint's moment was determined for every trial. The average of the peak values over the two trials for each condition was used to represent the maximum joint moment for that experimental condition.

Analyses of variance with repeated measures were adopted to examine the impact of vibration parameters on the joint moments. The two within-subject factors were the frequency (three levels: 10 vs. 20 vs. 30 Hz) and amplitude (three levels: 1 vs. 2 vs. 3 mm). The dependent variables included the peak GRF, ankle, knee, and hip joint moments. All statistical analyses were performed using SPSS 24.0 (IBM, NY), and a significance level of 0.05 was implemented throughout.

RESULTS AND DISCUSSION

Our results revealed that the peak GRF between the feet and the vibration platform rises with the increases in the frequency (p = 0.007) and the amplitude (p = 0.030, Fig. 1a). During all experimental conditions, the maximum loading at the ankle joint was a dorsiflexor moment; the knee experienced an extensor moment; and the hip joint displayed a flexor moment (Fig. 1b-d). These joint moments significantly increased with the increases in the vibration frequency (p = 0.002) and amplitude (p = 0.021). No significant frequency by amplitude interaction effect was noticed (p = 0.577).

Although it was qualitatively suspected that the joint loading increases positively with the vibration intensity, this study represents the first one that quantitatively tackles the relationships between lower limb joint moments and vibration intensity. It seems that the ground reaction force along with the joint moments changes monotonically and positively with the vibration frequency and the amplitude. These findings provide direct evidence and guidance of selecting vibration parameters when designing CWBV training protocol.

Our study had limitations. Firstly, only healthy young adults were enrolled in this study. It remains unknown if findings from this study could be generalized to other populations. Furthermore, the vibration frequencies and amplitudes in this study only represent a small portion of the ones used in the current research field. Lastly, only the acute effect of CWBV training was examined. The chronic or long-term effects due to CWBV training on joint moments are unanswered. More studies based on large sample sizes and other populations are desired to deepen our understanding of the influence of the vibration intensity on neuromuscular functions.

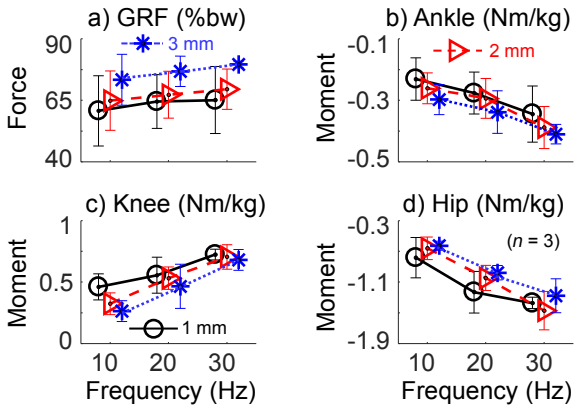

Figure 1: Comparisons of (a) the vertical interaction force (GRF) between the right foot and the platform expressed as the percentage of the body weight and the peak joint moment normalized to the body mass in Nm/kg at (b) the right ankle, (c) right knee, and (d) right hip joints. Positive values indicate extensor or plantar-flexor moment while negative ones mean flexor or dorsiflexor moment.

CONCLUSIONS

Overall, the loading at the lower limb joints increases with the increases in the vibration intensity, as indicated by the increments in either the vibration frequency or amplitude. The findings from this study could provide guidance for designing optimal vibration training protocols which maximize the effects of CWBV training in improving trainees' neuromuscular functions.

REFERENCES

1. Rittweger J. Eur J Appl Physiol. 2010.
2. Yang F, et al. Disabil Rehabil. 2018.
3. Rogan S, et al. Eur Rev Aging Phys Act. 2015.
4. de Leva P. J Biomech. 1996.
5. Winter DA. Biomechanics and Motor Control of Human Movement. 2009.

EFFECT OF POST ACTIVATION POTENTIATION ON KNEE ANGLE DURING REBOUND JUMPS

Katherine A. Walker, Ryan L. Meidinger and Randall L. Jensen

Northern Michigan University, Marquette, MI,
USA www.nmu.edu/hhp
Email: kawalker@nmu.edu

INTRODUCTION

Post activation potentiation (PAP) theory, states that once a participant completes a maximum voluntary isometric contraction (MVIC), their explosive movement performance will be enhanced. Numerous studies have been completed that show evidence that PAP may be beneficial to athletes [8].

Joint angles affect the length of the muscles during exercise. Tsoukas and coworkers found that at the start of a squat jump a knee angle of 165° caused the muscles to shorten and resist fatigue [10]. They also stated that a knee angle of 90° caused fatigue more quickly [10]. Gheller and colleagues stated that squat jumps that begin with a knee angle around 90° produce better performance than deeper or shallower jumps [5]. Therefore, more research must be done to conclude if there is an optimal knee angle for jump performance. The current study allowed the participants to self-select their knee joint angle during their jump.

The purpose of the current study was to examine the effect of PAP on knee angles during rebound jumping. The researchers hypothesized PAP would have an effect and cause the participants to obtain a more optimal knee joint angle.

METHODS

Three females and four males between the ages of 19 and 30 participated. They also were required to have at least 2 years of lower body resistance training to reduce the chance of injury and improve the chances of PAP occurring [7]. Each participant completed a Physical Activity Readiness Questionnaire (PAR-Q) [8] to ensure that they were healthy and signed an informed consent form. The study was approved by the university ethics board (HS17-843).

For 48 hours before the test, participants did not consume alcohol. They also did not consume caffeine on the day of the testing. These precautions were taken due to the effect caffeine may have on the central nervous system [4, 3]. On the left leg of each participant, a central marker was placed on the lateral epicondyle of the femur. Markers were also placed 13 cm above the central marker on the thigh in line with the iliac crest; and 13 cm below on the shank in line with the lateral malleolus of the fibula.

Testing consisted of three days of roughly three hours as follows: 15-20 minutes familiarization/baseline testing, and 30-45 minutes on each of the control and experimental testing days. Countermovement jumps (CMJ) were performed in the sledge, as presented by Comyns and colleagues [2]. After the CMJ, the participants were placed in the sledge and dropped from an estimated 75% of max CMJ height. For familiarization to jumping on the sledge, participants performed 3-5 rebound jumps prior to testing.

Participant order was randomized for control and experimental sessions to avoid a learning effect. On the control day, participants warmed up for 5 minutes on a bike ergometer. Following warm-up there was a 5 minute break for participants to get into the sledge. The participants then completed a 5 second MVIC after their knee angle was set for their loading position to an angle similar to that of their CMJ. Next, there was an 18 minute break to remove the effect of PAP [1, 11]. Participants were then dropped from 75% of their max CMJ height and continued to rebound jump until they failed to jump as high as 75% of their CMJ; or they chose to stop.

Participants began the experimental trial in the same manner as the control. After their original MVIC, they rested again for 6 minutes before completing 3

more MVICs with 5 seconds rest between each [1, 11]. The rest of the trial was performed identical to the control day.

Each trial was recorded on a video camera with a sagittal view and frame rate of 240 hz. The video data were analyzed through the online software Kinovea 0.8.15 to find the smallest knee angle relative to the thigh and shank at contact with the bottom of the sledge. The first and last three jumps of each trial were recorded and the mean of the jumps was used for each condition.

RESULTS AND DISCUSSION

Two-way Repeated Measures ANOVA revealed a significant difference ($p=0.036$) in the knee angles between the control and experimental trials. There was no difference ($p=0.329$) between the knee angles at the start of the individual trials compared to the end and no significant interaction (0.977). Table 1 displays mean ± standard deviation knee angle for each trial.

Table 1: Mean ± SD of the knee angles in rebound jumps for control and experimental trials.

Jump #	Degree of angle
Start control jumps	100.0 ± 8.3
End control jumps	90.4 ± 15.8
Start experimental jumps	97.3 ± 12.5
End experimental jumps	87.8 ± 15.1

Since there was no significant interaction, one can assume PAP was active throughout the entire experimental trial. An explanation for the significant difference in the control and experimental knee angles may be due to the fatigue of the stretch shortening cycle. Horita and colleagues found that at initial contact the knee joint angle is larger (around 140°) but then it collapsed to a smaller joint angle before takeoff as the participant fatigued [6]. This may explain why Tsoukos stated that a larger knee angle is more fatigue resistant than an angle around 90° [10].

CONCLUSIONS

The hypothesis that PAP affects knee angle was confirmed by the significant difference between the control and the experimental conditions. However, with limited participants, further research is suggested. Future research involving PAP should include similar studies with greater sample populations to provide better statistical power of the effects of PAP on knee angle changes.

REFERENCES

1. Chui, L.Z, Fry, AC, Weiss, LW, Schilling, BK, Brown, LE, & Smith, SL. *Journal of Strength and Conditioning Research, 17*(4), 671-677; 2003.
2. Comyns, TM, Harrison, AJ, Hennessy, L, & Jensen, R. L. *Journal of Strength and Conditioning Research, 6*(1), 59-70; 2007.
3. Davis, JM, Zhao, Z, Stock, HS, Mehl, KA, Buggy, J, & Hand, GA. *American Journal of Physiology: Regulatory, Integrative and Comparative Physiology, 284*, R399-R404; 2003.
4. Eckart, MJ, File, SE, Gessa, GL, Grant, KA, Guerri, C, Hoffman, PL, . . . Tabakoff, B. *Alcoholism: Clinical and Experimental Research*, 998-1040; 1998.
5. Gheller, RG, Pupo, JD, Ache-Dias, J, Detanico, D, Padulo, J, & Santos, SG.
6. Horita, T., Komi, P.V., Nicol, C. and Kyrolainen. Stretch shortening cycle fatigue: Unteractions among joint stiffness, reflex, and muscle mechanical performace in the drop jump. *European Journal of Applied Physiology*, 73: 393-403, 1996 *Human Movement Science,42*, 71-80; 2015.
7. Sale, DG. *Exercise and Sport Science Review, 30*(3), 138-143; 2002.
8. Thomas, S, Readings, J, & Shepard, RJ. *Canadian Journal of Sport Science,* 17(4), 338-345; 2002.
9. Tillin, NA & Bishop, D. *Sports Medicine*, 39(2), 147-166; 2009.
10. Tsoukos, A, Bogdanis, GC, Terzis, G, & Veligekas, P. *Journal of Strength and Conditioning Research, 30*(8), 2250-2257; 2016.
11. Wilson, J M, Duncan, NM, Marin, PJ, Brown, LE, Leonneke, JP, Wislon, S. M, . . . Ugrinowitsch, C. *Journal of Strength and Conditioning, 27*(3), 854-859; 2013.

VERBAL INSTRUCTION REDUCES PATELLOFEMORAL JOINT LOADING DURING BODYWEIGHT SQUATTING

Emily Watkins, Tricia Widenhoefer, Thomas Gus Almonroeder

Trine University, Doctor of Physical Therapy Program
Fort Wayne, IN, USA
email: almonroedert@trine.edu

INTRODUCTION

Patellofemoral pain is relatively common in young active females. The pathogenesis of patellofemoral pain is complex; however elevated patellofemoral joint forces and stress (i.e. the forces relative to the joint contact area) appear to be contributing factors [1, 2]. Weight-bearing lower extremity strengthening exercises, such as the bodyweight squat, are recommended for managing patellofemoral pain [3]. However, squatting can also place a substantial load on the patellofemoral joint. As a result, there is a need to explore how manipulating squat technique may influence patellofemoral joint forces and stress.

The position of the knees relative to the toes may be important to consider when analyzing squat technique. A recent study reported greater patellofemoral joint forces and stress when young females performed bodyweight squats where their knees were required to move past their toes, compared to squats where their knees needed to remain behind their toes [4]. Guide wires were used to direct/restrict knee motion during the squat trials for both conditions (i.e. knee past toes, knees behind toes). These results appear to support recommending that individuals limit anterior knee motion when squatting. However, exercise professionals often rely on verbal instruction to alter squat technique (vs. physical restrictions). To our knowledge there has not been an attempt to explore how verbal instruction influences patellofemoral joint loading during bodyweight squatting.

METHODS

This study included 11 females between the ages of 18 to 35 years old. At minimum, participants were required to engage in weight-bearing aerobic activity three times per week for a total of 60 minutes. Individuals were excluded from this study if they had a history of significant injury or surgery involving their back or lower extremities.

Following a brief warm-up, participants performed five bodyweight squats using their typical technique (baseline condition). They also performed additional sets of five squats after they received verbal instructions intended to limit anterior motion of their knees relative to their toes. Two different types of verbal instructions were used; one promoted an internal focus of attention (FoAin) and the other promoted an external focus of attention (FoAex). For the FoAin condition participants were instructed: 'try to prevent your knees from moving past your toes'. For the FoAex condition they were instructed: 'squat like you are sitting back into a chair'. The order of the FoAin and FoAex conditions was counterbalanced.

Participants performed the squat trials with their dominant limb (i.e. the leg used to kick a ball) on a force plate that measured ground reaction forces at 1000 Hz (OR6-7-2000, Advanced Mechanical Technology, Inc.). Retroreflective markers adhered to the participant's dominant lower extremity and pelvis were tracked simultaneously using a multi-camera motion capture system (Vicon Motion Systems, Inc.). Joint angles and net joint moments were calculated using the marker and force data via Visual3D software (C-Motion, Inc.).

The patellofemoral joint forces and stress were estimated during the squat trials using a previously described musculoskeletal model [1]. The model inputs were the knee flexion angles and the knee extension moments. The moment arm of the quadriceps was estimated as a function of the knee flexion angle. The quadriceps muscle force was estimated by dividing the knee extension moment by

this moment arm. A constant was multiplied by the quadriceps muscle force to determine the forces acting at the patellofemoral joint. The patellofemoral contact area was estimated as a function of the knee flexion angle. Patellofemoral joint forces were divided by the joint contact area to estimate the patellofemoral joint stress.

The primary dependent variables of interest were the peak patellofemoral joint forces and stress from the squat trials. In addition, we also tracked the vertical excursion of the center of mass of the pelvis using the motion capture system. A repeated-measures ANOVA was used to compare the variables across conditions (baseline, FoAin, FoAex). In the case of a significant omnibus test, Bonferroni post-hoc tests were conducted. An alpha of .05 was used for all significance testing.

RESULTS AND DISCUSSION

There was not a difference in pelvis excursion among the conditions ($p=.60$). As a result, any differences in patellofemoral joint mechanics were not due to a difference in squat depth.

There was a difference among the conditions for the patellofemoral joint forces ($p=.001$) and stress ($p<.001$). The post-hoc tests indicated that participants demonstrated lower patellofemoral joint forces for the FoAin ($p=.008$) and FoAex ($p=.03$) conditions compared to baseline (Fig. 1). They also demonstrated less patellofemoral joint stress for the FoAin ($p=.002$) and FoAex ($p=.03$) conditions (vs. baseline) (Fig. 2). There was not a difference between the FoAin and FoAex conditions for the patellofemoral forces ($p=.84$) or stress ($p=.41$).

Participants in our study demonstrated a reduction in patellofemoral joint forces and stress after receiving instructions intended to limit anterior knee motion during squatting. This is encouraging, as it appears that relatively simple verbal instructions can influence squat mechanics in a manner that could reduce patellofemoral joint loading.

Previous studies have indicated that instructions promoting an external focus of attention may result in better performance for a variety of movement tasks in comparison to instructions that promote an internal focus of attention [5]. However, our results indicate that instructions intended to promote an internal vs. external attentional focus had a similar influence on patellofemoral joint loading during squatting. Future studies should explore potential differences in retention of squat instructions that promote an interval vs. external focus of attention.

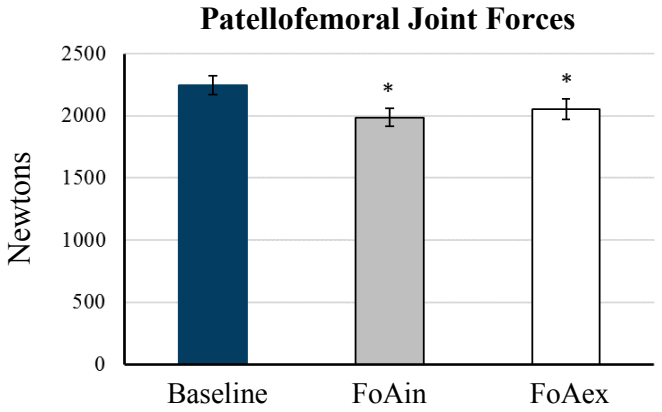

Figure 1: Mean patellofemoral joint forces for each condition. * indicates a reduction vs. baseline. Error bars reflect the standard error.

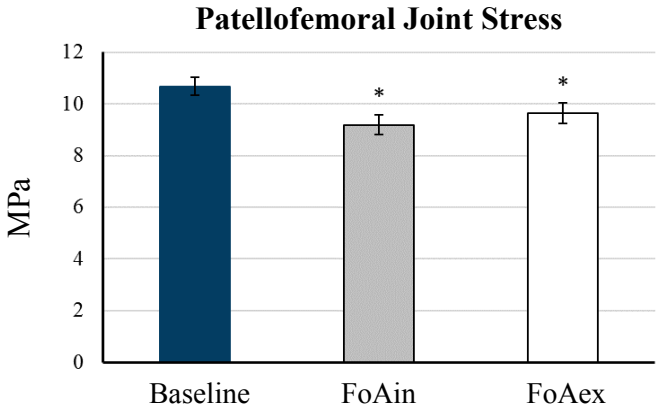

Figure 2: Mean patellofemoral joint stress for each condition. * indicates a reduction vs. baseline. Error bars reflect the standard error.

REFERENCES

1. Brechter & Powers. *Med Sci Sports Exerc*, **34(10)**, 2002.
2. Farrokhi et al. *Osteoarthritis & Cartilage,* **19(3)**, 2011.
3. Kooiker et al. *J Orthop Sports Phys Ther*, **44(6)**, 2014.
4. Kernozek et al. *J Sport Rehabil,* [Epub ahead of print].
5. Wulf et al. *Med Educ,* **44(1)**, 2010.

TESTING THE EFFICACY OF ACL INJURY PREVENTION PROGRAMS THROUGH OPENSIM

[1] Shunafrica C. White and Matthew B.A. McCullough

[1] North Carolina Agricultural and Technical State University, Greensboro, NC, USA
email: scwhite@aggies.ncat.edu

INTRODUCTION

Anterior cruciate ligament (ACL) injury is a common problem among active individuals [1]. There is approximated number of 200,000 to 400,000 cases per year in the United States with an estimated cost of diagnostics, treatment, and/or loss of salary or scholarships around $625 million to $1 billion annually [2]. Noncontact injuries account for majority of reported ACL injuries, which are sustained during tasks that involve sudden deceleration when running, changing direction, or landing from a jump [3]. These tasks paired with unbalanced muscle activation of quadriceps and hamstrings have been demonstrated as risk factors for ACL injuries. In efforts to prevent ACL injuries, researchers have developed and tested the effectiveness of multiple ACL injury prevention programs. However, research has still left some unanswered questions about how muscle forces can help to prevent ACL injury. Therefore, the primary objective of this study was to implement the basic component of neuromuscular ACL injury prevention programs, strength training of the lower extremities, and quantify knee valgus using kinematics based computational modeling.

METHODS

One participant, a young female recreational athlete, performed a jump landing task and a generic musculoskeletal model was developed in OpenSim to calculate knee valgus during that task. The model consisted of 23 degrees of freedom and 54 muscle tendons [3]. The model was scaled to match anatomical features of the participant and subjected to three scenarios: no change to the maximum isometric force of the biceps femoris (long and short heads), gracilis, and sartorius, a 20% increase to the maximum isometric force of the biceps femoris, and a 20% increase to the maximum isometric force of the gracilis and sartorius.

Analysis of variance was performed to determine differences in knee valgus for the three scenarios.

RESULTS AND DISCUSSION

There was no significant difference ($P = 0.99$) found in knee valgus between the model with no changes and the model with a 20% increase to the maximum isometric force of the biceps femoris. There was also no significant difference ($P = 0.99$) found in knee valgus between the model with no changes and the model with a 20% increase to the maximum isometric force of the gracilis and sartorius.

Increasing the maximum isometric force of the biceps femoris, gracilis, and sartorius, alone, did not improve knee valgus, and in fact there were no numerical differences in values among the three scenarios. The lack of differences among the three scenarios could be that 20% was too small of an increase to make any real impact on knee valgus. However, the knee valgus calculated in this study reflects what has been reported in literature [3, 4].

There were several limitations within this study. The kinematic data used was limited to only one trial from one participant of the jump landing task. Photographs from the motion capture could not be used to validate the scaled model, which could have eliminated large marker errors, the distance between the experimental marker and the corresponding virtual makers, during the inverse kinematics simulation. Lastly, the musculoskeletal model used in this study was very generic, and although this helps to hasten the calculations it does not help to reproduce realistic results to investigate ACL injury risk factors.

Focus for future work should be on conducting a kinematic analysis of a jump landing task in a

sample population that is reflective of the entire population. Furthermore, maximum isometric force should be increased to more than one level (e.g., 30%, 40%, 50). Lastly, future work should investigate how increasing the muscle strength of flexor muscles affect Hamstrings-to-Quadriceps ratios and the activation of muscle during landing.

CONCLUSIONS

Despite the many limitations of the study, the concepts are a good approach to determine if flexor muscles contribute to ACL injury risk factors and should be conducted again to account for the limitations of the current study. However, based on the results of the study it can be concluded that increasing the maximum isometric force of the biceps femoris, gracilis, and sartorius, in a young recreational female athlete does not improve knee valgus. Furthermore, there are no studies that have used OpenSim to consider how the strength of flexor muscles contribute to ACL injury risk factors.

REFERENCES

1. Joseph et al. *J Athl Train.* **48**(6), 2013.
2. Utturkat et al. *Annals of Biomedical Engineering,* **41**(1), 2013.
3. Kar et al. *Ann Biomed Eng*, **40**(8), 2012.
4. Hewett et al. *Am J Sports Med,* **33**(4), 2005.

Impact Attenuation of Biomechanics in Drop Landing on Synthetic Turf with Shock Pad

Songning Zhang[1], Thomas K. Elvidge[1], Kevin A. Valenzuela[2]
[1] Biomechanics/Sports Medicine Laboratory, Department of Kinesiology, Recreation and Sport Studies, The University of Tennessee, Knoxville, USA
[2] Department of Kinesiology and Health Promotion, California Polytechnic University, Pomona, USA
email: szhang@utk.edu, Web: http://krss.utk.edu/centers-labs/biomechanics-laboratory/

INTRODUCTION

Shock pad (PAD) has become a popular option as an underlayment installed under a synthetic turf (TURF) field [1]. Previous research has mostly focused on TURF surface only condition in cutting and landing movements [2]. Due to the practice of combination of TURF and PAD being relatively new, research on effects of this combination on impact related variables in landing movement is largely missing in literature. Therefore, purpose of this study was to examine impact attenuation related biomechanical characteristics of a drop landing on synthetic turf plus shock pad compared to synthetic turf only.

METHODS

Twelve recreational football and soccer players (age: 21.9 ± 2.7 years, height: 1.85 ± 0.06 m, mass: 78.5 ± 9.4 kg) participated in this study. They performed five successful drop landing trials from each of four test conditions, which include a combination of two heights: 0.4 and 0.6 m landing heights and TURF and PAD surfaces in a laboratory setting.

A 2" monofilament synthetic turf with 1/2" stitch gauge (PowerBlade Shaw Industries, Dalton, GA) was used in TURF only and PAD conditions. A foam based shock pad (POWERBASE/YSR, Brock International, Boulder, CO) was placed underneath the TURF in PAD conditions. Participants wore American football cleats (Nike Vapor Untouchable Pro, Nike) during testing. A 12-camera motion capture system (240Hz, Vicon, UK) and two force platforms (1200Hz, AMTI, USA) were used to collect 3D kinematic and ground reaction force (GRF) data, respectively. Anatomical markers and tracking markers were placed bilaterally on the trunk, pelvis, thighs, shanks, and cleats for kinematic data collection. Participants performed the five drop landing trials in each of four test conditions: a combination two landing heights 40 and 60 cm and two surfaces of TURF and PAD. The mean maximum knee flexion angles from each height were determined during practice trials. During the actual testing trials, the participant was asked to land within the range of mean maximum knee flexion angle ± 8°. The heights were first randomized and the surface conditions were randomized within each landing height.

Kinematic and GRF data were filtered using a low-pass fourth-order zero-lag Butterworth filter at a cutoff frequency of 8 Hz for joint kinetic calculation. GRF data were filtered separately with the low-pass filter at 50 Hz for obtaining GRF related variables. Visual3D (5.0, C-Motion, Inc.) was used to compute 3D kinematic and kinetic data. GRF and joint moments were normalized to body weight (BW) and mass (Nm/kg), respectively. A 2×2 (turf × height) repeated measures analysis of variance (ANOVA, $p<0.05$) was performed to detect differences between turf conditions and heights for kinematic and kinetic variables (Version 22, SPSS).

RESULTS AND DISCUSSION

Significant differences with respect to the landing height and turf main effects and their interactions were found in all sagittal plane related variables. Both peak vertical GRFs increased with increased landing height (Table 1). However, no interactive and turf effects were found. A significant turf effect was found for the peak knee extension moment and knee flexion range of motion (ROM), showing that knee extension moment was smaller ($p = 0.029$) while the knee flexion ROM was greater ($p = 0.037$), in the pad condition. This was especially the case at 40 cm landing where greater reduction was seen in the peak knee extension moment with the interaction of Turf and Height close to be significant ($p = 0.067$). Knee frontal-plane kinematic and kinetic variables were not different between the heights and surfaces. Significant height main effect was seen for the peak knee extension moment, eccentric power and flexion

ROM, suggesting that the values of these variables increased with the increased landing height.

No surface main effect was found for any ankle variables (Table 1). There was a significant interaction of Turf and Height for the peak plantarflexion moment and dorsiflexion ROM. The post hoc comparisons showed that the peak plantarflexion moment was greater for the TURF compared to the PAD at the 40 cm height ($p = 0.008$), and was smaller at 40 cm compared to 60 cm in the PAD condition ($p < 0.001$, Table 1). A significant height effect was also found for the peak plantarflexion moment, peak plantarflexion power, peak plantarflexion angle, and dorsiflexion ROM, indicating that the values of these variables increased with the increased landing height.

These results seems to suggest that adding the shock pad to the existing synthetic turf does not affect the overall loading to the body during the landing movement. Human body makes adjustments to adapt to changes in external loading during human movements. These adjustments are most evident in the ankle and knee related variables in the PAD conditions during drop landing. Significant interactions of the turf and landing height for the peak ankle plantarflexion moment and ankle dorsiflexion ROM and the post hoc results showed that the athletes exerted smaller peak ankle plantarflexion moment and had smaller dorsiflexion ROM in 40 cm than that in 60 cm drop landing on PAD. Additionally the athletes also exerted smaller peak knee extension moment in the PAD compared to the TURF conditions. This was especially the case for the 40 cm drop height and no difference in the 60 cm drop height between the two turf conditions was observed, with a marginal difference of the interaction ($p = 0.067$). These results suggest that the shock pad offers some protective effects to the knee and ankle joints, mostly at a moderate submaximal 40 cm landing height in landing related activities (e.g., landing from a jump). The protective effects seem to diminish at 60 cm height, which may be partially due to subjects' neuromuscular adjustments. The results from the study provide novel data in the biomechanics literature.

REFERENCES

1. McGhie, D., et al. (2013). *Am J Sports Med*, **41**, 177-185.
2. Brock E. et al. (2014). *Sports Biomech*, **13**, 362-379.

ACKNOWLEDGEMENT

Supported in part by Brock International.

Table 1. Peak Vertical GRF, and Knee and Ankle Kinematic and Kinetic Variables: Mean ± STD.

	TURF 40 cm	TURF 60 cm	PAD 40 cm	PAD 60 cm	*Interaction P value*	*Turf Effect P value*	*Height Effect P value*
1st GRF	0.611±0.176	0.918±0.141	0.579±0.114	0.882±0.171	0.794	0.500	**<0.001**
2nd GRF	2.182±0.525	2.618±0.688	2.216±0.458	2.554±0.644	0.418	0.928	**0.002**
Knee Joint –							
Eccentric Power	-20.036±5.947	-25.662±6.124	-17.542±4.764	-25.539±6.428	0.179	0.315	**<0.001**
Extension Moment	2.293±0.248	2.449±0.263	1.984±0.485	2.460±0.475	0.067	**0.029**	**0.019**
Abduction Moment	-0.259±0.225	-0.265±0.156	-0.375±0.173	-0.505±0.425	0.473	0.175	0.290
Flexion Angle	-76.463±13.997	-98.810±2.304	-78.377±8.090	-98.778±3.876	0.659	0.669	**<0.001**
Flexion ROM	-52.417±15.638	-73.723±6.702	-58.778±5.088	-76.930±7.637	0.454	**0.037**	**0.000**
Ankle Joint –							
Plantarflexion Eccentric Power	-11.400±3.240	-16.360±4.406	-8.736±3.849	-15.402±3.888	0.074	0.060	**<0.001**
Plantarflexion Moment	-1.370±0.266!	-1.500±0.372	-1.114±0.383^	-1.430±0.302	**0.022**	0.078	**<0.001**
Inversion Moment	0.164±0.114	0.170±0.094	0.218±0.187	0.197±0.123	0.641	0.427	**0.991**
Dorsiflexion ROM	46.376±10.786	49.956±8.118	42.451±11.778^	51.624±7.323	**0.023**	0.625	**0.002**

Note: ! – significantly different from PAD of the same height, ^ - significantly different from 60 cm of the same turf condition.

BIAXIAL CYCLIC LOADING OF SKIN

[1]Nazanin Afsar Kazerooni, [1]Arun Srinivasa and [1]John Criscione

[1] Texas A&M University, College Station, TX, USA
email: nazanin26@tamu.edu

INTRODUCTION

The largest organ in the body is skin. It is composed of several layers such as stratified, cellular epidermis, and an underlying dermis of connective tissue [1]. To measure the properties of anisotropic materials, biaxial tension tests are widely used, where Digital Image Correlation (DIC) technologies are often employed to measure the displacement fields [2]. In order to better understand the mechanical behavior of skin, it is important to run tests not only in uniaxial tension, but in biaxial tension too. This need becomes direr once it is realized that there are no experiments on investigation of Mullins effect on skin in biaxial testing. To that end, we have built a biaxial set that can be installed on conventional uniaxial Instron machine and tested skin under biaxial cyclic loading and using the data which were taken by DIC to find the deformation and strain field.

METHODS

Skin from the abdominal and back region of an adult pig was harvested in Veterinary School of Texas A&M University. In order to apply speckle pattern on skin to study the deformation field, hair was removed from the skin using a razor blade. In all samples, fat layer was removed and epidermis and dermis were studied. Sample were cut by scapula firstly. Since pig skin is very tough and it is very difficult to cut samples for biaxial testing, laser cutter was used to cut samples.

Figure 1: Skin sample after preparations

In order to prevent slipping of samples from grips, pieces of wood were stapled on both sides of samples. Next step is preparing samples for Digital Image Correlation. Since color of skin samples were dark gray, there is not enough contrast between speckles and background, therefore, black pigment was applied on samples as the background. Figure 1 shows a biaxial sample after preparation. In order to get random and uniform pattern, white pigment was sprayed by electric toothbrush on samples with black pigments. To get better speckle pattern, it is better to apply white pigment after gripping samples. In order to study mechanical behavior of skin and perform deeper investigations on mechanisms of tearing of soft tissue, biaxial set-up has been designed based on Brieu's design [3]. The main idea behind the designing of this new biaxial set-up is to build a low cost biaxial set-up which is adaptable to uniaxial tensile testing machines. Another advantage of this biaxial set-up is that it can be adjusted to be both equibiaxial and nonequibiaxial. Figure 2-a shows the schematic design of biaxial tensile test mechanism.

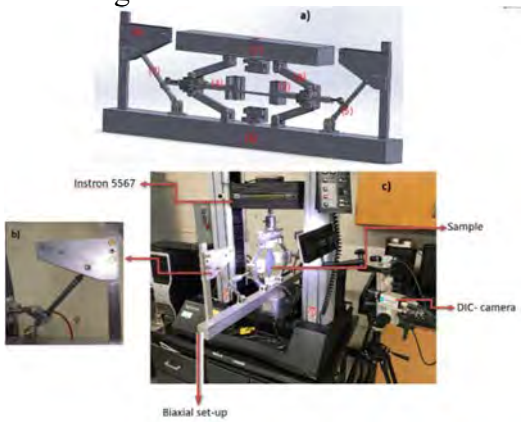

Figure 2: a) Schematic design of the biaxial tensile test mechanism, b) Horizontal displacement, adjusted for equibiaxial and non-equibiaxil set-up and c) Biaxial set-up on uniaxial tension machine (INSTRON 5567)

Cyclic tension loading was done on samples, in the biaxial fixture with the angle of 63.44 degrees. Once with the direction of vertical loading in the same direction as spine, and once perpendicular to it. Samples were tested at room temperature and the displacement rate of 30 (mm/min). Firstly, samples

were stretched to a specific elongation and then partially unloaded down to a certain elongation. In order to keep samples wet during the tension tests and prevent them from drying which affects the behavior of skin [4], Veterinary 0.9 percent Sodium Chloride solution was sprayed on each sample during the test. Then this strain controlled loading and unloading cycles were repeated for a few times and strain field was measured by Digital Imaging correlation (DIC). The DIC system used is Q-400 DIC system. The correlations are based on images taken with two video cameras and processed using Istra 4D software.

RESULTS AND DISCUSSION

Figure 3 shows the grids on sample during biaxial testing which were taken by DIC.

Figure 3: Grids on pig skin sample during biaxial testing.

Figure 4 shows the load measurements from load cells in both vertical and horizontal directions. It was observed that after first cycle softening happened and there is a reduction in load after first cycle at specific strain which is called Mullins effect. Figure 5 shows the engineering strain field on the sample and expresses the partially strain field. There are missing pieces because of the nature of skin which has wrinkles and it is difficult to get the full strain field data. These are the preliminary results but yet it is possible to extract the material parameters from these partial data by using Virtual Field Method (VFM)[5].

The two pieces of data, partial strain field through the body and forces of the both directions would be sufficient to extract the material properties.

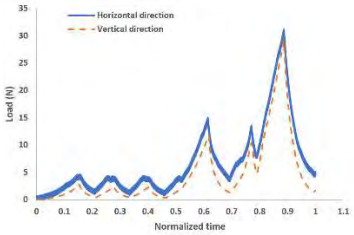

Figure 4: Loads in both horizontal and vertical directions.

CONCLUSIONS

According to this study, it was observed that under biaxial cyclic loading test, softening happens to skin and Mullins effect was observed. Also, by using VFM, we will extract material parameters of skin despite the missing pieces of data.

REFERENCES

1. McGrath, J.A., et al., Anatomy and Organization of Human Skin, in Rook's Textbook of Dermatology. 2010, Wiley-Blackwell. p. 1-53.
2. Goh, C.P., et al., Optics and Lasers in Engineering, 2017. 88: p. 167-177.
3. Brieu, M. et al. Journal of Testing and Evaluation, 2006. 35(4): p. 364-372.
4. Berardesca, E., et al., Bioengineering of the skin: methods and instrumentation. Vol. 3. 1995: CRC Press.
5. Grediac, M., et al., Strain, 2006. 42(4): p. 233-253.

ACKNOWLEDGEMENTS

The authors gratefully thank Dr. Terry Creasy for allowing us to use his facilities and Dr. Goenezen for lending us, the DIC.

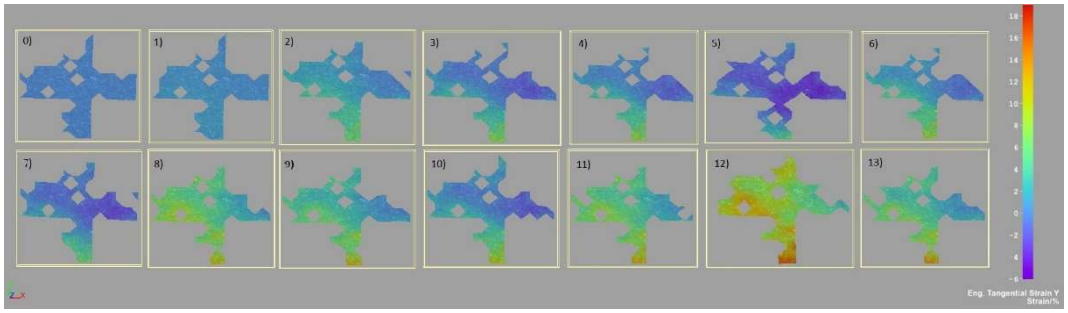

Figure 5: Engineering strain in y direction for each step during cyclic loading

Excursion of Individual Wrist Tendons Using a Joint Motion Simulator and Phantom Limb

[1] Drew A. Anderson, [1]Michele Oliver PhD, PEng., [1]Karen Gordon PhD, PEng.

[1] School of Engineering, University of Guelph, Guelph, ON, Canada
email: dander04@uoguelph.ca

INTRODUCTION

A greater understanding of the relationship between tendon excursion and wrist kinematics will benefit upper limb pathology treatment and prevention. The invasive nature of *in vivo* tendon force measurement underscores the need for alternative approaches such as *in vitro* simulation with cadaveric specimens, and/or musculoskeletal modelling.

Unfortunately, the wrist joint is an over-actuated system whereby the number of forearm muscles acting on the wrist exceed the degrees of freedom resulting in an indeterminate problem. Five main muscles flexor carpi ulnaris (FCU), flexor carpi radialis (FCR), extensor carpi ulnaris (ECU), extensor carpi radialis longus (ECRL), and extensor carpi radialis brevis (ECRB) exert a torque about the wrist as a function of the muscle's moment arm and tendon excursion. . Synergistic and antagonistic relationships between these muscles will result in varying tendon loading profiles. Previous work has applied optimization methods and physiologic parameters to determine loading profiles for sustained wrist postures and dynamic movement through flexion/extension and radial/ulnar deviation [1]–[4]. Variability in the results of these studies warrants further investigation.

This study uses a joint motion simulator (JMS) and a phantom wrist model to investigate the relationship between wrist flexion and extension and loading of the wrist tendons. While fresh-frozen cadaveric specimens are typically used in JMS studies, each specimen is highly valuable and has a limited timeframe for use. A phantom limb allows for repeated experimentation and the ability to modify anatomical characteristics such as tendon moment arms. For wrist flexion/extension (FE), individual tendons will be loaded against constant antagonistic forces to determine the excursion required of a single agonist to move the hand to a given posture. The aim of the study is to determine the contributions of each main wrist tendon to moving the wrist through ±30° of FE and validate the use of a phantom limb.

METHODS

Active Joint Motion Simulator

The study uses a custom-built in vitro JMS as pictured in Figure 1. The JMS was designed to actively manipulate the wrist joint concurrent with CT image acquisition. The JMS operates on the same basis as active wrist simulators previously described in literature whereby actuators act on tendons to simulate the action of the forearm flexor and extensor muscles. [1], [2]. Specifically, four electromechanical actuators vary the tendon excursion of the FCU, FCR, ECU and ECR (ECRL and ECRB coupled) tendons to generate desired tendon loading and wrist kinematics.

Phantom Limb

A phantom limb, designed to be representative of a 50th percentile male upper extremity, was mounted in the JMS. The phantom used in this study was machined in aluminum with stainless steel cables acting as tendons. A 2 degree-of-freedom universal joint permits wrist FE and RUD with the deviation axis distally offset by as distance of 5mm [5]. Hand, forearm, and upper arm segment lengths, as well as the hand COM were determined using anthropometric data for a 50th percentile male [6]. The tendon moments arms of the phantom limb were designed based on the mean moment values determined through passive wrist flexion and extension by Horii et al 1993 [7]. The hand is attached to a moving hand support which restricts the movement to a single degree of freedom and offers a small amount of resistance to replicate the passive tissues of the wrist.

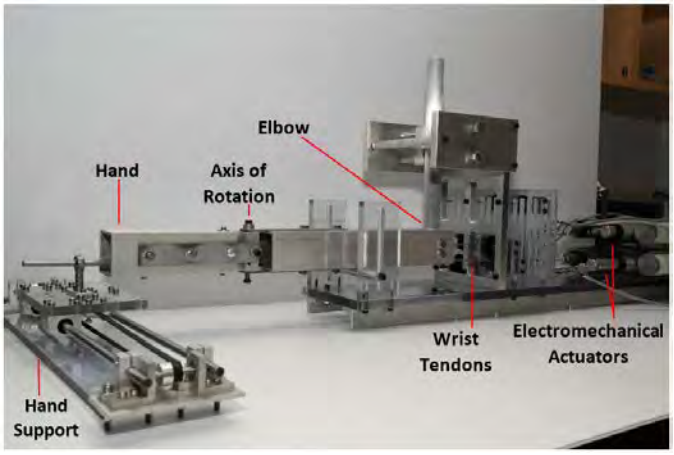

Figure 1: Phantom limb mounted and active joint motion simulator used to examine the relation between tendon excursion and wrist position

Test Procedure and Data Analysis

The upper arm segment and forearm of the phantom are rigidly secured to the JMS in a position representing 90° elbow flexion and 0° pronation. Trials of flexion and extension are conducted with 0° of RUD. Individual tendons are used to move the wrist through a range of motion against constant tone load of 10 N on each antagonist tendon. For example, a trial measuring the effect of the FCU on wrist flexion consists of moving the FCU actuator against 10 N of load on each of the ECU and ECR such that the wrist position moves from -30° to 30°. Therefore, a total of 4 test conditions are completed to test all tendons in FE; each condition is repeated 3 times. A single axis goniometer is used to record wrist position and the position of the actuator is used to record tendon excursion.

RESULTS AND DISCUSSION

The data from all three trials of each test condition is plotted in Figure 2. For each test condition, the relationship between tendon excursion and wrist flexion can be modelled by a linear equation with an R^2 value of 0.995 or greater. The slope for FCU is slightly greater than the slope of FCR, while the slope of ECR is greater than that of ECU. The greater slope of the FCU compared to the FCR indicates a greater contribution of the FCU towards wrist flexion. Likewise, the greater slope of the ECR reflects that the ECRB and ECRL are the greatest contributors to wrist extension. The relative relationship between the tendons is consistent with the findings of Horii et al 1993 [7].

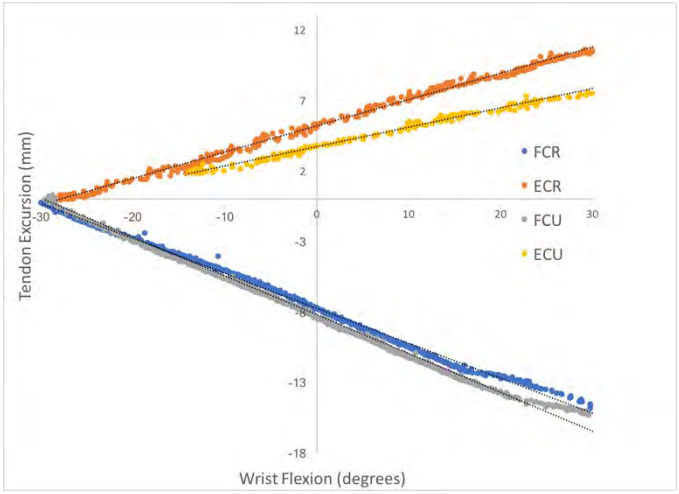

Figure 2: Relation between tendon excursion and wrist flexion angle for the loading of individual wrist tendons against constant antagonistic force.

The moment arm of the ECR tendon was determined by averaging the ECRL and ECRB moment arms. The result is a slope of 0.1863 mm of excursion per degree of flexion for the ECR which is within 0.08 of the slopes of ECRL and ECRB as determined by Horii et al. 1993 [7]. The maximum wrist extension achievable using the ECU was -15 degrees because of a physical limitation of the phantom limb and location of the ECU moment arm relative to the axis of rotation. The results of this investigation show that a phantom limb modeled after a 50th percentile male arm can produce tendon excursion results similar to those found experimentally with human specimens. The phantom limb will allow for future studies of biomechanical relations between wrist kinematics, tendon excursion, and tendon loading.

REFERENCES

[1] F. W. Werner et al., *J. Orthop. Res.*, 14(4), 1996.
[2] L. G. (2010). F.W. Werner et al., *J. Hand Surg. Am.*, 35(4), 2011.
[3] D. S. Shah et al., *J. Biomech.*, pp. 0–5, 2017.
[4] B. Goislard De Monsabert et al., 46(1), 2018.
[5] S. K. Charles and N. Hogan, *J. Biomech.*, 44(1), 2011.
[6] D. A. Winter, *Biomechanics and Motor Control of Human Movement*, John Wiley & Sons Incorporated, 2009.
[7] E. Horii, K. N. An, and R. L. Linscheid, 'Excursion of

prime wrist tendons', 1993.

QUANTIFYING THE SHOULDER WORKSPACE OF WHEELCHAIR USERS AND ABLE-BODIED CONTROLS USING IMUS

[1] Stephen M. Cain, [2] Emma Fortune, [2] Meegan Van Straaten, and [2] Melissa M. Morrow

[1] The University of Michigan, Ann Arbor, MI, USA
[2] Mayo Clinic, Rochester, MN, USA
email: smcain@umich.edu and morrow.melissa@mayo.edu

INTRODUCTION

Current understanding suggests that shoulder rotator cuff pathology in manual wheelchair (MWC) users is caused from wear and tear due to overuse of the shoulder soft tissues [1]. To advance our understanding of the mechanisms of shoulder overuse injury, it is important to understand the real-world use of the shoulder including the overall workspace and distribution of shoulder kinematic positions. Inertial measurement units (IMUs) provide a way to measure the acceleration and angular velocity of body segments in the real-world; these measurements can be used to estimate segment and joint kinematics [2]. Accurate estimation of real-world joint kinematics requires utilizing both a properly executed functional calibration and appropriate drift correction methods, which are often joint specific [3].

This study had two purposes: 1) to develop a methodology that uses body-worn IMUs to estimate the angle of arm elevation (θ) and plane of arm elevation (ϕ) [4] of MWC users and able-bodied age and sex matched controls during day-long data collections in their natural environments and 2) to explore how the estimates of θ and ϕ can be used to quantify and compare the shoulder workspace of MWC users and matched controls.

METHODS

In our IRB approved study, participants (Table 1) secured a total of three wireless IMUs (Opal, APDM, Inc.) to their left and right upper arms and thorax utilizing elastic hook and loop straps. A Kalman filter was used to estimate the orientation of each IMU relative to an inertial frame defined by the directions of gravity and magnetic north (similar to [2]). After donning the IMUs, participants followed an instructional video to perform a functional calibration. Most important were the following: static upright posture with upper arms pressed against thorax, right/left arm t-pose ($\theta \approx 90°$, $\phi \approx 0°$), and right/left arm straight in front of body ($\theta \approx 90°$, right $\phi \approx -90°$, left $\phi \approx 90°$). Using data from the functional calibration, we defined orientations of anatomical axes relative to the IMU-fixed reference frames [5], which enabled estimation of the orientation of each body segment in the inertial frame and calculation of θ and ϕ for both shoulders [4]. We used the functional calibration to ensure alignment between the inertial frames established by each IMU.

Table 1: Participant demographics, where numbers denote matched pairs (S indicates MWC user).

	Age	Sex	Injury Level	Dominant Arm	Current Shoulder Pain	Rotator Cuff Pathology on MRI
S004	56	M	T7 - T12	R	Yes: L	Yes: L & R
C004	55	M		R	No	Yes: L & R
S008	32	M	T4	R	Yes: R	Yes: R
C008	32	M		R	No	No
S010	25	M	T5	R	No	No
C010	24	M		R	No	No

Participants were in a variety of environments and experienced varying magnetic fields throughout the data collections, and therefore measurements of the magnetic field were not always suitable for correcting drift between the inertial frames established by each IMU (heading drift). To correct this drift, which pollutes the estimates of θ and ϕ, we assumed that the estimated heading angles of the arm-mounted IMUs should track that of the thorax IMU and that any drift between the inertial frames occurred at a frequency less than 0.01 Hz. By using corrected heading angles to correct the yaw angles of the IMU orientations, we were able to reduce the drift in our estimates of θ and ϕ, even in unreliable magnetic fields. In general, θ is less sensitive to drift in orientation estimates than ϕ.

RESULTS AND DISCUSSION

Histograms for the left and right angles of arm elevation (Figure 1) reveal varying elevation angle distribution patterns for the MWC users and controls with the majority of motion occurring between 0° and 100°.

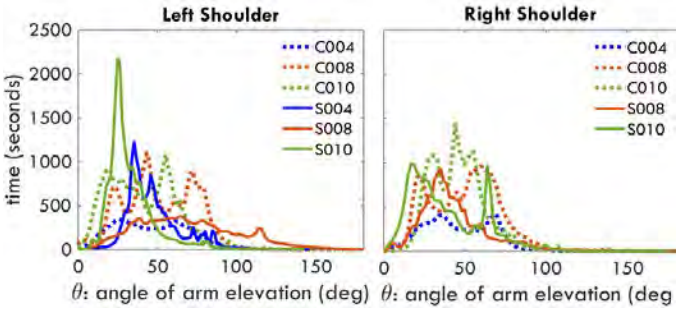

Figure 1: Histograms (smoothed using kernel density estimation) for the angles of arm elevation measured for each participant.

Figure 2 illustrates two-dimensional histograms (bin size 10°×10°) for the left and right shoulders of a MWC user (S010) and an able-bodied age and sex matched control (C010) for a 10.2 and 12.6 hour data collection, respectively. The highest density arm elevation for the control was similar between arms (~50°) while the dominant arm in the MWC user was ~60-70° and ~20-30° in the non-dominant arm. The dominant arm in the control and non-dominant arm in the MWC user functioned primarily in front of the body while the non-dominant arm of the control functioned closer to the abduction plane. While the correction of the heading angles removed much of the drift, it is noted that there is still potential for the plane of arm elevation to be polluted by drift.

CONCLUSIONS

This preliminary data set from a larger study demonstrates that shoulder motion (θ and ϕ) can be meaningfully quantified using IMUs in the real-world. Understanding of the kinematic workspace of the shoulder can be combined with knowledge of shoulder impingement across the workspace [6] to elucidate the potential for overuse injury in the rotator cuff.

REFERENCES

1. Requejo et al. *Top Spinal Cord Inj Rehabil* **13**, 86-119, 2008.
2. El-Gohary and McNames. *IEEE Trans Biomed Eng* **59**, 2635-2641, 2012.
3. Vitali et al. *Sensors* **17**(9), 1970, 2017.
4. An et al. *J Ortho Res* **9**(1), 141-149, 1991.
5. Cain et al. *ASB 2017*, Boulder, CO, USA, 2017.
6. Dal Maso et al. *Manual Therapy* **25**, 94-99, 2016.

ACKNOWLEDGEMENTS

This research was supported by the Eunice Kennedy Shriver National Institute of Child Health and Human Development of the National Institutes of Health (R01 HD84423).

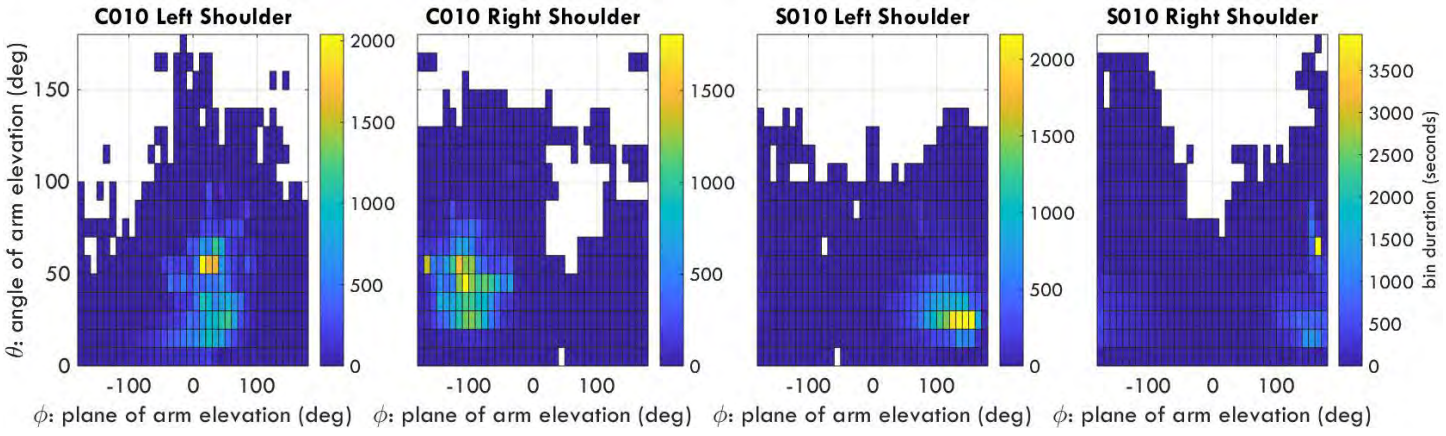

Figure 2: Two-dimensional histograms (bin size 10°×10°) for the left and right shoulders of C010 and S010 for a 12.6 and 10.2 hour long data collection, respectively. The histograms reveal the full shoulder motion functional workspace and frequently utilized shoulder positions (larger bin durations). Positive ϕ indicates that the arm is in front of the body for the left shoulder and behind the body for the right shoulder.

ACCURACY OF VIDEO ANALYSIS TO MEASURE THE INITIAL LEAN ANGLE, STEP LENGTH AND STEP VELOCITY FOR FORWARD LEAN RELEASES IN A CLINICAL SETTING

[1,2] Evelyne Carbonneau, [1,3] Kevin Lalanne, [1,3] Guillaume Léonard,
[4] Rubens A. da Silva and [1,2] Cécile Smeesters

[1] Research Center on Aging, Sherbrooke, QC, Canada
[2] Department of Mechanical Engineering, Université de Sherbrooke, Sherbrooke, QC, Canada
[3] School of Rehabilitation, Université de Sherbrooke, Sherbrooke, QC, Canada
[4] Department of Health Sciences, Université du Québec à Chicoutimi, Chicoutimi, QC, Canada
e-mail: Cecile.Smeesters@USherbrooke.ca, web: http://www.usherbrooke.ca/gmecanique

INTRODUCTION

The ability to recover balance and avoid a fall decreases exponentially with age, falling below one standard deviation (SD) of the mean value of 18-year-olds in individuals above 51.0yrs for forward lean releases [1]. Furthermore, in a 12-month prospective falls evaluation, while the maximum forward lean angle was shown to significantly predict a future fall in community-dwelling older adults (65-90yrs), postural sway and timed up and go measures were not predictive [2]. Finally, we have recently shown that simpler and lower-cost technologies to measure the maximum forward lean angle (load cell, inclinometer and protractor) are sufficiently accurate (Pseudo R^2>0.966) in a clinical setting, to potentially identify individuals at risk of falls or evaluate the effectiveness of exercise-based fall prevention programs [3]. The purpose of this study was thus to determine the accuracy of video analysis, compared to the current complex and costly gold standard, to measure, not only the initial lean angle, but also step length and step velocity for forward lean releases.

METHODS

As in our previous study [3], 12 healthy adults (mean±SD=27.4±10.1yrs; range=20-48yrs, 50% women) were instructed to recover balance using a single step, after first being leaned forward and then suddenly released from six randomly ordered initial lean angles (5-30deg or 10-35%BW in 5deg or 5%BW increments), using four different measurement methods (LabVIEW, load cell, inclinometer and protractor).

The following three variables [1] were calculated in post-processing from a) 2D video camera (scA640-120fc, Basler AG, Germany) recordings of the left side of the participant at 100Hz using a free video analysis tool (Tracker v4.9.7, https://physlets.org/tracker/) and b) 3D marker positions captured by four optoelectronic position sensors (Optotrak, NDI, Waterloo ON) at 100Hz and ground reaction forces captured by four force platforms (OR6-7, AMTI, Newton MA) at 1000Hz using Matlab (Mathworks, Natick MA), the gold standard:

- The **initial lean angle** in degrees was measured as the sagittal plane angle between the vertical and the line connecting the midpoints of the two lateral malleoli and the two greater trochanters prior to lean release. Only the left lateral malleolus and greater trochanter were used for the video analysis.
- **Step length** in meters was measured as the anterior-posterior displacement of the stepping foot lateral malleolus from heel strike (zero ground reaction force) to toe off (non-zero ground reaction force). The medial malleolus was used for steps with the right foot, and heel strike and toe off were determined by visual inspection for the video analysis.
- **Step velocity** in meters per second was calculated by dividing step length by step time, where step time was the time difference between heel strike and toe off.

RESULTS AND DISCUSSION

Unconditional growth linear regressions showed that, despite some residual SD ($p_{ResidualSD}$<0.001, Table 1), the three variables calculated using video

analysis were strongly correlated ($p_{Slope}<0.001$, Pseudo $R^2 \geq 0.977$, Figure 1) with the ones calculated using Matlab (gold standard) and did not have significant intercepts ($p_{Intercept} \geq 0.052$). The initial lean angle had the strongest correlation (99.6%) and a residual SD of only 0.9-1.6deg, which is smaller than the SD for the maximum forward lean angle of 4.7-8.7deg (younger-older adults) [1]. Furthermore, it is second only to the LabVIEW method from our previous study, which had a residual SD of 0.6-0.9deg [3]. Step length had a correlation of 97.7% and a residual SD of 0.039-0.046m, which is smaller than the SD for step length at the maximum forward lean angle of 0.130-0.240m (younger-older adults) [1]. Finally, step velocity had a correlation of 98.2% and a residual SD of 0.17-0.31m/s, which is much smaller than the SD for step velocity at the maximum forward lean angle of 0.68-1.23m/s (younger-older adults) [1].

Table 1: Unconditional growth linear regressions for the three variables calculated using video analysis and Matlab (gold standard)

	p-value		
Variable	**Intercept**	**Slope**	**Residual SD**
Initial lean angle *	0.332	**<0.001**	**<0.001**
Step length †	0.495	**<0.001**	**<0.001**
Step velocity †	0.052	**<0.001**	**<0.001**

Significant p-values ($p \leq 0.05$) are **bolded**. * N=286/288 and † N=281/288 (2 and 7 Matlab variables discarded due to post-processing errors, respectively).

The video analysis method is equal in complexity but takes more time than the gold standard Matlab method. Indeed, it requires the same types of calculations, but cannot be automated. However, the video analysis method (≈100$) is much less expensive than the Matlab method (≈100k$).

CONCLUSIONS

Therefore, to accurately measure the maximum forward lean angle, as well as step length and step velocity, in a clinical setting, the video analysis method appears to be a much less expensive alternative to current technologies. Lean releases could thus be used to identify individuals at risk of falls or to evaluate the effectiveness of exercise-based fall prevention programs.

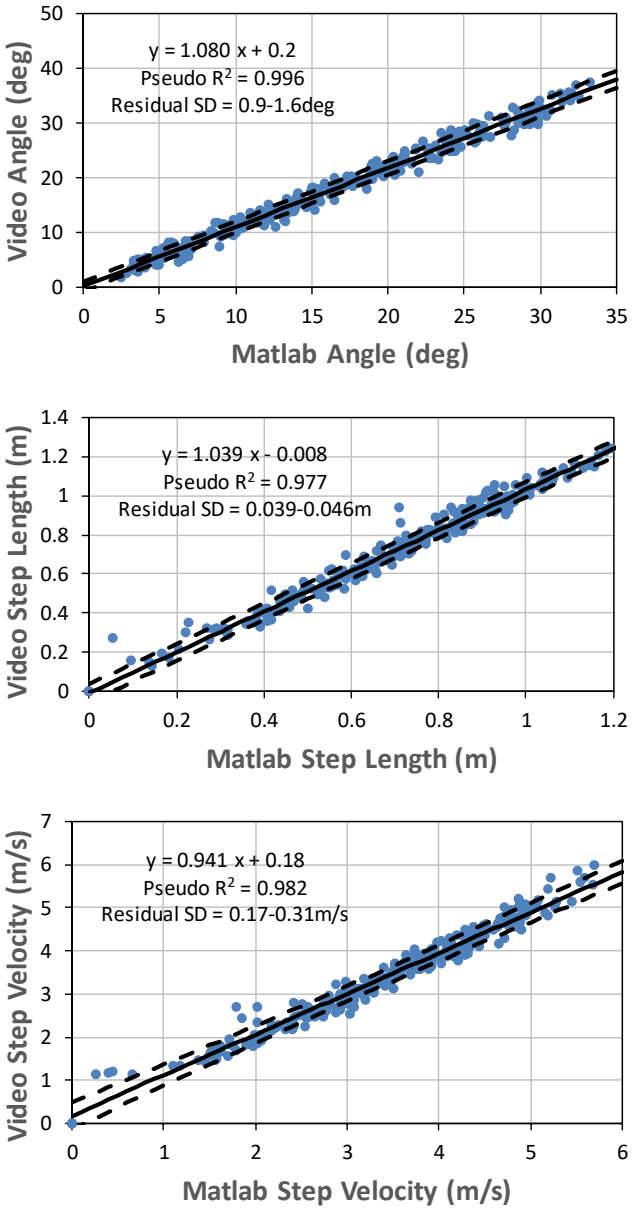

Figure 1: Unconditional growth linear regressions (mean±SD) for the three variables calculated using video analysis and Matlab (gold standard)

REFERENCES

1. Carbonneau E, Smeesters C. *Gait Posture* **39**, 365-371, 2014.
2. Carty CP, et al. *Age Ageing* **44**, 109-115, 2015.
3. Carbonneau E, et al., *41st Annu Meet Am Soc Biomech*, Boulder, CO, USA, 2017.

ACKNOWLEDGEMENTS

Antoine Guillerand for technical assistance, as well as a grant from the Ministère des Relations Internationales et de la Francophonie of the Quebec government for financial support.

INSTRUMENTATION OF A ROD ROTATION WRENCH FOR USE IN SCOLIOSIS SURGERY

[1]John M. Cummings, [1]Abdul A. Safi, [1]John Jacob Lopez, [1]Julia Noginova, [1]Sebastian Y. Bawab,

[1]Stacie I. Ringleb, and [2] H. Sheldon St. Clair

[1]Old Dominion University, Norfolk, VA, USA
[2]Children's Hospital of the King's Daughters, Norfolk, VA, USA
Email:SRingleb@odu.edu

INTRODUCTION

Scoliosis affects approximately 1.4 million children a year in North America; 3% of affected children require treatment, and 10% of them must undergo corrective surgery [1]. Scoliosis correction surgery is an invasive surgery which involves forming a rod to the patient's spinal curve and then adjusting it into the correct position using a variety of tools. One of the tools involved in the surgery is the Rod Rotation Wrench (RRW) (Alphatec Spine, Carlsbad, CA), which is used in conjunction with a rod gripper to rotate the spinal rods in the desired position. Because these tools are non-instrumented, surgeons do not have empirical data to help make surgical decisions. Therefore, the purpose of this project is to take the first step toward instrumentation of the wrench for use in surgery to accurately measure and display applied loads.

METHODS

A finite element model of the RRW was designed in SolidWorks (Dassault Systèmes, Waltham, MA) to find stress concentrations of the wrench. Stainless steel 465 was used for the tool's material property and was constrained at the open end in the XYZ direction. A distributed load of 50 lbf/in was applied toward the end of the wrench. Finer mesh elements were applied at the neck of the tool as it was predicted that stress would be condensed in that area. The analysis showed that the location of maximum strain was in the neck of the wrench. This was not an optimal location due to the dimension restrictions of the strains gauges, therefore, the strain gauges were placed at the top and bottom of the wrench at 0.04 meters from the center of the wrench head. (Fig. 1).

Figure 1: Strain gauge placement.

The RRW was then instrumented with 2 KFH-6-350-C1-11L3M3R strain gauges (Omega Engineering, Stamford, CT) placed on the top and bottom of the wrench in two NI-9945 quarter bridge completion circuits using a CompactDAQ Chassis (National Instruments Corp, Austin, TX) including NI-9237 and NI EDAQ-9172 modules. A custom LabVIEW VI (National Instruments Corp, Austin, TX) was constructed to display and collect strain data.

Calibration experiments for the RRW involved hanging weights on the wrench in 1 kg increments up to 5 kg (Fig. 2). Applied moments were calculated by multiplying the applied weight by the moment arm which was 0.181 meters. The resultant moment ranged from 0 to 8.87 Nm. The slope from the microstrain vs. applied moment curve displayed by the LabVIEW program was calculated to determine the multiplier that would be used to output moment from the strain gage readings.

The calculated moment from the calibration and moment calculations was then verified by measuring the applied moment with an ATI mini 58 six-axis force/torque transducer (ATI Industrial Automation, Apex, NC) and measured by the Motion Monitor (Innovative Sports Training, Chicago, IL). The fixture design for the verification experiment is

comprised of a spinal rod that is welded to a plate which was attached to the load cell (Fig. 2). The load was initially placed at the same location as in calibration (0.181 m moment arm) and then applied at 0.154 meters and 0.202 meters from the center of the wrench head, to verify that the location of the applied load will not affect the measured load.

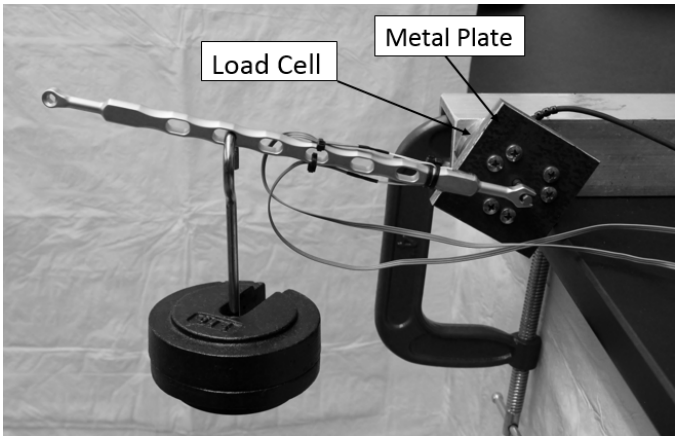

Figure 2: Testing setup and verification test

RESULTS AND DISCUSSION

The linear calibration factor was 46085 N-m/micro strain (Fig. 3). The offset in the calibration curves was addressed by performing an offset null calibration through the DAQ-assistant module in LabVIEW. The verification tests showed an average error of 2.99% between the reading from the load cell and the LabVIEW code (i.e., calculated from the strain gage measurements). The force input can be applied at any location due to the conversion factor being calibrated to the resultant moment at the axis/rotation instead of a specific force. This was verified by testing at a location closer to the strain gauge (0.154 m moment arm) which had an average error of 3.7% and at a location further from the strain gauge (0.202 m moment arm) with an average error of 1.3% .

The Bland-Altman method [2] identified a mean difference of -0.0015 N-m, with the mean +/- 1.96*SD from -0.348 N-m to 0.325 N-m (Fig 4). When used in practice, if a surgeon is comparing two different surgical procedures, if the difference between those loads are outside of the aforementioned confidence interval, then the variation in applied loads is worth considering in surgical decision-making.

The next steps to prepare this device for surgery is to develop a method for wireless signal transmission with instrumentation that can withstand the sterilization process.

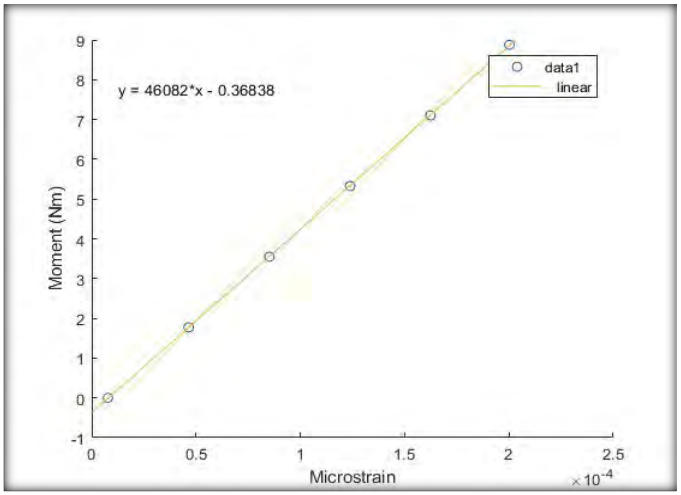

Figure 3: Sample Calibration Plot

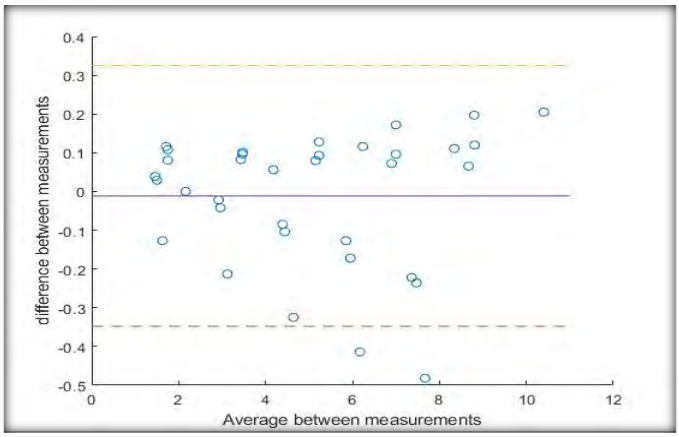

Figure 4: Bland Altman Plot comparing the measurement error between the Motion Monitor and LabVIEW

REFERENCES

[1] E. Lou et al. Proc IEEE Eng Med Biol 27th Annual Conference, Shanghai, China, 2006.

[2] Bland and Altman, *Lancet* . *327*(8476): 307-310, *1986.*

ACKNOWLEDGEMENTS

This project was funded by the Children's Health Foundation. We would like to thank Alphatec Spine for providing the wrench and Michael Polanco for his assistance with the experimental design.

REVISITING THE MINIMUM NUMBER OF STEPS TO ACCURATELY MEASURE STEP KINEMATICS DURING TREADMILL WALKING

David M. Desmet, Andrew B. Sawers, Mark D. Grabiner
University of Illinois Chicago, Chicago, IL, USA
Email: ddesme2@uic.edu

INTRODUCTION

More than 300,000 older adults suffer a hip fracture each year, over 95% of which result from a fall [1, 2]. Falls to the side increase the risk of hip fracture 6-fold [3], and the risk increases 30-fold if impact occurs directly at the hip [4].

Although the mechanisms responsible for falls to the side are unclear, step width and step width variability have been implicated to some extent. Step width variability has been prospectively associated with all-cause falls [5], while falls to the side have been specifically and prospectively associated with narrower step width compared to falls in other directions [6].

Further understanding of the relationship between step width, step width variability, and cause-specific or direction-specific fall-risk of older adults is reliant upon accurate and precise calculations of step width and step width variability. For young, healthy subjects walking on a treadmill, 400 consecutive steps was previously suggested as necessary to establish an accurate, subject-specific measure of step width and step width variability [7]. Beyond 400, and in the absence of potentially confounding variables such as fatigue, it was assumed that increasing the number of steps would only minimally affect the accuracy of the estimate.

There are populations for whom completion of 400 consecutive steps is not possible but for whom accurate measurement of step width and step width variability may be desirable. To our knowledge, there is no published evidence of how the accuracy (or precision) of step width calculations are affected by using less than 400 steps, or the extent to which 400 steps can be generalized to other populations. Therefore, the purpose of the present analysis was to assess the effect of using fewer than 400 consecutive steps on the calculation of step width and step width variability of healthy middle age and older women.

METHODS

The present study was a secondary analysis of step width data collected from twenty-four healthy women (59.5±6.8 yrs) who served as a control group in a previous study [8]. Following the acquisition of informed, written consent, and based on the assumption that 400 steps would be sufficient to acquire an accurate measure of step width [7], each woman walked on a microprocessor controlled, stepper motor-driven, dual belt treadmill for ten minutes at a self-selected speed. An eight-camera motion capture system operating at 120 Hz tracked the three-dimensional positions of 22 reflective markers, a subset of which were used to calculate step width.

The running mean and the associated running standard deviation functions of each step width time series were calculated. Estimates of step width or step width variability are said to be accurate when "the slope of the running function approaches zero" [7]. Therefore, we first applied a linear regression to the final 25% of each step width and step width variability running function to assess the extent to which the slope of each running function approached zero (Figure 1). The regression coefficient (slope) from each running function was extracted, from which the margin of error was computed for both step width and step width variability. The criterion for accuracy of step width and step width variability was considered to be met for those subjects whose regression coefficient fell within the margin of error.

For each time series found to have met the criterion for accuracy, the number of steps required to meet this criterion was then assessed. The mean and standard deviation of the final 25% of steps were calculated, allowing a range of ±3 standard

deviations about the mean to be established. A 50-point sliding window was used to iteratively progress through each running function. The first point of the first window for which all 50 points fell within the criterion range of ±3 standard deviations was established as the minimum number of steps required to meet the criterion for accuracy [7] (Figure 1).

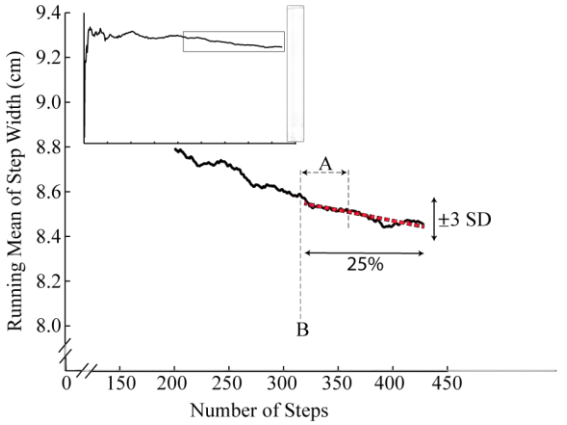

Figure 1: The insert depicts the full time series, while the body of the graph depicts the final 222 steps. A linear regression was applied to the final 25% of each time series (red dashed line), and the regression coefficient (slope) determined. If the slope coefficient was within the margin of error computed from all of the time series, a 50-point sliding window, starting at the first point, progressed through the time series (A) until all 50 points fell within three standard deviations of the mean value. The first point of this window was recorded as the required number of steps to reach an accurate and precise value for that subject and function (B).

RESULTS AND DISCUSSION

All step width time series were truncated to 422 steps, which was the fewest number of steps required by any subject to complete the ten-minute walking trial. Thus, the final 25% used to assess accuracy of each running function began at step 317.

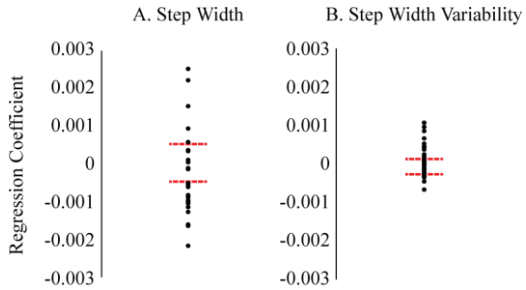

Figure 2: Regression coefficients calculated from the final 25% of the step width (A) and step width variability (B) running functions for each subject. The subjects with regression coefficients falling within the margin of error (red dashed lines) were determined to have met the criterion for accuracy for that running function.

Four-hundred consecutive steps of treadmill walking was insufficient to establish an accurate value for step width and step width variability for these healthy middle-age and older women. For step width, only 25 percent of the subjects met the criterion for accuracy (Figure 2a). For step width variability, only 42 percent of subjects met the criterion for accuracy and precision (Figure 2b).

Notably, those subjects who did meet the criterion for accuracy did so using fewer than the expected 400 steps. The number of steps required to calculate an accurate value was 264±55 for step width and 283±46 for step width variability.

CONCLUSIONS

The results suggest that the previously reported minimum of 400 steps necessary for an accurate estimate of step width and step width variability could not be generalized to middle age and older women during treadmill walking. Given the question of generalizability, and the potential importance of step width and step width variability to the issue of laterally-directed falls, further work to determine the minimum number of steps required for an accurate and precise estimate of step width and step width variability is warranted for all populations for whom step width and step width variability are thought to contribute to fall risk.

REFERENCES

1. *Hip Fracture among Older Adults* (Last updated September, 2016), cdc.gov
2. Pakkari J et al. *Calcif Tissue Int*. 65:183-187, 1999
3. Greenspan SL et al. *JAMA*. 271(2): 128-133. 1994
4. Nevitt MC & Cummings SR. *J Am Geriatr Soc*. 41(11): 1226-1234. 1993
5. Maki BE. *J Am Geriatr Soc*. 45: 313-320. 1997
6. Ko S et al. *J Aging Health.* 19(2): 200-212. 2007
7. Owings TM & Grabiner MD. *J Biomech*. 36: 1215-1218. 2003
8. Pater ML et al. *J Biomech*. 49:1128-1133. 2016

RELATIONSHIP BETWEEN REGIONAL LUMBAR POSTURES AND TRUNK MUSCLE FATIGABILITY DURING STANDING IN CHRONIC LOW BACK PAIN

[1]Eman A. Embaby, [1]Amira A. A. Abdallah, and [2]Mostafa A. Hegazy

[1] Cairo University, Giza, Egypt
[2] Southwest Minnesota State University, MN, USA
email: eman_ahmed@cu.edu.eg

INTRODUCTION

Low back pain (LBP) is a serious health problem affecting lumbar spine and adjacent joint mobility, leading to functional disability [1]. LBP is the most common cause of job related disability and missed word days [2].

Standing is a common working posture and is associated with an increased risk for non-traumatic low back pain secondary to cumulative sub-threshold loading of the spine [3]. Observational and biomechanical studies have shown that prolonged standing can cause a significant increase in intervertebral and vertebral endplate compression [4] as well as an increase in intradisc pressure [5], both of which are potential predictors of disc degeneration. Although numerous studies have reported an association between quickly fatiguing back muscles and LBP, these studies were based on endurance tests and not prolonged static postures adapted in the work place such as standing [6]. In addition, previous studies have focused on studying these relationships in manual labor workers ignoring other workers who also stand for prolonged periods of time, such as clinical instructors.

Thus, this study was conducted to: 1) compare lumbar spine posture in female clinical instructors with LBP and those with no LBP during prolonged standing, 2) investigate the relationship between regional lumbar spine postures and trunk muscle fatigue in the same two groups, and 3) investigate the ability of predicting muscle fatigue from lumbar spine postures.

METHODS

Fifteen female clinical instructors (age: 29.53±2.4 years, mass: 63.6±7 kg and height: 162.73±4 cm) with LBP that had existed periodically for at least six months and fifteen controls (age: 29.07±2.4 years, mass: 60±7.8kg, height: 162.8±6 cm) with no LBP. All participants were clinical instructors who stand 2-3 hours a day, 3-4 day per week.

Participants stood in a defined area (80x80cm) for thirty minutes while giving instruction about a bad posture. Sagittal plane upper (T12-L3), and lower (L3-S2) lumbar postures were recorded using 3D motion analysis (Qualisys, Gothenburg, Sweden) immediately before and after the standing task. Right erector-spinae (RES), left erector spinae (LES), right external oblique (REX), left external oblique (LEX), right rectus abdominis (RRA), and left rectus abdominis (LRA) muscle median frequencies were recorded using electromyography during the first and last five minutes of the 30-minute standing task.

A mixed design MANOVA was used to compare the two tested groups for median frequencies of the RRA, LRA, REX, LEX, RES, and LES during the first and last 5 minutes as well as the upper (T12-L3), and lower (L3S2) lumbar extension angles before and after performing the standing task. Furthermore, Pearson correlation coefficient was used to determine the relationships between the lumbar posture and median frequencies for all six muscles during the last 5 minutes of the standing task. Lastly, a multiple backward stepwise regression was used to predict muscle fatigue from lumbar spine position.

RESULTS AND DISCUSSION

Table 1 shows lumbar postures for both segments (upper, and lower). The greatest change observed in

the table is the greater L3-S2 angle in the LBP group compared to controls in post-testing. Indeed, this observation was confirmed by our MANOVA analysis which revealed a significantly greater L3-S2 extension posture in the LBP group (p=0.003). In addition, the LBP group showed significant increase in L3-S2 extension posture following the standing task (p=0.031). This increase in lower lumbar extension is most likely to reduce the load supported by the muscles and increasing that on passive structures.

Table 1: Mean ± standard deviation for lumbar segment angles pre- and post-standing

	T12-L3		L3-S2	
	Pre	**Post**	**Pre**	**Post**
LBP	15.5±3.4	16.1±6.4	17.8±5	20.7±6.8*~
Controls	16.4±5.4	15.8±5.1	15.9±6.4	14±4

*indicates significant LBP to controls difference
~ indicates significant pre to post difference

Table 2 shows the Pearson correlation between lumbar postures and median frequencies for all six muscles for both groups. For the LBP group, only T12-L3 showed significant moderate negative correlation with the right external oblique median frequency (r= -0.437, p=0.008). Regression analysis revealed that T12-L3 posture was the only significant predictor of the right external oblique median frequency (b= -2.642, p= 0.016) with no other significant predictors of trunk muscles' fatigability.

For the control group, only T12-L3 showed a significant weak negative correlations with LRA (r= -0.39, p=0.017).) and LES (r= -0.361, p=0.025). Regression analysis revealed that T12-L3 posture was the only significant predictor of the left rectus abdominis (b= -3.675, p= 0.01) median frequency with no other significant predictors of trunk muscles' fatigability.

Although it is well established that muscle fatigability has a direct impact on poor posture adjustment [7], there was only one significant correlation between lumbar posture and muscle fatigue for each group. This indicates that quantifying such relationships may be difficult especially when the objective is to predict muscle fatigue from lumbar posture. That may be due to several possibilities including natural variability of EMG signals as well as the different compensation mechanism for everyone. As individuals stand they tend to lean in different directions at any given point in time resulting in the need for different muscles to be active.

Any questions about this study should be addressed to:

Eman A. Embaby, PhD
eman_ahmed@cu.edu.eg

CONCLUSIONS

Patients with low back pain tend to adopt more extended lower lumbar posture during standing. Although trunk muscle fatigability is associated with adaptive changes in lumbar posture, quantifying this relationship during an occupation that involves prolonged standing may be difficult.

REFERENCES

1-Wong and Lee. *Hum Mov Sci,* 23, 2004
2-Van Nieuwenhuyse et al. Occup Med. 54, 2004.
3-Norman et al. Clin. Biomech. 13(8),1998.
4-Van Deursen et al. Clin. Biomech. 20, 2005.
5-Claus et al. J. Electromyogr. Kinesiol. 18:550e558, 2008.
6-Lee et al. J Rehabil Res Dev. 47(2), 2010
7. Embaby and Abdallah. Br J Sports Med. 47(10), 2013.

Table 2: Pearson correlation between lumbar postures and median frequencies for all six muscles

	LBP						Controls					
	RRA	**LRA**	**REX**	**LEX**	**RES**	**LES**	**RRA**	**LRA**	**REX**	**LEX**	**RES**	**LES**
T12-L3	0.17	0.09	-0.44*	0.30	0.11	-0.21	-0.27	-0.39*	-0.08	0.16	-0.02	-0.36
L3-S2	0.84	0.14	0.05	-0.004	-0.07	-0.31	-0.05	-0.15	0.09	-0.15	0.09	0.11

*indicates a significant correlation, correlation coefficients (r) are presented

CHARACTERIZATION OF A MINIATURIZED HORIZONTAL SLED FOR REPLICATION OF HEAD AND NECK ACCELERATIVE LOADING IN NOVEL LOW-ACCELERATION ENVIRONMENTS

[1,2]Patrick N. Estep, MS, [1,2]Adrienne M. Madison, PhD, [1,3]M. Reid Holderfield, [1]B. Joseph McEntire, and [1]Valeta Carol Chancey, PhD.

[1]U.S. Army Aeromedical Research Laboratory, Fort Rucker, AL
[2]Laulima Government Solutions, Orlando, FL
[3]Oak Ridge Institute for Science and Education, Oak Ridge, TN
Email: patrick.n.estep.ctr@mail.mil

INTRODUCTION

In the early 1980s, the U.S. Army Aeromedical Research Laboratory (USAARL) sought to develop a methodology to assess flight helmet retention systems under various scenarios [1]. The use of full horizontal sled test facilities with a complete anthropomorphic test device was deemed impractical due to cost and difficulties associated with inter-test reliability and repeatability. Other available methods lacked the capabilities to simulate inertial loading scenarios or non-severe accelerations. USAARL (J.L. Haley and B.J. McEntire) developed a mini-sled apparatus that provides controllable, realistic simulations of head and neck responses to non-destructive accelerative loading scenarios. It allows researchers to assess biomechanical parameters in surrogate heads and necks within and beyond levels that are suitable for human volunteer research.

The mini-sled apparatus is primarily comprised of five parts: (1) an impact pendulum, (2) a low-friction carriage, (3) a surrogate head and neck system, (4) a precision track, and (5) a braking mechanism.

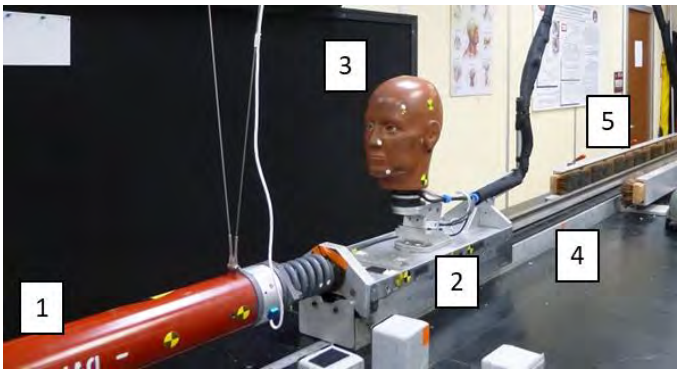

Figure 1: The mini-sled apparatus.

The pendulum is held by an electric magnet and is raised using an electric winch. The motor raises the pendulum to one of eight preset drop heights (ranging from 5.25 - 53.25 in. above the track), which controls the magnitude of acceleration input into the system. To simulate indirect impacts to the head, the pendulum impacts the carriage at the level equivalent to that of the seventh cervical and first thoracic vertebral junction [2]. Springs can be attached to the end of the pendulum facing towards the carriage assembly to buffer the impact between the pendulum and carriage, controlling the pulse shape applied to the sled.

Traditionally, the mini-sled has been used to assess scenarios relevant to high-acceleration aviation environments, including survivable aircraft crashes. Current volunteer research efforts at USAARL are focused on acute exposures and military operating environments with significantly lower inertial loading than previously tested on the mini-sled, specifically those related to dismounted Soldiers and parachutists.

The objective of this work was to characterize the range of achievable testing conditions of the mini-sled apparatus by varying the drop height and buffer spring to determine if non-aviation scenarios, such as dismounted and parachutist accelerative loadings, can be recreated in this controllable lab environment.

METHODS

Indirect impact testing was conducted starting with the lowest of the eight drop heights using four springs with different stiffness to produce resultant inertial loading scenarios. Drop heights were increased by one interval until all eight heights were assessed or the

spring fully compressed at impact. Each drop height and spring configuration was tested three times. The carriage was equipped with a Facial and Ocular CountermeasUres for Safety (FOCUS) headform and a Hybrid III neck. Headform accelerations and angular velocities, as well as neck forces and moments, were recorded at 20 kHz and filtered according to guidelines set forth by the Society of Automotive Engineers (SAE) J211-1. High-speed video was also recorded to track the angular displacement of the headform relative to the carriage.

RESULTS AND DISCUSSION

Peak sled accelerations ranged from 4.7 to 43.4 Gs. The range of standard deviations for peak sled accelerations across all test configurations was 0.02 to 1.08 Gs. The ranges of achievable peak conditions for the head and neck from the indirect impact testing on the mini-sled are reported below in Table 1.

Table 1: Range of absolute values achievable by the mini-sled.

Parameter	Range
Head Acceleration, X (G)	3.2 - 21.1
Head Acceleration, Z (G)	0.3 - 23.2
Head Angular Rate, Y (deg/s)	330.8 - 2294.1
Upper Neck Force, X (lbf)	26.6 - 192.0
Upper Neck Force, Z (lbf)	1.6 - 249.2
Upper Neck Moment, Y (lbf*in)	107.3 - 684.2
Lower Neck Force, X (lbf)	48.6 - 424.3
Lower Neck Force, Z (lbf)	18.8 - 197.0
Lower Neck Moment, Y (lbf*in)	355.3 - 2021.6
Forward Rotation (deg)	10.7 - 60.3
Backward Rotation (deg)	6.54 - 44.6

The lower levels of head acceleration responses are within the ranges observed in military environments related to parachutists and dismounted Soldiers [3]. The levels of achievable exposures on the mini-sled also fall within those observed in sports environments, such as head injuries in football [4]. Additional springs may be used to expand the range of testing to other applicable environments.

In the future, the mini-sled exposures can be used to validate the head and neck responses observed in current lab- and field-based volunteer research efforts at USAARL. Additional work will include the quantification of relationships between helmet stability and neck loading over a range of accelerations, as well as the development of a lower neck injury criteria for use in high acceleration aviation scenarios.

CONCLUSIONS

The USAARL mini-sled provides non-destructive, repeatable, controllable, realistic simulations of head and neck responses to various accelerative loading scenarios in many environments, including military operations and sports.

REFERENCES

1. Gruver, D.M. & Haley, J.L. Development of a Test Method for Evaluating the Effectiveness of Helmet Retention Systems, *USAARL Letter Report 88-5-4-3*. Fort Rucker, AL, 1988.

2. Brozoski, F.T. & Licina, J.R. Static and Dynamic Retention Assessment of the HGU-56/P Aircrew Integrated Helmet System Equipped with Quick-release ALPHA and Snap-fastener Retention Assemblies, *USAARL Report No. 2006-02*. Fort Rucker, AL, 2006.

3. Shivers, B.L., et al. Mass Properties Comparison of Dismounted and Ground-Mounted Head-Supported Mass Configurations to Existing Performance and Acute Injury Risk Guidelines. *Proceedings of American Society of Biomechanics 2017*. Boulder, CO, 2017.

4. Rowson, S. Linear and Angular Head Acceleration Measurements in Collegiate Football. *Journal of Biomedical Engineering*. Blacksburg, VA, 2009.

ACKNOWLEDGEMENTS

The authors would like to acknowledge Mike Henry and Jackson Hayes for their contributions during testing; Tyler Rooks, Joe McEntire, and Fred Brozoski for their guidance; and Dr. Bethany L. Shivers for making this work possible.

DETERMINING THE ODDS OF EXCEEDING NIOSH RECOMMENDED L5/S1 SPINAL COMPRESSION FORCE USING A BAYESIAN NETWORK IMPLEMENTATION OF A BIOMECHANICAL LIFTING MODEL

Richard E. Hughes

University of Michigan, Ann Arbor, MI, USA
email: rehughes@umich.edu

INTRODUCTION

Litigation support is one area biomechanical models of lifting are used. Occupational biomechanics models of lifting tend to be deterministic, which creates a challenge of developing an opinion to meet a stochastic legal standard of "more probable than not". A second challenge a biomechanics expert may face is that traditional job analysis methods do not explicitly include the injury status of the plaintiff, which is available to the biomechanics expert through reports, depositions, and testimony of medical experts. Hughes [1] published a Bayesian network implementation of an established lifting model [2] that incorporates disk injury addresses these challenges. The output of the model is the probability density function of L5/S1 compression force.

However, an expert submitting a report in a civil case regarding a low back disc injury faces the problem of developing an analysis that meets the standard of proof "more probable than not." The objective of this project was to adapt the Bayesian network model of lifting [1] to predict the probability of L5/S1 compression force exceeding 3400 N because the standard of proof required the probability to exceed 0.5. The model developed here is academic; it is not being used by the author for expert work.

METHODS

A static biomechanical lifting model for predicting L5/S1 compression and shear [2] was implemented as a Bayesian network (BN).[3] Nodes represened random variables, which can be external forces, joint moments, joint angles, or joint reaction forces. The arcs represented either probabilistic or deterministic relationships between nodes. Hand forces and joint angles were random inputs to the model. The example presented here is for a 50-percentile (height and weight) female. The directed acyclic graph inside the dotted box in Figure 1 shows the BN developed in [1].

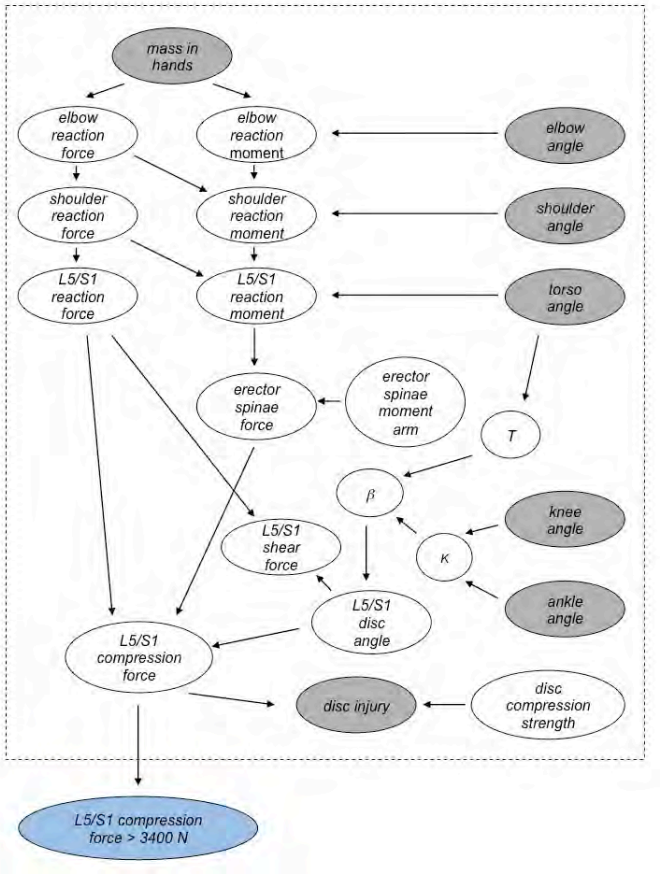

Figure 1: Bayesian network implementation of static two-dimensional lifting model. Gray, white, and blue nodes represent input, computational, and output nodes, respectively.

Errors in joint angle estimation were modeled as random variables. The average (SD) joint angles from horizontal were 82° (9.4°), 114° (9.4°), 40° (6.3°), 192° (7.9°), and -56° (11.8°) for the ankle, knee, torso, shoulder and elbow, respectively. The Mass in

the hands was simulated at 5 kgs increments from 0 to 70 kgs.

An interference model of structural reliability was implemented (two bottom nodes in Figure 1) to incorporate injury status into the model. For a full description of this Bayesian network model and its verification, see [1].

The BN model was augmented with a single node, *L5/S1 compression force > 2400 N*, representing a Boolean random variable that takes on a value of true if and only if the random variable *L5/S1 compression force* exceeds 3400 N. This full BN model was used for simulations presented in Figure 2, with probabilities expressed as odds. The threshold of 3400 N was selected because it was specified as a design limit in the 1981 NIOSH work practices guide [4] and cited as the basis for the revision of the NIOSH lifting equation [5]. The BN was implemented in AgenaRisk software (Agena, Cambridge, UK) and run on an iMac.

RESULTS AND DISCUSSION

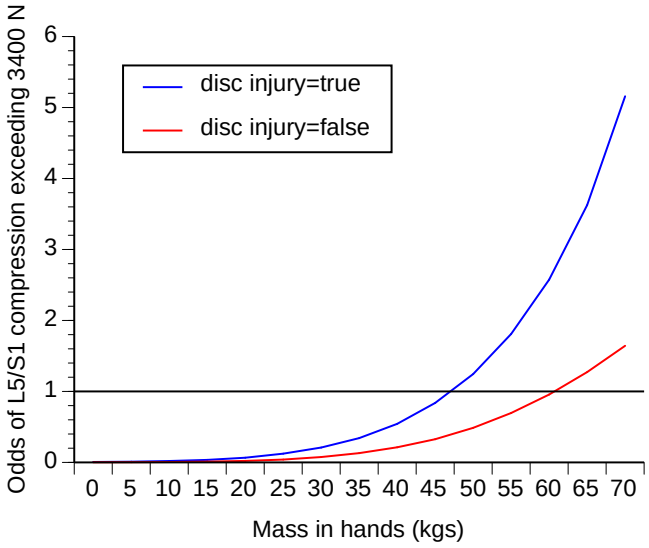

Figure 2: Odds of L5/S1 compression force exceeding 3400 N as a function of mass held in hands for two disc injury states (true and false).

Including injury status in the Bayesian network analysis strongly affects the odds of L5/S1 spinal compression force exceeding 3400 N (Figure 2). For the lift posture analyzed, the odds of exceeding the 3400 N threshold increased much faster with mass in hands when *disc injury* was set to true than when it was set to false. Below a hand load of 47.0 kgs the odds of exceeding the threshold was less than 1.0 for both *disc injury* states (true and false); similarly, above 60.7 kgs both disc injury states produced odds estimates greater than 1.0. Since an odds of 1.0 is the threshold for determining if an event is "more probable than not," the region between 47.0 kg and 60.7 kg would produce different opinions using that standard of proof. At a hand load of 55 kgs, for example, the odds would be 1.81 and 0.70 for the true and false *disc injury* states, respectively.

CONCLUSIONS

This model addresses the challenges a biomechanics expert may make in developing an opinion in a civil litigation case involving lifting. Specifically, it solves the problem of developing a stochastic estimate of whether spinal compression force exceeds a well-recognized threshold put forward by the NIOSH that can be used to directly address the "more probable than not" standard of proof expected in a tort law.[6]

CONFLICT OF INTEREST

The author has no conflict of interest to disclose. The author is not using the model in support of any legal cases.

REFERENCES

1. Hughes, RE. *Applied Bionics and Biomechanics* 2017:1-7, 2017.
2. Chaffin, DB *et al*. *Occupational Biomechanics*. John Wiley: New York, 2006.
3. Fenton, N and Neil, M. *Risk assessment and decision analysis with Bayesian networks*. Taylor and Francis: New York, 2013.
4. NIOSH. Work practices guide for manual lifting. DHHS: Cincinnati, 1981.
5. Waters, T. *et al*. *Ergonomics* 36:749-776, 1993.
6. Redmayne, M. *The Modern Law Review* 62:167-19, 1999.

NORMATIVE CERVICAL SPINE KINEMATICS OF A CIRCUMDUCTION TASK IN A HEALTHY COHORT

[1] Craig C. Kage, [1] Nathaniel E. Helwig, [1] Benjamin Hyatt, [1] Jessica Blaisdell, [1] Kayla Mabamba, [1] Lisa Nguyen, [1] Zachary Eitel, [1] Mary H. Foltz, [1] Arin M. Ellingson

[1] University of Minnesota, Minneapolis, MN, USA
email: ellin224@umn.edu, http://z.umn.edu/MRBL

INTRODUCTION

Neck pain prevalence in the adult population has been estimated to be as high as 30-50% annually [1]. Current clinical physical examination techniques are typically limited to basic cardinal plane range of motion (ROM) assessment and special tests with subjective interpretation. Additionally, existing diagnostic imaging techniques have been found to offer limited insight into true pathoanatomic causes of neck pain and are generally limited to two-dimensional, static analysis [2]. There is a growing need for dynamic, three-dimensional (3D), objective examination to better quantify cervical spine motion and function [3]. A better understanding of normative motion will allow for more effective comparisons to those with pathology. Recent work has utilized a novel, neck circumduction task (Figure 1) that incorporates all cardinal plane motions into one continuous head-rolling task to examine dynamic, 3D cervical spine kinematics at end range [4]. Furthermore, recent advanced statistical analyses have proven to be effective in the evaluation of continuous, functional biomechanical data beyond the standard and limited approach of only examining specific time points [5].

The purpose of this study was to establish normative and predictive intervals of cervical spine kinematics for a circumduction task in a healthy cohort. The goal of establishing normative cervical spine kinematics is to gain a better understanding of functional and dynamic motion for improved diagnosis, treatment, and comparative assessment of those with neck pain.

METHODS

Twenty subjects (26.5±7.1 years of age, 11 females, 9 males) were recruited on the University of Minnesota – Twin Cities campus. Participants were excluded if they had a history of neck pain, trauma, or conditions that might impair neck mobility. Two separate data collections were completed with 1-2 weeks between the initial and follow-up collection. Only the second session was analyzed to minimize potential learning effect. Data was collected at 100Hz within an eight-camera Vicon set-up in a standardized, seated position (Vicon Nexus software and MX40 camera system, Vicon, Oxford, UK). Retroreflective markers were secured to each subject to define the head and torso as separate rigid bodies. A custom helmet apparatus was used for the head and a custom-cluster consisting of four markers located at the sternum was used to define the torso (Figure 1). Additional anatomic markers were used to define each local coordinate system (Head: bilateral mandibular condyle, external occipital protuberance; Torso: suprasternal notch, xiphoid process, C7 and T8 spinous processes). Local coordinate system origins were assigned to the midpoint between bilateral mandibular condyles for the head and to the suprasternal notch for the torso with X positive anteriorly, Y positive to the left and Z positive superiorly for both (TheMotionMonitor Version 9.31, Innovative Sports Training, Inc. Chicago, IL, USA). Three trials each of left and right circumduction were completed at the participants' preferred pace.

Data were filtered (4th order, zero-lag, Butterworth filter with 6Hz cutoff frequency) and exported as a YXZ Euler sequence. To account for subject selected pacing, each circumduction trial was normalized by max flexion (0%, 100%), max lateral bending (25% and 75%; left and right), and max extension (50%) (Figure 1). (MATLAB, R2016B, The MathWorks, Inc., Natick, MD, USA). Two-way mixed effects smoothing spline analysis of variance (SSANOVA) was performed (time and direction as predictors) for all circumduction trials (R Core Team, 2017. R: A Language and Environment for Statistical Computing. R

Foundation for Statistical Computing, Vienna, Austria) [5-6].

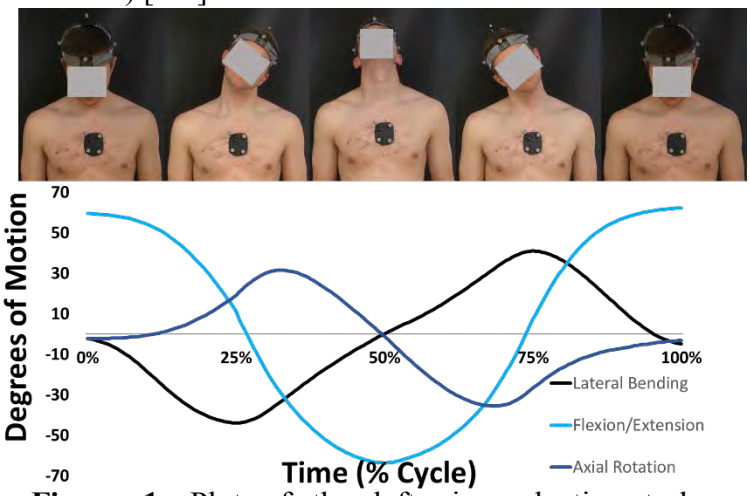

Figure 1: Plot of the left circumduction task, normalized and divided into cardinal plane components.

RESULTS AND DISCUSSION

Time-normalized circumduction results for all trials of session two (3 trials left, 3 trials right circumduction; 120 total trials) are divided into component cardinal plane motions and displayed in Figure 2 with 95% confidence (top) and prediction intervals (bottom). Confidence intervals represent the variability in the collected data. They were very narrow and comparable between left and right circumduction tasks. Prediction intervals represent the increased variability associated with predicting a new observation, and therefore were wider than the confidence intervals, as expected. For our particular circumduction data, lateral bending demonstrated the least amount of variability and was coupled with ipsilateral axial rotation. Lateral bending and flexion/extension motions approached expected end-range of motion values, whereas axial rotation did not approach typical end-range of motion values [7].

CONCLUSIONS

The results of this study demonstrate the feasibility of normalizing a cyclic, novel circumduction task into normative prediction intervals to assess cervical spine range of motion. Future work will focus on the full age spectrum and compare these normative values to a symptomatic cohort to determine possible diagnostic utility.

REFERENCES

1. Hogg-Johnson, et al. *Eur Spine J* **17**, S39-S51, 2008; 2. Nordin M, et al. *J of Manip. Phys Ther* **32**, S117-S140, 2009; 3. Andersson GB, et al. *JBJS* **88** 110-114, 2006. 4. Ellingson AM., et al. *Clin Biomech* **28**, 731-735, 2013; 5. Helwig NE, et al. *J Biomech* **49**, 3216-3222. 2016. 6. Helwig, N.E., 2017. bigsplines: Smoothing Splines for Large Samples. R package version 1.1-0.URL https://CRAN.Rproject.org/package=bigsplines 7. Ferrario VF, et al. *J of Orth. Res* **20**, 122-129, 2002.

ACKNOWLEDGEMENTS

This project was supported by NIH/NICHD K12HD073945, NIH/NIAMS T32 AR050938 Musculoskeletal Training Grant, and the University of Minnesota Institute for Engineering in Medicine Seed Grant Program.

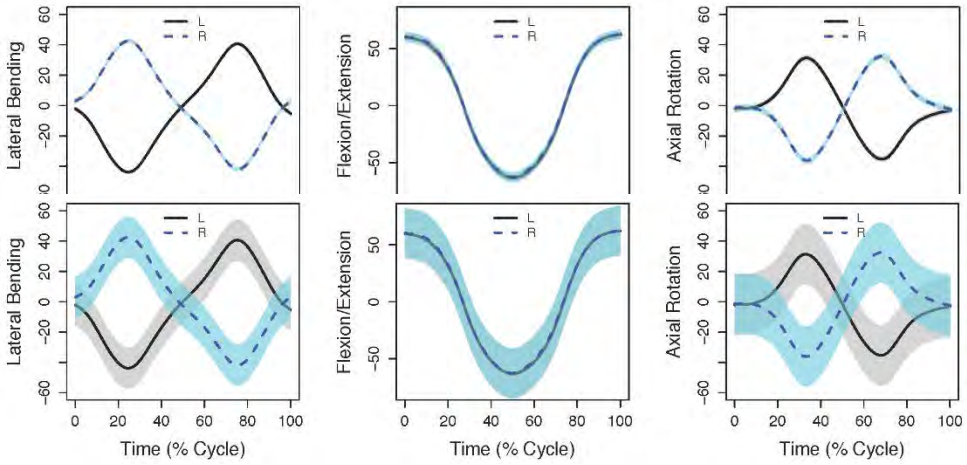

Figure 2: Normalized left and right circumduction tasks for all second session trials divided into component cardinal plane motions. (Top) 95% confidence intervals, (Bottom) 95% prediction intervals.

LUMBAR SPINE BIPLANE FLUOROSCOPY VALIDATION VIA AN AUTOMATED SHAPE-MATCHING ALGORITHM

[1]Craig C Kage, [2]Mohsen Akbari-Shandiz, [1]Mary H Foltz, [1]Rebekah L Lawrence, [1]Taycia Brandon, [1]Eric Twohey, and [1]Arin M Ellingson

[1] University of Minnesota, Minneapolis, MN, USA
[2] Mayo Clinic, Rochester, MN, USA
email: ellin224@umn.edu, web: http://z.umn.edu/MRBL

INTRODUCTION

Biplane fluoroscopy is an emerging imaging technology that has proven to be an accurate, valid method for non-invasively acquiring spinal motion at the segmental level [1-3]. Three-dimensional (3D), dynamic imaging such as this provides exquisite detail that can provide insight into motion patterns and pathways to enlighten clinical care for various spinal pathologies. Due to each biplane fluoroscopic imaging system's unique set-up, each laboratory and system set-up needs to be validated prior to data collection on human subjects. The ability to continuously track the vertebrae throughout the motion is often performed frame-by-frame through manual shape-matching. This process is very tedious, and accuracy can vary based upon the individual's familiarity with the anatomy when processing the data. Therefore, we aimed to develop an automated, customized shape-matching algorithm to assess continuous motion observed with biplane fluoroscopy and validate the accuracy against the golden standard, radiostereometric analysis (RSA), for lumbar spine kinematics.

METHODS

A fully intact fresh-frozen cadaveric specimen (55-year-old male) was used for data collection. Four tantalum beads were implanted into the posterior side of the lumbar vertebrae (L3 and L4) to facilitate RSA. Following bead placement, a computed tomography (CT) scan was obtained (Siemens Somaton Senation 64; Forchheim, Germany; 120 kVp; voxel size: 0.30×0.30×0.60mm). Dynamic fluoroscopic images were collected with our custom biplane fluoroscopy system (Imaging Systems and Services, Inc.; Painesville, OH, USA). The biplane system setup consisted of two 16″ image intensifiers (Thales 9447 QX; North American Imaging, OH, USA) with high-speed cameras capturing at 60Hz (Xcitex, ProCapture, Woburn, MA, USA). The two planes were offset by 90° from each other – one system was oriented in the sagittal direction (parallel to horizontal) and the second system in the anterior-posterior direction (8° above the horizontal), Figure 1. Source-to-image distance (SID) was 167cm. Acquisition parameters for the biplane were 80kV, 630 and 200mA (sagittal and anterior-posterior system, respectively), and 5.07ms. A radiographic wedge filter was positioned in the system set in the sagittal plane (Ferlic Filter LLC, White Bear Lake, MN, USA). The cadaveric specimen was inverted, and a handled apparatus was used to passively simulate lumbar flexion from an extended position. An attenuator was incorporated along the lumbar spine to minimize 'wash-out' of the vertebral bodies in the sagittal view [4].

From the CT images 3D bone models were reconstructed, the centroid of each bead was determined, and anatomic coordinates were established (Mimics; Materialise, Plymouth, MI, USA), Figure 1. Prior to shape-matching, the beads were masked to avoid potential bias throughout the shape-matching process (ImageJ/Fiji, US NIH, Bethesda, MD, USA).

Fluoroscopic images from a single trial of flexion (100 frames) were undistorted (XMALab, Brown University, RI, USA) and the 3D position of each bone model was set for an initial frame (AutoScoper, XROMM, Brown University). The subsequent frames were tracked with the automated shape-matching algorithm. The algorithm incorporated a standard ray casting approach to generate digitally reconstructed radiographs (DRR) and a 2D-3D image registration algorithm (Nelder-Mead Simplex optimization) applying a max correlation similarity measured to shape-match the DRR's onto the biplane radiographic projections based off of an initial frame. RSA was also performed for the trial (XMALab, Brown University, RI, USA)

Prior to statistical analysis, both the shape-matching and RSA output data were filtered with a low-pass, 4th order Butterworth filter (3Hz cutoff frequency) [3]. Filtered output from the shape-matching algorithm was directly compared to the RSA for both the rotation and translations at each level (L3 and L4) and intersegmentally (L3/L4). Bias, precision, and root mean square error (RSME) were calculated at each of the levels throughout the flexion motion trial and averaged across the levels.

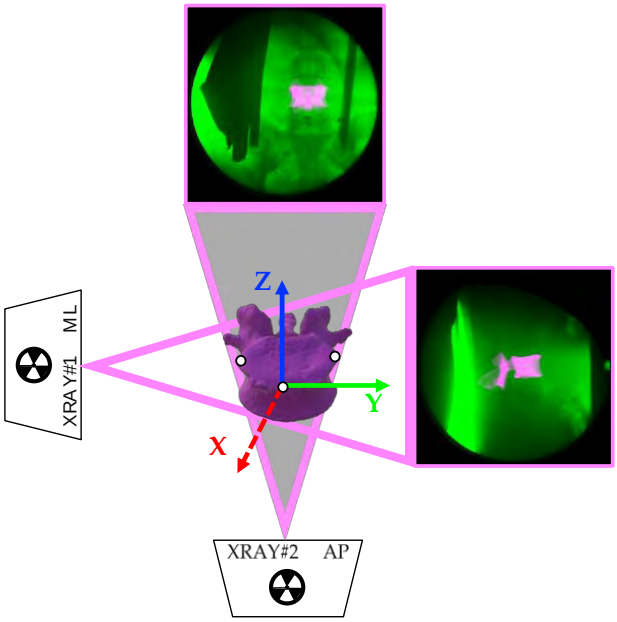

Figure 1: Reconstructed L4 CT bone model inset within the biplane fluoroscopic set-up for flexion motion; Medial-Lateral (ML), Anterior-Posterior (AP). Local coordinate system and anatomic landmarks (white) located on the superior endplate (anterior, lateral left, and lateral right).

RESULTS AND DISCUSSION

Table 1 displays the results of the bias, precision, and RSME calculations. Average segmental accuracy were sub-degree and sub-millimeter, and the intersegmental accuracy were sub-degree and sub-millimeter excluding translations in the Z-direction (-1.05mm). At the segmental level, the greatest error occurred about the Y-axis (FE) and in the X-direction (AP) for rotations and translations, respectively. This is likely because the anterior margin of the vertebral body is faint. The intersegmental accuracy had the greatest error about the Y-axis (bias), Z-axis (precision), and X-axis (RSME) for rotations. Intersegmental accuracy had the greatest error in the Z-direction. Maximum average RSME was determined to be less than 0.60° and 1.13mm. Bias and precision values are similar to previous publications for flexion of the lumbar spine [1-2].

CONCLUSIONS

Our results show that our biplane fluoroscopy system is within appropriate accuracy for the lumbar spine with our customized, shape-matching algorithm.

REFERENCES

1. Anderst et al. *The Spine Journal.* 8:991-7, 2008.
2. Wu et al. *Eur Spine J.* 23:2350-8, 2014.
3. Anderst et al. *Spine.* 36(6), E393-400, 2011.
4. Aiyangar et al. *J Biomed Eng.* 136:011004, 2014.

ACKNOWLEDGEMENTS

This project was supported by NIH/NICHD K12HD073945, F31HD087069, and the Minnesota Partnership for Biotechnology and Medical Genomics (MHP IF #14.02).

Table 1: Average kinematic summary of the bias, precision, and RMSE for segmental (L3 & L4) and intersegmental (L3/L4) motion. Lateral bending (LB), Flexion-Extension (FE), Axial Rotation (AR), Anterior-Posterior (AP), Medial-Lateral (ML), Superior-Inferior (SI).

	Segmental Accuracy			Intersegmental Accuracy		
Rotation (degrees)	**LB (X)**	**FE (Y)**	**AR (Z)**	**LB (X)**	**FE (Y)**	**AR (Z)**
Bias	-0.13	0.32	0.18	0.18	0.88	0.56
Precision	0.21	0.24	0.22	0.27	0.37	0.42
RMSE	0.26	0.51	0.36	0.60	0.18	0.29
Translation (mm)	**AP (X)**	**ML (Y)**	**SI (Z)**	**AP (X)**	**ML (Y)**	**SI (Z)**
Bias	-0.60	0.27	-0.37	0.33	-0.05	-1.05
Precision	0.22	0.16	0.28	0.18	0.24	0.43
RMSE	0.64	0.31	0.55	0.37	0.25	1.13

PASSIVE AND ACTIVE CHARACTERISTICS OF THE SMOOTH MUSCLE OF THE STOMACH AND ITS FINITE ELEMENT SIMULATION

[1] Jaemin Kim, [1] Hunhee Kim, [1] Taekyung Lee, [1] Youngho Lee, [1] Soonmoon Jung, [1] Beomgeun Jo, [1] Jeongwoo Lee and [1] Junghwa Hong

[1] Korea University, Sejong City, Republic of Korea
email: hongjh32@korea.ac.kr, web: http://kucie.korea.ac.kr/

INTRODUCTION

The smooth muscle which cannot do the conscious control as an involuntary muscle occurs in the stomach, intestines, bladder and blood vessel. The abnormal contraction of the smooth muscle has been reported to be the major cause of internal diseases such as high blood pressure, asthma and indigestion. For accurate diagnosis and treatment of internal diseases, detailed analysis of biomechanical behavior and physiological characteristics of the smooth muscle is required. The purposes of this study were to obtain the passive and active characteristics of the smooth muscle of the porcine stomach by the progress of in vitro experiments and to develop the smooth muscle FE (finite element) model to simulate active behavior of gastrointestinal tract.

METHODS

This study was conducted in two phases. In the first phase, to obtain passive and active characteristic of the smooth muscle, tensile, isometric contraction and isotonic contraction in-vitro experiments were performed on the porcine stomach. In the second phase, an active continuum smooth muscle model was developed based on the experimental results. The stomach was extracted from gnotobiotic pigs. The whole process of storage and specimen preparation (size: 3x1 cm) of the extracted stomach was conducted in PBS (Phosphate-buffered saline) solution with cold condition (2-5 ℃) in order to prevent loss of the energy source for the muscle contraction. The tensile test was done on a universal testing machine (displacement resolution 0.005 mm, sampling frequency 100 kHz, test speed 30 mm/min) to determine the passive one-dimensional stress-strain relationship. Isometric and isotonic tests were performed to measure the active material properties of the stomach tissues. The uppermost and lowermost stomach specimen were connected to the stainless steel jig and the jig at the lowermost region was fixed on the bottom of the organ bath shown in Figure 1. In the case of the jig at the uppermost region, it was connected the isometric sensor (TRI-201; Harvard Apparatus, Holliston, USA; range 0-5 gf, resolution 5 mgf) during isometric contraction experiment and the isotonic sensor (TRO-015; Harvard Apparatus, Holliston, USA; range ±24 mm, resolution 0.25 mm) during isotonic contraction experiment, respectively. Acetylcholine (1 mM, 300 µl) was used to produce muscle contraction and the few minutes of initial rest time for tissue relaxation were taken before inducing stomach muscle contraction. The smooth muscle FE model, which is presented in Figure 2, was developed by the combination of the continuum elements with passive muscle properties and the truss elements with active muscle properties. The passive properties were described by a QLV (quasi-linear viscoelastic) material model. The passive tensile response curve was employed for curve fitting and fitting data was used as input for initial values of the QLV material parameters. The active properties were described by a Hill-type muscle model. The isometric and isotonic experimental results were used as input for the muscle parameters.

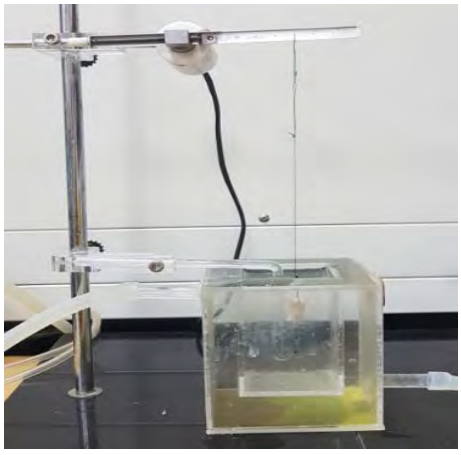

Figure 1: The organ bath for isometric and isotonic experiments of the porcine stomach specimen.

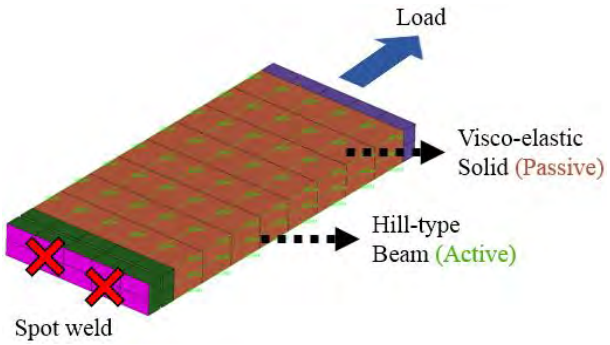

Figure 2: The smooth muscle FE model of the porcine stomach specimen.

RESULTS AND DISCUSSION

As a result of the tensile test, the tensile response, which is the stress-strain curve, showed non-linear, viscoelastic and hyperelastic material behaviors. The average ultimate stress was measured, 137 kPa at 0.56 strain. The isometric contraction experiment carried out showed that the maximum isometric contractile force on the force – relative length relationship curve was measured 14.9 mN at the relative length 1.0. The force – velocity relationship curve was derived from the results of the isotonic experiment which is another experiment performed on the porcine stomach specimen. The maximum muscle contractile velocity on the force – velocity curve was 64.8 μm/s.

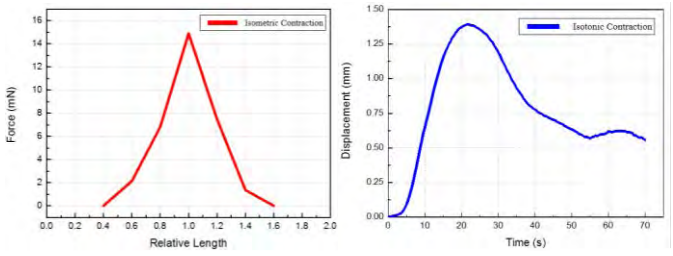

Figure 3: The results of the isometric (left) and isotonic (right) contraction test.

The specimen FE model of the smooth muscle was developed based on the results obtained from experiments. The results of smooth muscle simulation were agreed well with the experimental response including static tetanic muscle stimulation and relaxation, as well as dynamic stretch and release with muscle activation.

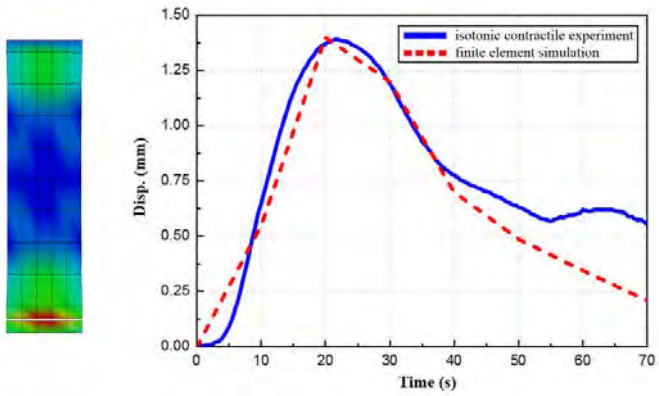

Figure 4: The validation results of the developed smooth muscle FE model.

CONCLUSIONS

Although the maximum muscle force varies, the overall passive and active response of the smooth muscle were similar with skeletal muscle. This study has significant implications for the understanding of the smooth muscle physiology. Based on the passive and active characteristics obtained from experiments, it will be possible to develop an active continuum smooth muscle model. Developed smooth muscle FE model will be suitable for use in analysis of the abnormality in the digestive system or stomach and development of new technology medical device.

REFERENCES

1. Fung, Yuan-cheng. *Biomechanics: mechanical properties of living tissues,* Springer Science & Business Media, 2013.
2. Hill, A. Vo. The heat of shortening and the dynamic constants of muscle. In *Proc. R. Soc. Lond. B.*, 126, 136-195, 1992.

ACKNOWLEDGEMENTS

ANALYSIS OF STRESS WAVE PROPAGATION BY AN ANATOMICAL FINITE ELEMENT MODEL OF THE SKULL WITH THE SUTURE

[1] Yoshimori Kiriyama, [1] Shunsuke Iwamoto, [1] Teppei Mano and [2] Kotaro Oshio

[1] Kogakuin University, Tokyo, JAPAN
[2] St. Marianna University, Kanagawa, JAPAN
email: kiriyama@cc.kogakuin.ac.jp, web: http://www.kogakuin.ac.jp

INTRODUCTION

The cranium in the skull is constructed with the frontal bone, parietal bone, temporal bone, occipital bone mainly. Also, the cross sections of these bones consist of three layers where the diploe as the cancelous bone is put between the external and internal tables as the cortical bone. At the suture region, there is not the diploe, and the external and internal tables make the serrate suture and squamous suture. This means that the skull has distribution of material properties at the suture region, and also stress would be distributed over the skull. In this study, we developed anatomical precise finite element model of the skull with the suture, and compared the difference of the stress wave propagation on the skull between with and without the suture.

METHODS

We obtained the skull structure without traumatic injury from CT images, and then constructed the finite element model of the skull. As shown in Fig.1, the diploe, and the external and internal tables were extracted from the images.
In this study, the sagittal suture, coronal suture and lambdoidal suture were reproduced. The suture regions of them were recognized as the overlapped part by both of the external and internal tables in the cross section of the CT images. Therefore, we extracted the suture region as one part with the overlapped width without separation of the external and internal tables as shown in Fig.1.
The skull surface with the suture region, we constructed the finite element model of the diploe with solid elements. Moreover, the external and internal tables were modeled as shell elements wrapping the diploe elements. The mesh size was 5.4 mm averagely. The coronal, sagittal, lambdoidal sutures were distinguished based on the extracted surfaces of the skull. The external and internal sutures were given Young's modulus of the cortical bone (ρ =2.0 × 10^3 kg/m^3, E= 15.0 GPa, ν =0.22), while the diploe was given the Young's modulus of the cancelous bone (ρ=1.3 × 10^3 kg/m^3, E=1.0 MPa, ν=0.24). In this study, we had two kind of the skull finite element models. One has the suture, and the other does not have the suture. The model with the suture was anatomical precise model and was assumed that the suture was combined with the cortical bones uniformly. Hence the diploe in the suture region was set as the cortical bone.
The bottom of the occipital bones was fixed completely. To apply load to the models, a sphere impactor (D=96 mm, m=1.213 kg) was dropped with 7.2 m/s from the superior to the top of the skull [1]. In the analysis, the impactor was used as a rigid body. We used RADIOSS (Ver.14, Altair Engineering) as a solver to analyze the stress, and dynamical solution was calculated explicitly.

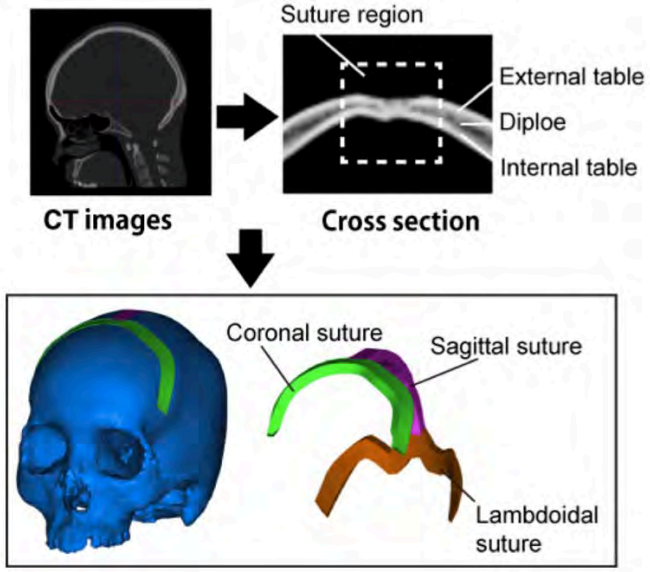

Figure 1: The skull finite element model with the suture constructed from CT images.

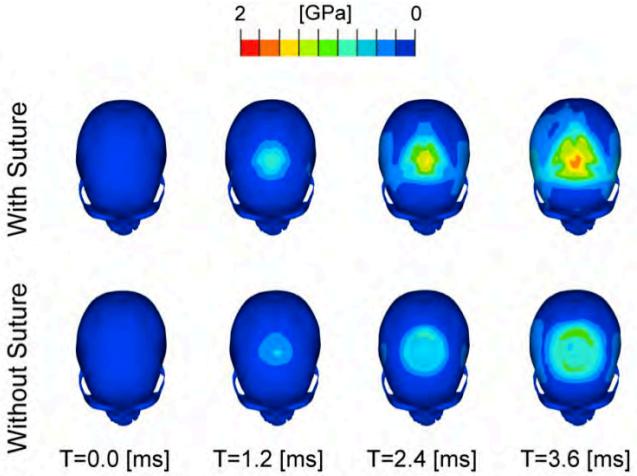

Figure 2: Difference of stress propagation between with and without the suture models. ***Note***: The below is the face side.

RESULTS AND DISCUSSION

Fig.2 shows the stress wave propagation in the model with and without the suture. In the model without the suture, the stress spreads radially from the impacted points, while the model with the suture shows different shape of the propagation. In the model with the suture, whole of the suture region was modeled as the same material properties as the cortical bone. Therefore, the impact stress transmitted along the suture once, and then the stress spread peripherally. As the result, the stress wave should form triangle shape from the top of view. Such difference of the stress propagation should come from the existence of the suture, and the modeling of the suture could be important to analyze stress wave propagation precisely and to investigate moderate disease without severe fracture. For quantitative evaluation of the stress propagation, the changes of the stress value along time at the four observation points, namely the parietal, sinciput, occipital, and left temporal points of the skull. In Fig.3, at the sinciput and temporal points, the transition of the stress on the external and internal table was almost same between the models with and without the suture. On the other hand, at the parietal and occipital points, the external and internal tables showed the same stress value in the model with the suture, while the internal table showed higher stress value than the external table in the model without the suture. Hence, hard and uniform material

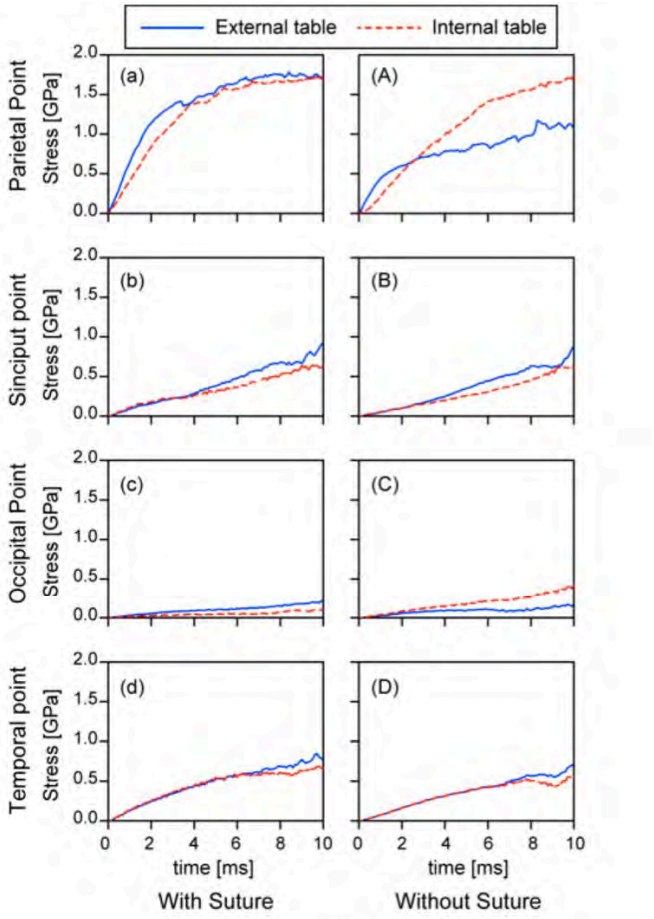

Figure 3: Stress changes along time after the impact at the four observation points.

property of the suture on the skull could show obvious difference of the stress distribution.

Our model doesn't have the brain in the skull, and this is a large limitation in this study. The presence of the brain might change the stress transition, especially on the internal table. Nevertheless, the existence of the suture affected the stress propagation. In this point, the anatomical skull model with the suture could be important to evaluate moderate disease on the skull.

REFERENCES

1. Yoganandan et al. J. Neurotrauma. 12(4), 1995.

ACKNOWLEDGEMENTS

This study was supported by Academic Open Program (AOP) in Altair Engineering Inc.

SOFT TISSUE STIFFNESS OVER THE HIP INCREASES WITH AGE AND ITS IMPLICATION IN HIP FRACTURE IN OLDER ADULTS: DATA FROM ONE HUNDRED FIFTY INDIVIDUALS

[1] KiTaek Lim, [1] Jieun Lee, [1] HaEun Park, and [1] Woochol Joseph Choi

[1] Injury Prevention and Biomechanics Laboratory, Department of Physical Therapy, Yonsei University, Wonju, South Korea
email: wcjchoi@yonsei.ac.kr

INTRODUCTION

Risk of hip fracture depends on the strength of bone as well as impact force delivered to the proximal femur during a fall [1]. Soft tissue (i.e., skin, fat, muscle, fascia) covering the proximal femur should play a role in attenuating the impact force during compression. A recent study has measured mechanical property of soft tissue (i.e., stiffness and damping) over the greater trochanter through vibration analysis using a single degree of freedom mass-spring-damper model with base excitation, and reported that shock-absorbing capacity of trochanteric soft tissue is more than three times smaller in older than young adults, explaining, in part, the exponential increase of hip fracture incidence with age [2]. We examined whether stiffness of soft tissue over the hip area is affected by age, gender, and different sites with respect to the greater trochanter.

METHODS

One hundred fifty healthy individuals (fifty young adults (aged between 19 and 29), fifty middle-aged (30 to 64), and fifty older adults (over 65)) participated. Each age group included 25 males and females. The study protocol was approved by the Institutional Review Board at Yonsei University Wonju Campus.

Participants lay sideways on a bed, exposing 12 points with respect to the greater trochanter (Figure 1). Stiffness of soft tissue over the 12 locations was measured through a hand-held indentation device (MyotonPRO, Myoton AS, Tallinn, Estonia). Five trials were acquired for each location and averaged for data analysis. Both left and right hips were measured.

ANOVA was used to test whether stiffness of soft tissue over the hip area was affected by age, gender and different sites with respect to the greater trochanter.

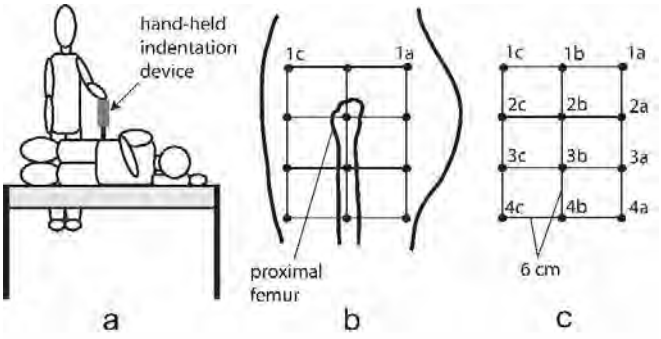

Figure 1: Experimental setup (a), measurement site with respect to the greater trochanter (b), and a 3 X 4 grid of markers spaced 6 cm apart that used to mark on skin surface.

RESULTS AND DISCUSSION

For both left and right hips, soft tissue stiffness associated with age ($p < 0.0005$), gender ($p < 0.0005$), and site ($p < 0.0005$) (Table 1). On average, the stiffness was 27% greater in older than young adults (321.5 versus 253.8 N/m). Furthermore, on average across 12 sites, our regression analysis indicated that the stiffness increases 1.37 N/m for every year while getting aged ("soft tissue stiffness over the hip = 1.37*age + 219.9"; R = 0.467, $p = 0.001$) (Figure 2). The stiffness was 18% greater in male than female (308.5 versus 262.1 N/m), and differed across 12 sites over the hip, being greatest (423.8 N/m) at site 2b (greater trochanter), and least (205.8 N/m) at site 1a (superior gluteal region).

We found, through clinical measures of large population with a hand-held indentation device, that soft tissue stiffness over the hip area increases with

age, which compared well with previous findings that stiffness and tone of skeletal muscles increase while aging [3,4]. However, our finding conflicts with a previous finding that stiffness of trochanteric soft tissue is three times smaller in older than young adults [2]. This may be explained by understanding of two different measurement approaches (techniques). While they minimized contribution of hard tissue (femur, pelvis and spine) in their quantification of trochanteric soft tissue stiffness, by modeling the hard tissues as a single moving mass, contribution of each bone during vibration was not clearly studied. Whereas, a hand-held indentation device allowed to characterize stiffness value contributed by soft tissue only, by applying low force (< 1 N) to soft tissue, which is critical to understand force attenuation characteristics of soft tissue as greater force magnitude (> 1 N) is transmitted to the bone [5].

We also found that soft tissue stiffness over the hip area differs across different sites with respect to the greater trochanter, being greater along the femur.

From a mechanical perspective, one can expect greater force attenuation (protection) or energy absorption from a stiffer protective gear. Soft tissue covering (i.e., skin, fat, muscle, fascia) over the hip is a natural padding device, and provides protection during a fall and impact. Our data suggest that the protective benefit of soft tissue increases with age. However, more studies are required to understand what that means in context of risk and mechanism of hip fracture during a fall.

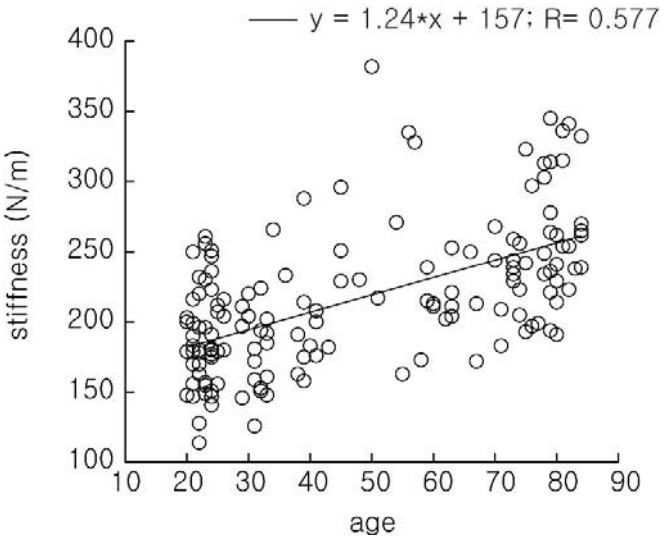

Figure 2: Effect of age on soft tissue stiffness over the location 3a of right hip.

REFERENCES

1. Bouxsein et al., J Bone Miner Res. **22**:825-831, 2007.
2. Choi et al., J Biomech. **48**:695-700, 2015.
3. Eby et al., Clinical Biomech. **30**: 22-27, 2015.
4. Kocur et al., Arch Gerontol Geriatr. **70**: 14-18, 2017.
5. Serina et al., J Biomech. **30**:1035-1040, 1997.

ACKNOWLEDGEMENTS

This work was supported by the National Research Foundation of Korea (NRF) grant funded by the Korea government (MSIT) (No. 2017-51-0082).

Table 1: Average values of stiffness over the hip (with SE shown in parentheses)

	Sex		Age		
	female	male	young	mid-aged	old
Left	264.6 (5.9)	309.2 (5.9)	254.2 (7.2)	283.2 (7.2)	323.4 (7.2)
Right	259.6 (5.7)	307.8 (5.7)	253.4 (7.0)	278.3 (7.0)	319.5 (7.0)

	Site											
	1a	1b	1c	2a	2b	2c	3a	3b	3c	4a	4b	4c
Left	208.5 (4.0)	288.7 (6.5)	314.2 (6.6)	222.2 (3.5)	430.1 (13.2)	318.4 (6.5)	222.2 (3.4)	311.4 (7.3)	285.0 (4.2)	231.5 (3.2)	303.1 (7.7)	307.9 (4.3)
Right	203.1 (3.2)	282.6 (6.6)	320.8 (7.9)	213.9 (3.3)	417.4 (12.3)	333.1 (6.8)	216.3 (3.5)	307.0 (7.0)	284.8 (4.7)	226.7 (3.3)	290.5 (6.8)	308.6 (5.1)

Anatomical Model Evaluation Using *In Vitro* Squat Simulation

[1] Kurt Manal, [2] Joshua Green and [2] Roger V. Gonzalez

[1] Mechanical Engineering, University of Delaware (UD)
[2] Joint Lab, The University of Texas at El Paso (UTEP), El Paso, TX, USA
email: manal@udel.edu, web: http://jointlab.utep.edu

INTRODUCTION

Medial and lateral knee contact force (MC & LC) can be computed knowing muscle forces crossing the knee and moment arms (MA) about medial and lateral points of contact. MA are derived from musculotendon lengths (L^{mt}) defined by muscle attachment points and wrapping surfaces collectively referred to as an "*anatomical model*". The 1990 anatomical model by Delp and colleagues has a long history of use in the biomechanics community [1]. It was updated by Arnold et al in 2010 to include more detailed muscle parameters and refined L^{mt} and MA [2]. It is unclear which anatomical model is better suited for studies examining MC and LC loading.

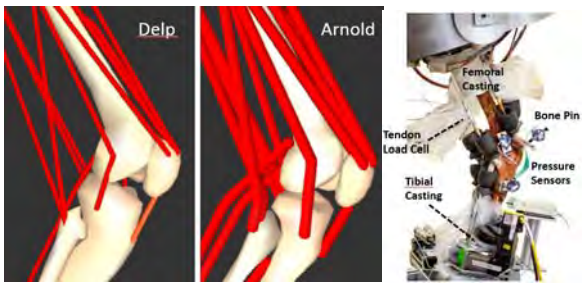

Figure 1. Delp (1990) and Arnold (2010) anatomical models. UTJLS robotic system used to recreate squat dynamics and record MC & LC force.

The University of Texas Joint Load Simulator (UTJLS) is a robotic system capable of recording articular contact pressures during synchronous real-time application of muscle forces, ground reaction forces (GRF), and joint kinematics [3]. The unique capabilities of the UTJLS were leveraged to simulate a squat exercise based on experimental data to evaluate which anatomical model yielded more accurate estimates of MC and LC loading.

METHODS

Anatomical model evaluation involved 4 distinct steps. **Step 1**: video-based motion capture with GRF and EMG recordings for a male (1.68 m, 51 kg) performing a squat exercise were collected at UTEP. The subject descended to approximately 100 degrees of knee flexion and then stood back up. **Step 2**: the squat data in conjunction with the Calibrated EMG-Informed Neuromusculoskeletal modeling toolbox (CEINMS) were used to compute muscle forces for the vasti medialis and lateralis (VM & VL), rectus femoris (RF), semimembranosus (SM), semi-tendinosus (ST), biceps femoris longus (BFL), and medial and lateral gastrocnemii (MG & LG). **Step 3**: Squat dynamics recorded in Step 1 were applied in real-time to a cadaveric knee (male, right leg) by the UTJLS including joint kinematics, GRF's, and muscle forces from Step 2. Muscle forces were scaled by 50% to minimize risk of tendon failure. Forces for the SM & ST were combined and applied to the SM tendon. MC and LC forces were simultaneously recorded using Tekscan pressure sensors (Teksan, Inc., Boston, MA). Pressure data were converted to relative MC and LC forces and reported as a percentage of total load. **Step 4**: The anatomical models were scaled to match tibial and femoral specimen length, and tibial plateau width. Medial and lateral contact points were set at ± 25% of the plateau width relative to the center of the knee. Medial and lateral MA for both models were combined with UTJLS muscle-actuated data to predict MC and LC force [4]. Contact force predictions were made "blind" without knowledge of the Tekscan loading data. MC and LC forces were reported relative to total load for comparison with the Tekscan recordings.

RESULTS AND DISCUSSION

There was strong temporal alignment between peak flexion angle, joint moments and quadriceps muscle-actuated forces (Figure 2). Loading during squat descent and ascent was greater for MC compared to

LC, with similar loading observed when flexed in the range of 90 - 100° (Figure 3, Tekscan MC & LC).

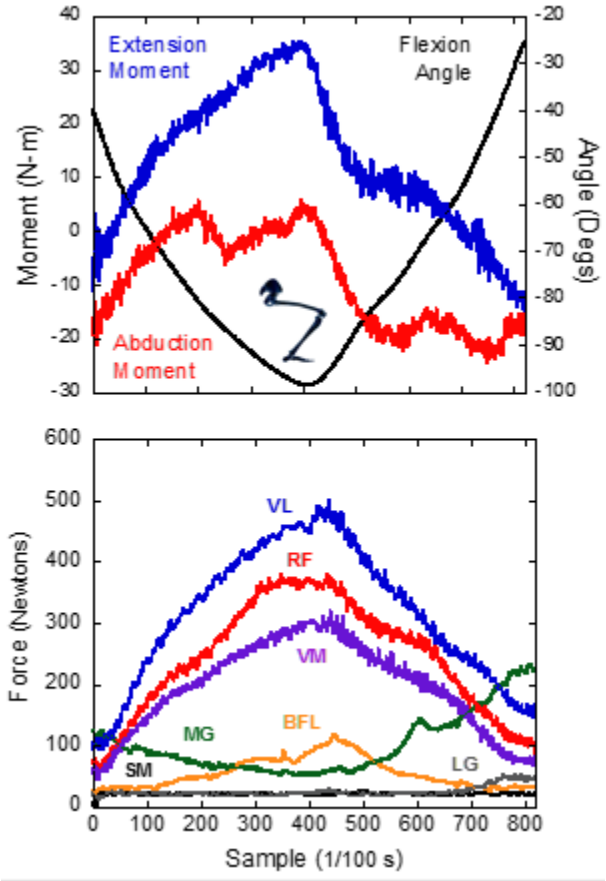

Figure 2: (A) Internal knee moments and flexion angle for the simulated squat exercise. (B) Muscle-actuated forces applied to the test specimen.

MC and LC forces estimates using frontal plane MA for the Arnold model (Figure 3B) were more closely aligned with Tekscan recordings compared to the Delp model. Differences can be traced back directly to the anatomical models since all other input data for MC and LC force estimates were identical.

CONCLUSIONS

Our findings suggest the anatomical model by Arnold et al is preferred for MC and LC force estimates specific to squatting maneuvers. Additional tasks including simulated walking will be evaluated using the UTJLS framework to better characterize which anatomical model is better suited for frontal plane force applications. The UTJLS is unique with potential to critically evaluate and to benefit applications of musculoskeletal modeling.

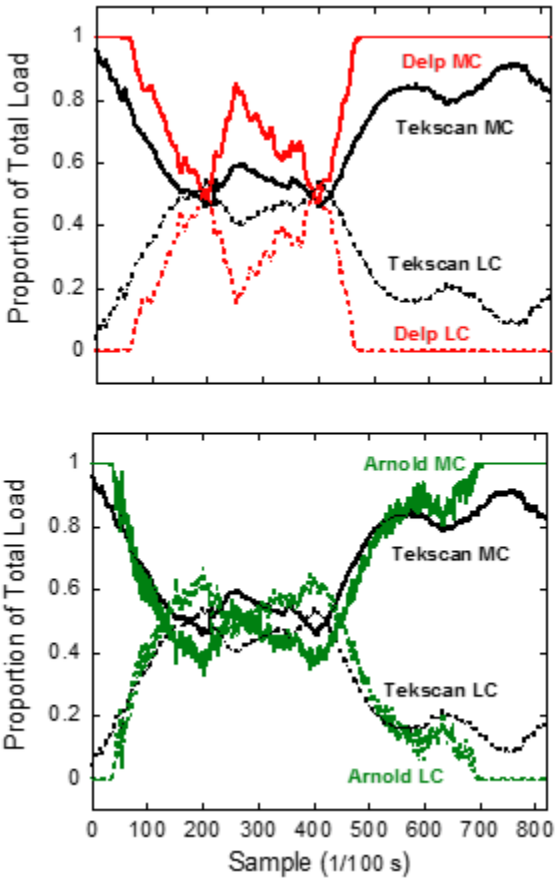

Figure 3. Relative MC & LC force estimates using MA computed from (A) Delp et al, and (B) Arnold et al.. The Arnold forces were much closer to the Tekscan recorded loading profile.

REFERENCES

1. Delp et al. *IEEE Trans Biomed Eng*. 37(8), 1990.
2. Arnold et al. *Ann Biomed Eng*. 38(2), 2010.
3. Green et al. *J Biomech Eng*. 139(12), 2017.
4. Winby et al. *J Biomech*, 42(14), 2009.

ACKNOWLEDGEMENTS

Rena Hale for collection of in vivo squat data and preparation of cadaver specimen. David Lloyd & research team at Griffith University for providing CEINMS muscle force estimates.

Effects of Age and Gender on Cervical Lateral Bending Injury Tolerance Corridors

[1,2] Sean Maroney and [1] Sean D. Shimada, Ph.D.

[1] Biomechanical Consultants, CA, USA
[2] Sacramento City College, CA, USA

INTRODUCTION

Currently, Hybrid III Anthropomorphic Test Devices (ATD) are used in automotive safety research to determine injury potential for human occupants. In part, the 50th percentile male Hybrid III ATD was based upon the anthropometric data from a 49 year-old male [1]. By following the guidelines set forth in the literature [2,3], the ATD was then scaled to different sizes to create the Hybrid III ATD family. The ATD family includes the 5th, 50th, and 95th percentile male and female devices. The scaling for the Hybrid III ATD family assumes that the anatomical soft tissue properties are the same for all individuals regardless of size, age, and gender. The cervical spine research literature reveals that females have a greater range of motion than males, while males on average tend to be stronger and have higher injury tolerances. Cervical moments generated by males were shown to be two times greater than females, but their mass and inertial properties are only 1.1 to 1.3 times greater [4]. As one ages, the moment generating capabilities of muscle decreases; however, females tend to better maintain and preserve muscle strength as they age. Throughout the aging process, a reduction in muscle and ligament strength leads to changes in impact injury tolerances. In order to increase the overall biofidelity of ATDs, factors such as age and gender need to be addressed. This study proposes a method to scale the 50th percentile male ATD to various sizes while also accounting for changes in anatomy due to age and gender. The proposed model would be used to redefine cervical spine injury tolerance corridors for lateral bending. The use of the enhanced injury corridors in the fields of biomechanics and accident reconstruction may increase the accuracy of injury prediction from lateral impacts.

METHODS

The anthropometric data for the standard 50th percentile male Hybrid III ATD was retrieved from the National Highway Traffic Safety Administration (NHTSA) database. The Irwin scaling method was implemented as a part of our proposed model to accommodate for various size individuals [2]. Data specific to muscle and ligamentous strength characteristics for age and gender were both assembled through a comprehensive search of the current research literature. Data was also complied for cervical range of motion changes due to age and gender. The data related to the effect of age and gender on cervical spine anatomy and range of motion was analyzed using a regression analysis. The regression analyses resulted in coefficients which were used in conjunction with the Irwin method [2] to redefine the cervical impact response corridors for lateral bending range of motion. The same procedure was carried out for the cervical moment producing/resisting capabilities.

RESULTS AND DISCUSSION

The resulting regressions for age and gender factors associated with muscle and ligament strength and range of motion were incorporated into the established Irwin scaling method [2]. In Figure 1, the resulting lateral bending range of motion data when age and gender is considered are compared to the ATDs described in Irwin et al. [2]. The results revealed that females generally have a greater range of motion than their male counterparts. Notably, range of motion decreases for both males and females over the course of a lifespan. Despite this, females had a slightly slower rate of decline, which indicates that they remain more flexible at ages above 70. The analysis also revealed that our proposed model more specifically represented the natural decrease in cervical range of motion as one ages when compared to no change in range of

motion when utilizing the Mertz [3] and Irwin [2] models.

Figure 2 shows a comparison of injury response corridors with the age and gender adjustments from a 49-year-old male to a 69-year-old. Generally, cervical spine tolerances to injury decrease with age, while the female musculature and ligamentous structures have lower strength properties than males. Nevertheless, the data revealed that females preserved their strength characteristics as they age when compared to males.

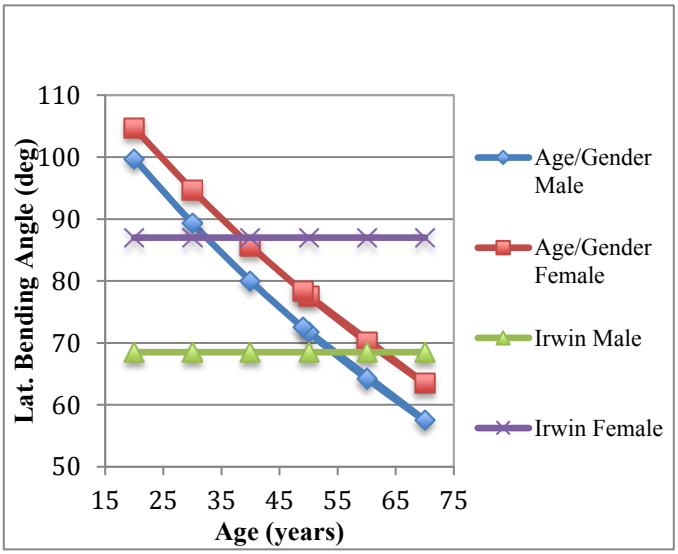

Figure 1: Gender/Age and Irwin Scaled ATD

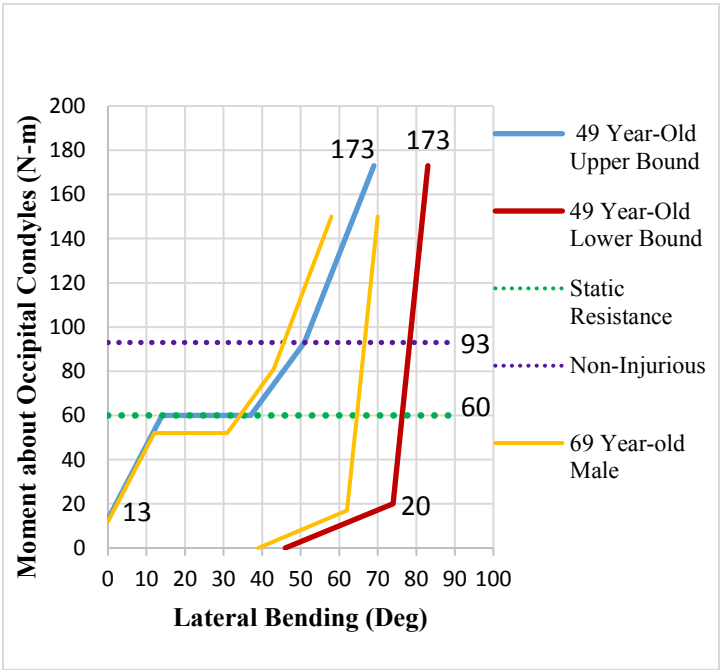

Figure 2: 49 and 69 Year-Old Scaled Injury Corridor

In Figure 2, the divergence between the two corridors can be observed in both cervical strength and range of motion due to the 20 year difference in age. As age increases the muscles no longer have the ability to laterally flex with the same strength in order to prevent excess lateral movement from an impact. Furthermore, the decrease in range of motion due to the aging process increases the stress on the cervical spine at an advanced rate.

CONCLUSIONS

The proposed injury response corridors resulted in differing cervical spine tolerances due to the inclusion of the age and gender characteristics into our model. The younger age groups have an increased ability to prevent excessive movement on their spine by contracting their contralateral flexors. Additionally, the younger age group has the ability to withstand increased lateral flexion because of their overall greater range of motion. The injury corridors for the current Hybrid III family can be improved by implementing the proposed model which accounts for the differences in gender and tissue changes over the course of the lifetime. The expanded injury tolerance corridor allow for scaling to any size, gender, and age adult occupant. The use of the model can ultimately improve biomechanical injury analyses by more accurately predicting injury thresholds for occupants exposed to lateral impacts.

REFERENCES

1. Mertz, H. and Patrick, L., “Strength and Response of the Human Neck," SAE Technical Paper 710855, 1971
2. Irwin, A., et al. *SCCJ*, 2002, v46, pp297-319.
3. Mertz, H. J., et al. 1989. “Size, Weight and Biomechanical Impact Response Requirements for Adult Size Small Female and Large Male Dummies,” *SAE Technical Paper Series*, 1989
4. Vasavada, A., et al. *Spine*, 2001, v26, n17, pp1904-1909.

CUSTOM SOFTWARE FOR CALCUATION OF SHEAR WAVE VELOCITY

[1]April L. McPherson, [1]Nathan D. Schilaty, and [1]Timothy E. Hewett

[1]Mayo Clinic Biomechanics Laboratories & Sports Medicine Center, Rochester & Minneapolis, MN, USA
email: mcpherson.april@mayo.edu

INTRODUCTION

Shear wave elastography (SWE) is an emerging ultrasound imaging technology that quantifies tissue stiffness properties. A shear wave is emitted by the transducer and propagates through tissue at different velocities depending on the tissue type. Shear wave propagation velocity can be easily converted to shear modulus and Young modulus by previously established mathematical relationships.[1] Young modulus (E) is a measure of the stiffness of a material.

Previously, SWE has been used in clinical settings to replace palpation and provide additional quantified data to clinicians. However, as SWE is being implemented in the research environment, large amounts of data are being generated that require measurement. Currently, the only available method to measure tissue stiffness in the region of interest is through the ultrasound machine interface. When being used in an investigational research study, the protocol can require the generation of thousands of images in order to determine the effects and relationships between multiple variables. Thus, a more efficient method to measure tissue stiffness is desirable and necessary. Accordingly, a custom, offline software was developed to batch process images and improve the efficiency of SWE data analysis.

METHODS

A General Electric LOGIQ E9 Ultrasound System (GE Healthcare, Wauwatosa, WI, USA) outfit with a 9L linear array probe with a 2-8 MHz frequency range was used for data acquisition. The musculoskeletal general exam model was selected. Using the B-mode image to localize the desired muscle tissue, a rectangular field of view was selected for SWE acquisition and stiffness distribution was displayed as a color map in the selected FOV (**Fig. 1**). The transparency setting on the ultrasound machine is pre-set to zero for all data acquisitions in the musculoskeletal general exam setting. DICOM files were exported from the ultrasound machine and imported onto a computer for analysis using the custom MATLAB software.

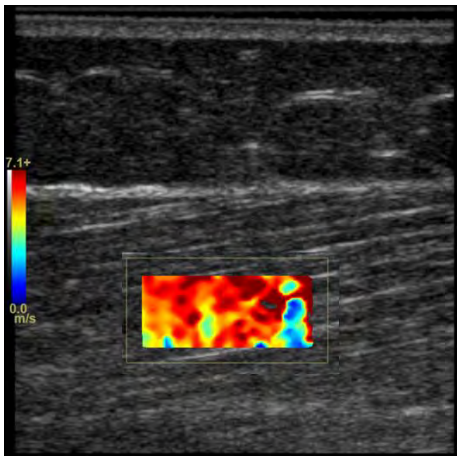

Figure 1: Example shear wave image color map

SWE data were acquired on several different muscles and for different conditions, including passive and active muscle contraction, in order to build a robust analysis algorithm that would encompass all stiffness values that may be observed in future analyses. During data acquisition, the transducer was aligned parallel with muscle fibers, as previous research has identified this as the optimal alignment.[1] Minimal pressure was applied to the transducer by the researcher in order to prevent tissue compression that would artificially influence measured tissue stiffness.

To build the software, the acquired images were measured on the GE ultrasound machine interface. These stiffness values were manually recorded and considered the "gold-standard" values for comparison against the custom software outputs. The custom software computes a shear wave velocity speed for each pixel in the image from the corresponding pixel RGB value in the SWE map.

Twelve critical RGB pixel value and corresponding shear wave velocities were provided by GE Healthcare, including the minimum and maximum speeds. For example, minimum shear wave velocity corresponds to RGB value (0, 0, 132) and maximum shear wave velocity 7.1 m/s corresponds to RGB value (128, 255, 128). Normalized values convert shear wave velocity from m/s; a normalized shear wave value 0 indicates 0 m/s and 255 indicates maximum speed. The images contain the standard 256 RGB pixel values (range 0-255). To create the required 256 RGB values for normalized shear wave velocity conversion, linear interpolation was performed using the twelve critical values (**Fig. 2**).

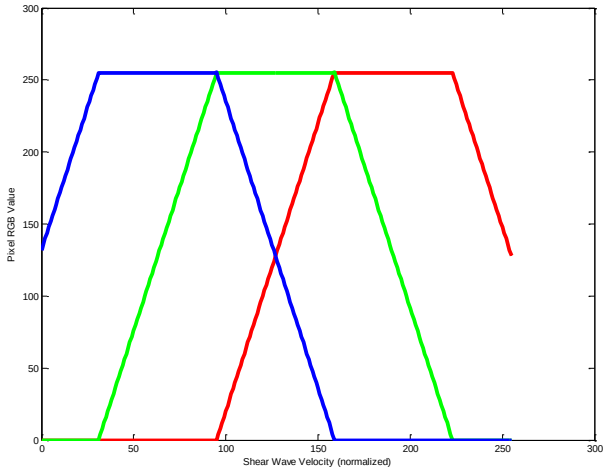

Figure 2: RGB pixel values and corresponding normalized velocity values.

The underlying black and white B-mode image was ignored and did not contribute to the computed shear wave velocity. After shear wave velocity was calculated for each pixel and saved in a matrix, the average shear wave velocity was computed. The shear modulus equation was then used to compute the shear modulus (Equation 1) where ρ was density and assumed to be 1000 kg/m^3 for all soft tissues and c was shear wave propagation velocity (m/s).[1] Stiffness (kPa) was computed using the shear wave modulus (Equation 2).[1]

$$\mu = \rho * c^2 \qquad \textbf{Equation 1}$$

$$E = 3\mu \qquad \textbf{Equation 2}$$

RESULTS AND DISCUSSION

To validate the custom software, we measured stiffness of images using the LOGIQ E9 stiffness measurement package and compared it to the stiffness output of the custom software.

The exported DICOM file from the ultrasound machine was known to be compressed and was susceptible to data truncation. Sole calculation of shear wave velocity from RGB pixel values yielded approximately a 10% error between gold standard stiffness values and the software output values. Thus, a linear correction equation was determined using 100 unique data points. The linear fit was determined to have r^2 of 0.95 (**Fig. 3**).

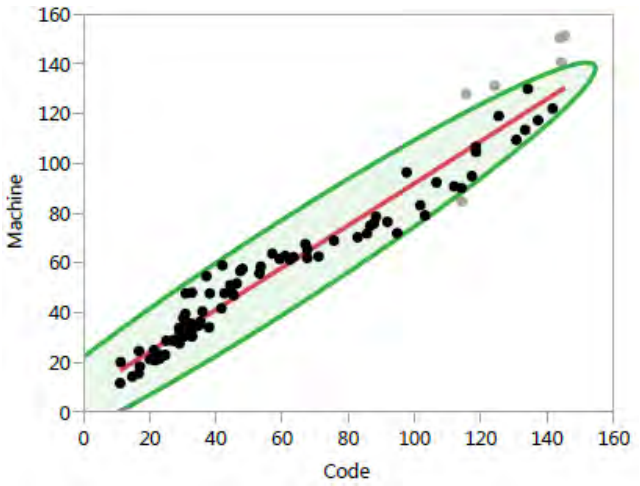

Figure 3: 95% confidence interval demonstrating agreement between custom software stiffness calculation and GE machine stiffness measurement.

CONCLUSIONS

The custom software demonstrated excellent agreement in stiffness calculation compared to the GE measurement system and can be used to enhance and batch data processing of DICOM SWE images from a GE LOGIQ E9.

REFERENCES

1. Eby et al. *J Biomech.* 46(14):2381-7, 2013.

ACKNOWLEDGEMENTS

Funding provided by an NBA/GE Grant. Fellowship funding (ALM) provided by the Mayo Clinic Graduate School of Biomedical Science. NIH funding include: K12HD065987 and L30AR070273 (NDS), and R01AR049735, R01AR055563, R01AR056259 (TEH).

VALIDATION of IMUs for TRUNK KINEMATICS DURING TREADMILL DISTURBANCES

[1] Emily J. Miller and [1] Kenton R. Kaufman, Ph.D.

[1] Motion Analysis Lab, Department of Orthopedic Surgery, Mayo Clinic, Rochester, MN, USA
email: Kenton.Kaufman@mayo.edu

INTRODUCTION

Individuals with lower limb amputation have a high risk for falling. It has been reported that 52% of lower limb amputees have fallen in the community [1]. Kaufman et al. have shown that task-specific fall prevention rehabilitation training reduces falls in individuals with lower extremity transtibial amputations [2]. Trunk flexion and velocity at recovery step determined the probability of a fall and are key outcome measures for fall prevention training [2, 3]. The Centers for Disease Control and Prevention (CDC) is working to make fall prevention a routine part of clinical care. Traditionally, motion capture systems have been used to measure joint kinematics, such as trunk angles and velocities, in a controlled laboratory setting. However, this equipment is expensive, requires a large, dedicated space and is operated by well-trained staff; all of which aren't practical for a routine clinical setting. Inertial measurement units (IMU) provide a better solution. They are commercially available, inexpensive, small and easily attached to key body segments by tape or elastic straps.

IMUs contain a gyroscope, accelerometer and magnetometer. The output can be combined to calculate joint segment kinematics. Previous studies have validated the accuracy of IMUs for upper extremity use [4, 5]. However, fall prevention training is conducted on a treadmill. Therefore, it is necessary to verify IMU function while being exposed to the high magnetic field generated by the treadmill during the rapid accelerations and decelerations implemented during the training protocol. The purpose of this study was to validate the IMU measurement of trunk flexion angles and velocities at recovery step against the gold-standard motion capture system during treadmill induced forward and reverse disturbances.

METHODS

Ten healthy young adults (5/10 female, age: 27.1 ± 4.2 years, BMI: 23.8 ± 2.7) were recruited for this study. Informed consent was obtained for each subject prior to data collection. A commercial IMU (OPAL, APDM, INC., Portland, OR) was secured to the sternum of each subject. Custom code was implemented to define the trunk coordinate system [6] and calculate trunk flexion angles and velocities at the recovery step as measured by the IMU. A 10-camera (Raptor-12, Motion Analysis Corporation, Santa Rosa, CA) motion analysis system was utilized to acquire kinematic parameters. Retro-reflective, 3D markers were placed bilaterally on the acromion processes and the anterior superior iliac spines to define the proximal and distal ends of the trunk segment. The local anatomical coordinate system was constructed using these landmarks, following the right hand rule. A triad of markers was also placed directly on the IMU to track the motion of the trunk segment. The 3D coordinates of the marker data were used as input to a commercial software program (Visual3D v6.01.07, C-Motion, Inc., Germantown, MD) to calculate the trunk flexion angles and velocities at the recovery step as measured by the motion capture system.

The participants stood in the center of the treadmill (DBCEEWI-Instrumented Treadmill, AMTI, Inc., Watertown, MA) facing the front of the treadmill. The participants wore a safety vest that was secured to a harness, which was attached to a track in the ceiling above the treadmill and had the freedom to slide forward and backward in the same direction as the treadmill belts. The harness was adjusted for each subject to ensure that the subject didn't impact the treadmill during the trial, but also had enough range of motion to sufficiently recover from the disturbance on their own.

The participants experienced a series of forward and reverse postural disturbances, generated using custom code, which caused trips and slips, respectively. The participants were instructed to take a step, if necessary, but to remain upright. A trial was considered a fall if the harness fully supported the participant after the induced disturbance. The direction of the disturbances was randomized and the magnitude increased each time the participant did not fall. When the participant fell three times in a given direction, it was considered a fail for that direction. The intensity was decreased for the fail direction and testing continued until the participant fell three times in the opposite direction.

Trunk flexion angle and angular velocity were calculated at recovery step for both the motion capture system and the IMU. Equivalence testing was performed to demonstrate that the two methods were equivalent, with alpha set to 0.05.

RESULTS AND DISCUSSION

The number of disturbances ranged from 27 to 49 trials (average: 36±6), while the magnitude of the forward disturbances ranged from 18 m/s^2 to 27 m/s^2 (average: 21.3 m/s^2 ± 2.7 m/s^2) and the magnitude of the backward disturbances ranged from 12 m/s^2 to 18 m/s^2 (average: 14.4m/s^2 ± 2m/s^2). The results of Equivalence Test (Table 1) demonstrated for both the trunk angle and angular velocity that the methods were equivalent. The 95% Confidence Intervals were within the equivalence interval and the P-Values were less than alpha.

Table 1: Equivalence Results

Variable	Equivalence Interval	95% CI for Equivalence	P-Value
Angle (deg)	[-2, 2]	[-0.605, 1.253]	0.005
Angular Velocity (deg/sec)	[-20, 20]	[0, 16.66]	0.011

The equivalence intervals for both the trunk angle and the angular velocity at foot contact were considerably less than the standard deviations of these variables presented by Owings et al. [2]. Therefore, the IMUs are an acceptable method for measuring trunk angle and angular velocities during clinical fall prevention rehabilitation.

CONCLUSIONS

IMUs are a valid method for measuring trunk flexion angles and angular velocity during forward and reverse treadmill disturbances in a clinic setting.

REFERENCES

1. Miller et al. *Arch Phys Med Rehabil*. **82**: 1031, 2014.
2. Kaufman et al. *Clin Orthop Relat Res*. **472**: 3076, 2014.
3. Owings et al. *Clin Biom.* **16**: 813, 2001.
4. Morrow et al. *J. App Biom*. **33**: 227, 2017.
5. Bauer et al. *J Elect & Kines*. **25**: 782, 2015.
6. Cain et al. *Gait & Posture*. **43**, 65, 2016.

ACKNOWLEDGEMENTS

Funding for the project was provided by the Department of Defense grant # W81XWH-15-2-0071. The views expressed are those of the authors and do not reflect the official policy or position of the Department of Defense or the US Government.

INTRASESSION RELIABILITY, PRECISION, AND BETWEEN-/WITHIN-SUBJECTS VARIABILITY OF HAMSTRINGS SHEAR WAVE ELASTOGRAPHY AT DIFFERENT POSITIONS

Takashi Nagai, April L. McPherson, Nathan D. Schilaty, Nathaniel A. Bates, Rena Hale, and Timothy E. Hewett

Mayo Clinic Biomechanics Laboratories & Sports Medicine Center, Rochester & Minneapolis, MN, USA
Email: nagai.takashi@mayo.edu

INTRODUCTION

Hamstrings strains are common sports-related musculoskeletal injuries in basketball players. A lack of hamstrings flexibility is believed to be one of the risk factors for hamstrings strains [1]. Clinically, hamstrings flexibility is commonly assessed with passive or active knee extension tests. More recently, local muscle tissue stiffness has been directly quantified by musculoskeletal diagnostic ultrasound shear wave elastography (SWE) [2]. SWE measures of muscle stiffness increase with a greater passive stretch of hamstrings muscles in young adults [3]. However, intrasession reliability and precision as well as variability within-subjects and between-subjects have not been established in high school basketball players. These parameters are important in developing research studies and help investigators to understand the associated within-subjects and between-subjects variation in SWE data [4]. Furthermore, the effects of different knee positions on muscle stiffness within-subjects during passive knee extension test are unknown.

METHODS

A total of 165 high school basketball players (106 females / 59 males, age: 15.7 ± 1.3 years, height: 173.6 ± 9.5 cm, weight: 68.4 ± 13.1 kg) participated in the study. Prior to their participation, informed consents were obtained from each player and his/her parent (only players under 18 years old). The study was reviewed and approved by the Mayo Clinic Institutional Review Board.

First, flexibility of the hamstrings was assessed with passive knee extension tests. Subjects lie supine with the examiner holding the subjects' testing thigh to keep the hip and the knee at 90°. Then, the examiner moved the testing shin toward full extension, without moving the thigh. A digital inclinometer (Johnson Level & Tool, Mequon, WI) was placed when the examiner determined the sacrum moved/max tension in hamstrings. The starting position (shin in horizontal position) was defined as 0 degrees. A full extension (knee completely straight) is read by the inclinometer as 90°. An average of three maximum flexibility values was used to determine the following testing positions: 80, 60, and 40% of maximum for ultrasound SWE acquisition.

Ultrasound images of the biceps femoris were acquired using the 9L-D transducer on the General Electric LOGIQ E9 Ultrasound System in SWE mode (GE Healthcare, Wauwatosa, WI). The biceps femoris was identified by finding the midway point between the greater trochanter and the lateral epicondyle of the femur. The transducer is aligned along the short axis of the muscle to visualize the long-head of the biceps femoris by moving toward the most posterior (slightly medial) of the thigh. Then, the SWE images were acquired with the transducer head aligned parallel with the biceps femoris.

Subjects were in the same supine position as passive knee extension testing for ultrasound acquisition. The examiner moved the subjects' leg to 80% of the maximal range-of-motion value while the second examiner acquired ultrasound images. After three SWE images were acquired, the first examiner moved the subjects' leg to the 60% and 40% positions. Muscle stiffness (kPa) was measured from the SWE color map using custom Matlab software.

Descriptive statistics (means and standard deviations) were calculated for each position (80, 60, 40%) on both left and right leg. Intrasession

Reliability, precision, and within-subjects (W/S) / between-subjects (B/S) variability were assessed using intraclass correlation coefficient (ICC Model 2.1), standard error of measurement (SEM), and coefficient of variation (CV in percent: %), respectively [4].

Within-subjects one-way analysis of variance (ANOVA) or nonparametric test was used to examine the effects of position in each leg. Significance was set at $p < 0.05$. If the ANOVA was significant; then, post-hoc analyses with Bonferroni adjustment ($p < 0.0167$) were performed to compare each position.

RESULTS AND DISCUSSION

The observed SWE values of hamstrings muscle in the current study were within the values reported by previous studies [5, 6]. Excellent reliability (ICC = 0.833 – 0.925) was observed. There was a consistent pattern of worse precision (Left 40%: SEM = 8.2 kPa vs. Left 80%: SEM = 12.2 kPa) and higher within-subjects variability/CV (Left 40%: CV = 12.6% vs. Left 80%: CV = 22.4%) and between-subjects variability/CV (Left 40%: CV = 63.1% vs. Left 80%: CV = 75.0%) at more stretched positions (80%). A lack of warmup or hysteresis property of musculotendinous tissue might explain why we observed lower SWE values and higher SEM and variability at 80% position (which is tested first after knee extension flexibility tests).

ANOVA revealed that there was significant among three positions on right leg ($p = 0.008$) and left leg ($p < 0.001$). Contrary to the hypotheses and previous studies [2, 3], stiffness at 80% was lower than at less stretched positions (40% and 60%). Post-hoc analyses revealed that on right leg, the stiffness at 60% was significantly higher than the stiffness at 80% (Right 60%: 47.8 ± 35.0 kPa, Right 80%: 38.1 ± 29.8 kPa, $p < 0.001$). Similarly, on left leg, the stiffness at 60% was significantly higher than the stiffness at 80% (Left 60%: 47.8 ± 33.7 kPa, Left 80%: 40.0 ± 30.0 kPa, $p < 0.001$). Additionally, the stiffness at 40% was also significantly higher than the stiffness at 80% (Left 40%: 47.2 ± 29.8 kPa, Left 80%: 40.0 ± 30.0 kPa, $p = 0.001$). All results are shown in Table 1.

Table 1. Descriptive Statistics of Intrasession Reliability, Precision, and Variability of Shear Wave Elastography Stiffness Values of the Biceps Femoris Muscle

Leg Positions	Left 40%	Right 40%
SWE - Group Average	47.2 ± 29.8 kPa*	41.7 ± 26.7 kPa
Intrasession ICC	0.925	0.854
Intrasession SEM	8.2 kPa	10.2 kPa
W/S Variability	12.6 ± 11.9 %	15.7 ± 13.7 %
B/S Variability	63.1%	64.1%
Leg Positions	**Left 60%**	**Right 60%**
SWE - Group Average	47.8 ± 33.7 kPa*	47.8 ± 35.0 kPa*
Intrasession ICC	0.897	0.918
Intrasession SEM	10.8 kPa	10 kPa
W/S Variability	17.2 ± 15.6 %	16.5 ± 15.3 %
B/S Variability	70.5%	73.1%
Leg Positions	**Left 80%**	**Right 80%**
SWE - Group Average	40.0 ± 30.0 kPa*	38.1 ± 29.8 kPa*
Intrasession ICC	0.838	0.833
Intrasession SEM	12.1 kPa	12.2 kPa
W/S Variability	22.4 ± 16.2 %	21.1 ± 19.0 %
B/S Variability	75.0%	78.3%

*represents significant SWE differences between Right/Left 60% and 80% and between Left 40% and 80% ($p = 0.001$). SWE: Shear Wave Elastography, B/S: Between-Subject, ICC: Intraclass Correlation Coefficient; SEM: Standard Error of Measurement, W/S: Within-Subject.

CONCLUSIONS

The current SWE procedures resulted in lower stiffness when the muscle was placed under greater tendon. The SWE is reliable within a session but lacks precision with large variability. Further refinement to improve SWE values should be considered to reduce variability.

REFERENCES

1. Gabbe et al. *J Sci Med Sport*, 2006: 327-333.
2. Eby et al. *Clin Biomech,* 2015: 30(1): 22-27.
3. Le Sant et al. *PLOS One,* 2015: 10(9): e0139272.
4. Hopkins WG. *Sports Med,* 2000: 1-15.
5. Miyamoto et al. *Scand J Med Sci Sports,* 2017: 27: 99-106.
6. Umegaki et al. *Man Ther,* 2015: 134-137.

ACKNOWLEDGEMENTS

Funding from the NBA & GE Healthcare Orthopedics and Sports Medicine Collaboration, and NIH grant funding R01AR056259 & R01AR055563 and T32AR056950.

LOAD CARRIAGE EFFECT ON THE ABILITY TO CONTROL DYNAMIC MOVEMENT

Bekah Perlin[1], John W. Ramsay[2], Katherine A. Boyer[1]

1. University of Massachusetts Amherst, Amherst, MA, USA
2. Natick Soldier Research, Development & Engineering Center, Natick, MA, USA

email: bperlin@umass.edu, http://people.umass.edu/mobl/

INTRODUCTION

Musculoskeletal injuries are a significant concern for infantry soldiers, most often occurring in the lower body and typically while lifting and marching long distances with heavy loads [1]. Knee injuries are the most common lower extremity injury in the U.S Army Special Operations Forces [2]. Locomotion with body-borne loads can cause biomechanical adaptations that may contribute to injury incidence. By quantifying the whole body biomechanical adaptations for heavy load carriage, injuries may be predicted and therefore potentially prevented.

Prior work on the effects of heavy load carriage on locomotion has found that in running the knee and the trunk flexion moments increase [3], as does total joint work (hip, knee, and ankle) and total positive joint work [4]. In a run to stop maneuver, individuals with body borne loads also experience an increase in the vertical and anterior-posterior ground reaction forces and peak knee joint contact forces [5]. This suggests there is a whole body adaptation in movement mechanics with heavy load carriage. The automatic recognition of movement patterns may be of importance to quantify and compare adaptations to new load carriage designs that may be more or less risky.

It has been suggested that the temporal and spatial information available from 3D marker trajectories may be sufficient for group differentiation. Prior work has used principal component analysis (PCA) feature extraction to successfully classify older and young gait [6], gait in different shoes at varying speeds [7] and to determine postural strategies to maintain balance [8]. The aim of this study was to use PCA feature extraction to quantify whole body 3D marker trajectory and whole body posture changes to load carriage.

METHODS

Data Collection. All participants completed three visits: an orientation session to collect participant characteristics and to practice movement tasks with the load; and then two load carriage visits where participants completed 3 – 5 runs at 4.0 m/s or at maximal speed on a 10m runway with an in ground force-plate while kinematic and kinetic data were captured. Markers were place on the head, trunk, pelvis, and right limb.

Load conditions. Two load conditions were tested. For each load condition, the volunteer wore and carried equipment weighing 6.17 kg, including a helmet, boots, spandex top and shorts, and a mock M16 weapon. For the heavily loaded (30% of BW) configuration, the participant also wore an adjustable weighted vest (V-FORCE®, WeightVest.com Inc. Rexburg, ID, USA), to add load to the torso.

Data Analysis. All calculations and statistical procedures were carried out in Matlab (Math Works Inc., USA). To prepare the data for PCA, three data conditioning steps were conducted. First, all marker coordinates were expressed in coordinates relative to the horizontal position of the pelvis. Second, the trajectories of all markers were resampled to 101 time points representing touch-down to take-off. Third, the influence of anthropometric differences between participants on marker trajectory variance was minimized by subtracting the mean over the stance phase and dividing by the standard deviation for each coordinate. The resultant normalized trajectories for all markers were then concatenated into one data vector with 7575 vector components (25 markers x 3D coordinates x 101 time points for each waveform) for each trial. A PCA was performed on the matrix formed by data vectors of all 24 trials (3 subjects x 4 trials per subject) yielding (a) principal component vectors (PCi) indicating the

direction of the largest variation in the data set; (b) eigenvalues (EVi) indicating the amount of variation in the data explained by a given PCi; and (c) weights, obtained by projecting individual trials on to the PCi. Each PCi represents a characteristic manner of how individual trials deviated from the average gait pattern. Characteristic differences between the gait patterns for the unloaded and loaded conditions were identified by comparing the scores of the first 11 PCi using a repeated measures ANOVA ($\alpha = 0.05$).

RESULTS AND DISCUSSION

Three male military personnel participated this study (mean age 19.3 years). There was a significant difference in the weights for the 5th PCi (PC_5) between the loaded and unloaded conditions ($P=0.05$). This suggests that the magnitude of the deviations from the mean represented by this PCi are greater for loaded condition.

To visualize and interpret the differences in movement represented by PC_5, the marker trajectories were reconstructed as the mean positions, plus the weighted PCi that identified group differences. Four time points were chosen to investigate the changes: touch down, 30% and 60% of stance, and toe off.

In the sagittal plane, participants tended to land with a more extended leg and anterior trunk lean followed by greater limb flexion through-out stance and more limb extension at toe-off (Figure 1). This suggests a greater range of flexion motion in the limb may be adopted to assist in the absorption of the impact.

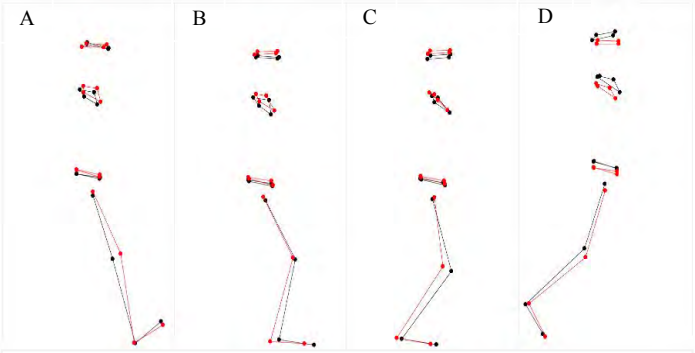

Figure 1: Comparison between sagittal plane reconstructed heavily loaded (black) and mean (red) marker positions. Clusters from top to bottom: helmet, shoulders, pelvis, right leg. For visualization purpose the weight factors were amplified by a factor of 10.

However, landing with a more extended limb may increase risk for non-contact anterior cruciate ligament injuries. In the frontal plane, there were very few deviations in the limb and trunk motions during the stance phase with the exception of a more medial limb position relative to the pelvis at take-off (Figure 2).

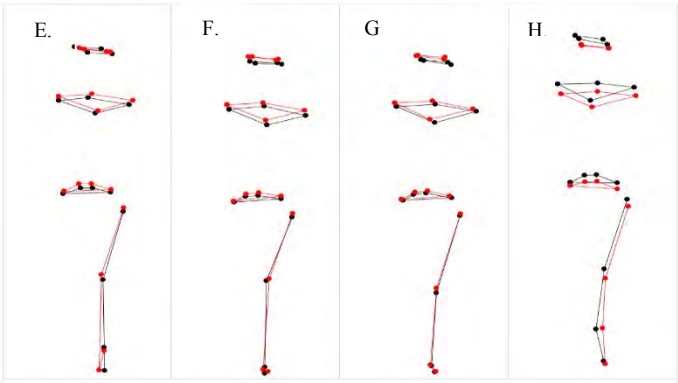

Figure 2: Comparison between frontal plane reconstructed heavily loaded (black) and mean (red) marker positions. Clusters from top to bottom: helmet, shoulders, pelvis, right leg. For visualization purpose the weight factors were amplified by a factor of 10.

CONCLUSION

Using PCA extracted features of the 3D marker trajectories, we were able to differentiate loaded and unloaded movement patterns for the stance limb and trunk. This analysis provided a visual representation of those aspects of movement that varied significantly with the addition of load. This visualization technique through PCA 3D marker trajectories may be relevant to industry, military officials, and coaches who have limited experience with the analysis of joint kinematic data.

REFRENCES

1) Kaufman et al. *American Journal of Preventive Medicine*, 2000.
2) Abt et al. *Military Medicine*, 2014.
3) Brown et al. *Gait & Posture*, 2014.
4) Liew et al. *Journal of Biomechanics*, 2016.
5) Ramsay et al. *Journal of Biomechanics*, 2016.
6) Eskofier et al. *Computer Methods in Biomechanics and Biomedical Engineering*, 2013.
7) Mauer et al. *Gait & Posture*, 2012.
8) Federolf. *Journal of Biomechanics*, 2016.

CLASSIFYING TYPE OF NATURAL GAIT USING ANN AND ANKLE-MOUNTED ACCELEROMETER DATA

[1]Matthew B. Rhudy and [1]Joseph M. Mahoney

[1]Mechanical Engineering, Penn State Berks, Reading, PA, USA
email: matthew.rhudy@gmail.com

INTRODUCTION

Due to rising health concerns across the world, activity monitoring has become increasingly popular to encourage movement. There are many existing activity monitoring devices often worn on the wrist or hip available to consumers with various capabilities such as step counting, calorie counting, and intensity of activity. Another feature that is growing in popularity among consumer activity monitoring devices is classifying activities into categories such as sitting, walking, running, and cycling [1]. While activity monitors, in general, utilize a range of sensor packages, accelerometers are commonly implemented within these devices and are often the primary signal used to identify types of activity. For classification purposes, research has studied the use of accelerometers strapped onto locations including arm, hip, thigh, chest, and ankle [1], or through a cell phone carried in a pocket [2]. Due to the necessity of leg motion for any ambulatory activity, the ankle has been identified as a more accurate sensor mounting location for activity classification [3]. Therefore, ankle mounted accelerometers were selected for this study.

In order to determine a classification from a data signal, it is desirable to reduce the raw data into a set of features. Many features have been considered for activity classification from both time-domain metrics, such as mean and standard deviation [2], and frequency-domain metrics, such as wavelet transform [3, 4] or Fourier transform [4] features. This work focuses on the use of time-domain features to classify the type of gait as either walk, jog, or run based on ankle-mounted accelerometer measurements. Time-domain features were selected because they correspond to relevant temporal parameters contained in gait cycles, such as heel strike and toe off [5].

METHODS

This IRB-approved study used an MBientLab MetaMotion R Inertial Measurement Unit (IMU) containing a BMI160 3-axis accelerometer sampled at 200 Hz with 16-bit resolution. The IMU was attached using an ankle strap on the lateral side of the left ankle of 15 healthy participants. Each participant completed three 90-second constant-speed conditions on a Quinton TM55 treadmill presented in random order: 1.21 m/s (walking), 2.01 m/s (jogging), and 2.68 m/s (running). Data collection was started after the participant was acclimated to the treadmill speed for each condition. Approximately 60 seconds of rest was given between trials.

After data collection, the three axes of accelerometer data were zero-lag filtered using a 4th order low-pass Butterworth filter with cutoff frequency of 4 Hz. These signals were then used to calculate the magnitude of the acceleration to remove any orientation dependence of the sensor. Gait cycles (from left foot heel-strike to the following heel-strike) were isolated by applying peak detection to identify heel strikes in the acceleration signal [6]. After parsing out each gait cycle for each participant, each cycle was normalized in time based on the duration of that cycle. A total of 2444 gait cycles were identified, with 954 walk, 923 jog, and 567 run cycles. These cycles were classified based on the treadmill speed. Additionally, the distinction between walking and jog/run was verified manually using the video recording. First, the mean of the acceleration magnitude for each motion type across these trials was calculated, as shown in Fig. 1.

A few observations were made from the data in Fig. 1. First, the run condition has the highest overall peak value and tends to be highest on average throughout the cycle. Similarly, the jog condition has a larger peak and average value than the walk

condition. From these observations, the maximum and mean values of these acceleration signals are expected to help to establish differences between the conditions. Additionally, the minimum acceleration magnitude of the walk condition appears significantly lower than the other two conditions. It was also observed through the standard deviation that there is more variation in the signals as the speed increases. The final metrics identified from the data in Fig. 1 were the acceleration and corresponding gait cycle percentage at toe-off, which is identified by the local maxima within the gait cycle (around 60% in Fig. 1). As an example of the metrics, the mean and standard deviation are shown in Fig. 2, which demonstrates clustering of the different categories based on these metrics.

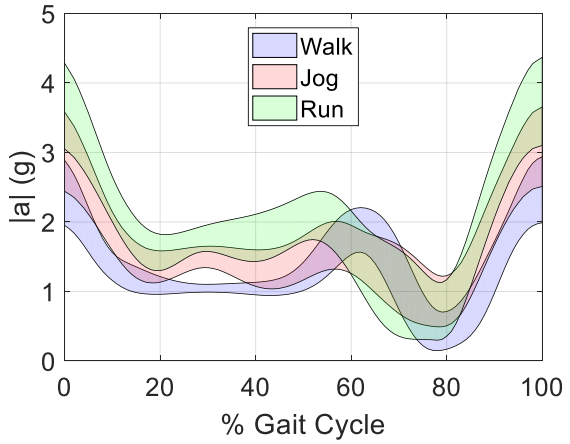

Figure 1: 95% CI of Acceleration over Gait Cycle

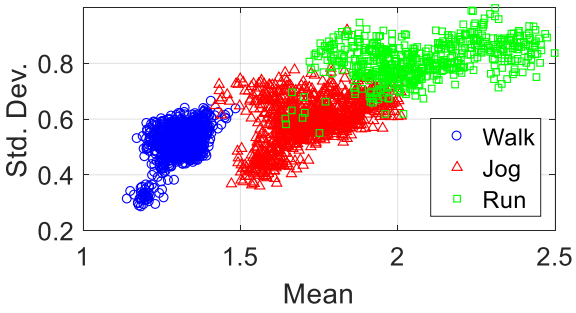

Figure 2: Clustering of Example Metrics used for Classification within the ANN

From these observations, an Artificial Neural Network (ANN) was designed with inputs of the mean, standard deviation, maximum, and minimum values of the acceleration magnitude, as well as the identified acceleration and percent gait cycle at toe-off. These six inputs were used within the ANN with a single hidden layer containing 15 neurons and a single output given as 1 for walk, 2 for jog, and 3 for run. The result of the ANN is rounded to determine the official classification. From the 2444 gait cycles, 85% were used to train the ANN, and the remaining 15% were used as validation data to verify the performance of the ANN.

The confusion matrix for the ANN is provided in Table 1. Overall, the ANN was determined to be 99.2% accurate in identifying the type of gait using the 367 validation gait cycles. It is shown in Table 1 that the walk cycle is able to be identified with 100% accuracy, while there is minimal confusion of the run cycles being interpreted as a jog. This is reasonable since the differences between jogging and running are ambiguous and can vary from person to person.

Table 1: Confusion Matrix for ANN Classifier

		Predicted		
		Walk	**Jog**	**Run**
Actual	**Walk**	137	0	0
	Jog	0	144	0
	Run	0	3	83

CONCLUSIONS

This work presented a method for classifying the type of gait cycle into categories of walk, jog, and run using an ANN with inputs derived from ankle acceleration data. The results showed good accuracy of the ANN in classifying each type of gait using the considered metrics.

REFERENCES

1. Cleland I, et al. *Sensors* **13.7**, 9183-9200, 2013.
2. Kwapisz JR, et al. *ACM SigKDD Explorations Newsletter* **12.2**, 74-82, 2011.
3. Mannini A, et al. *Med Sci Sports Exerc* **45(11)**. 2193-2203, 2013.
4. Preece SJ, et al. *IEEE T Bio-Med Eng* **56.3**, 871-879, 2009.
5. Lee J-A, et al. *J Med Syst* **34**, 959-966, 2010.
6. O'Connor, et al. *Gait & posture* **25(3)**, 469-474, 2007.

VALIDATION OF A NECK MODEL WITH MUCLE FATIGUE USING THE SORENSEN TEST

[1] Paulien E. Roos, [2] Nigel Zheng, [1] Timothy Zehnbauer, [1] Austin Mituniewicz, [1] Philip E. Whitley, and [1*] Xianlian Zhou

[1] CFD Research Corporation, Huntsville, AL, USA
[2] UNC Charlotte, Charlotte, NC, USA
*email: Alex.Zhou@cfdrc.com

INTRODUCTION

Prolonged use of head supported mass (sports, VR goggles and military applications) increases risk of chronic neck injury due to muscle fatigue. Although acute neck injury, such as whiplash, has been investigated extensively, chronic neck injury under long duration and low loading is less understood. The aim of this study was to validate a neck model with muscle fatigue, with the long term goal to develop a software tool that can predict neck injury (specific muscles) under different conditions (head supported mass; activities; and duration).

METHODS

Pilot data were collected on nine subjects (5 male; age: 21±2 years; mass: 80.2±31.4 kg; height: 1.71±0.16 m) while performing a neck Sorensen test [1] for up to 180 s. Subjects wore a helmet with added mass. Electromyographic (EMG) data were collected on four muscles: sternocleidomastoid, scalenus, trapezius, and splenius capitis (extensor). EMG data were analyzed for average activity level normalized to maximum voluntary contraction (MVC), and for muscle fatigue as the median frequency and mean amplitude [2]. Average median frequency and mean amplitude were calculated for 16.7% windows and the difference between the last and first window was calculated (ΔF and ΔA).

An adaptation of an existing neck model [3] was scaled to the subjects' anthropometry using in-house developed Anthropometry Model Generating software [4]. Simulations were performed using Cobi-Dyn (in-house developed biodynamics software). The model was placed in a prone position with the shoulders and torso fixed and the neck in a neutral posture. Simulations were performed for 180 s with a fatigable muscle model implemented [5].

RESULTS AND DISCUSSION

The sternocleidomastoid muscles were not activated much and therefore not included in further analysis (Fig. 1). As expected, neck extensors showed high activation. The trapezius showed relatively high and the scalenius showed medium activation. As both do not generate much neck extension moment, this was likely as co-contraction to stiffen the neck.

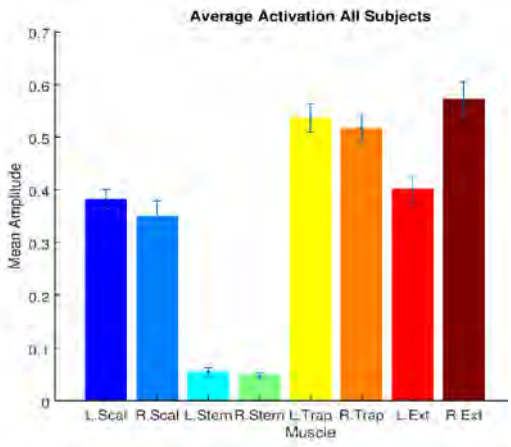

Figure 1: Mean amplitude of muscle activation, normalized to MVC and averaged over the whole fatigue trial, presented as the mean of all subjects with the standard deviation.

Visual inspection of median frequency and mean amplitude of individual trials showed fatigue mostly in the neck extensors and also some in the trapezius and scalenius muscles. A summary of the overall subject fatigue data (Fig. 2) shows that the largest overall decrease in median frequency (ΔF) was for the neck extensors, which also showed an increase in mean amplitude (ΔA), indicative of fatigue. For the scalenius and trapezius overall results were less indicative of fatigue due to large inter-individual variation. This suggests that some subjects stiffened their neck more than others resulting in fatigue, while the neck extensors fatigued for all subjects.

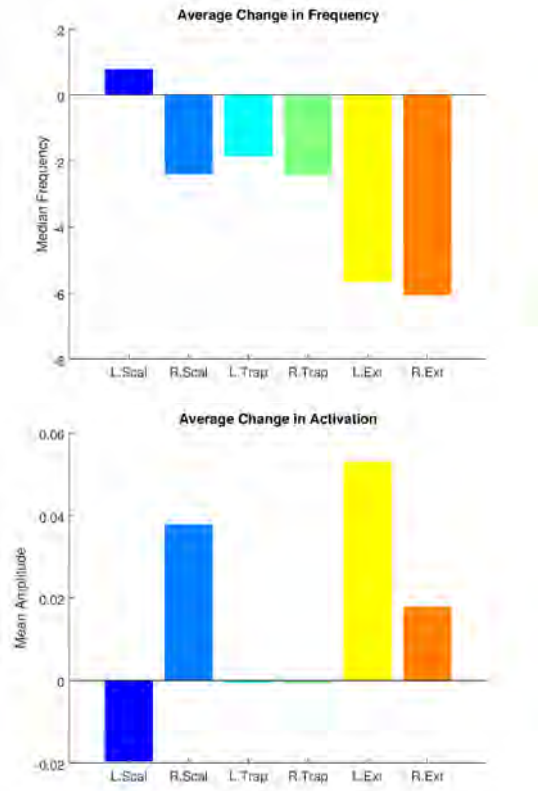

Figure 2: Change in median frequency (ΔF; top) and mean amplitude (ΔA; bottom) averaged over all subjects.

When comparing the simulation (Fig. 3) to the experimental results, the trapezius and sternocleidomastoid muscles show no fatigue for both simulations and experiments. In the simulations, the posterior scalenus shows fatigue and activation whereas the anterior and medial scalenus do not, which is reasonable since the posterior scalenus is a weak extensor while anterior and medial scalenus are not. The muscles that show the most activation and fatigue in the simulation are the extensor muscles. This is in agreement with experimental results where these are the only muscles to show a significant amount of fatigue. The top branches of splenius are less active than bottom branches at the beginning but later their activation are seen increasing as the bottom branches become more fatigued. Overall, the model was able to predict fatigue of neck extensors well, but co-activation of other muscles (trapezius and scalenius) was not predicted. This could be due to the scapula being fixed in this model, while it may require fixation/stiffening in real life.

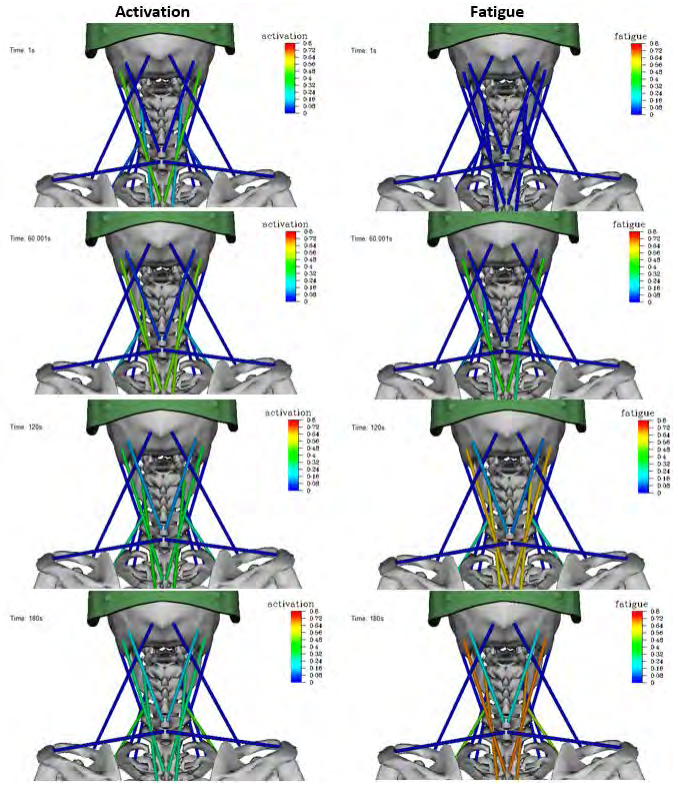

Figure 3: Left: Simulated activation of muscles measured experimentally at 1, 60, 120, and 180 s. Right: Muscle fatigue at said times. Warm colors are high fatigue. 0: no fatigue and 1: full fatigue.

CONCLUSIONS

This study provides preliminary validation of a neck model with fatigue for injury prediction. It was demonstrated that the model accounts for the main muscles that fatigue, but not for muscles that stabilize or stiffen the neck. This should be kept in mind in future work addressing risk of injury with head supported mass.

REFERENCES

1. Lee et al. *J. Manipulaive Physiol.,* 28, 2005.
2. Potvin and Bent. *J. Electromyo. Kinesol*. 7, 1997.
3. Vasavada et al. *Exp. Brain Res.,* 147, 2002.
4. Zhou et al. *Int. J. Digit. Hum.* 1, 2016.
5. Zhou et al. *Int. J. Hum. Factors Models.* 4, 2014.

ACKNOWLEDGEMENTS

Dr. Anita Vasavada for generously sharing her neck model, Mr. Shangcheng Wang and Zheng Xu for data collection.

ASSESSING FATIGUE AND STRETCHING AFFECT ON THE ACHILLES TENDON USING SURFACE WAVE ELASTOGRAPHY

[1] Muhammad Salman, [2] Karim G Sabra
[1] Kennesaw State University, Marietta, GA, USA
[2] Georgia Institute of Technology, Atlanta, GA, USA
[1]email: msalman1@kennesaw.edu
[2]email: karim.sabra@me.gatech.edu

INTRODUCTION

Currently, there's a lack of noninvasive cost-effective techniques that can quantify in-vivo non-uniform degradation of tendon's mechanical and structural properties associated with localized tendon injuries. This study will demonstrate the applicability of a novel cost-effective surface-wave elastography (SURF-E) method for quantifying fatigue and stretching effects of Achilles tendon in a much broader range of tendon stiffness with various positions and anatomical level than currently available elastography methods do such as Ultrasound (US) and MRI.

METHODS

Ten healthy men (age: 22 ± 5 years, height: 175 ± 9 cm, body mass: 72 ± 8 kg) were tested with no signs of neuromuscular diseases. The study was approved by the Institutional Review Board (IRB) of the Georgia Institute of Technology. The ankle joint was set to three different values 70°, 80° and 90° by the help of a goniometer (Fig. 1a). In order to have the data repeatability, leg was restrained in a fixture around calf (Fig. 1b) by the help of a strap and a tong clamp.

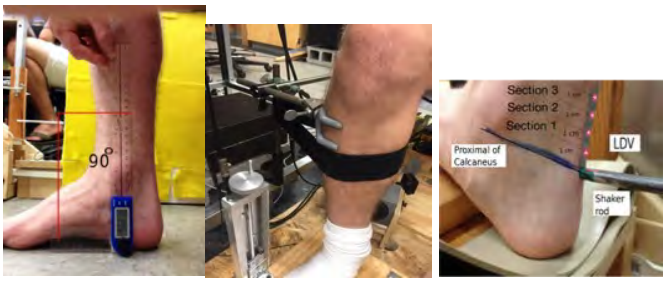

Figure 1: a) Ankle angle set by goniometer, b) Fixture around calf, c) Achilles Tendon setup with LDV and shaker rod.

Achilles tendon was marked by five anatomical landmarks each 1cm apart starting from the datum line parallel to the proximal of calcaneus bone (Fig. 1c). Three sections of AT starting from 1 cm above the datum line were quantified for elastic stiffness. The datum line was actuated by an electrodynamic mini-shaker (model 4810, Brüel & Kjær, Nærum, Denmark) to generate band pass filtered frequency (5 Hz-1000 Hz) impulses. Four LDV sensors (PDV 100, Polytec, Irvine, CA, USA) shone along a 5-6 cm long thin retro-reflective adhesive tape (*3M*). The tape was attached over the tendon from the datum line and 6 cm along the axis of the Achilles tendon. Subjects performed three series of brief contractions for each ankle. The measurements were made in a randomized order. The SURF-E measurements were performed on these ten subjects using the same procedure as described in details in Salman & Sabra and previously validated using soft gel samples.

RESULTS AND DISCUSSION

Fig. 2 illustrates the SURF-E method with results collected on one subject for a 70° ankle angle (dorsiflexion). Fig. 2a is the power spectrum of the shaker excitation and the four LDV sensors measurements where most of the energy is limited to 500Hz as higher frequencies are greatly attenuated by soft tissues. Fig. 2b displays typical surface waves propagating along the Achilles tendon, as measured by each of the 4 LDVs. The peak values of each waveform is used to determine arrival times and in turn the surface wave propagation velocity

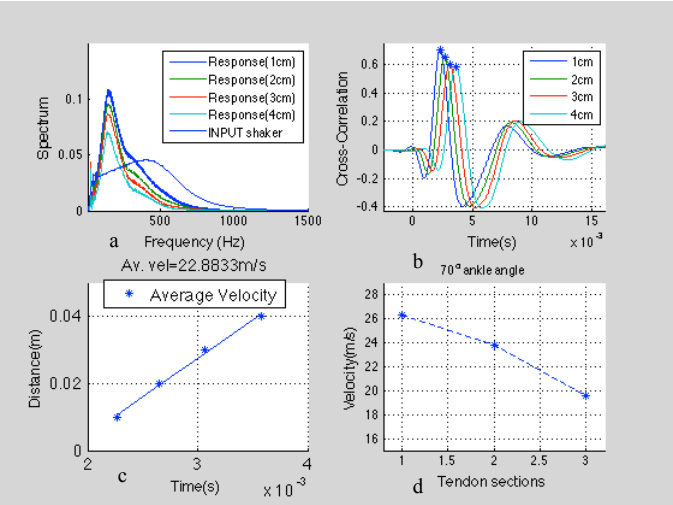

Figure 2: (Data analysis of a subject at 70º ankle angle) a) Power spectrum of the sensor and shaker, b) Cross-Correlation signal processing filter, c) Linear fit of four max. peaks in fig. 2b, e) Spatial velocity variaiton of the AT.

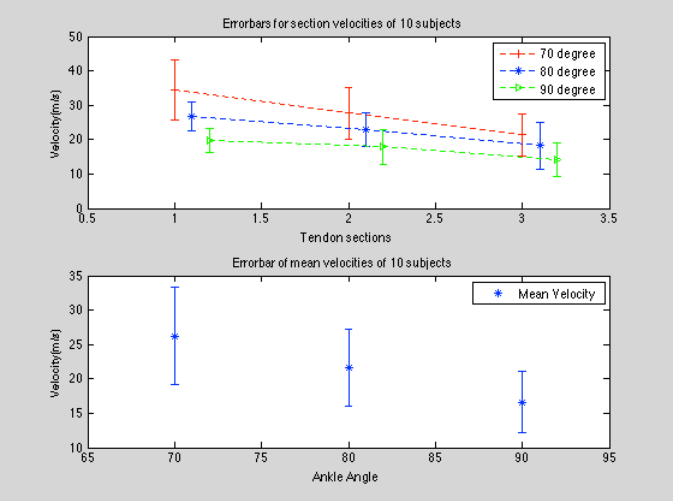

Figure 3: (Data analysis of 10 subjects) a) (Top) Spatial velocity variation of AT at three ankle positions. b) (Bottom) Mean of shear wave velocity along the AT.

When these peaks are linearly fit they give the slope of an average shear wave velocity as shown in Fig. 2c. When the difference of these peaks is taken the local spatial velocity variations of the AT as shown in Fig. 2d can be estimated in each of the 3 segments of the AT shown in Fig 1b. Fig. 3 is the result analysis of ten subjects for three different ankle positions. Fig. 3a shows a decreasing trend in the surface wave velocity along the AT going from section I of AT [1,2], proximal to calcaneus bone, up to section III which are near the calf muscle. Since a decrease in local surface wave propagation velocity is directly correlate with a local decrease in to stiffness of the AT [1,2] this indicates a non-uniform stiffening of the AT during dorsiflexion, therefore. Finally, Fig 3b shows the mean value of surface wave velocity, average over all 10 subjects, for three ankle positions. Again, here this indicates that the SURF-E method is capable of sensing the increase in AT stiffness as the ankle joint angle goes from neutral (90º) to dorsiflexion position (70º). High standard deviation in Fig 3a for 70º ankle position as compared to the other two shows the variability of stiffness of AT under high loading.

CONCLUSIONS

The large range of velocity values (10--38m/s) shown in Fig 3 indicates that the SURF_E technique can quantify stiffness variations of the AT is a much broader range than other techniques such as Ultrasound (US) and MRI techniques which have inherent limitations for high stiffness (typically propagation velocities less than 18m/s). [3,4] Future work will be done to assess stiffness variations of the AT during fatigue exercise and stretching. Developing a low-cost, single LDV-based SURF-E modality as an alternative to using expensive US scanner would broaden the acceptance and clinical usage of transient elastography methods for AT's diagnosis and monitoring the mechanical recovery of injured ATs. SURF-E method would assist the injury risk assessment and patient-specific selection of treatment plans for tendinopathy as well as the monitoring of the efficiency of therapeutic exercise programs which would diminish health care costs associated with the exponentially increasing number of AT injuries. As another advantage, SURF-E method can be performed in near real-time (<3 s) and thus could readily be used to monitor the evolution of the AT.

REFERENCES

[1] M. S. K. S. Muhammad Salman, "Assessment of muscle stiffness using a continuously scanning laser-Doppler vibrometer," *Muscle and Nerve,* vol. 50, p. 133–135, 2014.
[2] S. K. Muhamamd Salman, "Surface wave measurements using a single continuously scanning

Laser Doppler Vibrometer: Application to elastography," *Journal of Acoustical Society of America,* vol. 133, p. 1245–1254, 2013.

[3] Aubry, S., Risson, J. R., Kastler, A., Barbier-Brion, B., Siliman, G., Runge, M., & Kastler, B. (2013). Biomechanical properties of the calcaneal tendon in vivo assessed by transient shear wave elastography. *Skeletal radiology*, *42*(8), 1143-1150.

[4] Chen, X. M., Cui, L. G., He, P., Shen, W. W., Qian, Y. J., & Wang, J. R. (2013). Shear wave elastographic characterization of normal and torn Achilles tendons a pilot study. *Journal of Ultrasound in Medicine*, *32*(3), 449-455.

ADDED MASS EFFECTS ON TENDON VIBRATION UNDER AXIAL LOAD

[1] Dylan G. Schmitz, [1] Jack A. Martin, [1] Josh D. Roth, [1] Matt S. Allen, and [1] Darryl G. Thelen

[1] University of Wisconsin, Madison, WI, USA
email: dgschmitz@wisc.edu

INTRODUCTION

There is growing interest in the use of shear wave sensors to estimate tissue loading [1]. Recent work in our lab suggests there is a linear relationship between shear wave speed squared and tendon stress under functional loading conditions [2]. The constant of proportionality is the effective density, which would account for the tissue density and the added mass effects of adjacent tissues and fluid. Ideally, one could use geometric measures of the tissues and first principles to ascertain what the added mass is for a given tendon. Such an approach has been used to estimate added mass effects for a cantilever beam vibrating in a viscous fluid, as can occur in atomic force microscopy [3]. This approach can be extended to *ex vivo* tendon tests by assuming tendon behaves like a tensioned beam with an elliptical cross-section [2]. The purpose of this study was to compare tendon vibration in air and fluid to ascertain if the theoretical predictions of added mass effects are consistent with experimental observations.

METHODS

Model: We modeled tendon as a tensioned beam with elliptical cross-section and transversely isotropic material properties [2]. In this case, shear wave speed is dependent on axial stress $\boldsymbol{\sigma}$, the tangential shear modulus **μ,** a shear correction factor **k',** and the effective density $\boldsymbol{\rho_{eff}}$ [2]:

$$c^2 = \frac{\mu k' + \sigma}{\rho_{eff}} \quad (1)$$

If the tendon is subjected to pinned-pinned boundary equations, the shear wave speed, **c**, is given by:

$$c = \frac{2 \times f \times L}{n}, \ n = 1,2,3, \ldots \quad (2)$$

where **f** is the standing wave vibration frequency in Hz, **L** is the sample length, and **n** is the vibration mode.

Combining equations (1) and (2), one predicts that vibration frequency squared is inversely proportional to the effective density at a given stress magnitude.

$$f \propto \frac{1}{\sqrt{\rho_{eff}}} \quad (3)$$

For a tendon with an elliptical cross-section vibrating in fluid, the effective density is given as [3]:

$$\rho_{eff} = \rho_t + \rho_f \cdot AR \cdot \Gamma_r \quad (4)$$

where $\boldsymbol{\rho_t}$ and $\boldsymbol{\rho_f}$ are tendon and fluid densities, $\boldsymbol{AR}$ is the elliptical cross-section aspect ratio, and $\boldsymbol{\Gamma_r}$ is a frequency-dependent hydrodynamic function. From equations (3) and (4), one then obtains a prediction of the ratio of vibration frequencies between bath and air when a tendon is subjected to a stress $\boldsymbol{\sigma}$:

$$\frac{f_{bath}}{f_{air}} = \left(\frac{\rho_t + \rho_f \cdot AR \cdot \Gamma_r}{\rho_t}\right)^{-1/2} \quad (5)$$

Experiments: To evaluate the model prediction, we tested three fresh-frozen porcine digital flexor tendons in an electrodynamic testing system (MTS). Six axial loads, ranging from 50-300 N in 50 N increments, were applied (Fig. 1). Tendon vibration was induced by an impulsive tap (20-micron amplitude) from a piezoelectric actuator device positioned 8 mm above the lower grip. The tap induced a damped standing wave in the tendon. At each load, a laser Doppler vibrometer (Polytec) measured the transverse tendon velocity for 10 seconds at 50 kHz (Fig. 1). Spectral analysis was used to ascertain the dominant vibration frequency from the velocity records. Tests were repeated with the tendons placed in and outside of a saline bath (1 g/mL NaCl).

A least-squares linear regression was used to determine the slope between frequency squared and stress for each trial (Table 1, Figure 2). The square root of the regression slope between bath and air was used to compute the average frequency ratio for each tendon.

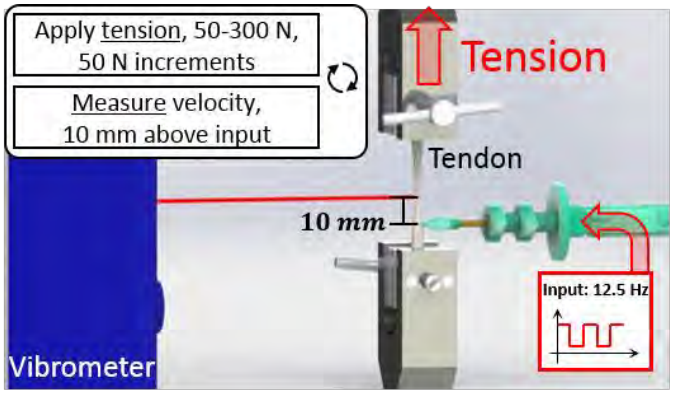

Figure 1: Experimental setup and procedure. A laser Doppler vibrometer measured transverse tendon velocity in response to an impulsive input tap.

RESULTS AND DISCUSSION

Frequency squared was strongly correlated with stress for both in-air and in-bath conditions (Fig. 2, R^2 = 0.96 ± 0.03). For all samples, the tendon vibration frequencies in-bath were significantly lower than in-air (p = 0.03, α = 0.05), as was predicted by the analytical model. The average frequency ratio between bath and air conditions was 0.83 ± 0.04. Assuming a hydrodynamic function $\mathbf{\Gamma}_r$ = 1.07 [3] and using the measured tendon aspect ratios, our analytical model predicted an average frequency ratio, 0.79, that was within 1 s.d. of the measured values.

These results support the use of analytical approaches to account for added mass effects of *ex vivo* tendons vibrating in fluid. The added mass effects due to hydrodynamics were substantial, increasing the effective density by ~60% and thereby decreasing the vibration frequency by 20%. Even greater added mass effects would be expected for tendon *in vivo*, where both surrounding tissue and hydrodynamic effects can increase the effective density. Such effects likely contribute to the lower shear wave speeds seen *in vivo* as compared to *ex vivo* at similar tendon stress magnitudes [2]. Additional work is needed to ascertain if added mass effects of adjacent tissues can be estimated based on geometry metrics and simplified models. These insights will be critical to transform noninvasive shear wave measures into a proxy of tendon loading during movement.

Table 1: Linear regression slopes and fit between squared wave speed and stress during both in-bath and in-air conditions. Model predicted and measured bath-to-air frequency ratios for each of the tendons.

	Slope (kHz^2/MPa)		R^2		Freq. Ratio f_{bath}/f_{air}	
Sample	Bath	Air	Bath	Air	Model	Exp.
1	16.5	10.1	0.97	0.98	0.77	0.78
2	12.0	8.21	0.92	0.99	0.80	0.83
3	7.68	5.78	0.97	0.95	0.79	0.87
Mean			0.95	0.97	0.79	0.83
(s.d.)			0.03	0.02	0.01	0.04

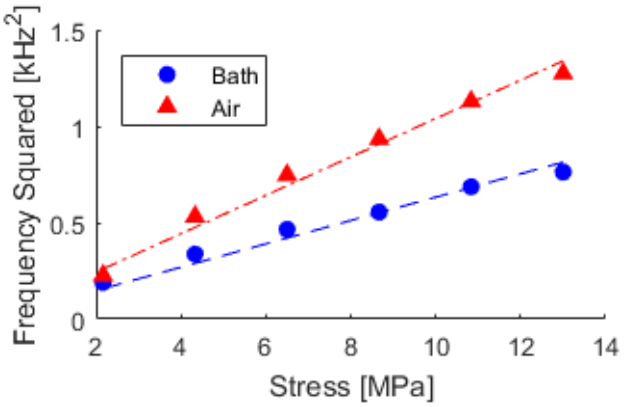

Figure 2: Strong, but distinct, linear relationships between vibration frequency squared and stress were observed for tendons vibrating in-bath and in-air.

CONCLUSIONS

A strong linear relationship between vibration frequency squared and axial stress was evident in tendon vibrating in both air and a saline bath. Vibration frequencies were 20% lower in the bath, a reduction that is consistent with predictions based on an analysis of the added mass arising from hydrodynamics. Future work will explore whether added mass effects due to adjacent tissues can similarly be modeled and the effects on vibration directly predicted.

REFERENCES

1. Hug et al. *Exerc. Sport Sci. Rev.* **2015**.
2. Martin et al. *Nat. Comm.* Accepted.
3. Allen et al. *J. Dyn. Syst. Meas. Control*. **2009**.

ACKNOWLEDGEMENTS

NIH AG051748, HD092697

RELIABILITY, VALIDITY, AND TORQUE-ANGLE CURVES OF HIP STRENTH MEASURED BY HAND-HELD DYNAMOMETRY

Kaitlin Squier and Dr. David Bazett-Jones

Carroll University, WI, USA
email: ksquier@pio.carrollu.edu

INTRODUCTION

Hip strength is often measured by hand-held dynamometry (HHD), however, the validity of this method compared to a gold-standard has received limited investigation [1-2]. Hip strength curves for abduction (ABD) and extension (EXT) have been recently published [3] but internal rotation (IR) and external rotation (ER) hip strength curves have not recently [4]. Therefore, the aims of this study are to 1) determine the intrarater reliability of the HHD for hip strength testing across the joint range of motion, 2) determine the validity of the HHD compared to isokinetic dynamometer (IKD) for hip strength testing across the joint range of motion, and 3) describe the torque-angle curves for each hip muscle group measured.

METHODS

Thirty healthy subjects (16 females, age=21.5±2.4 yrs, mass=76.7±24.1 kg, height=1.7±0.1 m) participated in this cross-sectional study. Participants completed 3 sessions of hip strength testing with at least 48 hours of recovery in between each session. Each session hip strength testing was measured at multiple angles throughout the range of motion. The first and third session were using a belt-stabilized HHD. The second session was using an IKD. In each session, ABD was tested in a side lying position at -10°, 0°, 20°, and 40°. IR and ER were measured in an upright seated position with 90° of knee flexion at -30°, -15°, 0°, 15°, and 30°. EXT was tested in a supine position at -10°, 0°, 30°, 60°, 90°, and 120°. Strength was tested twice at each angle and the average torque values were used for analysis.

Intrarater reliability of hip strength was analyzed using Intraclass Correlation Coefficients (ICCs), standard error of measurement (SEM; SEM=SD*√1-ICC), and minimal detectable change (MDC; MDC=SEM*1.96*√2). Strength of the reliability was categorized as poor (ICC<0.40), fair (0.70 > ICC $\geq$ 0.40), good (0.90 > r $\geq$ 0.70), or excellent (ICC $\geq$ 0.90). Validity of hip strength was analyzed using Pearson Correlations and dependent t-tests. The correlation was classified as low (r < 0.40), moderate (0.70 > r $\geq$ 0.40), or high (r > 0.70). The α level was set at 0.05.

RESULTS AND DISCUSSION

All tests of hip strength showed fair to excellent reliability across the full range of motion (ICC=0.620-0.900). Hip ABD strength was a valid (r=0.556-0.624, no significant differences) measure for all angles throughout the range of motion. Both ER and IR showed mostly low to moderate relationships between the measures (0.194-0.651 and 0.393-0.771, respectively) and torque values were significantly different (p<0.005) between HHD and IKD for all tests at all angles. Hip EXT strength showed poor relationships at -10 and 0 (-0.037 and 0.192, respectively); however, the values were not significantly different (p>0.05). At 60, 90, and 120, hip EXT strength showed strong relationships (0.648-0.794) but significant differences (p<0.05). At 30°, hip EXT strength was both moderately correlated (r=0.586) and not significantly different (p=0.612), showing the best position for testing hip EXT strength in supine.

Previous studies of reliability have only been performed at 0°. The results of this study at 0° are in agreement with previous research for all muscle groups [1-2].

Our results agree with the literature [1-2] in concluding that hip ABD is valid when measured by a HHD. In regards to ER and IR, our results are similar to previous research [1-2] that showed

moderate relationships between HHD and IKD but significant and large differences between the values [2]. The HHD measurement tool cannot be used interchangeably with the IKD since the HHD underestimates strength, calling into question its validity compared to the gold standard. For hip EXT strength, our poor relationship results are not in agreement with previous research at 0° [1-2]. This might be due to positioning participants in supine, whereas previous research has only used a prone position.

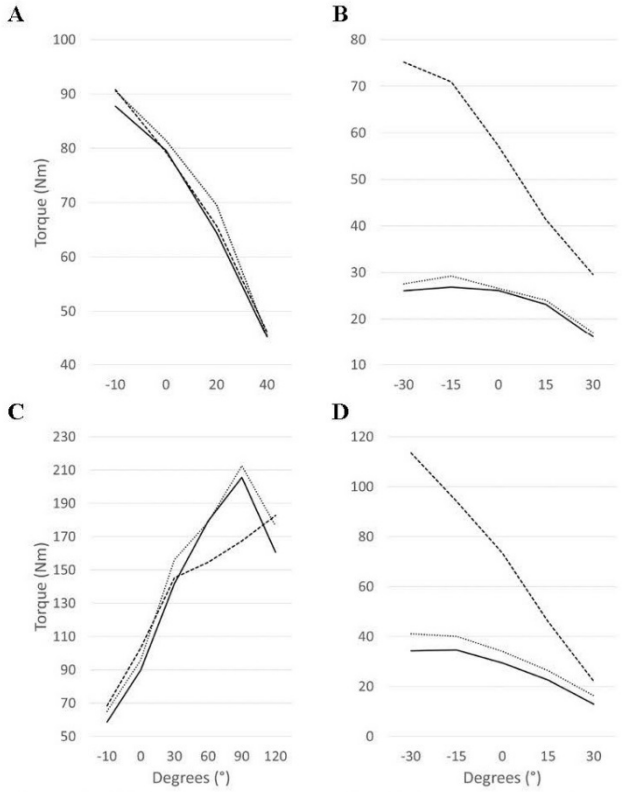

Figure 1: Hip torque-angle curves for A) abduction, B) external rotation, C) extension, and D) internal rotation. Solid line=Hand-held dynamometer (HHD) Test 1, Dotted line=HHD Test 2, Dashed line=Isokinetic dynamometer (IKD)

This study is unique in that it provides torque-angle curves throughout the full joint range of motion for hip ABD, ER, IR, and EXT (Figure 1). A recent study [3] demonstrated a similar relationship for ABD (as angle increased, torque decreased) and EXT (as angle increased, torque increased). This study was limited in that it only looked at 0-45° of hip flexion when testing EXT. Our findings are in agreement with these findings [3] for both ABD and EXT. In 1966, May [4] performed a similar investigation to ours on IR and ER, reporting that as muscle length increased, the force values increased as well. Our findings demonstrate that the ER, IR, and ABD muscles generate the highest torque value in a lengthened position. These results cause us to question the common testing position of neutral for hip IR and ER.

CONCLUSIONS

Strength measured with an IKD is considered the gold standard. HHD can be an effective tool for measuring strength under certain circumstances. When using a HHD to measure hip strength, users should be aware that a HHD will significantly underestimate strength compared to the IKD, except in ABD and EXT near neutral. EXT torque is greatest at 90° flexion and ER, IR, and ABD torque is greatest in their lengthened position.

REFERENCES

1. Martins, J., Silva, J. R., Silva;, M. R., & Bevilaqua-Grossi, D. (2017). Reliability and Validity of the Belt-Stabilized Handheld Dynamomter in Hip-and Knee Strength Tests. *Journal of Athletic Training, 52*(9), 809-819.
2. Katoh M., Hiiragi Y., & Uchida M. (2011). Validity of Isometric Muscle Strength Measurements of the Lower Limbs Using a Hand-held Dynamometer and Belt: a Comparison with an Isokinetic Dynamometer. *Journal of Physical Therapy Science, 23*(4), 553-557.
3. Kindel, C., Challis, J. (2017). Joint moment-angle properties of the hip abductors and hip extensors. *Physiotherapy Theory and Practice*, DOI: 10.1080/09593985.2017.1323357.
4. May, W. (1966). Maximum isometric force of the hip rotator muscle groups. *Journal of the American Physical Therapy Association*, 46, 233-238.

ACKNOWLEDGEMENTS

The Carroll University Pioneer Scholar Summer Undergraduate Grant Program funded this project. Stephanie Bandura assisted with data collection.

Comparing Inertial Measurement Unit and Optical Infrared Passive Marker-Based Motion Capture Systems: Studying the Effects of Subject Preparation Variability

Rafael Valbuena, Sarah Griffin, and Craig M. Goehler

Department of Mechanical Engineering and Bioengineering, Valparaiso University, Valparaiso, IN, USA
email: craig.goehler@valpo.edu

INTRODUCTION

The aim of this study was to compare the two most popular measurement systems for recording human motion kinematics: camera-based motion capture (MoCap) and inertial measurement units (IMUs). MoCap is generally regarded as a more accurate measurement system [1], but the need for Infrared (IR) cameras constrains the possibilities of conducting research programs outside of a controlled laboratory space. On the other hand, recent IMU-based portable systems like the the XSens MVN allow the user much more flexibility, eliminating the need for IR cameras and opening the possibility to study the motion of athletes in their natural environment (a soccer/football field, baseball diamond, basketball court, etc). However, IMU-based systems are anecdotally believed to provide less accurate results.

While the argument against the use of IMUs to obtain accurate data could potentially be reasonable, few efforts have been made to quantify the difference in accuracy between both systems in the context of injury prevention studies [2]. In a preliminary study, our group took the first steps to determine if it is appropriate to use IMUs to collect joint kinematic data while completing an injury prevention protocol, but at the time we were limited to a single assessment [3]. For this reason, we developed this updated study by expanding on our previous database, and studying the effects that different factors like marker placement have in the accuracy of our data.

METHODS

For this study, 1 male subject, age 22, participated in an IRB approved study that compared two quantitative techniques for human movement data collection. The subject was affixed with 28 passive reflective markers based on the anatomical locations specified in a previous study [3], and 17 IMUs at locations specified by XSens. The subject was brought in for five sessions and completed a series of motions from the Functional Movement Screening and Landing Error Scoring System tests. The subject performed each test three times per session.

MoCap data was collected using 11 VICON Bonita cameras. A subject-specific full-body model was used to calculate the inverse kinematics for each trial. IMU data was collected using the XSens Awinda station and MVN Studio. Kinematic data was calculated using the XSens internal model and exported directly from MVN Studio.

The first session was used as control, placing all of the markers in the recommended locations. In each of the following sessions, the Xsens sensors were systematically moved from their recommended place on the subject's anatomy while keeping the VICON markers as close as possible to their ideal anatomical locations.

RESULTS AND DISCUSSION

For this abstract, results from the deep squats and right and left in-line lunges were compared between the two systems. The data for hip and knee flexion was the focus of the study. The collected data was then plotted against normalized time so that it could be compared qualitatively. The MoCap and IMU data was paired for each trial so that the exact same movement was being considered each time. Figure 1 shows a representative sample of data collected by the two systems.

For the majority of the trials, the MoCap and IMU systems produced similarly shaped curves, but there were differences in the the maximum values and, in some instances, the shape of the graphs. Additionally, there were more inconsistencies in hip

flexion than in knee flexion. The graphs consistently showed this across all trials.

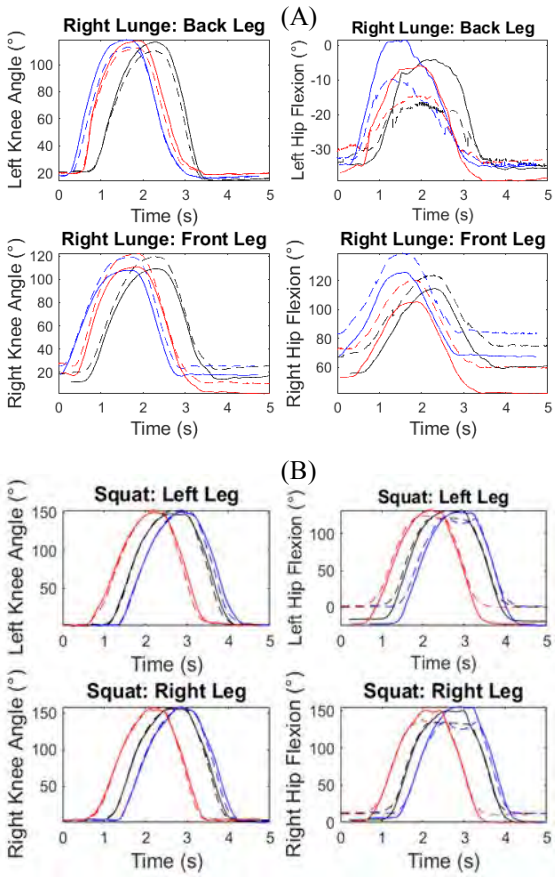

Figure 1: Comparison of the knee angle and hip flexion for MoCap (VICON), represented with dashed lines, and IMU (Xsens), represented with solid lines, during (A) left in-line lunge and (B) squat tests.

Because the simulation model for the IMUs is black boxed, it is difficult to say exactly why the differences occur; however, it can be hypothesized that it is due to the fact that the MoCap has more markers surrounding the hip than the IMUs do. Thus, the MoCap is likely more accurate. With the knee angles, the numbers of markers are nearly identical which could explain the similarities in results.

This study has shown that IMUs can be used to collect accurate information, but possibly not for all joint angles. The IMUs provide nearly the same information regarding the knee angles with both exercises. However, the inconsistencies between the hip flexion angles demonstrate that IMUs could be less valuable for certain degrees of freedom until a better understanding of the internal model can be obtained and utilized to create an effective mapping of the results.

The results regarding marker location variability where close to what we expected. Table 1 shows how the average RMS error increased significantly, in sessions 1-4, compared to the control. Moreover, we found that some joint angle calculations experienced different effects across the sessions because we shifted different IMU markers in various ways for each session. For example, in session 4 in which the Right Upper Leg marker was shifted inferior to its recommended location and the Left Upper Leg was shifted superior to it, the error for almost every angle increased, except for the Right Knee which showed a lower error than the control session. A theory to explain this behavior would be that when shifting the marker close to the Right Knee we actually got closer to the ideal theoretical location by "accident" while the others got further away. Even though each variable was affected differently, increasing error was consistent across all sessions in which the markers placements were shifted, which leads us to think that subject preparation plays a big role in the accuracy in the IMU-based system.

Future work will involve analysis of more joint angles and exercises to determine which joint angles demonstrate similar inconsistencies between systems so that users can know how to better collect and interpret data from IMUs.

REFERENCES

1. *Eichelberger P, et al. Journal of Biomechanics, **49**(10), 2085-2088, 2016.*
2. *Skogstad A, et al. SMC Conference 2011*
3. *Valbuena R*, et al. *Annual Meeting of ASB 2017.*

Table 1. Root Mean Square deviation between the VICON and Xsens measured maximum angles in the left lunge for each session

RMS Error	Control	1	2	3	4
Lknee [°]	4.15	11.22	3.16	2.88	10.46
Rknee [°]	2.14	4.63	2.06	9.35	1.15
Lhip [°]	4.27	15.19	22.35	4.55	18.18
Rhip [°]	1.78	13.46	19.54	6.77	11.62
Average [°]	3.09	11.13	11.78	5.89	10.35

CHANGES IN MUSCLE SHEAR WAVE PROPAGATION WITH ACTIVE AND PASSIVE FORCE GENERATION

[1,2] Allison B. Wang, [1,2] Eric J. Perreault, [1,2] Sabrina S. Lee

[1] Northwestern University, Evanston, IL USA
[2] Shirley Ryan AbilityLab, Chicago, IL USA
email: bwang15@u.northwestern.edu

INTRODUCTION

Skeletal muscles exhibit viscoelastic properties that arise from a network of active and passive structures that change during active contractions and externally imposed length changes [1]. These structures can be affected by neuromuscular diseases and injuries, leading to altered mechanical properties and impaired force generation capacity. Until recently, there have been no non-invasive techniques for quantifying the active and passive contributions to intrinsic muscle mechanics. Ultrasound-based shear wave elastography has emerged as a possible tool for characterizing muscle mechanics [2]; however, most previous applications have only considered the elastic properties of muscle, whereas muscle is viscoelastic, and viscoelastic characterizations in other biological tissues have been used to link microscopic structure to macroscopic properties.

The objective of this study was to evaluate how the viscoelastic properties of muscles, as measured by shear wave ultrasound elastography, vary with active and passive changes in muscle force. Since active and passive muscle tension govern the function of our daily movements, understanding how the viscoelastic properties differ under various force modulation will contribute to understanding of intrinsic muscle mechanics and the information can be useful for monitoring muscular adaptation due to aging, diseases and injuries, and rehabilitation.

METHODS

The data collection protocol was approved by the Northwestern University Institutional Review Board (STU00200422). Ten healthy adults (4 M and 6 F; mean±SD age 25±2.6 yrs, mass 62.2±9.9 kg, height 1.70±0.07m) participated in this study. Ultrasound data (Aixplorer V10, Supersonic Imagine, Aix-en-Provence, France) were collected at different active and passive muscle forces within the biceps brachii, as regulated by changes in activation and joint angle, respectively. Elbow flexion angles of (80°, 90°, 135°, and 180°) were used to change the length of the biceps brachii, and thereby passive muscle force. Active force was regulated by voluntary contractions at 0, 10, 20, and 30% of maximum voluntary contraction (MVC). All active measurements were made with the elbow in 90° of flexion. These submaximal activation levels were chosen to prevent muscle fatigue and to avoid saturation of the shear wave velocity measurements.

Shear wave phase velocities (V_ϕ) were estimated from the ultrasound data collected over a range from 0 - 800 Hz. A Voigt model was fit to these data to characterize the shear viscoelasticity of muscle [1]. This model relates shear wave phase velocity (V_ϕ) to shear elasticity (μ) and shear viscosity (η) using Eq. 1, where ρ is the density of muscle, ω is the angular frequency. A nonlinear least-squares method was used to estimate μ and η from V_ϕ. The dynamic properties of Voigt model were characterized by the time constant $\tau = \frac{\eta}{\mu}$. The effects of active and passive changes in muscle force on the estimated shear elasticity, viscosity, and time constant were tested using a linear mixed-effect model.

$$V_\phi(\omega) = \sqrt{\frac{2(\mu^2+\omega^2\eta^2)}{\rho(\mu+\sqrt{\mu^2+\omega^2\eta^2})}} \quad (1)\ [3]$$

RESULTS AND DISCUSSION

The estimated viscous and elastic properties of muscle increased with active and passive forces. Under active conditions, shear elasticity and shear viscosity increased by ~16x from 0% to 30% of MVC (Fig. 1a,b). A similar proportional increase in the elastic and viscous properties of muscle with active force was previously reported in animal studies where direct measurements could be made [4]. Across the range of tested passive conditions, shear elasticity increased by ~ 8x while shear viscosity increased only by ~ 2x (Fig. 1c,d). Such

length-dependent changes in viscoelastic properties has not been directly reported, although previous studies have separately confirmed the increase in elastic [5] and viscous properties [6] when muscle is passively lengthened.

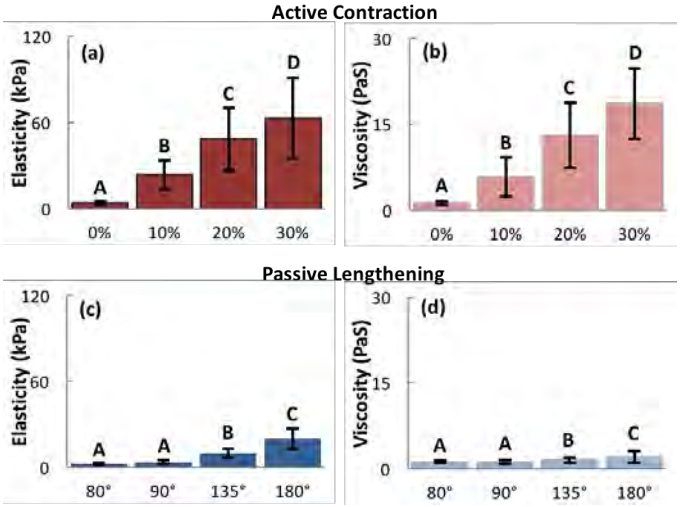

Figure 1: Shear elasticity (μ) and shear viscosity (η) extracted from Voigt model (mean and standard deviation across subjects) under active (a, b) and passive conditions (c,d). Groups that do not share a letter indicate statistical difference ($p<0.05$).

The time constant of the estimated Voigt model differed during active and passive force generation. The time constant remained nearly constant during active contractions of muscle (Fig. 2a,c). In contrast, the time constant changed significantly with changes in passive tension, regulated by changing muscle length. The time constant decreased for increasing muscle lengths, representative of changes in the estimated elasticity parameter that increased more rapidly than the estimated viscous parameter (Fig. 2b,d).

CONCLUSIONS

We demonstrated that the estimated elasticity and viscosity parameters characterizing shear wave propagation increased with increasing muscle force. However, the relationship between these parameters, quantified by the time constant, depended on how force was generated. The time constant remained nearly constant for actively generated forces, but decreased as passive forces increased.

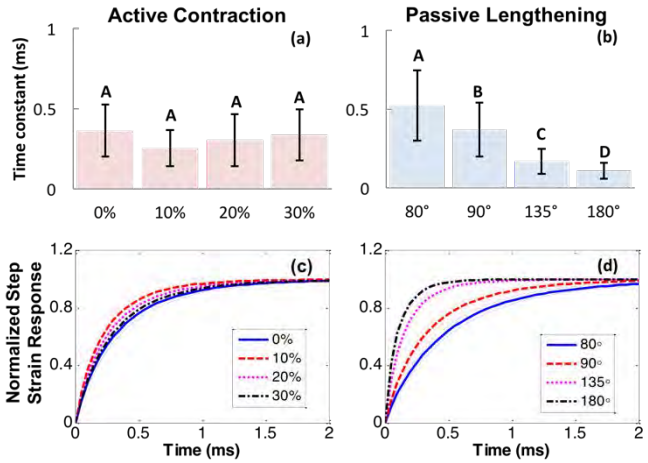

Figure 2: Average time constant under a) active and b) passive conditions across subjects (error bars: ± standard deviation). Groups that do not share a letter indicate statistical difference ($p<0.05$). (c, d) Simulated step strain response using time constant. The thin lines are 95% confidence interval.

The reported differences in the estimated time constant likely reflect differences in how force is transmitted in active and passive muscle. Structures such as the extracellular matrix, cross-bridges, titin and other load-bearing elements of muscle contribute differently to active and passive force transmission. Shear wave propagation appears to be sensitive to these differences, as summarized by the time constant for propagation. Previous studies have suggested that the viscoelastic time constant might be an important diagnostic index for pathological tissues [7]. Our results support that possibility, and clarify that this use may stem from a sensitivity to changes in the active and passive load-bearing structures in muscle.

REFERENCES

1. Fung YC. *Biomechanics Mechanical properties of living tissues,* New York: Spinger; 1993.
2. Bercoff et al. (2004) *IEEE Trans Ultrason Ferroelectr Freq Control*. 51: 396-409.
3. Chen et al. (2004) *J Acoust Soc Am*. 115:2781-85.
4. Halpern et al. (1971) *J Appl Physiol*. 31: 913-925.
5. Brown et al. (2012) *J Orthop Res*. 30: 1321 – 1326.
6. Meyer et al. (2011) *J Biomech Eng*. 133: 091007.
7. Palacio-Torralba et al. (2015) *J Mech Behav Biomed*. 41:149-160.

ACKNOWLEDGEMENTS

Funding: NIH R01 AR0711

VALIDITY OF THE OPTOGAIT PORTABLE PHOTOELECTRIC CELL SYSTEM FOR QUANTIFICATION OF SPATIAL-TEMPORAL PARAMETERS OF RUNNING GAIT

Amy Weart, Erin Miller, Gregory Freisinger, Michael Johnson, Donald Goss[1]

[1] United States Military Academy, West Point, NY, USA
email: amy.n.weart.ctr@mail.mil

INTRODUCTION

Gait analysis on a treadmill can be used to identify spatial-temporal parameters of gait in both healthy [1] and injured [2] individuals. Instrumented treadmills have been considered the gold standard for assessing certain running parameters; however, these treadmills are costly, require trained personnel to operate, and use custom code to calculate variables of interest from the raw data. The OPTOGait system is portable and can be used on any flat surface or treadmill to collect data. OPTOGait uses high-density photoelectric cells between transmitting and receiving bars which detect interruption in light signals due to a subject's foot and automatically calculates spatial and temporal parameters [3]. While convenient, the reliability of the OPTOGait system for the assessment of gait parameters during running has not been studied. The purpose of this study was to examine the validity of spatial and temporal gait parameters calculated by the OPTOGait compared to an instrumented treadmill system during running.

METHODS

Twenty-nine healthy runners (mean age= 31.1 ± 9.8 years, 23 males, mean weekly run mileage 11.3 ± 10.8 miles) at the United States Military Academy were recruited to participate in the study. Participants met the following inclusion criteria: 1) Run at least a 2.7 meter per second (m/s) pace for 5 minutes; 2) Between ages of 18-60 years; 3) Department of Defense beneficiary; 4) English speaking. Participants were excluded based on the following criteria: 1) Current pregnancy; 2) Lower extremity or back injury within previous 3 months; 3) Lower extremity or back surgery within previous 6 months.

All subjects ran for 5 minutes at a self-selected pace (mean 3.2 ± 0.3 m/s) on an instrumented treadmill (Bertec; Columbus, OH) with the OPTOGait 1-meter system (OPTOGait, Microgate S.r.l, Italy, 2010) mounted along the treadmill platform. Raw force data on the treadmill were collected at 1000 Hertz (Hz), low-pass Butterworth filtered at 35 Hz, and normalized to bodyweight. Spatial-temporal running variables of step rate, step length, and contact time were calculated using a custom Matlab script (Mathworks Inc., Natick, MA). OPTOGait collected data at 1000 Hz and all spatial-temporal running variables were calculated using OPTOGait Version 1.11.1.0 software (Microgate s.r.l, Italy). Data were collected during the final minute of running.

The level of agreement between the OPTOGait system and instrumented treadmill were analyzed using intraclass correlation coefficients ICC (3,1) for step rate, step length, and contact time using SPSS v 24. Pearson product moment correlation was conducted for contact time between OPTOGait and Bertec treadmill.

RESULTS AND DISCUSSION

Step rate demonstrated excellent reliability ICC=0.97 (95% CI=0.93-0.99). Step length demonstrated excellent reliability ICC= 0.99 (95% CI= 0.98-1.00). Contact time demonstrated moderate reliability ICC= 0.54 (95% CI= -0.23-0.84). Pearson product moment correlation coefficient for contact time was 0.81 (95% CI= 0.60-0.91).

The concurrent validity for step rate and step length was excellent, but the ICC for contact time was moderate (Table 1). The OPTOGait appears to be a valid instrument to measure step rate and step length for healthy runners during treadmill running.

Previous work supports these results with healthy young adults and stroke patients walking on a treadmill with ICCs demonstrating excellent concurrent validity and test-re-test reliability between OPTOGait and a Zebris instrumented treadmill [3].

Contact time demonstrated moderate agreement between the OPTOGait and instrumented treadmill. The scatter plot reveals that contact time was over-estimated for most subjects on the OPTOGait system (Figure 1). OPTOGait photoelectric cells are located 3 millimeters above the treadmill belt; this offset may account for additional time during heel strike and toe off that does not exceed the 50 Newton threshold that was used for foot strike on the instrumented treadmill. In healthy young adults and stroke subjects during walking on a treadmill, excellent agreement was found between the OPTOGait and instrumented treadmill ICC's= 0.85-0.99 [3]. The authors in this study did not define initial foot strike threshold value for the instrumented treadmill. Furthermore, Alvarez et al found no difference in contact time between OPTOGait and high-speed video analysis sampling at 1000 Hz for racewalkers walking on treadmill at speeds between 3.1-4.2 m/s [4]. Additional research is needed to look at subjects at different running speeds and inclines.

CONCLUSIONS

The present study validates the OPTOGait system as a method for analyzing step rate and step length. Increasing step rate and decreasing step length has been shown to reduce loading and joint moments at the hip and knee and may aid in the prevention of lower extremity running related injuries [5-6]. The OPTOGait system is a valid device that can be used clinically to evaluate step rate and step length without time or skill needed to reduce the data as in the case with the instrumented treadmill.

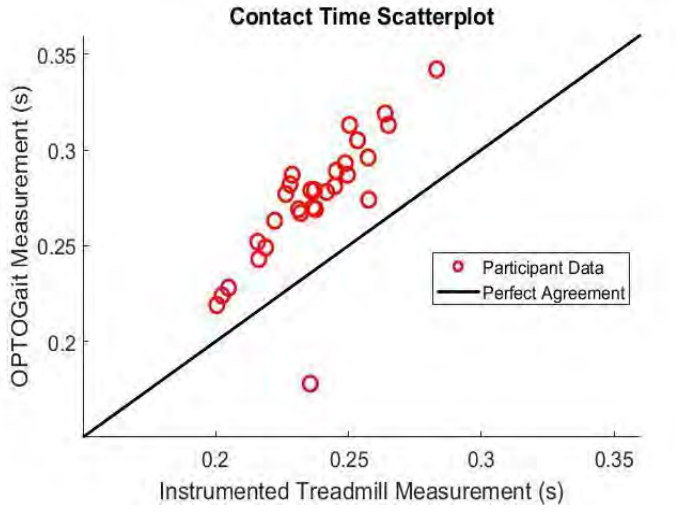

Figure 1: Relationship between OPTOGait and Bertec treadmill for contact time (seconds).

REFERENCES

1. Saleh M, Murdoch G. *J Bone Joint Surg Br*. 67B(2):237–241, 1985.
2. Lord SR et al. *J Gerontol*. 51(2):M64–70, 1996.
3. Lee MM et al. *J Phys Ther Sci.* 26(1):81-85, 2014.
4. Alvarez D et al. *ISBS Proceedings Archive*. 35(1):292-294, 2017.
5. Heiderscheit BC et al. *Med Sci Sports Exerc.* 43(2):296-302, 2011.
6. Thompson MA et al. *J Biomech.* 47(11):2745-2750, 2014.

Table 1: Means, standard deviations, and levels of agreement of gait parameters using OPTOGait and instrumented treadmill

	OPTOGait	Treadmill	ICC (95% CI)
Step Rate (steps/min)	173.13 ± 9.65	172.25 ± 9.01	0.97 (0.93- 0.99)
Step Length (centimeters)	111.94 ± 10.89	112.47 ± 11.90	0.99 (0.98- 1.00)
Contact Time (seconds)	0.27 ± 0.03	0.24 ± 0.02	0.54 (-0.23- 0.84)

DOES A ROTATING BAR AFFECT THE BODY KINEMATICS DURING A PENNY DROP MANUEVER?

Nicholas Yang, Lenka Stepan, Bethany Suderman, Irving Scher

Guidance Engineering, Seattle, WA, USA
email: yang@guidanceengineering.com, web: www.guidanceengineering.com

INTRODUCTION

Falls from equipment is one of the most common mechanisms related to playground injuries.[1,2] Turning and chinning bars are common playground structures and different maneuvers and calisthenics may be performed on these bars, including pull-ups or spinning maneuvers. One of the more advanced maneuvers that can be performed on a turning bar (with the potential for catastrophic injury) is a backward somersault while sitting on the top of the bar (also called a "penny drop"). Improper installation or lack of maintenance can cause chinning bars to rotate about their long axis. The objective of this study was to determine the influence of the chinning bar rotational state on body kinematics in a penny drop maneuver while sitting on the top of a chinning bar.

METHODS

A chinning bar system was setup in the Guidance Engineering laboratory in Seattle, Washington. The chinning bar was instrumented with strain gauges to determine the torque applied to the bar by the subjects during different maneuvers. The chinning bar was allowed to rotate freely about its long axis with a braking system used to control the motion of the chinning bar. In addition to the above instrumentation, the body motions of each subject were measured using an instrumented body suit (MVN Biomech Body Suit, Xsens Technologies, Enschede, Netherlands) containing 17 inertial measurement units. For each test trial, real-time video and high-speed video was recorded.

Three chinning bar conditions were tested: (A) *Fixed* – the chinning bar was held firmly in place and not permitted to rotate during the maneuver; (B) *Free* – the chinning bar was free to rotate during the entire test trial, including while the subject was sitting on the chinning bar; and, (C) *Released* – the chinning bar was held firmly in place until a specified torque was reached and then the chinning bar was released instantaneously and permitted to rotate freely. For the *Released* condition, the release torque was set to between 4 and 5 foot-pounds of torque. For all subjects, the *Fixed* tests were conducted prior to the other tests and the subjects were not aware that the chinning bar would be released (and allowed to rotate freely) for the *Released* tests.

Seven female subjects with no gymnastics or acrobatics training took part in the study; their average height was 5 feet 8 inches (range: 5 feet 6 inches to 5 feet 10 inches) and their average weight was 181 pounds (range: 141 to 204 pounds).

For each test trial, the peak torque on the chinning bar and angular velocity of the vector between the pelvis and head were ascertained. ANOVA and t-tests with a Bonferroni correction were used to determine statistical significance; a significance level of 0.05 was used for all statistical comparisons.

RESULTS AND DISCUSSION

A total of 78 penny drop tests were conducted: 32 with the *Fixed* bar condition, 23 with the *Free* bar condition, and 23 with the *Released* bar condition. For all test trials, the subjects completed successfully the penny drop maneuver. The general motion of the subjects was the same regardless of the bar condition.

During the penny drop test trials with the *Fixed* bar condition, the subjects applied a torque to the bar, but still rotated backwards. In the *Free* or *Released* (after the brake was released) condition, the bar rotated generally with the subject while the subjects were rotating backwards and did not rotate much more (if at all) after the subject's legs released from

the chinning bar (and her torso was in a generally inverted configuration).

In the *Fixed* bar condition, average peak torque applied to the chinning bar by the subjects was 11.9 foot-pounds (95% confidence interval: 10.5 to 13.4 foot-pounds). In the *Free* and *Released* bar condition, the average peak torque applied to the chinning bar by the subjects were 3.6 foot-pounds (95% confidence interval: 3.0 to 4.1 foot-pounds) and 7.8 foot-pounds (95% confidence interval: 6.7 to 9.0 foot-pounds). There were significant differences between the torque applied to the chinning bar based on the bar condition. It was hypothesized that a subject would apply less torque to the chinning bar when it was free to rotate throughout the test trial (the *Free* bar condition) when compared to the *Fixed* bar condition; the testing confirmed this hypothesis.

The angular velocity of subjects' COM varied throughout a test trial and data are presented for positions after initiation of the penny drop from a sitting position on the bar; *Back Horizontal*, *Back Below Horizontal, Back Vertical (inverted)*, and at *PT – Time of Peak Torque*. A typical time history of the angular velocity of the subject's COM can be observed below, see Figure 1.

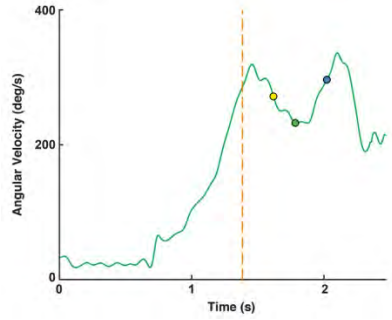

Figure 1: Typical time history of the angular velocity of the subject's COM during a penny drop maneuver. *Back Horizontal* position (yellow dot), *Back Below Horizontal* position (green dot), *Back Vertical* position (blue dot), or at the time of peak torque (dashed orange line).

The angular velocity in the *Back Horizontal*, *Back Below Horizontal*, and *Back Vertical* positions varied by subject and trial but were not significantly different between the *Fixed* and *Released* bar conditions. There was no significant difference between bar conditions for the angular velocity of a subject's COM at *PT – Time of Peak Torque* applied to the chinning bar. In all three cases, the subject rotated backwards and had similar angular velocities. Some subjects did not even realize that the bar had been allowed to rotate freely in the *Released* tests. Furthermore, all of the subjects indicated that it was easier (not more difficult) to execute successfully and fully the penny drop maneuver with the chinning bar in the *Released* or *Free* conditions when compared to the *Fixed* condition.

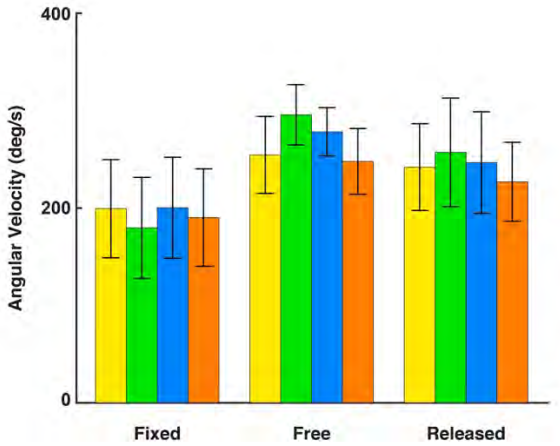

Figure 2: Average angular velocity of subject's COM by bar condition. For each bar condition, the four bars (from *Left* to *Right*) show the angular velocity at the *Back Horizontal* (yellow), *Back Below Horizontal* (green), *Back Vertical* (blue) positions and at the *Time of Peak Torque* (orange).

CONCLUSIONS

The female subjects applied less than 12 foot-pounds of torque on the chinning bar during the backward somersault (penny-drop) maneuver. During the penny drop maneuver, the angular velocity in the *Back Horizontal*, *Back Below Horizontal*, and *Back Vertical* positions varied by subject and trial but were not significantly different between the *Fixed* and *Released* bar conditions.

REFERENCES

1. Standard Consumer Playground Safety Performance Specification for Playground Equipment for Public Use, ASTM F1487-17
2. Fiissl et al. *Injury Prevention*. 11, 2005.

INVESTIGATION OF FATIGUE-ASSOCIATED MEASURES: AN EXPLORATORY FRAMEWORK USING SUPERVISED CLASSIFICATION APPROACH

*Liying Zheng, Xueyan S. Xu, Erik W. Sinsel, Daniel E. Welcome and John Z. Wu

Health Effects Laboratory Division, National Institute for Occupational Safety and Health (NIOSH), Morgantown, WV, USA.
*email: lzheng2@cdc.gov

INTRODUCTION

Understanding of fatigue implications in physically-demanding work has been one of the sustained interests in occupational research [1, 2]. Due to the complex cause and mechanism of fatigue, researchers face challenges to comprehensively "measure" fatigue [3, 4]. That complexity further makes it difficult to effectively evaluate certain ergonomic devices (such as industrial exoskeletons), which aim to reduce fatigue and to improve occupational safety.

Using machine learning algorithms, the goal of present study is to explore a framework that can detect most fatigue-relevant measures and monitor workers' fatigue level. In this exploratory study, we selected a simple isometric single-leg fatiguing exertion task as an example to demonstrate the framework with incorporating three categories of measurements—electromyography (EMG), near infrared spectroscopy (NIRS), and vibromyography (VMG).

METHODS

Four healthy subjects (male, 25 ± 6 years old, 85.9 ± 13.6 kg, and 1.72 ± 0.03 m) were consented to participate in this ongoing NIOSH Institutional Review Board-approved study. During the testing, subjects were instructed to sit upright with an approximate 90-degree knee flexion angle and to exert force on a non-elastic strap (Fig. 1a). Prior to the fatiguing trials, the reference trials of resting and maximal voluntary contraction (MVC) were conducted. Then subjects completed two randomized fatiguing tasks (two trials per task): maintaining the exertion level at 30% or 60% of their MVC until exhaustion.

Seven EMG sensors (Noraxon, Dual Ag/AgCl Electrode) were placed on the subject's right leg (on rectus femoris, vastus laterallis, rectus medialis, biceps femoris, semimembranosus, and lateral and medial gastrocnemius). Two NIRS sensors (Nonin, SenSmart, Model X-100) were placed on the subject's left forehead and right rectus femoris (Fig.

Figure 1. The experimental setup.

(a) A wooden box filled with heavy weights (the box could not be moved by the subject) were placed on the force plate, and a non-elastic strap was fixed and wrapped around the box. The subject was asked to exert force on the red strap. For submaximal tasks, subjects were asked to maintain the desired force level using graphical feedback on a monitor.

(b) EMG electrodes were placed on the quadricep muscles; NIRS and VMG sensors were both on rectus femoris muscle.

(c) VMG sensors were placed on the patellar bony area and the "fatty" adductor area of the thigh.

(d) NIRS sensor was on the left forehead (prefrontal cortex).

1b&d) to measure the oxygenation levels (Oxy). The VMG signals were measured using tri-axial accelerometers (Endevco, M35B, mass=0.55 g). The accelerometers were attached to the skin surface on rectus femoris muscle, the patellar bone and the adductor area of the thigh (often the "fatty" area) (Fig 1b&c). The leg pulling force was recorded by the force plate (Bertec, 4080-10) and for submaximal tasks, subjects were directed to maintain a force target using an unlabeled dial gauge displayed on a monitor. The Borg Rating of Perceived Exertion (RPE) scale [5] was explained beforehand and visible to the subjects during the test. The subjects were asked repeatedly (every 10-30 seconds) to give the RPE ratings of perceived exertion ("6" at rest; "20" at exhaustion) starting at each fatiguing task.

The recorded measurements were pre-processed and normalized to the reference values in the resting and the MVC trials (the selected normalized data of a representative subject shown in Fig. 2). The recorded data were split into 5-second windows. For each window, 67 fatigue-related feature candidates were calculated based on the suggestion from literature, including the signal information in time- and frequency-domains [1-2, 7-9]. Each window (i.e., observation) was labeled to a fatigue level according to the subjects' RPE values. The observations with the fatigue levels labeled as "light" (RPE<11) and "tired" (RPE>16) were chosen for classification and a total of 1184 observations were selected across all the subjects.

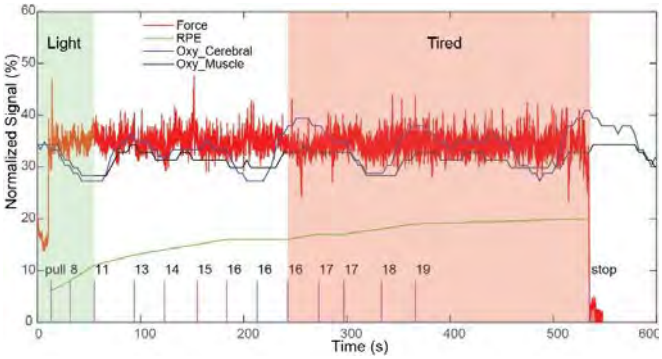

Figure 2: A representative fatiguing trial at 30% of the MVC. Fatigue levels ("light" or "tired") were labeled based on the subject's RPE values (the green curve and numbers indicated above). The normalized force and oxygenation ("Oxy") levels were shown.

The supervised classification algorithms were deployed in "Classification Learner" (Matlab, 2017b) with randomized 75% of data for training models and 25% for validation. The data were trained on all 23 types of available classifiers. An automated feature selection approach (Neighborhood Component Analysis) [6] was also performed to select a smaller subset of features with the majority of the predictive power based on the ranking of weights (i.e. those features may carry more information to differentiate subjects feeling "tired" from feeling "light").

RESULTS AND DISCUSSION

The Ensemble Model/Classifier (Boosted Trees) gave the best classification accuracy on the validation set (95%) using all the features. Using twelve auto-selected (high-ranked) features resulted in 94% classification accuracy with the same type of classifier. Those selected features happened to be cerebral and muscle oxygenation levels, and the median frequency of EMG and VMG data, which agreed with the previous studies [1-2, 7-9]. However, in order to put the trained models into practical applications, larger datasets would be required to avoid overfitting, and more comprehensive measurements (such as electrocardiogram (ECG), electroencephalography (EEG) etc.) would be explored to further reduce on the feature set.

This initial study provides a novel framework to explore and to potentially rank fatigue-associated measures for various physically or mentally demanding tasks at workplace. This machine-learning-guided framework will advance our understanding in fatigue mechanism and help us target key measures for monitoring fatigue level and evaluating ergonomic solutions.

REFERENCES

1. Ferguson, S. et al., *Human Factor* 55(6): 1077-1087, 2013.
2. Perrey S., et al., *Int J Ind Ergo,* 40:185-189, 2010.
3. Barry B., et al., *Integr Comp Biol* 47(4):465-473, 2007.
4. Enoka R., et al., *Med Sci Sports Exerc* 48(11): 2228-38, 2016
5. Borg GA, *Med Sci Sports Exerc* 14(5):377-81, 1982
6. Yang W., et al., *Journal of Computers,* 7 (1): 161-8, 2012.
7. Mannion A., et al., *Spine* 19 (11): 1223-1229, 1994
8. Zhang et al., *IEEE Trans Biomed Eng* 39 (10): 1045-52, 1992
9. Wu J., et al., *Neuroreport* 28(17):1134-38, 2017

DISCLAIMER

The findings and conclusions in this report are those of the authors and do not necessarily represent the official position of the National Institute for Occupational Safety and Health, Centers for Disease Control and Prevention.

DOES NECK MUSCLE FATIGUE AFFECT CERVICAL INTERVERTEBRAL KINEMATICS?

[1]Yu Zhou, [2]Ryan M. Byrne, [1]Suman K. Chowdhury, [1]Xudong Zhang

[1]Texas A&M University, College Station, TX, USA
[2]University of Pittsburgh, Pittsburgh, PA, USA
Email: xudongzhang@tamu.edu

INTRODUCTION

Work-related neck musculoskeletal disorders are highly prevalent across all occupations and populations [1]. To date, biomechanical studies have established the contribution of mechanical factors, such as sustained forceful exertions, in particular at non-neutral postures, to the pathogenesis of neck pain [1]. During sustained-until-exhaustion exertions, a continuous tradeoff in force generation between active and passive tissues has also been advocated in previous studies [2]. However, to our knowledge, whether and how the skeletal kinematics of the neck, (i.e., the intervertebral positions and orientations at individual or multiple vertebral levels as a whole) may change during sustained-till-exhaustion neck exertions remains unknown. Therefore, this study seeks to establish some initial evidence to support the hypothesis that neck muscle fatigue during sustained exertions at various postures would lead to different degrees of alteration in cervical intervertebral kinematics.

METHODS

We used data from six healthy male participants who performed sustained neck exertions at fifty percent of their maximal efforts while seated at three different neck postures (neutral, 40° extended, and 40° flexed). Using a gamut of biodynamic measurements (electromyography, surface-based motion capture, and load cell) and multimodality imaging (dynamic stereo-radiography (DSX) and CT imaging), we recorded *in vivo* cervical kinematics, neck muscle activity, and neck strength data during sustained-till-exhaustion neck exertions. The experimental setup and procedures were detailed in a prior publication [3]. Using the 3D vertebral models reconstructed from the participant's CT scan, along with the recorded radiographic images during exertion, a previously validated volumetric model-based tracking algorithm produced the 3D, *in vivo* kinematics at the initial (non-fatigue) and end (fatigue) instance of each exertion [4]. The convention and definition of the anatomical coordinate systems of the vertebrae and their kinematic computations were similar to our previous study [3]. The exertion duration and surface EMG data recorded from eight neck muscles (left and right sternocleidomastoid, left and right hyoid, left and right cervical trapezius, and left and right splenius capitis were used to evaluate neck muscle endurance capacity and muscle fatigue at three postures. Since the participants performed the exertions in the mid-sagittal plane, we speculated that there would not be any significant differences in muscle activation between left and right sides of the same muscle group. Therefore, the median frequency (MF) data, estimated at every 0.5s time interval of the total exertion duration, were pooled from both sides and averaged across all subjects. A decrease in MF data is used as a biomarker of muscle fatigue in previous studies [2,3]. Therefore, a linear regression line was fitted through MF data at every 10% increment of the total duration to assess neck muscle fatigue.

RESULTS AND DISCUSSION

The negative MF slope values indicated that the cervical muscles experienced a significant amount of fatigue during sustained neck exertions at all three neck postures (Table 1).

The flexion-extension (F-E) data of whole cervical spine (C1-C7) exhibited about 5% (from -53° to -55°) increase in extension motion, about 26% (from -28° to -35°) increase in extension motion, and about 186% (4.87° to 13.87°) increase in flexion motion at fatigue state compared to non-fatigue state during 40° extended, neutral and 40° flexed postures, respectively (Figure 1). The anterior-posterior (A-P) translation data of C1-C7 also showed that the

increase (227%; 12 mm) in anterior translation at fatigue state was substantially greater at 40° flexed posture compared to the increase (49%; 5 mm) and the decrease (10%; 3 mm) in posterior translation at neutral and 40° extended postures, respectively. The substantial increase in cervical kinematics at 40° flexed posture revealed that the sharing synergy and spinal tissue loadings mainly occur at a neck flexion posture.

Table 1: The median frequency (MF) slope values of sternocleidomastoid (SCM), trapezious (Trap), hyoid, and splenius capitis (SPL) muscle groups for all three postures. An asterisk (*) indicates a statistically significant (P≤0.05) trend. A negative slope value indicates a decrease in MF over time.

	SCM	Hyoid	Trap	SPL
40° Extension	-0.47*	-0.56*	-1.58*	-0.75
Neutral	-0.32	-0.82*	-1.93*	-0.34
40° Flexion	-0.54	-0.89*	-0.46	-1.17*

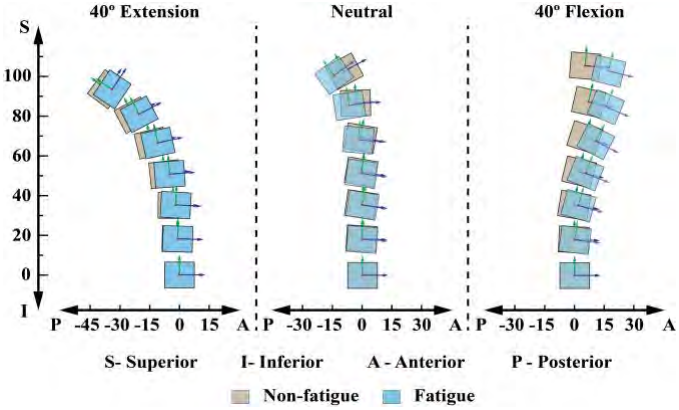

Figure 1: Sagittal view of the superimposed cervical vertebral orientation between fatigue and non-fatigue states at three different postures. The F-E of C1, C2, C3, C4, C5, and C6 levels were calculated with regard to C7. The units of S-I, and A-P translations are in millimeter.

The muscular endurance data showed a greater endurance time at 40° flexed posture (109.8±20.0s) compared to neutral (103.0±20.5s) and 40° extended (68.1±8.7s) postures. Since participants performed an 'extension' task during 40º flexed posture, a greater endurance time revealed higher endurance capacity of extensor (e.g., Trap and SPL) muscles compared to flexor (e.g., Hyoid and SCM) muscles, which are consistent to prior studies [5].

The changes in superior-inferior (S-I) translation between non-fatigue and fatigue state were minimally observed (1.7 mm) at 40° extended posture compared to neutral (3.0 mm) and 40° extended (2.6 mm) postures. Muscle fatigue data also showed a significant amount of fatigue at more muscles (3 out of 4) during 40° extended posture compared to that (2 out of 4) of neutral and 40° flexed postures. It leads us to conclude that when the fatigued cervical muscles were unable to maintain the forces, the passive elements of the spine compensated the required force, which was observed to be higher at a neck flexion posture and lower at a neck extension posture.

Interestingly, the spinal column translated anteriorly at the fatigue state of 40° extended posture and translated posteriorly at that of neutral posture, even though the participants performed 'flexion' tasks at both postures. Given that the superficial neck muscles are fatigued, an anterior translation of the cervical column at 40° extended posture hints that, the neck deep muscles compensated the required force and initiated a flexion motion to resist destabilization of the cervical column.

CONCLUSIONS

The results of this preliminary observation revealed that sustained submaximal neck exertion caused cervical muscle fatigue and altered cervical vertebral kinematics across all postures. The alterations in vertebral kinematics between non-fatigue and fatigue states were more saliently observed at 40° flexed posture compared to neutral and 40° extended postures. The findings are based on data from six male participants. To confirm these findings, future study should consider a larger sample size.

REFERENCES

1. Côté et. al., *Eur Spine J,* 17 (1): S60-S74, 2008.
2. Lee et. al., *J Phys Ther Sci*, 23: 599-601, 2011.
3. Chowdhury, S.K, et. al., *Pro of the HFES Annual Meeting*, 61(1), 986-990, 2017.
4. Bey et. al., *J of Bio Eng,* 128: 604-609, 2006.
5. Edmondston et. al., *Manual Therapy*, 16 (332-338), 2011

THE AFFECT OF NEUROMUSCULAR IMPAIRMENT ON MOTOR UNIT ACTIVATION IN CHILDREN WITH CEREBRAL PALSY

[1] Zachary J Adams, [2]Stephanie K Yeager, [2]Robert E Akins Jr and [1] Thomas S Buchanan

[1] University Delaware, Newark, DE, USA
[2] A.I. DuPont-Nemours Hospital for Children, Wilmington, DE, USA
email: buchanan@udel.edu

INTRODUCTION

Cerebral palsy (CP) is the most common neuromuscular movement disorder in children. While traditionally understood as a static injury in the central nervous system, recent literature has begun to observe peripheral neural and muscular irregularities that may progress over time [1]. Thus a new area of interest in CP research is the effects of the neural insults with respect to muscle activation.

One method to assess muscle activation is to observe motor unit recruitment and firing characteristics within a muscle. Understanding how children with CP recruit and activate motor units differently than healthy children would provide useful insights for rehabilitative strategies.

The aim of this study was to understand the relationship between muscle activation behavior and impairment in children with CP. We hypothesized that children with neuromuscular impairments associated with a diagnosis of CP would exhibit depressed motor unit activity as compared to controls. Similar activity has been observed in other populations with neurological impairments. [2]. By identifying changes in motor unit recruitment in the affected populations it would allow for earlier detection and treatment for children with CP.

METHODS

Ten children with CP (12-17 yrs, 4M, 6F) and ten healthy children (12-17 yrs, 6M, 4F) were selected to participate in a controlled elbow flexion task. All CP children had a GMFCS score of 3 or lower and were able to complete the task. Exclusionary criteria included: any patients with genetic mutations, syndromes, or chromosomal abnormalities, patients with neuromuscular diagnoses for controls, and if patients with CP had a classification of quadriplegia. All subjects agreed to consent approved by the IRB of the University of Delaware and the IRB of Nemours Alfred I duPont Hospital for Children.

Subjects performed an elbow flexion tracking task with their most proficient arm. The arm was constrained at 90 degrees elbow flexion and horizontal with the ground with the wrist in full supination. Specialized 5-pin (Delsys Inc.) surface electromyography (EMG) sensors were placed on the active arm's biceps (BB) and brachioradialis (BRA). Subjects tracked a trapezoidal shape on a screen by applying isometric flexion torques.

The surface signals from both muscles were decomposed using a high density spike analysis algorithm (Delsys, Inc.) to obtain individual motor unit spike trains from each contraction. These trains were converted to firing rate curves for analysis. All statistics were performed in JMP (SAS ®).

RESULTS AND DISCUSSION

Motor units in children with CP did have a slightly lower firing behavior than healthy children in both muscles (Fig 1.) While this was not significant (BB $p=0.15$, BRA $p=0.23$) many of the subjects were high functioning (GMFCS of 1). These children often have more normal functioning muscles and have shown to have less disorder in their neuromuscular junction (NMJ) [1].

Figure 2 shows the breakdown of motor unit firing activity, shown by the standard deviation of the firing rates, with respect to the GMFCS score for each subject. While the BB motor units showed no correlation between GMFCS ($p=0.68$), the BRA in patients with higher motor-affect/GMFCS scores

exhibited a significantly lower firing rate than controls (p=0.045). This may due to more distal muscles having greater muscular disorganization in populations with neural impairments.

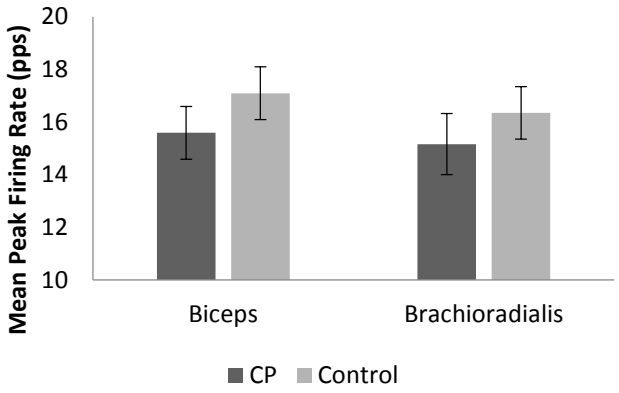

Figure 1: Mean peak motor unit firing rates (pulses per second, pps) and standard error (n=10) for the biceps (left) and brachioradialis (right).

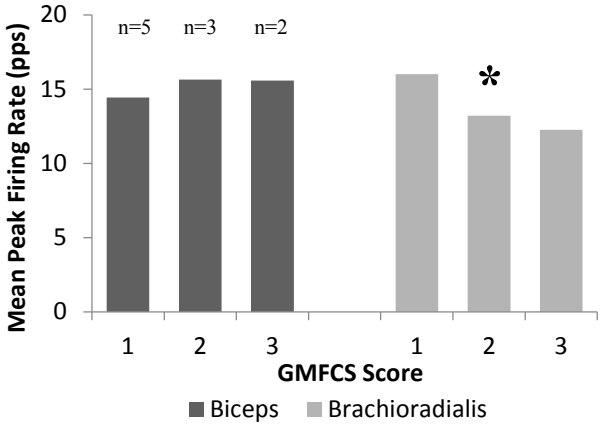

Figure 2: Mean peak motor unit firing rates (pulses per second, pps) organized by GMFCS score for both muscles in the 10 CP subjects: biceps (left) and brachioradialis (right). Number of subjects per GMFCS score indicated on the left columns. * indicates significance when compared to controls.

An alternate study has shown that rocuronium (ROC) does correlated with severity of motor affect/GMFCS score (unpublished). A subset of the subjects in the present study had a recent surgery at which their ROC dose was recorded. Because mechanism of action for ROC is at the NMJ, increased ROC doses may suggest altered NMJ morphology or function. Figure 3 shows an evaluation if mean firing rate correlates with ROC dose. In this correlation the standard deviation of the firing rates was used instead of the mean firing rate to encompass the makeup of the motor unit pool. For both muscles the more depressed muscle activity required higher ROC doses in both populations. While neither muscle showed a significant relationship (BB p=0.24, BRA p=0.12) it is interesting that the best fits and R^2 values are similar within both populations.

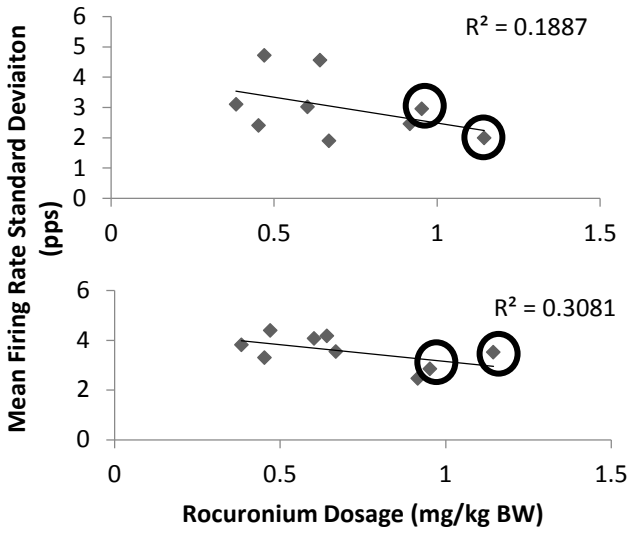

Figure 3: Mean peak firing rates standard deviation for the biceps (top) and brachioradialis (bottom). CP subjects (n=2) are circled.

The results here provide evidence that there may be a correlation between impairments in children with CP and motor unit activation. If this is sustained, it may assist in identifying at risk children and support the development of rehabilitative strategies.

REFERENCES

1. Robinson et al. *Plos* One, 8(8), 2013.
2. Mottram et al. *J* Neurophysiology, 111, 2014.

ACKNOWLEDGEMENTS

The authors recognize the Nemours Foundation and the Howard W. Swank, Alma K. Swank, and Richard Kemper Swank Foundation for their generous support to R.A.

Soleus T- and H-reflex Modulation When Performing an Unstable Stance

Gordon R. Chalmers

Western Washington University, Bellingham, WA, USA
email: gordon.chalmers@wwu.edu

INTRODUCTION

Reduced stance stability when on a narrow or unstable surface decreases soleus Hoffmann (H-) reflex amplitude due to greater pre-synaptic inhibition (PSI) of the Ia signal [1]. The only study of soleus T- reflex modulation comparing two stances of different stability levels reduced stance stability merely by removed hand support, finding a reduced stretch reflex [2]. Spindle sensitivity can increase in humans during seated precise ankle control [3, 4]. Concurrent examination of the H- & T-reflex may differentiate control of the Ia signal in the spinal cord versus at the spindle [5, 6], but such studies are lacking for challenges to stance stability.

The purpose of this study was to test the hypothesis that a challenging tandem stance would decrease the H-reflex, and increase the T-reflex (the latter due to enhanced attention to precise ankle position control), together suggesting an increased spindle sensitivity [5, 6], compared to a stable wide stance condition.

METHODS

Twenty nine subjects (mean (standard deviation): 23(5) years; 20F, 9M) were studied. Data were collected in a single session from the right leg. The soleus and tibialis anterior (TA) were instrumented for EMG recordings. Posterior tibial nerve stimulation elicited the H-reflex, and the H-reflex test stimulus strength used was on the mid portion of the ascending H-reflex recruitment curve, also producing a small M-wave used to monitor for consistency of the electrical stimuli intensity. A pendulum tendon tapper delivered Achilles tendon tap forces [7].

A random sequence of two stance positions was used. Stable stance: feet spaced a preferred distance apart, with the heel of the left foot in line with the front of the toes of the right foot. Tandem stance: left foot placed directly in front of, and with heel touching the toes of, the right foot.

When background EMG (bEMG) levels had been held steady for >1 sec., a silent electrical stimuli or tendon tap was delivered in a random sequence, with >15 sec between stimuli. If an electrical stimulus M-wave amplitude was not within ±15% of the standard for the subject, the measurement was rejected.

Data analysis: For electrical stimuli, the peak-to-peak amplitude of the M and H-reflex waves; for mechanical stimuli the peak-to-peak amplitude of the short latency T-reflex response, in the raw soleus EMG were measured. Rectified EMG was averaged 100 ms prior to each stimulus to determine bEMG.

For each subject and each stimulus type, only data points within the soleus bEMG range that was common to both of the stance positions for the same stimulus type in a subject were used for comparison across the stances, to ensure a similar level of motor neuron excitability. At least six of each reflex measures were required. For each of the stance positions within a subject the H-reflex, M-wave, and bEMG measures were each averaged. Likewise for T-reflex measures, without M-waves.

Statistical analysis: Two-tailed repeated measures t-tests determined differences between measures made in the wide and tandem stance positions (significance at $p < 0.05$). Cohen's d values were calculated for significant differences.

RESULTS AND DISCUSSION

Twenty five subjects were reported on, 21 for the H-reflex, 22 for the T-reflex. Four subjects were excluded because the minimum required six reflex

measures within the range of common background EMG for at least one of the two stances examined were not obtained for both the H- and the T-reflexes.

H- and T-reflex amplitudes were significantly lower in tandem compared to wide stance position, -9% & -23% respectively (Table 1).

The hypothesis that the unstable tandem stance would increase T-reflex amplitude due to enhanced attention to precise position demands was not supported by the 23% reduction in T-reflex amplitude. Previous studies reporting increased stretch reflex size under conditions requiring enhanced attention to precise position control were conducted on the finger [8], the ankle while seated [4], or for a stable sitting position transition to standing [9]. Difference in tasks examined and/or magnitude of the increase in position precision or attention enhancement demands in the more challenging conditions employed may explain increased stretch reflex size in other studies as opposed to the decrease found here.

The decrease in both T- and H-reflex amplitudes in the present study suggests that spindle sensitivity was not increased as hypothesized. The reduction in mean H-reflex amplitude in the tandem stance observed would be produced by an increase in PSI of the IA signal [1]. The T-reflex is less depressed by PSI than the H- reflex is [10]. Consequently, an increase in PSI in the narrow stance would be expected to produce less of a reduction in the mean T-reflex amplitude than in the H-reflex amplitude. The wide to tandem stance comparison, however, produced a greater percentage reduction (-23%) and a greater magnitude of effect (Cohen's d = 0.49) for the T-reflex amplitude than for the H-reflex (-9%, Cohen's d = 0.14). This pattern of the decrease of the mean T-reflex amplitude exceeding the decrease of the mean H-reflex amplitude suggests that the mean spindle response to the stretch was reduced when in the unstable stance

REFERENCES

1. Chen et al. *Gait Posture*. **33**(2), 2011.
2. Elner et al. *Agressologie*. **17**(1), 1976.
3. Hospod et al. J *Neurosci*. **27**(19), 2007.
4. Ribot-Ciscar et al. *J Neurophysiol*. **101**(2), 2009.
5. Nafati et al. *Brain Res*. **1018**(2), 2004.
6. Rossi-Durand. *Somatosens Mot Re*s. **19**(4), 2002.
7. Mildren et al. *Gait Posture*. **43,** 2016**.**
8. Akazawa et al. *J Neurophysiol*. **49**(1), 1983.
9. Obata et al. *J Electromyogr Kinesiol*. **22**(1), 2012.
10. Morita et al. *J Neurophysiol*. **80**(2), 1998.

Table 1: Mean reflex amplitudes, M-wave and background EMG levels (mV).

		H-reflex	M-wave	T-reflex
Wide stance	Reflex or Wave Amplitude	3.66(2.45)	0.63(0.35)	1.25(0.63)
	Soleus bEMG	0.02(0.01)	n/a	0.03(0.01)
Tandem stance	Reflex or Wave Amplitude	3.33(2.17)*	0.64(0.36)	0.96(0.56)$^{\#}$
	Soleus bEMG	0.02(0.01)	n/a	0.02(0.01)

Compared to same measure in wide stance: *$p<0.05$, Cohen's d = 0.14; $^{\#}p<0.01$, Cohen's d = 0.49; n/a: not applicable.

FATIGUE AFFECTS BALANCE CONTROL DIFFERENTLY DURING SINGLE- AND DUAL-TASK WALKING IN OLDER WORKERS

Szu-Hua (Teresa) Chen and Li-Shan Chou

Department of Human Physiology, University of Oregon, Eugene, OR, USA
email: szuhuac@uoregon.edu, web: http://choulab.uoregon.edu

INTRODUCTION

Older adults are more likely to perform daily physical activities or work at levels close to their maximal capabilities [1] and experience fatigue. Given the increasing participation rate in the labor force of older adults and the positive association between fatigue and fall injuries [2], it is important to investigate the effects of fatigue during walking, especially perturbed walking when falls most often occur. The impact of fatigue on gait performance could be amplified when cognitive demand increases [3]. This can be problematic for older adults as cognitive function deteriorates with aging. Walking and simultaneously performing an attention demanding task could occur with increasing fatigue at the end of a job performance. Therefore, the purpose of this study is to investigate the effect of fatigue on gait balance control during dual-task level walking and obstacle-crossing in older workers.

METHODS

Seven older workers (4 females, 61.4 ± 5.1 yrs) performed the following five tasks before and after a fatigue protocol in a random order: 1) walking at a self-selected comfortable speed along a 15-m walkway (WALK), 2) walking and crossing over an obstacle with height set at 10% of body height (OC), 3) sitting and performing a 3-back test, in which participants listened a series of digits over a loud speaker and were instructed to verbally respond "yes" whenever the digit matches the one from three steps earlier in the sequence (Nback), 4) dual-task: WALK+Nback, and 5) dual-task: OC+Nback. All participants were informed of the protocol and signed the consent form approved by the Institutional Review Board of the university.

A 30-minutes sit-to-stand task at a fixed pace was employed to induce fatigue as indicated by the participant's inability to continue or when the movement frequency falling below the prescribed pace after the examiner's encouragement. Once the protocol was terminated, participants were asked to estimate rate of perceived exertion (RPE) on a 6 to 20 Borg scale. The maximal voluntary isometric strength of knee extensors was assessed using a dynamometer immediately before and after the fatigue protocol and at the completion of the entire study protocol.

Whole body motion data were collected from a set of 29 retro-reflective markers placed on bony landmarks with a 12-camera motion system. The whole-body center of mass (CoM) was calculated as the weighted sum of 13 body segments. Gait balance control was examined using the total medial-lateral CoM displacement (M-L CoM), peak CoM medio-lateral velocity (M-L vCoM) and stride width during each of the walking conditions. A crossing stride was defined as the gait cycle during stepping over the obstacle between heel strikes of the trailing foot immediately before and after crossing the obstacle. Gait speeds were calculated as the average forward CoM velocity during a gait cycle. Dependent variables for crossing characteristics included the toe-obstacle clearance (TC) and foot placements (FP) before and after the obstacle. TC was calculated as the vertical distance between the obstacle and toe marker at the time of crossing. FP of trailing foot and leading foot were measured as the horizontal distance between the obstacle and toe marker and heel marker, respectively.

Two separate two-way ANOVAs with repeated measures were used to examine effects of fatigue (pre- and post-fatigue) and task (single- and dual-tasks) in walking and obstacle-crossing conditions. Alpha level was set at .05.

RESULTS AND DISCUSSION

An average of 11.0% reduction in knee extensor strength was observed immediately after the

completion of fatigue protocol, and it was recovered to approximately 5.8% by the completion of study protocol. The average time-to-fatigue during the sit-to-stand task was 23.0 minutes. The average RPE was 14 (somewhat hard).

WALK

Gait speed and M-L vCoM showed significant task main effects (Table 1). Participants walked slower but demonstrated a faster frontal plane sway when responding to a concurrent 3-back test than they did under single-task walking. M-L vCoM also showed a tendency toward a significant interaction effect, p=.067, η^2_p = .45 (Figure 1). No significant effects were detected for M-L CoM or stride width.

OC

Gait speed remained unchanged after fatigue (Table 1). M-L vCoM demonstrated a significant interaction effect (Figure 1). Participants swayed faster post-fatigue during the single-task obstacle crossing. However, when a concurrent cognitive demand was imposed, a slower frontal plane sway was observed after fatigue. The only task main effect in obstacle-crossing condition was found in TC of leading foot, where participants elevated the leading limb higher when crossing an obstacle in dual-task (18.9±1.3 cm) versus single-task (17.8±1.1 cm) conditions. No fatigue main effects were found in M-L CoM, stride width, and crossing behaviors.

CONCLUSIONS

Older workers demonstrated a faster sway in single- but a slower sway in dual-task obstacle crossing. The might be a result of that older adults prioritize gait balance over cognitive task performance. The central nervous system might anticipate that balance control would be disturbed after fatigue and, therefore, prioritize the effort to maintain dynamic balance during the dual-task obstacle-crossing condition.

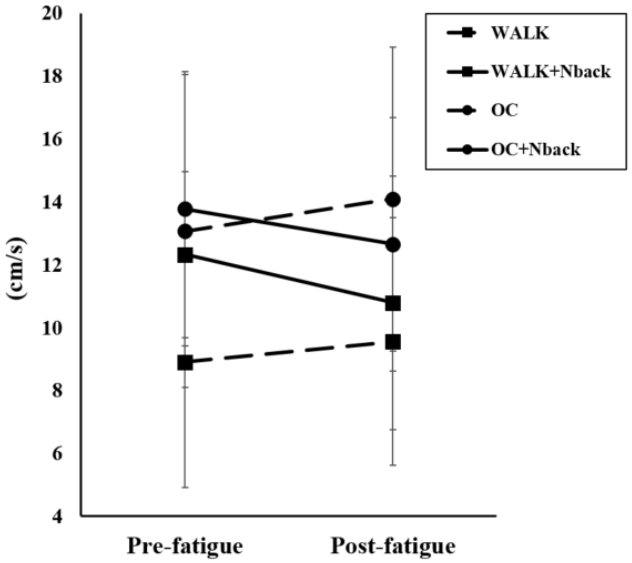

Figure 1. Peak medio-lateral velocity of center of mass (M-L vCoM).

The peak CoM medio-lateral velocity could be a sensitive measurement, which can be applied in occupational medicine to monitor fatigue status in older workers. More study participants are necessary to strengthen the current findings.

REFERENCES

1. Hortobágyi T et al. *J Gerontol A* **58**, M453–60, 2003.
2. Parijat P & Lockhart TE. *Ergonomics* **51**, 1873–84, 2008.
3. Lorist MM et al. The Journal of Physiology **545**, 313-9, 2002.

Table 1: Spatiotemporal and gait balance control parameters during walking and obstacle-crossing

		WALK		OC	
		Pre-fatigue	Post-fatigue	Pre-fatigue	Post-fatigue
Gait Speed (m/s)	Single	1.29±0.21[b]	1.29±0.21[b]	1.07±0.19	1.07±0.18
	Dual	1.16±0.19[b]	1.19±0.19[b]	0.98±0.19	1.00±0.16
M-L vCoM (cm/s)	Single	8.91±3.99[b]	9.56±3.94[b]	13.07±4.97 [a]	14.09±4.83[a]
	Dual	12.33±2.64[b]	10.79±4.04[b]	13.78±4.36[a]	12.66±4.03[a]
M-L CoM (cm)	Single	4.21±0.82	4.25±0.90	5.62±2.12	5.87±2.12
	Dual	4.05±0.80	4.46±1.19	5.06±1.33	5.57±1.78
Stride Width (cm)	Single	6.92±3.42	6.95±3.40	7.83±3.00	8.40±3.32
	Dual	6.36±2.80	6.83±3.52	8.35±3.68	8.34±3.47

Note. a: interaction effect (fatigue x task), b: condition effect (single versus dual-tasks)

Control of Motor Units and Strategies of Force Generation during Fatigue

[1] Paola Contessa, [1] John Letizi, [1] Gianluca De Luca, and [1] Joshua C. Kline

[1] Delsys and Altec Inc., Natick, MA, USA
email: pcontessa@delsys.com, web: http://www.delsys.com

INTRODUCTION

Most studies agree that the excitation to the motoneuron pool of a muscle increases to compensate for fatigue-induced decreases in force generating capacity and sustain force output at a constant level [1]. Yet, despite these increases in excitation, some studies have reported that the firing rates of earlier-recruited motor units may decrease during fatiguing contractions [2]. These observations contradict the known control mechanisms of motor unit firing behavior, by which motor unit firing rates increase in response to increasing excitation [3]. To explain these observations, it has been suggested that the control of motor units changes with fatigue so that the firing rates of earlier-recruited motor units are selectively inhibited by mechanically or metabolically sensitive afferents while the excitation to the motoneuron pool increases [2].

In this study, we investigated the firing rates of motor units in the First Dorsal Interosseous (FDI) muscle of the hand and the concurrent activation of forearm muscles during fatigue to identify whether changes in muscle co-activation may provide an alternative explanation for decreases in motor unit firing rates.

METHODS

Five subjects (4 males, 1 female; 22-34 years old) with no known history of neuromuscular disorders participated in the study. All subjects read, indicated they understood and signed the informed consent form approved by Western Institutional Review Board (Puyallup, WA).

During data acquisition, subjects were seated with their hand placed in a restraining apparatus that measured isometric index finger abduction force by means of a load cell (Interface Inc., AZ).

The fatigue protocol consisted of a series of isometric contractions performed by tracking a target force trajectory displayed on a monitor and repeated to the subject's endurance limit. The trajectory increased linearly up to 50% of the subject's maximal voluntary contraction (MVC) force, and was maintained at the target level for 10-s.

A dEMG array sensor (Delsys Inc., Natick, USA) was used to record 4 channels of surface electromyographic (sEMG) signals from the FDI. Signals were filtered between 20-450 Hz, sampled at 20 kHz, and decomposed into their constituent motor unit action potential (MUAP) shapes and firing trains [4]. For each motor unit, we calculated the MUAP amplitude, as the maximum amplitude of the positive and negative MUAP phases, and the average firing rate, as the inverse of the inter-pulse intervals between firings in a 5-s interval.

Because wrist abduction and forearm pronation may contribute to the measured force, we monitored the activation of the following forearm muscles: flexor carpi radialis (FCR), extensor carpi radialis (ECR), and pronator teres (PT). Muscle activation was measured as the root-mean-square (RMS) of the sEMG signals recorded using single-differential sEMG sensors (Delsys Inc., Natick, USA).

RESULTS AND DISCUSSION

Subjects performed on average 66±35 contractions prior to reaching their endurance limit. The fatigue protocol induced a decrease in MVC from 39.3±4.3 N pre-fatigue to 26.4±6.1 N post-fatigue.

We observed two general patterns of motor unit firing adaptations throughout the contraction series, which are shown in Fig.1 for a representative subject:

1) FDI motor unit firing rates (Fig.1A) increased significantly ($p<0.05$ for all subjects) from the first

contraction to a mid-fatigue contraction, when they reached the highest value during the fatigue protocol. Importantly, the progressive increase was always associated with a significant increase ($p<0.001$ for all subjects) in the sEMG RMS amplitude of the FDI muscle (Fig.1B).

These findings suggest that the excitation to the motoneuron pool of the FDI muscle increased to sustain the force output as fatigue developed, leading to increases in FDI motor unit firing rates.

2) FDI motor unit firing rates decreased from the mid-fatigue contraction to the last contraction in four of five subjects ($p<0.02$ for subjects 1, 2, 3; $p=0.49$ for subject 4). Importantly, the decrease was always associated with a decrease in the sEMG RMS amplitude of the FDI; and with a significant increase ($p<0.005$ for all subjects) in the sEMG RMS amplitude of the FCR, ECR, and PT (Fig.1C).

These findings suggest that the strategy for sustaining force output may have changed by increasing the contribution of concurrently active muscles while the excitation to the FDI decreased. Importantly, the adaptations in FDI motor unit firing rates were always associated with similar adaptation in FDI activation. Therefore, changes in motor unit firing rates were directly related to natural changes in the excitation to the motoneuron pool of the FDI.

CONCLUSIONS

During fatigue, decreases in motor unit firing rates may be explained by changes in the strategy for sustaining force output and increased co-activation of concurrently active muscles. Nonetheless, the adaptations in motor unit firing behavior are driven by changes in the excitation to the motoneuron pool of the muscle, and follow the well-known control mechanisms of muscle force generation [3].

REFERENCES

1. Bigland-Ritchie et al. *J Physiol*. Oct;379:451-9. 1986.
2. McManus et al. *J Neurophysiol*. 113(9):3186-96, 2015.
3. De Luca et al. *J Physiol*. Aug;329:129-42, 1982.
4. Nawab et al. *Clin Neurophysiol*. 121(10):1602-15, 2010.

ACKNOWLEDGEMENTS

Funding was provided in part by the National Institute of Neurological Disorders and Stroke (R43NS093651 and R44NS077526), and by the De Luca Foundation, MA.

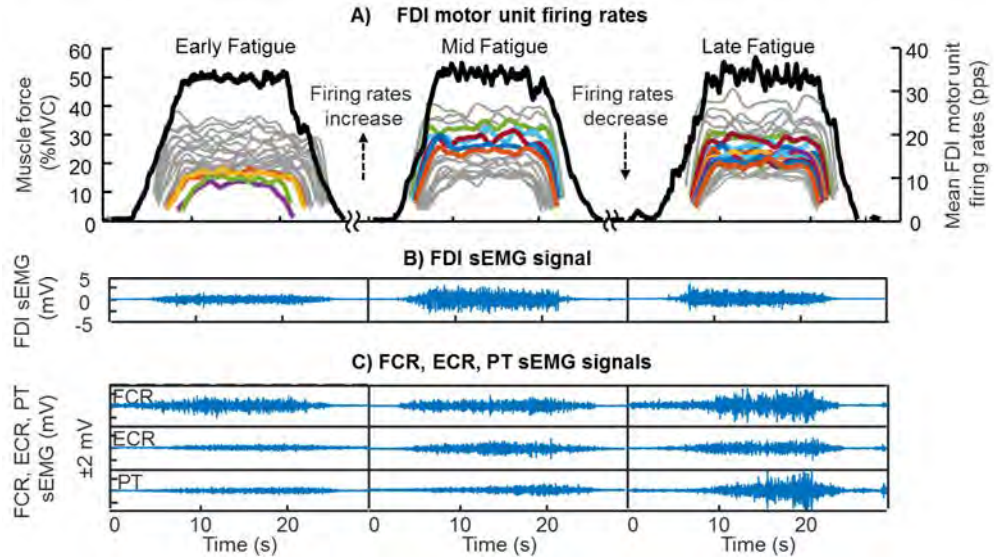

Figure 1: Muscle force (A, black line); FDI motor unit firing rates (A, grey and colored lines); and sEMG signal of the FDI (B), FCR, ECR, PT muscles (C) at the beginning, middle, and end of the fatigue protocol for a representative subject. Note that colored lines in (A) indicate motor units with similar MUAP amplitude.

MODELING MOTOR NOISE REGULATION IN A SIMPLE SHUFFLEBOARD MACHINE

Joseph P. Cusumano and Jonathan B. Dingwell

The Pennsylvania State University, University Park, PA, USA
Email: jpc3@psu.edu

INTRODUCTION

In a study of human shuffleboard playing [1], multi-trial time series of end-effector kinematic data were used to explain observed motor variability as arising from an inter-trial regulation process [2]. However, it is not immediately obvious that motor regulation at the neuromuscular level can be characterized using only task-level kinematics (e.g., position and velocity of the hand at puck release). We here use a physics-based model of a shuffleboard machine with inter-trial motor regulation to illustrate the relationship between the dynamics of task-level observables to those of internal motor variables. We show that, in principle, it is possible to characterize internal motor regulation using kinematic data of the type typically collected in human subjects experiments.

METHODS

A slider-crank mechanism represents the human arm (Fig. 1). It launches a puck toward a target under the action of an adjustable torque, $M(\theta)$, representing the output of muscle activations. The Newton-Euler equations lead to a dimensionless equation of motion:

$$\ddot{\theta} = \frac{9\,\dot{\theta}^2\,\sin(2\,\theta) - 6\,\mu\,\sin\theta + 3\,\cos\theta - 3\,M(\theta)}{9\,\cos(2\,\theta) - 11}\,.$$

For simulations, each trial starts from rest ($\dot{\theta}_0 = 0$) with $\theta_0 = \pi/2$. The applied torque is assumed to be well-approximated within one trial by

$$M(\theta) = M_0 + M_1(\theta - \theta_0) + M_2(\theta - \theta_0)^2\,. \quad (1)$$

We set $M_0 = -1$ to overcome friction from rest; (M_1, M_2) are treated as internal states of an inter-trial regulator. Each trial, the puck is released with position and velocity (x, v) when the reaction force between puck and cue drops to zero. The puck slides before stopping from Coulomb friction (Fig. 1). The goal equivalent manifold (GEM) [1] is thus found from the pairs (x, v) satisfying

$$v = \sqrt{\mu\,(x_T - x)}\,. \quad (2)$$

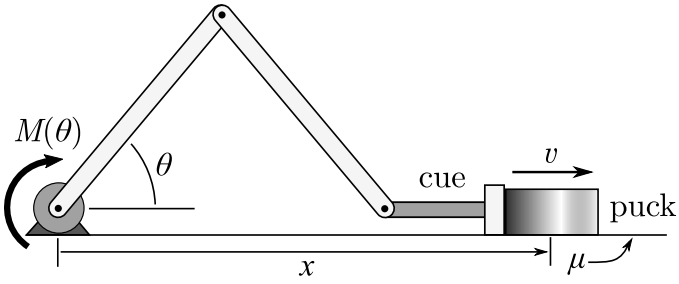

Figure 1: A simple two-link shuffleboard machine. Trial outcome is determined by internal parameters (M_1, M_2) in torque profile $M(\theta)$ of Eq. (1).

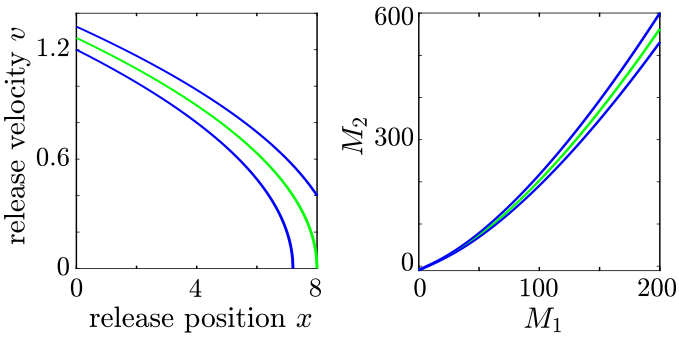

Figure 2: Plots of GEM (green) and ±10% error contours (blue): (*left*) in space of observable task variables (x, v); (*right*) in internal torque variable space, (M_1, M_2). In both plots, values on the GEM result in zero error at the target.

All trials (x, v) on the GEM (Fig. 2, left) perfectly hit the target at $x = x_T$. The (x, v) are in 1-1 correspondence with the (M_1, M_2) for each trial, thus we can compute the GEM in the internal variable space, as well (Fig. 2, right).

Motor noise perturbs the "planned" values of (M_1, M_2) in each trial. Following the minimum intervention principle (MIP) [3] we use a "GEM aware" regulator to mitigate the effects of this noise:

$$\begin{aligned} \delta_t(k+1) &= \lambda_t\,\delta_t(k) + \nu_t(k) \\ \delta_n(k+1) &= \lambda_n\delta_n(k) + \nu_n(k) \end{aligned} \quad (3)$$

where k indicates the trial, (δ_t, δ_n) are tangential and normal components of fluctuations in the torque parameters from an operating point on the GEM,

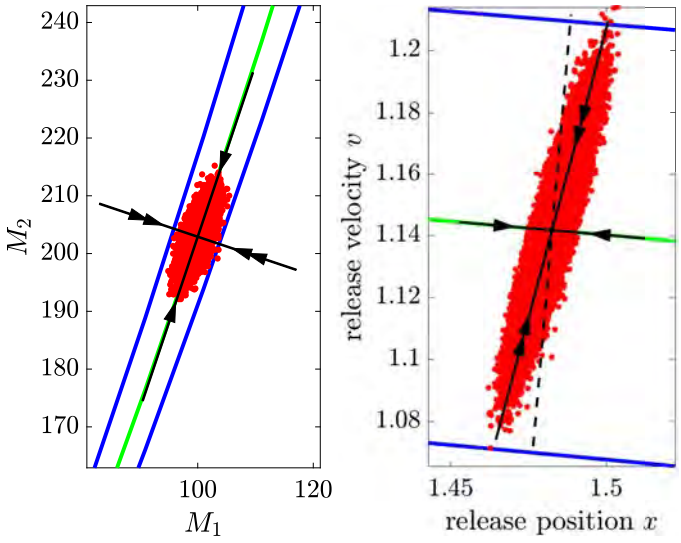

Figure 3: Theoretical scatter plots of 10^4 simulated trials of the MIP regulator (Eq. 3): data (red dots); GEM (green line); $\pm 10\%$ error contours (blue lines). Black lines indicate strongly stable ($\lambda_n = -0.2$, double arrow) and weakly stable ($\lambda_t = 0.8$, single arrow) directions. Dashed line indicates normal to GEM. RMS error at the target was set to about 5%. By design, variability cloud aligns with GEM in (M_1, M_2) space. This is not the case in the observable (x, v) space. However, geometric stability is consistent with GEM orientation in both spaces.

(ν_t, ν_n) the corresponding motor noise components, and (λ_t, λ_n) the strength of regulation in those same directions. Values of $|\lambda|$ closer to 0 (resp. 1) indicate stronger (resp. weaker) regulation [2]. To mimic typical human performance [1], for these simulations we set $\lambda_t = 0.8$, $\lambda_n = -0.2$.

RESULTS AND DISCUSSION

Numerical simulations were used to theoretically examine how variability is mapped between the internal (M_1, M_2) and observable (x, v) spaces (Fig. 3). We find the tangent (weakly stable) direction in (M_1, M_2) space remains tangent (weakly stable) in (x, v) space; the normal (strongly stable) direction is no longer normal to GEM. Significantly, the variability cloud does not align with (x, v) GEM, and hence is a poor indicator of its location. However, the geometrical relationship of the fluctuation dynamics to the GEM is preserved (see black arrows in Fig. 3). Furthermore, using simulated time series, we estimated the inter-trial dynamics exactly as for human subjects experiments [1, 2]. We find (Fig. 4) that this procedure can estimate the strength of the internal motor regulation process using only end-effector kinematic data.

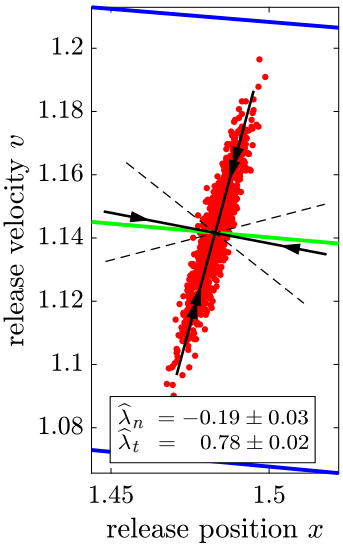

Figure 4: Regression on 10^3 trials used to recover theoretical stability multipliers $(\lambda_t, \lambda_n) = (0.8, -0.2)$ (Eq. 3) characterizing error regulation. Also estimated were dynamical eigendirections (compare to theory, Fig. 3, right): $\pm$ error estimates and dashed lines indicate 95% CI.

CONCLUSIONS

When playing shuffleboard, the neuromotor system does not determine hand movements directly but, instead, activates muscles that, in turn, create joint torques generating each shot of the puck. Thus, muscle activations must be regulated from one trial to the next to mitigate the effects of physiological noise. It is reasonable, therefore, to question if fluctuations in end-effector kinematic data can give us insight into the regulation of internal motor variables. In response to this question, our analysis of a simple shuffleboard-playing machine showed that this *is* possible, in principle. Specifically, we showed that using only directly observable task-level data it is possible to dynamically characterize the motor regulation operating on internal torque variables.

ACKNOWLEDGMENTS

NIH/NIA Grant #R01AG049735.

REFERENCES

1. J. John et al. *PLoS Comput Biol*, 12(9): e1005118, 2016.
2. J. P. Cusumano and J. B. Dingwell. *Hum Movement Sci*, 32(5):899 – 923, 2013.
3. E. Todorov. *Nat Neurosci*, 7(9):907–915, 2004.

INVESTIGATION OF OPTIMAL NOISE LEVEL FOR IMPERCEPTIBLE VIBROTACTILE STIMULATION

Courtney A. Haynes[1], Matthew S. Tenan[2], Antony D. Passaro[3], Andrew J. Tweedell[1]

[1]Human Research and Engineering Directorate, Aberdeen Proving Ground, MD
[2]Human Research and Engineering Directorate, Research Triangle Park, Durham, NC
[3]Human Research and Engineering Directorate, ARL West, Playa Vista, CA
email: courtney.a.webster2.civ@mail.mil

INTRODUCTION

In recent years, imperceptible noise stimulation has emerged as a possible intervention strategy to affect motor behavior and postural stability [1,2]. The stimulation is thought to improve the sensitivity of the somatosensory system affording better detection of postural deviations and more precise postural corrections [1,2]. Despite the increasing use of this technique for a variety of applications, there appears to be no consensus on the best "dosing" for noise stimulation. In some cases, stimulation level is prescribed as a percentage of an individual's sub-sensory threshold. However, work by the Kristeva group suggests that an individual's response to noise stimulation varies depending on its magnitude and that there may exist an optimal noise stimulation level which will elicit an individual's greatest performance benefits [3].

We explored this concept of optimal noise stimulation using a series of ramp-and-hold finger flexion trials while participants received imperceptible vibrotactile noise stimulation of varying levels. Task performance was quantified as a root mean squared (RMS) error between the target and generated force value. The goal of this study was to quantify performance differences under different stimulation levels to determine if the identified optimal stimulation level was similar between individuals.

METHODS

Participants included 18 young, healthy males (25.8 ± 6.2 years) with no history of pain, surgery, or injury to the dominant upper extremity. Participants completed all protocols seated at an adjustable height desk equipped with a custom instrumented finger flexion grip (LCM302-50, Omega Engineering, Inc., Stamford, CT). Grip and desk positions were adjusted to standardize posture for each participant. Participants engaged the finger flexion grip with the hand and wrist of the dominant hand in a supine position, and the second phalanx of the pointer finger was used to apply force to the grip.

A maximum voluntary contraction (MVC) protocol was completed to determine each participant's maximum finger flexion force. Participants then practiced the ramp-and-hold task which consisted of ramping up over a period of 2.5 seconds to produce force equal to 20% MVC and maintaining this force for a duration of 10 seconds. A visualization of the target force was provided along with visual feedback of the current finger flexion force. Following 10 practice trials, participants were fitted with a vibrotactile stimulator (BM1C, Tactile Labs Inc., Montreal, Canada) at the wrist. A second protocol was completed in which we identified each participant's sub-sensory vibrotactile threshold level. Participants then completed the ramp-and-hold task while receiving broadband (1-500Hz) Gaussian noise stimulation corresponding to 10, 20, 30, 40, 50, 60, 70, 80, 90, and 100% of their sub-sensory threshold level. The order of the stimulation levels was randomized, and sham (no stimulation) trials were completed before and after the noise stimulation trials. RMS errors were calculated between the generated finger flexion force and target force value for the middle 5 seconds of the sustained "hold" portion of the trial. RMS errors were used as the metric of performance for each applied stimulation level, and the stimulation level corresponding to the lowest RMS error was identified as an individual's optimal noise stimulation level.

RESULTS AND DISCUSSION

The identified optimal noise stimulation levels

varied between individuals such that when group means were considered, no differences in RMS errors were found between stimulation levels.

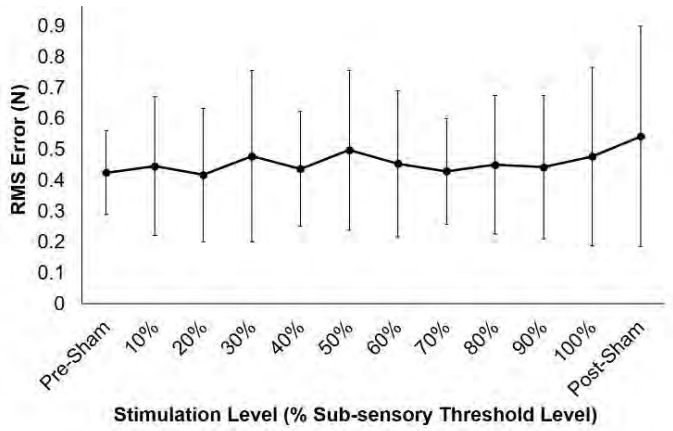

Figure 1. Mean and standard deviation force stabilization RMS errors versus applied noise stimulation level.

Note that the largest mean error and standard deviation occur for the final sham trial. This may illustrate the effect of removing noise stimulation following its repeated application. That is, performance may vary with noise magnitude, but its subsequent absence appears to result in a decrement of performance. Results suggest that the optimal stimulation level is highly variable between individuals (Figure 2). Among the 18 participants, each sub-sensory stimulation level elicited the lowest RMS error (best force stabilization) for at least one individual. Figure 2 presents the spread of errors recorded for each participant along with their 95% confidence interval (CI). The difference between a participant's lowest RMS error and their lower 95% confidence limit ranged from 0.005 N – 0.21 N with a group mean difference of 0.08 ± 0.06 N. Individual one-sided Dixon Q tests were completed for each participant to determine if the identified optimal stimulation level resulted in RMS error that would be considered an outlier. Only two participants (4 and 11) demonstrated RMS errors that were significantly lower ($Q = 0.50$, $p = 0.039$ and $Q = 0.54$, $p = 0.024$, respectively) than the remaining distribution of errors recorded for the other stimulation levels.

CONCLUSIONS

Results suggest that optimal stimulation levels vary considerably between individuals. The lack of

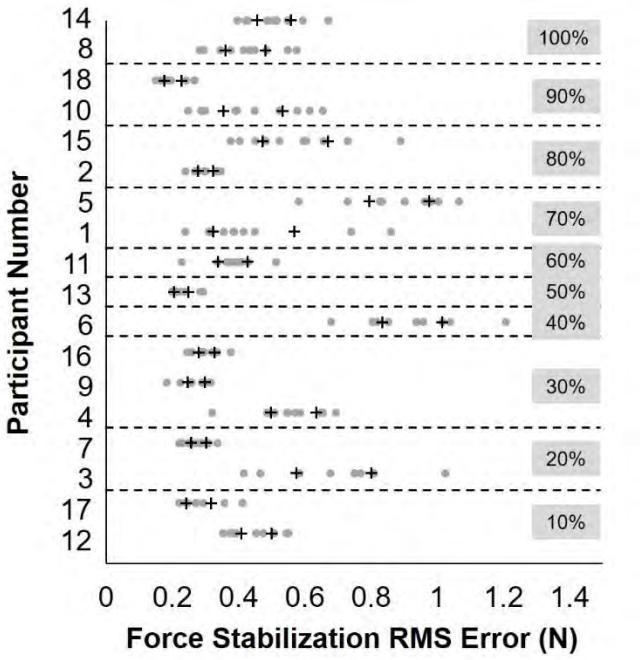

Figure 2. RMS errors recorded for all participants for each of the 10 stimulation levels. "+" symbols indicate the upper and lower limits of the 95% CI. Shaded values indicate the optimal stimulation level as a percent of individual sub-sensory threshold.

"outlier" performance with the optimal stimulation level may suggest that the benefits of optimal stimulation may only marginally outweigh the benefits of noise stimulation at an arbitrary level. More work is needed to determine the repeatability of the optimal noise stimulation level within individuals and determine if there are substantial benefits to identifying an optimal stimulation level. Developing a consistent and reliable methodology for identifying the optimal noise stimulation level would enable noise stimulation interventions to be customized to maximize the motor control benefits to the user.

REFERENCES

1. Priplata et al. *Phys Rev Let*. 89(23): 238101, 2002.
2. Ross & Arnold. *J Sport Health Sci*. 1: 102-106, 2012.
3. Mendez-Balbuena et al. *J Neurosci*. 32(36):12612-12618, 2012.

ACKNOWLEDGEMENTS

Many thanks to Mr. Mike Kosinski for his help with the fabrication of the testing apparatus.

UNIQUE ADAPTATIONS EMERGE FROM ACUTE EXPOSURE TO VARIABLE ASYMMETRIC SPLIT-BELT TREADMILL WALKING

[1,2] Jacob W. Hinkel-Lipsker and [2] Michael E. Hahn

[1] California State University, Northridge, CA USA
[2] University of Oregon, Eugene, OR USA
Email: jacob.hinkellipsker@csun.edu, web: http://bssc.uoregon.edu

INTRODUCTION

When a person makes an error during stepping, they must correct for it by adjusting the mechanical output of the lower limbs. These adaptations can become learned over time through repeated exposure to stepping errors [1]. Clarification of the relationship between specific stepping errors and locomotor adaptations has direct application towards enhancement of future gait rehabilitation paradigms.

Previous work has shown that increased variability of movement errors leads to improved learning outcomes across a variety of motor skills [2]. Further, we recently demonstrated that, when compared to less variable forms of practice, some variability in stepping errors during practice lead to improved transfer of balance control during performance of a novel asymmetric split-belt treadmill walking task [3]. Moving forward, we were interested in whether this improvement in balance control was accompanied by a differing mechanical walking strategy. Therefore, the purpose of this study was to compare how increased variability in stepping errors influenced lower-limb gait mechanics. We hypothesized that compared to more predictable forms of practice, a random practice group would demonstrate significantly different spatiotemporal, kinematic, and kinetic gait adaptations on a series of transfer tests. These results, then, would highlight how acute exposure to variable types of stepping errors would change the way that mechanical adaptations of the lower limbs are learned.

METHODS

Forty-eight able-bodied subjects (25 female/23 male, 24.0 ± 0.8 years old) were recruited for this study. All study protocols were approved by the university Institutional Review Board and all subjects gave written informed consent prior to enrollment.

Subjects attended two days of experimental testing, separated by exactly 24 hours. On the first day, they were randomly selected to undergo one of three practice paradigms on a split-belt treadmill. All paradigms involved walking for 720 strides with one limb being driven at a constant velocity (constant limb) and the other limb driven at a changing velocity (variable limb) according to the practice group. The serial practice group underwent a linear increase in velocity with every step for the 720 strides on the variable limb. The random blocked practice group was given a more unpredictable practice context where the variable limb belt changed velocities randomly every 20 strides. Finally, the random group had their variable limb undergo random velocity changes with every step, thereby inducing the most variable (and unpredictable) stepping errors. On the second day, subjects completed one of two 400-stride transfer tests that required walking with both belts at different constant velocities. In both cases, the variable limb was driven faster than the constant limb, but the velocity difference was less on one test (1.5:1 variable:constant; termed Transfer 1), and greater on another (2:1 variable:constant; termed Transfer 2). These tests were applied to measure how well subjects were able to generalize previously learned adaptations to new walking contexts.

During this process, three-dimensional marker coordinate data from 54 reflective markers applied to subjects' bony landmarks were collected at 60 Hz using an 8-camera motion capture system. Ground reaction force data were collected at 1200 Hz from two force plates, one under each treadmill belt.

Discrete lower-limb biomechanical variables were chosen and calculated based on previous work in gait

adaptation. These included spatiotemporal (step length asymmetry, double support asymmetry), kinematic (peak sagittal plane ankle, knee, and hip angles), and kinetic measures (GRF, internal hip and knee extensor moments).The main effects of practice group and limb on these discrete biomechanical variables were tested for using a series of multivariate analyses of variance ($\alpha = 0.05$), and follow-up Bonferroni-corrected pairwise comparisons were made where appropriate.

RESULTS AND DISCUSSION

A few statistically significant findings seem to best illustrate how variable stepping errors create new locomotor adaptations. The random practice group had many gait adaptations that were significantly different from the other practice groups during the acquisition phase, including an increased peak knee extensor moment and knee flexion angle during early stance on the constant limb. These adaptations were likely a way for subjects to avoid shifting their weight to the variable limb, where the treadmill belt was changing velocities randomly with every step. For the Transfer 1 test, there were no significant gait mechanical differences among groups. This suggests that when individuals are required to generalize their gait to a context close to that of what they have previously experienced, the mechanical output is universal, or not dependent on a previous exposure.

Finally, the random blocked practice group demonstrated a significantly shorter step length on the constant limb compared to the other practice groups during the Transfer 2 test. More surprisingly, the asymmetry between the limbs seemed to increase over time during the Transfer 2 test, with individuals spending more time on the variable limb compared to the constant limb (Figure 1). These findings are in contrast with previous work in split-belt treadmill walking, which has shown that walkers trend towards greater step length symmetry as they adapt their gait to constant asymmetric belt velocities [4]. These results indicate that those who underwent random blocked practice found a unique way to adapt their gait, where step length for each limb seems to scale with the associated belt velocity. This uncoupling of limbs during gait adaptation has been previously discussed only in terms of lower-limb kinetics [5].

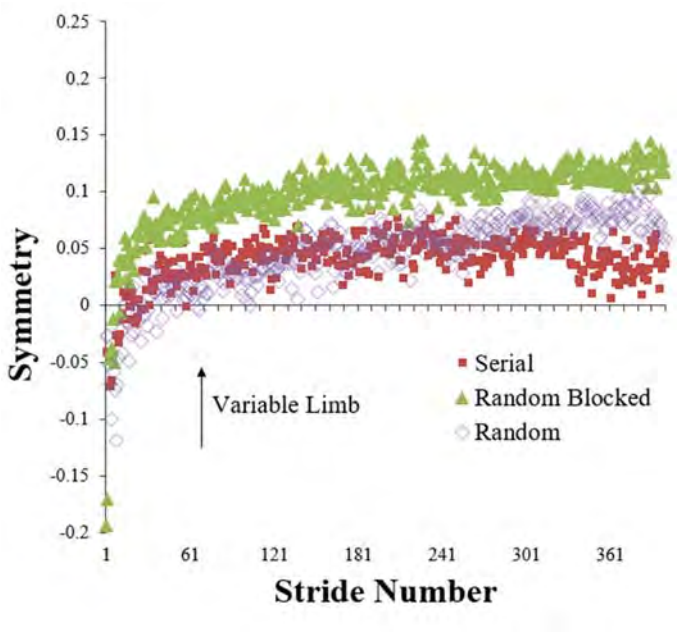

Figure 1: Step length asymmetry during a transfer test. All groups became more asymmetric over time, with longer step lengths on the faster moving belt (variable limb). Random blocked practice resulted in the largest asymmetry.

CONCLUSIONS

Previously, we showed that random blocked practice led to the best ability to generalize mediolateral balance control compared to the other two forms of practice. Our current analysis indicates that this superior balance control is accompanied by an uncoupling of limb step lengths when generalization of a gait patterns to a much different context is required. These results demonstrate a different spatiotemporal gait strategy than what has been previously reported for adaptation to asymmetric split-belt treadmill walking, and highlight that a moderate level of variability in stepping errors results in generalization of a unique gait adaptation.

REFERENCES

1. Prokop et al. *Exp Brain Res.* 106(3), 1995.
2. Lee and Magill. *J Exp Psychol Learn Mem Cogn*. 9(4), 1983.
3. Hinkel-Lipsker and Hahn. *Exp Brain Res*. 235(9), 2017.
4. Reisman et al. *J Neurophysiol*. 94(4), 1995.
5. Roper et al. *J Appl Biomech.* 33(4), 2017

MOTOR UNIT MEASUREMENT TECHNOLOGY FOR TRAINING, EXERCISE AND FUNCTIONAL ACTIVITIES

[1]Joshua C. Kline, [1]Bhawna Shiwani, [1]Serge H. Roy, [1]John P. Chiodini and [1]Gianluca De Luca

[1]Delsys, Inc. and Altec, Inc, Natick, MA, USA
email: jkline@delsys.com, web: http://www.delsys.com/altec/

INTRODUCTION

The mechanisms used by the central nervous system to regulate force and movement during training, exercise and functional activities remain poorly understood. Today the most common approaches for investigating the control of human movement either: 1) infer neural mechanisms from biomechanical measures using motion capture, instrumented force plates or inertial measuring systems; or 2) directly image the central nervous system using electroencephalography (EEG) or functional magnetic resonance imaging (fMRI) technology that are less practical for use outside of controlled laboratory settings. A more practical solution for accessing the neural mechanisms that regulate movement is to develop new ways of analyzing the surface EMG (sEMG) signal that can leverage the advanced capabilities and diverse applications of modern wireless sEMG systems. Over the past 3 decades, our group has been at the forefront of developing sensors and algorithms for automatically measuring the action potentials of individual motor units directly and noninvasively from the sEMG signal. But while current sEMG decomposition algorithms can be used to study motor units during isometric contractions or constrained cyclic contractions [1, 2], there remains an unmet need for directly measuring motor unit contributions during strength training, exercise and functional movement.

METHODS

To achieve this goal, we have developed new algorithms for extracting motor unit firings directly and noninvasively from the sEMG signal. Each algorithm component was strategically designed to solve each of the three challenges associated with sEMG decomposition during dynamic movement:

1) We developed clustering algorithms to track non-stationary changes in motor unit action potential shapes that occur when dynamic movement leads to slight changes in the relative position of the sEMG sensor with respect to the active muscle fibers during movement.
2) We implemented custom expectation maximization methods to improve the temporal resolution of motor unit firing rate measurements across dynamically varying functional activities.
3) We integrated error reduction algorithms to localize firing detections amongst complex superpositions of motor unit action potentials typically encountered in non-cyclic exercise.

To test these algorithms, we conducted a series of experiments involving n=10 volunteer subjects (5 males, 5 females, age range 22-68 y.o.) with no known history of neuromuscular disorders. The subjects participated in each of three test protocols: 1) strength training of the biceps brachii muscle; 2) exercises of the quadriceps muscle group; and 3) functional tasks of the extensor and flexor digitorum of the hand. During each activity, sEMG signals were recorded using a custom-designed dEMG sensor (Delsys Inc, Natick, MA). The recorded data were processed by the newly designed dEMG decomposition algorithms, validated to establish the accuracy of the firing detections and analyzed to investigate the motor control behavior.

RESULTS AND DISCUSSION

From over 278 contractions tested, the algorithms were able to identify a broad range of motor units ranging from approximately 6-34 above the 90% accuracy benchmark. These motor unit firing trains provided a rich data source for empirically investigating the motor control properties in each of the three applications tested. We observed:

1) During strength training of the biceps brachii, motor units showed clear differences in the progression of firing rates between concentric

and eccentric changes in elbow joint angle.

2) During exercises of the quadriceps muscle group, motor unit firing rates from the vastus lateralis manifested the greatest magnitude peaks when the knee joint angle increased from approximately 120 to 180 degrees.
3) In the flexor digitorum muscle of the fingers, motor unit firing rates indicated relatively high correlation with the finger force during functional drinking task.

CONCLUSIONS

These results mark a first step towards delineating the neural contributions associated with normal human movement. Further investigations using the dEMG technology will provide new research opportunities to modify exercise, guide new training modalities and tailor rehabilitation protocols based on the underlying motor unit-based outcome measures of neuromuscular control.

REFERENCES

1. De Luca et al. *J Neurophysiol* **96**: 1646-1657, 2006.
2. De Luca et al. J Neurophysiol **113**: 1941-1951, 2015.

ACKNOWLEDGMENTS

Research reported in this abstract was supported in part by the De Luca Foundation and by a grant from the National Institute of Neurological Disorders and Stroke of the National Institutes of Health under award number R43NS093651 and R44NS077526.

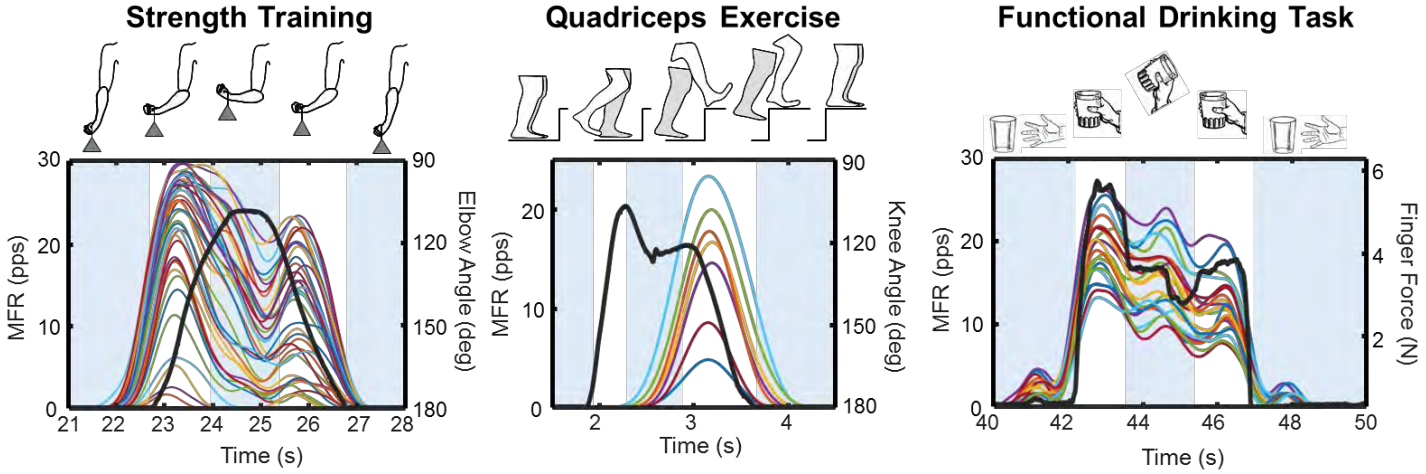

Figure 1. Motor unit mean firing rates (MFR) measured from A) the biceps brachii muscle during exercise, B) the vastus lateralis muscle during strength training, and C) the flexor digitorum muscle during a functional drinking task.

ACCURACY OF GROUP ANALYSES IN REPRESENTING SHOULDER MUSCLE COORDINATION PATTERNS OF THE INVIVIDUAL

[1] Joshua M. Leonardis, [2] Raina Coflin, and [1] David B. Lipps

[1] School of Kinesiology, University of Michigan, Ann Arbor, MI, USA
[2] Department of Mechanical Engineering, University of Michigan, Ann Arbor, MI, USA
email: jleo@umich.edu web: http://www.kines.umich.edu/research/mbil

INTRODUCTION

The neuromuscular system can recruit different combinations of muscles with varying magnitudes and durations of activity to achieve a given task [1]. Low-dimensional groups of muscles activated simultaneously, further referred to as coordination patterns, can be used to simplify this problem of redundancy. Non-negative matrix factorization (NNMF), a commonly-used electromyography (EMG) decomposition technique, has been used to identify these coordination patterns [2]. This approach has been used to characterize neuromuscular adaptations to neurological events such as stroke, and has also been utilized to investigate how the healthy nervous system adapts to changes in mechanical constraints [3,4]. NNMF is commonly used to describe individual subjects, but group analyses of coordination patterns have also been proposed [5]. Group analyses present a valuable tool for evaluating how the neuromuscular system responds to different surgical and rehabilitation treatments. It is unclear, however, if coordination patterns identified through group analyses sufficiently represent the coordination patterns of individuals within that group. We hypothesized that group analyses of shoulder muscle coordination patterns involving the use of individual data optimized to the group will 1) outperform group analyses that only use group data, and 2) provide results similar to individual analyses.

METHODS

We evaluated shoulder coordination patterns in 6 healthy adults (3M, 3F, age: 27 ± 5 yr, height: 1.75 ± 11 m, mass: 75 ± 15 kg). Participants' dominant arm was placed in a removable cast that was attached to a six-degree of freedom load cell while fixing their elbow at 90° and wrist neutral. Participants matched isometric shoulder torques for 5 seconds in 8 combinations of vertical add/abduction (Θ), internal/external rotation (Φ), and horizontal add/abduction (Ψ). The Θ, Φ, and Ψ components of each torque task were scaled to 20% of the participant's lowest maximal voluntary contraction. The 8 torque directions were repeated in 20 experimental arm postures, resulting in 160 total trials per participant. EMG data were collected from 9 upper extremity muscles: sternocostal (SC) and clavicular (CL) region of the pectoralis major; anterior (AD), medial (MD) and posterior (PD) deltoid; upper (UT) and lower trapezius (LT); latissimus dorsi (LD), and serratus anterior (SA). EMG data were processed using established parameters [6]. A custom-written algorithm adapted from a previously described framework was used to quantify individual and group coordination patterns (Figure 1) [5].

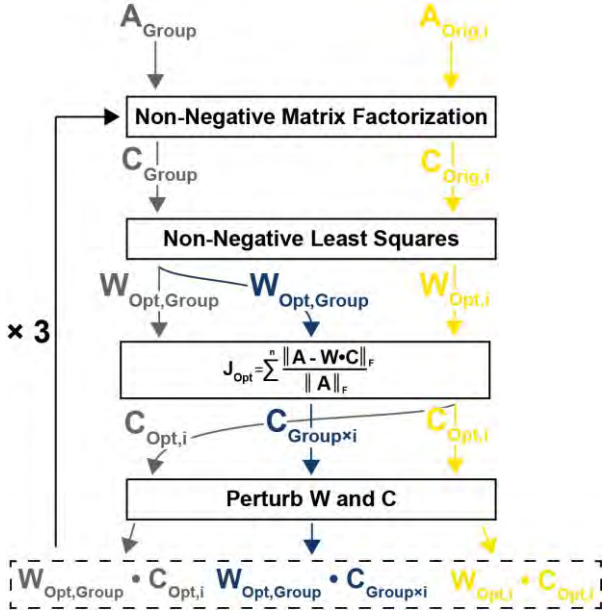

Figure 1: Framework for calculating weights and activations from original EMG data (A_{Group}, $A_{Orig,i}$). Method 1 (gray) used group optimized weights ($W_{Opt,Group}$) and activations optimized to each individual ($C_{Opt,i}$). Method 2 (blue) used group optimized weights and group activations optimized to each individual ($C_{Group\times i}$). Method 3 (maize) used weights ($W_{Opt,i}$) and activations optimized to each individual.

For each method, the variance accounted for (VAF) between the measured EMG data (A) and reconstructed EMG (W·C) was computed for each muscle and individual. Comparisons of the VAF generated by each method for each muscle were performed using univariate ANOVAs, where data reconstruction method was a fixed factor. Post-hoc analyses were completed using Bonferroni corrections with the significance set at $p < 0.05$.

RESULTS AND DISCUSSION

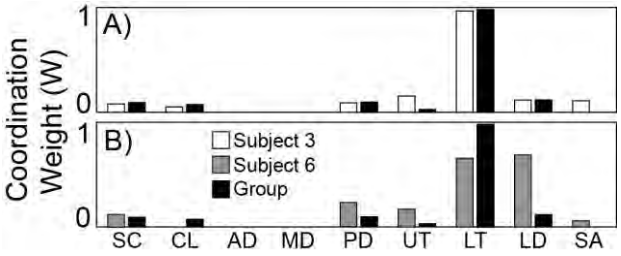

Figure 2: Representative coordination weights that show (A) good (r = 0.98) and (B) poor (r = 0.65) similarity between individual subjects and the same group coordination pattern.

Four muscle coordination patterns could describe >95% VAF for the group and all 6 individuals (Figure 2). Our statistical analyses revealed main effects for reconstruction method for the CL ($F_{(2,4)}$ = 25.43, p = 0.005), MD ($F_{(2,4)}$ = 949.2, p = 0.000), PD ($F_{(2,4)}$ = 48.44, p = 0.002), UT ($F_{(2,4)}$ = 11.18, p = 0.023), and SA ($F_{(2,4)}$ = 11.01, p = 0.024) muscles. Post-hoc analyses found that methods 2 and 3 reconstructed original EMG data similarly (Figure 3); both methods reconstructed data for the MD, PD, UT, and SA muscles better than method 1 (all $p < 0.05$). Additionally, no statistically significant difference existed between methods 2 and 3 for any muscle.

Our results suggest that group analyses of muscle coordination patterns can reconstruct individual data as well as individual analyses as long as the coordination activations used in the reconstruction are optimized to the group optimized coordination weights such as in method 2. Otherwise, group analyses do not result in reconstructed data that accurately reflect the individual.

Additionally, it appears that both group and individual muscle coordination analyses allow for the reconstruction of only a small number of muscles with high accuracy. Our results suggest group analyses can be used to accurately reflect underlying neuromuscular changes of individuals within a group, but will require additional optimization to an individual's muscle activations if the muscle(s) of interest include the medial or posterior deltoid, upper trapezius, or serratus anterior. Future work will apply these analyses to examine adaptations to surgical approaches that change biomechanical constraints at the shoulder, including muscle disinsertion for the use of myocutaneous flaps.

CONCLUSIONS

The use of data reconstructed using group coordination weights and individual activations optimized to the group sufficiently represent original EMG from individual participants by representing a small number of muscles with high accuracy.

REFERENCES

1. Bernstein, *Coor & Reg of Mvmnts*, 1965.
2. Ivanenko, et al. *J Neurophys*. **90**:3555-65, 2003.
3. Tresch, et al. *Nature Neuro*, **2**:162-7, 1999.
4. Hug, et al. *J Neurophys*, **106**:91-103, 2011.
5. Shourijeh, et al. *J EMG & Kines*, **26**:36-43, 2016.
6. Roh et al., *J Neurophys*, **109**:768-81, 2012.

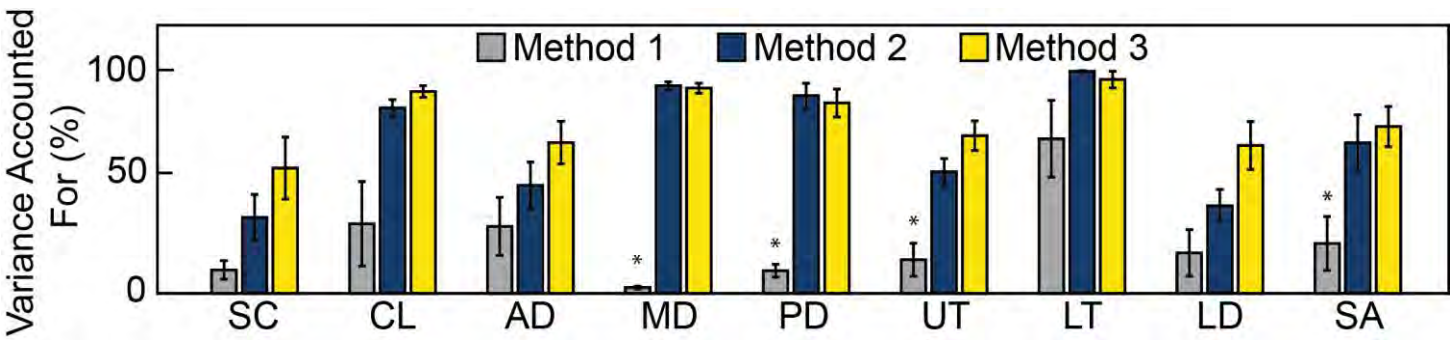

Figure 3: Variances accounted for (mean ± SE) by data reconstruction methods 1 (gray), 2 (blue), and 3 (maize) across all muscles. * indicates a significant difference from Method 3.

EFFECT OF VISUAL RHYTHMIC CUEING AND VISUAL FEEDBACK ON MOTOR CONTROL IN CHILDREN WITH AUTISM

[1] Daniel E. Lidstone, [1]Jeffrey D. Eggleston and [1] Janet S. Dufek

[1] Department of Kinesiology and Nutrition Sciences, University of Nevada, Las Vegas, NV, USA
email: daniel.lidstone@unlv.edu

INTRODUCTION

Autism Spectrum Disorder (ASD) is a developmental disability characterized by social and communication impairments and by restricted interests and repetitive behaviors [1]. In addition to core ASD symptomology, sensorimotor integration deficits are consistently observed in individuals with ASD [2]. Children with ASD show larger variability and errors on motor-synchronization tasks to auditory rhythmic cueing compared to children with typical development (TD) [3,4]. However, no study has examined sensorimotor integration using visual rhythmic cueing in children with ASD. Synchronizing two-legged hopping to a visual rhythmic cue requires effective integration of proprioceptive and visual input that may be impaired in children with ASD.

The primary aim of the current study was to determine the effect of increasing sensory integration demands on the variability of timing, kinetics, and kinematics of hopping in children with ASD. We hypothesized that children with ASD will show greater timing, kinematic, and kinetic variability as sensory integration demands increase.

METHODS

Three children (aged 13±2.5 years; 3 males; 47±16 kg; 1.62±0.19m) with a clinical diagnosis of ASD and three age-matched TD children (aged 13±2.2 years; 2 males, 1 female; 44±13 kg; 1.52±0.17m) were recruited for participation in this study.

Three-dimensional kinematic data were obtained using a 10-camera motion capture system (200 Hz, Vicon Motion Systems, Ltd.). Simultaneous kinetic data were obtained using two Kistler force platforms (1000 Hz) mounted flush with the floor side-by-side. Following a static calibration, the participants were familiarized with the two-legged hopping task and completed three 20 second hopping trials in each condition: (1) self-selected hopping without cueing (SS), (2) synchronous hopping to a 2Hz visual cue (VC), and (3) synchronous hopping to a 2Hz visual cue with visual feedback (VC+VF). The visual cue was a ball bouncing at 2 Hz, presented at eye-level using a custom-built game (Idoneus Digital®) developed in Unity™. In the VC+VF condition, the game integrated with Vicon to present visual feedback on the screen using the sacrum marker of the participant (Fig. 1). In the VC+VF condition, the participant was instructed to bounce both balls off the ground at the same time.

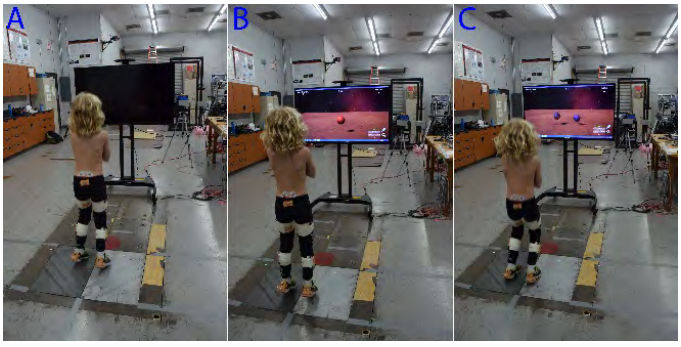

Figure 1: Experimental conditions (A = SS; B = VC, C = VC+VF)

All kinematic data (vertical sacrum marker excursion; knee and ankle angular joint positions) were computed in Visual 3D (C-Motion) and processed using custom MATLAB scripts. Marker trajectories and kinetic data were filtered using a low-pass Butterworth filter at 6 Hz and 25 Hz, respectively. A 25N cut-off was used to identify ground contact (GC) and toe-off. The first two hops of each trial were not included in the analysis. The subsequent twenty-five consecutive hops were selected for analysis within each trial. Each participant performed at least 25 consecutive hops in each trial without stopping. Hop frequency (Hz) was

calculated as the inverse of time in seconds (T) from GC to the subsequent GC (f=1/T).

The coefficient of variation [CoV; (SD/Mean)*100] was calculated, using the 25 hops, within each trial for hop frequency (Hz), maximal GRF (N), vertical sacral marker excursion (m), and right knee and ankle joint range of motion (deg). Effect size (ES; Cohen's d) was calculated to determine the effect of condition on movement variability between groups.

RESULTS AND DISCUSSION

Mean hop frequency for the ASD group during SS, VC, and VC+VF was 2.32±0.30, 2.32±0.34, and 2.50±0.24 Hz, respectively. Mean hop frequency for the TD group during SS, VC, and VC+VF was 1.92±0.18, 2.08±0.05, and 1.98±0.12 Hz, respectively.

Large CoV ES were found for each measured variable (ES>0.9) except for GRF CoV in SS (ES=-0.24) and knee angle in VC (ES=0.5) (Table 1). The large positive ES indicate larger CoVs in children with ASD vs. TD controls. The mean ES, collapsed across dependent variables within each condition, shows a nearly two-fold increase in ES during visual cueing conditions (VC and VC+VF) vs. no-cueing (SS) (Fig. 2).

The main finding in this exploratory study is that differences in movement variability between children with ASD vs. TD increased as sensorimotor integration demands increased. The sample of children with ASD in the study were more variable in hopping timing, kinetics, and kinematics than TD controls. These findings support previous research showing individuals with ASD are more variable in single and multi-joint rhythmic motor-synchronization tasks compared to TD controls [3,4]. Cerebellum structural and functional deficits are implicated in ASD core symptomology and may explain findings of motor coordination and sensorimotor integration deficits in this population.

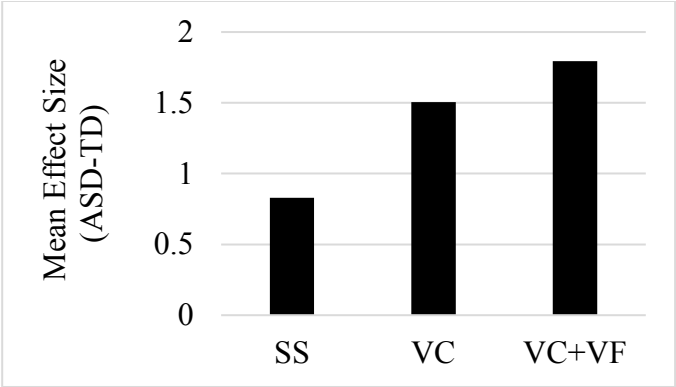

Figure 2: Mean CoV effect size (ASD-TD) within each condition (SS=self-selected; VC=visual cue; VC+VF=visual cue and visual feedback).

CONCLUSIONS

The present data suggest children with ASD are more variable in the timing, kinetics, and kinematics of two-legged hopping than age-matched TD children. These differences are magnified as sensory integration demands increase. Two-legged hopping is a simple whole-body motor task that may serve as a model to assess sensorimotor integration deficits in children with ASD and other neurodevelopmental disorders.

REFERENCES

1. Association AP. *American Psychiatric Association*, 2000.
2. Doumas et al. *J. Autism Dev. Disord*. 46(3), 2016.
3. Morimoto et al. *J. Autism Dev. Disord*. 0(0), 2017.
4. Moran et al. *Front. Integr. Neurosci*. 7, 2013.

Table 1: CoV (%) means and effect sizes (*ES*) for timing, kinetics, and kinematics [(ASD – TD)/SD *pooled*]

	Hop *f* (CoV)			**GRF (CoV)**			**Sacrum (CoV)**			**Knee Angle (CoV)**			**Ankle Angle (CoV)**		
	SS	**VC**	**VC+ VF**	**SS**	**VC**	**VC+ VF**	**SS**	**VC**	**VC+ VF**	**SS**	**VC**	**VC+ VF**	**SS**	**VC**	**VC+ VF**
ASD (%)	5.2	6.8	6.8	6.1	8.7	8.0	14.1	14.6	15.4	27.4	26.3	30.5	17.4	23.1	19.3
TD (%)	4.1	4.1	5.1	6.5	7.0	6.9	10.3	11.5	10.9	19.4	22.9	20.1	13.9	15.0	14.0
ES (*d*)	**0.91**	**2.51**	**2.12**	**-0.24**	**1.71**	**1.59**	**1.21**	**1.31**	**1.94**	**1.29**	**0.50**	**2.08**	**0.96**	**1.46**	**1.22**

Biomechanical Variability Among Individuals Following ACL Reconstruction and Rehabilitation

[1] Hadley Lindley [2] Shiho Goto [3] Joseph Hannon [4] Craig Garrison [5] James Bothwell [6] Adam King

[1] Texas Christian University, Fort Worth, TX, USA
[2]Texas Health Resources Ben Hogan Sports Medicine, Fort Worth, TX, USA
Email: Hadley.lindley@tcu.edu

INTRODUCTION

The neuromuscular system is a complex system with abundant degrees of freedom (DoF) available to perform a given motor task. With redundant DoF, movement variability is inherent throughout most motor tasks and also exists across different levels of analysis (joint space, segment space, muscular activity, etc.). Currently, it is unclear on what constitutes a healthy range of movement variability and the potential implications of high and low degrees of movement variability for injured populations and other motor disorders. Recent propositions suggest an optimal range of movement with low degrees of variability indicating rigid movement patterns and high degrees reflecting unstable movements [1]. Following lower extremity injuries, such as anterior cruciate ligament (ACL) tears, individuals often exhibit reduced movement variability that can be attributed to altered organization of DoF used to execute functional movements [2]. Following an ACL injury, surgical reconstruction and extensive rehabilitation aim to restore neuromuscular; however, injured individuals may not exhibit appropriate degrees of movement variability compare to pre-injury functionality states. The lack of movement variation potential limits adaptability to dynamic sport environments and may place individuals at a higher risk for re-injury.

Biomechanical analysis of neuromuscular control patterns includes the use of a motion capture system to measure various kinematic and kinetic variables throughout different motor tasks. Movement variability can be evaluated using common variables such as joint angle, segment angle, and joint moment [3]. Additionally, understanding the complex profiles of these variables will aid understanding how the neuromuscular system utilizes the redundant DoF.

Principal component analysis (PCA) is a data decomposition method that reduces a dataset containing a large number of variables into "principal components" (PCs) that account for the most variance. Further, PCA takes these PCs and determines the individual weightings each variable is contributing to the corresponding PC. In this way, PC gives us information about how individuals organize DoF in order to produce dynamic movements[4].

Provided the presence of abundant DoF across various sub-components of the neuromuscular systems, examining the mechanical properties (joint angle, segment angle, and joint moment) of the lower extremity during functional movement patterns can help identify individuals that at higher risk for injury [5].

The purpose of this study was to determine whether individuals following ACL reconstruction and rehabilitation exhibit consistent reduction of DoF across three different biomechanical variables.

METHODS

This study included 27 participants who had sustained a unilateral ACL tear. All participants had undergone at least six months of outpatient rehabilitation and were at the return to sport level at the time of testing. 33 reflective markers were attached to the bony landmarks/clothing of each subject with adhesive tape to create body segments. For the static trials, the sternum, bilateral acromion process, seventh cervical vertebra (C7), 12th thoracic vertebra (T12), lumbar spinal disc L4L5, bilateral posterior superior iliac spine (PSIS), bilateral sacrum, inferior sacrum, bilateral anterior superior iliac spine (ASIS), bilateral greater trochanter, bilateral thigh, bilateral medial and lateral epicondyles, bilateral shank, bilateral medial

and lateral malleoli, bilateral head of the 1st metatarsal (MT), bilateral head of the 5th MT, and bilateral calcaneus had reflective markers on them. For the dynamic jump-landing trials, the markers were removed from the medial epicondyle, medial malleolus, and ASIS. Each subject performed three jump-landing trials and were instructed to jump off of a 31cm high box and land on a bipedal force plate with both feet, and perform a maximal vertical jump, landing back down on the force platform. Each subject performed three jump-landing trials. The bipedal force platform was sampled at 1200 Hz (AMTI Force and Motion). The kinematics were measured using an eight camera motion analysis system, sampled at 120 Hz (Qualisys Motion Capture). Force platform data were used to define initial contact and take-off. Kinematic variables of segment angles (global coordinate system), joint angles, and joint moments were time normalized to the events of initial contact and take-off. Individual time series of each variable for a single trial were submitted to a principal component analysis. All statistical analysis was completed using MATLAB and Visual 3D.

A custom MATLAB code was used to apply PCA to the kinematic variables of interest. Data were then averaged to obtain the final values.

RESULTS AND DISCUSSION

The results of the principal analysis showed that components 1-3 accounted for an average of 92.1% of the joint moment variance. This was less than that of joint angles, 99.22%, and segment angles, 98.1%. The PCA analysis of joint angles accounted for the most variance using 3 PCs.

The purpose of our study was to determine whether individuals following ACL reconstruction and rehabilitation exhibit consistent reduction of DoF across three different biomechanical variables. The principal components (PCs) of the joint moment data differed the most from the other kinematic variables. The first PC accounted for an average of 52.04% of the variance in the dataset while the second PC accounted for an average of 30.32%. The first PC for the joint angle dataset accounted for 91.98% of the variance while the second one accounted for 6.07%. For the segment angle dataset, the first principal component accounted for 81.86% of the variance while the second one accounted for 11.97%. Figure 1 shows the first three principal components of the dataset.

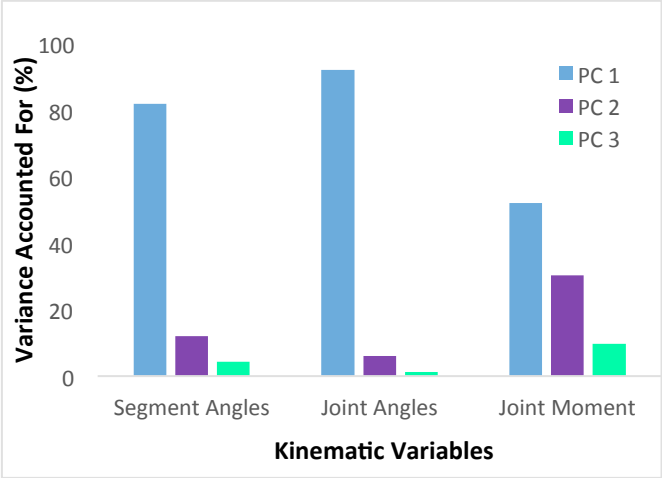

Figure 1: A comparison of Principal Component Analysis in the three kinematic variables. Principal Component one (PC1) accounted for the majority of the variance in segment angle, joint angle, and joint moment.

CONCLUSIONS

Individuals following ACL injury and reconstruction exhibit altered neuromuscular control patterns as a result of disrupted DoF organization. More variability is expressed in the biomechanical variables of joint and segment angles than that of joint moment, suggesting that these individuals organize their DoF more consistently with segment and joint loading. Further understanding how these individuals organize these DoF can help improve the rehabilitation process following ACL reconstruction.

REFERENCES

1. Lockhart, T., & Stergiou, N., *41*(8), 2013.
2. Trulsson, A. et al., *16*(1), 2015.
3. Hewett, T. E., et al., *33*(4), 2005.
4. Newell, K. M., et al., 2009.
5. Winter, David A., Wiley, 2009.

FEMOROACETABULAR IMPINGEMENT SYNDROME ALTERS THE KINEMATIC CONTROL STRATEGY DURING GAIT

[1, 2] Philip Malloy, [1] Donald Neumann, [3] John T. Heinrich, and [1] Kristof Kipp

[1] Marquette University, Milwaukee, WI, USA
[2] Rush University Medical Center, Chicago, IL, USA
[3] Milwaukee Orthopedic Group, Milwaukee, WI, USA
email: Philip_Malloy@rush.edu

INTRODUCTION

Arthroscopic hip surgery for femoroacetabular impingement syndrome (FAIS) has grown exponentially over the past 10 years [1]. Recent studies have found differences in the dynamic motor control strategy of gait in people with FAIS when compared to healthy controls [2-3]. The aim of the current study was to determine if arthroscopic hip surgery changes the kinematic control strategy of the hip joint during gait in people with FAIS. We hypothesized that before surgery, people with FAIS will demonstrate a more complex control strategy compared to controls, and that after arthroscopic hip surgery for FAIS this strategy will become more similar to the strategy used by controls.

METHODS

Six males and two females FAIS patients, who underwent arthroscopic hip surgery and eight sex, age, and body mass index (BMI) matched controls were enrolled in this study. Three-dimensional kinematic data were collected at 100 Hz using 3D motion capture techniques during five trials of level walking both before and greater than 1 year (15.2 ± 3.9 months) after arthroscopic hip surgery in people with FAIS, and at a single time point for controls.

Three-dimensional time normalized hip joint angle waveforms (X, Y, Z) were extracted for each trial and used as inputs for principal components analysis (PCA) [4]. All joint angle waveforms were z-scored prior to analysis. Eigenvalues and eigenvectors (i.e. principal components – PC) were extracted from the co-variance matrix of the 3D joint angles. The eigenvalues were used to calculate the proportion (%) of variance accounted for (VAF) by each of the principal components by dividing the eigenvalue for each PC by the sum of the all the eigenvalues. The VAF by the first and second eigenvectors were used to quantify the complexity of the kinematic control strategy. The contribution of each PC to the joint angle time series was also quantified by calculating the PC scores for each contributing joint angle. The PC scores thus represent how much each joint angle contributed to shaping the plane of covariation (i.e. kinematic pattern) and provides insight into the determinants of the control strategy. The 5-trial ensemble average for VAF for by each PC and the PC scores for each angle were calculated for each person in the FAIS group both before (Pre) and after (Post) surgery. The same procedures were used for the control group. All data analysis were performed with custom written MATLAB programs.

The dependent variables for analysis included: the ensemble averaged VAF (i.e. kinematic control strategy) and PC scores (i.e. joint-specific contributions). An independent sample *t*-test was used to determine between-group differences between the PRE time point of FAIS patients and healthy controls. A paired samples *t*-test was used to determine within-group differences between PRE and POST time points for FAIS patients. An *a-priori* alpha level of .05 was set for statistical significance. All statistical testing was performed using SPSS version 22 (IBM, Chicago, IL).

RESULTS AND DISCUSSION

There were no between-group differences in self-selected gait speed for the preoperative time point for FAIS group and healthy controls (PRE: 1.36 ± 0.10 m/s; Control: 1.40 ± 0.16 m/s; $p = 0.592$), or within-group differences before and after arthroscopic hip surgery (PRE: 1.36 ± 0.10 m/s; POST: 1.35 ± 0.06 m/s; $p = 0.704$).

A significant difference was found in the percent variance accounted for by each of the principal components between the preoperative time point for the FAIS group and healthy controls. The VAF by the first PC (PC1) for the preoperative time point of the FAIS group was significantly less than that of healthy controls (PRE: 77.2 (8.7) %; Control: 96.1 (2.8) %; p = .0001). Additionally, the VAF by the second PC (PC2) was significantly greater for the preoperative time point of the FAIS group when compared to healthy controls (POST: 22.8 (8.7) %; Control: 3.9 (2.8) %; p = .0001). Conversely no within-group differences were found between the VAF by PC1 (PRE: 77.2 (8.7) %; POST: 79.3 (11.1) %; p = .472) or PC2 (PRE: 22.7 (8.7) %; POST: 20.7 (11.1) %; p = .472), before and after arthroscopic hip surgery for FAIS. Despite no changes in the overall kinematic strategy after arthroscopic hip surgery, significant statistical differences were found in the joint-specific contributions to the kinematic control pattern after arthroscopic hip surgery for FAIS (**Table 1**).

Patients with FAIS demonstrated a more complex kinematic control strategy of hip joint motions than controls. In addition, the complexity of the kinematic control strategy did not differ from before to after arthroscopic surgery. However, at both time points the control strategy was more complex than the control group. Interestingly, the joint-specific contributions to the kinematic control strategy did change after surgery, which may indicate that patients with FAIS were still trying to achieve normal movement patterns. These results therefore indicate that 15 months may not enough to restore the kinematic control strategy in people with FAIS to a level that is comparable to healthy controls, which is consistent with previous research [5]. These findings thus provide important additional evidence about the length of time that may be required to effectively rehabilitate movement dynamics in people who underwent arthroscopic hip surgery for FAIS.

CONCLUSIONS

Arthroscopic surgery changed aspects of the kinematic control strategy of hip joint motions in people with FAIS. The changes associated with the surgery, however, were not enough to restore the control strategy to a level comparable to healthy controls, which may indicate the need for a longer rehabilitation period.

ACKNOWLEDGEMENTS

The Foundation for Physical Therapy (PODS II Scholarship) and CTSI Southeastern, WI (Grant Number 8UL1TR000055).

REFERENCES

1.Bozic K et al. *J Arthoplasty. 28(8),* 2013.
2.Samaan M et al. *Clin Biomech*. 30 (10), 2015.
3.Diamond LE et al. *J Orthop Res. 35 (7),* 2017.
4.Kipp K et al. *Clin Biomech*. 28 (5), 2013.
5.Kemp J. et al. *J Orthop Sports Phys Ther. 46 (11),* 2016.

Table 1: Mean (SD) contribution of each angle to shaping each principal component (PC) in the FAIS patients at the preoperative (PRE) and postoperative (POST) time points, and in the control group (Control).

PC	Hip Angle	PRE	POST	Control	*P*-value (PRE vs. Control)	*P*-value (PRE vs. POST)
PC 1	Flex/Ext	5.6 (2.7)	.91 (6.1)	.67 (15.7)	.352	.012*
	Add/Abd	-10.4 (2.2)	-1.5 (6.3)	-.74 (29.2)	.326	.005*
	IR/ER	4.6 (3.8)	2.4 (3.0)	.08 (13.7)	.796	.157
PC 2	Flex/Ext	-2.1 (5.1)	-.69 (2.3)	-.30 (3.9)	.391	.451
	Add/Abd	.37 (1.8)	-.22 (2.6)	-.06 (.56)	.579	.665
	IR/ER	1.7 (4.6)	.91 (3.1)	.36 (4.3)	.500	.654

Flex/Ext = Flexion/extension; Add/Abd = Adduction/abduction; IR/ER = Internal rotation/external rotation
* indicates statistical significance at $p < .05$

DYNAMIC ULTRASOUND ANALYSIS OF MEDIAN NERVE MAY DIFFERENTIATE CLINICALLY SIGNIFICANT CARPAL TUNNEL SYNDROME

Dominik Mattioli, Joseph A. Buckwalter, Ericka Lawler, Jessica E. Goetz
University of Iowa, IA
email: jessica-goetz@uiowa.edu, web: https://uiowa.edu/uiobl/

INTRODUCTION

Carpal tunnel syndrome (CTS) is among the most commonly encountered compressive peripheral neuropathies, with symptomatic patients complaining of pain, numbness, and paresthesia in the palm, thumb, index, and middle finger. Electrodiagnostic tests (e.g. motor/sensory nerve conduction and electromyography) can provide objective confirmation of a CTS diagnosis based on measurable degenerative abnormalities of median nerve signal conduction. However, in many patients with early-stage CTS, median nerve dysfunction may not be progressed to a point where changes in nerve conduction are consistently measurable.

A common feature of CTS is fibrosis of the subsynovial connective tissue surrounding the digital flexor tendons and the median nerve and thickening of the perineural tissue. This may limit mobility of the nerve within the tunnel, potentially increasing nerve compression and associated symptoms. Differences in nerve kinematics may develop before late stage nerve dysfunction, and therefore quantifying kinematic abnormalities may provide an objective measure of early-stage CTS. The goals of this work were to develop a methodology to track transverse-plane kinematics of the median nerve in the carpal tunnel using real-time ultrasound movies, and to pilot this technique to document CTS-related functional abnormality.

METHODS

Under IRB approval, 20 patients underwent ultrasound imaging of the carpal tunnel while performing a flexion of all 4 fingers simultaneously while holding the wrist straight. 10 of these subjects were individuals with clinically significant and electrophysiologically diagnosed CTS. These individuals underwent ultrasonographic data collection immediately prior to their carpal tunnel release. The other 10 participants were healthy individuals with no history of CTS. All data were captured in a single session using a Philips IU22 ultrasonography system and exported as .avi movies for analysis.

Ultrasound (US) movies were imported into MATLAB (The Mathworks, Natick MA) for analysis using a custom analysis routine developed for tracking the median nerve. The algorithm utilizes 2D image correlation to incrementally track the texture of a user-selected sub-region of the median nerve tissue through all sequential frames of the US movie. An anatomic reference point was similarly identified in every frame by tracking a user-selected sub-region of a carpal bone through each frame using the same correlation algorithm. This reference point was necessary due to the movement of the hand-held ultrasound transducer, which could cause calculation of artificial movement by the median nerve. The carpal bone reference point was used as a surrogate correction for translation of the ultrasound transducer movement during the flexion of the fingers, which would have remained in a consistent location within the image if the transducer could have been positioned without movement over the carpal tunnel during hand movement.

The algorithm permitted enhancement of image contrast to allow for more accurate calculation of image correlation. This process and analysis were automated within a Graphical User Interface (GUI) developed in MATLAB. For efficiency, the GUI provides user instruction and visual interpretation of real-time results when performing the analysis. Additionally, the GUI employs several automated image processing tools to reduce the extent of user input and computational time (Figure 2). To illustrate the use of the algorithm, velocity, acceleration, and total excursion of the median nerve relative to the carpal bones during active finger flexion was computed in the radial/ulnar and dorsal/palmar directions of each patient's wrist.

RESULTS AND DISCUSSION

Median nerve excursion in the radial/ulnar direction varied between the groups, with an average excursion of 4.6 +/- 2.7 mm in the healthy patient group and an average nerve excursion of 3.8 +/- 2.1 mm in the CTS group. Similarly, median nerve excursion in the dorsal/palmar direction averaged 1.5 +/- 0.6 mm in the healthy patient group and 1.6 +/- 1.6 mm in the CTS patient group (Figure 1).

The greater median nerve excursion in the healthy group was primarily a result of the nerve's considerable deformation in those individuals, whereas CTS patients' median nerves only minimally deformed as they were forced through a similar range of motion. It is worth noting that without an anatomic reference point these results are equivocal, as the total median nerve excursion in the radial/ulnar direction was not different between the groups (4.6 +/- 2.1 mm for the healthy patient group and 4.6 +/- 1.9 mm for the CTS patient group).

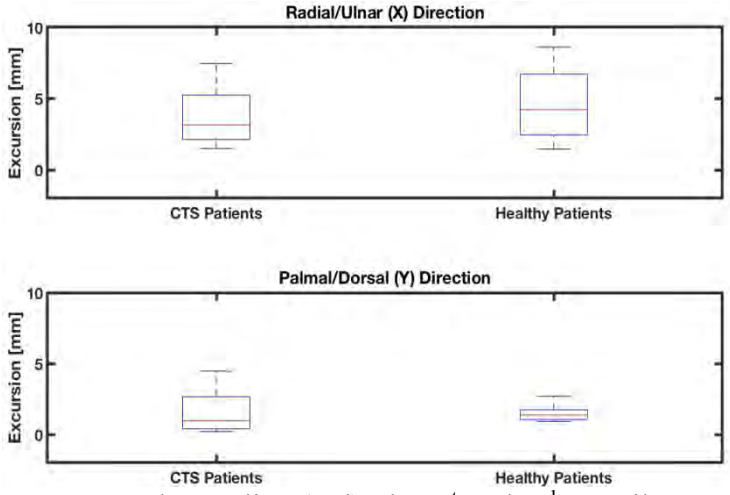

Figure 1: The median (red), the 1st and 3rd quartiles (blue), and the range (black) of median nerve excursion.

ACKNOWLEDGEMENTS

This work was funded by NIH grant R03 AR062729.

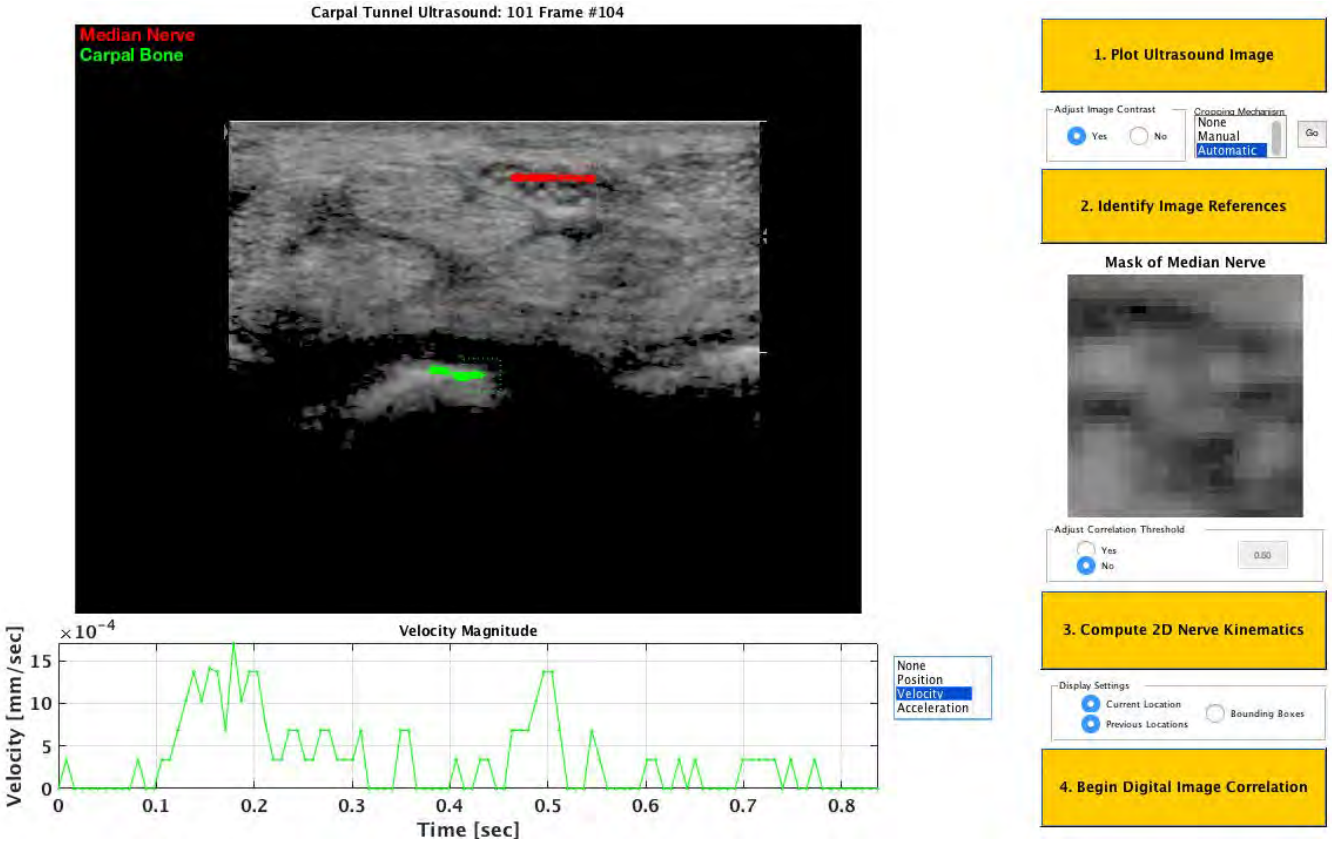

Figure 2: Appearance of the graphical user interface developed for tracking median nerve motion in US movies. Red and green asterisks indicate the tracked location of the median nerve and of a carpal bone (respectively) in each incremental frame. Total nerve excursion in the radial/ulnar and dorsal/palmar directions, and movement velocity and accelerations are quantified, and the motion path shown is for a healthy individual.

RELATIONSHIPS AMONG RESTING MUSCLE TENSION, SHORT-RANGE STIFFNESS, MOTION DETECTION, AND TIME TO PEAK TORQUE IN HUMAN KNEE JOINT

Takashi Nagai, Nathaniel A. Bates, Timothy E. Hewett, and Nathan D. Schilaty

Mayo Clinic Biomechanics Laboratories & Sports Medicine Center, Rochester & Minneapolis, MN, USA
Email: nagai.takashi@mayo.edu

INTRODUCTION

Skeletal muscles have the mechanical property to withstand rapid perturbation due to the resting cross-bridge linkage of the actin and myosin filaments of a relaxed skeletal muscle. Higher velocity perturbation is matched with higher forces. This rapid force production is commonly known as short-range stiffness (SRS) [1]. This is an important property for joint stability and injury prevention as the first line of defense against aberrant joint forces and moments [2]. It is also known that proprioceptive feedback from muscle spindles, Golgi-tendon organs, and other cutaneous and articular mechanoreceptors can directly influence the resting tone of skeletal muscles via α-γ motor neuron co-activation [2]. Habitual physical training can also influence this neural co-activation and function and result in increased maximal muscular force as well as the time to reach the maximal muscular force [3].

Traditionally, proprioception was measured using threshold to detect passive motion test (TTDPM) [4] while the time to peak torque was measured during the maximal voluntary isometric contraction [3]. We developed sensorimotor test to examine both proprioception with high-velocity (hvTTDPM) and reactive knee flexion (hamstrings) muscular strength to assess the time to peak torque [4] and tested on healthy individuals and individuals with anterior cruciate ligament-reconstruction (ACLR) surgery. This test also assesses the resting muscular tone and SRS within 50 milliseconds of the movement. It is innovative and exploratory until more data is available.

The purpose of the current investigation was to establish the relationship among SRS, resting muscle tone, hvTTDPM detection time, and the time for the maximal force. It was hypothesized that all four variables would be significantly related (higher resting tone, higher SRS, faster time at hvTTDPM, and faster time to peak torque).

METHODS

A total of 31 subjects participated in the study (16 males / 15 females, age: 21.4 ± 5.8 years, height: 174.7 ± 8.8 cm, weight: 73.3 ± 11.6 kg). Prior to their participation, informed consents were obtained from each subject. The study was reviewed and approved by the Institutional Review Board.

Subjects were seated on a HumacNORM dynamometer (CSMi; Natick, MA) with the knee joint axis rotation aligned to the axis of rotation of the dynamometer. The leg of the subject was then comfortably strapped to the dynamometer arm. The leg was then extended and anatomic zero recorded in the machine. The dynamometer acceleration was set for 500°/s and torque limit set to 60 Nm. For safety reasons, both mechanical and hardware limits of rotation were set at 30 and 70 degrees. The subject's leg was then rested on the 30 degree stop and a blindfold was placed over the subject's eyes.

The subject was instructed to relax the leg completely. The subject was instructed to resist forward motion as quickly and forcefully as possible when they became aware of acceleration. Then, the dynamometer accelerated at random points in time. The subject had 3 trials of randomized time intervals to respond to the perturbation. Based on previous piloting data, it was determined that subjects failed to react about 20% of time; therefore, only successful trials were used for analyses.

Joint position and torque values were collected at 1000 Hz with customized LabVIEW (National Instruments; Austin, TX) on a USB-1608G

(Measurement Computing; Norton, MA). Data was post-processed in customized LabVIEW software to determine joint position and torque values at initiation (0ms) and 50ms to calculate the SRS (ΔTorque/ΔPosition). The time to detect movement (Time at hvTTDPM) was defined as the point in which acceleration of the dynamometer began decreasing and when torque deflected greater than 10% over a 5ms interval. The time to reach peak torque was also calculated.

Based on the preliminary analyses, there were no side-to-side differences; therefore, each leg was analyzed together. Descriptive statistics (means and standard deviations) were calculated. Pearson correlational analyses or nonparametric analyses were used to establish the relationships among the following four variables: Torque at Initiation (Nm), SRS (Nm/°), Time at hvTTDPM (ms), and Time at Peak Torque (ms). Significance was set at $p < 0.05$.

RESULTS AND DISCUSSION

Descriptive statistics are shown in Table 1. The resting muscle torque was on average 4.3 ± 3.1 Nm. The torque and position at 50ms was 11.8 ± 3.5 Nm and 0.29 ± 0.09°, respectively. Based on the stiffness calculation, SRS was 29.4 ± 14.7 Nm/°. Subjects took on average 141.4 ms to detect movement. At this time point (hvTTDPM), the torque and position were 16.4 ± 3.5 Nm and 4.5 ± 1.3°, respectively. Time at peak torque was on average 321.6 ms. The torque and position at the peak torque were 62.5 ± 2.9 Nm and 23.6 ± 6.1°, respectively.

Table 1. Descriptive Statistics

	Mean	Standard Deviation
Torque at Initiation (Nm)	4.3	3.1
Short-Range Stiffness (Nm/°)	29.4	14.7
Time at hvTTDPM (ms)	141.4	16.9
Time at Peak Torque (ms)	321.6	32.4

For correlational analyses, the torque at initiation was significantly negatively correlated with the time to peak torque ($r = -0.453$, $p < 0.001$). There was a trend toward significant positive correlation between the torque at initiation and the SRS ($r = 0.242$, $p = 0.073$). There were no significant correlations associated with the time at hvTTDPM. Therefore, the hypotheses tested were partially supported.

Table 2. Correlation Matrix

		Short-Range Stiffness	Time at hvTTDPM	Time at Peak Torque
Torque at Initiation	Correlation	0.242	0.056	-0.453**
	p	0.073	0.685	0.000
Short-Range Stiffness	Correlation	-	0.075	-0.027
	p	-	0.584	0.844
Time at hvTTDPM	Correlation	0.075	-	0.156
	P	0.584	-	0.252
Time at Peak Torque	Correlation	-0.027	0.156	-
	p	0.844	0.252	-

CONCLUSIONS

The current study is the first to report the relationships among resting muscle tension, SRS, hvTTDPM, and time to peak torque in knee flexors (hamstrings). Further analyses showed that the magnitude of initial torque was significant predictor of torque values throughout the test (both passive torque: prior to hvTTDPM and active torque: after hvTTDPM). Hence, how fast individuals perceive the leg movement was less critical in the development of rapid muscular force development against perturbation and in voluntary reactive muscular force development.

Future investigations should explore different treatment options such as whole-body vibration and eccentric loading to alter the resting muscle tension. Our preliminary data indicate that the resting tension was actually higher in individuals with ACLR after their return-to-sport. This test could potentially be used to screen and monitor sensorimotor function of individuals at different ages or musculoskeletal conditions.

REFERENCES

1. Campbell et al. *J Physiol*, 1998: 941-962.
2. Nagai et al. *Sports Med,* 2018.
3. Aagaard P. *Exerc Sport Sci Rev*, 2003: 61-67.
4. Nagai et al. *J Athl Train*, 2013: 31-38

ACKNOWLEDGEMENTS

Funding from the NIH R01AR056259, R01AR055563, L30AR070273, K12HD065987, and the Mayo Clinic Kelly Orthopedic Fellowship.

THE EFFECT OF SURGICAL ALIGNMENT ON GAIT COMPLEXITY IN ADULT DEFORMITY PATIENTS - A NEUROMUSCULAR SYNERGY APPROACH

[1] Mohammad Moein Nazifi, [1] Pilwon Hur, PhD,[2] Theodore Belanger, MD,[3] Isador H. Lieberman, MD MBA FRCSC, and [4] Ram Haddas, PhD

[1]Texas A&M University, College Station, TX, USA
[2]Texas Back Institute, Rockwall, TX, USA
[3]Texas Back Institute, Plano, TX, USA
[4]Texas Back Institute Research Foundation, Plano, TX, USA
email: {moeinnazifi,pilwonhur}@tamu.edu, rhaddas@texasback.com

INTRODUCTION

Adult degenerative scoliosis (ADS) patients frequently suffer from impairments in mobility. Surgical intervention for ADS can improve gait, balance and other health related quality of life scores. Previous literature demonstrates that the central nervous system (CNS) might use an organization of muscle synergies to control a wide range of activities, e.g. walking [1]. The muscle synergy hypothesis claims that the CNS may use a single control input to activate a large group of muscles instead of controlling each muscle individually [2]. Hence, neuromuscular synergies may verify the ability of the CNS in generating independent control signals [3]. A lower number of muscle synergies during gait would imply inability of the CNS to generate independent control signals [3]. A greater number of muscle synergies represent more substantial gait complexity since more control inputs are required to achieve the same task [4].

Objective of this study is to compare number of muscle group synergies in ADS patients during gait both before and 3 months after surgery to detect significant differences.

METHODS

Clinical gait analysis was performed on thirteen ADS patients, one week prior and 3 months post-surgery. Five walking trials were performed at self-selected speed of the patients. Surface electromyography (EMG) electrodes were placed and recorded bilaterally from 16 trunk and lower extremity muscles: External Oblique, Gluteus Maximus, Multifidus, Erector Spinae, Rectus Femoris, Semitendinosus, Tibialis Anterior, Medial Gastrocnemius. EMG data was collected at 2000 Hz, high-pass filtered at 20 Hz, low-passed at 450 Hz, then rectified and low-passed at 35 Hz [5]. The data was then normalized to the maximum activity observed among all trials of each subject. The processed EMG was then fed into a non-negative matrix factorizer to extract synergies and their activation coefficients [2]. Mathematically, a higher number of synergies would always reduce the residual error between the reconstructed EMG and the original EMG [2]. The required number of synergies were defined as the minimum number of synergies that could reconstruct EMG signals with a VAF higher than 95%:

$$VAF = 1 - \frac{EMG_{processed} - EMG_{reconstructed}}{EMG_{processed}}$$

Equation 1: VAF definition.

After deciding the number of walking synergies required for each patient both pre- and post-surgery, a paired t-test was used to test the hypothesis (α=0.05) using SPSS.

RESULTS AND DISCUSSION

The results of the paired t-test revealed that surgical alignment cause a significant increase in number of walking synergies. The information regarding the number of synergies can be found in Table. 1 and Fig. 1.

The significant increase in number of walking muscle synergies post-surgery substantiates the improvements in gait quality and complexity for ADS patients following surgical interventions. More synergies can potentially show the ability of the CNS in generating independent control signals. An alternative interpretation of this result is that pain, as a crucial sensory input, has the potential to affect motor control and its complexity. Hence, it sounds cogent to assume surgery can potentially affect the motor control by reducing the pain experienced by subjects throughout walking.

The greater number of muscle group synergies post-surgery will result in a more elaborate gait pattern since more muscle group synergies (that can be considered as the basis vectors of a n-dimensional space) are present to rebuild the EMG signals (Eq. 1).
As an example, the inability of post-stroke patients to generate independent control signals for gait forces their CNS to activate numerous muscles with a single signal (at the same time), causing unwanted co-contractions that hinders their normal gait [3].

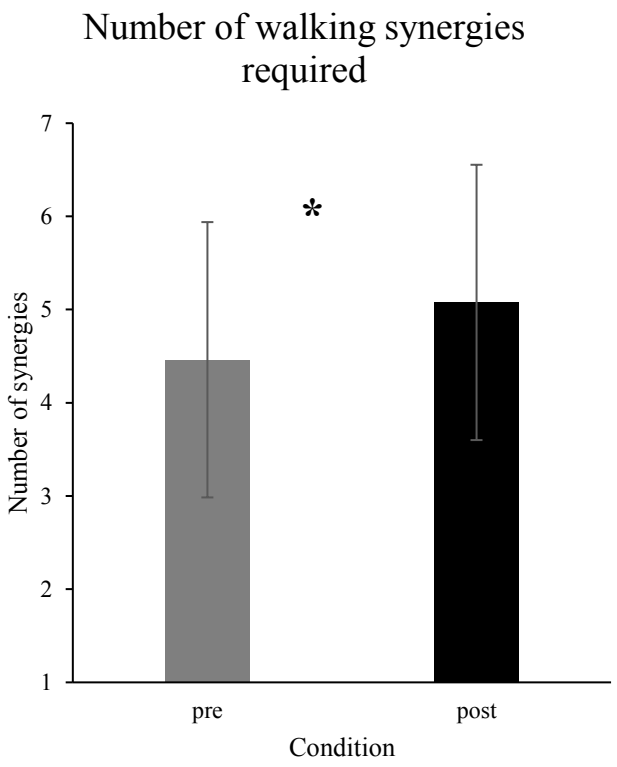

Figure 1: Number of synergies required for patients before and after surgery.

CONCLUSIONS

This study demonstrated an increase in gait complexity by virtue of the increased number of muscle group synergies following surgical intervention in ADS patients. The higher number of synergies observed in ADS patients following a surgery verifies the efficacy of this method in improving subjects' walking patterns/quality.

We recommend that spine care providers use gait analysis as part of their clinical evaluation to provide an objective measure of function and to better understand the effects of the disease and its treatment on their patients' gait, function, and, ultimately, quality of life.

REFERENCES

1. Nazifi et al. *Frontiers in Human Neuroscience,* **Vol. 11**, **No. 40**, 2017.
2. Ting et al. *Journal of Neurophysiology*, **93(1)**, 2005.
3. Clark et al. *Journal of Neurophysiology*, **103**, 2010.
4. Shuman et al. *American Society of Biomechanics*, Raleigh, NC, USA, 2016.
5. De Luca et al. *Journal of Neurophysiology*, **Vol. 43**, **No. 8**, 2010.

Table 1: Required number of walking synergies pre- and post-surgery, and t-test results.

	Pre-surgery	**Post-Surgery**	***p*-value**
Number of synergies (Mean ± SD)	4.54 ± 1.45	5.15 ± 1.46	0.04

EMG-DRIVEN MUSCULOSKELETAL SIMULATIONS USING A NEW THRESHOLD OPTIMIZATION TECHNIQUE

Kevin O'Brien & James Schmiedeler
University of Notre Dame, Notre Dame, IN, USA
corresponding email:kobrie23@nd.edu

INTRODUCTION

In gait analysis of individuals with neuromuscular disorders, the muscle forces required to generate observed experimental gaits are of interest. Since there are more muscles acting across a joint than there are degrees of freedom for that joint, these forces cannot be calculated directly [1]. OpenSim, an open-source neuromusculoskeletal system simulation tool, attempts to solve for individual muscle forces by minimizing an objective function at discrete time points in a given gait [2]. This objective function can be further refined by also considering EMG signals. When driving a simulation with EMG, this objective function is

$$J(t+T) = \sum_{i=1}^{m} V_i[a_i(t+T)]^2 + W_i[a_i(t+T) - \tilde{E}_i(t+T)]^2, \quad (1)$$

where V_i is the volume of muscle i, $a_i(t+T)$ is the activation of muscle i at time $t+T$ for a given muscle activation at time t, W_i is a weighting factor and $\tilde{E}_i$ is the normalized EMG signal for muscle i. The EMG, collected in mV, must be converted to a percentage of the maximum excitation in order to be compared with the simulated muscle activation. This conversion is commonly accomplished by recording the maximum voluntary isometric contraction (MVIC) for each muscle and normalizing the EMG data by this value [3].

For individuals with neurological disorders, damaged communication within the neuromuscular system can make MVIC difficult to determine. Instead, it may be possible to determine muscle activation by comparing the EMG signal during gait to a resting EMG signal. In order to run neuromuscular simulations for these individuals, the OpenSim protocol needs to be formulated in such a way that the results match the true activity as closely as possible.

METHODS

To determine the efficacy of using resting EMG signals, three simulation conditions were applied to the same experimental data: 10 trials of a healthy individual walking at a self-selected pace. First, the gait motion data were used to simulate the muscle activity with no EMG input. The subject was asked to run through an MVIC protocol to scale EMG data, and these data were then used in a second simulation of the same experimental data. Finally, resting EMG data were used to set a threshold for the proposed EMG thresholding objective function in a third simulation.

With the subject sitting down and motionless, the EMG signals of eight instrumented muscles for each leg were recorded. These resting EMG values provided a baseline signal from which the noise and bias of each sensor could be collected. A muscle activation threshold was set as

$$\lambda = mean(restEMG) + 2 * StDev(restEMG), \quad (2)$$

with any muscle whose EMG signal was above/below this threshold considered to be on/off.

The traditional EMG-driven optimization objective function could not be used with this new method of analyzing muscle activation. Instead, a new optimization parameter Γ, taking the form of a logistic function (Eq. 3), was introduced to drive muscles on/off based on the EMG threshold value. The slope and the continuous nature of the logistic function improve the optimizer's ability to find the global minimum within the simulation constraints at each time step.

RESULTS AND DISCUSSION

Figure 1 details the comparative results of these simulations in two muscles characteristic of what was found across the other muscles simulated. Across all muscles, the MVIC optimization condition most accurately followed the recorded EMG signal. This is not surprising, as the protocol for analysis allows for the direct relationship between the EMG signal and the simulation activations to be incorporated into the optimization. The EMG thresholding optimization had its most significant effect at the time points in which there was any EMG

$$J(t+T) = \sum_{i=1}^{m} V_i[a_i(t+T)]^2 + W_i * \Gamma,$$

$$\Gamma = \begin{cases} 0, & \text{for } E_i(t+T) \geq \lambda \text{ and } a_i(t+T) \geq 0.5 \\ \dfrac{e^4}{e^4 + e^{200*a_i(t+T)}} + 0.1(1 - a_i(t+T)), & \text{for } E_i(t+T) \geq \lambda \text{ and } a_i(t+T) < 0.5 \\ 0, & \text{for } E_i(t+T) < \lambda \text{ and } a_i(t+T) < 0.5 \\ \dfrac{e^{200*a_i(t+T)}}{e^{16} + e^{200*a_i(t+T)}} + 0.1 * a_i(t+T), & \text{for } E_i(t+T) < \lambda \text{ and } a_i(t+T) \geq 0.5 \end{cases} \tag{3}$$

activity and there was no simulated activity in the control simulation. This is most significant near the end of the gait phase for the Vastus Lateralis.

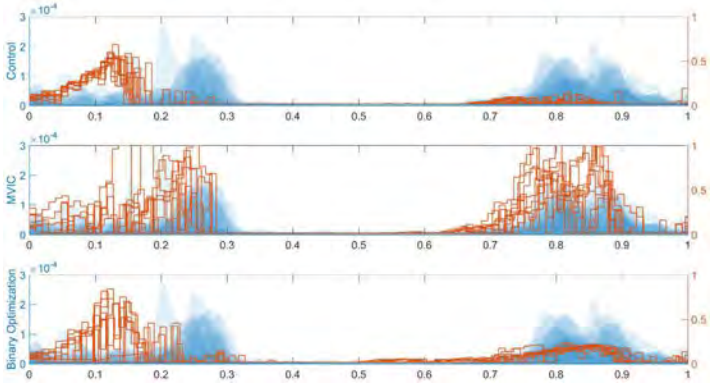

A. Vastus Lateralis

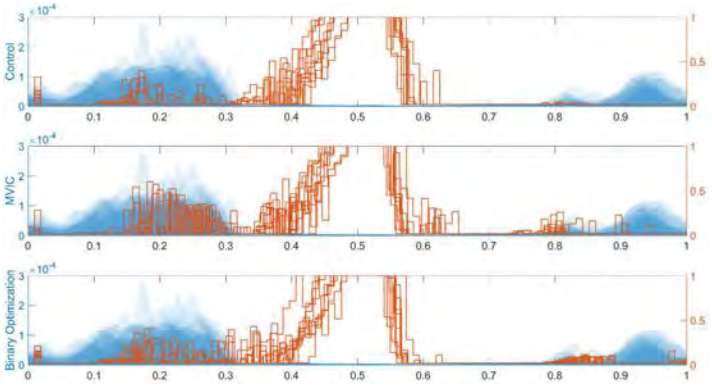

B. Soleus

FIGURE 1. Simulated muscle activity vs. percent of gait for optimization conditions: no EMG consideration, MVIC EMG normaliztion, and EMG threshold optimization. Blue shaded regions represent filtered EMG data from 10 steps of one subject. Orange trajectories are the simulated muscle activations.

One shortcoming of the simulations is that all three conditions predict the soleus to be active in propulsion, while the experimental EMG data indicate that it is active prior to propulsion (Figure 1). This relates to research into stretch-shortening cycles, in which energy is stored in the tendons during stance by controlling the activation of the ankle plantarflexors before releasing this energy during toe-off. This transient behavior is energetically more efficient [4], but due to the limitations of the forward dynamic simulation, does not appear in the results.

CONCLUSION

The results demonstrate that using resting EMG to set thresholds for the EMG signals provides a viable method for generating neuromuscular simulations. Further refining the optimization method may be necessary to ensure that muscle power results accurately reflect the true muscle powers. There is no reason to believe that the Thelen muscle model [5] used in OpenSim cannot perform the stretch-shortening cylces seen in experimentation, but the optimization strategy may need to be adjusted to consider the entire stride rather than each time step individually.

ACKNOWLEDGMENTS

This material is based upon work supported by the Indiana Clinical and Translational Sciences Institute (TL1 Program), Grant # TL1 TR001107 with partial funding from Grant # UL1 TR001108 (A. Shekhar, PI), 9/26/2013 4/30/2018.

REFERENCES

[1] MG Pandy. *Ann Rev Biomed Eng*, 3(1):245–273, 2001.
[2] S Delp et al. *IEEE: Biomed Eng*, 54(11):1940–1950, 2007.
[3] TS Buchanan et al. *J Appl Biomech*, 20(4):367–395, 2004.
[4] M Ishikawa et al. *J Appl Physiol*, 99(2):603–608, 2005.
[5] DG Thelen et al. *ASME: J Biomech Eng*, 125(1):70–77, 2003.

MODULAR CONTROL OF GAIT IN HEALTHY OLDER AND YOUNGER ADULTS

[1,3]Sarah A. Roelker, [2,3]Elena J. Caruthers, [3]Laura C. Schmitt, [3]Ajit M.W. Chaudhari, [3]Robert A. Siston

[1]The University of Texas at Austin, Austin, TX, USA; [2]Otterbein University, Westerville, OH, USA;
[3]The Ohio State University, Columbus, OH, USA
email: sarah.schloemer@utexas.edu

INTRODUCTION

Age-related changes in muscle function have been identified as the most important physiological change leading to functional limitations in older adults [1], and recent research demonstrated that impaired neuromuscular activity is responsible for this altered muscle function [2]. Current motor control theory suggests lower extremity muscle activity during gait can be modeled by a reduced set of principal activation patterns (modules); however, the literature lacks consensus as to whether aging alters the modular control of gait [3–5]. Identifying age-related changes in modular control may provide insight into the neurological mechanisms underlying functional limitations in older adults. Therefore, the purpose of this study was to determine if the modular control of gait differs between healthy young and older adults. We hypothesized that 1) healthy older adults would have the same principal patterns as young adults but 2) different muscle weights on the principal patterns.

METHODS

Ten healthy older (63.1±2.6 years; 7 female; 1.68±0.08 m; 71.8±12.2 kg) and ten young (23.9±2.8 years; 5 female; 1.76±0.07 m; 70.6±10.9 kg) adults provided written informed consent prior to walking at their self-selected speed while 3D kinematic and kinetic data were collected. Electromyography (EMG) data were simultaneously collected from the rectus femoris (RF), vastus lateralis (VL), vastus medialis (VM), biceps femoris (BF), medial hamstrings (MH), lateral gastrocnemius (LG), medial gastrocnemius (MG), and soleus (SO) on the participant's dominant leg. The EMG data were demeaned, passed through a 10-300 Hz sixth order Butterworth bandpass filter, and full wave rectified. The data were then passed through a sixth order Butterworth low-pass filter at 6 Hz to create linear envelopes. Each muscle's processed EMG was normalized by its maximum muscle activation in the trial. A 40ms delay was applied to the EMG to account for electromechanical delay [6].

For each participant, non-negative matrix factorization (NMF) [7] was used to extract modules from the original activation patterns (EMG_o). The number of modules required to produce adequately reconstructed activation patterns (EMG_r) was determined using the variability accounted for (VAF) by the modules. The VAF was calculated as $VAF = 1 - ((EMG_o - EMG_r)^2/EMG_o^2)$ and used as a measure of the agreement between EMG_o and EMG_r. The NMF began by extracting just one module. If the VAF was greater than 0.9 for each of the eight muscles, no additional modules were needed to represent the data. Otherwise, the number of modules extracted by NMF was increased by one until the VAF of all eight muscles was greater than 0.9 or until the VAF was greater than 0.8 and adding another module did not increase the VAF of the muscle with the lowest VAF by more than 5% [8].

To compare the principal patterns for each module across age groups, principal patterns for each participant were normalized to their peak value so that the magnitude of the patterns ranged from 0 to 1. Similarly, the weights of each muscle were normalized to the maximum weight of the muscle across all modules, resulting in a range of weights from 0 to 1 such that each muscle had a normalized weight of 1 for the module for which it had the greatest weight. Normalized principal patterns and muscle weights were averaged across participants within an age group to determine group means and standard deviations. Individual 2-sample t-tests assessed for age group differences in participant demographics and muscle weight factors on individual modules. A significance level of $\alpha<0.05$ was set a priori for all statistical tests.

RESULTS AND DISCUSSION

While height was significantly different between age groups ($p=0.016$), there were no significant

differences in mass, BMI, or stride length normalized to leg length ($p \geq 0.100$). Gait speed was not statistically different between older (1.17±0.20 m/s) and young (1.25±0.20 m/s) adults ($p=0.336$).

In support of our first hypothesis, the average number of modules required to reconstruct EMG_o with 90% VAF was the same in young (3.6±0.7 modules) and older (3.6±0.8 modules) adults. For the young adults, five participants required three modules, four participants required four, and one participant required five. For the older adults, one participant required two modules, three participants required three, five participants required four, and one participant required five. To compare modules between older and young adults, four modules were extracted from each participant. The modules' principal activation patterns were qualitatively similar between age groups (Figure 1A) and comparable to modules extracted from similar muscle sets in previous studies [3,8,9]. However, the older adults' muscle weights of MG on Module 2 ($p=0.041$), MH on Module 4 ($p=0.049$), and VL on Module 1 ($p=0.038$) were significantly smaller than those of young adults (Figure 1B), supporting our second hypothesis.

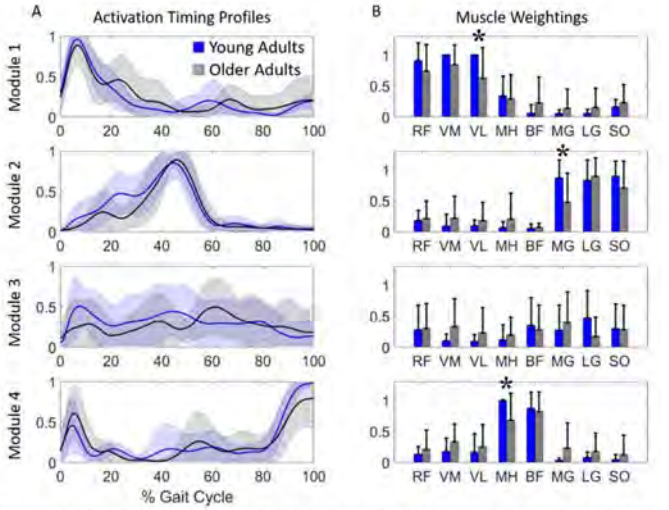

Figure 1: Average principal activation patterns and muscle weightings for four modules extracted from the EMG of young and older adults. A) The solid line represents the average activation pattern and the shaded region represents ± 1 standard deviation. B) Average normalized muscle weightings for the four modules. Error bars represent one standard deviation. All young Module 1 VM and VL weights equaled 1, resulting in a standard deviation of 0 for these muscles. * indicates statistically significant difference between age groups.

The decreased Module 2 MG weight observed in older adults compared to young adults may support the hypothesis of an age-related distal-to-proximal shift in motor control characterized by decreased plantarflexor power and increased hip extensor work [10]. Although the older adults' smaller Module 4 MH weight does not suggest increased hip extensor activity, EMG from gluteus maximus, the primary hip extensor, was not collected in this study. Future work should characterize differences in hip extensor modular organization between older and young adults, which may indicate a proximal shift in motor control strategy.

CONCLUSIONS

Although similar principal activation patterns were derived for each age group, the reduced muscle weights in the older adults suggests a diminished muscle response to the neural signal [8]. Altered modular control has been shown to be related to impaired function in post-stroke [8] and total knee arthroplasty [9] patients. The reduced muscle weights (response) suggest the older adults in this study may have used a different neuromuscular strategy than the young adults to achieve similar function (gait speed). These findings suggest future studies should investigate differences in the modular control of gait in older adults with different functional levels to determine the contribution of altered modular control to impaired walking ability.

REFERENCES

1. Pendergast et al. *J Gerontol.* **48,** 61-7, 1993.
2. Clark et al. *J Gerontol A Biol Sci Med Sci.* **66A,** 115-21, 2011.
3. Monaco et al. *J Neurophysiol.* **104,** 2092-102, 2010.
4. Wang et al. *Exp Brain Res.* **226,** 463-72, 2013.
5. Wang et al. *Eur J Appl Physiol.* **117,** 201-11, 2017.
6. Arnold et al. *J Exp. Biol.* **216**, 2150-60, 2013.
7. Lee & Seung. *Nature.* **401,** 788-91, 1999.
8. Clark et al. *J Neurophysiol.* **103,** 844-57, 2010.
9. Ardestani et al. *J Electromyogr Kinesiol.* **37,** 90-100, 2017.
10. DeVita & Hortobagyi. *J Appl Physiol* **88,** 1804-11, 2000.

ACKNOWLEDGEMENTS

We thank Drs. Jackie Lewis and Greg Freisinger for their help with data collection. This research was supported by National Science Foundation Graduate Research Fellowship Program Grants DGE-1343012 (SAR) and DGE-0822215 (EJC).

Kinematic Variability in Piano Performance

Anna-Marie Schmidt, Brent Russell, and Ronald Hosek

Life University, Marietta, GA, USA
email: anna-marie.schmidt@student.life.edu, web: http://www.ccr.life.edu

INTRODUCTION

We have developed a methodology utilizing kinematics to quantify the recovery process in pianists undergoing care for musculo-skeletal problems. The pressing of piano keys is the end result of the coordinated activity of many joints by multiple muscles, allowing for multiple degrees of freedom. When the key is pressed, there are potentially many combinations of motions in the kinetic chain and spine that may be utilized. If the same key is pressed multiple times, there may be variability in how it is done.

The aim of this study was to examine methods for analyzing motions, and variability of movement patterns of pianists performing a scale-based excerpt.

METHODS

All procedures were approved by our institution's IRB. Pianists were recruited via word-of-mouth within the university community. Participants were eligible if physically able to play and had reached an advanced technical playing level.

A MyoMotion inertial measurement unit (IMU) system (Noraxon; Scottsdale, Arizona) was used to track spinal and arm movements. Each pianist was outfitted with eight IMU sensors overlying the forearms, upper arms, back of the head, T1 and T12 vertebrae, and the sacrum.

Participants sat at an electronic keyboard and played a scale-based excerpt 12 times. The process was repeated on a second day. Bench height and tempo were participant-selected and remained constant. A metronome was used to maintain temporal consistency.

Calibration was done with participants seated, elbows flexed to 90 degrees. Data were recorded at 200 Hz and analyzed using a program custom-written by the 3rd author. Graphs were generated from running averages of consecutive 20-point samples for flexion-extension, lateral bending, and rotation of the cervical, thoracic, and lumbar regions; flexion-extension, abduction-adduction, and rotation of the shoulders; and flexion-extension of the elbows. Means and standard deviations for matched time points across all trials of a session were used to calculate Mean Coefficients of Variation over the entire waveform. Finally, we adapted a method previously described by O'Dwyer to characterize trial-to-trial motion pattern variability as a single value.[2]

RESULTS AND DISCUSSION

Results: Five participants completed a first recording session; four were available for a second. Methodological refinement was required with the first participant, much related to electromagnetic interference with the IMUs by the keyboard. We wrapped the keyboard's power supply in aluminum foil, experimented with locations within the lab, and instructed participants to not drop their hands below the level of the keyboard. A few trials were repeated immediately due to mistakes in mechanical execution. Later, during analysis, two trials were excluded as outliers because their graphic patterns were radically atypical for the session; these cases may have involved electromagnetic interference or participant discomfort.

Numeric values for variability were consistent with their graphic representations; that is, graphs that visually displayed widely-varying trial-to-trial motion patterns had high numeric values, and graphs displaying multiple tightly-grouped patterns always had smaller numbers. In general, there was a decrease in variability from the first to the second session.

In general, sagittal plane motions tended to be the most variable in both sessions, cervical flexion

particularly so; thoracic and lumbar flexion, and head and pelvis pitch were also among motions with highest variability. The least experienced participants had greater amounts of sagittal variability (e.g., Figure 1a).

Transverse plane motions, cervical rotation and head course (yaw), were among the more variable for most participants; thoracic and lumbar rotation tended to be lower, as did pelvic course (e.g., Figure 1b). The two least experienced participants demonstrated high variability of pelvic course. Pelvic roll and thoracic lateral bending were the least variable of all motions.

Discussion: Ultimately, data collection with IMUs worked well and numeric values produced by the analysis method appear to consistently represent the patterns recorded by the IMUs.

The length of the keyboard and hand placement have determining effects on motions in the coronal and transverse planes. Movements in the sagittal plane do not have such constraints but are affected by dynamics (loudness); the production of louder sounds involves playing with more force and larger-amplitude sagittal motions. Pianists were not given instructions about dynamics; inexperienced or less trained pianists may be unaware of or have less control of these motions. The constraints hold true for transverse plane motions occurring in the torso and pelvis, but less for cervical rotation and head course. Cervical and head positioning are less crucial, perhaps accounting for increased variability.

In classical training pianists are taught to not rotate the pelvis or slide along the bench to reach higher and lower octaves, instead, to rock onto the ischial tuberosity (coronal plane motion). Less experienced participants might not accomplish this motion**,** their greater variability in pelvic course, and somewhat in thoracic rotation**,** may represent compensation.

The first recording session was a new environment for participants in regard to instrument, room, and motion capture equipment, which may have contributed to higher variability. In the second session, the participant would have been more comfortable, leading to less variability.[3]

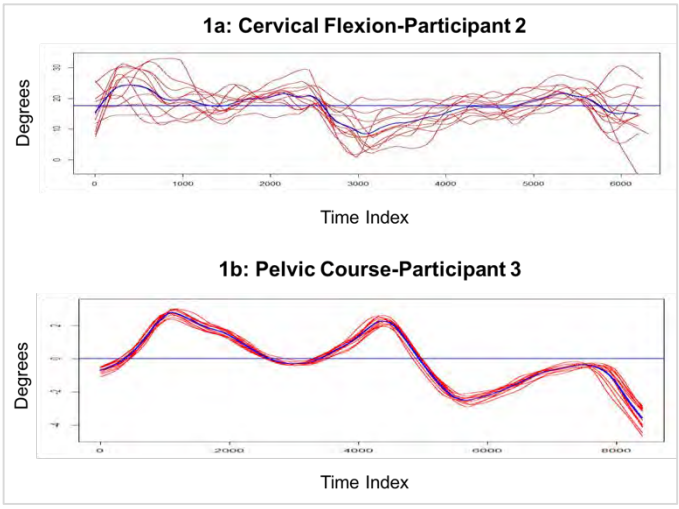

Figure 1: 12 trials for: (a) cervical flexion (note the high degree of variability). (b) pelvic course for (note the low degree of variability). Blue lines represent averages.

CONCLUSIONS

We are confident in our method's ability to accurately capture movement patterns of pianists. Analysis methods for determining and comparing variability seem appropriate for future use in studying the effect of chiropractic care on pianists with musculoskeletal injuries.

REFERENCES

1. O'Dwyer N, et al. Independent assessment of pattern and offset variability of time series waveforms. *Gait Posture.* 2009;29(2):285-9.
2. Davids K, et al. Dynamics of skill acquisition. Champaign, IL: Human Kinetics; 2008.

Table 1: Averaged participant MCVs for Session 1 and 2

	Average MCV's for Session 1 and 2														
	C-flex	C-lat	C-rot	L-flex	L-lat	L-rot	T-flex	T-lat	T-rot	HD course	HD pitch	HD roll	P-course	P-pitch	P-roll
Day 1	304%	68%	112%	166%	138%	57%	199%	44%	56%	130%	229%	93%	81%	290%	33%
Day 2	170%	80%	140%	138%	80%	77%	131%	35%	60%	133%	154%	94%	65%	140%	36%

INVESTIGATION OF WHOLE-LIMB MOTION AS A PRIMARY MOTOR GOAL DURING GAIT

Brittany N. Sommers, Andrew D. Shelton & Louis A. DiBerardino III

Ohio Northern University, Ada, OH, USA
email: l-diberardino@onu.edu

INTRODUCTION

Human gait is critical in daily locomotion and its study can result in greater understandings of restorative processes for normalization after injury. Lower-limb kinematics are frequently studied for these purposes. Lower limb kinematics are obtained with the use of three-dimensional motion capture systems to determine the joint and whole-limb angles through a single gait cycle (Figure 1).

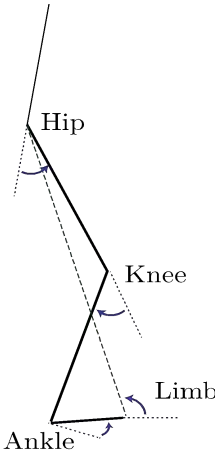

Figure 1: Joint and whole-limb angles.

A previous study conducted on a treadmill demonstrated that cycle-to-cycle variability was much lower for an individual's whole-limb angle than for their individual joint angles [1]. The Uncontrolled Manifold Hypothesis demonstrates how the Central Nervous System (CNS) uses redundant degrees of freedom to stabilize the performance of a motor task [2]. This maximum performance is achieved by neglecting the variance in parameters that do not influence the primary motor goal and minimizing variance in the parameters important to the goal.

There are differing opinions on whether sagittal-plane variability is similar between over-ground and treadmill walking, or whether a treadmill reduces the variability in individual joint angles, especially the ankle [3,4]. Therefore, the goal of this study is to determine if maintaining the whole-limb angle is a primary motor goal of over-ground gait. It is hypothesized that whole-limb angle variability will be lower than individual joint angle variability, but to a lesser extent than in treadmill gait.

METHODS

This study was approved by the Ohio Northern University Institutional Review Board. The following procedure has been completed for eight healthy, male, college-age subjects, all of whom provided informed consent.

A three-dimensional motion capture system (Cortex by MotionAnalysis) was used to create a 6-camera capture volume to record the over-ground gait. Retroreflective markers were placed on the subject's sacrum, bilateral ASIS, knee, ankle, heel, and toe to record position. The subject was asked to walk through the capture volume unrecorded to establish a comfortable pace. During each recorded trial the subject took a minimum of 3 steps before entering and after exiting the capture volume to reach a consistent gait [5]. The subject then made 30 recorded passes through the capture volume. The subject's pace was determined using a metronome, and the subject repeated the assessment while instructed to step in sync with beats played at their previous comfortable pace.

The Cortex software was used to produce three-dimensional positions for all markers throughout each trial. This data was then post-processed using MATLAB to calculate the whole-limb and joint angles for each trial. Each gait cycle was normalized to evenly spaced points from 0-100% using piecewise linear length normalization to align heel strike and toe off events. After normalization, cycle-to-cycle variability was calculated as the sum of standard deviations at each integer percentage of the gait cycle for each angle. Differences between whole-limb angle variability and each individual joint angle, as well as differences between condition for each angle, were tested using paired *t*-tests ($\alpha = 0.05$, Excel, Microsoft).

RESULTS AND DISCUSSIONS

Group means for cycle-to-cycle variability of each angle can be found in Table 1, including data from the 10 subjects of the previous study described above. For the current study, variances in the hip and knee were much greater than that of the whole-limb angle during the un-paced condition ($p = 0.025$ and $p < 0.001$, respectively). The ankle also showed increased variance, but it was not statistically significant ($p = 0.107$). For the paced (metronome) condition, all three joint angles were statistically higher than the whole-limb angle ($p < 0.005$). These trends are similar to those found in the previous study, except that all measures were lower in treadmill gait, and the whole-limb angle exhibited a more drastic decrease when compared to individual joint angles. None of the joint angle variability differences between the current un-paced and paced conditions proved statistically significant.

Table 1: Group mean of cycle-to-cycle variance of previous study (treadmill) [1] and current study (over-ground with/without metronome).

Sum of SD (deg)	**Angle**			
Group	**Limb**	**Hip**	**Knee**	**Ankle**
Previous	56.2	99.8	132.0	100.6
Current (no metronome)	89.4	114.0	166.1	105.8
Current (metronome)	96.2	130.8	178.1	114.9

In general, the whole-limb angle proves to have the least amount of cycle-to-cycle variability compared to the hip, knee, and ankle angles. This is similar to the previous study (Table 1), where the whole-limb also resulted in the lowest variability. This result helps support the hypothesis that the whole-limb angle is a primary motor goal during gait and the CNS performs to minimize its variance. To further emphasize this, when looking at individual subject data, all subjects had lower whole-limb variability than any joint angle except for one subject during only one condition (including the previous study).

Further work is certainly needed to solidify the proposal that whole-limb motion is a primary goal of gait. It would be prudent to repeat this study where the same subjects walk both over ground and on a treadmill. Also, if whole-limb motion was truly a goal of gait, then it's reduced variability should be insensitive to gait perturbations, where the CNS would adjust the individual joints to compensate and maintain normal whole-limb motion. This was seen in the previous study where an ankle injury was simulated, which increased ankle variability while whole-limb variability was maintained [1]. Finally, the hypothesis should be tested on subjects who walk over ground and are not instructed *anything*. Here they were instructed to walk at a comfortable pace, which may have led to an internal pacing similar to that provided by the metronome, or the treadmill of the previous study.

CONCLUSIONS

In cases where the brain is forced to think about the speed with which the body is walking, evidence suggests that whole-limb motion is a primary motor goal during gait, and the CNS functions to minimize those variances. This is supported by the previous treadmill study and the results of the current over ground study.

ACKNOWLEDGEMENTS

The authors wish to acknowledge Michael Potter and John Rasch for their help with the initial stages of this work.

REFERENCES

1. DiBerardino LA. *Neuromuscular control adaptation during recovery from injury* (Dissertation), University of Illinois, 2014.
2. Scholz JP & Schoner G. *Exp Brain Res* 126, 289-306, 1999.
3. Ivanenko YP et al. *J Neurosci* 27, 11 149-11 161, 2007.
4. Dingwell JB et al. *J Biomech Eng* 123, 27-32, 2000.
5. Mann RA et al. *J Bone Joint Surg Am* 61, 232-239, 1979.

MECHANISMS OF PREPARATION FOR TASK SWITCHING IN A FINGER PRESSING TASK

[1]Mitchell A. Tillman and [1]Satyajit S. Ambike

[1]Purdue University, West Lafayette, IN, USA
email: sambike@purdue.edu. web: https://www.purdue.edu/hhs/hk/Biomechanics-MotorBehavior/

INTRODUCTION

Ensuring the stability of motor behavior is crucial for successfully performing steady-state movements. However, when transitions between movement types are expected, maximizing the stability of the current movement will hinder the execution of the transition [1]. We recently demonstrated that in a four-finger, isometric force production task, stability of the total force of the four fingers is reduced solely in response to a cue that creates an expectation of force change in the future [2]. The distribution of the demeaned finger forces obtained from multiple trials changed across a cue condition (shift from the black ellipse to the red ellipse; Fig. 1) that indicated variance reduction along the task-irrelevant directions in the space of finger forces. That is, the nature of the co-variation between the finger forces changed to suit the expected task of changing total force rather than the current goal of maintaining total force. This general preparatory strategy was demonstrated by all young, healthy subjects.

The purpose of this study is to identify if the mean force shifts in response to a cue (black ellipse to blue ellipse; Fig. 1). Such a change would support the notion that, in addition to the change in coordination, subjects restrict the finger forces to a specific set of configurations in the finger-force space that are better suited for rapid changes in the total force. This optimal subspace would depend on neuromechanical properties of the finger muscles, and would likely be subject-specific.

METHODS

Twenty-four healthy subjects (6 male, 20.4±2.5 yrs) participated in the study after providing informed consent. Subjects were seated comfortably in a chair with their forearms resting on top of a table. They placed the distal phalanx of each finger of their dominant hand on one force transducer (Nano-17; ATI Automation). The transducers recorded each finger's downward vertical force at 1000 Hz. Visual feedback on the total force, F_T, was provided via a computer screen placed in front of the subject. F_T was computed as the sum of the vertical downward forces of all fingers ($F_T=\sum F_i$; i=1 to 4).

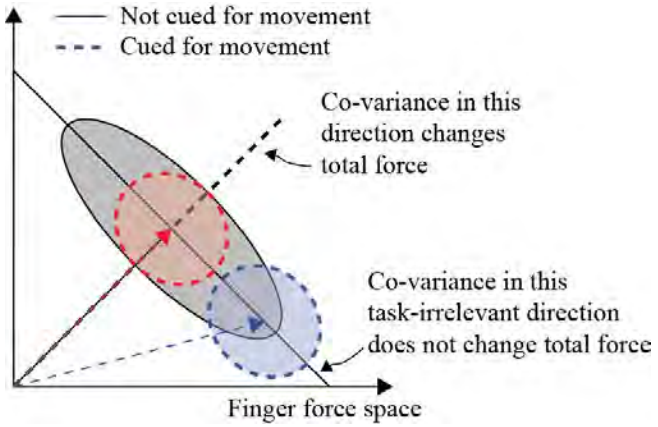

Figure 1: Distribution of demeaned finger forces changes in response to an expectation of movement (from the back to the red ellipse). Does the mean force also shift (black ellipse to blue ellipse)?

Subjects performed 16 trials in two experimental conditions. For the *steady* condition, subjects were instructed to produce a constant total force of 10% maximum voluntary contraction (MVC, measured earlier) for seven seconds. Finger forces from the last one second (6s – 7s) were isolated for analysis. For the *dexterous* condition, subjects tracked a variable target for 30 seconds. The force target moved unpredictably until at some point in every trial it stabilized at 10% MVC and remained there for at least 4 seconds, and then resumed its unpredictable movement. There were eight unique target traces for the dexterous condition, performed in a random order and repeated twice. The stationary portions of each dexterous trial were time-aligned to the first instant of constant force, and the mean of each finger force in the 3s – 4s

window were computed. Note that the current task definition is identical in the analysis window in both conditions, but the subject expects upcoming movement only in the *dexterous* condition. For each subject, the finger forces from the 16 trials of the *steady* and *dexterous* tasks were subjected to paired-sample t-tests. Thus, 96 (4 fingers x 24 subjects) t-tests were conducted. We also computed the mean finger forces across the 16 repetitions for each task, and conducted four (one per finger) paired-sample t tests using data from all subjects.

RESULTS AND DISCUSSION

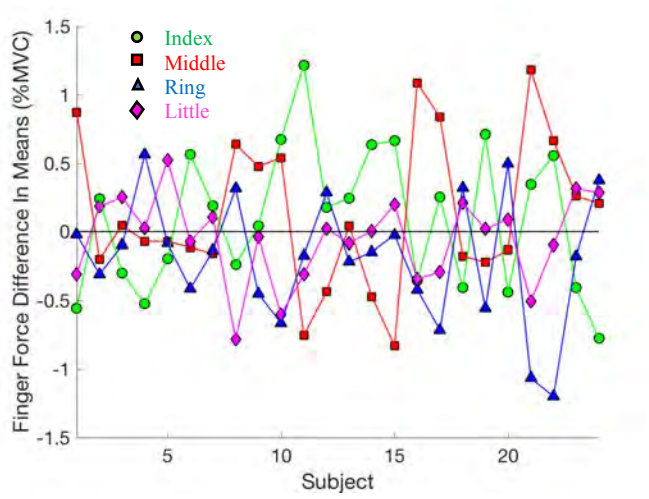

Figure 2: Difference in the mean finger forces for all subjects (n = 24). Means were computed across all trials of one task. Values shown are *steady* task mean force – *dexterous* task mean force for each finger.

Figure 2 shows the difference in the mean forces for all fingers and subjects. The error bars are omitted for clarity. The t tests for each subject consistently yielded differences in mean finger forces. Across conditions, 23/24 subjects significantly changed at least one finger force, 17/24 changed at least two, 8/24 changed at least 3, and 2/24 changed all finger forces ($p<0.05$).

Among only the significant changes in finger forces, the changes in the mean forces of the index and middle fingers ranged between 62% and 95% of their values for the *steady* task. More subjects decreased their index and middle finger forces (9/15 and 8/11, respectively). The change in force for the ring finger ranged between 26% and 89%, and for the little finger ranged between 4% and 81%. More subjects increased their ring finger force (9/15), and 5/9 subjects increased their little finger force.

In contrast to subject-specific comparisons, we did not observe significant changes in the mean finger forces between the two experimental conditions when data were pooled across subjects ($p>0.05$).

Based on these data, we claim that the expectation to change the total force produced by the four fingers prompts a change in the mean forces currently generated by the fingers to stabilize the current total force value. The change in mean is subject-specific. This is consistent with similar findings in adaptive locomotor studies: expectation to change the heading direction during forward locomotion leads to subject-specific changes in posture and gait patterns [3].

CONCLUSIONS

Preparation to transition between motor tasks consists of general and specific strategies. The general strategy is to change the coordination between input elements to suit the upcoming state transition. The specific strategy is to constrain the mean configuration of the input elements to an optimal subspace that is suited for the upcoming state change. In the present experiment, we hypothesize that the locations of these optimal subspaces depend on the impulse-production abilities of the individual fingers. This is a topic of our future research. Quantification of the mechanisms of motor preparation will facilitate the clinical evaluation of aberrant processes underlying deficits in motor transitions and assist in the development of rehabilitative strategies to address manual dexterity issues.

REFERENCES

1. Hasan Z, *J Mot Behav*, 37(6), 484-493, 2005.
2. Tillman and Ambike, *J Neurophysiol*, 119:21-22, 2018.
3. Wu et. al, *Plos One*, 10(7): e0132707, 2015.

ENERGETICS AND LEG STIFFNESS OF HOPPING WITH DIFFERENT EXOSKELETON SPRING STIFFNESS PROFILES IN PARALLEL TO THE LEGS

[1] Stephen P. Allen and [1,2] Alena M. Grabowski

[1] University of Colorado, Boulder, CO, USA; [2] VA Eastern Colorado Healthcare System, Denver, CO, USA
email: stephen.allen-1@colorado.edu

INTRODUCTION

During bouncing gaits such as hopping and running, the biomechanics of the body are well represented by a spring-mass model [1]. When people hop or run on compliant surfaces or with springs in-series to their legs, they adjust their leg stiffness in response to the surface stiffness to maintain invariant total stiffness across a variety of surfaces [1]. Recently, the development of a passive-elastic, full-leg exoskeleton (Exo) has provided the opportunity to study the effects of springs placed in-parallel to the legs during bouncing gaits. Research suggests that humans maintain a constant vertical stiffness by reducing their leg stiffness during hopping to compensate for the addition of springs in parallel to the legs [2]. Further, when hopping with a passive-elastic, full-leg Exo, the net metabolic power (P_{met}) required to hop is reduced by ~24% compared to normal hopping (NH) [2].

Though previous research used a degressive (stiff and then soft) spring stiffness for the in-parallel Exo, it is not clear if this stiffness profile is optimal for reducing the metabolic cost of bouncing gaits. The purpose of this study was to determine the metabolic and biomechanical effects of hopping with a full leg Exo using springs with three different stiffness profiles placed in parallel to the legs. We compared hopping in place with an Exo that had progressive (PG), linear (LN), or degressive (DG) springs stiffness profiles in parallel with the legs to NH (Fig. 1). We hypothesized that: 1) P_{met} for hopping would be lower when using each Exo compared to NH. 2) for a given center of mass displacement, elastic energy return (EE) would vary with each spring stiffness profile (Fig. 1); therefore, reductions in P_{met} would be lowest when using DG springs compared to LN and PG springs. 3) dimensionless vertical stiffness (K) for hopping would be the same when using each Exo compared to NH.

METHODS

10 healthy, active subjects [3F, 7M; Avg.±SD; 25.7±4.3 yrs; 69.1±6.4 kg; 1.73±0.07 m] hopped in place on both feet at 2.4, 2.6, 2.8, and 3.0 Hz to the beat of a metronome during 3 sessions. Subjects hopped in 4 conditions: NH, and using an Exo with DG, LN, and PG springs. Springs with a DG spring rate are stiff during initial compression and become more compliant. Conversely, springs with a PG spring rate are compliant during initial compression and become stiff. Finally, a LN spring rate has constant stiffness throughout compression (Fig. 1). Because DG and PG springs have a variable stiffness, we measured the stiffness of each spring at 10 cm of displacement, as this approximates center of mass displacement at a preferred hopping frequency [3], and was used previously to determine full-leg Exo stiffness [2].

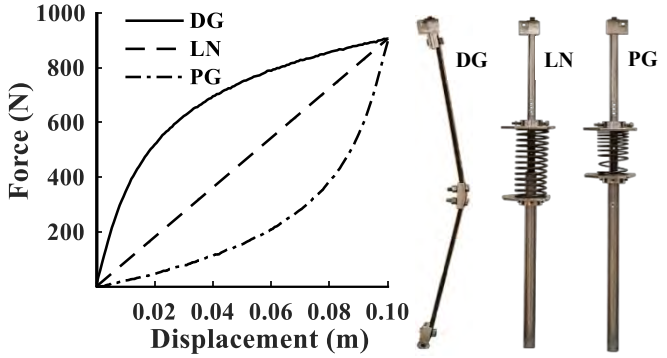

Figure 1: Representative DG, LN, and PG stiffness profiles (Force versus Displacement) for the Exo. The DG profile is created by fiberglass leaf springs, the LN profile is created by linear coil springs with even pitch and the PG profile is created by coil springs with variable pitch.

Each trial was 5 minutes long with 5 minutes rest between trials. We measured rates of oxygen consumption and carbon dioxide production (TrueOne 2400, Parvo, Sandy, UT) throughout each trial. We calculated P_{met} from the average of the last 2 minutes with a standard equation [4] and normalized to body mass. Subjects hopped on a force plate (Bertec, Columbus, OH, 1000 Hz), and ground

reaction forces were analyzed with a custom Matlab (Mathworks) code. We used center of mass displacement (ΔL) to approximate the compression of the legs and springs. Then, we matched ΔL to the corresponding force from the force-displacement curves attained from a materials testing machine (Instron Series 5859) to estimate *EE* from each Exo. We compared *K* across subjects by normalizing the peak vertical ground reaction force (F_{peak}) to bodyweight (*BW*), and ΔL to leg length (*l*) (Eq. 1):

$$K = (F_{peak}/BW) / (\Delta L/l) \quad (1)$$

We used a repeated measures ANOVA at each frequency to test for differences in P_{met} across all conditions, with Tukey HSD for pairwise comparisons when applicable. To test for differences in *K* between NH and Exo conditions, we used paired t-tests with a Bonferonni correction (p=0.0167).

RESULTS AND DISCUSSION

1 outlier (>3SD from the mean of *K*) was removed from analyses at 2.4 Hz. Compared to NH, use of the Exo with DG and LN springs decreased P_{met} across all frequencies by 12-24% and 4-11%, respectively, but use of the Exo with PG springs increased P_{met} by 5-9% at 2.4-2.8 Hz (Fig 2).

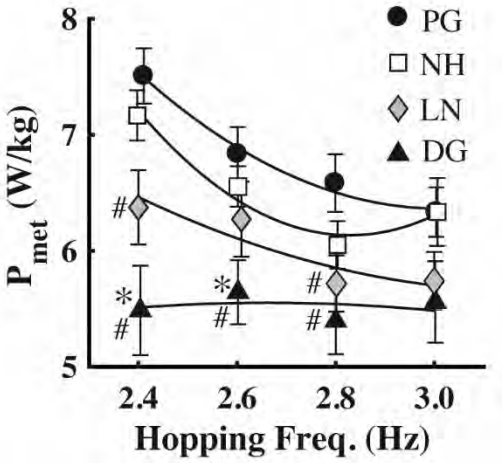

Figure 2: Avg ± SE net metabolic power (P_{met}) at average hopping frequencies. * indicates significantly different from NH. # indicates significantly different from the PG Exo.

K was the same across all conditions at each frequency except at 2.8 Hz, where *K* was 5% lower when using the Exo with DG and LN springs compared to NH (p<0.007; Table 1). *EE* for the Exo with DG, LN, and PG springs accounted for 65-74%, 37-51%, and 12-24% of total *EE* across all frequencies, respectively (p<0.001; Table 1).

We reject our first hypothesis, because not all spring stiffness profiles reduced P_{met} compared to NH. We partially accept our second hypothesis, because P_{met} for DG was lower than PG, but not LN despite large differences in *EE*. Finally, we accept our third hypothesis because *K* is invariant despite hopping with different spring stiffness profiles.

Table 1: Avg ± SD dimensionless stiffness (*K*) and elastic energy return (*EE)* in Nm at each hopping frequency. * indicates significantly different from NH, # from PG, ^ from LN, † from DG.

		Hopping Freq (Hz)			
		2.4	**2.6**	**2.8**	**3.0**
K	**NH**	27 ± 4	31 ± 4	36 ± 3	41 ± 4
	DG	24 ± 2	29 ± 3	34 ± 4*	40 ± 4
	LN	24 ± 2	32 ± 6	34 ± 4*	39 ± 4
	PG	26 ± 2	32 ± 4	35 ± 3	40 ± 3
EE	**NH**	-	-	-	-
	DG	59 ± 9#^	53 ± 10#^	43 ± 8#^	36 ± 6#^
	LN	44 ± 6#†	37 ± 7#†	27 ± 5#†	21 ± 4#†
	PG	21 ± 1^†	17 ± 2^†	10 ± 2^†	7 ± 1^†

In agreement with a previous study [2] that measured P_{met} while hopping at 2.0-2.6 Hz, hopping with springs in parallel to the legs reduces P_{met} at multiple frequencies, and DG spring stiffness profiles elicit the greatest metabolic reduction. We showed that PG stiffness profiles provided 12-24% *EE*, but increased P_{met} by 5-12%. This metabolic response is similar to hopping with added mass equivalent to that of the exoskeleton (~8% of body weight; [5]), suggesting that *EE* returned by the springs is not enough to offset the weight of the PG exoskeleton. Future exoskeletons utilizing springs to assist bouncing gaits should consider DG spring stiffness profiles, and not PG spring stiffness profiles. We also found *K* to be invariant between nearly all Exo conditions and NH. Humans maintain vertical stiffness in bouncing gaits despite changes to in-series or in-parallel stiffness [1,2]. Given that overall vertical stiffness depends on the torsional stiffness of the joints, future studies should examine changes in joint stiffness and joint mechanics while hopping with different spring stiffness profiles in-parallel to further understand how humans maintain constant vertical stiffness.

REFERENCES

1. Ferris and Farley. *J App Physiol*. **82**, 1997
2. Grabowski and Herr. *J Appl Physiol* **107**, 2009
3. Farley et al. *J App Physiol.* **85**, 1998
4. Brockway. *Hum Nutr Clin Nutr* **41**, 1987
5. Allen and Grabowski. *41st ASB [Abstract]*, 2017

COMPARISON OF MACHINE LEARNING ALGORITHMS FOR ACTIVITY CLASSIFICATION USING EMG

[1,2] Anthony Anderson, [1,2] Evan Schuster, [1,2] Andrea Willson, and [1,2] Patrick Aubin

[1] Department of Mechanical Engineering, University of Washington, Seattle, WA, USA
[2] VA Puget Sound RR&D Center for Limb Loss and MoBility (CLiMB), Seattle, WA, USA
email: ajanders@uw.edu, web: http://faculty.washington.edu/paubin/wordpress/

INTRODUCTION

Abundant wearable sensor data and advances in machine learning algorithms have made activity classification a viable technique for biomechanical studies. Research groups have used different classification algorithms to predict gait activities using lower-limb electromyography (EMG), but few studies have compared the effectiveness of common classification algorithms [1, 2]. The purpose of this experiment was to evaluate the predictive performance of four commonly used pattern recognition algorithms on a labeled EMG dataset of six mobility tasks of daily living.

METHODS

With approval from the VA Puget Sound Health Care System's IRB, EMG data was recorded for two subjects (male, age 24-27, height 5'10"-6'2") at the VA Center for Limb Loss and Mobility. For each subject, 16 EMG sensors (Delsys Inc., Natick MA) were placed on the right leg and lower abdomen. Ten of the sensors were placed on leg muscles commonly measured in EMG studies. These muscle locations were found via palpations and references to anatomical landmarks. The six remaining sensors were placed pseudo-randomly, without isolating specific muscles (Table 1). All sensors wirelessly streamed data to a desktop PC at 1200 Hz for the duration of the study. For both subjects, 150 trials lasting three seconds were recorded while the subject performed each of the following activities: standing, sitting, walking at a self-selected pace, walking at 175% of the self-selected pace, stair ascent, and stair descent.

Using MATLAB (MathWorks, Natick MA), each three-second recording was separated into 0.15-second windows. Each window contained signals from all 16 sensors and was labeled as one of the six activities. The following five features were then extracted for each sensor over each of the 0.15-second snapshots: mean average value, number of zero crossings, variance, number of slope sign changes, and waveform length. These five features across 16 sensors resulted in an 80-dimensional feature vector for each window.

The data was then randomly split into a training set (80% of data) and a testing set (20% of data). The training data was reduced via SVD to a collection of 40-dimensional feature vectors that retained 99% of the variance in the initial feature set. These labeled vectors were then used to train the following classification algorithms: a random forest (RF) with 40 decision trees, a linear support vector machine (SVM), linear discriminant analysis (LDA), and an artificial neural network (ANN) with 100 neurons in a single hidden layer. Each classifier was then tested on its ability to accurately predict the activities in the testing dataset.

This train-test process was repeated ten times with a different random 80-20 cut of the initial dataset each time. The classifiers were trained on an individual basis, i.e. trained with participant 1's data and tested with participant 1's data, as well as on a group basis where the classifiers were both trained and tested with both participants' data.

To determine how classification accuracy was impacted by removing sensors from the initial dataset, a backward-selection algorithm was implemented for each classifier. All classifiers were trained fifteen times, each time with a different sensor removed from the training and testing sets. The sensor that reduced the classifier accuracy by the least amount was then permanently removed from the set. This process was repeated until only one

sensor remained. Feature vectors were cast into SVD bases but were not truncated as before. This resulted in higher classification accuracies but substantially longer training times for the backward-selection algorithm.

RESULTS AND DISCUSSION

All the classifiers predicted the activities with high accuracy (>80%) (Figure 1). The classifier with the highest accuracy when trained and tested with data from both participants was the ANN at 94.95 ± 0.01%. In each case, classifiers trained and tested on Participant 2 outperformed the same classifiers trained and tested on Participant 1.

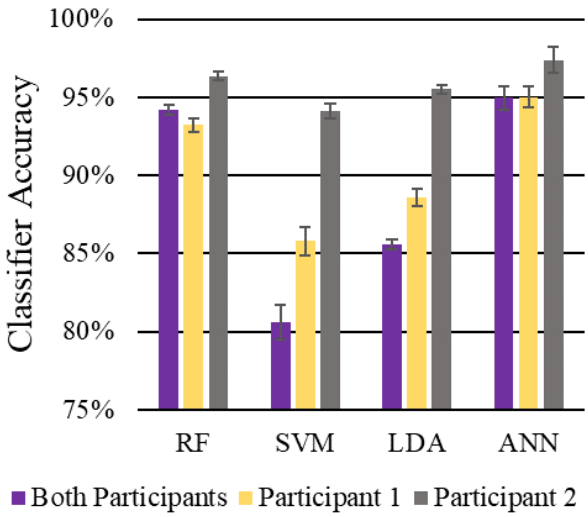

Figure 1: Mean classifier accuracies when trained on individual and combined subject data with all sensors. Each bar shows the mean of ten test-train cycles.

All classifiers decreased in accuracy when trained and tested on both participants except for RF. This may imply that the RF classifier is more generalizable between subjects within a population. While the accuracy of the ANN was slightly greater than the RF, the backward-selection algorithm showed the RF to be superior, as it could achieve over 90% accuracy with only the Tibialis Anterior and Posterior Mid Shank sensors. The ANN required seven sensors to reach a comparable classification accuracy (Figure 2).

The backward-selection algorithm also revealed that the classifiers did not rely exclusively on the sensors placed on muscle bellies but used information from the nonconventional sensor placements as well.

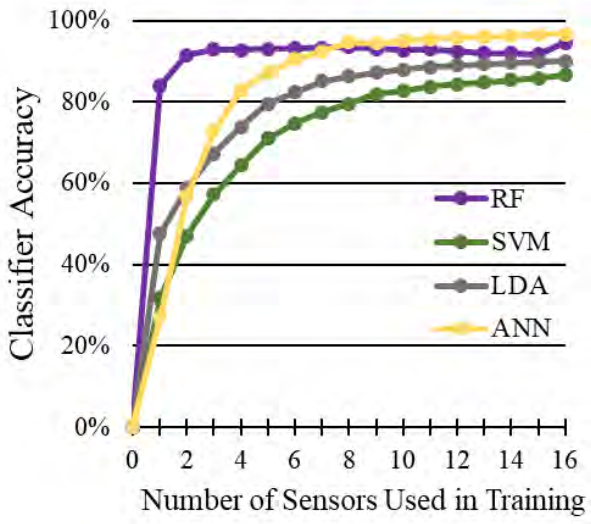

Figure 2: Classification accuracy for both participants as a function of number of sensors used to train the classifier.

These techniques could also be applied with sensors other than EMG, including IMUs, footswitches, heart-rate monitors, or a combination of sensor types to improve classifier accuracy. These results can inform future studies on supervisory prosthetic limb control or monitoring patient activity outside of the laboratory environment.

REFERENCES

1. Hargrove et al. *IEEE Transactions on Biomedical Engineering*. **56**(5). 2009.
2. Huang et al. *IEEE Transactions on Biomedical Engineering*. **58**(10). 2011.

Table 1: Sensor locations. Sensors with yellow shading were placed without regard to muscle location.

Sensor	1	2	3	4	5	6	7	8
Location	Tibialis Anterior	Posterior Mid Shank	Soleus	Medial Gastroc.	Vastus Medialis	Rectus Femoris	Bicep. Femoris L.H.	Fibularis Longus
Sensor	9	10	11	12	13	14	15	16
Location	Distal Tibialis Anterior	Bottom of Foot	Vastus Lateralis	Adductor Magnus	Superior Lateral Hamstring	External Abdominal Oblique	Tensor Fasciae Latae	Distal Vastus Lateralis

VERTICAL GROUND REACTION FORCES AND LOADING RATES WHEN RUNNING WITH RUNNING-SPECIFIC AND DAILY USE PROSTHESES

[1] Brian S. Baum, [2] Lauren A. Sepp; [1] Erika Nelson-Wong, and [2] Anne K. Silverman

[1] School of Physical Therapy, Regis University, Denver, CO, USA
[2] Department of Mechanical Engineering, Colorado School of Mines, Golden, CO, USA
email: bbaum@regis.edu

INTRODUCTION

High ground reaction forces (GRFs) and loading rates during running have been linked to overuse injuries [1-3]. GRFs and loading rates typically increase with running speed [4] suggesting that running faster increases the risk of these injuries. Running after amputation induces asymmetries that alter limb loading. Individuals with unilateral transtibial amputations using running-specific prostheses (RSPs) generate greater loading rates in their intact limbs than runners without an amputation, suggesting greater intact limb reliance and injury risk [3]. RSPs are not typically covered by insurance, introducing a financial barrier to running for exercise. Consequently, those without RSPs must run using their daily use (DU) prosthesis. However, loading rates while running with DU prostheses have not been investigated, so our knowledge of the injury risk potential when using these devices is limited.

Therefore, the purpose of this study was to determine how running with RSPs and DU prostheses affect GRFs and loading rates. We hypothesized that (1) GRFs and loading rates would increase with speed, (2) intact limb peak GRFs, average GRFs, and loading rates would be greatest when running in the DU prostheses followed by running in RSPs, and then control limbs; and (3) prosthetic limb peak GRFs, average GRFs, and loading rates would be greatest when running in the DU prostheses and control limb values would be greater than the prosthetic limb when running in RSPs.

METHODS

Seven healthy participants (5F, 2M, average age 31.0±8.0 years, height 1.71±0.04 m, and mass 64.5±8.3 kg) with unilateral transtibial amputation (TTA) ran with their own prescribed RSP and DU prostheses. Five healthy control participants (3F, 2M, average age 25.6±5.1 years, height 1.69±0.08 m, and mass 68.2±4.6 kg) also completed the experimental protocol.

Participants ran at six speeds (2.5, 3.0, 3.5, 4.0, 5.0, and 6.0 m/s) on an instrumented treadmill (Bertec, Columbus, OH) that collected GRF data at 2000 Hz. GRF data were filtered using a 4th order, low pass Butterworth filter with a cutoff of 30 Hz. Peak and average vertical GRFs were calculated from the stance phase data. Vertical average loading rates (VALR) were calculated for 20%-80% of the duration prior to the vertical impact peak [3].

Average and peak GRFs and loading rates were entered into a 2x2x6 (Group x Leg x Speed) repeated-measures ANOVA. When significant differences were identified from the full factorial model, pairwise comparisons with Bonferroni adjustments were performed. A significance level of α=0.05 was used for all statistical tests.

RESULTS AND DISCUSSION

Hypothesis 1 was supported as peak vertical GRFs, average vertical GRFs, and loading rates increased with running speed for all limb conditions ($P \leq 0.05$, Figs. 1A-C). This confirms observations from prior studies [3-4] and indicates that loads applied to the limbs increase with running speed and faster running may increase injury risk.

Intact limbs generated greater average GRFs and loading rates ($P<0.05$) in the RSP condition compared to control limbs, supporting our second hypothesis ($P<0.05$, Figs. 1A-C). When wearing DU prostheses, the intact limb generated greater

GRFs and loading rates than control limbs only at faster running speeds (5.0-6.0 m/s). These data support the idea that the intact limb may be overloaded and at greater injury risk when running with any prosthesis at faster speeds, but running with DU prostheses may not place the intact limb at greater risk at slower running speeds. Intact limb loading when running with DU prostheses was less than or equal to intact limb loading when running with RSPs, and thus hypothesis 2 was not supported.

Prosthetic limbs generated lower peak and average GRFs and loading rates in the RSP condition compared to control limbs, supporting our third hypothesis (P<0.05, Figs. 1A-C). The prosthetic limb joints may therefore be at reduced risk of injury when running with RSPs. The DU prosthetic limb generated greater loading rates compared to the prosthetic limb when running with RSPs (P<0.05), but peak and average GRFs were similar. Thus hypothesis 3 was only partially supported. The loading rate data suggest greater loading on the prosthetic limb and greater potential for injury risk in this limb when running with DU prostheses. However, DU prosthetic limb loads were less than control limbs at all speeds except for peak GRFs at the top running speeds. This supports that running with DU prostheses does not place undue loading on the prosthetic limb, so the risk of injury may not be higher compared to runners without an amputation.

CONCLUSIONS

Loading rates and peak and average vertical GRFs increase with running speed for all runners, which suggests injury risks are greater with faster running. Running with DU prostheses places similar loads on the limbs as running with RSPs. Intact limbs may have greater injury risk when running with RSPs at any speed or DU prostheses at faster speeds compared to uninjured runners. Overall, running at slower speeds (jogging, exercise, etc.) with DU prostheses does not appear to place the prosthetic or intact limb at greater risk of injury.

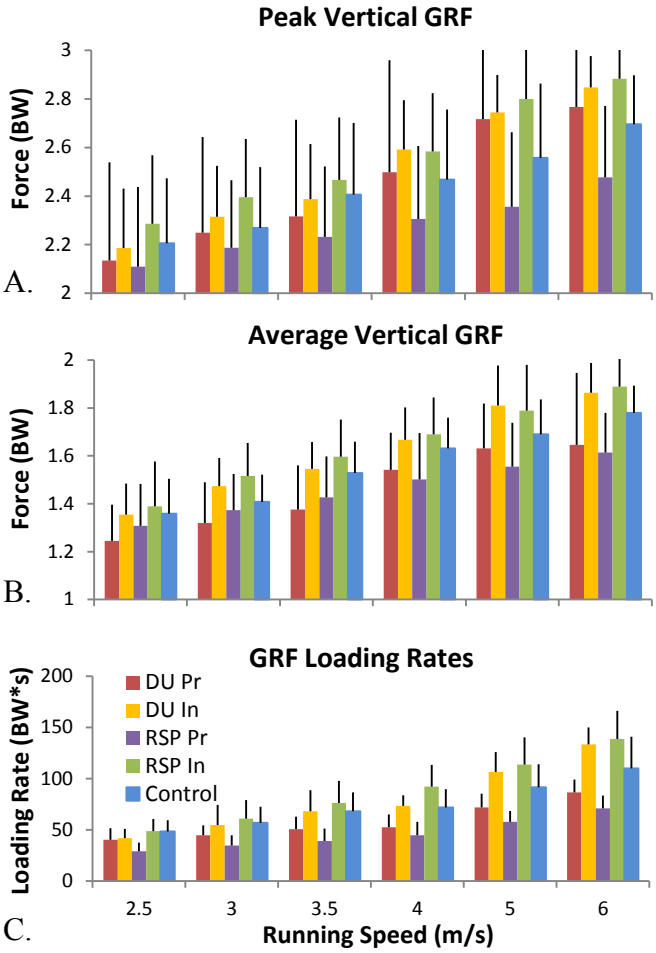

Figure 1: (A) Peak vertical GRF, (B) average vertical GRF, and (C) vertical average loading rates for each limb condition across running speeds. Error bars represent +1SD. BW=times body weight, DU=daily use prosthesis, RSP=running-specific prosthesis, Pr=prosthetic limb, In=intact limb, Control=control limbs.

REFERENCES

1. Zadpoor AA et al. *Clin Biomech*, **26**, 21-28, 2011.
2. Milner CE et al. *Med Sci Sports Exerc*, **38**, 323-328, 2006.
3. Hobara H, et al. *Gait Posture*, **39**, 386-390, 2014.
4. Munro CF et al. *J Biomech*, **20**, 147-155, 1987.

ACKNOWLEDGEMENTS

Funding and support for this study was provided by DoD grant #W81XWH-15-1-0518 and the Regis University Research and Scholarship Council.

AN ANKLE-FOOT ORTHOSIS IMMEDIATELY IMPROVES WALKING PERFORMANCE IN PATIENTS WITH PERIPHERAL ARTERY DISEASE

[1]Blake Beier, [1]Ben Senderling, [2,3] Holly DeSpiegelaere, [1]Mahdi Hassan, [2,3]Iraklis Pipinos, [2,3]Jason Johanning, [1,3]Sara Myers;

[1] The University of Nebraska at Omaha, Omaha, NE, USA
[2]University of Nebraska Medical Center, Omaha, NE, USA
[3]Omaha VA Medical Center, Omaha, NE, USA
email: bbeier@unomaha.edu, web: cobre.unomaha.edu

INTRODUCTION

Peripheral artery disease (PAD) is a common cardiovascular disease manifesting from atherosclerotic blockages in the arteries of the legs. The most prevalent symptom of PAD is intermittent claudication, defined as a cramping-like pain in the legs that is produced by physical activity and is relieved only through rest. Our research has documented significant deficits in gait; specifically, an inability of the ankle plantarflexors to generate normal torque and power [1]. There is a critical treatment gap for individuals whose disease presentations warrant a non-operative treatment plan but lack the motivation, time, access, and monetary resources for supervised exercise therapy. Using an ankle-foot orthosis (AFO) to offset ankle plantarflexor torque and power deficiency is a novel approach to increase the walking distances and physical activity levels in those with PAD.

Carbon-composite material AFOs exhibit spring-like properties, allowing energy storage at weight acceptance and return at the point of toe-off, when ankle plantarflexors propel into the next step. While AFOs have been shown to improve ankle kinetics and angular momentum in stroke patients, they have never been implemented in patients with PAD to improve forward propulsion [2]. This study investigated the effects of walking with an AFO on walking distance, ankle plantarflexor torque, and hip extensor torque in patients with PAD.

METHODS

Four male patients with PAD (Age: 66.0 ± 10.9 years; Body Mass: 84.3 ± 17.1 kg) completed testing of initial and absolute claudication distances while walking with and without an AFO. Using an instrumented treadmill, starting at 0% grade with a set speed of 2.0 mph, patients completed a progressive-load treadmill test. Every two minutes, the grade increased by 2%, up to a maximum of 15% grade. The first indication of claudication pain was recorded as initial claudication distance (ICD), while the total distance the patients could walk before stopping due to pain was the absolute claudication distance (ACD). Two patients walk first with the AFO, while the other two walked first without the AFO to counterbalance a potential fatigue effect.

To test the AFO's effect on ankle and hip torque, the same patients completed overground walking with and without an AFO. Using a twelve camera high speed digital motion capture system (Cortex 5.1, Motion Analysis Corp) and eight in-ground AMTI force platforms, three dimensional kinematics (60 Hz) and kinetics (ground reaction forces, 600 Hz) were collected while subjects walked with their self-selected pace through a ten-meter walkway. Reflective markers were placed at specific anatomical landmarks on the lower limbs. Joint torques were calculated using inverse dynamics for the hip and ankle during the stance phase of walking. Peak torque was calculated for the ankle at the end of the stance phase, and hip extensor torque was calculated from early stance in each trial.

RESULTS AND DISCUSSION

On average, the initial claudication distance was 140.1 ± 72.5 meters while walking without the AFO and 183.5 ± 121.2 meters while walking with the AFO (Figure 1). The average absolute claudication distance was 366.0 ± 118.3 meters without the AFO and 492.3 ± 66.8 meters with the AFO (Figure 1).

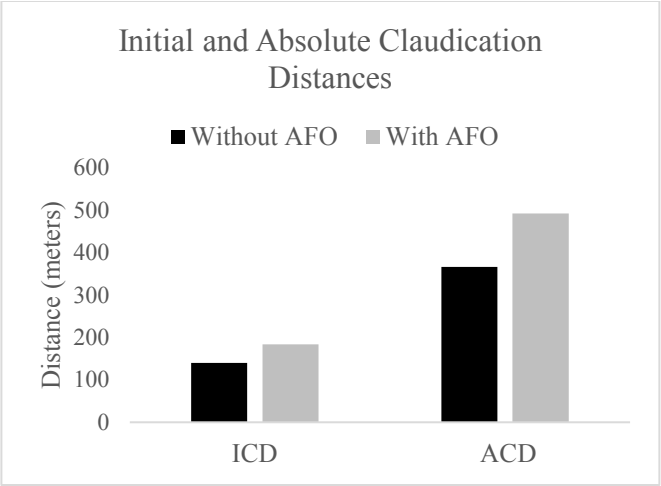

Figure 1: Initial (ICD) and absolute claudication distances (ACD) improve in patients with PAD when walking with an AFO.

Results from overground walking show that the ankle plantar flexor muscles contributed less torque while walking with the AFO, as the ankle plantarflexor torque decreased while wearing the AFO (Figure 2; 1.28 ± 0.14 Nm/kg without the AFO, and 1.22 ± 0.12 Nm/kg with the AFO). This decrease in ankle plantarflexor torque but maintenance of the overall torque profile (data not presented) is in line with previous studies of older individuals and patients with neuromuscular diseases [3]. This shift in torque production from biological muscles to the AFO is known as the substitution paradigm. Lowering the muscular demand slightly in each step likely reduces the ischemia by decreasing the demand for blood flow during walking. The AFO also helps to compensate for myopathy-related muscle weakness found in patients with PAD by providing propulsion torque at the end of stance.

Hip extensor torque increased when walking with the AFO (Figure 2; 0.602 ± 0.12 Nm/kg without the AFO, and 0.621 ± 0.12 Nm/kg with the AFO). This is consistent with the redistribution of torque from the ankle to the hip seen in healthy older individuals [4] and likely contributes to the overall increase in walking distances when wearing the AFO. Additional future studies will examine how the increased hip extensor torque contribute to increases in walking distances.

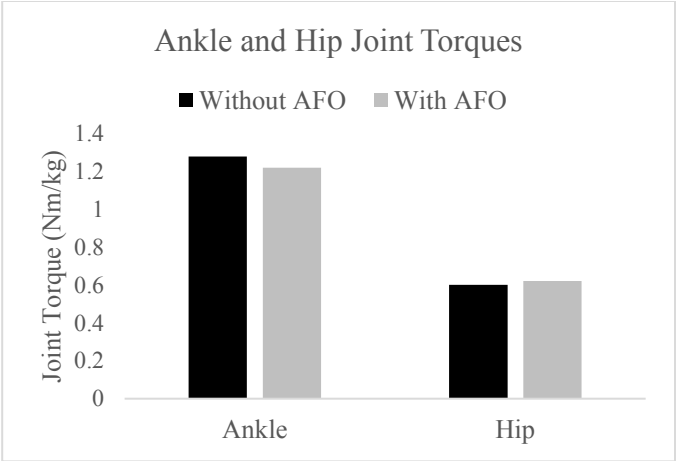

Figure 2: Wearing the AFO resulted in a decrease in ankle plantarflexor torque contribution during late stance, while increasing hip extensor torque during early stance.

CONCLUSIONS

AFOs are simple exoskeletons that are easily adjustable, affordable, and available to immediately be prescribed and worn by patients with PAD. An AFO is ideal for patients whose disease presentation warrants a conservative approach. These preliminary results show that increases in initial and absolute claudication distances while wearing an AFO are comparable to those seen after pharmacotherapy for six months [5]. Future studies should address how AFO use impacts muscle strength and activation, muscle oxygenation, and physical activity levels in patients with PAD.

REFERENCES

1. Wurdeman et al. *Gait Posture*, 2012 Jul; **36(3)**, pp. 506-509.
2. Danielsson et al. *Journal of Rehabilitation Medicine*, **vol. 36(4)**, 2004, pp. 165–168.
3. Bregman et al. *Prosthetics and Orthotics In,* **vol. 34(3),** 2010, PP. 293-304.
4. Devita et al. *Journal of Applied Physiology*, **vol. 88(5),** 2000, pp. 1804–1811.
5. Thompson et al. *The American Journal of Cardiology,* **vol. 90(12)**, 2002, pp. 1314-1319.

ACKNOWLEDGEMENTS

This work was funded by 1R01HD090333-01, 1R01AG049868, and 5U54GM15458.

A COMPARATIVE EVALUATION OF DIFFERENT WEARABLE DEVICES ON LOWER EXTREMITY KINEMATICS IN UPRIGHT KNEELING WHILE ON A ROOF

[1]Scott P. Breloff, [1]Erik W. Sinsel, [1]Christopher M. Warren, [1]Robert E. Carey, [2]Fei Dai, [2]Amrita Dutta, & [1]John Z. Wu

[1] National Institute for Occupation Safety & Health, Morgantown, WV, USA
[2] West Virginia University, Morgantown, WV, USA
email: sbreloff@cdc.gov, web: https://www.cdc.gov/niosh/

INTRODUCTION

Due to the unique work environment (sloped rooftops), roofers spend more than 75% of their working time in crawling, squatting, stooping, and kneeling posture. The cumulative effects of these awkward postures, combined with repetitive motions, may not only lead to low back pain, but also can increase the musculoskeletal loading in the lower extremity – factors leading to the initiation and development of osteoarthritis [1,2]. Because of this, roofers have the second highest incident rate of work-related musculoskeletal disorders (MSDs) among all construction sectors [3] and most of these MSDs are observed in the lower back and lower extremity [4].

When roofers are burdened with MSDs, they face work limitation, missed work, and/or reduced physical functioning, leading to premature departure from the workforce [5-6]. While numerous studies and protective wearable interventions exist to reduce musculoskeletal injury risk for construction workers, very few, if any, exist specifically for roofers. The purpose of this study was to determine if a third party device—designed to reduce MSD risk, within other occupations—is able to reduce MSD risk in a roofing environment.

METHODS

Nine male participants (height: 180.6±6.1cm, weight: 99.7±27.6kg, age: 26.1±5.6years)—with no roofing experience—participated in the study. All subjects were male, as 97% of roofers are male; and they were healthy and did not have any musculoskeletal or neurological disorders which would influence the outcome of the study. The test protocol was approved by the National Institute for Occupational Safety & Health's (NIOSH) Institutional Review Board (IRB) and subjects read and completed the informed consent.

Participants came to the NIOSH biomechanics laboratory for one testing day. Subjects changed into tight fitting clothing and were outfitted with 82 retro-reflective motion capture markers (9 mm diameter). Kinematic motion data were collected using 14 MX Vicon cameras (Oxford, England) at a sampling rate of 100 Hz. In a random order, subjects completed five trials of each of the 12 tasks on a roof simulator (Fig. 1).

Figure 1. Roofer simulator at three different pitches (from left to right: 0^0, 15^0, & 30^0).

The roof simulator had three different angles (0^0, 15^0, and 30^0) and four different intervention combinations (no wearable assist device [NO], knee pads only [KP], knee savers only [KS], and both knee pads and knee savers [BO]), resulting in 12 combinations. Subjects knelt in an upright static posture and data were collected for 5 seconds after the subject was set and comfortable in that posture (Fig 2).

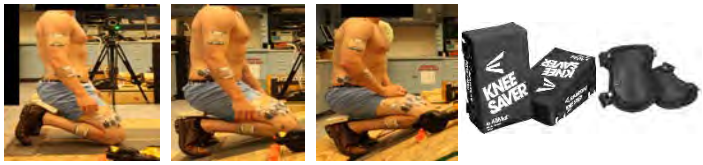

Figure 2. Left: Subject in upright posture at three different pitches on roofing simulator (from left to right: 0^0, 15^0, & 30^0). Right: Knee Pads and Knee Savers used in the study.

This posture was selected because it allowed interaction with the knee saver intervention. In a working posture, the knee flexion decreased and the thigh did not contact the shank. This was essentially described as a 'resting' posture roofers would take when not affixing shingles to the roof.

The kinematics of the lower extremity—ankle, knee, and hip—were analyzed with a two-way—4(intervention) X 3(slope)—repeated measure analysis of variance (ANOVA). Data analysis was completed using SPSS v22 and *p*-values were set to 0.05.

RESULTS AND DISCUSSION

The only measure that was statistically significant due to the various intervention and slope combinations was flexion—or sagittal plane—kinematics (Fig. 3; Table 1). There was a main effect of slope ($p \leq 0.001$) on ankle dorsiflexion. Ankle dorsiflexion on the zero degree surface ($43.37^0 \pm 4.76^0$) was significantly less than the fifteen degree ($64.58^0 \pm 3.55^0$) and thirty degree ($77.13^0 \pm 1.38^0$) sloped surface. Ankle dorsiflexion on the fifteen degree slope ($64.58^0 \pm 3.55^0$) was significantly less than the thirty degree ($77.13^0 \pm 1.38^0$) sloped surface. There was a main effect of intervention ($p \leq 0.001$) on knee flexion. Knee flexion with NO ($145.10^0 \pm 1.41^0$) was significantly larger than KS ($140.25^0 \pm 1.24^0$) and BO ($140.20^0 \pm 1.57^0$).

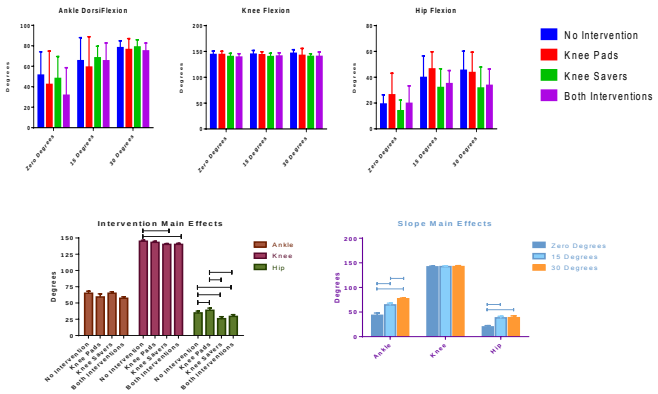

Figure 3. Top: Lower extremity flexion during multiple roofing slopes and interventions. Bottom: Intervention and slope main effects.

There was an interaction effect ($p=0.046$) on the hip and both main effects, slope ($p \leq 0.001$), and intervention ($p \leq 0.001$), were significant. Hip flexion on the zero degree surface ($19.83^0 \pm 2.54^0$) was significantly less than the fifteen degree ($38.32^0 \pm 3.16^0$) and thirty degree ($38.59^0 \pm 3.69^0$) sloped surface. The flexion of the hip with NO ($34.82^0 \pm 2.79^0$) was significantly smaller than KP ($38.81^0 \pm 3.40^0$), but significantly larger than KS ($25.89^0 \pm 3.05^0$) and BO ($29.47^0 \pm 2.59^0$). Hip flexion while using KP ($38.81^0 \pm 3.40^0$) was significantly larger than KS ($25.89^0 \pm 3.05^0$) and BO ($29.47^0 \pm 2.59^0$).

This study demonstrates that the introduction of sloped surfaces induces postural changes—particularly in the sagittal plane—of a kneeling roofer that prompts an awkward posture, which may lead to increased MSD risk [1-4]. A positive result from the current study is that the introduction of knee savers was able to reduce the extreme posture during the resting position of the roofers.

One limitation of the current study is the subjects are not experienced roofers. It is unclear if an individual with experience working on a sloped surface would have different kinematics than a novice.

CONCLUSIONS

The knee savers— despite not designed for use on a sloped surface—were able to stimulate a more neutral posture in the knee and hip. Although it was promising that current wearable devices are effective, the current models that we tested might not alter posture enough to have a clinical effect on MSD risk in roofers. Therefore, this project was a strong first step in roofer specific wearables for reducing MSD risks; a future project will focus on optimizing a knee saver for roofing specific activities.

REFERENCES

1. Wang et al. *Proceedings of Construction Specialty Conf.*, USA, 2015.
2. Wang et al. *Con. Eng.* 143(7), 2017.
3. BLS, *IIF*, 2013.
4. Holmstrom and Engholm. *A.J. Ind. Med.* 44(4), 2003.
5. Welch et al. *Scn. J. Wk, Env Hel*. 56-63, 2009
6. Welch et al. *A.J. Ind. Med*. 53(6), 200

DISCLAIMER

The findings and conclusions in this report are those of the authors and do not necessarily represent the official position of the National Institute for Occupational Safety and Health, Centers for Disease Control and Prevention

Table 1: Depicts statistical significance ($p \leq 0.05$) changes in flexion based on the various testing conditions. † indicates statistical significant interaction, ‡ is statistical significant slope main effect, and ǂ is a statistical significant intervention main effect.

		Interaction	Main Effect Slope	Main Effect Intervention
Flexion	Ankle		‡	
	Knee			ǂ
	Hip	†	‡	ǂ

How does touch influence postural stability of single leg stance?

[1]Megan Cabrales, [1]Becca Koppel, [1]Samuel Cauble, [1]Christopher Foster and [1]Rahul Soangra

[1] Department of Physical Therapy, Crean College of Health and Behavioral Sciences, Chapman University, Orange, CA, USA
email: soangra@chapman.edu, web: https://www.chapman.edu/our-faculty/rahul-soangra

INTRODUCTION

Single leg balance plays an important role in its clinical significance to patient recovery especially with functional performance and with activities of daily living. Clinically, it is used as a predictor of fall risk and injury prevention (Vellas et al., 1997). Touch (proprioceptive input) has been proven to be as effective as visual input at improving postural stability, suggesting that even light touch can have significant effects on balance (Riley et al., 1997). The benefits of touch are not due to mechanical support, but rather, sensory cue inputs from the fingertips (Kouzaki et al., 2008). It has been documented that light finger contact on a stationary surface could reduce postural sway in standing up to 50% (Krishnamoorthy, 2002), even though the touch force is much lower than what is required for physical support (Chen, 2015). The supplemental sensory information comes from the large density of cutaneous mechanoreceptors that go along with the kinesthetic receptors to provide information about the arm position (Baldan et al., 2014). This suggests that in addition to touch on stable surfaces, holding an object may provide enough sensory input to facilitate balance.

We hypothesize that holding the object will improve measures of postural stability when compared to balancing with no support, but will be less useful than touch on stable or unstable surfaces. In this experiment, we investigate whether holding onto an object in open chain can improve balance as much as placing a finger on a stable or unstable object resting on the ground and compare them with eyes closed to eyes open.

METHODS

Four participants were recruited in this study. Participant ages ranged from 23-26, and all participants were healthy with no neuromuscular or balance problems. The protocol for this study was approved by Chapman University Institutional Review Board (IRB#1718H020). All participants provided written informed consent prior to the experiment. All trials were performed without shoes and in single leg stance on the non-dominant (stance) leg, which was the left leg for all the participants.

Participants balanced for 60 seconds on their stance leg with i) an empty hand, ii) holding a stress ball (weighing 0.149 kg), iii) with a finger placed on the handle of a cane (weighing 0.910 kg; SPC – "single point cane" trials), and iv) with a finger placed on the back of a chair measuring 86 cm tall (for trials involving a stable object). Each of these four conditions were performed with eyes open and eyes closed. The right arm was maintained at 90 degrees in each trial for consistency. Participants were rested for 3 minutes after each trial.

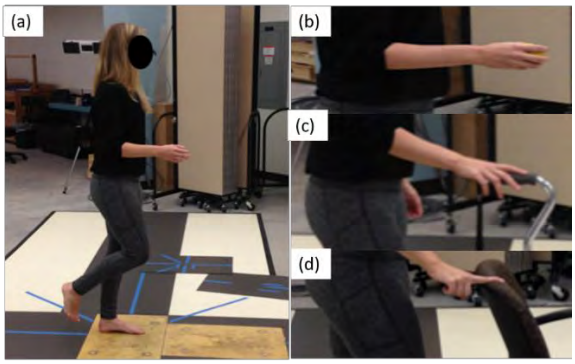

Figure 1 a) Arm at 90 degrees (Control); b) holding a stress ball c) Light touch on single point cane (d) Light-touch on a chair

A 40cm by 60cm Bertec force plate (BP4060, Bertec, Columbus, OH 43229 USA) was used with Motion Analysis Cortex software to measure center of pressure (COP) displacement over 60 seconds of participants balancing in single leg stance.

RESULTS AND DISCUSSION

We found that medio-lateral sway ranges were significantly different for eyes open versus eyes

closed condition.

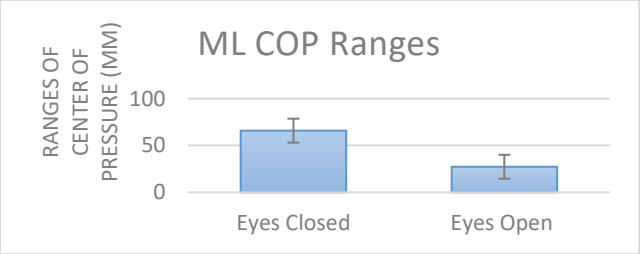

Figure 2: ML COP ranges in eyes open and eyes closed condition

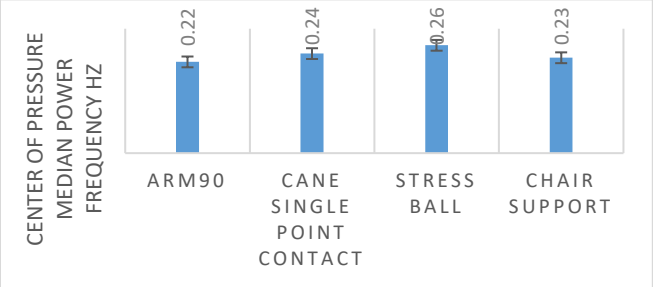

Figure 3: Median power sway frequency

Table 1: Tukey's HSD for Median power Frequency

	Tukey's HSD	Median power Sway Frequency
Stress Ball	A	0.26
Cane Single point contact	AB	0.24
Chair support	AB	0.23
Arm 90	B	0.22

We also found interaction effects between eyes open/close condition and 4 different conditions of touch for sway length.

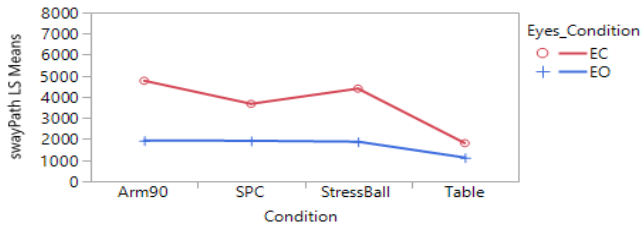

Figure 4: Sway path length

Sway Path was smallest when the subject was steadied upon a stable object such as a chair. Conversely, the Sway Path was largest when the subject had no balance assistance and simply had their arm in a 90-degree position. Romberg ratios were also calculated using the Sway Path data for further insight into the differences amongst the four conditions. Touch has been shown to positively affect balance, potentially as much as the presence of visual input (Riley, et al., 1997), and this was confirmed by the results. Overall, light touch conditions, whether using an unstable surface (cane) or stable surface (chair), were successful in reducing postural instability measured using sway path, ranges, and Median power frequency.

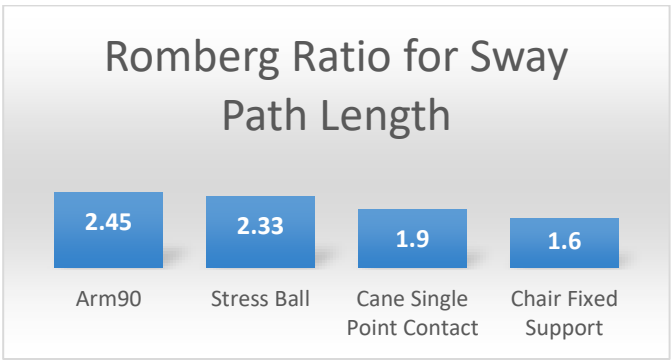

Figure 5: Romberg ratio for sway path length.

The eyes closed condition was more difficult under all touch conditions. The Romberg ratio, eyes closed over eyes open, is used in many studies to standardize the values of the touch conditions, accounting for both eye conditions while allowing direct comparison between touch conditions.

We found that the most stable (smallest sway path) condition was a finger on a stable chair, then a finger on a single point cane, then holding a stress ball, and the least stable (largest sway path) was the arm at 90 degrees position, which had no sensory or mechanical support.

CONCLUSIONS

Research investigating the effects of touch on postural stability has widespread applications in physical therapy. Many patients have decreased balance due to aging or pathologies, and extra somatosensory input provided through touch can improve balance among them.

The light touch has been previously reported to be beneficial to the older population as compared to young adults, suggesting that sensory cues from the fingers can counteract sensory loss in the lower extremity due to aging (Baccini, et al., 2007). The major benefit of light touch comes from the sensory input, and not the mechanical support available (Kouzaki, et al., 2008). In addition, studies have shown that light touch can be used as a training method to help improve postural stability (Oshita, et al., 2016).

REFERENCES

1. Baccini, M., Rinaldi L. A., Federighi, G., Vannucchi, L., Paci, M., Masotti, G. Age and Ageing. Volume 36, Issue 1, 1 January 2007, 30–35Bach et al. *Plos One*. 10(3): e0118797, 2015.

Comparison of constant weight compensation and inertia compensation for knee and ankle joints in wheel-type weight-bearing gait

[1] Wiha Choi and [1] Sehoon Oh

[1] Daegu Gyeongbuk Institute of Science and Technology (DGIST), Daegu, Korea
email: {choiwiha, sehoon}@dgist.ac.kr, web: http://control.dgist.ac.kr/

INTRODUCTION

Weight bearing gait is an effective method of walking rehabilitation. By reducing the load acting on the patient's lower extremity limb, it helps the patient practice walking without a large load on the joint. In general, the patient practices walking with the weight being compensated by a certain percentage of the patient's weight [1].
The weight compensation by the conventional weight bearing gaits tends to be static and constant, while new study investigated dynamic weight bearing considering the inertial force of the human body during walking [2].
In this study, the load on the knee and ankle joint during gait are investigated with dynamic weight bearing in two dimension (vertical and roll directions). The dynamic weight bearing in the two dimensions are provided by a force controlled weight bearing system [3] which can precisely control and compensate for the inertial force of walking.

METHODS

This experiment was performed on 6 male and 2 female subjects (169.43 ±7.01cm, 63.30 ±6.41kg, ages: 26~29) who had no past surgical history.
In this experiment, Vicon (MX-T10S, Vicon Co., Ltd) and force plate (OR6-6-2000, AMTI Co., Ltd) were used for motion capture as shown Figure 1. As shown on left side of Figure 1, each subject walks 2 m, with 10%, 20%, 30%, and 40% of their weight (force compensation mode) being compensated for. The robot provides constant levels of force during walking which are 10 to 40% of the weight. The order of degree of weight compensation was arbitrarily given. On the other hands, under the same experimental environment, gait experiments were carried out while compensating for 10%, 20%, 30% and 40% of the subjects' inertia (inertia compensation mode). The robot provides compensating force proportional to body acceleration as well as the constant forces. When the human weight is m, the gravitational acceleration is g, and the additional acceleration due to walking is a, the force compensation mode only compensates for mg, and the inertia compensation mode compensates for both mg and ma as shown on the right side of Figure 1. The markers for motion capture were attached according to Plug-in gait model (lower limb).
Experiments were performed three times in each weight compensation, and a 60-second rest interval was given between the weight compensations. Between the two modes, a 30 minute break was given. The protocol involved 2 conditions: barefoot, self-selected gait velocity.
The protocol was approved by the Daegu Gyeongbuk Institute of Science and Technology Science Ethical Committee (DGIST-170721-HR-020-01).

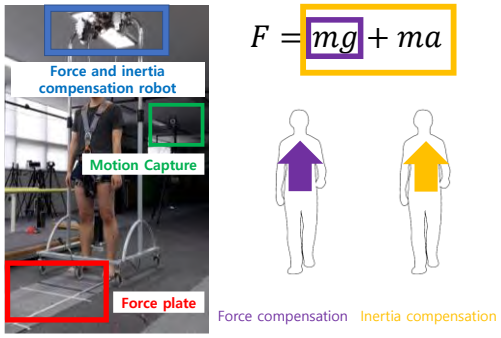

Figure 1: Experiment set-up and explain the difference between force compensation mode and inertia compensation mode. F means compensating force, m means mass, g means gravitational acceleration, and a means the acceleration from motion.

RESULTS AND DISCUSSION

It is well known that as the weight compensation progresses, the joint loads are reduced and the maximum lower extremity joint moment generated by the walking decreases [4].

In Figure 2, it can be seen that the maximum knee joint moment decreases as the weight compensation proceeds in both the force compensation mode and the inertia compensation mode. When the maximum knee moments are compared in two modes, there is a greater decrease in inertia compensation mode. The maximum moment of the knee joint occurs during the heel-strike process [5]. In other words, it slows down the speed of human walking. In this process, the human inertia itself is reduced, which reduces the load on the knee joint. In the case of 30% and 40% compensation, the difference between the two modes is statistically significant (p<0.05, paired t-test). In the force compensation mode, since only a certain weight is compensated, the force due to the acceleration caused by the walking cannot be compensated. This means that the inertia compensation mode can further reduce the load acting on the knee joint compared to the force compensating mode, especially, when it slows down the gait.

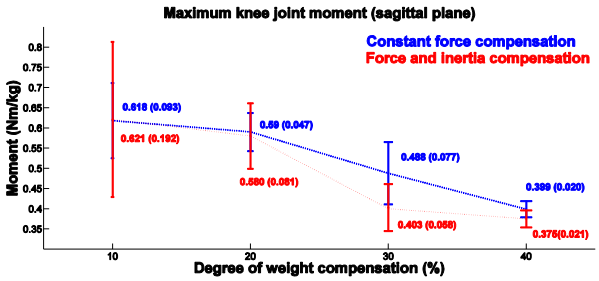

Figure 2: Maximum knee joint moment as weight bearing level increases and comparison of force compensation mode and inertia compensation mode.

In general, the maximum ankle joint moment appears in the toe-off process in the gait, that is, in the process of accelerating the gait [5]. However, in the case of ankle joint, the difference between the force compensation mode and the inertia compensation mode is not statistically evident (p>0.05, paired t-test) over the entire weight bearing levels as shown Figure 3.

From these experimental results, it can be seen that the maximum ankle joint moment is not significantly different from the force compensation in case of inertia compensation.

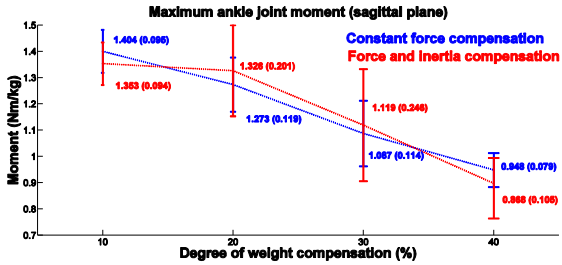

Figure 3: Maximum ankle joint moment as weight bearing level increases and comparison of force compensation mode and inertia compensation mode.

Before the experiment, the maximum ankle joint moment in the propulsion process of the gait was expected to decrease because it compensates for the inertia itself in the inertia compensation mode. However, unlike the knee joint, the ankle joint moment has no difference between the two modes, which is presumed to be due to the fact that the ankle must produce a certain amount of moment in order to produce the acceleration and force required for the gait during the propulsion process.

In conclusion, adding an inertia mode to the existing force compensation mode can reduce the load on the knee joint during gait rehabilitation.

REFERENCES

1. Frey, Martin et al. *IEEE Transactions on Neural Systems and Rehabilitation*. 14(3), 311-321, 2006.
2. Kammen et al. *Plos One*. 9(9): e107323, 2014.
3. Jihoo Kwak et al. *IECON 2017 – 43rd Annual Conference of IEEE Industrial Electronics Society*. 2017.
4. Goldberg et al. *Journal of biomechanics*. 46(6): 1176-1183, 2013.
5. Perry, J. *Gait Analysis: Normal and Pathological Function,* Slack Incorporated, 12(6) 1992.

ACKNOWLEDGEMENTS

This work was supported by the Robot industry fusion core technology development project through the Korea Evaluation Institute of Industrial Technology (KEIT) funded by the Ministry of Trade, Industry and Energy of Korea (MOTIE) (No.10080547).

MECHANICAL WORK ADAPTATIONS USING A TRANSTIBIAL PROSTHESIS DURING THE FIRST THREE MONTHS OF UNASSISTED AMBULATION

[1, 2] John-David Collins, [1]Trevor Kingsbury, and [1]Marilynn Wyatt
[1] Naval Medical Center San Diego, San Diego, CA, USA
[2] University of Delaware, Newark, DE, USA
email: john.d.collins1.ctr@mail.mil

INTRODUCTION

Learning to walk on a prosthetic ankle-foot system for the first time is challenging, and the adaptations required to rely on a mechanical interface to replace an anatomical structure pose many challenges after undergoing transtibial amputation (TTA) [1]. While the importance of understanding the process of learning to walk again is clear, few studies have attempted to quantify this adaptation process. As standard protocol in the unique clinical setting at the Comprehensive Combat and Complex Casualty Care (C5) program at the Naval Medical Center San Diego (NMCSD), all patients who have undergone amputation receive an Energy Storing and Returning (ESR) prosthetic ankle-foot device. Patients are studied in the gait laboratory at regular intervals, and thus, we are uniquely positioned to describe the adaptations of new users as they learn to utilize the mechanical properties of an ESR device.

The benefits of characterizing new users' adaptions go beyond the understanding of individual patient performance and provide insight and feedback into how patients adapt to the novel experience of relying on a mechanical device to walk again. ESR devices are designed to mimic natural anatomy and support and propel the body forward [2, 3]. In order to understand how new users utilize and adapt to their first ESR device, we examined changes in mechanical work of both the ESR device and their natural limb during gait at their self-selected (SS) speed from baseline gait study (0mo) and three months (3mo) after. The three months time point was selected because at this point, the focus of the NMCSD rehabilitation program shifts from walking to high-level activities [4], and patients often try different ESR device styles as it suits their new rehabilitation and mobility/functional goals. We hypothesize that on the prosthetic side, total negative and positive work will increase, and the work-ratio (positive work to magnitude of negative work) will increase, indicating an increase in utilization of ESR properties of the device. Additionally, we hypothesize that there will be decreases in both unaffected limb negative and positive work and an increase in SS gait speed.

METHODS

We performed a retrospective analysis of five patients (age: 25±5.1yrs, height: 1.75±0.07m, weight: 0mo: 90.6±23.44kg, 3mo: 91.62±23.52kg) with unilateral, transtibial amputation resulting from traumatic injury (Table 1) who underwent 3-D gait analysis as part of their routine clinical care at the NMCSD C5 Gait Lab (CIP# NMCSD.2014.0026). Patients walked at their own, SS speed across four AMTI (Watertown, MA) force plates embedded in a 10m walkway, with 12 Motion Analysis (Motion Analysis Corporation, Santa Rosa, CA) cameras. Six degrees of freedom data were processed with Visual3D (C-Motion Inc, Germantown, MD) and Unified Deformable segment analyses [5] were performed to investigate the changes in mechanical work on both the ESR device and intact ankle-foot during walking.

Each patient utilized their own clinically prescribed ESR device which was aligned and adjusted by one of two prosthetists at NMCSD and sockets were all fitting comfortably prior to data collection. All five patients maintained use of the same model prosthetic device for the baseline and three month data collection, and only two different devices were worn: VariFlex XC and ProFlex XC from Ossur® (Ossur Americas, Foothill Ranch, CA). For each limb, total negative and positive work, work-ratio, and SS speed were measured.

RESULTS AND DISCUSSION

Results of a one way repeated measures ANOVA with an alpha level of 0.05 reveal that there was not a significant change in any of the metrics we examined per side (Fig. 1). While not significant, it is important to note that these results are in line with those of Ray et al., 2018 [6] who recently reported similar negative and positive work values and work-ratios in experienced prosthetic users who had been given a new ESR device. Where they found significant increases in prosthetic and unaffected positive work, our data set lacks sufficient power to detect any significant change.

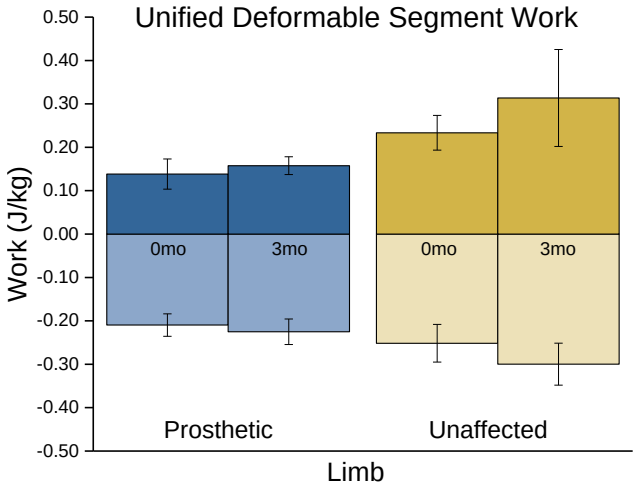

Figure 1: UD segment work for the prosthetic and unaffected limbs, at the baseline (0mo) and 3 month time points (3mo).

The intention of this abstract was to explore the adaptations made by new prosthetic users over the first three months of prosthetic use. It was hypothesized that after three months of use, an increase in prosthetic positive and negative work would occur, reflecting improved utilization of the energy return properties of the device. The observed increase in work-ratio indicates a more balanced magnitude of positive and negative work which is accompanied by comparable increases in positive and negative work.

Similarly to the prosthetic limb, unaffected limb positive and negative work increased at 3mo but was not significant. Along with the increases in work observed in the prosthetic, these increases could be paired with the average increase in SS gait speed observed at the 3mo time point.

SS gait speed is often an indicator of overall gait improvement and a reflection of increased comfort/ability in the prosthetic device. Despite not having significance, an increase in stature-scaled speed was found in this subject group.

CONCLUSIONS

This abstract is the first of its kind to describe the initial mechanical work adaptations when learning to walk in a prosthetic device. SS gait speed and the amount of positive and negative work in both the prosthetic and unaffected limbs were increased. This increased work-ratio, which reflects similar increases in both positive and negative work with the ESR device, may indicate the improved ability of the new prosthetic user to capitalize on the energy returning characteristics. Future work should investigate these parameters with a larger sample size as well as characterize the mechanical work adaptations at the knee and hip.

REFERENCES

1. Sanderson and Martin. *GAIPOS*. **6**(1), 1997.
2. Kepple, et al. *GAIPOS*. **6**, 1997.
3. Neptune, et al. *J Biomechanics*. **34**(11), 2001.
4. Kingsbury, et al. *MHSRS Proceedings '17, Kissimmee, FL, USA,* 2017.
5. Takahashi, et al. *J Biomechanics.* **45**(15), 2012.
6. Ray, et al. *JNER*. **15**(1), 2018.

ACKNOWLEDGMENTS

Many thanks to the NMCSD gait lab staff for the conversations and helpful input in shaping this abstract.

DISCLOSURE STATEMENT: The views expressed herein are those of the author(s) and do not necessarily reflect the official policy or position of the Department of the Navy, Department of Defense, or the U.S. Government.

Table 1: Mean and standard deviation results for the five patients

	Negative Work PROS (J/kg)	Positive Work PROS (J/kg)	Negative Work UNAFF (J/kg)	Positive Work UNAFF (J/kg)	Work-Ratio PROS	Work-Ratio UNAFF	SS Gait Speed (Stat/s)
Baseline	-0.21±0.03	0.14±0.03	-0.25±0.04	0.23±0.04	0.65±0.10	0.94±0.18	0.70±0.07
3mo	-0.23±0.03	0.16±.0.02	-0.30±0.05	0.31±0.11	0.71±0.09	1.04±0.29	0.76±0.06

POSITIONAL AND POSTURAL EFFECT OF A VISUAL BIOFEEDBACK DEVICE DURING ROLLATOR WALKER USE: A DEVICE VALIDATION

[1] Courtney Golembiewski, [1]John Schultz, [1]Kurt Jackson, [1]Harold Merriman, [1]Timothy Reissman, [1]Julie Walsh-Messinger, and [1]Kimberly Bigelow

[1] University of Dayton, Dayton, OH, USA
email: Kimberly.bigelow@udayton.edu, web: https://udayton.edu/stem-catalyst/recipients/smartwalker.php

INTRODUCTION

Approximately 6.5 million Americans over the age of 65 use a walker [1]. However, research suggests individuals often do not receive the appropriate training on using their walkers [2]. Rolling walkers can be pushed too far forward or roll forward unexpectedly, which raises risk of falling [3]. Nearly half of all rolling walker users also exhibit a forward lean, with this posture indicative of having a significantly higher incidence of falls ($p < 0.01$) than those who maintain a more erect, upright posture [2]. These needs drive the design of an effective sensor that can alert individuals when they have taken on an unfavorable position and posture.

METHODS

To address this, our team developed a biofeedback based electro-mechanical system that can clip onto a walker and provide visual feedback to the user to encourage proper positioning. Based on the measurement of an ultrasonic distance sensor as compared to a pre-programmed individualized threshold, a green (good position) or red (poor position) LED is illuminated to provide real-time feedback to the user. The system then records how often and how long users maintained a proper distance from the walker. We hypothesized that when positioned better, individuals would also exhibit a more erect posture.

To demonstrate feasibility of the device, 14 participants over the age of 65 who regularly used rolling walkers first performed tasks with the device recording but not providing feedback. Individuals then completed the same series of tasks while the device provided feedback based on a preset distance relative to the front walker crossbar. This distance was established by positioning the rear wheel axles at the 5th metatarsal heads and adjusting the handle height to allow 20-40 degrees of elbow flexion. In each condition, individuals completed three 10 meter walks at a comfortable pace and navigated through an 8 meter obstacles that consisted of thresholds and cones. Data was collected from the device as well as an Xsens 3D motion tracking system.

RESULTS AND DISCUSSION

Results demonstrated that individuals were able to attend to and appropriately respond to feedback from the device in both an ideal environment (10-meter walk) and while navigating environmental obstacles such as would be commonly faced during every day ambulation (obstacle course). During the 10 meter walks, individuals spent on average 90.0±7.12 percent of the time of the walk positioned within the preset threshold when feedback was provided, compared to 10.9±9.6 percent of the walk time when no feedback was provided ($p<0.001$). Gait speed did not differ between the conditions ($p=0.305$). During the obstacle course, individuals spent 63.1±21.13 percent of the walk time within the desired range when feedback was provided, compared to 5.5±7.1 percent of the walk time during the no feedback condition, $p<0.001$.

Figure 1 shows a representative plot of distance from the walker during the 10-Meter Walk as compared to the set threshold with and without feedback.

Joint angle analysis shows that the most notable adaptation used to move the walker closer to the target position was a decrease in shoulder flexion ($p<.001$). A significant increase in elbow flexion was also shown to be a method of correction in both the 10-Meter Walk and obstacle course trials ($p=0.013$). There was a small, but non-significant increase in trunk inclination angle (0.84±1.9^{o}) during the 10-

meter walk when feedback was provided (p=.141). During the obstacle course, the trunk inclination angle decreased by 1.52±2.0º when feedback was provided, which was a significant improvement to a more erect posture (p=0.016).

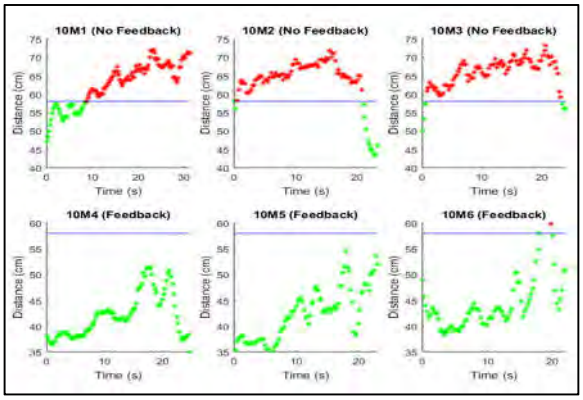

Figure 1: Distance from the walker (cm) tracked during 10-Meter Walk trial, with the green data points indicative of being within the desired position.

The T1C7 articulation flexion was also analyzed, and although a significant increase in flexion was seen during the 10-Meter Walk (*p*=.032) this increased flexion was not seen during the obstacle course where attention to the environment was crucial for task completion.

Figure 2 shows the avatar generated by the Xsens MVN Studio software for a subject that is representative of the study population displaying the common biomechanical correction methods.

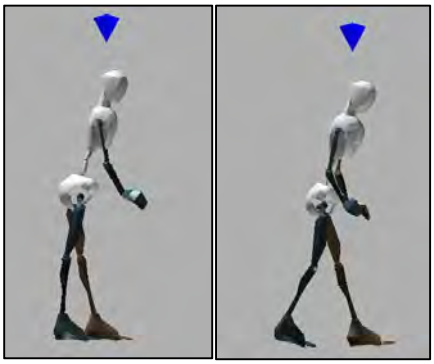

Figure 2: Xsens MVN Studio generated avatar for a subject representative of the study population during a 10-Meter Walk baseline (left) and feedback (right) trials

Together, these results indicate that the developed device was able to bring the individual's position relative to the walker to a position considered more clinically desirable. Such a position should improve overall stability and ability to quickly react. In order to change their position, individuals demonstrated several common changes to their posture. While it was hoped that the most notable of these changes would be a more upright posture, this was not observed and may warrant further device development to provide additional feedback not only on position, but on posture.

CONCLUSIONS

It was found that:

- The biofeedback-motivated position monitor encourages a significant and clinically relevant change in a user's distance from their walker.
- The change in walker distance is driven by a combination of decreased shoulder flexion, increased elbow flexion and in some cases decreased trunk inclination.
- The ability to observe surroundings is not impaired while monitoring visual cues from the positon monitor.
- The use of the position device does not impact gait speed.

As such the preliminary findings in this study merit further research on the impacts of this device. Future work should concentrate on longer term use, including examining habituation and training effects. Additionally, work is now necessary to ensure that the common changes to correct position are not unfavorable in the long-term.

REFERENCES

1. National Institutes of Health. https://www.nichd.nih.gov/health/topics/rehabtech/conditioninfo/Pages/people.aspx
2. Liu H. Geriatr. Gerontol. Int., 9(2), 2009.
3. Bradley and Hernandez. AAFP. 84(4), 2011.

ACKNOWLEDGEMENTS

This work was funded by the University of Dayton STEM Catalyst Grant.

MECHANICALLY PASSIVE PORTABLE SHOULDER EXOSKELTON: PRELIMINARY DESIGN AND BIOMECHANICAL ANALYSIS

Patrick T. Hall, Allison J. Nelson, and Dustin L. Crouch

University of Tennessee, Knoxville, TN, USA
email: phall8@vols.utk.edu, web: http://assistlab.utk.edu/

INTRODUCTION

Patients with chronic shoulder impairment due to neuromuscular disorders, such as peripheral nerve injury, may maintain some shoulder function and strength, though they are substantially diminished from that of a healthy shoulder [1]. Some disorders, such as rotator cuff tear, may also be associated with soft tissue injury, and biomechanical loads on the shoulder may increase severity and recurrence of injury [2]. Wearable portable exoskeletons are devices that could provide continuous mechanical assistance to the shoulder to augment movement ability and decrease biomechanical loads in soft tissues in patients with shoulder impairment. Some wearable shoulder exoskeletons rely on motors, controllers, and electrical power supplies to apply forces to biological joints [3], which make them relatively expensive and susceptible to electromechanical failure. Mechanically passive exoskeletons, which store and return energy in elastic springs to supplement muscle force, may be more affordable and reliable for continuous movement assistance. The purpose of our research was to develop and analyze the mechanical design of a passive portable exoskeleton that, like one reported in a previous study [4], uses a spring-pulley system and cam wheel gearing mechanism to provide gradually increasing mechanical assistance as the shoulder is elevated against gravity. We also implemented the exoskeleton in an upper limb musculoskeletal model to determine its effect on muscle contributions to a simulated movement.

MECHANICAL DESIGN ANALYSIS

The proposed mechanically passive exoskeleton incorporates a preloaded elastic spring (Fig 1). A cable transmits the spring force across the superior aspect of the shoulder, generating a positive shoulder elevation (SE) moment to counteract the negative SE moment caused by gravity. As SE angle increases, the spring tension *decreases* as it shortens despite an *increasing* SE moment due to gravity; thus, we incorporated a wrapped cam wheel as a variable gearing mechanism that increases SE assistance as SE angle increases.

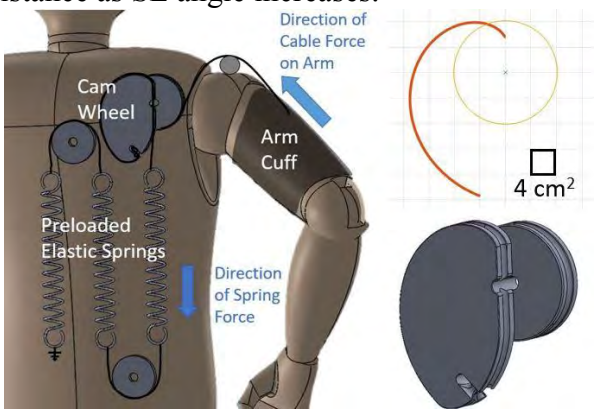

Figure 1: Left: Diagram of shoulder exoskeleton concept (posterior view on right shoulder); **Right:** cam wheel profile and CAD prototype

To counteract as much gravitational load on the shoulder as possible without overassisting, we deigned the exoskeleton's torque output (T_E) to be equal to the net SE moment needed to counteract gravity (M_G), which was calculated through an inverse dynamic analysis at static SE angles ranging from 0 to 90 degrees in the coronal plane. The moment was computed with the elbow completely extended using the inertial and anthropometric properties of 50th percentile adult males [5], though these properties could be changed to match any subject.

In MATLAB, we used a global optimization function (GlobalSearch) to compute exoskeleton design parameters that minimized the difference between M_G and T_E, with T_E being defined as:

$$T_E = \frac{ma_s}{ma_w} ma_c(\alpha)[k_e(x - \int_0^{\alpha} ma_c(\alpha)d\alpha)] \quad (1)$$

In Eq. 1, x is spring deflection at 0 degrees of shoulder elevation, k_e is equivalent spring stiffness, ma_s is the moment arm of the exoskeleton cable

about the shoulder joint, ma_w is the moment arm of the constant-radius wheel, α is the angular deflection of the cam wheel, and ma_c is the moment arm of the variable-radius cam wheel which was modeled as a sinusoid.

Table 1: T_E Optimized Parameters

X (cm)	K (N/m)	ma_s (cm)	ma_w (cm)	ma_c (m)
28.94	500	6.50	4.07	-.127sin(.218α)

With the computed parameters (Table 1), the exoskeleton torque was aligned with the moment required to counteract gravity (Fig 2).

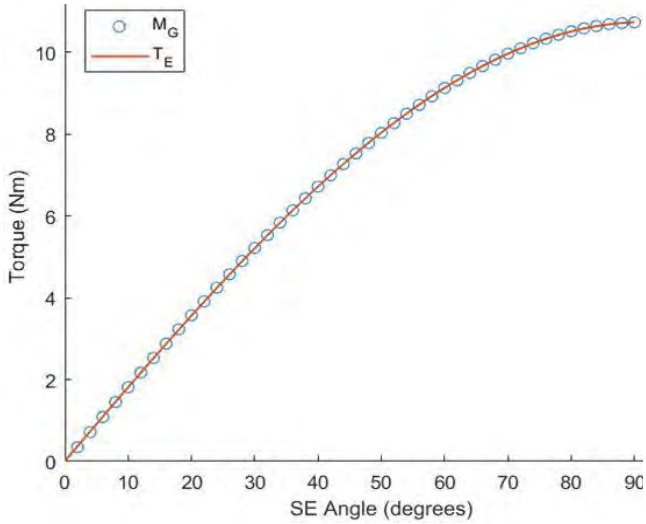

Figure 2: The gravitational moment on the shoulder (M_G) compared to the calculated output torque from the exoskeleton (T_E).

Using the parameters from T_E, we performed a numerical integration to calculate the profile of the cam wheel based on the cam moment arm. This cam profile was graphed with the concentric single radius wheel to create the entire cam gearing mechanism and develop a CAD prototype for the physical cam wheel (Fig 1).

BIOMECHANICAL SIMULATION

We incorporated the exoskeleton in a dynamic upper extremity musculoskeletal model in OpenSim [6] as a custom generalized coordinate force element, which applied the exoskeleton torque, T_E, to the SE moment as a function of SE angle. Using computed muscle control, we computed muscle activations during simulations of an abduction-adduction movement with the elbow extended, both with and without the exoskeleton. Muscles that generated positive SE moments had lower peak activations with the exoskeleton during the abduction phase of the movement Some muscles that generated negative SE moments had greater peak activations with the exoskeleton (Fig 3). The higher peak activations occurred at the start of the adduction phase.

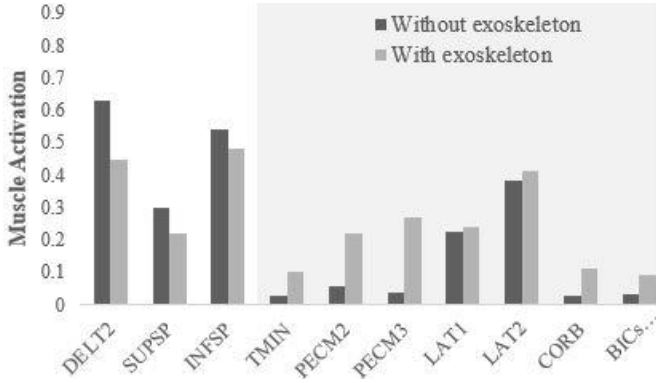

Figure 3: Peak muscle activations of muscles in the model that experienced >2% peak activation changes with the exoskeleton.

CONCLUSION

Our unique biomechanics-driven approach for computing exoskeleton design parameters ensures that the exoskeleton provides appropriate assistance and makes it easier to customize the device for individual users. The biomechanical simulation showed that our device effectively lowers peak activation in muscles with positive SE moments, verifying our expectation that the exoskeleton would assist in and reduce muscle contributions to elevating the shoulder against gravity. Constraining the simulations with and without the exoskeleton to the same kinematics may explain why peak activations were higher for some muscles; in future studies we will determine if human subjects adapt their movement when wearing the exoskeleton to prevent increasing muscle activations.

REFERENCES

1. Crouch DL, et al. *Gait Posture*, 44: 2016.
2. Galatz LM, et al. *JBJS Am,* 86A, 2004.
3. O'Neill CT, et al. *Proc ICORR*, 2017.
4. Schroeder J and Perry J, *Proc ICORR*, 2017.
5. McConville JT, et. al *AFAMRL Report*, 1980.
6. Saul KR et al, *Comput Methods Biomech Biomed Engin,* 18(13), 2015.

Improving quantitative predictions of a human-prosthesis simulation

[1] Matthew Handford and [2] Manoj Srinivasan

[1,2] The Ohio State University, Columbus, OH, USA
[1] email: handford.4@osu.edu, web: http://movement.osu.edu

INTRODUCTION

If we wish to use a simulation to study a human with a lower limb prosthesis, we typically start by building a simplified model of the person and replacing one of the limbs with a prosthesis. Then we simulate a walking gait through various objective functions and experimental tracking terms. However, by tracking experimental data, we assume that, regardless of the prosthesis used, the user will always walk with the same gait. As an alternative route, we developed a simulation through which we predict the interaction between a person and a robotic lower limb prosthesis without tracking experimental data. When we tested variety of controllers, we found a strong correlation between positive prosthesis work, large bilateral asymmetries, and decreasing metabolic cost (down to a minimum). These results suggest what features of control and human movement are important for minimum effort. However, our results do not quantitatively match what is seen in experiment. To improve our qualitative and quantitative predictions, we systematically test the effects of socket interaction, complex muscle models, muscle atrophy, and leg inertia properties.

METHODS

We made a planar simulation of a person with a robotic ankle-foot prosthesis, Figure 1, which uses energy optimality to predict the kinematics and dynamics of a periodic walking gait. We actuate this model using thirteen uni- and biarticular muscles which cross all of the biological joints (and a single prosthesis torque motor at the ankle of the affected limb). These muscles are simplified as piecewise linear force-sources in initial testing; however, recent tests also use a hill-type model to study activation dynamics. The muscle and prosthesis actuations are then determined by optimizing a metabolic cost function based on muscle activation, shortening velocity and max isometric force:

$$C_m = \int \sum \left[0.05(a + a^2) + a\phi\left(\frac{v}{v_{max}}\right)\right] F_{iso} v_{max}\, dt$$

This metabolic cost is augmented with a small muscle force rate cost to discourage erratic muscle activations. A more in-depth description of this model can be found in our previous work [1].

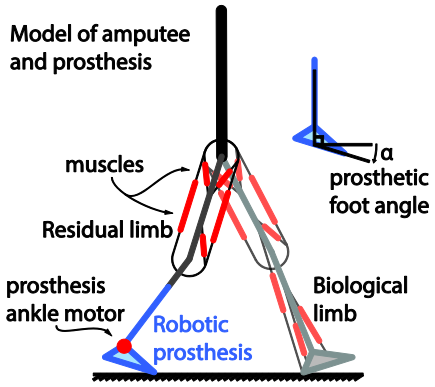

Figure 1: Sagittal plane model of human and prosthesis.

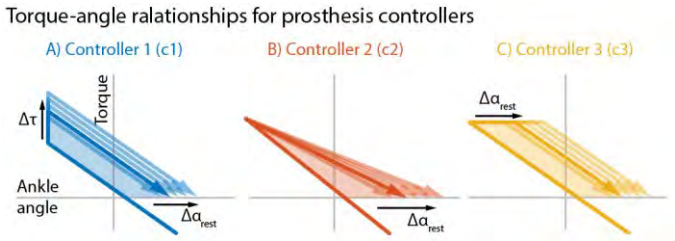

Figure 2: Prosthesis controller torque – prosthesis ankle angle relationship.

Using this planar model, we defined a series of simple prosthesis controllers, Figure 2, which are capable of applying positive or negative net prosthesis work at push off using three unique strategies: applying a constant torque (c1), changing the stiffness (c2), and holding a max torque (c3). Each of these controllers had the same dorsiflexion

stiffness and swing position control. We also simulated a passive SACH foot and a controller free optimized prosthesis torque to use for comparison.

RESULTS AND DISCUSSION

Testing each of the controllers with various levels of prosthesis work, we found a roughly quadratic relationship between the net prosthesis work and the human metabolic cost, Figure 3, and we find a linear relationship between net prosthesis work and stance time on the affected side, Figure 4. Despite the controllers applying work differently throughout push-off, the cost observed seems independent of the controller used while bilateral symmetry is dependent.

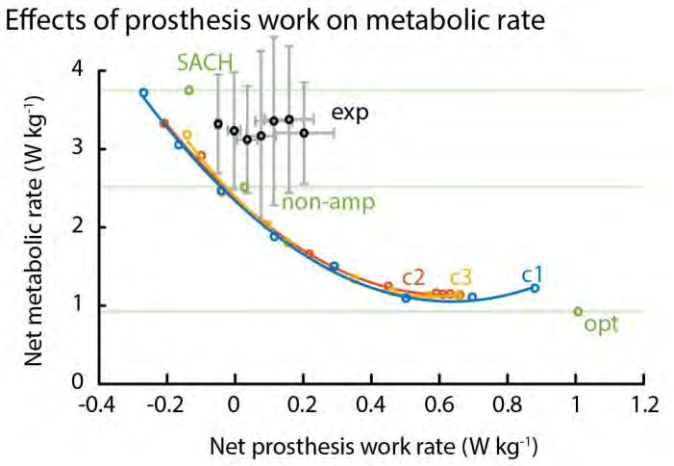

Figure 3: Metabolic rate due to various levels of work from all controllers. Experimental data [2] is shown black with standard deviation in gray.

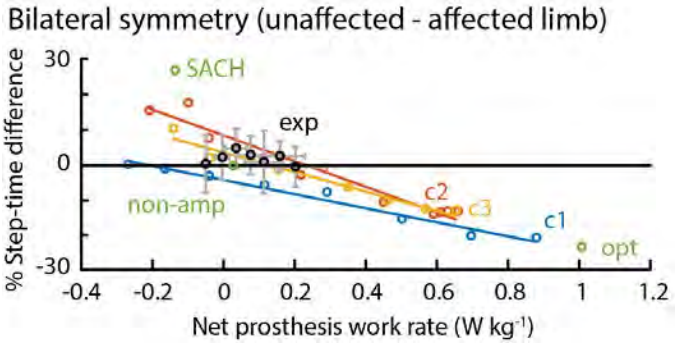

Figure 4: Bilateral symmetry of all controllers displayed as unaffected – affected side over the unaffected side step time.

When we compare these results to experiment [2], we don't see these same trends. Most experiments predict either no improvement in metabolic cost or a small decrease when adding work, and typically we do not see an increase in affected side stance time. This could be due to some of the simplifying assumptions made in our model, such as ignoring socket interactions while amputees have to deal with discomfort associated with socket loading. To account for this, recent tests add a socket torque, axial force, and/or shear force cost term in our optimization to penalize high socket loading [3]. We also seek to improve the prediction of the model through testing of other cost functions, more complex muscle models, adding activations dynamics as well as force-length/velocity relationships, and accounting for the change in inertial and muscle strengths properties on the affected side [4].

REFERENCES

1. M. Handford and M. Srinivasan, "Robotic lower limb prosthesis design through simultaneous computer optimizations of human and prosthesis costs," Sci. Rep., vol. 6, 2016.Gardner JG, et al. *J Biomech* **38**, 1861-1868, 2004.
2. Quesada, Roberto E., Joshua M. Caputo, and Steven H. Collins. "Increasing ankle push-off work with a powered prosthesis does not necessarily reduce metabolic rate for transtibial amputees." Journal of biomechanics 49.14 (2016): 3452-3459.
3. Koelewijn, A.D. and van den Bogert, A.J., 2016. Joint contact forces can be reduced by improving joint moment symmetry in below-knee amputee gait simulations. *Gait & posture*, *49*, pp.219-225.
4. Esposito, E.R. and Miller, R.H., 2018. Maintenance of muscle strength retains a normal metabolic cost in simulated walking after transtibial limb loss. *PloS one*, *13*(1), p.e0191310.

ACKNOWLEDGMENTS

This work was supported by NSF CMMI grant 1300655. We thank Steve Collins and Joshua Caputo for discussions informing this study.

EFFECT OF NIGHT VISION GOGGLE TECHNOLOGIES ON TASK PERFORMANCE DURING A SIMULATED ROOM CLEARANCE TASK

[1] Brian K. Higginson and [2] Jemma L. Coleman

[1] Gonzaga University, Spokane, WA, USA
[2] Australian Defence Science and Technology Group, Melbourne, Australia
email: higginson@gonzaga.edu

INTRODUCTION

Building and room clearance tasks are commonly performed by military and civilian law enforcement personnel to neutralize any potential threats contained within. Under ideal circumstances this task is performed with an adequate level of ambient light to maximize the amount of visual information available to the task performer. Recent modern conflicts have resulted in an increased reliance on night vision technologies to provide a tactical advantage to the user. Although these technologies allow the user to operate in an environment few others can, they do have their limitations. These limitations include tunnel vision, decreased visual acuity, compromised depth perception, and loss of peripheral vision. All of which can result in decreased task performance. Up until now, most research examining the effects of night vision goggles on military performance have focused on applications related to fixed and rotary wing pilots [1, 2]. Very little research has focused on performance outcome measures of soldiers performing tactical operations on the ground.

The purpose of this study was to determine the effects of various night vision technologies on time-to-target, target discrimination, and threat neutralization measures during a simulated room clearance task.

METHODS

Twelve Special Weapons and Tactics (SWAT) team members (Mean ± SD: 40.4±4.3 yrs, 180.3±6.8 cm, 93.5±10.3 kg) volunteered to participate in the study. The experimental protocol consisted of a simulated room clearance task that included an approach component, and a threat discrimination and neutralization component. The approach component required the subjects to navigate to the room to be cleared as quickly as possible. This component included four right angle corners, three steps, and an incline that had to be navigated, and was a total of 25 meters in length.

In each room clearance scenario, there were two individuals located within the room, with one holding a weapon pointed toward the entry door. Locations of the room occupants, as well as which individual was holding the weapon, were randomized across trials. Once at the target room, subjects were asked to discriminate friend from foe and neutralize the threat as rapidly as possible. This task was performed under four different conditions. The reference condition consisted of performing this task under ambient light in which all available room lighting was used to illuminate the approach and target areas. This condition was compared to three other conditions that were performed using three different types of night vision goggle (NVG) technologies. For these conditions, all ambient lighting was removed from the approach and target room. Two of the NVG's used the newer white phosphor intensifier tubes, whereas the third utilized older generation green phosphor intensifier tubes. Of the white phosphor technology NVG's, one was a monocular (WP-1) consisting of a single optical tube and single intensifier tube, whereas the other was a binocular (WP-2) unit consisting of dual optical and dual intensifier tubes. The green phosphor NVG consisted of a dual optical tube, and single intensifier tube design (GP-1).

The order of conditions were randomized across subjects, with each condition being repeated twice and outcome measures averaged within condition for analysis. In addition to wearing their standard issue body armor and ballistic helmet, all subjects performed the shooting task using their primary duty

weapon (M-4) equipped with an infrared laser shooting training ammunition (UTM simunition).

Outcome measures consisted of time-to-target (TT), engagement time (ET), and total time (TOT). Measures were derived from linear and angular measures of motion obtained from inertial sensors mounted to the rifle, body armor, and helmet of the subject. A one-way repeated measures ANOVA and Tukey's post-hoc test was used to detect differences in outcome measures between ambient light and NVG conditions (α=.05).

RESULTS AND DISCUSSION

All NVG conditions resulted in a significant increase in the time required to get to the target room (TT) when compared to the ambient lighting condition ($p<.001$). Specifically, the WP-2 NVG's resulted in an additional 1.84 ± 0.34 s ($p<.001$), the WP-1 NVG's resulted in an additional 2.73 ± 0.46 s ($p<.001$), and the GP-1 NVG's resulted in an additional 3.89 ± 0.66 s ($p<.001$) required to cover the 25 m to the target room.

Once at the target room doorway, engagement times (ET) increased for all NVG conditions ($p=.005$) from 1.19 ± 0.09 s for the ambient light condition, to 1.60 ± 0.13 s ($p=.010$) for the WP-2 condition, to 1.94 ± 0.19 s ($p=.020$) for the WP-1 condition, and 2.97 ± 0.43 s ($p=.002$) for the GP-1 condition. These data indicate that once the shooter has access to all visual information in the room, it takes 2.5 times longer to neutralize the threat with the worst performing NVG technology (GP-1), and almost 0.50 s longer with the best performing NVG technology (WP-2). Considering the implications of this task, these increases in task performance times while wearing NVG's has significant consequences relating to the survivability of the operator performing the task.

Looking at these individual TT and ET components in aggregate, the total time to complete the shooting task (TOT), from initiation of approach to threat neutralization, took 2.24 ± 0.34 s longer using the WP-2 NVG's, 3.48 ± 0.53 s longer using the WP-1 NVG's, and 5.66 ± 0.91 s longer using the GP-1 NVG's when compared to performing the same task in ambient lighting conditions ($p<.001$).

Although overall task performance took longer, to varying degrees, when NVG's were used, overall task outcomes remained unchanged. In all cases, target discrimination and threat neutralization remained at 100%. Previous studies [3] have shown that, for a given shooting task, more experienced shooters will compromise time to task completion to optimize task outcome (correct identification and neutralization of the threat). Less experienced shooters will tend to compromise task outcome for speed of task completion.

CONCLUSIONS

In the current study, it was found that NVG technology does, in fact, adversely affect performance during a room clearance task by increasing both approach and engagement times. The trained shooters used in the current study were able to maintain perfect task outcome (100% target discrimination and neutralization) at the expense of greater task completion times. It may be possible that with less skilled shooters, task completion times may increase along with an associated decrease in task performance outcome, as seen in previous studies. Future studies will focus on factors that are responsible for increased task performance times while wearing NVG's, and elucidate potential mechanisms responsible for compromised task performance to inform training in an attempt to minimize these factors.

REFERENCES

1. Ang, B. & Kristofferson, M. *Aviation and Space Environmental Medicine*, 84(2), 125-33, 2013.
2. Harrison et al., *Military Medicine,* 172(8), 864-70, 2007.
3. Fox et al. *International Journal of Exercise Science*, 8(5), 2017.

EFFECT OF TOE STIFFNESS ON THE PUSH-OFF AND JOINT TRAJECTORIES FOR THE POWERED TRANSFEMORAL PROSTHESIS: A PILOT STUDY

[1] Woolim Hong, [1]Shawanee Patrick and [1] Pilwon Hur

[1] Texas A&M University, College Station, TX, USA
email: [1]{ulim8819, shawaneepatrick, pilwonhur}@tamu.edu, web: http://hurgroup.net/

INTRODUCTION

A powered transfemoral prosthesis is an assistive device that has two actuators for ankle and knee joints to provide stable walking to the lower extremity amputees (above-knee). Transfemoral amputees commonly have gait abnormalities that can lead to long term problems, such as fatigue, arthritis and scoliosis [1]. Reducing these abnormalities could lead to a reduction in some of the long-term issues.

Human walking consists of several events: heel-strike, foot-drop, heel-off, push-off, and toe-off [2]. The entire stance phase comprised approximately 60% of the gait cycle [2]. Between heel-off and push-off, positive work is required to insert energy into the moving body and to transition from the stance phase to the swing phase [3]. To provide positive work to the user, a toe joint is essential for the foot; the toe joint lets the foot to bend naturally as the gait cycle progresses and provides appropriate push-off torque to the body [4]. However, no studies have investigated the effects of the toe stiffness in the gait characteristics of powered transfemoral prosthesis.

In this study, we investigated the effects of the toe stiffness modulation on the gait kinetics and kinematics of the powered transfemoral prosthesis. Specifically, joint trajectory profiles and the push-off force at the toe are examined while the toe stiffness was varied. It is hypothesized that providing appropriate toe stiffness will enhance the gait kinetics and kinematics of the powered transfemoral prosthesis compared with the rigid foot without a toe joint.

METHODS

We designed a foot with a toe joint as shown in Figure 1. The foot is composed of the toe joint and the foot base, connected by the hinge and flat shaped spring steel. The toe stiffness varies from 0 to 1 Nm/rad. The toe stiffness modulated by stacking multiple spring steel sheet. The decision of toe length was based on the human factor considering where the forefoot strike occurs [5].

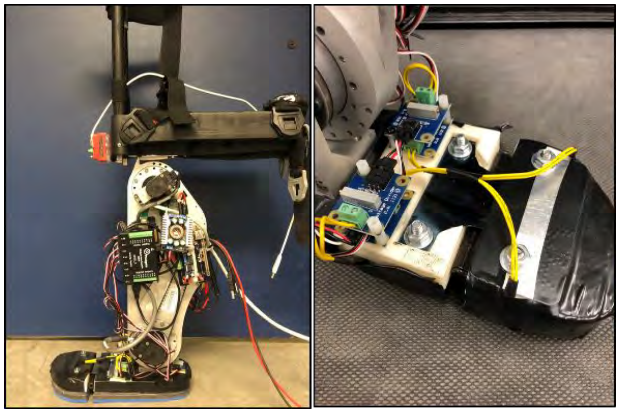

Figure 1: Human-inherent designed foot considering a toe joint with spring steel for providing required PO force.

A custom-built fully actuated powered transfemoral prosthesis (AMPRO II) was used. AMPRO II is the second generation of a powered prosthesis developed at Texas A&M University. AMPRO II utilizes feedback from the prosthetic leg and force sensors at the prosthetic foot to synthesize the control signals for the knee and ankle joints of AMPRO II. The device has a height of 470mm and weight of 4.5kg. The control framework of the prosthesis consists of two different strategies: impedance control and trajectory tracking. The impedance control was utilized during the stance phase, and the desired human joint angle trajectories were tracked by PD control during the swing phase.

The experiment was performed on one subject (age: 29 years, height: 175cm, weight: 75kg, healthy non-amputee male) who walked on a level-ground treadmill. We tested 5 different stiffnesses: no stiffness, 3 Nm/rad, 6 Nm/rad, 9 Nm/rad, and rigid foot. A treadmill speed was selected by user's preference (0.5 m/s). For each condition, the subject

walked 20 gait cycles. Kinematic data (i.e., knee and ankle joint angles of the prosthesis via the embedded encoder) and kinetic data (i.e., force at the toe) were measured. The subject used an adapter to simulate an amputee gait. In order to measure toe force data, 2 force sensors (FlexiForce, Phidgets Inc. Calgary, AB, Canada) were embedded at the prosthetic foot. A qualitative analysis for both the toe force profile and joint trajectories are performed without statistical analysis for this case study.

RESULTS AND DISCUSSION

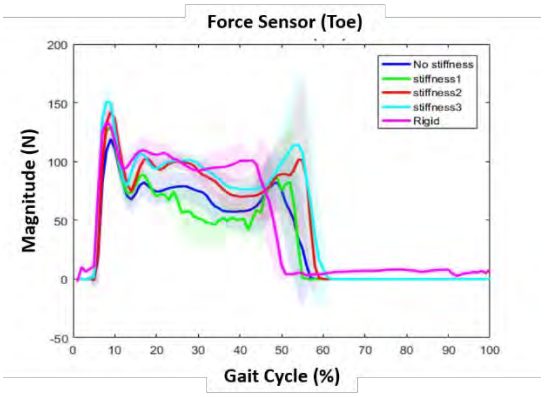

Figure 2: The bold lines are indicated the mean value of the toe force sensor data, and the shaded regions are indicated the range within one standard deviation.

Figure 2 shows the toe force profiles during the gait cycle with various toe stiffness conditions. During the foot-drop (around 10% of the gait cycle), there seems no prominent differences in the onset of first peak across the stiffness conditions. However, it is clearly observed that the onset of the second peak was delayed from 49% to 55% of the gait cycle as the stiffness increased from 3 Nm/rad to 9 Nm/rad. However, when the stiffness was infinite (i.e., rigid food), the onset timing did not follow this trend, but it happened too earlier (i.e., 43% of the gait cycle). Noting that the second peak of the vertical ground reaction force of normal human walking happens at around 50% of the gait cycle [5], toe joint contributes to the modulation of the timing of the push-off. Selecting appropriate toe joint stiffness will optimize the gait patterns of the powered transfemoral prosthesis.

Figure 3 shows the joint trajectories of both ankle and knee of the prosthesis. The dashed line is the trajectories for the normal healthy gait. Pearson correlation for the ankle trajectory was examined: r=0.90, 0.92, 0.89, 0.86, 0.88 for the five stiffness conditions. Pearson correlation for the knee trajectory was examined: r=0.97, 0.99, 0.96, 0.96, 0.96 for the five stiffness conditions. It was clearly seen that the correlation was the greatest when the stiffness was 3 Nm/rad whereas the correlation became the worse when the stiffness was too high (e.g., 9 Nm/rad or infinity).

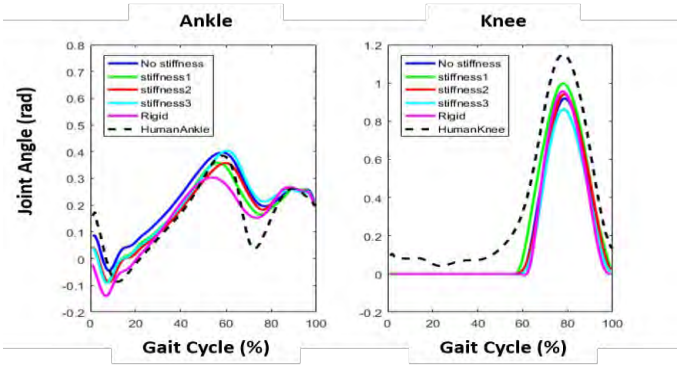

Figure 3: Ankle/Knee joint encoder data from the prosthesis compared to the human joint trajectories

CONCLUSIONS

In this pilot study, it was observed that the existence of the toe joint with appropriate stiffness enhanced both the onset timing of the push-off and the joint trajectory profiles for both ankle and knee. 3 Nm/rad was found to be optimal among 0, 3, 6, 9 and ∞ Nm/rad. We are now planning to conduct a systematic experiments with more number of subjects, motion capture system and force plates. We anticipate that optimal toe stiffness of the foot will provide optimal push-off with more normative joint trajectories for the powered transfemoral prosthesis.

REFERENCES

1. Gailey, et al., *J.Rehabil. Res. Dev.*, vol 45, no 1, pp15–30, 2008.
2. Neuman, *Kinesiology of the Musculoskeletal System: Foundations for Rehabilitation*, 2nd ed. St. Louis: Mosby, 2010.
3. Usherwood, et al. *Journal of The Royal Society Interface, 9.75, 2396-2402*, 2012
4. Honert, et al., *American Society of Biomechanics 2017*, 2017
5. Winter, *"The Biomechanics and Motor Control of Human Gait"*, University of Waterloo Press, 1987.

ACKNOWLEDGEMENTS

The authors thank to Namita Anil Kumar for the assistance to design a new prosthetic foot.

EFFECT OF A FOOT PAD ON THE PUSH-OFF AND JOINT TRAJECTORIES FOR THE POWERED TRANSFEMORAL PROSTHESIS: A PILOT STUDY

[1] Woolim Hong, [1]Shawanee Patrick and [1] Pilwon Hur

[1] Texas A&M University, College Station, TX, USA
email: [1]{ulim8819, shawaneepatrick, pilwonhur}@tamu.edu, web: http://hurgroup.net/

INTRODUCTION

A powered transfemoral prosthesis is an assistive device that has two actuators for ankle and knee joints to provide stable walking to the lower extremity amputees (above-knee). Transfemoral amputees commonly have gait abnormalities that can lead to long term problems, such as fatigue, arthritis and scoliosis [1]. Reducing these abnormalities could lead to a reduction in some of the long-term issues.

Human walking consists of several events: heel-strike, foot-drop, heel-off, push-off, and toe-off [2]. The entire stance phase comprised approximately 60% of the gait cycle [2]. Between heel-off and push-off, positive work is required to insert energy into the moving body and to transition from the stance phase to the swing phase [3]. Adding a pad to the rigid foot can modulate the stiffness and damping between the rigid foot and the ground, which can simulate the natural human foot during the walking [4]. However, no systematic studies have investigated the effects of the foot pads in the gait characteristics of powered transfemoral prosthesis.

In this study, we investigated the effects of the foot pad on the gait kinetics and kinematics of the powered transfemoral prosthesis. Specifically, joint trajectory profiles and the push-off force at the toe are examined while foot pad condition was varied. It is hypothesized that providing a foot pad will enhance the gait kinetics and kinematics of the powered transfemoral prosthesis compared with the rigid foot.

METHODS

A custom-built fully actuated powered transfemoral prosthesis (AMPRO II) was used. AMPRO II is the second generation of a powered prosthesis developed at Texas A&M University. AMPRO II utilizes

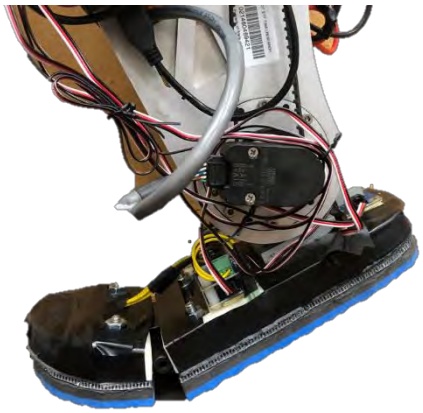

Figure 1: A foot considering a toe joint with spring steel for providing required push-off force. For this study, we constrained the toe joint with a rigid bar such that the stiffness of the foot was infinite. Please see the foot pad was attached to the existing foot of the prosthesis.

feedback from the prosthetic leg and force sensors at the prosthetic foot to synthesize the control signals for the knee and ankle joints of AMPRO II. The device has a height of 470mm and weight of 4.5kg. The control framework of the prosthesis consists of two different strategies: impedance control and trajectory tracking. The impedance control was utilized during the stance phase, and the desired human joint angle trajectories were tracked by PD control during the swing phase.

The experiment was performed on one subject (age: 29 years, height: 175cm, weight: 75kg, healthy non-amputee male) who walked on a level-ground treadmill. We tested 2 different conditions: no foot pad vs. foot pad. A treadmill speed was selected by user's preference (0.5 m/s). For each condition, the subject walked 20 gait cycles. Kinematic data (i.e., knee and ankle joint angles of the prosthesis via the embedded encoder) and kinetic data (i.e., force at the toe) were measured. The subject used an adapter to simulate an amputee gait. In order to measure toe force data, 2 force sensors (FlexiForce, Phidgets Inc. Calgary, AB, Canada) were embedded at the prosthetic foot. A qualitative analysis for both the toe

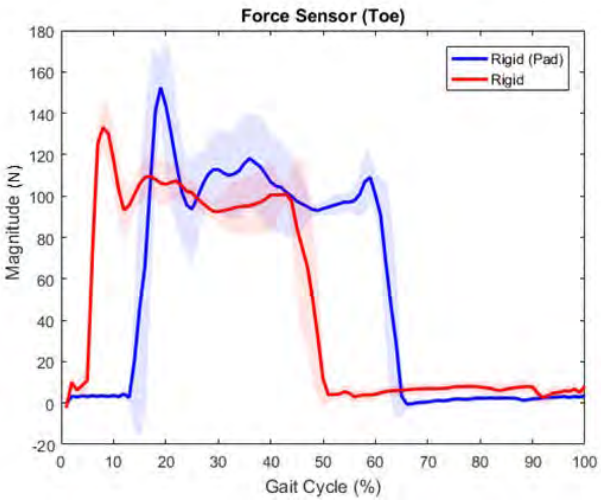

Figure 2: Force sensor (toe) data from 2 different cases: rigid foot with a pad vs. rigid foot without the pad. The bold lines are indicated the mean value of the sensor data, and the shaded regions are indicated the range within one standard deviation.

force profile and joint trajectories are performed without statistical analysis for this case study.

RESULTS AND DISCUSSION

Figure 2 shows the toe force profiles during the gait cycle with various foot pad conditions. For the rigid foot with no pad, the foot-drop happened around 10% of the gait cycle whereas for the rigid foot with a pad, the first peak happened around 20%. For the normal human gait, the first peak happens between 10% and 20% [5]. It is also clearly observed that the onset of the second peak was delayed from 43% to 60% for a rigid foot with a pad compared with a rigid foot without a pad. The delayed onset of the first peak is possibly due to the delayed transfer of the force to the force sensors due to the soft material of the pad. By varying the softness of the pad, the onset of the first and the second peaks seems to be modulated.

It is interesting to note that the second peak was delayed to 60%, suggesting that push-off may have occurred late compared with the rigid foot without a pad. Figure 3 supports this argument. When a foot pad existed, the push-off happened around 60% whereas when the pad was not used the push-off happened around 42% (Figure 3a). This was also supported by the ankle torque profile (Figure 3c). It was found from the literature that push-off usually happens between 50-60% of the gait cycle [5]. More

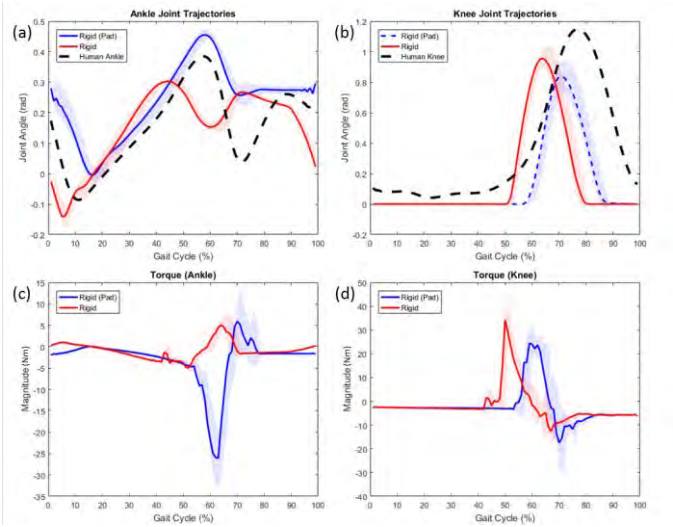

Figure 3: Ankle joint trajectory (a), knee joint trajectory (b), ankle torque (c), and knee torque (d) from 2 different cases: rigid foot with a pad vs. rigid foot without the pad. Dashed black line indicates the joint trajectory of the normal healthy gait.

interestingly, when a foot pad was used, the ankle and knee joint trajectories resembled the normal human walking with higher Pearson correlation (0.89 vs. 0.56 for ankle and 0.81 vs. 0.38 for knee).

CONCLUSIONS

In this pilot study, it was observed that the existence of the foot pad with appropriate softness enhanced both the onset timing of the push-off and the joint trajectory profiles for both ankle and knee. We are now planning to conduct a systematic experiment with more number of subjects, more conditions of the softness of the pad, motion capture system and force plates. We anticipate that optimal softness of the foot pad will provide optimal push-off with more normative joint trajectories for the powered transfemoral prosthesis.

REFERENCES

1. Gailey, et al., *J.Rehabil. Res. Dev.*, vol 45, no 1, pp15–30, 2008.
2. Neuman, *Kinesiology of the Musculoskeletal System: Foundations for Rehabilitation*, 2nd ed. St. Louis: Mosby, 2010.
3. Usherwood, et al. *Journal of The Royal Society Interface, 9.75, 2396-2402*, 2012
4. Honert, et al., *American Society of Biomechanics 2017*, 2017
5. Winter, *"The Biomechanics and Motor Control of Human Gait"*, University of Waterloo Press, 1987.

ACKNOWLEDGEMENTS

The authors thank to Namita Anil Kumar for the assistance to design a new prosthetic foot.

ENERGY EXPENDITURE DURING GEARED MANUAL WHEELCHAIR PROPULSION IN INDIVIDUALS WITH SPINAL CORD INJURY

[1] Omid Jahanian, [2,3]Barbara Silver-Thorn, [1] Scott J Strath, [3]Vaishnavi Muqeet, [4]Elizabeth T. Hsiao-Wecksler, and [1] Brooke A Slavens

[1] University of Wisconsin–Milwaukee, Milwaukee, WI, USA
[2]Marquette University, Milwaukee, WI, USA
[3] Medical College of Wisconsin, WI, USA
[4]University of Illinois at Urbana-Champaign, IL, USA
email: jahanian@uwm.edu, Web: www.uwm.edu/mobilitylab/

INTRODUCTION

Geared manual wheelchairs (GMWs) are a promising alternative propulsion mechanism for manual wheelchair users (MWUs) [1]. Similar to a multi-speed bicycle, they allow users to choose the option of wheeling in a lower gear. Previous studies [1-3] have suggested that using GMWs might be beneficial for MWUs to independently accomplish more strenuous tasks, while reducing the risk of secondary upper extremity injuries and pain. However, no research has evaluated the effects of using GMWs on energy expenditure and physical activity in manual wheelchair users. The purpose of this study was to investigate the effects of using GMWs on energy cost, and cost of transport of manual wheelchair propulsion in individuals with spinal cord injury (SCI).

METHODS

The study protocol was approved by the Department of Veterans Affairs (Milwaukee, WI) and the University of Wisconsin-Milwaukee (UWM) Institutional Review Boards. Ten adult male manual wheelchair users with SCI with an average age of 46.5 $\pm$ 13.6 years (ranging from 24 to 68 years) participated in this study. The average time as MWU for the participants was 14.4 $\pm$ 12.9 years (ranging from 7 months to 31 years); SCI levels ranged from T1 to L2. The average body mass index (BMI) was 25.7 $\pm$ 3.2 kg/m^2 (ranging from 22 to 31.7 kg/m^2).

Participants were instructed to refrain from caffeine and energy beverages for six hours and not to vigorously exercise for 12 hours prior to testing. Data collection was completed at the UWM Mobility Lab. Participants used their personal standard manual wheelchairs equipped with the IntelliWheels geared wheels (IntelliWheels, Inc., Champaign, IL) which allowed them to propel in direct drive (gear ratio of 1:1), or shift into a low gear (gear ratio of 1.5:1) [4]. Participants were asked to propel their wheelchair on a passive wheelchair ergometer instrumented with a speedometer for six minutes at their normal comfortable speed in both low gear (geared) and direct drive conditions, in random order. Ten minutes of rest separated each activity.

Oxygen consumption was measured using the $K4b^2$ portable gas analysis system (COSMED, Rome, Italy) during manual wheelchair propulsion. Cadence (stroke cycle frequency) during the tasks was calculated in Matlab based on the sagittal plane kinematics of a marker located on the third metacarpal recorded using a 3D Vicon T-series motion capture system (Vicon Motion Systems, Oxford, UK) [4]. The $K4b^2$ software was used to calculate the measures of energy expenditure, including oxygen uptake (ml/kg/min) and total energy expenditure (kcal). Cost of transport (cal/m) was calculated as the ratio of total energy expenditure to the travelled distance measured by the speedometer. As per Collins et al., one SCI metabolic equivalent (MET) was defined as oxygen consumption of 2.7 ml/kg/min, rather than standard one MET = 3.5 ml/kg/min in able bodied adults. The energy cost of manual wheelchair propulsion was reported in SCI METs [5]. For this purpose, oxygen consumption measured for 2-5 minutes (steady-state condition, coefficient of variation < 5%) were averaged across 30-second periods and divided by one SCI MET (2.7) [5]. Statistical analyses were completed with IBM SPSS software using separate

paired samples t-tests (significance level = 0.05).

RESULTS AND DISCUSSION

The results indicated that the travelled distance, propulsion speed, total energy expenditure, and energy cost were significantly less during the geared compared to direct drive condition (Table 1). The cost of transport was significantly higher during the geared condition. Gear ratio did not significantly affect cadence.

The energy cost results (Table 1) for both tasks indicate that propulsion on passive wheelchair ergometer was moderate intensity (3.0 – 6.0 METs) physical activity [6], similar to wheeling on carpet or grass [5]. The intensity of wheelchair propulsion was significantly lower during the geared condition. Significantly higher cost of transport during the geared condition demonstrate the lower energy efficiency in comparison to the direct drive condition, which may increase the physical activity and daily energy expenditure of MWUs with SCI. Increased energy expenditure in individuals with SCI may enhance overall health and decrease risk for cardiovascular disease [7]. The significantly decreased propulsion speed during the geared condition is primarily attributed to the reduction in the stroke distance, a direct effect of the gear reduction (1.5:1). Similar cadence in both wheel conditions indicate that participants perform both tasks at their comfortable cadence rather than comfortable speed.

CONCLUSIONS

The current investigation demonstrated that using GMWs at comfortable normal cadence may increase energy expenditure while decreasing the intensity of wheelchair propulsion. These results may be utilized to develop practical and accessible exercise recommendations based on manual wheelchair propulsion for individuals with SCI to maintain and promote their health. This work also has the potential to impact clinical decision making for wheelchair prescription and usage.

REFERENCES

1. Jahanian O, et al. *Proceedings of IEEE EMBC,* Orlando, FL, USA, 2016.
2. Howarth SJ, et al. *Clin Biomech* **25**: 21–28, 2010.
3. Finley M, et al. *Arch Phys Med Rehabil* **88**: 1622–1627, 2007.
4. Jahanian O, et al. *Proceeding of ASB'15*, Boulder, CO, USA, 2016.
5. Collins E, et al. *Med Sci Sports Exerc* ***42*****(4)**: 691-700, 2010.
6. Haskell W, et al. *Med Sci Sports Exerc* ***39*****(8)**: 1423-34, 2007.
7. Zachary L, et al. *J Spinal Cord Med* **39(1)**: 45-49, 2016.

ACKNOWLEDGEMENTS

The content of this work was developed under a National Institutes of Health (NIH) SBIR Phase II grant number 2R44HD071653- 02, and a student research grant from UW-Milwaukee College of Health Sciences.

Table 1: Mean and standard deviation of total energy expenditure, cost of transport, energy cost, total travelled distance, average propulsion speed, and cadence for direct drive and geared conditions.

	Direct Drive	**Geared**	**Statistical Results**	
	Mean ± SD	**Mean ± SD**	**t**	***p***
Tot. Energy Expenditure (kcal)	24.4 ± 6.1	21.1 ± 4.6	3.32	0.009 *
Cost of Transport (cal/m)	77.9 ± 23.8	101.2 ± 27.0	-8.81	< 0.001 *
Energy Cost (SCI MET)	4.5 ± 1.2	3.9 ± 0.9	3.17	0.011 *
Travelled Distance (m)	343.9 ± 140.1	227.0 ± 91.0	6.45	< 0.001 *
Propulsion Speed (m/s)	0.96 ± 0.39	0.64 ± 0.25	6.45	< 0.001 *
Cadence (1/min)	56.1 ± 9.2	55.5 ± 9.9	0.38	0.710

t = t-statistics; p = significance level; *: $p < 0.05$.

POWERED KNEE-ANKLE PROSTHESIS AND DUAL TASK WALKING IN UNILATERAL TRANSFEMORAL AMPUTEES: A PRELIMINARY INVESTIGATION

[1,2] Chandrasekaran Jayaraman, [1]Aileen Naef, [1]Shenan Hoppe-Ludwig, [1]Matt McGuire, [1,2] Arun Jayaraman

[1] Shirley Ryan Ability Lab, Chicago, IL, USA
[2] Department of Physical Therapy and Human Movement Sciences, Northwestern University, Chicago, IL, USA
email: chandrasekaran.jayaraman@northwestern.edu

INTRODUCTION

Gait deviations and the need to concentrate more on walking have been reported in individuals with transfemoral (above knee) amputation [1]. The need to concentrate more on walking could impede performance during demanding environments such as a concurrent walking and cognitive task (i.e. dual task (DT) paradigm). Gait deviations and need to concentrate on every step during walking have been identified as potential correlates to increase fear of falls in transfemoral amputees [1]. Consequently, any improvement to prosthetic design (mechanical or control system) that enables users to attain a gait behavior similar to healthy limb is beneficial. The Vanderbilt University powered knee-ankle prosthesis (Generation-3) (PKA), is currently one of the advanced prosthetic device for transfemoral amputees. The PKA has integrated communication between the knee and ankle joints have been shown to enable users to walk with a biomechanics similar to that of a healthy limb [2]. *However, it is presently not known if such a PKA could lead to normalized gait behavior during a DT walking paradigm. Consequently, the aim of this preliminary investigation is to compare the performance between the PKA and microprocessor knee (MPK) in DT walking paradigm*.

METHODS

Four transfemoral amputees (reason: cancer or trauma) currently use an advanced MPK were recruited and trained to use the PKA under various ambulatory environments (even and uneven surfaces, DT). All participants had the left side as their sound side (42.3(13.6) yrs; 3M/1F). Participants provided voluntary informed consent. An expert prosthesist ensured comfortable fit (customized socket) of the PKA for each participants. All participants' executed an elaborate device tuning with PKA and training protocol to use both the devices (their predicate MPK and PKA). This protocol has been extensively discussed elsewhere [2, 3]. On completion of the training (8-12 sessions), participants performed a DT walking test. Participants walked for 20 seconds along a 42 m walkway at their safest but fastest possible self-selected speed during the single task (ST) (only walking – 2 trials) and the DT (walking and serial subtraction by 7 from a random 3-digit number – 2 trials) with both devices (their predicate MPK and the PKA). Inertial measurement units (IMUs [3]) were placed at the ankles, knees and the sternum to measure the spatial-temporal gait parameters during the walking tasks. All IMUs were time synced with the atomic clock. Participants were instructed to give equal priority to both walking and the cognitive task during the DT walking. Sufficient rest was given between each walking trial.

10 healthy controls (HC) (25.3(3.1) yrs; 5M/5F) also performed the same ST and DT protocol in order for us to benchmark and compare the DT performance between healthy and the amputee group. The control did not use any by-pass or prosthetic device during the protocol.

Data analysis: Based on the DT literature [1] the following spatial-temporal gait parameters were extracted as outcome metrics from the post-processed IMU data at knees, (i) gait speed, (ii) cadence and (iii) stride time variability indexed as coefficient of variation of stride time (CV_{STime} %). A continuous wavelet transform was used to extract the spatial temporal parameters from the vertical acceleration of the knee IMU [3]. These outcomes metrics were extracted for the healthy controls and the amputee group from the ST and DT conditions. All data was averaged over 2 trials and each trial had 20 steps.

RESULTS AND DISCUSSION

Benchmarking protocol: For the HC, in comparison to the ST condition, (i) the mean gait speed(m/s) and mean cadence (steps/min) reduced ($p<.05$) and (ii) stride time variability ($CV_{STime\%}$) increased during the DT walking ($p=0.234$) (Table. 1, Fig. 1). These trends are consistent with DT literature [4]. This validates the efficacy of the DT protocol followed in this study.

Table 1: Speed and cadence comparison between ST and DT conditions.

Spatial-temporal variables	HC(mean(SE))		MPK(mean(SE))		PKA(mean(SE))	
	ST	DT	ST	DT	ST	DT
Speed (m/s)	2.22(.02)	1.95(.05)*	1.82(.02)	1.59(.01)	1.77(.01)	1.51(.04)
Cadence (steps/min)	144(.4)	134(.5)*	116(.8)	119(.4)	117(.3)	109(.5)
* p<.05 between ST and DT in HC						

Comparison prosthetic device performance: The group mean trends from the four participants with amputation are qualitatively compared with the group mean trends observed from the HC.

In the amputee group, while using the PKA device, the spatial-temporal gait parameters during the DT walking followed the same trend as that of HC group. However, this was not the case while using the MPK. In comparison to the ST condition, during the DT walking (i) the mean gait speed(m/s) reduced while using the MPK and PKA, (ii) the mean cadence (steps/min) reduced while using the PKA and increased while using MPK, and (ii) stride time variability ($CV_{STime}\%$) increased while using the PKA and reduced while using the MPK (Table. 1, Fig. 1).

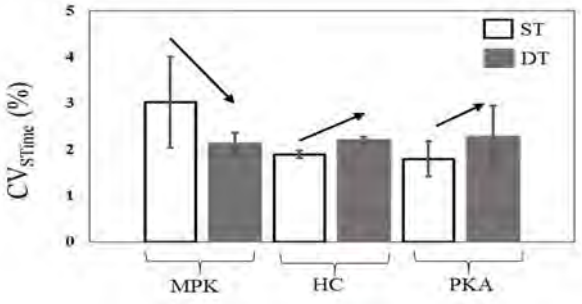

Figure 1: Qualitative comparison of trends for group mean stride time variability (CV_{STime}: mean(SE)) during ST and DT walking for HC and amputee group. The arrow mark shows that the $CV_{STime\%}$ trend is similar between HC and PKA for ST vs DT walking conditions. The MPK shows opposing trends.

The goal of this preliminary investigation was to compare the spatial-temporal gait characteristics during DT walking which using PKA. It was found that using the PKA enabled the four transfemoral participants to reproduce a mean gait behavior (deviation in spatial-temporal variables) that trended similar to HC during a DT paradigm. A potential reason for this is the PKA uses a powered knee and ankle, and the control system is designed to follow a preset trajectory that is similar to a healthy limb during the swing phase. The MPK is a passive device. Further the PKA also offers dynamic control (participant has partial control over cadence) to impart larger ranges of variable cadence than the MPK. These advantages while using the PKA could have led to spatiotemporal gait trends similar to HC. Participants showed near similar cognitive cost while using the MPK and PKA device. The DT paradigm was chosen to study the efficacy of this device because it closely emulates scenario that are often encountered in activity of daily living.

CONCLUSIONS

The PKA enabled individuals with unilateral transfemoral amputation to reproduce a gait behavior similar to HC during DT walking. The preliminary study shows the potential, such advanced device like the PKA offers over the MPK in a DT environment. These findings may hold potential for safer ambulation (fall risk) in individuals with unilateral transfemoral amputation when ambulating in different environments. The trends from this preliminary analysis is not broadly generalizable. However, this is a large ongoing clinical trial and these findings must be replicated with the larger sample. Further analysis to assess the implications of PKA for (i) fall risk and (ii) cognitive cost is warranted.

REFERENCES

1.Morgan et al. P & O International 2016, Vol. 40(4) 490 –496.
2.Lawson BE et al. IEEE Robotics and Automation Magazine 2014. 70-81.
3. C Jayaraman et al. Frontiers in Neuroscience 2018, (In press).
4. Dubost V et al. Gait & Posture 27 (2008) 138–143.

EFFECTS OF ISOKINETIC BI-AXIAL ANKLE MOVEMENT TRAINING ON ANKLE MUSCLE COACTIVATION PATTERN DURING BILATERAL STANDING IN THE ELDERLY WITH POST-STROKE HEMIPARESIS

[1]Hogene Kim, [1]Ji-Eun Cho, [1]Dohoon Koo,[2]Joon-Ho Shin

[1] National Rehabilitation Center Research Institute, Seoul, South Korea
[2] National Rehabilitation Center Hospital, Seoul, South Korea
email: hogenekim@korea.kr, web: http:// http://www.nrc.go.kr/nrc/english/

INTRODUCTION

Post-stroke hemiparesis is a major source of gait and balance impairments. Especially the foot drop syndrome, a more ankle extension (plantarflexion) along the talocrural (ankle) axis, causes an occasional failure of limb advancements during mid-swing phase of gait, and increases the trip-related fall risk and fall-related injuries [1].

Aiming at better gait and balance performance in the elderly with post-stroke hemiparesis, Ankle Movement Trainer (AMT) was developed to provide passive isokinetic bi-axial ankle movements along ankle (talocrural) and subtalar (talocalcaneal) axes while comfortably seated. The ankle movements are currently defined along 3 orthogonal axes [2]. However ankle movements approximately follow bi-axial movements along the ankle and subtalar joints, and the subtalar axis is naturally 42 degree tilted on average in sagittal plane [3,4]. The AMT was designed to move along the tilted subtalar joint axis during inversion/eversion.

The objective of this study investigated the effectiveness of four-week isokinetic passive bi-axial ankle movement training using AMT on ankle muscle co-activation pattern during bilateral standing. To evaluate the effectiveness of AMT ankle training, we evaluate normalized ankle muscle activation pattern during bilateral standing.

METHODS

Total 15 patients with post-stroke hemiparesis (6 females, age: 64.9±9.0yrs, duration: 9.5±5.6yrs) were recruited for this study. This study was approved by the NRC Institutional Review Board and all participants signed written informed consent form before the study (NRC2015-03-020).

The AMT exercise program consists of total 12 sessions (four week three sessions per a week) about 30 minutes per a session. A session consists of 20 repetitions of two simple movements (20 dorsi-/plantar flexion; 20 inversion/eversion) and 40 repetitions of two constrained movements (40 Dorsi-flexed Inversion/Eversion; 40 Everted Dorsi-/Plantar flexion) (Figure 1).

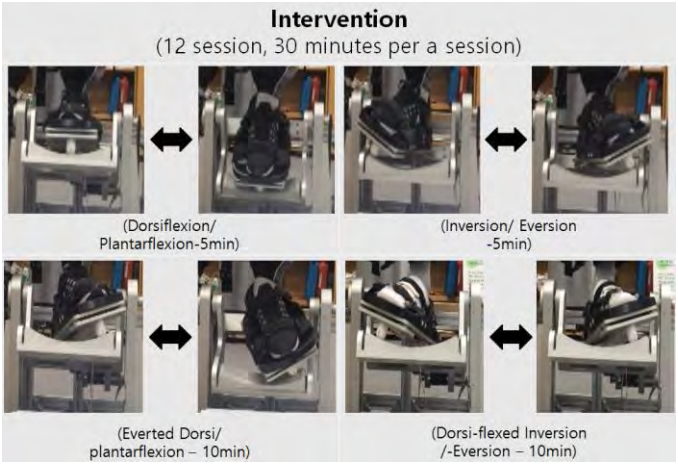

Figure 1 Experimental protocol of passive isokinetic bi-axial ankle movement training using Ankle Movement Trainer (AMT)

Wireless electromyography(EMG) electrodes measured four ankle muscles of Tibialis Anterior, Gastrocnemius, Medial Soleus, and Peroneus Longus while during bilateral standing. The normalized EMG activities were calculated by average EMG divided by maximum EMG before and after AMT training during 30 seconds bilateral standing.

In bilateral standing, subject comfortably stood with each foot on the force plates for 30 seconds with eyes open and closed. Balance performances of Pre-

and Post- AMT trainings were compared with paired-sample t-test (Significance level: $p<0.05$).

RESULTS AND DISCUSSION

Table 1 showed the normalized ankle muscle EMG activation pattern during 30 second bilateral standing. There was less muscle activation in stroke patients than healthy controls. The healthy control showed more muscle activation during eyes closed ($p<0.05$). The elderly with post-stroke hemiparesis showed there was AMT training effect on Tibialis Anterior that the muscle activation is significantly less during standing with eyes opened (Figure2).

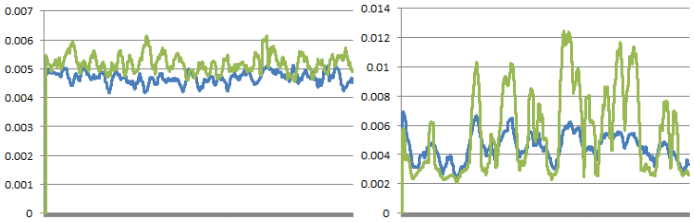

Figure 2 rms EMG muscle Activation Pattern in Tibialis Anterior(TA) during 30 second bilateral standing; Eyes closed (left) and open (right)

The Tibialis Anterior EMG activation patterns during passive isokinetic ankle movement in AMT are shown in Figure 3. While healthy control showed absent or less EMG activity around maximum dorsiflexion ROM, there were significantly elevated EMG activities during passive dorsiflexion compared to healthy controls. The increased EMG activity during passive dorsiflexion may indicate the shortened ankle muscle fiber in the elderly with post-stroke hemiparesis. The change in muscle property may affect the muscle activation pattern during bilateral standing.

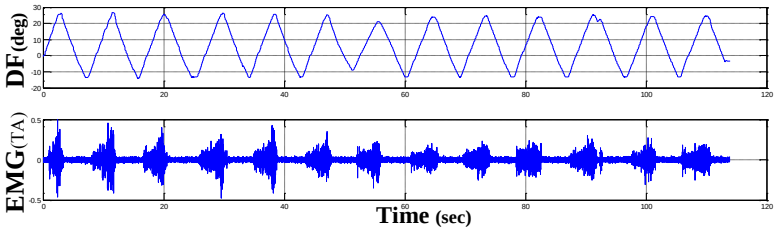

Figure 3 Muscle Activation Pattern (Tibialis Anterior, TA) during passive isokinetic ankle movement, DF denotes dorsiflexion (+ dorsiflexion, – plantarflexion)

In the future, the analysis on the ankle muscle EMG activation patterns during walking shows the synergetic relationship between balancing activity and gait performance, and the effectiveness of the AMT training that affects the fundamental changes in ankle structure in the elderly with chronic post-stroke hemiparesis.

REFERENCES

1. Thilmann AF, et al. *J Neurol, Neurosur & Psych* **54(2)**, 134-139, 1991
2. Letter to the editor. *J Biomech,* **35**, 543-548, 2002
3. Manter JT, *Ana Rec*, **80(4)**, 397-410, 1941
4. Jastifer JR et al. *Foot*, **24(4)**, 203-209. 2014

ACKNOWLEDGEMENTS

Translational Research Center for Rehabilitation Robots, Korea National Rehabilitation Center, Ministry of Health & Welfare, Korea (#NRCTR-IN16003,17004,18003).

Table 1: Normalized Ankle Muscle EMG activation pattern during 30 second bilateral standing. TA denotes Tibialis Anterior, GCM Gastrocnemius, mSOL medial Soleus, PL Peroneus Longus, EO Eyes Open, EC Eyes Closed

	Chronic Post-stroke Hemiparesis												Healthy Control		
	Before AMT training						After AMT training								
	Affected side			Non-affected side			Affected side			Non-affected side					
	EO	EC	p	EO	EC	p	EO	EC	p	EO	EC	p	EO	EC	p
TA	12.0	12.5	0.491	26.7	32.8	**0.040**	7.2	30.2	0.327	14.0	19.8	0.485	7.4	9.6	0.238
GCM	28.6	30.2	0.240	78.4	81.5	0.746	55.2	69.1	0.345	140.6	170.8	0.168	38.5	40.2	**0.028**
mSol	46.8	49.1	0.257	71.2	75.6	0.332	83.7	78.9	0.793	107.9	115.6	0.750	34.4	38.5	**0.004**

SIMULATED DEVELOPMENT OF AN ASSISTIVE DEVICE TO AID OLDER ADULTS IN ASCENDING STAIRS

[1]Anna Lee, [1,2]Anne Marie Jackson, [1,3]Elena Caruthers, [1,4]Sarah Roelker, [1]Laura Schmitt, [1]Ajit Chaudhari, [1]Robert A. Siston
[1]The Ohio State University, Columbus, OH, USA; [2]Ohio WillowWood, Mt Sterling, OH, USA
[3]Otterbein University, Westerville, OH, USA;[4]The University of Texas at Austin, Austin, TX, USA;
Email: lee.6339@osu.edu; web: https://nmbl.engineering.osu.edu/

INTRODUCTION

Up to 22% of older adults struggle ascending stairs [1]. Several devices exist that facilitate stair climbing such as the Stair Lift (a powered chair that carries users up stairs) [2], EZ-Step (a half sized step attached to a cane) [3], and the Honda Walking Assist (a motorized exoskeleton at the hips) [4], but devices assisting joints like the knee and ankle and inexpensive devices such as springs have not been investigated. Previous work suggests that maximal stair ascending velocity is highly dependent on knee and ankle power [5], demonstrating that knowledge of how assistive devices affect muscle forces and activations could improve the design of assistive devices for ascending stairs.

Musculoskeletal simulations have provided a powerful way to analyze how assistive devices impact muscle recruitment and energetic cost during running [6] and long jumping [7]. The effects of assistive devices during stair ascent have not been simulated. Therefore, the purpose of this study was to investigate the effects of simulated assistive devices on the muscle forces and metabolic cost of older adults ascending stairs.

METHODS

Four healthy participants (4 female, age = 65.00 ± 4.76 years, height = 1.61 ± 0.02 m, weight = 58.59 ± 6.11 kg) provided IRB-approved written consent. We applied markers to participants using the Modified Point Cluster Technique with additional markers on the iliac crests and upper limbs [8]. Marker data were collected at 150 Hz using 10 Vicon MX-F40 cameras (Vicon; Oxford, UK) and filtered using a fourth-order Butterworth filter at 6 Hz. Ground reaction forces were collected using Bertec 4060-10 force plates (Bertec Corp; Columbus, OH) at 1,500 Hz. Surface EMG data sampled at 1500 Hz were collected bilaterally from the rectus femoris, vastus medialis, vastus lateralis, medial gastrocnemius, lateral gastrocnemius, soleus, semimembranosus, and biceps femoris (Telemyo DTS, Noraxon USA, Inc; Scottsdale, AZ). Participants ascended the stairs at a self-selected speed, and one trial was selected for simulation.

We created individual models scaled from the Full Body Model 2016 in OpenSim 3.3 [9]. We used Inverse Kinematics (IK) to minimize the difference between experimental and virtual markers [9]. We reduced inconsistencies between IK model kinematics and experimental GRFs using the Residual Reduction Algorithm [9]. We ran Static Optimization (SO) to resolve joint torques into individual muscle forces [10]. The SO-simulated activations were compared with experimental EMG to verify the simulations [11].

We then added ideal massless torsional springs to one joint at a time at the ankle, knee, and hip. A total of sixty simulations, fifteen per participant, were run with spring stiffnesses for each joint varied by 1 Nm/deg increments from 1 to 5 Nm/deg. We again ran SO while maintaining the original kinematics and kinetics. We estimated metabolic cost using the sum of the activations squared of all of the assisted leg's lower extremity muscles. Changes in metabolic cost and muscle

forces estimated from SO were then compared to a baseline of the original unassisted participant.

RESULTS AND DISCUSSION

The average global metabolic cost increased for all passive elements. A torsional spring located at the ankle with stiffness k=1 Nm/deg increased global cost by 3±11%, while a spring with k=5 Nm/deg increased global cost by 138±91%. Two participants decreased in global metabolic cost when a 1 Nm/deg spring was at the ankle. At the knee, the least stiff spring increased global cost by 15±100% and the stiffest spring increased global cost by 1268±69%. When the 1 Nm/deg spring was at the hip, global cost increased by 15±25%, while the 5 Nm/deg spring increased global cost by 544±208%. One participant decreased in global cost when the 1 Nm/deg spring was at the hip.

The passive elements increased and decreased individual muscle forces depending on the assisted joint. The max force in the soleus (SOL) decreased by 13±6% compared to the unassisted participant when a 1 Nm/deg spring was at the ankle, but the max force in the tibialis anterior (TA), semimembranosus (SM), and vastus lateralis (VL) increased (Figure 1). A spring with k=5 Nm/deg at the ankle decreased max force in the SOL by 36±19%. A 1 Nm/deg spring at the knee decreased max force in the VL by 77±5%, while a 5 Nm/deg spring decreased max force in the VL by 92±9%, and increased max force in the gastrocnemius medialis (GMED), TA, and SM. When a 1 Nm/deg spring was at the hip, the max force in the SM decreased by 25±19%, while a 5 Nm/deg spring decreased the max force in the SM by 90±19% and increased the max force in the TA and GMED.

CONCLUSIONS

To our knowledge, this is the first study to examine the effects of simulated assistive devices on stair ascent. Our results demonstrate that a torsional spring at the ankle with k=1 Nm/deg was the least metabolically expensive simulated assistive device. However, overall metabolic cost increased when even the least stiff spring was applied to any joint. While previous studies showed a decrease in overall metabolic cost during assisted running [6], our results suggest that the use of a passive assistive device has the potential to reduce metabolic cost in only certain muscles and not overall during stair ascent. Further simulations of assistive devices on individuals with muscle weakness are needed to understand the impact of assistive devices on stair ascent in that population.

REFERENCES

1. Freedman, VA et al. *Am. J. Public Health.* **88**(10): 1457-1462, 1998.
2. https://www.bruno.com/products/stairlifts
3. http://www.ez-step.com
4. http://world.honda.com/Walking-Assist
5. Larsen, AH et al. *Scandinavian Journal of Medicine & Science in Sports.* **19**(5): 678–686, 2009.
6. Uchida, TK et al. *PLOS ONE.* **11**(9): 1-19, 2016.
7. Ong, CF et al. *TBME.* 1-10, 2014.
8. Jamison, ST et al. *J Biomech.* **46**(13): 2236-2241, 2013.
9. Delp et al. *IEEE Trans Biomed Eng.* **54**(11), 2007.
10. Crowninshield et al. *J Biomech.* **14**: 793–801, 1981.
11. Hicks, JL et al. *J Biomech Eng.* **137**(2): 0209051–02090524, 2015.

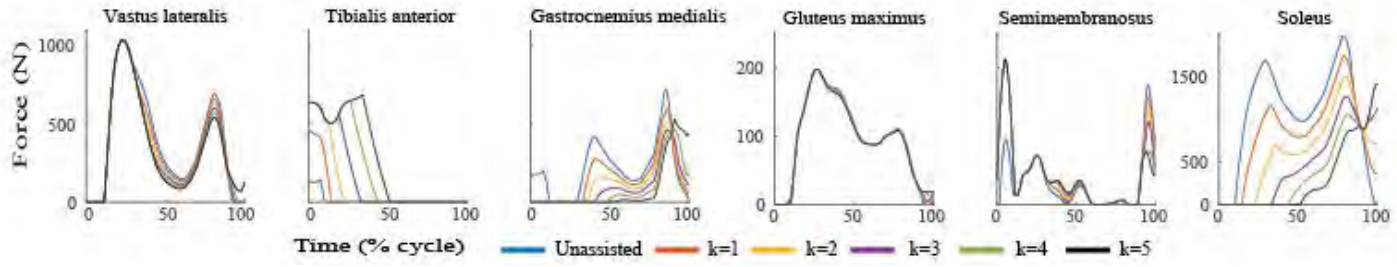

Figure 1: Selected muscle forces for one representative participant with varying spring stiffness at the ankle

Developing an Exoskeletal Device to Increase the Efficiency of Moderate Running

Alice Luanpaisanon, Michael Donovan, Peter Rhodes, and Craig M. Goehler

Department of Mechanical Engineering and Bioengineering, Valparaiso University, Valparaiso, IN, USA
email: craig.goehler@valpo.edu

INTRODUCTION

The ankle–foot complex plays an important role in human locomotion. It is also one of the most frequently injured joints in the body. The direct causes of the injuries vary, but often occur while running, jumping, or through general overuse of the joint. In particular, the ankle flexor is crucial to providing vertical support and forward progression of the body [1]. One possible method for minimizing the risk of ankle injury is the use of exoskeletal devices, which can potentially relieve some of the stress experienced by the ankle flexor. Ankle exoskeletons are already being used to help both impaired and unimpaired individuals augment their mobility [2]. Exoskeletons have the potential to improve and assist walking and running during a variety of exercises by providing additional energy for propulsion.

One of the major challenges of designing a wearable exoskeleton at the ankle joint is the fact that the device can often upset the wearer's natural gait [3]. The device may lead to a series of issues elsewhere, including greater reliance on other muscles or increased stress in the ankle joint due to an alternate gait and increased total weight of the orthosis and the limb. The goal of this research project is to develop an ankle-based exoskeletal device that will improve the efficiency associated with moderate running and lessen the strain on involved joints, with an emphasis on simplicity. The design will use mechanical power from the passive spring elements to capture energy of motion as well as energy of impact and return it to the wearer.

METHODS

Prior to determining a design, a literature review was performed in order to determine the movement style and gait patterns of intermediate level runners. This research helped to rule out initial design ideas of creating blade-like attachments to a wearable boot, as seen in Fig. 1, due to that method demonstrably affecting the user's natural gait [3].

Another possible design was an exoskeletal device that solely captured energy from the movement of the ankle. These kinds of devices generally attached easily to the wearer's shoe, and included an elastic element from the heel to the calf. However, these devices have no way of capturing the energy lost in the impact of the user's foot with the ground. We wanted to be able to capture both the impact energy and the energy associated with the ankle movement, while keeping the device simple.

Design ideas then centered on an assortment of springs being implanted into an enlarged sole of a shoe such that the user would be held only slightly off the ground. This would ensure that the user is still able to enjoy the benefits of increased force to propel them in the direction of their choosing, while minimizing the impact of the device on the user's natural gait. In order to reduce costs and maintain simplicity, the exoskeleton became an attachable sole for the shoe rather than the shoe itself. This allows for users to strap the sole on and off at their leisure while removing bulk, expense, and design complexity.

A concern was that the increased force resulting from the springs would inadvertently cause greater stress and fatigue to the muscles in the lower leg. The extra force could also directly translate into a user's foot and cause undue stress to joints. To account for the increased force, a surgical tubing "ligament" was added (component 3 in Figure 2). This ligament connects the extra sole to a strap right below the user's knee and acts as a supplementary "calf muscle" to reduce the force on lower leg muscles while spreading out the area the force from the ground is applied over. Importantly, this is also expected to reduce force over the ankle joint.

RESULTS AND DISCUSSION

The design we arrived at combines several approaches to capturing the kinetic energy of walking or running in order to be able to accommodate different types of motion. We also wanted the device to be built to accommodate a running shoe. This means the device does not need to be sized precisely to the individual wearer.

The final result is a device that straps onto the wearer's shoe and calf as seen in Figure 2. The device allows full mobility in the ankle joint. The design includes an array of compression springs on the sole of the boot. These springs absorb the energy of impact and return it to the wearer as kinetic energy. The actual sole is separated into two different sections to better adapt to terrain changes and to mimic foot flexion. The other energy storing element is a tensile spring that captures energy from ankle flexion and returns it as kinetic energy, essentially assisting the calf muscles.

Our goal for the first version of this prototype is to test our initial design and adjust it to optimize its function for an easy to moderate running speed. We would then like to test a modified elastic element on the ankle. This modified elastic element would allow for control of how and when energy is stored and released. The next goal, in the following iteration of the device, would be to design similar modified compression elements on the sole of the boot.

Figure 1: "Blade-design" exoskeletal device.

Figure 2: CAD model of the proposed device. (Components: 1 - Compressive elastic elements, 2 - Separated sole, 3 - Tensile elastic element, 4 - Shoe straps, and 5 - Calf straps)

FUTURE WORK

We intend to expand the scope of this project to a wider range of activities, including walking and sprinting. This will require the development of new techniques for passively storing and releasing energy; namely, elements that allow for control of how energy is stored and released. These new techniques could be used in applications beyond human locomotion, and potentially beyond the field of biomechanics. Practically, this will give people greater freedom to experience running and nature despite any physical limitations. In the future, this technology could be applied to people with limited locomotion abilities, such as the elderly, to improve their quality of life.

REFERENCES

1. *Jimenez R, et al. Medical Engineering and Physics,* ***34****(10), 397-408, 2012.*
2. *Steele K, et al, Journal of Biomechanics, 59, 50-58, 2017*
3. *Zhu A, "Run Like An Animal With Bionic Boots." Popular Science, 2015*

THE INFLUENCE OF RETURN TO RUN PROGRAM ON FOOT STRIKE AND LOADING RATE WHILE RUNNING USING A PASSIVE-DYNAMIC ANKLE-FOOT ORTHOSIS

Jenny Anne Maun, Katherine Sharp, Julianne Stewart, Kimberly Rowe, and Marilynn Wyatt
Naval Medical Center San Diego, San Diego, CA, USA
email: jennyanne.c.maun.ctr@mail.mil

INTRODUCTION

The Intrepid Dynamic Exoskeletal Orthosis (IDEO®) is a carbon fiber, passive-dynamic ankle-foot device that provides wounded servicemembers the ability to perform low- to high-level functional activities, such as walking and running [1,2]. After receiving their custom-made, energy-storing braces, IDEO users are required to participate in the Return to Run (RTR) Program [1]. This intense, sports medicine-based rehabilitation program was created to improve strength, power, multidirectional agility, and running technique in order to safely optimize energy return in the IDEO [1]. Optimal energy return in the IDEO occurs with a midfoot strike (MFS) to forefoot strike (FFS) due to the brace's plantarflexed position, allowing proper loading of the carbon fiber struts [1,2]. A rearfoot strike (RFS), however, creates a knee extensor moment by pushing the IDEO's tibial cuff posteriorly, causing a potential for injury [1,2]. Previous research has focused on IDEO running [2] but it is unknown whether the IDEO users' running mechanics were influenced by the amount of training completed in the brace at the time of the running study. Therefore, the purpose of this study was to determine if users with an increased number of RTR sessions were better able to adopt a MFS/FFS with low loading rate than those with a smaller number of RTR sessions. Variables investigated were strike index (SI) and vertical average loading rate (vALR).

METHODS

Overground self-selected jogging speeds (4.2±0.48m/s) were collected from five male, military servicemembers who use the IDEO due to lower-limb injuries (age: 30.6±5.5yrs; height: 1.8±0.04m; weight: 98.7±9.1kg). Patients provided written informed consent under a research study (CIP# NMCSD.2014.0026) approved by the Naval Medical Center San Diego Institutional Review Board. All patients were cleared for high-level activity by their providers and participated in the RTR Program. Patients ran through a mobile motion-capture system consisting of a 50m straightaway track with 12 Motion Analysis Corp. cameras (Santa Rosa, CA, USA) used for marker tracking and four embedded force platforms (Kistler Instrument Corp., Amherst, NY, USA) for analog data collection. A six degrees-of-freedom (6DOF) marker set was used with target and analog data processed in Visual3D (C-Motion Inc., Germantown, MD, USA) using a fourth order, Butterworth filter with cut-off frequencies at 8Hz and 50Hz, respectively. A successful session required a minimum of five strides and three clean force plate strikes per lower-limb.

SI was calculated at initial contact (RFS ≤33%; 33< MFS <68%; FFS ≥68%) from two additional markers on each shoe used to determine each patient's shoe length [3]. vALR was calculated from 20-80% between initial contact to impact peak of the vertical ground reaction force (vGRF) [3].

RESULTS AND DISCUSSION

Strike indices: There was no change in SI (Fig. 1) with an increased number of RTR sessions where Patient 3 had the most sessions and Patient 4 had the least sessions (Table 1).

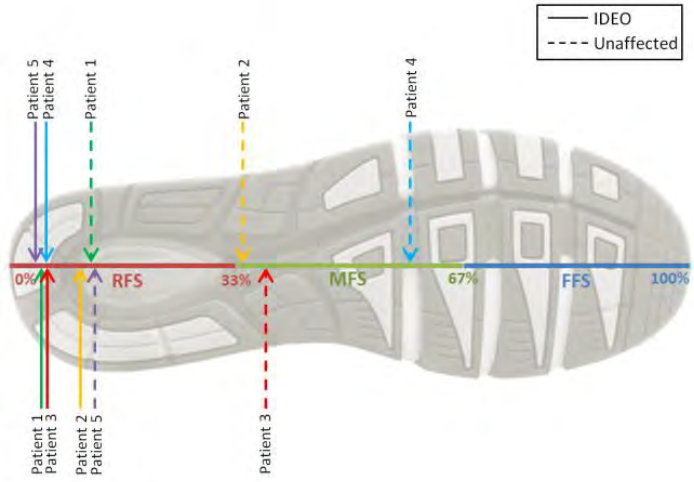

Figure 1: Location of all patients' SI on the bottom of a shoe with each patient in a different color and the heel at 0% and the toe at 100%.

All patients ran with a RFS on their IDEO limb (6.04±1.8%). Two of the five patients ran with a symmetrical foot strike pattern with a RFS on their unaffected limb (12.3±0.3%) while the other three patients ran with an asymmetrical foot strike pattern with a MFS on their unaffected limb (43.9±10.3%). Previous literature reported asymmetrical foot strike patterns exhibited by most of their IDEO users; those patients adopted a MFS on their IDEO limb, and used a FFS on their unaffected limb [2]. In this study, however, some patients that showed a symmetrical foot strike pattern were a RFS. A MFS only occurred on their unaffected limb. The lack of a MFS/FFS on their IDEO side in this study is interesting and circumstances influencing this are worthy of further investigation. Since a main goal of learning to use the IDEO is to adopt a MFS/FFS, more retraining time may be necessary to consistently optimize their energy return and reduce limb asymmetry while running [1,2].

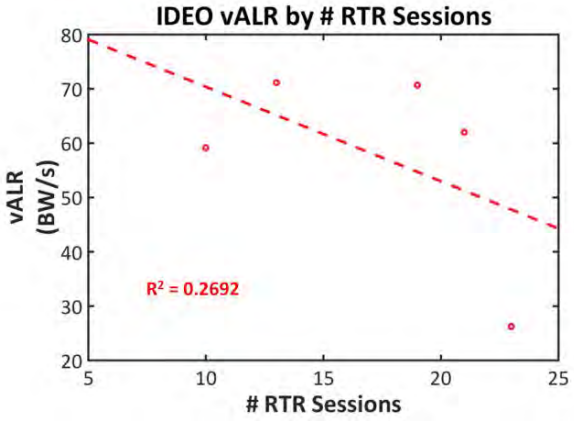

Figure 2: Relationship between vALR and # RTR sessions of the IDEO limbs using a linear fit line (dashed).

Vertical average loading rate: There was a trend in decreased vALR with an increase in RTR sessions (R^2 = ~0.27; Fig. 2) except with Patient 4 (Table 1). vALR decreased in both the IDEO (57.8±12.6BW/s) and unaffected (79.9±21.3BW/s) limbs. These results are similar to previous literuatre [2] where asymmetrical loading rates occurred between limbs with 43% higher loading on the unaffected limb than the IDEO limb. Although vALR decreased, patients in this study may still be at risk because four of the five patients' loading rates were similar to runners with tibial stress fractures that reported a vALR of ~78.9BW/s [3]. Therefore, changes to the rehabilitation protocol may help minimize loading rates which could decrease the risk of these overuse injuries [2,3].

CONCLUSIONS

This study aimed to determine whether IDEO users' ability to adopt a MFS/FFS and a low loading rate improved with increased RTR sessions. A trend revealed that vALR decreased with more RTR sessions. On the other hand, SI may need a longer retraining time before changes are observed. Future work will continue to measure these variables as more patients complete the RTR program, and will also look into power generation, kinematics, and potentially analyzing long-term IDEO users while running.

REFERENCES

1. Owens et al. *J Trauma*. **71**(1):S120-124, 2011.
2. Russell Esposito and Wilken. *Med Sci Sports Exerc*. **49**:30, 2017.
3. Milner et al. *Med Sci Sports Exerc*. **38**(2): 323-8, 2006.

ACKNOWLEDGEMENTS

The authors would like to thank Tatiana Djafar, Trevor Kingsbury, and John-David Collins for data collection, processing, and technical support and General Dynamics Information Technology. This work was supported (in part) by the Extremity Trauma and Amputation Center of Excellence.

DISCLOSURE STATEMENT: The views expressed herein are those of the author(s) and do not necessarily reflect the official policy or position of the Department of the Navy, Department of Defense, or the U.S. Government.

Table 1: SI and vALR of both limbs of all patients from most to least (left to right) number of RTR sessions.

		Patient 3	Patient 2	Patient 1	Patient 5	Patient 4
# RTR Sessions		**23**	**21**	**19**	**13**	**10**
SI (%)	**IDEO**	5.77	10.40	4.69	3.90	5.24
	Unaffected	37.83	34.50	11.91	12.59	59.23
vALR (BW/s)	**IDEO**	26.26	61.96	70.64	71.17	59.18
	Unaffected	40.43	81.51	84.31	126.96	66.04

DESIGN OF A FRAGILE OBJECT FOR EVALUATING GRIP PERFORMANCE WITH POWERED PROSTHESES

[1]Brian McCollough, [1]Andrew Thoreson, [1]Karen Andrews, [2]Marco Santello, [1]Kristin Zhao
[1]Mayo Clinic, Rochester, MN, USA
[2]Arizona State University, Tempe, AZ USA
email: zhao.kristin@mayo.edu

INTRODUCTION

User control over powered prosthetic devices has previously been evaluated by tasking the user to manipulate objects that are instrumented or have an engineered failure load [1, 2]. Manipulating these "fragile objects" without triggering the failure mechanism demonstrates fine control of the prosthetic and the ability to safely handle delicate items in tasks of daily living. Previous fragile object designs have included instrumentation with load cells that provide user feedback, and magnetic devices that disassemble when a load threshold is reached. Drawbacks to such designs include their weight and wiring that can interfere with device performance and increase test complexity.

The goal of this work was to create a wireless fragile object with a fuse having consistent mechanical strength to be used in a modified box and blocks test for prosthetic hand users [3]. The objective of the modified test is for the user to be able to perform tasks with the box without breaking the mechanical fuse inside. This is representative of handling breakable objects in everyday life.

METHODS

Design

The design objectives were to develop a fragile object that could be fabricated using primarily 3D printing manufacturing methods. The object was to break under a uniaxial load applied to one axis of the device with application of sufficient load. The dimensions of the device were to be approximately 50 mm x 50 mm x 50 mm.

Initial designs for the fuse were based on a column with stress riser features and proved to be too strong and ductile. A wishbone-shaped fuse design was demonstrated to behave like a beam subjected to three-point bending, and failed at levels that were much more appropriate for this application and in a more brittle manner. To tune the strength of the design, additional features were added to the center of the beam where stresses were highest, to further increase stress and reduce fuse strength (Figure 1). Two designs developed that had two distinctly different strength levels.

The box designed to hold the fuse included a top and bottom half, with slots and grooves on each of its four mating sides to align components and prevent binding. The top half includes a feature to hold the upper part of the fuse in place. The bottom half has guides to control the movement of the fuse to hold it in place (Figure 2).

Fabrication

All components were printed using a Maker Select 3D printer (Monoprice, Brea, CA) with polylactic acid (PLA) filament (3D Solutech, Seattle, WA). Autodesk Inventor (San Rafael, CA) was used to design the objects. Cura software (Ultimaker, Cambridge, MA) was used to convert STL code to g-code. The fuses used a 10% infill density, and the box used a 30% infill density. Each used 0.4 mm minimum side thickness and 0.6 mm top/bottom thickness guidelines. Each of these designs were fabricated and subjected to mechanical testing.

Testing

Fuse designs were tested using a servohydraulic mechanical loading frame (858 Mini Bionix II, MTS Systems, Eden Prairie, MN) under displacement control at a rate of 5 mm/min.

Each of the final fuse designs were tested within the box housing to confirm that failure strength was unchanged when added to the assembly. After each fuse failed it was placed back in the box and retested to examine the post failure compliance of the device.

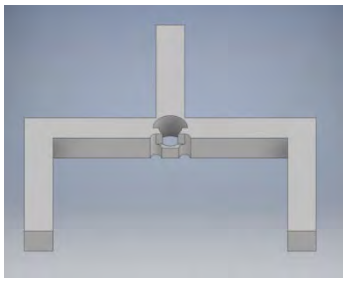

Figure 1: CAD rendering of the final high strength mechanical fuse.

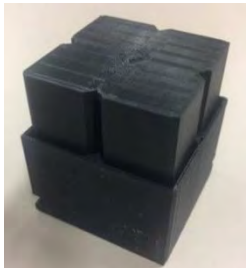

Figure 2: Photo of the box to hold the mechanical fuse.

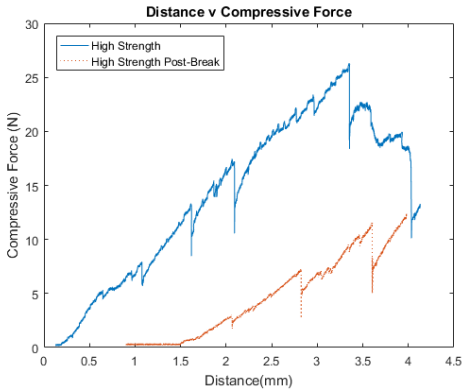

Figure 3: High strength test of mechanical fuse in box pre and post break.

RESULTS AND DISCUSSION

After the testing of the different types of mechanical fuses, two final designs were selected for their strengths; one design was shown to have a mean breaking strength of 9.24 ± 0.67 N, and the second a mean breaking strength of 26.49 ± 0.81 N. These two strengths were sought based on different markers. The lower strength of 9.24 N was sought to be similar to the strength of previous test boxes [1]. The higher strength of 25 N was selected based on the breaking strength of an egg during an egg drop test.

Each fuse was tested in the box to make sure the strength was not affected. The low strength fuse had a mean strength of 9.78 ± 0.78 N in the box, and a mean pre-break stiffness of 5.93 ± 0.91 N/mm. Post failure testing showed a mean post-break stiffness of 3.08 ± 0.39 N/mm. Failure was confirmed by opening the box and visually inspecting the fuse for a break.

The high strength fuse had a mean strength of 25.80 ± 1.31 N in the box, and a mean pre-break stiffness of 10.55 ± 3.30 N/mm. Post failure testing showed a mean post-break stiffness of 5.8 ± 0.54 N/mm (Figure 3).

In addition to MTS testing, each of the final fuses in box was physically handled to get a qualitative feeling of the fragile box, as its intended use will be a sensory test. Each box was able to be broken by hand. There was a resistance difference after breaking each of the fuses. For the weak fuse the difference was difficult to notice and the fuse could be easily broken without detection. In the case of the strong fuse there was a noticeable change in the resistance, as well as an audible cracking sound when the fuse broke.

CONCLUSIONS

The 3D printed mechanical fuses were demonstrated to have consistent breaking strength through multiple tests. We have demonstrated that a basic design with slight alterations of key features can result in two distinct breaking strengths, and that introducing them into the box housing does not greatly impact the fuse strength. While failure of the higher strength fuse is apparent, the failure of the lower strength fuse is more difficult to detect. Future work will include the reduction of friction inside the box and the testing of the box with a prosthetic hand.

REFERENCES

1. F. Clemente et al.: Non-invasive, Temporally Discrete Feedback of Object Contact and release Improves grasp control of Closed-Loop Myoelectric Transradial Prostheses, *IEEE Trans Neural Sys & Rehab Eng* 24, (12):1314-22, 2015.
2. S. Gorniak, V. et al.: Manipulation of a fragile object *Ex Brain Res* 202(2):413-30, 2010.
3. V. Mathiowetz, G. et al.: Adult norms for the box and block test of manual dexterity, *Am J. Occupat Ther* 39(6):386-91, 1985.

ACKNOWLEDGEMENTS

This work was supported by the Mayo Clinic-Arizona State University Team Science Grant Program.

RELIABILITY TESTING OF THE SMAPP DEVICE FOR CHARACTERIZING ANKLE FOOT ORTHOSIS STIFFNESS

Meghna Menon, Deema Totah, Robert Chisena, Albert Shih, Deanna Gates, Kira Barton

University of Michigan, Ann Arbor, MI, USA
email: menonmeg@umich.edu, web: http:// brg.engin.umich.edu/

INTRODUCTION

Ankle-Foot Orthoses (AFOs) are prescribed medical devices which provide support for patients with ankle impairment. The effectiveness of AFOs is dependent on their torsional stiffness. There are several existing devices that have been developed to measure AFO torsional stiffness [1], with each design having its own contributions and limitations. In reviewing these, the authors identified four key design features necessary for producing an accurate and versatile stiffness measurement device. To facilitate the development of a single cohesive device, the authors developed a novel Stiffness Measurement Apparatus (SMapp) that combines these four key features into a single framework:

1. **Applied Forces:** SMapp applies forces through a calf-surrogate ring [2] rather than directly at the ankle [3]. This allows the device to mimic loading during gait.
2. **Spurious Hysteresis Mitigation:** The calf-surrogate ring is positioned on a linear bearing [2], which prevents spurious hysteresis effects due to AFO slippage.
3. **Device Actuation:** SMapp is automatically actuated rather than manually-operated [2], allowing for accurate and customized movement control, and cyclic fatigue testing.
4. **AFO Diversity:** SMapp footplate clamp design allows for testing over a wide range of AFO sizes.

The purpose of this study was to determine the inter-operator, inter-day and intra-day reliability of the SMapp for a range of AFOs.

METHODS

Two operators were asked to measure the stiffness of three AFOs: two 3D printed (1 nylon and 1 carbon fiber) AFOs and one traditional thermoplastic AFO. Each operator tested each AFO for six deflection cycles on two separate days.

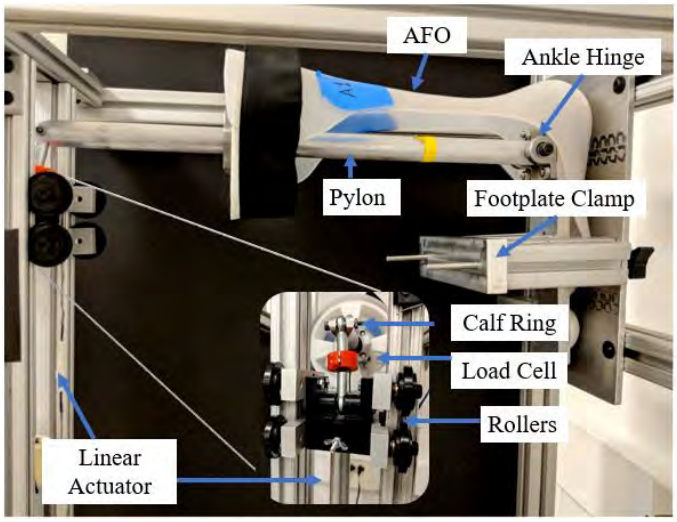

Figure 1: SMapp System with an AFO

The SMapp (Figure 1) consists of a linear actuator attached in series with a load cell. The linear actuator rotates the shank of the AFO about the ankle joint, mimicking gait. The angle of the shank is determined via user input and cycled between -4° (plantarflexion) and 23° (dorsiflexion) for this study.

Torque is calculated from tension and compression of a load cell placed in series with the pylon holding the AFO shank in place. The angular displacement of the linear actuator is measured via a potentiometer built into the linear actuator.

SMapp reliability was evaluated using an Intraclass Correlation Coefficient (ICC) to determine the data set correlations for inter-operator, inter-day and intra-day conditions. Torque and joint data were low-pass filtered, and the 2nd to 6th cycles were averaged for the inter-operator and inter-day analyses. Data were processed in Matlab and single-measures ICCs were calculated in SPSS using a two-way mixed model to test for absolute agreement. An ICC ≥ 0.75 was considered to indicate good reliability [4].

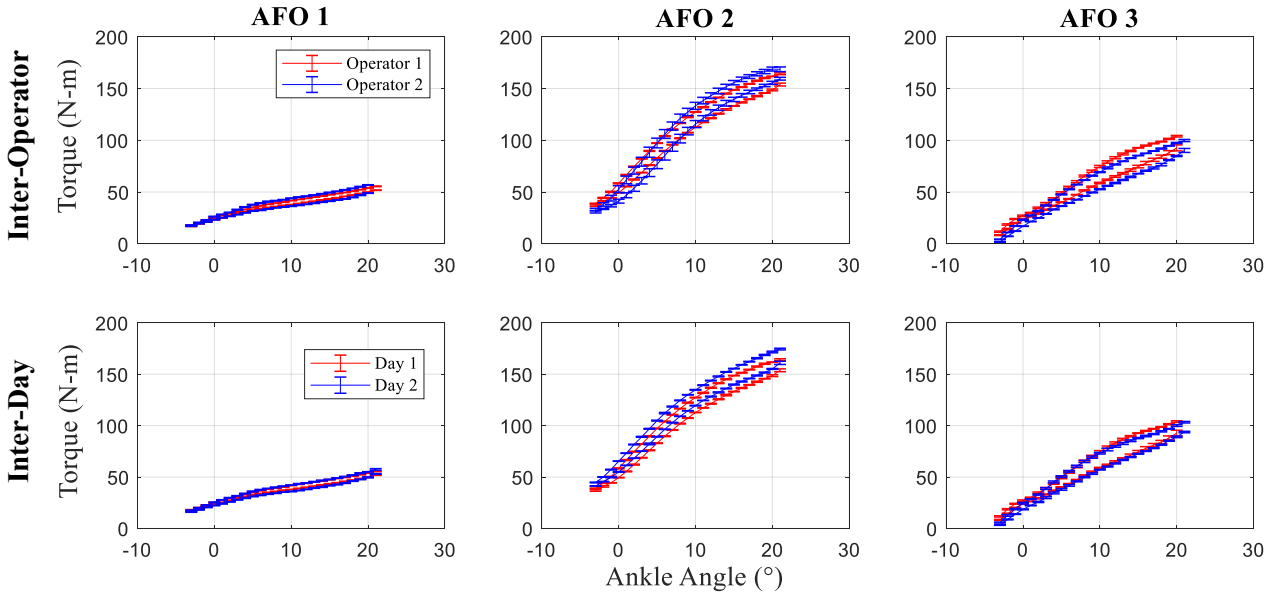

Figure 2: AFO stiffness curves for inter-day (with Operator 1) and inter-operator (on Day 2) tests

RESULTS AND DISCUSSION

Figures 2 shows the averaged stiffness curves of the three AFOs for inter-session and inter-operator evaluation. Each AFO presented shows a distinct stiffness mapping. The ICC results (Table 1) indicate high device reliability with ICCs ≥ 0.9 for inter-operator, inter-day, and intra-day correlations. Notably, the 95% confidence interval for AFO 3 was quite large for inter-day (Table 1). This AFO had a slightly plantarflexed neutral angle. This made it difficult to secure the AFO to the SMapp's footplate clamp consistently, which may explain the lower ICC value. Additionally, AFOs constructed asymmetrically may deform when actuated towards dorsiflexion in the SMapp. Adjusting the surrogate ankle hinge position may mitigate this deformation. It should also be noted that although each operator conducted their testing independently, both operators were familiar with the SMapp device and followed the same testing protocol.

Future work will include reliability testing with novice operators and employing the use of heel wedges when testing AFOs set in plantarflexion. Additionally, surrogate-ankle hinge position effects will be investigated.

REFERENCES

1. Kobayashi et al. (Review). *J. Rehabil. Res. Dev.* 38(5), 2011.
2. Bregman et al. *Gait and Posture*. 30(2), 2009.
3. Bedard et al. *J. Prosthetics Orthot.* 28(1), 2016.
4. Portney & Watkins. *Foundations of Clinical Research: Applications to Practice*, 2009

ACKNOWLEDGEMENTS

Thank you to Susannah Engdahl for advice on the statistical analysis and Dr. Leo Tse for feedback on the SMapp design.

Table 1: Intraclass Correlation Coefficients for each reliability condition

	ICC (95% Confidence Interval)			
	AFO 1	**AFO 2**	**AFO 3**	**All AFOs**
Inter-Day ICC	.992 (.982 - .996)	.997 (.974 - .999)	.967 (.075 - .993)	.994 (.956 - .998)
Inter-Operator ICC	.989 (.703 - .997)	.986 (.975 - .992)	.989 (.463 - .997)	.994 (.991 - .996)
Intra-Day ICC	0.999 (.998-.999)	1.000 (1.000 - 1.000)	0.999 (.998 - .999)	1.000 (1.000 - 1.000)

CHARACTERIZATION OF ECCENTRIC MOTOR DEFICIENCIES IN INDIVIDUALS WITH INCOMPLETE SPINAL CORD INJURY

Kevin O'Brien[1*], Lise Worthen-Chaudhari[2*], Timothy Faw[2], Albert Olszewski[1], Michael McNally[2], James Schmiedeler[1], & D. Michele Basso[2]
[1]University of Notre Dame, Notre Dame, IN, USA
[2]The Ohio State University, Columbus, OH, USA
[*]Co-first authors; corresponding email:kobrie23@nd.edu

INTRODUCTION

Approximately 17,000 Americans have a traumatic spinal cord injury (SCI) every year [1], and there remains wide variability in the success of current rehabilitation paradigms. Whereas many individuals improve functionally, others show little or no improvement [2]. As an example of a persistent deficit, individuals with incomplete SCI (iSCI) avoid walking strategies that require energy absorption at the joints by means of eccentric muscle activity. Eccentric muscle control requires unique muscle activity that can maximize forces while simultaneously decreasing fatigue [3]. Eccentric activity is particularly prevalent in the weight acceptance phase and important in the sagittal plane motion of the knee and the frontal plane motion of the hip [4].

For individuals with iSCI, rehabilitation techniques may benefit from addressing walking deficits by targeting eccentric activity. To further investigate potential effects that these rehabilitation techniques may have on the eccentric activity of muscles during the weight acceptance phase, the EMG signals and joint kinetics of individuals with chronic iSCI were compared with matched healthy controls. It is hypothesized that individuals with iSCI will exhibit significantly less eccentric activity during the weight acceptance phase, particularly avoiding sagittal plane eccentric activity at the knee and the frontal plane eccentric activity at the hip.

METHODS

Seven individuals (44 ± 10 years; 4 female) with chronic iSCI (ASIA Impairment Scale C or D classification; average of 7.18 years since injury) were matched with seven healthy controls (35 ± 7 years; 5 female) based on a least-squares matching of age and BMI. All subjects were asked to walk through a motion tracking setup at their self-selected pace while kinematics (Vicon, 200Hz, Butterworth 8Hz low pass filter), ground reaction forces (Bertec, 2000Hz, Butterworth 8Hz low pass), and EMG signals for the gluteus medius, vastus lateralis, tibialis anterior, and soleus (Delsys, 2000Hz, Butterworth 6Hz low pass) were collected.

When comparing motor control between pathologic and non-pathologic there is precedent for matching self-selected walking conditions [5]. Individuals with iSCI had 3 data collections over 16 weeks to account for known variability in motor performance. Individuals with assistive devices used their devices during the motion capture (see Tab. 1)

EMG signals of each muscle were recorded at the start of each day of motion capture testing while the subject was in a relaxed, seated position to determine a resting activation threshold for each muscle. Muscles were determined to be active when

$$V > mean(V_{resting}) + 2 * std(V_{resting}), \quad (1)$$

where V was the EMG signal in volts and $V_{resting}$ was the resting EMG signal for that same muscle. Inverse kinematics and kinetics were performed to determine joint velocities and torques (Visual3D). A muscle was determined to be acting eccentrically if the motion of the joint about which it acts indicated it was lengthening and the EMG signal exceeded the resting threshold.

Weight acceptance was defined to end at the first peak of the vertical ground reaction force for that leg. The area under the curve of the EMG signal quantified the eccentric contribution of each muscle while it was acting eccentrically during the weight acceptance phase.

The eccentric contribution of each muscle for individuals with iSCI was compared with the eccentric contribution of their matched healthy control using Welch's t-test with a 95% confidence level. The left and right sides of each subject were treated as independent samples to account for observed asymmetry in individuals

TABLE 1. Significant differences in eccentric muscle activity during weight acceptance for individuals with iSCI compared to matched healthy controls, where "+/-" means that the individual with iSCI exhibited significantly more/less eccentric activity ($p < 0.05$). For subjects using walkers, the number of wheels are included in parentheses (Note: Subject 5 primarily uses a manual wheelchair).

Subject #:	1		2		3		4		5		6		7	
Device:	walker (4)		Cane		walker (2)		walker (4)		walker (2)		None		None	
Side:	Left	Right	Left	Right	Left	Right	Left	Right	Left	Right	Left	Right	Left	Right
Glut Med			-	-	-	-	-	-	-	-	-		-	-
Vastus Lat	-	-	-	-	-	-	-	-	-	-	-		+	+
Tib Ant	-	-	-	-	-	-	-	-	-	-	-		-	-
Soleus	+	+	+	+	-	-	+	+		-	+	+	+	+

with iSCI (i.e. fourteen total samples). The left leg of each individual was compared with the left leg of their matched control (and the same for the right leg).

RESULTS AND DISCUSSION

Tab. 1 details the significant differences between the eccentric contribution of each muscle for individuals with iSCI and their matched control subject. For gluteus medius (representative example in Fig. 1), 11 of 14 iSCI samples demonstrated significantly less eccentric activity during weight acceptance. For vastus lateralis, 11 of 14 iSCI samples exhibited significantly less eccentric activity during weight acceptance, while 2 of 14 exhibited significanly more eccentric activity during weight acceptance. For the tibialis anterior, 13 out of 14 iSCI samples exhibited more eccentric activity during weight acceptance. And finally, for soleus, 10 of 14 iSCI samples exhibited more eccentric activity during weight acceptance, compared to 3 of 14 exhibiting less eccentric activity during weight acceptance.

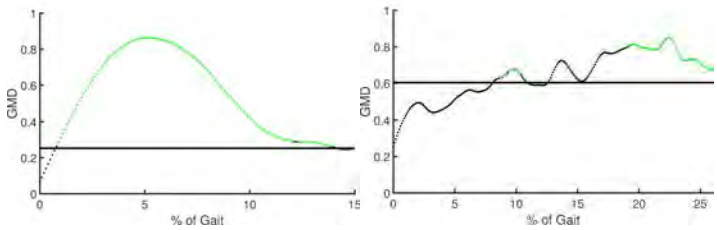

FIGURE 1. Representative examples of glut med eccentric activity for left legs of matched control (left) vs Subject #4 (right) during weight acceptance. Green data points represent eccentric muscle activity. Horizontal black line is the EMG activation threshold.

CONCLUSION

The results confirmed the hypothesis that individuals with iSCI exhibit significantly less eccentric muscle activity compared with their matched healthy controls. Traditionally, ankle dorsiflexors, hip abductors, and knee extensors provide support during weight acceptance [6]. Instead, these individuals with iSCI tended to absorb energy with the ankle plantarflexor. The observed differences in eccentric activity may be the result of differences in the self-selected speeds of the individuals with iSCI and the healthy controls and/or the use of assistive devices. Nonetheless, there is significant evidence that there are similarities in the most active muscles of motor modules used for walking at different speeds [7]. To further determine how speed plays a role, the muscle activity of individuals with iSCI compared with healthy control subjects walking at slower speeds will be the subject of future analysis.

ACKNOWLEDGMENTS

Research funded with support from NIH F31 NS096921 (TDF NRSA), NIH R21 HD082808 (DMB), 316282 Craig H. Neilsen Foundation (DMB), and Promotion of Doctoral Studies Level II Scholarship (TDF).

REFERENCES

[1] Nat SCI Stat Center. *Facts & Figs at a Glance*, 2016.
[2] JJ Buehner et. al. *Arch Phys Med and Rehab*, 93(9):1530–1540, 2012.
[3] RM Enoka. *J App Phys*, 81(6):2339–2346, 1996.
[4] L Worthen-Chaudhari et. al. *Gait & Pos*, 39(1):588–592, 2014.
[5] HB Hayes et al. *Clin Neurophysiol*, 125(10):2024–2035, 2014.
[6] FC Anderson et. al. *Gait & Pos*, 17(2):159–169, 2003.
[7] LH Ting et al. *Neuron*, 86(1):38–54, 2015.

PREDICTING INTERACTION FORCES BETWEEN UPPER EXTREMITIES AND SUPPORT DEVICES

[1]Brooke M. Odle, [1]Naji A. Alibeji, [1]Musa L. Audu, and [1,2]Ronald J. Triolo

[1] Case Western Reserve University, Cleveland, OH, USA
[2] Louis Stokes Cleveland Department of Veterans Affairs Medical Center, Cleveland, OH, USA
email: brooke.odle@case.edu

INTRODUCTION

Musculoskeletal models have been used extensively to design control systems for maintaining standing balance and providing propulsive power for walking after spinal cord injury (SCI). To prepare for a functional task or maintain balance in the presence of destabilizing postural disturbances while using these systems, individuals must rely on voluntary effort exerted by their upper extremities (UEs) on a support device, such as crutches, walker or countertop. In previous simulation studies [1], we modeled the interaction forces of the UEs and the support device by applying point forces to each of the model's shoulders. We assumed that the forces could be modeled as impedance forces, which were determined by a proportional-derivative controller that acted on changes in shoulder position and velocity as the model moved away from erect stance. Compared to baseline stimulation, simulation results suggested that the controller reduced UE effort by 34%. Although these findings were encouraging, our assumption may have oversimplified the UE contribution. To accurately predict the muscle forces and further advance the state of the art of control systems for standing and walking, a more accurate representation of the interactions of the UE forces and the support device is needed. The objective of this study is to develop and validate linear mathematical models that accurately account for intact volitional control exerted by the UEs on a support device.

METHODS

To develop preliminary models, experiments were conducted with a 24-year-old, able-bodied male volunteer. Prior to participating in the experiments, the volunteer signed informed consent forms approved by the Institutional Review Board of the Louis Stokes Cleveland Veterans Affairs Medical Center. The volunteer stood in an instrumented walker (80/20, Columbia City, IN) to measure UE forces (AMTI, Watertown, MA), and wore retroreflective markers (Vicon, Oxford, UK) on each shoulder. As the volunteer adjusted posture from an upright, erect stance to leaning in the forward, diagonal, and lateral directions, three-dimensional shoulder positions and UE forces were captured. A total of 14 trials were collected.

The data from the trials were divided in two groups: model identification and model performance (independent data set). The model identification data were further divided in half, with the first half selected to estimate the models and the latter half selected to validate the models. The System Identification App in MATLAB 2015b (The MathWorks, Natick, MA) was utilized to identify appropriate linear state-space models [2], via the subspace method [3], for each UE. The state-space model was parametric and had the following structure, which was governed by Equations (1) and (2):

$$\frac{dx}{dt} = Ax(t) + Bu(t) + Ke(t) \quad (1)$$

$$y(t) = Cx(t) + Du(t) + e(t) \quad (2)$$

where y(t) represents the output at time t, u(t) represents the input at time t, x is the state vector, and e(t) is the white noise disturbance. The state-space matrices A, B, C, D, and K were estimated by the System Identification Toolbox. It also automatically selected the model order, by optimizing the number of non-zero singular values [2].

For each model, the measured 3D components of shoulder position were the inputs and the magnitude of the resultant UE force was the output. After

identifying the model structure and parameters, the best fit between the model output and the measured data (estimation set) was computed. To validate the quality of the identified models, residual analyses were performed on the model output and the measured data (validation set).

To determine model performance, each model was imported from the MATLAB environment into a Simulink model for simulation with the independent data set. Linear regression analyses of the measured resultant force and the simulated force output from the models were computed.

RESULTS AND DISCUSSION

A fourth order state-space model was identified for the right UE and a second order model for the left UE. The best fit between the model output and the estimation set was 61.9% for the right UE and 59.3% for the left UE. The cross-correlation between the measured shoulder positions and the residuals of the predicted right resultant UE force were within the 99% confidence band for all lags, while those for the left UE were outside of the 99% confidence band. This suggests that right UE model is slightly better at describing how the resultant force is formed from the corresponding shoulder positions.

The resultant forces predicted by the simulated models and the measured resultant forces (from the independent data set) are displayed in **Figure 1**. The predicted force profiles have a trend similar to the measured forces. Linear regression analyses demonstrated a positive relationship between the predicted and measured resultant forces, with a regression value of 0.94 for the right UE and 0.93 for the left UE. Based on these encouraging findings, future work will further validate the models with data obtained from additional able-bodied volunteers and individuals with SCI that stand and lean with implanted neuroprostheses.

CONCLUSIONS

Preliminary models that predict the interaction forces between the right and left UEs of an able-bodied individual and a support device have been developed and validated. Given the 3D positions of the shoulders, these models can accurately predict the magnitude of the resultant force exerted by the right and left UEs, with regression coefficients as high as 0.94. These models will be invaluable in the design and deployment of advanced control systems for neural stimulation that are integrated with volitional control.

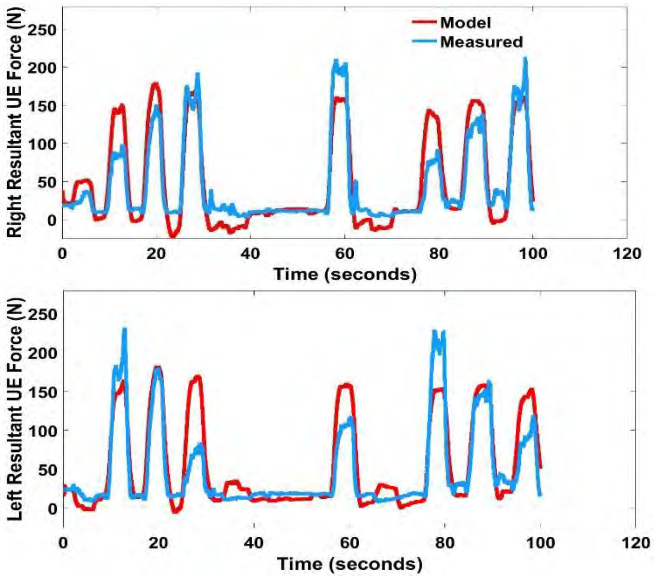

Figure 1: Model performance with independent data set. Predicted resultant force profiles (red) and measured resultant force (blue) for the right UE model (top) and left UE model (bottom), based on the independent data set.

REFERENCES

1. Audu et al. *JRRD*. **51(3)**: pp. 481 – 496, 2014.
2. Ljung, L. *System Identification: Theory for the User*, Appendix 4A, Second Edition, pp. 132-134. Upper Saddle River, NJ: Prentice Hall PTR, 1999.
3. Overschee, J and De Moor, B. *Subspace Identification of Linear Systems: Theory, Implementation, Applications*. Springer Publishing: 1996.

ACKNOWLEDGEMENTS

This work is funded by the Craig H. Neilsen Foundation, Grant #459308.

DIFFERENCES IN MECHANICAL DEMAND IMPOSED ON THE SHOULDER DURING MANUAL WHEELCHAIR PROPULSION IN THE COMMUNITY

Marisa Papp[1], Ian M. Russell[1], Philip S Requejo[2], Jan Furumasu[2], Carmen Muller-Karger[3], Mary M Rodgers[4], Jill L. McNitt-Gray[1]

[1] University of Southern California, CA, USA
[2] Rancho Los Amigos National Rehabilitation Center, CA, USA
[3]Florida International University
[4]University of Maryland School of Medicine
email: mpapp@usc.edu

INTRODUCTION

Manual wheelchair (WC) users with spinal cord injury (SCI) have high inclination for shoulder joint pain and fatigue due to increased reliance on the upper extremity during activities of daily living[1]. Modification in manual WC propulsion conditions (e.g. fast propulsion, graded) are known to affect push angle, reaction force (RF) magnitude, direction and time of peak RF during the push phase of WC propulsion[1]. The purpose of this study was to determine differences in mechanical loading of the shoulder when initiating manual WC propulsion than when maintaining horizontal velocity along a level sidewalk. We hypothesized the mechanical loading in the initial push cycle (1) would be significantly greater than during steady-state propulsion velocity at a self-selected fast speed due to an expected increase in push duration and more time spent with the RF acting posterior to the forearm in cycle 1.

METHODS

Nine individuals with paraplegia (T2-L3, 9 male) using a manual WC for mobility volunteered to participate in accordance with the Institutional Review Board of Rancho Los Amigos National Rehabilitation Center (RLANRC). Individuals were excluded from participation if they reported a history of shoulder pain that altered performance of daily activities or required medical treatment. All participants initiated self-selected fast WC propulsion from a stationary position in a courtyard outside of the Seating Center at RLANRC. RFs applied by the hand to the pushrim were measured using three strain gauge force transducers (240 Hz, SmartWheel). Two-dimensional segment kinematics were captured in the frontal and sagittal planes (60 Hz HD, JVC). This information was then used to determine RF orientation relative to the forearm and to calculate NJM contributions of the shoulder during the push phase (while elbow moment in the axis perpendicular to pushrim exceeded 5Nm for each participant).

RESULTS AND DISCUSSION

As hypothesized, hand contract with the pushrim was longer in duration when initiating WC propulsion (Cycle 1) than when maintaining self-selected speed (Cycle 3) (Table 1). Greater shoulder NJM impulse was also observed for Cycle 1 than for Cycle 3 across all participants (Figure 1). The difference in magnitude of the peak Shoulder NJM between Cycle 1 and Cycle 3 varied considerably between participants (Figure 2). These observed differences in Shoulder NJM between conditions were attributed to observed differences in the orientation of the RF relative to the forearm. RFs oriented posterior to the forearm center of mass contribute to the need for an elbow flexor NJM. Increase in the elbow flexor NJM contribute to increases in shoulder flexor NJMs[1,2].

Push Duration (s)	Cycle 1	Cycle 3
Participant 1	0.904	0.300
Participant 2	0.633	0.254
Participant 3	0.350	0.267
Participant 4	0.708	0.275
Participant 5	0.713	0.288
Participant 6	0.658	0.296
Participant 7	0.842	0.288
Participant 8	0.779	0.246
Participant 9	0.829	0.279

Table 1. Comparison of average push duration between Cycle 1 vs Cycle 3, within participant.

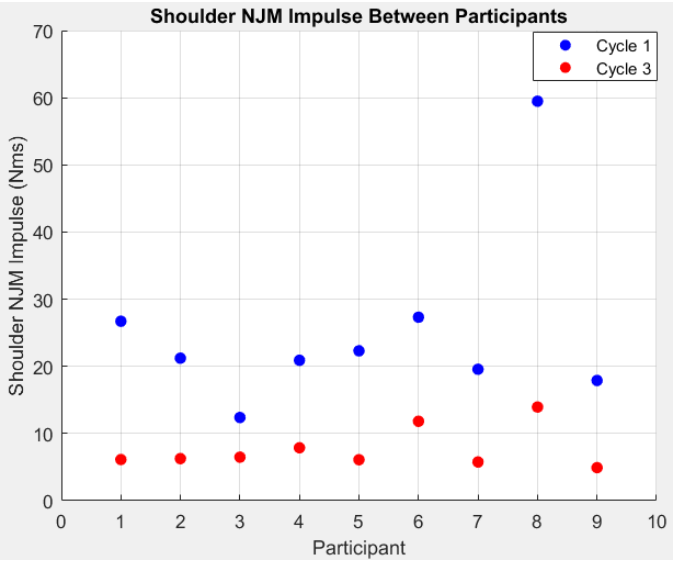

Figure 1: Comparison of shoulder NJM impulse between Cycle 1(blue) vs Cycle 3 (red) within participant.

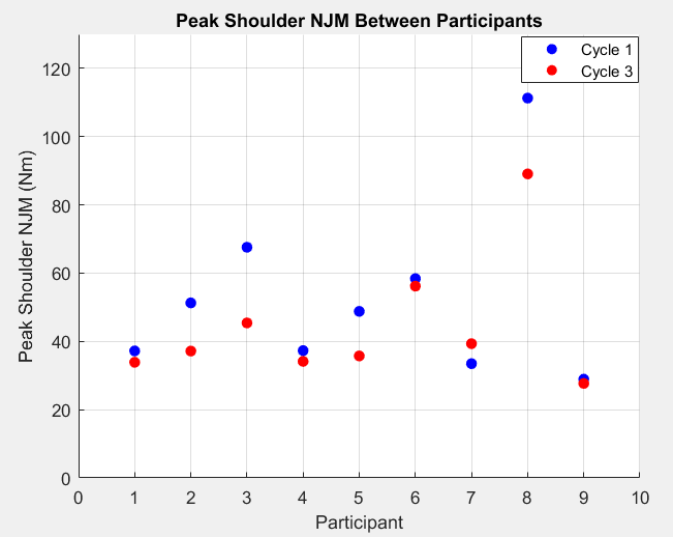

Figure 2: Comparison of peak Shoulder NJM during push between Cycle 1(blue) vs Cycle 3 (red) within participant.

CONCLUSIONS

The mechanical loading of the shoulder when initiating manual WC propulsion was found to be greater for participants in this study than when maintaining horizontal velocity at a self-selected fast speed in the community. The results indicate that all participants experienced substantial increases in Shoulder NJM impulse when accelerating the body-WC system. Differences in peak Shoulder NJMs between Cycle 1 and Cycle 3 varied across participants and reflect differences in the individual's WC propulsion technique. As found previously, the magnitude of the Shoulder NJM is sensitive to the orientation of the RF relative to the forearm and the adjacent elbow NJM[1,2]. When the RF acts anterior to the forearm, the extensor NJM at the elbow assist the shoulder flexor NJM during manual WC propulsion, thereby reducing the mechanical demand imposed on the shoulder. These observed differences in the type of mechanical loading imposed during different phases of manual WC propulsion is important when charactering load exposure during activities of daily living in realistic contexts.

REFERENCES

1. Russell IM, Raina S, Requejo PS, Wilcox RR, Mulroy S, McNitt-Gray JL (2015). *Modifications in Wheelchair Propulsion Technique with Speed.* Front Bioeng Biotechnol 3:171.
2. Munaretto, J., McNitt-Gray, J.L. & Flashner, H. (2013). Reconfiguration of the upper extremity relative to the pushrim affects load distribution during manual wheelchair propulsion, *Journal of Medical Engineering & Physics*, 35(8), 1141-9.

ACKNOWLEDGEMENTS

This work was supported by the Office of the Assistant Secretary of Defense for Health Affairs, through the Spinal Cord Injury Research Program under Award No. W81XWH-14-1-0560. Opinions, interpretations, conclusions and recommendations are those of the author and are not necessarily endorsed by the Department of Defense.

Optimizing a Variable Stiffness Transverse Plane Adapter for Lower Limb Amputees

Corey Pew[1, 2], Ava Segal[1] and Glenn K. Klute[1, 3]

[1] Center for Limb Loss and Mobility, VA Puget Sound, Seattle, WA,
[2] Department of Mechanical Engineering, University of Texas, Austin, TX,
[3]Department of Mechanical Engineering, University of Washington, Seattle, WA
email: gklute@u.washington.edu, web: www.amputation.research.va.gov

INTRODUCTION

Turning gait comprises a significant portion of daily steps [1] and requires varied transverse plane motion and loading in the lower limbs [2]. A fixed stiffness transverse plane adapter at the residual limb-socket interface has been shown to reduce amputee residual limb loading [2, 3], which may translate to reduced soft tissue damage and increased user comfort [2].

A variable stiffness torsion adapter (VSTA) has the potential to reduce transverse plane stiffness in the shank of a lower limb prosthesis during varied activities, which would reduce peak loading on the residual limb [4]. While initial results using the VSTA were promising, the optimal transverse plane stiffness levels for varying walking speeds and activities remains unknown. Additionally, it is unknown how stiffness and the specific locomotor activity affect user preference.

We hypothesize that reduced transverse plane stiffness will most benefit (reduced peak loading on the residual limb) turning gait vs. walking straight and that peak loading will increase with increased walking speed, independent of stiffness. Additionally, user preference for stiffness will vary based on walking speed and activity. Lastly, stability will not decrease with reduced stiffness as indicated by whole body angular momentum (WBAM) [5].

METHODS

An updated prototype of the VSTA, the VSTA II, was designed with five discrete stiffness settings ranging from 0.25-1.25 Nm/° in 0.25 Nm/° increments, plus a sixth fully locked setting. The VSTA II is 73 mm tall, weighs 0.88 kg and includes a stand-alone controller.

Seven male, unilateral transtibial amputees provided informed consent to participate in this IRB-approved protocol. Gait kinematics and kinetics were collected using a 12-camera Vicon system (Vicon, Centennial, CO), modified Plug-in-Gait model, 8 force plates (AMTI, Watertown, MA), and an iPecs 6-axis load cell (College Park, Warren, MI) installed on the distal end of the VSTA II to directly measure transverse plane loading of the residual limb (normalized by subject mass). Gait data were analyzed in Visual 3D (C-Motion, Germantown, MD) to determine the range of WBAM (normalized by subject height, mass and walking speed) [5].

Subjects performed testing to determine their stiffness preferences at three walking speeds (*self-selected*, *fast* and *slow*: +/- 20% of *self-selected*, respectively) and during three activities (straight walking, prosthesis outside turning, and prosthesis inside turning). Straight walking was performed over-ground along a 7-meter walkway and turning gait was simulated by walking around a 1-meter radius circle [3]. An 'A-B-C' testing series allowed subjects to identify their preferred stiffness setting (A: 0.25 Nm/°, B: 0.75 Nm/°, C: 1.25 Nm/°) during blinded testing for each speed-activity combination. For a given activity and speed, the user performed three trials each at settings A and C (random order) to give the highest contrast in stiffness. Subjects were then required to choose their preference (P1). The P1 setting was then compared to the middle, B, setting after three trials each (random order). The overall stiffness preference (P2) was chosen between B and P1. Nine preference testing series were completed for each subject (3 speeds for each of the 3 activities) over the course of two days. The order of stiffness settings within each round, speeds and activities were block randomized for each series and subject.

A linear mixed effects model with fixed effects for stiffness setting and walking speed and random effect for subject was used to test differences between varying stiffness settings and speeds on the peak transverse plane moment in the residual limb and the range of WBAM. An exact multinomial test was used to analyze difference between categorical subject preferences for varying stiffness.

RESULTS AND DISCUSSION

Significant reductions ($p<0.05$) in peak transverse plane moments (normalized by subject mass) were found for all three activities for the varying stiffness settings, contrary to our hypothesis (Table 1). Peak transverse plane moment was reduced by 4.0±1.5 Nm (3.1%, $p=0.025$), 3.5±0.8 Nm (7.2%, $p<0.001$) and 4.5±1.4 Nm (5.0%, $p=0.005$) between the A and C conditions for turning with the prosthetic limb on the inside, turning with the prosthetic limb on the outside and straight walking respectively. Significant increases in peak transverse plane moment were also related to increases in walking speed with increases of 9.2±1.6 Nm (7.0%, $p<0.001$) and 5.5±0.8 Nm (10.9%, $p<0.001$) between the *fast* and *slow* speed conditions while turning with the prosthesis on the inside and outside, respectively. However, during straight walking the *slow* walking condition represented a significant increase in peak transverse plane moment of 5.1±1.5 Nm (5.8%, $p=0.002$) and 8.0±1.4 Nm (9.4%, $p<0.001$) over the *fast* and *self-selected* conditions, respectively.

The range of WBAM was found to increase significantly between the C and A conditions in the coronal plane by 3.1% ($p=0.004$) for turning with the prosthesis on the inside and in the transverse plane by 7.7 % ($p<0.001$) when walking straight for decreasing transverse plane stiffness. Similar to previous studies, the range of WBAM decreased with increasing walking speed in all planes [5].

Lastly, preference results at this time do not show any significant trends (Table 2), however, it was generally found that individuals tend to pick the middle setting, B, more often when turning and the stiffest setting, C, when walking straight. Future work will aim to collect more subjects to better define the results.

CONCLUSIONS

Significant differences in peak transverse plane loading existed primarily between the extreme settings, A and C, which may indicate that two transverse plane stiffness settings (Low and High) are sufficient to optimize performance. However, the range of WBAM also increased at lower stiffness settings, which may suggest compromised stability. This finding may explain why subjects were reluctant to choose the lowest setting, A, and may indicate a setting between A and B is optimal.

REFERENCES

1. Glaister, et al., *Gait & Post.*, **25**(2), 2007.
2. van der Linden, et al.,*Pros. Orth. Int.*, **26**(1), 2002.
3. Segal, et al., *J. Rehab. Res. Dev.*, **46**(3), 2009.
4. Pew, et al., *Gait & Post.*, **51**, 2017.
5. Silverman, et al. *J. Biomech.*, **44**(3), 2011.

ACKNOWLDEMENTS

Dept. of Veteran Affairs, Rehab. Research & Development (RX001933, A9248-S, A9243C).

Table 2: Subject stiffness preferences over all speeds by stiffness and activities (straight (ST), prosthesis inside turns (PI) and prosthesis outside turns (PO)). Values represent the number of times each stiffness was chosen during each activity during all speeds.

Overall Stiffness Preferences			
	ST	PI	PO
Stiffness	All	All	All
A	3	6	6
B	8	10	11
C	10	5	4
p-value	0.145	0.475	0.206

Table 1: Peak transverse plane moment (PTPM) (Nm) ± standard error for varying stiffness and speed. Statistical comparison (Comp) between different stiffness settings (A: 0.25 Nm/°, B: 0.75 Nm/°, C: 1.25 Nm/°) and walking speeds (Fast Walking (FSW), Self-Selected Walking (SSW), Slow Walking (SLW)).

		Prosthesis Inside Turn			Prosthesis Outside Turn			Straight Walking		
		PTPM (Nm)	Comp	p-value	PTPM (Nm)	Comp	p-value	PTPM (Nm)	Comp	p-value
Stiff	A	123.2 ± 16.9	A-B	0.194	45.5 ± 5.0	A-B	0.284	86.5 ± 10.3	A-B	0.196
	B	126.1 ± 16.9	A-C	0.025	46.8 ± 5.0	A-C	<0.001	89.4 ± 10.3	A-C	0.005
	C	127.2 ± 16.9	B-C	0.809	49.01 ± 5.0	B-C	0.028	91.0 ± 10.3	B-C	0.531
Speed	SLW	121.7 ± 16.9	SLW-FSW	<0.001	45.1 ± 5.0	SLW-FSW	<0.001	93.4 ± 10.3	SLW-FSW	0.002
	SSW	121.7 ± 16.9	SLW-SSW	0.368	45.8 ± 5.0	SLW-SSW	0.662	85.3 ± 10.3	SLW-SSW	<0.001
	FSW	130.9 ± 16.9	SSW-FSW	<0.001	50.6 ± 5.0	SSW-FSW	<0.001	88.2 ± 10.3	SSW-FSW	0.151

DEVELOPMENT OF A SEMG-BASED SILENT SPEECH RECOGNITION SYSTEM

[1]Serge H. Roy, [2]Geoff S. Meltzner, [3]James T. Heaton, [4]Yunbin Deng, [1]Gianluca De Luca and [1]Joshua C. Kline

[1] Delsys, Inc. and Altec, Inc, Natick, USA
[2]Vocal ID, Inc, Belmont, USA
[3]Harvard Medical School Department of Surgery, MGH Voice Center, Boston, USA
[4]BAE Systems Inc, Burlington, USA
email: sroy@delsys.com, web: http://www.delsys.com/altec/

INTRODUCTION

Speech is among the most natural forms of human communication offering an attractive modality for human-machine interaction through automatic speech recognition (ASR). However, the limitations of ASR - including degradation in the presence of ambient noise, limited privacy and poor accessibility for those with significant speech disorders – have created a need for alternative non-acoustic modalities of subvocal or silent speech recognition (SSR). To meet this need we have designed, developed and empirically evaluated a new system of face- and neck-worn sensors and signal processing algorithms that recognize silently-mouthed words and phrases entirely from the surface electromyographic (sEMG) activity recorded from muscles of the face and neck.

METHODS

We conducted experiments to record sEMG signals from articulator muscles of the face and neck during subvocal speech tasks involving n=5 native English (American) speakers (3 females, 2 males; age range 23-35 y.o.). Custom-designed sEMG sensors (Delsys, Inc. Natick, MA) were strategically placed on 11 muscles of the face and neck (n=7 submental; n=4 on the face) previously identified as those most involved in the articulation of speech [1]. The subjects recited a series of 1,200 phrases of ~6 words/phrase from a 2,200-word vocabulary derived from these data sets: SX part of TIMIT data corpus, a special operations silent-speech data corpus, commonly used English phrases, a text-messaging corpus, and a custom corpus to cover phone calls, numbers, and dates for digit recognition. Words were presented in token sentences on a terminal for subjects to subvocally articulate by silently mouthing the words.

We developed and tested a two-stage speech recognition algorithm in which signal segments containing speech data were identified by a finite state Speech Activity Detection (SAD) algorithm and processed with speaker-dependent window lengths and frame rates to compute Mel-frequency cepstral coefficients (MFCC) [2]. Hidden Markov Models were used to develop multi-stage phoneme-based speech recognition models that incorporate MFCC features, NL Equivalence Grammar, as well as MLLR, HLDA and SGMM algorithm layers were empirically evaluated to configure the architectures with optimal model parameters [3]. These algrotihms were migrated into a system for practical use outside of the laboratory using subsets of the full array of 11 sensors, tested across the different data sets within the corpus.

RESULTS AND DISCUSSION

We evaluated the maximal speaker-dependent word error rate (WER), achieved by all speakers for different numbers of sensor subsets. The best

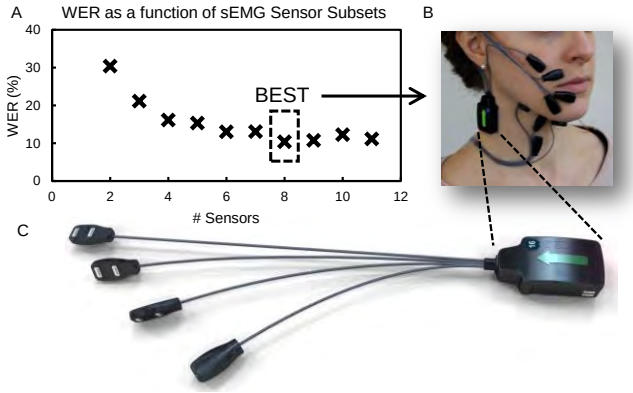

Figure 1. *A) The word error rate (WER) as a function of the best combination for each sensor subset. B) Depiction of the 8-sensor configuration on a subject. C) Rendering of the prototype sEMG facial sensor array Trigno™ Quattro (Delsys, Inc).*

performing sensor subset (Fig. 1A) was obtained with 8 sensors arranged on a single side of the face and neck as shown in Fig. 1B. With this sensor arrangement, we analyzed the recognition performance across 4 different data sets from the 1,200 continuous phrases tested (Table 1). Overall the average WER across all four data sets was 8.9%, with one subject reaching a WER as low as 1.4%.

Our ability to advance SSR performance through the development of an advanced SSR algorithm was aided by parallel efforts on our part to develop acquisition system hardware that is robust and unencumbering when interfaced with the geometrically complex and dynamically changing skin surface of the face and neck during mouthed speech. Fig 1C displays a 4-sensor cluster of sensors (Delsys Inc) with a miniaturized 1 cm x 2 cm contact footprint used to record sEMG signals. These multi-point 4-sensor sets are mated to a common wireless transceiver to achieve robust signal transmission using either a custom wireless protocol for enhanced bandwidth, or Bluetooth for portability and integration with a tablet or similar personal device.

CONCLUSIONS

Our work empirically demonstrates the advancements of a state-of-the-art sEMG-based SSR system. Developments in the signal parameterization schemes, recognition algorithms and phoneme model configurations enabled the system to function on a relatively large 2,200-word vocabulary of continuous phrases, and recognize vocabulary of both trained as well as untrained words with a WER of 8.9%.

The final system of recognition algorithms and miniaturized, conformable facial sensors has the potential to provide a much-needed means of human communication to individuals that are currently underserved by existing ASR technologies. These results demonstrate the viability of our system as an alternative modality of communication for a multitude of applications including: persons with speech impairments following a laryngectomy [3]; military personnel requiring hands-free covert communication [1, 2]; or the consumer in need of privacy while speaking on a mobile phone in public.

REFERENCES

1. Colby G, et al. *34th Annual IEEE ICASSP*, Taipei, Taiwan, 473-476, 2009.
2. Deng Y, et al. *Proc. 15th Annual Interspeech Conf*. Singapore, 1164-1168, 2014.
3. Meltzner et al. *IEEE/ACM Trans Audio, Speech, and lang Proc,* 25(12):2386-2398, 2017.

ACKNOWLEDGMENTS

Research reported in this abstract was supported in part by the De Luca Foundation and by a grant from the National Institute on Deafness and other Communication Disorders (NIDCD) of the National Institutes of Health under award R44DC014870.

Table 1. *The word error rate (WER %) of the final SSR system.*

Subject	Digits	Text Messages	Special Operations	Common Phrases	Mean
1	2.7	0.9	2.0	0.0	1.4
2	15.4	15.9	8.0	15.4	13.9
3	20.7	12.1	13.6	5.2	12.9
4	18.2	10.3	10.6	3.7	10.7
5	12.2	5.6	3.4	1.2	5.6
Mean	13.8	9.0	7.5	5.1	**8.9**
SD.	7.0	5.8	4.9	6.1	**5.3**

IMPACT OF FORCES ON PEDIATRIC POSTERIOR WALKER ON WORK IN CEREBRAL PALSY GAIT

Marshall W. Tumperi and Shawn D. Russell

Motion Analysis and Motor Performance Lab
Department of Aerospace and Mechanical Engineering
University of Virginia, Charlottesville, VA, USA
email: sdr2n@virginia.edu,
web: med.virginia.edu/orthopaedic-surgery/research/the-motion-analysis-and-motor-performance-lab/

INTRODUCTION

United Cerebral Palsy (UCP) reports that an estimated 764,000 individuals in the United States exhibit one or more symptoms of CP [1]. Children with CP are commonly prescribed walkers to maintain the stability required for ambulation. Posterior walkers improve posture and other gait parameters of the user in comparison to anterior walkers [2].

Children with CP typically are weaker and fatigue faster than their typically developed (TD) peers. Additionally they have been shown to do 59% more work per unit mass on average than TD children [3]. Children with CP rely on the walker during times of instability in their gait, but there is an energy cost to pulling the walker along causing them to be less efficient. Additionally, the kinetics of this interaction have not been quantified by previous studies. This work incorporates a dynamic model which includes the forces applied to the walker in addition to the traditional kinematics and GRF with which to address shortcomings of previous work.

METHODS

9 children (5 TD, 4 CP) were instructed to walk in a straight path at their self-selected comfortable walking speed without any assistive devices (prescribed afo's were used) (baseline) and our custom instrumented posterior pediatric walker (PPW) (Fig 1). The PPW was instrumented at the handles with two 6 DoF load cells (ATI) to capture all forces applied through the handles. For each walking trial kinematic data was collected at 100Hz using an 8 camera motion capture system (Vicon) and the full-body Plug-in-Gait AI functional marker set in tandem with the 5-point set for the walker located at each handle end (2), load cell location (2), and center cross bar (1).

Figure 1: Instrumented walker with five markers (left/right grip, left/right load cell, bar) and load cells at connection from handles to walker.

Kinetic forces, at the handles, and GRF's (5 bertec force plates) were collected at 1000Hz. Three trials of each condition, baseline and PPW were collected. The kinematics and reaction forces measured at the load cells and ground-embedded force plates were used to construct models in MSC ADAMS software. The models for gait with the PPW were run with and without the measured walker forces in order to observe the impact of the walker-subject interaction. Mechanical work for each trial was calculated using external force data and joint angle and torque data (Eq 1). A value of $p<0.05$ was considered to be significant in comparing the mechanical work across trials.

$$W_{mech} = \tau_{joint} * \Delta\theta \quad (1)$$

The anterior/posterior forces applied at the handles were used in conjunction with the kinematics of the load cells in order to calculate the mechanical work required to move the walker. This was done to quantify the work done by the user to pull the walker along.

RESULTS AND DISCUSSION

A model incorporating the load cell forces quantifying the walker-subject interaction was successfully created (Fig 3). The total work for instrumented CP PPW trials with load cell data was significantly greater than that of the trials without load cell data (Table 1). The difference of upper-body work was significant between the PPW trial types while the lower-body work difference was not significant. The PPW LC/PPW work difference for the upper body is greatest during times of weight acceptance, push off, and swing phases in gait when patients are least stable.

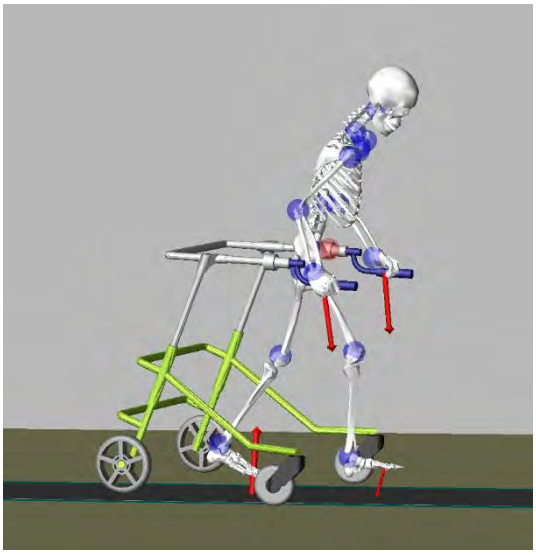

Figure 2: Modelled PPW trial with GRF and handle forces shown.

In both TD and CP cases, the instrumented PPW trials without load cells used less energy than in the baseline trials. A positive linear relationship has been reported for children with CP and TD children between mechanical cycle work and velocity [4]. During the instrumented walker trials, we believe the calculated lower work is a result of subject speed dropping in comparison to the baseline.

The full work done on the walker in both groups was greater than the difference between the full body PPW work with and without load cells. This and other changes in gait parameters cannot be explained with the current data. Other spatiotemporal factors are being examined for causes for the changes observed.

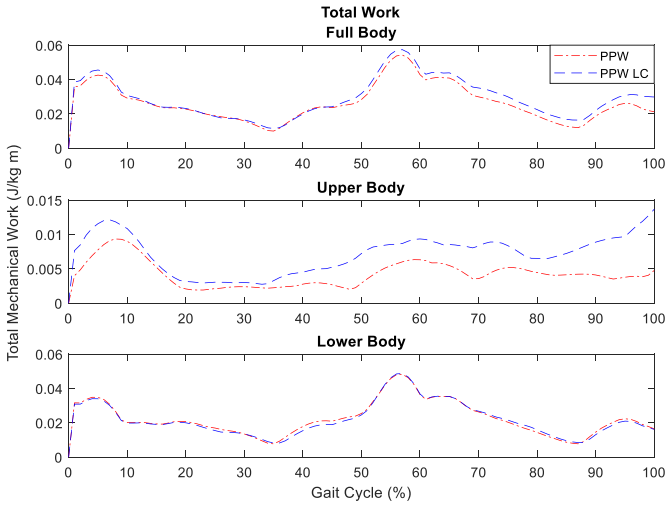

Figure 3: Normalized work of CP gait cycle from heel strike to heel strike with and without load cells.

CONCLUSIONS

The CP group was composed of children who could be or had been prescribed a walker to use for ambulation (GMFCS II/III). The results of mechanical work calculations allow individual joints or groupings to be observed and how the distribution of kinetics in the system changes.

Based on the differences between PPW without load cells and with load cells, the subject-walker interaction cannot be ignored when modelling the system. These forces must be accounted for when considering the dynamics of gait with a walker.

REFERENCES

1. Koman et al., *United CP,* 1997 (8-1-2005)
2. Park et al., *Yonsei Med J, 42*(2), (2001).
3. Russell et al., *J Biomech*, *27*, (2011).
4. Dziuba et al., *Acta of Bioeng and Biomech, 16*(3), (2014).

ACKNOWLEDGEMENTS

This work funded in part by a NIH phase I SBIR. The authors would like to thank the UVA Motion Analysis and Motor Performance lab for their continued assistance with data processing.

Table 1: Total work averages for subject groups, significance comparing to baseline (°), between with and without load cell (□), and between TD and CP (◊). Where t-test results of p<0.05 (*), p<0.01 (**), p<0.001 (***).

	Baseline	**PPW: Without Load Cell**			**PPW: With Load Cell**			**Walker**
	Full body (J/kg m)	*Full body (J/kg m)*	*Lower Body (J/kg m)*	*Upper Body (J/kg m)*	*Full body (J/kg m)*	*Lower Body (J/kg m)*	*Upper Body (J/kg m)*	*Full (J/kg m)*
TD	2.85±0.19	2.66±0.29°	2.45±0.27	0.21±0.064	2.63±0.32°	2.39±0.28	0.23±0.10□	0.25±0.30
CP	4.16±1.04	3.29±1.02°°	2.71±0.89	0.58±0.21	3.64±1.27□□□	2.68±0.98	0.96±0.39□□□	1.03±0.59◊◊◊

Simulating Ankle Torque during Walking Using a new Bioinspired Muscle Model with Application for Controlling a Powered Exoskeleton

[1] Safoura Sadegh Pour Aji Bishe, [1]Dan Rivera, [2]Katherine Strausser, [1]Kiisa Nishikawa, and [1]Zachary Lerner

[1]Northern Arizona University, Flagstaff, AZ, USA
[2]Ekso Bionics Company, Richmond, CA, USA
Email: zachary.lerner@nau.edu

INTRODUCTION

Human-like motion is a primary goal for many robotic assistive devices. Emulating the strategy of the human neuromuscular system may aid the control of such powered devices, yet many challenges remain.

Among all muscle models, Hill type models are the most commonly used for controlling assistive devices [1]. The Hill muscle model represents muscle function through two simple elements, and often fails to accurately predict muscle force in different situations [2]. Nishikawa et al. developed a novel ~~"~~winding filament" hypothesis for muscle contraction (Fig. 1-A) that incorporates a role for the giant titin protein in active muscle [3].

In this study, we investigated the potential for using the winding filament model (WFM) of muscle to predict the net muscle moment of the ankle. The long-term goal is to use this model to improve ankle control of a commercial powered exoskeleton.

METHODS

As biological tissues, muscle and tendon exhibit time dependent properties. However, Hill-type muscle models do not contain any time-dependent properties, suggesting that Hill models cannot accurately predict muscle function when time-dependent properties of muscle plays a significant role in motion. In contrast, the winding filament hypothesis incorporates time-dependent tissue behavior and may be more capable of capturing human-like actuation [3].

The WFM has a series-elastic passive component (tendon), represented by a spring in the mechanical model (K_{ss} spring in Fig. 2, similar to l^T in Hill model), in series with a pulley representing actin thin filaments. The contractile element is parallel to a damper (C_{ce}) that accounts for time-dependent properties of muscle. These two components, connected to the titin elastic element, also represented by a spring (K_{ts} spring in Figure 1-A).

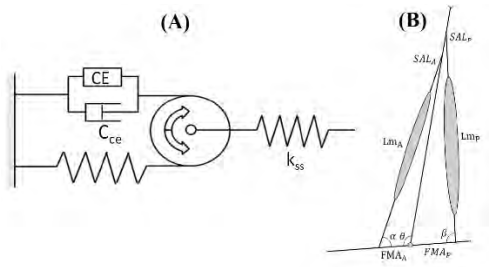

Figure 1: (**A**) Mechanical model of winding filament hypothesis, that contains two springs for representing the series elastic component (K_{ss}) and titin elastic component (K_{ts}). There is also contractile element (CE) parallel to a damper (C_{ce}). (**B**) Two virtual muscles used in model of ankle joint. One represents the anterior muscles (m_A), and the other one represents the posterior muscles (m_P). (Lm_A) and (Lm_P) are the length of virtual anterior muscle and virtual posterior muscle, respectively, calculated from the muscle attachments and ankle joint angle (θ).

We use lump-sum model design, where only two muscles were used, one representing all the anterior muscles that contribute to ankle dorsiflexion, and the other one represents all the posterior muscles (Figure 1-B) that contribute to plantarflexion.

The ability of our model to accurately predict the ankle moment was evaluated by adjusting only a single activation node of the muscle activation signal by comparing model output to the ankle

moment computed from Inverse Dynamics (ID) in OpenSim.

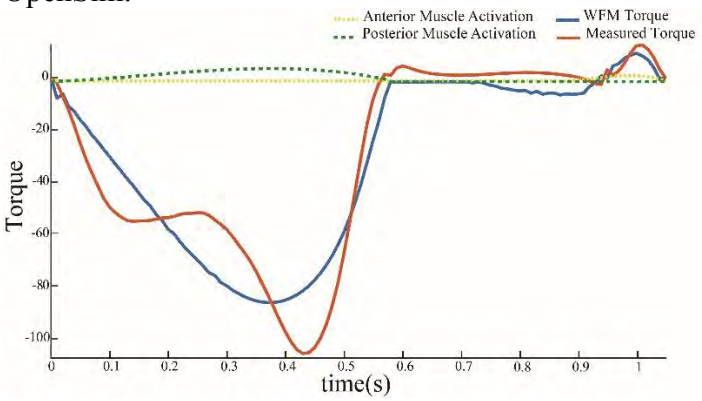

Figure 2: The result of optimization for one male subject. The blue line is the predicted torque by WFM, and the red line is the measured torque. The yellow and green dash point is the evaluated activation for anterior virtual muscle posterior one, respectively.

Particle Swarm Optimization (PSO) was used to minimize the root mean square error (RMSE) between the ankle moment from Inverse Dynamics and the output torque of the model. The optimization where done using the walking data of four healthy subjects (two male and two female) as training data, and then we test the results of optimization on another four subjects (one male and three female). The walking speed of all the patients were 125 (m/s).

RESULTS AND DISCUSSION

The control of exoskeleton should be designed generally for all populations, so the activation of muscles should be defined generally too. In this case, we designed a general shape for activation that is a function of subject's weight and gait cycle time. The result of the optimization shows that the best activation curve that fits for the training walking data of four subjects has the maximum activation of 0.05 for anterior virtual muscle, and 0.1 for posterior one. The shape of the resulting activations is also shown in Figure 2 by dash lines. Based on the result of optimization, the maximum force of the muscle was 5 times of subject's body weight in kilogram. The RMSE between WFM torque and Inverse Dynamics in OpenSim for test and train data are shown in Table 1.

The purpose of this study was evaluating two general activation curves that best fit the torque output of WFM model to the ID in OpenSim. It is expected that the RMSE of the WFM modeling be large, since it is a general model that should work for every different person with different pattern of walking. The important result of this study is that the test data have the same amount of RSME as the train data—the mean of RSME for train subject is 154.78, and for test subject 129.07. Comparing the RMSE of test and train data indicates that our model can predict the ankle joint torque of all populations with the same amount of error, which is acceptable for an exoskeleton.

REFERENCES

1. J. Rosen, M. B. Fuchs, and M. Arcan, "Performances of Hill-Type and Neural Network Muscle Models—Toward a Myosignal-Based Exoskeleton," *Computers and Biomedical Research,* vol. 32, pp. 415-439, 1999.Bach et al. *Plos One*. 10(3): e0118797, 2015.
2. G. I. Zahalak, "A distribution-moment approximation for kinetic theories of muscular contraction," *Mathematical Biosciences,* vol. 55, pp. 89-114, 1981/07/01/ 1981.
3. *K. C. Nishikawa, J. A. Monroy, T. E. Uyeno, S. H. Yeo, D. K. Pai, and S. L. Lindstedt, "Is titin a 'winding filament'? A new twist on muscle contraction," Proceedings of the Royal Society B: Biological Sciences, vol. 279, pp. 981-990, 09/07 06/22/received 08/17/accepted 2012.*
4. *E. M. Arnold, S. R. Ward, R. L. Lieber, and S. L. Delp, "A model of the lower limb for analysis of human movement," Ann Biomed Eng, vol. 38, pp. 269-79, Feb 2010.*

Table 1: The root mean square error (RMSE) between the torques calculated from WFM and ID in OpenSim.

Type of data	**Train**	**Train**	**Train**	**Train**	**Test**	**Test**	**Test**	**Test**
Subject number	1-F*	2-F	3-M*	4-M	1-F	2-F	3-M	4-F
RMSE	118.95	167.23	213.85	119.08	102.16	110.88	163.59	139.67

*F stands for Female subject, and M stands for male subject.

DEPENDENCE OF AGENCY AND PERFORMANCE ON VISUALIZED PRECISION PINCH FORCE

[1,2] Sean Sanford, [1,2]Aniket Shah, [1,2] Gabriella Borodyansky, [1,3] Vasundhra Srevatsan, [1,2] Raviraj Nataraj (PI)

[1]Movement Control Rehabilitation (MOCORE) Laboratory, [2]Department of Biomedical Engineering,
[3]Department of Mathematical Sciences, Stevens Institute of Technology, Hoboken, NJ, USA
email: ssanford@stevens.edu, web: http://www.mocorelab.com

INTRODUCTION

Hand grasp capabilities can be severely impaired by neuromuscular trauma such as amputation and spinal cord injury. Function may be restored using a prosthesis device. For upper-limb amputation, the device may be a sensory-driven motor prosthesis [1]. For spinal cord injury, it may be a hand neuro-prosthesis that uses functional neuromuscular stimulation to activate paralyzed muscles [2]. Physical rehabilitation with these devices may involve repetitive practice of a specific functional task for heuristic user learning and ad hoc tuning of device operation parameters. Methodology that identifies optimal device parameters to more naturally integrate the user and device and to make rehabilitation more efficient would be of great clinical value.

In this study, we investigate the potential role of cognitive agency in visualized grasp force. The sense of agency is the perception that one is the true author of one's actions [3]. We hypothesize that with a greater sense of agency, individuals will have improved functional capabilities in a visualized grasp force task. Such findings may provide a foundation to design rehabilitation paradigms that identify and relate agency to user-device parameters that accelerate rehabilitation progress. In this study, force is applied to a load-sensing apparatus with the thumb and index finger to match the applied force to a target ramp on a visual display. The display of the applied force is systematically modified to potentially alter agency and functional performance. Modified operational conditions on the visualized force include loading speed, the addition of random noise, and an automated condition to gradually complete ramp-tracking under present control. These conditions were chosen to consider common operational parameters for an assistive device to be tuned by a clinical engineer.

METHODS

A. Subjects

Ten volunteers (8 males, 2 females, 21 ± 3 years in age) have participated according to protocols approved by the local Institutional Review Board. Subjects were screened to be able-bodied, right-hand dominant, and to have no previous injury or surgery to the upper extremities, no cited neuromuscular disease, and correctable-to-normal vision.

B. Motion capture system

Hand movements were tracked using retro-reflective motion capture of marker clusters placed on each phalange and metacarpal of the index finger and thumb using nine infrared cameras (*Prime17, OptiTrack, Natural Point, Inc.,* Corvallis, OR). Motion capture data were sampled at 120Hz with *Motive* (*Natural Point, Inc.*). Kinematics were collected for subsequent processing of digit joint moments using a 3-D hand model in *OpenSim*, [4].

C. Pinch apparatus

A specialized pinch apparatus for two load cells (*Mini40, ATI Industrial Automation*, Apex, NC) was custom created for this experiment. The apparatus has extensions rigidly connected to the load cells for applying thumb and pinch forces in opposition. The extensions may slide and be re-fixed along a rail to adjust the pinch grip width relative to each subject's hand size. Data from the load cells were sampled at 120Hz using the *NI PXIe-6363* (*National Instruments*, Austin, TX) data acquisition system. The embedded computer real-time streams the force data in *Simulink* (*Mathworks Inc.*, Natick, MA) for visual display of the applied force and target ramp.

D. Protocol

Each subject participated in a two-hour session. Each trial involved applying force to affect a visualized dynamic force trace to match a preset target ramp

force (**Figure 1**) with peak at 5N. Performance was measured according to the mean absolute error between applied force and the ramp. Subjects also had to ensure they applied sufficient load at the top of the ramp, past a threshold line, to complete the 'action' for this trial. The subject was made aware of a sound (short beep) as a sensory 'consequence' of the 'action' at a variable time-interval (0 to 1 sec) following contact with the threshold line. To identify intentional binding between action and consequence as a measure of agency [3], the subject estimated the time-interval. It is inferred that with greater agency one would perceive a shorter time-interval [5].

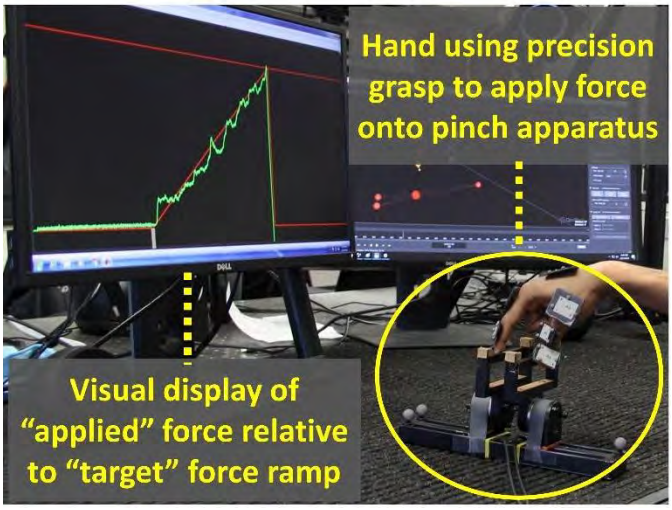

Figure 1: Hand applies force onto pinch apparatus to produce display of force against target ramp.

Twenty trials were done for each condition of visual representation of the force. The conditions were: (1) 'normal' (control) - force shown same as actual force applied, (2) 'slow' - force shown is 50% less than actual force, (3) 'fast' - force shown is 50% greater than actual force, (4) 'noisy' – force contaminated with bi-directional random noise (1.25N peak-to-peak), (5) 'auto' – visualized applied force under gradually greater, by linear progression, preset control to perfectly match ramp, (6) '1-phase loading' - no ramp as subject can immediately apply load to reach 5N threshold.

RESULTS AND DISCUSSION

Preliminary analysis (**Table 1**) shows that greater agency is observed for 'slow' and '1-phase'. These respective results suggest greater perception of control when applying higher loads or not being overly constrained by the task of following the ramp. The 'auto' case showed significantly worse performance from the control, suggesting performance trail-off with automation. Additional analyses will be performed to compute joint angles and moments and observe how joint mechanics may be a function of visualized loading and agency.

The next phase of this research will build upon the principles identified in this study that relate agency and performance to grasp force application. We seek to create virtual reality platforms that include force and electromyography signals to drive actions of devices within the VR environment to leverage agency and maximize functional performance. We expect related protocols to employ agency to optimize control systems of hand grasp assistive devices and rehabilitation protocols to accelerate functional gains.

REFERENCES

1. Kuiken et al. *Lancet*, 369(9559): 3-9, 2007.
2. Peckham et al. *Arch Phys Med*, 82(10): 1380-1388, 2001.
3. Moore and Obhi, *Consciousness and Cognition*, 21(1): 546-561, 2012.
4. Delp et al. *IEEE TBME*, 54(11): 1940-50, 2007.
5. Caspar et al. *Plos One*, 11(10): e0163892, 2016.

ACKNOWLEDGEMENTS

We would like to thank the Schaefer School of Engineering and Science at the Stevens Institute of Technology for providing faculty start-up support.

Table 1: Performance (mean force error, N) and agency (estimation time offset, msec) per operation condition

*p < 0.05 relative to "Normal"	PRECISION PINCH FORCE RESULTS					
	Normal	**Slow**	**Fast**	**Noisy**	**Auto**	**1-phase**
PERFORMANCE	0.40	0.38	0.36	0.35	0.55*	N/A
AGENCY	+14	+36*	+27	+9	-9	+36*

DISCRETE VISUAL FEEDBACK ON SHORT-TERM RETENTION OF LEARNED MOVEMENTS

[1,2]Sean Sanford, [1,2]Gabriella Borodyansky, [1,3]Thomas Selvaggi, [1,2]Corrine Rybarski,
[1,2]Aniket Shah, [1,2]Raviraj Nataraj (PI)

[1]Movement Control Rehabilitation (MOCORE) Laboratory, [2]Department of Biomedical Engineering,
[3]Department of Mechanical Engineering, Stevens Institute of Technology, Hoboken, NJ, USA
email: ssanford@stevens.edu, web: http://www.mocorelab.com

INTRODUCTION

Persons with traumatic injuries or neuromuscular deficits can benefit from well-targeted rehabilitation methods to accelerate functional recovery. During physical therapy, verbal or visual cues may be provided for more accurate performance of repetitive movements [1]. Such guidance is intended to build task-specific strength and functional ability while avoiding extreme joint motions that could create or exacerbate injury. The ultimate goal is for individuals to perform movements more effectively and independently. We are investigating the potential of various modes of visual feedback (VF) to maximize performance *and* learning of functional movements. We seek to create novel visually-driven rehabilitation paradigms that accelerate gains in neuromotor function. Previous studies have indicated trade-off in performance versus learning retention for concurrent versus terminal feedback, respectively [2]. Concurrent feedback is provided while performing the task, but terminal feedback provides knowledge of performance only after task completion. The guidance hypothesis states that continuous real-time feedback reduces learning potential by prohibiting intrinsic factors [3]. Visual feedback modes that co-maximize performance and learning may be a valuable foundation for designing more optimal movement rehabilitation protocols.

In this pilot study, we investigate the performance and learning potential of *discrete* feedback that presents concurrent but sparse points of reference. We hypothesize that selectively discretized feedback can offer both performance and retention benefits. This would suggest that a few well-posed reference points may accelerate movement rehabilitation. The squat was chosen as an initial test movement since it is well controlled and muscle activation changes are highly sensitive to small changes in a performance metric, such as squat depth [4].

METHODS

A. Subjects

Eight subjects (3 males, 5 females, 20±2 years in age) have participated according to protocols approved by the local Institutional Review Board. Subjects were screened to have no prior lower extremity nor spinal surgery and no cited neuromuscular disease.

B. Motion Capture (MoCap) System

Squat depth was tracked in real-time by retro-reflective MoCap of a marker-cluster placed at the femur *midpoint* (between the proximal head and lateral epicondyle). MoCap data were sampled by infrared cameras (*Prime17, OptiTrack, Natural Point, Inc.,* Corvallis, OR) at 120 Hz. Data were then streamed via broadcast ethernet to a remote computer with *MATLAB2017a* (*Mathworks, Inc.*, Natick, MA) for the visual feedback display.

C. Muscle Activations and Center of Pressure

Surface electromyography (EMG) and ground reaction data were collected using wireless electrodes and force sensitive resistor (FSR) sensors (*Trigno, Delsys, Inc.,* Natick, MA).

D. Protocol

Squat depth was defined as the vertical displacement of the femur marker cluster. The zero-position, z, for squat depth was calibrated while subjects stood upright. The max-position, m, was found from subjects holding a self-selected squat for 10 seconds comfortably while aligning thighs 'near parallel' to the ground. The squat depth trace to be tracked in subsequent visual feedback trials was computed as:

$$x(t) = A \sin\left(2\pi f t + \frac{\pi}{2}\right) - A$$

where $x(t)$ is the target squat depth with time; amplitude, $A = |z - m|/2$; frequency, $f = 1/3$ Hz. A single cycle of this sinusoid (**Figure 1**) was tracked each trial under one of three visual feedback (VF) modes: (1) *continuous* - concurrent feedback to show target and actual movement traces together in real-time, (2) *discrete* - concurrent feedback where target trace only has three points (start z, m, end z), and (3) *terminal* - visual display of actual versus continuous target trace shown right after movement completion.

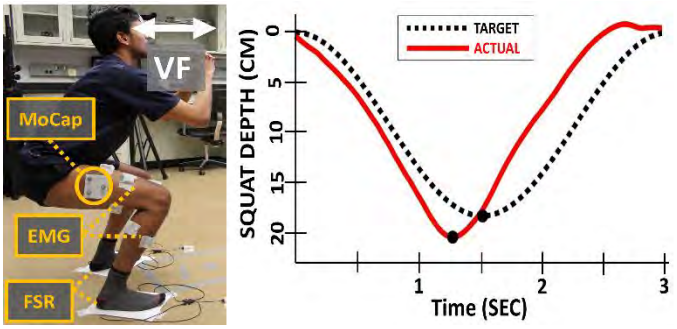

Figure 1: Subject executing squat (LEFT) with visual feedback (VF) of performance (RIGHT).

For each mode, a second "retention" trial was done at five seconds after the first VF "training" trial. For retention, the subject performed the squat with no visual feedback (NVF) during or after the trial. A total of 45 trial pairs (15 total for each mode) were performed in randomized order with each subject.

RESULTS AND DISCUSSION

ANOVA showed significant difference ($p < 0.05$) in NVF (retention) performance across the modes (**Table 1**). Post-hoc Tukey showed 'terminal' with the significantly lowest mean error for retention, confirming the guidance hypothesis for this study paradigm. No other significant differences were observed and may be attributable to only testing eight subjects. As is, the lowest *overall* (training and retention) performance error was seen with 'discrete' mode. With additional data, we aim to confirm this discrete mode result and also analyze changes in muscle activations and center of pressure across gradations of visual feedback modes.

In the next stage, we intend to develop a platform to drive more complex visual feedback paradigms that include performance matching across multiple degrees of freedom. Visual feedback will be provided on either two-dimensional projections or a virtual reality environment (*Multi-joint dynamics with Contact, Roboti LLC*, Redmond, WA). The final goal is to create a visual feedback platform that guides the user to produce "optimal" movements that inherently has several co-objectives. These objectives include achieving performance targets, maximizing activations of specific muscle groups, and minimizing joint stresses. Optimal movements will be identified through subject-specific musculoskeletal models (*Software for Interactive Musculoskeletal Modeling*, *Motion Analysis Corp.*, Santa Rosa, CA). Finally, visual feedback paradigms will be further developed to maximize motor integration between the user and an assistive device for human machine interface (HMI) rehabilitation.

REFERENCES

1. Sigrist et al. *Psych Bull Rev*, 20(1): 21–53, 2013.
2. Blandin et al. *J Exp Psych Learn Mem Cog*, 34(4): 994–1000, 2008.
3. Schmidt, *Tutorials in Motor Neuroscience*, 1991
4. Clark et al. *J Strength Cond Res*, 26(4): 1169–1178, 2012.

ACKNOWLEDGEMENTS

We would like to thank the Schaefer School of Engineering and Science at the Stevens Institute of Technology for providing faculty start-up support.

Table 1: Squat tracking **performance error (cm)** for various visual feedback modes and sub-cases:
(VF = visual feedback (training), NVF = no visual feedback (retention), OVERALL = mean of VF and NVF)

VISUAL FEEDBACK MODE								
CONTINUOUS			***DISCRETE***			***TERMINAL***		
VF	NVF	*OVERALL*	VF	NVF	*OVERALL*	VF	NVF	*OVERALL*
2.76	4.55^{+}	*3.65*	2.60	4.46^{+}	*3.53*	4.65	4.09^{+}	*4.37*
Note: $^{+}p < 0.05$ for post-hoc Tukey for terminal NVF versus both other NVF								

EFFECT OF FOOT PLATE LENGTH ON HEALTHY GAIT

David Schmitthenner and Anne E. Martin
The Pennsylvania State University
Email: dhs5071@psu.edu, aem34@psu.edu

INTRODUCTION

Assistive ankle devices such as braces often use a stiff foot plate to help constrain the motion of the ankle and restore a more typical gait [1]. Design of the foot plate is critical for powered assistive devices such as exoskeletons because of the greater force transfer. Given that the human foot does not function like a stiff plate during gait [2], it is unclear what affect a stiff plate has on the user's gait, independent of any other mechanical constraints or assistance. It is also unclear how the length of the foot plate affects gait. A longer plate allows the force to be distributed over a larger area but a shorter plate may have less undesirable effects because it constrains the foot less. In one of the few studies investigating foot plate length, [3] found that foot plate length does affect gait slightly for stroke victims wearing an articulated ankle-foot orthosis. However, this study primarily compared each orthotic condition to healthy speed-matched gait, making it difficult to determine what affect the foot plate itself had. The goal of this work is to quantify how different length foot plates, in and of themselves, alter gait.

METHODS

Four healthy young adult subjects (2 male) walked overground at their self-selected speeds while kinematic (Vicon, Oxford, UK) and kinetic (Bertec, Columbus, OH) data were collected. The subjects wore shoes in which the sole was replaced with a foot plate. Three conditions were tested – a foot plate ending just before the metatarsal joints (three quarters condition), a foot plate equal to the length of the foot (full condition), and an unmodified insole from the shoe (control condition). The foot plates were made of 5 mm thick Delrin and a thin 2 mm layer of foam rubber for comfort. For the three quarters condition, a denser 5 mm foam was used under the toes to maintain a constant insole height. Each subject completed 20 trials per condition, with each trial consisting of walking approximately 20 feet. The left

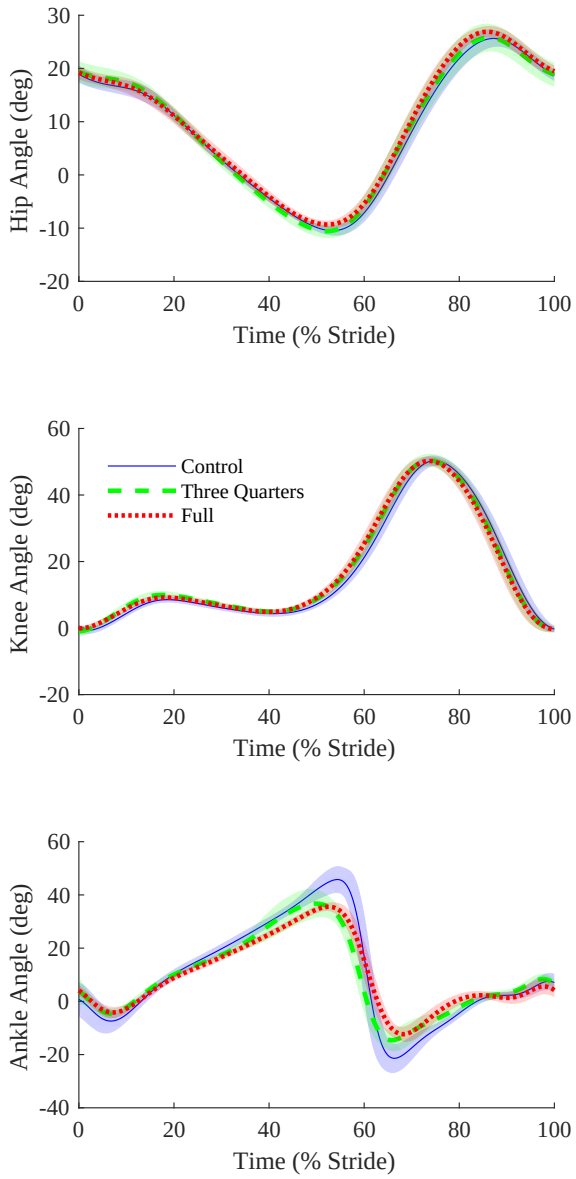

Figure 1: The hip, knee, and ankle joint trajectories for the three conditions for a representative subject. The ankle range of motion tends to decrease as the foot plate gets longer. The hip and knee trajectories are unaffected by a foot plate regardless of length. This suggests that any kinematic variation caused by the foot plate is accounted for at the ankle.

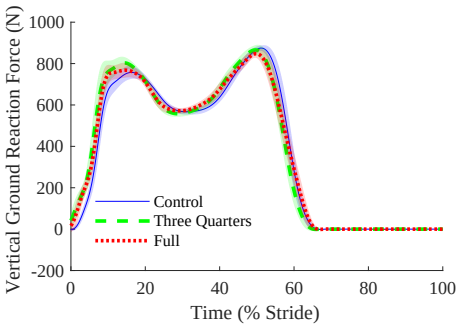

Figure 2: The vertical ground reaction force is unchanged by a foot plate.

and right legs were analyzed separately due to several of the subjects having a somewhat asymmetric gait. Data were tested for statistical differences and equivalence using standard t-tests and the two one-sided tests procedure [4]; $\alpha = 0.05$ and data were considered equivalent if they were within 6% of mean value of the no foot plate condition. A statistical difference indicates that the observed difference between conditions is not due to measurement noise, while statistical equivalence indicates that any changes are not meaningful. All statistical testing compared the control condition to the full plate or the three quarter plate conditions. P-values for statistical differences are indicated with p_d while p-values for statistical equivalence are indicated with p_e.

RESULTS AND DISCUSSION

The subjects walked at an average speed of 1.27 $\pm$ 0.10 m/s for the control condition, 1.32 $\pm$ 0.11 m/s for the three quarters condition, which is a significant change ($p_d < 0.05$), and 1.28 $\pm$ 0.13 m/s for the full condition, which is equivalent to the no plate condition ($p_e < 0.05$). For the three quarters condition, two subjects increased their speed significantly when wearing the three quarter foot plate by an average of 0.10 m/s while the other two subjects maintained their walking speed ($p_e < 0.05$). The faster walking speed may be caused by some energy storage and return in the foot plate. For all four subjects, their step cadence was statistically equivalent to their no foot plate conditions regardless of foot plate length ($p_e < 0.05$). The subjects walked with an average cadence of 0.94 $\pm$ 0.07 Hz for the control condition, 0.95 $\pm$ 0.07 Hz for the three quarters condition, and 0.93 $\pm$ 0.07 Hz for the full condition.

In general, the foot plate decreased ankle range of motion but had little effect on the hip and knee kinematics (Fig. 1). The timing of the trajectories are consistent across all conditions for all joints. Peak stance knee flexion increased ($p_d < 0.05$) in two subjects by an average of 1.9°, altering weight acceptance. For three subjects, the ankle range of motion decreased ($p_d < 0.05$) by an average of 8° for the full length foot plate. The longer foot plate is likely stiffer than the shorter plate, so these results are consistent with [5] in which progressively stiffer prosthetic feet led to a progressive decrease in the ankle range of motion. This suggests that the foot plate does influence gait somewhat but that most compensations are at the ankle, allowing relatively normal hip and knee kinematics. This is supported by previous findings that people adapt their ankle kinematics when walking with ankle exoskeleton assistance but do not alter their hip and knee kinematics [6].

The vertical ground reaction force is not statistically affected by the foot plate ($p_e < 0.05$, Fig. 2). Since a decreased ankle range of motion may reduce the push-off force, this suggests that the foot plate may provide some energy storage and return in the form of elastic bending. It further suggests that the human compensates for any energy storage in the foot plate.

CONCLUSIONS

The similarity in kinematics between the control and both foot plate conditions suggests that introducing a stiff foot plate has very little effect on gait. Some subjects speed up, but overall the effects appear minimal. This bodes well for exoskeleton design because there is little concern that even a long, stiff, mechanically-advantageous foot plate alters gait.

REFERENCES

[1] Tyson, SF, et al. *Clin Rehabil* **27**, 879–891, 2013.
[2] Carson, MC, et al. *J Biomech* **34**, 1299–1307, 2001.
[3] Fatone, S, et al. *Arch Phys Med Rehab* **90**, 810–818, 2009.
[4] Lakens, D. *Soc Psychol Pers Sci* **8**, 355–362, 2017.
[5] Klodd, E, et al. *J Rehabil Res Dev* **47**, 543, 2010.
[6] Kao, PC, et al. *J Biomech* **43**, 203–209, 2010.

A HAPTIC BIOFEEDBACK CANE TO REDUCE DEGENERATIVE LOADING IN THE ARTHRITIC KNEE

[1,2,3]Evan Schuster, [1,2,3]Rebecca L. Routson, [1,2,5]Mason Hinchcliff, [1,2,3]Karley Benoff, [2,4]Pradeep Suri, [1,2,4]Joseph M. Czerniecki, [1,2]Chris Richburg, and [1,2,3]Patrick M Aubin,
[1]Center for Limb Loss and Mobility (CLiMB), [2]VA Puget Sound Health Care System, Seattle, WA USA
Dept. of [3]Mech. Eng., [4]Rehab. Medicine and [5]School of Medicine, U of Washington, Seattle, WA USA
Email: eschu92@uw.edu, Web: http://faculty.washington.edu/paubin/wordpress/

INTRODUCTION

Osteoarthritis (OA) is the most common joint disorder and the leading cause of disability in adults [1]. It is thought that at least 37% of adults over the age of 65 exhibit evidence of knee OA [2]. Medial compartment knee loading is thought to play a key role in the development and progression of knee OA [3]. The knee adduction moment (KAM), a proxy for medial compartment loading, is associated with the rate of OA progression [4]. When properly used, walking canes can reduce the KAM [5], however most cane users under-load their cane and thus do not receive the maximum beneficial knee unloading [6].

To provide patients with a practical, intuitive solution to improve cane loading, we developed a walking cane with haptic biofeedback which alerts the user when the target amount of force has been applied to the cane. The purpose of this study is to compare the efficacy of the haptic cane to that of a traditional walking cane in terms of cane loading and KAM reduction. Proper and constant cane loading over time may slow the progression of OA, reduce pain, delay surgery, and improve mobility.

METHODS

Nineteen individuals who had experience using a walking cane and reported clinically diagnosed knee OA were recruited for the study. The average ± one standard deviation (SD) age, height, and weight was 60 ± 12.1 years, 1.79 ± 0.09 m, and 99.9 ± 21.3 kg. Participants had been living with diagnosed knee OA for an average of 12.5 ± 11.4 years with 5.25 ± 7.4 years of experience using a walking cane. Subjects were given the Western Ontario and McMaster Universities Osteoarthritis Index (WOMAC) questionnaire, commonly used to assess the impact knee OA has on day-to-day life [7]. The average score was 48.3 ± 19.7 (with 96, the maximum score, indicating extreme pain, stiffness, and difficulty). All subjects gave their informed consent to participating in the IRB approved study.

Participants attended a single lab session for collection of kinematic, kinetic, and biometric data. Participants changed into motion capture conducive clothing and retro-reflective markers were placed using a modified Plug-In-Gait model. During the data collections, participants were instructed to walk at SSW along an approximately 20-meter path containing five force plates (Bertec, Columbus, Ohio). Twelve Vicon motion capture cameras (Vicon Motion Systems, Oxford, United Kingdom) recorded marker positions. Walking trials were carried out under five conditions (Table 1).

Table 1. Descriptions of walking trial conditions.

Condition	Description
C1: Naive	Conventional cane with no instruction
C2.A: Scale Training	Conventional cane, scale training, & instruction on proper cane technique
Rest Period	5-minute break to test short-term instruction recall
C2.B: Scale Recall	Conventional cane with no further instruction nor practice
C3.A: Haptics Training	Haptic cane with instruction and a practice session
Rest Period	5-minute break to test short-term instruction recall
C3.B: Haptic Recall	Haptic cane with no further instruction nor practice.

The order of conditions C2 and C3 were randomized at the beginning of data collection to avoid a learning bias. During "scale training" participants practiced applying the suggested 20% BW to their canes using a beam scale that had been set to the correct weight,

until they felt comfortable recreating the technique (usually less than five minutes). Before the 'B' conditions, a five-minute break was taken to test short-term instruction retention. For each condition, between 5 and 8 successful walking trials were collected.

The KAM was calculated in Visual3D using standard inverse dynamics techniques and exported to MATLAB to determine the peak KAM (PKAM) and knee adduction angular impulse (KAAI), as well as their associated averages and SD's. Peak cane load averages and SD's were also calculated in MATLAB.

RESULTS AND DISCUSSION

Compared to naïve cane loading, both scale training and use of the haptic biofeedback cane significantly increased cane loading (Figure 1). Scale training had greater cane load variability than the haptic cane (Figure 1). Scale training and use of the haptic biofeedback cane reduced KAM across stance phase with the primary reductions occurring in late-stance (Figure 2).

The PKAM was reduced from 2.56 ± 0.94 %BW*Ht in the naïve condition to 1.86 ± 0.88 %BW*Ht after scale training (C2A) and 1.75 ± 0.84 %BW*Ht in trials using the haptic cane (C3A). The averages for the recall conditions (C2B, C3B) were 1.87 ± 0.95 %BW*Ht and 1.83±0.82 %BW*Ht, respectively. The KAAI had a similar significant reduction, from 1.38 ± 0.19 %BW*Ht*s (naïve) to 0.757 ± 0.20 %BW*Ht*s for scale training (C2A) and 0.553 ± 0.23 %BW*Ht*s for the haptic cane condition (C3A) (Figure 3).

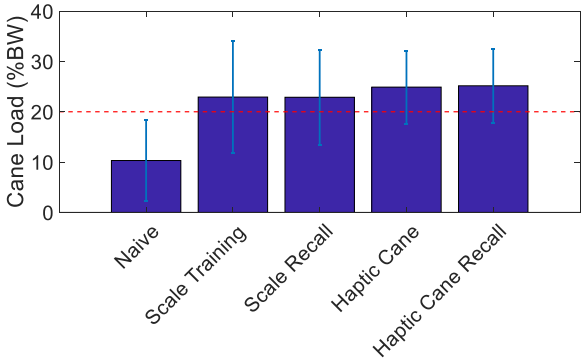

Figure 1. Mean cane load in %BW of 19 subjects' arthritic knee during stance phase, while walking with a cane. Dotted line indicates target of 20% BW.

The averages for the recall conditions (C2B, C3B) were 0.700 ± 0.23 %BW*Ht*s and 0.563 ± 0.19 %BW*Ht*s, respectively. We are currently performing multivariate statistical analyses to determine statistical significance. Improving the design, usability and efficacy of common walking aids through biofeedback serves those with OA improving conservative treatment options.

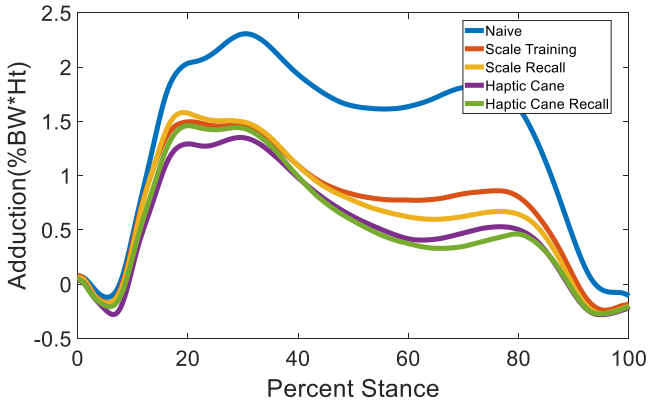

Figure 2. Mean KAM of 19 subjects' arthritic knee during stance phase across the tested conditions

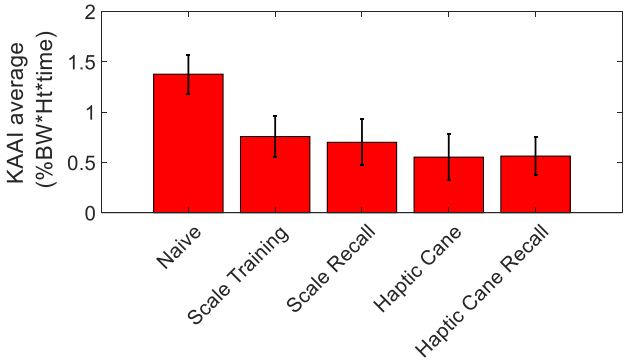

Figure 3. Mean KAAI normalized to %BW*Ht*stance-time of 19 subjects' arthritic knee during stance phase, while walking with a cane.

REFERENCES

[1] G. Peat, et al. *Ann. Rheum. Dis.*, **60**, 2001.
[2] C. F. Dillon, et al. *J. Rheumatol.*, **33**, 2006.
[3] D. E. Hurwitz, et al. *J. Biomech.*, **31**, 1998.
[4] T. Miyazaki, et al. *Ann Rheum Dis*, **61**, 2002.
[5] M. Simic, et al. *Osteoarthr. Cartil.*, **19**, 2011.
[6] R. L. Routson, et al. *IEEE (EMBC)*, 2016.
[7] N. Bellamy, et al. *J. Rheumatol.*, **15**, 1988.

ACKNOWLEDGEMENTS

This research was supported by VA RR&D Service Grants A9243C, RX002357, and RX001926.

Granular Jamming Foot Orthosis For Emulating A Range of Biomechanical Properties

[1] Emily Simonds, [2] Jonathan Colton, [3] Geza Kogler, [1,3] Young-Hui Chang

[1] Bioengineering, Georgia Institute of Technology, Atlanta, GA, USA
[2] Mechanical Engineering, Georgia Institute of Technology, Atlanta, GA, USA
[3] Biological Sciences, Georgia Institute of Technology, Atlanta, GA, USA

email: yh.chang@ap.gatech.edu

INTRODUCTION

Although foot orthoses are widely used to ease pain and treat pathologies of the foot, their efficacy is still being debated and there is an increasing demand to use international testing standards to assess their performance. The current standards of design and manufacturing for custom foot orthoses are time consuming and introduce potentially detrimental errors in fit [1]. Another issue with current foot orthoses is the lack of durability inherent with certain configurations of materials. Moreover, orthoses are generally designed for a specific purpose based on factors such as loading rate and magnitude.

The aim of this study was to develop and test a novel foot orthosis that uses granular jamming principles to provide rapid custom fit and emulation of a range of material properties. Granular jamming refers to a material phase transition where a fluid-like granular medium (e.g., sand) can become rigid when the fluid is considered jammed and there is no appreciable flow [2]. Granular jamming, which includes the principles of dilatancy, has already been implemented in prosthetics and orthotics [3,4] as well as in universal soft robotic grippers [2]. These applications take advantage of the rapid shape matching potential of jamming. Other applications such as the alteration of the material properties of an orthosis have not been explored. This novel approach would have the advantage of providing a single prefabricated device that can be quickly customized to a patient's foot and used immediately.

We designed and tested several new prototypes of a variable stiffness Foot Granular Orthosis (FootGO) that can be adjusted automatically with vacuum pressure. We predicted that the FootGO would be able to imitate the compression properties (stress-strain relationship and energy absorption) of a range of commercial foams commonly used in foot orthoses, while still maintaining or exceeding the durability of the commercial standard.

METHODS

Granular media were utilized in combination with negative pressure to create a variable stiffness capability. The FootGO consists of layered membranes that contain the granular media within a rectangular shape (size 10.5 men's shoe size) that allow for a vacuum seal to be made. Negative pressure was controlled using a custom microcontroller (Model Arduino Uno R3, Vilros, Brick, NJ) and a vacuum pump (Karlsson Robotics Model D2028, Tequesta, Florida) at a tested range of pressures from 0 to -50 kPa. A custom code was written to set, sense and maintain the internal pressure of the FootGO. Three types of granular media (rice, poppy seeds, and polystyrene beads) were used in different prototype configurations to study the effects of volume fill, particulate size, and granular media type.

A series of uniaxial compression tests were conducted on four types of common commercial orthotic foams (closed cell polyethylene, EVA, Polyurethane, and SBR), and eight different FootGO prototype configurations. ASTM standard testing protocols (D1621-16 and D3575-14) were chosen as reference standards upon which to base the methods we used to evaluate the material performance of both the commercial materials and the prototypes. Stress-strain curves were obtained from these tests at two different strain rates (0.001 s^{-1}, 0.1 s^{-1}). Energy absorption, U, was obtained by computing the area under the stress-strain curve up to the densification strain of the foam (Figure 1) for each foam sample and for each prototype.

RESULTS AND DISCUSSION

With a single FootGO prototype, we were able to adjust the negative pressure to match the range of material behaviors exhibited by multiple commercial foams (Figure 1). Generally, higher negative pressure resulted in an increasing stiffness of a given prototype configuration, with some exceptions.

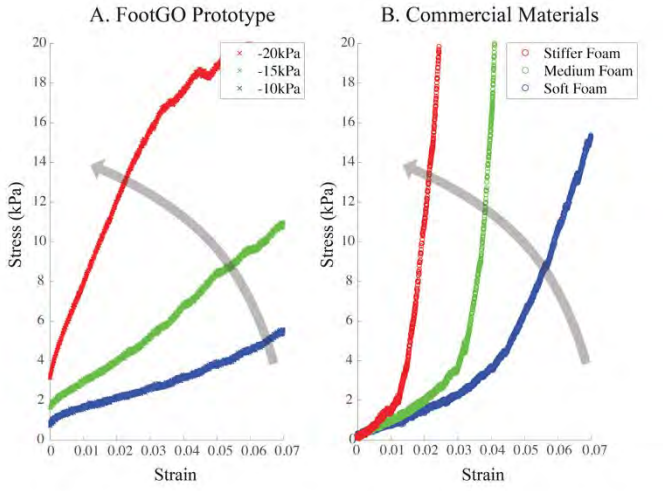

Figure 1: Stress-strain behavior of (A) a FootGO Prototype under three different negative pressures and (B) three different representative commercial foams at the same strain rate (0.1). Increased negative pressure of the FootGO prototype resulted in corresponding increases in orthosis stiffness. The gray arrows indicate general trends of increasing stiffness in both sample types.

Failure strains of the granular orthoses were always greater than those measured for the commercial foams. Commercial foams quickly reached failure strains (densification), whereas the granular orthoses often never reached densification in our tests.

By adjusting negative pressure, each of the different prototype configurations was found to span the full range of energy absorptions of all the commercial foams tested (Figure 2). The energy absorbed across all of the commercial foams never exceeded 250 J/m^3. In contrast, all of the FootGO prototypes exhibited ranges of energy absorption at different negative pressures that spanned the range of the foams and sometimes far exceeded this range in the case of the poppyseed and rice granules.

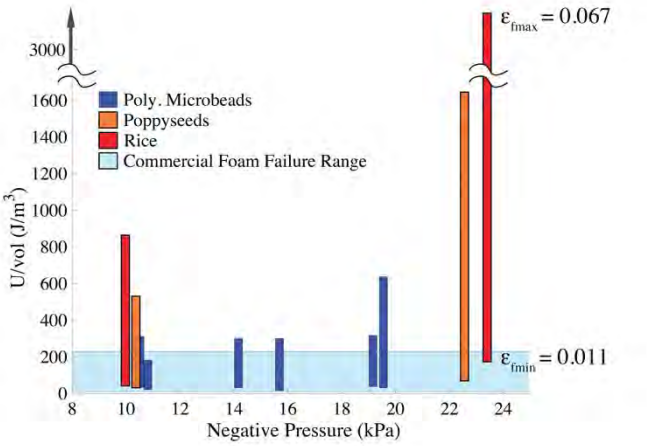

Figure 2. Minimum-maximum ranges of energy absorption (strain rate=0.001) of various FootGO prototype configurations. Each bar depicts the range of energy absorbed for each individual prototype compared to the minimum and maximum energy absorption values across all commercial foams tested (light blue band). The ranges of energy absorbed are obtained with respect to the minimum (0.011) and maximum (0.067) failure strains of all commercial foams tested. The performance of a given prototype configuration is shown at various negative pressures.

CONCLUSIONS

The principles of granular jamming can be implemented in prosthetic and orthotic applications when traits such as instant shape matching or adjustable material properties are desired. A single granular jamming foot orthosis can be rapidly tuned to imitate and surpass the energy absorption (i.e., shock absorption) capabilities of commercially available foams. This offers a wide variety of suitable applications from a single device orthotic device and the need for multiple custom orthoses per patient could be eliminated with a granular orthosis that can be adjusted (and re-adjusted) instantaneously to match desired properties.

REFERENCES

1. Laughton, et al. *JAPMA*., 2002; 92: 261-268.
2. Brown, et al. *PNAS*, 2010; 107: 18809-18814.
3. Sletto, et al. *POI*, 2016; 40: 409- 413.
4. Wu, et al. *POI,* 2009; *33*: 1-9

SUBTHRESHOLD VIBRATION DOES NOT AFFECT WALKING PERFORMANCE OF TRANSTIBIAL AMPUTEES

Ian Sloan [1], Jenny A. Kent[1], Shane R. Wurdeman[2], Adam L. Jacobsen[3], Kota Z. Takahashi[1], Nicholas Stergiou[1, 4]
[1]Department of Biomechanics, University of Nebraska at Omaha, Omaha, NE USA
[2]Department of Clinical and Scientific Affairs, Hangar Clinic, Houston, TX USA [3]Veterans Affairs Medical Center, Omaha, NE USA [4]College of Public Health, University of Nebraska Medical Center, Omaha, NE USA
Email: csloan@unomaha.edu
Presentation Preference: **Podium**

INTRODUCTION

Amputation below the knee causes a person to lose important pathways to the central nervous system used in sensation and balance [1]. A lack of sensation in the residual limb [2] has been shown to be a factor in poor balance [3]. The 'stochastic resonance' phenomenon, where the addition of subthreshold noise can enhance the detection of a weak stimulus, has been shown to improve sensation and subsequently balance [4]. The objective of this study was to explore if stochastic resonance can be used while walking to improve walking performance in transtibial amputees. White noise has been typically used in previous stochastic resonance studies; a random signal with equal intensity throughout its frequency spectrum. We chose to also investigate a pink noise (1/f) vibration structure based on the fact that is a structure that is more often seen in natural processes [5]. We hypothesized that stimulation would improve control of the prosthesis, which would be seen in increased step lengths and decreased step width, step length variability and step width variability. Further, we expected the change to be greater with the pink noise stimulation when compared with the white noise.

METHODS

Fourteen participants with a unilateral transtibial amputation (height 1.79m±0.07, weight 100.3kg±15.6, age 59.7±15.0) completed a series of walking trials at a self-selected pace across the laboratory, under three different vibration conditions; no vibration, pink noise vibration, and white noise vibration. Vibration was provided by a vibrating tactor and set on the thigh of the residual limb. The three conditions were randomized and the participant was not made aware of which condition was being used for each trial. The threshold for the two vibrations were set at the beginning of the session and vibration was set to 60-90% of this threshold to ensure that the participant could not feel the device. Kinematic data from at least ten traverses for each condition were collected at 100Hz with a twelve-camera motion capture system (Motion Analysis Corporation, Santa Rosa, CA). Step length and step width along with their standard deviations were computed for the first thirteen steps in each condition using Visual 3D (C-Motion, Germantown, MD). A 1-way Repeated Measures ANOVA was used to compare variables across different vibration conditions (3 levels: none, pink, white; $\alpha = 0.05$).

RESULTS AND DISCUSSION

There were no significant differences between conditions (Table 1), indicating that vibrating the residual thigh of transtibial amputees during walking does not affect their walking as evaluated by the selected dependent variables. There was also high variability among participants, reflecting the heterogeneity of the group.

CONCLUSIONS

Vibrating alternative body sites, applying longer duration of vibration, or potentially outside of the laboratory in the form of an intervention/training, and we will explore gait biomechanics with different dependent variables that examine kinematics and kinetics for the present experiment are of few of the alternatives we explore as our next investigative steps.

REFERENCES

1. Skidmore, FM et al. *J Neurol Nueorsurg Psychiatry* **80**(1), 569-570, 2009.
2.Quai, TM, et al. *Clin Rehabil*, **19**(6), 668-76, 2005.
3. Kavounoudias, A et al. *Arch Phys Med Rehabil*, **86**(4), 633-640, 2005.
4. Moss, F et al. *Clin Neurophysiol*, **115**(2), 267-281, 2004.
5. Stergiou, N et al. *Kinesiology Review* **5**(1), 15-22, 2016.

ACKNOWLEDGEMENTS

This work was supported by NIH P20GM109090 and NIH R15HD08682

Table 1: Applying the various vibration conditions had no significant effect on any of the walking measures examined. (n=14)

	Vibration Condition							
	None		Pink		White		Vibration Condition p (sig at 0.05)	
	Prosthetic	Sound	Prosthetic	Sound	Prosthetic	Sound	Prosthetic	Sound
Step Length (m)	0.688 ± 0.127	0.672 ± 0.106	0.692 ± 0.119	0.671 ± 0.102	0.687 ± 0.127	0.674 ± 0.109	0.242	0.517
Step Width (m)	0.175 ± 0.034	0.175 ± 0.034	0.171 ± 0.033	0.173 ± 0.034	0.178 ± 0.038	0.178 ± 0.039	0.216	0.238
Step Length Variability (m)	0.127 ± 0.005	0.106 ± 0.006	0.119 ± 0.007	0.102 ± 0.005	0.127 ± 0.005	0.109 ± 0.005	0.434	0.256
Step Width Variability (m)	0.033 ± 0.006	0.034 ± 0.007	0.032 ± 0.007	0.034 ± 0.007	0.038 ± 0.007	0.039 ± 0.007	0.098	0.353

DEVELOPMENT OF AN UPPERLIMB MUSCULOSKELETAL WHEELCHAIR PROPULSION MODEL TO ANALYZE THE INFLUENCE OF AXLE POSITION ON SHOULDER MOMENTS

Amy Strong[1,3], Nathan Hogaboom[2,3], Alicia Koontz[2,3], Michael Boninger[2,3,4]
[1]Department of Mechanical Engineering, Auburn University, Auburn, AL
[2]Department of Rehabilitation Science and Technology, University of Pittsburgh, Pittsburgh, PA
[3]Human Engineering Research Laboratories, VA Pittsburgh Healthcare System, Pittsburgh, PA
[4]Department of Physical Medicine & Rehabilitation, University of Pittsburgh, Pittsburgh, PA
email: aks0043@auburn.edu

INTRODUCTION

Manual wheelchair users often report shoulder pain, which can affect overall quality of life [1]. Clinical Practice Guidelines suggest minimizing forces exerted on the upper limbs during propulsion to prevent upper extremity pain [1]. The position of the wheelchair's axle affects rolling resistance and, therefore, the force required for a stroke [2]. Axle positioning has also been found to influence injuries to the median nerve [1]. To investigate this further we created a subject specific model in OpenSim to examine shoulder moments during propulsion in relation to position of the axle. This study asserts an axle position that is closer to the shoulder in the y-plane (POSY) and further in front of the shoulder in the x-plane (POSX) would correlate with lower shoulder moments in the frontal, sagittal, and transverse planes.

METHODS

Flyers, research registries, and word of mouth were used to recruit individuals with paraplegia between 18 and 65 years old. Participants were included if a wheelchair was their primary means of mobility, they had been injured after the age of 15, and they were injured for more than one year. Participants were excluded if they had a history of upper-extremity fractures or dislocations, were pregnant, did not have a "quick-release" axle, had upper-limb dysthetic pain from regional pain syndrome or syrinx, or had a history of cardiovascular or cardiopulmonary disease. Ethical approval was obtained, and participants gave informed consent prior to their participation.

Reflective markers were placed on participants head trunk, and shoulder and arm of their non-dominant hand [3]. Participants sat upright in their chair with arms to their sides for several seconds while VICON data was collected. The distance between the acromion and center hub markers in the x- (POSX) and y-planes (POSY) was used to calculate shoulder to hub distance. Arm length was determined by measuring and summing the distance between the acromion, olecranon process, and ulnar styloid.

A SmartWheel – a wheel capable of detecting forces and moments applied to the pushrim – was attached to the participants' wheelchair on the side of their non-dominant hand opposite a dummy wheel with identical tread and handrim. The participants propelled down a 15-meter tile floor at 1.5 m/s. A metronome ensured each participant propelled at a constant speed. Each participant completed five trials; only the middle three were analyzed to account for potential learning and fatigue effects. A twenty-camera VICON system collected kinematic data at 60 Hz. A 4th order zero-phase low pass Butterworth filter with a 7 Hz cutoff filtered the VICON data. The SmartWheel data collected at 240 Hz was processed with an 8th order zero-phase low-pass Butterworth filter with a 20 Hz cutoff frequency.

Virtual markers were placed on the OpenSim Upper Lower Body Model to match the marker placement on each subject [4]. The full body model accounted for muscles in the arm and shoulder, as well as the core. OpenSim's scaling feature created participant specific models (Figure 1). Kinematic data was input to perform inverse kinematics and create a motion file for three consecutive steady state strokes for each trial. The threshold to determine a stroke was a positive wheel torque greater than 0.4 Nm [5]. Kinetic data from the SmartWheel was input as the reaction forces in the arm, with the third metacarpal-phalangeal joint acting as the center of pressure [6]. Inverse dynamics was performed to find average maximum shoulder moments in the frontal, sagittal,

and transverse planes for each stroke. These planes represent shoulder abduction (+) and adduction (-), flexion (+) and extension (-), and internal (+) and external (-) rotation, respectively. Joint kinetics were averaged across three strokes and three trials.

Shoulder moments in each plane were normalized to subject bodyweight. Armlength influences the position of the axle, so the relationship between these moments and POSX and POSY were calculated using Pearson's partial correlation while controlling for armlength. $P<.05$ was considered significant.

Figure 1: Subject specific model created in OpenSim, using static VICON data.

RESULTS AND DISCUSSION

Models were successfully built for nine wheelchair users with paraplegia who were on average 38.8±10.5 years old, 16.2±8.6 years since injury, and weighed 77.3±24.3 kg. Mean POSX and POSY were 2.9±2.7 cm and 70.8±4.3 cm, respectively. Positive values of POSX indicate the axle was in front of the shoulder, and negative values behind.

A significant inverse correlation was found between POSX and the average maximum shoulder flexion moment (r=-.715, p<.05). Thus, participants with axles more forward relative to the shoulder used smaller flexion moments to propel their chairs. No significant correlations were found with respect to POSY; it is possible that the position of axle in the y-plane affects elbow positioning and loading more than the shoulder. Research has shown that POSX can affect both push frequency and force, while POSY affects only push frequency [2]. These results may have clinical implications, as reducing biomechanical loads can prevent pain and injury [1]. Furthermore, ultralight wheelchairs can be modified so that the axle position is moved forward and rolling resistance is diminished, while maintaining stability. The sample size was small due to modelling errors, which can introduce error and limit statistical power. Further development of this technique may yield more successful models.

CONCLUSIONS

OpenSim was used to create a biomechanical model of wheelchair propulsion. This application has the potential to provide more specific data such as modelling individual muscle forces. OpenSim should be considered for future research in the study of wheelchair propulsion biomechanics. It has the potential to provide insight into the impact of wheelchair setup on pathology and to prevent further injuries in wheelchair users.

ACKNOWLEDGEMENTS

This material was produced through the support of the National Science Foundation's REU QoLT grant (#1358903) and the Department of Veterans Affairs (Grant #B6252R). Any opinions, findings, and conclusions or recommendations expressed in this material are those of the authors and do not necessarily reflect the view of the NSF, Department of Veterans Affairs, or United States Government.

REFERENCES

1. PVA Consortium for Spinal Cord Medicine. *J Spinal Cord Med* **28**, 434–470, 2005.
2. Boninger, M.L. et al. *Arch Phys Med Rehabil* **81**, 608-613, 2000.
3. Wu, G. et al. J Biomech, **38**, 981-992, 2005.
4. Menegolo, Andrea. *Upper and Lower Body Model.* OpenSim Online Database, 2011.
5. Kulig, K. et al. *Clin Orthop Relat Res,* **354**, 132-143, 1998.
6. Sabick, M.B., et al. *J Rehabil Res Devel,* **38,** 57-68, 2001.

ADVANCED PROSTHETIC CONTROL FROM A NONINVASIVE NEURAL INTERFACE (MU DRIVE)

[1,2]Michael D. Twardowski, [1]Serge H. Roy, [2]Zhi Li, [1]Gianluca De Luca and [1]Joshua C. Kline

[1]Delsys, Inc. and Altec, Inc, Natick, MA, USA
[2]Robotics Engineering, Worcester Polytechnic Institute, Worcester, MA, USA
email: jkline@delsys.com, web: http://www.delsys.com/altec/

INTRODUCTION

Dating back to the introduction of electrically powered prostheses more than 65 years ago, surface electromyographic (sEMG) signals have served as the primary means of translating a user's intent into mechanical actuation of a myoelectric prosthesis. Yet previous investigations have shown that the amplitude of the sEMG signal is only an approximation of the intended neural control and is nonlinearly related to the actual force of the contracting muscle. Consequently, in spite of decades of development, myoelectric prosthetic controllers are prone to disproportional and highly variable control, leading to a relatively high-incidence of prosthesis abandonment among 23-35% of those with upper-limb-loss [1].

To improve neural interfaces beyond these limitations, research has focused on implanted electrodes within residual muscles or peripheral nerves to better interface with the underlying neural control sources. While some of these implantable technologies have shown promise for recording signals in human subjects, practical questions surrounding the implantation and maintenance of invasive neural interfaces remain, including: 1) the preservation of residual nerve or muscle integrity; 2) the management of increased health-risks to an aging population of people with limb-loss; and 3) the accommodation of substantially greater health costs to the prosthesis care system. Even if some of these practical concerns are mitigated over time, there remains an immediate need for a lower-cost, risk-averse, neural interface that can provide comparable access to the control information within the nervous system, but in a noninvasive configuration.

METHODS

To meet this need, we are developing new neural interface technology, referred to as motor unit drive (MU Drive), that is able to extract the firings of individual motor units both noninvasively and in real-time for prosthetic control. 23 volunteer subjects (13 trans-radial amputees and 10 controls with intact limbs, 13 male and 10 female; age range 26-74) participated in experiments to develop and evaluate the MU Drive control capabilities. We recorded sEMG signals using a noninvasive dEMG sensor array (Delsys Inc., Natick, USA) placed on the surface of the skin over each of four muscles associated with 4 actual (controls) or intended (amputees) movements: extension of the fingers, flexion of the fingers, pronation of the forearm and supination of the forearm. Movements for control subjects were measured using a custom Trigno™ data acquisition glove while those for amputees were facilitated by mirrored movements of the intact limb and sEMG biofeedback from the residual limb.

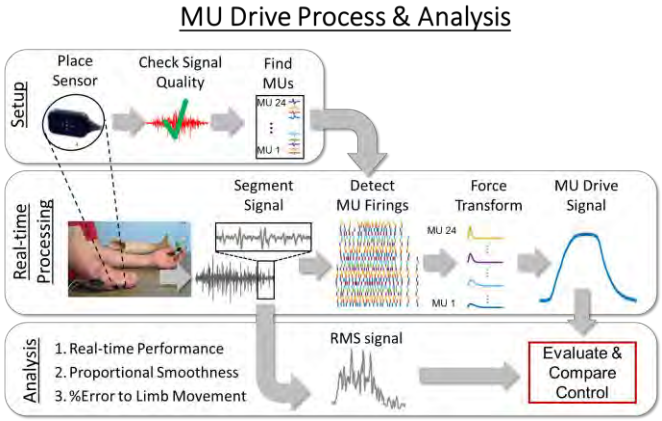

Figure 1. MU Drive algorithm for translating motor unit firings into real-time prosthetic control signals.

The sEMG signals recorded during the movement tasks were processed using newly developed MU Drive algorithms (Fig. 1) that measure the firings of a population of motor units in real-time and convert

the firing information into viable prosthetic control signals. The MU Drive algorithms were based on existing dEMG algorithms for measuring motor unit firings during dynamic exercises and functional activities [2] but implemented in a real-time rather than a post-processing architecture. We evaluated three primary characteristics of the MU Drive control signals measured from each muscle: 1) real-time performance; 2) proportional smoothness; and 3) replication of actual limb movement. The performance of MU Drive was compared with that of the Root Mean Square (RMS) of the sEMG signal, a typical amplitude estimate used for myoelectric control. A non-parametric Wilcoxon rank sum test was used to evaluate significant differences between the MU Drive and RMS-based control signals.

RESULTS AND DISCUSSION

We successfully measured MU Drive control signals from all 23 subjects and 4,942 voluntary contractions tested. When we compared MU Drive with typical RMS-based signals we observed 3 major findings in the control characteristics in both amputees and intact control subjects, described below and illustrated in Figure 2:

1) *Responsive, real-time processing* – Our algorithms were successful at providing an MU Drive signal with a real-time ratio of 1:4 (5 ms processing: 20 ms signal) and total delay of 25 ms; comparable to the time required to obtain a RMS-based control signal with a 25 ms window.
2) *Smooth, proportional control* – When we compared the MU Drive control signal with that of the RMS-based signal obtained with comparable time delay we found that MU Drive maintained consistently smoother proportional changes over the RMS-based signal. Specifically, across all subjects and muscles tested, the signal smoothness (measured from the Spectral Arc Length) averaged -10.4, more than 97.6% better than the -432.5 smoothness measured from the RMS-based signal and significantly closer to the -5.0 smoothness measured from the actual movement of the intact limb in control subjects.
3) *Replicates intended limb movement* – When we compared the MU Drive and RMS-based signals with the actual limb movement across multiple repetitions in control subjects, we found that MU Drive more closely replicated movement of the intact limb with an average Error of 31.3.0%, significantly lower than the 72.6% average error measured for the RMS-based signal.

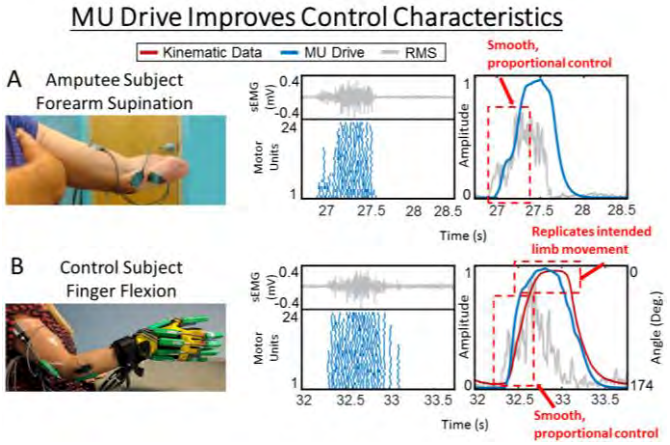

Figure 2. MU Drive control compared with typical myoelectric sEMG RMS-based control.

CONCLUSIONS

Our analysis establishes a vital proof-of-concept: MU Drive provides responsive real-time control with improved proportional smoothness, and replication of intended limb movement over current amplitude-based myoelectric methods. This innovation provides first-time, non-invasive access to the natural mechanisms of neural control for improving the sense of embodiment, increasing function and reducing prosthesis rejection for amputees while maintaining lower costs and reduced risks than implantable alternatives.

REFERENCES

1. Biddiss and Chau. *Prosthetics and Orthotics International*. **31(3)**: 236–257, 2007.
2. De Luca et al. *J Neurophysiol.* **113(6)**: 1941-1951, 2014.

ACKNOWLEDGMENTS

Research reported in this paper was supported in part by the De Luca Foundation and by a grant from the National Institute of Neurological Disorders and Stroke of the National Institutes of Health under award number R43NS093651.

MODIFICATIONS IN WHEELCHAIR PROPULSION MECHANICS AFTER WHEELCHAIR RECONFIGURATION

Casey Wiens[1], Ian M. Russell[1], Philip S. Requejo[1,2], Jan Furumasu[2], and Jill L. McNitt-Gray[1]

University of Southern California, Los Angeles, CA, USA
Rancho Los Amigos National Rehabilitation Center, Downey, CA USA
email: cwiens@usc.edu, web: http://asb2018.asbweb.org/

INTRODUCTION

Implementation of current guidelines for wheelchair (WC) seating tends to be iterative with emphasis on the individual's posture, pressure distribution, and stability requirements [1]. Personalizing the WC fit to achieves these needs remains highly dependent on the expertise of the clinician and their ability to account for multiple interacting factors.

Ongoing clinical research investigating the effect of WC seating on manual WC propulsion mechanics confirms that modifications to WC seating alter multiple factors known to affect upper extremity joint kinetics in individuals with paraplegia [2-7]. These factors include segment kinematics, reaction forces (RF) generated at the pushrim, and neuromuscular control. Modification in task performance conditions (e.g. fast propulsion, incline) are also known to affect push angle, RF magnitude, direction, and time of peak RF during the push phase of WC propulsion [8].

In this study, we used a within-subject experimental design to determine how WC reconfiguration affects posture, functional stability, and interaction with the pushrim during manual WC propulsion at self-selected fast speeds in the community after one month post-WC reconfiguration.

METHODS

Individuals with paraplegia (T2-L3, 13 male, 1 female) using a manual WC for mobility volunteered to participate in accordance with the Institutional Review Board of Rancho Los Amigos National Rehabilitation Center (RLANRC). Individuals were excluded from participation if they reported a history of shoulder pain that altered performance of daily activities or required medical treatment. Average (standard deviation) weight of participants was 81.08 (20) kg, average height was 1.77 (0.1) m and average age was 30 years (range: 18 to 47 years). The mean time since occurrence of the injury in relation to baseline data collection was 11.67 months (range: 2 to 25 months). Participants initiated self-selected fast WC propulsion from a stationary position in a courtyard outside of the Seating Center at RLANRC during (baseline) and post-WC reconfiguration (follow-up) propulsion trials. RFs applied by the hand to the pushrim during WC propulsion were measured using three strain gauge force transducers (240 Hz, SmartWheel). Upper extremity segment kinematics were captured in the frontal and sagittal planes (60 Hz HD, JVC) and using inertial measurement units (APDM). Segment kinematics and RFs were then used to determine RF orientation relative to the forearm during push. WC adjustments for 13 out of 15 subjects involved modifications to the seatback with the goal of supporting the lumbar region of the spine, encouraging neutral position of the pelvis, and allowing for the torso to sit more comfortably in an upright posture. The specific adjustments to the seatback varied depending on the baseline setup of the wheelchair, the subject's ability to use their core muscles, and individual's functional stability limitations when seated in the WC and during propulsion at self-selected free, fast, and graded conditions.

RESULTS AND DISCUSSION

Within-subject comparison of torso angle relative to the right horizontal at the start of elbow extension (start of push) revealed that 4 of 15 participants made significant shifts towards a more upright posture (90 deg) between baseline and follow-up propulsion cycles (no significant group difference ($p=0.411$, Fig. 1). One participant adjust further from 90 degrees.

Within-subject comparison of mean RF angle relative to the forearm during phase of elbow extension indicated 5 participants reoriented the RF. One to a more anterior orientation relative to the forearm, two shifted to less anterior, and another two to a less posterior orientation (Fig. 2) post-WC reconfiguration. Reorientation of the RF relative to the forearm to be less posterior or more anterior is expected to contribute to a smaller flexor/greater extensor elbow NJM which can reduce mechanical demand imposed on the shoulder.

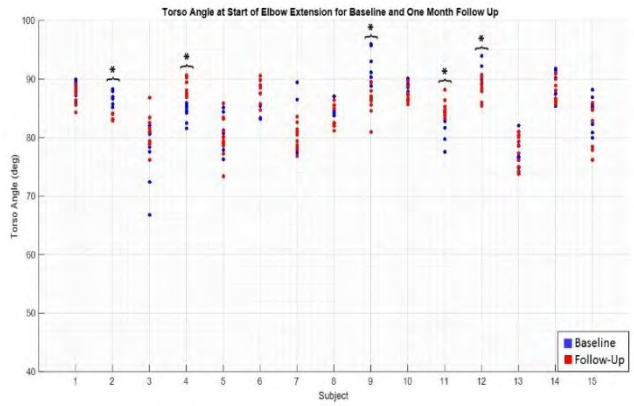

Figure 1. Subjects with significant changes in torso angle (5 of 15) between baseline and follow-up are signified with a curly bracket*.

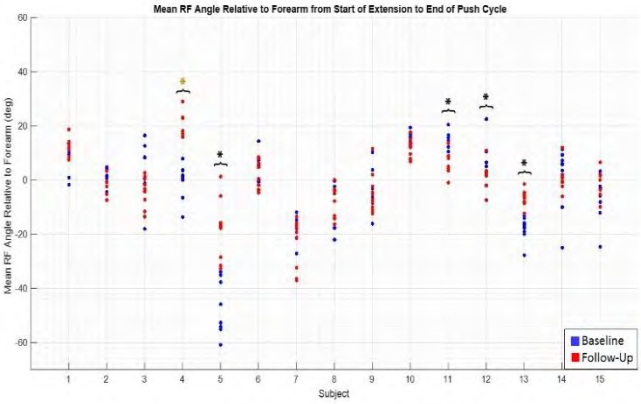

Figure 2. Subjects with statistically significant changes in RF angle relative to forearm during phase of elbow extension (5 of 15) are signified with a curly bracket* (black Cliff's step-down, gold Wilcoxon-Mann-Whitney).

Of the four participants that shifted towards a more upright posture (towards 90 degrees), a couple changes in the RF orientation occurred. One participant shifted from posterior to anterior and two shifted to less anterior (closer to inline with forearm). In total, three participants (subjects 4, 5 and 13) experienced a RF orientation after the WC reconfiguration that would be expected to create a smaller flexor/greater extensor elbow NJM. This can then lead to a reduction in the mechanical demand on the shoulder.

CONCLUSIONS

WC reconfiguration was found to significantly affect posture and interaction with the pushrim during manual WC propulsion at self-selected fast speeds in the community in one third of the participants one-month post-WC reconfiguration. These results suggest personalized WC fitting can contribute to improvements in posture and interactions with the handrim that can mitigate mechanical loading of the shoulder.

REFERENCES

1. Medicine PV of AC for SC. Preservation of Upper Limb Function Following Spinal Cord Injury: A Clinical Practice Guideline for Health-Care Professionals. *J Spinal Cord Med*. 2005;28(5):434-470.
2. Desroches G, Aissaoui R, Bourbonnais D. *J Rehabil Res Dev*. 2006;43(7):871.
3. Mulroy SJ, Newsam CJ, Gutierrez D, et al. *J Spinal Cord Med*. 2005;28(3):214-221. doi:10.1080/10790268.2005.11753815.
4. Hughes CJ, Weimar WH, Sheth PN, Brubaker CE. *Arch Phys Med Rehabil*. 2017;73(3):263-269.
5. Mâsse LC, Lamontagne M, O'Riain MD. *J Rehabil Res Dev*. 1992;29(3):12—28.
6. Majaess GG, Lee Kirby R, Ackroyd-Stolarz SA, Charlebois PB. *Arch Phys Med Rehabil*. 2017;74(9):977-982.
7. van der Woude L, Bouw A, van Wegen J, van As H, Veeger D, de Groot S. *J Rehabil Med*. 2009;41(3):143-149.
8. Russell IM, Raina S, Requejo PS, Wilcox RR, Mulroy S, McNitt-Gray JL. *Front Bioeng Biotechnol* 2015; 3:171.

ACKNOWLEDGEMENTS

This work was supported by the Office of the Assistant Secretary of Defense for Health Affairs, through the Spinal Cord Injury Research Program under Award No. W81XWH-14-1-0560. Opinions, interpretations, conclusions and recommendations are those of the author and are not necessarily endorsed by the Department of Defense. Thanks also to the Undergraduate Research Assistants who assisted with this project.

Technical, Clinical and Functional Considerations for the Development of 3D Printed Upper-Limb Prostheses

Keaton Young[1], Jean L. Peck[2], Rakesh Srivastava[3], James Pierce[1], Nicholas Stergiou[1], Jorge M. Zuniga[1].
1. University of Nebraska at Omaha, Department of Biomechanics, USA; 2. CHI Health Creighton University Medical Center, Omaha, USA; 3. Innovative Prosthetics & Orthotics, USA.

INTRODUCTION

The development of 3D printing for the manufacturing of prostheses and orthoses has resulted in cost reduction strategies, better accessibility and customization of prosthetic designs. The widespread use of 3D printing and the existence of myriad prosthetic designs available on the internet allows clinicians and researchers from different disciplines to manufacture their own devices. Given the dearth of studies discussing the practical application of 3D printed upper limb prostheses, the current paper describes the technical and clinical considerations for the implementation of these devices in rehabilitation and research settings. Specifically, considerations on fitting procedures, assembly, durability, regulatory implications, and patient functional outcomes are discussed.

METHODS

Subjects: Eleven children (five girls and six boys, 3 to 15 years of age) participated in this study and were fitted with a 3D-printed transitional wrist-driven and elbow-driven prosthesis.
Apparatus and Procedures: Gross manual dexterity was assessed using the Box and Block Test and wrist strength was measured using a dynamometer. This testing was conducted before and after a period of 24±2.61 weeks of using a 3D printed transitional prosthesis. The eleven children (five girls and six boys; 3 to 15 years of age) who participated in the study, were fitted with a 3D printed transitional partial hand (n=9) or an arm (n=2) prosthesis.
Data Analysis: Separate two-way repeated measures ANOVAs [2 x 2; hand (affected versus non-affected) x time (before and after)] were performed to analyze function and strength data. An alpha value of 0.05 was considered statistically significant for all comparisons.

RESULTS

There was a significant hand by time interaction for the function [$F(1,10) = 6.42$; $p = 0.03$, $\eta p2 = 0.39$], but not for the wrist flexion strength [$F(1,7) = 0.67$; $p = 0.44$, $\eta p2 = 0.02$], or for the wrist extension strength [$F(1,7) = 0.05$; $p = 0.40$, $\eta p2 = 0.1$]. There were significant main effects of function for the affected hand [$F(1,10) = 52.41$; $p = 0.01$, $\eta p2 = 0.84$] and the time [$F(1,10) = 37.31$; $p = 0.01$, $\eta p2 = 0.79$]. There were significant main effects of strength for time [$F(1,7) = 6.56$; $p = 0.38$, $\eta p2 = 0.48$].

	Box & Block Test (blocks per min)*				Flexors Strength (Kg)**			
	Non-affected		Affected		Non-affected		Affected	
ID	Before	After	Before	After	Before	After	Before	After
1	24	25	0	5	10	11.6	8.46	14.6
2	22	26	3	3	11.8	13.46	11.7	13.2
3†	26	27	0	3	---	---	---	---
4	36	38	13	19	4.2	10	5.2	7.6
5†	36	38	0	9	---	---	---	---
6	50	54	40	47	27.53	33.13	17.43	18.9
7†	60	66	0	3	14.8	14.7	25.2	22
8	60	62	13	16	15.7	17.8	12.3	19.46
9	53	53	0	17	24.4	19.4	20.46	22.46
10	69	68	0	9	10.8	10.1	8.3	12.16
11	75	75	0	12	---	---	---	---
M	**46.45**	**48.36**	**6.27**	**13.00**	**14.90**	**16.27**	**13.63**	**16.30**
SD	**18.67**	**18.34**	**12.31**	**12.70**	**7.70**	**7.62**	**6.83**	**5.24**

Figure 1: Table 1. Mean (±SD) for function and strength measurements before and after one to six months of using the 3D-printed hand prosthesis.

DISCUSSION & CONCLUSIONS

The increases in manual gross dexterity suggests that the Cyborg Beast 2 3D printed prosthesis can be used as a transitional device to improve function in children with traumatic or congenital upper-limb differences. The lack of significant increases in

strength of the affected lib after using the prostheses may be related to the small sample size and then large variability in the force production among children participating in the present study.

Although durability constraints are factors to consider when using 3D printed prostheses, the practicality and cost-effectiveness represent a promising new option for clinicians and their patients (1-3, 4).

CLINCIAL APPLICATIONS

The use of 3D printed transitional prostheses may improve manual gross dexterity in children after several weeks of using it. 3D printed transitional prostheses may play an important role in patient rehabilitation by familiarizing patients to the use and function of the prosthesis.

REFERENCES

1) Zuniga JM, Peck J, Srivastava R, Katsavelis D, Carson A. An Open Source 3D-Printed Transitional Hand Prosthesis for Children. JPO: Journal of Prosthetics and Orthotics. 2016;28(3):103-108.

2) Zuniga JM, Carson AM, Peck JM, Kalina T, Srivastava RM, Peck K. The development of a low-cost three-dimensional printed shoulder, arm, and hand prostheses for children. Prosthetics and orthotics international. Apr 26 2016.

3) Zuniga JM, Katsavelis D, Peck J, et al. Cyborg beast: a low-cost 3d-printed prosthetic hand for children with upper-limb differences. BMC research notes. Jan 20 2015;8(1):10.

4) Ten Kate J, Smit G, Breedveld P. 3D-printed upper limb prostheses: a review. Disability and rehabilitation. Assistive technology. Feb 02 2017:1-15.

VALIDATION OF AN INSTRUMENTED KNEE BRACE FOR TRACKING KNEE FLEXION/EXTENSION ANGLES DURING ACTIVITIES OF DAILY LIVING

Calvin Young[1], Michele L. Oliver[1], and Karen D. Gordon[1]

[1]University of Guelph, School of Engineering, Guelph, ON, CA
email: cyoung02@uoguelph.ca

INTRODUCTION

Gait assessment provides important insights into recovery progress after an anterior cruciate ligament (ACL) tear or reconstruction, yet recovery data lacks the resolution to describe day to day activity [1]. Current methods typically rely on clinical assessment during periodic visits. Characterization of gait using wearable devices would provide quantitative data to assess joint performance under free-living conditions. This would allow progress to be tracked at a much higher resolution than is currently possible.

The wearable device uses a rotary potentiometer mounted at the hinge of a commercially available ACL brace. It is expected that the proposed system will provide more accurate results with lower required computational overhead than inertial measurement unit based alternatives. The purpose of this study was to validate the instrumented knee brace against a gold standard optical motion capture system for tracking knee flexion/extension angles during three activities of daily living.

METHODS

8 subjects (3 female and 5 male, aged 25.0 ± 1.6 years) participated in this University of Guelph Research Ethics Board approved study. Knee flexion/extension angles were recorded using a DonJoy Armor ACL brace (DJO Global, CA, USA) instrumented with a 10kΩ linear rotary potentiometer (Canada Robotix, ON, CA) at the hinge (Figure 1). The voltage drop across the potentiometer was recorded using a Teensy 3.2 (PJRC, OR, USA) microcontroller with a 10-bit analog to digital converter.

Figure 1: Instrumented knee brace, rotary potentiometer labelled A

To validate the brace instrumentation, lower body kinematics were recorded using an optical motion capture system and the lower body Plug-in Gait marker set and model. (VICON, Oxford, UK) Data from the brace (potentiometer) and the VICON were collected at 100Hz

Three activities of daily living (ADLs) were performed by each subject:

1. Gait: Level walking at a self-selected pace over a distance of 5 meters.
2. Ascending and descending stairs: Ascending two stairs to a landing, turning 180º and descending two stairs (26.0cm rise, 19.0cm tread depth).
3. Stand-Sit-Stand: Sitting down on a stool at a participant selected height, followed by a brief pause, then standing up and stepping away from the stool.

Each task was performed five times with 8 seconds of data sampled mid-task. One example of each task was removed and combined to generate a calibration curve. This calibration was applied to the remaining trials. The resultant angular data were then analyzed using Python 2.7 and SciPy[2]

The angular data from the VICON and brace were synchronized using cross-correlation and filtered using a 4th order zero lag Butterworth filter with a

cutoff frequency of 10Hz. The angular data from both the VICON and the brace were correlated for each movement, and a linear regression was calculated (Figure 2). The cumulative root mean squared error (RMSE) and R^2 values were calculated to assess the accuracy and precision of the brace output.

RESULTS AND DISCUSSION

All three locomotor ADL showed a high degree of positive correlation, and a low RMSE (Table 1). The brace was capable of measuring knee flexion/extension angles within 3º of the VICON for all tasks with an average correlation coefficient (r) of 0.987. The highest correlation, and lowest RMSE was observed during the stand-sit-stand task, which is likely due to the stationary position held during the 'sit' portion of the task. This contrasts sharply with IMU based methods which require advanced post processing to mitigate integration drift [5].

Table 1: Summary statistics for brace performance

	RMSE	R^2	p-value
Gait	2.3º	0.970	$2.2x10^{-18}$
Stand to sit/sit to stand	2.3º	0.996	$2.2x10^{-18}$
Ascending and descending stairs	2.6º	0.985	$2.2x10^{-18}$

Conversely, the lowest correlation and highest error were observed during the gait task, however and R^2 value of 0.970 is still quite high. In addition, the RMSE and correlation for all cases exceed the performance of IMU based models and are well within the skin artifact error threshold for an optical motion capture system [3, 4].

This high correlation across multiple observations and participants suggests that the brace could successfully be used for monitoring small changes in gait over an extended period with the ability to provide quantitative data describing joint function for ADLs over long durations. This data could also be used for dynamic monitoring during a return to sport progression. This type of active monitoring would augment clinical assessment and provide opportunities for customized care and research.

REFERENCES

1. Gokeler et al. *International Journal of Sports Physical Therapy*, **8**(4), 441-451.
2. Walt et al. *Computing in Science & Engineering,* **13**(2), 22-30
3. Seel et al., *Sensors*, **14**(4), 6891-6909, 2014.
4. Benoit et al., *Gait & Posture*, **24**(2), 152-164, 2005.
5. Luinge et al., *Medical & Biological Engineering & Computing*, **43**(2), 273-282, 2005

ACKNOWLEDGEMENTS

The knee brace used in this project was provided by DonJoy (DJO Global, CA, USA)

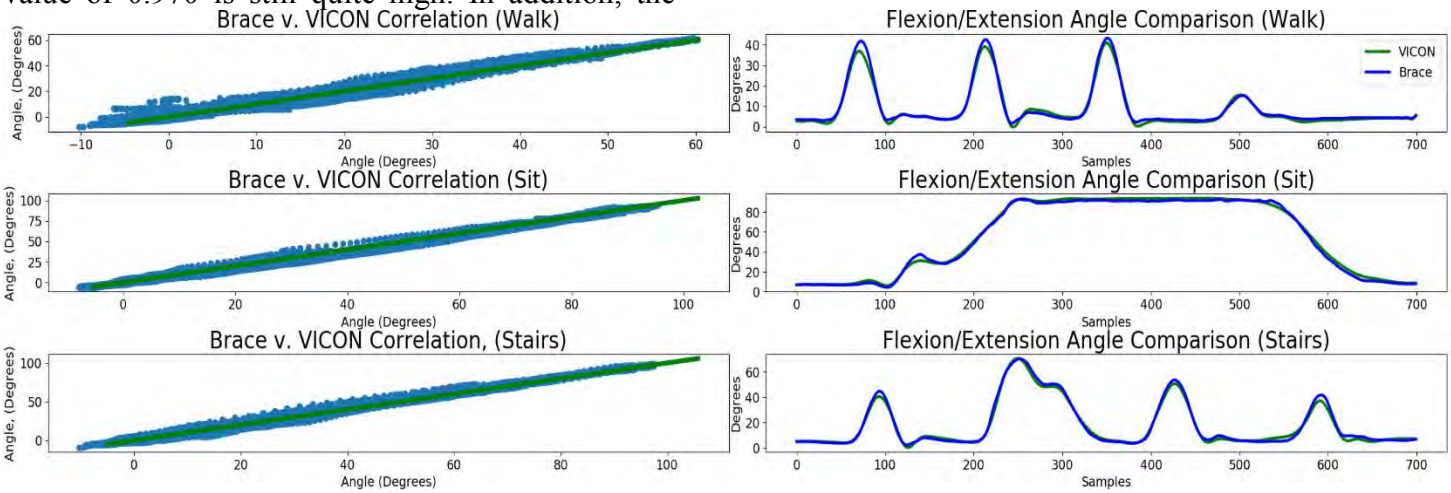

Figure 2: Correlation and linear fit for each of the locomotor activity of daily living (Left), and one representative segment of data for each task (Right)

AUTOMATED GAIT SEGMENTATION FOR A NOVEL GAIT TRACKING KNEE BRACE

Calvin Young[1], Michele L. Oliver[1], and Karen D. Gordon[1]

[1] University of Guelph, School of Engineering, Guelph, ON, CA
email: cyoung02@uoguelph.ca

INTRODUCTION

Return to normal gait is an important objective for recovery after an anterior cruciate ligament (ACL) injury. [1] A novel brace mounted sensor system has been developed to track gait for long durations during activities of daily living. One challenge associated with the implementation of such a device is the analysis of the large amount of data produced. This necessitates some form of automated processing to generate informative user feedback.

Here an automated segmentation algorithm is demonstrated, in conjunction with piecewise linear length normalization to produce a representative gait cycle from a series of gait recordings. [2] The ability to automatically segment and combine a series of gait cycles into one representative cycle, and subsequently detect deviations from that cycle, would enable clinicians and researchers to assess knee joint biomechanics outside of the clinic and research laboratory.

The purpose of this study was to compare the performance of the brace with a force plate for heel strike detection and to demonstrate the utility of an automated data processing pipeline for generating summary data from a series of gait cycles.

METHODS

Following provision of informed consent, 6 healthy subjects (3 male and 3 female;aged 25.3 ± 1.6 yrs) participated in this University of Guelph research ethics board approved study. Each participant walked over a level surface at a self-selected pace for 5 meters, followed by a 180º turn, and then walked 2 meters back. Data were recorded by an instrumented brace which included a rotary potentiometer (Canada Robotix, ON, CA) to record flexion/extension angles, and a LSM6DS3 inertial measurement unit (IMU) (STMicroelectronics, Geneva, CH) to record acceleration along the superior/inferior axis of the tibia. Midway through the trial, the subject stepped onto a force plate (Kistler, Winterthur, CH) which recorded the vertical ground reaction force (vGRF) using Nexus 2.6 (VICON, Oxford, UK). All data were sampled at 100Hz and analyzed using SciPy. [3]

Gait segmentation was performed using a modified peak finding algorithm to locate heel strikes in the IMU data, as explained below.

First the acceleration signal was normalized to zero mean and unit standard deviation (z-scores), per equation 1

$$p = \frac{p - \mu}{\sigma} \quad [\mathbf{1}]$$

where p is a time series, and μ and σ are the mean and standard deviation of p respectively (figure 1-A). A one standard deviation threshold filter and an event based low pass filter were applied, to equations 2 and 3 respectively, where p_i represents the i-th element of time series p (figure 1-B).

$$p_i = \begin{cases} 0\,, & |p_i|_i \leq 1 \\ p_i\,, & otherwise \end{cases} \quad [\mathbf{2}]$$

$$p_i = \begin{cases} 0\,, & p_{i-1} \wedge p_{i+1} = 0 \\ p_i\,, & otherwise \end{cases} \quad [\mathbf{3}]$$

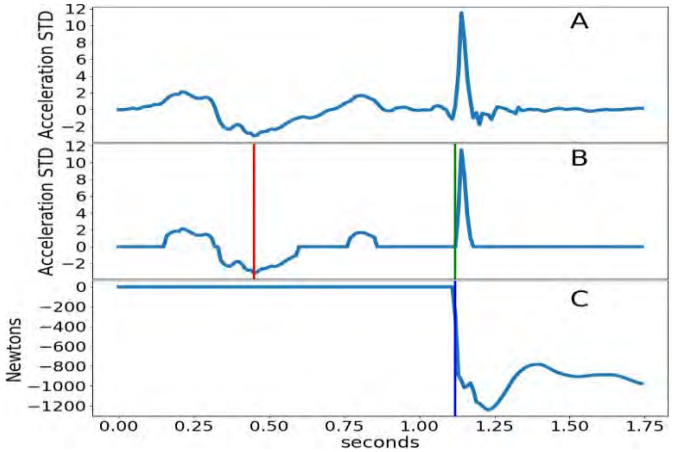

Figure 1 Superior/inferior tibial acceleration z-scores (A), 1 standard deviation threshold filtered tibial acceleration (B), vertical ground reaction force (C).

A peak finding algorithm was then applied to locate the local minima (figure 2-B in red). A 50-sample window was selected after each local minimum, and the maximum within that window was located. The leading edge of the event containing this maximum is selected as the heel strike (figure 3-B in green).

To validate the located heel strikes, the vGRF was used. Heel strike was selected as the first non-zero value in the vGRF signal (figure 1-C in blue).

The flexion/extension angles were then segmented based on the heel strikes detected by the accelerometer. The piecewise linear length normalization technique described by Helwig et al.[2] was then applied to normalize the length of each gait cycle, using the two maxima in the flexion/extension signal as points of interest. This method linearly compresses or extends the segments such that all segments share the same length. After synchronization, the individual cycles were combined to form the mean gait cycle ± standard deviation shown in Figure 2-C.

RESULTS AND DISCUSSION

The mean absolute error for heel strike identification was 2.45 samples (0.0245s), with a mode difference of 0 samples.

The low absolute error coupled with the high agreement between to the two measurement systems indicates that the combination of IMU and algorithm provide a good method of heel strike detection. This information enables the automated parsing of the remaining gait data into individual gait cycles.

Figure 2-A shows the result of the flexion/extension angle segmentation. Gait cycle duration ranges from 0.94s to 1.69s, and peak flexion ranges from 32º to 68º. Noticeable in both figure 2-A and B are distinct groupings of gait cycles in both duration (A), and magnitude (A, B). This likely is due to interparticipant gait differences.

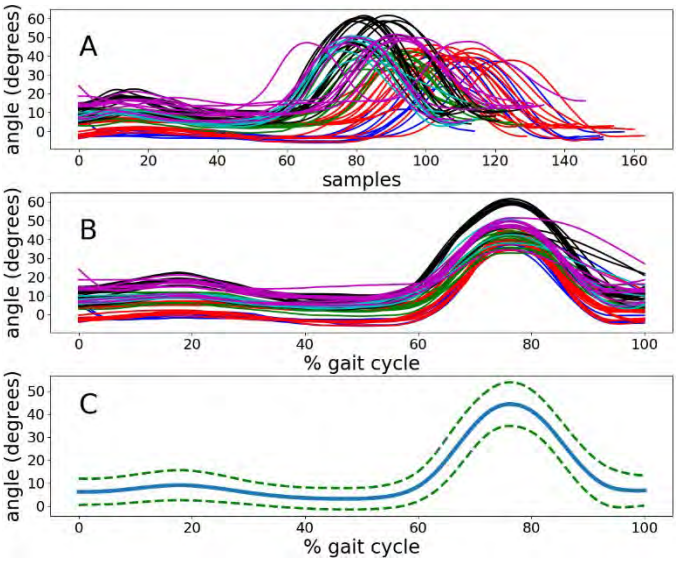

Figure 2: Flexion/extension angles segmented by heel strikes coloured by participant (A), piecewise linear length normalized gait cycles coloured by participant (B), mean gait cycle with ± 1 standard deviation.

CONCLUSIONS

The brace, in conjunction with relatively simple post processing techniques, was able to accurately identify heel strikes, when compared to a force plate. Segmentation in conjunction with piecewise linear length normalization was used to generate a representative gait cycle for six healthy subjects. Furthermore, after segmentation, interparticipant gait differences could be seen, demonstrating the capability of the brace hardware to capture subtle gait changes.

REFERENCES

1. Gokeler et al. *International Journal of Sports Physical Therapy*, **8**(4), 441-451.
2. Helwig et al. *Journal of Biomechanics,* **44**(3), 561-566.
3. Walt et al. *Computing in Science & Engineering,* **13**(2), 22-30

ACKNOWLEDGEMENTS

The knee brace used in this project was provided by DonJoy (DJO Global, CA, USA)

AGENT-BASED COMPUTATIONAL MODEL OF HUMAN SKELETAL MUSCLE ADAPTION TO CHANGES IN ACTIVITY

[1]Benjamin L. Anton, [1]Shayn M. Peirce, and [1] Silvia S. Blemker

[1] University of Virginia, Charlottesville, VA, USA

email: bla4jd@virginia.edu

INTRODUCTION

Skeletal muscle is a highly plastic organ with the ability to adapt to changes in activity. Mechanical overuse results in increases in muscle size (hypertrophy) while disuse results in decreases in muscle size (atrophy). Changes in skeletal muscle size are regulated by protein turnover—the balance between protein synthesis and degradation. Protein turnover is not pre-programmed but influenced by biomechanical and cellular signaling [1]. These behaviors have been observed in a vast number of experimental studies however, the underlying mechanisms are difficult to determine through individual experiments alone.

Computational modeling provides the opportunity to compile the vast number of individual experimental observations into a comprehensive framework with the ability to predict observed outcomes. However, the current modeling framework of skeletal muscle evaluate function at a prescribed timeframe with defined architectural parameters that remain constant. There is a need for novel computational modeling frameworks that can predict skeletal muscle adaptations to various states of activity and can treat each muscle cell type independently [1]. Agent-based modeling is advantageous because it has the ability to allow muscle fibers to act independently with its surroundings and incorporate complex biomechanical and cellular signaling to induce skeletal muscle adaptations. Previous agent-based models developed by group have accurately predicted rat and mouse skeletal muscle adaptations to disuse as well in disease states [2,3]. However, there is yet a computational model that predicts *human* skeletal muscle adaptation to various states of activity.

The goal of this study therefore was to develop an agent-based computational model of human skeletal muscle that will accurately predict experimental observations of skeletal muscle adaptation to changes in activity by correctly adjusting protein balance in individual muscle fibers.

METHODS

The agent-based model (ABM) was generated to create a cross section of a muscle fascicle (Fig 1). Euler method was used to calculate the new fiber cross-sectional area (CSA) at each time point:

$$\frac{dCSA}{dt} = \beta_s * timestep - \beta_d * CSA * timestep$$

Where β_s is the protein synthesis rate, β_d is the protein degradation rate, and the timestep is one hour.

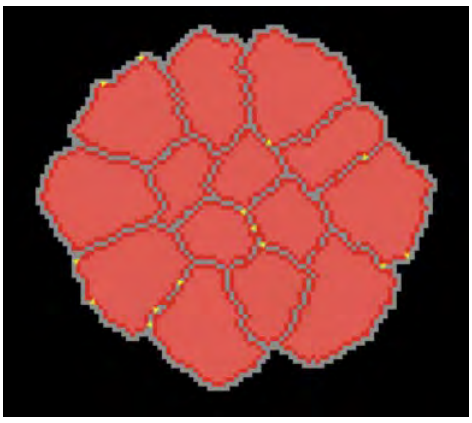

Figure 1: ABM of skeletal muscle fascicle cross section.

Baseline protein degradation and synthesis rates were determined using bed-rest atrophy studies of human skeletal muscle [4]. The model was simulated

over a period of 14 days using a range of protein degradation (β_d) (2.4—2.8 x 10^{-3}/h) and synthesis coefficients (β_s) (8.5—9.0 μm^2/h).

RESULTS AND DISCUSSION

Protein degradation and synthesis rates were varied until the percent error between the model fiber CSA and the experimental CSA after 14 days was <1% (Fig 2A). Type I fibers had β_d of 2.7 x 10^{-3}/h and β_s of 8.8 μm^2/h with a percent error of 0.06%. Type II fibers had a β_d of 2.7 x 10^{-3}/h and a β_s of 7.9 μm^2/h with a percent error of 0.07%.

These protein turnover rates were validated by computing soleus Type I fiber data as observed in Widrick et al. [5]. Fiber type distributions were assigned according to experimental measurements and previously determined protein turnover rates were assigned accordingly. After running the simulation for 17 days, the percent error between the model fiber CSA and the experimental CSA was 8% (Fig 2B). Further, the model illustrations the ability of the model to predict the varied responses of different muscles to immobilization-induced atrophy. In particular, it replicates the heightened sensitivity of the soleus muscle to disuse-induced atrophy as compared to most other muscles in the body.

CONCLUSIONS

This study proposed an agent-based modeling framework to comprehensively describe how human skeletal muscle fibers adapt to changes in activity. Currently, the model has been calibrated and validated based on experimental data of skeletal muscle atrophy during bed rest. Future work will include tuning the model to resistance exercise parameters in order to produce a comprehensive modeling framework that will adapt to use and disuse.

REFERENCES

1. Lieber et al. *Journal of NeuroEngineering and Rehabilitation*, 2017.
2. Martin et al. *J Appl Physiol* 118: 1299–1309, 2015.
3. Virgilio et al. *Interface Focus* 5: 20140080. 2015.
4. Bamman et al. *J. Appl. Physiol.* 84(1): 157–163, 1998.
5. Widrick et al. *Am. J. Physiol.* Vol 273:5. 1997

A)

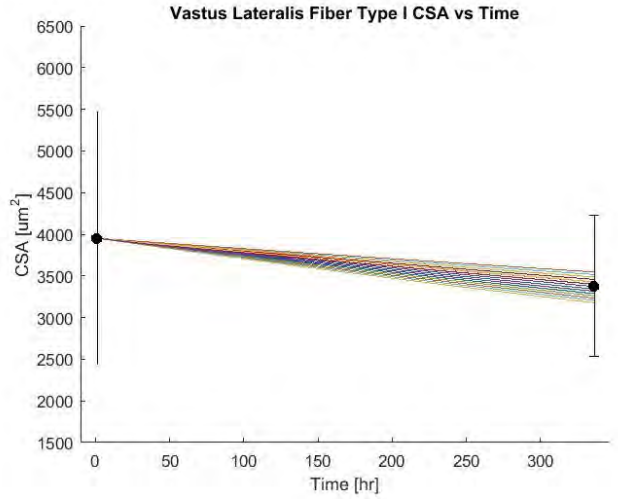

B)

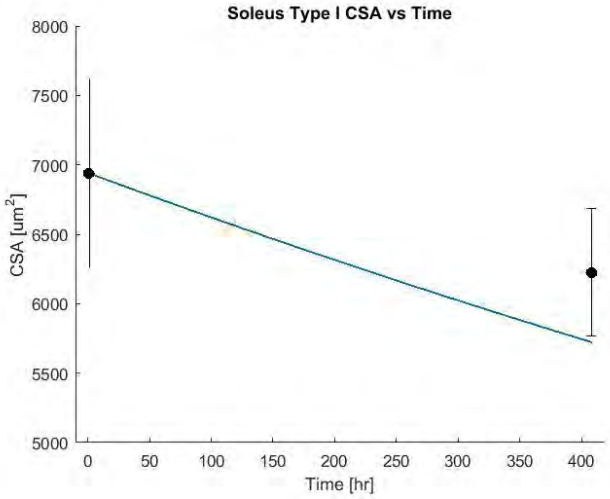

Figure 2: **A)** Determined protein turnover parameters for Type I (shown) and Type II fibers. **B)** Validated protein turnover parameters by simulating Vastus Lateralis atrophy after 14 days of bed rest.

EFFECT OF ARM MOTION ON STANDING LATERAL JUMP PERFORMANCE

Blake M. Ashby, Arif Ahmed Sohel, and Gordon J. Alderink

Grand Valley State University, Grand Rapids, MI, USA
email: ashbybl@gvsu.edu, web: http:// www.gvsu.edu/biomechanicslab/

INTRODUCTION

Many sporting events involve jumping in multiple directions. Jumping requires complex coordination of both upper and lower body segments to maximize performance. Previous studies have documented the performance improvements due to arm motion in standing jumps for height and forward distance [1-3], but no studies have examined the effect of arm swing on performance in standing lateral jumps. Various hypotheses have offered explanations for enhanced performance due to arm motion in standing long jumps. The "impart energy" hypothesis (i.e., swinging the arms allows more work to be done at the shoulder and elbow thereby increasing the total mechanical energy of the body) was the largest contributor to improved performance in a standing long jump simulation study [3]. The purposes of the present study were 1) to investigate the effect of arm motion on standing lateral jump performance and 2) to further explore proposed mechanisms that may explain differences in jump distance.

METHODS

Six physically active, adult men (mean ± standard deviation: mass = 85.5 ± 10.6 kg; height = 1.823 ± 0.097 m; age = 26.7 ± 2.4 years) performed a series of lateral jumps to the right for maximum distance. Each subject performed six jumps taking off and landing with two feet for each of two cases: 1) free arm jumps and 2) restricted arm jumps for which arms were held akimbo throughout the movement. The 3D positions of 53 passive reflector markers were recorded (120 Hz) throughout the jumping movements using an eight-camera Vicon motion capture system (Vicon Motion Systems Ltd., Los Angeles, CA). Two in-ground AMTI force platforms (Advanced Mechanical Technology Inc., Watertown, MA) recorded (1200 Hz) the 3D ground reaction forces, free moments, and center of pressure locations for each foot during the takeoff phase.

The body was modeled using a 3D, 12-segment, 11-joint model modified from previous work [4]. Inverse kinematics and dynamics analyses were performed using MATLAB R2017a (MathWorks, Natick, MA) to calculate segment angular velocities and accelerations, and net joint moments. "Bottom up" inverse dynamics was used to calculate ankle, knee, hip, and lower back moments and "top down" inverse dynamics was used to calculate elbow and shoulder moments. Over-determinacy of the system of equations resulting from the use of force plate data was resolved by disregarding the equations of motion from the head-neck-trunk segment [5]. Segment angular velocities and joint moments were used to calculate joint power and work for all jumps.

Jump distance was defined as the lateral distance between the right 5th metatarsal head marker at takeoff and the left 5th metatarsal head marker at touchdown. An increase in the body's center of gravity (CG) position in the vertical direction at takeoff or a decrease in the vertical CG position at landing results in additional lateral jump distance. The amount of this increase in lateral distance as a result of improvements in the vertical CG positions at takeoff and touchdown was calculated using standard projectile formulas.

SAS OnDemand for Academics (SAS Institute Inc., Cary, NC) was used to create repeated measures ANOVA models for comparisons between free and restricted arm jumps. Results are presented as least square means $\pm$ 95% confidence intervals. Statistical significance was indicated for $p < 0.05$.

RESULTS AND DISCUSSION

Free arm motion improved jump performance by 29% or 35.6 ± 7.1 cm (jump distances of 1.587 ± 0.141 m vs. 1.231 ± 0.141 m, $p < 0.0001$). Most (56% or 20.0 cm) of this improvement was due to a

13% increase in takeoff velocity (3.20 ± 0.17 m/s vs. 2.83 ± 0.17 m/s, $p < 0.0001$) in free arm jumps. Increased displacement of the CG relative to the right foot at takeoff in the lateral direction of 7.2 ± 2.3 cm ($p < 0.0001$) and vertical direction of 2.4 ± 0.9 cm ($p < 0.0001$) accounted for 29% (10.2 cm) of the improvement. The remaining 15% (5.4 cm) was due to the improved position of the CG relative to the left foot at landing in the lateral (4.1 ± 1.3 cm, $p < 0.0001$) and vertical (1.1 ± 1.0 cm, $p = 0.0335$) directions.

The improved takeoff velocity and position of the center of gravity at takeoff was due to a 126.5 ± 27.4 J or 33% increase ($p < 0.0001$) in the work done in jumps with free arm movement during takeoff (Table 1). In free arm jumps, significantly more work was performed over restricted arm jumps at the left and right ankle, left and right hip, lower back, left and right shoulder, and left elbow, with the largest differences (> 30 J) occurring at the lower back, right hip, and right shoulder (Table 1). In restricted arm jumps, significantly more work was performed over free arm jumps at the right knee and right elbow (Table 1).

The upper extremity joints (i.e., elbow and shoulder) combined did 41.6 ± 10.9 J more ($p < 0.0001$) work in free arm jumps demonstrating the impart energy mechanism's substantial contribution to performance improvement in standing lateral jumps. The remaining improvement in work done in free arm jumps occurred at the lower extremity joints (i.e., ankle, knee, and hip) (54.1 ± 16.8 J increase, $p < 0.0001$) and lower back (30.8 ± 8.1 J increase, $p < 0.0001$). "Joint torque augmentation" and "hold back" hypotheses offer explanations for why the lower extremity and lower back joints do more work in jumps with arm motion [1-3]. Further investigation in the form of computer simulations and/or experimental EMG studies could provide insight into whether these mechanisms can explain the cause of the increase in work at lower extremity and lower back joints with arm motion or if other mechanisms need to be proposed.

REFERENCES

1. Feltner, et al. *J Sports Sci* **17**, 449-466.
2. Ashby and Heegaard. *J Biomech* **35**, 1631-1637, 2002.
3. Ashby and Delp. *J Biomech* **39**, 1726-1734, 2006.
4. Hickox, et al. *J Biomech* **49**, 1085-1093, 2016.
5. Ashby, et al. *39th Annual Meeting of ASB,* Columbus, OH, USA, 2015.

ACKNOWLEDGEMENTS

Special thanks are given to the Statistical Consulting Center at GVSU for their help with the statistical analyses.

Table 1: Joint and Total Body Work for Free and Restricted Arm Lateral Jumps

Joint	Restricted Arms	Free Arms	Difference	*p*-value
Left ankle	70.8 ± 5.3 J	82.8 ± 5.3 J	12.0 ± 4.0 J	<0.0001
Right ankle	74.2 ± 5.5 J	83.2 ± 5.5 J	9.0 ± 2.8 J	<0.0001
Left knee	27.4 ± 14.3 J	21.9 ± 14.3 J	−5.5 ± 7.6 J	0.1455
Right knee	98.5 ± 16.3 J	80.9 ± 16.3 J	−17.5 ± 8.3 J	0.0002
Left hip	38.0 ± 9.7 J	60.3 ± 9.7 J	22.3 ± 10.4 J	0.0001
Right hip	50.8 ± 10.4 J	84.7 ± 10.4 J	33.8 ± 10.7 J	<0.0001
Lower back	21.6 ± 9.9 J	52.4 ± 9.9 J	30.8 ± 8.1 J	<0.0001
Left shoulder	2.2 ± 4.8 J	17.4 ± 4.8 J	15.1 ± 6.8 J	<0.0001
Right shoulder	−3.5 ± 5.3 J	35.4 ± 5.3 J	39.0 ± 7.5 J	<0.0001
Left elbow	1.1 ± 2.4 J	16.2 ± 2.4 J	15.1 ± 3.1 J	<0.0001
Right elbow	3.2 ± 12.5 J	−24.4 ± 12.5 J	−27.6 ± 17.2 J	0.0027
Total Body	384.5 ± 53.6 J	511.0 ± 53.6 J	126.5 ± 27.4 J	<0.0001

Differences in Knee Flexibility during Functional Movements between Track and Field Athletes Based on Event Participation

[1]Megan Austin, [1]Marlee Profitt, [2]Kelly Helm,
[3]Luis Prato, [4]Anthony Levenda, and [1]Craig M. Goehler

[1]Department of Mechanical Engineering and Bioengineering, Valparaiso University, Valparaiso, IN, USA
[2]Department of Kinesiology, Valparaiso University, Valparaiso, IN, USA
[3]Incremedical, Portage, IN, USA
[4]Lakeshore Bone and Joint Institute, Chesterton, IN, USA
email: craig.goehler@valpo.edu

INTRODUCTION

Lower extremity injuries have become increasingly common for young athletes. According to a 2017 study, anterior cruciate ligament (ACL) injuries have increased 2.3% per year in teens over the past twenty years [1]. Another study found that for ACL injuries, 72% resulted from noncontact and 28% from contact [2]. Extensive research has been conducted on contact and noncontact ACL injuries in high-risk sports such as football and soccer. Little is known about the prevalence of knee injuries in track and field events. Because noncontact ACL injuries are more likely, and track and field events are strictly noncontact, it is important to understand the effects of track versus field events and the kinematics of knee flexion associated with these events to prevent injury for athletes participating in this sport.

In this study, the kinematics of college track and field athletes were compared based on athletic event (track versus field). Track events include sprints and hurdles; field events include pole vault, high jump, long jump, and discus. The purpose of this study is to determine if track and field athletes can be equally assessed for risk of injury, or if one group requires a separate statistical metric from the other.

Using a data acquisition and analysis procedure previously created by our lab, the maximum knee and hip flexion angles (left and right) of the subjects were compared across three functional movements: left and right in-line lunges and deep squats [3].

METHODS

For this project, 12 subjects from the Valparaiso University track and field team (2 female, 10 male) between the ages of 18 and 22 were invited to participate in an IRB approved study. Each subject was affixed with 28 passive reflective markers on both the upper and lower extremities based on the anatomical locations specified in a previously developed musculoskeletal model [4]. The specific placements of these markers is

Figure 1: Reflective marker placement on subject performing squat exercise.

shown in Figure 1. The subjects completed the following exercises: lunges (right and left leg), squats, one-legged jumps (right and left leg), box jumps, and hurdle steps (right and left leg). Each exercise was completed until three successful trials were recorded.

The collected data files containing the three-dimensional positioning of each marker throughout each trial were processed, filtered, exported and converted to ensure compatibility with OpenSim. For each subject, a generic full body model was scaled using a static trial. The subject-specific model was then used to run inverse kinematic simulations to calculate the joint kinematics for each trial of each movement.

RESULTS AND DISCUSSION

For this abstract, results from the left and right in-line lunge and squat tests were analyzed and compared. Of the 12 subjects that participated in this study, 6 subjects were athletes who competed primarily in track events and 6 subjects were athletes who competed primarily in field events.

A preliminary statistical analysis of the data was performed to determine if there are any statistically significant differences across events. As seen in Table 1, there is a noticeable (but not significant) difference between the averages of the maximum hip flexion angles for the track and field athletes during the squat test for both the left and right legs. The field subjects appear to have exerted greater hip flexion when completing the squat test compared to the track subjects. However, further study of a larger group of athletes should be completed before such a claim can be effectively made from a statistical standpoint. Additionally, there were no statistically significant differences between corresponding hip flexion values for the lunge tests.

There are no statistically significant differences between left and right leg maximum knee flexion angles across the events for the three tests performed. Therefore, this preliminary study concludes that track and field athletes may be grouped into a common statistical metric for use in assessing risk of ACL injuries. As previously mentioned, additional studies including a larger group of athletes across track and field events should be completed to further confirm this conclusion. Since there were so few female participants in this current study, it would be interesting to also analyze future results to identify if any gender-based differences exist.

REFERENCES

1. Jenco, M. *American Academy of Pediatrics*, 2017.
2. Boden, B.P., et al. *Orthopedics*, 23, 573-578, 2000.
3. Miller, B., et al. *Annual Meeting of ASB 2016.*
4. Kozlowski, A., et al. *Annual Meeting of ASB 2015*.

Table 1. The average (standard deviation) maximum knee and hip flexion angles across all trials of the in-line lunge and squat tests. The results from the 6 track subjects and 6 field subjects are statistically compared.

		Track Athletes		**Field Athletes**	
		Left Leg	***Right Leg***	***Left Leg***	***Right Leg***
Knee Flexion	Left Lunge	121.42 (3.76)	112.51 (4.69)	124.47 (6.02)	109.58 (11.37)
	Right Lunge	107.97 (5.18)	124.38 (2.79)	105.65 (4.82)	124.33 (4.69)
	Squat	132.94 (11.38)	132.63 (10.35)	136.55 (8.23)	123.81 (61.00)
Hip Flexion	Left Lunge	88.33 (20.85)	13.72 (21.09)	100.37 (3.54)	21.26 (11.17)
	Right Lunge	4.73 (11.67)	90.09 (7.50)	12.12 (10.58)	95.78 (7.99)
	Squat	98.32 (9.18)	98.69 (8.68)	104.43 (1.47)	104.65 (0.27)

LABORATORY AND ON-FIELD RESULTS OF ATHLETE HEAD IMPACT MONITORING

[1]Adam Bartsch, [1]Rajiv Dama, [2]Sergey Samorezov, [2]Jay Alberts, [2]Edward Benzel, [3]Vincent Miele, [4]Alok Shah, [4]John Humm, [4]Michael McCrea, [4] Brian Stemper

[1] Prevent Biometrics, Minneapolis, MN, USA
[2] Cleveland Clinic, Cleveland, OH, USA
[3] University of Pittsburgh Medical Center, Pittsburgh, PA, USA
[4] Medical College of Wisconsin & Zablocki VA Medical Center, Milwaukee, WI, USA
email: abartsch@preventbiometrics.com

INTRODUCTION

Although concussion continues to be a major source of acute and chronic injury in automotive, athletic and military arenas, concussion injury mechanisms and risk functions are ill-defined. This lack of definition has hindered efforts to develop standardized concussion monitoring, safety testing and protective countermeasures. To overcome this knowledge gap, we have developed, tested and deployed a head impact monitoring mouthguard (IMM) system (**Figure 1**).

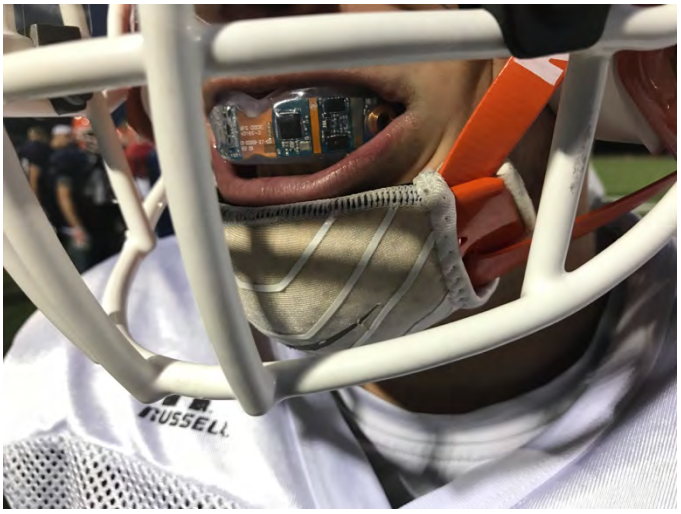

Figure 1: IMM System.

The IMM system was first calibrated in 731 laboratory tests against Hybrid III and NOCSAE headforms with Reference kinematic sensors. Next, during on-field play involving n=54 amateur American athletes in football and boxing, there were tens of thousands of kinematic signatures collected by the IMM. A total of 890 true positive head impacts were confirmed using a combination of signal processing and NINDS/NIH Common Data Elements methods [**1**].

METHODS

Laboratory tests were conducted using an American football helmet (n=451), padded headform (n=99) or bare head (n=181). Impacts were delivered using a linear pneumatic impactor and Hybrid III headform at Cleveland Clinic (n=366 football helmet, n=68 padded head and n=117 bare head; fixed mandible) and BioKinetics (n=54 football helmet and n=33 bare head; articulating mandible), as well as using a pendulum with NOCSAE headform at Virginia Polytechnic University (n=32 football helmet, n=32 bare head and n=32 padded; fixed mandible).

Each IMM had an embedded flexible printed circuit board hermetically sealed between layers of FDA-grade mouthguard material thermoformed to the upper dentition. The IMM included either 12 channels of linear acceleration ("12a", [**2**]) or 3 channels of linear acceleration and 3 channels of angular velocity ("3a3omega", [**3**]), along with associated microprocessor, battery and data storage. Peak linear acceleration (PLA) at headform center of gravity (cg) was compared in each test between Reference and IMM.

After calibrating the impact monitoring system in the laboratory, 54 amateur athletes in American football and boxing aged 11 to 22 were consented through Cleveland Clinic or Medical College of Wisconsin IRB. Events with cg PLA as low as 7g were collected during practices and games. Each event was time-synchronized to 30fps, 1080p video collected of each activity. Any events collected when the athlete was not actively participating were discarded. Any event when the athlete was participating but not being impacted in the head was also discarded. The remaining events were scrutinized to (a) confirm obvious head impact

occurred in the video and (b) the kinematic traces computed at the head center of gravity were physically realistic and mimicked the impact observed on video. The PLA and peak angular acceleration (PAA) were reported.

RESULTS AND DISCUSSION

In the laboratory testing, football helmet, padded and bare head impacts fit a linear model, with football helmet and padded impacts close to the ideal linear model of form y=x+0, R^2=1 (**Figure 2**).

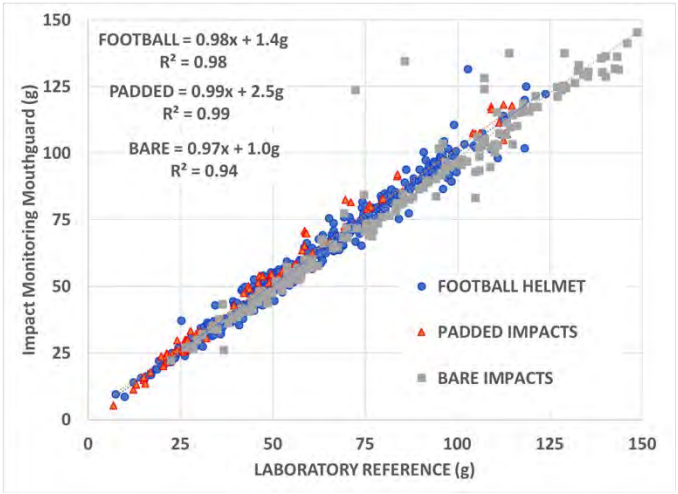

Figure 2: Laboratory PLA results.

Non-trivial processing algorithm, mouthguard customization, knowledge of accelerometer/gyro positions and orientations, and calibration of individual accelerometer/gyro outputs were required to achieve this level of accuracy.

During on-field data and video collection, there were more than 100,000 triggering events stored, with 890 true positives confirmed. "False positives", were triggered events on the IMM that generally contained high frequency kinematic data ~200Hz+ not indicative of head motion, or occurred during sequences where there was no head impact on video.

The median and 99th percentile of peak scalar linear acceleration (PLA) and peak angular acceleration (PAA) were 20g and 50g, and 1700rad/s^2 and 4600rad/s^2, respectively (**Figure 3**). Two-thirds of all true positives were to the face, facemask and front of helmet as indicated by component analysis of time traces of linear and angular acceleration.

There were no diagnosed concussions. One of the athletes was removed from competition by athletic training staff after a significant head impact.

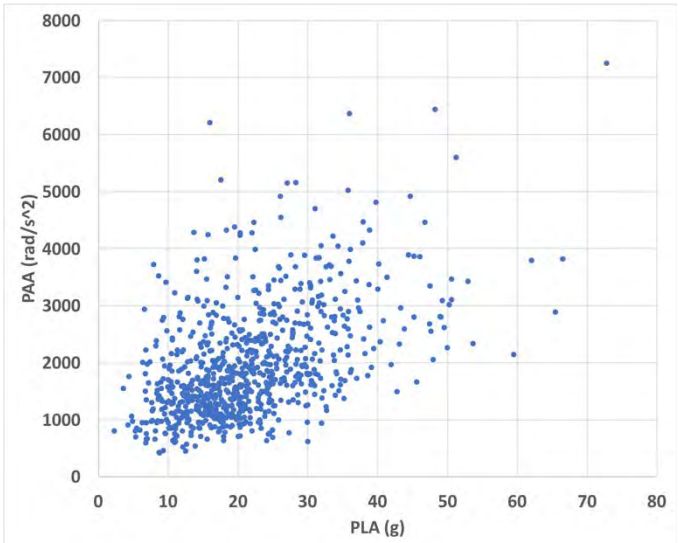

Figure 3: On-field PLA, PAA results.

CONCLUSIONS

While these data are useful for understanding human tolerance to head impact, a larger population must be studied to quantify real-world head impact dose-response thresholds accurately and precisely as a function of impact magnitude, direction, location and accumulation. This head impact dynamics data must also be correlated with sensitive and specific assessments of cognitive, executive, vision and balance parameters.

ACKNOWLEDGMENTS

This publication was supported by NIH NCATS Grants 8UL1TR000055 and 1UL1RR031973-01, NIH STTR Grant 1R41HD079158-01A1, NIH SBIR Grant 2R44NS076102-02A1, FAA DOT Grant 15-G-012, USAMRMC Award W81XWH-12-1-0004 and by the Defense Health Program under the DOD BAA Award No. W81XWH-14-1-0561. Its contents are solely the responsibility of the authors. Opinions, interpretations, conclusions and recommendations are those of the authors and are not necessarily endorsed by the NIH, DOT or DOD.

REFERENCES

1. Gay K, et al. *Amer. Acad. Neur.* 2018.
2. Bartsch AJ, et al. *Stapp Car Crash J* 2014.
3. Hedin DS, et al. *IEEE* 2016

KINETIC AND KINEMATIC DIFFERENCES IN WEIGHTLIFTING MOVEMENTS WITH AND WITHOUT THE USE OF A DOUBLE KNEE BEND

[1] Alexander M. Carnall, [1]Ramzi M. Majaj, [1]Maxime R. Paquette, [1]Douglas W. Powell

[1] University of Memphis, Memphis, TN, USA
Email: mcarnall@memphis.edu

INTRODUCTION

Existing research supports the notion that weightlifting training is associated with the development and improvement of multiple desirable physical qualities of athletes [2, 6, 10]. Since sport movements like sprinting, changing direction, throwing, and kicking involve contraction times between 50ms and 250ms, a high premium is necessarily placed on rate of force development as a desirable and trainable athletic quality. Weightlifting movements and their derivatives demand a unique blend of both high force production and high velocities [6, 10], which make them an obvious choice for strength and conditioning professionals. In support of this, agreement exists that exercise movements and programs are inherently more successful at improving athletic qualities if they prioritize force production intent, and rate of force generation [1, 4].

While strength and conditioning coaches have been quick to recognize the utility of these movements, some weightlifting coaches are critical of the techniques taught in athletic weight rooms [9]. Primarily this criticism stems from the observable absence of the double knee bend (DKB) in the cleans performed by non-weightlifting athletes. Early research confirms that the DKB is present in Olympic level weightlifters [3], and is observably absent in district level weightlifters as compared to those at the elite level [7].

In simplest terms, the DKB is a second knee bend as the barbell passes knee height in the clean pull. It is believed to be a learned technical adjustment whereby the lifter may shift from a hip and trunk extensor driven first pull to a knee extensor driven second pull. The purpose of the present investigation was to determine whether or not any significant differences in kinetic and kinematic variables exist in the presence or absence of the DKB technique.

METHODS

Kinetic and kinematic data were collected from three young, healthy, physically active males (Age: 27.0 ± 1.7 years, Height: 188.33 ± 14.84 cm, Weight: 122.0 ± 29.5 kg, 1RM Clean: 149.0 ± 9.6 kg) with experience using the double knee bend technique. A 20kg training bar and rubber training discs were used for all trials with retroreflective markers fixed to the end-cap of the barbell for motion capture tracking purposes. All trials were performed on two force platforms (1200Hz, AMTI, Watertown, MA).

Each participant performed trials as outlined in Table 1. Minimum two minutes rest between conditions was mandated.

Table 1: Trials Performed

	50% 1RM		70% 1RM	
Condition	No DKB	DKB	No DKB	DKB
Clean Pull	4	4	4	4
Clean	4	4	4	4
Hang Clean	4	4	4	4

Primary kinematic outcome variables included (1) peak barbell acceleration and (2) peak barbell velocity. Kinetic outcome variables included (3) athlete-barbell system weight normalized propulsive impulse, (4) rate of force development in first pull (RFD_1), and (5) rate of force development from knee to terminal force production (RFD_2). Paired t-tests were used to compare No DKB to DKB conditions.

RESULTS AND DISCUSSION

Preliminary findings are shown in table 2.

Table 2: Results of Primary Outcome Variables

	No DKB	DKB	Sig.
Peak Acceleration	6.40 ± 2.47	10.61±15.98	<.001*
Peak Velocity	1.99 ± 0.21	2.05 ± 0.16	0.011*
Propulsive Impulse	692.82 ± 189.13	709.69 ± 136.46	0.420
RFD_1	11.11 ± 14.50	12.15 ± 14.10	0.650
RFD_2	37.35 ± 18.27	51.91 ± 11.69	<.001*

Significantly greater peak barbell acceleration and velocity was found for trials in which the participants used the DKB technique. In addition, significantly greater RFD_2 was found in the DKB trials. Representative force-time curves are shown in Figure 1.

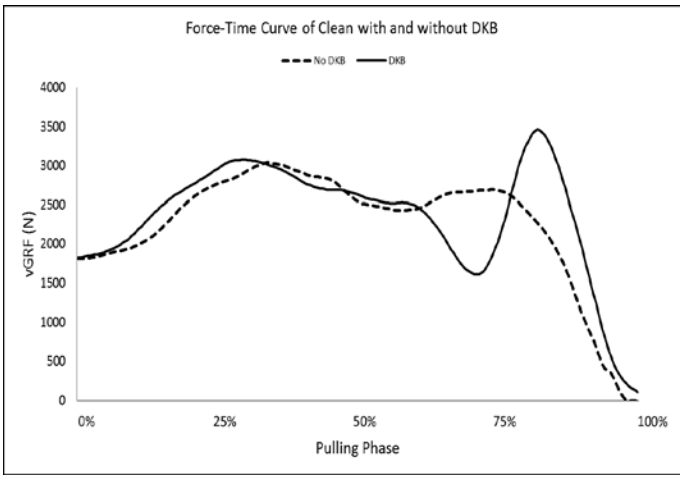

Figure 1: Differences in force-time curves for clean trials with and without use of the DKB technique.

With respect to the underpinning mechanism, there is general agreement that the first pull (RFD_1) is largely driven by hip and lumbar extensors, with the DKB serving to shift primary extensor torque obligations to the knees for the second pull [8]. This is supported by other findings identify this position as one in which knee joint angles are optimized to exert greatest concentric force [3].

Interestingly, significant differences were not found for RFD_1 or normalized propulsive impulse, suggesting that the DKB has no influence on total force generated or the mechanics of the first pull. Rather, it appears that the DKB allows the lifter to achieve greater peak vertical forces via manipulation of joint positions to optimize force output in the second pull.

CONCLUSIONS

To our knowledge, this is the first investigation to use a within-subjects design to examine the effects of two technical variants on kinetic and kinematic outcomes related to performance of the clean and its derivative movements. As such, we feel the clinical or practical significance of these findings are uniquely actionable.

The DKB appears to decrease the internal mechanical resistance of the clean movement and its derivatives by optimizing joint angles for force production during this dynamic movement. By learning this technique, the magnitude of the adaptive stimulus of training may be increased beyond what may be experienced using suboptimal movement strategies resulting greater likelihood of realizing the intended training effects.

REFERENCES

1. Aagaard, P. (2003). Training-induced changes in neural function. *Exercise and Sport Sciences Reviews,* ***31***(2), 61-67.

2. Chiu, L. Z., & Schilling, B. K. (2005). A primer on weightlifting: From sport to sports training. *Strength & Conditioning Journal,* ***27***(1), 42-48.

3. Enoka, R. M. (1979). The pull in olympic weightlifting. *Med Sci Sports,* ***11***(2), 131-137.

4. Garhammer, J., & Gregor, R. (1992). Propulsion forces as a function of intensity for weightlifting and vertical jumping. *J Appl Sport Sci Res,* ***6***(3), 129-134.

5. Hernández-Davó, J. L., & Sabido, R. (2014). Rate of force development: Reliability, improvements and influence on performance. A review. *European Journal of Human Movement, 33*, 46-69.

6. Hori, N., Newton, R. U., Nosaka, K., & Stone, M. H. (2005). Weightlifting exercises enhance athletic performance that requires high-load speed strength. *Strength and Conditioning Journal,* ***24***(4), 50.

7. Kauhanen, H., Hakkinen, K., & Komi, P. (1984). A biomechanical analysis of the snatch and clean & jerk techniques of finnish elite and district level weightlifters. *Scand J Sports Sci,* ***6***(2), 47-56.

8. Kipp, K., Redden, J., Sabick, M. B., & Harris, C. (2012). Weightlifting performance is related to kinematic and kinetic patterns of the hip and knee joints. *Journal of Strength and Conditioning Research,* ***26***(7), 1838-1844.

9. Takano, B. (1992). RESISTANCE EXERCISE: The power clean-perspectives and preparation. *Strength & Conditioning Journal,* ***14***(1), 68-71.

10. Tricoli, V., Lamas, L., Carnevale, R., & Ugrinowitsch, C. (2005). Short-term effects on lower-body functional power development: Weightlifting vs. vertical jump training programs. *Journal of Strength and Conditioning Research,* ***19***(2), 433.

Sex Differences in Joint Kinetics during a Restricted Vertical Jump

[1] Hailey J. Daugherty, [1]Doug W. Powell, [1]Max R. Paquette, [1]Lindsey E. Allison, [1]Lawrence W. Weiss
[1]Musculoskeletal Analysis Laboratory, University of Memphis, Memphis, TN, USA
email: dwpowell@memphis.edu, web: http://www.memphis.edu/shs/research/mal.php

INTRODUCTION

Vertical jumping tasks are common in sports are often an indicator of athletic performance (1). Kinetic variables, such as joint power and joint work, are often assessed as good measures of vertical jump performance (2). Sex differences in joint kinetics during landing tasks have been widely investigated; kinematically, Decker *et al.* (2003) found that females have a significantly greater ankle range of motion (ROM) than males during a drop-landing task. This suggests that if females have less relative ROM at the knee and hip joints, kinetically, females also may have reduced muscular power and vertical jump performance may be impaired.

Research often indicates sex differences in kinetic variables even when normalized to body mass (2). Differences in joint kinetics, such as muscular power, may be due to sex- related neuromuscular control strategies. Further, if sex- related differences could be identified, training could be altered to potentially increase performance and decrease the risk of injury (2,3).

There is limited research that investigates individual joint contributions relative body mass in vertical jump performance (4). Therefore, the purpose of this investigation was to evaluate sex differences in joint work contributions to a restricted vertical jump task when normalized to body mass and lean mass. We hypothesized that when normalized to lean mass, individual joint contributions would be similar between sexes.

METHODS

Fifty-five recreationally trained young adults (30 male and 25 female) recruited from a university population participated in this study (22.92±3.02yrs; 73.18±14.41kg; 1.71±1.24m; 17±7.7 % of body fat). Participants attended one testing session to perform maximal, restricted vertical jumps wearing their own footwear. All participants were instructed to refrain from exercise the day before the testing session.

Testing involved measurement of anthropometric variables (e.g. height, mass, body fat percentage), a general warm-up on a cycle ergometer, a dynamic warm-up including 10 bodyweight squats and 5 jump squats, and 3 maximal, restricted countermovement vertical jumps. The restriction in the vertical jump task was indicated by a standardized arm position, such that the nondominant hand was situated across the participant's chest. The restriction was designed to minimize the influence of the arms on the height of the vertical jump. A demonstration of the task to be completed was provided for each participant. Participants were provided practice trials until comfort in the task was reported. Rest intervals of 75 seconds were provided between each jump trial.

A 9- camera motion capture system (240Hz, Qualisys AB, Sweden) and force platforms (1200Hz, AMTI, Inc.) were used to collect kinematic and ground reaction force data, respectively. Visual 3D software (C-Motion, Germantown, MD) was used to process and analyze both kinematic and kinetic data. Newtonian inverse dynamics were used to compute internal joint moments (Nm). Angular joint powers (W) were computed as the product of joint moments and joint angular velocities. Joint work was calculated as the product of joint power (W) and time (s). The average of all biomechanical variables from each jumping trial during the concentric phase of jumping was used in statistical analyses. Paired Samples T Tests were used to compare lower extremity joint kinetics between normalization method (Body Mass vs. Lean Mass) and between sexes ($p<0.05$).

RESULTS AND DISCUSSION

As hypothesized, lower extremity joint kinetics between males and females were not significantly different when normalized to lean mass. There was a difference between normalization techniques (Body Mass vs. Lean Mass) ($p<0.05$) indicating that lower extremity joint kinetics (e.g. moments, powers, and work) significantly differed between normalization techniques. There was also a significant interaction between normalization techniques ($p<0.05$) indicating that the change (e.g. slope of the line) between normalization techniques differed between males and females. As expected, lower extremity joint kinetics did not significantly differ between males and females when normalized to body mass.

CONCLUSIONS

The findings from this investigation suggest that normalization techniques should be considered when comparing lower extremity joint kinetics between sexes. Although many factors are believed to result in sex differences in vertical jump performance, and therefore sport performance, body fat percentage depicts a factor that may be modifiable.

It is important to consider if body mass normalization provides useful information. In this investigation, females had lower total joint work compared to males when normalized to body mass, but when normalized to lean mass females and males had relatively similar total joint work during the restricted vertical jump task. This implies that females may produce similar relative muscular power as males, yet have an increased resistance (e.g. increased body fat percentage), which may impair performance. Therefore, if body fat percentage is a modifiable factor, females may be able to alter lower extremity joint kinetics such that sex differences diminish.

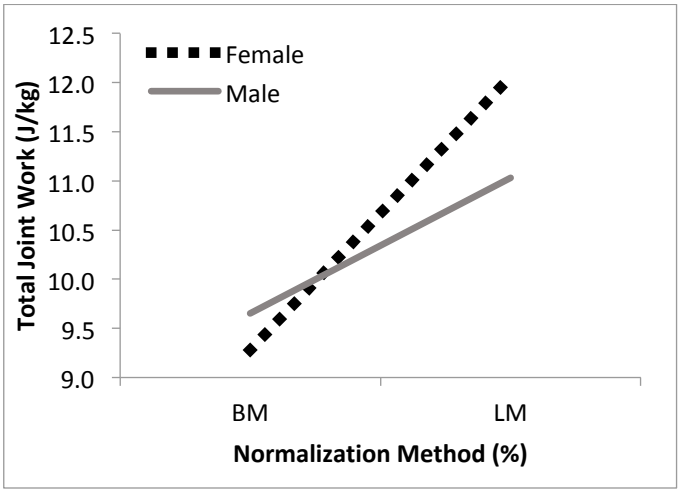

Figure 1: Total lower extremity joint work between normalization techniques (Body Mass vs. Lean Mass) and between sexes.

REFERENCES

1. Barker, M. et al. (1993). *Journal of Strength & Conditioning Research*, 7(4), 224-233.
2. Caserotti, P. et al. (2001). *Eur. J. Appl. Physiol.* 84: 206-212.
3. Decker, M. J. et al. (2003). *Clinical biomechanics*, *18*(7), 662-669.
4. Hubley, C. et al. (1983). *Eur. J. Appl. Physiol. Occup. Physiol.* 50:247-254.

Table 1: Comparison of joint moments (Mean±SD), powers (Mean±SD), and work (Mean±SD), normalized for body mass (BM) and lean mass (LM) between sexes.

		Moment (Nm)		Power (W)		Work (J/kg)	
Joint	**Sex**	**BM (kg)**	**LM (kg)**	**BM (kg)**	**LM (kg)**	**BM (kg)**	**LM (kg)**
Ankle	M	-1.68±0.27	-1.92±0.33	11.38±2.94	13.02±3.54	2.61±0.85	3.00±1.02
	F	-1.48±0.18	-1.92±0.22	10.35±1.95	13.42±2.46	2.55±0.78	3.32±1.05
Knee	M	1.86±0.31	2.12±0.38	13.73±2.56	15.62±2.73	3.54±1.38	4.05±1.59
	F	1.68±0.28	2.17±0.33	12.68±2.52	16.47±3.35	3.44±1.41	4.47±1.85
Hip	M	-2.35±0.52	-2.68±0.61	9.89±2.15	11.19±1.99	3.50±1.09	3.98±1.22
	F	-2.12±0.45	-2.75±0.56	9.42±2.13	12.20±2.61	3.29±1.34	4.27±1.74

Pacing Strategy Changes as Age Increases in Long Distance Runners

[1] Tyler Davis, [1] Kevin Krieg, [1] Cassandra Kuyawa, and [1] Cristine Agresta

[1] Michigan Performance Research Laboratory, University of Michigan, Ann Arbor, MI, USA
email: cagresta@umich.edu, web: http://www.mipr.kines.umich.edu/

INTRODUCTION

Pacing strategy varies depending on the race type and length. For distance running, performance is well known to decline with age, however world-class marathoners are often older than runners of shorter distance. This suggests that experience is an important factor.[1] The fastest times for elite marathon runners typically employ a "fast-slow-fast" pacing strategy where they run faster than their mean speed for the first part of the race, slow down below average pace in the middle and then have a final push that is above average pace for the end.[3] Significant age-related losses in performance for trained half-marathon and marathon runners do not occur until 50 years old. Males typically run about 10-13% faster than females.[2] Since this study incorporated novice and experienced runners of both genders, there is expected to be a larger difference. However, it is unclear whether older runners change their pacing strategies in addition to or as a result of slowing speed. Thus, the purpose of this study was to describe pacing strategies in distance runners of varying ages.

METHODS

Sixty runners (26 M, 34 F, 32.7 ± 10.3 years) participated in this study. Runners were free of injury or pain at the time of testing and all were within the first month of a half or full marathon training program. Participants ran a 5-min warm-up. Participants were allowed to rest before being asked to complete a self-paced 5-kilometer time trial (5KTT) on a pressure-sensing treadmill (h/p cosmos Quasar). The treadmill was set to 1% elevation. Participants had knowledge of current speed and total distance covered via display monitor and could freely adjust treadmill speed at any point during the trial. The participant's running speed was recorded every 30-seconds.

Participants were categorized into the following age groups: 18-24, 25-32, 33-40, and 41-55. The 5KTT duration for each subject was normalized on a 0-100% scale. Normalized 5KTT running speed was then sectioned into 10% increments by averaging all data points within 10% window.

For instance, a single ANOVA test was used to determine the averages of each group's pace with 1 standard deviation in 10% time increments. A two-way repeated ANOVA measures test compared each 10% increment with every other increment within each group to determine any significant changes. Statistical significance between groups or time increments was deemed significant at $P < .05$ and were calculated with SPSS (IBM) statistical package software. Subjects were sorted into their categories and then graphed means and standard deviations using Matlab software.

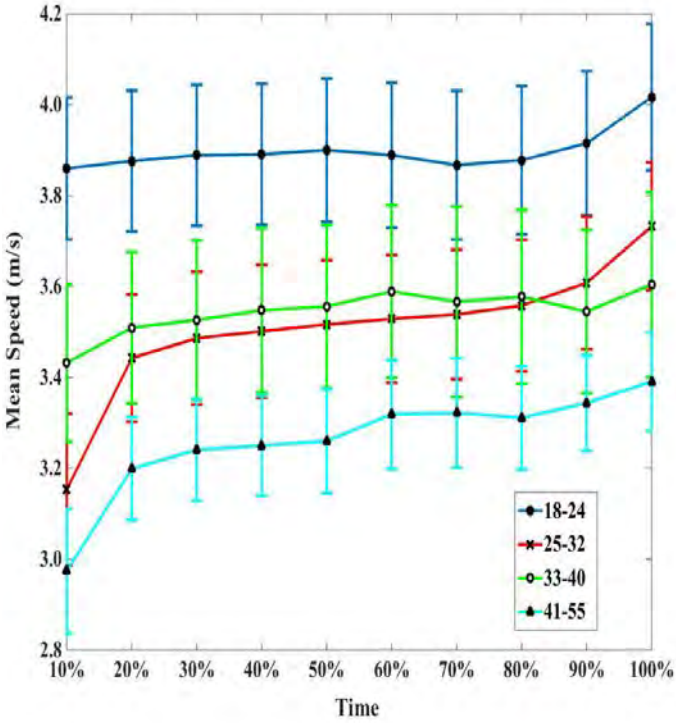

Figure 1: Mean running speed (m/s) during a 5km time trial for each age group: 18-24 years (blue line), 25-32 years (red line), 33-40 years (green

line), and 41-55 years (teal line). Errors bars (±1STD) are presented at each 10% interval.

RESULTS AND DISCUSSION

Mean running speed for 5KTT for all participants was 3.23 ± 0.24 m/s. Group data is available in Table 1. There was primarily significant change across all groups for all time increments except 70% and 80%. The 25-32 age group had the most significant changes within itself while 33-40 group had the least significant changes. There was only a significant decrease in speed between the 18-24 group and 41-55 group.

Results from this study are in agreement with previous findings that as the age groups get older, their speed decreases in general. There are some noticeable differences in patterns between each group as seen in Figure 1. However, these pacing strategies do not follow the "fast-slow-fast" strategy that is seen in world-record performances in marathon runners.[3] The data shows that recreational runners tend to slowly increase up to their average speed in the beginning of the race and try to maintain that pace until a final push at the end of the race.

CONCLUSIONS

Following previous literature [1], there is not enough data to determine a consistent effect on pacing as age increases for a recreational runner. There are several factors that could influence speed such as experience, age, and gender. However, coaches and runners can use this data as a general guide for trends of the recreational long distance runner.

REFERENCES

1. March, DS, Vanderburgh, PM, Titlebaum, PJ, and Hoops, ML. Age, sex, and finish time as determinants of pacing in the marathon. J StrengthCond Res 25(2): 386–391, 2011
2. Leyk, D, Erley, O, Ridder, D, Leurs, M, Ruther, T, Wunderlich, M, Sievert, A, Baum, K, and Essfeld, D. Age related changes in marathon and half marathon performances. Int J Sports Med 28:513–517,2007.
3. Hoos, O., Boeselt, T., Steiner, M., Hottenrott, K., & Beneke, R. (2014). Long-Range Correlations and Complex Regulation of Pacing in Long-Distance Road Racing. *International Journal of Sports Physiology and Performance,9*(3), 544-553. doi:10.1123/ijspp.2012-0334

Table 1. Mean running speed (m/s) for each 10% interval during 5KTT for all age groups.

	10%	20%	30%	40%	50%	60%	70%	80%	90%	100%	Overall
18-24	3.86 ± 0.63	3.88 ± 0.62	3.89 ± 0.62	3.89 ± 0.62	3.90 ± 0.63	3.89 ± 0.64	3.87 ± 0.65	3.88 ± 0.65	3.92 ± 0.64	4.02 ± 0.64	3.90 ± 0.04
25-32	3.15 ± 0.65	3.44 ± 0.54	3.49 ± 0.57	3.50 ± 0.57	3.52 ± 0.55	3.53 ± 0.54	3.54 ± 0.55	3.56 ± 0.56	3.61 ± 0.56	3.73 ± 0.54	3.51 ± 0.15
33-40	3.43 ± 0.49	3.51 ± 0.47	3.53 ± 0.50	3.55 ± 0.51	3.56 ± 0.51	3.59 ± 0.54	3.57 ± 0.59	3.58 ± 0.54	3.55 ± 0.51	3.60 ± 0.58	3.55 ± 0.05
41-55	2.97 ± 0.53	3.20 ± 0.44	3.24 ± 0.43	3.25 ± 0.43	3.26 ± 0.44	3.31 ± 0.46	3.32 ± 0.46	3.31 ± 0.44	3.34 ± 0.41	3.39 ± 0.42	3.26 ± 0.12

LOWER EXTREMITY BIOMECHANICS ARE ALTERED IN A SPORT-SPECIFIC VIRTUAL ENVIRONMENT

[1]Christopher A. DiCesare, [1]Adam W. Kiefer, [1]Scott H. Bonnette, [1]Gregory D. Myer

[1]The SPORT Center, Cincinnati Children's Hospital Medical Center, Cincinnati, OH
e-mail: christopher.dicesare@cchmc.org

INTRODUCTION

Biomechanical analyses of sport movements have classically been used to quantify kinematic (i.e., joint angular motion) and kinetic, (i.e., joint moments of force) factors in the context of task performance or injury risk. Specific movement patterns exhibited during the performance of various tasks, such as reduced knee flexion and excessive knee abduction during the drop vertical jump (DVJ) [1], and their associations with injury risk have been identified and used to inform neuromuscular training strategies aimed to target and ameliorate high risk biomechanics in susceptible populations (see [2] for a review). Classical biomechanical assessment is limited, however, in its generalizability to sport-specificity associated with actual sport competition.

Simulation of sport-specific environments through virtual reality (VR) can overcome the limitations of classical assessments by presenting virtual scenarios that facilitate real-world athletic performance [3]. The purpose of this study was to compare movement patterns exhibited by athletes during both a standard biomechanical assessment (i.e., DVJ) and a sport-specific VR-based assessment. It was hypothesized that the VR scenario would elicit increased magnitude of injury risk biomechanics compared to the standard biomechanical assessment.

METHODS

Thirty-eight healthy, female adolescent soccer athletes (M ± SD age = 16.0 ± 1.3 years; height = 1.65 ± 5.5 m; weight = 59.5 ± 9.9 kg) participated in this study. Athletes underwent a standard biomechanical assessment including performance of the DVJ task, as well as a VR-based assessment of jump-landing performance during a soccer-specific corner-kick scenario in which athletes headed a virtual soccer ball.

For both standard laboratory and VR assessments, each athlete was instrumented with 37 reflective markers with a minimum of 3 tracking markers per segment. For the VR assessment, athletes also wore a custom-built, wireless, head-mounted display with 5 additional markers attached for tracking of head position and orientation (see [3] for technical specifications). The three-dimensional marker trajectories were collected using a 39-camera passive optical motion capture system (Motion Analysis Corp., Santa Rosa, CA). From these measures, Cardan joint angles were calculated using a six-degree-of-freedom model in Visual3D (C-Motion Inc., Germantown, MD).

For the standard biomechanical assessment, athletes performed a minimum of 3 DVJ trials. The DVJ was performed by dropping off a 31-cm box with both feet at the same time, landing on the ground, and then performing a maximum vertical leap to reach for an overhead target. The VR assessment required athletes to head a virtual soccer ball that was kicked by a computer controlled non-player character toward a virtual goal. Athletes performed a minimum of 4 trials of a corner kick scenario counterbalanced so that the athlete performed two trials each in which they approached the ball from the left and right side of the goal.

Figure 1. The VR-based corner-kick soccer scenario.

Data from both the VR assessment and DVJ were extracted for both the stance phase before the jump, when the athlete was in contact with the ground before toe-off, as well as the second landing period after the jump. The stance phase was determined as the period of time between the heel strike and toe-off events immediately preceding the jump, and the landing period was determined as the period of time between the first heel strike after the jump to maximum knee flexion. Only VR trials in which double-leg jumps or landings occurred were considered, as these are the most directly comparable to the DVJ task in the standard assessment.

Data during the stance and second landing phases were normalized to 101 points (representing 0-100% of the phase), and peak sagittal and frontal plane hip, knee, and ankle joint angular measures were extracted for the respective phases. Pearson product-moment correlations were run between the variables for the standard and VR conditions for both phases and were compared using paired t-tests. The *p*-value was selected to be .05 to indicate statistical significance and adjusted using a Bonferroni correction for multiple comparisons.

RESULTS AND DISCUSSION

During the VR condition, athletes exhibited reduced sagittal plane joint motion for the stance phase (all $p < .0042$; Table 1). Sagittal plane joint motion during the second landing phase and frontal plane joint motion for both the stance and second landing phases were similar between the standard and VR conditions (all $p > .0042$ except for ankle dorsiflexion during the second landing; Table 1).

CONCLUSIONS

VR-based assessments can provide a sport-specific context in which to assess movement patterns that, while comparable to standard assessments, exhibit increased magnitudes of biomechanical deficits, particularly in the sagittal plane, that predispose athletes for lower extremity injury.

REFERENCES

1. Hewett et al. *Am J Sports Med*. 33(4): 492-501. 2005.
2. Sugimoto et al. *Br J Sports Med*. 46(14): 979-988. (2012).
3. Kiefer et al. *Proceedings of ICVR '17*, Montreal, Quebec, Canada, 2017.
4. Myer et al. *Br J Sports Med*. 42(7): 614-619. 2008.

ACKNOWLEDGEMENTS

The authors would like to thank Kim Barber Foss, Staci Thomas, Katie Kitchen, and Brooke Gadd for their assistance with data collection; Bernard Casey, Ian Anderson, and Chris Collins of the University of Cincinnati Simulation and Virtual Environments for the development of the VR scenario; and Matt Batie for the development of the head-mounted display.

Table 1: Means, standard deviations, Pearson correlation coefficients, and *p*-values of peak lower extremity joint angular motions during stance and second landing phases in the standard and VR conditions.

		VR		Standard			
Phase	**Joint Angular Motion**	**Mean**	***SD***	**Mean**	***SD***	*r*	***p***
Stance	Hip Flexion (°)	48.45	10.28	59.91	13.74	0.398	<.001*
	Hip Adduction (°)	3.41	4.77	1.89	3.99	0.241	.072
	Knee Flexion (°)	-68.54	8.91	-83.83	10.37	0.543	<.001*
	Knee Abduction (°)	-7.33	4.39	-7.66	5.36	0.759	.542
	Ankle Dorsiflexion (°)	21.12	5.49	29.21	4.85	0.567	<.001*
	Ankle Eversion (°)	-2.30	3.52	-1.98	4.59	0.464	.624
Second Landing	Hip Flexion (°)	30.38	14.57	42.36	21.40	0.378	.012
	Hip Adduction (°)	2.53	3.69	0.72	4.33	0.228	.096
	Knee Flexion (°)	-62.89	10.72	-70.27	15.76	0.444	.024
	Knee Abduction (°)	-6.47	4.54	-7.40	5.16	0.704	.249
	Ankle Dorsiflexion (°)	21.80	6.01	27.24	4.13	0.165	.001*
	Ankle Eversion (°)	-2.54	3.47	-1.16	4.46	0.200	.206

KINEMATIC AND KINETIC DIFFERENCES BETWEEN LEFT- AND RIGHT-HANDED PROFESSIONAL BASEBALL PITCHERS

[1]Alek Z. Diffendaffer,[1] Glenn S. Fleisig, [1] Brett Ivey and [1]Kyle T. Aune

[1]American Sports Medicine Institute, Birmingham, AL, USA
email:alekd@asmi.org, web: asmi.org

INTRODUCTION

While only 10% of the general population is left-handed, 27% of professional baseball pitchers are left-handed [1]. Due to the disproportionately high number of left-handed pitchers, biomechanical differences between left- and right-handed pitchers have previously been examined at the college level [2,3]. These studies identified several kinematic, kinetic and passive range of motion differences between left- and right-handed pitchers. Although these two studies were able to agree on certain findings, there were also inconsistencies which warrant further investigation to confirm meaningful biomechanical differences and refine the magnitude of these differences [4]. Furthermore, differences between left- and right-handed professional baseball pitchers have yet to be examined and may differ from the findings among the previously studied college pitchers. Therefore, the purpose of this study was to determine if kinematic and kinetic differences exist between left- and right-handed professional baseball pitchers. It was hypothesized that left-handed pitchers will display different kinematic and kinetic mechanics when compared to their right-handed counterparts.

METHODS

A retrospective review of the American Sports Medicine Institute (ASMI) pitching biomechanics database was performed. From 2002 to 2015, biomechanical data were collected on 399 healthy professional baseball pitchers. At the time of testing, each participant was outfitted with 23 retro-reflective markers and was then instructed to warm-up. After conclusion of the warm-up, data for ten full-effort fastballs were collected. Each pitch was thrown from a pitching mound towards home plate located 18.44 meters away, while ball velocity was measured by a radar gun (Stalker Radar, USA). For all trials, three-dimensional motion data were tracked with a 12-camera automated motion analysis system sampling at 240 Hz (Raptor System, Motion Analysis Corp., USA). From the captured motion data, 31 kinematic and kinetic variables were calculated for each pitch as previously described [5].

Of the 399 professional pitchers tested, 96 left-handed pitchers were identified. These 96 were then matched to 96 right-handed pitchers for age, height, mass and ball velocity.Two one-sided t-tests (TOST) for equivalence determined that age (RHP, 22 ± 2 yrs; LHP, 22 ± 2 yrs), height (RHP, 189 ± 5 cm; LHP, 189 ± 6 cm), mass (RHP, 93 ± 5 kg; LHP, 93 ± 9 kg), and ball velocity (RHP, 38 ± 1 m/s; LHP, 38 ± 2 m/s) were the same for the two groups. Independent two-sided Student t-tests were used to identify kinematic and kinetic differences between left- and right-handed professional pitchers.

RESULTS AND DISCUSSION

Of the 31 variables calculated, four kinematic variables were found to be statistically different (Table 1). At the point of foot contact, right-handed pitchers obtained more trunk ‘separation’ (axial rotation) and landed with their lead foot positioned more ‘closed’ or more toward their throwing arm side than their left-handed counterparts (Fig 1). Additionally, maximum shoulder external rotation and trunk forward tilt at the instant of ball release were significantly greater in right-handed pitchers. No significant differences in kinetic variables were identified between the groups.

The results from this study may imply that right-handed pitchers utilize more core and shoulder flexibility, while left-handed pitchers may adopt other techniques to maintain equivalent outcomes (ie. ball velocity). Possible reasons for the observed differences may be due to different in-game

strategies practiced by left-handed pitchers. For instance, since the trunk of a left-handed pitcher faces first base when pitching from the stretch, obtaining less trunk separation may be critical for holding a runner on first base to a shorter lead. Also, since all pitchers face a majority of right-handed batters, right-handed pitchers may benefit from landing with a closed lead foot position to throw inside to the batter, while left-handed pitchers may land with a more "open" lead foot position to gain a similar advantage.

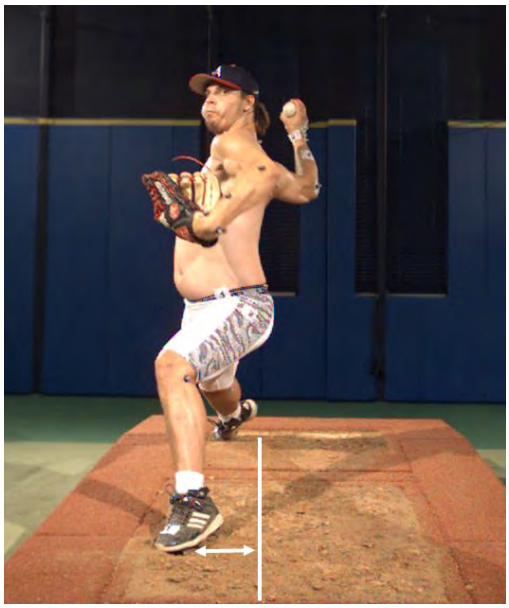

Figure 1: Lead foot position was defined as the distance between the lead ankle's position at the instant of foot contact and the back ankle's positon at maximum knee height, in the global y-direction. Positive ('closed') foot position was towards third base for a right-hander pitcher, and towards first base for a left-handed pitcher.

In general, differences found in this study were not reported in the previous two studies. When comparing all significant findings among the three studies, there were minimal consistent findings. For example, Werner et al. reported a drastic difference in shoulder abduction between right- and left-handed pitchers, while Solomito et al. reported a difference in elbow varus torque. Neither of these findings were supported by the current study. Additionally, the current study found no differences in arm angles at the instant of foot contact, while the previous two studies both reported that left-handed pitchers had more elbow flexion and less shoulder horizontal abduction.

CONCLUSIONS

Both Solomito and Werner proposed to establish normative data specifically for left-handed pitchers when assessing their biomechanics. The authors from the current study are not in agreement with this recommendation. The current study quantified kinematics and kinetics for highly skilled baseball pitchers (ie. professional). With a very large sample size and high statistical power, 27 of the 31 variables analyzed showed no differences. While the remaining four variables showed statistical significance, the magnitudes of these differences were relatively small and not consistent with the previous studies. Thus we conclude that any differences between left- and right-handed pitchers that exist are of minimal practical significance and left-handed pitchers should be biomechanically analyzed and coached no differently than their right-handed counterparts.

REFERENCES

1. Conte et al. *Am J Sports Med.* **43(7)**, 1764-1769, 2015.
2. Werner et al. *Am J Sports Med.***38(8)**, 1606-10, 2010.
3. Solomito et al. *Sports Biomechanics.***16(2)**, 143-151, 2017.
4. Knudson, D. *Sports Biomechanics.* **16(4)**, 425-433, 2017.
5. Fleisig et al. *J of App Biomech.* **(12)**, 207-224, 1996.

Table 1: Significant kinematic differences between left- and right-handed professional baseball pitchers.

Kinematic Variable	RHP	LHP	p-value
Lead Foot Position (in)	25 ± 11	21 ± 12	0.018
Trunk Separation (deg)	50 ± 10	45 ± 11	<0.001
Maximum Shoulder External Rotation (deg)	177 ± 9	174 ± 10	0.012
Trunk Forward Tilt (deg)	33 ± 7	31 ± 7	0.039

MODELLING TRACTION FORCES DURING STUDDED BOOT–SURFACE INTERACTIONS

Steph Forrester, James Montgomery and Paul Fleming

Sports Technology Institute, Loughborough University, UK
email: s.forrester@lboro.ac.uk, web: http://asb2018.asbweb.org/

INTRODUCTION

The use of cleated or studded footwear is common in sports played on third generation (3G) artificial turf and natural grass. They allow for improved performance through the generation of greater traction forces, however, injury risk is a limiting factor [1]. Foot fixation, due to excessive traction at the boot–surface interface, is considered a major contributor to ankle and knee injuries [1]. Previous studies have been empirical, using player or mechanical testing to quantify traction for various outsole and surface designs, but providing little insight to the mechanisms contributing to these forces. Ultimately, if boots and surfaces are to be designed which enable performance without compromising injury risk, a better understanding of how traction forces are generated is needed.

Given the complexity of boot–surface interactions, a simplified starting point is necessary. Thus, the purpose of this study was to develop an analytical model for the traction forces generated during a FIFA rotational traction test (RTT) on 3G turf (Fig. 1; [2]). This model can provide an important first step in the development of a model for the traction forces during real boot–surface interactions, and ultimately aid in reducing injury risk.

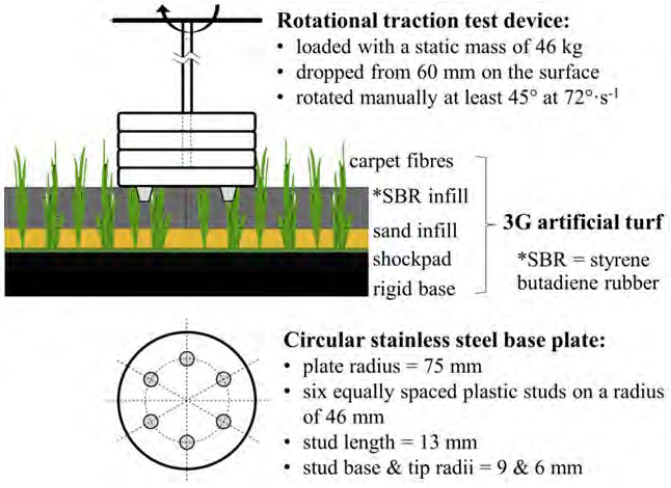

Figure 1. Schematic of the FIFA RTT device.

METHODS

The output from a FIFA RTT typically demonstrates an initial rapid rise in torque for angles up to ~5°, followed by a less rapid rise to ~30°, with peak torque reached at ~40° (Fig. 2). This peak is related to the leading edge of one stud overlapping the zone where the preceding stud has already disturbed the infill (stud lead to trail edge angle ~43°; Fig. 1). Traction is generated by both the base plate and studs interacting with the surface. Testing without studs can give the plate torque (Fig. 1), whilst the stud torque can be estimated by subtracting this plate torque from the total torque.

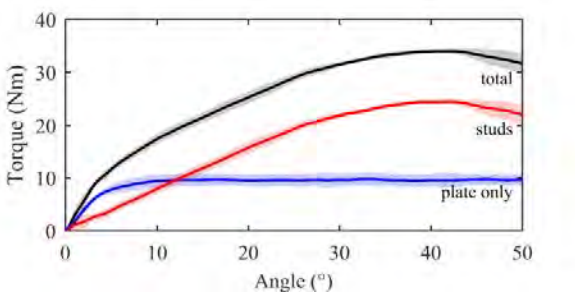

Figure 2: FIFA RTT torque–angle output: plate & studs (black), plate only (blue), studs (red: total–plate).

Plate–surface torque (T_P): Torsional shear until static friction is overcome:

$$T_{P,T} = (G \times J/L) \times \theta_P \quad (1)$$

where L is SBR infill depth, J is polar MoI, and G is shear modulus. G is a function of SBR infill properties, state and normal stress (solid SBR: G~0.3 MPa). Thereafter, dynamic friction:

$$T_{P,F} = (2/3) \times r_P \times \mu_{P-S} \times F_{P,N} \quad (2)$$

where r_P is base plate radius, $F_{P,N}$ is normal load and μ_{P-S} has a value between 0.2 (metal–polyethylene) and 0.7 (metal–rubber). Based on the above, overall plate–surface torque can be approximated by the upper half of a sigmoid curve (Fig. 2) where the rate of rise is determined by torsional shear (represented by p_1 in eq.(3)) and the upper plateau by friction:

$$T_P = [(2 \times T_{P,F}) / (1 + exp(-p_1 \times \theta_P))] - T_{P,F} \quad (3)$$

Stud–surface torque (T_S): Prior to stud interaction effects, compression of the SBR infill in front of the ploughing studs:

$$T_S = [(E \times A_S/l_0) \times n_S \times r_S^2] \times \theta_P \quad (4)$$

where A_S is stud frontal area, l_0 is no strain infill length, n_S is number of studs, r_S is radial position of the studs and E is Youngs Modulus. E is a function of SBR infill properties, state and normal stress (solid SBR: E~10 MPa). Stud–surface torque can be approximated by a power curve (Fig. 2) where the coefficient (s_1 in eq.(5)) relates to the rate of rise and the power exponent (s_2) accounts for any non-linearity in the infill response:

$$T_S = s_1 \times \theta_P^{s2} \quad (5)$$

Experimental: To assess how well the model represents the RTT, tests were conducted under four different normal loads of 451 N (FIFA standard; Fig. 1), 337 N, 286 N and 114 N. To provide an estimate for μ_{P-S}, the 451 N load was repeated with no studs. 3G turf preparations and all traction tests followed FIFA regulations (Table 1; [2]).

Table 1. 3G turf system tested.

Carpet	Polytan LigaTurf RS+ CoolPlus 260 16/4
Fibres	60 mm monofilament polyethylene
Stabilising infill	2EW sand; 15 kg·m^2 (depth 11±1 mm)
Performance infill	SBR 1–3 mm; 15 kg·m^2 (depth 22±2 mm)
Shockpad	None

RESULTS AND DISCUSSION

Model goodness of fit: The model provided a very good fit to the experimental data (RMSE<0.2 Nm) and consistent values for p_1, s_1, s_2 for fitting up to 30° (Table 2 & Fig. 3). Attempts to go beyond 30° saw rapidly deteriorating fit metrics. Since real boot rotations are typically <10° [3] the presented model appears relevant to player traction. Furthermore, the deteriorating fit beyond 30° suggests that a zone of infill ~13° (or ~10 mm) in front of the studs was affected by stud movement, i.e. the remaining angle through to the initial position of the preceding stud (Fig. 1).

Shear Modulus and Young's Modulus: Values of G ranged from 0.007–0.044 MPa (~2–15% of solid SBR) and E from 1.9–5.4 MPa (~19–54% of solid SBR) across the four normal load conditions (Fig. 4). Fitting a ramp function (from 0 MPa to the solid SBR value) to these values highlights that the surface response is highly sensitive to normal stress, particularly in relation to the compressive stiffness of the SBR infill (E in stud ploughing resistance). It is also of interest to note that the FIFA test operates at a normal stress of ~10% of those during real boot–surface interactions [3].

Table 2. Summary of the model fit parameters.

Load (N)	Plate (eq.(3))		Studs (eq.(5))		RMSE (Nm)
	p_1 (1/°)	μ_{P-S} (-)	s_1 (Nm/°)	s_2 (-)	
451	0.413	-	1.678	0.793	0.172
337	0.206	-	1.636	0.712	0.191
287	0.164	-	1.448	0.649	0.156
114	0.091	-	1.030	0.604	0.057
451 NS*	0.464	0.319	-	-	0.164

* NS = no studs on base plate

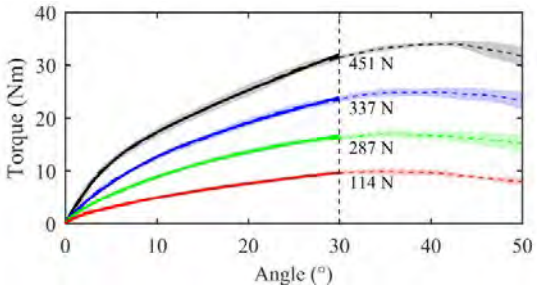

Figure 3: Model fit (solid lines) to experimental data (dashed lines) from 0° to 30° for the four normal loads.

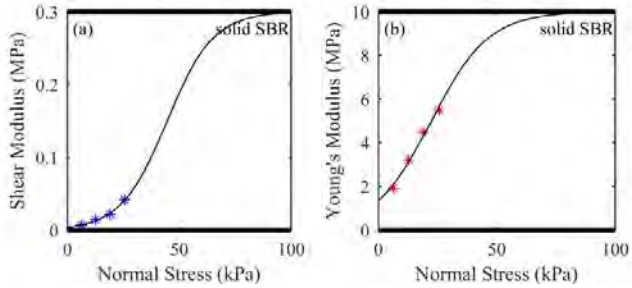

Figure 4: SBR infill: (a) G and (b) E vs. normal stress. * = model values; black lines = ramp function.

CONCLUSIONS

An analytical model for the traction forces during a FIFA RTT on 3G turf has been developed by considering the independent contributions of the plate–surface and stud–surface interactions. The model provides a good fit to experimental data for angles up to 30°. Thereafter, stud interaction effects occur which have not been included in the model. The predicted Young's Modulus for the SBR infill highlights the rapidly stiffening response with increasing normal stress which may have important implications for real boot–surface interactions.

REFERENCES

1. Lacovelli *et al. Br J Sports Med*, *47*, pp.789, 2013.
2. FIFA. *Quality Concept: Handbook of Test Methods*. www.fifa.com, 2015.
3. El Kati, R. *PhD Thesis*, Loughborough University, 2012.

A COMPARISON OF TOTAL BODY BAND-RESISTED EXERCISES ON GLUTEUS MEDIUS ACTIVATION

Kenzie B. Friesen, Kyle W. Wasserberger, Jessica L. Downs, Jessica K. Washington, Teasie K. Williams, and Gretchen D. Oliver

Auburn University, Auburn, AL, USA
email: gdo0001@auburn.edu, web: www.sportsmedicineandmovement.com

INTRODUCTION

Gluteus medius (GM) weakness can be a precursor for lower extremity pain through differed joint loading patterns and altered mechanisms of control [1]. As gluteal muscles strengthen, they can provide the necessary joint stability to resist injury [1] and help stabilize the pelvis [2, 3]. Such exercise programs focusing on gluteal muscle strength and activation may help with injury prevention and rehabilitation.

Jagger bands are a functional and widely used tool for warm-ups in throwing athletes. While Jagger bands are already popular in preparing overhead throwing athletes' upper extremities for activity, the use of such bands may also contribute to higher muscle activation of the lower body, thus preparing the lower extremity for activity as well. Gluteal muscle activation has been directly related to throwing velocity [2], and should therefore be considered during Jagger band warm-ups. Therefore, the purpose of this study was to compare the activation patterns of four preparatory total body exercises on bilateral GM muscle activation with and without the use of Jagger bands.

METHODS

Thirteen healthy and active individuals (177.4 ± 10.2 cm; 76.4 ± 14.2 kg; 21.8 ± 2.4 years) regardless of sex participated. Healthy was defined as having no history of upper or lower extremity injury within the past six months. Active was defined as 30 minutes of physical activity for most days of the week. The University Institutional Review Board approved all testing protocols.

Muscle activation data were collected using surface electromyography (sEMG). Following electrode placement, %MVIC data were measured using three, five-second manual muscle tests (MMTs). One investigator performed all electrode placements and MMTs. sEMG data were normalized as a percent of participant's maximum voluntary isometric contraction (%MVIC) prior to analysis.

Following the collection of %MVIC data, participants performed four total body exercises with and without Jaeger resistance bands (Jaeger Sports, Los Angeles, CA). The exercises performed were: airplane (AP), overhead squat (OH), lunge with "W" arm hold (WL), and single leg Romanian dead lift with horizontal row and external rotation (RDL). The OH, WL, and RDL were performed for one set of five repetitions. The AP was performed for one set of six repetitions. The first and last repetitions were excluded during statistical analyses. Ranges for muscle activation were defined as follows: low (<20% MVIC), moderate (21-40% MVIC), high (41-60% MVIC), and very high (>61% MVIC). All statistical analyses were performed using IBM SPSS Statistics 22 software (IBM Corp., Armonk, NY) with an alpha level set a priori at $\alpha = 0.05$.

RESULTS AND DISCUSSION

Prior to analysis, Shapiro-Wilk tests of Normality determined that muscle activation data were non-normally distributed and thus were transformed using a logarithmic transformation. A within-subjects 2 (muscle) x 2 (condition) x 4 (exercise) repeated measures ANOVA was used to identify significant differences between conditions and bilateral GM muscle activation during the four exercises. There were no statistically significant three-way interactions between muscle, exercise, and condition ($F = 1.416$, $p = 0.26$) (Figure 1). There was a statistically significant interaction between muscle and exercise. Post hoc pairwise comparison showed

that the RDL elicited the greatest activation of the GM. Dominant GM during the RDL had greater activation than the AP (p <0.001) and the WL (p <0.001). Non-dominant GM during the RDL had greater activation compared to the AP (p = 0.004) and the OH (p = 0.04) but not the WL (p = 0.68).

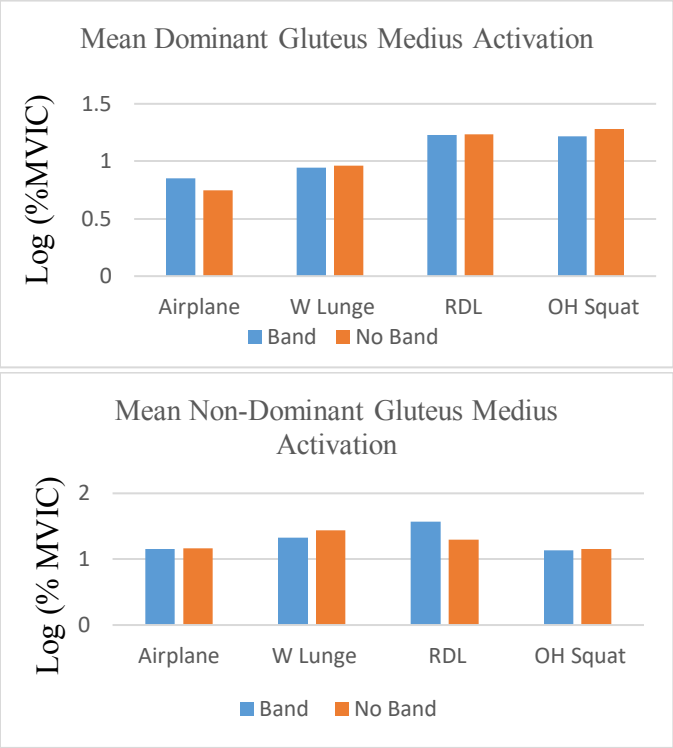

Figure 1: Log normalized means of dominant (top) and non-dominant (bottom) GM.

The results of this study indicate no significant increases of bilateral GM muscle activation during any of the four total body exercises. However, there were significant differences in muscle activation levels between exercises, particularly the RDL.

CONCLUSIONS

Literature suggests that the GM of the non-dominant leg acts as a point of stabilization for the femur and pelvis during weight bearing activities [3]. Overhead throwing requires a sequential pattern of movement involving the planting of the non-dominant leg prior to the release of the ball. Pelvis stability is a crucial link, connecting the lower extremity to the upper extremity. Thus efficient muscle activation of pelvic stabilizing muscles such as the GM is needed for adequate energy transfer for overhead throwing activities. Though much of the current research focuses on pre-game warm-up routines of the upper-extremity, the importance of lower extremity mechanics in throwing should prompt future research of lower extremity integration in pre-game total body warm-up routines. Specifically, the RDL should be considered in such programs since it produced statistically significant activation differences in both dominant and non-dominant GM. Additionally, future studies should investigate other exercises to determine if Jagger bands can increase muscle activations during different loading patterns in the dominant and non-dominant GM.

Limitations of this study include movement artifact with the sEMG because of the dynamic nature of the exercises, as well as the possibility of muscle crosstalk.

REFERENCES

1. Distefano et al. J. Orthop. Sports Phys. Ther. 39(7), 2009.
2. Oliver, G. Med. Biol. Eng. Comput. 52, 2014.
3. Gottschalk et al. Journal of Anatomy. 166, 1989.

Table 1: Means and standard error for non-transformed bilateral GM activation.

	Dominant Glute Med		Non-Dominant Glute Med	
	Band (%MVIC)	No Band (%MVIC)	Band (%MVIC)	No Band (%MVIC)
AIRPLANE	13.3 ± 3.60	9.46 ± 2.35	27.7 ± 8.80	26.8 ± 8.16
W LUNGE	13.6 ± 2.90	14.1 ± 2.88	40.2 ± 13.20	50.8 ± 16.10
RDL	27.7 ± 6.99	26.6 ± 5.24	57.2 ± 13.40	49.0 ± 13.10
OH SQUAT	28.1 ± 8.41	31.9 ± 10.50	28.4 ± 10.00	28.6 ± 10.3

EFFECT OF LATE TRAINING SESSIONS ON RECOVERY: A STUDY OF HEART RATE VARIABILITY IN WOMEN'S SOCCER

[1] Kayla Grotelueschen, [2] Devin Clark, and [1] Reva Johnson

[1] Valparaiso University, Valparaiso, IN, USA
[2] Zimmer Biomet, Warsaw, IN, USA
email: reva.johnson@valpo.edu
web: valpo.edu/college-of-engineering/reva-johnson

INTRODUCTION

Recovery is an essential component of training for all athletes. The physiological stresses of workouts and competition must be balanced with recovery that allows the body to adapt. One important factor in recovery is the timing and frequency of training sessions.

Recovery is governed by the autonomic nervous system and can be estimated by measuring heart rate variability (HRV) [1]. Parasympathetic activity increases HRV; sympathetic activity decreases HRV. Parasympathetic activity drives recovery, so recovery is associated with increased HRV. When monitoring athletes, low HRV can be used as a warning sign for inadequate recovery or high stress.

Inadequate recovery can lead to overtraining and injuries, which are particularly frequent in women's soccer [2]. Inadequate recovery is also a primary concern for collegiate athletes, who sometimes struggle with suitable nutrition and sleep. Most collegiate programs have fewer resources than professional sports organizations, which can result in training sessions very late or very early in the day. We hypothesized that late or early training sessions can negatively affect recovery in collegiate athletes.

In this study, we focused on one potential cause of inadequate recovery: beginning training sessions after 8:00pm. We used heart rate analyses to investigate the effect of late training sessions on the recovery of female collegiate soccer players.

METHODS

De-identified heart rate data was obtained from the training records of an NCAA Division I women's soccer team. Heart data had been recorded during all training sessions, matches, and daily recovery tests over a time period from April 2015 to May 2016. During that period, the team's training records included 27 women between the ages of 18 and 22. All heart rate data was recorded using Firstbeat heart rate belts and pre-processed using Firstbeat Sports algorithms (Firstbeat Technologies Oy; Jyväskylä, Finland).

A Recovery Index was calculated from each player's daily recovery test: five minutes of heart rate data recorded soon after waking up each day. The Recovery Index is a function of heart rate and heart rate variability, and is normalized to each individual's maximum score [3]. The scores are interpreted as shown in Table 1.

Table 1. Suggested interpretations of Recovery Index	
0- 30%	Poor
30-70%	Moderate
70-90%	Good
90-100%	Excellent

Because training load or intensity also affects recovery, our analysis considered the training load of each session. Training load was estimated using a metric called Training Impulse (TRIMP) [4]. A TRIMP score was recorded for each player in every training session studied.

The timing of training sessions was categorized into late training sessions and normal training sessions. Sessions starting after 8:00pm were considered late training sessions. All other sessions were considered normal training sessions.

To compare recovery after normal and late practices while controlling for training intensity, we used a

one-way analysis of covariance (ANCOVA). The dependent factor was the Recovery Index on day $(i+1)$. The independent factor was a binary variable indicating normal or late training session on day (i). The independent covariate was the training load index (TRIMP score) of the session on day (i).

RESULTS AND DISCUSSION

Figure 1 shows that the Recovery Index was significantly lower on the day after late practices, compared to the day after normal practices ($F = 5.737, p = 0.0168$). After controlling for training load, the mean Recovery Index on the day after late training sessions was 37.1%, whereas the mean Recovery Index the day after normal training sessions was 45.3%.

Training load, as measured by TRIMP scores, also had a significant effect on the Recovery Index ($F = 4.551, p = 0.0332$). This result is consistent with others that show that an increased training load decreases heart rate variability although there have been other conflicting results [1].

The decreased recovery after late practices could be due to several factors. One factor may be that the late practices cause a lack of sleep, which decreases recovery. Sleep is known to affect athletic performance; however, the relationship between sleep and recovery is not as well studied [5]. Another factor may be that the decreased recovery is caused by a shorter time between the late training session and the five-minute recovery test, which was typically applied in the morning.

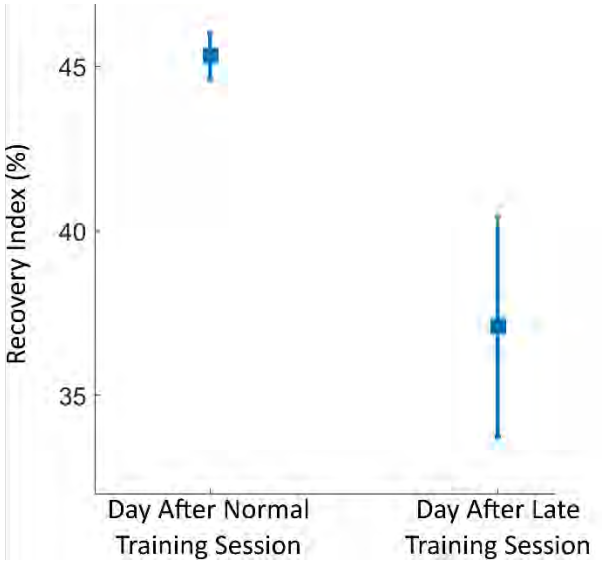

Figure 1: When players trained after 8pm, their average recovery was lower by 8.2% on the following day. This plot shows the adjusted mean Recovery Index scores after controlling for training load. Bars indicate standard error of the adjusted means.

There are several limitations of this preliminary study. First, we estimated recovery with heart rate data recorded over only five minutes in uncontrolled conditions (athletes independently recorded data for five minutes each morning). Second, we hypothesize that sleep quality, sleep duration, and nutrition quality (especially after training sessions) may be confounding variables. Third, we focused on collegiate female soccer players, and it is unclear how our results generalize to broader populations.

CONCLUSIONS

Our results suggest that late training sessions (past 8pm) caused decreased recovery after training for collegiate female soccer players. We plan to further investigate the relationship between sleep and recovery in several ways: continuously monitoring heart rate, recording sleep quality and duration, and documenting nutrition after training sessions.

REFERENCES

1. Plews *et al.*, *Sport. Med.* **43** (2013).
2. Yang *et al.*, *J. Athl. Train.* **47** (2012).
3. Firstbeat, "Recovery Analysis for Athletic Training Based on Heart Rate Variability" (2015).
4. Banister, in *Physiological testing of elite athletes* (1991).
5. Fullagar *et al.*, *Int. J. Sports Physiol. Perform.* **10** (2015).

ACKNOWLEDGEMENTS

The authors thank John Marovich for his collaboration and coaching perspective; and thank Morgan Manzke, Lauren Uhlean, and Bailey Flemming for their literature review.

Determining Kinematics Parameters that Dictate Successful Completion of the Hurdle Step Functional Movement

[1]Kathryn Harrold, [1]Rachel Noel, [2]Kelly Helm,
[3]Luis Prato, [4]Anthony Levenda, and [1]Craig M. Goehler

[1]Department of Mechanical Engineering and Bioengineering, Valparaiso University, Valparaiso, IN, USA
[2]Department of Kinesiology, Valparaiso University, Valparaiso, IN, USA
[3]Incremedical, Portage, IN, USA
[4]Lakeshore Bone and Joint Institute, Chesterton, IN, USA
email: craig.goehler@valpo.edu

INTRODUCTION

The Functional Movement Screen (FMS) assesses the quality of movement in athletes to determine if the athlete could be at risk for injury [1]. Jenkins et al. analyzed correlations between the FMS screening and hip mobility. They found that, "when used as part of a pre-season screening, the FMS can be used to determine potential functional limitations that may place an individual at risk for future injury." [2]

Traditionally the FMS is scored qualitatively on a scale from 0-3, where a "0" signifies that the athlete being evaluated experienced pain and a "3" signifies that the athlete was successful in the completion of the task without any compensation. The overall goal of this study is to create a metric to quantitatively assess risk of injury in the knees and hips using successful completion of the FMS hurdle step test.

METHODS

For this abstract, 16 subjects from the Valparaiso University swim and tennis teams (9 male and 7 female) aging from 18 to 22 years old participated in an IRB approved study by completing a Functional Movement Screen (FMS). Each subject was affixed with 28 passive reflective markers on the upper and lower extremity using hypo-allergenic adhesive. The markers were placed based on anatomical locations specified by a previously created musculoskeletal model [3]. The subjects completed a series of tests which included the hurdle step. Each test was performed three times.

To perform a hurdle step test, a measurement of the subject's tibia is taken to determine the height of the marking cord connecting the hurdle uprights. The subject is then asked to stand directly behind the hurdle base with their feet together and to hold the dowel across their shoulders below their neck. The subject is then instructed to step over the hurdle with one leg while balancing their weight on the stance leg. They must touch their heel on the ground in front of the hurdle while maintaining an upright posture and return their heel back to starting position.

The three dimensional position data from each of the subject's trials were processed and filtered in VICON Nexus. The resulting output files were converted to be compatible with OpenSim. In OpenSim, a scaled model of each subject was created. The subject specific model was then used to determine the inverse kinematics of the subject's hurdle step movements.

RESULTS AND DISCUSSION

The resulting joint kinematics from 11 swim and 5 tennis team subjects performing left and right hurdle steps were analyzed and compared. Hip and knee flexion were plotted versus time using a single trial from each of the subject's hurdle step tests (Figures 1 and 2). A chain connection of the sagittal plane movements relating the hip and the knee flexion during a hurdle step can be observed across all subjects. When the hip is maximally flexed, there is a corresponding knee flexion that allows the subject to clear the marking cord. A range of values denoting successful completion of the task was calculated by

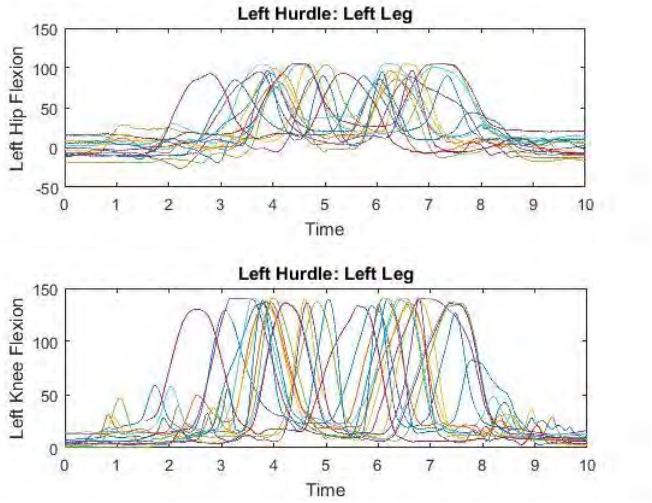

Figure 1: Left hurdle hip and knee flexion

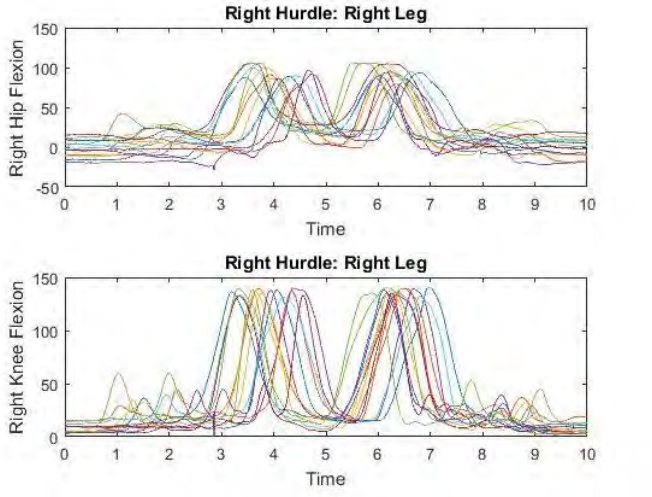

Figure 2: Right hurdle hip and knee flexion

determining the mean and standard deviation of all subjects' maximum hip flexion and the corresponding knee flexion (Table 1). Since there were no statistically significant differences between the ranges for right and left hurdle steps, an overall metric was calculated. The overall ranges of hip and knee flexion to successfully complete a hurdle step were calculated to be 87.2-102.7 and 113.5-126.8 degrees respectively.

This metric has the potential to be used as an indicator for risk of injury. Generally a tear in the medial collateral ligament (MCL) causes laxity in knee flexion [4]. A subject with a knee flexion value below the overall range in Table 1 may be an indicator of MCL tightness which in turn could suggest that the ligament is on the verge of tearing. This "red flag" could provide this athlete an opportunity to see a physical therapist or athletic trainer that can then design appropriate exercises for the athlete to minimize or even prevent future injury.

Additionally, a metric of this fashion which combines the ranges of hip and knee flexion needed to successfully complete a hurdle step can be used for older patients working on regaining or improving their lower extremity function through physical rehabilitation. Quantitatively using measurable variables instead of qualitatively using the hurdle and marking cord would reduce the risk of injury caused by incidences such as their foot getting caught on the marking cord causing them to stumble or fall.

While this method is a start to determining the range of hip and knee flexion necessary for a healthy athlete to successfully complete the hurdle step, a wider array of degrees of freedom must be considered. These remaining degrees of freedom could potentially allow better insight into how joints, other than the hip and knee, are used for compensation and to maintain balance. In the future the same process will be used to create similar metrics to quantify the landing error scoring system and box jump tasks.

REFERENCES

1. Cook G, et al. *International Journal of Sports Physical Therapy.* 9(3) 2014.
2. Jenkins, M, et al. *International Journal of Exercise Science* 10.4 2017.
3. Koehn R, et al. Annual Meeting of ASB 2016.
4. Chen L, et al. *Current Reviews in Musculoskeletal Medicine.* 1(2) 2008.

Table 1: The ranges of hip and knee flexion that represent successful completion of the left and right hurdle steps along with a combined overall metric to be used for the leading leg in either hurdle step test.

	Hip Flexion		**Knee Flexion**	
Test	Minimum	Maximum	Minimum	Maximum
Left Hurdle Step	86.9	102.6	113.7	128.6
Right Hurdle Step	87.3	102.9	113.5	124.6
Overall Hurdle Step	87.2	102.7	113.5	126.8

INVESTIGATING THE COMPLEXITY OF MOVEMENT PATTERNS DURING AMERICAN FOOTBALL COMPETITION

Ryan M. Hasenkamp and Jack W. Ransone

University of Nebraska, Lincoln, NE, USA
email: rhasenkamp@huskers.edu

INTRODUCTION

Dr. Yuri Verkhoshansky described sport competition as a problem-solving task which athletes must solve with movement solutions [1]. Thus, a holistic understanding of athletes' movement patterns during sport competition may lead to effective strategies in athletic development, preparation, and rehabilitation.

Dr. Nikolai Bernstein presented two major challenges in the study of human movement [2]. First, the human system has many redundant degrees of freedom available for which it may use to execute a given movement. How do we select which degrees of freedom to utilize during a given task (degrees of freedom problem)? Furthermore, how do we execute a movement task under complex external conditions which are constantly changing (context variability)?

Insight from motor control theory such as the Constraints-Led Approach from the work of Dr. Karl Newell suggests that movement outcomes emerge as a self-organizing process based upon constraints from the task, the individual, and the environment [3]. This is opposed to traditional, reductionist views of motor control in which the sum of the parts equals the whole: where large factors produce large outcomes and small factors produce small outcomes. Rather, human movement is a complex system where small, seemingly insignificant factors may play a large role in the outcome [2,3,4].

An American football game may be considered a complex, dynamical system as well. Over the course of competition, each play will not exhibit the same characteristics as each other, rather each one will present its own unique characteristics. While any particular play outcome may appear to a random occurrence, closer investigation may reveal a complex, ordered structure (where future events are uniquely correlated to past events i.e. the butterfly effect). During competition, the athlete must coordinate his movements to navigate the rich sport environment in order to achieve his goal.

Fractal analysis techniques are capable of identifying patterns within data series. One of these techniques, the detrended fluctuation analysis (DFA), is capable of demonstrating long-range correlations across different time scales in a time series, which is typical of complex systems. Such analysis of players' movement patterns during a competition may provide novel information about the athlete's performance. The purpose of this investigation is to determine the complexity, as quantified by long-range correlations through DFA, of movement patterns for an American football player during competition throughout a competitive season.

METHODS

The movement patterns for a single D-1 Collegiate athlete, a quarterback, were analyzed for each competition throughout a 12-game competitive season. Movement patterns were measured using a wearable GPS tracking system (Catapult, Chicago, IL). Raw resultant player accelerations (100 Hz) were analyzed to represent the player's movement patterns. The presence of long-range correlations over a wide range of time scales was evaluated by the scaling exponent, α, using DFA. The subject completed a consent form approved by University Institutional Review Board.

RESULTS AND DISCUSSION

Analyzed time series demonstrate self-similarity where seemingly repeated structures occur on smaller time scales (Fig. 1). These self-similar structures are demonstrated in the DFA calculation and resultant log-log plot with the scaling exponent, α (Fig. 2).

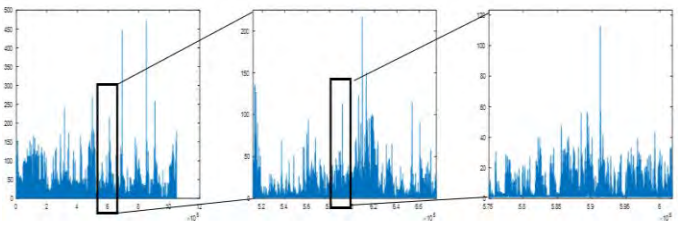

Figure 1: Time series of player acceleration, when magnified reveals self-similarity where a seemingly repeated structure occurs at smaller time scales.

Over the course of an entire season, the calculated scaling exponent resulted in an average of $\alpha = 0.90 \pm 0.01$, with individual game values shown (Fig. 3). In fractal analysis, noise colors describe the structure of a time series. White noise is said to represent random, incoherent movement. Brown noise is overly-constrained, periodic movement. Pink noise represents complex movement that is ordered and flexible and is representative of healthy human biology [4]. In terms of the scaling exponent, white noise is found near $\alpha = 0.5$, and brown noise is found near $\alpha = 1.5$. Pink noise is found near $\alpha = 1.0$ and may encompass values of $\alpha = 0.7 - 1.2$ [4]. Our values fall within the range of pink noise, meaning that there are persistent fractal correlations within our data set. This indicates that an increasing trend in acceleration is eventually followed by a similar increasing trend in acceleration. This finding thus, supports the notion that American football competition may be modeled as a complex system and provides quantification for the complexity through the scaling exponent $\alpha = 0.90 \pm 0.01$.

This complexity is thought to allow for flexibility and adaptability in an unpredictable environment.

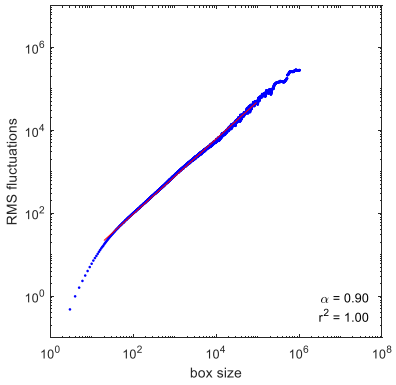

Figure 2: The scaling exponent, α revealed as the slope of the log-log plot from the DFA calculation.

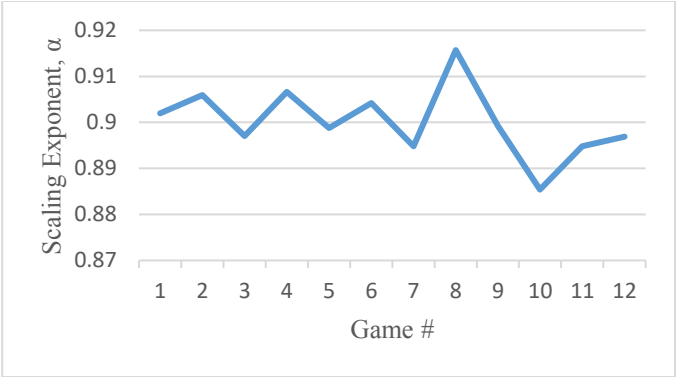

Figure 3: α values for individual games.

For a quarterback, each play presents its own unique dynamics for which he must adapt. Even if the exact same play is run, there will be unique aspects to the play that are different and unpredictable at some scale. Having access to an adaptable repertoire of movement solutions from which he can choose allows the quarterback to be able to perform within the complex environment that is the competition.

The implications of this finding may be far-reaching. Further research may investigate players of different skill level, positions, health, practice strategies, etc. However, before any of these avenues are explored it was necessary to first, establish the complexity of typical competition as has been done here.

CONCLUSIONS

This investigation reveals that an American football player's movement patterns during competition, as assessed by acceleration, demonstrates robust fractal correlations as characterized by the DFA scaling exponent $\alpha = 0.90 \pm 0.01$, supporting the idea of sport competition as a complex, dynamical system.

REFERENCES

1. Verkhoshansky, Y. *Supertraining*, Yerkhoshansky SSTM, 2009.
2. Bernstein N.A. *The co-ordination and regulation of movements*. Pergamon Press, 1967.
3. Newell, K. Constraints on the development of coordination. *Motor development in children: Aspects of coordination and control*, 1986.
4. Stergiou, N. *Nonlinear analysis for human movement variability*. CRC Press, 2016.

EFFECTS OF FINGER TAPING ON FOREARM MUSCLE ACTIVATION IN ROCK CLIMBERS

Julianna J. Johnson, Brynne C. Dyke, Gary D. Wiley Jr., Jun G. San Juan

Western Washington University, Bellingham, WA, USA
email: johns888@wwu.edu

INTRODUCTION

The increase of popularity of rock climbing has also led to prevalence of overuse injuries, with most common injury being of the hand and wrist [1]. Specifically, a flexor tendon pulley injury has become a large portion of rock climbers' injury, found in about 26% of competitive climbers [2,3].

The mechanism of a flexor tendon pulley injury or rupture in the fingers is a resultant of the flexor tendon sheath surrounding the Flexor Digitorum Superficialis (FDS) and Flexor Digitorum Profundus (FDP) muscles. Specific hand positions, such as the crimp position of hyperextension of distal interphalangeal joint and flexion at the proximal interphalangeal joint create this high force on the tendon pulleys [4,5].

Remarkably, various taping techniques among competitive rock climbers have been gaining recognition for reduction of this overuse injury. Recent studies on cadavers show the decrease in force applied to the tendon pulleys [6].

The purpose of this study was to investigate the effects of taping on muscle activation in the FDS and FDP muscles. With the understanding that the increase of the FDP in the crimp position is associated with flexor tendon pulley injury [7]. Two taping techniques were used based on previous studies [6,8].

METHODS

Thirteen subjects (20.9 ± 1.73 years; 1.83 ± 0.07 m; 70.9 ± 6.26 kg) participated in the study. Inclusion criteria of the study was for the climbers to had at least six months or more of climbing experience, along with climbing at least two hours a week, accomplishing a V4 level climbing route.

The following protocol was standardized for all participants. Two different sets of climbing holds were placed at a distance of 0.91 m apart and 1.22 m above the ground (Fig 1). A relative voluntary contraction (RVC) was done while performing isometric holds on a 7.0 cm wide, 2.0 cm lip and protruded 4 cm from the wall, large hold. The crimp position holds were 5.0 cm wide and protruded 2.0 cm from the wall.

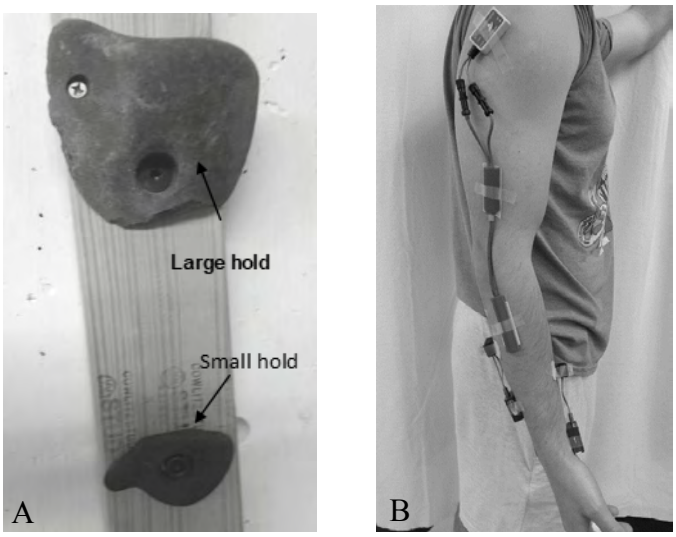

Figure 1. A) Large (used for warm-up and RVC trial) and small (used for experimental trials) holds. B) Subject with both EMG electrodes and electrogoniometer in correct positions.

Electromyography of FDS and FDP muscles were used to assess muscle activation at a frequency of 1500 Hz with a gain of 500 and CMRR > 100 dB. Electrodes were placed intramuscularly with a 27ga. 30 mm-paired wired for FDS and 25 ga. 50 mm-paired wires for FDP. An electric goniometer was also used for angular displacement of the elbow (Figure 1).

After placement of electrodes, subjects did an isometric hold with elbow flexion between 85 and 95 degrees on the large holds for 6 seconds to normalize

the EMG (RVC), followed by a 3-minute rest. This was then followed by 3 randomized trials of crimp position isometric holds with H-tape, circular tape or no tape on the subjects' middle and ring fingers, also for 6 seconds with 3-minute rests in between.

Two-way repeated measures ANOVA was used to determine significance between taping conditions and muscles for both average and peak activation values. Alpha level was set at 0.05.

RESULTS AND DISCUSSION

Average peak muscle activation of FDS and FDP muscles are in Table 1. Analysis revealed no significant interaction effect of taping condition and EMG muscle level ($F[2\text{-}18] = 0.225$, $\eta_p^2 = 0.024$, $p = 0.801$). Taping did not have a significant effect on average relative muscle activation of FDS and FDP muscles ($F[2\text{-}18] = 3.122$, $\eta_p^2 = 0.257$, $p = 0.069$). There was also no significant difference between FDS and FDP muscle during experimental trails ($F[1\text{-}9] = 0.053$, $\eta_p^2 = 0.006$, $p = 0.822$). No significant difference were found between the peak muscle activation of FDS and FDP muscles ($F[1\text{-}9] = 0.159$, $\eta_p^2 = 0.040$, $p = 0.699$), or peak relative muscle activation of FDS and FDP ($F[2\text{-}18] = 0.511$, $\eta_p^2 = 0.054$, $p = 0.608$).

Although previous studies have shown an increase in activation of the FDP and decrease in activation of FDS with the crimp position [7, 8], it was not found to be significant in the current study. Current study also did not find significance of the FDP tendon to have higher percent tension than in the FDS which does not support previous research [7]. In contrast, taping techniques used in the current study did support a previous finding of no significant decrease in the A2 pulley tendon [8] with either taping technique.

CONCLUSIONS

Results of this study suggests that taping fingers may not affect relative muscle activation of the FDS and FDP in an uninjured climber when executing a static hold in a crimp hand position. Effectiveness of the taping for the use of prevention of a flexor tendon pulley injury is not supported by the results of the study, but primarily due to the limitations of the study via testing procedure and subject demographics. Future research should continue to investigate the effect of taping on muscle activation during dynamic holds.

REFERENCES

1. Maitland. *J Orthoped Sports Phys Ther*, 16(2), 68-73, 1992.
2. Rohrbough et al. *Med Sci Sports Exerc*. 32(8), 1369-1372, 2000.
3. Bollen et al. *Br J Sports Med*. 24(1), 16-18, 1990.
4. Sheikh et al. *Plastic Surgery* 14(4), 227-231, 2006.
5. Schweizer, et al. *J Biomech*, 34(2), 217-223, 2001.
6. Schweizer. *J Hand Surg: Br Europ. V*, 25(1), 102-107, 2001.
7. Vigouroux et al. *J Biomech,* (14), 2583-2592, 2006.
8. Schöffl et al. *J Appl Biomech*, 23(1), 52-62, 2007.

Table 1: Mean peak muscle activations (% RVC) of the FDS and FDP muscle under all conditions.

Muscles	No Tape	H-Tape	Circumferential Tape
Flexor Digitorum Superficialis	125.5 ± 72.6	140.6 ± 75.8	124.6 ± 50.8
Flexor Digitorum Profundus	125.5 ± 65.9	127.3 ± 42.2	123.9 ± 73.8

Developing Methods of Fatigue Analysis and Injury Prevention in Baseball Pitchers: A Study Using Motus Sensors

Chet Joslyn, Jacob Larson, Wes Gordon, and Craig M. Goehler

Department of Mechanical Engineering and Bioengineering, Valparaiso University, Valparaiso, IN, USA
email: craig.goehler@valpo.edu

INTRODUCTION

Elbow injuries are the most common injury in baseball [1]. However, there are no current rules or regulations in the NCAA regarding a pitcher's inning limit or pitch count. Coaching staff judgement and traditional knowledge of pitcher fatigue is used to determine when to remove a pitcher from a game as well as how to train a pitcher during practice. These traditional methods of predicting pitcher fatigue are outdated, inaccurate, and place pitchers at unnecessary risk of injury. By using the MotusTHROW sensor, a more statistically reliable system can be developed to determine fatigue and avoid injuries for future generations of baseball players.

The MotusTHROW sensor is an Inertial Measurement Unit (IMU) which reports arm slot (angle of the forearm relative to the ground at pitch release), arm speed (peak rotational velocity of the forearm measured as RPM), shoulder rotation (maximum external rotation of the forearm relative to the ground), and elbow stress (the peak torque in Nm placed on the UCL during the pitch near the time of maximum shoulder rotation) [2].

Our study attempts to show that elbow stress variation over time can be used as a method of indicating fatigue and potential injury due to a change in pitching mechanics. A pitcher's throwing mechanics will correlate to a torque that is consistent as long as their mechanics are consistent. This trend over time of an individual pitcher's elbow stress could correlate to the health of that pitcher.

METHODS

For this study, 6 male subjects from the Valparaiso University Men's Baseball team ranging from 18 to 22 years of age, participated in an IRB approved study that utilized the MotusTHROW sensor to collect data for arm slot, arm speed, shoulder rotation, and torque.

Each subject was asked to wear a MotusTHROW sensor on their throwing arm each time they threw a baseball. The subjects were studied during an off-season time period during which simulated games, individual bullpens, and day-to-day catch was recorded. Using the output information from the Motus Dashboard, torque (Nm) was analyzed using MATLAB and plotted as a function of pitch count during individual bullpen sessions.

Data for this experiment was collected without interference to a normal practice schedule. Due to the nature of a collegiate baseball practice, the pitchers were not able to tag each individual throw but rather all throws from that day as having occurred during the same session. Only being able to tag a throwing session as one form of throw means that catch on a day where that pitcher threw a bullpen will be tagged as a bullpen. This causes our data to capture the steady increase in torque during the "warm-up" portion of the bullpen, rather than a pitcher

immediately throwing at his typical bullpen level torque.

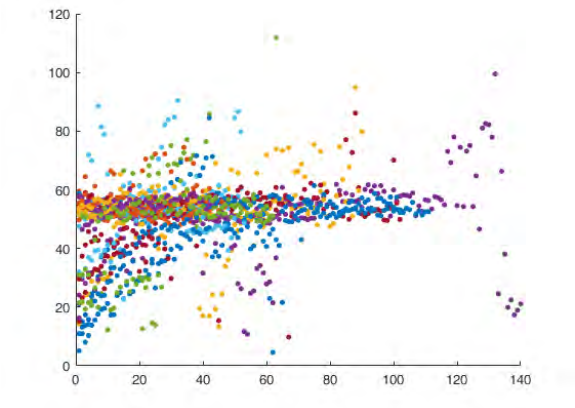

Figure 1: Subject 1 Torque (Nm) vs Bullpen Pitch Count

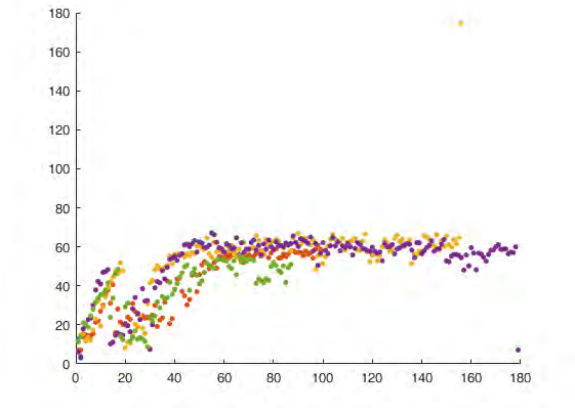

Figure 2: Subject 2 Torque (Nm) vs Bullpen Pitch Count

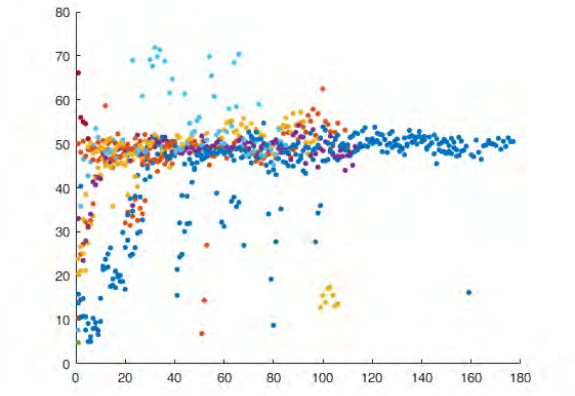

Figure 3: Subject 3 Torque (Nm) vs Bullpen Pitch Count

RESULTS AND DISCUSSION

During our research trials, we saw that pitchers slowly increased their varus torque for the first 30 pitches, after which point their torque values plateaued. This plateau of torque values is what would consider the normal performance torque for a pitcher during a bullpen session. For future studies, we would compare the deviation of torque values to this reference torque. Repeated bullpen sessions over a three month timespan showed that individual pitchers perform in a consistent range of torques which is unique from other subjects.

Figure 1 shows a subject who performs between 50 and 60 Nm; Figure 2 shows a subject who performs between 60 and 65 Nm; Figure 3 shows a subject who performs at approximately 50 Nm. Outliers can be seen in each of the three subjects. These outliers may be due to sensor reading errors or from throws at a low intensity level between pitches. An analysis of this torque over time can be done to show the variation away from the range of torque a pitcher typically performs at. A pitcher may be showing signs of fatigue and increasing his risk of injury as the variation increases or as the mean decreases.

Further testing in a controlled environment could confirm the study's hypothesis that torque variation is a precursor to fatigue and injury in pitchers. By asking pitchers to throw until they fully fatigue, we will be able to compare varus torque to previously established mean torque values. If this hypothesis is confirmed, a proposal to the NCAA Baseball Rules and Regulations Committee would be written to recommend a form of torque monitoring and analysis to be done for all collegiate baseball pitchers to reduce the risk of injury in pitchers.

REFERENCES

1. Contes, S., et al. *Am J Orthop (Belle Mead, NJ)*, 45(3): 116-123, 2016.
2. Bushnell, B., et al. *Am J Sports Medicine,* 38(4): 728-732, 2010

The Effect of Player Performance on Head Impact Exposure in Youth Football

[1]Mireille Kelley, [1]Derek Jones, [2]Christopher Miles, [1]Joel Stitzel, and [1]Jillian Urban

[1]Virginia Tech – Wake Forest University School of Biomedical Engineering and Sciences, Winston-Salem, NC
[2]Wake Forest School of Medicine, Department of Family and Community Medicine, Winston-Salem, NC
email: mekelley@wakehealth.edu

INTRODUCTION

Approximately 5 million athletes play organized football in the United States and youth football athletes make up approximately 70% of participants [1, 2]. The high concussion rate in football has prompted investigations into head impact exposure (HIE), with recent efforts focused on the youth population [1, 3]. Studies have shown that HIE increases with increasing level of play [1, 2]. However, HIE also varies considerably within a single team or level of play [1, 2]. Playing position may account for some of the variation; however, at the youth level, athletes often play a number of positions throughout the season. There are also considerable changes in body size, muscle mass, and physical ability among adolescents [4].

While physical performance measures have been evaluated in youth athletes, the relationship between performance and HIE has not been evaluated [4]. Therefore, the objective of this study was to evaluate the effect of performance measures on HIE in youth football players.

METHODS

This study collected head impact data from athletes participating on three separate youth football teams (A, B, and C). Head impact data were collected using the Head Impact Telemetry (HIT) System for all pre-season, regular season, and play-off practices and games. Video was also recorded for all sessions to confirm the times that the players were helmeted and impacts that occurred while the players were not helmeted were excluded. HIE was quantified in terms of total number of impacts in a season and median/95th percentile linear acceleration, rotational acceleration, and impacts per player per session. The HIE data was evaluated as a whole season and stratified by session type (i.e. practice or game).

Performance testing of athletes was completed in one session after the first week of pre-season conditioning. The performance tests included the vertical jump (VJ), shuttle run (SR), 3-cone drill (3C), and 40 yard sprint (40S). Each athlete completed 3 trials of the VJ and 2 trials of the SR, 3C, and 40S. The best trial from each performance test was used for statistical analysis.

Linear regression analyses were performed to evaluate the relationships between performance measures and HIE metrics of all athletes together and stratified by team. Secondary analyses were also performed to examine the effect of BMI on performance measures and HIE metrics. For each linear regression performed, the Cook's distance of each point was calculated and outliers were removed from analysis. Statistical analysis was performed using SAS version 9.4.

RESULTS AND DISCUSSION

HIE and performance measures were collected from 38 athletes on 3 teams (team A: N=15, team B: N=14, and team C: N=9). A demographic summary of all athletes is shown below (Table 1).

Table 1: Summary of player information stratified by team. Mean ± SD are shown.

	A	B	C
Age	13.3 ± 0.4	12.3 ± 0.6	11.6 ± 0.3
Height (cm)	65.6 ± 3.0	63.2 ± 2.4	58.7 ± 1.8
Weight (lb.)	136.2 ± 18.9	140.9 ± 38.6	97.1 ± 12.3
BMI	22.3 ± 3.3	24.7 ± 6.2	19.7 ± 2.0

There were 10,228 impacts collected during the season. The median [95th percentile] number of impacts per player was 196 [537] impacts. The

median [95th percentile] linear and rotational acceleration was 19.0 g [53.8 g] and 935.5 rad/s^2 [2,484.4 rad/s^2], respectively.

The results from the performance testing are summarized in Table 2. There were no significant associations among performance measures and HIE metrics when evaluating all athletes together. However, the relationship between the shuttle run time and 50th percentile rotational acceleration in practice was nearing significance (p=0.05). Player BMI was significantly associated with 95th percentile linear acceleration (p=0.001, r^2=0.27), median rotational acceleration in games (p=0.04, r^2=0.03), and 95th percentile linear acceleration in practices (p=0.02, r^2=0.16). There were also significant associations among all performance measures and BMI (all p<0.005).

Table 2: Summary of performance testing results stratified by team. Mean ± SD are shown.

	A	B	C
VJ (cm)	47.6 ± 10.3	34.9 ± 6.9	37.6 ± 5.7
SR (s)	5.1 ± 0.4	5.6 ± 0.5	5.4 ± 0.3
3C (s)	8.6 ± 0.6	9.6 ± 1.1	9.1 ± 0.5
40S (s)	5.6 ± 0.5	6.3 ± 0.7	6.0 ± 0.4

Due to variation in HIE and season length between teams, the results were stratified by team, which resulted in a number of significant associations between performance measures and HIE (Figure 1). The strongest relationship within team A was a positive correlation between 3C speed and median rotational acceleration in practice (p=0.001, r^2=0.59). Within team B, VJ height and 95th percentile linear acceleration were significantly positively correlated (p=0.0002, r^2=0.72). The strongest association within team C was a negative correlation between VJ height and median linear acceleration in practice (p=0.004, r^2=0.77).

CONCLUSIONS

This study demonstrates that performance and player size may be predictive of HIE. However, the trends differ by team and level of play. In the older athletes, teams A and B, increased power and agility was associated with increased HIE, whereas the opposite trend was observed in team C, the youngest team. This work is ongoing to include further performance testing and a larger sample size. The influence of other factors such as playing experience and position will be evaluated as well. Improved understanding of the factors that influence a football player's HIE will help in creating strategies to reduce HIE.

REFERENCES

1. Kelley et al. *J Neurotrauma*. 34(11), 2017
2. Cobb et al. *Ann Biomed Eng*. 41, 2013.
3. Bryan et al. *Pediatrics*. 138, 2016.
4. Caswell et al. *Orthop J Sports Med*. 4(8). 2016.

ACKNOWLEDGEMENTS

Research was supported by the NINDS of the NIH under Award Numbers R01NS094410 and R01NS082453. The content is solely the responsibility of the authors and does not necessarily represent the official views of the NIH.

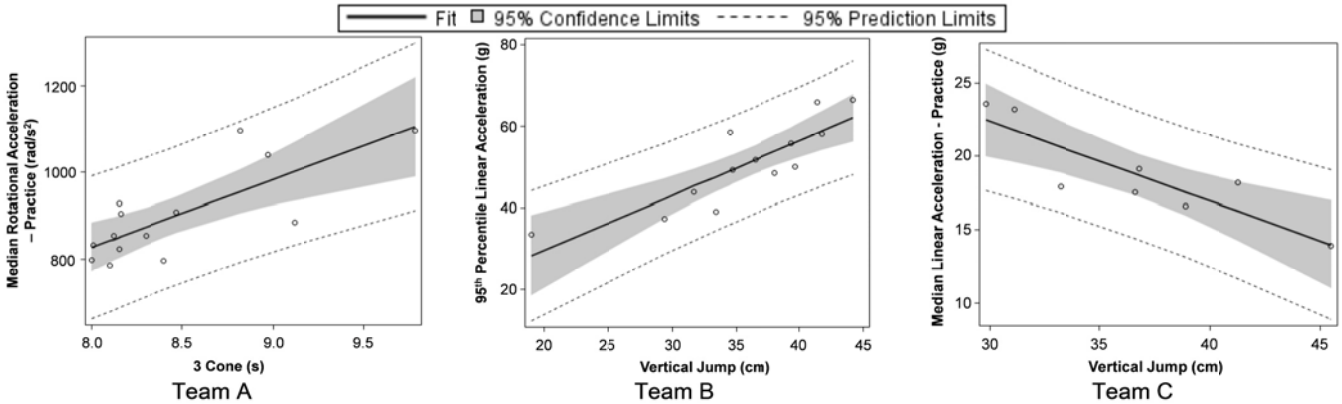

Figure 1: The strongest linear relationship between performance measures and HIE for each team.

Quantifying Human Motion in Swimmers using Inertial Measurement Units

Casey Main, Jacqueline Kitten, and Craig M. Goehler

Department of Mechanical Engineering and Bioengineering, Valparaiso University, Valparaiso, IN, USA
email: craig.goehler@valpo.edu

INTRODUCTION

The current methods for quantifying human motion in swimmers are not as advanced as those implemented for other athletes. While runners have a variety of sensors that can be attached to their body to measure joint flexure and gait, it is increasingly difficult to measure parts of the swim stroke due to the lack of waterproof sensors, and some sensors that are waterproof tend to be invasive in that they affect the stroke of the swimmer. The most common method for evaluating swimmers is qualitative observation from the pool deck and timing with a stopwatch [1], which is heavily influenced by refraction of light from the water and very unreliable. Current quantitative methods of measuring the biomechanics of swimmers include the use of Computational Fluid Dynamics to measure drag coefficients [2], tether cords to measure force [3], waterproof EMGs for muscle activation [4] and inertial magnetic measurement units for joint flexion [5], and accelerometers [6] in wearable technology to count strokes and laps.

The main objective of this study was to use a minimally invasive sensor to obtain basic "gait" patterns of swimmers swimming the front crawl. By identifying a general pattern across multiple swimmers, a base pattern can be determined and variations from that pattern can be identified and addressed. Also by identifying a general pattern, it may be possible to see if common variations from the pattern prove beneficial to certain types of events such as distance events or sprints.

METHODS

To determine the gait of front crawl, eleven female collegiate swimmers were gathered to swim a length of 200 yards (8 lengths), each with a Gait Up Physilog®5 motion sensor clipped to the back of her suit. These waterproof sensors measure acceleration in Cartesian coordinates along with gyration about each axis, pressure, and temperature. Participants were instructed to swim the 200 yards as if it were a warm-up, then to exit the pool so that the sensor could be removed.

The data from the sensors was then uploaded to the Physilog® software to display graphs from the accelerometer, gyroscope, pressure transducer, and thermometer. From the graphs, each swimmer's stroke count per lap could be determined along with the magnitude of rotation, the duration of time spent underwater after the flip turn, the quantity and magnitude of underwater dolphin kicks, and the sharpness of the turn. In addition, the data was uploaded to MATLAB for further analysis. Through MATLAB, the peaks in data can be more precisely visualized to determine how arm movement affects body rotation, average magnitude of rotation, motion forward per rotation, movement in other axes, effectiveness of underwater dolphin kick, and how breathing can affect body rotation.

RESULTS AND DISCUSSION

The front crawl gait can be characterized through periodic motion. The general pattern resembles a sine wave, as seen in Figure 1. However, there were variations across the eleven swimmers analyzed. For instance, two swimmers had a gallop in their stroke which means that their stroke was not symmetrical, and while their stroke was still periodic, it was not harmonic. An example of the gait of a swimmer with a gallop is shown in Figure 2. The presence of this gallop did influence time as illustrated in Table 1.

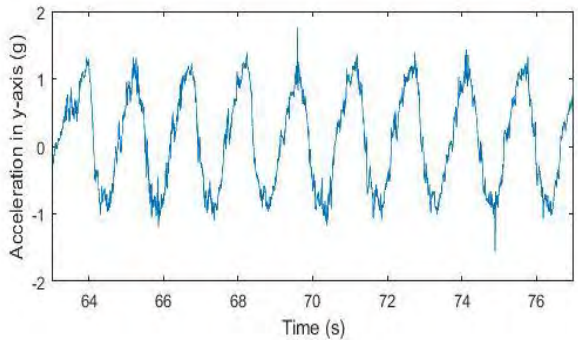

Figure 1: Acceleration in the y-axis (lateral direction) of a normal trial lap (25 yards) - appears to have harmonic motion.

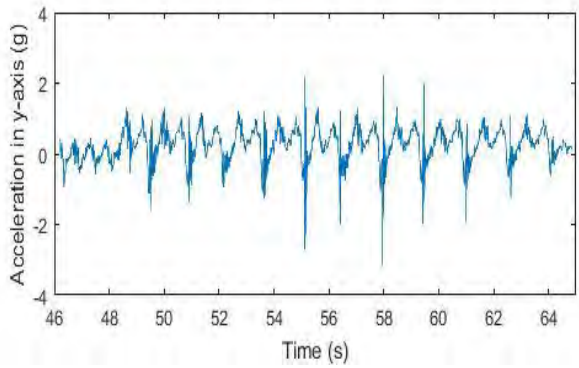

Figure 2: Acceleration in the y-axis (lateral direction) of a trial lap for a swimmer with a gallop. Appears to be periodic, but not harmonic.

Table 1: Average time of swimmers with and without a gallop.

	Gallop	No Gallop
Average Time (seconds)	180.9	159.4

For the swimmers that did rotate, it was determined that an increase in the number of strokes taken by a swimmer resulted in a larger amount of time taken to complete the laps. This matches with intuition because faster swimmers will be more efficient and pull more water per stroke, taking an overall lower number of strokes. However, in this study, it was determined that there was no correlation between number of underwater dolphin kicks and time. This does not align with the concept that underwater dolphin kicks should be more efficient than normal strokes due to streamlined body position. A possible reason for this is that the swimmers were told to treat the test as a warm up lap and not make use of their underwater dolphin kick as they normally would. Additionally, most research related to underwater dolphin kicks has been done on Olympic caliber swimmers who tend to have very different body types than the swimmers in this study.

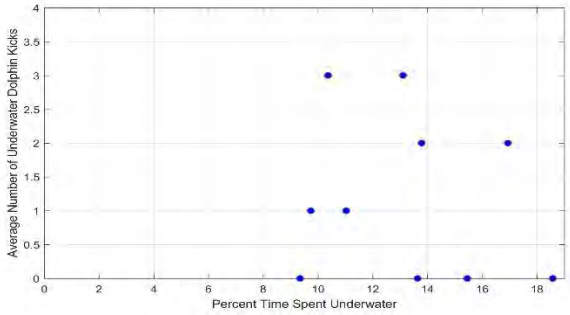

Figure 3. Amount of underwater dolphin kicks versus the percent of time spent underwater. Swimmers who took more kicks spent less time underwater.

As shown in Figure 3, swimmers who spent less percent of time underwater had more dolphin kicks, which may mean that the amount of time spent underwater and the amount of dolphin kicks are not as important as the efficiency of the time spent underwater. More controlled trials would be recommended to determine whether there is a correlation between underwater movement and overall time. As these trials are further analyzed, we aim to look further into how the stroke gait can be affected by numerous variables and establish a standardized gait that can be used as a basis for injury prevention analysis.

REFERENCES

1. Strzala M. et al, *Journal of Human Kinetics,* **60**(1), 51-62, 2017
2. Barbosa T. et al, *Journal of Sports Sciences*, **36**(5), 492-498, 2018
3. Gatta G. et al, *Journal of Sports Sciences*, **36**(5), 506-512, 2018
4. Yamakawa K. et al, *Human Movement Science*, **54**, 276-286, 2017
5. Mangia A. et al, *Sensors*, **17**(4), 927, 2017
6. Lecoutere and Puers. *Procedia Engineering*, **147**, 627-631, 2016

INDIVIDUAL CROSS PUNCH VERSUS COMBINATION CROSS PUNCH MECHANICS

Caitlin M. Mazurek and Arnel L. Aguinaldo

Point Loma Nazarene University, San Diego, CA, USA
email: cmazurek216@pointloma.edu

INTRODUCTION

Few studies have been conducted on striking mechanics, and even fewer have compared single strikes to strikes within combination [1]. Single maximal punches have been found to produce nearly twice as much impact force as punches in combination, though the mechanics have not been extensively compared [2]. The ability to compare and contrast different striking set-ups can affect combat athlete training and strategies for competition [3].

The objective of this study was to determine whether a difference exists in peak rear (dominant) hand wrist speed, mean center of mass (COM) acceleration, and peak vertical ground reaction force (vGRF) between an individual cross punch and cross punch within a jab-cross-lead hook combination in a group of experienced combat athletes.

METHODS

Twelve combat athletes (Table 1) with a minimum experience of 6 months training and 1 sanctioned amateur bout in boxing, kickboxing, Muay Thai, or mixed martial arts (Table 2) completed a series of individual cross punches, and a series of jab-cross-lead hook combination punches. Trials were completed while subjects were shoeless and wearing no additional equipment, following a 5-minute warm-up. Participants stood on two force platforms (AMTI, Watertown, MA) with one foot on each platform while kinematic and vGRF data were collected using an 8-camera 3D motion capture system (Motion Analysis, Santa Rosa, CA) with a 29-marker modified Helen Hayes marker set. Camera and analog data were captured at sampling rates of 240 Hz and 1200 Hz, respectively. Peak wrist speed, mean COM acceleration, and peak vGRF values were extracted and analyzed using paired t-tests at an alpha level of 0.05.

RESULTS AND DISCUSSION

Peak wrist speed (n = 12) was 6.4 ±1.1 m/s for the individual cross punch and 5.2 ±1.2 m/s for the combination cross punch (p = 0.011). Mean COM acceleration (n = 10) for the individual cross punch was 4.3 ± 1.7 m/s/s, while for the combination cross punch it was 4.8 ± 4.9 m/s/s (p = 0.804). Peak vGRF (n = 11; normalized by body weight) was .98 ± .2 BW for the individual cross punch, and 1.02 ± .2 BW for the

combination cross punch (p = 0.388). Differences in mean COM acceleration and peak vGRF were not statistically significant.

The result of mean peak wrist speed in the individual cross punch being higher than the combination cross-punch does not support a previous finding that combination punches have shorter delivery time than single punches [3]. This could be due to differences in measured variables as well as the parameters defining each event.

CONCLUSIONS

Individual cross punches and cross punches within a jab-cross-lead hook combination have similar COM acceleration and vGRF. Peak wrist speed is significantly higher in an individual cross punch than the cross punch within the combination.

This information is useful for further understanding the kinematics and kinetics of punches being delivered to an opponent's head or body, the subsequent injuries caused by such blows, and conversely, to improve the efficiency of a combat athlete's technique, offensive plan, and training regimen.

REFERENCES

1. Gartland et al, *British Journal of Sports Medicine*, 35(5), 308-313, 2011.
2. Pierce et al, *Journal of Quantitative Analysis in Sports,* 2(2), 3, 2006.
3. Piorkowski, Lees, & Barton, *Sports Biomechanics*, 10(01), 1-11, 2011.

Table 1: Demographic Data

Age (years)	**Height (in)**	**Weight (kg)**	**% Male [Female]**	**% Pro [Amateur]**	**% Orthodox [Southpaw]**
28 ± 9.8	70.80 ± 3.24	81 ± 18.98	83 [17]	50 [50]	83 [17]

Table 2: Demographic Data Continued - Discipline

Primary Discipline	Boxing	Kickboxing	Muay Thai	MMA
%	66	0	17	17

LANDING CHARACTERISTICS OF BEANBAG AND KOOSH BALL THROWS

Ben W. Meyer

Shippensburg University, Shippensburg, PA, USA
bwmeyer@ship.edu

INTRODUCTION

In recent years, much emphasis has been placed on using appropriate methods to measure and quantify error values in performance studies [1]. In a two-dimensional (2-D) error value study by Carter et al., participants tossed Koosh balls to a target painted on a gym floor [2]. Experimenters used a measuring tape to obtain X and Y coordinates of the tossed balls. Chiviacowsky and Wulf used a beanbag toss task in order to demonstrate that learning is facilitated if feedback is provided after good rather than poor trials [3]. Recent research has assessed the effectiveness of a target grid method to more easily obtain 2-D data in performance studies [4]. Figure 1 shows the 1.8 m by 1.8 m vinyl banner target grid with 10 cm distance between lines.

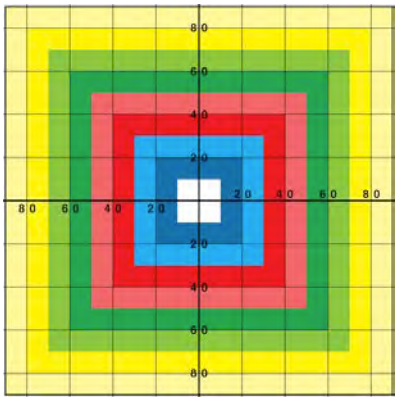

Figure 1: Target grid used in the present study.

Some studies have used the initial landing position of the tossed object as the performance measure, while other studies have used the final resting position. It can be difficult to accurately identify the initial landing position of a tossed object in real-time using only observer eyesight. Video cameras can be used to record all tosses, but the analysis of the footage can be time-consuming and tedious. A simpler way to collect data (as in classroom laboratory experiences) is to use the final resting position of the tossed object as the performance measure. However, little is known about the distance that a tossed object moves after its initial landing in studies that use Koosh balls and beanbags.

The main purpose of this study was to determine the distance traveled by Koosh balls and beanbags after initial contact with the target surface. In addition, comparisons will be made between types of throws (high trajectory and flatter trajectory). This information will be useful for practitioners who conduct research and perform experiential learning activities using these methods.

METHODS

Ten undergraduate students (age = 20 ± 1 yr; 5 male, 5 female) participated in the study. Participants performed underhand tosses with their dominant hand from a 5 m distance to the center of the floor-mounted target grid. The Koosh balls used in the study (3" diameter, 45 grams) were made of rubber filaments attached to a soft rubber core. The Baggo beanbags used by participants had a mass of 262 grams and 5.5" by 5.5" dimensions. Participants were given instructions that the measured location of the tossed object would be its final resting position, and that they should try to have the final resting position of the object be as close as possible to the center of the floor-mounted target grid (see Figure 1). Prior to the start of data collection, participants were allowed to warm-up and perform practice tosses with each object. Four conditions were tested: (1) Koosh ball lob (KBL); (2) Koosh ball roll (KBR); (3) beanbag lob (BBL); and (4) beanbag slide (BBS). In the lob conditions, participants were instructed to throw the object with a high trajectory, and have it drop close to the target. In the roll/slide conditions, participants were

instructed to use a flatter trajectory with a larger amount of object movement post-landing.

Each trial was recorded with a Casio Exilim EX-F1 camera at a sampling rate of 30 frames per second. The target grid has 10 cm dividing lines that were used to calculate reference distances for the trials. QuickTime Player software was used to analyze landing and final resting positions. The landing was considered to be the frame in which the object made its first contact with the floor surface. The final resting position after the object slid/rolled was recorded, and the distance between landing and final resting position was computed using Microsoft Excel. The mean, standard deviation, minimum and maximum post-landing distance were computed for each condition. Differences between measures were assessed using ANOVA tests with a cut-off for statistical significance set at $\alpha = 0.05$.

RESULTS AND DISCUSSION

Figure 2 shows that participants had, by far, the largest post-landing distance values using the beanbag slide technique (118 ± 47 cm). The Koosh ball roll (63 ± 19 cm) and beanbag lob (56 ± 34 cm) techniques yielded moderate post-landing distance values. The smallest post-landing distance values were obtained using the Koosh ball lob (33 ± 15 cm) technique.

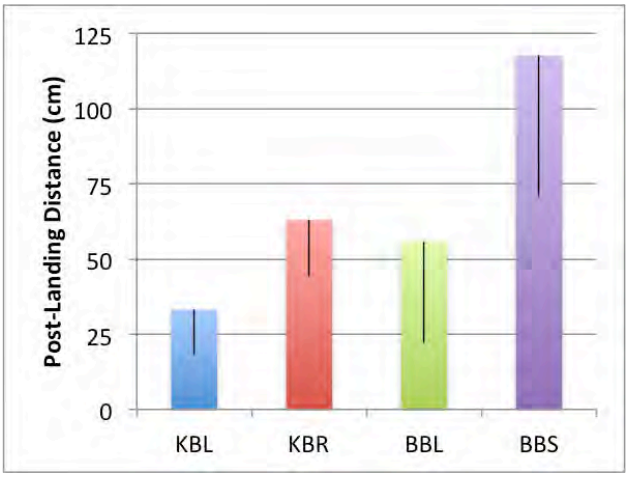

Figure 2: Post-landing distances for Koosh ball lob, Koosh ball slide, beanbag lob, and beanbag slide techniques.

The differences in post-landing distances between conditions were significant (except for KBR and BBL). In addition, the variability of post-landing distances was significantly larger using beanbags.

Figure 3 shows that, on average, the initial landing positions of the tossed objects were "undershot", with the BBS being the most undershot (-88 ± 32 cm). Participants landed the object closest to the target using the BBL technique (-13 ± 41 cm). The most accurate final resting positions were obtained using the KBL (-8 ± 43 cm) and KBR (-18 ± 27 cm) techniques.

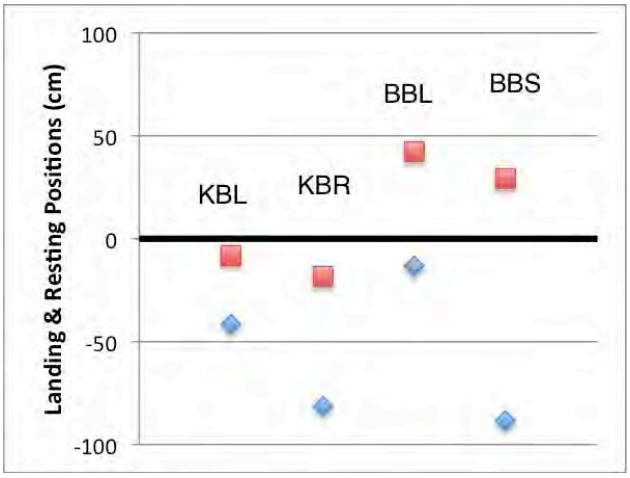

Figure 3: Initial landing and final resting positions of tossed Koosh balls and beanbags.

CONCLUSIONS

The results of this project indicate that the post-landing distance traveled by a beanbag on a floor-mounted vinyl target grid is quite large and variable. In studies that use the final resting position of a tossed object as a performance measure, it is advisable to use a Koosh ball lob technique in order to maximize the accuracy and consistency of participants' results.

REFERENCES

[1] Fischman MG. *Hum Mov Sci*, **42**, 225-231, 2015.

[2] Carter MJ, et al. *Hum Mov Sci*, **45**, 63-70, 2016.

[3] Chiviacowsky S, et al. *Res Quart Exer Sport*, **78**, 40-47, 2007.

[4] Meyer BW. *40th MARC-ACSM Meeting*, 2017.

EFFECTS OF SEX AND AGE ON HAMSTRINGS AND QUADRICEPS STRENGTH AND RATIO IN HIGH SCHOOL BASKETBALL PLAYERS

Takashi Nagai, Nathan D. Schilaty, Nathaniel A. Bates, April L. McPherson, Rena Hale, and Timothy E. Hewett

Mayo Clinic Biomechanics Laboratories & Sports Medicine Center, Rochester & Minneapolis, MN, USA
Email: nagai.takashi@mayo.edu

INTRODUCTION

The impact of hamstrings strains are significant as injuries typically result in persistent symptoms and lengthy recovery periods which limit an athlete's ability to participate. These injuries are additionally significant because hamstrings strains have high rates of re-injury [1].

Multiple risk factors for hamstrings strains have been identified. Perhaps the strongest modifiable risk factor associated with hamstrings strains is an imbalance between quadriceps and hamstrings strength, specifically the eccentric hamstrings and concentric quadriceps strength ratio [2]. However, strength data on high school basketball players is limited and normative values based on sex and age have yet to be established.

The purpose of this study was to examine the effects of age and sex on hamstrings and quadriceps strength and ratio in high school basketball players. The study aimed to establish normative strength values as well as compare those strength values among different ages and between sexes. The hypothesis tested was that male players would exhibit significantly greater strength than female players at all ages. It was further hypothesized that older high school athletes would be significantly stronger than younger high school athletes.

METHODS

A total of 97 female (age: 15.6 ± 1.3 years, height: 169.9 ± 8.3 cm, weight: 66.6 ± 14.3 kg) and 61 male (age: 15.9 ± 1.2 years, height: 180.9 ± 8.5 cm, weight: 73.2 ± 11.9 kg) basketball players were recruited from local high schools and participated in the study. Informed consents were obtained from each player Assent was obtained from legal guardians of players who were under 18 years old. The study was reviewed and approved by the Mayo Clinic Institutional Review Board.

Isokinetic concentric knee extension and flexion strength at 240°/sec and eccentric knee flexion strength at 30°/sec were assessed using the Humac Norm dynamometer (CSMi, Stoughton, MA). Subjects were seated on the dynamometer chair with straps around shoulder, waist, and thigh to minimize body movements during testing.

The testing leg was securely attached to the dynamometer around the distal shank 3 cm proximal to the lateral malleolus with the axis of the dynamometer aligned with the axis of flexion rotation in the knee. After familiarization trials, subjects were asked to extend and flex their knee as hard as possible for a full-range of motion for 10 repetitions. Subjects then performed eccentric contractions for the hamstrings. Eccentric trials started with the knee at full flexion Subjects were then asked to resist the dynamometer arm by flexing their knee as hard as possible while the dynamometer arm articulated their shank towards full extension [2]. Peak knee flexion torque was recorded during three trials. This methodology has previously reported good reliability [3].

For statistical analyses, the average of 10 and 3 trials were used for concentric and eccentric trials, respectively. The average peak torque (Nm) normalized to their body mass (kg) was used for analyses (%BM). The concentric hamstrings / concentric quadriceps strength ratio (HamC / QuadC) was calculated by the peak knee flexion torque divided by the peak extension torque multiplied by 100 in order to express a percentage.

The eccentric hamstrings / concentric quadriceps strength ratio (HamE / QuadC) was calculated similarly.

Descriptive statistics (means and standard deviations) were calculated for both left and right leg in each sex and age group. Independent t-tests and ANOVA (or nonparametric tests) were used to examine the sex differences within each age group and the effects of age within each sex, respectively. Significance was at $p < 0.05$ *a priori*.

RESULTS AND DISCUSSION

Descriptive statistics are shown in Table 1. There were multiple sex differences observed in muscular strength at 16yr, 17yr, 18yr, and all, partially supporting the hypothesis (quadriceps concentric: p = 0.001-0.314, hamstrings concentric: p = 0.001-0.676, hamstrings eccentric: p = 0.005-0.834). Fewer sex differences were observed in the strength ratios (HamC / QuadC: p = 0.142-0.995, HamE / QuadC: p = 0.008-0.878), which is contrary to previous literature [4]. Effects of age on strength were significant in males (p = 0.001-0.031), not in females except left quadriceps concentric strength (p = 0.048-0.856). There were no effects of age on strength ratio for both males (p = 0.148-0.290) and females (p = 0.783-0.941). Interaction effects on sex and age suggest that boys were gaining strength at ages 16 yr, 17 yr, and 18 yr while girls' strength was mostly unchanged throughout high school. The current findings align with our previous study that demonstrated a lack of strength changes in female players in middle/high school [5].

CONCLUSIONS

Significant strength differences between males and females, especially in quadriceps, become prominent over 16 years of age. Effects of intervention programs at earlier ages should be explored to minimize the observed strength deficits in females. Minimal effects of sex and age were observed in the hamstrings/quadriceps strength ratio in this population.

REFERENCES

1. Warren et al. *Br J Sports Med*, 2010: 415-419.
2. Croisier et al. *Am J Sports Med,* 2008: 1469-1475.
3. Habets et al. *BMC Res Notes,* 2018: 15.
4. Hewett et al. *J Sci Med Sport*, 2008: 452-459.
5. Hewett et al. *J Bone Jt Surg*, 2004: 1601-1608.

Table 1. Descriptive Statistics on Muscular Strength and Effects of Sex and Age

	Males		Females		
Age	Left and Right QuadC		Left and Right QuadC		Sex p (L/R)
14	125.5±30.4	125.5±34.8	112.1±19.6	114.1±23.2	0.167/0.314
15	141.3±33.0	139.8±25.9	121.9±16.6	122.4±21.1	0.071/0.032*
16	162.7±22.9	161.6±28.2	110.1±22.3	114.3±19.3	0.001*/0.001*
17	141.5±11.3	151.5±30.4	125.0±21.6	123.3±21.7	0.003*/0.003*
18	162.0±30.6	161.3±23.5	128.5±26.6	120.4±41.2	0.034*/0.034*
All	147.8±28.4	149.2±30.1	118.8±21.1	119.1±23.8	0.001*/0.001*
Age p	0.004*	0.031*	0.048*	0.580	
Age	Left and Right HamC		Left and Right HamC		Sex p (L/R)
14	61.9±13.8	56.7±20.4	55.2±12.0	53.9±14.0	0.281/0.676
15	62.3±15.3	65.9±15.9	56.9±17.4	55.4±17.4	0.302/0.053
16	77.8±15.8	75.1±17.8	53.6±12.8	59.3±13.4	0.001*/0.009*
17	68.7±15.1	64.4±12.0	59.0±12.4	60.5±16.1	0.048*/0.465
18	90.3±15.8	91.3±16.2	63.0±13.4	58.9±12.1	0.002*/0.001*
All	71.2±17.5	70.0±18.5	57.0±13.9	57.1±15.2	0.001*/0.001*
Age p	0.001*	0.001*	0.276	0.480	
Age	Left and Right HamE		Left and Right HamE		Sex p (L/R)
14	145.7±39.0	162.6±44.9	162.7±47.1	167.1±51.2	0.390/0.834
15	166.8±42.1	156.4±36.4	178.4±45.7	177.2±48.0	0.409/0.196
16	219.3±65.1	214.3±50.8	156.4±48.8	160.3±50.3	0.005*/0.005*
17	204.4±61.1	204.1±77.7	175.2±50.9	176.3±49.3	0.138/0.302
18	229.1±56.0	218.5±41.4	171.9±41.0	167.9±51.0	0.033*/0.051
All	194.2±60.4	190.5±57.7	169.5±47.1	170.9±49.1	0.024*/0.031*
Age p	0.005*	0.006*	0.579	0.856	
Age	Left and Right HamC/QuadC		Left and Right HamC/QuadC		Sex p (L/R)
14	51.4±14.0	48.8±20.3	50.0±10.2	48.8±14.4	0.762/0.995
15	44.8±10.4	47.3±9.0	47.4±15.3	46.4±15.3	0.540/0.823
16	48.3±9.6	47.7±13.9	51.1±17.8	52.9±13.0	0.573/0.287
17	48.6±9.9	43.4±8.1	48.2±12.0	49.6±13.1	0.933/0.131
18	56.3±8.2	57.5±13.0	50.5±12.7	60.1±47.5	0.311/0.142
All	48.7±10.6	47.9±12.6	49.1±13.4	50.0±19.4	0.870/0.834
Age p	0.148	0.213	0.874	0.783	
Age	Left and Right HamE/QuadC		Left and Right HamE/QuadC		Sex p (L/R)
14	118.2±27.1	136.1±40.3	145.7±35.5	147.0±36.0	0.069/0.496
15	119.7±25.3	114.3±31.1	148.0±41.0	146.4±38.0	0.015*/0.008*
16	134.6±34.3	134.7±32.2	147.2±52.8	140.5±40.7	0.425/0.882
17	143.7±37.6	132.7±30.8	141.7±38.6	144.8±40.6	0.878/0.361
18	141.6±23.2	135.4±17.0	141.7±57.5	154.8±69.1	0.351/0.483
All	131.3±31.6	128.8±31.6	145.2±42.1	146.1±41.4	0.061/0.017*
Age p	0.169	0.290	0.881	0.941	

QuadC = Quadriceps concentric strength, HamC = Hamstrings concentric strength, HamE = Hamstrings Eccentric Strength. *represents significance.

ACKNOWLEDGEMENTS

Funding from the NBA & GE Healthcare Orthopedics and Sports Medicine Collaboration, and NIH grant funding R01AR056259 & R01AR055563 and T32AR056950.

EFFECTS OF SEX AND AGE ON HIP FLEXORS AND HAMSTRINGS FLEXIBILITY IN HIGH SCHOOL BASKETBALL PLAYERS

Takashi Nagai, Nathan D. Schilaty, Nathaniel A. Bates, April L. McPherson, Rena Hale, and Timothy E. Hewett

Mayo Clinic Biomechanics Laboratories & Sports Medicine Center, Rochester & Minneapolis, MN, USA
Email: nagai.takashi@mayo.edu

INTRODUCTION

Clinical examinations of hamstrings flexibility are important because lack of hamstrings flexibility and hip flexors is associated with individuals with hamstrings strains [1]. Hamstrings strains are common sports-related musculoskeletal injuries in basketball players. Hamstrings flexibility can be influenced by sex as post-pubertal female athletes are more flexible and exhibit better stretch tolerance than male counterparts [2, 3].

Depending on stages of maturity [2] or age, hamstrings and hip flexibility can different. It is clinically important to establish the hamstrings and hip flexibility on high school basketball players as they are experiencing rapid growth of the musculoskeletal system between 14 and 18 years old. As a result, higher incidence of musculoskeletal injuries, including hamstrings muscle strains, can be observed.

The purpose of this study was to examine hamstrings and hip flexors flexibility in high school basketball players. The study aimed to establish normative values as well as compare those flexibility values among different ages and between sexes. It was hypothesized that female players would exhibit significantly greater hamstrings and hip flexors flexibility than male players at all ages. It was also hypothesized that older athletes would be significantly less flexible than younger athletes.

METHODS

A total of 108 female (age: 15.6 ± 1.3years, height: 170.2 ± 8.5 cm, weight: 66.4 ± 13.8 kg) and 64 male (age: 15.9 ± 1.2 years, height: 180.7 ± 8.6 cm, weight: 73.2 ± 11.9 kg) basketball players were recruited from local high schools and participated in the study. Informed consents were obtained from each player and his/her parent (only players under 18 years old). The study was reviewed and approved by the Mayo Clinic Institutional Review Board.

A Modified Thomas test was used to assess flexibility of hip flexors (iliopsoas and quadriceps muscles) [3]. Subjects were in a supine position while subject's ischial tuberosity was on the edge of treatment table. A clinician elevated both subject's legs simultaneously into hip flexion until neutral pelvis position was established. From this position, the clinician held the contralateral leg stable and slowly lowered the testing leg. The clinician placed a digital inclinometer (Johnson Level & Tool, Mequon, WI) on the top of thigh and shin to measure the iliopsoas and quadriceps flexibility, respectively. The flexibility values are set 0 degree at the level, and higher values represent greater iliopsoas and quadriceps flexibility.

Flexibility of posterior hip (gluteal and hamstrings muscles) and posterior knee (hamstrings muscles) was assessed using passive straight leg raise and passive knee extension, respectively [4]. For the passive straight leg raise, subjects laid supine while a clinician flexed their hip and kept their leg straight. Subject's pelvis was stabilized with a belt. An inclinometer was place on the top of the shin. The degree of flexibility from the horizontal position was measured (higher values represented greater flexibility). Similarly, passive knee extension was performed in a supine position with the testing leg positioned at 90 degrees hip and knee flexion [5]. Examiner clinician stabilized the testing leg's thigh vertically and moved the lower leg to a full extension. An inclinometer was placed on the top of shin to measure maximum flexibility (higher values represented greater flexibility). An average

of three flexibility trials was used for statistical analyses.

Descriptive statistics (means and standard deviations) were calculated for both left and right leg in each sex and age group. Independent t-tests or Mann-Whitney U tests were performed to examine the sex differences at each age group. In order to examine the effects of age within each sex, one-way between-subjects analysis of variance (ANOVA) or Kruskal-Wallis test were used. Post-hoc analyses were used to compare between each age group. Significance was at $p < 0.05$ *a priori*.

RESULTS AND DISCUSSION

Descriptive statistics are shown in Table 1. The hypotheses are partially supported. There were a few (5/24 comparisons) significant sex differences in hip flexors flexibility (p = 0.003-0.829). There were significant sex differences in hamstrings flexibility during passive straight leg raise and passive knee extension (p = 0.001-0.123) at almost all ages (20/24 comparison). The current findings are in agreement with a previous study [3]. Effects of age on flexibility are not significant. It is likely due to their age in the current study (older and post-puberty when compared to our previous study [2]).

Table 1. Iliopsoas and Quadriceps Flexibility during a Modified Thomas Test

	Males		Females		
Age	L/R Iliopsoas		L/R Iliopsoas		Sex *p* (L/R)
14	83.9±4.2	81.4±4.4	84.6±5.8	82.6±5.8	0.576/0.363
15	82.3±4.6	78.9±8.4	84.6±4.4	82.3±5.6	0.063/0.093
16	81.6±6.8	80.6±8.3	82.6±5.8	79.9±7.4	0.784/0.789
17	78.7±9.8	73.2±21.2	84.6±5.3	83.8±4.8	0.043*/0.006*
18	78.6±9.5	81.3±6.1	81.5±8.1	80.0±7.2	0.518/0.707
All	81.1±7.1	78.8±11.7	84.0±5.5	82.2±6.0	0.005*/0.011*
Age *p*	0.392	0.651	0.539	0.372	
Age	L/R Quadriceps		L/R Quadriceps		Sex *p* (L/R)
14	4.5±2.4	5.0±1.8	4.7±3.9	5.1±4.2	0.923/0.576
15	4.0±3.9	4.2±5.4	4.2±5.1	4.9±5.5	0.829/0.459
16	2.8±3.9	4.5±6.2	6.7±3.0	7.9±5.0	0.003*/0.091
17	5.9±12.7	6.5±9.7	5.0±3.4	6.0±5.7	0.721/0.603
18	4.4±4.2	5.1±4.4	3.7±2.3	5.8±6.2	1.000/0.813
All	4.2±6.5	4.9±6.3	4.8±4.0	5.7±5.2	0.105/0.164
Age *p*	0.394	0.956	0.151	0.393	

* represents significance. L: Left, R: Right.

Table 2. Flexibility during Straight Leg Raise (SLR) and Passive Knee Extension (PKE)

	Males		Females		
Age	L/R SLR		L/R SLR		Sex *p* (L/R)
14	61.4±6.1	64.3±6.1	74.9±8.2	75.5±8.6	0.001*/0.002*
15	66.9±8.5	68.1±8.2	75.2±10.7	74.9±9.0	0.007*/0.123
16	66.0±7.6	67.9±9.8	74.7±9.0	74.7±7.0	0.004*/0.029*
17	61.9±10.5	62.6±10.1	75.9±10.2	76.6±10.2	0.001*/0.001*
18	65.0±5.6	64.6±6.3	79.1±6.2	78.2±7.1	0.001*/0.001*
All	64.7±8.2	66.1±8.8	75.6±9.3	75.7±8.7	0.001*/0.001*
Age *p*	0.349	0.372	0.776	0.817	
Age	L/R PKE		L/R PKE		Sex *p* (L/R)
14	52.1±10.4	53.4±10.2	58.7±10.1	62.3±9.1	0.140/0.023*
15	50.0±9.1	53.0±8.1	57.1±10.7	61.6±8.8	0.023*/0.001*
16	52.2±9.3	53.7±7.5	57.5±7.5	61.7±6.9	0.080/0.003*
17	49.7±10.8	51.3±8.1	60.0±9.2	63.0±9.3	0.005*/0.001*
18	48.9±8.0	51.3±4.5	58.3±9.7	62.1±10.6	0.051/0.019*
All	50.7±9.4	52.7±7.7	58.3±9.6	62.1±8.8	0.001*/0.001*
Age *p*	0.890	0.912	0.864	0.984	

* represents significance. L: Left, R: Right.

CONCLUSIONS

Hamstrings flexibility assessments through single-passive straight leg raise and passive knee extension were sensitive to differentiate between sexes at each age group. There were fewer sex differences observed in iliopsoas and quadriceps flexibility during a Modified Thomas Test. Flexibility is consistent at all ages. The normative values can be used to screen individuals for future risk of injury and to individualize their training for hamstrings injury prevention or return-to-sport.

REFERENCES

1. Witvrouw et al. *Am J Sports Med*, 2003: 41-46.
2. Quantman et al. J Sci Med Sport, 2008: 257-263.
3. Marshall et al. *BMC Musculoskeletal Dis*, 2014.
4. Schneider-Kolsky et al. *Am J Sports Med,* 2006: 1008-1015.
5. Harvey D. *Br J Sports Med,* 1998: 68-70.
6. Reurink et al. *Am J Sports Med,* 2013: 1757-1761.

ACKNOWLEDGEMENTS

Funding from the NBA & GE Healthcare Orthopedics and Sports Medicine Collaboration, and NIH grant funding R01AR056259 & R01AR055563 and T32AR056950.

NEUROMUSCULAR CHARACTERISTICS OF HIGH SCHOOL BASKETBALL PLAYERS WHO LATER SUFFERED HAMSTRINGS STRAINS: PRELIMINARY FINDINGS

Takashi Nagai, Ryan R. Woods, Eric M. Crowley, Nathan D. Schilaty, Nathaniel A. Bates, April L. McPherson, Rena Hale, and Timothy Hewett

Mayo Clinic Biomechanics Laboratories & Sports Medicine Center, Rochester & Minneapolis, MN, USA
Email: nagai.takashi@mayo.edu

INTRODUCTION

Hamstrings strains are common sports-related musculoskeletal injuries in high school basketball players [1]. Hamstrings strength, strength ratio, and hip and knee flexibility have been reported in previous studies as risk factors [2,3]. More recently, muscle tissue stiffness was measured with musculoskeletal diagnostic ultrasound shear wave elastography (SWE). Stiffness increases with a greater stretch of hamstrings in young adults [4]. But, it is not known whether SWE stiffness can differentiate basketball players at higher risk of prospective hamstrings strains.

Therefore, the purpose of the study was to examine hip and knee flexibility, knee muscular strength, and SWE stiffness of the biceps femoris among high school basketball players at baseline and compare them between players who later suffer hamstrings strains and uninjured controls. The hypothesis tested was that players who later suffered hamstrings strains would exhibit less flexibility, strength, and SWE stiffness when compared to controls.

METHODS

This study was approved by the Institutional Review Board, and high school basketball players from local high schools were recruited for this study. All players (and parents if players were minor) were consented prior to the testing. All players were free of any musculoskeletal injuries at the time of testing and were cleared for full sport participation. Briefly, baseline neuromuscular tests consisted of three flexibility tests, two isokinetic strength tests, and SWE at three different knee flexion positions. Height and weight were also measured using a standard scale.

A Modified Thomas test was used to assess flexibility of hip flexors muscles. Passive straight leg raise and passive knee extension tests were used to test hip extensor and hamstrings. An average of three measurements in degrees (º) was used for analysis. Measures were performed with a digital inclinometer (Johnson Level & Tool, Mequon, WI).

For muscle strength tests, subjects were seated on a HumacNORM (CSMi, Stoughton, MA). Concentric quadriceps and hamstrings strength was assessed with isokinetic testing for knee flexion and extension at 240°/s for ten repetitions. Eccentric hamstrings strength was assessed by isokinetic knee flexion at 30°/s for five repetitions. An average of peak torque normalized to body mass (Nm/kg), expressed in percentage (%BM), was used for analysis.

For SWE tests, subjects were lying supine, and the clinician positioned the athlete's leg at 40, 60, and 80% of the maximum passive knee extension flexibility. An ultrasound probe (GE LOGIQ E9, 9L-D transducer; GE Healthcare, Wauwatosa, WI) was placed on the biceps femoris muscle parallel to the muscle fibers. An average of three SWE stiffness measures (kPa) was used for analysis.

A total of 172 high school basketball players (108 females / 64 males) were tested at baseline. Out of those players, three female basketball players later suffered hamstrings strains during their basketball season; therefore, they serve as injured group (n=3). The hamstrings injury was confirmed by the school's athletic trainer and/or sports medicine medical doctor. All uninjured female players who completed all parts of baseline tests (flexibility, strength, and SWE) were used as a control group (n=91). Demographics are shown in Table 1.

Table 1: Demographics

Demographics	Controls	Injured	*p*
Age (years)	15.6 ± 1.3	16.3 ± 2.1	0.471
Height (cm)	169.7 ± 8.2	173.0 ± 2.2	0.499
Weight (kg)	65.3 ± 13.2	79.6 ± 13.3	0.047

Descriptive statistics (means and standard deviations) were calculated. Group differences were assessed with Independent t-tests or nonparametric analyses. Within three injured players, paired t-tests were performed to compare between limbs. Significance was set at $p < 0.05$.

RESULTS AND DISCUSSION

Three female players who later suffered hamstrings strains had significantly higher weight than controls ($p = 0.047$). None of neuromuscular risk factors were significantly different between groups, rejecting hypotheses ($p > 0.05$).

Table 2: Flexibility Variables (in degrees)

Flexibility	Controls	Injured	*p*
Thomas Quad Left	84.2 ± 5.5	80.3 ± 7.6	0.250
Thomas Quad Right	82.2 ± 6.0	77.0 ± 9.6	0.259
Thomas Hip Left	4.9 ± 3.9	4.3 ± 3.1	0.824
Thomas Hip Right	5.7 ± 5.5	6.3 ± 3.1	0.730
Straight Leg Raise Left	75.1 ± 9.1	73.3 ± 10.1	0.791
Straight Leg Raise Right	75.4 ± 8.9	76.0 ± 8.2	0.911
Passive Knee Ext Left	58.8 ± 9.8	50.0 ± 7.2	0.111
Passive Knee Ext Right	62.3 ± 8.9	56.3 ± 3.5	0.249

However, when examined closely, there were potentially clinical significant neuromuscular deficits in hamstrings flexibility during passive knee extension test (9.6-15.0%, Table 2), less SWE stiffness values in all three positions both right and left leg (23.1-44.7%, Table 3), eccentric hamstrings strength (21.0-31.4%, Table 4) and the strength ratio of eccentric hamstrings and concentric quadriceps strength (20.1-27.2%, Table 4).

Table 3: Shear Wave Elastography Stiffness (in kPa)

Stiffness	Controls	Injured	*p*
40% Left	42.8 ± 25.8	29.4 ± 16.6	0.511
60% Left	40.7 ± 25.9	22.5 ± 11.2	0.287
80% Left	32.9 ± 21.7	18.8 ± 2.5	0.063
40% Right	36.8 ± 21.5	24.7 ± 17.9	0.224
60% Right	40.7 ± 29.2	31.3 ± 21.6	0.552
80% Right	31.0 ± 21.4	18.9 ± 7.6	0.164

Table 4: Strength Variables (strength are in %BM; ratios are in %)

Strength	Controls	Injured	*p*
Con Quad at 240°/s Left	119.4 ± 21.0	116.2 ± 18.1	0.796
Con Quad at 240°/s Right	119.5 ± 23.9	110.2 ± 13.0	0.505
Con Ham at 240°/s Left	57.2 ± 14.1	53.7 ± 10.0	0.714
Con Ham at 240°/s Right	57.5 ± 15.6	48.9 ± 2.7	0.344
Ecc Ham at 30°/s Left	171.5 ± 47.1	135.4 ± 39.1	0.193
Ecc Ham at 30°/s Right	173.2 ± 49.2	118.9 ± 26.1	0.061
Ratio ConHam/Quad Left	49.1 ± 13.7	46.1 ± 2.9	0.855
Ratio ConHam/Quad Right	50.2 ± 19.9	44.9 ± 7.3	0.567
Ratio EccHam/Quad Left	146.4 ± 42.7	117.0 ± 28.2	0.233
Ratio EccHam/Quad Right	147.7 ± 42.0	107.5 ± 16.6	0.060

Con: Concentric, Ecc: Eccentric, Quad: Quadriceps, Ham: Hamstrings.

Within the injured group, there were no statistically significant differences between injured limb and contralateral uninjured limb ($p > 0.05$). Interestingly, uninjured limb was 9 to 21% weaker than the injured limb, which may indicate systematic neuromuscular deficits in those injured individuals.

CONCLUSIONS

The current preliminary findings are the first prospective study to include all three neuromuscular characteristics (flexibility, strength, and SWE) in high school basketball players. Future investigations will increase the quantity of subjects in the injured group and explore efficacy of screening and interventions with various types of exercises to counter the above-mentioned neuromuscular risk factors for prevention and return-to-sport.

REFERENCES

1. Borowski et al. *Am J Sports Med*, 2008:2328-2335.
2. Croisier et al. *Am J Sports Med*, 2008:1469-1475.
3. Witvrouw et al. *Am J Sports Med*, 2003: 41-46.
4. Le Sant et al. *PLOS One,* 2015: 10(9): e0139272.

ACKNOWLEDGEMENTS

Funding from the NBA & GE Healthcare Orthopedics and Sports Medicine Collaboration, and NIH grant funding R01AR056259 & R01AR055563 and T32AR056950.

HOP DISTANCE AND LOADING SYMMETRY IN ACL RECONSTRUCTED ATHLETES DURING RETURN TO SPORT TESTING

[1] Alex Peebles, [1] Kristen Renner, [2] Thomas Miller and [1,2] Robin Queen

[1] Kevin P. Granata Biomechanics Lab, Virginia Tech, Blacksburg, VA
[2] Department of Orthopaedic Surgery, Virginia Tech Carilion School of Medicine, Roanoke, VA
email: apeebles@vt.edu, web: https://www.beam.vt.edu/granatalab/

INTRODUCTION

Between limb movement and loading asymmetries are present in athletes returning to sport following anterior cruciate ligament reconstruction (ACLR) and rehabilitation. These asymmetries are believed to be risk factors for secondary ACL injuries and long-term joint degeneration [1-3]. Following ACLR, athletes have significantly lower impact forces on their surgical limb and higher impact forces on their uninvolved limb when compared to healthy controls [1]. The offloading of the operative limb represents a movement compensation which is potentially dangerous to both limbs. Reducing between limb asymmetries may decrease the incidence of secondary injuries when returning to sport following ACLR.

Functional hop tests are commonly used clinically to evaluate the independent performance of the surgical leg relative to that of the nonsurgical limb following ACLR [2]. These tests are currently measured in hop distance, however, ACLR athletes with clinically normal hop distances (>85% of uninvolved limb) have been shown to still have altered lower extremity mechanics during single leg hops [3]. Differences in impact force symmetry between ACLR and healthy controls during clinical hop testing have yet to be determined.

The loadsol (Novel Electronics, St. Paul Minnesota) is a force-sensing insole which is wireless, relatively inexpensive, and simple to use during outpatient visits (Figure 1). Investigating impact forces during functional hop testing may help clinicians understanding movement quality in their patients and reduce asymmetry prior to return to sport. The first purpose of this study was to compare hop distance symmetry and loading symmetry between ACLR athletes at the time of return to sport and healthy recreational athletes. We hypothesize that both hop distance and loading symmetry would be worse in ACLR patients when compared to healthy controls. The second purpose of this study was to determine the correlation between hop distance symmetry and loading symmetry across both ACLR and healthy uninjured individuals.

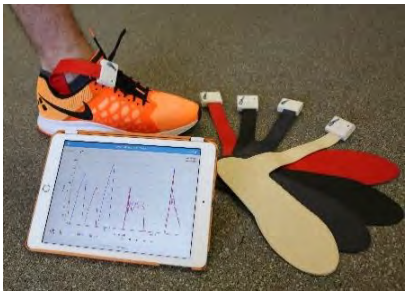

Figure 1: loadsol sensors shown and worn inside a running shoe with data collected via Bluetooth on an iDevice

METHODS

Twenty-five patients recovering from a primary unilateral ACLR (6 male/19 female, age: 18.7 ± 3.0, height: 1.73 ± 0.07 m, mass: 72.4 ± 14.3 kg) were included in the present study. All patients had been cleared for return to sport by their treating orthopedic surgeon and were tested at 6.95 ± 1.27 months following ACLR. 29 recreational athletes (11 male/18 female, age: 22.1 ± 3.5 years, height: 1.72 ± 0.08 meters, mass: 65.9 ± 10.2 kg) served as a control group. All participants signed institutional review board approved consent.

Each participant was fit with a pair of loadsol (Novel Electronics, St. Paul, MN) single sensor insoles (100 Hz) and neutral running shoes. Each participant completed 7 single hops (SH), 3 triple hops (TH) and 3 crossover triple hops (CH) for distance per limb using the standard clinical testing protocol. Impact peak, loading rate, and impulse were calculated during the first 200 milliseconds after initial contact for the SH and for the final landing of the TH and CH. A Limb Symmetry Index (LSI) was calculated as the ratio of the surgical (non-dominant) to non-surgical (dominant) limb for each trial pair and then averaged across trials for each task [1].

Shapiro-Wilk normality tests revealed non-normal distribution for multiple outcome measures, therefor

Mann-Whitney U-Tests were used to compare our outcome measures between groups and Spearman rank correlations were used to compare distance and loading symmetry metrics across all participants. Significance was set at 0.05. All statistical analysis was performed using SPSS (SPSS Version 24).

RESULTS AND DISCUSSION

ACLR patients were less symmetric in hop distance compared to healthy controls for the single hop, triple hop, and crossover hop (Table 1). Load-based outcome measures were also significantly different between groups, with lower symmetry values found in ACLR. These results are consistent with previous findings of reduced loading and distance symmetry during dynamic sport-related tasks in ACLR patients [1,2] and demonstrates differences in neuromuscular control on the surgical limb relative to the non-surgical limb as well as the differences between ACLR and control subjects.

Table 1: Comparison of hop distance and loading LSI between healthy controls (HC) and ACLR

	HC	ACLR	*p*-value
Single hop			
Distance	94.7 (10.7)	80.5 (12.4)	***p* < 0.001***
Impact peak	99.5 (16.9)	90.9 (19.9)	*p* = 0.126
Loading Rate	102.3 (24.6)	83.0 (33.8)	***p* = 0.020***
Impulse	99.3 (11.2)	93.5 (13.7)	***p* = 0.049***
Triple hop			
Distance	98.3 (8.7)	78.4 (11.9)	***p* < 0.001***
Impact peak	99.9 (22.1)	85.2 (15.2)	***p* = 0.014***
Loading Rate	103.7 (30.4)	88.2 (26.1)	*p* = 0.091
Impulse	100.8 (13.0)	88.9 (11.5	***p* = 0.001***
Crossover hop			
Distance	98.1 (12.8)	80.1 (17.2)	***p* < 0.001***
Impact peak	102.4 (28.1)	86.0 (19.4)	***p* = 0.017***
Loading Rate	110.0 (43.7)	87.6 (31.9)	***p* = 0.026***
Impulse	99.0 (11.4)	95.0 (16.4)	*p* = 0.115

All but one correlation between distance symmetry and loading symmetry measures were found to be significantly positively correlated (Table 2). This finding intuitively makes sense, as further jump distances are expected to generate more kinetic energy which needs to be dissipated at ground contact. However, all correlations were found to be weak-to-moderate (0.3-0.7), suggesting that hop distance symmetry and loading symmetry provide different information when assessing movement. For example, lower knee flexion angles at initial contact have been shown to result in larger impact peaks during single-leg vertical drop landings [4]. Future work should evaluate the relationship between the force attenuation measures used in the present study and lower extremity mechanics during functional hop testing in order to better understand how measures of loading symmetry are associated with movement asymmetries.

Table 2: correlation between distance and loading symmetry across all study participants. Values presented as correlation coefficient and *p*-value.

	Impact Peak	Loading Rate	Impulse
SH Distance	0.497 (<0.001)	0.435 (0.001)	0.560 (<0.001)
TH Distance	0.379 (0.003)	0.249 (0.059)	0.397 (0.002)
CH Distance	0.632 (<0.001)	0.609 (<0.001)	0.554 (<0.001)

CONCLUSIONS

The results of the present study reveal that hop distance symmetry and loading symmetry are both reduced in ACLR athletes who have been cleared to return to sport. Additionally, the present results document significant, yet moderate associations between hop distance symmetry and loading symmetry. Collectively, these results suggest that using force-sensing insole devices (Figure 1) may be a clinically feasible method for evaluating loading asymmetry during functional testing when making return to sport decision and could improve our ability to reduce the risk of secondary ACL injuries following return to sport.

REFERENCES

[1] Schmitt et. al., Med and Sci in Sport and Exercise 2015
[2] Barber-Westin and Noyes, The Physician and Sports Medicine, 2011
[3] Orishimo et. al., Knee Surgery, Sport Traumatology, Arthroscopy, 2010
[4] Padraza and White, The Knee, 2010

ACKNOWLEDGEMENTS

This work was funded in part by a grant from DonJoy Orthopedics.

Effects of Age on Skeletal and Muscular Contributions to Leg Stiffness

[1]Douglas W. Powell, [2]Jacqueline Morgan, [1]Max R. Paquette
[1] University of Memphis, Memphis, TN, USA
[2]Virginia Commonwealth University, Richmond, VA, USA
email: douglas.powell@memphis.edu, web: http://www.memphis.edu/shs/research/mal.php

INTRODUCTION

Advancing age is associated with general declines in functional performance. Remaining physically active across the lifespan is known to mitigate age-related declines in cardiovascular, neuromuscular and skeletal health (1-3). Running is a common form of physical activity that is inexpensive, readily accessible to most individuals and has been shown to ameliorate age-related declines in physiological function (1, 2). While running is known to benefit health and functional performance with advancing age, it is also associated with a high rate of musculoskeletal injury (4).

Middle-aged and older runners have greater injury rates compared to young runners (3, 4). These unique injury patterns can be related to factors that effect lower extremity stiffness including changes in muscle physiology (5-7), mechanical properties of the muscle-tendon unit (8,9) and altered neuromuscular strategies resulting in distinctive running biomechanics (10).

Stiffness is a composite measure of kinematic response to imposed kinetics describing the interaction of a load applied to a structure and that structure's response to that load (11,12). Functionally, leg stiffness is the result of the mechanical properties of the musculoskeletal structures including passive connective tissues as well as the active forces created by muscle activation. Previous research has differentiated leg stiffness into skeletal and muscular contributions during locomotion (13,14). While lower extremity stiffness has been differentiated into skeletal and muscular components during running (14), the effect of advancing age on components of leg stiffness during running remains unknown. Therefore, the purpose of the current study was to quantify muscular and skeletal contributions to leg stiffness in young compared to older runners at preferred and fixed running speeds. It was hypothesized that older runners would exhibit greater skeletal contributions and smaller muscular contributions to leg stiffness than young runners. It was further hypothesized that older runners would have greater relative contributions of the skeletal component and smaller relative contributions of the muscular component of leg stiffness than young runners.

METHODS

Twenty-one male runners (11 young, 10 older) performed two 30-second running trials on an instrumented treadmill (960 Hz, Treadmetrix) while ground reaction forces (GRFs) and kinematics (240 Hz, Qualisys Inc) were collected simultaneously. Participants ran at self-selected and matched (3.35 m/s) running velocities. Joint kinematics and kinetics were calculated using Visual 3D (C-Motion Inc.) while custom software was used to calculate leg stiffness (kLeg) as well as muscular (kMusc) and skeletal (kSkel) contributions to kLeg.

Leg stiffness was calculated as the peak GRF vector magnitude divided by the change in length of the lower extremity from initial contact to peak GRF vector magnitude. Skeletal and muscular components of leg stiffness were calculated as:

$$kLeg = kLeg \cos^2\phi + kLeg \sin^2\phi$$

where kLeg was leg stiffness, $kLeg \cos^2\phi$ was the skeletal contribution to leg stiffness and $kLeg \sin^2\phi$ was the muscular contribution to leg stiffness and ϕ was the angle between tibial orientation and the ground reaction force vector (Figure 1).

A repeated measures ANOVA was used to assess the effects of age and running speed on stiffness variables. In the presence of a significant interaction, post-hoc t-tests were conducted to determine the source of the interaction.

RESULTS AND DISCUSSION

No interaction effects were observed for any stiffness measures. Significant main effects for age were observed for kLeg and kMusc. Older runners had smaller leg stiffness values and smaller kMusc (Table 1). No differences were observed in kSkel.

These findings do not support the hypothesis that older runners would exhibit greater kSkel than younger runners. However, older runners do demonstrate a greater reliance upon skeletal structures to create leg stiffness compared to their younger counterparts. Therefore, these findings may identify a contributing factor to skeletal injury in older runners.

CONCLUSIONS

Older adults have a greater reliance upon skeletal structures during load attenuation during running. These altered mechanical strategies may underlie distinct injury patterns in older compared to young runners.

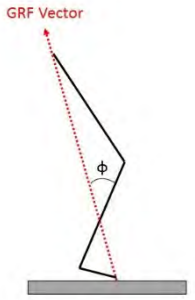

Figure 1. Skeletal and muscular components of leg stiffness (kLeg) were calculated as a function of the angle (φ) between the ground reaction force vector at the time of peak ground reaction force and the longitudinal axis of the leg with equation 1 presented in methods.

REFERENCES

1. Beck ON et al. Med Sci Sports Exerc. 2016;48(4):697-704.
2. Larsen RG et al. Appl Physiol Nutr Metab. 2012;37(1):88-99.
3. Nielsen RO et al. Int J Sports Phys Ther. 2013;8(2):172-9.
4. McKean KA et al. Clin J Sport Med. 2006;16(2):149-54.
5. Harbo T et al. Eur J Appl Physiol. 2012;112(1):267-75.
6. Hortobagyi T et al. J Gerontol A Biol Sci Med Sci. 1995;50(6):B399-406.
7. Narici MV et al. Br Med Bull. 2010;95:139-59.
8. Karamanidis K et al. J Biomech. 2006;39(3):406-17.
9. Karamanidis K et al. Gait Posture. 2007;25(4):590-6.
10. Devita P et al. Med Sci Sports Exerc. 2016;48(1):98-106.1.
11. Butler RJ et al. 2003;18(6):511-7.
12. Farley CT and Morgenroth DC. J Biomech. 1999;32(3):267-73.
13. DeVita P and Hortobagyi T. J Gerontol A Biol Sci Med Sci. 2000;55(12):B593-600.
14. Powell DW et al. Med Sci Sports Exerc. 2017;49(8):1662-7.2.

Table 2. Mean dependent variables in young and older runners when running at preferred (PREF) and fixed (FIX) speeds; mean (SD).

	PREF		FIX		*p*-values		
Dependent Variables	Young	Older	Young	Older	Inter.	Age	Speed
k_{leg} (kN/m) [b,c]	18.8 (2.8)	16.4 (1.5)	19.8 (3.8)	17.0 (1.7)	0.41	**0.03**	**0.006**
k_{skel} (kN/m) [c]	14.7 (2.2)	13.5 (1.3)	15.6 (3.3)	14.1 (1.4)	0.67	0.16	**0.012**
k_{musc} (kN/m) [b]	4.1 (0.8)	2.9 (0.4)	4.2 (1.0)	2.9 (0.8)	0.38	**0.001**	0.52

Notes: [a]: significant interaction effect; [b]: significant age main effect; [c]: significant speed main effect; leg stiffness (k_{leg}), skeletal (k_{skel}) and muscular (k_{musc}) contributions to leg stiffness.

CRITICAL FACTORS IN THE WEIGHT THROW FOR COLLEGIATE THROWERS

Cailyn Schroeder and James Becker

Montana State University, Bozeman, MT, USA
email: james.becker4@montana.edu, web: http://www.montana.edu/biomechanics

INTRODUCTION

Track and field competitions take place indoors and outdoors, with several events differing slightly between the two. The weight throw is one example, and is considered to be the indoor version of the hammer throw. Compared to the outdoor hammer implement, the indoor weight is heavier (9.09 kg vs. 4 kg for women and 15.09 kg vs. 7.26 kg for men). Despite these differences, the technique used in the two throws is similar, with the athlete completing three or four and half complete turns while moving across the throwing circle. As such, the indoor weight throw is often used as a training event for the outdoor hammer throw.

Several previous studies have examined critical factors for performance in the hammer throw. Critical variables influencing throw distance include: the release angle, height, and velocity, ball velocity on each turn, time in double and single limb support during each rotation, and path of the hammer [1, 2]. In comparison, the indoor weight throw is relatively unstudied. As such, despite the similarities in technique, it is currently unknown whether critical factors in the hammer throw are also critical factors for performance in the indoor weigh throw.

Therefore, the purpose of this study was to identify the critical kinematic factors of the weight throw, specifically in non-elite throwers. It was hypothesized that due to similar technique between the hammer and weight throw, that the critical factors will also be similar between events.

METHODS

Four throwers participated in this study (sex: 2 male, 2 female; age: 19.5 ± 2.3 years; experience: 2.0 ± 1.4 years). All participants were members of an NCAA Division I track and field team and active competitors in the weight throw. Each thrower used a 4-turn technique when throwing the weight.

Participants completed their own standard competition warm up followed by two maximal effort throwing trials. Three minutes of rest was taken between throws. Each throw was measured for distance and fouled throws were not included in the data set. Throwers used implements meeting NCAA competition standards for both men and women.

Forty-two reflective markers were placed on bony landmarks and six markers were placed on the weight throw implement. Whole body kinematics on each throwing trial were recorded using a 10-camera motion capture system (Motion Analysis Corp.) sampling at 250Hz. Marker trajectories were smoothed using a fourth order zero-lag low pass Butterworth filter with a 12 Hz cutoff frequency. Timing of the start of the throw, heel contact and toe off on each turn, and release were identified based on the motion capture data. The following kinematic variables were then calculated: release velocity, release height, velocity added to the implement during each turn, time spent in single and double limb support during the throw, and the average angle of the orbit of the weight relative to horizontal on each turn.

Data analysis was conducted as reported in studies identifying critical factors in other throwing events [3]. Pearson product moment correlations were conducted between all possible combinations of independent variables. Where two variables were highly correlated, only one was retained for inclusion in the regression. A stepwise linear regression was then performed to determine which variables were significant predictors of throw distance. All statistical analyses were performed using SPSS, with an alpha of $p < .05$.

RESULTS AND DISCUSSION

Mean throw distance for the analyzed throws was 16.05 (± 1.4 m) for the men and 9.26 (± 0.98 m.) for the women. The stepwise regression indicated that two of the fifteen parameters (Table 1) significantly predicted throw distance (F = 120.8, R^2 = .984, p < .001), with higher release velocities and a lower angle of the orbit on turn four predicting longer throws. Mean values for these parameters were 8.79 (± 1.53 m/s) for release velocity and 40.22 (± 8.06°) for the angle of the orbit on turn four.

Table 1. Results of the stepwise regression

Variable	Coefficient	p value
Intercept	-6.94	< .001
Release velocity	1.15	< .001
Angle of orbit on turn 4	-0.26	.040

Correlation analyses revealed that time spent in single limb support during the throw was negatively associated with increased release velocity (R = -.821, p = .023), while the angle of the orbit relative to horizontal on turns two (R = .759, p = .048) and three (R = .784, p = .037) were both positively associated with increased release velocity (Figure 1). None of the other kinematic variables were associated with the angle of the orbit on turn four.

Similar to previous studies on the hammer throw [2], the release velocity of the implement is a critical factor for the indoor weight throw as well. Hammer throw studies have also shown that minimizing the time spent in single limb support during the throw allows athletes to add velocity to the hammer on each turn [1,2]. While time spent in single limb support was not a direct predictor of weight throw distance, there was an association between less time in single limb support and increased release velocity, suggesting this could be an important parameter for coaching the weight throw.

There are several limitations which must be considered when interpreting these results. First, we used a small sample, and thus this should be considered an exploratory study. Second, as indicated by the mean throw distances and years of experience, the throwers in this study were non-elite collegiate throwers. Whether these results apply to more experienced or higher level throwers requires further investigation.

CONCLUSIONS

In non-elite collegiate throwers, weight throw distance is predicted by the velocity at release and the angle of the weight orbit on the fourth turn. Spending less time in single limb support during the throw and optimizing the angle of the weight orbit on the second and third turns may improve these parameters, and thus improve performance.

REFERENCES

1. Judge et al. *Int J Sport Sci and Coaching.* **3**, 477-488, 2008.
2. Mercedante et al. *Proc XXV ISBS Symposium* Ouro Preto, Brazil, 2007.
3. Young, M. et al. *Sport Biomech.* **4**, 131-148, 2005

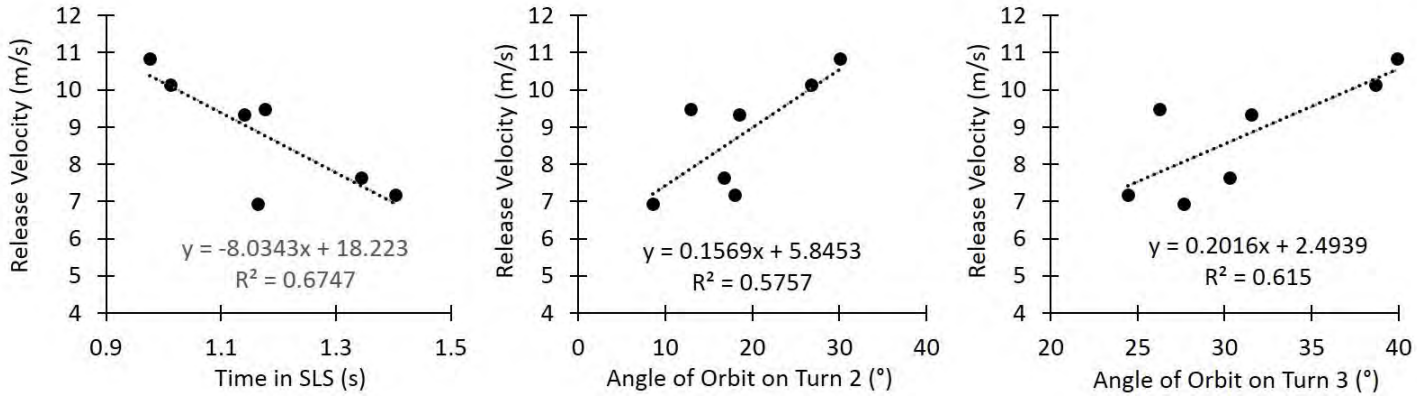

Figure 1. Correlations between time in single limb support during the throw, angle of the orbit on turn two, and angle of the orbit on turn three, and release velocity. All correlations were statistically significant at the p < .05 level.

WAVELET TRANSFORM ANALYSES OF COUNTERMOVEMENT JUMP PERFORMANCE

[1] Zhanxin Sha, [1] Zhaoxian Zhou, [2]Boyi Dai, [1]Gary Krebs, [1]Scott Piland

[1] University of Southern Mississippi, Hattiesburg, MS, USA
[2] University of Wyoming, WY, USA
email: zhanxin. sha@usm.edu

INTRODUCTION

Countermovement jump (CMJ) is a vertical jump that has been used very often to evaluate the ability of explosive force production, to identify athletes' strength and weakness, to monitor rehabilitation progress, and to measure the training progress. Previous researchers and investigators have studied ground reaction force (GRF) for quantifying and evaluating jump performance.

Temporal aspects of the jump include the slope of the GRF, area under the curve, rate of force development (RFD), time to peak force (tPF) and impulse. RFD and tPF were determined by muscle neural activation and highly correlated with athletes' explosive force production and CMJ performance [1, 2]. However, the RFD and tPF are associated with low test-retest reliability [1].

A frequency domain analysis is also a solution to describe rate of change [3]. High frequency signal means a fast rate of change from the system. The Fourier analysis is one typical method to decompose and transform time domain signal to frequency components. However, the Fourier analysis cannot provide time dimension information. This may not match the need of performance analyses. The wavelet transform can decompose a complicated signal into a finite number of frequencies. In addition, using basis functions, wavelet transform could locate time and frequency of non-stationary signals. At present there is a paucity of studies to explore wavelet analysis at GRF from CMJ. Therefore, the purpose of the current study was to analyze CMJ from wavelet transform analyses.

METHODS

Forty-four Division I football players (body mass 101 ± 18.96 kg, age 21 ± 2 years old) participated in the study. All athletes wore training shoes and thirty of them wore the same type of training shoes. The testing included three trials of a countermovement jump. Jumping and landing kinetic variables from dominant and non-dominant legs were measured from two force platforms (AMTI) at a frequency of 1000 Hz. Trials were considered to be valid only when both jump and landing were on the force platforms. Informed consent was obtained from each athlete in accordance with the protocol approved by the Institutional Review Board.

Many wavelet functions can be used in wavelet transform. In this work, we have selected Haar basis as our wavelet because they are multiresolution basis in the sense that the scaling function is orthogonal to its integer translates and the subspaces spanned by the scaling function at low scales are nested within those spanned at higher scale. The Wavelet transform analysis is implemented with function cwt in Matlab environment. DC components are subtracted from the combined forces from both left and right feet. We define mean frequency, in Hz, as the power weighted pseudo-frequencies corresponding to different scales, which is approximate relationship between scale and frequency. Jump height (JH) was calculated based on the takeoff velocity from impulse and momentum theorem. Mean frequency at the time where minimum force occurred from eccentric phase (Mf @MF_ECC) and mean frequency at time of peak force at concentric phase (Mf @PF_CON), and JH were used for further analysis. Pearson's product correlations were used to determine if any relationship existed between mean frequency and jump height. Coefficients of variation were calculated for each variable in order to determine

variability. The significance level was set at $p \leq .05$ for all statistical analyses. All statistical analyses were completed using MATLAB software.

RESULTS and DISCUSSION

Table 1 summarizes the means and standard deviations of the mean frequencies and jump height variables. Relationship between variables were listed in Table2, Mf @PF_CON positive correlated with JH. An example of the wavelet transform results is plotted in Figure 1. Mean frequencies demonstrated high test-retest reliability. Intra-participant CV were range between 0.20% - 10.00%. Current study indicated that wavelet transform is reliable and may valuable for analyzing GRF from both time and rate of change perspectives. Current study focused on wavelet transformation on CMJ and only pick two specific time points. Relationship between rate of force development and Wavelet transformation need to be investigated in future in order to establish reliable methods to investigate athletes' jump performance from a temporal perspective.

REFERENCES

1. McLellan, C. J Strength Cond Res, 25(2): 379-385, USA, 2011.
2. Laffaye, G and Wagner, P. Comput Methods Biomech Biomed Engin. 16 suppl: 82-83, 2013.
3. Sha, Z et al. Proceedings of ASB 16, Colorado. 2016.

Table 1: Descriptive statistics: mean ± SD values

Variables	Mean	± SD
Mf @MF_ECC (Hz)	2.61	0.48
Mf @PF_CON (Hz)	2.87	0.19
Jump Height (m)	0.51	0.11

Table 2: Correlation Matrix

	Mf @MF_ECC	Mf @PF_CON	Jump Height
Mf @MF_ECC	1	-0.03	-0.06
Mf @PF_CON	-0.03	1	0.31**
Jump Height	-0.06	0.31	1

** P=0

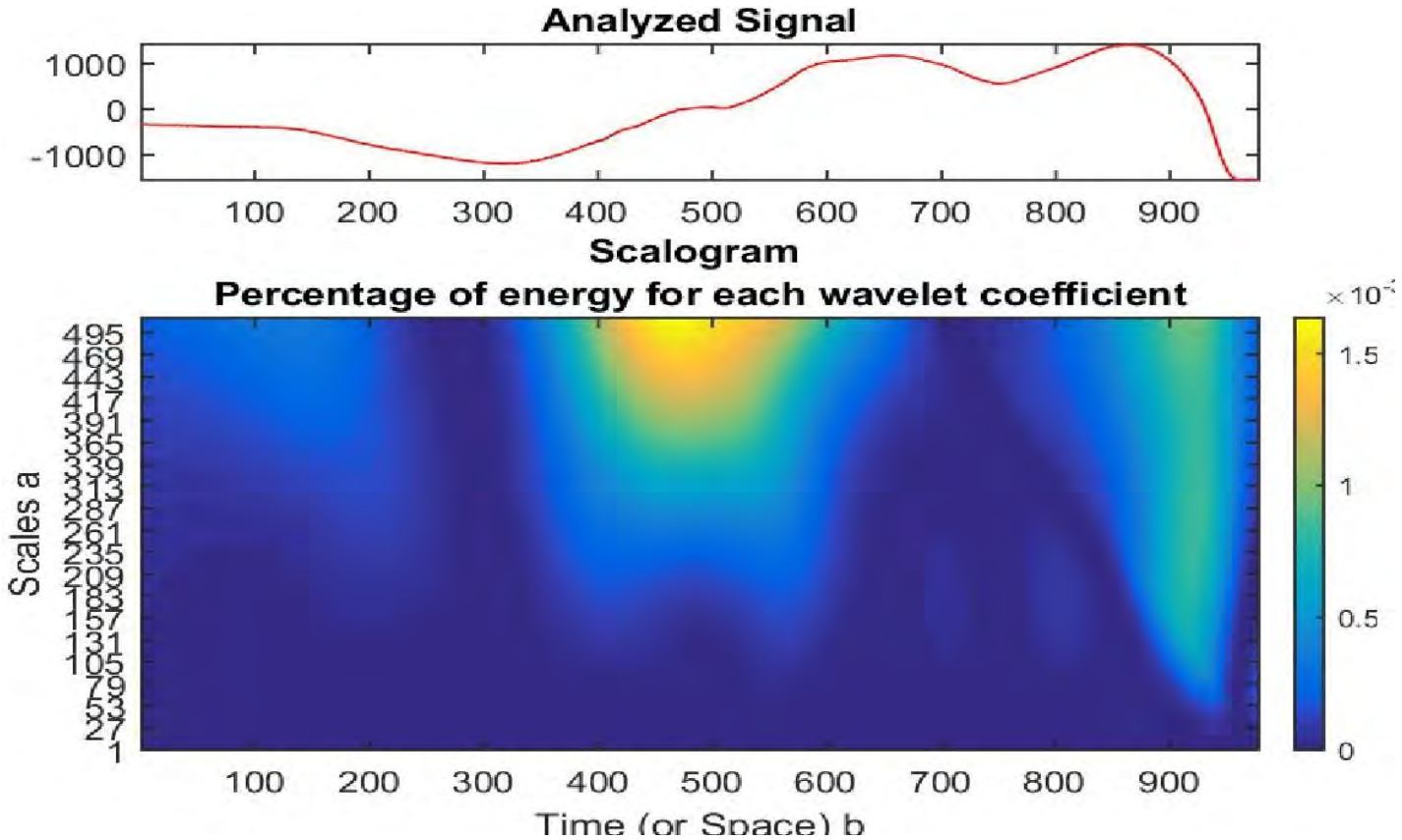

Figure 1. Frequency and power distribution from one participant.

MUSCLE ACTIVATION ANALYSIS WITH KINEMATIC COMPARISON BETWEEN WIND-UP AND STRETCH PITCHING WITH RESPECT TO THE UPPER AND LOWER EXTREMITIES

[1,2]Megan Smidebush, [2]Ethan Stewart, [2]Adam Knight, [2] Harish Chander [1]Robert Shapiro

[1]Department of Kinesiology and Health Promotion, University of Kentucky, USA
[2]Department of Kinesiology, Mississippi State University, USA
email: mmsm235@g.uky.edu, web: https://education.uky.edu/khp/laboratories/biodynamics-laboratory/

INTRODUCTION

Baseball pitching is considered one of the most intense aspects within the game of baseball, as well as the most complicated dynamic throwing task in all of sports. The biomechanics of pitching have been heavily investigated in an attempt to identify optimal pitching mechanics in terms of pitching performance. Previous quantified upper body kinetics research has concluded that improved muscle strength is needed in attempting to achieve adequate upper body kinetics and efficient pitching performances. Therefore, it is the purpose of this research study to compare the lower extremity muscle and upper extremity muscle activation patterns and kinematic variables associated with the curveball pitch and the fastball pitch when pitching from the wind-up and stretch position.

METHODS

Twelve skilled (competed at the NCAA collegiate level) baseball pitchers volunteered to be research subjects for this study. The participants were fitted with six surface electromyography (EMG) bipolar electrodes (Delsys Inc., Boston, Massachusetts) on the stride leg biceps femoris, medial gastrocnemius, ipsilateral side (throwing arm side) lower trapezius, upper trapezius, triceps brachii and biceps brachii. Each participant underwent maximum voluntary isometric contraction (MVIC) testing and then performed a pitching analysis. All variables of interest were normalized using MVIC data and then compared between pitching types and pitch delivery. Shoulder rotation, elbow flexion and extension, elbow angular velocity and pelvis rotation were all collected with Cortex (Motion Analysis Corp., Santa Rosa, SA) and processed using Visual 3D software (C-Motion Inc., Germantown, MD). Paired t-tests and factorial analyses were performed using SPSS ($p \leq 0.05$).

Table 1: Demographic data including age, height, weight & pitching dominate hand (Mean±SD).

	All Subjects	Right Handed	Left Handed
Age (years)	22.33±4.54	23.44±4.69	19±1.73
Height (m)	1.742±0.13	1.73±0.15	1.77±0.06
Weight (kg)	89.02±10.98	85.6±8.17	99.27±13.62

RESULTS AND DISCUSSION

Differences in the peak and mean muscle activity for the fastball and curveball pitched from the wind-up and stretch position were seen to have differences showing significance. These findings suggest that upper and lower extremity muscle activity could be associated with enhanced pitching technique and pitching performance. The following tables show visual representation of the muscle activity comparison between the pitch type and pitch delivery. Refer to Table 2-Table 5 below for mean muscle activity and refer to Table 6-Table 9 for peak muscle activity below.

Differences in the kinematic variables between the fastball and curveball from the wind-up and stretch were also seen showing significance. Pitching kinematic differences associated with the diverse pitch types as well as the multiple pitch deliveries may impact the overall "wear and tear" on a pitcher's health and pitching arm. Refer to Table 10-Table 13 for the kinematic variables.

CONCLUSIONS

Many differences were found, between both the pitching type and the pitching delivery as well as the kinematic variables. These findings suggest that upper and lower muscle activity could be associated

with enhanced pitching technique and pitching performance to keep a baseball pitcher healthy and on the pitching mound longer into the season, decreasing the rate of injury. Shoulder rotation as well as the elbow angular velocity and elbow flexion-extension have an impact on the pitcher's ability to stay of the disabled list and in the game longer. Determining pitch types along with delivery types that enhance the pitcher's ability to stay active without injury will provide a way to make the game of baseball safer for the future generation of all stars.

Table 2: Mean Muscle Activity (Mean ±SD) for Stretch Fastball

Stretch Fastball Mean Muscle activity (% MVIC)						
	Biceps Brachii	Triceps Brachii	Upper Trapezius	Lower Trapezius	Biceps Femoris	Gastrocnemius
Foot Contact	14.98±1.8	5.84±1.8	4.95±1.3	3.49±1.2	32.42±1.6	31.79±1.2
Maximal External Rotation	36.02±1.1	91.71±1.7	45.73±2.4	7.18±1.8	22.69±0.9	66.2±1.8
Ball Release	26.05±1.3	205.22±2.7	46.96±1.9	3.87±1.2	99.64±1.3	142.15±1.3
Maximal Internal Rotation	15.65±1.2	19.23±1.9	3.38±2.6	2.55±2.3	115.63±1.2	120.2±.75

Table 3: Mean Muscle Activity (Mean ±SD) for Stretch Curveball

Stretch Curveball Mean Muscle activity (% MVIC)						
	Biceps Brachii	Triceps Brachii	Upper Trapezius	Lower Trapezius	Biceps Femoris	Gastrocnemius
Foot Contact	13.34±2.4	4.84±1.3	3.96±1.2	2.61±1.1	29.23±1.6	29.41±1.4
Maximal External Rotation	34.18±1.0	92.60±1.6	44.44±2.3	6.30±1.7	20.84±0.9	65.32±1.84
Ball Release	23.87±1.3	203.33±2.8	45.97±1.9	2.99±1.2	97.44±1.3	140.15±1.3
Maximal Internal Rotation	14.77±1.2	16.05±1.7	2.41±0.9	2.01±1.3	110.8±1.9	118.75±1.2

Table 4: Mean Muscle Activity (Mean ±SD) for Wind-Up Fastball

Wind-Up Fastball Mean Muscle activity (% MVIC)						
	Biceps Brachii	Triceps Brachii	Upper Trapezius	Lower Trapezius	Biceps Femoris	Gastrocnemius
Foot Contact	12.96±1.5	5.08±1.1	3.97±1.0	2.60±1.0	14.77±1.8	30.50±1.4
Maximal External Rotation	34.18±1.0	91.00±2.1	44.45±2.3	6.30±1.7	21.46±0.9	65.20±1.8
Ball Release	23.88±1.3	202.24±1.6	45.97±1.9	2.99±1.2	98.36±1.3	140.3±1.3
Maximal Internal Rotation	11.21±1.4	11.21±1.3	1.99±3.1	1.91±1.2	105.9±2.3	109.0±0.9

Table 5: Mean Muscle Activity (Mean ±SD) for Wind-Up Curveball

Wind-Up Curveball Mean Muscle activity (% MVIC)

	Biceps Brachii	Triceps Brachii	Upper Trapezius	Lower Trapezius	Biceps Femoris	Gastrocnemius
Foot Contact	13.28±1.0	5.7±1.3	4.80±1.2	2.50±1.0	29.23±1.5	29.41±1.4
Maximal External Rotation	34.35±1.1	89.73±1.7	44.18±2.4	5.56±1.8	20.85±0.9	65.32±1.84
Ball Release	22.42±1.3	202.25±2.8	45.06±1.9	3.25±1.2	97.45±1.3	140.15±1.3
Maximal Internal Rotation	10.80±1.1	08.31±1.10	1.07±1.1	1.60±1.6	100.31±1.0	101.3±2.2

Table 6: Peak Muscle Activity (Mean ±SD) for Stretch Fastball

Stretch Fastball Mean Muscle activity (% MVIC)						
	Biceps Brachii	Triceps Brachii	Upper Trapezius	Lower Trapezius	Biceps Femoris	Gastrocnemius
Foot Contact	35.93±3.4	9.67±1.3	13.72±1.2	7.77±1.0	37.3±1.6	42.52±1.4
Maximal External Rotation	35.86±9.5	92.63±3.2	55.36±2.4	11.17±1.8	31.58±0.9	76.07±1.8
Ball Release	38.93±1.3	215.47±2.54	55.63±1.9	11.13±1.2	110.91±1.3	155.40±1.3
Maximal Internal Rotation	15.65±1.20	22.17±1.1	5.54±1.8	4.15±1.6	127.80±1.3	130.01±.98

Table 7: Peak Muscle Activity (Mean ±SD) for Stretch Curveball

Stretch Curveball Mean Muscle activity (% MVIC)						
	Biceps Brachii	Triceps Brachii	Upper Trapezius	Lower Trapezius	Biceps Femoris	Gastrocnemius
Foot Contact	27.76±1.8	8.73±1.3	7.75±1.2	6.28±1.0	40.6±1.6	43.19±1.4
Maximal External Rotation	34.18±11.7	92.60±3.4	44.45±3.6	6.30±2.0	35.57±0.9	75.99±1.8
Ball Release	32.56±1.3	215.98±2.8	57.25±1.9	8.53±1.2	97.45±1.3	150.21±2.0
Maximal Internal Rotation	31.51±1.2	47.59±1.1	20.92±12.5	13.92±6.6	139.3±1.3	140.50±1.0

Table 8: Peak Muscle Activity (Mean ±SD) for Wind-Up Fastball

Wind-Up Fastball Mean Muscle activity (% MVIC)						
	Biceps Brachii	Triceps Brachii	Upper Trapezius	Lower Trapezius	Biceps Femoris	Gastrocnemius
Foot Contact	23.74±1.8	12.09±1.3	11.49±1.2	9.94±1.0	38.7±1.2	30.50±1.4
Maximal External Rotation	44.10±1.5	103.05±1.7	56.66±2.4	16.64±1.8	29.62±1.9	65.20±1.8
Ball Release	37.28±3.7	218.53±2.8	65.94±1.9	17.17±1.2	109.61±1.9	140.27±1.3
Maximal Internal Rotation	24.05±1.20	34.28±1.1	11.34±1.9	8.95±16	132.31±1.25	139.68±0.94

Table 9: Peak Muscle Activity (Mean ±SD) for Wind-Up Curveball

Wind-Up Fastball Mean Muscle activity (% MVIC)						
	Biceps Brachii	Triceps Brachii	Upper Trapezius	Lower Trapezius	Biceps Femoris	Gastrocnemius
Foot Contact	24.55±1.8	14.60±1.3	12.57±1.2	11.39±1.0	24.87±1.8	41.89±1.4
Maximal External Rotation	45.80±2.2	101.00±1.7	53.41±2.4	12.12±1.8	30.46±0.9	75.43±1.8
Ball Release	33.16±1.3	217.93±2.8	55.94±1.9	10.71±1.2	106.60±1.3	151.60±1.3
Maximal Internal Rotation	24.84±1.2	34.77±1.1	11.95±1.93	8.66±1.6	134.48±1.30	152.99±4.9

Table 10: Stretch Curveball Mean Kinematic Data including Elbow Flexion, Elbow Angular Velocity, Shoulder Rotation & Pelvis Rotation

	Elbow Flexion (Degrees)	Elbow Angular Velocity (Degrees/sec)	Shoulder Rotation (Degrees)	Pelvis Rotation (Degrees)
Foot Contact	82.76±3.00	24.84±3.58	128.57±2.16	75.47±4.42
Maximal External Rotation	79.86±3.01	1.61±2.83	30.84±5.72	60.90±3.95
Ball Release	29.53±2.91	-1349.47±5.06	82.56±5.02	88.51±.4.08
Maximal Internal Rotation	57.17±1.9	774.10±3.24	173.24±6.36	88.89±3.21

Table 411: Stretch Fastball Mean Kinematic Data including Elbow Flexion, Elbow Angular Velocity, Shoulder Rotation & Pelvis Rotation

	Elbow Flexion (Degrees)	Elbow Angular Velocity (Degrees/sec)	Shoulder Rotation (Degrees)	Pelvis Rotation (Degrees)
Foot Contact	85.71±2.40	28.13±3.83	164.12±4.71	73.29±4.98
Maximal External Rotation	82.81±1.88	4.90±6.01	35.84±6.23	58.72±6.19
Ball Release	32.48±2.20	-1345.18±4.17	87.56±4.82	86.33±5.93
Maximal Internal Rotation	60.13±1.93	77.39±2.99	179.34±5.59	86.71±6.45

Table 4.12: Wind-Up Curveball Mean Kinematic Data including Elbow Flexion, Elbow Angular Velocity, Shoulder Rotation & Pelvis Rotation

	Elbow Flexion (Degrees)	Elbow Angular Velocity (Degrees/sec)	Shoulder Rotation (Degrees)	Pelvis Rotation (Degrees)

Foot Contact	33.74±2.59	37.90±7.24	154.90±3.18	79.47±5.83
Maximal External Rotation	92.41±2.01	6.76±5.90	35.51±4.47	93.99±6.01
Ball Release	33.68±2.48	-1078.21±7.96	69.60±5.02	96.72±5.97
Maximal Internal Rotation	55.08±1.92	308.96±8.64	140.92±3.96	91.89±6.78

Table 4.13: Wind-Up Fastball Mean Kinematic Data including Elbow Flexion, Elbow Angular Velocity, Shoulder Rotation & Pelvis Rotation

	Elbow Flexion (Degrees)	Elbow Angular Velocity (Degrees/sec)	Shoulder Rotation (Degrees)	Pelvis Rotation (Degrees)
Foot Contact	36.49±2.40	46.43±8.00	161.67±12.15	74.36±2.71
Maximal External Rotation	95.16±1.61	15.29±5.81	55.89±14.21	88.87±3.10
Ball Release	36.43±1.87	-1069.23±7.26	89.98±13.24	91.61±2.26
Maximal Internal Rotation	57.83±2.3	317.49±8.80	146.30±14.48	86.77±3.39

REFERENCES

1. Aguinaldo, A.L., J. Buttermore, and H. Chambers, *Effects of upper trunk rotation on shoulder joint torque among baseball pitchers of various levels.* J Appl Biomech, 2007. **23**(1): p. 42-51.
2. Campbell, B.M., D.F. Stodden, and M.K. Nixon, *Lower extremity muscle activation during baseball pitching.* J Strength Cond Res, 2010. **24**(4): p. 964-71.
3. Conte, S.A., et al., *Prevalence of Ulnar Collateral Ligament Surgery in Professional Baseball Players.* Am J Sports Med, 2015. **43**(7): p. 1764-9.
4. Cordo, P.J. and L.M. Nashner, *Properties of postural adjustments associated with rapid arm movements.* J Neurophysiol, 1982. **47**(2): p. 287-302.
5. Dillman, C.J., G.S. Fleisig, and J.R. Andrews, *Biomechanics of pitching with emphasis upon shoulder kinematics.* J Orthop Sports Phys Ther, 1993. **18**(2): p. 402-8.
6. Dun, S., et al., *Biomechanical comparison of the fastball from wind-up and the fastball from stretch in professional baseball pitchers.* Am J Sports Med, 2008. **36**(1): p. 137-41.
7. Ellenbecker, T.S., et al., *Glenohumeral joint total rotation range of motion in elite tennis players and baseball pitchers.* Med Sci Sports Exerc, 2002. **34**(12): p. 2052-6.
8. Erickson, B.J., et al., *Is Tommy John Surgery Performed More Frequently in Major League Baseball Pitchers From Warm Weather Areas?* Orthop J Sports Med, 2014. **2**(10): p. 2325967114553916.
9. Escamilla, R.F., et al., *Pitching biomechanics as a pitcher approaches muscular fatigue during a simulated baseball game.* Am J Sports Med, 2007. **35**(1): p. 23-33.
10. Fabricant, P.D., et al., *Return to play after anterior cruciate ligament reconstruction in*

major league baseball athletes. Arthroscopy, 2015. **31**(5): p. 896-900.
11. Fleisig, G.S., et al., *Risk of serious injury for young baseball pitchers: a 10-year prospective study.* Am J Sports Med, 2011. **39**(2): p. 253-7.
12. Fleisig, G.S., et al., *Kinetics of baseball pitching with implications about injury mechanisms.* Am J Sports Med, 1995. **23**(2): p. 233-9.
13. Fleisig, G.S., et al., *Kinematic and kinetic comparison of baseball pitching among various levels of development.* J Biomech, 1999. **32**(12): p. 1371-5.
14. Fleisig, G.S., et al., *Biomechanical comparison of baseball pitching and long-toss: implications for training and rehabilitation.* J Orthop Sports Phys Ther, 2011. **41**(5): p. 296-303.
15. Fleisig, G.S., et al., *Kinetic comparison among the fastball, curveball, change-up, and slider in collegiate baseball pitchers.* Am J Sports Med, 2006. **34**(3): p. 423-30.
16. Fronek, J., et al., *Shoulder functional performance status of Minor League professional baseball pitchers.* J Shoulder Elbow Surg, 2015. **24**(1): p. 17-23.
17. Hermens, H.J., et al., *Development of recommendations for SEMG sensors and sensor placement procedures.* Journal of electromyography and Kinesiology, 2000. **10**(5): p. 361-374.
18. Hirashima, M., et al., *Sequential muscle activity and its functional role in the upper extremity and trunk during overarm throwing.* J Sports Sci, 2002. **20**(4): p. 301-10.
19. Jobe, F.W., et al., *An EMG analysis of the shoulder in pitching. A second report.* Am J Sports Med, 1984. **12**(3): p. 218-20.
20. Keeley, D.W., G.D. Oliver, and C.P. Dougherty, *Shoulder kinematics during pitching: comparing the slide step and traditional stretch deliveries.* Hum Mov Sci, 2012. **31**(5): p. 1191-9.
21. Keller, R.A., et al., *Major League Baseball pitch velocity and pitch type associated with risk of ulnar collateral ligament injury.* J Shoulder Elbow Surg, 2016. **25**(4): p. 671-5.
22. Kibler, W.B., *Role of the scapula in the overhead throwing motion.* Contemp., 1991. **22**: p. 525-535.
23. Kibler, W.B., J. Press, and A. Sciascia, *The role of core stability in athletic function.* Sports Med, 2006. **36**(3): p. 189-98.
24. MacWilliams, B.A., et al., *Characteristic ground-reaction forces in baseball pitching.* Am J Sports Med, 1998. **26**(1): p. 66-71.
25. Matsuo, T., et al., *Contributions of factors based on kinematic relationship to the inter-subject variability of baseball pitch velocity.* J Appl Biomech, 2001. **17**(1): p. 1-13.
26. Matsuo, T. and G.S. Fleisig, *Influence of shoulder abduction and lateral trunk tilt on peak elbow varus torque for college baseball pitchers during simulated pitching.* J Appl Biomech, 2006. **22**(2): p. 93-102.
27. Matsuo, T., et al., *Optimal shoulder abduction angles during baseball pitching from maximal wrist velocity and minimal kinetics viewpoints.* Journal of Applied Biomechanics, 2002. **18**(4): p. 306-320.
28. McMullen, J. and T.L. Uhl, *A kinetic chain approach for shoulder rehabilitation.* J Athl Train, 2000. **35**(3): p. 329-37.
29. Murray, T.A., et al., *The effects of extended play on professional baseball pitchers.* Am J Sports Med, 2001. **29**(2): p. 137-42.
30. Myers, J.B., et al., *Scapular position and orientation in throwing athletes.* Am J Sports Med, 2005. **33**(2): p. 263-71.
31. Oliver, G.D. and D.W. Keeley, *Gluteal muscle group activation and its relationship with pelvis and torso kinematics in high-school baseball pitchers.* J Strength Cond Res, 2010. **24**(11): p. 3015-22.
32. Oliver, G.D. and D.W. Keeley, *Pelvis and torso kinematics and their relationship to shoulder kinematics in high-school baseball pitchers.* The Journal of Strength & Conditioning Research, 2010. **24**(12): p. 3241-3246.
33. Olsen, S.J., 2nd, et al., *Risk factors for shoulder and elbow injuries in adolescent baseball pitchers.* Am J Sports Med, 2006. **34**(6): p. 905-12.
34. Pappas, A.M., R.M. Zawacki, and C.F. McCarthy, *Rehabilitation of the pitching*

shoulder. Am J Sports Med, 1985. **13**(4): p. 223-35.
35. Pappas, A.M., R.M. Zawacki, and T.J. Sullivan, *Biomechanics of baseball pitching. A preliminary report.* Am J Sports Med, 1985. **13**(4): p. 216-22.
36. Reinold, M.M., et al., *Changes in shoulder and elbow passive range of motion after pitching in professional baseball players.* Am J Sports Med, 2008. **36**(3): p. 523-7.
37. Sabick, M.B., et al., *Humeral torque in professional baseball pitchers.* Am J Sports Med, 2004. **32**(4): p. 892-8.
38. Sabick, M.B., et al., *Valgus torque in youth baseball pitchers: A biomechanical study.* J Shoulder Elbow Surg, 2004. **13**(3): p. 349-55.
39. Stodden, D.F., et al., *Relationship of biomechanical factors to baseball pitching velocity: within pitcher variation.* Journal of applied biomechanics, 2005. **21**(1): p. 44-56.
40. Stodden, D.F., et al., *Relationship of pelvis and upper torso kinematics to pitched baseball velocity.* Journal of applied biomechanics, 2001. **17**(2): p. 164-172.
41. Watkins, R.G., et al., *Dynamic EMG analysis of torque transfer in professional baseball pitchers.* Spine (Phila Pa 1976), 1989. **14**(4): p. 404-8.
42. Werner, S.L., et al., *Biomechanics of the elbow during baseball pitching.* J Orthop Sports Phys Ther, 1993. **17**(6): p. 274-8.
43. Werner, S.L., et al., *Relationships between throwing mechanics and shoulder distraction in professional baseball pitchers.* Am J Sports Med, 2001. **29**(3): p. 354-8.
44. Yamanouchi, T., *EMG analysis of the lower extremities during pitching in high-school baseball.* Kurume Med J, 1998. **45**(1): p. 21-5.
45. Zattara, M. and S. Bouisset, *Posturo-kinetic organisation during the early phase of voluntary upper limb movement. 1. Normal subjects.* J Neurol Neurosurg Psychiatry, 1988. **51**(7): p. 956-65.

ON THE PLYOMETRIC NATURE OF OLYMPIC WEIGHTLIFTING

Antonio Squillante

A.T. Still University, Mesa, AZ, USA
email: anto.squillante@gmail.com

INTRODUCTION

Olympic-style weightlifting exercises have found their place in the training of speed and power athletes. Evidence in the most recent academic literature seems to suggest underlying similarities between performance in Olympic weightlifting and performance in sports; however, the assumption that Olympic-style weightlifting derivatives can be as effective, if not more effective, in improving performance on the field and on the court of play has resulted in a tendency to overlook some of the "*unique aspects in competitive weightlifting*" that can further benefit the development of well-rounded athletes. A better understanding of the nature of these explosive movements - snatch, clean and jerk - can provide more insights on the use of Olympic-style weightlifting exercises and their derivatives to improve performance in speed and power events

METHODS

A systematic review of the most recent academic literature provides kinetic and kinematic data to define the relationship between the change in vertical ground reaction force (GRF), peak vertical bar velocity, and the average joint angular displacement and angular velocity during the pull in Olympic-style weightlifting. A comparison between the biomechanical characteristics of the second pull in Olympic weightlifting and jumping mechanics provides a rational explanation for the positive transfer of training between Olympic-style weightlifting exercises and performance in activities involving sprinting, jumping and changing direction..

RESULTS AND DISCUSSION

Peak power output has long been considered as the main criteria to determine some degree of similarity between the pull in Olympic weightlifting and performance in sport. This approach originally proposed by Garhammer and Gregor in 1992 has eventually led to abandon the practice of competition lifts in favor of less complex, easier to learn variations of these movements such as pulls, high pulls, and power shrugs. By comparing the biomechanical model of the pull in Olympic weightlifting originally proposed by Enoka, Takano and Garhammer with the most recent data describing the change in vertical GRF, peak vertical bar velocity, average angular displacement and average angular velocity at the hip and knee joint during the snatch, clean and jerk it is possible to define important similarities between these explosive movements and jumping mechanics, the paradigm of athletic performance in speed and power events. This biomechanical model provides evidence on the plyometric nature of Olympic weightlifting, defining a rational explanation for the positive transfer of training between these competitive lifts and performance on the field and on the court of play. During the pull in Olympic weightlifting, by the time vertical GRF peaks - during the transition between first pull and second pull - knees bend under load of approximately 16.2 ± 6.64 degrees while the angle at hips progressively increases from 89.5 ± 2.47 degrees of flexion (with an angle at the knee joint of approximately 134 ± 7.59 degrees) to 58 ± 2.47 degrees of flexion (with an angle at the knee joint of approximately 117.8 ± 6.62 degrees). As knees are extending during the liftoff, hamstrings and glutes undergo a time of vigorous, violent eccentric contraction while their proximal insertion stays still to preserve the angle at the hip joint [1,2]. Dampening mechanics in weightlifting closely resemble the amortization phase in regular, standing vertical jumping as confirmed by the significant similarities between the power position in Olympic weightlifting and the take-off position in jumping mechanics; knee and

hip joint position at the beginning of the second pull (approximately 70 degrees of knee flexion and approximately 55 degrees of hip flexion) correspond with the knee and hip angle at the takeoff in jumping mechanics. Approximately 70 degrees of knee flexion and 55 degrees of hip flexion have been shown to provide the most significant mechanical advantage in the development of peak power output [2,3]. These findings have been previously validated in practical and mathematical models based on vertical jump mechanics, depth jump mechanics and sprinting mechanics, especially within the 10-30m distances more often common in sports. The transition between first pull and second pull only lasts for approximately 0.148 ± 0.015 seconds - less than 160 m/sec, the average coupling time in high power, plyometric activities as original confirmed by Bosco, Viitasalo, Komi, and Luhtanen - and it initiates the fast, concentric, muscle action of the lower extremities that results in a sudden increase in vertical bar velocity. From the power position, a higher degree of angular velocity at the hip joint compared to the knee joint - maximum hip extension velocity during the second pull of 460.7 ± 27 degrees·s-1 compared to maximum knee extension velocity during the second pull of 390 ± 49.4 degrees·s-1 - reveals a higher contribution of hamstrings and glutes over quadriceps, as a consequence of the stretch-shortening cycle taking place during the second knee bent [1,2,3]. This pattern confirms the proximal-to-distal activation sequence in the lower extremity described by Bobbert and van Ingen Schenau as the blueprint of power development in sports. Both kinetic and kinematic between the pull in Olympic weightlifting and jumping mechanics are further supported by the absolute level of peak power output and peak vertical bar velocity (compared to peak vertical velocity of the athlete center of gravity as measured in the countermovement vertical jump) achieved at the end of second pull: approximately 3000 N of vertical ground reaction force and bar velocity in excess of 1.32 m/sec. However, it seems reasonable to consider how the plyometric nature of Olympic weightlifting is inherent to the active transition from first to second pull whereas movements initiated at the power position (see hang power snatch and hang power clean, pulls and high pulls) rely on the ability to create a high level of starting strength without taking full advantage of the physiological stretch-shortening cycle involved in athletic-like activities.

CONCLUSIONS

Average knee and hip angular displacement in the snatch, clean and jerk has never been studied as a function of the different distribution of GRF and relative change in bar velocity during the entire pull. Models describing both kinetic and kinematic evaluation of the pull in Olympic weightlifting have been derived from hang power snatch and hang power clean without taking into consideration the different distribution of vertical GRF throughout the entire pull. This review provides a mechanical model that can be used to describe important kinetic and kinematic similarities between snatch, clean and jerk and jumping mechanics, the paradigm of power development in sports. These findings confirm the plyometric nature of Olympic-style weightlifting exercises, encouraging the use of full lifts (competition lifts) rather than Olympic-style weightlifting derivatives in the training of speed and power athletes.

REFERENCES

1. Gourgoulis, V., Aggeloussis, N., Antoniou, P., Christoforidis, C., Mavromatis, G., & Garas, A. (2002). Comparative 3-dimensional kinematic analysis of the snatch technique in elite male and female greek weightlifters. *The Journal of Strength & Conditioning Research*, **16(3)**, 359-366.
2. Kipp, K., Redden, J., Sabick, M., & Harris, C. (2012). Kinematic and kinetic synergies of the lower extremities during the pull in Olympic weightlifting. *Journal of applied biomechanics*, **28(3)**, 271-278.
3. Moolyk, A. N., Carey, J. P., & Chiu, L. Z. (2013). Characteristics of lower extremity work during the impact phase of jumping and weightlifting. *The Journal of Strength & Conditioning Research*, **27(12),** 3225-3232.

BIOMECHANICS DIFFER IN HIGH SCHOOL PITCHERS BASED ON INJURY HISTORY

[1] Aaron Struminger, [2] Alfred Atanda, [3] Thomas Buckley, [3] James Richards, [3] Charles Buz Swanik

[1] Eastern Michigan University, Ypsilanti, MI
[2] Nemours/Alfred I. DuPont Hospital for Children, Wilmington, DE
[3] University of Delaware, Newark, DE
email: astrumin@emich.edu

INTRODUCTION

Chronic, recurrent injuries in baseball pitchers may be a result of specific biomechanics which have been associated with excessive joint loading in the shoulder and elbow [1, 2]. Since pitching mechanics remain relatively consistent over time [3], injured pitchers could maintain those potentially harmful biomechanical patters after they have returned to play. Furthermore, injury could limit range of motion or strength, creating differences in the biomechanics of previously uninjured pitchers.

Two previous studies have examined biomechanics in post-surgical professional pitchers, but the athletes in those investigations had undergone surgery and typically have better access to coaching and rehabilitation specialists than high school athletes [4, 5]. Therefore, the purpose of this investigation was to determine whether pitching mechanics differ between high school baseball pitchers who have a history of injury and those who do not.

METHODS

High school aged, male baseball athletes (n = 43, age = 15.6 ± 1.3 years, height = 178.7 ± 6.1 cm, weight = 73.5 ± 12.4 kg) who had played the position of pitcher for at least two consecutive seasons participated in this investigation. Participants who reported a shoulder or elbow injury that caused them to miss at least one scheduled practice or game were placed into the injury group (n = 16). Participants who did not report any previous upper extremity injury were classified as uninjured (n = 27). All participants were not injured at the time of testing.

Three-dimensional coordinate data were recorded using a 12 camera motion-capture system (Motion Analysis Corporation, Santa Rosa, CA) collecting at a speed of 240 Hz. Retroreflective markers were placed over visual anatomical landmarks, which were then used to define joint centers and axes. Visual3D (C-Motion Inc, Germantown, MD) was used to calculate joint angles during specific phases of the pitching motion from the position of the retroreflective markers.

Each pitcher warmed up and threw at least 10 pitchers from the indoor mound at a regulation distance. The fastest 3 pitches thrown for strikes were used for analysis. The coordinate systems for each upper extremity joint were constructed via recommendations from the International Society of Biomechanics (ISB). The ball was added as a 142g point mass immediately anterior to the 3rd metacarpal marker and was removed from the model at ball release. Shoulder abduction, shoulder external rotation, shoulder horizontal abduction, elbow flexion, and trunk lateral flexion were calculated at five different points of the pitching motion (stride foot contact, maximum external rotation, ball release, maximum elbow varus moment, and maximum shoulder distraction force using recommended ISB rotation sequences.

One athlete in the uninjured group was removed from the analysis due to incomplete injury data. Binary recursive partitioning was performed in JMP to screen kinematic variables as well as height, weight, and ball velocity for a subsequent logistic regression. The logistic regression was performed in SPSS and evaluated how well the dependent variables predicted injury history.

RESULTS AND DISCUSSION

All 16 injured athletes reported missing at least one week of competition as a result of the reported injury. Even though no athlete underwent surgery, 11 of the

16 injured pitchers were instructed by medical professionals to refrain from, or drastically alter, overhead activity for at least three months following the injury. Athletes threw at a speed of 29.99 ± 2.63 meters per second (67.1 ± 5.9 miles per hour) with no differences between groups.

Binary recursive partitioning in JMP identified four variables (shoulder abduction at stride foot contact, lateral trunk tilt at maximum internal varus moment, shoulder abduction at maximum external rotation, and horizontal abduction at ball release) that were able to significantly improve the model. Results of the binary logistic regression showed a statistically significant improvement over the constant only model ($\chi^2 = 10.563$, df = 4, $p = .032$). The Nagelkerke R^2 indicated that the model accounted for 30.2% of the variance with an f^2 of .432, suggesting a large effect size of the four predictors in discriminating between pitchers with and without previous injury. Only one variable, shoulder abduction at the point of maximum external rotation, was identified as a statistically significant predictor (p = .026). Athletes who displayed less abduction at the time point of maximum external rotation were more likely to be placed in the injured group (Figure 1).

Predictive success was evaluated for cases used in the development of the model. Overall classification accuracy was 78.6%. Sensitivity was moderate (68.8%) and specificity was high (84.6%).

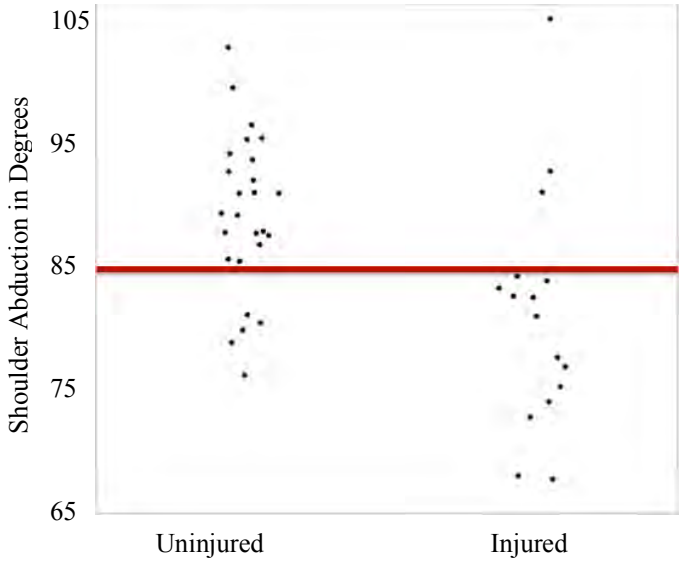

Figure 1: Shoulder abduction values at time of maximum external rotation

The restriction of abduction at maximum external rotation is commonly described by pitching coaches as "dropping the elbow." That biomechanical pattern can lead to increased medial elbow load [1], which could have predisposed the injured athletes towards elbow pain. Furthermore, a lack of shoulder flexibility and strength, as a result of the injury itself, could have led to the limited abduction in the injured group. That biomechanical pattern could been a compensation to prevent glenohumeral translation and reduce potential for rotator cuff tendon impingement and subsequent pain in those previously injured athletes.

CONCLUSIONS

This study contributes to the limited information on biomechanics in pitchers after injury. Shoulder abduction at maximum external rotation successfully grouped high school pitchers with and without previous injury history. Shoulder external rotation and horizontal abduction, elbow flexion, and lateral trunk flexion did not differentiate between groups at any time point during the cocking, acceleration, or deceleration phase. Height, weight, and ball velocity also did not accurately identify injury group.

Our results indicate athletes who have suffered a previous injury pitched differently than those with no injury history, even after they had been cleared for full competition. Therefore, clinicians, coaches, and parents may want to identify and begin conversations about injury in youth pitchers who throw with a reduced shoulder abduction angle to provide early interventions. Future studies should examine rehabilitation techniques that could help restore proper shoulder abduction angles in this population.

REFERENCES

1. Matsuo T and Fleisig GS. *J Appl Biomech*. **22** (2): 2006.
2. Sabick MB et al. *Am J Sports Med.* **32** (4): 2004.
3. Fleisig GS et al. *Am J Sports Med*. **46** (1): e0363546517732034, 2017.
4. Fleisig GS et al. *Am J Sports Med*. **43** (5): e0363546515570464, 2015
5. Laughlin WA et al. *Am J Sports Med.* **42** (12): e0363546514552183.

Upper Extremity Forces During Water Tubing

Bethany Suderman, Irving Scher

Guidance Engineering, Seattle, WA, USA
email: suderman@guidanceengineering.com, web: www.guidanceengineering.com

INTRODUCTION

Water tubing is a popular water sport, as it requires little skill on behalf of the rider. Injuries can occur due to collisions with other riders, impact with the water, or unsafe boat driving.[1] According to the National Electronic Injury Surveillance System between the years of 2002 and 2016 there were over 93,000 estimated injuries that occurred related to water tubing. Approximately 23% of these injuries were upper extremity injuries (finger, elbow, hand, lower arm, shoulder, upper arm and wrist). Riders must maintain a grip on the handles to stay on the tube and not fall.The loads on the upper extremities could be high in the event of the tube catching air and impacting the water or the tube being whipped back and forth. These injuries could occur due to the loads required to maintain a grip on the handle or due to falls when the rider can no longer maintain a grip and impacts the water. The purpose of this study was to determine the on-water loads on the upper extremity during water tubing. We hypothesize that forces on the upper extremity will increase with rider weight.

METHODS

Testing was conducted on a lake in the Conway chain in Orlando, Florida. All towable tubes were towed behind a 21-foot 2004 Super Air Nautique boat. Eight towable tubes were tested: two one-rider tubes, one two-rider tube, four three-rider tubes and one six-rider tube; see Table 1. The multi-rider tubes were tested with one, two and up to 5 riders where applicable. All tubes were towed with a 65-foot rope.

Table 1:Tube type and size.

	Donut	Cockpit	Deck	Sit-on -top	Total
1-rider	1		1		2
2-rider				1	1
3-rider		2	1	1	4
6-rider				1	1
Total	1	2	2	3	8

The boat was instrumented with a GPS data logger (G2X Extreme Data Logger 600-KT-G2XRND; Rancho Santa Margarita, CA). Boat position, and velocity were collected using GPS data. The force applied to each handle was measured with two single-axis load cells (WMC-500; Interface, Scottsdale, AZ) with a 2,224-N capacity.. Data were acquired at 2500 Hz.

Fourteen riders participated in the study (9 males; 5 females). The average age of the participants was 31.9 (std; ± 8.0) years; the average height was 1.78 m (std; ± 0.11 m) and the average weight was 72.7 kg (std; ± 15.0 kg). All participants provided written informed consent prior to participation.

For each test the boat driver was instructed to drive straight to bring the tube and rider to plane. After the tube and rider were brought to plane the boat driver drove the boat in semi-circle turns and brought the tube across wakes and bumps.

Handle force was filtered with a low-pass, 8th order, zero-phase shift butterworth filter with a cutoff frequency of 150 Hz. Total handle force was calculated by summing the two load cell forces on each handle to determine the total force acting on the upper extremity for each arm. Peak handle force was determined for each test. Peak handle force was plotted verse rider weight and fit with a linear fit.

RESULTS AND DISCUSSION

A total of 103 tests were completed. The peak overall handle force measured was 973 N. This occurred on the cockpit style tube during an event where the rider fell off of the tube and was dragged in the water for a short distance before letting go.

Peak handle force was compared to rider weight for each test; see Figure 1. A slight trend in increasing peak handle force with increasing rider weight can be seen; however, the R-squared coefficient for a linear fit was approximately 0.1.

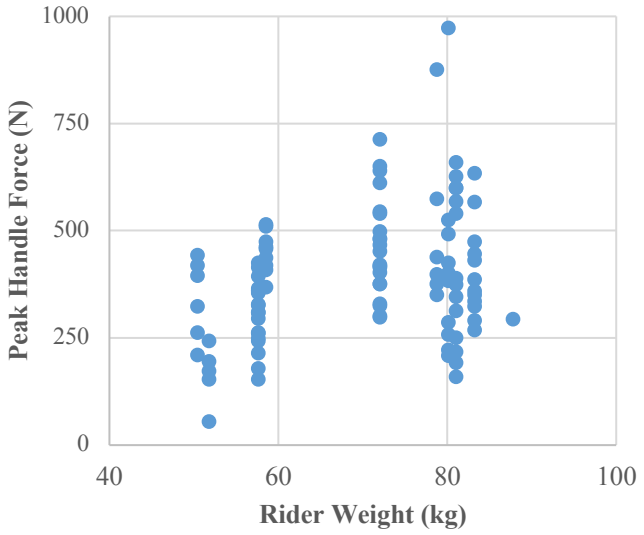

Figure 1: Peak handle force for each test plotted against rider weight.

The peak handle force is most likely related to both rider weight and the event at which time the peak handle force occurred. For example, the overall peak handle force measured occurred during an event in which the rider partially fell off of the tube and was dragged in the water. In order to best understand the effect of rider weight, peak handle forces should also be categorized by event; such as, tube whipped, tube caught air and hit water, rider partially fell or fully fell into water.

According to a study by Arcini et al. 2002, hand grip strength ranged from 38 to 160 kg (373 to 1570 N).[2] This suggests that the handle forces measured during some of the events on the tube may to be too great for some riders to maintain a grip and could lead to a fall and possible injury.

CONCLUSIONS

The correlation of peak handle force to rider weight was low. Tubing event should be taken into account along with rider weight to find a better correlation. The load required to maintain a grip on the handle of the tube to prevent a fall may be too large for some riders to maintain during certain events.

REFERENCES

1. Heinsimer et al. *Journal of Physical Activity & Health*. 10:2, 2013.
2. Incel et al. *Grip Strength: Effect of Hand Dominance*. Singapore Med J 43:5 2002.

MULTIVARIATE ANALYSIS OF THE MAGNITUDE AND TEMPORAL COMPONENTS OF GROUND REACTION FORCE DURING THE GOLF SWING: A PILOT STUDY

[1] Aaron T. Trunt, [2] Zadok J. K. Isaacs, and [1,2]Lisa N. MacFadden

[1] Department of Biomedical Engineering, University of South Dakota, Sioux Falls, SD, United States
[2] Sanford Sports Science Institute, Sioux Falls, SD, United States
email: aaron.trunt@coyotes.usd.edu

INTRODUCTION

The golf swing is a multifaceted kinetic movement utilizing all planes of motion that has been found to not only be reliant on the overall production of forces but also the timing of when this force production occurs. The force exerted from the ground on the golfer, or ground reaction force (GRF), is a popular area of study in golf biomechanics. However, using GRF to accurately predict golf performance has been difficult due to the complexity of the swing. Previous research suggests that since the golf swing is happening in multiple planes, analyzing just one component of the ground reaction force produced by the golfer is not a sufficient way to predict performance [1].

The purpose of this study was to assess the peak GRF produced in each direction during the golf swing as well as the timing of these forces and their respective relationship with performance (measured in club speed) for two different clubs.

METHODS

This study was approved by the Sanford Institutional Review Board. Nineteen (6 females and 13 males) golfers (age 14-30) of varying skill levels from middle school to professional participated in this study. Subjects were asked to hit 10 balls with a driver and a 6 iron in an indoor biomechanics lab. Swing data was recorded using two high speed 2-D cameras (one positioned down the line and one positioned anterior to the golfer recording at 200 Hz), a FlightScope Xi launch monitor, and two force plates (Bertec Co., Columbus Ohio) one placed under each foot of the golfer. Univariate as well as bivariate regression models were made to assess the relationships between normalized magnitude, time, and direction of GRF with club speed as the dependent variable. Figure 1 shows the GRF directions relative to each subject's feet on each force plate. All statistical analysis was performed in MATLAB (Mathworks, Natick MA).

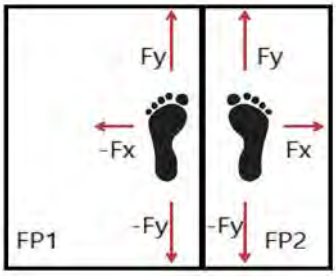

Figure 1: Force Plate Configuration: Fz is the vertical force (positive direction up from the plate).

RESULTS AND DISCUSSION

Table 1 shows the statistical results and variables used to predict performance as accurately as possible with the 6 iron. Although all models were significant on a 95% confidence interval (α=.05), univariate linear models were the worst predictors of performance for each GRF component. This suggests the relationship between club head speed and different GRF variables is not strongly linearly dependent and a simple linear increase in these variables would not have a large impact on club speed. Alternatively, quadratic models were much better predictors of club speed in the 6 iron using one variable (Table 1). These results suggest that there is a potential "sweet spot" regarding these GRF variables. For example, the most accurate predictor of club speed in the F_y direction was the amount of time between the back-foot peak GRF and ball contact in the quadratic model. Thus, if peak GRF was produced too early or too late in the F_y direction on the back foot this could cause a potential over-rotation or under-rotation of the trunk ultimately affecting club speed.
Furthermore, it was found that quadratic statistical models using more than one variable were even

better predictors of club speed than their univariate predecessors for the 6 iron. These bivariate models involve both a GRF peak variable and a temporal variable with high R^2 values (>0.88) for all directions except F_x. The quality of these models, along with the fact that a temporal and GRF peak component are utilized, show that club speed is dependent on both how much GRF a person can produce, and when that peak GRF is produced both in quadratic fashion. The results imply that too much as well as too little GRF production is not beneficial to club speed and instead there is an optimal amount of GRF a golfer should be producing at an optimal time to maximize club speed and, in turn, performance.

Conversely, similar models used to predict driver club speed were not as robust (R^2<0.2) when using them same methods. Previous research suggests that lower handicap golfers using less lofted clubs produce higher vertical GRF values and club speed [2]. However, while significantly higher club speed was produced in the driver ($p<0.001$), the vertical (F_z) GRF peaks on the lead foot were not significantly increased ($p=0.063$).

CONCLUSIONS

These findings, particularly in the 6 iron, support much of the previous golf GRF research as well as introduce some novel ideas for predicting performance based on temporal components and GRF magnitude. Because the GRF produced by the golfer needs to be kinetically transferred efficiently for a successful golf swing, regression models using only peak GRF and time of these peaks will never be able to perfectly predict performance. However, it is clear club speed is somewhat quadratically dependent on GRF and time of forces being produced. Further research should look to maximize the R^2 model values by using more variables to build the most accurate predictor of club speed.

With regard to the driver findings, it is possible that because these subjects varied in range of skill the results were not consistent with those found in low handicap golfers. Further research will be required to assess the biomechanical reasons for these results and look to build a more accurate regression model explaining driver club speed using similar methods.

Ultimately, these results need to be translated to a coach and/or golfer in a practical manner as a tool for success. Pressure mats are a golf teaching tool more widely accessible to golf coaches than force plates and some of these same trends may be relatable to pressure mat outputs, particularly the temporal components. Subsequent research will look to integrate force plate data with kinetic chain principles and other common theories pertaining to successful golf biomechanics to produce a particularly accurate model to predict performance. Nonetheless, the results show that GRF is indeed a satisfactory starting point for predicting performance across a wide age range and skill level of golfer, especially in the 6 iron.

REFERENCES

1. Williams and Cavanagh. *Medicine & Science in Sports & Exercise*, vol. **15**, 1983.
2. Richards et al. *Research Quarterly for Exercise and Sport*, vol. **56**, 1985.
3. Hume et al. *Sports Medicine*, vol. **35**, 2005.

Table 1: Assorted Model Best Fit Statistics for 6-Iron GRF Variables vs. Club Speed

GRF →	Fz		Fy		Fx		Resultant	
Model Type	**Fit**	**Variable(s)**	**Fit**	**Variable(s)**	**Fit**	**Variable(s)**	**Fit**	**Variable(s)**
Linear Univariate	R^2=.136	FPT	R^2=.306	BP	R^2=.157	BPT	R^2=.126	FPT
Quadratic Univariate	R^2=.560	FP	R^2=.591	BPT	R^2=.407	FP	R^2=.562	FP
Quadratic Bivariate	R^2=.895	BP BPT	R^2=.889	BP BPT	R^2=.480	FP FPT	R^2=.895	BP BPT

Variable Key: (FP = Front Foot Peak GRF, BP = Back Foot Peak GRF, FPT = Front foot peak GRF time relative to ball contact, BPT = Back foot peak GRF time relative to ball contact. All reported R^2 values are significant on a 95% confidence interval.)

THE EFFECTS OF RESISTANCE BANDS ON TRAPEZIUS ACTIVITY DURING FULL-BODY EXERCISES

Kyle W. Wasserberger and Jessica L. Downs, Teasie K. Williams, and Gretchen D. Oliver

Auburn University, Auburn, AL, USA
email: goliver@auburn.edu, web: www.sportsmedicineandmovement.com

INTRODUCTION

Scapular dyskinesis has been linked to abnormal muscle activation patterns between the upper (UT) and lower (LT) trapezius [1-5]. Specifically, overhead athletes that exhibit UT dominant activation profiles are more likely to have shoulder impingement due to excessive clavicle elevation on the thorax along with the increased anterior tilt at the scapulothoracic joint [3,5].

In the worlds of baseball and softball, resistance bands are a standard modality within strength and conditions programs for pre and post throwing programs. Because of the growing popularity, portability, and low cost, resistance bands are a great modality in the quest for injury prevention in overhead throwing athletes. Due to the prevalence of scapular dyskinesis in overhead throwing athletes as well as the rehabilitative focus on LT activation, understanding muscle activations of the UT and LT is imperative [1,2]. Thus, it was the purpose of this pilot study to quantify the activation patterns of the UT and LT during four full-body exercises with and without resistance bands. It was hypothesized that exercises which incorporated resistance bands would yield greater muscle activation and specifically, the LT would exhibit a greater %change (%CH) increase than the UT when adding a resistance band.

METHODS

Fourteen healthy active individuals (176 ± 10.7 cm; 75.3 ± 14.3 kg; 22.0 ± 2.50 years) regardless of sex volunteered. Healthy was defined as having no history of upper or lower extremity injury in the past six months. Active was defined as 30 minutes of physical activity for most days of the week. The University Institutional Review Board approved all testing protocols.

Muscle activation data were collected via surface electromyography (sEMG). All sEMG data were normalized as a percent of participant's maximum voluntary isometric contraction (%MVIC).

Subsequent to the collection of %MVIC data, participants performed four full-body exercises with and without the use of Jaeger resistance bands (Jaeger Sports, Los Angeles, CA). The exercises were airplane (AP), overhead squat (OH), lunge with "W" hold (WL), and single leg Romanian dead lift with horizontal row and external rotation (RDL). All exercises, except for the AP, were performed for one set of five repetitions. The AP was performed for one set of six repetitions. First and last repetitions were excluded during statistical analyses for all exercises. Ranges for muscle activation were defined as low (<20% MVIC), moderate (21-40% MVIC), high (41-60% MVIC), and very high (>61% MVIC).

Statistical analyses were performed using IBM SPSS Statistics 22 software (IBM Corp., Armonk, NY) with an alpha level set a priori at $\alpha = 0.05$. Prior to analysis, Shapiro-Wilk tests of normality determined that muscle activation data were normally distributed and %CH data were non-normally distributed. Dependent samples t-tests and Wilcoxon Signed Ranked tests were used to identify significant differences between conditions in muscle activation and %CH levels respectively.

RESULTS AND DISCUSSION

Dependent samples t-tests support the hypothesis that exercises which incorporated resistance bands would yield greater activation of both the UT and LT. Data revealed each exercise performed with the bands yielded at least moderate activation of both the LT and UT. During the band condition, the AP,

RDL, and OH elicited high UT activation while only the OH produced high LT activation. The OH yielded very high UT activation however no exercise achieved very high LT activation.

Means and standard error means for muscle activity during each exercise are shown in Table 1. No exercises elicited significantly greater LT activation when compared to UT activation. During the no band condition, the AP (df(13), $p = 0.004$) and OH (df(13), $p = 0.019$) showed significantly greater UT activation while only the OH showed significantly greater UT action during the band condition (df(13), $p = 0.024$).

The %CH was defined as the percent normalized quotient of the difference in activation levels between the two [(Difference/No Band)*100]. The effects of adding resistance bands on region-specific trapezius activation levels for a given exercise is quantified through %CH. Wilcoxon signed ranked tests showed significantly greater %CH for the LT when compared to the UT for the WL ($z = -2.17$, $p = 0.03$). No exercises showed significantly greater %CH for the UT. Thus, these data do not support the second hypothesis that all exercises would elicit greater change in LT activation than UT.

Although not all exercises elicited greater LT activation as hypothesized, it is still worth emphasizing that the WL not only elicited greater LT than UT activation during both conditions, but also had a statically significant greater %CH for the LT; possibly indicating an ability to target the LT when adding resistance bands.

CONCLUSIONS

Previous literature has stated the importance of exercises that increase LT while decreasing UT activation for those suffering scapular dyskinesis [1-5]. The current results add to the growing body of descriptive EMG data relevant to overhead throwing athletes. Through continuing quantification, coaches will be able to make increasingly informed decisions when designing training programs unique to each throwing athlete.

Using these data in conjunction with athlete-specific training considerations will allow the trained exercise or coaching professional to maximize performance and minimize risk of injury. Additionally, clinicians may use these exercises, specifically the WL and OH, in attempt to restore normal activation patterns between the LT and UT. However, caution must be used with the OH, as it also elicited significantly higher UT activation.

Limitations of this study include all traditional limitations of sEMG. Movement artifact may have occurred due to the dynamic nature of included exercises. Muscle cross talk may have also occurred. Finally, the use of healthy participants limits the generalizability of these data. Future studies should incorporate additional exercises and more diverse, pathological populations.

REFERENCES

1. Cools, A. *Am J Sport Med*. 35(10). 2007
2. Cools, A. *Braz J Phys Ther.* 19(5). 2015
3. DeMay, K. *J Sci Med Sport*. 16(1). 2013
4. Kibler, B. *Br J Sports Med*. 44(5). 2010
5. Ludewig, P. *Man Ther*. 16(1). 2011

TABLE 1

	Lower Trapezius			Upper Trapezius		
	Band (%MVIC)	No Band (%MVIC)	%Change	Band (%MVIC)	No Band (%MVIC)	%Change
AIRPLANE	36.6 ± 4.9	15.5 ± 1.9	164.0 ± 32.8	52.2 ± 6.0	30.0 ± 2.9	76.6 ± 12.0
W LUNGE	35.2 ± 6.3	23.1 ± 4.9	75.8 ± 23.7	28.6 ± 6.0	20.8 ± 3.2	27.2 ± 9.3
RDL	32.5 ± 3.6	23.9 ± 3.6	55.1 ± 16.1	40.2 ± 4.6	26.8 ± 3.1	54.3 ± 12.0
OH SQUAT	51.2 ± 7.1	25.8 ± 3.7	104.0 ± 19.1	78.2 ± 9.4	40.0 ± 5.4	107.0 ± 14.5

Asymmetries in knee extensor moments during fatigue in athletes who sustain bilateral ACL injuries

[1]Kate E Webster, [1]Jodie A. McClelland, [1]Luke Santamaria and [2]Julian A. Feller

[1]La Trobe University, Bundoora, VIC, AUS
[2] OrthoSport Victoria, Melbourne, VIC, AUS
email: k.webster@latrobe.edu.au

INTRODUCTION

Fatigue has been shown to lead to landing joint postures that increase the risk of anterior cruciate ligament (ACL) injury. There is less information about the effect of fatigue on landing biomechanics after ACL reconstruction surgery, or whether assessment of athletes in the fatigued state is of use for identification of those at risk of a second ACL injury (1-3).

The purpose of this study was to determine i) the effects of fatigue on hip and knee biomechanics during landing in athletes who had undergone ACL reconstruction surgery and ii) determine whether asymmetries during fatigued landing were associated with further ACL injury.

METHODS

Twenty four athletes (15 male, 9 female) who had undergone primary ACL reconstruction 12-18 months previously had three-dimensional lower limb kinematics and kinetics recorded during single limb landings, both before and during a protocol designed to induce localized fatigue of the quadriceps. The landing task was a vertical drop from a 30cm platform onto one leg. The cohort was followed for 8 years after biomechanical testing and any further ACL injuries were recorded. Repeated measures ANOVA was used to compare limb and fatigue conditions. Joint moment limb symmetry indices (LSI) were calculated and compared between athletes who did and did not go on to have further injury.

RESULTS AND DISCUSSION

Biomechanical testing showed that fatigue led to increased knee rotation and hip abduction and reduced knee joint moments in the ACL reconstructed limb compared to the contralateral limb. Four athletes (2 male, 2 female) sustained a contralateral ACL injury during the 8 year follow up period. These four athletes had significantly more asymmetrical external knee flexion moments at maximum fatigue compared to the athletes who did not go on to another ACL injury (Figure 1, $p<0.03$).

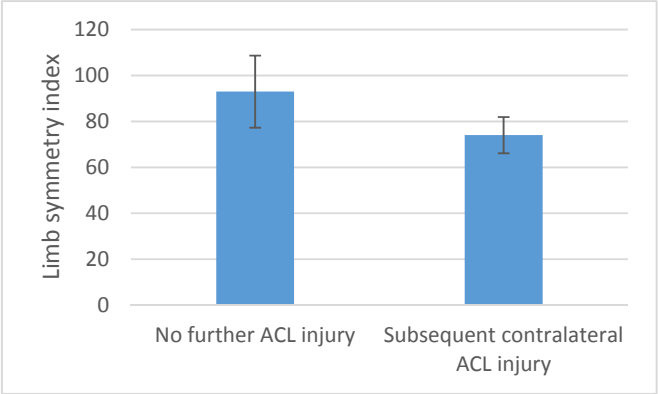

Figure 1. External knee flexor moment symmetry at maximum fatigue at biomechanical assessment 12-18 months post ACL reconstruction surgery. Athletes who sustained a subsequent contralateral ACL injury during the 8 year follow-up period had reduced symmetry at the 12-18 month assessment.

In all 4 cases the moment in the fatigued state was reduced on the operated side; and the LSI fell within the lowest third recorded for all athletes. There were no pre-fatigue differences, nor was peak knee adduction or hip moment asymmetry associated with further ACL injury.

CONCLUSIONS

Athletes who went on to suffer a second (contralateral) injury were found to have more asymmetrical knee extensor moments when fatigued. This may indicate a preference for shifting load to the contralateral side which over time, increases the risk of bilateral ACL injuries.

REFERENCES

1. Webster et al. Med Sci Sport Exerc, **44**, 2012
2. Oberlander et al. Med Sci Sport Exerc, **45**, 2013
3. Lessi et al. Knee Surg Sports Traumatol Arthrosc, **25**, 2017

IT MATTERS WHAT YOU CURL, BUT NOT TO THE BICEPS BRACHII

Wendi Weimar, Brandi Decoux, Christopher Wilburn, Lauren Brewer and Nicholas Moore

Auburn University, Auburn, AL, USA
email: weimawh@auburn.edu

INTRODUCTION

Previous literature has investigated the difference between the kettlebell swing and traditional free weight exercises, but these few studies have usually only considered lower extremity exercises and outcomes [1]. However, kettlebells and dumbells have not compared barbells, dumbbells, and kettlebells on the same task. While these authors accept that kettlebells and dumbells are not designed to be used in the same way, one can perform the same exercises with each lifting device. Furthermore, these devices alter the relationship between the center of gravity of the lifting tool and the hand placement and as a result, may place different demands on the lifter. Therefore, the purpose of this project was to compare the electromyography and kinematics of the bicep curl while utilizing these different implements.

METHODS

Sixteen individuals volunteered to participate in this project (10 M and 6 F, height 1.74 m, mass 81.02 kg). Each participant was asked to perform 3 repetitions of a bicep curl with each implement (barbell (BB), 2 handheld dumbbells (DB), a kettlebell held with one hand (KB1) and a kettlebell held in each hand (KB2)), at 65% of an estimated 1 repetition maximum. All lifts were performed while outfitted with a modified plug in gait marker arrangement, and kinematics were collected by 10 Vicon T-series cameras (Vicon, Los Angeles, CA). In addition, electromyography (EMG) was collected on the biceps brachii, erector spinae and the rectus abdominus, using a Noraxon Telemyo (Noraxon, Scottsdale, AZ). Data were analyzed by a 1 (variable) x 5 (lifting device) repeated measures ANOVA for each variable.

RESULTS AND DISCUSSION

Elbow motion was unremarkable. Significant differences were noted for the angular position of the shoulder at the beginning and top position of the biceps curl, in the sagittal plane. At the starting position KB1 caused the shoulder to be in a more flexed position than any of the other lifting devices ($p=0.000$ DB, $p=0.001$ BB, $p=.002$ KB2). At the top of the motion the KB1 condition also yielded more shoulder flexion ($p=0.00$ DB, $p=0.00$ BB, $p=0.000$ KB2). With regard to emg, no significant difference in average muscle activity was noted for the biceps brachii between lifting implements. However, both the erector spinae (ES) and rectus abdominus (RA) yielded larger percentages of MVIC (average) during the concentric portion of the movement during the KB1 condition (concentric ES: $p=0.005$ DB, $p=0.002$ BB, $p=0.001$ KB2, concentric RA:$p=0.028$ DB, $p=0.034$ BB, $p=0.029$ KB2). During the eccentric motion significance was only found for the erector spinae (eccentric ES: $p=0.008$ DB, $p=0.0027$ BB, $p=0.009$ KB2).

CONCLUSIONS

These implements place differing postural demands on the body. Specifically, holding a kettlebell with both hands requires more shoulder flexion, as the arms must be in front of the trunk in order to hold the handle. This arm arrangement moves the load further away from the trunk creating a larger moment increasing trunk stabilizing musculature involvement. The significant increase of RA would seem to suggest that it must either act to cancel any trunk extension, or is stabilizing the pelvis so that the ES has a more stable anchor from which to pull. Future research should aim to determine the role of the RA and investigate if the increase in shoulder flexion is more effectively contracting the biceps

brachii at both attachment sites, through the use of diagnostic ultrasound.

REFERENCES

1. Otto, W., et al. *J Strength Cond Res,* **26***,* 1199-1202, 2012.

THE EFFECT OF POWER AND CADENCE ON CENTER OF MASS MOVEMENT AND LOWER LIMB MECHANICS DURING STANDING CYCLING

Ross D. Wilkinson, Andrew G. Cresswell and Glen A. Lichtwark

The University of Queensland, Saint Lucia, QLD, AUS
email: r.wilkinson@uq.edu.au

INTRODUCTION

Cyclists often transition to a standing position when needing to produce high pedal torque and power (i.e. during steep climbs, accelerations and sprinting). Previous research and field observations of cyclists during these scenarios suggest that significant vertical displacement of the rider's center of mass (COM) occurs over each pedal cycle (1). Raising and lowering the COM against gravity is significant to the energetics of cycling because the total work required to do so comes at a cost to the rider. Thus, one could assume that riders choose to incur this cost as it may increase pedaling effectiveness while minimizing energy expenditure. Presently the impact of vertical COM displacement on lower limb mechanics during standing cycling remains unresolved. We speculate that different combinations of power output and cadence impact how a rider determines the optimal level of vertical COM displacement, thus the aim of this study was to test the effects of power output and cadence on vertical COM displacement during standing cycling. We hypothesize that vertical COM displacement would increase with power output. We also predict that the effect of power would be cadence dependent due to the increased cost of producing force at high velocity. Effective mechanical advantage (EMA) of the hip, knee and ankle, leg extension velocity and duty cycle were measured to compare the effects of power output and cadence on lower limb effectiveness.

METHODS

Nineteen subjects (17M; 2F) rode on an electronically braked cycle ergometer for all cycling trials. Subjects performed five maximal cycling trials of 3-s duration in a seated position to determine individual peak power output (PPO). Resistance for the sub-maximal trials was set to either 10% or 50% PPO as these levels sit either side of the reported threshold for the sit to stand transition (2). Cadence was set to either 70 rpm or 120 rpm as these are associated with the preferred cadence of cyclists during climbing and sprinting respectively. Participants performed the combinations of cadence (70 rpm: LC and 120 rpm: HC) and power output (10%: LP and 50%: HP) in a randomized order and were required to maintain these targets for a period of 10 seconds whilst kinematic and kinetic data was recorded. Crank angle and forces tangential and radial to the left and right crank were recorded at 100 Hz using instrumented cranks. The 3D trajectories of 46 passive, reflective markers placed across the lower limbs, torso and upper limbs were recorded at 200 Hz. Lower limb joint kinematics and net muscle moments were calculated using a scaled full-body model (3) within OpenSim v3.3. Data was calculated from five pedal cycles of the right leg. Processing of data was completed using custom scripts in MATLAB R2017a. A repeated measures, two-way ANOVA was performed to test for main effects of cadence and power and interaction effects (cadence x power). The alpha level for main and interaction effects was set at .0247 in order to minimize false positive risk. Whenever a main or interaction effect was found, Sidak's multiple comparisons test was used to detect the effects of factor/s within each condition. For main and interaction effects the F-value ($F_{(dof)}$), p-value (p), partial eta squared (η_p^2) and generalized eta squared (η_G^2) are provided. For multiple comparisons the t-statistic ($t_{(dof)}$), adjusted p-value (p), 95% confidence intervals (95% CI [Low-High]), and effect size (Cohen's d_{av}) are provided. All values are reported as mean±sd.

RESULTS AND DISCUSSION

Center of mass displacement: There was a main effect of power ($F_{(1,18)}$=33.53, p<.0001, η_p^2=.93505, η_G^2=.63149) and cadence ($F_{(1,18)}$=167, p<.0001, η_p^2=.9027, η_G^2=.8426) on the range of vertical COM

displacement. There was also an interaction effect between power and cadence ($F_{(1,18)}$=7.047, p=.0161, η^2_p=.2814, η^2_G=.1064). This resulted in the largest range of vertical COM displacement occurring during LC+HP (5.1±1.5 cm) and the smallest range during HC+LP (1.1±0.03 cm). Due to the larger effect of cadence, displacement during LC+LP (3.3±1.1 cm) was significantly higher than HC+HP (2.2±1.1 cm), $t_{(18)}$=3.223, p<.0047, 95% CI [0.387, 1.837], Cohen's d_{av}=1.046 (Fig. 1A).

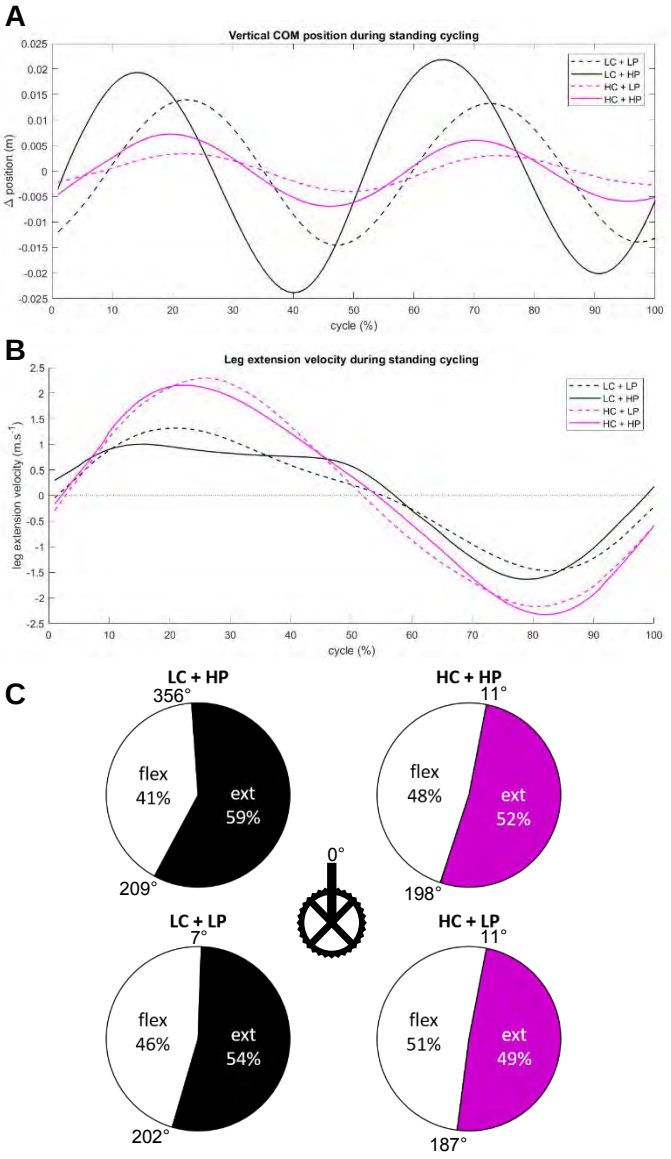

Figure 1: A. Mean vertical COM displacement over a full pedal cycle from top dead center to top dead center of the right crank. Note the significant effect of cadence by comparing both LC conditions (black) to the HC conditions (magenta). **B.** Mean extension velocity of the right leg. **C.** Mean flexion and extension phases of the right leg. The crank angle corresponding the start and end of the extension phase is given in degrees. Angles are relative to top dead center. Crank position at top dead center (0°) shown inset.

Lower limb mechanics: The only main effect on EMA was that of cadence on the hip ($F_{(1,18)}$=29.69, p=.0002, η^2_p=.7297, η^2_G=.3766). At low power, EMA of the hip was similar at low and high cadence. At high power, EMA at the hip was higher at low cadence (0.435±0.147) than at high cadence (0.311±0.091), $t_{(18)}$=3.116, p=.006, 95% CI [0.04, 0.2065], Cohen's d_{av}=1.011. Increasing power output lowered peak leg extension velocity at both low (LP=1.326±0.102 v HP=1.065±0.137 m.s^{-1}, $t_{(18)}$=6.661, p<.0001, 95% CI [0.179, 0.343], Cohen's d_{av}=2.161) and high cadence (LP=2.308±0.079 v HP=2.184±0.169 m.s^{-1}, $t_{(18)}$=2.897, p=.0096, 95% CI [0.034, 0.214], Cohen's d_{av}=0.94), but the effect was larger at low cadence (Fig. 1B). The ratio of time spent in extension versus flexion, known as duty cycle, was greatest during the LC+HP condition (1.43), while the only condition with a duty cycle <1.0 was the HC+LP condition (0.96) (Fig. 1C).

CONCLUSIONS

These results extend our understanding of how vertical COM displacement may impact pedaling mechanics as well as the energy fluctuations of the bicycle-rider system by highlighting the significant effects of power output and cadence. It appears that vertical displacement and rocking of the hips can be used by riders to increase EMA at the hip, knee and ankle. Raising the COM leads to a subsequent increase in the body's momentum during the down stroke of each pedal cycle, which extends the time spent using powerful anti-gravity muscles around the hip, knee and ankle. The interaction effects between power and cadence on COM movement and lower limb mechanics help to explain why the standing position is superior to the seated position for producing high torque and peak power. Our future research will focus on the possibility that lateral sway of the bicycle and elastic energy storage mechanisms within the lower limb also affect vertical COM displacement and lower limb mechanics during standing cycling.

REFERENCES

1. Hull et al. *Journal of Biomechanics.* 23(7), 1990.
2. Costes et al. *Journal of Biomechanics*. 48(12), 2015.
3. Rajagopal et al. *IEEE Transactions on Biomedical Engineering*. 63(10), 2016.

QUANTIFICATION OF THE SHOCK ABSORPTION PERFORMANCE OF CONSTRUCTION HELMETS IN TOP IMPACT

*John Z. Wu, Christopher S. Pan, and Bryan M. Wimer
National Institute for Occupational Safety and Health, Morgantown, WV, USA.
*Email: jwu@cdc.gov

INTRODUCTION

Traumatic brain injuries are among the most common severely disabling injuries in the United States. It is estimated that approximately 1.7 million cases occurred to civilians annually during 2002-2006 [1]. Work-related traumatic brain injury is one of the most common occupational injuries among construction workers [2, 3], resulting in extensive medical care and rehabilitation, multiple days away from work, permanent disability, or death. Industrial helmets are considered the most common and effective personal protective equipment available to protect against work-related traumatic brain injury [3]. There are numerous industrial helmets on the market, from basic models to advanced designs. Although all industrial helmets on the market are known to pass existing test standards [4-6], the shock absorption performance of them has not been quantified. In other words, the "two-level grading system" of pass/fail does not effectively characterize the performance of industrial helmets. The purpose of the current study is to develop an approach to characterize the shock absorption performance of industrial helmets.

METHODS

In the current study, we performed only Type 1 impact tests, i.e., the impact on the top crown of helmet shell. Helmet drop impact trials were performed using a commercial drop tower test machine (P. White Laboratory, MD, USA), which complies with the ANSI Z89.1 standard [4]. Twenty drop impact trials were performed; each dropped once at a particular height. The control parameter was the drop height; the acceleration of the impactor and the reaction force at the base of the headform (Fig. 1) were measured. The drop heights varied from 0.30 m (1 ft) to 2.23 m (7.33 ft), which resulted in impact velocities from 2.4 m/s to 6.6 m/s. The drop height was uniformly randomized within the range. The mass of the impactor was fixed at 3.6 kg. One representative Type 1 helmet model was used in this study. A Type 1 helmet is a basic helmet, and it is used widely at construction worksites. A Type 1 helmet is designed for the top impact protection only, not designed for the protection of the lateral impacts from the front, side, or rear.

RESULTS

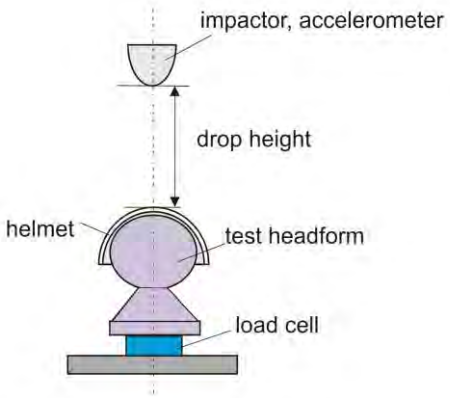

Figure 1. Schematic of the test procedure. The control parameter was the drop height; the accelerations of the impactor and reaction force at the base of the headform were measured.

The representative data plots of the force and acceleration generally show two peaks, corresponding to the initial and secondary impacts between the impactor and the helmet shell, as illustrated in Fig. 2. The magnitude of the peak force and acceleration decreased by about 70% and 50%, respectively, from the initial impact to the

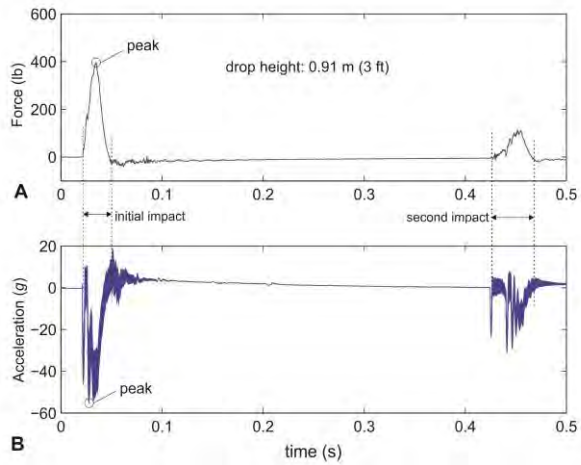

Figure 2. The representative time-histories of the force (A) and acceleration (B) around the impact.

second impact. In this study, we were mainly interested in the peak impact force and acceleration for the first impact.

For each of the force-time and acceleration-time curves, the peak forces and peak accelerations have been identified. The peak force and peak acceleration as a function of the drop height is shown in Fig. 3A and Fig. 3B, respectively. Our results show that both peak force and acceleration values increase gradually with the increase of the drop height, when the drop height is less than 1.75 m. When the drop height is above 1.75 m, both peak force and acceleration values increase dramatically.

DISCUSSION AND CONCLUSIONS

Our results indicate there exists a critical drop height, h_{cr} = 1.75 m, which is the cross point of the two regression lines (Fig. 3). The relationships of force-drop height and acceleration-drop height can be characterized by a flat toe region ($h < h_{cr}$), where the force or acceleration increases slowly with increasing drop height, and a steep linear region ($h > h_{cr}$), where the force or acceleration increases dramatically with even a slight increase in drop height (Fig. 3). The scattering of the test data is small when the drop height is below h_{cr}, and the pattern becomes large once the drop height is above h_{cr}, indicating mechanical characteristics

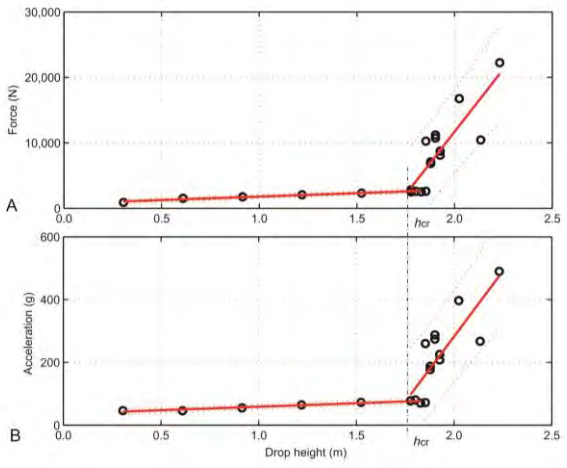

Figure 3. Peak force (A) and peak acceleration (B) as a function of the drop height. The data for the drop heights from 0.30 m to 1.75 m and from 1.75 m to 2.23 m were fitted using two separate lines (solid lines). The dotted lines are the 95% confidence intervals for the linear regressions.

became unstable once the drop height exceeds the critical height.

A helmet should never be subject to impacts beyond the critical drop height, not only because the transmitted impact force would increase dramatically, but also because of the compromised mechanical stability. Therefore, the critical drop height, h_{cr}, represents the shock absorption performance of a helmet. If a helmet passes a standard test, the safety margin of the helmet for that standard is defined based on the potential impact energy: $\rho = \left(\frac{h_{cr}}{h_{std}} - 1\right)\%$, with h_{std} being the drop height specified in the standard. For the current study, h_{cr} =1.75 m, $h_{\text{ANSI Z89.1}}$=1.54 m, and the safety margin of the helmet is 13.6%.

The advantage of the proposed approach over existing standard-based test methods is that the new approach can yield a performance spectrum of a helmet, and it can estimate the safety margin of the helmet if it passes the standardized tests. The proposed approach conceptually changed the conventional testing methods and would help improve helmet quality control and workers' safety.

REFERENCES

[1] CDC, 2007. Traumatic brain injury in the United States emergency department visits, hospitalizations, and deaths 2002-2006. US Department of Health and Human Service. Centers for Disease Control and Prevention. Washington D.C.

[2] Hino, Y., 2012. *Work* 41(Suppl 1):3339–42.

[3] Tiesman, H. M., Konda, S., Bell, J. L., 2011. *Am J Prev Med* 41(1):61–7.

[3] Kim, S., Ro, Y., Shin, S., Kim, J., 2016. *Int J Environ Res Public Health* 13:1063–78.

[4] ANSI, 2014. ANSI/ISEA Z89.1: American national standard for industrial head protection.

[5] BS, 2012a. EN 14052: 2012+A1: High performance industrial helmets.

[6] BS, 2012b. EN 397:2012+A1: Industrial safety helmets.

ACKNOWLEGEMENT: This project was made possible through a partnership with the CDC Foundation. We want to express our gratitude to Turner Construction Company, Liberty Mutual Insurance, Zurich Insurance Group, and ACE Group for their generous contributions to this project via the CDC Foundation.

DISCLAIMERS: The findings and conclusions in this report are those of the authors and do not necessarily represent the official position of the National Institute for Occupational Safety and Health, Centers for Disease Control and Prevention. Mention of any company or product does not constitute endorsement by the National Institute for Occupational Safety and Health, Centers for Disease Control and Prevention.

EFFECT OF SEX ON CENTRE OF MASS DURING SIDESTEPPING

[1]Hannah Wyatt, [1]Gillian Weir, [1]Carl Jewell, [2]Richard van Emmerik and [1]Joseph Hamill

[1]Biomechanics Laboratory, University of Massachusetts, Amherst
[2]Motor Control Laboratory, University of Massachusetts, Amherst
email: hwyatt@umass.edu

INTRODUCTION

It has been well established that female athletes have a greater risk of anterior cruciate ligament (ACL) injury compared to males [1]. Sidestepping is recognised as one of the most injurious sporting tasks for non-contact ACL injury occurrence, with greatest risk during the weight acceptance phase.

Knee valgus moments are a recognised predictor of ACL injury risk in female athletes [2]. Strategies for reducing peak knee valgus moments include redirection of the whole-body centre of mass (CoM) towards the desired direction of travel [3] and reduced displacement of the foot from the midline of the body [4]. To further understand the heightened risk of female athletes to ACL injury, much emphasis has been put on the investigation of lower-limb biomechanics, with little study of whole-body organisation.

To assist the development of tailored ACL injury prevention strategies, the purpose of this study was to investigate CoM orientation of female and male athletes during the stance phase of anticipated and unanticipated sidestepping manoeuvres. It was hypothesised that female athletes would display more at-risk strategies compared with males where: 1) their CoM would be less orientated toward the desired direction of travel; and 2) their foot placement would be further from the CoM.

METHODS

Nine female (age 20.6 ± 1.3 years, height 1.66 ± 0.05 m, mass 59.5 ± 5.5 kg) and nine male (age 21.2 ± 1.14 years, height 1.83 ± 0.10 m, mass 73.1 ± 8.5 kg) collegiate team sport athletes participated in a single biomechanics testing session. Participants performed a series of anticipated and unanticipated sidestepping trials, among a random distribution of straight line running and stopping trials, used to limit task predictability. Seven anticipated and seven unanticipated sidestepping trials were performed by each participant at 3.5-4.5 $m.s^{-1}$, with a desired direction of travel of 45° from straight line running.

Three-dimensional kinematic data were recorded at 240Hz synchronously with ground reaction forces at 1200Hz. Forty-two retroreflective markers were attached to specified landmarks allowing for the development of a bilateral eight-segment model in Visual 3D software (C-motion, Inc., Rockville, MD). Anterior-posterior whole-body CoM position was calculated relative to the head of the first metatarsal phalange; medio-lateral CoM position was determined relative to the first metatarsal base of the stance foot. Whole-body CoM velocity was additionally derived. Each variable were analysed for the duration stance, defined using a 10 N vertical ground reaction force threshold.

Two-tailed t-tests were used to compare CoM position and CoM velocity over stance between females and males. All statistical tests were completed using one-dimensional statistical parametric mapping (SPM1D) [5].

RESULTS AND DISCUSSION

Whole-body centre of mass orientation during anticipated and unanticipated sidestepping manoeuvres were compared between female and male athletes. Females displayed differing CoM position and velocity predominantly during weight acceptance compared with their male counterparts.

Female athletes had a greater degree of CoM anterior travel than males throughout the entire stance phase in anticipated (Fig 1; $P < 0.01$) and for the first 56% of stance in unanticipated sidestepping ($P < 0.01$). In consideration of previous research [3], the CoM path that female athletes utilise may contribute to increased knee valgus loading and subsequent ACL

injury risk. The respective finding may partially account for heightened ACL injury incidences in female athletes.

Females performed anticipated sidestepping with significantly less distance between CoM and stance foot in comparison with the male cohort (Fig 1, 0-46% stance, $P = 0.01$ and 81-100% stance, $P = 0.02$). In line with foot placement width findings [4], the technique used by females may reflect positively in the way of ACL risk, however, it is possible that the respective technique was achieved with increased lateral trunk lean which has been recognised to contribute to increased knee valgus load [4]. Further exploration of trunk kinematics may offer valuable insight into the strategies used by female athletes to achieve the evidenced narrow foot placement.

In comparison with their male counterparts, females performed both anticipated and unanticipated sidestepping manoeuvres with significantly lower CoM velocity during the weight acceptance phase. Significant differences for AP CoM velocity were found between 0-53% of stance in anticipated ($P = 0.01$) and 0-60% of stance in unanticipated sidestepping ($P < 0.01$). ML CoM velocity was significantly different at 0-41% ($P = 0.03$) and 0-44% of stance ($P = 0.02$) for anticipated and unanticipated sidestepping, respectively. As pre-contact speed was consistent across groups, it is potentially the case that injurious mechanisms (such as increased knee valgus moments) are more prominent in female athlete as a result of their endeavour to reduce CoM velocity. As is favourable for sidestepping performance, male athletes are able to re-orient their CoM at increased speeds in comparison with females. Both performance and injury risk reduction may be enhanced by the ability to re-orient the CoM towards the desired direction at a sustained CoM velocity.

CONCLUSIONS

Female athletes performed anticipated and unanticipated sidestepping with less orientation of the CoM towards the desired direction of travel at a decreased velocity during the weight acceptance phase as compared with males. Female-specific prevention strategies for ACL injury should work towards improving CoM redirection strategies during both anticipated and unanticipated sidestepping.

REFERENCES

1. Walén, M. et al., *Knee Surg. Sports Traumatol. Arthosc*, 19(1), 2011.
2. Hewett, T.E. et al., *Am. J. Sports Med,* 33(4), 2005.
3. Donnelly, C.J. et al., *J Biomech*, 45(8), 2012.
4. Dempsey, A.R. et al. Med. Sci. Sports Exerc., 39(10), 2007.
5. Pataky, T.C. et al., *J Biomech*, 46(14), 2013.

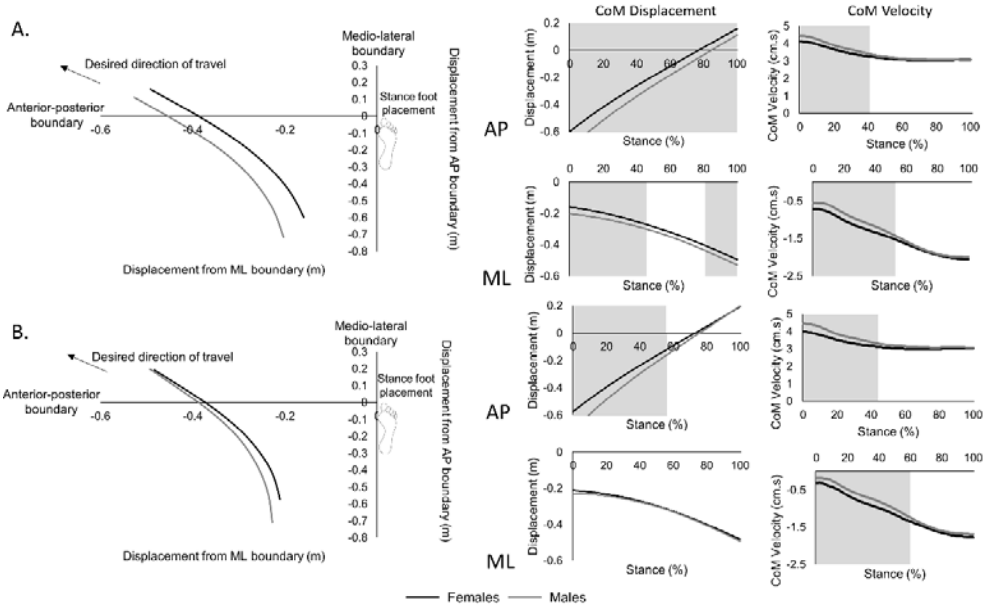

Figure 1. Whole-body centre of mass path in relation to stance foot placement and CoM velocity for both anterior-posterior (AP) and medio-lateral (ML) across stance (%) during anticipated (A) and unanticipated (B) sidestepping. Shaded regions indicate statistical significance from SPM1D ($P < 0.05$).

INFLUENCE OF CHINSTRAP ATTACHMENT LOCATION ON AMERICAN FOOTBALL HELMET IMPACT PERFORMANCE

Shayne York, Darcie L. Yount, Elizabeth D. Edwards, Mark Jesunathadas, Scott G. Piland, Trenton E. Gould

University of Southern Mississippi, MS, USA
email: Shayne.York@usm.edu

INTRODUCTION

Participation in the sport of American football carries the highest incidence of concussion across all sports in the United States [1]. In an effort to reduce the risk of this injury, helmet manufacturers have worked to introduce helmet designs purported to greatly reduce the accelerations of the head during impacts. With attention paid to shell design and energy mitigating liner systems, a paucity of research has been devoted to the role 4-point chinstrap attachment options may have upon head accelerations. Across all modern designs, wearers are afforded two options for attachment: high and low (see Figure 1). The different attachment locations change the direction of the line of pull of the chinstraps and thus, may influence the coupling of the helmet to the head and outcome accelerations of the head [2]. To date, it is unclear if varying attachment points influences the peak linear and angular accelerations of the head during blunt impacts. Therefore, the purpose of this study was to evaluate the influence of 4-point chinstrap attachment location on head peak linear and angular accelerations during blunt-force impacts to the helmet.

METHODS

Six new Schutt F7 helmets (Schutt Sports, Litchfield IL) with no prior impact history were separated into high chinstrap (n=3) and low chinstrap (n=3) location groups (Figure 1). Facemasks were removed, and helmets were fitted to a medium NOCSAE anthropometric test device (ATD) attached to a male 50% Hybrid III neck. Helmets were impacted at 6 m/s with a pneumatic linear impactor (15.55 kg), comprised of an

Figure 1: Left: High chinstrap configuration. Right: low chinstrap configuration.

aluminum and polyurethane head. The helmets were impacted twice at front, front boss, side, rear boss non-centroidal (NC), rear boss centroidal (CG) and rear locations according to the NOCSAE impact test method [3]. Nine accelerometers arranged in a 3-2-2-2 configuration measured the accelerations of the center of mass of the ATD headform [4]. Acceleration signals were sampled at 10 kHz and filtered with a CFC 180 filter with Biokinetics software (Ottawa, Ontario, CN), which was also used to calculate peak resultant linear and angular accelerations. High-speed video of a subset of impacts (18 videos out of 72 total impacts) for the low and high chinstrap configurations were captured at 6000 frames per second during the impact event using a Phantom V611 camera (Vision Research, Wayne, New Jersey). Separate two-way repeated measures ANOVAs (6 x 2, Impact Location x Chinstrap) for peak resultant linear and peak resultant angular acceleration were used to make comparisons between groups (SPSS v24, IBM Armonk, NY). Significance values were corrected with Huynh-Feldt adjustments for violations of sphericity. Simple effects analyses were used to explain the interactions between Impact Location and Chinstrap for peak resultant linear and angular accelerations. An alpha level of 0.05 is considered

significant. Data are reported as mean ±1 standard deviation (SD).

RESULTS AND DISCUSSION

Mean peak resultant linear acceleration for the high and low chinstrap groups were 69.93 ± 13.83 g and 71.19 ± 13.11 g, respectively. Mean peak resultant angular accelerations for high and low chinstrap groups were 7013.13 ± 3056.81 rad/s^2 and 6813.03 ± 3046.98 rad/s^2, respectively. An interaction effect between Impact Location and Chinstrap was found for peak resultant linear accelerations (p = 0.045, η^2 = 0.216), and angular accelerations (p = 0.023, η^2 = 0.224). There was no main effect of Chinstrap for peak resultant linear (p = 0.657, η^2=0.021) or angular accelerations (p = 0.169, η^2 = 0.180). Significant differences between Chinstrap groups for peak resultant linear accelerations were found at front (p = 0.007, η^2 = 0.538) and rear boss NC (p = 0.039, η^2 = 0.361; Figure 2) locations. A significant difference between Chinstrap groups for peak resultant angular acceleration was found at the front (p = 0.031, η^2 = 0.385; Figure 3) location.

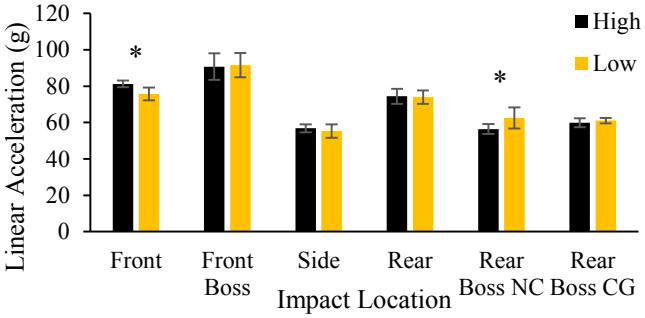

Figure 2: Peak resultant linear acceleration (mean ± 1 SD) between helmets with high and low chinstrap attachments. * significant difference between Chinstrap groups ($p \leq 0.05$).

High-speed video observations demonstrated deformation of the helmet shell, which led to buckling of the chinstraps for both high and low configurations. Chinstrap behavior was not measured and further analysis is needed to quantify the buckling across configurations and impact locations.

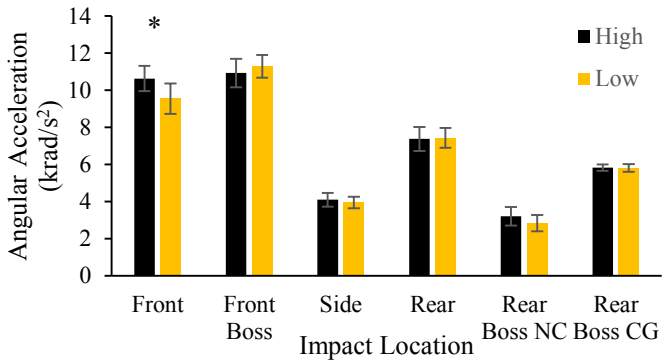

Figure 3: Peak resultant angular acceleration (mean ± 1 SD) between helmets with high and low chinstrap attachments. * significant difference between Chinstrap groups ($p \leq 0.05$).

CONCLUSIONS

Chinstrap configuration did influence peak headform acceleration measures, but in a minority of impact locations. The amount and nature of chinstrap buckling may have contributed to these differences. However, further research should investigate chinstrap buckling magnitude and tension as well as decoupling of the helmet and chinstrap from the headform in order to understand the role of chinstrap attachment location on head acceleration. Additional research is also needed to evaluate the influence of 4-point chinstrap attachment configurations across different helmet designs. An understanding of the role chinstrap attachment location has on coupling the helmet to the headform, may aid in understanding the factors that result in head injury in American football.

REFERENCES

1. Rowson et al. *Annals of Biomedical Engineering*, **40**(1): 1-13, 2012.
2. Cobb et al. *Journal of Sports Engineering and Technology*. **229**(1): 39-46, 2014.
3. NOCSAE. *DOC ND0081-14m15,* 2015.
4. Padgaonkar et al. *Journal of Applied Mechanics*, **42**(3): 552-556, 1975.

EFFICACY OF A NEW FOOTBALL HELMET LINER MECHANISM ON HEAD IMPACT ACCELERATIONS

Darcie L. Yount, Shayne York, Elizabeth D. Edwards, Mark Jesunathadas, Trenton E. Gould, Scott G. Piland

University of Southern Mississippi, Hattiesburg, MS, USA
email: darcie.yount@usm.edu, web: https://www.usm.edu/kinesiology/applied-biomechanics-research-laboratory

INTRODUCTION

Due to high participation and occurrence of high-energy impacts, American football has the highest prevalence of concussions in the U.S. [1]. In an effort to reduce concussions in sport, researchers and helmet manufacturers are investigating new mechanisms and technologies to mitigate linear and angular accelerations of the head upon impact. To this end a newly designed American football helmet, incorporates an additional slip liner called the Radian Diffusion System (RDS) between the comfort layer and primary cushioning layer in an attempt to reduce angular accelerations. Purportedly, the addition of a slip liner allows the helmet to move independently of the head on impact, resulting in reduced angular head accelerations. Despite these claims the efficacy of this mechanism is currently unknown. Therefore, the purpose of this study is to evaluate the efficacy of a new helmet liner system toward reducing peak resultant linear and angular accelerations.

METHODS

Six Schutt (Schutt Sports, Litchfield, IL) F7 American football helmets with (n = 3) and without (n = 3) the Radian Diffusion System liner were used in this study. Facemasks were removed, and helmets were fitted to a Medium NOCSAE headform, which was attached to a male 50% Hybrid III neck mounted to a sliding table. Helmets were impacted twice at six locations (front, front boss, side, rear, rear boss non-centric, and rear boss centric) at 6 m/s using a pneumatic linear impactor (mass 15.55 kg) comprised of an aluminum and polyurethane impactor head. A nine-accelerometer package (Endevco, Orange County, CA, USA) arranged in a 3-2-2-2 arrangement measured the dynamic headform response [2]. Acceleration data were sampled at 10 kHz and data were filtered using a CFC 180 filter to obtain peak resultant linear and angular accelerations (Biokinetics, Ontario, CN). A 6 x 2 (Location x Liner) repeated measures ANOVA compared accelerations between groups (SPSS v. 25, IBM Corp., NY). Simple effects analysis was performed to explain the interaction between Liner and Location. An alpha level of 0.05 was considered significant. Data are reported as mean ± 1 standard deviation (SD).

RESULTS AND DISCUSSION

Mean peak resultant linear accelerations across locations for helmets with and without the RDS liner were 69.93 ± 13.83 g and 72.13 ± 12.71 g, respectively. Mean peak resultant angular accelerations across locations for helmets with and without the RDS liner were 7013.13 ± 3056.80 rad/s^2 and 7162.46 ± 3392.08 rad/s^2, respectively. As sphericity was violated for angular accelerations (p = 0.003), univariate angular acceleration statistics are reported with Greenhouse-Geisser corrections. An interaction effect was observed between the factors Liner and Location for both linear (p = 0.001, η^2 = 0.403) and angular accelerations (p = 0.014, η^2 = 0.325). No main effect was observed for either peak linear (p = 0.15, η^2 = 0.195) or angular accelerations (p = 0.444, η^2 = 0.060). A comparison of peak linear and angular accelerations between helmet impacts with and without the RDS liner is shown in Figures 1 and 2, respectively.

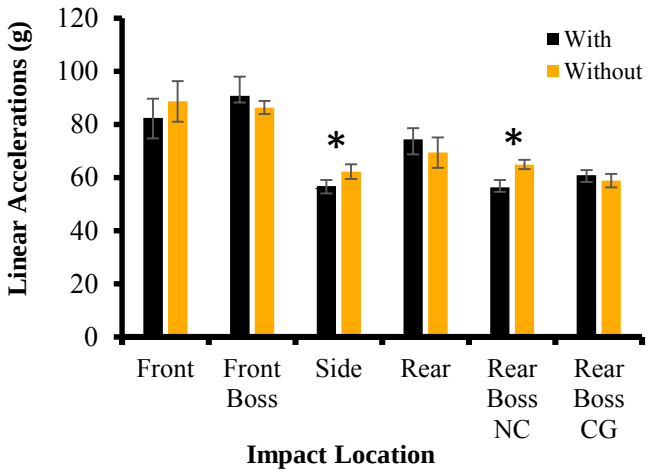

Figure 1: Linear accelerations (mean ± 1 SD) between helmets with liner and without liner. *significant at $p < 0.05$.

Simple effects analysis showed a significant difference in linear accelerations between helmets with the slip liner and those without at the side ($p = 0.004$, $\eta^2 = 0.583$) and rear boss non-centric ($p < 0.001$, $\eta^2 = 0.807$) locations; no difference was observed at any other impact site.

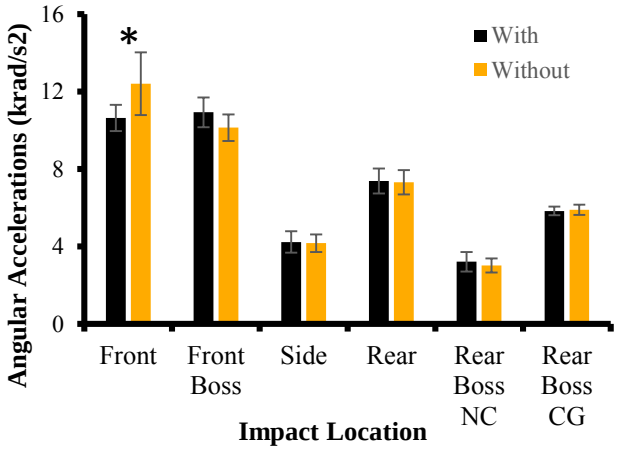

Figure 2: Angular accelerations (mean ± 1 SD) between helmets with liner and without liner. *significant at $p < 0.05$.

Simple effects analysis showed a significant difference in angular accelerations between groups at the front location ($p = 0.33$, $\eta^2 = 0.381$). No difference was observed at any other impact site.

CONCLUSIONS

The inclusion of the RDS liner did statistically reduce head linear and angular accelerations during impacts to some of the tested locations. The lack of reduction in peak angular accelerations at the majority of the impact sites indicates that the mechanism may not sufficiently decouple the movement of the helmet from the head. Further research is needed to determine if the RDS liner and similar technologies can reduce the angular accelerations of the head and consequently the risk for concussion in impact sports.

REFERENCES

1. Rowson et al. *Annals of Biomedical Engineering*, **40**(1): 1-13, 2012.
2. Padgaonkar et al. *Journal of Applied Mechanics*, **42**(3): 552-556, 1975.

ACKNOWLEDGEMENTS

This research was funded in part by the Department of Defense and U.S. Army Award #NSRDEC-W911QY-15-C-0038

DIVERSITY IN SHOULDER AND ABDOMINAL MUSCLE ACTIVATION PATTERNS USED DURING THE VOLLEYBALL SPIKE

Antonia M. Zaferiou, Christopher B. Knowlton, Matthew Perek, and Anthony A. Romeo
Rush University Medical Center, Chicago, IL, USA
email: Antonia_Zaferiou@Rush.edu, web: www.rushu.rush.edu/orthoresearch

INTRODUCTION

In both elite performers and clinical populations, subject-specificity in muscle activation patterns and movement mechanics calls us to carefully consider how to extract meaningful patterns across individuals [1-3]. This provides an exciting prospect for machine learning and cluster-analysis techniques to be applied to studies of elite athletes. Furthermore, shoulder dynamics are often represented using a 3-axis reference system, which is prone to cross-contamination across axes [4]. Recently, a four-axis shoulder dynamics parameterization has been developed in our biomechanics community [5-6].

The purpose of this study was to understand shoulder and abdominal muscle activation patterns and shoulder dynamics used during the volleyball spike. We hypothesized that we would identify subject-specific muscle activation and humeral dynamics.

METHODS

Five elite female volleyball players (15-18 yrs) provided informed consent/assent in accordance with the IRB. Participants performed five spikes while muscle activation was monitored using surface electromyography (EMG, 1500Hz, Noraxon, AZ) and an optical motion capture system (300fps, Optitrack, Corvallis, OR) measured whole body movement. Data were collected in the participants' practice gym and prioritized keeping the participants most comfortable/natural by allowing their coaching assistants to toss a live ball during their spike trials.

Data were processed using custom code in Matlab (Mathworks, Novi, MI), including shoulder angular dynamics, which followed methods described in [5-6]. These methods include using quaternions to determine the angular velocity between the humerus and trunk, isolating the angular velocity acting about the long axis of the humerus, then distributing the remainder of the angular velocity vector across the 3-axis of the trunk [5-6]. EMG data were filtered using a 4th order zero-phase butterworth band-pass filter (40Hz-400Hz) and quantified using root mean squared values in 20ms average bins that were normalized to the maximum bin during manual muscle tests (MMTs) or the maximum bin during spike trials for that individual ("within-spike-trials max"). Muscles monitored by EMG: Lower, Middle, and Upper Trapezius (LowTrap, MidTrap, UpTrap), Posterior and Anterior Deltoid (PostDelt, AntDelt), Pectoralis Major (PecMaj), External Oblique (ExtObl), Rectus Abdominus (RectAb). Initial ball-contact was determined using the video and became the time of synchronization time.

RESULTS AND DISCUSSION

Subject-specific muscle activation patterns were identified between take-off and landing (Figs1-2).

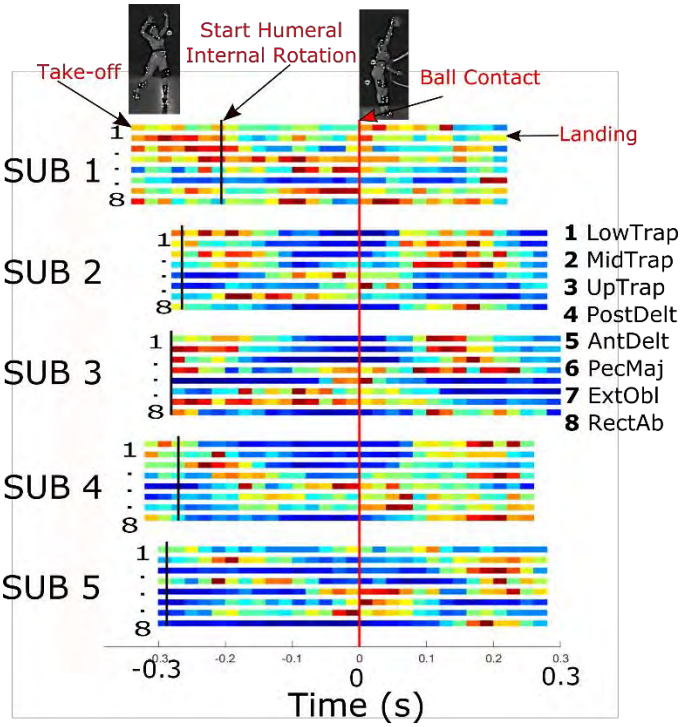

Figure 1: Muscle activation heatmap during the spike, normalized to the within-spike-trials max (maximum activation in dark red, minimum activation in dark blue).

An exemplar comparison of humeral dynamics is displayed in Fig. 3 below the muscle activation graph for Subject 1 and Subject 3. Other subjects used different arm swing techniques. Current efforts focus

on further understanding (1) how arm swing techniques, *including follow-through* relate to performance outcomes and shoulder joint kinetics and (2) how lumbo-pelvis dynamics relate to the activation of the abdominal muscles. Ultimately, as others have previously described, identifying the role of rotator cuff muscles and scapulo-humeral kinematics and kinetics would advance our understanding of volleyball player risk of shoulder injury.

CONCLUSIONS

Subject-specific muscle activation patterns and humeral dynamics were identified. The follow-through phase may present particular challenges to volleyball players (rapid arm deceleration, as in the baseball pitch [3], concurrent with net avoidance) which merits further analysis, especially given the arm swing technique shown in Fig3B.

An EMG representation that used "within-spike-trials max" and a 4-axis humeral dynamics approach provided useful alternatives to identify muscle activation patterns accounting for diversity in MMT as a normalization signal and for understanding humeral dynamics (e.g., Fig2 A vs Fig2B).

REFERENCES

1. Serrien et al. *Intl. J. of Hum. Mov.and Sports Sciences*, 2016.
2. Zaferiou et al. *J.Biomechanics,* 2017.
3. Erickson et al. *J Shoulder Elbow Surg*, 2017.
4. Woltring, *J.Biomechanics,* 1994.
5. Muller-Karger et al. *Proceedings ISB*, 2013.
6. Russel et al. J. *Proceedings ISB*, 2017.

ACKNOWLEDGEMENTS

We thank the participants and research assistants and the philanthropic support from grateful patients.

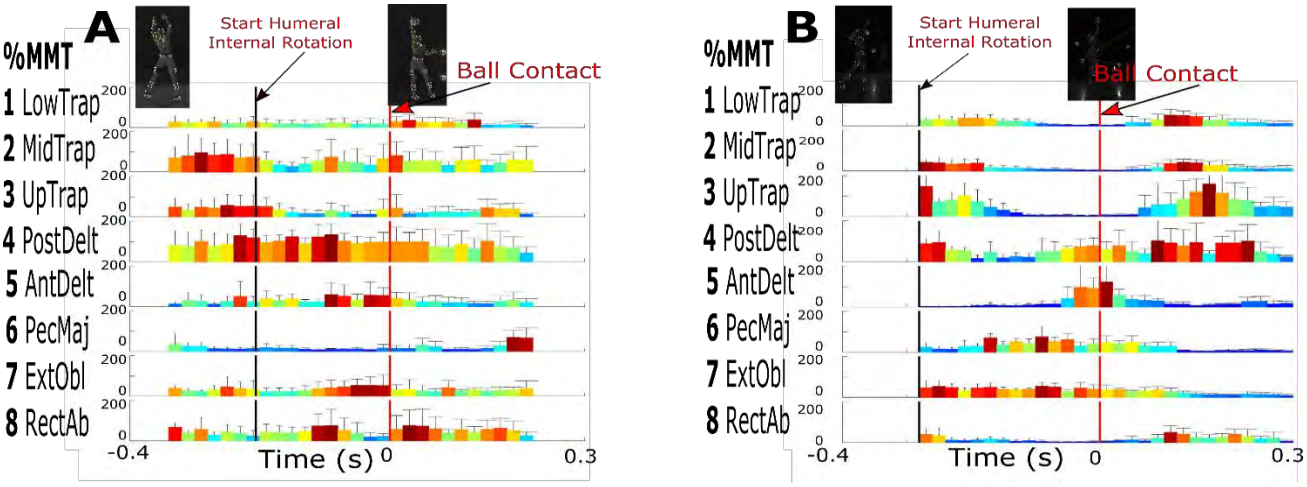

Figure 2: Exemplar mean (SD) binned muscle activation (%MMT) during the spike for Subject 1 (A) and Subject 3 (B). Color scale is normalized to the within-spike-trials max (max activation dark red, min activation dark blue).

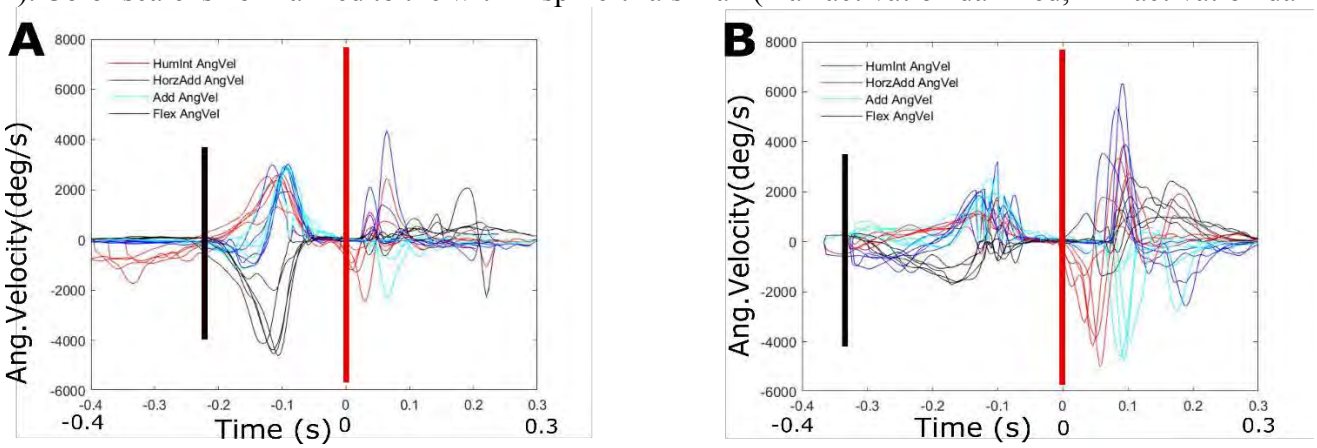

Figure 3: Exemplar angular velocity (**A**: Subject 1, **B**: Subject 3): humeral internal rotation (+,red), horizontal adduction (+, blue), adduction (+,cyan), and flexion (+,black). This figure is vertically aligned with Figure 2 to provide kinematic context for the muscle activation patterns shown above.

DESIGNING USABLE ASSISTIVE DEVICES IN A FIRST-YEAR ENGINEERING DESIGN CLASS: LESSONS LEARNED TO MAXIMIMIZE THE ODDS OF SUCCESS

[1] Kimberly E. Bigelow

[1] University of Dayton, Dayton, OH, USA
email: Kimberly.bigelow@udayton.edu, web: https://udayton.edu/engineering/research/biomechanics-lab/index.php

INTRODUCTION

In the engineering curriculum, senior capstone design courses serve as a way for students to synthesize their undergraduate learning to produce a real-world product or solution. The benefits of this experience have been well-recognized [1] and have led many institutions to begin to implement first-year cornerstone design courses so that students earliest in their career get hands-on exposure to engineering design. Often senior capstone design projects are industry-sponsored, where area companies provide the project description, financial support, and some level of mentorship with the expectation that a certain deliverable is produced at the end of the term. This arrangement is not as feasible for the cornerstone courses, as first-year students do not generally have the same preparation and skills to meet paying customers' expectations. Because of this, a community partnership approach can serve as a, perhaps even more meaningful, stand-in at the first-year level. This is especially true for implementing projects focused on the design of assistive technology. Such a focus is especially appropriate for students with an interest in biomechanics and has been shown to resonate especially well with females and other historically underrepresented minorities within the engineering profession [2], helping to diverse the pipeline. The aim of this work is introduce the model we have established at the University of Dayton for fostering a meaningful design experience in the first-year, while sharing lessons learned and example outcomes from the course.

METHODS

Engineering Innovation is a two-credit hour, single semester course that all first-year engineering students take. Students are placed into sections of approximately 24 students, each taught by one instructor. The project-based course covers the engineering design process, engineering innovation skills and entrepreneurial mindset development. It is up to the instructor to determine the focus of the course project and establish any necessary resources that they need. Since 2009, while the specific projects have differed, my course projects have always focused on designing assistive technology for individuals in our community with disabilities.

The most critical key to success of this project is identifying a community partner who can represent the needs of area individuals with disabilities and then establishing realistic expectations with that partner. There is a careful balance that must be reached where students are given enough freedom to be innovative (e.g. an open enough problem statement), sufficient information to design while respecting patient privacy and confidentiality, and encouragement to produce a fully functional, simple enough, safe product that can be used - with the understanding that this deliverable is not guaranteed. We have found our greatest success working with United Rehabilitation Services of Greater Dayton, a large non-profit facility that assists thousands of families with disabilities annually. We specifically work with an occupational therapist on staff who serves as our liaison to identify assistive technology needs. She also serves as the mentor to the class.

RESULTS AND DISCUSSION

A key obstacle to the success of an approach like this is that it is hard to guarantee a deliverable within the abilities and skills of a first-year student especially within the time and resource constraints of the class. We have implemented several practices that have helped increase the odds of completing the semester with successful prototypes and encourage other

instructors wishing to adopt a similar model to consider these lessons learned.

First, it is critical to work with the community partner to scope projects that are achievable within the abilities of the students in the course. In considering the appropriateness of projects, the end goal of having a product functional and safe enough for regular use must be given top-priority. The more complex or sophisticated the design, the less likely it is to be refined sufficiently within the semester to be useful (or even safe enough to test). Therefore designs that require complex mechanisms, electricity, or specialized safety requirements (e.g. pool flotation devices) have been found to be better to avoid. Devices that require interface with the body have often been achievable by having the occupational therapist prepare a splint and provide that to the students for incorporation into the final product. It is also helpful when the community partner is willing to forego requiring a product to be entirely innovative, choosing instead to reproduce the function of an available product, catered to the specific needs and limitations of an individual. Having a clearer starting point has helped students make sufficient progress in the time that they have. Examples of projects the first-year students have successfully pursued include: Knee abductor to assist with self-catheterization, wrist splint to assist with self-feeding, adjustable drawing easels, device to assist with drying hair with limited upper extremity function, and seating to help practice trunk control.

Giving students guidance about building their prototypes is another important step to success. Encouraging students to keep their devices simple enough that they can be well achieved and look refined is important. Students should be encouraged to use existing parts to the extent possible, but should recognize the desire to avoid a "Frankenstein"-looking assembly. Wood and PVC often lend themselves especially well for design at the first-year level, especially if basic woodworking and tool safety training can be incorporated within the curriculum. The increase in availability and exposure of 3D printing has also opened up options that have helped with the success of products. We provide student teams a $150 budget, which is more than the majority of teams need for a successful deliverable.

We also have begun having two teams in each class independently approach each design need (generally 3 total presented to the class). This helps increase the likelihood that at least one team will successfully build a product that will be deliverable at the end of the term. Teams are encouraged to consult with each other and during the conceptual design review are often steered in two different directions if the emerging solutions are too similar. This way if both products do end up being successful they meet different needs or meet the needs in different ways.

We have also begun having senior students with expertise in biomechanics participate in the conceptual design review which occurs about halfway through the project, before protoype building begins. The seniors sit with each team and review the proposed design alternatives, providing feedback, critique, and revisions. The seniors provide a valuable reality check about what is feasible within the time and abilities of the class and their input is generally very well adhered to.

Finally, we also have developed a pathway for those promising products that are not completed at the end of the semester to be seen through to completion. This occurs in a sophomore biomechanics course.

CONCLUSIONS

We have established several practices that have empowered our first-year engineering students to successfully deliver assistive technology products to individuals with disabilities in our community. This experience has been mutually beneficial to the students and to our community partner, while providing a real-world outlet for biomechanical design from the earliest years.

REFERENCES

1. Dutson et al. *JEE.* 86.1, 1997.
2. Buckley et al. ACM SIGCSE Bulletin. 36(1), 2004.

ACKNOWLEDGEMENTS

This work was funded by a National Science Foundation GARDE award (Award ID: 1510314).

SOFTWARE-BASED TRAINING CAN IMPROVE STUDENT LEARNING IN UNDERGRADUATE BIOMECHANICS CLASS

Angel Gonzalez[1], TeSean Wooden[2], Amelia S. Lanier[1], Michelle Friend[3], Anne Karabon[3], Neal Grandgenett[3] & Kota Z. Takahashi[1]
[1]Department of Biomechanics, University of Nebraska at Omaha, Omaha, NE, USA
[2]Department of Health and Kinesiology, University of Nebraska at Omaha, Omaha, NE, USA
[3]Department of Teacher Education, University of Nebraska at Omaha, Omaha, NE, USA
email: agonzalez@unomaha.edu

INTRODUCTION

Problem-based learning in biomechanics has been shown to effectively motivate student learning and increase knowledge retention [1]. Integrating software-based training through scaffolding techniques that encourages problem-solving into undergraduate courses may improve student learning [2]. At the University of Nebraska at Omaha, we have implemented software-based teaching into an undergraduate biomechanics course to supplement traditional lecture-based teaching. The course emphasized visual aids and numerical computations through software-training in weekly laboratory sessions to further enhance learning biomechanical concepts.

The purpose of this study was to examine the effect of software-based training of biomechanics on undergraduate student performance. We hypothesized that following the completion of the course, students will exhibit improved self-confidence of fundamental biomechanics' concepts. Moreover, we hypothesized that the performance in the laboratory section (i.e., software-based training) would have a stronger correlation with the students' perceived confidence compared to the performance in the lecture component of the course.

METHODS

The study was composed of 86 students from an undergraduate course. Informed consent was obtained prior to participating in the study. The research was approved by the Internal Review Board at the University of Nebraska Medical Center.

An undergraduate biomechanics course was redesigned by implementing software-based training, Visual 3D (C-Motion, Germantown, MD), into the laboratory component of the course. The lecture-based component was held twice a week for an hour while the laboratory section was held once a week for two hours.

Weekly laboratory sessions introduced software-based computations and emphasized application of fundamental concepts in biomechanics. Students were given existing data of human walking and were exposed to basic computational features of the software by computing biomechanical variables pertinent to human walking performance (e.g., ground reaction force, power, etc.). Then, students were asked to compare and contrast human walking with other modes of locomotion, such as during running and reduced gravity. The semester concluded with students working with existing data of patients with various movement pathologies. Students gave a final report to interpret their results along with recommendations for treatment/interventions by using their newly acquired knowledge of biomechanical principles.

To assess learning outcomes, students were given a questionnaire at pre- and post-semester. The questionnaire included Likert scale assessment questions to evaluate students' perceived confidence for understanding fundamental concepts in biomechanics. Although there were eight Likert questions, the question we chose to analyze was '*I am comfortable in describing how Newton's Laws play a role in human movement'* (1 = strongly agree; to 5 = strongly disagree). To compare perceived confidence level at pre- and post-semester, a paired t-test was used. To assess whether performance in the laboratory sessions and/or the lecture component influenced the students' perceived confidence, two separate Pearson's correlation analyses were

performed on the previously mentioned Likert-based question: 1) correlation between final laboratory grades and change in perceived confidence level (from pre- and post-semester), and 2) correlation between final lecture-component grades and change in perceived confidence level (from pre- and post-semester). Statistical significance was set at $\alpha = 0.05$.

RESULTS AND DISCUSSION

The results indicated that software based training improved students' self-confidence in biomechanics-based concepts, such as in describing Newton's Laws (Figure 1. $p<0.001$), supporting our first hypothesis. A significant positive correlation was found between student perceived confidence and performance in the laboratory component of the course (Figure 2a, $R^2=0.074$, $p=0.012$). However, no significant correlation was found between student perceived confidence and performance in the lecture section of the course (Figure 2b, $R^2=0.019$, $p=0.205$).

One limitation of our study design is that we did not include a control group (i.e., laboratory session that does not include software-based training), and thus we may not be able to identify the independent contribution of student learning from the software-based training. Yet, our analyses indicated that students have a higher association with perceived confidence due to the software-based training (laboratory) compared to the lecture component. Another limitation of the study included having two different instructors across three semesters in the lecture section of the course. However, the lab instructor did not change during the study.

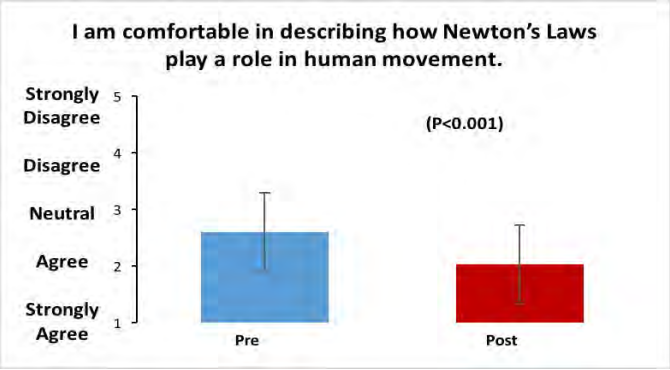

Figure 1: Following the completion of the software-integrated course, students showed improved perceived confidence on describing concepts fundamental to biomechanics (N = 86) between pre- and post-semester ($p<0.001$).

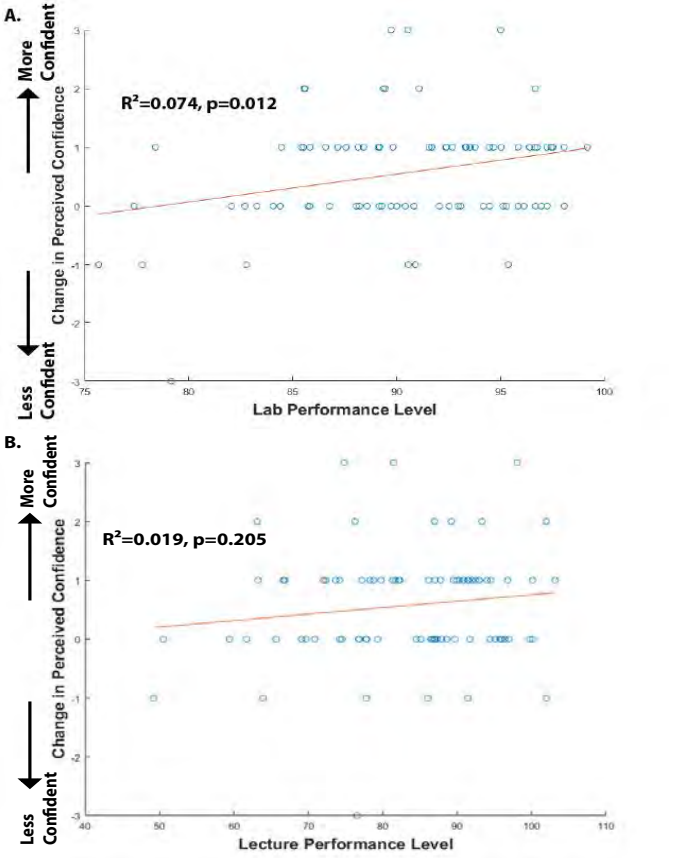

Figure 2: Students demonstrated a higher association with perceived confidence in the lab section of the course (a, $R^2=0.074$, $p=0.012$) compared to the lecture-based section (b, $R^2=0.019$, $p=0.205$). Change in perceived confidence was quantified as the difference in the previously mentioned Likert scale responses (Figure 1) from pre and post-semesters.

CONCLUSIONS

Our study demonstrates that there may be an association between software-based training and student perceived confidence. This data may indicate that integrating software-based training into undergraduate courses can improve student confidence on biomechanics-based concepts.

REFERENCES

1. Clyne AM, Billar KL. *J Biomech Eng* 2016.
2. Belland et al. *Rev Educ Res* 2017.

ACKNOWLEDGEMENTS

This study is supported by the funding from the University Committee for Advancement of Teaching (UCAT) at UNO and from NASA Nebraska Space Grant. This work was supported by the Center for Research in Human Movement Variability of University of Nebraska at Omaha, NIH (P20GM109090).

STUDENT PERCPETIONS OF ACTIVE LEARNING AND MASTERY IN BIOMECHANICS

[1] Duane V. Knudson and [2] Brian Wallace

[1] Texas State University, San Marcos, TX, USA
[2] University of Wisconsin-Oshkosh, Oshkosh, WI, USA
email: dk19@txstate.edu wallaceb@uwosh.edu

INTRODUCTION

Student difficulty mastering Newtonian mechanics and biomechanical concepts is common. Active learning pedagogies, however, have conclusively been shown to significantly increase mastery of biomechanical concepts [1], mechanical and other STEM subjects [2] over tradition lecture It is important to begin to examine what specific active learning exercise are most effective and that create the least initial resistance that is common in some students when active learning pedagogies are implemented. The present study documented which low-tech, easily implementable to lecture active learning tools may be preferred by introductory biomechanics students and if any of these preferences and student epistemology were related to learning biomechanical concepts.

METHODS

Students in two introduction biomechanics courses in kinesiology departments from two universities (comprehensive and research) agreed to participate following IRB approved protocol. The investigators implemented five low-tech active learning activities (Quizzes/Projects, Professional Issues Discussions, Think-Pair-Share, Hypothesize-Activity, and Self-Assessments) in their 3-credit courses. The instructors used between 34 and 60 short (3-10 minute) active learning exercises. Participants took the Biomechanics Concept Inventory (BCI) [3] the first day of the class, taking the test again along with 10 additional questions using a 6-point Likert scale on student perceptions of the active learning exercises at the end of the term. Descriptive data, correlations, and learning defined as normalized gain (g) score [4] were calculated. Preliminary results from the first semester of a planned two-semester study.

RESULTS AND DISCUSSION

Sixty-nine students were included in the preliminary analysis, with 23 being removed due to missing tests, dropping, or noncompliance. The mean BCI pre-test scores (M = 9.4 and 9.1) were qualitatively similar to previous studies of student knowledge entering introductory biomechanics courses using the BCI [3] so further statistical analyses were based on pooled data for both courses.

The low-tech active learning exercises used resulted in a mean post-test BCI score of 11.8 which corresponded to a mean gain score of 17%. Mean post-test scores and student learning in the present study were qualitatively higher than national mean g scores of 3-credit classes (11%), but were qualitatively lower than mean g scores of 4-credit courses (25%) with labs [5] or active learning (25-30%) physics classes [4].

Student perceptions of the low-tech active learning strategies were generally positive (Table 1), particularly for Quizzes/Projects and individual-oriented exercises (Hypothesize-Activity & Self-Assessments). Group active learning exercises were also positively perceived, although a slightly higher percentage of students (16-23%) tended to disagree. This was consistent research reporting some students are initially resistant to cooperative active learning, may not enjoy [6], and may have lower student perceived value of cooperative active learning than more individualized active learning [7]. A majority (85%) of students were comfortable using their biomechanical response systems (thumb) in public to answer instructor questions. A smaller majority (71%) of students liked that the instructors did not allow use of smart phones or computers in these classes.

Predominant student philosophy of learning was surprisingly constructivist. Most (85% agree to strongly agree) students reported they felt responsible for their own learning of biomechanical concepts and most (91% agree to strongly agree) believed that their learning was facilitated by interactions with peers and the instructor. This perspective was less pronounced in responses to the interval level question on epistemology where students reported that mean contributions to variance in learning were primarily due to the instructor (32%), themselves (28%), the book (21%), and finally interactions with other students (15%). Only one correlation of these student epistemology variables (percentage of variance of positive influence on learning from working with other students) had a significant, but weak negative correlation ($r = -0.36$, $p < 0.05$) with learning (g).

The study was limited due to the preliminary analysis of a small sample of volunteers in two intact classes. The investigators made no systematic effort to equalize the course content or exact values of each active learning exercise used. These limitations do not seriously influence the results, given previous research has reported that student factors like GPA, interest in the subject, and perception of application to future career account for much more variance in learning biomechanics concepts than instructor factors [9,8]. The participants had an exaggerated perception of the instructor's influence on student learning of biomechanical concepts. Future research should explore the interaction of student motivation, dosage and kinds of active learning exercises with biomechanics concept mastery.

CONCLUSIONS

The infusion of several low-tech active learning exercises in two introductory biomechanics courses appeared to slightly improve learning of biomechanical concepts over lecture alone. Most of the participants had positive perceptions of active learning exercises, particularly when working individually. About 16 to 23% of participants tended to dislike group active learning exercises, so a mix of individual and group experiences, along with progressive 'training' in group active learning over a term is recommended if more collaborative exercises are to be used.

REFERENCES

1. Riskowski *Sports Biomech.* **14**:168, 2015.
2. Freeman et al. *Proceed NAS*. **111**: 8319, 2014.
3. Knudson et al. *Sports Biomech.* **2**:267, 2003.
4. Haake *Am J Physics*. **66**:64, 1998.
5. Knudson et al. *Perc Mot Skills*. **108**:499, 2009.
6. Smith et a. *J Schol Teach Lrn* **11**:53, 2011.
7. Machemer et al. *Act Lrn High Ed.* **8**:9, 2007.
8. Hsieh et al. *Sports Biomech*. **7**:398, 2008.
9. Hsieh et al. *J Coll Sci Teach*. **41**:82, 2012.

Table 1: Student Perceptions of Active Learning Exercises and Epistemology of Learning

Question	Percentage			
	Strongly Agree	Mod. Agree	Agree	All Levels Disagree
Quiz/Projects aided learning	33	28	30	9
Pro. Issue Disc. aided learning*	25	21	37	16
Think-Pair-Share aided learning*	21	28	28	23
H_o –Activity aided learning	19	31	36	13
Self-Assessment aided learning	27	33	27	13
Like excluding phone/computer	16	14	41	29
Comfortable non-private answer	19	19	47	15
Believe construct own learning	24	31	30	15
Learning facilitated by student and instructor interaction	36	37	19	7

*Active learning exercises using small groups (2-3 students).

BIOMECHANICS TO ENGAGE ELEMENTARY STEM EDUCATION

[1,3] Amelia S. Lanier, [1,3] Kota Z. Takahashi, [2] Michelle Friend, [2] Anne Karabon, [4] Sarah Moulton, and [2] Neal Grandgenett

[1] University of Nebraska at Omaha, Department of Biomechanics, Omaha, NE, USA
[2] University of Nebraska at Omaha, Department of Teacher Education, Omaha, NE, USA
[3] Center for Human Movement Variability, University of Nebraska at Omaha, Omaha, NE, USA
[4] Moulton Editorial Services, Omaha, NE, USA
email: alanier@unomaha.edu, web: https://www.unomaha.edu/college-of-education/cobre/index.php

INTRODUCTION

As an inherently interdisciplinary field, biomechanics includes the intersection of several science, technology, engineering, and mathematics (STEM) disciplines making it an optimal context to engage students in STEM learning and enhance their interest in STEM occupations [1]. Furthermore, with its focus on the body in motion, biomechanics is particularly well suited to engaging young students, who naturally use their bodies to make sense of themselves and their surrounding environment [2, 3]. With a recent influx of new consumer-oriented and education-focused biomechanics technologies including smart watches, mobile health apps, wearable garment sensors, open-source video-analysis software, and low-cost sensor technology the ability to bring biomechanics to classrooms has drastically improved. Addressing this opportunity, researchers in both teacher education and biomechanics at the University of Nebraska at Omaha are beginning to utilize biomechanics in 3rd-6th grade classrooms as a vehicle for STEM learning and engagement.

The goal of this project is to use biomechanics as a context for increasing awareness of, interest in, and capability to participate in STEM education pathways among in elementary level students in the Omaha Metropolitan area.

METHODS

In an effort to promote biomechanics in elementary classrooms, this project will include a summer teacher institute, a summer student academy, professional development/support workshops, a biomechanics student fair, and engagement with STEM professionals. All teachers and students participating in these activities will be recruited from Omaha Public Schools (OPS).

The teacher institute will be centered on the development of teaching modules that utilize inquiry-based learning (IBL) as an approach to teaching biomechanics. The modules will cover topics such as balance (Fig.1), muscle activity, running mechanics, robotics, and spring mechanics, among others. IBL is a powerful and valuable learning strategy at the elementary level [4]. IBL invites students to ask questions, explore and investigate, analyze and describe, communicate, and reflect. This process not only aligns strongly with how successful biomechanists approach their research but also with K12 science education strategies recommended by the National Research Council [5].

Figure 1: Dr. Kota Takahashi demonstrates how foot sensation plays a role in human balance (picture from The Boy Scout Jubilee 2017). Angle of trunk lean indicated by orange vectors.

The student academy will engage students in the newly developed teaching modules generated at the summer teacher institute. The teacher workshops

will guide and support teachers as they plan and implement biomechanics modules in their classes. Throughout the duration of this project, student reported and teacher reported outcomes will be collected and analyzed.

RESULTS AND DISCUSSION

This project has the potential to develop more positive perceptions about STEM among participating teachers and students, which would have a strong future impact on STEM education in and around Omaha. As this project is currently in the planning phases, there is not data to report, and so the specific research questions and measures to be collected will be discussed. The data collection for the project is two-fold, being both educator- and student-centered.

Our teacher-centered research aims to address how learning biomechanics affects confidence and attitude towards STEM concepts, how teachers are able to introduce emerging technologies in a biomechanics context, and what barriers exist for integrating biomechanics and technologies. The authors will utilize STEM attitude and interest surveys, STEM teaching efficacy tests, interviews, teacher reflections, and classroom observations.

Our student-centered research aims to address how engaging in biomechanics curricular activities changes students' awareness of, interest in, and motivation to pursue STEM education pathways. Additionally, the authors will explore if student engagement in STEM relates to performance on state level science and math assessments. The authors will utilize STEM attitude and interest surveys, Nebraska State Accountability tests, and student interviews.

CONCLUSIONS

Taken together, the interdisciplinary STEM content, use of emerging technologies, and diverse career opportunities in biomechanics make it an excellent context for engaging students in STEM learning and enhancing their interest in STEM occupations. As this project moves forward, the teacher institute and student academy will be first implemented in Summer 2018, with the professional development/support workshops beginning in Fall 2018.

The project will directly impact an estimated 1,500 youth, most of whom reside in the diverse OPS district. In addition, the project will help engage elementary teachers, school districts, informal educators, and business professionals in the Omaha Metro Area, establishing long-term professional networks to support effective STEM teaching well into the future. Furthermore, successful implementation of this project will result in standards-based and culturally responsive curricular resources that can be easily adapted by elementary teachers across the country to reach students in diverse school contexts.

Overall, this project will help build awareness of the importance of STEM and will challenge stereotypical perceptions of what STEM is by demonstrating its real-world biomechanics integration across disciplines, including biology, engineering, physics, and mathematics.

REFERENCES

1. Drazan et al. *Conf Proc IEEE Eng Med Biol Soc,* 2014.
2. Piaget, J. *The psychology of the child*. New York: Basic Books.
3. Vygotsky, L. *Mind in Society: The development of higher psychological processes*, Harvard University Press, 1978
4. National Research Council. *Adding It Up: Helping Children Learn Mathematics*, National Academy Press, 2001.
5. National Research Council. *A Framework for K-12 Science Education: Practices, Crosscutting Concepts, and Core Ideas*, National Academy Press, 2012.

ACKNOWLEDGEMENTS

The authors would like to acknowledge NSF ITEST Grant 1759000 and RMC for their assistance with developing the evaluation plan for this project.

OPEN-ENDED DISCUSSION IN THE BIOMECHANICS CLASS

[1] Karen L. Troy and [2]Laurel Kuxhaus
[1] Worcester Polytechnic Institute, Worcester, MA, USA
[2]Clarkson University, Potsdam, NY, USA
email: ktroy@wpi.edu, web: http://wp.wpi.edu/MBL

INTRODUCTION

In a traditional biomechanics classroom, teaching typically focuses on technical content such as correctly calculating joint reaction forces and moments. Because classroom time is a finite resource, as teachers we often choose to spend time on this important technical material at the expense of covering more broad applications and implications. As a result, we graduate students who are technically proficient, but may lag in both the ability to identify opportunities to apply their knowledge or the confidence to do so.

In addition to the usual challenge of delivering an exciting and engaging class, many Universities have expanded the number of courses that are offered as online or blended courses. Others have encouraged the use of a "flipped" classroom so that more class time can be spent on engaging activities and discussions. Here, we present examples of open-ended discussion prompts; one uses an out-of-class, online, group discussion, and the other culminates in an in-class work session with discussion. These prompts were designed to enhance the "Entrepreneurial Mindset" of the students [1]. That is, they were intended to inspire curiosity and help students make connections between the course material and real-world applications.

METHODS

Discussion questions can be focused to expand either the breadth or depth of understanding about a particular topic. The examples presented here accomplish both, with Method 1 aimed at breadth, while Method 2 addresses depth.

Method #1: Brief Online Discussion Prompts

A total of four of online discussion prompts were presented to a junior/senior level biomechanics class taught within departments of Mechanical and Biomedical Engineering. The discussions were worth a total of 10% of the final course grade, with each discussion being worth 2%. The final 2% of the grade came from students' interactions with each other.

Discussion prompts were delivered approximately biweekly through the Discussion board feature on Canvas, the learning management system available at our University. To make interactions between students more manageable, students were divided into discussion groups of approximately 20 students.

The primary purpose of the discussion prompts was to encourage students to think creatively and critically about applications of biomechanics in the context of research and product design. Each discussion was delivered at a point during the course where it was most relevant.

The following instructions were provided to students:

- You are expected to respond to each question with an intelligent, detailed, and thoughtful post.
- The professor and TA will read and comment on student posts after the prompt has been "live" for 2-3 days. During the week, you should read and respond to each other's posts, and to questions or comments that are addressed to you.
- You are expected to read and comment thoughtfully on a classmate's post at least twice during the term. This accounts for the remaining 2% of the final grade.
- I expect that responses will be thoughtful, coherent, will cite references or web links where appropriate, and will, in part, demonstrate knowledge of biomechanics.
- All interactions with classmates will be respectful and constructive.

The full text of the prompts will be made available on the biomechanics teaching repository [2]. Here is one example, which served the dual-purpose of helping graduating seniors brainstorm potential job opportunities.

Osteoarthritis a major clinical problem and is big business for medical device companies. Identify a product or service related to osteoarthritis prevention or treatment. Briefly explain what it is and provide a link to the company information. Next, identify the key stakeholders who are invested in the development, deployment, and use of the product/service. For each stakeholder, explain their key objective/motivation. Explain how biomechanics and mechanobiology play a role.

Method #2: Open-ended Innovation Experience – "Why is ankle joint replacement so problematic and what can we do about it?"

This implementation of an open-ended discussion question occurred as a final "exam" in an upper-level undergraduate introductory biomechanics class (class size: 35) of predominantly mechanical and chemical engineering students. Students were instructed to prepare for this experience by performing independent learning (seeded by two review articles provided by the instructor) and brainstorm ways to improve total ankle arthroplasty (TAA). The general topic of joint replacements had received little prior attention during the course.

When students arrived to the final "exam" in Clarkson's innovation studio space, they were instructed to form self-selected interdisciplinary groups of 3-5 and work together for about an hour to prepare a two-minute presentation about their TAA innovation. The studio space included traditional presentation resources (projectors), and creativity-inspired items, such as play-doh, whiteboard walls, butcher paper, and other materials. The session culminated with these presentations, to communicate WHY the proposed innovation was necessary/ WHAT problem it would solve, WHAT the innovation was and why it was technically feasible, HOW it would be evaluated, and what BENEFITS it would have to the patient, surgeon, and/or supply chain. Each student was required to speak for a portion of their group's time.

Assessment of this activity (10% of the overall course grade) was as follows: 50 points for individual preparation as documented by the student in notes, citations, prose, or other means; 40 points for the presentation as assessed by a rubric; 10 points for filling out a feedback survey.

RESULTS AND DISCUSSION

Method 1 (KLT)

Students were generally happy with the discussions, One student wrote, "I really liked the discussions online. I thought it was really beneficial to have those discussions and be able to share ideas as well as read other people's ideas about real life applications of biomechanics."

Method 2 (LK)

Students generally enjoyed the activity, with many commenting that the lively environment was a welcome contrast to a written exam during the Final Exam period. Most students reported that the preparation was less work than preparing for a written exam. The instructor observed a high degree of synthesis and independent learning during the preparation phase – several students turned in preparation work that was, in essence, a 2nd literature review/term paper! Others focused more on brainstorming solutions. The general mood of the room during discussion time was one of amazement that TAA was so challenging from an engineering standpoint. The presentations were varied in format – some students made a few Powerpoint slides; others made play-doh/clay models to supplement white-board drawings. The most common suggestion for improvement from students was to permit preparation of the presentation in advance.

CONCLUSIONS

Open-ended discussion questions inspire students to learn independently and synthesize their own thoughts. These can be incorporated into biomechanics courses in several ways, and are critically important to the professional formation of the next generation of engineers.

REFERENCES

1. http://engineeringunleashed.com
2. Smeeters C, Bigalow K, ASB 2016

ACKNOWLEDGEMENTS

We thank the Kern Family Foundation for inspiring discussions of the Entrepreneurial Mindset

UPPER LIMB JOINT KINEMATICS DURING TOUCHSCREEN INTERACTION

[1] Deanna S. Asakawa, [1]Matthew G. Becker, [1]Jennifer M. Asaro and [1]Jennifer L. Hein

[1] California State University San Marcos, San Marcos, CA, USA
email: dasakawa@csusm.edu

INTRODUCTION

Human interaction with touchscreen computing technology has become common for work, personal and school use. Currently, there are ergonomic guidelines for desktop computer use, but similar guidelines do not exist for touchscreen mobile computing technology [1]. Contributions of the different joints of the upper limb have been studied for single-finger keyswitch tapping [2], and showed that wrist and elbow movements contribute to fingertip tapping. However, similar comparison of upper limb joint movement contribution has not been studied for tapping or gesturing on a touchscreen computing interface. Quantitative upper limb joint kinematics may assist design of software and ergonomic guidelines to help reduce repetitive stress injury from overuse of touchscreens [3].

The aim of this study is to determine the relative contributions of the shoulder, elbow, and wrist during different touchscreen gestures. Specifically, based on previous work [3], we hypothesized that gestures such as tap, pinch and stretch would involve more wrist motion than elbow or shoulder motion. Also, we hypothesized that swiping gestures would involve more shoulder motion than elbow or wrist motion.

METHODS

Ten right-hand dominant participants (4 male, 6 female; age 21-35 years) were seated at a table and completed 7 gestures on a 10.1 inch Galaxy Tab 4 touchscreen tablet (Samsung, Seoul, South Korea). Subjects ranged in height from a 1.63m female to a 1.85m male. All participants provided consent to forms and protocols approved by California State University, San Marcos. The touchscreen computing device was placed in landscape orientation on a small easel set on the table in front of subjects such that the top of the screen was reclined 20° from the vertical. The tablet computer dimensions were 24.3 x 17.6 x 0.8 cm. The center of the touchscreen was aligned with the center of the participant's sternum. The touchscreen was placed at a comfortable reaching distance, at 70-75% of the participants arm length as measured from the acromion to tip of the third digit with the arm outstretched. An 8-camera motion capture system (Qualisys AB Goteborg, Sweden) was used to measure the kinematics of the upper limb of participants during touchscreen interaction by tracking the three-dimensional positions of 16 passive reflective markers placed on bony landmarks of the upper limb and trunk. Motion capture data were recorded at 120Hz.

Gestures included index-finger tap, swipe left, swipe right, swipe down and swipe up. Two additional gestures, pinch (zoom out) and stretch (zoom in), were completed with the index finger and thumb. All participants had previous experience using touchscreen computing devices. Order of gestures was randomized. Participants repeated each gesture at a self-selected pace for 12 seconds per gesture. Visual 3D software (C-Motion, Inc., Germantown, MD) was used to compute shoulder flexion/extension, shoulder internal/external rotation, elbow flexion/extension, forearm rotation (pronation/supination) and wrist flexion/extension throughout each gesture. Three-dimensional marker positions were filtered with a low pass Butterworth 6Hz filter. When analyzing joint angle data for the repeated gesture motions, a minimum of three complete consecutive repetitions were analyzed for each subject for each gesture. The first and last repetitions completed by the participants were not used in data analysis. Mean joint excursions (± standard deviations) were computed for all participants for each gesture. Gestures and joint motions were compared using SPSS Statistics (IBM Inc, New York, NY) with two-way repeated measures analysis of variance and Bonferonni's post hoc comparison.

RESULTS AND DISCUSSION

Overall, joint excursions at the wrist, elbow and shoulder were less than 20° during the performance of the touchscreen gestures studied (Table 1). Individual participants demonstrated consistency in the repetitions of each gesture. Index finger tapping on the touchscreen demonstrated on average less than 6° of motion at the shoulder, elbow, or wrist joint. Joint excursions for tap were significantly different from joint excursions for all other gestures ($p \leq 0.005$).

For the gestures studied, wrist flexion/extension was significantly different than shoulder flexion/extension ($p<0.01$). As hypothesized, tapping involved significantly more wrist flexion/extension than shoulder flexion/extension and shoulder rotation. Also, to complete pinch and stretch, participants used significantly more wrist flexion/extension, as compared to flexion/extension joint excursion at the elbow or shoulder (Table 1).

Swiping gestures involved shoulder motion (Table 1). However, shoulder rotation excursion was significantly greater than wrist flexion/extension excursion for swipe right, but not for swipe left, up, or down. When comparing swiping gestures, the directions that were significantly different for joint excursions were slide left and slide down ($p<0.02$). These data show only swipe right involved more shoulder motion than wrist motion.

CONCLUSIONS

In conclusion, performance of touchscreen gestures differs in the amount of motion at the different joints of the upper limb. Results of this study suggest that gestures such as tap, pinch and stretch utilize wrist movement with little shoulder motion. Previously, finger joint motion has also been shown to contribute to tap, pinch and stretch gestures [3]. For the swiping gestures studied, shoulder motion contributed to completion of gestures.

Characterization of upper limb joint kinematics during touchscreen interaction may provide data needed to develop guidelines for ergonomic use of touchscreen devices. For example, interaction with a touchscreen on an easel is similar to a clerk/cashier or shopper actuating a touchscreen cash register. Therefore, these data suggest that risk of repetitive stress injury to the shoulder, elbow, and wrist may depend on the type of gesture being repeated during touchscreen use.

REFERENCES

1. Dennerlein. *Work*. 52:269-77, 2015.
2. Dennerlein et al. *J Biomech*. 40:3013-22, 2007.
3. Asakawa et al. *Applied Ergo*. 58:176-81, 2017.

ACKNOWLEDGEMENTS

We thank Devin L. Jindrich, T. Varner and N. Mendoza.

Table 1: Joint angle excursion in degrees reported as average (±standard deviation) for 10 participants. Values in bold show the greatest joint excursion measured for each gesture.

Gesture	Shoulder Flex/Ext (°)	Shoulder Rotation (°)	Elbow Flex/Ext (°)	Forearm Rotation (°)	Wrist Flex/Ext (°)
Tap	0.9(0.5)	1.3(0.5)	2.2(1.4)	2.4(1.4)	**5.7(2.2)**
Pinch	2.3(1.1)	3.4(1.5)	3.6(1.8)	9.4(2.2)	**13.4(5.1)**
Stretch	1.9(1.0)	3.9(1.9)	4.1(1.6)	8.2(2.1)	**13.5(5.3)**
Swipe Left	8.4(2.6)	**14.4(3.5)**	7.8(2.1)	5.4(2.4)	9.1(4.6)
Swipe Right	9.7(3.0)	**15.6(4.4)**	8.1(2.1)	4.9(1.7)	7.8(2.7)
Swipe Up	7.9(2.0)	**9.5(4.9)**	4.9(1.2)	4.7(2.0)	7.1(3.4)
Swipe Down	7.4(1.9)	7.2(4.4)	5.0(1.9)	5.1(2.4)	7.9(3.3)

SHOULDER MUSCLE ACTIVITY CHANGES IN PATIENTS AFTER INJECTION AND THERAPY

Jennie Cooper and Andy Karduna

University of Oregon, Eugene, OR, USA
email: jenniec@uoregon.edu, web: http://karduna.uoregon.edu/

INTRODUCTION

Shoulder pain is a common orthopedic ailment. There are a multitude of potential sources of pain and dysfunction in and around the shoulder, which can make both diagnosis and treatment a challenge. One common diagnosis is Subacromial Impingement Syndrome, in which the soft tissue inferior to the acromion process does not have sufficient space to slide unimpeded. This could be caused by joint narrowing, often from bone spurs, or from tissue inflammation. Regardless of the initiating mechanism, once the tissue is irritated it has even less space to slide so the likelihood of resolution without intervention is slim. A shotgun approach is often used to treat this syndrome, and it may include a cortisone injection, anti-inflammatory pills, ice, or physical therapy, or a combination [1].

While this intervention has generally been shown as effective, it does not resolve the syndrome for all patients [1]. Also, while multiple studies have investigated muscle activation differences between healthy subjects and those with subacromial impingement, results appear conflicting and require further investigation [2].

The purpose of this experiment is to determine the effect of a standardized treatment protocol on the neuromechanics of the shoulder. It is hypothesized that rotator cuff activation will increase both with pain relief and with physical therapy.

METHODS

Sixteen subjects age 21-65 (ten male, six female) have been recruited from the Slocum Center for Orthopedics. They were all being seen by an orthopedic surgeon for shoulder pain, which the surgeon assessed and determined was caused by subacromial impingement. Inclusion criteria were positive Neer, Hawkins, and Jobe tests and pain wsith active elevation; exclusion criteria included signs of a full-thickness rotator cuff tear, pain with cervical range of motion, positive Spurlings, history of shoulder surgery, or recent dislocation, instability, or injection. Once the subject consented to be included in the study, a subacromial injection was scheduled to be performed on a subsequent day.

Once the subject arrived for testing, pain measures were taken and the subject was instrumented with electromyography (EMG) sensors (six surface and two fine-wire; Delsys Inc. Boston, MA USA) on the anterior, middle, and posterior deltoid heads, upper trapezius, latissimus dorsi, serratus anterior, supraspinatus (fine-wire), and infraspinatus (fine-wire).

The subject performed two Maximal Voluntary Contractions (MVCs, full can and external rotation), followed by multiple dynamic contractions, including humeral elevation in the scapular plane.

The physician then administered a subacromial injection (6 cc 0.5% Marcaine with Epinephrine and 1 cc DepoMedrol). Pain was reassessed and the subject again performed the MVCs and dynamic contractions. Additionally, a submaximal (30%) absolute force was calculated for each subject and the isometric contractions were again performed at this force. This was done in order to have an absolute comparison value for post-physical therapy, at which point the MVC force will likely have changed.

The subject then attended six weeks of physical therapy using a standard protocol and home exercise program [3]. Following the last physical therapy session, the subject returned for testing. The same protocol was performed, including MVCs, dynamic contractions, and submaximal isometric contractions at the same force as before (30% of previous MVC).

Normalization of EMG was performed not to the MVCs, as they were anticipated to change with physical therapy, but to the absolute force determined by 30% of the post-injection MVC.

The three testing periods were designated T1 (before injection), T2 (after injection), and T3 (after physical therapy).

Custom Motion Monitor software (Innovative Sports Training Inc. Chicago, IL USA) was used to collect the data. EMG and Inertial Measurement Unit (IMU, Thales Visionix, Billerica, MA, USA) data were collected at 2000 Hz. EMG data were bandpass filtered for 20-450 Hz. The Common Mode Rejection Ratio of the system was >80 dB. EMG amplitude was smoothed using a root mean square (RMS) analysis with a sliding 50 ms window.

RESULTS AND DISCUSSION

Preliminary results from one subject are displayed in Figures 1 and 2. Figure 1 shows the supraspinatus activity during humeral elevation in the scapular plane, specifically calculated as an average across three trials at 30, 60, 90 and 120 degrees, at T1 (before the injection), T2 (after the injection), and T3 (after six weeks of physical therapy). Figure 2 shows the same for the infraspinatus.

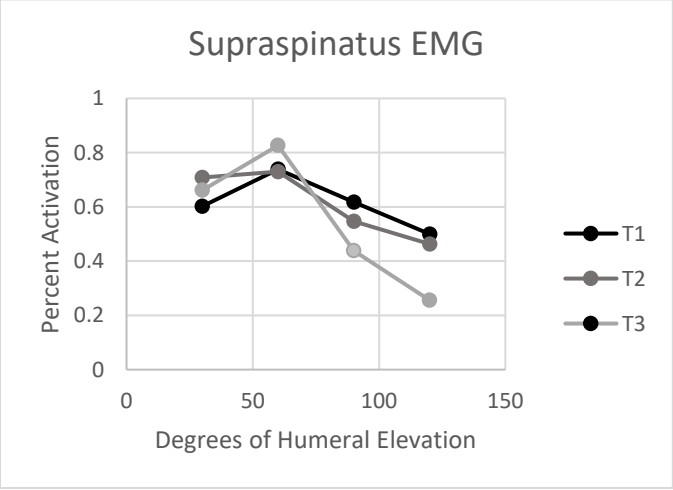

Figure 1: Supraspinatus activity at three time points

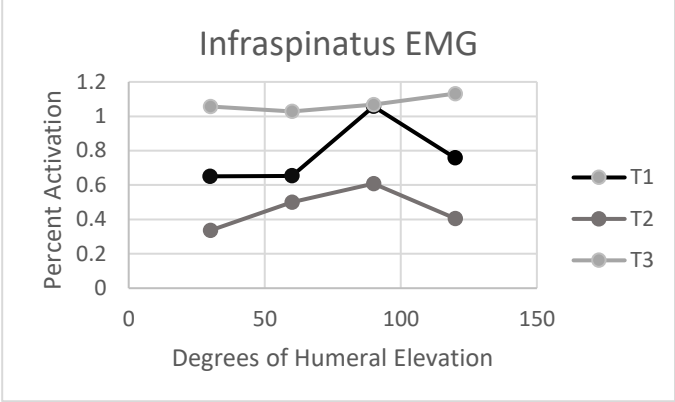

Figure 2: Infraspinatus activity at three time points

There are insufficient data at this point to determine what changes might be associated with the subacromial injection or with physical therapy.

In addition to the results being influenced by the intervention, we anticipate there potentially being differences in activity between patients and control subjects who are tested at the same three time points but without the injection or physical therapy.

CONCLUSIONS

There are currently insufficient data to attempt to draw any conclusions about the effect of subacromial impingement or treatment on the levels of muscle activation in the shoulder. Data collection and analysis are continuing. Additionally, the potential remains to compare "responders" with "non-responders" (those for whom the intervention does not resolve their dysfunction), since they might give a hint about the effect of physical therapy without pain reduction.

REFERENCES

1. Marinko et al. *Journal of Shoulder and Elbow Surgery,* 20(8), 2011.
2. Chester et al. *BMC Musculoskeletal Disorders*. 11(45), 2010.
3. McClure et al. *Physical Therapy,* 9(84), 2004.

ACKNOWLEDGEMENTS

Dr. Shapiro and his team at Slocum have been integral members of this study team.

QUANTIFYING GLENOHUMERAL JOINT STIFFNESS ACROSS DIFFERENT SHOULDER POSTURES

[1] Brian J. Diefenbach and [1] David B. Lipps

[1] School of Kinesiology, University of Michigan, Ann Arbor, MI, USA
email: dlipps@umich.edu

INTRODUCTION

The glenohumeral joint is stabilized by passive soft tissues and the coordinated activations of shoulder muscles [1]. Measures of joint stiffness can provide insights into the postural stability of the glenohumeral joint. Previous studies have individually estimated the stiffness of the glenohumeral joint in different postures, including with the arm abducted 90° at the side [2] or abducted 45° in the scapular plane [3]. However, it is unclear how changes in arm posture in a given individual affects glenohumeral joint stiffness. Quantifying stiffness in various shoulder postures provides insights into how changes in both the muscles recruited in a given posture and the fiber lengths of these muscles impact glenohumeral stiffness, and as a result postural stability of the shoulder. Therefore, the purpose of this study was to investigate the effect of arm posture within an individual on glenohumeral joint stiffness in the horizontal plane. It was hypothesized that (1) increasing shoulder elevation and plane of elevation would lead to increased glenohumeral stiffness in the horizontal direction and (2) higher volitional contractions and activation levels would increase glenohumeral stiffness.

METHODS

The right, dominant, shoulder of five healthy participants (4 M, 1 F; mean age: 20.8 ± 0.1 yr, weight: 77.1 ± 8.9 kg, height: 1.81 ± .04 m), with no history of shoulder injury was placed into a plastic removable cast that held the arm fixed at 90 degrees of elbow flexion. The plastic cast attached to the crank arm of a high-precision rotary motor via a six-degree of freedom load cell (JR3). The center of rotation of the glenohumeral joint was aligned with the motor axis. Subjects were perturbed in the horizontal plane with small, stochastic perturbations (amplitude = 0.06 rad) while the resultant torques were measured in all three degrees of freedom. During the 60-second experimental trials, participants were asked to remain at rest, or maintain constant shoulder torque scaled to ±10% or ±20% of their maximum voluntary contraction (MVC) in the horizontal plane. An LCD monitor was provided to allow for torque feedback to participants during the trial. Trials were repeated in four experimental arm postures: two vertical positions (arm elevated 45° (V45) or 90° (V90)) combined with two horizontal positions (plane of elevation of 0° (H0) or 45° (H45)) (Figure 1). Two trials were performed in each of the five activation conditions and four arm angles, yielding 40 total trials.

Stiffness was approximated by modeling the shoulder as a spring mass damper system. Joint impedance, the dynamic relationship between the torque response to an imposed change in joint position, was quantified using a frequency response function (FRF). The dynamic properties of the shoulder were approximated by fitting the FRF with a 2nd order linear system with inertial, viscous and elastic parameters [4]. The variance accounted for (%VAF) between the measured torque and the torque predicted by the parametric fit was calculated. The current study focused on the elastic parameter ("stiffness") as it is the most clinically relevant. A repeated-measures analysis of variance was

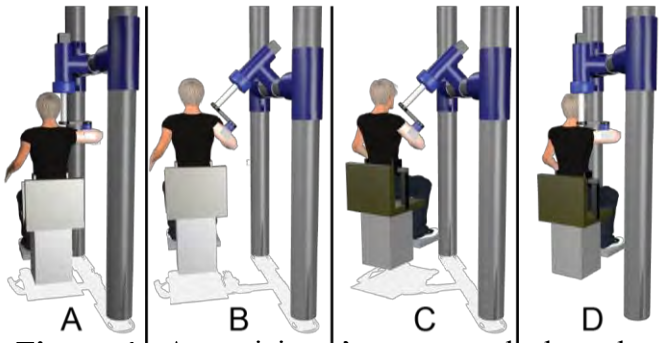

Figure 1: A participant's arm attached to the rotary motor at four different testing conditions. A. *V90_H0* B. *V45_H0* C. *V45_H45* D. *V90_H45*

performed where glenohumeral stiffness was our outcome measure and activation level, vertical position, and horizontal position were within-subjects factors. Post-hoc multiple comparisons with Bonferroni corrections were performed to investigate significant main effects.

RESULTS AND DISCUSSION

The overall %VAF for all subjects and trials was 87 ± 10%, indicating our parametric fits to estimate glenohumeral stiffness were robust. Our statistical analysis revealed main effects for activation level, ($F_{(4,9)}$ = 48.834, p<0.001), vertical position ($F_{(1,9)}$ = 18.046, p<0.02), and horizontal position ($F_{(1,9)}$ = 15.808, p<0.02). There were no significant interactions. Post-hoc analysis found that activation levels of ± 10% horizontal ab/adduction produced stiffness values that were significantly higher than the passive condition, but significantly lower than the ± 20% horizontal ab/adduction activation levels (all p < 0.05). Additionally, greater elevation of the arm (e.g. moving the arm upward) significantly reduced horizontal glenohumeral stiffness (p = 0.01), and increasing the plane of elevation of the arm (e.g. moving the arm forward) significantly reduced the horizontal glenohumeral stiffness (p = 0.01).

On average, altering the elevation of the arm had a larger effect on glenohumeral stiffness than altering the plane of elevation. One potential explanation for this result is that lowering the arm increases the contributions of gravity to stiffness at the glenohumeral joint, and should be taken into consideration in future work.

Overall, glenohumeral stiffness in the horizontal plane is sensitive to volitional contraction levels and the elevation and plane of elevation of the arm. Measuring glenohumeral joint stiffness in the horizontal plane provides important insight into one's ability to execute everyday tasks, as many such tasks destabilize the shoulder joint [5]. Our findings that certain glenohumeral joint postures have lower stiffness, and therefore lower postural stability, could indicate that the shoulder is more prone to injury in these specific postures. Further work is needed to determine how the injury progression and rehabilitation of different shoulder pathologies impacts glenohumeral stiffness throughout the entire range of motion.

CONCLUSIONS

Changing the elevation and plane of elevation of the arm impacts glenohumeral joint stiffness.

REFERENCES

[1] Bigliani et al. *Clin Orthop Relat Res,* **330**,13-30, 1996.
[2] Lipps, et al. *IFAC-PapersOnLine* **48,** 1369-1374, 2015.
[3] Zhang, et al. *J Orthop Res* **18,** 94-100, 2000.
[4] Perreault, et al. *Exp Brain Res* **141,** 312-23, 2001.
[5] Rancourt & Hogan. *J Mot Behav* **33(2),** 193-204, 20.

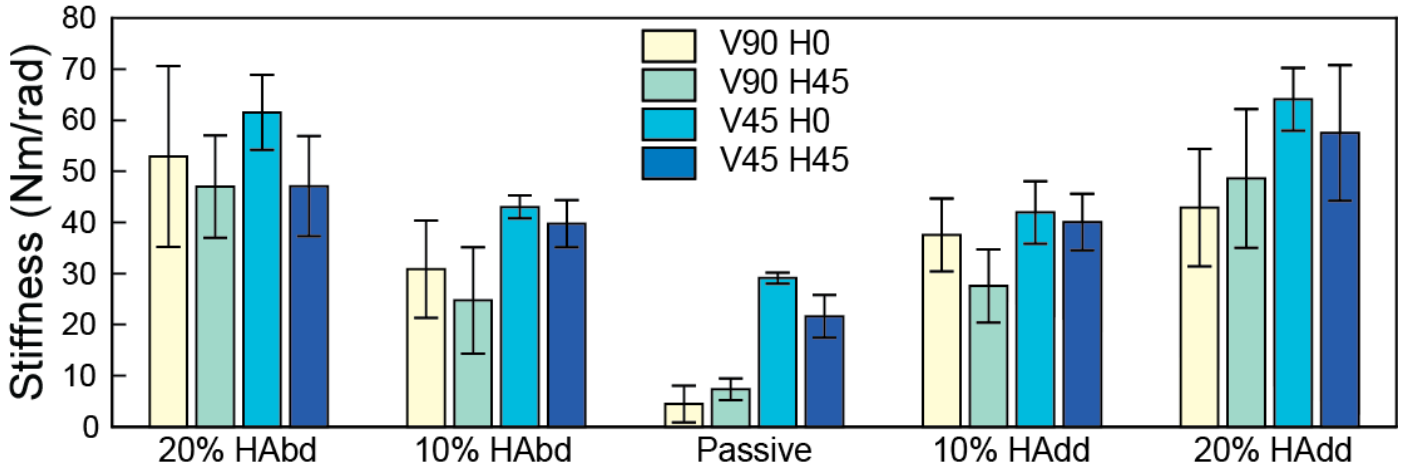

Figure 2: Horizontal glenohumeral joint stiffness (mean ± SE) across five torque conditions (20% horizontal abduction (HAbd), 10% HAbd, Passive, 10% horizontal adduction (HAdd), and 20% HAdd) and four arm positions (V90_H0, V90_H45, V45_H0, V45_H45).

ANALYSIS OF UPPER EXTREMITY MOMENTS DURING HAMMERING

[1] Sumaya Ferdous, [2] Nilanthy Balendra, [1] Joseph E. Langenderfer

[1] School of Engineering and Technology, and [2] Doctoral Program in Physical Therapy,
Central Michigan University, Mt. Pleasant, MI
email: ferdo1s@cmich.edu

INTRODUCTION

The overall inertia of an object and the symmetry of principal inertias affects ability to move the object. Previous work has shown that the relationship between the symmetry of inertia and overall inertia influence effectiveness as a hammering tool [1]. When the magnitude of overall inertia was increased relative to the symmetry of inertia, hammers were more effective. However, previous studies did not investigate biomechanics and did not describe or interpret the entire movement, but only measured vertical hammer motion and simple task outcomes. In our previous study of hammering kinematics [2] subjects performed the hammering motion with greater complexity when the hammer symmetry of inertia was increased. Others have hypothesized that symmetry may be important in determining how torques, and forces which cause the torques, must be directed. Symmetry may be related to the diversity of forces required to move the object, but this hypothesis is untested. Objects with larger symmetry require less diverse forces, and objects with smaller symmetry require diverse forces.

The purpose of this study was to describe moments of upper-extremity joints while subjects performed hammering with hammers of varying properties. The goal was to examine the role of hammer inertia and symmetry of inertia. The hypothesis was that more complex moments, as represented by the number of principal components required to explain moment variance, would be generated for hammers with greater symmetry of inertia.

METHODS

Data were collected using a 12 camera Vicon motion capture system with 13 markers on anatomical landmarks and three on the hammer as described in [1]. Inverse dynamics analysis of 19 male subjects hammering with four hammers was done using previously described procedure [1].

PCA was performed on the covariance matrix of concatenated moment data of all trials for all hammers, for each of the nine moments calculated from inverse dynamics following procedure described in [3]. Continuous hammering moment data were cropped into only one full swing and linear length normalized. The square of the correlation value is generally known as percent variance explained which is used to observe the differences in timing and magnitude of the relative contribution of a principal component to overall waveform (Fig-1). Reconstruction of the moment for each PC was performed by projecting moment data onto the principal components and analyzing the Q-statistic value of each PC with Q-critical. To assist in the interpretation of PCA, each principal component was portrayed about the mean moment curve of the original dataset for the four hammers. The high and low range of the mean curve was set by adding (+) and subtracting (-) 2.5 standard deviation to the mean curve (Fig-2). The PC scores and cumulative percent variances explained by each PC were analyzed separately with repeated-measures ANOVAs to detect differences between hammers.

RESULTS AND DISCUSSION

For elbow and wrist flexion moments, almost five principal components were required for reaching 90% of the total variance. Later PC's (>PC4) have smaller contribution in capturing variance and also are difficult to interpret in physical terms.

For the elbow flexion moment PC1 acts as a magnitude operator for the entire cycle and explains ~ 90% variance at the trial beginning and end, and also 60-85% variance in the middle of the cycle. PC scores are different for each hammer for PC1 (Table-

1). PC2 acts as an amplitude operator at discrete points, mainly at the global and local minimum and maximum points of the cycle and explains ~ 40-70% variance of the original data set at those points. For wrist flexion moment, PC1 explains about 95% variance at the starting and end of the cycle, and 20-30% variance during the middle of the cycle. Significant group differences in PC-scores are present between long handle and short handle hammers. PC2 explains around 20-70% variance from 20-85% of the cycle. PC3 retrieves 40-80% of variance at the discrete portions like at the beginning and 80-90% of the cycle. PC-scores are different for each hammer. Differences in moment complexity in swinging different hammers were found for lower PCs but after a certain percent variance explained, the differences among hammers were not significant (Fig-3). Other moments showed similar patterns.

Table-1: PC-1 scores (mean and standard error).

Moment	Hammer	Mean	SE	P value
Elbow flexion	1	50.06	2.91	<<0.001
	2	24.96	2.93	
	3	-30.87	2.89	
	4	-59.32	2.95	
Wrist flexion	1	-1.06	0.98	<<0.001
	2	-2.41	1.00	
	3	4.64	0.98	
	4	1.23	1.01	

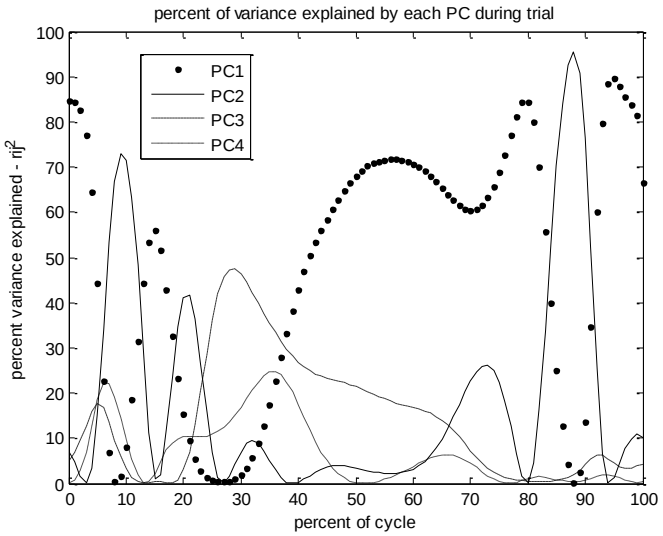

Figure 1: Percent variance explained by each PC for elbow flexion moment.

CONCLUSIONS

For these two moments, only one PC is required at the beginning and end of the cycle, to explain most of the variance of the original data set. Three or four PCs are required in the middle to explain the same level of variance. This result indicates that moment is more complex in the middle than at the starting or ending which are strike and follow through phase of the hammering motion. The additional complexity is associated with aiming and reaction of hitting the target.

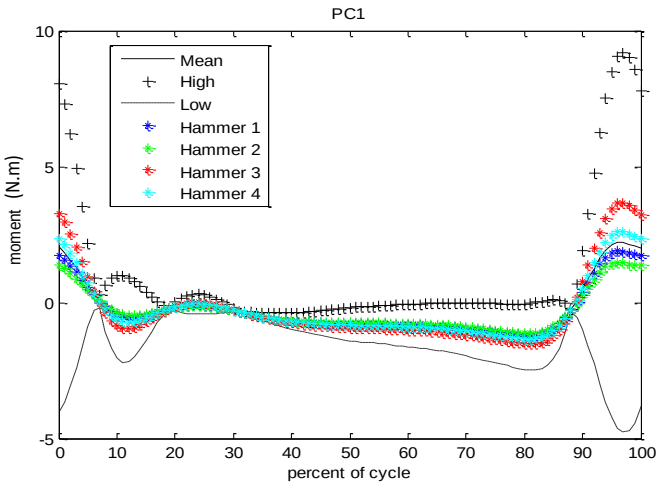

Figure 2: Average wrist flexion moment reconstructed with PC 1.

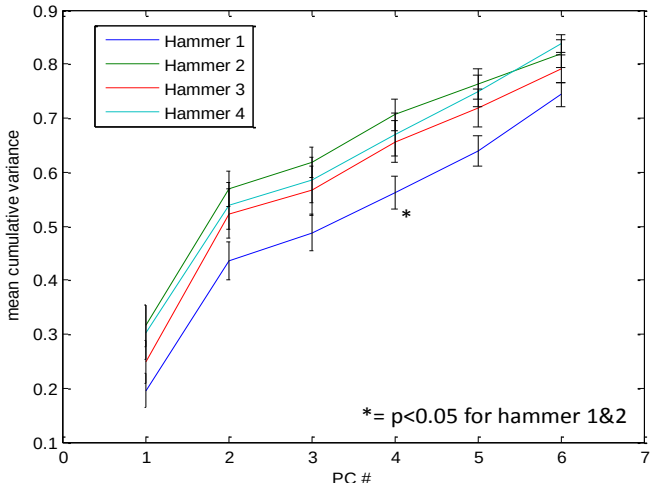

Figure 3: Mean cumulative variance for elbow flexion moment.

REFERENCES

1. Balendra, N. and Langenderfer, JE. *App Ergon* **60**, 231-239, 2017.
2. Ferdous, S. et al., ASB, 2017
3. Wrigley, A.T., et al., *Clin Biomech* **21**, 567–578, 2006.

SHOULDER MUSCLE ACTIVATION PATTERNS DURING MULTIPLANAR ARM ELEVATION

[1] Matthew M. Gibbs, [1] John T. Lowe, [2] Traci Bush, [3] David Stapleton, and [2,3] Vassilios G. Vardaxis

[1] College of Osteopathic Medicine, [2] Department of Physical Therapy, [3] Human Performance Laboratory
Des Moines University, Des Moines, IA, USA
email: vassilios.vardaxis@dmu.edu, web: http://asb2018.asbweb.org/

INTRODUCTION

Active arm elevations at different planes are regularly used during clinical assessment [1] and are often incorporated in rehabilitation protocols for patients with shoulder pain and dysfunction [2]. Such arm elevations are often performed interchangeably in the frontal, scapular, and sagittal planes for assessment and therapeutic exercise purposes. This equivalence is assumed despite evidence of differences in clavicular, scapular, and humeral kinematics during arm elevation between these planes [3]. The scapular plane has been suggested as the most appropriate plane that provides optimal bone and muscle functionality [4]. While scapular stability, position, and movement are essential to support the glenohumeral joint function for proper arm elevation, it is not known how muscle recruitment is influenced by the plane of arm elevation and its clinical impact.

Therefore, the aim of the current study was to investigate the recruitment of selected shoulder muscles during active arm elevation performed on selected planes between the sagittal and frontal.

METHODS

Twenty (20) right-handed male adults (mean age 24.4±1.27 years) with no history of shoulder pathology (mean BMI 25.6 kg/m²; range 20.4 to 33.4 kg/m²) participated in the study. Subjects performed arm elevation (elbow extended) to a target at 120° of arm elevation (while seated), on each of 13 randomly ordered elevation planes (0, 10, 20, 25, 30, 35, 40, 45, 50, 60, 70, 80, and 90°, to frontal). The subjects were asked to maintain their open palm on the plane of elevation with the thumb up (guided by the tactile sense of a string-net). The arm was weighted with a half-pound load taped to the dorsal aspect of the hand. Motion capture (10-camera Motion Analysis Corp. sampling at 120 Hz) was used to track the elevation of the arm (using planar projection of the upper arm on the elevation plane). Surface electromyography (sEMG) data for the upper, middle and lower trapezius (UT, MT, and LT), the anterior, middle and posterior deltoid (AD, MD, and PD), and the serratus anterior (SA) muscles was recorded using the MA-300 system (Motion Lab Systems, Inc.). The sEMG signals were differentially pre-amplified and sampled at 1200 Hz using a 16-bit A/D convertor. The activation patterns were demeaned, band-pass filtered (10-450 Hz), and RMS processed using MATLAB. Four trails were averaged to create an ensemble-average waveform for each muscle, plane, and subject [5]. The RMS data from all dynamic trials were normalized to the peak sEMG value recorded across all elevation planes, expressing the relative task specific activation intensity for each muscle. With this normalization technique: (1) all RMS data was at or below 100% activation intensity, and (2) the inter-participant variability was reduced [6]. The ensemble-average waveforms (between 0 and 90° of arm elevation) were segmented into three arm elevation levels (30° of elevation each), using motion capture. Two-way repeated measures ANOVA was used to examine the elevation plane and the arm elevation segment effects on the relative EMG muscle activation intensity (α=0.05).

RESULTS

Angle of arm elevation and task specific normalized relative EMG muscle activation intensity of seven muscles tested in 13 distinct planes of elevation between the frontal and sagittal were recorded. The average activation intensity for each of the three arm elevation segments for the AD, PD, SA, and MD across all planes of elevation are shown in Fig 1. As expected, we found an arm elevation segment main effect in the relative muscle activation intensity ($P <$ .001), indicative of the higher activation demand on all these muscles with arm elevation (Table 1).

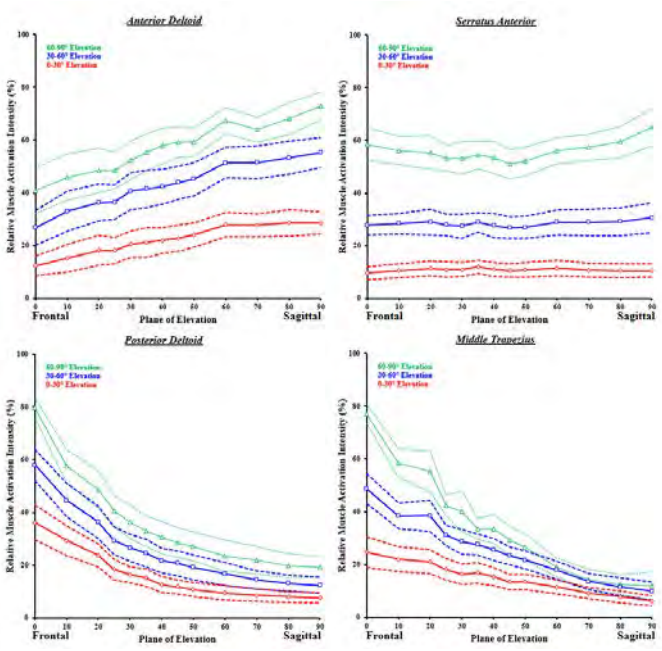

Figure 1: Muscle activation intensity of exemplar shoulder muscles. Mean (±1SD) are shown at 3 arm elevation segments (0°-30°, 30°-60°, & 60°-90°), for 13 planes of elevation between frontal and sagittal.

The two-way repeated measures ANOVA revealed significant interaction effects between arm elevation segment and elevation plane for all seven muscles. However, the activation intensity modulation by elevation plane and segment was highest for the MT, PD, and MD ($\eta_p^2 > 0.50$) and least for the LT, SA, and AD ($\eta_p^2 < 0.25$) (Table 1). There were also significant plane of elevation main effects for all muscles ($\eta_p^2 > 0.25$), other than the serratus anterior.

DISCUSSION AND CONCLUSIONS

A comprehensive muscle activation pattern of normal shoulder muscle activity was developed. Using the right shoulder of 20 participants on seven shoulder muscles, the relative intensity for each muscle was measured at three segments of arm elevation (0° to 90°) in thirteen planes of elevation between the frontal and sagittal. All muscles increased their activation intensity with arm elevation level. The AD and LT showed higher relative activation in the sagittal plane, whereas, the MD, PD, MT, and UT in the frontal plane. Interestingly the SA activation did not monotonically change with the plane of elevation, but rather showed higher activation closer to the cardinal planes. Understanding the activation intensity of shoulder muscles during the completion of tasks at various planes of motion can contribute to the optimization of examination tests, measures, and therapeutic exercise prescription.

REFERENCES

1. Magee, DJ. *Orthopedic Physical Assessment.* Elsevier Health Sciences, 2014.
2. Lee et al. *Arthroscopy* 28(1):34–42, 2012.
3. Ludewig et al. *J Bone Jt Surg* 91:378-89, 2009.
4. Alpert et al. *J Shoulder Elb Surg* 9:47-58, 2000.
5. Winter and Yack. *Electromyography and Clinical Neurophysiology* 67:402–11, 1987.
6. Cronin et al. Neuroscience 300:19–28, 2015.

ACKNOWLEDGEMENTS

Many thanks to Jeffrey Mann and Jordan Estes for their assistance with the data collection process.

Table 1: Statistical results of the two-way repeated measures ANOVA (Interaction effect size order)

	Relative EMG muscle activation intensity								
	Interaction Effect			**Main Effects**					
	Elevation Segment **x** Plane			Arm Elevation Segment			Plane of Elevation		
	P	Power	Partial η^2	P	Power	Partial η^2	P	Power	Partial η^2
Middle Trapezius (MT)	<.001[a]	1.000	0.771	<.001[a]	1.000	0.903	<.001[a]	1.000	0.883
Posterior Deltoid (PD)	<.001[a]	1.000	0.599	<.001[a]	1.000	0.881	<.001[a]	1.000	0.898
Middle Deltoid (MD)	<.001[a]	1.000	0.550	<.001[a]	1.000	0.925	<.001[a]	1.000	0.782
Upper Trapezius (UT)	<.001[a]	0.999	0.264	<.001[a]	1.000	0.816	<.001[a]	0.998	0.278
Lower Trapezius (LT)	<.001[a]	0.996	0.244	<.001[a]	1.000	0.776	=.001[a]	0.961	0.273
Serratus Anterior (SA)	<.001[a]	0.984	0.182	<.001[a]	1.000	0.977	=.059	0.698	0.104
Anterior Deltoid (AD)	=.006[a]	0.896	0.163	<.001[a]	1.000	0.937	<.001[a]	1.000	0.640

[a] Indicates difference

The Effect of Wrist Position on Tendon Loads Following Pulley Sectioning and Operative Reconstruction

[2]Mohammad M Haddara, [1,2]Brett Byers, [1,2]Nina Suh, and [1,2,3]Louis M Ferreira
[1]Roth | McFarlane Hand and Upper Limb Centre
[2]St Joseph's Hospital
[3]Western University
email: mhaddara@uwo.ca

INTRODUCTION

Isolated flexor tendon pulley ruptures following injury often require surgical reconstruction to prevent tendon bowstringing[1]–[3]. Post-operative rehabilitation is imperative and must balance potential rupture of the pulley reconstruction with aggressive therapy and tendon adhesion formation from overly cautious protocols. When undergoing therapy, clinicians typically fix the wrist in a neutral position. Frequently, this action is taken with insufficient justification that the position supports optimal outcomes.

This gap in clinical literature is concerning and consequently, should be explored. Therefore, the purpose of this study is to identify an optimal wrist position that rehabilitation should be undertaken to decrease the strain on pulleys following reconstruction surgery using tendon loads as a proxy for pulley strain.

METHODS

Fourteen digits, comprised of the index, long and ring fingers, were tested from 5 cadaveric specimens (age: 71.8±9.9 years; gender: 2 males, 3 females). All computed tomography (CT) scans of specimens were screened prior to testing for the presence of osteoarthritis (OA) at the metacarpal-phalangeal (MCP), proximal interphalangeal, (PIP), and distal interphalangeal (DIP) joints. Active (tendon-driven) finger flexion was simulated using a validated cadaveric motion simulator[4], utilizing servo-motors to generate motion through closed-loop control of tendon excursion and finger range of motion.

FDP tendon loads were measured sequentially with native intact pulleys, A2 and A4 pulleys sectioned, and finally with reconstructed A2 and A4 flexor tendon pulleys. Each pulley condition was tested in wrist neutral, and 30 degrees of wrist flexion and extension.

Pulley reconstructions were executed using a circumferential tendon graft technique. A tendon graft was looped twice around the proximal phalanx (A2 pulley reconstruction), and both the middle phalanx and extensor mechanism (A4 pulley reconstruction) for a double tendon thickness reconstruction. To adjust the tension of the reconstruction, a snap was placed between the tendon and the reconstructed pulley while it was sutured. The tension was tested by flexing and extending the digits under direction visual observation for free gliding of tendon and adjusted if required.

Using the simulator to measure FDP tendon load, the effects of wrist position on sectioned and reconstructed A2 and A4 pulleys were analyzed using multiple 1-way repeated-measures ANOVA.

RESULTS AND DISCUSSION

With the wrist in neutral, FDP tendon loads were 8.5N, 6.2N, and 7.8N with pulleys intact, sectioned, and reconstructed, respectively (Fig. 1). With a flexed wrist, the loads were 8.5N, 4.7N, and 5.4N. When the wrist was extended, the loads were 8.7N, 5.2N, and 6.7N.

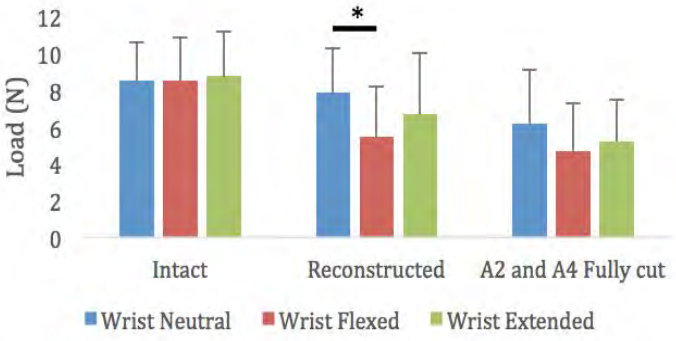

Figure 1: Maximum FDP Loads intact, sectioned and reconstructed pulleys as a function of wrist position.

With pulleys reconstructed, the wrist position had a significant effect on tendon load ($p=0.030$). The flexed wrist position resulted in a 31% reduction of FDP load compared to the neutral wrist position ($p=0.010$). Wrist extension also produced an apparent reduction, though not statistically significant.

The in-vitro finger motion simulator detected a significant decrease in FDP tendon loads caused by sectioning of A2 and A4 pulleys. Placing the wrist in 30 degrees of flexion decreased tension in the reconstructed FDP tendon compared to a neutral wrist. These results may suggest that rehabilitation of surgically reconstructed flexor tendon pulleys should be carried out with the wrist flexed in order to reduce strain on pulley reconstructions.

CONCLUSIONS

The use of active motion simulators to reanimate cadaver specimens have opened doors to attaining reliable data for the investigation of joint kinematics. The current gap in literature regarding the effect of pulley sectioning and subsequent reconstruction on tendon load was explored in this study. Our findings suggest that placing the wrist in 30° of flexion resulted in decreased tension in the FDP tendon compared to a neutral wrist following full reconstruction of the pulley. These results suggest that rehabilitation protocols should be carried out with the wrist flexed in order to reduce strain on pulley reconstructions. In addition, pulley reconstructions restored loads by not only reducing bowstringing but also restoring natural joint kinematics.

REFERENCES

1. J. Doyle, “Palmar and digital flexor tendon pulleys,” *Clin. Orthop. Surg.*, pp. 84–96, 2001.
2. T. Clark, K. Skeete, and P. Amadio, “Flexor tendon pulley reconstruction,” *J. Hand Surg. Am.*, no. 10.1016/j.jhsa.2010.07.029, p. 9, 2010.
3. V. Mehta and C. Phillips, “Flexor tendon pulley reconstruction,” *Hand Clin.*, no. 10.1016/j.hcl.2004.12.002, pp. 245–51, 2005.
4. M. Haddara, “Development of an Active Finger Motion Simulator: With In-Vitro Assessments of Tendon Loads and Joint Kinematics,” Western University, 2017.

The Effect of Sequential Flexor Tendon Pulley Sectioning and Reconstruction on Joint Range of Motion and Tendon Load

[2]Mohammad M Haddara, [1,2]Brett Byers, [1,2]Nina Suh, and [1,2,3]Louis M Ferreira
[1]Roth | McFarlane Hand and Upper Limb Centre
[2]St Joseph's Hospital
[3]Western University
email: mhaddara@uwo.ca

INTRODUCTION

A2 and A4 pulleys are known clinically to be the most important in maintaining independent interphalangeal joint function [1]. Injury to A2 and A4 flexor tendon pulleys are not uncommon following sharp lacerations or crush injuries. These defects are known to cause tendon bowstringing with subsequent range of motion (ROM) deficits of the affected finger. In response, deficient tendon pulleys are reconstructed in an effort to avoid these complications. However, it is unclear how deficient tendon pulleys and subsequent reconstructions affect actual tendon load in addition to joint ROM.

The purpose of this study is to characterize the effects of sequential A2 and A4 pulley sectioning and reconstruction on joint ROM and tendon load.

METHODS

Fourteen digits, comprised of the index, long and ring fingers, were tested from 5 cadaveric specimens (age: 71.8±9.9 years; gender: 2 males, 3 females). All computed tomography (CT) scans of specimens were screened prior to testing for the presence of osteoarthritis (OA) at the metacarpal-phalangeal (MCP), proximal interphalangeal, (PIP), and distal interphalangeal (DIP) joints.

Active (tendon-driven) finger flexion was simulated using a validated cadaveric motion simulator[2], utilizing servo-motors to generate motion through closed-loop control of tendon excursion and tendon load. Electromagnetic trackers were inserted lateral to the finger bones, close to each joint (MCP, PIP, DIP) to analyze proper ROM. Joint motion and tendon loads were initially measured with native intact pulleys, followed by A2 and A4 pulleys sequentially sectioned at 25% and 50% increments respectively, and finally with a full reconstruction of A2 and A4. Pulley reconstructions were executed by looping a tendon graft twice around the proximal phalanx (A2 pulley reconstruction), and both the middle phalanx and extensor mechanism (A4 pulley reconstruction) for a double tendon thickness reconstruction.

Each pulley conditions were tested with the wrist fixed in the neutral position, 30 degree flexed, and 30 degree extended. The effects of A2 and A4 pulley sectioning and their subsequent reconstructions were analyzed using a 2-way repeated-measures ANOVA.

RESULTS AND DISCUSSION

With the wrist in neutral, full sectioning of both A2 and A4 pulleys reduced MCP ROM and FDP tendon load by 9.1±7.1° ($p=0.016$) and 2.3±1.9N ($p=0.029$), respectively (Fig. 3).

With the wrist flexed, sectioning of both A2 and A4 had a significant effect on MCP ROM ($p=0.002$), FDP ($p=0.006$), and FDS ($p=0.002$) tendon loads. More specifically, MCP lost 7.4±6.3° of ROM ($p=0.009$) while FDP load was reduced by 3.6±3.5 N ($p=0.034$).

With the wrist extended, sectioning both A2 and A4 also had a significant effect on MCP ROM ($p=0.006$), FDP ($p=0.001$), and FDS ($p=0.046$) loads. The MCP experienced a loss of 7.2±7.3° in ROM ($p=0.024$), whereas FDP loads were reduced by 3.5±1.7 N ($p<0.001$). DIP and PIP ROM were not significantly altered.

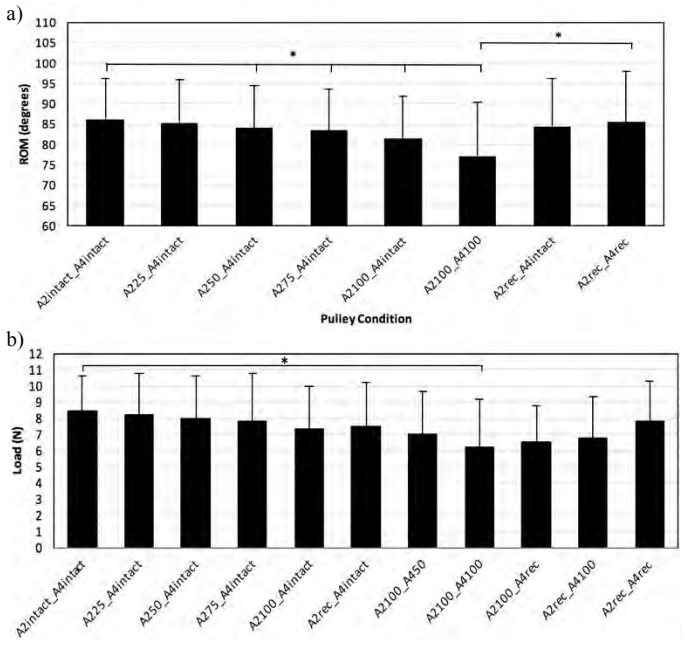

Figure 3: MCP ROM (a) and FDP Load (b) following Pulley Sectioning/Repair. Asterisk highlights PW comparison significances. Error bars represent the standard deviations between specimens (n=14)

Partial excision of the A2 pulley had the largest effect on MCP ROM (Fig. 3a). With wrist in neutral, MCP experienced a significant reduction in ROM of 3%, 3%, and 6% with every sequential 50%, 75%, and 100% A2 cut made, respectively, compared to the intact state. However, partial excision of the A4 pulley failed to reveal similar trends within our sample size. Full sectioning of both pulleys also revealed significant losses in tendon load. With the wrist in neutral, FDP suffered a 27% loss in load compared to the intact state. Furthermore, loads were reduced by 43% and 40% with the wrist in flexion and extension, respectively. Such significant losses in load due to partial and full excisions of the pulleys signify the true importance of having a functional A2 and A4 pulley on the kinematics of the finger.

Surgical pulley reconstruction is clinically common and valuable in reinstating proper kinematics of the finger. Following reconstruction of the A2 and A4, MCP ROM and FDP loads were restored to within 0.7° (10% increase) and 0.7N (19% increase) of the intact state respectively with the wrist in neutral, 2° (5% increase) and 3N (7% increase) with the wrist in flexion, and 2° (5% increase) and 1.8 N (19% increase) with the wrist in extension. As justified by the results of this study, sequential reconstruction of the pulleys restored normal kinematics to within no significant difference of the intact state; thus, supporting the decision to reconstruct.

CONCLUSIONS

The in-vitro finger motion simulator was successful in detecting significant changes in both load and ROM caused by the sectioning of A2 and A4 pulleys. As established within current clinical grounds, a patient can undergo a 50% cuts to both the A2 and A4 pulleys without significantly affecting the kinematics of the finger [3], [4]. These results were further strengthened within our study as minor changes in ROM and load were experienced up to 50% cuts, with an exception for the PIP and DIP joints. In addition, pulley reconstructions restored load and ROM with no significant difference compared to the intact state; increasing their function by not only reducing bowstringing, but by restoring natural joint.

REFERENCES

1. J. R. Doyle, “Anatomy of the flexor tendon sheath and pulley system: a current review.,” *J. Hand Surg. Am.*, vol. 14, no. 2 Pt 2, pp. 349–51, Mar. 1989.
2. M. Haddara, “Development of an Active Finger Motion Simulator: With In-Vitro Assessments of Tendon Loads and Joint Kinematics,” Western University, 2017.
3. M. Tomaino, G. Mitsionis, J. Basitidas, R. Grewal, and J. Pfaeffle, “The effect of partial excision of the A2 and A4 pulleys on the biomechanics of finger flexion.,” *J. Hand Surg. Br.*, vol. 23, no. 1, pp. 50–2, Feb. 1998.
4. S.-C. Lu, T.-H. Yang, L.-C. Kuo, I.-M. Jou, Y.-N. Sun, and F.-C. Su, “Effects of Different Extents of Pulley Release on Tendon Excursion Efficiency and Tendon Moment Arms,” *J. Orthop. Res.*, vol. 33, no. 2, pp. 224–228, Feb. 2015.

WEB-BASED VISUALIZATION OF 4DCT IMAGE DATASETS FOR ASSESSING WRIST INJURY

David Holmes, III, Mohsen Akbari Shandiz, Julie Adams, Sanjeev Kakar, Steven Moran, and Kristin Zhao

Mayo Clinic, Rochester, MN, USA
email: zhao.kristin@mayo.edu

INTRODUCTION

Four-dimensional CT (4DCT) is a new imaging technique used to assess joint motion. Multiple volumes of CT data are acquired and reconstructed. One of its applications is the assessment of ligament injury in patients with wrist injury[1]. Prior research initiatives included both the qualitative (i.e. visual) and quantitative assessment of wrist joint motion. One of the important observations of the work is that the standard clinical infrastructure (i.e. PACS systems and radiology workstations) are unable to be used by physicians in their assessment of patients. Instead, surgeons and other providers must visit a radiology reading room and learn the radiology workstation software in order to analyze the 4DCT data. In this abstract, we describe a web-deployed visualization platform which delivers the patient's motion movies of 4DCT scans of the wrist to the surgeon.

METHODS

Following IRB approval, patients who were identified for wrist surgery were enrolled into the 4DCT acquisition protocol. Each patient was scanned on a Siemens SOMATOM Force CT scanner (0.234 mm in-plane, 0.7 mm slice thickness). The protocol consists of acquiring a static CT scan and two motion sequences bilaterally. The subject was asked to complete a flexion-extension and radial-ulnar deviation motion within a two second time period. To the best of his/her ability, the subject was to complete a full range of motion at a constant velocity. Each arm was scanned independently and resulted in 15 different time points over the extent of the motion. After acquisition, the projection data was reconstructed using a Br44 (e.g. soft tissue) kernel.

After image archiving, the images were routed to a custom processing engine. The engine automatically sorted the image series and identified the motion image series. Volumetric representations of each time point were created. Volume rendering was used to generate a 3D visualization of the data. Renderings were generated every 10° from -180° to 180° by rotating the dataset around the long axis of the arm. The process was repeated with similar rotation perpendicular to the long axis of the arm. For these rotations, the data was rotated from -90° to 90° with renderings every 30°. All of the renderings were organized by both time point and rotation before serializing the stack of images (Figure 1)[2].

A web-interface was developed to allow an observer to interact with the dataset (Figure 2). PHP was used to serve the data to the client browser. Javascript was used for client-side programming. An HTML5 application was developed to present the user with the rendering data. The operator is able to drag the 3D model interactively and view the data over the rotational extent defined above. Additional controls are provided to play through the motion movies. The operator is able to view 1, 2 (e.g. left/right for the same motion), or 4 (left/right for both motions) series simultaneously. If desired, the visualization windows can be linked for synchronous viewing or unlinked for individual analyses. The client application functions on many modern web browsers, including Microsoft Edge, Google Chrome, and Safari (both iPad and iPhone).

RESULTS AND DISCUSSION

To date, four subjects (3M; 1F) have been enrolled into the study. The number of acquired slices and dataset size varies slightly. The smallest case contained 15,292 images; a single time point of the 4DCT scan had to be removed due to significant image artifact. The largest dataset consisted of 17,085 images. The dataset sizes corresponded to the number of images, ranging from 7.66 Gb to 8.70 Gb. Each of the 4D volumes was 928 Mb with the exception of the smallest scan, which had one 3D volume of 771Mb (due to the excluded time point).

The size of each rendered time point ranged from 63.4 Mb to 75.2 Mb. The combined size of all of the renderings per patient ranged from 253.6 Mb to 300.6 Mb. When loaded into a browser (Google Chrome, build 64.0.3282.140), all of the data from a single patient resulted in a 70Mb memory footprint.

One of the significant problems with deploying imaging solutions through a browser is the diversity of hardware and software that is currently available. Users expect a similar experience on all platforms regardless of the network connect (i.e. LAN or wifi) or the capabilities of the technology that they are on (i.e. processor, memory, etc.). Although network speeds continue to increase, it is largely impractical to serve nearly 1 Gb of data to a user and expect real-time performance. Additionally, very few hardware platforms are able to generate renderings in real time on the client system. By pre-rendering the data, we are able to achieve real-time interactivity with the data including rotations and motion playback. Additional benefits can be achieved in the web application and can be multi-threaded and support multi-socket connections.

CONCLUSIONS

One of the challenges of working with new imaging workflows is deploying these systems into the clinical practice. Standard clinical tools, such as EMR viewers, are limited in their functionality. Specialized tools, such as radiology workstations, are not available to most practitioners. As such, using widely deployed technology (i.e. web browsers) allows users to interact with the data without the need for specialized hardware/software. To make such solutions practical, it is necessary to take advantage of techniques which reduce the burden of data transfer and client-side processing.

REFERENCES

1) Zhao, Kristin, et al. J Biomech Eng. 2015; 137(7): 074501-074501-5.
2) Schubert, R., et al. Medicine Meets Virtual Reality: 62 (1999): 321.

ACKNOWLEDGEMENTS

The authors would like to acknowledge the efforts of the Mayo Clinic radiology technicians, the staff of the Biomedical Imaging Resource, and Adam Wright for development of the initial web interface. Research reported in this publication was supported by the National Institute of Arthritis and Musculoskeletal and Skin Diseases of the National Institutes of Health under Award Number R01AR071338. The content is solely the responsibility of the authors and does not necessarily represent the official views of the National Institutes of Health.

Figure 1 – Generating pre-rendered motion and rotation sequences. After generated a matrix of rendered images, the elements are sequentially formatted into a movie file.

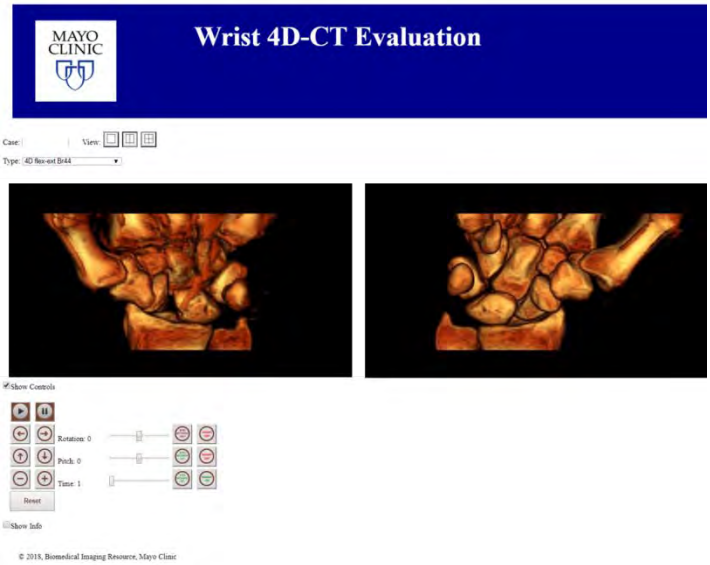

Figure 2 – The web interface allows for 1, 2, or 4, simultaneous visualizations. Each render can be rotated during motion playback. All visualization can be linked to allow for synchronous viewing.

CUMULATIVE LOAD EXPOSURE TO UPPER EXTREMITIES IN MANUAL WHEELCHAIR USERS IN THEIR FREE-LIVING ENVIRONMENTS

[1] Alexander W Hooke, [2,3] Emma Fortune, [3] Meegan G Van Straaten, [2,3] Melissa M Morrow

[1] Materials and Structural Testing Resource Core, Mayo Clinic, Rochester, MN
[2] Robert D. and Patricia E. Kern Center for the Science of Health Care Delivery, Mayo Clinic, Rochester, MN
[3] Rehabilitation Medicine Research Center, Mayo Clinic, Rochester, MN
email: hooke.alexander@mayo.edu

INTRODUCTION

Injury and pain in the upper extremities are commonplace in manual wheelchair (MWC) users. One recent systematic review estimated shoulder pain and injury prevalence in people with spinal cord injuries to be 37 to 84% [1], compared to 2.9% in the general population [2]. This pain is often caused by tendinopathies, subacromial bursitis and rotator cuff tears due to shoulder impingement in the subacromial space. Biomechanical loading at the shoulder joint is increased as ambulatory responsibility is shifted to the upper extremity, and weight relief exercises and transfer events become a part of daily living. This increase in loading is considered to be a primary causal element. However, little is known regarding MWC users' cumulative exposure to shoulder loading and its role in impingement risk.

While upper extremity loading in MWC users can be analyzed in the laboratory environment, previous studies have shown that clinically relevant biomechanical variables differ significantly in community settings [3]. The purpose of this study was to quantify upper extremity forces in MWC users during day-long collections in their free-living environment.

METHODS

Preliminary results from a longitudinal study are presented including 6 participants (3 MWC users with spinal cord injury (27±6 yrs, injury levels T4-T6, 1 F) and 3 (age and sex) matched able-bodied controls) that have completed the baseline field collection. The field collection consists of one typical day in the subject's natural environment while kinematic and kinetic data are collected. All participants wore a set of custom, force-sensing iGloves [4] to capture upper extremity loading. Each iGlove consisted of 3-4 force sensitive resistors stitched into the palm of the glove and a data logger box worn in a sleeve on the forearm (Figure 1). Data was sampled at 20Hz with gloves having a battery life of 10-12 hours. The primary variables of interest for this component of the study are the magnitude, frequency, and duration of proximally directed forces at the hand while performing activities of daily living.

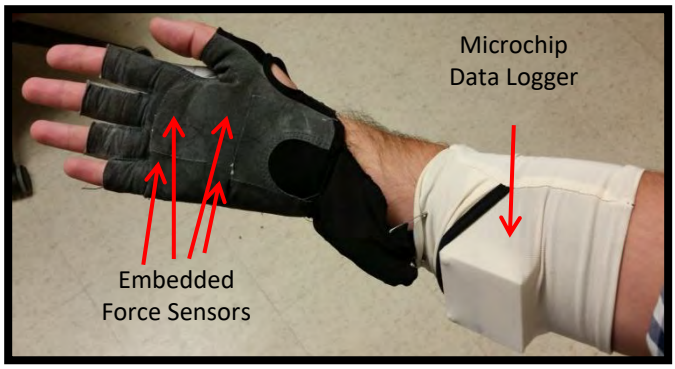

Figure 1: Instrumented glove with data logging box in arm sleeve

An algorithm to identify periods of active upper extremity loading was developed and applied to the data using MATLAB (Mathworks, USA). An active loading period is defined as a non-overlapping 15 second interval containing a minimum of 3 seconds of loading over 10N.

RESULTS AND DISCUSSION

The mean (SD) data collection duration was 10.6 (2.1) hours long. Histograms representing each MWC user and matched control subjects' loading distributions are shown in Figure 2, A and B. The frequency of higher loading events (>20N) are 1-2 orders of magnitude higher in the MWC users vs controls. This pattern is present across all subjects

analyzed at this time. The loading range experienced was 0 - 490N for the MWC users and 0 – 445N for the matched controls.

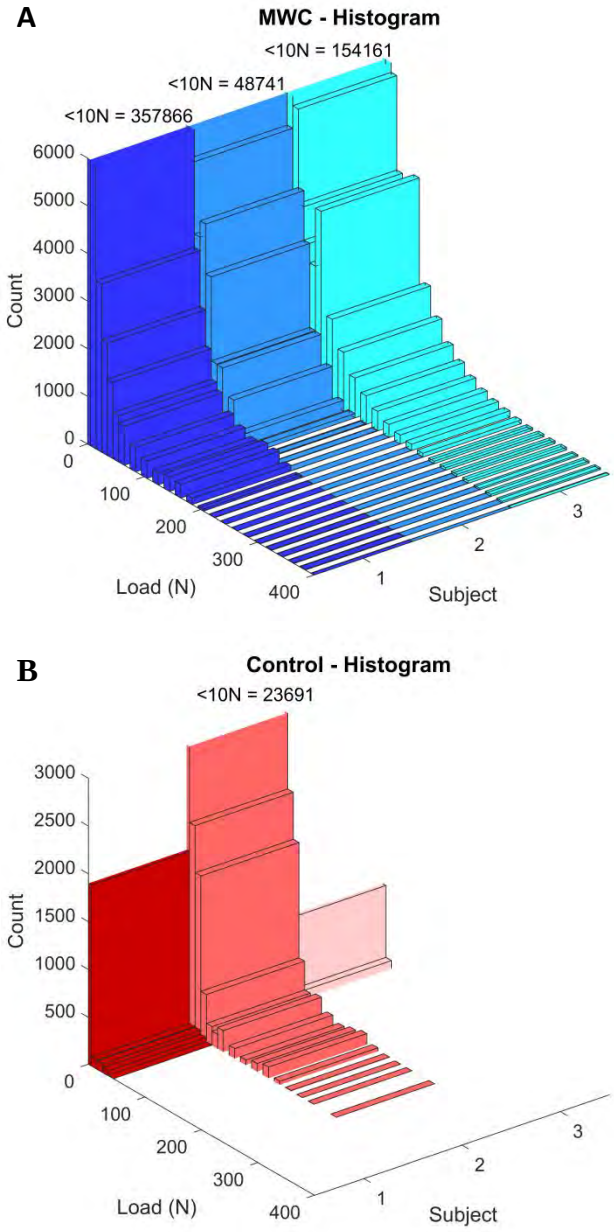

Figure 2: Histogram of each subjects' loading frequency distribution for a single day collection for a MWC user (A) and matched-control (B). Counts of loads <10N too large to fit on the scale are labeled directly.

While the magnitudes and frequency suggest that the cumulative loading exposure to the upper extremities is higher in MWC users than in able bodied persons, the total duration of loading during the day is an important consideration. MWC users experienced periods of loading during 3.5 (2.3) % of their day vs 0.16 (0.2) % in control subjects (Figure 3), or 0.38 (0.12) hours and 0.01 (0.01) hours, respectively. The exceptionally low duration of loading in controls is expected. It is unknown if 3.5 % of the day spent in loading will contribute to increased impingement risk in the shoulder of MWC users. In comparison, able-bodied lower extremity loading time during standing and/or moving while upright is 45.1% of the day [5]. However, the anatomy of shoulder is designed for a wide range of motion and not load bearing as in the hip.

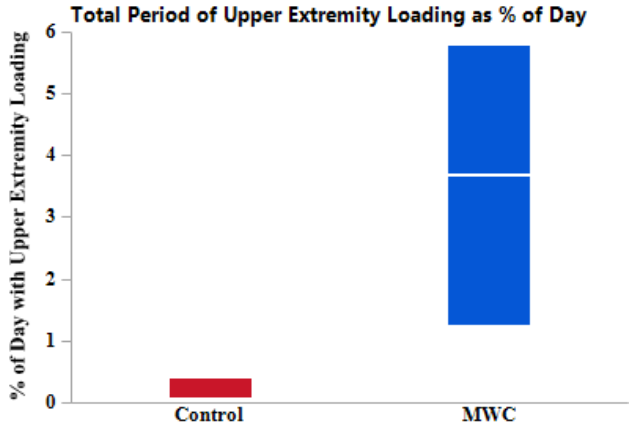

Figure 3: Total periods of upper extremity loading (>10N) as a percentage of day long collection.

CONCLUSIONS

Upper extremity kinetics can be measured in MWC users in their free-living environment. Preliminary data suggests that the magnitude, frequency, and duration of loads of the upper extremity are greater in MWC users than in healthy controls. This cumulative load analysis will be combined with kinematics captured via IMUs, radiological imaging, and survey data better understand the etiology of shoulder pain and injury in MWC users

REFERENCES

1. Silvestri. *Disabil Rehabil*. **39**: 82–90, 2017
2. Greving, K, et al. *Scand J Rheumatol*. **41**(2): 150-5, 2012
3. Hurd, W, et al. *J Electromyogr Kinesiol*. **19**(5): 942-47. 2009
4. Burns, AJ and Jayaraman, C, U.S. Patent Appl. No. 15/449,103, (filing date Mar. 7, 2017)
5. Matthews CE et al. *Am Jour Epidemiol*. **167**(7): 875-81. 2008

ACKNOWLEDGEMENTS

Funding provided by NIH (R01 HD84423) with support from the Mayo Clinic Materials and Structural Testing Core

Force Transmission Through the Elbow Joint Associated with Contact Pressure and Contact Area in a Cadaveric Model with Forearm Instability

Hwang, JT, PhD, MD[a,b]; Kim, YB, MD[a]; Shields MN, MS[a]; Bachman, DR, MD[a]; Berglund, LJ, BS[a]; Fitzsimmons, AT[a]; Fitzsimmons JS, BSc[a]; and O'Driscoll SW, PhD, MD[a]

[a]Department of Orthopedics, Biomechanics Laboratory, Mayo Clinic Rochester MN, United States
[b]Department of Orthopedic Surgery, Chuncheon Sacred Heart Hospital, Hallym University Medical College, Rep. of Korea

INTRODUCTION

The primary source of longitudinal forearm stability is the radial head. Secondary stabilizers include the triangular fibrocartilage complex (TFCC) and the interosseous membrane (IOM).[1-3] Disruption of any of these structures can lead to forearm instability. To our knowledge, there has not been a comparative study examining the axial force transmission through the elbow joint in the setting of forearm instability. Therefore, it is necessary to study the biomechanics of the axial force transmission through the elbow joint in an unstable forearm to better understand the forces contributing to ulnar load sharing. We hypothesized that an injury to the interosseous membrane has a greater influence on the radioulnar load sharing through the elbow joint compared to a distal radial ulnar joint (DRUJ) Injury. The objective of this study was to test this hypothesis by examining changes in elbow force transmission as they relate to contact area and pressure of the joint surface in the setting of forearm instability caused by the aforementioned conditions. These parameters were used to evaluate ulnar load sharing to better understand the impact the IOM versus an intact ulna has on axial load sharing through the elbow.

METHODS

Ten fresh-frozen cadaveric upper limbs were used for this study (8 males and 2 females). The hand distal to the carpometacarpal joint was removed. The proximal humeral and distal carpal ends of the specimen were then potted into cylindrical metal sleeves in parallel with the long-axis using polyurethane resin in order to fix the specimen and to load it onto the testing machine (Fig. 1). Once the specimen was placed in the testing machine, a transverse olecranon osteotomy was made at the apex of the ulnar bare spot to facilitate the placement of the pressure transducer. Each specimen was tested under four conditions: 1) INTACT, 2) DRUJ Injury, 3) IOM Injury, and 4) IOM + DRUJ Injury.

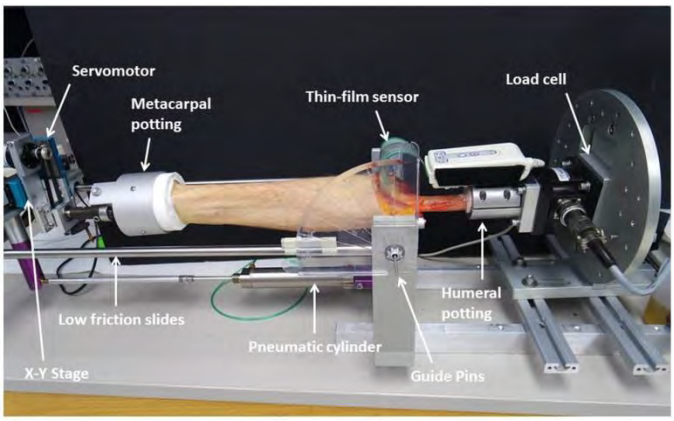

Figure 1: THE TESTING MACHINE. The custom-made apparatus that rotates the forearm while applying extrinsic loading across the cadaveric elbow joint.

Data were recorded at with a Tekascan 5051 sensor at 100Hz using the Tekscan software (I-Scan). Force, contact pressure, and contact area were calculated and presented as the mean ± standard error of the mean. The data from the first neutral position and those from the pronation and supination position in the third cycle were used for statistical analysis.

RESULTS AND DISCUSSION

The force across the radiocapitellar joint was significantly higher in the IOM + DRUJ Injury and the IOM Injury groups than those in the INTACT and DRUJ injury groups. The mean force across the RC joint was not significantly different between the

INTACT and DRUJ Injury groups, nor between the IOM + DRUJ injury and the IOM Injury groups. Forces across the ulnohumerual joint showed an inverse pattern to those in the radiocapitellar joint (Fig 2).

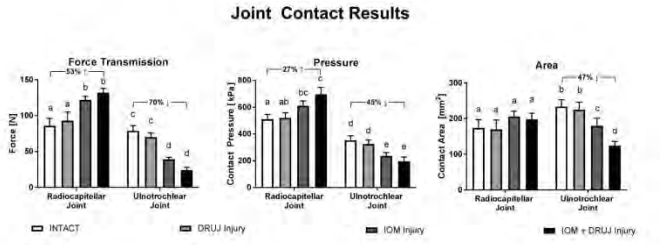

Figure 2: Mean force, contact pressure, and contact area at the elbow joint in pronation under the four testing conditions. **RC**: radiocapitellar, **UT**: ulnotrochlear. Lowercase letters represent the result of Least Squares *post-hoc* comparisons within either the radiocapitellar or ulnotrochlear regions ($p<0.05$). Columns with a letter in common are not statistically different from one another (i.e. $p>0.05$). Where statistically significant differences were detected between the INTACT and IOM + DRUJ Injury groups, relative percent increases (%↑) and decreases (%↓) are indicated.

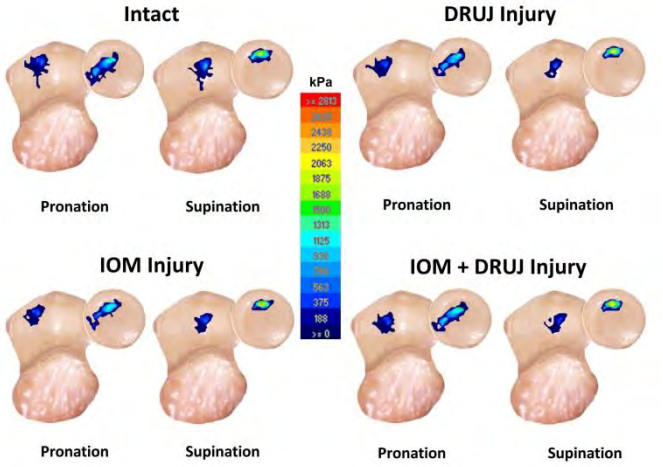

Figure 3: Schematic representation of contact pressure and contact area during forearm rotation. In general, the contact area of the radiocapitellar joint in pronation was larger than that in supination.

The contact pressure of the radiocapitellar joint in supination was higher than that in pronation. The contact area and contact pressure of the ulnotrochlear joint did not significantly change with pronation and supination. The contact pressure across the radiocapitellar and ulnotrochlear joints demonstrated a similar pattern to the differences in force (Fig. 3). Contact area measured across the RC joint was not significantly different in any of the testing conditions. Across the UT joint, the contact area in the INTACT and DRUJ Injury were not significantly different, however they were both significantly greater than contact area of the IOM Injury and IOM + DRUJ Injury ($P<0.0108$). Contact area of IOM Injury was greater than IOM + DRUJ Injury ($P=0.0012$) (Fig. 2 and 3). This study showed that disruption of the IOM had a greater impact than disruption of the DRUJ on load sharing across the elbow joint. It also showed that the resulting changes in force, contact pressure and contact area across the radiocapitellar articulation are accompanied by inverse changes across the ulnohumeral articulation. The highest mean force across the RC joint occurred when the forearm was in a pronated position in the IOM + DRUJ Injury and IOM Injury groups. The force across the RC joint was inversely proportional to the ability of the ulnotrochlear joint to share the load across the elbow.

CONCLUSIONS

These findings suggest that injury to the interosseous membrane contributes more to the disruption of the normal distribution of axial loads across the elbow than injury to the DRUJ.

REFERENCES

1. Adams JE, Culp RW, Osterman AL. Interosseous Membrane Reconstruction for the Essex-Lopresti Injury. J Hand Surg Am 2010; 35A:129-36. DOI: DOI 10.1016/j.jhsa.2009.10.007.
2. Gofton WT, Gordon KD, Dunning CE, Johnson JA, King GJ. Soft-tissue stabilizers of the distal radioulnar joint: an in vitro kinematic study. J Hand Surg Am 2004; 29:423-31. DOI: 10.1016/j.jhsa.2004.01.020.
3. Shepard MF, Markolf KL, Dunbar AM. The effects of partial and total interosseous membrane transection on load sharing in the cadaver forearm. J Orthop Res 2001; 19:587-92. DOI: 10.1016/S0736-0266(00)00059-0.

COMPENSATORY MUSCLE ACTIVATION INCREASES WITH ROTATOR CUFF TEAR SEVERITY: A SIMULATION STUDY

[1] Sujata Khandare, [2] Richard A. Arce and [1] Meghan E. Vidt

[1] Pennsylvania State University, State College, PA, USA
[2] Loughborough University, Leicestershire, UK
email: uuk72@psu.edu, web: sites.psu.edu/mvidt

INTRODUCTION

Rotator cuff tears (RCT) are a common musculoskeletal injury in the geriatric population. Up to 50% of those aged ≥65 years have a symptomatic RCT, and prevalence increases with age [1]. A primary role of rotator cuff muscles is maintaining the static and dynamic stability of the glenohumeral joint. Rotator cuff pathology is a major contributor to shoulder dysfunction in elderly patients and impacts their ability to perform daily functional tasks. However, how RCT severity influences loading at the glenohumeral joint or how muscles crossing this joint compensate for increased RCT severity is not known. A computational musculoskeletal model allows prediction of the role of unaffected compensatory muscles crossing the glenohumeral joint and identification of adaptive muscle activation strategies with increased RCT size. The goal of this study was to determine the effect of systematic variation of RCT severity on muscle activation using a simulation-based approach.

METHODS

The OpenSim (v.3.3) [2] computational musculo-skeletal model of the upper extremity [3] was used as a foundation. The model was modified to represent the muscle force-generating properties of a group of healthy older adult males [4]. Rotator cuff tear severity was represented by systematically reducing each rotator cuff muscle's peak isometric force to a percentage of the nominal model's value. Force values were modified for supraspinatus (S), infraspinatus (IS) and subscapularis (SS) muscles systematically to represent different tear scenarios with increasing severity. Eight configurations of muscle force distribution were evaluated, as shown in Table 1. Four static postures in the frontal plane were evaluated, including 30°, 45°, 60°, and 90° shoulder elevation, with elbow flexed to 90°, and forearm and wrist in neutral posture.

The Computed Muscle Control (CMC) and joint force analysis tools in OpenSim were used to perform computational simulations for 1sec. Static postures for model degrees of freedom were used as an input. Muscle excitation time histories calculated by CMC were used to calculate glenohumeral joint contact force with Opensim's joint reaction analysis tool for all time steps. The peak resultant joint contact force was identified in the last 0.25 sec of each simulation. Activation histories were evaluated for the same duration as it captured the static posture once it reached equilibrium. This was done for all permutations of tear scenarios and postures. Combined activations of primary glenohumeral anterior muscles were compared to the combined activation of primary muscles.

Table 1: Increased RCT severity was simulated by systematic reduction of peak isometric force for model muscle actuators. Percentages represent the proportion of the model's nominal peak isometric force, where 100% indicates nominal force.

Tear Scenario	S	IS	SS	TM
Baseline	100%	100%	100%	100%
S50	50%	100%	100%	100%
S0	0%	100%	100%	100%
IS75	0%	75%	100%	100%
IS50	0%	50%	100%	100%
IS25/SS75	0%	25%	75%	100%
IS25/SS50	0%	25%	50%	100%
IS25/SS25	0%	25%	25%	100%

RESULTS AND DISCUSSION

Glenohumeral joint force was reduced on average by 13% with increased RCT severity, and was un-changed (average 0.8% change) with increased elevation posture. CMC results revealed that, with an exception of TM in 90° elevation, IS, SS, and TM activations increased with greater RCT severity and with increase in elevation. Activation of IS, SS, and

TM showed a marked (~68%) escalation when major tearing of infraspinatus (IS50) and incorporation of subscapularis tear were introduced (IS25/SS75).

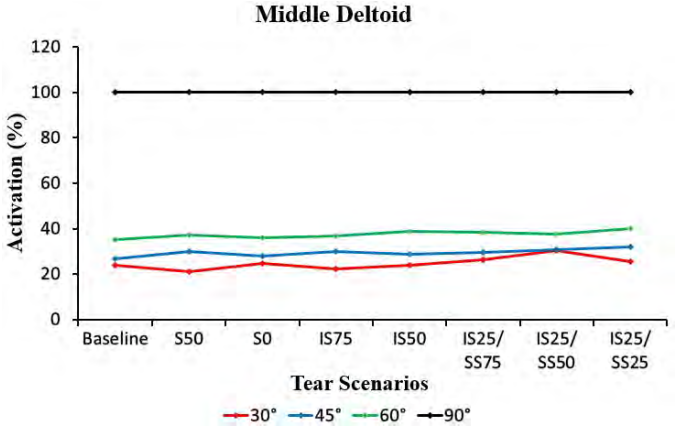

Figure 1: Activation pattern of middle deltoid muscle path.

Activation of anterior, middle, and posterior compartments of deltoid increased with an increase in thoracohumeral elevation, with middle deltoid showing maximum activation at 90° elevation (Fig.1). The activations of all compartments of deltoid in 90° of elevation were ~200% higher than activations in 60° of elevation for all tear scenarios. Teres major and latissimus dorsi (thoracic, lumbar and iliac compartments) activations across tear scenarios remained relatively constant (23% difference), but activation decreased an average of 40% with increases in thoracohumeral elevation. Pectoralis major (clavicular, sternal and rib compartments) activation also showed a similar trend with a 10% average change across tear scenarios, and an average 20% decrease with increased elevation.

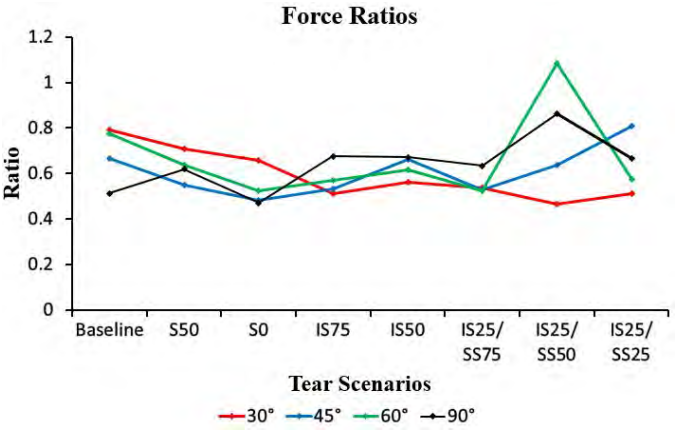

Figure 2: Ratios of primary anterior glenohumeral muscle forces to primary posterior muscles forces.

The ratios of combined activation of primary anterior glenohumeral muscles (anterior deltoid, subscapularis) versus combined activation of primary posterior glenohumeral muscles (posterior deltoid, infraspinatus, teres minor) remained relatively constant (Fig.2) across increased tear severity and elevation (average anterior:posterior force = 0.63±0.13). These results suggest that muscle force balance across the glenohumeral joint is prioritized even as joint contact force is reduced.

CONCLUSIONS

Study outcomes reveal that as humeral elevation and RCT severity increase, glenohumeral joint force is decreased and activation of unaffected muscles crossing the glenohumeral joint increases. This suggests that these muscles have an increasing compensatory role in stabilizing the glenohumeral joint. For RCTs beyond an isolated supraspinatus tear, joint instability becomes a prominent factor: when deltoid compensates for the net elevation (abduction) moment, adductor muscles, like subscapularis, increase activation to compensate.

Rehabilitation protocols can be improved by focusing on the muscles that are most affected by the loss of S, IS, and SS muscles to restore normal shoulder function. For example, this work identified that teres minor increases activation with increased tear severity, indicating its role in compensation, but it is not maximally activated, suggesting it may be a viable target for rehabilitation. Ongoing work is examining additional static postures and dynamic functional movements to achieve a more complete understanding of these compensation strategies and which targets should be prioritized in future development of rehabilitation protocols.

REFERENCES

1. Lin JC et al. *J Am Me Dir Assoc* **9**(9): 626, 2008.
2. Delp SL et al. *IEEE Trans Biomed Eng*, **54**(11): 1940, 2007.
3. Saul KR et al. *Comput Methods Biomech Engin* **18**(13): 1445, 2015.
4. Vidt ME *J Biomech* **45**(2): 334, 2012.

ACKNOWLEDGEMENTS

Funding for this project was provided by Penn State University start-up funds (Vidt) and a travel award to the OpenSim Advanced User Workshop.

The Effect of Material Heterogeneity on Trabecular Stiffness in Micro Finite Element Models

[1,3] Nikolas K Knowles, [1,3] Kenneth Ip, and [2,3] Louis M Ferreira

[1]Graduate Program in Biomedical Engineering, The University of Western Ontario, London, ON, CAN
[2]Department of Mechanical and Materials Engineering, The University of Western Ontario, London, ON, CAN
[3]Roth|McFarlane Hand and Upper Limb Centre, St. Josephs Health Care, London, ON, CAN
email: nknowle@uwo.ca

INTRODUCTION

Trabecular bone transmits loads to the outer cortical shell and is therefore most active in bone remodeling [1]. This remodeling alters the trabecular material strength thereby changing the bending stiffness [2]. In pathologic joints and/or joints with replacement components, variations in joint loads may increase trabecular fracture risk due to altered bone formation/resorption.

To determine variations in trabecular mechanical properties, linear and non-linear micro finite element models (μFEMs) have shown increasingly high correlations with empirical models [3]. As the initial input for many non-linear trabecular μFEMs, the apparent modulus (E_{app}) of experimentally tested bone cores are combined with linear elastic μFEMs E_{app} to determine an effective (homogeneous) tissue modulus [1,4]. An arbitrary tissue modulus E_i, is used to scale the ratio of experimental, E_{exp}, and finite element, E_{FEM}, to determine the 'real' effective tissue modulus, E_{tissue}.

$$E_{tissue} = \frac{E_{exp}}{E_{FEM}} E_i$$

These models then use this homogeneous effective tissue modulus in non-linear models for bone strength predictions and failure analysis [3]. *In-vivo,* trabeculae are heterogeneous, with increased tissue modulus at the core, and decreased modulus superficially, due to surface bone resorption/formation [1,2]. Accounting for trabecular material heterogeneity has been shown to improve empirical-μFEM correlations by allowing for more realistic trabecular bending stiffness [2].

In μFEMs to reduce computation time, region averaging is often used to scale image resolution, while maintaining the recommended one-fourth mean trabecular thickness for numerical convergence. This has been shown to have less than 7% error in mechanical properties when down-sampled to half the original scan resolution [5]. However, this region averaging not only alters the trabecular architecture, but inherently alters the CT-intensity of each trabeculae. In homogeneous μFEMs, this has been shown to have negligible effect on the stiffness and strength due to trabecular architectural changes [6]. However, the effect of CT-intensity variations on computationally derived E_{app} in heterogenous μFEMs has not been discussed. The objectives of this study were to compare trabecular E_{app} among i) hexahedral and tetrahedral μFEMs, ii) μFEMs generated from 32 μm, 64 μm, and 64 μm down-sampled from 32 μm μ-CT scans, and iii) μFEMs with homogeneous and heterogeneous tissue moduli.

METHODS

Fourteen cadaveric scapulae were denuded of soft tissue (7 male; 7 female; mean age 67 ± 8 years). Micro-CT scans at two spatial resolutions were acquired (Nikon XT H 225 ST, Nikon Metrology, NV) for each scapula (Table 1).

Table 1: Micro-CT scan parameters.

Parameter	Micro-CT Scans	
Voxel Size (isotropic) (μm^3)	32	64
Peak Voltage (kVp)	95	95
Current (μA)	64	64
Projections	3141	3141
Exposure (ms)	1000	1000

The raw DICOM images were filtered to remove high frequency noise (Gaussian filter: σ = 1.25, support = 2) (Mimics, Materialise, Leuven, BE).

Virtual bone cores were extracted from the glenoid vault, medial to the subchondral bone, maintaining the recommended 2:1 aspect ratio [7], to create μFEMs from the 32 μm, 64 μm, and 32 μm down-sampled to 64 μm scans. Custom code was used to generate μFEMs with 8-node hexahedral elements (HEX8), while maintaining the bone volume

fraction (BV/TV) of each HEX8 32 μm model (BV/TV=0.24±0.10). Each virtual core was also generated as a 10-node tetrahedral (TET10) μFEM. All μFEMs were given either a homogeneous tissue modulus of 20 GPa, or a heterogeneous tissue modulus scaled by CT-intensity [8]. All FEMs were constrained with identical boundary conditions and compressed to 0.5% apparent strain. The apparent modulus of each model was calculated and compared.

RESULTS AND DISCUSSION

The highest resolution (32 μm) HEX8 μFEMs provide the comparative 'gold standard,' for all other μFEMs. For each μFEM, linear regression of E_{app} and BV/TV was performed.
Models with a homogeneous tissue modulus showed almost no difference in the slope or intercept between HEX8 or TET10 μFEMs at 32 μm resolution (Table 2). These models also had the lowest standard error of regression divided by the mean E_{app}, or the best fit. Of the 64 μm μFEMs, the down-sampled HEX8 64 μm μFEMs most closely matched the HEX8 32 μm μFEMs. No other homogeneous model showed slopes or intercepts comparable to the gold standard μFEMs.

When heterogeneous tissue modulus was used in the μFEMs, none of the μFEMs were able to match the E_{app} of the HEX8 32 μm μFEMs (Table 3). This is concerning, considering μFEMs with heterogeneous tissue moduli are most representative of *in-vivo* trabecular bone [1, 2].

CONCLUSIONS

This study questions the ability to use a homogeneous effective tissue modulus in non-linear μFEMs. Additionally, this study shows that translation of stiffness from down-sampled scans are not equivalent to scans performed at the down-sampled resolution, or that account for trabecular material heterogeneity.

REFERENCES

1. Oftadeh et al. J Biomech Eng; 137:010802. 2014
2. Renders et al. J Biomech; 44:402-7. 2011
3. Bayraktar et al. J Biomech; 37:27-35. 2001
4. van Reitbergen. J Biomech; 28:69-81 1995
5. Niebur et al. J Biomech Eng; 121:629-35. 1999
6. Bevill and Keaveny. Bone; 44:579-84. 2009
7. Helgason et al. Clin Biomech; 23:135-46. 2008
8. Bourne & van der Meulen. J Biomech; 37:613-21. 2004

Table 2: Linear regression results for apparent modulus and volume fraction of homogeneous FEMs.

$E_{app} = m\frac{BV}{TV} + b$	r^2	m	b	SE	SE/mean
HEX8 – 32 μm	0.88	13685	-1433	383	20.2%
TET10 – 32 μm	0.89	13830	-1430	360	19.6%
HEX8 – 64 μm	0.89	12373	-1488	338	22.1%
TET10 – 64 μm	0.88	11701	-1228	310	22.4%
HEX8 – Down-sampled 64 μm	0.87	13674	-1650	391	23.8%
TET10 – Down-sampled 64 μm	0.88	14080	-1568	369	23.5%

Table 3: Linear regression results for apparent modulus and volume fraction of heterogeneous FEMs.

$E_{app} = m\frac{BV}{TV} + b$	r^2	m	b	SE	SE/mean
HEX8 – 32 μm	0.84	7054	-817	234	26.0%
TET10 – 32 μm	0.85	7429	-837	231	25.2%
HEX8 – 64 μm	0.88	6669	-856	188	24.5%
TET10 – 64 μm	0.87	6477	-720	176	24.3%
HEX8 – Down-sampled 64 μm	0.85	7463	-961	240	28.7%
TET10 – Down-sampled 64 μm	0.85	7830	-916	229	27.4%

Accuracy of Density-Modulus Relationships Used in Finite Element Modeling of the Shoulder

Nikolas K. Knowles[1,2,4], G. Daniel G. Langohr[1,2,4], Mohammadreza Faieghi[1], Andrew Nelson[3,4], Louis M. Ferreira[1,2,4]
[1]Department of Biomedical Engineering, The University of Western Ontario, London, ON, CANADA
[2]Roth|McFarlane Hand and Upper Limb Centre, St. Josephs Health Care, London, ON, CANADA
[3]Department of Anthropology, The University of Western Ontario, London, ON, CANADA
[4]Collaborative Training Program in Musculoskeletal Health Research, and Bone and Joint Institute, The University of Western Ontario, London, ON, CANADA
email: nknowle@uwo.ca

INTRODUCTION

Density-modulus relationships are often used to map the mechanical properties of bone based on CT-intensity in finite element models (FEMs). Although these relationships are thought to be site-specific [1], relationships developed for alternative anatomical locations are often used regardless of bone being modeled. Six relationships are commonly used in finite element studies of the shoulder [2-7]; however, the accuracy of these relationships have yet to be compared.

This study compares the accuracy of each of these six relationships ability to predict apparent strain energy density (SED_{app}) in trabecular bone cores from the glenoid.

METHODS

Quantitative-CT (QCT) (0.625 mm isotropic voxels), and µ-CT scans (0.032 mm isotropic voxels) were obtained for fourteen cadaveric scapulae (7 male, 7 female). Micro finite element models (µ-FEMs) were created from 98 virtual 'cores' using direct conversion to eight-node brick elements. Two µ-FEM cases were considered: homogeneous with a uniform tissue modulus of 20 GPa, and heterogeneous with a tissue modulus scaled by the CT intensity of the µ-CT images (196 models).

Each µ-FEM model was compressively loaded to 0.5% apparent strain and apparent strain energy density (SED_{app}) was calculated. Additionally, each of the six density-modulus relationships were used to map heterogeneous material properties to co-registered QCT-derived models (588 models in total) (Figure 1).

The loading and boundary conditions were replicated in the QCT-FEMs and the SED_{app} was calculated and compared to the µ-FEM SED_{app}. To account for more samples than donors, restricted maximum likelihood estimation (REML) linear fits compared µ-FEM SED_{app} and QCT-FEM SED_{app} for each relationship.

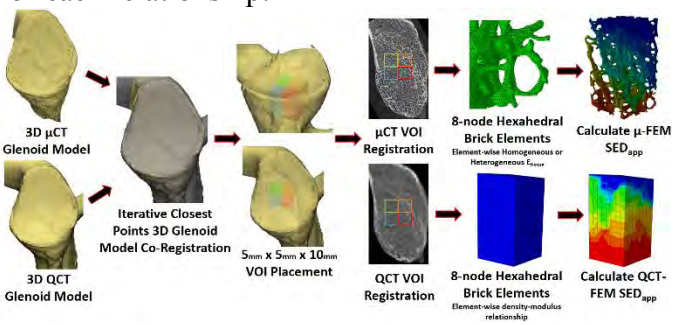

Figure 1: The workflow used to create QCT-FEMs and µ-FEMs. Three-dimensional models of the µ-CT glenoid and QCT-glenoid (gray) were co-registered. Rectangular volumes of interest (VOIs) were placed and co-registered with the µ-CT and QCT images. Hexahedral brick elements were created for each of the µ-FEMs and QCT-FEMs using custom code, and boundary conditions replicated between the µ-FEMs and QCT-FEMs.

RESULTS AND DISCUSSION

When considering comparisons between QCT-FEMs and µ-FEMs with a homogeneous tissue modulus, near absolute statistical agreement (Y=X) was observed between the µ-FEMs and the QCT-FEMs using the Morgan et al. (2003) pooled relationship (Table 1). Not surprisingly, due to the similarity between the two relationships, the Gupta & Dan (2004) and Carter and Hayes (1977) models showed near identical REML linear regression fit parameters. All relationships other than the Morgan et al. (2003) pooled relationship, greatly underestimated the µ-FEM apparent strain energy

density (SED_{app}) when considering a homogeneous tissue modulus in the μ-FEMs.

The same result with the pooled relationship did not hold true when heterogeneous tissue modulus was considered in the μ-FEMs. The Büchler et al., (2002) relationship most accurately predicted the SED_{app} for this comparison (Table 2). Interestingly, the Gupta & Dan (2004) and Carter and Hayes (1977) relationships again showed near identical REML linear regression fit parameters.

This study compared the six most common density-modulus relationships used to map mechanical properties of bone in shoulder FE studies. It was found that when considering a homogeneous tissue modulus for μ-FEMs, relationships pooled from alternative anatomical locations may accurately predict the mechanical properties of glenoid trabecular bone. However, when considering a heterogeneous, this did not hold true.

Further studies to determine if these relationships can be translated to whole bones may provide insight into the predictive capabilities of using pooled density-modulus equations in the mapping of mechanical properties in future FEMs of the shoulder.

CONCLUSIONS

This study suggests that density-modulus relationships developed from pooled anatomical locations may accurately predict trabecular strain energy density in alternate anatomical locations, when homogeneous effective tissue moduli are assumed. However, when considering material heterogeneity, consistent with *in-vivo* trabeculae, the Büchler et al., 2002 most accuretly replicated the μ-FEM SED_{app}.

REFERENCES

1. Schileo et al. J Biomech; 41:2483-91. 2008
2. Morgan et al. J Biomech; 36:897-904. 2003
3. Gupta & Dan. Trends Biomater Artif Organs; 17: 61-70. 2004
4. Büchler et al. Clin Biomech; 17:630-9. 2002
5. Carter & Hayes. J Bone Jt Surg; 59; 954-62. 1977
6. Schaffler & Burr. J Biomech; 21:13-16. 1988
7. Rice et al. J Biomech; 21:155-68. 1988

Table 1: Results from restricted maximum likelihood estimation linear regression fits of apparent strain energy (SED_{app}) predictions between QCT-FEMs and homogeneous tissue modulus μ-FEMs (20 GPa)

QCT-FEM SED_{app} = m μ-FEM SED_{app} + b	r^2	m	b	SE	SE/mean
(Morgan et al., 2003) Pooled	0.933	0.979	0.0066	0.0049	17.5%
(Morgan et al., 2003) Femur	0.937	0.739	0.0098	0.0037	14.4%
(Gupta and Dan, 2004)	0.891	0.326	-0.0013	0.0019	32.2%
(Büchler et al., 2002)	0.919	0.476	0.0026	0.0028	21.6%
(Carter and Hayes, 1977)	0.903	0.320	-0.0024	0.0018	31.4%
(Schaffler & Burr, 1988) (Rice et al., 1988)	0.940	0.105	0.0013	0.0005	13.7%

Table 2: Results from restricted maximum likelihood estimation linear regression fits of apparent strain energy (SED_{app}) predictions between QCT-FEMs and heterogeneous tissue modulus μ-FEMs

QCT-FEM SED_{app} = m μ-FEM SED_{app} + b	r^2	m	b	SE	SE/mean
(Morgan et al., 2003) Pooled	0.926	1.914	0.0091	0.0052	18.5%
(Morgan et al., 2003) Femur	0.928	1.431	0.0119	0.0040	15.4%
(Gupta and Dan, 2004)	0.892	0.638	-0.0010	0.0019	32.2%
(Büchler et al., 2002)	0.911	0.945	0.0013	0.0030	22.7%
(Carter and Hayes, 1977)	0.902	0.623	-0.0007	0.0018	31.9%
(Schaffler & Burr, 1988) (Rice et al., 1988)	0.948	0.211	0.0015	0.0005	12.9%

MUSCULAR DEMANDS ASSOCIATED WITH MANUAL PALLET WRAPPING TECHNIQUES

Jacquelyn M. Maciukiewicz, Kimberly B. Hogervorst and Clark R. Dickerson
Department of Kinesiology, University of Waterloo, Waterloo, ON, Canada
email: jmmaciuk@uwaterloo.ca

INTRODUCTION

Occupational tasks often include exposure to various ergonomic risk factors. Awkward or strenuous postures, high physical demands, and repetitive tasks all increase the occupational injury risk. Overexertion, repetitive motion, and bodily reactions accounted for 36% of the claims in 2012 [1]. For the upper extremity, large horizontal, forward or upward reaches are associated with increases in specific and overall muscular demands [2]. Wrapping a loaded pallet involves pushing and pulling a roll of film and potentially an additional device to secure cargo. Pallet wrapping entails reaching above shoulders, bending, twisting and extending reaching forwards. 8-10lbs (3.5-4.5kgs) of force is used to pull the film tight and create adequate tension to secure the load to the pallet [1]. Increased force requirements concomitantly raise muscle activations. Muscular responses were also sensitive to changes of technique at lower loads, where pushing required less muscular demand than pulling. However, in both pushing and pulling upper body muscles and erector spinae were engaged statically, increasing risk for fatigue [3].

Despite the adoption of various tools to assist in manual pallet wrapping, limited exposure quantification for workers using these devices exists. Therefore, the purpose of this study was to determine how pallet wrapping technique (using an assistive device or wrapping by hand) influences specific muscular demands across genders in a simulated workstation at three heights. It was hypothesized that males would exhibit lower muscular demands, and that interactions would exist between the height of the wrapping performed and technique. Specifically, using the tool would require less muscular demand across all heights compared to the bare roll.

METHODS

Fourteen healthy, university-aged participants completed this study (7M, 7F). A simulated pallet station was recreated in a laboratory setting. The workstation matched the dimensions of a standard pallet stacked with boxes (size: 122x122x154cm). A line was placed enclosing the pallet at approximately 60cm, as a guide to keep participants close to the pallet and mimic space confinements.

Six upper extremity and two torso muscles were measured bilaterally using surface electromyography (sEMG) with a Noraxon T2000 telemetered system sampled at 1500Hz (Noraxon Inc., Scottsdale, AZ, USA): deltoids (anterior and middle), biceps brachii, infraspinatus, supraspinatus, upper trapezius, and erector spinae (T8 & L3).

Prior to experimental trial data collection, participants completed two muscle specific maximum voluntary isometric contractions (MVCs) for each muscle. Participants were shown a training video for pallet wrapping with the bare roll and the device, and were given practice trials. For both scenarios participants wrapped twice at low, medium and high levels of the pallet.

Raw EMG signals were band pass filtered from 10-500Hz and differentially amplified (Common Mode Rejection Ratio (CMRR) >100dB at 60Hz, input impedance 100MΩ). Signals were full wave rectified then low pass filtered using a single pass, 2nd order Butterworth filter with a cut-off frequency of 3Hz [4] and normalized to muscle specific maximums. From each partial wrap trial, the mean normalized muscle activity was extracted. All statistical analyses were completed using JMP 12.0 software (SAS Institute, North Carolina, USA). Based on participant preference, muscles were split into support arm and top arm. A 3-way mixed effect ANOVA (gender, device, and task height) was used to detect main and 2-way interaction effects of each parameter on mean sEMG for each of the muscles.

RESULTS

Interactions between gender and tool type

The interaction of gender and tool existed for the top arm upper trapezius as well as the support arm biceps brachii,

anterior deltoid, middle deltoid, supraspinatus and infraspinatus. Females wrapping with the tool had more muscular activation of the top arm upper trapezius (~11% MVC) compared to any other scenario (~5-6% MVC). Similarly, females wrapping with the tool had more muscular activation of the middle deltoid (~8% MVC) and infraspinatus (~14% MVC) on the support arm than any other scenario (~2-5% MVC and ~5-8% MVC, respectively). Males performing hand wrapping required the least muscular activation of the supraspinatus (~2% MVC) compared to other scenarios (~5-6% MVC).

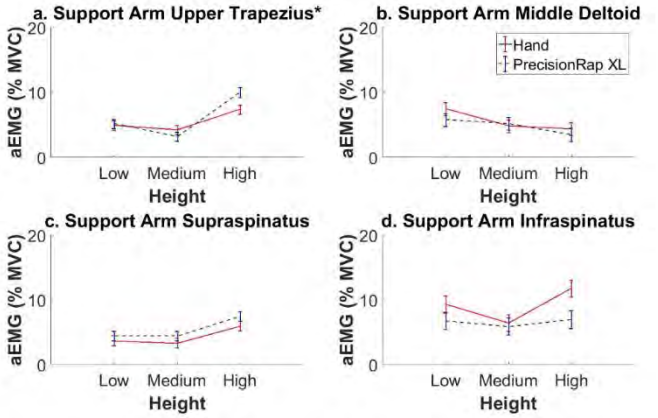

Figure 1: Interaction between height and tool for aEMG of the 4 of the support arm muscles. Significant muscles are denoted with an asterisk (*).

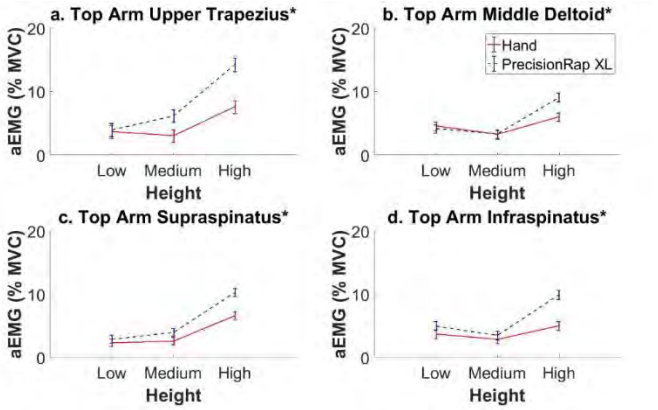

Figure 2: Interaction between height and tool for aEMG of the 4 of the top arm muscles. Significant muscles are denoted with an asterisk (*).

Interactions between height and tool

An interaction between height and tool existed for the upper trapezius of the support arm (Figure 1), as well as anterior and middle deltoid, upper trapezius, supraspinatus and infraspinatus of the top arm (Figure 2). Both the tool and hand wrapping required the greatest muscular activation at the highest height (7-10% MVC), compared to either of the other heights (3-5% MVC).

DISCUSSION AND CONCLUSIONS

Muscular activity can be altered by changing techniques associated with pulling tasks, such as pallet wrapping. However, in the current study, using a tool to alter technique resulted in similar muscular activity as wrapping with no tool. In some cases using the tool required more muscular activity for some muscles of the support arm, or the top arm (responsible for guiding the tool/bare roll). Although average muscular demands in the current project seem modest, they approach muscular demand limits that indicate risk for tasks completed for 1 hour/day (10% MVC) [5].

Previous work indicated that manual materials tasks that require pulling, such as wrapping a pallet, require adoptions of awkward postures that may increase muscular activity [6]. While a change of technique can potentially decrease muscular activity [3]. The tool was designed to reduce the pull, and allow the user to push when possible. However, the introduced tool increased muscular activity in some scenarios likely reflective of the added weight of the tool. A reduction was seen in the infraspinatus muscle of the support arm with the use of the tool. This could indicate a reduction in external rotation of the support arm. Further analysis on kinematic differences of this wrapping task continues to determine if more desirable postures are being adopted with tool use, potentially offsetting the higher muscular demand.

REFERENCES

[1] Workplace Safety & Prevention Services, 2012.
[2] McDonald et al., *Applied Ergo.* **43,** 2012.
[3] Bennett et al., *Work,* **28,** 2011.
[4] Winter. *4th Edition*. 2009.
[5] Jonsson. *J Human Ergol,* **11,** 1982.
[6] Hoozemans et al. *Occup Env. Med*, **56,** 2002.

ACKNOWLEDGEMENTS

The authors would like to acknowledge Ontario Centre of Excellence for funding support.

IMAGING-BASED QUANTIFICATION OF SHOULDER IMPINGEMENT DURING MANUAL WHEELCHAIR-BASED ACTIVITIES OF DAILY LIVING

Joseph D. Mozingo, Mohsen Akbari Shandiz, Naveen S. Murthy, Meegan G. Van Straaten, Beth A. Schueler, David R. Holmes III, Cynthia H. McCollough, and Kristin D. Zhao

Mayo Clinic, Rochester, MN, USA
Email: zhao.kristin@mayo.edu

INTRODUCTION

The majority of individuals with a spinal cord injury (SCI) who use a manual wheelchair (MWC) report shoulder pain [1]. This limits independence due to reliance on the shoulders for mobility and activities of daily living (ADLs). Shoulder mechanical impingement, caused by narrowing of the space between the humerus and scapula, is considered a primary factor associated with shoulder pain and rotator cuff pathology in this population [2]. Despite this link, the etiology of impingement is not well understood, in part due to the inability of previous technologies to provide arthrokinematic measures. Model-based tracking, using biplane fluoroscopy and computed tomography (CT), has become the gold standard for noninvasive in vivo quantification of bone motion. Investigators have demonstrated the utility of this technique for quantification of shoulder kinematics as well as changes in the subacromial space, primarily during simple arm elevation tasks in able-bodied individuals [3]. *Leveraging this technique, the goals of this work were: 1) Quantify dynamic changes in proximity between relevant sites on the humerus and scapula during functional MWC-based ADLs in individuals with a SCI, 2) Determine percent of total task associated with impingement.*

METHODS

Following IRB approval, informed consent was obtained for 10 individuals with paraplegia that use a MWC as their primary mode of mobility (ages 26 – 58, 1F/9M, injury levels T3 – T12). A licensed physical therapist conducted an upper extremity physical examination and participants underwent ultrasound, CT, and fluoroscopy examinations of the dominant arm.

A fluoroscopy examination was conducted to obtain dynamic images during functional activities. Imaging was completed with the participant seated in their MWC and the shoulder centered in the calibrated image volume of a clinical flat-panel biplane fluoroscope (Artis zee; Siemens Healthcare). Images were acquired at 15 frames/s per plane (48 cm FOV, 3.2 ms pulse width) during scapular plane elevation (scaption) to max elevation, a propulsion cycle, and weight relief raise (Fig. 1). Propulsion was carried out on a set of stationary rollers Imaging duration was approximately 3 – 4 seconds per activity, and motion speed was verbally guided.

Next, a CT scan (Definitions Flash, Siemens Healthcare) of the full humerus and scapula of the dominant shoulder was obtained (140 kVp, 0.75 mm slice thickness, 0.35 mm slice increment).The scapula and proximal humerus were imaged using a 250 quality reference mAs, and the remainder of the humerus was imaged at 20 quality reference mAs to acquire distally located anatomical landmarks and reduce radiation exposure. In order to create 3D models, the scapula and humerus were segmented from the image volume (AnalyzePro; Mayo Clinic). Additionally, the footprints of 3 rotator cuff tendons (supraspinatus, infraspinatus, subscapularis) were manually segmented from the humerus model. Similarly, the attachment sites of the coracoacromial ligament (CAL) onto the acromion and coracoid were manually segmented from the scapular model. To model the ligament, a planar mesh was created between the attachment sites.

Figure 1: Participant completing 3 tasks within image volume of clinical biplane fluoroscope.

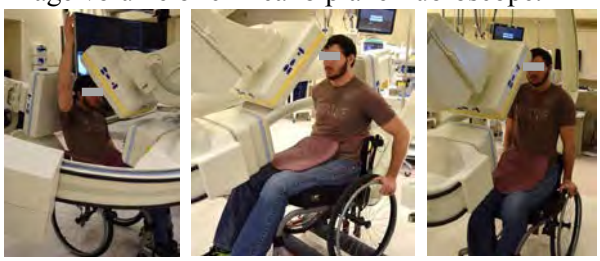

Scaption **Propulsion** **Pressure Relief**

Last, a musculoskeletal radiologist performed an ultrasound examination (LOGIQ E0; GE Healthcare) of the shoulder using a ML6-15 MHz probe (MSK setting). Standard imaging planes were employed including the modified Crass position for the supraspinatus and infraspinatus. Static images were obtained to measure the thickness of the rotator cuff tendons at their insertions.

After data collection, model-based tracking was used to register the 3D bone models to each fluoroscopic image pair using freely available software (Autoscoper; Brown University) and a custom semi-automated tracking algorithm. The pose of each model was adjusted such that its digitally reconstructed radiograph was optimally aligned with its fluoroscopic projection in each image plane. Global orientation and position data of the bone models were described in anatomical coordinate systems using landmarks established by the International Society of Biomechanics [4]. For each frame, kinematic data generated from model-based tracking was used to align the 3D bone models, tendon footprints, and CAL. The minimum Euclidean distance was then computed from the vertices that comprised each footprint to overlying scapular structures (coracoacromial arch [acromion, coracoid, and CAL]). For each task, impingement was defined by quantifying the percentage of the task for which proximity measures were below a tendon's measured thickness. Additionally, within these periods, the absolute minimum distance was determined.

RESULTS AND DISCUSSION

For the first subject, scaption was characterized by tendon compression for no less than 44% of the total task (Table 1). The reported minimum distances correspond to 77%, 63%, and 38% reductions in tendon thickness relative to the original thickness of the supraspinatus, infraspinatus, and subscapularis respectively. Considering the overlap in periods of compression for the separate tendons, 94% and 20% of scaption and propulsion respectively were characterized by impingement. None of the tendon footprints were in proximity to the scapula during the pressure relief. Analysis is ongoing for the other subjects.

Our preliminary results indicate that distinct kinematic phases of MWC-based ADLs are characterized by shoulder impingement (Figure 2). Additionally, this approach allowed us to delineate which tendons were susceptible, as well as the potential level of compression. For this first subject, the majority of scaption and the middle third of the propulsion cycle were characterized by periods of impingement. No structures were impinged during the full pressure relief. This knowledge can be used to inform MWC prescription and training in effective MWC use following SCI to lessen damage to the rotator cuff.

Figure 2: Proximity profiles for one subject. Points represent minimum distance between supraspinatus footprint and coracoacromial arch over course of activity. Dashed line indicates tendon thickness value.

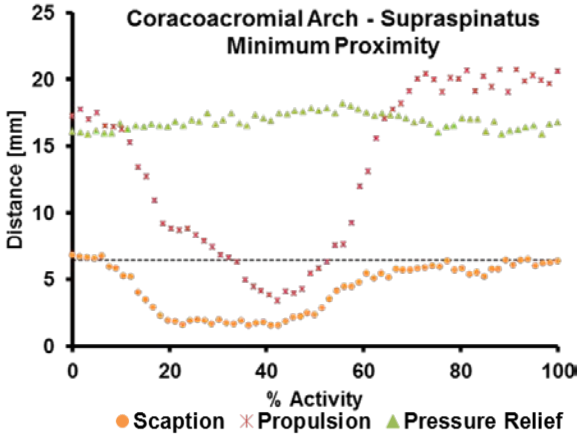

Table 1: Activity impingement characteristics for one subject. Values correspond to distance between footprint and nearest point on coracoacromial arch. A tendon was considered impinged when proximity was below measured thickness.

% Activity in impingement, Minimum distance in impingement [mm]			
	Supra	*Infra*	*Subscap*
Scaption	56.7, 1.5	79.1, 2.6	44.8, 3.1
Propulsion	20.0, 3.4	21.7, 4.1	0, N/A
Pressure Relief	0, N/A	0, N/A	0, N/A

REFERENCES

1. McCasland, L. *J Clin Rheumatol*, **12**, 179-186, 2006
2. Akbar M., et al. *J Bone Joint Surg,* **92**, 23-30, 2010
3. Baumer T., et al. *Orthop J Sports Med*, **4**, 2016
4. Wu G., et al. *J Biomech*, **38**, 981-992, 2005

ACKNOWLEDGEMENTS

We thank Mark Hindal for assistance with imaging, and NIH/NIAMS T32 AR56950 for supporting this work.

DISCRIMINATION BETWEEN HAND/WRIST OCCUPATIONAL TASKS AND INDIVIDUAL WORKERS THROUGH THE USE OF AN INSTRUMENTED WRIST BRACE

Bryan Piper MASc.,[1] Michele Oliver PhD, PEng.,[1] Karen Gordon PhD, PEng. [1]
[1] School of Engineering, University of Guelph, Guelph, ON, Canada
email: kgordon@uoguelph.ca

INTRODUCTION

Carpal Tunnel Syndrome (CTS) is an example of a repetitive strain injury that is often the cause of lost wages and medical expenses in major developed countries [1] . Certain occupations are associated with high risk of developing CTS, including occupations that involve manual labour, processing involving fine motor control, and typing [2].

Ergonomic assessment tools are often used in the workplace such as Strain Index, Threshold Limit Value for Hand Activity Level, and (modified) Rapid Upper Limb Assessment (RULA and mRULA) to quantify hand-wrist repetitive strain injury risk. These methods score a workplace task based on the relative postures, repetition of movements, and level of worker exertion. The results can be subjective and qualitative in nature. Wearable technology stands to improve the subjective nature of ergonomic assessment, and to provide valuable quantitative data.

To the authors' knowledge, there are currently no devices to aid in ergonomic assessment related to CTS. This study aims to implement a newly developed brace, capable of recording wrist kinematics, in a simulated workplace setting. The objective was to determine if the data from the brace could be used to differentiate between different tasks and different subjects. If significant differences were noted between subjects and tasks performed, the brace could be used in a personalized setting to provide a user with unique, customized biofeedback. We hypothesized that the data from the brace would reveal significant differences between subjects performing the tasks and between tasks being performed.

MATERIALS AND METHODS

An instrumented wrist brace was developed for the purposes of wrist kinematic tracking. The brace was modified from the DonJoy Functional Wrist Brace, provided by All Sports Dynamics Inc., Nacogdoches, Texas USA. Two braces were 3D printed to dimensions representing the 50th percentile male and female geometry [3]. Two rotary encoders (Nemicon, 7S, Tokyo, Japan) were placed at the anatomic centres of rotation for wrist flexion-extension (FE), and radial-ulnar deviation (RUD) in each brace. The encoders were selected for their size and resolution, 4.44 pulses per degree, allowing accurate recording of angular changes of magnitude less than one degree.

A Parallax Propeller Quickstart microcontroller was used to collect data in conjunction with the Excel DAQ. The data acquisition was limited by the Excel DAQ baud rate of 120 000 and resulted in an average collection rate of 35 Hz for all trials.

Thirteen right-hand dominant subjects (seven males, age 21.1 ± 2.81 years) were recruited for this University of Guelph REB approved study. An eight camera VICON Bonita Motion Capture System (Vicon Motion System Ltd, Oxford, UK) was used to record wrist kinematics at a sampling frequency of 100 Hz. Seven VICON motion capture markers were placed on the subjects' right upper limb [4]. All subjects performed a full ROM trial in FE and RUD, while wearing the brace and collecting VICON data. In addition, subjects completed (randomly) a typing task and an object placement task.

Brace and VICON data were imported into Matlab and filtered with a low-pass second order Butterworth filter at 10 Hz. Brace data was then converted from bits (encoder data) to angle using a subject-specific calibration determined from the full range of motion trial described above. A 25-30 second section of each task was then split into 5 second windows with 0% overlap. The total range of motion (maximum minus minimum angle) and average angle were calculated for both the brace and VICON for the typing and pick and place tasks for each window.

Factors of subject, gender, task (typing or pick and place) and motion (flexion extension or radial ulnar deviation) were included in a general

linear model ANOVA in Minitab 17, (Minitab Inc., Chicago, Illinois, USA).

RESULTS AND DISCUSSION

ROM data for flexion extension angle were not normally distributed, so a Johnson transformation was used. Mean RUD angle was significantly higher for typing than the pick and place task (p=0.005). RUD ROM was significantly higher for the pick and place task compared to typing (p=0.000). FEM ROM was significantly higher for pick and place compared to typing (p=0.00). No significant differences were noted for FE mean angle.

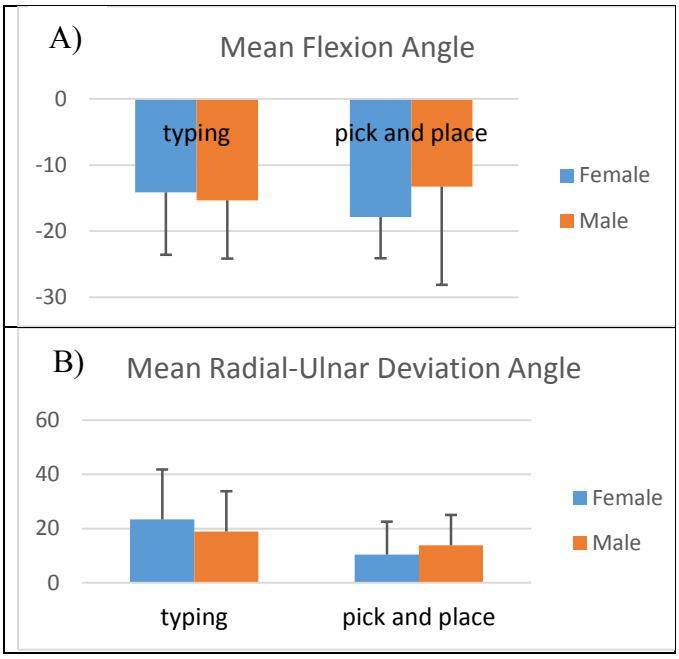

Figure 1: Mean Flexion Extension Angle (A) and Radial Ulnar Deviation Angle (B) (error bars represent standard deviations) by task and gender) (Negative values represent flexion and radial deviation).

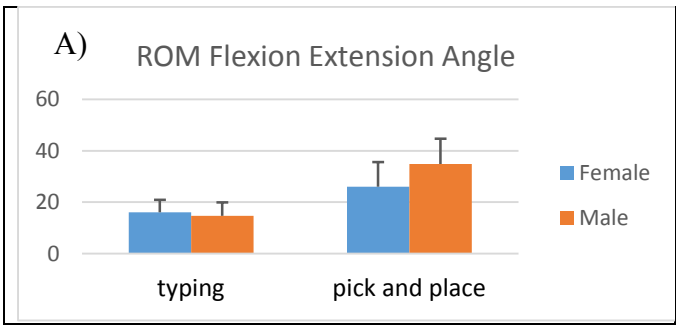

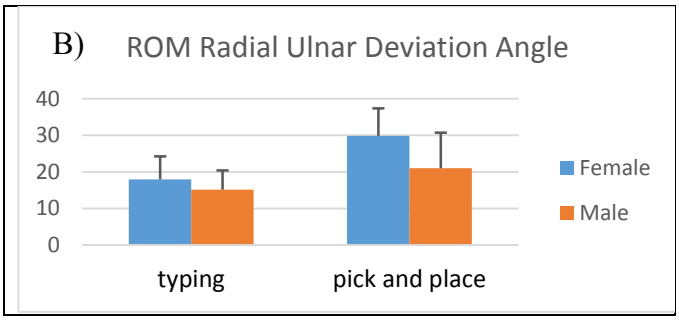

Figure 2: Mean ROM Flexion Extension Angle (A) and ROM Radial Ulnar Deviation Angle (B) (error bars represent standard deviations) by task and gender).

CONCLUSIONS

The results illustrated that significant differences could be found in kinematics from a simply designed wrist brace instrumented with a rotary encoder. Significant differences between two tasks (typing and a pick and place object task) were noted using simple measures such as mean angle and ROM. Future work with the brace and the data collected from the brace will involve more sophisticated detection algorithms, a higher data collection frequency, and a broader study with additional activities of daily living. The data from the brace has the potential to provide custom, real-time feedback for rehabilitation and ergonomic purposes.

REFERENCES

[1] K. T. Palmer, "Carpal tunnel syndrome: The role of occupational factors," *Best Pract. Res. Clin. Rheumatol.*, vol. 25, no. 1, pp. 15–29, Feb. 2011.

[2] A. Petit *et al.*, "Risk factors for carpal tunnel syndrome related to the work organization: A prospective surveillance study in a large workingpopulation," *Appl. Ergon.*, vol. 47, pp. 1–10, 2015.

[3] Tilly, Alvin R.; Henry Dreyfuss Associates, *The measure of man and woman: Human factors in design*, Revised Edition. New York: Wiley, 2002

[4] Murgia *et al.*, "Marker Placement to Describe the Wrist Movements during Activities of Daily Living in Cyclical Tasks." *Clin. Biomech.,* vol. 19, no. 4, pp. 248-54, 2004.

ACKNOWLEDGEMENTS

The wrist brace used in this project was provided by DonJoy (DJO Global, USA)

VALIDATION OF AN INSTRUMENTED BRACE FOR TRACKING WRIST KINEMATICS IN OCCUPATIONAL SETTINGS

Bryan Piper MASc.,[1] Michele Oliver PhD, PEng.,[1] Karen Gordon PhD, PEng. [1]
[1] School of Engineering, University of Guelph, Guelph, ON, Canada
email: kgordon@uoguelph.ca

INTRODUCTION

Carpal tunnel syndrome (CTS) is the most common entrapment neuropathy which affects approximately 5.8% of the population as a conservative estimate [1]. CTS is often the cause of lost wages and medical expenses in major developed countries [2] . CTS symptoms are associated with tasks involving high hand stress, repetition, and vibration coupled with extreme postures [3]. Jobs with high risk include manual labour, processing involving fine motor control, and typing [3].

Ergonomic assessment may be conducted to assess risk factors in the workplace, with measures such as Strain Index, Threshold Limit Value for Hand Activity Level, and (modified) Rapid Upper Limb Assessment (RULA and mRULA) used to quantify risk. These methods score a workplace task based on the relative postures, repetition of movements, and level of worker exertion. The results can be subjective with high variability between raters, considering the worst postures and capturing only snapshots of workplace task performance. Moreover, the act of being observed may alter the behaviour of the worker being assessed thus affecting test scores. Wearable technology stands to improve the subjective nature of ergonomic assessment.

To the authors' knowledge, there are currently no devices to aid in ergonomic assessment related to CTS. This study aims to develop and validate a method of wrist posture tracking with capabilities for real-time feedback. The data from a newly developed wrist brace was validated through comparison to the current gold standard (motion capture). We hypothesized that the brace would be able to track the kinematics of the wrist with a high degree of correlation to motion capture.

Materials and Methods

An instrumented wrist brace was developed for the purposes of wrist kinematic tracking. The brace was modified from the DonJoy Functional Wrist Brace, provided by All Sports Dynamics Inc. (Nacogdoches, Texas USA). Using hand and wrist anthropometric data for 50th percentile males and females [4], two modified braces were 3D printed from ABS (Acrylonitrile butadiene styrene) to custom dimensions (Figure 1). Two rotary encoders (Nemicon, 7S, Tokyo, Japan) were placed at the anatomic centres of rotation for wrist flexion-extension (FE), and radial-ulnar deviation (RUD). The encoders were selected for their size and resolution, 4.44 pulses per degree, allowing accurate recording of angular changes of magnitude less than one degree.

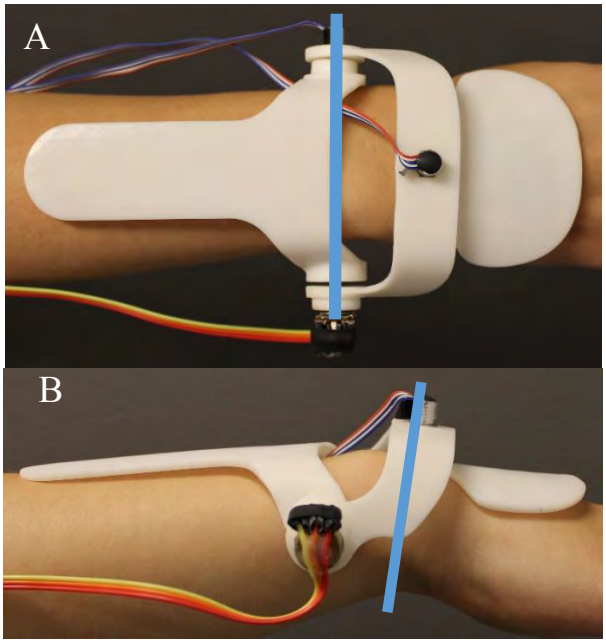

Figure 1: Dorsal (A) and lateral (B) views of brace on subject's right wrist indicating Flexion-Extension (A) and Radial-Ulnar (B) axes of rotation (blue).

A Propeller Quickstart microcontroller (Parallax Inc., CA) was used to collect data in conjunction with the Excel DAQ. The data acquisition was limited by the Excel DAQ baud rate of 120 000 and resulted in an average collection rate of 35 Hz for all trials.

Thirteen right-hand dominant subjects (seven males, age 21.1 ± 2.81 years) were recruited for this University of Guelph REB approved study.

An eight camera VICON Bonita Motion Capture System (Vicon Motion System Ltd, Oxford, UK) was used to record wrist kinematics at a sampling frequency of 100 Hz. Seven VICON motion capture markers were placed on the subjects' right upper limb [5]. All subjects performed a full ROM trial in FE and RUD, three times, while wearing the brace and collecting VICON data.

Data from the brace were filtered with a second order Butterworth low-pass filter, f_c =10 Hz. The VICON and brace data were synchronized by matching a known peak in the trial. Each encoder was calibrated separately for FE and RUD angles using the first ROM trial. Calibrated brace angles were compared to VICON angles using a Pearson Correlation test in Minitab 17, (Minitab Inc., Chicago, Illinois, USA).

RESULTS AND DISCUSSION

Two subjects were excluded from this analysis because markers from the VICON analysis were lost and the resulting VICON data was erratic. Figures 2 and 3 represent the results from the remaining 11 subjects.

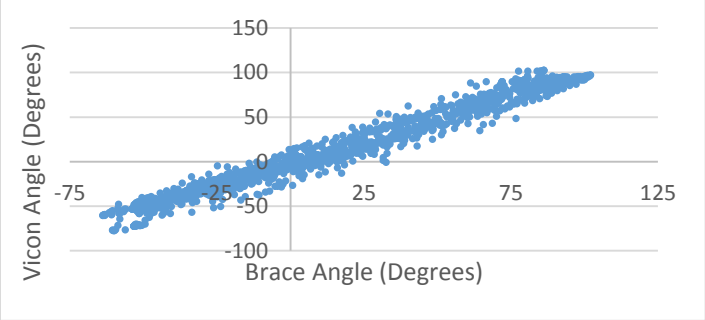

Figure 2: Correlation of Brace to VICON Flexion-Extension Angle (R^2 = 0.972, R = 0.986, p<0.001)

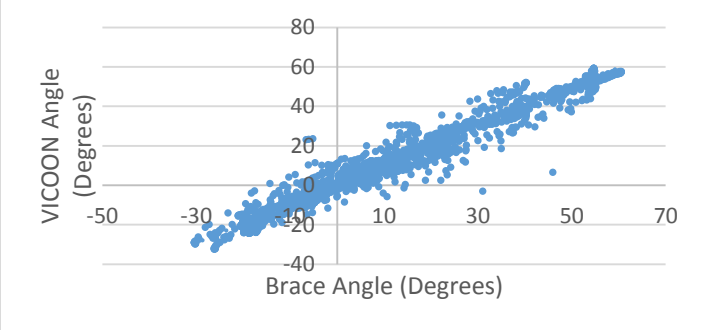

Figure 3: Correlation of Brace to VICON Radial-Ulnar Deviation Angle (R^2 = 0.957, R = 0.978, p<0.001)

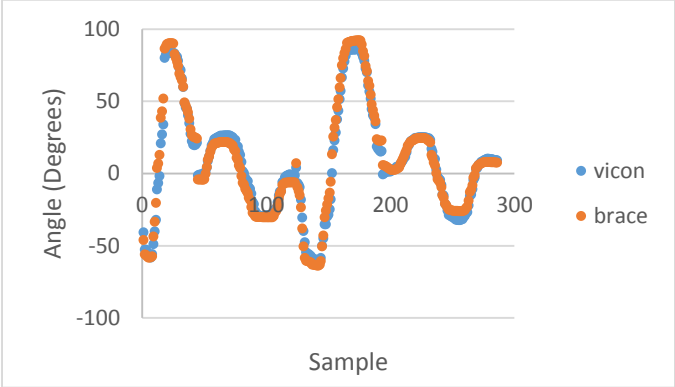

Figure 4: One representative subject illustrating VICON and brace output (Negative angle is wrist flexion, positive is wrist extension)

CONCLUSIONS

Results illustrate excellent agreement between the brace output and the VICON. However, when examining the data on a per-subject basis, larger differences between brace and VICON angles were noted at the extreme ranges of motion, and in regions of local maximum or minimum (Figure 4). It is anticipated that this could be improved with a more robust calibration procedure, including dynamic data. In addition, in future work, the data collection rate of the brace will be increased. While 35 Hz is adequate according to Nyquist criterion, a faster collection rate (100 Hz) in this study would have facilitated direct comparison between brace and VICON data.

The proposed brace shows promise for quantifying CTS occupational risk factors and other wrist pathologies and may provide a useful tool for long term ergonomic assessment, injury diagnosis and return to work progress.

REFERENCES

[1] M. De Krom, et al., *J. Clin. Epidemiol.*, vol. 45, no. 4, pp. 373–376, 1992. [2] K. T. Palmer, *Best Pract. Res. Clin. Rheumatol.*, vol. 25, no. 1, pp. 15–29, Feb. 2011. [3] A. Petit *et al.*, *Appl. Ergon.*, vol. 47, pp. 1–10, 2015. [4] Tilly, Alvin R.; Henry Dreyfuss Associates, *The measure of man and woman: Human factors in design*, Revised Edition. New York: Wiley, 2002 [5] Murgia *et al.*, *Clin. Biomech.,* vol. 19, no. 4, pp. 248-54, 2004.

ACKNOWLEDGEMENTS

The wrist brace used in this project was provided by DonJoy (DJO Global, USA).

PLANE OF ARM ELEVATION EFFECT ON SCAPULOHUMERAL RHYTHM (SHR)

[1] Jase A. Schossow, [1] Jacob R. Ahles, [2] Traci Bush, [3] David Stapleton, and [2,3] Vassilios G. Vardaxis

[1] College of Osteopathic Medicine, [2] Department of Physical Therapy, [3] Human Performance Laboratory
Des Moines University, Des Moines, IA, USA
email: vassilios.vardaxis@dmu.edu, web: http://asb2018.asbweb.org/

INTRODUCTION

Shoulder movement coordination is explicitly quantified in 3D by three angle-angle plots for the specific plane of arm elevation (frontal, scapular, and sagittal). This coordinated movement is clinically characterized by the scapulohumeral rhythm (SHR), a ratio of the glenohumeral and scapulothoracic contribution to humerothoracic elevation. The therapeutic management of patients with shoulder pathology includes assessment and interventions specific to SHR [1]. Several studies have reported altered SHR (reflecting shoulder dyskinesia) related to various pathologies [2-4]. Regardless the nature of the altered shoulder kinematics (compensatory or causative), addressing SHR is essential for optimal patient care [5]. Previous studies have focused SHR assessment on scapular and cardinal planes. Its consistency across planes of active arm elevation, however, remains unclear.

The purpose of this study was to test the hypothesis that SHR varies by plane and level of arm elevation during multiple dynamic humerothoracic elevations between the frontal and sagittal planes.

METHODS

Twenty healthy male volunteers (mean age 24.4±1.27 years) without upper extremity neuromuscular pathology (mean BMI 25.6 kg/m²; range 20.4 to 33.4 kg/m²) participated in the study. Participants were tested on the right-hand dominant side and were screened for pain free active shoulder elevation (>150°) in flexion and abduction by visual observation. The protocol consisted of arm elevations on thirteen randomly ordered planes (between the frontal at 0, 10, 20, 25, 30, 35, 40, 45, 50, 60, 70, 80, and 90° sagittal plane). Participants were instructed to maintain their trunk in a stable, upright posture (while seated) and to perform 4 trials of arm elevation per plane (guided by the tactile sense of a string-net to a target, at 120° elevation) at the controlled pace of approximately 3 seconds elevation and lowering of the limb. The palm was maintained on the plane of elevation with the thumb up and was weighted with a half-pound load taped to the dorsal aspect of the hand. A motion capture system with 10-cameras (Motion Analysis Corp.) running at 120 Hz was used to capture 3D data of reflective markers attached to the upper-limb and torso. Euler angles (per ISB recommendations [6]) were used to reference the 3D scapula position to thorax, humerus to scapula, and humerus to thorax. The glenohumeral and scapulothoracic motion was assessed between 16° and 105° of humerothoracic elevation and was divided into six separate segments of 15º each. Linear regression lines were fit at each segment of the scapular upward rotation versus the glenohumeral elevation. The dependent measure used in the analysis was the SHR, the slope of the linear fit for each arm elevation segment (Figure 1).

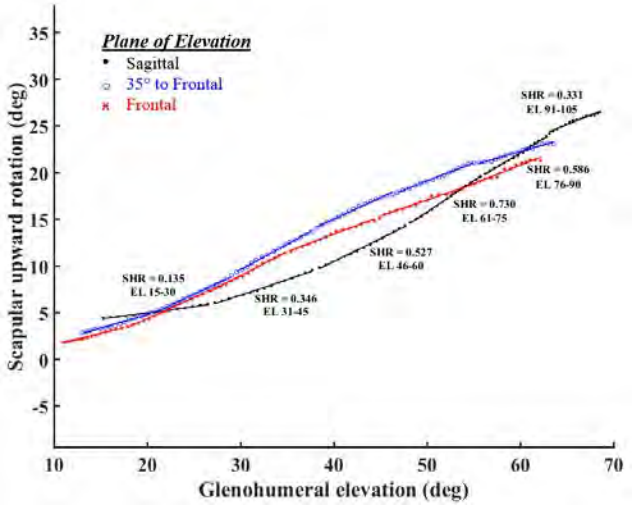

Figure 1: Scapular upward rotation and glenohumeral elevation at 3 elevation planes. SHR slopes on six (15°) humerothoracic elevation segments, from 16° to 105°.

A two-factor repeated-measures ANOVA, on the SHR slopes, was used to determine within factor effects for plane of elevation, arm elevation segment, and interaction. One-way repeated-measures

ANOVA models were used to test for arm elevation segment differences at each plane of arm elevation. Significance level was set at α=0.05. Bonferroni adjustments were used for multiple comparisons.

RESULTS

SHR slopes were calculated at each arm elevation segment for all planes. Motion below 16° and above 105° of thoracohumeral elevation was not analyzed. Exemplar data for the frontal, scapular (35° to frontal), and sagittal plane are shown in Figure 1. Larger SHR values are indicative of higher scapular upward rotation contribution to arm elevation.

A significant plane of elevation by arm elevation segment interaction effect was found for SHR slopes (P = 0.004, η_p^2=0.141). Whereas the scapular upward rotation contributions at (and close to) the frontal plane were larger than the sagittal plane for arm elevations below 60°, the opposite was true for arm elevations between 60° and 105° (Figure 2). Significant arm elevation segment (P = 0.004, η_p^2=0.245) and plane of elevation main effects (P = 0.019, η_p^2=0.158) were also found.

There were significant quadratic trends for SHR slopes across arm elevation segments for most of the arm elevation planes (12 out of the 13 planes) ($F_{(1,19)}$ > 4.279, P < .05, η_p^2 > 0.184).

DISCUSSION AND CONCLUSIONS

The results showed that during weighted dynamic humeral elevation the SHR varies with the level [7] and the plane of arm elevation [8,9]. In addition, the non-linear trend found in SHR with arm elevation is indicative of non-constant scapular upward rotation contribution across humerothoracic elevations 16° to 105°. Specifically, there were increasingly larger SHR values observed up to 60° of arm elevation (close to frontal plane) and up to 75° degrees (close to the sagittal plane), indicative of progressively higher scapular contribution. The scapular contribution decreased thereafter. More consistent scapular contribution (SHR values close to 0.5) was observed between 30° and 90° of humerothoracic elevation with arm elevations, on and close to the scapular plane.

Our findings are limited by the soft tissue artefact concern associated with the noninvasive approaches of the study of shoulder kinematics. Knowledge of the typical SHR and its variation with level of arm elevation and plane, could serve as the basis in understanding shoulder dyskinesis, as well as, the associated therapeutic assessment and intervention methods.

REFERENCES

1. Cutti et al. *J Biomech*, 47:1035-44, 2014.
2. De Baets et al. *J Electrom Kinesiol*, 23:3-13, 2013.
3. Robert et al. *J Sh Elbow Surg*, 25:1616-22, 2016.
4. Walker et al. *J Sh Elbow Surg*, 24:1129-34, 2015.
5. Kibler et al. *Br J Sports Med*, 47:877-85, 2013.
6. Wu et al. *J Biomech*, 38:981-92, 2005.
7. McQuade et al. *JOSPT,* 27:125-33, 1998.
8. McClure et al. *J Sh Elbow Surg*, 10:269-77, 2001.
9. Ludewig et al. *J Bone Joint Surg*, 91:378-89, 2009.

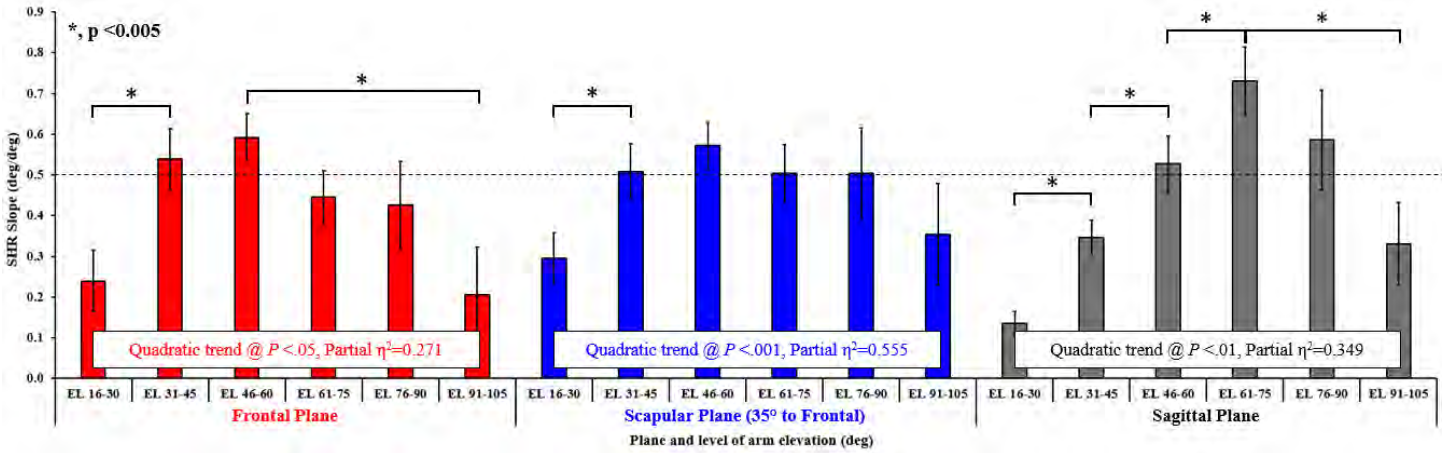

Figure 2: SHR (mean ±SEM) slope of scapular upward rotation versus glenohumeral elevation for each humerothoracic elevation segment on 3 exemplar planes of arm elevation (frontal, scapular, and sagittal).

THUMB FORCE AND ASSOCIATED ACTIVATION OF INDIVIDUAL THENAR MUSCLES DURING PIPETTING

[1]Narenraj Selvaraj, [1]Daniel Santana, [1]Carli Norman, [1,2,3]Zong-Ming Li
Hand Research Laboratory, Departments of [1]Biomedical Engineering, [2]Orthopaedic Surgery, and [3]Physical Medicine and Rehabilitation, Cleveland Clinic, Cleveland, OH, USA
email: liz4@ccf.org web: http://handlab.org/

INTRODUCTION

Pipetting is associated with high risk of musculoskeletal hand disorders due to the highly repetitive force produced by the thumb [1]. The mechanisms underlying this repetitive strain injury are unclear. The role of the thenar muscles during pipetting has been studied previously using electromyography [2] and inverse dynamic modeling [3], the latter of which estimated that the abductor pollicis brevis (APB) generates the greatest forces among the thenar muscles during plunger depression [3]. Additionally, ultrasonic imaging of muscle morphology has been shown to be related to muscle contraction [4]. The purpose of the present study is to investigate thumb force and associated thenar muscle activations during pipetting. Muscle activations of the APB, flexor pollicis brevis (FPB) and opponens pollicis (OPP) were quantified as the percentage change of cross-sectional area (CSA) relative to the resting state CSA. We hypothesized that at peak thumb force (1) the individual CSAs of thenar muscles would be larger than at rest, and (2) the APB would demonstrate a greater percentage change in CSA than FPB or OPP muscles.

METHODS

Ten healthy right handed volunteers (five male and five female subjects; mean age 25.6±2.0 years) participated in this study. Each subject sat next to the experimental setup with the right arm stabilized in an arm-wrist splint (Fig. 1a). An instrumented pipette (Pipetman P1000, Gilson, Inc., Middleton, WI, USA) with a Flexi-force sensor (A401, Tekscan Inc., South Boston, MA, USA) embedded within the plunger was grasped in the subject's hand to record pipetting thumb forces. Axial cross-sectional images of each thenar muscle (Fig. 1b,1c,1d) were obtained with a Siemens Acuson S2000 ultrasound system using an 18L6 HD linear array ultrasound transducer (Siemens Medical Solutions USA, Inc. Mountain View, CA, USA) positioned on the midpoint of and perpendicular to the first metacarpal. To acquire the optimal image of each muscle, the probe was rocked about the metacarpal axis until the muscle fascia of interest was clearly visible. The probe was oriented approximately perpendicular to the palm for imaging the OPP (Fig. 1c), rocked laterally for the APB (Fig. 1b), and rocked medially for the FPB (Fig. 1d). B-mode ultrasound video and thumb force data were collected simultaneously using a custom LabVIEW program while the subject performed the pipetting task. Each subject performed three pipetting trials with three consecutive cycles within a trial. A two-minute rest was provided between trials.

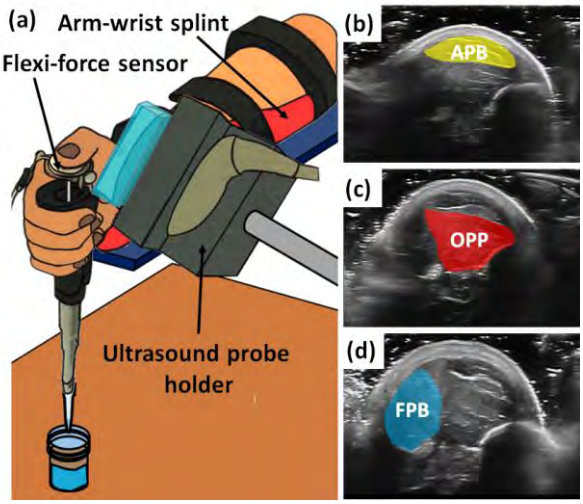

Figure 1: Experimental setup for pipetting and data collection (a) with highlighted ultrasound images of APB (b), OPP (c) and FPB (d).

Lucas-Kanade algorithm was used to track the thenar muscles in the ultrasound video. The CSA of each muscle was calculated in every frame. Thumb force data were synchronized with ultrasound video and one cycle from each trial was selected for analysis. A two-way repeated measures ANOVA was used to examine the dependence of CSA change on muscle (APB, OPP, FPB) and pipetting peak forces (air dispense and liquid dispense peak forces).

RESULTS

Thumb forces during a pipetting cycle (Fig. 2a) can be separated into six phases: air-dispense (t_1-t_2), aspiration (t_2-t_3), recess (t_3-t_4), liquid-dispense (t_4-t_5), blow-out (t_5-t_6), and release (t_6-t_7). The peak thumb forces were 6.5±1.5 N and 25.3±5.2 N for air dispense and blow-out phases, respectively. The pipetting phases were synchronized with the CSA change profiles of the thenar muscles (Fig. 2b).

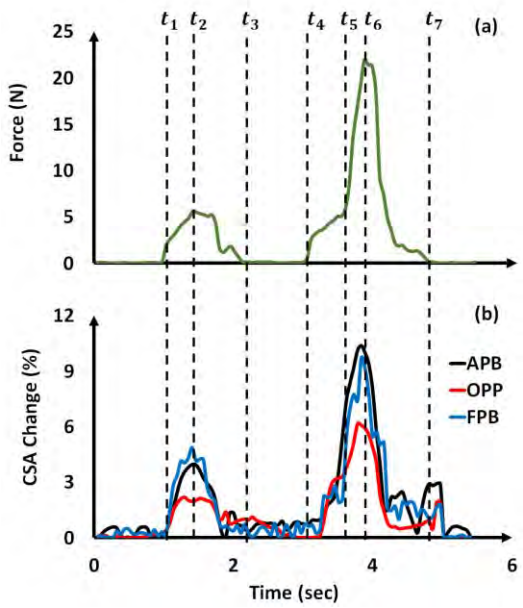

Fig. 2: Representative thumb force (a) and CSA changes (%) of thenar muscles (b) during a pipetting cycle

At rest, the CSAs of the APB, OPP, and FPB were 92.9±43.3 mm^2, 175.9±61.1 mm^2, and 123.1±28.4 mm^2, respectively. At air-dispense peak, the CSA changes were 6.4±3.4 mm^2 (7.9±4.9%) for APB, 4.8±2.3 mm^2 (2.8±1.1%) for OPP, and 6.6±2.9 mm^2 (5.6±2.5%) for FPB. At blow-out peak, the CSA changes were 12.4±6.8 mm^2 (14.6±7.0%) for APB, 10.8±5.7 mm^2 (6.2±2.4%) for OPP, and 13.9±5.9 mm^2 (11.2±4.2%) for FPB (Fig. 3). Significant differences in CSA change were observed between air-dispense and blow-out peaks in all the thenar muscles ($p < 0.001$). The OPP had a smaller CSA change than the APB at air-dispense ($p < 0.05$) and blow-out peaks ($p < 0.001$). However, the OPP was only significantly smaller than the FPB at blow-out peak ($p < 0.05$). There was no significant difference in CSA change between the APB and FPB at air dispense ($p = 0.85$) or blow-out ($p = 0.11$) peaks.

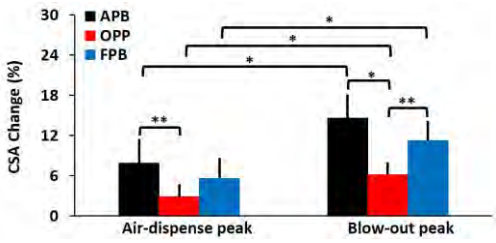

Fig. 3: Percentage change in CSA of APB, OPP, and FPB at peak forces. (*p<0.001, **p<0.05)

DISCUSSION

In this study, ultrasound captured the in-vivo behavior of the thenar muscles during thumb force production while pipetting. The measured thumb forces agree with previously reported values [2, 3]. Among the thenar muscles, OPP had the greatest CSA, followed by FPB and then APB, consistent with a previous cadaveric study [6]. At peak pipetting forces, the CSAs of each muscle were greater than at rest. Of the thenar muscles, the APB and FPB showed larger CSA changes than the OPP. Opposition of the thumb, the primary function of the OPP, may have less mechanical advantage in contributing to pipetting. The APB and FPB muscles did not show statistically different changes in CSA. Although inverse dynamic modeling estimated that the APB exhibits the largest peak muscle force, this value was only moderately higher than the FPB [3]. Therefore, our results agree with the modeling study. A limitation of this study is that the correlation between the CSA change of an individual muscle and its actual force is unknown. However, our results indicated a positive relationship between force and individual thenar muscle CSA changes. Knowledge of thenar muscle activation and associated tissue interaction helps understand the pathogenesis of tissue maladaptation and musculoskeletal disorders caused by repetitive hand use.

REFERENCES

[1] Harris-Adamson et al. Occup Environ Med. 2015, 72(1):33-41. [2] Asundi et al. Hum Factors. 2005 Spring, 47(1):67-76. [3] Wu et al. JBiomech. 2014 Jan 22;47(2):392-9. [4] Chen et al. 4th Int Conf BMEI, IEEE. 2011, 1:56-59. [5] Guo et al. Med Eng Phys. 2010, 32(9):1032-42. [6] Jacobson et al. J Hand Surg Am. 1992, 17(5):804-9.

FATIGUE OF THE LOWER TRAPEZIUS MUSCLE DECREASES SCAPULAR POSTERIOR TILT DURING ARM ELEVATION.

Mark K Timmons, Kristian Rigsby and Suzanne Konz

Marshall University, Huntington, WV, USA
email: timmonsm@marshall.edu

INTRODUCTION

Altered scapular kinematics during overhead arm motion have been associated with an increase incidence of shoulder pain however; the mechanisms that lead to the altered kinematic patterns are not well understood. During arm elevation contraction of the lower trapezius muscle helps produce scapular upward rotation and posterior tilt. Several authors have reported on scapular kinematic changes resulting from muscular fatigue. [1-3] Suggesting that muscular fatigue may produce scapular kinematic patterns that have been hypothesized to be a contributing mechanism for rotator cuff injury.

This investigation explored the effects of low trapezius fatigue on scapular kinematics in individuals without shoulder pain in order to better understand the mechanisms that lead to rotator cuff tendon injury.

METHODS

Thirty participants (170.9 ± 9.1cm, 70.5 ± 13.7Kg, 21.8 ± 1.7 years, 15 female, 15 male) took part in 1 testing session. All participants were free from shoulder pain and dysfunction, none were considered an upper extremity athlete. All measures of shoulder strength and kinematics were made on participants non-dominate side. Participants performed 5 repeated arm elevations. Three-dimensional scapular, and humeral positions were recorded during all 5 repetitions, the mean of the middle three repetitions were used for analysis. Strength and kinematic measurements were performed prior to and immediately following the fatigue protocol. Prior to the start of the testing session participants provided their written informed consent to participate, the Marshall University Human Subjects IRB approved this project.

The lower trapezius fatigue protocol consists of 2 exercises; exercise 1) participants lay prone with their arm abducted to 120°, they lift their arms off the table to approximately 2-3 inches, exercise 2) participants lay prone with their arm elevated to 120°and their elbows flexed to 90°, the participant then performs shoulder external rotation while holding the elbows on the table top. Participants performed 30 repetitions of each exercise. The strength of the low trapezius was measured immediately following the 30th repetition, if the participants low trapezius strength did not decrease by at least 20% the participant preformed another set of 15 repetitions of both exercises.

Scapular and humeral kinematics during arm elevation were measured using an Ascension TrackStar electromagnetic motion capture system (Ascension Technology, Shelburne, VT) and Motion Monitor software (Innovative Sports Training, Inc, Chicago, IL). Electromagnetic sensors were placed over the distal humerus, posterior lateral acromion, and the third thoracic vertebra. The digitization processed followed the International Society of Biomechanics (ISB) recommended protocol for sensor placement, creation of anatomical coordinate systems, and Euler angle rotation sequence. [4]

Pre-fatigue / Post fatigue differences were explored using paired t-test and repeated analysis of variance (ANOVA) were appropriate. All statistical analysis was performed with SPSS 21.0 (SPSS, Chicago, Il), statistical significance was determined at $p \leq 0.05$.

RESULTS AND DISCUSSION

Following the fatigue protocol shoulder strength decreased for all motions, 5.1 – 20.5%, decreases in force were all statically different from zero. The lower trapezius showed greatest decrease in force, 20.5% (mean = 6.5± 4.5N).

The fatigue main effect was significant for scapular upward rotation ($F_{(1,29)}$ = 22.733, p < 0.001) the scapula went into greater upward rotation after the fatigue protocol. The fatigue main effect was not significant for scapular external rotation, and posterior tilt. The fatigue by arm elevation angle interaction effect was significant for scapular upward rotation ($F_{(1,29)}$ = 7.728, p = 0.009), and posterior tilt ($F_{(1,29)}$ = 5.190, p = 0.030). (Fig's. 1 -3) Scapular upward rotation increased with arm elevation between rest and 45° pre and post fatigue protocol however there was a greater increase in scapular upward rotation at 45° (mean difference = 4.9±4.8°) than at rest (mean difference = 2.5±4.9°). Prior to the fatigue protocol the scapula went into increased posterior tilt (mean difference = 1.5±3.5°, t = -2.325, p = 0.027), after the fatigue protocol there was no difference in scapular posterior tilt with arm elevation from rest to 45°.

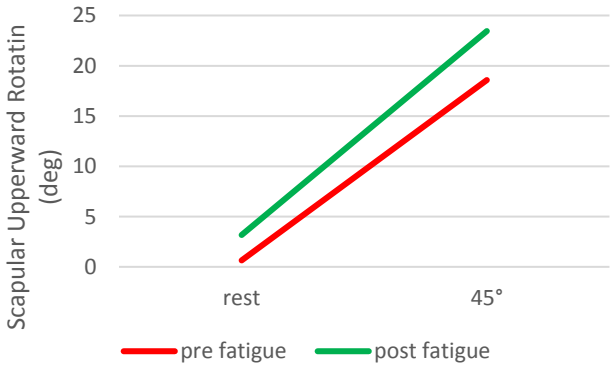

Figure 1: Scapular upward rotation, positive values refer to upward rotation of the scapula.

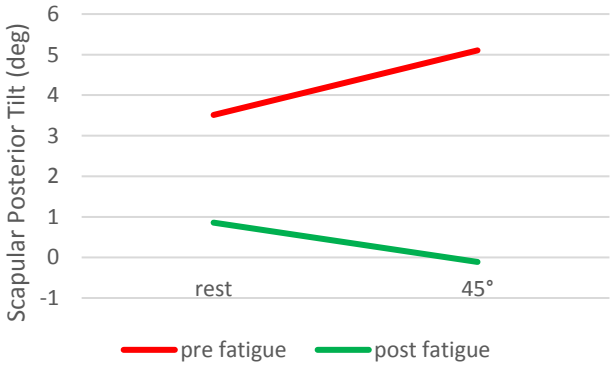

Figure 2: Scapular posterior tilt, positive values refer to posterior tilt.

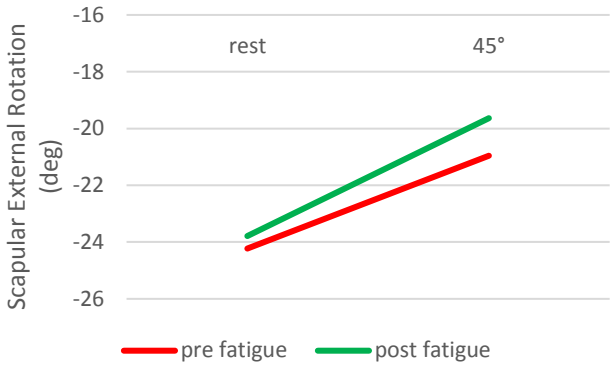

Figure 3: Scapular external rotation, positive values refer to external rotation.

CONCLUSIONS

The results of this investigation support the hypothesis that the reduce function of the low trapezius muscle results in decreased scapular posterior tilt and decreased AHD measurement during arm elevation. The reduced scapular posterior tilt during arm elevation observed after the fatigue protocol should result in the greater decrease in the AHD measurement during arm elevation following the fatigue protocol.

REFERENCES

1. Ebaugh, et al, *Scapulothoracic and glenohumeral kinematics following an external rotation fatigue protocol.* J Orthop Sports Phys.Ther., 2006. 36(8): p. 557-571.
2. Su, K.P et al., *Scapular rotation in swimmers with and without impingement syndrome: practice effects.* Med Sci.Sports Exerc., 2004. 36(7): p. 1117-1123.
3. Maenhout, A., et al., *Acromiohumeral Distance and 3-Dimensional Scapular Position Change After Overhead Muscle Fatigue.* J Athl Train, 2015. 50(3): p. 281-8.
4. Wu, G., et al., *ISB recommendation on definitions of joint coordinate systems of various joints for the reporting of human joint motion--Part II: shoulder, elbow, wrist and hand.* J Biomech., 2005. 38(5): p. 981-992.

THUMB KINETICS AND KINEMATICS IN OSTEOARTHRITIC AND HEALTHY PARTICIPANTS

[1,2] Amber R. Vocelle, [3] Gail A. Shafer, and [1] Tamara R. Bush
[1] Department of Mechanical Engineering, Michigan State University, East Lansing, MI, USA
[2] College of Osteopathic Medicine, [3] Mid-Michigan Center for Orthopedic Rehabilitation
email: cussenam@msu.edu, reditama@msu.edu

INTRODUCTION

The functionality of the thumb is determined by its ability to generate forces and motions. Thumb motion, in particular the motion that occurs at the carpometacarpal (CMC) joint, i.e., the base of the thumb, plays a critical role in one's ability to complete daily tasks [1]. Due to its saddle-like structure, motion at the CMC joint is difficult to measure, and gonoimeters, typically used to measure range of motion (ROM), have poor interrater reliability [2].

Thumb ROM and hand grip strength decline with age, and in nearly 50 % of adults over 65 years old, this functional loss is exacerbated by osteoarthritis in the CMC joint [3]. However, few studies have investigated the effects of aging and disease on thumb motions and forces. Indeed, little is known about the relationship between thumb forces and motions in a healthy population or disease state. The goal of this work was to quantify thumb motions and forces for three groups of participants.

METHODS

Thumb ROM, grip strength, and thumb force application was measured in five young healthy (ages 20-29, 3 male, 2 females, YH), five older healthy (ages 55-71, 2 males, 3 female, OH), and five osteoarthritic (ages 65-75, 2 males, 3 females, OA) participants. All individuals were right-handed and the thumb motions were tested in the right hand (Figure 1a-e). Motion data were collected with 15 reflective markers located on the hand and wrist (8 individual markers and 7 pods, Figure 1f).

Hand grip forces were measured using a Jamar dynamometer with handle distances set to 1 7/8" (grip #2) and 2 3/8" (grip #3). Thumb forces were measured using a custom build apparatus attached to a load cell (Figure 2). Forces were collected during thumb radial adduction, radial abduction, palmar abduction, and extension.

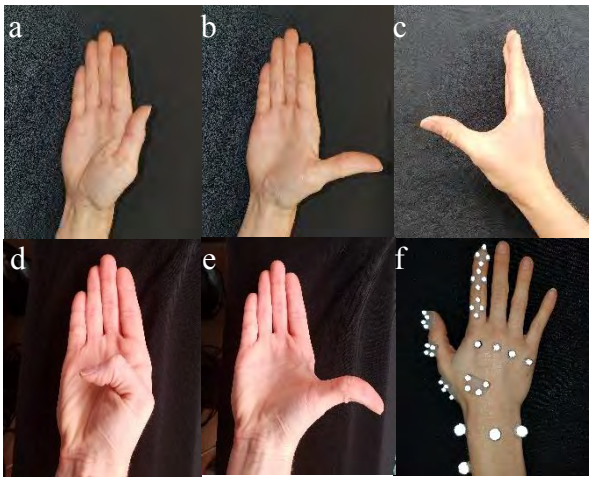

Figure 1. Thumb motion tested were a) adduction, b) radial abduction, c) palmar abduction, d) MP and IP flexion, and e) MP and IP flexion. f) Markers were placed on the hand and wrist.

RESULTS AND DISCUSSION

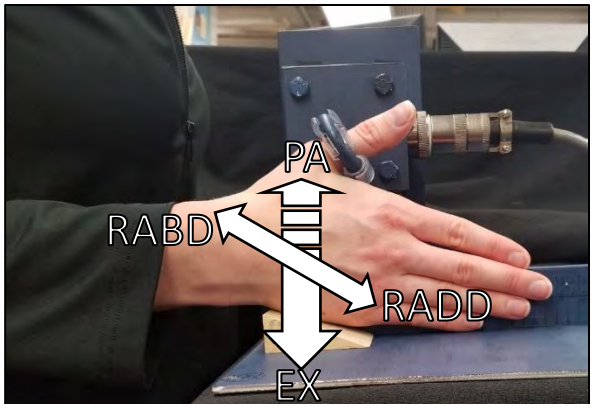

Figure 2. Load cell apparatus. The thumb can apply force to the ring attached to the load cell during thumb palmar abduction (PA), radial adduction (RADD), extension (EX), and radial abduction (RABD).

Each participant completed a series of thumb motions to determine ROM. During IP flexion-extension, the YH group had the largest ROM at 101°

(SD 9°), the OH group had 82.6° (18°), and the OA group had 92° (9°). During radial abduction-adduction, the OH group had the largest ROM at 58° (12°), the YH group had 55.3° (9°), and the OA group had 50 ° (12°). Interestingly, the OA group had a tendency to have a greater ROM during CMC palmar abduction-adduction, and MP flexion-extension than OH or YH groups.

OA participants had reduced radial abduction-adduction ROM, but did not exhibit reductions in palmar abduction-adduction or IP and MP flexion-extension ROM compared to the OH group. This suggests that OA may have an asymmetrical effect on CMC joint motion.

Hand grip strength and thumb forces are presented in Table 1. The YH group had a higher grip strength than OH and OA groups, and female OH participants had a higher grip strength than OA females.

Thumb force application was collected during thumb palmar abduction, radial adduction, extension, and radial abduction (Figure 2, Table 1). Forces were greatest during thumb radial adduction for most groups. Radial abduction forces were similar between OA and YH groups, and lowest in the OH group. In females, radial adduction force application was greatest in the YH group, but force application during radial abduction, palmar abduction, and extension were similar between YH and OA females. Extension forces were greatest in males in OA and OH groups.

The OA group had a lower grip strength than YH, and the female OA group had lower grip strength than OH, in line with trends found in known literature. One OA male had a larger grip strength than the other OA participants, so average grip strength in the OA male group was likely skewed because of this participant. However, the OA group exhibited similar or greater thumb forces during radial adduction and extension compared to the OH group, and females in these two groups had similar forces during radial adduction and palmar abduction. This suggests that there may not be an early, intrinsic loss of strength from the thumb itself during OA development.

Our pilot data demonstrated that use of motion capture and a load cell system can gather kinetic and kinematic data which can be used to quantify differences that occur during aging and osteoarthritis. A limitation to this work is the current sample size; our data collection is ongoing, and this abstract presents a sample of the work thus far.

REFERENCES

1. Arden N. *Best Pract. Res. Clin. Rheumatol* **20(1)**, 3-25, 2006.
2. Lewis E, et al. *Am J Occ Ther* **64**, 555-561, 2010.
3. Luker KR, et al. *Clin Orthop Relat Res* **472**, 1123-1129, 2014.

ACKNOWLEDGMENTS

Funding was provided by Blue Cross Blue Shield of Michigan and the Pearl J. Aldrich Endowment in Aging Related Research.

Table 1: Thumb force application during radial adduction (Radd), radial abduction (Rabd), palmar abduction (PA), and extension (EX) and hand grip strength (N). Values are recorded as average (standard deviation).

	Dynamometry (N)					
	Male YH	**Male OH**	**Male OA**	**Female YH**	**Female OH**	**Female OA**
Grip #2	430.0 (125.9)	360.3 (37.8)	400.3 (157.3)	318.0 (3.14)	274.3 (85.5)	227.6 (45.1)
Grip #3	495.2 (31.6)	373.7 (6.3)	404.8 (151.0)	291.4 (9.4)	277.3 (71.9)	241.7 (51.2)
	Thumb Force Application (N)					
	Male YH	**Male OH**	**Male OA**	**Female YH**	**Female OH**	**Female OA**
Radd	32.5 (9.5)	12.4 (2.8)	54.6 (2.3)	33.7 (15.0)	24.0 (5.7)	25.0(5.6)
Rabd	22.6 (3.0)	11.2 (4.6)	20.7 (10.5)	14.5 (6.4)	10.8 (3.9)	14.5 (7.5)
PA	18.6 (3.3)	22.7 (2.9)	29.7(1.4)	12.9 (1.5)	15.9 (7.1)	13.0 (3.9)
EX	19.2 (1.4)	24.3 (7.1)	24.9 (7.3)	18.2 (9.1)	18.7 (6.7)	20.9 (2.2)

HIP AND KNEE MOVEMENT PATTERNS PREDICT KINETIC RISK FACTORS ASSOCIATED WITH RUNNING RELATED INJURIES

Marwan Aljohani, Alec C. Miller, Hoon Kim, and Kristof Kipp

Marquette University, Milwaukee, WI, USA
email: Marwan.Aljohani@marquette.edu

INTRODUCTION

Tibial stress fractures and patellofemoral pain are among some of the most common running related injuries (RRI). Primary risk factors for overuse RRI include excessive impact kinetics, such as high rates of loading (ROL) and tibial impact shocks (TIS) [1, 2]. Research has therefore focused on identifying movement patterns associated with these risk factors [3].

A recent study investigated the association between sagittal plane hip / knee movement patterns and the peak impact force during running. No significant associations were found. The authors of that study used Continuous Relative Phase (CRP) to quantify movement patterns. CRP may, however, not be the best method to quantify the movement patterns. Vector coding may be more appropriate to investigate movement patterns, especially if the motions of interest are non-sinusoidal [4]. Not much is currently known about how movement patterns influence kinetic risk factors, such as ROL and TIS. This knowledge gap limits the ability of researchers and clinicians to screen for and/or target movement patterns that increase a person's risk of an RRI. The purpose of this study was to investigate the relationship between movement patterns and kinetic risk factors of RRI.

METHODS

Eleven healthy runners (4 males and 7 females) participated in this study (Table 1). All subjects were required to run >10 miles per week, have no pain while running, and have had no musculoskeletal or neuromuscular injury in the past 6 months.

A motion analysis system was used to collect three-dimensional kinematic data at 100 Hz. A pressure sensor instrumented treadmill and one triaxial accelerometer were used to collect vertical ground reaction force (VGRF) and tibial acceleration data, respectively. The treadmill data were collected at 100 Hz, the accelerometer data at 148 Hz. Thirty seconds of kinematic and kinetic data were collected as each subject ran at their long slow distance speed (LSD).

Table 1: Mean ± SD demographic data

Age (years)	21 ± 2
Mileage (miles)	35.6 ± 13.5
LSD Speed (mph)	6.8 ± 0.7
ROL (BW)	22.8 ± 5.2
TIS (g)	5.7 ± 1.7

A custom MATLAB program was used to process and filter raw kinematic and kinetic data. The same program was also used to define gait cycle events based on VGRF data. Initial contact and toe-off were defined as the points when the VGRF exceeded and fell below 10N, respectively. Dual-pass, 4th order low-pass Butterworth filters with cutoff frequencies of 13 Hz and 60 Hz were used to filter kinetic and acceleration data, respectively. The ROL was calculated as the peak VGRF derivative. Peak stance-phase TIS along the long-axis of the tibia was extracted from the filtered accelerometer data. Vicon Nexus was used to calculate relative joint angles. Coupling Angles (CA) were calculated with vector coding methods [4]. The CA of interest were the Hip sagittal/Knee Sagittal (HS/KS) and Hip frontal/Knee sagittal (HF/KS) combinations. Coordination patterns of each CA were divided into four different phase proportions to provide information about whether the proximal (Prox) or distal (Dist) joint was dominant, or whether the joints were moving in the same (In-Phase – InPhs) or opposite (Out-of-Phase – OutPhs) directions (Fig.1). Coordination patterns were expressed as a percentage of how much time each runner spent within each pattern during the gait

cycle [5]. Multi-linear regression models were used to investigate the ability of HF/KS and HS/KS movement patterns to predict TIS and ROL. All predictor variables were entered into the regressions models at the same time. It should be noted that the distal dominant movement patterns for HS/KS and HF/KS were excluded from all regression models because of excessive co-linearity (i.e., extremely low Tolerance).

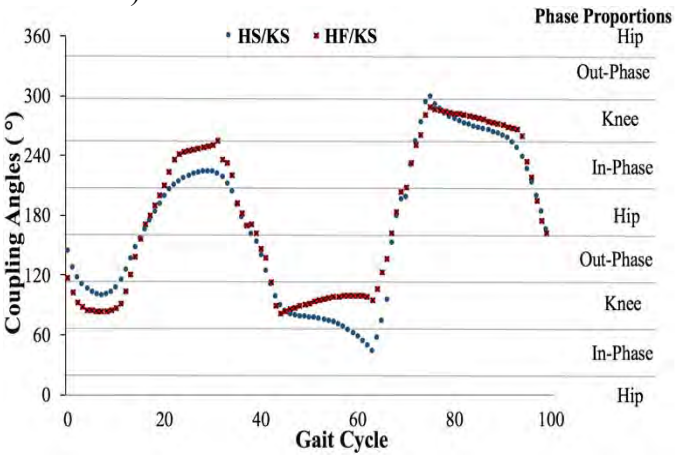

Figure 1: The averaged coupling angles and the four phase proportions of HS/KS and HF/KS.

RESULTS AND DISCUSSION

The average phase proportions are displayed in Table 2. Neither of the regression models for ROL were significant (Table 3). In contrast, both of the regression models for TIS were significant. Within each of these two models, significant individual predictors were the out-of-phase HF/KS movement pattern (p = 0.001) and the proximal HS/KS movement pattern (p = 0.027).

Table 2: Mean±SD phase proportions (%).

CA	Prox	Dist	InPhs	OutPhs
HS/KS	10 ± 1	47 ± 3	31 ± 1	12 ± 2
HF/KS	2 ± 1	77 ± 8	15 ± 6	6 ± 3

These results from the regression models suggest a relationship between hip and knee movement patterns and TIS during running. Specifically, runners with a higher proportion of proximal HS/KS movement pattern exhibited higher TIS. In addition, greater TIS were also observed in runners with greater out-of-phase HF/KS movement patterns. These finding are contrary to previous research where no significant relationships between impact kinetics and movement patterns of the lower extremities were found [3]. This discrepancy may be due to the methods that were used to quantify movement patterns (i.e., CRP vs. vector coding).

In conclusion, a more dominant sagittal plane hip / knee coupling, and out-of-phase frontal plane hip / sagittal plane knee coupling affect the magnitude of the impact shock experienced by the tibia during running. It might thus be important for researchers and clinicians to screen for these movement patterns as they are correlated with kinetic risk factors for RRI. However, future studies need to further investigate the association between these movement patterns and the incidence of RRI.

REFERENCES

1.Zadpoor AA, et al *Clin Biomech* **26**, 23-28. 2011.
2.Davis IS, et al. *Annual Meeting of the ASB. 2*010.
3.Wang L, et al. *Sports Biomech* 1-14. 2017.
4.Sparrow WA, et al. *J Motor Behav* **19**, 115-129. 1987.
5.Chang R, et al. *J Biomech* **41**, 3101-3105. 2008.

Table 3: Multi-linear regression models for kinetic risk factors with movement patterns as predictors.

Outcome	Predictors	R^2_{adj}	p-value
ROL =	-0.353·Prox_HF/KS + 0.043·InPhs_HF/KS + 0.583·OutPhs_HF/KS	0.04	0.398
ROL =	0.358·Prox_HS/KS - 0.347·InPhs_HS/KS - 0.721·OutPhs_HS/KS	0.23	0.202
TIS =	0.249·Prox_HF/KS - 0.25·InPhs_HF/KS + **0.88·OutPhs_HF/KS***	0.77	**0.003**
TIS =	**0.784·Prox_HS/KS*** + .041·InPhs_HS/KS + .059·OutPhs_HS/KS	0.53	**0.042**

* significant predictor variables where $p < 0.05$

Adnan Apti. (1), Nazif Ekin Akalan (1), Shavkat Kuchimov (2), Yener Temelli (3), Önder İsmet Kılıçoğlu (3), Aslıhan Kurt (4) Freeman Miller (5)

(1) Istanbul Kültür University, Faculty of Health Science, Physiotherapy and Rehabilitation Division, Istanbul, Turkey
(2) Bogazici University, Institute of Biomedical Engineering, Istanbul, Turkey
(3) Istanbul University, Istanbul Faculty of Medicine, Department of Orthopedics and Traumatology, Istanbul, Turkey
(4) Biruni University, Faculty of Health Science, Physiotherapy and Rehabilitation Division, Istanbul, Turkey
(5) Department of Orthopedics, Nemours/Alfred I. duPont Hospital for Children, Wilmington, Delaware, USA

Determination of biomechanical influences of increased femoral anteversion (twisted leg) on running for developing individual.

Introduction

Increased femoral anteversion is the forwardly rotated femoral head relative to transcondylar axis of the knee (1). Femoral anteversion angle, which is high in newborn, decreases by ages and reaches normal values by bone growth completes (2). Our previous work, demonstrated that increased femoral anteversion (IFA) not only augments internal hip rotation and foot progression but also reduces the peak knee extension and total knee range in sagittal plane for neurologically intact participators during gait (3). Moreover, children with IFA have some postural asymmetries such as lateral head, shoulder, scapular, knee malleoli-level and pelvic asymmetries. Although, there are reports IFA related gait and postural deviations in literature, there is no study investigating the IFA effect on sport activities such as running. The aim of this project was to investigate the biomechanical effects of IFA on neurologically intact children during running. The additional aim was to investigate if IFA has potential of contribute the anterior knee pain (AKP) in older ages of the individuals.

Methodology

In this study four typically developed children (TDC) (mean-age: 8.25±1.71, Weight: 26.70±5.96kg, Height: 129.25±7.27cm) with no IFA and six TDC with IFA (mean-age: 8.50±3.78, Weight: 30.30±11.67kg, Height: 134.67±17.4cm) were participated in this study. Femoral anteversion (FA) angle was examined by measuring internal and external rotation angle of each child on lying prone position (4, 5). For all children with IFA internal rotation angle were ≥70° and external rotation was ≤20° and for TDC group, hip internal rotation was ≤50°. Kinematic parameters during running were assessed by 3D motion capture system (ELITE2002; BTS, Milan, Italy) at a self-selected speed in Istanbul University, Orthopedics and Traumatology Department, Gait Analysis Laboratory. In order to understand the potential contribution of IFA on AKP, peak hip adduction, peak knee valgus, peak hip internal rotation angle and peak knee valgus moment in stance were investigated. Normality test (Shapiro–Wilk test) and student-t test were used for statistical analysis ($p<0.05$).

Results

Physical examinations showed that mean hip internal rotation 74.92±6.16° and 47.88±6.38°, mean hip external rotation 11.75±8.93° and 32±11.8° were found for IFA and TDC group respectively. The running velocities of both groups were found insignificant (2.42±0.29 m/sec for the IFA group and 2.18±0.14 m/sec for the TDC group p=0.16). During running, no difference was found between peak hip adduction angle (p=0.49), peak knee valgus angle (p=0.20 peak knee valgus moment (p=0.30) and peak pelvic obliquity (p=0.84) during the stance. Peak hip internal rotation angle (p=0.02), peak pelvic rotation (p=0.03) and peak knee varus angle (p=0.01) were significantly higher in IFA group than TDC group (Fig 1a-b-c).

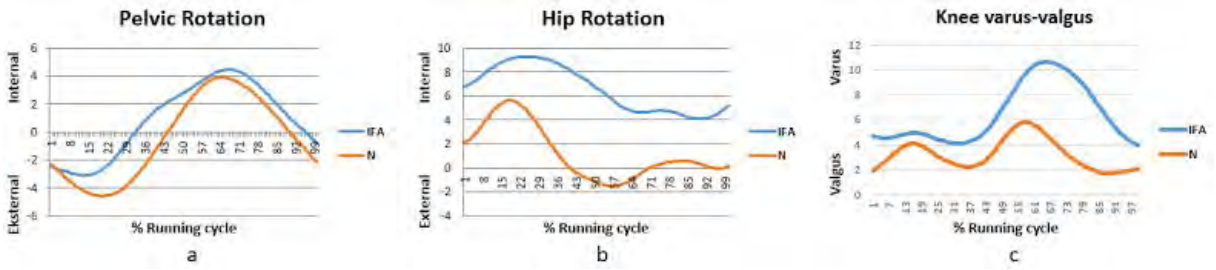

Figure-1: Running kinematics of normal (orange) and IFA (blue) group (a) pelvic rotation, (b) hip rotation, (c) knee varus-valgus.

Discussion

IFA alters the walking as well as running biomechanics(3). Previous reported studies show that stance phase hip adduction, hip internal rotation and knee varus angles were higher in adults with AKP at running (6,7,8). In this study, we underwent investigation on children to get biomechanical alteration during running. It is found that hip internal rotation and knee varus angles at stance phase were increased in IFA group then the control group. Those findings in IFA can be one of the predisposing factor for AKP and consequently knee osteoarthritis in future. There is no reports about changes those kinematics at later ages. Altered hip and knee biomechanics, IFA can facilitate overuse sport injuries that leads to reduce sport performance. Further researches are needed to investigate the effects of IFA on sport performance and the relation with overuse sports injuries. The present study is the first in literature which defines the biomechanical alteration of IFA during running.

References

1. Akalan NE, et al. Turk J Phys Med Rehabil 2009;55(4):135–40.
2. Horstman, et al. 2007
3. Akalan NE, et al. Gait & Posture 2017;57(1):1-367.
4. Ruwe PA, et al. J Bone Joint Surg Am 1992;74(6):820–30
5. Akalan NE, et al. J Hip Int 2013;23(5):492-499.
6. Ferber R, et al. Clin Biomech 2003;18(4):350-357.
7. Noehren B, et al. Clin Biomech 2012;27(4):366-371.
8. Willy RW, et al. Med Sci Sport Exerc. 2012;44(11):2165-2171.

EFFECT OF OBESITY ON TRUNK MUSCLE ACTIVITY DURING ONE-HANDED CARRYING

Mohamed Badawy, Mark C. Schall Jr., Jordan Coker, Richard F. Sesek, Gerard A. Davis, Michael E. Zabala, and Sean Gallagher

[1] Auburn University, Auburn, AL, USA
Email: msb0058@auburn.edu

INTRODUCTION

The percentage of obese adults in the American population has been increasing since the late 1980s [1], and is expected to keep increasing for the next several years [2]. One-handed carrying has been observed to result in increasing muscle activity of the lumbar paraspinal muscles on the contralateral side of the body [3]. It has also been associated with an increase in spinal compression and shear forces, compared with evenly distributing the load between both hands [4, 5]. However, the effect of one-handed carrying on trunk muscle activity among obese populations remains unclear. Accordingly, the objective of this study was to examine the differences in trunk muscle activity among obese individuals while carrying different loads in one-hand.

METHODS

Ten (10) right-hand dominant young adult males (mean age = 27.2 ± 3.82) were recruited and divided into two groups: obese (body mass index [BMI] ≥ 30 kg/m^2) and non-obese (BMI < 25 kg/m^2) following procedures approved by the Auburn University Institutional Review Board. Six paired surface electrodes were place on 6 trunk muscles (3 on each body side): right and left external oblique (REO and LEO), upper erector spinae (RUES and LUES), and lower erector spinae (RLES, and LLES) [5, 6].

Participants were asked to perform three replicates of three walking trials (total of 9). Trials were randomized and included walking while carrying different loads in the right hand (0 kg [none], 5.7 kg [12.5 lb., light], and 10.2 kg [22.5 lb., heavy]) for a distance of approximately 5 meters [4, 5]. Raw electromyography signals were sampled at 1,000 Hz. The root mean squares (RMS) of the walking data of each muscle were calculated using a 100-sample moving window with a 50-sample overlap [7], and normalized as percentages of maximum voluntary contractions (%MVC). MVC was obtained by considering the maximum muscle activity achieved during 11 different exercises [6]. The average %MVC during the stance phase of the left limb, contralateral to the loaded side, for two representative steady-state steps was calculated. Resulting values for each of the three trials of the different carrying conditions were averaged.

Shapiro-Wilk and Kolmogorov-Smirnov tests for normality suggested that the data were normally distributed. Also, the data had sufficiently equal variances according to Levene's test. Analysis of variance (ANOVA) following a split-plot factorial design was used to test for significance of the main and interaction effects of independent variables (obesity and load magnitude). Tukey honest significant difference (HSD) post-hoc tests were implemented to compare each pair of means of significant dependent variables.

RESULTS AND DISCUSSION

Carrying a load resulted in greater %MVC estimates on the contralateral side of the carried load for the oblique and lower erector spinae muscles and corresponding lower %MVC measurements on the ipsilateral side when compared to walking with no load (Fig. 1 and 2). However, %MVC for both LUES and RUES was greater when a load was carried (Fig. 3). In addition, %MVC on the contralateral side for both the light and heavy load conditions were larger for the non-obese group. The difference in %MVC between the two groups increased with increasing load magnitude. The largest difference in %MVC between the no-load and heavy-load conditions was 11.1% for the none-obese group (for LEO) and 5.5% for the obese group (for LLES), respectively.

A statistically significant main effect of load magnitude on %MVC for all 6 muscles was observed (p<0.01 for each). However, obesity had no statistically significant effect on any of them. The interaction effect of load magnitude and obesity had a statistically significant effect only on %MVC of the LEO (p<0.01). Results of the post-hoc Tukey HSD tests for the main effect of load magnitude on %MVC are presented in Fig.1-3.

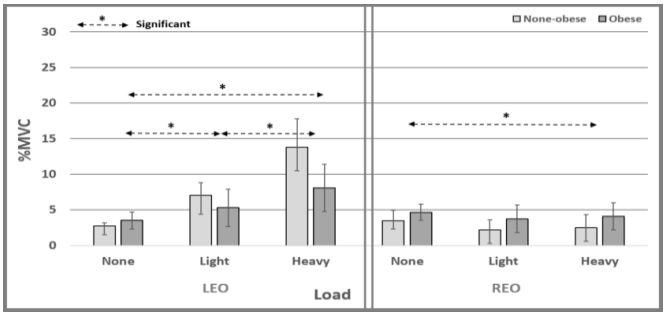

Figure 1: %MVC for LEO and REO.

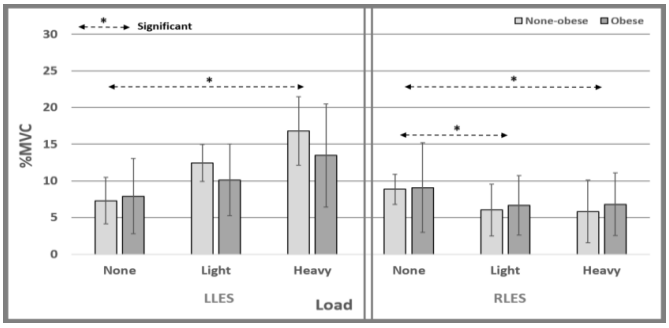

Figure 2: %MVC for LLES and RLES.

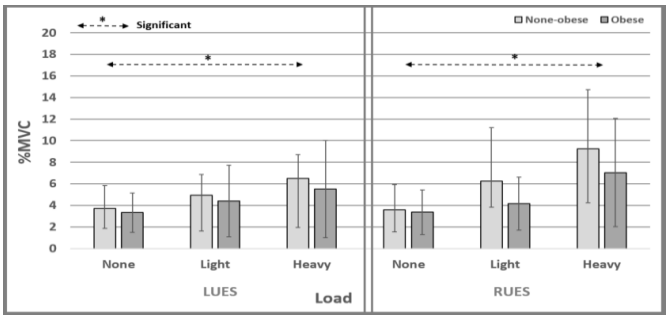

Figure 3: %MVC for LUES and RUES.

The increase in %MVC of the LEO and LLES may be because the muscles on the left side exert more force to counteract the load at the right side, whereas the %MVC of LUES and RUES did not follow this pattern. One possible explanation is that increased upper back muscle force may be necessary to keep the trunk upright while walking.

Two potential explanations for the small differences in %MVC in the obese group among load conditions are that obese people are already adapted to carry more body weight during normal walking, and they carried smaller percentage of body weight than the non-obese group did. Accordingly, results indicate that carrying a load of approximately 10 kg could be acceptable for obese individuals to carry in one hand. However, more research is needed to examine the impact of such load on spinal moments and forces, since one-handed carrying is not a preferred method for load carrying from a biomechanical perspective.

REFERENCES

1. Rosenthal, Morton, Brethauer, Mattar, De Maria, Benz, Titus, and Sterrett. *Surgery for Obesity and Related Diseases*, 13, 2017, 1643-51.
2. Finkelstein, Khavjou, Thompson, Trogdon, Pan, Sherry, and Dietz. *American Journal of Preventive Medicine*, 42 (6), 2012, 563-70.
3. Cook and Neumann. *Ergonomics*, 30 (10), 1987, 1413-23.
4. McGill, Marshall, and Andersen. *Ergonomics*, 56 (2), 2013, 293-302.
5. Rohlmann, Zander, Graichen, Schmidt, Bergmann. *Ergonomics*, 57 (2), 2014, 262-70.
6. McGill. *Journal of Orthopaedic Research*, 9 (1), 1991, 91-103.
7. Douphrate, de Porras, Nonnenmann, Hagevoort, Reynolds, Rodriguez, and Fethke. *Applied Ergonomics*, 58, 2017, 482-90.

ACKNOWLEDGEMENTS

The study was partially supported by the Deep South Center for Occupational Health and Safety, a National Institute for Occupational Safety and Health (NIOSH) Education and Research Center (Grant 2 T42 OH008436). The contents are solely the responsibility of the authors and do not necessarily represent the official views of the Deep South Center or NIOSH.

STEP WIDTH CHANGES WITH INCREASED BIMANUAL LOAD REGARDLESS OF SEX

[1] Sidney Baudendistel, [2]Adam Rosen, [3]Terry L. Grindstaff, and [2]Jennifer M. Yentes

[1] University of Florida, Gainesville FL, USA
[2] University of Nebraska at Omaha, Omaha, NE, USA
[3] Creighton University, Omaha, NE, USA
Email: sbaudendistel@ufl.edu

INTRODUCTION

The ability to perform activities of daily living such as bimanual carrying (e.g. handling groceries) is an important indicator of health in all individuals. However, load carrying has primarily focused on packs for military purposes with less emphasis on a general population [1]. Additional weight to the body causes compensation for the load including changes in kinematics and kinetics [1,2,3]. Specifically, with packs, decreased stride length has been seen with increased load and for females these decreases were exaggerated [2]. Bimanual carrying, which may be more common in activities of daily living, is less efficient than packs and therefore changes in walking may be more evident.

The purpose of this study was to explore the effect of bimanual loads on treadmill walking in healthy, young participants. The effect between sex was also explored. Healthy, young participants were hypothesized to show decreased stride length and stride time, and increased step width between each of the 3 conditions: no added weight (baseline), 5%, and 10% body weight. Females were hypothesized to be impacted more from the load than males.

METHODS

Fourteen healthy, young participants (Table 1) completed the experimental procedures. Participants were excluded if they had any major surgeries or injuries within the last year or current pain that affected their walking and/or ability to carry loads.

Table 1: Participant demographics [mean (standard deviation)].

N	Age (yrs)	Sex	Mass (kg)	Ht (m)
14	23.21(2.46)	M=8	73.09(8.12)	1.76(0.08)

Seated heart rate, using a heart rate monitor, and rate of perceived exertion (RPE), according to Borg scale, were measured for one minute. Then, participants walked on a treadmill for five minutes with no weight followed by walking for five minutes in two weighted conditions which were performed in random order. Trials were completed at a self-selected speed (average speed: 1.23±0.15 m/s) while 3D marker trajectories were recorded (120 Hz). Loads of 5% body weight and 10% body weight were split equally across both arms using wrist weights (2.5% and 5% per arm) (Figure 1). Participants completed a mandatory five minute rest between trials and proceeded to the next walking condition after heart rate and RPE returned to seated levels to minimize fatigue.

Figure 1: Attachment of weights to subject's arms.

Spatiotemporal measures were calculated using three-dimensional marker positions and included stride time, stride length, and step width. Mean, standard deviation (SD), and coefficient of variation (CoV) were calculated for time, length, and width. Sample entropy (m = 2, r = 0.2*SD, n = 442) was used to determine the regularity of stride length and width [4].

Mixed between-within subjects ANOVAs were performed to determine differences among the conditions of no weight, 5%, and 10% loads and to explore the sex × load interaction using SPSS (20, IBM, Armonk, NY).

RESULTS AND DISCUSSION

In contrast with our hypothesis, no significant differences existed between conditions for stride time (mean, SD, and CoV) and stride length (mean, SD, CoV, sample entropy). Further, our hypothesis was not supported as differences found for step width were opposite of what was hypothesized. Step width mean decreased and CoV increased significantly as load increased across all conditions, with large effect sizes ($p<0.001$, $\eta^2>0.50$) (Figures 2 & 3). Step width SD and sample entropy did not demonstrate significant differences.

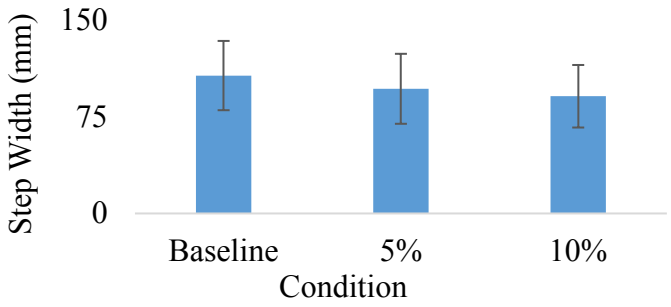

Figure 2: Step width significantly decreased between all conditions ($p<0.001$, $\eta^2=0.64$).

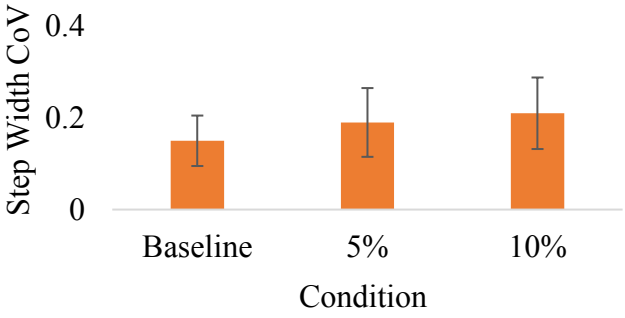

Figure 3: Step width CoV significantly increased between all conditions ($p<0.001$, $\eta^2=0.56$).

In addition, the sex × load interaction was not significant across any of the 11 gait parameters. Sample entropy step width was the largest interaction effect size ($\eta^2=0.15$), although not significant. The majority of effect sizes were below 0.02, indicating an effect well below small for any other interaction.

Overall, it appears that the hypotheses were not supported as stride length and time did not differ and the step width results were opposite of what was expected, regardless of sex.

Changes in step width are often related to increased risk in falling. Young adults displayed a narrower and less consistent step width, a pattern similar to older adults and fallers [5]. This may be due to a change in active control. Step width has been shown to require active control in forward walking, whereas step length does not [6]. In addition, the load grants additional momentum in the forward direction which may aid in the passive nature of forward walking needed in the anterior-posterior direction. Stride length and time are directly related on a treadmill, and young adults may alter time or distance to compensate in concurrent strides. However, the medial lateral direction of walking, step width, was significantly narrower as load increased. These differences were not altered by sex, but large effect sizes of load, regardless of sex, may warrant studies in additional populations. Between baseline and loaded conditions, healthy, young adults may have chosen a different strategy to maneuver the load, but this new strategy may be dangerous if adopted in older adults or pathologic populations.

CONCLUSIONS

Little to no research has been done on bimanual load carriage, despite being performed in everyday life. Healthy, young adults change their mediolateral stepping patterns as load increases, regardless of sex. This research should act as a call for additional studies in older populations to determine how walking may change with the addition of a bimanual load.

REFERENCES

1. Birrell and Haslam. *Ergonomics*. 52(10): 2009.
2. Martin and Nelson. *Ergonomics*. 29(10): 1986.
3. Krupenevich et al. *Mil Med.* 180(9): 2015
4. Yentes et al. Ann Biomed Eng. 41(2): 2013.
5. Maki, B. *J Am Geriatr Soc*. 45(3): 1997.
6. Bauby and Kuo. *J Biomech.* 33(11): 2000.

ACKNOWLEDGEMENTS

Funding for this work was supported by the University of Nebraska at Omaha Graduate Research and Creative Activity Fund, NASA Nebraska Space Grant Fellowship, and the NIH/NIGMS (P20 GM109090).

MUSCLE-TENDON UNIT PARAMETERS AFFECT SIMULATION RESULTS DURING WALKING

Josh R. Baxter and Michael W. Hast
University of Pennsylvania, Philadelphia, USA
email: josh.baxter@uphs.upenn.edu, web: www.med.upenn.edu/motionlab/

INTRODUCTION

Plantarflexor function is critical to locomotor performance in athletic, pathologic, and aging populations. Longer muscle fascicles allow for greater joint power, explaining performance differences between good and great sprinters. Tendon stiffness, a function of both its slack (resting) length and material properties, dictates the shortening demands of the plantarflexor muscles and impacts movement efficiency. While these musculoskeletal parameters have been studied in great detail, the multi-factorial implications of muscle-tendon properties on the efficiency of human walking are less explored.

The purpose of this study was to characterize the complex interactions between muscle and tendon parameters on muscle function during gait. Specifically, we tested the effects of plantarflexor fascicle length, Achilles tendon slack length, and Achilles tendon stiffness on the energetics of walking. These three parameters were selected because they have been documented to change in response to both training and injury. We hypothesized that (1) plantarflexor metabolic demands would be sensitive to each muscle tendon unit (MTU) parameter and (2) reduced muscle shortening during the second half of stance would explain reduced metabolic demands.

METHODS

Human walking was simulated using open-source musculoskeletal modeling software and publically available gait data [1]. Joints were constrained to move in the sagittal plane (gait10dof18musc) and the ankle was actuated by one dorsiflexor (tibialis anterior) and two plantarflexors (gastrocnemius and soleus). Muscle and tendon dynamics were simulated by implementing a computed muscle control (CMC) algorithm.

Simulations were performed over a range of optimal plantarflexor muscle-fiber lengths (0.8 – 1.2 length), Achilles tendon slack lengths (0.9 – 1.1 lengths), and Achilles tendon stiffness values (0.03 – 0.12 strain at isometric muscle force), which resulted in 250 simulations. Metabolic demands [2] and shortening dynamics of the plantarflexors were evaluated during each simulation to quantify the effects of varying muscle-fiber lengths, tendon slack lengths, and tendon stiffness. Multivariate linear regression defined the effect sizes of the three MTU parameters on plantarflexor metabolic demands during gait. Metabolic measurements were normalized to the calculated demands using the default model parameters.

RESULTS AND DISCUSSION

Plantarflexor metabolic demands were minimized when the muscle fascicles were their shortest (80% of default), the tendons were at its default slack length, and the tendons were stiffest (isometric muscle force at 3% strain). Tendon slack length had a strong effect on dorsiflexor metabolic demands during stance phase. This demand was so great that a 10% decrease in the plantarflexor tendon slack lengths resulted in simulations that could not run to completion – unless plantarflexor fascicles were increased in length by 20% - while a 5% decrease in plantarflexor tendon slack lengths increased the dorsiflexor metabolic demand 5-10 fold. Simulations that required more than 150% of the default dorsiflexor metabolic demands were excluded from all analysis.

Table 1. Effect of 1% change of MTU parameters on PF metabolics

	Δ PF metabolics
Fascicle length	1.9%
Tendon slack length	6.7%
Tendon compliance	0.2%

Plantarflexor metabolic demands were more sensitive to fascicle length and tendon slack length than tendon compliance (**Table 1**). Fascicle and tendon slack lengths had effect sizes there were 29 and 8 fold greater than tendon compliance on plantarflexor metabolics, respectively. Despite its small effect size on metabolic demands, tendon compliance demonstrated a parabolic effect on metabolics (**Fig. 1**). Conversely, tendon slack length and fascicle length both imposed additional metabolic demands with increased length (**Fig. 1**). These effects appear to have been caused by increased muscle shortening demands that were required to take the slack out of the muscle tendon units.

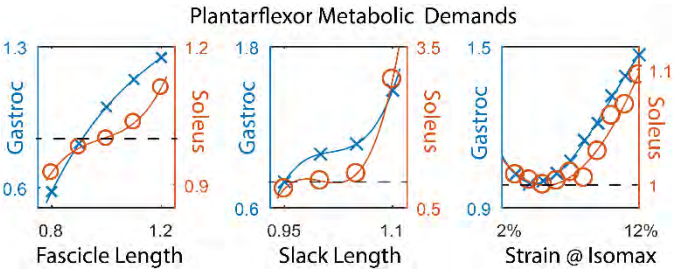

Figure 1. Small changes in MTU parameters had strong effects on the metabolic demands of both plantarflexor muscles (Gastroc-blue crosses, soleus-orange circles). Metabolic demands (Y-axis) normalized to the muscle metabolics calculated using default MTU parameters (dashed line).

Muscle activation was most sensitive to changes in MTU parameters during late stance (**Fig. 2**). Longer muscle fascicles and tendon slack lengths required greater muscle shortening in order to maintain the necessary tendon tension. Stiffer tendons reduced fascicle shortening during the second half of stance, suggesting that strain energy can be more efficiently stored.

Based on these simulation results, walking is most metabolically efficient when the plantarflexor muscles are short and the Achilles tendon is stiff. These findings agree partially with previous simulations [3], which found shorter fascicles in series with a more compliant Achilles tendon improves efficiency. Our model included an antagonistic-dorsiflexor muscle and satisfied the system dynamics using a CMC algorithm which may explain this disagreement between studies.

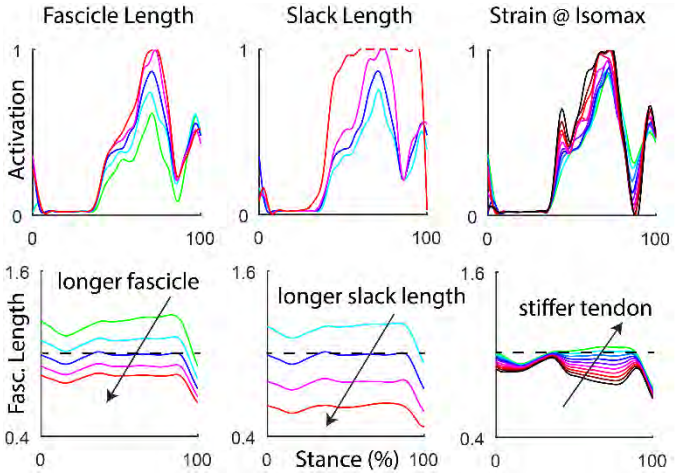

Figure 2. Gastrocnemius activation (top row) and normalized fascicle length (bottom row) throughout the stance phase was affected by optimal fascicle length (left), tendon slack length (middle), and tendon stiffness (right). Optimal fiber lengths (dashed line).

CONCLUSIONS

These findings highlight the importance of the parameters selected for the muscle tendon units in computational models. Small changes in muscle fascicle and tendon slack lengths have profound implications on simulation results (**Table 1**). Care should also be taken when considering how simulation results may explain plantarflexor pathology. Our group has identified muscle remodeling in response to tendon injuries as a potential mechanism to maintain tendon tension. Thus, we recommend that musculoskeletal models be tuned to maintain physiologic amounts of tendon tension under 'passive' conditions.

REFERENCES

1. Delp *et al. IEEE Trans. Biomed. Eng.*, vol. 54, no. 11, pp. 1940–1950, Nov. 2007.
2. Umberger, *et al. Comput. Methods Biomech. Biomed. Engin.*, vol. 6, no. 2, pp. 99–111, May 2003.
3. Lichtwark and Wilson. *J. Theor. Biol.*, vol. 252, no. 4, pp. 662–673, 2008.

FEMALES ARE MORE MECHANICALLY EFFICIENT THAN MALES DURING RUNNING

[1] Hunter J. Bennett and [2] Kevin A. Valenzuela

[1] Old Dominion University, Norfolk, VA, USA
[2] California State Polytechnic University, Pomona, CA, USA
email: hjbennet@odu.edu, web: https://sites.google.com/odu.edu/oduneuromechanicslab

INTRODUCTION

Males and females differ in running styles (e.g. stride lengths, cadences, etc.), which may be a result of anthropometric differences. In general, males and females differ in body mass and height. Males and females also differ in joint level kinematics [1], joint moments [2], and joint work [2].While it appears males and females utilize different movement strategies to perform running, the impact of their respective strategies on effort (work) to perform running tasks remains unknown.

Mechanical work can detail the total mechanical effort required to perform a task. Total work is the sum of the external and internal works performed during a task, such as walking and running [3,4]. External work is the muscular effort to raise and accelerate the center of mass, while internal work is the muscular effort to move the limbs in relation to the center of mass [3,4]. Mechanical work has been described from walking to sprinting [4], and compared between healthy and clinical populations [5,6]. However, mechanical work has not been previously compared between the sexes.

Therefore, the purpose of this study was to examine the differences between males and females in work during running at self-selected speeds. It was hypothesized males and females would have similar normalized work efforts.

METHODS

Fourteen healthy young adults (7 males and 7 females) were recruited for this study. Participant exclusion criteria included: any major lower extremity musculoskeletal injuries in the last six months, any prior lower extremity surgery or replacement, or any diagnosed joint disease. All participants signed approved consent forms.

Three-dimensional motion capture (200 Hz, Vicon) and ground reaction force data (2000 Hz, Bertec) were recorded while participants performed level ground running at self-selected speeds. Participants wore standard laboratory shoes and tight fitting clothing. Prior to data collection, participants performed a 5-minute warmup on a treadmill and several practice trials. Self-selected speeds were monitored and recorded during practice trials. Participants then performed 5 successful trials of running at ±5% average self-selected speeds.

Kinematics and GRFs were imported to Visual3d (C-Motion, Inc.) and filtered using 4th order Butterworth low pass filters at 15Hz. An 8-segment model was created from the kinematic data, which included: trunk, pelvis, and bilateral feet, shanks, and thighs. Total work was determined as the sum of external and internal works during 1 stride, and averaged for each subject [3,4]. External work was the integral of the center of mass's (COM) kinetic and potential energies, derived from GRF data (∑F=ma). External work was calculated using the equation [3,4]:

$$External\ Work = \int_1^n \left[\frac{1}{2} m v_{com}^2 + m g h_{com}\right]$$

where n: number of frames, m: total body mass, g: gravity, and v and h are the COM velocity and height. Internal work was the integral of segmental energies, calculated using the equation [3,4]:

$$Internal\ Work = \int_j^8 \left[\sum_i^n \left(\frac{1}{2} m v_{ij}^2 + \frac{1}{2} I \omega_{ij}^2 + m g h_{ij}\right)\right]$$

where i: frame, j: individual segment (e.g. foot), and I*ω: the segment's moment of inertia and angular velocity.

Mass, height, stride length, speed, and work (J/kg and J/kg*stride length) were compared between males and females using t-tests ($p<0.05$). Correlations were performed to determine the strength of relationships between anthropometric,

spatiotemporal, and work per unit mass for both sexes combined.

RESULTS AND DISCUSSION

Males were larger (mass: 81.6±15.2 vs. 66.5±5.0 kg, p=0.03; height: 1.77±0.07 vs. 1.65±0.06 m, p=0.01) and took longer stride lengths (2.44±0.21 vs. 2.04±0.21 m; p<0.01) than females. However, both sexes chose similar self-selected running speeds (2.94±0.39 vs. 2.82±0.21 m/s, p=0.47). Additionally, vertical excursion was similar between sexes (both 0.10±0.01 m, p=0.91).

Surprisingly, total work per unit mass was greater in males by 20% (Table 1, Fig 1.). External work per unit mass was also ~20% greater in males. As external work is derived from mass and accelerations of the center of mass/body (from GRFs), differences between sexes in work would seemingly be negated by normalizing to mass when running at similar speeds. However, as speeds did not differ, it appears running style may play a significant role in determining mechanical work during running.

Work per mass*meter was similar to those reported in the previous literature [3,4], but were not different between sexes (Table 1). A lack of differences found in work per mass*meter is likely due to the males' longer stride lengths (larger by 16%). Indeed, correlations show work per unit mass was strongly related to stride length overall (r=0.89). No other variables were strongly related to work (all r<0.40).

Although running speeds were similar between males and females, running style differences likely influenced total mechanical work. Males took longer stride lengths, requiring more effort to move their larger mass per stride. Therefore, it appears longer stride lengths decreased the males' efficiency during running. Extrapolated for 1 km at this speed, the males would take 413 strides and total 2379 J/kg, while the females would take 494 strides and total 2274 J/kg; thus, less work per unit mass for females.

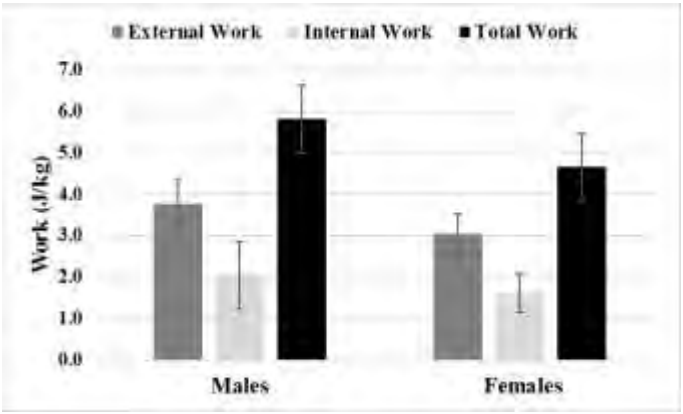

Figure 1. Average work per unit mass for males and females.

CONCLUSIONS

Despite males' longer stride lengths and size, females require less work per unit mass during running at self-selected speeds. Increases in males' work per unit mass are likely due to greater stride lengths. Therefore, energetic costs (per mass) during running are more affected by running style than mass. When increased mass is present, it may be beneficial to reduce stride length and increase stride rate in order to optimize energetic efficiency.

REFERENCES

1. Willson, J.D. et al. *Clin Biomech* 27(10), 2012.
2. Ferber, R.I. et al. *Clin Biomech*. 18(4), 2003.
3. Cavagna, G & Kaneko, A. *J Appl Phys* 268, 1977.
4. Willems, P.A. et al. *J Exp Biol* 198, 1995.
5. Mahaudens, P. et al. *Eur Spin J* 18, 2009.
6. Detrembleur, C. et al. *Gait Posture* 21(3), 2005.

Table 1. Differences in Work between males and females: mean±std.

	MALES	FEMALES	p-value	Effect Size
External Work ($J*kg^{-1}$)	3.77±0.60	3.04±0.50	**0.03**	**1.33**
Internal Work ($J*kg^{-1}$)	2.04±0.82	1.62±0.47	0.26	0.63
Total Work ($J*kg^{-1}$)	5.81±0.82	4.66±0.81	**0.02**	**1.41**
Total Work ($J*kg^{-1}m^{-1}$)	2.38±0.21	2.27±0.25	0.41	0.46

KNEE LOADS DURING RUNNING AT COMMONLY PRESCRIBED RUNNING PACES: A CASE STUDY

[1]Richard A. Brindle, [1]James M. Smoliga, [1]Kevin R. Ford
[1]High Point University, High Point, NC
Email: rbrindle@highpoint.edu

INTRODUCTION

Overuse injuries are common in competitive distance runners. In prospective studies of high school and collegiate cross country teams, approximately 29% to 74% of runners experienced an overuse injury each year [1, 2]. Overuse injuries may occur at any time during the season, however most have been reported at the beginning of the season [2]. The beginning of the season typically marks a change from low intensity running during base training to a mix of low, moderate, and high intensity running. This increase in running intensity may influence peak loading at the knee joint, which could lead to injury. The purpose of this study was to determine the peak total tibiofemoral contact force during commonly prescribed low, moderate, and high intensity running paces. We hypothesized that the change in peak total tibiofemoral contact force would be greater between low to moderate intensity running than moderate to high intensity running.

METHODS

An uninjured male runner participated in this study (19yr, 1.72m, 63.3kg, 56km per week). Before participating in the study, the runner gave written informed consent. A sixteen camera motion capture system recorded marker position at 200 Hz, while a force plate instrumented treadmill recorded ground reaction forces at 1200 Hz. For running trials, the participant wore laboratory footwear and reflective markers were placed on the trunk and lower extremity. Self-selected running velocity was determined using published protocol [3]. The runner's self-selected running velocity was operationally defined as the 'easy pace'. Based on the easy pace and Daniel's pace formulae [4], running velocity was determined for recovery, threshold, interval, and repetition paces which are commonly prescribed in individualized training programs. Two minutes of rest was allotted in between determining self-selected running velocity and data collection. For data collection, the participant ran continuously on the treadmill while treadmill speed was adjusted for each pace, from slowest to fastest, at one minute intervals. Additionally, one minute of recovery pace was included between paces. Five steps in the middle of each one minute interval were recorded. Right limb data were processed with three-dimensional gait analysis software using the joint coordinate system and inverse dynamics. Sagittal plane ankle, knee, and hip moment, knee and shank angle, and knee joint reaction forces were used to calculate gastrocnemius, quadriceps, and hamstrings muscle forces, and peak total tibiofemoral contact force [5]. The magnitude of change in tibiofemoral contact force between paces was determined using Cohen's d effect size. Percent differences in peak total tibiofemoral contact force between paces were considered important if greater than reported within-session minimal detectable change [6].

RESULTS AND DISCUSSION

Peak total tibiofemoral contact force increased more than the within-session minimal detectable change between easy, threshold, interval, and repetition paces. From easy to threshold pace, treadmill speed increased by 19.2% and peak total tibiofemoral contact force increased 10.6% which was a large effect size (ES = 6.1). From threshold to interval pace treadmill speed increased 8.2% and peak total tibiofemoral contact force increased 6.1% which was a large effect size (ES = 3.2). Between interval and repetition pace, treadmill speed increased 7.8% and peak total tibiofemoral contact force increased 2.5%, which was a large effect size (ES = 1.0). Peak total tibiofemoral contact force differed 1.3-3.0% across repeated recovery paces trials which were moderate to large effect sizes (ES = 0.6 to 1.7).

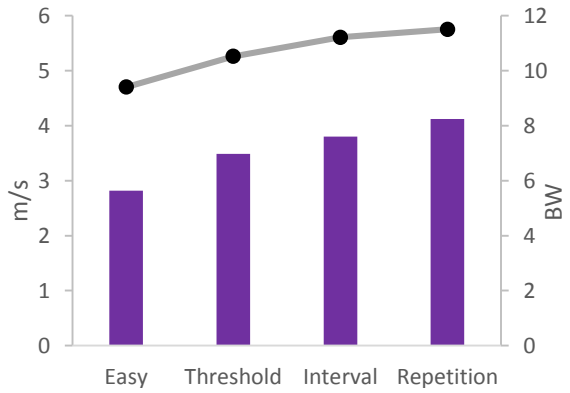

Figure 1: Peak total tibiofemoral contact force (line) across treadmill speeds (bars).

With this study, we sought to determine the influence of varying running paces on peak total tibiofemoral contact force. We hypothesized that the change in peak total tibiofemoral contact force during running would be greater between low to moderate intensity paces compared to moderate to high intensity paces. Our pilot data supports this hypothesis which should be confirmed in a larger sample. Incidents of overuse injuries in competitive runners are reported to be elevated at the beginning of the season, which coincides with an increase in running pace intensity [2]. Threshold pace may be similar to a runner's 5km or 10km race pace, and is often used during training. Overuse injuries in runners are most likely due to multiple intrinsic and extrinsic factors. The greater peak total tibiofemoral contact force during threshold pace compared to easy pace compounded with a sudden increase in prescribed threshold pace may contribute to the high injury rates at the beginning of the season.

CONCLUSION

The relative increase in peak total tibiofemoral contact force between low to moderate intensity was greater than that between moderate to high intensity running. Cumulative tibiofemoral load should be determined for these commonly prescribed running paces at relevant distances to further understand injury risk during training. Promoting moderate intensity running during the off-season may reduce the magnitude of change in peak total tibiofemoral contact force experienced at the beginning of the season.

REFERENCES

[1] Daoud, et al. *Med Sci Sports Exerc* 44, 1325-34, 2012.
[2] Rauh, et al. *J Clin Sport Med* **10**, 110-6, 2000.
[3] Ford, et al. *Med Sci Sports Exerc* **45**, 1125-30, 2013.
[4] Daniels. Daniels' Running Formula, 3rd Ed. *Human Kinetics* 2013.
[5] Willy, et al. *J Sports Sci* **34**, 1602-1611, 2016.
[6] Bowersock, et al. *Clin Biomech* **43**, 79-85, 2017.

SEX COMPARISON OF POST-ARTHROSCOPY GAIT MECHANICS FOR FEMOROACETABULAR IMPINGEMENT SYNDROME

[1]Lindsey Brown, [2]Brittany Schroeder, [1]Michael P McNally, [1]Jennifer Perry
[3]John Ryan, [4]Timothy E Hewett, and [1,2]Stephanie Di Stasi

[1] Sports Medicine Research Institute, The Ohio State University Wexner Medical Center, Columbus, OH, USA
[2] Division of Physical Therapy, The Ohio State University, Columbus, OH, USA
[3] Department of Orthopaedics, The Ohio State University, Columbus, OH, USA
[4] Mayo Biomechanics Laboratories and Sports Medicine Center, Mayo Clinic, Rochester, MN, USA
email: brown.4119@osu.edu

INTRODUCTION

Femoroacetabular impingement syndrome (FAIS) is a clinical condition of the hip identified by clinical signs, patient symptoms, and radiographic findings.[1] FAIS is associated with sex-dependent clinical features and functional deficits, as women present with greater passive hip motion and less severe bony abnormalities,[2] report worse pre- and post-operative hip function,[3] have lengthier recovery,[4] and are at greater risk for conversion to a total hip replacement.[5]

Women with FAIS demonstrate greater sagittal and coronal plane motion during a step-down task.[6] Understanding sex-specific movement mechanics during functional tasks may elucidate why abnormal movements persist even post-operatively for this population.[7] The purpose of this study was to evaluate sex differences in coronal plane hip mechanics during gait in persons post-arthroscopy for FAIS compared to healthy controls (HCs). We hypothesized that women in the FAIS group would exhibit greater peak hip abduction and adduction and greater peak external coronal plane hip moments compared to men, and these sex differences would not exist in HCs.

METHODS

Participants: Thirty participants with FAIS were recruited from a prospectively collected cohort of patients undergoing elective hip surgery at the study institution. 7 of 30 were removed from this analysis. Fifteen HCs were recruited via convenience sampling. Participants in the FAIS group were at least one year post-arthroscopy for FAIS (Figure 1); whereas, HC participants reported 0/10 hip pain in the month prior to data collection. Participants in either group were excluded if they reported a history of serious injury to the spine or lower extremity that required medical intervention.

Figure 1. Surgical Procedures

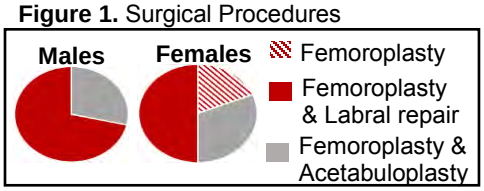

Gait Mechanics: All participants completed five walking trials at self-selected gait speeds. A standard 3-dimensional motion analysis system was used to capture kinematics and kinetics of the trunk, pelvis, and lower extremity. Only hip mechanics of the involved (or dominant for HC) were considered for this paper. Hip kinematics were calculated from a pelvic reference. Hip kinetics were calculated using a hip joint center determined from dynamic hip joint movement trials. Kinematic and kinetic data were filtered using 20hz and 50hz low-pass 4th order Butterworth filters, respectively. Kinetic data was normalized to participant body weight.

3 of 5 trials with acceptable data were averaged to provide time series gait data for coronal plane hip kinematics and kinetics, from which peak values were determined.

Table 1. Participant Demographics

	FAIS		HC		
	Male	Female	Male	Female	P=
N	7	16	5	7	--
Age (y)	35.8(8.5)	37.0(9.7)	38.2(9.0)	29.4(8.6)	0.29
BMI (kg/m^2)	24.8(1.9)	24.2(1.7)	27.1(2.2)	23.5(3.6)	0.07
Gait Speed (m/s)	1.49(0.12)	1.61(0.12)	1.67(0.35)	1.64(0.12)	0.27
Time post-op (y)	2.2(1.1)	2.7(1.5)	--	--	0.47
iHOT33	72.4(16.6)	76.7(18.9)	98.8(1.1)	97.6(4.8)	0.004

Mean(standard deviation); iHOT33 = 33-item International Hip Outcome Tool

Hip Function: Participants completed the 33-item International Hip Outcome Tool (iHOT33) to collect validated patient-reported hip function, used to evaluate group (FAIS vs HC) and sex differences as a secondary analysis.

Statistical Analysis: Two-way analyses of variance were used to evaluate for group and sex interactions for the primary variables of interest (peak hip abduction and adduction, peak external hip abduction and adduction moments; $P \leq 0.05$), co-varied by gait speed. If significant interactions were found, planned *post-hoc* t-tests were performed to determine effect of sex in each group. Significant main effects were reported if no significant interactions were found.

RESULTS AND DISCUSSION

Demographic variables were not significantly different between groups or sexes (Table 1), except for patient-reported hip function which was worse for the FAIS group (P=0.004), as expected. There were no significant interactions for any of the primary variables of interest (P>0.05); a significant main effect of sex was identified with respect to peak abduction (P<0.001), peak adduction (P<0.001), and peak external abduction moment (P=0.002).

Female participants had lower peak abduction, higher peak adduction, and lower peak external abduction moments compared to males (Figures 2 & 3). These findings differ from previous investigations that found healthy women exhibit greater coronal plane hip excursion during gait.[8]

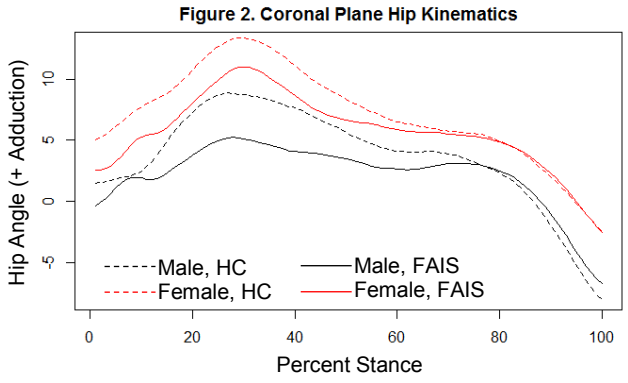

There was also a significant main effect of group for peak adduction (P=0.001). Participants in the FAIS group had lower peak adduction compared to HCs (Figure 2). These findings are consistent with previous literature that demonstrated reduced frontal and sagittal plane motion during gait both pre- and post-operatively for persons with FAIS.[7]

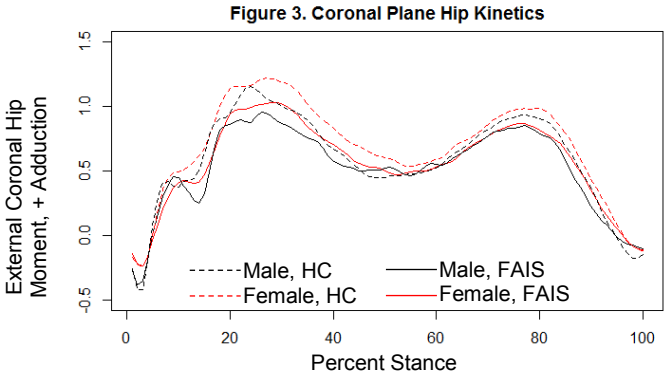

While age was not significantly different between sexes and groups, previous work has found that women older than 45 years report worse post-operative function than those younger than 30.[9] The current sample was too small to investigate any effect of age within each sex.

Any aberrant movement in the coronal plane during a sagittal plane tasks may help to explain any sex or group differences observed in patient-reported function. As expected, our FAIS group reported significantly (P=0.004); however, scores were similar between sexes.

CONCLUSIONS

The results of this study did not support the *a priori* hypotheses. The hypothesis tested was that sex differences would exist in the FAIS group but not the HC group for coronal plane hip mechanics. Based on the small cohort of participants, there does not appear to be sex-specific coronal plane gait mechanics for persons with FAIS that differ from HCs.

REFERENCES

1. Griffin D. *BJSM*. **50**(19), 1169-76, 2016.
2. Nepple JJ. *J Bone Joint Surg Am.* **96**(20):1683-9, 2014.
3. Glaws K. *APTA CSM.* 2018 [abstract]
4. Lee H. *Arthroscopy*. **26**(3):328-34, 2010.
5. Naal F. *AJSM*. **40**(7):1501-10, 2012.
6. Lewis CL. *JOSPT*. 1-31, 2018.
7. Brisson N. *Gait Posture.* **37**(2):258-63, 2013.
8. Bruening DA. *Gait Posture*. **41**(2):540-5, 2015.
9. Frank RM. *J Bone Joint Surg Am*. **98**(10):797-804, 2016.

SEX DIFFERENCES PERSIST ACROSS GAIT SPEEDS

Dustin A. Bruening, Andrew Baird, Kelsey Weaver, Kirk Bassett,
Weston Peine, Nick Macfarlane, Sarah T. Ridge

Brigham Young University, Provo, Utah, USA
email: dabruening@byu.edu, web: http://footankle.byu.edu

INTRODUCTION

Gait differences between sexes were first formally studied by sociologists in the 1960s and 70s, who showed that lay observers could distinguish sex by focusing on frontal plane torso and pelvis motion cues [1]. Despite a number of more recent biomechanics studies on sex differences in gait [2], it is still unclear to what extent these differences are due to structural, socio-cultural, or other factors. Previous research has almost exclusively investigated kinematic sex differences at unconstrained, self-selected walking speeds, which also differ between sexes [3]. A simultaneous investigation into the effects of sex, ambulation speed, and ambulation type (walking vs running) may provide additional insight into underlying sex differences in gait.

The identification and understanding of sex differences are of interest in a variety of fields. In clinical gait analysis, normative data is often pooled between sexes, but there may be instances that warrant separation. In addition to medicine, many applications in psychology, surveillance, targeted advertising, and animation may benefit from research on sex differences. Many of these applications rely on quick visual identification of subject sex, for which upper body motion cues may be ideal. Yet, the vast majority of the biomechanics literature on this topic covers only the lower extremities.

The purpose of this study was therefore to investigate the effects of speed and sex on several previously identified mid and upper body gait kinematic variables. We hypothesized that as task demand (i.e. gait speed) increased, these sex differences would diminish, indicating the presence of influences beyond anatomical structure.

METHODS

Forty-three university age students participated after providing informed consent (20 M, 23 F). Subjects wore standardized athletic shoes to walk and run on an in-ground treadmill. Sixty-one reflective markers were placed on the body to create a custom full-body model. Collection consisted of three walking and three running speeds, performed in order from slowest to fastest. To control for differences in subject height [3], speeds were non-dimensional, based on each subject's leg length:

$$F = \frac{v^2}{gl}$$

Where F = froude number, v = speed, g = gravitational acceleration, and l = leg length. Leg length was measured from ASIS to medial malleolus. The tested Froude numbers for walking were 0.32, 0.48, and 0.64, and for running 0.88, 1.12, and 1.36.

Marker trajectories were collected at 240 Hz and filtered at 10 Hz. Ranges of motion (RoM) throughout the gait cycle were calculated in Visual 3D software for three variables: 1) Frontal plane pelvis (wrt lab), 2) Frontal plane torso (wrt lab), and 3) Sagittal plane (left) shoulder motion [4]. Mixed model ANOVAs were run for each of the three variables to determine the effects of sex and speed on RoM.

RESULTS

Pelvic obliquity RoM increased with walking speed, but then returned to match slow walking following the walk to run transition (Figure). It again increased with running speed, but not to the extent that it did during walking. Sex differences were apparent across all speeds (Table), but slightly more so during walking. Torso sway RoM increased gradually as speed increased, but was not found to

be statistically different between sexes. Left shoulder RoM increased markedly as speed increased, with females having consistently greater RoM than males across all speeds (Figure, Table).

Table: ANOVA main effects p-values for each of the three dependent variables (α=0.05).

	Sex	Speed	Interaction
Pelvis	0.001	<0.001	0.057
Torso	0.195	<0.001	0.355
Shoulder	0.005	<0.001	0.094

DISCUSSION

Our RoM values during slow and medium walking for the most part closely match previous values from self-selected walking speeds [2]. One exception was not detecting a sex difference in torso sway. While this variable was identified as a main distinguishing characteristic in early literature, equivocal results across several modern studies suggest that sex differences in torso sway may be subtle.

Conversely, pelvis and shoulder RoM were substantially greater in females than males, even after controlling for speed and height differences. Differences in pelvic motion are not surprising, given the known distinctions in pelvis structure. The extent of shoulder motion differences, however, were unexpected, as these differences appeared to increase with walking speed (e.g. mean differences doubled between slow walking and fast running). While previous research on sex differences has focused primarily on frontal plane pelvis and torso motion, these results suggest that transverse plan rotation should be more fully investigated, as this typically drives passive arm swing.

CONCLUSIONS

Overall, our hypothesis was not supported, as sex differences in pelvis and shoulder RoM persisted across gait speeds. This may indicate large influences from known anatomical and structural differences between sexes, primarily originating in the pelvis. The relationship between transverse plane pelvis/torso motion and arm swing warrants additional investigation.

REFERENCES

1. Mather and Murdoch. *Proc. R. Soc. Lond. B*. 258 (1353): 273-279, 1994.
2. Bruening et al., *Gait Posture*. 41(2): 540-545, 2015.
3. Frimenko et al., *Physiotherapy*. 101(3): 266-272, 2015.
4. Kuhtz-Bushbeck et al., *Gait Posture*. 27(3): 447-454, 2008.

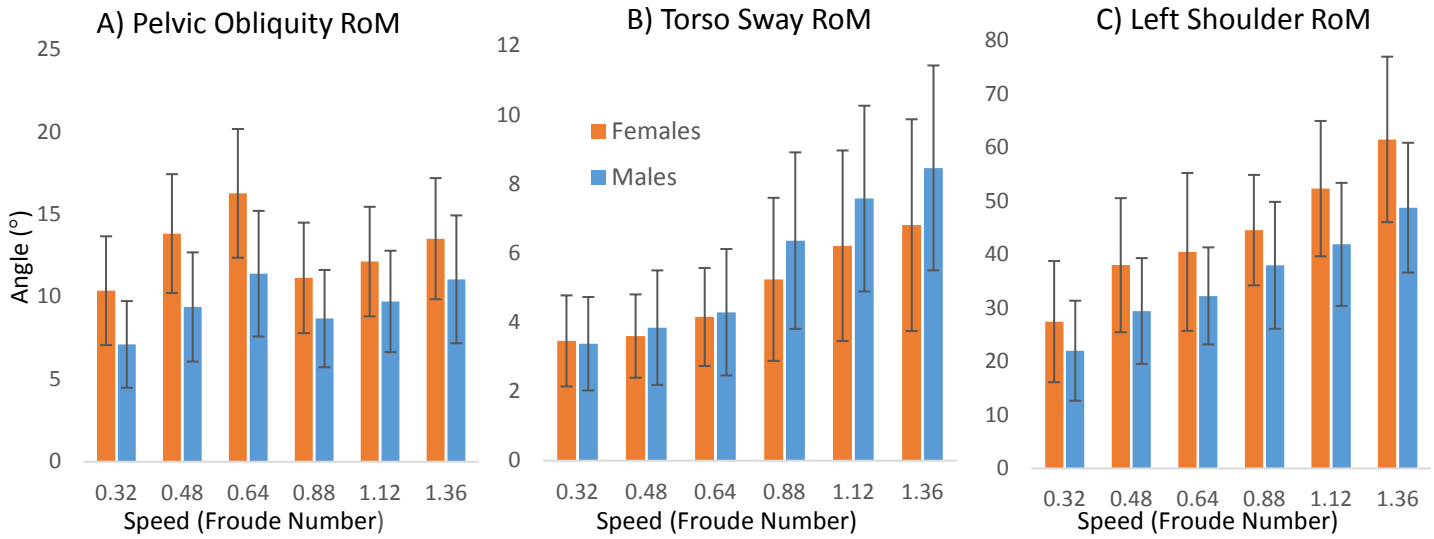

Figure: Aggregate data showing mean ± stdev for all female (orange) and male (blue) subjects across the six non-dimensional speeds (3 walking speeds and 3 running speeds).

TRANSITIONAL MOVEMENTS WITH BODY BORNE LOAD INCREASES ANKLE WORK

[1]Sarah E. Cameron, [1]Jonathan T. Kaplan, [2]Tyler N. Brown, [1]John W. Ramsay
[1]Natick Soldier Research, Development and Engineering Center (NSRDEC) Natick, MA, USA
[2]Dept. of Kinesiology, Boise State University, Boise, ID, USA
email: sarah.e.cameron20.civ@mail.mil

INTRODUCTION

In military operations, a soldier has to perform a transitional movement to quickly avoid or pursue enemy fire. A transitional movement necessitates a quick change in speed: such as a deceleration for run to walk (RTW) or an acceleration for a walk to run (WTR). In order to decelerate, the lower limb must absorb enough energy to produce an adequate breaking force. Likewise, to accelerate, the lower limb must generate enough energy to propel the body forward. Although lower limb energy does not change during steady state movements [1], it may be that dynamic tasks, such as a WTR or RTW, may require substantial lower limb joint power to successfully complete transitional maneuvers. In the military, these maneuvers are often performed while donning body borne load, sometimes in excess of 45 kg. These loads increase the mechanical work as well as muscle activity required to sustain velocity of a task [2]. Yet, it is unknown if muscle activity must increase to change speed of movement, particularly with body borne load. To stabilize the stance limb with body borne load, greater muscle activity, including cocontraction (i.e. the simultaneous activation of agonist and antagonist muscle pairs) may be required, potentially increasing lower limb work to perform the movement. To date, it is unclear how body borne load affects cocontraction of lower limb musculature and thereby joint work during RTW and WTR transitional movements.

METHODS

Twenty-one male military personnel (age: 21.6 ± 3.1 yrs, height: 1.77 ± 0.56 m, weight 79.9 ± 11.6 kg) participated in this study. For the WTR trials, 2 subjects' data was unavailable and the sample size was 19. Each participant completed the study maneuvers with three different load configurations: light (~6 kg), medium (15 % BW) and heavy (30 % BW). For the light load, participants wore military equipment (helmet, boots and mock weapon). For the medium and heavy loads participants added a weighted vest to the military equipment. With each load, participants completed five successful RTW and WTR maneuvers. The WTR required the participant to walk at 1.5 m/s before transitioning to a 4 m/s run when their dominant limb contacted a force platform. The RTW required the participant running at 4 m/s before transitioning into a 1.5 m/s walk when their dominant leg contacted the force platform

During each task, surface electromyography (EMG) quantified tibialis anterior (TA), lateral gastrocnemius (LG), vastus lateralis (VL), rectus femoris (RF), lateral hamstrings (LH), and gluteus medius (GM) muscle activation. Then, each EMG signal and cocontraction of TA-LG, VL-LH and RF-GM muscle pairs calculated, per Rudolph [3]. For the RTW, cocontraction was integrated over the breaking phase of the movement, the period of stance when apGRF was negative. For the WTR, cocontraction was integrated over the propulsion phase of the movement, the period of stance when apGRF was positive.

During each task, lower limb biomechanics were quantified from 3D trajectories of 36 reflective markers. A kinematic model, consisting of eight segments, was created from a static calibration using Visual3D (C-Motion, Rockville, MD). Synchronous ground reaction force (GRF) data and marker trajectories were low pass filtered with a fourth-order Butterworth filter (12 Hz). Filtered kinematic and GRF data were processed using conventional inverse dynamics to calculate joint power. Joint power was calculated and integrated with respect to time to obtain work during the RTW (negative work) and work during the WTR (positive work).

For both the RTW and WTR, TA-LG, VL-LH and RF-GM cocontraction and joint work were submitted to a RM ANOVA to test the effect of load configuration (LL, ML, and HL). Where statistically significant differences were observed ($p < 0.05$), a modified Bonferroni procedure was used.

RESULTS AND DISCUSSION

Body borne load increases the energy the lower limb must absorb to safely decelerate the center of mass. With borne load, the current participants exhibited a significant increase in ankle (P<0.001), but not hip (P=0.435) or knee (P=0.162) work to complete the RTW. Although participants increased ankle work to perform the RTW, a similar increase in ankle cocontraction (P=0.156) was not observed. Rather, cocontraction increased at the hip (P=0.010) and knee (P=0.036). Specifically, the RF-GM muscle pair that crosses the hip increased cocontraction between the light and medium load (P=0.045). Similarly, the cocontraction of the VL-LH muscle pair that crosses the knee increased between the medium and heavy loads (P=0.018). Considering adequate cocontraction is necessary to provide joint stability, it may be that sufficient hip and knee muscle activity is required to prevent collapse of the limb during a loaded RTW. Whereas, the primary function of the ankle and its associated musculature is to absorb kinetic energy and safely decelerate the center of mass during a RTW maneuver with body borne load.

Body borne load also increased the ankle work necessary to accelerate speed of movement. During the WTR, body borne load increased ankle work (P=0.032) but not hip (P=0.784) or knee work (P=0.475). The ankle is the primary generator of work during locomotion and responsible for propulsive forces necessary for acceleration [4]. With the heavy compared to light load (P=0.023), the ankle significantly increased the work produced at the joint to complete the WTR. Similarly, cocontraction of the TA-LG muscle pair that crosses the ankle increased with heavy compared to light body borne load (P=0.019). Greater ankle cocontraction may be necessary to stabilize the joint during propulsive phase of WTR with addition of load. But, additional efforts to understand how both the TA and LG muscles contribute to creating the propulsive forces required to complete the WTR with body borne load is necessary.

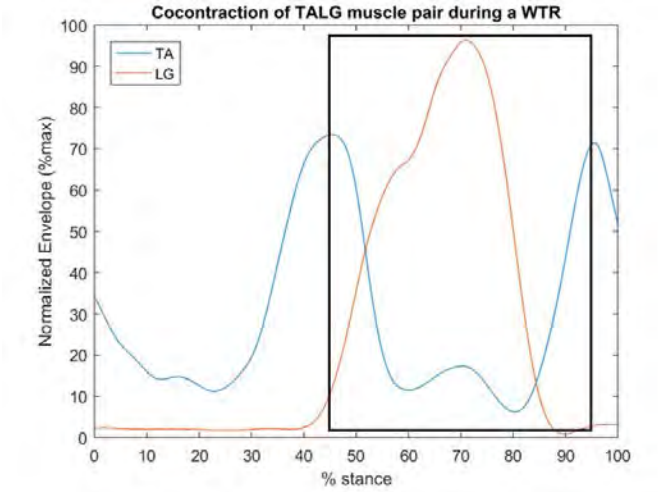

Figure 1: Depicts TA and LG muscle activity during WTR task. Box refers to time in stance where cocontraction occurs.

CONCLUSIONS

Body borne load had a significant effect on ankle work during both the RTW and WTR. The ankle and associated musculature may absorb and generate kinetic energy to safely perform transitional movements common to military activities. Improving our understanding of the role of the ankle joint and surrounding musculature may be a means to improve performance and reduce injury risk of military locomotor tasks.

REFERENCES

1. Brown et al. Gait Posture **40**, 237–242, 2014.
2. Huang et al. J.Exp.Biol **217**, 605–613, 2014.
3. Rudolph. Knee Surg Sport Trauma **8**, 262-269, 2000.
4. Herr et al. Proc. Biol. Sci. **279**, 457–464, 2012.

Table 1: Mean (± SD) cocontraction and joint work exhibited during the RTW and WTR with each load condition.

Cocontraction (%)	RTW			WTR		
	LL	**ML**	**HL**	**LL**	**ML**	**HL**
TALG	24.85±9.5	26.49±6.9	29.11±9.7	11.28±8.1$^{\$}$	11.53±4.9	19.70±10.5
VLLH	26.67±15.02	25.70±6.8$^{\wedge}$	31.92±9.2	32.97±15.9	33.27±12.7	39.17±11.2
RFGLMD	27.21±10.23*	31.09±9.6	34.79±10.8	25.51±5.9	29.85±9.4	34.98±8.8
Joint Work (J)						
Hip	-30.26±14.9	-30.76±12.9	-33.28±15.2	85.24±21.4	88.02±19.4	88.46±23.1
Knee	-148.79±36.9	-156.9±48.8	-162.8±48.1	50.65±14.7	50.65±14.7	53.65±16.1
Ankle	-46.86±7.2$^{\$}$	-51.22±9.9	-54.81±8.5	83.37±17.1$^{\$}$	86.27±18.3	89.04±24.6

For pairwise comparisons: *LL-ML, $^{\$}$LL-HL, $^{\wedge}$ML-HL denotes a significant ($p < 0.05$) main effect of body borne load

OLD AND YOUNG ADULTS DEMONSTRATE SIMILAR MUSCLE CO-CONTRACTIONS DURING WALKING

[1] Vishnu D. Chandran, [2,5] Philippe C. Dixon, [1] Jan A. Calalo, [2,6] Jack T. Dennerlein, [3] Xu Xu, [4] Chien-Chi Chang, [5] Jeffrey M. Schiffman, and [1] Saikat Pal

[1] New Jersey Institute of Technology, Newark, NJ, USA
[2] Harvard University, Boston, MA, USA
[3] North Carolina State University, Raleigh, NC, USA
[4] National Tsing Hua University, Hsinchu, Taiwan, ROC
[5] Liberty Mutual Research Institute for Safety, Boston, MA, USA
[6] Northeastern University, Boston, MA USA
email: pal@njit.edu

INTRODUCTION

The level of muscle co-contraction during walking reflects movement efficiency and joint stability. Excessive muscle co-contractions have been related to increased metabolic cost [1] and joint stiffening [2] in older adults. Some walking studies comparing young and old adults reported consistently higher muscle co-contractions in the lower extremity of older adults [3-5], while others reported higher muscle co-contractions in some joints but not other joints [1]. The evidence of greater muscle co-contractions in older adults remains inconclusive. The purpose of this study was to determine if there were differences in agonist and antagonist muscle co-contractions between young and old adults. We hypothesized that older adults have higher muscle co-contractions compared to young adults at the ankle and knee joints during walking.

METHODS

We recruited 17 (8M, 9F) healthy old adults (74.2 ± 6.3 years, 162.3 ± 8.8 cm, 71.4 ± 18.1 kg, 2.7 ± 1.8 hours exercise/week) and 13 (6M, 7F) healthy young adults (25.2 ± 4.2 years, 170.6 ± 9.3 cm, 69.7 ± 12.3 kg, 3.8 ± 1.8 hours exercise/week). There were no statistical differences in height, weight, or exercise time between the groups. Prior to participation, subjects were informed on all aspects of the study and provided written consent according to the policies of the local Institutional Review Board.

We analyzed each subject during walking at self-selected speeds in a gait lab, with simultaneous measurements of muscle electromyography (EMG) and ground reaction forces (GRF). We measured EMG from the tibialis anterior (TA), medial gastrocnemius (GAST), vastus lateralis (VL), and lateral hamstrings (HAMS) muscles. Although EMG from both legs were measured, only the leg with the greater number of successful trials (entire foot contacting a force plate) was included in this analysis. We ensured that there were a minimum of three successful trials from each subject. The EMG data were filtered [6] and dynamically normalized to muscle-specific maximum activations obtained from all successful trials. The EMG and GRF data were synchronized to determine heel strikes and toe off.

We calculated muscle co-contractions at the ankle and knee joints for each trial of each subject using:

$$\%\ \text{Co-contraction} = \frac{2*\text{common area A \& B}}{(\text{area A} + \text{area B})} * 100$$

where A and B were filtered and normalized EMG signals from muscle pairs (Figure 1) [6, 7]. Percent co-contraction values from individual trials were averaged for each subject and between the young and old groups. We analyzed percent co-contractions

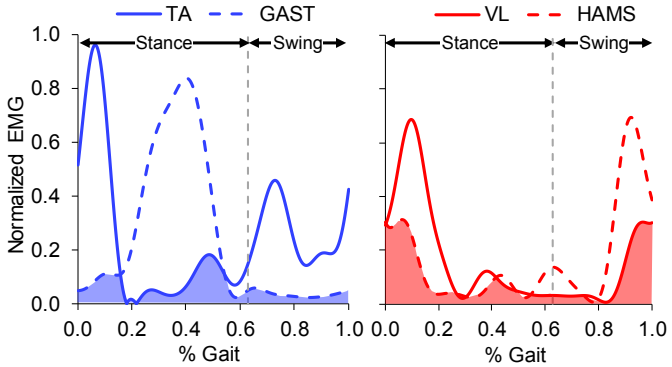

Figure 1: Filtered and normalized EMG from a representative walk trial. The shaded regions are the common areas between the muscle pairs at the ankle (left) and knee (right) joints. The vertical dashed lines indicate transition from stance to swing.

over the entire gait cycle, as well as during the stance and swing phases of gait. Significant differences between the young and old groups were assessed with 2-tailed, unpaired *t* tests with Bonferroni corrections for multiple comparisons.

RESULTS AND DISCUSSION

The results of this study demonstrate no differences in muscle co-contractions between young and old adults during walking. At the ankle joint, average (± standard deviation, SD) muscle co-contractions over the entire gait cycle were 38.8% (± 8.2%) and 41.7% (± 7.5%) for the young and old adults, respectively (Figure 2). At the knee joint, average (± SD) muscle co-contractions over the entire gait cycle were 65.0% (± 11.1%) and 63.0% (± 6.3%) for the young and old adults, respectively (Figure 3). Similar results were observed for muscle co-contractions during stance and swing phases of gait at the ankle (Figure 2) and knee (Figure 3) joints.

We observed large variabilities in muscle co-contraction in both young and old adult groups. At the ankle joint, muscle co-contractions over the entire gait cycle ranged from 27.0% to 56.4% for young adults, and 28.6% to 57.8% for old adults. At the knee joint, muscle co-contractions over the entire gait cycle ranged from 48.0% to 81.6% for young adults, and 55.1% to 78.1% for old adults. Similar variabilities were observed for muscle co-contractions during stance and swing phases of gait at the ankle and knee joints.

The results of this study do not support our hypothesis that older adults have higher muscle co-contractions compared to young adults during walking. A reason for this lack of difference between the young and old adult groups is the large variability in muscle co-contractions observed within each subject group. Our results contradict previous walking studies that reported higher muscle co-contractions in the lower extremity of older adults [1, 3-5]. These contradictions may be explained, in part, due to differing methods for calculating muscle co-contractions. Mian et al. [3] quantified co-contraction based on the time when antagonist muscle pairs were active. Hortobagyi et al. [4] measured timing and amplitude of antagonist muscle pairs. This reasoning, however, does not explain our differences with the Peterson and Martin [1] and Franz and Kram [5] studies, as we used a similar method to calculate muscle co-contraction as these two studies. It may be that the similar exercise levels in the old and young adults in our study minimized age-related increases in muscle co-contractions observed in previous older adult cohorts.

CONCLUSIONS

Muscle co-contraction has been used as a clinical tool to study changes in muscle strategies during gait due to aging and pathology. However, evidence in support of greater muscle co-contraction in older adults is sparse. Further investigation is required to understand the validity of this phenomenon.

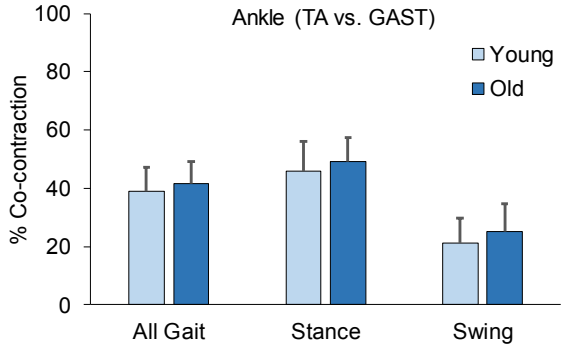

Figure 2. Average muscle co-contractions at the ankle joint for young and old adults. Error bars represent one standard deviation.

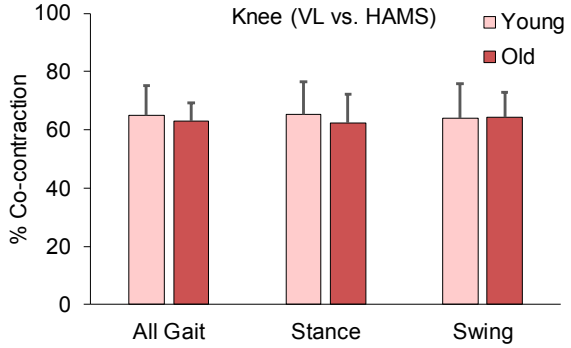

Figure 3. Average muscle co-contractions at the knee joint for young and old adults. Error bars represent one standard deviation.

REFERENCES

1.Peterson, D, et al. *Gait Posture*, 31(3), 2010.
2.Benjuya, N, et al. *J Gerontol A Biol Sci Med Sci*, 59(2), 2004.
3.Mian, O, et al., *Acta Physiol (Oxf)*, 186(2), 2006.
4.Hortobagyi, T, et al., *Gait Posture*, 29(4), 2009.
5.Franz, J, et al., *Gait Posture*, 37(3), 2013.
6.Lo, J, et al., *Gait Posture*, 53, 2017.
7.Hesse, S, et al., *Restor Neurol Neuros*, 17(1), 2000.

OLDER ADULTS OVERCOME THEIR DEFICITS TO YOUNG ADULTS WHEN PROPULSIVE DEMANDS OF WALKING ARE INCREASED TO THEIR MAXIMUM

Katie A. Conway, Randall Bissette, and Jason R. Franz

University of North Carolina at Chapel Hill and North Carolina State University, Chapel Hill, NC, USA
email: kaconway@unc.edu, web: http://abl.bme.unc.edu

INTRODUCTION

Reduced push-off intensity during walking, arising from diminished plantarflexor mechanical output and thus propulsive force generation, plays an important role in age-related mobility impairment [1]. Unfortunately, conventional interventions aimed at enhancing ankle power generation (e.g., resistance training) seem to convey benefits only during maximum speed walking [2]. Thus, improving maximum muscular capacity may fail to alter the instinctive utilization of that capacity, with limited improvements for habitual walking. As a potential explanation, evidence suggests that older adults retain the capacity to enhance push-off performance, for example to walk uphill or with biofeedback [3-4]. Thus, our working hypothesis is that many older adults retain a 'propulsive reserve' during normal walking that goes underutilized for reasons that are poorly understood (e.g., **Fig. 1A**). Understanding the emergence of these reserves, and thus the functional utilization of propulsive capacity during walking, is a critical step toward the strategic and discriminate prescription of resistance training complemented by innovative alternative therapies to restore walking ability in our aging population.

Therefore, our purpose was to gain an improved joint-level understanding of the utilization of propulsive capacity in older adults during walking, and thereby the availability of propulsive reserves, with a special emphasis on the plantarflexor muscles. We leveraged a motor-driven impeding force system and maximum speed walking to systematically increase the propulsive demands of walking to their maximum. We hypothesized: (*i*) that older adults would exhibit a diminished push-off intensity compared to their younger counterparts, but (*ii*) that older adults' propulsive reserve would allow them to overcome those deficits when the propulsive demands of walking are increased to their maximum.

METHODS

Twelve healthy older adults participated (age: 75.0±4.6 years, height: 1.71±0.1 m, body mass: 68.6±11.1 kg, 5M/7F). We first recorded subjects' preferred (1.28±0.2 m/s) and maximum (1.89±0.1 m/s) walking speeds using an instrumented walkway. Subjects then walked on a dual-belt instrumented treadmill (Bertec, Corp.) for 1 min at their preferred speed ("Pref"). In another

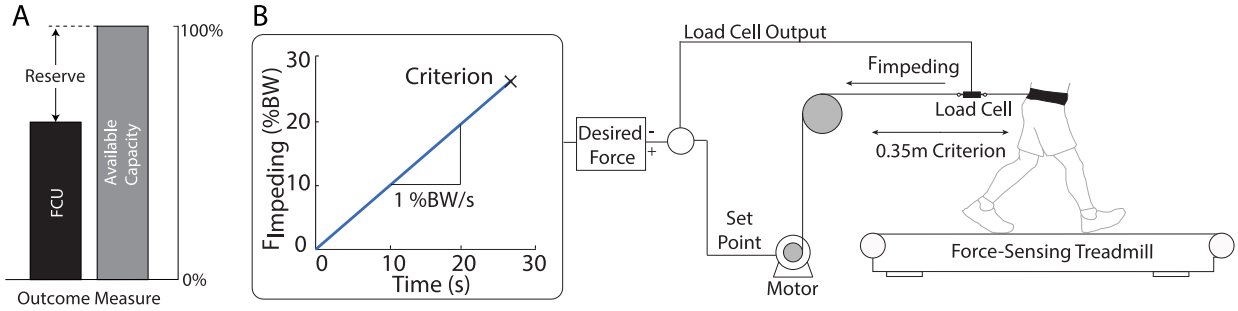

Figure 1. (A) Schematic showing our representation of propulsive reserves, shown here as the difference between functional capacity utilized (FCU) and maximum available capacity. (B) A motor-driven, feedback controlled impeding force system including load cell and motor increased the demand for propulsive forces at a rate of 1% BW/s until we observed an inexorable 0.35 m posterior displacement of the subject's pelvis.

trial, subjects walked on the treadmill at their maximum overground walking speed, which they maintained for approximately 10 s ("Fast"). Subjects also wore a waist belt that connected to a feedback-controlled, motor-driven system that prescribed horizontal impeding forces according to instantaneous measurements from a load cell (**Fig. 1B**). Specifically, while subjects walked at their preferred speed on the treadmill, a real-time controller increased the impeding force at a constant rate of 1 %BW/s ("Ramp"). The trial ended following a 0.35 m inexorable posterior translation of the subjects' center of mass, monitored using the motor's encoder. For all treadmill trials, we recorded the 3D trajectories of retroreflective markers on the pelvis and lower limbs using motion capture (Motion Analysis, Corp.) and used inverse dynamics to estimate leg joint moments and powers. Finally, we compared to reference data from young adults (24.5±5.5 years) walking at their preferred speed (1.35±0.2 m/s, p=0.281 vs. old).

RESULTS AND DISCUSSION

Older adults walked normally with 14% smaller peak propulsive forces (p=0.012) and 19% smaller peak ankle power (p=0.022) than young adults. However, these deficits disappeared as the propulsive demands of walking increased (**Fig. 2**). Compared to normal walking, older adults increased their peak propulsive force by an average of 42% and 68% during maximum speed and maximum ramp, respectively. (p<0.001). Interestingly, this ability to increase propulsive force to its maximum during preferred speed walking is nearly identical to that found previously for older adults walking at a 9° uphill grade (i.e., +69%), suggesting a functionally limiting environmental demand for older adults [3]. Peak ankle power, but not peak moment, also increased during these conditions, by 59% and 22% compared to Pref, respectively (p<0.021) (**Fig. 2**).

CONCLUSIONS

Using a ramped impeding force protocol, we have discovered preliminary evidence that older adults' propulsive reserve allows them to overcome apparent age-related deficits in push-off intensity, at least for peak propulsive force and ankle power generation. Interestingly, of the outcome measures used to characterize push-off intensity, peak ankle moment increased when walking faster but not when generating maximum propulsive forces. The emergence of propulsive reserves in elderly gait may facilitate the more discriminate prescription of interventions aimed at enhancing walking ability by increasing push-off intensity in older adults.

REFERENCES

1. Kerrigan et al. *Arch Phys Med Rehab*, **79**, 1998.
2. Beijersbergen et al. *Gait Posture*, **52**, 2017.
3. Franz. *Exer Sport Sci Rev*, **44**, 2016.
4. Franz and Kram. *J Biomech*, **46(3),** 2013.

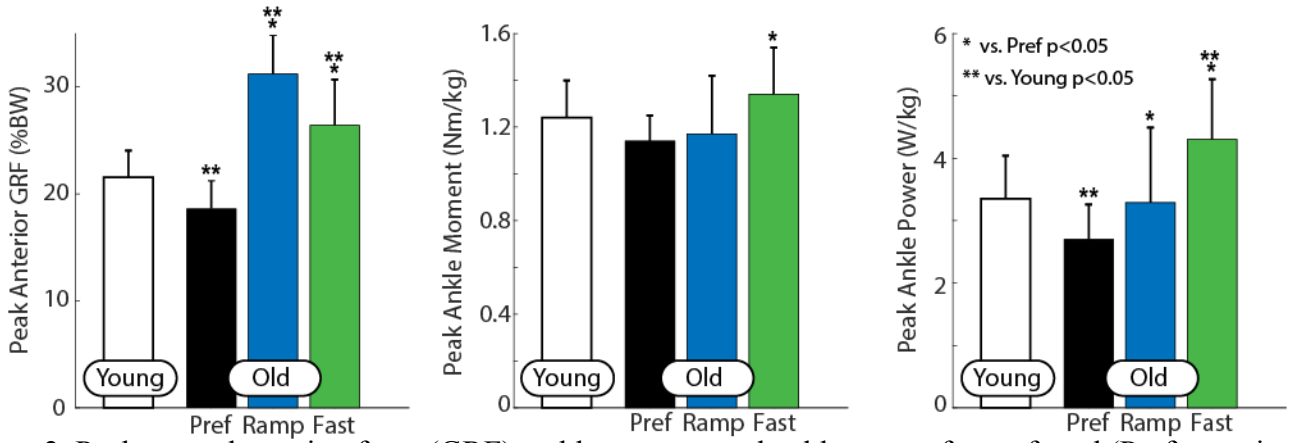

Figure 2. Peak ground reaction force (GRF), ankle moment and ankle power for preferred (Pref), maximum ramp (Ramp) and maximum speed (Fast) trials, compared to reference normal walking data for young adults (Young).

MODULATION OF NON-LINEAR STIFFNESS IN THE FOOT-SHOE COMPLEX DURING RUNNING

[1,2] Evan M. Day and [1,2] Michael E. Hahn

[1] Bowerman Sports Science Clinic, [2]Neuromechanics Lab, University of Oregon, Eugene, OR, USA
email: eday5@uoregon.edu, web: bssc.uoregon.edu

INTRODUCTION

The metatarsophalangeal (MTP) joint mechanically functions as a damper linking the metatarsal heads as the base of support during late stance in running gait.[1] The foot and shoe act in series to provide stiffness in the foot-shoe complex.[2] Increasing stiffness of the shoe increases the applied torque from the shoe during MTP plantar flexion in late stance, but may inhibit natural motion of the MTP joint.[3] Despite the growing interest in optimally tuning footwear bending stiffness to increase running performance[4], little is known about the individual contributions of the foot and shoe to MTP joint stiffness across running speeds. The purpose of this study is to determine the stiffness contributions and temporal behavior of the foot and shoe to MTP joint stiffness across running speeds.

METHODS

To date, eleven male runners (16:11 5000m best, 54mi/wk) have been analyzed. Written informed consent was provided prior to the IRB-approved protocol. Running trials were conducted on an instrumented treadmill (Bertec, Inc., Columbus, OH) at 3.89, 4.44, 5.00, 5.56, and 6.11 m/s. These velocities were chosen as they represent relevant training and racing paces for competitive distance runners. Data were collected for ten strides. Rest between conditions was self-selected. Subjects all wore the same footwear to control for the effects of varied longitudinal bending stiffness on MTP joint mechanics. Windows were cut in the shoes at the hallux, first and fifth metatarsals, and the medial, lateral, and posterior calcaneus for direct placement of markers on the foot. Marker coordinate data were collected at 200 Hz using an 8-camera motion capture system (Motion Analysis Corp., Santa Rosa, CA). Ground reaction force data were collected at 2000 Hz. Data were imported to MATLAB for analysis. Mechanical footwear testing data were obtained from the manufacturer.

A two-segment foot model was defined. The MTP joint was modeled as a hinge axis defined by the vector from the first to fifth metatarsal markers. Marker and ground reaction force data were filtered with a symmetric low-pass fourth-order Butterworth filter at 20Hz. The moment arm for kinetic analysis was defined as the perpendicular distance from the center of pressure to the MTP joint axis. The forefoot mass was considered negligible. Moments about the MTP joint were considered zero until the center of pressure acted distal to the MTP joint axis.

The slow (3.89 m/s), medium (5.00 m/s), and fast (6.11 m/s) speeds were analyzed. Two measures of joint stiffness, active ($K_{active}=\Delta M_{peak}/\Delta\Theta$) and critical ($K_{cr}=\Delta M/\Delta\Theta_{peak}$) were defined. These values represent stiffness of the foot-shoe complex. Instantaneous stiffness was calculated as the first derivative of the MTP joint angular load-displacement curve. Footwear stiffness ($K_{shoe}=\Delta M/\Delta\Theta$) was calculated from mechanical testing data provided by the manufacturer. Between speed effects were analyzed using a repeated measures ANOVA with Bonferroni adjustment.

RESULTS AND DISCUSSION

Data presented from three of five running speeds are part of an ongoing study. K_{cr} (N-m/kg/deg) was significantly higher during fast (0.0164±0.0045) compared to slow (0.0083±0.0034) and medium (0.0121±0.0059) running speeds ($p < .005$). K_{shoe} was linear from zero to 30 degrees of flexion, 0.0727 N-m/deg. K_{active} was not different between speeds ($p = .585$).

Critical stiffness (K_{cr}) defines the functional stiffness of the MTP joint, representing the total amount of energy available for push-off in late stance. K_{cr} is comprised of K_{shoe}, eccentric action of the toe-flexor musculature, and other soft tissue strain. K_{active} represents the initial loading of the MTP joint prior to energy dissipation. K_{shoe} was much smaller than K_{cr} and K_{active} at each speed, suggesting that stiffness of the foot-shoe complex is intrinsically modulated. While the MTP moment is greater at the fast speeds, K_{active} did not vary due to an accompanied increase in MTP dorsiflexion.

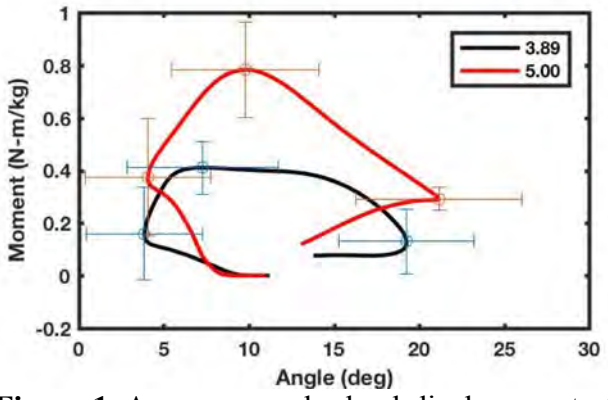

Figure 1. Average angular load-displacement of the MTP joint across speeds (m/s).

Stiffness of the lower extremity joints are commonly analyzed using linear equations. However, the MTP joint stiffness curve elicits a non-linear pattern (Figure 1). It may be more appropriate to utilize the derivative of the angular load-displacement curve to understand how MTP joint stiffness varies throughout stance. A linear increase in torque is required to bend the shoe to approximately 30 degrees, resulting in a constant shoe stiffness. However, instantaneous stiffness of the foot-shoe complex is much larger than the shoe and is variable throughout stance, suggesting that the foot modulates foot-shoe complex stiffness (Figure 2). While the stiffness values of the shoe and foot-shoe complex are approximately equivalent from 50-65% stance at slower speeds, the MTP moment is much larger than that required to bend the shoe. The low stiffness value is representative of little change in the MTP moment while MTP dorsiflexion increases.

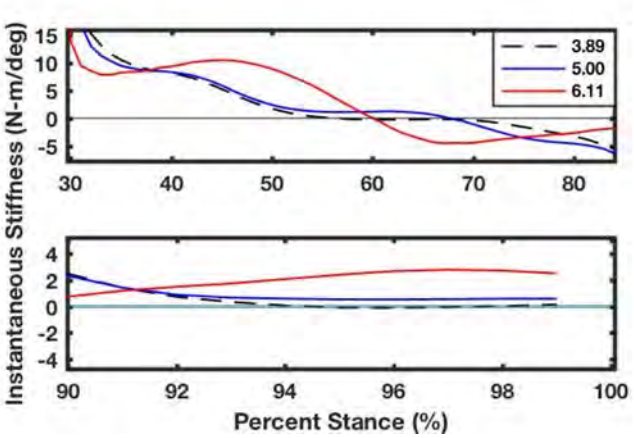

Figure 2. Instantaneous MTP joint stiffness across speeds (m/s) during loading (top) and push-off (bottom). Blue line represents footwear stiffness.

The instantaneous stiffness curve may be utilized to understand when varying amounts of work are being done on the shoe by the foot during stance phase. High stiffness represents phases when a large amount of work is being performed, whereas low stiffness represents energy dissipation. This analytical approach may be of use to footwear designers to understand which sections of a shoe should consist of high energy storage and return materials and which sections should facilitate a quick roll-through to minimize energy dissipation.

CONCLUSIONS

Examination of MTP joint stiffness during running suggests that the foot modulates complex stiffness and increases stiffness with running speed. A novel framework is also proposed for how to assess MTP joint function throughout stance. These results may be of use in footwear design.

REFERENCES

1. Stefanyshyn D., Nigg B. *JoB*. **30**, 1081-1085, 1997
2. Kelly et al. *J. R. Soc. Int.* **13**, 20160174, 2016
3. Oh K, Park S. *JoB*. **53**, 127-135, 2017
4. Hoogkamer et al. *Sports Med.* **47**, 1739-1750, 2017

ACKNOWLEDGEMENTS

Thank you to Brooks Sports for providing footwear for this study.

VALIDITY OF PRESSURE-MEASURING INSOLES IN QUANTIFYING CENTER OF PRESSURE

[1] Jessica DeBerardinis, [1] Conner Neilsen, [2] Daniel Lidstone, [2] Janet S. Dufek and [1] Mohamed B. Trabia

[1] Mechanical Engineering Department [2] Kinesiology and Nutritional Sciences Department
University of Nevada Las Vegas, Las Vegas, NV
email: deberj1@unlv.nevada.edu

INTRODUCTION

Center of pressure (COP) measurements can be useful in assessing gait pathology, effectiveness of foot orthotics, and the long-term effects of surgeries such as hip or knee arthroplasty [1]. COP can also be used to assess balance control and lower body joint kinetics [2-3]. The gold-standard method for measuring COP is the force platform; however, they are not portable and generally are not used to evaluate multiple consecutive steps. Pressure-measuring insoles overcome this limitation of force platforms due to their portability and their ability to record multiple consecutive steps. Several studies have compared the COP measurements between pressure-measuring insoles and force platforms to determine the validity of the insole measurements [4-7]. These studies have shown that the insoles provide a valid measure of COP compared to the force platform method. However, these studies were limited due to their small sample size (<50), the low resolution of the insole sensors (24), or sensor sensitivity to humidity. Additionally, the insoles were placed inside shoes in these experiments, which might have influenced measurements.

The purpose of this study was to examine the validity of the COP measurements obtained using pressure-measuring insoles compared to a force platform. This study was designed to simulate barefoot walking.

METHODS

A total of 65 participants (18 men, 47 women, 23.5 ± 5.1 yrs, 67.2 ± 19.3 kg, 1.64 ± 0.10 m) gave institutionally approved written consent to participate. Each participant was fitted with a pair of insoles (Medilogic®, Schönefeld, Germany, 60 Hz) that best matched their foot size.

The insoles were placed inside thin socks provided by the researchers, next to the skin, to simulate barefoot walking. After being fitted with the insoles and socks, the participants were asked to sit with their feet lifted off the ground. This was used to assess the level of noise from the unloaded sensors. The participants then were asked to stand and walk 5m over two consecutive force platforms (Kistler, 1000 Hz) at a self-selected speed. A total of three trials were collected for each participant with each foot having full and isolated contact with the corresponding force platform.

The raw insole data was summed at each time point to determine the times of the steps that occurred on the force platform. An adaptive threshold was used to determine the sensors that were active during stance phase [6]. The force platform COP and vertical ground reaction force (vGRF) data were filtered using a low pass Butterworth filter (cutoff of 125Hz). An onset threshold of 80N was used to identify times of heel strike and toe off within the vGRF data.

The active insole sensors were used to determine the COP location:

$$X_{Ins_t} = \frac{\sum_{i=1}^{n}(B_{t,i})(X_i)}{\sum_{i=1}^{n} B_{t,i}} \quad (1)$$

$$Y_{Ins_t} = \frac{\sum_{i=1}^{n}(B_{t,i})(Y_i)}{\sum_{i=1}^{n} B_{t,i}} \quad (2)$$

where $(X_{Inst,}, Y_{Inst})$ was the position of the insole COP at time instance t, n was the number of time instances of the data set, $B_{t,i}$ was the bit value of each sensor i at each time instance t, and (X_i, Y_i) was the position of sensor i with the origin set at the bottom medial side of the insole. For both COP data sets, insole and force platform, the first and last 5% of the data were eliminated. Both data sets were adjusted to start at

(0,0) and matrix rotation was used to orient the force platform COP curve with the insole COP data.

The path length and width were determined (Fig. 1) for both instruments and the difference between these variables, ΔL and ΔW, was determined:

$$\Delta L = L_{Ins} - L_{FP} \quad (3)$$

$$\Delta W = W_{Ins} - W_{FP} \quad (4)$$

where ΔL and ΔW are the difference between the path length and width of the insole (L_{Ins} and W_{Ins}) and the force platform (L_{FP} and W_{FP}), respectively. Average of ΔL and ΔW, combining both limbs, were calculated for the three trials of each subject. The correlation between the length and width measured by each instrument was determined.

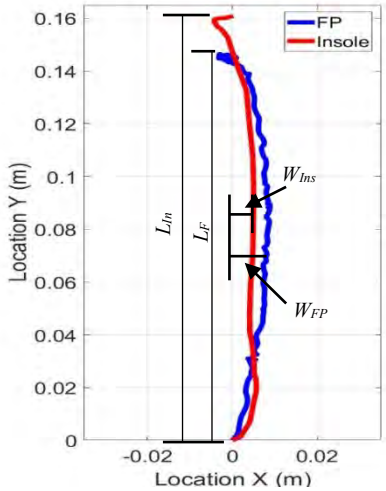

Figure 1: Exemplar COP force platform (FP) and insole curves.

RESULTS AND DISCUSSION

The differences between the insoles and force platform for the path length, ΔL, and path width, ΔW, are shown in Table 1 for each insole size and for all sizes combined. The averages did vary for each insole size, with large error for size 45-46. However, these may be due to the small number of participants and are on the similar order as the errors reported in previous literature [4-7].

There were strong correlations between the path lengths for the instruments (r=0.71) but a small correlation between the path widths (r=0.06). This indicates that the insoles were consistent in their measurements of path length but were not as accurate in their measurement of path width.

CONCLUSIONS

The Medilogic® insoles seem reasonably accurate in measuring COP when examining all the sizes of the insoles. However, there is a large variation in the errors for each insole. Further, the correlations show that the insoles are limited in measuring path width. Future experiments should only use the insoles for qualitative measurements of COP as each insole may respond differently.

REFERENCES

1. Laroche et al. *Osteoarthitis and Cartilage*. **23**:1357-1366, 2015
2. Zumbrunn et al. *Gait & Posture*. **34**(2):174-177, 2011
3. Dixit and Maiya. *J. Postgraduate Medicine*. **60**(1): 33, 2014.
4. Chumanov et al. *Proceedings of 30th Annual Meeting of ASB*. Palo Alto, CA, USA 2007.
5. Debbi et al. *The Foot*. **22**:269-275, 2012.
6. Chesnin et al. *Gait & Posture*. **12**(2):128-133, 2000
7. Cordero et al. *J. of Biomechanics* **37**(9):1427-1432
8. Lidstone et al. *SWACSM*. Long Beach, CA, USA 2017

ACKNOWLEDGEMENTS

The project described was supported by a grant from the National Institute of General Medical Sciences (GM103440).

Table 1: The mean and mean absolute deviation in the path length (ΔL) and the path width (ΔW) in millimeters.

Insole Size	35-36	37-38	39-40	41-42	43-44	45-46	All insoles
No. of Subjects	9	22	11	8	9	6	65
ΔL (mm)	-8.7 (11.6)	3.7 (9.6)	4.2 (7.6)	3.0 (14.6)	-4.7 (16.2)	17.4 (6.1)	1.7 (12.1)
ΔW (mm)	-5.8 (2.7)	-6.5 (2.8)	-3.1 (3.3)	-9.6 (3.5)	-2.0 (3.8)	-1.9 (3.6)	-5.3 (3.5)

ELLIPTICAL ESTIMATION OF PLANTAR CONTACT AREAS DURING WALKING

[1] Jessica DeBerardinis, [2] Daniel Lidstone, [2] Janet S. Dufek and [1] Mohamed B. Trabia

[1] Mechanical Engineering Department [2] Kinesiology and Nutritional Sciences Department
University of Nevada Las Vegas, Las Vegas, NV
email: deberj1@unlv.nevada.edu

INTRODUCTION

Plantar contact area (CA) has been used as a measure to examine the effectiveness of interventions to address injury risk in diabetic patients with neuropathy and used to classify foot structure [1-2]. Several methods have been used to measure CA. Electronic pedography using pressure-measuring insoles has the advantage of portability. Recently, it has been shown that these insoles can measure the CA accurately [3]. However, insoles pixelate the contact area due to the sensor resolution, which does not reflect the true shape of the contact area. While ellipses have been used in contact models [4], they have not been verified to be accurate measures of contact area.

It is proposed that ellipses fitted to the CA as defined by the insoles can better represent the shape of the CA of the foot. We present an approach to automatically fit ellipses to specific anatomical regions of the foot. The resulting elliptical CA was compared to the corresponding results from an optical pedography procedure.

METHODS

A single participant (21 yrs, 57 kg, 1.63 m) who wore an insole size of 39-40 (Euro) gave institutionally-approved written consent (IRB #772154) to participate. The data were collected using a previously described protocol [3]. In this protocol, the participant was dressed in black, with their right foot bare. Their left foot was fitted with an insole (Medilogic®, Schönefeld, Germany). The insole was placed inside a sock, provided by the researchers, to simulate barefoot walking. The participant was asked to walk across an elevated acrylic walkway while a camera captured the bare right foot compressing against the acrylic. The participant completed five practice walks and then data were collected for a total of 10 walking trials.

The insole data and the digital images of foot contact were processed as previously described [3]. The contact area of the insole was sorted into anatomical regions: heel, midfoot posterior, midfoot anterior, metatarsals 1-2, metatarsals 3-5, toes 3-5, toe 2, and toe 1 (Fig. 1).

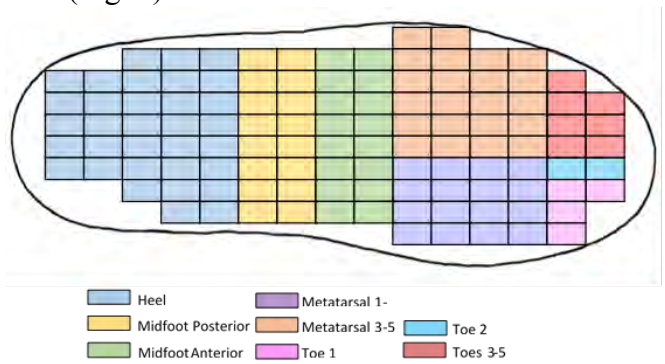

Figure 1: Example of the sensors organized into their respective anatomical regions.

In order to fit an ellipse, the CA of the insole for each region was assessed using four cases:
(1) Isolated Sensors: Isolated sensors were considered an anomaly and were not considered in this analysis. The only exceptions were isolated sensors in the heel at initial heel strike or in the toes.

(2) Rectangular CA: These areas were fitted with an ellipse with the same area and aspect ratio as the rectangle as follows:

$$a = \frac{N_r W}{\sqrt{\pi}} \quad (1)$$

$$b = \frac{N_c H}{\sqrt{\pi}} \quad (2)$$

where a is the radius of the ellipse in the x axis, b is the radius of the ellipse in the y axis, N_r is the number of sensors in a row, N_c is the number of sensors in a column, W is the width of the sensor of 0.75cm, and H is the height of the sensor of 1.5cm.

(3) Irregular CA: These areas were fitted by ellipses that best matched points placed around the boundary using a least squares method [5].

(4) Long Irregular CA: For areas with long aspect ratios, the methods of Case (3) resulted in large errors. In these cases, the radii along the long aspect ratio was adjusted using the equations:

$$a = (N_r + N_c - 1)\frac{W}{\sqrt{\pi}} \quad (3)$$

$$b = (N_r + N_c - 1)\frac{H}{\sqrt{\pi}} \quad (4)$$

The CAs for the ellipses in each region were identified and summed to determine the total CA for the entire foot during the stance phase.

The total CA from the ellipses, insole, and digital assessment were plotted against time. They were then compared to each other using the following variables from each measurement (Fig. 2):
(1) Midstance CA: The midpoint of the CA curve.
(2) Impulse CA – the integration of the CA-time curve.

These results of the techniques (Table 1) were compared using descriptive statistics. A qualitative assessment was also used to compare the general shape of the ellipses versus the results of the digital technique.

RESULTS AND DISCUSSION

The results show that the mid-stance CA and the impulse and of the three techniques were close. Qualitatively, it can be seen that the area measured by the ellipses is similar in shape to the area measured digitally.

Table 1: Comparison of the midstance and Impulse for each technique.

	Midstance CA (cm^2)	**Impulse ($cm^2 \cdot s$)**
Photography	80.88 (1.91)	41.78 (1.83)
Insole (Raw)	83.25 (2.25)	41.72 (1.52)
Insole (Elliptical Fitting)	84.15 (2.34)	41.93 (1.43)

Figure 2: A qualitative assessment of the accuracy of the ellipses to assess the contact area of the foot at midstance. Top: video images of the foot contacting the acrylic walkway; Middle: CA results of the digital technique; Bottom: insole sensors and the ellipses fitted to them.

CONCLUSIONS

The CA measured using an elliptical fit to the insole sensors resulted in areas that were relatively accurate for midstance and the overall impulse of the CA when compared to the digital technique. However, this experiment is limited to a single participant and does not assess the various phases of gait. Further experimentation is needed to examine the results at heel strike and toe-off and to assess if these results are consistent across multiple participants.

REFERENCES

1. Gus SA, et al. *Clin Biomec*. **19**:629-638, 2004.
2. Gutiérrez-Vilahú L, et al. *J Am Podiatr Med Assoc*. **105**:226-232, 2015.
3. Lidstone D, et al. *SWACSM.* Long Beach, CA, USA 2017.
4. Lopes D., et al., *Comp. Meth. Biomech. & Biomed. Eng.* **19(9):**954-963, 2015.
5. Brown R. *FITTELLIPSE: Least squares ellipse fitting.* 2007.

ACKNOWLEDGEMENTS

Partially supported by a grant from the National Institute of General Medical Sciences (GM103440).

ENERGY RETURN IN PROSTHETIC FEET FOR HIGH ACTIVITY USERS DURING WEIGHTED AND UNWEIGHTED WALKING

[1,2] Clifford A. Dellamano, [3] Samuel Ray, [3] Barri L. Schnall, [3,4,5] Brad D. Hendershot,
[1] Sara R. Koehler-McNicholas, [1,2] Andrew H. Hansen

[1] Minneapolis VA Health Care System, Minneapolis, MN, USA
[2] University of Minnesota, Minneapolis, MN, USA
[3] Walter Reed National Military Medical Center, Bethesda, MD, USA
[4] DoD-VA Extremity Trauma and Amputation Center of Excellence, USA
[5] Uniformed Services University of the Health Sciences, Bethesda, MD, USA
email: clifford.dellamano@va.gov

INTRODUCTION

Energy storage and return (ESAR) prosthetic feet enhance mobility and are the standard of care for highly active prosthesis users [1]. However, there are limited data comparing current commercially-available ESAR prosthetic feet for this population, and it is unclear how these devices react to weighted walking. This information could be highly valuable to clinicians to assist with the prescription of prosthetic feet. The goal of this study was to analyze the energy return capabilities of nine commercially-available prosthetic feet during weighted and unweighted walking conditions.

METHODS

This study was approved by the Institutional Review Board at the Minneapolis VA Health Care System. Three high functioning (K4) male subjects with unilateral transtibial amputation (age: 39 ± 6 yrs, mass: 85 ± 14 kg, height: 1.76 ± 0.05 m) were tested with nine commercially-available prosthetic feet: All Pro (Fillauer, Chattanooga, TN), Panthera CFII (mediUSA, Whitsett, NC), Renegade AT (Freedom Innovations, Irvine, CA), Rush Foot (Ability Dynamics, Tempe, AZ), Soleus Tactical (College Park, Warren, MI), Thrive (Freedom Innovations, Irvine, CA), Trekk (Makstride Prosthetics, Prescott, AZ), Triton Heavy Duty (Otto Bock, Duderstadt, Germany), and Variflex XC (Össur, Reykjavik, Iceland). Prosthesis order was randomized. Reflective markers were placed on subjects using a modified Helen Hayes marker set (Fig 1, left; [2]).

Subjects walked with and without a 22-kg weighted vest over a set of two AccuGait force platforms (AMTI, Watertown, MA, sampling rate=1200 Hz) at a constant, self-selected walking speed. Markers were tracked using an eight-camera Oqus 100 motion analysis system (Qualisys Motion Capture Systems, Gothenburg, Sweden, sampling rate=120 Hz) until three clean force platform contacts were obtained.

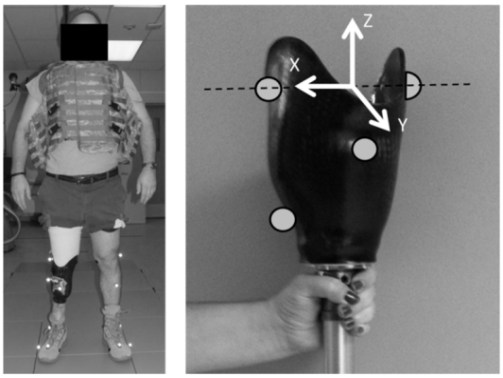

Fig 1. Marker placement used for the unified deformable segment analysis.

A unified deformable (UD) segment analysis [3] was used to calculate total energy return of the keel using Visual3D (C-Motion, Inc., Germantown, MD). Compared to a traditional inverse dynamics analysis, the UD segment analysis considers all components below a rigid prosthetic socket a deformable mass to more accurately capture the energetics of prosthetic structures. In this study, the proximal rigid segment was defined and tracked using markers on the residual limb socket (Fig 1, right).

Total energy return of the keel was quantified by integrating all power done by the prosthesis between zero crossings near the end of single support and at toe off. These data were then averaged for each foot and weight condition across their respective trials

and normalized by subject mass (including the 22-kg mass when relevant) to determine the average energy return values for each prosthesis in both the weighted and unweighted conditions. These averaged data were then compared to prosthetic forefoot stiffness in a region between body weight and body weight plus the added load (i.e., stiffness above body weight). The testing procedure to obtain these forefoot stiffness values has been detailed previously [4].

RESULTS

Energy return (normalized by mass) ranged from 0.09 to 0.22 J/kg across feet (Fig 2).

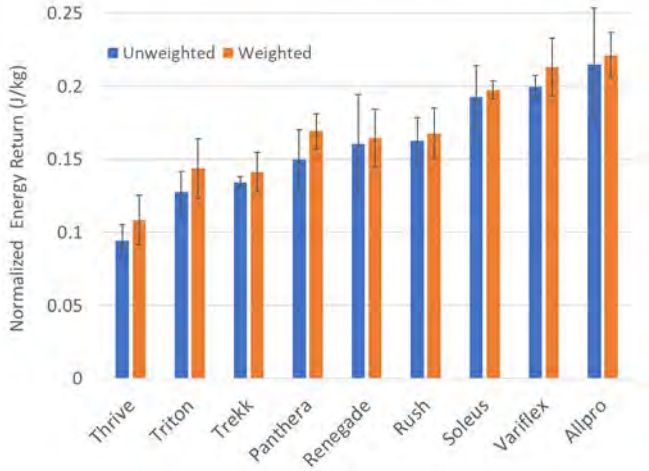

Fig 2. Mean (± 1 standard deviation) normalized energy return values across all ankle-foot systems.

Stiffness above body weight (normalized by body weight) ranged from 0.04 to 0.09 %BW/mm (Fig 3).

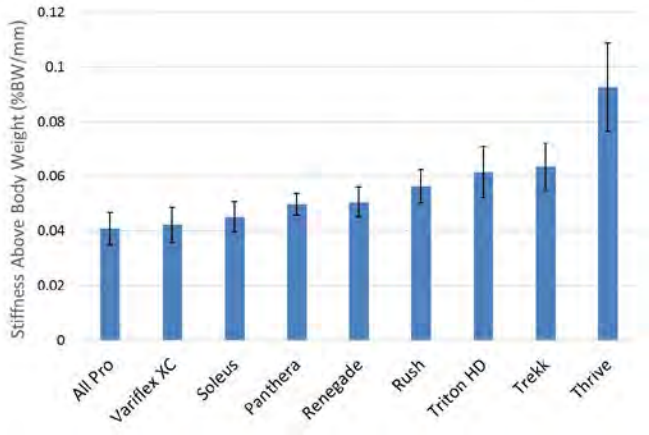

Fig 3. Mean (± 1 standard deviation) normalized stiffness above body weight across all ankle-foot systems.

DISCUSSION

Energy return may be a useful measure to guide the prescription of prosthetic feet, as increased energy return is thought to reduce the metabolic cost of walking and reduce sound limb loading [5]. The results of this study showed a wide range of energy return values across prosthetic feet. The prosthesis with the most energy return (All Pro) exceeded the foot with the least energy return (Thrive) by a factor of nearly 2.5. Energy return did not vary considerably in any of the ankle-foot systems tested under weighted conditions. As can be seen from Figs 2 and 3, the prosthetic feet with the lowest stiffness above body weight (e.g., Soleus, Variflex, and All Pro) yielded the highest normalized energy return. The feet with the highest stiffness above body weight (e.g., Thrive, Triton, and Trekk) yielded the lowest normalized energy return. The Thrive is designed with an additional strut to limit deflection, but this feature may limit energy return from the foot. It is possible that this feature may be more important when carrying heavier loads. Future research will determine the effect of stiffness above body weight on other functional outcomes of the prosthesis user.

REFERENCES

1.Hafner et al. *J Rehabil Res Dev* 39(1):1-11, 2002.
2.Kadaba et al. *J Orthop Res* 8(3):383-92, 1990.
3.Takahashi et al. *J Biomech* 45(15):2662-7, 2012.
4.Koehler-McNicholas et al. *Proceedings of ASB*, Boulder, CO, USA, 2017.
5.Caputo and Collins. *Sci Rep,* 4(7213):1-9, 2014.

ACKNOWLEDGEMENTS

We would like to thank Kyle Barrons, Spencer Mion, Eric Nickel, Kathryn Blaharski, and Billie Savvas Slater for their assistance with data collection. This work was supported by the BADER Consortium via the Congressionally Designated Medical Research Program (Award # W81XWH-11-2-0222).

The views expressed are those of the authors and do not reflect the official policy of the Department of Army/Navy/Air Force, Department of Defense, Department of Veterans Affairs, or any other branch of the United States Government.

Energetics and stability of running on rough terrains

Nihav Dhawale[1,2,†] and Madhusudhan Venkadesan [1]

[1]Department of Mechanical Engineering and Materials Science, Yale University, New Haven, CT, USA
[2]National Centre for Biological Sciences–Tata Institute of Fundamental Research, Bangalore, Karnataka, India,
[†]nihav.dhawale@yale.edu

Introduction

Better understanding of how humans run stably on rough terrains has implications for human evolution, sports and legged robotics. However, most studies on running have been performed on flat terrains [but see 1]. Studies like [1] that used step-like obstacles mimic some aspects of rough terrains, but lack sloping features that may have a significant impact on stability [2].

Dynamics and energetics of running on rough terrains that resemble natural trails is the topic of this study. Specifically, we test a hypothesis arising from previous mathematical analyses [2] that runners minimize the tangential collision with the ground to improve stability.

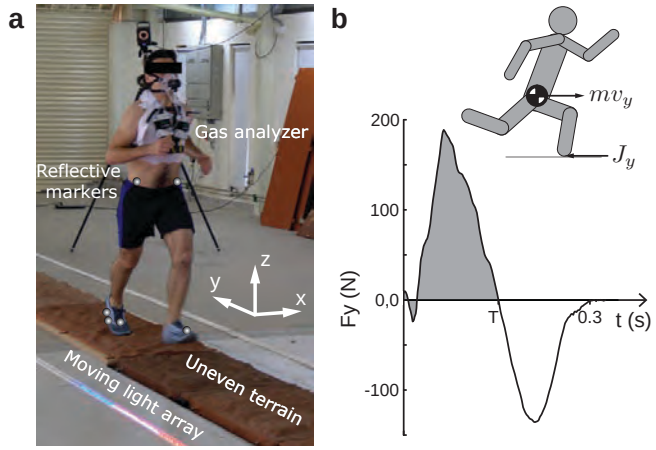

Figure 1: **a**, Experimental set up. **b**, Fore-aft ground reaction force during stance (+Y as in panel (a)). The area of the shaded region is the retarding impulse J_y.

Methods

Nine consenting and able-bodied runners (1 female, 23-45 yrs, approved by NCBS IRB), ran back-and-forth for 8–10 min on 3 different tracks of 24m length each. Two tracks were custom-made rough terrains (*Uneven II* rougher than *Uneven I*) and one flat track. Speed was controlled using lights moving at 3m/s on either side of the track (Fig. 1a).

We recorded kinematics of the hip and foot using an 8-camera motion capture system (Vicon Inc.), and ground reaction forces at the middle of the track using two force plates (AMTI Inc.). Mobile gas analyzers (Oxycon Mobile, CareFusion Inc.) recorded breath-by-breath respirometry data.

Baseline subtracted (quiet standing), steady state (first 3 minutes excluded) oxygen consumption rates were averaged and normalized by the runner's mass and speed.

Center of mass (CoM = average of the hip markers) trajectory during stance was fitted with a regression line in the horizontal plane, and twice the distance of nearest approach of the foot from this line is defined as the step width. Meander away from a straight trajectory is defined as $(d - d_0)/d_0$, where d is the distance traversed by the CoM in the horizontal plane during a single run across the length of the track, while d_0 is the track length.

The maximum retarding impulse J_y during stance is treated as a tangential collision (Fig. 1b), and the fractional loss $\hat{\epsilon}_\mathrm{t}$ of the forward momentum mv_y due to this collision is given by,

$$\hat{\epsilon}_\mathrm{t} = \frac{(mv_y - J_y)}{mv_y},\ J_y = \max_T \int_0^T F_y\, dt'. \qquad (1)$$

Forward speed v_y is the CoM's speed just before stance.

Comparisons of the mean and standard deviations of energetic, kinematic, and kinetic variables across terrain conditions are performed using a linear mixed-model (LMM) in R. Terrain is a fixed factor, subject a random factor, and multiple steps of a single run are treated as repeated measures. The significance threshold was 0.05. Post-hoc comparisons were performed when the LMM was significant.

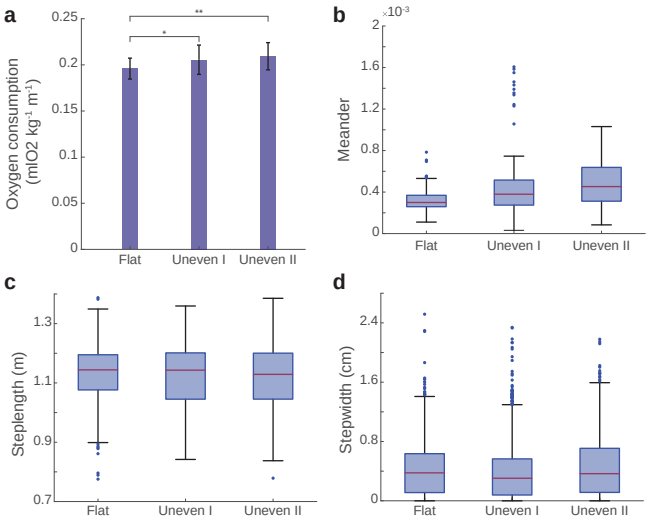

Figure 2: Energetics and kinematics. **a**, Oxygen consumption (whiskers: standard deviation). **b**, Meander. **c**, Step length. **d**, Step width. Boxes: interquartile range, horizontal line: median, whiskers: $1.5\times$ interquartile range, dots: outliers.

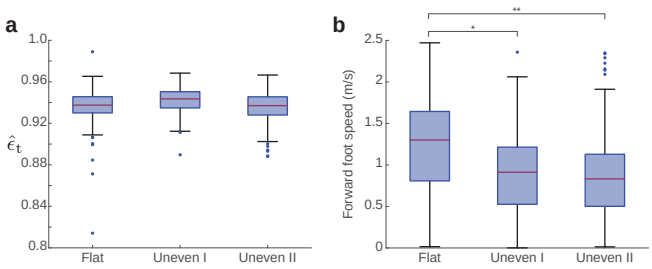

Figure 3: Control of tangential collisions. Boxes in all boxplots represent the interquartile range with the line in the box representing the median. Whiskers extend to $1.5\times$ the interquartile range. Filled circles denote outliers. **a**, On all terrains, $\hat{\epsilon}_t = 0.94 \pm 0.01$ (mean $\pm$ standard deviation). **b**, Forward foot speed at landing.

Results and Discussion

Oxygen consumption depends on terrain type ($p<0.05$). Compared to the flat track, oxygen consumption increased by 4.9%$\pm$2.4% on *Uneven I* ($p=0.06$, mean$\pm$std. error), and by 6.8%$\pm$2.5% on *Uneven II* ($p=0.01$, Fig. 2a). These resemble the 5% increase in O_2 consumption to run on step-like terrains [1], and are far smaller than the 28% increase reported [3] for walking on step-like terrains.

Meander was terrain independant and small, as subjects traversed a mere 1m extra per km of the track (Fig. 2b). Mean step length and width are terrain dependant ($p<0.01$ for both), while their standard deviation is not (Fig. 2c,d). However differences in mean step length are smaller than a foot length (Δ*Uneven I*=21$\pm$2mm, $p<0.01$ and Δ*Uneven II*=13$\pm$2mm, $p<0.01$). Mean step width differences were statistically significant, but barely greater than measurement resolution for this capture volume (Δ*Uneven I*=–2mm, $p<0.01$ and Δ*Uneven II*=6mm, $p<0.01$).

Mean foot speed at landing is terrain dependant ($p<0.01$, Fig. 3b) while its standard deviation is not. On *Uneven I*, the mean foot speed is lower than flat ground by (0.39$\pm$0.03) m/s, and on *Uneven II* by (0.38$\pm$0.03) m/s ($p<0.01$ for both). These differences are an appreciable fraction of the forward speed $\approx$3m/s.

As hypothesized by [2], runners maintained low tangential collisions on all terrains, losing only 6$\pm$1% (mean $\pm$ std. dev.) of their forward momentum during the retarding phase of each stance period (Fig. 3a). Mean $\hat{\epsilon}_t$, unlike $\hat{\epsilon}_t$ variability, was terrain dependant ($p<0.01$), although the difference in mean $\hat{\epsilon}_t$ values between flat and rough terrains was only $\sim 10^{-3}$. However, the low collision is not accounted for by control of leg retraction speed. An $\hat{\epsilon}_t \approx 1$ requires foot speed at landing to be $\leq$0.2 m/s, which is significantly lesser than the recorded speeds $\approx$1m/s (Fig. 3b). We speculate that runners use stiffness modulation at the joints of the foot and leg to mitigate tangential collisions.

The evidence supports the hypothesis that humans maintain low tangential collisions to run stably on rough terrains, rather than increasing or varying step width. The low tangential collisions are likely the result of maintaining soft joints in the legs and feet.

References

[1] Voloshina, A.S. and D. Ferris. *J Exp Biol*, vol. 218, no. 5, pp. 711–719, 2015.

[2] Dhawale, N. and M. Venkadesan. *ASB Annual Meeting '15*, Columbus, OH, 2015, Abstract 52BD.

[3] Voloshina, A.S. et al. *J Exp Biol*, vol. 216, no. 21, pp. 3963–3970, 2013.

Acknowledgements: Human Frontiers Science Program and the Wellcome Trust/DBT alliance for funding. Shreyas Mandre for guidance with the project.

KINETIC ANALYSIS OF RODENT GAIT AFTER VOLUMETRIC MUSCLE LOSS INJURY AND TREATMENT

Jack Dienes, Conrad Slater, Kevin Janson, Juliana Passipieri, Ph.D., Ellen Mintz, Paige Miller, George Christ, Ph.D., and Shawn Russell, Ph.D.

University of Virginia, Charlottesville, VA, USA
Email: sdr2n@virginia.edu

INTRODUCTION

Much research is currently underway to develop novel methods for the regeneration of functional muscle tissue as treatment of volumetric muscle loss (VML) injury. To date, the method for evaluating functional gain has primarily focused on the ability of the muscle to generate force. However, studies of human movement have shown that gains in strength do not necessarily result in improvements in movement function. To address this knowledge gap, we have developed a novel method to quantify the changes in gait for rats with tibialis anterior (TA) VML injuries that illustrates biomechanical changes in response to the injury as well as during recovery. The ability to measure changes in rat gait parameters will facilitate our ability to quantify relevant functional deficits that result from VML injury, as well as the functional effectiveness of regenerated muscle volume after treatment.

We are the first group to successfully collect kinetic data on rodents, and we were able to detect significant differences in joint moments post-VML injury. We also used this method to determine the efficacy of one state of the art muscle regeneration material for treatment of VML injury. This represents a breakthrough in rodent gait analysis, and now that we can see how and why function changes this method can be expanded to evaluate any other human pathologies modeled in the rat hindlimb in order to inform the development of more effective treatments.

METHODS

23 twelve (12)-week old female Lewis rats were divided into three groups: 8 healthy animals (Control), 8 who received a 20% by mass VML injury to their right TA with no repair (NR, injured) performed, and 7 who received the injury and were treated with tissue engineered muscle repair (TEMR, treated) technology. The TEMR [1] construct is a bioreactor preconditioned scaffold prepared from porcine bladder lamina propria and seeded with muscle progenitor cells. The TEMR was implanted immediately upon creation of the VML injury.

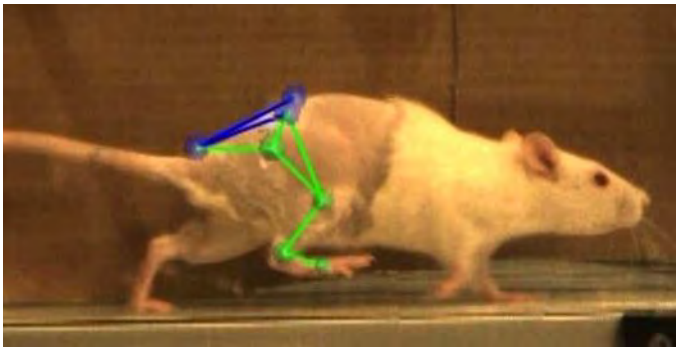

Figure 1. Overlay of 3-D markers, LASI, RASI, SPINE, TAIL, HIP, KNEE, and ANKLE on typical rat while walking on the treadmill. Marker locations shown as placed on test animals.

All animals were labeled with motion capture markers (Fig.1) and recorded using Vicon Nexus motion capture software as they voluntarily walked down an instrumented walkway at -1, 4, 8, and 12 weeks relative to their surgery date. The walkway contained two loadcells (ATI) centered in the collection space to record ground reaction forces. Marker locations were reconstructed in Nexus and transferred to OpenSim. Once in OpenSim, a modified version of an existing rat hindlimb model [2] was scaled to each individual rat at each timepoint. After model scaling, inverse kinematics and inverse dynamics were performed to calculate kinematic and kinetic curves for each animal. SPM1D statistical code was run in MATLAB to determine areas of significant difference between the kinetic and kinematic curves of the control, injured, and treated animals.

RESULTS AND DISCUSSION

Baseline sagittal plane kinematics [3] and measured ground reaction forces (GRFs) [4] were similar to previously reported data of normal gait in rats.

We were able to detect significant differences between all three treatment groups at the 12-week

timepoint at significance level 0.05 (Fig.2). As expected, there were differences in both the kinematics of hip flexion (HF), internal rotation (HIR), and adduction (HA) as well as kinetics (HF and HIR torques) for the NR animals as compared to the healthy controls. Also as expected, there were differences between the kinematics (HF, HIR, HA) of the NR group and the TEMR group, and no differences between the TEMR group and the Control group. However, there were differences between the kinetics (HF and HIR torques) of the TEMR group and the Control group and no differences between the kinetics of the NR group and the TEMR group, although there were areas approaching significance. This tells us that our kinetic data is still slightly noisy, and that we would benefit from higher power in the form of larger groups in future studies.

As a dorsiflexor, an injury to the TA causes a drop foot response in humans. There are two methods of compensating for drop foot, vaulting gait and circumduction, both of which were seen in our injured and treated groups. The results seen in the NR animals at the 4-week timepoint indicate a clear shift towards vaulting gait, as evidenced by increased hip flexion and hip flexion torque at toe-off. As the healing process continues our data shows a compensatory transition from vaulting gait to classic circumduction, an exaggerated external rotation of the hip to help clear the injured foot from the floor. Similarly, the TEMR animals exhibited classic circumduction throughout the 12-week observation period. Our healthy control animals showed no significant differences in their gait patterns throughout the duration of the testing.

CONCLUSIONS

The ability to model kinetics represents a breakthrough in the analysis of rodent gait biomechanics and advances the ability of researchers to evaluate the quality of their treatment methodologies. Whereas force generation and kinematics provide partial pictures about the functional recovery of an animal, kinetics ties the story together. With this information we get feedback on joint control, allowing us to understand how the body is utilizing new strength from regenerated muscle or lack of strength from a catastrophic injury and compare that information to a healthy baseline. This gives us the ability to confidently assess where and why functional differences are occurring, which will allow us to fine-tune therapies to address these differences. Ultimately, this research informs targeted treatments to facilitate a return to natural gait patterns rather than adoption of a pathologic gait.

REFERENCES

1. Corona et al, 2013, *Tis Eng Part A* 20(3-4) 705-15.
2. Johnson et al, 2008, *J Biomech* 41(3) 610-619.
3. Garnier et al , 2007, *Behav Brain Res* 186 57-67.
4. Howard et al, 2000, *J Biomech* 33(6) 751-757.

ACKNOWLEDGEMENTS

This work was supported in part by the AR^{3}T Pilot Funding Program.

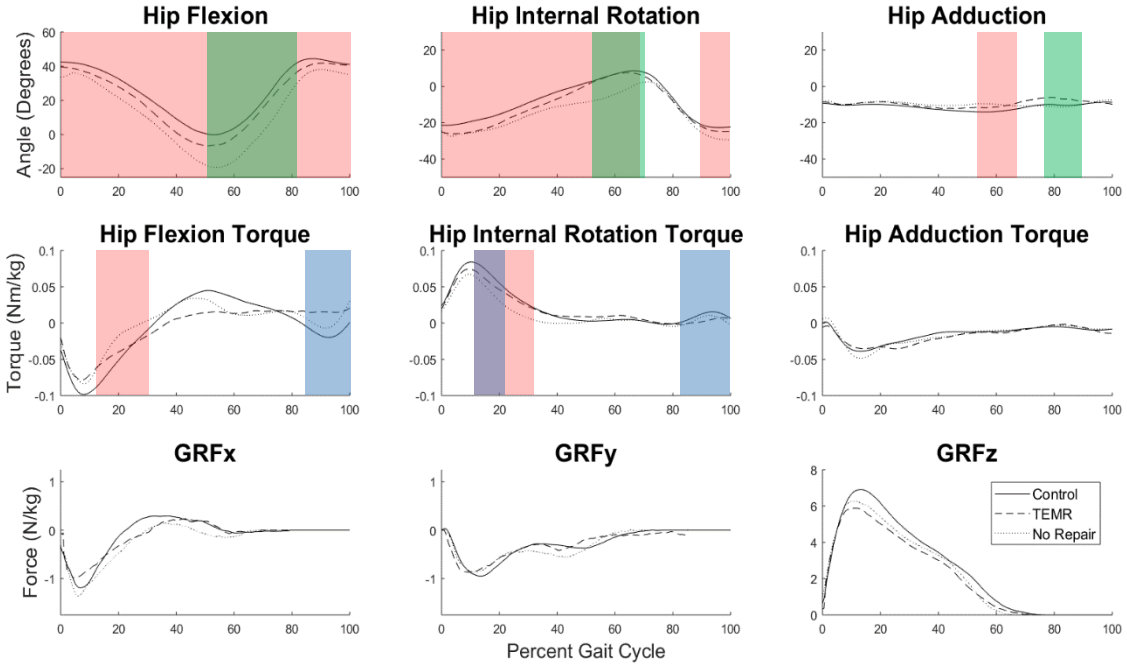

Figure 2.
12 week comparison of Control vs. NR vs. TEMR treated animals. Kinematics are shown in the top row, kinetics in the middle row, and GRFs in the bottom row. Shaded areas represent regions of significant difference (p=0.05). Red illustrates differences between Control and NR, blue is between Control and TEMR, and green is between TEMR and NR.

FOOTSTRIKE PATTERN EFFECTS ON SAGITTAL KNEE MECHANICS IN RUNNERS WITH TRANSTIBIAL AMPUTATION: INITIAL OBSERVATIONS

Tatiana Djafar, Katherine Sharp, Julianne Stewart, Jenny Anne Maun, Kimberly Rowe, John-David Collins, Trevor Kingsbury and Marilynn Wyatt
Naval Medical Center San Diego, San Diego, CA, USA
email: tatiana.e.djafar.ctr@mail.mil

INTRODUCTION

In recent years, able-bodied runners are more frequently categorized based on footstrike patterns – namely forefoot strikers (FFS) and rearfoot strikers (RFS) – in an effort to understand strike pattern's effects on running biomechanics and related risk of injury. However, there has been little research on these effects in the population of runners with amputation despite higher reported rates of injury, most commonly overuse injuries in the intact limb [1]. The purpose of this study was to compare sagittal knee mechanics – specifically knee flexion at initial contact (KF), peak knee flexion moment (KFM), and peak knee power absorption (KPA) – of runners with amputation using a FFS with their intact limb to those using a RFS with their intact limb. It was hypothesized that FFS would demonstrate increased KF, decreased peak KFM, and decreased peak KPA in their intact, unaffected limb compared to RFS as reported in able-bodied literature [2]. Additionally, it was hypothesized that FFS would present as more symmetrical between limbs in all variables due to the "forefoot" position and alignment of the prosthesis [3].

METHODS

Four subjects (age 32 ± 8years; height 1.8 ± 0.1m; weight 78.1 ± 15.8kg) with unilateral, transtibial amputation provided informed consent under a research study approved by the Naval Medical Center San Diego Institutional Review Board (CIP# NMCSD-2013.0109). All subjects had been medically cleared for high-level activity by their providers and were prescribed the same running specific prosthesis (Össur® Flex-Run™).

Data were collected overground using a mobile motion capture system which included 12 Raptor-E infrared cameras (Motion Analysis Corp., Santa Rosa, CA, USA) erected around four portable force plates (Kistler Instrument Corp., Amherst, NY, USA) embedded within a modular walkway. Frontal and sagittal high-speed videos (Nikon Corp., Tokyo, Japan) were taken for reference purposes. Three-dimensional marker positional data were sampled at 300Hz by the camera system, and the force plates sampled analog GRF data at 1800Hz. Kinematic and kinetic data were processed using Visual3D software (C-Motion Inc., Germantown, MD, USA), and a fourth-order, bi-directional Butterworth filter was applied with cut-off frequencies at 8Hz and 50Hz respectively.

The subjects were outfitted with a 6 degrees of freedom, full-body marker set and instructed to run through the capture volume at $3.5 m \cdot s^{-1} \pm 5\%$ during data collection, which concluded after a minimum of three clean force plate strikes and five complete gait cycles per leg were recorded within the specified velocity range. Group designation for three subjects was determined using strike index calculation at initial contact of the intact limb (FFS > 33%, RFS ≤ 33%) [4]. Sagittal reference videos confirmed calculated footstrike patterns and were also used to solely determine the footstrike pattern of one subject for whom strike index was unavailable. Using video, initial contact with the forefoot or midfoot was considered FFS while initial contact with the heel or hindfoot was considered RFS.

RESULTS AND DISCUSSION

Two subjects were identified as FFS, and two subjects were identified as RFS. Descriptive statistics are presented in Table 1. We found some disagreement with our hypothesis with regards to knee flexion at initial contact: while FFS landed with overall increased flexion compared to RFS as expected, both groups had symmetrical KF between limbs, which was unexpected.

Also contrary to our proposed hypothesis, similar values were observed for peak KFM between groups for both the affected and unaffected limbs (Fig. 1).

The unaffected limb of FFS demonstrated decreased peak KPA compared to the unaffected limb of RFS as hypothesized, and the FFS group displayed greater interlimb symmetry compared to the RFS group, though is notably still asymmetric (Fig. 1).

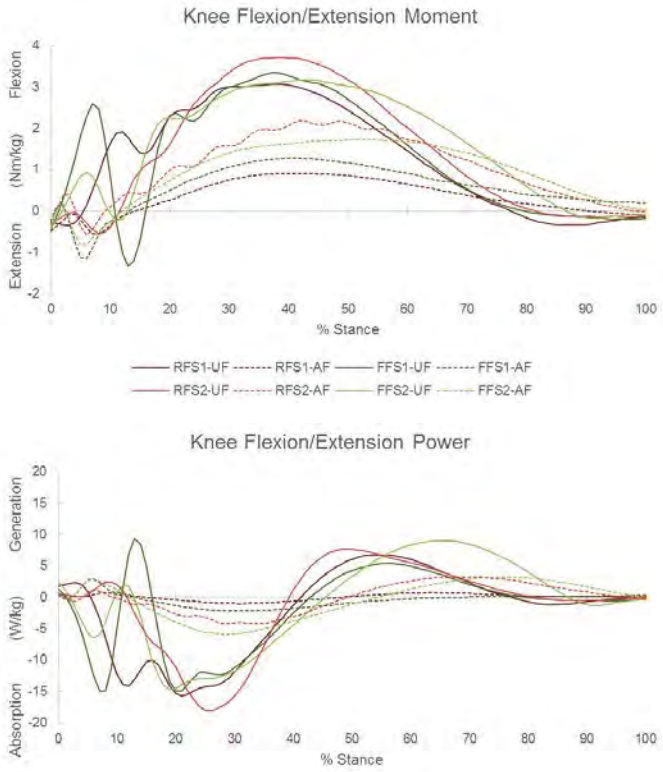

Figure 1: Signal means for Knee Flexion/Extension Moment (top) and Power (bottom) normalized to stance percentage for the affected (AF - dashed) and unaffected (UF - solid) limbs of FFS (green) and RFS (red) subjects

CONCLUSIONS

While the results presented here are preliminary in nature, there is evidence of inherent biomechanical differences between FFS and RFS in runners with amputation similar to those seen in able-bodied runners [2]. The decreased KPA of the unaffected limb for FFS in particular may be a factor in considering footstrike pattern conversion as a clinical intervention to reduce loading at the knee and potentially minimize overuse injury risk. However, more evidence is needed.

With two subjects in each group, sample size is the main limitation of this study. Future work will include additional runners with amputation as well as able-bodied runners using both footstrike patterns as a means of comparison. Other kinematic and kinetic measures will also be analyzed to determine additional interlimb asymmetries footstrike pattern may affect.

REFERENCES

1. Hobara H, et al. *Jpn J Biomech in Sports Exerc* **17**, 53-61, 2013.
2. Stearne S, et al. *Med Sci Sports Exerc* **46**, 1578-87, 2014.
3. Nolan L. *J Foot Ank Surg* **14**, 125-9, 2008.
4. Milner C et al. *Med Sci Sports Exerc* **38**, 323-8, 2006.

ACKNOWLEDGMENTS

Project was supported in part with resources provided by the Extremity Trauma and Amputation Center of Excellence (EACE).
DISCLOSURE STATEMENT: The views expressed herein do not necessarily reflect those of the Department of the Navy, Department of Defense, or U.S. Government.

Table 1: Descriptive statistics for the affected and unaffected limbs of FFS and RFS

	FFS		RFS	
	Affected	**Unaffected**	**Affected**	**Unaffected**
KF (°)	20.94 ± 0.52	23.26 ± 0.09	15.45 ± 0.02	16.89 ± 4.22
KF Difference (°)	2.32 ± 0.09		1.44 ± 4.24	
Peak KFM (Nm/kg)	1.50 ± 0.32	3.29 ± 0.06	1.50 ± 0.95	3.40 ± 0.44
Peak KFM Difference (Nm/kg)	1.79 ± 0.38		1.91 ± 0.52	
Peak KPA (W/kg)	4.00 ± 2.61	14.48 ± 0.25	2.64 ± 2.62	16.94 ± 1.53
Peak KPA Difference (W/kg)	10.49 ± 2.86		14.30 ± 1.08	

ALTERED KNEE LOADING PATTERNS OBSERVED IN CONTRALATERAL LIMB DURING MEDIAL KNEE THRUST

[1]Oladipo Eddo, [1]Bryndan Lindsey, [1]Matt Prebble, [1]Shane Caswell, [1]Nelson Cortes
[1]George Mason University, Manassas VA, USA
email: ncortes@gmu.edu, web: https://smartlab.gmu.edu/

INTRODUCTION

Joint load experienced during the load acceptance phase of stance has been shown to be strong predictor of medial compartment osteoarthritis (OA). [1] Numerous treatment and management options for knee OA have been recommended, including the use of non-pharmacologic, pharmacologic and surgical interventions with the goal of reducing symptoms and medial compartment loads. [2] Results from recent systematic reviews confirm the effectiveness of various gait modification strategies including reduced foot progression angle (FP), medial knee thrust (MKT), and trunk lean (TL) using real-time biofeedback (RTB) at reducing the magnitude of external knee adduction moment (KAM). [3,4] Despite the nature of these modifications, and their propensity to increase axial loading along the kinetic chain [1,3,4], potential effects on contralateral limb remains poorly understood. Therefore, the purpose of this study was to investigate the effects of MKT, TL, and FP strategies using RTB on the biomechanical parameters of the contralateral side. We hypothesized that implementing RTB would result in an altered loading pattern at the knee and hip of the contralateral side.

METHODS

Nineteen healthy participants (age 26.7±4.8 years; height 1.69±0.17 m; mass 72.3±11.8 kg) qualified for inclusion in the current study. Prior to data collection, dominant limb was established as the preferred swing leg in a kicking task. The biomechanics of the contralateral limb (non-dominant) was analyzed. Eight high-speed motion analysis cameras sampling at 200 Hz were used to track marker trajectory. Ground reaction force (GRF) was acquired using four floor embedded force plates located along a 6 meter walkway, and sampled at 1000 Hz. Fifty three retroreflective markers were attached to the trunk and lower extremity of participants.

Participants were instructed to complete 10 baseline gait trials along the laboratory walkway using a self-selected speed. Average walking speed was measured using timing gates positioned 2.4 meters apart, covering the length of the force plate area. Baseline trials were exported to Visual 3D for further processing.

Gait modification interventions

Ten trials were completed for each gait modification strategy using RTB ensuring joint angles fell within 1-3 standard deviations (SD) away from baseline average for the 1st 5 trials, and within 3-5 SD away from baseline average for the last 5 trials. RTB was delivered visually and projected as a line graph displaying the respective joint angle in real time during stance. Standardized verbal instructions were provided to participants before implementing each gait modification. Practice trials were allowed, and gait modification trials were valid if gait speed was within ±5% of average baseline speed (Table 1). The kinematic model created on Visual 3D was used to quantify the motion at the hip, knee, and ankle joints with rotations expressed relative to the static trial. Joint angles were measured in degrees (°), and all internal joint moments were normalized to mass and height (Nm/Kg.m). Ground reaction force data were normalized to body weight. Gait trials were normalized to the stance phase, and all variables were measured during the load acceptance phase. Repeated measures ANOVAs were performed to compare the results between gait conditions ($p<0.05$).

RESULTS AND DISCUSSION

Hip flexion at peak knee extension moment (PKeM) was significantly different from baseline to gait

modification conditions ($F_{6, 108}$ = 10.227, P<0.001). Participants walked with increased hip flexion angles at PKeM during both levels of MKT compared to baseline. MKT also resulted in increased knee flexion angles at PKeM compared to baseline ($F_{6, 108}$ = 11.528, P<0.001). For the MKT intervention, knee extension moment impulse was significantly greater compared to baseline ($F_{4.032, 108}$ = 5.437, P=0.001). Peak KeM significantly increased when using MKT compared to baseline ($F_{6, 108}$ = 8.323, P<0.001). Lastly, MKT gait intervention resulted in increased vertical ground reaction force at peak knee flexion on the contralateral side during MKT ($F_{6, 108}$ = 5.859, P<0.001).

Result from this study suggests compensatory gait changes on the contralateral side when adopting MKT strategies. The altered loading environment in the contralateral limb is potentially due to the medialization of the force vector from the limb undergoing gait modification and the center of mass.

CONCLUSIONS

Changes in the gait mechanics of the contralateral limb can be regarded as an attempt to attenuate the increased loads experienced on the contralateral side. Alternatively, these kinematic and kinetic changes could be as a result of compromised gait patterns adopted to facilitate the execution of the implemented modification.

Future studies should investigate both the acute and chronic changes to the loading environment of the contralateral side specifically in pathological populations.

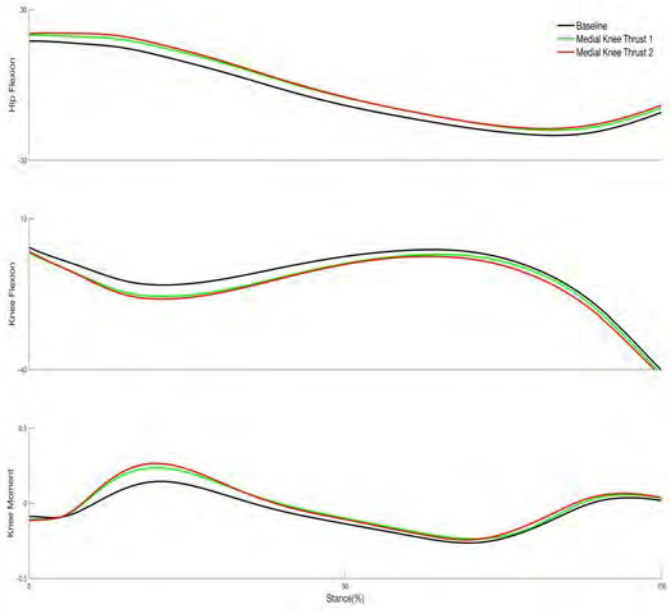

Figure 1: Effects of gait modification on hip flexion angle, knee flexion angle, and knee extension moment during stance.

REFERENCES

1. Simic M, et al. *Arthrit Care Res*., **63**(3): 405-426, 2011
2. Zhang W, et al. *Osteoarthritis and Cartilage*., **15**(9): 981-1000, 2007
3. Richards R, et al. *Osteoarthritis and Cartilage*., **24**(S1): S470, 2016
4. Eddo O, et al. *International Journal of Kinesiology and Sports Science*., **5**(3): 35–55, 2017

Table 1: Descriptive statistics (mean ± standard deviation) of gait speed and temporal spatial parameters across gait modification strategies. FP 1 = foot progression 1 to 3 SD, FP 2 = foot progression 3 to 5 SD, MKT 1 = medial knee thrust 1 to 3 SD, MKT 2 = medial knee thrust 3 to 5 SD, TL 1 = trunk lean 1 to 3 SD, and TL 2 = trunk lean 3 to 5 SD.

Gait characteristics	*Baseline*	*FP 1*	*FP 2*	*MKT 1*	*MKT 2*	*TL 1*	*TL 2*
Gait speed	1.34±.18	1.35±.19	1.34±.19	1.33±.19	1.33±.18	1.34±.19	1.34±.19
Stride length	1.41±.17	1.41±.18	1.40±.16	1.42±.18	1.43±.16	1.40±.17	1.41±.14
Stride width	0.13±.03	0.14±.03	0.14±.03	0.14±.03	0.13±.03	0.14±.03	0.14±.03

GAIT INITIATION: UNDERSTANDING BIOMECHANICS OF NON-STEADY MODULATIONS

Farzad Ehtemam

University of Maryland, College Park, MD, USA
email: fehtemam@umd.edu

INTRODUCTION

The assumption of steady-state gait has been used broadly in the study of human walking. While this has provided us with a simplified model of the system to work with, walking is an inherently non-steady motor output. Changing direction and speed of locomotion under normal and perturbed conditions is a control problem requiring real-time solutions from the nervous system. Recently we showed that perturbed walking exhibits control strategies not observable by applying common analysis methods to transient data (e.g. averaging over consecutive gait cycles) [1]. Equally important we believe is the understanding of the control process in transient phases of normal walking such as gait initiation and termination.

Gait initiation has been explored in a few studies in the past with analysis of changes in the ground reaction forces (GRFs) and kinematics [2-4]. It has been shown that people achieve their steady-state speeds within the first three steps during which center of pressure moves laterally. It is also known that this phase of the gait involves activation of tibialis anterior (TA) with a concurrent relaxation of bicep femoris and gluteus medius [5]. What is not clear however is the transient changes in muscle activations as a function of the phase of gait. A phase advance or a phase delay can reveal control strategies used during the initiation process. As a result, this study was designed to quantify transient patterns of muscle activity as a function of phase during each step.

METHODS

Fourteen college students (eight males) walked on an instrumented treadmill (Forcelink, Culemborg, Netherlands) for this experiment. Each trial started with a velocity ramp that went from zero to 1.3 ms^{-1} in 3 sec thus creating an acceleration of 0.43 ms^{-2}. The values for speed and acceleration were chosen based on reports of preferred walking speeds and accelerations in humans [6,7]. This acceleration phase was followed by 270 sec of walking at the steady speed of 1.3 ms^{-1} before the subject went through a deceleration ramp of 3 sec to come to a full stop. Kinematics was captured by tracking trajectories of twenty-seven reflective markers on the body using a motion capture system (Motion Analysis, CA, USA). A wireless sixteen channel TRIGNO system (DELSYS, MA, USA) was used to capture EMG signals from fourteen muscles. Data was recorded at the sampling rate of 1000 Hz.

We have developed a new method of organizing the gait data appropriate to analyze changes in initial steps during acceleration [8]. The start and the end of a step are defined as the anteroposterior alignment of the heel markers of both feet. Unlike the classical definition of a step which starts from heel-strike, our definition ensures the first step of movement which starts from both feet aligned to have the same temporal features as the following steps. Additionally, each leg during each step takes only the role of a leading leg (the leg that initiates the movement forward) or a trailing leg (the leg that has to catch up). This method has also the advantage of positioning the important events such as the heel-strike and the toe-off toward the middle of a step rather than at one end of the spectrum and this makes the understanding of modulations happening around these points easier.

RESULTS AND DISCUSSION

The step time, as well as timings of heel-strike and toe-off, reached their steady-state values within the first three steps (Figure 1). The initial step of the leading leg showed a delayed heel-strike while the initial step of the trailing leg went through a delayed toe-off. Transient modulations of TA activity in the figure for the leading leg shows an increase in the

activity around heel-strike (i.e. blue dots) and in the trailing leg TA activity increases after toe-off to provide support during the foot clearance.

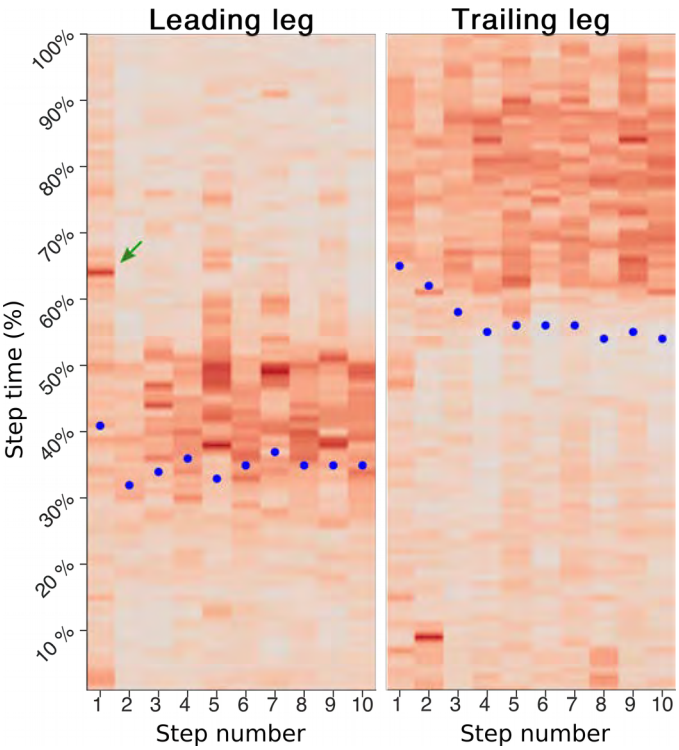

Figure 1: Transient modulation of TA activity during the first 10 steps after gait initiation. The horizontal axis shows the step number and the vertical shows the percentage of step time. The color is used as the third dimension to mark the changes in amplitude. *Left:* Changes during the steps for the leading leg averaged over subjects. The blue dots mark the timing of heel-strike for each step. The green arrow shows the peak of activity in the first step. *Right:* Changes during the steps for the trailing leg averaged over subjects. The blue dots mark the timing of toe-off for each step.

The activity of plantarflexors (see [8]) started to increase after the heel-strike for the leading leg and peaked before toe-off for the trailing leg. Quadriceps showed increased activity around heel-strike and hamstrings activities peaked during the late swing. These trends are in agreement with the roles traditionally assumed for different muscle groups in support and progression during steady-state walking. However, we also observed deviations from steady-state behavior for TA. Subjects consistently showed a delayed peak during the first step of the leading leg (the green arrow in the figure). Lack of a significant increase in the activity of TA around heel-strike is expected during the first step since the limb is experiencing low initial velocities and impact forces at the beginning compared to the following steps. However, an increase in the activity between heel-strike and mid-stance does not fit in the conventional role of TA which is stabilizing foot and ankle upon the impact during heel-strike. Further investigation is required to elucidate the role of TA in progression during transient modulations of gait. Of particular interest is a comparison of the changes presented here to those happening in gait termination.

The significance of the results presented here lies in the critical role of transient modulations in maintaining stability in gait initiation. Older adults and patients are at high risks of fall during this inherently non-steady phase of walking. A better understanding of functional roles of different muscles involved in this process is required in developing novel therapeutic approaches and designing new assistive devices.

REFERENCES

[1] F. Ehtemam, S. K. Hnat, T. Kiemel, and A. van den Bogert, *41st Annual Meeting of the ASB*, 2017.

[2] E.C. Wentink , S.I. Beijen, H.J. Hermens, J.S. Rietman and P.H. Veltink, *Gait & Posture*, 2013

[3] B.C. Muir, S. Rietdyk and J.M. Haddad, *Gait & Posture*, 2014.

[4] M. Anand, J. Seipel and S. Rietdyk, *the Royal Society*, 2017.

[5] S. Park, H. Choi, K. Ryu, S. Kim and Y. Kim, *J Mech Sci & Tech*, 2009.

[6] E. Bosina and U. Weidmann, *Physica A, vol. 468, no. C, pp. 1-29*, 2017.

[7] K. Teknomo, *Transportation Research Part F 9 15–27*, 2006.

[8] https://github.com/fehtemam/Gait_init/blob/master/Gait.Rmd

ACKNOWLEDGEMENTS

We would like to thank Dr. van den Bogert and his research team at Cleveland State University for their support and guidance during data collection.

Sex and Limb Impact Lower Limb Biomechanics During Loaded Single Leg Cuts.

Fain, A.C., Lobb, N.J., Seymore, K.D., Brown, T.N.
Dept. of Kinesiology, Boise State University, Boise, ID USA
email: auraleafain@u.boisestate.edu

INTRODUCTION

Female soldiers are two times more likely to suffer a musculoskeletal injury than males during military activities [1]. During military activities, soldiers wear heavy body borne loads that range between 20 kg and 40 kg, while performing dynamic tasks, such as a single-leg cut [2]. These body borne loads produce adaptations of lower limb biomechanics that elevate risk of musculoskeletal injury, including inducing neuromuscular patterns that reportedly increase proximal anterior tibial shear force and loading on the ACL [3]. During a single leg cut, body borne load reportedly produces a reduction in peak hip and knee flexion angle and an increase in associated hip and knee moments [4]. Females' injury risk may stem from a sex dimorphism in lower limb biomechanics evident during a single-leg cut. Females reportedly exhibit larger hip adduction and knee abduction angles and moments, biomechanics thought to increase risk of injury by producing valgus loading of the knee [5]. However, it is unknown if females exhibit a similar dimorphism of lower limb biomechanics during loaded single-leg cuts. Further, the non-dominant limb is reportedly weaker than the dominant limb [6], and may exhibit biomechanical adaptations that increase musculoskeletal injury risk during loaded single-leg cuts. This study sought to examine the impact of sex and limb on lower limb biomechanics during single leg cuts with heavy body borne loads.

METHODS

11 female and 17 male participants (1.74 ± 0.09 m, 75.69 ± 11.55 kg, 21.76 ± 2.66 years) had 3D lower limb biomechanics quantified during a series of single-leg cuts. Each participant performed the cut with four body borne loads (20, 25, 30 and 35 kg). For each load, participants carried a mock weapon, and wore a military issue helmet and weighted vest. The weighted vest was systematically adjusted to apply the load necessary for each condition. The single leg cut required participants run at 3.5 m/s ± 5%, before planting their foot (either dominant or non-dominant) on a force platform and cutting 45° towards the opposite limb. Participants completed five successful cuts off each limb.

During each single leg cut, lower limb biomechanics were quantified from 3D trajectories of 34 retroreflective markers and four virtual markers. A kinematic model, consisting of eight segments, was created from a static calibration using Visual3D (C-Motion, Rockville, MD). Synchronous ground reaction force (GRF) data and marker trajectories were low pass filtered with a fourth-order Butterworth filter (12 Hz). Filtered marker trajectories were processed to solve for 3D hip, knee and ankle rotations, while filtered kinematic and GRF data were processed using conventional inverse dynamics to calculate joint moments and knee joint forces. Proximal anterior tibial shear force was defined as the anteriorly directed y-axis force occurring at the proximal tibia. Forces were normalized to bodyweight, while joint moments were normalized to body mass multiplied by height.

Peak stance (0%-100%) hip and knee flexion, hip adduction and internal rotation, and knee abduction and external rotation angles and moments, and proximal tibial shear were quantified for analysis. Each variable was submitted to a RM ANOVA to test the main effect and interaction between load (*20 kg, 25 kg, 30 kg, 35 kg*), sex (*male, female*), and limb (*dominant, non-dominant*). Significant interactions were submitted to simple main effect analysis and a modified Bonferroni procedure was used for multiple comparisons. Alpha was set at $p < 0.05$.

RESULTS AND DISCUSSION

Body borne load may increase risk of knee injury during a single-leg cut. Specifically, peak proximal tibial shear force was significantly larger with the 35 kg compared to 20 kg ($p = 0.011$). An anteriorly directed knee shear force is thought to increase ACL

loading and increases risk of injury. But, this injury risk may differ between sexes. Loading of female's ACL may be more sensitive to body borne load, increasing their risk of injury during military activities. Females exhibited a significant increase in peak proximal tibial shear force with the 25 kg compared to 20 kg ($p = 0.028$), whereas, males did not exhibit a significant increase in proximal tibial shear until donning the 35 kg load configuration (compared to 20 kg: $p = 0.04$ and 25 kg: $p = 0.011$) (Fig. 1).

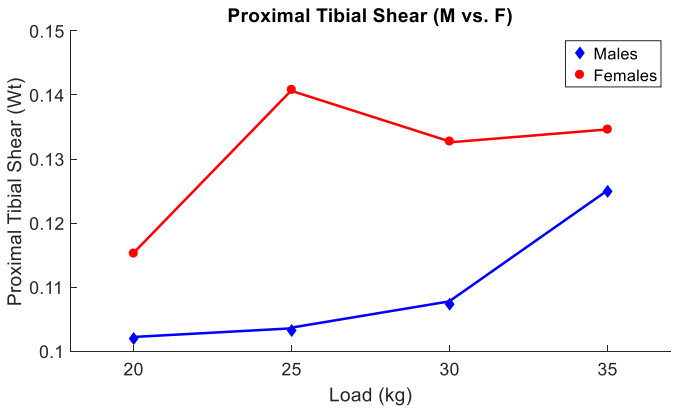

Figure 1: Depicts the peak proximal tibial shear for males (blue) and females (red) with each load condition (20 kg, 25 kg, 30 kg and 35 kg).

A sex dimorphism in lower limb biomechanics may further elevate females injury risk during the single-leg cut. Females exhibited hip and knee biomechanics related to dynamic knee valgus loads. Specfically, during the cut, females exhibited a significant increase in PS hip adduction angle ($p = 0.015$) and moment ($p < 0.001$), and knee external rotation ($p = 0.004$) moment compared to males. Both hip addution and knee external rotation are thought to increase valgus loading and injury risk at the knee. Males, however, relied upon larger sagittal plane hip and knee moments to complete the cut. Specficially, males significantly greater PS hip flexion ($p = 0.041$) and knee flexion moments – with 25 ($p = 0.040$) and 30 ($p = 0.022$) kg load configurations – compared to females. Larger sagittal plane hip and knee moments may affford males the ability to successfully execute the cutting maneuver, but aid in the transfer of high ground reaction forces and increase strain on the soft tisue structures of the limb.

Both limbs exhibited hip and knee biomechanics associated with dynamic valgus. During the single-leg cut, the dominant limb exhibited significantly greater PS hip adduction moment ($p = 0.010$), whereas, the non-dominant limb exhibited greater PS hip internal rotation angle ($p = 0.05$) and moment ($p = 0.07$), and knee abduction ($p = 0.047$) and external rotation ($p = 0.003$) moments. But, only the non-dominant limb exhibited a significant increase in biomechanical patterns reported to be a predictor of soft-tissue injury at the knee joint with the addition of load. Specifically, adding of body borne load produced a significant 40% increase in PS knee abduction moment in the non-dominant limb (Table 1; $p = 0.003$), but a similar increase was not evident in the dominant limb ($p = 1.000$).

Table 1: Peak knee abduction moments for each limb with each load configuration.

	Peak Knee Abduction Moment (Nm/kg*m)			
	20 kg	**25 kg**	**30 kg**	**35 kg**
Dom	0.313	0.265	0.312	0.331
Non*	0.280	0.353	0.331	0.396

* Denotes a significant load by limb interaction

CONCLUSIONS

Body borne load increase risk of knee injury during the single-leg cut. Participants exhibited a significant increase of the anteriorly directed tibial shear force with the addition of load. But, loading of females' ACL may be more sensitive to load compared to males. Further, both females and the non-dominant limb exhibit lower limb biomechanics thought to produce valgus loading of the knee and may have elevated injury risk. Future research is warrented to examine if body borne load produce knee valgus loading for both female military personnel and the non-dominnant limb in other military-related tasks.

REFERENCES

1. Bell NS, et al. *Am J of Prevent Med*, **18**, 141–6, 2000.
2. Dept. of Army Headquarters, *TB MED*, **592**, 2011.
3. Brown TN, et al. *J Sci Med Sport*, **17**, 408-13, 2014.
4. Brown TN, et al. *J Biomech*, **47**, 3494-501, 2014.
5. McLean SG, et al. *Clin Biomech,* **20**, 863-70, 2005.
6. McGrath TM, et al. *J Sports Sci*, **34**, 289-302, 2016.

DESTABILIZATION AFTER EXPECTED AND UNEXPECTED DISCRETE PERTURBATIONS DURING OVERGROUND GAIT

[1,2] Peter C. Fino

[1] Oregon Health & Science University, Portland, OR, USA
[2] Veterans Affairs Portland Health Care System, Portland, OR, USA
email: fino@ohsu.edu

INTRODUCTION

The ability to respond to small-scale perturbations and irregular surfaces is essential during daily locomotion, and techniques assessing the local dynamics of gait and response to small perturbations are increasingly used to quantify stability [1]. However, it is unclear how local dynamic stability relates to the response to discrete physical perturbations one may encounter during every-day, overground locomotion. Kim and Ashton-Miller used a novel perturbation device, embedded within a shoe, to deliver unexpected, discrete ankle inversion and eversion perturbations similar to stepping on a small rock [1]. They found changes in step length and step width for several steps following the perturbation, even in healthy young adults [2]. Yet, it is unclear the extent to which small perturbations destabilize the local dynamics of overground gait, and how knowledge of an upcoming perturbation affects the dynamic response following that perturbation. Here, a proof of concept if examined to characterize the dynamic response to discrete overground perturbations using a similar perturbation protocol to compare the responses following unexpected and expected perturbations.

METHODS

Two healthy adults (1F/1M, ages = 29/31 yrs.) performed a series of walking trials while instrumented with four inertial measurement units (IMUs) on the trunk, lumbar spine, and left and right feet (Opal v1, APDM, Inc.). Each participant wore a prototype of custom-built shoes capable of delivering a discrete ankle eversion or inversion perturbation through the deployment of an aluminum flap contained within a recess in the sole of the shoe (Fig 1) [2]. The flap was deployed during the swing phase of the foot using a servo motor embedded in the sole and controlled by an Arduino board affixed to the participant's shank just above the ankle. A speaker was connected to the control board to deliver a warning tone prior to some perturbations.

Figure 1: Left: The aluminum flap creating an inversion of the ankle. Right: The controller, containing a speaker was strapped on the shank above the ankle.

Participants walked for two-minutes at their comfortable pace between lines marked 9 m apart. Participants were informed there would be no perturbation during this trial. Following the baseline walk, participants completed three blocks of perturbation trials: unexpected, expected, and dual-task. Each block contained 6 trials with a perturbation (3 eversion, 3 inversion) and 9 trials where no perturbation was presented. Each trial consisted of walking down and back along the 9 m route. The perturbation was always delivered to the left foot, but the timing of the perturbation within the trial was random. During the expected perturbation block, the shoe delivered an auditory tone 1.5 strides prior to the perturbation. The auditory tone was delivered just prior to toe-off of the left foot. The order of the blocks was randomized across subjects. All procedures were approved by the Oregon Health & Science University Institutional Review Board.

Raw 3D accelerations were extracted from the trunk, lumbar, left and right foot IMUs for the baseline walk

and all blocked trials. Trials where the perturbation occurred within one step of the turn were excluded from this analysis, and only ankle inversion perturbations were considered in this proof of concept work. Left and right heel strikes (LHS, RHS) were determined using the frequency content of the accelerometer and gyroscopes on the left and right feet [3] and each stride was interpolated to normalize the duration of each gait cycle. For the baseline condition and each trial, a 9D state-space was constructed using the 3D accelerations and their twice time-delayed copies. To examine how the discrete perturbations alter body kinematics compared to a periodic attractor, the minimum Euclidean distance (d_{min}) to the baseline trajectory within the state space was computed for every point in each trial. d_{min} was descriptively compared across trials with expected, unexpected, and no perturbation.

RESULTS AND DISCUSSION

A total of 4 ankle inversion perturbations were retained (2 per participant) for analysis. Figure 3 displays average curves of d_{min} for unexpected and expected perturbations, respectively, compared to no perturbation.

Both unexpected and expected ankle inversion perturbations induced a divergence in the left foot away from normal gait, illustrated with the green arrows. However, only the unexpected perturbation appeared to influence the dynamics at the lumbar region representative of the center-of-mass. Additionally, the dynamics at the lumbar region appeared to only be altered by the unexpected perturbations at the weight transfer phase of gait surrounding heel contacts. These descriptive results also agree with previous studies that reported even small ankle perturbations may disrupt gait dynamics for several steps [2]. Ongoing and future work will examine how simultaneous cognitive tasks or neurological injury affect the dynamics following small unexpected and expected perturbations.

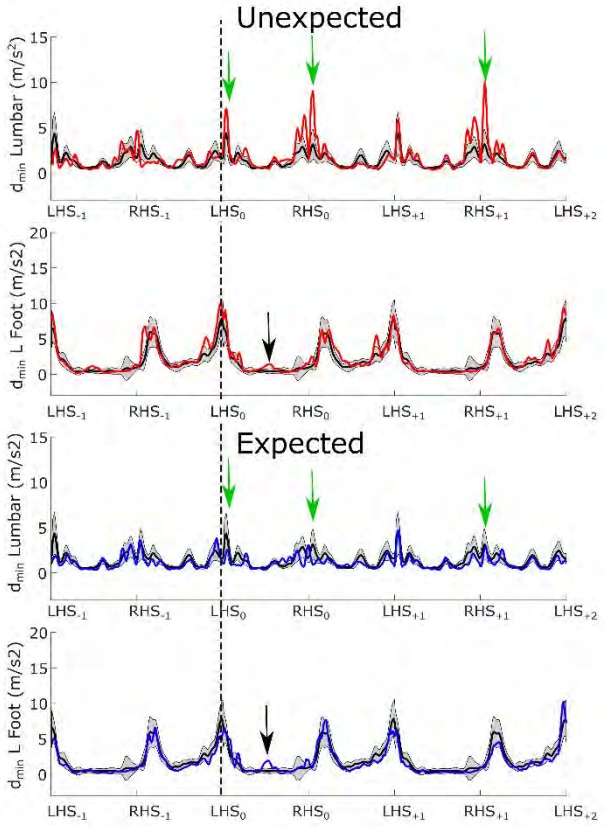

Figure 3: d_{min} for three consecutive strides during unexpected (red) and expected (blue) perturbation trials of the lumbar and left foot. The perturbed step began at LHS_0. Black line and shaded gray show mean and SD of trials with no perturbation. The black arrows indicate the small divergence directly caused by the ankle inversion. The green arrows indicate the larger response in the unexpected trials compared to the expected trials.

REFERENCES

1. Bruijn et al. *Journal of the Royal Society Interface*. 10:20120999, 2013.
2. Kim and Ashton-Miller. *Journal of Biomechanics*. 45:1850-1853, 2012.
3. Kim et al. *Gait & Posture*. 38:853-857, 2013.
4. Cain et al. *Proceedings of ASB'17,* Boulder, CO, USA, 2017.

ACKNOWLEDGEMENTS

Funding provided by the Medical Research Foundation of Oregon. Thank you to Drs. James Ashton-Miller and Hogene Kim for their insight during the designing and building of the shoes.

AN INITIAL LOOK AT GAIT STABILITY DURING OVER-GROUND WALKING IN CANCER PATIENTS

[1]Patrick D. Fischer, [1]Scott M. Monfort, [2]Maryam B. Lustberg, and [2]Ajit M.W. Chaudhari

[1]Montana State University, Bozeman, MT, USA; [2]The Ohio State University, Columbus, OH, USA
email: scott.monfort@montana.edu website: http://www.montana.edu/biomechanics/

INTRODUCTION

Cancer survivors are reported to be at an increased risk of falling [1], but little is known about the factors that drive this problem. Many falls occur during gait, suggesting that altered locomotion is an important consideration that needs better characterization in this population. One method of characterizing gait is through Lyapunov exponents, which quantifies local stability [2]. Potential factors that influence gait stability include chemotherapy and its side effects, such as chemotherapy-induced peripheral neuropathy (CIPN). Altered spatiotemporal gait characteristics associated with more cautious gait in cancer patients who received chemotherapy have been reported by us and others [3]. However, to our knowledge, gait stability measures have not been utilized to further characterize gait impairments in this population.

The purpose of this pilot study was to investigate the effects of chemotherapy on local stability during overground walking. The primary hypothesis was that patients receiving chemotherapy would exhibit decreased local stability when compared to a control group with no prior chemotherapy treatment.

METHODS

Seventeen cancer patients participated in the study after providing IRB-approved informed consent. Participants were divided into two groups: a control group having undergone no chemotherapy (f/m: 6/0; 59.3±9.7yr; 78.0±14.1kg; 1.62±0.05m) and a group having received taxane- or oxaliplatin-based chemo (f/m=9/2; 49.3±11.4yr; 81.7+13.6kg; 1.68±0.06m).

Participants were asked to walk at a self-selected speed around an indoor track; no additional task was required. Inertial measurement units (IMUs, IMeasureU) were attached to the L5 region of the lower back and the left ankle of each participant. Triaxial accelerometer and gyroscope data were recorded at a sampling rate of 500 Hz for the duration of a single five-minute trial.

Raw data from the IMUs were processed using a custom MATLAB program. A twelve-dimensional state space consisting of pelvis 3D linear accelerations and angular velocities with a single time delay copy was used [3]. 150 consecutive strides were considered from each trial, and each trial normalized to 15,000 data points. The maximum short-term (SLE) and long-term (LLE) Lyapunov exponents were calculated as measures of local stability [2], with greater Lyapunov exponent values indicating decreased local stability.

Participants also completed validated patient-reported outcomes (PROs) including the EORTC QLQ-CIPN20 [4] and EORTC QLQ-C30 [5]. These questionnaires assessed the severity of various symptoms associated with chemotherapy and CIPN.

Independent 2-sample t-tests and Wilcoxon Rank Sum tests were performed to identify differences for group demographics and PROs, respectively. Best subsets regression analyses were used to identify linear regression models that best explained the variance in Lyapunov exponents. Prior chemotherapy treatment, age, and average walking speed were considered as candidate predictors. Model performance was evaluated based on adjusted-R^2 and Mallow's C_p values. The top performing models were then analyzed. Significance was set at $p<0.05$. Corrections for multiple comparisons were not made due to the exploratory nature of this study.

RESULTS AND DISCUSSION

Patients who were treated with chemotherapy reported greater symptom severity compared to the control group (Table 1).

Table 1. Group demographics and select characteristics.

Patient Characteristic	Control Group	Chemotherapy Group	p-value
Age	59.3 ± 9.7	49.3 ± 11.4	0.079
CIPN Sensory [a]	1.06 ± 0.06	1.64 ± 0.77	0.063
Quality of Life [b]	6.25 ± 0.69	5.00 ± 0.81	0.008
Physical Function [c]	1.03 ± 0.08	1.67 ± 0.61	0.009

[a] EORTC QLQ-CIPN20 subscale (1-4: **higher=worse**)
[b] EORTC QLQ-C30 global health score (1-8: **lower=worse**)
[c] EORTC QLQ-C30 symptom subscale (1-4: **higher=worse**)

The best subsets analysis suggested that a model containing chemotherapy treatment and age best explained SLE. This model (R^2=47%, p=0.011) suggested that chemotherapy (β_{chemo}=-0.073, p=0.034) was associated with improved local stability even after controlling for age (β_{age}=-0.002, p=0.19). The effect of chemotherapy remained significant after adding average walking speed into the model (model: R^2=47%, p=0.035; β_{chemo}=-0.073, p=0.048). No other model coefficients were significant. Only age was a significant predictor for LLE, but explained a low amount of variability in LLE (model: R^2=27%, p=0.032, β_{age}=-0.0005).

Table 2. Group comparison of gait parameters

Gait Parameter	Control Group	Chemotherapy Group
Average Speed (m/s)	1.35 ± 0.12	1.22 ± 0.21
SLE	1.05 ± 0.03	0.96 ± 0.06
LLE	0.03 ± 0.01	0.04 ± 0.01

One possible explanation is the presence of some internal compensation exhibited by the group who received chemotherapy. Walking speed was previously shown to be a compensation in patients with diabetic peripheral neuropathy [6]; however, speed did not appear to be the driving compensation within our cohort. This study was not designed to identify specific compensations, but we speculate that the increased perception of chemotherapy-related symptoms and functional limitation in the chemotherapy group (Table 1) may be associated with those individuals adopting a more conscious strategy during gait. Increased cognitive attention may enable improved local stability during single-task gait, but could be potentially hazardous during distracted gait where this strategy would be hindered.

Several limitations of this study should be considered. Notably, the small sample size limits the conclusions that can be drawn. Additionally, single-task walking on an isolated track may not represent real world conditions. Due to these limitations, no definitive conclusion between chemotherapy treatment and local gait stability may be drawn. However, further investigation is warranted, and investigating dual tasks during overground walking may provide better insight into this effect.

CONCLUSIONS

This exploratory study investigated the possible relationship between chemotherapy and gait stability. Findings indicated participants receiving chemotherapy displayed improved gait stability over the control group, which was counter to our original hypothesis. No definitive connection between chemotherapy treatment and gait stability may be drawn; it is recommended that further studies be done, with more emphasis placed on dual-task studies to account for potential attentional compensatory strategies adopted during overground gait by participants receiving chemotherapy.

REFERENCES

1. Bao et al. *Breast Cancer Res Treat*, 159: 327-333, 2016.
2. Bruijn et al. *Annals Biomed Eng*, 38(8): 2588-2593, 2010.
3. Monfort et al. *Breast Cancer Res Treat*, 164: 1: 69-77, 2017.
4. Postma et al. *Eur J Cancer*, 41(8):1135-1139, 2005.
5. Aaronson et al. *J Natl Cancer Inst*, 85(5): 365-376, 1993.
6. Dingwell et al., *J Biomech*, 33(10): 1269-1277.

ACKNOWLEDGEMENTS

We would like to thank the study participants for donating their time, and our funding sources:

- NCI R03 CA182165-01
- NSF GRF DGE-1343

MISADVENTURES OF A BIOMECHANIST: A CLOSER LOOK AT KINEMATICS AND ULTRASOUND OF A HAMSTRING INJURY

Zachary B. Fox[1], Allison R. Altman-Singles[1,2] and Benjamin W. Infantolino[1]

[1] Kinesiology, Penn State Berks, Reading, PA, USA
[2] Mechanical Engineering, Penn State Berks, Reading, PA, USA
email: bwi100@psu.edu

INTRODUCTION

Hamstring strains are highly prevalent in sports involving high-speed movements, such as football, soccer and track; however, the mechanisms of hamstring injuries are complex and not well understood [1,2]. Attention has been drawn to the late swing phase as being the most vulnerable phase of the gait cycle for injury due to the eccentric contraction of the hamstring muscle to prepare for foot contact [3,4].

Few studies have *in vivo* experimental data of hamstring injuries in human subjects because of ethical reasons and the limited generalizability of anecdotal evidence. These studies reported decreased peak hip flexion angles during the swing phase as well as decreased torque and power at the hip and knee. Before the injury, there was an increased musculotendon stretch to the biceps femoris during the late swing phase. The studies concluded that injuries likely occur during the terminal swing phase [3,4].

Research using magnetic resonance and ultrasound imaging has shown that hamstring injuries most frequently occur to the biceps femoris. Edema, hemorrhaging and increased echogenicity can be noticed in ultrasound imagining in hamstring injuries. The size of the injury site has not been shown to correlate with injury severity [5].

The purpose of this research was to examine sagittal plane kinematics and spatiotemporal parameters of gait while sprinting. A second purpose of the study was to investigate the injury site using ultrasound to determine the extent of the muscular injury. By combining this information, this study provides insight into the mechanisms of a hamstring strain.

METHODS

A 31-year-old male (1.75 m height; 65.8 kg mass) with a history of hamstring injuries participated in a local 60-yard dash event. Towards the end of the sprint, the subject sustained a left semitendinosus injury as evaluated by a certified athletic trainer. Before and after the injury, knee range of motion (ROM) with a flexed hip was measured. After injury, the injury site was viewed using ultrasound.

A sagittal plane video captured the last three strides prior to the hamstring injury. The video was manually digitized to measure hip and knee angles as well as foot position.

RESULTS AND DISCUSSION

Based upon reviewing the video and speaking to the subject, the time of injury was determined (red box in Figure 1).

Joint kinematic data did not show any large changes in joint angles between strides when comparing the stride in which the injury occurred and the stride prior to injury. Peak foot velocity of the injured limb appeared to coincide with the timing of the injury (Figure 2).

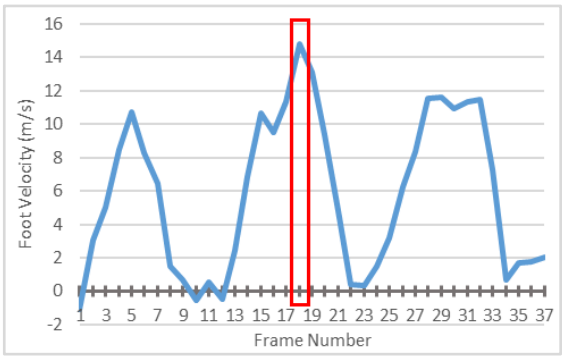

Figure 2. Left foot velocity during all analyzed frames (red box corresponds to time of injury)

Post-injury assessments revealed passive knee ROM decreased from baseline by 19 degrees. Subject's gait was visually affected in terms of walking speed and ability to climb stairs. Ultrasound of the painful area did not show any musculotendon injury based upon a lack of bleeding and structural deficit (Figure 3). However, an area of muscle in the painful area was seen to be twitching uncontrollably and continued for thirty minutes after the injury occurred (left red oval in Figure 3). Minimal effusion in the area was seen five days after the injury occurred (right red oval in Figure 3).

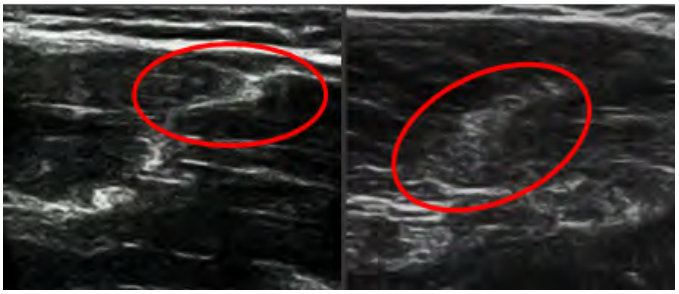

Figure 3. Ultrasound images of the intermuscular junction of the semitendinosus from day of (left) and five days post-injury (right)

To date, only two previous studies [3,4] have *in vivo* experimental data of hamstring injuries. In this present study, the hamstring injury occurred in the terminal swing phase which is in agreement with the previous research. In agreement with Petersen et al. (2013), no structural deficit was found with ultrasound, yet there was a functional deficit seen in ROM and gait. This suggests the pain and functional loss may be due to neurological factors more than muscle tissue damage. The increased foot velocity may have overstretched the muscle spindle afferents, causing the stretch reflex to be activated in the semitendinosus which lead to the semitendinosus strain. This increase in muscle afferent activity could explain the subsequent muscle twitch and pain as well as the lack of tissue damage.

The nature of a case study as well as the lack of EMG and three-dimensional kinematic data limits the ability to more precisely determine the mechanism of the hamstring injury. Another limitation is the uncertainty of whether foot velocity is the cause of or the result of the hamstring injury because of the difficulty in pinpointing the exact moment of injury.

This study is the first to assess semitendinosus strain in real time. These findings may suggest that prevention and rehabilitation techniques could focus on neuromotor control at the end range of motion.

CONCLUSIONS

These data indicate the functional deficit does not necessarily correlate with the presence of a muscular deficit. Kinematic data indicates the injury occurred at the peak foot velocity.

REFERENCES

[1] Dalton SL, et al. *Am J Sports Med* **43**, 2671-9.
[2] Erickson LN, et al. *J Sport Health Sci* **6**, 262-70.
[3] Heiderscheit BC, et al. *Clin Biomech* **20**, 1072-78.
[4] Schache AG, et al. *Gait Posture* **29**, 332-8.
[5] Peterson J, et al. *Am J Sports Med* **42**, 399-404.

Figure 1. Left foot contact before, at (red box) and after injury (numbers indicate frame numbers)

RUNNING TRAINING ALTERS LIMB STIFFNESS AND LOWERS THE COST OF LOCOMOTION

[1] Maria Fox, [1]Oshane Thomas, [2]Sarah P. Psutka, [3]Daniel E. Lieberman, [1]John D. Polk

[1] University of Illinois Urbana-Champaign, Urbana, IL, USA
[2]John H. Stroger Jr. Hospital of Cook County, Chicago, IL, USA
[3]Harvard University, Cambridge, MA, USA
email: jdpolk@illinois.edu, web: http://publish.illinois.edu/evolutionarybiomechanicslab/

INTRODUCTION

During running, the biomechanics of the stance limb can be modeled as a spring-mass system that stores and releases elastic strain energy [1–3]. Storage of elastic strain energy requires some joint flexion and recoil. If little flexion occurs, elastic storage and recovery savings may not be substantial. In contrast, during so-called 'Groucho' running when limb stiffness is decreased, there is limited vertical fluctuation in the body's center of mass (COM). This results in increased metabolic cost to prevent the limbs from collapsing combined with decreased elastic energy storage and return [2]. Similarly, increased vertical fluctuations of the COM and higher limb stiffness can also increase locomotor costs [4, 5].

While limb stiffness should affect locomotor costs, this relationship is rarely evaluated directly. This study tests how stiffness and vertical fluctuations vary with locomotor cost in trained and untrained female runners. Farley and González [3] distinguished spring constants associated with the fluctuations in limb length (k_{leg}) and fluctuations in body center of mass (k_{vert}). The angle swept by the limb during stance (excursion angle, ϕ) also influences the dynamics of the spring and force generation. Here we test the hypothesis that running training lowers the cost of locomotion and that this is reflected in limb stiffness and angular excursion.

METHODS

The Harvard University Institutional Review Board approved all protocols. Seventeen healthy adult female subjects ran on an instrumented, motorized treadmill: 2.5, 3, 3.5, 4, and 4.5 m/s. Subjects were classified into Trained (T) and Untrained (U) groups; trained runners had experience running competitively and had received instruction in running technique. Kinematic measurements were obtained using a 3-camera Qualisys motion capture system (Qualisys AB, Sweden), at 240Hz that tracked reflective markers placed on standard lower extremity landmarks. Peak vertical ground reaction forces (F) were recorded using Superscope (GWInstruments) and processed in IGOR (Wavemetrics) and Matlab (Mathworks, Natick MA). Cost of locomotion (COL) estimates were derived following Pontzer [4]. Limb spring stiffness was measured following [3] as $k_{vert}=F/\Delta y$, where Δy is the vertical fluctuation in COM during stance, and $k_{leg}=F/\Delta L$, where ΔL is the change in limb length between touchdown and midstance. Data were processed in Matlab and all statistical analyses were performed in R (R Core Team, 2017).

RESULTS AND DISCUSSION

Cost of locomotion increases linearly with speed ($r = 0.93$, $p < 0.001$, Fig. 1a). Training is a significant coefficient in a linear regression model that controls for speed ($p = 0.007$), and comparisons among estimated marginal means show that trained subjects have lower costs of locomotion than untrained subjects ($p = 0.007$).

Across all speeds, vertical stiffness (k_{vert}) increases linearly with COL ($r = 0.72$, $p < 0.001$). k_{vert} and its component Δy do not differ between trained and untrained individuals (Fig. 1b). However, leg stiffness (k_{leg}) and its component ΔL do differ significantly between training groups when controlling for speed ($p = 0.0456$, Fig. 1c). With greater leg stiffness, untrained runners experience higher locomotor cost compared to trained runners.

Excursion angle ϕ also increases with greater COL (Fig. 1d). At all speeds, trained runners have greater excursion angles than untrained runners ($p = 0.046$).

CONCLUSIONS

These results suggest that trained runners use both kinetic and kinematic mechanisms to reduce locomotor costs during running by increasing limb compliance (k_{leg}) and limb excursion (ϕ) during stance phase. Although differences between trained and untrained groups are small at each speed, they indicate that training does improve locomotor economy.

REFERENCES

1. McMahon, T. *Muscles, Reflexes, and Locomotion*. Princeton: Princeton University Press, 1984.
2. McMahon et al. *Appl. Physiol.*, **62**(6): 2326–2337, 1987.
3. Farley and González. *J. Biomech.*, **29**(2): 181–186, 1996.
4. Pontzer, H. *J. Exp. Biol.*, **210**(3): 484–494, 2007.
5. Willems et al. *J. Exp. Biol.*, **198**(2): 379-393.

ACKNOWLEDGEMENTS

We are grateful to Herman Pontzer, Andy Biewener, Suzy Cote, Elizabeth Lee, and Aron Tan. Research was supported by the Skeletal Biology and Biomechanics Lab at Harvard University and Evolutionary Biomechanics Lab at the University of Illinois at Urbana-Champaign.

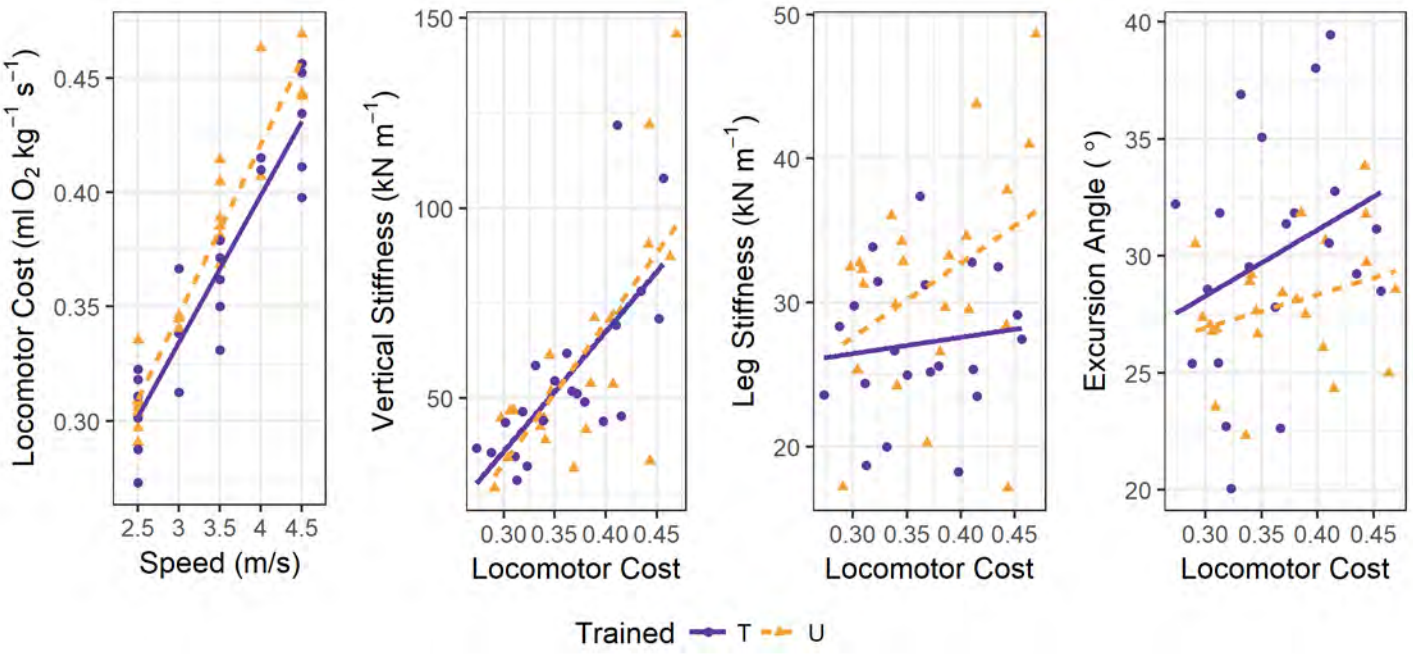

Figure 1: Relationships between locomotor cost ($mlO_2kg^{-1}s^{-1}$) and: a) speed (m/s), b) vertical stiffness (kNm^{-1}), c) leg stiffness (kNm^{-1}), d) and excursion angle (°) in trained (T) and untrained (U) runners.

SWING PHASE KINEMATICS AND PROSPECTIVE RUNNING INJURY DEVELOPMENT

Naomi E. Frankston, Ashley B. Nguyen, John J. Davis, and Allison H. Gruber

Indiana University, Bloomington, IN, USA
email: ahgruber@indiana.edu, web: https://iubiomechanicslab.weebly.com/

INTRODUCTION

Most gait studies traditionally report variables only from the stance phase of running despite swing phase representing a greater percentage of the gait cycle [1]. The focus on stance phase variables is most likely because tissue loading is greatest during stance and thus assessing stance phase variables may provide important information about the development of overuse injuries. Kinematic variables from stance phase previously associated with injury include peak hip adduction angle (HADD), knee flexion angle (KFLEX), and knee adduction angle (KADD) [2,3]. However, there is a lack of agreement between studies regarding the gait variables related to overuse running injuries. Given the lack of research on swing phase mechanics, it is possible that we are not accounting for a significant portion of motion that may be related to injury development.

Swing phase kinematics may be valuable to examine when evaluating injury risk. Joint angles tend to be greater during swing than during stance [1] which may cause a significant degree of tissue stress from moving closer to the limits of the allowable range of motion. Therefore, the purpose of this study was to examine kinematics during the swing phase of running to assess the feasibility of investigating swing and stance variables when studying overuse injury. We hypothesize that peak joint angles and excursions from the sagittal plane knee, frontal plane knee, and frontal plane hip during swing will be greater in subjects who develop a running-related overuse injury during a 12-month follow-up period compared with those who remain uninjured.

METHODS

Data were taken from a larger prospective running study of recreational and competitive runners. Twenty-eight subjects (18 female/10 male; age: 30.8 ± 9.4 years; BMI: 22.3 ± 2.3 kg/m^2; weekly mileage: 21.0 ± 12.4 miles) were grouped based on whether they developed a running injury within the 12-months following gait analysis (n = 14) or remained uninjured (n = 14). The groups were comparable in gender, age, BMI, and mileage ($p > 0.05$). The study was approved by the Indiana University IRB.

At enrollment, subjects ran overground at 4.0 ± 5% m·s^{-1} while nine motion capture cameras (Qualisys, Gothenburg, Sweden) collected bilateral 3D kinematic data at 240 Hz. Kinematic data were processed using Visual 3D (C-Motion, Germantown, MD, USA). Data were not normalized to the standing calibration. Peak joint angles and excursions were extracted from the sagittal plane knee, frontal plane knee, and frontal plane hip time series during both stance and swing phases. Swing and stance phases did not always occur in the same order within the trial collection volume. Therefore, swing and stance phases were analyzed as separate time series and time-normalized to 100% of the given phase. The right limb was assessed in the uninjured group and the injured limb was assessed in the injured group. Subjects responded to a weekly online survey to report running volume and injury. Injuries were defined as any musculoskeletal symptom of the lower limb which required a reduction or stoppage of normal training [4].

Two tailed independent t-tests were carried out in SPSS 24.0 (IBM, Armonk, NY, USA) to compare means between the uninjured and injured groups during stance and swing phase ($\alpha = 0.05$). Cohen's d and coefficient of variation (CV) were calculated to assess the effect of group differences and variation within groups, respectively.

RESULTS AND DISCUSSION

There were significant group differences for minimum KFLEX during swing phase ($p = 0.024$), with the uninjured group exhibiting a greater minimum KFLEX than the injured group (10.1 ± 3.5° vs 6.6 ± 3.4°). No significant differences between

groups were observed for any other hip or knee variables during stance or swing ($p > 0.05$).

For swing phase, a large effect size was observed for minimum KFLEX ($d = 0.99$) and a moderate effect size was observed for minimum knee frontal plane angle (KFRONT) ($d = 0.55$). Minimum hip frontal plane angle (HFRONT), peak KFLEX, and KFRONT excursion had effect sizes between $d = 0.41$-0.43. For stance phase, moderate effect sizes were observed for minimum HFRONT ($d = 0.55$), HFRONT excursion ($d = 0.52$), and peak KFLEX ($d = 0.58$). When comparing stance and swing phases, minimum KFLEX had a large effect size during swing but a small effect size during stance ($d = 0.25$). In terms of the timing, minimum KFLEX occurred around 90% of swing phase, which represents the transition from swing to stance. Maximum KFRONT occurred around 5% of swing, which is the transition from stance to swing. Thus, the transitions between stance and swing phases may useful when looking at injury.

The mean ± standard deviation of the coefficients of variation (CV) across variables were 75 ± 84% for the uninjured group and 96 ± 92% for the injured group ($p > 0.05$). There were no significant differences in CV between stance and swing phases.

More data are currently being collected and analyzed. A sample size estimate for each variable using the current data set revealed minimum sample sizes required for 0.8 statistical power of $n = 17$ per group for minimum KFLEX during swing.

CONCLUSIONS

Significant group differences and a large effect size were found for minimum KFLEX during swing phase. Moderate effect sizes were observed for minimum KFRONT during swing phase and for minimum HFRONT, HFRONT excursion, and peak KFLEX during stance phase. Our ongoing work will provide enough subjects to reach 0.8 statistical power and allow for a stepwise logistic regression analysis to determine causal relationships between gait kinematics and running injury risk. The preliminary results from this study suggest that swing phase kinematics should not be overlooked when assessing the relationship between running gait and injury.

REFERENCES

1. Novacheck, TF. *Gait & Posture.* 7:77–95, 1998.
2. Dierks, TA et al. *MSSE*. 43(4):693–700, 2011.
3. Baker, RL & Fredericson, M. *Phys Med Rehabil Clin N Am.* 27:53–77, 2016.
4. Eskofier, BM et al. *Comput Methods Biomech Biomed Engin*. 15(5):467-74, 2012.

ACKNOWLEDGEMENTS

Funding: School of Public Health – Bloomington Faculty Research Grant Program.

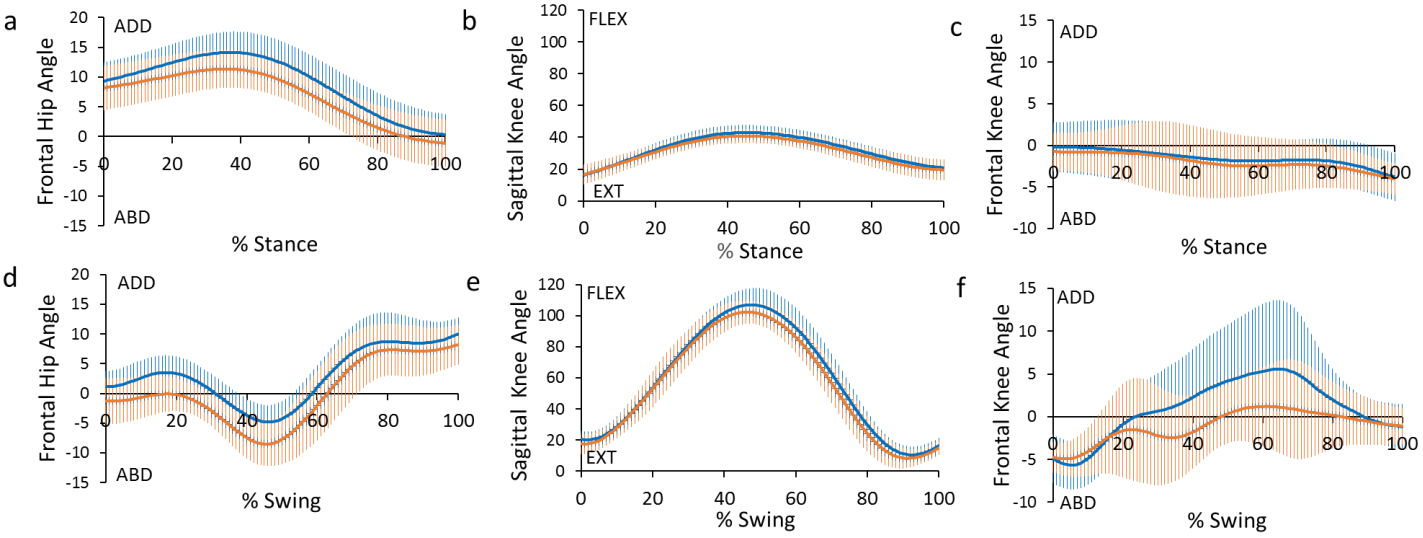

Figure 1: Frontal plane hip and knee angles (a, c) and sagittal plane knee angles (b) during stance. Frontal plane hip and knee angles (d, f) and sagittal plane knee angles (e) during swing. Adduction and flexion are positive and abduction and extension are negative. Blue lines represent the uninjured group and orange lines represent the injured group. Vertical bars represent the standard deviation.

KNEE DYNAMICS AND RUNNING CADENCE: A CONTROLLED CASE STUDY

[1,2] Jessica M. Fritz, [1] Nathaniel Ford, [2] Carolyn M. Meinerz, [1] Kristof Kipp, [2] Carole Vetter, and [1,2] Gerald F. Harris

[1] Marquette University, Milwaukee, WI, USA
[2] The Medical College of Wisconsin, Milwaukee, WI, USA
email: jessica.fritz@marquette.edu

INTRODUCTION

Approximately 56% of recreational runners suffer a running induced injury annually [1]. A cited method in reducing lower extremity injury is to reduce peak accelerations by decreasing the magnitude and rate of impact force loading to the lower leg [2-4]. The knee is one of the most common areas of injury in a runner [5]. While running, the knee experiences forces up to 7.6 times body weight and can suffer injuries such as patellofemoral pain syndrome (PFPS) [6]. One training approach for injury risk reduction is cadence manipulation through increasing the rate of footfalls of the individual by 10% or greater while maintaining a constant speed [1]. When increasing cadence, certain kinematic and biomechanical factors are altered and allow for a reduction of injury risk, especially at the knee. It has been reported that as cadence increases, the knee is more flexed at foot strike and less flexed during the stance phase [3]. This is primarily explained by the fact that as cadence increases while running velocity remains constant and, stride length decreases [3]. This change in kinematics has the effect of reducing center of mass excursion, as the legs of the runner are kept closer to the center of mass. Additionally, this causes a decrease in the maximum angular velocity experienced by the knee [3]. These factors reduce the overall energy absorption at the knee, and could play a large role in injury reduction [1]. The objective of this study was to examine the effects on running kinematics of the knee by increasing running cadence, and how these changes aid in injury risk reduction.

METHODS

This case study was part of a larger overall study examining the effects of using music set to specific beats per minute (bpm) as a means of cadence training in recreational runners. Of the 20 subjects who participated in our protocol, as approved by the Medical College of Wisconsin Institutional Review Board, only a single subject successfully increased his cadence while running to music with increased bpm. Inclusion criteria included running at least 10 miles/week, being comfortable running on a treadmill (self-rating of at least a 5 on a scale of 0-10 with 0 being uncomfortable/unfamiliar), being free of any cardiovascular condition and being free of any lower extremity injuries. The subject of this case study was a 25-year-old male (82.4 kg, 184.5 cm). After providing informed consent, the subject was fitted with 17 reflective markers on anatomical landmarks based on the modified Helen Hayes marker set for Vicon's Plug-in Gait model (Vicon Motion Systems, Ltd; Oxford, UK). Motion data for this study was collected at a sampling rate of 250 Hz in Nexus software (Vicon Motion Systems, Ltd; Oxford, UK). In addition to the markers, a triaxial accelerometer was secured against the anteromedial aspect of the distal tibia. The subject was given 10 minutes to warm up to a comfortable, 5K training run speed. Following warmup, baseline data was acquired for 10 strides to calculate the preferred cadence. The subject was instructed to run for 5 minutes to the beat of the music of a song that had a bpm 5% greater than their preferred cadence. This was repeated for an additional 5 minutes to a song that had a bpm 10% higher than their preferred cadence. Sagittal plane kinematics and temporal parameters were analyzed for six trials at each cadence level.

RESULTS AND DISCUSSION

The results of this case study indicate there was an increase in footsteps per minute experienced by the

runner between the three cadence levels. Additionally, as cadence increased from the preferred (176 steps/min) to 191 steps/min, and 200 steps/min there was a decrease in joint range of motion (Fig. 1, Table 1), though the changes were not statistically significant at an alpha level of 0.05. Additionally, decreases in flight time and stride time were observed as cadence increased. While not a focus of this analysis, peak vertical acceleration also decreased with increased cadence.

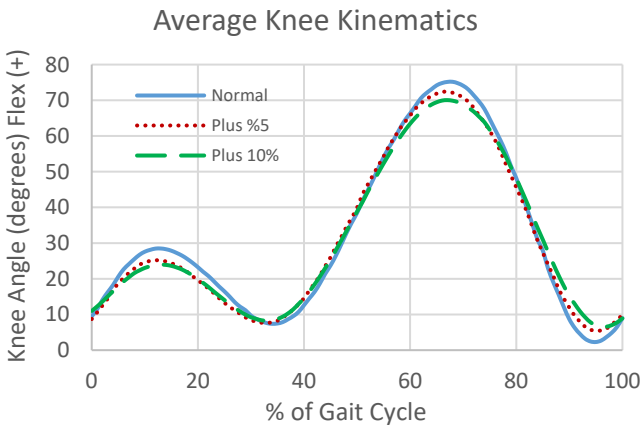

Figure 1. Average left knee kinematics for one full gait cycle across six trials for self-selected, plus 5%, and plus 10% cadence levels.

These findings are consistent with previous studies that showed the knee to be most affected by cadence manipulation; as cadence increases the knee is more flexed (less extended) at foot strike, and there is reduction in peak knee flexion in the stance phase, both of which were observed in our results (Fig. 1) [1]. As previously reported, we found a decrease in maximum hip flexion at loading response as well as more ankle plantarflexion at foot strike as cadence increases [1,3]. Biomechanical changes in the ankle such as the reduction of range of motion and a shift to greater plantarflexion, has the effect of reducing heel strike running patterns and encouraging midfoot and forefoot strikes. This, in turn, reduces peak positive accelerations and loading of the tibia, as seen in our subject's acceleration decreases, which could aid in preventing tibial stress fractures [4].

CONCLUSIONS

The findings from this case study demonstrate that increasing running cadence has significant effects on knee, hip, and ankle kinematics. These changes in joint kinematics have the effect of reducing stride length and encourage the runner to run closer to their center of mass, which in turn reduces the impact magnitudes and energy absorption of the lower limbs. Further study of cadence manipulation as an option to reduce risk of running injuries is supported by this pilot.

REFERENCES

1. Heiderscheit B et al. *Med Sci Sports Exerc*, **43**(2): 1-7, 2011.
2. Meinerz M et al. *Proceedings of the 40th Annual Meeting of the American Society of Biomechanics*, Raleigh, NC, USA, 2016.
3. Schubert A et al. *Sports Health*. **6**(3): 210-216, 2014.
4. Crowell H and Davis I. *Clinical Biomechanics*, **18**(6): 78-83, 2010.
5. Taunton J et al. *Br J Sports Med*, **36**(2):95-101, 2002.
6. Lenhart R et al. *Med Sci Sports Excerc*, 46(3):557-564, 2014.

ACKNOWLEDGEMENTS

This study was funded by an intramural grant from the Medical College of Wisconsin Department of Orthopaedic Surgery.

Table 1: Average running stride sagittal plane range of motion for all three running cadences.

Cadence	Hip Flexion/Extension	Knee Flexion/Extension	Ankle Flexion/Extension
Self-Selected	45.0	73.9	41.9
Plus 5%	41.8	68.5	37.3
Plus 10%	40.7	66.2	34.2

A PIPELINE FOR ANALYZING MOTION CAPTURE DATA USING OPENSIM

[1] Adam E. Galloy, [2]Dylan G. Scmitz, and [1] Kayt E. Frisch PhD

[1] Dordt College, Sioux Center, IA, USA
[2] University of Wisconsin, Madison, WI, USA
email: kayt.frisch@dordt.edu

INTRODUCTION

3D motion capture has applications in clinical and research settings and is especially powerful when supplemented with musculoskeletal simulations [1]. OpenSim (National Center for Simulation in Rehabilitation Research, Stanford, CA) is a readily available (and free) musculoskeletal simulation program that allows researchers to estimate joint angles, body forces and torques, and muscle parameters [2]. The user community actively participates in creating OpenSim documentation and currently a good set of tutorials guide new users in learning the program. However, the documentation needs additional resources guiding new users in importing their own motion capture data in the program. This abstract provides a template for a data analysis pipeline that will allow users to prepare and use 3D marker and force data for use in OpenSim analyses.

METHODS

Figure 1 summarizes the process of preparing data for use in OpenSim inverse kinematics (IK) and inverse dynamics (ID) analyses.

In order to analyze data in OpenSim, the user must begin by identifying an appropriate musculoskeletal model from the library of models available or create their own. The user will likely need to modify the model in order to use it for a specific study. Common changes include modifying the model's range of motion relative to the ground, adding a marker set to represent the marker set used by subjects during data collection, and adding/adjusting inertial parameters.

The first step in preparing experimental data is reformatting the data into appropriate file types and formats. Although many motion capture software packages output data in a .c3d file format, OpenSim

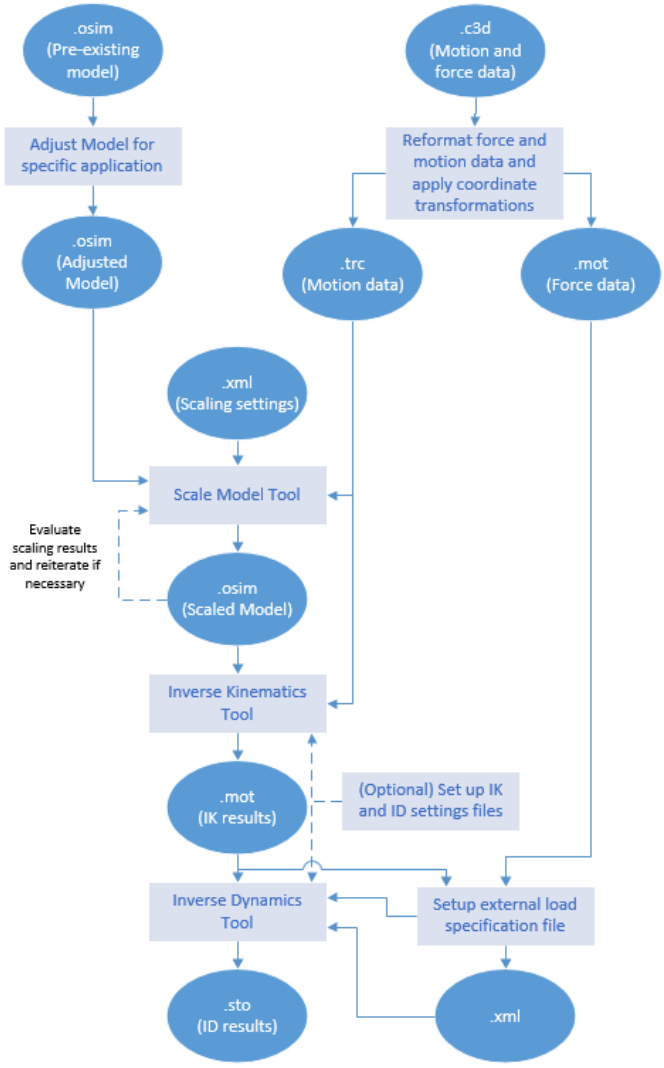

Figure 1: The workflow of musculoskeletal simulation with OpenSim. Arrows going in and out of the different steps represent input and output files for each step.

reads the 3D marker coordinate data from a csv formatted file with a .trc extension and force data from a similar formatted file with a .mot extension. Multiple options exist for parsing the marker and force data contained in the .c3d files to the .trc and .mot formats respectively. Two of the more common

options are the biomechanics tool kit (and companion software MOKKA), and the LabVIEW biomedical engineering tool kit. In order to ensure a smooth transition to OpenSim, coordinate transformations often need to be applied and data columns may need to be renamed, so it is important that the user consider their needs and look for options that provide the appropriate level of flexibility. Expectations for column organization is available on the OpenSim documentation website.

Once the user adjusts the model appropriately and prepares the data, they must scale the model to individual subjects using static pose data. The large number of settings that need adjusting for each model make this a potentially complicated process. The scale parameters for each body segment are determined by comparing model and physical marker locations and should be applied before scaling. Additionally, it is important to set marker weights to align the model with the subject's pose. These settings should be saved in a .xml scale settings file for making repeated scaling of a subject more consistent and convenient. Example settings files for various OpenSim tools are used extensively in OpenSim tutorials.

After completing scaling, the results must be evaluated. Scaling is often an iterative process and markers will need to be moved on the model and weights adjusted multiple times before the model is properly scaled. Keeping pictures of subjects with markers properly placed can aid the adjustment process. Additionally, overlaying the marker coordinate data on the model shows discrepancies more clearly, which can help improve scaling accuracy.

After the model is properly scaled, analysis of the motion capture data can begin. OpenSim's inverse kinematics (IK) tool calculates joint angles and body positions using the data supplied in the .trc file created from the 3D marker data and the scaled model. The results of this analysis are saved in a .mot file.

Once IK is completed, the generalized forces and torques for each degree of freedom in the model can be estimated using the inverse dynamics tool (ID). Running ID requires a .xml external loads specification file and the .mot results file from the IK analysis. The external loads specification files are created within the ID tool and are used to assign force data from the .mot files to the appropriate rigid bodies in the model. The results of the ID analysis are saved in a .sto file format. The resulting .mot and .sto files can then be opened by any software capable of reading .csv files. For both the IK and ID tools, settings and parameters used can be saved in .xml files for future use.

RESULTS AND DISCUSSION

The authors are currently working to add this analysis process (along with more detailed guidelines as appropriate) to the official OpenSim documentation website.

CONCLUSIONS

A well-documented pipeline for analyzing 3D motion capture data using OpenSim will help make motion capture techniques more accessible in clinical and research settings. The current OpenSim tutorials do an excellent job of introducing users to the analysis platform, but additional resources are needed to help new users translate their tutorial knowledge to their own data sets. By adding the workflow described here to the official OpenSim documentation, users will be able find more detailed and structured instructions in an easily accessible place.

REFERENCES

1. Reinbolt JA, et al. *Procedia IUTAM* **2** 186-198, 2011
2. Delp SL, et al. *IEEE Transactions on Biomedical Engineering* **54**, 1940-1950, 2007

ACKNOWLEDGEMENTS

The authors would like to thank the Dordt College Engineering Department, the Dordt College Center for Research and Scholarship, and the Carver Foundation.

RUNNING KINEMATICS AT SELF-SELECTED AND PRESCRIBED SPEEDS IN ADOLESCENT LONG-DISTANCE RUNNERS

Micah C. Garcia, Jeffery A. Taylor-Haas, and Jason T. Long
Cincinnati Children's Hospital Medical Center, Cincinnati, OH, USA
email: micah.garcia@cchmc.org, web: http://www.cincinnatichildrens.org/mal

INTRODUCTION

Running as an endurance sport continues to grow in popularity amongst middle- and high-school athletes, with nearly 500,000 young athletes participating in cross-country during 2016-2017 [1]. Unfortunately, the literature on pediatric running mechanics is sparse, especially when running at different speeds. Pediatric physical therapists, physicians, and athletic trainers currently apply adult literature on running mechanics to pediatric and adolescent runners. Previous literature on adults running at different speeds has reported increased cadence, stride length, and kinematic and kinetic peak values at faster speeds [2-4]. However, the potential confounding effects of growth and maturation on running biomechanics in children and adolescents may limit the generalizability of adult literature to this population. These topics warrant study in a younger population to better understand the effects of running speed on kinematics in pediatric and adolescent long-distance runners.

METHODS

Uninjured adolescents who participated in long-distance running activities were recruited for the study, and a subgroup of 21 runners (m = 10, f = 11, age = 14.66 ± 1.55 years) with a self-selected treadmill speed of at least 2.68 meters per second (m/s) were identified for analysis. Study participation required a single visit to the Motion Analysis Lab for testing. Subjects were instrumented with reflective markers [5] and tested using a 12-camera Raptor 4 system (Motion Analysis Corp.; Santa Rosa, CA). Kinematics were measured during self-selected (SS) and prescribed (PS) running speeds on a non-instrumented motorized treadmill (Biodex RTM-600; Biodex Medical Systems, Inc; Shirley NY). Prescribed speed was set to 3.57 m/s for all participants. Participants were provided a four-minute warmup on the treadmill with instructions to increase treadmill speed to SS by the end of the fourth minute. Participants ran at SS for an additional two minutes, followed by a treadmill speed adjustment to the PS for two more minutes. Kinematic data were captured using MAC Cortex software during the final minute of both SS and PS running and post-processed in Visual3D (C-Motion, Inc; Germantown, MD) and exported to MATLab (Mathworks, Inc; Natick, MA) for further analysis. Foot contact and toe-off events were determined based on algorithms from Leitch et al. [6] and Maiwaild et al. [7], respectively. Data from the right side were used for analysis. Variables of interest included joint angle at initial contact (IC), as well as maximum angle, minimum angle, and average angle during stance and swing phases. Data normality was established via the Lilliefors test, and differences between SS and PS were assessed using paired t-tests. The group was stratified into those runners for whom SS < PS ("*SpeedUp*" group) and those for whom PS < SS ("*SlowDown*" group). Differences between the *SpeedUp* and *SlowDown* groups were assessed using unpaired t-tests. Temporal-spatial significance threshold was set at $p<0.05$. Due to the large number of kinematic comparisons, the threshold for significance was adjusted *ad hoc* and set at $p<0.02$.

RESULTS AND DISCUSSION

Temporal-spatial analysis revealed increased cadence, stride length, and swing phase duration at faster speeds for each group (Table 1). No significant differences were measured at the PS between groups. These findings match the previous adult literature and demonstrate that pediatric and adolescent long-distance runners manipulate both cadence and stride length to adjust running speed. Further analysis revealed a greater change in stride length than cadence to adjust speed (*SpeedUp*: Δ cadence: 2.5%, Δ stride length: 10.8%; *SlowDown*: Δ cadence: -2.4%, Δ stride length: -6.9%). This matches prior reports of greater stride length than cadence manipulation in adults when increasing running speeds below 7 m/s [4].

Intergroup comparison of PS kinematics (Figure 1) revealed that the *SpeedUp* group demonstrated increased pelvic tilt at IC (*SpeedUp*: 20.0˚; *SlowDown*: 13.8˚) and an anteriorly tilted pelvic position throughout the stride (*SpeedUp*: 19.3˚; *SlowDown*: 12.6˚). The hip demonstrated increased

flexion at IC (*SpeedUp*: 42.5˚; *SlowDown*: 35.2˚) and a more flexed position during stance (*SpeedUp*: 21.9˚; *SlowDown*: 13.7˚). Greater peak knee flexion (*SpeedUp*: 43.2˚; *SlowDown*: 37.6˚) was measured during stance. Previous literature has reported a positive correlation between peak knee flexion and peak patellofemoral joint reaction force [8]. Considered with these findings, this suggests that increasing speed greater than a comfortable, self-selected pace may place additional and potentially detrimental demands on the knee. Further study with concurrent kinetics is warranted.

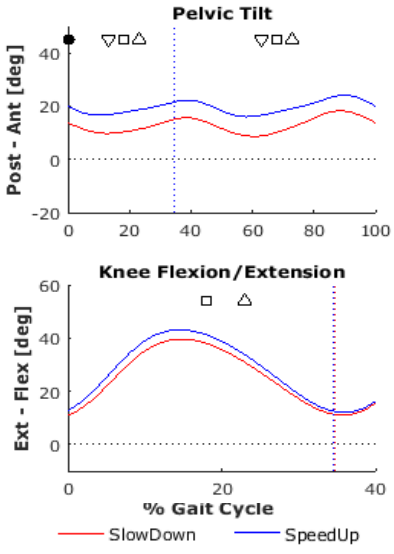

Figure 1: Sagittal pelvis and knee motion at PS for *SlowDown* and *SpeedUp* groups. (●) signifies difference at IC; (▽) signifies difference in minimum value within phase; (Δ) signifies difference in maximum value; (□) signifies difference in average position. ($p<0.02$ for all measures.)

When comparing SS and PS kinematics, significant differences were found in sagittal and coronal trunk motion; sagittal and transverse pelvis motion; and triplanar hip motion for the *SpeedUp* group. During PS, the trunk demonstrated greater anterior lean at IC (PS: 2.2˚; SS: 1.5˚) and greater peak anterior lean during stance (PS: 6.9˚; SS: 5.9˚). The pelvis demonstrated greater anterior tilt at IC (PS: 20.0˚; SS: 18.9˚) and an anteriorly tilted position throughout the gait cycle (PS: 19.3˚; SS: 17.9˚). Hip kinematics demonstrated greater flexion at IC (PS: 42.5˚; SS: 39.2˚) and greater sagittal plane ROM during stance (PS: 49.9˚; SS: 45.4˚) and swing (PS: 63.8˚; SS: 56.8˚). Increased peak knee flexion (PS: 99.9˚; SS: 93.0˚) and sagittal plane ROM (PS: 91.1˚; SS: 84.7˚) were measured during swing. Although the magnitudes of most differences were small, there are clinical implications associated with the repetitive and prolonged nature of long-distance running. These cyclic mechanics could result in an additive effect of increased demands on the body over time, increasing the risk of injury.

Fewer significant differences were noted for the *SlowDown* group. During PS, reduced hip flexion (PS: 35.2˚; SS: 37.2˚) was measured at IC as well as reduced sagittal plane ROM (PS: 70.2˚; SS: 64.7˚) during swing. Though not significant, a trend for reduced knee flexion (PS: 102.4˚; SS: 105.9˚) was measured during swing ($p=0.021$).

CONCLUSIONS

This study demonstrated kinematic and temporal-spatial adaptations associated with changes in running speed in adolescent long-distance runners. Greater changes were noted when increasing speed above SS, particularly during stance phase at the knee. These alterations may induce soft tissue stresses above a safe threshold, suggesting that increasing speed above a comfortable pace and may increase the risk of injury. Future studies should investigate changes in joint kinetics and muscle activity in adolescent long-distance runners to better understand how changes in speed impact the demands placed on the body.

REFERENCES

1. National Federation of High School Associations 2016-2017 Participation Survey. www.nfhs.org/ParticipationStatistics/ParticipationStatistics.
2. Fukuchi RK, et al. *PeerJ* 5:e3298, 2017.
3. Brughelli M, et al. *J Strength & Cond* **25**(4):933-9, 2011.
4. Dorn TW, et al. *J Exp Bio* **215**, 1944-56, 2012.
5. Ford KR. et al. *Med & Sci in Sports & Exercise* **45**(6):1125-30, 2013
6. Leitch J, et al. *Gait & Post* **33**, 130-2, 2011
7. Maiwald C. et al. *2009 ISB Conference*.
8. Wille C, et al. *JOSPT* **44**(10):825-30, 2014.

Table 1: Temporal-spatial parameters and SS and PS speeds for *SpeedUp* and *SlowDown* groups. Asterisk (*) indicates significant difference between running speeds ($p<0.05$).

Group	Condition	Running Speed (m/s)		Cadence (steps/min)		Stride Length (m)		Swing Duration (%)	
SpeedUp	*SS*	3.11 ± 0.2	*	170.3 ± 9.8	*	2.20 ± 0.2	*	62.3 ± 2.4	*
	PS	3.58 ± 0.0		174.6 ± 9.5		2.47 ± 0.2		63.8 ± 1.8	
SlowDown	*SS*	3.96 ± 0.3	*	178.3 ± 15.9	*	2.68 ± 0.3	*	64.5 ± 1.1	*
	PS	3.58 ± 0.0		174.0 ± 14.4		2.48 ± 0.2		63.2 ± 1.1	

Marathon Training and Perceived Exertion: Can Self-Evaluation Lead to Healthier Runners at the Starting Line?

[1] Alianna Gedlinske, [2] Stephen M Suydam and [1] Matthew Evans

[1] University of Wisconsin Eau Claire, Eau Claire, WI, USA
[2] Milestone Sports, Inc., Columbia, MD, USA
email: ssblemker@virginia.edu, web: http://asb2018.asbweb.org/

INTRODUCTION

Hundreds of thousands of runners sign up each year to participate in marathons, but a high percentage of those will retire from the race before the starting gun or show up injured [1,2]. Many theories have been presented with means to reduce injury including limited mileage increase per week and shoe rotation [3, 4]. Despite these efforts, a simple injury model to assist in injury prevention for the distance runner has yet to be determined. Other sports have adopted a rate of perceived exertion (RPE) index combining exercise intensity and duration [5]. The RPE is a subject measure of the difficulty of the activity, regardless of the duration or type of activity. This not only takes into account the strain of the activity (running in the case of this study), but the life stresses being placed on the runners as well, thus creating a cumulative load.

The purpose of this study is to determine if there is a connection between injury rates to self-identified exertion over extended durations while training for a long-distance road race (marathon or half marathon). We hypothesize the runners who report injury will have an increased RPE index the week they reported injury.

METHODS

108 runners (70 female and 38 male) are currently participating in a 13-week marathon training course at the University of Wisconsin-Eau Claire. Each runner read and signed an inform consent document provided by the University of Wisconsin-Eau Claire. Each week, runners meet for an hour to discuss race preparation including nutrition and cross training. The runners also meet each Saturday morning for their "long run," a guided, pre-set path with pacers to help the runners develop their mileage safely. In addition to their group runs, runners are encouraged to run an additional two or more times a week.

Each participant wears a shoe-mounted (MilestonePod, Milestone Sports Inc, Columbia, MD) device that uses a validated algorithm to estimate temporal and kinematic properties of a run. The MilestonePod will be used primarily to detect the time spent running. The MilestonePod is mounted to the runner's shoe and starts collecting data once it detects a running motion. Within the Milestone Sports Application, after each run, participants sync their run and rate their perceived exertion using the rate of perceived exertion scale (RPE scale) within the app. The scale has a range from 1 to 10 and is used to determine the intensity at which one is exercising. A score of one would be considered the least amount of effort, whereas a score of ten would be considered maximal effort.

Each week, participants take an online survey to self-evaluate injuries. Through this survey, they were asked about the parameters of their runs such as the surfaces they ran on, number of runs that week, weather conditions, running partners and if they cross-trained.

The duration of the run (in minutes) is multiplied by the RPE value to determine the RPE index, reported as a unitless value. The RPE index and the injury data is combined for analysis. Statistical measure will be performed through JMP (SAS Institute Inc.). Effect size of differences between the injured and un-injured group will be reported.

RESULTS AND DISCUSSION

Twenty-six of the 108 runners completed an injury and RPE log at least one week of the 5 weeks of which these data encompass. Each week, an

average of 4.5 injuries were reported from this group and an average RPE of 639.5 was reported thus far (Table 1).

There were not enough data to report statistical differences thus far, but trends are emerging. Each week, the RPE index increased, less one (Figure 1). This study concludes May, 6th, 2018

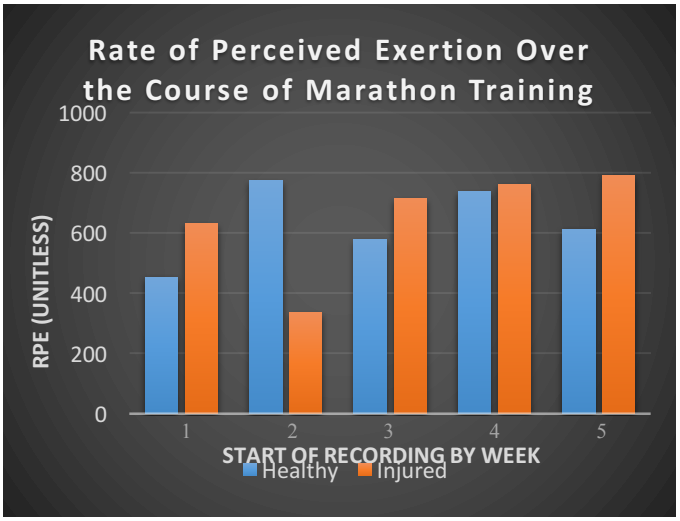

Figure 1. The reported rate of perceived exertion (RPE) displayed during each of the 5 weeks the study has been operating. Note the greater RPE index for the injured runners on 4 of the 5 weeks.

This study is evaluating a novel assessment tool of self-evaluation in a real-world scenario. The ease of determining one's own level of fatigue not only creates a more introspective analysis of a run but also may lead to a simple injury prevention guide. This evaluation in conjunction with the passive nature of the MilestonePod permits to have a means of truly running without interruption of personal assessment. The magnitude and duration of this study should lead to large scale implications for whether the RPE index is applicable to the greater population of runners.

CONCLUSIONS

Thus far, there has been a steady increase in rate of perceived exertion index with the increase of miles in preparation for the running of a marathon or half marathon distance. With a continuous increase in time throughout this training, it is highly likely for RPE to remain on a steady incline. What is less known for the future of this study are the injury outcomes. Currently, with only 17% of runners reporting injuries each week, it is well below the nation averages of 20-80%. This leads the authors to believe the injuries will also increase.

An increase of the RPE index for those with injuries would demonstrate a simple and understandable way for runners to see their load without reference to the miles they are running. There is currently no metric to understand not only physical training but also sleep, nutrition and life stress. The RPE has the ability to capture all of those through a personalized subjective measure and the potential to take more runners to the starting line.

REFERENCES

1. *2016 Running USA Annual Marathon Report*, (2017, June 15). www.runningusa.org
2. Van Gent et al. *Br J Sports Med*. **41**, 2007.
3. Malisoux et al. *Scand J Med Sci Sports*. 25 (1), 2013.
4. Malisoux et al. *J Sci Med Sport*. 18(**5**), 2014.
5. Gabbett, TJ. *J Strength Cond Res*. 24(**10**), 2010

ACKNOWLEDGEMENTS

Research funding for Alianna Gedlinske comes from the Blugold Fellowship at the University of Wisconsin- Eau Claire.

Table 1: Rate of perceived exertion by date for the duration of the marathon training class to date. Note the general increase of RPE with the increase in weeks. The authors of this paper expect this trend to increase.

Date	1/28/2018	2/4/2018	2/11/2018	2/18/2018	2/25/2018	**Average**
RPE	474.3	712.7	600.3	744.0	666.4	**639.5**

THE EFFECTS OF A CARBON FIBER SHOE INSOLE ON RUNNING MECHANICS

Robert W. Gregory, Robert S. Axtell, Marc I. Robertson, and William R. Lunn

Southern Connecticut State University, New Haven, CT, USA
E-mail: gregoryr3@southernct.edu, Web: http://www.southernct.edu/running-clinic/

INTRODUCTION

Athletes often select equipment, such as running shoes, that is designed to maximize energy storage and return. However, athletic footwear is typically characterized by poor energy storage and return (~1-2%) as a result of current technological limitations in the design of and material properties used in shoe midsole construction [1, 2]. As a result, most of the energy that is stored in a shoe midsole when the foot contacts the ground is lost through heat, friction, and vibrations and, thus, decreases the efficiency of the athlete.

There is limited research to date that has addressed the role of orthotics/shoe insoles on performance improvement. Increasing the bending stiffness of shoes (via the use of carbon fiber plates inserted either into the shoe midsole or under the shoe sock liner) has resulted in 1-4% improvements in running economy [3-5]. These changes in running economy have been accompanied by minor changes in gait mechanics [3-5] that may have secondary consequences. However, it is unknown if these (or other) changes in gait parameters will occur when using carbon fiber insoles with standard footwear in an attempt to improve running economy.

The purpose of this study was to examine the effects of a carbon fiber shoe insole on global alterations in running mechanics. The gait parameters assessed in this study were: stride length (SL), stride rate (SR), stride time (ST), stance phase %, swing phase %, vertical ground reaction force (vGRF), and rate of force development (RFD). Based on previous research investigating running footwear using carbon fiber plates inserted into the midsole, it was hypothesized that there would be increases in SL, ST, stance phase %, and vGRF and decreases in SR and swing phase % when using carbon fiber insoles.

METHODS

Twelve male distance runners and triathletes (age: 24.5 ± 6.4 yr, height: 177.9 ± 5.4 cm, mass 68.1 ± 5.5 kg) participated in this study. Participants provided informed consent according to the policies and procedures of the Institutional Review Board at Southern Connecticut State University.

The gait mechanics of the participants were analyzed while they performed running economy tests wearing a standard shoe insole and two different stiffness (medium and stiff) carbon fiber shoe insoles (VK Performance Insoles; VKTRY Gear; Milford, CT). The participants ran 15-20 km in both pairs of carbon fiber shoe insoles to become accustomed to the increased footwear bending stiffness during the two weeks prior to testing. All participants used the same model of racing shoe for test footwear (XC700v2; New Balance Athletics, Inc.; Boston, MA). Following a 10 min warmup run at a speed of 3.58 m/s (7:30/mile pace), the three running economy tests were performed at a speed of 4.47 m/s (6:00/mile pace) for 6 min. The three shoe insole conditions were presented in random order; all trials were separated by a period of 6 min to minimize the effects of fatigue.

Kinematic and kinetic data were collected during the last 90 s of each condition using an instrumented treadmill (FDM-T; Zebris Medical GmbH; Isny im Allgäu, Germany). A minimum of 60 strides were analyzed for all conditions. The following gait variables were measured: SL, SR, ST, stance phase %, swing phase %, peak vGRF, and average RFD. Descriptive statistics (mean and standard deviation) were calculated for all variables. A repeated-measures MANOVA was used to compare changes across the three shoe insole conditions; the level of significance was set at $p < 0.05$.

RESULTS AND DISCUSSION

Previous research has shown that increasing forefoot bending stiffness (via the use of carbon fiber plates inserted into the shoe midsole or under the shoe sock liner) can enhance running economy by 1-4 % [3-5]. However, the mechanism(s) behind the improvement in running economy (and the associated alterations in gait mechanics) need to be more fully investigated. While the use of carbon fiber plates incorporated into shoe midsoles or carbon fiber shoe insoles may improve performance in a relatively short laboratory-based running economy test, changes in running mechanics may lead to fatigue, decreased efficiency, or increased risk of injury in a longer duration real-world training or racing setting.

The use of medium and stiff flex carbon fiber shoe insoles did not result in any changes in SL, SR, ST, peak vGRF, or average RFD (Table 1). These findings contrast with increased SL and peak vGRF and decreased SR observed during running economy testing of Nike Zoom Vaporfly 4% footwear, which incorporates a carbon fiber plate in the shoe midsole [5]. Both medium and stiff flex carbon fiber shoe insoles resulted in a significant increase and decrease in stance phase % and swing phase % (both $p < 0.001$), respectively, when compared to a standard shoe insole (Table 1). These findings are in agreement with increased contact time observed during running economy testing of the Nike Zoom Vaporfly 4% [5].

CONCLUSIONS

A carbon fiber shoe insole has recently been developed to provide the same performance benefits (such as improved running economy) as carbon fiber plates inserted into a shoe midsole. The shoe insole form factor has two significant advantages over a plate incorporated into a shoe's construction: 1) more cost-effective (insoles can be used in multiple pairs of footwear), and 2) more adaptability (insole stiffness can be "tuned" to optimize performance under different conditions).

The use of a carbon fiber shoe insole to improve running economy does not cause any alterations in gait mechanics that would either decrease efficiency or increase risk of injury. Differences in gait parameters between footwear with carbon fiber shoe insoles and footwear with carbon fiber plates (such as the Nike Zoom Vaporfly 4%) may be due to differences in midsole compliance and resilience.

REFERENCES

1. Nigg BM, et al. *Biomechanics and Biology of Movement,* Human Kinetics, 2000.
2. Nigg BM. *Biomechanics of Sport Shoes,* Author, 2010.
3. Roy JPR, Stefanyshyn DJ. *Med Sci Sports Exerc* **38**, 562-569, 2006.
4. Madden R, et al. *Footwear Sci* **8**, 91-98, 2016.
5. Hoogkamer W, et al. *Sports Med* https://doi.org/10.1007/s40279-017-0811-2, 2017.

Table 1: A comparison of gait mechanics between footwear with a standard insole and footwear with medium (stiffness = 30 N/mm) or stiff (stiffness = 47 N/mm) carbon fiber shoe insoles during running economy testing.

Gait Variable	Shoe Insole		
	Standard	**Carbon Fiber Medium Flex**	**Carbon Fiber Stiff Flex**
Stride Length (m)	2.91 ± 0.19	2.90 ± 0.19	2.92 ± 0.18
Stride Rate (Hz)	1.52 ± 0.11	1.52 ± 0.11	1.52 ± 0.11
Stride Time (s)	0.66 ± 0.04	0.66 ± 0.04	0.66 ± 0.04
Stance Phase (%)	31.0 ± 2.1	32.2 ± 2.0	32.0 ± 2.2
Swing Phase (%)	69.0 ± 2.1	67.8 ± 2.0	68.0 ± 2.2
Peak vGRF (BW)	2.21 ± 0.17	2.08 ± 0.17	2.19 ± 0.15
Avg. RFD (BW/s)	33.2 ± 4.4	33.6 ± 5.6	34.9 ± 4.9

RUNNING GAIT COMPLEXITY INCREASES BEFORE INJURY IN COLLEGIATE RUNNERS

[1]Allison H. Gruber, [1]Jacob E. Vollmar, [2]Jake A. Melaro, [2]Douglas W. Powell, [3]Robert K. Boorsma, [1]Ashley B. Nguyen, [2]Max R. Paquette

[1] University of Indiana, Bloomington, IN, USA
[2] University of Memphis, Memphis, TN, USA
[3] University of Guelph, Guelph, ON, Canada
email: ahgruber@indiana.edu, web: https://iubiomechanicslab.weebly.com/

INTRODUCTION

Running-related overuse injuries (RROI) to the musculoskeletal system affect 26%–92% of runners annually [1]. RROI can largely be attributed to increased training volume and intensity without proper recovery [e.g. 2]. In collegiate runners, injury rates range between 4.66 to 5.85 injuries per 1000 athlete exposures in men and women, respectively, with the majority of injuries classified as overuse [3]. Musculoskeletal overuse injuries can lead to setbacks in training progression that may ultimately affect competitive performance. It is therefore of utmost important to identify early detection methods of overtraining and injury risks to help reduce the likelihood of injury onset.

Wearable sensor technology has been used to detect changes to whole-body movement complexity after a single fatiguing run [4]. This change in whole-body movement complexity may reflect an altered running gait pattern that may lead to RROI. We previously presented pilot data from novice runners that showed whole-body, center of mass (COM) movement complexity changes in response to a 3-week training program and the change in complexity might be associated with subjective measures of fatigue or overtraining [5]. However, the relationship between reductions in movement complexity caused by prolonged training and prospective development of RROI has not been investigated.

The purpose of this study was to test if COM acceleration complexity could be used to detect injury onset in collegiate distance runners. It was hypothesized that COM acceleration complexity would be lowest during runs preceding the onset of overuse injury in collegiate runners who sustained an injury compared with runners who did not develop an injury. Furthermore, the change in complexity would be greatest in the injured vs. uninjured groups.

METHODS

Thirty collegiate runners (12 women and 18 men) participated in the study. All runners received a wearable 3D accelerometer (GT3XP-BTLE, ActiGraph Corp, USA) at the start of their collegiate cross-country season (i.e., early September). Accelerometers were worn over the posterior aspect of their pelvis using an adjustable belt during continuous training runs for the entire cross-country season. Accelerometers were not worn during interval running sessions or races. The maximum sampling frequency of 100 Hz was used. At the start of the study, all runners completed a baseline run, which was an easy run on a known cross-country route. The length of this run varied among runners given that they all trained at slightly different weekly running volumes. However, the relative intensity of the run (i.e., low) was the same for all runners. Every day during the season, runners also completed an online survey to track injury or symptom onset and injury location and severity. When injuries were reported, the date of injury onset was recorded and accelerometer data during runs preceding injury onset were analyzed. The season length varied among runners depending on qualification to the collegiate championship and club championship.

Injured runners were matched with uninjured runners by gender and age to compare COM acceleration complexity between groups. The acceleration data collected during the baseline run were analyzed for all runners. Data from the last run prior to injury in the injured group were analyzed and compared with the data from the matched uninjured runners on the same date as the last run of the injured runners

preceding injury onset ('pre-injury'). The pre-injury run data were taken from the same dates within matched pairs to account for differences in cumulative fatigue at different times in the season.

The resultant value of the raw COM acceleration data was calculated for each instant of each analyzed run. Complexity of the resultant raw COM acceleration signal was calculated by control entropy with a 2-point window length [6]. Radius of similarity (r_e=0.001) was determined by calculating 15% of the standard deviation of the original signal. The length of the matching sequence that identifies regularity in the signal was set to a value of m = 2. The average control entropy of each analyzed run was used for statistical analysis.

Multivariate ANOVA was used for the following comparisons of interest: baseline vs. pre-injury complexity within groups as well as baseline, pre-injury, and change in complexity between groups (α=0.05). Cohen's *d* effect sizes were used to determine if the differences in complexity between groups and time points were meaningful.

RESULTS AND DISCUSSION

Of the 30 runners, one runner lost the accelerometer (the backpack containing the device was stolen), and seven runners developed an injury (3 males, 4 females; 18.7±1.0 years). Seven uninjured runners (3 males, 4 females; 18.7±1.1 years) were matched with the injured runners. These 14 runners were analyzed.

No significant differences in baseline vs. pre-injury complexity within groups were detected (injured p=0.23; uninjured p=0.81). However, the increase in complexity baseline vs. pre-injury in the injured group had a moderate effect size (*d*=0.74) but no effect was observed in the uninjured group (*d*=0.13; Fig. 1). No significant differences between groups were detected for baseline, pre-injury, or change in complexity (p>0.05; Fig 1). The effect size for baseline complexity between groups was low (*d*=0.29). The injured group experienced a greater change in complexity baseline to pre-injury than the uninjured group indicated by a large effect size (*d*=2.61). This large effect size provides merit to the hypothesis that the change in complexity from an early season baseline test to days before injury onset would be greater for injured vs. uninjured runners. However, the direction of the change in complexity was opposite than expected. The injured group had a moderately greater pre-injury complexity compared with uninjured (*d*=0.66; Fig. 1).

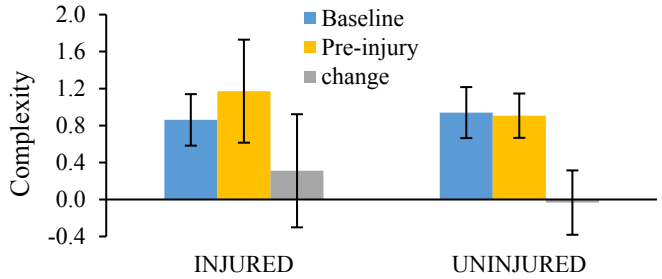

Figure 1. Mean±1SD complexity at the start of the cross-country season (baseline), from the dates associated with the run prior to injury in the injured group (pre-injury), and the change in complexity from baseline to pre-injury (negative indicates a decline).

CONCLUSIONS

Previous studies have shown lower complexity in older vs. young adults [7] and in disease states vs. healthy counterparts [e.g. 8]. Contrary to those cross-sectional findings but in support of our previous prospective work in novice runners [5], the current study suggests that an increase in complexity during a cross-country season may reflect an increased risk of injury in collegiate cross-country runners who were otherwise healthy.

REFERENCES

1. van Gent, R.N., et al., Br J Sports Med, **41**(8): 469-80, 2007.
2. Hespanhol Junior, L.C., et al., J Physiother, **59**(4): 263-9, 2013.
3. Kerr, Z.Y, et al., J Athl Training, **51**(1): 57-64, 2016.
4. McGregor, S.J., et al., Chaos, **19**(2): 026109, 2009.
5. Gruber, A.G., et al., ASB Proceedings, 2017.
6. Bollt et al., Math Biosci Eng, 6(1): 1-25, 2009.
7. Bisi, M., et al. *Gait Posture*, 2016, **47**, 37-42.
8. Costa, M., et al., *Phys Rev E Stat Nonlin Soft Matter Phys*, **71:** 021906, 2005.

ACKNOWLEDGMENTS

Funding for this study was provided by the American Athletic Conference Academic Research Consortium.

COORDINATION AND VARIABILITY DIFFER BY YEARS OF RUNNING EXPERIENCE

Jocelyn F. Hafer, Ronald F. Zernicke, and Cristine E. Agresta

University of Michigan, Ann Arbor, MI, USA
email: johafer@umich.edu, web: http://www.mipr.kines.umich.edu/

INTRODUCTION

Overuse injury is common in running, but individuals who have been running for fewer years have higher rates of injury compared to their more-experienced peers [1]. Because common running injuries have been associated with aberrant mechanics, differences in running mechanics between less- and more-experienced runners have been hypothesized to cause increased injury incidence in less-experienced runners. However, there is little evidence of differences across running experience level in commonly measured running mechanics such as joint angles at specific gait events or phases [2]. While it appears that less- and more-experienced runners produce similar joint kinematics, the coordination or flexibility of the running movement may differ by experience level, potentially affecting injury susceptibility.

Running injuries may be associated with lower segment coordination variability [3]. Further, less experience in running may be linked to altered coordination, as introduction of a novel running intervention has been shown to result in decreased coordination variability and different segment coordination [4]. Taken together, these studies suggest that decreased coordination variability and altered coordination could be present in a relatively novel task and could alter tissue loading in such a way to cause pain or injury. As a first step in testing whether less-experienced runners' higher injury rates are related to differences in movement organization or flexibility, the purpose of this study was to compare segment coordination and its variability between asymptomatic runners with differing years of running experience.

METHODS

Data were pooled from a database of previously-collected running data. Participants were included in the current analysis if they reported being a consistent runner for ≤ 2 years or ≥ 10 years and had no running injury in the previous 12 months. Descriptive statistics of the 20 more- and 21 less-experienced runners included in the analysis are reported in Table 1.

Kinematics were collected at 200 Hz using inertial measurement units (IMUs; Myomotion, Noraxon) as participants ran at self-selected comfortable training pace on a treadmill. Standard placement of IMUs was used across all participants for the left thigh (halfway along segment length on lateral aspect), shank (halfway along segment length on lateral aspect, aligned with thigh IMU), and foot (dorsal aspect of foot). Immediately prior to data collection, IMU alignment was calibrated to anatomical alignment during a static standing trial.

For each participant, sagittal plane segment angles were extracted and normalized to 101 points per gait cycle for 50 consecutive strides of data. Segment coordination and its variability were calculated for sagittal plane thigh vs. shank and shank vs. foot couples using a modified vector coding technique [5]. Coordination data were averaged during early, mid, and late (thirds of) stance, and terminal swing (last 15% of swing) and compared between groups for each segment couple using circular 1-way ANOVAs (Watson-Williams test) for segment coordination phase angles and t-tests for coordination variability with $\alpha=0.05$.

RESULTS AND DISCUSSION

More- and less-experienced runners had different phase angles during terminal swing and early stance for the shank vs. foot couple (Figure 1). However, these differences did not result in a significant group difference in coordination pattern, as more- and less-experienced runners were in-phase during both early stance and terminal swing. Less-experienced runners had lower coordination variability compared to more-experienced runners for the thigh vs. shank and

shank vs. foot couples during early and mid stance (Figure 2).

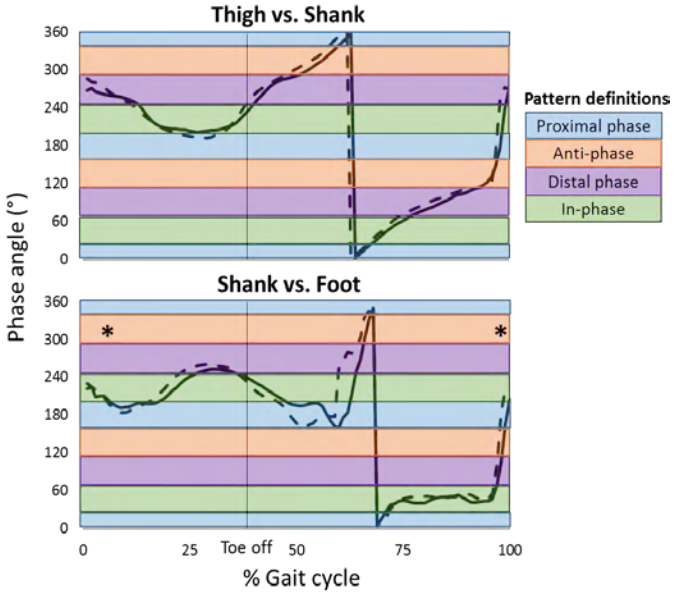

Figure 1: Segment coordination for more- (solid) and less- (dashed) experienced runners. Color indicates coordination pattern. *: significant difference between groups for phase of gait cycle.

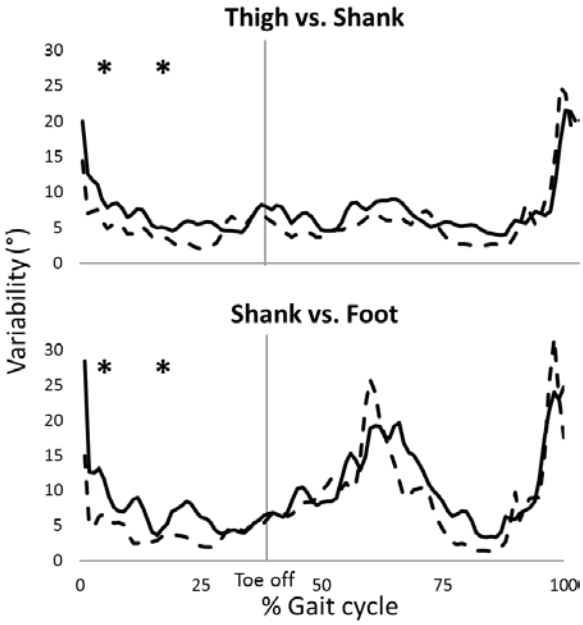

Figure 2: Coordination variability for more- (solid) and less- (dashed) experienced runners. *: significant difference between groups for phase of gait cycle.

The negligible differences in segment coordination by experience level suggest that less-experienced runners produced sagittal plane movement patterns about the knee and ankle that were similar to those of more experienced runners. The lower coordination variability during early and mid stance in less-experienced runners, however, suggested that individuals gain flexibility of these movement patterns with experience. The timing of decreased variability in early and mid stance may be important for injuries such as patellofemoral pain or tibial stress fractures, where distribution of loads across the patellar cartilage or tibia via movement variability may reduce tissue damage.

CONCLUSIONS

While less- and more-experienced runners did not appear to have different movement patterns about the knee and ankle, less-experienced runners produced these patterns with less movement flexibility. Lower coordination variability may contribute to the higher incidence of overuse injuries in less-experienced runners. These results reveal initial insights that may prove to be useful for developing studies to assess injury-prevention interventions or training strategies that focus more on neuromuscular control, rather than exclusively on running mechanics.

REFERENCES

1. Macera. *Sports Med*. **13**(1):50-57, 1992.
2. Agresta et al. *Gait Posture*. **61**:13-18, 2018.
3. Heiderscheit et al. *J Appl Biomech*. **18**:110-121, 2002.
4. Hafer et al. *J Sports Sci*. **34**(15):1388-1395, 2016.
5. Chang et al. *J Biomech*. **41**(14):3101-3105, 2008.

ACKNOWLEDGEMENTS

Funding provided by the Michigan Institute for Clinical Health Research grant UL1TR000433.

Table 1: Characteristics of more and less experienced runners. *: significant difference between groups.

	n (# male)	Running Years	Running Speed (m/s)	Age (yr)	BMI (kg/m^2)	Typical Weekly Mileage (miles)
More experienced	20 (16)	15.8±8.3*	3.2±0.3	38.2±10.9*	22.1±1.9	34.3±15.9
Less experienced	21 (17)	1.3±0.7	3.2±0.4	32.3±9.4	23.6±3.0	25.5±15.4

Examining the minute to minute predictability of walking distance and local joint stability across multiple surfaces

Tyler Hamer, Abderrahman Ouattas, Katlyn Nimtz, Brian A. Knarr
Department of Biomechanics, University of Nebraska at Omaha, Omaha, NE USA
Email: thamer@unomaha.edu, Web: https://www.unomaha.edu/college-of-education/cobre/

INTRODUCTION

The 6-minute walk test (6MWT) is useful for longitudinal assessment as well as monitoring treatment response and is considered a simple method for assessing exercise capacity at a submaximal level[1] . In recent years, we have begun to shorten the duration of clinical walking tests as correlations between duration of the test and findings become more apparent[2]. With findings that the 6MWT is more efficient than the original 12-minute walk test (12MWT), recent studies have explored further shortening the 6MWT for use in populations with walking impairments. However, it is important that a shorter duration test can accurately capture walking function compared to the 6MWT. Additionally, it is important that these findings accurately represent real-world walking, where surfaces are often less homogenous compared to a lab or indoor setting.

Therefore, the goal of the study is to determine the minute-to-minute changes in walking distance and kinematics during indoor and outdoor walking, and the ability for data collected at earlier minutes to accurately quantify walking function. Two primary measures will be assessed: walking distance, and local joint stability, as quantified by the maximum Lyapunov exponent. The Lyapunov exponent (LyE) is a measure of how infinitesimally close trajectories of dynamical systems vary or diverge in a certain dimension of phase space[5]. This is particularly effective in analyzing stride-to-stride fluctuations in gait patterns because it describes the overall consistency of a system by describing how similar gait kinematics are from one stride to the next[6]. A minimal level of variability, or a lower LyE value, in joint kinematics is necessary for adaptability and response to everyday perturbations, such as walking on uneven terrain. However, too much variability, or a higher LyE value, may be reflective of impaired motor control and can lead to irregular movement patterns[7]. We hypothesize that there are strong correlations between walking distances during the first three minutes and distances in the last three minutes of the test. Secondly, we hypothesize local joint stability will be consistent from minute to minute. This finding will suggest that underlying kinematics are consistent throughout the walking trials. Lastly, we hypothesize that the variation (standard deviation) between minutes in local joint stability is less than the differences between surfaces, such that surface changes would demonstrate statistically different LyE despite any between-minute variability.

METHODS

This study included 18 healthy adults between the age of 40 and 85 years old (Age 65.1±10.1, Mass 74.8±17.7). Subjects completed a walking trial on three different surfaces: an indoor track, an outdoor paved surface, and an outdoor unpaved surface. Sagittal plane joint angles were measured using an inertial sensor based motion capture system (Xsens Technologies). Sensors were attached bilaterally to the shank and thigh segments to capture knee joint angle. Subjects completed a 6MWT on an indoor track. Subjects then completed a 3MWT on a nearby circular sidewalk path outside and directly next to the sidewalk on the grass. The sidewalk and grass paths were chosen to preclude any stepping or turning patterns not typical of a standard 6MWT. To maintain consistency between subjects for the grass surface, collections did not take place within 24 hours of heavy precipitation, and an examination of the surface was made prior to data collection. The total distance walked was measured using a rolling measuring wheel alongside the participant. Distances were collected at every minute mark.

Linear regressions were performed to measure predictability of walking distance from minute to minute. R^2 values were calculated to signify predictive trends amongst each minute within the trials. A custom MATLAB code that uses the Wolf algorithm[4] was used to calculate the Lyapunov exponent. A repeated measures ANOVA was run on the minute to minute knee joint angle LyE over the three surface trials to determine differences in time and surface.

RESULTS AND DISCUSSION

Linear regressions revealed that distance within the first few minutes significantly predicted performance around the six-minute mark. Results indicated that very strong correlations between the mean distances walked across minutes appeared around the two-minute mark, with an R^2 value of .95 (Table 1). This suggests that while the first minute may be unreliable of 6-minute findings, the second minute onwards is highly predictive of the full 6MWT.

Table 1: Minute to minute correlations of distance walked.

	1 v. 3	2 v. 3	1 v. 6	2 v. 6	3 v. 6	4 v. 6	5 v. 6
Track	.69	.96	.64	.95	.98	.99	.99
Paved	.59	.99	-	-	-	-	-
Unpaved	.90	.96	-	-	-	-	-

Knee joint flexion LyE showed that the track surface was much less variable in knee flexion compared to the outdoor surfaces, with an average LyE of 1.37 across the six minutes. Unpaved surface trials contained the most variable gait pattern, with an average LyE of 3.94 (Table 3). The paved surface trials more closely resembled that of the track surface, displaying a LyE of 2.32.

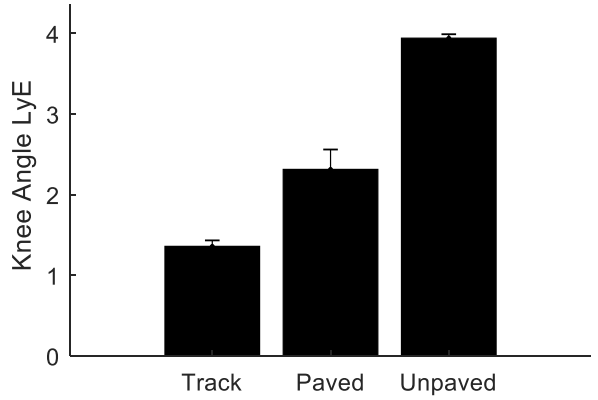

Figure 1. Knee joint angle LyE averaged across 1-minute interval for three different walking surfaces.

Standard deviations within trials are less than the differences in knee angle LyE across trials (Figure 1). For track, paved, and unpaved, minute-minute values were relatively consistent, with standard deviation values were 0.07, 0.24, and 0.05 respectively (Table 3). This coincides with our last hypothesis that there is less variability within a trial when compared to other trials on different surfaces. This is important to note, as the between minute variation would dictate the amount of change that is detectable across populations or conditions.

CONCLUSION

We hypothesized that correlations would be found between the first few minutes and last few minutes of a 6MWT. Strong R^2 developed at the two-minute mark and continued to strongly correlate with each passing minute. With other studies working with the 2-minute walk test (2MWT)[8,9], researchers have shown it may be possible to replicate 6MWT findings in shorter durations. Shortening these functional tests can help patients who struggle with various walking deficiencies as well as shortening exam research protocol altogether. When observing between total distance walked and the minute-to-minute variability in distance amongst participants, it was found that no correlation between the two variables exists. Similarly, we observed relatively consistent values of knee joint angle LyE within the individual trials, with intra-trial differences much less than the differences between surfaces. While these findings are relevant for healthy populations, further research needs to be conducted to elaborate on shortening the 6MWT in consideration to pathological populations, particularly those who may be easily fatigued.

REFERENCES

1. Lammers AE. Arch Dis Child. 2008;93: 464–468.
2. Enright PL. The six-minute walk test. Respir Care. 2003;48: 783–5.
3. Cutti AG. Med Biol Eng Comput. Springer-Verlag; 2010;48: 17–25.
4. Wolf A. Phys D Nonlinear Phenom. 1985;16: 285–317.
5. Kempski K. J Biomech. 2018;68: 1–5.
6. Wurdeman SR.J Rehabil Res Dev. 2013;50: 671–86.
7. Stergiou N. Hum Mov Sci. 2011;30: 869–888.
8. Connelly DM, Physiother Can. 2009;61: 78–87.
9. Leung ASY. Chest. 2006;130: 119–125.

ACKNOWLEDGEMENTS

P20GM109090

Chaotic behavior of peak ground reaction forces during gait

Jerome Hausselle and Eranda Ekanayake

BAMM Lab, Mechanical & Aerospace Engineering, Oklahoma State University, Stillwater, OK, USA
email: jerome.hausselle@okstate.edu, web: https://bammlab.okstate.edu/

INTRODUCTION

More than half of the Americans older than 65 suffer from osteoarthritis (OA). However, screening protocols and prevention strategies are still underdeveloped because of a lack of accurate predictive models. OA progression has been correlated with several anatomical, musculoskeletal, and mechanical factors, including higher-than-normal joint contact forces [1]. Nevertheless, the mechanisms associated with OA progression remain largely unknown.

Although peak ground reaction forces (GRF) undoubtedly influence peak joint contact forces and thus OA progression, we hypothesize that their dynamic fluctuations also play a key role. In this study, we aimed at quantifying the dynamic behavior of peak vertical GRF during gait and its dependence on speed and body mass index (BMI). This work is the very first step towards a more accurate predictive model of OA progression.

METHODS

Eleven healthy females (age: 21 ± 2 years old, BMI: 22 ± 3 kg/m^2) and eleven healthy males (age: 22 ± 1 years old, BMI: 25 ± 3 kg/m^2) participated in this study. The protocol was approved by the Institutional Review Board and each participant signed an informed consent form. The exclusion criteria were (1) lower limb surgeries, (2) diagnosed osteoarthritis, (3) diagnosed cardiac condition. Subjects walked barefoot at a self-selected speed on an instrumented treadmill (Noraxon, Scottsdale, AZ, USA) for 10 minutes. Plantar pressure distributions were continuously recorded at 100 Hz.

For each subject and side, we computed the vertical ground reaction force (vGRF) at each instant in time. The vGRF was filtered using a 4th-order low pass Butterworth filter with a cutoff frequency of 20 Hz [2]. Peak vGRF were determined for the heel strike and toe off phases. Finally, to assess the dynamic behavior of these peak forces, we performed detrended fluctuation analysis (DFA) on the original and randomly shuffled data [3]. The output of DFA is the fractal scalar index α. A series exhibiting a random behavior is characterized by $\alpha \approx 0.5$, whereas a series exhibiting a chaotic behavior is characterized by $\alpha > 0.5$ or $\alpha < 0.5$. We computed the mean of α for each side and gender.

We tested each α distribution for normality (Shapiro-Wilk test), and used t-test with a *p*-value at 0.05 to test for differences between side and gender. Finally, we performed a linear regression in Matlab with BMI and speed as independent variables and α of the peak vGRF at heel strike as the dependent variable, with a *p*-value at 0.05.

RESULTS AND DISCUSSION

Mean fractal indices varied between 0.83 and 0.96 (Fig. 1). We did not find any statistical differences between sides for each gender, and between genders for each side. Mean fractal indices for the shuffled data varied between 0.45 and 0.54, validating the efficacy of the DFA to detect chaotic behavior (Fig. 2). These results highlight the chaotic nature of the peak vGRF during the heel strike and toe off phases, regardless of gender, BMI, and gait speed. A fractal scaling index above 0.5 indicates long-range self-similar correlations, which means that the value of the peak vGRF at a specific time depends on all the previous values.

Although many studies analyzed single gait cycles, only a few included the fluctuations of gait variables over hundreds of cycles. Hausdorff et al. [3] showed that the fluctuations of a temporal gait parameter such as the stride interval exhibit a chaotic behavior. Moreover, age or diseases seem to disrupt the

fluctuation dynamics and lead to random behaviors [4]. This is one of the first studies to apply this approach to kinetic variables related to OA. Our results offer new insights for simulating OA progression since peak cartilage loading is likely neither cyclic nor random.

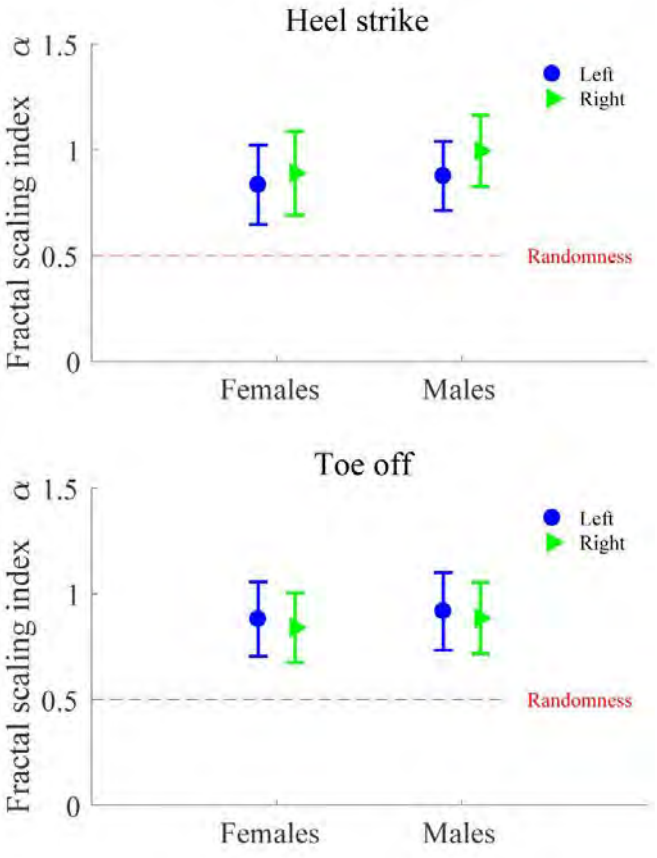

Figure 1. Mean fractal scaling indices of the peak vertical ground reaction forces during the heel strike and toe off phases, for both genders and both sides. Whiskers represent one standard deviation.

Self-selected speeds were 0.9 ± 0.2 m/s for female subjects and 1.0 ± 0.2 m/s for male subjects. Both the speed and the BMI were included ($p < 0.05$) in the model created using the linear regression. The peak vGRF value is related to the gait speed since the higher the speed the higher the breaking forces needed to decelerate the foot during the heel strike phase. The same reasoning can be applied to the BMI. However, our results show that speed and BMI not only influence the values of the peak vGRF, but also its dynamic behavior

Current work focuses on recruiting older subjects to assess the effect of age on the dynamic behavior of ground reaction forces during gait. We are also developing an OpenSim model [5] to compute joint contact forces and assess their dynamic behavior.

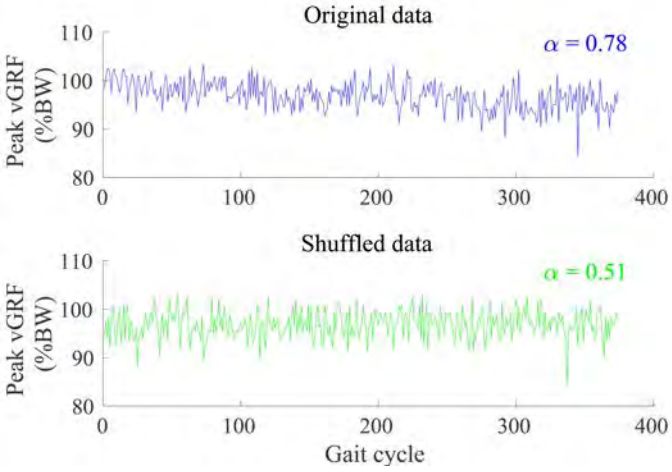

Figure 2. Example of an original signal of the peak vGRF at heel strike (α = 0.78) and the corresponding shuffled signal (α = 0.48).

CONCLUSIONS

Peak vertical ground reaction forces during gait exhibit a chaotic behavior, which depends on gait speed and body mass index. This study represents the first critical step towards the development of accurate predictive models to detect patients at risk of developing OA. Preventing OA would greatly enhance older adults' quality of life and reduce the burden placed on them, their families, and the overall health system.

REFERENCES

1. Neogi and Zhang. *Rheumatic Disease Clinics of North America*. 39(1): 1-19.
2. Kiss. *Medical Engineering & Physics*. 32(6): 662-667, 2010.
3. Hausdorff et al. *Journal of Applied Physiology*. 78(1): 349-358, 1995.
4. Hausdorff et al. *Physica A*. 302(1-4): 138-147, 2001.
5. Delp et al. *IEEE Transactions on Biomedical Engineering*. 54(11): 1940-1950.

Delayed Time to Fixation of an Intra-articular Fracture Does Not Cause Additional Limb Dysfunction in a Large Animal Model of Post-Traumatic Osteoarthritis

Christopher R. Heck, Austin M. Lauters, Nicole A. Watson, Douglas C. Fredericks, Jessica E. Goetz

University of Iowa, Iowa City, IA
email: christopher-heck@uiowa.edu, web: https://uiowa.edu/uiobl/

INTRODUCTION

The Yucatan minipig has been shown to replicate many characteristics of the human response to intra-articular fracture (IAF), including timeline to bone healing, acute inflammatory response, and eventual development of PTOA.[2] A limitation to that previous work was that the surgical fixation was performed immediately after fracture creation, which differs from a human treatment setting where surgical fixation is often delayed for several days or weeks in order to permit resolution of soft tissue swelling and reduce wound healing complications.

Investigating the effects of such a delay on joint degeneration in the minipig IAF model may be confounded by altered limb loading that may occur in an animal that is additionally lame after the trauma of a second surgery. The purpose of this study was to evaluate Yucatan minipig kinematics to determine if additional abnormalities beyond those that result from a surgically treated IAF develop as a result of a delay in surgical fixation after IAF.

METHODS

Under IACUC-approval, 16 skeletally mature (minimum 2 years of age) anesthetized Yucatan minipigs received an impact to the left distal tibia sufficient to cause an IAF.[3] Eight of these animals had the fracture fixed anatomically using a plate and screws at the time of fracture creation. To simulate the clinical practice of a delay between injury and fracture fixation, the remaining eight animals were casted in a flexed position after fracture to prevent weight bearing. Three days after IAF, the animals underwent a second surgery for fixation of the fracture using an identical plate and screw construct.

Gait analysis was performed preoperatively and again 1, 2, 4, 6 and 12 weeks postoperatively. Bony landmarks on each limb segment from the pelvis to tarsus were marked with 15-mm diameter reflective markers. Marker clusters (4 per cluster) were added to the femur and tibia to aid with visualizing segments with large amounts of soft tissue overlying bony landmarks. A total of 42 markers were tracked during walking using an 8-camera Vicon system. Marker data were captured at 120 Hz while the animals walked on a treadmill at 1.2 kph for approximately 15 seconds per trial. Marker coordinate data were exported to a custom program developed in MATLAB to solve Euler angles at each joint (pelvis center, hip, knee, and hock).

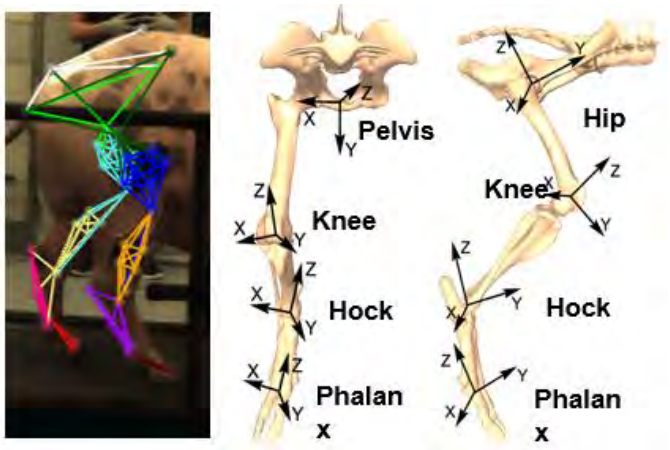

Figure 1: A Yucatan minipig at right leg toe touch with Vicon-labeled segments superimposed on the markers (left). Bony landmark-based individual joint coordinate systems (right).

Local bone coordinate systems (Figure 1) were established for each segment. Initial bone positions were calculated using singular value decomposition to calculate the rotation matrix required to relate each bony coordinate system to the world coordinate system, and each resulting rotation matrix was decomposed using YZX factorization. This process was propagated through each data capture on a frame-by-frame basis. Multiple steps from a trial were automatically parsed, and hock angular data for the multiple steps were averaged for each animal at

each time point. Stance and swing times were calculated from the average of the parsed steps for each postoperative time point.

RESULTS AND DISCUSSION

One week postoperatively, there was a 10 degree reduction in hock flexion angle relative to normal in both the immediate and the delayed fixation groups. At 2 weeks, there was a 10 degree increase in extension compared to normal. This trend was found in both the immediate and delayed fixation groups. At 4 and 6 weeks, the delayed groups re-approached the preoperative data whereas there was a slight increase in flexion in the immediate fixation group. Starting at 6 and by 12 weeks, both groups have re-approached the preoperative data.

At the early postoperative time points (1 and 2 weeks), there was increased hock adduction which resolved by 12 weeks. A similar trend was found for internal and external hock rotation, with early increases in internal rotation that return to normal by 12 weeks. All differences between operative groups were well within the group standard deviations indicating no significant difference in time to fixation on hock kinematics.

There were insignificant differences (<0.1 sec) in swing and stance time between the immediate and delayed fixation groups across all postoperative time points and in both the fractured and in the non-operative limb. Given these similarities in limb loading and hock joint kinematics, it would be expected that any notable differences in joint degeneration that may be found after a delay between fracture and definitive fracture fixation surgery in this animal model are not the result of significantly different limb loading.

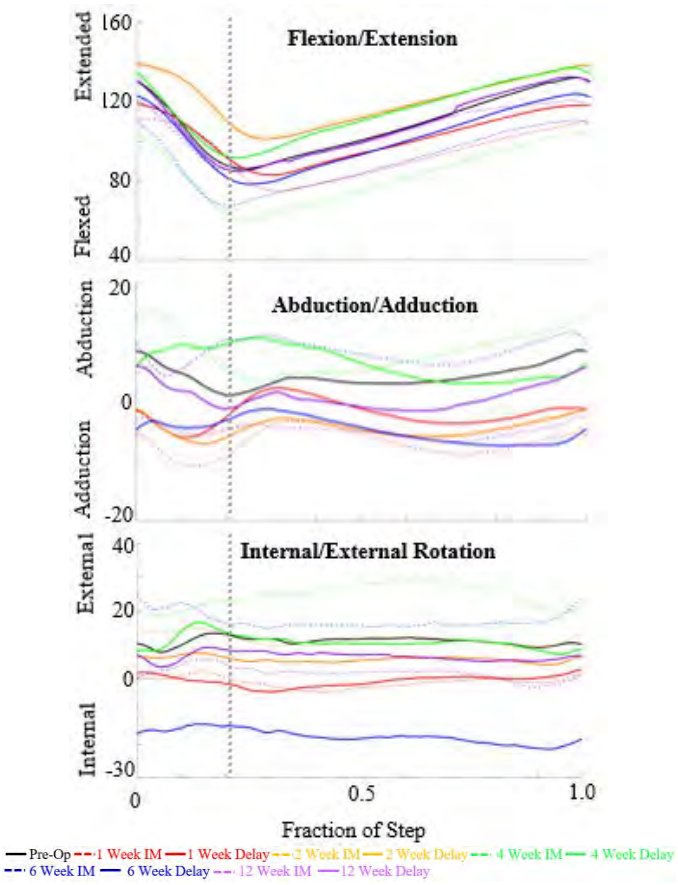

Figure 2: Group average hock angular data during walking gait at all postoperative time points.

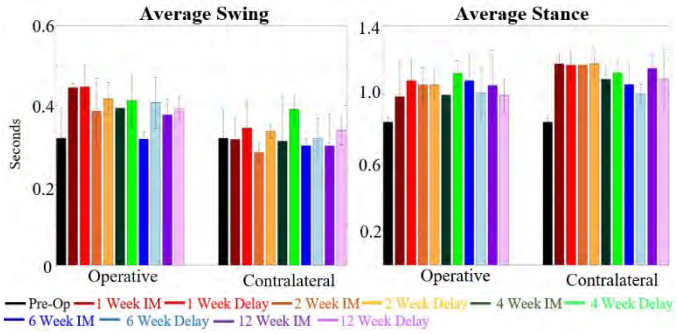

Figure 3: Average swing and stance time of the operative and non-operative limb show no consistent limb loading differences between groups.

REFERENCES

1. Teeny SM, & Wiss DA. *Clin. Orthop. Rel. Res.* 1993;108-117.
2. Matta JM. *J Bone Joint Surg. Am*. 1996;78:1632-1645.
3. Goetz JE, et al. *Osteoarthritis Cartilage*. 2015; 23(10):1797-805

ACKNOWLEDGEMENTS

This work was supported by Department of Defense award W81XWH-15-1-0642. Ms. Amie Pluskowski was instrumental during gait capture throughout the study.

Quantifying Changes in Gait Following Intra-articular Fracture in a Large Animal Model of Post-Traumatic Osteoarthritis

Christopher R. Heck, Austin M. Lauters, Nicole A. Watson, Douglas C. Fredericks, Jessica E. Goetz

University of Iowa, Iowa City, IA
email: christopher-heck@uiowa.edu, web: https://uiowa.edu/uiobl/

INTRODUCTION

The Yucatan minipig has been shown to replicate many characteristics of human response to intraarticular fracture (IAF), including timeline to bone healing, acute inflammatory response, and eventual development of PTOA.[1] In the initial characterization of the model, it was found that the minipig will load a fractured and surgically treated limb with approximately 45% of its preoperative value.[1] However, that work simply evaluated the load passing through the foot of the animal during ambulation, not the kinematics of the animal during gait. Gait asymmetry and abnormal kinematics are signs of pain in animal models who are very stoic and continue to use an injured limb. And subtle changes in gait pattern may have implications for limb loading, which may in turn affect the eventual development of PTOA in the model. The purpose of this study was to measure normal Yucatan minipig kinematics during normal walking gait and identify more subtle abnormalities in gait that result from an IAF that is treated surgically.

METHODS

Under IACUC-approval, formal gait analysis was performed in 16 skeletally mature (minimum 2 years of age) Yucatan minipigs. Eight of those animals then received an impact to the left distal tibia sufficient to cause an IAF while under anesthsia.[1] The resultant fracture was fixed anatomically using a plate and screws at the time of fracture creation. Gait analysis was performed 1, 2, 4, 6 and 12 weeks postoperatively in these animals.

During all gait analysis sessions, bony landmarks on each limb segment from the pelvis to tarsus were marked with 15-mm diameter reflective markers. Marker clusters (4 per cluster) were added to the femur and tibia to aid with visualizing segments with large amounts of soft tissue overlying bony landmarks. A total of 42 markers were tracked during walking using an 8-camera Vicon system. Marker data were captured at 120 Hz while the animals walked on a treadmill at 1.2 kph for approximately 15 seconds per trial. Marker coordinate data were exported to a custom program developed in MATLAB to solve Euler angles at each joint (pelvis center, hip, knee, and hock).

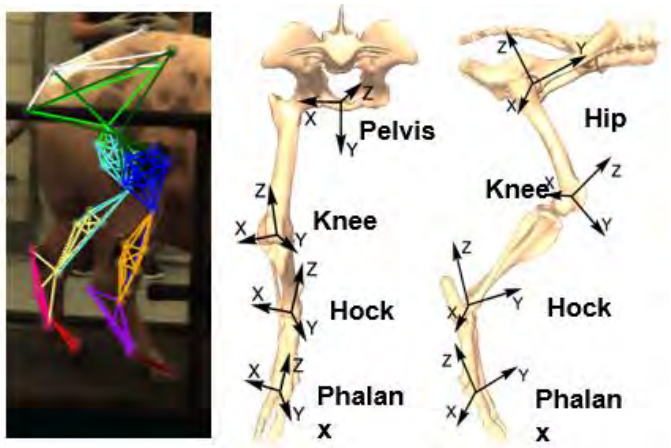

Figure 1: A Yucatan minipig at right leg toe touch with Vicon-labeled segments superimposed on the markers (left). Bony landmark-based individual joint coordinate systems (right).

Local bone coordinate systems (Figure 1) were established for each segment. Initial bone positions were calculated using singular value decomposition to calculate the rotation matrix required to relate each bony coordinate system to the world coordinate system, and each resulting rotation matrix was decomposed using YZX factorization. This process was propagated through each data capture on a frame-by-frame basis. Multiple steps from a trial were automatically parsed, and hock angular data for the multiple steps were averaged for each animal at each time point.

RESULTS AND DISCUSSION

One week postoperatively, there was a 10 degree reduction in hock flexion angle relative to normal. At

2 weeks, there was a 10 degree increase in extension compared to normal. At 4 and 6 weeks, there was a slight increase in flexion. Starting at 6 and by 12 weeks, the animal re-approached the preoperative data. In the corresponding abduction and adduction plot, the 1 week, 2 week and 6 week operative data for the left limb demonstrated an increase in adduction. By 4 weeks there was a notable increase in abduction by 10 degrees. By 12 weeks, the animal re-approached the normative data (Figure 2).

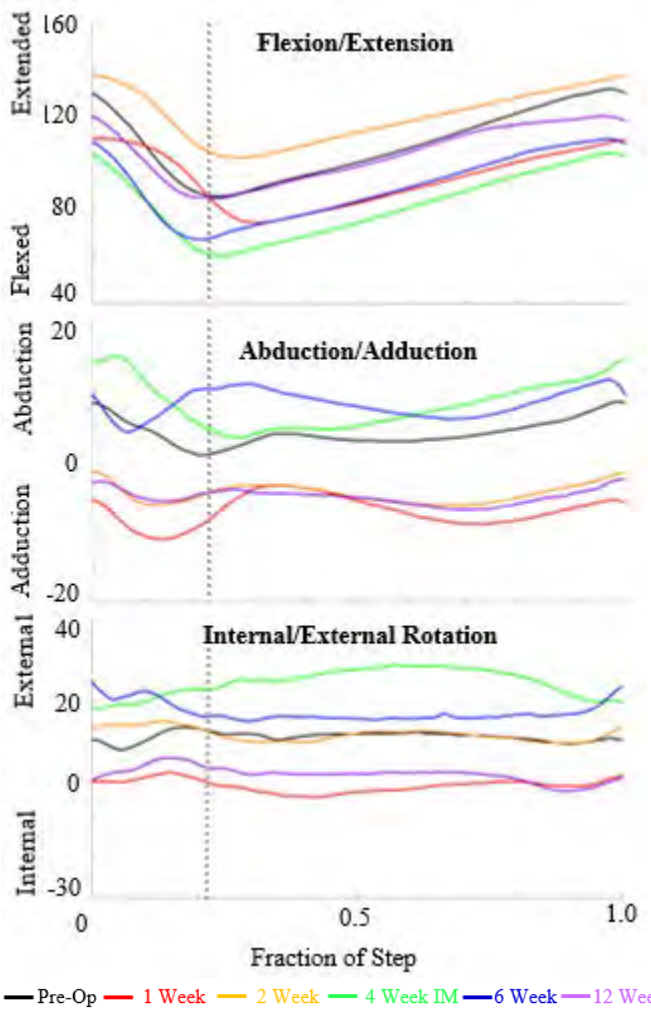

Figure 2: Group average hock angular data during walking gait at all postoperative time points. For the preoperative group, n = 30 and for the postoperative group n = 2-6.

There was a notable change in total knee, phalanx, and hip flexion in the 1 week posteoperative, indicating that the subject is compensating for injury by ambulating with less limb motion. The compensation for injury at the lower limb joints included an increase in pelvic tilt. The animal exhibited 5 degree, 8 degree and 10 degree increases in pelvis tilt at 1, 2 and 6 weeks respectively. By 12 weeks, pelvis tilt and rotation returned to the preoperative normal. Compensation for hock loading was more apparent on the non-operative side, for example, a large increase in phalanx range of motion. This suggests, as might be expected, that the animal is more weightbearing on its contralateral leg versus the operated leg. Further compensation can be observed in the differences in range of motion in Figure 3, especially at the 1 and 2 week time points in each joint, where there is at minimal, 20 degrees difference between limbs. On the operative side 6 week time points, the subjects have learned to swing their legs under their body and produce a more typical pattern at 6 weeks onward.

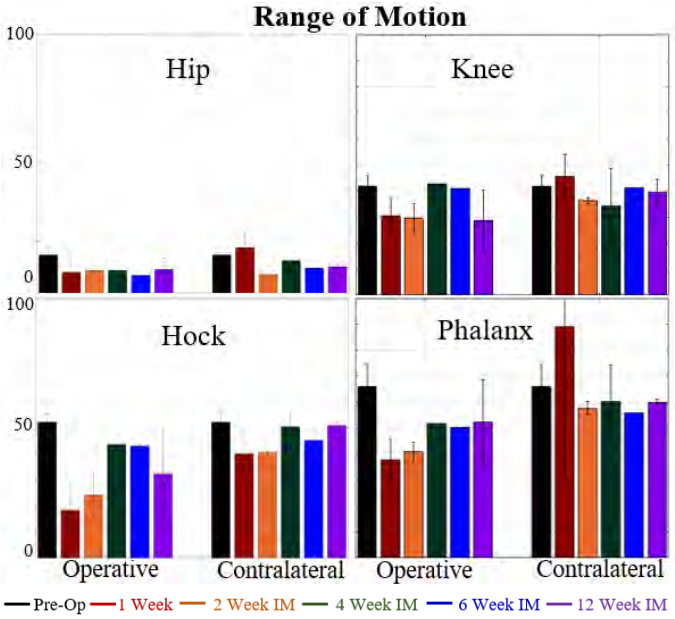

Figure 3: Range of motion of the operative and non-operative limb across all joints relative to peak extension.

REFERENCES

1. Goetz JE, et al. *Osteoarthritis Cartilage*. 2015; 23(10):1797-805

ACKNOWLEDGEMENTS

This work was supported by Department of Defense award W81XWH-15-1-0642. Ms. Amie Pluskowski was instrumental throughout the study.

HIP AND KNEE FORCES FOR TRANSTIBIAL AMPUTEES IN GAIT AND CYCLING

[1] Elizabeth A. Heyde, [1]Greg Orekhov, [2]A. Matt Robinson, [1]Scott J. Hazelwood, and [1] Stephen M. Klisch

[1] California Polytechnic State University, San Luis Obispo, CA, USA
[2] Hanger Clinic, San Luis Obispo, CA, USA
email: sklisch@calpoly.edu

INTRODUCTION

Abnormal biomechanics is thought to be related to high risk contralateral (intact) hip and knee osteoarthritis (OA) in transtibial (TT) amputees [1,2]. Biomechanical challenges exist for TT amputees in gait [3] and cycling [4] that depend on intensity and prosthetic design. Prostheses do not restore natural biomechanics in gait or cycling [5]. Cycling is a recommended exercise for TT amputees, but no studies exist for contralateral hip or knee loads in gait and cycling for the same subjects. Differences in hip and knee loads between TT amputees and controls may contribute to the increased OA risk for TT amputees.

The long-term goal of this study is to identify exercises that produce normal hip and knee joint biomechanics, and minimize OA risk, for TT amputees. The hypotheses were that hip and knee joint resultant forces and moments of the dominant (contralateral) leg were dependent on subject (TT amputee, control) and exercise (gait, cycling) type.

METHODS

Protocols were approved by Cal Poly's Human Subjects Committee. Kinematic data were collected using a multi-camera (9-12) motion analysis system with Cortex software (Motion Analysis Corp., CA, USA). An enhanced Helen Hayes marker set with 32 retroreflective markers was used to track kinematics. Five gait trials at self-selected speeds were conducted using 4 ground force plates (Accugait, AMTI, MA, USA). Three cycling trials at moderate cadence (70 RPM) and machine resistance level (10) were conducted using a stationary bike (Lifecycle GX, Life Fitness, IL, USA) retrofitted with custom pedals containing 6-axis load cells (AD2.5D, AMTI, MA, USA). Unilateral TT amputees (4 male, 2 female, aged 29-45, 3-13 years post-op, BMI 22.6-29.6) and control subjects (5 male, 1 female, aged 20-29, BMI 19.1-28.9) participated. Participants were screened for other known medical conditions/injuries that may bias results.

Cortex was used to post-process trials by identifying and tracking markers to generate body segments. Kinematic data were filtered (4^{th} order Butterworth, 6Hz cutoff frequency). Kinetic data were calculated using the KinTools RT engine in Cortex and were exported to MATLAB (MathWorks, MA, USA). Force and moment results were normalized by body weight (BW) and body mass times height, respectively, interpolated for one full gait cycle (0% = 1^{st} heel strike, 100% = 2^{nd} heel strike) or one full crank revolution (0% and 100% top dead center), and averaged across subjects. Two-factor repeated measures ANOVAs (subject and exercise types) and post-hoc Tukey tests were performed ($p<0.05$ significant) in Minitab (Minitab Inc., PA, USA) to compare peak hip/knee compressive (C) forces, shear (S) forces at peak C force time, and overall peak extension (E)/flexion (F) moments.

RESULTS AND DISCUSSION

Hip C forces ($p < 0.03$), knee C forces ($p < 0.009$), knee S forces at peak C force time ($p < 0.05$), and knee F moments ($p < 0.04$) were higher in gait than cycling for both control and TT amputee subjects (Figs. 1, 2), confirming the hypothesis that hip and knee joint resultant forces and moments of the dominant leg are dependent on exercise type. No differences were found due to subject group, refuting the hypothesis that subject type affects these joint forces and moments.

The results suggest that prostheses may restore natural biomechanics in gait and cycling, countering results from previous studies and indicating a need for future studies.

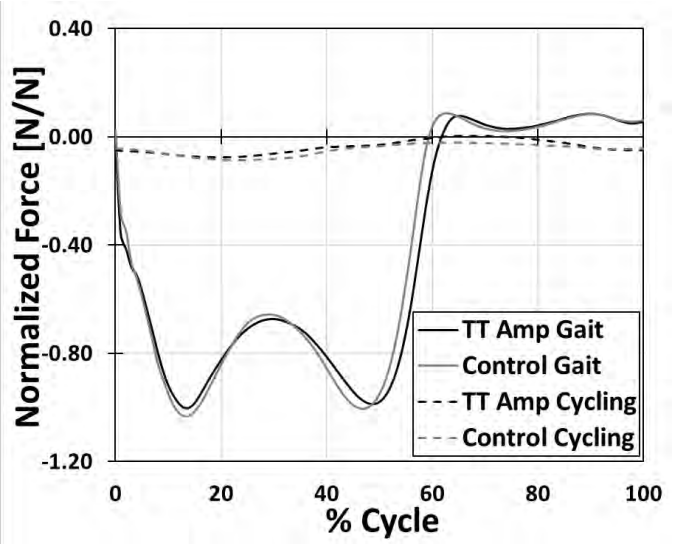

Figure 1: Mean normalized resultant knee compressive forces averaged across subjects for one full cycle in gait and cycling.

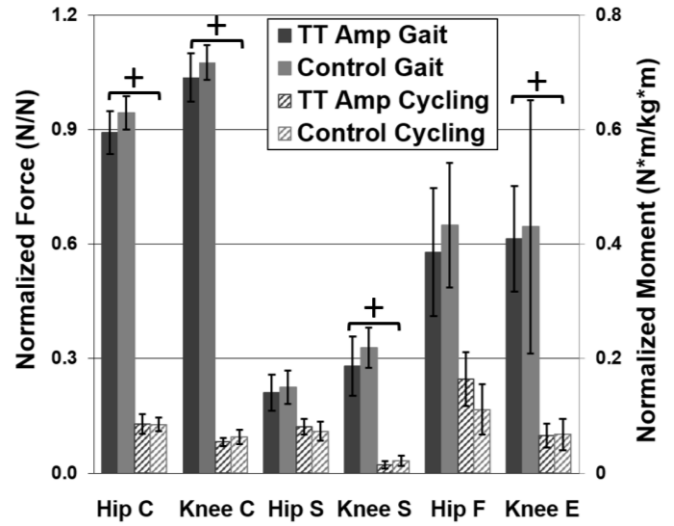

Figure 2: Mean ± 1 S.D. peak hip/knee compressive (C) forces, shear (S) forces at peak C force time, and overall peak extension (E)/flexion (F) moments. + indicates significant differences across exercise types.

CONCLUSIONS

The results reinforce that cycling may be a preferred exercise for limiting OA risk for TT amputees due to the lower joint resultant forces and moments when compared to gait. However, the results do not provide evidence of abnormal biomechanics in TT amputees in gait and cycling.

Limitations of the study included the small sample sizes, lack of kinematic analyses, and neglect of muscle forces in the analyses. Altered kinematics could indicate higher OA risk in these exercises. Joint contact loads, unlike resultant loads, take muscle forces into account and are applied directly to the cartilage surfaces making them better predictors of OA risk. Future studies should include kinematic and EMG-driven OpenSim Inverse Dynamic analyses to determine joint contact loads in TT amputees. Furthermore, future investigations should consider additional exercises to provide more accurate, evidence-based guidelines on the preferred fitness sustainment exercises for TT amputees.

REFERENCES

1. Andriacchi TP et al., *Current Opinion Rheumatology*, **18**(5): 514-18, 2006.
2. Ebrahimzadeh MH et al., *Military Medicine*, **174**(6): 593-7, 2009.
3. Snyder RD et al., *Journal of Rehabilitation Research and Development,* **32**: 309-15, 1995.
4. Gailey R et al., *Prosthetics and Orthotics International*, **33**(3): 242-55, 2009.
5. Versluys R et al., *Disability & Rehabilitation: Assistive Technology*, **4**(2): 65-75, 2009.

ACKNOWLEDGEMENTS

Supported by the Defense Health Program through the Department of Defense under Award No. W81XWH-16-1-0051 and Cal Poly's Donald E. Bentley Center. Opinions, interpretations, conclusions, and recommendations are those of the authors.

EFFECT OF FOOT POSITION ON KNEE MECHANICS IN OBESE YOUNG ADULTS

[1]Skylar C. Holmes, [2]Michael N. Vakula, [1]Steven A. Garcia, [1]Brett K. Post, [1]Derek N. Pamukoff
[1]California State University, Fullerton, [2]Utah State University
Email: sholmes@fullerton.edu

INTRODUCTION

Obesity contributes to the incidence and progression of knee osteoarthritis (OA) [1] partially due to altered loading patterns during gait. Body size and anthropometrics influence limb posture during locomotion [2]. Obese individuals exhibit less knee flexion throughout the early stance phase, which impairs force attenuation [3, 4]. Foot position also influences the magnitude and direction of knee moments during gait. Individuals with medial knee OA commonly walk with an externally rotated foot ("toe out") to reduce pain and attenuate knee joint loading when walking [5]. This strategy moves the line of action of the ground reaction force closer to the weight-bearing knee, reducing the external knee adduction moment (KAM). The KAM is a factor in the development and progression of knee OA [6], and higher peak knee adduction angles have been observed in obese individuals compared to controls [6]. A larger knee adduction angle contributes to a greater KAM, and the higher knee adduction seen in obese individuals may contribute to OA risk. Therefore, the use of a compensatory mechanism, such as a toe out foot progression angle (FPA) may be observed in these individuals. However, using a toe out FPA to reduce the KAM results in an increase in knee flexion moment (KFM) in patients with medial knee OA [7]. Increasing the KFM may simultaneously influence compressive loading in the patellofemoral joint [7].

Research has shown that a toe out FPA can decrease the KAM [5], but its effects on the KFM in an obese population has not been studied. Therefore, the purpose of this study was to evaluate the relationship between knee kinetics, kinematics and foot progression angle (FPA) during gait in obese and normal weight young adults. It was hypothesized that those with a toe out FPA would have a lower knee flexion angle (KFA) and a higher KFM.

METHODS

Table 1. Participant demographics (mean ± SD)

Group	Normal	Obese
Age (years)	22.0 ± 2.9	22.23 ± 3.7
Height (m)	1.68 ± 0.09	1.68 ± 0.09
Mass (kg)	61.5 ± 8.96	92.5 ± 15.00
BMI(kg/m^2)	21.5 ± 1.7	32.5 ± 3.7
Body Fat (%)	20.09 ± 6.99	37.98 ± 7.29

BMI: Body Mass Index

Eighty-one participants were recruited for this study: 39 normal weight (BMI 18.5-24.5), 42 obese (BMI 30-40) (Table 1). FPA (Figure 1) was calculated as the average position of the foot from 15-50% of stance phase ("flat foot") [8].

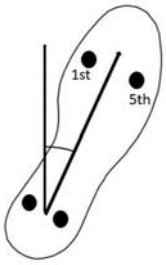

Figure 1. FPA was calculated as the angle of the longitudinal axis of the foot segment in the global (lab) coordinate system relative to the walking direction's axis (line of progression), negative values represent toe out. The foot model used was a modified virtual foot segment where a longitudinal axis was projected from the ankle joint center to the midpoint of the first and fifth metatarsal markers [8]. These markers were then projected to align with the world axis system, as to make the foot segment parallel with the ground

Three-dimensional gait biomechanics (Göteborg Sweden) were recorded as participants completed 5 walking trials across 2 force plates (AMTI, Watertown MA) along a 10-m runway at a self-selected speed. Five practice trials were performed to obtain preferred walking speed. Walking speed was kept within for each trial (±5%) and monitored using infrared photocells (model TF100, TrakTronix, Lenexa KS) that were positioned 2-m apart around

the force plates. Marker position and force plate data were sampled at 240 and 2400Hz respectively. Participants wore laboratory standard neutral cushion footwear (Nike Pegasus, Beaverton OR). Marker position and force plate data were exported to Visual 3D for model construction, and low pass filtered using a fourth order zero-phase lag Butterworth filter at 6Hz and at 50Hz, respectively. The external knee flexion moment was extracted from the time of heel contact, peak moment in the first 50% of stance, value at peak knee flexion angle in the first 50% of stance. Knee flexion angles (KFA) were calculated at heel contact (HC), and the peak in the first 50% stance. Joint moments were normalized to a product of body weight and height.

A chi-square analysis was used to compare the proportion of individuals who demonstrate toe out between groups. Toe out was defined as an angle greater than 10 degrees [8]. Partial correlation (r) was used to determine the relationship between FPA and lower limb kinetics and kinematics after accounting for self-selected gait speed.

RESULTS AND DISCUSSION

A chi-square analysis indicated a similar proportion of toe out participants between groups (X^2 =.301, p=.583), and thus groups were collapsed for correlational analyses. After controlling for gait speed, greater toe out FPA was associated with a larger knee flexion angle at heel contact (KFA at HC) ($p<0.001$, r =-0.42, a larger peak KFA ($p<0.001$, r=-0.40). There was no relationship between toe out FPA and KFM (p=0.25, r=-0.13) or KFM at peak KFA (p=0.25, r=-0.13).

Contrary to our hypotheses, these results indicate that individuals with more toe out FPA have higher knee flexion at heel contact and larger peak knee flexion angles. Previous research indicates that a toe out gait pattern shifts the KAM to a KFM in patients with knee OA [7], thus redistributing joint load away from the medial compartment. Greater medial compartment knee joint loading in obese individuals may be detrimental to joint integrity and influence OA incidence and progression [9]. Thus, the use of a strategy to shift joint load away from the medial compartment is beneficial to this population. As a larger KFA contributes to a larger KFM, the shift in joint load may be attributed to a larger joint angle. In addition to increased knee OA risk, obese individuals also have a higher risk of developing hip osteoarthritis [1]. The use of a toe out FPA can increase compressive loading at the hip [7]. Therefore, using a toe out FPA to decrease the KAM in this population may be beneficial if they do not have any hip impairments.

CONCLUSIONS

Individuals with greater toe out FPA during gait have higher peak knee at heel contact and peak knee flexion. The use of a toe out FPA in obese individuals may be a useful strategy to redistribute frontal plane loading to the sagittal plane. However, this may lead to increased hip joint compressive forces and may be detrimental to those with impairments at the hip.

REFERENCES

1.Felson, D.T., Annals of the Rheumatic Diseases, 1996. **55**(9): p. 668.
2.Gatesy, S.M. et al., J. Zool., 1991. **224**: p. 127-147.
3.Devita, P. et al. J. Biomech., 2003. **36**(9): p. 1355-1362.
4.Hora, M. et al., Folia Zoologica, 2012. **61**(3/4): p. 330-339.
5.Wang, J. et al., J. Bone and Joint Surgery-American Volume, 1990. **72A**(6): p. 905-909.
6.Lai, P.P.K., et al., Clinical Biomech., 2008. **23**: p. S2-S6.
7.Jenkyn, T.R., et al., J. Biomech., 2008. **41**(2): p. 276-283.
8.Hunt, M.A. et al., Archives of Phys Med and Rehab, 2014. **95**(10): p. 1912-1917.
9.Maly, M.R., Curr Opin Rheumatol, 2008. **20**(5): p. 547-52.

ACKNOWLEDGMENTS

This study was supported by the CSU-Fullerton Intramural Research Grant Program

RUNNING ECONOMY AND MARA THON RACING SHOES

[1] Iain Hunter, [1]Aubree McLeod, [1]Tyler Low, [1]Dru Valentine, [1]Jared Ward, and [1]Ron Hager

[1] Brigham Young University, Provo, UT USA
email: iain_hunter@byu.edu, web: https://biomechanics.byu.edu

INTRODUCTION

In May 2017, Nike hosted an event titled, "Sub 2". It was a project involving three of the top marathoners in the world with other elite distance runners pacing the marathoners in an ideal formation for pacing and drafting. Fluids were also allowed at any time. Nike was also testing a new shoe called the Nike Vaporfly 4% (VP). They believed it would significantly reduce metabolic cost by providing minimal weight with excellent energy return and optimal stiffness. The shoe design includes a lightweight responsive midsole along with a carbon fiber full-length plate that creates a stiff midsole with little added mass.

Eliud Kipchoge ran 2:00:25 in the attempt which led to a lot of enthusiasm for the new Vaporfly 4%. Measurements on a prototype shoe showed a 4% decrease in metabolic cost at 14, 16, and 18 km/hr in comparison with two of the most popular elite marathoning shoes [1].

Figur e 1: The three shoes used in this study (Nike Vaporfly 4%. Adidas Adios Boost, and Nike Zoom Streak.

Now that the VP shoe is available to the public, we replicated the prototype shoe study with some minor changes to investigate whether the shoes would indeed result in a 4% lower metabolic cost in comparison to the Adidas Adios Boost (AB) and the Nike Zoom Streak (ZS) (Figure 1). These shoes were chosen because of the success that elite marathoners wearing these shoes demonstrated in recent years (Table 1).

While we expected a decrease in metabolic cost, we were unsure whether the prototype shoe would react with the same metabolic cost differences as the publicly available shoes.

Table 1: Successes of the three shoes used in this study. Masses are of men's size 10 shoes.

Shoe	Stats
Adios Boost (230 gm)	Three most recent World Records (Berlin 2011, 2013, 2014)
Zoom Streak (192 gm)	3 different athletes 2:04:00 or faster
Vaporfly 4% (184 gm)	Out of the six 2017 World Majors marathons, 19 of the 38 top 3 finishes were in the Vaporfly 4%

METHODS

Nineteen subjects performed a warm up on a treadmill in the lab at 3.53 m/s for 5 min. Following the warm up, they were fitted with equipment for measuring oxygen uptake (TrueOne 2400, Parvo Medics, UT). After fitting shoes, testing continued using one of three shoe models in random order. They completed five-minute runs at 16 km/hr on an instrumented treadmill (AMTI Force Sensing Tandem Treadmill, MA) followed by five-minute breaks to change shoes until they had worn all three shoe models twice.

Sixteen km/hr was chosen since it matched one of the speeds used in the previous study and provided an intensity well-below the subjects' anaerobic threshold.

A Repeated Measures Mixed Model determined differences in oxygen uptake between shoe conditions. Correlations matrices on each subject were calculated based on a compound symmetry structure, and Tukey HSD adjustments were made for post-hoc comparisons between shoes.

RESULTS AND DISCUSSION

Oxygen uptake at 16 km/hr in the VP shoe showed a 2.8% lower metabolic cost than the AB shoe ($p<0.001$) and 1.9% lower metabolic cost than the ZS ($p<0.001$). The ZS shoe was 0.9% more economical than the AB shoe ($p=0.022$) (Table 2). All respiratory exchange ratios were below 0.9 and there was no difference between first and second trials in each shoe indicating the runs were below subject's anaerobic thresholds.

While the VP showed the lowest metabolic cost, the difference between shoes was smaller in this study compared with Hoogkamer [1]. The VP prototype shoes used in the previous study had different soles. Some of our subjects complained of slipping on the treadmill surface in the VP shoes. The surface of these shoes is relatively smooth compared with the AB and ZS. That could take away from some of the potential metabolic benefit of the VP. This may not be a problem in use on roads which would have a different coefficient of friction with the VP compared with the treadmill surface.

A difference was also observed between the AB and ZS. While this was only 0.9%, that may be enough for a runner to view as important. Knowing that physiological and mechanical factors affect performance times [2, 3], it is difficult to know how every individual will respond to the various footwear. However, efforts to understand the variations between shoes will gradually lead to customized footwear for performance improvements.

The midsole of the VP shoe includes a relatively stiff carbon fiber plate inside a thick midsole made with a lightweight responsive foam leading to a greater standing height with the shoes on. These shoe properties change the mechanical advantage of the foot and leg. The stiff midsole should bring the center of pressure during toe-off further forwards leading to a greater moment arm from the ankle. The greater shoe height will lead to a greater moment arm from the ground to the knee and hip. Additionally, the lower mass, and perhaps other factors could lead to improved running economy through mechanics in the VP shoe.

CONCLUSIONS

Use of the VP shoe resulted in lower metabolic cost when compared with the AB and ZS at 16 km/hr. The difference in marathon time or any other distance race is difficult to predict based purely on metabolic cost. However, it is likely that improvement in performance times will be attainable in the VP.

REFERENCES

1. Hoogkamer et al. Sports Med, Online, 2017.
2. Joyner MJ. J Appl Physiol, 1991.
3. Di Prampero PE, Atchou G, Bruckner JC, et al. Eur J Appl Physiol Occup Physiol. 1986.

Table 2: Tables may extend across both columns, and those should be included at the bottom of the abstract.

Shoe	Mean±SD	95 % Conf LB	95 % Conf UB	p-value to VP	p-value to AB
Adidas Boost	49.48±2.60	48.30	50.60	<0.001	NA
Zoom Str eak	49.05±2.55	47.84	50.15	<0.001	0.022
Vaporfly	48.11±2.49	46.86	49.17	NA	<0.001

GAIT BIOMECHANICS EARLY AFTER ACLR DO NOT PREDICT MEDIAL COMPARTMENT JOINT SPACE WIDTH 5 YEARS AFTER ACLR

Jessica L. Johnson[1], Jacob J. Capin[1], Ashutosh Khandha[2], Kurt Manal[3], Thomas S. Buchanan[2, 3], and Lynn Snyder-Mackler[1, 4]

[1]Biomechanics and Movement Science, University of Delaware, Newark, DE, USA
[2]Department of Mechanical Engineering, University of Delaware, Newark, DE, USA
[3]Department of Biomedical Engineering, University of Delaware, Newark, DE, USA
[4]Department of Physical Therapy, University of Delaware, Newark, DE, USA
Email: jljohn@udel.edu

INTRODUCTION

More than 20% (46.4 million) of American adults report doctor-diagnosed osteoarthritis (OA) and more than 5% (8.6 million) report daily disabilities because of OA[1], making it the most common cause of disability in adults. The prevalence of OA is significantly higher in people after anterior cruciate ligament reconstruction (ACLR) with more than 50% of participants showing signs of knee OA 10 years after ACLR[2]. Overall, the growing impact of OA needs to be anticipated so we are able to diagnose and intervene to reduce the impact on the public health and health care systems[1].

Changes in joint load-bearing position to areas not adapted to ambulatory loading secondary to altered kinematics and kinetics may be significant contributors to the development of joint degeneration and premature OA[3]. Higher peak knee adduction moment is associated with more baseline-2 year cartilage loss[4] and lower medial compartment contact forces early after ACLR are associated with early onset knee OA[5].

Tibiofemoral joint space width (JSW) in the medial compartment measured from plain radiographs has been shown to be a surrogate for cartilage loss[6] and an accepted marker for structure. The International Knee Documentation Committee (IKDC) radiographic scale was found to have the highest correlation to arthroscopic findings, with normal JSW $\geq$4mm and no osteophytes[7].

The purpose of this study was to determine if knee joint biomechanics, including medial compartment tibiofemoral loading, early after ACLR were associated with radiographic medial compartment joint space width 5 years after ACLR.

METHODS

As part of a prospective trial, 10 athletes (age 21.8 ± 5.5 years, 8 male) completed biomechanical gait assessment 24.4 ± 7.4 weeks after ACLR. Inclusion criteria included: age 13-55, $\geq$ 80% quadriceps strength index (QI), and prior participation in jumping, cutting, and pivoting sports $\geq$ 50 hours per year. We used an eight-camera motion capture system (VICON, Oxford, UK) at 120 Hz and an embedded force platform (Bertec Corp., Columbus, OH) at 1080 Hz to analyze over-ground walking at a self-selected gait speed (± 5% across trials) with 39 retroreflective markers on the bilateral lower extremities and pelvis. Data were processed using commercial software (Visual3D; C-Motion, Germantown, MD).

We collected surface electromyography from 7 lower extremity muscles per limb that were used to inform a previously validated patient-specific musculoskeletal modeling approach[8]. We used this model to compute medial compartment contact force and total tibiofemoral contact force. Loading variables were normalized by body mass. Variables of interest included: peak knee flexion angle (pKFA), peak knee flexion moment (pKFM), peak knee adduction moment (pKAM), peak medial compartment contact force (pMCCF), and peak total contact force (pTCF).

Weight-bearing posterior-anterior (PA) bent knee (30°) radiographs were completed 5 years after ACLR (5.12 ± 0.36 years). One reviewer (JLJ) read all images (SigmaView) for JSW in the medial compartment.

We used regression analyses (SPSS) with alpha set to 0.05 a priori.

RESULTS

The range for medial compartment JSW in the uninvolved limb (UN) was 5.3-7.0 mm (mean ± SD: 6.22 ± 0.6 mm) and the involved limb (INV) was 5.5-7.7 mm (6.45 ± 0.7 mm). The mean interlimb difference was 0.23 mm.

Table 1 Biomechanical Variables (mean ±standard deviation)

	UN	INV
pKFA (°)	-24.2 ± 6.1	-21.7 ± 7.7
pKFM (Nm/kg*m)	0.51 ± 0.10	0.41 ± 0.16
pKAM (Nm/kg* m)	-0.28 ± 0.06	-0.24 ± 0.08
pMCCF (Bodyweight)	3.0 ± 0.4	2.7 ± 0.6
pTCF (Bodyweight)	4.5 ± 0.5	4.3 ± 0.8

We found no statistically significant relationship between any biomechanical variable early after ACLR and ipsilateral medial compartment JSW 5 years after ACLR (Table 2).

Table 2 Regression Analysis

	UN		INV	
	R^2	p	R^2	p
pKFA	0.058	0.502	0.020	0.698
pKFM	0.067	0.470	0.000	0.963
pKAM	0.010	0.783	0.067	0.471
pMCCF	0.026	0.657	0.003	0.882
pTCF	0.001	0.918	0.023	0.672

DISCUSSION

While we did not find a relationship between any biomechanical variable early after ACLR and ipsilateral medial compartment JSW 5 years later, none of our participants were below the normal cutoff of <4mm of JSW per IKDC scale. This lack of variability in JSW may limit our findings. Because of the small sample size, we did not have enough variability to use the Kellgren Lawrence (KL) categorical grading scale, which had been used by other authors to determine presence of knee OA[2,5]. As such, we did not assess for presence of osteophytes or other joint changes indicative of OA.

Additionally, we are unable to assess change in JSW over time. While our participants did not fall below the 4 mm JSW IKDC cut-off score and the mean interlimb difference was 0.23 mm, there may have been a loss of JSW since injury. Additional radiographs at multiple time points would allow for assessment of possible change in JSW over time.

Limitations include small sample size, high percentage of men, and the use of radiographs and not MRI to detect early degenerative knee joint changes.

CONCLUSION

We did not find a statistically significant relationship between biomechanical variables early after ACLR and medial compartment JSW 5 years after ACLR. Future research with larger sample size, more variability in JSW, and radiographs at additional time points to assess change in JSW may be indicated.

REFERENCES

1. Helmick CG, et al. *Arthritis Rheum*. 2008
2. Barenius B, et al. *Am J Sports Med*. 2014
3. Erhart-Hledik JC, et al. *J Orthop Res*. 2016
4. Chang AH, et al. *Osteoarthr Cartil*. 2015
5. Wellsandt E, et al. *Am J Sports Med*. 2016
6. Buckland-Wright JC, et al. *Ann Rheum Dis*. 1995
7. Wright RW, MARS Group. *J Bone Jt Surgery-American*. 2014
8. Manal K, Buchanan TS. *J Biomech Eng*. 2013

ACKNOWLEDGEMENTS

Funding provided by the National Institutes of Health: R01-AR048212, R37 HD037985, P30-GM103333, U54-GM104941, and T32-HD00749. This work was supported in part by a PODS Level I Scholarship from the Foundation for Physical Therapy (JJC) and a University of Delaware Doctoral Fellowship Award (JJC). Thank you to Amelia Arundale, Ryan Zarzycki, Celeste Dix, Angela H. Smith, Naoaki Ito, Georgia Gagianas, P. Michael Eckrich, and Martha Callahan for their invaluable assistance.

COMPARISON OF GAIT KINEMATICS AND SPATIOTEMPORAL MEASURES BETWEEN LOCK AND PIN AND A NEW VACUUM SUSPENSION SYSTEM IN TRANSTIBIAL AMPUTEES

Vanessa Kellems, Gabby Rentuma, Jeremey D. Smith, & Abbie E. Ferris
School of Sport & Exercise Science, University of Northern Colorado, Greeley, CO
vanessa.kellems@unco.edu; www.unco.edu/biomechanics

INTRODUCTION

One factor of consideration of prosthetic prescription for individual's with transtibial amputation (TTA) is the choice of socket suspension system used to attach the residual limb to the prosthetic socket [1]. Two commonly used methods are: lock and pin (PIN) and vacuum. PIN systems use a gel liner with a metal pin attached to the distal end to mechanically lock into the distal socket [2]. Elevated Vacuum systems use a pump to withdraw air molecules from between the socket and liner to form a tight seal over the length of the residual limb. However, pressure tends to fluctuate throughout the day due to leaks [3,4].

Residual limb volume tends to fluctuate throughout the day while using PIN systems, thus making it very difficult to maintain a secure fit which can lead to secondary physical conditions (i.e. sores, ulcers) [5-7]. The SmartPuck™ (PUCK) is a newly designed, adaptable vacuum suspension system that is housed within the socket, which prevents loss in pressure. Maintaining constant pressure may facilitate socket fit by maintaining limb volume and preserving the health of the residual limb. Anecdotally, patients have preferred the PUCK to other systems.

TTAs have asymmetrical gait patterns due to the loss of the ankle and associated musculature and deficiencies of the prostheses [7,8]. Temporospatial asymmetries include: increased stance time on the intact limb, increased swing time, decreased step length and stride length on the amputated limb [5,7]. Kinematic asymmetries are also seen at the knee and hip.

The choice of socket suspension may contribute to these asymmetries [9]. Large movements within the socket can lead or pain or feeling as though the prosthetic is not firmly attached to the residual limb and may cause gait alterations. The purpose of this study was to determine if any differences in gait symmetry exist between PUCK and PIN systems while walking. We hypothesized no differences would be found between socket suspension systems.

METHODS

Individuals with TTA (n = 4; 89.1 ± 12.1 kg, 1.73 ± 0.08 m; 61.5 ± 4.5 years, K3 - K4) participated in this study. Inclusion criteria: traumatic amputation, currently wearing a PIN or PUCK, at least 6 months in their current prosthesis, no concomitant musculoskeletal injuries, healthy residual limb, able to walk continuously for 10 minutes without assistance, and no other health concerns that may limit function. The protocol consisted of two visits: 1) current suspension system; 2) alternate suspension system. Participants were allowed one week to acclimate to the new suspension system.

Participants were instrumented for motion capture (100 Hz, VICON, Oxford, UK) by placing reflective makers on anatomical landmarks on the lower extremities. Participants walked on a treadmill (AMTI, Watertown, MA) for 6 minutes at their self-selected speed. The last 30s of each trial were analyzed. Kinematic data were low pass (Fc = 6 Hz) filtered in (Visual 3D, C-Motion, Germantown, MD). Temporospatial measures and sagittal plane peak joint angles were calculated for the knee and hip from 3 gait cycles.

RESULTS & DISCUSSION

Self-selected walking speed was the same for each session. Knee joint angles were slightly reduced in the PUCK amputed limb during swing (Figure 1). During early stance, the intact limb had a greater knee flexion angle than the amputated limb for both conditions. PIN and PUCK amputated limb had greater values through mid-stance and swing compared to intact limb. Knee range of motion (ROM) was reduced in the PUCK amputated limb (Table 1).

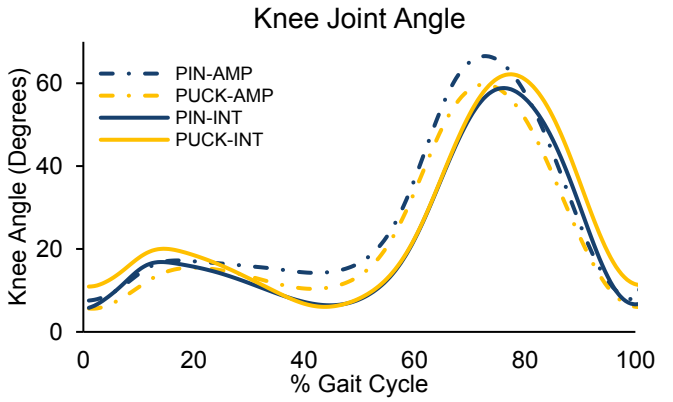

Figure 1. Knee joint angle for intact (INT) and amputated (AMP) limbs for both conditions.

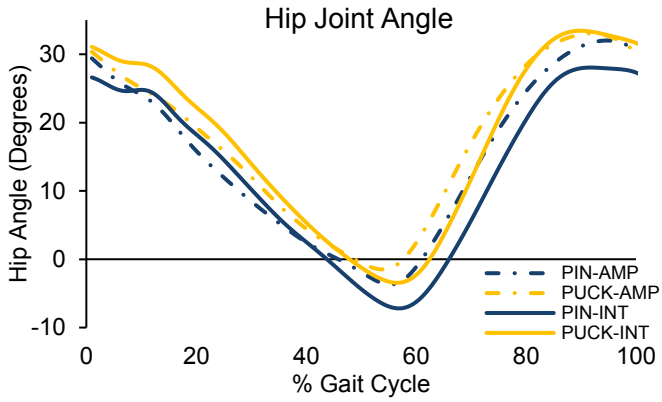

Figure 2. Hip angles for intact (INT) and amputated (AMP) limbs for both conditions

Early stance hip flexion angle was similar between limbs and conditions. Both conditions of PIN were greatest in mid stance compared to the PUCK conditions. Intact limb hip extension was slightly reduced in the PUCK compared the the PIN. Hip ROM was similar between both socket suspension systems.

Although large kinematic differences were not noted between systems, changes in the temporospatial measures were seen. Both conditions showed fairly symmetrical inter-limb temporospatial measures (Table 1). However, differences were noted between systems regardless of the fact that participants were walking at the same speed for both conditions. Stance and step time were longer for the PIN condition than the PUCK. Swing time was reduced for the PUCK. Further, stride length increased by ~0.06 m while wearing the PUCK.

Stride width (PIN: 0.14 ± 0.02 m, PUCK: 0.15 ± .02 m) and double limb support time (PIN 0.16 ± 0.04s, PUCK: 0.15 ± 0.04 s) were similar between conditions.

Table 1. Temporospatial measures for each limb while walking in the treadmill at self-selected pace. Data are shown as means ± SD.

Limb	Stance Time (s)	Step Time (s)	Stride Length (m)	Swing Time (s)
PIN Amp	0.70 ± 0.12	0.56 ± 0.09	1.07 ± 0.28	0.41 ± 0.07
PIN Int	0.74 ± 0.12	0.55 ± 0.08	1.06 ± 0.27	0.37 ± 0.05
PUCK Amp	0.65 ± 0.07	0.51 ± 0.02	1.13 ± 0.44	0.36 ± 0.04
PUCK Int	0.67 ± 0.05	0.50 ± 0.03	1.14 ± 0.44	0.34 ± 0.02

CONCLUSION

Our hypothesis was partially supported. Literature commonly reports that those with TTA exhibit an asymmetrical gait, these preliminary data suggest kinematic differences persist regardless of the choice of socket suspension system. Contrary to the literature, both systems showed symmetrical temporospatial measures.

Furthermore, the PUCK showed increased stride length and shorter stance and swing times which can be seen through increased flexion at the hip through gait. These differences may be seen due to the more secure fit between the residual limb and the socket while wearing the PUCK.

In contrast, the fit can change throughout the day in PIN systems due to the fluctuations in limb volume throughout the day leading to improper fit between the residual limb and the prosthetic socket. These preliminary data may suggest that these individuals were more comfortable in the PUCK than the PIN. As more data are added to this preliminary set, these differences may become more refined.

REFERENCES

1. Gholizadeh, H, et al. *PLoS ONE*, *9*(5), 1-9,2014.
2. Beil, T. L. et al. *J Rehabil Res Dev*, *41*(6A), 821–828. 2004.
3. Ferraro, C, et al. *J. Prosthet Orthot, 23*(2), 78–81. 2011.
4. Komolafe, O. et al. *J Rehabil Res Dev*, *50*(8), 1069-1078. 2013.
5. Board, W. et al. *Prosth & Ortho Inter*, *25*(3), 202–209. 2001.
6. Goswami, J. et al. *Prosth & Ortho Inter*, *27*(2), 107–113. 2003.
7. Gailey, R. et al. *J Rehabil Res Dev*, *45*(1), 15–29. 2008.
8. Su, P.F. et al. *J Rehabil Res Dev, 44,491*-501.2007.
9. Pitkin, M.R. *J Prosthet Orthot, 9,*113-122. 1997.

DYNAMIC STRUCTURE OF VARIABILITY OF JOINT ANGLES IN USER-DRIVEN TREADMILL WALKING

[1] Kelley M. Kempski, [1] Nicole T. Ray, [2] Brian A. Knarr, and [1] Jill S. Higginson

[1] University of Delaware, Newark, DE, USA
[2] University of Nebraska at Omaha, Omaha, NE, USA
Email: kelleyk@udel.edu

INTRODUCTION

Typical treadmills at fixed speed do not perfectly simulate an individual's typical overground locomotor patterns when being used for training interventions in affected populations. Statistically significant differences in kinematic and spatiotemporal parameters have been observed and, [1,2], specifically, it has been demonstrated that overground locomotion has higher variability and local dynamic stability than typical treadmill walking [2,3]. To minimize the differences between treadmill and overground locomotion, researchers are developing user-driven treadmill systems that adjust the speed of the treadmill belts in real-time based on how fast the subject is trying to walk [4].

The objective of this study was to determine how healthy subjects' dynamic structure of variability, quantified by the Lyapunov exponent, is changed on a fixed-speed treadmill and user-driven treadmill.

METHODS

Eleven healthy adults (age 23.4 ± 4.9 years, 3 males) were recruited for this study. Each subject walked on an instrumented split-belt treadmill (Bertec Corp., Worthington, OH) in its regular and user-driven modes while an 8-camera motion capture system (Motion Analysis Corp., Santa Rosa, CA) was used to locate the subject in 3-dimensional space and record kinematic data. The user-driven treadmill (UTM) control system used is unique because it updated the speed of the treadmill belts in real-time based on the subject's propulsive forces, location on the treadmill, step length, and step time. The speed of the two treadmill belts on the UTM were tied so at any time, the speed of the left belt was the same as the speed of the right belt. The subjects were asked to walk at their self-selected (SS) and fastest comfortable (fast) walking speeds. Additionally, the subjects walked on a regularly controlled treadmill (RTM) at the average speed from their UTM trials.

Continuous hip, knee, and ankle flexion/extension angles were calculated using Visual 3D (C-Motion, Inc, Germantown, MD). The continuous 1-minute trials were then run through a custom MATLAB code that utilized the Wolf algorithm [5] to calculate the maximum Lyapunov exponent. The Lyapunov exponent, often referred to as local stability of a joint in the context of walking kinematics or stride-to-stride variability, is a measure of how infinitesimally close trajectories of dynamical system vary or diverge in a certain dimension of phase space (Fig. 1) [5,6].

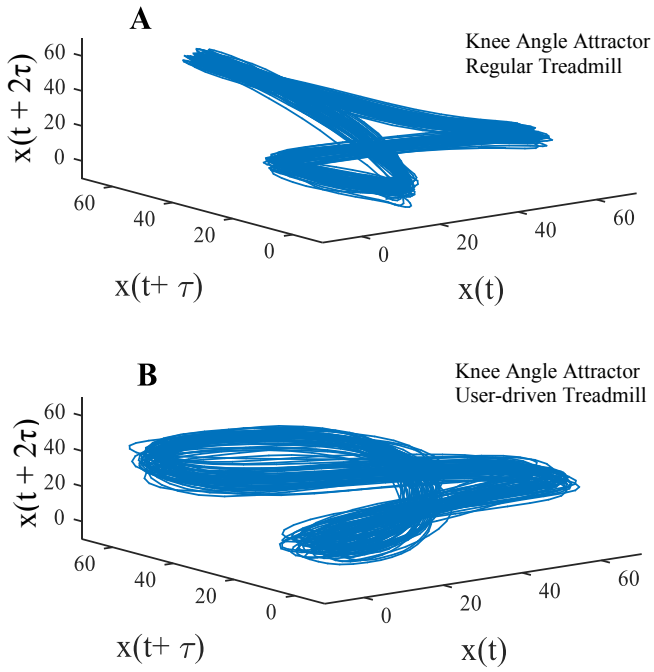

Figure 1: Reconstructed attractors for (A) regular treadmill (RTM) and (B) user-driven treadmill (UTM) knee flexion/extension angle, x(t), of subject 2 at SS speed, shown in three dimensions for visualization purposes. The attractor shown is

reconstructed in multiple dimensions using the measured knee flexion angle and time delayed copies of itself. Greater disorganization, as seen on the UTM, is indicative of greater divergence and greater positive LyE.

A 2x2 (speed x treadmill condition) repeated measures ANOVA and Student's t-test were run to determine if significant differences exist among joint angle LyE between walking speed on the regular treadmill and user-driven treadmill (JMP-13, SAS Institute, Cary, NC).

RESULTS AND DISCUSSION

The LyE was higher on the user-driven treadmill compared to the regular treadmill at SS speed for ankle ($p = 0.01$), knee ($p = 0.04$), and hip ($p = 0.01$) angles, and at fast speed for ankle ($p = 0.01$) and knee ($p = 0.03$) angles (Figure 2). Higher LyE is indicative of greater variability.

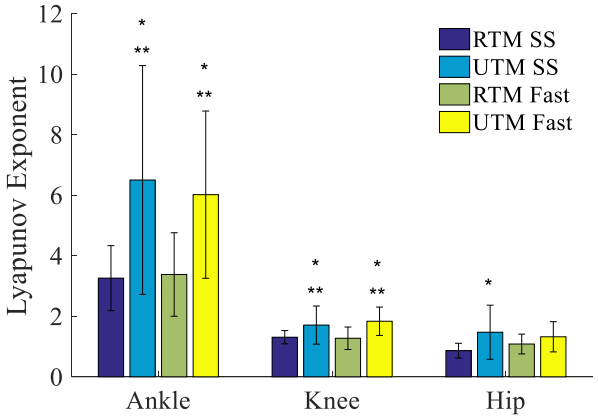

Figure 2: Mean LyE ± 1 standard deviation for ankle, knee, and hip sagittal plane angles.
* indicates significant difference from RTM SS.
** indicates significant difference from RTM Fast.
*** indicates significant difference from UTM SS ($p<0.05$).

The findings of our study agree and complement previous work which showed an increase in LyE from treadmill to overground walking. Furthermore, our study finds comparable results when moved distally, with the ankle showing the greatest changes between the user-driven and regular-controlled treadmills [3]. The increased dynamic structure of variability of sagittal plane angle observed on the user-driven treadmill compared to the regular treadmill suggests that the user-driven treadmill may be more comparable to overground walking than typical treadmill walking. Since the speed of the RTM was selected to match the average speed on the UTM, the change in variability can be attributed to the change in treadmill condition.

Future studies should explore the relationship between overground and user-driven treadmill locomotion using nonlinear analyses. The user-driven treadmill may be a better rehabilitation tool for improving gait, as it may minimize the misleading results that have been shown in regular-controlled treadmills [3]. This rehabilitation tool may be especially beneficial for affected populations that experience asymmetries in dynamic structure of variability such as individuals post-stroke and post-ACL injury [7,8].

CONCLUSIONS

There was increased LyE indicative of higher dynamic structure of variability in joint angles on the user-driven treadmill than the regular treadmill. This may indicate that the user-driven treadmill more closely resembles the variability experienced overground.

REFERENCES

1. Alton F. *Clin Biomech (Bristol, Avon)*. 1998;**13**: 434-440.
2. Hollman JH. *Gait Posture*. 2016; **43**:204-209.
3. Dingwell JB. *J Biomech.* 2001; **123**: 27-32.
3. Kim J. *IEEE Eng Med Biol Soc Annu Conf*. 2012;**2012**:3061-3064.
4. Wolf A. *Phys D Nonlinear Phenom*. 1985; **16**:285-317.
5. Cignetti F. *Ann Biomed Eng*. 2012;**40**:1122-1130.
6. Kempski K. *J Biomech.* 2018; **68**: 1-5.
7. Moraiti C. *Gait Posture.* 2010; **32**: 169-175.

ACKNOWLEDGEMENTS

NIH P30 GM 103333
NIH P20 GM 109090
Helwig Fellowship, University of Delaware
Department of Mechanical Engineering

DO PEOPLE WITH A TRANSTIBIAL AMPUTATION HAVE A ROUGHER RIDE ON UNEVEN TERRAIN?

[1] Jenny A. Kent, [1] Kota Z. Takahashi and [1,2] Nicholas Stergiou

[1] University of Nebraska at Omaha, Omaha, NE, USA
[2] University of Nebraska Medical Center, Omaha, NE, USA
email: jkent@unomaha.edu, web: https://www.unomaha.edu/college-of-education/cobre/

INTRODUCTION

The pursuit of activities outside the home frequently relies on an ability to ambulate on non-level surfaces. Walking on uneven terrain is a known challenge that can present a barrier to mobility and participation for people with a lower limb amputation [1]. Global changes in the step dynamics of lower limb amputees have been observed in medial-lateral and anterior-posterior directions in response to destabilizing environments (see, e.g. [2]). Manifestations of the deficits of the prosthesis on vertical dynamics during uneven terrain walking have received little attention, however. Prosthesis users lack the precise control and active propulsion of a natural ankle, and therefore an inability to control the vertical motion of the center of mass (COM) when changes in surface height are experienced may be contributing to the challenge. For example, an inability to lower the COM following a peak, or to raise the COM upwards following a dip may result in suboptimal energy transfer from step to step and a propensity for abrupt destabilizing interactions with the ground. The aim of this study was to investigate the vertical dynamics of walking on uneven terrain in people with and without a transtibial amputation.

It was hypothesized that, when walking on uneven terrain (UT) in comparison to flat terrain (FL), (i) amputees would exhibit more variable vertical excursions of their COM, and (ii) the vertical acceleration patterns of the lower extremity on contact with the ground would be more variable in comparison to controls. It was further anticipated that (iii) when stepping onto the sound limb, amputees would exhibit a relationship between the change in surface height and the vertical deceleration of the sound lower extremity on loading.

METHODS

Approval for the study was obtained from the Institutional Review Board of the University of Nebraska Medical Center. Eleven experienced prosthesis users with a transtibial amputation (TTA; 8M 3F; 56.6±12.6 yrs; 101.9±16.4 kg; 1.79±0.07 m, time since amputation: 10.3±7.7 yrs) and age- and gender- matched control participants (CON; 8M 3F; 56.0±13.3yrs; 76.9kg; 1.71±0.09m) were recruited. Participants walked on two treadmills: flat (FL; Tandem Treadmill, AMTI Inc, MA) and uneven terrain (UT; in-house built with maximum depth ~3cm) for two minutes each. Walking speed was set at preferred UT speed (TTA 1.0±0.2m/s; CON 1.1±0.2m/s). Kinematic data from markers on the legs, pelvis and trunk were recorded at 100Hz using a 12-camera motion capture system (Motion Analysis Corp., CA). Computations were performed in Visual3D (C-motion Inc, MD).

The peak vertical COM excursion (COM height) during single limb stance was estimated for 120 steps in each walking condition. The deceleration patterns of the ankle joint center were examined and the maximum vertical deceleration of the ankle joint center during loading estimated for each left and right step as an indication of control. The variability (standard deviation) of both measures was calculated. The height of the walking surface during each step was approximated from the vertical position of the stance limb ankle joint center during mid-stance and consecutive step heights subtracted to obtain surface height differences. COM height variability, and loading deceleration variability were examined using 1-factor (condition) and 2 X 2 (condition, limb) mixed ANOVAs respectively with a between-subject factor of group, and alpha at .05. A Pearson correlation was performed for each participant in the UT condition comparing change in

surface height to subsequent loading deceleration, using 60 steps on each limb.

RESULTS AND DISCUSSION

No significant differences between groups were observed for COM height variability (p=0.075) or loading deceleration variability (p=0.829). COM height variability increased on UT by ~2.3mm on average (p<0.001; Figure 1). A significant main effect of condition indicated an increase in loading deceleration variability (0.369m/s^2; p<0.001; Figure 2) on UT, again with no main effect of group nor interaction effects thus refuting our hypotheses. Weak and non-significant correlations were observed between surface height change and loading deceleration for all participants with the exception of one TTA and one CON with significant moderate relationships on the prosthetic (r=0.523, p<0.001) and right side respectively; r= 0.567, p<0.001).

The results suggest that the uneven surface evoked increases in the variability of the vertical movement of the COM, and of the decelerations of the lower extremity on loading during walking, but that on average these were no greater for TTA than for CON, and there was no notable difference across limbs. It is not clear whether this increased variability in itself may be more destabilizing for people with amputation. It is possible that our experienced participants with amputation have developed effective compensatory strategies for coping with modest changes in surface height. Further, effects may have been diluted by the inclusion of older adults in both cohorts. Finally, although surface height was investigated, no consideration was taken of surface contour, which may have acted to slow or propel shank movement, affecting subsequent swing foot impact.

CONCLUSIONS

The variability of vertical COM movement and loading decelerations on foot contact increase on uneven ground in both individuals with and without amputation. Future work will explore dynamics at an individual level with a focus on compensatory strategies, and include healthy young adults with no known deficits likely to compromise walking.

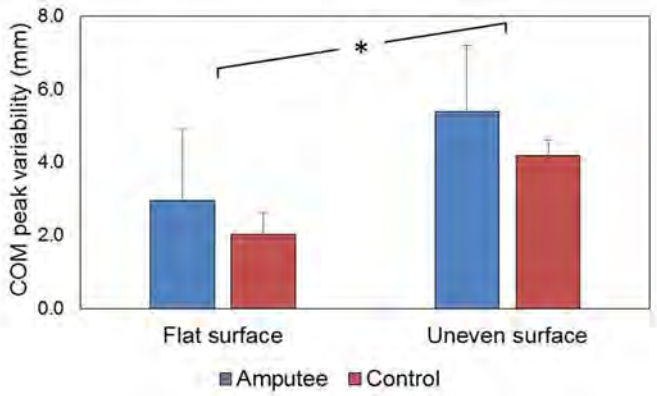

Figure 1. Variability of peak vertical height of the COM over 120 strides on flat and uneven terrain treadmills (amputee n=11, control n=11; * p<0.001)

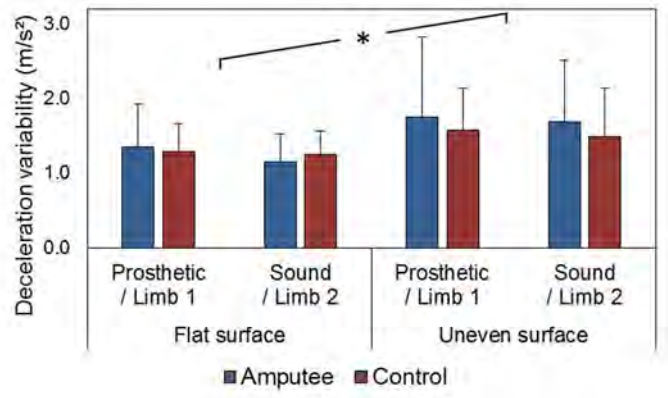

Figure 1: Variability of peak vertical ankle joint center deceleration in stance over 60 strides on each limb on uneven terrain (amputee n=11, control n=11; * p<0.001)

REFERENCES

1. Gauthier-Gagnon C, et al. *Arch Phys Med Rehabil* 80(6): 706-13, 1999.
2. Gates DH, et al. Gait Posture. Gait & Posture 38: 570–575, 2013.

ACKNOWLEDGEMENTS

This work was supported by NIH P20GM109090 and NIH R15HD08682.

WALKING WITH ADDED MASS INFLUENCES ANKLE AND MID-TARSAL JOINT QUASI-STIFFNESS

Andrew M. Kern[1], Nikolaos Papachatzis[1], Jeffrey Patterson[1], Dustin Bruening[2] & Kota Z. Takahashi[1]

[1]Department of Biomechanics, University of Nebraska at Omaha, Omaha, NE USA
[2]Exercise Science Department, Brigham Young University, Provo, UT USA
email: andrewkern@unomaha.edu, web: https://www.unomaha.edu/college-of-education/cobre/

INTRODUCTION

Mechanical behavior of the human foot is a complex interplay of joints and soft tissues that allow for adaptation to a wide range of environments and gait strategies. Quasi-stiffness (also called dynamic stiffness [1]), the ratio of the external joint moment and angle [2], is a property which characterizes the dynamic behavior of joints during locomotion. A deeper understanding of how the foot and ankle modulate quasi-stiffness across a wide range of locomotor activities may have implications for treatment of gait pathology, improvement of human performance, and design of assistive devices. Preliminary investigations have characterized quasi-stiffness of the human ankle, mid-tarsal and metatarsophalangeal joints in walking and running [1,2]. The effect of added body mass on quasi-stiffness during walking has not yet been quantified and is particularly important for the design of augmentative or assistive devices (e.g., prostheses, exoskeletons, shoes).

This study seeks to understand the relationship between carriage of additional body mass and quasi-stiffness of the human ankle and mid-tarsal joints during over-ground walking. We hypothesized that ankle and mid-tarsal joint quasi-stiffness will increase when walking with greater levels of added mass.

METHODS

Gait analysis was performed on 18 healthy subjects (age = 24.6 ± 2.8 years, height = 1.75 ± 0.06 m, mass = 85.3 ± 21.1 kg), while wearing three levels of weight added via a vest, 0%, 15% and 30% of body mass. Subjects were instrumented with 53 retro-reflective markers, allowing for motion analysis of the hips, knees, ankles and a multi-segment foot model [3]. All subjects were tested walking over-ground (at 1.25 m/s) with the three levels of mass, in randomized order.

Kinematic and force-plate data were processed in Visual3D (C-Motion, Germantown, MD) to determine joint angles and moments in the ankle, and mid-tarsal joints. Further processing was completed within a custom MATLAB (Mathworks, Natick, MA) script, which computed joint quasi-stiffness for two phases within stance. These phases form two predominantly linear regions of the moment-angle curve for both ankle and mid-tarsal joints [2]. The dorsiflexion phase (DF) corresponds to ankle

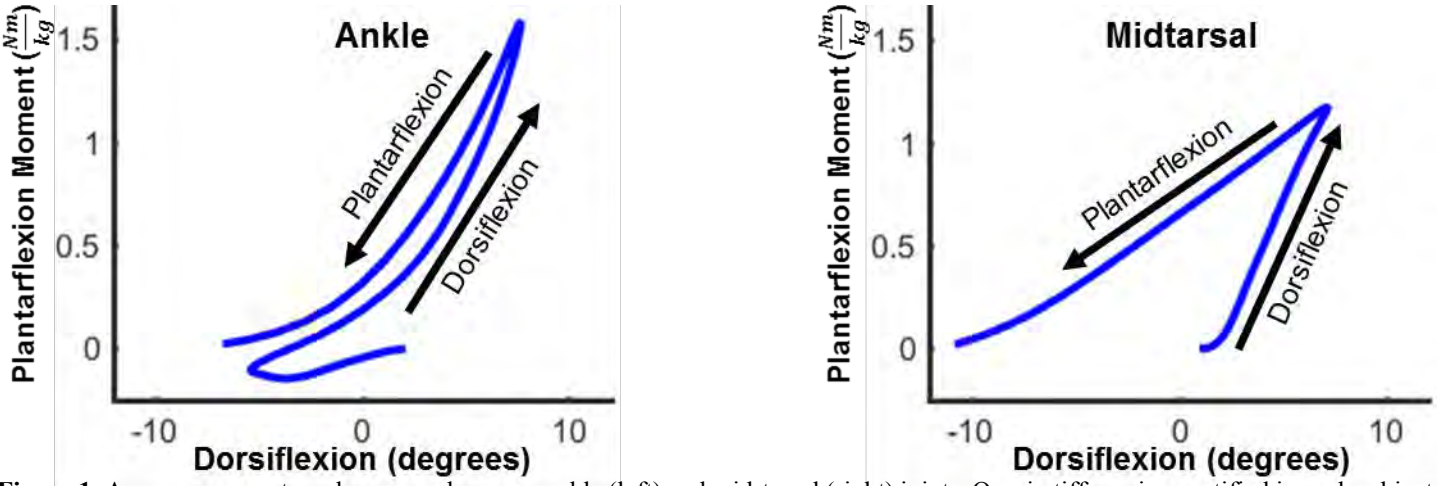

Figure 1: Average moment-angle curves shown on ankle (left) and mid-tarsal (right) joints. Quasi-stiffness is quantified in each subject using a linear fit in two phases of stance (shown above) where the slope is reported as stiffness.

dorsiflexion during mid-stance, and the plantarflexion phase (PF) corresponds to ankle plantar flexion during late-stance [2]. Joint quasi-stiffness was quantified as the slope of a linear fit to the moment-angle curve section within that phase (**Fig. 1**). Statistical analysis was performed with one-way repeated measures ANOVA and a pairwise post-hoc test using Bonferroni correction in JASP software.

RESULTS AND DISCUSSION

It was found that that quasi-stiffness increased significantly ($p<0.001$) with added mass in the ankle for DF and PF phases and in the mid-tarsal joint for PF. No statistical significance was found in the mid-tarsal joint during DF ($p = 0.181$). Pairwise tests revealed that in PF a 30% increase in body mass showed a significant increase in stiffness (from 0%) in both joints, however there was no significant increase from 15% to 30% (**Fig. 2**). These results support our hypothesis that ankle stiffness increases with added body mass, however an increase in mid-tarsal joint stiffness was only partially supported (no significant increase in DF).

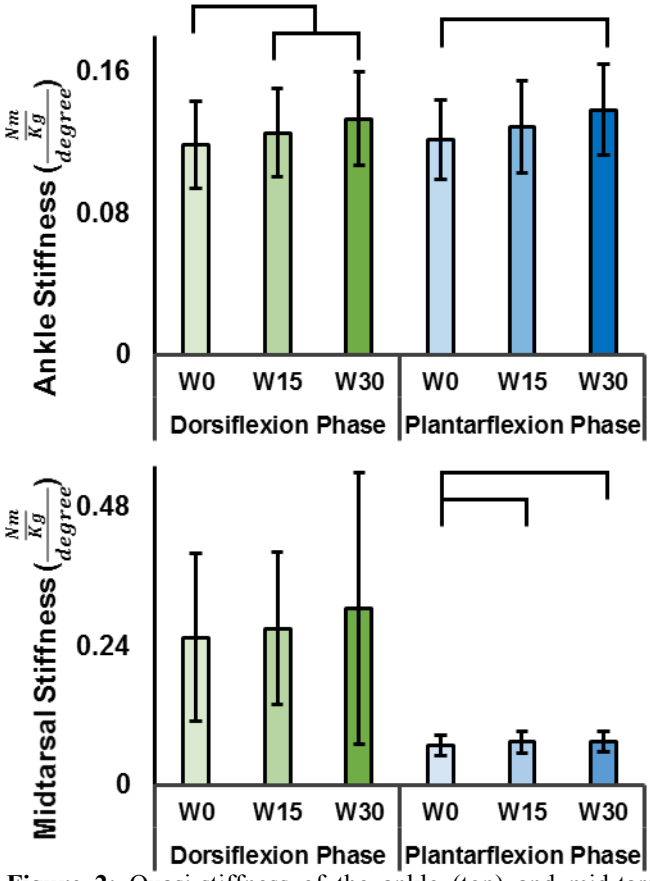

Figure 2: Quasi-stiffness of the ankle (top) and mid-tarsal (bottom) joints during **DF** and **PF** phases. Ankle quasi-stiffness is similar across both phases, whereas the mid-tarsal stiffness changes substantially. Brackets show statistical significance.

Interestingly, the mid-tarsal quasi-stiffness displayed a distinct difference in behavior between DF and PF phases with high variability between subjects in the DF phase, whereas the ankle joint was more uniform. This is corroborated by other work, which has shown large inter-subject variability in MT joint stiffness during mid-stance [1]. The source of this variability is currently unclear; however, it is possible that natural variation in tensile properties of the plantar aponeurosis and differences in muscle activation patterns play a role. Although muscle activation was not quantified in this study, other work has shown that contraction of the plantar intrinsic foot muscles can pose a significant alteration to the mechanical response of the foot at loads of up to 150% of body weight [4].

Though not yet fully understood, it is possible that modulation of quasi-stiffness in the ankle and foot is important for adaptation of locomotion to a variety of environments. This is supported by our results, which indicate that foot and ankle stiffness are altered due to external loading. This may be an active or passive response, due to muscle activation or non-linear properties of the soft tissue structures in the foot. It remains unclear however, whether these changes mediated significant alterations in other functional gait parameters. Ongoing analysis will investigate the relationship between quasi-stiffness in the foot and ankle, and the efficiency of gait. These findings inform our understanding of normal biomechanical function of the foot as well as how wearable devices may be tuned to accommodate variable walking and loading conditions.

REFERENCES

1. Sales E et al. *J. Am. Pod. Med. Assoc.* **106,1** 2016
2. Shamaei, K et al. *PLOS One,* **8,3,** 2013
3. Bruening DA et al. *Gait & Posture,* 2012
4. Kelly LA et al. *J. R. Soc. Interface* **11** 2014

ACKNOWLEDGEMENTS

This work was supported by the Center for Research in Human Movement Variability of University of Nebraska at Omaha, NIH (P20GM109090) and the University of Nebraska Collaboration Initiative.

Effect of Pediatric Obesity on Patellofemoral Joint Contact Force during Walking

[1] Namwoong Kim and [1] Zachary F. Lerner
[1] Northern Arizona University, Flagstaff, AZ, USA
email: nk379@nau.edu

INTRODUCTION

Pediatric obesity, one of the most serious public health concerns of the 21st century, increases the risk of developing musculoskeletal disorders particularly of the knee joint. The patellofemoral (PF) joint is considered to be the primary source of symptoms associated with knee pain. Patellofemoral pain (PFP) is the most common knee disorder in adolescents, and it may limit their daily activity.

The PF joint plays an important role in knee joint function to increase leverage of quadriceps, enhancing their mechanical advantage. PF joint contact forces range from 0.97 to 1.36 times body weight (BW) during walking in healthy populations, with loads up to 2 to 3 BW during daily activities involving high knee flexion in total knee replacement (TKR) patients. These are high loads considering that the joint contact force of the tibiofemoral joint, which is the primary weight bearing joint, ranges from 2 to 4 BW during daily activities in TKR patients. Obesity is associated with reduced knee angle, and it has been associated with an increased ground reaction force during stance phase. Furthermore, reduced knee flexion leads to reduced PF contact area. Given the implications, increased body weight may cause increased load on the PF joint, and it may lead to increased joint stress and structural joint alteration.

Physical activity is considered to be an effective and fundamental treatment for pediatric obesity. However, potential adverse effects of physical activity on the musculoskeletal system should be considered for obese children because abnormal joint loads may lead to musculoskeletal injury and pain, which can lead to more sedentary behavior. Knowledge of how pediatric obesity affects PF joint contact forces (PFJCF) during activities of daily life may contribute to understanding the mechanisms of musculoskeletal disorders of the knee joint in this population.

This study sought to identify how pediatric obesity affects PFJCF during walking. We hypothesized that obese children would exhibit larger absolute, but similar body weight normalized PFJCF compared to healthy-weight children.

METHODS

A total of 20 subjects, 10 obese (6 male) children with a body mass index (BMI) z-score greater than the 95th percentile and 10 healthy-weight (5 male) participated in a previously reported study[1,2]. We quantified body composition for the participants using dual x-ray absorptiometry (DXA) (Whole-Body Scan, Hologic Discover, Bedford, MA). A custom foot placement jig was used to standardize the orientation of each participant's lower extremity in the frontal-plane.

Subjects walked on an instrumented treadmill (Bertec Corp, Columbus, OH) at 1m/s. The experimental data collected for 6 minutes of walking was used in the computational analysis of this study. Ground reaction force data from an instrumented treadmill was collected at 1000 Hz and low-pass filtered at 12 Hz using a fourth order zero-lag Butterworth filter. A three-dimensional motion capture system (10 cameras, Nexus, Vicon, Centennial, CO) was used to collect marker trajectories at 100 Hz and low-pass filtered at 6 Hz using a fourth order zero-lag Butterworth filter.

A full-body musculoskeletal model was scaled for each participant using OpenSim. This model had 18 body segments, 21 degrees of freedom, and 92 muscle-tendon actuators. The model was modified to consider subject-specific lower-extremity alignment. PFJCFs were obtained using OpenSim's joint reaction analysis. The model used in this study has been previously validated[1,2].

Three representative gait cycles were averaged for each subject. Independent sample t-tests were used to determine the significance of differences between the obese and healthy-weight groups for PFJCFs, in which $p<0.05$ indicated statistical significance. Matlab version 2017a (Mathworks Inc.,

Natick, MA) was used to perform data analysis and statistical analysis.

RESULTS AND DISCUSSION

PFJCFs for the obese and healthy-weight children during walking are shown in Fig 1. First peak absolute PFJCFs were not significantly different compared to the healthy-weight participants (Table 1). Second peak absolute PFJCFs were 2.27 times greater in the obese participants compared to the healthy-weight participants ($p < 0.001$). No significant differences were found for first and second peak body-weight normalized PFJCFs between the two groups.

This study presented the first analysis of how pediatric obesity affects PFJCFs. The results indicated that obese children have greater absolute, but similar body-weight normalized PFJCF compared to healthy-weight children during walking. Greater PFJCF has been associated with cartilage degeneration and patellofemoral pain[3]. This information may help clinicians to develop exercise or rehabilitation programs for obese children. Since PF joint stress is dependent on PFJCF and PF joint contact area, future work will focus on incorporating estimates of PF joint contact area in our analysis of the joint loading environment.

REFERENCES

1. Lerner ZF, DeMers MS, Delp SL, Browning RC. *How tibiofemoral alignment and contact locations affect predictions of medial and lateral tibiofemoral contact forces,* Journal of Biomechanics. 48:644–650, 2015.
2. Lerner ZF, Board WJ, Delp SL, Browning RC. *Pediatric obesity and walking duration increase medial tibiofemoral compartment contact forces*, Journal of Orthopaedic research. 34:97–105, 2015.
3. Heino, J. B., & Powers, C. M. *Patellofemoral stress during walking in persons with and without patellofemoral pain*. Medicine and science in sports and exercise, 34(10), 1582-1593, 2002.

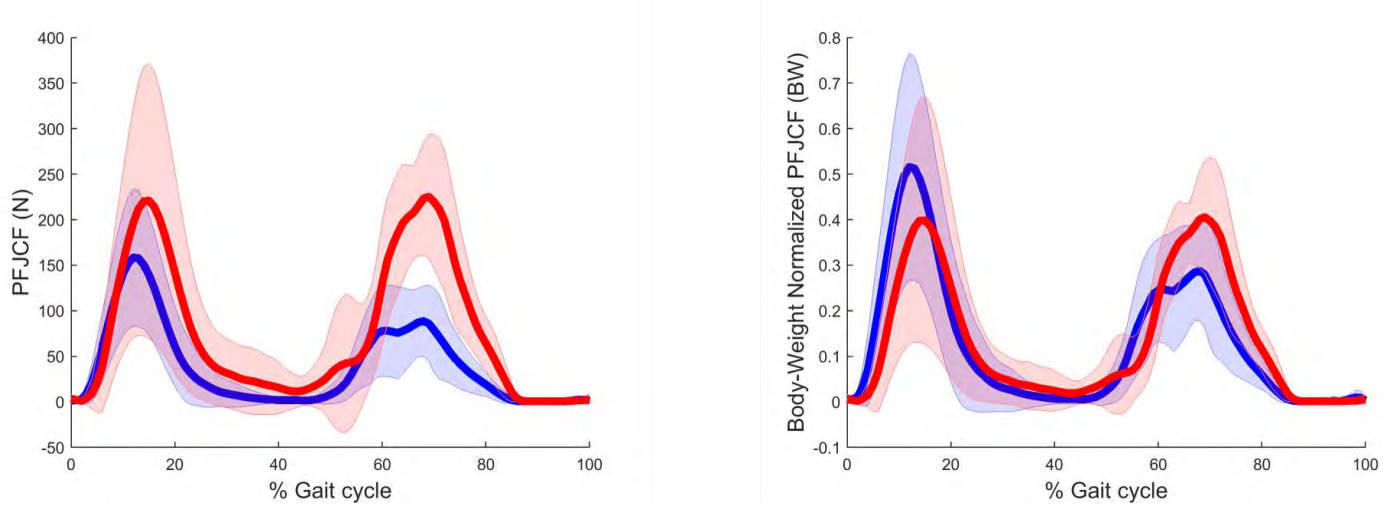

Fig. 1. Absolute (left) and BW normalized PF joint Contact force in the obese (red lines) and healthy-weight (blue lines) participants. The red and blue shading represents ±one standard deviation in the PF joint contact force.

Table 1. Mean (SD) of the PFJCF from the obese and healthy-weight participants.

	First peak (N)			Second peak (N)		
	Obese	Healthy-weight	*p*	Obese	Healthy-weight	*p*
Peak PFJCF (N)	232.3 (152.7)	160.3 (76.1)	0.20	246.5(75.3)	106.7 (42.9)	**<0.001**
Normalized PFJCF (N)	0.42 (0.28)	0.52 (0.25)	0.40	0.44 (0.12)	0.35 (0.11)	0.07

MOTOR LEARNING RESPONSE TO SPLIT-BELT TREADMILL WALKING AFTER NON-TRAUMATIC AMPUTATION

[1,2] Paul W. Kline, [3] Amanda M. Murray, [1,2] Matthew J. Miller, [2] Thomas Fields, and [1,2] Cory L. Christiansen

[1] University of Colorado Anschutz Medical Campus, Aurora, CO, USA; [2] VA Eastern Colorado Healthcare System, Aurora, CO, USA; [3] University of Toledo, Toledo, OH, USA
email: paul.kline@ucdenver.edu

INTRODUCTION

Step length asymmetry is common following transtibial amputation (TTA) [1, 2]. Split-belt treadmill walking with asymmetrical belt speeds can exaggerate step length asymmetry, forcing correction of the asymmetry by the neuromotor system through sensory feedback [3]. People with traumatic TTA demonstrate similar motor adaptability as healthy adults in response to asymmetrical split-belt walking [4]. However, individuals with non-traumatic TTA are typically older, more medically complex, and have greater disability than individuals with traumatic TTA [5]. Additionally, deficits in vascularity and limb sensation are hallmark characteristics of the non-traumatic TTA population, creating further sensory impairment that may influence response to split-belt walking. Thus, the purpose of this study was to evaluate the motor learning response to exaggerating asymmetrical step length through split-belt walking in patients with non-traumatic TTA, as measured by step length symmetry adaptation and retention.

METHODS

Eight males with 1) non-traumatic, unilateral TTA acquired within the past 1-5 years and 2) a diagnosis of diabetes mellitus and/or peripheral vascular disease were enrolled (age: 68.5 ± 4.8 years, height: 1.81 ± 0.09 m, weight: 94.8 ± 16.18 kg).

Participants completed the split-belt treadmill walking protocol (Fig. 1) on an instrumented treadmill (Bertec Corp, Columbus, OH) while outfitted with 3 reflective markers placed on bilateral feet. Three-dimensional kinematic data were collected (100Hz) and synchronized with two force plates imbedded in the treadmill (2000Hz) (Oxford Metrics, Oxfordshire, UK). Step length was calculated using the time and position of foot strike and toe off (8N threshold) using Visual 3D (C-Motion, Bethesda, MD). The treadmill protocol involved two conditions: belts moving together at the same speed (TIED), and belts moving at asymmetrical speeds (SPLIT). During TIED, the belts were set to 75% of each participant's self-selected walking speed, as determined using a GAITRite electronic walkway (CIR System, Inc., Franklin, NJ). During SPLIT, the faster belt was set to 75% of self-selected walking speed while the slower belt was set to 50% the speed of the faster belt (2:1 ratio). The limb with the shorter step length at baseline was assigned to the faster belt during SPLIT. After a 4-minute treadmill accommodation period, the two conditions were tested as follows: 2-minutes TIED (BASELINE), 3-minutes SPLIT for 2 sets (SPLIT1 & 2), 1-minute TIED (TIED1), 3-minutes SPLIT for 2 sets (SPLIT3 & 4), 1-minute TIED (TIED2), and 3-minutes SPLIT (SPLIT5) (Fig. 1).

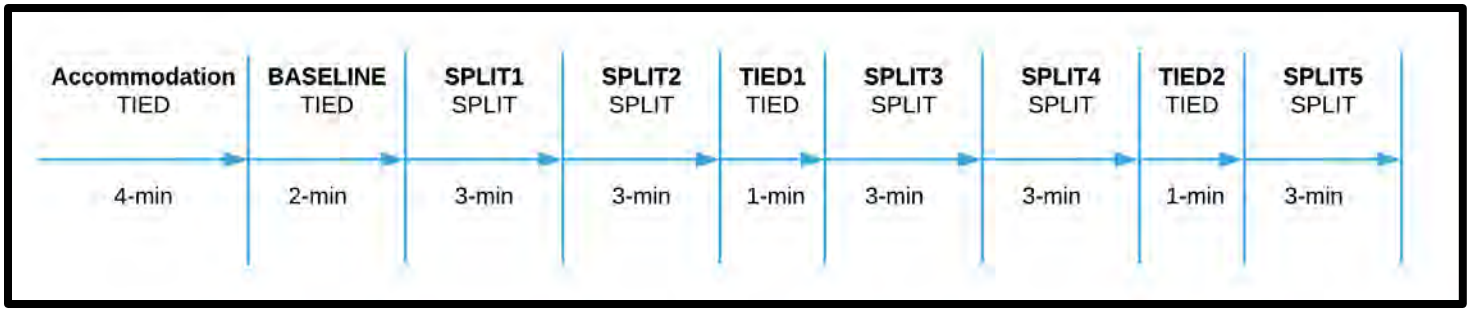

Figure 1: Schedule of treadmill protocol including duration of each TIED and SPLIT condition.

The first 5 strides and final 5 strides of BASELINE, SPLIT1, TIED1, SPLIT3, TIED2, and SPLIT5 were used to for data analysis.

Step length symmetry index (SI) was calculated as:

$$SI = 2*(Long-Short)/(Long+Short)*100$$

with "Long" and "Short" representing the longer and shorter step lengths at BASELINE. Using this formula, a value moving toward zero (perfect symmetry) indicates improved symmetry, while increasing magnitude in the positive or negative direction indicates worse symmetry towards either the "Long" (positive) or "Short" (negative) limb.

One-way repeated measures ANOVAs with post-hoc paired-samples *t*-tests were used to calculate differences in: 1) step length SI between BASELINE, TIED1, and TIED2; 2) step length SI during immediate exposure to SPLIT conditions; and 3) step length SI during the final five strides of SPLIT1, SPLIT3, and SPLIT5.

RESULTS AND DISCUSSION

Step length SI during TIED conditions significantly adapted at TIED1 (1.1 ± 2.6, p = .011) and TIED2 (-1.0 ± 5.9, p = .002) compared to BASELINE (7.5 ± 4.5). Step length SI during the first five strides of SPLIT3 (21.4 ± 3.7, p = .000) and SPLIT5 (15.2 ± 4.4, p = .006) were significantly improved compared to SPLIT1 (34.3 ± 5.1). Lastly, significant improvement in step length SI during the final five strides was observed with each additional exposure to the SPLIT condition: SPLIT1 (16.7 ± 2.7), SPLIT3 (10.4 ± 3.7, p = .009), SPLIT5 (3.6 ± 3.0, p = .034) (Fig. 2).

These results are consistent with a prior study of reactive adaptation to split-belt walking in individuals with traumatic TTA [4]. Furthermore, by incorporating multiple exposures to split-belt walking, the current results demonstrate that additional improvements in symmetry can be achieved with repeated dosage.

Future studies are needed to determine the effects of multi-day repeated sessions of split-belt walking and identify the duration of retention in step length symmetry. Additionally, evaluation of the necessary dosage required to retain long-term improvement in gait symmetry is needed. Limitations of this study include a lack of comparison group to determine if the magnitude of change or rate of adaptation in non-traumatic amputees differs compared to either those with traumatic amputation or healthy individuals.

CONCLUSIONS

Individuals with non-traumatic TTA and underlying vascular disease are: 1) capable of gait adaptation to split-belt walking, 2) retain motor adaptations after removal of the SPLIT condition, and 3) demonstrate continual improvement with additional dosing of the SPLIT condition.

REFERENCES

1. Prinsen et al. *Arch Phys Med Rehabil.* **92**, 2011.
2. Sagawa et al. *Gait Posture.* **33**, 2011.
3. Helm et al. *Phys Med Rehabil Clin N Am.* **26**, 2015
4. Darter et al. *PLoS One*. **12**: e0181120, 2017.
5. Gailey et al. *J Rehabil Res Dev.* **45**, 2008.

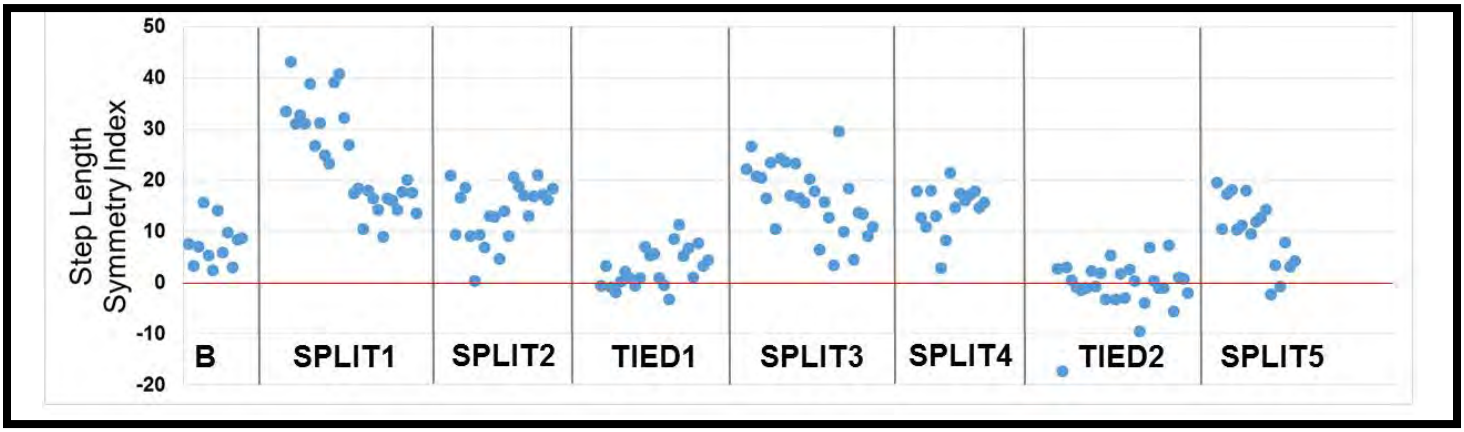

Figure 2: Step Length Symmetry Index at Baseline (B), SPLIT and TIED conditions demonstrating gait adaptation and retained motor learning response with repeated exposure to SPLIT conditions.

PROPULSION FORCE SYMMETRY DURING WALKING IN PATIENTS WITH PERIPHERAL ARTERY DISEASE

[1]Todd Leutzinger, [1]Mahdi Hassan, [2,3]Holly DeSpiegelaere, [2]George Casale, [2,3]Iraklis Pipinos, [1,3]Sara Myers

[1]Department of Biomechanics, University of Nebraska at Omaha, Omaha, NE USA
[2]College of Public Health, University of Nebraska Medical Center, Omaha, NE USA
[3]Omaha Veterans' Affairs Medical Center, Omaha NE USA
email: tleutzinger@unomaha.edu

INTRODUCTION

Peripheral artery disease (PAD) is an atherosclerotic disease affecting the arteries of the upper and lower extremities [1]. The primary manifestation of PAD is intermittent claudication, classified as walking-induced ischemic leg pain in the form of cramping, aching, tightness, and/or fatigue in the muscles of the calf, thigh, and/or buttocks. Individuals with PAD have demonstrated significant alterations in anterior-posterior peak propulsion force both before and after the onset of claudication pain [2]. Moreover, individuals with PAD also display differences in gastrocnemius strength between the most affected leg and the alternate leg [3]. The less affected leg is able to generate significantly greater force compared to the more affected leg. Gait symmetry is defined as the perfect, synonymous behavior between the two lower limbs during ambulation [4]. We investigated the anterior-posterior peak propulsion force symmetry in patients with bilateral PAD before and after the onset of claudication pain.

METHODS

Twenty-nine individuals with bilateral PAD (males: 28; females: 1; height: 1.75 ± 0.068 m; body mass: 88.80 ± 15.0 kg; age: 64.69 ± 8.29 years) and 29 healthy age matched controls (height: 1.74 ± 0.073 m; body mass: 80.37 ± 14.07 kg; age: 64.90 ± 10.06 years) walked 4.5 meters across eight AMTI (Watertown, MD, USA) in-ground force platforms. Subjects performed overground trials until five clean foot contacts with an individual forceplate were acquired for each leg. A one-minute rest period was observed between each trial to ensure the absence of claudication pain (PF). Patients with PAD then performed the six-minute walk test to induce claudication pain. During this test subjects walked as far as they could over a six minute time frame at their self-selected walking speed. After the completion of the six-minute walk test, subjects returned to the overground force platforms where they repeated the overground walking trials while experiencing claudication pain (P). No rest was given between pain trials to maintain claudication pain throughout. Healthy controls performed the PF trial only.

Anterior-posterior peak propulsion force data were calculated from a custom-made code in Visual 3D version 6 (Germantown, MD, USA). All forces were normalized by each subject's body weight (kg m/s^2) so results could be compared across participants. Propulsion force symmetry was calculated using the equation [5]:

$$\text{Symmetry index} = \left|\frac{2(F_n - F_i)}{F_n - F_i} \times 100\right|$$

Where F_i represents the peak propulsion force of each subject's most affected leg, and F_n represents the peak propulsion force of the subject's less affected leg. A value of zero indicates perfect peak propulsion force symmetry between legs. A paired samples t-test was used to determine differences in peak propulsion force symmetry between the P and PF walking trials. Separate independent t-tests were used to compare the PF and P conditions to healthy controls. Separate bivariate Pearson's correlations were used to correlate total walking distance in the six-minute walk test to the peak propulsion symmetry index of the P and PF conditions. Lastly, a one-sample t-test was used to compare the symmetry index in the P and PF conditions to perfect gait symmetry. The level of significance was $p<0.05$ for all comparisons.

RESULTS AND DISCUSSION

Subjects with PAD displayed a mean peak propulsion force symmetry index of 11.96 ± 10.25 when walking in the PF condition and 13.17 ± 8.93 when walking in the P condition. Control subjects reported a mean symmetry index of 7.76 ± 6.37 (Figure 1). No significant difference was found in peak propulsion force symmetry between the P and PF walking conditions. When walking in the P condition, the PAD subjects walked with a symmetry index that was significantly different from that of healthy controls (p=0.012). However, no difference was found between the PF condition and healthy controls (p= 0.072).

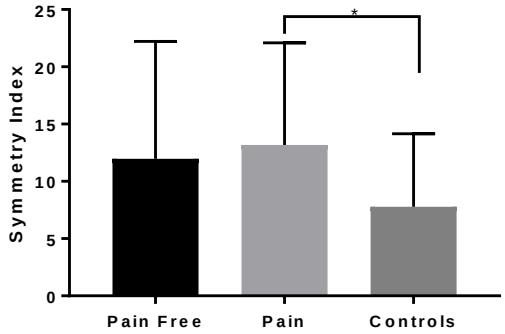

Figure 1. Average peak propulsion symmetry index of the pain (P) and pain free (PF) walking conditions for patients with PAD and data from healthy controls. An asterisk indicates a significant difference between groups ($p<0.05$).

Six-minute walking distance was not correlated with peak propulsion force symmetry in either the P (0.593) or PF (p=0.914) walking conditions indicating peak propulsion force symmetry is not a strong predictor of how far an individual with PAD can walk. The current data show a significant difference between perfect peak propulsion force symmetry and the average symmetry index of both the pain ($p < 0.01$) and pain free ($p < 0.01$) walking conditions. Bilateral PAD patients present more pronounced gait asymmetry than that of healthy age matched controls, particularly when walking in pain.

Previous work has determined that an asymmetrical gait pattern may increase the risk for joint pain, joint degeneration, and osteoarthritis in the less affected limb [6]. These complications are commonly observed in populations such as amputees and stroke patients who often ambulate with an asymmetrical gait pattern. It has also been suggested that an asymmetrical gait places individuals at higher risk of falling [7].

CONCLUSIONS

Patients with PAD have a less symmetrical gait compared to healthy aged matched controls, and this asymmetry increases following the onset of claudication pain. Future studies should investigate how gait asymmetry changes from the time claudication pain begins until the individual experiences maximal claudication pain while walking. Such data would give researchers and clinicians greater insight to the potential consequences of pain onset during gait. Data from this study were collected while the subjects experienced pain, but were not from the last steps subjects took before they had to stop walking. Unilateral PAD patients, disease severity, the effects of treatment, and the use of assistive gait devices should be included in future studies to investigate their effects on gait symmetry in individuals with PAD.

ACKNOWLEDGEMENTS

This work was funded by 1R01HD090333-01, 1R01AG049868, 5U54GM115458, and the University of Nebraska at Omaha GRACA

REFERENCES

1. Hiatt et al. *Circulation* **118**, 2826-2829, 2008
2. Scott-Pandorf et al. *Journal of Vascular Surgery* **46**, 491-499, 2007
3. Hiatt et al. *Circulation* **90**, 1866-1874, 1994
4. Herzog et al. *Medicine, Science, and Sports Exercise* **21**, 110-114, 1989
5. Nigg, Robinson, & Herzog *J.Manipulative Physiol.Ther.* **10**, 1987
6. Burke, Roman, and Wright *Annals of the Rheumatic Diseases* **37**, 252-254, 1978
7. Lewek, Bradley, Wutzke, & Zinder *Journal of Apllied Biomechanics* **30**, 31-36, 2014

SCALING FORCE IN THE FLEXOR DIGITORUM LONGUS TENDON USING A PASSIVE IMPLANTED MECHANISM: A PARAMETER SENSITIVITY ANALYSIS

[1] Hantao Ling and [2] Ravi Balasubramanian

[1] Oregon State University, Corvallis, OR, USA
email: lingh@oregonstate.edu, web: http://web.engr.oregonstate.edu/~balasubr/

INTRODUCTION

Posterior tibial tendon dysfunction is a common cause of adult acquired flatfoot deformity (AAFD). This condition results in a deformed and painful flatfoot. The tendon dysfunction can occur due to rupture or damage to the posterior tibialis (PT) tendon or through the process of tendinosis [1, 2]. A common surgical procedure used to treat this condition is a flexor digitorum longus (FDL) tendon transfer to PT tendon surgery in combination with a corrective osteotomy (see Fig. 1a) [2]. However, previous studies have shown that this procedure only partially restores the foot arch due to the reduced force capability of the FDL tendon (one-third the force capability of the PT tendon) [3]. Oftentimes, an additional osteotomy procedure is necessary for full restoration [2].

Motivated by this limitation, we previously explored the use of an implanted passive mechanism in between the FDL and the navicular in the tendon-transfer surgery to better restore the foot arch in the AAFD condition [4] (see Fig. 1b). When compared with directly suturing the FDL to the PT tendon, the implant would passively scale up the force transferred to the navicular.

Given the positive findings of the preliminary studies, this paper seeks to better characterize the surgical parameters that will help in customizing the level of force scaling to be most beneficial. Specifically, this paper evaluates the effect of the anchoring angle (theta) of the FDL tendon on the force scaling capabilities of the implant through a sensitivity analysis in an isometric biomechanical simulation (see Fig. 2).

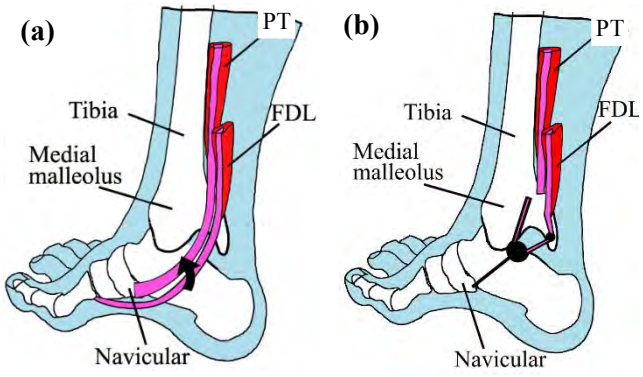

Figure 1: Foot drawings showing the relative locations of the PT tendon, FDL tendon, and the navicular bone for (a) the traditional tendon transfer surgery and (b) the proposed tendon transfer surgery with implanted passive mechanism.

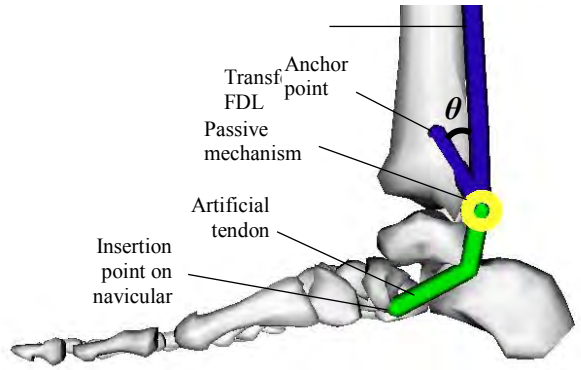

Figure 2: OpenSim model of the proposed surgical procedure for the correction of adult acquired flatfoot deformity using an implantable passive mechanism.

METHODS

A lower limb biomechanical model of an AAFD foot with our proposed surgical procedure was previously developed in the OpenSim software [5]. The model consists of four foot segments and four joints and includes the FDL tendon transfer surgery, our proposed implant and an artificial tendon [4]. In studying the effect of anchoring angle on force scaling, these model's joints were locked to allow for isometric muscle contraction. The anchoring angle is defined as the positive counterclockwise angle between the lines of action created by the transferred

FDL tendon coming into and out of the implant before being anchored to the tibia (see Fig. 2). For five anchoring angles (0°, 15°, 30°, 45°, 60°), a 10-second forward dynamic simulation was conducted and the resulting tendon forces in the transferred FDL and artificial tendons were recorded. Over the next 3 seconds, the FDL ramped up to 75% activation of the FDL's maximum isometric force. For the final 5 seconds, the activation of the FDL was held at 75% of the maximum isometric force. In each of the simulations, the FDL tendon slack length and artificial tendon were each held fixed across all anchoring angles.

The implant's force-scaling effect was calculated by dividing the average force in the artificial tendon by the average force in the FDL tendon over the final 4 seconds of simulation (see Table 1). This multiplier was plotted against $\cos\theta$, and a linear regression analysis was used to generate a relationship between $F_{artificial}$ and F_{FDL}.

RESULTS AND DISCUSSION

The simulated artificial tendon forces for each of the five anchoring angles are shown in Fig. 3. The FDL tendon force for each of the five models was nearly identical, so a representative trial is shown in the figure. For decreasing anchoring angles, there is an associated increase in tensile forces in the artificial tendon. This relationship, which defines the implant force scaling multiplier ($F_{artificial}/F_{FDL}$), can be characterized with the following equation.

$$\frac{F_{artificial}}{F_{FDL}} = 1.0169\cos\theta + 0.9628$$

The continued development of an accurate biomechanical model of our proposed surgical procedure will help to inform the procedure's parameters and the passive implanted mechanism's design. The anchoring angle is directly related to the force scaling multiplier provided by the passive implanted mechanism. The derived equation relating

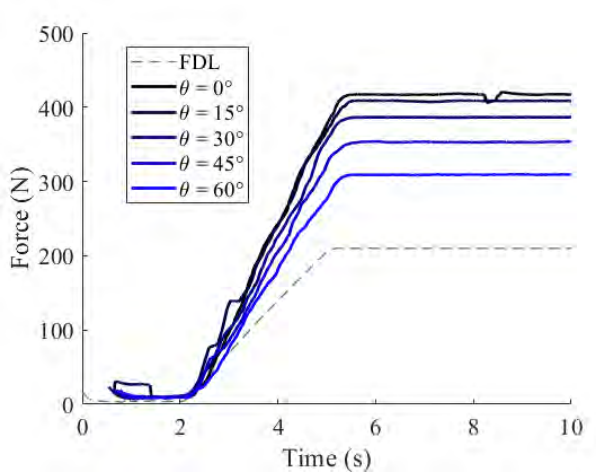

Figure 3: Tensile forces in the FDL (dashed) and artificial (solid) tendons over a 10-second forward dynamic simulation.

the anchoring angle to the implant force scaling multiplier allows for customizability of the force scaling effects of the implant. Understanding the relationship of these parameters and balancing the force-scaling benefits with the implant's range of motion limitations will specifically allow for more surgical treatment options for AAFD. The successful development of the force scaling passive implant, however, would be applicable a broad range of tendon networks in the human body. In future studies, we will conduct more sensitivity analyses in simulation to help us to determine whether this version of the tendon transfer surgery could eliminate the need for an additional corrective osteotomy in the treatment of AAFD.

REFERENCES

1. Niki H, et al. *Foot and Ankle Int* **22.4**, 292-300, 2001.
2. Kohls-Gatzoulis. *BMJ* **329**, 1328-1333, 2004.
3. Rosenfeld PF, et al. *Foot and Ankle Int* **26.9**, 671-674, 2005.
4. Ling and Balasubramanian. *Proceedings of ASB 2017*, Boulder, CO, USA, 2017.
5. Delp S, et al. *Biomed Engr*, IEEE Trans **54.11**, 1940-1950, 2007.

Table 1: Implant force scaling multipliers for varying anchoring angle.

Anchoring Angle	**0°**	**15°**	**30°**	**45°**	**60°**
Implant Force Scaling Multiplier (*N*/*N*)	1.982	1.945	1.840	1.681	1.472

FEMALES AND MALES USE DIFFERENT HIP MECHANICS IN RESPONSE TO MILITARY-RELEVANT LOADS

[1] Kari L. Loverro, MS, [2] Leif Hasselquist, PhD, and [1] Cara L. Lewis, PT, PhD

[1] Boston University, Boston, MA, USA
[2] Natick Soldier Research Development and Engineering Center, Natick, MA, USA
email: kloverro@bu.edu, web: http://sites.bu.edu/movement/

INTRODUCTION

Females now have access to all combat positions in the military, of which some require heavy load carriage. While previous research has indicated that wearing load affects gait mechanics [1], there are only a few studies comparing how females and males respond to load. A previous study found that females and males respond similarly to carrying loads that are a percentage of body mass [2], but in practice females carry the same load as males regardless of body mass. Investigating the effects of load on females is especially important due to their increased risk of musculoskeletal injury during training [3]. Specifically, females are at increased risk for femoral neck stress fractures that can occur during a loaded road march [4]. Differences in hip mechanics due to carrying standard loads may give insight into injury mechanisms.

Therefore, the purpose of this study was to determine if females and males use different hip mechanics in response to wearing standardized loads that are militarily-relevant.

METHODS

Fifteen females (age: 26.1±5.1yrs, height: 1.65±0.08m, mass: 67.8±9.4kg) and fifteen males (age: 26±4.8yrs, height: 1.78±0.08m, mass: 79.8±9.1kg) participated in the study. Participants were active and had no current injury or pain in the lower extremity, with no history of lower extremity surgery or stress fracture. All participants provided written informed consent prior to participation.

Participants competed two-minute walking trials on a treadmill (Bertec Corp.) at a single speed (1.35m/s) under three load conditions: 1) unloaded weight vest (1.7kg), 2) medium load (15kg), and 3) heavy load (26kg). The speed and load selected were based on army doctrine recommendations. At least 2-minutes of rest was given between each walking trial and ratings of perceived exertion were monitored to ensure that participants did not become fatigued.

Kinematic data were collected using a motion capture system (VICON Ltd.) and kinetic data were collected from the instrumented treadmill. Visual3D (C-Motion Inc.) was used to measure angular kinematics and kinetics of the hip for every stride of each 2-minute trial. Hip angles and internal moments occurring in the sagittal and frontal planes were time normalized to the gait cycle for each stride and exported for further analysis.

A custom MATLAB (The MathWorks, Inc) program was used to extract peak hip angles and moments, as well as to calculate angular excursion. Joint moments were normalized two ways: to body mass and to total mass, which included both the body mass and the added mass. Data from the participants' dominant limb was used for analysis.

For kinematic data, we used a 3x2 mixed design analysis of covariance with sex as a between subject factor, load as a within-subject factor, and unloaded body mass as a covariate (SPSS, IBM). This analysis was used to test for the main effect of sex. An additional analysis of variance (ANOVA) using the same 3x2 design was performed to test for the main effect of load and interaction of load and speed. Additional post-hoc tests were performed when significant interactions were detected. For kinetic data, we only ran a 3x2 mixed design ANOVA, with post-hoc tests for significant interactions. An ANCOVA was not needed for the kinetic data because the data are already normalized to mass.

RESULTS AND DISCUSSION

The results (Table 1) indicate that females and males use different hip mechanics when walking with standardized loads. Significant load-by-sex interactions were detected in the frontal plane. Compared to the unloaded condition, males had greater peak adduction angles ($p=0.007$) and frontal plane excursion ($p=0.002$) in the medium and heavy load conditions. Females did not change hip kinematics with increased load, but had 4.5° and 3.0° more hip adduction than males in the unloaded ($p=0.015$) and heavy ($p=0.036$) load conditions. In females, the peak hip abduction moment normalized to total mass decreased with each increase in load ($p<0.001$).

There were significant main effects of load at the hip including greater peak flexion angle ($p<0.001$) and excursion ($p<0.001$) with each increased load. When normalized to body mass, hip flexion, extension and abduction moments increased with increased load ($p<0.001$). Conversely, when normalized to total mass, hip flexion moments decreased with increased load ($p<0.001$).

Table 1: Mean±SD of hip kinematics and kinetics.

	Unloaded		Medium Load		Heavy Load	
Angles (°)	Female	Male	Female	Male	Female	Male
Sagittal Exc.*	43.7±3.7	42.5±2.3	44.6±3.8	43.7±2.6	46.0±3.6	44.5±2.6
Flexion*	39.2±8.4	33.4±6.1	39.9±8.0	34.3±6.0	41.2±7.8	34.7±5.9
Extension	4.5±8.1	9.1±6.7	4.8±8.0	9.4±6.4	4.8±8.0	9.8±6.0
Frontal Exc.‡	12.8±2.1	11.9±2.2	12.5±2.6	12.5±2.6	12.6±2.7	13.0±2.6
Adduction‡	7.1±2.7	3.7±2.6	7.1±2.6	4.1±2.7	6.9±2.8	4.3±2.8
Abduction	5.7±2.7	8.2±3.6	5.4±2.8	8.4±3.6	5.7±2.9	8.7±3.7
Moments (Nm/kg body mass)						
Flexion*	0.67±0.17	0.71±0.16	0.76±0.19	0.79±0.17	0.83±0.2	0.87±0.17
Extension*	0.7±0.11	0.85±0.14	0.77±0.12	0.81±0.14	0.85±0.14	0.87±0.15
Adduction	0.1±0.03	0.12±0.04	0.1±0.05	0.12±0.05	0.11±0.05	0.12±0.06
Abduction*	0.92±0.11	1.17±0.16	1.05±0.13	0.96±0.14	1.17±0.16	1.06±0.16
Moments (Nm/kg total mass)						
Flexion*	0.67±0.17	0.71±0.16	0.64±0.17	0.68±0.15	0.61±0.15	0.67±0.14
Extension*	0.7±0.11	0.62±0.1	0.65±0.1	0.7±0.13	0.62±0.1	0.66±0.12
Adduction*	0.1±0.03	0.12±0.04	0.09±0.04	0.1±0.04	0.08±0.04	0.09±0.04
Abduction‡	0.92±0.11	0.85±0.12	0.88±0.11	0.82±0.12	0.85±0.12	0.81±0.12

Note: *Indicates significant ($p < 0.05$) main effect for load, ‡Indicates significant ($p < 0.05$) load-by-sex interaction effect

CONCLUSIONS

When carrying load males were shown to make adaptations at the hip to keep joint moments constant, yet females did not show the same adaptation to loads. In fact, with increasing load, frontal plane kinematics of males become similar to female kinematics. This finding could suggest that females are already at the end range of frontal plane motion of the hip during unloaded walking. The difference in hip joint adaptations suggests that males and females use different gait controls strategies during load carriage and that the lack of kinematic adaptation made by females in the frontal plane may increase their risk of injury.

REFERENCES

1. Liew et al. *J App Biomech,* 32(6):614-629, 2016.
2. Silder et al. *J Biomech*. 46(14): 2522-8, 2013.
3. Bell et al., J. *Am J Pre Med,* 18(S3):141-6, 2000.
4. Kupferer et al. *Mil Med.* 176(1): 56-61, 2014.

ACKNOWLEDGEMENTS

This work was supported by the Dudley Allen Sargent Research Fund. Kari Loverro is supported by the SMART Scholarship-for-service program.

EMG-DRIVEN OPENSIM ANALYSIS OF KNEE FORCES IN NORMAL WEIGHT, OVERWEIGHT AND OBESE SUBJECTS DURING GAIT, CYCLING AND ELLIPTICAL EXERCISES

[1] Chiara Marino, [2]Megan V. Pottinger, [2]Scott J. Hazelwood, and [2] Stephen M. Klisch

[1] Polytechnic of Turin, Turin, Italy
[2] California Polytechnic State University, San Luis Obispo, CA, USA
email: sklisch@calpoly.edu

INTRODUCTION

Exercise has been recommended for preventing and treating obesity; however, obesity is a risk factor for knee osteoarthritis (OA) partly due to altered and/or increased mechanical loading [1, 2]. Thus, select weight control exercises may produce adverse loading conditions that cause injury and, ultimately, arthritis. Although biomechanical gait studies using inverse dynamics have been used to predict knee joint loading for normal weight and obese subjects [1], bicycling and elliptical training studies have not used inverse dynamics to predict knee joint loading for overweight and obese subjects.

Our hypothesis was that maximum knee compressive contact forces would depend on exercise and body types. The aims were to: (1) conduct motion analysis experiments with normal weight (NW), overweight (OW), and obese (OB) subjects during gait (G), cycling (C), and elliptical (E) exercises and (2) calculate and compare knee compressive contact forces using EMG-driven inverse dynamic analysis with OpenSim (Stanford, Palo Alto, CA, USA).

METHODS

Protocols were approved by Cal Poly's Human Subjects Committee. Kinematic data were collected using a 10-12-camera motion analysis system with Cortex software (Motion Analysis Corp., CA, USA). For G, kinetic data were obtained using 3 ground force plates (Accugait, AMTI, MA, USA). For C and E, a stationary bike (Lifecycle GX, Life Fitness, IL, USA) and an elliptical machine (XE-795, Spirit Fitness, AR, USA) were used with custom pedals containing load cells (AD2.5D, AMTI). EMG data were collected using 4 wireless sensors (Trigno, Delsys, MA, USA).

7 males and 2 females (22.7 ± 3.2 years old) participated (NW n=3, OW n=3, OB n=3). NW, OW and OB classification was determined by body mass index (BMI; kg/m^2) (22.7 ± 3.1 for NW, 27.4 ± 1.4 for OW, and 32.8 ± 1.3 for OB).

An enhanced Helen Hayes marker protocol, with 32 markers, was used. EMG sensors were placed on dominant leg muscles: vastus medialis, vastus lateralis, lateral gastrocnemius, and semimembranosus. Each subject underwent 3 G trials at a self-selected walking speed, and 3 C trials and 3 E trials both at 70 rpm with moderate machine resistance levels. A static pose trial was captured for model scaling.

Trials were processed with Cortex to obtain kinematics and kinetics files. Kinematic data were filtered (4^{th}-order Butterworth, 6 Hz cutoff frequency) in Cortex. Matlab (MathWorks, MA, USA) was used to filter forces (4^{th}-order Butterworth, 6 Hz cutoff frequency) and EMG data (bandpass filter of 20 Hz to 450 Hz) [3]. OpenSim analysis involved 5 steps: (1) model scaling with the static pose trial data, (2) Inverse Kinematics (IK) to calculate kinematics, (3) Residual Reduction Algorithm (RRA) to adjust kinematics based on the applied forces, (4) Computed Muscle Control (CMC) with EMG activation constraints to obtain muscle activations, and (5) Joint Reaction (JR) analysis to obtain joint contact forces.

A two-factor repeated measures ANOVA (body and exercise types) with post-hoc Tukey tests ($p<0.05$ significant) were performed in Minitab (Minitab Inc., PA, USA) to compare maximum TF compressive forces.

RESULTS AND DISCUSSION

The effect of exercise, but not body type, was statistically significant. In particular, TF compressive forces for C were lower than those for G and E for all three subject groups (Fig. 1). Also, TF compressive forces for OB subjects during G were higher than values for NW subjects during E.

The knee joint compressive contact forces were lowest during C. That result was expected and was likely due to the bike saddle partially supporting the body weight, thus reducing the forces supported by the knee joint. For each exercise, NW, OW and OB had similar TF compressive forces ($p=0.068$); however, that p value is nearly significant, so inclusion of additional subjects may detect significance.

There are a few limitations to this study. First, the samples sizes were small with only 3 subjects in each group and the differences between males and females were not evaluated. Second, body type was classified using BMI, not considering body fat percentage. Third, the bike and the elliptical machine were not instrumented in the seatpost and handlebars. Measurement of those forces could provide an experimental target for the residuals in the RRA tool. Regardless, this study's results suggest that cycling may be a preferred weight loss exercise to prevent overloading knee joints and, thus, minimizing OA risk in OW and OB subjects.

REFERENCES

1. Haight et al*., Journal of Orthopaedic Research,* 32(2): 324–330, 2014.
2. Messier*, SP et al., Arthritis & Rheumatism,* 52(7):2026-2032, 2005.
3. De Luca, C et al., *Journal of Biomechanics*, 43:1573-1579, 2010.

ACKNOWLEDGEMENTS

Funded by the Donald E. Bently Center and the W.M. Keck Foundation. We thank Professor Laura Gastaldi for supporting the student travel to the US for thesis project work.

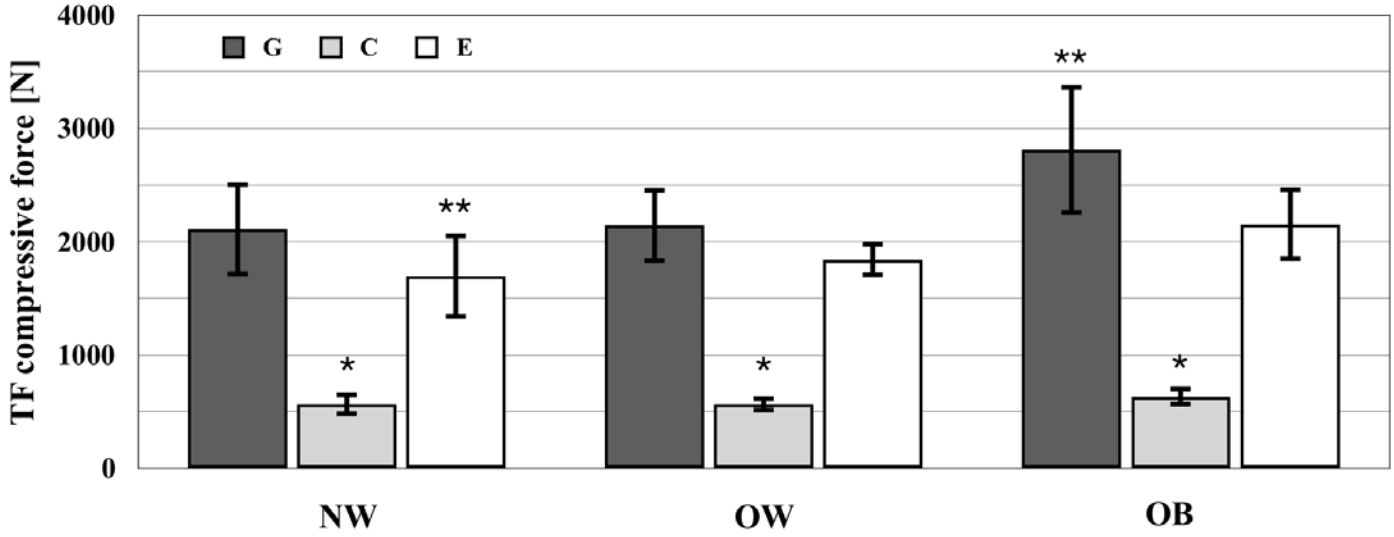

Figure 1: Mean ±1 S.D of maximum knee TF compressive force for normal (NW), overweight (OW) and obese (OB) subjects during gait (G), cycling (C) and elliptical (E) training. *= significantly different from all G, E values, **= significantly different between values.

Acute Effects of Distance Running on Healthy Femoral Condyle Cartilage Thickness and Volume: A Pilot Study

[1]Marlee A. Mason, [1]Alyssa Evans, [1]Sunku Kwon, [2]Merry Taylor, [2]Neal Bangerter, & [1]Matthew K. Seeley

[1]Department of Exercise Science; [2]Department of Electrical Engineering
Brigham Young University, Provo, UT, USA
email: marlee_m@byu.edu

INTRODUCTION

The influence of distance running on healthy knee articular cartilage is unclear. Some evidence indicates that distance running might temporarily decrease articular cartilage thickness [1]; however, long-term cartilage health might benefit from running, for some healthy asymptomatic individuals [2]. MRI is currently an acceptable method for quantifying articular cartilage morphology (i.e., thickness and volume), but current MRI methods of cartilage segmentation are quite time-consuming and sometimes unreliable.

The purpose of this pilot study was twofold: (1) to examine acute effects of running on femoral condyle articular cartilage morphology (thickness and volume), and (2) to evaluate two different methods of MRI quantification of femoral cartilage thickness and volume: a standard whole-cartilage method, and a novel abbreviated condylar method. We hypothesized that (1) distance running would acutely decrease cartilage thickness and volume, and (2) the aforementioned abbreviated analysis method would yield measures of cartilage morphology comparable to the standard method.

METHODS

Five subjects (2 Females; Age = 29 ± 7 years; Height = 176 ± 11 cm; Mass = 66.5 ± 12.9 kg) participated in this study. All subjects gave informed consent and data collection procedures were approved by the appropriate institutional review board before data collection. Subjects had no prior history of knee pain, injury, disease or surgery. MRIs were obtained for each subject immediately before and after a 30-minute run. The pre-run MRI was taken in the morning, after minimal weight-bearing activity. The post-run MRI was taken immediately after the run.

All MRIs were performed using a Siemens 3T Tim Trio with a designated 8 channel knee coil. For each MRI, a 3D DESS scan was obtained with the following parameters: TR/TE = 16.3/4.7ms, matrix = 384 × 307 with 160 slides, FOV = 140 × 140mm, flip angle = 25 degrees. DESS scans were segmented via a semi-automated technique, using COLIPE software (Qmetrics Technologies, Pitsford, NY, USA). Segmentations of cartilaginous regions were manually delineated and adjusted, slice by slice, to create an accurate 3D model of each subject's full knee cartilage before and after running.

A novel abbreviated segmentation method was used, in addition to the previously-described traditional 160-slide whole-cartilage method, to determine whether time spent in segmentation could be reduced, without a loss of accuracy for the present measures of femoral condyle cartilage morphology (thickness and volume). We hypothesized that, during running, the cartilage over the middle of the femoral condyles might bear the greatest load; consequently, we suspected that these areas might experience the greatest changes in volume and average thickness due to running. Therefore, cartilage from 20 slices of each femoral condyle region, totaling 40 slices, were chosen to represent the whole-cartilage and used in the novel abbreviated segmentation. The 20 slices from each condyle were chosen by determining the center of the condyle and segmenting 10 slices on each side of the center. After the pre-run and post-run segmentation models were created via both the traditional and abbreviated methods, each scan was individually run through a quantification program to calculate mean thickness and volume. Measures of mean cartilage thickness and volume were compared between pre- and post-run, and standard and abbreviated methods, using Wilcoxon signed-rank tests ($\alpha = 0.05$).

RESULTS AND DISCUSSION

The present results did not support our first hypothesis concerning potential effects of distance running on healthy femoral condyle articular cartilage: on average, the run did not significantly decrease mean cartilage thickness or volume, measured using either of the quantification approaches (Table 1). Both the standard and abbreviated approaches indicated that the run decreased mean thickness and volume for three subjects, while increasing mean thickness and volume for two subjects. However, the present results did support our hypothesis concerning the traditional and abbreviated quantification methods: they produced values that did not significantly differ (Table 1). Further, the present data (1) fit with existing literature indicating that running might not significantly alter knee cartilage morphology, and (2) are comparable to previously reported measures of femoral cartilage morphology [3-4].

The cause of the heterogeneous responses in cartilage morphology to the 30-min run, within our sample, is unclear. We speculate, however, that various factors, including subject physical activity habits are related; specifically, we hypothesize that cartilage might respond differently to running for habitual runners, compared to sedentary individuals or individuals who participate in exercise other than distance running. Further, we speculate that genetic predisposition, running biomechanics, and/or weight-to-cartilage ratio may influence response of cartilage morphology to distance running. Future research should be conducted to test these ideas.

The present abbreviated quantification approach reduces time required to segment a scan by approximately 75%, but does not appear to decrease accuracy. Consequently, in the future, this new approach could be helpful in this particular context (i.e., when evaluating the effect of physical activity on femoral condyle articular cartilage morphology). Additionally, although perhaps obvious, it should be emphasized that this sample is quite small and additional data collection is necessary to better understand exactly how distance running influences femoral cartilage morphology. Finally, it was surprising that, for certain subjects, changes due to the run occurred in different directions for mean thickness and volume. We plan to investigate this unexpected phenomenon further.

CONCLUSIONS

The influence of distance running on knee articular cartilage morphology remains unclear and deserves additional study. The novel abbreviated segmentation method, presently evaluated, appears to be a time-effective and viable approach to knee cartilage segmentation, in this context.

REFERENCES

1. Boocock et al. *Osteoarthritis and Cartilage.* **17**(7), 883–890, 2009.
2. Krampla et al. *Skeletal Radiol*. **30(**2), 72-76, 2001.
3. Subburaj et al. *Am J Sports Med.* **40**(9), 2134-2141, 2012.
4. Kauffmann et al. *IEEE Trans Biomed Eng.* **50**(8) 978-988, 2003.

Table 1: Changes (absolute and relative (%)) for mean cartilage thickness and cartilage volume, due to a 30-min run, calculated using two different quantification methods. Note: T = Traditional; A = Abbreviated; Diff = post-run value minus pre-run value.

	Volume (mm^3)				Thickness (mm)			
	T Diff	A Diff	T PDiff	A PDiff	T Diff	A Diff	T PDiff	A PDiff
Subject 1	2291	1075	19.8%	17.3%	0.1	0.1	6.3%	8.4%
Subject 2	-406	-114	-2.8%	-1.6%	0.2	0.3	11.4%	14.1%
Subject 3	-136	-56	-1.7%	-1.1%	0.2	0.3	17.9%	22.2%
Subject 4	740	316	9.9%	6.9%	-0.2	-0.2	-11.2%	-13.2%
Subject 5	-776	-414	-4.4%	-4.7%	-0.1	-0.2	-3.9%	-8.9%

A COMP ARISON OF RUNNING MECHANICS IN MARA THON RACING SHOES

[1] Aubree McLeod, [1]Luis Gonzalez, [1]Dru Valentine, [1]Jared Ward, [1]Ron Hager, and [1]Iain Hunter

[1] Brigham Young University, Provo, UT USA
email: aubreermcleod@gmail.com, web: http://biomechanics.byu.edu

INTRODUCTION

In November 2017, Shalane Flanagan crossed the finish line of the NYC Marathon in 2:26:53, becoming the first American woman to win the race since 1977. In addition to extreme dedication and hard work, Shalane's victory was aided by training and racing in Nike's new marathon racing shoe, the Nike Zoom Vaporfly 4%. Athletes wearing this shoe have dominated the past 6 world marathons, with 19 top finishes being by men and women in the Vaporfly shoe.

The Vaporfly 4% (VP) shoe has a unique design; including a carbon fiber plate contributing to longitudinal stiffness and a lightweight energy efficient foam. Initial studies on a prototype version of the VP shoe show a 4% reduced metabolic cost of running when compared to other common marathon shoes; Adidas Adios Boost (AB) and Nike Zoom Streak (ZS) [1].

20% of the metabolic cost improvement while wearing the VP shoe was attributed to changes in running mechanics [1]. The VP shoe was shown to decrease stride rate, and increase stride length, contact time, and peak force [1]. Though no research was done on joint kinematics, previous studies have shown increased knee flexion and leg stiffness when running on highly compliant surfaces, which lessens vertical displacement and stabilizes center of mass mechanics [2].

Initially, the Vaporfly 4% was only available to elite athletes. Now that a consumer version is available to the public, we replicated the initial study to examine changes in running mechanics, focusing on joint kinematics. We expect to observe similar changes as the initial study in stride and peak force. We also expect to see additional changes in joint kinematics to explain reduction in metabolic cost.

Figur e 1: The three shoes used in this study. (Nike Zoom Vaporfly 4%, Adidas Adios Boost, Nike Zoom Streak)

METHODS

Nineteen subjects were brought into a lab equipped with a treadmill force plate and motion capture cameras. Subjects tried on shoes for a good fit (sizes 9-12) and were then fitted with 35 reflective light markers on major body landmarks.

Subjects ran a 3 minute trial at 16 km/hr in the VP, AB, and ZS shoes in a randomized order. Force and 3D Vicon visual data was collected during the last 30 seconds of each trial.

3 minutes is adequate time to adjust running mechanics to a new condition [2]. 16 km/hr was chosen since it matched one of the speeds used in the VP prototype study and provided an intensity that subjects could maintain without difficulty or breakdown of running form.

We analyzed and compared peak force, ground time, stride length, vertical impulse, knee range, hip range, plantar flexion velocity, and center of mass vertical oscillation between the 3 shoes. Repeated measures multivariate ANOVA determined

differences in running mechanics between shoe conditions with Tukey HSD post-hoc tests.

RESULTS AND DISCUSSION

At 16 km/hr, the VP shoe was associated with significant changes in stride length, peak flexion velocity, and center of mass vertical oscillation.

The VP shoe was associated with a 1.2% increase in stride length when compared to AB. The VP shoe was also associated with a 10.6% decrease in plantar flexion velocity compared to ZS. Subjects in the VP shoe showed a 5.3% and 4.7% increase in CM vertical oscillation when compared to ZS and AB respectively. Other measures of running mechanics were not found to vary significantly between shoes (Table 1).

Our finding of an increased VP stride length correlates with the original prototype study [1]. We did not, however, observe the same increased peak force, and longer ground time [1]. This difference may be because the consumer version of the VP has a smoother sole than the originally tested prototype and some of our subjects noted slipping when running on a treadmill. It is possible that this smoother sole causes changes in mechanics that would not be observed when running on the road, which would have a different coefficient of friction.

Ferris et al. predicted decreased knee flexion when running on a highly compliant surface to stabilize center of mass oscillation [2]. In contrast, we observed unaltered knee flexion, and an increase in center of mass vertical oscillation in the VP shoe. The increased vertical oscillation may be explained by the greater stride lengths observed among the subjects in our study wearing the VP shoe.

As noted by Hoogkamer et al, the small changes noted in running mechanics are not enough to explain the reduction in metabolic cost seen in the VP shoes [1]. We agree with their conclusion that the improved energy properties of the foam sole provide the best explanation for the metabolic cost reduction. Typically, muscles contract to aide tendons in absorbing and returning energy during gait [3]. If the sole of an energy efficient shoe can do this instead, less muscle work is required, and thus less metabolic cost for the runner. Another potential benefit of the VP is the stiffness of the shoe due to the carbon fiber plate. This changes the mechanical advantage about the ankle. Our study does not show how much this would affect metabolic cost, but may be a contributing factor.

CONCLUSIONS

There are meaningful mechanical differences between the VP shoe when compared with the AB and ZS at 16 km/hr. These differences could help to explain some of the reduction in metabolic cost observed when running in these shoes.

REFERENCES

1. Hoogkamer et al. Sports Med, Online, 2017.
2. DP Ferris et al. J Biomech, Online, 1999.
3. Shorten. J Biomech, Online, 1993.

Table 1: Mechanical differences between shoes. Superscripts indicate significant difference from another shoe.

	AB	ZS	VP
Peak Force (N)	3.00 ± .33	3.05 ± .32	2.94 ± .23
Ground time (sec)	.190 ± .019	.190 ± .017	.190 ± .022
Stride Length (m)	3.03 ± .15 (NS, VP)	3.05 ± .15 (AB, VP)	3.07 ± .15 (AB, NS)
Vertical Impulse (Ns)	97.4 ± 20.8	100.7 ± 16.8	97.2 ± 13.1
Knee Range (degrees)	23.0 ± 4.2	22.8 ± 4.1	22.6 ± 5.6
Hip Range (degrees)	70.0 ± 3.7	70.0 ± 3.6	70.0 ± 3.4
Plantar Flexion Velocity (deg/sec)	222.2 ± 42.3 (NS, VP)	233.3 ± 34.5 (AB, VP)	208.4 ± 35.0 (AB, NS)
CM Vertical Oscillation (mm)	98 ± 30 (NS, VP)	98 ± 29 (AB, VP)	103 ± 31 (AB, NS)

FRICTIONAL RESPONSE OF MULTIPLE SLIP-RESISTANT FLAT AND BEVELED SHOES TO NORMAL LOADING

Seyed Reza M. Moghaddam, and Kurt E. Beschorner

The University of Pittsburgh, Pittsburgh, PA, USA

email: sem162@pitt.edu, web: http://www.engineering.pitt.edu/hmbl/

INTRODUCTION

Slips and falls are a serious occupational and health problem and cost the US economy $180B each year [1]. Amongst the biomechanical and environmental factors that influence slip and falls, shoe design is of great importance since it is a controllable factor that affects the available coefficient of friction (COF). Slip risk can be predicted as a function of the difference between the available COF and the required coefficient of friction (RCOF) to maintain walking [2].

Previous research by our group has demonstrated capability of computational modeling in predicting the available COF of shoes on contaminated surfaces [3]. Specifically, a multiscale finite element model of shoe-floor friction has been developed that calculates the available COF based on the microscopic and macroscopic features of the shoe and flooring such as surface roughness, shoe material properties, shoe-floor contact angle, shoe sliding velocity, normal loading, and whole shoe geometry.

Of the design characteristics affecting COF of the footwear, one that has not been thoroughly investigated is the effect of beveling of the shoe heel and how the COF of beveled and flat shoes respond to the changes in normal loading. The effects of normal loading on COF is relevant to understanding the impacts of a person's weight on the resulting COF and slipping risk. To the best knowledge of the authors, one experimental study has investigated the effect of beveled heel on slip-resistance of only one shoe design in one level of normal loading [4]. This abstract fills the knowledge gap by introducing a computational modeling methodology to investigate the effects of beveling shoe heels and kinetics (i.e. normal loading) on the available COF and potential slip-resistance performance of shoes.

METHODS

A multiscale finite element model of shoe-floor friction which simulates the contact between shoe and flooring surfaces in microscopic and macroscopic scales was utilized to investigate the effect of normal loading on shoe-floor COF (LS-Dyna®, LSTC, Livermore, California, USA). The microscopic component of the multiscale model calculates the microscopic COF as a function of contact pressure (*COF(p)*). The macroscopic component of the multiscale model calculates the contact pressure distribution over the macroscopic geometry of the shoe sole and uses the *COF(p)* from the microscopic models to calculate the whole shoe COF on contaminated surfaces.

The multiscale model was applied to simulate the friction between four existing shoe designs against a vinyl flooring at a sliding speed of 0.3 m/s and a shoe-floor angle of 7° consistent with the standard for shoe-floor friction measurement [5]. Four shoes (Fig. 1) that were considered included two flat heel shoes (F1 & F2) and two shoes with beveled heels (B1 & B2). Shore A hardness of the shoes was measured using a durometer and was used in models for quantifying material properties of the shoes (Table 1).

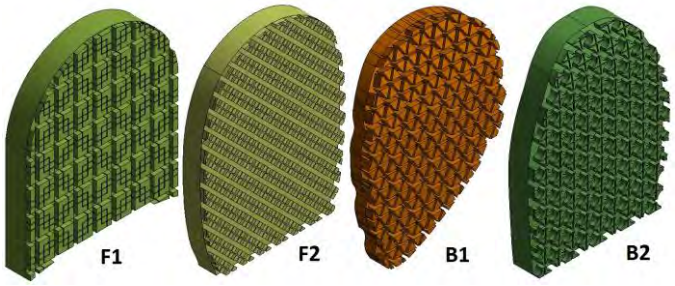

Figure 1: Geometries of the modeled shoes.

Simulations for each macroscopic shoe model were conducted over 10-11 normal load levels to generate a relationship between the normal loading and COF as well as contact area (A_{Model}). Contact area was chosen because higher contact areas between shoe and floorings are demonstrated to lead to a more distributed under-shoe contact pressure and correlate with a better slip-resistance performance [3].

RESULTS AND DISCUSSION

Computational models indicated that an increase in normal loading led to a decrease in COF (Fig. 2) and an increase in A_{Model} (Fig. 3). An exponential decay function (Eq. 1) and a power function (Eq. 2) described the variation in COF and A_{Model} with respect to the change in normal loading, respectively (R^2>0.99). In these equations, λ and b are coefficients that were determined using curve fitting techniques; COF_H and COF_L represent COF in high and low normal loads, respectively.

$$COF = COF_H + (COF_L - COF_H)e^{-\lambda F_{Normal}}, \text{ Eq. 1.}$$

$$A_{Model} = aF_{Normal}{}^{b}, \text{ Eq. 2.}$$

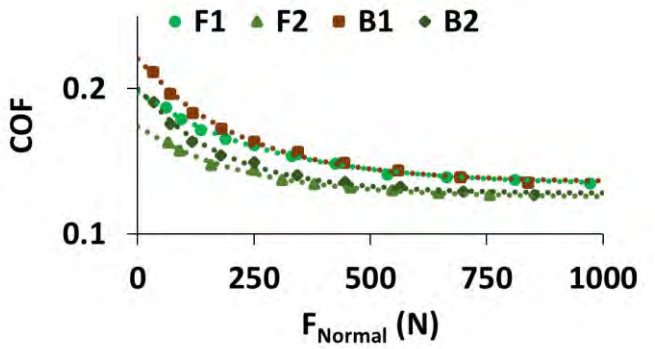

Figure 2: COF versus normal loading.

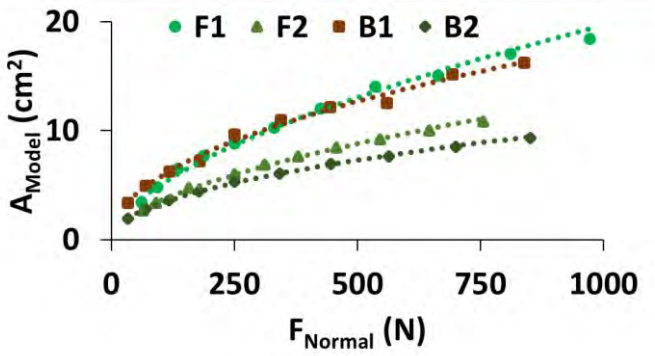

Figure 3: A_{Model} versus normal loading.

An analysis of the exponential decay coefficients in equation 1 (Table 1) revealed that the COF response (Fig. 2) of flat shoes was less sensitive to normal loading (smaller λ in Table 1). The contact area, A_{Model}, (Fig. 3) for flat shoes more closely simulated a linear curve compared to the beveled shoes (b values closer to 1, Table 1). These findings demonstrate a difference in response to normal loading between flat and beveled shoes.

Findings of this study can be applied to simulate the effect of a person's weight on slip-resistance performance. These findings suggest that while certain (beveled) shoes might have superior slip-resistance in lower normal loads, their performance might decay when a heavier person wears those and suggest that slip-resistance performance of flat shoes is less sensitive to a person's weight.

Although it is acknowledged that the range of the normal load that was used for this analysis might not fully represent the body weight of obese people, findings indicate a decrease in COF with increasing normal load, a phenomenon that could be partially responsible for the higher risk of falls in the overweight population [6]. It should be noted that overweight human subjects are reported to have a higher RCOFs in comparison to the non-obese subjects [7]. Therefore, the combination of reduction in COF (observed in the models) and the higher RCOF in overweight people (reported in the literature) is likely to explain the higher chance of slips and falls in overweight people given that the difference between the available COF and RCOF predicts the probability of slips and falls [2].

Table 1: Hardness and curve coefficients for shoes.

Shoe	Shore A Hardness	λ	b
F1	50	0.0035	0.59
F2	56	0.0044	0.56
B1	56	0.0045	0.48
B2	72	0.0054	0.49

REFERENCES

1. Florence C., et al. *MMWR Morb Mortal Wkly Rep,* **64** ,1074-82, 2015.
2. Hanson JP, et al. *Ergonomics,* **42**, 1619-33, 1999.
3. Moghaddam SRM, et al. *J Biomech,* **66**, 145-152, 2018.
4. Lloyd D, & Stevenson MG. *J Occup Health Saf*, **5**, 229-35, 1989.
5. ASTM F2913-11, *ASTM Intl.,* West Conshohocken, PA, 2011.
6. Fjeldstat, C, et al. *Dyn Med*, **7**, 2008.
7. Wu, X, et al. *J Biomech*, **45**, 1042-7, 2012.

Estimation of Dynamic Stability of Fallers and Non-Fallers Utilizing Long-term (3-Days) Wearable Sensor Data

[1] Seong Hyun Moon, [2] Timothy E. Hewett, [3] Hyunglae Lee, [4] Rahul Soangra,
[1] Chris Frames and [1] Thurmon Lockhart

[1] School of Biological and Health Systems Engineering, Arizona State University, Tempe, AZ, USA
[2] Department of Orthopedic Surgery, Mayo Clinic, Rochester, MN, USA
[3] School for Engineering of Matter, Transport, and Energy, Arizona State University, Tempe, AZ, USA
[4] Crean College of Health and Behavioral Sciences, Department of Physical therapy, Chapman University, Irvine, CA, USA

email: smoon13@asu.edu

INTRODUCTION

In 2014 alone, older adults in US experienced more than 29 million falls causing more than 7 million injuries and costing over $31 billion in annual Medicare costs [1]. Reducing fall rates is therefore an important goal for both individuals and the entire healthcare industry. Therapeutic techniques are being developed to help reduce fall risk, but their success depends both on accurately diagnosing fall prone individuals and on precisely assessing the benefits the techniques provide. Researchers are working towards providing these capabilities by studying the relationship between gait, posture, and falls. In this light, the local dynamic stability as measured by Maximum Lyapunov Exponent may be capable of differentiating fallers and non-fallers.

Although laboratory assessment of dynamic stability has been successfully implemented it is unclear if normal daily activities measures utilizing inertial measurement units (IMU) at their home can be used to assess dynamic stability by characterizing walking events and stitching it together (to veer away from "the white coat syndrome" from clinical environment, where subjects tend to perform irregularly during the data collection [2]). By observing and collecting 3 days continuous ambulatory data and characterizing walking events, we were able to use the stitched data to calculate dynamic stability of gait during normal daily activities. The hypothesis tested that dynamic stability measure assessed during normal ambulation at home can differentiate fallers and non-fallers.

METHODS

For this experiment, there were ten subjects, five fallers mean age 70 ± 12years, height 174.6 ± 7.8cm and weight 82.8 ± 15.7kg and five nonfaller subjects mean age 20 ± 2.6years, height 169.1 ± 9.4cm and weight 73.1 ± 13.3kg were recruited.

Subjects were asked to wear the DynaPort MM++ (triaxial accelerometer, tri-axial gyroscope, and Magnetometer) at the posterior lumbar region of the spine continuously for three days of data collection. Subjects were allowed to remove the device only for hygiene purpose and changing clothes.

With the collected long-term data, stitching algorithm [3] determined the Maximum Lyapunov Exponent. This value can determine the local divergence coefficient that quantifies the resistance to minute perturbations [4]. For the stitching process, the stitching algorithm was applied to attach acceleration signals [3]. The stitching signals part was at 50 percent of the last peak signal from the first walking data and other 50 percent from the first peak of second walking data set. This stitched data composed required minimum gait cycle to effectively calculate the Maximum Lyapunov Exponent. To measure the Maximum Lyapunov Exponent, first, time delayed coordinate needs to be determined [5]. This method was configured by Taken's theorem and reconstruction of multi-dimensional state space was performed with acceptable data from one of single dimensional time series measurement. To reconstruct the state space

X(t), the Initial single dimension time series data x(t), the minimum embedding dimension(d_E) and time delay(T) value are required. By using Auto Mutual Information approach and nearest false neighbors approach can determine d_E and T [3]. Equation for calculating state space is $X(t) = [x(t), x(t+T), x(t+2T), \ldots, x(t+(dE-1)T)]$. Determining state space, all the nearest neighbors were collected which has the closest distance from the stride trajectories in the state space. To calculate the Maximum Lyapunov Exponent, all the distance from nearest neighbors were measured and calculated the logarithmic divergence as function of time (higher slope – more trajectory divergence- less stable).

RESULTS AND DISCUSSION

The objective of this experiment was to determine the LDS with the stitching algorithm from 3days of Activity of Daily Living (ADL). It was performed to avoid "white coat syndrome" which may represent true stability characteristics at their own living environment.

The results indicated that the dynamic stability was significantly different for fallers and non-fallers utilizing long-term (3 days) ambulatory data (p value = 0.0252). The mean value of the nonfaller's Maximum Lyapunov Exponent was 1.322 and faller was 1.540. This result shows that fallers have higher Maximum Lyapunov Exponent compared to nonfaller as hypothesized. The minimum value of the faller is 1.422 and the maximum value of nonfaller is 1.480, this may indicate that nonfallers are less stable when walking. As shown in the Figure1, all nonfallers have higher value compared to fallers.

CONCLUSIONS

The objective of this study was to examine if the stitching algorithm was adequate to calculate the Maximum Lyapunov Exponent from 3-days of ADL data and determine the Local Dynamic Stability. Result indicated that calculated Maximum Lyapunov Exponent was possible to differentiate faller's from nonfaller. The stitching algorithm has the capability of encapsulating the exclusively required part of ambulatory data and preserve the integrity of the original data. For future studies, this algorithm will be implemented on various types of disease patients and age groups to contrast the Local Dynamic Stability differences among faller and non-fallers.

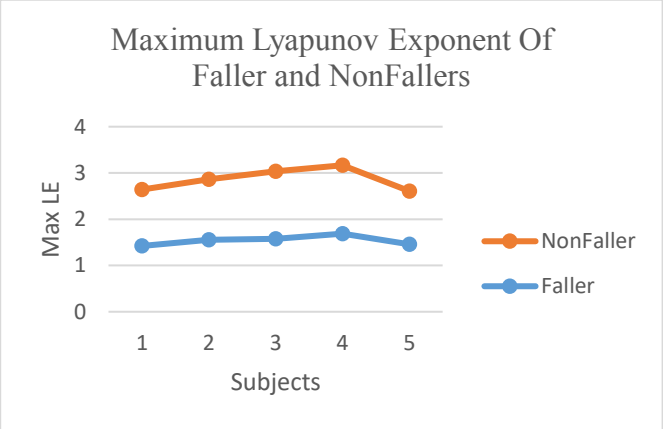

Figure 1: Maximum Lyapunov Exponent of each Faller and NonFaller subjects

REFERENCES

1. Centers for Disease Control and Prevention in this week's Morbidity and Mortality Weekly Report, 2017.
2. Weiss, A., Herman, T., Giladi, N., & Hausdorff, J. M. (2014). Objective assessment of fall risk in Parkinson's disease using a body-fixed sensor worn for 3 days. *PloS one*, 9(5), e96675.
3. Moon, S., Unpublished Thesis, 2017, ASU.
4. Rosenstein, M. T., Collins, J. J., & De Luca, C. J. (1993). A practical method for calculating largest Lyapunov exponents from small data sets. *Physica D: Nonlinear Phenomena*, 65(1-2), 117-134.
5. Lockhart, T. E., & Liu, J. (2008). Differentiating fall-prone and healthy adults using local dynamic stability. *Ergonomics*, 51(12), 1860-1872.

Teaching Older Adults How to Fall Safely

Yaejin Moon, Alka Bishnoi, Ruopeng Sun, Jong-Cheol Shin and Jacob J. Sosnoff

University of Illinois at Urbana-Champaign, Department of Kinesiology and Community Health, Urbana, IL
email: ymoon9@illinois.edu

INTRODUCTION

Given the frequency and severity of falls [1], insights are clearly necessary to decrease the risk of injury from falls. A novel approach that may augment current fall prevention practices is instructing older adults to fall safely. A recent systematic review paper found that tuck and roll strategy (Figure 1), which is characterized by knee flexion, rotation toward backward during descent to change a fall into rolling after an impact, was the most effective strategy to reduce impact severity [2]. Despite great promise, the majority of previous research examining safe landing strategies has methodological (young adults and self-initiated falls) and theoretical (lack of principles of motor learning) limitations. The purpose of the current study was to determine whether older adults can learn tuck and roll strategy in such a way that they reduce risk of fall related injuries. Consistent with the principles of motor learning [3], learning was quantified with changes in impact severity parameters following training (aim 1), transfer of the falling strategy to the untrained side (aim 2) and 1-week retention (aim 3). Additionally, the training group's ability to learn the tuck and roll strategy was quantitatively and qualitatively examined (aim4).

METHODS

Protocol (Figure 2)

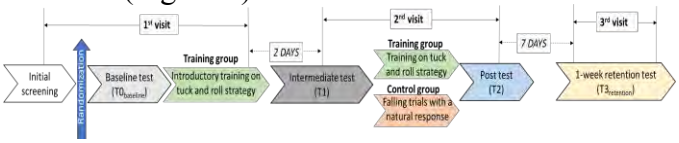

Figure 2: Experimental procedures

17 healthy older individuals participated (average age: 64.3±4.4 years, 14 males, 3 females). Participants were randomly assigned into one of two groups: (1) training group (n=9) who received two sessions of tuck and roll training on the right side falling (2) active control group (n=8) who had right-side falling trials without receiving instruction. All participants performed 6 trials of sideway falls (3 right-side, 3 left-side) for baseline ($T0_{baseline}$),

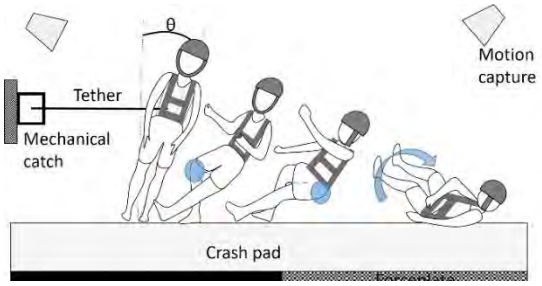

Figure 1: Schematic representation of tuck & rolling technique *and* experimental setup of a falling simulation

intermediate (T1), post (T2) and 1-week retention tests ($T3_{retention}$) (Figure 2).

Data collection

During the falling assessments, normalized hip impact force (=force/weight) was examined by forceplate (S-Mill, Motekforce Link, Amsterdam, the Netherlands, 500Hz). Also, a motion capture system (VICON, Oxford Metrics, Oxford, England, 100Hz) was used to collect kinematic data of the lower limb and the head using VICON plug-in-gait lower body® model. Subsequently, using a custom MATLAB script (MATLAB, MathWorks, Natick, MA), vertical hip impact velocity and vertical head impact acceleration were measured. Additionally, participants wore a wireless inertial sensor, BioStampRC (MC10, Inc., Lexington, MA, USA, 125Hz), on the lower back (L4) to estimate vertical hip impact acceleration. The acceleration measured in the inertial sensor was resolved into components associated with a global frame with a custom-made MATLAB [4]. We neglected horizontal components of the parameters since it has little effect on risk of bone fracture during a fall [5]. Lastly, tuck and roll performance was qualitatively (by a martial arts expert) and quantitatively (with knee flexion angle, hip rotation angle) examined.

Statistics

For short-term learning test (aim1), time (baseline, post)× group repeated-measures ANOVA was

performed. For bilateral transfer test (aim2), side × group repeated-measures ANCOVA was performed with baseline as covariate. For 1-week retention test (aim3), time (post, retention) × group repeated-measures ANCOVA was performed with baseline as covariate. Also, spearman's correlation analysis between qualitative/quantitative analysis and impact severity parameters was performed (aim4).

RESULTS AND DISCUSSION

Short-term acquisition (aim1)

Both group showed significant reduction of impact severity at post assessment compared to the baseline (*p's*<0.05). Additionally, the training group showed greater reduction than the control group in normalized hip impact force (training: 33%, control: 16% reduction), head acceleration (training: 59% reduction, control: no reduction) and hip impact acceleration (training: 38%, control: 18% reduction) (p's<0.05) (Figure 3).

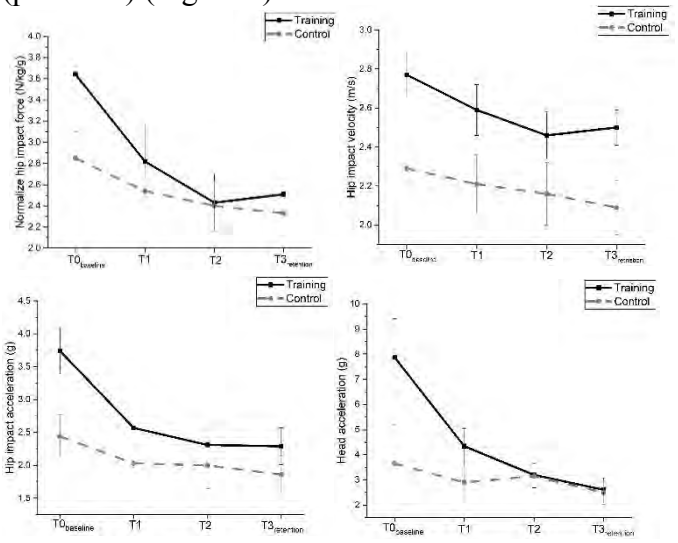

Figure 1: Impact severity measurements as a function of group × time of (a) normalized hip impact force (b) hip impact velocity (c) head acceleration (d) hip impact acceleration

Bilateral transfer (aim2)

There was no significant difference in all impact severity between right-side and left-side falls (*p's*>0.05) suggesting there was bilateral transfer effect.

1-week retention effect (aim3)

There was no significant difference between T2 and $T3_{retention}$ in hip impact velocity (p=0.15), head acceleration (p=0.09) and hip impact acceleration (p=0.33). However, there was significant difference between T2 and $T3_{retention}$ in normalized hip impact force (p=0.02) although hip impact at $T3_{retention}$ was still significantly less than that at $T0_{baseline}$ (p<0.01). Overall, the result suggests that there was partial 1-week retention effect.

Qualitative and quantitative evaluation on tuck and roll strategy (aim4)

Qualitative analysis showed that the training group had most difficulty in learning tucking chin in motion to protect their head when performing tuck and roll strategy. The qualitative analysis showed that the impact severity parameters had moderate to strong correlation with knee flexion angle when performing tuck and roll strategy (ρ=-0.44~-0.75) (Figure 4).

CONCLUSIONS

By comparing results of the training group with those of the active control group, we conclude that the reduction of impact severity measurements in the training group might be due to effectiveness of the tuck and roll strategy. Additionally, the subjects were able to utilize the strategy that was acquired through the right-side falling practice to the left-side falling. The observation regarding transfer effect is important in generalizing the effectiveness of training since a fall can happen in a multitude of ways [2]. Furthermore, the participants partially retained the effectiveness of tuck and roll strategy for 1-week. It is possible that if additional practice sessions ("overlearning") were provided, participants might have exhibited greater retention [6]. However, the current study also observed potential risks of the tuck and roll strategy, such as head impact, when the strategy was not performed properly. Given the promising results of the current study, developing comprehensive training program to teach the safe landing strategy for older adults is important to target fall related injury prevention.

REFERENCES

1. CDC, Ten Leading Causes of Death (chart), 2014
2. Moon et al. *Arch Phy Med Rehabil*., 2016
3. Newell, K.M., *Annu Rev Psychol,* 1991
4. McGinnis et al., *sensors,* 2012
5. Robinovitch et al., *J of Biomech,* 2004
6. McGaugh, J.L, *Science*, 2000

Relationship between Arch Structure, Mobility and Lower Extremity Injury in Runners

[1] Jacqueline Morgan and [2] D.S. Blaise Williams III
[1] Virginia Commonwealth University, Richmond, VA, USA
[2] Nike, INC, Beaverton, OR, USA
email: morganj3@mymail.vcu.edu web: https://khs.vcu.edu/about/vcu-run-lab

INTRODUCTION

Foot structure and mechanics have implications for running-related injuries. High arched (HA) runners experience greater bony and lateral injuries compared to low arched (LA) runners [1]. Potential mechanisms placing passive structures at increased injury risk are the high loading rates associated with HA [2,3] and greater contributions of passive tissues to force attenuation [4] seen in HA runners. Conversely LA runners experience greater soft tissue injuries [1] secondary to greater work requirement distally [5] and smaller leg and joint stiffness measures [3,5].

Limited arch mobility has also been implicated in increased injury risk as rigid arches are similarly linked to high loading rates and increased tibial internal rotation [6]. Conversely, decreased arch stiffness, defined as deformation of the arch relative to a change in load placed upon it, is associated with greater foot pronation and arch drop [7].

While the relationship between injury and foot mechanics is well-studied [1,2,8], no prospective studies have examined the effects of distance training on foot structure and mobility and injury risk in reactional runners.

Therefore, the purpose of this study was to examine the relationship between foot structure, mobility and risk of injury in recreational runners training for a half-marathon.

METHODS

Thirty-nine recreational runners training for a half-marathon [mean age 49.5 (5.1) years, height 1.68 (0.07) m, weight 67.6 (11.2) kg] were recruited from a larger study.

Baseline measures were collected at the start of training (Pre) and training and injury status were recorded daily for 16 weeks until the conclusion of training. Injury incidence was tracked using a daily questionnaire. Participants reported yes or no to their injury status and if they participated in running, cross training, or rest that day. Injury occurrence was defined as time lost to training secondary to reporting yes to injury. Initial injury developed was used for analysis.

Arch height index (AHI) was measured as the height of the dorsum of the foot at 50% total foot length divided by the truncated foot in weight bearing (WB) and non-weight bearing (NWB) [5]. Arch deformity was calculated as the difference AHI in WB and NWB. Arch heights and deformity were categorized into tertiles for high, normal and low arches (HA, NA, LA) as well as high, normal, low mobility (HM, NM, LM). Arch stiffness was calculated as 40% of the participant's body weight divided by the deformity of the arch [8].

Kaplan-Meier analyses were employed to investigate the time-to-event probability of developing an injury during the 16 weeks of training. Right-censoring was used to account for participants who dropped out or did not develop an injury after 16 weeks. Failure curves for all runners, those with HA, NA, LA and those with HM, NM, LM were created. A log rank test was employed for comparison of groups. Finally, a Cox regression analysis was employed to examine the relationship between predictor variables (foot structure, mobility, stiffness) and injury. Analyses was performed using SAS University, SAS Institute Inc, 2015. Significance was set at $\alpha < 0.05$.

RESULTS AND DISCUSSION

Overall, the probability of developing an injury after 16 weeks of training was 44.1%. At 4 and 8 weeks, the probability of developing an injury was 7.83% and 10.6%, respectively. A dramatic increase was seen at 12 weeks with a 30.2% probability. No differences between groups were found for foot

structure (p=0.63) or mobility (p=0.31) (Figures 1 and 2, respectively. The results of the regression model found no significant associations between foot structure, mobility, stiffness and injury risk (p=0.51).

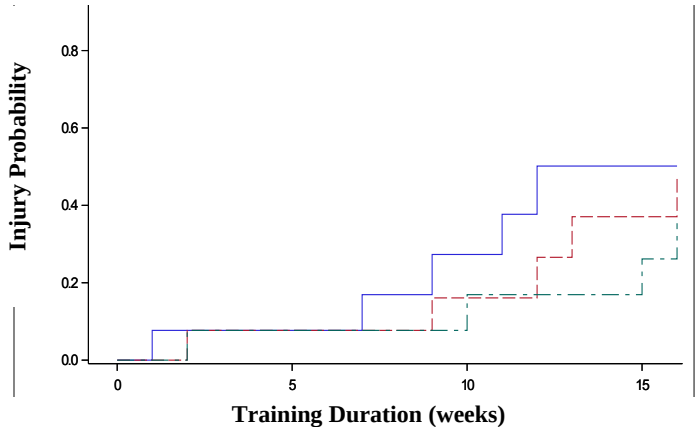

Figure 1: Failure curves for injury probability between those with high (solid blue), normal (dashed red) and low (dotted green) arches

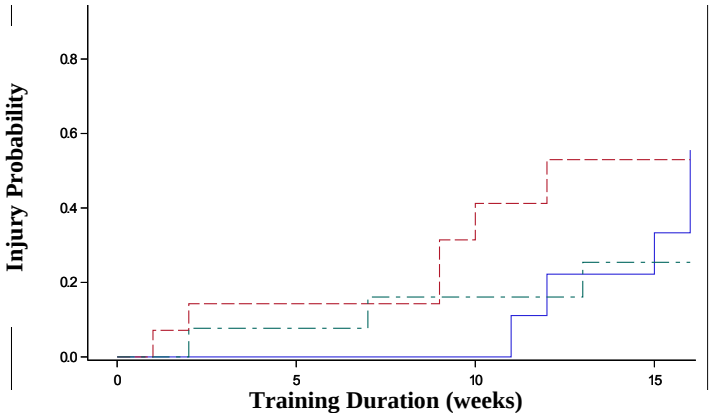

Figure 2: Failure curves for injury probability between those with high (solid blue), normal (dashed red) and low (dotted green) mobility

Overall, the probability of developing an injury during training was only 44% for all runners. The probability of developing an injury early on was relatively minimal, but increased during the second half of the training season. Participants with both high and low arches demonstrated no difference in injury risk compared to those with normal arches. Similar findings were for rigid and flexible arch types. These results are in contrast to previous investigations examining injury and foot type in runners retrospectively [1]. Surprisingly, no variables were found to be predictive of injury.

Previous studies have suggested positive associations between the extremes of arch height, rigid arches and running-related injuries [5,7]. One possible reason for these conflicting results may be a narrow range of arch heights. Previous investigations define HA as AHI>0.356 and LA as AHI<0.275 [5]. Using those requirements eight runners would have qualified as HA and seven as LA, creating very uneven groupings. Therefore, evenly numbered tertiles were created.

CONCLUSIONS

Thirty-nine recreational runners training for a half-marathon were recruited from a larger study. Diverging from previous studies analyses, extremes of foot type did not have an influence on injury risk suggesting additional factors may be important in injury risk in individuals with small differences in arch structure. Additionally, 16 weeks may not be long enough to see the influence of extreme arch types on overuse injury development. Future studies examining the effects of training programs on foot structure and its relationship to injury risk would benefit from recruiting a greater range of foot types and investigating runners over multiple training seasons. Additionally, examining changes to other variables shown to be associated with extreme arch types (leg and joint stiffness) during training may help to clarify the importance of foot structure to training and injury prevention.

REFERENCES

1. Williams III, DS., et al. *Clinical Biomechanics*, 16(4):341-347, 2001.
2. Butler, RJ., et al. *American Journal of Sports Medicine*, 18(6):511-517, 2003.
3. Williams, DS., et al. *Gait & Posture,* 19(3):263-269, 2004.
4. Powell, DW., et al. *Medicine & Science in Sports & Exercise,* 49(8):1662-1667, 2017.
5. Powell, DW., et al. *Human Movement Science,* 34:147-156, 2014.
6. Williams, DS., et al. *Journal of Athletic Training*, 49(3):290-296, 2014.
7. Song, J., et al. *Gait & Posture,* 60:175-180, 2018
8. Zifchock, RA., et al. *Foot and Ankle Int.*, 27(5):367-372, 2006

DISCREPANCIES IN KINEMATICS AND DYNAMICS OF MILD AND SEVERE SLIPPING

[1] Mohammad Moein Nazifi, [2] Kurt Beschorner, PhD, and [1] Pilwon Hur, PhD

[1]Department of Mechanical Engineering, Texas A&M University, College Station, TX, USA
[2]Department of Bioengineering, University of Pittsburgh, PA, USA
email: {moeinnazifi,pilwonhur}@tamu.edu, beschorn@pitt.edu, web: http://hurgroup.net

INTRODUCTION

Slips, trips, and falls were identified as the second leading cause of fatal occupational injuries during 2014-2015 [1]. These injuries cost over $180 billion damage each year, nationally [2]. Hence, studying slips and falls is necessary to avoid this damage. Additionally, studies have shown that slips can be classified into "mild" and "severe", where severe slips are more dangerous and more prone to result in a fall [1]. Consequently, methods that can help diagnose severe slippers are highly valuable.

Several studies have tried to use kinematic, dynamic, and neuromuscular variables to classify mild and severe slippers [3]. These methods targeted both gait and slipping behaviors of individuals to identify persons with high risk of fall. However, to the best of our knowledge no studies have tried to study the center of mass (COM) height, sagittal angular momentum (*H*, a representation of rotation of a body, equal to body's angular velocity multiplied to its inertia), and single/double support phase's length in different severity groups. These measures have been proven to be of crucial importance in gait control and may be critical in slip severity as well [4, 5].

The objective of this study is to compare COM's height, sagittal angular momentum, and single/double support (SS/DS) phase length between mild and severe slippers, during walking and slipping, to identify differences. We hypothesize that mild and severe slippers would differ in these measures, indicating their different gait and slip control.

METHODS

Eleven male and nine female healthy adults, free of gait disorders, participated in this IRB approved study by signing a written consent. Subjects first performed several walking trials in a long pathway at their convenient speed. After several walking trials, the pathway was contaminated to collect slip data. Subjects donned reflective markers (Vicon 612, Oxford, UK; collecting at 120Hz), PVC-soled shoes, and a harness throughout the experiment.

Markers' data was low-pass filtered at 10Hz, with a zero-lag second order Butterworth filter. Using markers data, subjects were classified to mild and severe slippers. A slip was considered severe if the Peak Heel Speed (PHS) exceeded 1.44 m/s [1]. COM and H were calculated using segmental analysis method, using markers and anthropometric data [4]. *H* was calculated as sum of the creoss product of the distance from COM to each limb's relative velocity (to COM) and mass. Also, heel strike and toe-off moments were identified and used to calculate the SS/DS lengths. These analyses were done for a full gait cycle before the slip initiation (i.e. heel strike on the slippery surface), and 30% of each individuals' gait cycle time length while slipping. The gait cycle was normalized to 100 points (percent) for everyone to facilitate the inter-subject comparisons. COM was normalized to subjects' height and reported as a percent of their height. *H* was reported as a dimensionless value, normalized to each individual's mass, height, and gait speed [5].

An independent *t*-test (SPSS, IBM, Chicago, IL) was performed on COM, *H* and support to check if the discrepancies between different severities are significant at level of 0.05.

RESULTS AND DISCUSSION

For COM height, there was no significant differences between mild and severe slippers preceding heel contact on the contaminant. However, severities differed post-slipping, starting during 24%-30% of the gait into slipping (Fig. 1a). Also, severe slippers had a significant larger post-slip angular momentum (Fig. 1b), from 3%-27%. There were also two gait discrepancies found in *H* presented in Fig. 1b. Lastly, mild slippers showed a

longer single support phase after slip initiation (Fig. 1c, SS2).

The results suggest a strong association between COM height post-slip and slip severity (Fig. 1a, *p*-value<0.05). Subjects who could maintain their COM experienced less severe slips. Previous research also claimed a significant height drop can be used to identify "falls" in presence of harness.

Sagittal angular momentum found to be different in two small windows (-93%~-81%) and (-26%~-23%) within the gait (pre-slip) (Fig. 1b, *p*-value=0.05), and a large window during slipping (3%~27%) (Fig. 1b, *p*-value<0.001). The values calculated for *H* stayed consistent with previous studies [5]. The post-slip difference, can clearly be due to rapid lower extremity movement in severe slippers. The excessive *H* seems to be eventually restrained around 27% post-slipping, which coincides with rapid counter-balance hand movements in subjects [6] to lower the excessive angular momentum. The pre-slip differences however, require further investigations in future studies.

Lastly, severe slippers exhibited a significant shorter single support post-slipping (Fig. 1c, *p*-value<0.001). This can be interpreted as an enforced "toe-touch" response [6] from the unperturbed limb as a measure to increase base of support to provide more stability throughout slipping, where mild slippers did not require such a support to maintain their balance.

CONCLUSIONS

This study examined COM height, sagittal angular momentum, and single/double support phase length in mild and severe slippers and found several significant differences. Mild slippers could maintain their COM higher and regulate their *H* compared to severe slippers. These differences may help understand the underlying causes of severe slipping to prevent them and eventually, prevent falls, and also be useful in designing preventive devices to warn severe slippers before fall incidents. Future work will investigate if these observed associations are causal for severe slipping or not.

ACKNOWLEDGEMENT

We appreciate Dr. Rakie Cham providing the data (collected under NIOSH R01 OH007592) for this analysis.

REFERENCES

1. Nazifi et al. *Front Human Neuroscience,* **Vol 11,** No 536, 2017b.
2. Beschorner et al. *Gait &* Posture, **Vol 48**, 256-60, 2016.
3. Cham et al. *J. of Biomechanics*, **Vol 34**, 1439-45, 2001.
4. Yang et al. *J. of Biomechanics*, **Vol 47**, 3807-12, 2014.
5. Herr et al. *J. of Experimental biology*, **Vol 211**, 467-81, 2008.
6. Marigold et al. *J. of neurophysiology*, **Vol 89**, No 4, 2003.

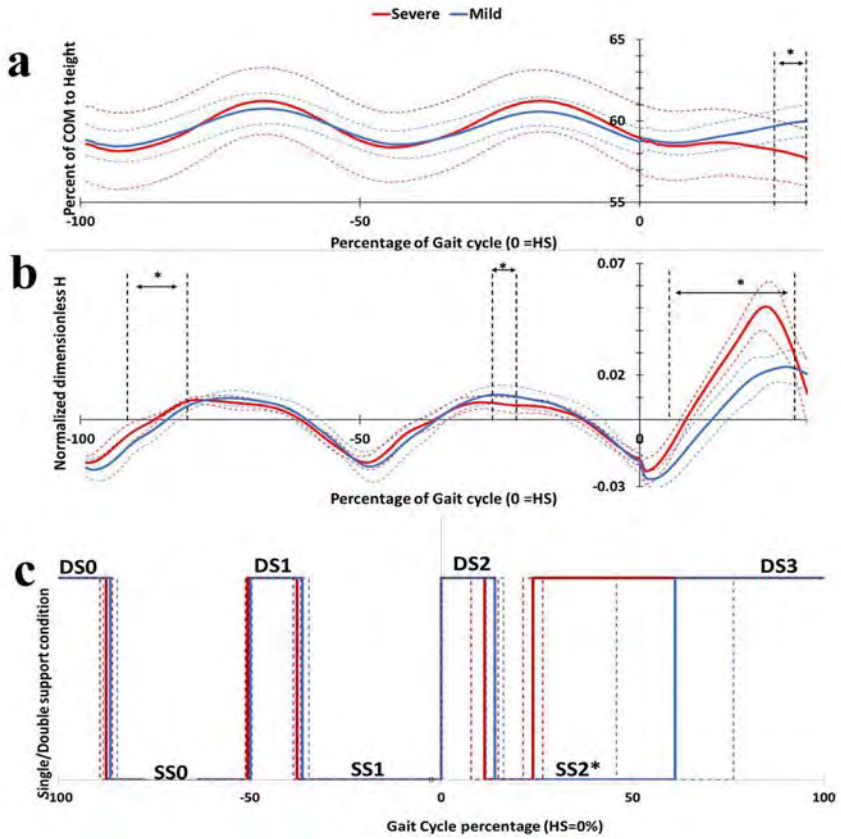

Figure 1: The COM height (a), sagittal *H* (b), and SS/DS (c) in mild and severe slippers. Asterisks show significant differences and dashed lines present SD.

The Influence of Spinal Cord Injury on Long-term Gait Variability

[1] Alireza Noamani, [2] Jean-François Lemay, [2,3] David Houston, [2,3] Janelle Unger, [2] Gunnar Schock, [2,3] Kristin Musselman, and [1] Hossein Rouhani
University of Alberta, Edmonton, AB, Canada
[2] Toronto Rehabilitation Institute-University Health Network, Toronto, ON, Canada
[3]Faculty of Medicine, University of Toronto, ON, Canada
email: hrouhani@ualberta.ca

INTRODUCTION

Fractal property of gait parameters characterized using detrended fluctuation analysis (DFA) has been investigated in the past. Previous studies have reported fractal dynamics and long-range correlation of the gait cycle time for healthy young adults [1]. The fractal-like property of gait parameters is of interest from a neurophysiological control perspective since it indicates long-term dynamics the locomotor system [2]. Gait stability is often affected following spinal cord injury (SCI) and can lead to an increased risk of falling. Despite impaired gait stability, clinical evaluation of gait parameters for individuals with SCI in long-term walking trials is yet to be studied. This study aimed to compare gait parameters in terms of mean, variability, and fractal property between individuals with SCI and able-bodied (AB) individuals during long-term (six minutes) over-ground walking using wearable sensors.

METHODS

Sixteen ambulatory individuals with chronic (at least one year post-injury) SCI, with ASIA Impairment Scale D (4 females and 12 males, age: 59.9±20.5 years, range 20 to 87 years) and seven AB individuals (4 females and 3 males, age: 35.0±21.8 years, range 24 to 84 years) participated in this study. All participants provided written informed consent prior to participating in the experiment. Research Ethics Board approval was received from the local ethics committee.

Participants were asked to walk at self-selected pace for six minutes in a hospital hallway. AB individuals performed only one trial and participants with SCI performed the experiment twice, spaced two weeks apart. Five inertial measurement units (IMUs) (Gait Up, Lausanne, Switzerland) were placed on the feet, shanks, and sacrum of each participant. Each IMU recorded three-dimensional (3D) acceleration and angular velocity of each body segment at the sampling rate of 256 Hz. The timing of heel strike, foot-flat, and toe-off were detected from the angular velocity signals based on the methods introduced by previous studies [3]. The instantaneous 3D trajectory of the feet during walking trials was determined via customized software according to the algorithm introduced by Mariani et al. [4]. Gait parameters (Table 1) were calculated based on the obtained foot trajectories for each participant.

The mean, variability, and fractal dynamics of the gait parameters were calculated for each participant and were compared between the AB and SCI groups. The variability of the gait parameters was represented by the coefficient of variation (CV), which is defined as the standard deviation normalized by the mean. The fractal dynamics can be quantitatively investigated using DFA such as a long-range correlation of gait variable [5]. The scaling exponent (α) resulting from DFA has been widely used to investigate the persistence of time-series [6]. A scaling exponent of $\alpha=0$ indicates uncorrelated data, $0.5<\alpha<1$ indicates a long-range persistent correlation, and $\alpha<0.5$ indicates anti-persistent correlation [5], [6].

The Kolmogorov-Smirnov test and Levene's test rejected the null hypothesis that the data for each gait parameter comes from a normal distribution with equal variances. Hence, we conducted a Wilcoxon rank-sum test on the mean, CV, and scaling exponent of the gait parameters to investigate any significant differences between AB and SCI participants. For all statistical analyses, the significance level was set at 0.05.

RESULTS AND DISCUSSION

Table 1 shows the mean, CV, and scaling exponent of the gait parameters presented as percentiles [25%, 50%, 75%] for the AB and SCI groups. Statistical analysis revealed no significant differences between AB and SCI groups for the mean values of the gait parameters. Significantly larger CV were observed for step height (p=0), stride length (p=0.01), and stride speed (p=0.007) of AB participants. Moreover, the scaling exponents of gait cycle time (p=0.006) and cadence (p=0.025) were significantly larger for the individuals with SCI compared to AB participants.

Previous studies revealed the fractal property of gait parameters and compared the scaling exponent of an AB young population to that of older adults, individuals with Huntington's disease [1], and people with Parkinson's disease. Our preliminary results indicate that although no significant difference was observed for the mean value, the fractal property of the gait parameter may distinguish the gait stability of SCI individuals from the AB population. However, more investigation is required to determine whether the fractal property of gait parameters is associated with clinical outcomes in the SCI population, such as the occurrence of falls.

REFERENCES

1. J. M. Hausdorff, S. L. Mitchell, R. Firtion, C. K. Peng, M. E. Cudkowicz, J. Y. Wei, and a L. Goldberger, "Altered fractal dynamics of gait: reduced stride-interval correlations with aging and Huntington's disease.," *J. Appl. Physiol.*, **82**(1), pp. 262–269, 1997.
2. J. M. Hausdorff, P. L. Purdon, C. K. Peng, Z. Ladin, J. Y. Wei, and A. L. Goldberger, "Fractal dynamics of human gait: stability of long-range correlations in stride interval fluctuations.," *J. Appl. Physiol.*, **80**(5), pp. 1448–1457, 1996.
3. A. Salarian, H. Russmann, F. J. G. Vingerhoets, C. Dehollain, Y. Blanc, P. R. Burkhard, and K. Aminian, "Gait assessment in Parkinson's disease: Toward an ambulatory system for long-term monitoring," *IEEE Trans. Biomed. Eng.*, **51**(8), pp. 1434–1443, 2004.
4. B. Mariani, C. Hoskovec, S. Rochat, C. Bula, J. Penders, and K. Aminian, "3D gait assessment in young and elderly subjects using foot-worn inertial sensors," *J. Biomech.*, **43**(15), pp. 2999–3006, 2010.
5. J. S. Choi, D. W. Kang, J. W. Seo, and G. R. Tack, "Fractal fluctuations in spatiotemporal variables when walking on a self-paced treadmill," *J. Biomech.*, **65**, pp. 154–160, 2017.
6. J. B. Dingwell and J. P. Cusumano, "Re-interpreting detrended fluctuation analyses of stride-to-stride variability in human walking," *Gait Posture*, **32**(3), pp. 348–353, 2010.

Table 1: The mean, CV, and scaling exponent of gait parameters were calculated for each participant. The results are presented as [25%, 50%, 75%] percentiles among all participants for each group (AB and SCI). **Bold** values and shaded cells indicate a significant difference between AB and SCI groups with p-value < 0.05.

Parameters	Mean		CV%		Scaling Exponent (α)	
	AB	SCI	AB	SCI	AB	SCI
Gait Cycle Time (s)	[1, 1.1, 1.1]	[1, 1.1, 1.2]	[5.8, 6.6, 15.6]	[4, 5.51, 7.54]	**[0.44, 0.52, 0.6]**	**[0.61, 0.7, 0.8]**
Stance Phase (%)	[55.4, 56.4, 59.2]	[57.5, 59.3, 61.1]	[3.7, 4.2, 4.4]	[2.87, 3.5, 4.97]	[0.51, 0.54, 0.67]	[0.53, 0.58, 0.62]
Double Support(%)	[10.7, 12.9, 18.6]	[14.9, 18.5, 22.2]	[31.9, 35.9, 40.2]	[23.19, 33.34, 45.26]	[0.45, 0.49, 0.63]	[0.51, 0.55, 0.6]
Swing Phase (%)	[40.8, 43.6, 44.6]	[38.9, 40.7, 42.5]	[4.7, 5.2, 6.4]	[4.3, 4.97, 7.16]	[0.51, 0.54, 0.67]	[0.53, 0.58, 0.62]
Cadence (step/min)	[112.8, 115.4, 119.5]	[104.8, 114.4, 120.4]	[4.4, 5.3, 6]	[4.28, 5.21, 7.59]	**[0.51, 0.6, 0.68]**	**[0.63, 0.76, 0.84]**
Step Height (m)	[0.1, 0.1, 0.3]	[0.1, 0.1, 0.2]	**[23.4, 32.9, 54]**	**[6.01, 9.89, 12.24]**	[0.53, 0.64, 1.19]	[0.52, 0.56, 0.62]
Stride Length (m)	[1, 1.1, 1.3]	[1.1, 1.2, 1.4]	**[15.1, 25.4, 32.2]**	**[11.4, 12.73, 15.11]**	[0.51, 0.66, 1.06]	[0.54, 0.61, 0.75]
Stride Speed (m/s)	[1, 1.1, 1.3]	[1, 1.2, 1.3]	**[16.8, 26.3, 33.1]**	**[13.12, 13.73, 15.86]**	[0.55, 0.64, 1.06]	[0.59, 0.66, 0.78]

EXAMINING THE EFFECTS OF LEG STIFFNESS ON VERTICAL GROUND REACTION FORCES USING A DUAL SPRING LOADED INVERTED PENDULUM MODEL

Kevin O'Brien & James Schmiedeler
University of Notre Dame, Notre Dame, IN, USA
corresponding email:kobrie23@nd.edu

INTRODUCTION

How humans select their method of locomotion is a long-standing topic of study, with researchers early on recognizing that minimizing energy expenditure was particularly relevant [2]. A number of models have been developed as a method of exploring this observation, often emphasizing how energy is exchanged between potential and kinetic energy. Cavagna et al. [3] proposed that walking could be modeled as an inverted pendulum, where a stiff leg supporting a mass exchanges potential and kinetic energy to move forward. Similarly, Blickhan proposed a spring-mass model for running, where elastic energy is exchanged with both potential and kinetic energy [4]. Geyer et al. [1] developed the dual spring-loaded inverted pendulum (dual-SLIP) model, combining the attributes of the two simpler models (Figure 1). With the added complexity of a second leg, this model can account for both single-leg and dual-leg stance in the gait cycle.

A defining characteristic of vertical ground reaction forces (GRFs) in human walking is an M-shaped curve (as seen in Figure 2a), where the force peaks after stance leg touchdown, dips in midstance, and peaks again as the stance leg propels the body forward. Figure 2 also demonstrates how the vertical GRF can vary significantly for (b) healthy individuals walking at reduced speeds or for (c) individuals following incomplete spinal cord injury (iSCI). This force trajectory can be replicated using the dual-SLIP model. By varying the system energy, leg stiffness, and angle of leg impact, this research seeks to investigate how the observed GRF behavior may be the result of altered gait characteristics or the effective stiffness of the joints.

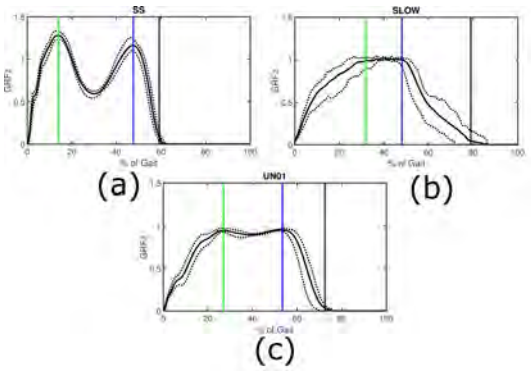

FIGURE 2. Vertical GRF (normalized) for (a) healthy subject walking at self-selected speed (1.42 ± 0.03 m/s), (b) healthy subject walking at slow speed (0.13 ± 0.01 m/s), and (c) individual with iSCI walking at self-selected speed (0.77 ± 0.03 m/s).

METHODS

To investigate how the vertical GRF may vary for a dual-SLIP model, the leg stiffness (k), leg angle at impact (α_0), and average horizontal velocity ($\bar{\dot{x}}$) of the model were varied to find viable gaits. The mass ($m = 80kg$), gravitational constant ($g = 9.81\frac{m}{sec^2}$), and free leg length ($l_0 = 1m$) were kept constant across all generated gaits. To ensure gait feasibility, the following constraints were enforced.

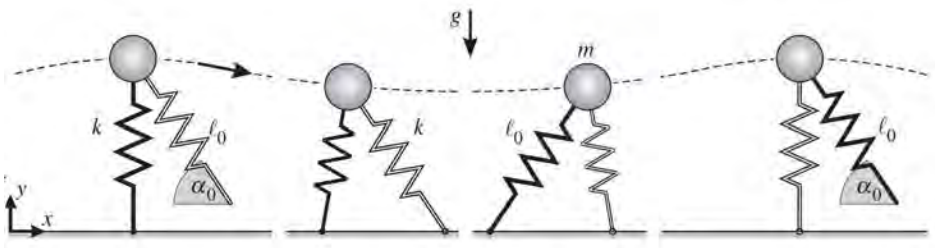

FIGURE 1. Dual spring-loaded inverted pendulum (dual-SLIP) model from [1]. 4 parameters (m, l_0, g, and k) can be varied at different speeds to generate gaits.

$$
\begin{aligned}
y_f &= y_0, \\
\dot{y}_f &= \dot{y}_0, \\
x_f &= x_c + l_0 \cos(\alpha_0), \\
\dot{x}_f &= \dot{x}_0,
\end{aligned}
$$

where x and y are the coordinates of the center of mass, 0 subscripts indicate initial positions, f subscripts indicate final positions, and c subscripts indicate positions at leg contact (second image of Figure 1).

Based on results presented in [1], the stiffness of the model was tested at fifteen values in the range $5,000 - 50,000 \frac{N}{m}$, the impact angle at ten values spanning $50° - 80°$, and the model speed at ten values between 0.6 and $1.6 \frac{m}{sec}$.

Finally, the vertical GRF of every feasible gait was evaluated. The GRFs were normalized to the bodyweight ($m * g = 784.8N$) for comparison with the observations from Figure 2. The difference between the peak and central valley of the vertical GRF curve (Δ vertical GRF) for each gait was then calculated.

RESULTS AND DISCUSSION

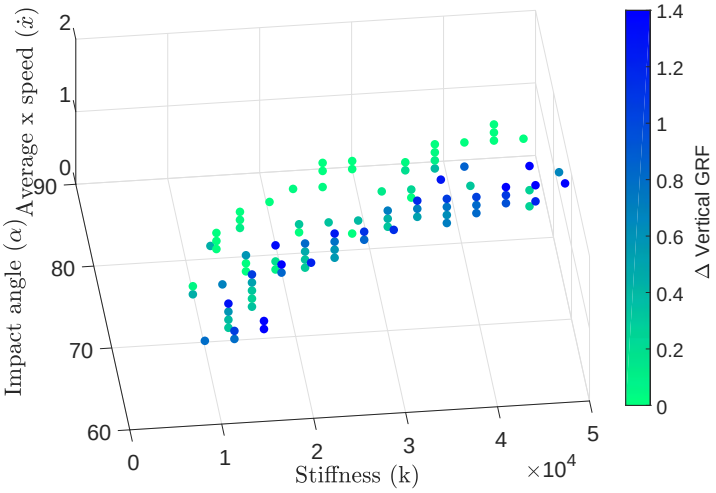

FIGURE 3. Viable dual SLIP gaits at given stiffnesses, impact angles, and speeds to demonstrate how GRF peaks vary across gaits.

Figure 3 presents the feasible gaits generated across the three varied parameters. These results demonstrate that for a given speed, as leg stiffness increases, the leg impact angle must also increase. These results match the results presented in [1]. Additionally, for a given stiffness, decreasing the impact angle increases the difference between the peaks and valleys of the vertical GRF. Moreover, for a given impact angle, decreasing the stiffness increases the difference between the peaks and valleys of the vertical GRF. These two trends are further emphasized in Fig. 4, where the gaits with the largest difference between the peak vGRF value and the vGRF value at the valley in vertical GRF and the smallest difference between the peak vGRF value and the vGRF value at the valley in veritcal GRF are presented. The gait with the median change in vertical GRF is also presented in Fig. 4, which more closely resembles the vertical GRF of the healthy individual walking at a self-selected pace.

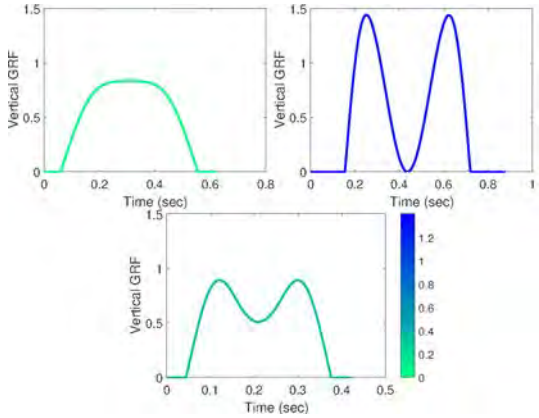

FIGURE 4. Three examples of Vertical GRF (Stiffness, Speed, Angle). Top Left: Smallest Δ Vertical GRF (11,429 N/m; 1.38 m/s; 70°); Top Right: Largest Δ Vertical GRF (17,857 N/m; 1.38 m/s; 67°); Bottom: Median Δ Vertical GRF (37,143 N/m; 1.04 m/s; 80°)

CONCLUSION

The dual SLIP model provides a simplified method for determining how leg stiffness, impact angles and walking speed can affect observed vertical GRFs. The presented results suggest that the GRF characteristics observed in Figure 2 may be the effect of more than just decreased speed. A smaller step size would lead to a greater impact angle, while increased muscle co-contraction would increase leg stiffness. For a given speed, increasing the impact angle and decreasing the stiffness leads to flatter vGRF curves. The model presented here is entirely passive, so the total model energy is constant through the entire gait. Nonetheless, comparing how different gaits convert energy from one form to another within the system may provide insight into the relative efficiencies of different gaits.

REFERENCES

[1] H Geyer et al. *Proc R Soc Lond B Biol Sci*, 273(1603):2861–2867, 2006.

[2] HJ Ralston. *Eur J Appl Physiol Occup Physiol*, 17(4):277–283, 1958.

[3] GA Cavagna et al. *J Physiol*, 262(3):639–657, 1976.

[4] R Blickhan. *J Biomech*, 22(11-12):1217–1227, 1989.

Pre-Operative Hamstring Length and Velocity Do Not Explain The Reduced Effectiveness Of Repeat Hamstring Lengthening To Correct Crouch Gait In Children With Cerebral Palsy

[1] Melisa Osborne, [2] Nicole Mueske, [2] Susan Rethlefsen, [1,2] Robert Kay, and [1,2] Tishya Wren

[1] University of Southern California, Los Angeles, CA, USA; [2] Children's Hospital Los Angeles, CA, USA
email: twren@chla.usc.edu

INTRODUCTION

Crouch (flexed knee) gait is a movement disorder frequently seen in children with cerebral palsy (CP) that progresses in severity with age and growth. To correct crouch gait, patients may undergo hamstring lengthening surgery (HSL). Despite the overall effectiveness of HSL, hamstring contractures and crouch gait can recur over time. Although repeat HSL is often performed, a recent study showed gait routinely improved after primary, but not repeated, HSL [2]. The causes of recurrent crouch gait and the lower effectiveness of repeat HSL are unclear. This study aimed to use musculoskeletal modeling to determine if outcome differences could be due to pre-operative dynamic muscle-tendon length and/or lengthening velocity. We hypothesized that patients who underwent primary HSL had short and/or slow hamstrings that would benefit from lengthening, while patients who underwent repeat HSL did not, thereby explaining differences in surgical outcomes.

METHODS

A retrospective chart review was conducted to identify children with CP under 15 years of age who had primary or repeat HSL with pre- and postoperative gait analyses at our institution between November 2005 and March 2016. A control group of typically developing children with no history of lower extremity pathology was also included. Gait analysis data were collected from a 3-D motion capture system using a modified conventional gait model. Marker position data were collected during barefoot walking at a self-selected speed and analyzed in OpenSim [3], a musculoskeletal modeling system, to calculate joint angles and muscle-tendon lengths. Joint angles during a single representative trial of walking were calculated using inverse kinematics in reference to a generic model [4] scaled to each participant. Muscle-tendon length of the semimembranosus (SM), chosen because it is one of the most frequently lengthened hamstring muscles in CP and has a length highly correlated with length of other hamstring muscles, was determined across the gait cycle for each surgical and control limb. SM length was smoothed with a 4th order Butterworth filter and normalized by SM length with the scaled model positioned in the anatomic position. SM lengthening velocity was calculated by numerically differentiating SM length with respect to time. Participant characteristics were compared among the control, primary HSL, and repeat HSL groups using ANOVA with Bonferroni adjusted post-hoc t-tests and Fisher's exact tests. ANOVA with Bonferroni adjusted post-hoc t-tests was also used to compare groups pre- and postoperatively. Pre- to postoperative change was evaluated within each HSL group using one-sample t-tests and between groups using two-sample t-tests.

RESULTS AND DISCUSSION

26 patients and 10 controls were included in this study. 15 patients had undergone primary HSL (13 bilateral), and 11 had repeat HSL (8 bilateral). Groups did not differ in terms of sex or Gross Motor Function Classification System (GMFCS) level (3 GMFCS I, 13 II, 10 III). Compared to controls, the primary and repeat HSL groups had higher preoperative initial contact knee flexion and minimum stance phase knee flexion, with lower peak hamstring length and hamstring lengthening velocity ($p<0.001$, Figure 1, Table 1). In both surgical groups, all limbs had hamstrings that were dynamically shorter and/or slower than controls by at least 1 standard deviation (SD). In pre- to postoperative analysis, the primary HSL group showed improvement in popliteal angle, initial contact knee flexion, minimum stance knee flexion, and hamstring length while the repeat HSL group only showed improvement in hamstring length. Postoperatively, both groups still had greater knee

flexion at initial contact and in the stance phase of gait compared to controls, as well as lower peak hamstring length and lengthening velocity ($p<0.001$). The repeat HSL group showed higher postoperative knee flexion at initial contact and less knee extension in stance than the primary group ($p\leq0.003$).

CONCLUSIONS

The results of this study suggest the lower effectiveness of repeat HSL is not related to pre-operative hamstring length and velocity. Almost all patients in both the primary and repeat HSL groups had shorter and slower than normal hamstrings, and both groups remained significantly shorter and slower than controls postoperatively. Therefore, the poor outcomes after repeat HSL are likely due to other factors. Potential causes include lever arm dysfunction due to femur and/or tibia rotational malalignment, fixed knee flexion contracture, quadriceps weakness due to patella alta, weak calf muscles, or the natural history of CP. Consequently, interventions other than repeat HSL may be preferable for treating recurrent crouch after primary HSL.

REFERENCES

1) Rethlefsen et al. J Pediatr Orthop 33:510-504, 2013. 2)Delp et al. IEEE Trans Biomed Eng 54:1940-1950, 2007. 3)Arnold et al. Ann Biomed Eng 38:269-279, 2010. 4) Arnold et al. J Biomech 39:1498-1506, 2006.

Table 1. Comparison of outcome measures within and between groups

	Control (N=20 sides)	Primary HSL (N=28 sides)				Repeat HSL (N=19 sides)				
		Pre	Post	Change	*P* Change	Pre	Post	Change	*P* Change	*P* Change Between Groups
Knee Flexion at Initial Contact (°)	11.4 (6.2)	40.6 (12.0)*	26.3 (10.4)*	-14.3 (12.6)	<0.0001	41.2 (10.8)*	38.1 (15.4)*†	-3.1 (12.7)	0.30	0.005
Min Knee Flexion Stance (°)	-0.1 (10.0)	27.0 (13.1)*	15.4 (9.7)*	-11.6 (12.8)	0.0001	30.3 (12.0)*	28.6 (15.8)*†	-1.8 (10.4)	0.47	0.008
Max Hamstring Length (normalized)	1.08 (0.03)	1.02 (0.03)*	1.05 (0.02)*	0.03 (0.03)	<0.0001	1.02 (0.04)*	1.03 (0.04)*	0.02 (0.03)	0.02	0.06
Max Hamstring Velocity (normalized length/sec)	0.87 (0.13)	0.40 (0.16)*	0.45 (0.17)*	0.05 (0.13)	0.06	0.39 (0.15)*	0.41 (0.14)*	0.02 (0.15)	0.56	0.52

Results are presented as mean (SD); * indicates $p<0.05$ vs. Control; † indicates $p<0.05$ vs. Primary

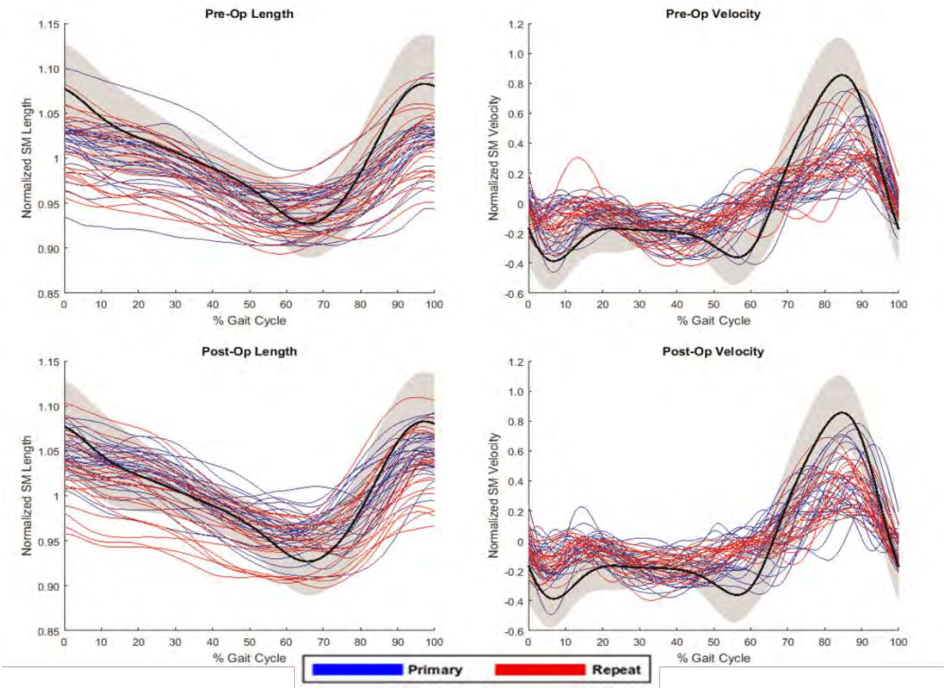

Figure 1. Normalized hamstring length and velocity for primary and repeat HSL.

KNEE ADDUCTION AND FEMORAL CARTILAGE CHARACTERISTICS IN OBESE AND NORMAL WEIGHT ADULTS

[1] Derek N. Pamukoff, [2]Michael N. Vakula, [1] Eric Shumski, [1]Steven A. Garcia, [1]Skylar C. Holmes, [1]Brett K. Post
[1] California State University, Fullerton, Fullerton, CA, USA; [2] Utah State University, Logan, Utah, USA
email: dpamukoff@fullerton.edu

INTRODUCTION

Obesity is a risk factor for knee osteoarthritis (OA), partially due to alterations in walking biomechanics [1]. Knee OA is characterized by a decline in articular cartilage health. Among those with knee OA, the external knee adduction moment (KAM) prospectively predicts medial compartment cartilage loss and OA progression [2]. Early cartilage changes involve compositional alterations with minimal change in structure (i.e. thickness) [3]. However, cartilage composition is assessed using magnetic resonance imaging (MRI) [4], which is cost-prohibitive. Ultrasound (US) imaging is an economical and portable method that may provide an indication of cartilage composition [5]. Analysis of cartilage cross-sectional area (CSA) also measures echo-intensity (EI), which is commonly used to measure composition and water content in skeletal muscle [6]. Comparatively, the relative water content within articular cartilage influences its ability to attenuate shock and respond to acute joint loading [5]. As such, cartilage EI may provide a novel method to assess early cartilage adaptations in obese individuals that are at high risk for knee OA. Therefore, the purpose of this study was to (1) compare femoral cartilage characteristics between obese and normal weight adults using US imaging and (2) evaluate the influence of deleterious gait biomechanics on femoral cartilage characteristics. We hypothesized that obese adults would have smaller cartilage, and higher EI (i.e. lower relative water content) compared to normal weight adults. We further hypothesized that a larger KAM and knee adduction angle (KAA) would be associated with smaller cartilage and higher EI.

METHODS

Thirty-eight normal weight and thirty-nine obese individuals participated in this study (Table 1), and were grouped based on body mass index (BMI).

Table 1. Subject Demographics (mean ± SD)

Group	Normal	Obese
Age (years)	21.9 ± 2.8	22.8 ± 3.6
BMI (kg/m^2)	21.5 ± 1.7	32.9 ± 4.2
Female (n)	23	23
Body Fat (%)	19.9 ± 6.9	38.1 ± 7.4

US imaging was conducted following a 30-minute resting period in a supine position to unload the articular cartilage. Femoral cartilage of the dominant limb was assessed in 140° of knee flexion [7]. The US probe was placed transversely in line with the medial and lateral femoral condyles above the superior border of the patella. Three images were obtained for each participant and analyzed using ImageJ software. The investigator analyzing all US images was blinded to BMI group. Cartilage thickness (mm) was assessed at the midpoint of the upslope of the medial femoral condyle as the straight-line distance between the cartilage bone and synovial space cartilage interfaces (Fig. 1) [5]. CSA (mm^2) and EI were extracted by tracing the femoral cartilage of the medial femoral condyle starting from the intercondylar notch (Fig. 1) [5]. EI refers to the average gray scale value of each segmented pixel on a scale of 0 (black) to 255 (white) [6].

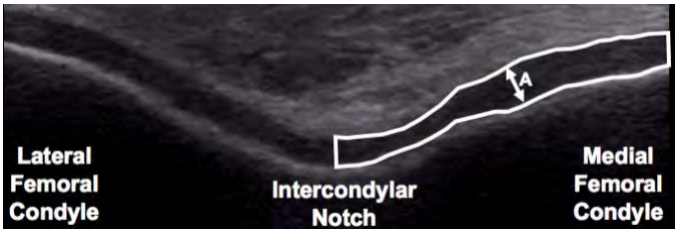

Fig. 1: Sample US image assessment and outcome variables. (A) represents cartilage thickness, and the traced region of interest provides the CSA and EI.

Bilateral static markers were placed on the greater trochanter, iliac crest, anterior superior iliac spine, medial and lateral femoral epicondyles, medial and lateral malleoli, 1st and 5th metatarsals, and calcanei, and were removed after calibration. Rigid clusters

of 4 markers were placed on the sacrum, and bilaterally on the thighs, shanks, and feet. Three-dimensional walking biomechanics were assessed as participants walked across a 10m runway at a self-selected speed wearing laboratory standard neutral cushion footwear. Participants' completed 5 trials, and trials were accepted if they were within ±5% of their self-selected speed and participants' feet made full contact with consecutive force plates located at the center of the runway. Marker position and force plate data were sampled at 240Hz and 2400Hz, respectively. All data were exported to Visual 3D for model construction, and further analyzed using a custom LabVIEW program. KAM was normalized to a product of body weight and height, and was quantified using the first (KAM_1) and second (KAM_2) peaks, and angular impulse (KAM_i). Cartilage outcomes (thickness, CSA, and EI) were compared between groups using one-way MANOVA. Partial correlation was used to assess the relationship between gait and cartilage outcomes after controlling for self-selected gait speed.

RESULTS AND DISCUSSION

There was no difference in cartilage outcomes between groups ($F_{3,65}$=0.65; Pillai's Trace=0.03; p=0.58). As no group differences were found, groups were collapsed for correlational analyses. Larger KAA (r=0.33, p<0.01), KAM_1 (r=0.40, p<0.01), and KAM_2 (r=0.34, p<0.01) were associated with higher EI. No associations were found between gait outcomes and thickness or CSA.

These findings suggest that larger KAA and KAM characteristics are associated with higher EI in normal weight and obese young adults. Echo intensity is used to measure tissue composition and relative water content in skeletal muscle [6], and has been used to assess femoral cartilage function in normal weight individuals [5]. Early stages of cartilage breakdown are characterized by altered composition and water content, which are typically assessed using advanced MRI techniques such as T2 relaxation time [8]. Moreover, KAM_1 and KAM_i are associated with medial compartment T2 relaxation time in other populations at risk for knee OA [8]. Future studies are needed to validate the use of US EI to other assessment methods.

Contrary to our hypotheses, we observed no relationship between gait outcomes and femoral cartilage thickness or CSA. Previous research suggests that greater KAM predicts cartilage loss and disease progression in obese individuals with knee OA [2]. The KAM is a surrogate for medial compartment knee joint loading, and likely contributes to the discrepancy in medial compared to lateral compartment knee OA incidence. The discrepancy in our findings compared to others [2] may be due to the population. Our sample of normal weight and obese participants did not have a diagnosis of knee OA, and thus may not have overt reductions in cartilage size. Collectively, our findings suggest that US EI may be a more sensitive measurement to detect early cartilage breakdown.

CONCLUSIONS

Findings indicate that a larger KAA and KAM are associated with higher US EI. A higher US EI may be indicative of altered tissue composition and water content, and could be used as a cost-effective and portable alternative method to MRI to assess early cartilage changes in high-risk groups.

REFERENCES

1. Silverwood, V., et al., Osteoarthritis Cartilage, 2015. **23**(4): p. 507-15.
2. Brisson, N.M., et al., J Orthop Res, 2017. **35**(11): p. 2476-2483.
3. Buckwalter, J.A. and H.J. Mankin, Instr Course Lect, 1998. **47**: p. 487-504.
4. Eckstein, F., et al., Anat Embryol (Berl), 2001. **203**(3): p. 147-73.
5. Harkey, M.S., et al., Ultrasound Med Biol, 2018. **44**(2): p. 311-320.
6. Pillen, S., I.M. Arts, and M.J. Zwarts, Muscle Nerve, 2008. **37**(6): p. 679-93.
7. Pamukoff, D.N., et al., Med Sci Sports Exerc, 2018. **50**(2): p. 211-217.
8. Kumar, D., et al., Knee, 2014. **21**(5): p. 881-5.

ACKNOWLEDGEMENTS

This study was supported by the California State University Fullerton Intramural Research Grant Program.

MODULATION OF FOOT MECHANICAL WORK DURING WALKING WITH ADDED MASS

Nikolaos Papachatzis[1], Philippe Malcolm[1], Carl A. Nelson[2] & Kota Z. Takahashi[1]

[1]Department of Biomechanics, University of Nebraska at Omaha, Omaha, NE, USA
[2] Department of Mechanical and Materials Engineering, University of Nebraska-Lincoln, Lincoln, NE, USA
email: npapachatzis@unomaha.edu, web: https://www.unomaha.edu/college-of-education/cobre/

INTRODUCTION

The human foot contains a mixture of structures that can perform a variety of mechanical work profiles. The foot can absorb or dissipate energy (e.g., fat pad, soft tissue), and generate positive work either through elastic energy return (e.g., plantar fascia) or active muscles (e.g., force generation).

An informative way to examine the mechanical function within the foot is by examining how individual structures respond in the presence of varying mechanical force demands. For example, the plantar aponeurosis can stretch (store energy) under load and recoil (return energy) [1,2]. The surrounding muscles of the longitudinal arch can actively control stretch and stiffness as the load increases [3]. The structures within the metatarso-phalangeal joint can dissipate mechanical energy as the ground reaction forces increase [4]. When accounting for all structural components, the human foot appears to perform net negative work during level-ground walking [5]. An objective analysis of the combined mechanical work within the structures of the foot can expand our understanding of foot's function.

Here, we used walking with added mass as a way to increase the force demand of the foot, and investigated how the foot would modulate its overall mechanical work production. During walking with added mass, the musculo-tendon structures surrounding the hip, knee, and ankle modulate their work production [6]. Similarly, added mass could cause a variety of changes to the foot's work profiles, and examining these changes may reveal insights regarding the foot's functional capacity. For example, when walking with greater levels of added mass, the human foot structures could: 1) increase the magnitude of net negative work, which may highlight the foot's role as a shock-absorber, 2) increase the positive mechanical work to generate net positive work, which may reveal the foot muscles' potential to actively produce work, or 3) increase similar magnitudes of positive and negative work and maintain roughly equal net work, which could indicate that elastic structures play a prominent role in work production.

We hypothesized that walking with greater levels of added mass would increase the magnitude of both negative and positive work. Furthermore, we hypothesized that the increase in magnitude of negative work will be greater than the increase in positive work, such that net work will be more negative.

METHODS

Eighteen healthy, young participants completed barefoot over-ground walking in three randomized loading conditions wearing a weight vest (0%, +15%, and +30% of added body mass). The participants targeted a walking speed of 1.25 m/s. We quantified the mechanical power of the foot during the over-ground trials using a unified deformable segment analysis by modeling all structures distal to the calcaneus as a deforming body [5]. We quantified the negative and positive mechanical work over stance, by integrating the positive and negative portions of the mechanical power data over time, respectively. To determine the effect of the added mass on the dependent variables (negative, positive, and net mechanical work), we used one factor (3 levels: 0%, 15%, & 30% added mass) repeated measures ANOVAs. When we found a significant main effect, we conducted a Bonferroni post-hoc analysis for pair-wise comparisons. The significance level was set to $\alpha = 0.05$.

RESULTS AND DISCUSSION

The added mass produced increases in vertical ground reaction forces during walking, and thus increased the force demand on the foot (Figure 1). Walking with added mass had a significant effect on the magnitude of positive work ($p = 0.004$), including

a 16% increase between 0 and 30% added mass conditions ($p < 0.001$). There was no significant effect of added mass on negative work ($p = 0.126$) or net work ($p = 0.423$) (Figure 2). The results supported one of our hypotheses that the foot would increase positive work, but failed to support the other hypotheses, as the foot preserved similar amounts of net negative work across varying levels of added mass.

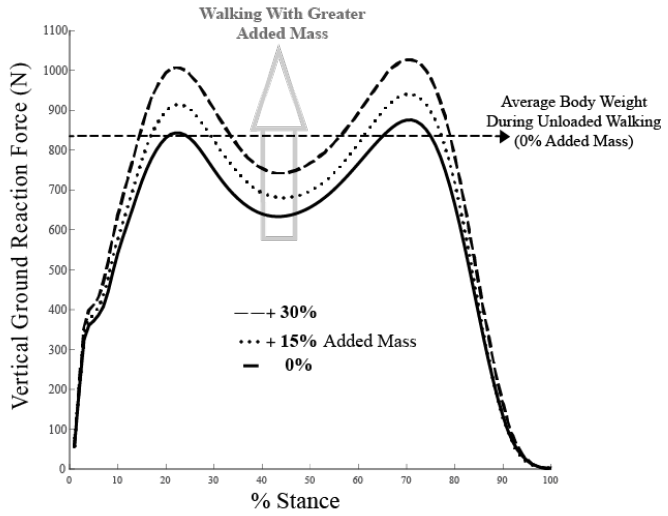

Figure 1. Average vertical ground reaction forces during stance phase (N=18). Each solid line represents the average vertical ground reaction force of all participants for each walking condition (0, 15 & 30% added mass). The dashed line represents the average body weight of all participants. Walking with added mass increased vertical ground reaction forces.

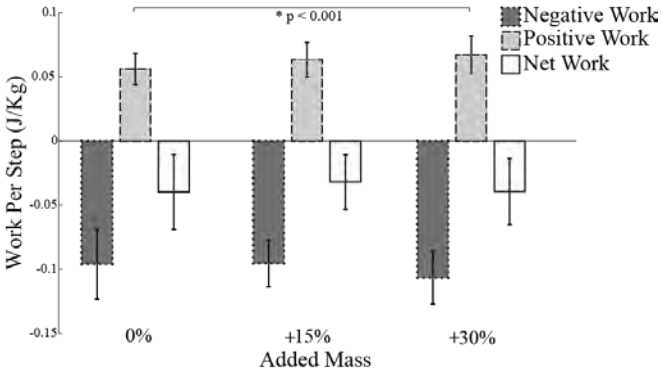

Figure 2: Negative, positive and net work produced by the foot structures normalized by each participant's body mass (not including added mass). Walking with added mass significantly increased the magnitude of positive work (16% increase between 0% and 30% added mass). Walking with added mass had no significant effect on negative work ($p = 0.126$) or net work ($p = 0.423$).

One plausible explanation behind the increase in foot positive work production (when walking with added mass) might be that the foot's intrinsic muscles increased their activation to produce greater positive work. A recent study has shown that the foot's intrinsic muscles can control the longitudinal arch motion when subjected to greater force demands [3], and thus it may be feasible that these muscles could actively produce work. Another plausible source for the increased foot positive work could be due to greater energy return from elastic structures, such as the plantar fascia. However, given that the magnitude of negative work (i.e., energy storage) did not increase significantly, it seems unlikely that elastic structures could account for this increased positive work production.

Despite the increased foot positive work, the net negative work remained the same across all levels of added mass. These results may indicate that the foot has a functional behavior analogous to a shock absorber-spring complex (i.e., overall dissipative), but the exact source of the mechanical work production would likely contain a combination of active (i.e., muscles), elastic and viscous structures. Our future experiments will investigate the functional role of the foot's net negative work – specifically, whether this energy is important for mobility, and/or stability.

REFERENCES

1. Ker RF, et al. *Nature*, 325: 147-149, 1987
2. Wager JC, et al. *Journal of biomechanics*, 49(5), 2016
3. Kelly LA, et al *Journal of The Royal Society Interface*, 12 (93), 20131188, 2014
4. Rolian C, et al. *Journal of Experimental Biology*, 212(5), 2009
5. Takahashi KZ, et al. *Scientific Reports*, 1 (1), 20017.
6. Griffin TM, et al, *Journal of Applied Physiology*, 95(1), 2003
7. Péter AHA, et al. *Scandinavian Journal of Medicine & Science in Sports*, 2017

ACKNOWLEDGEMENT:

This work was supported by the Center for Research in Human Movement Variability of the University of Nebraska at Omaha, NIH (P20GM109090) and the University of Nebraska Collaboration Initiative.

THE INFLUENCE OF ARCH TYPE AND WALKING SPEED ON PEAK PLANTAR PRESSURES

[1]Max R. Paquette, [1]Ross E. Smith, [1]Jake A. Melaro, [1]Douglas W. Powell
[1] University of Memphis, Memphis, TN, USA
email: mrpqette@memphis.edu, web: http://www.memphis.edu/shs/research/mal.php

INTRODUCTION

Fitness walking as a mode of aerobic exercise is popular among adults. During fitness walking, individuals walk faster to increase metabolic expenditure [1] with no relative increase in impact forces [2]. Gait speed has a near linear influence on the magnitude of peak plantar pressures under the heel, central and medial forefoot, medial and central metatarsal heads and toes [3, 4]. However, no pressure increases are observed under the lateral and medial arch, lateral metatarsal, and lateral midfoot and forefoot [3, 4]. The morphology of the foot, and specifically the medial longitudinal arch, can influence peak plantar pressures during walking [5, 6]. At a set gait speed, low arched individuals walk with lower peak pressures under the lateral forefoot compared to normal arched individuals [5]. High compared to normal and low arched individuals walk with higher pressures under the great toe, 2nd and 3rd metatarsal heads and, heel [6]. These combined findings on speed and arch type effects on plantar pressures demonstrate distinct loading patternsin different arch types which, as speed increases, could indicate distinct foot injury risks.

The objective of this work was to assess the interaction of speed and foot arch type on peak plantar pressures under different foot areas during walking. We hypothesized that faster walking speeds would increase peak pressures under all medial aspects of the foot areas, and that these pressure increases would be largest in low and normal arched compared to high arched individuals.

METHODS

Thirty-four young adults (Table 1) with low (6 women), normal (6 women), and high (5 women) arches [7] performed treadmill walking at four different walking speeds while plantar pressures were measured using a pressure insole system (Pedar, Novel Electronics, USA) under the following plantar areas: medial and lateral heel; medial and lateral midfoot; medial, middle, and lateral forefoot; hallux; and 2nd to 5th toes.

Table 1. Participant characteristics (mean±SD).

	Low (n=12)	Normal (n=12)	High (n=10)
Age (yrs)	25±4	25±6	25±6
Mass (kg)	73.8±14.5	75.5±10.9	65.9±14.9
Height (m)	1.70±0.10	1.74±0.09	1.70±0.11
Speed (m/s)	1.2±0.2	1.2±0.2	1.3±0.1

Notes: Speed: self-selected speed.

The four walking speeds included: 1) self-selected (**SS**), 2) SS+10% (**SS10**), 3) SS+20% (**SS20**), and 4) SS+30% (**SS30**). All participants wore the same footwear (NB690, New Balance, USA) during testing to remove any footwear effects from the experiment.

A mixed-design ANOVA was performed on the average values of all plantar pressure areas with speed as the within-subject factor and foot arch group as the between-subject factor (24.0, IBM SPSS, Chicago, IL). When interaction effects were observed, *post-hoc* paired t-tests were used to compare within group speed effects while independent t-tests were used to compare group differences ($p<0.05$). Cohen's d effect sizes were also reported to further assess arch type and speed differences.

RESULTS AND DISCUSSION

Preferred walking speed was not different between arch groups ($p>0.05$, $d<0.80$; Table 1). Contrary to our hypothesis, faster walking speeds did not show larger increases under medial aspects in low and normal compared to high arched individuals. A speed by arch type interaction was observed for peak plantar pressure under the medial forefoot ($p=0.041$). *Post-hoc* analysis revealed that pressure under the medial forefoot was higher in high compared to low arched individuals at the SS20 ($p=0.012$; $d=1.23$) and SS30 ($p=0.007$; $d=1.35$) speeds only (**Fig. 1**). This finding suggest that high arched individuals walk

with higher medial forefoot pressures at faster speeds but only compared to low arched individuals. Therefore, insoles with medial forefoot cushioning may help attenuate these higher peak pressures at faster speeds for high arched individuals only.

Speed effects for peak pressure were observed for the medial heel, lateral heel, medial midfoot, lateral midfoot, middle forefoot, lateral forefoot, and 2nd to 5th toes (Table 1). At SS20 and SS30, an increased peak pressure was observed under most plantar areas compared to SS (Table 1). At SS10, pressures were only increased under the lateral forefoot and toes compared to SS. Pressures under the midfoot increased with each speed. Contrary to previous findings [8], our results suggest that the midfoot may be most susceptible to increases in plantar pressures with increased speed and thus, fitness walking insole cushioning should mostly target the midfoot.

An arch group effect was only observed for peak pressure under the lateral heel (p=0.031) with higher pressure in the high (228.4±55.0 kPa) compared to normal (183.9±48.1 kPa; p=0.05; d=0.91) and low (168.6±45.5 kPa; p=0.01; d=1.25) arched groups. An arch group effect nearly reached significance for medial heel pressure (p=0.075), and *post-hoc* tests revealed higher pressure in the high (223.3±46.5 kPa) compared to low arched group (176.8±46.8 kPa; p=0.025; d=1.05). These findings are in agreement with previously reported higher heel pressures in high compared to low arched adults during walking [6]. Thus, strategies to reduce pressures under the heel should be considered in high arched individuals.

CONCLUSIONS

Our findings suggest that high arched individuals may be at a higher risk of increased medial forefoot pressures with increasing walking speed, and higher heel pressures at all speeds. Thus, insole designs may aim to specifically reduce pressures under the heel and medial forefoot of high arched individuals who take part in fitness walking. Finally, insoles designed to reduce midfoot pressures for fitness walkers (i.e., fast speed walking) of all arched types may be advisable.

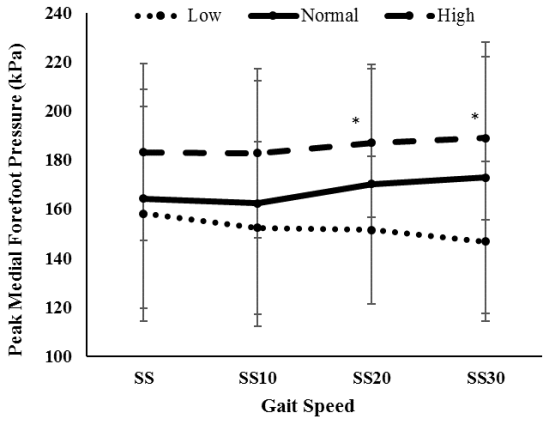

Figure 1: Peak medial forefoot pressures at all four walking speeds for all three arch groups (mean±SD). *: difference between high and low arched groups within specified speed.

REFERENCES

1. Bunc and Dlouha. *J Sp Med Phys Fit*, 1997. 37(2): p. 103-9.
2. Swain et al. *J Strength Cond Res*, 2016. 30(4): p. 1042-9.
3. Segal, et al. *Foot Ankle Int*, 2004. 25(12): p. 926-33.
4. Warren, et al. *Gait Posture*, 2004. 19(1): p. 91-100.
5. Chuckpaiwong, et al. *Gait Posture*, 2008. 28(3): 405-11.
6. O'Brien and Tyndyk. *Acta Bioeng Bio*, 2014. 16(2): 131-5.
7. Zhang, et al. *in Foot Biomech Symposium*. 2007. Taiwan.
8. Pataky, et al. *J Biomech,* 2008. 41(9): p. 1987-94.

FUNDING

Funding for this study was provide by Bayer HealthCare.

Table 2: Speed effects for all peak plantar pressures under all foot areas (mean±SD)

Plantar Pressures (kPA)	SS	SS10	SS20	SS30	p
Medial Heel *	189.1±44.1	194.6±51.8	197.9±50.5 [a]	203.0±55.0 [a,b]	0.005
Lateral Heel *	185.7±50.8	190.6±61.2	193.2±57.8 [a]	196.9±58.4 [a,b]	0.014
Medial Midfoot *	108.8±32.1	109.9±36.3	113.7±35.7 [a,b]	118.7±40.8 [a,b,c]	<0.001
Lateral Midfoot *	111.4±30.5	116.1±32.4	118.5±31.5 [a,b]	122.5±34.5 [a,b,c]	<0.001
Medial Forefoot	167.6±41.9	164.8±41.5	168.5±39.3	168.4±44.4	0.452
Middle Forefoot *	178.6±47.8	180.9±45.9	182.4±45.6	185.5±49.9 [a,b]	0.016
Lateral Forefoot *	166.6±46.8	171.4±44.6 [a]	172.0±44.9 [a]	173.5±48.5 [a]	0.024
Hallux	216.4±56.0	219.0±66.6	228.6±67.1	228.6±67.4	0.112
2nd-5th Toes *	179.7±54.8	186.0±56.6 [a]	190.9±59.0 [a,b]	195.6±58.3 [a,b]	<0.001

Notes: *: speed effect; [a]: different than SS; [b]: different than SS+10%; [c]: different than SS+20%; [#]: d>0.80; [$]: d>1.2 p<0.05. SS: self-selected; SS10: SS+10%; SS20: SS+20%; SS30: SS+30%.

ALTERATIONS IN LOWER-EXTREMITY FRONTAL PLANE JOINT MOMENTS DUE TO EXPERIMENTAL KNEE PAIN AND/OR EFFUSION DURING WALKING

[1]Jihong Park, [2]Matthew K. Seeley, and [3]Devin Francom, [2]J. Ty Hopkins

[1] Kyung Hee University, Yongin, Korea
[2] Brigham Young University, Provo, USA
[3] Los Alamos National Laboratory, Los Alamos, USA
email: jihong.park@khu.ac.kr

INTRODUCTION

Quadriceps dysfunction (e.g. altered activation and strength) is a common consequence in people with knee joint injuries and can cause deviations in the lower-extremity kinetic chain. Persistence of these abnormal movement mechanics might affect long-term joint and cartilage health, and finally result in knee joint degeneration [1].

Considering various onset, magnitude (volume), and duration of pain and joint effusion may confound the results, experimental knee pain [2] and joint effusion [3] models have been used. Since knee joint injuries typically accompany pain and joint effusion how these two stimuli, relatively or additively, alter functional movements is important.

Therefore, we were interested in observing the lower-extremity compensatory strategies in terms of net internal joint moments due to isolated and/or combined induced knee pain and joint effusion during walking. We hypothesised that both pain or effusion stimulus independently alters gait pattern. In case of the pain and effusion combined condition, we expected to see an additive effect.

METHODS

The independent variables were condition (pain, effusion, pain+effusion, and control) and time (pre, condition, and post). Prior to data collection, nineteen able-bodied subjects (10 males and 9 females; age: 22 ± 2 years; height: 1.73 ±0.10 m; mass: 73 ± 16 kg) gave informed consent approved by the appropriate institutional review board.

For each condition, subjects performed three walking trials at an intentional walking speed at each time point (pre: prior to injection; condition: 3-min post injection; and post: 30-min post injection). A successful walking trial was defined as each foot fully stepping on each force platform. Every two minutes, subjects rated their pain perception via a 10 cm visual analogue scale (VAS).

For the pain condition, we injected 1 mL of 5% sodium chloride into the infrapatellar fat pad [1]. For the effusion condition, we injected 2 mL of 1% lidocaine (for anesthetic purpose) and 50 mL of 0.9 sodium chloride into the superolateral knee joint [2]. For the pain+effusion condition three injections were performed in the order of 1% lidocaine, and 0.9% and 5% sodium chloride. All injections were performed on the right leg. The control condition consisted of no injection.

We used a standard inverse dynamics approach, combining joint kinematics (200 Hz), ground reaction force (2,000 Hz), and anthropometric data to calculate 3D net internal joint moments. In this abstract, we only reported the results of knee and hip joint.

A 4×24 mixed model analysis of variance and Tukey-Kramer pairwise comparisons were used to compare perceived pain. A functional analyses of variance [4] were used to compare joint moments, which allowed us to evaluate when differences existed, across the entire stance phase of gait, as well as the magnitude of the detected differences (p<0.05 for all comparisons).

RESULTS AND DISCUSSION

Subjects under the conditions with experimental pain models immediately felt knee pain, compared to the control condition ($F_{69,1242}$=12.36, p<0.0001; Figure

1). In a comparison of the pain and the pain+effusion condition, magnitude of pain perception was similar (4.1 vs. 3.9 cm in VAS, respectively). However, the pain+effusion condition induced a longer painful period (22-min), compared to the pain alone (14-min). Effusion condition induced pain for 8-min (average pain intensity: 1.9 cm in VAS).

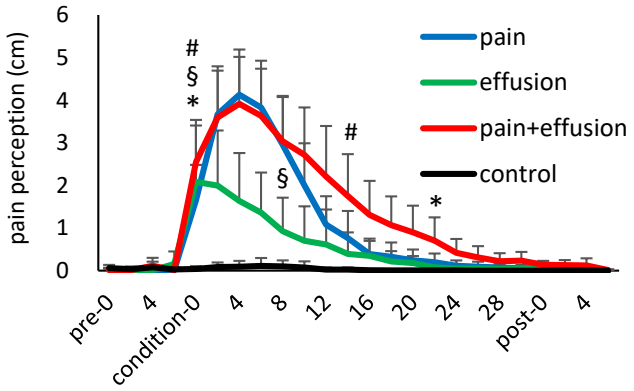

Figure 1: Perceived pain for each condition across time. Note that time points between the same symbols indicate statistical difference (#: pain; §: effusion; *: pain+effusion, $p<0.05$)

Subjects under the conditions with the injury model(s) walked with less hip and knee moments. A decreased knee moment is a common in patients with medial compartmental osteoarthritis [5]. Since mechanical changes are implicated in the progression of joint degeneration, our data may suggest that pain and joint effusion are potential mechanism for knee osteoarthritis.

The pain+effusion condition resulted in the greatest alterations although the patterns were similar to the effusion condition. When pain (e.g. nociceptors) is added on effusion (e.g. Ruffini endings) it appears to produce a summative effect. Presence of pain does not seem to shift a normal gait pattern.

The greatest joint moment alterations occurred around the same time as the peak impact and push-off in the vertical ground reaction force. This may indicate that joint moment alterations could be a compensatory strategy to manage external force, in the presence of pain and/or effusion stimuli.

CONCLUSIONS

Combination of experimental knee injury models produced a summative effect on gait deviations, similar patterns observed in patients with knee osteoarthritis. To avoid abnormal joint loading, pain and joint effusion should be controlled in all stage of rehabilitation.

REFERENCES

1. Felson et al. *Ann Intern Med*. **133**, 635-646, 2000
2. Hodges et al. *Arthritis Rheum*. **61**, 70-77, 2009.
3. Rice et al. *Arthritis Res Ther*. **16**, 502, 2014.
4. Park et al. *J Hum Kinet*. **60**, 39-49, 2017.
5. Astephen et al. *J Ortho Res*. **26**, 332-341, 2008.
6. Kulmala et al. *J Ortho Res*. **31**, 1013-1019, 2013.

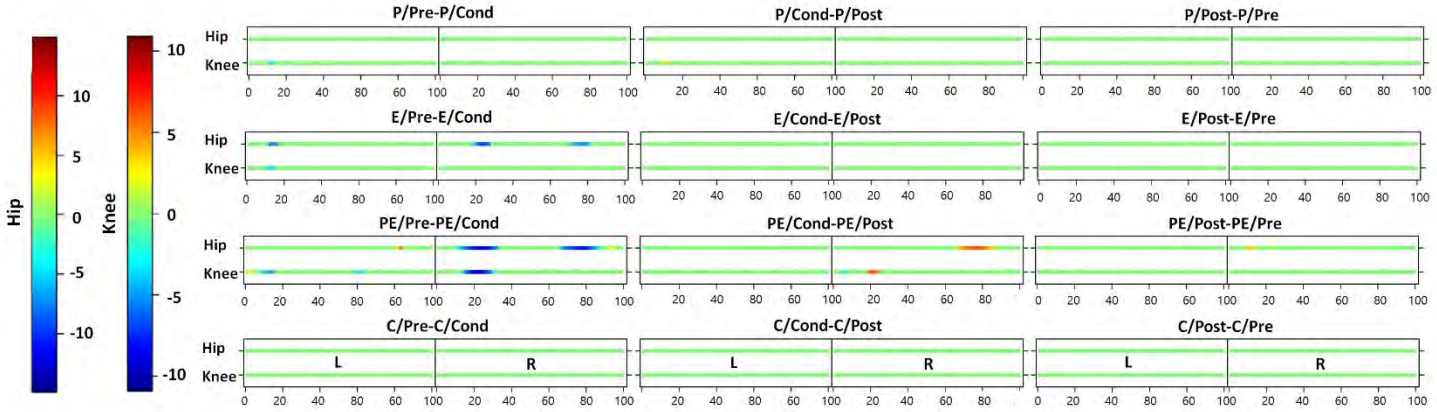

Figure 2: Summary of functional analysis of variance. L: left; R: right; P: pain; E: effusion; PE: pain+effusion; C: control; 0 to 100 indicate % stance phase. Colours other than green, indicate locations and magnitudes of differences between time points within a condition. For example, under the effusion condition, right knee and hip internal moments were less under the condition of pain+effusion during loading response.

THE RELATIONSHIP BETWEEN THE FOOT'S MECHANICAL ENERGY AND HEAT

[1]Jeffrey M. Patterson, [1]Nikolaos Papachatzis, [1]Andrew Kern, [2]Dustin R. Slivka, [3]Iraklis I. Pipinos, & [1]Kota Z. Takahashi
[1] Department of Biomechanics, University of Nebraska at Omaha, Omaha, NE, USA
[2] School of Health and Kinesiology, University of Nebraska at Omaha, Omaha, NE, USA
[3]Department of Surgery, University of Nebraska Medical Center, Omaha, NE, USA
Email: jmpatterson@unomaha.edu, web: cobre.unomaha.edu

INTRODUCTION

The foot and ankle produce nearly equal amounts of positive and negative work during normal walking [1]. However, when the mechanical behavior of the foot is analyzed separately from the ankle, it has been found that the foot produces net negative work during normal walking [1]. The implications of this net negative work production in the foot are poorly understood. While it has been shown that energy can be transferred proximally through musculotendinous structures crossing the ankle and foot, this effect is small [2]. It is plausible that some of this net negative work at the foot may be dissipated as heat which could potentially explain the increases in foot temperature experienced during walking [3].

In the present study, we attempted to manipulate the amount of work that the foot produces by adding mass to individuals during walking. It was hypothesized that additional mass would: 1) lead to greater increases in foot temperature, 2) increase the magnitude of net negative work at the foot, and 3) the greater temperature increase (with added mass walking) would be correlated with increased magnitude of net negative work.

METHODS

18 healthy subjects (age = 24.6 ± 2.8 years, height = 1.75 ± 0.06 m, mass = 85.3 ± 21.1 kg) walked over-ground on force plates and for 10 minutes on a treadmill (both at 1.25 m/s) while wearing added mass (0%, 15%, and 30% of body mass added via weight vest). A 53 marker lower-extremity marker set was used to track the motion of the hips, knees, and ankles, and to define a multi-segment foot model [1] during the over-ground trials. Four markers were used at the heels and toes of each foot during the treadmill trials to get step kinematics data.

Temperature measurements were taken immediately prior to and after each treadmill condition at four locations on the bottom of the right foot (hallux, head of the 1st and 5th metatarsals, and heel pad) which were averaged and presented here as "plantar". Isopropyl alcohol was sprayed on the right leg and foot and a 30-minute waiting period was given prior to the first and after each treadmill condition to allow the lower limbs to stabilize to a baseline temperature.

Kinematic and kinetic data were processed with Visual3D software (C-Motion, Germantown, MD) and custom MATLAB scripts (Mathworks, Natick, MA). The mechanical power of the foot was quantified using a unified-deformable analysis [4], and positive and negative work were calculated by integrating power during the stance phase of walking with respect to time. An estimate of the total work over the 10 minutes of treadmill walking was calculated by multiplying the average net work per step measured in over-ground trials by the number of steps taken in 10 minutes of treadmill walking. The difference between the change in temperature of the plantar foot between the 30% and 0% added mass conditions is "delta plantar temperature". A one-way repeated measures ANOVA was used to test the effects that added mass had on foot net work and on change in temperature. A Pearson correlation was used to identify the relationship between the foot's mechanical work and temperature changes between added mass conditions by correlating the change in "total net work" between the 30% and 0% added mass conditions with the change in the delta plantar temperature from the same conditions.

RESULTS AND DISCUSSION

The plantar temperature increased after each added mass condition (Figure 1), and there was a significant effect of added mass on change in plantar

temperature (p = 0.019), however post-hoc tests using the Bonferroni correction revealed no significant effect of levels of added mass. There was no effect of added mass on total net work after 10 minutes of treadmill walking (p = 0.400).

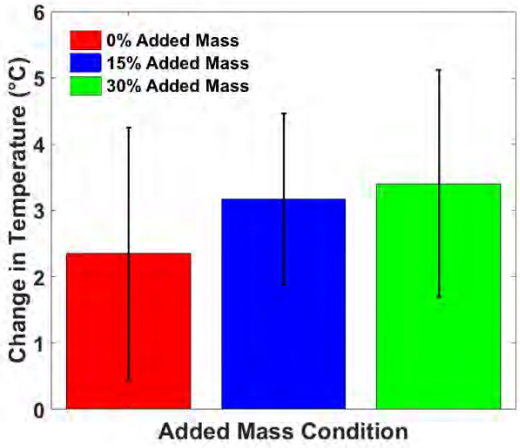

Figure 1: The plantar foot temperature increased after 10min. of walking with each added mass, but there was no significant effect of added mass on change in plantar foot temperature (p = 0.052).

There was no significant relationship between the change in the foot's net mechanical behavior between the 30% and 0% added mass conditions and the change in delta temperatures between the 30% and 0% added mass (Figure 2, $R^2 = 0.02$, p = 0.57).

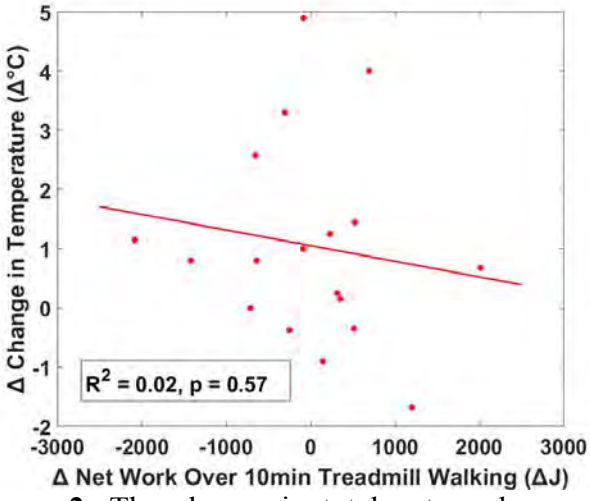

Figure 2: The change in total net work over 10 minutes of treadmill walking between the 30% and 0% added mass conditions was not correlated with the change in delta plantar foot temperatures between the 30% and 0% added mass conditions (p=0.57).

We performed calculations to estimate the theoretical expected amount of temperature increase at the foot with 30% added mass. The net work per step measured from the over-ground trials and number of right foot strides from 10 minutes of treadmill walking, across all participants, was -3.20 J and 568.34 strides, respectively. This gives a "net energy loss" of about 1817 J. We used the equation $q = \Delta T * C * m$ to compute the expected temperature change in the foot, where q represents the 1817 J dissipated as heat, ΔT represents the change in foot temperature, C represents the specific heat capacity of muscle [5], and m is the muscle mass in foot [6]. It was estimated that the foot would heat up by ~2.3 °C, which falls within the range of temperature values we found (~2.3 - 3.4 °C). The difference between the expected and actual values may be due to numerous other factors, including the role that shear stress at the foot plays in increasing foot temperature [7], as well as several physiological mechanisms like increased blood flow and sweating.

CONCLUSIONS

Our hypothesis was not supported as the foot temperature during walking was not correlated with the foot's net negative work. We are currently investigating alternative hypotheses to determine whether other factors could explain increases in foot temperature, such as shear force [7], heat due to energy expenditure from muscular force and work production, and increased blood flow. Our findings may be a result of the healthy foot accommodating to weight-bearing, whereas pathological populations (e.g., diabetics, peripheral artery disease) may not exhibit the same responses.

REFERENCES

1. Takahashi KZ, et al. *Sci Rep*, **7**, 15404, 2017.
2. Honert EC, et al. *PLoS One*, **11**, e0163169, 2016.
3. Reddy PN, et al. *Gait & Posture*, **52**, 272-9, 2017.
4. Takahashi KZ, et al. *J Biomech*, **45**, 2662-7, 2012.
5. Giering K, et al. *Proc. SPIE*, **2624**, 1996.
6. Clarys JP, et al. *Ergonomics*, **37**, 217-229, 1994.
7. Yavuz M, et al. *J. Biomech*, **47**, 3767-70, 2014.

ACKNOWLEDGEMENTS

This work was supported by the Center for Research in Human Movement Variability of the University of Nebraska at Omaha, NIH (P20GM109090) and the University of Nebraska Collaboration Initiative.

RATE OF FORCE DEVELOPMENT OF THE KNEE EXTENSOR MOMENT DURING LOADING PHASE OF GAIT IS NOT ASSOCIATED WITH PHYSICAL FUNCTION

[1]Richard E. Pimentel, [1]Alex Tagawa, [1]Lucas Moore, [1]Meghan Colip, [1,2]Amy W. Bodkin, [2]Patricia Heyn, [1,2]James J. Carollo

[1] Children's Hospital Colorado, Aurora, CO, USA
[2] University of Colorado Denver, Anschutz Medical Campus, Aurora, CO, USA
email: Richard.Pimentel@childrenscolorado.org, web: www.childrenscolorado.org/gaitlab

INTRODUCTION

Ability to generate force rapidly may be more important overall muscle strength in individuals with cerebral palsy (IwCP). Rate of force development (RFD) measured during maximum voluntary isometric contraction (MVICs) of the quadriceps are significant correlates of functional ability [1, 2] in IwCP. However, it is unclear if measurements of RFD during MVICs, a highly controlled and atypical kinesiologic task, are applicable to human movements during other activities.

The purpose of this study is to determine if RFD can be estimated walking and if it correlates to other measures of physical ability. The loading response phase of gait is selected for analysis due to timing of maximum demand from the knee extensors during weight acceptance. RFD will be assessed by estimating knee extension torque and correlating it with MVIC data, measures of walking ability, spasticity, gross motor function classification scale (GMFCS), and surveyed physical function.

METHODS

This work was part of a larger study to investigate relationships between gait, overall health, and risk for secondary health conditions in IwCP. This subset of participants included 50 young adults with cerebral palsy (27 female, age = 24.1, GDI = 78.7, GMFCS I-II) whose instrumented gait analysis data contained at least 5 barefoot walking trials without assistive devices and performed ≥ 3 MVIC trials.

The instrumented gait analysis consisted of 13 Vantage (Vicon, Oxford, UK) optical motion capture infrared cameras and 10 Bertec 4060-10 (Columbus, OH, USA) force platforms sampling at 120 and 2160 Hz respectively. Participants donned passive reflective markers consistent with the modified Helen Hays marker set. Kinematic trajectories were identified, gap filled, and filtered using Nexus 2.5 (Vicon). Foot/floor gait events were identified manually. The Plug in Gait model (Vicon) was used to estimate joint torques. Custom Matlab code (Mathworks, Natick, MA, USA) identified clean stance phase kinetics and parsed knee extension torques across the multiple walking trials for each participant (Figure 1). Gait RFD was determined by computing the first derivative of knee extension torque with respect to time and finding the maximum during the loading response phase of gait.

Seated MVIC of the knee extensors was performed bilaterally on a Human Norm isokinetic dynamometer (CMSI Inc, Stoughton, MA, USA) with 60° of knee flexion and 85° of hip flexion, sampling at 100 Hz. Participants started from rest and sustained the MVIC for 5 seconds. MVICs were measured 3 times, with the peak RFD values determined from the maximum slope following initial contraction.[1]

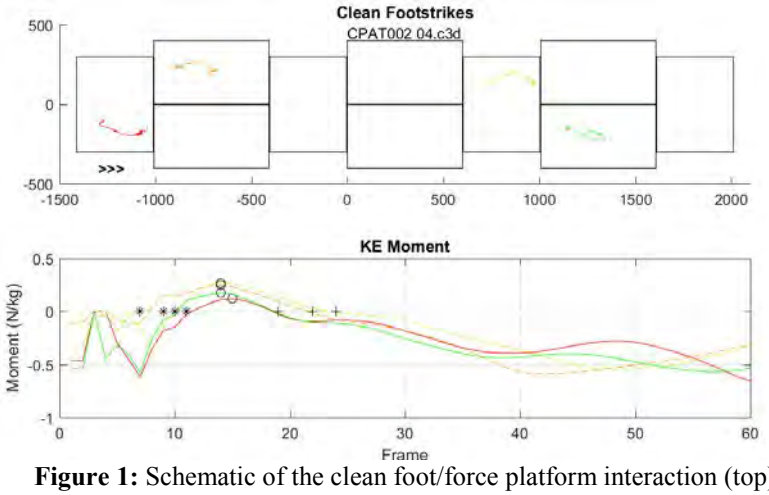

Figure 1: Schematic of the clean foot/force platform interaction (top) and extraction of knee moment after initial contact (bottom).

Physical activity was surveyed using the physical function total score of the PROMIS-57. GMFCS and quadriceps spasticity were evaluated by a trained physical therapist. Spasticity levels were classified using the Modified Ashworth Scale. Using Matlab, spearman rank-order correlations identified associations between gait parameters and function measures.

RESULTS AND DISCUSSION

Gait RFD did not correlate with isometric measures of RFD or any other measure of physical function other than average step length (Table 1). Peak knee extensor torque during gait also did not correlate with any of the other measures, except for nondominant peak knee extensor torque correlating with hamstring spasticity on the dominant side (Table 1). Knee extensor RFD during gait does not seem to be a useful measure of physical function in this cohort. Other studies have shown that isometric RFD correlates with physical function (more strongly than raw strength) and proposed that RFD may be more important than raw strength for overall functional ability. [1, 2]

CONCLUSIONS

Knee extensor MVIC RFD in IwCP is a unique biomarker of physical function that cannot be approximated by knee extension torque during walking. In IwCP with GMFCS levels I-II, knee extensor RFD during gait cannot be calculated from gait measurements and is not a useful measure of functional ability.

REFERENCES

1. Moreau NG, Falvo M, Damiano DL (2012) Gait Posture 35:154–158.
2. Carollo JJ, Colip M, Tagawa A, et al (2018) Gait Clin. Mov. Anal. Soc. Annu. Conf.

ACKNOWLEDGEMENTS

This work was supported by grants NIDRR #H133G130200, NIDILRR #90IF0055-01, and NIH/NCRR Colorado CTSI Grant Number UL1 TR001082 (REDCap). Additional support is provided from the J. T. Tai & Company Foundation.

Spearman Correlations	Dominant Peak RFD		NonDominant Peak RFD		Dominant Peak KE Torque		NonDominant Peak KE Torque	
	P	*R*	*P*	*R*	*P*	*R*	*P*	*R*
GMFCS Level	0.809	0.045	0.310	-0.188	0.840	-0.038	0.310	-0.188
Peak Humac RFD Non-Dominant Leg	0.884	0.027	0.668	0.080	0.967	0.008	0.788	0.050
Peak Humac RFD Dominant Leg	0.855	0.034	0.139	0.272	0.448	0.142	0.887	0.027
GMFCS Level	0.809	0.045	0.310	-0.188	0.840	-0.038	0.310	-0.188
Average GDI	0.201	-0.236	0.554	0.110	0.115	-0.289	0.283	0.199
Walking Speed	0.419	-0.151	0.082	0.318	0.586	0.102	0.097	0.303
Average Step Length	0.506	-0.124	**0.047**	**0.360**	0.403	0.156	0.089	0.310
Cadence	0.412	-0.153	0.789	0.050	0.296	-0.194	0.702	0.071
PROMIS physical function total score	0.712	-0.069	0.195	0.239	0.141	0.271	0.786	0.051
Quadriceps Spasticity Dominant	0.415	0.152	0.180	-0.247	0.536	0.116	0.290	0.196
Quadriceps Spasticity NonDominant	0.963	0.009	0.643	-0.087	0.600	0.098	0.255	0.211
Quadriceps Strength Dominant	0.458	-0.138	0.223	-0.225	0.440	-0.144	0.738	0.063
Quadriceps Strength NonDominant	0.321	0.184	0.967	0.008	0.078	0.322	0.080	0.319
Hamstrings Spasticity Dominant	0.950	0.012	0.718	-0.067	0.826	0.041	**0.030**	**0.389**
Hamstrings Spasticity NonDominant	0.834	0.039	0.671	0.080	0.475	-0.133	0.600	0.098
Hamstrings Strength Dominant	0.229	-0.222	0.468	0.135	0.343	-0.176	0.790	-0.050
Hamstrings Strength NonDominant	0.066	-0.334	0.707	-0.070	0.784	0.051	0.417	-0.151

AVERAGE AND MAXIMAL LOADING RATES DURING HILL RUNNING ARE GREATER ON A SOFT, GRASS SURFACE COMPARED TO A HARD, GRAVEL SURFACE

Heather J. Porter, Jinger S. Gottschall and Samuel E. Masters

Department of Kinesiology, The Pennsylvania State University, University Park, PA, USA
email: hjp9@psu.edu

INTRODUCTION

The popularity of recreational running is steadily increasing, with an estimated 40 million people participating in sanctioned events annually. Despite advances in equipment and technology, running-related overuse injuries continue to affect 30% to 70% of runners every year [1].

Several factors contribute to the development of injury, including high average loading rate (aveLR) and maximal loading rates (maxLR), both components of the vertical ground reaction force (GRF). Runners who remain injury free have significantly lower loading rates than those with a history of musculoskeletal injury [1]. Coaches and clinicians often name hard surfaces, such as concrete, as the culprit for high injury rates and frequently prescribe a running regimen with more variety in surface stiffness. Though this theory makes sense given current literature on GRFs in running [2], it has not yet been validated due to barriers of testing surface type in a natural running setting. Previously, GRFs have been studied with force plates using a limited number of steps or force treadmills in a laboratory [2,3]. Only recently has the ability to measure GRF in natural settings become available [1].

The purpose of this study was to determine if running on a soft (grass) surface produced lower loading rates compared to a hard (gravel) surface on level ground, as well as two hill grades. Our hypothesis was that loading rates (average and maximum) while running on a soft surface would be less than loading rates on a hard surface.

METHODS

Four subjects (ages 21 to 28 years) who run recreationally at least 10 miles per week were recruited to participate in this pilot study. Novel Loadsol® insoles, which measure GRFs normal to the plantar surface of the foot with separate sensors in three regions (rearfoot, medial forefoot, lateral forefoot), were placed in the subject's normal running shoes. An iPhone recorded the plantar forces while running and was placed into a sleeve to wear on the arm. Subjects completed a series of running trials on the two different surfaces, both uphill and downhill, at an imposed cadence of 160 steps/minute (3.1 m/s). Time to reach incline transition and trial completion were synchronized to insole data.

The 170 m experimental area was divided into 3 different segments for both uphill and downhill running; level (< 2 degrees), moderate (4-6 degrees) and steep (~8 degrees) yielding 6 conditions. Ground reaction forces were normalized to body weight and loading rates were normalized for each condition to the level segment of the uphill trial. A Student's paired t-test was performed to determine differences between hard and soft surface conditions ($p<0.05$).

RESULTS AND DISCUSSION

Overall, we reject our hypothesis that aveLR and maxLR during running on soft surfaces would be less than hard surfaces at an imposed cadence. For example, during all of the downhill segments (steep, moderate, flat), both loading rate variables were significantly *greater* on the soft surface compared to the hard (Figure 1). However, in agreement with our hypothesis, during the steep uphill condition, both aveLR and maxLR were significantly less on the soft surface (Table 1). In parallel to previous literature on GRF during hill running, aveLR and maxLR were correlated to surface grade with lower loading rates during uphill running and higher rates during downhill [3].

Subjects predominantly initiated ground contact with their forefoot on the level and uphill grades but switched to a heel strike pattern on the downhill. Maximum peak force at the heel was significantly greater on the soft surface. The heel loading rate contribution, calculated as the impulse of the heel loading rate over the impulse of the average loading rate during the first 5% of stance, was significantly greater on the soft surface. This has implications for running injury; when individuals run downhill on a softer surface, they make less protective kinematic adjustments based on leg compression adjustments, and force transmission up the kinematic chain may be more damaging [4].

CONCLUSIONS

Our findings have implications for injury risk in runners due to surface-dependent changes in loading rates. Predominantly forefoot strikers landed with a heel strike pattern when running downhill, which was more pronounced on the soft surface. This result indicates that benefits from running downhill on more compliant surfaces may not exist since loading rates were greater. This persisted as an after-effect as aveLR and maxLR remained elevated once subjects had reached the level ground after the conclusion of the hill.

REFERENCES

1. Hreljac, et al. *Medicine & Science in Sports & Exercise*. **32**(9): 1635–1641, 2000.
2. Cavanagh & Lafortune. *Journal of Biomechanics.* **13**(5): 397-406, 1980.
3. Gottschall & Kram. *Journal of Biomechanics*. **38**:445-452, 2005.
4. Ferris et al. *Proceedings of the Royal Society B: Biological Sciences.* **265**(1400): 989-994, 1998.

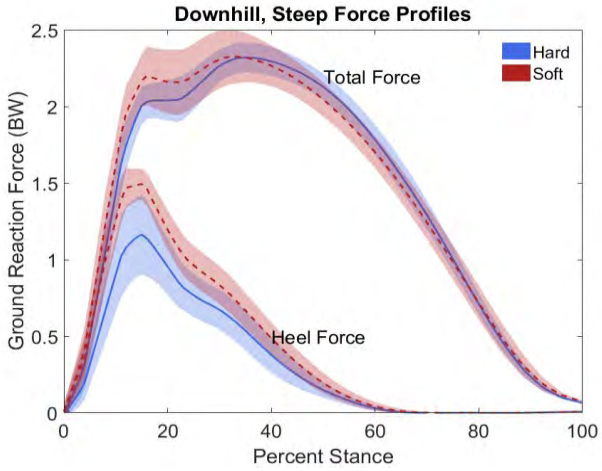

Figure 1: Representative profile of the total plantar surface force and heel force contribution on the steep downhill condition normalized to bodyweight.

Table 1: Percent differences (± standard deviation) of each hill condition normalized to UP level. An * indicates a significant difference between hard and soft surfaces ($p < 0.05$).

	UP moderate	UP steep	DN steep	DN moderate	DN flat
Hard Surface					
Average Loading Rate	-24.79 (9.86)*	-36.96 (13.59)*	35.35 (7.33)	21.49 (10.49)*	7.33 (3.93)*
Maximum Loading Rate	-24.27 (9.18)*	-35.41 (13.49)*	34.28 (7.88)*	22.34 (6.86)*	8.54 (2.68)*
LR Heel Contribution	-9.44 (8.64)	-37.81 (25.95)	-4.19 (11.90)*	-5.82 (12.28)*	0.80 (17.34)
MLR Heel Contribution	-11.46 (10.43)	-40.17 (20.41)	0.01 (6.33)*	-1.69 (6.86)*	-1.02 (9.74)*
Max Peak Heel	-22.47 (12.35)	-46.88 (22.52)	29.71 (15.13)*	19.38 (13.27)*	8.48 (5.50)*
Soft Surface					
Average Loading Rate	-9.50 (7.63)*	-41.89 (11.30)*	48.15 (6.53)*	43.38 (6.04)*	18.60 (4.67)*
Maximum Loading Rate	-12.42 (8.19)*	-40.19 (11.75)*	46.81 (4.53)*	39.47 (8.30)*	19.08 (7.89)*
LR Heel Contribution	-10.22 (12.54)	-46.68 (26.83)	22.09 (24.13)*	15.52 (17.83)	13.55 (16.87)
MLR Heel Contribution	-10.17 (6.48)	-46.32 (25.78)	19.05 (19.07)*	16.28 (15.07)*	11.93 (10.50)*
Max Peak Heel	-15.65 (8.06)	-51.39 (25.53)	59.27 (8.70)*	44.17 (13.55)*	23.15 (7.30)*

THE INFLUENCE OF BODY SIZE, SEX, AND GAIT SPEED ON PLANTAR FLEXOR MOMENT AND PROPULSIVE FORCE

[1] Brett K. Post, [2]Michael N. Vakula, [1]Steven A. Garcia, [1]Skylar C. Holmes, and [1] Derek N. Pamukoff
[1] California State University, Fullerton, CA, USA, [2]Utah State University, Logan, UT, USA
Email: brpost@fullerton.edu

INTRODUCTION

Declines in walking speed are associated with mortality and morbidity risk [1]. Walking speed is partially attributable to propulsive force (PF) production (i.e., the positive portion of the anteroposterior ground reaction force) during the push-off phase of mid-to-late stance [2]. Propulsive force generation can largely be attributed to plantar flexor muscle force production, especially when walking speed is increased [3]. However, PF and plantar flexor moments (PFM) are influenced body mass index (BMI), sex, and gait speed. For instance, obese individuals (BMI ≥30.0) have lower normalized peak PF when compared to non-obese individuals (BMI 18.0-25.0) [4]. Amongst healthy older populations, sex influences walking speed, with older women walking slower than older men [5]. However, the interaction of BMI, sex and gait speed on PF and PFM in young healthy adults is not well understood Additionally, understanding the influence of BMI and sex on gait biomechanics may be beneficial when constructing clinical interventions to moderate declines in walking speed. Therefore, the purpose of this study was (1) to investigate the influence between BMI, sex, and gait speed on PF and PFM; and (2) assess the relationship between PF, PFM, and walking speed. We hypothesized that (1) peak PFM and PF would be lower in obese subjects when compared to non-obese participants matched on age and sex, (2) there would be an interaction between BMI, sex, and gait speed on normalized peak PF and PFM values, and (3) that higher PF and PFM would be associated with faster SS gait speed in both sexes and BMI groups.

METHODS

Thirty-nine non-obese and forty-three obese individuals were recruited for this study (Table 1). Retro-reflective marker position and force plate data were collected using a 9-camera motion capture system and 2 AMTI force plates. Participants completed 5 walking trials in laboratory-standard neutral cushion footwear for two separate speed conditions (self-selected [SS] and a pre-determined (PD) speed (1 m/s)). Speeds were evaluated in a block-randomized order. Speed during each condition was monitored using timing gates and was within ±5% of their SS or PD speed. Marker position and force plate data were exported to Visual 3D and low pass filtered at 6Hz and 50Hz, respectively, utilizing a zero phase-lag, 4th order Butterworth filter. Stance phase was defined as the time between ground contact and toe off with the threshold set at 20N. Variables of interest were extracted using a custom LabVIEW program (peak PFM and PF during the second half of stance phase). Peak PF was normalized to bodyweight (N), while peak PFM was normalized to the product of bodyweight and height. A 2 (sex) by 2 (BMI) by 2 (speed) mixed model ANOVA was used to evaluate influence of sex, BMI, and gait speed on peak PF and PFM. Tukey's HSD was used for *post hoc* comparisons where a significant interaction was found. Pearson correlation was used to examine the relationship between PF and PFM, and SS speed (α=0.05).

Table 1. Subject Demographics (mean ± SD)

Group	Non-Obese	Obese
Age (years)	22 ± 2.89	22.25 ± 3.7
Female (N)	23	23
BMI (kg/m^2)	21.48 ± 1.74	32.46 ± 3.67
Body Fat (%)	20.09±6.99	37.98±7.29

RESULTS AND DISCUSSION

There was a significant interaction between sex, BMI, and speed on peak PF ($F_{1, 78}$ = 11.66, p= 0.001). There was a main effect of speed ($F_{1, 78}$ = 195.33, p<0.001), but not for sex (p= 0.25) and BMI (p= 0.18). Peak PF was larger at the SS compared to the PD speed (0.21 (0.20, 0.22) vs. 0.17 (0.16, 0.18) BW, p<0.001). *Post hoc* analyses indicate that non-obese

males at SS walking speed produced more peak PF than non-obese females at SS speed (0.24 (0.22, 0.26) vs. 0.20 (0.18, 0.21) BW). Non-obese males produce more PF compared to obese males at SS speed (0.24 (0.22, 0.26) vs. 0.19 (0.17, 0.21)). No differences were observed between non-obese and obese females at any speed.

There was a significant interaction between sex, BMI, and speed with regards to peak PFM ($F_{1, 78}$ = 3.79, p= 0.05). There was a main effect of BMI ($F_{1, 78}$ = 22.31, p<0.001) and speed ($F_{1, 78}$= 89.45, p<0.001), but not for sex (p= 0.41). The obese group had a lower PFM compared to the non-obese group (-0.086 (-0.088, -0.084) vs. -0.079 (-0.081, -0.077) %BW*Height), while PFM was greater at SS compared to PD speed (-0.086 (-0.088, -0.084) vs. -0.080 (-0.081, -0.078) %BW*Height). *Post hoc* analyses indicate that non-obese males at PD speed produced more peak PFM when compared to obese males at PD speeds (-0.083 (-0.086, -0.080) vs. -0.078 (-0.081, -0.075) %BW*Height). Additionally, non-obese females produced more peak PFM when compared to obese females in both SS (-0.088 (-0.092, -0.085) vs. -0.082 (-0.085, -0.079) %BW*Height) and PD speeds (-0.084 (-0.086, -0.081) vs. -0.074 (-0.077, -0.077) %BW*Height). Larger peak PF was associated with faster gait speed (r= 0.34, p= 0.04) in the non-obese group. A larger peak PF (r= 0.82, p < 0.001) and peak PFM (r= -0.48, p= 0.001) were associated with faster gait speed in the obese group.

We hypothesized that (1) peak PF and PFM would be lower in the obese compared to non-obese participants, (2) the interaction between BMI, sex and gait speed would influence peak PF and PFM values, and (3) larger peak PF and PFM will relate to SS gait speed in both sexes and BMI groups. Firstly, non-obese participants (both male and female) produced more peak PF and PFM compared to obese participants. This finding is supported by previous literature [4] and suggests that lower PFM and PF is a compensatory strategy to reduce compressive forces at the knee joint [6]. A larger PFM reduces tibial deviation with respect to the vertical, and thereby allows for greater joint reaction forces to align with the femur, thus increasing compressive forces [6]. Secondly, there was an effect of sex and gait speed on peak PF and PFM production. Non-obese males produced higher peak PF than non-obese females at SS speeds. However, peak PF was similar between sex in the obese group across both SS and PD speeds. Interestingly, obese participants generated less PFM than non-obese participants at standardized PD speeds. This finding suggests that obese young adults alter gait biomechanics to compensate for impaired propulsive characteristics indicative of elderly [2] and osteoarthritic populations [6]. The findings of Robon et al. [6] suggest that this these gait alterations include greater hip flexor moments to compensate for reduced PFM. Additionally, both peak PF and PFM were larger at SS when compared to PD speed [2]. On average, participants' SS speed was faster than the PD speeds, which may explain the larger peak PF and PFM observed at SS speeds. Lastly, the relationship between SS speed and peak PF and PFM among obese participants suggest that these variables are significant to gait speed. As such, peak PF [2] and PFM may be relevant targets for intervention regarding long-term health and quality of life.

CONCLUSIONS

The results of this study suggest that slower gait speed due to PF and PFM are multi-factorial and are influenced by BMI and sex. Future research should investigate these associations and evaluate their clinical relevance to long-term health outcomes.

REFERENCES

1. Newman, A.B., et al., Jama, 2006. **295**(17): p. 2018-26.
2. Browne, M.G. and J.R. Franz, J Biomech, 2017. **55**: p. 48-55.
3. Winter, D.A., Clin Orthop Relat Res, 1983(175): p. 147-54.
4. de Castro, M.P., et al., Res Q Exerc Sport, 2014. **85**(2): p. 188-97.
5. Bogen, B., et al., Gait Posture, 2018. **61**: p. 479-482.
6. Robon, M.J., et al., Clin Biomech (Bristol, Avon), 2000. **15**(7): p. 522-7.

ACKNOWLEDGMENTS

This study was supported by the CSU-Fullerton Intramural Research Grant Program.

Medial and Lateral Knee Joint Contact Forces While Walking at Different Speeds

[1] Matt Prebble, [1] Qi Wei, [1] Siddhartha Sikdar, [1]Shane Caswell, and [1] Nelson Cortes

[1] George Mason University, Fairfax, VA, USA
email: ncortes@gmu.edu, web: https://smartlab.gmu.edu/

INTRODUCTION

Unbalanced distribution of joint contact forces in the medial and lateral tibiofemoral compartments contributes to the development of pathological conditions such as knee osteoarthritis [1]. Computational models are a primary approach for estimating knee joint loads during gait [2-4]. Previous gait simulation research reported that tibiofemoral contact forces increase with increased gait speed [5] and that subject-specific models provide improved accuracy over models with generic parameters [1 6]. The purpose of this study was to estimate medial and lateral knee joint loads during four gait speeds. We hypothesized that greater speed will lead to increased contact forces in the medial and lateral compartments.

METHODS

A full-body OpenSim model was used to compute contact forces in the tibiofemoral joint of the dominant limb during gait [6]. The model has a modified knee joint that incorporates subject-specific tibiofemoral alignment and geometric parameters to calculate joint contact forces in the medial and lateral compartment of the knee.

Experimental data was captured from a healthy male participant (25 years, 1.9 m, 110.3 kg) who was free of current or recent lower extremity injury. Three trials each of walking at four speeds: preferred (PS), fast (FS), slow (SS), & very slow (VSS) were completed. Speed was determined using timing gates (Power Systems Brower) placed 2.4 meters apart on the lab walkway. The participant started by performing three trials walking at a self-selected "preferred" speed. The range for each speed was then determined by measuring a percentage of the participants average PS during the first three trials: FS = (120 ± 5%), SS = (80 ± 5%), and VSS = (50 ± 5%). If the speed was outside the allotted standard deviation, verbal feedback (speed up, slow down) was provided to the participant and the trial was repeated until deemed successful.

Forty-two reflective markers were attached to the participant's body as previously described [7]. Kinematic data was collected using eight high-speed motion analysis cameras (Vicon, Oxford, England) sampling at 200 Hz. Ground reaction force (GRF) data was measured using four floor embedded force plates sampling at 1000 Hz (Bertec, Columbus, OH). A static trial and a functional hip trial were obtained, prior to the dynamic tasks, for estimation of hip joint centers [7]. For static capture the participant stood in anatomical position on a force plate with the arms abducted ninety degrees and held motionless. For the functional hip trial the arms were abducted ninety degrees and the participant performed three hula circles with the hip in a clockwise direction [7].

The kinetic and kinematic data were processed in visual 3D and exported to OpenSim format. Implementation of the gait model followed the approach documented by Lerner et. Al [6] and the medial and lateral contact forces where estimated with the OpenSim Joint Reaction function.

RESULTS AND DISCUSSION

The average speed for the FS, PS, SS and VSS conditions where 1.35 m/s, 1.21 m/s, 1.00 m/s, and .83 m/s, respectively. The estimated joint loads in the medial and lateral compartment of the knee during gait are depicted in figure 1. The model predicted that in the early stance phase medial compartment joint contact forces decreased as speed increased (figure 1-top). The peak force also shifted later in the gait cycle for the SS and VSS conditions. However, in the late stance phase there was little difference between the four conditions. In contrast, the lateral compartment experienced

increased joint loads during the early phase of gait for the FS and PS conditions compared to the SS and VSS conditions (figure 2-bottom). However, in the late stance phase the FS and VSS conditions had a high joint contact force in the lateral compartment. Inspection of the ground reaction force (GRF) data for the participant indicated that there was little difference in the vertical GRF between the FS and PS and between the SS and VSS.

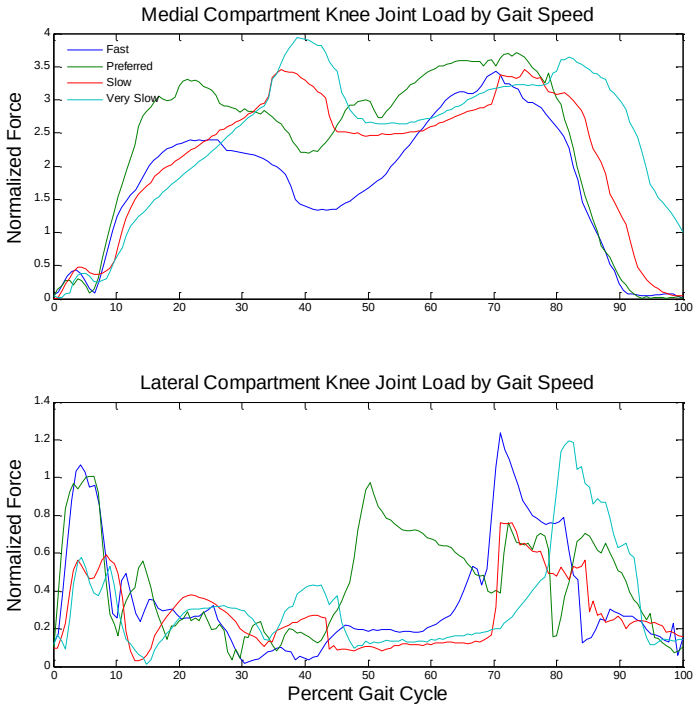

Figure 1: Medial (top) and lateral (bottom) compartment tibiofemoral contact forces at different gait speeds.

This contradicts previous research that showed an increase in compressive force in the tibiofemoral joint when gait speed increased from .75 m/s to 1.50 m/s [5]. This difference may be due to the knee model used in our study, which separates the joint forces into the medial and lateral compartments. Our results also indicated that the peak force shifted later in the gait cycle for the SS and VSS conditions and that in the late stance phase there was little difference between the four conditions.

One factor that may contribute to these findings is the stride length used during each condition. For FS and PS the subject walked with a more extended leg at foot contact which places greater force on the lateral side of the knee at foot contact. As they progressed through the gait cycle, forces shifted from the lateral to medial side. When walking with a SS and VSS the subject's stride was shorter with the leg in a less extended position at foot contact. This may lead to a greater force being placed on the medial side of the knee in the early stance phase. Another factor that may contribute to the results is the sensitivity of the model to knee alignment [5]. The model allows customization of the knee angle in the frontal plane and the locations of the medial and lateral knee compartments, relative to the knee joint center. We lacked the necessary radiographic images to customize the model accordingly.

CONCLUSIONS

This study indicates there may be a complex interaction between gait speed, stride length, and the distribution of forces between the medial and lateral compartments of the tibiofemoral joint. Further research should be conducted to clarify the effect of gait speed on the distribution of joint loads in the medial and lateral compartments. Future work will incorporate subject specific parameters including the angles between the knee and the femur and tibia as well as the location of the medial and lateral compartments in the knee joint model.

REFERENCES

1. Gerus P, Sartori M, Besier TF, et al. *J Biomech* 2013;**46**(16):2778-86.
2. Lin YC, Haftka RT, Queipo NV, Fregly BJ. *Med Eng Phys* 2010;**32**(6):584-94.
3. Serrancoli G, Kinney AL, Fregly BJ, Font-Llagunes JM. *J Biomech Eng* 2016;**138**(8).
4. Miller RH. J Biomech 2014;47(6):1373-81.
5. Lerner ZF, Haight DJ, DeMers MS, et al. *J Appl Biomech* 2014;**30**(2):197-205.
6. Lerner ZF, DeMers MS, Delp SL, Browning RC. *J Biomech* 2015;**48**(4):644-50.
7. Greska EK, Cortes N, Van Lunen BL, Onate JA. *Journal of strength and conditioning research* 2012;**26**(6):1609-19.

COMPARISION OF SOCKET SUSPENSION SYSTEMS DURING STAIR ASCENT IN INDIVIDUALS WITH TRANSTIBIAL AMPUTATION

Gabrielle M. Rentuma, Vanessa A. Kellems, & Jeremy D. Smith, Abbie E. Ferris
School of Sport & Exercise Science, University of Northern Colorado, Greeley, CO
Gabrielle.Rentuma@unco.edu; www.unco.edu/biomechanics

INTRODUCTION

Socket suspension systems have an important role in an amputee's ability to perform functional tasks. A suspension system that provides secure attachment to the residual limb can be beneficial in carrying out activities of daily living (ADL) such as level-ground walking and stair negotiation [1-2]. However, stair negotiation is a more demanding task than level-ground walking. The loss of lower-extremity muscles places more demand on the prosthetic for successful stair ambulation. Previous literature has primarily focused on the effects of prosthetic feet (powered and unpowered) [3-5] during stair ascent, however, there has been little research investigating the role of suspension systems during stair ascent.

Two main modes of suspension utilized by transtibial amputees (TTA) are lock and pin (PIN), and elevated vacuum. A newly designed vacuum suspension system, SmartPuck™ (PUCK), has recently been developed. It is unique in its ability to maintain a constant pressure since the vacuum is internal to the socket, which prevents loss of pressure throughout the day compared to other systems. Thus, it has been suggested this could combat daily residual limb volume fluctuations [6], which could improve functional abilities, such as stair climbing. Previous literature has reported during the swing phase of gait, the PIN suspension system applies tension distally, while compression is applied proximally [7]. Since differences are reported during gait, there could be differences between systems during stair negotiation.

The purpose of this study was to compare PUCK and PIN suspension systems during stair ascent. The goal of this study was to understand if differences exist between socket suspension systems and if functional ability improves through use of the PUCK. A null hypothesis was established; there would be no differences in joint angles between PIN and PUCK suspension systems.

METHODS

Four unilateral transtibial amputees (62.5 ± 4.5 years, 89.03 ± 12.1 kg, 1.73 ± 0.08 m) participated in this study. All amputees had an amputation due to trauma. Inclusion criteria included: At least 6 months of experience in their current lower-limb prosthesis, TTA resulting from trauma, bone cancer, or birth defect, and rated at levels K3 and K4 of function. Participants were fit with a new socket by a certified prosthetists and were tested in a PIN and PUCK system. Following the initial visit in the lab, participants were fit with the alternate suspension system and allowed to become comfortable with the other suspension system before retesting occurred.

An instrumented staircase was constructed in the lab and consisted of four steps with the first step having an embedded AMTI force plate (Figure 1). The staircase was placed over an instrumented treadmill to allow for force measurements on the ground (GROUND) prior to stepping onto the first stair (STAIR). The dimensions of the staircase were 19.5 cm (riser) by 27.5 cm (tread) and 1 m wide.

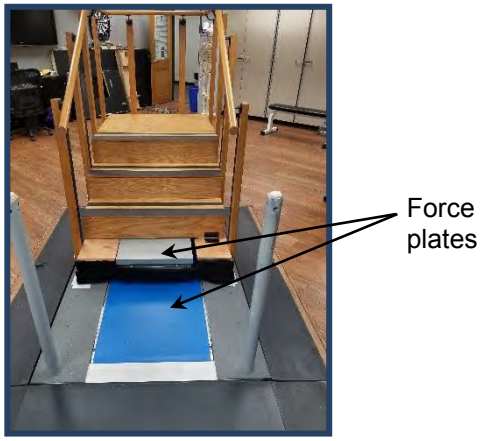

Figure 1. Configurations for stairs The "blue" force plates are mounted in the bed of our instrumented AMTI treadmill.

Participants were instructed to approach and ascend the stairs at a freely chosen speed (as they would normally ascend a staircase). Three trials were analyzed with the amputated limb on the STAIR, and three trials were collected with the intact limb on the STAIR. Trials were considered acceptable if the individual was able to ascend the stairs without using the handrails. Motion capture data were collected (VICON, 100 Hz) for each trial. Kinematic variables were analyzed for the ankle, knee, and hip joints for the GROUND and STAIR condition. As these data are preliminary, no statistical analyses were performed.

RESULTS & DISCUSSION

In general, during the GROUND and STAIR condition, the amputated limb showed a trend towards reduced range of motion (ROM) for knee and hip while wearing the PUCK (Table 1). Specifically, the amputated limb had a reduced knee ROM compared to the intact limb for both suspension systems. The reduction in knee ROM was primarily due to a decrease in knee flexion angle during swing. The reduction in knee flexion angle during swing (while wearing the PUCK) may have been exaggerated by the additional neoprene sleeve that is worn over the liner to create the vacuum seal.

At the hip, ROM was reduced in the PUCK for both the GROUND and STAIR steps compared to the PIN condition. However, asymmetries still persisted between the intact and amputated limbs in the PUCK and PIN conditions. The amputated limb showed an increased hip ROM compared to the intact limb. In general, this was driven by an increase in hip flexion during swing in the amputated limb. On the GROUND step, the PUCK amputated limb showed an increase in hip extension during push-off. This may indicate these individuals felt comfortable supporting themselves on the limb to propel themselves onto the STAIR.

CONCLUSION

Stair ascent is a demanding task, and requires an increased ROM and concentric muscle actions to complete the task [8]. From the general findings reported here, there is a reduction in ROM from PIN to PUCK at the knee. Further, the hip ROM suggests that the PUCK and PIN utilize different strategies to ascend a staircase.

These initial findings suggest that kinematic differences may exist between the PUCK and PIN suspension systems. These differences may be driven by several factors: 1) the addition of the neoprene sleeve on the PUCK may limit knee joint ROM, 2) the PUCK may reduce limb volume loss thereby improving the fit of the prosthetic socket. These factors may have conflicting effects, the reduction of knee ROM could be detrimental to functional performace whereas the improved fit may improve the ability to stand on the amputated limb as individuals ascend a staircase. Clearly, these results will become more clear as we add more participants to the current dataset.

REFERENCES

1. Beil, T. L. *et al.* Journal of Rehabilitation Research and Development, 2002, **39**(9): p. 693-700.
2. Board, W. J. *et al.* Prosthetics and Orthotics International, 2001, **25**: p. 202–209.
3. Dillingham, T. R. *et al.* American Journal of Physical Medicine & Rehabilitation, 2001 **80**(8): p. 563–571.
4. Ferraro, C. JPO Journal of Prosthetics and Orthotics, 2011, **23**(2): p. 78–81.
5. Fradet, L. *et al.* Gait & Posture, 2010, **32**: p. 191-198.
6. Torburn, L. *et al.* Clinical Orthopaedics and Related Research, 1994, **303**: p. 185–192.
7. Beil, T. L. *et al.* Journal of Rehabilitation Research and Development, 2004, **41**(6): p. 821-828.
8. Andriacchi, T.P. *et al.* Journal of Bone and Joint Surgery, 1980, **62**: p. 749-757.

Table 1. Knee and hip angles (mean ± SD) for the ground (GROUND) and the stair (STAIR) step for both systems and limbs (intact – INT, amputated – AMP).

			KNEE			HIP		
Condition	**Suspension System**	**Limb**	**Peak Swing Flexion**	**Late Stance Extension**	**ROM**	**Peak Swing Flexion**	**Peak Stance Extension**	**ROM**
GROUND	**PIN**	**Amp**	83.80 ± 11.22	5.03 ± 5.65	75.25 ± 10.80	78.62 ± 16.69	1.90 ± 20.93	76.71 ± 6.04
		Int	92.30 ± 6.63	9.10 ± 7.18	76.61 ± 14.56	83.80 ± 11.22	5.03 ± 5.68	78.76 ± 13.81
	PUCK	**Amp**	76.94 ± 9.81	6.60 ± 7.68	67.61 ± 10.61	63.05 ± 15.78	-7.96 ± 14.38	71.02 ± 6.19
		Int	91.53 ± 6.17	2.49 ± 5.56	76.03 ± 6.59	58.36 ± 10.38	-1.20 ± 10.38	59.56 ± 6.48
STEP	**PIN**	**Amp**	90.15 ± 10.80	14.88 ± 3.78	78.76 ± 13.81	75.33 ± 20.65	14.60 ± 19.51	63.73 ± 4.68
		Int	95.25 ± 6.93	11.74 ± 6.66	83.19 ± 6.02	65.36 ± 16.99	16.34 ± 16.99	55.06 ± 2.36
	PUCK	**Amp**	80.00 ± 10.61	12.27 ± 9.47	70.34 ± 9.61	63.23 ± 15.41	2.26 ± 12.39	60.78 ± 4.75
		Int	95.24 ± 6.59	12.53 ± 3.80	89.92 ± 5.73	54.47 ± 14.43	6.70 ± 11.21	52.52 ± 4.75

THE INFLUENCE OF LOCALIZED KNEE FATIGUE ON LOWER LIMB DYNAMICS DURING WALKING

[1]Nathan J. Robey, [1]Katie L. Boncella, [1]Margaret M. Ault, [1]Yute Wang, [1]Gary D. Heise and [1]Jeremy D. Smith

[1]University of Northern Colorado, Greeley, CO, USA
email: nathan.robey@unco.edu web: http://www.unco.edu/biomechanics Twitter: @UNCBiomechanics

INTRODUCTION

Knee joint injuries lead to changes in neuromuscular control and biomechanics of the lower limb, which may contribute to the development of osteoarthritis (OA) [1]. The exact cause of the cartilage degeneration in knee OA remains unclear in the literature as several potential contributors exist (e.g., previous joint injury, gender, etc.) [1]. However, one theory suggests that an increased rate of loading during gait may promote the development of OA [2,3].

Radin et al. (1991) analyzed loading rates in individuals with and without knee pain [3]. They suggested that individuals who had knee pain prior to the study had significantly higher loading rates. Individuals without knee pain used their quadriceps muscle group to control the rate of foot descent prior to heel contact, whereas this muscle function in individuals with knee pain was diminished, causing them to strike the ground harder [3].

Muscular strength around the knee joint has been identified as a potential contributor to the development of knee OA, specifically quadriceps strength [2]. Fatigue of the quadriceps may also lead to changes in knee loading during activities of daily living [4,5]. Previous literature is mixed on the exact effects of fatigue on lower limb kinetics and kinematics, as fatigue protocols vary between studies [4,5].

The purpose of this study was to determine how fatigued quadriceps and hamstring muscles influence kinematics and kinetics of the lower limb during walking.

METHODS

Eleven healthy, physically active females (n = 11) volunteered for this study (22 ± 2 years, 62.1 ± 8.4 kg, 167.0 ± 7.1 cm). Participants were free of any lower extremity injury for at least 6 months prior to participation. Participants wore socks during all walking trials [6], which occurred at 1.3 m/s on an AMTI tandem-belt treadmill (Watertown MA, USA).

A 6-min accommodation period was completed prior to data collection and served as a warm-up for each participant. A 3-min walk was performed prior to inducing fatigue in the quadriceps and hamstrings of the dominant leg. Maximal voluntary concentric actions on an isokinetic dynamometer were used to induce fatigue (Biodex, Shirley NY, USA). Baseline peak torque values for both knee flexion and extension were used to calculate the required fatigue level of 50% peak torque [7]. Fatigue was operationally-defined as the point where the first 5 consecutive maximal voluntary concentric repetitions were below the established 50% of initial peak torque values after returning from a 20-s rest period [7]. Once fatigue was achieved, a 3-min post-fatigue walking analysis was completed.

A total of 20 strides were analyzed for each participant during the walking trials. Joint kinematics and kinetics were determined. In addition, vertical loading rate (AVLR) was calculated between 20 and 80% of the slope of the weight acceptance phase of the vertical ground reaction force (VGRF) [8]. Repeated measures (pre- vs post-fatigue) ANOVAs ($\alpha = 0.05$) were performed to identify significant effects of fatigue and limb (control vs fatigued) (SPSS 24, IBM, USA).

RESULTS AND DISCUSSION

Following the fatigue protocol, both limbs exhibited increased power generation at the hip in early stance ($p = .035$) and late stance ($p = .018$), increased AVLR ($p = .034$), and increased VGRF during weight acceptance ($p = .028$) (Figures 1 & 2). In addition, two limb differences were observed when collapsed across pre and post fatigue: 1) the limb that was fatigued had greater ankle range of motion ($p = .048$) and 2) the fatigued limb generated more power at the hip during late stance ($p = .004$).

Our loading rates were significantly lower (Pre-fatigue = 6.23, Post-fatigue = 7.22 BW/s) than in individuals with knee pain (~68 BW/s) and controls (48 BW/s) that were reported by Radin et al. [3]. To some extent this may be due to the evaluation of GRFs during treadmill walking and overground walking. Where Radin [3] consistently observed a transient VGRF peak during weight acceptance, this transient peak only appeared in a few trials for some subjects. Thus, we chose to quantify the AVLR a little differently since we did not have that sharp transient peak in most of our trials. However, our method of quantifying the loading between 20-80% of the first VGRF peak might also be contributing to our lower AVLR values. Using a smaller window earlier in the slope of the VGRF may provide higher AVLR values.

CONCLUSIONS

Fatiguing the hamstrings and quadriceps of one limb led to increased reliance on the hip in both limbs for power generation during walking. Additionally, increased loading rates occurred in both limbs, which based on Radin et al. [3], may increase the risk of developing knee OA in both limbs with continued activity in the fatigue state.

REFERENCES

1. Thomas A, et al. *J Athl Train* **52**, 491-496, 2017
2. Mikesky A, et al. *J Orthop Res* **18**, 171-175, 2000.
3. Radin E, et al. *J Orthop Res* **9**, 398-405, 1991.
4. Murdock G, et al. *Eur J Appl Physiol* **112**, 439-449, 2012
5. Longpré H, et al. *Clin Biomech* **28**, 441-447, 2013
6. Zhang X, et al. *J Foot Ankle Res* **6**, 45, 2013
7. Thomas A, et al. *J Appl Biomech* **26**, 159-170, 2010
8. Milner C, et al. *Med Sci Sports Exerc* **38**, 323-328, 2006

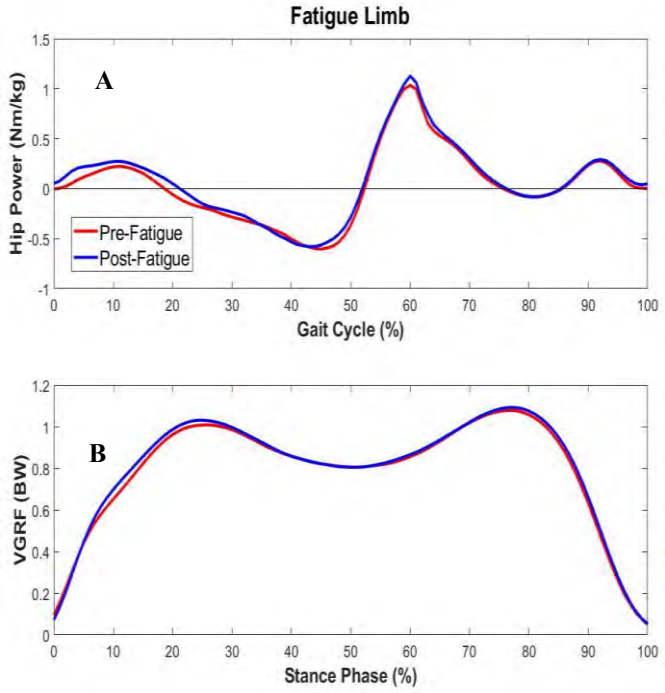

Figure 1. Mean hip joint power (A) and VGRF (B) across all subjects for the limb that was exposed to the fatiguing protocol.

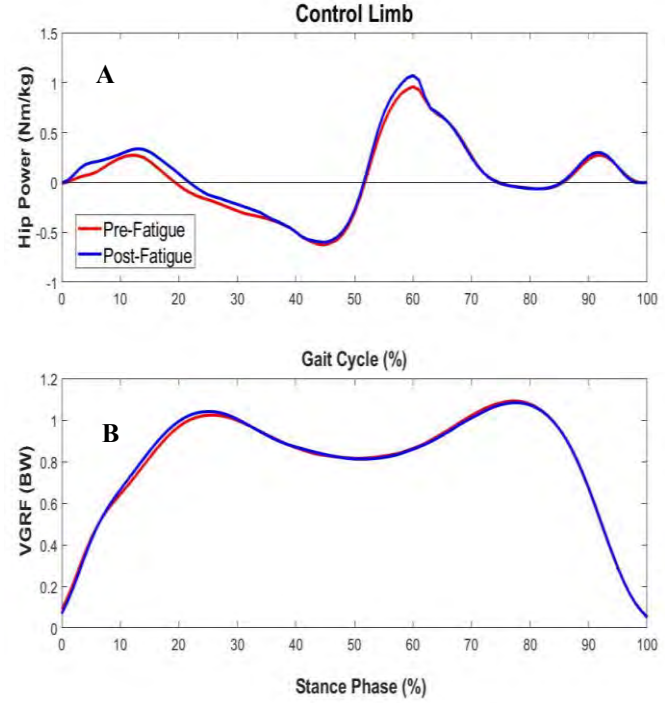

Figure 2. Mean hip joint power (A) and VGRF (B) across all subjects for the limb that was not exposed to the fatiguing protocol (i.e., control limb).

HAPTIC FEEDBACK DURING STAIR DESCENT

[1,2] Nataliya Rokhmanova and [1,2] Eric S. Rombokas

[1] Department of Mechanical Engineering, University of Washington, Seattle, WA, USA
[2] Center for Limb Loss and MoBility (CLiMB), Department of Veterans Affairs, Seattle, WA, USA
email: nrokh@uw.edu web: rombolabs.github.io

INTRODUCTION

With the loss of a limb comes not only the loss of function; the rich sensory experience of navigating the world is lost as well. Though great strides have been made in replacing sensation in missing upper limbs in a variety of contexts [1], development of sensory feedback in lower-limb prostheses has been largely stagnant. Without robust sensory feedback suited for a variety of environments, everyday tasks such as negotiating the stairs remain challenging and attention-consuming.

To maintain balance and mobility, it is possible to rely on other sensations: sight, sound, the pressure of the residuum against the socket. However, there is unique difficulty associated with stair descent, such as the absence of tactile sensations at the bottom of the foot, insufficient prosthetic ankle dorsiflexion, and undesirable energy release at the end of stair stance phase, as prostheses are generally optimized for flat-ground walking. This results in inefficient compensatory strategies of the knee and hip.

Here we describe a revised boot and electronic system based on our previous work [2,3] providing vibrotactile cues of foot placement during stair descent. We have created a simple and robust electronics package, and we use a ski boot in place of the medical walking boot. The new system provides more accurate readings of foot placement, eliminates the possibility of sensation through the boot, and provides reliable stimulation.

METHODS

The system consisted of an insole with force sensors, and electronics for logic and driving the motors. The insole may be attached to the bottom of a standard ski boot or worn under the prosthesis in a shoe. Our previous design used piezoelectric stimulators, which are potentially very expressive, but require custom drivers and are not commercially available. Here we use eccentric rotating mass (ERM) motors instead. We have also replaced the powerful BeagleBone computing system with a lightweight, inexpensive, and robust Arduino-based computing system. The previous system was integrated with a medical walking boot, which did not eliminate all sensation of plantar forces and featured a rounded sole, which complicated force sensing in the insole [3]. In the present study we used a stiff ski boot with a flat sole. The updated device has been evaluated so far on 4 participants without amputation (ages 20-26, 2 female). All participants consented under IRB approval.

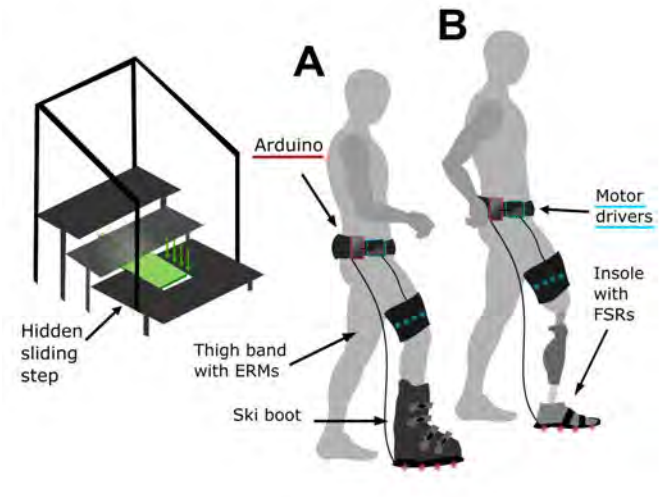

Figure 1: The hidden-step stair and haptic feedback system, worn by a subject in a ski boot (A) or prosthesis user (B).

The insole (Fig. 1) consisted of four force-sensitive piezoresistors (FSRs) arranged from toe to heel. The forces were read from each sensor at 10Hz. The Arduino coordinated with the motor drivers (I2C digital bus) to output a vibration pattern on the ERM stimulators on the thigh band. The ERMs vibrated at 70Hz, each corresponding to a single FSR when it senses a force exceeds a hand-tuned

threshold. The neoprene thigh band held four ERM motors, encased in an ABS housing with hook Velcro on the back, allowing for any spatial motor arrangement. The motor housings (2cm x 2cm) were in direct contact with the skin, spaced 7cm apart to ensure discriminability [4]. Motors were arranged medio-laterally, corresponding to the anterior-posterior arrangement of the FSRs.

Task 1 measured how well the subject can distinguish individual motor vibrations. The subject donned the thigh band and noise-cancelling headphones as the experimenter pressed a random sequence of FSRs on the insole one by one. The subject indicated which of the motors they felt vibrating. **Task 2** was to discern the vibration of the motors during a stair stepping task. The staircase (Fig. 1) had a sliding step hidden under a black felt sheet. The subject donned the thigh band, ski boot, and noise-cancelling headphones, and stood with both feet on either side of the hidden step. The experimenter locked the position of the step corresponding to one of the four toe overhang positions at each FSR, out of sight of the subject. The subject stepped onto the target foot outline and indicated which motors they felt vibrating.

RESULTS AND DISCUSSION

The results of the first task (Fig. 2a) across all four subjects show that the correct ERM was identified 93.1% of the time on average, and 82.9% of the time on average in the second task (Fig. 2b). Though performance decreased in the second task, errors were almost all a confusion of neighboring motors. The average performance in Task 1 was 5.9% greater than in our previous study [3], suggesting the ERMs and improved driver electronics resulted in greater perception accuracy.

Across all subjects, in both trials, identifying the vibration of the first ERM was easiest. It was placed on the inner thigh, which may be an optimal location for the placement of motors in future studies. The decreased performance between the two tasks can be partially attributed to poor boot fit in subjects with small feet, as well as varying levels of subcutaneous fat that made discerning vibration difficult in the more physically demanding second task. Additionally, the simultaneous stimulation of motors in the second task may make discrimination more difficult than in individual stimulation.

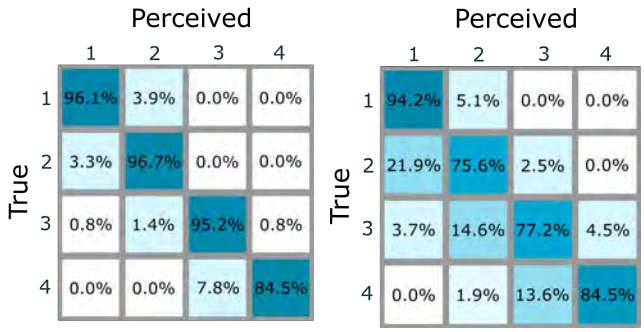

Figure 2: Average accuracy across all trials for true versus perceived results, in simple discrimination (a) and stair discrimination (b) tasks, respectively.

CONCLUSIONS

The improved performance of participants in this study justify the revisions of our haptic feedback system. This pilot study provides confidence that the system is ready to deploy for prosthesis users. Future studies will also investigate the effect of different spatial motor orientations on perception, as well as the impact of cueing foot placement on the speed of stair descent and user confidence. This method of sensory feedback may be well-suited for subjects that have undergone Targeted Reinnervation (TR) surgery.

REFERENCES

1. C. Antfolk, M. D'Alonzo, B. Rosén, G. Lundborg, F. Sebelius, C. Cipriani. "Sensory feedback in upper limb prosthetics." *Expert Review of Medical Devices*, 10:1, 45-54, 2014.
2. A. Sie, J. Realmuto, E. Rombokas. "A Lower Limb Prosthesis Haptic Feedback System for Stair Descent." *Design of Medical Devices*. 2017
3. A. Sie, D. Boe, E. Rombokas. "Design and Evaluation of a Wearable Haptic Feedback System for Lower Limb Prostheses during Stair Descent." 2018 IEEE BioRob, Enschede, The Netherlands, 2018. (under review).
4. S. Weinstein. "Intensive and extensive aspects of tactile sensitivity as a function of body part, sex, and laterality." *The Skin Senses.* Thomas Books: Springfield IL, 1968.

WALKING WITH VISUAL CUEING AFFECTS CORTICAL HEMODYNAMICS

Douglas A. Rowen[1], Joao R. Vaz[1], Brian Knarr[1], and Nicholas Stergiou[1,2]

[1]Department of Biomechanics, University of Nebraska at Omaha, Omaha, NE USA
[2]College of Public Health, University of Nebraska Medical Center, Omaha, NE USA
email: darowen@unomaha.edu, web: https://www.unomaha.edu/college-of-education/cobre/

INTRODUCTION

Walking is one of the most important activities of daily life and is needed to maintain independence and quality of life. A common rehabilitation approach to improve walking involves using auditory or visual cueing (e.g metronome) that has no variability in its presentation. Such cueing provides patients with spatial or temporal information on when or where to step. Previous research has shown that individuals are capable of synchronizing their steps with such cueing [1,2] and in pathological populations, improvements to gait characteristics, such as gait symmetry, gait velocity, and stride length, have been identified [3]. More recently, variable cueing has been used where cues are provided based on a pink-noise type of a distribution [1,4]. This type of cueing also improves gait characteristics and is hypothesized to be advantageous, providing greater improvements than non-variable cueing, as pink noise better resembles the distribution of the variations found during healthy natural gait. Thus a dilemma exists regarding what should be preferred for training patients, variable or non-variable cueing.

Previous research on gait variability have utilized functional Near Infrared Spectroscopy (fNIRS) to examine its relationship with sensorimotor cortical activity [5]. A positive strong relationship has been reported between gait variability and brain activation in the primary motor cortex and supplementary motor areas. We believe that such an investigative approach can also be utilized to allow us to provide additional insights regarding the above presented dilemma. Thus, the aim of this study was to investigate the differences in brain activation as a result of walking with different types of cueing.

METHODS

Four subjects (age 25.5 ± 5.25 yrs., 4 male) walked four 10-minute trials on a treadmill while wearing a 4x4 functional Near Infrared Spectroscopy (fNIRS) probe set (Hitachi ETG-4000) to measure brain activity. The fNIRS probes measured both deoxygenated and oxygenated blood flow at 690 nm and 830 nm with a source-detector separation distance of 3 cm. The fNIRS was placed using the 10/20 system for EEG placement and measured blood flow in the prefrontal cortex (PFC), supplementary motor areas (SMA), and the primary motor cortex (MC). FNIRS data was recorded and filtered using a low pass filter at 0.5 Hz. The subjects matched their heel-strikes to three different continuous visual cueing: non-variable, variable using a white-noise distribution and variable using a pink-noise distribution. Prior to the trials, a ten minute walking trial was recorded to determine the cadence and deviation for the metronomes. In addition, Noraxon footswitches were worn to determine gait events. Footswitch data was recorded to accurately identify heel-strike events. Inter-stride intervals were then calculated from heel-strike times and compared with the different conditions to determine if each subject matched the cueing. Detrended Fluctuations Analysis (DFA) exponent [6] was used for these evaluations. DFA estimates the relationship between the size of fluctuations $F(n)$ within a time series for windows of observation of size n. A linear slope in bi-logarithmic coordinates reveals a power-law relationship, such that $F(n) \sim n^{\alpha}$, where α is the slope or scaling exponent. An $\alpha > 0.5$ reflects persistent fluctuations while $\alpha < 0.5$ reflects anti-persistent fluctuations, and $\alpha = 0.5$ indicates randomness.

RESULTS AND DISCUSSION

The results of the present study are in line with the previous literature [1] showing that the DFA exponent of variable pink-noise cueing (0.95±.16) is

similar to the self-paced (0.82±.09) condition in young adults, while variable white-noise cueing (0.53±.07) and non-variable cueing (0.34±.09) exhibit lower values (Figure 1). Although this is a preliminary analysis of hemodynamic data, all three cueing conditions resulted in an increase of blood flow across the three regions of interest (Figure 2). The non-variable metronome had the least amount of increase in the prefrontal cortex. This may indicate that less concentration is needed to match to this cueing since it has no temporal variance.

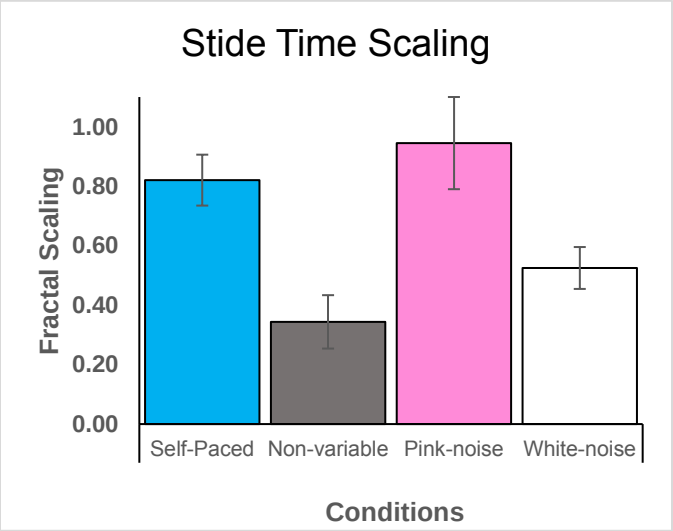

Figure 1: The average DFA exponent values for the self-paced and the three cueing conditions.

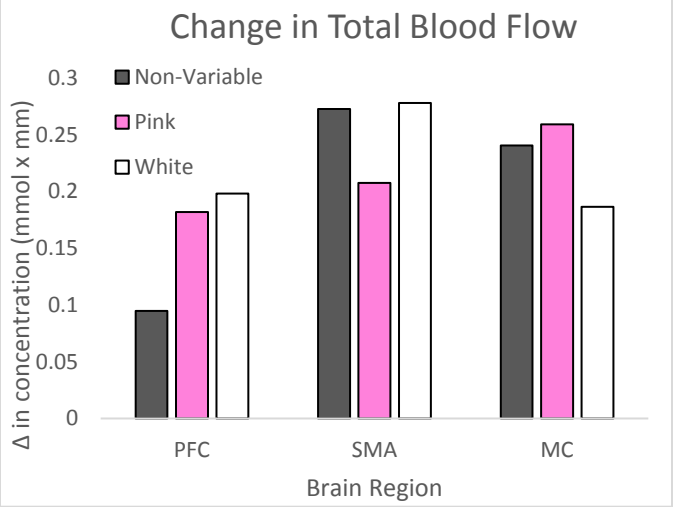

Figure 2: The change in the concentration of blood flow in the three regions of interest for the three cueing conditions. This represents the increase in blood flow seen during walking for each condition based on the self-paced walking condition.

The increases in the PFC were most likely due to the fact that walking with cueing may resemble a dual task activity which results in additional brain activity in the prefrontal region [7].

The cueing conditions exhibit similar levels of blood flow in the SMA and MC (Figure 2). This may mean that the changes in walking, away from the self-paced condition, are similar for all three cueing conditions. The SMA and MC are used in the initiation and control of movement so it may be useful to investigate if there are differences between the cueing conditions during the initiation of walking.

CONCLUSIONS

Regardless of the temporal structure of the cues, the blood flow increased in all three regions of interests. More data need to be collected to understand if the current preliminary findings are significant and correlate with changes in gait variability. Changes in the temporal structure of cueing may impose different attentional demands for an individual to remain synchronized with the presented cues.

REFERENCES

1. Kaipust JP, et al. *Ann Biomed Eng* **224**, 507-518, 2012.
2. Marmelat V. et al. *PLoS One* **9**, e91949, 2014.
3. Whittwer JE. et al. *Disabili Rehabil* **35,** 164-176, 2013
4. Hunt N. et al. *Scientific Reports* **4,** 5879, 2014.
5. Kurz MJ. et al. *NeuroImage* **59,** 1602-1607, 2012
6. Peng CK. et al. *Chaos* **5,** 82-87, 1995.
7. Herold F. et al. Neurophotonics **4,** 041403, 2017

ACKNOWLEDGEMENTS

This work was supported by NIH P20GM109090 and NIH R15HD0868.

Comparison of Three-dimensional Ankle and Foot Kinematics between Leardini and Oxford Multi-Segment Foot Models in Active, Healthy Elders

[1] Skylar A. Schoen and [1] Gordon Alderink

[1] Grand Valley State University, Grand Rapids, MI USA
email: aldering@gvsu.edu

INTRODUCTION

Despite the frequent use of multi-segment foot models (MSFM) in clinical and research settings, very few studies exist regarding kinematic variables derived from use of MSFMs in assessment of the well-elderly population. This study compared nine kinematic variables of the foot/ankle across two validated MSFMs: Oxford Foot Model (OFM) and Leardini, while simultaneously creating a controlled data set of kinematic gait variables for both models in a healthy, elderly sample, aged 70-85.

METHODS

This study was approved by the University institution review board (Ref#:14080H). The 18 healthy adults (7 females, 11 males, 78.1 ± 4.0 years, height = 169.9 ± 11.9 cm, mass = 72.3 ± 10.2 kg, BMI = 25.1± 2.6 kg/m^2) who participated were part of a larger convenient sample of normal, healthy adults aged 18-85 years that comprised a control gait data set. Participants were a sample of convenience and gave consent prior to participation. Inclusion criteria were absence of: significant medical condition, e.g., uncontrolled high blood pressure, unstable heart disease, respiratory disease, or neurological condition, e.g,. multiple sclerosis, significant orthopedic injury within the past six months, and reconstructive surgery e.g., ACL, to the joint(s) involving the lower extremity. Prior to data collection, each participant was given a medical and surgical questionnaire, and underwent a physical screening and anthropometric measures examination, which also served to screen individuals for normality.

Data were collected using two different full body models, Mary Free Bed Rehabilitation Hospital (MFB) with modified Leardini foot model [1] and Vicon Plug-in Gait (PIG) with Oxford Foot Model (OFM) [2].

The choice of which model to apply first was random. A single investigator attached markers using two-sided, hypoallergenic tape. Nine-millimeter diameter retro-reflective markers were used on the feet, and 14 mm markers on all other segments. Prior to walking, a standing static subject calibration data collection and reduction was completed, and modeled markers, i.e., joint centers, were checked for their presence. Each subject completed walking trials over a 10m walkway, until five successful force platform foot strikes were collected for each extremity. After a short break, the first model marker set was removed and replaced by the other marker set, followed by a second static calibration and set of successful walking trials.

Kinematic data were collected using eight MX-T40 cameras (120 Hz) and Nexus motion capture software v1.8.4 (Vicon Motion System Ltd., Oxford Metrics, UK). Synchronized ground reaction force data were collected (1200 Hz) with two AMTI force plates (Advanced Mechanical Technology Inc., Watertown, MA) embedded in the walkway.

Static and dynamic trials were reconstructed, and marker positions labeled using Vicon Nexus v 1.8.4. Marker trajectories were edited in Nexus using one of three gap-filling methods: spline fill, pattern fill, or rigid fill. Raw trajectory data were filtered using Woltring MSE 15 [3]. Visual 3D Professional (C-Motion, Germantown, MD) was utilized for dynamic processing.

SAS JMP 13.0 Statistical analysis software was used to complete a multivariate regression analysis of variance (MANOVA) for the nine separate kinematic variables.

RESULTS AND DISCUSSION

Given there is a paucity of published data on healthy elderly individuals using multi-segment foot models, the aims of this study were: 1) to create a control data set of ankle/foot motion related to walking, and 2) to compare ankle/foot joint angles determined from two frequently used multi-segment foot models. Our results showed significant kinematic differences in all nine ankle/foot variables.

There were significant differences between models for all 9 variables. The OFM showed greater range of motion (ROM) angles for ankle dorsiflexion/plantarflexion, ankle inversion/eversion, tibia/hindfoot dorsiflexion/plantarflexion, tibia/hindfoot abduction/adduction, and hindfoot/forefoot dorsiflexion/plantarflexion, while Leardini showed greater ROM angles for hindfoot/forefoot abduction/adduction, hindfoot/forefoot inversion/eversion, and foot progression angle.

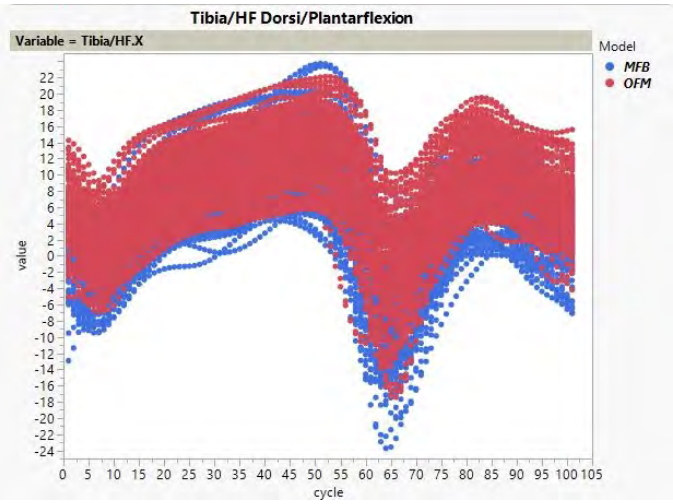

Figure 1: Data comparison of one of the nine kinematic variables (Tibia/HF Dorsi/Plantarflexion) that were analyzed.

Kinematic gait variables differed significantly across models. It's likely that differences were related to 1) marker definition and 2) how foot segments were defined [1,2]. Differences in foot motion in our use of the Leardini model and published values may rest in the modifications we made in heel marker placement. Knowing the trends of these differences in MSFMs will help clinicians and researchers choose which model to use when performing ankle/foot gait analysis.

CONCLUSIONS

Although the Oxford Foot Model and the Mary Free Bed/Leardini multi-segment foot model contain markers that allow for measurement of the same ankle/foot kinematic variables, the two produce significantly different joint angles when compared across nine commonly analyzed variables. . These data could serve as control data sets for the analysis of pathological gait in elders. Our results highlight the crucial role of marker placement, as well as the need for further examination of the potential causes for differences in gait variables between these two validated multi-segment foot models.

REFERENCES

1.Leardini A, Benedetti M, Berti D, Bettinelli D, Navito S, Giannini S. Rear-foot, mid-foot and fore-foot motion during the stance phase of gait. Gait Posture 2007;25(3):453-462.

2.Carson MC, Harrington ME, Thompson N, O'Connor JJ, Theologis TN. Kinematic analysis of a multi-segment foot model for research and clinical applications: a repeatability analysis. J Biomech 2001;34(10):1299–307.

3.Woltring HJ. A FORTAN package for generalized cross-validatory spline smoothing and differentiation. Adv Eng Softw 1986;8(2):104-113

ACKNOWLEDGEMENTS

David Zeitler, PhD, Statistical Consultant

COMPARISON OF SUBJECTIVE ELECTROMYOGRAPHIC ONSET DETERMINATION TO OBJECTIVE TECHNIQUES DURING RUNNING

[1] Barbara J. Schornstein, [2] Kevin D. Dames, [1]Jeremy D. Smith, and [1] Gary D. Heise

[1] University of Northern Colorado, CO, USA
[2] SUNY Cortland, NY, USA
email: barbara.schornstein@gmail.com

INTRODUCTION

There is not a universal standard for identifying onset and offset of electromyographic (EMG) activity during running. While many methods exist to achieve this goal, there has been a lack of consistency even when replicating studies [1,2,3]. The most common method used to determine onset and offset is manual determination [1,2], however this approach is time intensive and rater dependent. Being rater dependent, it can be highly subjective; however, objective techniques can produce false positives of muscle onset. The purpose of this study was to compare three techniques of EMG data analysis for determining muscular activity onset and offset during the stance phase of running to manual onset and offset detection.

METHODS

For this study that was approved by the Institutional Review Board, participants (11 women, 11 men; aged 31±10 years (mean ± standard deviation (SD))) ran on a treadmill at three speeds (3.3, 3.5 and 3.7 $m \cdot s^{-1}$). Motion (100 Hz), force (2000 Hz), and EMG data (2000 Hz) from rectus femoris (RF), biceps femoris (BF) and lateral gastrocnemius (LG) were recoded from the right leg only while running. Motion and force data were imported into Visual 3D (C-Motion) to determine stance phase for five consecutive strides. Foot strike data were then imported into MATLAB (MathWorks) for further analysis along with EMG data.

Manual determination of muscle onset during stance after full-wave rectification and a low-pass filter (f_c=15 Hz) [1,2] was considered the reference technique. This technique was used as the comparator as it was used in the original reference articles [1,2]. While it is the most subjective technique as it is rater dependent, it reduces the likelihood of false positives that may occur in automated approaches.

The second technique (Moore) was also used in previous running research [3]. A Root Mean Square (RMS) filter with a 50 ms sliding window was applied. A threshold as a percentage of max amplitude from a single stance phase was set (7% for RF and LG, 10% for BF) to determine when in stance was the onset of muscle activity [3].

The third technique (TKEO) was a five-step process and novel to running:

(1) High-pass filtering (f_c=10 Hz)
(2) Energy operator conditioner was applied:
$$\Psi[x(n)] = x^2(n) - x(n+1) * x(n-1)$$
where x is the EMG amplitude value and n is the sample number
(3) Full-wave rectification
(4) Low-pass filter (f_c=50 Hz)
(5) Threshold of 15 SD above the lowest mean baseline

The baseline was calculated by a sliding window of 10% advanced point-by-point over the gait cycle [4].

The fourth technique (AGLR) consisted of a whitening filter followed by a log-likelihood ratio test. A sliding window was advanced point-by-point over the entire EMG signal, calculating the variance in each of the windows. The window was set to 300 frames. If the ratio of variance between the baseline window and the testing window exceeded 20, the testing window was marked for post-processing. Next, a maximum likelihood function was run through the windows marked for post-processing and the variance levels were plotted in a histogram where onset was determined visually where a break in the variance levels occurred, which suggested a difference between the baseline activity and the onset

of muscle activity [5]. This technique was also novel to running.

All muscle activity durations were collapsed across speed and the interquartile ranges were calculated to demonstrate the variability in activity due to technique differences. Pearson's correlation coefficients were calculated between the manual, subjective approach and the three other techniques (Moore, TKEO, and AGLR).

RESULTS AND DISCUSSION

The largest interquartile range was for the BF with the AGLR technique at 32% of stance phase; however, BF had large interquartile differences regardless of technique as the mean range was 21.7% of stance phase (Figure 1). LG had the lowest mean interquartile range (11.9%) and suggests that the determination of onset and offset was easily detectable (Figure 1).

Data from all three speeds were collapsed and correlated with the manual technique. AGLR has the highest correlations with the manual technique (Table 1). This suggests that while manual methods are most commonly used, this novel technique removes some of the subjectivity that different raters can introduce. AGLR also had some subjective and visual parts of the method; however, the rater is guided through the process using computerized, objective techniques.

CONCLUSIONS

The AGLR method treats EMG data most similarly to manual determination. AGLR, then, is suggested as the best technique to use in determining onset and offset of muscular activity as it removes most of the inter- and intra-rater subjectivity that manual methods can introduce.

Table 1: Pearson's correlations between manual and the other three techniques of onset and offset determination for each muscle duration (RF, BF, and LG), collapsed across the three running speeds.

	Moore		TKEO		AGLR	
Muscle	r	*p*-value	r	*p*-value	r	*p*-value
RF	.17	.17	.13	.30	**.33**	**.01**
BF	.22	.08	**.30**	**.02**	**.25**	**.04**
LG	**.52**	**<.001**	**.28**	**.02**	**.85**	**<.001**

Note: **Bold**=significant $p \leq .05$

REFERENCES

1. Heise, Morgan, Hough, & Craib. *Int J Sports Med,* **17(2)**:128-133, 1996.
2. Heise, Morgan, & Binks. *Int J Sports Med*. **29(8)**: 688-691, 2008.
3. Moore, Jones, & Dixon. *J Sci Med Sport.* **17(6)**:671-676, 2014.
4. Solnik, Rider, Steinweg, DeVita & Hortobági. *Eur J Appl Physiol*. **110(3)**:489-498, 2010.
5. Staude & Wolf. *Med Eng Phys* **21(6-7)**:449-467, 1999.

ACKNOWLEDGEMENTS

Drs. Moore and Staude were helpful in responding to personal inquiries about and clarifications of their methods.

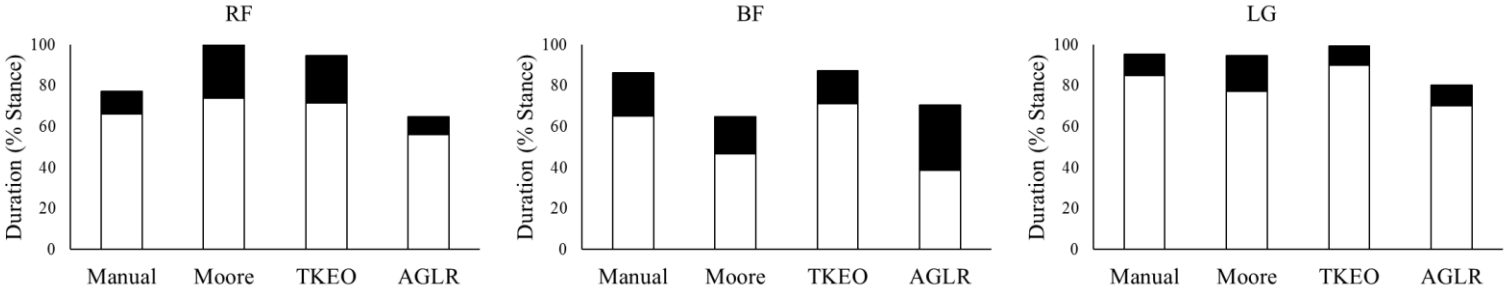

Figure 1: The interquartile range of duration in muscular activity collapsed across the three speeds of running during stance for all participants in each technique. The shaded black region represents the interquartile range.

Sex Impacts Frontal Plane GRF and Knee Biomechanics during Drop Landing with Body Borne Load

Kayla D. Seymore, AuraLea C. Fain, Nick J. Lobb and Tyler N. Brown
Dept. of Kinesiology, Boise State University, Boise, ID, USA
email: kaylaseymore@boisestate.edu

INTRODUCTION

Military personnel commonly suffer musculoskeletal injuries at the knee joint. These knee injuries occur during military activities when personnel repeatedly land with heavy body borne loads. During landing, these heavy body borne loads increase the risk of knee musculoskeletal injury by placing larger ground reaction forces (GRF) and subsequent loads on the joint. Female military personnel are twice as likely to sustain a training-related musculoskeletal injury compared to their male counterparts. Females' injury risk may be attributed to the use of larger GRFs and greater dynamic knee valgus (abduction motions and loads) during landing compared to males [1,2]. Landing with a laterally-directed GRF vector acts to push the knee further into dynamic valgus [3], increasing risk of injury by elevating the hazardous loads place on the joint. To reduce their risk of musculoskeletal injury, military personnel, particularly females, may need to increase lower limb flexion during landing, as it is reported to increase energy absorption and may decrease GRFs and loads placed on the knee. However, it is currently unclear if using greater lower limb flexion when landing with heavy body borne loads is attainable, or whether it reduces risk of musculoskeletal injury by decreasing magnitude and direction of GRFs associated with landing. As such, the purpose of this study was to determine whether using greater lower limb flexion when landing with body borne load decreases the magnitude and lateral-direction of GRFs for both male and female military personnel.

METHODS

Thirty-two (20 male and 12 female) participants had 3D lower limb biomechanics quantified during a series of drop landings. Each participant performed the drop landings with four load conditions: 20 kg, 25 kg, 30 kg and 35 kg. For each load, participants carried military equipment (mock weapon and helmet) and donned a weighted vest, which was systematically adjusted to apply the load necessary for each condition. Each participant performed five trials of two types of landings: normal (NL) and flexed (FL). The NL required participants to step off a 30-cm box and land with each foot on a separate force platform. Following the NL, participants performed the FL. For the FL, participants were instructed to step off a 30-cm box and exaggerate lower limb flexion upon landing.

During each drop landing, GRFs and knee biomechanics were quantified. During each trial, synchronous GRF data and trajectories of 32 retroreflective markers were low pass filtered with a fourth-order Butterworth filter (12 Hz). Filtered marker trajectories were processed to solve knee joint rotations using Visual 3D (C-Motion, Rockville, MD). Filtered kinematic and GRF data were processed using conventional inverse dynamic analysis to obtain knee joint moments. From the filtered GRF data, peak vertical GRF (vGRF), and the magnitude (GRF_{mag}) and direction (GRF_{ang}) of the GRF vector in frontal plane were calculated using the following standard trigonometry equations:

$$GRF_{mag} = \sqrt{F_x^2 + F_z^2}$$

$$GRF_{ang} = tan^{-1}\frac{F_x}{F_z}$$

where Fz and Fx represent the vertical and mediolateral GRF vectors, respectively [3]. Positive GRF_{ang} indicated a laterally-directed GRF. GRFs were normalized to bodyweight (BW), while joint moments were normalized to body mass by height.

For analysis, peak stance (PS, 0% - 100%) knee sagittal and frontal plane angles and moments, vGRF, GRF_{mag} and GRF_{ang} were quantified. Each variable was submitted to a repeated measures ANOVA to test the main effect and interaction between load (*20 kg, 25 kg, 30 kg, 35 kg*), sex (*male, female*), and landing condition (*NL, FL*). Significant interactions were submitted to a simple effects analysis, and a Bonferroni correction was used for multiple comparisons. Alpha was $p < 0.05$.

RESULTS and DISCUSSION

Landing with body borne load may increase risk of knee musculoskeletal injury by placing larger impact forces on the joint. Participants exhibited a significant increase in both peak vGRF and GRF_{mag} with each incremental addition of load ($p < 0.05$). But, body borne load had no significant effect on GRF_{ang} ($p = 0.754$). These elevated landing forces may act to increase injury risk by creating valgus loads at the females' knee. Specifically, females exhibited greater PS knee abduction moment with the 20 kg ($p < 0.001$), 25 kg ($p = 0.030$), and 35 kg ($p < 0.001$) loads compared to males, but only during the NL landings (Fig. 1).

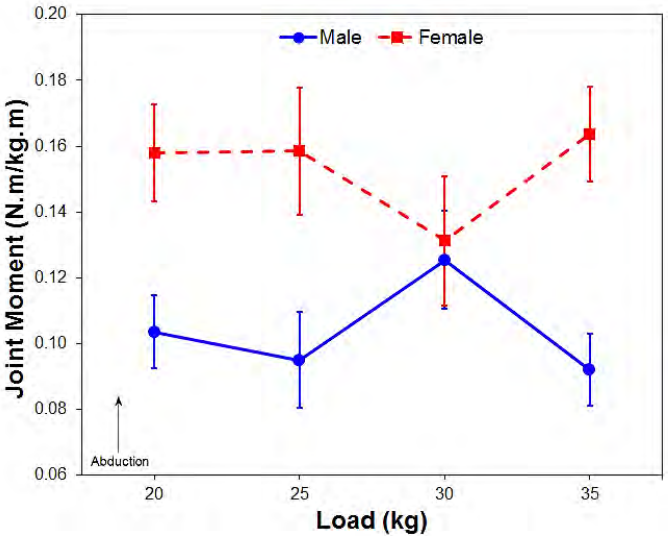

Figure 1: Peak (mean ± SE) knee abduction joint moment exhibited by males and females during NL for each load condition.

Using greater lower limb flexion when landing with load is attainable and may decrease injury risk. Participants exhibited a significant increase in PS knee flexion during the FL compared to NL landings ($p < 0.001$). However, the reduction in injury risk may depend on sex. The ANOVA revealed a significant landing type versus sex interaction for PS knee flexion ($p = 0.003$), vGRF ($p = 0.009$), and GRF_{mag} ($p = 0.005$). Both sexes increased PS knee flexion ($p < 0.001$), and decreased vGRF ($p<0.001$) and GRF_{mag} ($p < 0.001$) during the FL compared to NL landings. But, females may have greater risk of injury during the FL landings, as they exhibited greater vGRF ($p = 0.003$, Fig. 2) and GRF_{mag} ($p = 0.005$) compared to males. Using greater flexion during landing may also prevent the GRFs from pushing the knee into dynamic valgus and further increase injury risk. Participants decrease PS knee abduction moment ($p < 0.001$) during the FL compared to NL landings. Additionally, the GRF_{ang} was more medially-directed during the FL compared to NL ($p = 0.010$), but only with loads greater than 25 kg ($p < 0.05$).

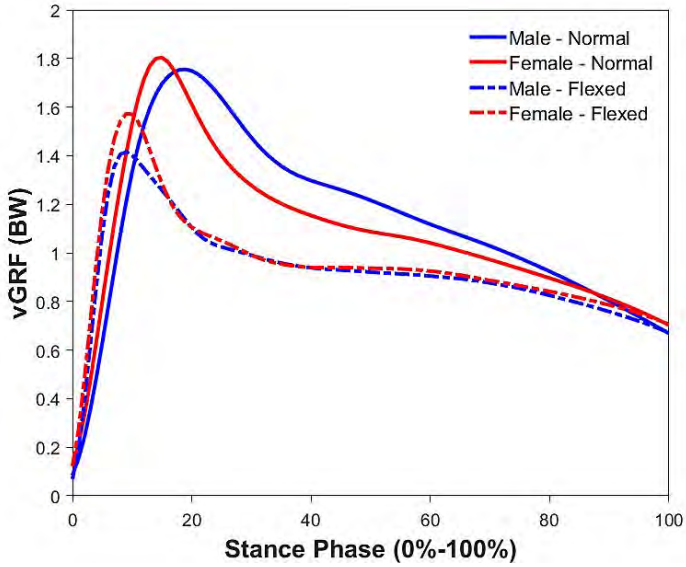

Figure 2: Peak vGRF exhibited by males and females during each landing type (NL and FL).

CONCLUSIONS

Heavy body borne load increased participants' risk of knee musculoskeletal injury. A reduction in this injury risk may be attainable by landing with greater knee flexion. Using greater flexion during landing was, indeed, attainable and reduced the ground reaction forces and frontal plane loading placed on the lower limb. However, females may have an elevated risk of injury, as they exhibited larger ground reaction forces and knee abduction moments during landing.

REFERENCES

1. Pappas E, et al. *J Sci Med Sport* **15**, 87–92, 2012.
2. Hewett TE, et al. *AJSM* **33**, 492–501, 2005.
3. Creaby M, et al. *MSSE* **40**, 1669–1674, 2008.

SAGITTAL PELVIC MOTION OF PATIENTS WITH UNILATERAL, TRANSTIBIAL AMPUTATIONS COMPARED TO HEALTHY MILITARY CONTROLS WHILE RUNNING OVERGROUND

Katherine Sharp, Julianne Stewart, Jenny Anne Maun, Kimberly Rowe, John-David Collins, Tatiana Djafar, Trevor Kingsbury, and Marilynn Wyatt

Naval Medical Center San Diego, San Diego, CA USA
email: katherine.sharp5.ctr@mail.mil

INTRODUCTION

Pelvic motion in the sagittal plane (anterior pelvic tilt) while running is one of various kinematic measures that can determine level of injury risk. Excessive anterior tilt at the pelvis has been linked to injuries including hamstring strain and low back pain, making it an important variable to consider during running training and evaluations [1]. The current study measured the sagittal pelvic motion of patients with unilateral, transtibial amputations (TTA) while running overground and compared it to uninjured, active-duty military controls (CTRL). It was hypothesized that TTAs would exhibit increased anterior pelvic tilt compared to CTRLs. Whether or not the hypothesis is supported, this work provides preliminary values of sagittal pelvic motion for this patient population, as well as reinforces previously published data regarding uninjured populations.

METHODS

Four male patients with TTA (age 32±6.8yrs, height 1.8±0.1m, weight 78±13.7kg) were compared to ten male CTRL subjects (age 30±6.1yrs, height 1.8±0.1m, weight 82.9±8.2kg). All participants provided written informed consent prior to the study (CIP #NMCSD-2013.0109) which was previously approved by the Naval Medical Center San Diego IRB. Patients wore their own running shoe on their unaffected side, and all donned a prosthetic running leg with a custom socket on their affected side. Controls ran in their own running shoes.

A six degrees of freedom (6DoF) marker set was used for this study (Fig. 1). Anatomical markers were placed on the following bony prominences: bilateral second and fifth metatarsal heads, calcaneus at the height of the marker of the second metatarsal head, medial and lateral malleoli, medial and lateral femoral condyles, anterior superior iliac spines (ASIS), and posterior superior iliac spines (PSIS). Clusters of markers used for tracking segments were placed bilaterally on the thigh and shank (or prosthetic socket). On the affected leg of TTA patients, markers were placed on the prosthetic running blade.

Figure 1: TTA patient donning all markers prior to data collection session

The motion capture system was set-up on a 50m section of track. It consisted of 12 Raptor-E motion capture cameras (Motion Analysis Corp., Santa Rosa, CA) collecting 3D kinematic data at 300Hz and four portable force plates (Kistler Instrument Corp., Amherst, NY) synced to the motion capture system collecting kinetic data at 1800Hz. The kinematic data were processed using Visual 3D software (C-Motion Inc., Germantown, MD, USA) and a 4th order, low-pass Butterworth filter with a cutoff of 8Hz was applied. Pelvic motion was defined as movement of the pelvic segment with respect to the lab coordinate system.

Participants were asked to jog down the capture volume repeatedly at a speed of 3.5m·s^{-1} (±0.2m·s^{-1}) until at least three clean force plate strikes and at least six full gait cycles on each limb were achieved. Speed was monitored using a Cortex (Motion Analysis Corp., Santa Rosa, CA) presentation graphs tool and force plate strikes were used to determine gait events. Anterior pelvic tilt from initial contact (IC) of affected leg of patients with TTA to subsequent IC on the same limb was compared to the right limb of CTRL subjects.

Pelvic tilt angles at toe-off were statistically compared using independent, two-tailed t-tests between TTA and CTRL groups with a significance level of 0.05.

RESULTS AND DISCUSSION

Patients with TTA had an anterior pelvic tilt angle that was significantly increased ($p<0.001$) compared to the CTRL group at toe-off. The max anterior pelvic tilt at toe-off on the affected limb of patients with TTA was 23.8° (±1.8°) and 19.3° (±1.6°) for the CRTL group. Sustained increased anterior pelvic tilt for patients with TTA can be observed throughout the gait cycle in Figure 2.

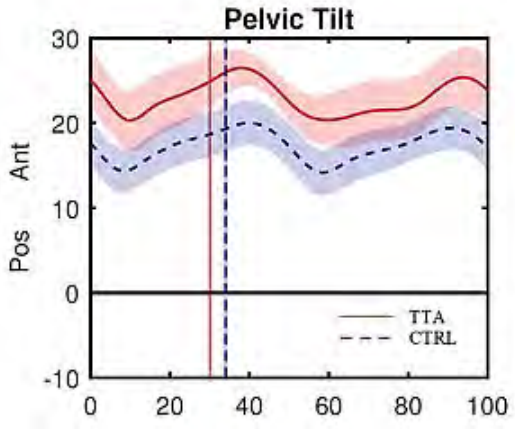

Figure 2. Pelvic tilt of affected limb of TTA group (red) and right limb of CTRL group (blue) over 100% of the gait cycle from IC to IC. Vertical lines represent toe-off for each group.

A top priority of patient care is to avoid movement patterns that increase injury risk. Therefore, it's important to consider the relationship between increased anterior pelvic tilt and stress on the low back. This is an important concern for the general population, and even more so for patients with TTA, as they demonstrate a high incidence of back pain from walking alone [2]. Now knowing that they are susceptible to increased anterior pelvic tilt while running as well, providers can attempt to prevent it through early practice of proper running mechanics and preparatory stretching and strengthening exercises.

Although this data set includes a limited number of patients with TTA, it can be viewed as the beginning of a knowledge base on pelvic tilt in runners with amputation that is not currently available [2]. Future work with runners with TTA will allow us to understand the connection between musculoskeletal restrictions (i.e. tight hip flexors, restricted hip capsule or ligamentous structures, etc.) and increased anterior pelvic tilt. This, in turn, can direct rehabilitation and training efforts to avoid excessive anterior pelvic tilt in both groups.

CONCLUSIONS

Patients with TTA demonstrated significantly increased anterior pelvic tilt at toe-off while running compared to their uninjured, active-duty military peers, thus supporting our hypothesis. Future work will focus on the continued collection of kinematic and kinetic data on this patient population. Additional kinematic variables and their possible relationship with range of motion, strength, and pain values will also be collected and evaluated to give further insight on this matter.

REFERENCES

1. Schache AG, et al. *Hum Mov Sci* **21**, 273-293, 2002.
2. Gailey R, et al. *J Rehabi Res Dev* **45**, 15-30, 2008.

ACKNOWLEDGMENTS

This work was supported (in part) with resources provided by the Extremity Trauma & Amputation Center of Excellence. And thanks to General Dynamics Information Technologies for their support.

DISCLOSURE STATEMENT: The views expressed herein do not necessarily reflect those of the Department of the Navy, Department of Defense, or U.S. Government.

DO ATHLETES MAXIMIZE GROUND REACTION FORCES AND POWER WHEN ACCELERATING?

[1] Alison L. Sheets and [1] Andrea Vinet

[1] Nike, Inc., Beaverton, OR, USA
email: Alison.sheets@nike.com, web: https://about.nike.com/pages/nike-explore-team-sport-research-lab

INTRODUCTION

Acceleration and top speed sprinting capabilities differentiate athletes in a wide variety of sports, including track and field, soccer, football, and basketball. In these sports, the limits of performance continue to be expanded as athletes and coaches refine sprint training and technique, and as equipment becomes more technical and specialized. Despite these advances, biomechanical limits to performance remain largely unknown.

Numerous researchers have found a positive correlation between horizontal ground reaction forces (GRF) and acceleration performances, and have suggested that GRF magnitude is less important than the horizontal GRF orientation during acceleration [1-6]. These relationships were found by comparing measurements across subjects with different abilities at discrete points in the acceleration [1-3], or by measuring every step over at least a 40m acceleration [4-6]. Due to the experimental designs, it is unknown whether athletes produced maximum GRF during each step of the acceleration, as has been suggested during top speed sprinting [7]. Another study of the 1st step in an acceleration reported that athletes can produce larger forces when wearing a weight vest [8].

The goal of this experiment was to measure whether athletes could produce larger GRF and more power during a maximum effort linear acceleration by adding mass to the torso. If larger GRF cannot be generated when increasing the mechanical demands of the task, it would suggest that maximal effort acceleration performances may also be limited GRF generation capabilities.

METHODS

Eight male athletes (mass: 70.33 ± 8.90 kg, ht: 1.77 ± 0.03 m, age: 23.6 ± 3.2 yrs) performed at least three maximal effort, 10 m accelerations from a standing position with and without approximately 10% (9.9 ± 2.17 %) body mass (BM) added to the torso. Prior to the data collection, athletes warmed up for at least 15 minutes and completed one maximal effort 10 m acceleration. The 10% BM was chosen to attempt to sufficiently alter the mechanical demands of the acceleration without large changes in speed and joint kinematics, and a weight vest was used to minimally alter whole body angular momentum. Condition order was randomized and balanced, and all subjects wore Nike Zoom Streak LT 2 racing flats during testing.

Ground reaction forces (GRF) were measured at approximately 8 m into the acceleration using two 90 x 60 cm piezoelectric force plates (2500 Hz) embedded in a Mondo track surface, and pelvis position was measured simultaneously using a passive, optical, three-dimensional motion capture system (500 Hz). Only trials in which an athlete's dominant foot contacted within the boundary of the force platform were considered.

The external mechanical work performed during stance was estimated using the 3D GRF. Stance occurred when the vertical component of the GRF was larger than 30N. Center of mass (CoM) acceleration was calculated from GRF, and then integrated over time to calculate changes in CoM velocity during contact [9]. Initial CoM velocity was estimated by differentiating the average position of markers placed on the left and right ASIS and PSIS.

RESULTS AND DISCUSSION

There were no differences in the peak resultant GRF (Figure 1), peak CoM power (Figure 2), or average resultant GRF in stance (control: 1.90 ± 0.12, mass: 1.92 ± 0.10) during maximal effort accelerations with (mass) and without (control) mass attached to the torso. Propulsive impulses when normalized to BW in the control, and BW+10% in the mass

condition were positively correlated with speed ($p<0.05$, Pearson correlation coefficient).

The average speed at 8 m into the acceleration was 5.07 ± 1.36 % slower with the added mass (control: 7.13 ± 0.44 m/s, mass: 6.77 ± 0.41 m/s), and contact time increased by 7.06 ± 3.07 %.

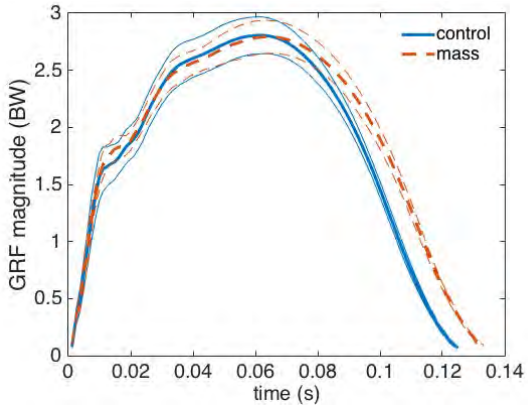

Figure 1: Average resultant GRF normalized by BW. Thicker lines denote population means. Thin lines show ± 1 SD within each athlete.

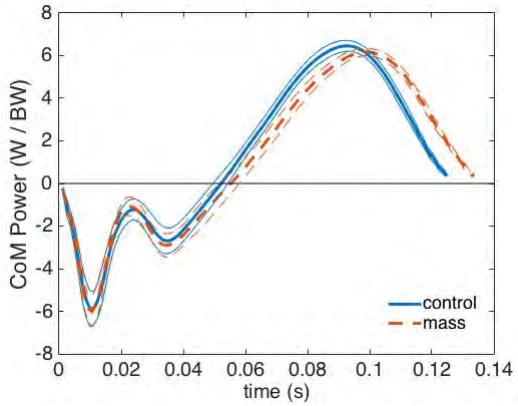

Figure 2: Average center of mass power normalized by BW. Thicker lines denote population means. Thin lines show ± 1 SD within each athlete.

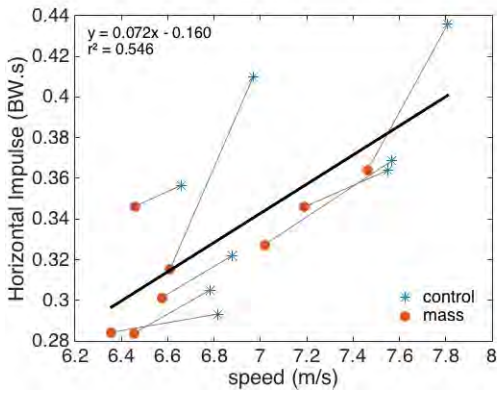

Figure 3: Propulsive impulse was linearly correlated with speed ($p<0.05$) across the population and within each individual (thin lines).

Results from this experiment suggest that at 8 m into a maximum effort acceleration, athletes are generating their maximum GRF and power, and neither increase when the mechanical demands of the movement are increased. Instead, each subject slowed with the added mass, which supports the hypothesis that GRF generation capability relative to BM affects acceleration. It is possible that the ability to generate larger GRF and powers would increase an athlete's acceleration capability. This hypothesis could be tested by reducing the mechanical demands of accelerating (or by increasing athlete capabilities through a training program) and measuring performance changes. Additionally, the previously reported [1-6] positive relationship between horizontal impulse and speed was confirmed.

CONCLUSIONS

Athletes could not generate larger GRF and power when mass was added to the torso, and all slowed in the mass condition; therefore, GRF and power likely limit maximal effort accelerations, and to get faster athletes would benefit from increasing their capacity for force production.

REFERENCES

1. Kawamori et al. *The J of Strength & Cond Research* 27(3), 2013.
2. Hunter, et al. *Journal of Appl Biomech* 21(1), 2005.
3. Kugler and Janshen. *Journal of Biomechanics*, 43(2), 2010.
4. Morin et al. *Med Sci Sports Exerc*, 43(9), 2011.
5. Morin et al. *European J of Appl Phys,* 112(11), 2012.
6. Rabita et al. *Scandinavian J of Med & Sci in Sports* 25(5), 2015.
7. Weyand et al. *Journal of Applied Physiology* 89(5), 2000.
8. Luo and Stefanyshyn. *Sports Performance*, Ch 22, 2015.
9. Donelan et al. *Journal of Biomech* 35(1), 2002.

ACKNOWLEDGEMENTS

This research was supported by Nike, Inc.

EFFECT OF AGE AND BODY MASS INDEX ON MOBILITY IN MIDDLE-AGED TO OLDER ADULTS WITH AND WITHOUT LOWER LIMB AMPUTATION

[1] Hui-Ting Shih and [1] Szu-Ping Lee

[1] Department of Physical Therapy, Clinical Locomotor Neuromechanics Laboratory, University of Nevada, Las Vegas, Las Vegas, NV, USA
email: shihh1@unlv.nevada.edu, web: https://unlvptlabs.com/clnl/

INTRODUCTION

Age and BMI are critical to functional mobility, influencing both daily activities and endurance. The impact has been recognized in individuals with lower limb loss [1] as well as able-bodied older adults [2], and the general trend is that with older age and higher BMI, both populations demonstrate degraded functional mobility. However, the rate of mobility decline and onset of increased fall risk have not been compared between the amputee and non-amputee populations. In the current study, we aim to predict functional mobility levels in individuals with and without amputation using a multiple regression model that included both the age and BMI.

METHODS

Twenty middle-aged to older individuals with amputation (13 transtibial, 6 tranfemoral, 1 hip disarticulation amputee, age from 36 to 70 years), and 243 age-similar adults (age from 31 to 70 years) participated. Both groups must be able to walk independently for at least 50 meters, and did not have any transient health conditions that would affect functional mobility, such as acute ankle sprain. For better generalizability, amputation levels and any permanently mobility-altered diseases were all included.

Timed up-and-go (TUG) was utilized to examine different aspects of functional mobility. TUG measures an individual's ability to perform sit-to-stand, level walking, turning, and stand-to-sit, mimicking the required movement in daily activities. An instrumented stool designed to accurately measure the TUG performance was utilized (**Figure 1**). Force as applied to the stool when the subject sits on the stool was used to determine the start and the end of a trial [3]. Specifically, the start was defined as the instant when 90% of the subject's bodyweight is removed; the end was when 90% of the weight was returned, indicating that the subject has sat down.

Figure 1: Instrumented stool [3]

Multiple linear regression analysis was conducted. We regressed TUG time on age and BMI for both groups in order to identify significant models and predictors of functional mobility. The α level was set at .05.

RESULTS AND DISCUSSION

In people with lower limb loss, a significant regression model with age and BMI was found for TUG (F (2,17) = 4.574, p = .026, R^2 = 0.350):

$$Amputee\_TUG = -13.768 + 0.219*Age + 0.406*BMI \quad \textbf{(Equation 1)}$$

Age and BMI were significant predictors of TUG in the amputee population. For every one-year increase in age, we estimated 0.219 seconds increase in TUG time. For each unit increase in BMI, TUG time was predicted to increase by 0.406 seconds.

In able-bodied adults, a significant equation was found for TUG (F (2,240) = 24.347, p < .001, R^2 = 0.169):

$$NonAm\_TUG = 0.198 + 0.052*Age + 0.134*BMI \quad \textbf{(Equation 2)}$$

Age and BMI were significant predictors of TUG in able-bodied adults. After accounting for BMI, for every one-year change of age, we estimated 0.052 seconds change on TUG. Alternatively, after accounting for age, for every unit increase in BMI, we estimated 0.134 seconds increase in TUG.

The age-related rate of increase in TUG in amputees is 4.2 times greater than able-bodied adults. With the same 10-year increase of age, the corresponding increase of TUG time in amputees would be 2.19 seconds, while the able-bodies adults would experience only 0.52 seconds change. On the other hand, the BMI-related change rate in TUG is 3 times greater in amputees than in able-bodied adults. With the same 5-unit increase in BMI, amputees would increase 2.03 seconds, while able-bodied adults would just increase 0.67 seconds in TUG time.

The cut-off points of TUG in screening high fall risk ranges from 7.94 to 31.9 seconds across a wide variety of clinical populations [4]. Given the high fall risk in amputees [5], using 8 seconds as the threshold and a BMI range from 25 to 35 kg/m^2, a person with lower limb loss would be under the risk of falling around ages 34 to 53. At the age of 65, people with lower limb loss will likely have elevated risk to fall regardless of their BMI.

CONCLUSIONS

In middle-aged to older people with and without amputation, age and BMI are significant predictors of TUG performance. Comparatively, the onset of fall risk in amputees is much earlier than age-matched or BMI-matched cohorts.

REFERENCES

1. Norvell DC. *Defining successful mobility after lower extremity amputation for complications of peripheral vascular disease and diabetes*. J. Vasc. Surg.**54(2), 412–419 (2011)**.
2. Launer LJ. *Body Mass Index, Weight Change, and Risk of Mobility Disability in Middle-aged and Older Women*. JAMA.**271(14), 1093 (1994)**.
3. Lee S-P. *Influence of Procedural Factors on the Reliability and Performance of the Timed Up-and-go Test in Older Adults.* Int. J. Gerontol.**10(1), 37–42 (2016).**
4. Timed Up and Go | AbilityLab [Internet]. Available from: https://www.sralab.org/rehabilitation-measures/timed-and-go#.
5. Dite W. *Clinical Identification of Multiple Fall Risk Early After Unilateral Transtibial Amputation*. Arch. Phys. Med. Rehabil**.88(1), 109–114 (2007)**.

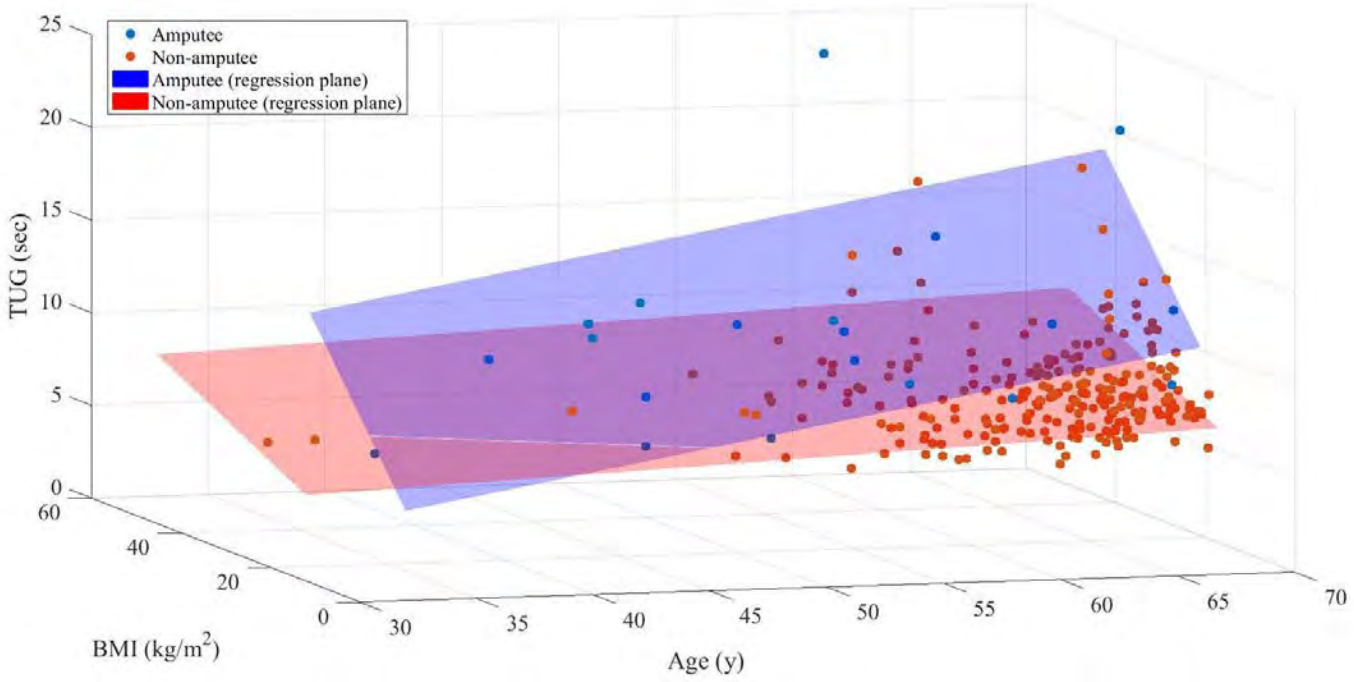

Figure 2: Age, BMI, and Timed up-and-go performance with regression planes across two groups.

EFFECTS OF DIFFERENT STEP WIDTHS DURING GAIT REVEAL ALTERED TRUNK KINEMATIC COORDINATION DURING LOW BACK PAIN REMISSION

Hai-Jung Steffi Shih and Kornelia Kulig

University of Southern California, Los Angeles, CA, USA
email: haijungs@usc.edu, web: http://pt.usc.edu/Hai_Jung_Shih/

INTRODUCTION

Persons with long-lasting back pain may have learned to utilize difference trunk control than back-healthy controls, which may contribute to long-term adverse consequences such as recurrence [1, 2]. However, there is insufficient research investigating whether altered trunk kinematic coordination is purely an effect of active pain, or if it persists beyond symptom duration, the latter indicating a relatively permanent "learned" effect.

Trunk control plays an important role in walking gait as it contributes to the stabilization of the center of mass, pelvis, and head. Gait is passively unstable in the mediolateral direction, therefore altering step width may place a higher demand on postural control of the trunk [3]. While a healthy person may be able to modulate trunk coordination according to various step width with ease, a person with a history of recurrent low back pain (hxLBP) may either require a larger change in trunk control to compensate for their impaired dynamic balance [4], or exhibit impaired ability to modulate trunk coordination according to external demands [1].

The purpose of this study was to investigate the persistence of altered trunk kinematic coordination during walking associated with low back pain by 1) comparing an asymptomatic person with hxLBP to a back-healthy control and 2) examine the modulation of trunk coordination to different step width in those two subjects.

METHODS

One participant with hxLBP and one back-healthy control (both female, both 23 years old) participated in this pilot experiment. The participant with hxLBP have had recurrent low back pain for 5 years, and was not in pain for a week at the time of the study. After giving informed consent, the participants walked on a treadmill with their preferred speed, and a range of prescribed step width was implemented using real-time visual feedback on a screen.

Reflective markers were instrumented on the participants' trunk and lower extremity. Kinematic data were captured by an 11-camera motion capture system (Qualisys, Gothenburg, Sweden) at 250 Hz. Trunk kinematic coordination between the thorax and pelvis in the transverse and frontal planes were analyzed using the vector coding approach.

RESULTS AND DISCUSSION

In the transverse plane, the person with hxLBP had a higher proportion of in-phase coordination and a lower proportion of pelvic-phase coordination compared with the back-healthy control, regardless of step width. This is consistent with the literature that persons with chronic or recurrent low back pain utilize a stiffening strategy perhaps by co-contracting the trunk muscles and maintaining a high degree of thorax-pelvis coupling during submaximal tasks such as walking.

There is a subtle decrease in in-phase coordination and increase in pelvic-phase coordination in the transverse plane when step width is increased or decreased from preferred, but only seen consistently in the person with hxLBP. This is consistent with the notion that persons with hxLBP may require a larger change in trunk control to adjust for altered step width than back-healthy controls. It appears that narrower and wider widths have similar effects on transverse plane trunk coordination in this person.

In the frontal plane, the person with hxLBP had a higher proportion of pelvic-phase coordination than the control at the preferred step width. Although counterintuitive in the "stiffening" standpoint,

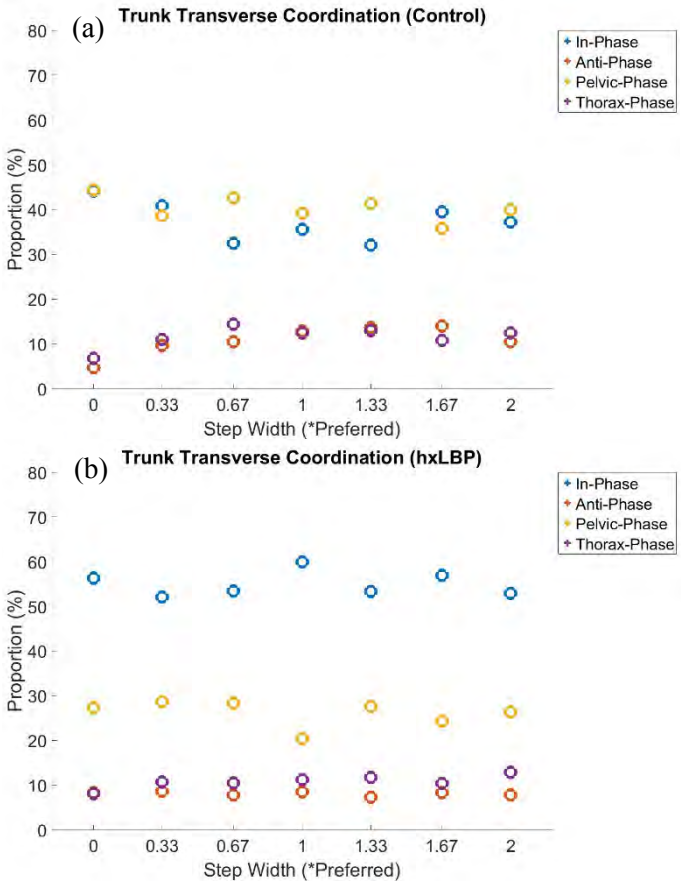

Figure 1: Transverse plane trunk coordination during different step widths of the (a) control and the (b) hxLBP participant. Colored circles indicate the proportion of each of the four coordination patterns.

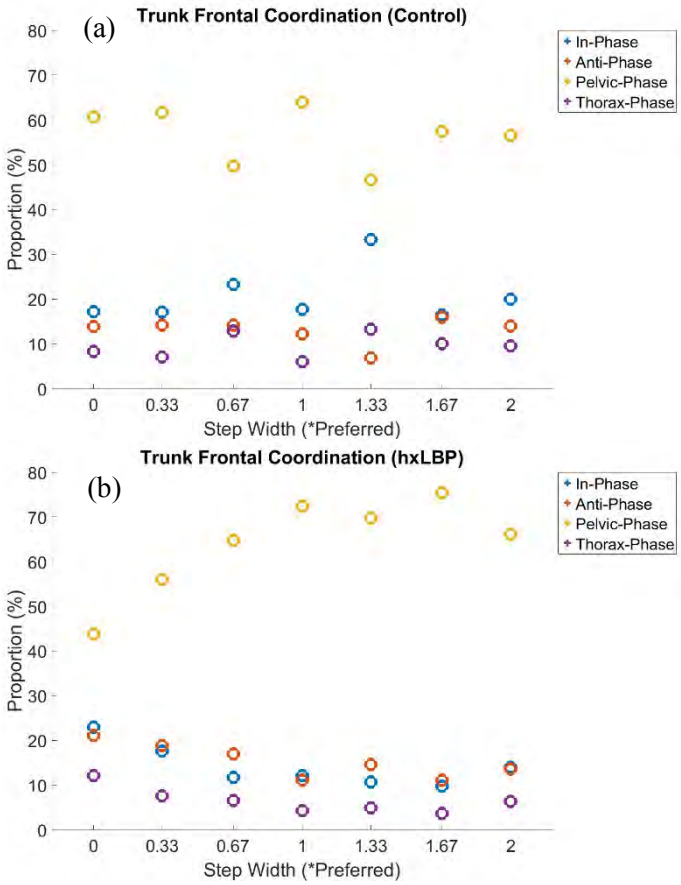

Figure 2: Frontal plane trunk coordination during different step widths of the (a) control and the (b) hxLBP participant. Colored circles indicate the proportion of each of the four coordination patterns.

greater pelvic drop could potentially be due to weaker hip abductors or altered control, which is often reported in persons with chronic low back pain.

There is a decrease in pelvic-phase coordination and increase in in-phase coordination in the frontal plane when step width is increased or decreased in the back-healthy control, which may be a strategy to adapt to altered step widths. The person with hxLBP demonstrated a similar strategy as the control when step width is narrower than preferred, but exhibited minimal changes in frontal plane trunk coordination in wider step widths. These findings support the speculation that the person with hxLBP has a weaker hip abductor since she was not able to further stabilize her pelvis at wider step widths.

Continuation of current study will elucidate trunk control in hxLBP, thus inform rehabilitation and prevention strategies for low back pain.

CONCLUSIONS

Persistent changes in trunk coordination were seen in a person during the pain-free period of recurrent low back pain. Larger sample size is needed to draw meaningful conclusions.

REFERENCES

1. van Dieën et al. *Exerc Sport Sci Rev.* 45(4): 223-229, 2017.
2. Hodges et al. *J Biomech*. 42(1): 61-66, 2009.
3. Donelan et al, *J Biomech.* 37(6): 827-835, 2004.
4. Hooper et al, *Phys Ther Sport. 22: 29-34, 2016.*

ACKNOWLEDGEMENTS

This work is supported by the International Society of Biomechanics Dissertation Matching Grant.

THE INFLUENCE OF ACL RETENTION IN TOTAL KNEE REPLACEMENT ON WALKING AND STAIR CLIMBING MECHANICS

Jacqueline C. Simon, Craig J. Della Valle, Markus A. Wimmer
Rush University Medical Center, Chicago, IL, USA
Email: markus_a_wimmer@rush.edu

INTRODUCTION

Bicruciate retaining (BiCR) TKRs were designed to allow for better functional activity due to the presence of the anterior cruciate ligament (ACL). Here we determine whether subjects with BiCR TKRs exhibit more normal knee mechanics during level walking and stair climbing than subjects with posterior cruciate retaining (PCR) TKRs. Our hypothesis is that the BiCR subjects will display normal biomechanics during both activities, while the PCR subjects will show the altered gait and moment patterns typical for TKR patients [1].

METHODS

Sixteen subjects (4/12 m/f, 65±3 years, 30.7±7.0 BMI, 8/8 R/L) with BiCR TKRs and 17 subjects (2/15 m/f, 65±7 years, 30.4±5.1 BMI, 7/10 R/L) with PCR TKRs were tested 8-24 months post-operatively. PCR subjects without an existing ACL preoperatively were excluded. Thirteen age-matched healthy control subjects (7/6 m/f, 58±9 years, 26.4±4.4 BMI, 8/5 R/L) were also included; limb tested was randomly selected for control subjects. Motion data were collected during level walking and stair ascent using 12 optoelectric cameras (Qualisys, Gothenburg, Sweden) and two force plates (Bertec, Columbus, OH). The point cluster marker set was used [2,3]. Five trials were collected per activity. For stair, a 2-step staircase (step height: 22.6cm) was positioned with the first step on a force plate. Subjects began on a flat 'step' in front of the staircase, took the stairs one at a time starting with their test limb, and came to rest on the second step. Knee kinematic and kinetic data were calculated in BioMove (Stanford University, Stanford, CA); kinetics were time-normalized to 100% stance and normalized to percent bodyweight times height (%BW*HT). Motion data were time-normalized to 100% gait cycle for level walking and 100% stance for stair ascent. One-way ANOVA tests with post-hoc Games-Howell analysis were used to compare subject demographics, spatiotemporal parameters, and peak knee kinematics and kinetics between groups. Kinematic and kinetic waveforms were evaluated using statistical nonparametric mapping (SnPM) [4,5].

RESULTS

PCR subjects trended to be older and have higher BMIs than the control group ($p=0.053$, 0.077); otherwise, there were no significant differences in age or BMI between groups ($p\geq0.099$). During level walking, BiCR subjects were significantly slower, had a shorter stride length, and had less extension than the controls ($p\leq0.012$, Table 1). Both TKR groups showed significantly less sagittal plane range of motion ($p\leq0.019$, Table 1) and had significantly lower peak extension, internal rotation, and external rotation moments than the controls ($p\leq0.019$, Table 1). During stair ascent, all TKR subjects had significantly reduced flexion moment peaks than subjects from the control group ($p\leq0.004$, Table 1), BiCR subjects had significantly reduced adduction moment peaks than the controls ($p=0.031$, Table 1), and PCR subjects had significantly lower extension moment peaks than control subjects ($p=0.014$, Table 1). There were no significant peak differences between TKR groups ($p\geq0.169$). SnPM analysis showed a difference in the knee rotation angle pattern during stair ascent; the BiCR group had significantly more external rotation of the tibia during 3-17% stance ($p=0.004$) (Fig. 1B). PCR subjects also showed a similarly altered rotation pattern, but it was not significant. Furthermore, the BiCR group had a significant increase in knee abduction angle during 36-55, 66-88% stance ($p=0.006$, 0.004), and both TKR groups showed a pattern of increased knee abduction overall compared to the control subjects (Fig. 1C).

DISCUSSION

As expected from the literature, the PCR subjects showed decreased flexion range of motion during level walking and altered flexion moment patterns overall. They showed significantly decreased sagittal plane range of motion and peak internal rotation and external rotation moments during level

walking, flexion moment peaks for stair ascent, and extension moment peaks overall compared with the control group. However, these decreases were largely seen in the BiCR group as well. This may indicate that TKR patients overall have some inherent weakness in the extensor mechanism, possibly induced by osteoarthritis, that is not related to the presence or absence of the ACL.

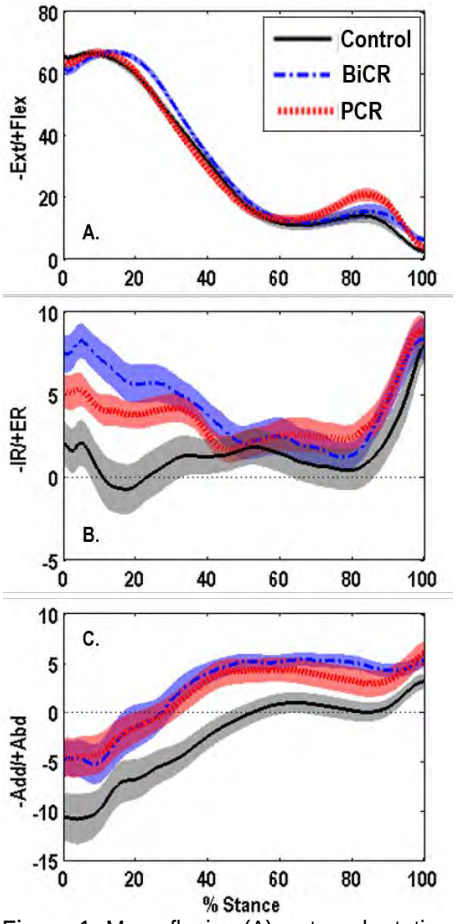

Figure 1: Mean flexion (A), external rotation (B), and abduction (C) angles (degrees) during stair ascent. Shaded region is ± 1 standard error.

SnPM analysis identified differences in secondary knee kinematics during stair climbing. Both TKR groups showed increased external rotation of the tibia in early stance (Fig. 1B), though only significant for the BiCR group. The differences in rotation angle decrease with decreasing flexion until approximately 50% stance, where rotation was similar for all three groups. For the remainder of stance, the BiCR curve closely matches the shape of the control curve, while the PCR curve appears to follow a different slope. Interestingly, at this 50% stance cutoff point, subjects from all three groups were in about 15° knee flexion. Previous studies have shown that during knee extension, the ACL begins to engage at 45° and reaches its maximum force at 15° [6,7]. This indicates that there may be some TKR related effects that are mechanically dominant at high flexion angles while the ACL is inactive, but which are corrected where the ACL is functional.

CONCLUSION

ACL retention in TKRs does not correct sagittal plane kinematic and kinetic gait alterations commonly seen in TKR populations. However, it appears to normalize knee rotation patterns at flexion angles for which the ACL is functional.

REFERENCES

[1] Andriacchi et al. *J. Bone Jt. Surg. Am.* 1982.
[2] Andriacchi et al. *J. Biomech. Eng.* 120. 1998.
[3] Alexander and Andriacchi. *J. Biomech.* 2001.
[4] Pataky, T. *J. Biomech.* 43(10). 2010.
[5] Pataky et al. *J. Biomech.* 48(7). 2015.
[6] Sakane et al. *J. Orthop. Res.* 15(2). 1997.
[7] Fujimaki et al. *Am. J. Sports Med.* 2015.

Table 1: Peak kinematics and kinetics during level walking and stair ascent. P-values from post-hoc tests between each TKR group and the HC group. Significant and trending values in **bold**.

	Level Walking				Stair Ascent			
	PCR	BiCR	HC	p-value PCR v HC, BiCR v HC	PCR	BiCR	HC	p-value PCR v HC, BiCR v HC
Speed (m/s)	1.19 ± 0.16	1.11 ± 0.19	1.32 ± 0.14	**0.071, 0.006**	--	--	--	--
Stride Length (m/m)	0.75 ± 0.15	0.72 ± 0.13	0.85 ± 0.06	**0.068, 0.009**	--	--	--	--
Max Knee Flexion (deg)	60.7 ± 4.2	61.8 ± 4.2	63.0 ± 3.7	0.264, 0.679	69.1 ± 5.5	69.4 ± 3.8	69.0 ± 6.1	0.999, 0.979
Min Knee Flexion (deg)	-2.6 ± 4.5	-0.9 ± 4.1	-6.2 ± 4.9	0.112, **0.012**	1.9 ± 4.0	1.9 ± 3.5	-0.68 ± 3.5	0.172, 0.168
Knee Sagittal Plane ROM (deg)	63.3 ± 5.6	62.9 ± 5.8	69.2 ±5.4	**0.019, 0.015**	67.4 ± 5.7	67.5 ± 4.4	69.7 ± 5.9	0.501, 0.520
Ext. Moment (%BW*HT)	-2.45 ± 0.85	-2.39 ± 0.81	-3.80 ± 1.05	**0.003, 0.002**	-1.41 ± 0.64	-1.67 ± 0.72	-2.13 ± 0.61	**0.014**, 0.179
Flex. Moment (%BW*HT)	1.65 ± 0.70	1.38 ± 1.09	2.16 ± 1.22	0.389, 0.197	3.54 ± 1.17	3.55 ± 1.28	5.14 ± 1.09	**0.002, 0.004**
Add. Moment (%BW*HT)	-2.39 ± 0.62	-2.32 ± 0.63	-3.24 ± 1.18	**0.076, 0.054**	-2.40 ± 0.58	-2.29 ± 0.55	-3.07 ± 0.90	**0.072, 0.031**
IR Moment (%BW*HT)	-0.75 ± 0.30	-0.76 ± 0.19	-1.08 ± 0.31	**0.019, 0.010**	-0.53 ± 0.21	-0.49 ± 0.19	-0.60 ± 0.24	0.667, 0.360
ER Moment (%BW*HT)	0.11 ± 0.07	0.075 ± 0.063	0.21 ± 0.10	**0.011, 0.001**	0.21 ± 0.15	0.19 ± 0.11	0.19 ± 0.10	0.868, 0.997

KNEE ANGLE AND AXES CROSSTALK CORRECTIONS IN GAIT, BICYCLING AND ELLIPTICAL EXERCISES USING PRINICPAL COMPONENT ANALYSIS

Jordan M. Skaro, Scott J. Hazelwood and Stephen M. Klisch

California Polytechnic State University, San Luis Obispo, CA, USA
email: sklisch@calpoly.edu

INTRODUCTION

Crosstalk is a leading source of error in motion analysis that results in a non-physiological correlation between flexion-extension (FE) and adduction-abduction (AA) angles due to marker placement error [1-2]. Principal Component Analysis (PCA) has been proposed as a post-hoc correction for crosstalk in gait [1-2], but studies have not proposed a method to determine PCA corrected knee axes nor investigated using a standardized set of PCA corrected knee axes for exercises other than gait where a natural FE-AA coupling may exist for high flexion angles [3] or when the subject's feet are constrained to the pedals.

We hypothesized that: 1) PCA corrects for crosstalk in gait (G), cycling (C), and elliptical (E) exercises and 2) PCA corrected FE and AA axes are different for G, C and E exercises. The aims were to: 1) assess PCA's ability to reduce crosstalk for the 3 exercises; 2) calculate PCA corrected knee axes for the 3 exercises; and 3) propose standardized knee axes to determine subject-specific PCA corrected knee angles for the 3 exercises.

METHODS

Subjects. Subjects were male (n=9) and female (n=6), 18-26 years of age, without prior leg injuries or malalignment, and both right (n=11) leg and left (n=4) leg dominant. Protocols were approved by Cal Poly's Human Subjects Committee.

Experimental Protocol. An enhanced Helen Hayes marker set and a 12-camera motion capture system with Cortex software (Motion Analysis, Santa Rosa, CA, USA) were used to record marker position and process kinematic data. Following static pose trials to obtain static offset angles, G trials with a full cycle of the dominant leg were captured. Then, C and E trials were captured with the subject pedaling at 70 rpm for 15 seconds. Static pose offset was calculated by subtracting static pose knee angles from dynamic knee angles.

The custom angles and axes calculations described below used MATLAB (MathWorks, MA, USA).

PCA Analysis. PCA was implemented to reduce crosstalk by conducting a coordinate system transformation of calculated knee angles that minimizes FE-AA correlations [3]. A covariance matrix [$\boldsymbol{S}$] was calculated:

$$[\boldsymbol{S}] = \frac{\mathbf{1}}{\boldsymbol{n-1}}[\boldsymbol{X_{centered}}]^{\boldsymbol{T}}[\boldsymbol{X_{centered}}] \qquad (1)$$

where [$\boldsymbol{X_{centered}}$] contains the $n \times 3$ matrix of original knee angles, [$\boldsymbol{X}$], for n-time points, rows, and 3 knee angles, columns, minus the means of each knee angle. An eigendecomposition of matrix [$\boldsymbol{S}$] was calculated to produce a matrix of column eigenvectors, [$\boldsymbol{P}$], according to

$$[\boldsymbol{S}] = [\boldsymbol{P}]^{\boldsymbol{T}}[\boldsymbol{X}][\boldsymbol{P}]. \qquad (2)$$

Finally, the original knee angles, [$\boldsymbol{X}$], were projected onto a new set of axes as defined by the eigenvectors in matrix [$\boldsymbol{P}$]. This results in an $n \times 3$ matrix [$\boldsymbol{Z}$] which contains n-time points and the PCA corrected FE, internal-external rotation (IR), and AA angles in the rows and columns, respectively:

$$[\boldsymbol{Z}] = [\boldsymbol{X}][\boldsymbol{P}]. \qquad (3)$$

Crosstalk is quantified using the coefficient of determination (R^2) and the correlation coefficient (R). Larger and smaller R^2 indicate greater and lesser crosstalk, respectively.

PCA Corrected Knee Axes. PCA corrected knee axes were determined using a non-linear solver by finding the axes that, when used with PCA corrected angles, resulted in equivalent thigh, shank and ankle trajectories calculated by Cortex (which used the

experimental marker data). A floating axis knee coordinate system was used [4].

Cycling and Elliptical Angles with Corrected Gait Axes. Using corrected knee axes found for G, a similar process was used to find new angles for C and E exercises using a non-linear solver. The knee angles were determined by finding the angles that, when used with the PCA corrected knee axes for G, resulted in equivalent thigh, shank and ankle trajectories calculated by Cortex.

Statistics. Regression analyses were performed on FE vs. AA angles before and after PCA correction to assess crosstalk in the 3 exercises. A paired multivariate Hotelling's T-squared test was performed on the PCA corrected G, C, and E knee axes to test for similarities with G axes used as reference. An ANOVA test was used to determine differences between Cortex, PCA corrected, and angles from the PCA corrected G axes for C and E. The significance levels used were 0.05 (regression analysis, T-squared test) and 0.0056 (ANOVA with Bonferroni correction).

RESULTS AND DISCUSSION

Regression analyses found reduced correlations (Table 1) for FE-AA angles (Fig. 1) in G ($p<0.001$ for Cortex [strongly correlated] and $p=0.85$ for PCA corrected [not correlated]), C ($p=0.01$ for Cortex and $p=0.77$ for PCA corrected), and E ($p<0.001$ for Cortex and $p=0.77$ for PCA corrected). The paired multivariate Hotelling's T-squared test found no similarities in PCA corrected knee axes between G and C nor between G and E ($p<0.0014$). The ANOVA test found no similarities between Cortex, PCA corrected, and C and E knee angles from the PCA corrected G axes ($p<0.0056$).

Table 1: R^2 values (mean ± sd) for FE-AA angles for gait (G), cycling (C), and elliptical (E) exercises.

Group	G	C	E
Cortex	0.61 ± 0.29	0.41 ± 0.29	0.80 ± 0.21
PCA	<0.01 ±	<0.01 ±	<0.01 ±
Corrected	<0.01	<0.01	<0.01

The results demonstrated substantial crosstalk for G, C, and E exercises, which can be corrected using PCA. Further, the corrected knee axes were not similar between G, C, and E exercises. Using PCA corrected knee axes from G to calculate new C and E angles produces dissimilar angles from the Cortex and PCA corrected C and E angles. Thus, when using PCA to correct for crosstalk error in subjects performing exercises other than G, a standardized set of knee axes from G is suggested to determine the knee angles.

REFERENCES

[1] Jensen, E. et al., *J Biomech*, 49: 1698-1704, 2016. [2] Shlens, J., *arXiv*:1404.1100, 2014. [3] Wilson, D. R., Feikes, J. D., Zavatsky, A. B., O'Connor, J. J., *J Biomech*, 33: 465-473, 2000. [4] E. S. Grood and W. J. Suntay, *J Biomech Eng*, 105: 136-144, 1983.

ACKNOWLEDGEMENTS

W.M. Keck Foundation, Donald E. Bently Center, and Defense Health Program through the DoD Broad Agency Announcement for Extramural Medical Research Program #W81XWH-BAA-14-1 under Award No. W81XWH-16-1-0051. Opinions, interpretations, conclusions and recommendations are those of the authors. We thank Dr. Jeffrey Sklar (Cal Poly) for guidance on statistical methods.

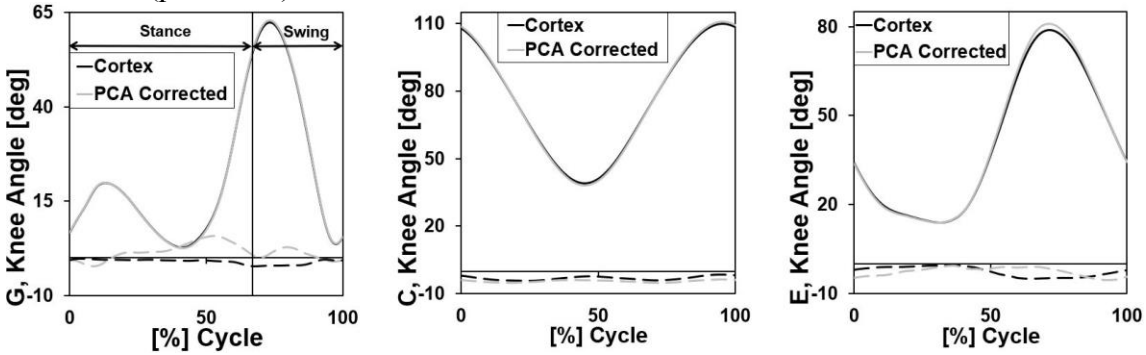

Figure 1: Averaged knee angles for G, C, and E exercises. Solid/dashed = FE/AA.

Can Changing Running Shoes Immediately Reduce the Risk of Tibial Stress Fractures?

[1] Jenny Tavares, [1]Tyler Jost, and [1] Jonathan Rylander

[1] Baylor University, Waco, TX, USA
email: Jonathan_Rylander@baylor.edu

INTRODUCTION

Running is an increasingly popular sport worldwide, both as a recreational activity and to improve overall health. However, stress fractures are one of the most common running-related injuries [1]. The most common site of stress fractures in runners is the tibia [2]. Risk factors for tibial stress fractures (TSF) include a rearfoot strike (RFS) pattern [3], pronation [4], increased vertical loading rate [5], and increased vertical ground reaction force [5]. With a variety of running shoes on the market it is possible that these biomechanical risk factors may be altered through a change in running shoe. While previous studies have been performed in this area, few include 3D kinematics, kinetics, and muscular activation data for use in direct comparison between multiple categories of commercially available running shoes. The purpose of this investigation is to determine the effects of various commercially available running shoes (minimalist, maximalist, neutral, and stability) on muscle activation patterns, kinetics, and kinematics as they relate to known risk factors for TSF.

METHODS

23 healthy runners (29±9 y.o) were enrolled in this study after completing IRB approved informed consent forms. The Baylor BioMotion Lab in the Baylor Research and Innovation Collaborative was the location of all testing. Testing included the use of 3D motion capture (Vicon Vantage), force plates (AMTI), and EMG (Noraxon). Ankle kinematics, ground reaction forces, and muscle activation for the left and right tibialis anterior (TA, dorsi-flexor), and the medial and lateral gastrocnemius (GM and GL, plantar-flexors) were collected.

Subjects ran in five running conditions: Barefoot (BF), minimalist (Nike Free), neutral (Nike Pegasus), maximalist (Hoka Bondi 5), and stability (Nike Structures). Running mechanics for each condition were compared to the neutral shoe which served at the baseline measure.

Between each running condition, the subject was asked to run for two-minutes on a treadmill to acclimate to the shoes. Subjects ran across a 12.5 m runway over the force plates at 3.35 m/s (±10%). During post processing, subjects were categorized as rearfoot strikers (RFS) or forefoot strikers (FFS) based on visual inspection of high speed video cameras. Running mechanics and EMG for each subject for each condition were compared to the neutral shoe which served at the baseline measure. Comparisons between RFS and FFS for various known tibial stress risk factors were calculated using ANOVA analyses.

RESULTS AND DISCUSSION

RFS and FFS showed trends toward different responses in the maximalist and stability shoes (Fig. 1). RFS had similar levels of ankle plantar flexion across all shod conditions while FFS showed a decrease in ankle plantar flexion in the maximalist and cushioned shoes. This corresponded to a decrease in GL activation in the maximalist and stability conditions and an increase in TA activation in the stability condition. Furthermore RFS appeared more responsive to changes in ankle eversion and internal rotation than their FFS counterparts (Fig. 2 and 3). However, these observed differences were fairly small within this group of runners.

Also analyzed were transient vertical ground reaction forces (TVGRF) and vertical instantaneous loading rate (VILR), but these results are not presented here.

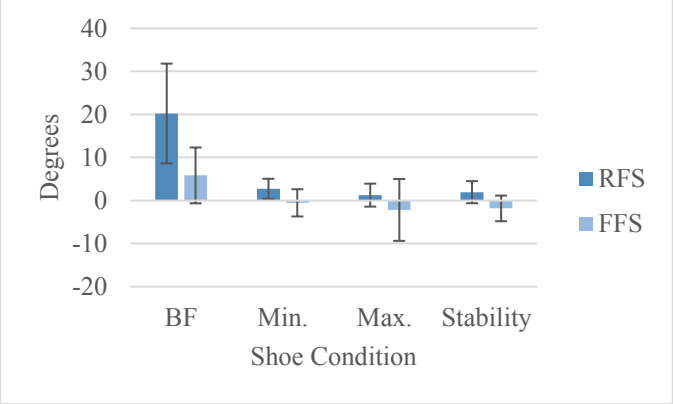

Fig. 1: Change in Ankle Plantar/Dorsiflexion Compared to Neutral Shoe Condition

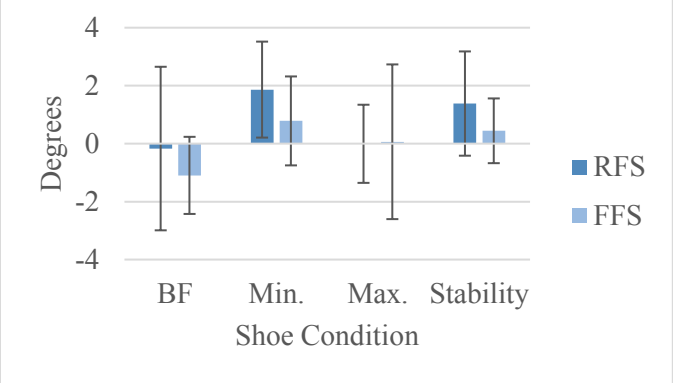

Fig. 2: Change in Peak Eversion Compared to Neutral Shoe Condition

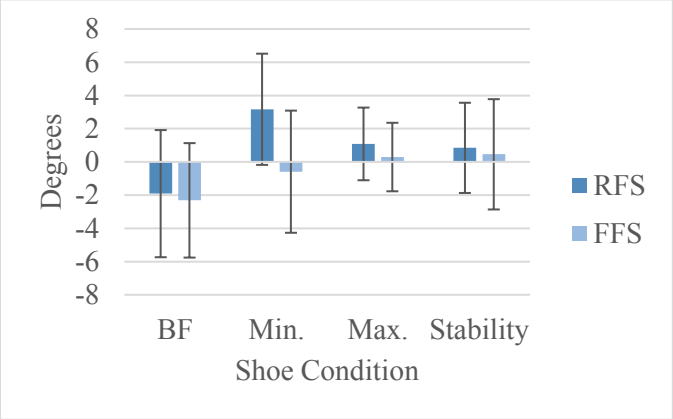

Fig. 3: Change Ankle Internal Rotation Compared to Neutral Shoe Condition

CONCLUSIONS

While numerous studies have been performed outlining the kinematic, kinetic, and muscular differences of various running shoes, few have provided an in depth analysis of multiple commercially available shoe types. Even fewer have involved the use of 3D kinematics, kinetics, and EMG. This particular study was focused on risk factors for TSF. This will be beneficial for coaches, physical therapists, and runners alike to alleviate the risk factors of TSF. Only a subset of the results are presented in this abstract.

FFS were not as influenced with regard to pronation (eversion and internal rotation) as their RFS counterparts. This suggests that the stability features in motion control shoes are not as beneficial for FFS and may instead cause them to adopt a RFS pattern. Additionally, FFS indicated a reduction in plantar flexion when running in the maximalist and stability shoes, indicating that they might eventually adopt a RFS pattern in these shoes, especially if they became fatigued. However, overall, the various shoes did not significantly reduce the risk factors of TSF and did not alter running mechanics by a substantial amount. The findings suggest that strike pattern and foot alignment rather than shoes are the determining factors in eliminating TSF risk factors under non-fatigued running conditions. These results are for runners who are not fatigued. It is very possible that the shoes will have a much larger impact on running mechanics once the muscles are fatigued, which is the focus of ongoing research in the lab.

REFERENCES

[1] Chen, T. L., et al., 2016, "Immediate Effects of Modified Landing Pattern on a Probabilistic Tibial Stress Fracture Model in Runners," Clin. Biomech., **33**, pp. 49–54.

[2] Matcuk, G. R., et al., 2016, "Stress Fractures: Pathophysiology, Clinical Presentation, Imaging Features, and Treatment Options," Emerg. Radiol., **23**(4), pp. 365–375.

[3] Nunns, M., et al., 2016, "Four Biomechanical and Anthropometric Measures Predict Tibial Stress Fracture," Br. J. Sports Med., **50**(19), pp. 1206–1210.

[4] Milner, C. E., et al., 2010, "Distinct Hip and Rearfoot Kinematics in Female Runners With a History of Tibial Stress Fracture," J. Orthop. Sports Phys. Ther., **40**(2), pp. 59–66.

[5] Milner, C. E., et al., 2006, "Biomechanical Factors Associated with Tibial Stress Fracture in Female Runners," Med. Sci. Sports Exerc., **38**(2), pp. 323–328.

APPLIED GAIT PATTERN INFLUENCES SPATIAL CHANGES IN CONTACT STRESS CALCULATED FOR DYSPLASIA PATIENTS FOLLOWING PERIACETABULAR OSTEOTOMY

Holly D. Thomas, Michael C. Willey, and Jessica E. Goetz
University of Iowa, Iowa City, IA
email: holly-thomas@uiowa.edu, web: https://uiowa.edu/uiobl/

INTRODUCTION

Acetabular dysplasia, characterized by the presence of a shallow acetabulum that inadequately covers the femoral head, is a common cause of hip pain and degeneration in the young adult population [1]. The altered force transfer through the hip joint resulting from dysplastic deformity elevates cartilage contact stresses, which may accelerate osteoarthritis (OA) progression [2]. Accurate quantification of these cartilage contact stresses would improve our understanding of the role of dysplasia in hip OA development.

The use of discrete element analysis (DEA), a rapidly-executing computational modeling method, permits analysis of larger populations of patients, which permits the ability to establish direct relationships between cartilage contact stresses and patient outcomes [3]. Our custom DEA technique has been previously validated in cadaveric hips [4], and we have previously shown [5] that that there are significant ($p < 0.001$) differences in the computed contact stresses when loading our patient-specific models with forces and rotations obtained from instrumented total hip data measured from patients with osteoarthritic hip joints [6], a gait pattern measured using motion capture in hip dysplasia patients [7], and a gait pattern measured in young, healthy individuals [8, 9]. However, that previous work only investigated the maximum contact stress at any location within the acetabular cartilage, which did not account for how the maximum contact stress shifts spatially throughout the cartilage as a result of gait loading differences or as a result of multiplanar acetabular reorientation that occurs as a result of surgical treatment of a dysplastic deformity using a periacetabular osteotomy (PAO). The purpose of this study was to evaluate spatial differences in pre- and post-operatively joint contact mechanics calculated when simulating stance phase of all three gait patterns.

METHODS

Under IRB approval, femoral, pelvic, and spinal bony geometry was segmented from pre- and post-operative CT scans of five PAO patients using a semi-automated program developed in MATLAB (Mathworks, Natick, MA). The acetabular and femoral cartilage surfaces were approximated with 1-mm uniform projections of the subchondral bone surfaces, which were then smoothed toward sphericity utilizing a custom-written algorithm. Each patient-specific model was aligned to the hip joint coordinate system defined by Bergmann *et al*. [6] and subjected to forces and rotations from arthritic [6], dysplastic [7], and normal [8, 9] gait patterns. The forces applied to each model were scaled based on the patient's body mass. For each model, the acetabular cartilage was divided into anterior, superior, and posterior regions (Figure 1) such that each region contained an equal number of triangular elements. The maximum contact stress was computed for each region to assess spatial stress differences.

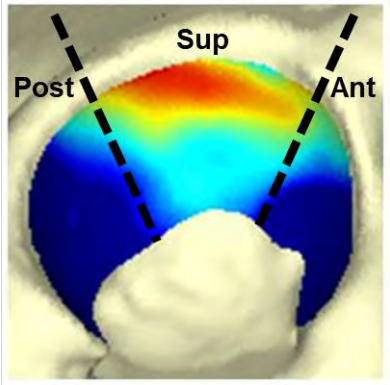

Figure 1: Acetabular cartilage geometry was divided into anterior, superior, and posterior regions to assess spatial contact stress differences.

RESULTS AND DISCUSSION

Pre-operative DEA models calculated the highest maximum contact stress when loaded with the dysplastic gait pattern (Figure 2). The highest pre-operative maximum contact stress was in the

superior region when models were loaded with the dysplastic (7.8 ± 3.5 MPa) and normal (7.4 ± 0.9 MPa) gait patterns. When pre-operative models were loaded with the arthritic gait pattern, the maximum contact stress was nearly equivalent in both the superior (5.7 ±1.2 MPa) and posterior (5.8 ± 0.8 MPa) regions. Following PAO, maximum contact stress increased in all three regions for models subjected to the arthritic and normal gaits; however, in models loaded with the dysplastic gait pattern, the maximum contact stress decreased in the superior region and increased in the anterior and posterior regions. When models were loaded with the normal gait pattern, there was a significant (p = 0.039) increase in maximum contact stress in the anterior region following PAO. Models loaded with the normal gait pattern also had significantly (p = 0.036) higher maximum contact stress in the superior region than models loaded with the arthritic gait pattern.

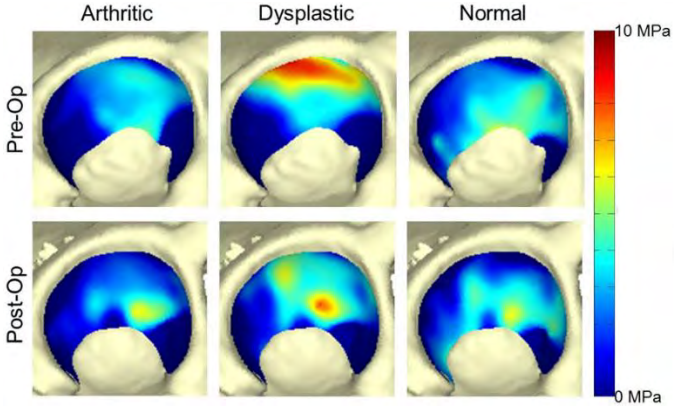

Figure 2: Representative contact stress distributions from DEA analysis of pre- and post-operative models of a single hip dysplasia patient subjected to an arthritic, dysplastic, and normal gait patterns.

CONCLUSIONS

We have previously shown that loading DEA models of this population of hip dysplasia patients with a dysplastic gait pattern significantly influences the DEA-computed contact stress [5]. The strongest finding of this work was the tendency for the highest maximum contact stresses to appear in the superior region of the acetabulum, which agrees with clinical findings of greater cartilage loading and wear superiorly. The strongest finding of this work was the tendency for PAO to decrease maximum contact stress when models used dysplastic gait compared to corresponding increases when models used arthritic gait. Additionally, PAO tended to decrease maximum contact stress superiorly only when models were subjected to a dysplastic gait pattern. These results further support the use of a dysplastic gait pattern when evaluating contact mechanics in this population and indicate that spatial changes in contact stress should be considered to accurately understand the role of dysplasia in cartilage damage and OA progression.

SIGNIFICANCE

This work will assist in understanding how pre- and post-operative contact mechanics relate to OA progression in hip dysplasia patients.

REFERENCES

1. Hadley NA, et al. *J Orthop Res* **8**, 1990.
2. Mavcic B, et al. *Clin Orthop Relat Res* **466**, 2008.
3. Kern AM and Anderson DD. *J Biomech* **48**, 2015.
4. Townsend KC, et al. *J Biomech* **67**, 2018.
5. Thomas HD, et al. Podium presentation at 41st Annual ASB Meeting, August 8-11, 2017.
6. Bergmann G, et al. *J Biomech* **34**, 2001.
7. Skalshoi O, et al. *Gait & Posture* **42**, 2015.
8. Anderson FC and Pandy MG. *J Biomech Eng* **123**, 2001.
9. Correa TA, et al. *J Biomech* **43**, 2010.

Table 1: Average pre-operative and post-operative maximum contact stresses for the five PAO patients selected from the larger cohort for this investigation. Pre-operative and post-operative models were subjected to arthritic, dysplastic, and normal gait patterns, and maximum contact stresses were assessed in the anterior, superior, and posterior regions of the acetabular cartilage. *p < 0.05, pre-op normal anterior vs. post-op normal anterior. #p < 0.05, post-op arthritic superior vs. post-op normal superior.

	Anterior Max Stress (MPa)			Superior Max Stress (MPa)			Posterior Max Stress (MPa)		
	Arthritic	**Dysplastic**	**Normal ***	**Arthritic**	**Dysplastic**	**Normal #**	**Arthritic**	**Dysplastic**	**Normal**
Pre-Op	4.7 ± 1.1	5.0 ± 1.1	5.4 ± 1.3	5.7 ± 1.2	7.8 ± 3.5	7.4 ± 0.9	5.8 ± 0.8	6.1 ± 2.0	6.8 ± 1.2
Post-Op	6.9 ± 1.4	6.8 ± 1.2	11.8 ± 4.9	7.1 ± 1.8	7.6 ± 1.0	13.3 ± 6.2	5.9 ± 1.9	7.0 ± 1.3	11.7 ± 6.1

THE IMPACT OF MECHANICAL LOAD CARRIAGE ON GAIT MECHANICS IN AN AGRARIAN SAMPLE

[1] Taylor P. Trentadue and [1] Daniel Schmitt

[1] Animal Locomotion Lab, Department of Evolutionary Anthropology, Duke University, Durham, NC, USA
e-mail: ttrentadue@bwh.harvard.edu, web: http://animallocomotionlab-duke.blogspot.com

INTRODUCTION

The prevalence of musculoskeletal (MSK) pathologies is increasing in the global population, including in Madagascar [1]. These conditions are especially acute in the predominantly agricultural SAVA Region, where most material transport occurs on foot, thus raising questions about the impact of load carriage on mechanics and MSK health. Previous studies suggest that the impacts of habitual load carrying are managed through gait and posture. Kenyan women transport head-supported mechanical loads up to 20% of body weight without expending additional energy [2]. Nepalese porters carry a wide range of head-supported mechanical loads without decreased muscular efficiency [3]. In posterior backpack carriage with loads up to 20.4 kg, the amplitudes of the relative maxima of vertical ground reaction forces (VGRFs) increased with load, while the timing of the relative maxima and minimum did not vary with additional weight [4].

We explored this question in Madagascar using Fourier analysis of VGRF waveforms produced during head- and shoulder-supported load carriage. Fourier analysis of VGRFs offers quantitative insight into limb kinetics and is useful in the absence of high-resolution video or kinematic data [5]. This analysis provides insight into COM motion, timing of relative maxima and minima, and peak forces during stance phase in these subjects.

METHODS

We collected survey, biometric, and VGRF data from subjects in Mandena, Madagascar. Mandena is an agrarian society in the northeast with a population of 4,000 and an area of 1 km^2.

We included individuals that reported carrying mechanical loads related to ADLs. Participants were provided the option of a head-supported basket or bamboo pole with hanging baskets and weights. Subjects were asked to fill the apparatus to a weight representative of that transported in daily tasks.

Subjects were asked to walk at self-selected speeds across a force platform (PASCO PS-2142, PASCO Scientific, Roseville, CA) normally and then under the mechanically loaded condition. We collected five steps from each limb under each condition.

To characterize and compare the shape of VGRF waveforms, we normalized the forces to body weight (BW) or BW plus load and filtered the data using a fourth-order low-pass Butterworth filter with a frequency of 10 Hz. The data were zero-padded to twice the length of the vector. We used MATLAB to fit an eight-term Fourier model with period $\omega=\pi/$contact time. We used dependent t-tests in R to compare the coefficients for each individual limb under the normal and loaded conditions.

RESULTS AND DISCUSSION

Twenty-four subjects (13 female) participated in this study. The mean (±SD) age and BMI were 36.5 (±8.2) years and 20.5 (±2.3) kg/m^2. The majority of participants (n=23) reported being farmers. The most common sites of pain were upper and lower back (each 63.6%) in males and lower back (76.9%) and neck (38.5%) in females.

Females carried head-supported loads, while males transported loads on their shoulders. On average, females carried 17.4% (±3.4%)—up to 24.9%—of BW. Males carried 28.7% (±5.4%)—with a maximum of 36.4%—of BW.

We calculated mean Fourier coefficients for all conditions and reconstructed representative VGRF curves (Figure 1).

In males, there were no significant differences in contact time between the normal versus loaded

conditions (p=0.1573). Four Fourier coefficients (a_3, b_5, a_6, b_8) were significantly different between the normal and loaded conditions (p=0.0027, p=0.0047, p=0.0269, and p=0.0336, respectively). Coefficients a_3, b_5, and a_6 drive the amplitude of the local maxima and minima. Additionally, a_3 relates to the time between the first relative maximum and the local minimum. Coefficient b_8 is related to the time elapsed from initial contact to local minimum. In males, the shape of the VGRF curve changed (Figure 1): the minimum was raised and the maxima lowered during load carriage, suggesting a more compressed leg spring while walking [6, 7].

In females, contact time was significantly longer in the normal versus the loaded condition (t=2.32, p=0.0283). Three Fourier coefficients (b_1, b_6, b_8) were significantly different between the normal and loaded conditions (p=0.0347, p=0.0103, and p=0.0012, respectively). Coefficient b_1 is related to the relative amplitudes of the maxima and local minimum, and b_6 drives the time elapsed from the local minimum to the end of stance phase, reflected as a change in the timing of the second maximum associated with longer contact time (Figure 1).

CONCLUSIONS

At relatively low loads, representative of those carried in ADLs, Fourier analysis of VGRF waveforms distinguished mechanical differences in walking in the normal versus loaded conditions. In males, who used shoulder-supported load carriage, the VGRF shape is a flatter curve with amplitudes of the relative maxima lower and local minimum higher, suggesting increased leg spring compression under moderate loading. In females, longer contact time appears to be a mechanism to manage load on the lower limb. Given the high prevalence of axial MSK pain in this population, this analysis of VGRFs offers insight into alterations in lower extremity kinetics as well as mechanical alterations for load carriage in an agrarian sample.

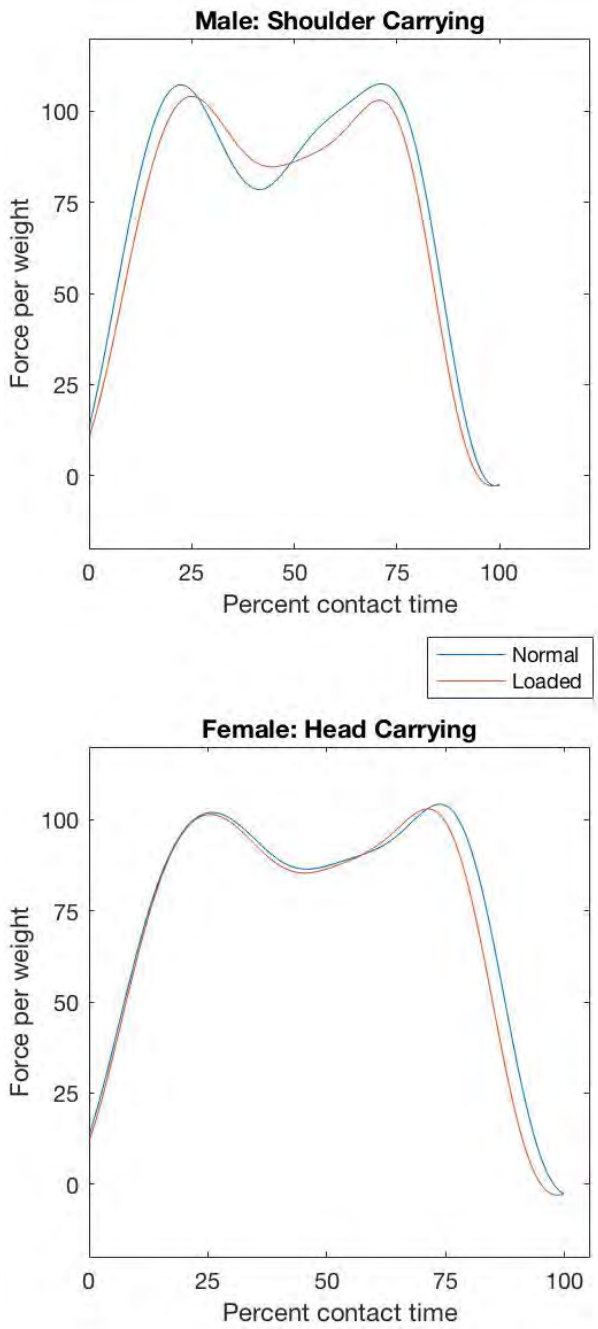

Figure 1: Reconstructions of vertical ground reaction forces (VGRFs) for males and females (top and bottom panels, respectively) using mean coefficients per condition. Blue lines represent normal and orange represent loading. VGRFs were normalized to static BW or BW plus load weight.

REFERENCES

1.Masquelier et al. Glob Health Action. 7:23237, 2014.
2.Heglund et al. Nature. 375(6526):52-4, 1995.
3.Bastien et al. J Exp Biol. 219(Pt 22):3626-34, 2016.
4.Huang and Kuo. J Exp Biol. 217(Pt 4):605-13, 2014.
5.Li et al. Folia Primatologia. 66:137-59, 1996.
6.Cavagna and Margaria. J Appl Physiol. 21(1):271-8, 1966.
7.Alexander and Jayes. J Zool (Lond). 185:27-40, 1978.

ACKNOWLEDGEMENTS

Duke Deans' Summer Research Fellowship, Duke URS Grants, and the Duke Bass Connections Program supported this research. We thank Melissa Manus for her assistance during data collection.

LONG-RANGE CORRELATION IN HUMAN JOINT-ANGLE VARIABILITY DURING WALKING

Dorothea J. Tsang, Meghan E. Lukac, and Anne E. Martin
Pennsylvania State University
Email: djt5071@psu.edu, mpl5351@psu.edu, aem34@psu.edu

INTRODUCTION

Human walking exhibits long-range correlation between stride durations [1]. These correlations measure how variation in one step influences variation in later steps. For example, a quick step will tend to be followed by more quick steps if the gait has a long-range correlation. These correlations are altered with age and some diseases and may provide information about walking ability [1]. The variability in stride durations occurs at least in part due to variation in joint angles [2]. It is not clear, however, if the joint angle variability also exhibits long range correlations given that these correlations can arise from the controller [3] or the natural dynamics of the system [4]. This study begins to quantify the long-range correlations in the joint angles during healthy human walking.

METHODS

Two healthy young adult females walked on a treadmill (Bertec, Columbus, OH) for ten minutes at an average speed of 1 m/s while kinematic data were collected at 100 Hz (Vicon, Oxford, UK). Prior to the experiment, each subject chose a comfortable speed. All data was processed using Nexus (Vicon, Oxford, UK) with the plug-in gait model and standard filtering parameters. For gaps of less than 20 frames, the cyclic method was used to fill the gap, while the spline method was used to fill longer gaps. Data was divided into stance and swing periods, and the periods were analyzed separately. The left and right legs were also analyzed separately. For each joint, the per-subject mean angle was subtracted from the total angle for each step to obtain the joint variability. To parameterize the variability mathematically, a second- (stance) or first- (swing) order Fourier series was fit to the variability [2]:

$$\begin{aligned} q_{vij}(t) =& a_{0ij} + a_{1ij}\cos\omega_{ij}t + b_{1ij}\sin\omega_{ij}t \\ &+ a_{2ij}\cos 2\omega_{ij}t + b_{2ij}\sin 2\omega_{ij}t \end{aligned}$$

where q_{vji} is joint j's variability for step i. For each step, the Fourier series is described by frequency (ω_{ij}) and magnitude (a_{0ij}, a_{1ij}, b_{1ij}, a_{2ij}, b_{2ij} where $a_{2ij} = b_{2ij} = 0$ for the swing joints) coefficients. Long-term correlations in frequency indicates that the timing of the variability is correlated while correlations in the magnitude coefficients indicates that size of the variability is correlated. To quantify the long-term correlations, detrended fluctuation analysis was performed [5] using 19 sample sizes ranging from 4 to 128 steps. For each sample size, data was divided into equal, non-overlapping segments, and the local root-mean-square (RMS) was computed. The slope of the linear regression line of the average RMS versus the segment sample sizes in log-coordinates is the Hurst exponent. A Hurst exponent of 0.5 indicates white noise and no long-term correlations. A Hurst exponent of > 0.5 indicates long-term correlations. The Hurst exponent for each frequency and magnitude coefficient was calculated separately. The Hurst exponent for stride duration was also found.

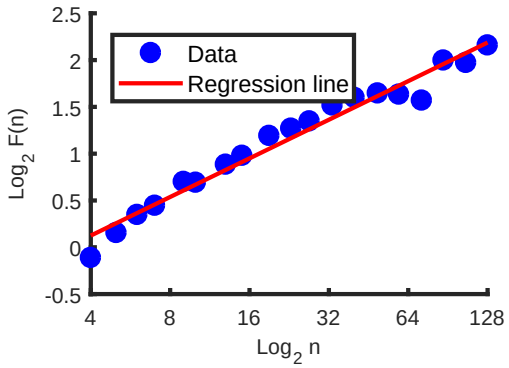

Figure 1: Average RMS vs. segment sample size in log-coordinates for the right stance hip frequencies of subject 1. The data is well fit by a line. The Hurst exponent is 0.41, indicating no long-range correlations.

RESULTS AND DISCUSSION

The subjects took 503 and 549 strides respectively. For scales of 4 to 128 steps, linear regression lines well fit the average RMS with R^2 values consistently ≥ 0.97 (Fig. 1). A scale exceeding 128 steps resulted

Table 1: Hurst exponents for the joint angle magnitude and frequency coefficients. The range of values for each coefficient is given. The data appears random with no long-term correlations regardless of period and joint.

	$\mathbf{a_0}$	$\mathbf{a_1}$	$\mathbf{b_1}$	$\mathbf{a_2}$	$\mathbf{b_2}$	ω
Stance Hip	0.53 - 0.59	0.50 - 0.58	0.46 - 0.53	0.50 - 0.60	0.48 - 0.56	0.41 - 0.50
Swing Hip	0.54 - 0.59	0.52 - 0.55	0.57 - 0.66	-	-	0.52 - 0.54
Stance Knee	0.51 - 0.64	0.51 - 0.62	0.52 - 0.58	0.56 - 0.61	0.55 - 0.64	0.48 - 0.58
Swing Knee	0.52 - 0.59	0.51 - 0.60	0.52 - 0.63	-	-	0.48 - 0.54
Stance Ankle	0.46 - 0.55	0.52 - 0.58	0.44 - 0.55	0.47 - 0.55	0.48 - 0.61	0.47 - 0.54
Swing Ankle	0.48 - 0.58	0.45 - 0.55	0.51 - 0.65	-	-	0.50 - 0.64

in RMS points that deviated from the trend apparent at smaller scale segments, suggesting insufficient data for the larger scales. There are clear long-term fluctuations in stride duration (Fig. 2). The average Hurst exponent was 0.75 which aligns closely to values reported in literature [6]. In contrast, the joint variability magnitude and frequency coefficients do not appear to exhibit long-range correlations (Fig. 2). This is confirmed with Hurst exponents ranging from 0.41 to 0.66 (Table 1). In all cases, both subjects and the left and right sides had similar values. The average Hurst exponent for the frequency coefficients over all joints and periods and for both subjects is 0.52. The average Hurst exponent for the magnitude coefficients over all joints and periods and for both subjects are 0.55 for a_0, 0.55 for a_1 and b_1, and 0.53 for a_2 and b_2. Since the Hurst exponents are all approximately 0.5, this indicates that joint variability may just be white noise. These results agree with the observation that long-term fluctuations in step duration occur with white noise in a push-off force [4].

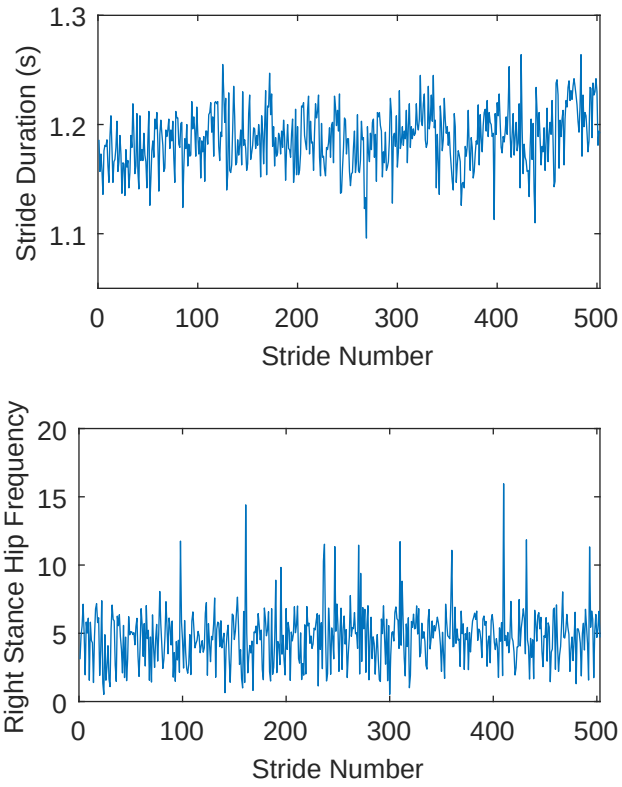

Figure 2: Stride duration (top) and right stance hip frequencies (bottom) vs. stride number for subject 1. The stride durations exhibits long-term correlations while the frequencies are random with no long-term correlations. The plots for the other frequencies and magnitudes coefficients for both subjects are similar.

CONCLUSIONS

In contrast to the stride duration variability, the joint angle variability does not appear to exhibit long-range correlations. Instead, it has an anti-correlated, time-independent structure, at least when each coefficient is analyzed independently. This suggests that the long-term correlations in stride duration may arise from the natural dynamics of the system rather than from correlations in the leg kinematics.

REFERENCES

[1] Hausdorff, JM. *Hum Movement Sci* **26**, 555–589, 2007.

[2] Martin, AE, et al. *J Biomech* **49**, 3298–3305, 2016.

[3] Dingwell, JB & Cusumano, JP. *PLOS ONE* **10**, e0124879, 2015.

[4] Ahn, J & Hogan, N. *PLOS ONE* **8**, e73239, 2013.

[5] Ihlen, EAF. *Front Physiol* **3**, 141, 2012.

[6] Rhea, CK, et al. *Hum Movement Sci* **36**, 20–34, 2014.

KNEE ANGLES WITH SOFT TISSUE ARTIFACT CORRECTION FOR NORMAL WEIGHT, OVERWEIGHT AND OBESE SUBJECTS IN GAIT AND CYCLING

[1]Sam Tucker, [2]Valentina Profiti, [1]Scott J. Hazelwood, and [1]Stephen M. Klisch
[1] California Polytechnic State University, San Luis Obispo, CA, USA
[2] Politecnico di Torino, Torino, Italy
email: sklisch@calpoly.edu

INTRODUCTION

Obesity is a risk factor for knee osteoarthritis (OA) [1] and has reached epidemic proportions in the US. Knee angles for normal weight (NW) and obese (OB) subjects have been reported in gait [2]. However, previous studies with OW and OB subjects have not reported knee angles for other exercises (e.g. cycling) nor corrected for soft tissue artifact (STA), a primary source of error using skin-based marker systems. The objective of this study was to correct for STA in gait and cycling using pseudo-rigid body (PRB) [3] and Procrustes solution (PS) [4] methods. The hypothesis was that knee angles would differ due to subject type (NW, OW, OB) in gait but not in cycling.

METHODS

Cal Poly's Human Subject Committee approved all protocols. NW (n=6, aged 18-25, BMI = 21.8±2.5), OW (n=6, aged 18-25, BMI = 27.8±1.4), and OB (n=3, aged 18-25, BMI = 32.7±1.4) participants performed 3 trials for each exercise. An enhanced Helen Hayes marker set with 32 markers and 2 clusters of 7 randomly spaced markers on the thigh and shank were placed on the participants. Kinematic data were captured using a 10-camera motion analysis system with Cortex software (Motion Analysis Corp., CA, USA). Kinetic data were collected using 3 ground force plates (Accugait, AMTI, MA, USA) for gait experiments and a stationary bike (Lifecycle GX, Life Fitness, IL, USA) retrofitted with custom pedals with 6-axis load cells (AMTI, MA, USA). A static trial capture was used to identify marker reference configurations. Gait experiments were conducted at self-selected walking speeds and cycling experiments were conducted at 70 RPM with a moderate machine resistance level. Kinematic and kinetic data were processed in Cortex and filtered (4^{th} order Butterworth, cutoff frequency 6 Hz). Custom codes (Matlab, MA, USA) were used for all subsequent analyses.

The 7-marker clusters were used to obtain STA corrected body segment orientations. For the PRB method [3], each 7-marker cluster was partitioned into sub-clusters of 3 markers. Sub-clusters were modeled as Triangular Cosserat Point Elements (TCPEs). Using a director vector approach, a deformation gradient tensor, a Finite Lagrangian strain tensor, and a translation vector were calculated. The translation vector was defined for a TCPE's centroid relative to the knee joint center. Using the right polar decomposition, a TCPE's rotation tensor was calculated from the deformation gradient tensor. TCPEs whose strain tensors and translation vectors had the lowest magnitude and whose rotation tensors were most consistent with other TCPEs were then selected using a filtering algorithm. From the selected TCPEs (and, thus, from a subset of the 7-marker clusters), thigh and shank rotation tensors were determined.

For the PS method [4], a Singular Value Decomposition (SVD) was used. This method assumed all markers of a 7-marker cluster move together as a rigid body and minimized the least squared error of all 7 marker positions in the cluster from a configuration defined by an optimized rigid body rotation tensor for the thigh or shank.

With the thigh and shank rotation tensors obtained as described above, a floating axis coordinate system [5] was used to define knee angles: flexion/extension (FE), internal/external (IE) rotation, and adduction/abduction (AA). Results were normalized to 101 time points corresponding to 0-100% of a gait/cycling cycle. Significant differences were investigated using 1-way ANOVAs and post-hoc Tukey tests ($p < 0.05$ significant).

RESULTS AND DISCUSSION

In gait, maximum IE (p=0.045) and AA angles (p=0.047) differed between NW and OW subjects. Minimum IE angles differed between NW and OB (p=0.021) and OW and OB (p=0.034) subjects. There existed no differences between NW, OW, and OB angles in cycling.

The results confirmed the hypothesis that knee angles varied due to subject type in gait and did not vary between subject type in cycling. In gait, OW and OB subjects experienced an external rotation offset that may be linked to high OA risk [6]. Furthermore, the differing NW and OW knee angles in gait suggests altered kinematics, related to excess body weight, may occur before BMI reaches OB status. Although the results suggest that cycling may maintain knee angles at normal levels for OW and OB subjects, this study was limited by a relatively low number of subjects and that limitation should be addressed in a future study.

The PRB and PS methods predicted qualitatively similar results, and statistical significance did not change between methods. An advantage of using the PRB method is that it incorporates the use of scalar optimization parameters that model the amounts of 3 distinct STA modes (i.e. homogeneous deformation, rigid body rotation, rigid body translation), allowing for a physiological description and quantification of STA. Since the PRB and PS methods produced similar knee angles, the PRB method may be considered the preferred algorithm for STA correction, but further work needs to be done to better interpret its scalar optimization parameters.

CONCLUSIONS

Novel results of this study were STA corrected knee angles for OW and OB participants in gait and cycling. Results of this and previous studies suggest that cycling may be a preferred weight-loss exercise for OW and OB patients due to maintenance of normal knee biomechanics [1].

REFERENCES

1. Issa, et al., *Current Opinion in Rheumatology,* 18:147-56, 2006.
2. Lerner, AL. et al., *Journal of Pediatric Orthopedics*, 25:763-8, 2005.
3. Solav, D. et al., *International Journal of Engineering Science*, 85:1-9, 2015.
4. Söderkvist, I. et al., *Journal of Biomechanics*, 26:1473-1477, 1993.
5. Wu-Cavanaugh, *Journal of Biomechanics*, 10: 1257-1261, 1995.
6. Andriacchi et al., *Journal of Orthopedic Research* 22: 794-800, 2004.

ACKNOWLEDGEMENTS

Supported by the Donald E. Bently Center, W.M. Keck Foundation, and the Defense Health Program through the Department of Defense under Award No. W81XWH-16-1-0051 and Cal Poly's Donald E. Bentley Center. Opinions, interpretations, conclusions, and recommendations are those of the authors.

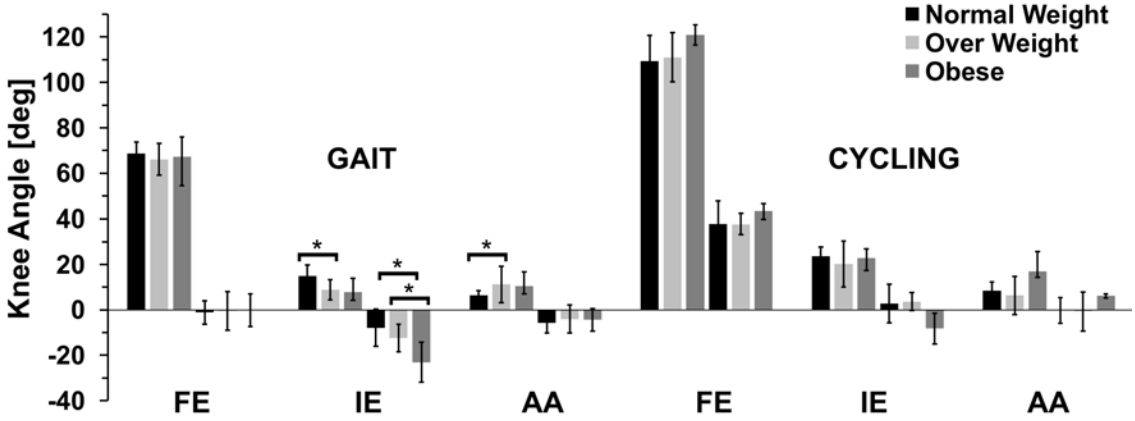

Figure 1. PRB predicted maximum/minimum FE, IE, and AA angles in gait and cycling averaged over all NW (n=6), OW (n=6), and OB (n=3) subjects. Mean ±1 S.D. shown. * indicates significance.

THE BENEFIT OF DIFFERENT MARA THON SHOES THROUGH VARIOUS RUNNING MECHANICS

[1]Dru Valentine, [1]Aubree McLeod, [1]Neal Anderson, [1]Jared Ward, [1]Ron Hager, and [1]Iain Hunter

[1] Brigham Young University, Provo, UT USA
email: valentinedru04@gmail.com, web: http://biomechanics.byu.edu

INTRODUCTION

In the 2014 Berlin Marathon, Adidas elite runner, Dennis Kimetto, broke the marathon world record with a finishing time of 2:02:57. This facilitated the race between Nike and Adidas to create a shoe that would enable an athlete break the 2-hour marathon barrier. Adidas released the Adidas Adios Boost (AB); worn by Kimetto during the Berlin marathon. Nike then followed with the launch of the "Breaking2" project, focused on the Vaporfly 4% (VP).

Both Adidas and Nike took different approaches when designing their sub-2 marathon shoes; attempting to find the optimal energy cost point between mass, cushioning and stiffness. AB is lightweight, with a minimal cushioning design (23mm heel), similar to the Nike Zoom Streak (ZS), which contributed to success for marathon runners in recent years. The VP is also lightweight, however, the shoe includes a high heel (31mm) with the new ZoomX foam and a full-length carbon fiber plate.

Figur e 1: The Nike Vaporfly 4%, Adidas Adios Boost, and Nike Zoom Streak used in this study.

Initial VP prototype testing resulted in a 4% lower metabolic cost compared to both the AB and NS, 20% of which was attributed to the change in running mechanics, such as ground contact time [1]. Runners with a shorter ground contact time (a more midfoot or forefoot strike), also have a lower metabolic cost [2].

The article by Hoogkamer [1] used a prototype version of the VP shoe, and reported force measures, but did not report kinematics. We utilized similar methods, but took kinetic and kinematic measures into account on a second day of testing in the consumer version of the VP shoe compared to the AB and ZS. We expected to observe similar results to Hoogkamer while adding new information about kinematics.

METHODS

Nineteen subjects participated in a two-day data collection. On the first day, subjects did a 5 minute warm-up at 3.54m/s. After warm-up, each subject was fitted for the AB, NS, and VP. They were also fitted for equipment that measured oxygen uptake (TrueOne 2400, Parvo Medics, UT).

Each subject completed a 5 minute run at 16 km/hr in each shoe, with a 5 minute break between the runs to change shoes. The subject wore AB, NS, and VP once, in a randomized order, and then cycled through each shoe again with the same protocol.

On the second day of data collection, subjects were measured for force and kinematics using Vicon Plug-in Gait (Vicon, Oxford, UK). Subjects ran for 3 minutes in each shoe model at 16 km/hr on a instrumented treadmill (AMTI Force Sensing Tandem Treadmill, MA). Data was only collected during the last 30 seconds of each trial.

The dependent variables listed in Table 1 were computed within Vicon Nexus. A regression analysis determined which of these variables were correlated with each subject's percent of oxygen uptake benefit due to wearing the VP shoe in comparison to the AB. The comparison of VP to AB was chosen rather than VP to ZS since the oxygen uptake benefit of the VP to AB (2.8%) was greater than that of VP to ZS (1.9%) as shown through repeated measures ANOVA with Tukey HSD post hoc tests.

RESULTS AND DISCUSSION

The percent benefit of the VP shoe over the AB shoe was predicted only by ground time ($F=7.082$, $p=0.012$, $R^2=0.164$). Other variables were non-significant (Table 1 & Figure 2). The prediction equation for the percent oxygen uptake benefit by ground time was VO_2 benefit (%) =
$-0.357 \times GT + 0.092$.

Table 1: Independent variables tested for correlations with the percent benefit in oxygen uptake while using the VP shoe.

Variable	p-value
Ground Time (s)	0.010
Stride length (m)	0.261
Vertical Impulse (Ns)	0.639
Knee flexion range of motion during ground contact (deg)	0.282
Hip flexion range of motion through full stride (deg)	0.446
Plantar flexion velocity from maximum flexion to toe off (deg)	0.446
Vertical oscillation of center of mass (cm)	0.126

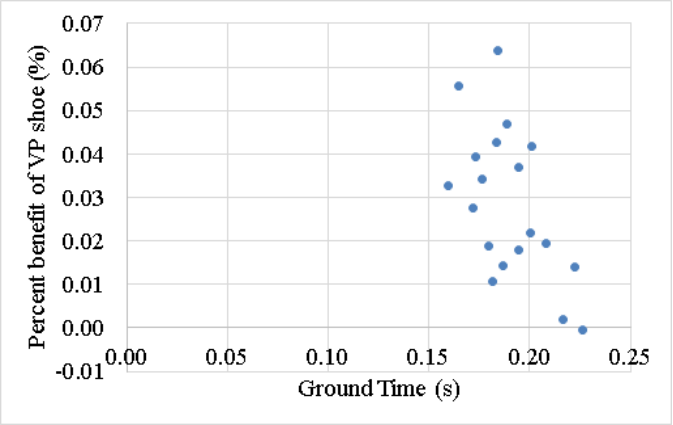

Figure 2: Percent VO2 benefit of VP over AB versus ground time.

While ground time was the only significant variable to the VP energy cost benefit in our study, Hoogkramer's study found that only peak force was significant in VP energy cost benefit. The difference between the studies could possibly be explained by the differences between Hoogkramer's prototype VP and the consumer VP. In our study, some subjects commented on the lack of grip between the treadmill belt and sole of the VP shoes.

Ground time only explained 16% of the variance, and while the other independent variables were not significant. So, the question of which shoe will be most effective for which runner remains only partly explained.

CONCLUSIONS

Considering both Hoogkamer and our study there seems to be an interaction between the ground and the VP shoe, which is connected with amount of energy benefit individual runners gets from the VP shoe.

REFERENCES

1. Hoogkamer et al. Sports Med, Online, 2017.
2. Chapman et al. Medicine & Science in Sports & Exercise, 2012

SEX DIFFERENCES IN GLUTEAL MUSCLE FORCES DURING RUNNING

[1] C. Nathan Vannatta and [2] Thomas W. Kernozek

[1] Gundersen Health System, La Crosse, WI, USA
[2] University of Wisconsin – La Crosse, La Crosse, WI, USA
email: cnvannat@gundersenhealth.org

INTRODUCTION

Injury trends appear to differ between males and females for a variety of sport related activities, but research surrounding these differences is sparse [1]. During running, specific injuries (i.e. patellofemoral pain and iliotibial band syndrome) are reported as more common in females [2,3].

To aid our understanding and investigate potential factors in the etiology of such running injuries, studies examining sex differences in running gait mechanics have been conducted. Females have been reported to demonstrate greater hip adduction and internal rotation range of motion and hip frontal and transverse plane negative work during running [4]. In addition to these mechanical factors, females also appear to show greater EMG activity in the gluteus maximus compared to males [5].

These previous findings suggest that differences in gluteal muscle function may be present between sexes. However, no studies have investigated differences in gluteal muscle forces between male and female runners.

METHODS

Twenty-one healthy male and female runners were recruited for this study. All participants ran >10 miles per week, had a self-reported rear-foot strike pattern, and were free from any injury to the lower extremity in the past six months.

Each participant was outfitted with 47 retroreflective markers necessary to calculate a 44 degrees of freedom musculoskeletal model with 18 rigid segments (HBM Motekforcelink, Amsterdam, Netherlands). A standing neutral pose was completed to determine body weight, calibrate and scale the model, and establish global and joint coordinate reference frames.

Participants were then allowed several practice trials to familiarize themselves with the runway. Five trials were collected for the right leg as the participant ran at a controlled speed of 3.52-3.89 m/s. Each leg made one foot contact with a force platform mounted within the runway. Motion capture data were completed via 15 high speed cameras. Analog data were captured at 1800 Hz and synchronized to kinematic data at 180 Hz. Each of these data were filtered at 15 Hz. Muscle forces were estimated from the joint moments by minimizing a static cost function where the sum of squared muscle activations is related to maximum muscle strengths.

Peak muscle force for the gluteus maximus, gluteus medius, gluteus minimus, and hamstrings were compared between genders using a multi-variate analysis of variance with an alpha set to 0.05. Hip kinematics and kinetics were also compared.

RESULTS AND DISCUSSION

Age and activity level was similar between males and females. Males had greater average height and mass. Females demonstrated 71.3% greater gluteus medius force and 86.8% greater gluteus minimus force (Table 1). However, gluteus maximus force was 58.17% less in females compared to males (Figure 1). Females also had 4.5° less peak hip flexion, 5.5° greater peak hip adduction, and 4.2° less anterior pelvic tilt. No differences were observed in hip internal rotation or pelvic drop between sexes (Figure 2).

The reduced gluteus maximus force observed in females was unexpected based on the previous literature reporting increased gluteus maximus EMG activity in running compared to males [5]. The greater EMG activity (found previously) in conjunction with reduced force generation

(observed in this study) may allow one to hypothesize that motor unit recruitment, or synchronization, may be different in females and result in less force production. This hypothesis requires further investigation.

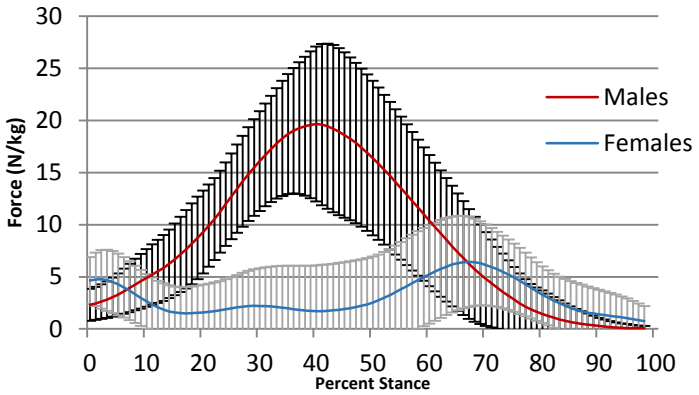

Figure 1: Comparison of gluteus maximus muscle force during the stance phase of running between males and females.

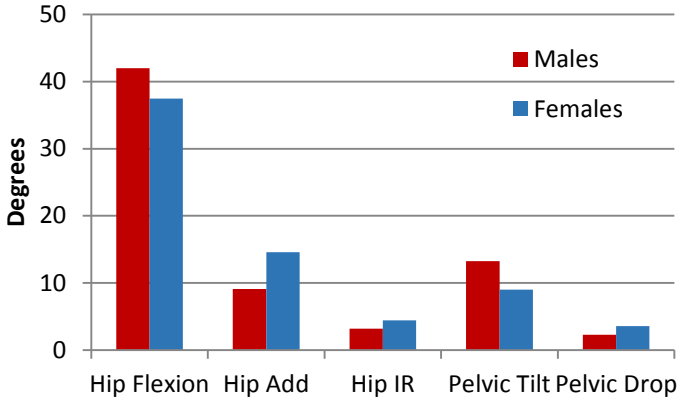

Figure 2: Comparison of peak kinematics of the hip and pelvis during the stance phase of running between males and females.

Additionally, females demonstrated greater hamstring muscle force. This may indicate a compensation in force production from the hamstrings to account for the reduced gluteus maximus force. Alternatively, this may suggest a different muscle force strategy to produce hip extension moment in females.

The increase in hip adduction seen in females may further explain the larger gluteus medius and minimus muscle force values. Greater hip adduction may lead to a larger external moment being applied therefore requiring a larger hip abduction moment [4]. Since the gluteus medius and minimus are the prime movers to produce this moment, they may have been required to produce more force.

CONCLUSIONS

Differences in gluteal muscle forces and hip kinematics were observed between male and female runners. Further understanding of underlying muscle forces and tissue specific stresses may assist in explaining the disparity between injury rates between males and females. As there are few studies which have investigated the role of individual muscle forces and running related injury, this appears to be an area needing further investigation.

REFERENCES

1. Hewett, Schilaty, & Bates. *J Sci Med Sport*. Nov. 3: doi. 10.1016, 2017.
2. Boling et al. *Scand J Med Sci Sports*. 20: 2010.
3. Phinyomark et al. *Scand J Med Sci Sports*. 25: 2015.
4. Ferber et al. *Clin Biomech*. 18: 2003.
5. Willson et al. *Clin Biomech*. 27: 2012.

ACKNOWLEDGEMENTS

We would like to acknowledge Drew Rutherford and Nagmeh Gheidi for their assistance in data collection and processing.

Table 1: Comparison of peak muscle forces in the stance phase of running between males and females.

Muscle Force (N/kg)	Females	Males	Difference	Effect Size	F- Statistic (1,40)	p-value
Gluteus Maximus	8.50 (sd 4.11)	20.32 (sd 7.68)	-11.82	2.00	39.430	<0.001
Gluteus Medius	63.84 (sd 11.01)	37.26 (sd 9.36)	26.58	2.60	70.132	<0.001
Gluteus Minimus	12.01 (sd 2.53)	6.43 (sd 1.68)	5.58	2.86	84.480	<0.001
Hamstrings	36.03 (sd 8.77)	28.14 (sd 5.31)	7.89	1.12	-	<0.001

THE EFFECT OF GRADE ON JOINT MECHANICS DURING DOWNHILL RUNNING IN FEMALE DISTANCE RUNNERS

[1,2] Meredith Wells, [2]D. Clark Dickin, [2]Jennifer Popp, and [2]Henry Wang

[1]Georgia State University, Atlanta, GA, USA
[2]Ball State University, Muncie, IN, USA
email: mwells19@student.gsu.edu

INTRODUCTION

Vast numbers of people run because it provides a variety of health benefits and can be done anywhere. Long distance runners have an increased likelihood of running up and down hills during long runs, and hill training is a key technique used to build strength and speed. Despite the health benefits of long distance running, anywhere from 27 to 79 percent of distance runners will sustain an overuse injury over the course of a year [1].

Some of the most common overuse running injuries are patellofemoral pain syndrome (PFPS) and iliotibial band friction syndrome (ITBFS) [2]. Previous research has shown that decreased hip and knee flexion at initial contact, and a greater range of motion (ROM) at the knee has been associated with PFPS and ITBFS [3]. However, the research regarding lower extremity joint moments and powers, muscle activity, and spatiotemporal parameters is conflicted.

Although numerous studies have been conducted on level running, there is limited research available regarding downhill running. No downhill running studies have been conducted looking at specifically females, yet females are at an increased risk of injury due to anatomical differences [4]. Therefore, the purpose of this study was to analyze the joint mechanics of female distance runners at five different grades with regards to the risk of injury. It was hypothesized that the steeper declines would show decreased hip and knee flexion at initial contact, greater moments at the knee and ankle, and altered spatiotemporal parameters.

METHODS

Fifteen healthy, female distance runners (Age: 23.5 ± 4.9 years, Ht: 1.7 ± .06m, Wt: 57.8 ± 6.8kg, weekly mileage: 35 ± 13 miles) participated in this study. All participants signed an informed consent, and IRB approval was received. Participants were provided compression clothing and standardized athletic shoes. Anthropometric measurements were taken and reflective markers were placed on anatomical landmarks following a modified plug-in-gait model.

Participants warmed up for 5 minutes on a level surface before being fit with a harness attached to the ceiling as a safety precaution. Each participant ran on an AMTI force-instrumented treadmill (Advanced Mechanical Technology, Inc., Watertown, MA, USA) at 0%, -5%, -10%, -15%, and -20% grades for 2 minutes at 4.0 m/s in a randomized order with 5 minutes of rest between conditions.

Kinematic data were collected using 15 VICON infrared cameras (Oxford Metrics, Oxford, UK), sampling at 200 Hz. Kinetic data was sampled at 2000 Hz. Vicon Nexus 2.5, Visual 3D, and Matlab were used to process the data and calibrate the treadmill. Statistical significance was determined using repeated measure MANOVAs in SPSS with an alpha level of .05.

RESULTS AND DISCUSSION

Ankle ($p<.01$) and hip ($p<.05$) ROM decreased, and knee ($p<.02$) ROM increased in the sagittal plane during downhill running. Trunk extension at initial contact increased from level to each of the grades as well ($p<.001$). Hip adduction angle at initial contact and peak hip adduction angle decreased in a dose-response relationship as the grade declined.

Peak knee adduction ($p<.01$), and peak hip adduction ($p<.05$) moments increased, and the peak knee abduction ($p<.01$) moment decreased in the downhill conditions compared to level.

Ankle and knee power absorption increased while ankle and knee power propulsion decreased as the grade declined ($p<.001$) (Figure 1).

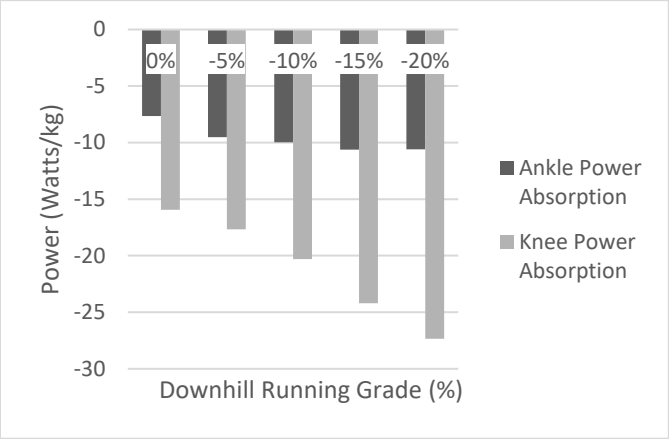

Figure 1: Power absorption at the ankle and knee at each running grade.

There were no significant differences in stride rate or stride length at any of the grades ($p>.05$).

The dose-response relationship between the decline and the power absorbed by the knee joint may be the reason for the significant soreness often felt by runners when training downhill. The increased ROM at the knee and the decreased knee flexion at initial contact are risk factors for knee pain such as in PFPS and ITBFS. The increased knee and hip adduction moments may lead to increased lateral knee pain. Overall, there appears to be a greater risk for sustaining an injury when running downhill.

CONCLUSIONS

There is a chance that running downhill at steep grades for an extended period of time may increase the risk of sustaining a running related injury. This was not a prospective study, so it cannot be stated that downhill running causes injuries. Additionally, downhill running is a necessary part of distance training, and should not be eliminated. Rather, runners and coaches need to be aware of the potential risks associated with downhill running, so that they may be considered when creating training programs so that injuries may be avoided.

REFERENCES

1. Lun V. et al. *Br J Sports Med* **38,** 576-580, 2004.
2. Taunton J, et al. *Br J Sports Med* **36,** 95-101, 2002.
3. Buczek F & Cavanagh P. *Med Sci Sports Exerc* **22,** 669-677.
4. van Gent R, et al. *Br J Sports Med* **41,** 469-480, 2007.

ACKNOWLEDGEMENTS

Ball State University Graduate Student ASPIRE Grant.

Table 1: Average lower extremity sagittal plane joint angles at each treadmill grade.

	Grade				
Joint Position (degrees)	**0%**	**-5%**	**-10%**	**-15%**	**-20%**
Peak Ankle Dorsiflexion	25.4	23.4	21.9	21.3	19.8
Peak Ankle Plantarflexion	-14.4	-11.3	-8.9	-4.9	-4.8
Knee Flexion at Initial Contact	16.7	11.7	9.8	9.3	10.1
Peak Knee Flexion	42.4	41.5	42.4	44.4	47.8
Hip Flexion at Initial Contact	42.7	39.1	37.5	36.2	35.4
Peak Hip Extension	-7.9	-7.6	-6.4	-4.4	0.6
Trunk Extension at Initial Contact	-14.0	-16.9	-18.8	-19.6	-19.5

Gait Modification when Decreasing Double Support Percentage

Daniel S. Williams and Anne E. Martin
Pennsylvania State University
Email: dmw5737@psu.edu, aem34@psu.edu

1 INTRODUCTION

Humans naturally modify the percentage of time they spend in the double support (DS) phase of gait as they modulate their speed, but this change is done unconsciously. As humans walk faster, the DS phase decreases, both in time and as a percentage of step duration. In addition, peak knee angle increases in both stance and swing, and the range of motion at both the hip and ankle increases [1, 2]. However, it is unknown which changes are explicitly due to a change in DS percentage and which are simply adaptations to the change in speed. In this study, subjects directly modulated their DS fraction while holding speed constant, and the change to their gait was analyzed. The analysis of these changes can be used to develop a better understanding of the role of the DS period in gait.

2 METHODS

The results presented herein are part of a larger study. Kinematic data (Vicon, Oxford, UK) were collected from 7 health adults (3 male) walking on a split-belt instrumented treadmill (Bertec, Columbis, OH). One additional subject's data were collected, but are omitted because the subject did not complete the task requirements. Subjects chose a slow, comfortable pace; this speed was used for all four one-minute trials and this natural step frequency was specified in two trials. Subjects then walked with a normal or decreased DS fraction and were given time to adapt to each gait before data collection. During the first two trials, one for each DS condition, no feedback was provided. During the last two trials, a metronome dictated step frequency and visual feedback indicated DS fraction. The order of the trials within each block was randomized. Normal DS with feedback is the control condition because it ensures the gait's spatial temporal values are identical to normal walking before subjects modified their gait. Comparisons are with respect to this trial. All values presented are statistically significant at $\alpha = 0.05$.

3 RESULTS AND DISCUSSION

As expected, when walking with a normal DS percentage, subjects maintained their normal step frequency within $\pm 4\%$, and feedback had almost no effect on gait. All subjects decreased their DS fraction, both when provided with feedback and without feedback. When shortening DS percentage with feedback, all subjects maintained their normal step frequency within $\pm 5\%$. When shortening DS percentage without feedback, step frequency decreased by $14\% \pm 12\%$. The DS percentage decreased by $25\% \pm 11\%$ (feedback) and $31\% \pm 12\%$ (no feedback). DS time decreased by $25\% \pm 11\%$ with feedback and $22\% \pm 12\%$ without feedback and single support (SS) time increased by $11\% \pm 8\%$ with feedback and $32\% \pm 19\%$ without feedback. Without the step cadence constraint, subjects achieved a shorter DS percentage by substantially increasing SS time. Adding the step cadence constraint forced subjects to reduce SS time, and they decreased DS time to compensate and achieve the desired DS percentage.

FOOT HEIGHT When decreasing DS percentage, swing foot height increased (Fig. 1). The peak height of the swing foot, measured at the heel, increased by

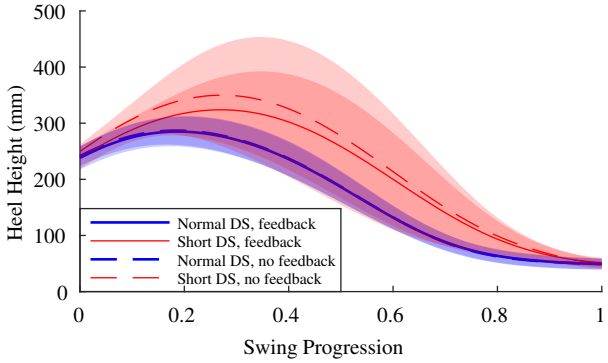

Figure 1: Swing foot height over normalized swing period. Shaded areas represent one standard deviation. Reducing the DS percentage increased swing foot height.

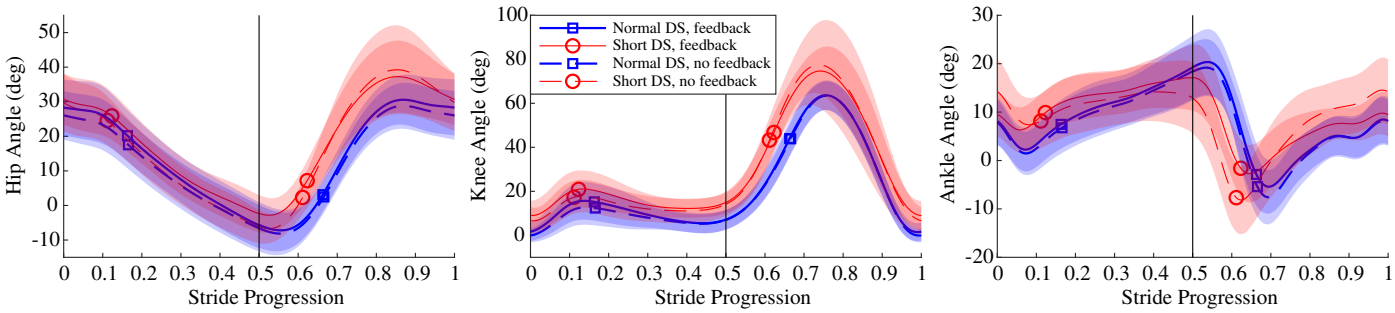

Figure 2: Joint angles. Markers represent contralateral and ipsolateral toe off, the vertical line represents contralateral heel strike, and the shaded areas represent one standard deviation from the mean. Conscious modification of the DS period affected a noticeable change in joint angle trajectories while feedback had a smaller effect.

$14\% \pm 21\%$ (feedback) and $25\% \pm 29\%$ (no feedback). The timing of the peak foot height relative to the total step time did not significantly change. This change in foot height indicates that subjects chose to lift their feet higher to increase the time spent in SS, rather than slow their foot velocity and maintain the same foot trajectory.

KINEMATICS Hip angle from heelstrike to contralateral heelstrike was similar between conditions (Fig. 2). Hip flexion from contralateral heelstrike through the swing phase increased, with the peak hip angle increasing by $31\% \pm 41\%$ without feedback, but the increase was not statistically significant with feedback. Similar to the hip angle, the knee angle from heelstrike to contralateral heelstrike was similar between conditions, although the shortened DS gaits have more knee flexion on average. Knee flexion from contralateral heelstrike through the swing phase significantly increased, with the peak knee angle increasing by $18\% \pm 16\%$ (feedback) and $25\% \pm 29\%$ (no feedback). Interestingly, the knee angle at contralateral toe off did not change as much, only differing by $\pm 4\%$. This suggests that toe-off may be driven by the trailing knee angle [3]. When shortening DS percentage, ankle range of motion from heelstrike to contralateral heelstrike decreased by $30\% \pm 29\%$ with feedback and $28\% \pm 30\%$ without feedback. In both cases, peak dorsiflexion shifted earlier so that it occurred just before toe off. Adding feedback allowed subjects to see how well they were achieving the goal but added a step cadence constraint. This addition significantly affected the swing foot height, which was decreased $9\% \pm 17\%$ compared to the short DS without feedback trial. It also significantly affected ankle angle from contralateral toe off through ipsolateral toe off, decreasing peak dorsiflexion by $6^\circ \pm 6^\circ$. Thus, as expected, subjects modified their gait differently when step cadence was or was not specified. The changes in the joint trajectories are similar to changes made when walking faster [2], but consciously shortening the DS percentage resulted in a more substantial change during swing and a less substantial change during stance. This may be because average hip velocity must match average walking speed. Altering stance leg kinematics will also alter hip velocity, thus making it difficult to maintain the given walking speed. In contrast, adjusting swing leg velocity is much easier [4].

4 CONCLUSIONS

To accommodate a shortened DS fraction without changing walking speed, subjects increased swing knee flexion, reduced ankle range of motion, and increased swing foot height. The changes are distinct from those made when increasing walking speed and affect the swing leg far more than the stance leg.

REFERENCES

[1] Murray, MP. *Am J Phys Med Rehab* **46**, 290–333, 1967.

[2] Han, Y & Wang, X. *Sci China Technol Sci* **54**, 983–991, 2011.

[3] Holden, JP, et al. *Clin Biomech* **12**, 375–382, 1997.

[4] Martin, AE, et al. *Int J Robot Res* **33**, 1530–1543, 2014.

COMPARISON OF PATIENT-REPORTED OUTCOME AND PERFORMANCE-BASED OUTCOME MEASURES OVER THE RETURN TO RUN PROGRAM FOR LOWER EXTREMITY INJURIES

Amanda Wingate, BA, Julianne Stewart, PT, DPT, John David Collins, MA, Trevor Kingsbury, MA and Marilynn Wyatt, PT, MA

Naval Medical Center San Diego, San Diego, CA
email: afwingate@gmail.com

INTRODUCTION

Patient-reported outcome (PRO) and performance based, functional outcome measures are important parameters to track during rehabilitation of servicemembers (SMs) with lower extremity injuries. Presently, little research has looked at the ability of SMs to return to a high-level of activity after injury. At the Naval Medical Center San Diego (NMCSD) Gait Analysis Laboratory, quantitative and qualitative measures are collected at multiple time points as part of routine patient care to support the rehabilitation process and document outcomes. The Return-to-Run (RTR) Program is for those SMs who have had a traumatic/high-energy injury to their lower extremity. The RTR program is an intense rehabilitation program designed to improve strength, power, multidirectional agility, and running technique to optimize energy return and safety in the IDEO brace. SMs receive the Intrepid Dynamic Exoskeletal Orthosis (IDEO) brace to help restore lost energy [1] and participate in the RTR program to adjust to using this brace.

Two qualitative measures are used to evaluate a patient's overall opinion of his or her health: the PROMIS® Global Health, a 10-item instrument scored into two subscales: physical health and mental health [2] and the Short Musculoskeletal Function Assessment (SMFA), a 46-item instrument that measures perceived functional status by two subscales, one a dysfunction index and the other a bother index [3]. The Four Square Step Test (FSST) is a functional outcome measure that is used to quantify the physical balance and agility of patients and is a sensitive and specific test for impaired mobility [4]. The comprehensive high-level activity mobility predictor (CHAMP) is used to measure the changes in high-level mobility by administering four physical performance subtests: Single limb stance (SLS) assesses balance, Edgren side step test (ESST) assesses lateral speed and agility, and the T-test and Illinois Agility Test (IAT) assesses multi-directional speed and agility [5].

The primary purpose of this study is to evaluate the effect of time through the return to run rehabilitation program on PROs and functional outcome measures for SMs with lower traumatic injuries. Correlations between PRO and performance measures were investigated to see if there are predictable behaviors of good rehabilitation outcomes.

METHODS

Twenty-three male SMs who sustained a lower limb high-energy injury were identified through an IRB approved retrospective analysis of 2014-2017 clinical records at NMCSD. The mechanism of injury ranged from high-energy activities and motor vehicle accidents to combat blasts. As part of their RTR rehabilitation process, SMs underwent CHAMP, FSST, and PRO collection (SMFA and PROMIS® Global Health) at preRTR and at postRTR. At preRTR, patients were participating in the RTR program for 6.1+2.5 weeks. During each visit, patients completed two qualitative PROs: SMFA and PROMIS® Global Health; and two quantitative functional measures: FSST and CHAMP. For comparison purposes, the focus was on the subtests scores and not the overall CHAMP score. One way ANOVAs were performed to examine the effect of time on each PRO and functional measure with a $p < 0.05$. If a main effect was found, Tukey post hoc tests were used to determine where differences occurred. Pearson correlation coefficients were computed for all PRO and functional outcome variables.

RESULTS AND DISCUSSION

Descriptive statistics are reported in Table 1 for PROs and Table 2 for performance-based, function outcome measures. There was not a main effect of time through RTR program for any of the PRO measures (SMFA Dysfunction $p = 0.26$, SMFA Bother $p = 0.26$, PROMIS PH $p = 0.13$, PROMIS MH $p = 0.18$). There was a significant effect of time on one functional measure (FSST $p < 0.01$). None of the PRO measures were significantly improved, however all SMs PRO scores were trending toward improvement. The overall CHAMP scores were impacted by the SLS. SMs have a hard time standing still for any length of time on the foot with the IDEO. There were no correlations between the two functional measures and the between the PROs.

CONCLUSIONS

The purpose of this study was to report on PRO and functional outcome measures throughout return to run rehabilitation program and to determine how the qualitative and quantitative measures may correlate with each other. It appears that the functional measures have better sensitivity to change compared to the PRO measures in relatively low patient numbers. As more patients are added to this preliminary study, some of the trends toward PRO and CHAMP improvement may become statistically significant. Also, more time points could be examined; for instance, at 6-months, 1-year, and every year after to see if there are improvements and whether or not the SMs maintain their conditioning. In addition to attempting to understand the relationship between PRO measures and functional outcomes, future research could examine more the differences between patients that would make the variability of PROs so large. That in turn may help explain the changes, or lack thereof, in the SMFA across time in RTR rehabilitation in SMs with lower extremity injuries. The addition of other PROs may be able to predict the functional outcomes.

REFERENCES

1. Owens JG, et al. Trauma, **71**, S120-4, 2013.
2. Hayes RD, et al. Qual Life Res **18**, 873-80, 2009.
3. Swiontkowski MF, et al. J Bone Joint Surg **81**, 1245-60, 1999.
4. Dite W, et al. Arch Phys Med Rehabil, **83**, 1566-71, 2002.
5. Gailey RS, et al. JRRD, **50**, 905-18, 2013.

ACKNOWLEDGEMENT

Thank you to the NMCSD Gait Lab, the Physical Therapy Department, and the Prosthetics/Orthotics Department.

DISCLOSURE STATEMENT

The views expressed herein are those of the author(s) and do not necessarily reflect the official policy or position of the Department of the Navy, Department of Defense, or the United States Government. All data collection and analysis was performed under IRB protocol NMCSD.2014.0026.

Table 1: Descriptive statistics (mean ± standard deviation) of patient-reported outcomes over Return-to-Run Program.

	SMFA Dysfunction	SMFA Bother	PROMIS Physical Health	PROMIS Mental Health
PreRTR	32.7±23.1	26.4±21.1	43.7±6.3	48.7±7.6
PostRTR	25.0±20.9	19.7±16.7	46.7±6.9	52.1±8.9

Table 2: Descriptive statistics (mean ± standard deviation) of performance-based outcomes over Return-to-Run Program. Bold/italic indicates significant differences $p < 0.05$.

	FSST	SLS	ESST	T-Test	IAT
PreRTR	6.7±1.2	30.3±5.8	16.0±3.6	22.0+5.8	29.2±5.6
PostRTR	***5.2±1.2***	32.5±4.3	20.9±3.0	15.5+2.4	22.6±2.7

Knee Joint Loading during Gait in Independently Ambulatory Children with Spina Bifida

[1,2] Tishya Wren, [2] Nicole Mueske, [1,2] Deirdre Ryan, and [3] Katherine Steele

[1] University of Southern California, Los Angeles, CA, USA
[2] Children's Hospital Los Angeles, CA, USA
[3] University of Washington, Seattle, WA
email: twren@chla.usc.edu

INTRODUCTION

Children with spina bifida have altered walking patterns due to varying degrees of weakness in trunk and lower extremity muscles. These walking patterns can lead to pain and possibly premature joint degeneration. The purpose of this study was to use gait analysis and musculoskeletal modeling to examine knee joint loads applied to the tibia in children with myelomeningocele, the most severe type of spina bifida. We hypothesized that knee joint loads would be elevated in children with myelomeningocele due to abnormal gait patterns.

METHODS

31 independently ambulatory children with myelomeningocele (14 female; mean age 10.0 years, SD 2.2, range 6-13; 15 sacral, 5 low lumbar, 11 mid lumbar) and 16 controls (7 female; mean age 10.1, SD 1.7, range 7-12) underwent motion analysis testing walking at a self-selected speed with or without braces and shoes as needed. Retro-reflective markers were placed on the trunk and lower extremities following a modified Plug-in-Gait model. Data were collected at 120 Hz by an 8-camera motion capture system (Vicon, Oxford, UK). Synchronized ground reaction force data were collected by four floor-embedded force plates (AMTI, Watertown, MA) at 2520 Hz. Knee joint reaction loads were calculated from the motion analysis data using OpenSim [1]. First, a musculoskeletal model of the full body less arms [2] was scaled to each participant. Joint angles were calculated using inverse kinematics, and the residual reduction algorithm was used to improve dynamic consistency by making small changes to the torso mass center and kinematics. Muscle activations and forces were estimated from static optimization, which minimizes the sum of squared muscle activations. Knee joint reaction loads on the tibia were determined using joint reaction analysis. Data from 1-5 gait cycles were analyzed for each limb depending on the data available. Peak axial compressive and shear loads normalized to body weight were compared between children with spina bifida and controls using 2-sided t-tests with significance at $\alpha < 0.05$.

RESULTS AND DISCUSSION

Knee joint reaction loads showed good consistency between trials in controls and children with spina bifida (Figure 1). Compressive and shear forces were lower in the spina bifida group compared with the control group ($p<0.03$) (Figure 2). This was likely due to slower walking speed in the spina bifida group (1.1 ± 0.1 vs. 1.3 ± 0.1 m/s, $p<0.0001$).

Based on the current analysis, it appears that knee joint loads tend to be reduced, rather than elevated, in children with spina bifida. While this might lessen the risk of developing premature osteoarthritis due to overloading, the reduced loading may also contribute to lower bone mass and increased susceptibility to fractures. These findings should be considered preliminary, however, since the current analysis has several limitations. First, the model used does not have an independent degree of freedom for knee varus/valgus (this motion is coupled with knee flexion) and therefore cannot fully model the valgus thrust often observed in children with spina bifida. Also, with the current model we can only examine the resultant joint load and not the distribution of loading, which might fall disproportionately on the lateral condyle. Also, loads are higher than measured in vivo, though the effect should affect both groups similarly allowing valid comparison between groups. Finally, muscle weakness was not explicitly modeled, and muscle

forces and activations have not yet been examined in detail. However, preliminary analysis indicates that even without reducing optimal muscle forces, estimated gastroc-soleus activation is much lower than normal in the children with spina bifida, as would be expected, increasing confidence in the simulation results. Despite these limitations, this study provides new insight into joint loading during gait in ambulatory children with spina bifida, which cannot be directly measured.

CONCLUSIONS

Our results suggest that knee joint loads tend to be reduced, rather than elevated, in independently ambulatory children with spina bifida, likely due to reduced walking speed. This might lessen the risk of developing joint problems and osteoarthritis due to overloading, but could also contribute to lower bone mass and increased fracture risk.

Figure 1: Consistency of joint reaction loads among multiple trials for two subjects

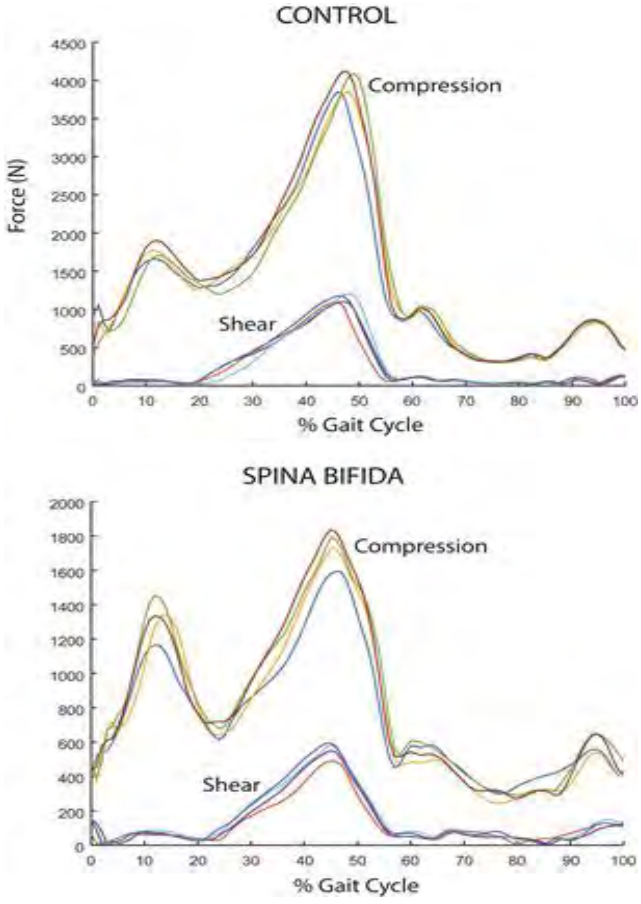

REFERENCES

1. Delp et al., IEEE Trans Biomed Eng 54, 1940-50, 2007.
2. Rajagopal et al., IEEE Trans Biomed Eng 63, 2068-79, 2016.

ACKNOWLEDGEMENTS

Funding provided by NIH-NICHD Grant # 5R01HD059826

Figure 2: Comparison of joint reaction loads between control and spina bifida groups

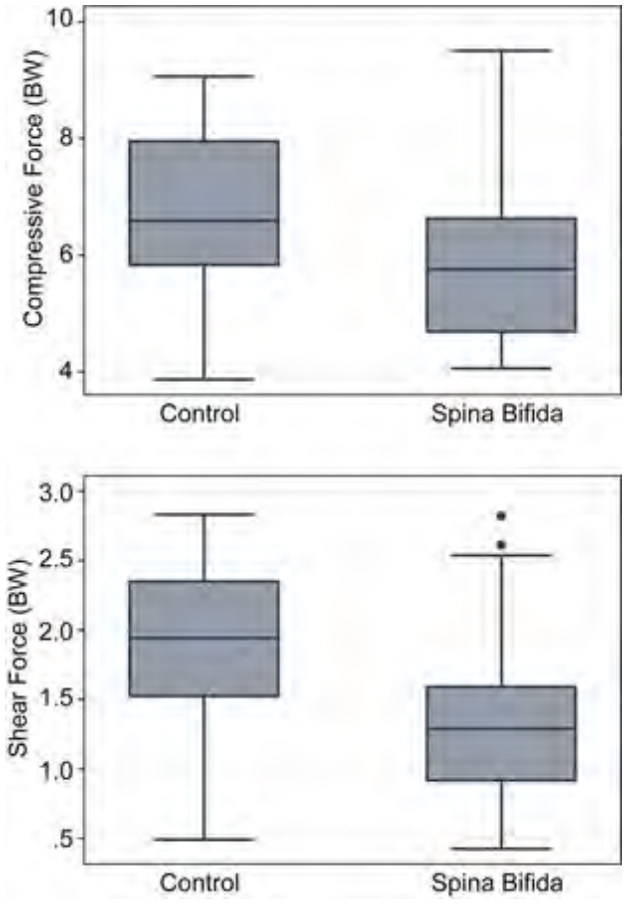

COMPARING TWO MEASURES OF KNEE VALGUS ANGLE

[1]Taylor Wright, [1]Scott Kennedy, [1]Megan Young, [1,2]Michael Goodlett, [1]Michael Zabala

[1] Auburn University, Auburn, AL, USA
[2]Edward Via College of Osteopathic Medicine (VCOM), Auburn, AL, USA
email: zabalme@auburn.edu, web: http://eng.auburn.edu/sites/aubelab/

INTRODUCTION

It is well known that anterior cruciate ligament (ACL) ruptures are prevalent in athletics [1,3]. Even with extensive research on this topic, the injury remains common in sports such as soccer and basketball [1,3]. ACL injuries not only affect the athlete's immediate lifestyle, but oftentimes continues to cause medical issues into their future through early onset osteoarthritis and potentially early knee replacement [6].

Kinematic measures, such as knee valgus angle during drop-jumps (Fig. 1), have demonstrated correlations with ACL rupture [2,5]. With this knowledge, field-screening tests, involving drop-jumps, have been developed to aid in prediction of an individual's risk of undergoing an ACL rupture [8]. In addition, preventative programs, covering a range of topics such as strength and motor learning, have been developed to reduce the number of ACL injuries [8]. However, ACL ruptures continue to occur [3].

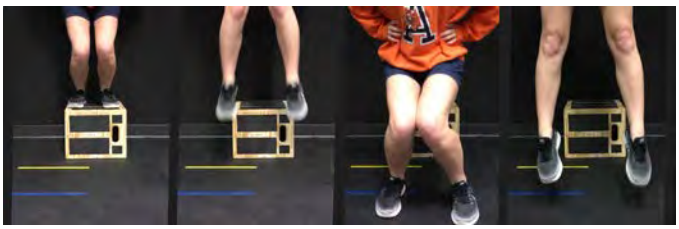

Figure 1: Drop jump test.

Perhaps the most widely used measure for knee valgus angle was developed in 1983 by Grood and Suntay [4]. This method of measuring knee valgus angle (KVA) is a mathematical approach relating the orientation of the shank with respect to the thigh by utilizing transformation matrices for 3D kinematic analysis [4]. Hewett, et al. provides a simpler approach to interpreting the KVA by measuring the shank with respect to the vertical axis perpendicular to the floor plane [2,5]. This implied knee valgus angle (IKVA) can be measured in 3D and 2D, and allows for easier use in clinical and athletic training settings. This measure has been shown to have a significant correlation to ACL rupture when assessed during the drop jump test (Fig. 1).

The purpose of this study is to analyze the difference between IKVA and KVA in order to determine whether a relationship between the two exists during a drop-jump test.

METHODS

A total of 20 division 1 women's soccer and women's basketball and club soccer athletes were recruited to participate in the study from Auburn Athletics and Auburn Club Sports (mean age 19.8±1.6 years, height 172.5±8.9 cm, and weight 67.9±7.2 kg). The athletes were not excluded by past injuries; two athletes had previous ACL injuries and reconstructions. The athletes performed the Landing Error Scoring System (LESS) drop-jump test three times [7]. For this test, the subject jumps from a height of 12 inches to a distance away of one-half their height. They were instructed to stand with their hands above their head before the test, so the arm countermovement would be similar for each subject. The trials were recorded using a Vicon motion capture system with 10 cameras and 2 AMTI force plates. The average IKVA and KVA of the three trials was calculated for each subject using Visual 3D. A linear regression test was used to analyze the max IKVA and the KVA at max IKVA. The Auburn University Institutional Review Board approved all study procedures.

RESULTS AND DISCUSSION

No significant correlation was found between the two values, (R^2 = 0.0345, p = 0.211) (Fig. 3). This shows the KVA does not have a large effect on the IKVA.

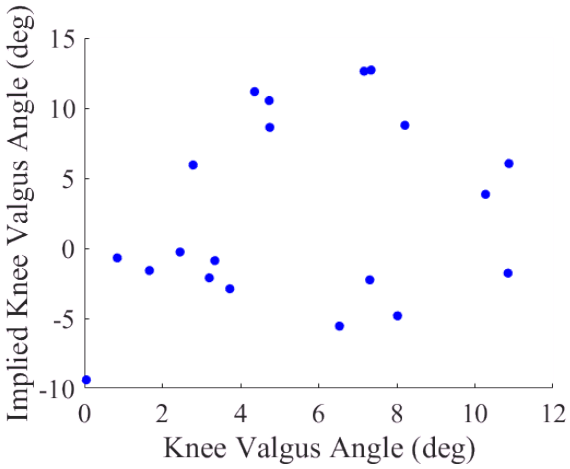

Figure 1: IKVA vs. KVA at maximum IKVA.

Although a simplified version of the KVA, IKVA, is beneficial to understanding ACL injury risk, it is important to be aware that this method does not take into consideration the effects of parameters such as stance width, hip and ankle rotation, hip ab/adduction, and toe-out angle. These variables will influence the IKVA but may have no direct effect on the KVA. For example, if both the hip and ankle rotate simultaneously, the IKVA will change, but the KVA may not (Fig. 2).

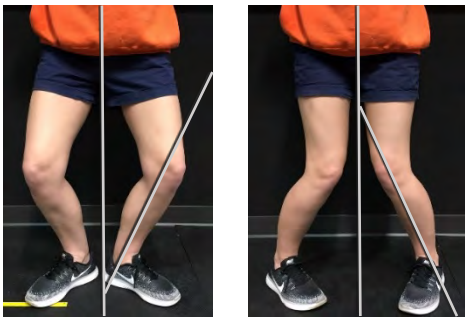

a **b**

Figure 2: IKVA angles **a)** varus **b)** valgus.

The IKVA has shown to be a valuable risk factor for ACL ruptures. However, addition analysis should be conducted to determine the contributions of additional parameters to IKVA. Further analysis of this type will serve to improve ACL injury risk analysis and preventative training techniques.

REFERENCES

1. Beynnon, et al. *The effects of level of competition, sport, and sex on the incidence of first-time noncontact anterior cruciate ligament injury*, Am J Sports Med 42, 1806-12, 2014.
2. Ford, K, et al. *Valgus knee motion during landing in high school female and male basketball*, Med Sci Sports Exerc. 35, 1745-50, 2003.
3. Gornitzky, AL, et al. *Sport-specific yearly risk and incidence of anterior cruciate ligament tears in high school athletes: a systematic review and meta-analysis*, Am J Sports Med 44, 2716-2723, 2016.
4. Grood, ES; and Suntay, WJ. *A joint coordinate system for the clinical description of three-dimensional motions: application to the knee*, J Biomech Eng 105, 136-44, 1983.
5. Hewett, TE, et al. *Biomechanical measures of neuromuscular control and valgus loading of the knee predict anterior cruciate ligament injury risk in female athletes: a prospective study*, Am J Sports Med 33, 492-501, 2005.
6. Lin, SH, et al. *Association of anterior cruciate ligament injury with knee osteoarthritis and total knee replacement: A retrospective cohort study from the Taiwan National Health Insurance Database*, PLoS One, 12, 2017
7. Padua, DA, et al. *The Landing Error Scoring System (LESS) is a valid and reliable clinical assessment tool of jump-landing biomechanics*, Am J Sports Med, 37, 1996-2002, 2009
8. Swart, ES, et al. *Prevention and screening programs for anterior cruciate ligament injuries in young athletes*, J Bone Joint Surg Am 96, 705-11, 2014.

ACKNOWLEDGMENTS

We would like to thank the Auburn Athletic Department for their assistance in this project. This work was supported by Edward Via College of Osteopathic Medicine (VCOM) Research Eureka Accelerator Program (REAP).

The Contribution of Frontal Hip Power to Slope Walking

[1,2] Zihan Yang, [2] Feng Qu, [1] Chuyi Cui and [1] Shirley Rietdyk

[1] Health and Kinesiology, Purdue University, West Lafayette, IN, USA
[2] College of Sport science, Beijing Sport University, Beijing, CHINA
email: yang1566@Purdue.edu

INTRODUCTION

More than 30% of the older population aged above 65 in the USA fall at least once during a year [1]. The risk of falling in the elderly is increased when facing increased challenges to balance control while walking on uneven terrains such as up stairs and slopes [2]. The task demands for slope walking result in changes in lower limb kinematics and kinetics, but little is known about how power in the frontal plane changes with slope. During level walking, 23% of the total hip work is done in the frontal plane [3]. It is reasonable to expect that slope walking will place greater demands on the hip in the frontal plane to control the pelvis and trunk against gravitational forces in downslope walking, and to help lift the trunk in upslope walking. Therefore, the purpose of this abstract is to fully describe the change with the frontal of hip joint powers during slope ascent and descent, and to quantify total work done in the frontal of the hip joint.

METHODS

Nine healthy male adults (23.8±1.1years) were fitted with 29 retroreflective markers (Helen Hayes Marker Set). Each participant read and signed an informed consent form approved by the Institutional Review Board of Beijing Sport University. Participants were habituated to the walkway area and then performed at least three walking trials at each of seven grades (+20°, +12°, +6°, 0°, -6°, -12°, -20°). Each participant walked at a self-selected speed. Each subject took at least two steps on the slope before and after contacting the force platform. The kinect data and kinematic data were captured with a mounted force-platform (Kistler 9281CA, Switzerland) and an 8 camera 3D Optical Capture system (Motion Analysis Raptor-4, USA). Major gait events (heel strike and toe off) for each foot were visually identified. Kinetic data were filtered using a 4th order zero-lag Butterworth filter at 15 Hz [3].

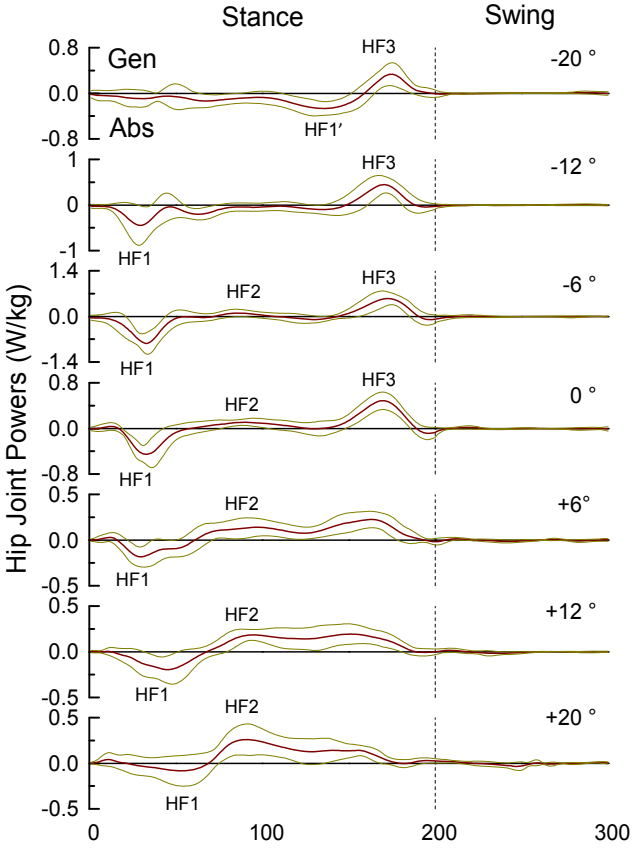

Figure 1: Frontal hip powers as a function of slope averaged for nine subjects.

The time integral of the power curves (i.e. work) was calculated (a) over one stride and (b) for each phase of the hip frontal power (HF1, HF2 and HF3; Fig. 1). The total work over the stride was the sum of the positive work and the negative work [4]. This paper focused on the comparisons within the upslope and downslope conditions (including level condition), but not between upslope and downslope. Thus, a one-way ANOVA was used to determine differences of hip frontal work within upslope and downslope, with Tukey post hoc tests; alpha level was set at 0.05.

RESULTS AND DISCUSSION

For energy absorption at early stance (HF1), significant differences were observed during upslope between 0° and 20° (p=0.04), and during downslope between 0° and -6° (p=0.02), and -6° and -20° (p=0.05). For energy generation during mid and late stance (HF2 and HF3), significant differences were observed during downslope between 0° and -20° (p=0.01, and -6° and -20° (p=0.03)) (Fig. 1).

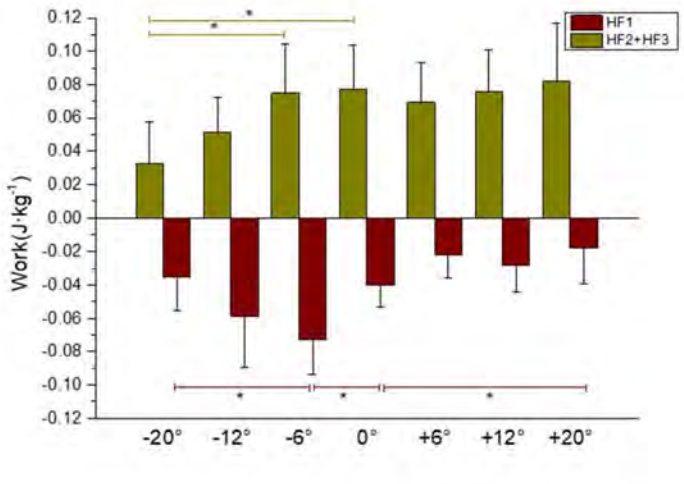

Figure 2: Average work for hip frontal power bursts. Asterisk (*) indicates p<0.05

During level walking, HF1 absorption is the eccentric control of the dropping pelvis during weight acceptance, and the HF2 and HF3 generation bursts raise the pelvis during midstance and push off phases [4].

During downslope walking, HF1 absorption increased for the -6 degree slope, but was not different from level walking for the steeper slopes (Fig. 2). The increased absorption at -6 degrees acts to control the dropping pelvis and was expected due to the greater downward distance traveled. Note HF2 generation during level walking becomes absorption (HF1′) in the most extreme slope (-20 deg., Fig. 1). HF1′ lasted from early stance phase to push-off phase; these the changes are consistent with higher demands associated with dropping pelvis. However, the work of HF1 was not greater than that during level walking (Fig. 1). The power phase HF2 generation decreased as expected, but only in the most extreme slope (-20 deg., Fig. 1). Overall, to accomplish downslope walking, relative to level walking, there was more energy absorption on the -6 degree slope, after that, energy absorption was decreased, and less energy generation in the hip frontal plane allows the pelvis and trunk to drop.

During upslope walking, HF1 absorption decreased as expected, but only in the most extreme slope (+20 deg., Fig. 2). It is interesting to note that the power phases HF2 and HF3 become one phase with increasing gradient (Fig. 1). The combined power bursts were consistent with higher demands associated with raising the pelvis to accomplish upslope walking. However, the total combined work of HF2 and HF3 was not greater than during level walking (Fig. 2). Overall, to accomplish upslope walking, relative to level walking, there was less energy absorption and similar energy generation in the hip frontal plane to elevate the pelvis and trunk.

CONCLUSIONS

To accomplish upslope walking, less energy absorption in the hip frontal plane was required, for downslope walking, less energy generation was required, but more energy absorption was required on -6 degree. The power bursts changed when facing different gradient slopes, indicating complex strategies to accomplish these locomotor tasks. Further research should examine other joint powers and compare upslope and downslope in order to gain insight into causes of stumbles, slips and falls. These observations could be used to improve design of biped robots and prosthetic devices.

REFERENCES

1. Chang et al. *JAMA*. 303(3): 288-288. 2010.
2. Honeycutt Ramsey. *Geriatr Nurs*. 23(5):250-257. 2002.
3. Hong, et al. *Gait Posture*. 42(4):523-528. 2015.
4. Eng Winter. *J Biomech*. 28(6):753-758. 1995.

WIDE STEP WIDTH ALTERS KNEE LOADING DURING STAIR DESCENT IN OBESE PARTICIPANTS

[1] Derek Yocum, [1] Joshua T. Weinhandl, [1] Jeffrey T. Fairbrother, [1] Songning Zhang
[1] Department of Kinesiology, Recreation and Sport Studies, University of Tennessee, Knoxville, TN, USA
email: dyocum@vols.utk.edu, web: http://krss.utk.edu/centers-labs/biomechanics-laboratory/

INTRODUCTION

Chronic overload of the knee joint due to obesity may lead to medial compartment knee osteoarthritis (OA) [1]. Due to difficulty in *in vivo* collections of joint contact force, the internal knee abduction moment (KAbM) is often used as a surrogate. However, consideration of the knee extension moment (KEM) is also of significance when estimating changes in joint loading [2]. Obese participants display an increase in non-normalized peak KEM and KAbM, compared to healthy-weight individuals [3].

During stair descent phase of stair negotiation, participants experience greater loading-response peak vertical ground reaction force (GRF) [4], and KAbM, compared to ascent and level walking [5].

Increasing step-width (SW) reduces KAbM during level walking, and stair descent [6, 7]. However, this has not been studied in an obese population. The purpose of this study was to determine the effects of increased SW on the KEM and KAbM of obese participants in comparison with healthy-weight participants.

METHODS

Fourteen healthy-weight (age: 21.6±0.5 years, height: 1.7±0.1 m, mass: 66.3±9.3 kg, BMI 22.5±1.9 kg/m^2) and ten obese (age: 25.7±5.8 years, height: 1.7±0.1 m, mass: 100.6±12.6 kg, BMI 32.8±2.7 kg/m^2) participants were recruited to participate in the study. Obese participants had a BMI between 30.0 and 39.9 kg/m^2, while healthy weight participants were between 18.0 and 24.9 kg/m^2.

A 12-camera motion analysis system (120 Hz, Vicon Motion Analysis Inc., UK) collected three-dimensional kinematics during the test. Retroreflective markers were placed on both sides of feet, ankles, legs, knees, thighs, and hips. Participants performed five successful trials each of stair descent at preferred and wide SW. Mediolateral distance between the center of masses of both feet during midstance defined SW. The wide SW was set as twice the participant's preferred SW, which reduces loading-response knee abduction moment [6]. SW was calculated using the second and first steps. Participants walked at their preferred walking speed. A speed range, average speed ±5% of their preferred speed, was used to monitor the speed of movement trials.

A low-pass 4th order Butterworth filter at a cutoff frequency of 8 Hz for kinematic and joint moment calculations, and 50 Hz for GRF calculations. A 2 x 2 (Group x SW) mixed design analysis of variance (ANOVA) was performed to analyze selected variables (22.0 IBM SPSS, Chicago, IL). An *a priori* alpha level with Bonferroni adjustment was set to 0.05 for all statistical tests.

RESULTS AND DISCUSSION

Obese participants descended with a wider SW ($p = 0.047$) and 0.05 m/s slower ($p = 0.038$). A significant interaction was found for SW ($p = 0.006$). Post-hoc results indicated that obese participants had a larger increase in their SW from preferred to wide SW trials.
Increasing SW reduced push-off peak vertical GRF ($p=0.048$), as well as loading-response and push-off peak medial GRF (both $p<0.001$, Table 1).

Significant Group x SW interactions were observed for peak loading-response vertical and medial GRFs (both $p<0.001$) and push-off peak medial GRF ($p=0.015$, Table 1). The post hoc comparisons showed an increase in peak loading-response vertical GRF for obese participants, but a decrease for healthy participants. Additionally, obese participants had greater peak medial GRF increases with increased SW. Obese participants had higher vertical and medial GRFs during loading-response and push-off (all $p<0.001$).

Increasing SW led to increased peak loading-response ($p<0.024$) and push-off KEM ($p<0.001$, Table 1). An interaction ($p=0.030$) for push-off response KEM indicated that KEM was affected differently between groups. Post-hoc results indicated that KEM increased more greatly for healthy-participants ($p<0.001$) compared to obese ($p=0.023$). Loading-response and push-off response KAbMs were reduced ($p=0.048$ and $p<0.001$, respectively). Obese participants had a higher ($p = 0.047$) push-off KAbM.

Decreased loading-response and push-off peak KAbM through SW manipulation may indicate that this modification may decrease loading in the medial compartment of the knee; however, there was an increase in KEM. This increase may result in undesirable increases in knee joint loading, despite reductions in KAbM.

CONCLUSION

This investigation is a first step in analyzing the effects of SW on knee joint loading during stair descent in an obese population. However, due to the limitations of inverse dynamics, investigations on the impact of SW modification may benefit from musculoskeletal modeling techniques to determine loading at the knee joint. An investigation into the effectiveness of SW modification as an intervention to promote knee joint health in obese population may be warranted.

REFERENCES

1. Felson, D. (2013). *Osteo and Cart*, **21**,10-15.
2. Walter J., et al. (2010). *J Ortho Res,* **28**, 1348-1354,.
3. Blazek, K., et al. (2013). *J Orthop Res,* **31**, 1414-1422.
4. Protopapadaki, A., et al. (2007). *Clin Biomech*, **22**, 203-210.
5. Nadeau, S., et al. (2003) *Clin Biomech*, **18**, 950-959.
6. Paquette, M., et al., (2014). *Knee* **21**, 821-826.
7. Zhao, D., et al. (2007). *J Orthop Res,* **25**, 789-797.

Table 1: Peak Mediolateral and Vertical GRFs (N), Knee Extension and Knee Abduction Moments (Nm): mean ± STD.

	Healthy		Obese		Int.	Grp	SW
Variable	Preferred SW	Wide SW	Preferred SW	Wide SW	p	p	p
LR Vertical GRF	1093.4±132.7[a,#]	1023.6±170.1[#]	1480.7±206.0[a]	1555.9±226.6	**0.001**	**<0.001**	0.889
PO Vertical GRF	576.0±127.0[a#]	610.0±143.7[#]	826.8±106.0	834.9±116.2	0.211	**<0.001**	**0.048**
LR ML GRF	-94.9±25.0[a, #]	-146.6±31.0[#]	-148.3±39.5[a]	-253.1±57.0	**<0.001**	**<0.001**	**<0.001**
PO ML GRF	-63.8±19.3[a,#]	-111.2±32.7[#]	-110.3±25.5[a]	-175.5±35.1	**0.015**	**<0.001**	**<0.001**
LR Knee Extension Moment	57.0±21.2[#]	64.4±25.3[#]	109.5±26.4	118.8±26.9	0.787	**<0.001**	**0.024**
PO Knee Extension Moment	59.7±21.1[a,#]	75.5±24.2[#]	100.4±26.9[a]	106.6±24.9	**0.030**	**0.001**	**<0.001**
LR Knee Abduction Moment	-49.2±8.7	-47.0±8.4	-66.4±28.0	-63.3±30.3	0.721	0.051	**0.048**
PO Knee Abduction Moment	-31.7±11.0[a,#]	-26.2±12.3	-45.2±14.3[a]	-35.4±16.7	0.140	**0.047**	**<0.001**

[a]: Significantly different from Wide SW of the same subject group, [#]: Significantly different from Obese of the same SW, ML: Mediolateral, LR: Loading Response, PO: Push-off Response, GRF: Ground Reaction Force, Int.: Interaction, Grp.: Group, SW: Step Width, Bold: p-values indicate significance.

INDEPENDENT METABOLIC CONTRIBUTIONS OF SUPPORTING BODY WEIGHT AND ACCELERATING BODY MASS DURING WALKING ON UPHILL/DOWNHILL SLOPES

[1] Claire Z. Zai and [1,2] Alena M. Grabowski
[1] University of Colorado Boulder, Boulder, CO, USA
[2] Eastern Colorado Healthcare System, Department of Veterans Affairs, Denver, CO, USA
email: Claire.Zai@colorado.edu

INTRODUCTION

The biomechanics of the single leg support phase of level-ground walking have been described as an inverted pendulum (1), where center of mass (CoM) energy is conserved, the leg muscles generate force to support body weight (BW), and thus incur a metabolic cost (6). During the step-to-step transition, the leg muscles produce work to redirect and accelerate the CoM upward and forward, and thus incur a metabolic cost (5). During level-ground walking, ~28% of the net metabolic power (NMP) is due to BW support and ~45% is due to CoM work (3,5).

The independent metabolic effects of BW and mass (M) during uphill and downhill walking have not yet been determined. This information would help improve the control and design of assistive devices such as powered orthoses and prostheses for sloped walking. The overall NMP required to walk changes for uphill and downhill slopes, but does not exhibit a linear relationship across slopes (9). During the single support phase of walking, greater positive mechanical work is performed to walk uphill and greater negative mechanical work is absorbed to walk downhill (4), which results in asymmetric CoM energy fluctuations relative to the walking surface (2,4). The unequal exchange of kinetic and gravitational potential CoM energies changes the NMP required for sloped walking. During the step-to-step transition, individual leg power increases from downhill to uphill slopes (-9° to +9°) (2,7). Both legs simultaneously produce more positive power during uphill walking and both legs simultaneously absorb more negative power during downhill walking (8). It is possible that these differences in individual leg work and power during uphill and downhill walking incur and save similar amounts of metabolic power, respectively, and thus the percentage of NMP due to M redirection does not change across slopes.

Uphill walking requires more force to overcome gravity and downhill walking requires less force to resist gravity compared to level-ground walking; thus, the percentage of NMP due to BW support is likely greater on uphill and less on downhill slopes compared to level ground. The purpose of this study was to determine the independent percentages of NMP for supporting BW and redirecting M on slopes. We hypothesized that the percentage of NMP for BW support would increase with slope and the percentage of metabolic power for M redirection would not change across slopes during walking.

METHODS

10 healthy subjects (5F) participated (Avg±SD: age 24.5±4.5 years, body mass 56.6±2.9 kg, height 161.0±2.3 cm) and gave informed consent per the University of Colorado Institutional Review Board approved protocol. Subjects completed 5 sessions, each corresponding to one slope (0°, ±3°, ±6°). During each session, we measured rates of oxygen consumption and carbon dioxide production using indirect calorimetry (ParvoMedics TrueOne 2400, Sandy UT) throughout each 6-minute trial while subjects stood in place and walked on a dual belt force-measuring treadmill (Bertec Corp., Columbus, OH). On each day, subjects walked 1.25 m/s on one slope at 7 conditions per slope, combinations of added mass (M), reduced weight (W) and added W (1.0 W and 1.0 M; 0.75 W and 1.0 M; 0.50 W and 1.0 M; 1.0 W and 1.25 M; 1.0 W and 1.5 M; 1.25 W and 1.25 M; 1.5 W and 1.5 M). We randomized the trial order each day. We calculated metabolic power using a standard equation (2) and averaged metabolic rates from the final two minutes of each trial (minutes 4-6). Then, we subtracted standing metabolic power from each trial to determine NMP.

Conditions: We reduced W via a modified climbing harness that surrounded the torso and was attached

above to a frictionless pulley system, nylon cord, elastic rubber tubing, and a ratchet (Fig 1A) (5). To add W, subjects wore a padded waist belt with lead strips wrapped tightly at their CoM. We added M alone using a combination of added load and reduced W. To calculate the percentage of NMP allocated to BW support we found the y-intercept of the line for reduced gravity (0G) and NMP, subtracted this from the unaltered walking (UW) NMP and divided by UW NMP.

$$\frac{UW - 0G}{UW} x\ 100 = \%\ of\ NMP\ to\ support\ BW \quad (1)$$

To calculate the percentage of NMP allocated to M redirection, we calculated the ratio of NMP for added mass (AM) to NMP for added weight (AW):

$$\frac{AM}{AW} x\ 100 = \%\ of\ NMP\ to\ redirect\ mass \quad (2)$$

We compared the percentage of NMP due to W and M at each slope to level ground using paired t-tests. We adjusted for multiple comparisons with Bonferonni corrections ($p<0.025$).

RESULTS AND DISCUSSION

Overall average NMP increased from 1.37 W/kg at -6° to 6.38 W/kg at +6. The percentage of NMP allocated to BW support was greater for +3° and +6° compared to level-ground walking ($p<0.0005$) (Fig. 1B). There were no significant differences in the percentage of NMP for BW support and M redirection on downhill slopes compared to level-ground walking. The percentage of NMP allocated to M redirection was lower for slopes of +3° and +6° compared to level-ground walking ($p<0.05$) (Fig. 1).

Based on our results, we partially accept our hypothesis that generating force would incur a greater percentage of NMP during uphill and a lesser percentage of NMP during downhill compared to level ground walking. We reject our hypothesis that performing work would require the same percentage of NMP for uphill, level, and downhill slopes. We found that the percentage of NMP for BW support was the same at downhill slopes, but increased for uphill slopes compared to level ground.

These data provide information to inform the development and design of assistive devices for walking on uphill and downhill slopes. Increases in the percentage of NMP for BW support implies that more force is needed to overcome gravity and thus biomimetic prostheses, for example, should be designed to provide force, presumably at the ankle, during uphill walking to reduce the metabolic cost. Decreases in the percentage of NMP for mass redirection implies that a lower percentage of mechanical work is needed for the step-to-step transition phase on uphill slopes. The remaining percentages of NMP for walking on level ground and slopes are likely due to balance and internal work (i.e. leg swing).

REFERENCES

1. Cavagna G et al. *Am J Physiol* **233**: R243-261, 1977.
2. Brockway Hum Nutr Clin Nutr. **41** 463-471, 1987
3. Franz J et al. *J Biomech* **45**: 257-262, 2012.
4. Gottschall J & Kram R. *J Appl Physiol* **94**: 1766-1772, 2003.
5 .Gottschall J & Kram R. *J Exp Biol* **209**: 4895-4900, 2006.
6. Grabowski A et al. *J Appl Physiol* **98**: 579-583, 2005.
7. Griffin T et al. *J Appl Physiol* **95**: 172-183, 2003.
8. Jeffers J et al. J Biomech **48** 2919-2924,2015.
9. Minetti A et al. *J Appl Physiol* 93: 1039-1046, 2002.

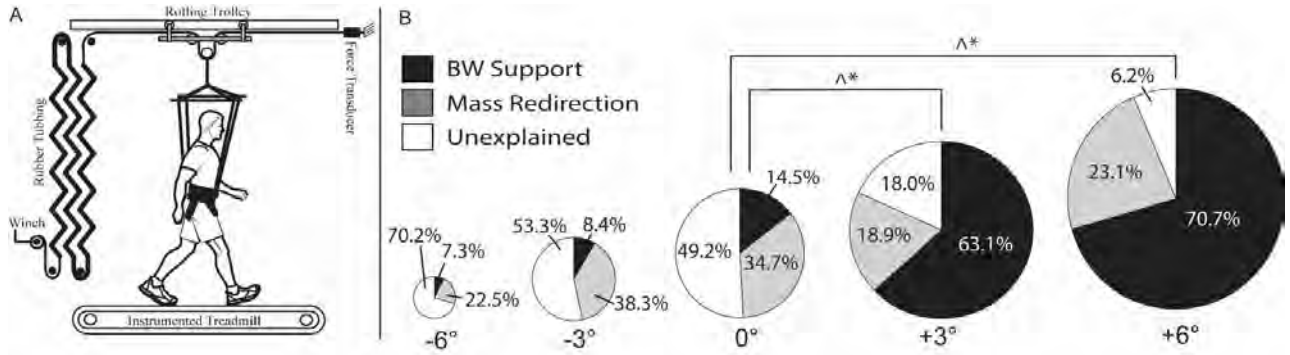

Fig. 1A: The simulated reduced gravity apparatus, including a winch, rolling trolley, force transducer, and rubber tubbing for walking on an instrumented treadmill. **B**: Pie chart of the percentage of NMP due to generating force to support BW (black) and redirecting mass (light gray) across slopes. *Significant difference from 0° (p-value<0.025) for mass redirection. ^Significant difference from 0° (p-value < 0.025) for BW support.

EFFECT OF ENVIRONMENT ON GAIT AND GAZE DURING WALKING IN OLDER ADULT FALLERS

[1] Lisa A. Zukowski, [2] Carol Giuliani, and [2] Prudence Plummer

[1] High Point University, High Point, NC, USA
[2] University of North Carolina at Chapel Hill, Chapel Hill, NC, USA
email: lzukowsk@highpoint.edu

INTRODUCTION

Environmental hazards have been identified as a major cause of falls in healthy, older adults [1], yet traditional fall-risk assessments do not adequately take into account the role of distractions and hazards experienced in everyday life. Compared to the low-distraction setting of a laboratory, the real world is a highly distracting environment with constant demands on visual attention to avoid hazards and falling. A better understanding of the differences between older adults at risk of falling and older adult non-fallers during walking in the real world, relative to a lab setting, may improve fall-risk evaluation.

The purpose of this project was to identify the effect of the environment on gait and gaze behavior during walking in older adult fallers relative to non-fallers. We hypothesized that 1) relative to the lab, in the real world older adults would exhibit greater gait variability, greater fixation durations (indicative of less or slower active scanning), and more frequent fixations on the travel path, and 2) the environmental influence on gait and gaze would be more pronounced in fallers than non-fallers.

METHODS

Thirteen older adult fallers (76.8±9.4 years of age, 10 females, 16.8±3.3 years of education) and 13 older adult non-fallers (78.3±7.3 years of age, 9 females, 16.7±2.3 years of education) were recruited from the local community. Fallers were defined as those reporting 2 or more falls within the past 12 months; non-fallers reported no falls in the last 12 months.

Participants performed 2 walking task trials for 1 minute in both a real-world environment (busy hospital lobby) and laboratory setting. We recorded spatiotemporal gait parameters using the LEGSys 5-node wireless ambulatory system (100 Hz, Biosensics, Cambridge, MA) and gaze behavior using wireless eye tracking glasses (60 Hz, SensoMotoric Instruments, Boston, MA) during each walking task. The surrounding environment was recorded with a video camera during each walk.

The dependent variables were coefficient of variation of stride length and stride duration, stride velocity, percentage of total time fixating on 6 areas of interest (AOIs, i.e., far environment (FE), far walking path (FW), far people (FP), near environment (NE), near walking path (NW), and near people (NP)), and average duration of fixation on the 6 AOIs. For each dependent variable, we computed the average across the 2 walking trials in each environment. From each video recording, we quantified the environmental busyness during each walk (number of people in and outside of participant's walking path).

Independent samples t-tests were utilized to compare fallers and non-fallers based on age, sex, and years of education. A paired samples t-test was utilized to compare the environmental busyness of the lab relative to the lobby, and independent samples t-tests were utilized to compare the environmental busyness between fallers and non-fallers in both testing environments. A repeated measures ANOVA was utilized to compare average walking performance and gaze behavior for fallers and non-fallers in the laboratory and hospital lobby settings (Group x Environment). All statistical procedures were performed using SPSS 24 and α=0.05.

RESULTS AND DISCUSSION

There were no significant differences between fallers and non-fallers in terms of age, sex, or years of education. Thus, the only difference between the two groups was fall history.

The real-world environment was significantly busier (22.4±7.7 individuals) than the lab setting (1.1±1.0 individuals) in terms of people walking in and outside of the walking path ($p<0.001$). However, there were no significant differences in busyness of either environment between fallers and non-fallers. Thus fallers and non-fallers were presented with similarly challenging lab and real-world environments to navigate.

In contrast to our hypothesis, we did not find a significant effect of environment on gait variability or gait speed. In other words, there were no differences in gait between the environments. However, non-fallers walked 0.2 m/s faster than fallers ($p=0.03$), which is in agreement with previous research that shows that a fall history is related to slower walking speeds [2]. There were no differences between the groups in terms of gait variability.

We found a significant effect of environment on gaze behavior, but in contrast to our hypothesis, older adults fixated 32.3% less frequently ($p<0.001$) and for 67.0 ms less time ($p=0.001$) on FW and 6.6% less often on the NW ($p=0.002$) in the lobby relative to the lab (Fig. 1). From the lab to the lobby, they also fixated 38.8% more frequently on FP and 2.27% more often and for 139.1 ms longer on NP (all $p<0.001$, Fig. 1). Thus participants appeared to prioritize visually attending to people within and adjacent to their walking path, who represent environmental hazards, as opposed to their actual walking path or more varied visual scanning of the environment. This finding is supported by the work of Di Fabio et al. [3] who determined that age-related changes in spatial information processing impact fixation duration on hazards within the walking path. Our secondary hypothesis was partially corroborated by the greater 214.8 ms decrease in time spent fixating on the NE in the lobby by fallers, relative to the 38.8 ms decrease by non-fallers ($p=0.01$, Fig. 1). Fallers may have been less comfortable in diverting attention from urgent environmental hazards to look at the near environment in the lobby than non-fallers.

CONCLUSIONS

Gait performance did not differ between the environments. However, relative to the lab, in a real-world setting older adults fixated more frequently and for longer on people in their environment, and fallers decreased their fixation time on their near environment. Thus, the addition of moving hazards and distractions to fall-risk assessments may provide new means of evaluating fall-risk status.

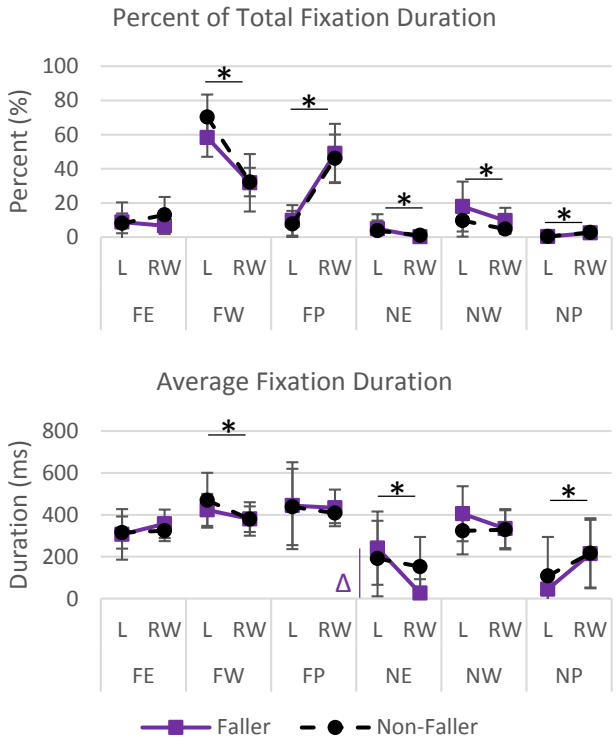

Figure 1: Gaze behavior on the 6 AOIs (FE, FW, FP, NE, NW, and NP) of fallers and non-fallers in the lab (L) and real-world (RW) environments. Significant differences between environments (*) and a Group x Environment interaction effect (Δ) are indicated.

REFERENCES

1. Rubenstein and Josephson. *Clin Geriatr Med*. **18**, 141-58, 2002.
2. Verghese et al. *J Am Geriatr Soc*. **50**, 1572-6, 2015.
3. Di Fabio et al. *Neurosci Lett*. **339(3)**, 179-82, 2003.

ACKNOWLEDGEMENTS

The project described was supported by the National Center for Advancing Translational Sciences (NCATS), National Institutes of Health, through Grant Award Number UL1TR001111. The content is solely the responsibility of the authors and does not necessarily represent the official views of the NIH.